

Uncorrected Proof

---

Lucas F. M. da Silva • Andreas Öchsner  
Robert D. Adams  
Editors

# Handbook of Adhesion Technology

Second Edition

Volume 1

With 919 Figures and 106 Tables



Springer



*Editors*

Lucas F. M. da Silva  
Department of Mechanical Engineering  
Faculty of Engineering  
University of Porto  
Porto, Portugal

Andreas Öchsner  
Faculty of Mechanical Engineering  
Esslingen University of Applied Sciences  
Esslingen, Baden-Württemberg, Germany

Robert D. Adams  
Department of Mechanical Engineering  
University of Bristol  
Bristol, UK

Department of Engineering Science  
University of Oxford  
Oxford, UK

ISBN 978-3-319-55410-5      ISBN 978-3-319-55411-2 (eBook)  
ISBN 978-3-319-55412-9 (print and electronic bundle)  
<https://doi.org/10.1007/978-3-319-55411-2>

Library of Congress Control Number: 2018940005

1st edition: © Springer-Verlag Berlin Heidelberg 2011

© Springer International Publishing AG, part of Springer Nature 2018

This work is subject to copyright. All rights are reserved by the Publisher, whether the whole or part of the material is concerned, specifically the rights of translation, reprinting, reuse of illustrations, recitation, broadcasting, reproduction on microfilms or in any other physical way, and transmission or information storage and retrieval, electronic adaptation, computer software, or by similar or dissimilar methodology now known or hereafter developed.

The use of general descriptive names, registered names, trademarks, service marks, etc. in this publication does not imply, even in the absence of a specific statement, that such names are exempt from the relevant protective laws and regulations and therefore free for general use.

The publisher, the authors and the editors are safe to assume that the advice and information in this book are believed to be true and accurate at the date of publication. Neither the publisher nor the authors or the editors give a warranty, express or implied, with respect to the material contained herein or for any errors or omissions that may have been made. The publisher remains neutral with regard to jurisdictional claims in published maps and institutional affiliations.

Printed on acid-free paper

This Springer imprint is published by the registered company Springer International Publishing AG part of Springer Nature.

The registered company address is: Gewerbestrasse 11, 6330 Cham, Switzerland

---

## Second Edition Preface

50

51 The first edition of *Handbook of Adhesion Technology* has been very well accepted  
52 by the adhesion community with over 25,000 downloads per year. This was the main  
53 motivation for the preparation of this 2nd edition. Also, there has been a general  
54 increase of the scientific and industrial community in this technology, which justifies  
55 an update. There are more papers published every year, there are new journals related  
56 to the field, there are more national and international conferences, and there are more  
57 applications. A revolution is currently taking place in the transport industry where  
58 fuel is being replaced by electric power. This change means that lighter structures  
59 need to be manufactured with the use of light materials and more efficient joining  
60 methods such as adhesive bonding. But, the use of adhesive bonding is not limited to  
61 the transport industry, and there are several other applications described in this  
62 handbook such as the use of adhesives in medicine.

63 This 2nd edition of *Handbook of Adhesion Technology* is a complete revision of  
64 the 1st edition with an update of the methods that have been investigated recently,  
65 which are now fully accepted by the adhesion community. Themes that are now  
66 included in more detail include, for example, hybrid adhesives used for automotive  
67 applications, ecofriendly surface treatments, damage mechanics, joint durability  
68 prediction, functionally graded joints, adhesive selection for space applications,  
69 and, lastly, trends in bioadhesion. There is also a new chapter related to the  
70 application of adhesives in the oil industry. Besides these content changes, there  
71 has been a complete revision of all chapters in terms of text, figures, tables, and  
72 references for a more didactic character of this reference book.

73 The editors would like to thank the authors for their patience with the preparation  
74 of this handbook. Finally, the editors especially thank Dr. Christoph Baumann,  
75 Ms. Tina Shelton, and Ms. Monika Garg, Springer editors, who helped enormously  
76 toward the success of this handbook.

77  
78 Department of Mechanical Engineering  
79 Faculty of Engineering  
80 University of Porto  
81 Porto, Portugal

Lucas F. M. da Silva

85 Department of Mechanical Engineering  
83 University of Bristol  
84 Bristol, UK

Robert D. Adams

88 Department of Engineering Science  
86 University of Oxford  
87 Oxford, UK

91 Faculty of Mechanical Engineering  
89 Esslingen University of Applied Sciences  
90 Germany

Andreas Öchsner

Uncorrected Proof

Adhesives have been used for thousands of years, but until 100 years ago, the vast majority was from natural products such as bones, skins, fish, milk, and plants. Since about 1900, adhesives based on synthetic polymers have been introduced, and today, there are many industrial uses of adhesives and sealants. It is difficult to imagine a product—in the home, in industry, in transportation, or anywhere else for that matter—that does not use adhesives or sealants in some manner.

Adhesion technology is nowadays a common approach to many joining situations. There are many books and several international journals dealing with this subject. However, when the end-user needs to apply this technology, he does not have the time or the resources to thoroughly study the various technologies related to adhesives and sealants. It is not practical to go through volumes of text and product information looking for the specific methods or processes to apply. However, such information should be close-by if the need arises. The *Handbook of Adhesion Technology* is intended to fill a gap between the necessarily simplified treatment of the student textbook and the full and thorough treatment of the research monograph and review article. The subject is treated very comprehensively and with the most up to date information so that the end-user has in a single book a proper guidance and fundamental knowledge required for many adhesive bonding or sealing applications.

The *Handbook of Adhesion Technology* is intended to be a book of reference in the field of adhesion. Essential information is provided for all those concerned with the adhesion phenomenon. Adhesion is a phenomenon of interest in diverse scientific disciplines and of importance in a wide range of technologies. Therefore, this handbook includes the background science (physics, chemistry, and materials science), engineering aspects of adhesion, and industry specific applications. It is arranged in a user-friendly format with ten main sections: theory of adhesion, surface treatments, adhesive and sealant materials, testing of adhesive properties, joint design, durability, manufacture, quality control, applications, and emerging areas. The sections contain each about five chapters written by internationally renowned authors who are authorities in their fields.

This Handbook is intended to be a reference for people needing a quick, but authoritative, description of topics in the field of adhesion and the use of adhesives and sealants. It is intended for scientists and engineers of many different backgrounds who need to have an understanding of various aspects of adhesion

technology. These will include those working in research or design, as well as others involved with marketing services. It is expected to be a valuable resource for both undergraduate and research students.

The editors would like to thank the authors for their patience with the preparation of this Handbook. Finally, the editors especially thank Christoph Baumann and Tina Shelton, Springer editors, who helped enormously toward the success of this Handbook.

Porto, Portugal  
Skudai, Johor, Malaysia  
Oxford, UK

Lucas F. M. da Silva  
Andreas Öchsner  
Robert D. Adams

---

# Contents

139

## 140 Volume 1

141	<b>1 Introduction to Adhesive Bonding Technology</b>	1
142	Lucas F. M. da Silva, Andreas Öchsner, and Robert D. Adams	
143	<b>Part I Theory of Adhesion</b>	<b>9</b>
144	<b>2 Theories of Fundamental Adhesion</b>	11
145	David E. Packham	
146	<b>3 Forces Involved in Adhesion</b>	43
147	Maurice Brogly	
148	<b>4 Wetting of Solids</b>	71
149	Martin E. R. Shanahan and Wulff Possart	
150	<b>5 Spreading of Liquids on Substrates</b>	101
151	Günter Reiter	
152	<b>6 Thermodynamics of Adhesion</b>	115
153	Wulff Possart and Martin E. R. Shanahan	
154	<b>Part II Surface Treatments</b>	<b>129</b>
155	<b>7 General Introduction to Surface Treatments</b>	131
156	Gary Critchlow	
157	<b>8 Surface Treatments of Selected Materials</b>	163
158	Guy D. Davis	
159	<b>9 Surface Characterization and Its Role in Adhesion Science and Technology</b>	197
160	John F. Watts	
161		

162	<b>10 Use of Surface Analysis Methods to Probe the Interfacial</b>	
163	<b>Chemistry of Adhesion</b> .....	227
164	John F. Watts	
165	<b>11 Organosilanes: Adhesion Promoters and Primers</b> .....	257
166	Marie-Laure Abel	
167	<b>Part III Adhesive and Sealant Materials</b> .....	<b>281</b>
168	<b>12 Classification of Adhesive and Sealant Materials</b> .....	283
169	Erol Sancaktar	
170	<b>13 Composition of Adhesives</b> .....	319
171	Hyun-Joong Kim, Dong-Hyuk Lim, Hyeon-Deuk Hwang, and	
172	Byoung-Ho Lee	
173	<b>14 Adhesive Families</b> .....	345
174	Eric Papon	
175	<b>15 Pressure-Sensitive Adhesives (PSAs)</b> .....	373
176	Charles W. Paul and Eric Silverberg	
177	<b>16 Selection of Adhesives</b> .....	409
178	Ewen J. C. Kellar	
179	<b>Part IV Testing of Adhesive Properties</b> .....	<b>431</b>
180	<b>17 Physical Properties</b> .....	433
181	David A. Dillard	
182	<b>18 Thermal Properties of Adhesives</b> .....	459
183	John Comyn	
184	<b>19 Failure Strength Tests</b> .....	489
185	Lucas F. M. da Silva, R. J. C. Carbas, and M. D. Banea	
186	<b>20 Fracture Tests</b> .....	523
187	Bamber R. K. Blackman	
188	<b>21 Impact Tests</b> .....	555
189	Luca Goglio	
190	<b>22 Special Tests</b> .....	593
191	David A. Dillard and Tetsuo Yamaguchi	
192	<b>Part V Joint Design</b> .....	<b>613</b>
193	<b>23 Constitutive Adhesive and Sealant Models</b> .....	615
194	Erol Sancaktar	

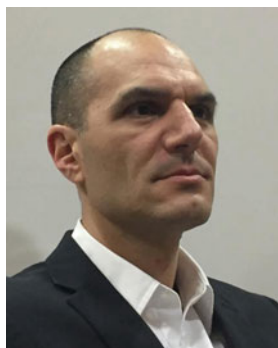
195	<b>24 Analytical Approach</b>	665
196	Liyong Tong and Quantian Luo	
197	<b>25 Numerical Approach: Finite Element Analysis</b>	701
198	Ian A. Ashcroft and Aamir Mubashar	
199	<b>26 Special Numerical Techniques to Joint Design</b>	741
200	Andreas Öchsner	
201	<b>27 Design Rules and Methods to Improve Joint Strength</b>	773
202	Lucas Filipe Martins da Silva, E. A. S. Marques, and R. D. S. G.	
203	Campilho	
204	<b>28 Design with Sealants</b>	811
205	Gregory L. Anderson	
206	<b>29 Design for Impact Loads</b>	829
207	Chiaki Sato	
208	<b>30 Vibration Damping of Adhesively Bonded Joints</b>	853
209	Robert D. Adams, Duncan G. A. Cooper, and Stuart Pearson	
210	<b>Volume 2</b>	
211	<b>Part VI Durability</b>	<b>877</b>
212	<b>31 Effect of Water and Mechanical Stress on Durability</b>	879
213	Ian A. Ashcroft, John Comyn, and Aamir Mubashar	
214	<b>32 Adhesives in Space Environment</b>	915
215	Sabine Dagrás, Julien Eck, Claire Tonon, and Denis Lavielle	
216	<b>33 Fatigue Load Conditions</b>	941
217	Ian A. Ashcroft	
218	<b>34 Creep Load Conditions</b>	975
219	Paul Ludwig Geiß and Melanie Schumann	
220	<b>35 Durability of Nonstructural Adhesives</b>	1009
221	James D. Palmer	
222	<b>Part VII Manufacture</b>	<b>1029</b>
223	<b>36 Storage of Adhesives</b>	1031
224	Hans K. Engeldinger and Cai R. Lim	
225	<b>37 Preparation for Bonding</b>	1051
226	Andreas Lutz	



227	<b>38 Equipment for Adhesive Bonding</b>	1091
228	Manfred Peschka	
229	<b>39 Environment and Safety</b>	1117
230	Ansgar van Halteren	
231	<b>Part VIII Quality Control</b>	<b>1127</b>
232	<b>40 Quality Control of Raw Materials</b>	1129
233	Kazutami Wakabayashi	
234	<b>41 Processing Quality Control</b>	1151
235	Kosuke Haraga	
236	<b>42 Nondestructive Testing</b>	1171
237	Robert D. Adams	
238	<b>43 Techniques for Post-fracture Analysis</b>	1195
239	R. Créac’hadeac	
240	<b>Part IX Applications</b>	<b>1233</b>
241	<b>44 Adhesively Bonded Joints in Aircraft Structures</b>	1235
242	L. John Hart-Smith	
243	<b>45 Aerospace Industry</b>	1285
244	Christian Désagulier, Patrick Pérès, and Guy Larnac	
245	<b>46 Automotive Industry</b>	1333
246	Klaus Dilger, Bernd Burchardt, and Michael Fraunhofer	
247	<b>47 Adhesive Bonding for Railway Application</b>	1367
248	Yasuaki Suzuki	
249	<b>48 Marine Industry</b>	1391
250	Peter Davies	
251	<b>49 Civil Construction</b>	1419
252	Stefan Böhm, Martin Kahlmeyer, Andreas Winkel, and Ilko Hartung	
253	<b>50 Electrical Industry</b>	1449
254	Kwang-Seok Kim, Jong-Woong Kim, and Seung-Boo Jung	
255	<b>51 Shoe Industry</b>	1483
256	José Miguel Martín-Martínez	
257	<b>52 Oil Industry</b>	1533
258	Silvio de Barros, Luiz C. M. Meniconi, Valber A. Perrut, and Carlos E.	
259	Reuther de Siqueira	

260	<b>Part X Emerging Areas</b> .....	<b>1557</b>
261	<b>53 Molecular Dynamics Simulation and Molecular Orbital</b>	
262	<b>Method</b> .....	<b>1559</b>
263	Ya-Pu Zhao, Feng-Chao Wang, and Mei Chi	
264	<b>54 Bioadhesives</b> .....	<b>1597</b>
265	Katharina Richter, Ingo Grunwald, and Janek von Byern	
266	<b>55 Biological Fibrillar Adhesives: Functional Principles and</b>	
267	<b>Biomimetic Applications</b> .....	<b>1641</b>
268	Stanislav N. Gorb and Lars Heepe	
269	<b>56 Adhesives with Nanoparticles</b> .....	<b>1677</b>
270	Ambrose C. Taylor	
271	<b>57 Adhesive Dentistry</b> .....	<b>1703</b>
272	John W. Nicholson	
273	<b>58 Adhesion in Medicine</b> .....	<b>1729</b>
274	Robin A. Chivers	
275	<b>59 Recycling and Environmental Aspects</b> .....	<b>1751</b>
276	Chiaki Sato	
277	<b>60 Adhesion Technology Recap: Current and Emerging Areas</b> .....	<b>1775</b>
278	Lucas F. M. da Silva, Andreas Öchsner, and Robert D. Adams	
279	<b>Index</b> .....	<b>1785</b>

## About the Editors



**Lucas F. M. da Silva** is currently Associate Professor with Aggregation at the Department of Mechanical Engineering of the Faculty of Engineering of the University of Porto and Director of the Integrated Master in Mechanical Engineering. He obtained his Ph.D. in bonding of composites from the University of Bristol (UK) in 2004. He leads the Adhesives Group, composed of post-docs, Ph.D. students, and M.Sc. students. He has published 206 ISI papers (174 as author and 32 as editor) and 23 books (9 as author and 14 as editor) mainly on adhesive joint mechanics. His papers were cited 4690 times and correspond to an h-index of 37 (SCOPUS, 06/02/2018).

One of his papers obtained the SAGE Best Paper Award 2010 and Donald Julius Groen Prize 2010 (both awards given by the Institution of Mechanical Engineers). He received in 2013 and 2018 the Award of Scientific Excellence by the Faculty of Engineering of the University of Porto.

He is editor-in-chief of *The Journal of Adhesion*, *Proceedings of the Institution of Mechanical Engineers, Part L: Journal of Materials: Design and Applications*, and *University of Porto Journal of Engineering*. He is also co-editor of two Springer book series (*Advanced Structured Materials* and *Springer Briefs in Engineering: Computational Mechanics*). He is member of the editorial board of *International Journal of Adhesion and Adhesives* and *Journal of Adhesion Science and Technology*. He is reviewer of 60 ISI journals.

He organizes international conferences on adhesive bonding (*Structural Adhesive Bonding* every odd year and *Industrial Applications of Adhesive Bonding* every even year) and materials (*Materials Design and*

Applications every even year), and founded the Portuguese Adhesion Society that belongs to European Adhesion Societies Group (EURADH).

He has seven pending patents. He developed a software for designing adhesive joints available online (*jointdesigner*). He is consultant of several international companies (e.g., Alstom, Nagase Chemtex, John Deere).



**Andreas Öchsner** is Full Professor for lightweight design and structural simulation at the Esslingen University of Applied Sciences, Germany. Having obtained a Diploma Degree (Dipl.-Ing.) in Aeronautical Engineering at the University of Stuttgart (1997), Germany, he spent the time from 1997 to 2003 at the University of Erlangen-Nuremberg as a research and teaching assistant to obtain his Doctor of Engineering Sciences (Dr.-Ing.). From 2003 to 2006, he worked as Assistant Professor in the Department of Mechanical Engineering and Head of the Cellular Metals Group affiliated with the University of Aveiro, Portugal. He spent 7 years (2007–2013) as a Full Professor at the Department of Applied Mechanics, Technical University of Malaysia, where he was also Head of the Advanced Materials and Structure Lab. From 2014 to 2017, he was a Full Professor at the School of Engineering, Griffith University, Australia, and Leader of the Mechanical Engineering Program (Head of Discipline and Program Director). His research interests are related to experimental and computational mechanics, cellular metals and thin structures and interphases. He has published over 450 scientific publications, comprising 13 research monographs, 23 book chapters, and four teaching books on finite element methods. He obtained more than 3000 citations in Google Scholar. He is the general Chairman of 12 international conferences on computational and experimental engineering (ACE-X series) and 14 international conferences in the area of heat and mass transfer (DSL series). His editorial work comprises posts as editor-in-chief of the international journal *Continuum Mechanics and Thermodynamics* (Springer), editor-in-chief of the Springer book series on Advanced Structured Materials, and editor of *SpringerBriefs in Applied Sciences and Technology: Computational Mechanics*.

His research activities were recognized in 2010 by the award of a higher doctorate degree (D.Sc.) by the University of Newcastle, Australia.



**Robert D. Adams** got his first degree, in Mechanical Engineering, from Imperial College, London, in 1962, and his Ph.D. from Cambridge University in 1967 and an Sc.D. in 2017. He was awarded a D.Sc. (Eng) from London University in 1986. Most of his academic career (1967–2005) was at Bristol University where he was made Full Professor in 1986. He was Head of the Department of Mechanical Engineering from 1994 to 1998 and Graduate Dean from 1998 to 2004. In 1991, he was awarded the Visiting Foreign Franqui Chair and Medal at the Free University of Brussels (VUB). He is now an Emeritus Professor of Applied Mechanics at the University of Bristol and a Visiting Professor at the Universities of Oxford and Oxford Brookes. He has published and edited several books and published about 200 papers in international refereed journals.

In 2011, he was awarded the R.L. Patrick Fellowship of the US Adhesion Society. He is active in organizing conferences and publishing and was a founder member of EURADH and WCARP, the main European and World series on Adhesion. He has been joint editor-in-chief of the *International Journal of Adhesion and Adhesives* since 1999. His main research area is on adhesively bonded joints, and he pioneered the application of finite element analysis for determining the stresses, strains, and strength of such joints. In addition to his adhesives research, he has also worked extensively on vibration properties in composites and developed low-velocity impact tests for nondestructively testing composites and sandwich structures.

- 393 **Marie-Laure Abel** Faculty of Engineering and Physical Sciences (A1), University  
394 of Surrey, Guildford, Surrey, UK
- 395 **Robert D. Adams** Department of Mechanical Engineering, University of Bristol,  
396 Bristol, UK
- 397 Department of Engineering Science, University of Oxford, Oxford, UK
- 398 **Gregory L. Anderson** R&D Laboratories, Propulsion Systems – Launch Systems  
399 Group, Orbital ATK, Corinne, UT, USA
- 400 **Ian A. Ashcroft** Faculty of Engineering, University of Nottingham, Nottingham,  
401 UK
- 402 **M. D. Banea** CEFET/RJ – Federal Center of Technological Education in Rio de  
403 Janeiro, Rio de Janeiro, Brazil
- 404 **Bamber R. K. Blackman** Department of Mechanical Engineering, Imperial  
405 College London, South Kensington Campus, London, UK
- 406 **Stefan Böhm** Department for Cutting and Joining Manufacturing Processes, Uni-  
407 versity of Kassel, Institute for Production Technologies and Logistics, Kassel,  
408 Germany
- 409 **Maurice Brogly** ENSCMu – LPIM – Equipe Chimie et Physico-Chimie des  
410 Polymères, Université de Haute Alsace, Mulhouse, France
- 411 **Bernd Burchardt** Weiningen Zürich, Switzerland
- 412 **R. D. S. G. Campilho** Instituto Superior de Engenharia do Porto (ISEP), Instituto  
413 Politécnico do Porto, Porto, Portugal
- 414 **R. J. C. Carbas** Institute of Science and Innovation in Mechanical and Industrial  
415 Engineering (INEGI), Faculty of Engineering, University of Porto, Porto, Portugal
- 416 **Mei Chi** State Key Laboratory of Nonlinear Mechanics (LNM), Institute of  
417 Mechanics, Chinese Academy of Sciences, Beijing, China
- 418 **Robin A. Chivers** York, North Yorkshire, UK

- 419 **John Comyn** Materials Department, Loughborough University, Leicestershire, UK
- 420 **R. Créac'hcadec** ENSTA Bretagne, Institut de Recherche Dupuy de Lôme, FRE  
421 CNRS 3744, Brest, France
- 422 Assemblages Multi-Matériaux, Institut de Recherche Dupuy De Lôme, Brest, France
- 423 **Duncan G. A. Cooper** Department of Mechanical Engineering, University of  
424 Bristol, Bristol, UK
- 425 **Gary Critchlow** Department of Materials, Loughborough University, Loughbor-  
426 ough, Leicestershire, UK
- 427 **Lucas F. M. da Silva** Department of Mechanical Engineering, Faculty of Engi-  
428 neering, University of Porto, Porto, Portugal
- 429 **Sabine Dagrás** Airbus Defence and Space, Toulouse, France
- 430 **Peter Davies** Materials and Structures Group, Marine Structures Laboratory, Brest  
431 Centre, IFREMER, (French Ocean Research Institute), Plouzané, France
- 432 **Guy D. Davis** ElectraWatch, Inc., Linthicum Heights, MD, USA
- 433 **Silvio de Barros** Department of Mechanical Engineering, Federal Center of Tech-  
434 nological Education in Rio de Janeiro – CEFET/RJ, Rio de Janeiro, RJ, Brazil
- 435 **Carlos E. Reuther de Siqueira** Department of Offshore Engineering, Petróleo  
436 Brasileiro S.A. – PETROBRAS, Rio de Janeiro, RJ, Brazil
- 437 **Christian Désagulier** ArianeGroup, Les Mureaux, France
- 438 **Klaus Dilger** Institute of Welding and Joining, TU Braunschweig, Braunschweig,  
439 Germany
- 440 **David A. Dillard** Biomedical Engineering and Mechanics Department, Virginia  
441 Polytechnic Institute and State University, Blacksburg, VA, USA
- 442 **Julien Eck** Airbus Defence and Space, Toulouse, France
- 443 **Hans K. Engeldinger** Product Development HAF Tapes, tesa SE, Norderstedt,  
444 Germany
- 445 **Michael Frauenhofer** Audi AG, Ingolstadt, Germany
- 446 **Paul Ludwig Geiß** Faculty of Mechanical and Process Engineering, Workgroup  
447 Materials and Surface Technologies (AWOK), University of Kaiserslautern, Kai-  
448 serslautern, Germany
- 449 **Luca Goglio** Department of Mechanical and Aerospace Engineering, Politecnico di  
450 Torino, Torino, Italy
- 451 **Stanislav N. Gorb** Department of Functional Morphology and Biomechanics,  
452 Zoological Institute at the University of Kiel, Kiel, Germany

- 453 **Ingo Grunwald** Department of Adhesive Bonding Technology and Surfaces,  
454 Adhesives and Polymer Chemistry, Fraunhofer Institute for Manufacturing Technol-  
455 ogy and Advanced Materials (IFAM), Bremen, Germany
- 456 **Kosuke Haraga** Tapes and Adhesives Department, Electronic Materials Division,  
457 Electronic Materials Business Unit, Denki Kagaku Kogyo Kabushiki Kaisha, Chuo-  
458 ku, Tokyo, Japan
- 459 **L. John Hart-Smith** Boeing Company, Long Beach, CA, USA
- 460 **Ilko Hartung** Dr. Kornder Anlagen- und Messtechnik GmbH & Co. KG,  
461 Bergheim, Germany
- 462 **Lars Heepe** Department of Functional Morphology and Biomechanics, Zoological  
463 Institute at the University of Kiel, Kiel, Germany
- 464 **Hyeon-Deuk Hwang** Laboratory of Adhesion & Bio-Composites, Program in  
465 Environmental Materials Science, Seoul National University, Seoul, Republic of  
466 Korea
- 467 **Seung-Boo Jung** School of Advanced Materials Science & Engineering,  
468 Sungkyunkwan University, Suwon, Gyeonggi-do, Republic of Korea
- 469 **Martin Kahlmeyer** Department for Cutting and Joining Manufacturing Processes,  
470 University of Kassel, Institute for Production Technologies and Logistics, Kassel,  
471 Germany
- 472 **Ewen J. C. Kellar** TWI Ltd. (The Welding Institute), Cambridge, Cambridgeshire,  
473 UK
- 474 **Hyun-Joong Kim** Laboratory of Adhesion & Bio-Composites, Program in Envi-  
475 ronmental Materials Science, Seoul National University, Seoul, Republic of Korea
- 476 **Jong-Woong Kim** School of Advanced Materials Engineering, Chonbuk National  
477 University, Jeonju, Jeollabuk-do, Republic of Korea
- 478 **Kwang-Seok Kim** Carbon & Light Materials Application Group, Korea Institute of  
479 Industrial Technology, Jeonju, Jeollabuk-do, Republic of Korea
- 480 **Guy Larnac** ArianeGroup, Saint Médard en Jalles, France
- 481 **Denis Lavielle** Airbus Defence and Space, Toulouse, France
- 482 **Byoung-Ho Lee** Laboratory of Adhesion & Bio-Composites, Program in Environ-  
483 mental Materials Science, Seoul National University, Seoul, Republic of Korea
- 484 **Cai R. Lim** Research & Development, tesa SE Hamburg, Norderstedt, Germany
- 485 **Dong-Hyuk Lim** Laboratory of Adhesion & Bio-Composites, Program in Envi-  
486 ronmental Materials Science, Seoul National University, Seoul, Republic of Korea
- 487 **Quantian Luo** School of Aerospace, Mechanical and Mechatronic Engineering,  
488 The University of Sydney, Sydney, NSW, Australia



- 489 **Andreas Lutz** Automotive, Dow Europe GmbH, R&D Automotive Systems,  
490 Horgen, Switzerland
- 491 **E. A. S. Marques** Instituto de Ciência e Inovação em Engenharia Mecânica e  
492 Engenharia Industrial (INEGI), Porto, Portugal
- 493 **José Miguel Martín-Martínez** Adhesion and Adhesives Laboratory, University of  
494 Alicante, Alicante, Spain
- 495 **Luiz C. M. Meniconi** Research and Development Center, CENPES, Petróleo  
496 Brasileiro S.A. – PETROBRAS, Rio de Janeiro, RJ, Brazil
- 497 **Aamir Mubashar** Mechanical Engineering, Middle Eastern Technical University,  
498 Northern Cyprus Campus, Akara, Turkey
- 499 **John W. Nicholson** Bluefield Centre for Biomaterials, London, UK  
500 Dental Physical Sciences, Institute of Dentistry, Queen Mary University of London,  
501 London, UK
- 502 **Andreas Öchsner** Faculty of Mechanical Engineering, Esslingen University of  
503 Applied Sciences, Esslingen, Baden-Württemberg, Germany
- 504 **David E. Packham** Materials Research Centre, University of Bath, Bath, UK
- 505 **James D. Palmer** Staffordshire, UK
- 506 **Eric Papon** Laboratoire des Polymères Organiques – UMR CNRS 5629, Univer-  
507 sity of Bordeaux, Pessac, France
- 508 **Charles W. Paul** Henkel Adhesives, Bridgewater, NJ, USA
- 509 **Stuart Pearson** Department of Mechanical Engineering, University of Bristol,  
510 Bristol, UK
- 511 **Patrick Pérès** ArianeGroup, Saint Médard en Jalles, France
- 512 **Valber A. Perrut** Research and Development Center, CENPES, Petróleo Brasileiro  
513 S.A. – PETROBRAS, Rio de Janeiro, RJ, Brazil
- 514 Metallurgical and Materials Engineering Department, Federal University of Rio de  
515 Janeiro, Rio de Janeiro, Brazil
- 516 **Manfred Peschka** Fraunhofer Institute, Bremen, Germany
- 517 **Wulff Possart** Lehrstuhl Adhäsion und Interphasen in Polymeren, Universität des  
518 Saarlandes, Saarbrücken, Germany
- 519 **Günter Reiter** Physikalisches Institut, Fakultät für Mathematik und Physik,  
520 Albert-Ludwigs Universität Freiburg, Freiburg, Germany
- 521 **Katharina Richter** Department of Adhesive Bonding Technology and Surfaces,  
522 Adhesives and Polymer Chemistry, Fraunhofer Institute for Manufacturing Technol-  
523 ogy and Advanced Materials (IFAM), Bremen, Germany

- 524 **Erol Sancaktar** Department of Polymer Engineering, University of Akron, Akron,  
525 OH, USA
- 526 **Chiaki Sato** Precision and Intelligence Laboratory, Tokyo Institute of Technology,  
527 Midori-ku, Yokohama, Japan
- 528 **Melanie Schumann** Faculty of Mechanical and Process Engineering, Workgroup  
529 Materials and Surface Technologies (AWOK), University of Kaiserslautern, Kai-  
530 serslautern, Germany
- 531 **Martin E. R. Shanahan** Institut de Mécanique et d'Ingénierie-Bordeaux (I2M),  
532 CNRS UMR 5295, Université de Bordeaux, Talence, France
- 533 **Eric Silverberg** Henkel Adhesives, Bridgewater, NJ, USA
- 534 **Yasuaki Suzuki** Suzuki Adhesion Institute of Technology, Ichinomiya, Aichi,  
535 Japan
- 536 **Ambrose C. Taylor** Department of Mechanical Engineering, Imperial College  
537 London, London, UK
- 538 **Liyong Tong** School of Aerospace, Mechanical and Mechatronic Engineering, The  
539 University of Sydney, Sydney, NSW, Australia
- 540 **Claire Tonon** Airbus Defence and Space, Toulouse, France
- 541 **Ansgar van Halteren** Industrieverband Klebstoffe e.V. RWI-Haus, Düsseldorf,  
542 Germany
- 543 **Janek von Byern** Austrian Cluster for Tissue Regeneration, Ludwig Boltzmann  
544 Institute for Experimental and Clinical Traumatology, Vienna, Austria
- 545 Faculty of Life Science, Core Facility Cell Imaging and Ultrastructure Research,  
546 University of Vienna, Vienna, Austria
- 547 **Kazutami Wakabayashi** APS Research Co Ltd, Osaka, Japan
- 548 **Feng-Chao Wang** State Key Laboratory of Nonlinear Mechanics (LNM), Institute  
549 of Mechanics, Chinese Academy of Sciences, Beijing, China
- 550 **John F. Watts** The Surface Analysis Laboratory, Faculty of Engineering and  
551 Physical Sciences, University of Surrey, Guildford, Surrey, UK
- 552 **Andreas Winkel** Department for Cutting and Joining Manufacturing Processes,  
553 University of Kassel, Institute for Production Technologies and Logistics, Kassel,  
554 Germany
- 555 **Tetsuo Yamaguchi** Machine Elements and Design Engineering Laboratory,  
556 Department of Mechanical Engineering, School of Engineering, Kyushu University,  
557 Fukuoka, Japan
- 558 **Ya-Pu Zhao** State Key Laboratory of Nonlinear Mechanics (LNM), Institute of  
559 Mechanics, Chinese Academy of Sciences, Beijing, China

# Introduction to Adhesive Bonding Technology

1

Lucas F. M. da Silva, Andreas Öchsner, and Robert D. Adams

## Contents

1.1	Background .....	2
1.2	Definitions .....	4
1.3	Motivation .....	5
1.4	Organization of the Handbook .....	6
References	.....	7

## Abstract

This introductory chapter gives a brief description of adhesive bonding and adhesion-related phenomena. The major definitions of the terms associated to this technology such as adhesion, cohesion, adhesives, sealants, and adherends are given so that there is uniformity of language throughout the handbook. The reasons that drove the editors to prepare and revise this book are explained. Finally, the organization of the book is described.

L. F. M. da Silva (✉)

Department of Mechanical Engineering, Faculty of Engineering, University of Porto, Porto, Portugal

e-mail: [lucas@fe.up.pt](mailto:lucas@fe.up.pt)

A. Öchsner

Faculty of Mechanical Engineering, Esslingen University of Applied Sciences, Esslingen, Baden-Württemberg, Germany

e-mail: [andreas.oechsner@gmail.com](mailto:andreas.oechsner@gmail.com)

R. D. Adams

Department of Mechanical Engineering, University of Bristol, Bristol, UK

Department of Engineering Science, University of Oxford, Oxford, UK

e-mail: [r.d.adams@bristol.ac.uk](mailto:r.d.adams@bristol.ac.uk)

© Springer International Publishing AG, part of Springer Nature 2018

L. F. M. da Silva et al. (eds.), *Handbook of Adhesion Technology*,

[https://doi.org/10.1007/978-3-319-55411-2\\_1](https://doi.org/10.1007/978-3-319-55411-2_1)

## 1.1 Background

Adhesives have been used for thousands of years, but until 100 years ago, the vast majority was from natural products such as bones, skins, fish, milk, and plants. Since about 1900, adhesives based on synthetic polymers have been introduced, and today, there are many industrial uses of adhesives and sealants. It is difficult to imagine a product – in the home, in industry, in transportation, or anywhere else for that matter – that does not use adhesives or sealants in some manner.

It is possible to distinguish three stages in the formation of a bonded joint. Initially, the adhesive must be in the solid state so that it can spread easily on the surface and wet properly the adherends to be bonded so that an intimate molecular contact is created between the adhesive and the surface. Secondly, in order for the adhesive to support the loads that it will encounter in service, the liquid adhesive must harden. Often, the adhesive is initially in the form of a monomer and polymerizes into a polymer with a high molecular weight. Pressure-sensitive adhesives are an exception in that they do not harden but remain permanently sticky. Finally, it is necessary to understand that the capacity of the joints to carry the load and the durability of the joint are affected by various factors such as the joint design, the way the loads are applied, and the environment that the joint will be subjected to. Thus, to obtain good results with adhesive bonding technology, it is necessary to have knowledge in various sciences including surface chemistry, chemistry and physics of polymers, materials engineering, mechanical engineering, etc. (Petric 2000).

Adhesively bonded joints are an increasing alternative to mechanical joints in engineering applications and provide many advantages over conventional mechanical fasteners. They provide a more uniform stress distribution along the bonded area which enables to have a higher stiffness and load transmission, reducing the weight and thus the cost. Figure 1 shows how the stress distribution in a bonded joint can give a higher stiffness and more uniform stress distribution in relation to a riveted joint. Due to the polymeric nature of the adhesive, adhesive joints provide good damping properties which also enable to have high fatigue strength. Adhesives can bond dissimilar materials with different coefficients of thermal expansion because the adhesive flexibility can compensate the difference. They bond thin plates very efficiently being one of the major applications of structural adhesives. Adhesives have a strength well below that of metals; however, when used to bond thin plates with a large bearing area, the strength of the adhesive is sufficient for structural applications. The adhesive application can be very efficient because it is easy to create an automatic process. The joint design is very flexible and new concepts and materials can be introduced. A good example is the sandwich structures where the core is made of honeycomb and the skin of a composite. They enable to have very smooth surface finishes because they avoid the use of holes for rivets or bolts or welding marks. They create an intimate contact between the bonded surfaces which is good in structural terms and also for corrosion resistance.

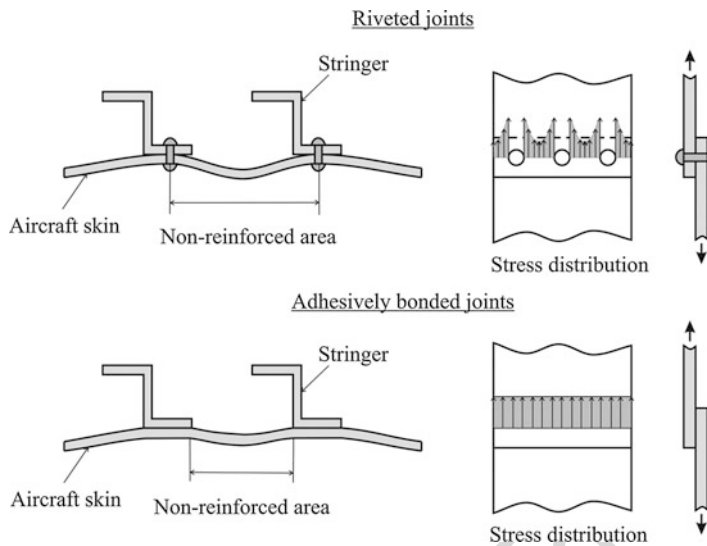


**Fig. 1** Improved stiffness (left) and stress distribution (right) of adhesively bonded joints in relation to riveted joints

Adhesive bonding is also associated to some disadvantages that leave room for more technological research and development. It is necessary to reduce the peel and cleavage stresses because they concentrate the load in a small area giving poor joint strength. They have limited resistance to extreme temperature and humidity conditions due to the polymeric nature of the adhesive. The bonding is usually not instantaneous which requires the use of tools to maintain the substrates in position. In addition, the hardening needs temperature for many adhesives. This is a big economical disadvantage. To have a good interfacial strength and a durable joint, a careful surface preparation is necessary such as solvent cleaning, mechanical abrasion, or chemical treatments. The quality control is more difficult than mechanical fasteners because it is not possible to dismantle an adhesive bond. However, a series of nondestructive techniques are now available. The joint design tends to be complex in many cases. There are no simple rules such as in the case of bolts, rivets, or welding, and design engineers still do not trust this technique, especially when it comes to long-term strength.

Applications related to adhesive bonding are today very diverse and can be found in virtually all types of industry. The aeronautical industry is one of the precursors of this technology and increasingly uses adhesives as more composites are introduced in airplanes. The rail and automotive industry is also turning to adhesives to produce lighter vehicles. Civil construction, shoes, and electronics are other examples. Emerging fields such as biology and medicine are also using developing processes based on cell adhesion and protein adhesion on surfaces which are important issues in, for example, biocompatibility of materials for prosthetics, artificial organs, and surgical glues.

This handbook is focused on adhesion science and technology. The topics of particular interest are surface preparation, joint configuration, adhesive properties, environmental conditions, analytical and finite element analyses of joints, and test methods.

## 1.2 Definitions

Adhesives have been used for many centuries. However, this method of joining only evolved significantly in the last 70 years. The main reason is because adhesives used in advanced technological applications are based on synthetic polymers whose development only occurred in the middle of the 1940s. The synthetic polymers possess properties that enable them to adhere easily the most materials and a strength capable to transmit considerable loads. According to Kinloch (1987), an adhesive may be defined as a material which when applied to surfaces of materials can join them together and resist separation. However, there are other substances which are outside this definition but which show the phenomenon of adhesion; these include paints and printing inks. A structural adhesive is an adhesive that can resist substantial loads and that is responsible for the strength and stiffness of the structure (Adams et al. 1997). The shear strength can vary from 5 MPa for a polyurethane to 50 MPa for an epoxy. Sealants are also an important part of this handbook and work under the same principles of adhesives. However, in this case the objective is to bond two surfaces, filling the gap between them and forming a barrier or protective layer. The materials to be bonded are called substrates. However, after bonding, the term generally used is adherend. Both adhesives and sealants work by adhesion phenomena. Adhesion is the attraction between two substances resulting from intermolecular forces that establish between them. This concept is different from that of cohesion which only involves intermolecular forces inside one substance. The intermolecular forces that exist in adhesion and cohesion are mainly van der Waals-type forces. Mechanical, electrical, and diffusion phenomena may also occur at the adhesion level (Possart 2005). Figure 2 illustrates the difference between adhesion and cohesion. Materials bonded with adhesives or sealants break by adhesion, cohesion, or a combination of the two. The region between the adhesive and the adherend is referred as the interphase. The interphase has chemical and physical characteristics different from those of the bulk adhesive or adherend. The nature of the interphase is a critical factor in the determination of the mechanical properties of the adhesive bond. The interface, different from the interphase, is a plane of contact between the surface and the two materials. It is within the interphase. It is useful to define and measure the surface energy. The interface is also designated by boundary layer. In the interphase, there might be several interfaces between different materials localized between the adhesive (or sealant) and the adherend. A primer is a substance which is often applied on the substrate to improve adhesion or protect the surfaces until the adhesive or sealant application. The joint is the whole part formed by the adherends, the adhesive or sealant, the primer (if present), and the interphases and interfaces associated to it, as shown in Fig. 3.

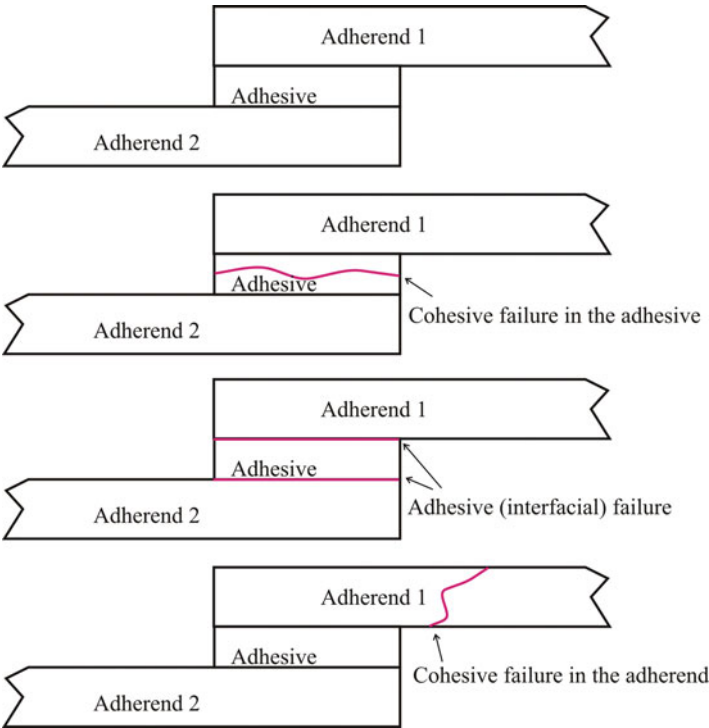
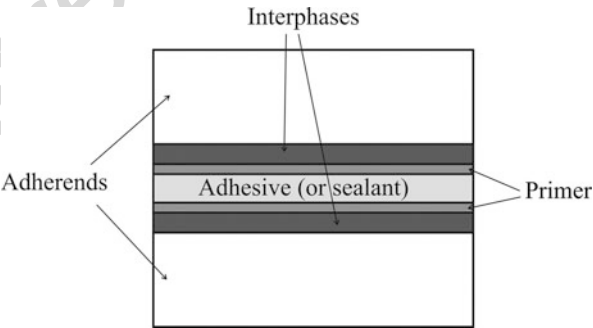


**Fig. 2** Examples of cohesive and adhesive failures

**Fig. 3** Adhesive joint



### 1.3 Motivation

The adhesion technology is nowadays a common approach to many joining situations. There are many books such as those of Kinloch (1987), Dostal (1990), Adams et al. (1997), Petrie (2000), Packham (2005), Adams (2005), Possart (2005), Lacombe (2006), Tong and Steven (1999), Ebnesajjad (2008), da Silva and Öchsner

(2008), da Silva et al. (2011, 2012), and da Silva and Sato (2013), and several international journals (*International Journal of Adhesion and Adhesives*, *The Journal of Adhesion*, *Journal of Adhesion Science and Technology*, *Applied Adhesion Science*, and *Reviews of Adhesion and Adhesives*) dealing with this subject. However, when the end user needs to apply this technology, he does not have the time or the resources to thoroughly study the various technologies related to adhesives and sealants. It is not practical to go through volumes of text and product information looking for the specific methods or processes to apply. However, such information should be close by if the need arises. The *Handbook of Adhesion Technology* (second edition) is intended to fill a gap between the necessarily simplified treatment of the student textbook and the full and thorough treatment of the research monograph and review article. The subject is treated very comprehensively and with the most up-to-date information so that the end user has in a single book a proper guidance and fundamental knowledge required for many adhesive bonding or sealing applications.

This book is intended to be a reference for people needing a quick, but authoritative, description of topics in the field of adhesion and the use of adhesives and sealants. It is intended for scientists and engineers of many different backgrounds who need to have an understanding of various aspects of adhesion technology. These will include those working in research or design, as well as others involved with marketing services. It is expected to be a valuable resource for both undergraduate and research students. The first edition of 2011 is already 6 years old, and the editors felt the necessity to update the whole book and include new material. The fact that the book has been of great interest to the adhesion community was also an important motivation for a complete review.

---

## 1.4 Organization of the Handbook

The *Handbook of Adhesion Technology*, second edition, is intended to be a book of reference in the field of adhesion. Essential information is provided for all those concerned with the adhesion phenomenon. Adhesion is a phenomenon of interest in diverse scientific disciplines and of importance in a wide range of technologies. Therefore, this handbook includes the background science (physics, chemistry, and materials science), engineering aspects of adhesion, and industry-specific applications. It is arranged in a user-friendly format with ten main sections: theory of adhesion, surface treatments, adhesive and sealant materials, testing of adhesive properties, joint design, durability, manufacture, quality control, applications, and emerging areas. The sections contain each about five chapters written by internationally renowned authors who are authorities in their fields. The last chapter gives a brief summary of each chapter with information about the main changes in relation to the first edition. Every chapter has been arranged so that it can be studied independently as well as in conjunction with the others. For those who are interested in in-depth information, numerous sources have been listed at the end of each chapter. The references listed serve as both bibliography and additional reading sources.



## References

- Adams RD (ed) (2005) Adhesive bonding: science, technology and applications. Woodhead Publishing Limited, Cambridge
- Adams RD, Comyn J, Wake WC (1997) Structural adhesive joints in engineering, 2nd edn. Chapman & Hall, London
- da Silva LFM, Öchsner A (eds) (2008) Modeling of adhesively bonded joints. Springer, Heidelberg
- da Silva LFM, Sato C (eds) (2013) Design of adhesive joints under humid conditions. Springer, Heidelberg
- da Silva LFM, Pirondi A, Öchsner A (eds) (2011) Hybrid adhesive joints. Springer, Heidelberg
- da Silva LFM, Dillard D, Blackman B, Adams RD (eds) (2012) Testing adhesive joints – best practices. Wiley, Weinheim
- Dostal CA (ed) (1990) Engineered materials handbook, vol 3: Adhesives and sealants. American Society for Materials, Metals Park
- Ebnesajjad S (ed) (2008) Adhesives technology handbook, 2nd edn. William Andrew Inc, New York
- Kinloch AJ (1987) Adhesion and adhesives: science and technology. Chapman & Hall, London
- Lacombe R (2006) Adhesion measurement methods – theory and practice. Taylor & Francis, New York
- Packham DE (2005) Handbook of adhesion, 2nd edn. Wiley, Chichester
- Petrie EM (2000) Handbook of adhesives and sealants. McGraw-Hill, New York
- Possart W (2005) Adhesion – current research and application. Wiley-VCH Verlag GmbH & Co. KGaA, Weinheim
- Tong L, Steven GP (1999) Analysis and design of structural bonded joints. Kluwer Academic, Boston

Uncorrected Proof

David E. Packham

**Contents**

2.1	Introduction .....	12
2.1.1	Practical and Fundamental Adhesion .....	12
2.1.2	Fracture Energy .....	13
2.1.3	Fracture Stress .....	14
2.1.4	Structure of This Chapter .....	15
2.2	Adsorption Theory .....	15
2.2.1	Contact and Bond Formation .....	15
2.2.2	Strength of the Adhesive Bond .....	19
2.2.3	Environmental Stability .....	19
2.2.4	Kinetic Effects .....	20
2.2.5	Rough Surfaces .....	20
2.3	Mechanical Theory .....	21
2.3.1	Macro and Microroughness .....	21
2.3.2	Mechanism of Adhesion to Rough Surfaces .....	23
2.4	Electrostatic Theory .....	25
2.4.1	Early Formulation .....	25
2.4.2	Particle Adhesion .....	27
2.5	Diffusion Theory .....	27
2.5.1	Origins: Voyutskii and Colleagues .....	27
2.5.2	Polymer–Polymer Compatibility .....	28
2.5.3	Interfacial Strength and Interdiffusion .....	30
2.5.4	Interfaces Between Incompatible Polymers .....	32
2.5.5	Copolymer Compatibilizers .....	33
2.5.6	Diffusion Theory: Conclusion .....	35
2.6	Weak-Boundary-Layer Theory .....	36
2.6.1	Practical Adhesion .....	36
2.6.2	Polymer Surfaces .....	37

D. E. Packham (✉)

Materials Research Centre, University of Bath, Bath, UK

e-mail: [D.E.Packham@bath.ac.uk](mailto:D.E.Packham@bath.ac.uk)

31	2.6.3 Formation of Weak Layers During Bonding .....	37
32	2.6.4 The Legacy of Bikerman .....	37
33	2.7 Conclusions .....	38
34	References .....	40

## Abstract

The historical development and current status of the four classical theories of adhesion are first reviewed. The *adsorption theory* emphasizes the point that once adhesive and substrate come into contact forces of attraction will act between them. As long as the extent of wetting is good, these forces, whether primary bonds, such as covalent, or secondary van der Waals forces, are generally considered sufficient to give a high bond strength. Primary bonding may be necessary to achieve bond durability in a hostile environment.

The *mechanical theory* focuses on interlocking between adhesive and a rough substrate surface. Again good wetting is required, or surface roughening is likely to lead to poor bond strength. It has been shown to apply to some surfaces rough on a macroscale as well as to microfibrinous and microporous surfaces, such as anodized aluminum. The enhanced adhesion is associated with increasing plastic energy dissipation during fracture in the bulk adhesive.

The *electrostatic theory* points to electrical phenomena such as sparking, which may be observed during the destruction of an adhesive bond, and consider the transfer of electrostatic charge between the adhesive and substrate. It regards the adhesive-substrate system as analogous to a parallel plate condenser. Estimates of the energy associated with this process are generally small compared with adhesion fracture energies, and the theory is much less vigorously supported than was the case some 50 years ago.

The *diffusion theory* has attracted increasing interest since the development of reptation theory of polymer chain dynamics. It provides a model for polymer-to-polymer adhesion, and gives an explanation of the time and molecular weight dependence of adhesion to polymers of various compatibilities.

The role of *weak boundary layers* is discussed with emphasis on the importance of careful investigation of the locus of failure of an adhesive bond.

In conclusion it is argued that the classical theories are best regarded as emphasizing a different aspect of a more comprehensive model which, in principle, relates molecular dispositions in the region of the interface to macroscopic properties of an adhesive joint.

## 2.1 Introduction

### 2.1.1 Practical and Fundamental Adhesion

The phenomenon of adhesion has been of interest for tens of thousands of years. Our remote ancestors were concerned to stick pigments to walls for cave painting and flint and bone to wood for tools and weapons (Pascoe 2005; Wadley et al. 2009).

Aristotle remarked on the gecko's ability to adhere to vertical surfaces; both Galileo and Newton were fascinated by the high forces of adhesion that could be observed in certain surfaces in intimate contact.

As Newton realized, there are two different types of question to be asked about the phenomenon of adhesion. The *first* type asks about the forces and so on which have to be applied to *separate* the bonded components; the *second* concerns what holds the components together in the first place. These two types of question respectively concern *practical* and *fundamental* adhesion. Some authors have written as if they thought that fundamental and practical adhesion were the same. This tendency was more prevalent in the past, but is still occasionally encountered.

Practical adhesion, then, is concerned with the magnitude of mechanical force or the quantity of energy which has to be applied to break an adhesive bond. It is relevant whether an adhesively bonded component breaks under load in service, or in some test machine in the laboratory. Practical adhesion is clearly of enormous importance and is considered in detail in this *Handbook* in ► Chaps. 20, "Fracture Tests," ► 21, "Impact Tests," ► 22, "Special Tests," and ► 23, "Constitutive Adhesive and Sealant Models." This chapter is concerned with fundamental adhesion. It is concerned with forces and mechanisms on, or approaching, the molecular scale, which are involved in holding together the different components of an adhesive bond. Newton recognized that the forces concerned in fundamental adhesion could be very large and challenged "experimental philosophy" to discover what they were! (Newton 1730).

Serious scientific concern with fundamental adhesion is usually dated back to the classic work of McBain and Hopkins in the 1920s, and to the various theories were advanced during the middle part of the last century. There was a strong tendency during much of this period to regard different theories as rival explanations of the same phenomena, rather than as complementary aspects of a broader rationalization. Much of the literature of the time, and even some of the literature today, reflects this approach, and therefore it is appropriate, if somewhat anachronistic, in this chapter first to consider different theories individually. A synthesis will be given in the conclusions.

It is obvious that adhesion at the fundamental level is a prerequisite for the existence of practical adhesion. What is the relationship between fundamental and practical adhesion? The answer to this question is by no means simple; indeed some authorities in the past have considered that there was no relation between the two. It is not appropriate here to attempt a detailed answer, but a simple, indeed simplified, account will be presented now.

Practical adhesion is generally assessed in the laboratory by loading an adhesive joint and observing the force required to produce failure, cf. ► Chaps. 20, "Fracture Tests," ► 21, "Impact Tests," and ► 22, "Special Tests." In some tests, the numerical value representing practical adhesion is a fracture energy (per unit area); in other tests, a fracture stress. Let us consider each in turn.

### 2.1.2 Fracture Energy

When an adhesive joint fails energy will have to be supplied to break the bonds where the joint fails, creating two new surfaces. These bonds broken may be,

according to circumstances, primary or secondary bonds. This energy required to form new surfaces is surface energy. If the failure is at the interface between phases 1 and 2, the appropriate surface energy term is the work of adhesion,  $W_A$ ,

$$W_A = \gamma_1 + \gamma_2 - \gamma_{12} \quad (1)$$

where  $\gamma_1$  and  $\gamma_2$  are the surface energies of materials 1 and 2 respectively in contact with air, and  $\gamma_{12}$  is the interfacial energy between phases 1 and 2.

An adhesive joint often fails cohesively within one component, rather than at the interface. Under these circumstances, the corresponding term will be the work of cohesion,  $W_C$ , given (for failure in phase 1) by

$$W_C = 2\gamma_1 \quad (2)$$

The work of adhesion and work of cohesion have been defined and discussed more fully in ► [Chap. 5, “Spreading of Liquids on Substrates.”](#)

In practice the magnitude of the fracture energy,  $G$ , is (almost) always considerably greater than that of the surface energy term  $W_A$  or  $W_C$  (now written as  $G_0$ ), given by Eqs. 1 or 2.  $G_0$  may be some average of  $W_A$  or  $W_C$ , depending on the locus of failure. These Eqs. 1 and 2, are thermodynamic equations; however, fracture of an adhesive bond will rarely, if ever, be reversible as thermodynamics require. Moreover, during the fracture process other energy absorbing processes occur, for example, plastic and viscoelastic deformation. Thus

$$G = G_0 + \psi \quad (3)$$

where  $\psi$  represents these other energy absorbing processes.

From a simple standpoint, Eq. 3 can be taken as representing the relationship between practical adhesion (represented by the measured  $G$ ) and fundamental adhesion associated with molecular forces at the interface,  $G_0$ . To repeat, usually  $\psi$  is very much larger than  $G_0$ , and so practical fracture energies for adhesive joints are almost always orders of magnitude greater than work of adhesion or work of cohesion.

It might be thought from this that the surface energy term  $G_0$  was not important as its magnitude was small. However  $G_0$  and  $\psi$  are coupled: as  $G_0$  increases  $\psi$  gets larger as well. Put simply, a very weak interface (low  $G_0$ ) would not be able to transmit a high stress needed to produce high  $\psi$ , say by plastic deformation. In some mechanically simple adhesive bonds, the loss term is directly proportional to the surface energy term. If  $G_0$  is doubled,  $\psi$  also is doubled, so the overall fracture energy,  $G$ , becomes twice as large.

### 2.1.3 Fracture Stress

Where the measure of practical adhesion is a fracture stress, similar considerations apply. A simple treatment of the physics of fracture (Griffith-Irwin theory, v. Good 1972) shows that the fracture stress  $\sigma_f$  also depends on the fracture energy  $G$ :

$$\sigma_f = k(EG/l)^{\frac{1}{2}} \quad (4)$$

where  $k$  is a constant,  $l$  is the length of the critical crack which leads to fracture, and  $E$  is the effective modulus. When this equation was first put forward, it was considered that the term  $G$  was the surface energy, but it was soon recognized that this led to strength predictions which were much too low. It was realized that  $G$  represented the sum of all the energy absorbing processes involved in the fracture, i.e., once again Eq. 3 applied. Practical adhesion (now represented by  $\sigma_f$ ) is related to fundamental adhesion through Eqs. 3 and 4.

## 2.1.4 Structure of This Chapter

Contemporary discussion of the fundamentals of adhesion generally reflects the historical development of the subject. For convenience, this approach will be adopted here. Early work in the 1920s discussed two kinds of adhesion. Where surfaces were smooth what would now be described as *Adsorption Theory* applied, with rough or porous surfaces *Mechanical Theory*. The next two Sects. 2 and 3, of this chapter discuss these in turn.

These theories were challenged by work originating in the Soviet Union. The *Electrostatic Theory*, considered in Sect. 4, laying emphasis on the transfer of charge across an interface, was put forward by Deryagin in the 1940s. A different challenge came from a different Soviet school which insisted on the fundamental importance of diffusion across an interface. The *Diffusion Theory* is the subject of Sect. 5.

The *weak-boundary-layer theory* is essentially a theory of fracture, rather than of fundamental adhesion. However it is frequently discussed along with these other theories, so consideration is given to it here in Sect. 6.

A great deal has been discovered about the mechanisms of adhesion since the middle years of the last century when the “classic” theories of adhesion were first proposed. The concluding section of the chapter will reassess them in the light of present understanding and question whether emphasis on one theory at the expense of another is still a useful way of rationalizing the results of experimental research in adhesion.

## 2.2 Adsorption Theory

### 2.2.1 Contact and Bond Formation

It is clear that the adhesive and substrate must come into contact for the possibility of the formation of an adhesive bond to exist. By far, the most common situation is one where a liquid adhesive comes into contact with a solid substrate. (That obviously means close contact on a molecular scale.) Factors that affect the extent of wetting and spreading of a liquid drop on a solid surface are, therefore, of primary

importance in any consideration of theories of adhesion. It is appropriate, then, that two other chapters in this handbook are devoted to these considerations.

As these other chapters show, there is a well-developed thermodynamic theory of wetting and spreading. This relates surface energies and surface tensions to contact angles and extent of wetting. Where the relevant surface energies and contact angles are known, or can be deduced, the extent of contact between a specific adhesive and substrate at equilibrium can be predicted. *The essential idea of the adsorption theory of adhesion is that whenever there is contact between two materials at a molecular level, there will be adhesion.*

When two materials come into contact, there will be forces of attraction between them. What those forces will be will depend on the chemical nature of the surfaces of the materials concerned. If this is known, it may be possible to postulate, or even to prove experimentally, the formation of a specific type of bond. Thus, metallic bonds may be involved in contact between a metallic solder and substrate metal (Some authors discuss secondary bonding in adhesion under the heading "Adsorption Theory," and treat primary bonding under a different heading, e.g., "Chemical Adhesion.").

Strong evidence for the presence of covalent bonds has been found, e.g., from some studies of the action of organosilane adhesion promoters used in bonding epoxies and other adhesives to metal and glass surfaces. It has long been suggested that the effectiveness of silanes was, in part, associated with covalent bond formation between the silane and a metal or glass surface, as indicated schematically in Fig. 1. Secondary ion mass spectroscopy (SIMS), which enables molecular fragments from

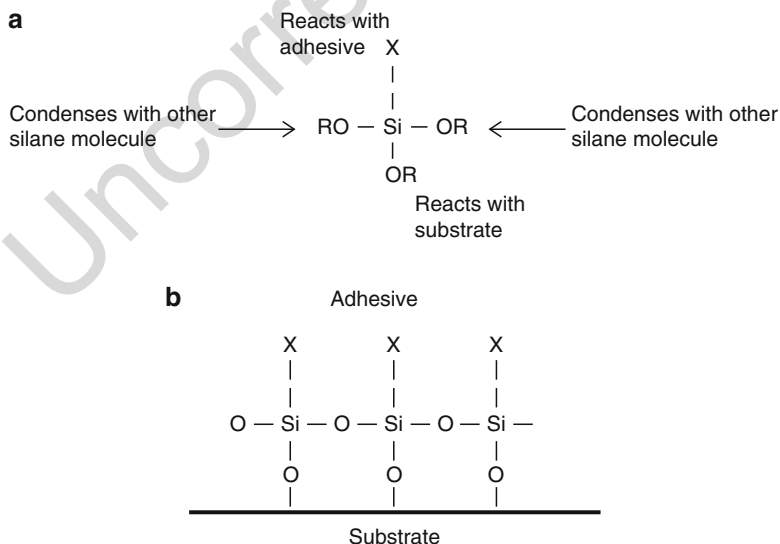


**Fig. 1** Typical structure (a) and postulated mode of action (b) for a silane adhesion promoter



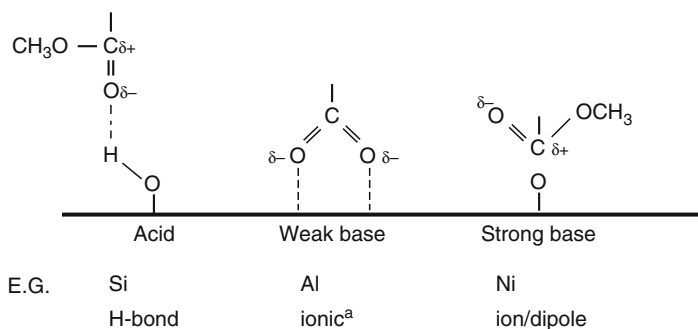


**Fig. 2** Interaction between PMMA and surfaces of differing acidic and basic nature (After Leadley and Watts (1997)). <sup>a</sup>Indicating hydrolysis of the ester and adsorption through the carboxylate anion

an interface to be examined, has produced evidence of the presence of such silicon-oxygen-metal covalent bonds.

Using high-resolution X-ray photoelectron spectroscopy (XPS), small changes can sometimes be detected in the molecular bonding of a chemical group at the interface. Leadley and Watts (1997) used the technique to examine the interface between polymethylmethacrylate (PMMA) and oxidized surfaces of metals or silicon. They found evidence for hydrogen bonding, ionic bonding, and ion-dipole interactions, depending on the strength of the acid or basic nature of the mineral surface (Fig. 2). All three are examples of electron donor-acceptor (i.e., Lewis acid-base) interactions.

A broadly similar conclusion was reached by a different route by Schneider et al. (2002). Maleic anhydride is used as a curing agent for some types of epoxy resin. The authors studied its interaction with a model system consisting of a thin aluminum layer deposited on a silicon wafer. The aluminum was allowed to oxidize and was then equilibrated with a laboratory atmosphere, before a monolayer of maleic anhydride was deposited from solution in acetone. Reflection-absorption intra-red spectroscopy indicated that the anhydride was hydrolyzed to the acid and adsorbed onto the oxidized aluminum surface. As a result of comparing the observed absorption frequencies with those calculated by quantum mechanical modeling for various plausible structures, the authors argued for the presence of three different adsorption structures (Fig. 3) in the ratio 6:1:1 for Fig. 3a-c. The dominant structure involved a carboxylate ion adsorbed on two neighboring aluminum ions. Figure 3b shows similar carboxylate ion adsorption with additional hydrogen bond adsorption involving the second carboxylic acid group of the maleic acid molecule. The third structure, Fig. 3c, involves interaction between the carbonyl oxygen and aluminum in the substrate surface. All three structures again involve electron donor-acceptor (i.e., Lewis acid-base) interactions.

Weak, secondary forces, resulting from molecular dipoles, also act between materials. They are often classified according to the nature of the interacting dipoles. Keesom orientation forces act between permanent dipoles, London dispersion forces

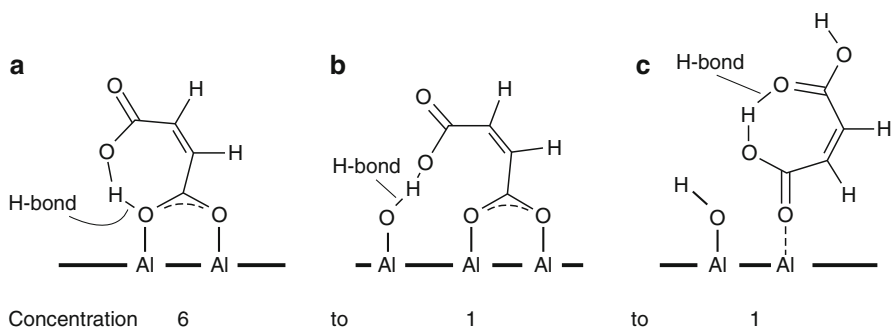


**Fig. 3** Adsorption of maleic acid on model-oxidized aluminum surface (After Schneider et al. (2002))

**Table 1** Classification of secondary forces

			Dipolar interaction
<b>Van der Waals</b>	London	Dispersion	Transient/transient
	Debye	Induction	Permanent/induced
	Keesom	Orientation	Permanent/permanent

**Table 2** Alternative classification of secondary forces (N.B. some authors, especially in earlier literature, have used t upon specifi to include hydrogen bonding and other electron donorersion forces are universal. They only require

			Dipolar interaction
<b>Van der Waals</b>	London	Dispersion	Transient/transient
<b>Polar forces</b>	Debye	Induction	Permanent/induced
	Keesom	Orientation	Permanent/permanent

between transient dipoles, and Debye induction forces between a permanent and an induced dipole, see Tables 1 and 2. These are collectively known as van der Waals forces (but note alternative usage of this term, Table 2) and occur widely between materials. They are much less dependent upon specific chemical structure than primary bonds. Indeed, dispersion forces are universal. They only require the presence of a nucleus and of extranuclear electrons, so they act between all atomic and molecular species.

Thus, whenever there is contact between two materials at a molecular level, there will be adhesion. Physical adsorption or chemical adsorption (chemisorption) will occur. Specific types of bonding may be present, but there will always, at least, be London dispersion forces. That is the essential idea of the adsorption theory of adhesion.

### 2.2.2 Strength of the Adhesive Bond

Elementary chemistry books give bond dissociation energies for bonds of different types. Primary bonds are typically of the order of hundreds of kilojoules per mole, van der Waals bonds tens of kilojoules per mole. It is natural then that many have supposed that an adhesive bond involving primary bonds at the interface will be stronger than one relying simply on van der Waals interactions. However, Eq. 3 above implies that the situation is not so simple. The “strength of an adhesive bond” (practical adhesion) depends not just on the interfacial forces (reflected in  $G_0$ ) but also on other energy terms ( $\psi$ ), and these latter are usually much greater in magnitude.

It is possible to calculate the energy of interaction between model molecules, representing adhesives, and model surfaces. When the results of such calculations are compared with corresponding practically measured adhesion, the predicted strength is found to be much higher than the measured strength. Even when dispersion forces are the only interactions considered, the calculated value is generally an order of magnitude higher than the measured strength. This has led to the conclusion that dispersion forces alone are more than sufficient to account for practical strengths of adhesive bonds. The question to be answered when considering the strength of adhesive bonds is not “why are they so strong?” but “why are they not stronger?” Of course, an analogous question occurs when considering the strength of materials in general, and much of the science of materials is devoted to answering it!

### 2.2.3 Environmental Stability

The discussion so far points to the critical importance of wetting in the formation of an adhesive bond. Once wetting occurs, there are adhesive–substrate interactions – adsorption of some sort has occurred, and dispersion forces alone will be sufficient to give a strong bond.

In a practical context, van der Waals adsorption may not form the basis for a satisfactory adhesive bond. The bond may not be stable in the service environment. This can be seen from a discussion of the work of adhesion considered above.

If the work of adhesion (as defined in Eq. 1) is positive, the adhesive will make contact with the adhesive and adsorption will take place. However, in the presence of a medium  $m$ , Eq. 1 has to be modified, and the work of adhesion now becomes

$$W_{A/m} = \gamma_{1m} + \gamma_{2m} - \gamma_{12} \quad (5)$$

where  $\gamma_{1m}$  is the surface energy of material 1 in the presence of the medium  $m$ . If  $\gamma_{1m}$  and/or  $\gamma_{2m}$  are sufficiently low, the work of adhesion (Eq. 5) may now become negative, and the bond fails.

A widely encountered “medium” is water, either liquid or vapor, and this is strongly adsorbed onto many high-energy surfaces, lowering their surface energy.

There are many examples of adhesive bonds that fail in a humid environment because the adhesive is displaced by this mechanism from the substrate.

Thus dispersion force adsorption may be sufficient, in principle, to provide good fundamental adhesion. In practice, it is often necessary to produce stronger bonds that are less susceptible to attack by medium  $m$ , e.g., less susceptible to hydrolysis. Silane adhesion promoters, discussed above, increase the hydrolytic stability of interfaces between adhesives and glass or metals through covalent bond formation.

#### 2.2.4 Kinetic Effects

At the start of Sect. 2, it was pointed out that thermodynamic theories of wetting (cf. ► Chap. 6, “Thermodynamics of Adhesion”) enable a prediction to be made of the extent of contact between a liquid adhesive and a given substrate, provided information relating to interfacial energies and contact angles was available. Obviously a thermodynamic theory predicts the equilibrium state, and in practice, it is important to consider whether equilibrium will be attained.

Typically, adhesives are liquids that solidify following application to the substrate. There is no reason to suppose that equilibrium wetting will always be achieved before they set. Whether equilibrium will be attained will depend on the relation between such factors as the forces causing the adhesive to spread and the rate of increase in viscosity with time. Moreover, the surface energy of the solidified adhesive will differ from that of the liquid, changing the equilibrium conditions. Such considerations are relevant to the application of the adsorption theory of adhesion.

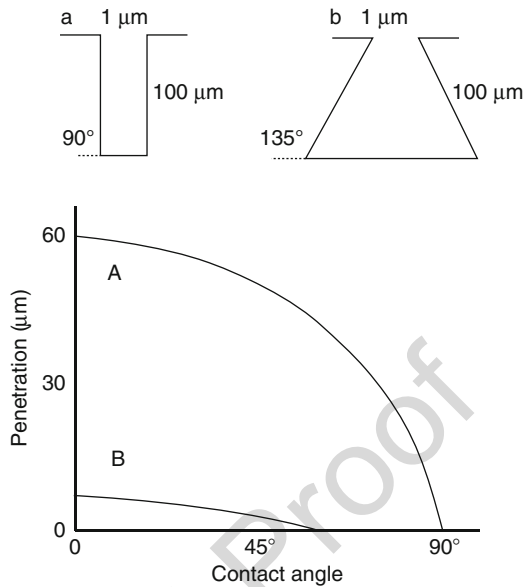
#### 2.2.5 Rough Surfaces

Rough surfaces are central to the concept of the mechanical theory of adhesion, discussed in Sect. 3. However, practical surfaces are always rough to some degree, and the discussion of the adsorption theory so far has tacitly assumed that the surface to be bonded was smooth.

If this roughness is not very great, its effect on wetting will be small, but some of the surfaces used in adhesion technology are extremely rough on a macro or microscale. Significant roughness can seriously reduce the extent of wetting achieved at equilibrium. If wetting is reduced, adsorption, and as a consequence fundamental adhesion, will be reduced also. The extent of this effect depends on the roughness features. It is possible, with plausible assumptions about surface tension and contact angle, to calculate equilibrium contact with model rough surfaces. Figure 4 shows some results after the classic work of de Bruyne (1956). Obviously a reentrant (“ink bottle”) pore is particularly difficult to wet.

The calculations on which Fig. 4 is based assume that equilibrium will be established. Considerations of the rate of setting of the adhesive and of its effect on viscosity and contact angle are relevant here. Depending on these factors, contact

**Fig. 4** Equilibrium penetration of a liquid into cylindrical and g will be small, but some de Bruyne (1956)



between an adhesive and a particular rough surface may be further inhibited by kinetic effects (Packham 2002).

### 2.3 Mechanical Theory

#### 2.3.1 Macro and Microroughness

Many of the features of the adsorption theory of adhesion, just discussed, can be traced back to McBain and Hopkins' classical work in the 1920s, where they are referred to it as "specific adhesion" (McBain and Hopkins 1925; Packham 1998, 2002, 2003). They also described "mechanical adhesion" to porous substrates, such as wood, unglazed porcelain, pumice, and charcoal. They regarded it as obvious "that a good joint must result whenever a strong continuous film of partly embedded adhesive is formed in situ." This is, in essence, the mechanical theory of adhesion.

Clearly, this mechanical adhesion relies on contact between adhesive and substrate, and therefore adsorption forces, described in Sect. 2, will act between the two materials.

Despite the "obvious" nature of the mechanical theory of adhesion, by the 1950s, the validity of the mechanism was largely denied by scientists working on adhesion. This denial was based on the results of studies in which adhesion to similar surfaces with different degrees of roughness was reported. These generally showed an inverse relationship between roughness and practical adhesion.

These results, no doubt, bore witness to the difficulty of obtaining good wetting of a rough surface by a viscous adhesive, cf. Fig. 4. Thus, many joints to rough surfaces

have voids at the interface and asperities will act as points of stress concentration, which can lower the practical adhesion with a brittle adhesive. However, there are now many examples in the literature where good wetting is obtained with rough surfaces, and, indeed, stress concentrations can even enhance practical adhesion with a ductile adhesive, but initiating local plastic deformation, which increases the energy dissipated during failure –  $\psi$  in Eq. 3.

Many successful prebonding treatments produce rough, microfibrinous, or microporous surfaces. Some of these are shown in Fig. 5. The integrity of a sizable proportion of the world's civil aviation fleet relies on adhesive bonding to anodized aluminum (Fig. 5a). A black, microfibrinous oxide coating on copper is often used as a pretreatment for bonding in electronic applications (Fig. 5c). PTFE is notoriously difficult to bond. Figure 5d shows the surface resulting from a successful bonding pretreatment involving irradiation by argon ions. Figure 5e shows an example, on a somewhat coarser scale, where the poor adhesion of copper to silica has been

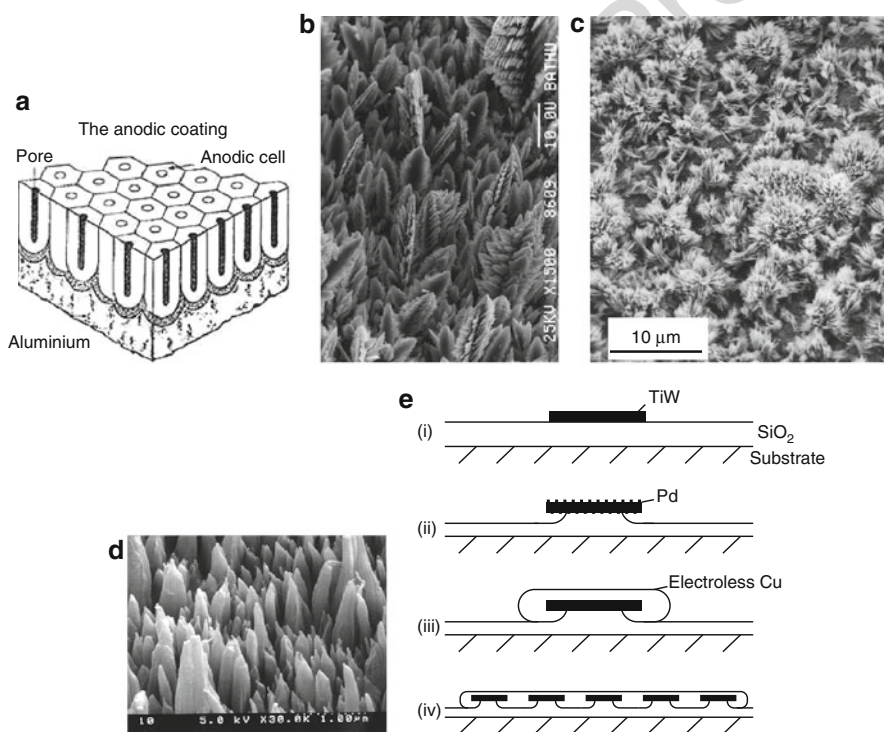


**Fig. 5** Some rough surfaces resulting from pretreatment prior to adhesive bonding: (a) porous anodic oxide on aluminum (schematic); (b) dendrites of zinc electrodeposited onto a zinc surface; (c) black CuO layer produced on copper; (d) PTFE irradiated by argon ions (After Koh et al. 1997); (e) adhesion of copper to silica using a mechanical key (van der Putten 1993). (i) TiW islands deposited; (ii) Pd activator adsorbed and HF etching; (iii) electroless Cu deposited; (iv) Cu electrodeposited

overcome by anchoring the copper to the silica surface using titanium tungstide “keys.”

Control experiments have shown scientifically that very rough surfaces, such as those illustrated in Fig. 5, give high adhesion under circumstances where adhesion to a corresponding smooth surface is low. So it could reasonably be said that the mechanical theory of adhesion applies in these cases. Of course, this does not necessarily mean that the high adhesion is the only technological reason for using the pretreatment. For example, the anodization of aluminum enhances durability of an adhesive bond in humid environments: in the aviation context, this is more important than the actual level of practical adhesion achieved.

### 2.3.2 Mechanism of Adhesion to Rough Surfaces

On the phenomenological level, it is clear that there are many rough surfaces known to adhesion science and technology where the surface roughness plays an essential role in adhesion: the mechanical theory of adhesion applies. Rather than simply ascribing adhesion to “mechanical effects,” it is useful to explore *why* roughness can lead to good adhesion.

Consider again Eq. 3. The surface energy term  $G_0$  is, from the standard definition of surface energy, the excess energy in the surface of the material, over that in the bulk material. In a simple way, this excess energy can be thought of as the energy necessary to break those bonds needed to produce the surface. Compare the bulk atom (B) in Fig. 6, with an atom S on a plane surface. In this schematic two-dimensional diagram, where the material is represented as a close-packed array of spherical atoms, B is bonded to six nearest neighbors, but S is only bonded to four. By extension of this argument, it can be seen that an atom (A) on an asperity will have a still higher surface energy. Thus, a rough surface, especially a very rough surface such as those illustrated in Fig. 5b–d, will have a higher surface energy than a corresponding smooth surface.

Returning to Eq. 3, it must be remembered that the fracture energy  $G$  is fracture energy *per unit area*. Obviously,  $G_0$  and  $\psi$  are also energies per unit area. The area relevant here is the formal (ideal) area, i.e., the macroscopic area of the interface, assuming that there was no roughness. For a rough surface, the “true” area will be greater and the surface energy term ( $G_0$ ) will consequently be higher. For moderate increases in surface roughness, a proportional increase in adhesion (practical adhesion) has been demonstrated (Gent and Lai 1995).

For very rough microporous and microfibrinous surfaces, the effective increase in area becomes enormous:  $G_0$  can be raised to a very high value indeed. Many engineering surfaces are fractal in nature: for such surfaces, the “area” is, in principle, indefinitely large. The practical adhesion to such surfaces does not become indefinitely large, because a joint with a strong interfacial region will fail cohesively in some other region where  $G_0$  is locally smaller.

The results presented in Table 3 show this effect in practice. Much higher fracture energies are found for adhesive bonds made to microfibrinous surfaces than to

**Fig. 6** Local environment of an atom in the bulk of a material (*B*), on a plane surface (*S*), and on an asperity on a rough surface (*A*) (Schematic representation)

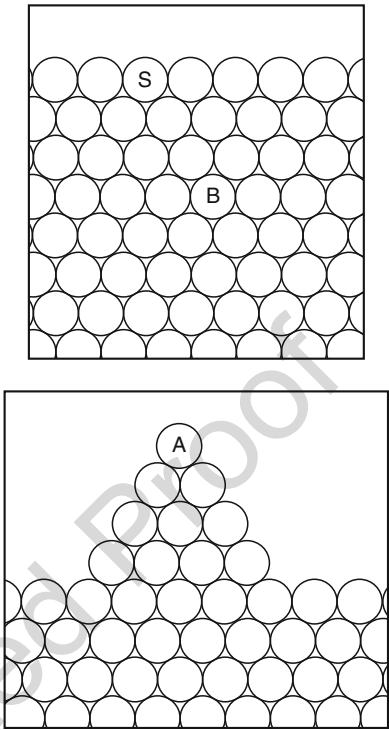


**Table 3** Adhesion of low density polyethylene (*LDPE*) to copper and of epoxy resin to electro-formed zinc, assessed, respectively, by peel and single edge notched (*SEN*) tests (Evans and Packham 1979; Hine et al. 1984)

Polymer	Substrate	Test	Fracture energy <sup>a</sup> J/m <sup>2</sup>	Fracture surface
LDPE	Copper (polished)	180° peel	210 ± 60	Close to substrate
LDPE	Copper (microfibrous <sup>b</sup> )	180° peel	1,620 ± 140	Plastic deformation of PE
Epoxy (unmodified)	Zinc (flat)	SEN	105 ± 30	Apparently adhesive
Epoxy (unmodified)	Zinc (dendritic <sup>c</sup> )	SEN	670 ± 290	Cohesive above dendrite tips
Epoxy (toughened <sup>d</sup> )	Zinc (flat)	SEN	700 ± 200	Adhesive with residual polymer areas
Epoxy (toughened <sup>d</sup> )	Zinc (dendritic <sup>c</sup> )	SEN	2,548 ± 515	Cohesive

<sup>a</sup>95% confidence limits given  
<sup>b</sup>cf. Fig. 5c  
<sup>c</sup>cf. Fig. 5b  
<sup>d</sup>15% CTBN rubber toughening agent incorporated



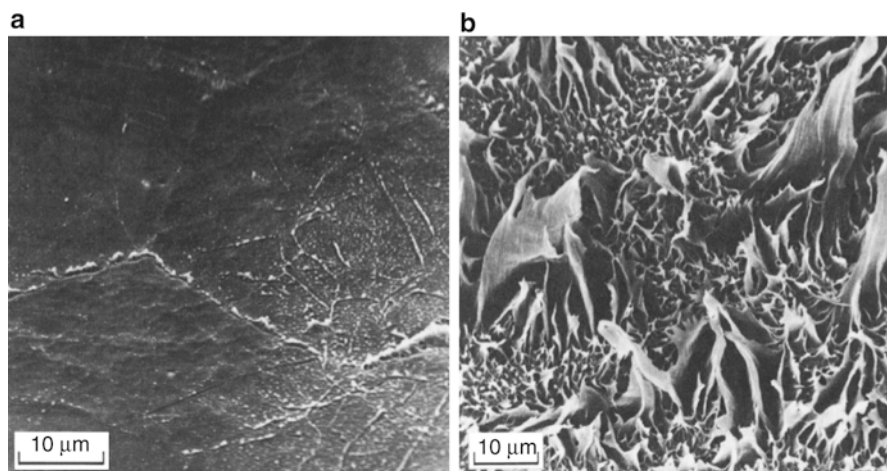


**Fig. 7** Adhesion of polyethylene to copper. Substrate surface after peeling from (a) polished copper and (b) copper with a microfibrinous oxide surface

corresponding smooth surfaces. For the smooth surfaces, stresses are concentrated at the interface, and failure occurs at or close to the interface with little plastic energy dissipation (Fig. 7a); for the microfibrinous surfaces, the stresses are concentrated at the fiber or dendrite tips causing yielding, which moves into the polymer, giving cohesive failure and higher fracture energy associated with the plastic deformation involved (Fig. 7b). It is interesting to note that, even with the brittle unmodified epoxy resin, cohesive failure occurs showing signs of plastic deformation associated with the dendrite tips (Fig. 8).

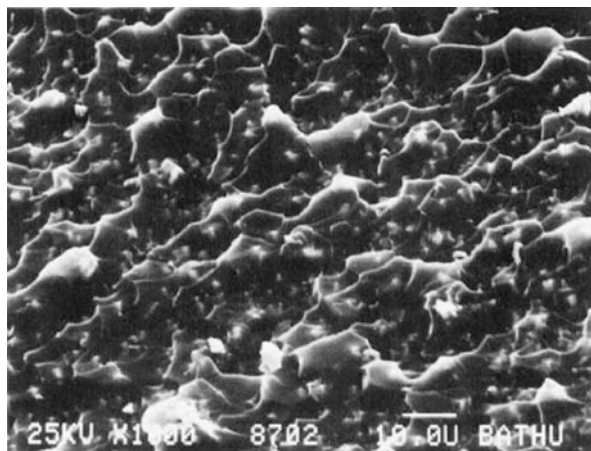
Thus, the basic ideas, related by McBain and Hopkins in the 1920s, underlying both the adsorption and mechanical theories of adhesion still provide useful models for rationalizing observations in adhesion science. Two further adhesion theories, the electrostatic and diffusion theories, emerged from the Soviet Union in the middle of the twentieth century. We now turn to consider them, and how they are regarded today.

## 2.4 Electrostatic Theory

### 2.4.1 Early Formulation

The electrostatic theory was put forward in the 1940s by Deryagin (alternative transliteration Derjaguin) and colleagues in the Soviet Union (Deryagin and Krotova 1948). The interface is seen as analogous to the plates of an electrical condenser across which charge transfer occurs. A physical model was introduced representing the electric double layer as a three-dimensional region at the polymer–solid contact (Deryagin et al. 1973).

**Fig. 8** Zinc with a dendritic surface bonded with unmodified epoxy resin: fracture surface showing plastic deformation of the epoxy just above the dendrite tips (Hine et al. 1984)



The basis of the theory is that free charges exist to some extent in any condensed material, even in the best dielectrics, and there will always be an electrochemical potential difference across the interface between two materials in contact, e.g., adhesive and substrate. Free electronic or ionic charge carriers will tend to move across the contact interface, and an electric double layer is established. This mechanism is considered quite distinct from any charge transfer, which may be associated with bonding at the interface, as discussed in Sect. 1.1.

Electrical phenomena (e.g., sparking) can often be demonstrated to accompany the destruction of an adhesive bond. The work of separation of the plates of a condenser depends upon rate of separation and ambient gas pressure. Measured peel energy certainly depends on rate of separation, and some published results indicate a dependence upon gas pressure. Deryagin argued that this supported the electrostatic theory of adhesion. He published results showing good correlation between measured peel energy and condenser discharge energy, but the details of his argument have been the subject of adverse criticism, see, e.g., Wake (1982) and Kinloch (1987).

More recently, Possart has used potential contrast scanning electron microscopy to study electric double layer formation associated with the interface between a thin layer of solvent-cast low-density polyethylene and aluminum (Possart 1988). While arguing that the electrical discharge energy of the double layer makes a contribution to the fracture energy, this study accepts that many other energy mechanisms also contribute. The work spent in mechanical testing surmounts the electrostatic interaction energy in the double layer by several orders of magnitude. The work of peeling was measured to be  $1 \text{ J/m}^2$ . The specific electrostatic work of separation was calculated as  $247 \text{ J/m}^2$ .

There was a period in the mid-years of the last century when its supporters presented the electrostatic theory as a comprehensive theory of adhesion, replacing the adsorption theory. Many critics of the theory pointed out examples where a change of filler or of polymer might lead to the absence of electrical phenomena,

despite there being similar levels of measured adhesion: most cases of conventional adhesion, it was argued, could be explained without recourse to the electrostatic theory. By the 1970s, Deryagin himself was prepared to accept that “an adhesive bond is always caused by either the forces of chemical bonding or by so-called van der Waals forces.” (Deryagin et al. 1978). The present writer’s perception is that the widely held view is that electrostatic contributions in conventional adhesion are likely to be small; this view, however, is not universally accepted.

## 2.4.2 Particle Adhesion

Although the detailed mechanism is distinct from that just discussed, it is relevant to note that electrostatic forces are still considered to be of relevance in adhesion of small particles. An advantage of this sort of adhesion is that it may be possible to manipulate the charged particles by external electric fields. Electrostatic precipitation is a well-established industrial technique. It is used to remove dust particles from a gas flow, e.g., from flue gases in a power station. Electrically charged dust particles are attracted to an electrode surface and are thus removed from the gas stream. In a similar way, the application of a strong field across the open base of a silo can be used to prevent the egress of charged dust particles.

The modern photocopier relies for its function on both electrostatic and van der Waals forces. Charged toner particles initially adhere to charged regions on a moving photoconductor belt and are subsequently transferred by electrostatic forces to a paper sheet on which they are fused (Kendall 2001).

## 2.5 Diffusion Theory

### 2.5.1 Origins: Voyutskii and Colleagues

The second adhesion theory to emerge from the Soviet Union in the mid-years of the twentieth century was the diffusion theory. The basic principles were set out by S.S. Voyutskii and his colleagues. Their compatriot, R.M. Vasenin, contributed to its quantitative development using Fickian diffusion theory (Voyutskii 1963; Wake 1982).

Much of Voyutskii’s original work was done on the self-adhesion (called autohesion) of unvulcanized rubbers. It was subsequently extended to polymer adhesion, more generally. The theory postulates that the molecules of the two parts of the specimen interdiffuse, so that the interface becomes diffuse and eventually disappears. For polymers in contact, Voyutskii studied the effects on adhesion of such variables as time, temperature, contact pressure, molecular weight, polarity, and crosslinking. He argued that the results proved that the adhesion was associated with the interdiffusion of polymer chains.

Voyutskii’s 1963 book, *Autohesion and Adhesion of High Polymers*, is the locus classicus for the exposition of his ideas in English. Here he takes a robust,

comprehensive view of the scope of the diffusion theory arguing that it is superior both to adsorption theory and electrostatic theory. He even argues for its application to the adhesion of polymers to metals.

As already indicated, the mid-decades of the twentieth century were the time when many authorities in the field of adhesion took an exclusive approach to theories of adhesion: if one theory was correct, another must be incorrect. In contrast, it is now much more widely recognized that different theories may have different areas of applicability, or even be better regarded as emphasizing a particular feature of a broader, overarching understanding.

Consistent with the spirit of the 1950s and 1960s, the diffusion theory generally got an unsympathetic reaction among supporters of the adsorption theory, i.e., mainly workers in the West. But attitudes changed, and by 1970, the position could probably be summarized by saying that diffusion was generally accepted as a mechanism for adhesion between samples of the same polymer (autohesion) or between very similar polymers (Wake 1982), but it was not more broadly accepted, even for polymer–polymer adhesion.

The reluctance to accept the applicability of diffusion theory to adhesion between chemically different polymers was because mutual solubility (emphasized by Voyutskii) was regarded as an essential feature of the mechanism, and most polymer pairs were known to be incompatible.

## 2.5.2 Polymer–Polymer Compatibility

It is often important to know whether two phases are mutually soluble, i.e., will mix on the molecular level to form a true solution. The question of mutual solubility – compatibility – can be approached in terms of thermodynamic criteria. The two phases will be compatible if the Gibbs free energy for mixing is negative. The Gibbs free energy of mixing  $\Delta G_m$  is related to the enthalpy (heat) of mixing  $\Delta H_m$  and entropy of mixing  $\Delta S_m$  by the usual second Law equation:

$$\Delta G_m = \Delta H_m - T\Delta S_m \quad (6)$$

where  $T$  is the absolute temperature. As mixing always increases disorder,  $\Delta S_m$  is positive, it follows that the  $-T\Delta S_m$  term is always negative, and therefore favors mixing. However, where polymers are involved, the long chain molecules mean that the entropy gain is much smaller than when compounds with small molecules are mixed. The  $-T\Delta S_m$  term, although negative, tends to be small in magnitude.

One approach to the discussion of compatibility in polymer systems is the Flory-Huggins theory (Berg 2002). This considers the number of ways in which chain segments of the polymers may be distributed among identical unit cells in a hypothetical lattice. The theory gives an expression for the free energy of mixing of polymers 1 and 2 (volume fractions  $\phi_1$  and  $\phi_2$ , degrees of polymerization  $x_1$  and  $x_2$ ) in terms of the Flory-Huggins interaction parameter,  $\chi$ . It may be written as:

$$\Delta G_{\text{mix}} = kT[\chi\phi_1\phi_2 + (\phi_1/x_1)\ln\phi_1 + (\phi_2/x_2)\ln\phi_2] \quad (7)$$

$$\frac{\Delta G_{\text{mix}}}{kT} = \underbrace{\chi\phi_1\phi_2}_{\text{enthalpy}} + \underbrace{(\phi_1/x_1)\ln\phi_1 + (\phi_2/x_2)\ln\phi_2}_{\text{configurational entropy}} \quad (8)$$

where  $k$  is Boltzmann's constant and  $T$  absolute temperature. In this particular form of the equation, the free energy change is expressed per total number of polymer chain segments. The interaction parameter,  $\chi$ , is a dimensionless temperature-dependent parameter.

The last two terms in Eqs. 7 and 8, involving  $\ln \phi$ , represent the configurational entropy of mixing. This is negative and so favors the formation of a solution, but, as explained, it is small in magnitude because of the limited potential gain in entropy in mixing long chain molecules. The first term, involving  $\chi$ , was originally conceived as expressing the enthalpy of mixing and is usually positive, meaning that for most polymer–polymer combinations  $\Delta G_{\text{mix}}$  overall is positive, and so the mixture is heterogeneous. Even polymers as similar as polyethylene and polypropylene are incompatible: the value of  $\chi$  at 140 °C has been calculated to be 0.011.

Such thermodynamic treatments point to the incompatibility of most polymer/polymer combinations, and practical studies with polymer blends lead to the same conclusion. Mutual solubility, regarded as an essential feature of the diffusion theory, would rarely be achieved, restricting the applicability of the theory to autohesion, and perhaps to adhesion between polymers of closely similar chemical structure.

## Developments in Molecular Dynamics

Following the work on molecular dynamics by de Gennes (1998) and by Doi and Edwards (1986) leading to the development of reptation theory, a much more detailed description of the motion of polymer chains can now be given (Wool 1995, 2002, 2005). Consider two samples of an amorphous polymer brought into contact above the glass transition temperatures. The conformations of the chains at the interface will tend to relax. Five different mechanisms of relaxation can be identified, corresponding to five different time scales. In order of increasing relaxation time, they are: (1) short-range Fickian diffusion of individual chain segments, (2) Rouse relaxation between chain entanglements, (3) Rouse relaxation of the whole chain, (4) reptation diffusion, and (5) Fickian long-range diffusion.

It is the reptation region (4) of diffusion of chain segments to a depth of the order of the radius of gyration that is considered to be the most important in discussing the development of strength of interfaces. This is illustrated for the autohesion of polystyrene at 118 °C by the data of Table 4 (Wool 2005). It can be seen that reptation leads to considerable interpenetration of the chains and, as discussed below, to significant strength.

The reptation model envisages the polymer chain to be enclosed within an initial tube out of which it gradually escapes by wriggling in a snake-like manner (“reptating”: *reptare* to creep). The reptation relaxation time  $T_r$  corresponds to the time when about 70% of the chain has escaped from the initial tube. During this time,

**Table 4** Chain relaxation and diffusion mechanisms: relaxation time ( $\tau$ ) and molecular weight ( $M$ ) relationships.  $M_c$  is molecular weight between chain entanglements,  $\tau_c$  is the Rouse relaxation time between chain entanglements,  $\tau_{RO}$  is the Rouse relaxation time of the whole chain,  $T_r$  is the reptation relaxation time

Mechanism	Relation between relaxation time and molecular weight	Relaxation time <sup>a</sup>	Average diffusion distance <sup>a</sup> at $\tau$
Rouse relaxation between chain entanglements	$\tau_c \sim M_c^2$	10 s	30 Å
Rouse relaxation of the whole chain	$\tau_{RO} \sim M^2$	21 min	60 Å
Reptation	$T_r \sim M^3$	1,860 min	110 Å

Numerical data<sup>a</sup> refer specifically to polystyrene ( $M = 245,000$ ) welded to itself at 118 °C

the interfacial thickness increases with time  $t$ , in proportion to  $t^{1/4}$ , in contrast with the  $t^{1/2}$  relationship for Fickian diffusion. The relaxation time  $T_r$  is proportional to the cube of molecular weight.

**2.5.3 Interfacial Strength and Interdiffusion**

The fracture strength of a polymer depends on molecular weight, the chain length, and in a similar way, the fracture of a polymer–polymer adhesive bond depends on the length of the chain, which has diffused across the interface.

Figure 9 shows the molecular weight dependence of the fracture energy for polystyrene. It can serve as a focus for consideration of the mechanisms involved in polymer–polymer adhesion. Two characteristic molecular weights are involved in this discussion:  $M_c$  and  $M^*$ .  $M_c$  is the average molecular weight between chain entanglements, the critical entanglement molecular weight. It represents the onset of the well-known zero shear viscosity law

$$\eta \sim M^{3.4} \tag{9}$$

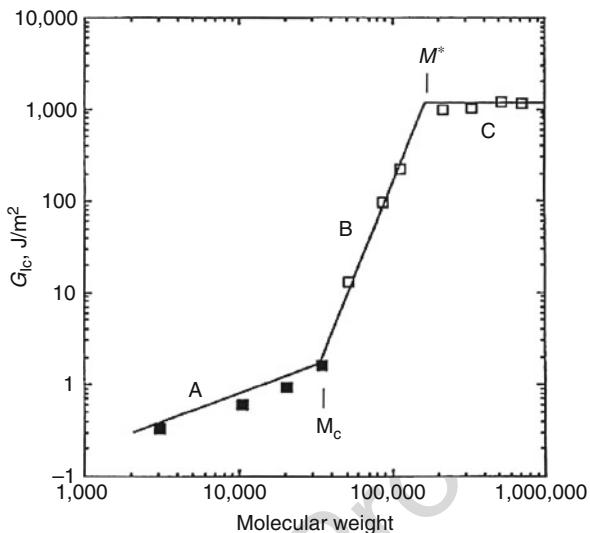
and the molecular weight at which the dynamics change from Rouse to reptation. In contrast,  $M^*$  is the value above which the molecules are too long for chain disentanglement (or pullout) to occur. They are related approximately by:

$$M^* \approx 8M_c \tag{10}$$

*Low molecular weight* When  $M < M_c$  (region A, Fig. 9) only short lengths of polymer chain are involved in the fracture process, which occurs by chain pullout. The fracture energy is low, up to about 1 J/m<sup>2</sup>.

Fracture behavior in this region can be treated using the “nail solution” where the weak interface is modeled as if the two sides were nailed together with  $\Sigma$  nails per unit area, each of length  $L$ . The analysis shows that the fracture energy associated

**Fig. 9** Fracture energy versus molecular weight for polystyrene in the virgin state (After Wool 2005).  $M_c$  is the average molecular weight between chain entanglements;  $M^*$  is the average molecular weight above which the molecules are too long for chain disentanglement (or pull-out) to occur



589 with chain pullout,  $G$ , increases with  $L^2$  and with  $\Sigma$ . To this “friction” term must be  
 590 added a surface energy term, so that

$$G_{1c} \sim 2S\gamma + kL^2\Sigma \quad (11)$$

591 where  $S$  depends on surface roughness ( $S = 1$  for a perfectly flat fracture surface) and  
 592  $k$  is a constant related to the “friction” involved in chain pullout. The term “friction,”  
 593 of course, refers to inter- and intramolecular attractions, such as van der Waals  
 594 forces.

595 *Intermediate molecular weight* When  $M_c < M < M^*$  (region B, Fig. 9), the chains  
 596 are long enough for entanglement to occur and the fracture energy rises progres-  
 597 sively. Fracture in this region occurs by disentanglement and chain pullout: bond  
 598 rupture is not considered to be significant.

599 Fracture in this region can be treated by the vector percolation theory, which  
 600 models the polymer as a three-dimensional network, the links of which are progres-  
 601 sively broken (here by chain disentanglement) until a critical value, the percolation  
 602 threshold, is reached, and the whole net fractures (Wool 2005).

603 *High-molecular weight* Here,  $M > M^*$  (region C, Fig. 9) and the dominant fracture  
 604 mechanism becomes bond rupture. Vector percolation theory predicts extensive  
 605 bond rupture throughout a significant volume of the polymer before failure occurs.  
 606 With glassy polymers, this is often associated with crazing. The fracture energy is  
 607 high tending to a limit, according to the Flory equation for molecular weight  
 608 dependence:

$$G_{1c}/G_{1c}^* = [1 - M_c/M] \quad (12)$$

609 where  $G_{1c}^*$  represents the fracture energy at high molecular weight.



To summarize, for autohesion (polymer–polymer welding), there will be rapid (Rouse) interdiffusion, which occurs to distances comparable to the radius of gyration of the entanglement molecular weight,  $M_e$ , say 3 nm (Table 4). The interface is very weak and could be described in terms of the nail solution, with chain pullout being the dominant fracture mechanism.

As welding proceeds, chains diffuse by reptation diffusion, and the failure mechanism then involves chain disentanglement and, with more extensive diffusion at longer times, bond rupture dominates. When bond rupture begins to dominate, the weld will appear fully healed, even in the absence of full interpenetration. There is a rate effect here. At high test rates, chains may not have time to disentangle and may rupture instead. This will give a high fracture toughness,  $G_{1c}$ , but at much lower deformation rates, weld weakness may be apparent. Wool (2002) cites, as an example, welding of a particular polystyrene at 125 °C, where essentially full (short time) weld strength would be obtained in 156 min, but the fatigue strength would be about one-fifth of its virgin value. For complete welding, a reptation time of 435 min, the relaxation time for reptation, would be needed. The importance of this observation for the molding of thermoplastics is obvious.

#### 2.5.4 Interfaces Between Incompatible Polymers

Despite macroscopic thermodynamic incompatibility, Sect. 5.2, an atomically sharp interface between two such polymers will not be stable. Although there is an enthalpy debt to be paid if a chain of polymer 1 starts to diffuse into polymer 2, there is an entropy gain. Helfand and Tagami (1972, Helfand 1992) introduced a model, which considered the probability that a chain of polymer 1 has diffused a given distance into polymer 2 when the interactions are characterized by the parameter  $\chi$ . They predicted that at equilibrium, the “thickness,”  $d_\infty$ , of the interface would depend upon the interaction parameter and the mean statistical segment length,  $b$ , as follows

$$d_\infty = 2b/(6\chi)^{\frac{1}{2}} \quad (13)$$

Thus, despite the argument in Sect. 5.2, some interdiffusion can be expected between formally incompatible polymers. The extent will depend on the extent of incompatibility, e.g., on the value of the interaction parameter: the smaller the  $\chi$ , the greater the possibility of interdiffusion.

Different mechanisms were discussed above (Sect. 5.3) in the context of autohesion. Depending on the extent of interdiffusion, fracture may occur at low energy by chain pullout or by chain disentanglement with bond rupture accompanied by crazing giving the highest fracture energies corresponding to the greatest extent of interdiffusion. In principle, the same considerations should apply to adhesion between different polymers.

The toughness of an interface will be expected to be related to the depth of interpenetration of the chains. Wool (1995) has argued that the fracture energy,  $G$ , for



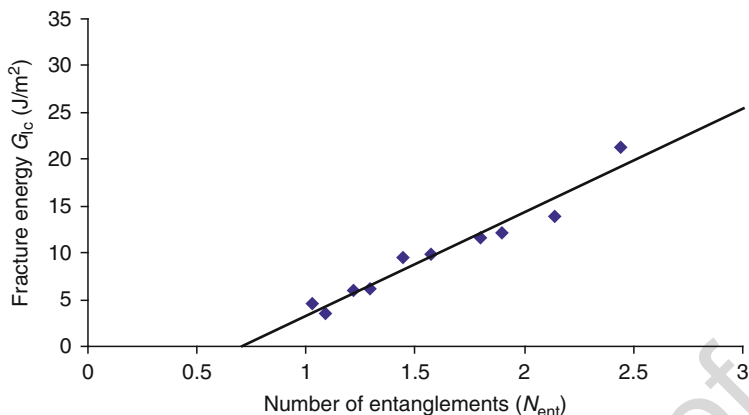


**Fig. 10** Fracture energy  $G_{Ic}$  of bonds between a range of immiscible polymers as a function of number of entanglements (After Wool 2005)

chain pullout, is proportional to the square of the interface thickness, which, via Eq. 6, gives

$$G \propto d_{\infty}^2 \propto 1/\chi \quad (14)$$

cf. Eq. 13 above.

For higher fracture energies, a linear relationship with the number of chain entanglements,  $N_{ent}$ , has been found for a range of polymer pairs, Fig. 10.

### 2.5.5 Copolymer Compatibilizers

Much higher adhesion may be obtained between incompatible polymers through the use of copolymer compatibilizers. If an AB diblock copolymer is introduced at the interface between two incompatible polymers A and B, the interface may be toughened by diffusion of the copolymer ends into the respective homopolymer. Much ingenuity has been employed in developing this type of compatibilizer.

A range of fracture toughness values ( $G_c$ ) may be obtained. The general principles are similar to those discussed in Sect. 5.3. For diblock copolymers, both surface density ( $\Sigma$ ) and degree of polymerization ( $N$ ) of the blocks are important. For example, if the degree of polymerization of the A block were shorter than the entanglement length, but that of the B block longer, interdiffusion could occur at the interface, but the bond would be weak with chain pullout of the A part of the copolymer from polymer A. Typical results are illustrated schematically in Fig. 11 (cf. Creton et al. 1994a): strength of the bond increases both with surface density of copolymer and with segment chain length (here segment A). However, as all the lengths of segment A are below the entanglement length, the fracture energy corresponds to chain pullout and is low.

**Fig. 11** Adhesion between incompatible polymers A and B. Interface reinforced by diblock copolymer AB, with A-block length below entanglement length

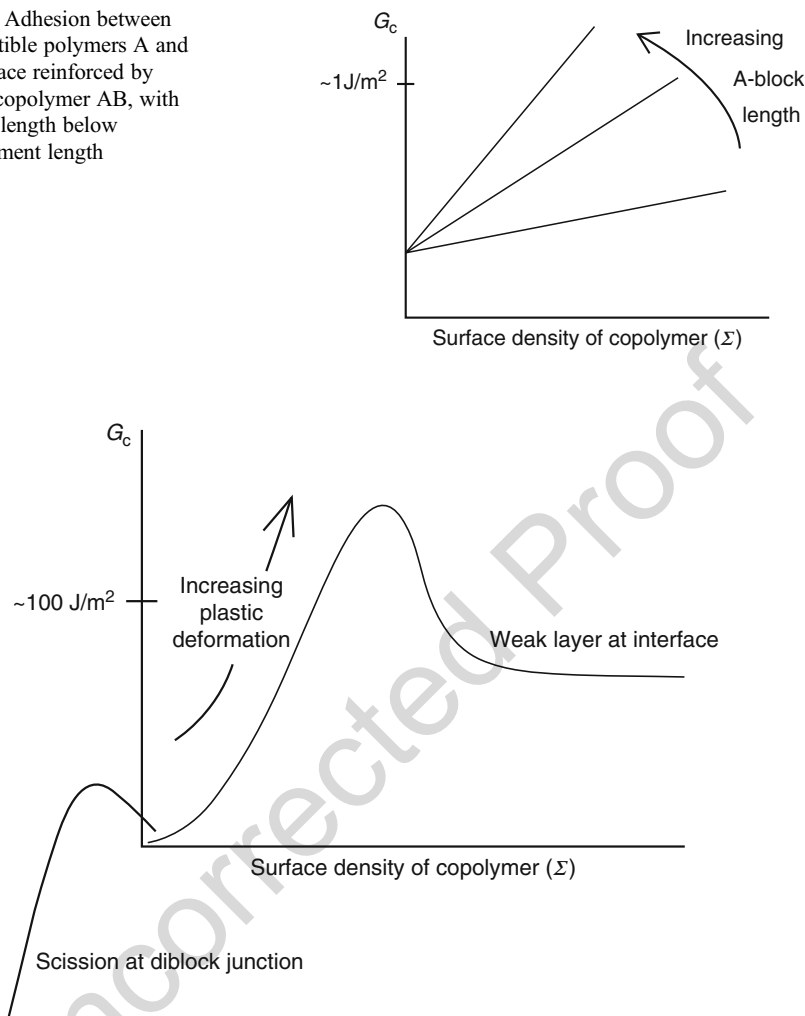


**Fig. 12** Adhesion between incompatible polymers A and B. Interface reinforced by long chain length diblock copolymer

With greater degrees of polymerization, chain entanglement can take place, Fig. 12. At low surface density ( $\Sigma$ ), chain scission will occur close to the junction of the diblock, with each fragment remaining on the “correct” side of the interface. The fracture energy is low. As the copolymer surface density increases, fracture energy rises steeply with plastic deformation, e.g., crazing, occurring in the polymer followed by chain scission or pullout. If an increase in copolymer surface density continues, eventually the surface becomes saturated and a weak layer forms at the interface with fracture energy falling toward a limiting value (cf. Creton et al. 1994b).

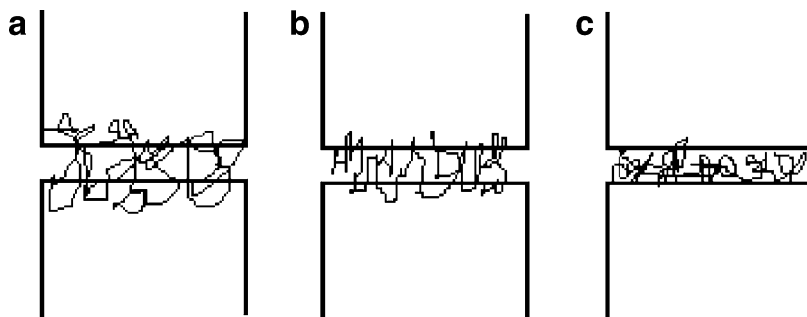


**Fig. 13** Schematic representation of a random copolymer at the interface between two incompatible homopolymers. Incompatibility increases in the order (a), (b), and (c)

Toughening of a polymer–polymer interface with random copolymers can sometimes be more effective than with diblocks, provided the polymers are not too incompatible. This is of industrial, as well as of scientific, interest as random copolymers are usually cheaper to produce.

Each molecule in diblock copolymers will form a single, strong chemical linkage across the interface. However if the incompatibility between the homopolymers is not too large, a molecule of a random copolymer will form coils wandering many times across interface, forming many “stiches.” At larger incompatibilities, the random copolymer will no longer describe coils, but the homopolymers will still be linked by “loops.” If the incompatibility is too large, the copolymer will simply form collapsed globules at the interface, a weak boundary layer giving no enhancement of adhesion, cf. Fig. 13.

As with block copolymers, the important parameters are the surface density and length of the copolymer chains. Toughening of the interface may occur as a result of pullout or scission of the connector chains, or of fibril or craze formation in the matrix. This last mechanism gives the highest fracture toughness,  $G$ , and tends to occur at high surface density of chains.

Needless to say, implicit in the general discussion of Sects. 5.4 and 5.5 is that the time and temperature of contact are such that the degree of interdiffusion discussed can occur. The lowering of temperature, and the shortening times will lead to kinetic inhibition.

### 2.5.6 Diffusion Theory: Conclusion

The ideas advanced by Voyutskii and his colleagues over half a century ago have now been developed far beyond what was possible at the time. It is now possible to relate with some clarity the circumstances where interdiffusion plays a significant part in adhesion, and plausible molecular models have been developed, which go a long way to describe it, relating joint strength to interfacial structure. These scientific developments have important technological implications for the development of new multicomponent polymer materials and for the recycling of mixed plastics waste.

## 2.6 Weak-Boundary-Layer Theory

### 2.6.1 Practical Adhesion

This article is concerned with *theories of fundamental adhesion*, i.e., with theories concerned with the reasons for two materials holding together in an adhesive bond, however weak. In contrast, a weak boundary is a cohesively weak layer in the interfacial region (some authors use the term “interphase”) of an adhesive joint, which may cause the joint itself to be weak, i.e., to fail at a low stress or with low fracture energy. So the question of weak boundary layers occurs when the level of practical adhesion is under consideration, and may form part of an answer to a question such as “why did this joint fail at such and such a stress?”

However, 50 years ago, when there was considerably less basic understanding, and more confusion, in the study of adhesion than there is now, “weak boundary layer theory” would often be discussed alongside theories such as the adsorption theory and the electrostatic theory. The tendency to group theories of adhesion in this way has persisted, and so it may now be useful to discuss the significance of weak boundary layers.

#### Need for Pretreatment

At one level, the existence of weak boundary layers and their deleterious effect on adhesion is obvious. Surface pretreatments, prior to adhesive bonding, are almost always a prerequisite for success. That is, because almost all surfaces will be contaminated to some degree from the environment to which they have been exposed. Generally speaking, extensive cleaning under conditions of ultrahigh vacuum is required to remove such contamination and to maintain a molecularly “clean” surface. Good adhesion is aided by high-substrate surface energy, partly to aid wetting (see ► Chap. 4, “Wetting of Solids,” ► 5, “Spreading of Liquids on Substrates,” and ► 6, “Thermodynamics of Adhesion”) and partly to increase fracture energy  $G$ , see Eqs. 1 and 3. The universal tendency for high-energy states to move toward lower-energy states is manifested here by adsorption onto a high-energy substrate surface of extraneous material. This can come from other solids or liquids with which the surface has been in contact, as well as from the atmosphere. Thus the surface of a metal, which, outside the realms of surface science might be described as “clean,” will be covered by complex layer including an oxide, probably partly hydrated, perhaps carbonated, adsorbed water, residual lubricant, and processing aids. Such a layer, in molecular terms, will be thick. It is unlikely to have good wetting properties and is likely to be cohesively weak. Unless removed by pretreatment, it is likely to form a weak boundary layer and to give poor practical adhesion. A successful pretreatment is very unlikely to produce a molecularly “clean” surface, but the surface produced will not suffer from the same cohesive weakness and lyophobicity of the original. Polymers are also likely to require pretreatment, because their surfaces usually carry complex layers, chemically different from the bulk material. The formation of these layers is now considered.

## 2.6.2 Polymer Surfaces

Few, if any, polymers in commercial practice are used without the incorporation of a range of additives. These may include antioxidants, processing aids, perhaps plasticizers and lubricants. Elastomers are likely to be based on even more extensive formulations including a complex vulcanization mixture.

In Sect. 5.2, the question of polymer–polymer compatibility was considered, and it was argued that the majority of binary polymer blends will be two phased because the component polymers are incompatible, the free energy of mixing,  $\Delta G_m$ , will be positive. Essentially, the same argument applies when polymer additive solutions are considered. The physical chemistry is similar: the entropy term will be small compared with that for a low-molecular-weight solvent–solute combination, and the enthalpy term is likely to be positive (cf. Eqs. 6–8). Most polymer-additive systems are thermodynamically unstable: the additive will tend to migrate out of the polymer. Loss of plasticizer from PVC (polyvinyl chloride) is a widely experienced phenomenon. The mode of action of antistatic agents depends on their progressive migration to the polymer surface.

Most adhesives are polymeric and set during the bonding process by loss of solvent, by solidifying from the melt, or by some form of cross-linking or polymerization reaction. In all of these solidification processes, there is the potential for low-molecular-weight additives to migrate to the substrate–adhesive interface and to form a weak boundary layer. Moreover, almost all polymers have a distribution of molecular weights, and there will be a similar tendency for low-molecular-weight fractions of the polymer itself to be rejected to the interface during solidification, especially during cooling from the melt.

## 2.6.3 Formation of Weak Layers During Bonding

The need for pretreatment to remove weak surface layers is widely understood. More subtly, other weak layers can form during the bonding process by the migration of low-molecular-weight species to the interface: sometimes these can lead to poor joint performance.

Many examples in the literature show that these effects occur. Classic experiments include removing low-molecular-weight fractions from a polymer, and observing increased adhesion, and complementarily, adding low-molecular-weight fractions, and observing a reduction in adhesion (Bikerman 1961). In Sect. 5.5, examples were given of weak boundary layers formed by copolymer compatibilizers.

## 2.6.4 The Legacy of Bikerman

Much of the early work on weak boundary layers was done by Bikerman and his colleagues in the 1950s and 1960s. His frequent observation of cohesive failure close

to the interface, combined with direct demonstration of a weak boundary layer mechanism in specific examples, led him to take up an extreme position (Bikerman 1961). This insisted on (1) the widespread occurrence of weak boundary layers, (2) the impossibility of adhesive (i.e., interfacial) failure, and (3) the practical strength of an adhesive bond depended on the rheology of the joint, not upon the forces at the interface.

Although Bikerman's position would not be supported today, it stimulated developments in the understanding of theories of adhesion, which can, to some extent, be regarded as his legacy. The potential for the formation of weak boundary layers (1) is well established, and much of the technique of adhesive bond preparation is designed to avoid them.

*Locus of failure* Where weak boundary layers exert an effect on adhesion behavior, failure typically occurs within the weak layer, close to the adhesive–substrate interface. The boundary layer will often be very thin, in macroscopic terms, and there are large numbers of examples where workers have reported the adhesive (i.e., interfacial) failure of a joint, when in fact it could be shown that failure was cohesive within a boundary layer. Bikerman's insistence (2) that adhesive failure could not occur had the beneficial effect of concentrating attention on the locus of failure. Careful examination of locus of failure is an important technique – still sometimes neglected – in the study of adhesive bonds. Modern methods of surface analysis are appropriate here. They have established that, although adhesive failure may be rare, it does occur sometimes.

In considering locus of failure, it must be emphasized that observation of cohesive failure close to the adhesive–substrate interface does not, itself, prove the presence of a weak boundary layer. The idea that an adhesive joint “fails at its weakest link” is naïve. The locus of failure of a joint depends in a complex way on the chemical and physical properties of the materials in the joint, and on the way the stress is applied to them. Cohesive failure close to an interface is entirely possible in the complete absence of weak interfacial layers (Good 1972). Dillard has demonstrated how failure can change between cohesive, interfacial, and oscillating for exactly the same joint, depending on how the stress is applied (Chen and Dillard 2002).

*Practical bond strength* Bikerman was right (3) in insisting on the importance of joint rheology in determining the practical strength of an adhesive bond. It was an important point to make at the time. However, he was wrong to say that interfacial forces were irrelevant. The connection between the two, expressed in a simple form in Eq. 3, is discussed in detail elsewhere in this handbook (► Chap. 3, “Forces Involved in Adhesion”).

---

## 2.7 Conclusions

A theory in science is a model that aims to order the experimental results in a field and, for a fruitful theory, to suggest new experiments and their outcome. We do not look to theories for immutable truths: we expect them in time to be modified and discarded (Popper 1959; Khun 1970).

In the light of our present understanding of adhesion, what can be said about the “classical” adhesion theories? On one level, it could be said that the adsorption, mechanical, and diffusion theories (and some would add electrostatic theory) maintain their importance undiminished. It is still acknowledged that adsorption plays a vital role, that there are examples where diffusion is crucial and so forth. However, the classic theories originated at a time when there were few, if any, experimental techniques available to study surfaces and interfaces at the nanometer level. We now benefit from several decades of results from scanning probe technologies and surface analysis and theoretical advances in contact mechanics and molecular chain dynamics. We have direct evidence for the presence of particular groups on a surface, for the effects of variations of topography and chemical nature over small distances on a surface. Consequently, in many cases, we have a much clearer understanding of what is happening in the interfacial region, and of how it affects adhesion.

One consequence of this understanding is that we can often make plausible suggestions about adhesion mechanisms without having to hide behind broad-brush statements about “mechanical effects” or “chemical activation.” We should also recognize now that the mechanisms characteristic of classical theories are not completely distinct. This is our contemporary answer, no doubt provisional, to Newton’s challenge (Sect. 1.1).

A good example of such an approach to theories of adhesion is provided by a recent extensive review of fracture and adhesion of soft materials by Creton and Ciccotti (2016). Nowhere in their review of adhesion mechanisms do Creton and Ciccotti find it necessary to refer to “classical” theories of adhesion, adsorption, mechanical, and so on. However, they discuss the use and range of validity of equations for fracture energy applicable to some of the soft materials which is their concern. These include equations which are much more specific versions of the general Eqs. 3 and 4 above.

It is recognized that the practical surfaces used in adhesion are always to a degree rough: the only question is “how rough?” As the roughness of a surface changes, so must the chemical environment of its surface atoms and molecules. Thus, changing the roughness changes the local chemistry, which will affect the adsorption properties of the surface. The scale of roughness of surfaces encountered in adhesive joints varies from the macroscopic through to the nano- and molecular scale, from the classic realm of the mechanical theory to that of the diffusion theory. The energy expended in peeling strands of rubbery polymer from a macroporous surface has been successfully analyzed in essentially the same way as the pullout of individual polymer chains by the “nail” model in diffusion theory (Sect. 5.3) (Gent and Lin 1990). In principle, the range of types of forces that may act between adsorbate and adsorbed molecule on a nominally flat surface are the same as those that may act between diffusing molecules.

Moreover, the way in which adhesion is enhanced is essentially the same whether we think in terms of adsorption, diffusion, or roughening. These provide mechanisms whereby the energy dissipation ( $\psi$  in Eq. 3) is enhanced. Whether the focus is on enhanced chemical interaction, surface roughening, or interdigitation of polymer chains, a common consequence is increased plastic or viscoelastic losses and crazing.

Each of the classical theories is best regarded as emphasizing a different aspect of a more comprehensive model, which, in principle, relates molecular dispositions in the region of the interface to macroscopic properties of an adhesive joint. It would be a mistake today to lay too much emphasis on the distinction between classical theories, although this has been valuable at various times during the last 80 years in stimulating the development of new concepts and in suggesting fruitful experiments.

## References

- Berg JC (2002) Semi-empirical strategies for predicting adhesion. In: Chaudhury MK, Pocius AV (assoc ed) *Adhesion science and engineering*, vol II, Surfaces, chemistry and applications. Elsevier, Amsterdam, pp 1–73
- Bikerman JJ (1961) *The science of adhesive joints*. Academic, London
- de Bruyne NA (1956) *Aero Res Tech Notes Bull* 168
- Chen B, Dillard DA (2002) Crack path selection in adhesively bonded joints. In: Dillard DA, Pocius AV (eds) *Adhesion science and engineering*, vol I. Elsevier, Amsterdam, pp 389–442
- Creton C, Ciccotti M (2016) *Rep Prog Phys*:79. <https://doi.org/10.1088/0034-4885/79/4/046601>
- Creton C, Brown HR, Shull KR (1994a) *Macromolecules* 27:3174
- Creton C, Brown HR, Deline VR (1994b) *Macromolecules* 27:1774
- Deryagin BV, Krotova NA (1948) *Doklady Akad Nauk SSSR* 61:849
- Deryagin BV, Krotova NA, Smilga VP (1973) “Adgezija tverdyck tel,” *elIzdvo*. Nauka, Moskva
- Deryagin BV, Krotova NA, Smilga VP (1978) *Adhesion of solids*. Consultants Bureau, New York/London, p ix. (Translation of original Russian version of 1973)
- Doi M, Edwards SF (1986) *The theory of polymer dynamics*. Clarendon, Oxford
- Evans JRG, Packham DE (1979) *J Adhes Dent* 10:177–191
- de Gennes P-G (1998) Simple views on condensed matter, *Series in modern condensed matter physics*, vol 8. World Scientific, Singapore
- Gent AN, Lai SM (1995) *Rubber Chem Technol* 68:13
- Gent AN, Lin CW (1990) *J Adhes Dent* 32:113
- Good RJ (1972) *J Adhes Dent* 4:133
- Helfand E (1992) *Macromolecules* 25:1676
- Helfand E, Tagami Y (1972) *J Chem Phys* 56:3592
- Hine PJ, El Muddarris S, Packham DE (1984) *J Adhes Dent* 17:207–229
- Kendall K (2001) *Molecular adhesion and its applications*. Kluwer, London
- Khun TS (1970) *The structure of scientific revolutions*, 2nd edn. Chicago University Press, Chicago
- Kinloch AJ (1987) *Adhesion and adhesives*. Chapman and Hall, London
- Koh SK, Park SC, Kim SR, Choi WK, Jung HJ, Pae KD (1997) *J Appl Polym Sci* 64:1913
- Leadley SR, Watts JF (1997) *J Adhes Dent* 60(10e):175–196
- McBain JW, Hopkins DG (1925) *J Phys Chem* 29:188
- Newton I (1730) *Optics*, 4th edn, bk 3, pt 1, William Innys, London.
- Packham DE (1998) The mechanical theory of adhesion – a seventy year perspective and its current status. In: van Ooij WJ, Anderson HR Jr (eds) *First international congress on adhesion science and technology: invited papers*. VSP, Utrecht, pp 81–108
- Packham DE (2002) Surface roughness and adhesion. In: Chaudhury MK, Pocius AV (assoc ed) *Adhesion science and engineering*, vol II, Surfaces, chemistry and applications. Elsevier, Amsterdam, pp 317–349
- Packham DE (2003) Mechanical theory of adhesion. In: Pizzi A, Mittal KL (eds) *Handbook of adhesive technology*, 2nd edn. Marcel Dekker, New York



- 923 Pascoe MW (2005) Adhesives - historical perspective. In: Packham DE (ed) Handbook of adhesion,  
924 2nd edn. Wiley, Chichester
- 925 Popper KR (1959) The logic of scientific discovery. Hutchinson, London
- 926 Possart W (1988) *Int J Adhes Adhes* 8(2):77–83
- 927 van der Putten AMT (1993) *J Electrochem Soc* 140:2376
- 928 Schneider B, Hennemann OD, Possart W (2002) *J Adhes Dent* 78(9):779–797
- 929 Voyutskii SS (1963) Autohesion and adhesion of high polymers. Interscience, New York
- 930 Wadley L, Hodgskiss T, Grant M (2009) *Proc Natl Acad Sci U S A*. 106(24):9590–9594. [https://doi.](https://doi.org/10.1073/pnas.0900957106)  
931 [org/10.1073/pnas.0900957106](https://doi.org/10.1073/pnas.0900957106)
- 932 Wake WC (1982) Adhesion and the formulation of adhesives, 2nd edn. Applied Science, London
- 933 Wool RP (1995) Polymer interfaces: structure and strength. Hanser, Munich
- 934 Wool RP (2002) Diffusion and autohesion. In: Chaudhury MK, Pocius AV (assoc ed) Adhesion  
935 science and engineering, vol II, Surfaces, chemistry and applications. Elsevier, Amsterdam, pp  
936 351–402
- 937 Wool RP (2005) Polymer diffusion: reptation and interdigitation/Polymer-polymer adhesion: incom-  
938 compatible interfaces/Polymer-polymer adhesion: models/Polymer-polymer adhesion: molecular  
939 weight dependence/Polymer-polymer adhesion: weld strength. In: Packham DE (ed) Handbook  
940 of adhesion, 2nd edn. Wiley, Chichester

Maurice Brogly

## Contents

3.1	Introduction .....	44
3.2	Physical Forces and Chemical Interactions: Basic Terms and Knowledge .....	45
3.2.1	van der Waals Forces .....	45
3.2.2	Acid-Base Interactions .....	48
3.2.3	Chemical Forces and Covalent Bonding .....	51
3.3	Experimental Determination of Adhesion Forces .....	54
3.3.1	Adhesion Forces Contribution to the Work of Adhesion .....	54
3.4	Case Study: In Situ Determination of the Work of Adhesion .....	64
3.4.1	Force – Distance Experiments on Self-Assembly Monolayers (SAMs) .....	64
3.4.2	Influence of Capillary Forces on Adhesion Forces .....	66
3.5	Conclusions .....	68
	References .....	68

## Abstract

The establishment of interfacial bonds through forces at the interface causes materials to attract one another. Therefore adhesion between materials and adhesive in assemblies are intimately related to the interatomic and intermolecular interactions at the interface of the two considered surfaces. Describing the mechanism responsible for adhesion in simple terms is difficult due to the complexity and evolving understanding of the subject. Nevertheless, when considering adhesion phenomena it is important to consider both the bulk and surface

M. Brogly (✉)

ENSCMu – LPIM – Equipe Chimie et Physico-Chimie des Polymères, Université de Haute Alsace, Mulhouse, France

e-mail: [maurice.brogly@uha.fr](mailto:maurice.brogly@uha.fr)

mechanical properties of the materials in contact and the type of interfacial forces established at the interface. High adhesion can only be obtained if the interface can sustain sufficient stress to induce dissipative forms of deformation, such as flow, yield, or crazing, in the polymer. Under most circumstances such dissipative processes can only be obtained when the interface is coupled with sufficient density of bonds. This chapter focuses on the description of the main forces responsible for adhesion, from strong covalent bonds to weak van der Waals forces, also considering some more specific interactions such as acid-base (like hydrogen bonding) or capillary forces (that could, as an example, influence adhesion of nanoparticles). The second part of this chapter concerns recent developments in experimental scanning probe techniques that may give access to direct adhesion forces determination at the nanoscale. A case study is presented.

### 3.1 Introduction

The term of adhesion between two objects appears confusing or ambiguous, because generally it is employed to describe: first, the formation of the interface between a pair of materials, i.e., the establishment of interfacial bonds through forces at the interface which cause materials to attract one another and second, the breaking stress or energy required to break the assembly. One can easily understand that both interfacial forces and mechanical properties of adherends in the vicinity of the interface and in the bulk contribute to the global mechanical response of the assembly. Such a fundamental issue reflects a paradox that has stimulated intensive research for decades: if adhesion is only a matter of thermodynamics, the work needed for separation would be close to the surface energies of the adherends, which are typically  $10^{-2}$ – $10^{-1}$  J/m<sup>2</sup>. Practical work of separation can be  $10$ – $10^6$  greater! On the other hand, separation has often been viewed as involving processes at the molecular level. The force needed for separation should then be as large as  $10^8$  N/m<sup>2</sup>– $10^9$  N/m<sup>2</sup>. Therefore the first part of this chapter relates more precisely to the question: what, precisely, is the role of interfacial forces in determining the mechanical strength of bonded structures such as adhesive joints, composites, coatings, etc.? In other words, do interfacial forces determine, by their “weakness” or “strength,” the “weakness” or “strength” of joint systems? A related question is: how to access adhesion forces at a local scale? In recent years, atomic force microscopy (AFM) has become a powerful tool, sensitive enough, to detect small surface forces and to study adhesion at the nanoscale. Adhesion forces and surface mechanical properties of surfaces can be achieved with such a nanometer probe even if quantitative results need important calibration procedures. The purpose and scope of the second part of this chapter is to give highlight to the experimental methods that enables one to measure adhesion forces on the basis of AFM force-distance experiments. Relationships are proposed that give a complete understanding on how capillary and van der Waals forces contribute to adhesion forces at a local scale.

## 3.2 Physical Forces and Chemical Interactions: Basic Terms and Knowledge

### 3.2.1 van der Waals Forces

The first forces subject to discussion are long-range van der Waals forces that include dispersion and polarization forces that arise from dipole moments induced in atoms and molecules by the electric fields of nearby charges and permanent dipoles.

#### Dispersion, Orientation, and Induction Forces

Dispersion forces (London 1937) represent the most important contribution to van der Waals forces between atoms and molecules. They are always present, act between all atoms and molecules (including totally neutral ones), and generally exceed the dipole-dependent induction and orientation forces except for small highly polar molecules (Israelachvili 1991). Even if they are of weak intensity, the perturbation responsible for dispersion forces is the existence of a finite dipole moment (given by the fluctuation of instantaneous positions of the electrons relative to the nuclear protons) that will generate an electric field that polarizes any nearby neutral atom, inducing a dipole moment in it. The same is for the second interacting atom. As a consequence, the resulting instantaneous dipole-dipole interaction gives rise to an instantaneous attractive force, called dispersion force. London has established using quantum mechanical perturbation theory the famous expression for the dispersion interaction energy ( $E_{\text{Disp.}}$ ) between two atoms or molecules (Eqs. 1 and 2) as follows:

$$E_{\text{Disp.}} = -C_{\text{Disp.}}/r^6$$

$$= (-3h\nu_1\nu_2\alpha_1\alpha_2)/\left[2(4\pi\epsilon_0)^2(\nu_1 + \nu_2)r^6\right] \approx (-\alpha_1\alpha_2)/r^6 \quad (1)$$

where  $r$  is the separation distance and  $C_{\text{Disp.}}$  is a constant proportional to the product of the polarizabilities ( $\alpha$ ) of the considered atoms or molecules,  $h$  is Planck's constant,  $\nu$  is electronic absorption frequency, and  $\epsilon_0$  is the dielectric permittivity in vacuum. The main features of dispersion forces may be summarized as follows (Israelachvili 1991):

- Dispersion forces are long-range forces and can be effective from large distances ( $>10$  nm) down to interatomic distances;
- Dispersion forces may be repulsive or attractive. Expression of the dispersion force does not follow a simple power law;
- Dispersion forces can also align or orient molecules, though this effect is usually weak;
- Dispersion interaction between two bodies is affected by the presence of other bodies nearby (nonadditivity interaction).

For larger molecules, with diameters greater than about 0.5 nm, the London equation can no longer be used. As molecules grow in size, their center-to-center

distance ceases to have any significance as regards the strength of cohesive energy. Likewise, the London equation cannot be applied to asymmetric (nonspherical) molecules such as polymers. Under such conditions, the exact dispersion interaction is difficult to compute. It is important then to consider that London theory must be modified and a complete description can be found in Spruch (1986) to account for the interaction between molecules at large distances ( $>10$  nm). A retardation effect occurs because a finite time is required for an electromagnetic wave to be propagated through the medium the atoms or molecules are situated in. As a consequence, the dispersion energy drops-off with distance ( $E_{\text{Disp.}}$  vary with  $1/r^7$  rather than  $1/r^6$ ) when the retardation effect comes into play. In the limit of very large separations, retarded dispersion interaction is given by the Casimir – Polder equation (Casimir and Polder 1948):

$$E_{\text{Disp.}} = (-23hc\alpha_1\alpha_2)/(8\pi^2r^7) \approx (-\alpha_1\alpha_2)/r^7 \quad (2)$$

where  $c$  is the speed of light in vacuum. Besides the most basic and predominant nonpolar interactions (dispersion forces), there are polarization or polar interactions between molecules of counter bodies, such as dipole-dipole interactions (Keesom 1922) and dipole-induced dipole interactions (Debye 1921). The essential difference between dispersion and polarization forces is that, while the former involve simultaneous excitation of both molecules, those for the latter involve only a passive partner. The Keesom orientation interaction energy between two molecules with permanent dipoles is temperature dependent and proportional to the dipole moments as follows:

$$E_{\text{Orient.}} = -C_{\text{Orient.}}/r^6 = -(\mu_1^2\mu_2^2)/(3kT(4\pi\epsilon_0)^2r^6) \approx -(\mu_1^2\mu_2^2)/r^6 \quad (3)$$

where  $r$  is the separation distance, and  $C_{\text{Orient.}}$  is a constant proportional to the temperature ( $T$ ), Boltzmann constant ( $k$ ), and the square product of the dipole moments ( $\mu$ ) of the considered molecules.

Debye argued that if the attraction energy was simply due to a Keesom effect then the interaction energy should be drastically reduced at high temperatures. Since experimental results were contrary to the prediction, he concluded that an additional attractive effect should be involved. He showed that an additional polar interaction should be induced between a permanent dipole and an induced dipole. The Debye induction interaction energy between two molecules with permanent dipoles is proportional to the square of the dipole moments and to the polarizabilities as follows:

$$\begin{aligned} E_{\text{Induct.}}(r) &= -C_{\text{Induct.}}/r^6 = -(\alpha_1\mu_1^2 + \alpha_2\mu_1^2)/[(4\pi\epsilon_0)^2r^6] \\ &\approx -(\alpha_1\mu_2^2 + \alpha_2\mu_1^2)/r^6 \end{aligned} \quad (4)$$

where  $r$  is the separation distance, and  $C_{\text{Induct.}}$  is a constant proportional to the sum of the square dipole moments ( $\mu^2$ ) times the polarizabilities ( $\alpha$ ) of the considered

molecules. If one of the interacting molecules has no permanent dipole (say the second), the term  $(\alpha_1\mu_2^2 + \alpha_2\mu_1^2)$  is reduced to  $(\alpha_2\mu_1^2)$ .

Finally the total van der Waals free energy of interaction has the following form:

$$E_{wdw}(r) = -C_{wdw}/r^6 = -[C_{\text{Disp.}} + C_{\text{Orient.}} + C_{\text{Induct.}}]/r^6 \quad (5)$$

An interesting property of van der Waals interactions must be considered that is the general dominance of dispersion forces in Eq. 5 except for highly polar molecules (i.e., water). Nevertheless rigorous computation of van der Waals force remains difficult.

### van der Waals Forces Between Macroscopic Bodies

To calculate the contribution of van der Waals forces in the interaction energy between macroscopic bodies one may sum the energies of all the atoms in one body with all the atoms in the other and thus obtain the “two-body” interaction energy. The resulting interaction laws are given in terms of a characteristic constant, namely, Hamaker constant (Hamaker 1937). The Hamaker constant is defined as:

$$A = \pi^2 C_{vdw} \rho_1 \rho_2 \text{ and } C_{vdw} \approx \alpha_1 \alpha_2 \quad (6)$$

where  $C_{wdw}$  is the coefficient in the atom-atom pair van der Waals interaction energy, and  $\rho_1$  and  $\rho_2$  are the numbers of atoms per unit of volume in the considered macroscopic bodies. Typical values for the Hamaker constants of condensed phases (liquid or solid) are about  $10^{-19}$  J for interactions in vacuum or air. Computation of Hamaker constants for polymers and various other materials could be found in Hough and White (1980). The nonretarded van der Waals interaction free energy between bodies of different geometries on the basis of pairwise additivity is given in Fig. 1. Direct applications are possible considering experiments such as surface force measurements with surface force apparatus (SFA) or adhesion force measurements with atomic force microscope (AFM).

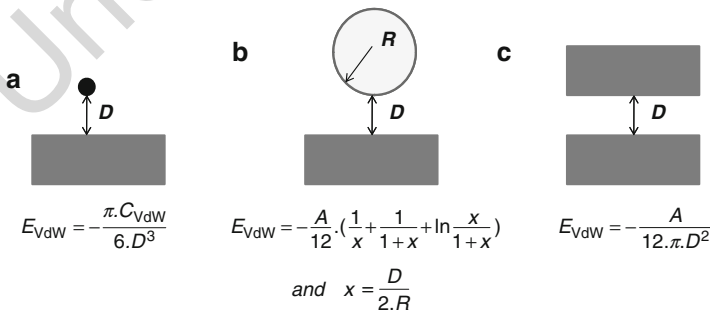


**Fig. 1** van der Waals free energy of interaction between interacting bodies ((a) atom – plane, (b) sphere – plane, and (c) plane – plane)

### 3.2.2 Acid-Base Interactions

#### The Original Lewis Definition

The Lewis definition of acid-base interactions are now over a half century old. Nevertheless they are always useful and have broadened their meaning and applications, covering concepts such as bond-formation, central atom-ligand interactions, electrophilic-nucleophilic reagents, cationoid-anionoid reagents, charge transfer complex formation, donor-acceptor reactions, etc. In 1923, Lewis reviewed and extensively elaborated the theory of the electron-pair bond (Lewis 1923). He states that a basic substance is one which has a lone pair of electrons which may be used to complete valence shell of another atom (the acid) and that an acid substance is one which can employ a lone pair from another molecule (the base) in completing the valence shell of one of its own atoms. Hence, the shared electron-pair bond model explains the existence of both nonpolar bond and polar link from the same premises. As the electrochemical natures of two atoms sharing an electron pair began to differ more and more, the pair should become more and more unequally shared, eventually becoming the sole property of the more electronegative atom and resulting in the formation of ions. Ionic and nonpolar bonds appear as logical extremes of a continuum of intermediate bond type. Differences in the continuum are only attributable to variations in the electron-pair donation, i.e., in the way in which the charges are localized within the molecule. As a consequence the distinctions between salts, acids, and bases; coordination compounds; and organic compounds are not of fundamental nature.

#### Molecular Orbital (MO) Approach of Acid-Base Reactions

Translated into the idiom of molecular orbital theory (Mulliken and Pearson 1969), the acid-base definitions should be read as follows:

- A base is a species which employs a doubly occupied orbital in initiating a reaction.
- An acid is a species which employs an empty orbital in initiating a reaction.

The donor orbital is usually the highest occupied molecular orbital HOMO, and the acceptor orbital is usually the lowest unoccupied molecular orbital or LUMO. Thus it is important to understand that considering the interaction between two species, the acid is always defined relatively to the base and the base relatively to the acid. The molecular orbital definitions have a number of important consequences:

First, it is not necessary that the donor and acceptor orbitals be localizable on a single atom or between two atoms, as implied by Lewis dot structures. That is, the orbitals may be multicentered even in a relatively localized representation. Thus donor-acceptor interactions involving delocalized electron systems ( $\pi$ -ring) (Hawthorne and Dunks 1972) are naturally assumed by the definitions. The same is for numerous organic or polymer molecules involving delocalized electrons. Second, the HOMO or donor orbital on a base is likely to be either bonding or nonbonding in character, the latter always being the case for monoatomic species. The LUMO or acceptor orbital of an acid is likely to be either antibonding or

nonbonding in character, the latter always being the case for monoatomic species. Third, all degrees of electron donation are possible, ranging from zero to the complete transfer of one or more electrons from the donor to the acceptor. This continuity can be represented (Eq. 7) by wave functions (Klopman 1974) where the degree of donation increases as  $(a/b)^2$  does ( $a$  and  $b$  are weighting coefficients).

$$\psi_{AB} = a\psi_A + b\psi_B \tag{7}$$

where  $\psi_{AB}$  is the wave function of the acid-base one-to-one adduct,  $\psi_A$  is the ground state wave function of the acid, and  $\psi_B$  the ground state wave function of the base.

Table 1 reports the possible adducts classified in terms of the bonding properties of the donor and acceptor orbitals of the acid and base. Complete description of the mechanisms involved during the following adducts formation can be found in Jensen’s complete review (Jensen 1979).

Even if the nature of an acid or a base is highly relative, a brief classification based on bonds properties and orbital symmetry can be proposed (where  $n$  represents the nonbonding orbital,  $\sigma$  represents the sigma orbital, and  $\pi$  the pi orbital.  $\sigma$  and  $\pi$  orbitals are also called bonding or antibonding orbitals if they address to a base or an acid, respectively).

- $n$  donor: Lewis bases, complex and simple anions, carbanions, amines, oxides, sulfurs, phosphines, sulfoxides, ketones, ethers, alcohols, etc.
- $\pi$  donor: Unsaturated and aromatic hydrocarbons having electron donor substituents, etc.
- $\sigma$  donor: Saturated hydrocarbons, CO, single links like C-C, C-H, polar links like NaCl, BaO, silanes, etc.
- $n$  acceptor: Lewis acids, simple cations, etc.
- $\pi$  acceptor:  $N_2$ ,  $SO_2$ ,  $CO_2$ ,  $BF_3$ , dienic and unsaturated and aromatic hydrocarbons having electron acceptor substituents, etc.
- $\sigma$  acceptor: Brönsted acids, boranes, and alkanes having strong acceptor substituents like  $CHCl_3$ , halogens, etc.

Table 1 Possible acid-base adducts in terms of orbital properties

			Acceptor Orbital of the Acid		
			Non-bonding	Anti-bonding	
			n	$\sigma^*$	$\pi^*$
			n.n	n. $\sigma^*$	n. $\pi^*$
Donor Orbital of the Base	Non-bonding	n	n.n	n. $\sigma^*$	n. $\pi^*$
	Bonding	$\sigma$	$\sigma$ .n	$\sigma$ . $\sigma^*$	$\sigma$ . $\pi^*$
		$\pi$	$\pi$ .n	$\pi$ . $\sigma^*$	$\pi$ . $\pi^*$



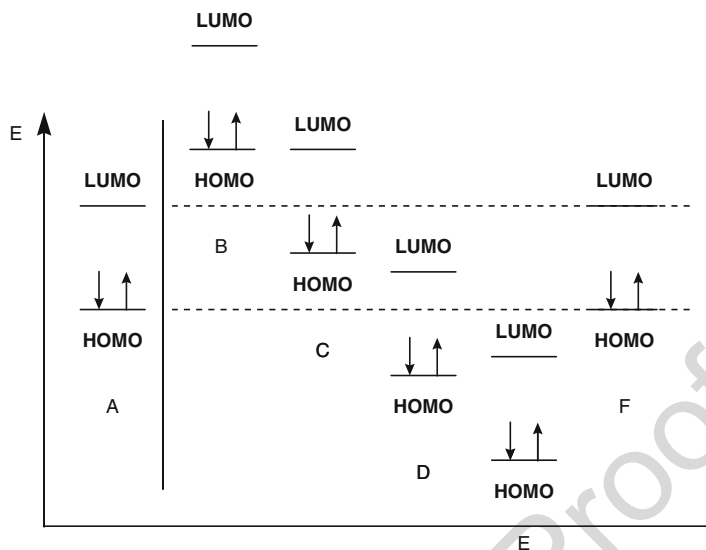


**Fig. 2** Donor-acceptor molecular orbital interactions. HOMO represents the highest occupied molecular orbital and LUMO the lowest unoccupied molecular orbital

To summarize how acid-base reactions do work on the basis of molecular orbitals perturbation theory, the relative energies of the frontier orbitals HOMO and LUMO of a hypothetical species A and of the frontier orbitals of several hypothetical reaction partners B, C, D, E, and F are reported in Fig. 2. This figure is intended to represent possible variations of donor-acceptor properties in the broadest possible way.

According to Fig. 2, with respect to B, complete electron transfer from B to A will be favorable and A will act as an oxidizing agent. With respect to C, the A(LUMO)-C(HOMO) perturbation will be favorable and A will act as an acid. With respect to D, the A(HOMO)-D(LUMO) perturbation will be favorable and A will act as a base. Lastly, with respect to E, complete electron transfer from A to E will be favorable and A will act as a reducing agent. For F species, the frontiers orbitals energies are identical with those of A. Here neither species is clearly the donor or acceptor and species may display both behaviors simultaneously (case of multisite interactions encountered in concerted organic cycloaddition reactions).

### The Case of Hydrogen Bonding

In extension to the general discussion relative to Lewis acid-base interactions, it is important to understand that hydrogen bonding represents a typical example acid-base interaction. According to Pauling (1960), hydrogen bonding is partly covalent and partly ionic (polar). Nevertheless, it is obvious that electrostatic and charge transfer interactions are predominant for hydrogen bonds. In most cases, the principal charge transfer contribution is derived from the proton acceptor-proton donor charge transfer complex through the  $\sigma$ -type interactions.

247 To conclude, the chemical phenomena subsumed by the category of acid-base  
248 reaction are the following:

- 249 – Systems governed by the Arrhenius description, solvent system, Lux-Flood, and  
250 proton acid-base definitions.
- 251 – Traditional coordination chemistry and “nonclassical” complexes.
- 252 – Solvation and ionic dissociation phenomena in both aqueous and nonaqueous  
253 solutions.
- 254 – Electrophilic and nucleophilic reactions in organic and organometallic chemistry.
- 255 – Charge transfer complexes, molecular addition compounds, weak intermolecular  
256 forces, hydrogen bonds.
- 257 – Salt melting and salt formation.

### 258 **3.2.3 Chemical Forces and Covalent Bonding**

259 The last case that should be considered in order to describe adhesion improvement is  
260 the possibility to form chemical bonds between adherends. Even if covalent bonds  
261 are just one variety in the continuum of bond types introduced before, it would be  
262 discussed in a special section as covalent bonding is in numerous cases required  
263 when high level of adhesive strength and durability of adhesive joints are required.  
264 Chemical bonds formed at an interface can greatly participate to the level of  
265 adhesion. The short-range forces involved in chemical bonding are quantum  
266 mechanical in nature and generally attractive. These bonds are generally considered  
267 as primary bonds in comparison with physical interactions such as van der Waals,  
268 which are called secondary interactions. The typical strength of a covalent bond is of  
269 the order of 100–1000 kJ/mol, whereas that of van der Waals interactions and  
270 hydrogen bonds does not exceed 50 kJ/mol. Chemical bonds depend strongly on  
271 the reactivity of both adhesive and substrate. To obtain strong adhesion, it is  
272 necessary that stress transfer could be achieved across the adhesive/substrate inter-  
273 face, so that cohesive failure is obtained. This stress transfer across the interface can  
274 be achieved by (i) chemical reaction to form coupling chains at the interface,  
275 (ii) the use of coupling chains placed at the interface, or (iii) chain interdiffusion,  
276 if the materials are sufficiently miscible.

#### 277 **Chemical Reaction to Form Coupling Chains at the Interface**

278 One of the most important adhesion fields involving interfacial chemical bonds is the  
279 use of adhesion promoter molecules, so-called coupling agents, to improve assembly  
280 joint strength. These species are able to react chemically on both ends (on one side  
281 with the adhesive, on the other side with the substrate). Silane-based promoter  
282 molecules are the most common type of coupling agent, widely employed in systems  
283 involving thermoset adhesives and glass, silicon oxide, silica, aluminum, or steel  
284 substrates. A complete review is available by Plueddemann (1982). Studies of the  
285 impact on epoxy fracture energy of model silanes (APS, GPS, MPS, AEAPS, PAPS)  
286 adsorbed on silicone oxide surface were done in Kramer’s group (Nakamura et al.

287 2007). The influence of chemical bonds on the joint strength ( $W$ ), and more precisely  
288 on the intrinsic fracture energy ( $G_0$ ), of a glass/elastomer interface was investigated  
289 (Gent and Ahagon 1975). They have shown that  $G_0$  increases linearly with the  
290 surface concentration of vinylsilane coupling agent, between the glass substrate and  
291 the cross-linked elastomer. A second system that has been studied extensively  
292 because of its technical importance is the adhesion between epoxy resins and  
293 glass, particularly glass fibres. To improve the hydrolytic stability of the composite,  
294 the glass surfaces are normally modified by covering them with a thin layer of a  
295 silane-adhesion promoter. These silanes are well known to self-assemble into mono-  
296 molecular and multi-molecular layers on surfaces (Flinn et al. 1994). Studies of the  
297 impact on epoxy fracture energy of model silanes (APS, GPS, MPS, AEAPS, PAPS)  
298 adsorbed on silicone oxide surface were done in Kramer's group (Nakamura et al.  
299 2007). One end of the silane molecule typically has di or tri methoxy or ethoxy  
300 functionality whilst the other end normally has amine or epoxy functionality. The  
301 ethoxy functionality is believed to condense with the hydroxyl functionality on  
302 the surface of the glass whilst the amine functionality can react with the epoxy.  
303 The amount of silane typically used is much too great to form a monolayer. Also,  
304 as the silane has multimethoxy or multiethoxy functionality, it can self-condense.  
305 The relatively thick layer of silane is believed to form a network and then the epoxy  
306 both mixes into and reacts with the network. Although it is clear that the silane  
307 causes covalent bonding between the glass and the epoxy, there is no simple way to  
308 estimate the actual density of coupling produced. Moreover, the silane condensed  
309 layer can be viewed as a rather porous layer (low degree of condensation) in which  
310 small molecules or additives have the possibility to diffuse. Similar silanes are also  
311 used as adhesion promoters on silicon dioxide.

312 A second commonly used strategy to couple two bulk polymers is to introduce  
313 into one or both of the materials a small percentage of chemically modified chains  
314 (Lewis and Natarajan Gounder 1991; Tao et al. 2001) that can react with the other  
315 polymer to form coupling chains at the interface. A classic example (Laurens et al.  
316 1994) is the introduction into polypropylene of some maleic anhydride grafted  
317 polypropylene chains to induce coupling with a polyamide such as Nylon 6. The  
318 maleic anhydride functionality can react with hydroxyl end groups on the polyamide  
319 chain to form a graft or block copolymer at the interface. The molecular mechanism  
320 of interfacial failure can be either pullout or scission of these coupling chains.  
321 Pullout at low force can occur if either one of the blocks in the copolymer formed  
322 at the interface is rather short or if there are too many coupling chains at the interface.  
323 In systems where multiple grafts are possible on a single chain, then the coupling  
324 chains can become so densely packed at the interface that they exclude other chains  
325 and so cannot entangle well with the bulk material, causing pullout failure. This  
326 situation has been observed when the chains themselves were long enough to  
327 entangle.

### 328 Coupling Chains Placed at Polymer-Polymer Interfaces

329 Another case of interest concerns the adhesion between immiscible polymers.  
330 Adhesion is improved by the presence of diblock copolymers (Tirrel et al. 2001)

or grafted chains (Brochart-Wyart et al. 1994) at the interface. The diblock is chosen so as that each block dissolves in the respective homopolymer. The forces involved are in most cases physical like van der Waals interactions which drive the mixing of each of the blocks across the polymer-polymer interface. Blocks should also have masses higher than the critical molecular weight between entanglements ( $M_e$ ) of the respective homopolymer. The form of coupling, that is to say the mechanism of interface failure, has been found to depend on the molecular weight of the coupling chains. Short chains can pull out of the bulk material at a force that increases with the length of the pulled-out section. As the length of the chains increases to somewhere between one and four times the length required to form an entanglement in the melt, the force required for pullout becomes greater than the force to break chains, so they fail by scission of covalent bonds. The extent of adhesion is strongly affected by the molecular failure mechanism as tough interfaces are normally only obtained when the failure is by scission. However, scission failure does not guarantee a tough interface. Nevertheless, Brown has proposed a molecular interpretation of the toughness of glassy polymers (Brown 1991) which can be applied to the failure of interfaces between reinforced immiscible polymers, for which a covalent scission (Brown et al. 1989) of the copolymer chains is observed at the interface. Assuming that entangled chains in the material are drawn into fibril, the fracture energy  $W$  is found proportional to:

$$W \approx \nu^2 f^2 D / S \quad (8)$$

where  $\nu$  is the surface density of entangled chains,  $f$  is the force required to break a polymer chain,  $D$  is the fibril diameter and  $S$  is the local stress applied at fibril-bulk interface.

Moreover the chemist has the possibility to graft reactive functional groups on the blocks to promote chemical reactions between the blocks and the surrounding chains of the hosting polymer to improve adhesive strength by covalent bonding.

### Coupling Polymers Chains by Interdiffusion

Coupling by chain interdiffusion (Wool 1995) can occur if two polymeric materials are miscible in each other, or at least sufficiently miscible to form an interphase. Welding is the most common form of interdiffusional coupling, but chain interdiffusion is also important in solvent bonding. Polymer diffusion normally occurs by the process of reptation in which the chain moves a long 'tube' formed by its entanglements with all the other chains. Hence interface coupling is formed by a chain end initially crossing the interface and then slowly more of the chain following it across. Failure after short joining times is thus expected to be by chain pullout; Even if polymer chain interdiffusion is based on physical interactions that give rise to the original differences of the chemical potentials which drive the mixing, chain scission failure occurs (i.e., chemical bonds rupture) as the diffusion distance increases. Even if it is not the main topic of this chapter, there has been a considerable amount of work on polymer chain reptation concept (de Gennes and Léger 1982) and on the kinetic aspects of chain coupling but the problem is not

solved, as the location of chain end groups with respect to the interface is not easy to determine.

### 3.3 Experimental Determination of Adhesion Forces

#### 3.3.1 Adhesion Forces Contribution to the Work of Adhesion

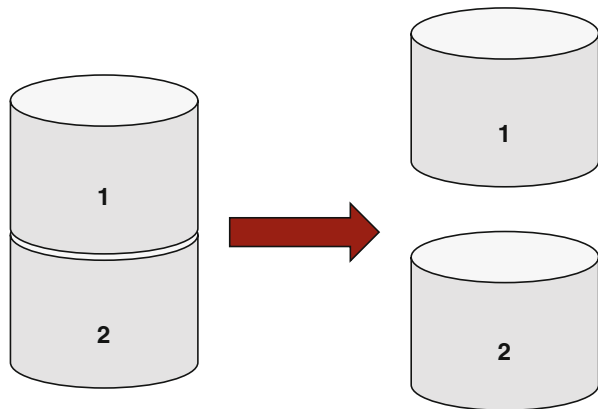
The magnitudes of forces responsible for adhesion (van der Waals, acid-base) can generally be related to fundamental thermodynamics quantities, such as surface free energies and work of adhesion. The work required to separate reversibly the interface between two bulk phases 1 and 2 from their equilibrium interacting distance to infinite one (Dupré 1869), represented on Fig. 3, is termed the “work of adhesion” and is equal to:

$$W_{12} = \gamma_1 + \gamma_2 - \gamma_{12} \quad (9)$$

where  $\gamma_1$  and  $\gamma_2$  are the surface free energies of phases 1 and 2, respectively, and  $\gamma_{12}$  is the interfacial free energy between phases 1 and 2. The work of adhesion is the decrease of Gibbs free energy per unit area when an interface is formed from two individual surfaces. Thus, the greater the interfacial attraction, the greater the work of adhesion will be and the smaller the interfacial free energy between phases 1 and 2 will be. Thereby,  $\gamma_{12}$  can be linked to the properties of the two individual phases. In the specific case of solid-liquid contact, phases 1 and 2 are commonly denoted phases S (solid) and L (liquid) and neglecting the spreading pressure of the vapor phase (V) of the liquid onto the solid, the solid-liquid work of adhesion ( $W_{SL}$ ) is:

$$W_{SL} = \gamma_S + \gamma_{LV} - \gamma_{SL} = \gamma_{LV}(1 + \cos \theta) \quad (10)$$

**Fig. 3** Representation of Hertz and Johnson-Kendall-Roberts (JKR) contact shapes



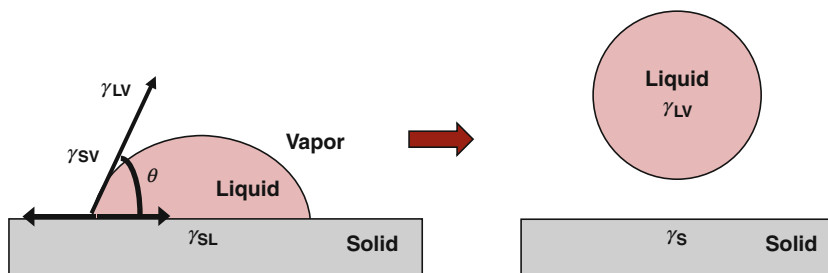


**Fig. 4** Reversible separation of two interacting bodies. The corresponding work is called “work of adhesion”

where  $\theta$  is the equilibrium contact angle at the three-phase contact point (Young 1805) as represented in Fig. 5. The first part of Eq. 10 is known as Dupré equation and its physical meaning is also represented in Fig. 4. More detailed consideration on wetting phenomena, surface energies, and thermodynamic of adhesion are presented in chapters relative to “Wetting” and “Work of adhesion” of this handbook. The subsections below will expose some experimental possibilities available to assess adhesion forces and interactions energies.

### van der Waals Forces Contribution to the Work of Adhesion

To reflect the contribution of the fundamental nature of the long-range interaction forces across the interface, it was suggested (Fowkes 1964) that surface free energies and work of adhesion may be expressed (Eq. 11) by the sum of two terms: the first one representative of London’s dispersion interactions (superscript D) and the second representative of non-dispersion forces (superscript ND), this latter include Debye induction forces, Keesom orientation forces, and acid-base interactions.

$$\gamma = \gamma^D + \gamma^{ND} \quad \text{and} \quad W_{12} = W_{12}^D + W_{12}^{ND} \quad (11)$$

Fowkes proposes that the London dispersive part of the work of adhesion is quantified as twice the geometric mean of the dispersive component of the surface energy of solid 1 and 2. The total work of adhesion reduced to:

$$W_{12} = 2(\gamma_1^D \gamma_2^D)^{1/2} + W_{12}^{ND} \quad (12)$$

If only London’s forces are present across the interface, the work of adhesion is fully determined because the nondispersive part is equal to zero. Indeed  $\gamma_1^D$  and  $\gamma_2^D$  can be easily determined by wettability experiments (Wu 1982). The only existence of London interactions at the interface between two adherends leads to:

$$W_{12} \approx W_{12}^D \quad (13)$$

### Dispersive Work of Adhesion ( $W^D$ ) and Adhesive Contact Theories (Hertz, DMT, JKR)

These theories concern the description of the contact between two homogeneous elastic bodies, usually two hemispheres or one hemisphere and one flat. Considered forces at the interface are only physical (van der Waals interactions). Hertz firstly describe such an elastic contact (Hertz 1896). He makes the hypothesis that solids are elastic, have smooth surfaces, and have small contact area with respect to solids dimensions, and finally have negligible adhesion and no friction. Outputs of Hertz theory are the shape of contact area, the load dependence of contact radius and stresses and strains in the contact zone. Johnson-Kendall-Roberts (JKR) extended the Hertz theory for the shape of two contacting but non-adhering elastic spheres to solids that do adhere (Johnson et al. 1971). Contact shapes are represented in Fig. 5 for Hertz and JKR approaches. The adhesion is due to the fact that real solids possess a finite surface tension. In the JKR theory, the attractive forces between the spheres are of infinitely short range and, hence, these forces manifest themselves only in the contact area. Derjaguin-Muller-Toporov (DMT) argue that since the attractive forces between the surfaces have a finite range, these forces also act in a region outside the contact zone where the surfaces are only a small distance apart (Derjaguin et al. 1975). The magnitude of these attractive forces outside the region of contact is responsible for deformation within the contact zone and determines the contact radius. Both theories show that the pull-off or adhesive force depends only on the interfacial tension and the radius of curvature of the undeformed surface and is independent of the contact radius and the elastic constants of the material such as the Young's modulus and the Poisson's ratio.

From the JKR theory, the pull-off force or adhesion force of a sphere (radius  $R$ ) from a flat is  $3\pi R\gamma$ , where  $\gamma$  is the interfacial tension between the solid and the indenting sphere. The DMT theory predicts that the pull-off force is  $4\pi R\gamma$ , i.e., greater by a factor of  $4/3$  than the adhesion force predicted by the JKR theory. The two

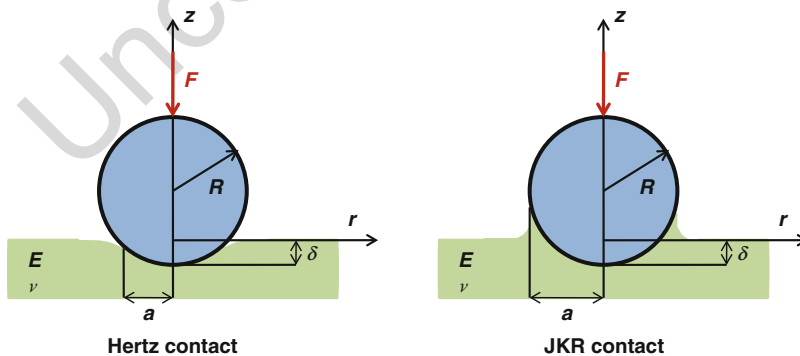


**Fig. 5** Reversible separation of a liquid droplet from a surface. The corresponding work satisfies Dupré equation

theories thus disagree in their predictions of interfacial tension from force measurements by this constant. However, there are two major differences between the theories that can be tested experimentally. One is the shape of the interface in contact under no load conditions and the second is the contact radius at which the surfaces separate. The JKR theory predicts that when the pull-off adhesion force equals  $3\pi R\gamma$ , the surfaces separate from a finite area of contact and the radius at pull-off is 0.63 times the radius under no load conditions. On the other hand, the DMT theory predicts that at the instant of separation, the contact radius is 0, i.e., the surfaces separate only at the point where they have achieved their original undistorted shape.

More interesting DMT and JKR theories give access to the thermodynamic work of adhesion. Indeed, based on different attractive stress distributions, established elastic theories for spherical contact, JKR and DMT, prescribe the adhesion force,  $F_{Adh}$ , in two different ways as  $F_{Adh} = 3/2\pi RW_0$  and  $F_{Adh} = 2\pi RW_0$ , respectively, with  $R$  is the sphere radius and  $W_0$  is the thermodynamic work of adhesion between bodies in contact. The debates on the validity of these two theories continued until Maugis showed that these two competing models are the limiting cases of his self-consistent transition model (Maugis 1992). This model adopts an adhesive potential between the surfaces exterior to the contact that exerts a constant stress,  $\sigma$ , until a critical separation distance,  $h$ , is reached (Dugdale approximation). Typically the value of  $h$  is chosen such that  $W_0 = \sigma h$  matches that of a potential describing van der Waals interactions between the surfaces. Nevertheless two important considerations must be outlined concerning the validity of these contact theories. The first one is that the considered solids in contact are purely elastic. Therefore the viscoelastic character of polymers still causes big difficulties in that context. The same is for the contact between a liquid adhesive and a solid substrate. As a consequence, experimental conditions have a major influence on the validity of the obtained results. Loading and unloading must be achieved in the linear elastic strain regime (first step of the loading regime for instance). The second point concerns the thermodynamic equilibrium of the contact. Experiments should be done as close as possible to equilibrium, i.e., close to zero strain rate. Making experiments at different strain rates and considering extrapolation to zero strain rate, one can assess the thermodynamic (reversible) work of adhesion (Amouroux and Léger 2003). If it is not the case, experiments will give the integral work of contact disruption (out of equilibrium).

### Complications Arising from Capillary Forces

The presence of liquid vapors in atmosphere can significantly affect the adhesion properties of bodies in contact. The major effect concerns the capillary condensation of water around surface contact sites. Liquids that easily wet surfaces (small contact angles) will spontaneously condense from vapor into surface pores and cracks as bulk liquid. As a consequence, a liquid meniscus can be formed between interacting bodies. This effect can strongly influence the adhesion of systems where the contact area is smaller than the capillary length (contact between a nanometer probe (AFM, nano-indentation) and a surface, adhesion of nanoparticles, etc.) At equilibrium, the meniscus curvature is related to the



relative vapor pressure. For surfaces interacting via discrete contacts in ambient conditions, the validity of Dupré's equation (Dupré 1869) is not obvious as the homogeneity of the medium is broken by the formation of water meniscus. Hence, neither the Dupré equation nor elastic continuum theories can be used to describe a meniscus-mediated contact. The equilibrium meniscus radius ( $r$ ) is described by the Kelvin equation,  $r = \gamma_{LV} V/kT \ln(p/p_{sat.})$ , where  $\gamma_{LV}$  is the surface tension of water,  $V$  is the molar volume of water,  $k$  is the Boltzmann constant,  $T$  is temperature, and  $p/p_{sat.}$  is the relative vapor pressure. The validity of the equation was experimentally verified by using a surface force apparatus (Fisher and Israelachvili 1979), where the effect of surface roughness is minimized by using smooth mica surfaces. The results imply that the Laplace pressure,  $P_L = 2\gamma_{LV}/r$ , acting inside a meniscus results in the capillary force between two contacting bodies. Thus, the maximum attractive adhesion force between a spherical body (radius  $R$ ) and a flat surface due to the liquid bridge, at zero separation distance, and considering the direct solid-solid contact adhesion force inside the liquid annulus is (Israelachvili 1991):

$$F_{adh} = 4\pi R(\gamma_{LV} \cos \theta + \gamma_{SL}) = 4\pi R\gamma_{SV} \quad (14)$$

## 500 Acid-Base Forces Contribution to the Work of Adhesion

### 501 Acid-Base Work of Adhesion

The knowledge of both the strength of acid-base interaction, i.e., the enthalpy of interaction, and the number of moles of acid or base functional groups interacting per unit area across the interface allow the determination of the reversible acid-base work of adhesion. In the particular case of adhesion between solids, it rapidly appears (Israelachvili 1991) that the contribution of the polar interactions (Keesom, Debye) to the thermodynamic work of adhesion could be neglected compared with both dispersive and acid-base contributions as experimentally confirmed (Fowkes et al. 1984). The acid-base component of the work of adhesion can be related to the variation of enthalpy per mole of acid-base interfacial adducts interaction,  $\Delta H_{12}^{AB}$ , as follows:

$$W_{12}^{ND} \approx W_{12}^{AB} = f(-\Delta H_{12}^{AB})n_{12}^{AB} \quad (15)$$

where  $n_{12}^{AB}$  is the number of mole of acid-base bonds per unit interfacial area and  $f$  is equal to:

$$f = [1 - d(\ln W_{12}^{AB})/d(\ln T)]^{-1} \quad (16)$$

$f$  is taken equal to unity in the case of the nondependence of  $W_{12}^{AB}$  with temperature.

The quantitative determination of these quantities can be either theoretical or experimental.

Theoretical determinations are mainly based on the assumption that the initial perturbation of the orbital of interacting species determines the course of a reaction or an interaction. In terms of equation of state, the perturbation theory was firstly developed. In terms of energy gap between HOMO and LUMO, acids and bases were defined by their hardness and softness. The Hard-Soft Acid-Base principle (Pearson 1963) describes some basic rules about kinetics and equilibrium of the acid-base interactions. The HSAB principle will be described as it has evolved in recent years on the basis of the density-functional theory (Parr and Yang 1989). For organic interactions, the following statements were proposed:

- A hard acceptor has a high energy LUMO and usually a positive charge.
- A soft acceptor has a low energy LUMO but does not necessarily have a positive charge.
- A hard donor has a low energy HOMO and usually a negative charge.
- A soft donor has a high energy HOMO but does not necessarily have a negative charge.

The principle states that hard acid prefers to interact with a hard base, and vice versa, a soft acid with a soft base. A hard-hard interaction is fast because of large Coulombic attraction; a soft-soft interaction is fast because of large orbital overlap between HOMO and LUMO. However, the problem is what is the physical meaning of hardness?

Berkowitz and Parr (1988) give a theoretical support to the absolute hardness,  $\eta$ . The absolute hardness determines the resistance of species to lose electrons. According to frontier orbital method, the relationship between  $\eta$  and the HOMO and LUMO energies is reduced to:

$$\eta = -1/2[E_{\text{HOMO}} - E_{\text{LUMO}}] \quad (17)$$

where  $\eta$  is the absolute hardness,  $E_{\text{HOMO}}$  is the energy level of the HOMO orbital, and  $E_{\text{LUMO}}$  is the energy level of the LUMO orbital.

Moreover, the absolute softness is defined as the reciprocal of the absolute hardness. The apparent success of the density-functional theory is to provide two parameters from which we can calculate the number of electrons transferred resulting mainly from the charge transfer between two molecules, i.e., from electrons flow until chemical potential reaches an equilibrium. As a first approximation, the number of electron transferred ( $N_{\text{Trans}}$ ) is given by (Shankar and Parr 1985):

$$N_{\text{Trans}} = [\mu_B - \mu_A]/2(\eta_A - \eta_B) \quad (18)$$

where  $\mu_A$  is the chemical potential of the acid,  $\mu_B$  is the chemical potential of the base,  $\eta_A$  is the absolute hardness of the acid, and  $\eta_B$  is the absolute hardness of the base. Calculation for various solid polymers could be found in a paper of Lee (1991).

The subsections below will emphasize the experimental options for getting quantitative data on adhesion interaction enthalpy ( $\Delta H^{AB}$ ).

### Effect of Ionocity and Covalency: Drago's Concept

Similar to the perturbation theory, Drago and Wayland proposed a four-parameter equation for predicting reaction enthalpies between acid and base species (Drago and Wayland 1965). Both species are each characterized by two independent parameters: an  $E$  value which measures their ability to participate in electrostatic bonding, and a  $C$  value which measures their ability to participate in covalent bond, leading to:

$$-\Delta H^{AB} = E_A E_B + C_A C_B \quad (19)$$

where  $\Delta H^{AB}$  is the enthalpy of acid-base adduct formation,  $E_A$  is the ability of the acid to participate in electrostatic bonding,  $E_B$  is the ability of the base to participate in electrostatic bonding,  $C_A$  is the ability of the acid to participate in covalent bonding, and  $C_B$  is the ability of the base to participate in covalent bonding.

A self-consistent set of  $E$  and  $C$  values is available (Drago 1973) for 33 acids and 48 bases, allowing  $\Delta H^{AB}$  prediction for over 1584 adducts. It is assumed that the conditions under which measurements are made (gas phase or poorly coordinating solvents) give rather constant entropy contribution and that most of the adducts are of one-to-one stoichiometry. The validity of Eq. 19 was clearly evidenced for polymer adsorption on various substrates.

Even if Drago's concept is an attempt to circumvent the quantum mechanical consideration of bond formation, the major importance of the above four parameters is their relationship with the HSAB principle. Actually, through the plot of  $E_A$  versus  $C_A$  for several liquids on a solid, one can obtain indirectly the values of the chemical softness  $1/\eta$  from the slope of  $C/E$ , as represented by the following equation:

$$E_A = [-\Delta H^{AB}/E_B - C_A C_B/E_B] \quad (20)$$

With the chemical hardness  $\eta$  and the chemical potential, one can easily apply the HSAB principle to acid-base interaction and calculate the number of electron transferred (Eq. 18).

### Effect of Amphotericity of Acid-Base Interaction: Gutmann's Numbers

Solvation, solvolysis, and ionic dissociation phenomena, in both aqueous and nonaqueous solutions are subsumed by the Lewis definitions. In addition to the previous discussion of the dual polarity character of Lewis acids and bases, it should be noted that many of them are amphoteric, by definition. Donor number,  $DN$ , were developed (Gutmann 1977) in order to correlate the behavior of a solute in a variety of donor solvents with a given basicity or donicity. A relative measurement of the basicity of a solvent is given by the enthalpy of its reaction with an arbitrarily chosen reference acid ( $\text{SbCl}_5$  in Gutmann's scale). Latter, an acceptor number  $AN$  was introduced as the relative  $^{31}\text{P}$  Nuclear Magnetic Resonance (NMR) shift induced by triethylphosphine, and relative to acidic strength ( $AN = 0$  for hexane and 100 for

SbCl<sub>5</sub>). These  $AN$  numbers were modified (Riddle and Fowkes 1990) to express them in the correct enthalpic unit (kcal/mol).

The most important assumption of Gutmann's approach is that the order of base strengths established remains constant for all other acids (solutes), the value of the enthalpy of formation of a given adduct being linearly related to the donor number of the base (solvent) through Eq. 21:

$$-\Delta H^{AB} = a_A DN_B + b_A \quad (21)$$

where  $\Delta H^{AB}$  is the enthalpy of acid-base adduct formation,  $DN_B$  is the donor number of the base, and  $a_A$  and  $b_A$  are constants characteristic of the acid.

Graphically, this means that a plot of  $DN_B$  for a series of donor solvents versus  $-\Delta H$  of their adduct formation with a given acid gives a straight line, allowing the determination of  $a_A$  and  $b_A$ . By experimentally measuring the enthalpy of formation of only two adducts for a given acid, one can predict, through the resulting  $a_A$  and  $b_A$  values, the enthalpy of adduct formation of this acid with any other donor solvent for which  $DN_B$  is known. Gutmann also proposes that the enthalpy of acid-base interaction could be approximated by a two-parameter equation of the form:

$$-\Delta H^{AB} = (AN_A DN_B) / 100 \quad (22)$$

where  $\Delta H_{AB}$  is the enthalpy of acid-base adduct formation,  $DN_B$  is the donor number of the base, and  $AN_A$  is the acceptor number of the acid.

The factor of 100 convert the  $AN_A$  value from a percentage of the SbCl<sub>5</sub> value to a decimal fraction. But one had to remind that on the 171  $DN_B$  values reported in the literature (Marcus 1984), only 50 were determined precisely, i.e., by flow microcalorimetric experiments.

Nevertheless Gutmann's approach has some limitation in the way it constitutes rather a prediction concept than an absolute way of determination of  $\Delta H^{AB}$ . Indeed this concept can be used to assess the determination of  $\Delta H^{AB}$  for probed liquids on a solid surface to assess the acid-base nature of the surface.

### IR Spectroscopic Tools to Assess Acid-Base Strength

For specific functional groups involved in acid-base interaction, the enthalpy of acid-base adduct formation is related to the infrared wavenumber shift,  $\Delta\nu$ , of its absorption band (Fowkes et al. 1984) according to the following equation:

$$\Delta H^{AB} = k_{AB} \Delta\nu_{AB} \quad (23)$$

Where  $\Delta H^{AB}$  is the molar enthalpy of acid-base adduct formation,  $\Delta\nu_{AB}$  is the infrared wavenumber shift, and  $k_{AB}$  is a correlation constant between IR wavenumber shift and enthalpy.

$k_{AB}$  is a characteristic constant of the functional group determined on the basis of compared infrared and microcalorimetric results of adduct formation. As an example, for the carbonyl functional group, C = O,  $k_{AB}$  is equal to  $-0.99 \text{ kJ/cm/mol}^{-1}$ .

The stretching wavenumber of the C = O vibration band is decreased by an amount  $\Delta\nu_{AB}$  proportional to the enthalpy of acid-base bonding  $\Delta H^{AB}$  according to  $k_{AB}$ . Such a methodology has been confirmed and case studies are available not only for polymer-solvent adduction but also for polymer/ polymer (Coleman et al. 1991) and polymer/metal adduction (Brogly et al. 1996, 1997). Moreover, infrared shifts can be used to determine Drago's  $E$  and  $B$  constants of unknown polymers or substrates. If a test acid of known  $C_A$  and  $E_A$  gives a  $\Delta\nu_{AB}$  shift allowing the determination of  $\Delta H^{AB}$  then Eq. 19 is reduced to:

$$E'_B = -\Delta H^{AB}/E_A - C'_B(C_A/E_A) \quad (24)$$

where  $E'_B$  and  $C'_B$  are "trial" values. The actual values of  $E_B$  and  $C_B$  occur at one point on the straight line obtained from Eq. 24. The use of multiple test acids shows that straight lines intersect at  $E_B$  and  $C_B$ .

Concerning the limitation of this approach, one must consider that best results are obtained from infrared transmission spectra. This technique is well adapted for the study of solution (polymer/solvent acid-base interactions) or thin films (polymer/polymer acid-base interactions). In the case of polymer/metal acid-base interaction, one can prefer infrared reflexion-absorption spectroscopy (IRAS) or polarization modulated infrared reflexion-absorption spectroscopy (PM-IRAS). Nevertheless this approach is a continuum-based (i.e., macroscopic) approach and it is important to understand that adhesion forces are not specified explicitly even if acid-base interactions contributed to  $\Delta H^{AB}$ .

### Adhesion Forces Measured by Atomic Force Microscopy

Advances in nanotechnology and miniaturization of devices have led to the requirement of an increased understanding of the interactions and adhesion phenomena present in nanoscale contacts. The forces involved include van der Waals forces, hydrogen bonds, electrostatic forces, as well as chemical bond in some cases. Although van der Waals forces are only short range (nanometer range), they often rule the adhesion between two materials and are therefore responsible for contact interactions. In recent years, Atomic Force Microscopy (AFM) has become a powerful tool, sensitive enough, to detect small surface forces and to study adhesion at the nanoscale. Retraction profiles from Force-Distance AFM measurements provide quantitative, chemically sensitive, adhesion information at the nanoscale between probe tips and sample surfaces. Information about local adhesion, friction, or surface stiffness is readily obtainable. The purpose and scope of this section is to describe the experimental method that enables one to assess nanoadhesion forces. Indeed, the quantitative determination of the work of adhesion gives rise to numerous experimental and theoretical approaches. Nevertheless, all these approaches are mainly macroscopic and not made "in situ." As a consequence, characterizations of local properties have stimulated widespread interest. Recent works have contributed to the understanding of adhesion mechanisms at a local scale. Burns et al. (1999) have demonstrated the influence of adhesion on sliding and on friction forces on chemically modified surfaces. Jones et al. (2002) have studied the effects of relative

humidity, roughness, and surface treatment on adhesive properties of glass-glass contact. But few studies have been devoted to the contact between a local probe and a chemically modified surface or polymer surface. Dissipative phenomena in the adhesive contact by using dynamic AFM were nevertheless studied (Boisgard et al. 2002). Finally Brogly et al. (2009) have done experiments on chemically modified polymer surfaces in order to investigate the interplay between surface chemistry and mechanical properties at a local scale.

### Force Versus Distance Measurements with an AFM

Force measurements with AFM, in the contact mode, consist in detecting the deflection of a spring (or cantilever) bearing tip at its end, when interacting with the sample surface. The deflection of the cantilever is detected by an optical device (four quadrant photodiode) while the tip is vertically moved forward and backward thanks to a piezoelectric ceramic (or actuator). Thus, provided that the spring constant of the cantilever is known, one can obtain a Deflection-Distance (DD) curve and then a Force-Distance (FD) curve, by using Hooke's law. The DD curves presented in this chapter were performed in air. A schematic representation of a DD curve obtained when probing a hard surface is reported in Fig. 6.

In zone A, the cantilever is far from the surface and stays in a state of equilibrium (no interaction with the surface). The cantilever deflection is zero. During the approach toward (or withdrawal from) the surface, the tip interacts with the sample and a jump in (or jump-off) contact occurs (zones B (for loading) and E (for unloading)). These instabilities take place because the cantilever becomes mechanically unstable. Usually, for undeformable surfaces, because of mechanical instabilities, jump-in contact is not significant to determine attractive van der Waals forces. When in contact, the cantilever deflection is equal to the piezoelectric ceramic displacement provided no indentation of the substrate occurs (zones C (for loading) and D (for unloading)). An undeformable reference sample (cleaned silicon wafer) is used to scale the DD curve in deflection by fixing to unity the slope value of the

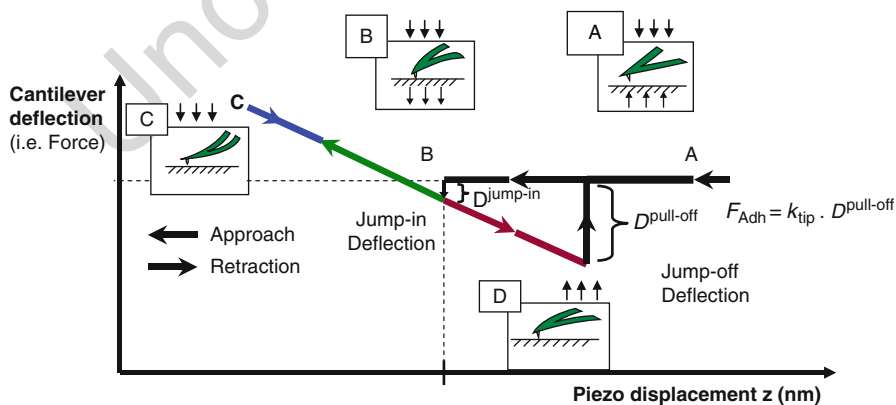


**Fig. 6** Schematic representation of a Force-Distance curve

contact line. Due to adhesion forces during contact, the jump-off is more interesting than the jump in and occurs in position D. Considering the cantilever like a spring, knowing its spring constant, one can obtain the adhesion force ( $F_{\text{Adh.}}$ ) between the tip and the sample by using Hooke's law:

$$F_{\text{Adh.}} = k_{\text{tip}} \cdot D^{\text{pull-off}} \quad (25)$$

where,  $k_{\text{tip}}$  represents the spring constant of the cantilever and  $D^{\text{pull-off}}$  represents the jump off deflection during retraction of the tip from the surface. The DMT theory also establishes a relationship between the adhesion force ( $F_{\text{adh}}$ ), the tip radius ( $R$ ), and the thermodynamic work of adhesion ( $W_0$ ):

$$F_{\text{adh}} = 2\pi R W_0 \quad (26)$$

Strictly speaking, experimental measurement is made out of equilibrium leading determination of the integral work of disruption rather than reversible work of adhesion. On the basis of this relation, one can deduce  $W_0$  from experimental adhesion forces. In order to carry out a quantitative analysis, different experimental points should be taken into consideration such as: selection of tips that possess apex spherical shape (SEM imaging), cantilever spring constant, tip radius, linearity of the photodiodes, piezodriver hysteresis, cantilever and piezo thermal stabilities and tip contamination (Noel et al. 2004).

### 3.4 Case Study: In Situ Determination of the Work of Adhesion

#### 3.4.1 Force – Distance Experiments on Self-Assembly Monolayers (SAMs)

In order to quantitatively and in situ measure the work of adhesion between an AFM tip and a given surface, one has to proceed according to a proper procedure that enables to control surface chemistry and thus surface forces. Organosilane molecules spontaneously organize to form self-assembly monolayers (SAMs). Such a self-organizing process gives rise to the elaboration of homogeneous model surfaces of controlled surface chemistry. Three different techniques are frequently used to obtain SAMs: Langmuir-Blodgett techniques, involving an air-water interface to transfer the assembled film to a solid substrate, solution adsorption of film molecules onto the substrate, and vapor-phase molecular self-assembling technique, which uses vapor deposition of the film onto the substrate. This last technique should be preferred, because the lack of solvent prevents the SAMs of a possible incorporation of small solvent molecules contamination and defects. Molecular films prepared with this method are homogeneous, stable, and resistant. Hydrophobic model surfaces could be prepared by using hexadecyltrichlorosilane ( $\text{C}_{16}\text{H}_{42}\text{Cl}_3\text{Si}$  or  $\text{Si}_{\text{CH}_3}$ ) and 1H,1H,2H,2H-perfluorodecylmethyldichlorosilane ( $\text{C}_{11}\text{H}_7\text{Cl}_2\text{F}_{17}\text{Si}$  or  $\text{Si}_{\text{CF}_3}$ ) and

**Table 2** Water contact angles and surfaces energies of self-assembly monolayers (SAM) on silicon wafers substrates (From Noel et al. 2004)

Substrates	Contact angle of water (°)	Surface energy (mJ/m <sup>2</sup> )
Si-CF <sub>3</sub>	106 ± 2	21 ± 1
Si-CH <sub>3</sub>	103 ± 2	22 ± 1
Si-COOR	71 ± 2	43 ± 1
Si-NH <sub>2</sub>	57 ± 2	53 ± 1
Si-OH	6 ± 2	76 ± 1

t.1  
t.2  
t.3  
t.4  
t.5  
t.6

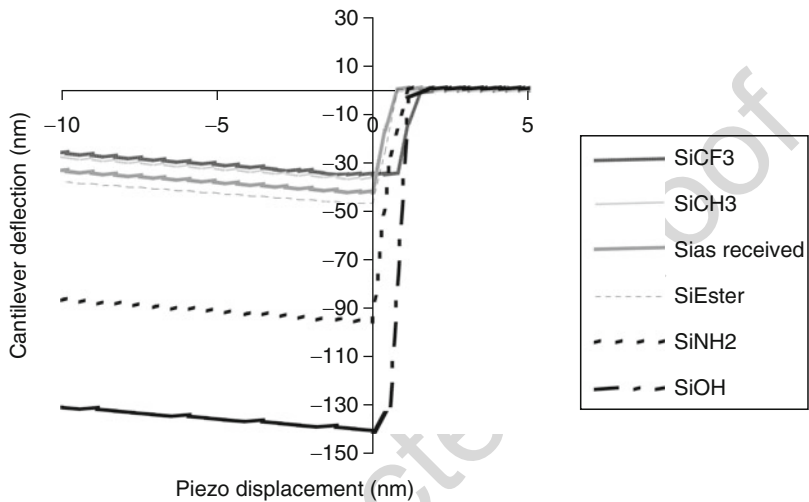


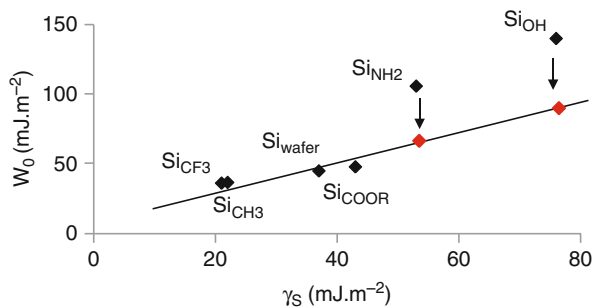
**Fig. 7** Experimental Deflection-Distance curves (retraction) on functionalized silicon wafers

hydrophilic model surfaces by using (6-aminohexyl)-aminopropyltrimethoxysilane ( $C_{12}H_{30}N_2O_3Si$  or  $Si_{NH_2}$ ) and 2(carbomethoxy)ethyltrichlorosilane ( $C_4H_7Cl_3O_2Si$  or  $Si_{ester}$ ), for instance. Equilibrium contact angle measurements with water droplets and surface energy (determined by wettability using various probed liquids (water, tricresyl phosphate,  $\alpha$ -bromonaphtalene, diiodomethane)) values obtained on silicon wafer grafted with such organosilanes are gathered in Table 2. It is important to note that surface roughness is extremely low ( $<0.2$  nm) and that the wetting liquids do not modify the physicochemical properties of the SAMs.

Table 2 shows that surface energy can be easily tuned, from highly hydrophobic to highly hydrophilic, in an elegant way by grafting SAMs on a dedicated surface. Fig. 7 shows AFM Deflection-Distance curves during retraction of the AFM tip from SAM modified silicon wafers. Results show clearly that force-distance curves are sensitive to a surface chemical modification by organosilane grafting. It is important to understand that during retraction of the cantilever, deflection is equal to the piezoelectric ceramic displacement (slope equal to unity) provided no indentation of the substrate occurs. On Fig. 7, all the experimental curves were horizontally shifted on the x-axis in order fix the beginning of pull-off at a value of x equal to zero.



**Fig. 8** Thermodynamic work of adhesion ( $W_0$ ) deduced from AFM (Derjaguin – Muller – Toporov (DMT) theory) versus surface energy of self-assembly monolayers (SAMs)



When jump-out of contact occurs, the corresponding pull-off deflection is measured. Pull-off deflection values ( $D^{\text{pull-off}}$ ) increases in the following order:

$$D^{\text{pull-off}}_{\text{SiCF}_3} < D^{\text{pull-off}}_{\text{SiCH}_3} < D^{\text{pull-off}}_{\text{SiCOOR}} < D^{\text{pull-off}}_{\text{SiNH}_2} < D^{\text{pull-off}}_{\text{SiOH}}$$

Knowing the pull-off deflection, one can easily deduce (Eq. 25) the adhesion force, knowing the cantilever spring constant  $k_{\text{tip}}$ . The pull-off deflection and thus the adhesion force value increases with the hydrophilicity of the surface. The measured adhesion force depends strongly on the tip radius in the case of purely rigid substrates (for which the slope in the deflection vs. piezo displacement is equal to unity, i.e., for 1 nm of piezo displacement the tip is deflected of 1 nm), the adhesion force being proportional to the tip radius. The DMT theory, also establish a relationship (Eq. 26) between the adhesion force ( $F_{\text{adh}}$ ), the tip radius ( $R$ ), and the work of adhesion ( $W_0$ ). On the basis of this relation one can deduce  $W_0$  from experimental adhesion forces. Fig. 8 shows that the work of adhesion,  $W_0$ , is proportional to the surface energy deduced from classical wettability measurements. If both the AFM tip and the silicon wafer are grafted with the same self-assembly monolayers, then the  $W_0$  should be equal to twice the surface energy (either of the wafer or the tip). Such an experiment (Noel et al. 2006) is an elegant way to demonstrate the possibility that give AFM to quantitatively measure both adhesion forces, work of adhesion and surface energy.

### 3.4.2 Influence of Capillary Forces on Adhesion Forces

In the case of hydrophilic surfaces (Si-NH<sub>2</sub>, Si-OH), the AFM tip interacts with the water layer adsorbed on the surface and the measured adhesion force results from the adhesion between water adsorbed on the both surfaces (tip and sample) and from the adhesion force due to the van der Waal forces between the NH<sub>2</sub> or OH sites existing at the grafted wafer surface. On the contrary, during wettability experiments the water droplet deposited on the surface is not sensitive to OH sites existing at the hydroxylated wafer surface but only to water molecules adsorbed on the hydroxylated surface.

Under these conditions, the influence of the capillary forces cannot be neglected. When AFM experiments are conducted in air medium, one has to suspect the existence of a capillary bridge (Kim et al. 2008). On the theoretical point of view, the minimum thickness of the water capillary film is expressed as (de Gennes 1985):

$$e = a_0(\gamma_w/S) \quad (27)$$

Where  $e$  is the film thickness,  $\gamma_w$  the surface tension of water,  $a_0$  a capillary length, and  $S$  the spreading coefficient ( $S = \gamma_S - \gamma_{SL} - \gamma_L$ ). As a consequence, the force measured by AFM includes the contribution of van der Waals and capillary forces. The total adhesion force is given by the following expression:

$$F_{adh} = F_{cap} + F_{VDW} \quad (28)$$

One can wonder about considering forces or energies. As in the present case, the slope in the deflection vs. piezo displacement is equal to unity during tip retraction is obvious, to a first approximation that the adhesion force (proportional to pull-off deflection) and energy of contact disruption (integral work of contact disruption) vary in proportion. Work will be done on forces. The capillary condensation induces the formation of a meniscus between the two surfaces and generates a capillary force which is given in the case of sphere-plane contact, by (Riedo et al. 2002):

$$F_{cap} = 2\pi R\gamma_w(\cos \theta_{w/tip} + \cos \theta_{w/wafer}) \quad (29)$$

where  $\gamma_w$  is the surface tension of water,  $R$  the tip radius, and  $\theta$  the contact angle between water and the tip or between water and the wafer. One can wonder about the possibility to apply Eq. 29, which derive from macroscopic considerations, to the case of nanoscopic measurements. In fact Environmental scanning electron microscopy can be used (Weeks et al. 2005) to image water meniscus formation between an AFM tip and a surface. Values of  $W_0$  obtained after correction from capillary force contribution on Si-NH<sub>2</sub> and Si-OH hydrophilic surfaces are represented by black circles in Fig. 8. Values of capillary force and van der Waals forces in the case of hydrophilic contacts were gathered in Table 3.

Taking into account the contribution of capillary forces, Fig. 8 shows that a good correlation is observed between the work of adhesion ( $W_0$ ) and the surface energy of the chemically modified solids ( $\gamma_s$ ). As a consequence, these results demonstrate that AFM Force-Distance experiments could be used to determine quantitatively the contribution of van der Waals forces and capillary force to the adhesion force.

**Table 3** Contribution of capillary force ( $F_{cap}$ ) and van der Waals forces ( $F_{vdw}$ ) to adhesion force ( $F_{adh}$ ) and work of adhesion ( $W_0$ )

Substrates	$F_{adh}$ (nN)	$F_{cap}$ (nN)	$F_{vdw}$ (nN)	$W_0$ (mJ/m <sup>2</sup> )
Si-NH <sub>2</sub>	33	17	16	52
Si-OH	45	27	18	60

t.1

t.2

t.3

### 3.5 Conclusions

Adhesion is a complex phenomenon and cannot be interpreted using a single model in view of the diversity of forces, materials, and process involved. However, the forces developed during adsorption and molecular contacts are believed to be one of the most important mechanisms in achieving adhesion. Diffusion and wetting are merely kinetic means to obtain good adsorption at the interface. By diffusion and wetting, the adsorbed molecules can reach an intimate contact with the substrate and allows the van der Waals and/or acid-base interactions to take place, which are predominant in numerous situations. Nevertheless, rigorous computation of van der Waals forces remains difficult. The same is for acid-base interaction energies on the basis of molecular orbital approach or quantum mechanical consideration. Thus, the knowledge of the surface properties of materials on the bases of continuum-based theories (hence macroscopic) allows an estimation of solid-solid or solid-liquid interfacial interactions, which is a necessary condition prior to any study on adhesion. In that sense, understanding the fundamentals of forces involved in adhesion helps to create conditions that will promote or reduce the attractive forces between interacting bodies and thus control adhesion. Development of local probe techniques (surface force apparatus (SFA), atomic force microscopy (AFM)) allows accessing directly adhesion force measurements. But one has to remind that the influence of capillary forces is obvious considering the nanometric size of the probes (nanoindentation, AFM). Other successful methods to quantify specific (acid-base) interaction energies are based on enthalpy or heat of adsorption measurements. Flow microcalorimetry, inverse gas chromatography (IGC), and spectroscopic techniques (FTIR) are particularly dedicated. To conclude one has also to consider that the specific case of biological adhesion was not treated in this chapter. Many other forces should then be involved in biological adhesion such as solvation, hydrophobic, entropic, and nonequilibrium forces.

### References

- Amouroux N, Léger L (2003) Effect of dangling chains on adhesion hysteresis of silicone elastomers, probed by JKR test. *Langmuir* 19:1396
- Berkowitz M, Parr RG (1988) Molecular hardness and softness, local hardness and softness, hardness and softness kernels, and relations among these quantities. *J Chem Phys* 88:2554
- Boisgard R, Aime JP et al (2002) Surface mechanical instabilities and dissipation under the action of the oscillating tip. *Surf Sci* 511:171
- Brochart-Wyart F, de Gennes PG et al (1994) Adhesion promoters. *J Phys Chem* 98:9405
- Brogly M, Nardin M et al (1996) Evidence of acid-base interfacial adducts in various polymer/metal systems by IRAS: improvement of adhesion. *J Adhes* 58:263
- Brogly M, Grohens Y et al (1997) Influence of tacticity on the conformation and development of acid-base adducts of PMMA homopolymers adsorbed on aluminium mirrors. *Int J Adhes Adhes* 17:257
- Brogly M, Awada H et al (2009) Contact atomic force microscopy: a powerful tool in adhesion science, Nanaoscience and technology, applied scanning probe methods XI. Springer, Berlin

- 843 Brown HR (1991) A molecular interpretation of the toughness of glassy polymers. *Macromolecules*  
844 24:2752
- 845 Brown HR, Deline VR et al (1989) Evidence for cleavage of polymer chains by crack propagation.  
846 *Nature* 341:221
- 847 Burns AR, Houston JE et al (1999) Molecular level friction as revealed with a novel scanning probe.  
848 *Langmuir* 15:2922
- 849 Casimir HBG, Polder D (1948) The influence of retardation on the London-van der Waals forces.  
850 *Phys Rev* 73:360
- 851 Coleman MM, Graf F et al (1991) Specific interactions and the miscibility of polymer blends.  
852 Technomic Pub, Basel
- 853 Debye PJW (1921) Molekularkräfte und ihre Elektrische Deutung. *Phys Z* 22:302
- 854 de Gennes PG (1985) Wetting: statics and dynamics. *Rev Mod Phys* 57:827
- 855 de Gennes PG, Léger L (1982) Dynamics of entangled polymer chains. *Annu Rev Phys Chem*  
856 33:49
- 857 Derjaguin BV, Muller VM et al (1975) Effect of contact deformations on the adhesion of particles.  
858 *J Colloid Interface Sci* 53:314
- 859 Drago RS (1973) Quantitative evaluation and prediction of donor-acceptor interactions. *Struct*  
860 *Bond* 15:73
- 861 Drago RS, Wayland B (1965) A double-scale equation for correlating enthalpies of Lewis acid-base  
862 interactions. *J Am Chem Soc* 87:3571
- 863 Dupré A (1869) *Théorie Mécanique de la Chaleur*. Gauthier-Villars, Paris
- 864 Fisher LR, Israelachvili JN (1979) Direct experimental verification of the Kelvin equation for  
865 capillary condensation. *Nature* 277:548
- 866 Flinn DH, Guzonas DA et al (1994) Characterization of silica surfaces hydrophobized by octa-  
867 decyltrichlorosilane. *Colloids Surf A* 87:163
- 868 Fowkes FM (1964) Attractive forces at interfaces. *Ind Eng Chem* 56:40
- 869 Fowkes FM, Tischler DO et al (1984) Acid-base complexes of polymers. *J Polym Sci: Polym Chem*  
870 22:547
- 871 Gent AN, Ahagon A (1975) Effect of interfacial bonding on the strength of adhesion. *J Polym Sci*  
872 *Polym Phys* 13:1285
- 873 Gutmann V (1977) *The donor-acceptor approach to molecular interaction*. Plenum Press, New York
- 874 Hamaker HC (1937) The London – van der Waals attraction between spherical particles. *Physica*  
875 4:1058
- 876 Hawthorne MF, Dunks GB (1972) Metallocarboranes that exhibit novel chemical features. *Science*  
877 178:462
- 878 Hertz H (1896) *Miscellaneous papers*. Macmillan, London
- 879 Hough DB, White LR (1980) The calculation of Hamaker constants from Lifshitz theory with  
880 applications to wetting phenomena. *Adv Colloid Interf Sci* 14:3
- 881 Israelachvili JN (1991) *Intermolecular and surface forces*. Academic Press Ltd, London
- 882 Jensen WB (1979) *The Lewis acid-base concepts: an overview*. Wiley, New York
- 883 Johnson KL, Kendall K et al (1971) Surface energy and the contact of elastic solid. *Proc R Soc A*  
884 324:301
- 885 Jones R, Pollock HM et al (2002) Adhesion forces between glass and silicon surfaces in air studied  
886 by AFM: effects of relative humidity, particle size, roughness, and surface treatment. *Langmuir*  
887 18:8045
- 888 Keesom WH (1922) Die Berechnung der molekularen Quadrupol- momente aus der Zustands-  
889 gleichung. *Phys Z* 23:225
- 890 Kim DI, Grobelyny J et al (2008) Origin of adhesion in humid air. *Langmuir* 24:1873
- 891 Klopman G (1974) *Chemical reactivity and reaction paths*. Wiley-Intersciences, New York
- 892 Laurens C, Creton C et al (1994) Adhesion promotion mechanisms at isotactic polypropylene/  
893 polyamide 6 interfaces: role of the copolymer architecture. *Macromolecules* 37:6814
- 894 Lee LH (1991) *Fundamentals of adhesion*. Plenum Press, New York
- 895 Lewis GN (1923) *Valence and the structure of atoms and molecules*. The Chemical Catalog Co,  
896 New York

- 897 Lewis AF, Natarajan Gounder RT (1991) In: Patrick RL (ed) Treatise on adhesion and adhesives,  
898 vol 5. Arnold, Cop, New York, p 313
- 899 London F (1937) The general theory of molecular forces. *J Chem Soc Faraday Trans* 33:8
- 900 Marcus Y (1984) The effectivity of solvents as electron pair donors. *J Solut Chem* 13:599
- 901 Maugis D (1992) Adhesion of spheres: the JKR-DMT transition using a Dugdale model. *J Colloid*  
902 *Interface Sci* 150:243
- 903 Mulliken RS, Pearson WB (1969) Molecular complexes: a lecture and reprint volume.  
904 Wiley-Intersciences, New York
- 905 Nakamura S, Pavlovic E et al (2007) Fracture energy of epoxy interfaces with layers of different  
906 silane coupling agents. *J Adhes* 83:351
- 907 Noel O, Brogly M et al (2004) In situ determination of the thermodynamic surface properties of  
908 chemically modified surfaces on a local scale: an attempt with the atomic force microscope.  
909 *Langmuir* 20:2707
- 910 Noel O, Awada H et al (2006) Force curve measurements with the AFM: application to the in situ  
911 determination of grafted silicon-wafer surface energies. *J Adhes* 82:649
- 912 Parr RG, Yang W (1989) Density functional theory of atoms and molecules. Oxford University  
913 Press, New York
- 914 Pauling L (1960) The nature of chemical bond. Cornell University Press, New York
- 915 Pearson RG (1963) Hard and soft acids and bases. *J Am Chem Soc* 85:3533
- 916 Plueddemann EP (1982) Silane coupling agents. Plenum Press, New York
- 917 Riddle FL Jr, Fowkes FM (1990) Spectral shifts in acid-base chemistry. 1. van der Waals contri-  
918 butions to acceptor numbers. *J Am Chem Soc* 112:3259
- 919 Riedo E, Levy F et al (2002) Kinetics of capillary condensation in nanoscopic sliding friction. *Phys*  
920 *Rev Lett* 88:185505
- 921 Shankar S, Parr RG (1985) Electronegativity and hardness as coordinates in structure stability  
922 diagram. *Proc Natl Acad Sci USA* 82:264
- 923 Spruch L (1986) Retarded, or Casimir, long-range potentials. *Phys Today* 11:37
- 924 Tao G, Gong A et al (2001) Surface functionalized polypropylene: synthesis, characterization, and  
925 adhesion properties. *Macromolecules* 34:7672
- 926 Tirrel M, Falsafi A et al (2001) Role of chain architecture in the adhesion of block copolymers.  
927 *Macromolecules* 34:1323
- 928 Weeks BL, Vaughn MW et al (2005) Direct imaging of meniscus formation in atomic force  
929 microscopy using environmental scanning electron microscopy. *Langmuir* 21:8096
- 930 Wool RP (1995) Polymer interfaces. Hanser, Berlin
- 931 Wu S (1982) Polymer interface and adhesion. Marcel Dekker Inc, New York
- 932 Young T (1805) An essay on the cohesion of fluids. *Phil Trans R Soc A* 95:65

Martin E. R. Shanahan and Wulff Possart

## Contents

4.1	What Is Wetting? .....	72
4.2	Thermodynamics of a Phase Boundary: An Introduction .....	74
4.2.1	Brief Description of Gibbs' Model for a Phase Boundary .....	75
4.2.2	Energy Balance for a Two-Phase System: Thermodynamic Potentials .....	82
4.3	Thermodynamic Equilibrium of Three Phases: Basics .....	84
4.4	Experimental Aspects of Static Wetting .....	86
4.4.1	Liquid Surface Tension .....	87
4.4.2	Contact Angle .....	91
4.5	Free Energy Balance of Wetting .....	95
4.6	Concluding Remarks .....	99
References	.....	100

## Abstract

The contact between a solid and a liquid involves the phenomenon of wetting. This is the intuitive, intimate contact between the two phases. We consider here thermodynamic aspects of wetting, which involves three phases in fact, since the environment must be taken into account. Methods for determining wetting characteristics are discussed.

M. E. R. Shanahan (✉)

Institut de Mécanique et d'Ingénierie-Bordeaux (I2M), CNRS UMR 5295, Université de Bordeaux, Talence, France

e-mail: [martin.shanahan@u-bordeaux.fr](mailto:martin.shanahan@u-bordeaux.fr)

W. Possart

Lehrstuhl Adhäsion und Interphasen in Polymeren, Universität des Saarlandes, Saarbrücken, Germany

e-mail: [w.possart@mx.uni-saarland.de](mailto:w.possart@mx.uni-saarland.de)

## 4.1 What Is Wetting?

When you “wet” your hands under the tap, or in a bowl of water, you are implicitly assuming that the water is directly, intimately, contacting your skin. Water is wet, apparently even etymologically. The Indo-European root of water is \*wed-, “wet.” However, this important, implicit connotation of the term wetting clearly fails if you are so unlucky as to break an old mercury thermometer or barometer and get the liquid on your skin. The mercury tucks itself up into little beads and apparently does not “wet” your skin. What is the fundamental difference? This can be explained by the concept of “contact angle,”  $\theta$ . For present purposes, it will suffice to discuss the “static” contact angle,  $\theta_0$ . Let us consider the case of a small drop of liquid deposited on a flat, solid surface (Most real solid surfaces are, of course, rough. The consequences will be considered below in Sect. 5), from an intuitive viewpoint. A *meniscus* (Greek: *mēniskos* = crescent), corresponding to the liquid/air environment, is formed. After *spreading* (cf. chapter Spreading of Liquids on Substrates) to rest (equilibrium) has occurred, a *sessile* (“sitting”), static drop of the liquid is present. Angle  $\theta_0$  is that subtended between the solid/liquid interface and the tangent to the liquid/air interface, as shown schematically in Fig. 1. It is measured perpendicularly both to the solid surface and to the triple line of contact where solid, liquid, and air come together. (For definiteness, the surrounding medium is regarded as “air.” More precisely, the surrounding gas, air or otherwise, *always* contains vapor of the liquid and, in principle, of the solid. However, the vapor pressure of most solids is very low.)

Of course, the gas phase could be a second liquid, provided it has a miscibility gap with the first liquid. Henceforth, the envrioning phase will generally be referred to as “vapor” while bearing in mind the previous comment. Referring to Fig. 1, it may be seen that the case on the left represents a contact angle of less than  $90^\circ$  ( $\pi/2$  rad), and may be called “good wetting,” whereas that on the right is such that  $\theta_0 > 90^\circ$ , and this represents “poor wetting.” In the extreme case of  $\theta_0 \rightarrow 0$ , the liquid becomes a thin film (e.g., oil deposited on a steel sheet). This is often called

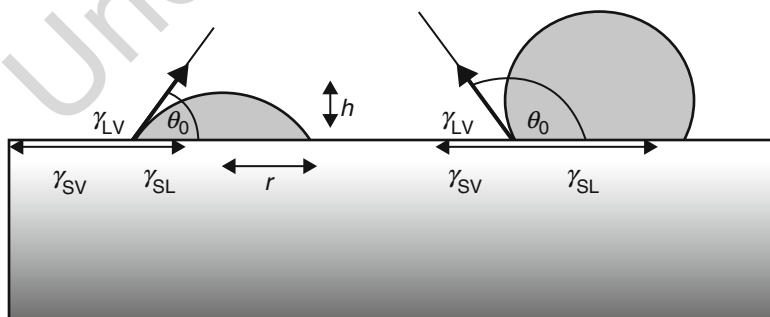


**Fig. 1** Schematic representation of low (*left*) and high (*right*) static contact angles,  $\theta_0$ . Interfacial tensions are represented by *arrows* and termed  $\gamma_{ij}$  (*S* solid, *L* liquid, *V* vapor/surrounding fluid phase)

*spreading*. Although it will not be treated here, the thickness of such films depends on long-range molecular forces, which may span the entire liquid thickness of the film, leading to what is effectively “interference” between the two interfaces, liquid–solid and vapor–liquid (cf. chapter Spreading of Liquids on Substrates). However, this is beyond the scope of the present chapter as such spreading is fundamentally different from simple wetting. At the other extreme, the case of  $\theta_0 \rightarrow 180^\circ$ , non-wetting, may be considered. This cannot, in fact, exist if the solid is truly smooth and if the environment is only gaseous but can in some cases when two liquids are involved (Shanahan et al. 1982). The importance of contact angle is that it determines the extent of (solid) surface coverage by a liquid. It is intuitively clear that the interfacial area covered by a sessile drop of given, fixed volume  $V$  of liquid increases as contact angle decreases, but this may be readily written formally in the case of a spherical, cap-shaped drop of contact radius  $r$  and height  $h$ . Writing  $t = \tan(\theta_0/2) = h/r$ , and with a standard trigonometric formula for the volume,  $V$ , of a spherical segment:  $V = \pi h(3r^2 + h^2)/6$ , it is readily shown that the contact area,  $A$ , is given by

$$A = \pi \cdot r^2 = \pi^{1/3} \left[ \frac{6V}{t(3 + t^2)} \right]^{2/3} \quad (1)$$

In the range of possible contact angles,  $0^\circ \leq \theta_0 \leq 180^\circ$ ,  $t$  is a monotonically increasing function of  $\theta_0$ , and therefore,  $A$  increases as  $\theta_0$  decreases, at constant  $V$ .

So, decreasing  $\theta_0$  implies better coverage, or wetting, but what controls  $\theta_0$ ? Between the solid and liquid and liquid and vapor phases, there are *phase boundaries* of the different substances. These can be imagined as 2D faces, or interfaces, but nature is never so clear-cut, and a vague transition zone, the interphase, typically of the order of a few nm (nanometers) or a few tens of nm thick constitutes the changeover. It has to be mentioned that an interphase and its width is not a uniquely defined thing as it has to be attributed to the macroscopic physical or chemical quantity of interest. In other words, each thermodynamic quantity of a heterogeneous system can possess its particular spatial function across its own interphase. The interphase will be considered in Sects. 2 and 3. However, accepting as a first approximation that 2D interfaces separate phases, it can be seen in the typical case exemplified in Fig. 1 that there are three *interfaces*: SL, LV, and SV (S, solid; L, liquid; V, vapor/surrounding medium), each of which has associated with it an *interfacial tension*  $\gamma_{IJ}$  where  $I$  and  $J$  refer to S, L, and V (see Sect. 2 for definition). Note that the very concept of “force/distance” is meaningless in absolute terms, since the force will have no area to “pull” or “push” on: the idea of a “stress” becomes vague. In fact, it is Gibbs’ concept of “surface excess” (cf. Sect. 2) that allows one to see that the forces are, in fact, acting over a thin layer at the interface, and thus the concept of stress is still valid. The three phases, and therefore interfaces, meet at the drop periphery, at what is termed term the *triple line* or *contact line*. Again, this is not really a line, but a “tube,” but the concept of line is adequate in Gibbs’ treatment. A force balance between the various  $\gamma_{IJ}$  exists at the triple line, and, at equilibrium, this is principally what governs the value of  $\theta_0$  (see below for details).



Accepting the concept of contact angle, its importance may be appreciated in many sectors, biological and industrial. Without resorting to equations, it is intuitive (and correct) to realize that it is more difficult to remove an oil film from steel (contact angle ca.  $0^\circ$ ) than a drop of mercury from glass (contact angle ca.  $130^\circ$ ). Not only is adherence of the oil intrinsically better, but for a given volume, coverage is superior. The same, of course, has to apply to paints and inks. If an insecticide is applied to a leaf, it is clearly inefficient if, when the leaf slopes, the liquid simply rolls off. Therefore, a small, preferably zero, contact angle is required. In the case of adhesives, this significant coverage and propensity to wet the solid in contact is crucial in forming a good bond as it gives the molecules the *opportunity* to form adhesive interactions, even if the “true,” chemical, bond is produced later by hardening of the adhesive (drying, chemical reaction, cooling). If the surface is rough, the same wetting tendency will help ensure filling the interstices. This not only increases true contact area, but reduces stress concentrations, liable to be crack initiators.

There are, of course, many cases where *poor* wetting is required. Nature masters this beautifully in the case of, for example, duck feathers and lotus leaves (Zhang et al. 2009). Mankind attempts to exploit it with PTFE and other polymers as cooking utensil coatings and raincoat treatments.

The main objective of this chapter is to consider in more detail the phenomenology of wetting, specifically in the static case (kinematics are covered in chapter Spreading of Liquids on Substrates). In other words, the triple phase line will principally be considered to be at rest. The description will now be couched in terms of the needs of thermodynamic equilibrium.

## 4.2 Thermodynamics of a Phase Boundary: An Introduction

As mentioned above, the boundary between two thermodynamic phases must be a vague transition zone for any physical quantity because nature does not like sharp steps. Hence, in principle, any real phase boundary extends in three dimensions – the *interphase* (cf. Fig. 2a). This apparently innocent comment has the important result that all extensive thermodynamic quantities, such as concentrations, energies, entropy, etc., will depend on position across the interphase. This causes trouble when it comes to an exact description of a thermodynamic system with more than one phase, because there is virtually no experimental access to the spatial dependence of thermodynamic quantities across the phase boundary. Moreover, the beauty of classic thermodynamics is very much due to the assumption that parameters remain constant across a phase. The exact volume  $V$  of such a two-phase system is given by the total

$$V = V_A + V_B + V_{\text{Interphase}} \quad (2)$$

where the terms on the right-hand side refer, respectively, to the two “bulk” phases and to the interphase. Hence, a method to circumvent the problem is needed. A pioneer in this subject (among many others!) was J.W. Gibbs, who introduced in a standardized way the notion of a “discontinuity” (Bumstead and Van Name 1961;

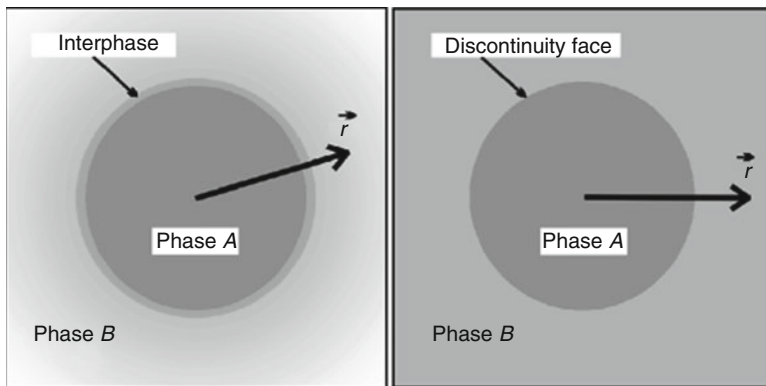


**Fig. 2** Schematic drawing for an interphase in a radially configuration of spherical symmetry of two phases  $A$  and  $B$ . The interphase shown in (a) (left) is replaced by the 2D discontinuity face (b) (right) in interface thermodynamics

Gaydos et al. 1996). A brief version of this thermodynamic description for phase boundaries is now introduced.

#### 4.2.1 Brief Description of Gibbs' Model for a Phase Boundary

The “real” interphase (Bakker 1902) is replaced by the “artificial” *discontinuity face* (D-face) with a certain area  $A_{AB}^D$  – cf. Fig. 2b. (For example, see (Rusanov 1978; Rusanov and Prokhorov 1996) for more details.) The position of the D-face can be chosen *arbitrarily, but only once*, from the theoretical point of view or, in measurements, is fixed by the experiment itself. Indeed, the experimenter is unable to select the position of the D-face deliberately. Usually, he does not know that position exactly. Although the D-face and the interface are very similar in many cases, the term “D-face” will be used here because similarity does not mean identity from the theoretical viewpoint. As a first consequence, (2) must be replaced by

$$V = V_A + V_B \quad (3)$$

for the two-phase system, i.e., the interphase volume  $V_{\text{Interphase}}$  is “eliminated,” being arbitrarily attributed partially to each of phases  $A$  and  $B$  according to the given position of the D-face.

Moreover, the balance of any extensive thermodynamic quantity,  $Y$ , in the two-phase system is no longer

$$Y = Y_A + Y_B + Y_{\text{Interphase}} \quad (4)$$

but is written as

$$Y = Y_A + Y_B + Y_{AB}^D \quad (5)$$

Here,  $Y_{AB}^D$  denotes the *excess of*  $Y$  with respect to the D-face. It is a correction that guarantees the correct value for  $Y$  in the whole two-phase system after the interphase has been ignored. Note that any excess quantity can adopt positive and negative values as well. The extensive  $Y$  can be referred to the D-face area  $A_{AB}^D$ , thus providing the corresponding intensive quantity  $y$

$$y = \frac{Y}{A_{AB}^D} = y_A + y_B + y_{AB}^D \quad (6)$$

For example, the number of moles  $n_i$  of a component  $i$  in the system

$$n_i = n_{i,A} + n_{i,B} + n_{\text{Interphase}} \quad (7a)$$

$n_{i,A}$ ,  $n_{i,B}$ ,  $n_{\text{Interphase}}$  = number of moles of component  $i$  in phases  $A$  and  $B$  and in the interphase is replaced by

$$n_i = n_{i,A} + n_{i,B} + n_{i,AB}^D = c_{i,A} \cdot V_A + c_{i,B} \cdot V_B + n_{i,AB}^D \quad (7b)$$

$n_{i,AB}^D$  = excess number of moles of  $i$  for the given D-face

$c_{i,A}$ ,  $c_{i,B}$  = concentrations of  $i$  (mole  $\text{m}^{-3}$ ) in phases  $A$  and  $B$

A simple rearrangement of (7b) provides the definition of the *absolute adsorption of component  $i$*  in a thermodynamic system with  $N$  components

$$\Gamma_{i,AB}^D \stackrel{\text{def}}{=} \frac{n_{i,AB}^D}{A_{AB}^D} = \frac{n_i - c_{i,A} \cdot V_A - c_{i,B} \cdot V_B}{A_{AB}^D} \quad \text{with } i = 1 \dots N \quad (8)$$

Indirectly, these  $N$  excess quantities replace the concentration profiles of all components in the system. Obviously, the value for any of the  $\Gamma_{i,AB}^D$  depends on  $A_{AB}^D$  and hence on the position for the D-face. As that position can be chosen only once for a given phase boundary, only one of the  $\Gamma_{i,AB}^D$  can be made zero, while all other  $(N - 1)$   $\Gamma_{j,AB}^D$  adopt nonzero values. (This naïve statement will be important for the coming discussions.)

The *interfacial tension* is another important quantity for the thermodynamics of interfaces. The starting point stems from continuum mechanics for deformable solids where the balance of forces at point  $\vec{r}$  in the solid is given by

$$\frac{d \vec{F}(\vec{r})}{dV} = \vec{f}(\vec{r}) = \text{Div } \vec{\sigma}(\vec{r}) \quad (9)$$

$\vec{f}(\vec{r})$  = density of the external force that deforms a solid

$\vec{\sigma}(\vec{r})$  = tensor of internal stresses in the deformed solid

171 and the mechanical work of deformation  $\Delta W$  of the volume  $V$

$$\Delta W = \int_V \sum_{i,k} (\sigma_{ik} \cdot \delta e_{ik}) dV \quad (10)$$

172  $\sigma_{ik}$ ,  $\delta e_{ik}$  = components of the stress and the deformation tensors,  $\vec{\sigma}(\vec{r})$ ,  $\vec{e}$   
 173  $(\vec{r})$ , respectively.

174 In thermodynamics, pressure is preferred, but now it is a tensor which is defined  
 175 as

$$\vec{e}(\vec{r}) = -\vec{\sigma}(\vec{r}) \quad (11)$$

176 All three tensors  $\vec{\sigma}(\vec{r})$ ,  $\vec{p}(\vec{r})$ ,  $\vec{e}(\vec{r})$  are symmetric, and hence they can be  
 177 transformed into diagonal form, provided a suitable system of coordinates is chosen.  
 178 Then, the analysis of (10) for the boundary between the two phases will provide a  
 179 definition for interfacial tension. As an illustration, the derivation is considered for  
 180 the case of an *isotropic horizontal planar phase boundary*. The D-face spans the  $x,y$ -  
 181 plane of the Cartesian coordinate system, and the  $z$ -axis is parallel to, but in the  
 182 opposite direction to, the gravitational force which is the external field here

$$\vec{f}(z) = -g \cdot \rho(z) \cdot \vec{k} \quad (12)$$

183  $g$  = gravity acceleration

184  $\rho(z)$  = mass density

185  $\vec{k}$  = unit vector for  $z$ -direction.

186 From (Eqs. 9, 11, and 12), it follows that

$$\text{Div} \begin{pmatrix} p_{xx} & 0 & 0 \\ 0 & p_{yy} & 0 \\ 0 & 0 & p_{zz} \end{pmatrix} = \begin{pmatrix} \frac{\partial p_{xx}}{\partial x} \\ \frac{\partial p_{yy}}{\partial y} \\ \frac{\partial p_{zz}}{\partial z} \end{pmatrix} = \begin{pmatrix} 0 \\ 0 \\ -g \cdot \rho(z) \end{pmatrix}$$

187 and hence

$$p_{xx}(z) = \text{const}; \quad p_{yy}(z) = \text{const}; \quad p_{zz}(z) - p = -g \cdot \int_{-\infty}^z \rho(z) dz \quad (13a - c)$$

188  $p$  = isostatic external pressure.

The two tangential pressure components  $p_{xx}$  and  $p_{yy}$  have to be equal for any  $z$ , by symmetry

$$p_{xx}(z) = p_{yy}(z) \equiv p_T(z) \quad (13d)$$

$p_T$  = pressure in the  $x,y$ -plane at  $z$

Usually, the interphase is very thin ( $d \approx 10^{-9}$ – $10^{-7}$  m) and (13c) can be approximated by

$$g \cdot \int_{-\frac{d}{2}}^{\frac{d}{2}} \rho(z) \, dz \approx 0 \rightarrow p_{zz}(z) \equiv p_N \approx p = \text{const} \quad (13e)$$

$p_N$  = pressure component in  $z$ -direction.

With (13), (10) is now

$$\begin{aligned} \Delta W &= - \int_V [p_T \cdot (\delta e_{xx} + \delta e_{yy}) + p \cdot \delta e_{zz}] \, dV \\ &= - \int_V [p_T \cdot (\delta e_{xx} + \delta e_{yy}) - p \cdot (\delta e_{xx} + \delta e_{yy}) + p \cdot (\delta e_{xx} + \delta e_{yy}) + p \cdot \delta e_{zz}] \, dV \\ &= \int_V [(p - p_T) \cdot (\delta e_{xx} + \delta e_{yy})] \, dV - p \cdot \int_V (\delta e_{xx} + \delta e_{yy} + \delta e_{zz}) \, dV \end{aligned}$$

and for small deformations

$$\Delta W = \Delta A_{AB}^D \cdot \int_{-\infty}^{\infty} (p - p_T) \, dz - p \cdot \Delta V \quad (14a)$$

The second term is the well-known work of volume expansion, while the first term

$$\Delta W_{AB}^D = \Delta A_{AB}^D \cdot \int_{-\infty}^{\infty} (p - p_T) \, dz \quad (14b)$$

gives the work for increasing the area of the D-face by  $\Delta A_{AB}^D$ .

Equation (14) implies the definition of the *interfacial tension for the* chosen isotropic planar D-face:

$$\gamma_{AB}^D \stackrel{\text{def}}{=} \int_{-\infty}^{\infty} (p - p_T) \, dz \quad (15a)$$

201 With an assumed *spherical shape for the isotropic interphase*, a similar mathe-  
 202 matical treatment provides the *interfacial tension for the spherical D-face of*  
 203 *radius  $r_D$*

$$\gamma_{AB}^D = \frac{1}{r_D^2} \left[ \int_0^{r_D} (p_A - p_T) r^2 dr + \int_{r_D}^{\infty} (p_B - p_T) r^2 dr \right] \quad (15b)$$

204  $p_A, p_B$  = isostatic pressures inside the phases A and B. They are different due to the  
 205 curved interphase.

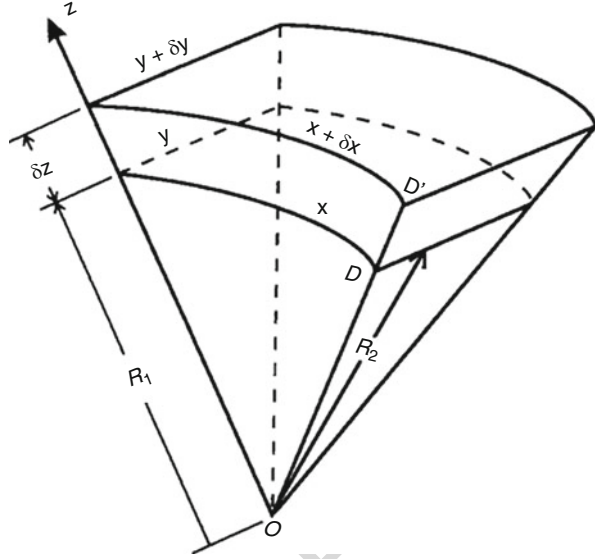
206 These two examples illustrate that  $\gamma_{AB}^D$  is, in general, an excess quantity for a  
 207 given D-face. As a consequence of this result, there is no physical difference  
 208 between interfacial and surface tension in thermodynamic equilibrium. In the  
 209 literature, the term surface tension is attributed to the D-face, or interface, between  
 210 a condensed phase and the corresponding vapor phase. Some authors define the  
 211 surface tension as the interfacial tension of a condensed phase in contact with  
 212 vacuum. This is incorrect in the framework of equilibrium thermodynamics. A  
 213 condensed phase will fill a vacuum with its vapor phase to be at thermodynamic  
 214 equilibrium. Hence, any interfacial tension results from a defined pair of phases,  
 215 never from a single phase, and they need to be marked by the subscript “AB” or  
 216 similar. Otherwise, the interfacial tension would be ill-defined.  $\gamma_{AB}^D$  accounts for  
 217 the real distribution of pressure or stress inside the phase boundary. It is called a  
 218 tension because it possesses the dimension of a force per unit length [ $\text{N m}^{-1}$ ] in  
 219 the 2D space of the D-face and indeed acts somewhat like the tension in a  
 220 membrane (except that there is no elastic proportionality between the tension  
 221 and extension). Moreover, (15b) reveals that the value for  $\gamma_{AB}^D$  usually depends on  
 222 the position, here  $r_D$ , chosen for the given D-face.  $\gamma_{AB}^D$  is always positive. This is a  
 223 condition of stability for the interphase and hence for the phase itself, and it is  
 224 proven by experiment and also by statistical mechanics calculations. The value  
 225 remains almost constant when  $p$  decreases. Therefore,  $p_T$  must be negative, at least  
 226 inside the dominant part of the interphase, and as a consequence, the interphase  
 227 and the corresponding D-face will adopt the minimum volume and area,  
 228 respectively.

229 To apply thermodynamic energy balances (first law), knowledge of how *mechan-*  
 230 *ical work* changes the state of the system must be available. As the phase boundary is  
 231 included, the usual equations have to be revised. Figure 3 depicts the situation for the  
 232 volume expansion  $\delta V$  of the phase A that is accompanied by a change of the principal  
 233 radii of curvature from  $R_1, R_2$  to  $(R_1 + \delta z), (R_1 + \delta z)$ , respectively. Now, the  
 234 mechanical work can be split into *four parts*. The first one comes from the work  
 235 of volume expansion

$$\delta W^V = -p_A \cdot dV_A - p_B \cdot dV_B \quad (16a)$$

236 Part two results from the corresponding increase of area of the D-face according to (14b)

**Fig. 3** Geometric scheme for the of the volume increase  $\delta V$  of a phase  $A$  with a curved D-face ( $D \rightarrow D'$ )



$$\delta W_{AB}^D = \gamma_{AB}^D \cdot dA_{AB}^D \quad (16b)$$

237 The increase of D-face area can be accompanied by a change of the radii of  
 238 curvature. This corresponds to the third contribution to the mechanical work:

$$\delta W_{\text{curvature}}^D = A_{AB}^D \cdot C_1 \cdot d\left(\frac{1}{R_1}\right) + A_{AB}^D \cdot C_2 \cdot d\left(\frac{1}{R_2}\right) \quad (16c)$$

239  $C_1, C_2 =$  proportionality factors.

240 The fourth and last part is related to the action of external forces such as gravity.

241 The D-face possesses the total excess mass

$$m_{AB}^D = \sum_{i=1}^N m_{i,AB}^D = \sum_{i=1}^N M_i \cdot n_{i,AB}^D = A_{AB}^D \cdot \sum_{i=1}^N M_i \cdot \Gamma_{i,AB}^D$$

242 which is raised by a height  $dh$  when the D-face shifts in the gravitational field.

243 Hence, the corresponding work is

$$\delta W_{\text{gravitation}}^D = A_{AB}^D \cdot \sum_{i=1}^N \left( M_i \cdot \Gamma_{i,AB}^D \right) \cdot g \cdot dh \quad (16d)$$

244 The total work is equal to

$$\begin{aligned}
\delta W = & -p_A \cdot dV_A - p_B \cdot dV_B + \\
& + \gamma_{AB}^D \cdot dA_{AB}^D + A_{AB}^D \cdot C_1 \cdot d\left(\frac{1}{R_1}\right) + A_{AB}^D \cdot C_2 \cdot d\left(\frac{1}{R_2}\right) + \\
& + A_{AB}^D \cdot \sum_{i=1}^N \left( M_i \cdot \Gamma_{i,AB}^D \right) \cdot g \cdot dh
\end{aligned} \tag{16f}$$

245 In this equation, however, the work would seem to depend on  $A_{AB}^D$  and hence on the  
 246 arbitrarily chosen position of the D-face. This is impossible from a physical point of  
 247 view and terms of (16f) must clearly correct for this implicitly. The paradox is  
 248 revealed from a virtual displacement  $\delta N$  of the D-face along its normal  $\vec{N}$ . The  
 249 corresponding virtual mechanical work is  $\delta W = 0$ . Another expression available is

$$\begin{aligned}
\delta V_A = A_{AB}^D \cdot \delta N, \quad \delta V_B = -A_{AB}^D \cdot \delta N, \quad dA_{AB}^D = A_{AB}^D \left( \frac{1}{R_1} + \frac{1}{R_2} \right) \delta N, \\
\delta N = \delta R_1 = \delta R_2
\end{aligned}$$

250 and (16f) now provides the *generalized Laplace equation*

$$p_A - p_B = \gamma_{AB}^D \left( \frac{1}{R_1} + \frac{1}{R_2} \right) - \frac{C_1}{R_1^2} - \frac{C_2}{R_2^2} + \sum_{i=1}^N \left( M_i \cdot \Gamma_{i,AB}^D \right) \cdot g \cdot \cos \varphi \tag{17a}$$

251 where  $\varphi$  = angle between  $\vec{N}$  and vertical direction.

252 The complete condition for mechanical equilibrium of a two-phase system with a  
 253 curved phase boundary in a gravitational field is now available. It shows that the  
 254 pressure difference between two curved phases depends on the properties of the  
 255 D-face: interfacial tension, curvature, and adsorptions  $\Gamma_{i,AB}^D$ . Usually, the absolute  
 256 adsorptions  $\Gamma_{i,AB}^D$ , as well as  $C_1$  and  $C_2$ , are small. Then, the following approximation  
 257 of (17a) can be used:

$$p_A - p_B = \gamma_{AB}^D \left( \frac{1}{R_1} + \frac{1}{R_2} \right) \tag{17b}$$

258 This is known as Laplace's equation.

259 For an *anisotropic* phase boundary such as in the case of oriented molecules, the  
 260 interfacial tension becomes a diagonal tensor

$$\vec{\gamma}_{AB}^D = \begin{pmatrix} \gamma_{11} & 0 \\ 0 & \gamma_{22} \end{pmatrix} \tag{18a}$$

261 and the trace of the tensor provides the value for the interfacial tension

$$\gamma = \frac{1}{2} (\gamma_{11} + \gamma_{22}) \tag{18b}$$



262 Finally, the corresponding forms of Equation (17) become

$$p_A - p_B = \frac{\gamma_{11}^D}{R_1} + \frac{\gamma_{22}^D}{R_2} - \frac{C_1}{R_1^2} - \frac{C_2}{R_2^2} + \sum_{i=1}^N \left( M_i \cdot \Gamma_{i,AB}^D \right) \cdot g \cdot \cos \varphi \quad (19a)$$

$$p_A - p_B = \frac{\gamma_{11}^D}{R_1} + \frac{\gamma_{22}^D}{R_2} \quad (19b)$$

263 With these results, the energy balance of the two-phase system can be evaluated  
264 in detail.

### 265 4.2.2 Energy Balance for a Two-Phase System: Thermodynamic 266 Potentials

267 The *thermodynamic potential for the internal energy*  $U$  in any thermodynamic  
268 system provides the starting point

$$dU = T \cdot dS + \delta W + \sum_i \mu_i \cdot dm_i$$

269  $T$  = absolute temperature

270  $S$  = entropy  $\mu_i$ ,  $m_i$  = chemical potential and mass of component  $i$ .

271 Using (5 and 16f) for a system with the isotropic phases A and B, the following  
272 relation is obtained

$$\begin{aligned} dU &= dU_A + dU_B + dU_{AB}^D \\ &= T \cdot (dS_A + dS_B + dS_{AB}^D) - p_A \cdot dV_A - p_B \cdot dV_B \\ &\quad + \gamma_{AB}^D \cdot dA_{AB}^D + A_{AB}^D \cdot C_1 \cdot d\left(\frac{1}{R_1}\right) + A_{AB}^D \cdot C_2 \cdot d\left(\frac{1}{R_2}\right) \\ &\quad + A_{AB}^D \cdot \sum_{i=1}^N \left( M_i \cdot \Gamma_{i,AB}^D \right) \cdot g \cdot dh + \sum_i \mu_i \cdot (dm_{i,A} + dm_{i,B} + dm_{i,AB}^D) \end{aligned} \quad (20)$$

273 The terms for the D-face are easily identified. For clarity and brevity, however, the  
274 following treatment is restricted to a *plane interface* and *neglect gravity*. Then, (20)  
275 reduces to

$$\begin{aligned} dU &= dU_A + dU_B + dU_{AB}^D = T \cdot (dS_A + dS_B + dS_{AB}^D) - p_A \cdot dV_A - p_B \cdot dV_B + \\ &\quad + \gamma_{AB}^D \cdot dA_{AB}^D + \sum_i \mu_i \cdot (dm_{i,A} + dm_{i,B} + dm_{i,AB}^D) \end{aligned} \quad (21)$$

Integration provides the full internal energy of the two-phase system

$$U = T(S_A + S_B + S_{AB}^D) - p_A V_A - p_B V_B + \gamma_{AB}^D A_{AB}^D + \sum_i \mu_i \cdot (m_{i,A} + m_{i,B} + m_{i,AB}^D) \quad (22)$$

and the *excess internal energy of the force-free plane D-face*

$$U_{AB}^D = T \cdot S_{AB}^D + \gamma_{AB}^D A_{AB}^D + \sum_i \mu_i \cdot m_{i,AB}^D \quad (23)$$

Now, *specific* quantities are introduced

$$u_{AB}^D = \frac{U_{AB}^D}{A_{AB}^D} = T \cdot s_{AB}^D + \gamma_{AB}^D + \sum_i \mu_i \cdot \Gamma_{i,AB}^D \quad (24)$$

$s_{AB}^D = \frac{S_{AB}^D}{A_{AB}^D}$  = specific excess entropy of the D-face

in order to get intensive thermodynamic quantities.

Moreover, the *excess Helmholtz free energy* is

$$F_{AB}^D = U_{AB}^D - T \cdot S_{AB}^D = \gamma_{AB}^D A_{AB}^D + \sum_i \mu_i \cdot m_{i,AB}^D \quad (25)$$

with the corresponding *specific excess Helmholtz free energy*

$$f_{AB}^D = \frac{F_{AB}^D}{A_{AB}^D} = u_{AB}^D - T \cdot s_{AB}^D = \gamma_{AB}^D + \sum_i \mu_i \cdot \Gamma_{i,AB}^D \quad (26)$$

These results give access to the *interfacial tension as a thermodynamic excess quantity of the force-free plane D-face*. Note that the interfacial tension and the absolute adsorptions of all components contribute to the interfacial energy, both the specific excess internal energy and the specific excess Helmholtz free energy. At a first glance, this statement is very natural, indeed. In the literature, however, interfacial tension and interfacial energy are very often considered as synonymous. This is incorrect.

Finally, the total differential for (23) is derived and compared with the corresponding terms in (21). This yields the *Gibbs adsorption equation*

$$d\gamma_{AB}^D = -s_{AB}^D dT - \sum_i \Gamma_{i,AB}^D d\mu_i \quad (27)$$

Equation (27) depicts the interfacial tension as a function of temperature and, via the chemical potentials, of pressure and composition of the two-phase system.

### 4.3 Thermodynamic Equilibrium of Three Phases: Basics

From Sect. 1, it is clear that wetting and the contact angle depend on all *three* contacting phases. Hence, the Gibbs concept of excess quantities as thermodynamic quantities for phase boundaries has to be extended in an appropriate way. For a sessile drop on a *flat, homogeneous* solid, the situation is illustrated in Fig. 4. The three phases create a new microscopic boundary region at their “line” of common contact. For the sessile drop, this region forms a curved tube along the rim of the drop on the solid. Inside the tube, the three D-faces for the three two-phase boundaries respond by deforming, shown very much exaggerated in the drawing.

The real three-phase region (tube) is replaced by a *triple line* (TL) as the new model element for thermodynamic considerations. In theory, its position results from the extrapolation of the three *undisturbed* D-faces to their common intersection. Accordingly, the tangent lines on these extrapolated D-faces  $D_{SL}$  and  $D_{LV}$  to the point of intersection lead *by definition* to the *thermodynamic contact angle*  $\theta_e$ . For reasons of exactness,  $\theta_e$  is introduced for the thermodynamic equilibrium of the three-phase system. The static contact angle  $\theta_0$  in Sect. 1 refers to the triple line at rest, i.e., to mechanical equilibrium which is a necessary but insufficient condition for thermodynamic equilibrium.  $\theta_e$  is the first excess quantity for the TL. As the position of any of the three D-faces can be chosen arbitrarily, the position of the TL and the value for  $\theta_e$  are arbitrary too. Fortunately, this vagueness is of no serious consequence as long as the two-phase and three-phase boundaries possess microscopic thicknesses. Note that  $\theta_e$  is a *local property* of the given TL in thermodynamic equilibrium. Hence, for isotropic phases,  $\theta_e$  possesses one and only one value!

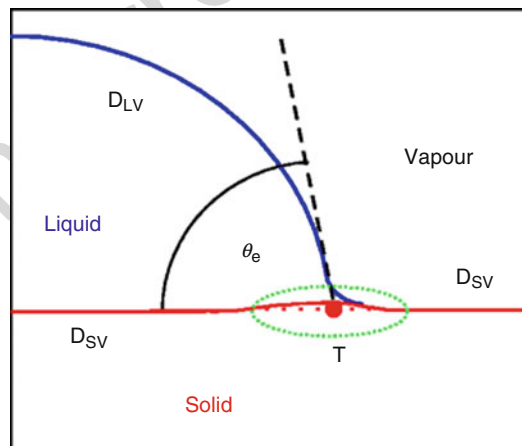


**Fig. 4** Sketch of the cross section through a sessile drop of liquid L on a *flat* solid S, both immersed in their common vapor atmosphere V. The D-faces  $D_{LV}$ ,  $D_{SV}$ , and  $D_{SL}$  describe the corresponding phase boundaries. T marks the triple line as the new model element for the three-phase boundary region (---) between the phases S, L, and V.  $\theta_e$  = contact angle in thermodynamic equilibrium

The pressure tensor  $\vec{p}$  will also vary in the three-phase region as compared with the two-phase boundary. Hence, a *line tension*  $\kappa_{\text{SLV}}$  has to be introduced as the corresponding excess quantity for the TL. Although the mathematical derivation is omitted here,  $\kappa_{\text{SLV}}$  follows from the same physical arguments that resulted in the definition of the interfacial tension in Sect. 2. It acts along the tangent of any point of the TL and has the dimension of a force as it refers to a tension in a 1D space.

By analogy with a D-face, new excess quantities have to be introduced for all extensive thermodynamic quantities with respect to the TL. Details are not given here. For brevity, only a result of consideration of the Helmholtz free energy for a three-phase system in thermodynamic equilibrium *under the influence of gravity* is mentioned. It leads to a condition for the *mechanical equilibrium at the TL on a solid with an arbitrary surface profile (roughness)*:

$$\gamma_{\text{SV}} = \gamma_{\text{SL}} + \gamma_{\text{LV}} \cdot \cos \theta_e + \left( \frac{\kappa_{\text{SLV}}}{R_0} + \frac{d\kappa_{\text{SLV}}}{dR_0} \right) \cdot |\cos \varphi_s| \quad (28)$$

$\gamma_{\text{LV}}$  = interfacial tension of the  $D_{\text{LV}}$ -face far from the TL

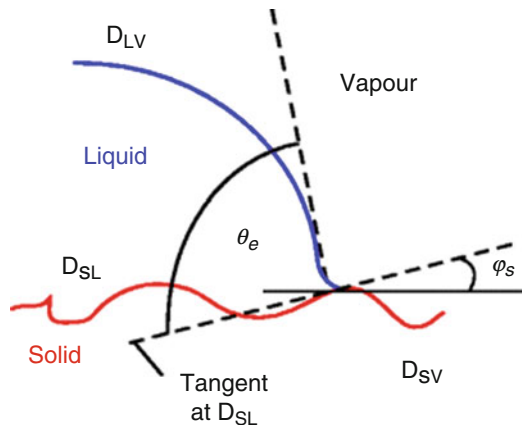
$R_0$  = radius of curvature in the considered point of the TL

$\varphi_s$  = angle of inclination of the extrapolated  $D_{\text{SV}}$ -face in the considered point of the TL.

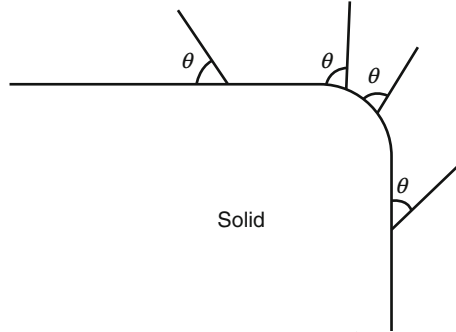
Accordingly,  $\theta_e$  does not only depend on the three interfacial tensions but also on the line tension and on the curvature of the TL.  $\kappa_{\text{SLV}}$  is of the order of  $10^{-10}$  N for solids in general. Nevertheless, it deserves attention when the phases are soft and one of the contacting phases becomes very small.

Figure 5 illustrates the situation for a sessile liquid drop on a *rough homogeneous* solid surface.  $\theta_e$  is defined as before. However, the true value of  $\theta_e$  cannot be obtained from the plane optical projection of the sessile drop anymore as the experimenter cannot look into the local surface profile in order to get the local inclination of the tangent on the  $D_{\text{SL}}$ -face.

**Fig. 5** Schematic cross section through a sessile liquid drop on a *rough* solid, both immersed in their common vapor. Now, the tangent on the extrapolated  $D_{\text{SL}}$ -face at a selected point of the TL is inclined according to the solid surface profile.  $\theta_e$  is defined as before



**Fig. 6** Schematic cross section through a sharp solid edge with the constant local  $\theta_e$  of a moving TL (liquid meniscus not shown)



Experimentally, it seems as if the contact angle varies substantially whenever the TL moves over a sharp edge. Figure 6 shows that this is just an optical illusion because the experimenter cannot resolve the local microscopic curvature of the edge. At a *very* sharp, angle on the solid, the contact angle may be considered to become indeterminate, an effect known as *canthotaxis*. However, this proposition assumes continuum mechanics, which clearly breaks down at this scale.

#### 4.4 Experimental Aspects of Static Wetting

In Sects. 2 and 3 the concept of interfacial tension and interfacial free energy was defined, and their importance in wetting was noted, without going into details.

For TLs with large radii of curvature ( $R_0 > 10^{-6}$  m), (28) can be approximated by

$$\gamma_{SV} = \gamma_{SL} + \gamma_{LV} \cdot \cos \theta_e \quad (29)$$

The thermodynamic contact angle is still a local excess property of the TL. Treating the  $\gamma_{LJ}$  as tensions (i.e., with dimensions of force/distance or mass/time<sup>2</sup> in some old literature!), as opposed to energies (i.e., dimensions of energy/area), in Fig. 1a balance of tensions at the triple line may be considered. This results directly in (29). This classic equation is usually referred to as *Young's* equation, although Thomas Young never, in fact, wrote the expression in his often-cited paper (Young 1805)! If it is preferred to treat the  $\gamma_{LJ}$  as interfacial free energies, and apply a simple argument of “virtual work,” the same relation is obtained. Having applied a force balance horizontally, this must be possible vertically, so what “resists”  $\gamma_{LV} \sin \theta_e$ ? Strictly, the action of tensions at the TL, specifically  $\gamma_{LV}$ , deforms the solid surface, but it is only under conditions in which the solid is very soft that the effect is noticeable. The slight “bump” on the solid in Fig. 4 has a height given approximately by  $\gamma_{LV} \cdot \sin \theta_e / G$ , where  $G$  represents the (elastic) shear modulus of the solid. Simple insertion of typical values shows that the effect becomes noticeable only for  $G < \approx 1$  MPa (Shanahan and de Gennes 1986).

As an example, aluminum has a value of  $G$  of ca. 25 GPa, and for water  $\gamma_{LV}$  is ca. 70 mN m<sup>-1</sup>. Taking  $\sin \theta_e$  as 1, it is found that the “wetting ridge” height is

ca.  $3 \cdot 10^{-12}$  m: well below atomic dimensions and thus meaningless in a continuum approach! In general, the effect perpendicular to the solid is negligible. However, the wetting ridge can be significant on soft solids and even modify wetting kinetics (Shanahan and Carré 1995).

In (29), it may be noted that each surface tension has two suffixes representing two of the three, S, L, and V, although the use of  $\gamma_{LV} = \gamma_L$  or  $\gamma_{SV} = \gamma_S$  often found in the literature. In the case of the solid,  $\gamma_{SV}$  changes a lot when it shares a common vapor phase with a liquid because the significant part of the surrounding vapor is due to the liquid. In the above thermodynamic treatment, allowance is already made for this effect. However, many workers prefer to adopt the alternative notion of equilibrium spreading pressure,  $\pi_e = \gamma_S - \gamma_{SV}$ , where  $\gamma_{SV}$  means the solid surface tension in presence of a liquid now.  $\pi_e$  is often considered negligible for low activity solids, such as polymers. (Figure 15 demonstrates that this assumption should be checked!)

The importance of (29) is that it may, in principle, allow one to estimate the surface tension of a solid,  $\gamma_{SV}$ , albeit indirectly, from knowledge of the surface tensions,  $\gamma_{LV}$ , of “probe” liquids and their contact angles on the solid surface in question. Knowledge of  $\gamma_{SL}$  is required too, and the problem is considered in Sect. 5 and chapter Thermodynamics of Adhesion.

Whereas liquid surface tension is readily measured (see below), that of a solid is inaccessible directly from experiment due to the intrinsic lack of molecular mobility. Firstly, liquid tension will be considered.

#### 4.4.1 Liquid Surface Tension

##### Maximum Bubble Pressure

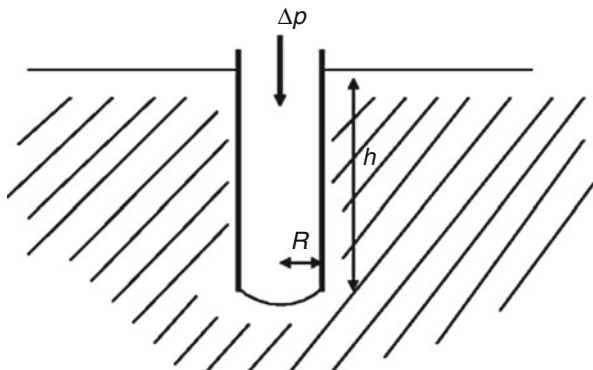
If a tube of radius  $r$  is immersed vertically in a liquid to a depth  $h$ , the local pressure will be  $\rho gh$ , where  $\rho$  is liquid density (more precisely, the difference between liquid density and that of the local vapor environment, but the difference is generally negligible) and  $g$  is gravitational acceleration. When air is blown through the tube, it will cause bubbles to form at the immersed end of the tube. Laplace’s equation (17b) relating the excess pressure on the curved side of the meniscus,  $\Delta p$ , to the principal radii of curvature  $R_1$  and  $R_2$  (both equal to  $R$  for a spherical surface) is given by

$$\Delta p = \gamma_{LV} \left( \frac{1}{R_1} + \frac{1}{R_2} \right) = \frac{2\gamma_{LV}}{R} \quad (30)$$

The internal bubble pressure is therefore  $\Delta p + \rho gh$ . When the bubble first starts to grow, it will have a large value of  $R$ , which will then decrease until the bubble becomes a hemisphere. Thereafter, the radius grows again. Thus, when the bubble is a hemisphere, of radius  $r$ , the pressure is maximal. Thus maximal bubble pressure,  $p_{\max}$ , is given by

$$p_{\max} = \frac{2\gamma}{R} + \rho gh \quad (31)$$

**Fig. 7** Schematic representation of maximum bubble pressure method



If the air line is fitted to a pressure gauge, the value of  $p_{\max}$  may be measured and the value of liquid surface tension,  $\gamma_{LV}$ , then readily calculated (Fig. 7).

### Drop Weight

An appealingly simple, but rather inaccurate, method to obtain liquid surface tension values is that of letting a drop accumulate at the end of a circular orifice of radius  $R$ , mounted horizontally like a tap. When sufficiently large, the drop will drop. On weighing the fallen liquid, a pseudo-equilibrium may be drawn between drop weight at separation,  $mg$ , and the hitherto surface tension-based retaining force,  $2\pi R\gamma_{LV}$ . Since some liquid is generally left behind, and since it is not entirely clear that the correct surface tension term to be used is that given above, generally a correction factor,  $\phi$ , is invoked where typically  $1 < \phi < 2$ . Surface tension is then estimated from

$$\gamma_{LV} = \frac{mg\phi}{2\pi R} \quad (32)$$

There is also a method for estimating  $\gamma_{LV}$  from the shape of a hanging, or pendent, drop *before* it falls, invoking the conflicting effects of gravity and surface tension (Padday 1971; Hartland and Ramakrishnan 1975). However, the mathematical complexities put this beyond the scope of the present text. Briefly, Laplace's equation (17b), allowing for *changing* pressure with height within the drop (hydrostatic head), can be rewritten as a second-order differential equation. It is this which is solved when drop size is comparable to capillary length (see chapter Thermodynamics of Adhesion). The resulting drop profile forms as a "compromise" between gravity (flattening) and surface forces (minimizing surface area and therefore seeking sphericity) (Fig. 8).

### Capillary Rise

A thin, circular capillary tube, of internal radius,  $R$ , may be immersed in a liquid vertically, and the height of ascension of the liquid within,  $h$ , can be used to calculate the surface tension of the liquid, with the proviso that the solid of the tube inner is completely wet by the liquid (i.e., zero contact angle). This is generally assumed for

**Fig. 8** Schematic representation of drop weight method

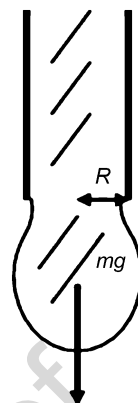
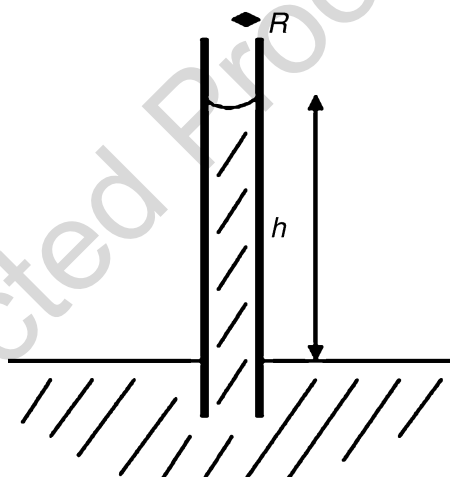


**Fig. 9** Schematic representation of capillary rise method



organic liquids, at least, by using glass tubes which have recently undergone some aggressive internal cleaning treatment, such as that by sulfochromic acid or similar. The liquid rises in the tube in order to counteract Laplace's reduced pressure in the meniscus by hydrostatic pressure. For thin tubes, those of interest, having the greatest capillary rise, deviation of the meniscus shape from sphericity may be neglected, and the resulting expression for surface tension is

$$\gamma_{LV} = \frac{R\rho gh}{2} \quad (33)$$

where  $\rho$  is liquid density and  $g$ , as before, is gravitational acceleration (Fig. 9).

### Wilhelmy Plate

If a smooth, flat solid is immersed in a wetting liquid (i.e.,  $\theta_0 < 90^\circ$ ), such that its surface is perpendicular to the horizontal, liquid surface, a meniscus forms toward



**Fig. 10** Schematic representation of Wilhelmy plate

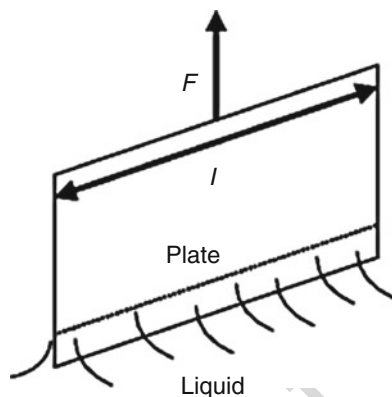
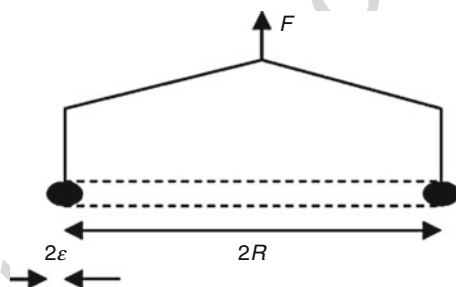


**Fig. 11** Schematic representation of du Noüy ring



the upper size, whose effective downward force, or “weight” is given by  $\gamma_{LV} \cdot \cos \theta_0$  per unit length measured along the triple line cf. Fig. 10. Provided a “high surface tension” solid is chosen, in general, a platinum plate that has been pre-roughened and pre-cleaned (e.g., by flaming in a Bunsen flame), the contact angle is zero and thus the “weight” per unit length is simply  $\gamma_{LV}$ . If the plate is thin and of length  $l$  (along the triple line), the upward meniscus force,  $F$ , is  $2l\gamma_{LV}$ , neglecting plate thickness. The method described wherein such a platinum blade is attached to a fine balance and meniscus weight evaluated, leading to  $\gamma_{LV} = F/2l$ , is known as the Wilhelmy plate technique. It is simple, but complications can however arise. If the plate is too thick, buoyancy must be allowed for acting on the submerged part of the plate (see [Fibers](#) below). In some cases, whether the blade is *immersed* or *emersed* from the liquid, it can give different results, due to wetting hysteresis (see below).

### Du Noüy Ring

This technique (Fig. 11) is a variation on the Wilhelmy plate, requiring a smaller quantity of expensive platinum! Notwithstanding, the platinum must be correctly formed into the shape of a circular ring of radius  $R$ . The ring is made from circular, platinum wire of sectional radius,  $\epsilon$ .

The primary part is thus a torus, although it is attached symmetrically to a small frame allowing it to be attached to an accurate balance. The principle is that when the ring is emersed from a liquid, a meniscus will form on both sides of the wire and all

459 around the ring. Neglecting difference in radius for inner and outer circles ( $R \gg \varepsilon$ ),  
460 it may be expected that the upward meniscus force will be given by  $F = 4\pi R\gamma_{LV}$  (see  
461 [Wilhelmy Plate](#)). However, spurious effects occur (interference across the ring  
462 diameter?) leading to the adoption of an empirical correction factor,  $\beta$ . Liquid  
463 surface tension is then given by

$$\gamma_{LV} = \frac{\beta F}{4\pi R}$$

(34)

464 where  $\beta$  is a function of  $R$  (and  $\varepsilon$ ). Table 1 gives a few examples of  $\beta$  as a function of  
465  $R$  and  $\varepsilon$ .

466 **4.4.2 Contact Angle**

467 Contact angle is the angle subtended, in the liquid, between the tangent to the liquid/  
468 vapor interface and the solid/liquid interface at the triple, or three-phase, line, in the  
469 plane perpendicular to this line. In Sect. 3, it was shown from thermodynamics that  
470 the contact angle at thermodynamic equilibrium,  $\theta_e$ , is a function of many quantities:  
471 the interfacial tensions of the three D-faces, line tension, the curvature of the triple  
472 line, and surface profile (cf. 28). For real solids in wetting experiments, the list of  
473 influences can be extended by surface heterogeneity in terms of locally varying  
474 interfacial tension, by adsorption layers, and by other “imperfections.” As a result,  
475 measured static contact angles *always* show some hysteresis  $\Delta\theta$ . The so-called static  
476 advancing contact angle  $\theta_{e,a}$  measured after the triple line has advanced onto a  
477 previously unwetted surface area is always larger than the so-called static receding  
478 angle,  $\theta_{e,r}$ , found after the triple line has receded onto a solid surface region that was  
479 previously in contact with the liquid

$$\Delta\theta = \theta_{e,a} - \theta_{e,r} > 0$$

(35)

480 Static contact angle hysteresis summarizes the difference in wetting of real  
481 surfaces and of ideally smooth homogeneous solids. The hysteresis can be even  
482 larger under dynamic measuring conditions. The static contact angle hysteresis does  
483 not depend on the experimental setup used for contact angle measurement provided  
484 the same solid and the same liquid are used and equilibrium is attained. As a  
485 consequence, the simplified equation (29) cannot be applied before the thermody-  
486 namic contact angle for the corresponding smooth solid has been deduced from  $\theta_{e,a}$   
487 and  $\theta_{e,r}$ . It should be mentioned that the contact angle hysteresis is not a consequence  
488 of (28) only. Moreover, gravity causes some kind of stick–slip behavior that depends

**Table 1** Two examples of  $\beta$  for different values of  $R$  and  $\varepsilon$  for the du Noüy ring

$R$ (cm)	$\varepsilon$ (cm)	$\beta$	t.1
1	0.02	0.93	t.2
1.85	0.03	0.88	t.3

on the slope of the roughness asperities when the three-phase boundary moves over the rough solid surface. It can be shown that static contact angle hysteresis depends upon this effect (e.g., Bartell and Shepard 1953a, b; Johnson and Dettre 1964; Busscher et al. 1984; Bischof et al. 1988).

Various propositions, such as

$$\cos \theta_{\text{meas}} = r \cdot \cos \theta_e; \quad r = \frac{A_{\text{true}}}{A_{\text{geom}}} \quad (36)$$

(Wenzel 1936)

$A_{\text{geom}}$  = macroscopic area of the solid surface, i.e., width by length

$A_{\text{true}}$  = microscopic area due to surface roughness within  $A_{\text{geom}}$ .

$$\theta_e = \theta_{e,a} \quad (37)$$

(Thiessen and Schoon 1940)

$$\theta_e = \frac{1}{2} (\theta_{e,a} + \theta_{e,r}) \quad (38)$$

(Adam and Elliott 1962)

have been proposed in the literature to tackle this problem. However, inspection of experimental data reveals that none of these formulae solves the problem totally and satisfactorily – cf. Fig. 12 as an example.

Instead, it is clear from experimental results that the functions  $\theta_{e,a}(\Delta\theta)$  and  $\theta_{e,r}(\Delta\theta)$  follow straight lines

$$\theta_{e,a} = \theta_e + a \cdot \Delta\theta \quad (39)$$

$$\theta_{e,r} = \theta_e - b \cdot \Delta\theta \quad (40)$$

As roughness is a major cause of  $\Delta\theta$  on homogeneous solids, the intersection of these lines with the ordinate is the value  $\theta_e$  being sought (Schulze et al. 1989). Hence, the equilibrium contact angle can, in principle, be determined from a suitable experiment.

In the following sections on experimental methods for contact angle measurement, we shall summarize  $\theta_{e,a}$  and  $\theta_{e,r}$  as  $\theta_0$ , for brevity. Of course, both advancing and receding angles must be measured for a complete appraisal.

## Goniometry

Contact angles may be assessed by various techniques, of which a few of the better ones will be mentioned. The simplest involves a plane optical projection of the three interfaces and the triple line. The tangent to the projection of the liquid/vapor interface at the triple line is estimated and the angles measured relative to the flat

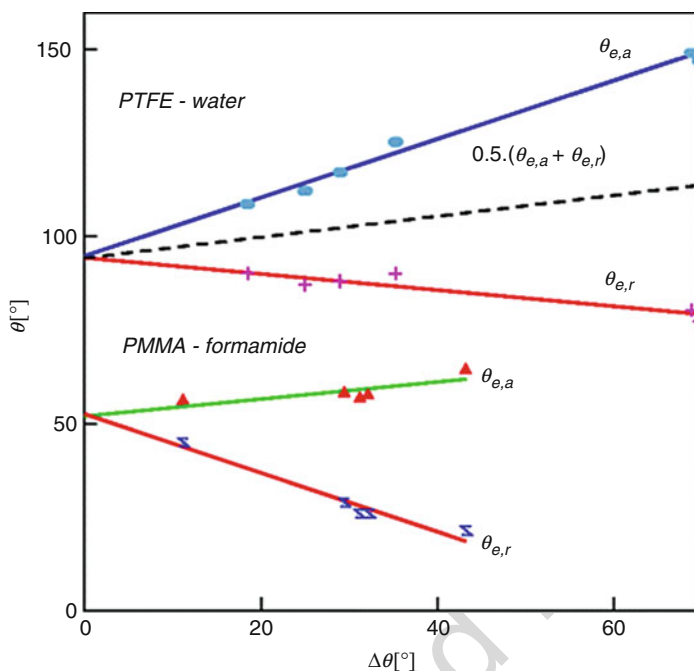


**Fig. 12**  $\theta_{e,a}$  and  $\theta_{e,r}$  data measured with various liquids on homogeneous polymer surfaces after stepwise increases of roughness following grinding with abrasive cloth of increasing grade

projection of the possibly rough solid surface. There is equipment available on the market to do this, using in the simpler cases an eyepiece with two, independent goniometers, one to align with the projection of the solid surface and one to form the tangent to the projection of the liquid/vapor interface. It is relatively easy to set up an optical bench arrangement, either to observe the drop directly or to project its magnified image onto a screen, and then to draw the requisite tangents.

However, placing a tangent to a curve is always somewhat subjective. An alternative method is to use the following procedure. Firstly, when posing a drop on the flat, horizontal surface, ensure from the top that its contact area is circular. (This may be done with a transparent slide, onto which are printed circles of various diameters. By adjustment of drop-to-transparent distance, it is possible to find a position at which a circle should coincide with drop circumference.) Any deviation of the triple line from a circle is a clear proof that the solid surface is either rough or inhomogeneous. The surface tension,  $\gamma_{LV}$ , of the liquid (necessary anyway, to exploit (29)) and also its density,  $\rho$  are required. Large drops tend to flatten (“puddles”), whereas small drops stay as spherical caps (“dew drops”). The approximate contact radius,  $r \approx a$ , below which the drop is sufficiently close to sphericity, is given by the liquid’s capillary length:  $a = (\gamma_{LV}/\rho g)^{1/2}$  where  $g$  is gravitational acceleration. For water, for example,  $a$  is ca. 2.8 mm. Having checked circularity of the contact area and droplet size,  $\theta_0$  can be readily estimated from the simple formula for a spherical cap:

$$\tan\left(\frac{\theta_0}{2}\right) = \frac{h}{r} \quad (41)$$

where height,  $h$ , and radius are as shown in Fig. 1.

### “Puddle”

At the other extreme from “dew drops,” a “puddle” may form (see Fig. 13). If the drop radius,  $r$ , considerably exceeds  $a$ , gravity flattens the liquid bulk. If  $\gamma_{LV}$  is known, e.g., by one of the above methods, then the contact angle may be calculated from a measurement of drop height (in the flat part):

$$\cos\theta_0 = 1 - \frac{\rho g h^2}{2 \gamma_{LV}} \quad (42)$$

As for the pendent drop (above), there exists an intermediate size range between the “dew drop” and the “puddle” for which  $\gamma_{LV}$  may be estimated from drop shape (slightly deformed from sphericity), but its treatment is beyond the scope of this chapter (Padday 1971; Hartland and Ramakrishnan 1975). Modern equipment on the market comes with software that approximates the projection of the liquid meniscus to a solution of the corresponding differential equations.

### Capillary Rise and Wilhelmy Plate

The principle here is the same as discussed above, the only differences being that the liquid surface tension is assumed to be known and that the contact angle is nonzero. If the  $\theta_0$  are greater than zero, capillary rise in a tube is less marked, and may even become capillary *descent*, if  $\theta_0 > \pi/2$ . The liquid level in the tube is lower than the surrounding liquid bath. When the  $\theta_0$  are nonzero, (33) includes a term in  $\cos\theta_0$ , and, after rearrangement, the following expression is obtained:

$$\theta_0 = \cos^{-1} \frac{R \rho g h}{2 \gamma_{LV}} \quad (43)$$

In much the same way, the Wilhelmy plate technique may be used, where force,  $F$ , becomes  $2 l \gamma_{LV} \cos\theta_0$ . The disadvantage for both of these is that the solid of interest must be made into a suitable geometric form, which is not always convenient or even possible!

### Fibers

The special case of fibers will be given, since knowledge of their surface properties is essential in composite technology. In principle, the method for obtaining contact

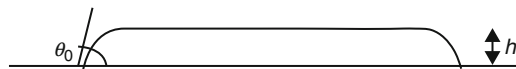


**Fig. 13** Schematic representation of “puddle” of height  $h$  and contact angle  $\theta_0$

angle on a fiber is the same as for the Wilhelmy plate: A liquid meniscus forms round the fiber immersed in a liquid bath, and its weight, detected by a microbalance, can be used to obtain  $\theta_0$ . It is assumed, for simplicity, that the fiber is of circular section of radius  $r$ . With  $F_0$  being the force on the balance corresponding to the weight of the fiber before immersion, and  $F$  that measured with the fiber partially immersed, vertically, axis perpendicular to free liquid surface and to depth,  $l$ , an expression for the difference,  $\Delta F$ , is obtained given by

$$\Delta F = F - F_0 = 2 \pi r \gamma_{LV} \cos \theta_0 - \pi r^2 l \rho_L g \quad (44)$$

In this equation,  $\rho_L$  is liquid density (or more precisely, the difference between density of liquid and air), and thus the right-hand term is a buoyancy correction. Since the surface tension term scales with  $r$ , and the buoyancy term with  $r^2$ , clearly the correction becomes very small for thin fibers. (The same basic argument is used when employing a thin Wilhelmy plate, above.)

## 4.5 Free Energy Balance of Wetting

With the thermodynamic background (cf. Sects. 2 and 3) and with the experimental steps for getting  $\theta_{e,a}$ ,  $\theta_{e,r}$  and the thermodynamic contact angle for the smooth homogeneous solid,  $\theta_e$ , (Sect. 4), the picture can now be completed by discussing the excess Helmholtz free energy of wetting which is often called the Helmholtz free energy of adhesion. Wetting is indeed the adhesion of a liquid on a solid.

Figure 14 illustrates the situation before and after wetting at thermodynamic equilibrium. For simplicity, consider a solid with at least one smooth and flat part of its surface. In the initial state (superscript 1), the solid has a phase boundary with the common vapor only. Hence, there are two D-faces with the areas  $A_{SV}^1$ ,  $A_{LV}^1$  in the initial state. The solid is lowered until the flat part of its surface is just isothermally wetted at constant pressure by the flat liquid meniscus. This is the final state (superscript 2) with three D-faces (areas  $A_{SV}^2$ ,  $A_{LV}^2$ ,  $A_{SL}^2$  and one triple line. (Any immersion of the solid into the liquid would simply create new area of the D-faces.

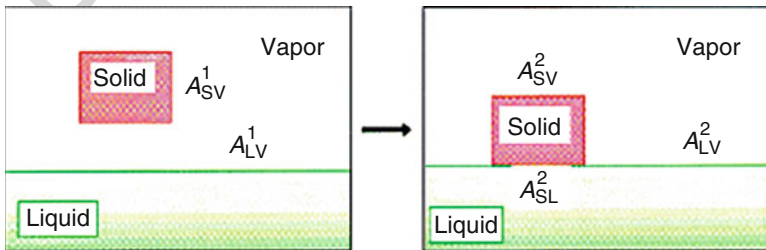


**Fig. 14** Schematic representation of a solid in vapor (*left*) being led to contact a liquid surface (*right*).  $A_{LV}^1, A_{LV}^2$  denote the areas of the corresponding D-faces

Such motion only complicates the thermodynamic free energy balance without giving any additional insight.)

Note that the constitution of the system, i.e., the components, their number  $N$ , their concentrations, and chemical potentials  $\mu_i$  as well as pressure and temperature is the same in the initial and the final state. Hence, the state of the bulk phases does not change. Moreover, the interfacial tensions  $\gamma_{SV}$  and  $\gamma_{LV}$  and the  $2N$  values for the absolute adsorptions  $\Gamma_{i,SV}$ ,  $\Gamma_{i,LV}$  will not change either.

Now (26) is employed and the excess Helmholtz free energies of all five D-faces may be written

$$F_{SV}^1 = \gamma_{SV} A_{SV}^1 + \sum_i^N \mu_i \Gamma_{i,SV} A_{SV}^1 \quad (45a)$$

$$F_{LV}^1 = \gamma_{LV} A_{LV}^1 + \sum_i^N \mu_i \Gamma_{i,LV} A_{LV}^1 \quad (45b)$$

$$F_{SV}^2 = \gamma_{SV} A_{SV}^2 + \sum_i^N \mu_i \Gamma_{i,SV} A_{SV}^2 \quad (45c)$$

$$F_{LV}^2 = \gamma_{LV} A_{LV}^2 + \sum_i^N \mu_i \Gamma_{i,LV} A_{LV}^2 \quad (45d)$$

$$F_{SL}^2 = \gamma_{SL} A_{SL} + \sum_i^N \mu_i \Gamma_{i,SL} A_{SL} \quad (45e)$$

where  $\Gamma_{i,IJ}$  = absolute adsorption of component  $i$  on the D-face  $IJ$ .

A relationship between the areas of the D-faces exists

$$A_{SL} = A_{LV}^1 - A_{LV}^2 = A_{SV}^1 - A_{SV}^2 \quad (46)$$

Therefore, wetting is considered to be an isothermal, isochoric, and isobaric change of state, and the contribution from the triple line is neglected. As a result, the change of Helmholtz free energy of the whole system is given by the change of the excess Helmholtz free energy at the D-faces

$$F^2 - F^1 = F_{SV}^2 - F_{SV}^1 + F_{LV}^2 - F_{LV}^1 + F_{SL}^2 \equiv F^{\text{wett}} \quad (47)$$

That is the *excess Helmholtz free energy of wetting*. Inserting (Eqs. 45 and 46), the following equation is obtained

$$F^{\text{wett}} = -(\gamma_{SV} + \gamma_{LV} - \gamma_{SL}) A_{SL} - A_{SL} \cdot \sum_i^N \mu_i \cdot (\Gamma_{i,SV} + \Gamma_{i,LV} - \Gamma_{i,SL}) \quad (48)$$

and for the specific value (per unit area)

$$f^{\text{wett}} = \frac{F^{\text{wett}}}{A_{\text{SL}}} = -(\gamma_{\text{SV}} + \gamma_{\text{LV}} - \gamma_{\text{SL}}) - \sum_i^N \mu_i \cdot (\Gamma_{i,\text{SV}} + \Gamma_{i,\text{LV}} - \Gamma_{i,\text{SL}}) \quad (49)$$

which is usually called the *adhesion energy* for the liquid–solid contact.

The first term on the right-hand side corresponds to the so-called reversible specific or thermodynamic, work of adhesion (to within a sign change)

$$W^{\text{adh}} = \gamma_{\text{LV}} - \gamma_{\text{SL}} \quad \text{Dupre's rule} \quad (50)$$

as introduced by Dupré (1869). Note that Dupré formulated his rule on an empirical basis long before Gibbs developed the thermodynamics for interfaces in the form used here.

However, there is a second term that covers the energetic contribution from the composition of the three-phase boundaries (via the absolute adsorptions), and hence the specific Helmholtz free energy of wetting may not be reduced to a balance of the interfacial tensions involved.

A simple experimental test can be used to demonstrate that this is more than just a theoretical statement. Figure 15 depicts the change of the wetting equilibrium of polymer samples at a Wilhelmy balance (cf. Fig. 10) owing to a slight compositional change of the common vapor phase. The sample plate at the fine balance consists of either polymer A or polymer B, the test liquid is water, and there is the common gas phase in the compartment (Fig. 15, left scheme). At the starting point  $t = 0$  min (Fig. 15, plot on the right), the plate just touches the water surface for wetting. The capillary in the setup is still empty so that the common gas phase consists of air and water vapor only. For that equilibrium, the wetting causes a certain force change  $F_{\text{meas}}(t = 0)$  as compared to the dry polymer sample A or B. As the next step ( $t > 0$ ), only the vapor phase is contaminated by a small amount of n-octane evaporating from a pendent drop hanging from the glass capillary now (cf. Fig. 15, left). n-Octane is “immiscible” with water. (N.B. According to thermodynamics, all substances mix, at least to some extent. Hence, the word “immiscible” corresponds to common usage.) As a saturated hydrocarbon, n-octane forms only weak physical interactions with water and the polymers. Nevertheless, the wetting force  $F_{\text{meas}}(t)$  at the Wilhelmy balance changes immediately and significantly whenever a small amount of n-octane vapor is added and then removed! This is due to a change of the wetting equilibrium which in turn is determined by the three D-faces LV, SV, and SL. In fact, this is the type of experiment that may be used to introduce the convenient “spreading pressure,” representing reduction in surface tension due to adsorption, as mentioned earlier.

For wetting, the extra force acting on the Wilhelmy balance is

$$F - F_0 = L \cdot (\gamma_{\text{SV}} - \gamma_{\text{SL}}) - \text{buoyancy of the sample} \quad (51)$$



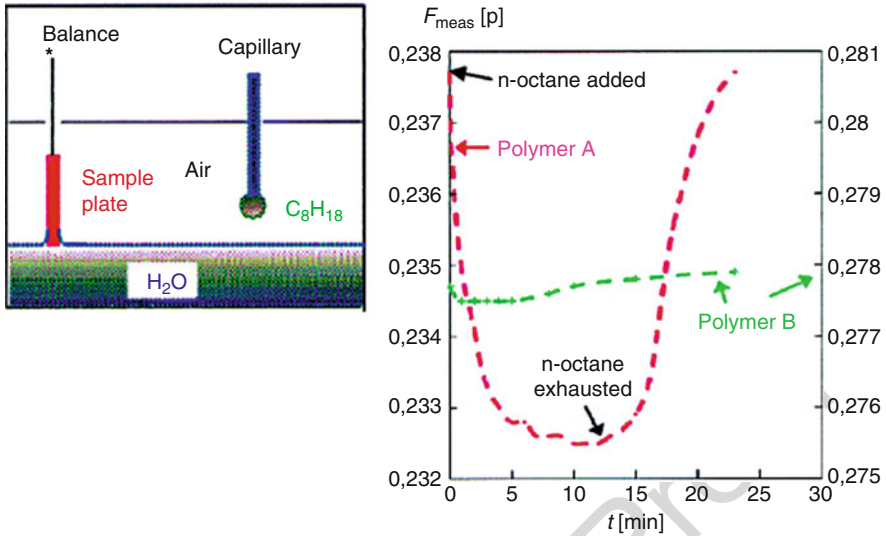


**Fig. 15** Sketch (*left*) for the Wilhelmy balance with sample plate and a capillary for n-octane evaporation into the common gas phase (air) above the wetting liquid (water).  $F_{\text{meas}}$  = load change in gram force  $p$  as measured at the balance. For two polymers A and B (different types of cellulose), the right-hand graph shows the quick response of the wetting equilibrium when a little amount of octane is evaporated into the gas phase at  $t > 0$  min and when the atmosphere is replaced by fresh air after some time (return of  $F_{\text{meas}}$  to the initial value)

$F_0$  = force due to the weight of the dry polymer sample before wetting

$L$  = length of the TL on the wetted polymer sample.

The sample immersion depth does not change when n-octane is added to the composition of the vapor phase, and hence the measured change of force is

$$\Delta F = L \cdot (\Delta\gamma_{\text{SV}} - \Delta\gamma_{\text{SL}}) = L \cdot [\Delta\gamma_{\text{LV}} \cdot \cos\theta_0 + \gamma_{\text{LV}} \cdot \Delta(\cos\theta_0)] \quad (52)$$

Since  $\Delta\gamma_{\text{SL}} > 0$ , according to (26), the change of the wetting equilibrium is accompanied by a change of the specific excess Helmholtz free energy of each D-face:

$$\Delta f_{\text{D}}^{\text{D}} = \Delta\gamma_{\text{D}}^{\text{D}} + \sum_i \left( \Delta\mu_i \cdot \Gamma_{i,\text{D}}^{\text{D}} + \mu_i \cdot \Delta\Gamma_{i,\text{D}}^{\text{D}} \right) \quad (53)$$

Therefore, the addition of n-octane to the vapor phase not only changes the interfacial tensions *but* also the chemical potential (via the compositional change) and the absolute adsorptions (mainly for the LV and SV interfaces).

As the consequence, an error results from utilizing Dupré's rule (50) instead of the full expression (49) for the specific Helmholtz free energy of wetting. The magnitude of the error cannot be deduced from wetting experiments since they do not provide information on adsorption at the D-faces in the system.

## 4.6 Concluding Remarks

It may be seen from the preceding sections that a variety of methods are available to obtain both liquid surface tensions and static contact angles. Some are cheap, or easily constructed, others less so. They all have their various merits, depending on the (geometric) presentation of the solid to be characterized. They also have their respective disadvantages, e.g., the sessile drop technique is simple, but care must be exercised in assuring correct drop size range and circularity of the triple line; the maximum bubble pressure is precise and capable of measurement of transient surface tensions but generally requires relatively advanced apparatus.

All techniques for contact angle measurement are prone to static wetting hysteresis effects. Wetting hysteresis has its origins in surface roughness, microheterogeneities, and other “imperfections” and can be of the order of 10 s of degrees. It is rarely less than  $2^\circ$  or  $3^\circ$ , so the commonly seen habit of specifying contact angles to one, sometimes two, decimal places is pointless. This leaves another question: If static advancing and receding contact angles are measured, what is the equilibrium value  $\theta_e$  on a flat smooth homogeneous surface? It is  $\theta_e$  that is needed for Young’s equation. The experimental procedure described in the context of (39 and 40) provides the answer.

Bearing in mind the limitations and approximations made for Dupré’s rule (50) and Young’s equation (29), finally consider the common treatment of contact angle data which makes use of the combination of the two equations:

$$W^{\text{adh}} = \gamma_{\text{LV}}(1 + \cos \theta_e) \approx -f^{\text{wett}} \quad (54)$$

This is the *estimated* specific wetting energy, provided that the surface tension  $\gamma_{\text{LV}}$  of the wetting liquid is measured using one of the techniques mentioned and that equilibrium contact angle for the flat surface  $\theta_e$  is derived correctly from the contact angle hysteresis. Nevertheless, it is unclear whether it is justified to neglect the adsorption terms in the energy balance.

Additional conditions needed for such interpretation of wetting data are as follows:

Pure liquids that neither swell nor dissolve the solid must be used.

Solids should be “ideal” (flat, homogeneous, etc.).

Small curvature of the triple line must be ensured.

Interfacial tension is an excess property of the phase boundary of *two* phases and responds remarkably to minute changes of the composition!

The use of literature data for  $\gamma_{\text{LV}}$  of liquids should be avoided. Conditions of use can vary.

Finally, there is another price to be paid for using (54): The interfacial tensions  $\gamma_{\text{SL}}$  and  $\gamma_{\text{SV}}$  of the solid have been eliminated, and hence, they cannot be deduced from wetting experiments. This obstacle was the reason for the development of so-called thermodynamic adhesion theories which introduce various proposals for a

relationship between the liquid–solid interfacial tension  $\gamma_{SL}$  and the surface tensions  $\gamma_{LV}$  and  $\gamma_{SV}$ . These theories are considered in chapter Thermodynamics of Adhesion.

## References

- Adam NK, Elliott GEP (1962) Contact angles of water against saturated hydrocarbons. Theory of the capillary layer between the homogeneous phases of liquid and vapour II. *J Chem Soc* 2206–2209. <https://doi.org/10.1039/JR9620002206>
- Bakker G (1902) Theory of the capillary layer between the homogeneous phases of liquid and vapour II. *Z Phys Chem Stoichiometrie Verwandtschafts* 42:68
- Bartell FE, Shepard JW (1953a) Surface roughness as related to hysteresis of contact angles I. The system paraffin–water–air. *J Phys Chem* 57:211
- Bartell FE, Shepard JW (1953b) Surface roughness as related to hysteresis of contact angles II. The system of paraffin–4M–calcium chloride solution–air and paraffin–glycerol–air. *J Phys Chem* 57:455
- Bischof C, Schulze RD, Possart W, Kamusewitz H (1988) The influence of the surface state of polymers on the determination of the contact angle. In: Allen KW (ed) *Adhesion*, vol 12. Elsevier Appl Sci, London/New York, pp 1–16
- Bumstead HA, Van Name RG (eds) (1961) *Scientific papers of J Willard Gibbs*, vol 2. Dover, New York
- Busscher HJ, van Pelt AWJ, de Boer P, de Jong HP, Arends J (1984) The effect of surface roughening of polymers on measured contact angles of liquids. *J Coll Surf* 9:319
- Dupré A (1869) *Théorie mécanique de la chaleur*. Gauthiers-Villars, Paris, p 369
- Gaydos J, Rotenberg Y, Boruvka L, Chen P, Neumann AW (1996) The generalized theory of capillarity. In: Neumann AW, Spelt JK (eds) *Applied surface thermodynamics*. Marcel Dekker, New York, pp 1–51
- Hartland S, Ramakrishnan S (1975) Determination of contact angles and interfacial-tension from shape of sessile interfaces. *Chimia* 29:314
- Johnson RE, Dettre RH (1964) Contact angle hysteresis. I. Study of an idealized rough surface. *Adv Chem Ser* 43:112
- Padday JF (1971) The profiles of axially symmetric menisci. *Philos Trans R Soc A* 269:265–293
- Rusanov AI (1978) *Phasengleichgewichte und Grenzflächenerscheinungen*. Akademie-Verlag, Berlin
- Rusanov AI, Prokhorov VA (1996) Interfacial tensiometry. In: Möbius D, Miller R (eds) *Studies in interface science*, vol 3. Elsevier, Amsterdam/Lausanne/New York/Oxford/Shannon/Tokyo
- Schulze RD, Possart W, Kamusewitz H, Bischof C (1989) Young's equilibrium contact angle on rough solid surfaces – I. An empirical determination. *J Adhes Sci Technol* 3:39–48
- Shanahan MER, Carré A (1995) Viscoelastic dissipation in wetting and adhesion phenomena. *Langmuir* 11:1396
- Shanahan MER, de Gennes PG (1986) The ridge produced by a liquid near the triple line solid/liquid/fluid. *C R Acad Sci Paris* 302:517
- Shanahan MER, Cazeneuve C, Carré A, Schultz J (1982) Wetting criteria in 3-phase solid/liquid/liquid systems. *J Chim Phys* 79:241
- Thiessen PA, Schoon E (1940) Besetzung und Adhäsionsarbeit von Oberflächen fester organischer Verbindungen. *Z Elektrochem* 46:170
- Wenzel RN (1936) Resistance of solid surfaces to wetting by water. *Ind Eng Chem* 28:988–994
- Young T (1805) Cohesion of fluids. *Philos Trans R Soc A* 95:65–87
- Zhang J, Sheng X, Jiang L (2009) The dewetting properties of lotus leaves. *Langmuir* 25:1371–1376

Günter Reiter

## Contents

5.1	Introduction .....	101
5.2	Equilibrium Conditions .....	102
5.3	The Spreading Coefficient .....	103
5.4	The Flow Profile and Energy Dissipation .....	104
5.5	The Dynamic Contact Angle .....	106
5.6	The Rate of Spreading .....	108
5.7	Dewetting .....	110
5.8	Concluding Remarks .....	111
	References .....	112

## Abstract

A short overview of relevant processes and parameters in spreading of liquids on substrates is presented. In a simplified view, the dynamics of these processes can be understood as being controlled by the balance of driving forces and resistance due to dissipative processes. Analogies between spreading and dewetting are discussed.

## 5.1 Introduction

Spreading of a liquid on a substrate represents an elementary step in many processes like adhesion, coating, or painting. Spreading is the dynamic route of covering a substrate with a liquid up to the point when an equilibrium state is reached (Dussan 1979; de Gennes 1985; Cazabat 1987; Good 1992; Leger and Joanny 1992; Blake 2006; De Coninck and Blake 2008; Bonn et al. 2009; Marmur 2009). Many practical

G. Reiter (✉)

Physikalisches Institut, Fakultät für Mathematik und Physik, Albert-Ludwigs Universität Freiburg, Freiburg, Germany

e-mail: [guenter.reiter@physik.uni-freiburg.de](mailto:guenter.reiter@physik.uni-freiburg.de)

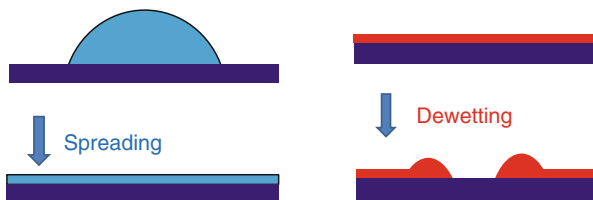


**Fig. 1** Schematic side-view representation of spreading of a drop toward a thin film (*left*) and dewetting of an unstable thin film via nucleation and growth of a dry patch surrounded by a rim (cross-sectional view) collecting the removed liquid

applications require the knowledge of how fast a liquid droplet, once deposited on a substrate, can spread out and cover a given area of the substrate.

Because the complementary process to spreading, that is, the retraction or dewetting of a liquid from a substrate (see Fig. 1), is determined by the same intermolecular forces and the corresponding dissipation routes, both processes can be treated in analogous ways (de Gennes 1985; Brochard-Wyart and de Gennes 1992).

Of course, the properties of the substrate represent equally relevant parameters as can be demonstrated by modifying the surface chemistry by standard chemical means (e.g., silanization, plasma treatment) (Israelachvili 1995). The process of liquid spreading is determined by short-ranged surface forces mainly controlled by surface chemistry but also by forces acting over longer distances up to some tens of nanometers (long-ranged forces). Moreover, chemical and physical heterogeneities are responsible for hysteretic behavior (Dussan 1979), which can significantly affect spreading and dewetting up to the point of prohibiting it. Generally, all spreading phenomena are governed by the interplay of surface and interfacial interactions, in particular in the region where the liquid meets the yet uncovered solid, the region of the three-phase contact line (de Gennes 1985).

## 5.2 Equilibrium Conditions

As stated already in 1805 by Thomas Young (1805), at thermodynamic equilibrium (no temperature gradients, concentration gradients, i.e., no net forces acting) the three surfaces that meet at the three-phase contact line define an equilibrium contact angle ( $\theta_{eq}$ ). Using a vector description for the forces (per unit length of the contact line), which are balanced at their contact, it can be seen that the surface tension ( $\gamma_{SV}$ ) between substrate and the surrounding medium (which is often the vapor of the liquid in question) has to be equal to the interfacial tension ( $\gamma_{SL}$ ) between substrate and liquid plus the projection of the interfacial tension ( $\gamma_{LV}$ ) between liquid and the surrounding medium onto the  $\gamma_{SL}$ -vector, resulting in the Young-equation:

$$\gamma_{SV} = \gamma_{SL} + \gamma_{LV} \cos \theta_{eq} \quad (1)$$

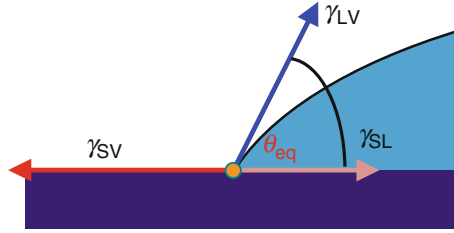


**Fig. 2** Schematic representation of the balance of interfacial forces (represented by the arrows for  $\gamma_{SV}$ ,  $\gamma_{LV}$ , and  $\gamma_{SL}$ , which meet at the contact line (indicated by a small circle)). This force balance determines the equilibrium contact angle  $\theta_{eq}$

Using Young's Eq. 1 and knowing  $\gamma_{SV}$  and  $\gamma_{LV}$ ,  $\gamma_{SL}$  may be obtained by measuring the contact angle  $\theta_{eq}$  (see Fig. 2) (Zisman 1964).

It should be noted that the equilibrium contact angle is a direct consequence of the balance of molecular interactions among the three materials at the contact line. At equilibrium, the contact line will not be set in motion and a drop will never spread. On the contrary, spreading occurs for a closed nonequibrated system that tries to reach equilibrium. Alternatively, a liquid may be forced to spread under the influence of an external force.

From a mechanical point of view, the balance of forces within the plane of the substrate neglects the force component  $\gamma_{LV} \sin \theta_{eq}$  in the direction normal to the substrate. Usually one assumes that the substrate is completely rigid and not deformable. Thus, this vertical force component is balanced by a reaction force of the solid, which is equal to  $-\gamma_{LV} \sin \theta_{eq}$ . Furthermore, it is assumed that the solid is not generating a force component parallel to the surface when getting in contact with a liquid. In such a situation, the forces acting at the contact line could be balanced by any value of the contact angle (Dussan 1979). On liquid or deformable (e.g., thin membranes or elastomers) substrates, however, this normal force component leads to a vertical displacement of the contact line, that is, the formation of a wetting ridge (Shanahan and Carré 1995; Carré et al. 1996). The Neumann triangle construction can account for this case (Chen et al. 1996).

### 5.3 The Spreading Coefficient

Based on these three interfacial tensions, a spreading coefficient  $S_{eq}$  may be defined, which characterizes the tendency of a liquid to spread out (or not) on a substrate:

$$S_{eq} = \gamma_{SV} - (\gamma_{SL} + \gamma_{LV}) \quad (2)$$

Using Eq. 1, this relation may be rewritten as:

$$S_{eq} = \gamma_{LV} (\cos \theta_{eq} - 1) \quad (3)$$

As pointed out by de Gennes (1985), in equilibrium,  $\gamma_{SV}$  can never be larger than  $\gamma_{SL} + \gamma_{LV}$ . If it were, the total free energy of the system could be lowered by removing the solid–vapor interface, that is, by coating the substrate with a (thick) layer of liquid. Then only a solid–liquid and a liquid–vapor interface would remain, that is, the solid is wetted (coated) by the liquid. In other words, the “true” equilibrium value of  $\gamma_{SV}$  is identical to  $\gamma_{SL} + \gamma_{LV}$ . However, if the solid to be coated is initially not in equilibrium with the surrounding vapor, the initial spreading coefficient  $S_{in}$  may be larger than zero.

In particular for nonvolatile liquids (these cannot reach equilibrium by evaporation and condensation but only by diffusion on the surface of the substrate)  $S_{in}$  can be defined by referring to the interfacial tension  $S_{SO}$  between the dry substrate and vacuum.

$$S_{in} = S_{SO} - (\gamma_{SL} + \gamma_{LV}) \quad (4)$$

In equilibrium, some molecules from the liquid will be adsorbed on the substrate, lowering  $\gamma_{SO}$  to  $\gamma_{SV}$ . Consequently,  $S_{in}$  is larger than  $S_{eq}$  and accordingly, after depositing a drop of liquid onto a dry substrate, flow will start (the drop spreads) until the equilibrium value of the contact angle is reached.  $\theta_{eq}$  may well be zero representing the situation where the liquid will cover the substrate by a film of homogenous thickness.)

## 5.4 The Flow Profile and Energy Dissipation

In spreading, the whole liquid wedge close to the contact line moves with the velocity  $U$  of the contact line. A standard boundary condition for liquid flow on solid substrates is typically the no-slip at the substrate. Liquid molecules at a solid substrate experience (significant) interactions responsible for adhesion. Thus, in contrast to liquid molecules in contact with other liquid molecules, they are not moving easily on this substrate. As a consequence, the velocity of these molecules is approximated by zero velocity (= no-slip boundary condition). However, applying this boundary condition strictly would not allow for any displacement of a liquid on a solid substrate. Thus, to account for the experimental fact that contact lines can and do move, various assumptions, partially based on molecular mechanisms, have been proposed (see, e.g., Bonn et al. 2009). In general, a cutoff length, typically as small as the size of the molecules, has to be introduced (de Gennes 1985; Huh and Scriven 1971).

For small contact angles (allowing to approximate  $\sin\theta_{eq} \approx \theta_{eq}$  [in radians]), the flow pattern close to the contact line (the wedge region) can be approximated by the so-called lubrication approximation, which compares the flow in the wedge with flow in a thin film: the velocity of fluid molecules is only determined by their distance  $z$  to the substrate, that is, the molecules move preferentially in the  $x$ -direction parallel to the substrate and less in the direction away from the substrate.

Thus, at any point  $x$  from the contact line the velocity  $v(z)$  is only a function of  $z$  [ $v_x(z) = v(z)$ ; see Fig. 3].

As interactions between liquid molecules, and thus their viscosity  $\eta$ , are assumed to be independent of the distance  $z$  to the substrate also the relative velocity difference between molecules should be constant. Thus, in a film of local thickness  $h(x)$  that moves at the mean velocity  $U$  of the contact line, a decrease in velocity is found when going from the film surface toward the substrate with a velocity gradient  $dv(z)/dz$  inside the film. Thus,  $U$  is the average along the normal to the surface, that is, the  $z$ -direction, of this velocity profile

$$U = h^{-1} \int_0^h dz \, v(z) \quad (5)$$

Accordingly, a parabolic velocity profile is obtained (de Gennes 1985) (with the boundary conditions that the velocity vanishes at the solid side and the derivative of the velocity at the liquid/gas interface is zero, that is, there is no tangential stress):

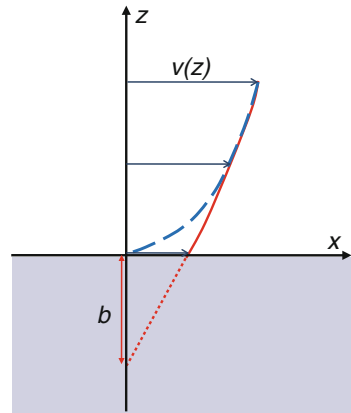
$$v(z) = \frac{3U}{2h^2(x)} (-z^2 + 2h(x)z) \quad (6)$$

and the rate of viscous dissipation (within one slice of the film) due to viscous friction of the liquid molecules that are moving past each other, integrated over the film depth  $h(x)$ :

$$\int_0^{h(x)} dz \, \eta \left[ \frac{dv_x(z)}{dz} \right]^2 = \frac{3\eta U^2}{h(x)} \quad (7)$$

Integration now over the whole moving object, from its lowest thickness at the contact line having a minimum thickness of  $h_{\min}(x)$  to its thickest part with the maximum thickness of  $h_{\max}(x)$ , using the approximation  $h(x) \approx x \cdot \theta_{\text{dyn}}$  (with  $\theta_{\text{dyn}}$

**Fig. 3** Schematic representation of the velocity profile of liquid flow within a thin film (lubrication approximation). For the no-slip boundary condition (broken line) the velocity at the substrate ( $z = 0$ ) is zero. In the case of slippage (full line), the liquid velocity is not zero at the substrate surface and only extrapolates to zero at a distance  $b$  ( $=$  slippage length) within the substrate





being the dynamic contact angle at the contact line) yields the total viscous dissipation per unit time and unit length of the contact line during spreading (Bonn et al. 2009):

$$D_{\text{diss}} \cong \int_{h_{\min}}^{h_{\max}} \frac{3\eta U^2}{h(x)} dx = \frac{3\eta U^2}{\theta_{\text{dyn}}} \ln \frac{h_{\max}}{h_{\min}} \quad (8)$$

Clearly, if  $h_{\min}$  would be zero the dissipated energy would be infinite. However, such a value is not physical because the smallest lengthscale in the problem is related to the moving molecules. Thus, it is plausible to set the lower cutoff length proportional to the size of the molecules.

Basically, the same procedure can be applied to the case where the liquid is slipping on the substrate by introducing an extrapolation length (slippage length)  $b$  within the substrate (see Fig. 3) where the flow velocity would be zero, that is, the nonslip boundary would be reached at a virtual interface inside the solid. Thus, one expects  $h_{\min} \sim b$  (de Gennes 1985). Slippage is particularly relevant in the case of entangled polymer melts spreading or dewetting on a smooth surface (de Gennes 1985; Reiter and Khanna 2000a, b). A large number of experimental studies on slippage have been recently reviewed (Neto et al. 2005).

## 5.5 The Dynamic Contact Angle

While a well-defined equilibrium situation allows a clear characterization of  $\theta_{\text{eq}}$ , the displacement of the contact line (which evidently implies a velocity of displacement) requires a deviation from this value, resulting in a dynamic contact angle  $\theta_{\text{dyn}}$  (see Fig. 4). In fact, whenever on ideal surfaces the contact angle deviates from  $\theta_{\text{eq}}$  (which represents the absolute minimum in free energy of the system) the contact line will show the tendency to move in order to try to reestablish equilibrium. In

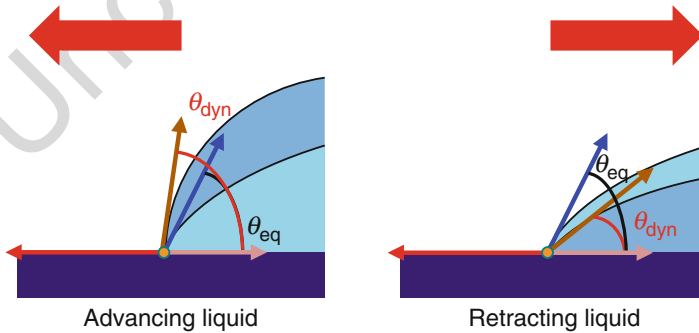


**Fig. 4** Schematic representation of the difference between the equilibrium contact angle  $\theta_{\text{eq}}$  and the dynamic contact angle ( $\theta_{\text{dyn}}$ ). In equilibrium, the force vectors for  $\gamma_{\text{SV}}$ ,  $\gamma_{\text{LV}}$  and  $\gamma_{\text{SL}}$  add up to zero within the plane of the substrate. However, in the case of an advancing (left) or retracting (right) liquid front a net force remains, indicated by the big (red) arrows on top

general, the stronger  $\theta_{\text{dyn}}$  deviates from  $\theta_{\text{eq}}$ , the faster will be the movement of the contact line (see Fig. 5). Thus, for  $\theta_{\text{dyn}} \neq \theta_{\text{eq}}$ , instead of a perfect balance of interfacial tensions at equilibrium, a net force  $F$  (per unit length of the contact line) remains:

$$F = -\gamma_{\text{SV}} + \gamma_{\text{SL}} + \gamma_{\text{LV}} \cos \theta_{\text{dyn}} \quad (9)$$

Using Eq. 1,  $(-\gamma_{\text{SV}} + \gamma_{\text{SL}})$  can be replaced by  $(-\gamma_{\text{LV}} \cos \theta_{\text{eq}})$  and finally the so-called unbalanced Young force is obtained (Brochard-Wyart and de Gennes 1992)

$$F = \gamma_{\text{LV}} (\cos \theta_{\text{dyn}} - \cos \theta_{\text{eq}}) \quad (10)$$

For small contact angles the cos-term can be approximated by the first term of its series expansion, that is,  $\cos \theta \sim 1 - \frac{1}{2}\theta^2$ . This leads then to

$$F = \frac{1}{2}\gamma_{\text{LV}} (\theta_{\text{eq}}^2 - \theta_{\text{dyn}}^2) \quad (11)$$

If the viscous forces are significantly smaller than the surface tension (as expressed by a capillary number  $Ca$  much less than 1:  $Ca = U \cdot \eta / \gamma_{\text{LV}}$ , with  $U$  being the velocity of the contact line and  $\eta$  the viscosity of the liquid), the shape of

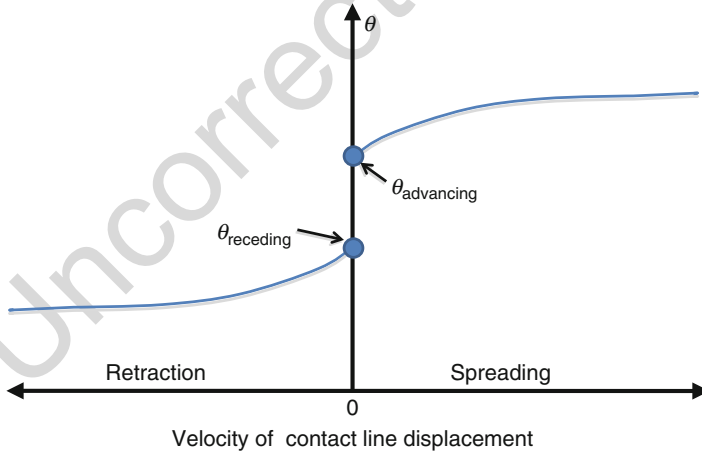


**Fig. 5** Qualitative representation of the variation of the contact angle as a function of the contact line velocity (a negative velocity represents retraction, a positive velocity represents spreading). On heterogeneous substrates, a difference between the values of the contact angle at zero velocity will be observed, depending on how zero velocity is approached, in the advancing ( $\theta_{\text{advancing}}$ ) or receding ( $\theta_{\text{receding}}$ ) direction. Contact angle hysteresis is defined as:  $\Delta\theta = \theta_{\text{advancing}} - \theta_{\text{receding}}$ . In some cases, for example, when heterogeneity is caused by substrate roughness, the equilibrium contact angle may be approximated by  $\theta_{\text{eq}} = \frac{1}{2}(\theta_{\text{advancing}} + \theta_{\text{receding}})$ . However, this last relation is not generally applicable

the drop can be reasonably well approximated by a spherical cap. Laplace pressure  $P_L(P_L = 2\gamma_{LV} \cdot C$ , for a spherical cap of radius  $R$  the curvature  $C = 1/R$  and thus  $P_L = 2\gamma_{LV}/R$ ) will be able to assure the same curvature everywhere, except for the region very close to the contact line, where long-range molecular interactions, for example, van der Waals forces, become important. At a macroscopic level, a spreading drop, for example, on a wettable substrate, can be well described by an apparent contact angle  $\theta_{ap} = 4V/\pi R^3$  (valid for small values of this contact angle): as the drop spreads, the apparent contact angle decreases as  $1/R^3$ .

## 5.6 The Rate of Spreading

The speed of spreading is determined by the balance of driving forces (corresponding to surface energy, represented by the contact angle, and, for big drops, gravity) and velocity-dependent dissipative forces. In many cases, the major contribution to dissipation originates from the velocity gradient experienced by the liquid molecules moving in the wedge region close to the contact line. The diverging increase of dissipation as the contact line is approached (see Eq. 8) represents the most important mathematical problem in the context of moving a three-phase contact line, as first pointed out by Huh and Scriven (1971).

For the complete wetting case ( $S \geq 0$ ), a thin film of dynamical origin (off-equilibrium) forms ahead of the apparent contact line of the drop. The formation of a precursor film avoids that viscous dissipation diverges near the (geometrically apparent) contact line. Thus, macroscopic spreading of a droplet of a nonvolatile liquid (with surface tension  $\gamma_{LV}$ ), which wets the substrate, proceeds via the formation of such a thin precursor film ahead of the “visible” (apparent) contact line (Checco 2009). The thickness of this precursor film is truncated at a value given by:

$$h_0 = a\sqrt{2\gamma_{LV}/2S_{in}} \quad (12)$$

with the molecular length scale  $a = \sqrt{2A/\gamma_{LV}}$  (where  $A$  is the Hamaker constant for the liquid on the substrate).  $h_0$  is usually larger than the molecular size  $a$ , because typically  $\gamma \gg S_{in}$ . In the equilibrium situation (after spreading being completed),  $h_0$  represents the final thickness of the so-called final pancake, that is, the resulting wetting film, which can be easily derived from the free energy  $\mathcal{F}$  of an initial droplet of volume  $\Omega$  (Brochard-Wyart et al. 1991):

$\mathcal{F} = \mathcal{F}_0 - A \cdot S_{in} + P(h) \cdot A$  with the constraint that  $\Omega = A \cdot h$ .  $\mathcal{F}_0$  is the free energy of the system without droplet,  $A$  is the area covered by the droplet,  $S_{in}$  is the initial spreading coefficient, and  $P(h)$  is the contribution to the free energy that arises as the thickness is less than infinity. Thus, the limiting values of  $P(h)$  are:  $P(h \rightarrow \infty) = 0$  and  $P(h \rightarrow 0) = S_{in} = \gamma_{SO} - \gamma_{SL} - \gamma_{LV}$ . For cases where van der Waals forces dominate the long-range interaction,  $P(h) = A/12\pi h^2$  is obtained. Minimization of  $\mathcal{F}$  with respect to  $h$  leads to Eq. 12 ( $h_0 = \sqrt{A/4\pi S_{in}} = a\sqrt{3\gamma_{LV}/2S_{in}}$ ).

A typical spreading experiment starts by depositing at time  $t = 0$  a spherical liquid droplet of volume  $V$ , characterized by the base radius  $R_0$ , onto an ideal, planar, and horizontal substrate, either solid or liquid. Suppose that the liquid is nonvolatile and that the initial shape of the now sessile droplet is part of a sphere with a macroscopic contact angle  $\theta_0$  (for simplicity, the case of  $\theta_0 \leq \pi/2$  is assumed). This droplet is surrounded by a nonreactive and nonmiscible fluid phase (either gas or liquid). When  $S \geq 0$ , the droplet spreads spontaneously and tends to separate solid and surrounding fluid phase. For a finite volume of the initial droplet, spreading continues only until the liquid layer, covering the solid surface reaches a mesoscopic or microscopic thickness controlled by the disjoining pressure (originating from long-range forces like van der Waals forces), which in most cases tends to thicken this layer, and which effectively competes with the capillary forces. Thus, the final thickness of the extended liquid structure is determined by the interplay between the spreading power and the liquid/gas interfacial tension (see Eq. 12).

For negative values of the spreading coefficient ( $S < 0$ ), the liquid droplet only partially wets the solid. If the liquid was forced to cover the substrate, it will retract (dewet) from it until one or many (macroscopic) liquid droplets with the equilibrium shape of a spherical cap have formed. If the liquid is deposited as a spherical droplet, it will spread out until it reaches its equilibrium shape, characterized by  $\theta_{eq}$ .

In describing spreading and the local molecular processes directly at the contact line, two different types of descriptions of sessile droplet spreading exist: hydrodynamic and molecular kinetic, which differ from each other mostly in the consideration of the dominant dissipation channel (de Gennes et al. 1990; Cazabat et al. 1997; Blake 2006).

In the molecular kinetic theory of Eyring, adapted to describe the kinetics of wetting phenomena (Blake and Haynes 1969; Blake 2006; de Coninck and Blake 2008), the focus is put on the dissipative processes occurring in the vicinity of advancing contact line, mainly due to the attachment/detachment processes of molecules from the liquid onto the solid. This approach yields for the dynamics of the base radius  $[R(t)]$  and contact angle  $[\theta_{dyn}(t)]$ ,  $R(t) \sim t^{1/7}$  and  $\theta_{dyn}(t) \sim t^{-3/7}$ , respectively.

When dissipation is due to viscous flows generated in the core of the spreading droplet, a relation (see Eq. 8) between spreading velocity  $U$ , viscosity  $\eta$ , surface tension  $\gamma_{LV}$  of the liquid (all represented by the capillary number  $Ca = U \cdot \eta / \gamma_{LV}$ ), and the value of the contact angle  $\theta_{dyn}(t)$  as a function of spreading time  $t$  can be formulated. This relation yields simple scaling laws determining the time evolution of the contact angle and of the droplet's base radius  $R(t)$ . For the case of spreading of circular droplets, one finds  $R(t) \sim t^{1/10}$  and  $\theta(t) \sim t^{-3/10}$ . These scaling laws have been examined experimentally and shown to agree fairly well with experimental data for many liquid/solid systems (Tanner 1979; de Gennes 1985; Cazabat and Cohen Stuart 1986; Brochard-Wyart et al. 1991; Marmur 1997).

De Gennes (1985) suggested that during the spreading process, the energy resulting from the unbalanced Young force is balanced by the total energy dissipation in the core of the droplet, at the advancing contact line and in a precursor film. Balancing the corresponding capillary driving force (given by Eq. 11) with the viscous force acting at the contact line (related to Eq. 8:  $D_{diss} = F_{visc} \cdot U$

(de Gennes 1985) with the viscous force  $F_{\text{visc}}$  being proportional to viscosity  $\eta$  and the velocity  $U$  at which the liquid moves) leads then to:

$$\frac{1}{2}\gamma_{LV}(\theta_{\text{dyn}}^2 - \theta_{\text{eq}}^2) = -(\eta \cdot U / \theta_{\text{dyn}}) \ln \frac{h_{\text{max}}}{h_{\text{min}}} \quad (13)$$

## 5.7 Dewetting

When a liquid is forced to cover a substrate, which it does not like to wet, the film is either metastable or completely unstable (de Gennes 1985; Brochard-Wyart and de Gennes 1992; Leger and Joanny 1992). Initiated by a defect or some other perturbation, a hole may be nucleated and grow in diameter. The liquid removed from the dry circular spot (the hole in the liquid film) is collected in a liquid ridge (the “rim”) (see Fig. 1). The shape of this rim may be described approximately as a portion of a cylinder that is characterized by two contact angles  $\theta_{\text{dyn}}$  and  $\phi$  (see Fig. 6).

In analogy to the complete wetting (see Eq. 13), for the movement of the contact line (position F) in the partial wetting case (with dewetting velocity  $V$ ), the following relation may be obtained:

$$\gamma_{LV}(\theta_{\text{dyn}}^2 - \theta_{\text{eq}}^2)\theta_{\text{dyn}} = -L_F \cdot \eta V \quad (14)$$

Here,  $L_F$  is an abbreviation for  $\ln \frac{h_{\text{max}}}{h_{\text{min}}}$  evaluated at the position F.

For hole diameters much larger than the width of the rim, both ends of the rim (denoted by F and R in Fig. 6) move at approximately the same velocity. Moreover, at the position R the equilibrium value of the contact angle is zero (rim in contact with the film of the same liquid) and thus yields:

$$\gamma_{LV}\phi^3 = -L_R \cdot \eta V \quad (15)$$

Here,  $L_R$  is an abbreviation for  $\ln \frac{h_{\text{max}}}{h_{\text{min}}}$  evaluated at the position R.

For large rims, small values of  $Ca = U\eta/\gamma$  and assuming that Laplace pressure is the same everywhere within the rim (i.e., the same curvature is assumed to exist everywhere in the rim) requires that  $\phi \cong \theta_{\text{dyn}}$ . As can be seen from Eqs. 8 and 13, the values of  $L_F$  and  $L_R$  are representing the logarithmic factor  $\ln \frac{h_{\text{max}}}{h_{\text{min}}}$ . While the

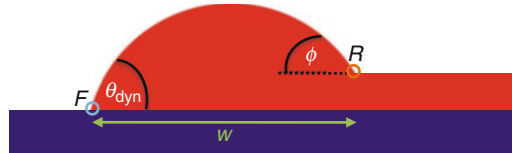


**Fig. 6** Schematic representation of the rim forming in the course of dewetting of a thin liquid film. At the front position F of the rim, the contact angle assumes its dynamic value  $\theta_{\text{dyn}}$  and at the rear position R it takes the value  $\phi$ . The width of the rim is given by  $w$

maximum size is represented by width of the rim and is the same for both values, the minimum length scale is different for the positions F (proportional to the size of the molecules) and R (proportional to the thickness of the film). Thus, for very thin films in the nanometer range, this difference between of  $L_F$  and  $L_R$  is small as the width of the rim is typically much larger than the film thickness or the size of the molecules. Consequently, a highly useful relation is obtained between dynamic and equilibrium contact angle for the case of viscous dewetting:

$$\gamma_{LV}(\theta_{\text{dyn}}^2 - \theta_{\text{eq}}^2)\theta_{\text{dyn}} = \gamma_{LV}\phi^3 \quad (16)$$

$$\phi \cong \theta_{\text{dyn}} \quad (17)$$

$$\theta_{\text{dyn}} = \theta_{\text{eq}}/\sqrt{2} \quad (18)$$

and a constant dewetting velocity of

$$V \sim \frac{\gamma_{LV}}{\eta} \cdot \theta_{\text{eq}}^3 \quad (19)$$

or with  $V^* = \gamma_{LV}/\gamma$

$$V \sim V^* \cdot \theta_{\text{eq}}^3 \quad (20)$$

It should be noted that a constant dewetting velocity, as predicted by Eq. 20, will only be observed as long as the assumption of nonslip boundary conditions applies, that is, main dissipation in the liquid wedge close to the contact line that is independent of the actual size of the rim. However, in the case of slippage as it occurs for polymer melts on “ideal” substrates (Reiter and Khanna 2000a, b), dissipation occurs over the whole moving interface that is proportional to the width of the moving rim. Thus, as the size of the rim increases in time, dissipation increases also. The driving capillary force, however, is constant and consequently the dewetting velocity is decreasing in time.

## 5.8 Concluding Remarks

The above presented concepts of liquid spreading and dewetting apply only in situations where the substrates are “perfect,” that is, chemically homogeneous and physically smooth. For example, on rough substrates spreading (Cazabat and Cohen Stuart 1986; Rolley et al. 1998) and dewetting (Zhang et al. 2005) dynamics will be modified. Moreover, in contrast to spreading of pure and simple fluids, the process can also be quite different for mixtures or solutions. For example, polymer solutions (Fondecave and Brochard-Wyart 1998) or surfactant solutions (Troian et al. 1990; Nikolov et al. 2002) can exhibit quite complex spreading behavior. Spreading will

become even more complex when a chemical reaction between liquid and substrate is involved like in reactive spreading (Eustathopoulos 1998).

In addition to spreading and dewetting driven by capillary forces, these processes may be “forced” by applying an external electric field like in “electrowetting” (Vallet et al. 1999; Verheijen and Prins (1999), Mugele and Baret 2005) or a mechanical force by inclining or moving the substrates. The latter process is highly relevant in coating technologies, for example, in the paper industry.

As a general summary, the dynamics of spreading and dewetting is controlled by the balance of driving forces (e.g., capillary forces, gravity, or electric forces) and resistance due to dissipative processes that may be increasingly more complicated when complex fluids rather than simple ones are used.

## References

- Blake TD Haynes JM (1969) Kinetics of liquid-liquid displacement. *J Coll Interf Sci* 30:421
- Blake TD (2006) The physics of moving wetting lines. *J Coll Interf Sci* 299:1
- Bonn D, Egges J, Indekeu J, Meunier J, Rolley E (2009) Wetting and spreading. *Rev Mod Phys* 81:739
- Brochard-Wyart F, di Meglio JM, Quéré D, de Gennes PG (1991) Spreading of nonvolatile liquids in a continuum picture. *Langmuir* 7:335
- Brochard-Wyart F, de Gennes PG (1992) Dynamics of partial wetting. *Adv Coll Interf Sci* 39:1
- Carré A, Gastel JC, Shanahan MER (1996) Viscoelastic effects in the spreading of liquids. *Nature* 379:432
- Cazabat AM, Cohen Stuart MA (1986) Dynamics of wetting: effects of surface roughness. *J Phys Chem* 90:5845
- Cazabat AM (1987) How does a droplet spread?. *Contemp Phys* 28:347
- Cazabat AM, Gerdes S, Valignat MP, Villette S (1997) Dynamics of wetting: from theory to experiment. *Interf Sci* 5:129
- Checco A (2009) Liquid spreading under nanoscale confinement. *Phys Rev Lett* 102:106103
- Chen P, Gaydos L, Neumann AW (1996) Contact line quadrilateral relation. Generalization of the neumann triangle relation to include line tension. *Langmuir* 12:5956
- De Coninck J, Blake TD (2008) Wetting and molecular dynamics simulations of simple liquids. *Annu Rev Mater Res* 38:1
- De Gennes PG (1985) Wetting: statics and dynamics. *Rev Mod Phys* 57:827
- De Gennes PG, Hua X, Levinson P (1990) Dynamics of wetting: local contact angles. *J Fluid Mech* 212:55
- Dussan EB (1979) On the spreading of liquids on solid surfaces: static and dynamic contact lines. *Ann Rev Fluid Mech* 11:371
- Eustathopoulos N (1998) Dynamics of wetting in reactive metal/ceramic systems. *Acta Mater* 46:2319
- Fondecave R, Brochard-Wyart F (1998) Polymers as dewetting agents. *Macromolecules* 31:9305
- Good RJ (1992) Contact angle, wetting, and adhesion: a critical review. *J Adhesion Sci Tech* 6:1269
- Huh C, Scriven LE (1971) Hydrodynamic model of steady movement of a solid/liquid/fluid contact line. *J Coll Interf Sci* 35:85
- Israelachvili J (2011) Intermolecular and surface forces, 3rd edn. Academic Press
- Leger L, Joanny JF (1992) Liquid spreading. *Rep Prog Phys* 55:431
- Marmur A (1997) Line Tension and the Intrinsic Contact Angle in Solid–Liquid–Fluid Systems. *J Coll Interf Sci* 186:462
- Marmur A (2009) Solid-surface characterization by wetting. *Annu Rev Mater Res* 39:473

- 345 Mugele F, Baret JC (2005) Electrowetting: from basics to applications. *J Phys Condens Matter* 17:  
346 R705
- 347 Neto C, Evans DR, Bonaccorso E, Butt H-J, Craig VSJ (2005) Boundary slip in Newtonian liquids:  
348 a review of experimental studies. *Rep Prog Phys* 68:2859
- 349 Nikolov AD, Wasan DT, Chengara A, Koczo K, Policello GA, Kolossvary I (2002) Superspreading  
350 driven by Marangoni flow. *Adv Coll Interf Sci* 96:325
- 351 Reiter G, Khanna R (2000a) Real-time determination of the slippage length in autophobic polymer  
352 dewetting. *Phys Rev Lett* 85:2753
- 353 Reiter G, Khanna R (2000b) Kinetics of autophobic dewetting of polymer films. *Langmuir* 16:6351
- 354 Rolley E, Guthmann C, Gombrowicz R, Repain V (1998) Roughness of the contact line on a  
355 disordered substrate. *Phys Rev Lett* 80:2865
- 356 Shanahan MER, Carré A (1995) Viscoelastic dissipation in wetting and adhesion phenomena.  
357 *Langmuir* 11:1396
- 358 Tanner LH (1979) The spreading of silicone oil drops on horizontal surfaces. *J Phys D* 2:1473
- 359 Troian SM, Herbolzheimer E, Safran SA (1990) Model for the fingering instability of spreading  
360 surfactant drops. *Phys Rev Lett* 65:333
- 361 Vallet M, Vallade M, Berge B (1999) Limiting phenomena for the spreading of water on polymer  
362 films by electrowetting. *Eur Phys J B* 11:583
- 363 Verheijen HJJ, Prins MWJ (1999) Reversible electrowetting and trapping of charge: model and  
364 experiments. *Langmuir* 15:6616
- 365 Young T (1805) An essay on the cohesion of fluids. *Philos Trans R Soc Lond* 95:65
- 366 Zhang F, Barilia G, Boborodea A, Bailly C, Nysten B, Jonas AM (2005) Partial dewetting of  
367 polyethylene thin films on rough silicon dioxide surfaces. *Langmuir* 21:7427
- 368 Zisman WA (1964) Chapter 1: Relation of the equilibrium contact angle to liquid and solid  
369 constitution. In: *Contact angle, wettability, and adhesion. Advances in chemistry series,*  
370 *vol 43. American Chemical Society, Washington, DC, pp 1–51*



Wulff Possart and Martin E. R. Shanahan

## Contents

6.1	Introduction .....	116
6.2	A Few Aspects of Intermolecular Interactions .....	117
6.3	Thermodynamic Models of Adhesion .....	119
6.3.1	The Zisman Approach .....	120
6.3.2	The Concept of Girifalco and Good .....	121
6.3.3	The Fowkes Approach and Its Modifications .....	123
6.3.4	Neumann's Approach .....	126
6.4	Conclusions .....	127
References	.....	128

## Abstract

Although practical adhesion depends on more than just interfacial bonds, clearly the latter are fundamental: the stronger the links, the higher the adhesion. In many cases, interfacial bonding is of a physical nature and is closely akin to wetting, with the same types of physical phenomena occurring. These can be treated from a thermodynamic standpoint. Wetting data may be used to *estimate* the thermodynamic energy of adhesion, provided certain assumptions are made and suitable models constructed for, in particular, a relationship between interfacial tensions. Several models have been established with greater or lesser success. The main ones are reviewed here, underlining their essential assumptions.

W. Possart (✉)

Lehrstuhl Adhäsion und Interphasen in Polymeren, Universität des Saarlandes, Saarbrücken, Germany

e-mail: [w.possart@mx.uni-saarland.de](mailto:w.possart@mx.uni-saarland.de)

M. E. R. Shanahan

Institut de Mécanique et d'Ingénierie-Bordeaux (I2M), CNRS UMR 5295, Université de Bordeaux, Talence, France

e-mail: [martin.shanahan@u-bordeaux.fr](mailto:martin.shanahan@u-bordeaux.fr)

## 6.1 Introduction

As measured by mechanical tests, adhesion strength is not a quantity of reversible thermodynamics. This is due to various factors but mainly related to the dissipation of energy connected with the *irreversible* process of separation. The act of separation induces local stresses, and if the intrinsic adhesion is sufficiently strong, these are often sufficient to lead to irreversible, or at least time-dependent reversible, strain in one or both members in contact. Anyway, the deformation beyond strictly elastic behavior leads to an input of energy that is not restituted mechanically at all as it dissipates in part as heat or in an entropy term. Another part may be returned on a longer time scale than the separation process. This means that the actual, pragmatic energy of adhesion, as measured in a macroscopic mechanical test, is often far greater than the energy required theoretically for reversible separation at the interface between adhesive and adherend. The effect was shown initially by Gent and Petrich (1969) and later found by many others. Moreover, it has to be pointed out that for the majority of mechanical adhesion tests, the fracture face is not located at that interface. Some residual adhesive is often found on the adherend (or vice versa) as can be shown by surface-sensitive experimental techniques such as infrared external reflection spectroscopy, X-ray photoelectron spectroscopy, thermo-desorption mass spectrometry, secondary ion mass spectroscopy, etc. Nevertheless, the stresses responsible for this behavior require an interfacial linkage or adhesive bonding mechanism (cf. ► Chaps. 2, “Theories of Fundamental Adhesion” and ► 3, “Forces Involved in Adhesion,” of this book). In cases of good adhesion, this may be due to chemical bonds, but in many cases, physical interactions may be adequate to withstand the applied stresses.

It is only the energy for the *reversible* separation at the very interface that is considered within the framework of thermodynamics. As a starting point, the thermodynamic equations, considered in ► Chap. 4, “Wetting of Solids” for wetting (this book), can be easily adopted by replacing the liquid by a solid adhesive  $S_1$  and considering the former solid as the adherend  $S_2$  now. Hence, the specific energy of adhesion,  $f_{S_1S_2}^{adh}$ , for the solid–solid contact takes the form

$$f_{S_1S_2}^{adh} = \frac{F_{S_1S_2}^{adh}}{A_{S_1S_2}} = -(\gamma_{S_1V} + \gamma_{S_2V} - \gamma_{S_1S_2}) - \sum_i^N \mu_i \cdot (\Gamma_{i,S_1V} + \Gamma_{i,S_2V} - \Gamma_{i,S_1S_2}) \quad (1)$$

where  $F_{S_1S_2}^{adh}$  is excess Helmholtz free energy of adhesion and  $A_{S_1S_2}$  is D-face area between solid adhesive  $S_1$  and adherend  $S_2$ . The D-face describes the true interphase (cf. ► Chap. 4, “Wetting of Solids”),  $\gamma_{IJ}$  = interfacial tension for the D-face IJ,  $\mu_i$  = chemical potential of component  $i$  in the system, and  $\Gamma_{i,IJ}$  = absolute adsorption of component  $i$  on the D-face IJ.

Clearly, the interfacial tensions and the adsorption state of all three D-faces contribute to this specific excess Helmholtz free energy of adhesion. In comparison, Dupré’s rule (Dupré 1865) for the *reversible* specific work of adhesion

$$W_{S_1S_2}^{adh} = \gamma_{S_1V} + \gamma_{S_2V} - \gamma_{S_1S_2} \approx -f_{S_1S_2}^{adh} \quad (2)$$

considers the part from the interfacial tensions only. As shown in ► Chap. 4, “Wetting of Solids”, it is hard to verify this approximation, and hence a considerable portion of energy could be disregarded without notice.

Notwithstanding, three unknown quantities still remain in Eq. 2: the solid interfacial tensions. In ► Chap. 4, “Wetting of Solids”, a way to estimate the specific wetting energy from contact angle measurement is given provided the same level of approximation is chosen and Young’s equation is employed. This was the origin of the idea to deduce the reversible work of adhesion with Dupré’s rule by exploiting wetting experiments in a clever way. A number of such so-called thermodynamic adhesion models can be found in the literature, and they will be discussed in Sect. 3 of this chapter. However, before doing this, it is helpful to have a closer look at the very nature of the problem. Assuming that some test liquid, L, is used to characterize the wetting of both the solid adhesive and adherend, two Young’s equations are obtained:

$$\gamma_{S_1V} = \gamma_{S_1L} + \gamma_{LV} \cos \theta_{e,S_1L}$$

$$\gamma_{S_2V} = \gamma_{S_2L} + \gamma_{LV} \cos \theta_{e,S_2L}$$

where  $\theta_e$  refers to equilibrium contact angle. Note that the vapor phases are not exactly the same as the solids vary. Moreover, it should be pointed out again that Young’s equation applies neither to advancing nor to receding contact angles. The equilibrium contact angle,  $\theta_e$ , is needed (cf. Sects. 3 and 4 in ► Chap. 4, “Wetting of Solids” of this book).

Equation 2 becomes

$$W_{S_1S_2}^{adh} = \gamma_{S_1L} + \gamma_{LV} \cos \theta_{e,S_1L} + \gamma_{S_2L} + \gamma_{LV} \cos \theta_{e,S_2L} - \gamma_{S_1S_2}$$

Obviously, the reversible work of adhesion cannot be estimated because the solid interfacial tensions  $\gamma_{S_1V}$  and  $\gamma_{S_2V}$  cannot be deduced explicitly from wetting measurements as outlined at the end of ► Chap. 4, “Wetting of Solids”. Even if they could,  $\gamma_{S_1S_2}$  would remain as an unknown quantity. Obviously there are simply less physical equations than unknowns to be found. This has motivated researchers to propose model equations that are supposed to solve this dilemma. These model equations make use of some general features of physical interactions that are summarized in Sect. 2.

## 6.2 A Few Aspects of Intermolecular Interactions

Molecular interactions inside a phase boundary are the microscopic driving forces for the formation of the interphase as introduced in Sect. 2 of ► Chap. 4, “Wetting of Solids.” Energies are additive, and hence the contributions from any type of physical and chemical interaction sum up to the internal energy of the phase boundary. As outlined in ► Chap. 3, “Forces Involved in Adhesion”, the theory of physical

interactions (also known as van der Waals interactions due to their “prediction” in his well-known modification to the ideal gas equation) between *two* free molecules *A* and *B* provides the approximate equations for the interaction energy of dipolar, induction, and dispersion forces, respectively:

$$E_{AB}^{dipole} = -\frac{C_{AB}^{dipole}}{R^6} \quad \text{with} \quad C_{AB}^{dipole} = \frac{2\vec{p}_A^2 \vec{p}_B^2}{3(4\pi\epsilon_0)^2 kT} \quad (3)$$

$\vec{p}_J$  = permanent dipole moment of molecule *J*,  $\epsilon_0$  = absolute dielectric constant,  $k$  = Boltzmann constant,  $T$  = absolute temperature

$$E_{AB}^{induction} = -\frac{C_{AB}^{induction}}{R^6} \quad \text{with} \quad C_{AB}^{induction} = \frac{\vec{p}_A \vec{\alpha}_B \vec{p}_A + \vec{p}_B \vec{\alpha}_A \vec{p}_B}{(4\pi\epsilon_0)^2} \quad (4)$$

$\vec{\alpha}_J$  = electric polarizability tensor of molecule *J*

$$E_{AB}^{dispersion} = -\frac{C_{AB}^{dispersion}}{R^6} \quad \text{with} \quad C_{AB}^{dispersion} = f(\vec{\alpha}_A, \vec{\alpha}_B, \text{other parameters}) \quad (5)$$

They all possess the same dependence on the distance,  $R$ , between the *two* molecules, and hence they sum up to the energy of an attractive physical interaction:

$$\begin{aligned} E_{AB}^{phys \text{ interact}} &= E_{AB}^{dipole} + E_{AB}^{induction} + E_{AB}^{dispersion} \\ &= -\frac{C_{AB}^{dipole} + C_{AB}^{induction} + C_{AB}^{dispersion}}{R^6} \end{aligned} \quad (6)$$

In addition, theory shows that the interaction constants,  $C_{AB}$ , can be estimated by

$$C_{AB} = \sqrt{C_{AA} \cdot C_{BB}} \quad (7)$$

from the interactions between equal molecules A-A and B-B. (In the literature, the harmonic mean is found instead of the geometric mean sometimes.)

Starting from these microscopic pair interactions, the Hamaker concept (Hamaker 1937) provides the approximate interaction energy per contact area of the *macroscopic* phases A and B at distance,  $d$

$$u_{AB}^{phys \text{ interact}} = -\left(C_{AB}^{dipole} + C_{AB}^{induction} + C_{AB}^{dispersion}\right) \cdot f(d) \quad (8)$$

Equation 8 gives the contribution of intermolecular physical interactions to the specific internal energy,  $u_{AB}$ . (Things become more complicated when the intermolecular distance,  $d$ , is of the order of a few molecular diameters.)

Correspondingly, the specific excess internal energy of a D-face owing to physical interaction can be written as

$$u_{AB} = u_{AB}^{dipol} + u_{AB}^{ind} + u_{AB}^{disp} \quad (9)$$

with

$$u_{AB}^{dipol} \approx 2\sqrt{u_{AA}^{dipol} \cdot u_{BB}^{dipol}}, \quad u_{AB}^{ind} \approx 2\sqrt{u_{AA}^{ind} \cdot u_{BB}^{ind}}, \quad u_{AB}^{disp} \approx 2\sqrt{u_{AA}^{disp} \cdot u_{BB}^{disp}} \quad (10)$$

The interaction energies of chemical bonds are additive, too. It is important to note, however, that no such formulae as Eqs. 3, 4, 5, 6, and 7 apply in general. Hence, Eq. 8 must not simply be extended by another additive term for chemical bonds.

Finally, an entropy balance is needed for a complete description of the thermodynamic equilibrium. The specific excess entropy,  $s$ , of the D-face between the two phases  $A$  and  $B$  cannot be deduced from the concept of summation of pair interactions described. Statistical mechanics concepts are needed, which have still not been developed to the necessary quantitative level.

In conclusion, only the specific internal energy part,  $u$ , of the specific excess free Helmholtz energy for a given D-face

$$f_{AB} = u_{AB} - T \cdot S_{AB} = \gamma_{AB} + \sum_i \mu_i \cdot \Gamma_{i,AB} \quad (11)$$

can be described, while the specific entropy part,  $Ts$ , is still missing.

### 6.3 Thermodynamic Models of Adhesion

All thermodynamic models of adhesion aim to exploit wetting experiments on solids for a determination of the surface tension of solids and, as far as possible, of the thermodynamic energy of adhesion. As mentioned briefly in Sect. 1, the wetting experiment provides only the difference

$$\gamma_{SV} - \gamma_{SL} = \gamma_{LV} \cos \theta_{e,SL} \quad (12)$$

thus leaving us with the two unknown interfacial tensions  $\gamma_{SV}$  and  $\gamma_{SL}$  of the solid.

Clearly, an additional equation of state

$$\gamma_{SV} = f(\gamma_{SL}, \gamma_{LV}) \quad (13)$$

is needed to solve the problem. The existence of such an equation can be shown by thermodynamics, but it cannot be given explicitly. That is the starting point for the thermodynamic adhesion models: An explicit expression for Eq. 13 is constructed that should possess general validity. It should nevertheless be noted that none of the models is universally accepted and research continues in this field.

This issue and the common thermodynamic adhesion models will be discussed below. But as a first illustration, the widely forgotten approach by Antonov (1907) will be considered here. Antonov's empirical rule for low energy solids ( $\gamma_{LV} > \gamma_{SV}$ )

$$\gamma_{SL} \approx \gamma_{LV} - \gamma_{SV} \quad (14)$$

is such an assumption for the equation of state (13). Inserting Eq. 14 into Eq. 12 results in

$$\cos \theta_0 \approx \frac{2\gamma_{SV}}{\gamma_{LV}} - 1 \quad (15)$$

Accordingly, the solid surface tension  $\gamma_{SV}$  may be estimated from the wetting experiment with a single liquid but advancing and receding contact angle are not distinguished.

### 6.3.1 The Zisman Approach

In the light of the inaccessibility of two  $\gamma$  terms in Eq. 12, Fox and Zisman (1952) (Zisman 1962) postulated the following approach. The idea is based on the concept of *critical* surface tension (of the solid),  $\gamma_C$ . They took a homologous series of liquids, e.g., *n*-paraffins,  $C_nH_{2n+2}$ , in their liquid state at ambient temperature with  $n = 5-16$  and measured their equilibrium contact angle,  $\theta_0$ , on a given solid. It is not reported if these were the advancing or the receding contact angles. Now,  $\gamma_{LV}$  increases with  $n$ , and values are known. Plotting  $\cos \theta_0$  versus  $\gamma_{LV}$  for the various liquids, they obtained a straight line with slope ( $-k$ ) and constant term  $a$ :

$$\cos \theta_0 = -k \cdot \gamma_{LV} + a \quad (16a)$$

whose *extrapolated* value of  $\gamma_{LV}$  for  $\cos \theta_0 = 1$  was termed the critical surface tension,  $\gamma_C$ , of the solid. With that, Eq. 16a changes into

$$\cos \theta_0 = -k \cdot \gamma_{LV} + k \cdot \gamma_C + 1 \quad (16b)$$

and Young's Eq. 12 reduces to

$$\gamma_{SV} - \gamma_{SL} = \gamma_{LV} \equiv \gamma_C \quad (17)$$

Zisman also mentioned, however, that it depends very much on the chosen set of liquids whether the plot of  $\cos \theta_0$  versus  $\gamma_{LV}$  provides a straight line. Curves or even irregular scattering are also sometimes observed. Moreover, Eqs. 16 presume a straight line for  $\cos \theta_0$  versus  $\gamma_{LV}$  while Eq. 15 does so for  $\cos \theta_0$  versus  $\gamma_{LV}^{-1}$ .

Zisman was careful to avoid saying this was the true solid surface tension, although it should be close. In fact, the hypothetical liquid *just* spreading on the solid should indeed have a surface tension close to that of the solid, provided  $\gamma_{SL}$  is

quite small (cf. Eq. 17). This last supposition is plausible if the liquids and solid are chemically similar. To give two examples, it was found that polyethylene had a  $\gamma_C$  of ca. 31 mN·m<sup>-1</sup> and poly(tetrafluoroethylene), ca. 18.5 mN·m<sup>-1</sup>.

As a next step, Zisman combines Dupré's rule with Eqs. 12 and 17 to give

$$W_{SL}^{adh} = \gamma_{LV}(1 + \cos \theta_0) = -k\gamma_{LV}^2 + (2 + k\gamma_C)\gamma_{LV} \quad (18a)$$

This reversible work of wetting possesses a maximum at

$$\gamma_{LV}^{max} = \frac{1}{k} + \frac{\gamma_C}{2}, \quad W_{SL}^{adh, max} = \frac{1}{k} + \gamma_C + \frac{k}{4}\gamma_C^2 \quad (18b)$$

By way of a prediction, Zisman considered this particular liquid as the optimal adhesive provided it retains all its interfacial interactions when it solidifies.

### 6.3.2 The Concept of Girifalco and Good

Although Zisman's approach had the merit of originality, it clearly was not general. Despite being rarely true, Antonov's rule (14) inspired Girifalco and Good (1957, 1960) to follow a suggestion by Berthelot (for molecular attractions) and write  $\gamma_{SL} \approx \sqrt{\gamma_S \gamma_L}$ . However, the interfacial interaction should surely include additive contributions from each contiguous phase, and thus they arrived at

$$\gamma_{SL} = \gamma_S + \gamma_L - 2\sqrt{\gamma_S \gamma_L} = \left(\gamma_S^{1/2} - \gamma_L^{1/2}\right)^2 \quad (19)$$

Indeed, Eq. 19 goes back to Rayleigh (1890). It predicts zero interfacial tension if  $S$  and  $L$  are identical, as would be expected. All this assumed equal molecular sizes for  $S$  and  $L$ . If different, allowance had to be made, and the final version became

$$\gamma_{SL} = \gamma_S + \gamma_L - 2\phi\sqrt{\gamma_S \gamma_L} \quad (20a)$$

The dimensionless interaction parameter,  $\phi$ , expresses implicitly the effect of all interactions in the given interphase on the interfacial tension,  $\gamma_{SL}$ . In the framework of the Girifalco–Good concept, Eq. 20a represents the form proposed for the equation of state (13). Hence, Eq. 20a has to refer to *all* phases involved and should be written more precisely as

$$\gamma_{SL} = \gamma_{SV} + \gamma_{LV} - 2\phi_{SL}\sqrt{\gamma_{SV}\gamma_{LV}} \quad (20b)$$

Good pointed out himself that he had reduced the subscripts only for convenience. Equation 20b clearly shows that the parameter  $\phi$  refers to two well-defined phases in a wetting experiment. Experiments with two “immiscible” liquids serve to estimate  $\phi$  because  $\gamma_{SV}$  is replaced by the known surface tension  $\gamma_{L_2V}$  for the second liquid.  $\phi_{AB} > 1$  indicates that intermolecular interactions appear in the interphase

$A-B$ , which are not present inside the phases. Specifically  $\phi_{L_1L_2}$  is found to vary from 0.32 to 1.17 for 137 pairs of liquids. However, only 15% of these  $\phi_{L_1L_2}$  values are in the interval  $0.95 \leq \phi \leq 1.05$  (Girifalco and Good 1957).

Moreover, it is obvious that Eqs. 20 do not solve the problem of the missing equation of state (13) because a new unknown is introduced, viz.,  $\phi_{SL}$ .

This point will be considered more closely below. Here it is asked first how Eq. 20b relates to the balance of the excess energy for the interface and what the consequences for the wetting experiment are. These questions are important since the specific interactions in an interphase add their interaction *energies* to the balance, not the corresponding *forces*. For a liquid wetting a solid, the specific excess Helmholtz free energy of the SL interface is given by (cf. Sect. 2 of ► Chap. 4, “Wetting of Solids”)

$$f_{SL} = \gamma_{SL} + \sum_i \mu_i \cdot \Gamma_{i,SL} \quad (21)$$

where  $\mu_i$  is chemical potential of component  $i$  and  $\Gamma_{i,SL}$  is absolute adsorption of component  $i$  at the SL interface.

Therefore, consideration of only the interfacial tensions with Eqs. 20 means that the effect of adsorption is neglected in the Girifalco–Good concept:

$$f_{SL}^D \approx \gamma_{SL}^D \quad (22)$$

If this approximation is accepted, Young’s and Dupré’s equations may be again introduced in Eq. 20b yielding

$$\phi_{SL} \sqrt{\gamma_{SV}} = \frac{1 + \cos \theta_e}{2} \sqrt{\gamma_{LV}} \quad (23a)$$

Again, Eq. 23a reveals the problem. The wetting experiment with one test liquid  $L$  does not provide  $\gamma_{SV}$  since  $\phi_{SL}$  cannot be derived independently from wetting data. To circumvent the problem, Good proposed to combine a series of test liquids and to plot  $\cos \theta_e$  versus  $\gamma_{LV}^{-0.5}$  according to Eq. 23a rewritten in the form

$$\cos \theta_e = 2\phi_{SL} \sqrt{\gamma_{SV}} \cdot (\sqrt{\gamma_{LV}})^{-1} - 1 \quad (23b)$$

A straight line passing through  $(-1)$  on the ordinate should be obtained if  $\phi_{SL}$  possesses the same value for all the liquids used. This cannot be true in a strict sense since, by definition,  $\phi_{SL}$  cannot be independent of the given liquid. Moreover, the Good plot implies that the changes in the common vapor phase V can be ignored when the test liquid is changed in the experiment. It was shown in Sect. 4.5, however, that these changes may not be neglected. Also, it has to be noted that Good et al. ignore the difference between the measured static contact angles  $\theta_a$ ,  $\theta_r$  and the equilibrium contact angle  $\theta_e$ . If, in addition,  $\phi_{SL}$  is assumed to be close to one, an approximate value for  $\gamma_{SV}$  follows from the slope of the straight line.



In the literature many authors have followed Good's advice, but there is no way reliably to find the resulting error for  $\gamma_{SV}$ . An additional and significant source of error is the use of the advancing (or receding) contact angle instead of  $\theta_e$ .

Finally, Dupré's reversible work of adhesion is considered in the framework of the Girifalco–Good concept. Assuming that the surface tensions  $\gamma_{S_1V}$  and  $\gamma_{S_2V}$  of the solid adhesive and of the solid adherend, respectively, were estimated from wetting experiments in the way described above, Eq. 20b is modified to

$$\gamma_{S_1S_2} = \gamma_{S_1V} + \gamma_{S_2V} - 2\phi_{S_1S_2} \sqrt{\gamma_{S_1V}\gamma_{S_2V}} \quad (20c)$$

It has to be noted in passing that the vapor phase has changed again. It does not contain the components of the test liquid anymore.

Dupré's Eq. 2 becomes

$$W_{S_1S_2}^{adh} = \gamma_{S_1V} + \gamma_{S_2V} - \gamma_{S_1S_2} = 2\phi_{S_1S_2} \sqrt{\gamma_{S_1V}\gamma_{S_2V}} \quad (24)$$

Obviously, the dilemma still exists: The new interaction parameter  $\phi_{S_1S_2}$  is not available, and the specific reversible work of adhesion is inaccessible. In Good and Elbing (1970) and Good (1977), Good et al. derive an equation that can be written in a generalized form as

$$\phi_{AB} \approx \frac{C_{AB}^{dipole} + C_{AB}^{inductive} + C_{AB}^{dispersion}}{\sqrt{(C_{AA}^{dipole} + C_{AA}^{inductive} + C_{AA}^{dispersion})(C_{BB}^{dipole} + C_{BB}^{inductive} + C_{BB}^{dispersion})}} \quad (25)$$

for the calculation of  $\phi_{AB}$  for the interface between phases *A* and *B* using the basic formulae of intermolecular physical interactions (cf. Eqs. 3, 4, and 5). However, this is also another approximation.

### 6.3.3 The Fowkes Approach and Its Modifications

Fowkes (1962, 1963, 1964, 1967) provided another approach for the analysis of wetting experiments by proposing that a surface tension  $\gamma$  (solid or liquid) may be expressed as the sum of a number of various components:

$$\gamma = \gamma^d + \gamma^p + \gamma^i + \gamma^C + \dots \quad (26a)$$

where the superscripts refer to contributions due to the intermolecular interaction forces of various types: dispersion, dipoles, induction interactions, covalent contributions, etc. In practice, he stopped after polarity, assuming most wetting interactions will not involve significant induction or chemical contributions:

$$\gamma = \gamma^d + \gamma^p \quad (26b)$$

At this point, it must be emphasized again that a surface or interfacial tension is a tensor by its physical origin (cf. ► Chap. 4, “Wetting of Solids”) and hence it may not be split into additive scalar components in general. Such additivity holds for the energy, and referring again to Eq. 11 for the specific excess free Helmholtz energy for a surface of phase  $A$  in equilibrium with its vapor phase

$$f_{AV} = u_{AV} - T \cdot S_{AV} = \gamma_{AV} + \sum_i \mu_i \cdot \Gamma_{i,AV} \quad (27)$$

It is seen that one formally arrives at

$$f_{AV} \approx u_{AV} \approx \gamma_{AV} \quad (28)$$

only by neglecting the specific excess entropy  $s_{AV}$  and all absolute adsorptions  $\Gamma_{i,AV}$ .

Using Eq. 9,  $u_{AV}$  is now written as

$$u_{AV} = u_{AV}^p + u_{AV}^i + u_{AV}^d \approx \gamma_{AV}^p + \gamma_{AV}^i + \gamma_{AV}^d \quad (29)$$

and with Eqs. 28 and 26, one gets

$$u_{AV}^p = \gamma_{AV}^p, u_{AV}^i = \gamma_{AV}^i, u_{AV}^d = \gamma_{AV}^d \quad (30)$$

Hence, Eqs. 28, 29, and 30 provide justification for the Fowkes Eqs. 26, and they illustrate the implied approximations.

As his explicit version for the general equation of state (13), Fowkes assumes that only dispersion interactions are present in the interphase, and he proposes (for the case of wetting)

$$\gamma_{SL} = \gamma_{SV} + \gamma_{LV} - 2\sqrt{\gamma_{SV}^d \gamma_{LV}^d} \quad (31)$$

We add the subscript V here for the sake of correctness. In the original work, no reference is made to the corresponding vapor phase that must exist for thermodynamic equilibrium at the surface of any condensed phase (cf. Sect. 4.2).

Obviously, Eq. 31 refers to the dispersion components of the solid and the liquid surface tensions that are new unknown quantities. Fowkes deduces the polar components  $\gamma_{LV}^d$  of the surface tensions for a series of liquids from mutual liquid–liquid wetting experiments, and  $\gamma_{LV}^p$  is determined from Eq. 26b. It is noted that the vapor phase is specific for any pair of liquids. Hence, the values derived for  $\gamma_{LV}^d$  and  $\gamma_{LV}^p$  depend on the partner liquid too! The results reported by Fowkes indicate that this is proven in his liquid–liquid wetting experiments.

However, if additional interactions (e.g., induction) contribute to the state of the liquid–liquid interphase, there are again more unknowns than equations!

Following Fowkes proposition, various workers postulated, more or less successfully, extensions to Eq. 31 in order to include other types of interphase interactions. It

must be emphasized that the term “extended Fowkes equations” is really a misnomer, since Fowkes did not condone their use. However, the two best-known versions are attributable to Owens and Wendt (1969):

$$\gamma_{SL} = \gamma_S + \gamma_L - 2\sqrt{\gamma_S^d \gamma_L^d} - 2\sqrt{\gamma_S^p \gamma_L^p} \quad (32)$$

and to Wu (1971):

$$\gamma_{SL} = \gamma_S + \gamma_L - \frac{4\gamma_S^d \gamma_L^d}{(\gamma_S^d + \gamma_L^d)} - \frac{4\gamma_S^p \gamma_L^p}{(\gamma_S^p + \gamma_L^p)} \quad (33)$$

These two variants, based on geometric and harmonic means for the surface tension components according to Fowkes, are often used, but their theoretical basis is questionable as will be shown below.

A further variant of Fowkes early work is due to van Oss et al. (1988). It is based on the concept that weak acid–base interactions (of the Lewis type) may contribute to interfacial tensions. Couched in a formalism inspired by Fowkes’ earlier work, it is proposed that a (general) surface tension may be written as

$$\gamma = \gamma_{LW} + \gamma^{AB} \text{ where } \gamma^{AB} = 2\sqrt{\gamma^+ \gamma^-} \quad (34)$$

In Eq. 34,  $\gamma^{LW}$  represents the dispersion and polar components of Fowkes’ expression (26b), all together, and  $\gamma^{AB}$  is the acid–base, or electron acceptor/donor, contribution. The terms  $\gamma^+$  and  $\gamma^-$  represent electron acceptor and electron donor characteristics of the phase. After some algebra, it is shown that in this approach, the expression for  $\gamma_{SL}$  becomes

$$\begin{aligned} \gamma_{SL} = & \left( \sqrt{\gamma_S^{LW}} - \sqrt{\gamma_L^{LW}} \right)^2 + 2 \left( \sqrt{\gamma_S^+ \gamma_S^-} + \sqrt{\gamma_L^+ \gamma_L^-} \right) \\ & - 2 \left( \sqrt{\gamma_S^+ \gamma_L^-} + \sqrt{\gamma_S^- \gamma_L^+} \right) \end{aligned} \quad (35)$$

The second term on the right amounts to the *internal* acid–base interactions, and the last is due to *interfacial* acid–base interactions. Some doubt has been cast on the validity of this formulation, but the intrinsic physical chemistry of allowing for electron acceptor and electron donor characteristics seems sound.

Let us now look at the implications of Eqs. 31, 32, and 33. Using Eqs. 9, 10, and 28, the specific excess Helmholtz free energy can be expressed as

$$f_{SL} \approx u_{SL} = u_{SL}^p + u_{SL}^i + u_{SL}^d = 2\sqrt{u_{SV}^p \cdot u_{LV}^p} + 2\sqrt{u_{SV}^i \cdot u_{LV}^i} + 2\sqrt{u_{SV}^d \cdot u_{LV}^d} \quad (36)$$

Dupré’s reversible work of wetting is introduced as

$$W_{SL}^{adh} = \gamma_{SV} + \gamma_{LV} - \gamma_{SL} \approx -f_{SL} \approx -u_{SL} \quad (37)$$

and with Eq. 30 follows

$$W_{SL}^{adh} = \gamma_{SV} + \gamma_{LV} - \gamma_{SL} \approx -2\sqrt{\gamma_{SV}^p \cdot \gamma_{LV}^p} - 2\sqrt{\gamma_{SV}^i \cdot \gamma_{LV}^i} - 2\sqrt{\gamma_{SV}^d \cdot \gamma_{LV}^d} \quad (38)$$

which is a generalized form of Eqs. 31 and 32. A corresponding form for Eq. 33 would follow by replacing geometric by harmonic means. As before,  $W_{SL}^{adh}$  could be obtained from a proper wetting experiment.

All these concepts suffer from the same problem as the thermodynamic adhesion model proposed by Girifalco and Good. Provided that attention is confined to polar and dispersion interactions and the use of the values for  $\gamma_{LV}^d$  and  $\gamma_{LV}^p$  from the liquid–liquid wetting is made, one still has two unknowns in Eq. 38:  $\gamma_{SV}^d$  and  $\gamma_{SV}^p$ .

In the literature, this problem is circumvented (but not solved!) by incorporating the wetting results from a second liquid (or even a series of test liquids) for the data analysis: With any additional liquid, Eq. 38 can be rewritten, thus expanding the starting point from a single equation into an unlimited system of simultaneous equations. Although mathematically correct, this procedure is inconsistent with several aspects of the fundamental thermodynamic concept of the interphase and its corresponding D-face or interface (cf. ► Chap. 4, “Wetting of Solids”). As a result, the reliability of data deduced for  $\gamma_{SV}^d$ ,  $\gamma_{SV}^p$ ,  $\gamma_{SV}^i$ , and hence  $\gamma_{SV}$  cannot be assessed.

Bearing this in mind, now a brief look at the work of adhesion between solid adhesive and adherend in the framework of Fowkes’ general approach is taken. Equation 38 is of the form

$$\begin{aligned} W_{S_1S_2}^{adh} &= \gamma_{S_1V} + \gamma_{S_2V} - \gamma_{S_1S_2} \\ &\approx -2\sqrt{\gamma_{S_1V}^p \cdot \gamma_{S_2V}^p} - 2\sqrt{\gamma_{S_1V}^i \cdot \gamma_{S_2V}^i} - 2\sqrt{\gamma_{S_1V}^d \cdot \gamma_{S_2V}^d} \end{aligned} \quad (39)$$

Obviously,  $W_{S_1S_2}^{adh}$  is as much in doubt as the components of the solid and liquid surface tensions. These are the physical limits of all these concepts.

### 6.3.4 Neumann’s Approach

Neumann et al. (1974) have adopted the stance of considering the *advancing* contact angle to be related to an equation of state. He followed the evolution of  $\gamma_L \cos \theta_a = f(\gamma_L)$  for a series of liquids on eight fluoropolymer surfaces. Thus, Neumann follows the lines of his predecessors. Combining the results of wetting experiments with an arbitrary choice of test liquids on a small number of polymer surfaces, he considers the phenomenological relationships found for that data pool as generally applicable. The treatment ignores the fact that all wetting pairs represent independent thermodynamic systems.

Neglecting spreading pressure,  $\pi_e$ , he observed a linear variation of  $\phi$  of the Girifalco–Good equation (20a). Combining this linearity with Girifalco and Good’s relation, he arrived at the following expression for Eq. 13:

$$\gamma_{SL} = \frac{[\sqrt{\gamma_S} - \sqrt{\gamma_L}]^2}{1 - A \cdot \sqrt{\gamma_S \gamma_L}} \text{ with } A = 15 \text{ m} \times \text{N}^{-1} \quad (40)$$

This relation is purely empiric and thus valid for the cases where it has been established. In another attempt, Li and Neumann (1990) used arguments based on the theory of intermolecular physical interactions along the lines of Eqs. 3, 4, 5, 6, and 7. Following Fowkes’ concept, they derived the expression

$$\gamma_{SL} = \gamma_{LV} + \gamma_{SV} - 2\sqrt{\gamma_{LV}\gamma_{SV}} \cdot e^{-\beta(\gamma_{LV}-\gamma_{SV})^2} \quad (41)$$

as an alternative version for the equation of state (13). Here, the model parameter  $\beta$  is the newly introduced unknown. From a pool of wetting data,  $\beta$  was derived to be equal to  $124.7 \text{ m}^2 \cdot \text{N}^{-2}$  (Li and Neumann 1992). Hence, this relation is purely empirical, too.

## 6.4 Conclusions

All thermodynamic adhesion models start with the idea that wetting experiments with suitably chosen test liquids could provide the surface tension,  $\gamma_{SV}$ , of the wetted solid.

As shown in the previous sections of this chapter, numerous approximations are made in each of these evaluations of the wetting data. Let us mention three of the more important simplifications: (a) the thermodynamic adhesion models blur the physical distinction between interfacial tension and thermodynamic excess energy of an interface; (b) they neglect the contribution of the interphase composition (i.e., the role of the absolute adsorptions  $\Gamma_i$ ); and (c) they ignore the fact that an interfacial tension belongs to *two* contacting phases in the framework of thermodynamics. In many published papers, the problem of how the thermodynamic contact angle is derived from measured advancing or receding angles is overlooked. These and more approximations are needed to handle the key problem of the overall situation: How should an explicit form for a general equation of state be constructed that is only implicitly given by theory  $-\gamma_{SV} = f(\gamma_{SL}, \gamma_{LV})$ ? The models vary considerably as can be seen by comparing Eqs. 17, 20, 31, 32, 33, 35, 40, and 41. Moreover, it is not presently possible to assess the accuracy of any of these approximate equations. Nevertheless, thermodynamic adhesion models are widely used in the literature.

In conclusion, it must be emphasized that wetting experiments do not provide enough information on interphases for deducing the interfacial tensions,  $\gamma_{SV}$ ,  $\gamma_{SL}$  of a solid, or, even worse, for the reversible work of adhesion,  $W_{S_1S_2}^{adh}$ . As far as future work is concerned, it would be a challenging goal to find an experiment enabling direct measurement of the specific excess free Helmholtz energy of adhesion  $\Delta f^{adh}$ .

## References

- Antonov GN (1907) Sur la tension superficielle à la limite de deux couches. *J Chim Phys* 372:5
- Dupré A (1869) *Théorie Mécanique de la Chaleur*. Gauthier-Villars, Paris, p 369
- Fowkes FM (1962) Determination of interfacial tensions, contact angles, and dispersion forces in surfaces by assuming additivity of intermolecular interactions in surfaces. *J Phys Chem* 382:66
- Fowkes FM (1963) Additivity of intermolecular forces at interfaces. I. Determination of the contribution to surface and interfacial tensions of dispersion forces in various liquids. *J Phys Chem* 2538:67
- Fowkes FM (1964) Attractive forces at interfaces. *Ind Eng Chem* 40:56
- Fowkes FM (1967) In: Patrick RL (ed) *Treatise on adhesion and adhesives*, vol 1. Marcel Dekker, New York, pp 325–449
- Fox HW, Zisman WA (1952) The spreading of liquids on low-energy surfaces. III. Hydrocarbon surfaces. *J Coll Interface Sci* 428:7
- Gent A, Petrich RP (1969) Adhesion of viscoelastic materials to rigid substrates. *Proc Roy Soc A* 433:310
- Girifalco LA, Good RJ (1957) A theory for the estimation of surface and interfacial energies. I. Derivation and application to interfacial tensions, *J Phys Chem* 904:61
- Good RJ (1977) Surface free energy of solids and liquids: thermodynamics, molecular forces and structure. *J Coll Interface Sci* 398:59
- Good RJ, Elbing E (1970) Generalization of theory for estimation of interfacial energies. *Ind Eng Chem* 3 (54):62
- Good RJ, Girifalco LA (1960) A theory for estimation of surface and interfacial energies. III. Estimation of surface energies of solids from contact angle data. *J Phys Chem* 561:64
- Hamaker HC (1937) The London – Van Der Waals attraction between spherical particles. *Physica* 1058:4
- Li D, Neumann AW (1990) A reformulation of the Equation of State for interfacial tensions. *J Coll Interface Sci* 304:137
- Li D, Neumann AW (1992) Contact angles on hydrophobic solid surfaces and their interpretation. *J Coll Interface Sci* 190:148
- Neumann AW, Good RJ, Hope CJ, Sejpal M (1974) An equation-of-state approach to determine surface tensions of low-energy solids from contact angles. *J Coll Interface Sci* 291:49
- Owens DK, Wendt RC (1969) Estimation of the surface free energy of polymers. *J Appl Polym Sci* 1741:13
- Rayleigh (Strutt JW) (1890) LII. On the theory of surface forces. *Phil Mag Ser 5* 456:30
- van Oss CJ, Chaudhury MK, Good RJ (1988) Interfacial Lifshitz-van der Waals and polar interactions in macroscopic systems. *Chem Rev* 927:88
- Wu S (1971) Calculation of interfacial tension in polymer systems. *J Polym Sci C* 19:34
- Zisman WA (1963) Influence of constitution on adhesion. *Ind Eng Chem* 10(19):55

Uncorrected Proof

Gary Critchlow

## Contents

7.1	Introduction .....	132
7.2	The Problem with Surface Contamination .....	133
7.3	Removal of Surface Contamination .....	137
7.3.1	Degreasing Metallic Adherends .....	137
7.3.2	Polymer Treatment: Removal of Contamination and Surface Functionalization .....	141
7.4	Mechanical Treatments and the Role of the Interphase .....	142
7.5	Chemical Treatments .....	145
7.5.1	Chemical Treatments for Metallic Adherends .....	145
7.5.2	Chemical Treatments for Polymeric Adherends .....	148
7.6	Electrochemical Treatments .....	149
7.6.1	Introduction to Anodizing .....	149
7.6.2	Structure and Composition of Anodic Films .....	151
7.6.3	Physical Factors Affecting Anodic Oxides .....	153
7.6.4	Alternatives to Phosphoric and Chromic Acid Anodizing .....	153
7.6.5	Alternating (AC) Current Anodizing .....	155
7.6.6	Alternating Current–Direct Current Anodizing (ACDC Anodizing) .....	156
7.7	Conclusions .....	159
	References .....	160

## Abstract

The use of surface treatments to optimize adhesion has been well established. In this chapter, the main treatment methods for metals and polymers will be considered in terms of how such processes are carried out and their influence on surface physical and chemical properties. Consideration has been given to a range of treatments from simple degrease options to the more highly complex multistage

G. Critchlow (✉)

Department of Materials, Loughborough University, Loughborough, Leicestershire, UK

e-mail: [g.w.critchlow@lboro.ac.uk](mailto:g.w.critchlow@lboro.ac.uk)



processes. An attempt has been made to relate the changes in physicochemical properties to adhesion performance, and, where relevant durability.

## 7.1 Introduction

It is usually recommended that some degree of modification or treatment is applied to all surfaces prior to adhesive bonding. This is particularly important if structural or semi-structural bonding is to be carried out. Some examples of specific surface treatments and their influence on initial adhesion and durability are given later in this section and, more extensively, in ► [Chap. 8, “Surface Treatments of Selected Materials.”](#) The particular surface treatment applied in any given situation will depend upon the requirements of the bond and the service conditions that it will experience and will generally be chosen on a “fit-for-purpose” basis. Additional factors such as the adherend type and geometry and production constraints, including cost considerations, may also be relevant factors when selecting a treatment process.

In simple terms, treatments are required to make the surface receptive to the applied adhesive. A treatment may also be required to provide a mechanically sound surface to be bonded and one which will also minimize the potentially damaging influence of external factors such as environmental ageing, corrosion, or applied loading. From the relevant literature, it is clear that the main function of any treatment on any surface is to provide desirable physical and chemical properties to that surface which will achieve the above-mentioned objectives. To do this, a particular treatment will facilitate one or more of the following functions:

- To remove, or prevent the formation of, any weak boundary layer on the adherend surface. Examples of weak boundary layers include machine oils, weak oxides or hydroxides, and airborne contamination on metals, or, internal segregants from within polymers. A simple degrease may fulfill this requirement. Alternatively, mechanical or deoxidizing treatments may be required if friable, inorganic layers are present.
- To maximize the degree of intimate molecular contact between the adhesive or primer and the adherend during the bonding and curing processes. This usually involves the creation of a high-surface free energy and the introduction of specific functional groups.
- To generate a specific structure or texture on the adherend surface. Even though mechanical interlocking may not be responsible for primary bonding, the complex structures present on, for example, conversion-coated or anodized surfaces may help increase joint fracture energies by redistributing the stresses away from any interphasial polymer. These structures also create an extended surface area, which may be utilized if the adhesive is able to flow into, for example, the pores on anodic oxides.
- To passivate the surface of the adherend prior to adhesive bonding. This is paramount for high-energy adherends as these are not only receptive toward the adhesive but also to all forms of contamination. This contamination may be

organic or inorganic and can influence the adherend in a number of ways, including by a reduction in its surface free energy, gross contamination, or corrosion. Passivating processes offer protection of the surface after bonding by providing electrochemical and barrier corrosion resistance to the substrate material.

The minimum preparation which is usually carried out on adherend surfaces might include a simple degrease to remove processing aids and contaminants. There does, however, exist a hierarchy of treatments. It is generally thought that mechanical processes such as abrasion or grit-blasting offer improved bonding surfaces compared with degreasing-only and, in some cases, offer adequate levels of adhesion either alone or with coupling agents applied. Further information on the role of coupling agents is given in ► [Chap. 11, “Organosilanes: Adhesion Promoters and Primers.”](#) Similarly, simple chemical treatments such as acid etching tend to offer further enhanced bond performance compared with mechanical treatments. However, it is recognized that the current state-of-the-art processes, particularly those for structural or semi-structural metal bonding and which are highly complex, multistage treatments, including chemical conversion coating and anodic oxidation of metals perform best of all. The more advanced processes provide the adherend surface with all of the required physical and chemical properties mentioned above to obtain optimized initial adhesion and, importantly, durability.

This chapter will firstly consider the problems associated with bonding as-received surfaces and the problems caused by the presence of contamination. Following this, details will be given of different surface treatment methods in terms of how they modify the above-mentioned surface physical and chemical properties, and how these changes impact upon the measured adhesion levels. In some cases, consideration has been given to alternative environmentally friendly surface treatments which might be considered as drop-in replacements for the current industrial standards. Many of the currently used processes are detailed further in ► [Chap. 8, “Surface Treatments of Selected Materials.”](#) This chapter will focus on the modification or treatment of metallic and polymeric adherends. It is, however, recognized that adhesion to other materials such as wood, ceramics, and glasses are industrially significant, and mention of relevant treatments for these materials are given in ► [Chap. 8, “Surface Treatments of Selected Materials.”](#)

---

## 7.2 The Problem with Surface Contamination

The removal of preexisting contamination, which often comprises low energy and friable material, to facilitate bonding to a mechanically sound surface is a fundamental requirement in establishing good adhesion. The requirement to remove such material is often overlooked, but it is, in fact, an essential stage in the more complex processes such as anodizing also.

It is important at this stage to note that when considering polymers, it is possible that internal migration of low-molecular-weight materials or processing aids can

occur to create a highly modified surface layer. This layer might be considered as comprising internal contaminants. A simple illustration of this has been given by Ansanfar et al. (2009) in their consideration of natural rubber (NR) and NR-sytrene-butadiene rubber blends. In this study, internal migration of paraffin wax, a processing aid, was directly observed, which led to poor self-adhesion between these polymers. In addition to influencing the surface thermodynamics, such internal contaminants may also form weak boundary layers; this topic has been extensively discussed following the early studies by Brewis (1982). The removal of such internal contaminants will be considered later in this section.

Following is a consideration of external contaminants on adhesive joints. There are many possible forms of external contamination; a reasonably comprehensive list is given by Averill et al. (1998).

For simplicity, surface contaminants can be considered to fall within two broad groups: organic and inorganic materials. The removal of the organic compounds can, generally, be achieved using simple degrease processes, whereas the inorganic compounds might require a combination of degrease, desmut and, in extreme cases, deoxidizing solutions.

As previously mentioned, substrate contamination can have a major effect upon the resultant quality of the bond due to the influence of the contaminant reducing the surface free energy. Naturally, in any conscientious facility that undertakes adhesive bonding, contamination will be reduced to an absolute minimum. In one study, Smith and Crane (1980) looked at the influence of controlled levels of contamination from various sources and determined their effects upon adhesive bond strength using aluminum alloy adherends. Ellipsometry and water contact angle measurements were used to study a range of process variables and contaminants. Aluminum panels treated by phosphoric or chromic acid anodizing (PAA or CAA) were contaminated with materials likely to be introduced by human error, including finger prints, cigarette smoke, and mucous, along with drink residues. Contaminants originating from a factory environment were also considered, including lubricating oils and silicone grease. In all cases, ellipsometry and water contact angles were able to detect the presence of these materials. In this study, it was noted that the presence of a level of 10 nm, and above, of lubricating oils had no effect upon the lap shear strength of joints made with a single part epoxide adhesive, even though an increase in the water contact angle was observed. Increasing the levels of oil did result in an increase in water contact angle toward 100°. Silicone grease was also introduced and evaluated; in this case, a more dramatic effect was noted in that a significant decrease in lap shear strength was observed. In an assessment of the sensitivity of the two types of surface treatment, small amounts of silicone grease, from 3.5 to 20 nm, were found to increase the water contact angle value and, using lap-shear testing, this was accompanied by a significant reduction in the failure load. Almost total apparent interfacial failure was noted for the silicone-contaminated joints.

Significant work carried out to evaluate the effects of contamination has also been conducted in the area of automotive bonding, where adhesion to lubricated surfaces is desirable. Research carried out principally on behalf of the automotive industry has studied the ability of adhesives to absorb or displace contaminants to facilitate

the formation of bonds with the underlying substrate. In one study carried out on electrogalvanized steel adherends, Hong and Boeno (1995) showed that the adhesive formulation can play a key role in successfully accommodating oils on such surfaces. In a related study, Minford (1981) looked at the effects of lubricants as contaminants on bonded and spot-welded aluminum substrates. For the substrates, he used 2036 T4 aluminum lap-shear joints bonded with a single part hot-curing epoxide. Surface contamination was controlled by immersing the substrates to be bonded in varying concentrations of an emulsified forming lubricant. Durability was tested by exposing joints to 52 °C and 100% relative humidity and measuring residual failure loads. Joints were also subjected to a 3.5% salt fog for 16 h in a 24-h cycle. Both simulated service conditions were assessed against freshly prepared joints. Other than the joints that were deliberately contaminated, all adherends received no other treatment. It was found that the adhesive was able to accommodate up to 0.82 mg/cm<sup>2</sup> of oil before any loss of strength was noticeable. At the 0.95 mg/cm<sup>2</sup> level, there was a significant loss in strength from 10 to 6 MPa and a shift in the locus of failure dropping from over 90% cohesive to demonstrate a mixture of 60% cohesive and 40% apparent interfacial failure. For the environmental ageing of joints, specimens were exposed to either humidity or salt-spray conditions for up to 180 days. Joints were periodically removed and loaded to 50% of their original bond strength and then finally tested to destruction after 280 days of exposure. Joints retained their original strengths with up to 0.62 mg/cm<sup>2</sup> level of contamination. At 0.71 mg/cm<sup>2</sup>, a reduction to 45% of the original joint strengths was observed and at 0.82 mg/cm<sup>2</sup>, the results became variable. Paradoxically, contaminated joints exposed to salt-spray conditions seem to perform better than the as-milled substrates which failed at 2% of their original joint strength after only 90 days exposure. The only contaminated joints that performed worse than this were the ones prepared at the 1.05 mg/cm<sup>2</sup> level. Overall, it was this latter level of contamination that caused the most detrimental effect upon the fresh and aged specimens.

Debski et al. (1986) have tried to explain the mechanisms by which the adhesive is able to function even through oily layers by investigating the ability of an epoxide adhesive to either displace or absorb such contamination. They determined the surface free energies for a diglycidyl ether of bisphenol A (DGEBA) based epoxide resin on ASTM 3 grade oil, plain steel, and a zinc-coated steel. Utilizing these surface free energy values, they investigated the thermodynamic possibility of the epoxide adhesive displacing a layer of an apolar oil on a steel surface. The model was that of a drop of resin spread over a layer of oil upon a metal substrate. Assuming that the resin remained geometrically constant they concluded that, theoretically, the oil could be displaced if the substrate was flat and determined that no oil could become entrapped within surface crevices. To deal with this entrapped oil, they assumed that any oil trapped beneath the adhesive was absorbed into the epoxide matrix. Using differential scanning calorimetry (DSC), they monitored the cross-linking kinetics of an adhesive containing 6% dicyandiamide and of the adhesive with the same formulation but with the addition of a CaCO<sub>3</sub> filler. They found that the effect of the increase in oil content was to lower the glass transition temperature ( $T_g$ ) during the cross-linking process. However, the  $T_g$  of the fully cross-

linked adhesive was unaffected even at the highest levels of oil contamination. Similar trends were also noted for the unfilled epoxide adhesive. Thermal gravimetric analysis (TGA) was also conducted to evaluate the levels of oil that were lost due to evaporation from the free surfaces of the adhesive samples. The filled and unfilled adhesives both containing 10% oil were monitored at 210 °C for weight loss alongside control samples containing no oil. After 1 h of heating, no loss of weight was recorded for either control sample; however, the unfilled sample with oil lost approximately 3% the filled version lost 1% and a pure oil sample lost 36% of its original weight. This study demonstrated the capacity of an epoxide adhesive to accommodate oil from substrates in one of three ways; the displacement, absorption, and “digestion” by the filler and absorption followed by evaporation at free surfaces. However, the latter would be a second-order mechanism in real joints as the free surface to volume ratio would be significantly lower than that present in the experiments conducted.

Anderson (1993) also discovered that contaminated bondlines can behave differently under different loading conditions. He studied the effects of HD-2 grease upon steel butt joints and tapered double cantilever beam test specimens that were bonded together with either Hysol EA946 or EA 913 epoxide adhesives. The substrates were prepared by vapor degreasing, grit-blasting, and a final vapor degrease prior to bonding. For the contaminated joints, varying solutions ranging from 0.5% to 2% of HD-2 grease were prepared by thinning down in 1,1,1 trichloroethane, which was then sprayed onto one of the substrates from a bonded pair. The test results from the tensile butt joints showed that there was a change of failure mode from that of cohesive to one of near interfacial even for the lowest levels of contamination. Joints prepared with the EA 913 adhesive lost approximately 50% of their overall tensile strength at a contamination level of 400 mg/m<sup>2</sup>, while EA946 was hardly affected. The results for the tapered double cantilever beam trials were somewhat different, and significant effects were noted for both adhesives. The EA946 results were significantly reduced from approximately 1,200 N/m to around 600 N/m at the 100 mg/m<sup>2</sup> level. The EA913 results were also similarly affected and were significantly reduced from an initial value of 400 N/m for the uncontaminated specimens to approximately 20 N/m at the lowest levels of contamination, 50 mg/m<sup>2</sup>. Trials were repeated for the EA 946 adhesive but with the addition of a silane primer to the bondline. The silane was applied by spraying a solution of 5% A187 in 40% toluene, 40% absolute ethanol, 5% butoxy ethanol, 5% deionized water, and 5% n-butanol. The results of both the tensile butt joint and cantilever beam trial showed improvements in the resistance to contaminant levels. For the butt joint trials, only a small loss of strength was observed up to the 200 mg/m<sup>2</sup> contaminant level. There was also a notable improvement in the fracture toughness values from a value of 1,200 to 4,000 N/m for the uncontaminated test specimens. Losses were again noted at the 100 mg/m<sup>2</sup> level of contamination.

In the above studies, the influence of various deliberately introduced chemical contaminants on the prebond condition of the adherends has been studied. Also of significance is the influence of prebond handling and the ability of some surface treatments to accommodate physical damage as well as contamination; this aspect has been investigated by McNamara et al. (1979).

It is clear that the role of surface contamination and its effects upon the resultant joint strength is complex; this point has been further highlighted in the work of Olsson-Jacques et al. (1996) who studied the influence of adsorbed aviation fuel on various differently treated surfaces. It is, however, important to note that the degree of degradation is a function of the specific adhesive-primer-treatment-adherend combination used. Therefore, to ensure good adhesion, in the general case, it is recommended that contamination is removed prior to adhesive application. Some methods to achieve this for metallic and polymeric adherends are discussed in the following sections.

## 7.3 Removal of Surface Contamination

### 7.3.1 Degreasing Metallic Adherends

For metals, an atomically clean surface will have a positive spreading coefficient, so wetting by a subsequently applied adhesive will occur; this topic has been dealt with elsewhere in this book and previously by Shanahan (2005). A large spreading coefficient is particularly important if complete wetting of highly textured surfaces is to be achieved. Note that the texture produced by various treatments may vary from the macro- or microscale created by grit-blasting to the nanoscale porosity present on anodized surfaces. Surface cleanliness, surface free energy, and wettability are intimately linked as has also been discussed, for example, by Rance (1985). Degreasing is the simplest possible method of achieving a clean surface and thereby increasing its surface free energy and spreading coefficient.

The simplest form of degreasing, involving the use of organic solvents, is used as a stand-alone treatment and as the first stage in a wide variety of multistage processes. Degreasing methods can range from simple immersion or wiping techniques to vapor degreasing or ultrasonic cleaning. The solvents industrially employed include isopropyl alcohol, acetone, methyl ethyl ketone, perchloroethylene, trichloroethylene, or 1,1,1 trichloroethane. However, environmental as well as health and safety legislation is rapidly reducing the range of solvents that can be used for this method (Averill et al. 1998). Furthermore, some standards agencies no longer advocate the use of solvents for the degreasing and cleaning of substrates to be bonded, preferring instead detergent degreasing or alkaline cleaning. For example, Lesley and Davies screened a range of approximately 150 solvents and degreasing agents in the search for a cleaner to replace the preexisting chlorinated vapor degreasing of aluminum and steel components for adhesive bonding. They concluded that substrates treated with aqueous cleaners resulted in surfaces with less residual organic matter than with any of the organic solvents they reviewed. Extensive studies have been carried out by Thiokol on replacements for methyl chloroform (TCA) for the cleaning of large-scale parts with great success achieved by various aqueous-based cleaners.

Alternatives to the commonly used degreasing processes are sought for many reasons, for example: established processes may not be adequate for difficult-to-



**Table 1** A summary of cleaners studied code to treatments

Code No.	Process description
1	Untreated
2	20% Circamax 103 alkaline cleaning solution
	2% Domestic detergent 1 solution
3	2% Domestic detergent 2 solution
4	2% Domestic detergent 3 solution
5	2% NMR Sea Power 100 solution
6	2% NMR Sea Power 100 solution +1% sodium hydrogen orthophosphate solution
7	2% NMR Sea Power 100 solution +1% sodium hydrogen orthophosphate +1% sodium metasilicate solution
8	0.5% NMR Sea Power 100 solution +1% sodium hydrogen orthophosphate solution
9	5% Domestic detergent 4 + 1% sodium hydrogen orthophosphate solution
10	1% Domestic detergent 4 + 1% sodium hydrogen orthophosphate solution
11	20% Circamax 103 alkaline cleaner solution followed by 20% Circamax 115 acid cleaner
	2% NMR Sea Power 100 solution +1% sodium hydrogen orthophosphate solution followed by a 4% sulfuric acid solution

remove materials or the processes may use undesirable volatile organic compounds (VOCs); alternatively, they can be carcinogenic or ozone depleting. In a study by Smith et al. (2000), a range of aqueous-based cleaners was evaluated in terms of their effectiveness on stainless steel. The usefulness of contact angle analysis was also demonstrated in this work. It is recognized that a monolayer of organic material present on metal surfaces will, typically, give a water contact angle between 55° and 95°. If the organic layer is effectively removed, the contact angle will be reduced to zero. Contact angle measurements can provide a simple method to assess the effectiveness of various cleaning agents. Smith et al. considered a range of cleaners on as-received stainless steel; the cleaners are detailed in Table 1. It was shown that the detergents were moderately effective in removing organic material from the stainless steel as can be seen from the much reduced contact angles in Table 2, compared with the untreated control. However, they were not as effective as the proprietary metal cleaner. Of particular interest, a natural detergent based on seaweed proved very effective in removing organic material as was confirmed using Auger electron spectroscopy (AES), particularly when used in combination with sodium hydrogen orthophosphate. As would be expected, the degree of cleaning increased with treatment time. Ultrasonics also significantly increased the effectiveness of the proprietary cleaner and the rate of cleaning. The alkaline and acid-based cleaners were also shown by AES to modify the surface oxide by enrichment of chromium, and the thickness of the oxide layer was reduced by both the alkaline and the acidic etches. The latter point may be relevant in terms of the durability of subsequently produced bonds.

For the removal of strongly adsorbed or chemisorbed contamination, simple solvent cleaning may not be effective. Litchfield et al. (2006) have detailed a

t.1
**Table 2** Summary of contact angle data

t.2	Pretreatment						
t.3	Code	Ultrasonics	Contact angles after x minutes in cleaning solution				
t.4			0	2	5	10	20
t.5	1	–	89				
t.6	2	√		14	11	9	5
t.7	2	–		23	14	17	10
t.8	3	√		–	36	37	–
t.9	4	√			31	22	–
t.10	5	√		–	42	28	–
t.11	6	√		–	72	83	–
t.12	7	√		53	36	23	16
t.13	8	√		33	19	10	13
t.14	9	√		50	41	17	20
t.15	10	√		15	12	30	30
t.16	11	√		54	21	20	15

312 range of processes for the removal of cross-linked epoxide resins from both metal  
313 and composite surfaces. Methods such as sodium hydride immersion, CO<sub>2</sub>-  
314 cryoblasting, and laser ablation all proved highly effective. In a further study, the  
315 efficacy of CO<sub>2</sub>-laser ablation was also demonstrated in terms of its ability to  
316 produce atomically clean surfaces with a resultant increase in surface energy and  
317 observed initial single lap shear (SLS) joint strength and durability, as measured  
318 using statically stressed SLS joints (Critchlow et al. 1997) with metallic adherends.  
319 In a related study by Bedwell et al. (1998), CO<sub>2</sub>-laser ablation was studied to  
320 establish the effectiveness of simply removing adventitious organic contamination  
321 from industrially sourced hot dipped galvanized (HDG) mild steel. This laser-based  
322 process was demonstrated to be more effective than double-degreasing combined  
323 with ultrasonic immersion in acetone for the removal of organic contamination from  
324 a previously oil-contaminated surface. In addition, the TEA CO<sub>2</sub>-laser was shown to  
325 modify both the near surface chemistry and the topography; the precise modifica-  
326 tions being dependent upon the degree of treatment used. Importantly, in bond  
327 durability trials, the changes introduced to the laser-treated HDG surface were  
328 shown to provide equivalent or better adhesion levels compared with degreased-  
329 only adherends; see Table 3. Furthermore, in durability trials, using statically  
330 stressed SLS joints immersed in hot water, a commercially available phosphate-  
331 based, chemical conversion coating was shown to provide bond durability signifi-  
332 cantly inferior to the TEA CO<sub>2</sub>-laser treatment. It should be noted though that a  
333 chromate-based process gave markedly superior bond durability in these trials; see  
334 Table 4. Lu and Aoyage (1994) also confirmed the effectiveness of laser cleaning on  
335 various substrates using a KrF excimer source.

336 Another process which is gaining popularity is the use of CO<sub>2</sub>-cryoblasting as  
337 discussed by Brewis et al. (1999). The combined thermomechanical action of solid  
338 CO<sub>2</sub> particles impacting upon surfaces combined with the effective solvent action



t.1 **Table 3** Initial joint strengths (kN) of SLS joints as a function of surface treatment

t.2	Treatment	Joint strength (kN), $\pm 1$ standard deviation
t.3	Double degrease	$4.4 \pm 0.08$
t.4	Gardobond 250	$4.5 \pm 0.22$
t.5	Gardobond 4504	$4.5 \pm 0.23$
t.6	Gardobond 250 + 4504	$3.6 \pm 0.11$
t.7	TEA CO <sub>2</sub> -laser treatment – 10 pulses	$3.9 \pm 0.31$
t.8	TEA CO <sub>2</sub> -laser treatment – 20 pulses	$4.0 \pm 0.56$
t.9	TEA CO <sub>2</sub> -laser treatment – 30 pulses	$4.1 \pm 0.22$

t.1 **Table 4** Mean times-to-failure,  $t_f$ , of SSLS joints immersed in water at 60 °C at applied loads of 0.2 and 0.5 kN as a function of surface treatment

t.2	Treatment	Applied load (kN)	Mean $t_f$ value (h) $\pm 1$ standard deviation
t.3	Double degrease	0.2	$163 \pm 32$
t.4		0.5	$85 \pm 12$
t.5	Gardobond 250	0.2	$90 \pm 16$
t.6		0.5	$27 \pm 7$
t.7	Gardobond 4504	0.2	$235 \pm 36$
t.8		0.5	$172 \pm 6$
t.9	Gardobond 250 + 4504	0.2	$198 \pm 53$
t.10		0.5	$27 \pm 7$
t.11	TEA CO <sub>2</sub> -laser treatment – 10 pulses	0.2	$177 \pm 38$
t.12		0.5	$37 \pm 11$
t.13	TEA CO <sub>2</sub> -laser treatment – 20 pulses	0.2	$217 \pm 30$
t.14		0.5	$79 \pm 30$
t.15	TEA CO <sub>2</sub> -laser treatment – 30 pulses	0.2	$162 \pm 30$
t.16		0.5	$58 \pm 18$

339 means that highly contaminated surfaces can be readily cleaned very quickly and  
340 over large areas. This process was shown by Brewis to effectively leave an atomi-  
341 cally clean surface on previously contaminated aluminum and to introduce some  
342 surface texture. SLS joint testing was carried out using aluminum 5251 alloy  
343 adherends and, in terms of creating initial adhesion, this treatment proved better  
344 than simple ultrasonic degreasing and as effective as grit-blasting. A further devel-  
345 opment by Deffeyes et al. (1997) is the use of cryoblasting followed by ultraviolet-  
346 light irradiation which proved to be highly effective at removing oils and waxes from  
347 aluminum surfaces. This combination process was shown to produce a zero-degree  
348 water contact angle on the treated surface, indicating complete removal of the  
349 preexisting contaminants.

350 In summary, although externally sourced surface contamination can be accom-  
351 modated by some adhesive-substrate combinations, it is generally regarded as good  
352 practice to remove such material prior to adhesive application. There are many  
353 treatments which will achieve this outcome; the preferred one will depend upon a

number of factors, including the chemical nature of the contaminant and adherends. Some degrease options can be considered as reasonably effective stand-alone treatments. In general terms though, mechanical, chemical, electrochemical, and some alternative treatments tend to give improved levels of adhesion and durability compared with simply degreasing.

### 7.3.2 Polymer Treatment: Removal of Contamination and Surface Functionalization

As previously mentioned, the surface of polymers can comprise contaminant from both internal and external sources. The aim of many polymer pretreatments is often to remove such material and to introduce or to expose desirable chemical functionality. This topic has been extensively covered by Brewis (1982) and Brewis and Briggs (1985); note that many of the treatments considered in Brewis' early work are now favored by industry and so are relevant to this book.

For some polymers, a solvent wipe will suffice to remove, for example, plasticizers, which have migrated to the air interface. However, not all solvents are compatible with all polymers, so care must be taken to select the most appropriate solvent.

Polymers which are difficult to bond such as polyolefins and elastomers may require the removal of such weak boundary layers and also the introduction of relevant functional groups; these are often oxygen-containing. The most favored methods to achieve this result include: flame treatment, corona discharge treatment, and plasma treatment. These are all dry processes which can oxidize a range of polymers by using excited gases, ions, neutrals, electrons, or free radicals. An illustration of the usefulness of plasma treatment to treat fluoropolymers, namely poly (vinyl fluoride) (PVF) and polytetrafluoroethylene (PTFE), has been given by Brewis et al. (1995). In this example, argon, oxygen, air, and nitrogen plasmas were used. In the case of PTFE, there was no significant change in surface chemistry observed by XPS; however, SLS joint strengths increased from 420 to 1,860 N following argon plasma treatment for 30 s. This result was explained as due to the removal of a preexisting weak boundary layer. In contrast, with PVF, XPS showed the various plasma types to increase oxygen levels in the surface from 0.8 up to 12.4 atom %, in the case of the oxygen plasma. The introduction of this level of oxygen functionality resulted in an approximate tenfold increase in initial adhesion. Similar large increases in adhesion are observed in many studies of polymer–polymer adhesion, these are explained in terms of the removal of weak boundary layers, an increase in surface functionality or free energy, or enhanced roughening of the polymeric substrate using these methods. A recent study by Stewart et al. (2005) has demonstrated the effectiveness of air plasma treatment of polypropylene as applied to complex shapes; in this case, a car bumper, which, with an optimized treatment condition, demonstrated good adhesion post treatment.

As an alternative to the above-mentioned treatments, Charbonnier et al. (2001) discussed the use of excimer laser and ammonia gas treatment for the

functionalization of polycarbonate and polyimide. In their study, a large increase was observed using X-ray photoelectron spectroscopy (XPS) in the levels of nitrogen, from 6.4 to 17.6 atom%, with no great change in the levels of oxygen as a result of a 3 min treatment. The improved adhesion of a subsequently applied palladium complex was attributed to this increased level of nitrogen, given the affinity of palladium to form “N-Pd” bonds.

Note that a consideration of plasma polymerized coatings, which is a related technology, is outside of the scope of this contribution; attention is drawn, however, to the relevant book by Strobel et al. (1994).

## 7.4 Mechanical Treatments and the Role of the Interphase

Mechanical treatments generally remove friable surface layers and generate macro-rough surface texture on metallic surfaces. They are generally combined, before and after, with a simple degrease process.

The penetration of polymers into the asperities on, or within, surfaces has been well discussed in the literature; an early study was carried out by Packham et al. (1974a) who investigated the keying of polyethylene into the pores present on anodized aluminum. The effect of such polymer penetration and the importance of mechanical interlocking with such highly textured surfaces which will facilitate energy dissipation within bondlines was further discussed by Packham et al. (1974b) and, amongst others, Rider and Arnott (2001). One important conclusion from such studies is that the stresses applied to joints containing highly rough adherends are potentially no longer concentrated at the surfaces, but are then distributed more widely within the bondline, enabling more plastic energy dissipation to occur and increased observed levels of adhesion. Photoelastic (Packham 2010) and Moiré interferometry (Asundi 1987; Sargent and Ashbee 1985) studies have directly observed the nonuniform stress distributions within bondlines and in the region of surface asperities. One advantage of creating such asperities is that stresses are then potentially dispersed into and away from the “interphasial” region.

It has been acknowledged for some years now that there is a zone between the substrate and adhesive within the bondline that is different to that of the bulk adhesive. In an early study, Allen et al. (1972) noted thin glassy layers remaining on titanium alloy lap joints after testing, free from the filler and pigmentation associated with the bulk of the adhesive. Similarly, Sharpe (1972) in 1972 commented upon the fact that, at that time, the components within a bonded system were treated as discrete entities, when, in fact there are many more layers present in a bonded joint. Since this pioneering work, many other workers have begun to study the interphasial chemistry. For example, Fondeur and Koenig (1993) conducted Fourier transform infrared (FTIR) microscopy studies on aluminum substrates coated with a dicyandimide cured epoxide adhesive. They found that there was a variation of the dicyandiamide concentration with thickness through the adhesive layer. Using both the nitrile and carbonyl peaks, they found that for untreated aluminum substrates, there was a comparatively high level of dicyandimide near

to the substrate surface that coincided with a high level of carbonyl material. The opposite was observed for chromic acid anodized adherends, where the dicyandimide content was at a minimum close to the substrate.

Similarly, Nigro and Ishider (1989) conducted FTIR reflectance absorption spectroscopy on an epoxide resin with a BF<sub>3</sub>-monoethylamine catalyst system applied to polished 1008 Drawing Quality steel substrates. They studied the degree of conversion of the oxirane (epoxide) ring as a function of depth and found that epoxy conversion rates were higher closest to the steel substrate. The epoxy prepolymer was also applied onto the steel surface without hardener and the same phenomenon was still observed. They suggested that the steel might, in some way, interact with the epoxide adhesive causing homopolymerization of the epoxide resin at the surface of the substrate.

Likewise, Roche et al. (2002) studied the resultant interphase of a DGEBA epoxide when combined with either an aliphatic, aromatic, or cyclic diamine curing agent and then applied onto aluminum or titanium surfaces. They found differences through the thickness of the adhesive layer: the  $T_g$  was lower at the interphase for both substrates and the stoichiometric ratio was higher nearer to the substrate, with an amine to epoxy ratio of 1.2 as opposed to 1 within the bulk region. Placing the DGEBA and IPDA individually in direct contact with the aluminum and titanium substrates, they found that dissolution of the metal oxides occurred in the basic IPDA liquid. Taking samples of the reacted IPDA liquor and combining them with DGEBA, they measured the  $T_g$ , Young's modulus, and the epoxide amine ratio. They compared this with the properties of the interphasial regions and bulk polymer regions. What they found was that the modified IPDA system had the same properties as the thin layer samples with reduced  $T_g$  and differing Young's moduli.

Safavi-Ardebili et al. (1997) conducted experiments upon acid etched A1100 aluminum substrates bonded with an epoxide adhesive, Hysol EA-9346. Sectioning the joints at varying angles, they examined the bondline with EDS, they measured the interphasial region, and found that this layer was irregular in thickness ranging from  $2 \times 10^{-6}$  to  $6 \times 10^{-6}$  m. Nano indentation revealed that there was a gradient of the Young's modulus, which increased by approximately 13% in the interphasial region when compared to the values obtained within the bulk of the bondline.

Likewise, Kollek (1985) used FTIR diffuse reflectance analysis to study the absorption chemistry of epoxide and phenolic resins on aluminum substrates. He observed that both the curing agent and the epoxy resin monomer were adsorbed on the aluminum oxide surface. They found that the dicyandiamide monomer was adsorbed by the oxide layers of the substrate and was attributed to the acid proton of the aluminum oxide reacting with and reducing the observed nitrile peaks. For the epoxide monomer, less adsorption was observed, and it was suggested that this occurred by the opening of the epoxide ring.

More recent studies have further added to the understanding of polymer-metal interactions and confirm the highly variable chemical nature of the polymer-metal interphase (Gaillard et al. 1994; Bistac et al. 1997; Roche et al. 2006); particular attention is drawn to the work of Possart in this area (Possart 2005). Of critical importance, the interphase comprises a region whose chemical composition might be

very different from the bulk polymer. The mechanical properties of the interphase might, as a consequence, be different as observed by many of the workers in this area mentioned above. The extent of the polymer-metal interphase is also the subject of some discussion with some researchers focusing attention on the polymer up to a few nanometres from the metal surface, whereas others maintain that the region of modified chemistry and properties extends up to many micrometres. What is clear is that the chemistry and resultant mechanical properties of the interphasial polymer are very different from the known bulk polymer properties; hence, the ability of this material to sustain loads and resist the initiation of damage and its reaction to moisture, all factors which might influence failure in the interphasial region, are more difficult to predict than the bulk polymer. Other complications arise when, for example, water interacts with the interphasial polymer and accelerated corrosion can be initiated.

In summary, the creation of rough surfaces provides the possibility of redistribution of stresses away from the interphasial polymer and into the bulk adhesive. This, in addition to the fact that rough surface have much higher specific surface areas for adhesive interaction and texture for mechanical attachment, means that the creation of such surfaces is highly desirable.

The simplest form of mechanical treatment is to hand abrade using dedicated abrasive pads or papers, followed by a solvent, or similar, wipe to help remove residues. This process may be effective but can also introduce contamination and may be nonuniform in application (Bishopp et al. 1988). On an atomic scale, the surface can retain contaminating residues from the pads or papers which cannot easily be removed. In terms of resultant texture, on the macroscale, the hand-abraded surface tends to comprise broad flat areas of unaltered surface in between the grooves created by the treatment. The ratio of the surface area exhibiting these features is clearly dependant on the degree of treatment applied.

A more controlled method of surface treatment is by grit-blasting or slurry-blasting followed by degreasing. Frequently, coupling agents are also applied post grit-blasting. This topic will be covered in greater detail in ► [Chap. 11, “Organosilanes: Adhesion Promoters and Primers.”](#) During grit-blasting, the abrasive media, which usually comprises alumina, chilled iron, or silica, is propelled to the surface under pressurized air, while in slurry-blasting alumina is usually used, which is transported via high pressure water jets. Clearly, treatment parameters such as pressure, times, and blast media can be optimized to produce the desired surface texture. In one study of the grit-blasting treatment, Critchlow and Brewis (1995a) quantified the degree of enhanced roughness created using various grades of alumina from 40/60 to 320, using profilometry, and changes to the surface chemistry, using AES. With 5251 grade aluminum alloy, grit-blasting did improve adhesion, but the importance of post cleaning to remove embedded grit and to create a subsequently wettable surface was emphasized. In general, the enhanced surface features created by grit-blasting provide reasonable levels of initial adhesion, Critchlow and Brewis (1996) in a review article identified a number of studies where this was the case. However, it should be noted that the very thin oxide-remaining post grit-blasting leaves metals susceptible to corrosion, and durability in hot-wet environments can

be poor. Bishopp illustrated this point by immersion of aluminum 2024-T3 clad alloy joints in 85% RH at 70 °C and measuring the fall-off in peel strengths with time (Bishopp et al. 1988). Under these conditions, joints incorporating grit-blasted adherends retained only 20 N/25.4 mm compared with anodizing which retained up to ~180 N/25.4 mm after 10 days exposure. Bishopp suggested that in some cases, surfaces can be “too rough,” allowing air to be trapped at the adhesive-metal oxide interface, i.e., there is incomplete wetting with poor durability resulting.

The possibility of using power beams for surface texturing has been originally discussed by Tavakoli (1994). In this sense, the term “power beams” includes the use of laser and electron beams for the texturing of surfaces. Significant work has been carried out in this area with the establishment of the Surfi-sculpt® and Comeld® processes. Some details of the structures generated by electron beam bombardment have been discussed by Tu et al. (2010). Such processes look highly promising for the generation of highly complex structures up to millimeters in scale on metallic, polymeric, and composite surfaces.

In summary, good initial levels of adhesion can be observed using metallic adherends post-mechanical treatment due to the ability of such surfaces to partially negate any adverse influence of the interphase and to provide desirable texture. However, the thin oxides present after such treatments tends to cause mechanically treated joints to perform badly, particularly in durability tests carried out under hot-wet conditions. The application of primers and coupling agents is usually carried out to obviate this poor performance. Also, the use of chemical treatments can be carried out if enhanced durability is required, as discussed in the following section.

The use of such mechanical methods on polymers is, to some extent, limited. Mechanical treatments such as grit-blasting can introduce high stress and damage into the substrate which metals can accommodate, but some polymers cannot. However, this is not always the case and grit-blasting is routinely used to treat carbon fiber-reinforced polymer (CFRP) composites. Attention is drawn to work of Belcher at NASA who reported that grit-blasting of CFRP performed similarly to the use of peel ply or laser ablation. The importance of using optimized mechanical methods though has been highlighted by Stone (1981) in his study on the influence of abrasion on CFRP adherends.

---

## 7.5 Chemical Treatments

### 7.5.1 Chemical Treatments for Metallic Adherends

These are invariably aqueous-based processes which may be applied from spray or full immersion. Importantly, surfaces are generally degreased prior to chemical treatment. In practical terms, this is to reduce drag-out contamination passing from stage-to-stage and so obviating the possibility of contamination present in the final solution. Chemical treatments can be considered as etchants or, alternatively, used to produce chemical conversion coatings.



Etch solutions invariably utilize strong single or mixed acids, although, in some rare instances, strong alkaline solutions can be used. The purpose of such etchants is to remove friable organic or inorganic layers, including loosely bound oxides, hydrated oxides, or other corrosion products, and to leave an enhanced surface topography. In principle, with metallic adherends, after rinse operations, the surfaces should also be of a high surface energy being atomically clean. Depending upon the treatment conditions used, i.e., solution type, time, and temperature along with substrate characteristics such as the alloy type and thermal history, the resultant topography can vary from macro- to nano-rough. The nanoscale features being regarded as particularly useful to enable the creation of a “micro-composite interphase.” The benefits of such topography have been discussed above and an illustration of the commonly used Forest Products Laboratory (FPL)–etched aluminum surface is given in ► [Chap. 8, “Surface Treatments of Selected Materials.”](#) Many of the common acids used for the prebond treatment of metallic adherends have been reviewed by Minford (1993) in the case of aluminum alloys and Critchlow and Brewis (1995b) for titanium alloys. The aforementioned works by Minford and Critchlow indicate that, as with mechanical treatments, acid etching can produce excellent initial levels of adhesion but, again, a relatively thin oxide is present after such treatments so that durability can be compromised. Chemical conversion coating is the simplest method of producing thicker, passivating films on metal surfaces.

Chemical conversion coatings develop a passivating film by means of a complex growth and deposition mechanism. The degree of roughness introduced by such conversion coatings on surfaces can be highly variable. For example, on medium carbon steel, this variability was illustrated in the work of Critchlow et al. (2000). In this study, a range of chromate-free conversion coatings were compared with chromate-containing processes. The best-performing process, Bonderite 901-Pyrene 8–90, provided a thick, mixed oxide extending to approximately 150 nm, which was highly nodular on the nanometre scale and which contained polymeric functionality in its outer layers. It was concluded that these physicochemical properties were responsible for the excellent adhesion performance: with the nodular surface capable of interphase formation, some epoxide component possibly present to react with the adhesive and good barrier corrosion protection afforded by the oxide. With this treatment combined with a single part epoxide mean initial SLS strengths of 57.9, MPa were measured. Significantly, after 8 weeks of immersion in water at 60 °C, these joints retained approximately 80% of their initial joint strength. Due to the complex nature of the conversion coating process, it should be noted that although the aforementioned Bonderite 901-Pyrene 8–90 process worked well for medium carbon steel, it will not necessarily be applicable to other adherends. There are, however, many available conversion coatings some of which are detailed below.

Phosphate coatings are widely used in the automotive industry due to their ability to treat both aluminum and steel. These coatings offer good levels of adhesion and, although the corrosion resistance is generally regarded as marginally lower than that of chromate-containing coatings, joints produced offer good environmental stability. A study of chromate-phosphate-based conversion coatings has been carried out by Maddison and Critchlow (1996). This study showed that the preexisting oxide

on aluminum 5251 alloy was removed within the first few seconds of treatment followed by a controlled film formation up to a thickness of approximately 1,000 nm with extended treatment times up to 60 s. The resultant film composition was highly complex comprising Al, O, P, and Cr. Importantly, with reasonable treatment times, the chromate-phosphate treatment demonstrated excellent durability with a single part epoxide in impact testing carried out on SLS joints which had been immersed in water at 75 °C prior to testing. In this experiment, the chromate-phosphate-treated joints absorbed over five times more energy than alkaline-cleaned controls.

Underhill and Rider (2005) propose an interesting alternative: a simple hot-water conversion coating. They have shown this method to have understandably low processing costs as well as suggesting successful adhesive performance. The same group has also demonstrated the effectiveness of boiling water treatment-applied post grit-blasting and subsequently followed by epoxide-functional silane application (gamma-GPS).

Molybdenum-based coatings have been considered as alternatives due to molybdenum having an electronic structure similar to that of chromium. Molybdates are known to be corrosion inhibitors. When incorporated within aluminum oxide films, the molybdate ( $\text{MoO}_4^{2-}$ ) is regarded as providing excellent corrosion resistance to pitting. The high cost of molybdenum conversion coatings is a possible explanation for their lack of popularity.

Of particular note are the titanium-zirconium-based solutions which are the basis of many commercial conversion coating systems due to their ease of application. These coatings, for example, are widely used to help attain good lacquer adhesion in the canning industry. Titanium-zirconium coatings produce thin films in very short application times, in the order of a few seconds, and good adhesion and corrosion performance is reported for a range of aluminum alloys. On some aluminum alloys, namely 6060, preferential deposition has been found to cause localized variations in film thickness which, when coupled with the fact that these processes produce colorless films, makes quality control assessments very difficult, however. For example, Schram et al. (1995) showed such conversion coatings to extend to about 10 nm in thickness independent of treatment time. Using AES, the same workers identified a duplex structure to the coating with a simple oxide present adjacent to the aluminum 1050 alloy substrate, but a more complex aluminum oxide-zirconium fluoride plus polymer present in the outer nanometres of the film. Critchlow and Brewis (1997) also studied such films on aluminum and confirmed the highly complex, duplex nature of the resultant films. These workers demonstrated that static-stressed SLS joints immersed in water at 60 °C had much greater times to failure compared with degreased-only or grit-blasted controls. Subsequent studies have shown the best-performing conversion coatings, on aluminum alloys, at least match the durability performance of the best acid etches, such as the FPL. However, the use of hot-water immersed static SLS joints has demonstrated that titanium-zirconium conversion coatings to be less durable than the phosphoric acid anodizing (PAA) treatment.

Cerium-based conversion coating processes are thought to precipitate Ce (III) hydroxide at regions of high pH. This precipitation gives the coating corrosion inhibiting properties similar to that of titanium-zirconium-based coatings. The



inhibition is believed to decrease the rate of cathodic oxygen reduction. A multistage process combining chemical and electrochemical treatments based on cerium and molybdenum has been studied and is shown to enhance the corrosion protection in the high-copper-content aluminum alloys, for example, the aerospace 2024 and 7075 alloys. The combined process offers good levels of adhesion on the 2xxx series alloys but mixed results are obtained on other alloys. One disadvantage of this process is the extended time taken to produce the coating, which increases production costs.

In summary, the chemical treatments when applied to metals do remove preexisting friable oxides or hydrated oxides in the early stages of the treatment followed by controlled film formation. The films can offer the advantages of increased surface free energy or, in the case of conversion coatings, the possibility of polymeric functionality introduced. The conversion coating processes, in particular, can provide corrosion protection via a number of mechanisms; the result of which is the observed increase in durability of such treated adhesive joints exposed to hot-wet conditions. A range of surface morphologies can be generated by both etch and conversion coating processes, and techniques such as electron and atomic force microscopy (AFM) can be used to monitor these treatments to provide optimized surface texture which will facilitate interpenetration of the polymer into the asperities of the treated surface. Whilst, chemically treated surfaces do offer a range of physicochemical properties which enhance adhesion, the electrochemical processes generally provide the best bonding surfaces for aluminum and titanium; these are discussed in the following section. Note that anodizing of steels is not possible.

## 7.5.2 Chemical Treatments for Polymeric Adherends

In addition to the dry processes detailed previously, wet chemical processes can also be used to modify polymeric surfaces to introduce desirable physicochemical properties. For example, chromic acid has been used as an oxidizing agent to this end for some time (Brewis and Mathieson 2001). Given the concerns over the usage of hexavalent chromium in this field, there are ongoing efforts to find suitable replacements. In one study by Brewis et al. (1995), a proprietary etchant, Tetra-Etch, was used to treat two fluorinated polymers, PTFE and PVF. The results of this treatment are given in Table 5. XPS showed Tetra-Etch caused the PTFE surface to lose almost all of its surface fluorine with a short treatment time of 10 s. This was accompanied by a large increase in the surface oxygen levels from zero to 11.6 atom%. This increase in useful oxygen-containing functional groups enabled a tenfold increase in measured adhesion in the SLS configuration. The PVF, however, required longer treatment times with the best results observed after 60 min immersion in Tetra-Etch. Again, a large increase in adhesion was observed from 360 to 3,020 N, but in this case, there was relatively little surface modification observed by XPS. This result was attributed to the removal of a potential weak boundary layer by the Tetra-Etch treatment.

Similarly, Dahm et al. (2005) studied a range of wet chemical treatments, including various oxidizing and halogenating agents on both additive-free and fully formulated

t.1 **Table 5** To show surface compositions and SLS joint strength of PTFE and PVF polymers following Tetra-Etch treatment for various times (Brewis et al. 1995)

t.3	Polymer/treatment	XPS (atom%)			Failure load (N)
		C	F	O	
t.4	PTFE none	38.4	61.6	—	420
t.5	PTFE 10 s	37.6	0.8	11.6	4,280
t.6	PTFE 1 min	82.2	0.9	16.9	4,260
t.7	PVF none	70.4	28.8	0.8	360
t.8	PVF 10 s	72.4	26.7	0.9	800
t.9	PVF 1 min	75.4	23.0	1.6	2,080
t.10	PVF 60 min	87.3	11.4	1.3	3,020

700 elastomers. Of particular interest were styrene butadiene (SBS) and ethylene-  
701 propylene-dimer terpolymers (EPDM). In this study, extensive use was again made  
702 of XPS to relate changes in surface chemistry to SLS strength determined using a  
703 composite SLS joint. As with polyolefins, elastomers proved highly receptive to  
704 oxidizing agents, showing a large increase in surface oxygen content with, for  
705 example, potassium permanganate, potassium dichromate, Fenton’s reagent, and  
706 other such treatments. In general, however, the oxidizing agents provided only a slight  
707 increase in observed adhesion; this being attributed to the production of a layer of low  
708 cohesive strength at the surface of the elastomers. In particular, static secondary ion  
709 mass spectrometry (SSIMS) was used to study the SBS surface following potassium  
710 permanganate treatment, and it could be inferred that this treatment did cause some  
711 chain scission of the elastomer surface. In contrast, a number of chlorinating agents,  
712 including sodium hypochlorite solution, Chloramine-T, and trichloroisocyanuric acid  
713 (TCICA) were studied, and these also created highly modified SBS and EPDM  
714 surfaces. With these treatments, however, a large increase in adhesion was observed,  
715 by a factor of approximately x4 to x20, depending upon the specific treatment on SBS.  
716 The mechanisms by which this was achieved have been discussed by Dahm et al.  
717 (2005). In summary, wet chemical treatments can be highly effective on a range of  
718 polymers by the removal of weak layers and the introduction of desirable chemistry.  
719 As with dry processing of polymers, there is always the potential for over-treatment,  
720 causing chain scission and a net reduction in adhesion levels. For this reason, such  
721 treatments should always be optimized for a specific application.

722 **7.6 Electrochemical Treatments**

723 **7.6.1 Introduction to Anodizing**

724 Regarding the higher treatments, and the anodizing processes in particular, these can  
725 be applied to a number of metals but are mostly carried out on aluminum and  
726 titanium and their alloys. These treatments are in the main complex, time consuming,  
727 and costly to carry out. There are also legislative drivers which make the use of some

processes, especially those which utilize hexavalent chromium, highly undesirable. Other factors such as energy and chemical disposal costs also deserve consideration. However, for structural metal bonding, these treatments are highly recommended as they impart all of the fundamental physicochemical properties required to provide the best initial levels of adhesion and durability of any treatments, namely, wettability, micro- and nano-roughness, mechanical stability, and passivation. Note that to take full advantage of the porosity present on anodic oxides, it is often recommended that primers are used in combination.

There exists extensive literature on this topic and attention is drawn to the highly relevant book by Minford (1993) and to ► Chap. 8, “Surface Treatments of Selected Materials” of this handbook. It is widely reported, and further discussed in ► Chap. 8, “Surface Treatments of Selected Materials,” that the most successful treatments for aluminum and titanium include direct current (DC) anodic oxidation in chromic, phosphoric, or sulfuric acid electrolytes (CAA, PAA or SAA). It is, of course, recognized that other electrolytes are used, some of which will be discussed later in this section. The Bengough–Stuart 40/50 V CAA process is currently the preferred pretreatment of European aerospace manufacturers, and on clad aluminum alloy produces a porous surface oxide typically 2–3  $\mu\text{m}$  thick with a pore diameter of approximately 25–35 nm. This oxide offers possibly the best levels of adhesion and environmental resistance. PAA, as a prebond process, is preferred by Boeing Commercial Airplane Company. Boeing claim good in-service durability performance with adherends using this pretreatment. The oxide produced is described as being 400–800 nm thick incorporating 100 nm of small outwardly protruding fibrils. The phosphate content of the oxide improves stability toward water and therefore improves the hydration resistance as discussed in the following section. PAA is considered to be very tolerant to variations in processing parameters compared to CAA. PAA is claimed by Boeing to provide the most durable joints but, in some studies, it is shown to be comparable to or even worse than CAA.

Sulfuric acid anodizing (SAA) has also been widely compared to CAA, PAA, and FPL etches in the review by Critchlow and Brewis (1996). As indicated by Critchlow and Brewis, SAA prepared joints usually demonstrate moderate initial joint strength and relatively poor long-term joint durability. In general, SAA-treated adherends are significantly out-performed by CAA and PAA but perform similarly to FPL etched adherends. The oxide thickness associated with SAA is of the order of 10  $\mu\text{m}$  and is significantly thicker than oxides produced during other anodizing processes. For this reason, it is ideally suited to corrosion protection applications. SAA followed by a phosphoric acid dip has been shown to improve joint performance by the opening up of the otherwise highly dense porous oxide.

Alternating current (AC) anodizing produces a similar but thinner surface oxide structure to the aforementioned direct current (DC) treatments, but with the advantage of the adherend being electrolytically deoxidized on the negative half of the applied voltage cycle. This reduces the importance of the preceding degrease and alkaline cleaning usually associated with conventional DC anodization. This, however, comes at a cost. The solution–adherend resistance is much less on the cathodic half of the cycle than it is on the anodic half. Consequently, the current density is

much larger and can potentially cause an undesirable effect known as “burning” or “powdering” on the surface. A compromise must be struck between treatment time, temperature, and applied voltage in order to minimize this effect. The thinner resultant surface oxide and limited applications are consequences of this. The two main electrolytes, indicated in the literature as being used for AC anodizing, are phosphoric acid and sulfuric acid. A number of workers have investigated both electrolytes and found promising results indicating that AC anodizing was suitable as a prebond process. Further details of this treatment, including a consideration of the mechanisms of anodic film formation, follow.

## 7.6.2 Structure and Composition of Anodic Films

It has been accepted for some time that an anodic oxide formed on the surface of an aluminum alloy typically consists of an inner, thin, compact oxide layer, called the barrier layer, and a porous outer oxide displaying a honeycomb-like hexagonal close-packed structure, as illustrated in Fig. 1. The thickness of the barrier layer is approximately 0.1–2.0% of the overall film thickness and is dependent upon the electrolyte concentration and the applied anodic voltage. Several authors propose the dependency to be close to 0.01 nm/V. It is suggested that the idealized honeycomb arrangement is due to repulsive interactions between the pores during anodic film growth, and that a mechanical stress resulting from the volume expansion of the forming oxide causes these repulsive forces. In doing so, the formation of a hexagonal arrangement during nucleation occurs. Production rates of between 1 and 5  $\mu\text{m/h}$  are typical. Factors such as the alloy type, the thermal history of the metal, deoxidizing process used, and electrolyte agitation can be a very important factor in the formation of ordered pore arrays.

When an anodic voltage is applied to aluminum in an electrolyte, a current will flow through the electrolyte to the anode and aluminum oxide or hydrated aluminum oxide will be produced on the surface. If this oxide is soluble or partially soluble in the electrolyte, then dissolution will occur creating the porous oxide layer. The porosity of the oxide will therefore be a function of the solubility of the oxide in the electrolyte, and the film will only grow if this rate of dissolution is less than the rate of oxide production. An important realization is that the oxide grows from the bottom of the film rather than being deposited on the outer surface as in electrodeposition. For this reason, it is pivotal in the understanding of porous oxides that the outer surface, being formed first, has been in contact with the electrolyte for the longest time and may have been notably modified.

The growth of the oxide film is reported to be made possible by the solid-state migration of the  $\text{Al}^{3+}$  and  $\text{O}^{2-}$  ions which move outward and inward, respectively, through the film. This movement is driven by the electric field created during anodization. The development of the new material at the metal/film interface is due to oxidation of aluminum atoms to form  $\text{Al}^{3+}$  combining with the  $\text{O}^{2-}$  ions present in the electrolyte. This migration results in new material being formed in two places, the metal/film and the film/electrolyte interfaces. The second phase elements

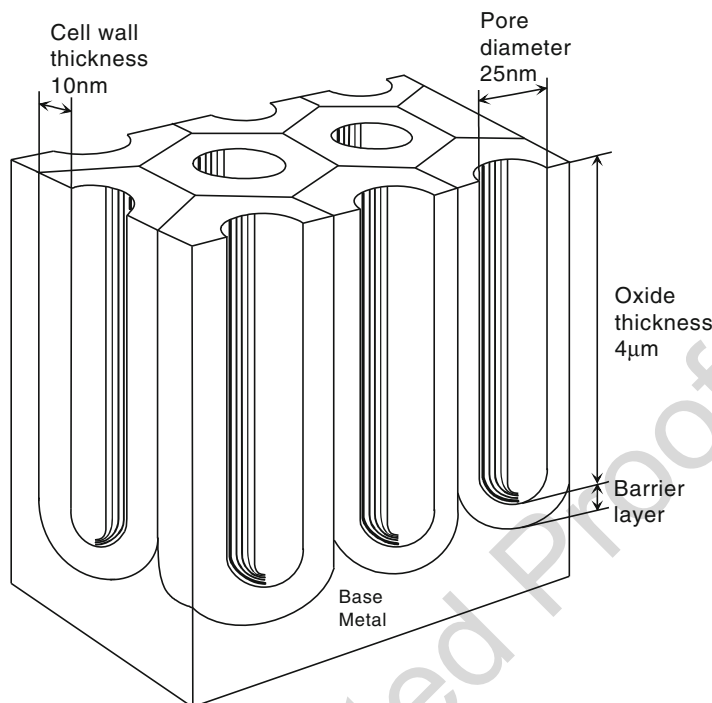


**Fig. 1** To show the idealized cell structure of a porous aluminum oxide grown post chromic acid anodization

present on the alloy surface are either removed or oxidized along with the aluminum. A further mechanism, field-assisted dissolution, may occur due to the of the electric field concentration across the barrier layer which is thermally enhanced due to localized Joule heating and the aforementioned ionic mobility. This effect causes the aluminum to oxygen bonds in the oxide lattice to weaken, resulting in a dissolution at the oxide/electrolyte interface. The chemical and field-assisted dissolution take place with widely differing rates, with the field-assisted being reportedly up to 3,000 times greater. Note that the electrolytically driven growth competes with these dissolution mechanisms to produce the final anodic film under steady-state conditions. The resultant surface features associated with the anodizing are further detailed in ► [Chap. 8, “Surface Treatments of Selected Materials.”](#) It is, however, sufficient to state that the microscopically rough features produced can increase the specific surface area of an anodized adherend by a factor of several hundred. It is widely accepted that wetting by an adhesive, or primer, into a porous anodized structure such as the PAA oxide or the CAA oxide is possible and is necessary for the formation of a strong bond via the formation of a “micro-composite” region due to this penetration of adhesive into the oxide. The microstructure generated by the CAA process on both bare and clad aluminum alloy is illustrated in Fig. 2. Note the non-idealized structure which is typical of that on the higher aluminum alloys.

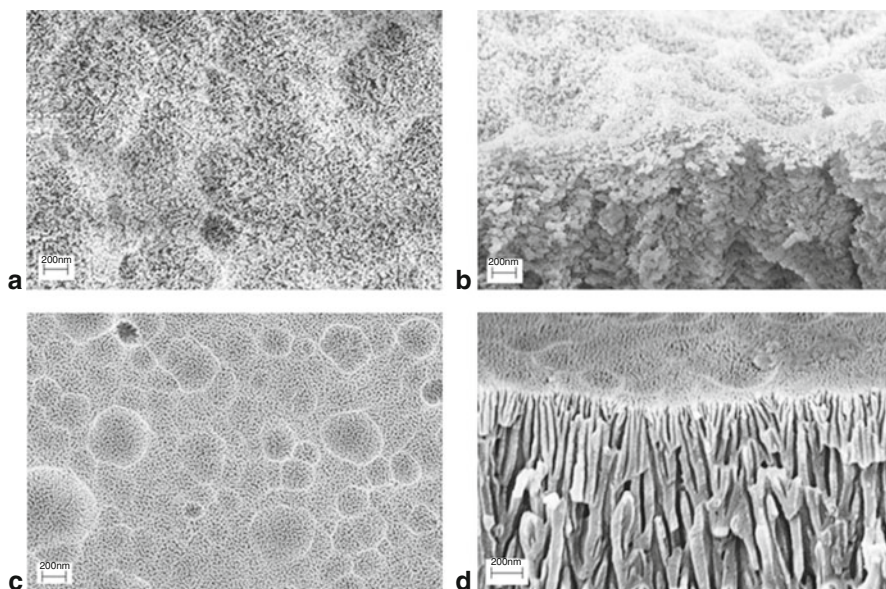


**Fig. 2** CAA 40/50 V processed, 2024-T3 bare; plan view (a) and cross-section (b), 2024-T3 clad; (c) plan view and (d) cross-section

### 7.6.3 Physical Factors Affecting Anodic Oxides

Physical properties such as the temperature of the electrolyte and the anodizing voltage have been shown to have a marked effect on the anodic oxide film formation. For example, an increase in local temperature due to convection heat transfer enhances the field-assisted dissolution at the pore bases and results in an increase in current density. The anodizing voltage has been shown to affect most of the overall film properties such as the barrier layer thickness, cell wall thickness, pore diameter, and the overall thickness of the oxide layer. The electrolyte temperature also has an effect on these properties due to its influence over the dissolution power of the solution. Increasing the temperature produces thinner porous and barrier layers, larger pore diameters, and thinner cell walls. Reducing the temperature has the opposite effects. The alloy used also affects the oxide composition. The copper rich 2xxx series alloys adversely affect the film morphology and integrity. The oxidation of copper and the inclusion of  $\text{Cu}^{2+}$  in the anodized alumina is associated with  $\text{O}_2$  evolution which causes localized film cracking and can lead to nonuniform current flow through the film.

### 7.6.4 Alternatives to Phosphoric and Chromic Acid Anodizing

As detailed above, anodizing of aluminum and titanium alloys provides a surface that is corrosion resistant and which may be receptive to applied organic layers. Such



functionality is achieved by engineering a hydrated oxide film with controlled nanometre-scale porosity within an adherent coating measuring typically 2–3.5  $\mu\text{m}$  in thickness. The 20–30 nm diameter ( $\Phi$ ) pores created during chromic acid anodizing (CAA), for example, enable interphase formation with the organic layer giving excellent adhesion, while the oxide present provides barrier corrosion protection. There is, however, a conflict between the requirement for good corrosion resistance, which dictates a compact pore structure with thick cell walls and small diameters, and adhesion, which requires good interlocking and a large pore diameter. The former case is satisfied by the sulfuric acid anodizing (SAA)–based processes with  $\Phi \sim 5$  nm, and the latter by phosphoric acid–based processes, where  $\Phi \geq 50$  nm. The CAA process, in some respects, provides a compromise; it is, however, very widely used but for a number of reasons drop-in replacements are being sought (Critchlow et al. 2006).

One option is the use of a more benign electrolyte, such as boric-sulfuric acid. In one study on boric-sulfuric acid anodizing (BSAA), Critchlow et al. (2006) modified a standard process by varying the deoxidizing stage prior to anodizing, and introduced a post-treatment stage in order to optimize structural adhesion between a range of aluminum alloys and a single part epoxide. It was shown that BSAA could provide all of the physicochemical parameters required for excellent adhesion being capable of replacing CAA for adhesively bonded components. The conclusions from the study by Critchlow et al. (2006) were that increasing the temperature of the electrolyte from room temperature to 35 °C increased the pore diameter of the BSAA oxide film, which allowed more complete surface wetting by the adhesive/primer and maximized the pore penetration depth of the primer. This resulted in joints which replicated CAA for environmental durability and adhesion performance.

Importantly, however, duplex structures offer the advantages of a large pore diameter in the outer layers of the anodic oxide and very small pores in the inner layer close to the metal to give the optimum adhesion and corrosion performance. There are a number of methodologies which might be used to achieve a resultant duplex structure. Yendall (unpublished work) has investigated the use of an electrolytic deoxidizing process (EPAD) followed by a conventional SAA. Figure 3 shows

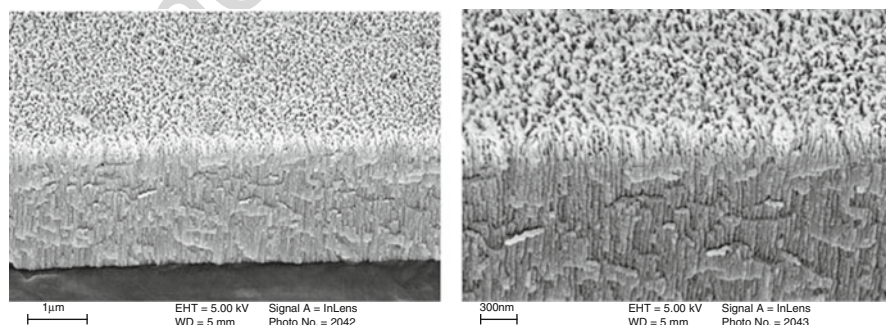


**Fig. 3** (a) Low-magnification FEGSEM image to show the through thickness duplex structure of the EPAD plus SAA oxide on clad 2024-T3 aluminum, and (b) the surface region at high magnification

the structure formed using an optimized EPAD plus SAA process. A number of process variables, for example, immersion times and temperatures plus acid electrolyte types and concentrations were considered to achieve this optimized structure. 2024-T3 clad aluminum alloy bonded with the BR127/FM73 primer/adhesive system (Cytec) exposed to 60 °C and tested using the standard wedge test configuration showed comparable results, with optimized processes, to CAA-treated controls. In contrast, the SAA only treated aluminum alloy performed very unfavorably in this test due to the lack of primer penetration; see Fig. 4. Other electrolytes have also attracted much recent attention such as the tartaric-sulfuric-based process. Although DC anodizing does provide many of the desirable features required for optimized bonding, alternating current (AC) or combined AC then DC combination processes do offer some further advantages and will be discussed in the following sections.

### 7.6.5 Alternating (AC) Current Anodizing

Apart from the obvious use of alternating current, the main difference between AC and DC anodizing is the increased porosity and ductility of AC films. The formation of the oxide is essentially the same as for direct current anodizing with the exception of the extra time during the cathodic half-cycle when extra field-assisted dissolution can take place, this being the cause of the increased porosity. Fortunately, this dissolution reaction is not as efficient as the anodic production reaction and dissipates much of the energy input by means of hydrogen evolution and heat. This results in an overall film thickening during AC anodizing. The proposed reactions for AC anodizing in a sulfuric acid electrolyte are given below [1] and [2]:

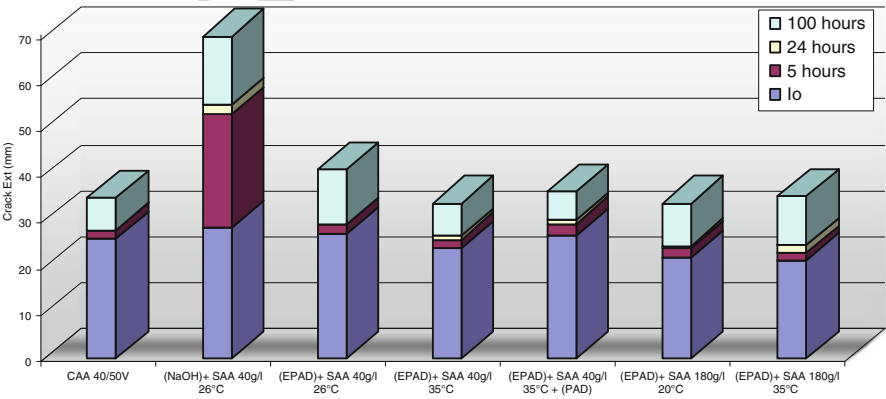
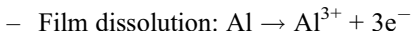


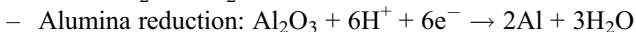
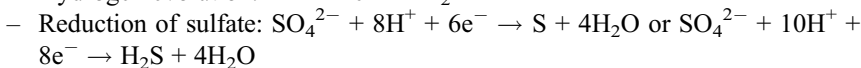
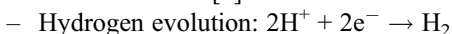
**Fig. 4** To show the results of wedge testing with clad 2024-T3 aluminum exposed to deionized water at 60 °C



• Anodic reactions [1]:



• Cathodic reactions [2]:



There is a tendency during AC anodizing for compounds from the electrolyte to be deposited within the anodic film, this can be an advantage if, for example, phosphates ions are incorporated, for reasons discussed in the following section. The oxide morphology of an AC anodized surface does not differ widely from the oxide produced using a DC counterpart when using either sulfuric or phosphoric acid electrolytes. The oxide retains the columnar porous structure with the only differences being the reduced thickness and increased pore diameter due to the extra dissolution time allowed on the cathodic part of the voltage cycle.

The overall thickness of the oxide is dependent on the electrolyte composition, but more importantly on the electrolyte temperature as this has, by far, the greatest effect in increasing the dissolution rate of the oxide. Specifically, with electrolytes comprising of sulfuric acid, there are two main processing difficulties; the discoloration of the oxide due to the deposition of sulfur compounds and the difficulty in growing a thick oxide layer without burning the surface.

AC anodizing in hot sulfuric and hot phosphoric acids gives clear advantages compared with conventional DC treatments. During the cathodic half-cycle, hydrogen evolution produces a cleaning effect of the surface of the substrates, possibly reducing or even eliminating the need for multistage degreasing and deoxidizing steps. The resultant anodic films are produced in treatment times typically in the order of 10 to 60 s. Hot AC SAA is typically conducted in an electrolyte of 15% sulfuric acid at a temperature of around 80 °C, whereas hot AC PAA has parameters of 10% acid concentration and 50 °C. The current densities for both these processes are held at 10<sup>3</sup> A/m<sup>2</sup> rms. Work by Johnsen et al. (2004) has shown AC anodizing to be comparable in mechanical performance to DC anodizing in equivalent electrolytes.

### 7.6.6 Alternating Current–Direct Current Anodizing (ACDC Anodizing)

The duplex structure created by first AC anodizing aluminum followed by a DC anodize was optimized by Cartwright (2005). Figure 5 shows the evolution of

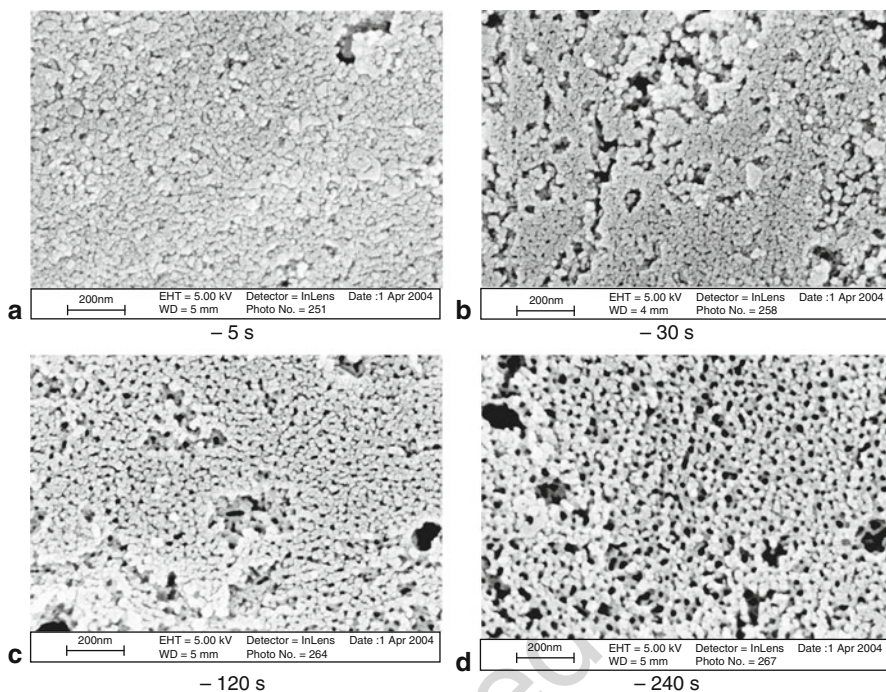
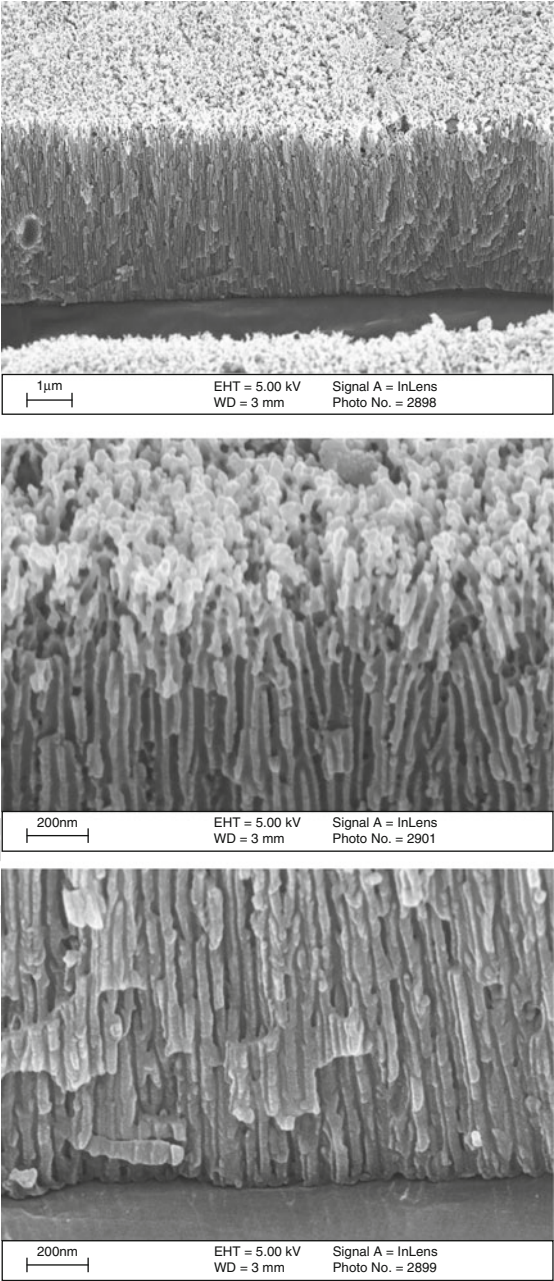


**Fig. 5 (a–d)** FEGSEM micrographs showing the development the AC anodized 2024-T3 clad aluminum alloy surface with application periods ranging from 5 to 240 s in the phosphoric/sulfuric acid electrolyte

the honeycomb-like porous oxide created by the AC phase. Figure 6 shows the fully formed optimized ACDC structure in cross-section at various magnifications. A range of tests have been conducted using 2xxx (clad and bare), 5xxx, 6xxx, and 7xxx (clad and bare) aluminum alloys. These tests include measurement of both adhesion and corrosion performance. In all cases, with all alloys, the ACDC process performed favorably compared with either SAA or CAA controls. Examples of wedge test data are presented by Cartwright (2005); see Table 6 which compares wedge test data for various ACDC parameters against the 40/450 V Bengough–Stuart CAA process. Note, however, that peel, butt, lap-shear (static exposed and fatigue) tests have also been carried out. All tests indicating comparable levels of adhesion between ACDC and CAA treated alloys (Shenoy 2009). Similarly, linear polarization and other corrosion studies have shown that the ACDC process gives comparable corrosion resistance to the CAA. Importantly, the ACDC process is carried out in a weak acid electrolyte with only a 5% total acid content and containing no hexavalent chromium. Furthermore, the total processing time for ACDC is approximately one tenth of that required to anodize to the standard CAA specification. These advantages make the ACDC anodizing process of industrial interest (Cartwright 2005).

**Fig. 6** FEGSEM images to show the structure of optimized ACDC oxides on clad 2024-T3 clad aluminum. Top image shows the through thickness, middle image the outer oxide, bottom image the inner oxide



t.1 **Table 6** Wedge crack length data to show the influence of varying the AC anodizing parameters and electrolyte temperature for the ACDC process; note a 10 m, 20 V DC process has been deposited beneath each AC film (Cartwright 2005)

t.2	AC anodizing parameters	Exposure time (h)							
t.3			1	4	8	24	48	72	96
t.4	10 V 120 s 35 °C	Mean crack length (mm)	33.25	33.25	33.25	35.00	35.38	35.50	35.50
t.5		Σ	0.82	0.82	0.82	0.74	0.75	0.54	0.54
t.6	10 V 120 s 50 °C	Mean crack length (mm)	31.33	31.50	31.58	32.83	33.33	33.33	33.33
t.7		Σ	0.37	0.41	0.45	1.07	1.18	1.18	1.18
t.8	10 V 240 s 35 °C	Mean crack length (mm)	31.33	31.42	31.42	33.00	33.33	33.42	33.42
t.9		Σ	0.56	0.69	0.69	0.79	0.95	0.99	0.99
t.10	10 V 240 s 50 °C	Mean crack length (mm)	33.50	33.67	33.67	34.50	34.83	35.25	35.42
t.11		Σ	0.19	0.25	0.25	0.84	0.45	0.69	0.91
t.12	15 V 120 s 35 °C	Mean crack length (mm)	31.33	31.67	32.25	33.08	33.25	33.25	33.25
t.13		Σ	0.82	1.25	2.07	1.65	1.57	1.57	1.57
t.14	15 V 240 s 35 °C	Mean crack length (mm)	31.92	32.17	32.58	33.58	34.08	34.25	34.92
t.15		Σ	0.29	0.56	0.75	1.11	0.90	1.11	1.41
t.16	40/50 V CAA	Mean crack length (mm)	31.50	33.10	33.35	33.90	34.45	34.45	34.45
t.17		Σ	0.95	1.09	0.84	1.37	1.90	1.90	1.90

965 **7.7 Conclusions**

966 A large range of processes exist which might be used to modify the surface of  
967 adherends prior to the application of an adhesive. All such treatments modify the  
968 surface physical and chemical properties to one degree or another. Important surface  
969 properties which might be modified include: wettability, roughness, mechanical, and  
970 electrochemical stability. The last point is particularly significant if joints are to  
971 experience environmental ageing under corrosive conditions.

972 The requirements of a particular treatment depends upon the demands put upon  
973 the joint; a simple degrease operation may suffice, and, alternatively, a more  
974 complex process may be required with well-defined surface topography and chem-  
975 istry to meet the demands of structural bonding.

976 Importantly, legislative drivers intended to reduce operator health and safety risks  
977 or environmental impact are currently in place which promote the need for more  
978 acceptable surface treatments such that the range of options available today may be  
979 reduced in the near future. Extensive efforts are, of course, ongoing to help develop

drop-in replacements particularly for the high-performance chromate-containing treatments. A number of drop-in replacements do, however, exist today which provide all of the functionality of the chromate-containing treatments and are likely to see further industrial usage.

## References

- Allen K, Allen HS et al (1972) Faraday special discussion. Chemical Society, London, p 38
- Anderson G (1993) *J Adhes* 41:129
- Ansanfar A, Critchlow G et al (2009) *Rubber Chem Technol* 82(1):113
- Asundi A (1987) *Int J Adhes Adhes* 7(1):39
- Averill A, Ingram J et al (1998) *Trans Inst Met Finish* 76(3):81
- Bedwell K, Critchlow G et al (1998) *Trans Inst Met Finish* 76(5):203
- Bishopp J, Kim E et al (1988) *J Adhes* 26:237
- Bistac S, Vallat M et al (1997) *Appl Spectrosc* 51(12):1823
- Brewis D (1982) Surface analysis and pretreatment of plastics and metals. Applied Science Publishers, London
- Brewis D, Briggs D (eds) (1985) Industrial adhesion problems. Orbital Press, Oxford
- Brewis D, Mathieson I (2001) Adhesive bonding to polyolefins. *RAPRA Rev Report* 12(11)
- Brewis D et al (1995) *Int J Adhes Adhes* 15:87
- Brewis D et al (1999) *Int J Adhes Adhes* 19:253
- Cartwright T (2005) PhD thesis, Loughborough University
- Charbonnier M, Romand M et al (2001) *J Adhes* 75:381
- Critchlow G, Brewis D (1995a) *Int J Adhes Adhes* 15(3):161
- Critchlow G, Brewis D (1995b) *Int J Adhes Adhes* 15(3):173
- Critchlow G, Brewis D (1996) *Int J Adhes Adhes* 16(4):255
- Critchlow G, Brewis D (1997) *J Adhes* 61:213
- Critchlow G, Cottam C et al (1997) *Int J Adhes Adhes* 17:143
- Critchlow G, Webb P et al (2000) *Int J Adhes Adhes* 20:113
- Critchlow G, Yendall K et al (2006) *Int J Adhes Adhes* 26:419
- Dahm R, Brewis D et al (2005) *J Adhes* 81:59
- Debski M, Shanahan M et al (1986) *Int J Adhes Adhes* 6(3):145
- Deffeyes J, Lilenfield H et al (1997) *SAMPE J* 33(1):58
- Fondeur F, Koenig J (1993) *J Adhes* 43:236
- Gaillard F, Romand M et al (1994) *J Adhes* 46:227
- Hong S, Boeno F (1995) *J Adhes* 49:133
- Johnsen B, Lapique F et al (2004) *Int J Adhes Adhes* 24:153
- Kollek H (1985) *Int J Adhes Adhes* 5:75
- Litchfield R, Critchlow G et al (2006) *Int J Adhes Adhes* 25(5):295
- Lu Y-F, Aoyage Y (1994) *Jpn J Appl Phys* 33(2B):430
- Maddison A, Critchlow G (1996) *J Adhes* 55:273
- McNamara D, Venables J et al (1979) In: Proceedings of the national SAMPE conference, p 740
- Minford J (1981) *Aluminium* 57(10):657
- Minford J (1993) Handbook of aluminum bonding. CRC Press, Boca Raton
- Nigro J, Ishider H (1989) *J Appl Polym Sci* 38:2191
- Olsson-Jacques C, Wilson A et al (1996) *Surf Interface Anal* 24:569
- Packham D (2010) *J Adhes* 86:1231
- Packham D, Bright K et al (1974a) *J Appl Polym Sci* 18:3237
- Packham D, Bright K et al (1974b) *J Appl Polym Sci* 18:3249
- Possart W (ed) (2005) Adhesion: current research and applications. Wiley, Weinheim

- 1028 Rance D (1985) Thermodynamic approach to adhesion problems. In: Brewis D (ed) Industrial  
1029 adhesion problems. Orbital Press, Oxford
- 1030 Rider A, Arnott D (2001) *J Adhes* 75:203
- 1031 Roche A, Bouchet J et al (2002) *Int J Adhes Adhes* 22:431
- 1032 Roche A, Aufrey A et al (2006) *J Adhes* 82(9):867
- 1033 Safavi-Ardebili V, Sinclair A et al (1997) *J Adhes* 62:93
- 1034 Sargent J, Ashbee M (1985) *J Adhes* 18(3):217
- 1035 Schram T, Goeminne G et al (1995) *Trans Inst Met Finish* 73(3):91
- 1036 Shanahan M (2005) In: Packham D (ed) *Handbook of adhesion*, 2nd edn. New York, Wiley
- 1037 Sharpe L (1972) *J Adhes* 4:51
- 1038 Shenoy V (2009) PhD thesis, Loughborough University
- 1039 Smith T, Crane R (1980) In: *Proceedings of the national SAMPE symposium*, p 25
- 1040 Smith B, Brewis D et al (2000) *Trans Inst Met Finish* 78(2):56
- 1041 Stewart R, Goodship V et al (2005) *Int J Adhes Adhes* 25:93
- 1042 Stone M (1981) *Int J Adhes Adhes* 5(1):271
- 1043 Strobel M et al (eds) (1994) *Plasma surface modification: relevance to adhesion*. VSP, Utrecht
- 1044 Tavakoli S (1994) *Assem Autom* 14(4):36
- 1045 Tu W, Pihua W et al (2010) In: *Proceedings of the world congress on engineering*, London
- 1046 Underhill P, Rider A (2005) *Surf Coat Technol* 192:199

Guy D. Davis

## Contents

8.1	Introduction: Requirements of Surface Treatments .....	164
8.1.1	Surface Pretreatment Steps .....	165
8.1.2	Degradation Processes .....	167
8.1.3	Processability Issues .....	173
8.2	Specific Metal Treatments .....	174
8.2.1	Aluminum .....	174
8.2.2	Titanium .....	181
8.2.3	Steel .....	184
8.3	Other Materials .....	188
8.3.1	Composites .....	188
8.3.2	Plastics .....	189
8.3.3	Ceramics .....	190
8.3.4	Wood .....	191
8.4	Conclusions .....	192
References	.....	193

## Abstract

Proper treatment of an adherend surface is one of the most important factors in assuring high initial strength and extended durability of high-performance adhesive joints. There are several requirements for a good surface preparation: (1) The surface must be cleaned of any contamination or loosely bound material that would interfere with the adhesive bond. (2) The adhesive or primer must wet the adherend surface. (3) The surface preparation must enable and promote the formation of chemical and/or physical bonds across the adherend/primer–adhesive interface. (4) The interface/interphase must be stable under the service conditions for the lifetime of the bonded structure. (5) The surface formed by the treatment must be reproducible.

G. D. Davis (✉)  
ElectraWatch, Inc., Linthicum Heights, MD, USA  
e-mail: [gddaccosci@aol.com](mailto:gddaccosci@aol.com); [guyddavis@verizon.net](mailto:guyddavis@verizon.net)



In this chapter, high-performance surface treatments for several metals and other materials are discussed. Surface treatments of aluminum and other metals are used to illustrate how proper surface preparations meet these requirements.

## 8.1 Introduction: Requirements of Surface Treatments

Proper treatment of an adherend surface is one of the most important factors in assuring high initial strength and extended durability of high-performance adhesive joints (Landrock 1985; Kinloch 1987; Clearfield et al. 1990; Minford 1993; Pocius 1997; Chaudhury and Pocius 2002; Davis 2003). Surface general principles, treatments, and assessments are treated in ► Chaps. 7, “General Introduction to Surface Treatments,” ► 9, “Surface Characterization and Its Role in Adhesion Science and Technology,” and ► 10, “Use of Surface Analysis Methods to Probe the Interfacial Chemistry of Adhesion” respectively. In the present chapter, surface treatments of selected materials are given.

In the case of a structural bond, a strong adhesive is of little value unless the stresses can be transferred via the adhesive from one adherend to the other. The interface or interphase (a three-dimensional interfacial region with properties different from those of either material) between the adhesive and the adherend is critical to this stress transfer. The goal of a surface treatment is to form a strong and stable interface or interphase that is stronger and more durable than the adhesive being used so that joint failure is cohesive within the adhesive, both initially and throughout the joint’s service lifetime.

There are several requirements for a good surface preparation: (1) The surface must be cleaned of any contamination or loosely bound material that would interfere with the adhesive bond. (2) The adhesive or primer must wet the adherend surface. (3) The surface preparation must enable and promote the formation of bonds across the adherend/primer–adhesive interface. These bonds may be chemical (covalent, acid–base, van der Waals, hydrogen, etc.) or physical (mechanical interlocking) in nature. (4) The interface/interphase must be stable under the service conditions for the lifetime of the bonded structure. A stable interface/interphase is critical for structures expected to be in service for a long time, e.g., aircraft, but is less critical for structures whose lifetime is expected to be short, e.g., some packaging, or if the bond will be protected from the environment over its lifetime. (5) The surface formed by the treatment must be reproducible. Reproducibility requires that the prepared surface be independent of material variables, such as surface contamination, mill scale, and, ideally, even alloy or heat treatment. Reproducibility is facilitated if the treatment has wide processing windows so that processing variables, such as pH, solution contamination, solution chemistry, temperature, and time, do not have to be narrowly controlled. The robustness provided by the wide processing windows increases reliability and decreases costs associated with stringent process controls and parts scrapped due to out-of-specification processing.

Different industries assign different roles to surface preparation. The aerospace industry, with relatively low throughput, but long expected lifetime (several decades), carefully prepares the surface prior to bonding during original manufacture



and repair to assure the best practical durability. The automotive industry, with high throughput, prefers almost no surface preparation and uses contamination-tolerant adhesives and overdesign of joints. The construction industry follows a similar approach. The packaging industry, with very high throughput but relatively low requirements for stress and durability, also minimizes surface preparation by using relatively pure aluminum that reportedly can be more easily wetted and bonded by adhesives. This chapter will focus on surface treatments used for high-performance bonds, primarily in the aerospace industry.

### 8.1.1 Surface Pretreatment Steps

Cleaning the surface of undesirable organic and inorganic material is the first step in preparing an adherend for bonding. The organic contamination originates from rolling oils at the mill, oils and greases applied for corrosion protection, machining oils and release agents used during fabrication, and contamination from the atmosphere. Unless the adhesive is specifically designed to absorb this material, such contamination will prevent wetting and formation of strong bonds across the interface and the joint will perform poorly.

The amount of acceptable contamination varies and can be very small. Silicones and other mold-release agents are designed to be very effective at preventing adhesives and primers from wetting the surface. Even small amounts can cause bond failure. Aluminum surfaces with one third to one molecular layer of silicone will not bond well. Unfortunately, silicones are very mobile and can readily migrate during solvent cleaning, transfer from tooling or handling, or diffuse during curing operations at elevated temperatures. Silicones and silicone-containing materials, such as certain pressure-sensitive adhesive tapes and mold-release agents, need to be carefully marked and kept away from bonding operations.

The sensitivity of a system to contamination depends on many factors. Rubbers are more tolerant of contamination than epoxies. Rougher surfaces can be more tolerant than smoother surfaces. In general, waterborne or high-solid adhesives and primers are more sensitive to organic surface contamination than solvent-borne materials. Thus, contamination may become a greater issue as environmentally acceptable adhesives and coatings are introduced. This is illustrated in Fig. 1, which shows the solvent-borne system to be very tolerant of grease, while the aqueous system is more sensitive. The type of contamination is also important as illustrated in Fig. 2, which shows that some contamination will cause the rubber-steel peel strength to decrease by 50% at levels less than  $1 \mu\text{g}/\text{cm}^2$  while others require more than  $100 \mu\text{g}/\text{cm}^2$  or even enhance the bond strength. Because one must always assume the contamination to be detrimental, the first step in an adherend preparation process is usually a degreasing step. Traditionally this was done with chlorinated solvents, but regulations have required substitution of more environmentally acceptable cleaners.

In addition to organic contamination, most as-received metal alloys have a thick oxide/hydroxide film formed during heat treatment, fabrication, and other processing.

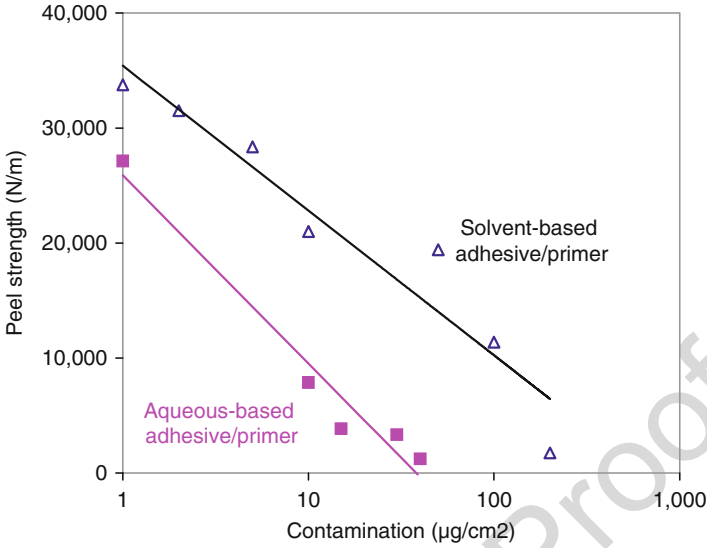


**Fig. 1** Peel strength of nitrile butadiene rubber (NBR) as a function of grease contamination level on grit-blasted steel using a solvent-borne primer/adhesive and an aqueous primer/adhesive

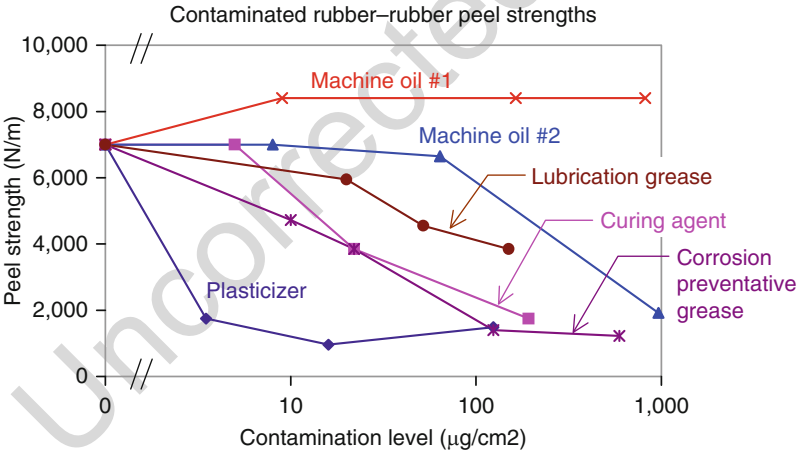


**Fig. 2** The effect of surface contamination on the peel strength of rubber-steel bonds (Adapted from Davis 1993)

The coating's composition, morphology, thickness, and mechanical properties will vary from fabricator to fabricator and from lot to lot. In the case of aluminum alloys containing magnesium, such as the 5000, 6000, and 7000 series alloys, the mill scale can be all or mostly MgO because of the high mobility of Mg in the alloy and its preferential oxidation when exposed to the atmosphere at high temperatures. In copper-containing alloys, such as the 2000 and 7000 series, there often is a buildup

of copper at the oxide/metal interface as aluminum is preferentially oxidized. This copper can serve to promote corrosion via galvanic coupling with the aluminum and reduce bond durability. The effect of magnesium is less clear and differences in surface morphology and other variables may have played a role in conflicting results. To assure reproducible bonding surfaces, the second step in treatment process is generally a deoxidizing step so that oxidizing or coating process begins with bare metal (or a thin native oxide).

The final step in providing an acceptable bonding surface is to grow or deposit an oxide or other surface film designed to promote good, stable bonds with the primer or adhesive. As mentioned earlier, the bonding can be either chemical or physical. Durable covalent chemical bonding across the interface can be achieved with phenolic adhesives, but not the more common epoxy adhesive without the use of coupling agents or sol-gel films. In the other cases, suitable surface morphology to promote physical bonding (mechanical interlocking) is critical. This is discussed below.

### 8.1.2 Degradation Processes

For most structural joints using epoxy adhesives and metallic adherends, secondary or dispersive bonds are the only ones formed across the interface. Because metal oxide surfaces are polar, they attract water molecules that can disrupt these dispersive bonds across the interface. This disruption can be seen thermodynamically by the work of adhesion in an inert medium,  $W_A$ , which can be represented as (Kinloch 1987)

$$W_A = \gamma_a + \gamma_s - \gamma_{as} \quad (1)$$

where  $\gamma_a$  and  $\gamma_s$  are the interfacial free energies of the adhesive and substrate, respectively, and  $\gamma_{as}$  is the surface free energy. In the presence of a liquid such as water, the work of adhesion  $W_{A1}$  becomes

$$W_{A1} = \gamma_{a1} + \gamma_{s1} - \gamma_{as} \quad (2)$$

where  $\gamma_{a1}$  and  $\gamma_{s1}$  are now the interfacial free energies of the adhesive/liquid and substrate/liquid interfaces, respectively. In an inert environment, the work of adhesion for a bonded system will be positive, indicating a stable interface, whereas in the presence of water, the work of adhesion may become negative, indicating an unstable interface that may dissociate. Table 1 shows, in fact, that moisture will displace epoxy adhesives from iron (steel) and aluminum substrates and promote disbonding (Kinloch 1987). In contrast, although moisture weakens epoxy/carbon fibers bonds, these remain thermodynamically stable. Experience with both metal and composite joints confirms these predictions.

The data presented in Table 1 illustrate the potential disastrous results when relying solely on dispersive bonds across the interface between an epoxy adhesive

**Table 1** Work of adhesion for various interfaces (Kinloch 1987)

Interface	Work of adhesion (mJ/m <sup>2</sup> )		Interfacial debonding after immersion
	In inert medium	In water	
Epoxy/ferric oxide	291	−255	Yes
Epoxy/alumina	232	−137	Yes
Epoxy/carbon fiber	88–90	22–44	No

and metals or ceramics. Even though good initial bond strengths may be obtained with cohesive failure (within the adhesive), bond durability in the presence of moisture is likely to be poor with interfacial failure. To illustrate this danger, demonstration specimens can be produced that exhibit good initial strength, but fall apart under their own weight when a drop of water is placed at the crack tip.

Because moisture will break the dispersive interfacial bonds, mechanical interlocking on a micro- or nanoscopic scale is needed between the adhesive/primer and adherend for good durability. In these cases, even if moisture disrupts interfacial chemical bonds, a crack cannot follow the convoluted interface between the polymer and oxide and the joint remains intact unless this interface or the polymer itself is destroyed. In addition, the micro- or nanocomposite interphase formed with the polymer and oxide allows a gradient of mechanical properties between the adhesive and the metal so that there is less buildup of interfacial stresses.

The scale of the microscopic surface roughness is important to assure good mechanical interlocking and good durability. Although all roughness serves to increase the effective surface area of the adherend and, therefore, to increase the number of primary and secondary bonds with the adhesive/primer, surfaces with features on the order of tens of nanometers exhibit superior performance to those with features on the order of microns. Several factors contribute to this difference in performance. The larger-scale features are fewer in number for a given area and generally are smoother (even on a relative scale) so that interlocking is less effective. Depending on the particular treatment used, there may also be loosely bound material that prevents bonding to the integral adherend surface. In addition, the larger-scale roughness frequently allows trapped air and surface contaminants to remain in the microscale valleys. These unbonded regions limit joint performance by reducing both chemical and physical bonds and serving as stress concentrators. In contrast, smaller-scale micro- or nanoroughness tends to be more convoluted in morphology and generates strong capillary forces as the primer wets the surface, drawing the polymer into all the “nooks and crannies” of the oxide and displacing trapped air and some contaminants to form a micro- or nanocomposite interphase. Indeed, cross-sectional micrographs show complete filling of the nanopores (Venables 1984; Clearfield et al. 1990).

This dependence on the degree and scale of roughness is illustrated in Fig. 3, which shows wedge test results of titanium bonds with several surface preparations (Brown 1982). Because the titanium surface is stable under these conditions, differences in the joint performance can be attributed solely to differences in the polymer-to-oxide bonds and correlate very well with adherend roughness. The poorest

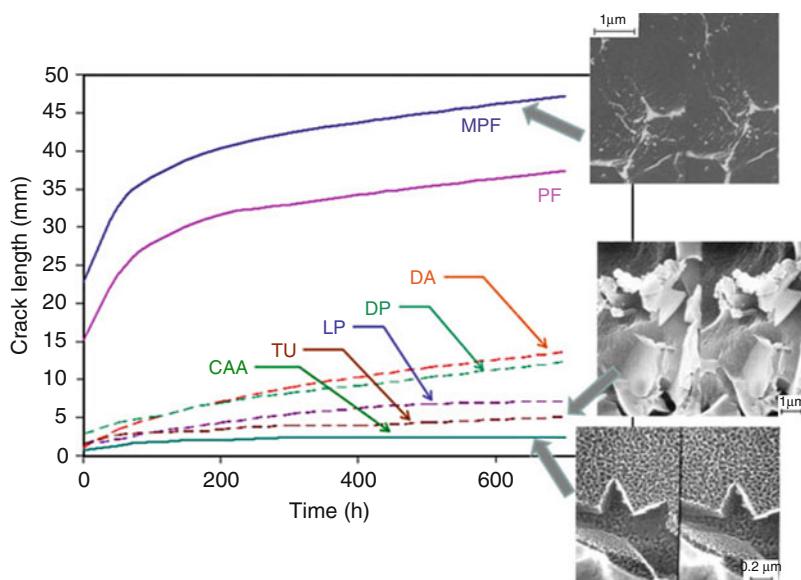


**Fig. 3** Wedge test results for Ti adherends with several different surface treatments having differing degrees and scales of roughness. Also shown are micrographs of selected specimens showing improved bond performance with increasing micro- or nanoroughness. Specimens were exposed to 100% relative humidity at 60 °C. Treatment key: phosphate fluoride (PF), modified phosphate fluoride (MPF), Dapcotreat (DA), dry hone Pasa Jell (DP), liquid hone Pasa Jell (LP), Turco (TU), and chromic acid anodization (CAA) (Wedge test data are from Brown (1982))

performing group of pretreatments (Class I: phosphate fluoride [PF] and modified phosphate fluoride [MPF]) produced relatively smooth surfaces. The intermediate group (Class II: Dapcotreat [DA], dry hone Pasa Jell [DP], liquid hone Pasa Jell [LP], and Turco [TU]) exhibited macrorough surfaces with little microroughness. They had significant improvements in durability over the smooth adherends, but not as good as the Class III pretreatment (chromic acid anodization [CAA]), which provided a much evolved nanoroughness. Because of the importance of nanoscale roughness, high-quality micrographs with magnifications in the order of 50,000X are critical in evaluating surface morphology.

Once high-quality physical bonds are formed across the interface, the interphase will not fail unless the polymer disengages from oxide or the interphase degrades in some manner to break the interlocking or allow crack growth through the oxide or at the oxide/metal interphase. The mechanism of degradation will depend on the adherend material and the exposure conditions. For aluminum adherends, moisture causes hydration of the surface, i.e., the  $\text{Al}_2\text{O}_3$  that is formed during the surface treatment is transformed into the oxyhydroxide  $\text{AlOOH}$  (boehmite) or trihydroxide  $\text{Al}(\text{OH})_3$  (bayerite) (Davis et al. 1982; Venables 1984). The transformation to the hydroxide leads in an expansion of the interphase (the volume occupied by the hydroxide is larger than that originally occupied by the  $\text{Al}_2\text{O}_3$ ). This expansion and the corresponding change in surface morphology and structure induce high stresses

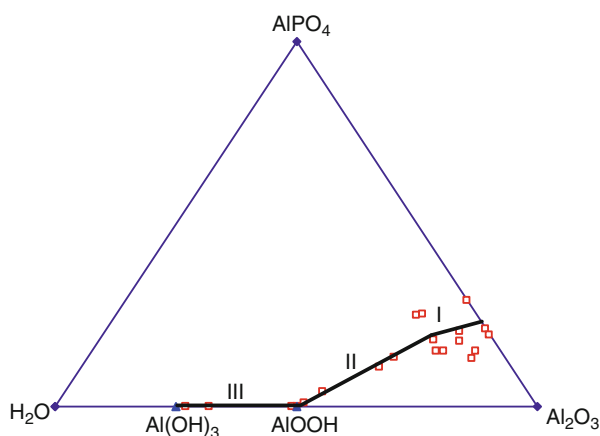
at the bondline. These stresses coupled with the poor mechanical strength of the hydroxide, promote crack propagation near the hydroxide/metal interface.

The rate of hydration of the aluminum oxide depends on a number of factors, including surface chemistry (treatment), presence of hydration/corrosion inhibitors in the primer or applied to the surface, temperature, and the amount of moisture present at the surface or interface. One surface treatment that provides an oxide coating that is inherently hydration resistant is phosphoric acid anodization (PAA). Its stability is due to a monolayer of phosphate incorporated into the outer  $\text{Al}_2\text{O}_3$  surface during anodization; only when this phosphate layer goes into solution does the underlying  $\text{Al}_2\text{O}_3$  hydrate to  $\text{AlOOH}$ . The hydration process is illustrated in the surface behavior diagram of Fig. 4 (Davis et al. 1982; Davis 1986). It shows hydration to occur in three stages: (1) a reversible adsorption of water, (2) slow dissolution of the phosphate layer followed by rapid hydration of the freshly exposed  $\text{Al}_2\text{O}_3$  to  $\text{AlOOH}$ , and (3) further hydration of  $\text{AlOOH}$  to  $\text{Al}(\text{OH})_3$ .

Although the evolution of surface chemistry depicts the hydration of bare surfaces, the same process occurs for buried interfaces within an adhesive bond. This was first demonstrated by using electrochemical impedance spectroscopy (EIS) on an adhesive-covered Forest Products Laboratory (FPL, a sodium dichromate + sulfuric acid etch) aluminum adherend immersed in hot water for several months (Davis et al. 1995b). EIS, which is commonly used to study paint degradation and substrate corrosion, showed absorption of moisture by the epoxy adhesive and subsequent hydration of the underlying aluminum oxide after 100 days (Fig. 5). At the end of the experiment, aluminum hydroxide had erupted through the adhesive. Later, cross-section micrographs of bonded tapered double-cantilever beam specimens cyclically loaded during immersion in water revealed the very early stages of hydration (prior to substantial changes in the oxide morphology and volume) in advance of the crack tip (Kinloch et al. 2000). Similar early stages of hydration have also been seen using high-frequency dielectric spectroscopy (Affrossman et al. 2000).

Subsequent investigations proved that identical hydration reactions occur on bare aluminum surfaces and bonded surfaces, but at very different rates of hydration

**Fig. 4** Surface behavior diagram showing hydration of the phosphoric acid anodized (PAA) aluminum surface. Hydration occurs in three stages: I. Reversible adsorption of moisture; II. hydration of the  $\text{Al}_2\text{O}_3$  to  $\text{AlOOH}$ ; and III. further hydration to  $\text{Al}(\text{OH})_3$  (Data are from Davis et al. (1982) and Davis (1986))



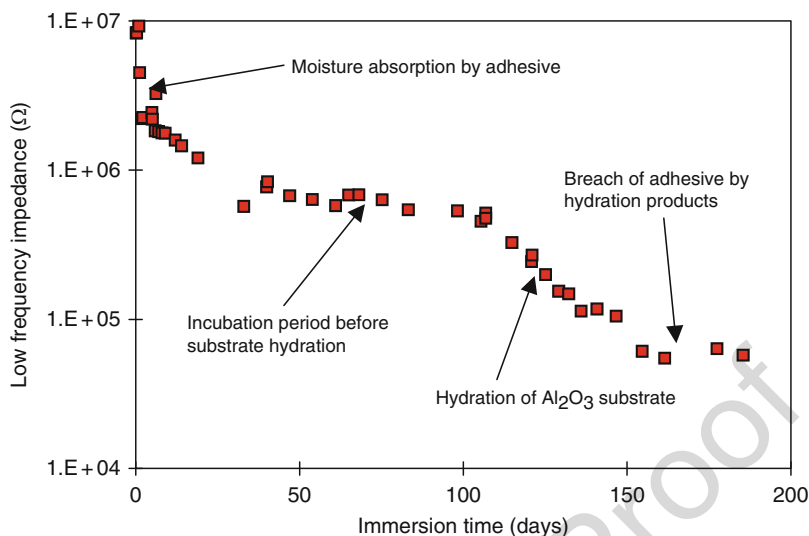


**Fig. 5** Low-frequency electrochemical impedance of an epoxy-coated Forest Products Laboratory (FPL)-etched aluminum adherend as a function of immersion time in 50 °C water (Adapted from Davis et al. (1995b))

(Davis et al. 2000). An Arrhenius plot of incubation times,  $t_i$ , prior to hydration of bare and buried FPL surfaces, for the equation

$$\frac{1}{t_i} \propto k = Ae^{-E_a/RT}, \quad (3)$$

where  $R$  is the universal gas constant and  $T$  is the absolute temperature in Kelvin, showed that the hydration process exhibits the same energy of activation,  $E_a$ , ( $\sim 82$  kJ/mole) regardless of the bare or covered nature of the surface (Fig. 6). On the other hand, the pre-exponential factor,  $A$ , and the rate of hydration vary dramatically, depending on the concentration of moisture at the oxide interface/surface available to react. The epoxy-covered surfaces have incubation times (and rate constants,  $k$ ) three to four orders of magnitude longer than bare, immersed specimens, reflecting the limited amount of moisture absorbed by the epoxy and free to react with the oxide.

The slow rate of hydration for buried surfaces is good from a service point of view, but makes the study and evaluation of the durability of surface treatments difficult unless wedge tests (ASTM D3762) or similar tests are used to accelerate the degradation. The stress at the crack tip of a wedge test specimen, together with the presence of moisture at the tip, serves to make this test specimen more severe than soaked lap-shear specimens or similar types for which moisture must diffuse from an edge and is only present at the interface in relatively low concentrations. As a result, the wedge test is a better laboratory evaluation of relative durability. Furthermore, from a production perspective, Boeing has correlated the results of wedge tests from

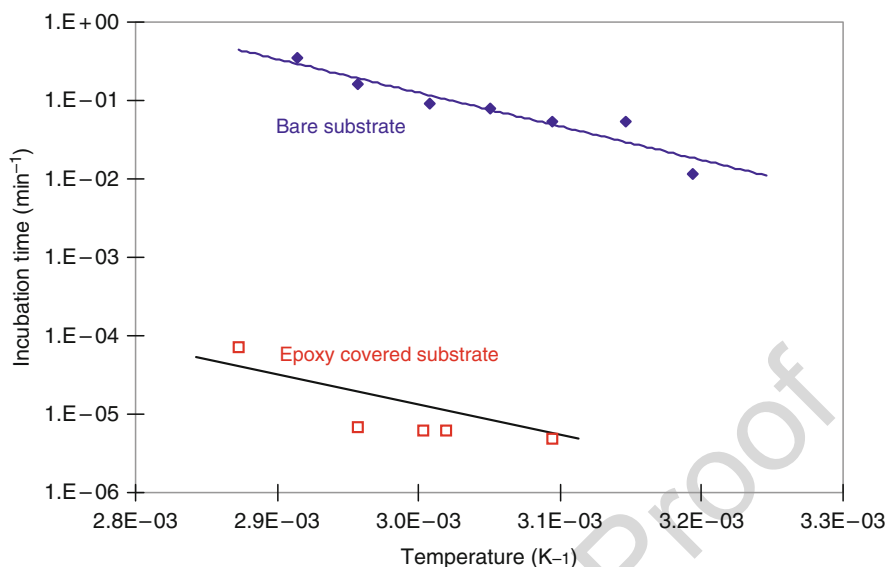


**Fig. 6** Arrhenius plot of incubation times prior to hydration of Forest Products Laboratory (FPL)-etched aluminum under various conditions (Adapted from Davis et al. (2000) with additional data)

actual aircraft components with their in-service durability (Marceau and Thrall 1985). Specimens fabricated from aircraft components that had exhibited service disbonds showed significant crack growth during the first hour of exposure whereas those fabricated from good components showed no crack growth during this time period. In contrast, lap-shear specimens and porta shear specimens all demonstrated high bond strengths regardless of the service conditions. Wedge tests can be used as a quick quality control test in the production facility (crack length after 1 h must be below a given value) or the laboratory to study long-term stability of a surface/interface. In principle, lap shear or similar tests can also be used to obtain the same information. However, the time for moisture to diffuse into these specimens and for the specimens to come into equilibrium with the test environment is so long that most investigators stop the test before useful durability information is obtained.

Unlike aluminum, titanium adherends are stable under conditions of moderately elevated temperatures and humidity. In the wedge test results of Fig. 3, the adherend surfaces underwent no change in morphology. Failure of the CAA specimens remained within the adhesive, with the physical bonds provided by the microscopically rough oxide remaining intact. For moderate conditions, the key requirement for a titanium treatment is a convoluted nanorough surface to promote physical bonding.

At elevated temperatures where titanium alloys would be the adherend of choice, a different failure mechanism becomes important. Because the solubility of oxygen in titanium increases with temperature, the oxygen in a CAA or other oxide dissolves into the metal, leaving voids or microcracks at the metal-oxide interface and embrittles the surface region of the metal. Consequently, stresses are concentrated at small areas at



the interface and the joint fails at low stress levels. Such phenomena have been observed for adherends exposed to 600 °C for as little as 1 h or 300 °C for 710 h prior to bonding (Clearfield et al. 1989) and for bonds using a high-temperature adhesive cured at elevated temperatures. To prevent this failure mode, thick oxides, such as those grown by CAA, should be avoided in high-temperature applications.

### 8.1.3 Processibility Issues

For a surface treatment process to be practical, not only does it have to produce a clean, stable surface suitable for bonding to the primer/adhesive, but it must be able to do this reliably in a production environment. An important aspect of processibility is the acceptable windows for the different process variables. That is, how much can a parameter vary from its nominal value before the performance of the bonded structure is compromised and degraded? The narrower the acceptable window, the tighter the processing controls must be. Tight controls, in turn, are associated with high cost for implementation of the controls, the inspection of the part or processing variable, and the waste from out-of-specification parts that must be reprocessed or discarded. In contrast, a robust process will have wide processing windows so that the prepared surface will still be acceptable despite the inevitable processing discrepancies that occur.

The critical processing parameters (those which must be controlled most closely) will depend on the specific process, the material, and the performance requirements. Typical parameters include solution composition/concentration, pH, temperature, and contamination of cleaning, deoxidizing, etching/anodization/deposition, and rinsing solutions, time of each step and time between each step, anodization voltage and current, ambient temperature and humidity, and airborne contamination.

An example of process controls is the acidification of rinse water baths following FPL or other chromic acid etches (CAE). Due to the nature of the processing, some etch solution drag-out is inevitable as parts are transferred from the etch bath to the rinse bath. In such cases, the pH of the rinse bath in the vicinity of the aluminum surfaces can be quite low. If low pH rinse water is allowed to dry on the oxide, the surface may become sufficiently acidic to react with the amine-curing agents that typically are in epoxy primers, leading to an undercured epoxy at the oxide interface (McNamara et al. 1983). Similar surfaces bonding with a partially cured (b-staged) film adhesive do not suffer bonding problems, presumably because the curing agent in these films is not sufficiently mobile to diffuse to the interface and be neutralized. Because the acidic residue cannot usually be detected on the surface during production, a two-step rinse after etching/anodizing is recommended.

Because of the critical nature of adhesive bonds in the aerospace industry, among others, it is essential to inspect the process to assure quality. This inspection can involve monitoring the critical process parameters, testing of witness specimens prepared at the same time as the structure, or evaluating the surface to be bonded. The best surface to inspect is the actual surface to be bonded, but techniques available for inspection are limited. Witness specimens allow a broad range of

techniques, including those requiring small sizes, vacuum, or highly trained personnel. They also allow bonding and destructive testing.

The most common inspection of actual bonding surfaces is the water-break test. Water, being a polar molecule, will wet a high-energy surface, such as a clean metal oxide, but will not wet a low-energy surface, such as most organic materials and will “bead up.” As a part is removed from a rinse bath or spray, if the water flows uniformly over the entire surface, the surface is clean. However, if the water beads up or does not wet an area, that area likely has an organic contaminant that must be cleaned.

A separate set of processability issues involves health, safety, and environmental concerns. Ozone-depleting compounds (ODCs), such as trichloroethane and trichloroethylene, have been banned. Hexachromium is a carcinogenic toxin and is heavily regulated. Disposal is becoming increasingly difficult and expensive. Other materials are either strong acids or strong bases and require appropriate safety precautions. As a result, considerable research has aimed at developing more environmentally acceptable and less hazardous processes. These will be discussed below along with the more conventional treatments.

---

## 8.2 Specific Metal Treatments

In this section, the most common or promising new treatments for aluminum, titanium, and steel are discussed. For more details, the reader is referred to books such as Wegman (1989), Cagle (1973), and Minford (1993) and review articles such as Crithlow et al. (2006) for comprehensive descriptions of the most relevant processes.

### 8.2.1 Aluminum

Aluminum surfaces are most commonly prepared for adhesive bonding in aerospace applications either by etching or anodization in acid solutions. (For less stringent strength and durability requirements, mechanical abrasion can be adequate.) Common preparations result in nanorough adherend morphologies, which studies have shown yield the best overall bond durability. The two widely used treatments are phosphoric acid anodization (PAA) and chromic acid anodization (CAA). Other treatments include Forest Products Laboratory (FPL) etch, or similar chromic acid etches (CAE), P2 etch, and the boric acid/sulfuric acid anodization (BSAA). These treatments are summarized in Table 2. In addition, sol-gel or grit blasting/silane coupling agent treatments are showing promise as environmentally acceptable processes that can be used for repair.

#### Anodization

Phosphoric acid anodization was developed by Boeing to improve the performance of bonded primary structures. Bonds formed with PAA-treated adherends exhibit

t.1 **Table 2** Selected surface treatments for aluminum adherends

t.2	Process	Solution	Process parameters
t.3	PAA	$\text{H}_3\text{PO}_4$	20–25 °C, 25 min, 10 V
t.4	CAA	$\text{H}_2\text{CrO}_4$	32–38 °C, 8 V/min to 40 V, hold 55 min
t.5	BSAA	$\text{H}_2\text{SO}_4 + \text{B}_2\text{O}_3 + \text{H}_2\text{O}$	25–30 °C, ramp to 15 V, hold 20–25 min
t.6	FPL	$\text{Na}_2\text{CrO}_7 \cdot 2\text{H}_2\text{O} + \text{H}_2\text{SO}_4 + \text{H}_2\text{O}$	68 °C, 15–30 min
t.7	P2	$\text{FeSO}_4 + \text{H}_2\text{SO}_4 + \text{H}_2\text{O}$	60–70 °C, 8–15 min

superior durability during exposure to humid environments compared to those formed with FPL-treated adherends, especially when epoxy adhesives are used. In addition, PAA bonds are less sensitive than FPL bonds to processing variables, such as rinse-water chemistry and time before rinsing. As a result, the PAA procedure has become the treatment of choice in the USA for critical applications.

Chromic acid anodization is widely used to improve the corrosion resistance of aluminum surfaces. The use of the good protective coating on the aluminum protects the metal interface and increases the bond durability of the joint. CAA is widely used for aerospace applications in Europe, although it is not as popular as PAA in the USA.

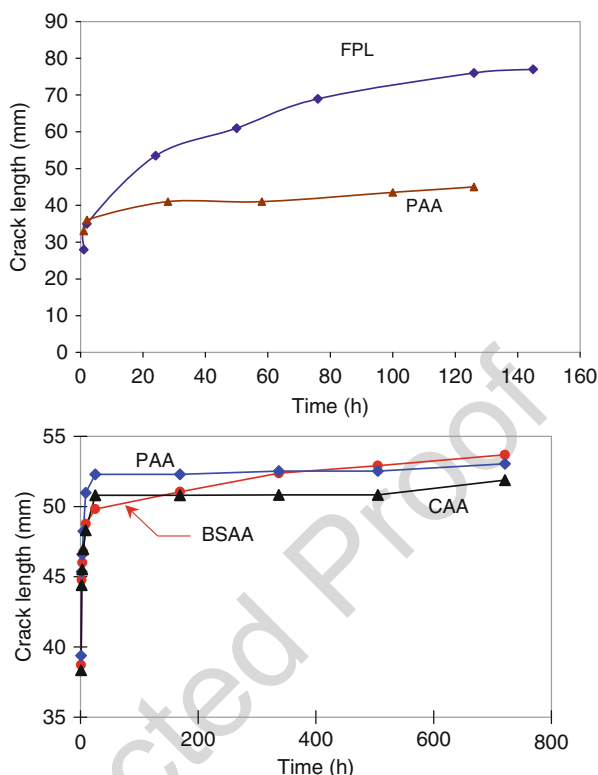
Boric acid/sulfuric acid anodization also avoids the chromates of the older processes. It provides an oxide similar to the CAA oxide – thick relative to PAA (~0.5  $\mu\text{m}$ ) with thick cell walls and narrow pores. Wedge test results indicate durability similar to CAA and PAA.

Although there are some differences in detail among the anodization processes used commonly for Al adherend preparation, they share many common features: cleaning, deoxidizing, and anodization. The anodization step for PAA is performed at a constant voltage, whereas for CAA, voltage is applied to the adherend in a gradual or stepwise fashion until the maximum voltage is reached, and is then held for roughly 30 min. Both anodization processes are more costly and time-consuming than the FPL process but are justified by the increase in bond durability as shown by the wedge test results of Fig. 7.

The PAA oxide morphology has an open nanorough morphology consisting of narrow-walled pores with whiskers sticking up above the pores, as the isometric drawing (adapted from Venables et al. (1979)) and the high-resolution stereo scanning electron micrograph (SEM) in Fig. 8 show. The total oxide thickness is ~400 nm. This type of nanoroughness can provide more mechanical interlocking than most other treatments for improved bond strength and durability, but this increase occurs in the interlocking only if the polymeric polymer or adhesive completely wets and penetrates the pores of the oxide. The nanoscale pores create capillary forces that help this penetration. Cross-sectional SEM views of PAA coated with typical epoxy primers show such penetration (Venables 1984). In such cases, strictly interfacial bond failure is very unlikely.

Chemically, the PAA film is amorphous  $\text{Al}_2\text{O}_3$  (Venables 1984) with the equivalent of a monolayer of phosphate incorporated onto the surface (Davis et al. 1982). Alloying constituents of the adherend are not generally found in the as-anodized

**Fig. 7** Wedge test results for Forest Products Laboratory (FPL)-etched and phosphoric acid anodized (PAA) adherends (*above*) and PAA, chromic acid anodized (CAA), and boric-sulfuric acid anodized (BSAA) adherends (*below*). The upper wedge test involved FM-123 adhesive; the lower wedge test involved FM-94 adhesive so the crack lengths cannot be compared from one test to the other. Exposures were 50 °C at 95% relative humidity (RH)



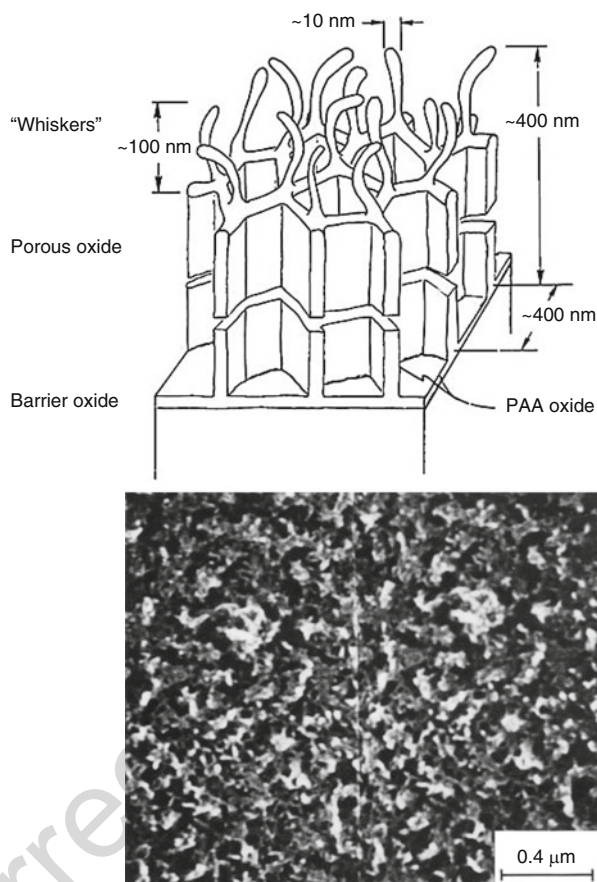
oxide. Depending on the storage conditions, some water can adsorb on the surface, but is readily removed by heating or storing in a dehydrating environment.

The morphology of the CAA oxide duplicates the morphology of the surface prior to anodization as oxidation occurs at the interface without dissolution of the existing oxide. The total oxide thickness is 1–2  $\mu\text{m}$ , which is much greater than that provided by PAA. The barrier layer at the bottom of the columns is also relatively thick ( $\sim 40$  nm), due to the high anodization voltages used. The CAA oxide is  $\text{Al}_2\text{O}_3$ ; the upper portion is amorphous but the lower part may be crystalline. In contrast to the phosphate incorporated in the PAA oxide, little Cr is incorporated into the CAA oxide.

Because the morphology of the outer surface of the CAA oxide is strongly dependent on the process steps used just prior to the CAA treatment, the type of pretreatment can be chosen to enhance the bonding. Samples that are FPL-etched and then anodized have a typical FPL shallow cell-and-whisker morphology. Surfaces that are PAA treated before the CAA anodization have a deeper cell structure, typical of PAA. Finally, surfaces that have a smooth tartaric acid-anodized (TAA) oxide before CAA treatment retain a smooth surface which is typical of the TAA treatment.

The morphology of CAA oxides can also be altered by varying the processing conditions, including using higher temperature anodizing solutions and post-anodizing phosphoric acid etches (Arrowsmith and Clifford 1985). One advantage

**Fig. 8** Phosphoric acid anodized (PAA) aluminum morphology. *Above*: Isometric drawing adapted from Venables et al. (1979). *Below*: High-resolution stereo scanning electron micrograph (SEM). Note: viewing this stereo micrograph and others in this chapter with a stereo viewer provides a 3-D image of the surface



to the CAA process is that the oxide is less friable, i.e., less susceptible to mechanical damage, than the PAA oxide.

Bonds made with PAA adherends exhibit excellent inherent durability with failure normally occurring within the adhesive (Venables 1984; Chaudhury and Pocius 2002) due to both the hydration resistance of PAA surfaces and the evolved nanoroughness and subsequent interlocking that occurs between the oxide and the adhesive (Venables 1984). Hydration of PAA surfaces occurs via a three-step process, as discussed above. It is the second step (hydration to boehmite) that causes crack propagation. The initial stability of the PAA surface results from the very thin layer of phosphate ions that is incorporated into the oxide during anodization. FPL oxides with an adsorbed layer of phosphonate-containing hydration inhibitor derive their hydration resistance from a similar mechanism (Davis et al. 1985). In all cases, the bond-degradation processes can be retarded by using moisture-resistant adhesives or primers.

CAA oxides protect the metal surface from hydration because of their inherent thickness; the important factor for bond durability is the stability of the outer oxide

structure when water diffuses through the bondline to the polymer/oxide interface. Because hydration rates are a function, in part, of the thickness of the barrier layer (which is directly proportional to the anodizing voltage), typical CAA processes yield oxides that are more resistant to hydration than FPL surfaces. Direct comparisons of the normal surface treatments based on durability tests show that CAA adherends and PAA adherends perform equally well (Fig. 7).

## Etches

The FPL and other chromic-sulfuric acid etching procedures are the oldest surface pretreatments for aluminum adherends other than simple degreasing or mechanical abrasion. In addition to being used as a complete adherend pretreatment, FPL was used as the first step in other pretreatments, such as PAA and CAA although it has largely been replaced as part of the PAA process for environmental reasons.

The presence of hexavalent chromium in the FPL/CAE and CAA solutions led to alternative treatments, such as P2 and BSAA and, later, sol-gel processing. The P2 etch, avoids the use of toxic chromates, but still provides the complex oxide surface morphology that is crucial to a “mechanically interlocked” interface and strong bonding. Ferric sulfate is used as an oxidizer in place of sodium dichromate (Rodgers 1981). The P2 solution produces an oxide morphology similar to what is seen on chromic-sulfuric acid etch surfaces over a broad range of time-temperature-solution concentration conditions. Mechanical testing indicates that P2-prepared surfaces are equivalent to FPL-prepared specimens.

The FPL oxide morphology is shown in the isometric drawing (adapted from Venables et al. (1979)) and high-resolution SEM stereo micrograph in Fig. 9. The oxide consists of a network of shallow pores and protrusions or whiskers on top of a thin barrier layer. This nanoroughness provides some mechanical interlocking between the adhesive and the oxide surface that is critical for the durability of epoxy-bonded structures, but is not sufficient to avoid interfacial failure if the oxide is stable enough to hydration (Davis et al. 1982). Chemically, the FPL film is amorphous with varying quantities of adsorbed water that can be removed by heating, vacuum exposure, or adsorption with certain organic hydration inhibitors.

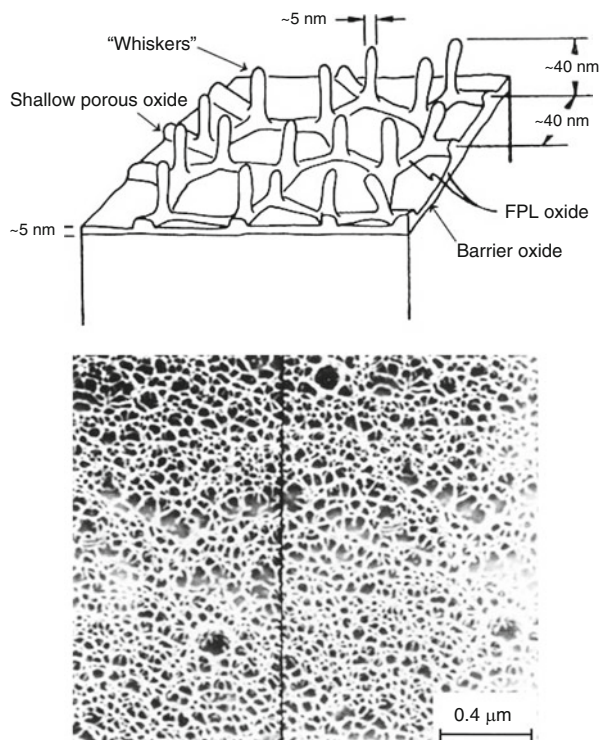
## Other Treatments

### Sol-Gel Processing

Sol-gel or “solution-gelation” is based on hydrolysis and condensation reactions to form inorganic polymer networks. The coating is schematically shown in Fig. 10. The Boegel process involves a dilute aqueous alkoxide solution containing zirconium isopropoxide (tetra-n-propoxyzirconium, TPOZ) and a silane coupling agent (Blohowiak et al. 1996; Park et al. 2000). The silane constituent can be chosen to be compatible with the primer and to form strong, durable chemical bonds. A glycidoxyl group, such as that of glycidoxymethoxysilane (GTMS), is typically used for epoxies. The hydrolyzed aluminum oxide surface promotes the condensation reactions. The part to be treated can be sprayed, drenched, or immersed. No rinsing is required.



**Fig. 9** Forest Products Laboratory (FPL)-etched aluminum morphology. *Top*: Isometric drawing adapted from Venables et al. (1979). *Bottom*: High-resolution stereo scanning electron micrograph (SEM)



A thin film (typically 50–200 nm) serves as a hybrid inorganic/organic interphase between the metal (oxide) surface and the organic primer or adhesive. The surface is silane-rich and the interface near the metal substrate is zirconia-rich with Zr-O-metal substrate chemical bonds formed with the substrate. The graded coating allows covalent bonding throughout the deposited interphase film. In this way, the sol-gel treatment differs from the traditional oxide treatments discussed above in that chemical bonding and not physical bonding governs joint strength and durability. Sol-gel films deposited on a grit-blasted aluminum surface give performance close to PAA bonds with little crack growth (Fig. 11). Failure is generally cohesive.

### Silane/Grit-Blast Treatment

The grit-blast/silane (GBS) treatment was developed in Australia for use with bonded repair patches. One example is the repair of outer wing fatigue cracks, in which over 1,000 bonded doublers have been applied to primary structure with no crack growth or patch failures for 20 years. The US Air Force has extended the technology and optimized a grit-blast/silane surface treatment for patching other aircraft.

In contrast with the oxide treatments discussed above where mechanical interlocking is the key to obtaining good bond strength and durability, the GBS treatment utilizes the functionality of the silane to form chemical bonds with both

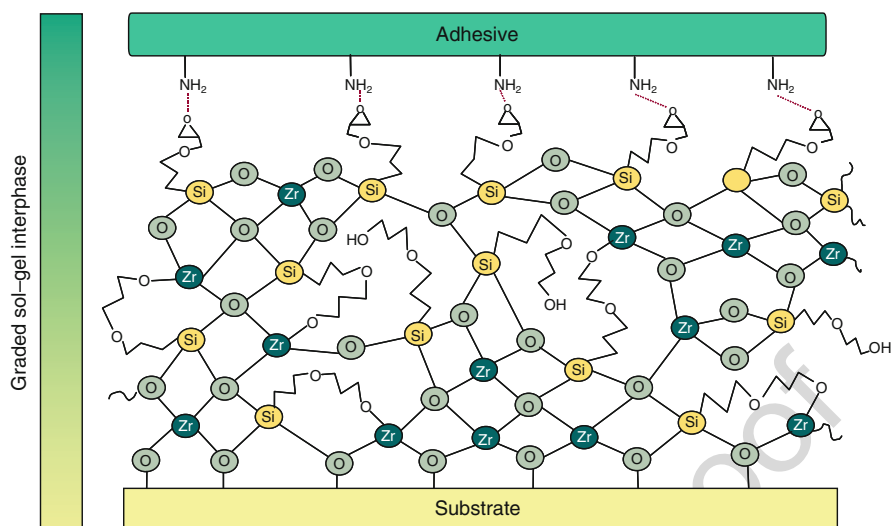


**Fig. 10** Schematic of sol-gel surface (Adapted from Blohowiak et al. (1996))

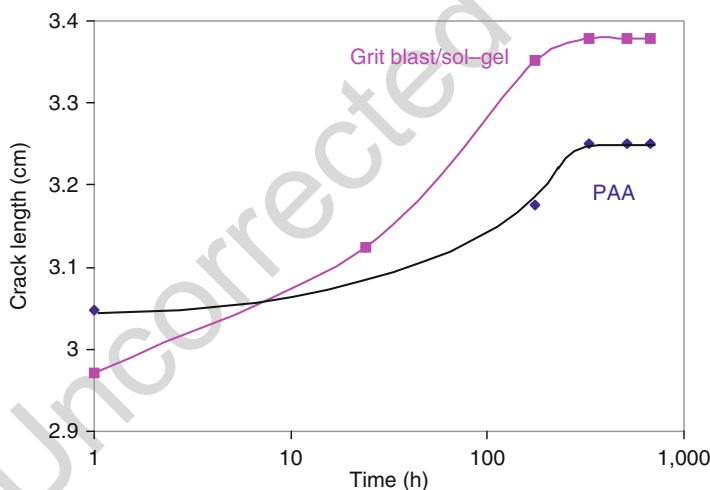


**Fig. 11** Wedge test results for Phosphoric acid anodized (PAA) and grit-blasted sol-gel treated aluminum adherends. Note the expanded crack-length scale (Data are from Blohowiak et al. (1998))

the surface and the adhesive/primer to couple the two materials (Plueddemann 1982; Bascom 1990). Silane coupling agents have the form  $R-SiX_3$ , where R is an organic function group and X is a hydrolysable group. The GBS treatment uses  $\gamma$ -glycidoxypopyltrimethoxy silane ( $\gamma$ -GPS), in which R is an epoxy group connected to the Si by a propylene chain and X is a methoxy. In an aqueous solution, the methoxies hydrolyze to form the trisilanol ( $R-Si(OH)_3$ ). For this application, the



epoxy group reacts with epoxy adhesive while the silanols react with the metal oxide surface. These bonds are stable against moisture attack and can provide excellent bond durability.

One issue with silane-coupling treatments is that the performance can be highly dependent on processing conditions, especially hydrolysis and drying conditions. Nonetheless, process controls suitable for field application of bonded repair patches are possible. With such controls, Optimized grit-blast/silane treatments can provide wedge test durability as good as PAA with failure entirely cohesive within the adhesive.

8.2.2 Titanium

Titanium alloys are particularly attractive for aerospace structures due to their high strength-to-weight ratio. In addition, they retain their mechanical properties at high temperatures, so that they can be used as components in structures where operating temperatures up to 370 °C (700 °F) are expected for short times or up to 177 °C (320 °F) for extended times. The desire to use adhesively bonded titanium structures at elevated temperatures has been a driving force in the development of high-temperature adhesives (those curing at temperatures up to 400 °C). In this section, surface preparations for titanium and the durability of the subsequent adhesive bonds are described. Selected treatments are shown in Table 3.

Like Al, durable surface preparations for titanium can be achieved by forming oxides in anodizing and/or etching solutions. Typically, anodization results in the best bond durability for Ti alloys, primarily due to the nanorough surface morphology that results from the treatment. The most commonly used anodization process is CAA (but in a different form than for aluminum adherends) (Venables 1984; Clearfield et al. 1990). The Pasa Jell 107 and Turco 5578 etches are also commonly used.

In early studies, the durability of Ti-6Al-4V adherends was determined as a function of surface preparation for ten adherend preparations (Brown 1982) and was discussed above (Fig. 3). The general result was that surface preparations that produce oxides with no roughness (macro- or micro-) yield the poorest bond durability; those that produce a large degree of macroroughness, with little or no micro- or nanoroughness, fall into an intermediate class of moderate-to-good durability; and those preparations that produce oxides with significant nanoroughness

Table 3 Selected surface treatments for titanium adherends

Process	Solution	Process parameters
CAA	CrO <sub>3</sub> + NH <sub>4</sub> HF <sub>2</sub> + H <sub>2</sub> O	20–25 °C, 10 V for 20 min
AP	NaOH + H <sub>2</sub> O <sub>2</sub>	65 °C for 20 min
Turco 5578	Proprietary, includes NaOH	80–95 °C for 15 min
Pasa-Jell 107	Proprietary	<38 °C, for 15–20 min

lead to the best durability. The morphology and bond durability of the most common treatments are described below.

The general steps used to provide an anodized surface on titanium adherends are similar to those used for aluminum adherends. Initially, the adherend must be degreased to remove organic contaminants. Degreasing is followed by an acid etch to remove the oxide scale. The anodization (if used) is done at constant voltage and the adherend is rinsed and dried.

The oxide formed by the CAA process is shown as an insert in Fig. 3. A two-level large-scale morphology is evident. This is typical of CAA-treated Ti-6Al-4V and is due to the two-phase nature of the alloy – large grains of the aluminum-rich alpha phase with an intergranular, vanadium-rich beta phase. At high magnifications, a honeycomb-like structure consisting of amorphous  $\text{TiO}_2$  is evident (Venables 1984; Clearfield et al. 1990). The cell diameters are on the order of 30–40 nm, with wall thicknesses about 5–10 nm. The thickness of the oxide depends on the concentration of the solution and the anodization voltage used. Typically, a 5%  $\text{CrO}_3$  solution (10 V, 20 min at room temperature) is used. This results in an oxide that is 120–130 nm thick. Cross-sectional transmission electron micrographs reveal that the honeycomb structure is on top of a thin, dense barrier layer (20–30 nm).

Turco 5578 (shown in insert of Fig. 3) and Pasa Jel 107 surfaces exhibit a roughness on the order of microns. At smaller scales (down to ~20 nm), the Pasa Jel surface is largely featureless while the Turco surface exhibits shallow oxide protrusions.

Surface preparations for Ti-6Al-4V that result in thick oxide films are limited to moderate temperatures over long times because the oxide is dissolved into the alloy at high temperatures. For instance, the failure mode in CAA lap-shear specimens (bonded with a thermoplastic polyimide) changed from cohesive to adhesive after 5,000 h of aging at 232 °C (Progar and St. Clair 1986). Oxide failure in CAA adherends that were exposed to high temperatures prior to bonding with epoxy was also observed. Although dry, high-temperature environments have little or no effect on CAA morphology, bonds formed after such exposures to high temperatures failed under minimal force. In these cases, the failures occurred at the oxide–metal interface, caused by the dissolution of the oxide into the base metal at the exposure temperature. Any stress applied to the adherend after exposure would then be concentrated at the weakened interface. Under these conditions, very little tensile force would be needed to pull the oxide away from the metal. This phenomenon has been observed for an adherend exposed in vacuum at 400 °C for as little as 1 h prior to bonding. Testing of bonded structures at lower temperatures, e.g., 177 °C, requires longer testing times for the same processes to occur. Such times reduce the feedback needed to optimize a surface treatment and make development slower, but are necessary to obtain valid testing.

Thus, for high-temperature applications, alternative surface treatments are necessary. Sol–gel processes similar to those for aluminum appear the most promising. Several different sol–gel chemistries have been described: the TPOZ/GTMS chemistry used for aluminum, an aromatic silane (m- and p-aminophenyltriethoxysilane), an aliphatic silane (3-aminopropyltriethoxysilane), and polyimide-silica hybrids (pendent

phenylethynyl imide oligomeric disilanes/tetraethoxysilane or PPEIDS/TEOS and phenylethynyl terminated imide oligomer/aromatic phenylethynyl imide silane/TEOS or PETI-5/APEIS/TEOS) (Blohowiak et al. 1996; Park et al. 2000). The later chemistries include high-temperature-stable components similar to those used in high-temperature adhesives. The surface morphology has not been investigated and reported in as much detail as CAA and the other oxide surfaces. However, Cobb et al. describe it as being similar to that of Turco 5578 provided that the Turco process is used as a precursor to the sol-gel process (Cobb et al. 1999). Because it relies on chemical bonding between the adhesive and the hybrid organic/inorganic structure, it does not require the fine microscopic features to form physical bonding that the anodized surface does. Exposure to 177 °C for up to 2,000 h has little effect on the lap-shear strength and locus of failure of PPEIDS/TEOS sol-gel treated bonds (Fig. 12). Other studies show that bonds prepared with the sol-gel treatments retain significantly more fracture toughness than bonds treated with Turco 5578 or Pasa-Jell 107 (Cobb et al. 1999).

Another high-temperature-compatible surface treatment is a microrough titanium coating deposited by plasma spraying. In plasma spraying, an electric arc is struck between a cathode and an anode (nozzle). A working gas, typically a mixture of argon and hydrogen (or nitrogen and hydrogen), is forced through the arc, creating a plasma. A powder of the material to be deposited is injected into the plasma either within or downstream from the nozzle, and the plasma softens or melts the powder in flight. The molten particles, traveling at supersonic velocities, strike the substrate and splat cool. The result is a microrough, metallic coating.

At high magnification, the microroughness of the plasma-sprayed surface is more random than that produced by any chemical process. The pores are quite deep, and many knob-like protrusions can be seen. These protrusions result from the splat

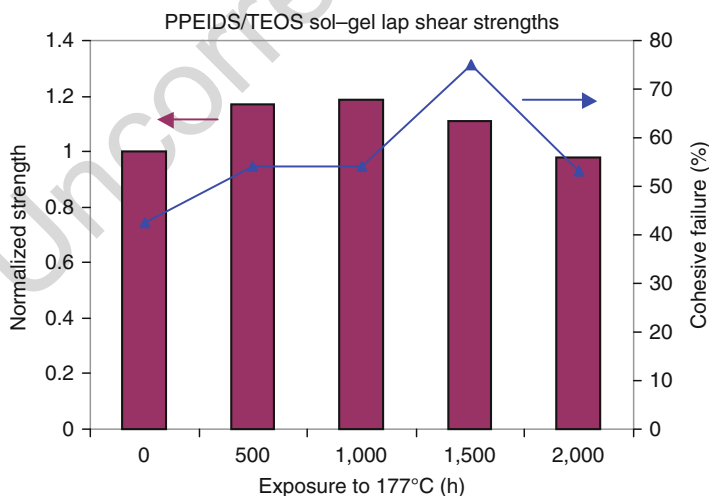


**Fig. 12** Normalized lap-shear strengths as a function of exposure to 177 °C for pendent phenylethynyl imide oligomeric disilanes/tetraethoxysilane (PPEIDS/TEOS) sol-gel treated titanium bonds. Also shown is the percentage of cohesive failure (Data are from Park et al. (1999))

cooling and rapid solidification of the Ti-6Al-4V droplets as they strike the substrate. At lower magnifications, some macroscopic inclusions are evident.

Plasma-sprayed adherends were exposed in vacuum at temperatures up to 800 °C for 1 h. No changes were observed at temperatures of 650 °C and below. Above 650 °C, changes in the bulk microstructure, and hence the surface morphology, were observed. At all temperatures, the coating remained adhered in tensile-button tests when the stubs were bonded following the high temperature exposure.

### 8.2.3 Steel

Although there is significant commercial interest in the adhesive bonding of steel structures, no general-purpose pretreatments for steel substrates have been developed (McNamara and Ahearn 1987; Clearfield et al. 1990). There are several reasons for this.

- For industries like the automotive industry, the focus has been on developing adhesives and processes that require minimal surface preparation.
- Unlike aluminum and titanium, iron does not form coherent, adherent oxides, so that it is difficult to grow a stable film with the fine micro- or nanoroughness needed for good adhesion.
- Different alloys can require different pretreatments so that a process that may give good performance for one alloy may give very different results for other alloys.

Grit blasting is commonly used as a pretreatment. Although it is adequate in many applications, it may not be suitable for cases where the bonded structure is exposed to severe environments.

The variety and complexity of steel microstructures greatly complicate the task of developing a universal surface treatment. Although several cleaning treatments and chemical etchants have been used for low-carbon and stainless steels, none has been widely adopted or shown to be superior to grit blasting. There have been encouraging results for stainless steels, but an effective etch or anodization process for low-carbon steels has not been developed. The best approach for preparing low-carbon steels appears to be the deposition of a more durable and bondable coating, such as a conversion-coating treatment.

As with aluminum and titanium, the most critical test for bonded steel joints is durability in hostile (i.e., humid) environments. Pocius et al. illustrated the difficulty of forming durable bonds on steels (Pocius et al. 1984b). They compared solvent-cleaned (smooth) 1,010 cold-rolled steel surfaces with FPL aluminum (nanorough) substrates. Although the dry lap-shear strengths were not markedly different, stressed lap-shear joints of steel adherends that were exposed to a humid environment failed in less than 30 days, whereas the aluminum joints lasted for more than 3,000 days.

Virgin alumina grit-blasted steel surfaces showed poor durability, as well, in wedge tests where specimens exhibited rapid crack growth (Trawinski et al. 1984).

Electron micrographs of opposing failure surfaces taken in the crack-growth region showed purely interfacial failure. The metal surface had not been corroded, nor was there visual evidence of moisture attack on the polymer during the relatively short test period. Gledhill and Kinloch investigated joints immersed in water and found a similar displacement of adhesive-to-metal bonds and concluded that thermodynamics considerations, such as those given in Table 1, indicate that water will virtually always displace an organic adhesive from a smooth metal oxide surface (Gledhill and Kinloch 1974). This suggests that simply cleaning the adherend surface is not an adequate treatment for structural bonding applications.

Other mechanical cleaning operations are no better and often worse than grit blasting. The best results were obtained when the grit size was matched to the size of the filler material in the adhesive.

Although chemical treatments for cleaning steel surfaces have been widely used for many years, there are no general chemical treatments designed to prepare steels for adhesive bonding. One of the main problems with chemical-etch treatments of low-carbon steels is the formation of a loosely adhering layer of iron oxide “smut” on the adherend surface. The oxide is difficult to remove before bonding even with vigorous rinsing, but easily pulls away with the adhesive when the joint is stressed. The formation of the smut can be suppressed by using acid etches in alcohol solutions. Although such solutions were reasonably effective, the treatments were no better than grit blasting in stressed durability testing. In many applications, a treatment that is “as good as grit blasting” is still acceptable.

Another major problem with chemical etches is that the resulting morphology is a function of the metallurgy of the substrate. Even though ASTM A606 and A514 substrates are chemically similar high-strength, low-alloy steels, their phosphoric-acid etched surfaces offer different bonding/interlocking potentials because different heat treatments are used to purposely change their microstructure (McNamara and Ahearn 1987). In both, the acid primarily attacks grain boundaries, etching out surface grains. However, the A606 surface has smooth-sided, dimpled morphological features, similar to grit-blasted surfaces, whereas the A514 surface has small crevices that can allow adhesive penetration. Etched A514 performs much better than either grit-blasted A514 or etched A606 surfaces in wedge tests.

The adherend metallurgy also indirectly determines the degree of smut buildup because the rate of smut formation is proportional to the etch rate (McNamara and Ahearn 1987). For instance, the etch rate of A606 is four times greater than that of A514, due to differences in grain size, etc. As a result, a different etch treatment is required for each. In general, the roles of alloy and heat-treatment differences have not been widely investigated in bonding research on steel; details of the substrate metallurgy are usually not reported.

Although chemical surface treatments can improve the substrate bondability of stainless steels, there is no general agreement on which is the best. One etchant commonly used with stainless steels is an  $\text{HNO}_3$ -HF mixture (Bottrell 1965; David 1974); another is chromic acid. Various solutions based on sulfuric acid have also been beneficial (Allen 1977), and several researchers investigated a wide variety of solutions based on acids with dichromates added, with and without anodization

(Haak and Smith 1983; Pocius et al. 1984a). They all used highly concentrated, very active solutions that attacked grain boundaries and the chromium-poor regions around chromium carbide particles. However, a treatment judged to be the best by one researcher did not receive the same ranking from another and the differences were probably related to the precise metallurgy of the samples investigated, which varied from one group to another. One common finding was that surface roughness correlated with peel test performance. Pocius et al. (1984a), for example, noted that peel performance could be correlated to the microscopic surface roughness.

A better approach to forming durable bonded joints with steels is to use a conversion-coating process to deposit a rough, corrosion-resistant layer on the adherend (Crithlow et al. 2000). To achieve such a coating, zinc and iron phosphate solutions are used to precipitate crystallites onto the steels. This can provide good bonding morphology if the process forms small crystallites (McNamara and Ahearn 1987). Large crystallites, on the other hand, can allow crack propagation within the conversion coating. Trawinski and coworkers demonstrated that lap-shear strengths using carefully controlled zinc-phosphate treatments were equivalent to those on grit-blasted steel substrates, but wedge test performances were greatly improved (Fig. 13) (Trawinski et al. 1984). To achieve this performance, the crystallites in the coating must be small. If the grain size is not controlled, the coating becomes too thick with phosphate crystallites precipitating on others, and a weak interface is introduced. As with chemical etches, optimum conversion coatings depend on the microstructure of the steel.

An alternative means of depositing a bondable coating onto steel that is largely independent of substrate metallurgy is thermal spray, such as plasma spray. The

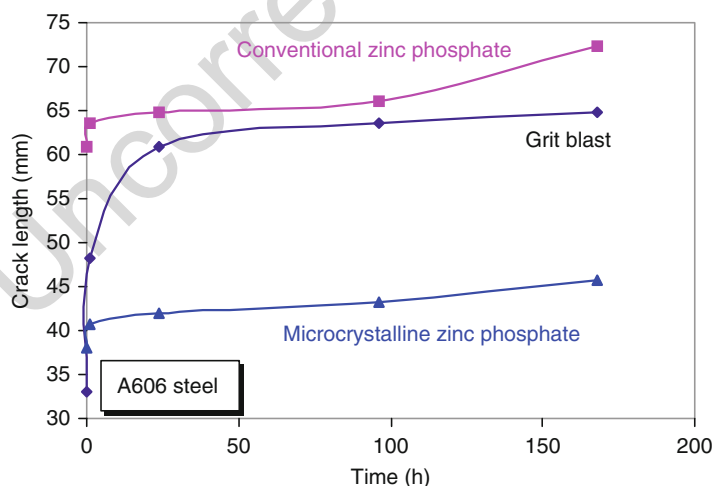


**Fig. 13** Wedge test results for ASTM A606 steel for grit-blasted and conventional and microcrystalline zinc phosphate conversion coatings. Failure of the microcrystalline zinc phosphate was 100% cohesive; that for the grit blast and conventional zinc phosphate was 100% adhesive (Data are from Trawinski et al. (1984))

chemistry and morphology of such coatings can be engineered for given applications. Plasma spray coatings of Ni-Cr, Ni-Cr-Al, and Ni-Cr-Zn exhibit excellent corrosion protection of the substrate and bondability to epoxy and rubber (Davis et al. 1995a, 1997). Additions of small amount of Zn provide cathodic protection of the substrate, much like galvanized coatings, and prevented substrate corrosion under a variety of aggressive conditions. Although the Zn component undergoes corrosion to protect the steel surface, the Ni-Cr or Ni-Cr-Al component provides a stable coating structure or framework so that adhesive bonds made after the corrosion tests using epoxy adhesive tensile buttons failed within the adhesive.

These plasma sprayed coatings also exhibit significant tolerance to oil and grease contamination of rubber bonds. In investigations using contamination-tolerant rubber materials, the plasma-sprayed surfaces retain high peel strengths and cohesive failure for more than double the grease level at which the grit-blasted surface begins to show degraded performance (Fig. 14). This increased tolerance is likely a result of a greater roughness and complexity of the plasma-sprayed surface compared to the grit-blasted surface.

In many high-volume production applications (i.e., the automotive and appliance industries), elaborate surface preparation of steel adherends is undesirable or impossible. Thus, there has been widespread interest in bonding directly to steel coil surfaces that contain various protective oils (Charnock 1985; Debski et al. 1986). Adhesives, particularly those curing at high temperatures, can form suitable bonds to oily steel surfaces by one of two mechanisms: (1) thermodynamic displacement of the oil from the steel surface and (2) absorption of the oil into the bulk adhesives (Debski et al. 1986). The relative importance of these two mechanisms depends on

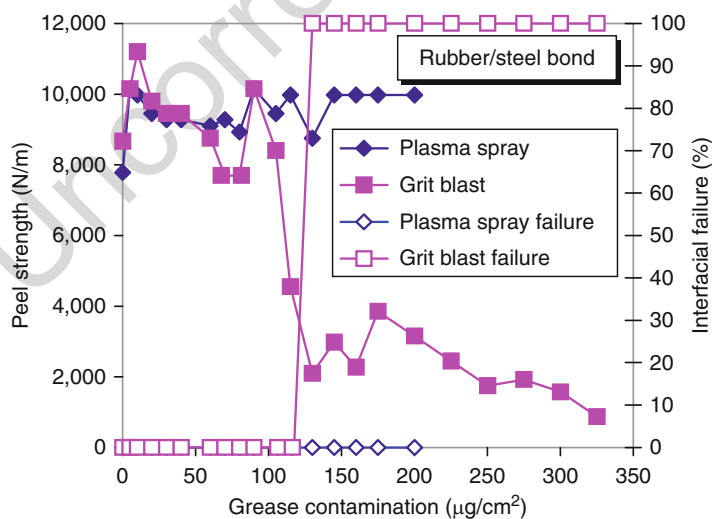


**Fig. 14** Peel strength of rubber–steel bonds contaminated with grease. Two different surface treatments were used: plasma spray and grit blast. Also shown are the loci of failure



the polarity of the oil and the surface area/volume ratio of the adhesive (which can be affected by adherend surface roughness).

Lap-shear bond strengths of joints made from steel substrates coated with a variety of oils and waxes ( $\sim 6 \text{ mg/cm}^2$ ) and joined with room-temperature curing acrylic adhesive have been reported to be up to 15 MPa (Charnock 1985). Very little degradation was seen after 1,000 h of exposure at 40 °C and 95% relative humidity. However, the shear strength dropped by roughly half when the joints were subjected to a 30 min bake at 200 °C. Although the bond strengths do not approach those reported for Al or Ti adherends, they were adequate for the intended application.

---

## 8.3 Other Materials

### 8.3.1 Composites

Bonding high-performance composite structures, such as those in aerospace, are very different than bonding metal structures in that the matrix polymer, such as epoxy, bismaleimide, or polyimide, can be used as the adhesive as well so that there is excellent chemical compatibility and good adhesion between the substrate and the adhesive (Pate 2002). Therefore, there is much less reliance on mechanical or physical bonding.

Often the adhesive and the adherends are cured simultaneously. This procedure reduces the cost of multiple curing cycles and promotes extensive chemical bonding and interdiffusion of polymeric chains during the curing process when the chains are mobile and the interface is under compressive forces.

Co-bonding (bonding cured parts to uncured parts) and secondary bonding (bonding fully cured parts) are also performed, especially for complex or large structures. In these cases, surface preparation of the composite surface is necessary to chemically reactivate surface and remove any surface contamination that might have occurred. One particular class of contamination of concern is mold-release agents. These agents are applied to the mold or tool surfaces to prevent the composite from bonding to the mold and to facilitate removal of the composite. By necessity, these agents are designed to prevent chemical bonding and must be removed prior to any subsequent bonding operation.

Peel plies are generally the preferred means of achieving a suitable surface. A peel ply is a sacrificial layer of dry or resin-impregnated tightly woven fabric that is added to the composite's surface during initial part fabrication. It is designed to form a weakened bond to the composite. The peel ply is peeled off just before the secondary bonding operation to expose a clean, active surface for bonding.

The alternative approach is surface abrasion or grit blasting to remove the outermost layer of matrix resin. However, this can be labor-intensive for large structures and exhibits two areas of concern: nonuniformity and the inherent balance of removing enough material to eliminate surface contamination while not damaging the fibers in the composite. There is also the possibility of abrasion of merely smearing contamination from one area to another.



A special example of secondary bonding is the repair of an existing structure. Once the damaged material has been removed, the structure’s surface area to be bonded is clean (if proper precautions are taken), activation is desired to promote chemical bonds. Silane coupling agents (discussed above) are one successful means to form interfacial chemical bonds.

Composites can also be treated with the same processes described below for plastics. This would be especially helpful when the composite resin is not compatible with the adhesive used.

8.3.2 Plastics

Unlike composites, most plastics have chemistries that are not suitable as adhesives. They typically have low surface energy while adhesive materials have high surface energy. Consequently, the high-surface energy adhesives do not wet and bond to the plastic surface. Furthermore, most plastic surfaces contain low-molecular weight material and contaminants, such as lubricants or mold-release agents, from the fabrication process. Thus, surface preparation is needed to prepare a reproducible clean and activated surface that is suitable for forming chemical bonds with the adhesive (Pocius 1997). An example of the need to change the surface chemistry is illustrated in Table 4 from Chew et al. (1986). Very little adhesion is observed between the epoxy adhesive and the unmodified polyethylene adhesive. However, surface carboxyl or ketone groups significantly increase the adhesion.

There are two classes of surface treatments for plastics: physical and chemical (Pocius 1997). Both classes alter the surface chemistry of the plastic but the distinction is that the physical methods involve some form of high-energy radiation while the chemical ones involve wet chemistry.

Perhaps the most common surface treatment for plastic films is Corona Discharge Treatment (CDT). In CDT, a high-frequency, high-voltage electrode serves to ionize the gas, normally air, above a plastic film. In air, a blue glow or corona appears

**Table 4** Effect of surface chemical functionalization of the adhesion of an epoxy to modified polyethylene surfaces<sup>a</sup>

Surface chemical functionality	Butt tensile strength (MPa)
–CH <sub>2</sub> –	1.4
–CH <sub>x</sub> CBr <sub>y</sub> –	6.7
–CH=CH–	3.7
–CH <sub>2</sub> –HC–OH	4.6
–CH <sub>2</sub> –C–CH <sub>2</sub>    O	11.3
–CH <sub>2</sub> –C–OH    O	15.7

<sup>a</sup>From Chew et al. (1986)

around the powered electrode. The ionized air oxidizes the plastic surface giving it a higher surface energy suitable for bonding. For polyethylene and polypropylene, the principal oxidation product is carbonyl (Cooper and Prober 1960; Carlsson and Wilson 1970). Because the treatment is at atmospheric pressure and film can advance rapidly on rollers, the CDT process can treat large areas of plastic very effectively.

Flame Treatment is the second most common surface treatment for plastics based on area treated (Pocius 1997). As with CDT, the plastic film passes over a roller or drum in air. Instead of a high-voltage electrode creating a corona or plasma, flame from a series of gas burners treats the plastic surface. The gas/air ratio, the distance of the burners from the film, and film speed are all important factors that govern the oxidization and activation of the film surface.

Plasma treatment is the third form of physical surface treatment. Here a radio-frequency (RF) or microwave generator ionizes a reduced-pressure gas to generate a plasma. Several different gases can be used to generate different chemistries on the surface. A principal disadvantage of most plasma processes is the partial vacuum required and the need for batch processing. This significantly increases the costs for high-volume operation. However, for low-volume specialty production, increased flexibility in surface chemistry with the use of different gases may warrant this approach.

Wet chemical treatments involve applying a solution to the plastic surface. Solvent cleaning is the simplest approach, but it alone is not usually effective in improving adhesive bonding. One of the oldest wet chemical surface treatments of polyethylene is exposure to oxidizing acids, such as chromic acid. A solution of sodium naphthalenide in tetrahydrofuran is useful in treating polytetrafluoroethylene (PTFE) (Benderley 1962). The very low surface energy of PTFE creates many uses for the polymer, but makes adhesive bonding problematic. For bonding, the surface energy can be increased by defluorination and subsequent oxidization of the surface. Roughening of the surface also occurs. As a result of this treatment, the bond strength can be up to seven times greater than that of the untreated PTFE.

### 8.3.3 Ceramics

Bonding to ceramics commonly relies on mechanical interlocking if the surface is porous or can be made porous, although chemical bonding can also contribute. Examples of ceramic bonds include dentistry, tiles on the Space Shuttle Orbiter, and ceramic armor for military vehicles.

In dentistry, bonding includes orthodontic or restorative dentistry to teeth (Barnes and Newsome 1996). The desired bonding can be temporary in the case of brackets for braces or permanent in the case of crowns, veneers, or bridges. The tooth enamel comprises many interlocking fine prisms of hydroxyapatite (calcium phosphate). Although temperature extremes are limited, the constant moisture in the mouth is a bonding challenge as is the need to achieve a good bond in a short time.

To accomplish adhesive bonding, the enamel is commonly etched by one or more acids, such as phosphoric, maleic acid, nitric acid, tartaric acid, sulfosalicylic acid, polyacrylic acid, citric acid, oxalic acid, and lactic acid, in various commercial formulations. The acids dissolve some of the hydroxyapatite crystals and remove 5–60  $\mu\text{m}$  of enamel surface and create a 5–50  $\mu\text{m}$  deep porous layer (Paradella and Fava 2007; Shinya et al. 2008). Generally, a higher acid concentration or a longer etch time produces deeper porosity. The dental adhesive then can flow into these pores for retentive tags or mechanical bonding. In some cases, the etching and bonding processes are combined as self-etching adhesives to simplify the process and make it quicker.

Other applications generally follow similar approaches. A clean, porous or rough surface, provided by either inherent porosity, etching, or grit blasting, is highly desired, but silane coupling agents or sol–gel treatments can provide chemical bonds to augment or replace physical bonding. They can also help “cure” surface-flaw damage caused by grit blasting (Bujanda et al. 2008).

Depending on temperature variations or extremes, differences in expansion due to differences in the coefficient of thermal expansion (CTE) may need to be considered with graded or intermediate interlayers being used as necessary. This is also true if the ceramic is being bonded to a structure subject to load deformation or other strain. For the Space Shuttle Orbiter, the thermal protection tiles are isolated from the aluminum frame with Nomex felt pads.

In the case of high operating temperatures where ceramics can be the material of choice, inorganic adhesives must be used and the surface preparation suitable to them is needed.

### 8.3.4 Wood

Wood is different from the materials discussed above in that it is a natural, heterogeneous material that exhibits variability of properties according to wood species, according to the cut of the wood, and according to specific wood specimen. Adhesion to wood most often relies on both physical (mechanical interlocking) and chemical bonds. Being inherently porous, the adhesive will normally penetrate into the wood several cells deep for excellent mechanical interlocking, but the most durable bonds to wood occurs when the adhesive diffuses into cell walls to make chemical bonds with the hemicellulosics and celluloses of the wood (Vick 2007). Adhesive penetration into sound wood can form an interphase that is stronger than the wood itself. To achieve such properties, the liquid adhesive must wet the wood surface with good capillary action to penetrate the sound wood structure, while displacing and absorbing air, water, and contaminants at the surface. Normally pressure is applied to facilitate this bonding process.

Surface treatment of the wood is intended to promote this bonding. Wood surfaces should be macroscopically smooth, flat, and free of surface irregularities, including planer skips and crushed, torn, and chipped grain. The surface should be free of burnishes, exudates, oils, dirt, and other contamination (Vick 2007). The best

surface treatment for wood is normally a smooth knife cut that avoids crushing or burnishing the surface and reduces adhesive wetting and penetration. This cut should be performed no earlier than 24 h before bonding. However, other surfacing procedures have been used successfully for certain types of adhesive joints, including sawing for furniture and millwork, knife-cutting for veneer, and abrasive-planning for panels.

Overdrying should be avoided as it can force hydrophobic extractives that can interfere with bonding to the surface (especially for resinous species) or can close some of the natural pores. Preservatives and fire retardants can also serve to fill natural pores and reduce the opportunities for good bond formation.

The density and, hence, the porosity of wood varies from species to species. As density increases, the ease of successful adhesive bonding decreases as opportunities for adhesive penetration decreases. Examples of easily bonding wood include basswood, fir, and pine. Examples of difficult to bond wood include persimmon, rosewood, and teak (Vick 2007).

As with metals, moisture is a major limiting factor in the durability of wood adhesive bonds. Dimensional changes (swelling or shrinking) of the wood adherend create significant changes vary with the orientation, type of wood specimen, and difference in moisture levels, but it can be up to 5–10% (Frihart 2009). Different adhesives handle this dimensional change in different ways. Frihart classifies the adhesives into two groups based on how swelling or shrinking affects the bond: in situ polymerized adhesives (phenolics, amino resins, isocyanates, and epoxies) have a rigid backbone and are usually highly cross-linked when cured, while prepolymerized adhesives (poly(vinyl acetate), polyurethane, emulsion polymer isocyanate, and proteins) have some backbone flexibility and a lower degree of cross-linking. In the first group, the adhesive achieves a durable bond by distributing the swelling strain across the wood interphase region (i.e., the region of the interphase in the wood where the adhesive has penetrated to lower interfacial stress). The flexibility of the second group of adhesives allows them to distribute strain in the adhesive interphase (i.e., the region of the adhesive near the wood). Both approaches decrease interfacial stress and allow dimensional changes to be handled.

---

## 8.4 Conclusions

High-performance, durable adhesive bonds to metal adherends require suitable surface preparation prior to bonding. The surface treatment cleans the surface of contamination that could prevent the adhesive or primer from bonding to the metal (oxide) surface. It also removes mill scale or other uncontrolled oxides that may be unsuitable for bonding or may represent a weak boundary layer. Finally, the treatment forms a new oxide or other film that provides physical (mechanical interlocking) or chemical bonding to the adhesive or primer. This oxide or film needs to be stable in the service environment for the life of the bond. It often forms a graded interphase between the polymer and the metal, thus minimizing stress concentrations at the boundary. This interphase can consist of a nanocomposite of

a porous oxide with the polymer penetrating into the pores or “nooks and crannies” of the oxide or a graded composition film.

The conventional surface treatments of aluminum, titanium, and steel were described. Environmentally benign treatments that are still being developed or are less common were also described. It is expected that these new treatments will see increasing use as environmental and health/safety regulations become stricter.

Similar approaches to preparing the adherend surface of other materials are also used although the details vary. The key aspects are to prepare a stable interface/interphase with either chemical or physical bonds that is stable under service conditions and able to handle stresses that arise from structural loading or from difference in material properties.

---

## References

- Affrossman S, Banks WM, Hayward D, Pethrick RA (2000) Non-destructive examination of adhesively bonded structures using dielectric techniques: review and some results. *Proc Inst Mech Eng C* 214:87
- Allen KW (1977) Surface preparation of a stainless steel for adhesive bonding. *J Adhes* 8:183
- Arrowsmith DJ, Clifford AW (1985) A new pretreatment for the adhesive bonding of aluminium. *Int J Adhes Adhes* 5:40
- Barnes IE, Newsome PRH (1996) The adhesive revolution of restorative dentistry. *Hong Kong Med J* 2:181
- Bascom WD (1990) Primers and coupling agents. In: Brinson (ed) *Engineered materials handbook: adhesives and sealants*, vol 3. ASM International, Metals Park, p 254
- Benderley AA (1962) Treatment of teflon to promote bondability. *J Appl Polym Sci* 6:221
- Blohowiak KY, Osborne JH, Krienke KA, Sekits DF (1996) Sol-gel surface treatments for adhesive bonding of titanium and aluminum structures. In: *Proceedings of the 28th international SAMPE technical conference*. SAMPE, Covina, p 440
- Blohowiak KY, Krienke KA, Osborne JH, Greeger RB (1998) Applications of sol-gel molecularly engineered surfaces on adhesively bonded aerospace hardware. In: *Proceedings of workshop on advanced metal finishing techniques for aerospace applications*, Keystone
- Bottrell NL (1965) Preparation of surfaces for adhesive bonding. *Sheet Metal Ind* 42(461):667
- Brown SR (1982) An evaluation of titanium bonding pretreatments with a wedge test method. In: *Proceedings of the 27th national SAMPE symposium*. SAMPE, Azusa, p 363
- Bujanda A, Copeland C, Dibelka J, Forster A, Holmes L, Jensen R, Kosik W, McKnight S, Koellhoffer S, Gillespie J Jr (2008) Analysis of adhesively bonded ceramics using an asymmetric wedge test, U.S. army research laboratory report ARL-TR-4665
- Cagle CV (ed) (1973) *The handbook of adhesive bonding*. McGraw Hill, New York
- Carlsson DJ, Wilson DM (1970) Surface studies by attenuated total reflection spectroscopy. I. Corona treatment of polypropylene. *Can J Chem* 48:2397
- Charnock RS (1985) Structural acrylic adhesives for the sheet steel fabrication industries. *Int J Adhes Adhes* 5:201
- Chaudhury M, Pocius AV (eds) (2002) *Adhesion science and engineering-2 surfaces, chemistry and applications*. Elsevier, Amsterdam
- Chew A, Dahm RH, Brewis DM, Briggs D, Rance DG (1986) Adhesion to polyethylene studied by means of a reversible bromination reaction. *J Colloid Interface Sci* 110:88
- Clearfield HM, Shaffer DK, VanDoren SL, Ahearn JS (1989) Surface preparation of Ti-6Al-4V for high-temperature adhesive bonding. *J Adhes* 29:81

- 977 Clearfield HM, McNamara DK, Davis GD (1990) Surface preparation of metals. In: Brinson HF  
978 (ed) Handbook on engineered materials: adhesives and sealants, vol 3. ASM International,  
979 Metals Park, p 259
- 980 Cobb TQ, Johnson WS, Lowther SE, St. Clair TL (1999) Optimization of surface treatment and  
981 adhesive selection for bond durability in Ti-15-3 laminates. *J Adhes* 71:115
- 982 Cooper GD, Prober M (1960) The action of oxygen corona and of ozone on polyethylene. *J Polym*  
983 *Sci* 44:397
- 984 Crithlow G, Webb PW, Tremlett CJ, Brown K (2000) Chemical conversion coatings for structural  
985 adhesive bonding of plain carbon steels. *Int J Adhes Adhes* 20:113
- 986 Crithlow G, Yendall KA, Bahrani D, Quinn A, Andrews F (2006) Strategies for the replacement of  
987 chromic acid anodising for the structural bonding of aluminium alloys. *Int J Adhes Adhes*  
988 26:417
- 989 David GL (1974) Adhesive joining of stainless steels. Pt. 2. *Met Deform* 26:45
- 990 Davis GD (1986) Use of surface behavior diagrams to study surfaces and interfacial reactions. *Surf*  
991 *Interface Anal* 9:421
- 992 Davis GD (1993) Contamination of surfaces: origin, detection, and effect on adhesion. *Surf*  
993 *Interface Anal* 20:368
- 994 Davis GD (2003) Durability of adhesive joints. In: Mittal KL, Pizzi A (eds) Handbook of adhesive  
995 technology, 2nd edn. Marcel Dekker, New York, p 273
- 996 Davis GD, Sun TS, Ahearn JS, Venables JD (1982) Application of surface behavior diagrams to the  
997 study of hydration of PAA surfaces. *J Mater Sci* 17:1807
- 998 Davis GD, Ahearn JS, Matienzo LJ, Venables JD (1985) Use of hydration inhibitors to improve  
999 bond durability of aluminum adhesive joints. *J Mater Sci* 20:975
- 1000 Davis GD, Groff GB, Biegert LL, Heaton H (1995a) Plasma spray treatments for steel adherends.  
1001 *J Adhes* 54:47
- 1002 Davis GD, Whisnant PL, Venables JD (1995b) Plasma sprayed coatings as surface treatments of  
1003 aluminum and titanium adherends. *J Adhes Sci Technol* 9:433
- 1004 Davis GD, Groff GB, Zatorski RA (1997) Plasma sprayed coatings as treatments for aluminum,  
1005 steel, and titanium adherends. *Surf Interface Anal* 25:366
- 1006 Davis GD, Krebs LA, Drzal LT, Rich MJ, Askeland P (2000) Electrochemical sensors for nonde-  
1007 structive evaluation of adhesive bonds. *J Adhes* 72:335
- 1008 Debski M, Shanahan MER, Schultz J (1986) Mechanisms of contaminant elimination by  
1009 oil-accommodating adhesives part 1: displacement and absorption and part 2: a model of the  
1010 processes involved. *Int J Adhes Adhes* 6:145, 150
- 1011 Frihart CR (2009) Adhesive groups and how they relate to the durability of bonded wood. *J Adhes*  
1012 *Sci Technol* 23:601
- 1013 Gledhill RA, Kinloch AJ (1974) Environmental failure of structural adhesive joints. *J Adhes* 6:315
- 1014 Haak RP, Smith T (1983) Surface treatment of AM355 stainless steel for adhesive bonding. *Int J*  
1015 *Adhes Adhes* 3:15
- 1016 Kinloch AJ (1987) Adhesion and adhesives: science and technology. Chapman & Hall, London
- 1017 Kinloch AJ, Little MSG, Watts JF (2000) The role of the interphase in the environmental failure of  
1018 adhesive joints. *Acta Mater* 48:4543
- 1019 Landrock AH (1985) Adhesives technology handbook. Noyes, Park Ridge
- 1020 Marceau JA, Thrall EW (1985) Environmental-durability testing. In: Thrall EW, Shannon RW (eds)  
1021 Adhesive bonding of aluminum alloys. Marcel Dekker, New York, p 177
- 1022 McNamara DK, Ahearn JS (1987) Adhesive bonding of steel for structural applications. *Int Mater*  
1023 *Rev* 32:292
- 1024 McNamara DK, Matienzo LJ, Venables JD, Hattayer J, Kodali SP (1983) Effect of rinse water pH  
1025 on the bondability of FPL-pretreated aluminum surfaces. In: Proceedings of the 28th national  
1026 SAMPE symposium. SAMPE, Azusa
- 1027 Minford JD (1993) Handbook of aluminum bonding technology and data. Marcel Dekker,  
1028 New York

- 1029 Paradella TC, Fava M (2007) Bond strength of adhesive systems to human tooth enamel. *Braz Oral*  
1030 *Res* 21(1):4
- 1031 Park C, Lowther SE, Smith JG Jr (1999) Organic-inorganic hybrids using novel phenylethynyl  
1032 imide silanes. In: *Proceedings of the polymer materials science and engineering*, vol 81.  
1033 American Chemical Society, Washington, DC, p 403
- 1034 Park C, Lowther SE, Smith JG Jr, Connell JW, Hergenrother PM, St. Clair TL (2000)  
1035 Polyimide-silica hybrids containing novel phenylethynyl imide silanes as coupling agents for  
1036 surface-treated titanium alloy. *Int J Adhes Adhes* 20:457
- 1037 Pate KD (2002) Applications of adhesives in aerospace. In: Chaudhury M, Pocius AV (eds) *Adhesion*  
1038 *science and engineering-2 surfaces, chemistry and applications*. Elsevier, Amsterdam, p 1129
- 1039 Plueddemann EP (1982) *Silane coupling agents*. Plenum, New York
- 1040 Pocius AV (1997) *Adhesion and adhesives technology*. Hanser/Gardner, Cincinnati
- 1041 Pocius AV, Almer CJ, Wald RD, Wilson TH, Davidian BE (1984a) Investigation of variability in the  
1042 adhesive bonding characteristics of 301 stainless steel. *SAMPE J* 20:11
- 1043 Pocius AV, Wangness DA, Almer CJ, McKown AG (1984b) Chemistry, physical properties  
1044 and durability of structural adhesive bonds. In: *Proceedings of the adhesion society meeting*,  
1045 Jacksonville
- 1046 Progar DJ, St. Clair TL (1986) Evaluation of a novel thermoplastic polyimide for bonding titanium.  
1047 *Int J Adhes Adhes* 6:25
- 1048 Rodgers NL (1981) Pre-production evaluation of a nonchromated etchant for preparing aluminum  
1049 alloys for adhesive bonding. In: *Proceedings of the 13th national SAMPE technical conference*.  
1050 SAMPE, Azusa, p 640
- 1051 Shinya M, Shinya A, Lassila LVJ, Gomi H, Varrelä J, Vallittu PK, Shinya A (2008) Treated enamel  
1052 surface patterns associated with five orthodontic adhesive systems—surface morphology and  
1053 shear bond strength. *Dent Mater J* 27(1):1
- 1054 Trawinski DL, McNamara DK, Venables JD (1984) Adhesive bonding to conversion coated steel  
1055 surfaces. *SAMPE Q* 15:6
- 1056 Venables JD (1984) Adhesion and durability of metal-polymer bonds. *J Mater Sci* 19:2431
- 1057 Venables JD, McNamara DK, Chen JM, Sun TS, Hopping RL (1979) Oxide morphologies on  
1058 aluminum prepared for adhesive bonding. *Appl Surf Sci* 3:88
- 1059 Vick CB (2007) Chapter 9. Adhesive bonding of wood materials. In: *Encyclopedia of wood*.  
1060 US Department of Agriculture, Washington, DC, p 9-1
- 1061 Wegman RF (1989) *Surface preparation techniques for adhesive bonding*. Noyes, Park Ridge

# Surface Characterization and Its Role in Adhesion Science and Technology

9

John F. Watts

## Contents

9.1	Introduction .....	198
9.2	Surface Topography .....	199
9.2.1	Scanning Electron Microscopy .....	199
9.2.2	Atomic Force Microscopy .....	201
9.2.3	White Light Interferometry .....	204
9.3	Surface Energetics .....	205
9.3.1	Simple Test Methods .....	205
9.3.2	Contact Angle .....	207
9.3.3	Inverse Gas Chromatography .....	209
9.4	Surface Chemical Analysis .....	212
9.4.1	X-ray Photoelectron Spectroscopy .....	213
9.4.2	Auger Electron Spectroscopy and Scanning Auger Microscopy .....	216
9.4.3	Time-of-Flight Secondary Ion Mass Spectrometry .....	221
9.5	Conclusions .....	225
	References .....	226

## Abstract

This chapter reviews a variety of methods of surface characterization that have been found to be useful in the study of adhesion. The methods considered can be conveniently classified in three groups: those that provide information regarding surface topography (scanning electron microscopy and atomic force microscopy [AFM]); those that probe the surface-free energy of a material (measurement of contact angles and inverse gas chromatography, in addition to simple test methods such as the water break test and dyne inks); and those that provide a surface-specific chemical analysis (X-ray photoelectron spectroscopy, Auger

J. F. Watts (✉)

The Surface Analysis Laboratory, Faculty of Engineering and Physical Sciences,  
University of Surrey, Guildford, Surrey, UK  
e-mail: [j.watts@surrey.ac.uk](mailto:j.watts@surrey.ac.uk)



electron spectroscopy, and time-of-flight secondary ion mass spectrometry). All provide surface-specific information and this is essential for adhesion investigations as the forces responsible for adhesion operate over very short length scales and for any analysis to be meaningful the analysis technique must probe depths of a similar order of magnitude. These methods are used in all types of adhesion investigations, which, in general, can be considered in one of three areas of endeavor. The analysis of the unbonded surface and the relationship of surface characteristics to performance such as strength or durability, the forensic analysis of failed joints with a view to defining the exact locus of failure and any interfacial phenomena that may have exacerbated failure, fundamental studies of adhesion carried out with a view to gaining a fuller understanding of the interfacial chemistry of adhesion.

---

## 9.1 Introduction

The last three decades have seen many advances in our understanding of fundamental aspects of adhesion. This has led to a large body of data in the open literature that relates the surface characteristics of substrates and polymeric overlayers to the interfacial chemistry of adhesion, which, in turn, is used to establish structure/property relationships based on measurements of a performance parameter, at the fundamental level (such as the thermodynamic work of adhesion, see ► [Chap. 6, “Thermodynamics of Adhesion”](#)). For applied investigations, surface data will be related to more pragmatic quantities such as the performance of an organic coating in a salt spray test or the strength and more importantly the durability of a structural adhesive joint. One thing is clear, however, and that is the surface characteristics of the two phases have a profound influence on the formation of the interface, which in turn governs performance. Adhesion relies on the establishment of intermolecular forces between a substrate and the polymeric adhesive itself. To this end it is invariably necessary to pretreat the solid substrate in some manner to confer the required surface properties; this may be a simple abrasion treatment or a more sophisticated method such as acid anodizing. In a similar vein, chemical methods such as a corona discharge treatment and flame treatment used on polyolefins or the application of a primer solution based on an organosilane adhesion promoter may be used to ensure the required durability of an adhesive joint. In all cases the performance of the adhesive joint is directly related to the successful application of such a pretreatment, and an important part of the development of a new pretreatment procedure or the quality assurance of an established process is the assessment of the surface characteristics, both in terms of topography and chemistry.

The characterization that is necessary in order to begin to appreciate the complexities that exist at the polymer/metal oxide junction relates to both surface chemistry and topography. The aim of this chapter is to introduce methods that are now well established in the adhesion field; although it is not possible to provide a complete description of these techniques, the aim is to provide a general background of what can be achieved and indicate why such methods have become widely used in

adhesion investigations. At this juncture it is worth reflecting on what exactly one hopes to achieve by carrying out such investigations, a review of the literature establishes quite clearly that adhesion studies that involve surface characterization techniques essentially break down into three clear areas:

- The investigation of surface characteristics prior to bonding and correlation with some form of performance parameter
- The forensic investigation of failed adhesive joints and once again correlation of failure characteristics with a chosen performance parameter (see ► Chap. 43, “Techniques for Post-fracture Analysis”)
- The use of sophisticated specimen preparation or modeling approaches to investigate the interfacial chemistry of adhesion

Such a list reflects the timeline along which adhesion science has developed in terms of surface characterization with the examination of the unbonded substrate being achieved first, then forensic analysis of failures and the determination of the interfacial chemistry of adhesion still being a significant challenge for many systems. Indeed the attainment of such a goal is in some ways the holy grail of adhesion science as it opens up the possibility of engineering the interface to provide a specific set of properties in terms of strength, toughness, and durability. Much headway has been made in this area in recent years but it is still a topic in which results are hard won and thus by definition very resource intensive.

The techniques by which such surface characteristics can be explored will be described in this chapter and a further chapter in this book will review the manner in which these methodologies are used in adhesion science (► Chap. 10, “Use of Surface Analysis Methods to Probe the Interfacial Chemistry of Adhesion”). The methods discussed will provide information regarding surface topography (SEM and AFM) as well as surface chemistry (XPS, ToF-SIMS, and AES). Surface thermodynamics is important at both a fundamental and an applied level and the use of wetting (see ► Chap. 4, “Wetting of Solids”) and spreading (see ► Chap. 5, “Spreading of Liquids on Substrates”) concepts such as contact angle and surface-free energy and inverse gas chromatography will also be considered.

---

## 9.2 Surface Topography

### 9.2.1 Scanning Electron Microscopy

Most laboratories engaged in adhesive bonding research and/or development will have ready access to scanning electron microscopy, and it is widely used to investigate both substrate surfaces prior to bonding and the characteristics of interfacial failure surfaces from adhesive bonds following a mechanical test. Optical or light microscopy is not really sufficient, not because it lacks the range of magnification of an SEM, although this is an important feature, but because of its poor depth of field and depth of focus. In optical microscopy features not in the image plane appear either under- or over-

focused (i.e., blurred) whereas an SEM is able to accommodate very large depths of field as exemplified by SEM images of small insects that often appear in the popular press. Having said that, the rigor of using digital photography to record all failure surfaces after test cannot be overemphasized to provide archival data that may provide important evidence once a program of testing has been concluded. As the general operating principles of an SEM are generally well appreciated, they will not be repeated here but the reader who needs a brief overview of operating principles is referred to standard texts such as Goodhew et al. (2001). The importance of surface topography is illustrated in Fig. 1. This shows a hot-dipped galvanized steel surface that has been temper-rolled (skin-passed) in readiness for a coil coating process. The surface rugosity is clearly observed at a scale of several tens of micrometers. As will be shown later in this chapter, the temptation to assume a homogeneous surface, although very natural, should be avoided as such mechanical treatment can lead to a well-defined heterogeneous surface.

It is very often convenient to use SEM to examine failure surfaces of joints as indicated above. The micrograph of Fig. 2 is the failure surface of an aluminum substrate bonded with a structural adhesive. Although on the basis of the microscopy one would tend to classify this as an interfacial failure, there are a few small islands of adhesive left on the metal side of the failure that vary in size from a few micrometers up to around 100  $\mu\text{m}$ . As the polymer is an insulating material, it will generally charge during electron microscopy and this is evident in the micrograph of Fig. 2 as darker contrast around the adhesive residue. As ► Chap. 10, “Use of Surface Analysis Methods to Probe the Interfacial Chemistry of Adhesion” will indicate, the definition of the locus of failure is a rather complex task and depends on the level of sophistication of the assessment methods available, but for the time being the example of Fig. 2 will be considered an interfacial failure. Some pre-treatments lead to characteristic morphologies on a very fine length scale that can only be clearly defined by high-resolution SEM. The most widely cited example of this type of surface is the classic work of Venables (1984) on the morphology of acid anodized aluminum. The approach taken by these authors was to record stereo pair

**Fig. 1** Scanning electron micrograph of a hot-dipped galvanized steel surface

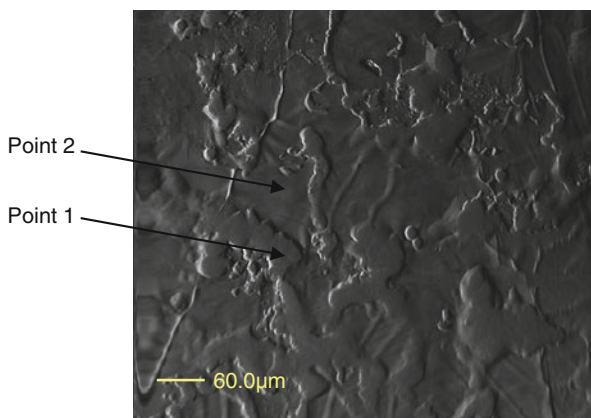
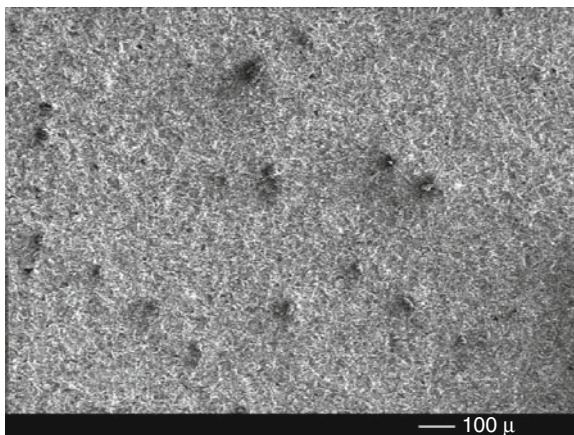


**Fig. 2** The interfacial metal failure surface from an adhesively bonded aluminum test piece. The substrate has been grit blasted with 50  $\mu\text{m}$  alumina grit prior to bond fabrication



SEM micrographs and present these along with an isometric drawing of the supposed morphology. These micrographs are, quite rightly, regarded as classics in the adhesion bonding literature and interested readers are referred to the above review of this work for further information.

In the case of polymeric substrates SEM is not quite so useful. The modifications brought about are quite subtle and the need to coat the insulating surface with carbon, gold, gold palladium, or a similar material to prevent electrostatic charging can add another level of complexity to sample preparation. Although useful for identifying debris at a surface or delamination in the case of composite materials, atomic force microscopy is generally preferred to SEM for the examination of polymer surfaces. SEM used in conjunction with energy dispersive X-ray analysis (EDX) will, however, always have a place in adhesion investigations as a result of the ready bulk analysis that can be undertaken, which will identify, for example, pigmentation in a coating or adhesive.

### 9.2.2 Atomic Force Microscopy

AFM is one of a family of techniques referred to by the generic name of scanning probe microscopy (SPM). These all have their genesis with the scanning tunneling microscope first developed by Binnig et al. (1982).

A schematic of an AFM is shown in Fig. 3, and although closely related to the STM the basic principle relies on the attraction between a sharp tip (often of silicon nitride) and the surface under examination. The tip is located at the free end of a cantilever of low spring constant (ca.  $1 \text{ Nm}^{-1}$ ). The force between the tip and the sample cause the cantilever to deflect. A detector arrangement, based on a laser reflecting from the cantilever and a quadrant array photodetector, records the deflection of the cantilever as the tip is scanned relative to the sample. The extent of deflection of the cantilever can then be used to produce an image of surface

**Fig. 3** Schematic of an atomic force microscope

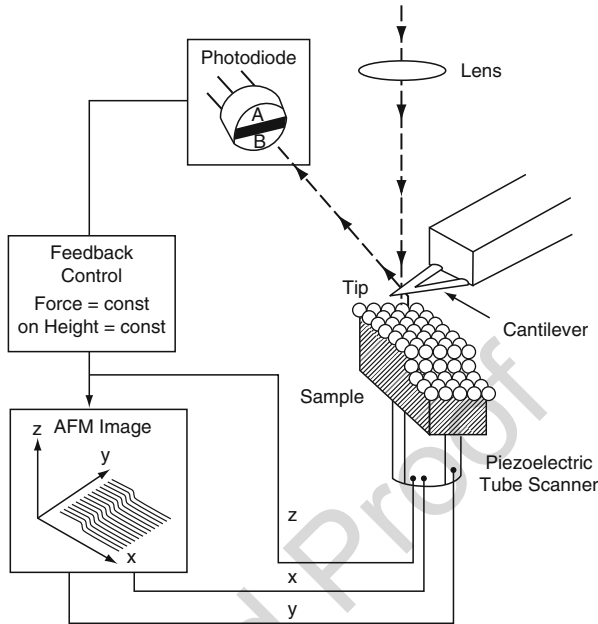
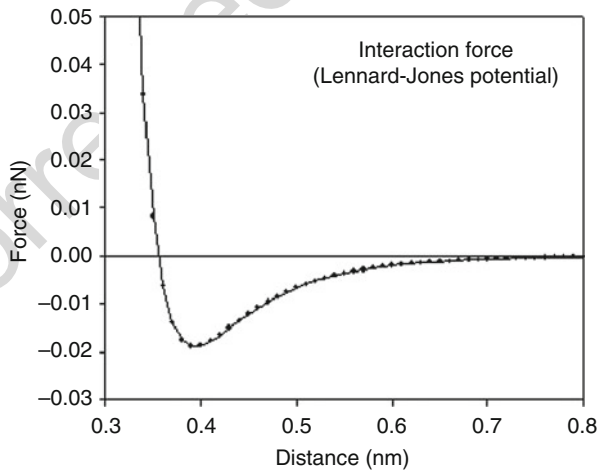


**Fig. 4** Force curve showing interatomic force, between tip and specimen, as a function of distance



topography. The forces involved are repulsive at very close proximity (ca. 0.1 nm) but as the cantilever is withdrawn they become attractive as shown in Fig. 4. This leads to the definition of two forms of AFM operation, contact (ca. 0.2 nm distance on Fig. 4) and noncontact AFM (0.4–0.6 nm). In contact AFM, the tip makes gentle contact with the sample and, in the case of very soft or delicate samples (e.g., pressure sensitive adhesive tape) may indent the surface giving erroneous results, if any at all. To overcome this problem the tip may be vibrated near the surface

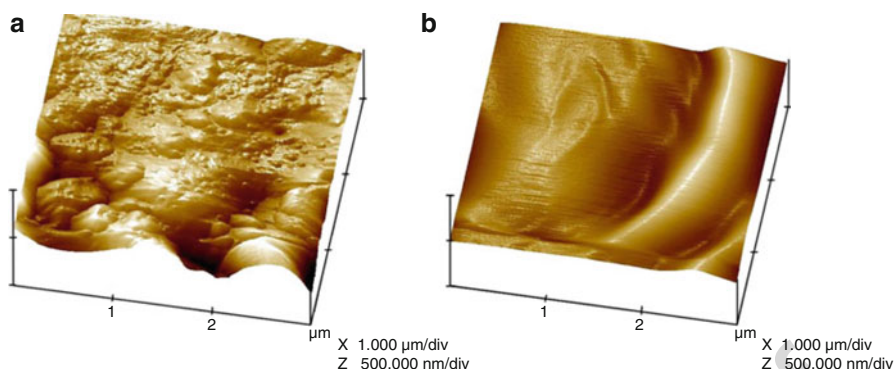


**Fig. 5** Tapping mode AFM image of a commercial PVC extrudate: (a) before treatment and (b) after flame treatment

(1–10 nm); however, the force between tip and sample may be very small (10–12 nN) making it more difficult to measure than the force in the contact mode, which is several orders of magnitude higher. There is also the possibility of the tip being pulled into the sample so stiffer cantilevers are required. A compromise between these two modes of operation is tapping mode AFM (TM-AFM) in which a sinusoidal vibration is applied to the tip and it gently taps against the surface; as shear and lateral forces are reduced, sample damage is, in most cases, negligible. An example of TM-AFM is shown in Fig. 5, which illustrates the topography of a poly (vinyl chloride) (PVC) surface before and after energetic surface treatment.

AFM has a wide range of magnifications from close to atomic resolution to a magnification of approximately 500 times; so in many ways it competes with the SEM as a method of assessment of surface topography. The complementarity of AFM and SEM have been discussed at some length by Castle and Zhdan (1997). Instruments are now available in portable format, low cost versions, geometries to accommodate very large specimens, and a plethora of different versions handle difficult samples such as cells and wet surfaces, making it a very versatile technique indeed. As far as those involved in adhesive bonding are concerned, the advantages of an AFM over other forms of surface characterization are threefold: Firstly, all samples, metal, polymer, ceramic, viscoelastic adhesives, and so on, can be handled successfully without the need for further sample processing. Secondly, by processing the image data as a line scan it is possible to carry out a “sectional analysis” that is essentially stylus profilometry, as described in BSI (2010) at the nanometric scale. The third is rather more specialized but if one measures forces directly one can use the AFM to monitor forces and thus use it as a localized surface forces apparatus, probing the adhesion properties of a polymer blend, for instance. In a similar manner force modulation can be used to probe localized elastic properties in the cross section of a polymer composite, or adhesive joint, and in this manner an interphase zone can be identified mechanically. Such modes of operation complement the traditional ways of probing surface-free energy, which are discussed in the following section.

### 9.2.3 White Light Interferometry

Although AFM has much to recommend itself as a technique for surface characterization, its primary role in most areas of research is, as its name suggests, that of a sophisticated microscope for the elucidation of surface topography. As a means of the determination of surface roughness it remains something of “an overkill,” but in addition it has two significant disadvantages for roughness measurement. Firstly, AFM is still some way off becoming a routine tool for quality assurance with a high level of operator skill being required, in addition the speed with which data is produced is not high and given the choice of an SEM or AFM for initial assessment of a surface many operators would resort to the rapidity of the former. The upper bounds of measurement achievable may also be a problem with samples exhibiting coarse features, as for AFM the scan area in the x and y directions is limited to tens or at best hundreds of micrometers and in the z direction only a few micrometers. The solution to the need to acquire statistically meaningful measures of surface roughness over relatively large areas has been driven by the microelectronics industry, which has the need to assess large wafers at roughnesses of much less than 1 nm. The solution to this need has been the development of the well-established technique of white light interferometry (WLI) into a routine quality assurance procedure, with large ranges available in all axes and superb height resolution (0.01 nm are quoted for the latest instruments). The area where AFM outperforms WLI is in lateral resolution, although for many measurements of relevance to adhesive bonding this will not present a problem.

The background to optical interferometry is well known and is based around the spitting of a beam from a single light source into two separate beams using a beam splitter: one of the beams acts as a reference and follows a well-defined path and the other is reflected from the sample surface. At some point in the optical path, the two beams recombine to form an interference pattern of light and dark fringes. This is then magnified by the detector optics and finally imaged using a suitable device such as a CCD (charge-coupled device) camera. If at the same time the objective lens is moved vertically (to change path length between sample and beam splitter), with a high-resolution device such as a piezoelectric drive system, a series of dynamic interference fringes will be observed. Constructive interference will lead to a brightening of the image and, provided the movement of the objective lens is known accurately, this can be mapped back to a position on the sample surface via the establishment of the brightest point on each element of the CCD array. In this way it is possible to create a three-dimensional image of the sample surface by recording the position of the objective that gives the brightest image at each point on the CCD. Data from WLI is often presented in the form of a color-coded topographic plot or a pseudo three-dimensional plot, forms that are familiar to many as a result of their popularity with AFM manufacturers. Roughness values will be reported usually as an average over the entire field of view rather than the one-dimensional line familiar from stylus profilometry or sectional analysis in the AFM.



## 9.3 Surface Energetics

### 9.3.1 Simple Test Methods

Surface energetics is the behavior of gas and liquid molecules on solid surface and the relationship to the surface-free energy of the solid and liquid phases. The three-dimensional equilibrium packing of solids and liquids cannot be maintained at the surface and this less-than-satisfactory situation gives atoms at the surface a greater free energy than those in the bulk. This excess energy is known as the surface-free energy and has the units of energy per unit area, and using the SI notation surface-free energy, represented by the symbol  $\gamma$ , is always reported in  $\text{mJm}^{-2}$ . In liquids the surface-free energy gives rise to the well-known phenomenon of surface tension and, indeed, the values of surface-free energy and surface tension are numerically equal, although surface tension has the units of force per unit length, in the SI notation  $\text{mNm}^{-1}$ . It is incorrect to refer to the surface tension of a solid and terms such as wetting tension, interfacial tension, and so forth are now regarded as deprecated. The value of surface-free energy can vary widely: solid polymers represent the lowest class of solid materials with values in the range of  $20\text{--}50 \text{ mJm}^{-2}$ , inorganic solids have values in the range of  $100\text{--}200 \text{ mJm}^{-2}$ , while clean metal surface (which are not achieved in practice except for the noble metals) are in the range of  $1000\text{--}2000 \text{ mJm}^{-2}$ . Liquid water, as a result of the hydrogen bonding present, has an unusually high-value surface-free energy for a liquid at  $72 \text{ mJm}^{-2}$  (or a surface tension of  $72 \text{ mNm}^{-1}$ ). Solid polymers on the other hand are characterized by very low values of surface-free energy as the surface of polymers generally do not contain broken bonds (or unsatisfied valencies) but merely loops resulting from the folding of the macromolecules making up the polymer structure. Thus the energy difference between bulk and surface is relatively small leading to a small value of surface-free energy.

As with bulk surface thermodynamics there is a driving force to reduce the surface-free energy of a material. For a solid such as a metal oxide this is readily achieved by the adsorption of a monolayer of organic vapor from the ambient. As surface practitioners are only too aware, any high-energy surface will adsorb such a monolayer spontaneously and all samples of this type analysed by X-ray photoelectron spectroscopy (or other methods for surface chemical analysis) will show tell-tale signs of the adsorption of adventitious carbon in the spectrum. The reduction of surface-free energy is the driving force for the deposition of a well-defined hierarchy of layers as discussed in detail by Castle (2008).

Any technique that probes explicitly, or at least gives an indication of the value of surface-free energy, has the potential to provide information regarding the behavior when a solid surface is coated with a liquid such as an adhesive or organic coating. Such measurements will be extremely surface sensitive, mostly providing information about the outer one or two atomic layers. Such methods can be used in a very pragmatic manner for quality assurance and also in a much more sophisticated manner using well-established protocols to evaluate surface-free energy and deduce the contribution to the parameter from various bonding types.



In the category of simple quality assurance methods, there are two widely used tests that provide straightforward information about the fitness of a solid surface (inevitably after treatment) for further processing: dyne pens and the water break test. Dyne pens are used for the assessment of polymeric surfaces where pretreatment has been carried out to increase the surface-free energy of the material by the incorporation of more polar functional groups. The concept of dyne markers is extremely simple (the term dyne is the cgs unit of force, surface tension having the units of  $\text{dyne cm}^{-1} = \text{mNm}^{-1}$ ;  $1 \text{ N} = 10^5 \text{ dyne}$ ; this system of units is based on centimeter-gram-second units and was the predecessor of the SI or mks system based on meter-kilogram-second units). They are usually supplied as a kit containing pens with “inks” of well-defined surface tensions, usually between 30 and  $60 \text{ mNm}^{-1}$ . In order to assess the surface under test, and they are used almost exclusively to establish the printability of polymer surfaces following surface treatment, the marker pen is applied to the substrate, and if it marks (i.e., the liquid wets) the surface then the substrate has been treated to a level required for wetting to take place. These markers will always have a dye included in the liquid so they can be used in the conventional sense as marker pens for product identification. In general these markers will be used as a go/no-go during processing or to identify the treated side of a polymer film. By using a range of dyne pens, it is possible to estimate the surface tension of a liquid that will just wet the surface and thus gain an indication of the level of treatment of the polymer surface. The advantage of this system is that it is quick, cheap ( $<£10$  per pen), easy to use, and, if the pen is new, can provide quite accurate results. The drawbacks are the short shelf life of pens, easy contamination of the liquid, and the lack of a numerical value relating directly to substrate properties – only a relative ranking order can be deduced. Notwithstanding such shortcomings, dyne markers will continue to play an important role in the surface treatment industry.

The other widely used simple test method is the water break test as described in ASTM (2002). The purpose of this test is to assess the efficacy of a cleaning process of a metal substrate. Here the requirement is exactly the opposite to that for the assessment of polymers in that an oxidized metal surface will have a high surface-free energy that may be compromised by the adsorption, or indeed a deliberate application of organic vapors or liquids. Cleaning is required to remove such extraneous material, which leads to a higher surface energy, and the successful removal of contamination is easily recognized by this test. Such carbonaceous films will be hydrophobic (non-wetting) in nature and the test involves withdrawing the metal panel under test from a container full to the brim with distilled water. On withdrawing a clean substrate, the water will drain uniformly over the surface. In the presence of residual contamination the draining water film will break up into a discontinuous layer around the contaminated regions. Although this is a very subjective test it is quick to carry out and lends itself to process control purposes. One form of the test is embodied in an international standard.

However, it is the measurement of contact angle that provides the most sensitive method and one that can be adapted to provide a quantitative measure of surface-free energy.

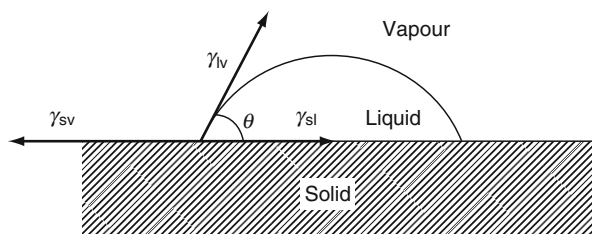
### 9.3.2 Contact Angle

The observation of contact angle ( $\theta$ ) can be related to the surface-free energies of solid substrate ( $\gamma_{\text{solid}}$ ) and wetting liquid ( $\gamma_{\text{liquid}}$ ), along with the interface free energy ( $\gamma_{\text{interface}}$ ) by the well-known Young Equation:

$$\gamma_{\text{solid}} = \gamma_{\text{liquid}} \cos \theta + \gamma_{\text{interface}} \quad (1)$$

which by the simple expedient of resolution of forces about the triple point relates the surface and interface free energy terms to the observed contact angle as shown in Fig. 6. This observation of a sessile drop is frequently used as a quality assurance measure as a very low water contact angle indicates a hydrophilic surface (i.e., one with a relatively high surface-free energy) and a high contact angle indicates a hydrophobic surface (low surface-free energy). The observed contact angle is simply a measure of the propensity of the liquid (generally water in a simple test) to bond with itself compared with the solid substrate. For a hydrophobic substrate the hydrogen bonding between water molecules is much greater than the association between water and the substrate; in the case of a hydrophilic substrate, the association between water molecules and substrate is sufficient to overcome the hydrogen bonding responsible for the self association between water molecules. The direct observation of a large sessile drop (several millimeters in diameter) is readily accomplished in a production environment but the results obtained are only representative of the actual surface-free energy of the substrate if the substrate is homogeneous; heterogeneities in either topography or composition may prevent equilibrium being attained as required by the Young Equation. This may lead to the periphery of the drop departing from the circular and such behavior also manifests itself as contact angle hysteresis. This is often the case and the use of a sessile drop deposited by syringe or pipette has limited the use of contact angle measurement in such environments. Recently, however, the concept of ballistic sessile drop deposition, in which a stream of nanoliter volume drops are deposited on the surface and then coalesce into a single drop with a volume of several microliters, has been investigated and developed to the point that such a device is now available commercially under the name Surface Analyst<sup>TM</sup> from Brighton Technologies Group Inc. (2010). The output from the device is the diameter of the drop deposited in this manner, typically of the order of several millimeters. Initial results are extremely promising and show that such a device is able to separate

**Fig. 6** The equilibrium that exists between a sessile drop and a solid surface, indicating the contact angle



composite panels prepared for adhesive bonding and then contaminated with a range of typical liquids found in a production plant (Dillingham et al. 2010).

As discussed above the surface-free energy of the probe liquid will influence the extent of solid–liquid interactions which will be observed as the contact angle. By the simple expedient of using a range of liquids with different surface-free energies and bonding types, it is possible to use such an approach to determine the surface-free energy of the solid. Many commercial instruments are available and all will be supplied with a dedicated computer that will contain the necessary software to make calculations of surface-free energy and related parameters, although all software should be supplied with a health warning for the inexperienced user! It is possible to assess the surface-free energy by extending the Young Equation, above, and recognizing that the surface-free energy can be subdivided into components that represent the degree bonding attributable to dispersion forces ( $\gamma^D$ ), polar forces ( $\gamma^P$ ), hydrogen bonding ( $\gamma^H$ ), and so forth, such that:

$$\gamma = \gamma^D + \gamma^P + \gamma^H + \dots \quad (2)$$

where the exact number of components depends on the material type and thus the bonding types involved. It is possible to arrive at the following relationship, the derivation of which is given by Packham (2005):

$$1 + \cos \theta = 2 \frac{(\gamma_L^D \gamma_S^D)^{1/2}}{(\gamma_L)} + 2 \frac{(\gamma_L^P \gamma_S^P)^{1/2}}{(\gamma_L)} \quad (3)$$

where the subscripts S and L represent the solid substrate and wetting liquid, respectively. The approach involves the use of a series of liquids of known values of the dispersive and polar contributions to surface-free energy, to measure the contact angles on the solid substrate of interest. This then yields a number of simultaneous equations of the type shown above. As they contain only two unknowns, the dispersive and polar contributions of the surface-free energy of the substrate, these can be readily evaluated. An alternative approach is to rearrange the equation in the form:

$$\frac{\gamma_L(1 + \cos \theta)}{2(\gamma_L^D)^{1/2}} = (\gamma_S^D)^{1/2} \left[ \frac{(\gamma_L^P)^{1/2}}{(\gamma_L^D)^{1/2}} \right] + (\gamma_S^P)^{1/2} \quad (4)$$

The equation is now in the form of  $y = mx + c$ , and a graph of  $\gamma_L(1 + \cos \theta)/2(\gamma_L^D)^{1/2}$  plotted versus  $[(\gamma_L^P)^{1/2}/(\gamma_L^D)^{1/2}]$ , the gradient of the best-fit line will be  $(\gamma_S^P)^{1/2}$ , and the line intercept  $(\gamma_S^D)^{1/2}$ . The surface energy of the unknown solid,  $\gamma_S$ , is then the sum of the two terms,  $\gamma_S = \gamma_S^D + \gamma_S^P$ . The form of plot obtained using this approach is illustrated in Fig. 7, which represents data obtained from a poly (dimethyl siloxane) surface using water, di-iodomethane, and hexadecane as probe liquids that gave mean contact angles of 119°, 79°, and 37°, respectively.

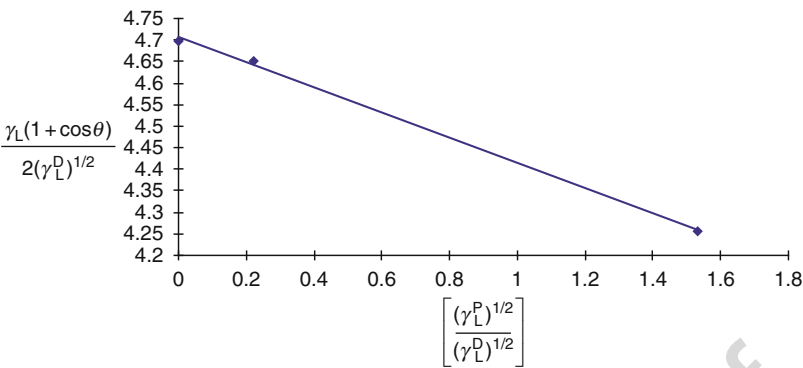


**Fig. 7** Wetting data for poly(dimethyl siloxane) (PDMS) probed by water, di-iodomethane, and hexadecane

**Table 1** Surface-free energies of liquids used in the wetting experiment of Fig. 7

Probe liquid	$\gamma^D$ (mJm <sup>-2</sup> )	$\gamma^P$ (mJm <sup>-2</sup> )	$\gamma$ (mJm <sup>-2</sup> )
Water	22	51	73
Di-iodomethane	28	0	28
Hexadecane	2	49	51

The relative contributions of dispersion and polar bonding to these three liquids are shown in Table 1. The value of surface-free energy obtained in this way was 22 mJm<sup>-2</sup> (Choi 2003).

### 9.3.3 Inverse Gas Chromatography

As shown above the use of contact angle measurements provides a relatively straightforward manner in which to assess the surface energetics and wetting characteristics of a solid surface. It is particularly attractive as it can be used on several levels of complexity ranging from a qualitative assessment of surface behavior (hydrophobic or hydrophilic) through to its use for the determination of surface-free energy and relative contributions to that parameter from dispersion and polar bonding. In spite of these obvious advantages it remains a macroscopic measurement and invariably represents the value over a large area, and application to rough surfaces will suffer from excessive amount of contact angle hysteresis unless some form of ballistic drop deposition is employed. An alternative approach to assessment of surface-free energy of solids is the use of inverse gas chromatography (IGC). The term inverse is used in the title to indicate that the material of interest is the stationary phase in the gas chromatography column rather than the volatile species injected into the column. (In the usual mode of operation for gas chromatography the volatile species is the phase under investigation and a standard stationary phase is employed.) The major restriction of IGC is that the solid phase under investigation

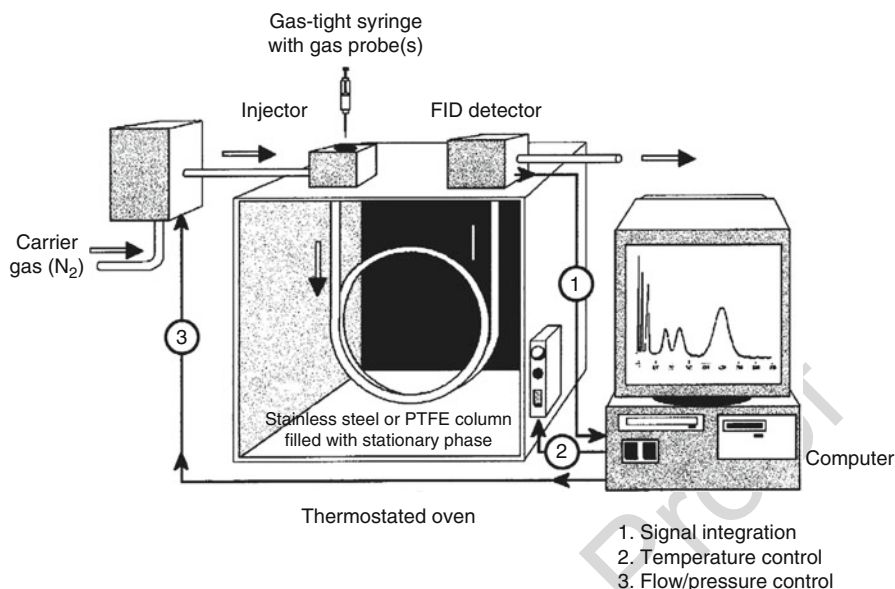


**Fig. 8** Schematic diagram of the experimental configuration used for inverse gas chromatography (Reproduced from Abel and Watts 2005a with permission)

must be in a form suitable for incorporation into a column a few millimeters in diameter. This limits the physical form to coarse powders and fibers. As the stationary phase is usually conditioned at elevated temperature (ca. 120 °C) before injection of probes, this provides the driving force to desorb adventitious contamination and water so that adsorption of the probes is carried out on a cleaner surface than contact angle measurements. One advantage of IGC is that the high-energy sites on the surface are probed preferentially and rough surfaces can be investigated; indeed the comparison of results from long chain and branched isomers of the same molecule (usually an alkane) enable roughness to be elucidated.

The form of a typical IGC arrangement is shown in Fig. 8 and is readily carried out using standard GC equipment although specialized IGC equipment is available that allows the control of relative humidity and automated operation (Surface Measurement Systems 2010). A column of stainless steel or poly(tetra fluoroethylene) (PTFE) is packed with the solid of interest and loaded between the injector and the detector. The analytical measurements consist of injecting, sequentially, a series of volatile probes of known properties through the column along with an inert carrier gas. The retention time for each probe is related to the surface properties of the stationary phase. The usual practice is to carry out a series of injections with a homologous series of nonpolar organic probes such as the n-alkanes. This gives information about the interactions between the probes and the stationary phase associated with dispersion forces (sometimes referred to as Lifshitz–van der Waals forces). When a parameter derived from the observed retention time is plotted against probe boiling point, a logarithmic relationship can be observed which can be used to calculate the dispersion

441 bonding contribution to surface-free energy (Abel and Watts 2005a). Alkane probes  
442 are apolar molecules only able to interact with solid surfaces through dispersion  
443 bonding and for this reason they only probe dispersion interactions with the stationary  
444 phase enabling the contribution of this bond type to surface-free energy to be assessed.  
445 In order to assess the contribution of acid–base (or polar) interactions it is necessary to  
446 use polar probes, the magnitude of the deviation from the linear relationship referred to  
447 above being a measure of the magnitude of acid–base interaction between the station-  
448 ary phase and the polar probes (Abel and Watts 2005b). The effect on retention time of  
449 the probe properties is illustrated in Fig. 9, which is an inverse gas chromatogram  
450 achieved by simultaneously injecting five probes (two alkanes and three polar probes)  
451 and methane as a noninteracting marker to define zero time. The substrate is hydrated  
452 alumina. A typical plot achieved in this manner is shown in Fig. 10 for an aromatic  
453 methacrylate resin (the parameter  $V_N$  in the ordinate is the net retention volume which  
454 is calculated from the net retention time, the primary measurement in IGC, illustrated  
455 in Fig. 9). The three polar probes are a combination of acidic and basic types:  
456 trichloromethane is acidic, ethyl acetate amphoteric but predominantly basic, and  
457 tetrahydrofuran is basic. The fact that significant deviations are seen from the reference

**Fig. 9** IGC data recorded for hydrated alumina treated with an organosilane adhesion promoter when five probes are injected simultaneously to illustrate the effect of probe characteristics on retention time (Reproduced from Chehimi et al. 2001 with permission of The Royal Society of Chemistry)

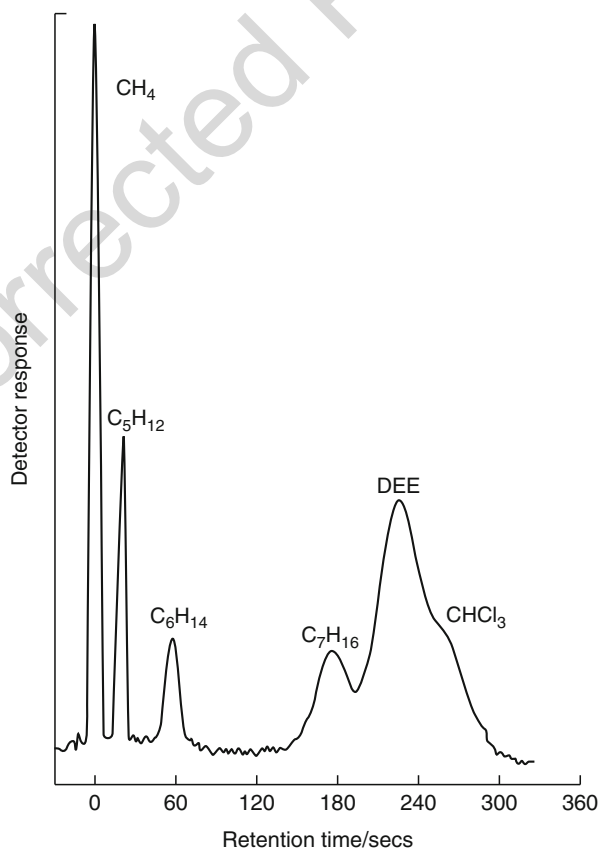
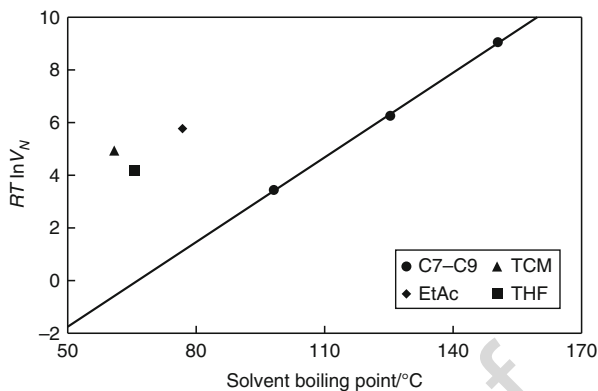


**Fig. 10** Adsorption of apolar and acid base probes on an aromatic methacrylate resin. *TCM* chloroform, *EtAc* ethyl acetate, *THF* tetrahydrofuran (Reproduced from Taylor et al. 1995 with permission)



alkane line indicates that the substrate has both acidic and basic sites. This illustrates one of the strengths of IGC; by the informed choice of polar probes it is possible to probe polar sites on the stationary phase and furthermore estimate the extent of acidic and basic contributions.

## 9.4 Surface Chemical Analysis

As the forces responsible for adhesion between substrate and adhesive or organic coatings operate over very short distances, the requirement for a chemical analysis method that can provide information regarding the nature of interfacial bonding, or indeed the presence of species that will compromise it, along with an exact definition of where failure occurs, needs to have a characteristic sampling depth of similar dimensions. This requirement is met by techniques that fall into the category of those that provide a surface chemical analysis. Although there are a number that can be placed in this category, or other methods that can be modified so as to provide surface-specific information, the term “surface chemical analysis methods” is currently taken to mean three methodologies: X-ray photoelectron spectroscopy (XPS); Auger electron spectroscopy (AES) and its chemical imaging variant scanning Auger microscopy (SAM); and time-of-flight secondary ion mass spectrometry (ToF-SIMS). The methods have all been commercially available for many years and can now be considered as mature analytical techniques that are fairly readily available in universities, corporate research laboratories, and organizations providing contract analysis. XPS and AES are based on the energy analysis of low-energy electrons while SIMS makes use of mass spectrometry of the sputtered surface ions (both positive and negative) to achieve surface mass spectrometry. The analysis depth is of the order of 5 nm for the electron spectroscopies and rather less for SIMS. Their application, particularly of XPS, in adhesion studies has been reviewed by the current author several times in the past (Watts 1988, 2009, 2010) and the current section is intended to provide a very brief overview of these methods and their application in adhesion-related studies. For further details the interested reader is referred to introductory



(Watts and Wolstenholme 2003; Vickerman and Gilmore 2009) or more advanced texts (Briggs and Vickerman 2001; Briggs and Grant 2003) on these topics.

### 9.4.1 X-ray Photoelectron Spectroscopy

XPS has been widely used in many areas of materials science, chemistry, and physics over the 40 years since it first became commercially available. The application of XPS to adhesive bonding studies and adhesion science in general was well established by the late 1970s and by 1980 there were four research groups with a strong presence in this area, two in the USA and two in Europe, interestingly enough three of these were based in corporate research laboratories with only one in academia (Castle's Group at the University of Surrey). The enthusiasm with which XPS has been adopted by the adhesion community springs, to a large extent, from the important role that surface and interfacial phenomena have to play in the adhesion process. The characteristic length scales over which bonds form, or indeed can be compromised or enhanced by the presence of additional molecules (e.g., contamination or adhesion promoters), are consistent with the analysis depth that is probed by XPS, as well as the other surface analysis techniques.

The heart of the XPS experiment is the irradiation of a solid sample with soft X-rays, usually  $\text{AlK}\alpha$  with a photon energy of 1486.7 eV. This leads to the emission of photoelectrons that are then injected into an energy analyzer/detector arrangement that will determine their intensity as a function of energy. The primary measurement made by the spectrometer is the kinetic energy ( $E_k$ ) of the outgoing electrons; this is not a characteristic material property but is a function of the photon energy ( $h\nu$ ) employed in the XPS experiment. The fundamental property is the electron binding energy ( $E_b$ ), in simple terms the energy with which a particular electron is bound into its electronic orbital. This quantity is related to the experimental observable and photon energy by the following equation:

$$E_b = h\nu - E_k - \omega \quad (5)$$

where  $\omega$  is a constant term, the spectrometer work function. The output of an XPS system is the X-ray photoelectron spectrum and Fig. 11 indicates the survey spectra obtained from clean aluminum foil and foil that has been handled prior to analysis. The spectra contain peaks that are assigned to Al (2p and 2s), Si (2p and 2s—contaminated sample only), C (1s), and O (1s); in addition there are Auger transitions associated with the de-excitation of the C1s and O1s core holes. These spectra are readily quantified to provide a surface chemical analysis in atomic percent, the carbon level having doubled on handling and silicon having appeared on the surface at a concentration of 6.3%. The silicon is present as a silicone oil (most likely from a personal care product) and provides an example of the type of adventitious material present on a surface that may compromise the bonding process and the performance of the adhesive joint.

As well as ready quantification XPS can provide chemical state information by inspection of the exact binding energy of the XPS peak. This so-called chemical shift



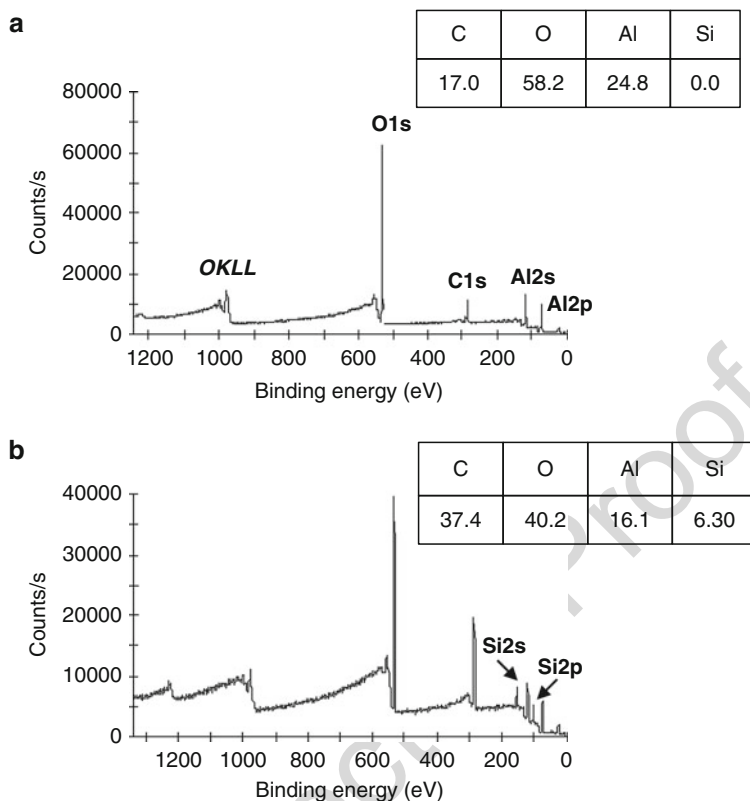


**Fig. 11** XPS survey spectra of aluminum foil recorded in the (a) as-received condition, and (b) following handling contamination. The quantitative surface chemical analyses (in atomic percent) is given in the inset boxes on each spectrum

is the cornerstone of XPS and provides a powerful means of assessing the valence state of metallic and nonmetallic species and the bonding types in organic and polymeric molecules. Figure 12 illustrates this aspect of XPS with a high-resolution Al2p spectrum showing components assigned to metallic aluminum ( $\text{Al}^0$ ) and the oxide ( $\text{Al}^{3+}$ ). The intensity of electrons ( $I_d$ ) emitted as a function of depth ( $d$ ) is described by the well-known Beer–Lambert Equation:

$$I_d = I_\infty \exp(-d/\lambda \cos \theta) \quad (6)$$

where  $I_\infty$  is the intensity from an infinitely thick sample of the same composition,  $\lambda$  is the electron attenuation length (the effective scattering length of electrons of a particular energy in the solid of interest that will be 1–3 nm), and  $\theta$  is the electron take-off angle relative to the sample surface normal. The variation of the intensity with depth is shown in Fig. 13, which illustrates quite clearly the exponential decay of the signal as a function of depth. This form represents the intensity for a solid with a thin attenuating overlayer (such as an oxide on a metal) and relates to the signal

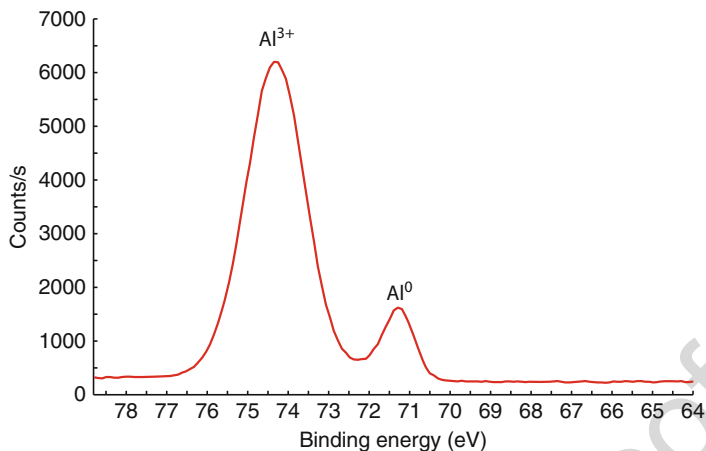


**Fig. 12** High-resolution Al<sub>2</sub>p spectrum showing metallic and oxidic components of the spectrum

from the substrate. The Beer–Lambert Equation can also be written in terms of a thin overlayer (such as the oxide on a metal) where the signal considered is that from the thin overlayer. The equation then becomes:

$$I_d = I_\infty [1 - \exp(-d/\lambda \cos \theta)] \quad (7)$$

This provides a useful approach for calculating the thickness of thin layers on substrates such as a thin adhesive residues or the thickness of a contaminant layer. In the case of a thin metal oxide, the two equations can be combined to provide a ready means of estimating the oxide thickness from the intensity of the cationic ( $I^{\text{ox}}$ ) and metallic ( $I^{\text{me}}$ ) components of the spectrum:

$$d = \lambda \cos \theta \ln[(I^{\text{ox}}/I^{\text{me}}) + 1] \quad (8)$$

For the spectrum of Fig. 12, an oxide thickness of 4.2 nm is calculated using this method.

The geometric term,  $\theta$ , in Eq. 6 indicates the variation of electron yield with the take-off angle and this provides an important way in which the depth of analysis can be varied by recording spectra at different take-off angles. This is known as angle-resolved XPS (ARXPS) and by combining the ARXPS data set with suitable software it is possible to use this method to produce shallow compositional depth profiles in the range 0–5 nm. This is particularly useful for investigating the surface segregation of minor components to free surfaces or, indeed, interfacial failure surfaces.

Thus, XPS provides a quantitative surface analysis method that is applicable to all solid materials, so long as they are stable within the ultra-high vacuum environment of the spectrometer, and the high-resolution spectra provide chemical information for all elements in the periodic table with the exception of hydrogen. Traditionally XPS is considered to be an area-integrating technique as the photoelectron spectrum is

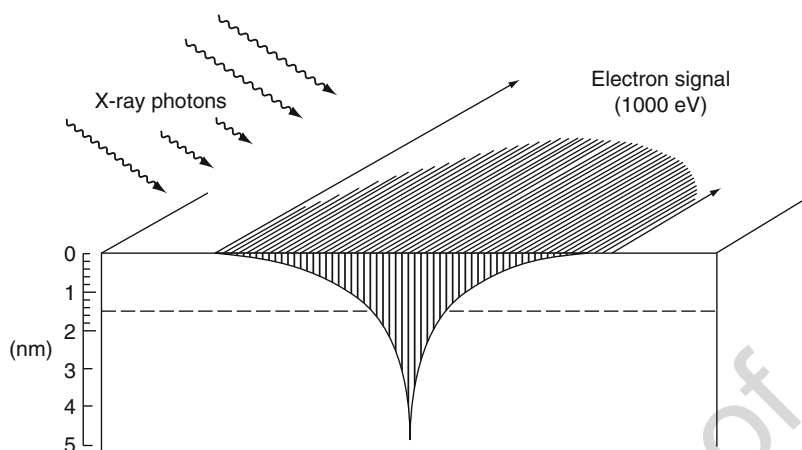


**Fig. 13** Variation of electron emission as a function of depth for a typical XPS experiment

acquired over a relatively large area of several square millimeters. Modern instruments, however, are able to record complete spectra at high spatial resolution (the best currently available is 10  $\mu\text{m}$ ) or produce elemental or chemical maps similar in appearance to those produced in electron probe microanalysis (EPMA). Such improvements have come about as a result of the development of microfocus X-ray monochromators and analyzers that allow the acquisition, in parallel or serial format, of images at the detector. A current state-of-the-art XPS system will be equipped with a monochromatic  $\text{AlK}\alpha$  X-ray source and imaging facilities by either parallel (at the detector) or sequential (rastering either specimen stage or X-ray spot) acquisition. The two approaches to imaging XPS both have their advantages; parallel imaging is much faster and allows assessment of the specimen to be made as the XPS images develop, but extraction of chemical state information requires a number of sequential energy-selected maps to be acquired. With serial mapping (analogous to the EPMA approach) a full spectrum can be acquired at each pixel point as the position of analysis moves sequentially across the specimen. The data set can then be integrated and spectra at each pixel point peak fitted or used to contribute to a quantitative analysis or overlayer thickness map. The disadvantage of such a method is that it is very time consuming. Figure 14 illustrates the small spot XPS system in the author's laboratory (which uses serial acquisition for imaging) and provides parallel ARXPS data. The XPS images from a failed adhesive joint obtained with this system are shown in Fig. 15.

#### 9.4.2 Auger Electron Spectroscopy and Scanning Auger Microscopy

AES and SAM are both based on the use of a finely focused electron beam to provide a surface analysis. The division between the two techniques is largely arbitrary nowadays but the configuration of a scanning Auger microscope will have, in appearance,

**Fig. 14** Modern XPS system with serial imaging and parallel ARXPS capabilities



much in common with a scanning electron microscope and at its heart will be a high-resolution electron gun, typically giving sub 10 nm resolution, and a high transmission electron energy analyzer. Such systems can usefully form the basis of sophisticated multi-technique instruments and Fig. 16 shows the Auger microscope in the author's laboratory that was specified in this way. As well as featuring high-resolution Auger analysis, this instrument also has facilities for energy dispersive X-ray analysis (EDX), XPS, and backscattered electron detection. The provision of AES and EDX without the need to relocate the sample is extremely useful as it provides analysis in surface and bulk regions (5 nm cf. 1  $\mu$ m). In contrast to scanning Auger microscopy, AES is taken to mean the provision of electron-induced Auger spectra, often in the form of an ancillary technique on an XPS system (as the analyzer used is the same) or process systems (where deposition quality may need to be monitored) where the need for the ultimate spatial resolution is not paramount. Electron guns for this application will range in spot size from 5  $\mu$ m down to 100 nm, still much better than the spatial resolution that can be achieved by XPS.

The generation of an Auger electron is a three-electron process involving the removal of a core electron to leave a core hole, the filling of the hole by an electron from outer level and the emission of an electron (often from the same outer level) as an Auger electron. The nomenclature employed for Auger transitions identifies the element and the energy levels involved in the three-electron process, for example, Zn  $L_3 M_{4,5} M_{4,5}$ . The Auger process achieves the same relaxation effect as the emission of an X-ray photon (indeed they can be considered as competitive processes) but

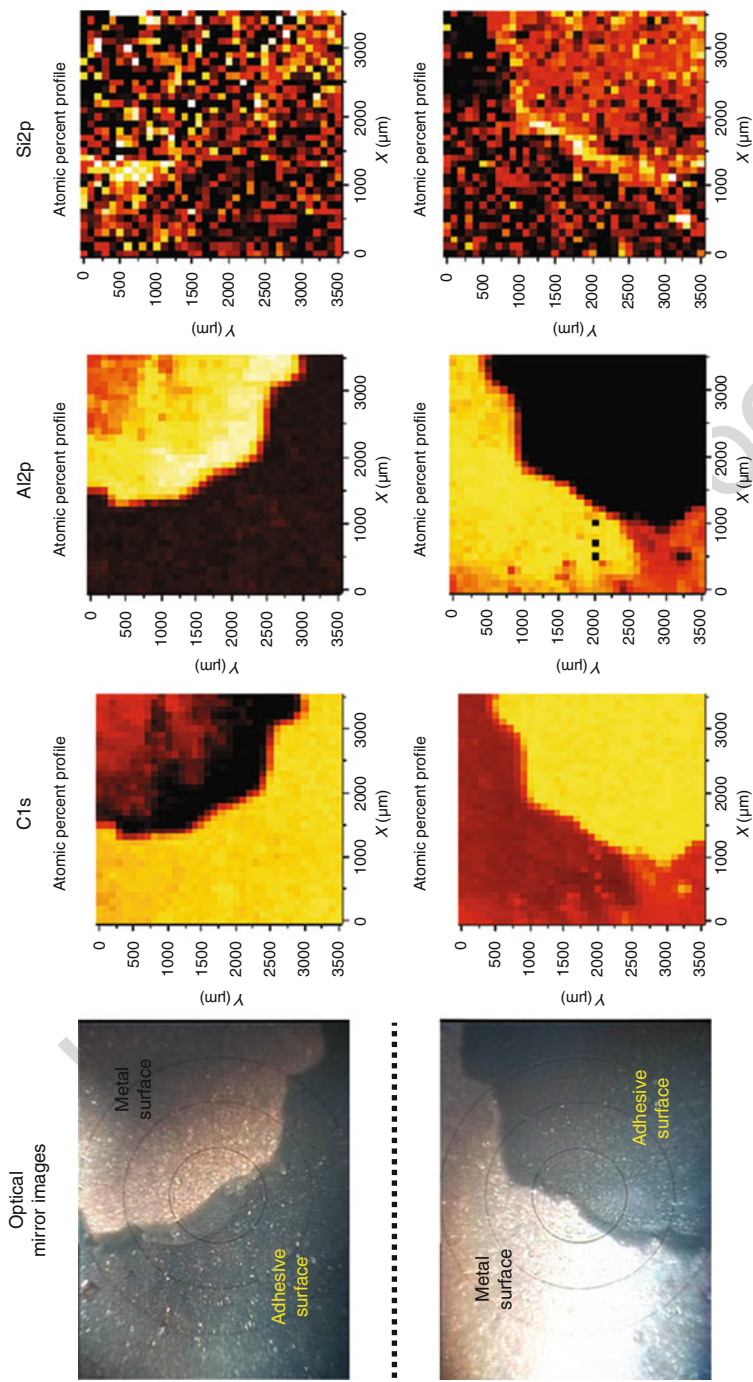
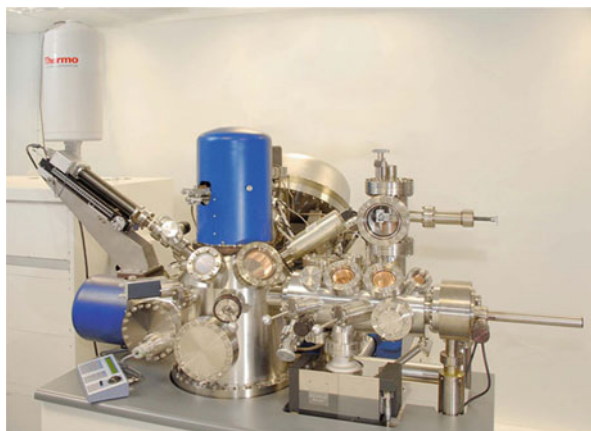


**Fig. 15** XPS images recorded from the interfacial failure surfaces of an adhesively bonded aluminum joint, prepared using an organosilane primer, with an instrument of the type shown in Fig. 14. The optical mirror images are complementary views of the fracture surfaces and are mirrored along the dotted line. Visually the failure appears to be interfacial with the fracture path moving from one interface to the other at the boundary between metal and adhesive interfacial failure surfaces

**Fig. 16** A multi-technique analytical system (AES, SAM, SEM, XPS, EDX, BSE) based around a high-resolution scanning Auger microscope



fortuitously Auger cross sections are good where X-ray ones are less favorable and vice versa. The nature of the Auger emission process means that very light elements do not show Auger transitions but elements from beryllium onward all yield Auger spectra. As an example of Auger spectra, Fig. 17 shows Auger spectra taken from the points identified in the SEM image of Fig. 1. The two survey spectra show clear differences in the Zn spectra with the data from Point 1 being much better defined than Point 2. The high-resolution Al KLL spectra provide an example of the chemical shift (seen in all elements in XPS), in AES; Point 2 shows both metallic and oxide contributions but Point 1 only shows evidence of aluminum oxide. The Auger chemical effect is generally only observed for transitions in which all three electrons can be considered to be core electrons. If valence band electrons are observed, the band structure is reflected in the shape of the Auger peak that becomes broad and degenerate and yields little chemical information.

It is usual for XPS and AES/SAM systems to be fitted with an inert gas ion gun which can be used for sputtering the surface layers of metallic and inorganic samples. When such sputtering is interspersed with surface analysis it is straightforward to produce a compositional depth profile. Figure 18 indicates a very high quality Auger sputter depth profile obtained from a multilayer structure provided as a standard reference material. In order to get very good interface definition from these 5-nm thick metallic layers, various parameters were optimized including ion beam energy, and specimen geometry, which was rotated during sputtering to avoid the development of ion beam-induced topography. By combining depth profiling with SAM it is possible to obtain a three-dimensional nanoscale representation of the near-surface region of a specimen.

SAM is a technique that can sample extremely small volumes of material (probably the smallest of any technique without the need for extensive sample preparation) and for this reason the choice of sample and the manner in which the analysis is carried out is extremely important. As with any electron microscopy-based analysis method, the need to acquire data from a representative sample of the specimen must be uppermost in the mind of the analyst. As SAM is an electron beam technique it is really only applicable to conductors or semiconductors, a useful guide being that if the specimen



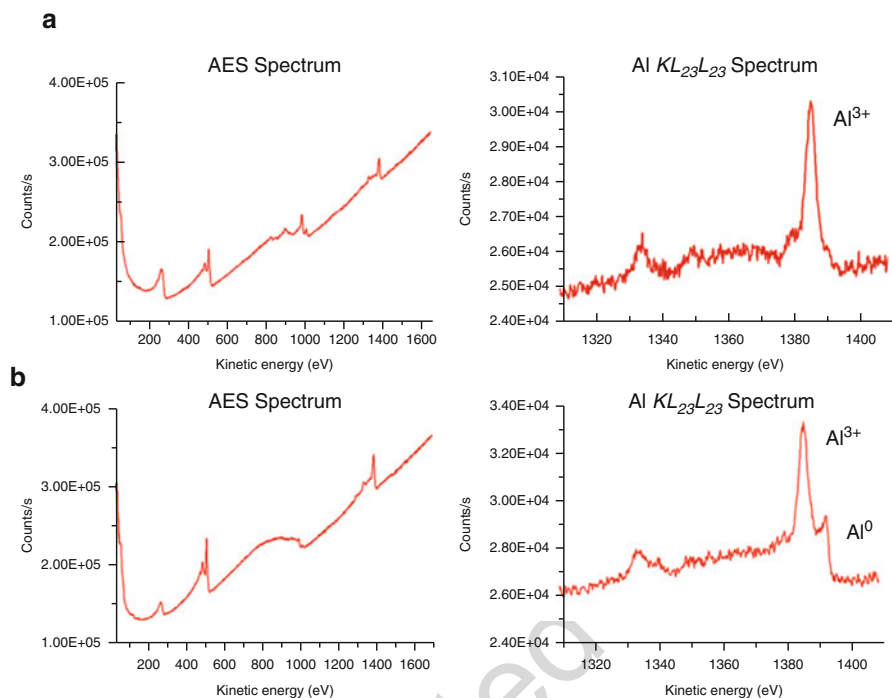


**Fig. 17** AES point spectra from the regions identified in the SEM image of Fig. 1. **(a)** Point 1 of Fig. 1, **(b)** Point 2 of Fig. 1

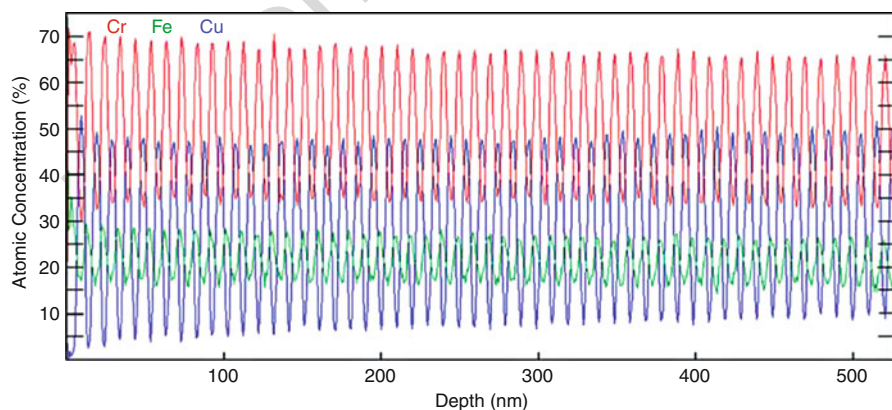


**Fig. 18** AES sputter depth profile through an iron/copper/chromium multilayer structure. Each layer is 5 nm thick (Courtesy of Thermo Fisher Scientific)

can be imaged in an SEM without sample charging SAM will be possible. For these reasons the role of AES/SAM in adhesion studies is restricted to the analysis of metallic substrates and pretreatment layers. There are ways in which it is possible to apply the technique to insulators (Baer et al. 2010) but analysis of polymers by AES is not practicable the usual approach being to use XPS or ToF-SIMS.

### 9.4.3 Time-of-Flight Secondary Ion Mass Spectrometry

In recent years SIMS has become a widening field with many types of ion sources and mass spectrometers being used to provide surface mass spectrometry. In ToF-SIMS the solid sample under investigation is bombarded by a beam of primary ions that sputters atomic ions, cluster ions, and neutrals from the surface. The secondary ions (either cations or anions depending on whether a positive or negative ToF-SIMS spectrum is being acquired) are extracted by high voltage extraction optics and injected into a time-of-flight mass spectrometer. The flight time of the ions is proportional to their mass, once energy distribution has been normalized by the use of an ion mirror, and the time taken to reach the detector is then converted to mass to charge ratio. Modern ToF-SIMS systems can operate at extremely high mass resolution and peak positions can be recorded with an accuracy of  $\pm 0.001$  Da, and this together with high transmission and parallel detection of all masses makes this analyzer the one of choice for surface analysis by SIMS. It should be noted that Dalton (Da) is the preferred unit in mass spectrometry indicating unified mass/charge ( $m/z$ ). The unified mass unit is not the same as atomic mass unit as the former is relative to the  $^{12}\text{C}$  isotope while the latter is relative to the  $^{16}\text{O}$  isotope. The difference between the two however is small at 318 ppm. As the SIMS process is a destructive one, in that material is removed from the surface as it is irradiated with the primary ions, by collecting the secondary ion signals as a function of sputter time it is possible to construct a compositional depth profile. This forms the basis of a technique known as dynamic SIMS, used for profiling dopant concentration in semiconductors and the like. For surface analysis by SIMS it is important that the spectrum is recorded from the undisturbed surface and the general rule of thumb is that the surface remains in this state if the total ion dose during the acquisition of the spectrum is  $<10^{13}$  ions  $\text{cm}^{-2}$ . When SIMS is carried out under these conditions it is known as static SIMS and the critical ion dose is referred to as the static limit.

A top end ToF-SIMS instrument, of the type shown in Fig. 19, is a very complex analytical system that provides the analyst with many choices relating to the manner in which the spectrum or image is acquired. Does one optimize spectral resolution or spatial resolution? Which ion source should be employed as the primary beam and, if required, which for sputtering to produce a depth profile? One of the key decisions to be made is in the choice of ion source; this can be monoatomic in nature (e.g.,  $\text{Ga}^+$ ,  $\text{Bi}^+$ ,  $\text{Cs}^+$ ,  $\text{Ar}^+$ ), but a major advance over the last decade has been the routine availability of cluster (i.e., polyatomic) ion sources. These are particularly useful in the ToF-SIMS analysis of polymers as they increase the yield at high masses and there is also increasing evidence that they increase the yield of nitrogen-containing



**Fig. 19** A modern ToF-SIMS instrument featuring multiple ion sources and preparation chamber



fragments (which occur at even masses if there are an odd number of nitrogen atoms in the cluster), which is particularly useful for the analysis of amine-cured epoxy adhesives. The choice of cluster ions available from ToF-SIMS manufacturers is currently based around liquid metal ion sources for high spatial resolution; for example, a bismuth source of this type can provide elemental ion ( $\text{Bi}^+$ ) or  $\text{Bi}_3^+$ ,  $\text{Bi}_5^+$ , or  $\text{Bi}_7^+$  cluster ions. There is a very slight reduction in spatial resolution of bismuth trimers compared with elemental ions, the best available currently being of the order of 100 nm. The other cluster ion source that has gained increasing popularity in the last few years is Buckminster Fullerene,  $\text{C}_{60}$  and while the resolution is of a few micrometers it is widely used as a primary source in biological studies although the mode of operation preferred for polymeric samples is to use the  $\text{C}_{60}$  source for sputtering and the Bi source for analysis. This combination indicates one of the strengths of the  $\text{C}_{60}$  source, which is its ability to sputter profile some polymeric materials without the damaging effects that are normally observed when profiling with inert gas ions such as  $\text{Ar}^+$ . Such profiling can be carried out by XPS as well but is restricted to certain commercial systems, whereas in ToF-SIMS the depth profiling of polymers is becoming a routine undertaking. Figure 20 illustrates such a depth profiling experiment on a poly(vinylidene fluoride) coating to which an acrylic flow aid had been added. The negative ToF-SIMS spectrum (Fig. 20a) was obtained after a short (<500 ms) sputter with 8 kV  $\text{C}_{60}$  ions. The depth profile of Fig. 20b shows how the acrylic specific ions peak at a sputter time of 1 s and then decreases as the PVdF ions reach a maximum at the same time. Angle-resolved XPS indicates that the surface segregated layer is about 1.5 nm thick so the seven second depth profiles represent about 10 nm in depth. The high-resolution spectra of Fig. 20c, recorded from the acrylate-rich subsurface and the PVdF bulk material from deeper in the profile, indicate the ease with which two ions of nominal mass

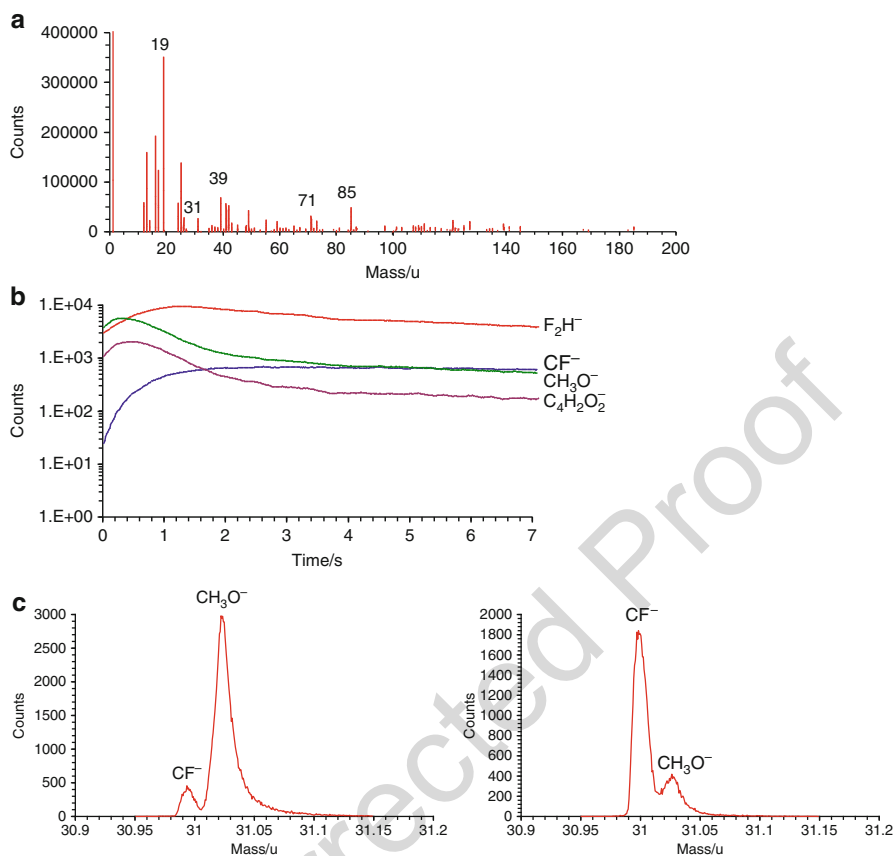


**Fig. 20** ToF-SIMS depth profile experiment of a PVdF organic coating. **(a)** Negative ToF-SIMS spectrum from a subsurface region of the materials showing the presence of acrylate ions in the spectrum, **(b)** molecular depth profiling showing PVdF and acrylate specific ions, **(c)** high-resolution negative ToF-SIMS in the nominal 31 u region of the spectrum

31 u can be resolved in the high-resolution mode. The exact masses of the two ions are 30.9984 u ( $CF^-$ ) and 31.0184 u ( $CH_3O^-$ ), the separation of 0.02 u quite easily achieved with the experimental conditions used.

ToF-SIMS can also be operated in a mode that provides spatially and mass-resolved chemical images referred to as imaging SIMS. The usual manner of operation is to collect full sets of mass spectra at each pixel point and post-acquisition processing is undertaken to assemble the mass-selected images of interest. A very simple manner in which variations of two mass fragments can be compared is by the use of a scatter ratio diagram, a technique developed many years ago for the processing of scanning Auger microscopy data. In the creation of a scatter ratio diagram, from ToF-SIMS data, two mass-selected images are compared and at each pixel point the intensity of the two ions are plotted on orthogonal axes. This enables the analyst to identify clusters of pixels that have similar compositions. These pixels are then highlighted

on a false color image to enable these regions to be visualized in x:y space. The scatter ratio diagram contains only compositional, but no direct positional, information while the false color image correlates positions of similar compositions. This can be illustrated by data obtained from a galvanized steel sample similar to that illustrated in Fig. 1. ToF-SIMS data was acquired in the usual way from a region  $500 \times 500 \mu\text{m}$  in size. The intensity of the  $^{27}\text{Al}^+$  and  $^{64}\text{Zn}^+$  ions were compared at each pixel point and the scatter ratio diagram of Fig. 21 produced. From this diagram it can be seen that the data falls into two distinct regimes, those with a low  $^{64}\text{Zn}^+$  intensity (outlined in dark grey) and those where the  $^{64}\text{Zn}^+$  intensity is significantly higher (outlined in light grey). If a false color map is now constructed with pixels in the low zinc region coded dark grey and those from the higher zinc region coded light grey, the characteristic topography of the steel sheet is revealed (Fig. 21b), indicating the regions that are low in zinc (dark grey) and those where the surface zinc concentration is higher (light grey).

Of course as with all forms of microscopy there is the trade-off of spatial resolution with intensity, which, in the case of ToF-SIMS, invariably compromises the spectral resolution. Although the ultimate spatial resolution may be of the order of 100 nm, the spectral resolution at this level will only be around unit mass resolution; if one optimizes spatial resolution the mass resolution has to be degraded to several micrometers in order to get adequate counting statistics. Fortuitously for the analyst instrument manufacturers provide a mode of operation that offers middle ground in forms of both spatial and spectral resolution.

The manner in which a ToF-SIMS data set is collected, with complete spectra at each pixel point, means that a single image, from perhaps a  $100 \times 100 \mu\text{m}^2$  or  $500 \times 500 \mu\text{m}^2$  field of view comprising of a  $128 \times 128$  pixel array, will contain

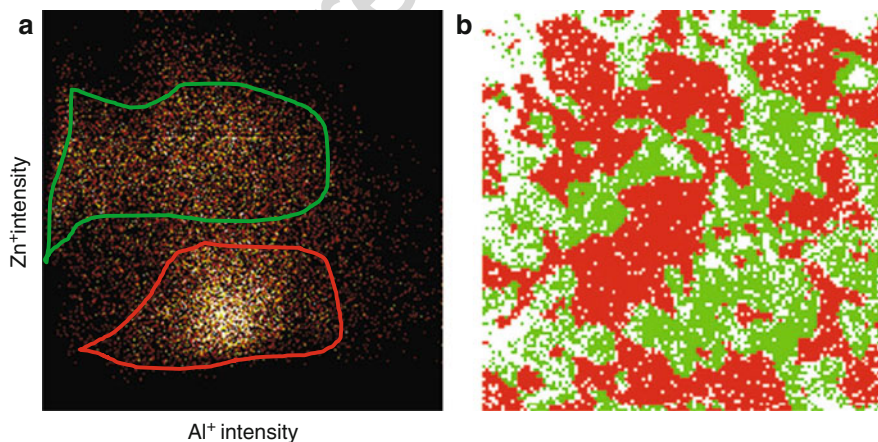


**Fig. 21** ToF-SIMS analysis of a galvanized steel sample. (a) is the scatter ratio diagram constructed from the intensities of the  $^{27}\text{Al}^+$  and  $^{64}\text{Zn}^+$  ions and regions of higher (light grey) and lower (dark grey) zinc concentration are readily identified, (b) grey scale ToF-SIMS image constructed using the dark and light grey regions of Fig. 21a, which now indicates the areas on the sample surface enhanced and deficient in zinc

more than 16,000 individual spectra; added to this is the possibility of depth profiling with 100 analysis points into the sample and the number becomes well over one million in the data set! With so many spectra the examination and interpretation of each individual spectrum becomes impossible; the univariate analysis approach will not work so one must resort to multivariate analysis (MVA) techniques. These are now widely applied in ToF-SIMS as well as many other forms of materials analysis and form part of an area of endeavor known as chemometrics. Commercial ToF-SIMS data systems now have MVA software included, but it is still often necessary for the analyst to buy in specific software suites and adapt for ToF-SIMS use. Popular MVA methods used to process ToF-SIMS data include principal component analysis, multivariate curve resolution, and partial least squares regression. Recent literature in the area has been augmented by an extremely comprehensive review article by Lee and Gilmore (2009) and also a special two-volume issue of the journal *Surface and Interface Analysis* (2009a, b) dealing MVA in surface analysis.

In adhesion research one of the options that has become achievable at last with the latest generation of ToF-SIMS instruments is the ability to track reaction chemistry on surfaces; in this manner it is possible to study how components present in an adhesive formulation may interact with the solid surface, and in this manner it has become possible to start to unravel the interface chemistry of adhesion from very complex multicomponent systems. Other important applications in adhesion include the identification of minor components of an adhesive at fracture surfaces and the ability to visualize such residues at a resolution of significantly less than 1  $\mu\text{m}$ .

---

## 9.5 Conclusions

There are a wide variety of procedures and analytical methods that can be used to assess the surface characteristics of a solid surface relevant to adhesive bonding. These range from the relatively simple and inexpensive such as the water break test through to the extremely complex and expensive such as ToF-SIMS. Some will be required for quality assurance purposes and some belong in a research environment; the surface characteristics that require assessment may be surface topography (AFM or SEM might be used), surface energetics (contact angle measurements or IGC), or surface chemical analysis (XPS, AES/SAM, or ToF-SIMS). It is unlikely that any one laboratory will have access to all such techniques and thus those readily available will be pressed into service. Some laboratories will carry out commercial consultancy activities for all-comers and this is often a cost-effective way to obtain electron microscopy and surface analysis services. This is often a way to gain familiarity with advanced techniques and added value is often obtained from experienced analysts who will be responsible for instrument operation.

In order to obtain a clear, concise, and accurate picture of the surface under investigation, there will almost certainly be the need to resort to more than one of the methods described in this chapter. The choice will be influenced by the nature of the material, the type of investigation, and other variables. In adhesive bonding research one thread that runs through virtually all work, be it quality assurance, development,

or research, is to relate surface characteristics to a performance measure of the bonded structure. This may be joint strength or toughness but more usually, and particularly for structural adhesive bonding, attempts will be made to correlate the surface and interface characteristics with joint durability.

## References

- Abel M-L, Watts JF (2005a) Inverse gas chromatography. In: Packham DE (ed) Handbook of adhesion. Wiley, Chichester, pp 252–254
- Abel M-L, Watts JF (2005b) Inverse gas chromatography and acid-base interactions. In: Packham DE (ed) Handbook of adhesion. Wiley, Chichester, pp 255–257
- ASTM (2002) F 22–02 Standard test method for hydrophobic surface films by the water break test. ASTM, West Conshohocken
- Baer DR, Lea AS, Cazaux J, Geller JD, Hammond JS, Kover L, Powell CJ, Seah MP, Suzuki M, Wolstenholme J, Watts JF (2010) J Elec Spec 176:80–94
- Binnig G, Rohrer H, Gerber C, Weidel E (1982) Phys Rev Lett 49:57
- Briggs D, Grant JT (2003) Surface analysis by Auger and x-ray photoelectron spectroscopy. IM Publications and Surface Spectra, Chichester
- Briggs D, Vickerman JC (2001) ToF-SIMS: surface analysis by mass spectrometry. IM Publications and Surface Spectra, Chichester
- Brighton Technologies Group Inc (2010) <http://www.btgnow.com/SEP.html>
- BSI (2010) British Standard 1134:2010, Assessment of surface texture. Guidance and general information
- Castle JE (2008) J Adhes 84:368
- Castle JE, Zhdan PA (1997) J Phys D Appl Phys 30:722
- Chehimi MM, Abel M-L, Watts JF, Digby RP (2001) J Mater Chem 11:533
- Choi JW (2003) The plasma treatment of poly(dimethylsiloxane) for enhanced surface properties. PhD thesis, University of Surrey
- Dillingham RG, Oakley BG, Renieri M, Salah L (2010) From bond gap thickness effects to geometric transferability of fracture parameters in structural adhesives. In: Proceedings 33rd annual meeting of the adhesion society inc, Daytona Beach, 21–24 Feb 2010, pp 217–219
- Goodhew PJ, Humphreys J, Beanland R (2001) Electron microscopy and analysis, 3rd edn. Taylor & Francis, London
- Lee JLS, Gilmore IS (2009) The application of multivariate data analysis techniques in surface analysis. In: Vickerman JC, Gilmore IS (eds) Surface analysis: the principal techniques. Wiley, Chichester, pp 563–612
- Packham DE (2005) Surface energy components. In: Packham DE (ed) Handbook of adhesion. Wiley, Chichester, pp 517–520
- Surface and Interface Analysis (2009a) Special issues on multivariate analysis 41(Pt 1):75–142; (2009b) 41(Pt II): 633–703
- Surface Measurement Systems (2010). [http://www.thesorptionssolution.com/Products\\_IGC.php](http://www.thesorptionssolution.com/Products_IGC.php)
- Taylor AM, Abel M-L, Watts JF, Chehimi MM (1995) Int J Adhes Adhes 15:3
- Venables JA (1984) J Mater Sci 19:2431
- Vickerman JC, Gilmore IS (2009) Surface analysis: the principal techniques. Wiley, Chichester
- Watts JF (1988) Surf Interface Anal 12:497
- Watts JF (2009) Adhesion science and technology. In: Riviere JC, Myhra S (eds) Handbook of surface and interface analysis: methods for problem solving. CRC Press, Boca Raton, pp 5651–5656
- Watts JF (2010) Role of corrosion in the failure of adhesive joints. In: Richardson JA et al (eds) Shreir's corrosion, vol 3. Elsevier, Amsterdam, pp 2463–2481
- Watts JF, Wolstenholme J (2003) An introduction to surface analysis by electron spectroscopy. Wiley, Chichester

# Use of Surface Analysis Methods to Probe the Interfacial Chemistry of Adhesion

10

John F. Watts

## Contents

10.1	Introduction .....	228
10.2	Substrate Characterization .....	229
10.2.1	Metallic Substrates .....	229
10.2.2	Polymer Substrates .....	231
10.3	Forensic Investigation of Failed Joints .....	233
10.3.1	Failure Prior to Environmental Exposure .....	235
10.3.2	Failure Following Environmental Exposure .....	237
10.4	Probing the Buried Interface .....	241
10.5	Model Systems .....	246
10.5.1	Adsorption Isotherms .....	246
10.5.2	Direct Interphase Analysis .....	249
10.6	Conclusions .....	254
References	.....	254

## Abstract

This chapter explores the manner in which the surface analysis methods of X-ray photoelectron spectroscopy (XPS) and time-of-flight secondary ion mass spectrometry (ToF-SIMS) can be used to extract information regarding the interfacial chemistry of adhesion from polymer/metal systems such as adhesive joints. It will be shown that the analysis of a failure interface is an uncertain method to extracting interface chemistry but in certain situations, where a very thin layer of polymer remains on the metal oxide surface, this provides spectra characteristic of the interphase. In most situations, some form of chemical or mechanical sectioning is necessary, and microtomy and dissolution methods are described

J. F. Watts (✉)

The Surface Analysis Laboratory, Faculty of Engineering and Physical Sciences, University of Surrey, Guildford, Surrey, UK

e-mail: [j.watts@surrey.ac.uk](mailto:j.watts@surrey.ac.uk)



as ways in which chemical information at high depth resolution can be extracted from the interphase zone.

An alternative manner in which interphase chemistry can be examined is by the use of model specimens consisting of thin layers of polymer deposited on the metal substrate. The construction of an adsorption isotherm from the liquid phase is a useful precursor to such studies as it provides an indication of the solution concentration at which monolayer coverage occurs. The shape of the isotherm can provide invaluable information regarding the adsorption of various components from a formulation on the substrate, indicating which component(s) has(have) the greatest affinity with the metal oxide. Specimens from the plateau region of the isotherm will have a monolayer of polymer deposited on them, and XPS and ToF-SIMS can be used to probe the interphase region through this very thin layer. This provides a powerful method for the elucidation of the specific interactions, such as covalent bonds, that are responsible for the forces of adhesion. Examples are given in this chapter of a range of systems featuring iron, zinc, aluminum, and ceramic substrates and polymeric systems as diverse as radiation-cured coatings and adhesives, through structural adhesives to an isocyanate-based systems turning finally to the fracture and analysis of a polyester-based nanocomposite.

---

## 10.1 Introduction

The surface chemical analysis methods of X-ray photoelectron spectroscopy (XPS), Auger electron spectroscopy (AES), and time-of-flight secondary ion mass spectrometry (ToF-SIMS) are introduced in ► [Chap. 9, “Surface Characterization and Its Role in Adhesion Science and Technology.”](#) The aim of the current chapter is to review the use of these techniques in adhesion science research paying particular attention to the contribution that they have to make toward unraveling the interfacial chemistry of adhesion. Surface analysis has been applied to adhesion investigations for more than three decades with a great deal of success, and their application in this field can be divided into three distinct areas:

- The investigation of surface characteristics prior to bonding and correlation with some form of performance parameter.
- The forensic investigation of failed adhesive joints and once again correlation of failure characteristics with chosen performance parameters.
- The use of sophisticated specimen preparation or modelling approaches to investigate the interfacial chemistry of adhesion.

This hierarchy also follows the chronology in which surface analysis has been applied with the three levels representing increasingly difficult situations for the analyst. As with most areas of science, however, the development of procedures and methodologies that provide a greater level of information occurs in parallel with advances in instrument design, operation, and data interpretation. XPS, AES, and ToF-SIMS are now mature analytical techniques but experience and specialist

knowledge are needed to get the best from them in adhesion research. The aim of this chapter is to illustrate the manner in which this can be achieved.

Adhesion science research covers adhesion between a number of polymeric and inorganic phases and has direct relevance in the areas of adhesive bonding, sealant chemistry, organic coatings, and composites manufacture. The work described in this chapter has developed from initial work on coatings and adhesives into the interface chemistry of fiber-reinforced composites.

The format of this chapter will follow the areas identified above with sections devoted to the analysis of substrate surfaces, the forensic analysis of failed adhesive joints and organic coatings, and a final section that will look at the methods in which the interfacial chemistry can be probed directly. Specimen preparation is an important part of this last section, and the particular methods relevant to adhesion research will be considered in some detail. The tenor of this chapter is to provide the adhesion scientist with an overview of the different hierarchies of information that can be obtained using surface analysis methods, throughout which there will be illustrations of work from the author's laboratory.

---

## 10.2 Substrate Characterization

### 10.2.1 Metallic Substrates

The use of XPS, and particularly AES, to assess the surface cleanliness of sheet steel in the automobile industry was one of the first applications of surface analysis in adhesion research. Forty years ago, the traditional manner to assess the level of carbonaceous contamination on steel stock, generally residues from processing aids or temporary corrosion protectives, was to use a glass fiber pad to remove as much of the residue as possible and then analyze for carbon by combustion methods. The level of carbon was then reported in units of mass per unit area (often  $\text{mg cm}^{-2}$ ), and correlations made with performance of the painted steel in a standard test. Once variations in steel performance were investigated in this rather crude manner it became clear that there was a strong correlation between the concentration of surface carbon and poor performance of the painted steel. Although a combustion test is perfectly adequate when it comes to assessing very high levels of carbon concentration (panels that feel greasy to the touch), at low levels where performance in a salt spray test is seen to be very variable for low concentrations of carbon, this approach is rather insensitive, as seen in Fig. 1. This changed in the mid-1970s when XPS and AES were applied to the assessment of surface cleanliness. The story that emerged was that adventitious carbon had the potential to interfere with the formation of the chemical conversion coating, an inorganic coating based on zinc phosphate, that is routinely applied to steel stock in the automobile and other industries prior to the application of the organic coatings system. The study undertaken by Iezzi and Leidheiser (1981) illustrates the strength of scanning Auger microscopy for the characterization, at high spatial resolution, of metal substrates prior to coating. A useful postscript to this is the recognition by Smith (2005) that the surface



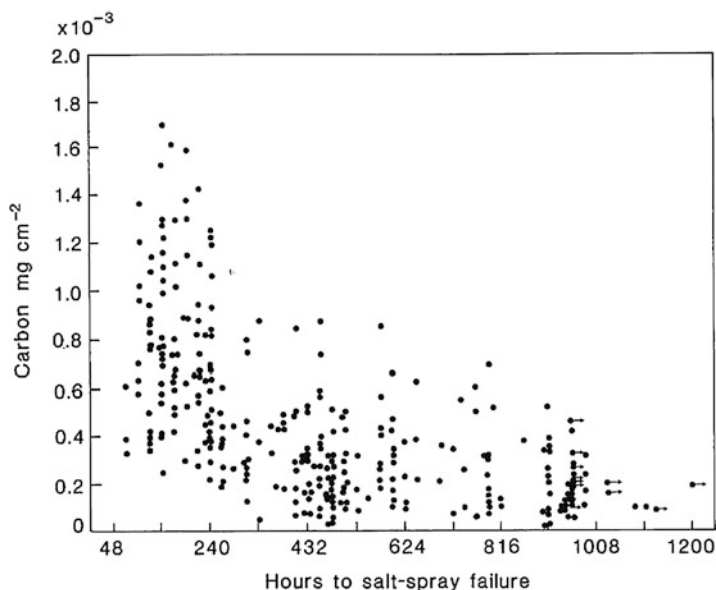


**Fig. 1** Correlation of steel surface cleanliness (determined by a combustion method) with time to failure in a salt spray environment. Although the general trend is clear, there is not sufficient discrimination at low carbon concentrations

concentration as measured by XPS can be converted directly to an overlayer thickness,  $d$ , in nanometers, by the use of a modified form of the Beer–Lambert Equation:

$$d = -\lambda \cos \theta \ln(1 - 0.01x) \quad (1)$$

where  $\lambda$  is the electron attenuation length,  $\theta$  is the electron takeoff angle relative to the sample normal, and  $x$  is the surface concentration of carbon in atomic percent determined by the usual method included in the software provided by the manufacturer of the data system.

An example of the manner in which XPS can be used to differentiate between surfaces that are notionally clean is provided in Fig. 2, which illustrates the XPS survey spectra from two steel surfaces prepared by different methods. Using Smith's approximation (above) the thickness of the adventitious carbon layer is 0.92 nm for the sample with the lower surface concentration (31 at%) and 2.46 nm for the other (63 at%).

Some alloys have minor components that show a propensity to segregate to the surface under certain process conditions which, in turn, can compromise the adhesion of a coating or adhesive. In the case of aluminum alloys, even very low levels of magnesium in the alloy may segregate to the surface during closed coil annealing to form a friable layer of MgO at the surface. This is readily identified by XPS or AES but if not removed prior to bonding will lead to poor performance. The

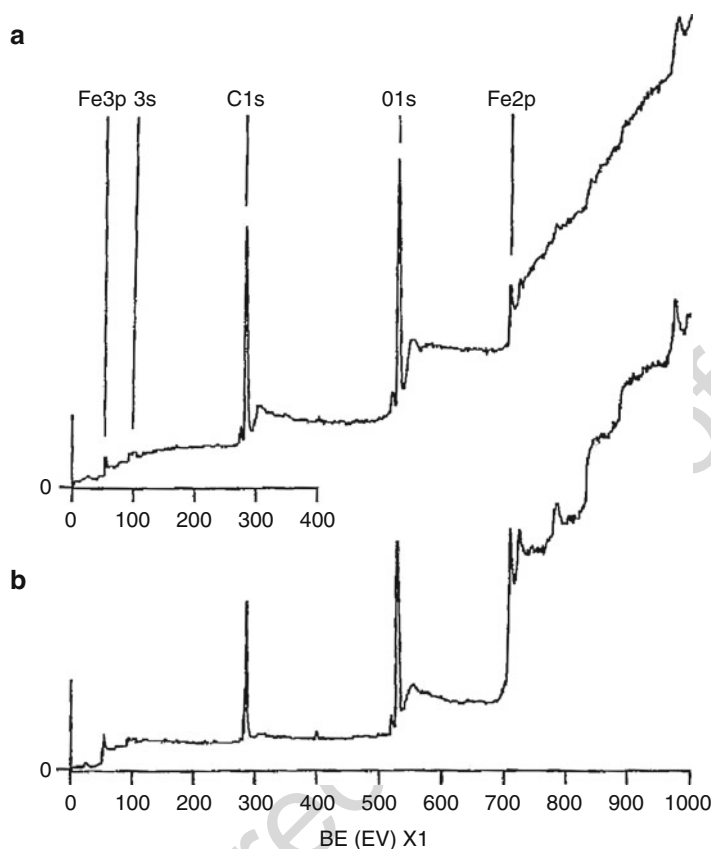


**Fig. 2** XPS survey spectra of low carbon steel sheet following (a) alkali cleaning and (b) energy abrasion. Note that the abrasion process, which removes the near-surface material, results in a much cleaner surface

128 detection of magnesium by surface analysis is not always a cause for concern as  
129 if the element is immobilized, in an anodic oxide layer, for example, satisfactory  
130 performance may result.

### 131 10.2.2 Polymer Substrates

132 In the case of metallic substrates the problem that is encountered which will  
133 compromise bond performance is often the presence of hydrocarbon contamination  
134 which as well as having the potential to act as a weak boundary layer will also reduce  
135 the surface free energy of the substrate from a high value (many hundreds of  $\text{mJm}^{-2}$ )  
136 to a value lower than  $100 \text{ mJm}^{-2}$ . In the case of polymers the surface energy is  
137 intrinsically low, of the order of  $20\text{--}50 \text{ mJm}^{-2}$ , as a result of chain folding rather  
138 than unsatisfied valencies at the material surface observed in metals and inorganic

materials. As a result, many pretreatments of polymers rely on increasing the surface functionality, and thus the surface free energy of the substrate by using methodologies that incorporate oxygen into the polymer surface, such as corona discharge and flame treatments, see ► Chap. 8, “Surface Treatments of Selected Materials.” There are, however, two process-related phenomena observed in polymers that have the potential to compromise bond performance. One is the segregation to the free surface of low molecular weight species (such as oligomers of the bulk polymer) that lack sufficient mechanical integrity with the bulk and lead to premature failure. The other is the segregation of minor components such as processing aids to the surface during production. A classic example is the surface segregation of the familiar plasticizer di-iso octyl phthalate to the surface of poly(vinyl chloride) (PVC). This can readily be identified by ToF-SIMS and is a familiar, along with poly(dimethyl siloxane), as a contamination to all ToF-SIMS users. The spectrum of the external surface of a PVC tube, widely used for many laboratory applications, is shown in Fig. 3 with the peaks assigned to the plasticizer labeled, which indicates the high concentration of material that can exist at a polymer surface. The presence of such additives at the surface of

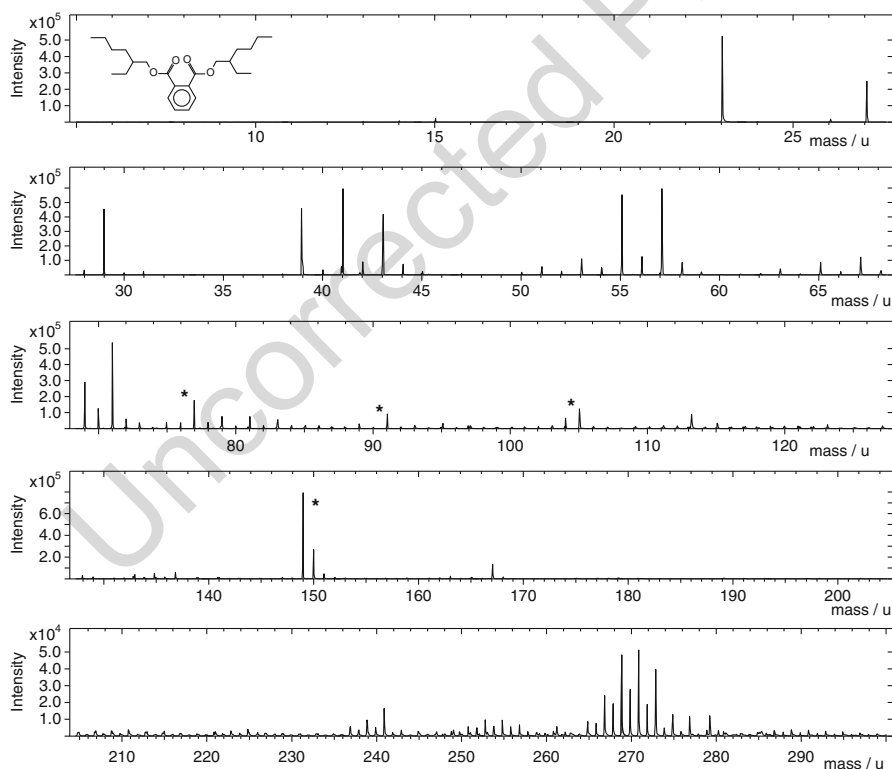


**Fig. 3** The positive ToF-SIMS spectrum of the external surface of laboratory PVC tubing. The peaks marked with an asterisk are those attributed to the plasticizer di-iso octyl phthalate. The structure of this molecule is shown in the inset, and the dominate ion at  $m/z = 149$  u is C<sub>8</sub>H<sub>5</sub>O<sub>3</sub><sup>+</sup>

mass-produced polymers is a familiar observation, and additives are readily detected and identified by ToF-SIMS. They can, however, be a source of a weak boundary layer when attempting to print or bond such substrates, and the application of some pretreatments to polymers may merely remove the aggregation of these extraneous materials at the surface, thus increasing the surface free energy, rather than modifying the base polymer by the incorporation of oxygen. Such an observation also indicates why samples for surface analysis should always be provided packaged in aluminum foil or glass containers of known cleanliness and never in crimp top plastic bags, as plasticizer and the like can all too easily contaminate the surface intended for analysis!

As indicated above, the surface treatment process may be responsible for the removal of such material and exposing the bulk of the polymer underneath the segregated layer. Such a situation can be illustrated by the XPS spectra of Fig. 4 from PVC in its extruded form and after flame treatment. The extrudate is protected by a thin film of low density polyethylene (LDPE), and upon removal of this film the spectrum (Fig. 4a) is dominated by carbon and oxygen with significant contributions from PVC-specific elements such as chlorine, lead, and zinc. On flame treatment (Fig. 4b), the carbon level is reduced to a certain extent (from 82% to 70%), while the oxygen increases from 12% to 22%, and the chlorine and inorganic ion concentration is broadly similar between the two, however, the water contact angle reduces from 91° to 59° showing that the flame treatment has increased the surface free energy significantly. This presumably reflects the manner in which the flame treatment has reduced organic material incorporated into either the PVC or LDPE formulations that have segregated to the interface on processing. For a spectrum of the bulk of the PVC, obtained by sectioning the PVC extrudate is shown in Fig. 4c and the intensity of the major peaks (C1s, O1s, Cl2p) are in the expected ratios for a commercial PVC, with approximate concentrations of carbon = 64%, chlorine = 26%, and oxygen = 10%. The inorganic contributions to the survey spectrum of Fig. 4c are attributed to fillers, anti-oxidants, and the like added to the formulation.

### 10.3 Forensic Investigation of Failed Joints

The investigation of a failed adhesive joint can be approached by many methodologies and these are considered at length in ► Chap. 43, “Techniques for Post-Fracture Analysis.” The aim of this section is to explore the utility of this approach to the understanding of the interfacial chemistry of adhesion for a particular system. As a starting point the application of surface analysis methods, particularly XPS and ToF-SIMS, has much to commend in the definition of the locus of failure of an adhesive joint, and the provision of important information at the molecular scale. For instance, XPS is able to deduce the thickness of organic overlayers up to a thickness of about 10 nm (more if XPS is used in conjunction with cluster ion bombardment for depth profiling) and the presence of unexpected ions at the failure interface, perhaps resulting from a corrosion-induced failure where an excess of anions (e.g., Cl<sup>-</sup>) will indicate that anodic conditions prevailed prior to failure or

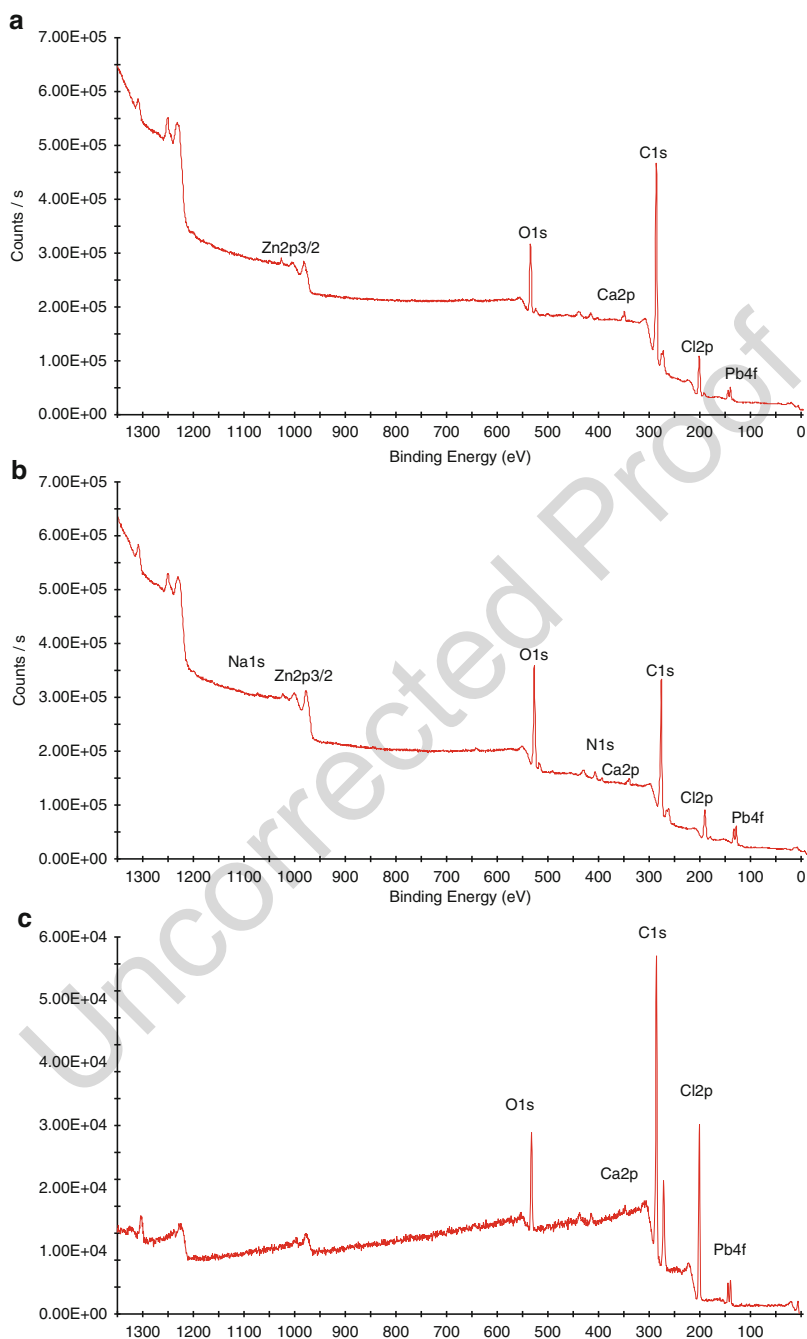


**Fig. 4** XPS survey spectra of commercial PVC extrudate. (a) As extruded, (b) following flame treatment, (c) bulk analysis following sectioning by microtomy

cations (e.g.,  $\text{Na}^+$ ), which are diagnostic of cathodic activity. ToF-SIMS is particularly valuable as it is able to differentiate unambiguously between minor components of an adhesive formulation. This is particularly useful in the identification of instances where the segregation of such species to an interface has compromised joint performance. Two examples of this will be provided later in this section.

### 10.3.1 Failure Prior to Environmental Exposure

As a general rule, and a phenomenon that can be predicted by surface thermodynamics, a joint that is tested in dry air, and that has not received exposure to an aggressive environment such as water, will fail in the bulk of the adhesive. This may be at the center of the glue-line in which case the locus of failure is easily defined using the naked eye. As the locus of failure moves toward a substrate/polymer interface, however, one must resort to increasingly sophisticated methods for an exact definition of the fracture locus. If adhesive residues cannot be observed with the naked eye the next observational methods should be optical microscopy, followed by electron microscopy. Many investigators will stop at this point but an adhesive layer of 10 nm or so will not be distinguishable in a scanning electron microscope (SEM) although it will appear as a uniform polymeric layer by XPS. Thus, XPS has an important role to play in the definition of failure when the residual layer of adhesive is extremely thin. Indeed by resorting to microscopy methods alone it is all too easy to assign a failure as interfacial when it is actually cohesive but very close to the substrate/polymer interface.

As an example of such a forensics analysis the following example relates to the joining of a nylon structure to epoxy-coated steel substrate by thermal bonding. The central photographs provide a visual appreciation of the appearance of the failure surfaces, and the spectra are taken from equivalent locations on the two sides of the failure. This is a standard approach in the analysis of the failure surfaces from adhesive joints, and surface analyses are sometimes referred to as mirror image surface analyses. The left hand failure surface shows characteristics of the coated steel, and at the bottom right hand corner there is a region where the epoxy lacquer appears to have been removed from the steel. The right hand failure surface confirms this with the regions of nylon in white and the peeled epoxy being darker (golden) in color. Turning to the XPS survey spectra of Fig. 5 it is clear that those from both interfacial failure surfaces of the peeled lacquer are very similar with C1s and O1s peaks dominating the spectra and no sign of metallic elements that might be expected from the steel surface. This is clearly indicating that the failure of the epoxy coating has occurred within the lacquer itself but close to the metal/coating interface. The other pair of spectra tell a similar story with failure having occurred in the nylon phase, although visual inspection would indicate failure to be between nylon and the epoxy coat.

Although the definition of the exact locus of failure is a crucial part of any failure investigation, and the examination of complementary surfaces as described above can be very informative, the situation that exists in a dry joint is generally rather

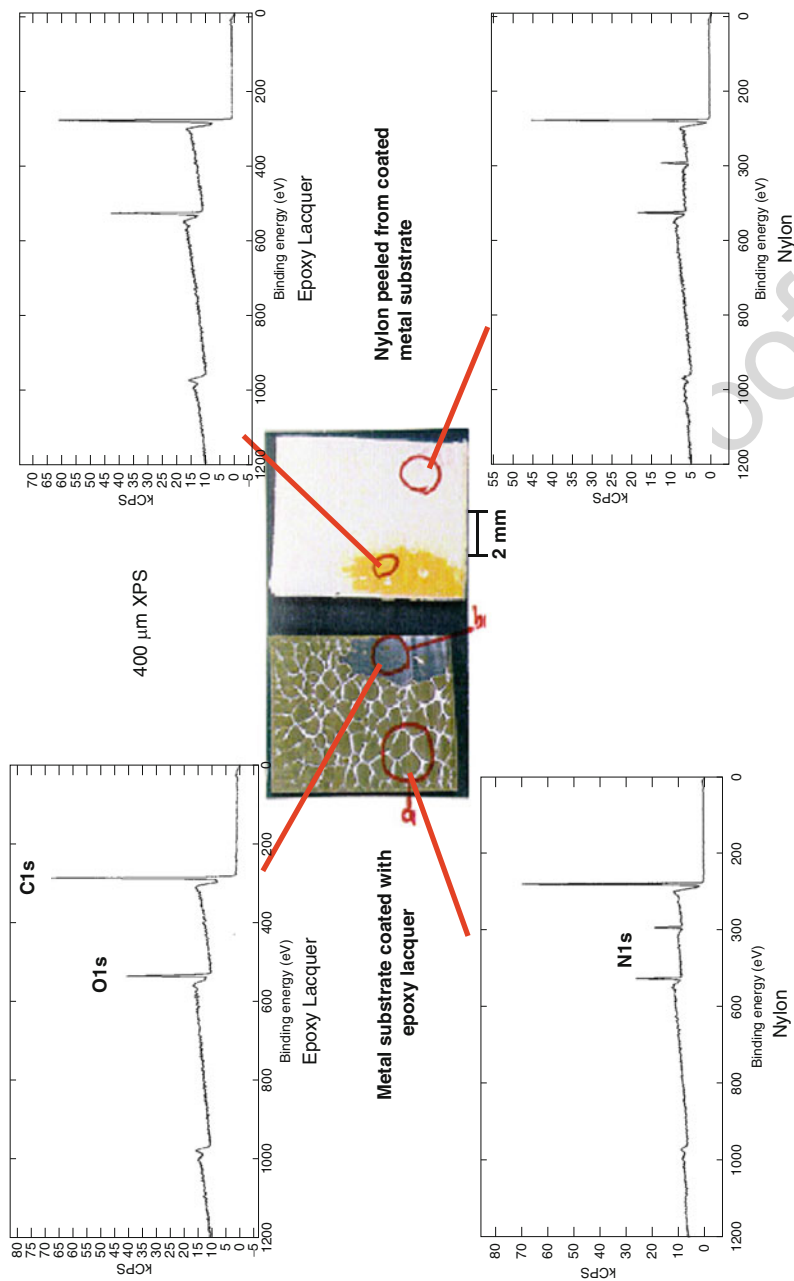


**Fig. 5** The XPS survey spectra from the failure of the bond between epoxy-coated steel and nylon. The upper two spectra are characteristic of the epoxy coating while the lower are typical of nylon. This shows that the two distinct failure regions both exhibit cohesive failure but in the epoxy lacquer (near to the epoxy steel interface) or the nylon (near to the epoxy nylon interface)

straightforward. It is once that the failure has occurred as a result of environmental exposure, particularly if water is involved, the elucidation of failure mode is to an extent more difficult as segregation or degradation process may have occurred during exposure. In the following section, the manner in which the nature of the locus of failure varies will be explored according to system type and also the possibility of using the analyses from failed systems to deduce the interfacial chemistry of adhesion.

### 10.3.2 Failure Following Environmental Exposure

When a coated metal is exposed to water there is always the possibility of corrosion of the metal substrate, particularly when the edge of the metal is exposed. The role of corrosion in the failure of adhesive joints is explored extensively elsewhere (Watts 2010), the most important aspect being that the behavior at cathodic and anodic areas is very different. At the cathodic areas the reduction of water and oxygen leads to the production of hydroxide ions and the generation of a higher pH locally. This in turn leads to a phenomenon known as cathodic disbondment (Watts 1989), which is readily observed by XPS as the failure will be truly interfacial, and cations in the test solution (e.g.,  $\text{Na}^+$ ,  $\text{Ca}^{2+}$  and the like) will decorate the cathodic regions. If gross corrosion occurs beneath the adhesive, failure will occur in the corrosion product itself which is of course the result of the anodic half reaction and the failure surfaces will be decorated with anions such as chloride. This latter failure type is exemplified by the spectra of Fig. 6, which represent complementary failure surfaces from a galvanized steel substrate and the organic phase. As can be seen both spectra are dominated by the Zn2p and Zn LMM (Auger) spectra at 1020–1050 eV and 450–700 eV respectively, and in the case of the zinc surface, the level of carbon is extremely low (typical of adventitious contamination on a voluminous corrosion product) but there is a significant concentration of chlorine (indicated by the Cl2p at a binding energy of 199.5 eV); the chemical shift on the Cl2p confirms the chlorine species as the chloride ion diagnostic of anodic activity. The sample was exposed to a salt spray environment so that there was an ample supply of chloride ions to label these regions. The spectrum from the organic phase is very similar but with an increased concentration of carbon, and a small amount of nitrogen, both elements indicate that the amount of zinc corrosion product is relatively modest with a signal from the organic coating also being present in the spectrum. Although such an investigation is very informative regarding the locus of failure, it provides no information about the interfacial chemistry of the system prior to failure. In more advantageous situations, the spectra of failure surface can provide detailed molecular relating to the interfacial chemistry of the systems.

Radiation-cured coatings have been under development for some time and are now commercially widely available for a variety of applications. In the early years of development of this technology, a prototype system (designed for eventual commercial exploitation) exhibited good dry adhesion but when exposed to water vapor the adhesion was significantly compromised (Leadley et al. 1998). XPS and ToF-SIMS



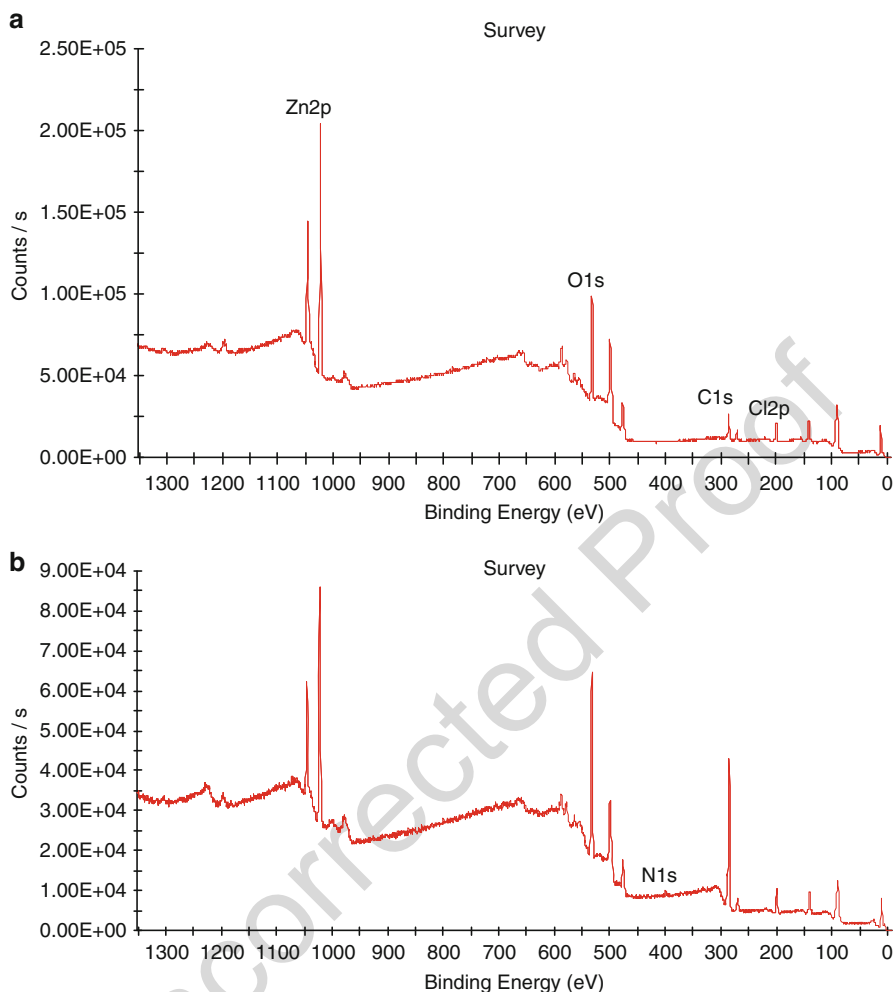


**Fig. 6** XPS survey spectra from a coated galvanized steel panel exposed to salt spray. Both surfaces, (a) metal substrate failure surface and (b) coating failure surface, show extensive mounts of zinc corrosion product and the Cl2p peak (present in both spectra) shows that failure has occurred in the layer of corrosion product

spectra were recorded from the interfacial failure surfaces of both the galvanized steel substrate and the polymer coating. The XPS spectra, together with that of the bare substrate are presented in Fig. 7. Comparison of the two interfacial surfaces appears to indicate an interfacial surface with a fairly clean zinc substrate (aluminum is present as it is a standard addition to the galvanizing bath), Fig. 7a, and a polymer surface showing no signs of any metal transfer, Fig. 7b. When the metal surface is compared with the as received steel surface, Fig. 7c, it is clear that the fluorine detected on the failure surface was not present on the initial surface. ToF-SIMS

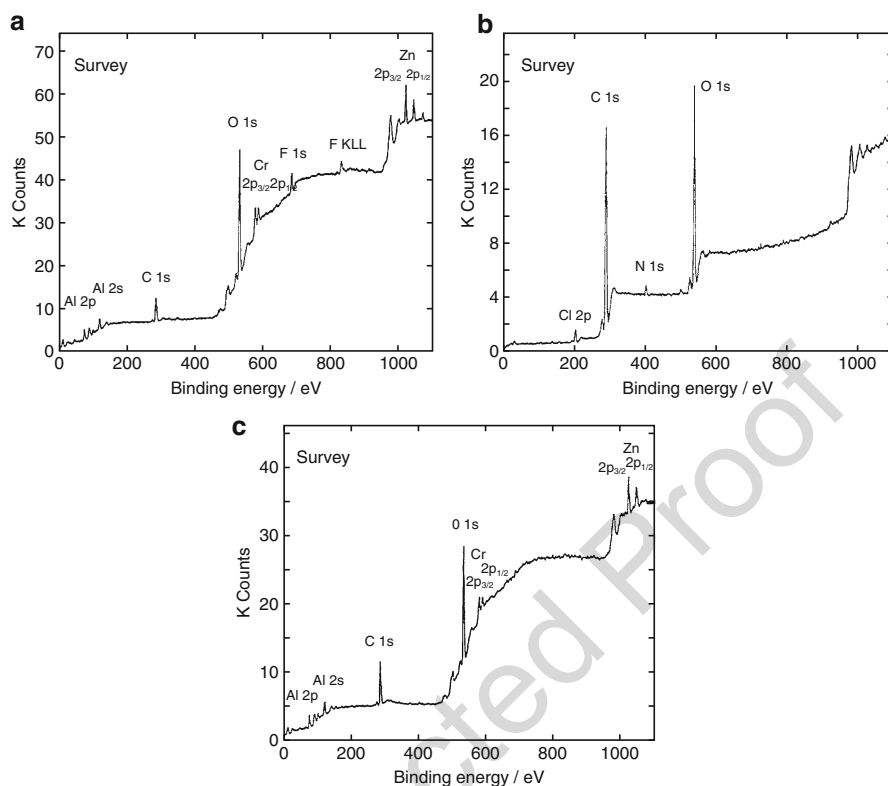


**Fig. 7** XPS survey spectra from a UV-cured coating applied to galvanized steel that has then been exposed to water vapor. (a) Interfacial failure substrate surface, (b) interfacial failure coating surface, and (c) steel surface prior to coating (Reproduced from Leadley et al. (1998), with permission)

analysis confirmed that the fluorine was associated with a  $\text{PF}_6^-$  ion, which is the anionic part of the radiation-curing package, and that the cation is a triaryl sulphonium species. The conclusion from this analytical data is that there is the segregation of the curing agent to the interface either during application or prior to the cure process. When the system is tested dry there is sufficient mechanical integrity but on exposure to water vapor the region between the segregated cure package and the bulk of the coating provides a hydrophilic interface along which water can diffuse easily, leading to premature failure. The solution to this short coming was to reformulate the system with a significant reduction in the amount of the cure package in the coating.

This example relies on the identification of an element at the failure interface that can be used as a marker for a particular component in the formulation. More usual is the need to resort to high resolution spectroscopy. The data of Fig. 8 relates to a radiation-cured adhesive being developed for the bonding of components to ceramic substrates for surface mount technology. Once again water reduced the adhesion

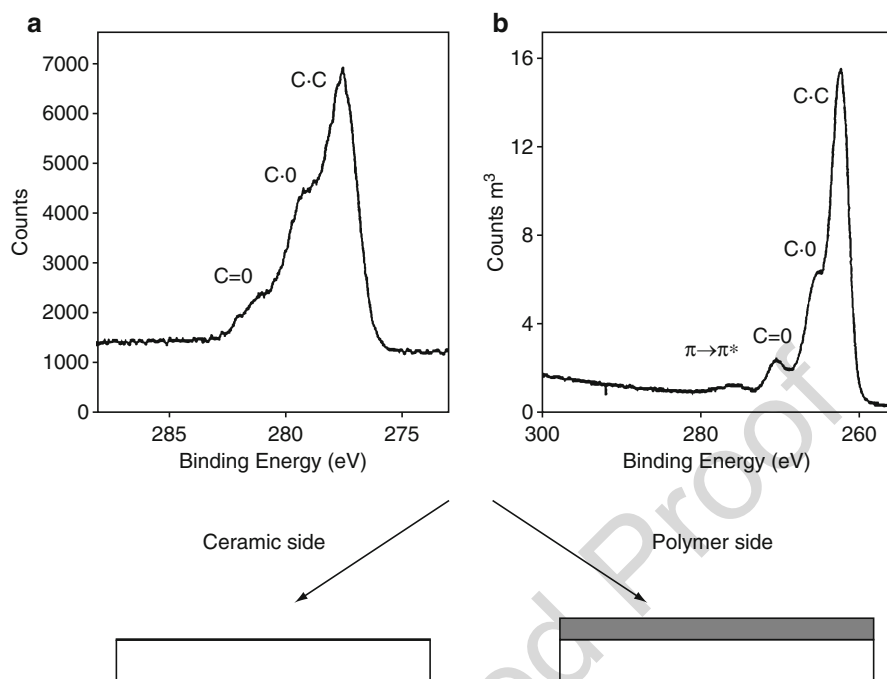


**Fig. 8** High resolution C1s spectra from the failure interfaces of an alumina system bonded with a radiation-cured adhesive. (a) Alumina side of the failure that exhibits a thin (ca 1 nm) layer of adhesive, (b) bulk adhesive layer. Note the presence of the  $\pi \rightarrow \pi^*$  shake-up satellite in the spectrum of the bulk adhesive but its absence from the very thin residual adhesive layer of (a) (Reproduced from Watts and Taylor (1995), with permission)

below an acceptable level and XPS and ToF-SIMS analysis of the failure surfaces provides an indication of the cause of the failure. The adhesive has two major components: an aromatic adhesive part and an aliphatic reactive diluent. Inspection of the high resolution C1s spectra from the adhesive side of the failure shows the expected  $\pi \rightarrow \pi^*$  shake-up satellite diagnostic of the aromatic component of the adhesive (Watts and Taylor 1995). The ceramic failure surface shows a small amount of carbon at a thickness of approximately 1 nm (determined by angle-resolved XPS) but the high resolution spectra show no sign of the expected aromatic component of the adhesive. ToF-SIMS identified the adsorbed layer on the ceramic as the reactive diluent while molecular dynamics modeling indicated that this molecule would adsorb on the ceramic surface to provide a monolayer some 1 nm in thickness (Taylor et al. 1995). This information combines to provide a very clear view of the interfacial chemistry and, indeed, why failure occurred. During application of the adhesive there is the segregation of a monolayer of the reactive diluent to the ceramic surface which in turn forms an interface with the bulk adhesive. On exposure to water the situation is similar to that described for Fig. 7, the water can readily diffuse along the interface leading to failure. The solution to improving the performance is

also similar, the concentration of reactive diluent in the formulation being reduced. Such a course of action improves the durability of the joint although, unfortunately, it also changes the viscosity of the adhesive that precludes its use in certain applications.

From the above examples it can be seen that the locus of failure generated by a mechanical test, either before or after environmental exposure is an uncertain route to exposing surfaces that will allow the elucidation of interface or interphase chemistry directly. In the following sections, a number of methods are described that allow the interfacial chemistry of adhesion to be examined directly by analytical methods. They fall into two categories: those in which a real interface is sectioned to allow surface analysis and other methods to probe the interfacial region, and those which make use of model systems, often in the form of very thin (<2 nm) films of adhesive where the interphase chemistry is directly accessible by surface analysis methods.

## 10.4 Probing the Buried Interface

In a review of polymer-to-metal adhesion, of more than two decades ago (Watts 1988), a variety of mechanical and chemical methods that would potentially enable the interface region of a coated or bonded system to be investigated were documented. Although the capabilities of the analytical techniques themselves have improved tremendously in the intervening years, the preparation methods themselves are essentially the same. Of the four methods mentioned one, the analysis of a simple metallographic cross section in the SEM, was discounted for not having the required spatial and chemical resolution. This is still the case, and although SEM remains an invaluable method to provide high quality images, the spatial resolution attainable in X-ray analysis by EDX or WDX is limited by the size of the electron beam interaction with the specimen (of the order of 1  $\mu\text{m}$  in both lateral and depth resolution); similarly these techniques only provide elemental analysis with no chemical resolution. The other three are in use and involve sectioning the specimen or chemical dissolution.

The sectioning of a specimen by microtomy to provide an electron transparent section for TEM microscopy and analysis is widely used in many areas of materials science. The use of TEM images in adhesion studies was first demonstrated by Thompson et al. (see, for example, Bishopp and Thompson 1993), and the addition of analysis by parallel electron energy loss spectroscopy (PEELS) provides a powerful technique as illustrated by Kinloch et al. (2000). The TEM images of Fig. 9 are false-color elemental images (obtained by PEELS) of the interfacial region of an aluminum alloy treated by phosphoric acid anodizing to develop a porous film, bonded with an epoxy paste adhesive. In Fig. 9a, the adhesive has been applied directly to the anodic oxide layer and there is very little penetration of the adhesive into the porous oxide. If a primer is applied, however, there is a significant interpenetration of the organic and inorganic phases to form a microcomposite interface as shown in Fig. 9b. The durability performance of these two systems can be related

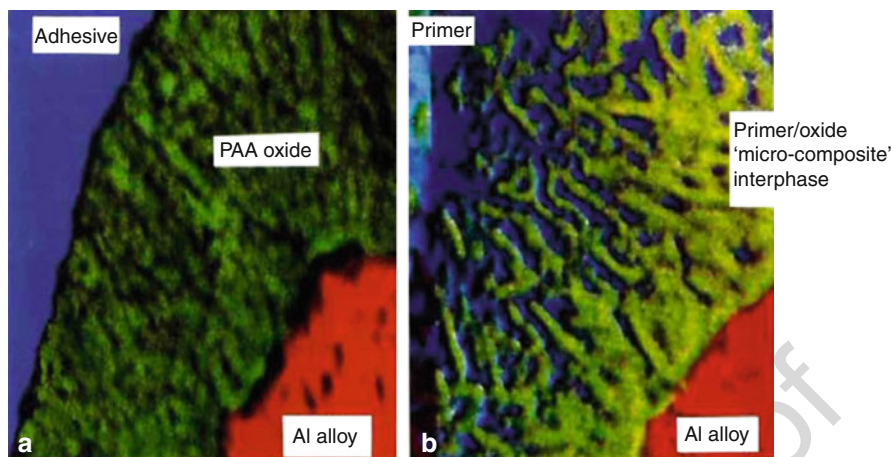
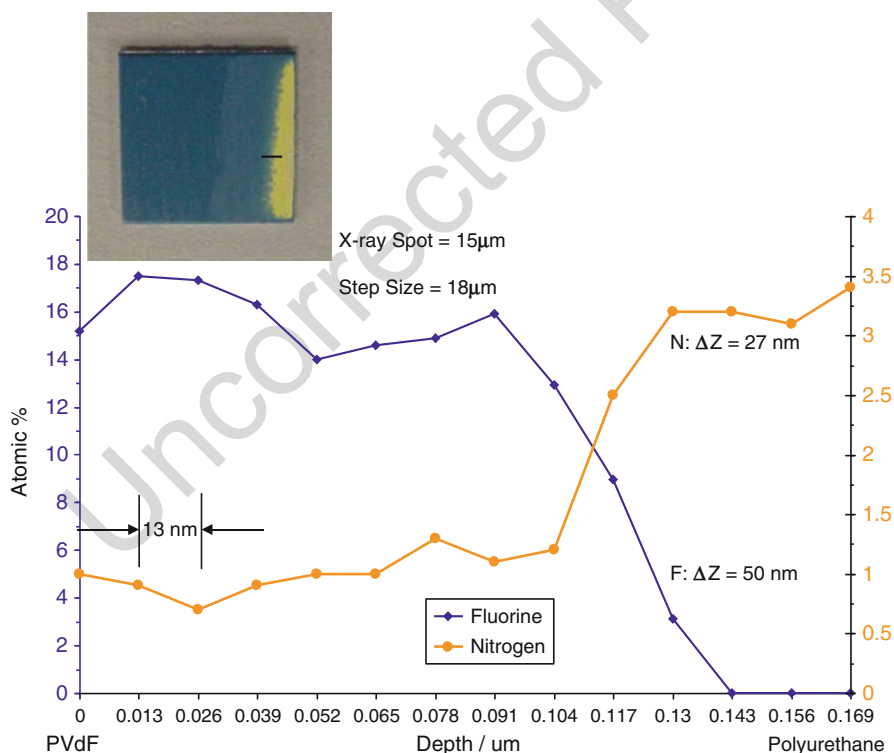


**Fig. 9** False color PEELS images of the interphase region of adhesive joints manufactured from aluminum alloy treated by chromic acid anodizing. (a) Paste adhesive applied directly to the anodic pretreatment layer, which yields a very abrupt interface between organic and inorganic phases, (b) application of a primer prior to adhesive bonding that leads to interdiffusion of organic and inorganic phases and the resultant microcomposite interphase (Reproduced from Kinloch et al. (2000), with permission)

directly to interphase characteristics with the system without primer (which yields a planar interface between organic and oxide) being poor but the system that makes use of a primer (and generates a microcomposite interphase) showing excellent performance. This method has been used to good effect by Bertho et al. (2010) to study the fate of an organosilane adhesion promoter incorporated into an epoxy formulation, and the development of a chemical interphase some 20 nm in thickness at the metal/adhesive interface.

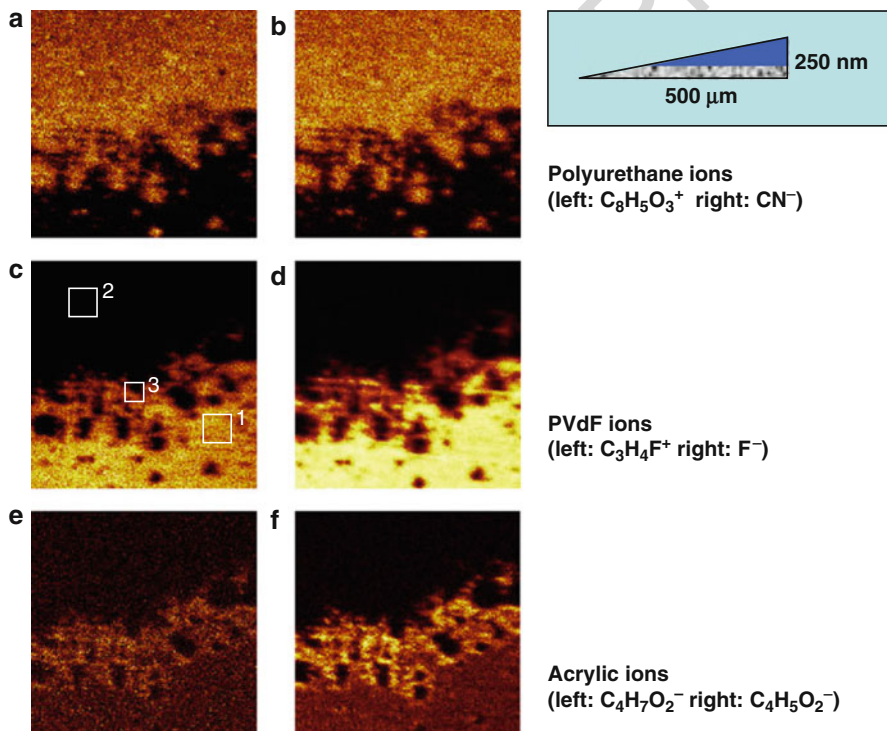
An alternative manner in which the interface region can be approached is by the production of very gentle ( $<5^\circ$ ) taper sections so that the interphase and its environs are magnified making them amenable to direct analysis by XPS or SIMS. Initial work with this approach made use of an ultra high vacuum mechanical taper sectioning rig, with a cryo-stage, that could be directly attached to the preparation chamber of the spectrometer. Although successful, this method has now been superseded by the use of a technique known as ultra-low angle microtomy (ULAM) (Hinder and Watts 2004; Hinder et al. 2004, 2005). This method makes use of a histological microtome and employs stainless steel spacer blocks between microtome bed and sample so that extremely low angles are subtended between sample surface and microtome blade ( $0.03^\circ$ – $0.33^\circ$ ). In this way it is possible to use a high spatial resolution surface analysis method to provide extremely good depth resolution (Hinder et al. 2004). For example, using the lowest angle of  $0.03^\circ$  and a small X-ray spot of 15  $\mu\text{m}$  for XPS, a depth resolution of 13 nm is theoretically attainable; if the spot size is increased to 100  $\mu\text{m}$  the depth resolution is reduced to 60 nm. An example of how a depth profile can be obtained using this method is provided in

Fig. 10, the specimen is a polyurethane primer on a metal substrate overcoated with a poly(vinylidene fluoride) plastisol layer. The specimen prepared by ULAM is shown in the upper left of Fig. 10, and the microtome cut, exposing the lighter (yellow) primer below the darker (dark blue) topcoat can be clearly seen. The black solid line represents the location of the XPS line scan that was carried out with a spot size of 15  $\mu\text{m}$  and a step size between analyses of 18  $\mu\text{m}$ . The compositional line scans for fluorine and nitrogen concentrations are presented on an abscissa that has been converted from distance along the specimen to depth toward the interface from an arbitrary position on the PVdF coating (on the black line of the specimen image of Fig. 10). The analysis depth considered in Fig. 10 is some 170 nm and the interdiffusion of fluorine and nitrogen is readily appreciated. The interface widths ( $\Delta Z$ ) of the nitrogen and fluorine profiles are 27 nm and 50 nm, respectively, indicating some diffusion of the PVdF into the primer coating. A reasonable observation as the primer would have been cured prior to the application of the topcoat. Although such a line scan provides useful information, the analysis of a similar region by ToF-SIMS enables additional information to be extracted (Hinder et al. 2004). Mass-selected ToF-SIMS images with a 500  $\mu\text{m} \times 500 \mu\text{m}$  field of view from the



**Fig. 10** Depth profile obtained by small spot XPS and ultra-low angle microtomy at the interface region of a PVdF coating applied to a polyurethane primer (Reproduced from Hinder and Watts (2004), with permission)

interphase region of the same sample are shown in Fig. 11 with pairs of images chosen to represent the polyurethane primer (Fig. 11a, b), the PVdF top coat (Fig. 11c, d) and also ions representing a minor component in the formulation of the PVdF plastisol, an acrylic co-polymer. It can be seen that although the acrylic material is distributed uniformly through the PVdF layer, its presence is enhanced at the interface between primer and topcoat. The depth dimension of the field of view is shown in the schematic of Fig. 11g, which indicates that the region of enhanced acrylic material concentration at the interphase is about 50 nm in thickness. The acrylic component is added to the formulation to enhance the adhesion of the plastisol to the primer and it appears that this is achieved by the development of an acrylic-rich interphase some 50 nm in thickness. The study of interactions with metals using this method is perfectly feasible so long as thin metal foils or vacuum-deposited layers are used as the substrate. Recent unpublished work carried out in the author's laboratory has shown that iron foil as thick as 25  $\mu\text{m}$  can be sectioned successfully by microtomy.



**Fig. 11** Mass-selected ToF-SIMS images of the PVdF/PU interface of Fig. 10. The field of view is 500  $\mu\text{m}$ , which is equivalent to a height difference of 250 nm from top to bottom of image. Images shown represent PU (a & b), PVdF (c & d), and acrylic adhesion promoter that segregates to the interface (e & f). Both positive (a & c) and negative (b, d, e & f) images are shown (Reproduced from Hinder et al. (2004), with permission)



In addition to microtomy it is possible, in some systems, to dissolve the metallic substrate (but not the oxide) and then use surface analysis in conjunction with sputter depth profiling, to approach the interphase between oxide and adhesive. This method has been used to good effect to study the interphase between a low carbon steel substrate and a polybutadiene coating (Watts and Castle 1983). In this work, the steel was dissolved in a methanolic iodine solution, and the subsequent duplex film of a thin oxide supported on the polymer was mounted oxide uppermost for analysis by XPS with sputter depth profiling. The depth profile showed a change in the shape of the  $\text{Fe}2p_{3/2}$  spectrum as the interphase was reached; in the oxide the iron was exclusively in the  $\text{Fe(III)}$  state but at the interphase some  $\text{Fe(II)}$  was seen in the spectrum as shown in Fig. 12. The presence of the  $\text{Fe(II)}$  component in the interphase is the result of the reaction between the polybutadiene (which cures by oxidation) and the native oxide on the steel substrate during cure. At the boundary between polymer and oxide the polymer acts as a reducing agent for the iron oxide leading to the production of an organometallic complex involving the reduced form of the oxide,  $\text{Fe(II)}$ .

A similar method has been used to investigate the interfacial characteristics of laminated aluminum systems used for beverage cans. When produced by this process a stock laminate is punched into blanks and the can body produced by deep drawing and wall ironing. To investigate the polymer/oxide interface the aluminum is dissolved in sodium hydroxide solution, and to study the polymer surface the oxide can be removed by treating with hydrofluoric acid. To investigate the metal/oxide region, as the oxide will undergo much fragmentation during the deep drawing process, the polymer is removed with trifluoroacetic acid. In this work,

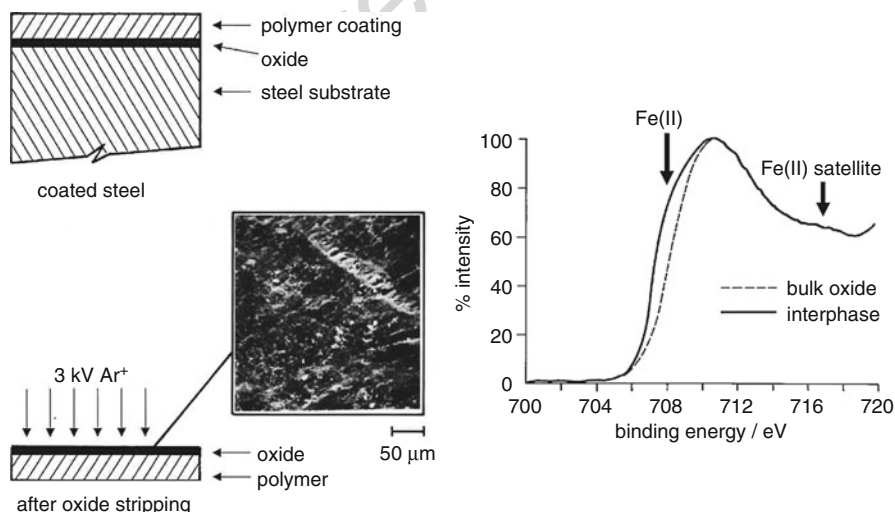


**Fig. 12** XPS examination of the interphase between a polymer coating and low carbon steel. The preparation method is shown schematically on the left hand side; the change in shape of the  $\text{Fe}2p_{3/2}$  spectrum, as the interphase is approached showing significant  $\text{Fe(II)}$  character, is shown on the right



the emphasis was to study the interphase morphology but if chemical information is required it is always important to establish that the reagents used for dissolution are not, themselves, reacting with the system to change the chemistry at the interphase.

## 10.5 Model Systems

### 10.5.1 Adsorption Isotherms

The determination of adsorption isotherms to study the reaction of gas phase molecules with a solid substrate is a well-established procedure in traditional surface chemistry. This method can be successfully adopted to study the adsorption of molecules incorporated in an adhesive formulation on a metal, or other, substrate (Watts and Castle 1999). The uptake of adsorbate from liquid solution as a function of solution composition is monitored by XPS or ToF-SIMS on a series of substrate coupons. The adsorption isotherm is plotted in the same manner as a conventional gas phase study but with surface composition (determined by XPS or ToF-SIMS) being plotted against solution concentration. In this manner, the adsorption of adhesive components can be compared on the same substrates, or the same adsorbate compared on different substrates such as metals with and without pretreatment (Rattana et al. 2006). An example of such an investigation is shown in Fig. 13, where the adsorption of adhesive components diglycidyl ether of bisphenol A (DGEBA – the epoxy building block) and the curing agent (toluene diisocyanate – TDI – urone) are compared on bare aluminum and aluminum that has been treated with an epoxy tipped adhesion promoter (glycidoxo propyl trimethoxysilane – GPS) (Watts et al. 2004). Figure 13a shows the adsorption of the epoxy component (DGEBA) from the adhesive solution, and it can be seen that there is very little difference in adsorption characteristics between the bare aluminum and the substrate

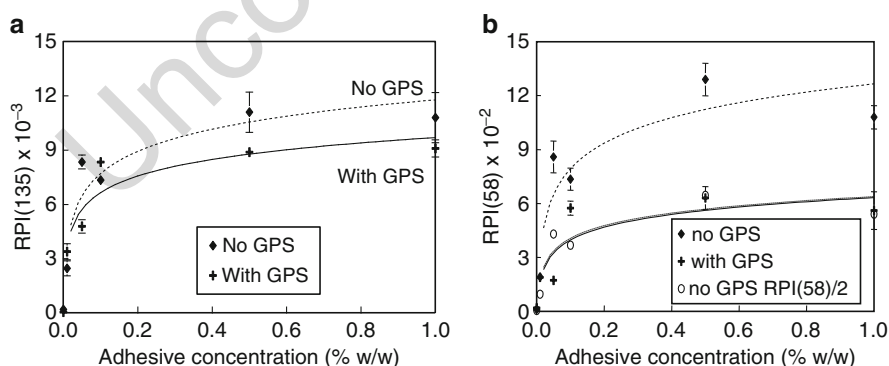


**Fig. 13** Adsorption of the epoxy component (a) and the curing agent (b) from dilute solutions of adhesive onto bare aluminum (“No GPS”) and aluminum treated with an organosilane adhesion promoter (“With GPS”). In (b) the data from the bare aluminum is shown divided by two as “no GPS RPI(58)/2” to illustrate the close match with the data from the silane treated substrate

466 treated with the organosilane. The situation is very different, however, for the  
467 toluene diisocyanate urone curing agent, where it is clear that the adsorption on  
468 the bare aluminum is significantly more than that of the GPS-treated substrate. A  
469 clue to the source of the large difference can be found if the data for the bare  
470 aluminum is divided by two and replotted (as the “no GPS RPI(58)/2” curve) and  
471 it is now coincident with the data set from the substrate treated with GPS. The reason  
472 for this becomes clear when the molecular architecture of the curing agent is  
473 considered. TDI urone is a symmetrical molecule. And in the case of the bare  
474 aluminum, it is weakly adsorbed on the substrate by donor–acceptor interactions,  
475 and both ends of the molecule can yield the  $m/z = 58$  ion ( $\text{CH}_3\text{NHCO}^+$ ) used in the  
476 analysis of this adsorption process. In the case of the GPS-treated aluminum, one end  
477 of the molecule can interact directly with the strained oxirane ring (epoxy group) of  
478 the organosilane adhesion promoter. It is more likely that there is now only one  
479 amine functionality to generate the diagnostic fragment. In this manner, it is  
480 possible to deduce the nature of the bonding between silane and curing agent, and  
481 specific ions indicative of such an interaction were also seen in the ToF-SIMS  
482 spectrum (Rattana et al. 2002).

483 In addition to providing information regarding the capacity of the solid surface for  
484 the liquid phase adsorbate, the adsorption isotherm can also provide valuable  
485 conformational and thermodynamic information. The data of Fig. 14 presents the  
486 adsorption isotherms for poly(methylmethacrylate) (PMMA) on oxidized aluminum  
487 and silicon surfaces (Watts et al. 2000). Figure 14a shows the behavior at low and  
488 medium concentrations, and this follows the expected form for chemisorption. The  
489 data at higher concentration, Fig. 14b, shows a sharp rise in adsorption that is  
490 consistent with multilayer rather than monolayer adsorption. The answer, however,  
491 lies in the conformation of the molecules; at low concentrations they are in an  
492 extended form (illustrated by the schematic inset of Fig. 14a), while at higher  
493 concentrations they are in a more compact form and pack more efficiently on the  
494 surface (shown in the schematic of Fig. 14b). Another useful feature that can be  
495 established qualitatively from inspection of the isotherms of Fig. 14a is the heat of  
496 adsorption. The sharpness of the “knee” at low concentration provides an indication  
497 of this value, thus for the data of PMMA on aluminum and silicon the heat of  
498 adsorption for PMMA on aluminum is more exothermic than on silicon. This is as  
499 one would expect as the silicon surface will be rich in acidic silanol groups very  
500 receptive to the basic PMMA, whilst the aluminum oxide surface is amphoteric and  
501 will not react so readily with PMMA.

502 The plateau of the adsorption isotherm indicates the concentration(s) at which all  
503 adsorption sites for the adsorbing species are occupied, in surface chemistry terms the  
504 fractional surface coverage of the substrate by the adsorbate is unity. Such a specimen  
505 provides an ideal opportunity to probe the interfacial chemistry of adhesion directly  
506 using what is sometimes referred to as the thin film approach. As the layer of organic  
507 material, such as adhesive, is very thin (as a result of monolayer coverage) the  
508 contribution of interfacial chemistry at the interface will be maximized in the resultant  
509 XPS or ToF-SIMS spectrum. For this reason, the construction of adsorption isotherms  
510 is often used as a precursor to direct interphase analysis in this manner.

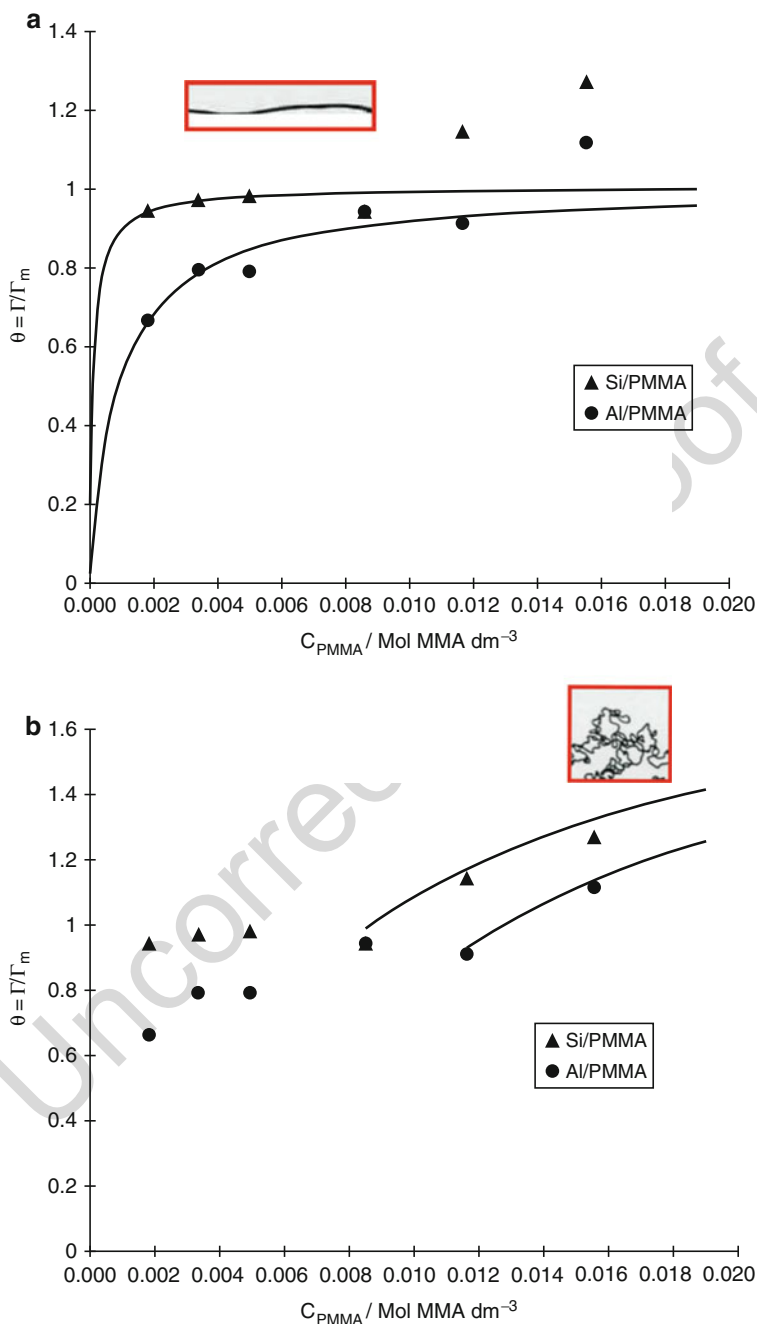


**Fig. 14** Adsorption of PMMA onto oxidized aluminum and silicon. (a) Shows the behavior of molecules at low concentrations when they are extended while (b) indicates the apparent deviation from monolayer coverage at high concentrations as a result of the molecule adopting a more compact form (Reproduced from Watts et al. (2000), with permission)

## 10.5.2 Direct Interphase Analysis

The concept that by carrying out a surface analysis on a model specimen one can obtain direct access to the interphase chemistry is a potentially very exciting and rewarding idea. The interaction of PMMA with various metals (as exemplified by Fig. 14 above) has been studied in some detail using high resolution XPS (Leadley and Watts 1997). In this work the manner in which PMMA formed specific interactions with oxidized metal surfaces was studied by the nature of the fine structure in the XPS spectrum. In this manner, it was possible to show that the polymer formed hydrogen bonds with oxidised silicon (an acidic substrate), a bidentate structure with oxidised aluminum (an amphoteric substrate) and would undergo acyl nucleophilic attack with oxidised nickel (a basic substrate).

In the case of the GPS organosilane adhesion promoter applied to aluminum (and used as a substrate in the data of Fig. 13), ToF-SIMS has established the formation of a covalent bond between the GPS molecule and the oxidized aluminum substrate (Abel et al. 2000). The chemistry leading to the formation of the diagnostic fragment ( $\text{Al-O-Si}^+$  at  $m/z = 70.9534$  u) and the high resolution spectrum at a nominal mass of 71 u is shown in Fig. 15. The formation of the specific bond is associated with good durability of the resultant bond, and examination of the fracture surfaces of failed joints shows that the presence of the ion in the ToF-SIMS spectrum correlates well with good durability.

ToF-SIMS has been used in a similar manner, in the work of Shimizu et al. (2010) to identify the specific interaction between aluminum and polymeric methylene diphenyl diisocyanate (PMDI). A series of ToF-SIMS spectra from the region of nominal mass  $m/z = 102$  u is shown in Fig. 16, and the spectra have been peak-fitted which is not a standard practice in ToF-SIMS (first demonstrated by Abel et al. 2009), although it is readily accomplished using standard XPS software such as CasaXPS (CasaXPS 2009). These range from a concentrated solution (Fig. 16a, 5 v/v%) through to a dilute solution and the bare aluminum substrate (Fig. 16e, f, respectively). For the two most concentrated solutions (Fig. 16a, b) a thick layer is deposited and the only fragment in this region of the spectrum is  $\text{C}_7\text{H}_4\text{N}^-$  characteristic of the PMDI material. The two dilute solutions show fragments from the substrate ( $\text{Al}_2\text{O}_3^-$ ) and the PMDI but also an ion at  $m/z = 101.9772$  u indicative of the  $\text{AlCHNO}_3^-$  ion, which results from the formation of a covalent bond between the aluminum substrate and PMDI. A possible structure of this ion is shown in the inset to Fig. 16d.

## In Vacuo Testing for the Provision of Interfacial Failure Surfaces

Almost all investigations seeking to elucidate mechanisms of adhesion, or define the locus of failure, are carried out on specimens which are generated outside the ultra-high vacuum of the surface analysis systems. For the most part this works extremely well, and the distinction between adventitious hydrocarbon materials and residual, vanishingly thin, layers of adhesive or organic coating are made in quite a straightforward manner. This is particularly true with the molecular specificity of ToF-SIMS that enables the individual components of the formulation of adhesive or coating to

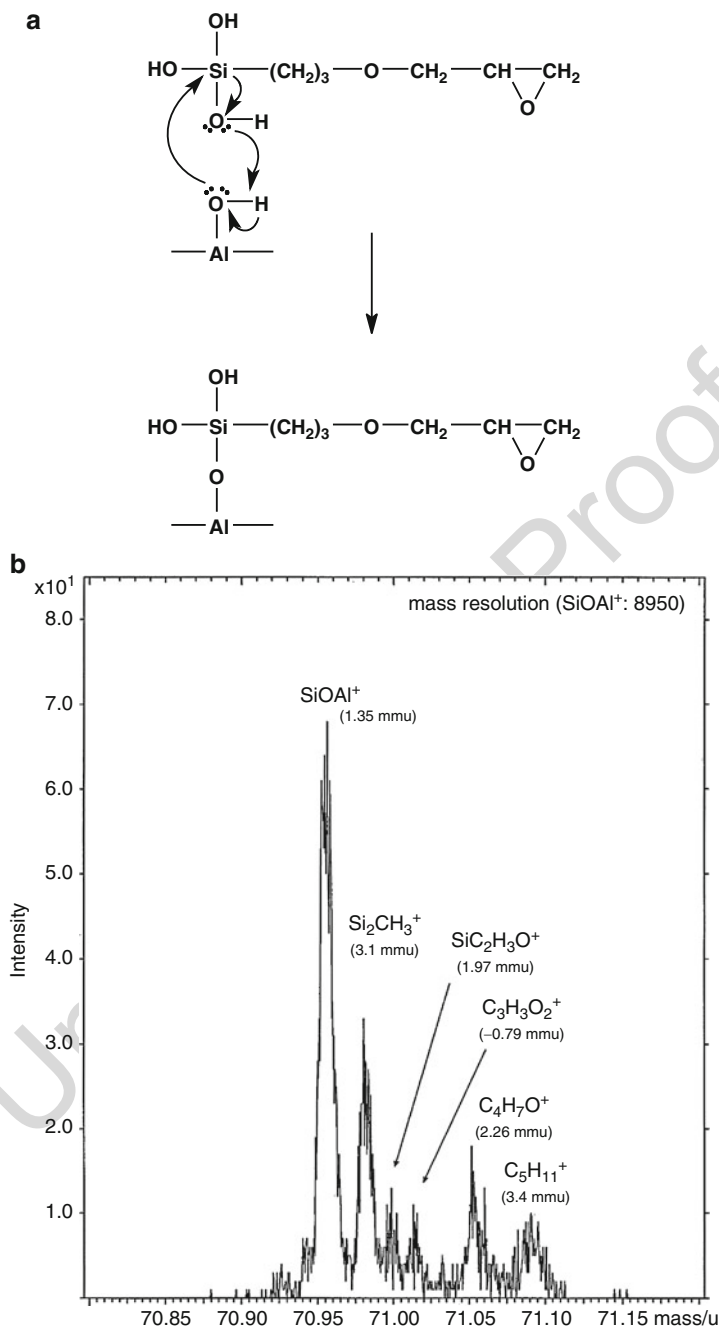


**Fig. 15** The specific interaction of glycidy propyl trimethoxysilane with hydrolyzed aluminum. **(a)** Reaction mechanism, **(b)** high resolution ToF-SIMS spectrum of  $m/z = 71$  u region showing the  $\text{SiOAl}^+$  fragment attributed to the specific bond

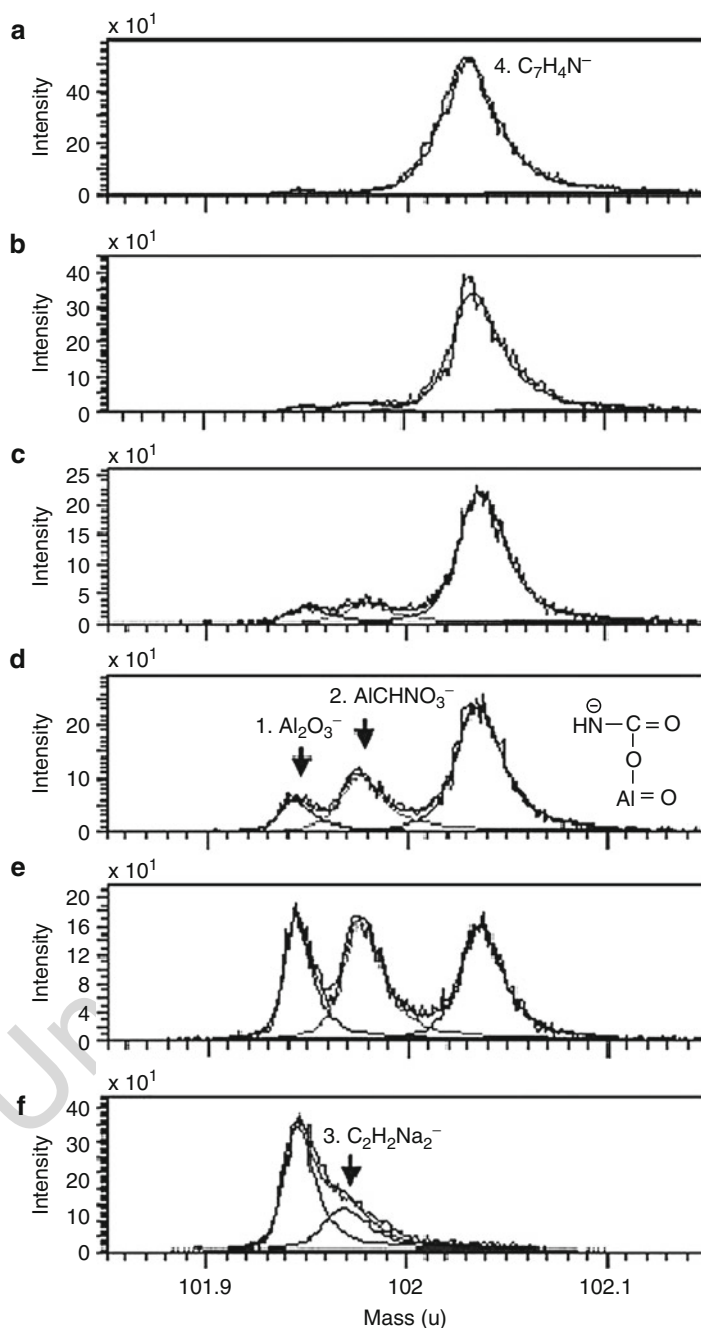


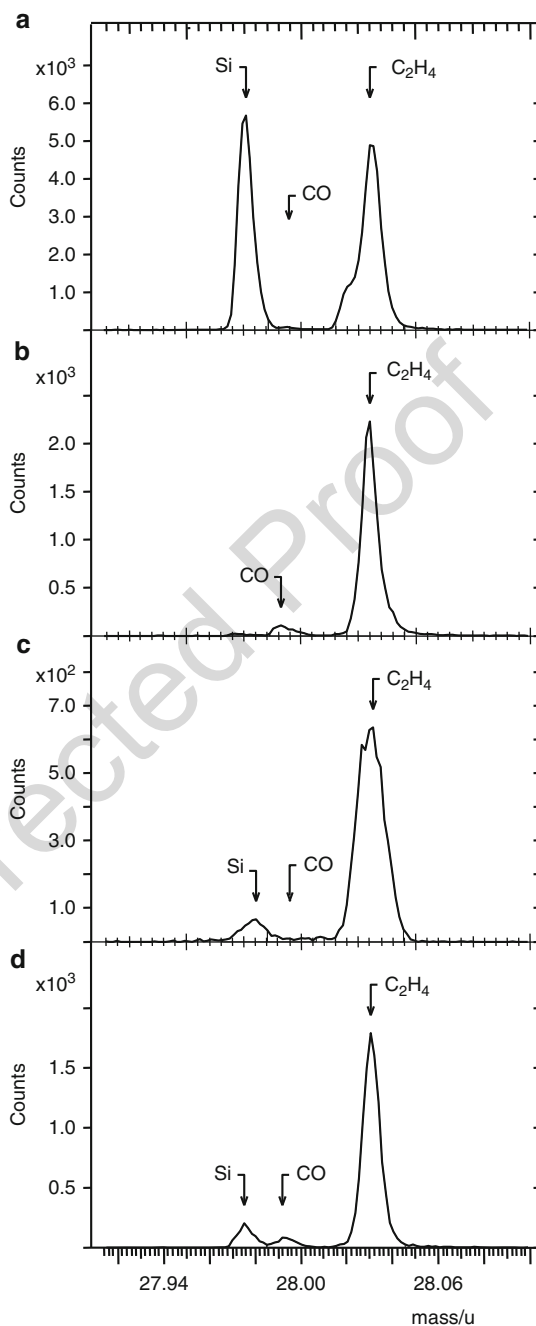
**Fig. 16** Specific interaction of polymeric methylene diphenyl diisocyanate (PMDI) with aluminum. Negative ToF-SIMS spectra at nominal mass  $m/z$  102 u from aluminum treated with PMDI of varying solution concentration. (a) 5 v/v%, (b) 0.5 v/v%, (c) 0.35 v/v%, (d) 0.1 v/v%, (e) 0.05 v/v%, (f) no PMDI (Reproduced from Shimizu et al. (2010), with permission)

be identified explicitly. There are situations when it is desirable and sometimes essential, to carry out the fracture process in a chamber of the spectrometer under UHV, clean conditions. There may be a number of reasons for the need to proceed in this manner; fracture may be thought to occur at a metal–oxide interface (of an anodic layer, for example), and the metal substrate will oxidize on air exposure making the failure indistinguishable from one that is within the oxide layer; an unfunctionalized carbon component in the formulation (a wax for example) may be thought to segregate to the interface forming a weak boundary layer that will be spectroscopically indistinguishable from adventitious hydrocarbon; there may be concerns about post-failure contamination of the surface by airborne material that is also in the organic material formulation.

The concept of *in vacuo* fracture as a means of sample preparation for adhesion studies has been developed in the author's laboratory in a gradual manner over many years. Initial studies made use of an impact fracture stage designed to provide an Izod (three-point bend) geometry for use with metallic samples that yielded intergranular fracture at cryogenic temperatures. This was modified for composites research. And small samples that are 30 mm in length and some 2 mm square (with fibers oriented in the 2 mm direction) could be accommodated in the stage using small sleeves, and fracture could be generated at, or around, the fiber–matrix interface at room temperature. The resulting fracture surfaces could then be examined by XPS, ToF-SIMS, or AES. The disadvantage of these early experiments were that it was not possible to control strain rate or loading geometry and the next step of development was the design of a controlled strain rate stage that could be arranged for Mode I or Mode II loading of the samples as described by Prickett et al. (2001). This established the concept of controlled geometry of loading but neither the applied load nor the strain rate was monitored in this intermediate fracture stage. The current solution to *in vacuo* fracture is a fully instrumented fracture stage, interfaced to a personal computer, that allows the strain rate to be controlled as the load applied is recorded (Wood et al. 2008). The use of this stage is illustrated below with an example involving the reinforcement of an unsaturated polyester resin (of the type used as a matrix in glass fiber–reinforced composites) with organically modified silica nanoparticles (ormosil).

The specimen geometry was a miniature compact tension specimen and samples were made of the unmodified polyester resin and polyester resin with ormosil added at a level of 1 v/v%. In order to compare the efficacy of the fracture stage a comparison was first made between surfaces produced in the fracture stage firstly at ambient atmosphere and then when the stage is pumped down to ultra-high vacuum and the fracture surfaces produced in these clean conditions (Wood et al. 2009). The high resolution ToF-SIMS spectra from the  $m/z = 28$  region of the spectrum shows clear differences between the spectra from these two surfaces. The spectrum from the sample fractured at ambient pressure shows a significant intensity of the  $^{28}\text{Si}^+$  ion (Fig. 17a), while the surface fractured in UHV shows no sign of silicon contamination, confirmed as poly(dimethyl siloxane) by the inspection of the complete ToF-SIMS spectrum. Turning now to the spectra from the fractured ormosil modified polyester fracture surfaces, it can be seen that the  $^{28}\text{Si}^+$  ion

**Fig. 17** ToF-SIMS spectra of nominal mass  $m/z = 28$  u for the polyester/ormosil system. (a) Polyester fractured in air, (b) polyester fractured in vacuo, (c) polyester + ormosil fractured in air, (d) polyester + ormosil fractured in vacuo (Reproduced from Wood et al. (2009), with permission)





intensity is significant on both surfaces (Fig. 17c, d, respectively). The question is, of course, the source of the silicon on these two surfaces as both have the potential to be from either PDMS or the SiO<sub>2</sub>-based ormosil particles. The resolution of this quandary, of course, lies in the information provided by the spectra of Fig. 17a, b, which indicate that fracture in situ will be PDMS-free but when fractured in air there is always the possibility of contamination by airborne PDMS. This example illustrates in a very powerful manner the benefit of in vacuo sample preparation. The source of the PDMS is thought to be personal care products used by many within the laboratory and the local environment.

---

## 10.6 Conclusions

The use of XPS and ToF-SIMS has much to recommend for the investigation of the interfacial chemistry of adhesion. In the most advantageous cases the analysis of fracture surfaces has the potential to provide such information but one must ensure that failure has occurred within the interphase; this will not always be the case and the onus, as always, is on the researcher rather than the analyst, to interpret the analytical data correctly in the context in which the analysis was made. If fracture surfaces do not provide access to the interphase it is necessary to resort to sectioning of the system to expose, possibly with sputter depth profiling, the interphase region itself for analysis. An alternative method is to use dilute solutions, based on either individual components of a formulation, or the complete adhesive or coating itself. This allows the determination of adsorption isotherms that measure the capacity of a solid surface for adsorbates in the liquid phase, and also confirms the development of monolayer coverage. By the analysis of a specimen from the plateau region of an isotherm, it is possible to probe the interfacial region with XPS or ToF-SIMS that allows spectroscopic identification of the interphase to be achieved. ToF-SIMS with its molecular specificity is particularly informative in this regard and may enable the nature of the bond to be identified explicitly if spectra are recorded at very high mass resolution.

---

## References

- Abel M-L, Fletcher IW, Digby RP, Watts JF (2000) *Surf Interface Anal* 29:115
- Abel M-L, Shimizu K, Holliman M, Watts JF (2009) *Surf Interface Anal* 41:265
- Bertho J, Stolojan V, Abel M-L, Watts JF (2010) *Micron* 41:130
- Bishopp JA, Thompson GE (1993) *Surf Interface Anal* 20:485
- CasaXPS (2009). <http://www.casaxps.com/>. Accessed 1 Mar 2011
- Hinder SJ, Watts JF (2004) *Surf Interface Anal* 36:1032
- Hinder SJ, Lowe C, Maxted JT, Watts JF (2004) *Surf Interface Anal* 36:1575
- Hinder SJ, Lowe C, Maxted JT, Watts JF (2005) *J Mater Sci* 40:285
- Kinloch AJ, Little M, Watts JF (2000) *Acta Mater* 48:4543
- Iezzi RA, Leidheiser H (1981) *Corrosion* 37:28

- 638 Leadley SR, Watts JF (1997) *J Adhes* 60:175  
639 Leadley SR, Watts JF, Rodriguez A, Lowe C (1998) *Int J Adhes Adhes* 18:193  
640 Prickett AC, Smith PA, Watts JF (2001) *Surf Interface Anal* 31:11  
641 Rattana A, Hermes JD, Abel M-L, Watts JF (2002) *Int J Adhes Adhes* 22:205  
642 Rattana A, Abel M-L, Watts JF (2006) *Int J Adhes Adhes* 26:28  
643 Shimizu K, Phanopoulos C, Loenders R, Abel M-L, Watts JF (2010) *Surf Interface Anal* 42:1432  
644 Smith GC (2005) *J Electron Spectrosc* 148:21  
645 Taylor AM, McLean CH, Charlton M, Watts JF (1995) *Surf Interface Anal* 23:342  
646 Watts JF, Castle JE (1983) *J Mater Sci* 18:2987  
647 Watts JF (1988) *Surf Interface Anal* 12:497  
648 Watts JF (1989) *J Adhes* 31:73  
649 Watts JF, Castle JE (1999) *Int J Adhes Adhes* 19:435  
650 Watts JF, Leadley SR, Castle JE, Blomfield CJ (2000) *Langmuir* 16:2292  
651 Watts JF, Rattana A, Abel M-L (2004) *Surf Interface Anal* 36:1449  
652 Watts JF, Taylor AM (1995) *J Adhes* 55:99  
653 Watts JF (2010) Role of corrosion in the failure of adhesive joints. In: Richardson JA et al (eds)  
654 Shreir's corrosion, vol 3. Elsevier, Amsterdam, pp 2463–2481  
655 Wood AR, Benedetto N, Hooker N, Scullion E, Smith PA, Watts JF (2008) *Surf Interface*  
656 *Anal* 40:1409  
657 Wood AR, Abel M-L, Smith PA, Watts JF (2009) *J Adhes Sci Technol* 23:689

# Organosilanes: Adhesion Promoters and Primers

# 11

Marie-Laure Abel

## Contents

11.1	Introduction	258
11.2	What Silanes are and Where do they Come from	259
11.2.1	Definition	259
11.2.2	The Origin of Organosilanes	259
11.2.3	Silanes Chemistry	260
11.2.4	Reactions in Solution	261
11.2.5	Specific Interactions at the Interface	265
11.2.6	Interactions with a Polymer or Polymeric Substrate	266
11.2.7	Reactions when Not in Solution	268
11.3	Uses of Organosilanes Other than Adhesion Promoter	268
11.4	Selection of a Coupling Agent	271
11.5	Organosilanes as Primers	271
11.5.1	Organosilanes as Adhesion Primers	272
11.5.2	Organosilane as Corrosion Protection Films	274
11.6	Silanes in Formulations	275
11.7	Non-silane Coupling Agents and/or Adhesion Promoters	277
11.7.1	Metal-Based Coupling Agents: Example of Zirconium and Titanium	278
11.7.2	Other Silicon-Based Coupling Agents	278
11.8	Conclusions	279
	References	279

## Abstract

Being amongst the most versatile molecules available to promote adhesion, organosilanes nonetheless remain a bit of a conundrum for some as one needs to know their chemistry thoroughly in order to utilize them in a useful fashion. In the first instance, this work starts with a short presentation of organosilanes defining this class of chemicals as well as explaining their genesis followed

M.-L. Abel (✉)

Faculty of Engineering and Physical Sciences (A1), University of Surrey, Guildford, Surrey, UK  
e-mail: [M.Abel@surrey.ac.uk](mailto:M.Abel@surrey.ac.uk)

immediately by a section of this chapter dedicated to their chemistry which includes a few words of warning. Closely related are the necessary interactions that such molecules have to develop on materials in order to fulfill their main role as adhesion promoters, and this is described too but more particularly when considering metallic substrates and polymers. Reactions in a medium are also covered briefly as silanes are commonly included in a matrix which precludes a more comprehensive section of silanes behavior in formulations later on in this document. Is also covered other usages of silanes than as adhesion promoters together with principles to follow in order to chose a silane for a particular application. The following section is concerned with the use of silanes as primers particularly where the user aims to improve adhesion or protect from corrosion. To complete this work, a small section covers some other organic or nonorganic adhesion promoters.

---

## 11.1 Introduction

Although initially the development of organosilanes adhesion promoters was a response to a technological need, more recent developments in the use of such molecules illustrate the reflection of recent legislation and need for more “green” materials. This is true in particular when considering such applications as replacements for chromic acid rinses used in the aerospace industry or corrosion protection where silanes are used as primers in the purest sense of the word. Unfortunately or fortunately, what lies at the heart of this class of molecules is their chemistry. It is both the tenor of their flexibility and complexity, and full understanding of such matters is of foremost importance. As such, explanations of the various intrinsic reactions they may undergo together with a review of how such molecules interact with a variety of materials is essential. The obvious next step from using silanes as adhesion promoters/primers consists into incorporating the silane within a formulation in order to interact with a surface while saving a step in the process. For example, an adhesive formulation may already contain a silane which is destined to diffuse and bond with the surface of choice. Apart from the obvious economy of time, one can anticipate large savings of a more real nature. This chapter will therefore also cover reactions of silanes when not in solution, i.e., for organosilanes incorporated in formulations such as inks or adhesives. Another major part is concerned with the parameters which influence the deposition of organosilanes as primers, some of which are often overlooked, as well as with the various uses of silanes either as adhesion promoters or otherwise including their sometimes controversial usage as corrosion protection coatings. One part is also dedicated to the manner in which one should choose one’s silane, although this section is certainly not exhaustive. The ultimate in the matter remaining a series of tests and experiments for the particular system considered. However, the present author acknowledges that this is not always timely or practical, especially when one considers the resources required and, hence, some pointers are provided to perform an adequate selection. Finally, and although this chapter will examine primarily organosilane adhesion

promoters as well as their use as primers, and within formulations, a short summary of other available adhesion promoters will also be presented at the end of the chapter.

## 11.2 What Silanes are and Where do they Come from

### 11.2.1 Definition

Organosilanes are hybrid molecules with at least one hydrolysable alkoxy silane. They usually bear the alkoxy silane functionality at one end and an organic functionality at the other end. The general formula is  $R'-Si(OR)_3$ , where  $R'$  corresponds to the main chain as well as any desired functionality, while  $OR$  is the hydrolysable alkoxy functionality. However, it is possible to find bis-silanes with alkoxy silanes at both ends of the molecules and one functionality within the middle chain. Various combinations of such structures may also be purchased according to the particular application sought after and/or the type of usage. There are many silanes available, but the most used bear the following organic functionalities: vinyl ( $-C=C-$ , double bond), epoxy, amino (primary amine as well as others,  $-N-$ ) and mercapto ( $-S$ ). They may be applied from solution as well as incorporated in formulations. They may be used on their own or in conjunction with other silanes. They can be deposited on several substrates: glass, metallic, as well as, more recently, organic. Their applications are vast and include composites, paints, adhesives, paints, and inks, and they can impart many properties on and to the materials they are used with, including hydrophobicity, temperature, and abrasion resistance. But mostly, what organosilanes are most famous for is their usage as primers and adhesion promoters where their role is to promote and improve adhesion between two dissimilar and/or incompatible materials.

### 11.2.2 The Origin of Organosilanes

The thought of creating such molecules originated from the will to render glass and an organic matrix compatible as well as to increase the durability of glass fibers-based composites. Indeed, although such composites were exhibiting strong initial strength, they would “fall apart” once introduced into a humid and hot environment. The debonding was attributed to water ingress and hydrolysis of glass. These composites were also exhibiting problems with stresses across the interface because of the very different properties of the glass and the matrix in terms of thermal expansion (Pluedemann 1991). A hybrid molecule with chemistry similar to glass on the one hand and similar to an organic matrix on the other hand was needed. A few organic reactions later, the first silane was born, itself a composite of the chemistry of glass (alkoxy silane part hydrolyzing into a silanol) and any chosen matrix (organic functionality born on the molecule in order to interact with a matrix). This was of course a major contribution to the world of chemistry and science by Edward D. Pluedemann, probably better known as “Mr Silane.” They

were obviously used on glass first, but their usage subsequently progressed onto the surface of metals and a lot recently on polymeric materials too (Pluedemann 1991, Smith 1999). The chemistry of those molecules is at the origin of their being but is also at the very root of their flexibility and the many domains in which they find valuable applications. Therefore, the following section will cover the chemistry of organosilanes and what other reactions they can undergo, including how they interact with other media be it with their surfaces or matrices.

### 11.2.3 Silanes Chemistry

First and foremost, one should make the distinction between all silanes molecules and the more specific organosilanes which are used in solutions or formulated systems as adhesion promoters. The former are basically any molecule-containing silicon, carbon, hydrogen, and possibly oxygen, and encompass both organosilanes and more simple gaseous silicon-based molecules mostly used for plasma deposition of silica or silicone like films. The molecules considered here are more complex as is explained further up in this paragraph. Organosilanes can undergo several types of reactions; they can be summed up as follows: hydrolysis, condensation (either between themselves or with a substrate) and, finally, less likely but nonetheless possible, alcoholysis. Organosilanes usually bear three alkoxy functionalities but may bear only one or two or present functionalities on both sides of the molecule or more. Examples of various silane structures are provided in Fig. 1 where one can see examples of silanes with either three (Fig. 1a) or more (Fig. 1b) alkoxy functionalities. An overview with a few vignettes is provided here, but for a more comprehensive review, one could consult the excellent work by Osterholtz and Pohl in particular where reactions in solution are concerned (Pohl and Osterholtz 1992).

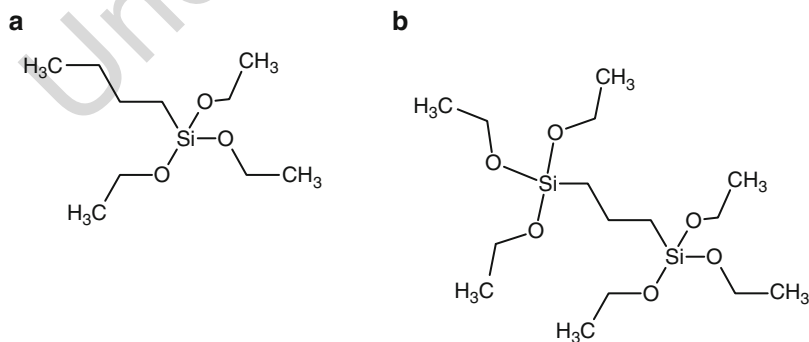


**Fig. 1** General silane structure (a) one-sided silane molecule and (b) organosilane with multiple silane functionalities

## 11.2.4 Reactions in Solution

**Hydrolysis**

Hydrolysis is the conversion of the alkoxy present on the silane molecule in silanols and leads to the production of the alcohol corresponding to the alkoxy present in the silane. This reaction is illustrated in Fig. 2a for an aminosilane,  $\gamma$ -aminopropyl triethoxysilane (APS), and many factors can influence it. This is an important reaction because it is usually preferable, though not compulsory, that the molecule should hydrolyze prior to bonding. The kinetics of hydrolysis depend on how easily the alkoxy to hydrolyze may be approached. One the factors to be considered is therefore steric hindrance. Initially and usually, three alkoxy are present on the molecule. It has been shown that the first one will take longer to hydrolyze followed by increasing kinetic constants for the two left. It also depends on the actual type of alkoxy (methoxy, ethoxy, or longer) as well as the length of the chain connected to the silicon atom, and this has been shown by Arkles et al. who compared the kinetics of hydrolysis for i-butyltrimethoxysilane and i-butyltriethoxysilane (Arkles et al. 1992). Another factor includes the type of functionality attached at the other end of

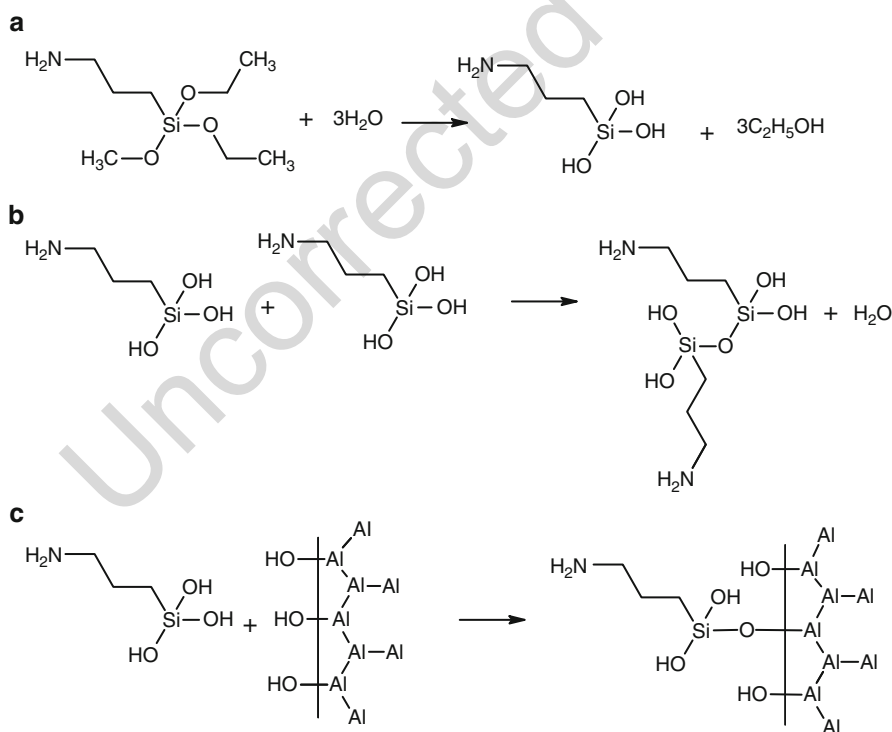


**Fig. 2** (a) Schematic of APS organosilane hydrolysis, (b) schematic of APS organosilane self-condensation, and (c) APS organosilane condensation with aluminum surface

the organosilane chain and one can demonstrate that, by example, an amino functionality tends to be self-catalyzed compared to an epoxy or a vinyl as in the work by Blum et al. as seen in Fig. 3, where the study was performed using proton nuclear magnetic resonance ( $^1\text{H}$ -NMR) (Blum et al. 1991): (A) represents the signal of methoxysilane (reactant) and (B) the resonance of methanol. The decrease of A versus the increase of B indicates that hydrolysis is taking place. Once the intensity of B is constant, the reaction is complete. This work is also a very good illustration of the rapidity with which amino-functionalized silanes can hydrolyze. It is very important to isolate them from water if not in use as they are autocatalyzed for both hydrolysis and condensation to such an extent that such molecules will even react with the air moisture and absorb  $\text{CO}_2$ . Such reactions can be controlled better paradoxically if performed in an aqueous solution as one can monitor the kinetics of reaction using catalysis by setting the pH of the solution. The catalysis for hydrolysis is usually acidic, although it is possible to use basic catalysis which is usually preferred for condensation, particularly self-condensation. A small paragraph on catalysis will be provided at the end of this section.

In addition, one should also emphasize one particular aspect of organosilane hydrolysis: the effect of other solvents and more particularly that of alcohol, understood as the organic class of molecules of course. It is often advised as

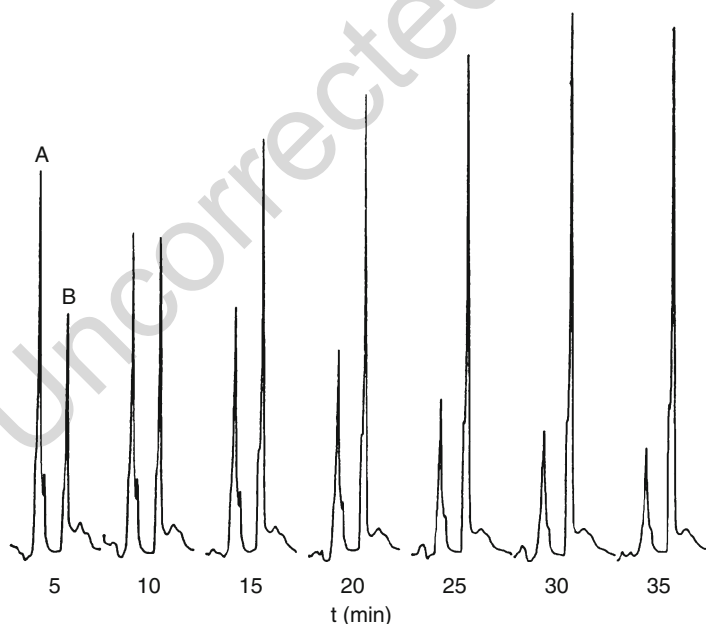


**Fig. 3** Illustration of hydrolysis: A represents the methoxysilane signal and B the methanol resonance in an extract of a nuclear magnetic resonance spectrum. The decrease of A versus the increase of B indicates that hydrolysis is taking place. Once the intensity of B is constant the reaction is complete



largely seen in the literature to proceed to the hydrolysis of a silane in aqueous solution; often also, one is advised to use an alcohol together with water as another solvent, and many authors happily mention using a mixture of water and either methanol or ethanol while waiting for a given time (of say 20–30 min) for hydrolysis. This is rather contra-intuitive as this clearly contradicts Le Chatelier principle. Indeed, hydrolysis of alkoxy functionalities should lead to the production of the corresponding alcohol. By example, an ethoxy will produce ethanol. Hence, adding the correct alcohol (only correct by the virtue that it will allow avoidance of alcoholysis, see below) can only slow down or even stop the hydrolysis reaction. Such problem has been illustrated clearly by some work where the hydrolysis is shown to clearly being extremely or even on existent when methanol is added to a solution of  $\gamma$ -glycidoxy propyl trimethoxysilane (GPS) (Abel et al. 2006). Again, NMR was used, and it was possible to show that adding methanol in solution was significantly slowing down the hydrolysis reaction even if only added at a concentration of 10% (v/v) in solution. However, notwithstanding the problem of volatile organics, one can comprehend that in some cases, it is preferable to use an organic solvent because it evaporate faster but remains the problem of controlling hydrolysis. A good answer to the conundrum would be to use a concentrated aqueous solution at ideal pH (see Sect. 2.4.4 below) and then diluting in an organic solvent once hydrolysis has occurred in order to obtain a solution in which the monomer is stable, i.e., with a longer shelf life. This is not valid though for aminosilanes.

### Condensation

Two types of condensation are possible. One is self-condensation, while the other corresponds to condensation with a substrate of choice such as a metallic substrate. The latter will be covered in more detail in another section below. By definition, condensation corresponds to the reaction of two hydroxyls ( $-\text{OH}$ ) functionalities, leading usually to the formation of water and an ether bond; there is a possibility, however, that condensation may occur before hydrolysis has taken place, but this is not as likely unless catalysis is being used. Figure 2b illustrates the reaction. Similar to hydrolysis, condensation and particularly condensation as oligomer formation is influenced by the value of the pH of the aqueous silane solution. Both condensation and hydrolysis can be controlled using catalysis, although, as mentioned before, amino-functionalized silanes are autocatalyzed with an extremely rapid tendency to polymerize and are also influenced by the amount of silanols present. Condensation is mostly performed under basic catalysis. One of the interests of the users would be of course to be able to establish whether a solution of silane has polymerized without resorting to complex and often expensive tools. One of the recommendations on the silane “grapevine” is to check whether the solution has gone cloudy. This, however, is not valid if the silane polymerizes clear, which is indeed the case of  $\gamma$ -GPS but not of  $\gamma$ -aminopropyl triethoxysilane (APS) or vinyl silanes which polymerize cloudy. One should also be aware that in spite of the opinion of various authors on the subject, organosilanes will not always go down happily on a surface in order to form

bonds. In the case of oligomeric solutions, this is totally false and can lead to premature bond failure if used as a primer.

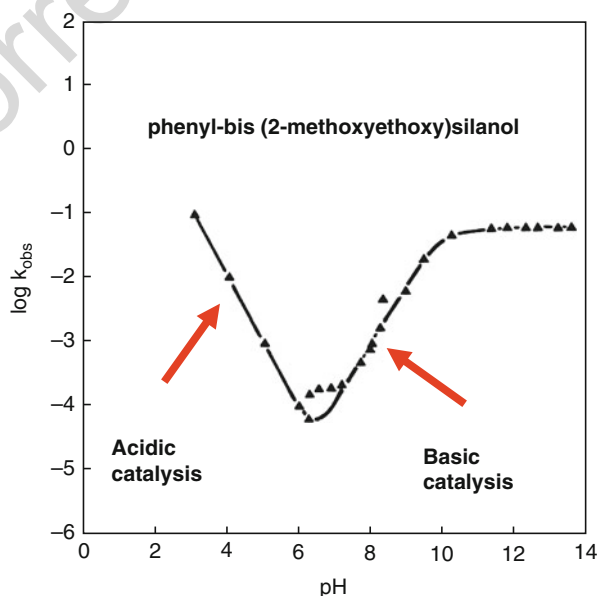
### Alcoholysis

Alcoholysis is the exchange of the alkoxy borne on the silane with the corresponding alcohol functionality if alcohol molecules are used within a silane solution. By example, if the silane is an ethoxy and that a solution containing methanol is made, then there is a possibility that the ethoxy may substitute for a methoxy.

### Catalysis

Either hydrolysis or condensation may be controlled using acidic or basic catalysis. Essentially, when examining these two reactions, one would ideally like to be able to freeze them in time in order to obtain solutions with long shelf life. Although this is only possible by, for example, cooling down a solution/mixture, it is preferable to use a solution of monomeric-hydrolyzed silanes as a primer solution and catalysis conveniently allows this. The kinetic constant of the hydrolysis and/or condensation reaction vary as a function of the pH of the solution. If acidic catalysis is examined for hydrolysis, then the constant, plotted as  $\log k$  as a function of pH, exhibits a “V-shaped” curve with a minimum specific value of pH. This value corresponds to the slowest kinetics of the reaction, usually around pH 6 for hydrolysis and 10 for condensation. Figure 4 shows an example of such a shape. The position of the minimum of the curve will itself depend on the structure of the molecule.

**Fig. 4** Illustration of the pH dependence of the kinetics of hydrolysis for phenyl-bis (2-methoxyethoxysilanol). On the left of the triangle, one can see acidic catalysis, while on the right, basic catalysis occurs



## 11.2.5 Specific Interactions at the Interface

### Interactions with a Metallic Substrate

As far as metallic substrates are concerned, the anticipation is that the silane will react with hydroxyls functionalities present at the surface in a reaction similar to that of self-condensation. An example of APS bonding on aluminum is given in Fig. 2c. It is important to point out that such interaction will be facilitated by a prior hydrolysis, but this is not necessarily compulsory, as silanes can even hydrolyze within a formulation and subsequently condense. This, for example, is particularly easy for aminosilanes which are autocatalyzed for both hydrolysis and condensation. A silane film is often shown as a “clean” monolayer being deposited on the surface of choice. This is far from reality, and often the film deposited on a substrate will represent several layers and have formed cross-linking of its own. This said, it is possible to deposit very thin films as well as monolayers in order to study the interaction of a possible silane with a substrate. Such methods include the use of adsorption isotherms, for example, as described by Watts in ► Chap. 10, “Use of Surface Analysis Methods to Probe the Interfacial Chemistry of Adhesion” of the present volume, or modelling of a silane layer using adequate softwares. Davis et al. showed that some silanes form a stable interaction when presented with a model aluminum surface; depending on the molecule, the interaction can occur via the silanol, the organic functionality, or forming a bridge while interacting with both sides of the molecule (Davis 1997). Kinloch et al. have also shown that the order, meaning geometry, in which silane will deposit on a surface is correlated with the length of the chain attached to the silane part, where it is above a length of 20 carbon atoms. At certain lengths, the molecules will order with a particular angle to the surface of choice, something not seen for short silane chains or below a length of 10 carbons (Hobbs and Kinloch 1998). Another example where the directionality of the interaction can be demonstrated is shown in the work of George et al. (George et al. 1996). In order to understand the interfacial chemistry of certain joints formed in the semiconductor industry and using angle-resolved x-ray photoelectron spectroscopy, George et al. have studied the interactions of APS with a silicon wafer as well as with Pyralin, a polyimide precursor. Their work shows that APS absorbs CO<sub>2</sub> indeed and can interact on both sides of the molecule with the substrate. The most interesting feature of the article is the demonstration that under a temperature of 125 °C, a thin APS film (1.5 nm) can “flip” from one side to the other (from –NH<sub>2</sub> interacting to silanol interacting), an interesting fact as most drying and cure processes will involve a step at temperature usually preferably above a threshold that will rid of most of the water present in the film. What remains is demonstrating the existence of bond formation. While acid-base type of bonds can sometimes be determined using x-ray photoelectron spectroscopy, showing the presence of covalent bond formation can be readily achieved by various methods such as time of flight secondary ion mass spectrometry (ToF-SIMS) but also with more accessible and cheaper techniques such as infrared spectroscopy (Abel et al. 2000, 2004). Figure 5 shows the region of nominal mass 71 in a positive mass spectrum (ToF-SIMS) for a GPS-coated grit-blasted aluminum where the fragment illustrating a bond formation between aluminum and a silanol is clearly visible, as shown by the fragment  $\text{AlOSi}^+$ . This was initially shown by Gettings and Kinloch at nominal

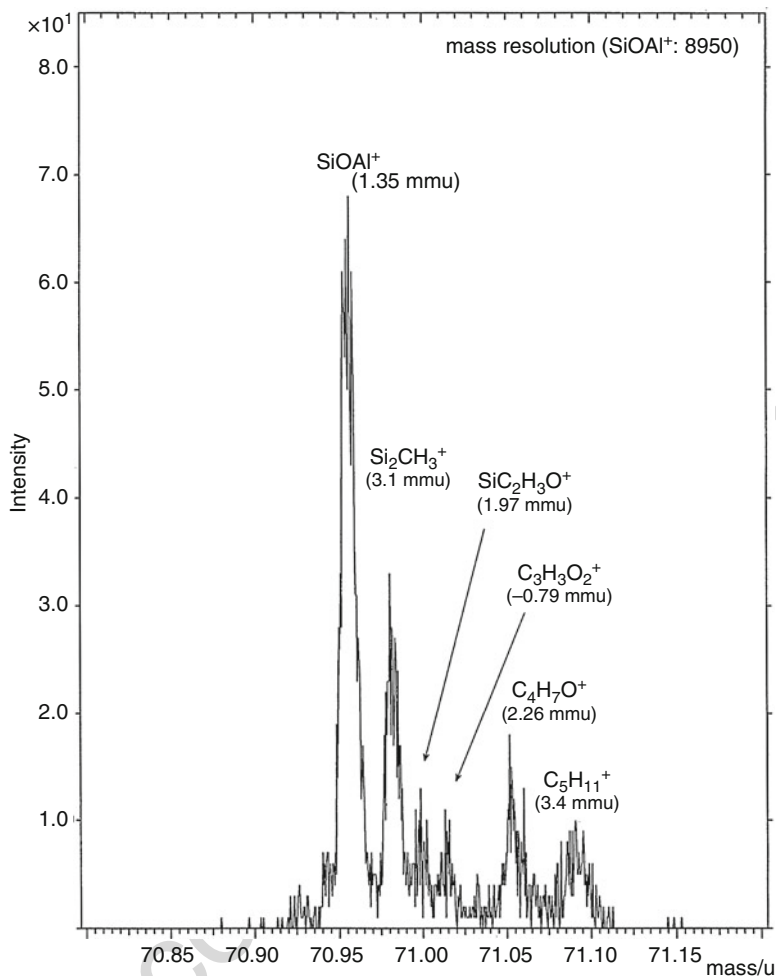


**Fig. 5** High-mass resolution of ToF-SIMS spectrum in the positive mode of grit-blasted aluminum coated with GPS at nominal mass 71. The most intense peak may be assigned to  $\text{AlOSi}^+$  and provides proof of silane bonding to aluminum substrate. The difference in mass between assignments and recorded masses is provided in mμ

280 mass  $m/z = 100u$  for  $\text{FeOSi}^+$  easier to demonstrate in spite of the lack of mass  
 281 resolution because of its occurrence at an even mass which is unusual for most organic  
 282 fragments, as shown in Fig. 6 (Gettings and Kinloch 1977).

### 283 11.2.6 Interactions with a Polymer or Polymeric Substrate

284 Although the interaction of organosilanes to metals or more generally surface-  
 285 bearing hydroxyl functionalities is usually well known, it is another matter when

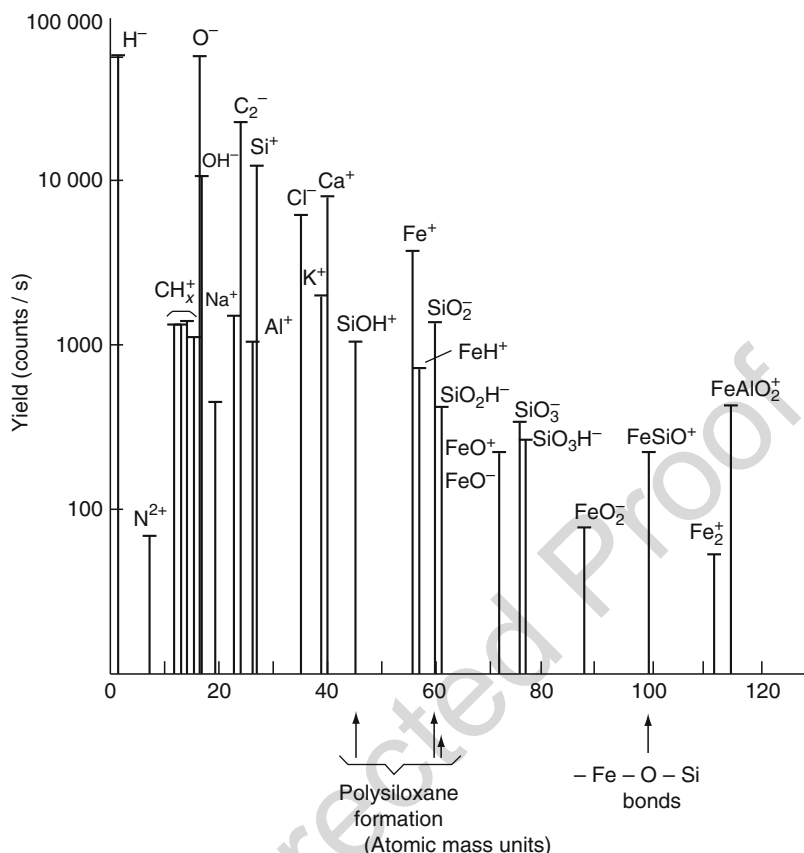


**Fig. 6** ToF-SIMS spectrum in the positive mode of detection of steel coated with silane, showing the presence of an ion at nominal mass  $m/z = 100u$  and indicating the presence of  $FeOSi^+$  resulting from bond formation of steel with silanols

interactions of the same molecules to polymer are concerned. If the silane has been selected properly, it is usually anticipated that the organic functionality borne by the silane will interact with the polymer of choice in some way either by forming a covalent bond or a Lewis (electronic type of interaction) acid-base type of bond. This is exemplified easily when a silane is incorporated in an epoxy resin; as most structural adhesives contain an epoxy part and an amine curing agent, one can see that an aminosilane will also react with the epoxy resin, and that an epoxy silane (such as  $\gamma$ -glycidoxo propyl trimethoxy silane or GPS) will react with the curing agent. Such a reaction was shown to occur by Rattana et al. using thin film deposition of an amine-curing agent on the top of an epoxy silane. The reaction mechanism is the same as seen for the curing of the resin itself (Rattana et al. 2002). Other authors have shown similarly that a methacrylate-functionalized silane will bond to an unsaturated polyester resin (Dow Corning 2011). Just as for any interactions with

metals, any film formed by the silanes on polymeric surfaces cannot be assimilated to a simple monolayer and, in the case of two organic materials (polymer/silane), this leads to the hypothesis proposed initially by Pluedemann that a silane coupling agent can form an interpenetrating network as a possible mechanism of adhesion (Pluedemann 1991). This provides another mode of interaction between silanes and polymers, where no chemical reaction is necessary.

### 11.2.7 Reactions when Not in Solution

Silanes can be incorporated in formulations as will be discussed later in this work. However, and for the sake of clarity, reactions in a bulk material will be briefly covered here. Silanes used in formulations can be used for different purposes but, most of the time, they are present in order to aid bonding between the matrix of choice (whether adhesive, ink, or else) and the chosen substrate. In order to do so, they have to undergo the exact same reactions that a silane and/or a primer prepared from a solution should, namely hydrolysis and condensation. The particular difficulty resides in the observation of reactions within a system which may contain other sources of silicon and where the silane is introduced at small concentrations of the order of 1% (w/w). Abel et al. have had some success in observing the reactions undergone, in particular, by an aminosilane within an epoxy system. Using ToF-SIMS, it was possible to observe peaks which are indicative of hydrolysis at nominal mass 79 ( $\text{Si}(\text{OH})_3^+$ ) as well as other fragments characteristic of condensation on both substrate (bonding) and as self (polymerization) (mass 71 and 72, for respectively  $\text{AlOSi}^+$  and  $\text{Si}_2\text{O}^+$ ). In these figures, two superimposed spectra are shown, and they correspond to two different regions close to the interface of an adhesive-containing APS deposited on aluminum foil. An example of such fragments is shown in Figs. 7, 8, and 9, where high-mass resolution spectra are shown for the masses mentioned above, together with other fragments present at the same nominal mass. The lower spectrum corresponds to the region closer to the substrate for nominal mass 79 and 72 while  $\text{AlOSi}^+$  was only observed for this region. For such reactions to occur, water must be present in some form; the most obvious way in which water may be found in a system is within the matrix itself or adsorbed on the substrate. Increase of temperature when curing an adhesive, for example, may be a further incentive for bond formation, be it covalent bond formation with the substrate or self-condensation. When an aminosilane is used, there is no doubt that the autocatalysis is aiding the reactions to occur as well as their identification.

## 11.3 Uses of Organosilanes Other than Adhesion Promoter

It is actually useful to look at the actual application for which organosilanes can be used rather than a particular field as well as the actual properties of materials provided by silanes. The major use of silane is obviously in the context of adhesion and very specifically as an adhesion promoter; however, this concept can be turned on its head and provide functionalized surfaces where silanes do not interact or with

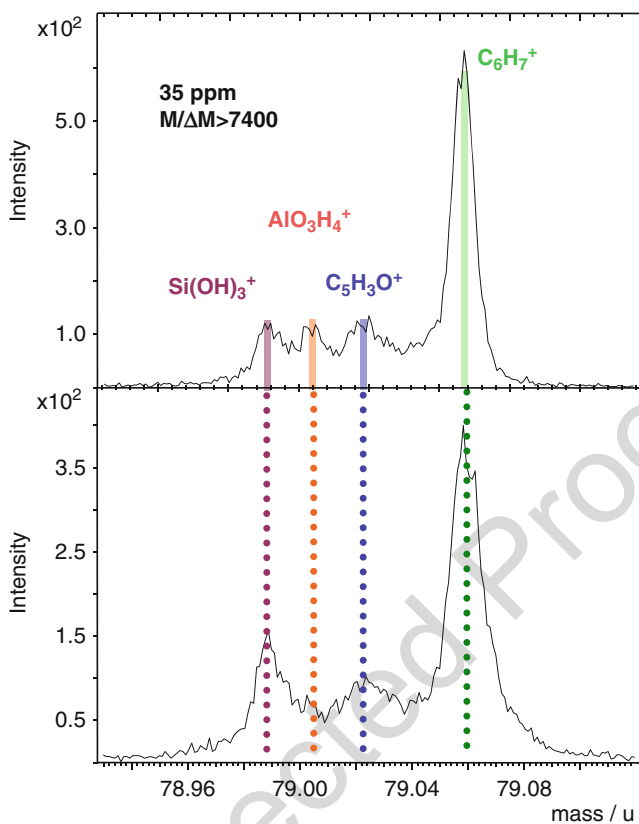


**Fig. 7** High-mass resolution at nominal mass 79, showing the presence of  $\text{Si(OH)}_3^+$  and indicating that the silane incorporated in the formulation has hydrolyzed

very small interactions. Most silanes bear alkoxy silanes and another functionality; usually the latter is designed to interact with another material, but it is possible to prepare silanes bearing an alkyl chain opposite to the alkoxy. This results in a molecule only capable to interact with van der Waals interactions. Such molecules when grafted/bonded to a surface of choice may therefore be used as water repellent and contribute to properties of materials in this manner. Apart from the obvious usage, this may, for example, provide such properties as thixotropy to adhesive and paints and also help in increasing toughness of materials as a “non-interaction” as the interface of two dissimilar materials can provide a deflection path for a fracture crack and hence increase resulting toughness. Another application uses the same concept as an adhesion promoter, and this is when a silane is used as a cross-linker. The very same functionalities used to promote adhesion can also be used within a matrix or formulation and promote cross-linking by forming bonds with neighbouring functionalities. Silanes can also impart temperature resistance, and to do so, the organic

**Fig. 8** High-mass resolution at nominal mass 71, showing the presence of  $\text{AlOSi}^+$  and indicating that the silane incorporated in the formulation has bonded with the substrate

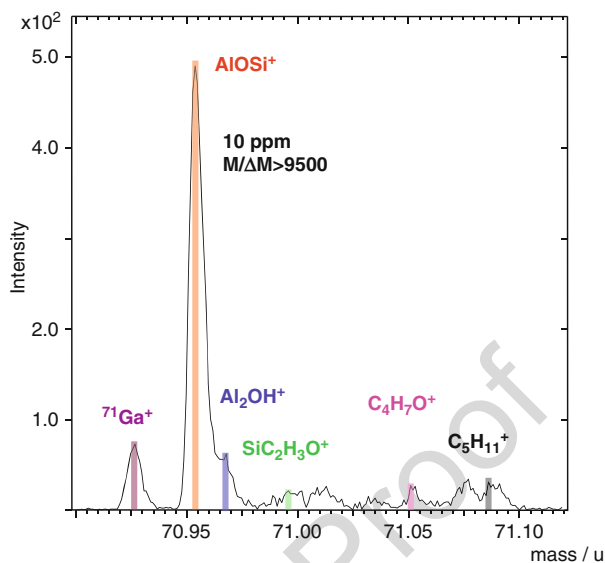
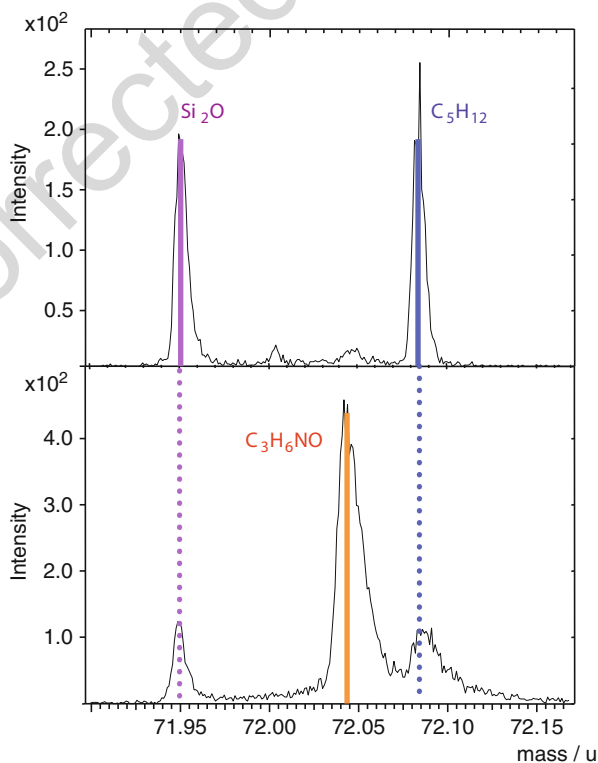


**Fig. 9** High-mass resolution at nominal mass 72, showing the presence of  $\text{Si}_2\text{O}^+$  and indicating that the silane incorporated in the formulation has polymerized





functionalities that the silane must bear are very specific. A good example of this is a phenyl functionality, which is not surprising as such chemistry also provides higher temperature resistance to molecules that bear it. Other applications include mechanical improvement with abrasion resistance as well as corrosion protection which will be described in more detail in Sect. 2.4 as it is invariably connected to adhesion.

---

## 11.4 Selection of a Coupling Agent

The general rules when choosing a silane is to work with a molecule which will be compatible with the system considered. This is why often the chemistry of the silane used will be considered and will provide a fairly good rule of thumb for selection. Examples include epoxy silane for epoxy adhesives, although an aminosilane can work as well, and vinyl can be used for rubber. The compatibility in the chemistry goes further than just exhibiting similar functional groups. Another way to choose a silane is of course to consider which type of reaction such molecule may undergo. For example, a vinyl silane will be compatible with a system that reacts through free radical process/polymerization. In that sense, an epoxy silane such as  $\gamma$ -glycidoxypentyl trimethoxy silane is compatible with an epoxy resin not only on the account of similar chemistry but because it will undergo the exact same reaction through the epoxy ring than cure reactions based on the same functionality in the resin/adhesive.

---

## 11.5 Organosilanes as Primers

When a material is to be bonded to another, various case scenarios may be considered. One would, of course, like to improve adhesion between these materials by treating the surface in some way which can be observed macroscopically by increased wetting. However, other considerations include protection of the substrate against corrosion or oxidation, especially but not only if metallic, as well as increasing the surface area available for bonding. These aims may be achieved in many ways with a treatment of the surface to bond. Abrasive mechanical, chemical, plasma, flame and coatings treatments are available and produce surfaces with improved, often combined characteristics (like higher surface energy and increased surface area by example), and properties which vary in benefit according to whatever technique is used and which effect is desired as well as how some of these methods are combined (abrasion plus primer).

One method that combines in attaining several of the properties considered in the previous paragraph is the application of a primer. This is achieved by depositing a relatively thin film of material, usually in liquid form, on the material to be bonded or coated. The role of the primer is to act as some kind of barrier (against possible corrosion for example) and/or to provide functionalities for bonding and hence make the two surfaces to be bonded more compatible. One particular type of molecules which seems to be used with some success in both cases is organosilanes. The use of silanes in such applications is popular because of its relative harmlessness compared

to for example chromium VI based treatments. They can also be prepared in aqueous solutions and this helps for applications where volatile organic compounds are either prohibited or reduced considerably as indicated by recent European Directives making them a good application in an industrial context. As described above these molecules were designed in order to compatibilize glass and coatings and in particular in order to increase durability of matrix to glass fibers in composites acting in stopping untimely hydrolysis of the glass acting therefore both as a barrier and providing ideal chemistry at the interface. Subsequently it was also found that silanes could be used on metals and more recently on polymers. Their use will be examined in the light of two of the mains aims for primers: as a barrier and creation of functionalities/compatibilization with other materials. In other words in two domains where silanes have potentially a great importance: adhesion and corrosion sciences.

### 11.5.1 Organosilanes as Adhesion Primers

Many parameters may influence the mechanical properties of a joint formed with a silane primer and the interactions formed when depositing the silane. One can roughly divide them in three categories prior to implementation in the field. Firstly, the solution used initially, then the application, and finally the curing of the coating and/or adhesive deposited on the top of the silane layer. If one considers the solution first, the tenor of using a silane primer or coating properly is to know the chemistry. One point which is never emphasized enough is that one should advise strongly to use a solution which only contains monomers of the hydrolyzed silane of choice or failing that a solution that does not contain oligomers of the silane of choice. Bertelsen and Boerio have shown quite cleverly using both fracture mechanics as well  $^{29}\text{Si}$  NMR and vibrational spectroscopy that poor durability of a joint formed with an epoxy adhesive and a hydrolyzed epoxy silane could be explained by the oligomerization of the solution used which is related with time and hence shelf life (Bertelsen and Boerio 2001). Figure 10 shows the relationship between the amount of polymerization present in the solution and the correlation with the onset of the increase of the crack length of a test joint. In other words, the higher the amount of oligomers/polymerization in the solution, the least durable is the joint. Similarly, other coworkers have shown that the amount of adsorption of  $\gamma$ -GPS decreases as a function of hydrolysis time which is consistent with Bertelsen and Boerio's studies (Abel et al. 2000). This also undoubtedly illustrates the importance of the hydrolysis parameters in solutions which include, to name but a few, hydrolysis time, pH of the solution, concentration of silane-used solvents (from aqueous only to mixtures of alcohol). Porrit underwent a very exhaustive study of the parameters which can influence durability when a particular silane primer is used in an epoxy adhesive joint (Porrit 2001). The parameters considered included details concerning the solution used (as exemplified by the sentence above) but also considered the substrate surface treatment prior to coating the silane solution, mode of deposition such as dipping or brushing the solution on, as well as time and temperature of cure for the adhesive. In his work, the durability tests were performed using the

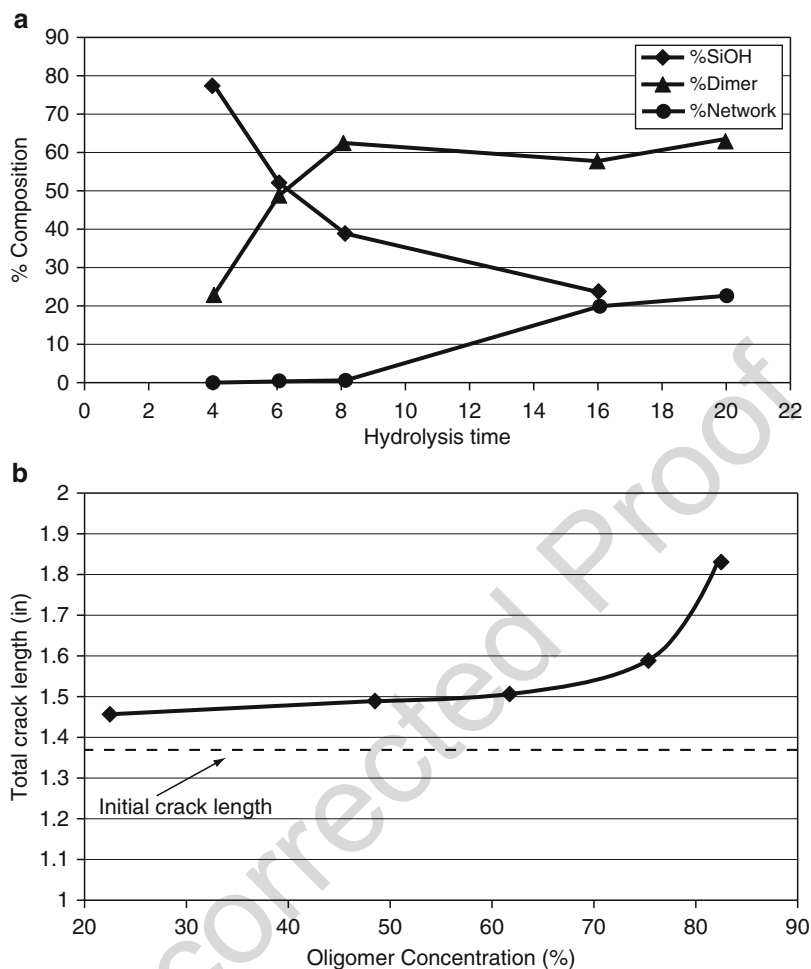


**Fig. 10** (a) Relationship between composition and hydrolysis time for a 10% solution of  $\gamma$ -GPS in water. (b) Relationship between the composition in a 10% solution and total crack length of wedge test specimens prepared from adherends treated with a 1%  $\gamma$ -GPS solution

rather convenient and quick Boeing wedge test, and he was able to eliminate unfavourable conditions and obtain the optimum concentration of silane, time, and pH of hydrolysis for an aqueous solution, lag time between drying and bonding, mode of deposition, time and temperature of drying. Parameters considered for the surface treatment included type of cleaning and, type of surface roughening. This shows that to obtain the full benefits of silane usage, one must know in detail not only the chemistry but also the favourable or unfavourable conditions such application may encounter once deposited on a substrate. This section is going to review some of these parameters.

First and foremost, the cleanliness of the substrate should be of uppermost importance but is not always necessary, which confuses the silane application issue further. Usually, one should deposit a coating or film on a clean surface to avoid any weak boundary effect, but it is not unusual to see that some adhesives and/or coatings subsequently deposited on a surface can absorb the contaminants or displace them (usual culprits include and not particularly in industry only polydimethyl siloxane (PDMS) and materials akin to polytetrafluoroethylene better known under the designation Teflon™ or PTFE). For example, Watts and Prickett have shown that adhesion to composite samples exhibiting PDMS on their surface can be good and explained this fact by assuming that the contaminant was being absorbed by the adhesive (Prickett 2003). Producing a similar final effect, it is assumed that silanes deposited on a surface can displace contamination. This is probably true of organics but is not the case for salts such as carbonates, and one should be aware that anything present on the surface prior to bonding may compromise strength and/or durability of a joint.

Another point of importance is the roughness of the substrate. It is usually thought that the rougher the surface, the better the adhesion or at least the mechanical anchorage of the coating on a substrate. Actually, what roughening produces is indeed an increase in surface area available for any coating, but this translates in particular into an increased number of available bonding sites. This is one of the reasons why phosphoric or chromic acid anodizing are so attractive for aluminum-based alloys notwithstanding their barrier properties. When Porritt studied the effect of surface preparation on the durability of joint prepared, the best effect was reported for a “boiled” aluminum surface where the microstructure obtained resembles that of phosphoric acid anodizing albeit at a smaller scale. The various parameters that were shown to be of importance were as follows: pH of the water used to hydrolyze GPS, time of hydrolysis, conditions of deposition, temperature of drying, and concentration of the solution. Figure 11 shows the results of the measurements of the fracture energy resulting from the optimized surface treatment using  $\gamma$ -GPS. This figure actually shows two optimized treatments: one optimized treatment corresponds to the best parameters as cited above, while the best treatment utilizes the same parameters and 1 h hydration (“boiling”) of the aluminum prior to deposition of the silane primer. It is rather remarkable that this final treatment happens to exhibit even better durability than the system usually assumed to be the best in terms of aluminum-based alloys for aerospace, namely chromic acid anodizing and phosphoric acid anodizing.

### 11.5.2 Organosilane as Corrosion Protection Films

The advantage of a protective coating containing silanes is supposed to be twofold: it can protect the metal on which the film will be applied, and it is also supposed to interact chemically with both substrate and covering coating. The treatment usually consists into the application of a mixture of silanes as it has been shown that a mixture exhibits a better performance in terms of corrosion protection than a single

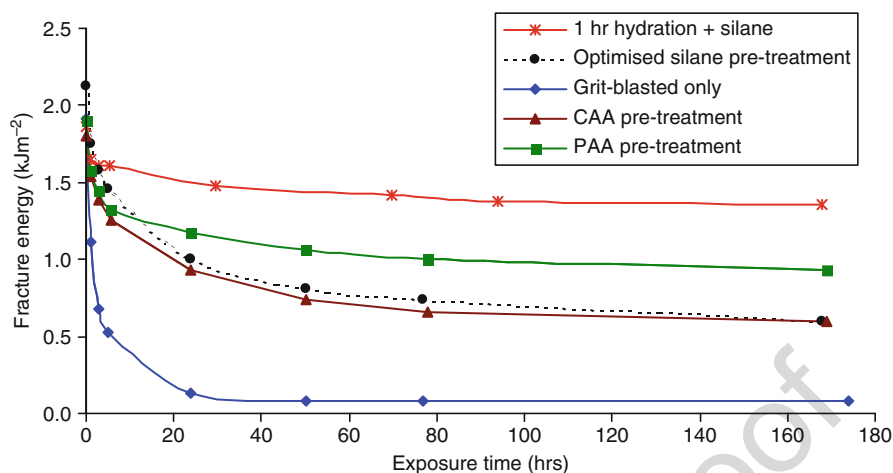


**Fig. 11** Fracture energy comparison for several treatments, including two optimized silane treatments. CAA denotes chromic acid anodizing, while PAA means phosphoric acid anodizing

silane solution (van Ooij et al. 2005). Much has been done to ascertain the efficacy of such corrosion protection primers as shown by one of the main protagonist of such methods, Win van Ooij based at the University of Cincinnati (van Ooij et al. 2005; Zhu and van Ooij 2004).

The mixture is typically a combination of “monosilanes” and “bis-silanes,” where the formula of the former is  $X_3Si(CH_2)_nY$  and the later is  $X_3Si(CH_2)_nY(CH_2)_mSiX_3$  (or even  $X_3Si(CH_2)_mSiX_3$ ). X represents the hydrolysable group and Y a functional group such as an amine or vinyl. The bis-silanes provide a pronounced hydrophobic polysiloxane layer resulting from SiOSi linkages. Unfortunately, such molecules are usually fairly hydrophobic and make the use of other solvents than water necessary, which is a clear handicap for the use of such solutions. Such systems include the use of bis-[triethoxysilyl]ethane (BTSE,  $(OC_2H_5)_3Si(CH_2)_2Si$ ). However, bis-silanes functionalized with amines are compatible with aqueous solutions and have allegedly shown the same resistance to corrosion as chromate based systems. Such systems are tested for corrosion resistance using various methods, mostly electrochemistry based.

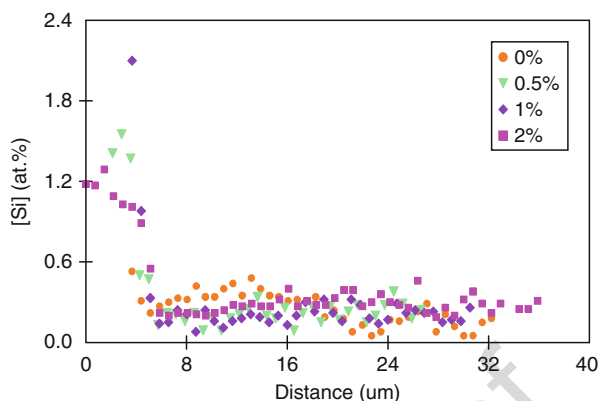
## 11.6 Silanes in Formulations

Silanes can be used in various ways, but when it comes to adhesion, they are either deposited as a coating or are incorporated within formulations. Those formulations include adhesives, coatings, and inks, but the list is not exhaustive. The intention is for these molecules to find their way toward the substrate and help bonding at the interface by rendering the substrate and the material deposited on it more compatible. This kind of application is important as it helps reducing time of application and

hence saves money but also because silanes are considered as a substitute to many other not so green materials. Using silanes in such a way can be considered as a “built-in” (within adhesive or coating for example) primer deposition as it is possible to show that a silane incorporated within a formulation will diffuse toward the desired interface. This is why relevant research will be described in this section.

The main problem encountered here is that there is hardly any control of the rate of the reactions happening within the system and similarly no control of the diffusion be it rate amount, type, etc. To confuse the issue further, many manufacturers will incorporate several organosilanes within a system on the off-chance that they have “missed something” without regard for the possible consequences on the interactions at the interface and durability of such joints. Although not many studies have been performed on the subject due to the intrinsic difficulty of the research, two were performed at the University of Surrey with two very different materials. One was concerned with the adhesion of polyamide coatings to steel in order to protect such items as dishwasher baskets from damage and corrosion; the other with the adhesion of an epoxy-based adhesive on aluminum to avoid the use of a silane (or other) primer. In both cases, only one organosilane was incorporated, and the aim was for the durability and/or protection resistance of the coating to be improved compared to a formulation without silane. In accordance with the general rules of silane choice, an epoxy functionalized (GPS) was chosen for the epoxy adhesive or an aminosilane (APS) for either the adhesive or the polyamide material (Guicheney et al. 2004, 2006a, b). In both cases, it was found that the addition of a silane is beneficial to durability and/or corrosion resistance. It was also possible to follow the diffusion of respective silanes using the now well-known method of ultralow-angle microtomy (ULAM) which allows access, amongst other advantages, to the still bonded material and hence the intact interface between either epoxy adhesive and aluminum or polyamide and steel (Hinder et al. 2005). Figure 12 shows an example of reconstructed diffusion profile of the concentration of silicon from the interface (distance zero) with the substrate toward the bulk of materials for an epoxy system. The analysis was performed using XPS after microtoming samples and calculation of the actual depth covered through ULAM cut (this is achieved through a simple trigonometry calculation, for more details see (Hinder et al. 2005)). Silicon is obviously used as a marker for the silane, and all precautions have been taken to eliminate other sources of silicon, including the silica (incidentally functionalized with an alkyl silane), usually included in the formulation to achieve thixotropy of the adhesive. One can see that the concentration of silicon is higher toward the substrate for aluminium whereas it has been shown that it increases also for while it was shown to be higher toward the steel and the air/polyamide interface in Guicheney et al.’s work (Guicheney et al. 2004, 2006a, b). This indicates that the silane has indeed diffused toward the desired interface but also toward the external surface of the coating. One can point out that the diffusion seems to occur in a similar way and achieve similar concentration of silicon at interfaces around 1–2 at.%. In the two examples provided, only the silanes are identical, while all other materials and conditions are totally different: two different substrates, a thermoplastic versus a thermoset as polymeric matrix which implies that the factors determinating the

**Fig. 12** Schematic indicating diffusion of silane within a formulation. On the left is the interface with aluminum and, on the right, the bulk of the adhesive



diffusion are similar and correspond to the molecule properties and behavior rather than anything else. This diffusion is most likely to occur when either material is still in a liquid/soft form with the difference that the temperature used is not the same, although it does not seem to be reflected in the diffusion.

Several driving forces can be invoked here. In order for the molecule to segregate to the interface with the substrate, it has to be mobile enough, and the local enrichment has to be driven by thermodynamic considerations. They have been described in detail by Abel and Watts as well as by Guicheney (2006b), but they can be summed up here. The metallic substrate capable of forming bonds with the silane may act as a sink for the silane molecules, solubility parameters should be considered also to assess the compatibility of matrix to silane to check on exclusions mechanisms as well as possible of interdiffusion with matrix as shown by Gentle et al. (1992). Another possible explanation lies into the value of the chemical potential (partial molar Gibbs free energy) of the silane, within the matrix considered as flow will occur spontaneously from a region of high chemical potential to a region of low chemical potential.

Several concentrations were tested, and one can find that if such a system is to be used, the concentration to be used has to be optimized and most likely will go an optimum then exhibit a detrimental effect on the properties considered. For example, adhesives containing a range of concentrations of GPS or APS were tested, and it became clear that too much silane within a formulation can exhibit similar properties to a formulation without silane, exemplifying beautifully the famous saying of “overegging the pudding.”

## 11.7 Non-silane Coupling Agents and/or Adhesion Promoters

Although silane adhesion promoters are probably the most known, used, and versatile, there are many others. Some are based on titanium, chromium, or zirconium, while others, still based on silicon chemistry totally differ in their structure



from regular organosilanes. This section will highlight briefly a few examples with their chemistry, mechanisms, and fields of applications.

### 11.7.1 Metal-Based Coupling Agents: Example of Zirconium and Titanium

Together with titanium, zirconium has a similar chemistry to that of silicon because of the group they belong to in the periodic table of elements. Zirconium tends to form polymeric species both in aqueous and solvent-based solution chemistry with a clear tendency to form bonds with oxygen. The zirconium compounds are classified as either anionic cationic or neutral. If organic species are involved in a system, it is generally admitted that zirconium will react readily with carboxyl groups rather than oxygenated functions such as an ether compound. They find applications, for example, in the industry of printing inks, lithographic printing plates for which they also contribute to corrosion resistance, aluminum drinking cans and pigment coating, as well as dental coupling agent between enamel polymeric filler. Several mechanisms can be put forward, and they include hydrogen bonding with zirconium as well as reactions with carbonyl functionalities. Titanium complexes on the other hand are believed to interact through surface hydroxyl groups. Other adhesion promoters based on other metals are also available, including one of the earliest known in the field dating from the 1960s and based on a methacrylate-chrome complex (Volan<sup>®</sup>).

### 11.7.2 Other Silicon-Based Coupling Agents

Some other coupling agents more recently highlighted include molecules which are again based on silane chemistry but do not have the same structure as organosilanes. Such an example is the use of cyclic azasilanes in particular in the field of micro-electronics and optoelectronics. The interest resides in a usage for a field in which the presence of water is totally undesirable and allows the avoidance of parasite by-products with the surface of nano-objects. Another reason for which the conventional adhesion promoters cannot be used is the propensity of organosilanes to self-condense or polymerize, inducing the creation of nanoscale domains thus potentially creating disturbances in the system or compromising its properties. For such an application, volatile molecules are needed to be able to use vapor phase deposition, one of the main deposition methods at the nanoscale. Another factor consists into the poor amount of sites functionalized using conventional silanes. If one considers pyrogenic silica, for example, only half at most will be functionalized which is far from desirable. Arkles et al. (2004) have shown the potential of such molecules and synthesized seven of this type with various functionalities on both the silicon and nitrogen atoms, including alkoxy functionalities with either one or two cycles in their structures. Cyclic azasilane molecules have been used to modify fillers with a showing higher bonding efficiency than a linear analogue (Vendamuthu et al.



2002), achieving a high-density monolayer deposit. The authors also concluded that although nitrogen had a catalytic action on bonding, further activity is provided by a ring-opening reaction.

## 11.8 Conclusions

Many parameters can influence the application of organosilane to whichever system is of interest. The major obstacle in their use is often the lack of knowledge of their mechanism as well as their chemistry, and although one would like to be able to pick any molecule and get on with work, this is not truly possible when using silanes. The only true answer is to test the system, coating, or formulation of interest to ascertain which are the optimum conditions to use a silane or even a mixture as is often done for corrosion protection for example or for formulations sometimes on the "of chance" to miss something out!!! However, when chosen carefully, silanes can provide an exceptional primer treatment even more performing than accepted though soon to be redundant surface treatments such as chromium VI based rinses. Testing does not have to always involve complex instrumentation, and often industry will use simple tests to decide on optimum conditions and concentrations. These molecules can find applications in so many domains that a little care and dispersing a few myths is well worth the effort and, hopefully, this work will have helped in achieving this goal.

## References

- Abel M-L, Digby RP, Fletcher IW, Watts JF (2000) *Surf Interface Anal* 29:115
- Abel M-L, Watts JF, Digby RP (2004) The influence of process parameters on the interfacial chemistry of  $\gamma$ -GPS on Aluminium: a review. *J Adhes* 80:291
- Abel ML, Joannic R, Fayos M, Lafontaine E, Shaw SJ, Watts JF (2006) Effect of solvent nature on the interaction of  $\gamma$ -glycidoxy propyl trimethoxy silane on oxidised aluminium surface: a study by solution chemistry and surface analysis. *Int J Adhes Adhes* 26:16
- Arkles B, Steinmetz JR, Zazyczny J, Metha P (1992) Factors contributing to the stability of alkoxysilanes in aqueous solution. *J Adhes Sci Technol* 6:193
- Arkles B, Pan Y, Larson GL, Berry DH (2004) In: Mittal KL (ed) *Silanes and other coupling agents*, vol 3. VSP, Utrecht, pp 179–192
- Bertelsen CM, Boerio FJ (2001) Linking mechanical properties of silanes to their chemical structure: an analytical study of  $\gamma$ -GPS solutions and films. *Prog Org Coat* 41:239
- Blum FD, Meesiri W, Kang H-J, Gambogi JE (1991) Hydrolysis, adsorption, and dynamics of silane coupling agents on silica surfaces. *J Adhes Sci Technol* 5:479
- Coming D (2011) A guide to silane solutions. [http://www.talleresnorte.com.ar/pdf/pinturas/silanos/silane\\_guide.pdf](http://www.talleresnorte.com.ar/pdf/pinturas/silanos/silane_guide.pdf). Accessed 01 Apr 2011
- Davis S (1997) PhD dissertation, University of Surrey
- Gentle TM, Schmidt RG, Naasz BM, Gellman AJ (1992) Organofunctional silanes as adhesion promoters: direct characterization of the polymer/silane interphase. *J Adhes Sci Technol* 6:307
- George I, Viel P, Bureau C, Suski J, Lecayon G (1996) Study of the silicon/ $\gamma$ -APS/Pyralin assembly interfaces by X-ray photoelectron spectroscopy. *Surf Interface Anal* 24:774

- 659 Gettings M, Kinloch AJ (1977) Surface analysis of polysiloxane/metal oxide interfaces. *J Mater Sci*  
660 12:2511
- 661 Guicheney M (2006) PhD thesis dissertation, University of Surrey
- 662 Guicheney M, Watts JF, Abel M-L, Brown AM, Audenaert M, Amouroux N (2004) Enhancement  
663 of the durability of a polyamide coating: incorporation of an aminosilane into the powder  
664 formulation. *Surf Interface Anal* 36:685
- 665 Guicheney M, Watts JF, Abel M-L, Audenaert M (2006) Mechanism of delamination of a  
666 polyamide coating modified with an aminosilane. *Surf Interface Anal* 38:168
- 667 Hinder SJ, Lowe C, Maxted JT, Watts JF (2005) The morphology and topography of polymer  
668 surfaces and interfaces exposed by ultra-low-angle microtomy. *J Mater Sci* 40:285
- 669 Hobbs PM, Kinloch AJ (1998) The computational molecular modelling of Organosilane primers.  
670 *J Adhes* 66:203
- 671 Pohl ER, Osterholtz FD (1992) Kinetics of the hydrolysis and condensation of organofunctional  
672 alkoxysilanes: a review. *J Adhes Sci Technol* 6:127
- 673 Porrit N (2001) PhD dissertation, University of Surrey
- 674 Prickett A (2003) PhD dissertation, University of Surrey
- 675 Rattana A, Hermes J, Abel M-L, Watts JF (2002) *Int J Adhes Adhes* 22:205
- 676 Smith JA (1999) PhD dissertation, University of Surrey
- 677 van Ooij WJ, Zhu D, Stacy M, Seth A, Mugada T, Gandhi J, Puomi P (2005) Corrosion protection  
678 properties of Organofunctional Silanes - an overview. *Tsinghua Sci Technol* 10:639
- 679 Vendamuthu M, Painter S, Ancheta J, Blitz J (2002) *J Undergrad Chem Res* 1:5
- 680 Zhu D, van Ooij WJ (2004) Corrosion protection of metals by water-based mixtures of  
681 bis-[trimethoxysilylpropyl]amine and vinyltriacetoxysilane. *Prog Org Coat* 49:42

**Adhesive and Sealant Materials**

Uncorrected Proof

# Classification of Adhesive and Sealant Materials

# 12

Erol Sancaktar

## Contents

12.1	Introduction .....	284
12.1.1	Classification of Engineering Polymers .....	285
12.1.2	Man-Made Fibers .....	288
12.1.3	Natural Adhesives .....	289
12.2	Function .....	290
12.2.1	Structural Adhesives .....	291
12.2.2	Hot-Melt Adhesives .....	291
12.2.3	Pressure-Sensitive Adhesives .....	291
12.2.4	Water-Base Adhesives .....	291
12.2.5	UV/Electron Beam-Curing Adhesives .....	292
12.2.6	High-Temperature Adhesives .....	292
12.2.7	Sealants .....	293
12.2.8	Conductive Adhesives .....	293
12.2.9	Nanocomposite Adhesives .....	294
12.3	Methods of Reaction .....	295
12.3.1	Thermosets .....	297
12.3.2	Thermoplastics .....	297
12.3.3	High-Temperature Adhesives .....	297
12.3.4	Elastomers .....	298
12.3.5	Sealants .....	298
12.3.6	Conductive Nanocomposite Adhesives .....	299
12.3.7	Other Types of Adhesives .....	299
12.3.8	Primers .....	300
12.4	Chemical Families and Physical Forms .....	301
12.4.1	Thermosets .....	301
12.4.2	Thermoplastics .....	305
12.4.3	Elastomers .....	306
12.4.4	Sealants .....	308

E. Sancaktar (✉)

Department of Polymer Engineering, University of Akron, Akron, OH, USA

e-mail: [erol@uakron.edu](mailto:erol@uakron.edu)

33	12.4.5	Important Moisture Curing Adhesives: Cyanoacrylate Adhesives .....	310
34	12.4.6	Conductive Adhesives .....	310
35	12.4.7	Physical Characteristics of Various Types of Adhesives .....	311
36	12.5	Methods of Application .....	312
37	12.5.1	Thermosets .....	313
38	12.5.2	Thermoplastics .....	313
39	12.5.3	High-Temperature Adhesives .....	314
40	12.5.4	Water-Base Adhesives .....	314
41	12.5.5	UV/Electron Beam Curing Adhesives .....	314
42	12.5.6	Sealants .....	314
43	12.5.7	Conductive Adhesives .....	314
44	12.5.8	Anaerobic Adhesives .....	315
45	12.5.9	Moisture Curing Adhesives .....	315
46	12.5.10	Primers .....	315
47	12.6	Conclusions .....	315
48		References .....	316

## Abstract

In this chapter, classification of adhesive and sealant materials is presented. For this purpose, various categories are considered depending on the polymer base (i.e., natural or synthetic), functionality in the polymer “backbone” (i.e., thermoplastic or thermoset), physical forms (i.e., one or multiple components, films), chemical families (i.e., epoxy, silicon), functional types (i.e., structural, hot melt, pressure sensitive, water-base, ultraviolet/electron beam cured, conductive, etc.), and methods of application. The classification covers high-temperature adhesives, sealants, conductive adhesives, nanocomposite adhesives, primers, solvent-activated adhesives, water-activated adhesives, and hybrid adhesives.

## 12.1 Introduction

This chapter aims to provide general information about the structure, properties, and applications of polymers and their composites that are used in the production of adhesives and sealants. The chapter is divided into six parts including: Function; Method of reaction; Physical form; Method of application; Conclusions, and References.

As discussed in earlier reviews, such as those by De Lollis (1980), Shields (1985) and Brinson (1987a, b, c), adhesive and sealant materials are classified using categories based on the nature of the following:

- Polymer base, i.e., natural or synthetic
- Functionality in the polymer “backbone,” i.e., thermoplastic or thermoset
- Physical forms, i.e., one or multiple components, films
- Chemical families, i.e., epoxy, silicon
- Functional types, i.e., structural, hot melt, pressure sensitive, water-base, ultraviolet/electron beam cured, and conductive

In order to be able to describe polymers and their composites which are used in the production of adhesives and sealants, a general classification of engineering polymers need to be considered first. The nature of a polymer defined as a plastic, an elastomer (rubber), or a fiber depends on the strength of its intermolecular bonds and molecular structure. At temperatures above their  $T_g$ , elastomers (rubbers) are typically noncrystalline polymers with weak intermolecular forces. Polymers with moderate intermolecular forces are classified as “plastics” at temperatures below their  $T_g$ ’s. On the other hand, polymers with strong hydrogen bonds and, especially, those with high crystallinity can be made into strong fibers, which are usually used to reinforce elastomers and plastics (Fig. 1). Furthermore, rubbery polymers that are flexible and readily deformable can acquire a reversibly elastic property by a cross-linking process. Many other processes are available to alter or transform the basic structure of a polymeric adhesive to suit a specific design need; e.g., an adhesive’s thermal insulating efficiency can be increased, if necessary, by foaming it with an appropriate cell structure, such as in polyurethane foam adhesives (Klepner and Frisch 1991).

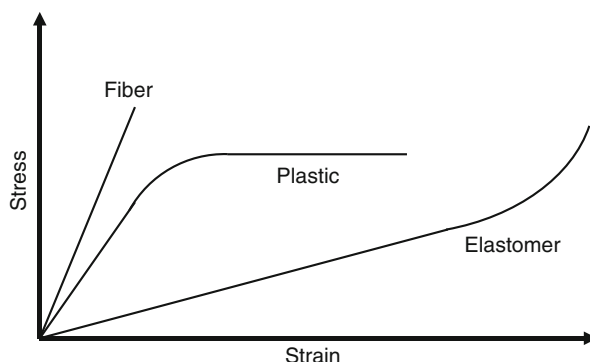
## 12.1.1 Classification of Engineering Polymers

### Thermoplastics

#### High-Performance Thermoplastics

- Polyamides (nylon)
- Polyamide-imide
- Polyarylates
- Polyaryletherketones
- Polyarylsulfones
- Polybenzimidazoles
- Polyetherimides
- Polysulfones

**Fig. 1** Stress–strain behaviors of typical fiber, plastic, and elastomer materials



For example, polyamides are typically applied as one part hot melts but are also available in alcohol base solution. Blending of polyamides with other polymers is frequently used to obtain tack and other required properties. For example, blending of amorphous polypropylene enhances peel adhesion to acrylic and canvas, and blending of phenolic resin produces high peel adhesion to plasticized polyvinyl chloride (PVC), porous materials, and metals.

### Other Thermoplastics

- Acetals
- Acrylics
- Acrylonitrile-butadiene-styrene
- Polycarbonates
- Polyethylene
- Polyethyleneterephthalates
- Polystyrene
- Polyvinylchloride

For example, tackified ethylene-vinyl acetate hot-melts are mostly used in the manufacture of exterior grade plywood, where water resistance is required, as well as in other general wood-bonding applications. They are also used in book binding, carton and case sealing, shoe manufacture, carpet seaming, as well as pressure-sensitive adhesives.

Polyvinyl acetate (PVA), used in emulsion form and sometimes called “white glue” has a glass temperature ( $\sim 28^\circ\text{C}$ ) above room temperature, thus requiring the addition of plasticizers to its formulation. This type of adhesive is typically used in packaging, for bonding paper, book binding, carton sealing, bag seaming, tube winding, cup adhesives, remoistenable adhesives (stamps), and in furniture industry.

Polyvinyl acetals, which are derived from the reaction of polyvinyl alcohol (a by-product of PVA) with formaldehyde, can be applied from solution as a one- or two-part system. Plasticizers (phosphates) can be added to improve their impact strength. These adhesives are typically used in the structural bonding of metals and auto safety glass. Hybrids of polyvinyl acetals with epoxies are used in structural bonding. Hybrids with phenolics (vinyl phenolic) are used in honeycomb manufacture for the aircraft industry, and also in printed circuits.

Higher  $T_g$  acrylic polymers are used for bonding of ceramic tiles, lamination of aluminum foil or plastic films to paper and wood, and in the treatment of textiles. The lower  $T_g$  (tacky) versions of the polymer, where the acrylic component is secondary to the elastomeric-based adhesive component, are used in pressure-sensitive adhesive applications.

Polyvinyl chloride copolymers are typically used in solution form for bonding PVC films to metals, paper, cloth, leather, and also used for foam lamination on plastics. PVC blended with plasticizers are used in automotive industry in adhesive form for bonding inner and outer hood and roof panels, and as a gap-filling adhesive.

## Thermosets

### General-Purpose Thermosets

- Amino
- Phenolics
- Polyesters
- Acrylics

For example, amino-resins are water-based condensation products of formaldehyde in urea or melamine. They are typically used for bonding wood, particle board, and decorative laminates.

Phenolic resins may be blended with elastomers, epoxies, and vinyl acetal resins to obtain versatile hybrid adhesives, especially to increase bond strength at elevated temperatures. Phenolic powders are also used as binding agents between glass and mineral fibers in the manufacture of thermal insulators. Fabrics, mats, and papers can be manufactured in laminate form by impregnating the sheets with a phenolic resin. Multiple layers of these products can be molded into various shapes, such as gears and cams, subsequent to drying. Phenolics are also used as binders in abrasive devices, such as grinding wheels.

Polyester resins can be used as a hot melt adhesive in shoe and textile industries.

Cyanoacrylates and anaerobic adhesives are the cross-linked versions of acrylic-based adhesives, cured by catalyst reactions.

### Engineering Thermosets

- Epoxy
- Polyurethane

For example, one-component isocyanate-terminated polyurethane prepolymers in solution are cured by reaction with moisture in 2–24 h, depending on bond thickness. Carbon dioxide is released during this cure, causing porosity in the bond and making them not suitable for structural adhesive applications. Consequently, they are mainly used in the packaging industry due to compatibility with cellophane, nylon, and polyester. On the other hand, two-component cross-linking urethane adhesives are used as structural adhesives in automotive and construction industries for plastic-to-metal and plastic-to-plastic bonding.

Thermoplastic and aqueous forms of the polyurethane-based adhesives are also available. Thermoplastic polyurethanes are soluble polymers, depending on the starting materials and differing greatly in their degree of crystallinity. For adhesives with high crystallinity, heat activation is required for adequate bonding resulting in high peel strength and high softening temperatures. These types of adhesives are typically used for bonding plastics, rubbers, leather, wood, vinyls, and metals. Aqueous forms of polyurethanes are applied with the use of compounded surfactants.



Epoxies provide good adhesion to a large spectrum of substrates and exhibit low shrinkage, low creep, the ability to formulate at 100% solids, and a large number of co-reactants. For example, its hybrids can be obtained with phenolics, polyamids, and elastomers.

### Specialty Thermosets

- Silicone
- Polyimide

For example, silicone adhesives can cross-link with moisture or with catalyzers, providing high elongation, chemical inertness, and heat resistance. On the other hand, silicones are used more as sealants than as adhesives and can also be prepared as pressure-sensitive adhesives.

### Elastomers (Rubbers)

- EPDM (Ethylene-Propylene)
- Fluorocarbons
- Natural
- Nitrile (Acrylonitrile butadiene)
- Polybutadiene
- Silicon

For example, polychloroprene/neoprene, with the addition of casein, provides adhesives for high-speed laminating of aluminum foil to paper. They are typically used in the automotive and construction industries for plastics-to-wood bonding (Formica), and also used as contact cements in the shoe industry. These adhesives typically crystallize from solution.

Elastomeric adhesives can be prepared by emulsion polymerization of nitrile rubber films. Blending of nitrile emulsions with phenolic resins, casein, and tackifiers produce “latex adhesives.”

Butyl Rubbers are noncrystallizing materials used in pressure-sensitive applications, such as bonding polyethylene tapes to steel pipes.

Styrene butadiene rubber (SBR) is heavily tackified and compounded with fillers, to be used in pressure-sensitive and spray applications, as construction adhesives in bonding plastic tile, panel, and floor adhesives in solution form and also as tire thread adhesives.

### 12.1.2 Man-Made Fibers

- Carbon
- Glass
- Aramid

### 12.1.3 Natural Adhesives

Adhesives are also obtained from natural resources in the following forms:

1. Starch form is basically made of carbohydrates ( $C_6H_{10}O_5$ ), found in many vegetables. When heated in water, starch swells into granules which disperse to a gel form. Modification with tackifying inorganic salts, fillers, and plasticizers is necessary for obtaining useful adhesive forms.

2. Dextrin is derived from starch by hydrolysis and is also marketed as gums. These adhesives are typically used in cellulose-based applications such as tube forming and laminating.

Starch-based adhesives degrade in humid service environments.

3. Protein-based glues typically cure with loss of water and require plasticizers such as glycerol. They are made of the following types: (a) Fish glues usually need glyoxal or formaldehyde addition due to their water solubility. They are compatible with acrylate and other emulsions. (b) Animal hide glues produce good tensile and shear properties in bonded joints. They are typically applied for binding in book and sandpaper production, as well as production of furniture, boxes, and gummed tapes. (c) Casein-based adhesives are often compounded with calcium hydroxide and/or formaldehyde for moisture/water resistance. These types of adhesives are mostly used in bonding wood. (d) Blood glues typically need addition of formaldehyde, manganese, and calcium salts for moisture resistance and have been steadily replaced by phenolic adhesives. They are mainly used in plywood and veneering applications. (e) Soybean adhesives are made of a combination of protein and carbohydrates and form a cross-link structure. They are mostly used in wood bonding.

4. Resins are bitumen (hydrocarbon), shellac, pitch, and drying oils.

5. Natural rubber is an elastomer, which is naturally tacky in dry form. With the use of additional tackifiers it acquires serviceable adhesion to itself and other surfaces. For example, in pressure-sensitive applications, the addition of tackifiers in a 40–60% proportion is usually necessary to increase bond strength. One area of application is in shoe manufacture.

Section 1.1 of this chapter classifies adhesives according to functional types including, structural, hot-melt, pressure sensitive, water-base, ultraviolet/electron beam cured, conductive, high-temperature, and sealant type.

Classification with respect to the methods of reaction is discussed in Sect. 1.2 to include thermosets, thermoplastics, high-temperature adhesives, elastomers, sealants, anaerobics, moisture curing adhesives, and primers.

In section “[Thermoplastics](#),” the physical form of adhesives is used for classification purposes and specific adhesives are discussed for each class of adhesives to provide more insight on adhesive categories including chemical families. This is because, many adhesives have cross-category characteristics, as

already illustrated with some of the above listed adhesive examples. Additional examples are epoxies, which are typically listed as structural adhesives, but are also available in “elastomer-epoxy” forms; high-temperature thermoplastic polyimide adhesives, which are also available in cross-linked forms; silicon, which can be used both as a sealant as well as an adhesive; hot-melt adhesives, which are typical thermoplastic resins, but can also be made into pressure-sensitive adhesives; and adhesives, such as epoxy, which can be used as primers subsequent to modification. Consequently, section “[Thermoplastics](#)” starts with the presentation of thermosets with the important example, epoxy. Structure and properties of epoxy are presented, followed by brief descriptions of “nylon-epoxies” and “elastomer-epoxies”; epoxy applications and comparison with other adhesives follow. Thermoplastics are discussed next with the important example, polyimides. Polyimide chemistry and properties, thermoset versions of polyimides, and polyimide applications are presented next. For the “elastomer” types, the important example of polyurethane is presented. Polyurethane chemistry and properties and its applications are discussed next. For the “sealant” category, silicone is discussed as an important example, providing silicone chemistry and properties, followed by its product forms and applications. For that purpose, “silicone fluids,” “room temperature vulcanizing silicones,” “one-part silicones,” “two-part silicones” and “heat-curable rubber types” are described. Cyanoacrylate adhesives are presented next as an important example of “moisture-curing adhesives.” “Advantages” and “limitations” of the different “functional types” presented in Sect. 1.1 are also discussed in section “[Thermoplastics](#),” with respect to their physical characteristics.

Section “[High-Performance Thermoplastics](#)” discusses common methods of application for various types of adhesives and the conclusions are presented in section “[Other Thermoplastics](#).”

---

## 12.2 Function

Adhesives and sealants are usually designed to have different properties even though they are often formulated using the same type of polymeric materials. Adhesives typically have high tensile and shear strengths. They are used to replace or reinforce mechanical fasteners in load-bearing applications. Sealants, on the other hand, typically have lower strength. They are flexible materials used to prevent the passage of liquids, vapors, gases, and solids. Sealants are also used to protect electronic components in aerospace, automotive, and appliance industries. Acrylics, silicones, urethanes, polysulfides, epoxies, and unsaturated polyesters are the primary sealant materials used in these applications. When vibration resistance and impact strength are required, or when materials with different coefficients of thermal expansion are bonded, a flexible sealant-type material is often the adhesive of choice.

The functionality of adhesives and sealants are generally categorized as follows:

### 12.2.1 Structural Adhesives

Structural adhesives are used to transfer loads between adherends in their service environments. They are typically cross-linked/thermosetting polymers, even though some thermoplastic polymers, such as acrylics, are also used in some structural load transfer applications.

### 12.2.2 Hot-Melt Adhesives

Hot-melt adhesives are 100% solids that include all thermoplastics. Hot-melt adhesives have versatile applications and can be used to bond many types of substrates, including metals, plastics, glass, ceramics, rubbers, and wood, in applications generally not requiring the transfer of high loads as in the case of structural adhesives. Applications include industrial and assembly bonding such as packaging, book bonding, and general household usage.

### 12.2.3 Pressure-Sensitive Adhesives

Pressure-sensitive adhesives (PSAs) are typically used to hold objects together by bringing the surfaces into contact under pressure, applied briefly at room temperature. Natural rubber, styrenebutadiene (SBR), butadiene-acrylonitrile rubber, thermoplastic adhesives, polyacrylates, and silicones are the typical materials used for pressure-sensitive adhesive applications. These materials have viscous properties to provide flow while resisting excessive flow, partial elastic behavior to be able to carry some load, the ability to store energy to provide peel and tack, and the capability to dissipate energy during usage. Tack may be obtained by the use of resinous softeners such as pine tar or rosin esters, by the use of mineral fillers and various coal tar or petroleum derivatives.

PSAs are typically supplied in the form of film, fabric, paper, two-face, electrical, and corrosion protection tapes.

Contact adhesives, which are manufactured using materials similar to the PSAs, typically, require little or no pressure to bond.

### 12.2.4 Water-Base Adhesives

Water-base adhesives are made of materials that can be dissolved or dispersed in water. Both natural (cellulosic, dextrin, starch) and synthetic (phenol formaldehyde, polyvinyl acetate, styrene-butadiene rubber, nitrile rubber) polymer materials are used in manufacturing water-base adhesives. Their primary application is in packaging, with a much smaller percentage usage in construction. Their share of the

market, however, has been increasing due to health concerns associated with some of the solvents used in organic-solvent adhesives.

### 12.2.5 UV/Electron Beam–Curing Adhesives

Specially formulated, 100% reactive liquids can be rapidly converted to solids using radiation curing with the inclusion of a photo initiator. Energy sources used for this purpose include ultraviolet (UV), electron beam (EB), visible (IR), and microwave sources. These adhesives are typically used as coatings, inks, sealants, and potting compounds, as well as for bonding purposes. The main advantage of UV/EB-curable adhesives is rapid curing at room temperature. Therefore, they can be used to bond heat-sensitive substrates, such as polyvinyl chloride. Furthermore, the rapid cure process increases production rates. UV/EB-cured adhesives are typically of the cross-linking type (acrylic acid esters of various forms or combinations of acrylates with aliphatic or aromatic epoxies, urethanes, polyesters, or polyethers) and provide good heat, chemical and abrasion resistance, toughness, dimensional stability, and adhesion to a spectrum of substrates. Unlike thermal curing, with UV/EB curing, the depth of penetration, and consequently, the depth of cure can be controlled, providing a distinct advantage over thermal curing. On the other hand, EB equipment and some UV equipment are expensive.

EB-curable adhesives are used in magnetic tape and floppy disk production to bond magnetic particles to films, as well as in packaging applications, such as tapes and labels. The UV-curable adhesive applications include electronics, automotive, medical, optical, packaging industries, as well as usage in tapes and labels.

### 12.2.6 High-Temperature Adhesives

Service temperature ranges for adhesives can be categorized as follows:

1. Low Temperature (under 121 °C): polyurethanes, polyesters, allyls (diallyl phthalate)
2. Medium Temperature (121–260 °C): epoxies, phenolics, silicones
3. High Temperature (over 260 °C): polyimides, bismaleimides, polybenzimidazoles

Advanced aircraft, space vehicles, satellites, missiles, electronics, and automotive industries often have applications requiring high-performance/high-temperature adhesives. Such adhesives are typically used to join plastics, metals, ceramics, and composites, while usage as insulators and coatings are also needed where adherence to the substrate, rather than the joining of two components, is desired. Applications in the aircraft and aerospace industries typically require bonding metals and composites which will be exposed to temperatures of 260 °C or higher. On the other hand, a high-temperature adhesive for missile applications must

perform at very high temperatures ( $\sim 760^\circ\text{C}$ ) for short periods of time, in the order of seconds. For advanced aircraft applications, however, the adhesive must perform satisfactorily for tens of thousands of hours over the temperature range of  $-54^\circ\text{C}$  to  $260^\circ\text{C}$ . Furthermore, the adhesives must resist degrading effects, such as aircraft fuels, hydraulic fluids, and moisture.

In applications involving orbital vehicles such as satellites and instrument platforms, high-performance/high-temperature adhesives may be expected to endure thermal cycling in the temperature range of  $-160^\circ\text{C}$  to  $125^\circ\text{C}$ . Furthermore, in such applications, the adhesive must resist ionizing radiation, such as radiation from photons, electrons, and ultraviolet rays.

In high-temperature applications, it is desirable to have a good match between the coefficients of thermal expansions for the adhesive and the adherend(s), as well as low moisture absorption, high strength and toughness, and high resistivity and stability in an electric field.

### 12.2.7 Sealants

Sealants are used to fill joints, gaps, and cavities between two or more similar or dissimilar substrates in contrast to adhesives which are used to bond two materials together, and usually with a much thinner bondline. Polymers typically used in sealant applications include silicones, urethanes, polysulfides, solvent acrylic, and butyls. Polysulfides, polyurethanes, and silicones are used more in bonding applications.

Sealants are also used to protect electronic components that are used in aerospace automotive and appliance equipment.

### 12.2.8 Conductive Adhesives

Electrical and/or thermal conductivities are the main requirements in these types of adhesives, and conductive (metallic or metal coated) fillers are used for this purpose. Most fillers that provide electrical conductivity in an adhesive also contribute to its thermal conductivity. On the other hand, thermally conductive adhesives are also available for electrically insulating purposes. Electrically conductive adhesive applications include the attachment of lead wires in hybrid and integrated circuits (dies).

Polymer materials which are most often used to provide electrical and/or thermal conductivity include epoxies, polyurethanes, silicones, and polyimides – epoxies being the most commonly used.

For die attach purposes, filled epoxies and polyimides are usually the adhesives of choice. They seem to meet the material requirement for die attach adhesives including the absence of resin bleed before or after cure, good elevated temperature strength after a short cure period, thermal stability, absence of out-gassing, and the presence of minimum ionic impurities.

Conductive adhesives are generally expensive due to the use of silver, gold, or palladium conductive fillers in high loadings (up to 85 wt%). Silver, either in flake or powder form is used in majority of applications because of its lower cost in comparison to gold or palladium, typically providing  $\sim 0.001 \Omega\text{-cm}$  volume resistivity in epoxy matrix. On the other hand, with silver-filled adhesives, migration of silver to the surface can occur under humid environments with direct current (Sancaktar et al. 2005). Uses of gold or silver-coated copper fillers may alleviate this problem. Other fillers that provide electrical conductivity include nickel, copper, aluminum, and carbon particles.

For thermal conductivity, oxide fillers, such as alumina, can be used. The most commonly used filler for this purpose is alumina (aluminum oxide), which is fairly inexpensive. Alumina fillers can be added to epoxies in amounts as high as 75% by weight to result in thermal conductivities, typically ranging from  $\sim 1.38$  to  $\sim 2.73 \text{ W/m-K}$  ( $\sim 3.31$  to  $\sim 4.13 \times 10^{-3} \text{ cal/cm-s } ^\circ\text{C}$ ).

Adhesives can prevent electrochemical corrosion in joints between dissimilar metals. They may also act to dampen vibrations, thus reducing fatigue failures. Changing a property in an adhesive, such as adding fillers, generally produces change in other properties of the joint, such as tensile or shear strength, elongation or resistance to peel.

## 12.2.9 Nanocomposite Adhesives

With the advent of “nanotechnology,” nanocomposite adhesives are fast appearing for many improved applications in aerospace, automotive, medical, and construction industries. For nanofiber-reinforced styrene-butadiene rubber, Kim and Reneker (1999) reported that the Young’s modulus of the nanofiber composite was tenfold greater than the pure material at 10 phr nanofiber content. On the other hand, information on the mechanical properties of nanofibers and nanofiber composites has so far been limited (Sancaktar and Aussawasathien 2009).

Qian et al. (2000) reported that nanotubes increase the composite strength by as much as 25%. However, multiwall nanotubes (MWNTs) are limited in their applications because of weak inter-shell interaction (Yu et al. 2000). Single-wall carbon nanotubes (SWCNTs) on the other hand are quite expensive and difficult to manufacture. Alternative reinforcement materials for nanocomposites include graphitic carbon nanofibers (GCNFs) and graphite nanoplatelets. GCNFs also have excellent properties and can be used as reinforcements in various kinds of matrices. They offer chemically facile sites that can be functionalized with additives thereby resulting in a strong interfacial bond with the matrix.

Wang et al. (1996, 1998, 2000) report that layered silicate nanolayers can be used as alternative inorganic components for the construction of nanostructured hybrid composites. The clay silicate nanolayers possess stable Si–O bonds and high particle aspect ratios comparable to conventional fibers. Their interlayer surface is easily modified by ion-exchange reaction, and the gallery can be intercalated by organic polymer precursors for the formation of organic–inorganic nanocomposites. The

intercalation chemistry of layered silicate clays plays an important role in the formation of polymer-clay nanocomposites. Exfoliated clay composites contain single,  $\sim 1$  nm thick layers of clay dispersed in the polymer matrix. Owing to the platy morphology of the silicate layers, exfoliated clay nanocomposites can exhibit dramatically improved properties such as barrier and mechanical properties that are not available for conventional composite materials. Wang et al. extended the exfoliation chemistry of smectite clay in an epoxy matrix to include the layered silicate magadiite with a layer thickness of 1.12 nm. The chemistry elucidated for magadiite is likely to be applicable to other members of this mineral family for the formation of polymer-inorganic nanolayer composites.

Previous work by Sancaktar and Kuznicki (2006) also showed reduction in water uptake in nanoclay/epoxy composites, specifically when stressed to stagger the clay layers with the action of strain that squeezed the layers to a smaller interlayer distance, thus producing a more effective barrier against water diffusion into the nanocomposite adhesive. This trend was not observed in the unfilled epoxy system, in which barrier properties were not affected by stressing below the yield point.

Use of nanotubes have been reported by Ge et al. (2007) in enhancing adhesion by “gecko-inspired adhesion” in production of “carbon nanotube-based synthetic gecko tapes,” and by Sethi et al. (2008) in the production of “gecko-inspired carbon nanotube-based self-cleaning adhesives.” More information about nanocomposite adhesives can be found in chapter □ 55.

---

### 12.3 Methods of Reaction

Except for pressure-sensitive adhesives, which undergo no phase change for application, adhesives are typically applied as low-viscosity liquids to wet adherend surfaces and to flow into their crevices and asperities. Liquid forms of adhesives are typically obtained by three methods: (1) heating the solid adhesive to the point of facile flow, (2) dispersing/dissolving the adhesive material in a solvent, and (3) starting with the adhesive material in liquid monomer form which is subsequently polymerized. These liquid forms are subsequently solidified by: (1) cooling, (2) solvent evaporation, and (3) chemical reaction.

Therefore, adhesives can be classified based on the method of “activation” as follows:

- Solvent-activated: These types of adhesives become tacky when wetted with an organic solvent. The presence of an organic solvent, however, may present fire and health hazards.
- Water-activated: These types of adhesives are generally based on polyvinyl alcohol, starch or protein glues.
- Heat-activated non-tacky solids: Adhesives based on rubber, vinyl polymers, phenoxies, cellulose, and PVC may be activated by heat.



- 489 • Hot melts: These adhesives are generally thermoplastic 100% nonvolatile  
490 materials heated to a melt to be applied to the substrates. With these types of  
491 materials, the adhesive bond is primarily mechanical, as achieved after  
492 solidification.
- 493 • Film adhesives: They resemble hot melts and heat-activated adhesives in the  
494 sense that heat is used for activation with a subsequent cure schedule, which may  
495 include additional heat application under pressure. They may contain lightweight  
496 fabrics, nylon, polyester, glass mats in the form of “carrier cloth.” Thus, the  
497 adhesive thickness may be controlled uniformly. Epoxies, phenolics, nitrile-  
498 elastomers, polyamides, PVC, polyvinyl butyl, ethylene-carbolic acid copoly-  
499 mers are available in film form with or without carrier cloths.

500 Additional classification is based on the physical form of the adhesive prior to  
501 application, but not much different than the classification based on activation:

- 502 • Solutions: Adhesives of this type have solid contents varying from 5% to 95%,  
503 with 20–50% being the most common.
- 504 • Adhesive solutions in organic solvents include: acrylics, polyurethanes, poly-  
505 amides, phenoxies, polyvinyl acetate, along with natural rubber and other  
506 elastomers.
- 507 • Adhesive solutions in water include: phenolics, amino-resins, methyl ether,  
508 polyvinyl alcohol, protein-based products such as blood and fish glues.

509 All thermosets which form high molecular weight or molecular network struc-  
510 tures after application fall into the classification of “polymerizing types”:

- 511 • Step-growth polymers: Step-growth polymerization starts with liquid monomers  
512 mixed with catalysts, curing agents, or co-reactive additions for step-growth  
513 polymerization. Condensation polymerization is the most common type of step  
514 reaction. The monomers used in this type of reaction are difunctional, i.e., they  
515 have chemically active group on each end of the molecule. Since polymerization  
516 occurs in consecutive reactions, the degree of polymerization and the average  
517 molecular weight increase as the reaction proceeds. The rate constant for the  
518 reaction is determined by the mobility of the ends of the growing molecule, and  
519 not by its size. High molecular weight is attained only at the very end of the  
520 reaction.
- 521 • Chain growth polymers: Chain or addition polymerization typically involves  
522 opening of a double bond by the action of an initiator thus generating an active  
523 site, which propagates down a growing chain. Three types of active sites can be  
524 used for addition reactions: anionic, cationic, and free radical. Chain growth is a  
525 fast polymerization process, which can be 10,000 times faster in comparison to  
526 the condensation polymerization. Addition polymerization may leave a larger  
527 number of monomers behind, thus resulting in a larger polydispersity in compar-  
528 ison to the step-growth polymerization. Cyanacrylates and anaerobic acrylics fall  
529 into the addition polymerization category.

- Aqueous dispersions: Emulsion polymerization is used to prepare this type of adhesives, mostly made of acrylics, chloroprene, and polyvinyl acetate. High shear dispersion can also be used in the presence of surfactants to obtain water borne formulations, as with polyurethanes, epoxies, silicones, and some elastomers.
- Radiation curable adhesives: Inclusion of a photo initiator in some one-component-type resins allows initiation of cure by ultra-violet or visible light, or by an electron beam.

As seen so far, the most descriptive classification method for adhesives and sealants is by physicochemical nature of the base resin. Thus, methods of reaction for different types of adhesives and sealants can also be summarized as follows:

### 12.3.1 Thermosets

As discussed by Lin and Pearce (1993), thermosetting materials consist of three-dimensional cross-linked networks of infinite or immeasurably high weight molecules. Thermosetting resins cure by cross-linking of reactive low molecular weight oligomers or by cross-linking reaction of high molecular weight polymers with reactive functional groups. Subsequent to such thermosetting cure processes, these resins become infusible, insoluble materials.

### 12.3.2 Thermoplastics

Thermoplastics are high molecular weight (ranging from 10,000 or more to several millions), linear polymers (more or less) that can be redissolved and re-fused.

Thermoplastic materials are capable of being repeatedly softened by an increase in temperature and harden by a decrease in temperature. This transition is marked by a particular glass transition temperature,  $T_g$ , for each (amorphous) polymer. This transition involves physical rather than chemical changes and therefore enables shaping of such polymers into articles by molding or extrusion processes in the softened stage. For crystalline polymers, the crystallization temperature,  $T_{cr}$ , and the melt temperature,  $T_m$ , constitute important thermal parameters defining the formation and the destruction of the crystalline structure.

### 12.3.3 High-Temperature Adhesives

Synthetic organics having aromatic (benzene) and/or heterocyclic rings in the main structure (i.e., imidazoles and substituted imidazoles) are used to produce structural adhesives having high-temperature resistance. These prepolymers have open-ring structures which close upon the application of heat during a condensation reaction,

resulting in a highly cross-linked system. Such high-temperature, structural adhesives are available in liquid and film forms.

High-temperature adhesives, including polyimides and polybenzimidazoles, are high-cost materials. They are typically difficult to handle and require long cure times during which volatiles must be released. Polyimides provide superior performance in long-term strength retention at elevated temperatures. At 260 °C in air, polyimides have higher bond strength than do epoxyphenolics, but strength retention following exposure to water is better with epoxyphenolics. Polybenzimidazoles are stable in air for short term exposure up to 288 °C. Both polyimide and polybenzimidazoles are moisture sensitive. Polyquinoxalanes provide another choice with good peel strength on titanium.

#### 12.3.4 Elastomers

As discussed by Morton (1987) and White (1995), rubbery polymers which are flexible and readily deformable can be made into reversibly elastic by a cross-linking process. Generally, such cross-linking reaction is carried out using sulfur along with “accelerators,” which act through the double bonds in the structural units. Elastomers may crystallize if they have regular structure involving the same repeated structural unit. For example, polyethylene, pure stereoisomeric forms of polybutadiene, polyisoprene, and polyisobutylene all crystallize.

Production of materials containing flexible elastomeric segments bound together by thermoplastic segments in the form of ABA sequence block copolymers, by Shell Development Company under the commercial name, Kraton, resulted in “thermoplastic elastomer” materials. These materials possess melt flow properties similar to thermoplastics along with solid properties resembling vulcanized rubber. For example, plasticized polyvinyl chloride, a partially crystalline material, which dissolves into amorphous regions when solvent is added, possesses elastomeric properties. It is also possible to directly blend elastomers with thermoplastics while the elastomer is vulcanized during the blending process. For example, polypropylene and ethylene-propylene terpolymers (EPDM) can be blended while the EPDM vulcanizes. Regular plastics manufacturing equipment such as extruders are used to process thermoplastic elastomers, rather than the use of rubber processing machinery providing a large advantage in manufacturing.

#### 12.3.5 Sealants

Adhesives and sealants may often have the same type of polymeric material formulations but sealants are usually designed to have different properties. Such properties are determined by the selection of ingredients such as fillers, plasticizers, adhesion promoters, and stabilizers. For example, if silicone polymers are fully cured and cross-linked without additives, they result in a soft polymer with very low tensile strength. Silicones have exceptional thermal stability up to 250 °C and remain

flexible at low temperatures ( $-60^{\circ}\text{C}$ ). Silicones exhibit very low shrinkage upon curing and are available in single-component moisture-cured version (known as room temperature vulcanizing, RTV) or in faster-curing two-component version.

Typically, sealant materials used to protect electronic components in aerospace automotive and appliance equipment are acrylics, silicones, urethanes, polysulfides, epoxies, and unsaturated polyesters. Liquid forms of these materials can be irreversibly converted to the solid form with no significant weight loss. These types of sealing processes are called potting and encapsulating.

Polysulfides can be used as sealants and/or adhesives over a temperature range from  $-57^{\circ}\text{C}$  to  $135^{\circ}\text{C}$ .

For polyurethane adhesives, primer use is recommended for improved durability.

### 12.3.6 Conductive Nanocomposite Adhesives

Submicron-size fillers, including electrospun conducting fibers have large specific surface area and tend to form high interconnecting network. These characteristics are expected to enhance the electrical conduction of polymer-matrix nanocomposites to be manufactured using such fillers (Wei and Sancaktar 1996; Sancaktar and Wei 1996).

Aussawasathien and Sancaktar (2008) showed that when carbon nanofiber (CNF) mats were used to render epoxy resins electrically conductive, the rate of cure reaction for CNF mat-epoxy nanocomposites was higher than that for the neat epoxy resin at low curing temperatures, due to the high aspect ratio, high interconnecting network and high thermal conductivity of CNF mats. Compared with the neat epoxy resin, the presence of nonwoven CNF mat in composite form enhanced the cure reaction in terms of residual heat, heat flow rate, reaction rate, and conversion at the initial stages of cure for given cure temperature and time conditions. The full cure of CNF mat-epoxy composites could be achieved at shorter times for given cure temperatures, in comparison to neat epoxy. However, at high CNF mat loading, the cure reaction was retarded since the amount of epoxy and hardener decreased at high CNF's weight fractions when combined with the hindering effect of the CNF mat to the diffusion of epoxy resin and curing agent, leading to low cross-linking density. The cure kinetics of CNF mat-epoxy nanocomposites could be predicted well by curve fitting with Kamal's model (1974).

Zhou and Sancaktar (2008) observed that incorporation of Ni nanopowders in an epoxy suspension resulted in a stable capillary flow at 75 wt% of Ni. Occurrence of agglomerates, however, somewhat nullified this advantage.

### 12.3.7 Other Types of Adhesives

Adhesives which have unique cure mechanisms and applications can be considered under this category.

### **Anaerobic Adhesives**

These types of adhesives remain fluid in the presence of oxygen but cure to solids in its absence. The simplest anaerobic adhesive consists of dimethyl acrylate ester with the peroxide catalyst system and accelerator. They cure by free-radical polymerization in the absence of oxygen. Anaerobic adhesives have strength characteristics equivalent to those of the structural adhesives. One-part anaerobic adhesives cure at room temperature in several hours, but their cure can be accelerated to minutes by high-temperature cure and by the use of certain primers/accelerators. Such elevated temperature, primer/accelerator-assisted cure is especially recommended when anaerobic adhesives are used on inactive surfaces, such as unclean metals or plastics, or inhibiting surfaces such as plated surfaces, chromates, oxides, and anodized surfaces.

### **Moisture Curing Adhesives**

These types of adhesives cure in the presence of moisture. For example, cyanoacrylates cure in an extremely short period (typically 10–15 s) if confined in a thin film between close-fitting parts. The mechanism of cure is an anionic polymerization induced by the presence of a base. A thin film of moisture usually present on bonding surfaces and exposure to normal atmosphere is generally sufficient to harden these materials if they are squeezed to a thin film. Methyl cyanoacrylates provide high strength when bonding rigid substrates such as metals. Ethyl cyanoacrylates, on the other hand, provide durability and high strength in bonding plastics and rubbers. Certain types of polyurethanes and silicones also cure in the presence of moisture.

### **Inorganic Adhesives**

This class of adhesives mostly includes soluble silicates and zirconia. Silicate-based adhesives are typically modified by adding clays to reduce shrinkage, protein glues for water resistance, starch for thickening, surfactants as wetting agents and humectants to increase tackiness and to increase application time. These types of adhesives are used for bonding paper, wood, glass, and metal. Refractory types are used for high-temperature applications involving 1000 °C or higher. They are based on mixtures of soluble zirconia or mixtures of silicates with sand, silicon carbides, clays, and other inorganic salts and oxides. Inorganic adhesives are also available for dental applications in combinations of silicates with zinc phosphates.

## **12.3.8 Primers**

High surface energy adherends such as metals, glasses, and ceramics with tendencies for chemical reactions which can replace existing chemical bonds with adhesives (i.e., hydration, oxidation) are recommended for primer applications prior to bonding. Primers are expected to interact between the substrate and the adhesive by having chemical features which provide chemical bonding for improved adhesion. Thus, primers serve several functions in adhesive bonding, principally by improving

adhesion displayed by improvement in shear, peel, and tension. They are typically applied as thin films on the substrates prior to bonding and are not expected to have high cohesive strength in bulk form. Their function is mainly by chemical bonding in the thin film form, with physical effects such as surface tension and dipole interactions taking the center stage. Thus, primers commonly used as metal surface conditioners mainly serve as adhesion promoters and surface protectors.

Primers used in structural bonding are typically composed of the following five types of materials: (1) resin, (2) curing agent, (3) film former (to promote the integrity of the film by improving the wetting of the primer), (4) corrosion inhibitor, and (5) solvent carrier.

Primers used for surface protection in structural bonding are essentially adhesives in solution. They protect the adherend from contamination or from changes in adherend surface chemistry between the cleaning/surface treatment and the bonding operations. Therefore, the base chemistry of a primer system is often the same as that of the adhesive to be used for bonding and, commonly, it is a one-part system in an organic solvent, usually at low solids content. There are a number of primers that are thermosetting types, in solution with low solid levels. Some of these are two-part and applied similarly, but have limited working life after mixing. Their cure may be accomplished at ambient or elevated temperatures.

---

## 12.4 Chemical Families and Physical Forms

### 12.4.1 Thermosets

Thermosetting adhesives are typically available in liquid, paste, and solid forms. The liquid form is generally one- or two-part system which may contain solid fillers and colorants. The paste form typically exhibits flow behavior different from those of the unfilled or highly filled liquids. Certain pastes are modified to be thixotropic, which are gel-like materials at rest but act as fluid when agitated. Possession of such solid-like yielding behavior allows an unstrained mass of adhesive not to sag or flow unless forced to do so by mechanical action, such as by spreading with a spatula.

Thermoset materials either exist or are converted to liquids of low molecular weight at early stage in their application. They are subsequently cured by heat and/or chemical catalysts, attaining very high molecular weight and a three-dimensional structure. They have outstanding mechanical strength, and thus used as structural adhesives. They do not easily solvate; have low creep and survive in temperature environments moderately above their cure temperatures.

Cross-linking of thermoplastics such as rubbers or vinyl polymers also yield rigid thermoset materials.

Thermosetting adhesives are also available in film form of various thicknesses. These films may be provided in composite reinforced form as supported by synthetic, woven or nonwoven fabrics of nylon, polyesters, etc. Such films are flexible and their drape ability allows them to conform to a particular joint subsequent to cutting or punching to shapes. Film adhesives are typically supplied containing

latent hardeners which are dormant at low temperatures but become active and initiate cure when brought to cure temperature. Refrigeration increases storage life for this type of adhesive.

### **Important Thermosets: Epoxies**

Epoxy adhesives are the most important and versatile of the structural adhesives family. As thermosetting, cross-linked resins, they are strong and brittle, but they can be formulated to be flexible and/or tough without loss of tensile strength by a variety of procedures, including nitrile rubber or thermoplastic toughening, cure control, and solvent addition. Epoxy adhesives are successfully used to bond a variety of substrates, and can be formulated to cure at a range of temperatures: room temperature and higher, and under dry or wet conditions. Service temperature range is  $-55$ – $121$  °C, but temperatures up to  $260$  °C can be tolerated for short periods.

### **Epoxy Polymer Structure**

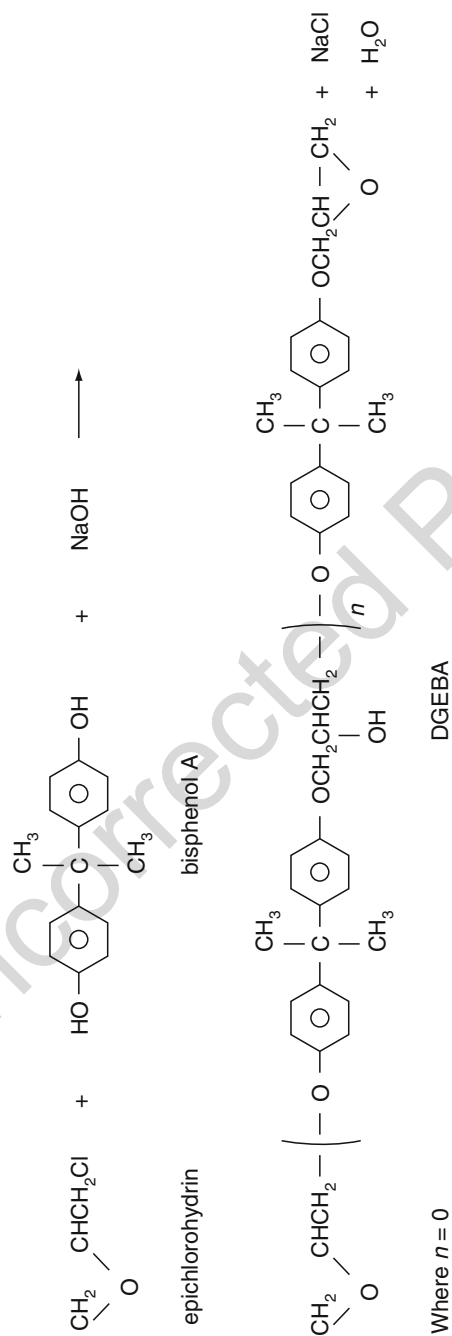
The main component of epoxy resins is the epoxy or oxirane group which is converted into three-dimensional structures by a variety of curing reactions. In the synthesis of epoxies, the liquid resins are typically obtained by using an excess of epichlorohydrin with respect to bisphenol A in the presence of sodium hydroxide as shown in Fig. 2.

### **Epoxy and Cure Agent Properties**

A two-component epoxy system consists of a resin and a hardener, along with possible additives such as accelerators, reactive diluents, resin modifiers, plasticizers, and fillers. Typical hardeners include aliphatic polyamines, which cure at room temperature or at slightly elevated temperatures; polyamides, which provide flexibility and are widely used; aromatics, which are solid; and anhydrides, which require elevated temperature cure and produce thermally stable but brittle adhesives. Low molecular weight epoxies are liquid and are usually cured by amines, carboxylic acid anhydrides, and Lewis acid and base catalyst. Higher molecular weight epoxies are cured through their hydroxyl groups. Cure of epoxies involves an exothermic reaction.

### **Nylon-Epoxies**

Nylon-epoxy is typically used in film and tape adhesive applications and has maximum service temperature of  $\sim 138$  °C, compared with  $177$  °C for unmodified epoxies. The addition of nylon provides increased flexibility and peel strength compared to unmodified epoxies. Nylon-epoxy is a tough material with excellent tensile lap shear strength and good fatigue and impact resistance. However, the addition of nylon results in deterioration in creep resistance and poor peel strength at low temperatures. Furthermore, the hydrophilic nature of nylon imparts poor moisture resistance in both uncured and cured forms of the resin. Consequently, nylon-epoxies are not as durable as elastomer-epoxies or other thermoplastic modified epoxies.

**Fig. 2** Synthesis of diglycidyl ether of bisphenol A (epoxy)



## **Elastomer-Epoxies**

Elastomer-epoxies are prepared mostly by nitrile rubber addition as the elastomeric component and are usually called “modified” or “toughened” epoxy. The bond strengths of elastomer-epoxies are lower in comparison to those of nylon epoxies. Their durability with respect to moisture resistance is better, but not as good as those of vinyl phenolics or nitrile-phenolics. A wide application is in films and tapes. Elastomer-epoxies typically cure at low pressures and temperatures, and over short cure periods, by adding a catalyst to the adhesive formulation.

## **Epoxy Applications**

Epoxies are typically used as adhesives, in coatings, composites, in electrical and electronic applications, and building materials, and civil engineering applications.

The wide usage of epoxies in coatings is due to their excellent adhesion, toughness, and corrosion and chemical resistance. The second wide usage of epoxies is as encapsulating materials for electrical and electronic devices.

Reinforced epoxy adhesives provide high strength and desired thermal and electrical properties. For example, fiber reinforcement, such as glass, carbon, and aramid fiber reinforcements, provide higher mechanical properties and render epoxies suitable for many versatile structural applications. Addition of powdered metal fillers provides electrical/thermal conductivity; alumina fillers provide thermal conductivity; mica provides electrical resistance; silica and calcium carbonate provide cost reduction; and graphite powders provide low friction. Silver-coated glass spheres can be used to replace the expensive silver powder to provide electrical conductivity in epoxy systems. Furthermore, the use of fillers can also serve to raise  $T_g$ , increase the thermal conductivity and thermal resistance of the composite, and to reduce shrinkage. The rheological behavior, and thus, the wetting/spreading behavior, pore penetration, and the yield behavior of the filled resin depends on the amount and the type of filler used.

Epoxy resins see large applicability in the aerospace and defense sector for a large number of structural applications as adhesives, as coatings, and in composite forms. Epoxies are used in composite manufacture and repair, missile manufacture, and bonding of aluminum skins to the aircraft body.

## **Comparison of Epoxy with Other Adhesives**

Unsaturated polyester resins provide properties somewhat competitive with the thermosetting epoxies, and are widely used for composite applications because of their low cost.

Vinyl esters are derivatives of epoxy resins and provide improved thermal performance and chemical resistance over the standard unsaturated polyester adhesives.

Phenolic adhesives provide better thermal resistance in comparison to epoxy adhesives, but require elevated temperature cure, while epoxies can be cured at room temperature. Phenolics produce volatiles during cure. Silicones also have thermal resistance characteristics similar to those offered by phenolics compared with epoxies.

Cyanoacrylates and acrylics provide fast cure and good strengths in comparison with epoxies, but they cost more.

## 12.4.2 Thermoplastics

Thermoplastic polymers are available in various molecular weight ranges with varying melt viscosity values. Their tensile modulus and strength values and impact resistance also exhibit a wide variation. Softening points are in the 100–200 °C range, and application times are 15–90 s.

Thermoplastic adhesives are typically available in liquid and solid forms similar to the thermosets, except for the paste form. In the liquid form, a solution and/or dispersion of the base thermoplastic polymer and other compounding ingredients are used.

Some widely used thermoplastic adhesives are polyvinyl acetate, polyurethane, polyamides, and aromatic polyamides.

### Important Thermoplastics: Polyimides

Fully imidized aromatic thermoplastic polyimides (TPI) are linear polymers with good thermomechanical performance, used in high-temperature (>230 °C) applications. PIs based on aromatic diamines and dianhydrides exhibit excellent heat resistance. In addition to their outstanding high-temperature resistance (Sancaktar et al. 1984; Sancaktar and Schenck 1985; Sancaktar and Dembosky 1986), toughness and good dielectric properties, low flammability, and high radiation resistance are desirable characteristics for this class of adhesives.

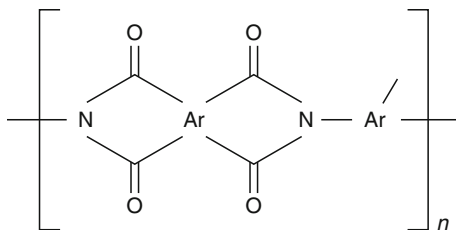
### Polyimide Chemistry and Properties

Aromatic TPIs are typically produced by condensation reaction of aromatic dianhydrides with aromatic diamines or aromatic diisocyanates (Fig. 3). An important advantage of the TPIs over their thermoset counterparts is that no further chemical reactions occur during their processing.

### Thermoset Versions of Polyimide Adhesives

Linear TPI materials are increasingly used in various fields, including advanced composites applications, in which both resistance to high-temperature environments and good mechanical performance are required. There are, however, serious

**Fig. 3** General structure of aromatic TPI materials



limitations with linear aromatic, condensation type TPIs, as they are difficult to process, typically requiring high temperatures (315–400 °C) and high pressures. They also degrade easily by solvents. Because of these limitations, addition type TPI's with monomeric or oligomeric imide compounds containing reactive end groups (maleimide, norbornene, acetylene) are cross-linked by curing process and offered as an improved version of the linear thermoplastic TPIs. Compared to the high molecular weight linear PIs, these adhesives are comparatively easy to manufacture by melt or solution processes, thanks to their low molecular weights. The asymmetric diaminophenylindane isomeric mixture is incorporated in the PI backbone as shown in Fig. 4.

### Polyimide Applications

PIs are finding increased use in aerospace and automotive applications as structural adhesives due to their excellent mechanical property retention at elevated temperatures. Another major area of PI usage is the electronics/electronics industry. They are used as thermal and electrical insulators due to their excellent hard radiation resistance and good insulation characteristics.

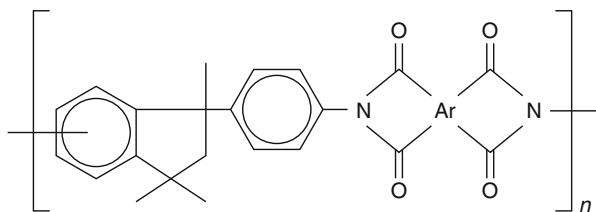
### 12.4.3 Elastomers

Elastomers are polymers with rubberlike properties. The word “elastic” refers to the ability of a material to return to its original dimensions when unloaded, and the term “mer” refers to the polymeric molecular make up in the word “elastomer.” Vulcanized rubber materials typically have more than 200% elongation in a tensile test and are capable of returning rapidly and forcibly to their original dimensions when load is removed. This elastic response is due to the three-dimensional cross-linked network molecular structure they have. An elastomer, on the other hand, typically has elongation rates of 100% or more and a significant amount of resilience. Resilience is represented by the area under the elastic portion of the stress–strain curve, and therefore, refers to a material's ability to undergo elastic deformations.

### Important Elastomer Adhesives: Polyurethanes

As discussed by Woods (1990), polyurethane resin systems are usually formed by addition polymerization involving the reaction between alcohols with two or more reactive hydroxyl groups per molecule (polyol or diols) and isocyanates that have

**Fig. 4** A typical structure in which the asymmetric diaminophenylindane isomeric mixture is incorporated in the PI backbone



more than one reactive isocyanate group per molecule (a diisocyanate or polyisocyanate).

### Polyurethane Chemistry and Properties

Polyurethane is produced by the reaction of isocyanate group ( $-\text{N}=\text{C}=\text{O}$ ) with hydroxyl groups as shown in Fig. 5.

All polyurethanes are based on toluene diisocyanate (TDI) and polymethylene diphenylene isocyanate (PMDI). MDI is produced from aniline and formaldehyde, reacted together using hydrochloric acid as a catalyst, under a condensation reaction producing a complex mixture of polyamines, which are phosgenated to obtain a polyisocyanate mixture. The polymeric MDI product is mainly used for rigid foam manufacture. The polyisocyanate mixtures can be formulated to possess a range of differing functionalities, which are the average number of chemically reactive groups on each individual molecule. The polyol structure also plays an important role in determining the final urethane properties. The size and flexibility of polyol molecular structure and its functionality (i.e., the number of isocyanate-reactive hydroxyl groups per molecule of polyol) controls the degree of cross-linking achieved in the polymer formed by the reaction with the polyisocyanate. The degree of cross-linking has a dominant effect on the stiffness of the polymer. In order to obtain a more flexible polymer, a proportionally lesser degree of cross-linking is needed. The “hydroxyl value” is used as a measure of the concentration of isocyanate-reactive hydroxyl groups per unit weight of the polyol, and it is related to molecular weight and functionality of the polyol.

Moisture-curing polyurethane coatings can be produced by mixing polyisocyanate and solvent while excluding moisture. A moisture scavenger, such as paratoluene sulfonyl isocyanate (pTSI) can also be added during this stage along with polyol and other additives for the mixture to be stored in a dry, airtight container.

### Polyurethane Applications

Polyurethane is supplied in elastomer form, as flexible and rigid forms and as a liquid for coatings, adhesives, binders, sizing fibers, sealant, and biomedical applications. The elastomer form of polyurethane can be used for applications requiring high toughness and resistance to tear and abrasion and for high impact and flexibility characteristics under cold temperature. Applications include flexible and wear-resistant coatings on textiles, floors, and outer skins of aircraft, as adhesives, and

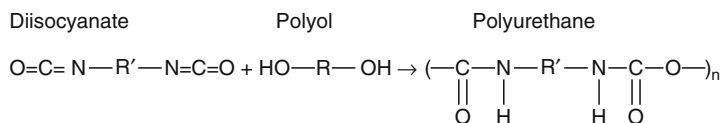


**Fig. 5** Reaction of isocyanate group ( $-\text{N}=\text{C}=\text{O}$ ) with hydroxyl groups for polyurethane production

in paints. They are also widely used as finishes on automobiles. Polyurethanes in coating form are generally based on TDI formulation.

#### 12.4.4 Sealants

Typically, adhesives have high tensile and shear strengths and are used to replace or reinforce mechanical fasteners in load-bearing applications. Sealants, on the other hand, typically have lower strength. They are flexible materials that are used as barrier to the passage of liquids, vapors, gases, and solids. When vibration resistance and impact strength are required or when materials with widely differing thermal coefficients of thermal expansion need to be bonded, a flexible sealant type material is often the adhesive of choice. Application size and complexity, function of the structure, movement capability of sealant, cost, and life expectancy play an important role in sealant selection.

##### Important Sealants: Silicones

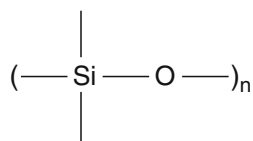
The chemical structure of silicon is different from that of carbon-backbone-based (organic) polymers with C–C repeat units. Specifically, the polymer chain backbone consists of repeat units shown in Fig. 6.

The Si–O bond is stronger and more flexible than the C–C or the C = C bond. Thus, silicon polymers are physically stronger and more flexible than typical organic polymers. Furthermore, silicone possesses rubber elasticity due to its organic functionality allowing limited cross-linking between polymer chains.

##### Silicone Chemistry and Properties

Most commercial silicones are made from a chloro-alkyl, a silicon-metal, and a catalyst and/or pressure. This reaction produces low molecular weight silanes and linear and cyclic siloxane as intermediates products. Silanes are widely used as adhesion promoters in organic and inorganic polymers, adhesion primers, coupling agents for custom reaction syntheses, and coupling agents to promote bonding of fillers to polymer matrices in composite materials. Silicones are typically formulated to provide a three-dimensional network of siloxane. Hydrocarbon radicals such as methyl, phenyl, vinyl, fluoro, amino, hydroxy, ethoxy, and other organic groups are attached to the silicon atom under heat, frequently combined with the action of metal catalysts, such as tin or platinum compounds, to condense the polymer into a rigid thermoset material. Use of functional vinyl improves compression set resistance and provides higher cross-linking density. Use of functional fluoro increases chemical and ozone resistance and provides higher temperature resistance. It also decreases

**Fig. 6** Silicone polymer chain backbone



polymer opacity by preventing haze-causing crystallinity with increased steric hindrance along the polymer chains. Silicon can also be synthetically polymerized with starting materials of quartz (sand) and chlorine and an organometallic reagent.

Silicons have excellent thermal and oxidative stability at high temperatures, up to 260 °C, and remain flexible at temperatures down to -75 °C. They possess excellent electrical properties, including resistance to corona breakdown. They exhibit general inertness, exhibited as resistance to weathering, ozone, and many chemicals and also exhibit general noncorrosiveness to other materials, with the exception of some construction adhesives in contact with ferrous alloys in closed, moist environments. They are inherently nonflammable and have self-extinguishing properties. Silicons exhibit lubricity and other unusual surface properties, such as low surface tension of the fluid resin, and the capability of preventing other materials from sticking, as well as very low water absorption. Even though its tensile strength is lower than most organic rubbers at room temperature, silicon rubber has higher tensile strength than most organic polymers at 204 °C.

### **Silicone Product Forms and Applications**

Silicon fluids: Methylsilicone fluid is the most common product, with relatively constant viscosity over a range of temperatures and it exhibits shear stability with high pumping pressure. Industrial applications of silicon fluids include uses in fermentation adhesives, and sealant manufacturing.

Room temperature vulcanizing (RTV) type: RTV silicon rubbers are used as one- and two-part adhesives and sealants. Applications include bonding of metals, polymers, and ceramic substrates, as well as formation of sealant barriers against liquids and certain vapors. RTV rubber cures by either a condensation or an addition reaction. In the condensation cure, the basic polymer is a silicon fluid in either one-part or two-part form. Vulcanization chemistry of RTV materials must be kept in mind during material selection since some condensation cure reactions release acetic acid and ammonia vapors which can be corrosive. Alternatively, natural-curing RTV materials are available with alcohol, oxime, platinum, and tin vulcanizate reactions. Rheologically, RTV materials range from a flowable, pourable consistency to the thixotropic paste form.

One-part type: For one-part-type silicones, both the catalyst and the cross-linking agent are incorporated in the base compound at the time of manufacture, which involves compounding a silanol-stopped silicone polymer with an excess of cross-linker. The one-component silicones typically cure with moisture. Exposure to atmospheric moisture causes further curing of the silicone rubber to take place. Diffusion of moisture into the rubber progresses vulcanization from the surface inward. One-part component type silicones are excellent adhesive sealants and can be formed in place as gaskets. They can also be used to form films by solvent dispersion.

Two-part type: As for one-part-type silicones, both the catalyst and the cross-linking agent are incorporated in the base compound just before use. They are generally silanol polymers, cross-linked with alkoxy silane or oligomers and organic

tin compound catalyst. Two-part-component-type silicones are typically used for applications in coatings, adhesives, and encapsulants.

Heat-curable rubber (HeR): These are typically silicon rubber compounded with catalyst, color, and additives mixed and milled into siloxane polymers. HCRs are often used in molded parts for high-temperature service or in applications that utilize their chemical and weathering resistance, but also see applications as seals and gaskets.

#### 12.4.5 Important Moisture Curing Adhesives: Cyanoacrylate Adhesives

Cyanoacrylate adhesives are single-part, solvent-free polymerizable adhesives. They start to cure within seconds by adsorbed moisture or by alkaline sites on the substrate, which can be nearly any solid or semisolid material. They have the advantage that no by-products are released during cure.

##### Cyanoacrylate Chemistry, Properties and Applications

The general structure of cyanoacrylate esters is:  $\text{H}_2\text{C} = \text{C}(\text{CN})(\text{COOR})$ . Most cyanoacrylate adhesives are based on either methyl-2-cyanoacrylate or ethyl-2-cyanoacrylates. Methyl cyanoacrylates yield better strengths when bonding metals or other rigid surfaces. In addition, impact resistance is slightly better. Ethyl cyanoacrylates are stronger and more durable when bonding rubber or plastic substrates.

In general, cyanoacrylates cure rapidly at room temperature, and exhibit excellent tensile strength and good shelf life. They have long pot life and good adhesion to metal. Limitations include high cost, poor peel strength, brittleness, limited elevated-temperature properties, and capability to fill only small gaps. Substrates need to be mated as quickly as possible to reduce the possibility of contamination and premature cure or vapors. Cyanoacrylate bonds are typically capable of withstanding long-term exposure to temperatures up to  $82^\circ\text{C}$  and can maintain their strength at temperatures as low as  $-54^\circ\text{C}$ .

The cured cyanoacrylate adhesives are brittle, high tensile polymers. These polymers show strong adhesion to metals, plastics, rubber materials, and wood. Initial strength of bonds between these materials is often higher than the strength of material itself. Cyanoacrylate adhesive bonds are typically durable, and bonds often show no significant change in strength over a period of years, under ambient indoor conditions.

#### 12.4.6 Conductive Adhesives

It is well known that metallic materials are excellent conducting fillers commonly used for improving the electrical properties of polymer composites, when included above their percolation threshold. A large portion of such applications include electrically conductive adhesives as illustrated by Sancaktar and Dilsiz (1997,

1014 1999a, b), Wei and Sancaktar (1996), Sancaktar and Wei (1996), and Sancaktar  
1015 et al. (1996).

1016 Metal-coated nonconductive or low-conduction fillers can also be used to induce  
1017 electrical conductivity in polymer composites. Dilsiz et al. (1997) coated spindle-  
1018 type hematite and magnetite particles and nickel filaments with silver by using  
1019 chemical reduction. The concentration of the reactants, the reaction time, and the  
1020 type of reducing agent greatly influenced the morphology of the silver coating and  
1021 the conductivity of the coated particles.

1022 Submicron-size fillers, including electrospun conducting fibers have large spe-  
1023 cific surface area and tend to form high interconnecting network. These character-  
1024 istics are expected to enhance the mechanical properties of polymer-matrix  
1025 nanocomposites to be manufactured using such fillers (Sancaktar and  
1026 Aussawasathien 2009; Sancaktar et al. 1996; Sancaktar and Zhang 1990).

## 1027 12.4.7 Physical Characteristics of Various Types of Adhesives

### 1028 Structural

1029 These are mostly one- or two-component thermosetting resins. They can be cured at  
1030 room or elevated temperatures. Joints bonded with these adhesives can be stressed to  
1031 a high proportion of maximum failure load under service environment.

- 1032 • Advantages: Resistance to elevated temperatures, solvents, and creep.
- 1033 • Limitations: Two-component systems require careful metering and mixing. Some  
1034 types are difficult to remove and repair, have poor peel strength, require heat to  
1035 cure, and some produce hazardous products during cure.

### 1036 Hot Melt

1037 These are typically 100% solids, rapid setting thermoplastics, which do not require  
1038 cure. They are typically compounded with additives for tack and wettability, and can  
1039 be produced into pressure-sensitive forms. They abruptly melt into a low-viscosity  
1040 liquid, which can be applied to substrate surfaces. Consequently, melt viscosity is an  
1041 important consideration with these types of adhesives.

- 1042 • Advantages: They require no solvents (100% solids), exhibit fast bond formation,  
1043 gap-filling capability, barrier properties, and wide deformability range.
- 1044 • Limitations: Thermoplastic properties, resulting in limited elevated temperature  
1045 resistance, poor creep resistance, limited penetration to substrate due to fast  
1046 viscosity increase upon cooling, and limited toughness with solid viscosity.

### 1047 Pressure Sensitive

1048 These adhesives are typically used to hold substrates together after brief application  
1049 of moderate (manual) pressure at room temperature. They are typically available in  
1050 organic solvent-base, water-base, or hot melt forms. They are primarily used in tapes  
1051 and labels, as well as in medical applications.



- 1052 • Advantages: They are easy to apply, have uniform thickness, permanent tack at  
1053 room temperature, and no activation is required by heat, water, or solvents.
- 1054 • Limitations: They are largely based on rubbers, requiring compounding; they  
1055 have limited heat resistance and poor gap-filling ability.

### 1056 **Water-Base**

1057 These include adhesives dissolved or dispersed (latex) in water. The water solvent  
1058 needs to be absorbed or evaporated for bonding. On nonporous substrates, water  
1059 must be removed prior to bonding. They are mostly used in non-pressure-sensitive  
1060 applications, but pressure-sensitive forms are also available.

- 1061 • Advantages: They have low cost, long shelf life, good solvent resistance, and are  
1062 nonflammable high molecular weight dispersions with high solids content and  
1063 low viscosity.
- 1064 • Limitations: They are slow drying, have limited heat resistance, poor creep and  
1065 water resistance. They exhibit shrinkage with certain substrates in supported films  
1066 and tapes and have tendency to freeze.

### 1067 **UV/Electron Beam Curing**

1068 These are typically 100% reactive liquids cured to solids. One substrate must be  
1069 transparent for UV cure, except when used in coating applications. Absorption  
1070 coefficient of the top substrate material affects penetration of the UV/EB irradiation.  
1071 Curable formulations are used in laminating, PSA, and some medical applications.

- 1072 • Advantages: They cure fast (2–60 s), require no mixing and contain no solvents.  
1073 They are typically one component liquids, yield high tensile strengths and have  
1074 the ability to bond heat-sensitive substrates at high production rates.
- 1075 • Limitations: They need expensive processing equipment, have high material cost,  
1076 limitation of UV transparent substrates. They possess application difficulties on  
1077 parts with complex shapes and the possibility of continued curing when exposed  
1078 to UV rays (sun exposure) may render them excessively brittle.

---

## 1079 **12.5 Methods of Application**

1080 The method of application for adhesives depends on several factors, including: the  
1081 type and rheological characteristics of the adhesive used, whether it is one- or  
1082 two-part type, the geometry of the parts to be bonded and the rate of their assembly.

1083 In many cases, manual application is employed with the use of: spatulas, squeeze  
1084 bottles, tubes, rollers, brush, mechanically fed brushes, and glue guns.

- 1085 • Applications requiring speed and/or precision over large flat areas utilize roll  
1086 contact.

- 1087 • One-part liquid adhesives can be applied by atomization using air or airless  
1088 spraying.
- 1089 • Two-part adhesives must be metered or mixed first.
- 1090 • Robotic applications have also become popular in many industries.

### 1091 **12.5.1 Thermosets**

1092 Small quantities are typically hand-mixed for two-part types, and heat-cured  
1093 versions are typically delivered directly from tubes or cartridges. For industrial  
1094 applications involving two-part forms, metering and mixing equipment are used.

1095 Since heat and pressure need to be used in advanced aircraft/spacecraft, military  
1096 etc., applications, usually involving long-fiber composite substrates, special auto-  
1097 clones or vacuum bag techniques are used.

### 1098 **12.5.2 Thermoplastics**

1099 Thermoplastic adhesives are available in liquid or solid forms. In liquid form, they  
1100 are dissolved and/or dispersed in solvent, which needs to be evaporated to obtain the  
1101 solid form of the resin and, consequently, proper bonding.

1102 In solid form, thermoplastic adhesives are available as unsupported or  
1103 supported films, granules, and in lengths of extruded, flexible, cordlike materials.  
1104 The fluid form is obtained for bonding by either solvent or heat activation. Heat  
1105 activation requires substrates which can withstand the required temperatures.  
1106 If the resin compound also contains a thermosetting resin, heat application  
1107 is continued to cross-link it. Solvent activation, on the other hand, requires  
1108 substrates to permit the release of the solvent by diffusion if the bonding area is  
1109 large.

### 1110 **Hot-Melt Adhesives**

1111 Thermoplastic adhesives which are applied in viscous fluid form obtained by heating  
1112 are called hot melt adhesives. They, typically, do not contain any heat-reacting resin  
1113 and are especially suitable for use with high-speed application machinery. Hot-melt  
1114 adhesives are frequently modified with plasticizers, tackifiers, antioxidants, and  
1115 fillers.

1116 In general, hot-melt adhesives are in solid form at temperatures below 79 °C,  
1117 and as the temperature is increased beyond this point, the solid adhesive material  
1118 rapidly melts to a relatively low-viscosity fluid that can be applied easily. Upon  
1119 cooling, the adhesive solidifies rapidly. Since these adhesives are thermoplastics,  
1120 the melting/resolidification process is repeatable with subsequent heating/  
1121 cooling cycles. Consequently, these adhesives allow reworking of the bonded  
1122 parts, when necessary. Typical application temperatures of hot-melt adhesives are  
1123 149–188 °C.

### 1124 **12.5.3 High-Temperature Adhesives**

1125 High-performance/high-temperature adhesives are developed, formulated, and  
1126 applied according to their specific applications. For example an adhesive used to  
1127 join honeycomb structure to face sheets has flow requirements that are different from  
1128 one designed for metal-to-metal bonding. In honeycomb structures, the adhesive  
1129 must flow sufficiently to form fillets at the honey comb cell/face sheet boundaries  
1130 under relatively mild pressures.

### 1131 **12.5.4 Water-Base Adhesives**

1132 When water-base adhesives are applied to a substrate, they simply set upon removal  
1133 of water. Some water-base adhesives (rubber-based adhesives) can be vulcanized or  
1134 cross-linked by the application of heat or by activation provided by catalyst.

### 1135 **12.5.5 UV/Electron Beam Curing Adhesives**

1136 Most UV/EB adhesives are based on an addition polymerization curing mechanism.  
1137 Materials consist of acrylic acid esters of various forms or combinations of acrylates  
1138 with aliphatic or aromatic epoxies, urethanes, polyesters, or polyethers.

### 1139 **12.5.6 Sealants**

1140 All sealants used for electrical encapsulation or joint sealing purposes must fill a  
1141 specific space to create a seal, form a barrier impervious to fluid flow, and maintain  
1142 the seal in operating environments.

1143 An important sealing application utilizes techniques known as potting and encaps-  
1144 ulating to protect electrical/electronic devices and components from the environ-  
1145 ment, to allow the heat generated by the device to dissipate and, sometimes, to mount  
1146 these devices/components. In these techniques, the liquid forms of sealant materials  
1147 are converted irreversibly to solids with no significant weight loss. Potting involves  
1148 placing a device or component in a container, or pot. The container is then filled with  
1149 potting sealant material, which becomes the exterior wear surface of the component  
1150 or device. Encapsulation involves protecting an electronic or electrical device or  
1151 component with a sealant which forms a thick protective envelope around it.

### 1152 **12.5.7 Conductive Adhesives**

1153 Zhou and Sancaktar (2008) observed polymer binder migration under static pressure  
1154 for epoxy-based conductive adhesives with 50 wt% of etched Ni flake particles,  
1155 during cure. Such binder migration led to unstable flow and electrical conductivity

1156 gradients after extrusion. Lower resin viscosity and shear rates facilitated the flow  
1157 instability and filtering of polymeric binder during dynamic capillary flow of epoxy/  
1158 Ni suspensions with 75 wt% of Ni, thus leading to a change in the bulk electrical  
1159 conductivity during processing. As the shear rate increased, the average plunger  
1160 force and force oscillation frequency increased. Ni concentrations of 70 and 62.7 wt%  
1161 gave rise to stable flows in these systems.

1162 Incorporation of Ni nanopowder in the suspension resulted in a stable capillary  
1163 flow at 75 wt% of Ni. Occurrence of agglomerates, however, somewhat nullified this  
1164 advantage.

### 1165 12.5.8 Anaerobic Adhesives

1166 Anaerobic adhesives are typically applied using bottles, cartridges etc., made for  
1167 specific applications. Since air exclusion is imperative for premature polymerization,  
1168 metering and dispensing equipment is designed specially to prevent contact of  
1169 anaerobic adhesives with air, prior to use.

### 1170 12.5.9 Moisture Curing Adhesives

1171 As with the anaerobic adhesives, moisture-curing adhesives, such as cyanoacrylates,  
1172 are typically applied using bottles, cartridges etc., made for specific applications.  
1173 Since moisture exclusion is imperative for premature polymerization, metering and  
1174 dispensing equipment is designed specially to prevent contact of moisture-curing  
1175 adhesives with air, prior to use.

### 1176 12.5.10 Primers

1177 Primers can be applied by either dipping the part in primer solution or by spraying it  
1178 with air gun. Spraying appears to be the most popular technique used in structural  
1179 bonding. Higher solid-level primers are typically applied by brush. In certain  
1180 applications, settling of the insoluble inorganic chromate corrosion inhibitor needs  
1181 to be avoided by agitation during primer application. Since peel performance  
1182 typically decreases with increasing primer thickness, proper pigment suspension,  
1183 and the control of film thickness and uniformity must be assured during primer  
1184 application.

---

## 1185 12.6 Conclusions

1186 Adhesive bonding has many advantages, including more uniform stress distributions  
1187 in comparison to the use of mechanical fasteners such as bolts, rivets, etc. Adhesives  
1188 provide full contact with mating surfaces, thus forming a barrier to fluids and gasses

which may cause degradation in the assembled structure. Adhesives can also function as electrical and/or thermal insulators or conductors in joints.

As described in this chapter, adhesives can be classified based on their chemical type and physical form, and their reaction/processing conditions. Such classification helps in determination of the method of application and setting of the adhesive, as well as in assembly and fixturing as they relate to the nature and purpose of the objects to be bonded. Therefore, attention to classification facilitates adhesive selection.

## References

- Aussawasathien D, Sancaktar E (2008) Effect of non-woven carbon nanofiber mat presence on cure kinetics of epoxy nanocomposites. *Macromol Symp* 264:26–33
- Brinson HF (1987a) Engineered materials handbook, Composites, vol 1. ASM International, Materials Park
- Brinson HF (1987b) Engineered materials handbook, Engineering plastics, vol 2. ASM International, Materials Park
- Brinson HF (1987c) Engineered materials handbook, Adhesives and sealants, vol 3. ASM International, Materials Park
- De Lollis NJ (1980) Adhesives, adherends, adhesion. Krieger Publishing Company Inc., Malabar
- Dilsiz N, Partch R, Matijevic E, Sancaktar E (1997) Silver coating of spindle- and filament-type magnetic particles for conductive adhesive applications. *J Adhes Sci Technol* 11:1105–1118
- Ge L, Sethi S, Ci L, Ajayan PM, Dhinojwala A (2007) Carbon nanotube-based synthetic gecko tapes. *Proc Natl Acad Sci USA* 104:10792–10795
- Kamal MR (1974) Thermoset characterization for moldability analysis. *Polym Eng Sci* 14:231–239
- Kim JS, Reneker DH (1999) Mechanical properties of composites using ultrafine electrospun fibers. *Polym Comp* 20:124–131
- Klepner D, Frisch KC (1991) Polymeric foams. Hanser, New York
- Lin S-C, Pearce EM (1993) High performance thermosets. Hanser, New York
- Morton M (ed) (1987) Rubber technology, 3rd edn. New York, Von Nostrand Reinhold
- Qian D, Dickey EC, Andrews R, Rantell T (2000) Load transfer and deformation mechanisms in carbon nanotube-polystyrene composites. *Appl Phys Lett* 76:2868–2870
- Sancaktar E, Aussawasathien D (2009) Nanocomposites of epoxy with electrospun carbon nanofibers: mechanical behavior. *J Adhes* 85:160–179
- Sancaktar E, Dembosky SK (1986) The effects of molecular weight on the single lap shear creep and constant strain rate behavior of thermoplastic polyimidesulfone adhesive. *J Adhesion* 19:287–308
- Sancaktar E, Dilsiz N (1997) Anisotropic alignment of nickel particles in magnetic field for electronically conductive adhesives. *J Adhes Sci Technol* 11:155–166
- Sancaktar E, Dilsiz N (1999a) Pressure dependent conduction behavior of various particles for conductive adhesive applications. *J Adhes Sci Technol* 13:679–693
- Sancaktar E, Dilsiz N (1999b) Thickness dependent conduction behavior of various particles for conductive adhesive applications. *J Adhes Sci Technol* 13:763–771
- Sancaktar E, Kuznicki J (2006) Stress-induced reduction of water uptake in clay-reinforced epoxy nanocomposites. *Curr Nanosci* 2:351–357
- Sancaktar E, Schenck SC (1985) Material characterization of structural adhesives in the lap shear mode, part II: the effects of rate. *Ind Eng Chem Prod Res Dev* 24:257–263
- Sancaktar E, Wei Y (1996) The effect of pressure on the initial establishment of conductive paths in electronically conductive adhesives. *J Adhes Sci Technol* 10:1221–1235

- 1236 Sancaktar E, Zhang P (1990) Nonlinear viscoelastic modeling of the fiber-matrix interphase in  
1237 composite materials. *Trans ASME. J Mech Des* 112:605–619
- 1238 Sancaktar E, Schenck SC, Padgilwar S (1984) Material characterization of structural adhesives in  
1239 the lap shear mode, part I: temperature dependent delayed failure. *Ind Eng Chem Prod Res Dev*  
1240 23:426–434
- 1241 Sancaktar E, Wei Y, Gaynes MA (1996) Conduction efficiency and strength of electronically  
1242 conductive adhesive joints. *J Adhesion* 56:229–246
- 1243 Sancaktar E, Rajput P, Khanolkar A (2005) Correlation of silver migration to the pull out strength of  
1244 silver wire embedded in an adhesive matrix. *IEEE Trans Compon Packag Technol* 28:771–780
- 1245 Sethi S, Ge L, Ci L, Ajayan PM, Dhinojwala A (2008) Gecko-inspired carbon nanotube-based self-  
1246 cleaning adhesives. *Nano Lett* 8:822–825
- 1247 Shields J (1985) *Adhesive handbook*, 3rd edn. Butterworth & Co Ltd, London
- 1248 Wang Z, Lan T, Pinnavaia TJ (1996) Hybrid organic-inorganic nanocomposites formed from an  
1249 epoxy polymer and a layered silicic acid (magadiite). *Chem Mater* 8:2200–2204
- 1250 Wang Z, Lan T, Pinnavaia TJ (1998) Hybrid organic-inorganic nanocomposites: exfoliation of  
1251 magadiite in an elastomeric epoxy polymer. *Chem Mater* 10:1820–1826
- 1252 Wang Z, Lan T, Pinnavaia TJ (2000) Epoxy-clay nanocomposites. In: Pinnavaia TJ, Beall GW (eds)  
1253 *Polymer-clay nanocomposites*. Wiley, Hoboken
- 1254 Wei Y, Sancaktar E (1996) Dependence of electric conduction on film thickness of conductive  
1255 adhesives: modeling, computer simulation, and experiment. *J Adhes Sci Technol* 10:1199–1219
- 1256 White JL (1995) *Rubber processing*. Hanser, New York
- 1257 Woods G (1990) *The ICI polyurethanes book*, 2nd edn. Wiley, Hoboken
- 1258 Yu MF, Lourie O, Dyer M, Moloni K, Kelly T, Ruoff RS (2000) Strength and breaking mechanism  
1259 of multiwalled carbon nanotubes under tensile load. *Science* 287:637–640
- 1260 Zhou JG, Sancaktar E (2008) Stable and unstable capillary flows of highly-filled epoxy/nickel  
1261 suspensions. *J Adhes Sci Technol* 22:983–1002

Hyun-Joong Kim, Dong-Hyuk Lim, Hyeon-Deuk Hwang, and  
Byoung-Ho Lee

## Contents

13.1	Introduction .....	320
13.2	Primary Resins .....	321
13.3	Solvents .....	323
13.4	Fillers .....	325
13.5	Plasticizers .....	331
13.6	Reinforcements .....	332
13.7	Other Additives .....	336
13.8	Conclusions .....	339
	References .....	342

## Abstract

Adhesives and sealants are generally developed and prepared for many applications such as packaging, construction, automobile, electronic, etc. An adhesive formulation will depend on the base materials and requirements of a particular application. Development managers or formulators have to have a public knowledge about the chemical composition and role of many components for reducing trials and errors. This chapter focuses on the definition and function of adhesive composition such as primary resins, solvents, fillers, plasticizers, reinforcements, and various additives.

H.-J. Kim (✉) · D.-H. Lim · H.-D. Hwang · B.-H. Lee

Laboratory of Adhesion & Bio-Composites, Program in Environmental Materials Science, Seoul National University, Seoul, Republic of Korea

e-mail: [hjokim@snu.ac.kr](mailto:hjokim@snu.ac.kr)

13.1 Introduction

An adhesive is a polymer mixture or polymerizable material in a liquid or semiliquid state that adheres substrates together (Petrie 2000). Adhesives may be composed of many components such as polymer, oligomer, filler, and additives from either natural or synthetic sources. It is very important to understand the components for adhesive formulation. The information of composition gives us an adhesive selection guide based on functional properties, curing mechanisms, and other relevant information supplied by the adhesive manufacturer.

An adhesive is a complex formulation of many components that have a unique function. The adhesive manufacturer or developer selects actual ingredients depending on the end-user requirement, the application, processing requirement, and the cost as shown in Fig. 1. The various components of an adhesive formulation include the following: primary resins, solvents, fillers, plasticizers, reinforcements, thickeners and thixotropic agents, film formers, antioxidants, antifungal agents, emulsifiers, and wetting agents (Petrie 2000).

The adhesive formulator gets a lot of information from raw material suppliers, books, papers, and patents. The number of possibilities for innovation seems to be endless. However, the formulation of an adhesive is fixed according to the formulator's experience and education. Knowledge of how to incorporate ingredients together into a practical, workable formulation is also required.

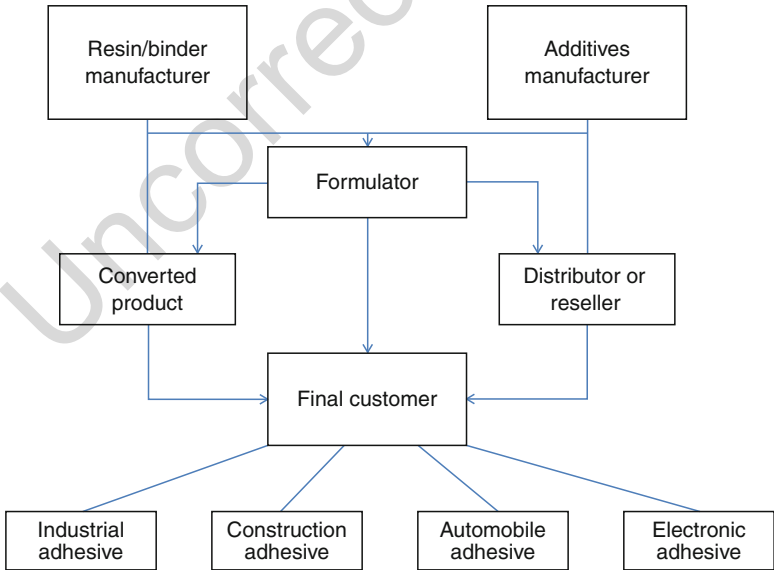


Fig. 1 Flow chart of adhesive applications



13.2 Primary Resins

The primary resins of adhesives and sealants are the principal component that provides a lot of characteristics such as wettability, adhesion strength, thermal property, chemical resistance, and environmental resistance. The word “resin” means a hydrocarbon secretion of many plants, particularly coniferous trees. In the adhesive industry, the primary resin means a polymer that is the main chain in the adhesive molecular structure. The understanding of primary resins is essential for adhesive curing, application, reliability, and adhesion failure analysis. For example, a modified epoxy acrylate is one of the primary resins for the main sealants of the liquid crystal display (LCD) (Park et al. 2009). The main sealants are used to adhere the thin film transistor and the color filter. To produce sealants for LCD, the primary resins have to have absolutely high purity to prevent pollution of the liquid crystal. However, some primary resins have a large range of performance depending on molecular weight, molecular structure, additives ratio, etc. Table 1 gives a classification of applications and primary resins (Dostal 1990).

Adhesives are classified by many methods such as dispensing method, application, and primary resin. The classification by primary resin is very useful to select a good

**Table 1** Various adhesive classifications and primary resins

Main category	Subcategory	Primary resins
Characteristics	Anaerobic adhesive	Polyester, urethane, epoxy, silicone, acrylate
	Elastic adhesive	Silicone, urethane, polysulfide
	Conductive adhesive	Epoxy, acrylate, polyimide, silicone, EVA, phenol
	Flame-retardant adhesive	Polybenzimidazole, polyquinoxazoline, polyphenylquinoxazoline, polyimide, bismaleimide, epoxy
	Damping adhesive	Silicone, polyvinylalchol
Curing methods	Quick-drying-glue	Cyanoacrylate
	UV-curable adhesive	Acrylate, polyene
	EB curable adhesive	Acrylate
	Visible light curable adhesive	Acrylate, polyene, polythiol
	Hotmelt adhesive	SBC, polyamide, polyacrylate, EVA
Applications	Medical adhesive	Fibrin, gelatin, cyanoacrylate, polyurethane
	Shoe adhesive	Polyurethane, phenol, SBR, rubber latex
	Structural adhesive	Phenol, epoxy, nitrile-phenol, vinyl phenol, epoxy, urethane, acrylate

*EVA* ethylene-vinyl acetate, *EB* electron beam, *SBC* styrene block copolymers, *SBR* styrene-butadiene-rubber

adhesive for a given application, because the name of the primary resin involves the chemical structure of the back bone and the sketchy properties such as adhesion strength and heat resistance. In this chapter, the classification of primary resins by chemical composition consists in thermosets, thermoplastics, and elastomeric resins. A thermosetting resin is a prepolymer in a soft solid or viscous state that changes irreversibly into an insoluble polymer network by curing, which can be induced by the action of heat or radiation, or humidity. Thermosetting materials are generally stronger than thermoplastic materials due to 3-D network of bonds, and are also better suited to high-strength and high-temperature applications. Table 2 shows some typical thermosetting resins and their characteristics for adhesives and sealants (Dostal 1990). A thermoplastic resin is a polymer that can turn to a melting liquid when it is heated and returns to solid when it is cooled down. Table 3 shows some thermoplastic resins and their properties (Dostal 1990). The molecular structure of thermoplastic resins is linear or branched. Linear and branched polymers are often soluble in solvents such as

**Table 2** Typical thermosetting resins for adhesives and sealants

	Advantages	Limitations
Epoxy	<ul style="list-style-type: none"> <li>• high strength</li> <li>• good solvent resistance</li> <li>• good gap-filling capabilities</li> <li>• good heat resistance</li> <li>• wide range of formulations</li> <li>• relatively low cost</li> </ul>	<ul style="list-style-type: none"> <li>• exothermic reaction</li> <li>• exact proportions needed for optimum properties</li> <li>• short pot life</li> </ul>
Polyurethanes	<ul style="list-style-type: none"> <li>• various cure times</li> <li>• tough</li> <li>• excellent flexibility even at low temperature</li> <li>• one- or two-component, room- or elevated-temperature cure</li> <li>• moderate cost</li> </ul>	<ul style="list-style-type: none"> <li>• both uncured and cured are moisture sensitive</li> <li>• poor heat resistance</li> <li>• may revert with heat and moisture</li> <li>• short pot life</li> <li>• special mixing and dispensing equipment required</li> </ul>
Cyanoacrylates	<ul style="list-style-type: none"> <li>• rapid room-temperature cure</li> <li>• one-component system</li> <li>• high tensile strength</li> <li>• long pot life</li> <li>• good adhesion to metal</li> <li>• dispense easily from package</li> </ul>	<ul style="list-style-type: none"> <li>• high cost</li> <li>• poor durability on some surfaces</li> <li>• limited solvent resistance</li> <li>• limited elevated-temperature resistance</li> <li>• bonds skin</li> </ul>
Modified acrylics	<ul style="list-style-type: none"> <li>• good flexibility</li> <li>• good peel and shear strengths</li> <li>• no mixing required</li> <li>• will bond dirty(oily) surfaces</li> <li>• room-temperature cure</li> <li>• moderate cost</li> </ul>	<ul style="list-style-type: none"> <li>• low hot-temperature strength</li> <li>• slower cure than with cyanoacrylates</li> <li>• toxic</li> <li>• flammable</li> <li>• odor</li> <li>• limited open time</li> <li>• dispensing equipment required</li> </ul>
Phenolics	<ul style="list-style-type: none"> <li>• good heat resistance</li> <li>• good dimensional stability</li> <li>• inexpensive</li> <li>• modification of toughness by adding elastomeric resins</li> </ul>	<ul style="list-style-type: none"> <li>• brittle</li> <li>• possibility of pollution due to formaldehyde as curing agent</li> </ul>

**Table 3** Typical thermoplastic resins for adhesives and sealants

	Advantages	Limitations
Acrylate	<ul style="list-style-type: none"> <li>• good UV resistance</li> <li>• good hydrolysis resistance (better than rubber)</li> <li>• good solvent resistance</li> <li>• good temperature use range (−45~260 °C)</li> <li>• good shear strength</li> <li>• long service life</li> </ul>	<ul style="list-style-type: none"> <li>• poor creep resistance</li> <li>• fair initial adhesion</li> <li>• moderate cost</li> </ul>
Polyvinyl alcohol	<ul style="list-style-type: none"> <li>• water soluble resin</li> <li>• good wettability to porous substrate such as wood</li> <li>• quick set</li> <li>• heat seal available</li> <li>• good oil/grease resistance</li> <li>• odorless/tasteless</li> </ul>	<ul style="list-style-type: none"> <li>• poor water resistance</li> <li>• poor heat resistance</li> <li>• poor creep resistance</li> </ul>
Ethylene vinyl acetate	<ul style="list-style-type: none"> <li>• application to hotmelt</li> <li>• good wetting and adhesion</li> <li>• good flexibility</li> </ul>	<ul style="list-style-type: none"> <li>• poor heat resistance</li> <li>• poor creep resistance</li> </ul>
Polyamide	<ul style="list-style-type: none"> <li>• application to hotmelt</li> <li>• good heat resistance (better than ethylene vinyl acetate)</li> <li>• good resistance to dry cleaning fluids</li> </ul>	<ul style="list-style-type: none"> <li>• expensive</li> <li>• low flexibility</li> <li>• poor resistance to impact</li> </ul>
Styrene block copolymer	<ul style="list-style-type: none"> <li>• cheap</li> <li>• good heat resistance</li> <li>• good toughness</li> <li>• low water absorption</li> </ul>	<ul style="list-style-type: none"> <li>• poor adhesion to nitrile, neoprene, natural rubber</li> </ul>
Polyolefins	<ul style="list-style-type: none"> <li>• good wettability to various substrates due to low surface energy</li> <li>• excellent peel strength</li> <li>• various applications</li> <li>• heat seal available</li> </ul>	<ul style="list-style-type: none"> <li>• low molecular weight constituents for commercial grade</li> <li>• no tacky</li> </ul>
Polysulfone	<ul style="list-style-type: none"> <li>• high heat resistance</li> <li>• very tough</li> <li>• high strength</li> <li>• excellent creep resistance</li> <li>• good chemical resistance to strong acid and alkali</li> </ul>	<ul style="list-style-type: none"> <li>• poor chemical resistance to polar organic solvent and aromatic hydrocarbons</li> <li>• low processability</li> </ul>

chloroform, benzene, toluene, and tetrahydrofuran (THF). More detailed information for each primary resin is given in ► [Chap. 14, “Adhesive Families.”](#)

### 13.3 Solvents

Solvents are liquids comprising one or more components that are volatile under the specified drying conditions and can dissolve film-forming agents purely and physically without chemical reactions (DIN EN 971-1 1996). Solvents can lower the

viscosity of the formulation to make it easier to apply and to help liquefy the primary resin so that the other additives may be easily incorporated into the formulation (Petrie 2000).

Diluents are defined as ingredients used in conjunction with the true solvent to increase the bulk of another substance without causing precipitation (LeSota 1995). Diluents are mainly used to lower the viscosity and modify the processing conditions of adhesives and sealants. Diluents participate in the partial components of the final adhesives because they have a lower volatility than solvents.

Solvents are used to control the viscosity of the adhesives so that they can be applied more easily. They are also used to aid in formulating the adhesive by reducing the viscosity of the primary resin so that additions of other components and uniform mixing may be achieved more easily. When solvents are used in the adhesive formulation, the similarity of the solubility parameter between the solvent and the primary resin is very important.

The solubility parameter ( $\delta$ -value) is divided as the following equation:

$$\delta_{\text{total}} = \sqrt{\delta_D^2 + \delta_P^2 + \delta_H^2} \quad (1)$$

$\delta_D$  = parameter for nonpolar contribution;  $\delta_P$  = parameter for polar contribution;  $\delta_H$  = parameter for hydrogen bridges contribution.

The indices relate to the nonpolar dispersion forces, the dipole forces, and the interactions caused by hydrogen bridges. Table 4 lists the solubility parameters of various solvents (Goldschmidt and Streitberger 2007).

The prediction of the miscibility between the polymer (primary resin) and solvent can be allowed from a comparison of the solubility parameters of the polymer ( $\delta_{\text{polymer}}$ ) and solvent ( $\delta_{\text{solvent}}$ ) because  $\delta$  is a measure of the interaction forces between molecules of the material. Therefore, the difference of solubility parameter ( $\delta_{\text{polymer}} - \delta_{\text{solvent}}$ ) should be small for good miscibility.

Solvents can be classified into some categories by their chemical character into groups with common features: aliphatic, cycloaliphatic, and aromatic hydrocarbons, esters, ethers, alcohols, glycol ethers, and ketones. Table 5 shows the important physical performance indicators of solvents used for the coatings or adhesives such as the density, refractive index, boiling temperature or boiling ranges, and the vapor pressure or evaporation time. In addition, the flash point, ignition point, and explosion limits must also be needed for safety reasons (Goldschmidt and Streitberger 2007).

General solvent contents used for typical sealants are shown in Table 6 (Petrie 2000).

The use of excessive solvent may cause a shrinkage problem when the sealant cures. Volume shrinkage will always be greater than the weight percent of solvent due to its much lower density than other components in the sealant. Toluene, xylene, petroleum spirits, water, and others are used as solvents in sealant formulations. In case of solvent mixtures, the balance of volatility between solvents is very important to avoid a trouble such as the sealant's skin drying problem.

**Table 4** Solubility parameters  $\delta_{\text{total}}$  of different solvents and their disperse contribution  $\delta_{\text{D}}$ , polar contribution  $\delta_{\text{P}}$  and hydrogen bridging contribution  $\delta_{\text{H}}$ , (unit in  $[\text{J}/\text{cm}^3]^{1/2}$ ) (Goldschmidt and Streitberger 2007)

	$\delta_{\text{total}}$	$\delta_{\text{D}}$	$\delta_{\text{P}}$	$\delta_{\text{H}}$
n-Hexene	14.9	14.7	0	0
Cyclohexane	16.8	16.8	0	0
Toluene	18.2	18.0	1.4	2.0
Xylene	18.0	17.8	1.0	3.1
Ethylbenzol	18.0	17.8	0.6	1.4
Styrene	19.0	18.6	1.0	4.1
n-Propnol	24.3	15.1	6.1	17.6
Isopropanol	23.5	15.3	6.1	17.2
n-butanol	23.3	16.0	6.1	15.8
Isobutanol	21.9	15.3	5.7	15.8
2-Ethylhexanol	19.4	16.0	3.3	11.9
Cyclohexanol	23.3	17.4	4.1	13.5
Diacetonealcohol	18.8	15.8	8.2	10.8
Acetone	20.5	15.6	11.7	4.1
Methylethylketone	19.0	16.0	9.0	5.1
Methylisobutylketone	17.2	15.3	6.1	4.1
Cyclohexanone	19.8	17.8	7.0	7.0
Ethylacetate	18.6	15.1	5.3	9.2
Butylacetate	17.4	15.1	3.7	7.6
Butylcellosolve	18.2	16.0	6.3	12.1
Ethylidiglycol	19.6	16.2	7.6	12.3
Butyldiglycol	18.2	16.0	7.0	10.6
Water	47.8	14.3	16.3	42.6
Polystyrene	19.0	17.5	6.1	4.0
Polyvinylacetate	23.0	18.9	10.1	8.1
Polymethacryladid methylester	22.0	18.7	10.1	8.5
Polyvinylchloride	22.4	19.1	9.1	7.1
Epoxy resin	23.4	17.3	11.2	11.2

**13.4 Fillers**

Fillers are generally relatively non-adhesive materials added to the adhesive formulation to enhance mechanical strengths, thermal properties, adhesion performance, etc. Common fillers in conductive adhesives are listed in Table 7. One of the purposes of using fillers is lowering the cost. The incorporation of fillers into the adhesive reduces the resin content and thus the product cost is also reduced. However, fillers can change adhesive properties. Filler selection and loading level are very important in formulation of adhesive because adhesive properties depend on filler type, size, shape, and volume contents. Common fillers are metal powder, kind of clay, dust, glass fiber, alumina, and so on. Sometimes fillers act as extenders or reinforcement materials.

**Table 5** Physical and safety-related data of important solvents (Goldschmidt and Streibberger 2007)

Type of solvents	Mol. Mass	Boiling point/region (°C)	Density at 20 °C (g/cm <sup>3</sup> )	Refractive index at 20 °C	Evaporation number	Vapor pressure at 20 °C (hPa)	Flash point (°C)	Ignition temperature (°C)	Explosion limit (Vol %)
Aliphatic hydrocarbons and mixture									
n-Hexane	86.2	65–70	0.675	1.372	1.4	190	–22	240	1.2/7.4
Solvesso 100	123	155–181	0.877	1.502	40–45	3	41	>450	0.8/7.0
Solvesso 150	135	178–209	0.889	1.515	120	1	62	>450	0.6/7.0
Solventnaphtha	123	150–195	0.870	1.500	40–45	3	41	>450	0.8/7.0
Benzine 135/180	131	135–175	0.766	1.428	25–30	70	~22	210	0.6/7.0
Cyclohexane	84.2	80.5–81.5	0.778	1.426	3.5	104	–17	260	1.2/8.3
Aromatic hydrocarbons									
Xylene	106.2	137–142	0.874	1.498	17	90	25	562	1.0/7.6
Toluene	92.1	110–111	0.873	1.499	6.1	290	6	569	1.2/7.0
Styrene	104.2	145	0.907	1.547	16	60	31	490	1.0/6.3
Alcohols									
Propanol	60.1	97.2	0.804	1.386	16	19	23	360	2.1/13.5
n-Butanol	74.1	117.7	0.811	1.399	33	6.6	34	360	1.4/11.3
Isobutanol	74.1	107.7	0.802	1.396	25	12	28	410	1.5/12
Ethylhexanol	130.2	183.5–185	0.833	1.432	600	0.5	76	250	1.1/12.7
Isotridecylalcohol	200.2	242–262	0.845	1.448	>2000	<0.01	115	250	0.6/4.5
Glycol ether									
Butylglycol	118.2	167–173	0.901	1.419	163	1	67	240	1.1/10.6
Propylglycol	104.2	150.5	0.911	1.414	75	2	51	235	1.3/15.8

t.23	Hexylglycol	146.2	208	0.887	1.429	ca. 1200	0.08	91	220	1.2/8.4
t.24	Methyldiglycol	120.2	194.2	1.021	1.424	576	0.3	90	215	1.6/16.1
t.25	Butyldiglycol	162.2	224–234	0.956	1.431	>1200	0.1	98	225	0.7/5.3
t.26	Methoxipropanol	90.1	122.8	0.934	1.403	25		38	270	1.7/11.5
t.27	Ethoxipropanol	104.1	132	0.896		33	<10	40	255	1.3/1.2
t.28	Esters									
t.29	Butylacetate	116.2	123–127	0.880	1.394	11	13	25	400	1.2/7.5
t.30	Ethylethoxypropionate	146.2	170	0.943		96	2	59	327	1.05/
t.31	Ethylacetate	88.1	76–78	0.900	1.372	2.9	97	–4	460	2.1/11.5
t.32	Isobutylacetate	116.2	114–118	0.871	1.390	8	18	19	400	1.6/10.5
t.33	Ethoxypropylacetate	146.2	158	0.941	1.405		2.27	54	325	1.0/9.8
t.34	Methoxypropylacetate	132.2	143–149	0.965	1.402	33	4.2	45	315	1.5/10.8
t.35	Pentylacetate	130.2	146	0.876	1.405	14	6	23	380	1.1/
t.36	Butylglycolacetate	160.2	190–198	0.945	1.415	250	0.4	75	280	1.7/8.4
t.37	Ketones									
t.38	Methylisobutylketone	100.2	115.9	0.800	1.396	7	20	14	475	1.7/9.0
t.39	Acetone	58.1	56.2	0.792	1.359	2	245	–19	540	2.1/13
t.40	Cyclohexanone	98.2	155	0.945	1.451	40	3.5	44	455	1.1/7.9
t.41	Methyl ethylketone	72.1	79.6	0.808	1.379	2.6	96	–14	514	1.8/11.5
t.42	Isophorone	138.2	215	0.922	1.478	230	3	96	460	0.8/3.8
t.43	Others									
t.44	Water	18	100	1.000				–	–	–
t.45	Propylencarbonate	102.2	242	1.208		>1000		123		

**Table 6** General solvent contents for typical sealants (Petrie 2000)

Base resin	Solvent content,%	Polymer content,%
Acrylic	20–40	35–45
Latex emulsion	35–45	35–45
Polysulfide	0	30–45
Silicone	0	60–85
Urethane	0	30–45

**Table 7** Filler for conductive adhesive in common adhesive formulations

Filler	Improvement in adhesive formulation
Aluminum	Electrical conductivity, thermal conductivity
Silver	Electrical conductivity
Carbon black	Electrical conductivity, color
Graphite	Electrical conductivity, lubricity
Copper	Electrical conductivity, machinability
Nickel	Electrical conductivity
Iron	Electrical conductivity, abrasion resistance
Chromium	Electrical conductivity
Molybdenum	Electrical conductivity
Tungsten	Electrical conductivity

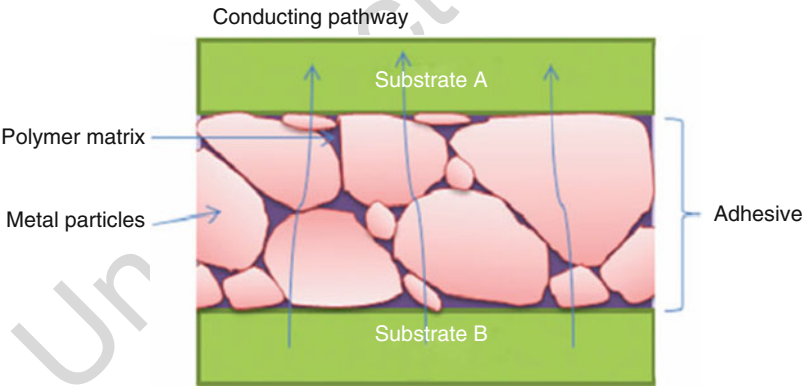
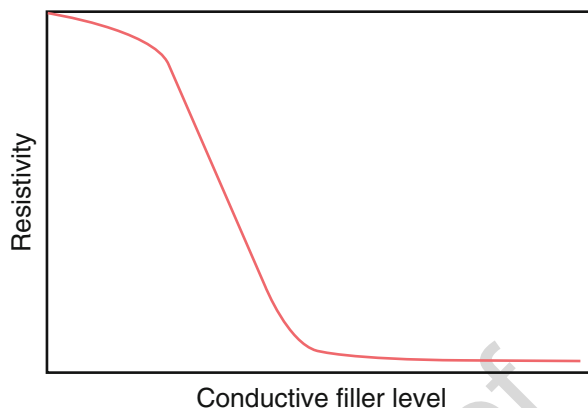


**Fig. 2** Conductivity depends on contact between filler particles within the adhesive (Petrie 2008)

Normally, adhesive can be conductive by adding conducting filler particles. The resin provides an interaction bond between substrates and conducting fillers as well. However, it is the conducting filler that provides the desired electrical interconnection path as depicted in Fig. 2. To make conducting adhesives, the fillers must be in physical contact with each other. Thus, the electrical conductivity increases sharply when a percolation threshold level of well-dispersed conducting filler is accomplished. Figure 3 shows the resistivity versus conductive filler level (Petrie 2008).



**Fig. 3** Conductive filler level versus resistivity in conducting adhesive formulation (Petrie 2008)



Alumina particles are one of the commonly used fillers for improving the thermal conductivity of adhesives in particular insulation adhesives. Aluminum and silver powders or flakes are used to improve the thermal and electrical conductivities for adhesives intended to be an electrical or thermal path. The filler volume content level is very important to get sufficient conductivity. However, excessive filler content might cause degradation in mechanical properties of the adhesives (Kahraman and Al-Harhi 2005; Kahraman et al. 2008).

One of the most effective techniques used to improve the electrical conductivity of polymers is the incorporation of conductive fillers in the polymer matrix. The most popular electrically conductive filler is silver due to its moderate cost and superior conductivity. Silver-coated inorganic particles and fibers are superior compared to carbon particles and fibers as components in epoxy-based adhesives regarding the electrical conductivity of the composite; because the electrical conductivity of silver is much higher than that of carbon. In addition to the high electrical conductivity of silver, the addition/application of silver-plated particles and fibers also leads to composites with high mechanical strength and modulus, low weight, and a high ratio of metal-plated fibers (Novák et al. 2004).

Among the various conductive particles, silver particle is probably the most common filler because of its excellent conductivity and chemical durability. Silver particles are easy to precipitate into a wide range of controllable sizes and shapes, so it can be used to change the percolation threshold of the adhesive formulation. Silver also exhibits high conductivity; however, the silver filler is expensive (Lin et al. 2009).

Graphite is usually used as an electro conductive filler due to its low cost and natural electrical conductivity. It also has a positive influence on the mechanical properties, as well as thermal and dimensional stability (Lin et al. 2009). Substitution of carbon black with renewable filler has been investigated in recent years. Carbon black has some advantages such as low cost, low density, high electrical conductivity, and, in particular, specific structures that enable the formation of conductive network (Wan et al. 2005; Jong 2007).

**Table 8** Filler for other function in common adhesive formulations

Filler	Improvement in adhesive formulation
Aluminum oxide	Flame retardant
Lead	Radiation shielding
Mica	Electrical resistance
Phenolic microspheres	Decrease density
Silica sand	Abrasion
Silicon carbide	Abrasion resistance
Titanium dioxide	Color
Zinc	Corrosion resistance

**Table 9** Fillers commonly used in sealants

Filler	Improvement in sealant formulation
Calcium carbonate	Adjustment of mechanical properties, thixotropic agent
Silica	Common for silicon resin
Clay	Mechanical modifier
Titanium dioxide	Colorant (for white)
Carbon black	Colorant (for black)
Iron oxides	Colorant
Glass fiber	Thixotropic agent

Copper has good electrical conductivity and high adhesion property in conductive adhesive systems. However, copper tends to form a nonconductive oxide surface layer (Zhao et al. 2007).

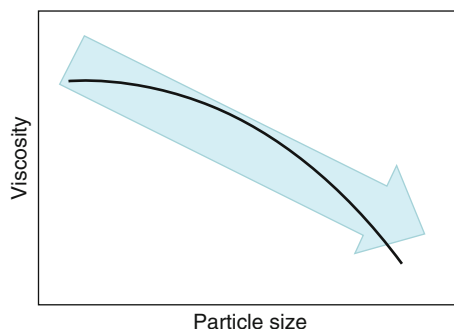
Nickel is a good nominee for conductive filler in conducting adhesives because of the numerous benefits it possesses. Nickel shows chemical stability and oxidizes relatively slowly compared to copper. But, nickel has disadvantages compared to silver: nickel has a higher electrical resistance than silver (about 25% of silver). However, it is less expensive than silver filler (Goh et al. 2006).

There are many conducting fillers for adhesive formulation. Apart from the ones mentioned above, iron, chromium, molybdenum, tungsten, and other metal particles can be used as fillers for conducting adhesives.

Many other inorganic fillers are used for adding a function to adhesive. Table 8 shows the additional function of fillers. Aluminum oxide (flame retardant), lead (radiation shielding), mica or clay (electrical resistance), and silica and silicon carbide (abrasion resistance) are used to add additional function to the adhesive formulation.

Generally, fillers in sealant formulation are used as additives to boost the viscosity of the sealant and get better gap-filling properties and to reduce the material cost of the sealants. In sealant formulation, fillers cannot affect reinforcement and improved strength. However, they can affect other properties such as water resistance and hardness, etc. The most common filler used in sealant is calcium carbonate, because of its many advantages such as abundant resource, low cost, and stability. Other fillers are clays, silica, titanium dioxide, carbon black, and iron oxide. Table 9 lists commonly used fillers in sealant formulations and functions in sealant systems.

**Fig. 4** The viscosity versus particle size in common adhesives (Chew 2003)



Fillers represent the largest part in terms of weight for many sealants. Calcium carbonate is the most widely used filler for sealant formulations. As a filler for sealants, calcium carbonate acts as an inert extender to reduce formulation cost, modifier for mechanical properties, and a rheological modifier. Normally, properties of fillers such as particle size, shape, and surface properties are very important factors for sealant properties. Figure 4 shows the typical effect of particle size on the viscosity in common adhesives (Chew 2003). Filler volume contents can vary significantly with being dependent on the primary resin and the formulation.

### 13.5 Plasticizers

Plasticizers are substances of low or negligible volatility that lower the softening range and increase workability, flexibility, or extensibility of a polymer (ASTM D907-08b 2008). The main purpose of plasticizers is to modify the property of adhesives and sealants. The addition of plasticizers causes the improvement of flow and flexibility, but the reduction of the elastic modulus, stiffness, hardness, and the glass transition temperature ( $T_g$ ). As a result, the processibility and extrudability of adhesives and sealants can be improved by addition of plasticizers (Tracton 2007; Stoye and Freitag 1998).

Plasticizers also affect the adhesion property. Addition of plasticizer to the adhesive will always lower the cohesive strength, generally reduce the peel adhesion, and will have a variable effect on the tack depending on the type of plasticizer used (Satas 1999). Plasticizers must be compatible with other adhesive ingredients because of their inherent chemical characteristics and nonreactivity with other components (Petrie 2000).

Plasticizers and solvents are governed by the same laws of solubility and have the ability to increase the free volume of the polymer. However, solvents mostly serve as viscosity modifiers and plasticizers are used to modify the properties of the adhesives or sealants, such as softening and lowering the  $T_g$  (Petrie 2000).

Plasticizers have polar and nonpolar components in the molecular structure. The polar components interact with the polar groups of the primary resins. Otherwise, the nonpolar components prevent the intermolecular interaction between plasticizers

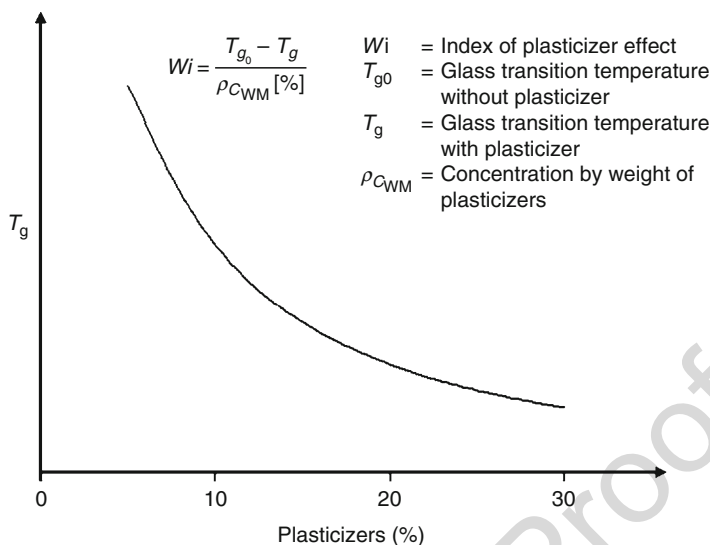


**Fig. 5** Lowering the glass transition temperature ( $T_g$ ) of a polymer by a plasticizer (Goldschmidt and Streitberger 2007)

and the molecules of primary resins by steric hindrance. As a result, the mobility of adhesives or sealants can be promoted. Due to the same reason,  $T_g$  is shifted to a lower temperature with an increase of the plasticizer content as shown in Fig. 5 (Goldschmidt and Streitberger 2007).

When a compatible oil is added to an elastomer such as natural rubber, it acts as a plasticizer. The storage modulus ( $G'$ ) of a natural rubber/aliphatic oil adhesive decreased at all frequencies with the increasing amount of plasticizing oil as shown in Fig. 6 (Satas 1999).

A variety of plasticizers can be used in adhesives and sealants as to their primary resin type. Paraffinic oils, phthalate esters, and polybutenes are typical plasticizers (Dostal 1990). Plasticizers for natural rubber adhesives, such as mineral oil or lanolin, are used to reduce the cost of the adhesive mass, and have a depressing effect on the peel adhesion (Satas 1999). Phthalates, chlorinated hydrocarbons, and aliphatic hydrocarbons are commonly used as plasticizers in urethane sealants (Dostal 1990). Most of sealants, except for silicones, contain plasticizers in their formulations. Silicone sealants can be plasticized only by low molecular weight silicone oils (Petrie 2000).

## 13.6 Reinforcements

Reinforcements are used to enhance mainly mechanical properties. Many reinforcements are now available, and some are designed for a particular primary resin. There are various reinforcements for adhesive formulation. Generally,

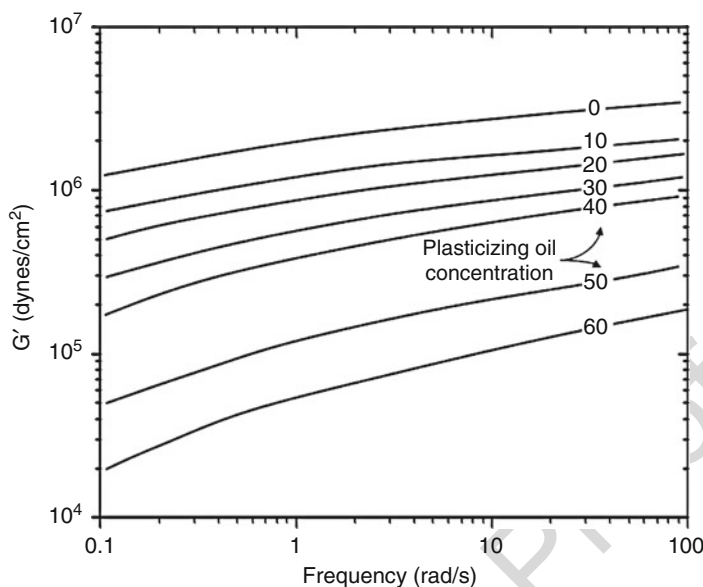


**Fig. 6** Effect of plasticizing oil on the storage modulus ( $G'$ ) of natural rubber/aliphatic oil as function of frequency at 25 °C (Satas 1999)

reinforcements act as the polymer resins in an adhesive system and reinforcing the internal bonding strength of the adhesive. Figure 7 depicts a schematic diagram of an adhesive with reinforcements. Reinforcements act like crosslink agents. It means that the reinforcement reduces the strain in a shear test and can enhance the mechanical strength of the adhesive. The main reinforcements in adhesive formulations are listed in Table 10.

Recently, reinforcement agents in adhesive formulations have received attention due to very high reinforcement ability, simple preparation, and cost. One of the agents is inorganic clay which acts as a modifier of the mechanical and barrier properties. However, clay has some disadvantages for application as a reinforcement agent because of aggregation in the polymer resin. Therefore, many researchers have modified the surface of the clay. Figure 8 shows the clay loading contents versus lap shear strength. It can be seen that the modified clay gives an improved lap shear strength in relation to that of the pure clay (Maji et al. 2009; Osman et al. 2003).

Carbon nanotube (CNT) has excellent mechanical properties. CNT is very similar to graphite. A single-walled carbon nanotube (SWCNT) can be seen as a rolled sheet of graphite, while a multi-walled carbon nanotube (MWCNT) can be viewed as layers of many graphite sheets. Moreover, the stiffness is very high: SWCNT's Young's modulus is about 1 TPa and the shear modulus to be 0.45 TPa. Many researchers have used CNT to enhance the mechanical properties of adhesives.

**Fig. 7** Schematic diagram of adhesive at shear strength test: (a) without reinforcement and (b) with reinforcement

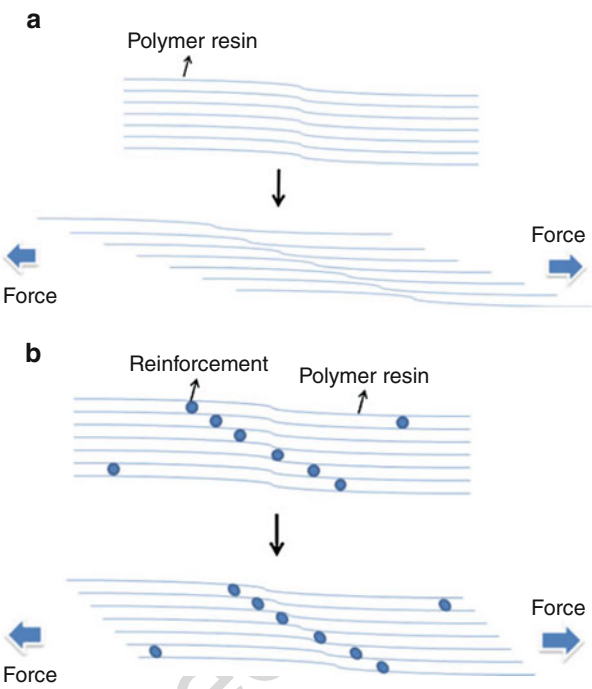


**Table 10** Common reinforcement agents

Reinforcement	Main function
Clay	Mechanical modifier
CNT	Mechanical modifier, electrical conductivity
Graphite	Mechanical modifier
Carbon black	Mechanical modifier, colorant

Figure 9 depicts the shear strength of an epoxy adhesive with different MWCNT contents (Hsiao et al. 2003).

Sometimes, the reinforcement is a carrier in the adhesive composition such as in tapes and films. A carrier is usually a thin fiber fabric, cloth, or paper material. In pressure sensitive adhesives, the carrier is a backing substance for the adhesive being applied. Usually, the backing materials are used for functional or decorative reasons. Glass, nylon fabric, polyester, and paper are common carriers for adhesives. In this case, the carrier acts as a “reinforcement” to ease the use of adhesive. Figure 10 shows a schematic diagram of the carrier for an adhesive tape or film. A carrier is very useful to b-staged adhesive systems because of their semi-cured formulation. The carrier can act as support for adhesive.

**Fig. 8** Lap shear strength versus clay contents in polyurethane adhesive between aluminum and aluminum with PU adhesives (Maji et al. 2009)

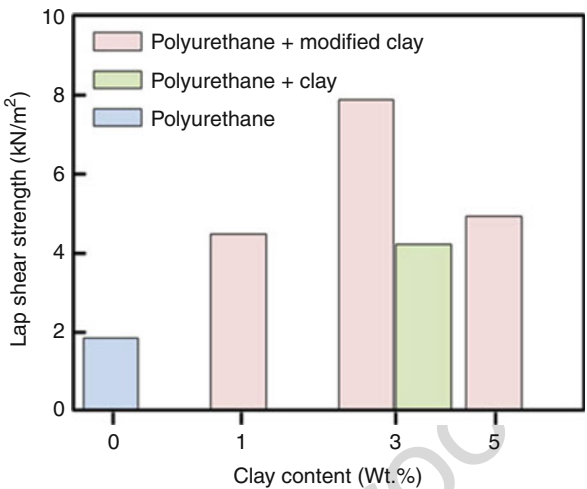


**Fig. 9** The average shear strength of epoxy adhesive with different MWCNT weight fraction (Hsiao et al. 2003)

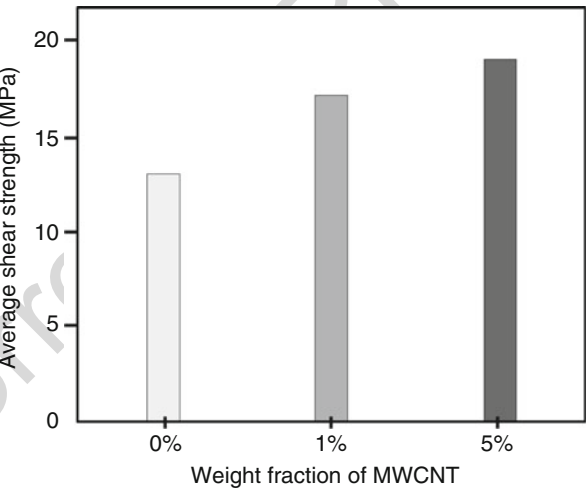
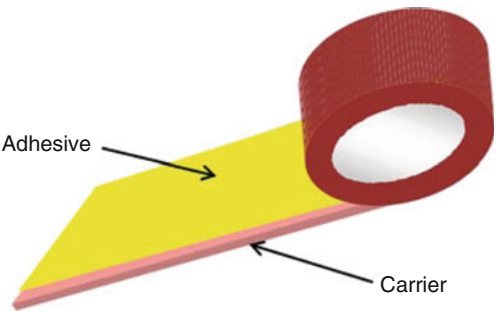


**Fig. 10** Carrier for adhesive



## 13.7 Other Additives

Additives are functional chemicals added to adhesives to ease the process and improve some properties. Many additives, like antioxidants, thermal stabilizers, UV stabilizers, polymer processing aids, anti-blocking additives, slip additives, antifogging agents, antistatic additives, flame retardants, and colorants, have been used for centuries. Recently, additives are used as special functional materials to improve important properties of final products; hence additives application technology is essential for adhesive development.

Antioxidant is any substance that delays or inhibits oxidation during the adhesive manufacturing process, storage, and application. Oxidation is a chemical reaction that transfers electrons from a substance to an oxidizing agent. As a result, reaction produces free radicals (Zweifel 2004). Oxidation during compounding or processing can cause problems such as loss of strength, breakdown, or discoloration. Oxidation can also occur in the final product causing discoloration, scratching, and loss of strength, flexibility, stiffness, or gloss. Antioxidants have some ability to terminate radical chain reactions by removing free radical intermediates or inhibiting other oxidation reactions. Antioxidants can be classified by the chemical structure such as phenol type, aromatic amine type, thioester type, phosphate type, etc.

For example, hotmelt adhesives are 100% solid thermoplastic compounds that are solids at room temperature, but they are changed to liquid when heated to the melting temperature. When applied, hotmelts bond and cool rapidly. To make EVA based hotmelt adhesives, mixing process at high temperature is essential. To reduce the thermal degradation of hotmelt adhesives, 1–2 parts of a phenolic antioxidant by weight were used as a thermal stabilizer (Park et al. 2003, 2006).

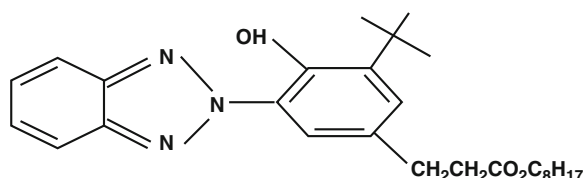
A UV stabilizer is a substance to prevent discoloration, surface crack, and decreasing of the mechanical properties by UV radiation that has a high energy wave in the range of 290–400 nm. In particular, UV stabilizers are essential additives for transparent plastics for outdoor application. UV stabilizers can be classified by chemical reaction, such as UV absorption, quenchers, and HALS (hindered amine light stabilizer). UV absorbers absorb the harmful UV radiation and dissipate it so that it does not lead to photosensitization. Typical UV absorbers are hydroxyl benzophenone, benzotriazoles, and modified acrylate. Quenchers are light stabilizers that are able to take over the energy absorbed by the chromophores present in plastic material (Bellus 1971). HALS is a radical scavenger that represents the most important development in light stabilization for many polymers. HALS acts by scavenging the radical intermediates formed in the photo-oxidation process. HALS' high efficiency and longevity are due to a cyclic process wherein the HALS is regenerated rather than consumed during the stabilization process. HALS also protects polymers from thermal degradation and can be used as a thermal stabilizer.

Table 11 shows an example of formulation of the UV-curable coatings, which is composed of isocyanate and acrylated urethane oligomers (Lee and Kim 2006). In

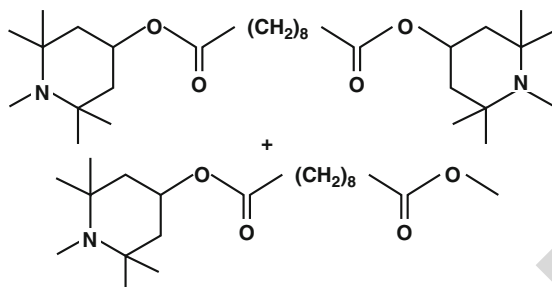


**Table 11** Formulation of UV-curable coatings

Components		Compositions (wt.%)						
		Sample #1	Sample #2	Sample #3	Sample #4	Sample #5	Sample #6	Sample #7
t.1	Oligomers	Ebecryl 210	—	57	55.2	55.2	55.2	45
t.2		Ebecryl 270	57	—	—	—	—	—
t.3	Monomer	Miramir M200	38	38	36.8	36.8	36.8	30
t.4	Photoinitiator	Micure CP-4	5	5	3	3	3	3
t.5		Irgacure 819	—	—	2	2	2	2
t.6	Light stabilizer	Tinuvin 384-2	—	—	3	2	2	—
t.7		Tinuvin 292	—	—	—	3	1	—
t.8	Pigment	Dupont R706	—	—	—	—	—	20
t.9	Total (wt.%)	100	100	100	100	100	100	100
t.10	Ebecryl 210 (aromatic urethane diacrylate)							
t.11	Ebecryl 270 (aliphatic urethane diacrylate)							
t.12	Miramir M200 (1,6-hexanediol diacrylate)							
t.13	Micure CP-4 (1-hydroxy-cyclohexyl-phenyl-ketone)							
	Irgacure 819 (bis(2,4,6-trimethylbenzoyl)-phenylphosphine oxide)							
	Tinuvin 384-2(95% benzene propanoic acid, 3-(2H-benzotriazol-2-yl)-5-(1,1-dimethylethyl)-4-hydroxy-, C7e9-branched and linear alkyl esters, 5% 1-methoxy-2-propyl acetate (UV absorber type))							
	Tinuvin 292 (mixture of bis(1,2,2,6,6-pentamethyl-4-piperidinyl)-sebacate and 1-(methyl)-8-(1,2,2,6,6-pentamethyl-4-piperidinyl)-sebacate (hindered amine light stabilizer type))							
	Dupont R706 (titanium dioxide)							



95% benzenepropanoic acid, 3-(2H-benzotriazol-2-yl)-5-(1,1-dimethylethyl)-4-hydroxy-, C7-9-branched and linear alkyl esters, 5% 1-methoxy-2-propyl acetate (Tinuvin 384-2)



Mixture of bis (1,2,2,6,6-pentamethyl-4-piperidiny) sebacate and 1-(methyl)-8-(1,2,2,6,6-pentamethyl-4-piperidiny) sebacate (Tinuvin 292)

**Fig. 11** Chemical structures of light stabilizers

addition, Fig. 11 shows chemical structures of light stabilizers. UV-cured film with both Tinuvin 384-2 and Tinuvin 292 showed the slight change of optical and mechanical properties. In the case of most UV-cured films, using a UV stabilizer is helpful to discoloration, gloss, and hardness properties after weathering.

Flame retardants are materials that inhibit or resist the spread of fire. Flame retardants can remove thermal energy from the substrate by functioning as a heat sink or by participating in char formation as heat barrier. The additives can also provide flame retardancy by conduction, evaporation, or mass dilution or by participating in chemical reactions (Zweifel 2004).

Adhesives can be separated into two general classes: thermoplastics and thermosets. Thermoplastics can be formulated with halogen-containing and non-halogen-containing additives. Thermosets are commonly treated by adding flame retardants that chemically react with a resin precursor. Table 12 lists flame retardants that are typically used.

Tackifiers are used in formulating rubber based on adhesives to improve the tack property. Tackifiers are low molecular weight compounds with high  $T_g$ . There are two classes of tackifiers: the rosin derivatives and the hydrocarbon resins. The rosin derivatives include the rosins, modified rosins, and rosin ester. The hydrocarbon resins consist of low molecular weight polymers derived from petroleum, coal, and plants. The miscibility between tackifiers and the adhesives is important to choose a tackifier. The viscoelastic property of adhesives can be modified by blending of a miscible tackifier.

**Table 12** Common flame retardants used within thermoset plastics

Resin	Flame retardant	Flame retardant level
Epoxy	Tetrabromobisphenol-A	18 wt.% Br
Unsaturated polyester	Tetrabromophthalic anhydride Chlorendic acid/anhydride	10~22 wt.% Br 15~29 wt.% cl
Polyurethane	Tetrabromophthalate diols Pentabromodiphenyloxide Dibromoneopentylglycol	15~28% 6~18% 5~15%

A curing agent or hardener is a substance added to an adhesive to promote the curing reaction. These affect curing reaction by chemically combining with the base resin and becoming part of the final polymer molecule. They are specifically chosen to react with a certain resin (ASTM D907-08b 2008). Curing agents will have an important effect on the curing features and on the fundamental properties on the adhesive system. A polyamide resin that is used in room-temperature curing epoxy adhesive system is an example of a curing agent (Petrie 2000). Polyamide curing agents are used in most “general-purpose” epoxy adhesives. They offer a room-temperature cure and bond well to many substrates that include elastomers, glass, and plastics. The polyamide-cured epoxy also provides a comparatively flexible adhesive with moisture resistance, fair peel strength, and thermal cycling properties. In general, mixing ratio is not critical. Within limits, the greater the quantity of polyamide in an epoxy formulation, the greater the flexibility, impact strength, and peel strength. However,  $T_g$  is decreased as are the shear strength and temperature resistance. There are some polyamides with changing viscosity. The reaction with conventional di-glycidyl ether of bisphenol A (DGEPA) epoxy resins yields a comparatively low degree of exotherm. In Table 13, the distinct features of curing agents used with epoxy resins in adhesive formulations are briefly stated (Petrie 2000).

Catalysts are substances that markedly speed up the cure of an adhesive when added in a minor quantity compared to the amounts of the primary reactants (ASTM D907-08b 2008). Solidification and crosslink of the primary resins are caused by catalysts. The commonly used catalysts are acids, bases, salts, sulfur compounds, and peroxides. To influence curing, only small quantities are needed (Petrie 2000). Table 14 shows the lists of some catalysts and the reactions they catalyze (Hare 1994). The curing of the adhesives or sealants by transformation into a hardened state is fulfilled by chemical methods, for instance, oxidation, vulcanization, polymerization, or by physical action, such as evaporation of the solvents (Cognard 2005).

### 13.8 Conclusions

There are various commercial adhesives in the market area and various requirements for a specific application: controlling flow, extending temperature range, improving toughness, lowering the coefficient of thermal expansion, reducing shrinkage,

**Table 13** Characteristics of curing agents used with epoxy resins in adhesive formulations

	Curing agent	Physical form	Amount required <sup>a</sup>	Cure temp (°C)	Pot life at 24 °C <sup>b</sup>	Complete cure conditions	Max use temp
t.1							
t.2	Triethylenetetramine	Liquid	11–13	21–135	30 min	7 days (24 °C)	71
t.3	Diethylenetriamine	Liquid	10–12	21–93	30 min	7 days (24 °C)	71
t.4	Diethylaminopropylamine	Liquid	6–8	28–149	5 h	30 min (24 °C)	85
t.5	Metaphenylenediamine	Solid	12–14	65–204	8 h	1 h (85 °C) 2 h (163 °C)	149
t.6							
t.7							
t.8	Methylene dianiline	Solid	26–30	65–204	8 h	1 h (85 °C) 2 h (163 °C)	149
t.9							
t.10	Boron trifluoride monoethylamine	Solid	1–4	135–204	6 months	3 h (163 °C)	163
t.11	Methyl nadic anhydride	Liquid	80–100	121–38	5 days	3 h (160 °C)	163
t.12	Triethylamine	Liquid	11–13	21–135	30 min	7 days (24 °C)	82
t.13	Polyamides						
t.14	Amine value 80–90	Semisolid	30–70	21–149	5 h	5 days (24 °C)	c
t.15	Amine value 210–230	Liquid	30–70	21–149	5 h	5 days (24 °C)	c
t.16	Amine value 290–320	Liquid	30–70	21–149	5 h	5 days (24 °C)	c
t.17							

<sup>a</sup>per 100 parts by weight; for an epoxy resin with an epoxide equivalent of 180–190

<sup>b</sup>Five hundred gram per batch; with a bisphenol A-epichlorohydrin derived epoxy resin with an epoxide equivalent of 180–190

<sup>c</sup>Highly dependent on concentration

t.1 **Table 14** Catalysts and reaction catalyzed

t.2	Catalyst	Reaction catalyzed
t.3	Base	
t.4	Tris (dimethylaminomethyl phenol) (and its tri-2 ethylhexanoic acid salt)	Epoxy/polyamide, epoxy/polyamine, epoxy/novolac, epoxy/polysulfide, epoxy/epoxy
t.5	Dimethylaminomethyl phenol	Epoxy/polyamide or polyamine, epoxy/novolac, epoxy/polysulfide, epoxy/epoxy
t.6	Diazabicycoundecene and its ethyl hexanoic salt	Epoxy/novolac, epoxy/anhydrides
t.7	Nonyl phenol, phenol	Epoxy/polyamide, epoxy/polyamine
t.8	Benzyl dimethylamine	Epoxy/polyamide
t.9	1-Propylimidazole, 2-methylimidazole	Epoxy/epoxy, epoxy/dicyandiamide, epoxy/anhydride
t.10	2-Ethyl-4-methyl imidazole and derivatives	
t.10	Triethylene diamine	Epoxy/epoxy, epoxy/novolac, epoxy/amine, epoxy/acrylic, epoxy/polyester, isocyanate/hydroxyl (polyesters and acrylics)
t.11	Quaternary bases (benzyltrimethylammonium chloride)	Epoxy/dicyandiamide, epoxy/anhydride, epoxy/phenol
t.12	Acid	
t.13	Paratoluene sulfonic acid (and its morpholine salt)	Epoxy/amino, epoxy/phenolic resole, alkyd/amino
t.14	Phosphoric acid	Epoxy/amino, epoxy/phenolic resole, alkyd/amino
t.15	Butyl phosphoric acid	Epoxy/amino, epoxy/phenolic resole, alkyd/amino
t.16	Acid ethyl phosphate	Epoxy/amino, epoxy/phenolic resole, alkyd/amino
t.17	Boron trifluoride monoethylamine	Epoxy/epoxy, epoxy/anhydride
t.18	Salicylic acid	Epoxy/amine (particularly cycloaliphatic and aromatic amines)
t.19	Metallics	
t.20	Dibutyl tin dilaurate	Isocyanate/hydroxyl
t.21	Cobalt naphthenate, octoate systems, etc.	Isocyanate (aromatic)/hydroxyl, oxidizing, vinyl ester, acrylated epoxies and acrylated urethanes, silicone/silicone, polyester/polyester, cyanate ester trimerization, cyanate ester/epoxy
t.22	Tin naphthenate, octoate, etc.	Isocyanate/hydroxyl
t.23	Zinc naphthenate, octoate systems, etc.	Isocyanate (aromatic)/hydroxyl, oxidizing, cyanate ester trimerization, silicone/silicone, cyanate ester/epoxy
t.24	Manganese naphthenate, octoate, etc.	Isocyanate/hydroxyl, oxidizing system, cyanate ester trimerization, silicone/silicone, cyanate ester/epoxy
t.25	Zirconium naphthenate, octoate, etc.	Isocyanate/hydroxyl, oxidizing system
t.26	Acetylacetonates of aluminum, chromium, iron, cobalt, copper acetylacetonates of zinc, copper, iron	Polyester, vinyl ester and acrylate polymerization and crosslinking, epoxy/epoxy

(continued)

**t.27 Table 14** (continued)

t.28	Catalyst	Reaction catalyzed
		vinyl ester (catalyzed with metallics) urethane reactions
t.27	Acetylacetonates of zinc	Trimerization of nitriles, epoxy/cyanate ester
t.28	Acetylacetonates of aluminum, copper, vanadium	Esterification reactions
t.29	Peroxides (as initiators)	
t.30	Methyl ethyl ketone peroxide	Polyester/polyester, vinyl ester, acrylated epoxies and urethanes (catalyzed with metallics)
t.31	Cumene peroxide Acetylacetonates of zinc, copper, iron	Polyester/polyester acrylated epoxies and urethanes, vinyl ester (catalyzed with metallics)

increasing tack, modifying electrical and thermal conductivity, etc. To meet specific requirements, the selection of a primary resin and its minor components is very important. Understanding the chemical composition of an adhesive or sealant is very useful to R&D centers, suppliers, and customers of the adhesives.

## References

- ASTM D907–08b (2008) Standard terminology of adhesives. ASTM International, West Conshohocken
- Bellus D (1971) Photo-fries rearrangement and related photochemical [1,j] -shifts (j = 3, 5, 7) of carbonyl and sulfonyl groups. *Adv Photochem* 8:109
- Chew MYL (2003) The effects of some chemical components of polyurethane sealants on their resistance against hot water. *Build Environ* 38(12):1381
- Cognard P (2005) Adhesives and sealants: basic concepts and high tech bonding. Elsevier, Oxford
- DIN EN 971-1 (1996) Paints and varnishes – terms and definitions for coating materials – part 1: general terms; trilingual version EN 971–1. German Institute for Standardization, Berlin
- Dostal CA (1990) Engineered materials handbook: adhesives and sealants, vol III. ASM International Handbook Committee, Materials Park
- Goh CF, Yu H, Yong SS, Mhaisalkar SG, Boey FYC, Teo PS (2006) The effect of annealing on the morphologies and conductivities of sub-micrometer sized nickel particles used for electrically conductive adhesive. *Thin Solid Film* 504(1-2):416
- Goldschmidt A, Streitberger HJ (2007) BASF handbook on basics of coatings technology, 2nd edn. Vincentz Network, Hannover
- Hare CH (1994) Protective coatings: fundamentals of chemistry and composition. Technology Publishing, Pittsburgh
- Hsiao KT, Alms J, Advani SG (2003) Use of epoxy/multiwalled carbon nanotubes as adhesives to join graphite fibre reinforced polymer composites. *Nanotechnology* 14(7):791
- Jong L (2007) Use of epoxy/multiwalled carbon nanotubes as adhesives to join graphite fibre reinforced polymer composites. *Compos Part A* 38(2):252
- Kahraman R, Al-Harathi M (2005) Moisture diffusion into aluminum powder-filled epoxy adhesive in sodium chloride solutions. *Int J Adhes Adhes* 25(4):337

- 398 Kahraman R, Sunar M, Yilbas B (2008) Influence of adhesive thickness and filler content on the  
399 mechanical performance of aluminum single-lap joints bonded with aluminum powder filled  
400 epoxy adhesive. *J Mater Process Technol* 205(1–3):183
- 401 Lee BH, Kim HJ (2006) Influence of isocyanate type of acrylated urethane oligomer and of  
402 additives on weathering of UV-cured film. *Polym Degrad Stabil* 91:1025
- 403 LeSota S (1995) *Coatings encyclopedic dictionary*. Federation of Societies for Coatings Technol-  
404 ogy, Blue Bell
- 405 Lin W, Xi X, Yu C (2009) Research of silver plating nano-graphite filled conductive adhesive.  
406 *Synth Metals* 159(7–8):619
- 407 Maji PK, Guchhait PK, Bhowmick AK (2009) Effect of nanoclays on physico-mechanical proper-  
408 ties and adhesion of polyester-based polyurethane nanocomposites: structure–property correla-  
409 tions. *J Mater Sci* 44(21):5861
- 410 Novák I, Krupa I, Chodák I (2004) Electroconductive adhesives based on epoxy and polyurethane  
411 resins filled with silver-coated inorganic fillers. *Synth Metals* 144(1):13
- 412 Osman MA, Mittal V, Morbidelli M, Suter UW (2003) Polyurethane adhesive nanocomposites as  
413 gas permeation barrier. *Macromolecules* 36(26):9851
- 414 Park YJ, Kim HJ, Rafailovich M, Sokolov J (2003) Viscoelastic properties and lap shear strength of  
415 EVA/aromatic hydrocarbon resins as hot-melt adhesives. *J Adhes Sci Technol* 17(13):1831
- 416 Park YJ, Joo HS, Kim HJ, Lee YK (2006) Adhesion and rheological properties of EVA-based  
417 hot-melt adhesives. *Int J Adhes Adhes* 26(8):571
- 418 Park YJ, Lim DH, Kim HJ, Park DS, Sung IK (2009) UV- and thermal-curing behaviors of dual-  
419 curable adhesives based on epoxy acrylate oligomers. *Int J Adhes Adhes* 29(7):710
- 420 Petrie EM (2000) *Handbook of adhesives and sealant*. McGraw-Hill, New York
- 421 Petrie EM (2008) Methods for improving electrically and thermally conductive adhesives. *Met*  
422 *Finish* 3:40
- 423 Satas D (1999) *Handbook of pressure sensitive adhesion technology*, 3rd edn. Satas & Associates,  
424 Warwick
- 425 Stoye D, Freitag W (1998) *Paint, coatings and solvents*, 2nd edn. Wiley, Weinheim
- 426 Tracton AA (2007) *Coatings materials and surface coatings*. CRC, Boca Raton
- 427 Wan Y, Xiong C, Yu J, Wen D (2005) Effect of processing parameters on electrical resistivity and  
428 thermo-sensitive properties of carbon-black/styrene–butadiene–rubber composite membranes.  
429 *Comp Sci Technol* 65(11–12):1769
- 430 Zhao HS, Liang TX, Liu B (2007) Synthesis and properties of copper conductive adhesives  
431 modified by SiO<sub>2</sub> nanoparticles. *Int J Adhes Adhes* 27(6):429
- 432 Zweifel H (2004) *Plastics additives handbook*, 5th edn. HANSER, Munich

Eric Papon

**Contents**

14.1	Introduction .....	346
14.2	Systematic Classification of Adhesives .....	347
14.3	Adhesives Implemented Via a Physical Process .....	350
14.3.1	Liquid-Phase Adhesives .....	350
14.3.2	Solid Phase Adhesives: Hot-Melts .....	356
14.4	Adhesives Implemented Via a Chemical Bonding .....	357
14.4.1	General Principles Underlying the Use of AICPs .....	358
14.4.2	Step-Growth Polymerization AICPs .....	359
14.4.3	Chain Polymerization Adhesives .....	366
14.5	Pressure-Sensitive Adhesives – PSAs .....	369
14.6	Conclusion .....	369
Appendix	.....	371
References	.....	371

**Abstract**

Adhesive bonding, which addresses applications in an ever-growing number of industrial, handicraft and service sectors, does not exist as a specific research activity in its own right. Every user of bonding technology – from surgeon and handyman to car manufacturer and aeronautical launch vehicle designer – has specific needs, especially in the area of adhesives. In order to answer to these needs, suppliers are diversifying and extending their product ranges in terms of conditioning and bonding processes. This results in some very difficult choices, making it necessary to have at one's disposal “navigational tools” in an extremely complex network (Fabris and Knauss 1990; Pocius 2002). Because the basis of adhesive formulation is inevitably macromolecular in nature, polymer science is

E. Papon (✉)

Laboratoire des Polymères Organiques – UMR CNRS 5629, University of Bordeaux,  
Pessac, Francee-mail: [papon@enscpb.fr](mailto:papon@enscpb.fr); [eric.papon@u-bordeaux.fr](mailto:eric.papon@u-bordeaux.fr)



likely to shed valuable light in this area. By using our knowledge of the principles underlying these formulations, and also the basic physical chemistry rules that apply, we can establish a general classification system, allowing us to direct our decision-making processes toward those product “classes” best suited to each specific application. On this basis, adhesives can be presented according to the following main discussion:

- The basic rules to establish a classification system based on the process used to achieve the transformation of an adhesive into a bonded joint.
- The main characteristics of adhesives for which the transformation is based on a physical phenomena.
- The main characteristics of adhesives for which the transformation is based on a chemical process.
- The main properties of adhesives used as Pressure-Sensitive Adhesives.

---

## 14.1 Introduction

Adhesives can be classified according to their areas of application, the nature of the materials that need bonding or the physical state at the time of application. However, none of these classifications allow commercial products to be adapted to specific applications or studies, nor do they enable us to determine the optimum conditions or limitations when using these products. To achieve these additional stages, we need to understand the physical and chemical behavior of the raw materials used as base components of these adhesives and to take an active interest in major developments regarding their formulation. Indeed, the raw materials are responsible for the general adhesive and cohesive properties of the bonded joints, while the “art” of adhesive formulation helps to find the most diverse potential applications possible for products prepared using these raw materials.

An adhesive (or a glue, both terms are used interchangeably, except by certain suppliers, who use the term “adhesive” exclusively for tape, labels, dressings and other types of auto-adhesive film) is a chemical substance used to join materials (substrates), either identical or different, by their surfaces. The key part of the adhesive assembly is the joint, a thin region (rarely more than 50  $\mu\text{m}$  thick) characterized by its cohesion and by its adherence to the substrates. This represents an interface phenomenon, although interactions normally occur within very thin hybrid areas (interphase) (typically less than 10  $\text{nm}$  thick). The very high surface to thickness ratio of the joints distinguishes adhesives from sealants for binders, products of a similar nature, but which are used in significant quantities with the filling of cracks or cavities as an end goal.

Certain adhesives, used to join substrates with a high degree of mechanical resistance, are able to ensure over potentially long periods of time, the survival of the joints, described as structural, under normal conditions of use while exposed to relatively high degrees of stress. Contrary to certain statements made, the minimum level mechanical strength is not quantifiable, if for no other reason than it would

mean having to quantify the amounts involved, the condition of the surface of the substrates, the temperature, etc., indeed all the parameters that determine whether a joint will “hold” or “not hold.” Of more interest is the observation that a structural joint is only able to fulfill its role if it is, itself, mechanically strong and therefore if it is a material with a three-dimensional structure. On the other hand, softer adhesives can be used with the aim to be more or less easily removed from one of the substrates after a certain time, depending on the application.

The multiple physical, rheological, mechanical, and chemical abilities that we demand of adhesives and glued joints can be boiled down to two essential characteristics: adhesion and cohesion.

Adhesion describes the ability of an adhesive to establish and maintain interactions with the substrates. This property corresponds mainly to wetting tendency, which describes how a liquid spreads spontaneously on the surface of a substrate. The laws of thermodynamics describe the wetting of surfaces, but the crucial practical condition for an adhesive to spread on a surface is that it should be in a sufficiently fluid state at the time it is applied. In terms of this concept, the adhesive behave like a liquid.

Although the idea of morphological stability of the assemblies is easier to picture in the case of structural bonding, the need for sufficient cohesion of the joint is, in the same way as the fluidity of the adhesive, a simple question of common sense. This cohesion determines the ability of the joint to contribute effectively to the solidity of the assembly (although liquids, water, for example, are capable of developing strong interactions with many substrates, it is impossible to imagine creating assemblies with them that would present any degree of solidity). In terms of this concept, the joint is a solid. But it is not, however, just any type of solid. It cannot, for example, be a crystalline system since the joint must not be anisotropic. In fact, we generally require that the joint provides the assembly with a minimum degree of flexibility or, at least, of reversible deformability (in order to endure the constraints relating to the differences in size variation of the assembled materials, to absorb the vibrations, to resist to “fatigue,” etc.). The joint should be capable, to a greater or lesser extent, of visco-elastic dissipation of the energy resulting from the stresses to which the assembly is subjected. To this end, it can only be a polymer, either linear (more or less rigid thermoplastic), or three-dimensional (chemically cross-linked, vulcanized, etc. ...).

---

## 14.2 Systematic Classification of Adhesives

The two contradictory requirements – adhesive applied in sufficiently fluid state and joint consisting of a solid visco-elastic state polymer – provides the basis for a classification into three broad groups:

- Adhesives where the polymer is preexisting (and must be placed beforehand in fluid form: solution, emulsion, or “melt” state).

- Adhesives where the polymer is formed during the course of a reactive process, polymerization, at the time as the bonding process itself.
- The particular category of Pressure-Sensitive Adhesives (PSA's) where the polymer exhibit visco-elastic properties able to develop adhesion during the bonding step as well as cohesion to resist to the debonding. No physical or chemical transformation of the adhesive is required to form the bonded joint.

Generally speaking, the polymers belonging to the first group are soluble in various solvents are dispersible in non-solvents or are liable to become fluid at a variable raised temperature. As a result, these are linear polymers, and these rarely produce highly cohesive materials. On the other hand, in the second group, the need to undertake polymerization processes based on monomer or oligomer precursors means mainly that three-dimensional lattices are produced, which in theory are highly cohesive and are capable of withstanding severe mechanical constraints. Therefore, structural bonding adhesives tend to come mostly from this group. Finally, adhesives from the third group exhibit a visco-elastic behavior that answers to the PSA's criteria (Creton and Fabre 2002).

According to the proposed classification, the classes from the first group of adhesives can be distinguished by the way in which the polymer is returned to a solid state (evaporation of the solvent, water diffusion, cooling): we therefore talk about Adhesives Implemented via a Physical Process (AIPPs). In the second group, the distinction tends to be according to the way in which the polymerization or cross-linking process occurs, and we talk about Adhesives Implemented via a Chemical Process (AICPs) (Fig. 1).

A third group is distinguished by the fact that the polymer exhibit particular visco-elastic properties able to develop adhesion during the bonding step as well as cohesion to resist to the debonding: we talk about Pressure-Sensitive Adhesives (PSA's) in that case. The Fig. 2 places the main classes of adhesive within either of these three broad groups.

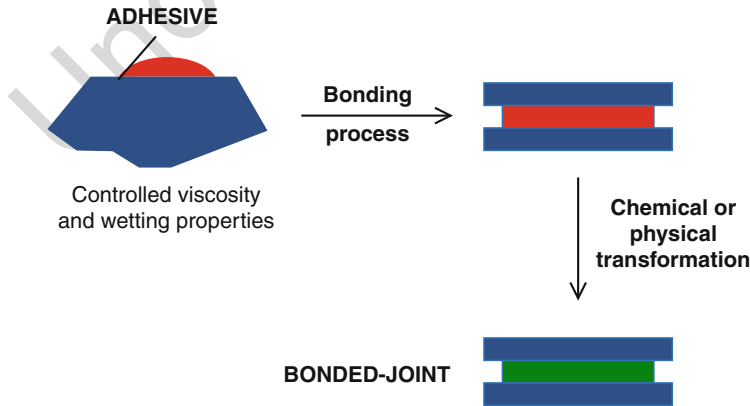


**Fig. 1** Main route to implement adhesives

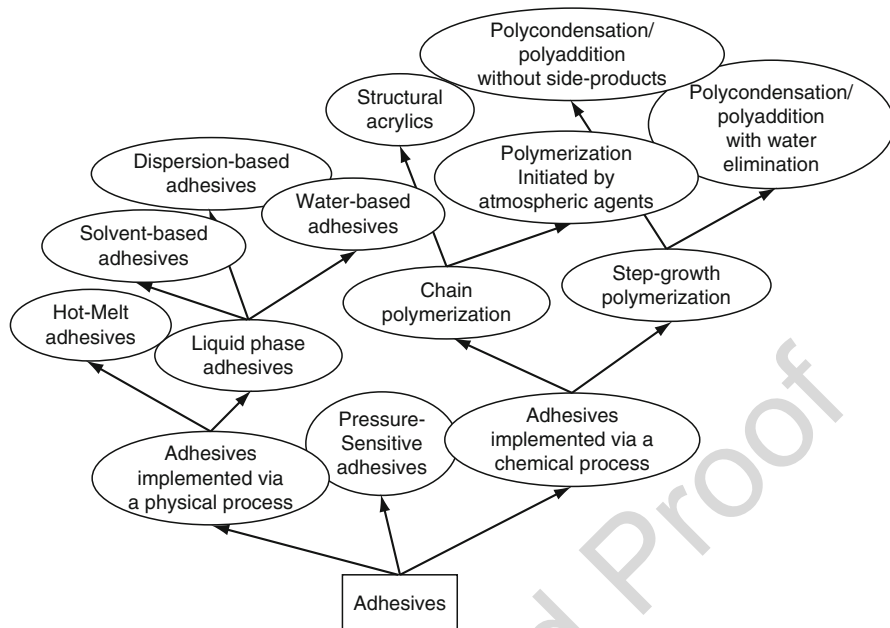


**Fig. 2** Adhesive “zoology”

Remark on the adhesive formulations. When adhesives are applied, the different steps, including preparation of the surfaces, application of the adhesive, assembly, etc., consist of key points, which will determine the quality and the result of the bonding process. The importance of these key points can often be explained by the nature of the formulation of the adhesives itself, with similarities but also significant differences between the three groups.

For both adhesive groups, the nature of the formulation reflects the concern that the products should be adapted as much as possible to the various applications for which they will be used. Across the different adhesive compositions, therefore, one can identify concerns relating to the setting process, to the mechanical behavior of the assemblies and to their durability. These concerns lead manufacturers to combine, with the raw polymer materials (or polymer precursors), various additives (products that mix at the molecular level) and types of filler (non-mixable materials dispersed in various-sized particles, from tens of nanometer to tens of micrometer).

There are numerous formulation rules, often driven by empirically concerns, but the most general one is that the mixture of a macromolecular compound with any additive or filler, regardless of how carefully mixed it is, while able to improve several properties, almost always results in a decrease in cohesion and often a lowering of the level of adhesiveness. This justifies, for theoretical approaches, efforts involving the development, via direct synthesis, of macromolecular systems liable to reproduce the behavior of various types of adhesive formulation. It is this research into models that is able to mobilize all the resources of macromolecular chemistry.

Remark on the comparison between adhesives and sealants. One can consider that even if the main properties of sealants differ from the ones addressed by glued joints the mechanisms involved to create the bonding are the same. Controlled chemistry is needed to reach the best level of interactions and formulations are improved to reach the required visco-elastic properties. The mechanism involved in the building of the joint is mainly based on chemical reactions. Nevertheless, the major difference between sealants and adhesives concerns the properties of the resulting joints that are not only adhesion properties. The fact that (1) the sealant joints are much more thicker than glued joints and that (2) additional properties such as, for example, watertightness or vibration absorbing lead us to separate the sealant family from the adhesive classification.

The “philosophy” behind a description of adhesives via their raw polymer materials differs according to whether the area of interest is AIPPs or AICPs. For the first category, the polymer is present within the adhesive formulation, and the adhesive and cohesive properties must be acquired before being dissolved, being made into an emulsion, or being melted. In that case, research and development is aimed at the development of linear macromolecular compounds, endowed with specific properties. Technically, the preoccupation is in the area of chemical engineering, with the solvent dissolution-evaporation, “emulsification”-coalescence, melting-solidification pairs. In the case of AICPs, the polymer is developed in situ in contact with the surface. Research and development efforts are focused on the precursors and on the types of chemical process. Technically, the crucial aspect is the control of polymerization occurring in undefined reactors, often open, where temperature is not regulated, unstirred, but working in thin films. Each class of adhesive meets certain specifications, and examining these helps to illustrate the influence that a number of elements, constituent or environmental, may have.

In the case of PSA’s, the polymer is formulated with additives such as waxes and plasticizers in order to govern at the same time instantaneous adhesion and visco-elastic dissipation and to satisfy a huge variety of bonding processes and performance requirements.

---

## **14.3 Adhesives Implemented Via a Physical Process**

### **14.3.1 Liquid-Phase Adhesives**

Bonding, achieved using single (coating of one substrate only) or double bonding, the spread (mass of “dry” adhesive per unit area) determines the future thickness of the joint. The speed of bonding is linked to the speed of setting of the adhesives, with the significant parameter being the work time, the period between the “gumming time” (after which the adhesion can occur), and the “open time” (after which cohesion becomes too strong, and negates any possible adhesiveness). The set of tools to deposit the adhesives, drying, the environment, the actions of the operators also play a key role, and it is important to take into account the fact that the behavior of adhesives, AIPPs (but also AICPs), is influenced to a much greater extent by the

technical bonding parameters than by the characteristics of their own base polymers. The storage conditions for the liquid-phase adhesives must obviously ensure airtight packaging (to avoid the evaporation of the solvents or to protect against the effects of humidity) and protect against extremes of temperature (especially damaging to emulsions), but do not differ, for example, for a vinyl polymer-based adhesive versus a polyurethane-based one. As a corollary to storage, the removal from storage (the amount of adhesive required for a single unit of work time) is a general parameter that must be carefully managed.

Packaging can occur in volumes ranging from a few tens of millimeters to several hundreds of liters. They can be prepared in units of production or on the site where they are to be used. But there is one parameter that remains constant that stems from the physical chemistry of polymers: as these have many more non-solvents than solvents, the dilution or the return to solution of an adhesive formulation is a risky process, very often doomed to failure.

### "Water-Based" Adhesives

For the most part, adhesives in aqueous solution are natural products, originating from plants (starches, (Fig. 3) (Kennedy 1987) and other starchy substances), from animals (casein, originating from milk, glycogen, taken from bones, from the skin of fish, etc.), or from minerals (silicates).

These are often forgotten because they have been known about for an "eternity"; they have been replaced by synthetic adhesives for more advanced uses, they are not very "media-friendly" and are not suitable for structural bonding. Nonetheless, they represent the largest quantity of adhesive product currently consumed in the world in terms of tonnage. Aqueous glues are often used to assemble together porous materials (paper, cardboard, plaster, wood (Johnson and Karuke 1985), etc.) through which water can easily diffuse. It is rare for the natural hydrophilic polymers to dissolve completely in water. Instead, it is more likely that the polymers will swell (especially the more ramified among them) or that colloidal dispersion will form. Generally, the result is that compositions said to be thixotropic are obtained (do not flow when not exposed to shearing stress), which can justify the use of hydrophilic polymers as thickening agents.

**Fig. 3** Macromolecular structure of starch

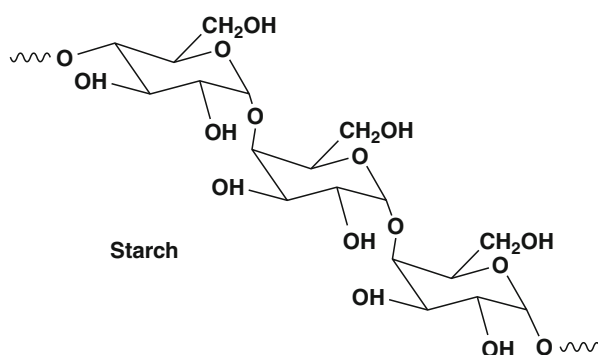
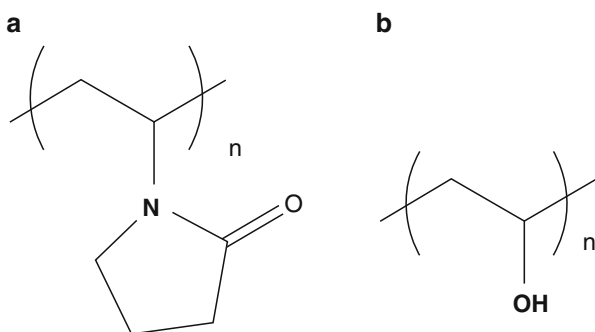


**Fig. 4** Chemical structure of polyvinylpyrrolidone (**a**) and polyvinyl alcohol (**b**)



There are also synthetic polymers that are soluble in water or highly hydrophilic: polyvinylpyrrolidone (Fig. 4a), polyvinyl alcohol (Fig. 4b), polyoxyethylene, etc.

As with their natural counterparts, these are important constituents of adhesive formulations used in the presence of water, for example in the paramedical field (Tan and Pfister 1999); it is these substances that make adhesion to humid surfaces, especially the skin, possible.

In spite of its value in terms of safety, toxicity and environment, water is not a very useful adhesive formulation solvent. During the bonding process, it can favor the establishment of interactions with certain substrates, thus depositing itself at their surface and forming layers with no cohesion. In terms of bonding, the water can accumulate near the polar groups of the polymer joints, weakening their adhesive interactions and their cohesion and potentially leading in the long term to their deterioration through hydrolysis.

Porous substrates (paper, cardboard, wood, plaster, etc.) allow the total elimination of water in the formulations, through diffusion. These are the materials that are best suited to water-based formulations. With substrates that are non-permeable to water (hydrophobic polymer films, metals, etc.), water evaporation is the only solution, but it is difficult to ensure that it is achieved completely, due especially to the very strong interactions that occur between the water and the adhesives' polar groups. Optimized formulations, with high "dry matter rates" (60%, even 70% or 75%), as well as specially developed applicator equipment (hot air drying tunnels, infrared radiation, microwave radiation, etc.) are designed to solve this problem.

The absorption of humidity by the joints is one of the main causes of ageing, physically to begin with, often involving the elimination of the plasticizers and other additives or impurities, and possibly chemically as well, with hydrolysis phenomena. This suggests that controlling the reduction in adhesive properties, an active area of research and development across many industries could be achieved through a regulated absorption of humidity.

### "Solvent-Based" Adhesives

A number of linear polymers are soluble in organic solvents that are able to be eliminated rapidly (through evaporation) after the adhesive has been deposited. This

**Fig. 5** Chemical structure of poly( $\beta$ -pinene)

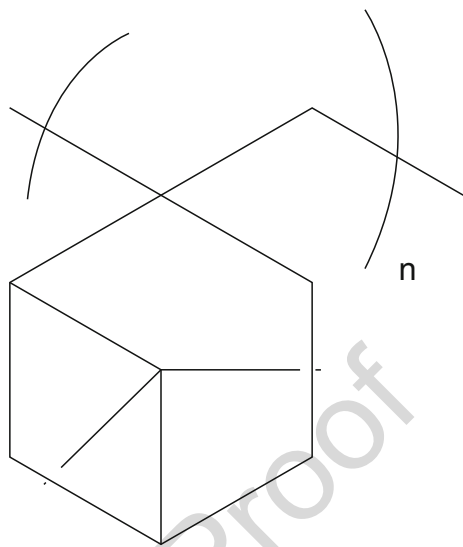
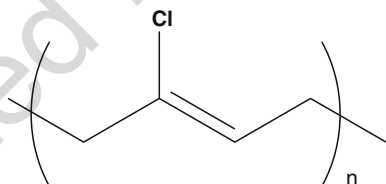


**Fig. 6** Chemical structure of polychloroprene



is the case, for example, for poly( $\beta$ -pinene) (Fig. 5) which, dissolved in methyl ethyl ketone, has for a long time been the basis of “universal glues” (Scotch<sup>®</sup> by 3 M).

The most typical “adhesive solvents” are those based on elastomers, compounds characterized by the fact that they have a strong natural adhesiveness, especially in respect of themselves (the phenomenon of self-adhesion, the instantaneous adhesion of two films of glue after almost total evaporation of the solvent, is the basis for the composition of the “contact glues” especially neoprene-based (Fletcher 1971)). The basic chemical composition of neoprene synthetic rubber is polychloroprene (Fig. 6). The polymer structure can be modified by copolymerizing chloroprene with, for example, 2,3-dichloro-1,3-butadiene to yield a family of materials with a broad range of chemical and physical properties.

They also produce highly flexible joints, providing excellent resistance to peeling. In general terms, the elastomers only display their elastic properties after having been vulcanized. In the case of polydienes, especially (polybutadiene, polyisoprene, neoprene, styrene-butadiene copolymers (Stricharczuk and Wright 1977), etc.), vulcanization occurs spontaneously on contact with the oxygen in the air as a result of a radical-based process or on contact with vulcanizing agents such as sulfurs or phenols.



**Fig. 7** Nano-organization of semicrystalline thermoplastic elastomer

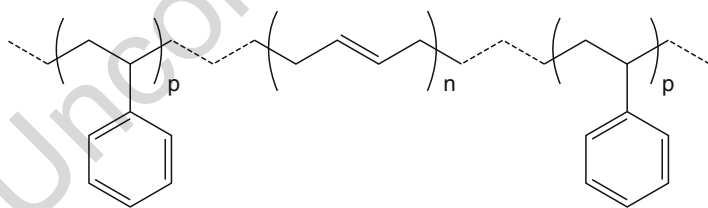
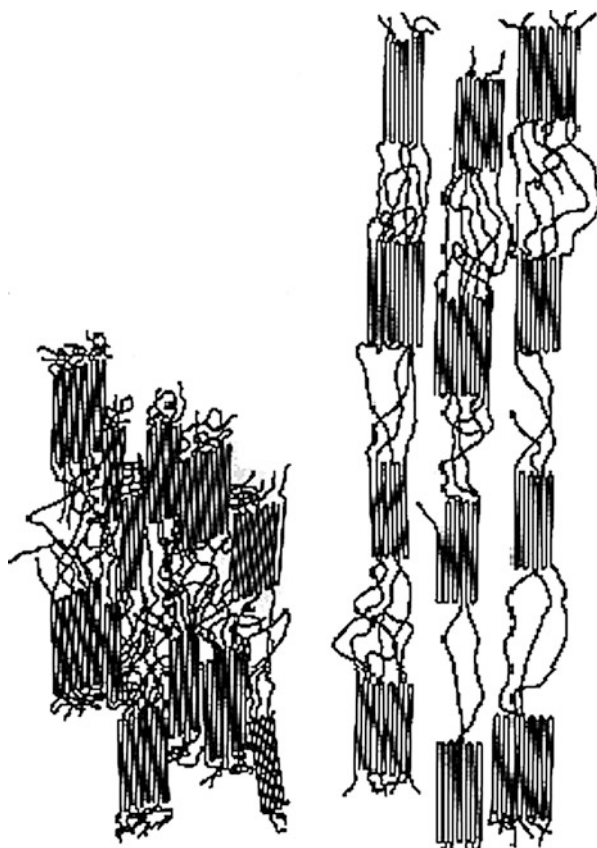


**Fig. 8** Chemical structure of poly(styrene- b-butadiene- b-styrene)

The thermoplastic elastomers (Legge et al. 1987) have the advantage that no vulcanization is required since the cross-linking points are provided by the thermoplastic micro-domains (in the order of 20–40, up to more than 500 nm in diameter), formed due to the non-miscibility of the two phases, elastomer and glassy (Fig. 7).

The thermoplastic elastomers, i.e., poly(styrene- b-butadiene- b-styrene): SBS (Fig. 8) and poly(styrene- b-isoprene- b-styrene): SIS. For a long time, the patent

belonging exclusively to SHELL (Holden and Milkovitch 1966) are now produced by various suppliers and have found highly diverse applications as Hot-melt or Pressure-Sensitive adhesives.

The thermoplastic polyurethane elastomers (Chen et al. 1992) exhibit very similar morphologies to that of the SBS or SIS and, similarly to them, allow the characteristics of both phases, crystalline and glassy, to be combined. Polyurethane adhesives can also be classified in the “Adhesives implemented by Chemical Process” category that can induce certain confusion. To be consistent with our classification one must consider that two types of polyurethane-based adhesives can be commercially available: the ones that exhibit semicrystalline properties that can be implemented via a physical process, and the seconds with dormant reactive functions that can react via a chemical process to lead to a network.

Similarly, although most vinyl and acrylic type polymers could be used as the basis of solution adhesives, it would seem more appropriate to describe them as emulsion adhesives. Other polymers (polyesters, polyamides) would seem to be more appropriately categorized within the Hot-Melt adhesive class.

The impact of the organic solvents on the environment (toxicity, flammability, pollution) is now well known. But there are a large number of elastomer-based adhesives that continue to be essential, in such a way that their disappearance, although a reality for applications involving the general public, is not on the agenda in the sector involving self-adhesive products (tapes, films, labels, bandages, skin patches, etc.). The only obligation is to have in place systems for recovering the solvents and, as much as possible, for recycling.

### “Dispersion-Based” Adhesives

In theory, any vinyl polymer that can be obtained through radical polymerization can be prepared directly in emulsion form (Lovell 1997). However, the most common formulations are the polyvinyl acetate and acrylic emulsions.

While the polyvinyl acetate-based emulsions have multiple applications (office glues, wood glues, packaging industry, etc.), the acrylic emulsions are used mainly for the production of auto-adhesive films and tapes or for other labels (see PSAs part); their main value therefore lies in the large variety of formulations accessible (using variable composition copolymers) and in the good tolerance they demonstrate toward the plasticizers present in certain substrates (bonding of polyvinylchloride films for example).

The ability of the water emulsions to resolve the problems of safety and protection of the environment, combined with the inherent problems associated with the use of dispersions, is leading to highly active research, both theoretical and applied. We are now able to master to a greater and greater extent:

- “Core-shell” materials, which are molecular objects combining flexible polymer cores and rigid shells (sometimes the opposite)
- “Micro-encapsulation” of various substances, finely dispersed, in polymer shells
- Emulsion “creaming,” which increases the stability by increasing the viscosity and which aims to increase as much as possible the dry final content

- The emulsification of various polymers, starting from their organic solutions or even in “molten” phase

On the other hand, there is still work to be done regarding:

- The emulsion stability with regard to “flocculation” – the speed of coalescence during application
- The elimination of the water
- The purity of the materials that come from polymers in emulsion
- The cost price, paradoxically much higher than that of corresponding formulations in solution.

Surfactants, which are essential during polymerization in emulsion or for emulsification, can have a very harmful effect on the durability of certain bondings. They illustrate very well the problem caused by the surfactants present in the joints (as well as remains of initiators or transfer agents, photo-sensibilizers, plasticizers, etc., in relatively great proportions: 1% by mass correspond to amounts of the order of 1,000% in terms of molar fraction, which explains the sensitivity of the materials to the presence of such “remaining chemical species”). For the surfactants, the poor performance of bonded joints exposed to the “humid cataplasma” test, which gives a picture of the resistance to ageing through humidity (used particularly in the car industry), significantly limits the development of “exterior” uses for emulsion adhesives. As a result, there is still very active research into the “neutralization” of surfactants in joints (for example, via the use of “surfmers” capable to polymerize).

### 14.3.2 Solid Phase Adhesives: Hot-Melts

For the adhesive to be capable of wetting the surface of the substrates, bonding must occur at a temperature greater than the melting point temperature. Using semicrystalline-based polymers, “Hot-Melt” adhesives are thus developed (Landrock 1985).

The “melting” of certain thermoplastic polymers, which often corresponds to a softening (going beyond the flow threshold) due to the application of heat, is a reversible phenomenon. Thus a solid adhesive mass, deposited using a hot-melt gun, can “set” while cooling down. Three types of compounds are representative of “Hot-Melt” adhesives: the ethylene vinyl acetate (EVA) copolymers (Fig. 9), the polyamides (referred to as “food adhesives”), and the polyesters (tend to be reserved for high temperature applications).

A concern for obtaining bonded assemblies that are resistant to high temperatures, but that remain “modifiable” has led to research aimed at developing more thermostable thermoplastic adhesives. Bonded joints that are reversible at high temperatures have already been obtained with the following types of compounds: polyether ether ketones, polyether sulfones, etc. Melt viscosity, one of the most important properties, influences the spreading of the adhesive and the wetting of the surfaces is

**Fig. 9** Chemical structure of ethylene vinyl acetate (EVA) copolymers

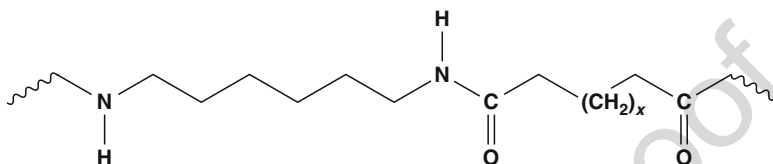
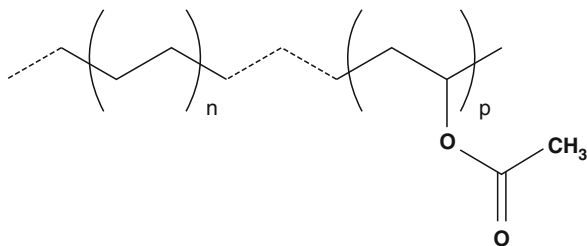


**Fig. 10** Chemical structure of polyamides –  $x$  is the number of methylene units that can affect the viscosity and the melting temperature

governed by the ratio between polar and nonpolar moieties. The design of polyamide (Fig. 10) or polyester backbones may give the appropriate properties: flexibility of the joint as well as low viscosity for an easier spreading.

One major drawback for this adhesive family is the lack of adhesion with the substrates. Generally speaking, one considers that a competition occurred between the maintaining of interfacial interactions that have been created during the bonding step and the developing of inter-macromolecular interactions due to the crystallization during the cooling-down step. This competition improved the lack of adhesion described by users.

## 14.4 Adhesives Implemented Via a Chemical Bonding

Conceptually, the AICPs are polymer precursors. They illustrate well the dichotomy between:

- Adhesive (liquid state and chemical activity in order, on the one hand, to ensure wetting of the substrates [by establishing with them adhesive interactions], and on the other hand to allow the formation of the joint through polymerization)
- Joint (solid state and chemical inertness in order to ensure the mechanical soundness and the durability of the assembly).

Because the synthesis of a linear polymer in situ is not of much value compared to the physical bonding of this same polymer, AICPs are really more three-dimensional network precursors. They are the products that are associated with the idea of structural assembly.

The capacity for the AICPs to wet the substrates is generally not a problem. The questions that arise relate more to the cohesion development processes, through polymerization. The two alternative approaches, step-growth polymerization (condensation or addition processes) and chain-growth polymerization, have to be conducted in an “undefined” reactor, unstirred, open (in contact, except in specific situations, with the air and humidity), without the possibility of recovering and possibly recycling the reagents or the light products, etc. The options available (excluding specific installations) are therefore limited, in the case of step-growth polymerization to total condensation reactions (without the formation of secondary products), preferably self-catalyzing, and in the case of chain-growth polymerization to free-radical chemistry.

Within these limits and as long as the basic rules of macromolecular synthesis are respected, the chemistry of bonding is a process “that works well.” The main reason for this is its nature, involving a thin film process, which allows it to regulate its own temperature (substrates serving as radiators) and which benefits from the very high degree of reactivity of the outer surface of the solids. Surface treatments that consist of grafting short chains with end groups of the same nature as the adhesive’s constituents are excellent ways of organizing this reactivity.

#### 14.4.1 General Principles Underlying the Use of AICPs

The first problem involved in chemical bonding is the competition that exists between adhesion and polymerization, which is caused by the need to initiate the polymerization process, by mixing the reagents, before the coating of the surfaces of the substrates to be assembled. Most of the methods for applying the AICBs aim to respond in the best way possible to the two conflicting imperatives: the creation of interactions strong enough with respect to the needed performance and the building of the polymer backbone. They essentially concern the activation of the reagents in conditions that respect the rules of macromolecular synthesis and that, at the same time, allow any operator to “do chemistry” without knowing it.

#### Polymerization Initiation – Temperature Effects

The processes vary intrinsically in terms of speed. Some can be accelerated, using catalysts. But all of them tend to slow down as they progress due to the decrease in concentration of the reagents and to the significant increase in viscosity (in such a way that the kinetics are often controlled by the diffusion of the reagents, which is very slow). Generally, viscosity and concentrations in the reactive phase cannot be kept constant (except in the case of a joint with a constitution that is completely non-miscible). To compensate for the slowing down process, the polymerizations can be completed by raising the temperature during the “post-curing” cycles (hence the label “thermal hardening”) that is applied to adhesives as well as to polymers. People need to understand how to vary the viscosity, the molar masses of polymer backbones, the cohesion with the rate of polymerization, and the overall percentage of monomer conversion. For that purpose, an interesting approach proposed in the

early 1980s (Guilham 1983) consists in the building of a “phase diagram,” i.e., a simplified time-temperature-transformation TTT diagram, that shows the evolution of  $T_g$  and the visco-elastic behavior versus the time (equivalent to the conversion). The time of gelation can give interesting information on the window in which adhesive is still processable.

### Relative Proportions of the Reagents

For chain-growth polymerizations, the initiators represent only a few fractions of a percentage in comparison with the monomers or prepolymers; it is difficult under these conditions to achieve homogenous mixtures according to target. Other difficulties occur as a result of the presence, at the surface of the substrates, of impurities that can act as inhibitors (acid traces that can improve transfer or termination reactions) or, on the contrary, as accelerators (very fast reaction speeds, which equate to low levels of polymerization, limiting the work time available, in a way that is sometimes highly problematic in the context of industrial applications, and not allowing the formation of joints with satisfactory cohesion). Initiation via electromagnetic radiation (photo-initiation, “ionization” with X-ray or electron beams) allows, in theory, the “adhesive setting” speeds to be managed. But it is not universally applicable for technical reasons (UV initiation is not possible in the case of nontransparent substrates, something that is fairly common), or for combined technical and economical reasons (cost and limited access to installations using ionizing radiation).

For step-growth polymerizations, it is necessary to respect the stoichiometry between the number of reactive functions of each of the two partners, bi- or multifunctional, involved in the reactions following Carother’s assumptions (Carothers 1936); even a slight imbalance leads to the formation of joints that are not properly polymerized, i.e., molar mass not large enough, with poor cohesion. To avoid bonding errors, the “two-part” formulations come in dual body systems that are equipped with static mixers; the two parts have distinct colors, so that a visual check can be made to ensure they are properly mixed. “One-part” systems involve either processes where the initiator or the reagent is an atmospheric agent (oxygen, humidity), or systems where the initiator, the catalyst, or one of the reagents has been hidden (latent initiator in the case of anaerobic adhesives, crystallized polyamine in the case of “high temperature” epoxy adhesives, hidden isocyanates in the case of polyurethane adhesives, etc.). Based on these systems, “pre-impregnated” tapes or tissues are particularly convenient, to the extent that with these, the users are likely to forget fundamental rules of use, for example, the necessity to store the “one-part” formulations at a low temperature ( $-15\text{ }^{\circ}\text{C}$  to  $-18\text{ }^{\circ}\text{C}$ , typically).

### 14.4.2 Step-Growth Polymerization AICPs

These represent the class with the most types of adhesive, for the most part identified with structural assembly products. Two groups can be distinguished, depending on whether the polymerization is accompanied by the formation of water (which needs to be steadily eliminated) or whether it involves the formation of the polymer only.

### Polymerized Adhesives with Elimination of Water

Aminoplasts (urea formol, melamine formol, and MUF: melamine urea formol) and phenoplasts (phenol formol) have been known about for a very long time and are used as binders in pressed wood panels, as adhesives in plywood panels, and as “coating agents” for paper and cloth (Robins 1986). They are characterized by their reasonable cost and, especially, by their excellent performance in extreme temperatures and fire (the aminoplasts are self-extinguishing in air at atmospheric pressure). The production of the polymer lattices occurs in several stages, passing through intermediary stages such as methylolurea or methylolmelamine and, for the phenolic glues, RESOL issued from acidic conditions or NOVOLAC from basic conditions (Fig. 11).

The intermediary stages often constitute the base components of the adhesives, with the subsequent condensation (still associated with the elimination of water

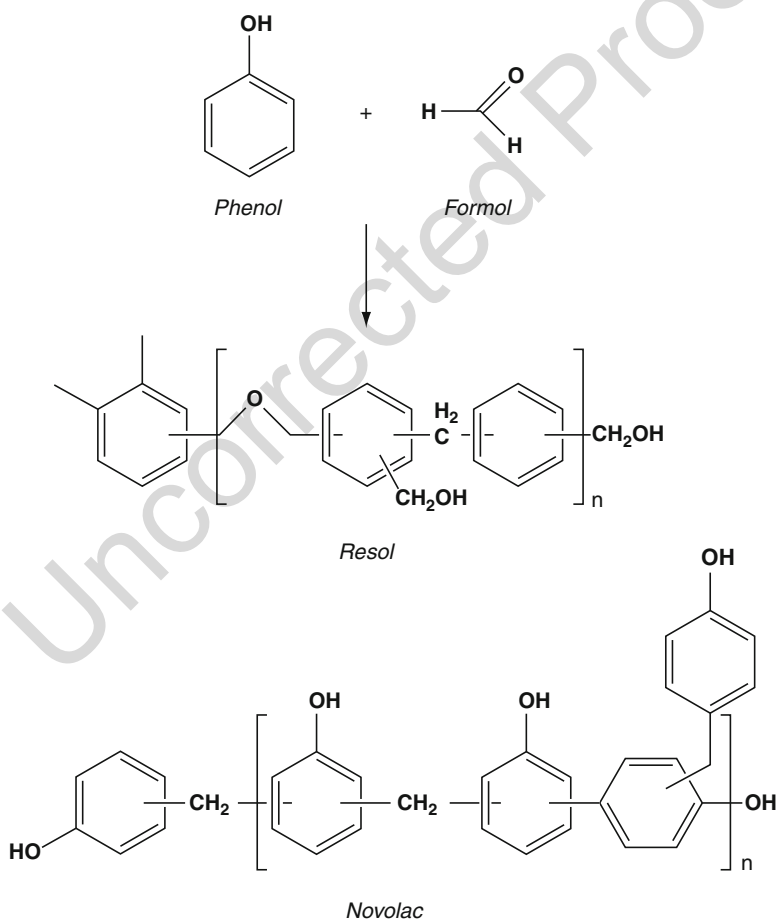
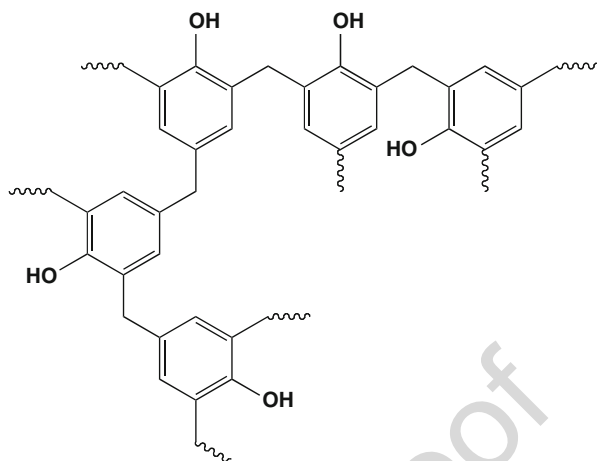


**Fig. 11** Chemical structure of formo-phenolic resin precursors

**Fig. 12** Schematic representation of a formo-phenolic network



at high temperature up to 200 °C), leading to complex three-dimensional networks (Fig. 12).

Having been somewhat eclipsed in the past, the phenolic adhesives are benefiting from renewed interest, which is linked to their heat stability and fire resistant characteristics, as well as to their compatibility with a large number of other polymers. The formo-phenolic precursors are “hybrid adhesive base components of choice that lead to interpenetrated polymer network-type joints (“IPN” epoxy–phenolic) or semi-interpenetrated ones (elastomers–phenolics), characterized by an excellent resistance to shocks, to vibrations and to shearing stresses” (Robins 1986). The characteristics of the phenolic glues means that they can be used in areas where no other adhesive can compete with them: break-pad assemblies, coating of abrasive substances to their support material, assembling of molds in foundries, bonding of surface panels and edges in furniture manufacturing, aeronautical equipment, etc. There are, however, limits to their applications, relating to the difficulties involved in applying them (elimination of water and heating necessary), their unpleasant odor, and their possible toxicity especially the degradation products.

### Full-Condensation Adhesives

These are high performance adhesives, used in small quantities, for “top of the range” applications that are emblematic of structural-based assembly.

#### Epoxy Adhesive (Wright and Mugge 1986)

Most of the epoxies are heat hardening adhesives, where cross-linking achieves high degrees of advancement only after heating (“curing”) at temperatures as high as 200 °C. Their components are more or less complex prepolymer resin-based mixtures, generally fluid, of type DGEBA: diglycidyl ether of bisphenol acetone (condensation product of epichlorohydrine of the glycerol on the hydroxyls of the bisphenol A, itself a condensation product of two molecules of phenol and one molecule of acetone) (Fig. 13).



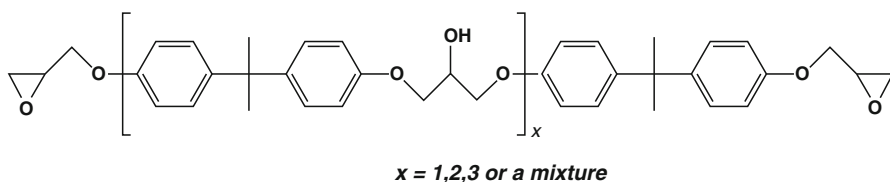


**Fig. 13** Chemical structure of diglycidyl ether of bisphenol A (DGEBA)

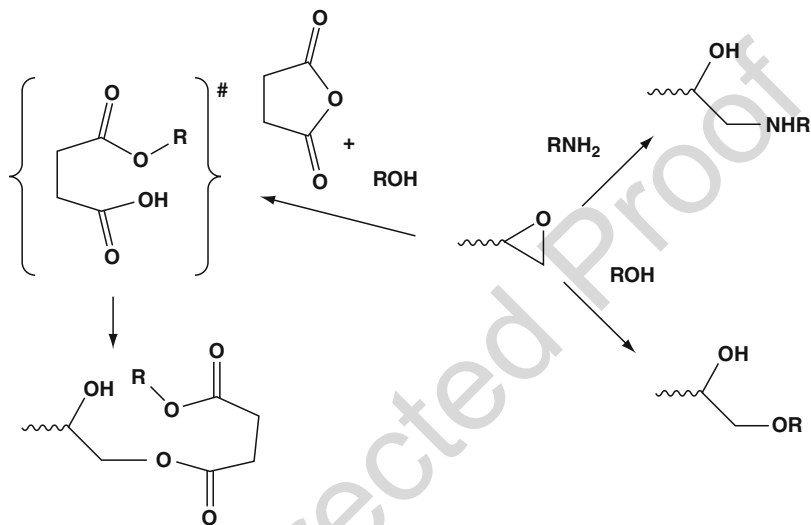


**Fig. 14** Most common chemical reactions involving epoxies: addition of amine ( $\text{RNH}_2$ ), addition of alcohol ( $\text{ROH}$ ), or addition of alcohol in presence of anhydride

The epoxy adhesives produce, with limited contraction, joints whose main characteristic is an absence of creep at high temperatures (mechanical strength is maintained up to temperatures of 100–150 °C). Epoxy groups exhibit a high reactivity with many antagonistic functions, mainly amines, but also alcohols, anhydrides, and carboxylic acids (Fig. 14).

When you add to this quality a high degree of cohesion (linked to the density that the three-dimensional lattice can achieve in the case, for example, of the polyamine-type hardening agents), which allows thick joints to be achieved and therefore the remediation of surface faults, good adhesiveness on a very diverse range of materials (combined with potential reactions of active sites of surfaces with the oxiran groups and with the reconstitution of a polar hydroxyl group each time one of these rings opens) and a great deal of inertness with regard to humidity and to chemical agents, it is understandable that the epoxy adhesives represent the classic structural (and even thermal-structural) adhesive.

For the “low temperature” epoxies (“setting” at between 0 °C and 50 °C), two-part formulations, the hardening agents are di- or polyamines (diethylene-triamine, for example). For the “high temperature” epoxies (“setting” at above 100 °C), one- or two-part formulations, the hardening agents are acid anhydrides (in the presence of tertiary amine catalysts), resols or novolacs (also in the presence of tertiary amine catalysts) or crystallized polyamines, insoluble in the oligomer except after melting (at a high temperature) (Wright and Muggee 1986).

The diversity of the range of epoxy adhesives, linked to a multitude of base constituents, hardening agents, and catalysts available, is increased by the possibility of formulating numerous hybrid adhesives (with the polyamides, the acrylics, the polysulfurs, the phenolic adhesives). You can find suitable epoxy adhesive formulation for virtually any glue-based assembly problem. This applies equally to conducting glues in microelectronics, to high thermal stability adhesives in space construction, and to “for all time” adhesives for the repair of works of art.

The excellent reputation of the epoxy adhesives is justified, and their applications in industry and at home are without question. But they can also be penalized because they are too high quality. Indeed, “indestructible” joints are in contradiction with the present need for recycling of materials, and as a result current research is aimed at finding tools to manage deterioration of the epoxy adhesives, rather than at improving them.

### Thermo-Structural Adhesives

Intended for limited “high performance” applications, the thermal-structural adhesives are the adhesives of the aeronautics and aeroballistics industries, where specifications are expressed in duration of resistance (maintenance of the majority of the mechanical properties) at a determined temperature, such as those decreed by the American Space Agency:

- Between 150 °C and 260 °C: several 1000 h
- Between 260 °C and 320 °C: several 100 h
- Between 320 °C and 350 °C: several tens of hours
- Above 350 °C: between a few hours and a few minutes (1 h at 535 °C; 5 min at 815 °C).

Besides the epoxies and certain phenolic adhesives, some compounds have gone beyond the stage of secret application (polybenzimidazole, polyimides (Fig. 15), polyarylsulfones), but in most cases, the formulations are adapted by the users (secretly in general) to specific problems.

We can, however, note that an adhesive intended for thermal-structural applications has a prepolymer with a thermostable structure as a base component, which will carry chemical functions that will allow its cross-linking (as widely as possible) at a high temperature. The main difficulty involved relates in fact to the small difference in temperature (“processability” range) between the softening of the prepolymers and the cross-linking reaction: typically 30° between 130–160 °C and 160–190 °C.

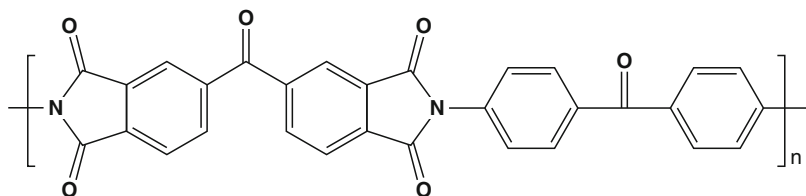


**Fig. 15** Chemical structure of LaRC-TPI (Linear Aromatic Condensation-Thermoplastic Imide) (Bell et al. 1976)

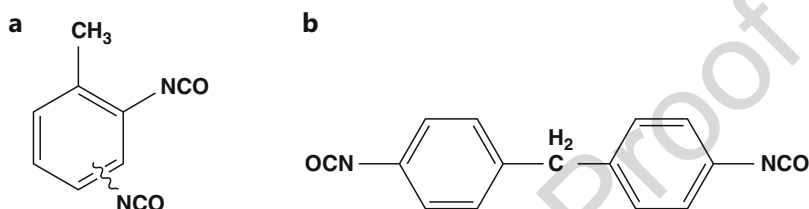


**Fig. 16** Chemical structures of toluene diisocyanate (a) and diphenylmethane diisocyanate (b)

### Polyurethanes (Chen et al. 1992)

Due to its richness and diversity, this class of compounds, that results from the polycondensation of di- or multi-isocyanates and of di- or polyols (of di- or polyamines the case of the polyureas), is one of the hardest to place in a classification. Indeed, polyurethanes are just as much elastomers, presented in solution, possibly in emulsion or in the form of structures that are self cross-linking (through atmospheric humidity), as they are structural adhesives, where the polymer networks are obtained from two-part and one-part formulations (with hidden isocyanate functions).

In the case of the elastomers, formulations that use diisocyanates (Fig. 16) and mixtures of long diols (oligomers of polybutadiene, polycaprolactone, or polyoxyethylene) and short diols lead to thermoplastic elastomer behavior, with physical cross-links (rigid sequences) finding themselves associated, dispersed in micro-domains, with a continuous elastomer phase (flexible sequences).

A certain degree of cross-linking can be obtained by using oligomers or triol-like extenders, but the three-dimensional polyurethanes tend rather to be produced in situ from formulations with two parts: prepolymers diisocyanate-diol oligomer (average degree of polymerization that does not exceed 3–5 with isocyanate chain ends) firstly, and secondly, primary diamine-type chain extender. The high degree of reactivity of the amine functions (and also the amide) with the isocyanates allows cross-linking to occur in short periods of time. In the presence of humidity, the diisocyanate-diol oligomers can be used as one-part formulations. Indeed, the action of water gives carbamic acid that decarboxylises spontaneously into primary amine, which reacts immediately with isocyanate groups (faster reaction than that involving water) causing the cross-linking (Fig. 17).

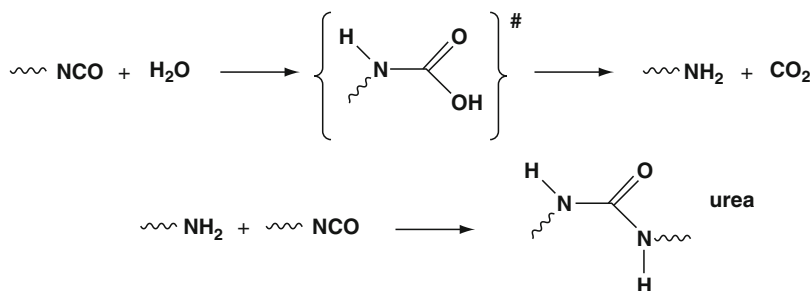


**Fig. 17** Schematic representation of the reaction of isocyanate groups with water

One-part polyurethane adhesives can also correspond to prepolymers with isocyanate functions blocked reversibly (due to reaction with oximes, phenols, etc.). The isocyanate groups are then regenerated, either by heating to a more or less high temperature, or by substitution of the blocking agent by a diol (oligomer, at least partly) (Fig. 18).

The reactivity of water with isocyanate functions, used to produce polyurethane foams (“foaming” from released  $\text{CO}_2$ ), can be a real disadvantage for the adhesive formulations since the reactions with water are in competition with the reactions with diols leading to poor performing joints due to an incomplete polymerization.

### Polymerization Through the Action of Atmospheric Agents

The cross-linking of the polyurethane prepolymers through the action of humidity is an example of adhesive – joint chemical transformation where one of the reagents involved is an atmospheric agent (Fig. 17). Another example involves the silicone adhesives, where water plays a catalytic-type role (in the sense that it is permanently regenerated).

### Silicone Adhesives (Owen 2004)

Due to their very weak surface energy, which allows them to completely wet virtually all substrates, but which then prevents their own wetting by virtually all the adhesives, the silicones are considered, rightly, to be anti-adhesion agents; they are often used as mold release agents. But silicon-based formulations are also used, increasingly, as specific adhesives, especially for applications requiring good performance at a high temperature (oven door windows) and as sealing agents (headlamp assemblies for the car industry). Vulcanization occurs through the action of humidity for the “one-part” formulations, with polydimethylsiloxane oligomer carrying hydrolysable end groups as base components. Hydrolysis releases the “blocking” group, explaining, for example, the release of acetic acid that is characteristic of certain formulations. The spontaneous dehydration of the silanol groups causes the cross-linking while, at the same time, regenerating the water necessary for the hydrolysis of new groups (Fig. 19). The process then carries on gradually.

Cross-linking, at high temperature, of the “two-part” formulations is not related in any way to the action of humidity. The basic process is an addition on an

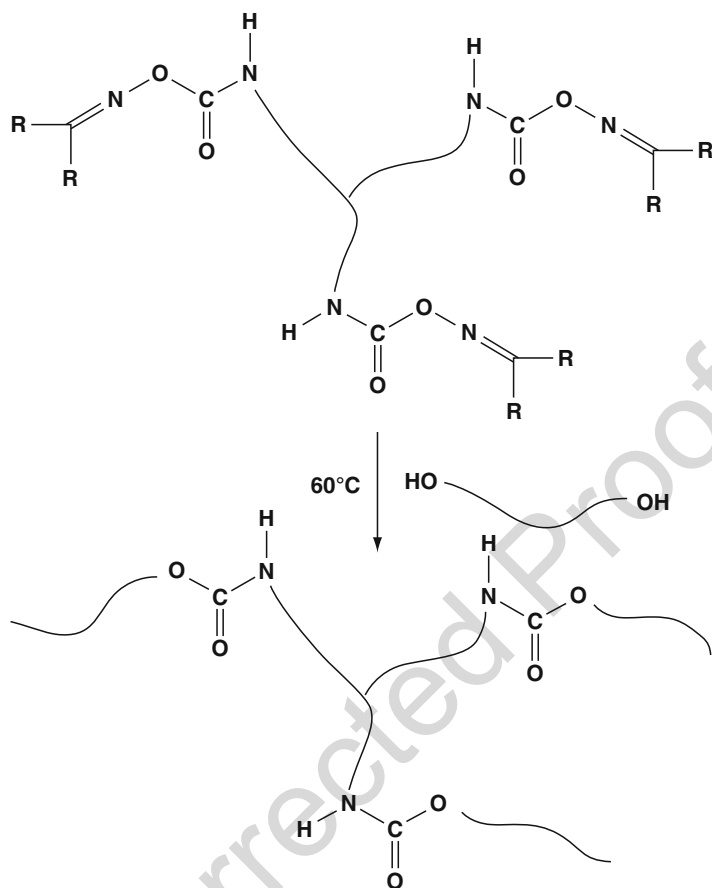


**Fig. 18** Mechanism of deprotection of oxime-functionalized polyurethanes

unsaturated site, which depends on the presence of catalysts. This leads to formulations that are difficult to use, and there is a tendency to replace these with silicone-acrylate type adhesives (polydimethylsiloxanes  $\alpha,\omega$ -acrylate), just as effective but easier to use. The problems associated with use do not arise with the humidity cross-linking formulations. But with these formulations, the operating conditions are neither easy to master (too much water can have a very negative effect), nor are they conveniently reproducible.

#### 14.4.3 Chain Polymerization Adhesives

The typical image of the “polymerizable” adhesives is provided by the structural acrylic adhesives, which include several classes, but which are all bi- or multi-acrylic monomer based.

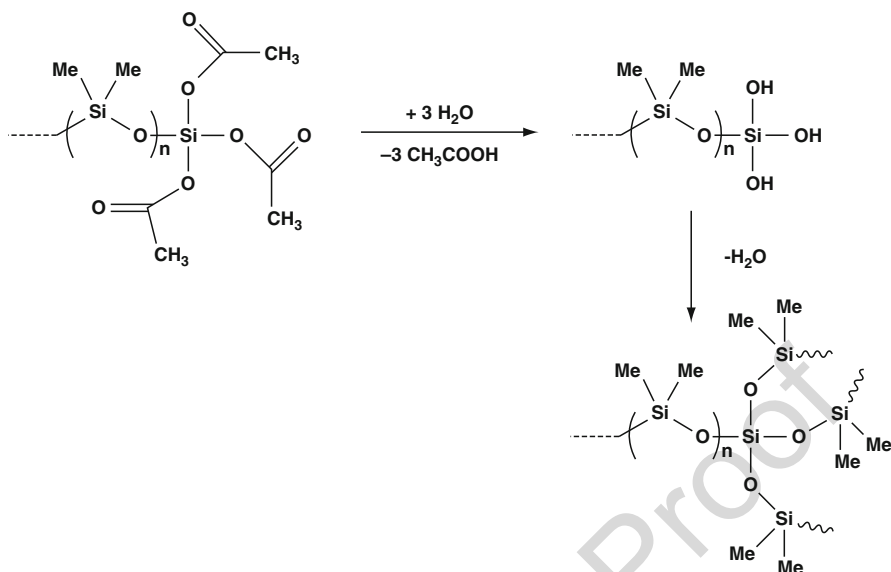


**Fig. 19** Schematic representation of cross-linking reactions of polydimethylsiloxanes

### “Structural” Acrylics

The chemical reaction leading to the joint is a radical polymerization, initiated by a peroxide (or an azonitrile) or, when it is possible, by electromagnetic radiation (polymerization under UV, polymerization under radiation, etc.). In the second case, the formulations, one-part type adhesives, do not pose any storage problems (stable in the absence of the initiator) and are easy to use (presentation as liquids, pastes, impregnated films, etc.). In the case of the chemical initiation, the formulations are two-part-type adhesives, the dissymmetry between the quantities is mitigated by mixing the initiator together with the additives and fillers (copolymers acrylate-methacrylate, notably). In this case as well, it is easy to use.

Flexibility of use is a major benefit of the acrylic adhesives in applications such as structural assembly. It allows them to be applied to a very diverse range of materials, in difficult climatic conditions (bonding in water or repairing concrete structures in winter). Performances (sufficient mechanical strength and flexibility) are similar to that of the epoxy formulations, especially since the appearance of the second generation structural acrylic adhesives: hybrids consisting of elastomer nodules distributed throughout the acrylic network. Compatibility is thus ensured by a grafting of the polymethacrylate chains on to the elastomer chains, achieved in situ by using a solution of elastomer in the monomer.

### Bonded Joints Obtained by the Action of Atmospheric Agents

Oxygen in the air, whether in combination with light or not, is capable of causing cross-linking of certain elastomers (dienic polymers and copolymers with residual

double-bonds). Similarly, the polysulfur type adhesives (“thiokols”) are vulcanized by oxygen. However, in both cases, the processes cannot be controlled and no optimization is possible. The situation is different with the particular acrylic formulations made up of the cyanoacrylate adhesives and the anaerobic adhesives.

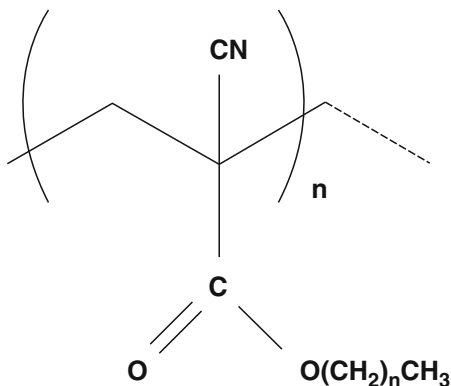
### Alkyl Cyanoacrylate Type Adhesives

The electron depletion of the site unsaturated by the nitrile and carboxyl groups is such that a process of anionic polymerization can be initiated, at room temperature, simply by traces of humidity (Fig. 20).

Polymerization then occurs very quickly, requiring that major precautions must be observed when this type of adhesive is applied (instant adhesion to the moist skin, but polymerization can be prevented from occurring by immersing in water). The adhesive power of the cyanoacrylates is very strong, although their cohesion is weak (they are linear polymers); this implies that bondings should be done using the thinnest films possible. Under these conditions, almost all materials can be bonded; the assemblies are strong, but they are sensitive to shocks (they can be made more flexible by combining ethyl and butyl cyanoacrylates with methyl cyanoacrylate, the base component of the formulations) as well as ageing under the effect of humidity.

The use of cyanoacrylates does not pose any sensitive problems, whether in automated industrial applications, that use formulations which are often very fluid, or in “household” applications, for which there are more and more gels with slightly longer “setting” times. However, the use of the cyanoacrylates requires, more than that of any other type of adhesive, the understanding of a few principles of chemistry. Thus, the application of cyanoacrylate glues on to “activated” metals or cleansed of fatty residues using PLASMA, LASER, or CORONA treatments (the effect of all of which is to completely dry the surfaces) leads to failures, often not properly explained. The same thing is true for bonding attempts on surfaces that have undergone “acid” treatments before the bonding step, since the anionic polymerization of cyanoacrylate is not compatible with the presence of electrophilic substance residues.

**Fig. 20** Chemical structure of polycyanoalkylacrylate  $n$  is the number of methylene units  $-\text{CH}_2-$



### Anaerobic Adhesives

These are oligomer dimethacrylate based formulations containing latent initiating systems (hydroperoxides in the presence of donor–acceptor systems, of the benzosulfimide type (saccharine) – di-methyl- p-toluidine) that are inhibited as long as they remain in contact with the oxygen in the air.

Away from it and when in contact with certain metal ions (iron and copper in particular), the radical polymerization occurs spontaneously, giving mechanically strong three-dimensional lattices. The anaerobic adhesives are used for the creation of mechanical assemblies (to seal or immobilize nuts) and gaskets (cylinder head gasket); they can be used in relatively thick coats. In this last case, they are capable of tightening up assemblies and behaving as an anti-corrosion barrier.

## 14.5 Pressure-Sensitive Adhesives – PSAs

Pressure-sensitive adhesives (PSAs) (Creton and Fabre 2002), “soft” visco-elastic solids that are able to develop adhesive interactions instantly with the pressure of a finger (exerted on the rear of the material being affixed), are generally applied at room temperature.

These polydiene-, polyacrylate- or silicone-based adhesives are generally formulated products (with waxes in order to lower the glass transition temperature, and tackifying resins to provide tack), used as self-adhesives, coated to materials such as paper, films, and polymer tapes, etc. The term Pressure-Sensitive Adhesive relates to the fact that pressure from a finger on the rear of the material to be affixed is all that is required in order to allow the adhesive mass to wet the substrate sufficiently and to adhere to it more or less strongly. Depending on the visco-elastic properties and the adhesion forces developed at the interface, various behaviors can be reached from nonpermanent in the case of Post-it<sup>®</sup> to semipermanent in the case of dressings.

The description of the behavior of the PSAs take into account the instantaneous adhesion ability as well as the cohesion developed during the separation of the substrates (for example, by peeling) with or without leaving residue. This property is called tack and can serve to describe, for example, the behavior of the repositionable adhesives. Polyacrylates are good examples to illustrate what kind of chemical structure can provide basic tack properties (Fig. 21).

The molar mass, the molecular distribution, the chemical nature of the monomer units, their distribution on the polyacrylate backbone will govern the raw-visco-elastic properties as well as the capacity to create more or less strong interaction with the surface. This behavior will be deeply discussed in ► Chap. 15, “Pressure-Sensitive Adhesives (PSAs).”

## 14.6 Conclusion

A presentation, even in organized and summarized form, of the famous classes of adhesives reveals the considerable diversity of applications that can be proposed for most compounds. When faced with a problem with an assembly, there is normally a



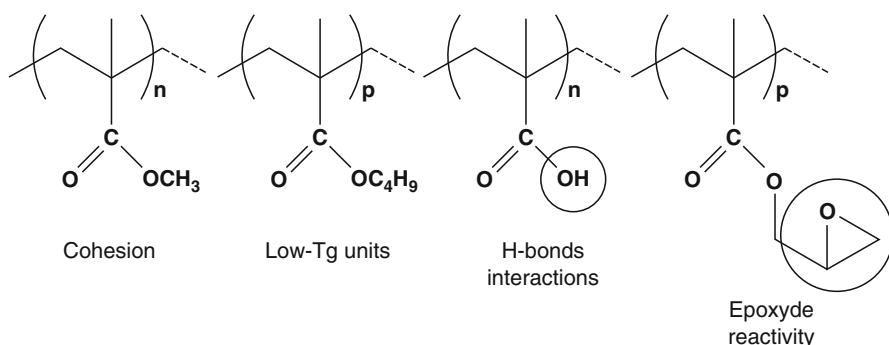


**Fig. 21** Schematic representation of acrylate-based monomer units with various properties

clear optimum solution in terms of the geometry of the joint or the preparation of the surfaces, but there are always several credible answers in terms of the choice of adhesive. Each one has advantages and disadvantages, in such a way that the solution to these problems is often sought in the multiple basic properties of adhesives that all differ in nature. If in the past, technical solution to enhance the bonding performances have been provided by playing with the composition of basic polymer structures, the effort achieved in the polymer science especially in the macromolecular engineering are capable of offering an approach to design multi-functional oligomer molecules, that can associate complex backbone architectures with alcohol, amine, isocyanate, acrylate, or epoxy reactive groups controlled in terms of distribution or concentration; the approaches to “chemical hybrid” adhesives are tending to grow and grow leading to a more complex adhesive classification. The “classical” routes of formulation adds to this richness by giving access to “physical hybrid” adhesives, in such a way that in order to find increasingly high-performance adhesives, one is not relying so much on the discovery of new molecules anymore, but on the right combination of systems, macromolecules, or groups already discovered.

Under these conditions, a chemist’s approach to polymers allows a specific solution to be offered to virtually any assembly problem. Whether this solution will be applicable or not depends afterwards on the correlations between structural and morphological characteristics of the raw polymer materials, physical properties, the mechanics or thermo-mechanics of the formulations, and the characteristics of the joint (via the characteristics of the assemblies). In this regard, we know that:

- The intrinsic properties of the raw components have less influence on the behavior of the adhesives and the joints than the formulation parameters.
- The usage conditions of the adhesive formulations can be the key elements of their behavior.

It is on this last point that one should probably focus: both the academic research aiming to understand the adhesion phenomenon, and the applied research on optimal

and reproducible performance of the adhesives. It is on this basis also that one can ask, going beyond current industry trends and developments, about the principles behind the development of future adhesives:

- Able to preserve the environment (and thus releasing neither volatile solvents, nor unfixed surface active agents)
- Free of industrial and toxicological risk (and therefore negligible volatility, nonexplosive, low combustibility, and also insoluble in water, all of which characteristics are presented by most of the  $\alpha,\omega$  -functionalized oligomers)
- Convenient to use (and so behaving like the AIPPs, but able, through heating or through some other stimulation, electromagnetic, for example, to achieve the three-dimensional structure, with strong cohesion, of the AICPs)
- Able to give strong assemblies, possibly structural and durable (with a premium given to systems with durability that is predictable and, if possible, manageable)
- But also allowing the “repair” of the assemblies as well as the recycling of the materials assembled (the bonding reversibility achieved with certain PSAs is obviously not possible for the structural assemblies performed with AICPs; the solution is, therefore, either to bring about the deterioration of the lattices, thus lowering the cohesion of the joints, or to “invent” a way to disrupt the interactions between joints and substrates).

---

## Appendix

Main ideas can be reached using former published books and handbooks in which readers can obtain an overview on the science of adhesives in Polymer synthesis, P. Rempp, E.W. Merill (1986), Huetig and Wepf Verlag Basel, Heidelberg, NY, Adhesive Technology Handbook (1985), Noyes Publications, Park Ridge, NJ, Handbook of Adhesives, 2nd Ed. (1985), Van Nostrand Reinhold, NY, Encyclopedia of Polymer Science & Engineering, 2nd Ed. (1989), B. Hardman and coll., John Wiley & Sons, NY, Toughened plastics I: Science and Engineering (1993), American Chemical Society, Washington, Adhesion and Adhesive Technology (2002), Marcel Dekker ED., NY, Adhesion Science and Engineering, Vol. I. and Vol. II The Mechanics of Adhesion (2002), D.A. Dillard and A.V. Pocius Eds., Elsevier.

---

## References

- Bell UL, Stump BL, Gager H (1976) J Polym Sci Chem Ed 14:2275
- Carothers W (1936) Trans Faraday Soc 32:39
- Chen W, Frisch KC, Wong S (1992) In: Frisch KC, Klempner D (eds) Advances in urethane science and technology, vol 11. Technomic, Lancaster. Chapter 3
- Creton C, Fabre P (2002) Tack. In: Dillard DA, Pocius AV (eds) Adhesion science and engineering, vol 1, The mechanics of adhesion. Elsevier, Amsterdam, p 535
- Fabris HJ, Knauss WG (1990) In: Aggarwal SL (ed) Comprehensive polymer science, vol 7, Speciality polymers & polymer processing. Pergamon, New York, p 131

- 791 Fletcher WP (1971) In: Blow MC (ed) Rubber technology and manufacture. CRC, Cleveland, p 111  
792 Guilham JK (1983) In: Seferis JC (ed) Proceedings of the joint U.S. – Italy symposium on composite  
793 materials. Plenum, New York, p 127  
794 Holden G, Milkovitch R (1966) US Patent, 3,265,756  
795 Johnson SE, Karuke FA (1985) For Prod J 44(3):46  
796 Kennedy MH (1987) ACS Symp Ser 385:386  
797 Landrock AH (1985) Adhesive technology handbook. Noyes, Park Ridge, p 154  
798 Legge NR, Holden G, Schroeder HE (1987) Thermoplastic elastomers, a comprehensive review.  
799 Hanser, Munich  
800 Lovell PA (1997) In: Lovell PA, El-Aasser MS (eds) Emulsion polymerization and emulsion  
801 polymers. Hoboken, Wiley. Chapter 7  
802 Owen MJ (2004) Encyclopedia of materials: science and technology, Chapter 15, p 2480  
803 Pocius AV (2002) Adhesion and adhesive technology. Marcel Dekker, New York  
804 Robins J (1986) In: Hartshorn SR (ed) Structural adhesives – chemistry and technology. New York,  
805 Plenum  
806 Strichartzuk PT, Wright DE (1977) In: Skeist I (ed) Handbook of adhesives, 2nd edn. Van  
807 Nostrand, New York, p 293  
808 Tan HS, Pfister WR (1999) Pharm Sci Technol Today 2(2):60  
809 Wrieth CD, Muggee JM (1986) In: Hartshorn SR (ed) Structural adhesives – chemistry and  
810 technology. New York, Plenum

Charles W. Paul and Eric Silverberg

**Contents**

15.1	Introduction .....	374
15.2	Tack and Adhesion .....	374
15.2.1	Tack: Soft Enough for Rapid Wet-Out .....	374
15.2.2	Bonding: Driven by Molecular Interactions (and Air Elimination), Resisted by Entropy Loss, and Delayed by Viscosity .....	375
15.2.3	Peel Adhesion (Resistance to Debonding) .....	376
15.2.4	Performance Test Methods and Variables .....	377
15.2.5	Rheological Tests .....	380
15.2.6	Optimizing Performance: General Principles .....	386
15.2.7	Other Characterization Methods .....	388
15.3	Backings and Release Liners .....	390
15.4	Acrylics .....	392
15.4.1	Monomer Composition .....	392
15.4.2	Molecular Weight and Solvents .....	393
15.4.3	Crosslinking .....	394
15.5	Rubber Based .....	399
15.5.1	Natural Rubber .....	400
15.5.2	Styrenic Block Copolymers .....	400
15.5.3	Tackifiers and Oils .....	402
15.6	Summary .....	405
References	.....	407

**Abstract**

The basic concepts, formulations, and test methods of pressure-sensitive adhesives are presented. The importance of interfacial interactions, viscous loss, and extensibility is stressed. The common rheological tests are described, and the equivalence of deformation rate and test temperature is emphasized. The much

C. W. Paul (✉) · E. Silverberg

Henkel Adhesives, Bridgewater, NJ, USA

e-mail: [charles.paul@henkel.com](mailto:charles.paul@henkel.com); [eric.silverberg@henkel.com](mailto:eric.silverberg@henkel.com)

longer time scale for bond formation versus the rate of deformation upon debonding in peel or tack is exploited by the formulator to optimize properties. The formulation principles and common ingredients for preparing acrylic and rubber-based adhesives are described, and the performance capabilities of these two types of pressure sensitives are contrasted.

---

## 15.1 Introduction

Pressure-sensitive adhesives (PSAs) are ubiquitous. They are the adhesive of choice for most office applications and for many industrial assembly operations. Consumer applications include common office tape (Scotch<sup>®</sup>), masking tape, packing tapes (for case and carton sealing), sticky notes (Post-it<sup>®</sup>), postage stamps, medical bandages or plasters (Band Aid<sup>®</sup>), and paper labels. Industrially, pressure sensitives are used for most product labels, decals and commercial graphics, protective and tinting window films, and two-sided tapes are used for a variety of product assembly applications such as the bedding of windows into their frames and the assembly of multilayered panels for semi-structural walls. (Scotch and Post-it are registered trademarks of 3M company. Band Aid is a registered trademark of Johnson & Johnson Corporation.)

Pressure-sensitive adhesives are unique in that they form a strong bond with only finger pressure. They exhibit this immediate grab of a substrate (also called “tack”) *without* the need for activation (e.g. heat, water, solvent, etc.). What distinguishes a pressure-sensitive adhesive from other merely “tacky” materials such as molasses or peanut butter is that they have adequate cohesion to hold the bond they form during service, i.e., labels do not slide around on bottles, packing tapes cannot be removed without tearing the cardboard, etc. Pressure-sensitive adhesives are solids. What gives these solids tack? In a word – *softness*. A solid which is soft enough will be tacky, and if it has adequate cohesion, it can be used as a pressure-sensitive adhesive. The demarcation line for adequate softness was discovered by Dahlquist (1966) and is discussed below.

---

## 15.2 Tack and Adhesion

### 15.2.1 Tack: Soft Enough for Rapid Wet-Out

To enable rapid and intimate wet-out of a surface by a film of adhesive requires only that it be sufficiently soft. Dahlquist found that materials with a dynamic shear modulus (stiffness) of less than  $3 \times 10^6$  dynes/cm<sup>2</sup> ( $10^5$  Pa) when deformed in 1 s will exhibit “tack.” When the application requires tack to develop either faster or slower than in a typical finger pressure test, the criterion will obviously be shifted – to higher stiffness values for longer dwell times and lower values for shorter ones or rougher surfaces. Nonetheless this simple criterion provides critical guidance for developing new pressure-sensitive adhesives. Note that nothing about the composition

of the material or the substrate is needed. All materials exhibit tack if made soft enough. The level of tack, however, will vary widely depending on the other characteristics of the material and substrate as described in more detail below.

15.2.2 Bonding: Driven by Molecular Interactions (and Air Elimination), Resisted by Entropy Loss, and Delayed by Viscosity

The Dahlquist criterion says simply that if an adhesive is soft enough, it will bond rapidly when deformed against a substrate with light pressure, and it will maintain this bond when the pressure is released and thus resist debonding with a force known as the tack force. Why does the adhesive not debond spontaneously when the pressure is released? The bond is maintained by the molecular interactions developed across the interface between the adhesive and substrate. These may be strong, such as hydrogen or ionic bonding, or they may be weak van der Waals forces, but they are always stronger than the interaction of the adhesive and substrate with air – which is roughly 1/1,000 as dense as any solid material. Thus any molecular interactions between adhesive and substrate are preferred to air (virtually no interactions).

The strength of the bond that develops depends on many factors, firstly the strength of the molecular interactions. Many acrylic adhesives, for instance, contain acrylic acid groups, and these are known to provide strong interactions with glass, inorganic, and metallic surfaces, since most of these are basic or amphoteric (Pocius 2002). The strength of the bond thereby increases with time as these acid groups find the substrate surface (see Table 1). In addition, while 1 s of finger pressure may

**Table 1** Properties of commercial pressure-sensitive adhesives at 25 μm thickness on a 50-μm-thick PET (polyethylene terephthalate) backing film

Adhesive type	Loop tack (N/25 mm)	180° peel (N/25 mm)				Shear <sup>a</sup>		
	Stainless steel	Stainless steel		High-density polyethylene		Stainless steel		
		20 min	24 h	20 min	24 h	RT (hours)	70 °C <sup>b</sup> (hours)	SAFT <sup>b</sup> (°C)
Acrylic A untackified	11	8.3	11.1	1.7	1.9	>50	10	149
Acrylic B (tackified A)	23	24	27	13	13	10	0.6	94
Styrenic block copolymer based	32	36	39	23	23	>50	NA	77 (500 g)

<sup>a</sup>RT shear at 22 °C using a 25-mm-high, 12-mm-wide overlap bond and a 1 kg weight  
70 °C testing used the same weight, but with a 25-mm-high and also 25-mm-wide overlap  
SAFT testing used the same configuration as at 70 °C, but the temperature was ramped 2.8 °C/min until failure. With the SBC sample, the weight was 500 g instead of 1 kg  
<sup>b</sup>50-μm-thick coating

provide wet-out, it is unlikely to be complete, especially if the substrate is rough and/or the adhesive layer is thin. The adhesive will try to continue to wet out the surface but will be slowed by the creep viscosity of the adhesive and inhibited by the entropy loss associated with deforming the polymer network in the adhesive layer. Pressure-sensitive adhesives gain their cohesion from polymer entanglements and crosslinking, but these same features limit their ability to wet out completely. There is a trade-off between the ability to build adhesion through more complete wet-out of the surface over time and the cohesive strength of the pressure-sensitive adhesive.

### 15.2.3 Peel Adhesion (Resistance to Debonding)

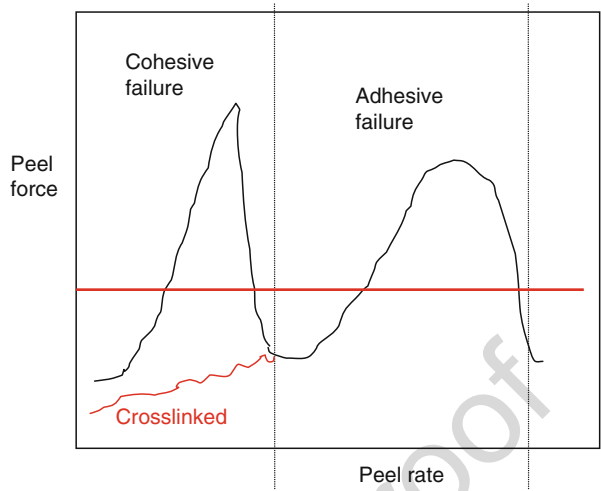
Why are pressure sensitives able to bond with minimal pressure but very difficult to debond? And what determines the level of resistance (force)? For one thing, thermodynamics drives bonding as air is displaced and thus must be overcome upon debonding. But more importantly, the time scales for bonding and debonding are quite different. The adhesive is given at least a second to bond (note Dahlquist criterion above) and often longer. However peeling or debonding involves much shorter time scales – typically about 0.01 s. It is this difference in time scale between bonding and debonding that is responsible for the high peel forces that can be obtained upon debonding.

The time scale for debonding may seem slow. Instrumented test frames typically pull the tape off the substrate at a standard speed of 2.5 mm/s (5 mm/s of crosshead speed). One watching the test would think it slow, but at the peel front of the adhesive, things are happening very fast. The time scale for adhesive deformation in the peel front is roughly the thickness of the adhesive/the speed of testing. For a typical 25- $\mu$ m-thick adhesive layer pulled at 2.5 mm/s, this is 0.01 s or 100 times faster than a typical finger bonding process. Because of this at least 100-fold difference in time scale between bonding and debonding, it is the viscoelastic properties that are critical for designing a high performance PSA. The ideal is an adhesive layer which is very soft and liquid like during bonding ( $\geq 1$  s deformation) for complete and irreversible wet-out but which should become much stiffer when deformed quickly (0.01 s) while remaining highly viscous and extensible to maximize the work done on the adhesive.

It is a common misconception that for high peel force an adhesive must be very strong. To the contrary, often weaker adhesives exhibit much higher peel. Peel force is a measure of the work done while removing the adhesive; its units are force/width of tape. This corresponds to the energy consumed on peeling per unit area of adhesive bond:

$$\begin{aligned}
 \text{Peel} &= \text{force/width} \\
 &= (\text{force} \times \text{distance peeled})/(\text{width} \times \text{distance peeled}) \\
 &= \text{energy consumed/area peeled}
 \end{aligned} \tag{1}$$

**Fig. 1** Peel force versus peel rate. For a given peel force, four peel rates are possible. The two with negative slopes are unstable since any fluctuation in peel rate will accelerate the crack to the next stable solution at higher peel rate. Most industrial adhesives are adequately crosslinked, either physically or chemically, so as to avoid cohesive failure in use



As the peel speed increases, the peel force generally also increases until it drops precipitously when the adhesive becomes very stiff and elastic at the pull speed (see Fig. 1). Since the failure is normally interfacial at all test speeds, yet the peel varies dramatically with speed and substrate (see Table 1), peel is clearly not a measure of the strength of the adhesive but rather of the work done on it under a particular set of conditions.

**15.2.4 Performance Test Methods and Variables**

A variety of tests have been developed and standardized. The details vary depending on the standards agency. Numerous customer-specific tests are also used. A comprehensive set of test methods are available from the Pressure Sensitive Tape Council (PSTC 2007). Usually polished stainless steel (S.S.) is employed as the substrate, but for specific applications, the actual substrate is often used instead. The backing is also important as its behavior under stress also contributes to the performance of the tape.

**Tack**

Tack is the force required to debond an adhesive after it has been bonded with low force for a brief time. Tack is also called “quick stick,” and the most common method is the uninstrumented “finger tack” – which is often the most important from a practical standpoint. Instrumented methods to characterize tack are numerous, but the most common are the rolling ball, loop tack, and probe tack methods. The rolling ball test (**PSTC-6**) is the least intuitive measure and the hardest to relate to actual use. A steel ball is rolled down an incline onto a tape of the adhesive at the bottom. The distance the ball travels along the adhesive before stopping is inversely related to its “tack.” The loop tack method (**PSTC-16**) takes a loop of tape, adhesive side



facing out, and brings it down onto a substrate, but not so far as to compress the loop entirely. The maximum bonding force is determined by the stiffness of the tape. The instrument then reverses and pulls the loop off of the substrate. The maximum force upon debonding is recorded as the loop tack value. The width of the loop is about 25 mm (1 in.) as is the width of the substrate, thus the contact area is roughly  $25 \times 25$  mm, and therefore loop tack is often reported in units of force/inch<sup>2</sup> or as force/inch width of tape. Probe tack is the most meaningful measure of tack. A cylindrical probe with a rounded edge is compressed briefly into the adhesive and removed (ASTM D-2975), much like one would do with their finger. The maximum force during removal is reported as the tack value. Probe tack is gaining popularity in usage with the advent of newer machines, such as the texture analyzer from Stable Micro Systems, which can measure the entire force displacement curve during the test.

Typically the tack level of the adhesive will increase with the thickness of the adhesive layer and show a maximum with testing temperature (see Fig. 2). Smoother substrates or those of higher surface energy show higher tack values.

## Peel

Peel resistance is a critical performance property (PSTC-101). The tape is bonded by first laying it down gently on the substrate, then pressing it twice with a standard weight roller (2 kg) moving at a standard speed (10 mm/s), and then allowed to stand for a specified time, which is commonly 20 min for initial peel and a week or more – perhaps at elevated temperature and humidity – for a measure of aged peel. The free end of the tape is gripped and the tape pulled off of the substrate at an angle by an automated tester with a load cell at a crosshead (grip) speed of 5 mm/s. Most common are peel tests conducted at 90° or 180° (most common; this is where the tape is peeled back on itself). The former generally yields higher peel values partly because at the same pull rate on the tape, the speed at which the peel front moves is twice as fast when pulled at 90° (this results because the bonded substrate is moved on a sled horizontally at the same speed as the crosshead moves vertically, in order to

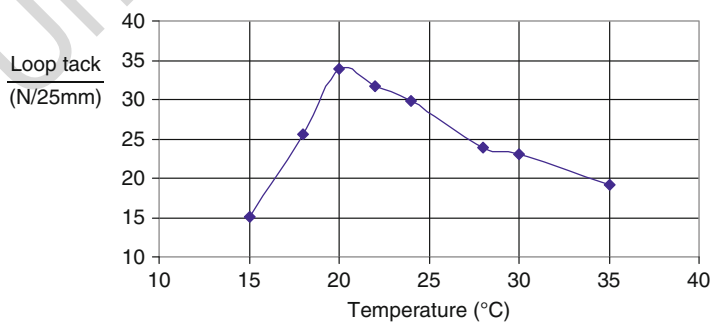


**Fig. 2** Loop tack (N/25mm) versus temperature for a pressure sensitive adhesive based on a styrenic block copolymer

maintain the 90° configuration, whereas the substrate is fixed in the lower grip in the 180° test).

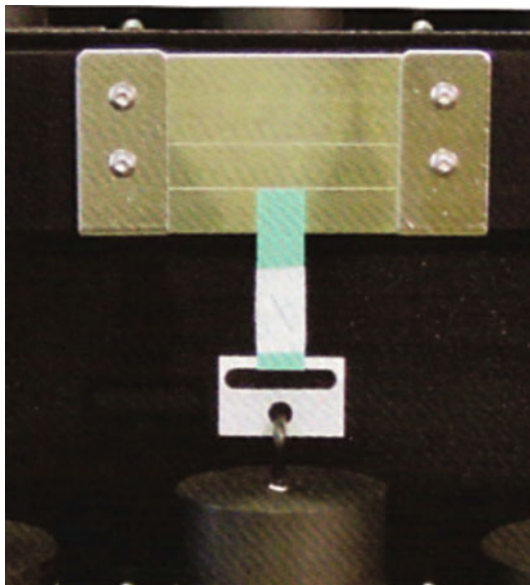
The peel test measures the work done on the entire tape. If the backing is stiff and elastic, such as polyethylene terephthalate (PET), no work will be done on the backing, and the peel force is unaffected. However, if the backing can also yield, such as aluminum, then the peel value will be increased in proportion to the work done. If the tape is curled or otherwise distorted after the test, then some work has been consumed in the backing. Even if the backing does not deform, its thickness can have an effect on the peel force since it changes the precise angle at the peel front which influences how the adhesive deforms and thus the work done on it. Peel increases with adhesive thickness, but not proportionately, provided that the whole adhesive layer becomes deformed during the test, which is usually the case. Peel also increases with peel rate until the peel becomes unstable and the force is no longer constant. This occurs as the peel rate crosses over the second maximum shown in Fig. 1. At this point a slip-stick behavior is observed and heard. With each “slip” of the bond, a snapping noise is emitted. The substrate will usually have thin lines of adhesive residue, equally spaced, remaining after the test from each sticking period during peel. Further increasing the peel rate increases the spacing of the stick lines and further lowers the average peel force.

As shown in Fig. 1, uncrosslinked adhesives can exhibit two maxima in peel force with peel rate. At slow peel rates, they will fail cohesively. When pulled sufficiently fast, their failure becomes adhesive, and the peel force drops but then rises with peel rate – as with crosslinked adhesives – until falling again when slip-stick failure occurs. Commercial styrenic block copolymer-based adhesives can exhibit high peel force cohesive failure at standard test speeds when bonded to high-energy substrates like polished steel.

## Shear

The shear holding power of pressure sensitives is low in comparison to other adhesives due to their softness and low strength. Thus, they are limited to low load applications. Failures can occur within the adhesive itself (cohesive failure) or through peel initiated by stress concentrations at the corners of the bond. Pressure sensitives are normally tested in static shear – fixed load – whereas most structural adhesives are tested in dynamic shear, fixed deformation rate (see ► Chap. 19, “Failure Strength Tests”). Two types of fixed load tests are most common: (1) time to failure at fixed load and temperature and (2) temperature of failure at fixed load and temperature ramp rate (known as the SAFT – shear adhesion failure temperature). The first of these gauges whether the bond can resist persistent loads in use, whereas the second provides a measure of the maximum use temperature. Shear bonds are made on clean polished stainless steel – identical to that used in peel and tack tests. The overlap depends on the test and customer requirements. The PSTC standard (PSTC -107) is 12 × 12 mm. The panel is tilted at a slight angle (2°) off of the vertical and away from the tape, to eliminate peel at the bottom edge of the tape (see Fig. 3). However, there are always peel stresses at the top edge of the tape. While shear loads are normally reported in units of force/area, the specific configuration of

**Fig. 3** Shear holding test with  $12 \times 12$  mm overlap bond (Reproduced with permission from the Pressure Sensitive Tape Council)



the bond is very important since it affects the magnitude of the stress concentrations and peel forces at the top edge of the bonded area. As much as an eightfold difference in shear hold time has been observed for the same nominal load/area by simply changing the dimensions of the overlap. This is much the same situation as with structural bonds, where doubling the length of a lap shear bond will not double the dynamic strength (failure load/bonded area). As with any adhesive test, failure analysis is the starting point for understanding how to improve the bond.

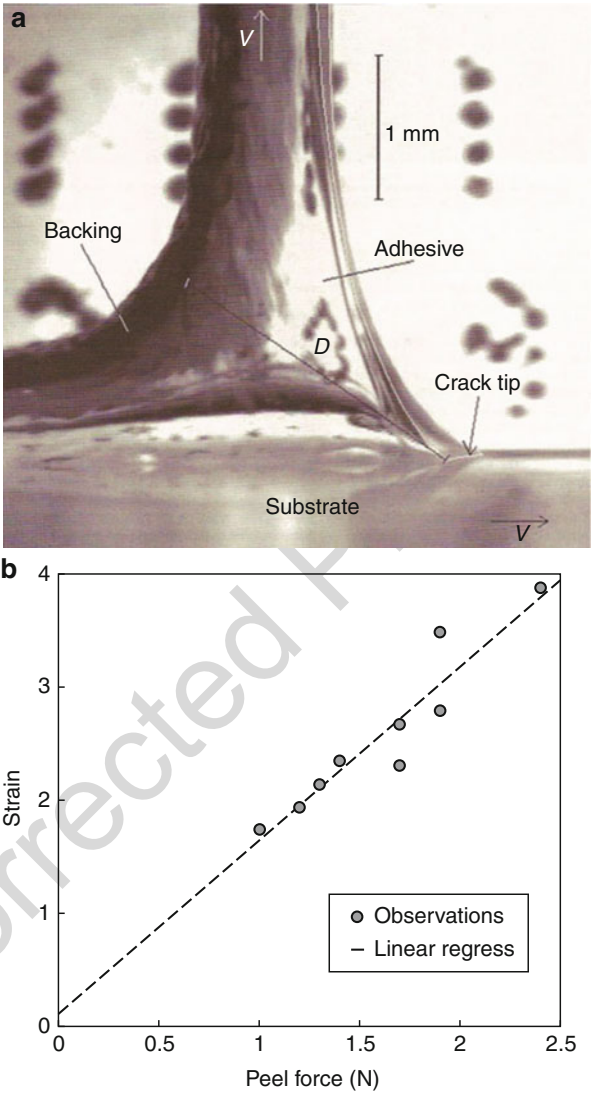
Typically, with lightly crosslinked materials, the shear failure is cohesive. This is also the case for physically crosslinked materials such as styrenic block copolymers, particularly at elevated temperatures. However, as the cohesive strength of the PSA increases and/or as the resistance to peel adhesion falls, the mode of failure will tend to switch to adhesive, normally initiated as a delamination from the substrate at the corners of the tape. As the delamination grows and the stress builds, failure can be rapid and catastrophic with the debond crack traveling interfacially, alternately along the substrate and the backing interface.

Thicker bonds fail more easily in shear whether adhesive or cohesive. For cohesive failure this is undoubtedly due to the narrower gap through which the adhesive is flowing. For adhesive failure, it is presumably due to an increase in peel forces at the top of edge of the bond.

### 15.2.5 Rheological Tests

The work consumed in deforming the adhesive (and backing) determines the peel force and shear resistance of the adhesive. Detailed observations of adhesive

**Fig. 4** (a) Side view of PSA tape being peeled at 90°. Note the extensive tensile deformation of the adhesive at the crack tip (Reproduced with permission from Christensen et al. (1998), copyright Elsevier). (b) Adhesive deformation (strain) measured optically versus recorded peel force (Reproduced with permission from Christensen et al. (1998), copyright Elsevier)



deformation during peel have shown that the adhesive is deformed in tension at the peel front (see Fig. 4a) and that the level of deformation can be as high as 1,000%. The peel force is directly proportional to the degree of deformation (see Fig. 4b). Thus the large deformation properties are critical to performance. Unfortunately, to measure the large deformation properties requires extensive testing since separate samples are needed for each test. Where this has been done, and the properties have then been used for finite element analysis of the peel process, good models have been generated. From a practical standpoint, such extensive testing and modeling are more burdensome than simply running the actual performance tests themselves.

Therefore, many have sought instead to correlate the low deformation, linear elastic, behavior of the adhesive with performance. With such tests, a single sample can be used to collect a vast quantity of data. These efforts have been very successful but still have their limitations, and pitfalls, inherent in the assumption that linear elastic properties can be used to predict nonlinear elastic properties.

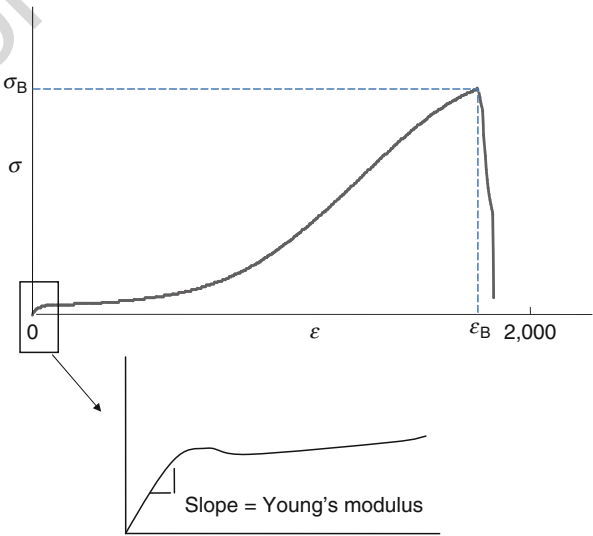
In this section, the concepts of viscoelasticity and linear elasticity are introduced. Then the common rheological tests conducted on pressure sensitives are described, followed by examples of how these tests are used in practice.

**Linear Elasticity and Viscoelasticity**

As mentioned above, the tensile properties of pressure sensitives dominate their peel performance. The tensile stress-strain curve on pressure sensitives has a shape similar to pure rubber (see Fig. 5). The linear elastic region is the low strain region where stress is proportional to strain (the proportionality constant is the modulus), and the material will recover fully when the stress is released. Beyond this point, the slope first decreases substantially with strain, or effectively the adhesive softens. This softening blunts the cracks that form on debonding and enables the high strain necessary to obtain high peel by fibrillation of the adhesive. At sufficiently high strains, the adhesive again hardens as the molecules become completely stretched to the limit of their covalent bonds. The strain range over which linearity is maintained will vary greatly with temperature and strain rate. Ordinarily the linear region is below 0.05% in the glassy state (low temperature), a few percent in the rubbery region, and below 30% in the melt or flow region (see Fig. 6 and explanation below). These deformations are all far below what the adhesive experiences during peel.

The measurement of the linear elastic properties is normally done through oscillatory measurements where strain, frequency, and temperature are controlled.

**Fig. 5** Tensile stress ( $\sigma$ ) versus strain ( $\epsilon$ , in %) for a styrenic block copolymer based adhesive (Reprinted with permission from Hu and Paul (2009), copyright Taylor and Francis)



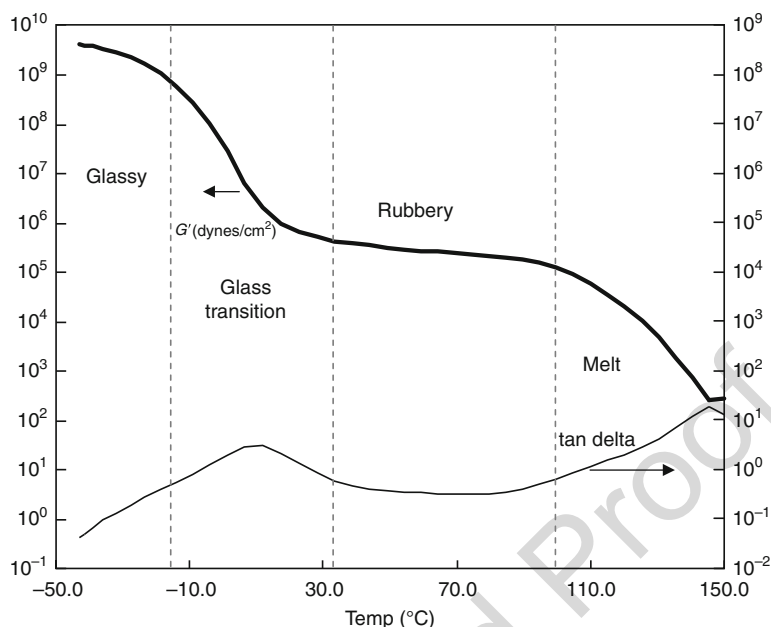


**Fig. 6** Modulus and tan delta versus temperature for a typical styrenic block copolymer-based adhesive (Reprinted with permission from Hu and Paul (2009), copyright Taylor and Francis)

If the material behaves perfectly elastically, then the stress recorded is in phase with the applied strain. If the material has no elasticity, but instead behaves perfectly viscously, then the recorded stress will be proportional to the strain rate, which is  $90^\circ$  out of phase with the applied strain, peaking where the strain is 0 in each sinusoidal cycle. Pressure sensitives are viscoelastic materials, and thus the recorded stress will peak in each cycle somewhere between  $0^\circ$  (in phase) and  $90^\circ$  (out of phase) with the applied strain. The tangent ( $\sin/\cos$ ) of this phase angle  $\theta$  is a measure of the relative viscous to elastic contributions to the adhesive's stress response. When a material approaches, its Tg "tan delta" (tangent  $\theta$ ) increases. The temperature at which tan delta reaches a maximum is very commonly defined as the material's Tg. The in-phase contribution to the stress ( $\text{maximum stress} \times \cos \theta$ ) provides the elastic modulus once divided by the applied strain. These experiments are normally conducted with parallel plate rheometers, and thus it is the elastic modulus in shear,  $G'$ , which is measured. The out-of-phase contribution to the stress ( $\text{maximum stress} \times \sin \theta$ ) yields the shear loss modulus,  $G''$ , when divided by strain. Note that these calculations are only valid in the linear elastic region where stress is assumed to be proportional to strain, and thus a single constant of proportionality (modulus) defines the material's response.

From such simple oscillatory measurements, a wealth of information is obtained. By scanning the temperature, a plot such as Fig. 6 is recorded. From this it can be determined: (1) the material should be tacky at room temperature ( $G'$  is below the

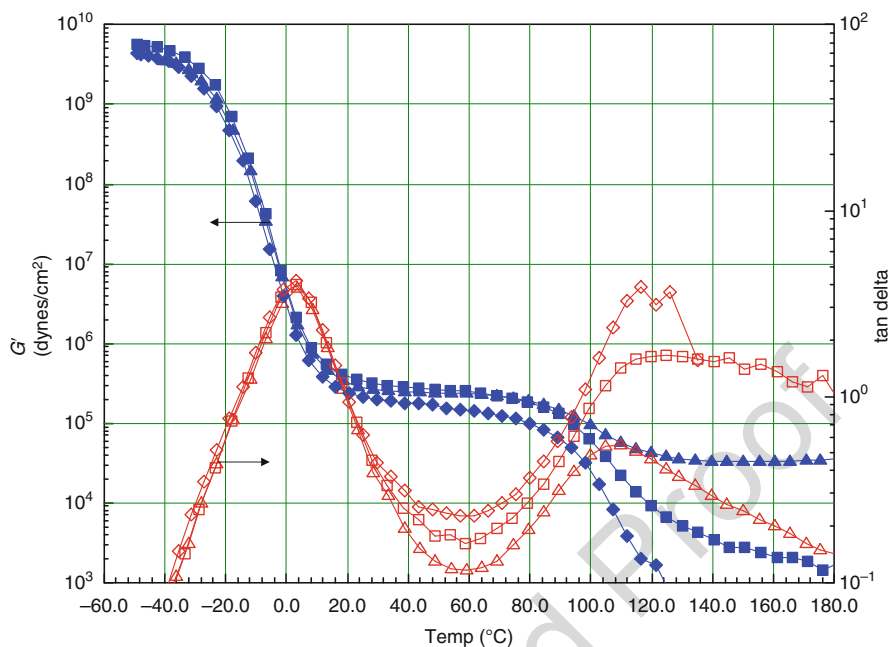


**Fig. 7** Styrenic block copolymer – based adhesive with various levels of UV-crosslinking: none ( $\diamond, \diamond$ ), low dose ( $\blacksquare, \square$ ), and high dose ( $\blacktriangle, \triangle$ )

299 Dahlquist criterion of  $3 \times 10^6$  dynes/cm<sup>2</sup>), (2) about 10 °C is the minimum tem-  
 300 perature at which the material will exhibit tack (very close to the T<sub>g</sub>), (3) the material  
 301 will begin to flow at about 105 °C (this is where tan delta = 1 ( $G'' = G'$ )) and thus  
 302 above this temperature it will behave more like a liquid (viscous) than a solid  
 303 (elastic)), and (4) if the T<sub>g</sub> has been optimized to maximize peel at the use  
 304 temperature (i.e., could the T<sub>g</sub> be increased without the peel becoming zippy?).  
 305 Comparing such curves is very useful. For example, the level of cure is easily gauged  
 306 by the magnitude of the modulus at elevated temperatures (see Fig. 7). When new  
 307 materials are added to the formulation or substituted for others, the effects on T<sub>g</sub> and  
 308 the rubbery plateau modulus are readily apparent. From rubber-elasticity theory, the  
 309 relationship between the  $G'$  in the rubbery region (see Fig. 6), the volume fraction of  
 310 polymer ( $V_p$ ), and the molecular weight between entanglements for the pure poly-  
 311 mer ( $M_e$ ) is

$$G'(\text{rubbery plateau region}) \sim V_p^2 / M_e \quad (2)$$

312 With multiphase materials, such as adhesives based on block copolymers, a  
 313 temperature scan is a sensitive although indirect gauge of morphology. The temper-  
 314 ature scan is also a useful fingerprint for a particular adhesive which is extremely  
 315 valuable for quality control.

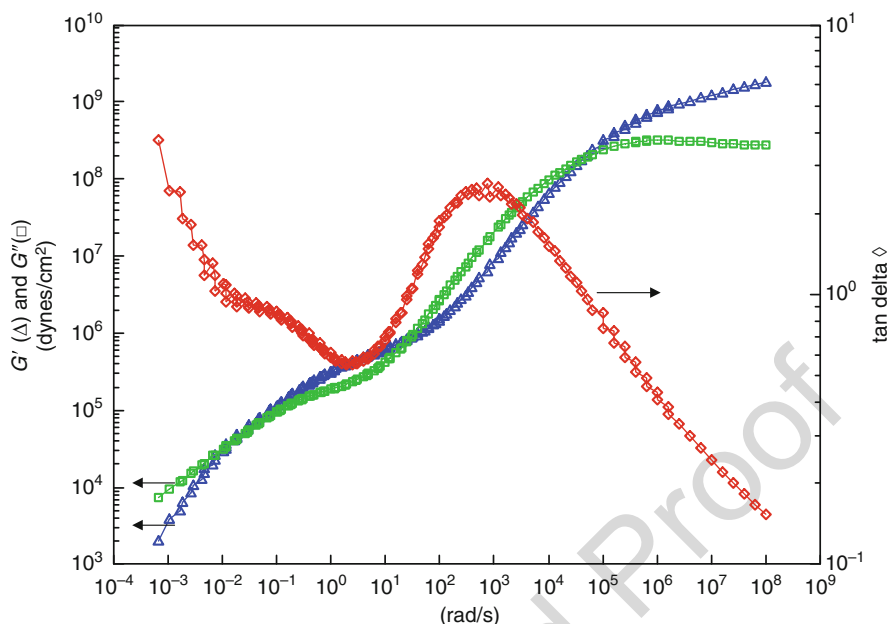


**Fig. 8** Elastic ( $G'$ ) and loss ( $G''$ ) moduli and their ratio ( $G''/G' = \tan \delta$ ) versus frequency at 25 °C for a styrenic block copolymer-based adhesive. Constructed via time-temperature superposition

Frequency scans are also useful. These are conducted at several temperatures and then via time-temperature superposition can be extrapolated to very low and high frequencies as was done in Fig. 8. This same type of data can be converted to a series of temperature scans at different frequencies as shown in Fig. 9. From this curve it can be determined that at a peel rate of about 100/s, the adhesive will become zippy and the peel force will drop at room temperature (this occurs at approximately the frequency at which the material becomes glassy at the temperature of the peel test). Another common use of the frequency curve is to look at the ability of the adhesive to damp vibrations at various frequencies. Tan delta is a direct measure of this capability.

Stiffness values at low frequencies have also been used as a relative measure of creep resistance for adhesives. A better way of gauging creep resistance is by direct measurement. Direct measurement has the advantage of extending the data beyond the linear elastic region, which is the region of interest when adhesive failure in creep is a possibility. Such measurements are made by applying a fixed stress and monitoring the strain. An example of the data obtained is shown in Fig. 10. The slope of the curve after the initial strain is a measure of the creep viscosity. The flatter the curve, the higher the creep viscosity. Upon removing the stress, the recovery of strain should mirror the creep viscosity. Notice that the strain values can reach several hundred percent in this test, which is far beyond the linear elastic region and more representative of the scale of deformation in the shear hold test.



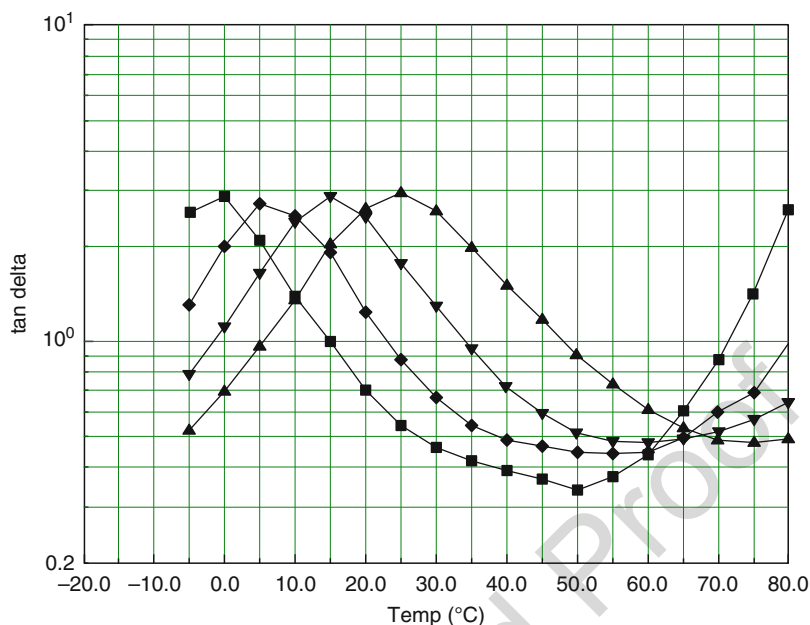


**Fig. 9** Tan delta versus temperature at  $10\times$  frequency intervals from 0.1 rad/s (■) to 100 rad/s (▲) via time-temperature superposition for a general purpose tape adhesive based on styrenic block polymers

### 15.2.6 Optimizing Performance: General Principles

There is often much confusion about what determines adhesion. The word adhesion intuitively seems to imply some measure of molecular interactions across an interface. Whereas, in practice we are referring to some measure of the overall bond strength. How important are the molecular interactions in comparison to the adhesive's bulk properties? Obviously both are quite important. The same acrylic PSA tape can yield peel forces that differ by several multiples depending on the substrate to which it is bonded (see Table 1). For pressure sensitives it is normally assumed that the peel force is proportional to both the level of specific interactions across the interface and some function of the adhesive's rheological response to peel:

$$\text{peel force} \sim \text{specific interactions} \times \text{rheological function} \quad (3)$$

The strength of the interfacial bond determines at what stress the substrate lets go. The higher this stress, the more work can be done on the adhesive before it debonds. The more the work done on the adhesive, the higher the peel. Because pressure sensitives have  $T_g$  values below their application temperature, there is substantial mobility within the adhesive. Thus there is an opportunity for specific interactions between the adhesive and substrate to build over time. A few acid groups attached to the polymer, for instance, can serve this purpose on metals and

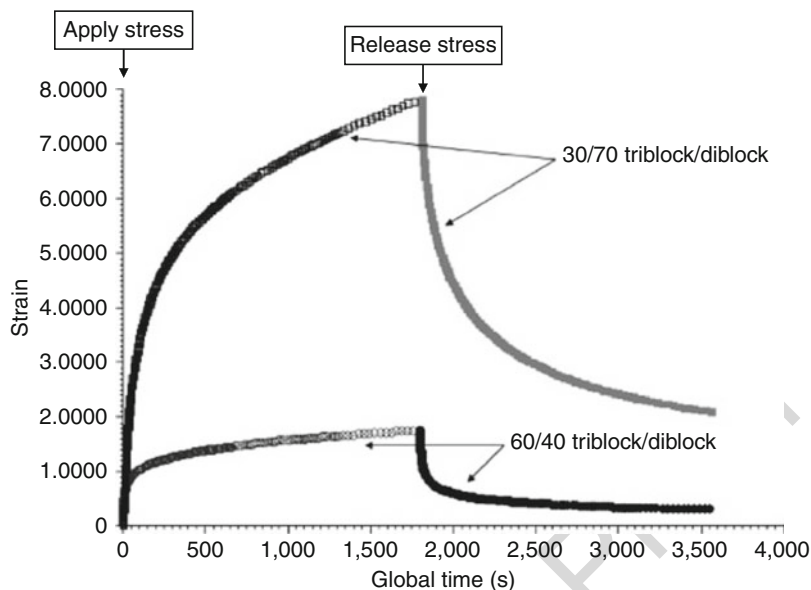


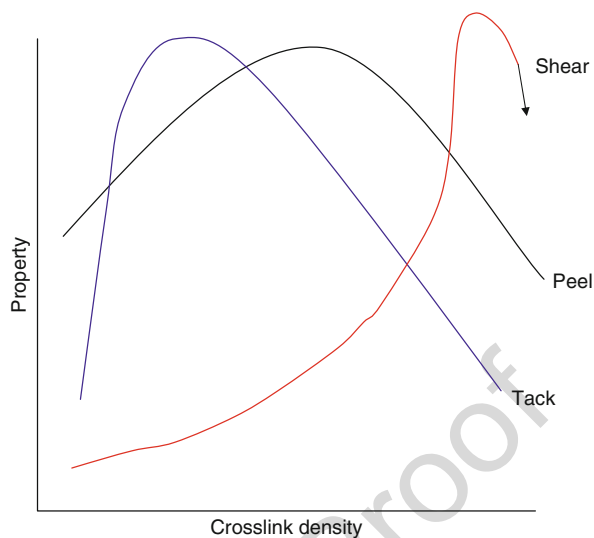
**Fig. 10** Creep and recovery for two styrene block copolymer-based hot melts (SHM) with different levels of diblock and triblock, but the same total amount of polymer. A higher level of triblock dramatically improves the creep resistance (Reprinted with permission from Hu and Paul (2009), copyright Taylor and Francis)

glass. A few basic groups can help build adhesion to polyvinyl chloride. Epoxy or silane groups can build adhesion to glass through covalent bonding. Two part systems such as isocyanate-cured materials can do the same. Ingredients within the adhesive, such as tackifiers, can partially solvate substrates such as plastics and thus help the adhesive to form a diffuse interface with it.

As noted earlier there is often a conflict between the capability of the adhesive to wet out the substrate completely and rapidly and its capacity to resist shear. This dependency follows the form indicated in Fig. 11. As the adhesive becomes stronger through physical or chemical crosslinks, the tack will first increase, until the molecular weight exceeds the capability to relax on the tack time scale (1 s for wet-out). Since the adhesive is normally given much longer to wet out prior to peel testing (typically 20 min for initial peel values and a week for ultimate values), adequate wet-out is achievable even with a much stiffer, lower tack adhesive. The increased stiffness with crosslinking will normally translate into increased peel, until the level of extensibility of the adhesive is reduced. Thus the peel force will peak at a higher level of crosslinking than the tack. Shear increases continuously with crosslinking provided the failure is cohesive. However, at a sufficiently high level of crosslinking, the mode of failure will switch to adhesive – or peel-initiated failure. At this point shear will fall with increased crosslink density just as the peel does.

Considering only the bulk adhesive properties, the ideal pressure-sensitive adhesive would have a broad molecular weight distribution with a fraction at very high

**Fig. 11** Tack, peel, and shear versus crosslink density of the adhesive



375 molecular weight but lightly crosslinked. Such a material will be highly extensible  
376 but unable to flow. It will provide rheological loss over a broad spectrum of  
377 relaxation times and thus be resistant to flow on various time scales  
378 (or alternatively temperatures). The  $T_g$  of the adhesive should be selected such  
379 that it is sufficiently below the lowest temperature/deformation rate it will experience  
380 in use. In later sections, how these principles translate into specific adhesive design  
381 and are reconciled with processing and interface issues will be discussed.

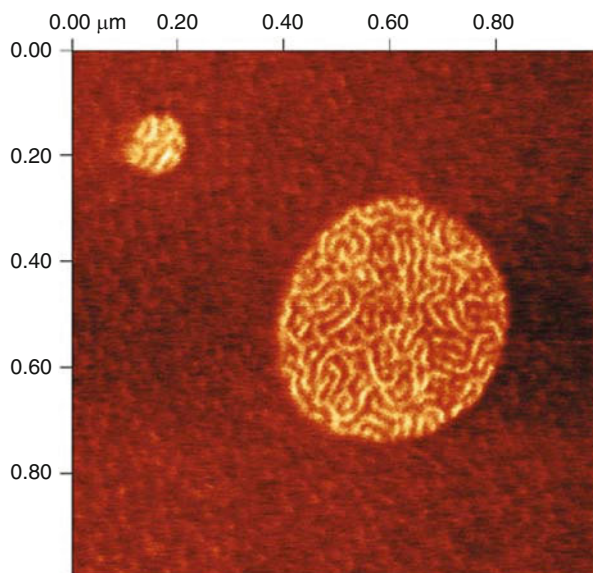
## 382 15.2.7 Other Characterization Methods

383 Beyond performance testing, there are a number of very useful ways of character-  
384 izing adhesives to better aid in their design. These methods have been used to gauge  
385 the uniformity of the adhesive, its morphology, specific interactions across inter-  
386 faces, and the mechanics of debonding at the peel front. These methods will not be  
387 described in detail.

388 Crosslinked adhesives are frequently characterized by conventional solvent-  
389 swelling methods. The adhesive is placed in a suitable solvent where it swells and  
390 would dissolve if not for chemical crosslinks. This is often the solvent from which it  
391 is applied. The amount the material swells is an inverse measure of the crosslink  
392 density and proportional to its extensibility. The soluble fraction is also then col-  
393 lected, dried, and weighed. For conventional acrylics about one third of the material  
394 remains soluble after crosslinking.

395 Adhesive morphology can be imaged using newer atomic force microscopes.  
396 This method has revealed the tendency for certain tackifiers to separate over time. It  
397 has also been used to study blends, as shown in Fig. 12. As the technique is further  
398 developed, its use in pressure sensitives is expected to expand. This method can

**Fig. 12** Atomic force microscopy (AFM) image of a pressure sensitive containing a blend of incompatible block copolymers. One of the block copolymers forms a separate macrophase, within which its hard and soft phases are evident as *light* and *dark* co-continuous domains



easily spot surface segregation. A cruder traditional method for analyzing surface segregation is attenuated total reflectance infrared spectroscopy. This technique often reveals some level of surface segregation of lower molecular weight materials such as tackifiers and can be used to spot transfer of silicone release resins to the adhesive surface.

Methods for characterizing specific interactions are few. Contact mechanics has been applied using the JKR (Johnson–Kendall–Roberts) methodology with some success using acrylic PSAs (Garif et al. 2002). This method involves bonding and debonding the materials at a very slow rate such that rheological loss can be ignored. Academic labs are applying it to characterize bioadhesion in particular. While collaborations with industry have borne fruit, it has not been adopted as an in-house technique. More common in industry is computer modeling of specific interactions.

Of most impact over the past decade has been the application of instrumented probe methods with direct visualization of the interface (Creton and Shull 2009). This simple technique has been used to study the tensile debonding process that occurs at the peel front. Using this method, the importance of the adhesive's ability to cavitate to form fibrils and for these fibrils to remain adhered to the interface while being highly extended has been solidly established. The dependence on adhesive composition and the substrate interface has been studied as well. These studies have demonstrated the validity of probe methods to characterize both tack and immediate peel in one test. The peak force upon probe removal is used as a measure of tack (similar to the normal probe tack measurement), whereas the area under the force displacement curve (a measure of the work of debonding) is a measure of peel resistance at short bonding times. The use of such methods in industrial labs is

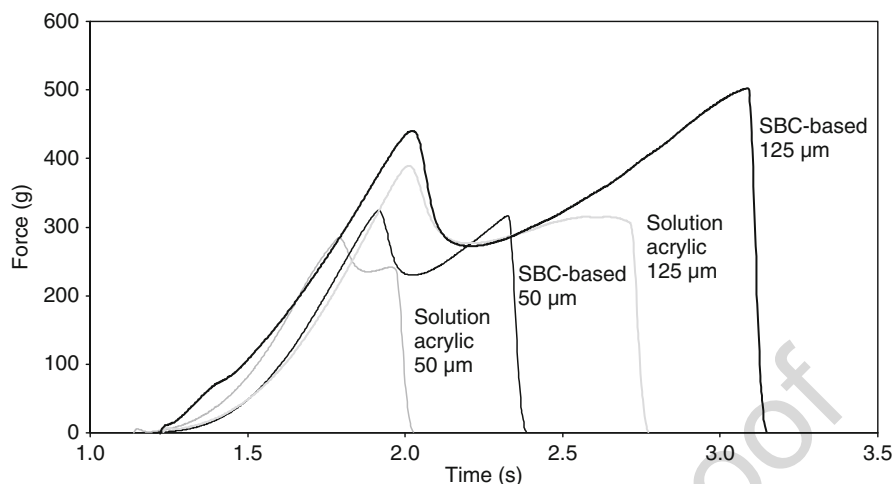


**Fig. 13** Instrumented probe test using a Texture Analyzer to record force versus time during debonding for a styrenic block copolymer (SBC) – based adhesive (dark lines) and a solution acrylic adhesive (gray lines) at thicknesses of 50 µm and 125 µm

gaining momentum. Stable Micro Systems offers an inexpensive instrument for this purpose and a variety of probe materials. (Visualization of the debonding process is not offered.) These devices are now in widespread use. An example of the data generated is shown in Fig. 13.

### 15.3 Backings and Release Liners

During adhesive development it is common to use polyethylene terephthalate (PET) film as the backing. This rigid plastic film has normally been corona treated to eliminate surface contaminants and increase the surface energy of the film. Adhesive failure from the backing, known as “transfer,” fails to give information about the adhesion to the substrate of interest. If substrate adhesion is very strong, it may be necessary to apply the adhesive directly to the backing in solvent or the melt state to ensure strong adhesion and avoid transfer. PET has the advantages of a  $T_g$  above room temperature, a high level of crystallinity, and high modulus. The high  $T_g$  and crystallinity help to prevent migration of the adhesive into the backing that would affect the adhesive properties. The high modulus of this backing film makes it rare for it to deform permanently in a peel test, and thus it will not contribute to the work done in peeling. For these reasons it is an ideal backing for measuring the properties of the adhesive itself.

While some applications use PET backings, most use less expensive materials such as oriented polypropylene (OPP), polyvinyl chloride (PVC), paper, and aluminum foil. The most common issue with backings is migration. PVC backings are heavily plasticized. These plasticizers are often compatible with acrylic and rubber

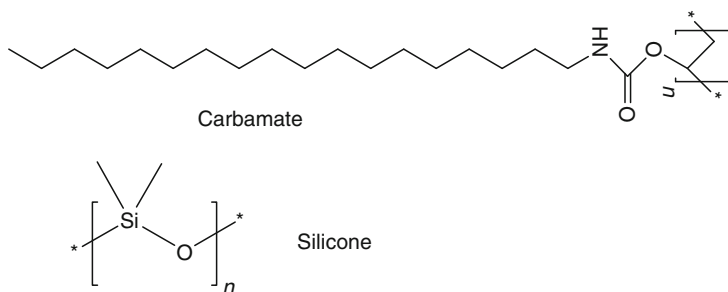


**Fig. 14** Structures of common release layers

adhesives. In the former, they tend to reduce the peel values, while in the latter they tend to destroy the cohesion by attacking the styrene domains. OPP and other olefin films are normally unplasticized; however, they can absorb tackifiers and oils from adhesives. Papers too can absorb these materials leading to not only a change in adhesive properties but also an increase in the transparency of the paper due to this “staining” by the adhesive. Primers or coatings on the backing have been used to block migration.

Unbacked, two-sided tapes can be adhesive alone or more commonly two adhesive layers with a central core reinforcement layer of paper, fabric, or foam. These are commonly called “transfer tapes” and are used in a variety of product assembly applications in industry and around the home.

The release layer is ordinarily a vinyl carbamate or a silicone (see Fig. 14). The primary requirements for good release are (1) the complete incompatibility between the adhesive and release layer and (2) the lack of specific interactions or covalent bonding across the interface. For cured silicones, the likely presence of some unreacted groups such as acrylate ends (UV cured) or hydrosilane (Si-H) groups (hydrosilylation cure) must be considered. The side chains of the vinyl carbamate release coatings are uniform in length which allows them to crystallize to a high degree. This high level of crystallinity ensures that the adhesive does not interpenetrate, so long as the temperature of the tape remains below the melting point of the crystals. Silicones are quite different. They are amorphous and very low in  $T_g$  which provides a smooth and noiseless release even when removed rapidly. The immiscibility of silicones with common adhesives prevents interpenetration without the necessity of crystallinity. Silicone PSAs (not discussed in this chapter) require a different release material; ordinarily fluorosilicones are used to achieve immiscibility between the adhesive and the release layer.

Crystalline vinyl carbamate release coatings are commonly called “low adhesion back-size coatings” or LAB, because they are used almost exclusively on the back side of the backing to allow self-wound tapes to release smoothly (Kinning and Schneider 2002). Silicones provide release at lower force levels and with less noise. They are applied neat or from solvent and are heat or UV cured on the support (paper, PET, or polyethylene-coated paper primarily) to create a release liner.

The level of release can be increased by using additives which co-cure with the silicone and raise its  $T_g$ . By using such a “tighter” release liner on one side with a “lighter” release on the other, a transfer tape will selectively release from one liner, after which it can be applied to a substrate, and then have the other release liner cleanly removed.

In the vast majority of tape and label applications which use a release liner, the adhesive is applied to the release liner and then nipped to the backing. This method does not optimize adhesion to the backing but does prevent its exposure to heat (from hot adhesive or subsequent solvent/water removal). The release liner is normally quite stiff because of its paper or PET support layer and is more resistant to heat than many backings (most liners have already been exposed to the oven cure of the silicone layer). In addition, the silicone layer is mirror smooth which yields a correspondingly smooth exposed adhesive layer for the tape or label.

---

## 15.4 Acrylics

In contrast to common rubbers, the entanglement molecular weight,  $M_e$ , of most acrylics is sufficiently high that without dilution they meet the Dahlquist criterion discussed earlier ( $G' < 3 \times 10^6$  dynes/cm<sup>2</sup>,  $10^5$  Pa) and exhibit tack. With little or no crosslinking, the neat polymers form a pressure-sensitive adhesive with some cohesion. To obtain adequate cohesion, it is common to use polar monomers which can form hydrogen bonds and usually also some level of crosslinking. (Acrylics are also discussed in ► [Chap. 14, “Adhesive Families”](#).)

### 15.4.1 Monomer Composition

Acrylic pressure-sensitive polymers consist mainly of a “soft” monomer with a low  $T_g$  and high  $M_e$ . The three most common soft monomers are butyl acrylate, iso-octyl acrylate, and 2-ethylhexyl acrylate. All three have a  $T_g$  below  $-40^\circ\text{C}$  and an  $M_e$  above 15,000 Da; see Table 2. When polymerized on their own, they meet the Dahlquist criterion at room temperature and well below. To increase peel, often a “hard” monomer is incorporated. These are high  $T_g$  monomers, and most are low  $M_e$ . By moving up the  $T_g$  of the overall polymer, these hard monomers increase the viscous loss and thus the peel force, much in the same way as increasing the rate of peel. In addition, the lower  $M_e$  hard monomers, such as MMA, also increase the stiffness of the adhesive which further increases the peel force. Polar monomers are invariably incorporated to increase cohesive strength through intermolecular hydrogen bonding and to increase the potential for specific adhesion with the substrate. These polar monomers are also generally “harder” (higher  $T_g$ , lower  $M_e$ ) than the soft monomers and so increase the peel in a similar manner. A wide variety of monomer blends are employed in practice to suit various applications. However, in its simplest form, a good pressure-sensitive adhesive is made from 95% of a soft monomer and 5% of acrylic acid with light crosslinking as described below.

**Table 2** Acrylic monomers and their T<sub>g</sub>, M<sub>e</sub>, and typical weight percent addition into an acrylic pressure-sensitive adhesive

		Monomer	T <sub>g</sub> (°C)	M <sub>e</sub> (Da)
<b>Soft monomers</b>	<b>70–90%</b>	2-ethyl hexyl acrylate	–65	35,000
		n-butyl acrylate	–50	17,000
		Iso-octyl acrylate	–70	
<b>Hard monomers</b>	<b>0–30%</b>	Methyl methacrylate	105	5,000
		Methyl acrylate	9	11,000
		Vinyl acetate	32	11,400
		Styrene	100	18,000
		Vinyl neodecanoate	–3	40,000
<b>Polar monomers</b>	<b>3–10%</b>	Acrylic acid	106	
		2-hydroxy ethyl acrylate	–15	
		N-vinylpyrrolidone	180	

## 15.4.2 Molecular Weight and Solvents

The vast majority of acrylic pressure sensitives are polymerized by free radical polymerization. Emulsion, solution, and neat polymerization are in widespread practice. Emulsion polymerization is the least expensive. While this method enables very high molecular weight polymers, usually lightly crosslinked, the necessity of surfactant in the formulation to create the emulsion results in adhesives with less water resistance and generally less heat resistance than those made in solution or neat form. The surfactant creates an obstacle to complete coalescence of the emulsion particles. Various techniques, such as polymerizable surfactants, have been employed to mitigate this issue. Nonetheless, homogenous films are never obtained starting from emulsions, and superior performance is delivered by solution acrylics which do form homogenous films and are devoid of surfactants.

A further disadvantage of emulsion-based systems is the difficulty of drying them. The high heat of vaporization of water makes it impractical to dry films above 50 µm since inordinately long dryers would be required. Such thick films, common in industrial tape applications, are not required for the majority of labels or graphic films. Here emulsion acrylics, coated to about 25 µm, find wide use.

The molecular weight of solution acrylic polymers is limited by the need to coat the adhesive, which requires a viscosity less than 10,000 cP, and the desire to minimize the amount of solvent that must be evaporated. Solid levels are normally kept above 20%, with 40–50% typical. Molecular weight is determined by the same factors which control any free radical polymerization. Thermal initiators are most common, such as azo and peroxide types. Polymerization can be done under pressure, allowing independent temperature control, but is more commonly done under reflux. Solvent choice is therefore critical for fixing the temperature of polymerization. Polymerization is normally done at a solids level above that of the final product. The polymerization solvents are chosen based on the desired reflux temperature, the solubility of the polymer, and their effects on polymer viscosity,



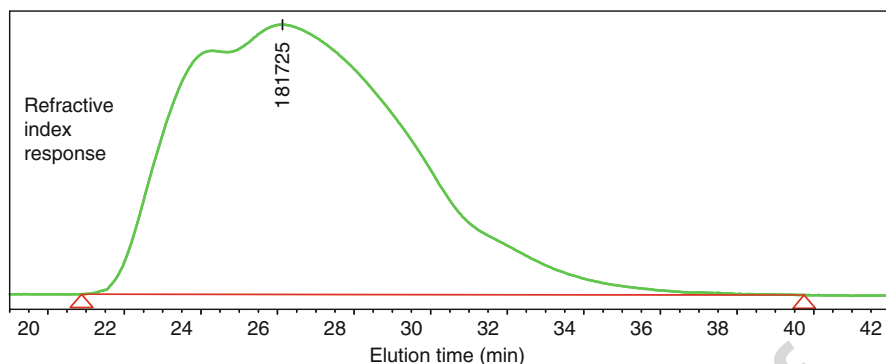


**Fig. 15** Gel permeation chromatography (GPC) trace of a typical solution acrylic polymer in dimethyl acetamide. The number average molecular weight,  $M_n$ , is 58 kDa, and the weight average molecular weight,  $M_w$ , is 312 kDa, based on polystyrene standards and using the integration points and baseline as shown. The molecular weight at the peak detector response is indicated

MW (through their tendency toward chain transfer), their health and safety profile, and their effect on the coatability of the final solution. A typical polymerization solvent would be a blend of ethyl acetate and heptane or isopropanol. The concentrated polymer solution is then diluted to achieve the desired stability and coating performance. Most solution acrylics are crosslinked via their acrylic acid groups using metals such as aluminum or titanium. These metals are incorporated into the adhesive in chelated form. To ensure shelf stability, extra chelation agent is often added to the mix, such as 2, 4-pentanedione. To minimize intermolecular hydrogen bonding in the solution and thus reduce viscosity, isopropyl alcohol is added. Toluene is also sometimes added to prevent bubbling on drying due to its higher boiling point which prevents the film from forming a solid skin as the more volatile solvents (ethyl acetate and heptane) are removed.

To consume the last traces of monomer, a final shot of initiator is often added at the end of the polymerization. This last step produces a small portion of very low molecular weight polymer. The final polymer often has a bimodal molecular weight distribution with a number average degree of polymerization of only about 40,000 Da but a weight average of four to eight times higher; see Fig. 15. This broad molecular weight distribution is beneficial as it provides a wide range of relaxation times and therefore viscous dissipation over a broad range of temperatures/peel rates. This breadth of relaxation times is evident in the dynamic mechanical temperature scan. As shown in Fig. 16, solution acrylics have a high tan delta, i.e., a large portion of its response to stress is viscous, over a very broad temperature range in comparison to a typical rubber-based PSA.

### 15.4.3 Crosslinking

To obtain an adequate level of shear and clean removal from substrates, some level of crosslinking is necessary. With water-based adhesives, this is accomplished by

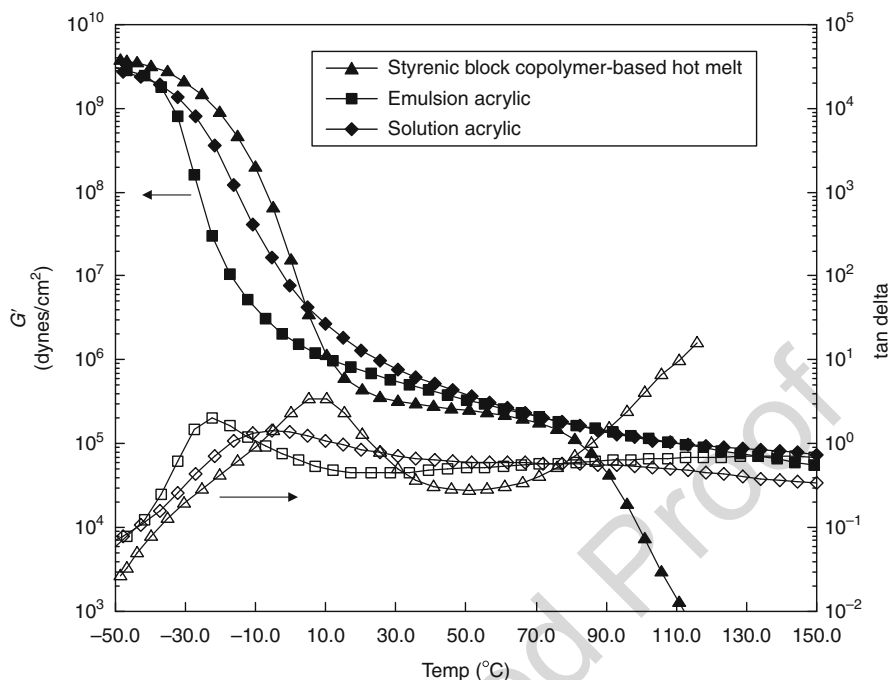


**Fig. 16** Comparison of  $G'$  and  $\tan \delta$  ( $G''/G'$ ) versus temperature for a styrenic block copolymer (SBC) – based PSA, a solution acrylic PSA, and an emulsion acrylic PSA (Reprinted with permission from Hu and Paul (2009), copyright Taylor and Francis)

using a portion of difunctional monomer and thus crosslinking during polymerization or by post-adding a crosslinker just prior to coating such as a polyisocyanate or most often a polyaziridine. The former reacts with alcohol groups on the polymer and the latter with acid groups. These same crosslinkers can be employed with solution acrylics to produce covalently bonded polymers. However, in most applications a one-part system is preferred. For these, metals are used, most commonly titanates and aluminum acetylacetonate (acac). The metal's ligands evaporate on drying liberating the metal to chelate with the acid groups and/or hydroxyl groups of the polymer. These metal oxygen crosslinks are labile at very high temperatures, whereas covalent crosslinks are not.

Another way to covalent crosslinks from a one-part system is to use electron beam or ultraviolet light radiation, by adding such a curing station at the end of the coating line. The need for inerting and the high capital cost of electron beam have driven the decision to favor UV curing.

Alternatively, neat polymerization is practiced in-house by several tape makers, using a complex UV-initiation process (Martens et al. 1980). Typically the monomer syrup is applied and polymerized very slowly under nitrogen using black lights. Slow polymerization provides high molecular weight – higher than can practically be obtained via solution polymerization. Some portion of difunctional acrylate is

included to provide a very low level of covalent crosslinking. This method provides a covalently crosslinked structure with outstanding shear hold. However, it is not practical to remove all traces of residual monomer, and thus such tapes are only suitable for industrial use.

The issue of residual monomer can be avoided, by using preformed and purified reactive oligomers such as epoxy or urethane diacrylates. This method has the advantages of formulation flexibility and low viscosity and the ability to be coated by a wide variety of methods including screen printing. However, these systems typically trade off pressure-sensitive properties for these processing advantages. To form an infinite network from such lower molecular weight precursors invariably results in a more tightly crosslinked network. Extensibility and thus viscoelastic loss are compromised, and peel, tack, and hold are reduced. In some cases excellent properties are obtained, but then over only a narrow temperature range. Such oligomer-based formulas have had success in removable labels and other low performance applications.

Nonetheless, the industry is moving toward 100% solid systems, driven by environmental considerations and the much lower capital and operating costs of such systems. By moving from liquid systems based on oligomers to solid hot-applied systems, the crosslink density can be lowered, and the performance of the pressure sensitive is significantly improved. Formulation techniques can further mitigate the difference between 100% solid UV-cured hot melts and conventional solution acrylics.

Photoinitiators are necessary for UV cure systems in order to initiate chain extension and/or coupling of chains. There are various types of photoinitiators to choose from based on whether cure follows free radical or cationic chemistry (see Figs. 17 and 18). The photoinitiators shown are formulated into the system; however, they can also be chemically bound to the base polymer (see Fig. 19).

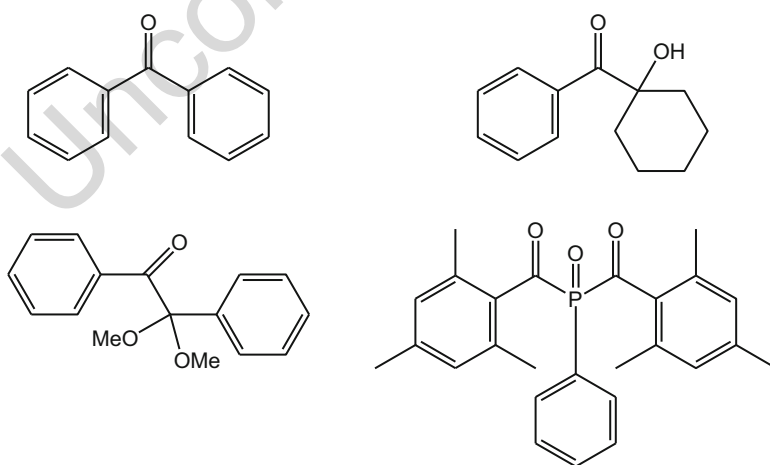


**Fig. 17** Photoinitiators for free radical UV cure

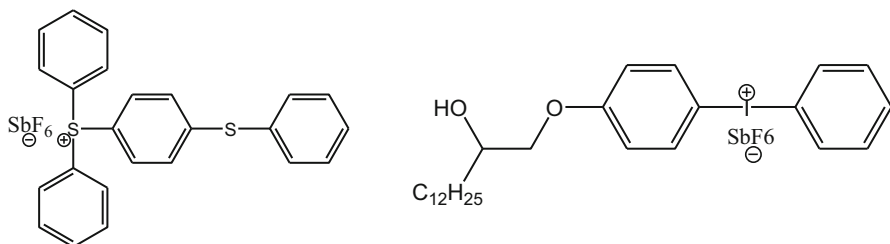
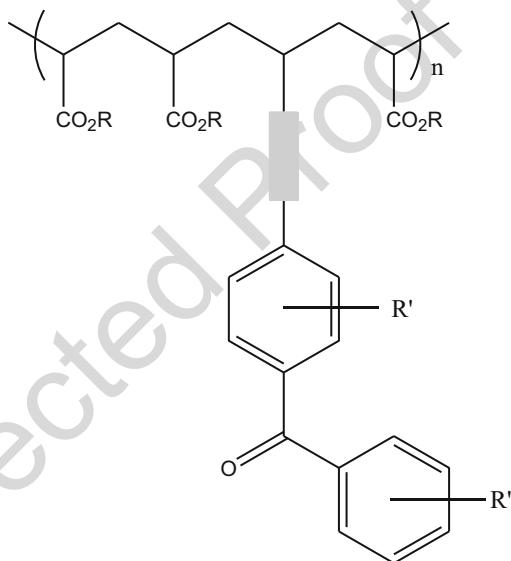


**Fig. 18** Photoinitiators for cationic UV cure

**Fig. 19** Polymer bound photoinitiator



A common commercial set-up is a slot-die hotmelt coater equipped with UV lights across the web just prior to lamination. There are a number of UV light choices available on the market today including microwave, arc, and LED. The microwave and arc systems contain lamps with broad spectral output including H bulb, H+ bulb, and D bulbs. LED bulbs by contrast exhibit a single narrow emission peak. It is important to match the photoinitiator UV absorption spectrum with the output from the UV light(s) in order to get maximum cure at the lowest dose.

A final consideration for UV cure is how Beer's law impacts the UV cure process. Photons are absorbed as they move through the film, and the intensity of the light is diminished, decreasing exponentially through the depth of the film. For this reason, UV free radical cure is usually limited to a thickness of about 5 mil (125  $\mu\text{m}$ ).

Thicker coatings can be obtained using UV-initiated cationic cure. In cationic cure, the UV light triggers the photoinitiator to form a super acid which in turn starts the cationic polymerization of cyclic ethers such as epoxides and oxetanes. These

reactive species do not couple and extinguish themselves like free radicals, or react with oxygen, but rather remain active until water or other basic impurities are encountered, or side reactions occur. Thus cationic polymerization can continue after the UV light source is removed, which is referred to as dark cure. Very thick pressure-sensitive films can be cured using cationic chemistry.

## Tackification

While tackifiers are not required to achieve pressure sensitivity in acrylic polymers, they are used to improve tack and peel, with some sacrifice in shear (see Table 1). Tackifiers have a higher  $T_g$  than the base polymer and much lower molecular weight, typically below 2,000 Da. These materials increase the  $T_g$ , pushing it toward room temperature and thus increasing the viscous loss and consequently the peel and tack (see Fig. 20 and Table 1). However, this comes at a sacrifice in low temperature performance. Tack is increased at room temperature because despite the higher  $T_g$ , the dilution of the entanglements softens the adhesive providing improved wet-out. The higher  $T_g$  increases the resistance to debonding in the tack test much as it does in peel. However, this can be carried too far. As the level of tackifier is raised further, eventually the  $T_g$  becomes too high and the adhesive too stiff. Tack will drop and then, at a somewhat higher level of tackifier, peel will drop as slip-stick behavior begins.

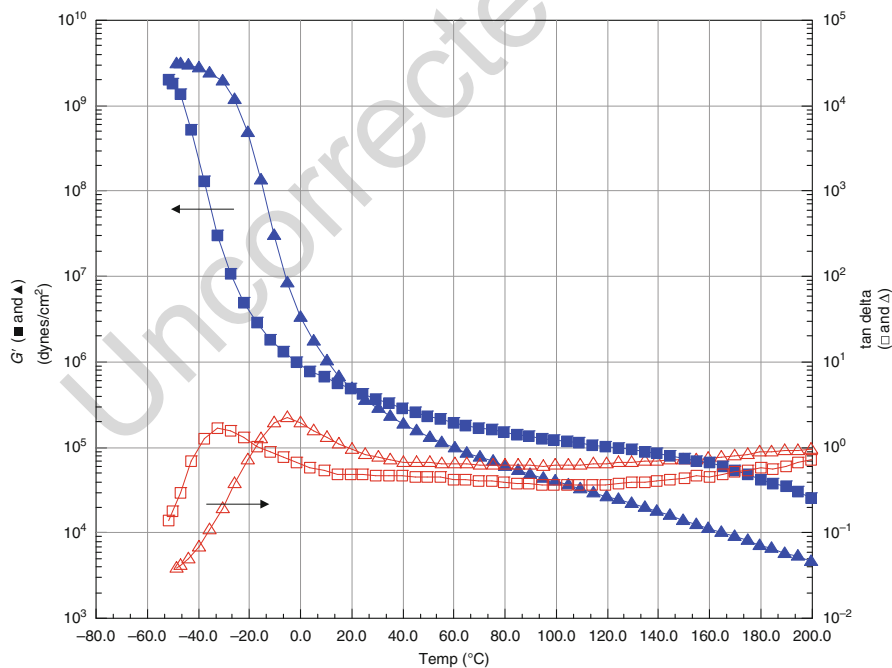


**Fig. 20** Dynamic mechanical properties versus temperature for untackified (acrylic A: ■, □) and tackified (acrylic B (tackified A): ▲, Δ) acrylic polymers. Adhesive properties are in Table 1

The loss in entanglement density upon tackification decreases the shear adhesion failure temperature and the hold at elevated temperatures (see Table 1). Hold at room temperature may also decrease, as it does for acrylic B in Table 1, but may not always due to the counterbalancing influence of the increase in Tg.

The most common reason tackifiers are added is to improve the adhesion to nonpolar plastics; see Table 1. Rosin ester tackifiers added at 15–30% will normally increase the peel several fold on polyethylene and polypropylene surfaces. For more polar surfaces, terpene phenolic or styrene phenolics are added. Tackifiers are discussed in more detail in the section on rubber-based adhesives below. Acrylics are compatible with only a narrow range of commercial tackifiers. Tackifier dispersions are available for water-based adhesives.

## 15.5 Rubber Based

The words “rubber” and “tackifier” imply physical effects materials can display. They are not linked directly to any specific chemical structures. “Rubbery” materials are defined by ASTM (D1566) as those which will have less than 50% permanent set after 1 min when recovering from a strain of 100% applied for 1 min. This is a physical, not chemical, definition. Any lightly crosslinked polymeric material (through physical or chemical crosslinks) of sufficient molecular weight to withstand a 100% deformation, and with a matrix phase Tg below room temperature (to allow rapid deformation and recovery), is a rubber (Rubbers are also treated in chapters ► “Adhesive Families,” and ► “Sealant Families”). Conventional “natural rubber,” if degraded to very low molecular weight and uncrosslinked, is not a rubber anymore but a liquid. Liquid rubber is an oxymoron, but one in common usage. From a historical perspective, rubbers were made from crosslinked polydienes (polyisoprene or polybutadiene) via sulfur crosslinking primarily, and so these early polymers – and butyl as well (polyisobutylene) – are often referred to as “rubber” even when they are not in this state.

In contrast to acrylics, the Me of all the low Tg rubber monomers are below 10,000 Da (see Table 3). Thus the polymers must have their entanglement density reduced to exhibit tack. This reduction in entanglements is accomplished by diluting the high molecular weight base polymer with materials that are less entangled or incapable of entanglements. These diluent materials can include low MW oligomers

**Table 3** Tg and Me of monomers in common rubbers

	Tg (°C)	Me (Da)
Isobutylene	−30	9,000
Ethylene propylene	−55	1,700
Ethylene butylene	−55	1,700
Isoprene	−60	7,000
Butadiene	−85	1,700
Styrene	100	18,000

of the base polymer itself (“liquid rubbers”), but more commonly are tackifiers and oils. These additives will be discussed in more detail below.

### 15.5.1 Natural Rubber

The rubbers in common use for pressure-sensitive adhesives are natural rubber and styrenic block copolymers. Natural rubber, cis-polyisoprene, is obtained as a latex from the rubber tree. To render it processible, it is degraded by shear, dissolved in solvent, and formulated with tackifiers and sometimes curing agents such as sulfur or phenolic resin (Eaverarts and Clemens 2002). The level of tackifier is about the same as the amount of rubber in the formula. Similar to the acrylics, the molecular weight distribution is broad, which provides adhesion over a broad range of temperatures/shear rates. However, unlike acrylics, these materials do not have polar groups attached to the polymer and consequently do not build adhesion to polar surfaces to the same extent. Due to their unsaturation, natural rubbers also have poor thermo-oxidative stability and so are not used in durable applications such as graphics. They find application instead for temporary bonding as masking and medical tapes.

### 15.5.2 Styrenic Block Copolymers

Styrenic block copolymers consist of high Tg polystyrene end blocks coupled to soft, low Tg mid-blocks made primarily of polybutadiene or polyisoprene. The end and mid-blocks are miscible with one another in solution or at high temperature but are sufficiently different in polarity that they phase separate upon drying or cooling. The hard styrenic end blocks thus physically crosslink the soft mid-blocks at their ends, providing them with heat and creep resistance.

Styrenic block copolymers are synthesized by anionic polymerization (Jagisch and Tancrede 1999). The high Tg polystyrene end blocks are polymerized first, followed by polymerization of the soft, low Tg mid-block. Next these diblocks are either (1) further polymerized with styrene or (2) reacted with a coupling agent to link two or more of these diblocks together. Normally 2 or sometimes 4 diblocks are linked; however, as many as 8–12 have been combined to produce so-called “star” polymers. The first process, called “sequential polymerization” can produce pure triblock copolymers for maximum strength and temperature resistance. The second process, coupling, is never 100% complete, so some diblock is always present. Heat resistance and strength are somewhat compromised, but peel and tack generally are increased by the presence of diblock. The amount of diblock can reach as high as 80 or even 100% if the polymer is high in styrene content and molecular weight. The upper limit for a particular starting diblock is set by the need to provide the final polymer in a readily dispersed form, either free-flowing pellets or a friable crumb. These forms permit the polymers to be dissolved or masticated quickly during the compounding of solvent-based or hot melt adhesives, respectively. By contrast,

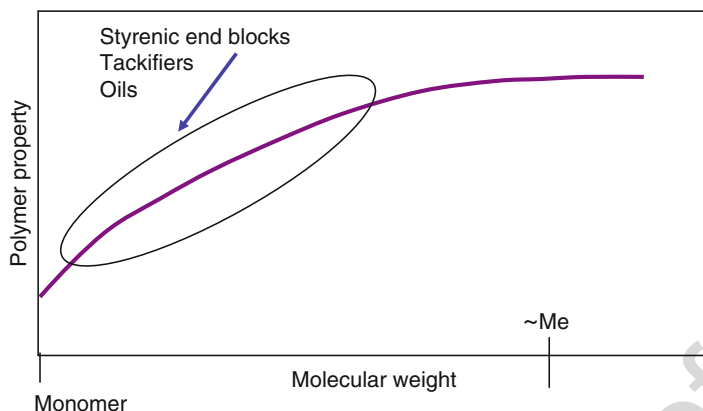


**Fig. 21** Polymer property versus molecular weight, where Me is the molecular weight at which the polymer chains become mechanically entangled (Reprinted with permission from Paul (2002), copyright Elsevier)

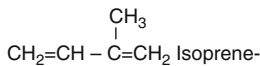
conventional non-blocky rubbers come in bales of about 20 kg each which the adhesive manufacturer must break apart using specialized equipment before blending with the other adhesive ingredients, and even then these conventional rubbers require extended mixing time. Thus a key advantage of the styrene block copolymers over conventional non-blocky rubber polymers is the ease of manufacturing adhesives from them.

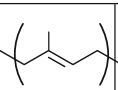
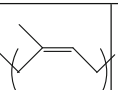
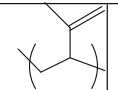
The polymerization of styrene anionically produces an atactic block. The typical end-block molecular weight for polymers used in pressure sensitives is below the 18,000 Da entanglement molecular weight of polystyrene (see Table 3). Thus the softening point of these polymers is less than that of pure polystyrene. Like the tackifiers and oils discussed below, the polystyrene end blocks are in the oligomeric region where properties still depend on molecular weight (see Fig. 21).

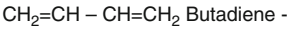
The soft block monomers are primarily isoprene and butadiene. These diolefins can each polymerize in one of three ways: (1) trans 1,4 addition, (2) cis 1,4 addition, or (3) across a terminal double bond to produce a pendant vinyl side chain (1,2 or 3,4 addition for butadiene or isoprene, respectively), as described in Fig. 22. The typical proportions of each and their Tg and Me (where available) are also shown. These proportions are easily varied by changing the polymerization solvent or adding complexing agents. The level of “vinyl” in the butadiene block is normally increased from 10% to 30% if this block is subsequently to be hydrogenated, otherwise the mid-block is prone to crystallization.

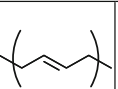
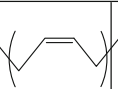
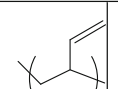
Styrene-isoprene-styrene (SIS) is the most common base polymer for pressure sensitives. The higher Me of isoprene versus butadiene permits higher levels of polymer to be used while maintaining adequate softness to meet the Dahlquist criterion. In addition, the overall polymer is higher in molecular weight for the same solution or melt viscosity. The lower solubility parameter for isoprene versus butadiene means that good phase separation between the hard and soft domains is





				For typical wt.%
	trans 1,4	cis 1,4	"vinyl" 3,4	
Typical wt. %	20	73	7	
Tg pure (°C)	-66	-71	20	-60°C
Me (Da)	NA	NA	NA	7,000



				For typical wt.%
	trans 1,4	cis 1,4	"vinyl" 1,2	
Typical wt. %	50	40	10	
Tg pure (°C)	-83	-95	-10	-85°C
Me (Da)	NA	2,900	1,700	1,700

**Fig. 22** Tg and entanglement molecular weight, Me, for isomers of polybutadiene and polyisoprene, and for typical average isomeric compositions in styrenic block copolymers (Reprinted with permission from Paul (2002), copyright Elsevier)

achieved at lower weight percentage of styrene. The lower styrene content of the adhesive produces a softer adhesive or alternatively enables additional polymer to be incorporated while maintaining tack. Peel and creep resistance benefit from the higher overall molecular weight and higher polymer content obtainable with SIS. Nonetheless, through careful formulation excellent pressure sensitives are made from SBS. These formulas have the advantage of being generally less expensive and significantly more thermo-oxidatively stable.

Hydrogenation of SIS and SBS produces SEPS (ethylene-propylene mid-block) and SEBS (ethylene-butylene mid-block), respectively. These saturated mid-blocks have relatively low Me values, similar to butadiene (see Table 3). Pressure sensitives based on SEPS and SEBS are generally inferior to those based on SIS and SBS in terms of peel, tack, and shear. However, formulations adequate for many applications have been developed. These polymers are used in removable applications such as for sanitary napkins which must adhere to undergarment fabrics and for attaching inserts into magazines or credit cards into mailers. Their superior thermo-oxidative stability and capacity for holding high levels of diluents are their key advantages in these and their other niche applications.

**15.5.3 Tackifiers and Oils**

Without dilution both natural rubber and styrenic block copolymers are stiffer than the Dahlquist criterion and therefore have no tack. Tackifiers gained their name

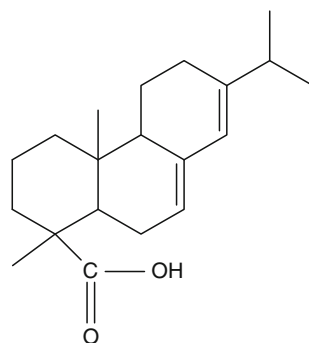
because of their capacity to render materials tacky when added. Tackifiers and oils are lumped to together in this section because they serve the same basic purposes in adhesive formulation:

- Reduce the entanglement density
- Lower the viscosity at a given solids level
- Adjust the  $T_g$
- Improve wet-out at a molecular level

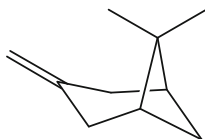
Both materials achieve these ends because they are amorphous and of sufficiently low molecular weight that they are unentangled. Where they differ is that oils are of low  $T_g$ , comparable to the soft phase of the base polymer, and tackifiers are of higher  $T_g$  than the base polymer. Together, they are used to optimize the full set of properties for a given application, including optimizing the formulation  $T_g$  and cost. The cost of most tackifiers is below that of most polymers, while oil is invariably the least expensive ingredient.

The range of commercial tackifier choices is extensive and growing. They are derived from trees or petroleum. From trees (stumps, sap, citrus oils, or pulpwood) are derived rosin and terpene monomers (see Figs. 23 and 24). From petroleum are derived various aliphatic monomers (principally piperylene and dicylopentadiene)

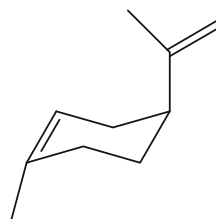
**Fig. 23** Abietic acid, the largest component in most rosin acids



$\alpha$ -Pinene



$\beta$ -Pinene



Dipentene (limonene)

**Fig. 24** Terpene monomers

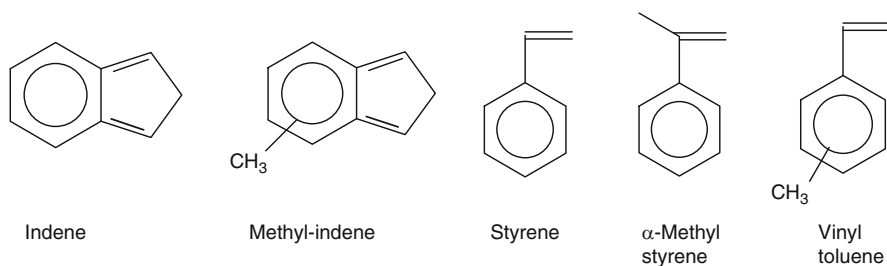


**Fig. 25** Vinyl monomers in the  $C_8 - C_{10}$  feed stream which polymerize to “ $C_9$ ” resins

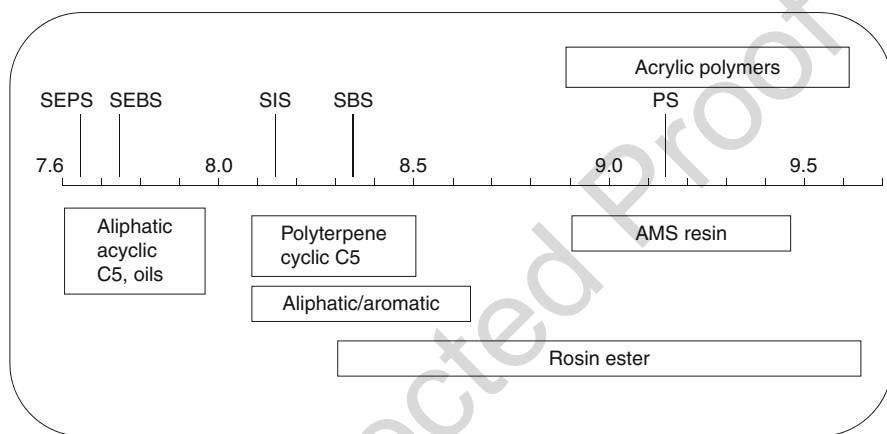


**Fig. 26** Solubility parameters of common tackifiers and polymers (Reprinted with permission from Hu and Paul (2009), copyright Taylor and Francis)

and aromatic monomers (see Fig. 25), and phenol. These materials are polymerized or copolymerized to obtain the desired polarity and Tg. More detailed descriptions are available elsewhere (Paul 2002). Rosin is the only material that can be used as a tackifier without modification. However, it is normally esterified with glycerin or pentaerythritol. As shown in Fig. 26, rosin esters offer the broadest range of compatibility. They are one of the few tackifiers compatible with acrylics. The excellent solvency power of rosin esters is likely why they are so effective in improving the adhesion of acrylic pressure sensitives to polyolefins. The more polar terpene phenolics and alpha-methyl styrene phenolics improve specific adhesion to polar surfaces and dilute entanglements with less of an effect on heat resistance due to their capacity for strong hydrogen bonding with the acrylic ester groups.

For styrenic block copolymers, the tackifier is normally chosen to be either mid-block (soft block) or end-block selective. For SIS, SEBS, or SEPS, the mid-block selective tackifiers are primarily aliphatic materials. For SBS, higher polarity is needed for the mid-block. Tackifiers composed of up to 30% aromatic

monomers are used. Rosin ester can be used with any of these polymers but in all cases is not entirely mid-block selective. A portion of the rosin ester will be incorporated into the styrenic end block leading to a decrease in softening point but an extension of the adhesive's open time. More details can be found in Hu and Paul (2009). The level of mid-block tackifier in PSAs based on styrenic block copolymers is very high, often more than half the formula and twice the amount of rubber.

The end-block selective tackifiers are usually added at a low level, 3–10%, to reinforce the end block. In a formulation with 30% polymer, containing 20% styrene, there is only 6% of the end-block phase. By adding 5% of end-block resin, this minor phase is reinforced, becoming more creep resistant. End-block tackifiers with  $T_g$ 's close to that of the polymer end block or higher are chosen to ensure the softening point is not compromised. Usually, for a given tackifier type, a range of softening points are offered, differing only in molecular weight not chemical composition. The higher the molecular weight, the higher the softening point ( $T_g$ ) since tackifiers are oligomeric materials and thus they are on the upward sloping portion of Fig. 21.

Oils, like tackifiers and styrenic end blocks, are oligomeric materials with molecular weights below Me. The majority of oils used in practice are petroleum derived with molecular weights between 300 and 600 Da. The higher the molecular weight, the higher the  $T_g$  and the lower the solvency power. These are hydrofinished to eliminate all but traces of aromatics, which are converted to cycloparaffins. The amount of linear, branched, and cyclic fractions of the oil depends primarily on the petroleum source. The more cyclics, the higher the  $T_g$  and solvency power and the less tendency to crystallize (Paul 2002). Low MW polyisobutylene oligomers are sometimes used in place of petroleum-derived oils. The amount of oil used in adhesives based on styrenic block copolymers ranges from none to as much or somewhat more than the rubber content. Typically oil is present at from 50% to 100% of the level of rubber.

In acrylic adhesives, plasticizers are rarely used. Conventional oils are incompatible due to their low polarity. A variety of other polar plasticizers are compatible such as phthalates, adipates, trimellitates, benzoates, and phosphates.

---

## 15.6 Summary

For a material to be tacky and thus pressure sensitive, it must be sufficiently soft (the Dahlquist criterion of  $G' < 3 \times 10^6$  dynes/cm<sup>2</sup> ( $10^5$  Pa) on a time scale of 1 s). Some polymers are sufficiently unentangled that they can meet this criterion without dilution. Acrylics based primarily on high Me, low  $T_g$  monomers such as butyl acrylate, 2-EHA, or iso-octyl acrylate, are in this class. Styrenic block copolymers and natural rubber are not and require dilution with tackifiers and/or oils. To qualify as a pressure-sensitive adhesive – a solid material and not merely a pressure-sensitive liquid – some minimum level of cohesion is required for clean peel and

adequate hold. This cohesion is obtained in acrylics through the use of hydrogen bonding monomers and also usually crosslinking, either covalently or by metal complexation of acrylic acid groups. Natural rubber also requires crosslinking, usually through sulfur, but styrenic block copolymers (SBC) rely only on the physical crosslinks provided by their high  $T_g$  end blocks which phase separate on cooling. However, this characteristic compromises the temperature resistance of SBC-based adhesives ( $SAFT \leq 110^\circ C$ ) in comparison to acrylics, where  $SAFT$  values can often reach above  $150^\circ C$ .

Optimization of properties generally involves trade-offs between tack, peel, and shear. Because peel and tack involve deformation of the adhesive on a relatively fast time scale,  $\sim 0.01$  s, raising the  $T_g$  of the matrix phase tends to improve both properties, up to a point. Once the failure becomes slip-stick, i.e., the material behaves rigidly during debonding, the average peel and tack drop. Tack drops first, because the time scale for initial wet-out is much shorter – 1 s versus typically at least 20 min for peel samples. The level of peel depends on the work that can be done on the tape.

To maximize the work done, the adhesive must hold onto the substrate strongly, i.e., the strength of the interaction with the substrate is critical. The work done on the adhesive depends on the force required to deform it (the level of viscous dissipation at a given strain rate) and the distance over which it is deformed (the extensibility of

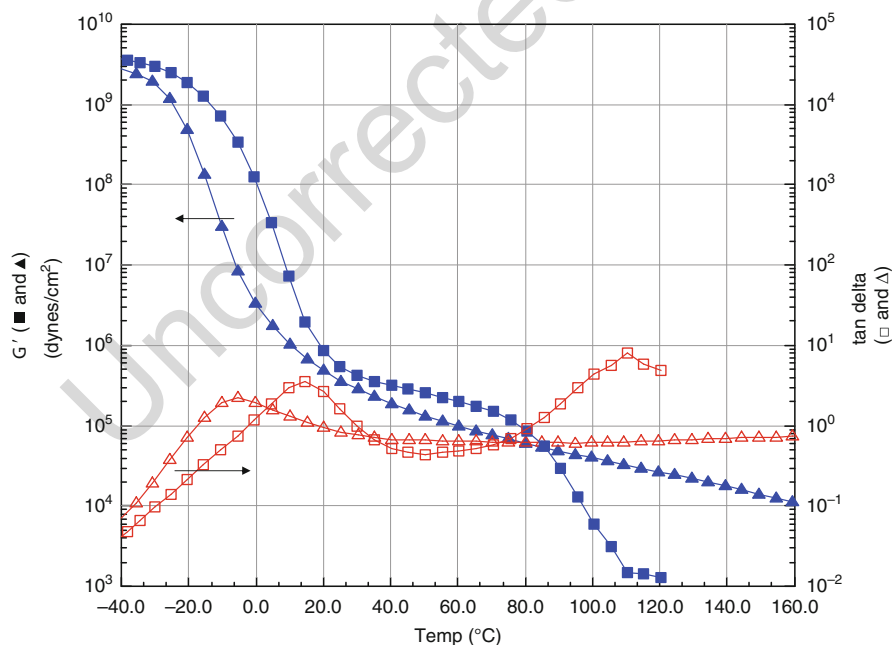


**Fig. 27** Dynamic mechanical properties versus temperature for tackified solution acrylic (acrylic B:  $\blacktriangle$ ,  $\triangle$ ) and a solution rubber adhesive, also tackified, based on styrenic block copolymers ( $\blacksquare$ ,  $\square$ ). Adhesive properties are listed in Table 1

the adhesive) as the peel front passes through. Thus peel is optimized with a strong interface, a high level of viscous loss as the adhesive is deformed, and a high level of extensibility (maximizing the total work done on each area of contact). Any permanent deformation of the backing also contributes.

Shear resistance increases with  $T_g$  (particularly the room temperature shear holding power), the level of crosslinking, and the polymer molecular weight, until again, failure occurs interfacially starting from the stress concentrations at the top edge of the tape. At this point the peel resistance dominates.

With acrylic adhesives the viscous dissipation of energy input, as characterized approximately by  $\tan \delta$ , is high over a much broader range of temperature than with rubber-based adhesives. Thus acrylics are chosen where a wide range of temperatures are expected. On the other hand, the sharper  $T_g$  and greater extensibility of rubber-based adhesives provides the highest levels of peel at an optimum temperature. This sharpness in  $T_g$  also contributes to their higher tack (see Fig. 27 and Table 1).

The selection of an adhesive for a specific application often hinges on the level of durability required. Untackified solution acrylics are chosen where durability is paramount.

---

## References

- Christensen SF, Everland H, Hassager O, Almdal K (1998) Observations of peeling of a polyisobutylene-based pressure-sensitive adhesive. *Int J Adhes Adhes* 18:131
- Creton C, Shull KR (2009) Probe tack. In: Benedek I, Feldstein MM (eds) *Handbook of pressure-sensitive adhesives and products, fundamentals of pressure sensitivity*. CRC Press, New York, pp 6-1-6-26
- Dahlquist CA (1966) Tack. In: The Ministry of Technology (ed) *Adhesion: fundamentals and practice*. Gordon and Breach, New York, pp 143-151
- Eaverarts AI, Clemens LI (2002) Pressure sensitive adhesives. In: Chaudhury M, Pocius AV (eds) *Surfaces, chemistry and applications: adhesion science and engineering*. Elsevier Science B.V, Burlington, pp 465-534
- Garif YS, Gerberich WW, Macosko CW, Pocius AV (2002) Proceedings of the 25th annual meeting of the adhesion society, pp 156-158
- Hu Y, Paul CW (2009) In: Benedek I, Feldstein MM (eds) *Handbook of pressure-sensitive adhesives and products, technology of pressure-sensitive adhesives and products*. CRC Press, New York, pp 3-1-3-45
- Jagisch FC, Tancrede JM (1999) Styrenic block copolymers. In: Satas D (ed) *Handbook of pressure sensitive adhesive technology*, 3rd edn. Warwick, Rhode Island, pp 346-398
- Kinning DJ, Schneider HM (2002) Release coatings for sensitive adhesives. In: Chaudhury M, Pocius AV (eds) *Surfaces, chemistry and applications: adhesion science and engineering*. Elsevier Science B.V, The Netherlands, pp 535-571
- Martens JM, Clemens LM, Zigman AR (1980) US patent 4,181,752
- Paul CW (2002) Hot melt adhesives. In: Chaudhury M, Pocius AV (eds) *Surfaces, chemistry and applications: adhesion science and engineering*. Elsevier Science B.V, Burlington, pp 711-757
- Pocius AV (2002) *Adhesion and adhesives technology*, 2nd edn. Hanser, Munich, p 151
- Pressure Sensitive Tape Council (2007) *Test methods for pressure sensitive adhesive tapes*, 15th edn

Ewen J. C. Kellar

## Contents

16.1	Introduction .....	410
16.2	Joint Performance .....	412
16.3	Joint Design .....	414
16.4	Pretreatments .....	414
16.5	Substrate Type .....	415
16.6	Adhesive Form .....	418
16.7	Application Requirements .....	418
16.8	Manufacturing Needs/Constraints .....	419
16.9	Aesthetics .....	419
16.10	Costs .....	422
16.11	Fabrication Issues (Jigging, Curing, Environmental Control, etc.) .....	423
16.12	Other Sources of Assistance .....	424
16.12.1	Adhesive Manufacturers/Suppliers and Trade Bodies .....	424
16.12.2	Consultancy and Academic Research Organizations .....	425
16.12.3	Online Assistance .....	429
16.13	Conclusion .....	429
References	.....	430

## Abstract

Selection of the correct adhesive for an application can be a daunting task due to the many types commercially available, ranging from different chemistries through different forms to almost a continuum of material properties. It is critical therefore to take a logical approach to this task and apply deselection criteria wherever possible. The needs of the final application are paramount and often a

E. J. C. Kellar (✉)

TWI Ltd. (The Welding Institute), Cambridge, Cambridgeshire, UK

e-mail: [ewen.kellar@twi.co.uk](mailto:ewen.kellar@twi.co.uk)

detailed review of the requirements can provide the engineer with some key selection needs or constraints which in turn may enable large groups of adhesives to be eliminated from consideration at an early stage in the process. It is also important to appraise aspects related to manufacturing, in terms of product volume, handling issues, curing equipment, dispensing equipment, etc. An apparently perfect adhesive with suitable mechanical properties may not be suitable for the application for one or more reasons such as not being able to be dispensed easily/rapidly enough, having a curing temperature that is too high for the substrate to tolerate, curing too fast for a large area joint etc.

Although the initial adhesive selection process is “only” a desktop exercise, the need to be efficient and identify only those candidates with the greatest property match requires that this activity be given a high level of importance. Almost every application will require a bespoke approach at some level and this will necessitate practical testing and trials to be carried out to verify suitability. Selection of unsuitable adhesives at the outset can be very costly in the long run.

---

## 16.1 Introduction

A quick search online or via textbooks in the library shows that there are many types of adhesives available to use, ranging in type from simple paper bonding adhesives to high-performance aerospace materials. Indeed if the reader considers the fact that in some cases the same generic adhesive will be sold under license to different suppliers or will be based upon common formulations, then there are probably hundreds if not thousands of adhesive products available worldwide to choose from. The situation is further complicated by the fact that the same adhesives can often be classified in several different ways; the main classifications being:

- Chemistry – epoxy, acrylic, polyurethane, etc.
- Form – two part (2K), single part (1K), paste, film, tape, etc.
- Function – wood bonding, metal bonding, multipurpose, rapid cure, etc.
- Cure type – room temperature (RT) cure, UV cure, moisture cure, pressure sensitive, etc.
- Specific property – high strength, electrically or thermally conductive, toughened, heat resistant, etc.
- Part name or number – VHB PSA, ESP110, Scotchweld DP8005, etc.

So it is not surprising to find the same adhesive being described as an RT curing two-part epoxy, as a metal bonding paste adhesive, Araldite 2015, or some other combination. Indeed it may well be that the standard titles do not convey or assist with the specific nature of the application in mind. Such a situation has the potential to make selection of the correct adhesive for the task in hand a potentially challenging activity. However, if the user follows a logical set of choice paths, then the task can be simplified considerably, Fig. 1. Key factors to consider include:



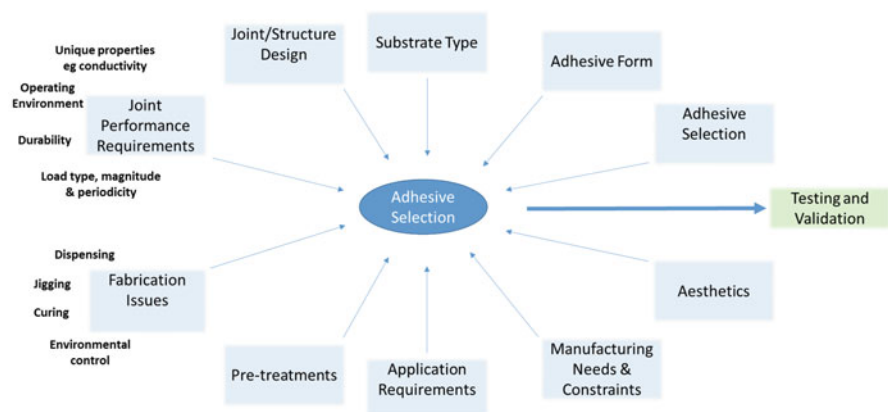


**Fig. 1** Primary influencing factors to consider when selecting an adhesive

- Joint performance requirements in terms of load type, magnitude, and periodicity; operating environment; unique properties (e.g., electrical conduction, low shrinkage); durability; etc.
- Joint/structure design
- Pretreatment type which often affects durability
- Substrate type(s), i.e., metal, polymer, ceramic, etc.
- Adhesive form
- Application requirements
- Manufacturing needs/constraints
- Aesthetics
- Cost
- Fabrication needs (dispensing, jigging, curing, environmental control, etc.)

As will be seen, it is important to understand from the outset what the key selection parameters are. Quite often the apparent key parameter can be superseded by another less obvious requirement. An example of this could be the physical form of the adhesive, i.e., whether it is a paste or a film which may turn out to be more important than the original selection parameter such as the mechanical strength of the joint. Both single-part paste and film adhesives can provide high strength joints, but while using a standard high strength paste, adhesive may be simpler and relatively cheaper per unit volume. Accurate rapid placement of the adhesive is critical to the manufacturing process which may require a significant amount of additional capital investment in terms of automated metering and dispensing. In contrast, a precut sheet of film or tape adhesive, although materially more expensive, is easy to handle and extremely quick to place in position prior to curing thereby potentially lowering costs while maintaining performance. Another example could be the need to identify adhesives that cure very slowly so that a large joint area can be bonded before the adhesive starts to gel or harden, over bond strength or cost.

The key parameters described above are often interrelated and it is therefore very important to stress that adhesive selection is often an iterative process where the first question must relate to what is required of the structure and the associated joints. This in turn will allow the engineer to start defining limits/requirements for the potential adhesive candidates. Often, whole families of adhesives can be eliminated early on in the process due to a single property such as pot-life duration, temperature of cure, shrinkage, or substrate type (Lees 1984). It is rare though, for there to be only one type or even only one specific product for an application. The inherent diversity of adhesives and the creativity of the chemists/formulators normally ensure a wide palette of adhesives from which to choose.

---

## 16.2 Joint Performance

When asked to design a structure or device, the engineer will normally always want to consider performance as a key initial selection criterion, but it should be remembered that “performance” is an umbrella term that covers many factors including:

- Mechanical strength – ultimate failure load, working load, toughness, etc.
- Loading conditions – static, impact, fatigue, intermittent peak, etc.
- Environmental tolerance – heat, cold, chemicals (acids, bases, solvents, gases, etc.), radiation, mechanical erosion, etc.
- Durability – prediction (how strong, how long?)
- Structural properties – conduction (thermal, electrical), self-repair, structural stability, etc.

Mechanical strength must not be oversimplified. The need for a strong joint can be subjective as there are adhesives which will provide very high bond strengths but at the cost of very low strain to failure values (e.g.,  $<0.05\%$ ). So while a headline peak failure load value may be impressive, say 40 MPa, the joint may well be very brittle and fails catastrophically when the peak load is exceeded with little or no indication. In contrast, a joint made using a toughened adhesive may be shown to fail at 20 or 25 MPa but at 5% strain, thereby demonstrating a much higher energy absorption capacity and a greater resistance to damage, especially with respect to impact loading. Such properties will significantly affect the types of applications for which an adhesive may be used. In the case of the first example (high strength and low strain to failure), it may be best suited to aerospace applications whereas the toughened system (lower strength and high strain to failure) is much more likely to be the adhesive of choice for an automotive application.

Loading conditions can be regarded as an extension of mechanical strength in that the form and type of load that the joint is designed for will also affect adhesive choice. Very high static loading conditions will require adhesives with high creep

resistance whereas “softer” more elastomeric adhesives will be better suited to fatigue cycling.

The core chemistry of an adhesive will have the largest effect on the environmental resistance of the adhesive. Epoxy-based systems are extremely tolerant of a wide range of chemicals either by resisting their uptake or by allowing free diffusion through the polymer structure whereas cyanoacrylates have a lower tolerance to water exposure. Polyurethanes and to a lesser extent toughened acrylics will start to thermally degrade above 160 °C while there are epoxies that will survive continuous exposure to temperatures of 250 °C or greater and some cyanate esters or aromatic polyimides systems which can be used continuously in environments of 320 °C or more. The majority of adhesives are chemically cross-linked rendering them stable but irreversible in structure but there are some which are not cross-linked, termed thermoplastics, which can be remelted or reformed. Examples of thermoplastic adhesives include hot-melts, cyanoacrylates, and polyvinyl acetates (PVA). Although limited in terms of temperature and chemical solvent tolerance, they do offer the benefit of reworkability and recyclability, useful green credentials in a modern world.

Probably the most common and important question that arises in the engineer’s mind when selecting an adhesive is how long will the adhesive joint last and will it be as strong in 5 or 15 years as it is at the start? Absolute life prediction of a bonded structure is still some way off and the adhesive is only one component within the joint. It should be remembered that the term “joint” refers to a system including the substrates (often termed adherends), the adhesive, and the surface pretreatment(s), or a primer or adhesion promoter applied to the substrates prior to bonding. The joint will only be as strong as the weakest link and if the pretreatment is inappropriate or the substrate has low cohesive strength, then the ultimate performance of the joint will have little to do with the adhesive selected. In the majority of cases, the stability of the modern adhesive will be sufficient to last at least as long as the substrates. Studies of bonded steel joints which had been aged in a marine environment have shown that in some instances the steel substrate corrodes much more quickly than the rate at which the adhesive degrades. See Part F “Durability,” for more information.

Almost all adhesives are complex mixtures, where the base resin will dictate many of the underlying properties, but which are modified to a greater or lesser extent by varying amounts and types of additives. Such components can increase toughness, reduce shrinkage, speed up or slow down cure rates, change rheology, change structure, provide new properties such as conduction (thermal/electrical) or self-repair, or simply reduce costs by acting as a simple bulking agent. Small amounts of highly specialized chemicals can enhance adhesion or increase tolerance to surface contamination.

It is hoped that the reader will now have an understanding that adhesive selection based purely upon performance can be daunting, but if a key, perhaps very specific parameter, can be identified such as electrical conductivity, then the adhesive selection process can be made much simpler.

### 16.3 Joint Design

The design of a joint can have a significant effect upon the type of adhesive that can be selected for two key reasons. The first and the most important being the way in which load passes through the joint, i.e., a joint which will see significant levels of peel and/or cleavage will require a toughened system that is resistant to such loads whereas high levels of shear or tension may be better addressed with a more rigid system. More information is given in Part E “Joint Design.” The other reason relates more to the way in which the joint requires to be assembled. If the joint is very large in size, then the adhesives selected will have to have a working life prior to cure (often termed as pot life) that is sufficiently long to allow for the application time especially if this is a manual operation. Examples would include either very slow cure mixed materials or single-part adhesives where cure is initiated by a controllable external source such as heat or radiation. This method of assembly assumes that the adhesive is applied prior to the structure being assembled and that the adhesive is of a form that will not move or migrate to any extent once applied, i.e., in a viscous liquid/paste or a solid state.

Some structures are better fabricated by applying the adhesive after the parts are brought together. In this case, the adhesive must be of sufficiently low viscosity that it can enter the joint area either through gravity/capillary action or by pumping.

### 16.4 Pretreatments

Critical to the success of an adhesive bonding operation is the type of surface pretreatment that is used. If the pretreatment (or lack of it) is not matched to the application and the substrate(s), then it is extremely likely that the joint will be compromised in a number of ways including initial strength, durability, environmental resistance, and substrate damage. As described in more detail in Part B “Surface Treatments,” there is a wide range of surface pretreatments from which to choose, each having distinct attributes, in particular being compatible with the substrate and ideally also with the adhesive.

Basic pretreatments are highly generic and very substrate/adhesive nonspecific; they typically include degreasing, washing, and abrasion, although care must be taken with selecting the correct abrasive medium for metallic materials to avoid the potential for contamination and possible galvanic corrosion, i.e., steel shot should never be used on lighter alloys (aluminum, magnesium, etc.). However, more complex pretreatments based upon chemical processes (etching, oxide growth, chemical conversion, etc.) and energetic physical processes (plasma, flame, corona, and laser) can be substrate specific. The final state of the pretreated surface may have an effect upon the type of adhesive that is selected in terms of adhesion properties such as wettability, mechanical interlock, polar attraction, chemical reaction, etc. Furthermore, if a primer or adhesion promoter is also used, then the likelihood of specific adhesive compatibility increases significantly. Examples include silane systems, often called coupling agents, where the silane molecule has two sites of

different chemical reactivity, one for reaction/interaction with the substrate surface and the other which can chemically react with the adhesive resin. It is therefore important to match the silane reactivity to the adhesive/substrate chemistry for the highest levels of adhesion. The most common type of silane reactivity is based upon the epoxide group. In the case of primers, it is also advisable to select similar chemistries where possible.

## 16.5 Substrate Type

The type of substrate or adherend that is required to be adhesively bonded may have an effect upon the type of adhesive to select for the task. This is especially true for thermoplastic polymers where either the adhesive may have a detrimental effect upon the polymer such as crazing, swelling, or in some cases dissolution or there may be an incompatibility that renders the adhesive incapable of bonding. Examples of the detrimental effects would be the use of some types of acrylic-based adhesives with polycarbonate or polystyrene where both crazing and dissolution are common or cyanoacrylates for acrylic systems where crazing often called fogging can be an issue. Incompatibility is especially relevant when trying to bond low energy polymers such as fluoropolymers (e.g., polytetrafluoroethylene [PTFE]) or the polyolefins (polyethylene and polypropylene). In the case of fluoropolymers, only specific surface pretreatments can be used to achieve any type of adhesion whereas polyolefins can now be bonded with some speciality-toughened acrylic systems.

In the case of metals, sensitivity is not quite so marked, although some adhesives in the anaerobic class are sensitive to the presence of certain metal ions, in particular copper which can act as a cure inhibitor. In contrast, the presence of other metal ions on the surface is essential for the curing process to occur at all and anaerobic adhesives will not work to bond together nonmetallic substrates. A simple selection guide is provided in Table 1.

All of the examples cited above have been specific to the chemistry of the substrate but the physical form can also have an effect, in particular porosity. Some adhesives are aqueous suspensions, e.g., poly vinyl acetates (PVAs), and others rely upon adsorbed moisture or ease of moisture transport to the bond-line for cure to occur, examples being single-part polyurethanes and silicones. In the case of PVA usage, it is important for either one or both of the substrates to be porous in nature, e.g., wood, paper, masonry, etc.

Extreme selection examples would be the ability to bond to materials in very nonideal conditions, e.g., wet/damp surfaces, underwater, or to very "contaminated" surfaces where oils are present. In such cases, the adhesives have been carefully formulated to address these requirements but the products are very specialized and come from limited sources/suppliers.

Another factor to consider relates to the mode of cure and the effect this may have on the substrate. The use of an ultraviolet (UV) curing adhesive on opaque materials is not going to be satisfactory as UV energy from the UV source can be absorbed or

**Table 1** Adhesive selection based on substrate type to bond (Shields 1984)

	Epoxy	Nitrile-phenolic	Vinyl-phenolic	Neoprene-phenolic	Resorcinol formaldehyde	Phenol formaldehyde	Melamine formaldehyde
Metals	×	×	×	×			
Ceramics	×						
Wood	×	×			×	×	×
Paper				×			
Leather		×					
Textile							
Elastomers							
Neoprene							
Silicone							
Polyurethane							
Thermoplastics							
PVC (flexible)							
PVC (rigid)	×						
Cellulose acetate					×	×	
PE (film)							
PE (rigid)	×	×					
PP (film)							
PP (rigid)	×	×					
PC	×						
Teflon®	×					×	
PS	×						
PA	×	×			×	×	
Thermosetting							
Epoxy	×				×	×	
Phenolic	×	×		×			
Polyester	×						
Ethylene polyterephthalate							
Polyaromatics	×						

Urea formaldehyde	Polyaromatic	Polyester	Polyurethane	Anaerobic	Cyanoacrylate	Modified acrylic
	×		×	×	×	×
			×	×	×	×
×			×			×
			×			
			×			×
			×		×	
						×
						×
			×			×
			×		×	
			×	×	×	×
×			×	×	×	×
		×				
		×				
	×					

blocked preventing the adhesive to cure within the joint where the adhesive is hidden.

There are probably two main adhesive classes which rarely exhibit substrate sensitivity: the two-part epoxies and the two-part polyurethanes; both rely upon internal curing mechanisms and do not contain solvent-like agents.

---

## 16.6 Adhesive Form

Adhesives are available in a wide variety of forms such as liquids of varying viscosity, pastes, semisolid films, and solids (powders, granules, chips, blocks, etc.). The form of the adhesive will dictate how the adhesive is dispensed/applied and the way in which the joint is designed and the structure manufactured (Table 2). For example, a low viscosity liquid is not easily applied to a joint oriented in an overhead or vertical position, whereas a paste adhesive would be a good choice. However, the same liquid system would be better suited to application over a large flat area or one which is very small and constrained with regard to access. Film adhesives are excellent for precise positioning in joints which are prepared to very high tolerance limits but are very poor for more variable structures where additional adhesive may be required to fill larger gaps or variations along the bond-line, whereas a paste adhesive would be much better suited for this application.

Another quite specific aspect relates to the use of adhesives in a film form such as pressure-sensitive adhesives or thermosetting systems such as epoxies. Such materials can appear to be quite expensive when compared to similar liquid/paste analogues, but there are many obvious benefits to using precut “dry” systems which can be easily handled and laid directly into the joint area before assembly. Often, especially in the case of pressure-sensitive systems, the adhesive can be supplied precut, ready for use with little or no wastage. Such properties enable the manufacturer to minimize assembly time, increase tolerances, and reduce rework which can have a significant effect on cost reduction thereby justifying the higher relative price of the adhesive used.

---

## 16.7 Application Requirements

Due to the inherent diversity of adhesives and potential for almost infinite formulations, these materials can offer a wide range of additional properties over the “simple” requirement to form a load bearing, structural joint. Such properties can include high compression strength, toughness, abrasion/erosion resistance, stiffness/elasticity, optical properties, anisotropic properties, tolerance to extreme temperatures (high and low), conductivity (thermal and/or electrical), dielectric properties, acoustic damping, chemical resistance, tolerance of contaminated surfaces, biocompatibility, bioactivity, etc. It may well be, therefore, that the initial requirement to select an adhesive to bond two substrates with a particular strength may be overridden by another more specific property such as one those listed above.



Indeed for some applications, the bond strength may be completely secondary to another function, e.g., a bioactive agent may be incorporated into an adhesive to ensure that rejection or infection are reduced/eliminated or for electrically conductive adhesives the level of resistivity may dominate the selection and ultimate function of the adhesive.

---

## 16.8 Manufacturing Needs/Constraints

Manufacturing requirements also have an impact upon the form of adhesive used, especially in terms of the number and size of products to be produced. The use of a single-part system will allow a simpler mode of dispensing to be employed, i.e., no mixing and subsequent replacement of mixing nozzles, but in turn such systems may be more restrictive with regards to curing time, i.e., they may cure very rapidly (cyanoacrylates) or they may require heat (epoxies) or radiation (acrylics). In contrast, a two-part system can be formulated to cure at different rates. If external curing stimuli such as heating or radiation is needed, then this can add to the total capital expenditure of fabrication although it may offer additional manufacturing control to the product assembly, i.e., assemble a number of separate products and then cure all of them at once using UV radiation. Alternatively adhesives can be selected so that they can be cured using a process normally assigned to another function (e.g., to cure a paint or other coatings). Examples of this include the ability to cure flange adhesives in car body structures at the same time as the paintwork is being cured or curing of electronic bonding adhesives on a circuit board during the solder reflow process.

Rapid cure systems are usually suited to small precision bond-lines such as medical or electronic products, whereas long cure time adhesives are used either for much larger structures where a large area has to be covered with adhesive before the two parts are brought together – a good example would be the assembly of a deck to the hull of a large yacht where the joint could be many meters in length – or where the joint is part of a more complex assembly and cure is required to be carried out at a later stage of the fabrication process.

If a small number of components are required to be adhesively bonded together, then it is most likely that the process will be manual in type as the cost of automation would not be justifiable. A key benefit of adhesive bonding is that it is fully scalable, enabling initial prototypes to be manually assembled, but as volumes increase, more and more of the bonding operations can be automated. See Part G “Manufacture” for more information on manufacturing.

---

## 16.9 Aesthetics

In some instances (bonding transparent materials or for visual impact), there may be a need for the adhesive to be seen as part of the structure, deliberately or otherwise. In such circumstances, care must be taken to select adhesives that have the correct

t.1 **Table 2** Adhesive selection based upon the form and processing conditions (Petrie 2007)

t.3	Type of adhesive	Common forms available				Solvent solution, emulsion
		Solid	Film	Paste	Liquid	
t.4	Epoxy (polyamine)			×	×	
t.5	Epoxy (polyanhydride)	×	×	×	×	
t.6	Epoxy (polyamide)			×	×	
t.7	Epoxy-phenolic		×	×		
t.8	Epoxy-nylon		×			×
t.9	Epoxy-polysulfide		×	×		
t.10	Nitrile-phenolic		×			×
t.11	Vinyl-phenolic		×			
t.12	Neoprene-phenolic		×			×
t.13	Resorcinol formaldehyde				×	
t.14	Phenol formaldehyde				×	
t.15	Melamine formaldehyde	×				
t.16	Urea formaldehyde	×			×	
t.17	Polyimide		×			×
t.18	Bismaleimide		×	×		
t.19	Polybenzimidazole		×			
t.20	Polyester + isocyanate		×			×
t.21	Polyester + monomer			×	×	
t.22	Polyurethane			×	×	×
t.23	Cyanoacrylate				×	
t.24	Acrylic			×	×	

Cure method		Processing conditions			
Solvent release	Chemical reaction	Room temperature	High temperature	Pressure required	Pressure not required
	×	×	×		×
	×		×		×
	×	×	×		×
	×		×	×	
	×		×	×	
	×	×			×
	×		×	×	
	×		×	×	
	×		×	×	
	×	×	×	×	
	×	×	×	×	
	×		×	×	
	×	×	×	×	
	×		×	×	
	×		×	×	
	×		×	×	
	×		×	×	
×	×	×	×	×	
	×	×	×		×
×	×	×			×
	×	×		×	
	×	×			×

visual characteristics. This might be relatively simple such as using a water-clear adhesive to bond transparent plastic/glass or perhaps as a design statement as shown in the Lotus Elise chassis where the adhesive is now a characteristic blue color (it used to be orange). For such applications, the adhesive must be applied very carefully and the final cured bond must be made to be aesthetically acceptable, with attention given to ensuring that the form and profile of the edge fillet is even and defect free.

Where transparent joints are required, the choice of adhesives can be significantly reduced as fully transparent systems will not be able to contain much, if any, filler or additives. Such a constraint will limit properties such as rheology, toughness, thermal conductivity, etc.

---

## 16.10 Costs

Costs are always never far from a manufacturer's mind and as before, adhesives offer a number of choices. Ultimately, almost all adhesives are derived from oil products and are therefore subject to world oil price fluctuations, but some systems are inherently more expensive than others. However, while base feed-stock prices will have some effect, much more cost is associated with manufacturing activity, functionality, quality, and ultimately the markets for which they are destined.

Aerospace film adhesives demand specific specialized processing equipment, high performance, consistent high quality, and careful transport and storage requirements. The demands are ultimately defined by the end users but no adhesive manufacturer would want a substandard product on an aircraft. In order to deliver such a product, it has to be tested and assessed at each stage. All of this work has a cost which is ultimately passed on to the consumer. Other areas where performance is critical are the medical sector and electronics applications. The former requires a product of extremely high quality and often high purity whereas the latter may contain high value additives such as silver to ensure the highest levels of electrical conductivity. Due to the very precise nature of the applications described, adhesive volumes are not necessarily that high but the consequences of failure are, making the adhesives used, high value components.

In contrast, industry sectors where higher volumes of adhesive are used may demand lower costs with little compromise to quality; examples would include the automotive sector and shipbuilding. Tolerances are often much lower, although the structural needs are still great. In these areas, a greater design leeway is factored into the structure allowing for more adhesive to be used. The costs associated with the additional testing and properties required by the end users are offset against the higher volumes of adhesive sold with lower margins. There are also many other factors which can affect cost of an assembly; these include storage, handling, drying, degassing, or dispensing of an adhesive or the substrate, type of surface preparation and cost of associated materials used (e.g., primers), fixing and assembly of the joint, type of curing method used, and cost of labor for each of these steps.

### 16.11 Fabrication Issues (Jigging, Curing, Environmental Control, etc.)

To enable effective fabrication using adhesive bonding, a wide range of factors must be considered which relate to the process of creating the bonded joint, most normally within a manufacturing environment. Examples of which include some areas already covered previously, such as joint design and assembly needs and within those processes adhesives have to be suitable to either remain in situ when applied (thixotropic pastes) or flow into inaccessible areas when the joint is formed. They have to cure in a controlled fashion either from an internal chemical reaction (room temperature systems) or by some external stimulus such as heat or light.

Considerations also need to be taken with regard to the mechanical performance of the joint and the potential sensitivity the adhesive is to bond-line thickness (BLT). Some adhesives are much more tolerant of BLT than others and can be used within variable tolerances in some instances up to and even greater than 1 mm (e.g., epoxies and polyurethanes), whereas others benefit from very low BLT values/ranges in the order of 20–50  $\mu\text{m}$  (e.g., cyanoacrylates). To ensure that such BLT values can be attained, four strategies can be considered:

- Joint tolerance – depending upon the substrates to be bonded, careful design, machining, and alignment are critical in achieving consistent BLT values.
- Jigging/fixtures – external jigging and fixtures such as clamping, tailored frames, fasteners, etc. will ensure that the parts are held closely together with little or no chance of movement while the adhesive cures.
- Joint features – in tandem with joint tolerance and jigging is the inclusion of features within the joint area such as ridges or localized protuberances which will hold the joint apart to a specific tolerance.
- Internal adhesive components – a relatively simple approach to achieving BLT control is by selecting an adhesive that has an internal additive/filler of sufficient dimensions to limit the minimum value of BLT. Normally such fillers are added by the adhesive manufacturer but the end user can also add material such as glass beads (ballotini).

Joint tolerance limits can have a significant impact upon adhesive selection. Different adhesive types will respond to the above approaches in different ways. For example, epoxy adhesives show little shrinkage upon cure and therefore are relatively insensitive to additives or external joint factors, whereas toughened acrylic adhesives can exhibit considerable shrinkage ( $\sim 10\%$ ) and if the joint cannot move sufficiently to accommodate this, then local voids can be formed and residual stresses can be very high. Moisture curing systems (e.g., polyurethanes and silicoes) require a relatively large BLT to enable the movement of water vapor into the adhesive and a thin BLT will significantly inhibit or slow the rate of cure.

Adhesive choice can therefore be influenced by actual joint tolerance control and dimensions and where a cyanoacrylate or an anaerobic adhesive might be ideal (polymeric substrates or a threaded metallic joint, respectively), the measured bond

421 gap may be too large and an alternative adhesive such as a polyurethane or an epoxy  
422 may be better suited.

---

## 423 16.12 Other Sources of Assistance

424 Assistance with adhesive selection may in the first instance come from asking others  
425 who have more experience with specific adhesives or with adhesives in general.  
426 Typically such help will come from a variety of sources, the main ones being:

- 427 • Adhesive manufacturers/suppliers and trade bodies (direct but product-specific  
428 information)
- 429 • Consultancy organizations (direct but product-neutral, i.e., no product preference)  
430 including universities and research and technology organizations (RTOs)
- 431 • Online resources (indirect and both specific and nonspecific information,  
432 depending upon reference source)
- 433 • Reference books

### 434 16.12.1 Adhesive Manufacturers/Suppliers and Trade Bodies

435 Every adhesive product should have a technical datasheet (TDS) and must have a  
436 materials safety data sheet (MSDS) to comply with international regulations. How-  
437 ever, as suppliers often have a wide range of products all differing slightly in  
438 properties such as substrate preference, viscosity, bond strength, environmental  
439 tolerance characteristics, and even color in some instances, it is often quite difficult  
440 to determine which is potentially best suited to the application in hand. Looking at the  
441 data supplied in the TDS may be confusing and may not highlight the key property  
442 required. It is therefore extremely useful to discuss the application requirements  
443 directly with company representatives, either within the sales team or if possible  
444 with the technical group. In that way, valuable time can often be saved by allowing a  
445 rapid, targeted product selection to be made. Most reputable suppliers will only try to  
446 promote the best potential products for the application as it does their reputation no  
447 good to sell inappropriate materials. However, supplier guidance must be treated with  
448 caution in that the recommendations will be product/brand specific and will not  
449 always be completely unbiased, although communication is most often direct and  
450 free evaluation material is often provided. In some instances, suppliers may offer to  
451 carry out test trials and supply additional test data, especially if the application volume  
452 has the potential to be large resulting in significant adhesive consumption/sales.

453 Sometimes, when a particularly demanding or unique application is sought  
454 where specialist materials are used, identification of a particular adhesive  
455 manufacturer/supplier may not be easy. In this instance, the use of a trade body  
456 which represents many industrial players may be another option to consider. Trade  
457 bodies represent a wide number of companies, normally on a region or country basis.  
458 Additionally, they serve as useful feedback/information centers to flag up legislative

issues such as REACH, H&S, and other regulatory concerns which may have a direct impact upon the use of adhesives. Examples of trade bodies include:

- ASC (Adhesive and Sealant Council, North America) – [www.ascouncil.org](http://www.ascouncil.org)
- ASMAC (Adhesive and Sealants Manufacturers Association of Canada, Canada) – [asmac.net](http://asmac.net)
- BASA (British Adhesives and Sealants Association, UK) – [www.basaonline.co.uk](http://www.basaonline.co.uk)
- CATIA (China Adhesives and Tape Industry Association, China) – [www.cnaia.org](http://www.cnaia.org)
- DETIC (Association Belgo-Luxembourgeoise des Producteurs et des Distributeurs de Savons, Cosmétiques, Détergents, Produits d'Entretien, d'Hygiène et de Toilette, Colles et Produits Connexes, Belgium) – [www.detic.be](http://www.detic.be)
- FEICA (Federation Europeenne des Industries de Colles et Adhesifs, Europe) – [www.feica.eu](http://www.feica.eu)
- JAIA (Japan Adhesive Industry Association, Japan) – [www.jaia.gr.jp](http://www.jaia.gr.jp)
- KAIA (Korea Adhesive Industry Association, Korea) – [www.kaia.kr](http://www.kaia.kr)
- PACIA (Plastics and Chemical Industry Association, Australia) – [www.cas.com.au](http://www.cas.com.au)
- PSTC (Pressure Sensitive Tape Council, North America) – [www.pstc.org](http://www.pstc.org)
- TASA (The Adhesives and Sealants Association, India) – [www.tasaindia.org](http://www.tasaindia.org)
- VLK (Vereniging Lijmen en Kitten, Netherlands) – [www.vlk.nu](http://www.vlk.nu)

## 16.12.2 Consultancy and Academic Research Organizations

There are a wide variety of consultancy bodies, often called research and technology organizations (RTOs) and universities who can offer a range of services from simple adhesive searching and material screening activities through adhesive bonding trials to fundamental modeling and phenomenological studies and failure investigation. RTOs are more industry focused and are therefore more sensitive to the budget and timescale requirements of industry, but services will often be priced at a higher level than those offered by universities due to the specific nature of the work and the allocation of specific resource to the client's needs. Examples of RTOs include:

- AIMEN (Spain) – provides technological services and engages in R&D&i activities in different areas such as high performance materials, smart manufacturing, laser based manufacturing, laser-assisted manufacturing, micro and high precision manufacturing, environmental technologies – [www.aimen.es](http://www.aimen.es)
- AIRTO (UK) Association for Innovation, Research and Technology Organisations – assists members to network and engage collectively with government and policy makers in the UK's R&D landscape on matters of mutual interest, including research policy, innovation strategy – [www.airto.co.uk](http://www.airto.co.uk)
- BATTELLE (USA) – conducts research and development, manages laboratories, designs and manufactures products, and delivers critical services for its clients – [www.battelle.org](http://www.battelle.org)

- 498 • Cambridge Consultants (Global) – innovative product development in a wide  
499 range of industrial sectors including medical technologies, consumer products,  
500 industrial products, smart metering, defense and securing, wireless, semiconduc-  
501 tor, transport, and clean-tech – [www.cambridgeconsultants.com](http://www.cambridgeconsultants.com)
- 502 • ChemQuest Inc. (USA) – is an international strategic business management  
503 consulting firm specializing in paints, coatings, resins, polymers, adhesives, and  
504 sealants industries – [www.chemquest.com](http://www.chemquest.com)
- 505 • EARTO (EU) European Association of Research and Technology Organisations –  
506 a nonprofit international association established in Brussels to promote and  
507 defend the interests of RTOs in Europe by reinforcing their profile and position  
508 as a key player in the minds of EU decision-makers and by seeking to ensure that  
509 European R&D and innovation programs are best attuned to their interests –  
510 [www.earto.eu](http://www.earto.eu)
- 511 • Element – previously MERL Ltd (Global) – R&D, laboratory testing, and  
512 consultancy services on polymer materials for engineering systems and structures  
513 – [www.element.com](http://www.element.com)
- 514 • Fraunhofer (Bremen, Germany) Institute for Manufacturing Technology and  
515 Advanced Materials (IFAM) – undertakes research and development work in  
516 the following areas: shaping and functional materials and adhesive bonding  
517 technology and surfaces – [www.ifam.fraunhofer.de](http://www.ifam.fraunhofer.de)
- 518 • HORIBA MIRA (UK) Motor Industry Research Association – is an automotive  
519 engineering and development consultancy company headquartered near Nuneat-  
520 on in Warwickshire, United Kingdom. It provides product engineering, research,  
521 testing, information and certification services to the automotive sector – [www.horiba-mira.com](http://www.horiba-mira.com)
- 522 • ISQ (Portugal) – founded in 1965, ISQ is a private and independent company  
523 providing inspection, testing, training and technical consultancy – [www.isq.pt](http://www.isq.pt)
- 524 • NPL (UK) – National Physical Laboratory is a world-leading center of excellence  
525 in developing and applying the most accurate measurements standards, science  
526 and technology – [www.npl.co.uk](http://www.npl.co.uk)
- 527 • PA Consulting Group (Global) – offers technology development and technology  
528 consulting services across a broad range of sectors including life sciences and  
529 health care, consumer products, communications and electronics, public sector,  
530 defense, energy, and transport – [www.paconsulting.com](http://www.paconsulting.com)
- 531 • SATRA (UK) – is an independent research and testing organization established in  
532 the UK in 1919. It has technical facilities in Europe and China serving customers  
533 throughout the world and is considered a leading technical authority for footwear  
534 and leather – [www.satrapra.com](http://www.satrapra.com)
- 535 • Smithers RAPRA (Global) – world-leading independent rubber, plastic, and  
536 composite consultants providing services including testing, analysis, processing,  
537 and research for the polymer industry and industries using plastics and rubber in  
538 any component, product, or production process – [www.smithersrapra.com](http://www.smithersrapra.com)
- 539 • TWI Ltd. (UK) – Global leader in technology engineering with key expertise in  
540 the welding and joining of all types of materials. The ACS (adhesives, compos-  
541 ites, and sealants) section provides assistance to industrial members in all aspects  
542



of adhesive and adhesion-related matters including material selection, surface preparation, design, testing, and training – [www.twi-global.com](http://www.twi-global.com)

• VTT (Finland) – is the leading research and technology company in the Nordic countries – [www.vttresearch.com](http://www.vttresearch.com)

• WMG (UK) Warwick Manufacturing Group – WMG was founded by Professor Lord Kumar Bhattacharyya in 1980 to help reinvigorate UK manufacturing. From its inception WMG's mission has been to improve the competitiveness of organizations through the application of value adding innovation, new technologies and skills deployment, bringing academic rigor to industrial and organizational practice. Today, the Group has grown into an international role model for how universities and business can successfully work together – [www2.warwick.ac.uk](http://www2.warwick.ac.uk)

Universities often can offer highly technical or scientifically focused work and access to sensitive instrumentation, but sometimes their priorities in relation to delivery timescales are less well aligned to the needs of industry. Confidentiality can also often be an issue in that universities will see a high throughput of students and possibly staff making it harder to control and maintain confidentiality. This is due to the fact that academic institutions have two primary functions, i.e., teaching and research. In view of this, specific services to industry will have a lower priority unless a dedicated capability is created, such as spin-out consultancy services.

Both RTOs and academic organizations can offer considerable assistance to the end user, but care is often needed when determining who to go to. Where a decision has been made to invest in a long-term study of a particular area and time is not critical, looking to a university and/or perhaps funding a student for a doctorate or master's degree in that area may be the best solution. This approach may provide significant benefits to the company funding the work but the timescale will be in years and the work will be often limited to generic models as there will be a requirement for the student to publish in the open literature.

At the time of writing, universities with a significant track record in adhesives research include:

#### UK

- University of Birmingham, Department of Chemical Engineering (K Kendall – contact mechanics), School of Dentistry (W Palin – dentistry adhesives)
- University of Glasgow, School of Engineering (M Cowling – adhesive bonding of ship-related structures)
- Imperial College, London, Department of Mechanical Engineering (A Kinloch – fatigue and durability of adhesive joints, B Blackman – studies and testing of structural adhesives, A Taylor – nanocomposites research, F Guild – joint mechanics)
- Loughborough University, Department of Materials (G Critchlow – surface analysis, A Ansarifard – bonding to rubber, J Comyn – curing and cross-linking of adhesives and sealants)
- University of Nottingham, Faculty of Engineering (I Ashcroft – mechanics and stress analysis of joints)

- Oxford Brookes University, Department of Mechanical Engineering and Mathematical Sciences (A Hutchinson – wide variety of adhesive-related areas including civil structure repair, bonding, and sealing), Joining Technology Research Centre (J Broughton – analysis of bonded and sealed joints, structural repair, durability, timber bonding, R Adams – mechanics of adhesive joints)
- University of Oxford, Department of Engineering Science (R Adams – mechanics of adhesives joints)
- Strathclyde University (R Pethrick – dielectric studies of adhesive joints and their durability to water)
- University of Surrey Department of Mechanical Engineering Sciences (J Watts – surface analysis, A Crocombe – stresses in joints), Department of Physics (J Keddie – pressure-sensitive adhesion)

#### Europe

- Saarland University, Saarbrücken, Germany (W Possart – adhesion, adhesion)
- University of Alicante, Spain (J M Martinez – shoe industry)
- University of Bordeaux, France (E Papon – adhesives, M Shanahan – adhesion, fracture)
- Technical University Braunschweig, Germany (K Dilger – adhesives technology in industry)
- IFREMER, Brest, France (J Y Cognard – joint mechanics)
- University of Kaiserslautern, Kaiserslautern, Germany (PL Geiss – durability)
- Laboratoire Génie de Production (LGP) – Ecole Nationale d'Ingénieurs de Tarbes – France (J A Petit – electronics and durability)
- University of Porto, Portugal (LFM da Silva – joint mechanics)
- University of Turin, Italy (L Goglio – joint mechanics)

#### USA and Canada

- Virginia Tech, USA (D Dillard – joint mechanics)
- University of Akron, USA (E Sancaktar – adhesives)
- University of Toronto, Canada (J Spelt – joint mechanics)

#### Asia

- Hiroshima University, Japan (T Sawa – joint mechanics)
- Korea Advanced Institute of Science and Technology, Korea (D G Lee – joint mechanics)
- Tokyo Institute of Technology, Japan (C Sato – joint mechanics)

In contrast, if the research is time critical and/or commercially very sensitive, then a dedicated RTO may be the most appropriate solution. Such organizations have experience managing such industrial needs and will fully respect the confidentiality that often accompanies such activities. Some organizations often specialize in one

industrial sector or manufacturing activity, whereas others will be more broad-based. In some instances, it may be possible to obtain economic assistance from national or local government to fund specific topics.

### 16.12.3 Online Assistance

One of the most significant developments in recent years is the rise of the Internet and the wealth of information that can now be obtained from this ever-expanding resource. Virtually all adhesives companies and suppliers have an online presence where product information (MSDS, TDS, etc.) can be accessed and downloaded. Many companies also offer adhesive selection facilities, though the majority of these still take the format of a requirements form which needs to be filled in and sent to the technical team where a human response will be made in due course. While this is a pragmatic approach and may well result in contact being made with an adhesives expert who should be able to offer good advice, the advice will be company product biased. The end user will therefore have to make calls to a range of adhesive suppliers to ensure that a full market appraisal has been achieved. Alternatively, one can find a small number of web sites where the end user can learn more about adhesives and associated design issues from a more neutral stand point. In some instances, some rudimentary design elements can even be applied to provide an initial sanity check to determine whether a design or an adhesive choice has viability. Examples of such sites include:

- Adhesives Toolkit – originally a UK government-funded project designed to assist adhesives end users with most adhesives-related topics including selection, design, and test standards – [www.adhesivestoolkit.com](http://www.adhesivestoolkit.com)
- Adhesives.org – a web site developed and supported by the Adhesives and Sealant Council and ChemQuest; it provides many useful areas of help including supplier links, introductions to adhesives, and articles on markets and applications – [www.adhesives.org](http://www.adhesives.org)
- GlobalSpec – specialized vertical search information services, and e-publishing company serving the engineering, manufacturing, and related scientific and technical market segments. The web site provides searching facilities for key industrial adhesive suppliers with a wide range of links, mostly USA based – [www.globalspec.com](http://www.globalspec.com)
- Specialchem4adhesives – an informative web site which primarily serves the adhesives industry, but many of the articles on the site provide useful background reading for anyone wanting to become more informed on adhesives matters – [www.specialchem4adhesives.com/index.aspx](http://www.specialchem4adhesives.com/index.aspx)

### 16.13 Conclusion

Adhesive selection can be a complex and sometimes frustrating task, with so many products to choose from and an almost infinite range of properties at one's disposal. However, with a logical approach and following some straightforward principals as

outlined in this chapter, it is possible to arrive at a sensible number of candidates relatively easily. It is normally easy to adopt a deselection approach where one identifies and ranks key selection parameters and their limits. The critical selection path will rest upon those parameters and it is strongly advised that sufficient time is devoted to this initial task. The actual initial selection activity is essentially a desktop exercise, aided by personal experience, searching technology and a network of experts to draw upon. Once practical trials begin, timescales and resource start to escalate rapidly and selection of the wrong adhesive(s) can be costly. It should also be mentioned that when comparing published adhesives data from different suppliers, care must be taken to check how the data was derived as the units used for each data set may be different or the joint strength may be obtained from tests on different substrates with different surface conditions or aging data reported may have been obtained in different environments.

Finally, it must be stressed that in virtually every new case where adhesives are to be employed, there will be sufficient differences to make it necessary for at least some practical trials to be carried out. The results made come out as predicted but it is better to reinforce confidence and minimize risk. Full details of the types of testing that can be carried out are discussed in Part D and also in Part F.

Books provide an excellent starting point to become acquainted with the very diverse world of adhesives and adhesion-related phenomena, but due to the rapidly changing world in terms of industrial takeovers, etc., books will rarely be able to provide the most up-to-date information on specific adhesive products. Direct contact with suppliers, experts/consultants, and use of the Internet are currently still the best ways to keep on top of adhesive selection when it comes to identification of specific products.

The range of reference books available to the reader is very large. Some are very generic while others are highly specialized.

---

## References

- Adams RD (2005) Adhesive bonding: science, technology, and applications. CRC Press, Boca Raton
- Dillard D (2010) Advances in structural adhesive bonding. Woodhead Publishing, Cambridge, UK
- Dunn D (2004) Engineering and structural adhesives. iSmithers Rapra Publishing, Shrewsbury, UK
- Ebnesajjad S (2008) Adhesives technology handbook, 2nd edn. Academic, London
- Goss R (2010) Practical guide to adhesive bonding of small engineering plastic and rubber parts. iSmithers Rapra Publishing, Shrewsbury, UK
- Lees WA (1984) Adhesives in engineering design. Springer, London, UK
- Petrie E (2007) Handbook of adhesives and sealants, 2nd edn. McGraw Hill, New York
- Pizzi A, Mittal K (2003) Handbook of adhesive technology, 2nd edn. CRC Press, Boca Raton
- Shields J (1984) Adhesives handbook, 3rd edn. Elsevier, London

**Testing of Adhesive Properties**

Uncorrected Proof

David A. Dillard

**Contents**

17.1	Introduction .....	434
17.2	Density .....	435
17.2.1	Experimental Methods for Polymer Density Measurements .....	437
17.2.2	Factors Affecting Polymer Densities .....	438
17.3	Viscosity .....	443
17.3.1	Newtonian Behavior .....	443
17.3.2	Non-Newtonian Behavior .....	446
17.3.3	Material Dependence .....	449
17.3.4	Adhesive Viscosity Measurements and Applications .....	452
17.4	Stress-Strain Behavior .....	453
17.5	Conclusion .....	455
References	.....	456

**Abstract**

A number of physical properties are relevant and important for characterizing adhesives, providing insights into the underlying behavior of the base polymer(s) as well as the effects that fillers, additives, and other factors may play on the behavior of the uncured adhesive, and also the quality and performance of bonded joints that may result. Characterizing these adhesive properties, interpreting the results, and understanding the implications provide important insights for assuring quality control, for improving bond performance, for assessing the relative merits of adhesive options for a given application, and for understanding the polymer more completely. This chapter addresses several

D. A. Dillard (✉)

Biomedical Engineering and Mechanics Department, Virginia Polytechnic Institute and State University, Blacksburg, VA, USA

e-mail: [dillard@vt.edu](mailto:dillard@vt.edu)

relevant physical properties of bulk adhesives, including viscosity, density, and stress-strain behavior. Methods of characterizing these properties are discussed, along with insights for interpreting these quantities and their implications for polymeric adhesive systems.

## 17.1 Introduction

The formation of satisfactory adhesive bonds normally involves the adhesive being applied in or changed to a liquid state to enable it to flow and wet the adherends, and then become a solid to resist loads associated with the service conditions (The exception being pressure-sensitive adhesives, which do not undergo the liquid to solid transition, but their high compliance is sufficient to wet the substrate (Dahlquist criterion), and their stiffness, strength, and energy dissipation capabilities are sufficient to resist removal.). Characterization of physical properties over this range of states from liquid to solid, as well as of a function of time, temperature, and often other factors, is of critical importance for formulating and selecting adhesives, optimizing fabrication techniques, and predicting performance. Excellent sources on a wide range of physical properties of polymers are available, including Ferry (1980), Osswald and Menges (1995), van Krevelen (1997), Rubinstein and Colby (2003), Ward and Sweeney (2004), and Mark (2007).

Density is a common physical property of interest, and although unlikely to be the determining factor in adhesive selection, density is an important indicator of the nature of a polymer, including chemical family, morphology, and filler or void content. While other physical properties such as moduli can vary over several orders of magnitude, density variations are typically much more subtle. While relatively simple methods are sufficient to characterize polymer density for some purposes, more precise methods are sometimes needed to ascertain quantitative attributes of the polymer in question. This chapter will review some of the methods for characterizing both liquid and solid polymer density and also some of the information that can be gleaned about a given material from careful density measurements.

Modulus and viscosity are two other important physical properties, representing the limiting idealizations of solid and liquid behavior. Recognizing their inherent viscoelastic nature, a particularly important aspect of any polymeric material is the time scale involved for the various transitions that occur. The time dependence of inorganic materials usually arises through the involvement of a very limited number of atoms, in mechanisms associated with the movement of dislocations as well as of bulk and grain boundary diffusion. For polymeric materials, however, time dependence is often associated with the complex movement of very large macromolecules or portions thereof, especially when flow of the liquid or uncured adhesive is involved. Depending on the scale of motion, a very wide range of characteristic times can be involved, ranging from short times associated with a limited number of atoms (e.g., crankshaft motion or the rotation of a side chain) to very long times required for entire molecules to slide or reptate past one another in a cooperative manner (Ferry 1980; Rubinstein and Colby 2003). Any one transition mechanism

can be considered to have an associated characteristic time,  $\tau$  (though the behavior may be spread over a number of decades). In considering the response of these time-dependent materials in light of experimental methods used for characterization, a useful concept is the Deborah number (Goodwin and Hughes 2000) defined as:

$$D_e = \frac{\tau}{t} \quad (1)$$

where  $t$  is the time of an experiment. For  $D_e \gg 1$ , the experiment may not adequately capture the time dependence of the respective transition, which occurs at much longer times than the experimental window. When  $D_e \ll 1$ , the experiment also may fail to capture important time-dependent deformation, which occurs much faster than the measurement capabilities of the instrument. When the Deborah number is on the order of unity, however, a well-designed experiment can capture this portion of the time-dependent behavior. Accelerated characterization techniques, such as the time temperature superposition principle (TTSP), can be employed to capture behavior that might otherwise be missed. TTSP involves the use of elevated temperature characterization to accelerate the polymer response into the experimental window, for predicting long-term response that is not experimentally feasible, or decelerate rapid polymer response to quantify very short time response not otherwise measurable in the test equipment (Ferry 1980; Rubinstein and Colby 2003) (► Chap. 18, “Thermal Properties of Adhesives”). Recognition of this viscoelastic response, including the use of appropriate experimental and interpretation techniques to properly characterize this behavior, is required. Because the characteristic times of complex polymeric materials often span many orders of magnitude, typical stress-strain behavior often exhibits significant rate dependence and viscosity experiments are complicated by the elastic component of seemingly liquid-like materials. With this as a background, characterizing viscoelastic materials from both the solid and liquid perspectives can be approached by addressing two different but related methodologies, both of which are discussed herein. Both approaches can, in principle, capture manifestations of the same viscoelastic nature of polymeric behavior, though in practice TTSP or other means are required to elucidate the full range of time-dependent mechanical properties.

## 17.2 Density

The *density* of a material, defined as the mass divided by the volume, is an important material property:

$$\rho = \frac{m}{V} \quad (2)$$

*Specific volume* is the reciprocal of the density. *Relative density* is the ratio of the density of a material to that of a reference material; for *specific gravity*, the reference material is water (Often the reference is water at 4 °C, when its density is greatest.) (Kholodovych and Welsh 2007). *Bulk density* is used to characterize the density of discretized forms of adhesives such as pellets and powders, where packing results in



large amounts of voids. Density typically decreases with increasing temperature and increases with pressure, although the latter dependence is very weak over commonly encountered pressures, except for foamed, pelleted, or granular forms of a material. *Physical aging* of glassy amorphous polymers is used to describe the time-dependent densification toward the equilibrium configuration.

Density may be measured through several means. In the direct measurement approach, the mass of a regular-shaped object is measured and the volume is calculated from known dimensions. This method is easily extended to liquid adhesives by determining the additional mass of a liquid used to fill a container of known volume. Indirect methods, useful for any solids, but especially for objects of irregular shapes, involve the use of a fluid or gas and include the volume and mass displacement techniques. In the volume displacement method, the amount of a fluid displaced by immersion of an object of interest provides a volume for the density calculation. This volume may be measured by the rise of the fluid in a graduated cylinder or the effluent from a container filled to the brim. The mass displacement method is based on Archimedes principle, which states that the buoyant force is the difference between the weight of an object measured in air and measured when immersed in a liquid of known density. Since the buoyant force is equal to the weight of the liquid displaced, one can determine the density of the object if the density of the liquid is known. Density columns have also been used to characterize polymer density, utilizing discrete or continuous gradients. A sequence of immiscible liquids, for example, will stratify into discrete layers, a popular classroom demonstration. Precise measurements can be obtained when polymer samples are allowed to drop to an equilibrium position in continuous gradient columns resulting when two miscible liquids with different densities are mixed under carefully controlled conditions (ASTM-D1505-03 2003).

Although seemingly a simple measurement, accurate density measurements require considerable care, especially since significant changes in formulation, processing, morphology, and physical aging, which, may of interest, typically result in relatively small changes in density. Thus, density is not particularly sensitive for reflecting a range of differences, so considerable precision is often required for meaningful quantitative studies. The density of polymeric samples, as well as fluids used for the indirect methods and even the containers in which such measurements are performed, are temperature dependent, so careful temperature control may be needed. Since mass is typically measured in air, the buoyant force of air should be recognized and included for precise density determinations. Voids or porosity within the polymer liquid or solid sample can significantly affect the measured density, as can the presence of bubbles on the walls of containers in the volume displacement method. Buoyant bubbles can also form around polymer samples when they are weighed in a liquid or dropped into a density column, effectively reducing their apparent density. Furthermore, the fluids used in the indirect methods should be chosen so that they have minimal interaction with the polymer samples. Measurements of displaced fluids flowing from a full container are complicated by surface tension of the fluid, so small mouths or capillary tubes are desired for escaping effluent. Considerable variation in reported densities can be found in

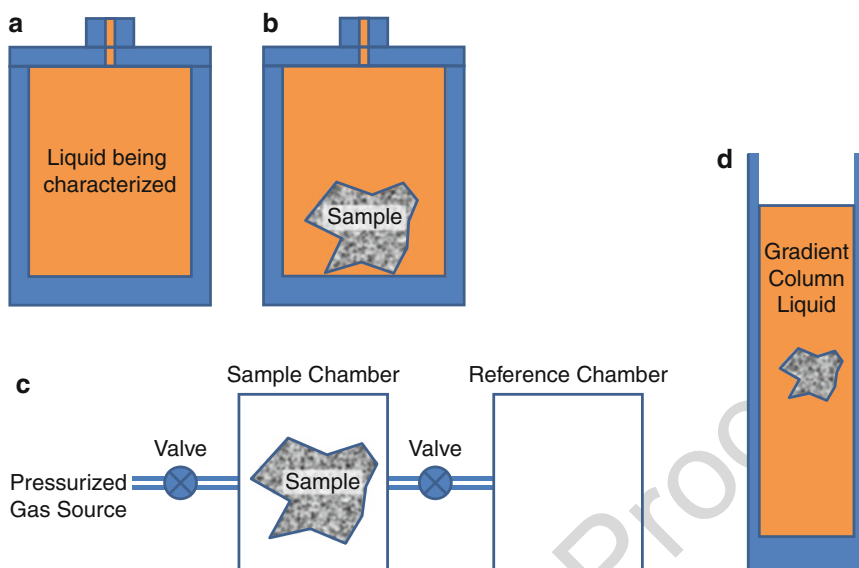


**Fig. 1** Illustrations of several methods to determine specimen volume or density: (a) pycnometer for liquid samples, (b) pycnometer for solid samples, (c) gas pycnometer, and (d) density gradient column showing sample suspended in liquid

the literature for a given polymer, due in part to the methods and equipment used, the skills of the operator, and whether appropriate corrections were made for buoyancy and other factors. Much of the variation, however, may be due to real differences associated with molecular weight, purity, processing conditions, physical aging, and the thermal, chemical, and mechanical history of the samples (Kholodovych and Welsh 2007). For porous materials, the measured density will depend on the method used and the nature of the porosity. If all pores are open to the outside and a gas is used to probe volume, the density of the polymer itself is obtained; if volume is directly measured from linear dimensions, the total volume of the foamed or porous material is obtained. When some pores are not open to the outside, or when the gas or liquid does not penetrate or wet the pores completely, intermediate values of density are obtained. Additional details on several popular methods (illustrated in Fig. 1) for determining polymer density are given in the following section.

### 17.2.1 Experimental Methods for Polymer Density Measurements

In practice, a pycnometer can be used to measure the density of liquid polymers by placing them in a cup of known volume and mass. A cover containing a capillary through which the overflow can pass for removal is typically added. Since both the volume of the cup as well as the density of the liquid adhesive are temperature dependent, accurate readings require that temperature be carefully controlled for the

test. The standard cup can be filled with a liquid adhesive that is below the desired test temperature. Then the cup and adhesive are heated to the temperature at which the density is to be determined, and the mass is determined after the excess overflow is wiped from the overflow orifice (ASTM-D1875-03 2003).

Pycnometers can also be used to measure the displacement of a gas or fluid from a container of fixed volume when a solid sample is added. Fluid-based pycnometers typically involve accurate mass measurements of the container when filled only with the fluid and when the sample is added. Knowing the density of the fluid and the mass of the polymer sample, one can then determine the density of the polymer sample. Commercial units are available, although standard laboratory equipment can also be used. Because the density of the fluid may be quite temperature dependent, care must be used to control temperature and use the density of the fluid at the test temperature, and care is also needed to avoid bubbles attached to the sample or container walls.

Gas pycnometers are popular because they avoid wetting and bubble issues. Because of this, they work well on materials with porosity and on granular and powdered materials, as well as on materials that might absorb, be dissolved in, or otherwise be affected by fluids used in fluid pycnometers. In constant volume gas pycnometers, a fixed amount of pressurized gas is introduced into a chamber containing the sample. A valve is then opened to permit this volume of gas to expand to fill a second or reference chamber as well. In a properly calibrated system, the pressure difference for the gas in the first chamber and then in both chambers, coupled with Boyle's law, allow one to measure the volume of the sample (ASTM-D6226 2005).

Continuous density gradient columns can be built and are commercially available. When a sample is dropped into the column, it will fall until it reaches the region of the column containing the same density. From the equilibrium position of the material and its relation to reference floats, the density can be accurately determined (ASTM-D1505-03 2003; ISO-1183-1:2004 2004). Organic solvents or salt solutions can be used to form the gradient column, but the liquids should be chosen so that they will easily wet the sample but not swell or dissolve the sample (Kholodovych and Welsh 2007).

## 17.2.2 Factors Affecting Polymer Densities

Polymer densities range significantly for common polymers, from as low as 0.6 g/cm<sup>3</sup> for thermoplastic polybutylene to 2.28 g/cm<sup>3</sup> for polytetrafluoroethylene (Kholodovych and Welsh 2007). Obviously, the atomic mass of the elements present in a molecule will affect the density, as well as their respective atomic radii. Thus, hydrocarbon polymers tend toward the lower range of density, whereas molecules containing large molar fractions of the halogens have larger densities. Density is affected by the relative rigidity of the molecule and the size and flexibility of side chains, which affect chain conformations and the resulting density.

## Crystallinity

Since the crystalline phase of a semicrystalline polymer is typically packed more efficiently, its density may be as much as 15% higher than the density of the corresponding amorphous region (Kholodovych and Welsh 2007). van Krevelen (1997) suggests that the density of a semicrystalline material,  $\rho_{sc}$ , may be estimated by

$$\rho_{sc} = \rho_a(1 + 0.13x_c) \quad (3)$$

where  $\rho_a$  is the density of the amorphous material and  $x_c$  is the degree of crystallinity, but the accuracy depends on the actual density difference between amorphous and crystalline regions, which can vary somewhat (Kholodovych and Welsh 2007). Density measurements have been useful for ascertaining the degree of crystallinity, but are complicated by the precise density measurements required to detect changes in crystallinity and the need to know the density of the crystalline and amorphous states, which can be difficult to determine in materials that are naturally semicrystalline. X-ray scattering differential scanning calorimetry (DSC), and other experiments provide capable alternatives for measuring polymer crystallinity, and are often preferred.

## Fillers and Foamed Materials

In addition to density variations among neat resins, significant density variations arise when these resins are formulated to contain fillers, which are often heavier inorganic materials, such as silica, calcium carbonate, aluminum, or even silver for electrically conductive adhesives. Where filler and polymer densities are considerably different, the density of the composite material can be used to determine filler content quite accurately, provided no voids are present. Voids will reduce the apparent density of a polymer, regardless of whether intentionally added or unintentionally introduced through the mixing process. Lower density adhesives can be produced when foaming agents are included or for syntactic foams containing microballoons. Foamed adhesives can provide lower weight, reduced stiffness, lower thermal conductivity, reduced coefficient of thermal expansion, altered response to ultrasonic energy, and flame retardant and ablative properties. These and other physical characteristics are often directly related to the density, making it an important quantity for estimating other physical properties (Gibson and Ashby 1999).

## Temperature Dependence

As with gases, the densities of solids and liquids also depend on the temperature and pressure at which measurements are made. Polymers expand more with temperature than most other engineering materials, having coefficients of thermal expansion that may be an order of magnitude larger than common metals, and as much as two orders of magnitude higher than some ceramics. In light of this, the density of polymers is significantly more temperature dependent. Dimensional changes associated with linear and volumetric expansion coefficients of materials arise from the asymmetry of the energy well associated with atomic spacing. Stronger interatomic forces, such as seen in ceramics and metals, typically result in deep energy wells with steep walls

and small coefficients of thermal expansion. The intermolecular forces between polymer molecules are typically weaker secondary interactions (e.g., van der Waal's or hydrogen bonding), resulting in shallow energy wells with considerable asymmetry about their equilibrium separation distance. Further complicating dimensional changes and their effect on polymer density, unlike gases, glassy solids in particular are often characterized in nonequilibrium thermodynamic states, resulting in a time dependence of density as well.

In understanding the role that temperature, pressure, and time have on polymers, the partitioning of volume within a polymer is important to understand. The majority of the space within a polymer is *occupied volume*, corresponding to the volume occupied by the individual atoms. The remainder of the space is *free volume*, an important quantity that significantly affects many of the physical, mechanical, and dielectric properties of a polymer, and is discussed further in ► Chap. 18, “Thermal Properties of Adhesives.” Polymers contain significantly more of this unoccupied space than other materials because the macromolecular chains have much more limited degrees of freedom than individual atoms due to the required continuity of the backbone, the bulky nature of side chains, steric hindrance, and other factors. For materials such as metals and ceramics, which do not contain significant amounts of unoccupied volume, the temperature dependence of density is quite small, with expansion corresponding primarily to expansion of the occupied volume associated with increasing atomic spacing. In polymers, however, the expansion of the free volume with temperature is much more significant, and in fact can be the dominant portion of polymer thermal expansion with temperature. Because the mobility of polymer chains requires free volume, the properties of polymers change significantly with temperature, especially about transition regions such as the *glass transition temperature*,  $T_g$ , which is the temperature at which molecular mobility changes dramatically as the polymer goes from glassy to rubbery behavior. Interestingly, this important transition occurs at fractional free volumes of about 2.5% for many polymers (Ferry 1980). In essence, once any polymer has about 2.5% fractional free volume, the molecules will have enough mobility to transition from glass-like to liquid-like (for very low molecular weights) or rubber-like (for high molecular weights with chain entanglements or in cross-linked systems) properties. Figure 2 shows the specific volume (reciprocal of density) as a function of temperature for a typical polymer, showing (specific) occupied, free, and total volume (Kovacs 1964). The expansion of free volume is seen to be responsible for a significant portion of the increase in total volume. Furthermore, there is a rapid increase (often about threefold) in the coefficient of thermal expansion, and because of its dominant effect, the total volume, as one passes through  $T_g$  (Ferry 1980). In light of this, the density of polymers is seen to be considerably more temperature dependent than metals and ceramics, and even more so for polymers above their glass transition temperature. Useful discussions of the temperature dependence of polymer density can be found in Ferry (1980) and Orwoll (2007).

Density measurements associated with temperature changes can often be measured through either volumetric or linear dilatometry, noting that the volumetric coefficient of thermal expansion is three times the linear coefficient of thermal

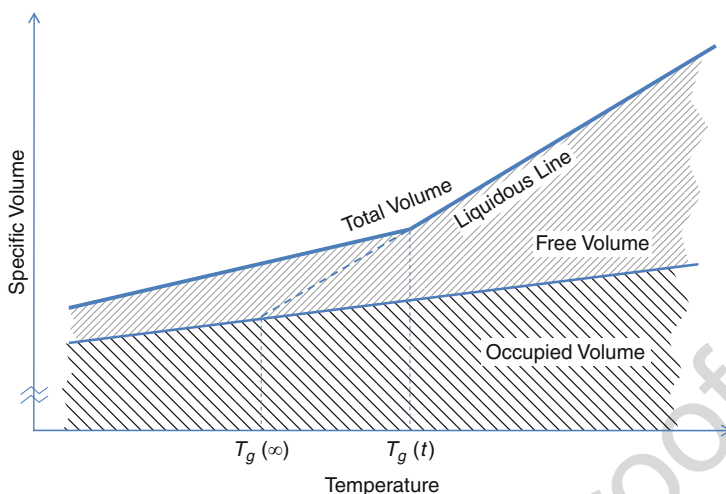


**Fig. 2** Illustration of total, free, and occupied specific volume in a polymer showing a  $T_g$  for samples cured at finite and infinitesimally slow rates

expansion. The latter is often measured in instruments such as thermal mechanical analysis (TMA) equipment that are fabricated with low expansion materials and carefully calibrated to correct for instrument dimensional changes. Additional methods to measure CTE and the associated stress-free temperature and residual stress state are discussed in ► Chap. 22, “Special Tests.” Mercury dilatometry is briefly discussed in ► Chap. 18, “Thermal Properties of Adhesives”; this can be useful to examine first-order (e.g., melting) and second-order (e.g.,  $T_g$ ) transitions in polymers, as well as explore physical aging and kinetics of equilibration in temperature jump experiments.

### Pressure Dependence

While doubling the pressure of an ideal gas will double the density according to Boyle’s law, pressure has much less effect on the density of solids and liquids, including polymers. Since the occupied space is filled with atoms whose size is barely affected by practical pressures, changes in density in polymers are often more associated with changes in the free volume. Free volume does contract when pressure is applied (Ferry 1980) and can reduce mobility and retard viscoelastic relaxations (Knauss and Emri 1987). The compressibility of polymers is very low, however. Even rubber, which is often referred to as “incompressible” (because elastomers deform in shear so much easier than volumetrically), is two orders of magnitude more compressible than steel. Thus, polymer density variations due to pressure are typically significant only when relatively high pressures are encountered in highly constrained configurations (Lai et al. 1992; Yu et al. 2001; Dillard et al. 2008; Tizard et al. 2012) or with foams or other products containing a significant fraction of voids. More detailed discussions of the pressure dependence of density can be found in Ferry (1980) and Orwoll (2007).

### Time Dependence

Although not often considered, density can be a time-dependent property in non-equilibrium systems such as amorphous regions of polymers below their glass transition temperature ( $T_g$ ), which is discussed in more detail in ► Chap. 18, “Thermal Properties of Adhesives.” In the rubbery region, a change in temperature or hydrostatic stress state results in a nearly immediate change in volumetric strain and density. For the case of a glassy polymer, however, the restricted mobility means that a portion of the response will be delayed, requiring convolution integrals to properly characterize the material’s behavior (Christensen 1982) and conveying the importance of the prior thermal and mechanical history on measurements of density. Of specific interest for density measurements is the process of physical aging associated with the gradual densification of a glass toward the equilibrium state (Kovacs 1964; Struik 1978). When an amorphous polymer is cooled from a cure or processing temperature through the glass transition temperature, the polymer density increases at a relatively constant rate until reaching  $T_g$ , below which the temperature dependence weakens significantly, as shown in Fig. 2 in terms of the specific volume. The polymer is unable to continue densifying along the liquidous line because of the reduced mobility (Matsuoka 1992; Shaw and MacKnight 2005). The liquidous line, however, remains the equilibrium configuration toward which molecular motion tends. The deviation from the equilibrium state explains why the Williams-Landel-Ferry (WLF) relationship for thermal shift factor breaks down below  $T_g$  (Struik 1978). Over time, the polymer will slowly continue toward the equilibrium configuration, as illustrated in Fig. 3. Upon heating, the polymer expands until it reaches the vicinity of  $T_g$ , where a step-like increase in volume can occur. Such behavior is a mechanical manifestation of the enthalpic anomalies that occur in DSC characterization of polymers (► Chap. 18, “Thermal Properties of Adhesives”). Physical aging usually occurs fairly slowly, often in a logarithmic time fashion (Struik 1978). Density measurements can be affected by physical aging, with

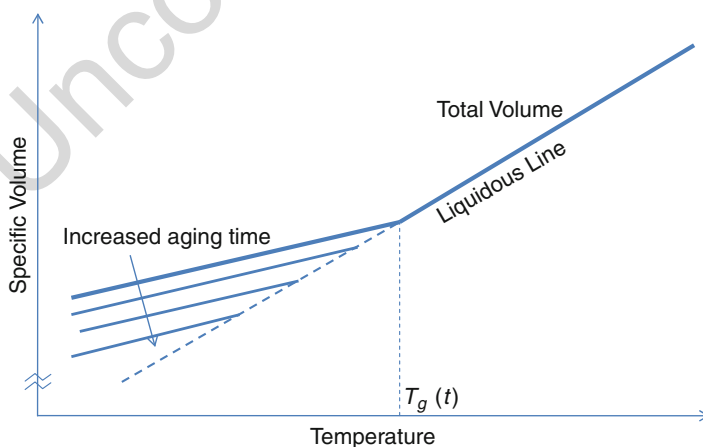


**Fig. 3** Illustration of physical aging as the reduction in excess free volume with aging time



volumetric changes occurring most rapidly right after being cooled from above the glass transition temperature. By heating physically aged materials above their glass transition temperature, polymers can be rejuvenated, in that physical aging can effectively be erased (Kovacs 1964; Struik 1978). When cooled, the density and other physical properties can return to the original values encountered when the polymer was first made, unless chemical or other degradation has occurred. Dropping the temperature below  $T_g$ , however, will restart the physical aging clock and its associated time dependence.

## 17.3 Viscosity

Viscosity is a very important property of adhesives, especially in their uncured fluid state, providing information that is of significant importance for mixing, pumping, and dispensing purposes (see Part G Manufacture), as well as for more fundamental understanding of the polymer itself. Relatively simple viscosity measurements can also be useful as a relatively sensitive metric for quality control, indicating changes in formulation, processing, and aging. More sophisticated techniques can provide important insights into the chemical structure, time and temperature dependence, and other properties, providing fundamental understanding of the polymer and allowing for accurate predictions of flow in complex systems. This chapter outlines some of the basic information relevant to viscosity as applicable to adhesive materials, but more detailed discussions should be examined for a thorough treatment of viscosity and the more comprehensive field of rheology (Bird et al. 1987; Larson 1988; Macosko 1994; Goodwin and Hughes 2000; Berker 2002; Han 2007).

### 17.3.1 Newtonian Behavior

The concept of viscosity is credited to Newton, who observed that the resistance to deformation of a fluid is proportional to the rate of change of deformation (Macosko 1994). Just as the elastic modulus is associated with the resistance of a solid to deformation, viscosity is a measure of a fluid's internal resistance to flow or deformation rate. *Viscosity* is defined as the ratio between the shear stress and the shear strain rate:

$$\eta = \frac{\tau}{\dot{\gamma}} \quad (4)$$

where  $\tau$  is the shear stress and  $\dot{\gamma}$  is the time rate of change of the shear strain,  $\frac{dv}{dy}$ , where  $v$  is the velocity and  $y$  is the coordinate perpendicular to the velocity, as illustrated in Fig. 4. Viscosity has traditionally been reported in poise or centipoise, but the SI units are *Pascal · seconds* [ $\text{Pa} \cdot \text{s}$ ], where  $1\text{Pa} \cdot \text{s} = 10\text{poise} = 1000\text{centipoise}$ . Viscosity as defined above is also referred to as the *absolute viscosity*. A related quantity, the *kinematic viscosity*, traditionally reported in Stokes,  $1\text{Stoke} = 10^{-4}\text{m}^2/\text{s}$ ,



**Fig. 4** Illustration of fluid element being sheared by a velocity difference

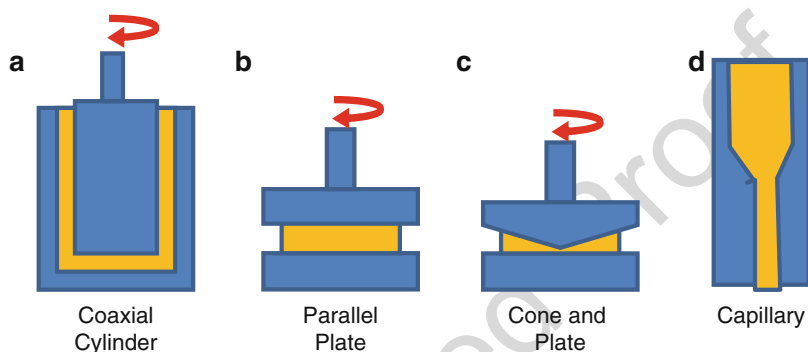
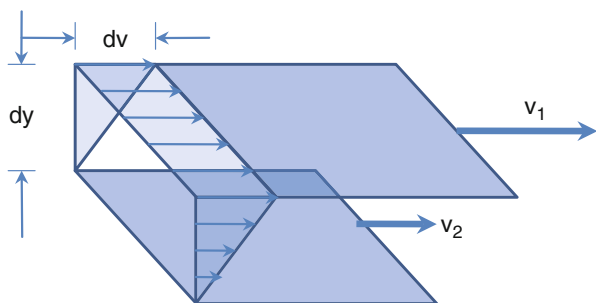


**Fig. 5** Illustration of several types of viscosity measurement configurations: (a) coaxial cylinder, (b) parallel plate, (c) cone and plate, and (d) capillary

is the absolute viscosity divided by the density of the fluid, resulting in a quantity that is particularly useful when relating viscous to inertial forces.

Viscosity may be physically measured in a number of ways. Some of the simplest and oldest methods rely on the time required for a given amount of liquid to flow from a chamber through an orifice or capillary. Such methods remain popular for quality control evaluation of materials because of their simplicity and ease of use. Some techniques span a range of applied pressures as the pressure head drops with flow, while in other tests, a constant pressure is applied. Steady-state flow methods work on the basis of applying a constant velocity difference across a known gap, and often involve the use of a rotating cylinder, plate, or cone. The torque required to maintain flow at this rate is measured and used to characterize the viscosity. A third primary method is the use of oscillatory methods to characterize the dynamic or complex viscosity. This method is seen as a bridge to the characterization of solid materials, which are often tested in a similar fashion. These methods, several of which are illustrated in Fig. 5, are described briefly in the following sections.

### Steady-State Rotation Rheology

Steady-state shear flow behavior can be measured with rotational equipment operating at prescribed angular velocities. The cone and plate configuration is commonly used (Han 2007), resulting in a relatively uniform shear rate within the test section

provided the angle between the cone and flat plate is relatively small (on the order of several degrees). Couette or concentric cylinder, Mooney, and double gap configurations have also been used (Goodwin and Hughes 2000). A variety of commercial instruments are available to characterize viscosity using this approach, many with interchangeable spindles to allow one instrument to be useful over a wide range of polymer viscosities.

### Capillary and Slit Rheometry

A number of rheometers have been developed based on flow through an orifice or capillary. Simple viscometers based on flow through a capillary involve flow of a fixed volume of fluid from a container. Instrumented versions include plunger-type capillary rheometers, in which a piston is used to force a fluid through a capillary. An inert pressurized gas can also be used to achieve the desired flow. Essentially, the pressure difference between the plunger and exit can be used to determine the relationship between the shear stress and strain rate at the walls of a capillary of known diameter and length. Corrections for end effects are often required to account for entrance losses, effectively lengthening the capillary by some fictitious distance, as can be determined with Bagley plots. Continuous-flow capillary rheometry allows one to not only measure the shear viscosity but also obtain the normal stress differences within a steady-state shear flow (Han 2007). Flow through a slit rather than a capillary has also been used, offering some advantages for certain situations (Han 2007).

### Dynamic or Complex Viscosity

In addition to their viscous properties, real liquids often exhibit elastic properties as well, meaning that if the applied stress is suddenly removed, stored elastic energy remains and can drive a partial recovery of the deformation. This combination of viscous and elastic behavior constitutes the class of viscoelastic materials. The limiting cases of solids and liquids correspond with materials that have either high or low Deborah numbers, the dimensionless ratio of characteristic material time to the time of the experiment. The time dependence of solid-like materials can be characterized through transient tests such as relaxation, in which the relaxation of stresses after a fixed strain is suddenly imposed; creep, in which the time-dependent strain is measured after a constant stress is suddenly imposed; and ramp tests, in which either stress or strain is increased at a constant rate (see ► Chap. 34, “Creep Load Conditions” in 1st edition). Characterization of the relaxation modulus and creep compliance can be made through either relaxation tests or ramp strain loading conditions, or through creep or ramp stress loading, respectively. Alternatively, linear viscoelastic behavior is often characterized through small strain, steady-state oscillation experiments, often using commercial dynamic mechanical analyzers (DMA), as also discussed in ► Chap. 18, “Thermal Properties of Adhesives.” Assuming a shear loading mode, the imposed stress and the resulting strain are given by the real parts of the complex shear stress,  $\tau^*(i\omega)$  and complex shear strain,  $\gamma^*(i\omega)$ , as:

$$\begin{aligned}\tau(t) &= \Re[\tau^*(i\omega)] = \Re[\hat{\tau} \cdot e^{i\omega t}] \\ \gamma(t) &= \Re[\gamma^*(i\omega)] = \Re[\hat{\gamma} \cdot e^{i(\omega t - \delta)}]\end{aligned}\quad (5)$$

441 where the carat denotes the amplitudes of the shear stress or strain,  $\omega$  is the angular  
 442 frequency of oscillation,  $i = \sqrt{-1}$ , and  $\delta$  is the phase lag of strain behind stress. The  
 443 complex shear modulus of viscoelastic materials can be defined in terms of the ratio of  
 444 complex stress to strain and expressed as a combination of storage and loss shear moduli:

$$G^*(i\omega) = \frac{\tau^*(i\omega)}{\gamma^*(i\omega)} = G'(\omega) + iG''(\omega) \quad (6)$$

445 If one approaches the constitutive characterization from the perspective of mea-  
 446 suring the viscosity rather than the modulus, however, replacing the complex strain  
 447 by the complex strain rate, the analogous complex viscosity is obtained:

$$\eta^*(i\omega) = \frac{\tau^*(i\omega)}{\dot{\gamma}^*(i\omega)} = \eta'(\omega) - i\eta''(\omega) \quad (7)$$

448 where  $\eta'$  is the in-phase component corresponding to the viscous contribution to the  
 449 dynamic viscosity and  $\eta''$  is the out-of-phase or elastic contribution. (The negative  
 450 sign in Eq. 7 arises to maintain a nonnegative value of  $\eta''$ .) One can easily go back  
 451 and forth between the dynamic modulus and viscosity using:

$$\begin{aligned} \eta'(\omega) &= \frac{E''}{\omega} \\ \eta''(\omega) &= \frac{E'}{\omega} \end{aligned} \quad (8)$$

452 The loss tangent can be defined as the ratio of loss to storage components in either  
 453 designation:

$$\tan \delta = \frac{\eta'(\omega)}{\eta''(\omega)} = \frac{G''(\omega)}{G'(\omega)} \quad (9)$$

## 454 **Extensional or Elongational Viscosity**

455 Capillary, rotational, and dynamic methods mentioned above are used to characterize  
 456 the shear viscosity of liquids. Extensional viscosity is also of significant interest,  
 457 including applications relevant to adhesive dispensing processes such as blade and  
 458 curtain coating (Goodwin and Hughes 2000). Beyond the scope of this chapter,  
 459 extensional characterization is discussed in sources such as Macosko (1994),  
 460 Goodwin and Hughes (2000), and Han (2007).

## 461 **17.3.2 Non-Newtonian Behavior**

462 Although Newtonian behavior is a useful starting point for many systems, more  
 463 complex behavior is very common, especially in formulated adhesives that  
 464 often have high solids content, contain fillers and flow controllers, or consist of

high-molecular-weight hot-melts. When materials are non-Newtonian, it is appropriate to refer to the measured viscosities as apparent viscosities in recognition of the more complex rate-dependent behavior.

### Shear Rate Dependence

Non-Newtonian behavior results when a material's viscosity varies with the imposed strain rate. Use of rotational viscometers described above have been advocated to address this issue for adhesives, wherein the rotational speed is varied from lowest to highest and back to lowest speed, all without stopping the instrument (ASTM-D2556-93a 2001).

Over a significant range of relevant shear rates, many polymers exhibit a simple power-law dependency of the form (Berker 2002):

$$\eta = m\dot{\gamma}^{n-1} \quad (10)$$

where  $m$  is known as the consistency index and  $n$  the power-law index. Such materials are referred to as Ostwald-De Waele fluids. For cases where  $n > 1$ , the material is referred to as dilatant, whereas for  $n < 1$ , the behavior is called pseudoplastic. In spite of the popular shear thickening example of the increasing viscosity with shear rate in corn starch and water dispersions, dilatant behavior is less common, applying principally to systems containing close-packed particles. Pseudoplastic behavior, on the other hand, is widely observed in many polymer products including adhesives. This shear thinning behavior is important for sag control of paints, coatings, adhesives, sealants, and even ketchup. The Bingham plastic fluid, represented by a viscous dashpot in parallel with a Coulomb (sliding or yield) element, can be thought of as a limiting case of a pseudoplastic material, in which a yield stress must be exceeded before viscous behavior is observed. Figure 6 illustrates Newtonian and non-Newtonian behavior, including pseudoplastic, dilatant, and Bingham response.

Caution is needed in using the power-law relationship of Eq. 10, however, as it cannot model the extreme rates, such as encountered near walls, for example (Berker 2002). Non-Newtonian behavior can be represented by a number of other representations that incorporate limiting values of viscosity at low shear rates, such as the Zaremba-Fromm-DeWitt (ZFD) model, which can be expressed as (Han 2007):

$$\eta(\dot{\gamma}) = \frac{\eta_0}{1 + (\lambda\dot{\gamma})^2} \quad (11)$$

where  $\eta_0$  is the limiting viscosity at zero shear rate and  $\lambda$  is a time constant. Forms that capture both the low and high shear rates include models such as the three-parameter Oldroyd, the four-parameter Carreau, and the five-parameter Elbirli-Yasuda-Carreau models, the latter of which is given by (Berker 2002):

$$\frac{\eta - \eta_\infty}{\eta_0 - \eta_\infty} = [1 + (\lambda\dot{\gamma})^a]^b \quad (12)$$

**Fig. 6** Illustration of non-Newtonian fluid behavior as well as a Bingham plastic fluid

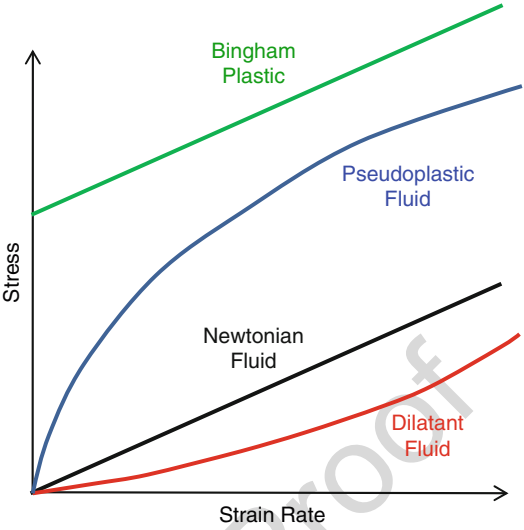
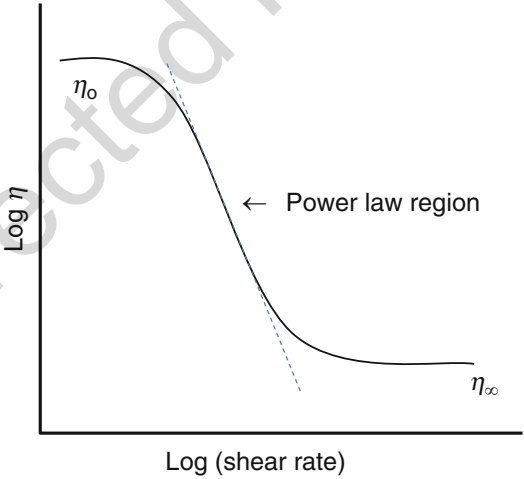


**Fig. 7** Representations of pseudoplastic or shear thinning material response



where the rate-dependent viscosity,  $\eta$ , is given in terms of the limiting viscosities at zero shear rate,  $\eta_0$  and “infinite” shear rate,  $\eta_\infty$ . Here,  $b$  is the slope of the power-law region of the behavior, and  $a$  characterizes the width of the transition from Newtonian to the power-law region. Figure 7 illustrates the common shear thinning behavior of many polymeric melts, solutions, and dispersions, along with limiting values that might be encountered.

**Time Dependent non-Newtonian Behavior**

Another common aspect that complicates the characterization and analysis of viscosity is time-dependent behavior. As a material cures, for example, the viscosity

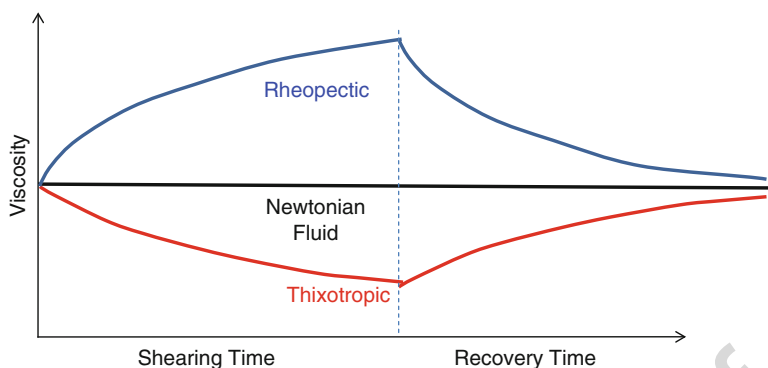


**Fig. 8** Effect of shearing time and recovery time on viscosity of rheopectic and thixotropic fluids

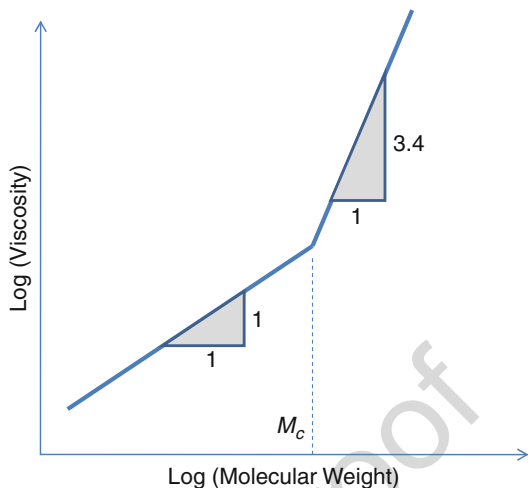
will change dramatically, making viscosity a useful metric in characterizing chain extension, crosslinking and other chemical structural changes. Other types of time dependence are also seen, however, and are associated with the length of time that a material has been sheared. For *rheopectic* materials, the viscosity increases over time with stirring or other forms of shearing. Examples of this include printer inks and body armor. *Thixotropic* materials exhibit a decrease in viscosity with shearing and is often observed in gels, colloids, clays, and drilling muds. For both of these time-dependent behaviors, there is typically a gradual recovery to the original viscosity if the shearing is stopped for a period of time. Figure 8 schematically illustrates such behavior.

### 17.3.3 Material Dependence

#### Dilute Solution Viscosity

To understand polymer structure, polymers are often dissolved in appropriate solvents, allowing molecular weight or degree of polymerization to be determined from dilute solution viscosity. The *relative viscosity*,  $\eta_{rel}$ , is the ratio of solution viscosity to that of the solvent. The *specific viscosity*,  $\eta_{sp}$ , is the ratio of the difference in solution and solvent viscosities divided by the solvent viscosity. These dimensionless quantities are often divided by the mass concentration of the polymer to obtain several additional terms that have units of dilution or volume per unit mass concentration: the *reduced viscosity*, which is ratio of the relative viscosity to the concentration; the *inherent viscosity*, which is the ratio of the natural logarithm of the relative viscosity; and the *intrinsic viscosity*,  $[\eta]$ , which is the common limiting value of the reduced (Huggins' definition) or inherent (Craemer's definition) viscosity at infinite dilution of the polymer. The intrinsic viscosity can be used to estimate molecular weight of a polymer through the Mark-Houwink equation. These solution viscosities are often measured with capillary viscometers.

**Fig. 9** Effect of molecular weight on viscosity, showing sharp transition at  $M_c$



### Molecular Weight Dependence

Viscosity is often strongly dependent on the molecular weight of the polymer. The zero-shear rate viscosity of many polymer melts has been shown to scale according to (Han 2007):

$$\eta_0 = \begin{cases} K \cdot M & \text{for } M \leq M_c \\ K \cdot M^{3.4} & \text{for } M > M_c \end{cases} \quad (13)$$

where  $K$  is a constant of proportionality,  $M$  is the molecular weight, and  $M_c$  is the critical molecular weight. Figure 9 is representative of such behavior. Since the transition appears to result from the onset of topological restrictions of chain movement, the process is often attributed to entanglement effects (Han 2007).  $M_c$  is believed to be related to the molecular weight between entanglements,  $M_e$ , through  $M_c \approx 2M_e$ , and appears to be the lower limit of molecular weight that can induce non-Newtonian behavior (Han 2007). Equation 13 can be extended to polydisperse polymers if  $M$  is replaced by the weight-average molecular weight,  $M_w$ .

### Dependence on Filler Content

Viscosity can depend strongly on fillers added to provide a range of mechanical, transport, electrical, magnetic, or other physical properties. The well-known Einstein-Guth relationship, for example, provides the viscosity of a dilute suspension of rigid spheres, obtaining the bulk or effective viscosity of a suspension as:

$$\eta_s = \eta(1 + 2.5\phi + 14.1\phi^2) \quad (14)$$

where  $\eta$  is the viscosity of the liquid and  $\phi$  is the volume fraction of the spheres. To be applicable, the initial liquid must behave in a Newtonian fashion and the concentration of particles must be very low (Han 2007). Other models have been

introduced to account for fillers that are not spherical but have other aspect ratios. At significant filler concentrations, the Guth and Gold equation and other relationships have been suggested, and yield phenomena are often observed (Goodwin and Hughes 2000). Extensions to nanocomposites have been reviewed (Han 2007).

### Temperature-Dependent Viscosity

For homopolymers, the Ostwald-De Waele power-law relationship may be extended to include temperature dependence as (Han 2007):

$$\eta(\dot{\gamma}, T) = K(T)\dot{\gamma}^{n-1} \quad (15)$$

where  $K(T)$  is the temperature-dependent consistency index. In addition to other forms cited earlier, the truncated power-law model can be used to capture the viscosity below some critical shear rate,  $\dot{\gamma}_0$ , below which the viscosity is not rate dependent (Han 2007):

$$\eta(\dot{\gamma}, T) = \begin{cases} \eta_0(T) & \text{for } \dot{\gamma} \leq \dot{\gamma}_0 \\ \eta_0(T)(\dot{\gamma}/\dot{\gamma}_0)^{n-1} & \text{for } \dot{\gamma} > \dot{\gamma}_0 \end{cases} \quad (16)$$

For many simple polymeric systems, thermal shift factors can be used to model the temperature dependence using:

$$\eta_0(T) = k_0 e^{(E/RT)} \quad (17)$$

where  $k_0$  is a pre-exponential factor,  $E$  is the shear flow activation energy,  $R$  is the universal gas constant, and  $T$  is the absolute temperature. The thermal shift factor can be expressed as the ratio of zero-shear rate viscosities at two temperatures:

$$a_T(T) = \frac{\eta_0(T)}{\eta_0(T_{\text{ref}})} \quad (18)$$

where  $T_{\text{ref}}$  is a reference temperature. For linear flexible homopolymers, Arrhenius and Williams-Landel-Ferry (WLF) relationships have been found useful as follows (Han 2007):

$$\log a_T(T) = \begin{cases} \frac{E}{R} \left[ \frac{1}{T} - \frac{1}{T_{\text{ref}}} \right] & \text{for } T > T_g + 100^\circ \text{C} \\ \frac{-C_1(T - T_{\text{ref}})}{C_2 + T - T_{\text{ref}}} & \text{for } T_g < T \leq T_g + 100^\circ \text{C} \end{cases} \quad (19)$$

where  $C_1$  and  $C_2$  are WLF constants (Ferry 1980) (also discussed in ► Chap. 18, “Thermal Properties of Adhesives”). Using the shift factor allows one to generate reduced shear rate or viscosity master curves spanning a wide range of rates and applicable for a range of temperatures by using the corresponding thermal shift factor plot. The master curve and shift factor plots are prepared with respect to the



chosen reference temperature,  $T_{\text{ref}}$ . Although such techniques are often extended to more complex material systems, the accuracy or appropriateness of these relationships for such systems should be carefully examined.

### 17.3.4 Adhesive Viscosity Measurements and Applications

In addition to the general approaches for measuring viscosity discussed earlier in this chapter, certain methods have been standardized specifically for adhesive materials. ASTM D1084 (ASTM-D1084-08 2008) describes four different methods for viscosity measurements for self-leveling adhesives (eliminating thixotropic or plastic materials where rate of stirring and prior history affect the behavior). Method A involves the use of viscosity cups with orifices that are several millimeters in diameter. Using accurate temperature control, acceptable readings are obtained when 50 mL of sample flow through the orifice in 30–100 s. Method B involves the use of a Brookfield rotational viscometer in which spindles outfitted with a disk appropriate to the viscosity being measured are rotated within a container of the liquid being characterized. Torque measurements associated with given angular velocities can be used to determine viscosity. Method C is based on the use of a Stormer rotational viscometer in which the time required for a spindle (equipped with paddles and loaded by a constant torque) to turn 100 revolutions. Method D quantifies the time required for a fixed volume of adhesive to flow through a properly sized orifice in a Zahn viscosity cup, which can simply be dipped into the adhesive for filling.

The viscosity of an adhesive can change significantly when solvent or dispersant evaporates, when chain extension or crosslinking occur, or when other changes take place over time. This sensitivity makes viscosity measurements popular for assessing the detrimental effects of storage life (ASTM-D1337-96 2001) (see ► Chap. 36, “Storage of Adhesives” in 1st edition), for characterizing the allowable working life of an adhesive (ASTM-D1338-99 2001), and to determine the heat stability of hot-melt adhesives (ASTM-D4499-95 2001) using (ASTM-D3236 2001). These measurements detect changes that take place with aging.

All of these test methods obtain viscosities at relatively low shear rates, and because of the sensitive to temperature and solvent content, means are required to maintain the desired temperature and minimize solvent loss during testing. Such viscosities may be relevant for low speed mixing, pumping, and dispensing methods, but may be insufficient for higher speed processing conditions. More sophisticated viscosity measurements are most easily performed with more elaborate equipment that allows for imposing a wide range of flow rates in a carefully controlled temperature environment. Because of the strong rate-dependence of many formulated adhesives, it is important that one characterize the viscosity at the temperature and rate conditions that the adhesive will experience during flow through the dispensing equipment and application to the adherends. Processing and dispensing or application methods cover a wide range of effective shear rates, such as indicated

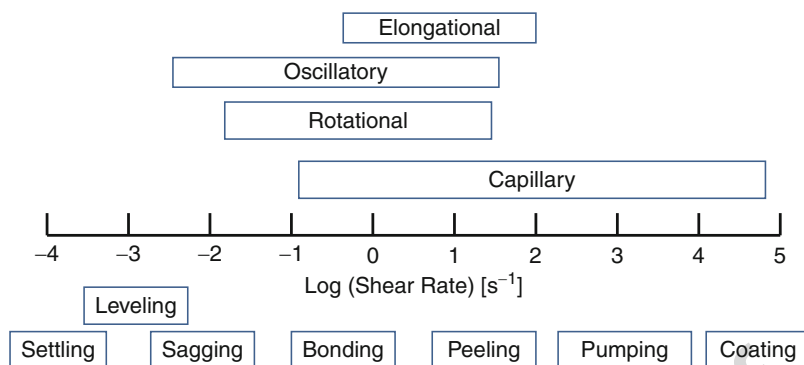


**Fig. 10** Approximate relative ranges of shear rates for rheometers (*above*) and polymer processing or adhesive applications (*below*)

in Fig. 10, which also suggests relevant rates of some of the viscosity measurement equipment discussed above.

## 17.4 Stress-Strain Behavior

While viscosity measurements are typically carried out on uncured adhesives that are still in their liquid state or on partially cured materials that can still exhibit flow, measuring the basic stress-strain behavior is one of the most fundamental tests conducted on polymeric adhesives in their cured or solid state. In their simplest form, these tests are intended for characterizing materials with very large Deborah numbers, where the time scale of the test is short compared to any relaxation times within the material, or for cross-linked materials tested at time scales much longer than their characteristic times. Just as with viscosity tests and because of the very broad characteristic time scale of typical polymers, however, stress-strain tests are often conducted in a manner that captures some of the inherent time dependence of the materials being evaluated.

The stress-strain behavior of a material provides important information relevant to its range of applicability. Load bearing applications may require certain stiffness or strength properties, the latter of which has been addressed in ► [Chap. 19, “Failure Strength Tests.”](#) For strain-controlled loading modes experienced by sealants, the modulus must be sufficiently low and the strain capabilities sufficiently high to provide adequate flexibility to meet the mechanical or thermally driven deformations. Due in part to the popularity of screw-driven test frames, most stress-strain characterization experiments have traditionally been carried out at a constant cross-head displacement rate, effectively straining the specimen at the desired rate. Results obtained are often quite rate- and temperature dependent, so care is needed in reporting these details.

Stress-strain behavior can be obtained with a variety of specimen configurations depending on the properties desired, the nature of the material being tested, and the available equipment. Perhaps the simplest and most common means to determine stress-strain behavior is in uniaxial tension, using either straight-sided or dogbone-shaped specimens. Straight-sided specimens are useful in some situations, especially if properties are only being measured to a fraction of the breaking strain and when appropriate extensometry equipment is not available. In such cases, the strain of straight-sided specimens can be estimated by dividing the crosshead displacement by the length of the specimen as measured between the grips. The aspect ratio of the specimens should be sufficient that end effects are negligible – suspended length-to-width ratios approaching 10 or more are preferred. Care should be used to make sure that specimen slippage within the grips does not affect strain measurements made in this manner. Where failure properties are important, waisted configurations, known as dogbone or dumbbell specimens, are favored for bulk polymer or adhesive samples. The higher stresses within the region of reduced cross section will typically induce failures within these regions, avoiding failures at the grips, as often occurs with straight-sided specimens. Engineering stress is characterized by dividing the applied axial force (typically measured by a load cell) by the original cross-sectional area of the specimen. Other stress metrics are also useful, including true stress, which is the applied load divided by the current cross-sectional area (Dowling 2007).

Strains can be measured by a number of techniques. The simplest technique is to divide the crosshead displacement by the gage length of the specimen, as mentioned before. Specimen slippage and load frame compliance can both affect the apparent strains determined through this method. Mechanical extensometers have been widely used, measuring a displacement over a given gage length and reporting the quotient as an average strain. Strain gages can be applied directly to specimens to measure strain, although the effects of reinforcement, local heating, and shear lag issues make these less appropriate for measuring strains on neat polymer samples. Optical techniques for characterizing strains are becoming increasingly popular. High resolution capabilities are available in the form of interferometric Moiré and other techniques, but for many applications, less resolution is acceptable. Optical methods have the advantage of being essentially noncontact techniques, a distinct advantage when working with small specimens that might be affected by the weight of a mechanical extensometer or the presence of their knife edges or contact points. Equipment based on several different principles is available. Examples include laser extensometers, which scan a laser beam along the length of the specimen to determine the location of two or more targets on the specimen. For uniaxial loading configurations, these methods normally report only the axial strains averaged over the distance between pairs of targets. Full field methods are also popular, including digital image correlation (DIC) techniques, which can provide measures of the full in-plane strain states across the specimen and, in three-dimensional systems, out of plane displacements as well. Such methods may require that the surface of the specimen be speckled with a paint or ink spray to provide a random pattern of features that can be tracked during the deformation process (Chu et al. 1985).

A number of metrics can be assessed from stress-strain behavior (Dowling 2007). Properties that are often evaluated include the modulus (initial modulus, or secant modulus evaluated to some specific strain), the yield stress, the yield strain, the ultimate strength, and the strain at break, as have been discussed in ► Chap. 19, “Failure Strength Tests.” The area under the curve, known as the modulus of toughness, has physical units of energy per unit volume, which are equivalent to force per unit area, the units of stress and modulus.

The initial modulus, ideally from the linear portion of the stress strain diagram, is known as Young’s modulus (or modulus of elasticity) for uniaxial tensile loading or shear modulus (or modulus of rigidity) for shear loading, assumes linear elastic behavior. This may be reasonable at rates much faster than the characteristic relaxation times of the material (i.e., glassy state) or at times much larger than these characteristic times (i.e., the rubbery state), provided the strains are small. Since polymeric adhesives are all time-dependent viscoelastic materials, however, the resulting modulus is, in general, a function of the rate of the test, as well as the test temperature and perhaps moisture or diluent content. Thus, modulus is a function of the test rate. The apparent linearity of the stress strain behavior breaks down as the strain rate approaches characteristic relaxation times of the material, resulting in nonlinear stress strain curves for even linear viscoelastic materials (Brinson and Brinson 2007). One particularly useful means to utilize the apparently nonlinear stress-strain response, resulting when time-dependent materials are characterized in constant strain rate experiments, is to obtain the viscoelastic relaxation modulus for either extension or shear, respectively:

$$E(t) = \frac{1}{\dot{\epsilon}} \frac{d\sigma}{dt} \quad G(t) = \frac{1}{\dot{\gamma}} \frac{d\tau}{dt} \quad (20)$$

where  $\sigma$  and  $\tau$  are the normal and shear stresses and  $\dot{\epsilon}$  and  $\dot{\gamma}$  are the imposed constant normal and shear strain rates, respectively. Since  $E(t)$  and  $G(t)$  are linear viscoelastic properties, the limits of linearity must be established through conducting tests at several rates or through other means (Brinson and Brinson 2007). Analogous forms for creep compliances can also be obtained for the less common loading cases of constant imposed stress rates (see ► Chap. 34, “Creep Load Conditions” in 1st edition). Equation 20 clearly illustrates that the stress-strain response for constant strain (or stress) rate loading is inherently nonlinear for viscoelastic materials, reminding practitioners of the complications that arise when the characteristic times of the material and test are of the same magnitude.

## 17.5 Conclusion

Many physical properties are of importance in the characterization, enhancement, and selection of adhesives for the wide range of uses that they enjoy. This chapter has highlighted just a few of these relevant properties and pointed reader to other sources for information. The density of polymers spans a relatively narrow range, and small

variations can provide significant insights into the behavior of a polymer. In formulated adhesives, density can provide information about the filler content or void content of liquid adhesives or solid parts. Viscosity is a very sensitive metric of a very important polymer property. A number of techniques have been developed to characterize viscosity over different viscosity ranges and shear rates. Viscosity is often significantly affected by temperature, shear rate, time of shearing, and other factors, so care is recommended in selecting appropriate viscosity measurement methods to provide behavior relevant to the applications being used. The stress-strain behavior of polymers, adhesives, and sealants is often important information for selecting and using adhesives. This chapter has provided a short section on several aspects of these tests to complement other related coverage in this book.

---

## References

- ASTM-D1084-08 (2008) Standard test methods for viscosity of adhesives. ASTM, West Conshohocken
- ASTM-D1337-96 (2001) Storage life of adhesives by consistency and bond strength. ASTM, West Conshohocken
- ASTM-D1338-99 (2001) Working life of liquid or paste adhesives by consistency and bond strength. ASTM, West Conshohocken
- ASTM-D1505-03 (2003) Standard test method for density of plastics by the density-gradient technique. ASTM, West Conshohocken
- ASTM-D1875-03 (2003) Standard test method for density of adhesives in fluid form. ASTM, West Conshohocken
- ASTM-D2556-93a (2001) Standard test method for adhesives having shear-rate-dependent flow properties. ASTM, West Conshohocken
- ASTM-D3236 (2001) Standard test method for apparent Viscosity of hot-melt adhesives and coating materials. ASTM, West Conshohocken
- ASTM-D4499-95 (2001) Standard test method for heat stability of hot-melt adhesives. ASTM, West Conshohocken
- ASTM-D6226 (2005) Standard test method for open cell content of rigid cellular plastics. ASTM, West Conshohocken
- Berker A (2002) Rheology for adhesion science and technology. In: Dillard DA, Pocius AV (eds) Adhesion Science and engineering – I: the mechanics of adhesion, vol 1. Elsevier, Amsterdam, pp 443–498
- Bird RB, Armstrong RC, Hassager L (1987) Dynamics of polymeric liquids: fluid mechanics. Wiley, New York
- Brinson HF, Brinson CL (2007) Polymer engineering science and viscoelasticity: an introduction. Springer, New York
- Christensen RM (1982) Theory of viscoelasticity: an introduction. Academic Press, New York
- Chu TC, Ranson WF, Sutton MA, Peters WH (1985) Applications of digital-image-correlation techniques to experimental mechanics. *Exp Mech* 25(Copyright 1986, IEE):232–244
- Dillard DA, Mallick A, Ohanehi DC, Yu JH, Lefebvre DR (2008) A high precision experimental method to determine poisson's ratios of encapsulant gels. *J Electron Packag* 130(3):0310061
- Dowling N (2007) Mechanical behavior of materials. Pearson Prentice Hall, Upper Saddle River
- Ferry JD (1980) Viscoelastic properties of polymers. Wiley, New York
- Gibson LJ, Ashby MF (1999) Cellular solids: structure and properties. Cambridge University Press, Cambridge
- Goodwin JW, Hughes RW (2000) Rheology for chemists: an introduction. Royal Society of Chemistry, Cambridge

- 776 Han CD (2007) Rheology and processing of polymeric materials: volume I: polymer rheology.  
777 Oxford University Press, Oxford
- 778 ISO-1183-1:2004 (2004) Plastics – methods for determining the density of non-cellular plastics –  
779 part 1: immersion method, liquid pycnometer method and titration method. International  
780 Standards Organization, Geneva
- 781 Kholodovych V, Welsh WJ (2007) Densities of amorphous and crystalline polymers. In: Mark JE  
782 (ed) Physical properties of polymers handbook. Springer, New York
- 783 Knauss WG, Emri I (1987) Volume change and the nonlinearly Thermoviscoelastic constitution of  
784 polymers. *Polym Eng Sci* 27(1):86–100
- 785 Kovacs A (1964) Glass transition in amorphous polymers: a phenomenological study. *Adv Polym*  
786 *Sci* 3:394–507
- 787 Lai YH, Dillard DA, Thornton JS (1992) The effect of compressibility on the stress distributions in  
788 thin elastomeric blocks and annular bushings. *J Appl Mech Trans Asme* 59(4):902–908
- 789 Larson RD (1988) Constitutive equations for polymer melts and solutions. Butterworths, Stoneham
- 790 Macosko CW (1994) Rheology – principles, measurements and applications. Wiley, New York
- 791 Mark JE (ed) (2007) Physical properties of polymers handbook. Springer, New York
- 792 Matsuoka S (1992) Relaxation phenomena in polymers. Hanser, Munich
- 793 Orwoll RA (2007) Densities, coefficients of thermal expansion, and Compressibilities of amor-  
794 phous polymers. In: Mark JE (ed) Physical properties of polymers handbook. Springer,  
795 New York
- 796 Osswald TA, Menges G (1995) Materials science of polymers for engineers. Hanser Publishers,  
797 Munich
- 798 Rubinstein M, Colby RH (2003) Polymer physics. Oxford University Press, Oxford
- 799 Shaw MT, MacKnight WJ (2005) Introduction to polymer viscoelasticity. Wiley, Hoboken
- 800 Struik LCE (1978) Physical aging in amorphous polymers and other materials. Elsevier Scientific,  
801 Amsterdam
- 802 Tizard GA, Dillard DA, Norris AW, Shephard N (2012) Development of a high precision method to  
803 characterize Poisson's ratios of encapsulant gels using a flat disk configuration. *Exp Mech*  
804 52(9):1397–1405
- 805 van Krevelen DW (1997) Physical properties of polymers: their correlation with chemical structure:  
806 their numerical estimation and prediction from additive group contributions. Elsevier,  
807 Amsterdam
- 808 Ward IM, Sweeney J (2004) An introduction to the mechanical properties of solid polymers. Wiley,  
809 Chichester, West Sussex
- 810 Yu JH, Dillard DA, Lefebvre DR (2001) Pressure and shear stress distributions of an elastomer  
811 constrained by a cylinder of finite length. *Int J Solids Struct* 38(38–39):6839–6849

John Comyn

## Contents

18.1	Introduction .....	460
18.2	Shelf-Life .....	460
18.3	The Hardening (Curing) Process .....	461
18.3.1	Hardening by Evaporation of Solvent or Water .....	461
18.3.2	Minimum Film-Formation Temperature of Latex Adhesives .....	462
18.3.3	Hardening by Cooling .....	463
18.3.4	Hardening by Chemical Reaction .....	463
18.4	Thermal Properties of Cured Adhesives .....	467
18.4.1	The Glass Transition Temperature .....	467
18.4.2	Melting of Semicrystalline Polymers .....	472
18.4.3	Viscoelastic Properties of Adhesives .....	475
18.4.4	Thermal Conductivity of Adhesives .....	479
18.4.5	Thermal Expansion of Adhesives .....	479
18.5	Breakdown of Adhesives .....	479
18.5.1	Oxidative Degradation .....	479
18.5.2	High Temperature Limits of Adhesives .....	482
18.5.3	Low Temperature Limits of Adhesives .....	483
18.5.4	Loss of Additives .....	483
18.5.5	Thermally Reversible Adhesive .....	483
18.6	Measurement of Thermal Properties .....	483
18.6.1	Differential Scanning Calorimetry .....	484
18.6.2	Dynamic Mechanical Thermal Analysis .....	484
18.6.3	Thermogravimetric Analysis .....	485
18.7	Conclusion .....	486
	References .....	486

J. Comyn (✉)

Materials Department, Loughborough University, Leicestershire, UK

e-mail: [gloojc@gmail.com](mailto:gloojc@gmail.com)

---

**Abstract**

The thermal properties of adhesives affect the rate of cure, whether the latter is by evaporation, cooling, or chemical reaction. In the latter case, cure may not go to completion in the sense that not all monomer is reacted, or may not be possible at all above a ceiling temperature. The heat of polymerization is a useful guide to what may happen.

The glass transition temperature of a cured adhesive is of critical importance in that although there are both sub-T<sub>g</sub> and super-T<sub>g</sub> adhesives, crossing T<sub>g</sub> in service is not acceptable. T<sub>g</sub> also has a role in latex adhesives forming cohesive films. Water plasticizes epoxide adhesives and so lower T<sub>g</sub>. Some adhesives are partially crystalline with a melting point T<sub>m</sub>.

Adhesives exhibit a mixture of viscous and elastic properties and obey the WLF equation. This indicates that the fraction of free volume at the glass transition is 2.5%.

Consideration is given to thermal conductivity and thermal expansion, and the breakdown of adhesives at elevated temperatures. Shelf-life and pot-life vary with temperature.

The main methods of obtaining thermal information on adhesives are reviewed; these are differential scanning calorimetry (DSC), dynamic mechanical thermal analysis (DMTA), and thermogravimetric analysis (TGA).

---

**18.1 Introduction**

Polymers are the major components of all adhesives and thus have a dominant influence on their properties. There is relatively little specific information in the literature on the thermal properties of adhesives; therefore, we must depend on the properties of the polymer to tell us about an adhesive. Examples are that polymethyl methacrylate can be used as a model for reactive acrylic adhesives, polydimethylsiloxane for silicone adhesives, and nylons for polyamide hot melts.

---

**18.2 Shelf-Life**

The period over which a packaged adhesive retains satisfactory properties is known as the shelf-life. Adhesives are based on organic chemicals, and provided they are kept in containers which exclude oxygen and UV-light; they have very long, perhaps indefinite, shelf-lives. Examples are epoxides, where resin and hardener are packed separately, hot melts, and adhesives which are solutions of polymers in organic solvents.

Exceptions include latex adhesives, reactive acrylics, and one-part epoxides. Freezing of latex adhesives causes the water phase to solidify and the particles to agglomerate irreversibly. Freeze-thaw stability can be improved by using carboxylate comonomers and adding antifreezes such as ethane diol or glycerol. Blackley (1997) has written a full account of this topic.



One-part epoxide adhesives contain resin and hardener, and can be supplied in the form of a film. The hardeners are such that high cure-temperatures are needed, and to slow down cure during storage and so lengthen shelf-life, such adhesives are stored at low temperatures where shelf-lives are between 6 and 12 months. The hardener dicyandiamide is insoluble in epoxides at low temperatures, but dissolves at cure temperatures; such adhesives are regarded as being completely stable below 40 °C.

Structural acrylic adhesives contain monomer, and cure is by a redox system which generates free radicals which cause cure by addition polymerization. Redox systems have two components, one being dissolved in the adhesive and the other in the hardener or “catalyst.” Once mixed, cure is rapid. Examples are cumene hydroperoxide and N,N-dimethyl aniline. Should the peroxide be in the adhesive, then it will slowly decompose to give free radicals, which will cause cure and eventually terminate the shelf-life, which is typically 12 months. Chemical reactions obey the Arrhenius relation (Eq. 1). Here  $k$  is the rate constant,  $A$  represents the total number of collisions between reacting molecules,  $E$  is the activation energy,  $R$  the universal gas constant, and  $T$  the absolute temperature.

$$k = A \exp(-E/RT) \quad (1)$$

Lowering temperature is thus a means to extend shelf-life.

Water vapor from the atmosphere is the curing agent for some silicone and isocyanate adhesives. Adsorbed surface water causes the cure of cyanoacrylates. Such adhesives are often packed in polyolefin containers which are naturally permeable to water. Hence, the passage of water through the container wall has the possibility to shorten shelf-life.

Hussey and Wilson (1996) have compiled some data which includes shelf-lives.

## 18.3 The Hardening (Curing) Process

At the time of application, an adhesive is a liquid, which is sufficiently mobile to wet the adherends. The process which follows is known as hardening or curing, and converts the liquid into a cohesive solid. Pressure-sensitive adhesives are an exception in that they remain viscous liquids. Hardening can be by loss of solvent, loss of water, cooling, or chemical reaction.

### 18.3.1 Hardening by Evaporation of Solvent or Water

The saturated vapor pressure of a liquid ( $p_o$ ) depends strongly on temperature according to Eq. 2, where  $\Delta H_e$  is the heat of evaporation,  $T$  the absolute temperature, and  $R$  the universal gas constant. Some values for water and for some solvents commonly used in adhesives are shown in Table 1.

$$d \ln p_o / d(1/T) = -\Delta H_e / R \quad (2)$$

**Table 1** Heat of evaporation of solvents

Solvent	$\Delta H_e/J\text{ g}^{-1}$
Water	2440
Acetone	534
Ethyl acetate	404
n-hexane	508
Tetrachloroethylene	242
Toluene	413

There is now much pressure from environmental and health and safety regulators to reduce or eliminate the use of solvents in adhesives, and the industry is responding by developing water-based systems to replace them. However, a fundamental problem is the low rate at which water evaporates because of its high heat of evaporation, which is about five times greater than for common solvents.

**18.3.2 Minimum Film-Formation Temperature of Latex Adhesives**

Latex adhesives consist of particles of polymers with diameters of the order of 1  $\mu\text{m}$  suspended in an aqueous medium. Surfactant molecules such as anionic soaps, which are adsorbed on the surfaces of the particles, maintain the particles in solution, and so stabilize the latex. Stabilization can also be gained by the presence of a soluble polymer in the aqueous phase which increases viscosity. The volume fraction of the phases is about 50%. Current adhesives include the latices of natural rubber, styrene-butadiene random copolymer, polyvinyl acetate, and its copolymers with ethylene and vinyl chloride. For any further information on polymer latices, the reader is directed to the three volumes of Blackley (1997).

Latex adhesives are applied to the substrate and the water is allowed to dissipate; this can be by evaporation, or in the case of porous substrates such as paper and wood, by passage into the adherend. To obtain a cohesive adhesive, it is necessary for the particles to coalesce, and this can only occur above a critical temperature (which is different for each latex) known as the minimum film-formation temperature MFFT; this is the lowest temperature at which the latex can form a film.

MFFT and glass transition temperature  $T_g$  are close but not identical. Brodnyan and Konen 1964 have measured and compared MFFT and  $T_g$  for a number of latices, and data are shown in Table 2.

A common viewpoint is that MFFT is usually lower than  $T_g$ , and this is due to plasticization by the dispersion medium, particularly water. This is contradicted by most of the data of Brodnyan and Konen, which show that MMFT exceeds  $T_g$ .

MFFT can be lowered by adding an organic plasticizer to the latex, or copolymerizing with a monomer whose homopolymer has a lower  $T_g$ . These phenomena are respectively termed internal and external plasticization and examples are the use of di-n-butyl phthalate, and the copolymerization of methylmethacrylate with ethyl acrylate (Protzman and Brown 1964).

t.1 **Table 2** Comparison of MFFT and Tg for some latex polymers

t.2	Polymer with molar ratios	MFFT °C	Tg °C	(MFFT – Tg) °C
t.3	Copolymer of styrene and n-butyl acrylate (75/25)	58	48	+10
t.4	Poly-n-butylmethacrylate	30	22	+8
t.5	Copolymer of styrene and n-butyl acrylate (55/45)	23	17	+6
t.6	Copolymer of methylmethacrylate and ethyl acrylate (50/50)	27	30	–3

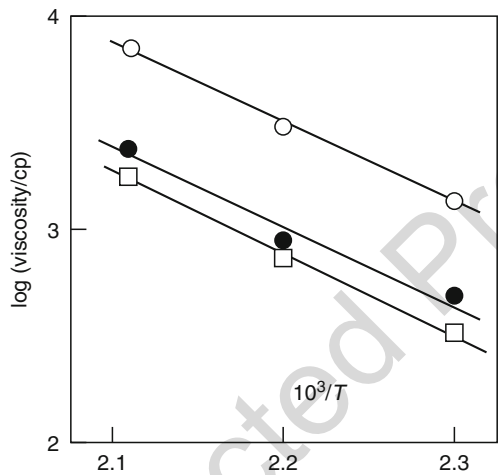


**Fig. 1** Dependence of melt viscosity upon temperature for three EVA hot melt-adhesives. Data replotted from Park and Kim 2003. The adhesives contain 50% by weight of EVA with different melt-flow indices, which were ○ 100 g min<sup>-1</sup>, ● 180 g min<sup>-1</sup>, and □ 200 g min<sup>-1</sup>

133 **18.3.3 Hardening by Cooling**

134 Hot melt adhesives harden by cooling, and it is first necessary to heat them to a  
135 sufficient temperature for flow, and for wetting of the adherends. Melt-viscosity fits  
136 the Arrhenius equation. Data for some ethylene vinyl acetate copolymer EVA hot  
137 melts are shown in Fig. 1 (Park and Kim 2003). Hardening is a rapid process which  
138 is primarily controlled by the flow of heat from the thin bondline. However,  
139 crystallization may increase after cooling. There can be a problem in using them  
140 on metals, in that rapid cooling prevents adequate wetting.

141 **18.3.4 Hardening by Chemical Reaction**

142 Where the hardening of an adhesive or sealant proceeds by chemical reaction, the  
143 rate will increase with temperature in accordance with the Arrhenius equation.  
144 Such materials include epoxides, structural acrylics, cyanoacrylates, silicones, and

high-temperature adhesives. Hence, pot-life and cure time will show the following proportionality.

$$\log t \propto 1/T \quad (3)$$

Lapique and Redford (2002) used differential scanning calorimetry to measure rates of cure for the epoxide paste-adhesive Araldite 2014, finding E to be 34.6 kJ mol<sup>-1</sup>. The equation also applies to other time-dependent processes such as diffusion and viscous flow.

### Pot-Life

Pot-life is the time available between mixing an adhesive and its application and the concept applies to adhesives where two components are mixed shortly before use. Examples are two-part epoxides, some silicones, reactive adhesives for wood based on formaldehyde condensates, some isocyanates, and polysulfides. Polymerization commences on mixing and crosslinking occurs in all cases. Both processes cause viscosity to increase, and this will begin to hinder the wetting of the adherends. A critical point however is the gel-point, where the viscosity increases very greatly, due to the adhesive becoming completely crosslinked. The gel-time is thus the upper limit of shelf-life, but in practical terms, the latter will be significantly less than the former. For some isocyanate and acrylic adhesives, pot-life can be only a few minutes. Where cure is rapid, the reaction exotherm can cause heating which accelerates the cure process. Such an effect will depend on the ability of the assembly to dissipate heat.

An adhesive which cures rapidly will have a relatively short pot-life; a prolonged cure is related to a long pot-life. Hussey and Wilson (1996) have compiled some data which includes pot-lives.

Factors other than pot-life can affect the working time of an adhesive or sealant. Some silicones and isocyanates are cured by moisture which causes a skin to form on the surface, the thickness of which increases in proportion to the square root of time. Solvent-based adhesives can suffer from rapid evaporation which limits their ability to wet the substrates. Hot melt adhesives are prone to oxidative degradation at temperatures of application.

### Ceiling Temperature

For thermodynamic reasons, some adhesives may not cure at all above a critical temperature, which is known as the ceiling temperature, and may only partially cure at lower temperatures. This particularly applies to adhesives which harden by polymerization of monomers with C = C bonds, such as acrylates, methacrylates, and cyanoacrylates.

The free energy of polymerization  $\Delta G_p$  is related to the heat  $\Delta H_p$  and entropy  $\Delta S_p$  of polymerization by Eq. 4.

$$\Delta G_p = \Delta H_p - T\Delta S_p \quad (4)$$

**Table 3** Some Thermodynamic Parameters for Polymerization

Monomer	$\Delta H_p/\text{kJ mol}^{-1}$	$\Delta S_p/\text{J mol}^{-1} \text{K}^{-1}$	$T_c/^\circ\text{C}$
Methylmethacrylate	-55.5	$-117 \pm 6$	201
Methyl cyanoacrylate	-42		
Ethyl cyanoacrylate	-47, -53, -54		
n-Decyl cyanoacrylate	-69, -74		217
Ethylene oxide	-94.6		-86
Styrene	-68.6, -70, -73	-104	387, 400, 429
$\alpha$ -Methylstyrene	-37	-110	61

Heat is evolved on polymerization, so  $\Delta H_p$  is negative. When monomer molecules which can move independently are captured in a polymer chain, there is an increase in order and therefore a decrease in entropy. At equilibrium,  $\Delta G_p = 0$  so the ceiling temperature  $T_c$  is given by Eq. 5.

$$T_c = \Delta H_p / \Delta S_p \quad (5)$$

Entropy of polymerization does not vary widely for  $C = C$  monomers; it is usually in the range of  $100\text{--}125 \text{ J mol}^{-1} \text{K}^{-1}$  for liquid monomers. This is because in each case, the dominant factor is the loss of transitional freedom that occurs when a monomer molecule is incorporated into a polymer chain. Table 3 gives some values for entropy of polymerization.

In contrast, heats of polymerization do vary from monomer to monomer. One factor which is particularly important in causing monomers to have different values of  $\Delta H_p$  is steric hindrance in the polymer chain caused by larger substituent groups. Table 3 gives some values for heat of polymerization. Changes in heat, rather than entropy of polymerization, cause polymers to have different ceiling temperatures. Some ceiling temperatures are given in Table 3.

The heat of curing for a fast curing two-part epoxide has been measured as  $494 \text{ J/g}$  (Keller et al. (2016)). Samples in aluminum molds were heated at  $80$  or  $100^\circ\text{C}$ .

And those which were  $4 \text{ mm}$  thick at  $100^\circ\text{C}$  reached a peak temperature of  $176^\circ\text{C}$  in about  $30 \text{ s}$ . Samples  $3 \text{ mm}$  thick cured at  $80^\circ\text{C}$  showed a rise of about  $40^\circ\text{C}$  in the same time. These rises will not be typical of adhesive joints with thin gluelines, and would be reduced by the presence of fillers and conductive adherends.

### Kinetic Approach to Equilibrium

The polymerization process can be represented as



where  $M^*$  is a polymer chain with an end group which is an active center (free radical, anion or cation) and  $M$  is monomer.  $M^*$  appears on both sides of the equation, but there is the actual difference in that the one on the right contains one more monomer unit than that on the left.

209 The rate of the forward polymerization reaction is

$$R_p = k_p[M^*][M] \quad (6)$$

210 The rate of the reverse depolymerization reaction is

$$R_d = k_d[M^*] \quad (7)$$

211 Here,  $k_p$  and  $k_d$  are the respective rate constants. At equilibrium, the rates of  
212 forward and reverse reactions are the same, so that

$$k_p[M^*][M]_e = k_d[M^*] \quad (8)$$

$$K = k_p/k_d = 1/[M]_e \quad (9)$$

213 Here,  $K$  is the equilibrium constant and  $[M]_e$  is the monomer concentration at  
214 equilibrium.

215 The Arrhenius equation can be substituted for the rate constants in Eq. 9, giving

$$A_p \exp(-E_p/RT) [M]_e = A_d \exp(-E_d/RT) \quad (10)$$

$$T = (E_p - E_d) / (R \ln A_p/A_d + R \ln [M]_e) \quad (11)$$

216 Equation 12 follows from the fact that heat of polymerization is the difference in  
217 the activation energies of the forward and reverse reactions. Here,  $R$  is the universal  
218 gas constant.

$$T = \Delta H_p / (R \ln A_p/A_d + R \ln [M]_e) \quad (12)$$

219  $A_p$  and  $A_d$  are related to the total number of collisions between reacting mole-  
220 cules, and to the entropies of activation. This leads to

$$T = \Delta H_p / (\Delta S_p^\circ + R \ln [M]_e) \quad (13)$$

221 Here,  $\Delta S_p^\circ$  is the entropy change in the standard state.

222 What this means is that at temperature  $T$ , a polymerization will continue consum-  
223 ing monomer, until the monomer concentration falls to  $[M]_e$ ; it will then cease. At  
224 the actual ceiling temperature,  $[M]_e$  = the bulk concentration of monomer.  $T_c$  will be  
225 less if the monomer is diluted.

226 The data in Table 3 have been compiled from a number of sources, and most are  
227 for the conversion of a liquid monomer to an amorphous polymer. The exception is  
228 ethylene oxide where the polymer is semicrystalline; the heat and entropy of  
229 crystallization will contribute to the parameters for this monomer.

230 The data illustrate some matters which have already been noted. One is that the  
231 entropies for the  $C = C$  monomers are very similar. Another is that the addition of a  
232 methyl group to styrene leads to increased steric hindrance in the polymer, so

lowering  $-\Delta H_p$  and ceiling temperature. If the methyl groups were replaced by the larger phenyl group (to give 1,1-diphenyl ethylene), the monomer would not polymerise at all! The first three monomers in the table are used in adhesives, and the ethylene oxide ring reacts in epoxide adhesives, which can cure by addition polymerization when certain hardeners are used (e.g., tertiary amines).

### Curing by Reaction with Water Vapor

Moisture curing adhesives and sealants consisting of low molar mass polymers with specific end-groups, hardened by reacting with water from the atmosphere. The end-groups include acetate, ethoxide and butanone ketoxime on silicones, and isocyanates. Cure proceeds by a skin forming on the surface, which then grows in thickness, such that the depth of cure ( $z$ ) is given by the following equation (Comyn et al. 1998).

$$z = (2PpVt)^{1/2} \quad (14)$$

Here,  $p$  is the vapor pressure of water,  $V$  is the volume of sealant which reacts with a unit of water, and  $t$  is the time.  $P$  is the permeability coefficient of water in the cured material and this in turn is the product of the diffusion coefficient  $D$  and solubility coefficient  $S$ . Thus, Eq. 14 can be modified to Eq. 15, where  $r.h.$  is relative humidity.

$$z = (2DSp(r.h./100)Vt)^{1/2} \quad (15)$$

The dependence of the rate of cure on temperature is thus controlled by three heats, which are the heat of evaporation of water, the activation energy for diffusion, and the heat of solution of water in the cured material.

For water in a silicone with ethoxy end-groups,  $P$  was found not to obey the Arrhenius equation, and to decrease slightly as the temperature rose; this is shown in Fig. 2 (Ashcroft et al. 2009). This was ascribed to many of the water molecules not being dispersed in the adhesive, but being isolated in droplets or clusters. A similar situation occurs for some isocyanate-ended automotive windscreen adhesives (Ashcroft et al. 2009), and the main factor which causes cure rate to increase with temperature was the increasing vapor pressure of water. Figure 3 shows that the actual Arrhenius plot was linear for the overall cure process.

## 18.4 Thermal Properties of Cured Adhesives

### 18.4.1 The Glass Transition Temperature

At low temperatures, all polymers are in the glassy state, by which it is meant that they are relatively hard and inflexible. At some temperature, which is characteristic for each polymer, the material becomes soft and flexible, and so enters the rubbery or leathery state. This change is the glass transition, and it occurs at the glass transition temperature  $T_g$ .

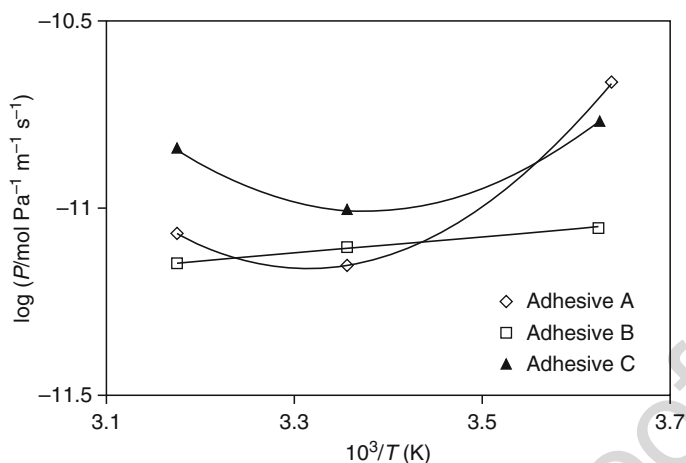


**Fig. 2** Dependence of water permeability for three automotive windscreen adhesives upon temperature (Ashcroft et al. 2009)

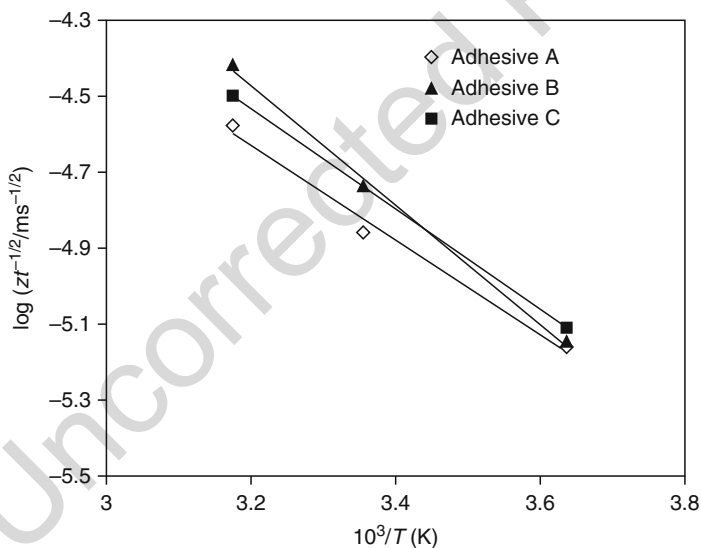


**Fig. 3** Dependence of rate of cure upon temperature for three isocyanate-based water-reactive automotive windscreen adhesives (Ashcroft et al. 2009)

Most polymeric adhesives are amorphous rather than semicrystalline, and the glass transition is a property of the amorphous phase. It is caused by changes in molecular motion, such that in the glassy state the polymer backbone is not free to move in translation, but it is free to do so in the leathery state.

T<sub>g</sub> can be measured by thermal analysis, dilatometry and mechanical damping. Heat distortion temperature, brittle point, and softening point are closely related to



T<sub>g</sub>. For a given polymer, these three temperatures will be similar, but not usually identical, because of the use of different heating rates and the fact that the phenomena are pressure sensitive.

Sun et al. (2014) used DMA to measure the effect of heating rates on the T<sub>g</sub> of an epoxy adhesive. A heating rate of 0.5°C min<sup>-1</sup> gave a T<sub>g</sub> of 61°C, whereas at 10°C min<sup>-1</sup>, T<sub>g</sub> was 64°C.

Both glassy and leathery polymers are used as adhesives. Examples of the former are epoxides, phenolics, and reactive acrylics; rubber-based adhesives are examples of the latter. However, because of the large changes in mechanical properties, it is unacceptable for the glass transition temperature to exist in the same region of temperature in which an adhesive bond has to operate.

### Free Volume Theory

The free volume theory is a simple and effective means of accounting for T<sub>g</sub>. Free volume increases on thermal expansion, and once it reaches a critical amount, the backbone is free to move and the polymer is transformed into a rubber or leather.

Thus, the effect of pressure will be to reduce free volume and so increase T<sub>g</sub>. The chemical structure of a polymer affects its T<sub>g</sub>. Intermolecular forces are attractive and so reduce free volume. Polar groups cause polymer chains to be mutually attractive and so increase T<sub>g</sub>, while large nonpolar side chains tend to hold them apart and so lower T<sub>g</sub>. Table 4 shows the T<sub>g</sub> of polymethylmethacrylate (PMMA) to be 105 °C, but replacement of the ester methyl groups with 2-ethylhexyl lowers it to -50 °C. Poly 2-ethylhexyl-methacrylate is used in pressure-sensitive adhesives. Polymethyl acrylate has a T<sub>g</sub> of about 10 °C, but that of polyacrylic acid is much higher as intermolecular hydrogen bonds will reduce free volume. The sodium salt of the polyacid has a much higher T<sub>g</sub> of 230 °C, caused by the much stronger ionic attractions between chains. Starch is extensively hydrogen-bonded and so has a high T<sub>g</sub>. The polar carbon-chlorine bond in polychloroprene gives it a higher T<sub>g</sub> (-46 °C) than poly-*cis*-1,4-isoprene (c -70 °C), which closely resembles natural rubber. Crosslinking ties chains together so limiting molecular motion and increasing T<sub>g</sub>. The data in Table 4 are taken from a compilation (Andrews and Grulke 1999); some are T<sub>g</sub>s and others are brittle points and softening temperatures. In some cases, there are multiple entries.

Brittle points for some polyacrylates and polymethacrylates are shown in Fig. 4. At first, the brittle point falls as the number of carbon atoms in the side-chain (n) increases. The side-chains are alkyl groups which are nonpolar and flexible, and they act as internal plasticizers. A minimum temperature is reached when n reaches 8 with the polyacrylates and 12 with the polymethacrylates; beyond this, the brittle point rises and this is caused by partial crystallization of the side groups.

End groups introduce extra free volume, and hence T<sub>g</sub> falls as molar mass decreases. Often data fit Eq. 16, where T<sub>g</sub><sup>h</sup> is the glass transition temperature of very high molar mass polymer, M is molar mass, and A is a constant.

$$1/T_g = 1/T_g^h + A/M \quad (16)$$

**Table 4** Glass transition temperatures of some polymers and adhesives

Material	T <sub>g</sub> /°C
Polyacrylic acid	75,106
Polychloroprene	−46
Polydimethylsiloxane	−127
Poly-2-ethylhexylacrylate	−50
Poly <i>cis</i> -1,4 isoprene	−73, −70, −69
Polymethylacrylate	9, 10, 11, 19
Polymethylmethacrylate	105
Polypropylene (atactic)	−3 to −17
Poly sodium acrylate	230
Polystyrene	100
Polyvinyl acetate	32
Polyvinyl alcohol	85
Starch (dry)	165–185
Starch (humid)	95–135
Styrene-butadiene rubber	−61

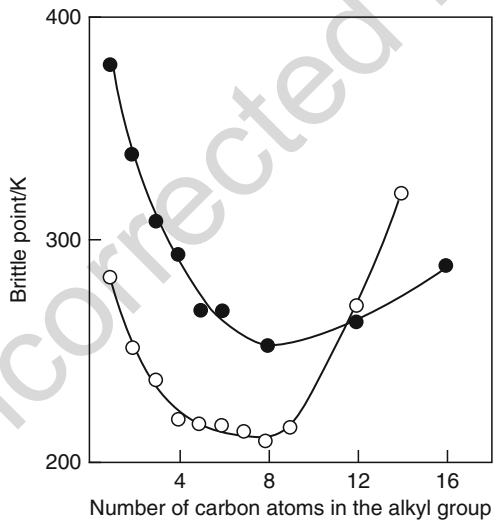


**Fig. 4** Brittle points of poly-*n*-alkyl acrylates ○ and methacrylates ● (Data taken from Andrews and Grulke 1999)

In most cases, the T<sub>g</sub> of a random copolymer is between those of the corresponding homopolymers, and if T<sub>g</sub> is plotted against composition for the series of copolymers, it is a straight line or gentle curve linking the homopolymer T<sub>g</sub>s. In such cases, the Fox equation (Eq. 17, Fox 1956) is moderately successful in accounting for the T<sub>g</sub>.

$$1/T_g = w_1/T_{g1} + w_2/T_{g2} \quad (17)$$

Here,  $w_1$  and  $w_2$  are the weight fractions of the two components, and  $T_{g1}$  and  $T_{g2}$  are the glass transition temperatures of the homopolymers. The equation assumes that free volume contributions are additive. There are exceptions such as the copolymers of ethyl acrylate and vinylidene chloride. Here, the  $T_g$ s of both homopolymers are about  $-25^\circ\text{C}$ , while the equimolar copolymer has a  $T_g$  of about  $25^\circ\text{C}$ . Other copolymers show  $T_g$  minima (Comyn and Fernandez 1975).

Cured rubber-modified structural adhesives have a glassy matrix and a disperse phase of small rubber particles, which have a reinforcing action. Such materials have two  $T_g$ s, a higher one associated with the matrix and a lower one for the rubber particles. The  $T_g$  of the rubbery phase represents a lower temperature limit for these adhesives.

Block copolymers of styrene with either butadiene or isoprene are used in pressure-sensitive adhesives. These are three-block copolymers of type ABA where A are polystyrene blocks and B are polydienes. The two phases are incompatible, each phase having a separate glass transition temperature. The rubbery phase is continuous and the styrene phase consists of small particles 20–30  $\mu\text{m}$  diameter. The styrene content is generally above 25%. The  $T_g$  of the polybutadiene phase is about  $-80^\circ\text{C}$ , and it is about  $-50^\circ\text{C}$  for polyisoprene. The  $T_g$  of polystyrene is about  $100^\circ\text{C}$ , and this temperature must be exceeded in thermal processing. They are also used as thermoplastic rubbers.

The addition of a liquid to a polymer causes an increase in free volume and lowers  $T_g$ . Liquids have relatively high amounts of free volume; they might be present in adhesives by design or chance, examples of the latter being water and plasticizers. The phenomenon is generally known as plasticization, and may be quantified by the Fox equation, where  $w_2$  and  $T_{g2}$  are the weight fraction and  $T_g$  of the plasticizer. Pressure-sensitive adhesives generally have a low  $T_g$  and additives such as tackifiers have a high  $T_g$ .

### Dry and Wet Epoxides

The diglycidyl ether of bisphenol A DGEBA is widely used as a resin in epoxide adhesives. The three principal groups of compounds that are used to cure such epoxide adhesives are aliphatic amines, aromatic amines, and acid anhydrides. Cure with aliphatic amines occurs at lower temperatures than that with aromatic amines and acid anhydrides. This temperature difference is reflected in the  $T_g$  of the cured adhesive. Also epoxides cured with aromatic amines have higher  $T_g$ s than those with aliphatic amines, as the former have less flexible molecules than the latter. This is illustrated in Table 5 where DAPEE and TETA are aliphatic and DAB and DDM aromatic.

Brewis et al. (1982) measured heat-distortion temperatures  $T_d$  of a range of epoxide adhesives, both dry, after reaching equilibrium when immersed in water, and after a total of 10 months immersion. Their data which appear in Table 5 show that distortion temperatures are all initially lowered in water, but all increase on immersion for 10 months. The latter may be due to further crosslinking between

t.1 **Table 5** Heat distortion temperatures of some dry and wet epoxides

t.2	Hardener eqn	Equilibrium water absorption at 25 °C	Td/°C			Td depression/°C	
			Dry	Wet	10 Months	Actual	Fox
t.4	DAPEE	5.0	67	37	49	30	23
t.5	TETA	3.8	99	86	111	13	23
t.6	DAB	2.3	161	143	157	18	22
t.7	DDM	4.1	119	110	130	9	27
t.8	DMP	4.4	68	51	54	17	21
t.9	BF <sub>3</sub> MEA	2.3	173	155	18	22	

t.10 Hardeners are DAPEE = di(1-aminopropyl-3-ethoxy)ether, TETA = triethylenetetramine, DAB = 1,3-diaminobenzene, DDM = 4,4'-diaminodiphenylmethane, DMP = tris(dimethylaminomethyl)phenol, BF<sub>3</sub>MEA = borontrifluoride monoethylamine

360 unreacted groups in the water-plasticized adhesive. The actual changes after initial  
 361 immersion were compared with that predicted by the Fox equation. In some cases,  
 362 the two values are in reasonable accord. Except with DAPEE hardener, the actual  
 363 depression of Td is less than that predicted by the Fox equation; this can readily be  
 364 explained by some of the water not being molecularly dispersed in the resin and so  
 365 not plasticizing it, but instead being isolated in clusters.

366 Use of the Fox equation in this manner requires a value for the glass transition  
 367 temperature of water. This has been reported in the range –134 to –138 °C using  
 368 differential thermal analysis and other methods (McMillan and Los 1965, Sugisake  
 369 et al. 1968, Rasmussen and Mackenzie 1971).

## 370 18.4.2 Melting of Semicrystalline Polymers

371 While the glass transition is of very great importance in adhesives, crystalline  
 372 melting is not. This is because the polymers in most adhesives are totally amorphous,  
 373 which in turn is due to the lack of molecular regularity. Stereoregular polymers can  
 374 be made from vinyl and vinylidene monomers with the employment of organome-  
 375 tallic initiators, but these are not used when such monomers are converted into  
 376 polymers which are used in adhesives. The latter are atactic and examples are MMA  
 377 copolymers in structural acrylic adhesives, amorphous polypropylene, polyacrylic  
 378 pressure-sensitive adhesives, and polycyanoacrylates.

379 Adhesives which exhibit some degree of polymer crystallinity include EVA and  
 380 polyamide hot melts, polyvinylalcohol, polychloroprene, polyurethanes, polyureas,  
 381 and starch.

### 382 Ethylene Vinyl Acetate EVA Hot Melts

383 The melting point of low-density polyethylene is about 117 °C, and its degree of  
 384 crystallinity will depend on its thermal history. When copolymerized with vinyl  
 385 acetate, molecular regularity is diminished and there is a large reduction in degree of

crystallinity. EVA random copolymers containing up to 30% vinyl acetate are used. Further information has been provided by Eastman and Fullhart 1990. The thermal properties of an EVA hot melt adhesive with an aromatic hydrocarbon tackifier have been examined in detail by Park and Kim (2003).

### Polyamide Hot Melts

The melting points of polyamides are affected by the ability of amide groups to form hydrogen bonds. The melting points of some polyamides made from aliphatic diacids and diamines are plotted in Fig. 5. Melting point does not change smoothly as the number of methylene groups increases, and polymers with even numbers of carbon atoms are at the peaks of the zig-zag, because the number of intermolecular hydrogen bonds is greater. The matter has been detailed by Comyn (1997).

This is illustrated from diamines and diacids in Fig. 6, where four pairs of molecules are shown. In each case, there are a pair of polymer molecules, and the issue of concern is whether all the carbonyl and amine groups inside the pair are so placed that they can form a hydrogen bond  $>\text{CO} \cdots \text{HN}<$ . This happens for all the groups when all the carbon atoms are in even numbers, but in all the other cases in Fig. 6, only 50% can do so. This means that in Fig. 5 the peak temperatures are when there are an even number of carbon atoms in the diacid, and the tetramethylene diamine has higher melting points the pentamethylene. Similar trends occur with polyureas and polyurethanes, and smoothed plots are shown in Fig. 7, where the asymptote is the melting point of polyethylene. There is a reverse trend for aliphatic polyesters, which can be major components in polyurethanes. An explanation for this is the higher flexibility of the C-O linkage which so gives the molten molecules a

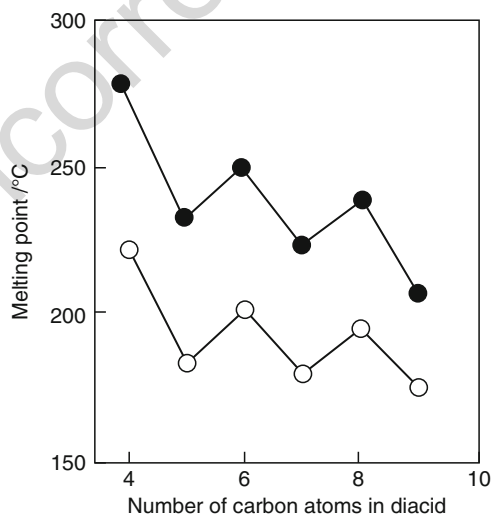


**Fig. 5** Melting points of polyamides formed from ● tetramethylenediamine, ○ pentamethylenediamine, and diacids (Comyn 1997)

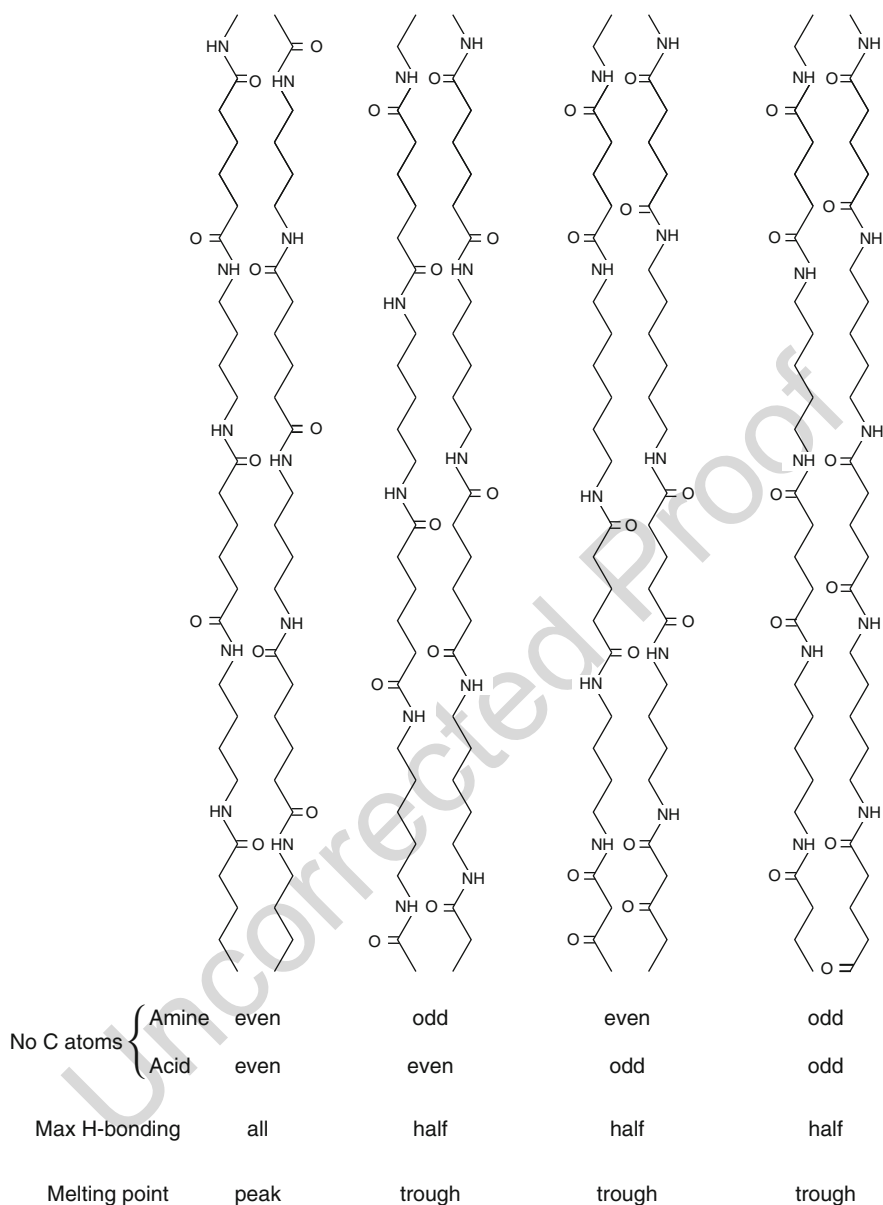


**Fig. 6** Hydrogen bonding in polyamides derived from diacids and diamines

409 higher number of configurations, and so increasing the entropy of fusion. Melting  
 410 point  $T_m$  is controlled by the heat and entropy of fusion  $\Delta H_f$  and  $\Delta S_f$  by Eq. 18,  
 411 which is really a restatement of Eq. 5.

$$T_m = \Delta H_f / \Delta S_f \quad (18)$$

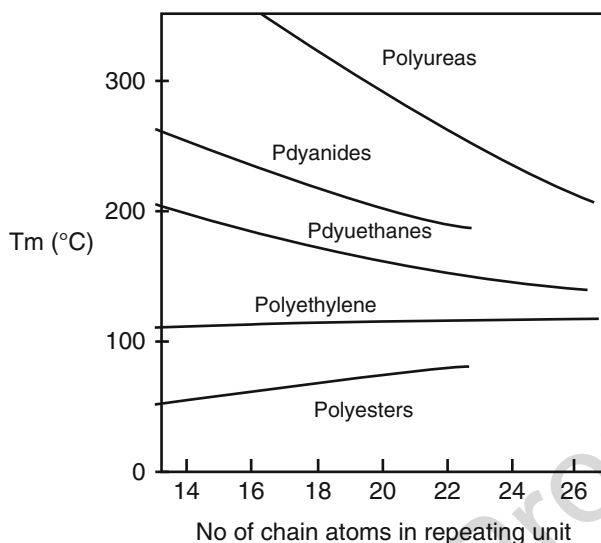


**Fig. 7** Smoothed plots of melting points of linear aliphatic heterochain thermoplastics

The use of mixed monomers in polyamide hot melts increases disorder, so lowering the extent of hydrogen bonding and melting point. Homopolyamides have melting points that are too high for hot-melt adhesives; for example, nylon 6 melts at 225 °C, nylon 66 at 264 °C, and nylon 12 at 180 °C. Their melt viscosities are also high for this particular application. However, copolymerization and terpolymerization give products with less regular structures and reduced levels of intermolecular hydrogen bonding, therefore yielding lower melting points. The polyamide terpolymers 6,6-6,6-10,6-6,12,6-6,6-12, and 6,6-9,6-12 are used for bonding textile fabrics, where they are resistant to washing and chlorinated dry cleaning solvents. Polyamide adhesives have been reviewed by Rossitto (1990).

### 18.4.3 Viscoelastic Properties of Adhesives

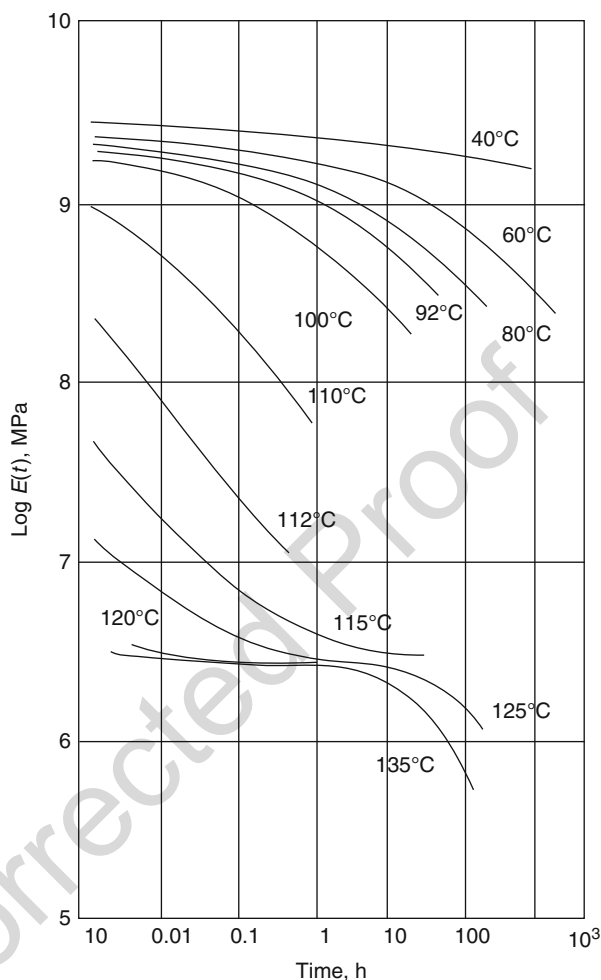
Polymers, and therefore adhesives, have a combination of the viscous properties of a liquid and the elastic properties of a solid. In a structural adhesive the elastic properties are dominant, whilst the viscous component is evident in pressure-sensitive adhesives.

#### Stress Relaxation

Viscoelasticity is manifest in creep and stress relaxation, which both depend on time and temperature.

If a constant strain is applied to a polymer at a fixed temperature, then the stress needed to maintain that strain will decrease with time. The time-dependent stress can be

**Fig. 8** Dependence of relaxation modulus upon time for polymethylmethacrylate, at temperatures between 40 and 135 °C (Comyn 1990, but original data from McLoughlin and Tobolsky 1952)



expressed as the relaxation modulus  $E(t)$ . The dependence of  $E(t)$  on time for PMMA at a number of temperatures is shown in Fig. 8. Using the principle of time-temperature superposition, the time range of the data in Fig. 9 can be extended both to longer and shorter times at any chosen temperature. According to this principle, any locus can be slid horizontally along the log (time) axis until it superimposes and extends its Neighbour; thus, data at a temperature below the reference temperature can be used to extend to shorter times, whereas data at higher temperature can be used to reach to longer times. The symbol for these shift-factors is  $\log a_T$ . This shifting has been done on the lines in Fig. 8 keeping 110 °C as the reference temperature, and the result is shown in Fig. 9.

The result of this operation is a single locus of  $\log E(t)$  against  $\log (\text{time})$  at a single temperature (here, 110 °C), which extends over a wider time range. A further consequence of time-temperature superposition is that plots of  $\log E(t)$  against temperature, at constant time, are similar in shape to those of  $E(t)$  against log (time).



**Fig. 9** Dependence of relaxation modulus upon time for polymethylmethacrylate, at 110 °C (Comyn 1990)

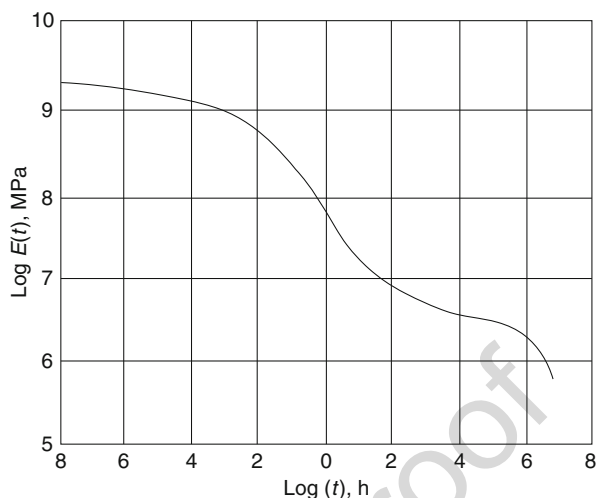
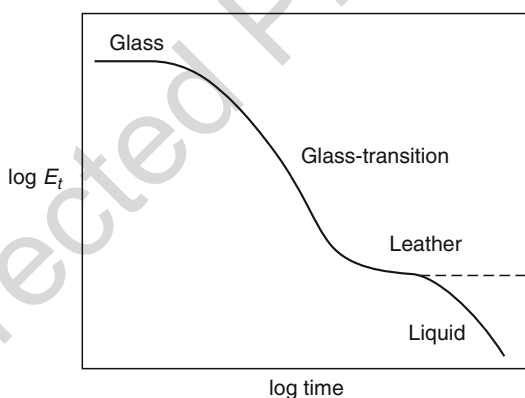


**Fig. 10** Dependence of relaxation modulus upon time for linear (continuous line) and crosslinked (broken line) polymers, showing four regions of viscoelastic behavior



For all amorphous polymers, values of  $\log a_T$  are an approximate fit to the following Eq. (19), which is widely known as the WLF equation after its originators Willams, Landel, and Ferry.

$$\log a_T = \frac{C_1(T - T_g)}{C_2 + (T - T_g)} \quad (19)$$

Here,  $C_1$  and  $C_2$  are empirical constants with the respective values of  $-17.44$  and  $51.6$ .

Figure 10 shows the modulus-temperature plot of a linear polymer, which has four regions of viscoelastic behavior. At the lowest temperatures, the material is a high-modulus glass. As temperature increases, it passes through the glass transition region and its modulus falls to that of a leathery material. It holds a stable modulus over a modest

region of temperature, but then enters a region of flow. The main difference between this case and that of a crosslinked polymer is that the crosslinks prevent the polymer from flowing.

A further empirical Eq. (20) due to Doolittle relates the viscosity of a liquid ( $\eta$ ) to its free volume. Here, A and B are constants and f is the fraction of free volume.

$$\log_e \eta = \log_e A + B/f \quad (20)$$

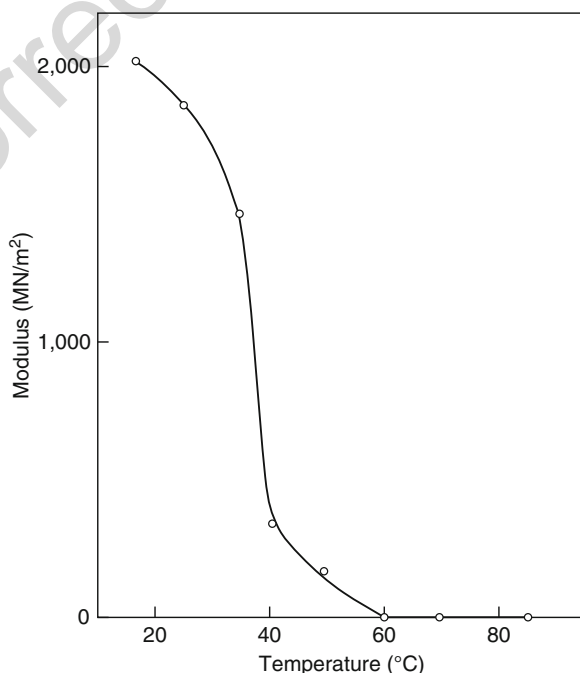
As stress relaxation is a manifestation of viscous flow, the WLF equation can also be applied to polymer viscosity, and comparison with the Doolittle equation shows that  $B/2.303 f = 17.44$ . If the value of B is unity, which is demonstrated by some of Doolittle's data, then the value of f is 0.025. This indicates that the free volume fraction at Tg of any polymer is 2.5%.

Further details of these matters have been given by Sperling (2006).

### Data for Adhesives

Brewis et al. (1982) reported the dependence upon temperature of the tensile modulus of the epoxide-polyamide adhesive FM1000, which has a Tg of 40 °C. Data which appear in Fig. 11 show typical viscoelastic behavior. The same authors (1983) showed similar data for an aliphatic amine-cured epoxide adhesive, which has a Tg of 65 °C. Changes in the strengths of lap-joints with increasing temperature fell in the same manner as the modulus and tensile strength of the adhesive, as in shown in Fig. 12.

**Fig. 11** Effect of temperature on the modulus of the epoxide-polyamide adhesive FM 1000 (Brewis et al. 1983)



#### 18.4.4 Thermal Conductivity of Adhesives

Adhesives are poor conductors of heat and electricity, but both can be increased by filling with powdered metals, especially silver. To increase thermal conductivity alone, metal oxide fillers can be used. The most effective of these is beryllium oxide, which is both toxic and expensive; aluminum oxide is a practical alternative. Some values of thermal conductivity are collected in Table 6.

Kilik et al. (1989) have measured thermal conductivities of a toughened epoxide adhesive filled with copper and aluminum powders. The effect of the size and shape of particles is less significant than the amount of filler used. Al-Samhan and Darwish (2005) showed that the thermal conductivity of an adhesive was increased from 1.06 to 1.81 W m<sup>-1</sup> K<sup>-1</sup> when filled with copper. Morriche et al. (2016) added graphene platelets of average thickness 6–8 nm to an epoxide cured with an aromatic amine which increased thermal conductivity by as much as 200–300%.

#### 18.4.5 Thermal Expansion of Adhesives

Unless polymers are the substrates, linear thermal expansion coefficients of adhesives are generally much greater than those of the materials being bonded. Some comparative data are shown in Table 7. When large areas are being bonded, these differences can lead to significant and damaging interfacial stresses as the temperature changes. Expansion coefficients of adhesives can be reduced by the addition of mineral fillers.

Expansion coefficients of polymers are greater in the rubbery state than in the glass. Some data appear in Table 8.

Metal cutting tools can reach very high temperatures (400 °C), and Al-Samhan and Darwish (2005) have used finite element stress analysis to examine the case of tungsten carbide tips bonded to a steel support. Here, the linear expansion coefficients were 12.1 × 10<sup>-6</sup> K<sup>-1</sup> for steel, 60 × 10<sup>-6</sup> K<sup>-1</sup> for the tip, and 40 × 10<sup>-6</sup> K<sup>-1</sup> for the adhesive. The use of cutting fluids much reduced the stresses.

Da Silva and Adams (2007) predicted advantages in using two adhesives in metal-composite double lap joints which had to operate over a temperature range of –55 to 200 °C, as might be the case in supersonic aircraft. A ductile adhesive was present to cope with low temperatures and a brittle adhesive for the high ones.

### 18.5 Breakdown of Adhesives

#### 18.5.1 Oxidative Degradation

Oxygen in the atmosphere generally attacks polymers. In many cases, the rate of attack, even at ambient temperatures, necessitates the use of stabilizing additives. Examples of adhesives that normally contain antioxidants are hot melts, those based on natural and synthetic rubbers, and pressure-sensitive adhesives.

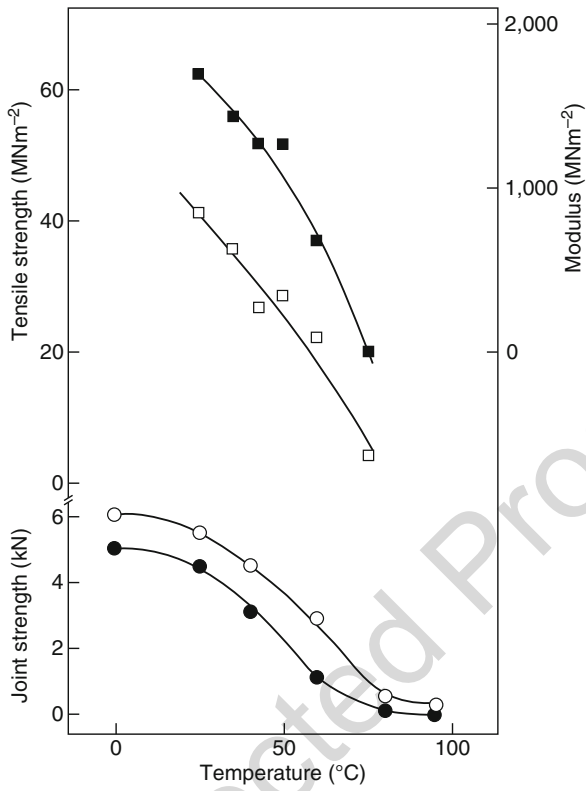


**Fig. 12** Comparison of dependence on temperature of joint strengths with mechanical properties of the adhesive. ○ dry joints, ● joints stored for 1000 hours at 100% relative humidity and 50 °C. ■ adhesive modulus, □ adhesive tensile strength. The adhesive is DGEBA cured with DAPEE (Brewis et al. 1983)

**Table 6** Thermal conductivities of fillers and adhesives

Material	W m <sup>-1</sup> K <sup>-1</sup>
Silver	410
Copper	370
Aluminum oxide	34
Unfilled epoxide	0.7–0.26
Epoxide with 25% by weight of alumina filler	0.34–0.51
Epoxide with 50% by weight of alumina filler	0.51–0.68
Epoxide with 75% by weight of alumina filler	1.3–1.7
Epoxide with 50% by weight of aluminum	1.7–3.4

Although all polymers will degrade at elevated temperature in the absence of air, the rate of degradation is generally increased when there is a supply of oxygen. In adhesive joints, the supply of oxygen will depend on the oxygen permeabilities of

**Table 7** Coefficients of linear thermal expansion of various materials

Material	$10^{-6} \text{ K}^{-1}$
Low-density polyethylene	100
High-density polyethylene	130
Polymethylmethacrylate below T <sub>g</sub>	260
Polymethylmethacrylate above T <sub>g</sub>	530
Polystyrene	60–80
Aluminum	29
Steel	11
Titanium	9
Soda-glass	8.5
Wood (along grain)	3–5
Wood (across grain)	35–60

**Table 8** Coefficients of linear thermal expansion of adhesives and polymers, both below and above T<sub>g</sub>.

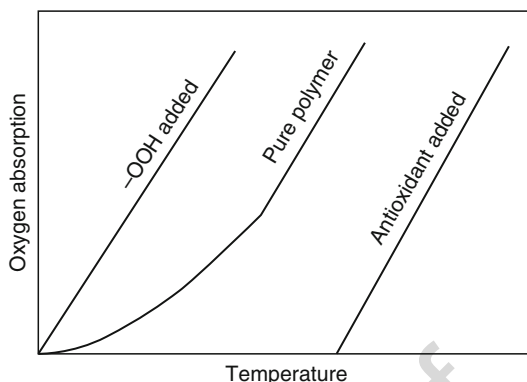
Hardener	Below T <sub>g</sub> /10 <sup>-4</sup> K <sup>-1</sup>	T <sub>g</sub> /°C	Above T <sub>g</sub> /10 <sup>-4</sup> K <sup>-1</sup>
<b>Epoxide adhesives with hardeners</b>			
BF <sub>3</sub> .Amine	0.63	141	1.7
Diethylenetetramine	0.60	122	1.8
1,2-diaminobenzene	0.57	190	2.1
Methylene bis(1-chloroaniline)	0.83	149	1.9
<b>Polymers used in adhesives</b>			
Polyvinyl acetate	2.1	29	6.0
Polymethylmethacrylate	2.6	105	5.1

both the adhesive and the adherends, and on the distance that oxygen must diffuse in either of these. Metallic, ceramic, and glass adherends are impermeable to oxygen and therefore represent a complete barrier to it, but composites with polymeric matrices are permeable to atmospheric gases. However, the rate of oxygen diffusion into adhesives at elevated temperatures will probably be sufficiently high for impermeable adherends to offer little protection against oxidative degradation.

Oxygen is a diradical and can participate in polymerization and degradation reactions by acting as an initiator. Oxygen is absorbed by the polymer to form a hydroperoxide that subsequently decomposes to give radicals that then initiate degradation.

Figure 13 shows the amount of oxygen absorbed by a typical polymer in air as the temperature is raised. The pure polymer has a buildup period in which the hydroperoxide is formed, but this is absent in the polymer in which hydroperoxide groups have previously been added. In the presence of an antioxidant, there is a long induction period in which the stabilizer scavenges any free radicals. The end of the induction period marks consumption of the stabilizer. Oxidative degradation is a complex series of chain reactions. Karger-Kocsis et al. (1980) have demonstrated induction periods in the oxygen uptake of a number of hot-melt adhesives.

**Fig. 13** Oxygen absorption by a polymer



The excellent resistance to oxidation possessed by high-temperature adhesives such as polyimides, polyquinoxalines, and polybenzamidazoles is due to their high content of aromatic groups.

Polymers are also attacked by ultraviolet (UV) radiation. The combined effects of UV radiation and oxygen are particularly damaging. However, unless one adherend is transparent to UV rays, this is not a factor in the weakening of polymer adhesives.

## 18.5.2 High Temperature Limits of Adhesives

The temperatures at which different types of adhesives will survive in service for a period of 1 year will vary somewhat among particular materials, but the following general guidelines can be used. The upper limit for acrylates and cyanoacrylates is 80 °C, whereas epoxides cured with polyamides have a service limit of 65 °C. Epoxides cured with aliphatic amines have an upper limit of 100 °C, whereas this limit is 150 °C for those cured with acid anhydrides. The surface temperature is 200 °C for silicones and 260 °C for polyimides. Many of these adhesives can be exposed at higher temperature for shorter periods without detrimental effects.

Kadiyala and Bijwe (2016) employed high-temperature thermoplastic polymers as adhesives for steel. The polymers were polyethersulfone (PES), polyetheretherketone (PEEK), and polyetherketone (PEK). The latter pair was about 30% crystalline with respective melting points of 343 and 372C. Lap shear strengths were measured at temperatures of 25, 150, 225, and 300C, and strength retention at 300C was about 30% for PES, 65% for PEK, and 70% for PEEK. Degradation temperatures for all adhesives were about 440–450C. Reiss et al. (2015) measured mechanical properties of an amine-cured toughened adhesive at temperatures between 25 and 130C. Both modulus and tensile strength fell by about half and in a linear manner.

Rubbery adhesives and rubber-modified structural adhesives have lower temperature limits (the glass transition temperature). In many cases, the development of thermal mismatch stresses upon cooling will increasingly weaken joints.

### 18.5.3 Low Temperature Limits of Adhesives

Adhesives are used to bond an insulating layer to the steel hull of ships for transporting liquefied natural gas which has a boiling point of  $-161.5^{\circ}\text{C}$ . A two-part epoxide and a two-part polyurethane were examined at temperatures of  $23$  and  $-100^{\circ}\text{C}$  by Crocker et al. (2016). Tensile strengths for the epoxy at these temperatures were  $35$  and  $38 \pm 3$  MPa and  $8$  and  $37\text{--}71$  MPa, respectively. Coefficients of thermal expansion were much reduced at the lower temperature ( $82$  to  $38 \times 10^{-6}/\text{K}$  for the epoxide and  $121$  to  $48 \times 10^{-6}/\text{K}$  for the polyurethane).

### 18.5.4 Loss of Additives

Additives in adhesives can be there for a number of reasons, one of which is to act as a stabilizer. Tarragrosa-Coque et al. (2011) looked at the effect of temperature on the migration of low molar mass additives to the surface of a crosslinked styrene-butadiene rubber. The additives of interest were paraffin wax and zinc stearate, and the main tool of investigation was ATR spectroscopy. Below the melting point of paraffin wax ( $c67^{\circ}\text{C}$ ) the amount of this additive increased at the rubber surface. The wax was removed by sublimation at temperatures in the range  $80$  to  $120^{\circ}\text{C}$  and so exposed the zinc stearate. Above  $130^{\circ}\text{C}$ , both additives sublimated.

### 18.5.5 Thermally Reversible Adhesive

Aubert (2003) has described a thermally reversible adhesive rubbery adhesive ( $T_g = -40^{\circ}\text{C}$ ) where chains can be separated or linked in the Diels-Alder reaction between a furan and a maleimide shown in Fig. 14. Above  $90^{\circ}\text{C}$ , the links are broken, but the process is reversed on cooling.

## 18.6 Measurement of Thermal Properties

Differential scanning calorimetry (DSC) and dynamic mechanical thermal analysis (DMTA) are the favored methods to obtain thermal data and are described below, together with thermogravimetric analysis. Modern instruments will be linked to a computer both for control and data collection and processing. Historical methods to measure both  $T_g$  and  $T_m$  include dilatometry and the use of a torsion pendulum to

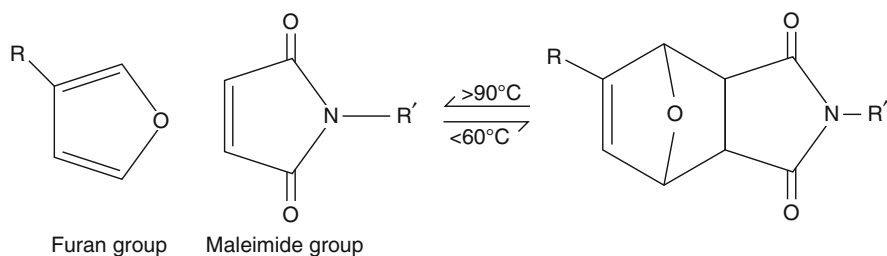


**Fig. 14** Reversible Diels-Alder reaction

measure damping. The practice of dilatometry involves containing the polymer in mercury in a sort of overgrown thermometer; it measures changes in volume.

### 18.6.1 Differential Scanning Calorimetry

Differential scanning calorimetry (DSC) examines how the heat capacity at constant pressure ( $C_p$ ) of a material changes with temperature. A sample is heated or cooled at a constant rate and changes in  $C_p$  are recorded. Rates can be in the range  $0.1\text{--}100\text{ K min}^{-1}$ .

A diagram of the scan of a semicrystalline adhesive is shown in Fig. 15. At low temperatures, the adhesive is in the glassy state and the slope of the line  $dH/dT$  gives its  $C_p$ . At the glass transition temperature ( $T_g$ ), the abrupt increase in slope is due to the higher heat capacity of the leathery adhesive. At a higher temperature  $T_m$ , the crystalline regions begin to melt, and a peak is observed due to heat being supplied to the sample, the area of which is measured in joules, and can give the degree of crystallinity of the adhesive. This requires the value of the heat of fusion of totally crystalline adhesive, which can only be obtained indirectly from the depression of melting point caused by diluents. Indium can be used as a calibrant for heat of fusion and synthetic sapphire for  $C_p$ .

If the sample is then cooled, it will eventually crystallize and the exotherm will be seen. This will be at a lower temperature than  $T_m$  due to supercooling. The area enclosed in the valley is related to the degree of crystallinity developed on cooling.

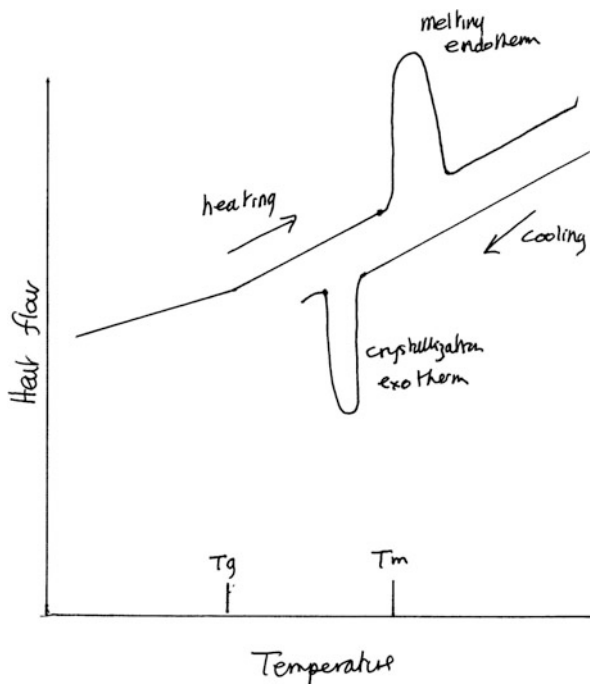
The cure of chemically reactive adhesives is exothermic and this permits DSC to follow cure, and also to measure the final to extent of cure. Kwon and Paik (2004) employed DSC to measure the extent of cure for an electrically conductive adhesive.

### 18.6.2 Dynamic Mechanical Thermal Analysis

Here, the sample is subjected to sinusoidal or other distortion at a fixed frequency and measurements are made over a range of temperatures. What is measured is stiffness and damping. The former is a measure of stored energy which is reported as



**Fig. 15** DSC thermogram for a semicrystalline adhesive, on heating followed by cooling



modulus; the latter is a measure of energy lost and is often reported as  $\tan\delta$ . The frequency range of commercial instruments is typically 0.001–1000 Hz and standard instruments have a temperature range of  $-190$  to  $400$   $^{\circ}\text{C}$  and heating rates are up to  $20$   $\text{K min}^{-1}$ . Samples can be maintained in inert gases, liquids, or humid air.

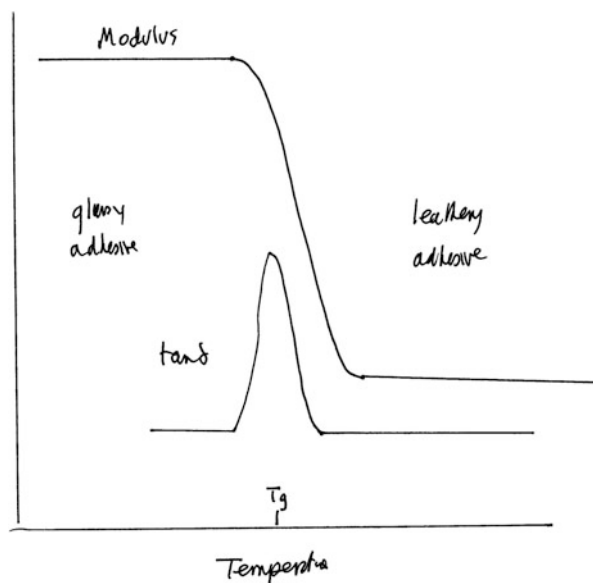
The diagram of a DMA record for a typical adhesive is shown in Fig. 16. It shows a loss peak centered on  $T_g$ . For adhesives which have two phases, such as block copolymers of dienes and styrene, both glass transitions are detected, one being about  $-70$   $^{\circ}\text{C}$  for the dispersed diene phase and the other at about  $100$   $^{\circ}\text{C}$  for the continuous polystyrene phase. Glass transition temperatures increase with frequency.

### 18.6.3 Thermogravimetric Analysis

Here, the sample is suspended from a balance and located in an oven. Weight changes are recorded as temperature increases. Its particular use is in observing thermal degradation of adhesives. Controlled atmospheres can be used. Typical temperature ranges are ambient to  $1000$   $^{\circ}\text{C}$  and heating rates  $0.1$ – $200$   $^{\circ}\text{C min}^{-1}$ .

An example is taken from the work of Xu and Dillard (2003). Data are for three epoxide adhesives made electrically conductive by the addition of about 80% by weight of powdered silver. They all begin to decompose at about  $400$   $^{\circ}\text{C}$ .

**Fig. 16** DMTA scan for a polymeric adhesive



## 18.7 Conclusion

Thermal properties of adhesives affect their behavior in a number of diverse ways. Firstly, cure processes, pot-life, and shelf-life depend on temperature. High temperatures can limit the lives of adhesives by causing chemical degradation, and in some cases by introducing stresses due to differences in thermal expansion. Glass transition is the most important temperature for an adhesive, in that it demarcates rubbery adhesives from rigid ones, and is something to be avoided in service.

## References

- Al-Samhan A, Darwish SM (2005) *Int J Adhes Adhes* 25:379
- Andrews RJ, Grulke EA (1999) In: Brandrup J, Immergut EH, Grulke EA (eds) *Polymer handbook*, 4th edn. Wiley, New York
- Ashcroft IA, Comyn J, Tellwright S (2009) *Int J Adhes Adhes* 29:155
- Aubert JH (2003) *J Adhesion* 79:609
- Blackley D C (1997) *Polymer latices, science and technology*, 2nd edn, vol 1, Fundamental principles, vol 2, Types of latices, vol 3, Applications of latices. Chapman & Hall, London
- Brewis DM, Comyn J, Shalash RJA, Tegg JL (1982) *Int J Adhes Adhes* 2:215
- Brewis DM, Comyn J, Shalash RJA (1983) *Polymer* 24:67
- Brodnyan JG, Konen T (1964) *J Appl Polym Sci* 4:687
- Comyn J (1990) *Engineered materials handbook series, Adhesives and Sealants*. ASM International, Materials Park, p 617
- Comyn J (1997) *Adhesion science*. Royal Society of Chemistry, Cambridge
- Comyn J, Fernandez RA (1975) *Europ. Polym J* 11:149

- 656 Comyn J, Day J, Shaw SJ (1998) *J Adhes* 66:289
- 657 Crocker LE, Duncan BC, Broughton WR (2016) *Int J Adhes Adhes* 70:126
- 658 Da Silva LFM, Adams RD (2007) *Int J Adhes Adhes* 27:362
- 659 Eastman EF, Fullhart L Jr (1990) Ch 23. In: Skeist I (ed) *Handbook of adhesives*, 3rd edn. Van  
660 Nostrand Reinhold, New York
- 661 Fox TG (1956) *Bull Amer Phys Soc* 1:123
- 662 Hussey B, Wilson J (1996) *Structural adhesives, directory and Databook*. Chapman and Hall,  
663 London
- 664 Kadiyala AK, J Bijwe J (2016) *Int J Adhes Adhes* 70:90
- 665 Karger-Kocsis J, Senyei Z, Hedvig P (1980) *Int J Adhes Adhes* 1:17
- 666 Keller A, Masania K, Taylor AC, Dransfield C (2016) *J Mater Sci* 51:236
- 667 Kilik R, Davies R, Darwish SMH (1989) *Int J Adhes Adhes* 9:219
- 668 Kwon W-S, Paik K-W (2004) *Int J Adhes Adhes* 24:135
- 669 Lapique F, Redford K (2002) *Int J Adhes Adhes* 22:337
- 670 Morriche R, Prolongo SG, Sanchez M, Jimenez-Suarez A, Chamizo FJ, Urena A (2016) *Int J Adhes*  
671 *Adhes* 68:407
- 672 McLoughlin JR, Tobolsky AV (1952) *J Colloid Sci* 7:555
- 673 McMillan JA, Los SC (1965) *Nature* 206:806
- 674 Park Y-J, Kim H-J (2003) *Int J Adhes Adhes* 23:383
- 675 Protzman TF, Brown GL (1964) *J Appl Polym Sci* 4:81
- 676 Rasmussen DH, Mackenzie AP (1971) *J Phys Chem* 75:967
- 677 Reiss JML, Amorim FC, da Silva AHMFT (2015) *Int J Adhes Adhes* 58:88
- 678 Rossitto C (1990) Ch 28. In: Skeist I (ed) *Handbook of adhesives*, 3rd edn. Van Nostrand Reinhold,  
679 New York
- 680 Sperling LH (2006) *Introduction to Physical Polymer Science*, 4th edn. Wiley, Hoboken, pp  
681 384–389
- 682 Sugisake M, Suga H, Seki S (1968) *Bull Chem Soc Japan* 41:2591
- 683 Sun W, Vassilopoulos AP, Keller T (2014) *Int J Adhes Adhes* 52:31
- 684 Tarragrosa-Coque R, Alvarez-Garcia S, Martin-Martinez JM (2011) *Int J Adhes Adhes* 31:20
- 685 Xu S, Dillard DA (2003) *J Adhes* 79:699

Lucas F. M. da Silva, R. J. C. Carbas, and M. D. Banea

## Contents

19.1	Introduction .....	490
19.2	Tensile Tests .....	491
19.2.1	Bulk Specimens .....	491
19.2.2	Axially Loaded Butt Joints .....	498
19.3	Compressive Tests .....	500
19.4	Shear Tests .....	502
19.4.1	Bulk Specimens .....	503
19.4.2	Joint Specimens .....	507
19.4.3	Recommendations .....	516
19.5	Relation Between Tensile, Compressive, and Shear Properties .....	517
19.6	Conclusions .....	518
References	.....	519

## Abstract

Failure strength tests are used for quality control, for adhesive properties development, and for design purposes. Typically, manufacturers provide the average single-lap joint (SLJ) shear strength and the peel strength. However, these are not

L. F. M. da Silva (✉)

Department of Mechanical Engineering, Faculty of Engineering, University of Porto, Porto, Portugal

e-mail: [lucas@fe.up.pt](mailto:lucas@fe.up.pt)

R. J. C. Carbas

Institute of Science and Innovation in Mechanical and Industrial Engineering (INEGI), Faculty of Engineering, University of Porto, Porto, Portugal

e-mail: [rcarbas@fe.up.pt](mailto:rcarbas@fe.up.pt)

M. D. Banea

CEFET/RJ – Federal Center of Technological Education in Rio de Janeiro, Rio de Janeiro, Brazil

e-mail: [mdbanea@gmail.com](mailto:mdbanea@gmail.com)

intrinsic adhesive properties and are of limited use for design purposes. The prediction of the joint strength based on stress or strain limit criteria needs the adhesive stress–strain curve. In this chapter, the most important tests for the determination of the adhesive mechanical properties are described. Tests for the three basic loading modes – tension, compression, and shear – are discussed, indicating for each case the advantages and disadvantages. Reference is made to the corresponding standards according to the major standard-setting organizations such as the American Society for Testing and Materials (ASTM) and the International Standards Organization (ISO). Within each category (compression, tension, and shear), tests on bulk specimens and those on joints are compared. Recommendations to select the most suitable test are given, and it is shown that a reasonable relationship exists between adhesive properties measured in compression, tension, and shear.

---

## 19.1 Introduction

Failure strength tests are carried out for different purposes. During the formulation and development stage, manufacturers need to certify their products, and the commonly used tests are failure strength tests. These can be related to the application for which the adhesive is designed using loadings and adherends found in a particular application. Also, some manufacturers provide standard tests that are universal and can be used not only for qualitative but also for design purposes. In many cases, manufacturers provide limited information in the adhesive data sheet, and it is therefore necessary for the joint designer or the researcher to carefully test the adhesive properties. There is a wide variety of standard tests available in different countries (the USA, Britain, France, Germany, and Japan) that are also provided by many organizations at the international level, such as the International Standards Organization (ISO) and the European Standards (EN) Organization (da Silva 2012). Wherever available, adhesive testing standards from these organizations and others are given in this chapter.

When a complex joint is to be introduced in a structure, the ideal situation is to test that specific joint. However, this approach is very expensive. Before real joints or prototypes are built, the designer should first come up with a good prediction of the failure load based, among other things, on the basic mechanical properties of the adhesive. The basic properties can mean the elastic properties, such as Young's modulus and Poisson's ratio in case the analysis is linear elastic. However, for the more realistic theoretical methods that take into account the nonlinear behavior of the adhesive, the yield stress, the ultimate stress, and the failure strain are necessary. The stress–strain curve of adhesives is necessary for designing adhesive joints in order to compute the stress distribution and apply a suitable failure criterion based on continuum mechanics principles.

The tensile stress–strain curve on bulk specimens is generally the most common test used. This test is sufficient if the yield behavior of the adhesive is assumed to be of the von Mises type. However, it is known that adhesive yielding is better

described by more complex yielding criteria (Drucker and Prager 1952; Raghava et al. 1973; Dolev and Ishai 1981) (see ► Chap. 23 “Constitutive Adhesive and Sealant Models”) for which an additional test under a different loading condition is required. Shear tests are usually preferred because the compressive test is more difficult to perform. There are many test methods for the determination of failure strength data. They can be divided into two main categories: tests on bulk specimens and tests in a joint or in situ. Tests in the bulk form are easy to perform and follow the standards for plastic materials. However, the thickness used should be as thin as possible to represent the thin adhesive layer present in adhesive joints. Tests in situ more closely represent reality, but there are some difficulties associated with accurately measuring the very small adhesive displacements of thin adhesive layers. Moreover, the adhesive stress distribution is not perfectly uniform, and the failure mode may not be the same as that found in real joints. Another important point is that the adhesive strength measured in a joint depends on the surface preparation. This is not only critical for the short-term strength but even more so for the long-term strength, especially if aggressive environments are present. Also, there might be a region close to the interface with chemical and physical characteristics different from those of the bulk adhesive or adherend, leading to the formation of an interphase. There has been intense debate about the most appropriate method and whether the two methods (bulk and in situ) can be related. Some argue that the properties in the bulk form may not be the same as in a joint because the cure in the bulk form and the cure in a joint (thin film) may not be identical. In effect, the adherends remove the heat produced by the exothermic reaction associated with cure and prevent overheating. However, many studies have shown that the relation is reasonable, taking into account all the differences associated with each method (Jeandrau 1991; Lilleheden 1994; da Silva and Adams 2005). The truth is that there is no perfect test for the determination of failure strength properties. The designer needs to select the most appropriate test for a given application and understand what the results mean (Adams 1990).

---

## 19.2 Tensile Tests

### 19.2.1 Bulk Specimens

One of the most common types of tests for determining the strength properties of adhesives is the tensile test on bulk specimens. The specimens and the test methods are comparable to those used for plastic materials. The properties determined are intrinsic to the material: they are obtained under a uniform and uniaxial state of stress, with no influence of the adherends.

The manufacture of the bulk specimen is usually done by pouring or injecting the adhesive into a mold with the final shape (Fig. 1) or by applying pressure between plates (Fig. 2). The first method is suited to one-part adhesives that are relatively liquid. The mold can be open, but it can also be a closed cavity, in which case the adhesive needs to be injected (Fig. 1). When the adhesive is viscous, in the form of a

**Fig. 1** Tensile bulk specimens obtained by pouring

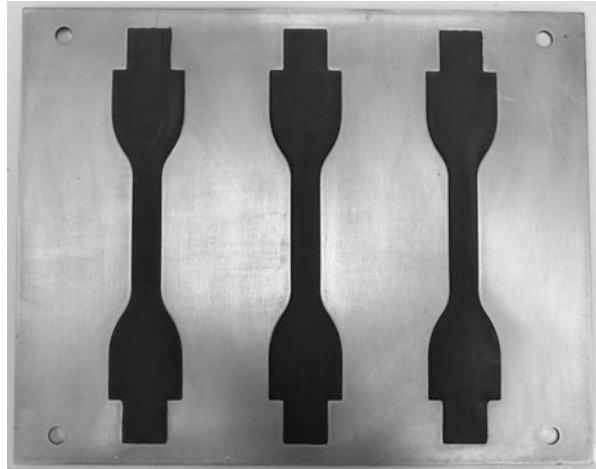
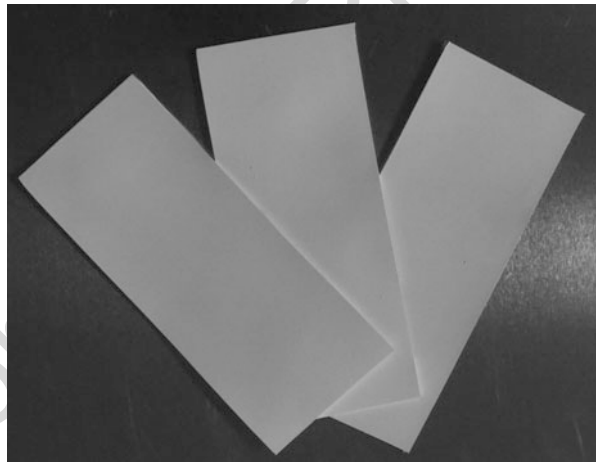


**Fig. 2** Bulk plates obtained by high pressure



film or of two components, the second method generally gives better results. If the adhesive is viscous or in film form, the pouring (or injection) phase is difficult or impossible. On the other hand, the mixing of two-part adhesives introduces voids. If the adhesive is liquid, the air bubbles can be removed by vacuum. If the adhesive is viscous, modern sophisticated machines that allow mixing at high speed under vacuum can ensure that the adhesive is void free. If the voids have been removed properly, the adhesive can be manufactured by pouring or injection. If not, the voids can be removed by high pressures. The technique described in the French standard NF T 76-142 works particularly well for producing plate specimens without porosity. It consists of curing plates of adhesive in a mold with a silicone rubber frame under a high pressure (2 MPa or 20 atm). The pressure is calculated using the dimensions of the silicone rubber frame. The technique, shown schematically in

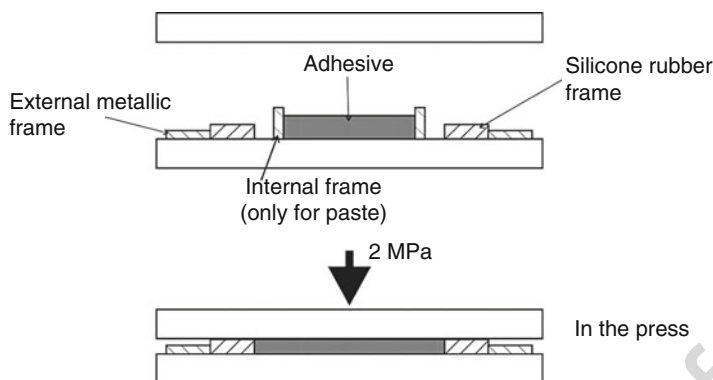


**Fig. 3** French method (NF T 76-142) to obtain plates without porosity (da Silva et al. 2004)

Fig. 3, consists of placing in the center part of the mold a quantity of adhesive slightly greater than the volume corresponding to the internal part of the silicone rubber frame. There is a gap, at the beginning of the cure, between the adhesive and the silicone rubber frame. At the moment of the application of the pressure, this gap enables the adhesive to flow (until the mold is completely filled) and avoids gas entrapment. This technique is suitable for any type of adhesive, i.e., liquid, paste, or film. The plates are then machined according to the dimensions used for tensile testing or for other types of geometry (see Sects. 3 and 4). The geometry generally used for tensile specimens is the dog-bone-shape specimen according to standard EN ISO 527-2, which is represented in Fig. 4. Long specimens (Fig. 4a) are used for rigid adhesives (e.g., epoxies) where the displacements are small, whereas short specimens (Fig. 4b) are more suited for flexible adhesives (e.g., polyurethanes). The geometry described in ASTM D 638 (tensile properties of plastics) can also be followed. Alternatively, standard ASTM D 3039 (tensile properties of fiber-resin composites) can be used when working with supported film adhesives. It is important to specify the thickness of the plate because the adhesive properties will depend on it, especially if there are many voids in the specimen. The ideal method would be to work with very thin samples to reproduce the adhesive layer in a joint, but this is very difficult due to the high flexibility of the adhesive. Generally, a thickness of 2 mm is used; larger thicknesses can be used, but the exothermic reaction during the cure can cause adhesive burning in some adhesives. Round solid bar tension specimens have also been used by some authors (Grant et al. 2009). The specimens should be conditioned under controlled temperature and humidity because these factors influence the mechanical properties of the adhesive, especially for polyurethane adhesives. This is valid for any type of test.

The test consists in loading the specimen in a longitudinal direction until failure. The test speed generally used is 1 mm/min for the determination of Young's modulus, but higher rates can be used for failure testing. The strain rate of the adhesive measured in bulk should be similar to the strain rate the adhesive has in the joint, especially if the adhesive is close to its glass transition temperature ( $T_g$ ). The



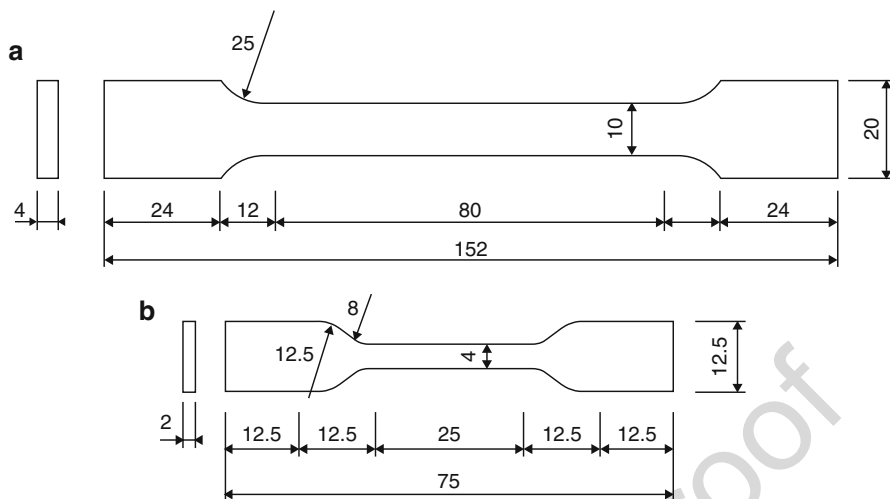


**Fig. 4** Tensile specimens according to EN ISO 527-2 (dimensions in mm): **(a)** long specimen and **(b)** short specimen

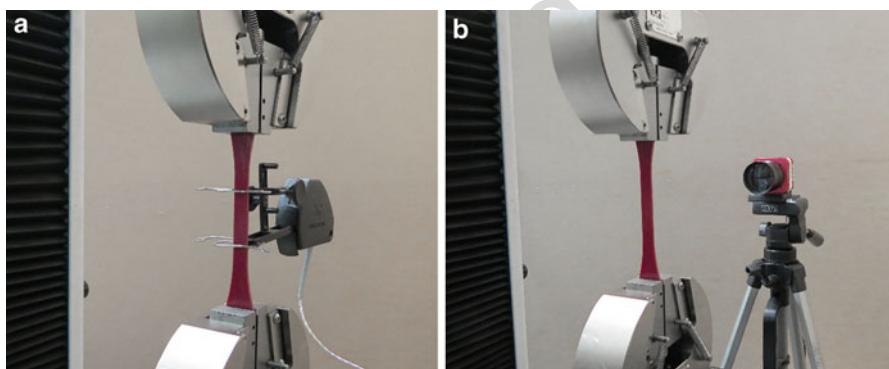


**Fig. 5** Adhesive displacement measurement with clip gauges or strain gauges **(a)** and with an optical method **(b)**

temperature and humidity of the test should also be recorded. Small deviations from typical laboratory conditions (25 °C and 50% relative humidity) can cause an important variation in the mechanical properties, especially if the adhesive  $T_g$  is in that range. The load and the displacement are measured, which can then be used to determine the stress-strain curve. Measurement of the adhesive displacement is relatively easy using clip gauges or strain gauges (see Fig. 5a). However, whenever possible, it is recommended to use noncontacting devices to avoid any interference of the extensometer with the material behavior, especially for flexible and ductile adhesives. Optical (see Fig. 5b) or laser methods are widely used. Video extensometers are not accurate enough for strains below 1%. However, other methods based

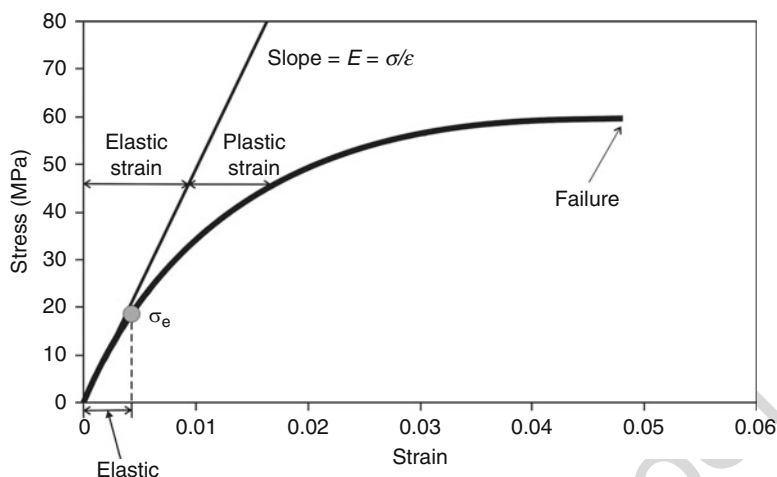


**Fig. 6** Typical tensile stress–strain curve of an adhesive with the definition of the mechanical properties

on optical data treatment such as digital image correlation (DIC) enable one to measure strains below 1%. The displacement of the crosshead can also be used to estimate the adhesive strain. However, this requires a correction as the adhesive displacement in the calibrated area is not the same as that between the grips. For highly deformable adhesives, the crosshead displacement is good enough, especially for the nonlinear part of the curve.

A typical tensile stress–strain curve is shown in Fig. 6. The stress–strain curve can be used to determine Young’s modulus, the tensile strength, and the failure strain. There are several methods to calculate Young’s modulus. Standard EN ISO 527-2 recommends determining Young’s modulus between points at 0.05% and 0.25% strain. This range generally falls in the elastic range of structural adhesives. Table 1 shows Young’s modulus of different types of adhesives below  $T_g$ . Stiff adhesives are in the range of 4–5 GPa (e.g., epoxies or polyaromatics). Flexible adhesives for structural use such as polyurethanes are in the range of 0.1 GPa. For flexible and ductile adhesives such as polyurethanes, the material is nonlinear even for these small deformations. Other methods such as the secant modulus or the tangent at the origin may be used. For flexible adhesives such as polyurethanes, because the displacement rate is constant, there is time for the load to relax through the test. In order to avoid this phenomenon, a test under constant strain rate should be done.

The tensile and compressive properties were obtained in the bulk form, and the shear properties were obtained with the thick adherend shear test (TAST). ( $E$  Young’s modulus,  $\sigma_y$  yield strength,  $\sigma_t$  strength,  $\varepsilon_t$  tensile failure strain,  $\tau_y$  shear yield strength,  $\tau_r$  shear strength,  $\gamma_y$  shear failure strain,  $\nu$  Poisson’s ratio).

Poisson’s ratio can be determined provided the adhesive displacement is measured in the longitudinal and transversal directions. This property is very difficult to measure experimentally, especially in the elastic range. For polymers, Poisson’s ratio

t.1 **Table 1** Mechanical properties of various adhesives below the glass transition temperature

t.3	Adhesive	Manufacturer	Tension		Compression			Shear		$\nu$			
			E (MPa)	$\sigma_y$ (MPa)	$\sigma_c$ (MPa)	$\epsilon_c$ (%)	$\sigma_y$ (MPa)	$\sigma_c$ (MPa)	$\tau_y$ (MPa)		$\tau_r$ (MPa)	$\gamma_r$ (%)	
t.4	Epoxies												
t.5	Araldite AV138	Huntsman	4,590	41.0	41.0	1.30			1,559	25.0	30.2	5.50	
t.6	Hysol EA 9394	Loctite	4,420	31.0	59.8	4.64	35.9	68.9	1,140	25.0	40.4	8.36	
t.7	Hysol EA 9321	Loctite	3,870	22.0	46.0	3.80	34.0		1,030	20.0	33.0	6.35	
t.8	Supreme 10HT	Master Bond	3,240	25.0	45.5	2.00			1,460	37.1	37.1	16.1	0.30
t.9	Araldite AV 119	Huntsman	3,450	67.1	67.1	4.10			1,260	47.0	47.0	50.7	0.37
t.10	Hysol EA 9150	Loctite	2,852		79.0	5.00		99.9	1,056				0.35
t.11	Hysol EA 9359.3	Loctite	2,650	42.5	42.5	4.50		145	660.0	35.3	35.3	63.0	
t.12	Hysol EA 9330	Loctite	2,646		38.6	2.40		53.1	965.0				0.37
t.13	Hysol EA 9628 <sup>f</sup>	Loctite	2,377		51.7	7.50		79.3	624.0				
t.14	Araldite 2015	Huntsman	1,850		22.5	4.40			560.0	14.0	20.0	40.3	
t.15	Redux 810	Hexcel comp.	1,730		40.0	5.53							
t.16	02 Rapid	Delo	1,000		24.0	20.0							
t.17	Hysol EA 9361	Loctite	670		7.99	44.0							

t.18	Araldite 420	Huntsman	1,850	30								35		
t.19	AF 163-2K	3 M	1,522	46.9								46.9		
t.20	SikaPower 4720	Sika	2,171	25.8			3.4							
t.21	XNR6852	Nagase Chemtex	1,176	59.9			100							
t.22	XNR6852-3	Nagase Chemtex	1,728	51.5			15				665	45		
t.23	XN1244	Nagase Chemtex	5,872	68.2			8.05				2,150	32		
t.24	Polyurethanes													
t.25	Araldite 2026	Huntsman	200			18.0	50.00							
t.26	Sikaflex 256	Sika									1,351	8.26	8.26	330
t.27	Bismaleimides													
t.28	Redux HP655	Hexcel comp.	3,620	80.7		80.7	2.39							
t.29	Redux 326	Hexcel comp.	4,850	50.9		50.9	1.28				1,615	37.9	37.9	3.70
t.30	Modified acrylics													
t.31	DP-8005	3M	590			13.0	5.30				178.6	5.3	8.40	180
t.32	Araldite 2024	Huntsman	760			20.0	42.5							

t.33 The tensile and compressive properties were obtained in the bulk form, and the shear properties were obtained with the thick adherend shear test (TAST)  
*E* Young's modulus, *σ<sub>y</sub>* yield strength, *σ<sub>r</sub>* strength, *ε<sub>r</sub>* tensile failure strain, *τ<sub>y</sub>* shear yield strength, *τ<sub>r</sub>* shear failure strength, *γ<sub>y</sub>* shear failure strain, *ν* Poisson's ratio)

varies between 0.3 and 0.5. For temperatures below the glass transition temperature ( $T_g$ ), the value is close to 0.3. When the adhesive is above  $T_g$  or in the plastic region, Poisson's ratio is about 0.5. Table 1 gives the values for several adhesives. One way to determine Poisson's ratio is to deduce it from the measurement of Young's modulus and the shear modulus (see Sect. 5).

It is generally easy to find the yield stress of metals because there is usually a clear transition between elastic and plastic behavior. However, for polymers, the elastic region may not be linear, and it is difficult to find the value of the stress corresponding to the initial yielding. Various authors have proposed methodologies to find the yield stress. Young and Lovell (1991) state that the exact position of the yield point is very difficult to estimate, and so they define yield as the maximum point on the stress–strain curve. This procedure is valid when the adhesive behaves elasto-plastically. For strain-hardening adhesives, it is convenient to take the yield stress as the intersection of a line tangent to the linear elastic region and a line tangent to the nonlinear plastic region of the actual stress–strain curve, such as in the bilinear model (Hart-Smith 1973). The traditional 0.2% offset method may also be used for this effect for glassy polymers. Table 1 gives yield strength values for several adhesives. The strongest adhesive is in the order of 60 MPa. This is well below the yield strength of a low-strength steel, which is approximately 180 MPa. However, when loaded in shear over a large area, the adhesive can deform plastically the steel.

The strain to failure is highly dependent on the presence of defects such as voids and micro-cracks. In tension, once a crack is triggered next to a void, the specimen often fails there due to the high stress concentration. Generally, the strain to failure presents a very large dispersion, unless the manufacture is very well controlled. Table 1 presents values of the failure strain in tension and shear. Generally, adhesives are much more ductile in shear than in tension. For ductile adhesives, the difference can be of one order of magnitude. Stiff and strong adhesives have generally a limited ductility of the order of 1% or 2%, especially in tension. On the other end of the scale, failure strains of up to 300% can be obtained with polyurethane adhesives.

### 19.2.2 Axially Loaded Butt Joints

The tensile properties can also be measured with the adhesive in a thin layer between two steel substrates as in the butt joint (also called the “poker chip” test). There are two ASTM standards for this type of test. The first, ASTM D 897, uses short circular specimens made of metal or wood, and the second (ASTM D 2095) is more general and includes round and square geometries (Fig. 7). Other standards include ISO 6922, BS EN 26922, and BS 5350 – Part C3. A mold is presented in ASTM D 2095 for controlling the adherend alignment and adhesive thickness. The stress is obtained by dividing the load by the loaded area. Apparently, the stress state is of uniform tension. However, some authors (Adams and Coppendale 1977, 1979) have shown that the stress distribution is nonuniform due to the constraining effect of the substrates or slight misalignments. The lateral contraction of the adhesive does not occur

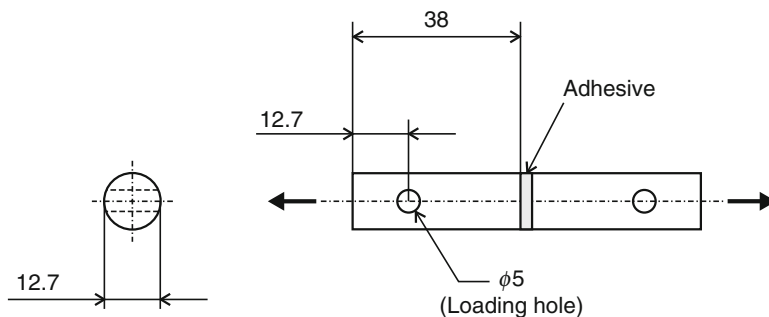
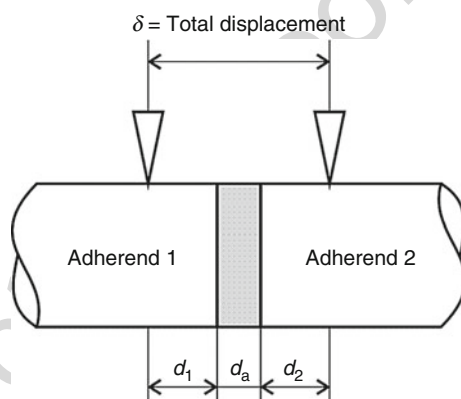


**Fig. 7** Butt-joint geometry (dimensions in mm) (ASTM D 2095)

**Fig. 8** Gauge length and displacements in the axially loaded butt joint



freely, which introduces additional radial and circumferential stresses, especially at the edges of the joint. In addition to the constraining effect of the substrate, misalignments can occur during fabrication or testing, which introduce bending in the adhesive.

The adhesive displacement can be measured by extensometers attached to the adherends, in which case a suitable correction is necessary. Taking the case illustrated in Fig. 8 and given by Adams et al. (1997), the extensometer displacement  $\delta$  is given by

$$\delta = \delta_1 + \delta_a + \delta_2 = \epsilon_1 d_1 + \epsilon_a d_a + \epsilon_2 d_2 = \epsilon_1 (d_1 + d_2) + \epsilon_a d_a \quad (1)$$

where  $\epsilon$  is the strain and  $d_1$ ,  $d_a$ , and  $d_2$  are defined in Fig. 8. If  $d_1$  and  $d_2$  are of the order of 1 mm and  $d_a$  (adhesive thickness) is of the order of 0.1 mm, then the displacements in the adhesive and in the adherend are of the same order. This correction is necessary for all the extensometers that measure not only the adhesive displacement but also the adherend displacement. This is a big disadvantage associated with adhesive joints and extensometers.

According to Adams and Cripps (1977), the elastic properties (Young's modulus,  $E$ , and Poisson's ratio,  $\nu$ ) can still be determined using this test. They defined a relation between the "apparent"  $E_a$  measured in the test and the real  $E$ . If the substrate is infinitely rigid in relation to the adhesive, the relation between  $E_a$  and  $E$  is given by

$$\frac{E_a}{E} = \frac{(1 - \nu)}{(1 + \nu)(1 - 2\nu)} \quad (2)$$

where  $\nu$  is Poisson's ratio of the adhesive. Another equation proposed by Kuenzi and Stevens (1963) gives Poisson's ratio of the adhesive, if the shear modulus of the adhesive is known, and the adherend elastic properties.

The stress-strain curve obtained with this test is not representative of the intrinsic adhesive behavior due to the adherend constraining effect described above and cannot be correlated with the adhesive bulk properties. An extensive study carried out by several laboratories and led by Centre Technologique des Industries Mécaniques from France (Jeandreau 1993) has shown that the reproducibility associated with this test is quite low, despite the use of a precise and specially designed extensometer.

### 19.3 Compressive Tests

This test is less common than the tensile or shear tests. Usually, it is assumed that the adhesive follows the von Mises model and, therefore, the compressive and tensile properties are the same. However, since adhesives depend on the hydrostatic stress component, the compressive strength properties differ from those obtained in tension. The ratio of the yield stress in compression to the yield stress in tension varies typically between 1.2 and 1.4 (Adams et al. 1997). There are various types of compressive tests on bulk specimens. The most common compressive test uses parallelepipedic (square or rectangular base) bulk specimens. The French standard NF T 51-101 recommends a square base (Fig. 9a), whereas ASTM D 695 (Fig. 9b) and ISO 604 use a rectangular base. In the case of ISO 604, the preferred specimens are  $50 \times 10 \times 4 \text{ mm}^3$  for modulus and  $10 \times 10 \times 4 \text{ mm}^3$  for strength. Cylinders can also be used and are 12.7 mm (1/2 in.) in diameter and 25.4 mm (1 in.) long according to ASTM D 695 (Fig. 10a). Gali et al. (1981) also used tubular specimens (Fig. 10b) with good results.

The specimen is placed between compressive plates parallel to the surface. The specimen is then compressed at a uniform rate. The maximum load is recorded along with stress-strain data. An extensometer attached to the front of the fixture is used to measure the adhesive displacement. The stress-strain curve is used to determine the properties of interest. Various authors have shown that Young's modulus in compression obtained by this method and that obtained with bulk tensile specimens correlate well. However, it is difficult to determine the failure stress and strain in

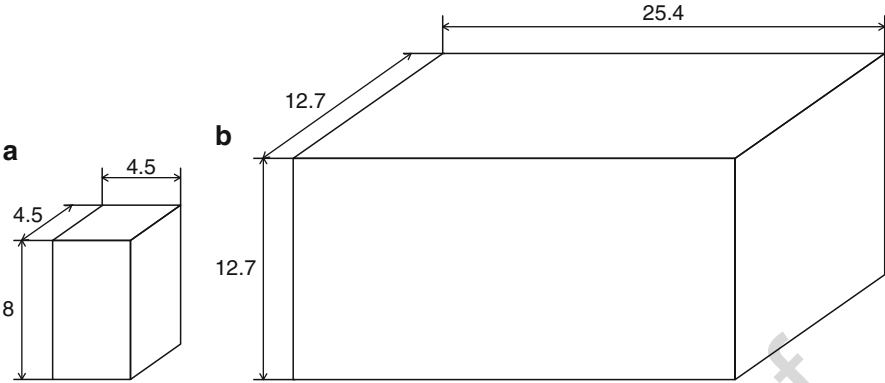
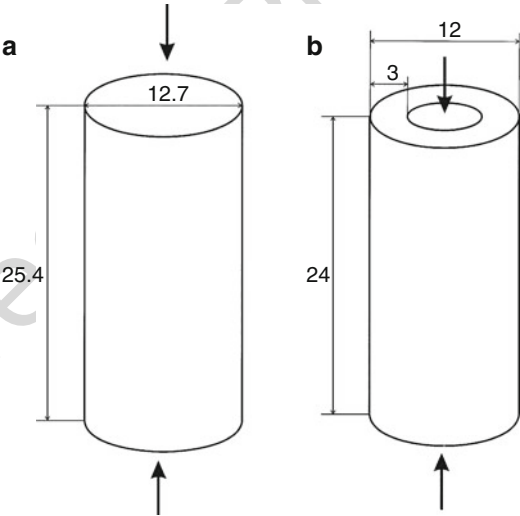


**Fig. 9** Bulk specimens for compressive testing using parallelepipedic specimens (dimensions in mm): (a) according to NF T 51-101 and (b) according to ASTM D 695

**Fig. 10** Bulk specimens for compressive properties using (dimensions in mm): (a) cylindrical (ASTM D 695) and (b) tubular specimens (Gali et al. 1981)



compression because the adhesive keeps deforming without breaking (Jeandreau 1993).

ASTM D 695 standard also describes a procedure using a plate specimen similar to the bulk tensile test (Fig. 11a). This method is valid only for rigid adhesives. However, special care must be taken to avoid buckling of the specimen, as shown in Fig. 11b. The machining of ends is particularly important to ensure they are smooth, flat, and parallel, with sharp and clean edges. Testing is done by placing a small specimen between the two blocks as shown in Fig. 11c and slowly compressing it until the point of fracture. Some of the results of this test include compressive strength, compressive yield strength, offset yield strength, and modulus of elasticity. Unpublished results by the author have shown that the values of the modulus



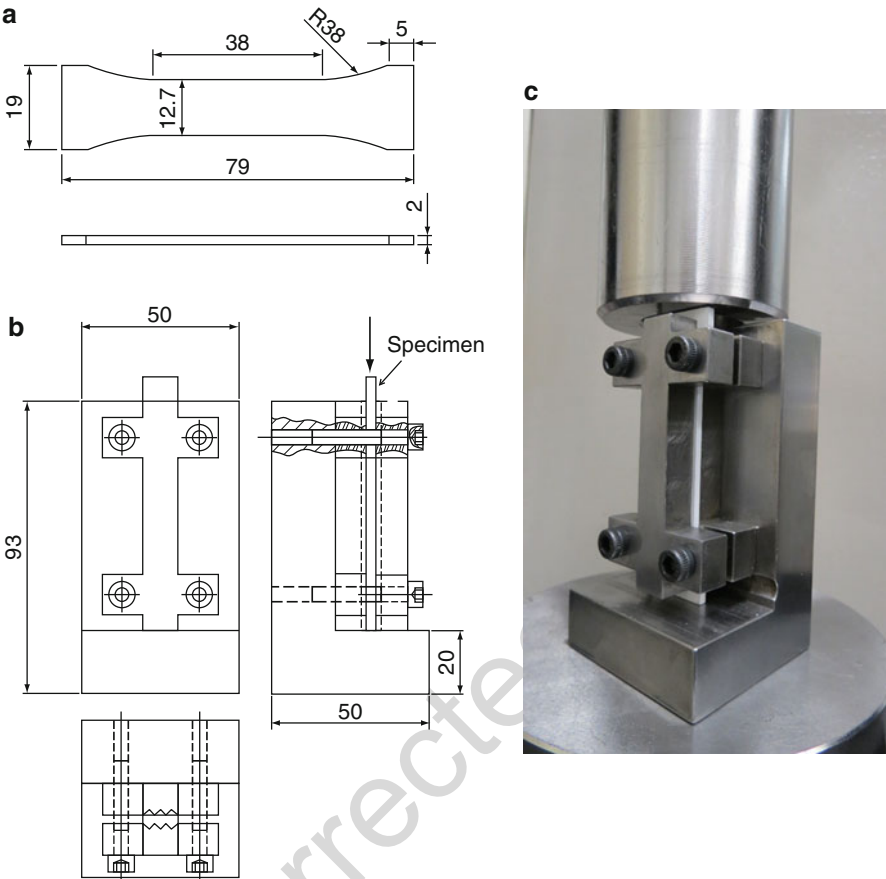


**Fig. 11** Bulk specimen for compressive properties according to ASTM D 695 (dimensions in mm): (a) specimen geometry, (b) blocks to avoid specimen buckling, and (c) loading jig

obtained with this type of test are comparable to those obtained using the bulk tensile test. The nonlinear part of the stress–strain curve should, however, be analyzed with caution because the two blocks used to avoid buckling might stiffen the adhesive.

### 19.4 Shear Tests

As with tensile tests, shear tests can be divided into bulk and joint tests. The adhesive displacement in joint tests is very small, and it is therefore more difficult to measure accurately. Bulk specimens give more accurate results because the gauge length is higher. However, it can be argued that the size and thickness of the specimens used are not representative of the adhesive properties in a joint. The National Physical Laboratory and other British laboratories (Dean et al. 1996) have carried out an

extensive theoretical and experimental study on various shear test methods. Many of their findings are well accepted by the adhesive community and are also presented here.

**19.4.1 Bulk Specimens**

**Bulk Torsion**

The shear properties of the adhesive can be obtained with solid or tubular bars in torsion. The dimensions of the specimen vary from author to author. An example is given in Fig. 12a (Chen et al. 2011) for solid bars. The specimen manufacture depends on the type of adhesive and is described above in Sect. 2.1. The round shape needs to be obtained by machining, which might not be possible with very flexible adhesives. Alternatively, round specimens can be cast in a centrifuge. The square sections at the two ends are used to locate into the grips of the test machine and to transmit the torque. The round shape is free of stress concentrations, and therefore the true adhesive properties can be measured with this test. Due to this advantage, torsion testing machines are used to characterize adhesives and are also continuously being improved. As an example, a new type of torsion testing machine concept was recently proposed to a provisional Portuguese patent to test specimens under torsion loads (Guimarães et al. 2016). The torque and the relative twist ( $T - \varphi$ ) along the gauge length of the specimen are recorded. The shear stress  $\tau$  and shear strain  $\gamma$  are obtained from the  $T - \varphi$  curve using the following equations:

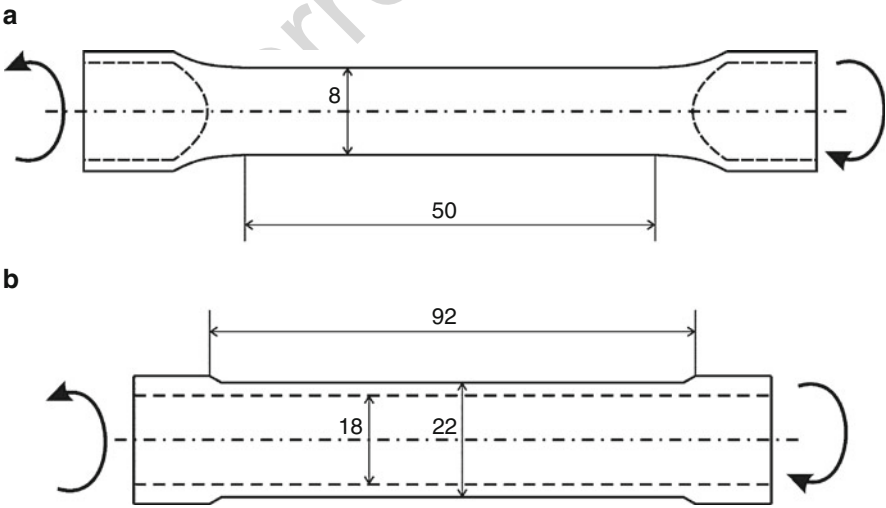


**Fig. 12** Bulk torsion specimens (dimensions in mm): (a) solid bar torsion specimen (Chen et al. 2011) and (b) tubular specimen (Gali et al. 1981)

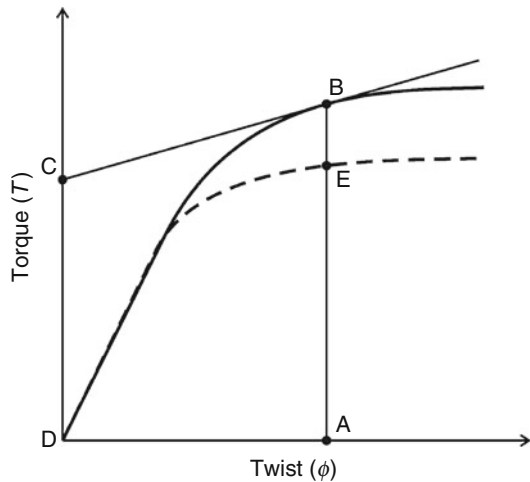
$$\tau = \frac{Tr}{J} \quad (3)$$

$$\gamma = r \frac{\phi}{l} \quad (4)$$

where  $r$  is the radius,  $l$  is the gauge length, and  $J$  is the polar moment of inertia. Contacting extensometers are used to measure the angular rotation of a known gauge length of the specimen. The use of large gauge length enables high accuracy with this test. In case the specimen is sensitive to the extensometer, the rotation of the specimen clamps can be used. For this type of solid bar, the shear strain varies linearly along the radial direction with zero strain at the center. The shear strain at the outside surface can be derived from the measured twist. However, the stress distribution is linear only if the material is absolutely linear elastic. Nonlinear behavior is bound to occur, especially in the pure shear state. Departure from linearity will redistribute the stress in such a way that some load carried by the most-stressed material at the outside surface (in the elastic case) shifts to the material inside. The graphical correction method due to Nadai (1931) can be applied to the recorded torque–twist curve to derive the shear stress–strain response at the surface of the specimen. The correction is illustrated in Fig. 13 (Adams et al. 1997). A tangent to the curve is made for any point of the nonlinear part. For example, the correction to the height AB is made by subtracting one quarter of the intercept height DC, giving the corrected height AE. The relevant properties are determined from the shear stress–strain curve.

Tubular specimens (thin walls) can also be used and do not require a Nadai correction (Nadai 1931). The specimen geometry used by Gali et al. (1981) is presented in Fig. 12b. Again, relevant properties are determined from the shear stress–strain curve.

**Fig. 13** Nadai correction



### V-Notched Beam Shear Method (Iosipescu)

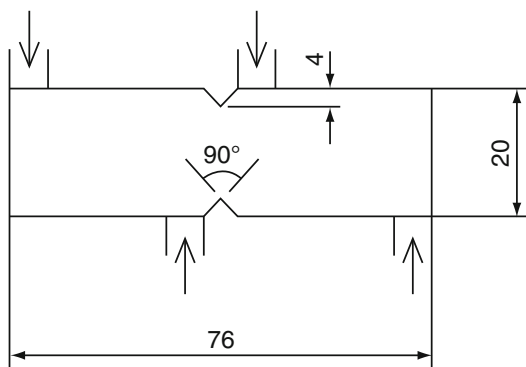
The V-notched beam shear method (or Iosipescu) and the notched plate shear method (or Arcan) are two methods of measuring the shear properties in bulk. The two methods are similar, differing only in the type of loading and geometry. Both test methods were made so that a conventional tensile testing machine can be used to apply shear. This test was originally developed for metals (Iosipescu 1967), but it has been adapted for laminated composites in the standard ASTM D 5379 following developments by Adams and Walrath (1987). The specimen is rectangular with two V notches at its center, as shown in Fig. 14. The geometry is usually 75 mm wide, 20 mm high, and at least 4 mm thick. The specimen is loaded in four points, creating an area with uniform shear between the notches since the bending moments from both sides cancel each other. Since the specimen is loaded at the edges, this can cause bending of the specimen along its longitudinal axis. To reduce this problem, thick specimens are recommended (3–4 mm). For very flexible adhesives such as polyurethanes, the testing method may not be adequate even with thick specimens. There is a stress concentration at the notch root, but the shear stress calculated with the force and the cross-sectional area is a good approximation. Alternatively, a correction can be applied with a finite element (FE) analysis. For brittle adhesives, the stress concentration at the root of the notch might be sufficient to induce premature failures and give only part of the stress–strain curve. That is one of the main disadvantages of this type of test. The same thing happens with the Arcan test. The shear displacement can be measured by strain gauges mounted at  $+45^\circ$  and  $-45^\circ$  with the specimen axis. If  $P$  is the load applied,  $t$  the specimen thickness, and  $h$  the distance between the notches, the shear stress  $\tau$  is given by

$$\tau = \frac{P}{th} \quad (5)$$

and the shear modulus  $G$  by

$$G = \frac{P}{th(\epsilon_{45} - \epsilon_{-45})} \quad (6)$$

**Fig. 14** V-notched beam shear method (or Iosipescu) specimen dimensions (in mm) and loading



where  $\varepsilon_{45}$  and  $\varepsilon_{-45}$  are the strains measured by the strain gauges bonded at  $+45^\circ$  and  $-45^\circ$  with the specimen axis. However, as in the tensile bulk test, strain gauges tend to stiffen the adhesive and have a limited strain limit (typically 10%). Alternatively, noncontacting devices, such as digital image correlation, can be used. The stress–strain curve can be used to determine the shear modulus, strength, and ductility.

**Notched Plate Shear Method (Arcan)**

The notched plate shear method, also called Arcan, is used to obtain the shear properties on bulk specimens. The specimen geometry looks like a butterfly (Fig. 15), and the test is also known as the butterfly test (Voloshin and Arcan 1980). The specimen contains two symmetric notches at  $90^\circ$  with a radius of curvature of 1.5 mm to minimize the stress concentration. The holes on the sides of the specimen allow the application of a shear loading (Fig. 16) that is uniform between the two notches. This loading arrangement avoids the problem of instability at the edges that occurs in the Iosipescu test and enables to work with thinner specimens. This is useful for flexible adhesives or for adhesives that have a big exothermic reaction during cure. There are, however, stress concentrations near the notches that can induce premature failures, especially for brittle adhesives (Dean et al. 1996). The stress is obtained dividing the load by the resistant area between the two notches. The displacement in the uniform shear deformation zone between the two notches can be measured with extensometers mounted on the specimen, with strain gauges bonded at  $+45^\circ$  and  $-45^\circ$  with the loading axis, or with noncontacting methods (Pinto et al. 2010). Dean et al. (1996) have developed an extensometer that

**Fig. 15** Notched plate shear method (or Arcan or butterfly) (dimensions in mm)

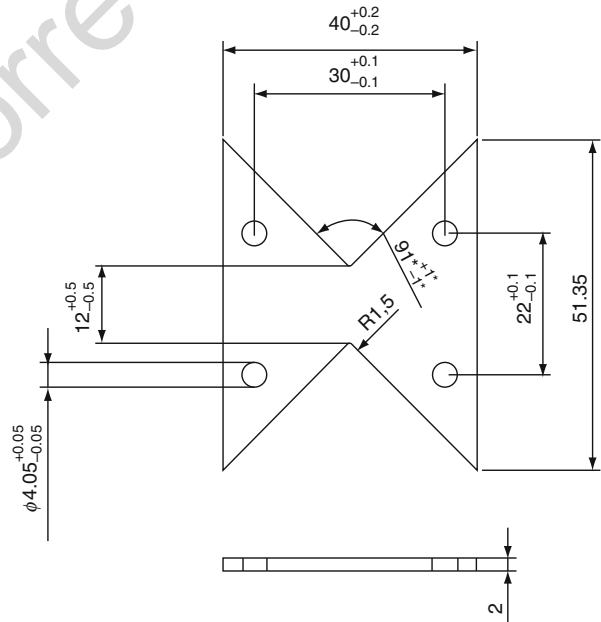
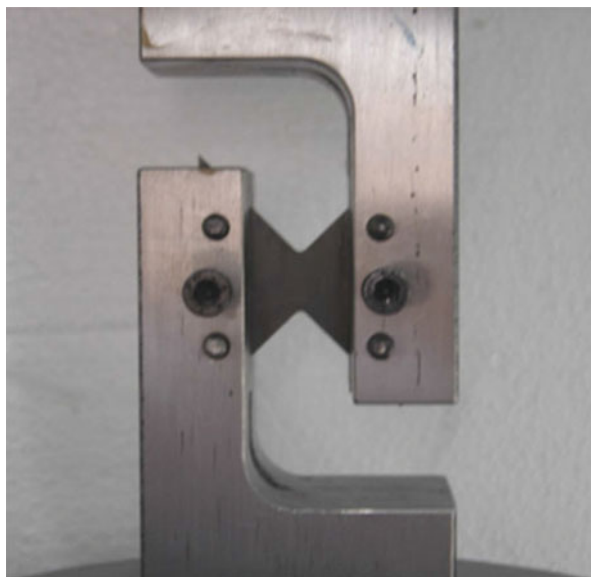


**Fig. 16** Loading jig of the Arcan specimen



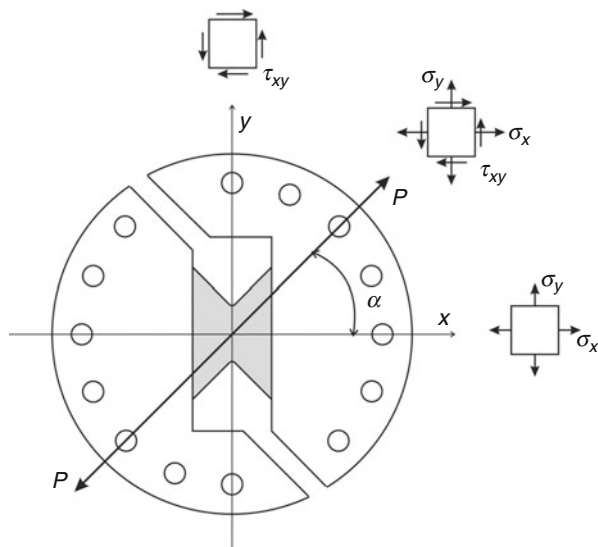
is mounted on the specimen and which consists of a pair of levers and displacement transducers. The extensometer is fixed to the grips and contacts the specimen at two points near the specimen center. For large strains (typically 20%), instabilities due to the loading arrangement make the results unreliable.

Arcan et al. (1978) proposed a biaxial fixture, commonly known as the Arcan fixture, to produce biaxial states of stress. The compact nature of the Arcan fixture enables obtaining the shear properties in all in-plane directions in a relatively simple manner. The Arcan fixture can be used to apply both shear and axial forces to the test specimen. The adhesive characterization in mixed mode loading allows for the generation of the yield surface of the adhesive in the hydrostatic versus the von Mises plane, which enables one to develop more accurate adhesive models for better simulations. Several modifications to the original test fixture have been proposed to include compression, such as that by El-Hajjar and Haj-Ali (2004). A scheme of the test fixture is shown in Fig. 17.

#### 19.4.2 Joint Specimens

One can argue that the adhesive properties measured in a joint are more representative. Furthermore, the fabrication and testing procedure is relatively simple, especially for the case of the thick adherend shear test (TAST). However, the main disadvantage is the need for high-precision measurement devices due to the low adhesive displacements. In many cases, extensometers that measure both adherend and adhesive displacements are used, which means that a correction is necessary to

**Fig. 17** Modified Arcan fixture for mixed loading



remove the adherend displacement. Another feature common to all joint tests is the fact that for a constant test speed, the strain rate in the adhesive will increase when the adhesive deforms plastically, which will increase the yield stress of the adhesive compared to a test carried out under constant strain rate.

### Arcan and Iosipescu Joint Methods

The Arcan and Iosipescu specimens can also be used as a joint where the adhesive is in a thin layer between two substrates. The test methodology is very similar to the bulk version. The adhesive displacement can be measured by noncontacting devices or extensometers of the type proposed by Dean et al. (1996). For devices that measure the adhesive and adherend displacement, a correction must be applied to have only the adhesive displacement. The stress distribution is not perfectly uniform, and an FE analysis can be used to have the value at the center of the specimen where the strain is obtained. Grabovac and Morris (1991) and Wycherley et al. (1990) used the Iosipescu method where two shaped adherends are bonded together. Weissberg and Arcan (1988) proposed a joint test based on the Arcan configuration. Cognard et al. (2005) proposed an Arcan joint method to produce not only shear but also biaxial stress states. The number of available loading directions is given by the number of holes on the modified Arcan device (Fig. 18b). There are two important parameters in this test: the geometry of the substrate (beaks machined on the substrates to reduce edge effects as illustrated in Fig 18a) and the geometry of the joint near the edge. A special system to guarantee an accurate control of the thickness and avoid misalignments is used (Fig 18c). However, the modified Arcan test is very sensitive to misalignments of the specimen regarding the direction of the applied load, and the procedure to control this aspect is very time-consuming which limits the application of this test in industry.

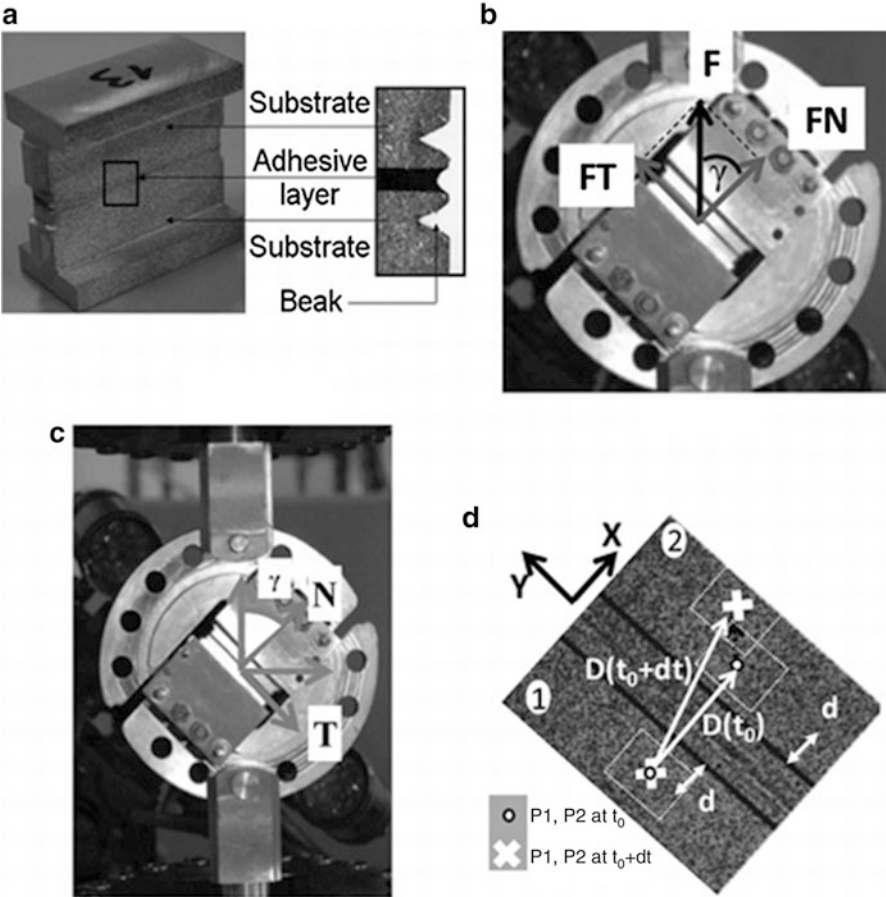


**Fig. 18** Modified Arcan test: (a) sample geometry with beaks, (b) recorded force divided into normal and tangential parts, (c) testing device, and (d) post-processing step to retrieve the normal and tangential displacements (Cognard et al. 2011)

More recently, improvements of the modified Arcan test were proposed by Créac'hadeac et al. (2015). The test substrate is a one-piece substrate that includes the bonding system and a new geometric beak.

Arnaud et al. (2014) used tubular bonded joints which enable a wide range of loadings, between tension, torsion, compression, and mixed loadings. Compared to the modified Arcan test, it has the advantage to allow nonproportional loadings and offers a continuous and infinite domain of mixed loadings.

### Butt Joint in Torsion

The butt joint with solid substrates or tubes can be used. The geometry of the specimen is represented in Fig. 19 for the butt joint with solid substrates (Adams and Coppendale 1977). As in the bulk torsion method, this test is free of stress



**Fig. 19** Butt joint in torsion with solid adherends (dimensions in mm) (Adams and Coppendale 1977)

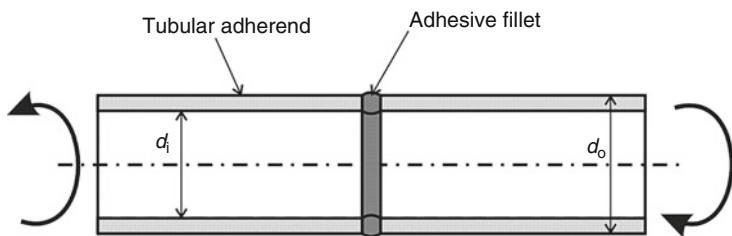
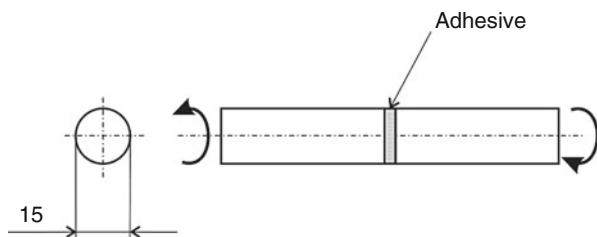


**Fig. 20** Napkin-ring test specimen

concentrations, which enables having larger strain to failures than other types of tests where stress concentrations exist. Also, the adhesive displacement generated is higher, which gives a higher accuracy for the strain than other joint methods. If the same dimensions are used as the bulk torsion test, the same test apparatus can be used. Contacting extensometers used for the bulk torsion test are also applicable to the butt joint, but a correction is needed to remove the displacement of the substrates, especially if the adhesive is strong and stiff (Adams et al. 1997). As in the bulk torsion test, the shear stress–strain curve obtained must also be corrected as in the bulk torsion method (Nadai 1931). The manufacture can be difficult when an adhesive of low viscosity is used because it is difficult to fill the bonded area properly. Adams and Coppendale (1977) designed a jig to produce fully filled joints with low-viscosity adhesives.

Another type of butt-joint test in torsion is the napkin ring where the adhesive is in a thin layer between two tubular substrates. ASTM E 229, ISO 11003-1, and DIN 54451 describe this method (Fig. 20). Because tubes are used, the adhesive is essentially at the same shear stress, since the shear stress is proportional to the radius  $r$  (see Eq. 3). Althof and Neumann (1974) have shown that the napkin-ring test and the thick adherend shear test (see Sect. 4.2.3) give a very similar shear stress–strain curve. The main disadvantage of this type of test is the difficulty of manufacture. In case the adhesive has low viscosity, the manufacture is particularly difficult because the adhesive will not stay in position. In the napkin-ring test, the adhesive fillets inside and outside should be removed because they make the calculation of the shear strength and modulus less exact. The outer fillet is easy to remove. However, the inner fillet is impossible to clean away. If the thickness of the tubes is thin enough, the effect of the fillet can be neglected.

### Thick Adherend Shear Test

The thick adherend shear test (TAST) is one of the most popular types of failure strength test because it is easy to make and test the specimens. Shear properties obtained with this test are presented in Table 1. The conventional single-lap shear joint, which is mostly used for comparison and quality control of adhesives, puts the adhesive in a complicated state of stress (see Sect. 4.2.4). Therefore, it is not suitable for the determination of the true adhesive properties. When stiff and thick metallic adherends are used, the adhesive is in a state of essentially uniform shear over most of the overlap, and peel stresses are reduced. Two forms of the TAST are used, as developed by Krieger (1988) (ASTM D 3983), in the USA, and Althof and Neumann (1974) (ISO 11003-2), in Europe. The main difference between the two tests is the size of the specimen: the Althof specimen is half the size of Krieger's. They both developed extensometers for measuring the very small displacements across the bond line (Fig. 21). The extensometer measures not only the displacement of the adhesive but also the displacement of the adherend (Fig. 22). Therefore, it is necessary to apply a correction to the measured displacements. According to ISO 11003-2, the correction should be deduced from the measurement of the shear strain on a “dummy” specimen consisting of the adherend material alone. Vaughn (1998)

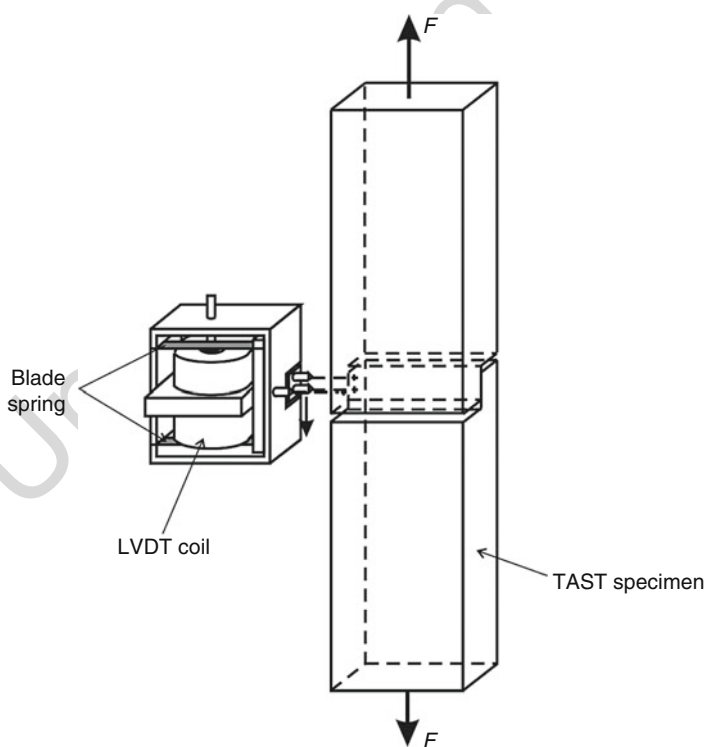


**Fig. 21** Thick adherend shear test (TAST) extensometer

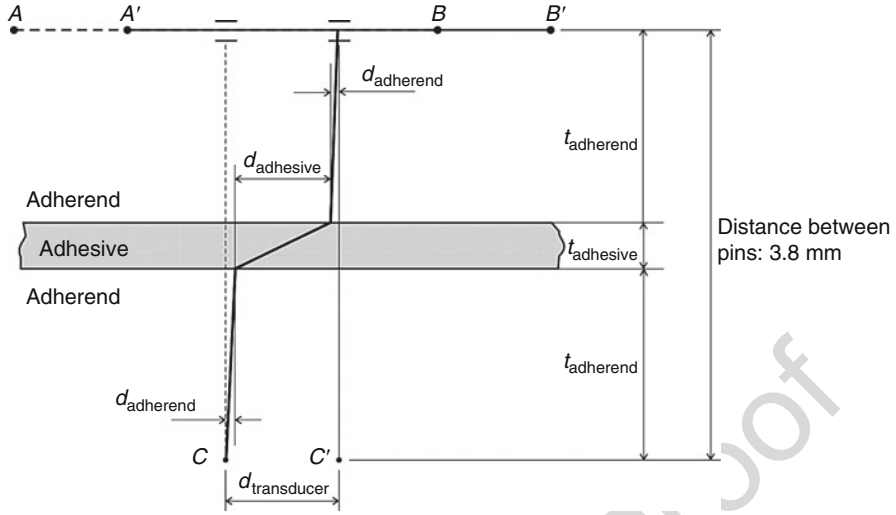


**Fig. 22** Thick adherend shear test (TAST) transducer measured displacement

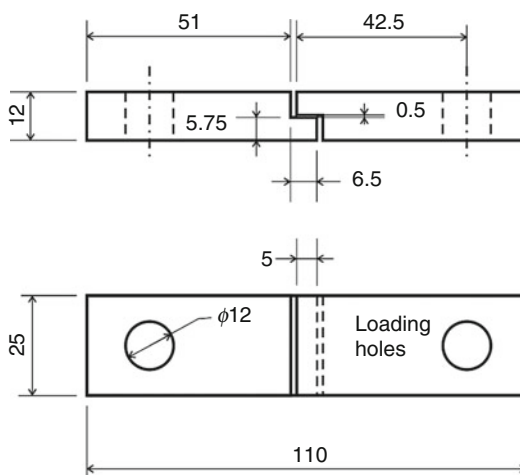
modeled the TAST specimen and the “dummy” specimen. The predicted profile of shear stress along the centerline of the adhesive is almost constant. Conversely, the shear stress distribution in the “dummy” is not uniform, so the correction cannot be deduced from that specimen. As part of a project to evaluate the relative performance of shear tests, Vaughn (1998) suggests that the adherend correction can be derived from simple elasticity assuming that the adherends experience pure shear only:

$$\begin{aligned} d_{\text{adhesive}} &= d_{\text{transducer}} - 2 \times d_{\text{adherend}} \\ 2 \times d_{\text{adherend}} &= \frac{2 \times t_{\text{adherend}} \times P}{G_{\text{adherend}} \times l \times w} \\ 2 \times t_{\text{adherend}} &= 3.8 \text{ mm} - t_{\text{adhesive}} \end{aligned} \quad (7)$$

where  $d$  is the thickness (mm),  $P$  the load (N),  $G$  the shear modulus (MPa),  $l$  the length of the overlap (5 mm), and  $w$  the width (25 mm). However, an FE analysis shows that direct axial stress is also carried by the adherend. Thus, an accurate correction cannot be properly calculated assuming that the adherends experience only pure shear. Taking this into account, it is better to use an FE analysis correction. Nevertheless, a simple elasticity correction is shown to be acceptable as long as the adhesive thickness is not too small. The adhesive displacement can also be measured with a conventional clip gauge used for tensile testing (da Silva et al. 2008). However, a correction is also needed. Optical methods such as image correlation analysis are probably the best because they give the adhesive displacement directly and do not interfere with the adhesive behavior (Pinto et al. 2010).

Despite the almost uniform stress distribution in the adhesive, stress concentrations still exist, especially at the edges of the overlap close to the interface. Several researchers have proposed modifications of the TAST geometry to reduce these

**Fig. 23** Thick adherend shear test (TAST) (dimensions in mm)



effects, including Lilleheden (1994) and Cognard et al. (2008), who propose the use of specially shaped adherends to reduce these stress concentrations. However, the machining cost is quite substantial. Another alternative is to use a spew fillet to reduce stress concentration, which avoids premature failures and enables the determination of the maximum of the stress–strain curve.

As regards the specimen manufacture, ISO 11003-2 recommends machining the specimens from two plates bonded together. However, this technique has disadvantages such as the effect of cutting in the highly stressed region at the end of the adhesive layer where initial failure is likely to occur. Vaughn (1998) proposed that a better solution was to machine the adherends to the correct dimensions before bonding (Fig. 23). The bending stiffness is higher than when the joint is composed of two bonded bars and, therefore, reduces the peel stresses. A specially built jig was designed for aligning and holding the specimens. To control the overlap and fillet, steel shims were inserted into the gaps once the adherends were brought together.

The test speed recommended by the standard ISO 11003-2 is 0.5 mm/min. However, a constant crosshead displacement rate will induce an accelerating strain rate in the adhesive once it starts yielding, influencing the yielding properties. This is a common feature of all the joint tests, contrarily to the bulk tests where the strain rate is much more constant for a given crosshead rate. To have a constant adhesive strain rate, the crosshead speed can be controlled using the adhesive displacement measurements.

### Tests with Thin Sheet Adherends

Tests with thin sheet adherends, and in particular the single-lap joint (SLJ) test, are very common in the industry. This has to do with the fact that it reproduces joints encountered in aeronautical structures that were the pioneers of adhesive bonding technology. The SLJ is described in ASTM D 1002 and ISO 4587. The usual dimensions are indicated in Fig. 24a. These standards recommend cutting specimens

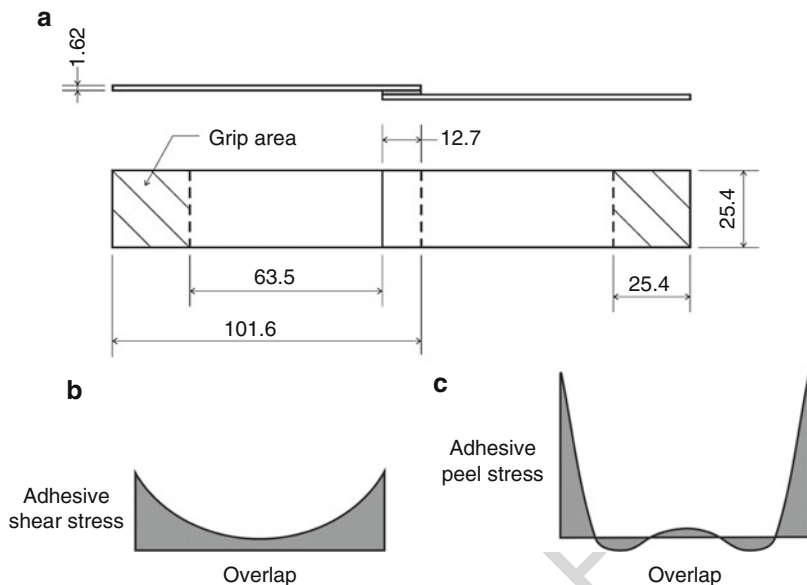


**Fig. 24** Single-lap joint: (a) dimensions in mm (ASTM D 1002), (b) adhesive shear stress distribution along the overlap, and (c) adhesive peel stress distribution along the overlap

from two bonded plates 178 mm (7 in.) wide. However, the joints can be made individually in a mold, reducing the defects introduced by cutting. As seen in Part E, the SLJ is in a complex state of stress. Due to the load misalignment, even if tab ends are used, and due to the differential adhesive straining effect (Volkersen 1938), the adhesive is subjected to a state of nonuniform shear and peel stresses (see Fig. 24b, c). Nevertheless, the ASTM D 1002 standard recommends reporting the results as the average shear stress at failure (maximum load divided by bond area). It is important to choose adherends that do not yield prior to joint failure. Otherwise, what causes the failure of the joint is the yielding of the adherend. In other words, the yielding of the adherend is being measured and not the actual strength of the adhesive.

The SLJ has the advantage of being simple and cheap. It is widely used and gives an idea of the adhesive shear strength. Valuable information is contained in the lap shear strength. The lap shear strength depends, among other things, on the yield strength of the adherends and the overlap length as shown schematically in Fig. 25. For the mild steel adherends, as the overlap increases, there is some increase in strength, but a plateau is reached quickly. In this case, the plastic deformation of the mild steel controls failure. As for the hard steel, the adherends remain elastic, and the strength increases almost linearly as the overlap increases, especially if the adhesive is ductile. An interesting result is that the slope of the tangent to the curves (as indicated in Fig. 25) gives a shear strength ( $\tau = \text{load}/(\text{overlap length} \times \text{joint width})$ ) equal to the maximum shear stress given by a shear stress–shear strain curve. Therefore, the lap shear strength gives an approximate value of the shear strength of

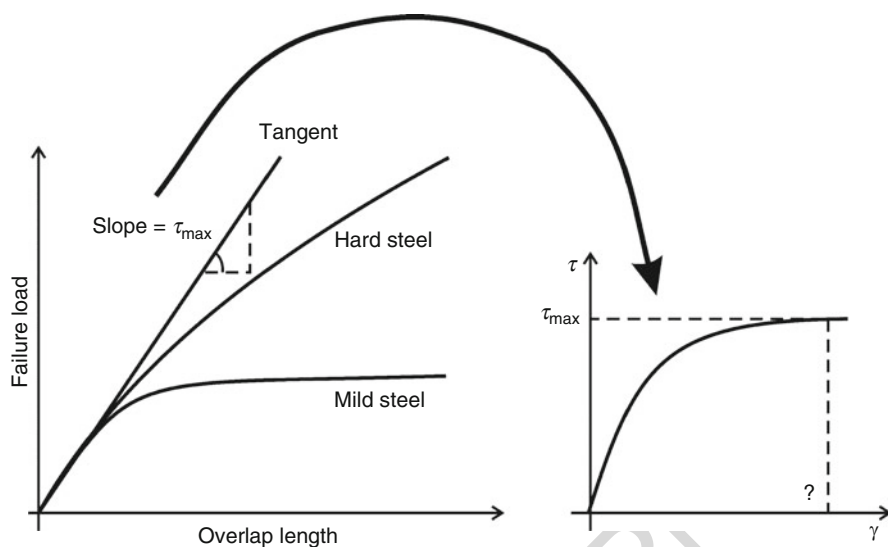


**Fig. 25** Lap shear strength versus overlap strength

the adhesive, provided high-strength adherends are used (with no yield) (Banea and da Silva 2009). Another factor that should be taken into account is the adhesive thickness. It has been shown experimentally by many authors that the joint strength decreases as the adhesive thickness increases. Also, the effective strain rate at constant displacement rate is affected by adhesive thickness. Therefore, it is important to indicate the adhesive thickness used. This is valid for all the joint tests. For relatively thin values (0.1–0.4 mm), the SLJ strength variation is not substantial (Adams and Peppiatt 1974, da Silva et al. 2006). The SLJ test does not give the shear strain at failure. The adhesive must be tested in uniform shear to obtain the shear stress–shear strain curve.

Other tests with thin sheet adherends have been used to have a more uniform adhesive stress distribution along the overlap, such as the laminated joint shown in Fig. 26a according to ASTM D 3165. The bending moment is largely reduced, but the differential straining is still present. The double-lap joint (Fig. 26b) also reduces the peel stresses due to the alignment of the load. Internal bending effects in the joint cause peel stresses at the ends of the internal adherend. Another type of double-lap joint, also called double-strap joint, can be used. Here again, despite the reduction of the peel stresses, the adhesive shear stress is still not uniform due to the differential straining effect.

### Pin-and-Collar Test

Standards ASTM D 4562 and ISO 10123 describe a shear test in which the specimen is a pin bonded inside a collar. The test uses a press to force the pin through the collar, which rests on a support cylinder. The test results are the load required to initiate failure divided by the bonded area between the pin and the collar. This type of

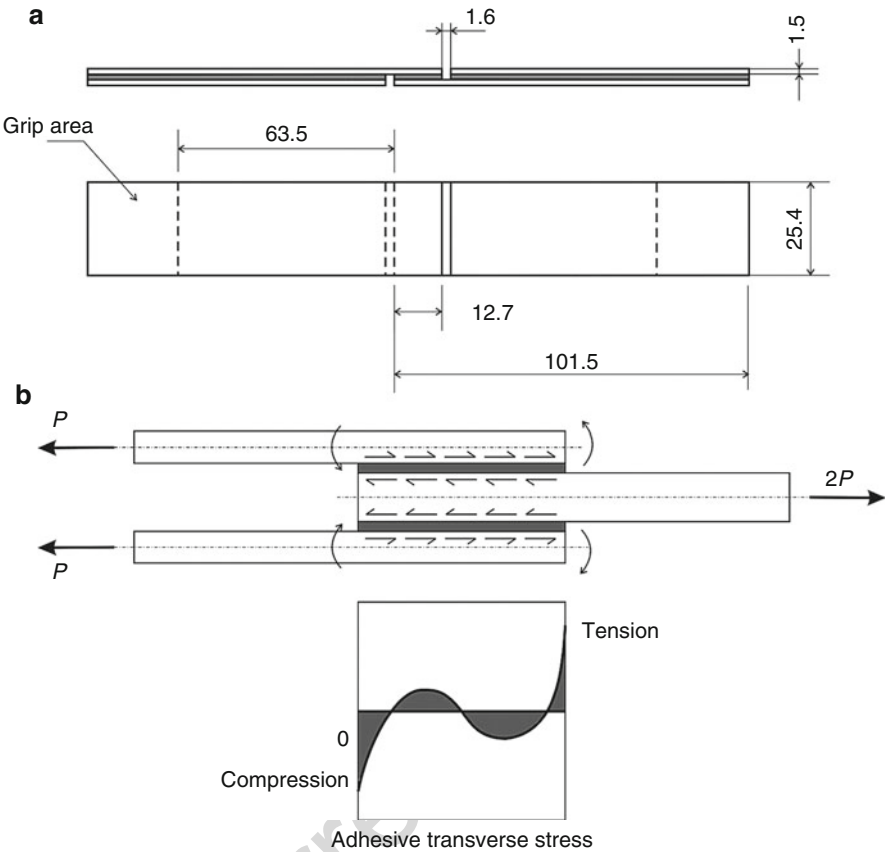


**Fig. 26** (a) Laminated joint (ASTM D 3165) and (b) double-lap joint with stress distribution (ASTM D 3528) (dimensions in mm)

test is particularly suited to test anaerobic adhesives. The shear strength determined with this test is only an average value because the stress distribution is not uniform along the overlap (Nemeş et al. 2006; Martínez et al. 2008). ASTM E 229 also uses a pin-and-collar type of specimen except that here torsional loadings cause failure. The adhesive stress distribution in this case is more uniform and may be used to determine the adhesive shear modulus and strength. However, the standard was withdrawn in 2003.

### 19.4.3 Recommendations

The most recent literature shows that all the test methods described above do not show a systematic variability in the shear stress–strain curves (Althof and Neumann 1974; Jeandreau 1993; Dean et al. 1996; da Silva and Adams 2005). The differences

can be attributed to material variability and different precision associated with each test method and manufacture.

The test that offers the most accuracy is the bulk torsion test in case of bulk specimens and the butt joint in torsion for the joint tests. However, torsion devices are not common in most laboratories. The bulk torsion specimen is also limited to adhesives that are sufficiently rigid to be machined. For example, it is not applicable to a silicone or a polyurethane.

In case a torsion machine is not available, the TAST is probably the simplest and most reliable technique to use. The Arcan joint is also a good alternative and is easily adaptable to mixed loading, which is very important for the proper adhesive yielding failure envelope.

---

## 19.5 Relation Between Tensile, Compressive, and Shear Properties

---

As described above, there is a wide range of test methods available, and it is difficult to make the right choice. However, the properties obtained in compression, tension, and shear can be related. One of the objectives of the adhesive characterization is to generate test data for constitutive modeling. If a von Mises-type criterion is used, then only one type of test is sufficient. Generally, in such a case, the bulk tensile test or the TAST is used. But other tests such as the bulk torsion test can also be used. However, if a more refined yielding model is used such as that of Dolev and Ishai (1981), then the properties of the adhesive in at least two loading modes are necessary. In this case, the tests generally chosen are the bulk tensile test and the TAST. Various authors have shown that the elastic properties obtained by each method correlate reasonably well. For a homogeneous material, the relation between Young's modulus  $E$  and the shear modulus  $G$  is

$$E = \frac{G}{2(1 + \nu)} \quad (8)$$

where  $\nu$  is Poisson's ratio. If  $E$  is taken from the bulk tensile test and  $G$  from a shear test such as the TAST, values of  $\nu$  between 0.3 and 0.5 are obtained for most adhesives (Lilleheden 1994; Dolev and Ishai 1981; Jeandrau 1991; da Silva and Adams 2005). Figure 27 shows on the same graph three stress–strain curves obtained by compression on bulk specimens (ASTM D 695), tension on bulk specimens (EN ISO 527-2), and shear using the TAST (ISO 11003-2). The predicted shear stress–strain using a modified von Mises model (Dolev and Ishai 1981) curve from the compressive and tensile results is also shown. The agreement with the experimental shear curve is very good. However, if the shear stress–strain curve of the same epoxy adhesive were to be predicted using the conventional von Mises model, then the predicted curve would be below the experimental one (also shown in Fig. 27). Adhesive properties in tension, compression, and shear are therefore well correlated provided a model that takes into account the hydrostatic stress component



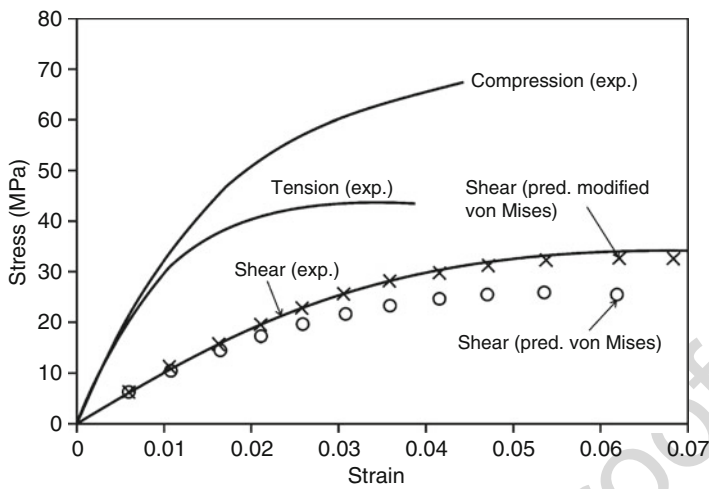


**Fig. 27** Basic stress–strain data curves under uniaxial loading in tension and compression and under shear for an epoxy adhesive

is used. However, the prediction of the shear strain to failure does not compare well with the experimental value. The shear strain to failure is the most difficult parameter to obtain in terms of both accuracy and precision. It is highly dependent on the type of loading and the quality of the specimen. The adhesive has a different behavior when loaded in shear and in tension in the presence of defects such as voids. In tension, once a crack is triggered next to a void, the specimen fails due to the high stress concentration. In shear, even if a crack is triggered, the remaining area is capable of further deformation, especially if the adhesive is ductile. For example, in bulk tension, a small void will cause a premature failure, whereas in the TAST, the presence of a void is not as critical. There have been recent advances in this area where the same type of specimen is used for all loadings giving very good results up to the failure strain (Cognard et al. 2010).

### 19.6 Conclusions

This chapter describes the major failure strength tests used to determine intrinsic adhesive properties. Tensile, compressive, and shear tests are described with reference to major international standards. Bulk and in situ (adhesive in a joint) tests are discussed and related. The major conclusions that can be drawn are the following:

1. The elastic properties can be determined by any test except tests with thin adherends or the pin-and-collar test.
2. In tension, the recommended test is the bulk tensile test. The axially loaded butt joint has poor repeatability and suffers from constraining effects.

3. Compressive tests are, in general, difficult to perform, and little data exists in the literature. Bulk specimens are commonly used, but the failure stress and strain are difficult to measure.
4. There is a wide variety of shear tests. All the test methods described in this chapter do not show a systematic difference in the shear stress–strain curves. Torsion tests are the most accurate. However, torsion devices are not common in most laboratories. In case a torsion machine is not available, the TAST is probably the simplest and most reliable technique to use.
5. Adhesive properties (except the strain to failure) in tension, compression, and shear can be correlated, provided a model that takes into account the hydrostatic stress component is used.
6. The shear strain to failure is the most difficult parameter to obtain in terms of both accuracy and precision. It is highly dependent on the type of loading and the quality of the specimen.
7. Devices based on Arcan and TAST geometries are being developed that can apply mixed loadings to the same type of specimen. The results obtained show that even the strain to failure can be related.

---

## References

- Adams RD (1990) Failure strength tests and their limitations. In: Dostal CA (ed) *Engineered materials handbook*, vol 3: adhesives and sealants. American Society for Materials, Metals Park, pp 325–335
- Adams RD, Comyn J, Wake WC (1997) *Structural adhesive joints in engineering*, 2nd edn. Chapman & Hall, London
- Adams RD, Coddendale J (1977) The elastic moduli of structural adhesives. In: Allen KW (ed) *Adhesion 1*. Applied Science, London, pp 1–17
- Adams RD, Coddendale J (1979) The stress–strain behaviour of axially-loaded butt joints. *J Adhes* 10:49
- Adams RD, Peppiatt NA (1974) Stress analysis of adhesive-bonded lap joints. *J Strain Anal* 9:185
- Adams DF, Walrath DE (1987) Current status of the Iosipescu shear test method. *J Compos Mater* 21:494
- Althof W, Neumann G (1974) Verfahren zur ermittlung von schubspannungs–gleitungs–diagrammen von konstruktionsklebstoffen. *Materialprüf* 16(12):387
- Arcan M, Hashin Z, Voloshin A (1978) A method to produce uniform plane stress states with applications to fiber reinforced materials. *Exp Mech* 18:141
- Arnaud N, Créac'hacdec R, Cognard JY (2014) A tension/compression–torsion test suited to analyze the mechanical behaviour of adhesives under non-proportional loadings. *Int J Adhes Adhes* 53:3
- Banea MD, da Silva LFM (2009) Mechanical characterization of flexible adhesives. *J Adhes* 85:261
- Chen Z, Adams RD, da Silva LFM (2011) Fracture toughness of bulk adhesives in mode I and mode III and curing effect. *Int J Fract* 167(2):221
- Cognard JY, Créac'hacdec R, da Silva LFM, Teixeira FG, Davies P, Peleau M (2011) Experimental analysis of the influence of hydrostatic stress on the behaviour of an adhesive using a pressure vessel. *J Adhes* 87:804
- Cognard JY, Créac'hacdec R, Maurice J, Davies P, Peleau M, da Silva LFM (2010) Analysis of the influence of hydrostatic stress on the behaviour of an adhesive in a bonded assembly. *J Adhes Sci Technol* 24:1977

- Cognard JY, Créac'hacdec R, Sohier L, Davies P (2008) Analysis of the nonlinear behavior of adhesives in bonded assemblies – comparison of TAST and Arcan tests. *Int J Adhes Adhes* 28:393
- Cognard JY, Davies P, Gineste B, Sohier L (2005) Development of an improved adhesive test method for composite assembly design. *Compos Sci Technol* 65:359
- Créac'hacdec R, Sohier L, Cellard C, Gineste B (2015) A stress concentration-free bonded arcan tensile compression shear test specimen for the evaluation of adhesive mechanical response. *Int J Adhes Adhes* 61:81
- da Silva LFM (2012) Testing adhesive joints: best practices. Wiley-VCH, Weinheim
- da Silva LFM, Adams RD (2005) Measurement of the mechanical properties of structural adhesives in tension and shear over a wide range of temperatures. *J Adhes Sci Technol* 19:109
- da Silva LFM, Adams RD, Gibbs M (2004) Manufacture of adhesive joints and bulk specimens with high temperature adhesives. *Int J Adhes Adhes* 24(1):69
- da Silva LFM, da Silva RAM, Chousal JAG, Pinto AMG (2008) Alternative methods to measure the adhesive shear displacement in the thick adherend shear test. *J Adhes Sci Technol* 22:15
- da Silva LFM, Rodrigues TNSS, Figueiredo MAV, de Moura MFSF, Chousal JAG (2006) Effect of adhesive type and thickness on the lap shear strength. *J Adhes* 82:1091
- Dean GD, Duncan BC, Adams RD, Thomas R, Vaughn L (1996) Comparison of bulk and joint specimen tests for determining the shear properties of adhesives. NPL Report CMMT(B)51. National Physical Laboratory, Teddington
- Dolev G, Ishai O (1981) Mechanical characterization of adhesive layer in-situ and as bulk material. *J Adhes* 12:283
- Drucker DC, Prager W (1952) Soil mechanics and plastic analysis or limit design. *Q Appl Math* 10:157
- El-Hajjar R, Haj-Ali R (2004) In-plane shear testing of thick-section pultruded FRP composites using a modified Arcan fixture. *Compos Part B* 35:421
- Gali S, Dolev G, Ishai O (1981) An effective stress/strain concept in the mechanical characterization of structural adhesive bonding. *Int J Adhes Adhes* 1:135
- Grabovac I, Morris CEM (1991) The application of the Iosipescu shear test to structural adhesives. *J Appl Polym Sci* 33:2033
- Grant LDR, Adams RD, da Silva LFM (2009) Experimental and numerical analysis of single lap joints for the automotive industry. *Int J Adhes Adhes* 29:405
- Guimarães AFC, Gonçalves JA, Carbas RJC, Lopes AM, da Silva CM, da Silva LFM (2016) Torsion machine for adhesive joints. Provisional Patent Application Portuguese, n. 109717 D
- Hart-Smith LJ (1973) Adhesive bonded double lap joints. NASA CR-112235
- Iosipescu N (1967) New accurate procedure for single shear testing of metals. *J Mater* 2:537
- Jeandrou JP (1991) Analysis and design data for adhesively bonded joints. *Int J Adhes Adhes* 11:71
- Jeandrou JP (1993) Technologie du collage structural pour les applications en mécanique. Centre Technique des Industries Mécaniques (CETIM), Senlis. ISBN 2-85400-255-5
- Krieger RB (1988) Stress analyses concepts for adhesive bonding of aircraft primary structure. In: Johnson WS (ed) *Adhesive bonded joints; testing, analysis and design*. American Society for Testing and Materials, Philadelphia, pp 264–275
- Kuenzi EW, Stevens OH (1963) Determination of mechanical properties of adhesives for use in design of bonded joints. US Forest Products Service Research Note FPL-011. US Department of Agriculture, Madison
- Lilleheden L (1994) Mechanical properties of adhesives in situ and in bulk. *Int J Adhes Adhes* 14:31
- Martínez MA, Velasco F, Abenójar J, Pantoja M, Del Real JC (2008) Analytical solution to calculate the stress distribution in pin-and-collar samples bonded with anaerobic adhesives (following ISO 10123 standard). *Int J Adhes Adhes* 28:405
- Nadai A (1931) *Plasticity: a mechanics of the plastic state of matter*. McGraw-Hill, New York
- Nemeş O, Lachaud F, Mojtabi A (2006) Contribution to the study of cylindrical adhesive joining. *Int J Adhes Adhes* 26(6):474

- 747 Pinto AMG, Magalhães AG, Campilho RDSG, da Silva LFM, Chousal JAG, Baptista APM (2010)  
748 Shear modulus and strength of an acrylic adhesive with the notched plate method (Arcan) and  
749 the thick adherend shear test (TAST). *Mater Sci Forum* 636–637:787
- 750 Raghava RS, Cadell R, Yeh GSY (1973) The macroscopic yield behaviour of polymers. *J Mater Sci*  
751 8:225
- 752 Vaughn LF (1998) Measurement of basic mechanical properties of adhesives for design use. PhD  
753 thesis, Department of Mechanical Engineering, University of Bristol
- 754 Volkersen O (1938) Die nietkrafteerteilung in zubeanspruchten nietverbindungen mit konstanten  
755 loschonquerschnitten. *Luftfahrtforschung* 15:41
- 756 Voloshin A, Arcan M (1980) Pure shear moduli of unidirectional Fiber-Reinforced Materials  
757 (FRM). *Fiber Sci Technol* 13:125
- 758 Weissberg V, Arcan M (1988) A uniform pure shear testing specimen for adhesive characterisation.  
759 In: Johnson WS (ed) *Adhesively bonded joints: testing, analysis and design*, ASTM STP 981.  
760 American Society for Testing and Materials, Philadelphia, pp 28–38
- 761 Wycherley GW, Mestan SA, Grabovac I (1990) A method for uniform shear stress–strain analysis  
762 of adhesives. *J Test Eval* 18:203
- 763 Young RJ, Lovell PA (1991) *Introduction to polymers*, 2nd edn. Chapman & Hall, London

Bamber R. K. Blackman

**Contents**

20.1	Introduction .....	524
20.2	Fracture Tests on Bulk Adhesive Specimens .....	526
20.3	Fracture Tests on Adhesive-Joint Specimens .....	529
20.3.1	The Mode I Double Cantilever Beam (DCB) Test .....	529
20.3.2	The Mode I Tapered Double Cantilever Beam (TDCB) Test .....	534
20.3.3	Mode II Adhesive-Joint Tests .....	535
20.3.4	Mixed-Mode I/II Adhesive-Joint Tests .....	540
20.3.5	Effects of Adhesive Layer Thickness .....	543
20.4	Peel Testing .....	543
20.4.1	Introduction to Peel Testing .....	543
20.4.2	Geometry-Dependent Peel Tests .....	544
20.4.3	Geometry-Independent Peel Tests .....	545
20.5	Relationship Between $G_c$ (Bulk, Fracture, and Peel) .....	550
20.6	Conclusions .....	551
	References .....	552

**Abstract**

This chapter considers first the fracture in a bulk adhesive specimen under mode I, that is, tensile opening loading conditions. Then, the testing of adhesive joints using a linear-elastic fracture mechanics approach is considered. In these tests, the substrates are assumed to only deform in a linear-elastic manner, and any permanent deformation of the substrates is avoided. In adhesive joints, due to the directional constraint of the failure path that is often observed, it is common to encounter failures in other loading modes, in addition to mode I. Thus, mode II (in-plane shear) and mixed-mode I/II testing of adhesive joints are also

B. R. K. Blackman (✉)

Department of Mechanical Engineering, Imperial College London, South Kensington Campus,  
London, UKe-mail: [b.blackman@imperial.ac.uk](mailto:b.blackman@imperial.ac.uk)

considered. There is often the need to measure the resistance to fracture in a joint with flexible substrates. In this case, the assumptions of linear elastic fracture mechanics may no longer be valid, and permanent deformation of the substrates may occur. One such test is the peel test and some variants of the peel test are considered in the present chapter, with a focus on the recent development of a geometry-independent peel test.

---

## 20.1 Introduction

Fracture tests are performed on bulk adhesive specimens and on adhesive joints for a number of reasons. Bulk adhesive specimens are frequently studied as part of the materials development process. For paste adhesives, the bulk specimens are usually formed by casting the paste into a mold and then curing the specimens according to the manufacturers' instructions. For film adhesives, bulk specimens can be prepared by carefully stacking multiple layers of film and applying pressure in a mold during cure. (It should be noted, however, that the use of multiple layers of film adhesive is not common in industry. If thicker layers are needed, a thicker film is usually used.) The cured plates may be machined into standard compact tension (CT) or single-edge notched bend (SENB) test specimens for subsequent fracture mechanics testing to determine the fracture toughness,  $K_{Ic}$ , or fracture energy,  $G_{Ic}$ , using standard techniques developed for polymers (ISO 2000). The manufacture of bulk adhesive specimens is not a trivial exercise; there is the need to minimize the presence of air voids, the need to obtain complete mold fill, and also the need to avoid uncontrolled exothermic degradation of the adhesive during cure. However, the testing of bulk adhesive samples isolates the adhesive from the interface or interphase regions and from the presence of substrates and so focuses entirely on the cohesive fracture properties of the adhesive. Such bulk tests have been used extensively in the literature to study; for example, the effects of combining different resins and hardeners, the effects of adding toughening particles to the adhesive formulation, and bulk specimens have been used to determine fracture resistance under different loading conditions, for example, quasi-static and fatigue and also to investigate the effects of test rate, temperature, and environment.

In practice, however, adhesives are usually applied as thin layers with the purpose of joining different substrates together to resist separation. Thus, in their common application, the adhesive exists as a thin layer, typically in the range of 0.1–2.0 mm thick and forming part of a system incorporating the adhesive, the substrates, and a region in between these, described as the interphase. Whereas the interface has only two dimensions, the interphase has three dimensions, potentially extending through an oxide layer on a metallic substrate or into the adhesive. The adhesive, as present in the cured joint, may possess different properties to the adhesive in a cured bulk specimen. This is because the adhesive may have cured under different conditions in the joint compared to the bulk. An equivalent temperature cycle applied to joints and to bulk specimens will be likely to induce different rates of heating and cooling of the

adhesive. This can lead to subtle changes in the microstructure. The measurement of thermal properties such as the glass transition temperature may detect when this has occurred. In addition to changes in the properties between bulk and joint, the behavior of the adhesive in the joint is influenced by the presence of the nearby substrates. This can limit the size of the plastic zone forming at the crack tip and can thus limit the toughness of the joint. Studies investigating the effect of bondline thickness on the toughness of adhesive joints frequently show a critical thickness at which the toughness of the joint reaches a maximum limiting value (Kinloch 1987). This limiting value is frequently equivalent to the value measured in the bulk adhesive.

Another important aspect of testing the adhesive as part of an adhesive-joint system is that the joint presents a number of “options” for the location of the failure path. Failure may be cohesive in approximately the center of the adhesive layer. It may be cohesive but near the interface as is often seen in peel testing. It may be interfacial along the adhesive–substrate interface or it may run entirely within an interphase, for example, within a metal oxide/adhesive interphase region. The failure path could run cohesively through the substrate, for example, the crack could run in the interlaminar region of a fiber-reinforced polymer composite substrate (Kinloch et al. 1992). Finally, some combination of the above could occur. Each of these options for the failure path may lead to a different fracture resistance being measured and thus adhesive-joint tests and their interpretation are necessarily more complex than bulk adhesive studies.

A final point is that a crack in a bulk material will always tend to run under local mode I tensile opening conditions. Thus, a crack loaded in, for example, the in-plane shear mode (mode II) will deviate to run locally in mode I. However, in the adhesive layer of a joint, the direction of the crack and the resulting failure path are usually constrained and thus cracks may truly propagate under mixed-mode and mode II loading conditions. Indeed, modes I and II and combinations of I and II have received the most attention in the literature and are considered in the present chapter. The out-of-plane shear mode (mode III) is less important and is not discussed in this chapter.

Adhesive-joint tests that have been developed to measure fracture resistance under these various loading modes have typically relied on the concepts of Linear Elastic Fracture Mechanics (LEFM), which imposes the restriction that the deformation of the substrates remains linearly elastic and that any plasticity is limited to a small region ahead of the crack tip. This requirement may not be met in the case of high elongation adhesives such as polyurethanes and also when substrates consisting of relatively thin materials, for example, sheet materials, are used. This is a common problem with peel testing: very frequently there is permanent plastic deformation of the peel arm during the test. As such, the concepts of elastic–plastic fracture mechanics need to be invoked and, for example, the energy dissipated in the plastic bending of the peel arm should be deduced and should be subtracted from the total work done on the joint during peeling. Without such correction, the peel strength of an adhesive joint may be manipulated simply by, for example, changing

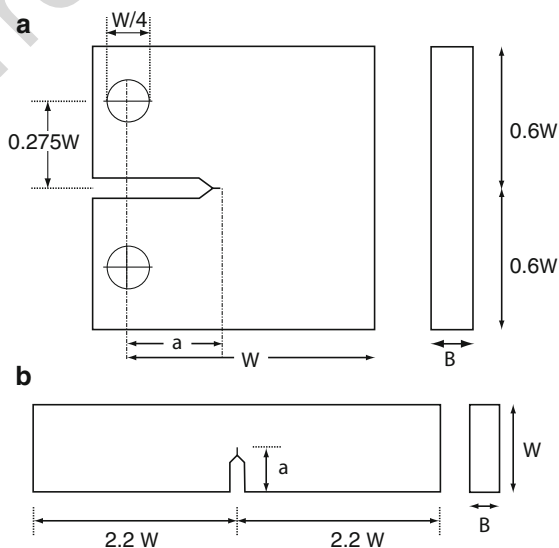
the thickness of the substrate material to invoke more plastic energy dissipation in the joint.

## 20.2 Fracture Tests on Bulk Adhesive Specimens

Mode I fracture tests on bulk adhesive samples may be carried out according to the international test standards for the determination of the fracture toughness ( $K_{Ic}$  and  $G_{Ic}$ ) for plastics – an LEFM approach. The ISO method is ISO 13586 (ISO 2000) and the equivalent ASTM method ASTM D5045 (ASTM 1999) are commonly employed. The standards specify that either compact tension (CT) or single-edge notched bend (SENB) specimens be prepared. These Linear Elastic Fracture Mechanics (LEFM) standards require a natural crack to be positioned in the specimen and then the tests specify the conditions for the reinitiation of this crack.

The choice of whether to use the CT or SENB test is influenced by several factors. First, the amount of material available: CT specimens are larger than SENB specimens so if the quantity of adhesive is limited, this would favor the SENB test. Second, the type of crack propagation observed: the tests are quasistatic and unstable crack initiation from the initial defect is intended in the test. If stable growth is obtained, the CT specimen will usually permit a greater length of crack propagation to occur than the SENB test. Figure 1a shows the CT and Fig. 1b shows the SENB test specimens. For either, it is necessary to mold bulk adhesive samples with sufficient dimensions to satisfy the validity criteria (see below) and to be sufficiently void free (see ► Chap. 19, “Failure Strength Tests” for more details on how this can be achieved for common adhesive types).

**Fig. 1** (a) Compact tension (CT) specimen used for bulk adhesive fracture testing. (b) Single-edge notched bend (SENB) specimen used for bulk adhesive fracture testing





Typically, the plates of bulk adhesive are prepared and then they are machined to size using a saw and a mill. A chevron notch is also machined into the specimen, and from this, a natural precrack is grown ahead of the initially machined notch by a razor tapping or sliding approach. The results obtained in the tests are critically dependent upon the quality of the precracks obtained. The initial dimensioning of the specimens is described in the standards. The size criteria for test validity are designed to ensure that LEFM conditions pertain and that the specimen is in a state of plane strain. A further restriction on the test is that the maximum force value obtained should not exceed 110% of the force at the 5% compliance offset point. This ensures the loading conditions are linear in the test. Obtaining sufficient thickness of the specimen,  $B$ , is usually the most difficult dimension to achieve, so the specimen thickness is usually given by the thickness of the prepared plate. For both specimens, the ratio of crack length to specimen width is given by:

$$0.45 < a/W < 0.55 \quad (1)$$

and  $W = 2B$  initially. The dimensions are defined in Fig. 1.

The success of the test depends very largely on the quality of the natural precrack obtained ahead of the machined notch. The precrack can be obtained using fatigue loading but it is usually more convenient to obtain a natural crack by lightly tapping a razor blade into the tip of the machined crack such that crack extension ahead of the razor blade is obtained. This requires some skill and practice is needed before satisfactory precracks are obtained. The cracks grown should be several times longer than the original notch tip radius. For brittle adhesives, razor tapping too firmly may cause the crack to run through the entire specimen, or the precrack may be otherwise too long or not straight. For tough adhesives, it may not be possible to obtain any crack growth ahead of the machined notch by razor tapping. In that case, razor tapping should be abandoned, as residual compressive stresses may be introduced by the tapping which will lead to artificially high values of  $K_{Ic}$  and  $G_{Ic}$  being deduced. In such cases with tough adhesives, it is recommended that a razor blade is drawn across the notch tip to create a precrack. The sliding action of the blade minimizes the introduction of compressive stresses ahead of the precrack.

The standards specify that the specimens should be tested at a temperature of 23 °C and with a loading rate of 10 mm/min. The loading time should be recorded. The loading supports for the SENB test should not be constrained but should be free to roll and should be of sufficient diameter to avoid plastic indentation into the specimen. The displacement of the specimen during the test can be obtained either by measuring the crosshead displacement of the test machine (which then requires a machine compliance correction to be performed as described in ISO 13586 (ISO 2000) and ASTM D5045 (ASTM 1999)), or by directly using a displacement transducer mounted at the load point. For the CT test, the displacement should be obtained using a clip gauge mounted close to the pins. For the determination of  $K_{Ic}$ , only the force and the specimen dimensions are required, but for  $G_{Ic}$ , the displacement is needed, and if only the

crosshead displacement is recorded, then machine compliance and pin indentation corrections are required to obtain accurate results.

A provisional value of the fracture toughness,  $K_Q$ , is determined at the intersection of the 5% compliance offset line with the force–displacement curve,  $P_Q$ . The provisional value is calculated from:

$$K_Q = f \frac{P_Q}{B\sqrt{W}} \quad (2)$$

where  $f$  is the geometry factor (a function of  $a/W$ ) given in the standards. The linearity of the loading (i.e., the cross-check on LEFM conditions) is assessed by determining the value of  $P_{\max}/P_Q$  and the criterion is passed if:

$$\frac{P_{\max}}{P_Q} < 1.1 \quad (3)$$

that is, up to a 10% nonlinearity is permitted. The attainment of plane strain conditions is assessed via the three size criteria. These are given by:

$$B, a, (W - a) > 2.5 \left( \frac{K_Q}{\sigma_y} \right)^2. \quad (4)$$

If the linearity criteria is violated, a possible option is to increase  $W$  for the same value of  $B$ . Values of  $W/B$  up to 4 are permitted. The uniaxial tensile yield stress  $\sigma_y$  is required for the assessment, and for polymers this is conventionally taken at the maximum load in the tension test, as described in ► [Chap. 19, “Failure Strength Tests”](#). If the linearity and size criteria are met, then  $K_Q$  is recorded as  $K_{Ic}$ , that is, the plane strain value. The corresponding fracture energy,  $G_{Ic}$ , can be obtained using:

$$G_{Ic} = \frac{K_{Ic}^2 (1 - \nu^2)}{E} \quad (5)$$

provided that Young’s modulus,  $E$ , and Poisson’s ratio,  $\nu$ , are obtained at the equivalent rate and temperature. However, there are many uncertainties when using this technique to obtain  $G_{Ic}$  (Williams 2001) and it is considered far preferable to measure the energy,  $U$ , directly from integrating the corrected load versus load-point displacement diagram (ISO 13586) and thus:

$$G_{Ic} = \frac{U}{BW\phi}, \quad (6)$$

where  $\phi$  is a calibration factor, a function of compliance,  $a$  and  $W$ . Round-robin testing by the ESIS TC4 group on various polymers found that the methods have a reproducibility of 5% in  $K_{Ic}$  values and 12% in  $G_{Ic}$  values (Williams 2001).

201 **20.3 Fracture Tests on Adhesive-Joint Specimens**

202 **20.3.1 The Mode I Double Cantilever Beam (DCB) Test**

203 The mode I fracture resistance of adhesive joints is most commonly determined  
204 using the double cantilever beam (DCB) test. This test was initially described in the  
205 ASTM standard (ASTM 1990) and has been developed more recently in the British  
206 standard (BSI 2001) and the international standard (ISO 2009). The original ASTM  
207 test standard specified metallic substrates and the critical strain energy release rate in  
208 mode I,  $G_{Ic}$ , was determined for repeated crack initiations using a version of simple,  
209 shear-corrected beam theory. The later standards additionally accommodate nonme-  
210 tallic substrates and employ corrected beam theory to determine values of  $G_{Ic}$  at both  
211 crack initiation and during steady-state crack propagation.

212 The DCB adhesive-joint test specimen, as shown in Fig. 2, comprises two sub-  
213 strates (the double cantilevers) bonded together with a thin layer of adhesive to form  
214 the joint. During joint fabrication, an initial crack is formed at one end of the joint. In  
215 the ASTM method, this can be achieved by positioning a shim at one end of the joint  
216 and having an area over which no adhesive is applied. In the BS and ISO standards,  
217 the initial crack is formed by placing a releasing film centrally in the adhesive layer  
218 during joint fabrication. This film, typically a fluoropolymer and 12–14  $\mu\text{m}$  in  
219 thickness, is then molded into the joint during adhesive cure. The ASTM test  
220 specimen comprises of substrates 300 mm long, 25 mm wide, and 12.7 mm high  
221 ( $24 \times 1 \times 0.5$  in). These are cut out from a larger bonded panel. The BS and ISO  
222 standards are more flexible on the substrate dimensions allowed, but have a require-  
223 ment that plastic deformation of the substrates must always be avoided. Typically,  
224 those following the BS and ISO test standards manufacture smaller test specimens  
225 than specified in the ASTM standard. They may either be fabricated individually, or  
226 by cutting from a larger bonded panel.

227 The surface pretreatment applied to the substrates prior to bonding is an important  
228 aspect of joint preparation. Usually the intention is to avoid interfacial crack growth  
229 between the adhesive and the substrate and as such, a surface pretreatment is carried  
230 out on the substrates prior to bonding. This may involve simply cleaning the surfaces  
231 to remove contaminants such a mill oils, greases, or release agents, but may  
232 additionally involve abrasion and/or a more detailed surface pretreatment incorpo-  
233 rating acid etching or anodizing in the case of metallic substrates and plasma or  
234 corona treatments in the case of polymeric substrates. Readers are referred to specific  
235 procedures for surface pretreatments prior to adhesive bonding (see ► Chap. 8,  
236 “Surface Treatments of Selected Materials” and BSI 2009) and a number of excellent

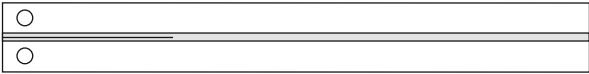


**Fig. 2** Mode I double cantilever beam (DCB) adhesive-joint specimen

review publications on this subject, for example, Molitor et al. (2001), Baldan (2004), and Bishopp (2005).

Once the substrates have been prepared, the adhesive layer is applied to the joint. If film adhesive is being used, the films are cut to size and applied to the substrates. The substrate can often be used as a cutting template in this procedure. The thickness of the adhesive layer applied to the joint is another important parameter. The thickness may be obtained using a single layer of film (applied to one substrate only), or may be obtained by using two or more film layers stacked inside the joint. For example, two layers of film are achieved by placing a single film layer on each substrate, four layers of film are achieved by placing two layers per substrate, etc. It should be noted that in most industrial applications using film adhesives, only a single layer of film is applied to the joint, and that stacking of multiple film layers may result in effects not seen when only single layers are used. If paste adhesives are being used, it is necessary to apply an adhesive bead to each substrate (or panel) and typically this is spread over the surface area of the substrates prior to closing the joint. Shims may be placed at either end of the joint to control bondline thickness, or ballotini (glass spheres) may be added or mixed into the adhesive paste formulation.

Once the joint is formed, the adhesive is cured according to the manufacturer's instructions. Adhesive data sheets usually specify a recommended cure schedule (temperature and time) and often a recommended pressure to be applied to the joint. Sometimes a range of cure schedules are quoted. It is important to ensure that the adhesive layer (as opposed to just the oven or even the jigging) reaches the cure temperature for sufficient time for full cure to be achieved. Massive jigs and large metallic substrates can very much increase the thermal inertia of the joint and the time taken for full cure to be achieved. A thermocouple wire placed in one end of the bondline can be used to confirm the thermal history of the adhesive layer during manufacture. When the cure is complete, the joints are removed from the jig and the adhesive fillets are removed to make a joint with smooth sides.

The DCB test requires that the initial crack in the joint introduced by the presence of the disbond or releasing film be extended by applying a load to the substrates. The load can be introduced via circular holes drilled through the end of the substrates, or via circular holes through the center of metallic load blocks bonded to the ends of each arm. In the ASTM method, load is applied until crack growth occurs, at which point the loading is stopped until the crack length stabilizes. The load is then increased until the crack grows again and this process is repeated a number of times. Repeated values of the load to initiate crack growth and for crack arrest are thus recorded, together with the corresponding crack lengths. In the BS and ISO methods, the loading is applied at a constant applied displacement rate until the crack initiates, at which point the loading is stopped and the specimen is fully unloaded. This is the precracking stage. The specimen is then reloaded at constant applied displacement rate. In this cycle, the crack initiates from the mode I precrack formed previously. This is the testing stage. After a specified length of crack propagation, the joint is fully unloaded. Both the loading and unloading force-displacement traces are recorded via analog or digital means. The resistance to both crack initiation from the precrack and for steady-state crack propagation is determined.

Upon unloading the joint, the force–displacement trace not returning to the origin may indicate that plastic deformation of the substrates has occurred; see ISO (2009) for full procedures. Such an occurrence would invalidate the values of  $G_{Ic}$  determined. The presence of stick-slip crack propagation in the continuously loaded BS or ISO methods requires some special considerations to be taken into account. Again, full details are provided in ISO (2009). Under these conditions, steady-state propagation values of  $G_{Ic}$  are not determined, instead values at crack initiation and crack arrest are obtained.

The fracture tests developed for modes I, II, and mixed-mode I/II loading require the measurement of the load, load-point deflection, and usually crack length together with some beam dimensions (e.g., thickness and width) and sometimes Young's modulus of the substrate. The use of the  $G$  rather than the  $K$  parameter has become common place for adhesive joints. The analysis methods referred to here assume that the adhesive layer makes negligible contribution to the overall compliance of the joint. The analysis schemes proceed by either using experimental compliance methods or by using simple or corrected beam theory. The fracture resistance in any mode may be determined using the Irwin–Kies equation:

$$G_c = \frac{P^2}{2B} \cdot \frac{dC}{da}, \quad (7)$$

and then the analysis proceeds by experimentally determining  $dC/da$  (experimental compliance methods) or by modeling the  $C(a)$  function using beam theory. The beam theory approach requires corrections to be implemented to take account of the ways in which the test specimens differ from the “simple beams” assumed in the analysis. Thus, “corrected beam theory” analyses are commonly employed.

The analysis methods developed assume that the adhesive layer is thin and that the adhesive has a low value of Young's modulus compared to the substrate material. Thus, the contribution of the adhesive layer to the overall beam compliance is assumed to be negligible. In the ASTM method for mode I (ASTM 1990),  $G_{Ic}$  is determined using simple, shear-corrected beam theory:

$$G_{Ic} = \frac{4P^2m}{E_sB^2}, \quad (8)$$

where  $P$  is the load,  $E_s$  is the axial modulus of the substrate,  $B$  is the substrate width, and  $m$  the geometry factor given by:

$$m = \frac{3a^2}{h^3} + \frac{1}{h}, \quad (9)$$

where  $a$  is the crack length and  $h$  is the height of one substrate. The first term in the above expression represents the contribution to the displacement from bending, and the second term the contribution from shear. The rationale for presenting the analysis in this form was that an alternative test specimen was identified with a constant value

of the geometry factor, making the values of  $G_{Ic}$  independent of crack length (see Sect. 3.2). However, a limitation of this approach is that the bending analysis assumes the DCB arms to behave as perfectly built-in cantilevers. Such an assumption can lead to significant errors, although the  $G_{Ic}$  values deduced in this way are usually conservative. The corrected beam theory analysis for the DCB test was initially outlined by Williams (1988) and was applied to fiber-reinforced polymer composites (Hashemi et al. 1990) and was shown to be valid for adhesively bonded joints (Blackman et al. 1991). During the development of a standardized DCB test for adhesively bonded joints via the British Standards Institution and ISO, a series of interlaboratory round-robin tests were performed on adhesively bonded joints using various substrate materials. The results of this program demonstrated the utility and reproducibility of the test method (Blackman et al. 2003b).

In the BS and ISO methods, additionally an experimental compliance and a corrected beam theory analysis are specified for the determination of  $G_{Ic}$ . The experimental compliance method is based on Berry's method (Berry 1960) and is given by:

$$G_{Ic} = \frac{nP\delta}{2Ba}, \quad (10)$$

where  $P$  is the load,  $\delta$  the displacement,  $B$  the specimen width, and  $a$  the crack length. The parameter,  $n$ , is determined from a linear regression to the log compliance versus log crack length data, recorded during the test. The corrected beam theory method is given by:

$$G_{Ic} = \frac{3P\delta}{2B(a + \Delta)} \frac{F}{N}, \quad (11)$$

where  $\Delta$  is the crack length correction term, accounting for the beam root rotation and deflection effects (incorporating those due to shear);  $F$  is a large-displacement correction factor (accounting for the shortening of the moment arm as the substrates deform elastically in bending); and  $N$  is a correction factor applied if end blocks are used (to account for the potential stiffening effect of the blocks and their rotation). The round-robin interlaboratory test program (Blackman et al. 2003b) indicated that the experimental compliance and corrected beam theory analyses yield  $G_{Ic}$  values in close agreement.

The definition of crack initiation has been a contentious issue in the formation of the DCB test standards. In line with the mode I test published for fiber-reinforced polymer composites (ISO 2001), three different definitions of crack initiation have been established and are now embodied in the BS and ISO standards. The first relates to the instant when the load–displacement trace deviates from linearity. This definition is termed the nonlinear (NL) initiation point. The second relates to the point when the crack is seen to grow ahead of the initial precrack. This definition is termed the visual (VIS) initiation point. Third, in line with earlier fracture mechanics test standards, initiation has also been defined as corresponding to when the initial

compliance of the test specimen has increased by 5%. This is termed the 5% offset value. To limit the potential magnitude of this value, it is a requirement that it precedes the point of maximum load. This initiation point is therefore called the Max/5% initiation point; the value taken is the one occurring first (the max point or the 5% offset point).

Various studies, for example, Blackman et al. (2003b), have shown that the nonlinear definition of crack initiation usually results in the lowest initiation values of  $G_{Ic}$  and is subject to the largest degree of scatter. Indeed, there is evidence to suggest that this point corresponds to the initial growth of the crack across a limited section of the joint width and as such NL values of initiation may not be true  $G_{Ic}$  values. The visual initiation point is more popular but remains operator sensitive, depending upon such factors as the magnification of the traveling microscope or video camera used to measure the crack length and eye sight! The Max/5% initiation point is usually the least conservative and the most reproducible.

In the continuously loaded DCB test (ISO 2009), the steady-state propagation value of  $G_{Ic}$  is the value most commonly reported in the research literature. When, following crack initiation, the values of  $G_{Ic}$  do not tend to change significantly with increasing crack length, a flat resistance curve (R-curve) results. In this case, the mean propagation value of  $G_{Ic}$  can be deduced from an average of the propagation points and is termed  $G_{Ic}$ -mean propagation. However, when following crack initiation, the values of  $G_{Ic}$  increase with increasing crack length, this is referred to as rising R-curve behavior and the determination of a characteristic “propagation” value becomes more difficult to define. If a constant, steady-state propagation value is eventually reached, then this may be defined as a plateau value of  $G_{Ic}$  and may be termed  $G_{Ic}$  plateau. If the R-curve continues to rise and fails to reach a steady state, it may be beneficial to manufacture a longer test specimen such that a steady state might be reached. If continuously rising R-curve behavior cannot be avoided, and thus a steady state is not achieved, the significance of the  $G_{Ic}$  values measured become questionable and great care is required in the interpretation of such data. Figure 3 shows the R-curve behavior for a typical brittle epoxy adhesive.  $G_{Ic}$  has been determined using simple, shear-corrected beam theory (SBT), which shows an apparent rising R-curve, but when calculated using either corrected beam theory (CBT) or the experimental compliance method (ECM), the variation in  $G_{Ic}$  with crack length largely disappears resulting in a flat R-curve being measured. In this case, the mean propagation value of  $G_{Ic}$  was approximately 380 J/m<sup>2</sup>. This type of flat R-curve behavior is typical for many structural epoxy adhesives tested in mode I.

Another commonly encountered feature of mode I DCB testing is the occurrence of nonsteady, discontinuous crack growth behavior. This is usually referred to as stick-slip crack propagation as the crack grows in a series of rapid bursts, interspaced by periods of crack arrest. The reasons for such crack growth behavior are complex but are thought to originate from an imbalance between the resistance of a crack to initiation versus its resistance to continued propagation. This imbalance results in there being an excess in available strain energy in the specimen arms once the crack has initiated, resulting in an unstable burst of growth. (This concept is analogous to that of static vs. kinetic coefficients of friction.) A consequence of stick-slip behavior



**Fig. 3** Typical resistance curve (*R*-curve) for a DCB specimen bonded with a brittle epoxy adhesive ( $G_{Ic}$  values have been deduced using simple beam theory (*SBT*), corrected beam theory (*CBT*), and the experimental compliance method (*ECM*))

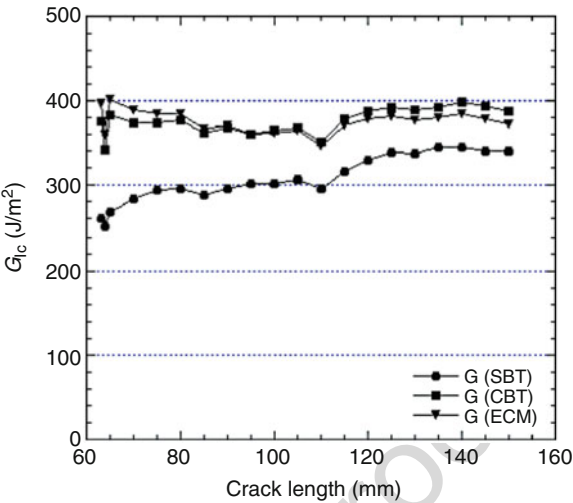
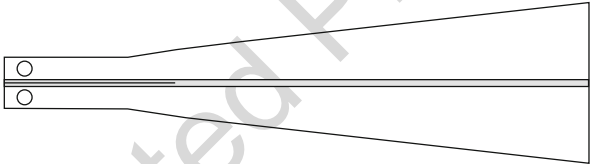


**Fig. 4** Mode I tapered double cantilever beam (*TDCB*) test specimen



is that it is not possible to record crack growth increments every 5 mm as required in the standard. However, a series of initiation and arrest points can be identified in the force–displacement traces and the crack lengths associated with the “stick” and “slip” points can frequently be identified on the fracture surfaces. The mode I DCB standards require that only the stick points (i.e., the initiation points) be used for the analysis to determine  $G_{Ic}$  values and that all the slip points (i.e., the arrest points) be disregarded. The rationale for disregarding the arrest points is that these points are influenced by such factors as the kinetic energy in the moving substrate arms and as such the arrest points are substrate dependent. When stick-slip crack growth occurs, the use of simple beam theory is recommended.

### 20.3.2 The Mode I Tapered Double Cantilever Beam (TDCB) Test

The tapered double cantilever beam (TDCB) adhesive-joint specimen was initially developed as a means to perform long-term, environmental crack growth studies, without the need to measure crack length (Ripling et al. 1964). The height of the beam is tapered to provide a constant rate of change in compliance with crack length, that is, the value of  $dC/da$  is a constant. The TDCB joint is shown in Fig. 4. An advantage of the TDCB test specimen is that the increasing height provides a greater resistance to plastic deformation in the specimen arms as the increased height



reduces the applied bending stresses in the arms. As such, it may be easier to maintain LEFM conditions in joints using the TDCB rather than the DCB specimen. However, the TDCB specimens are more expensive to manufacture; the nonlinear height profile is best achieved using a computed numerically controlled (CNC) milling machine. The mode I standards describe corrected versions of the analysis to deduce  $G_{Ic}$  values from the TDCB test, which take into account (1) the effects of the discontinuous profile used in the joints and (2) the beam root rotation effects in the joint. The original TDCB analysis assumed that the taper continued all the way back to the loading point, where a zero beam height would be implied. The analysis proceeds as follows. Values of  $G_{Ic}$  are determined using simple beam theory via:

$$G_{Ic} = \frac{4P^2m}{E_sB^2}, \quad (12)$$

where  $P$  is the load,  $E_s$  the substrate modulus,  $B$  the substrate width, and  $m$  the geometry factor defined previously. A more accurate, corrected beam theory analysis has been developed, which may be applied to the data (Blackman et al. 2003a). Using corrected beam theory, values of  $G_{Ic}$  are determined via:

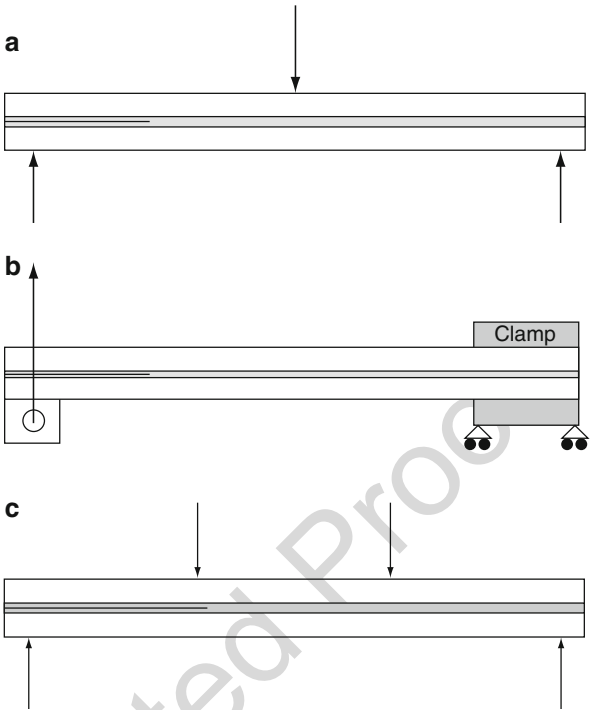
$$G_{Ic} = \frac{4P^2}{E_sB^2} \cdot m \cdot \left[ 1 + 0.43 \left( \frac{3}{ma} \right)^{\frac{1}{3}} \right], \quad (13)$$

where the second term in square brackets represents the correction for the beam root rotation effects. It should be noted that this more accurate expression requires the crack length,  $a$ , to be determined during the test. Finally, the values of  $G_{Ic}$  can be deduced directly from Eq. (7) as the value of  $dC/da$  is a constant for this test geometry and the value can be deduced from a linear regression of the measured compliance versus crack length data. When using beam theory to determine  $G_{Ic}$  for an adhesive joint, it is important to check that the geometry factor  $m$  is indeed a constant along the length of the substrate over which it is tapered. It is also important to ensure after the test that the substrates have not deformed plastically, as such deformation would violate the assumptions of linear-elastic fracture mechanics. Any plastic deformation may be observed in the substrates after the test via careful visual inspection, or may be evident from the load–displacement traces not returning to the origin upon unloading the joint.

### 20.3.3 Mode II Adhesive-Joint Tests

The mode II fracture testing of adhesive joints is significantly more complex than mode I testing and is yet to be standardized. The later development of mode II fracture tests reflects a greater skepticism held within the scientific community regarding the significance and uniqueness of mode II fracture. Such skepticism was well voiced by O'Brien in his "Shear measurement or Sheer Myth?" paper on

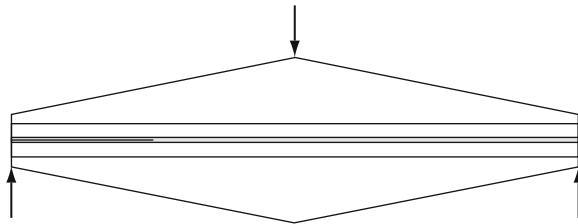
**Fig. 5** (a) Mode II, end-notched flexure (ENF) test specimen. (b) Mode II, end-loaded split (ELS) test specimen. (c) Mode II, four-point loaded end notched flexure (4-ENF) test specimen



mode II (O'Brien 1998). Despite the arguments that still exist surrounding the origins, true meaning, and uniqueness of mode II fracture, there is clearly a need to characterize how joints fail when mode II loading is applied to a joint, and there is a corresponding need to determine the fracture resistance in mode II.

In pursuit of this measurement, a number of different tests have been proposed and used by various researchers to obtain mode II fracture in adhesive joints. However, to date, no single method has proved entirely satisfactory. The most popular tests used have been the end-notch flexure (ENF) test (Fig. 5a), and the end-loaded split (ELS) test (Fig. 5b). Both of these are currently under consideration for standardization of mode II delamination toughness testing in fiber-reinforced polymer composites, and they have also been applied to study the fracture of structural adhesive joints. In both cases, a nonadhesive insert film is placed in the center of the adhesive layer during the manufacture of the joint and this then acts as the crack starter in the subsequent mode II test. The ENF test was used by Chai in his detailed study of mode II fracture in adhesive joints (Chai 1986, 1988). The ELS test requires the test specimen to be clamped on a linear bearing trolley which is free to slide in a horizontal direction. The specimen can be designed such that stable crack growth is achieved following initiation. The sliding trolley removes the horizontal forces which would otherwise develop during the test. In the ELS test, the specimen is loaded vertically via a load-block, and the load, beam displacement, and crack length are measured during the test. In the ENF test, the specimen is loaded in simple

**Fig. 6** Mode II, tapered end-notched flexure (TENF) test specimen



three-point bending and the position of the initial crack is usually such that  $a/L = 0.5$ , the specimen is centrally loaded, and the support span is  $2L$ . A disadvantage of the ENF test is that the fracture tends to be unstable, with the crack growing instantly to the central loading point after initiation, that is, to  $a = L$ . Thus, only an initiation value of  $G_{IIc}$  is determined, whereas a complete R-curve may be obtained from the ELS test.

A version of the ENF test using four-point loading was described by Martin and Davidson (1999) for composite delamination (Fig. 5c) and this has also been applied to adhesive joints. This test is commonly referred to as the 4-ENF test, and it has the advantage that stable fracture is achieved, circumventing the limitation in the conventional 3-ENF test. However, a limitation is that the test requires larger forces to be applied, and as a consequence, the frictional forces acting on the faces of the initial and subsequently grown fracture surfaces are greater than in the 3-ENF. As work is done against friction as the substrates shear relative to one another, then this leads to an increase in the “apparent” value of  $G_{IIc}$  that is determined.

Measuring crack length in a mode II test has posed significant difficulties. No beam opening occurs and shear fractures usually propagate in a complex manner, often via a microcracking mechanism. The experimental uncertainty associated with the measurement of the crack length in mode II can be significant. Some researchers have tackled this problem by using height contoured beams for substrates. The development of tapered ENF (TENF) specimens (Fig. 6) has been reported by some researchers, for example, Edde and Verreman (1995) and Qiao et al. (2003a, b), but their use has not become widespread.

A modified version of the ELS test has been under development in Europe, led by the European Structural Integrity Society’s Technical Committee 4 (ESIS/TC4) on Polymers, Composites, and Adhesives. An interlaboratory round-robin test program investigated the use of the ELS test using an effective crack length approach. In the effective crack length approach, there is no need to measure mode II crack lengths: rather the crack length is determined by changes in compliance in the specimen. The use of such procedures (Blackman et al. 2005) requires that the clamp used in the test be calibrated, such that the measured compliance can be accurately converted to crack length. There has been significant recent interest in effective crack length approaches with the concepts being extended to model damage zones in mode I, to analyze mixed-mode loading (see below), and also in fatigue crack growth studies (Brunner et al. 2009).

Summarizing the analysis methods for mode II, for the ELS test,  $G_{IIc}$  can first be determined from experimental compliance. If the relationship between compliance and crack length is assumed to be of the form:

$$C = C_o + ma^3, \quad (14)$$

where  $C$  is the compliance,  $a$  the crack length, and  $C_o$  and  $m$  are constants, then on substitution into Eq. 7:

$$G_{IIc} = \frac{3P^2 a^2 m}{2B}. \quad (15)$$

Second, simple beam theory can be applied, which leads to:

$$G_{IIc} = \frac{9P^2 a^2}{4B^2 h^3 E_s}, \quad (16)$$

where  $E_s$  is the substrate modulus. Third, corrections to this equation lead to:

$$G_{IIc} = \frac{9P^2 (a + \Delta_{II})^2}{4B^2 h^3 E_s} \cdot F, \quad (17)$$

where  $\Delta_{II}$  corrects for crack tip rotation, deflection, and shear effects, and  $F$  corrects for large beam displacements (Davies et al. 2001). It is noteworthy that all three analysis schemes require a measured crack length and indeed the experimental compliance method is most sensitive to measured crack length errors due to the dependence of  $m$  upon crack length.

Considering the 3-ENF test, first  $G_{IIc}$  may be deduced using the experimental compliance method. If a relationship between the compliance and crack length is assumed of the form:

$$C = C_o + C_1 a^3, \quad (18)$$

then

$$G_{IIc} = \frac{3P^2 a^2 C_1}{2b}. \quad (19)$$

Second, via simple beam theory:

$$G_{IIc} = \frac{9P^2 a^2}{16B^2 E_s h^3}. \quad (20)$$

And third, via corrected beam theory (Hashemi et al. 1990)

$$G_{IIc} = \frac{9P^2(a + \Delta_{II})^2}{16B^2h^3E_s} \cdot F. \quad (21)$$

The data reduction reported for the 4-ENF test uses an experimental compliance approach (Martin and Davidson 1999). For this test, the compliance is assumed to be a linear function of crack length, that is:

$$C = C_o + ma, \quad (22)$$

and thus  $dC/da$  is given directly by  $m$ , hence:

$$G_{IIc} = \frac{P^2}{2B} \cdot m. \quad (23)$$

The data reduction for the tapered ENF (TENF) specimen can take the form of an experimental compliance or a simple beam theory approach, as reported by Edde and Verreman (1995) or a corrected beam theory approach following the work of Qiao et al. (2003b), using a beam on an elastic foundation model. These authors showed that substrates with a linear taper gave an almost linear relationship between compliance and crack length, within a certain range of crack lengths.

The ELS method may be employed together with an effective crack length approach to circumvent the need to measure crack length in the test (Blackman et al. 2005). This requires a calibration of the clamping fixture by use of the so-called inverse ELS test. In this procedure, the test specimen is fixed in the clamp with the cracked portion of the specimen held fully within the clamp. The free length is varied through a range and the values of  $C^{1/3}$  are plotted against the free length,  $L$ . Such plots are usually linear, with a negative intercept on the  $L$  axis which is termed  $\Delta_{\text{clamp}}$ , as shown in Fig. 7. In the ensuing mode II fracture test, the effective crack length is determined for each experimentally determined value of compliance using beam theory and an independently measured value of substrate modulus. Using this scheme, the effective crack length is given by:

$$a_e = \left[ \frac{1}{3} \left\{ 2Bh^3E_sC - (L + \Delta_{\text{clamp}})^3 \right\} \right]^{\frac{1}{3}}, \quad (24)$$

and the mode II fracture resistance is then given by:

$$G_{IIc} = \frac{9P^2a_e^2}{4B^2h^3E_s}. \quad (25)$$

545

As discussed above, this scheme has the advantage of being independent of measured crack length. When the above analysis scheme is used, many adhesives

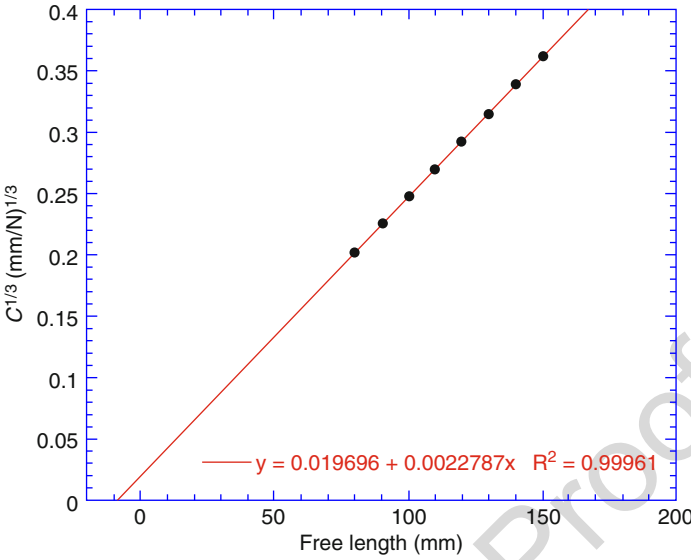


**Fig. 7** Graph of  $C^{1/3}$  versus clamp length in the inverse ELS clamp calibration procedure (The negative  $L$  intercept gives the value of the clamp correction,  $\Delta_{\text{clamp}}$ )

exhibit strong rising R-curve behavior in mode II. This is thought to be due to the development of the damage zone and microcracking of the adhesive layer. Usually,  $G_{\text{IIc}}$  values lie in the range of  $\times 1-2G_{\text{Ic}}$  for crack initiation, and then rise to as much as  $\times 7G_{\text{Ic}}$  during crack propagation (Blackman 2008). Table 1 shows some typical values of  $G_{\text{Ic}}$  and  $G_{\text{IIc}}$  reported in the literature for various adhesive joints.

**20.3.4 Mixed-Mode I/II Adhesive-Joint Tests**

In addition to pure modes I and II testing, there is considerable interest in determining the fracture resistance of joints subject to mixed-mode (I/II) loading as adhesive joints in engineering structures will frequently experience such mixed-mode conditions in service. There has also been a significant effort in the literature directed toward developing mixed-mode failure criteria for adhesively bonded joints, such that fracture resistance envelopes might be predicted if the resistance to the pure modes is known.

The experimental tests developed to measure mixed-mode fracture resistance use similar test specimens to the pure mode I and II tests, often developed originally from composite delamination tests. Some are shown schematically in Fig. 8. Test methods include the fixed-ratio mixed-mode (FRMM) test, also known as the asymmetric double cantilever beam (ADCB) test; the mixed-mode flexure (MMF) test (also known as the single leg bend test); and the mixed-mode bending (MMB)

t.1 **Table 1** Values of  $G_{Ic}$  and  $G_{IIc}$  reported in the literature for various adhesive joints

t.2	Adhesive and manufacturer (reference)	Substrate material and adhesive thickness where known	J/m <sup>2</sup>	
			$G_{Ic}$	$G_{IIc}$
t.4	Epoxy Cybond 4523GB	AA (7075-T6)	213 ± 19	577 ± 68
t.5	American Cyanamid (Fernlund and Spelt 1994)	$h_a = 0.4$ mm		
t.6	Epoxy ESP310	AA (7075-T6)	794	5,605
t.7	Permabond (Papini et al. 1994)			
t.8	ESP110, Bondmaster Plc, UK (Blackman et al. 2005)	CFRP	945 ± 28	2,672 ± 534 <sup>a</sup>
t.9		$h_a = 0.4$ mm		4,280 ± 128 <sup>b</sup>
t.10	FM300, American Cyanamid (Liechti and Freda 1989)	AA	1,120	1,400
t.11	AF126, 3M Inc. (Blackman et al. 2005)	CFRP	1,449 ± 113	1,624 ± 520 <sup>a</sup>
t.12		$h_a = 0.08$ mm		3,381 ± 372 <sup>b</sup>
t.13	Dow Betamate 4601	AA (5754-0) – no surface treatment	2,657	3,229
t.14	Essex Speciality Products (Liu et al. 2002)			
t.15		$h_a = 0.254$ mm		
t.16	Epoxy, Goodrich (Swadener et al. 1999)	GFRP	4,000	4,000

t.17 Notes: AA, aluminum alloy;  $h_a$ , adhesive layer thickness, where known  
<sup>a</sup> $G_{IIc}$  at crack initiation (defined as a 5% change in initial compliance of the joint)  
<sup>b</sup>Mean plateau value of  $G_{IIc}$  measured on the  $R$ -curve

567 test. As the name implies, the FRMM test provides a single mixed-mode ratio of  $G_I/$   
568  $G_{II} = 4/3$  for a joint with equal thickness substrates. The same ratio is achieved with  
569 the MMF test. However, the MMB test provides the option to change the mixed-  
570 mode ratio almost without limit between the pure mode I and pure mode II loading  
571 conditions, as the upper two loads are applied via a lever arrangement. This test is  
572 now standardized by ASTM for mixed-mode delamination testing (ASTM 2004b).  
573 In addition to the tests listed above, various other fixtures have been employed to  
574 obtain mixed-mode loading conditions including use of the ARCAN loading fixture,  
575 and other variable mode-mix loading frames, for example, as reported in Fernlund  
576 and Spelt (1994).

577 As with mode II, a common feature of mixed-mode testing is that the failure path  
578 is usually not in the center of the adhesive layer, but deviates to run close to the  
579 interface with the upper substrate. It has been shown that this makes only a very  
580 small difference to the applied mixed-mode ratio, but the locus of failure being close  
581 to an interface may have other effects on the test (Dillard et al. 2009). It is interesting  
582 to note that such studies highlight that profound effects can be observed if the mode  
583 mix alters the path taken by the crack. A fracture path between the adhesive and the  
584 carrier in a film adhesive, or within a polymeric fiber-composite substrate, can have a  
585 significant and deleterious effect on the fracture resistance of a joint.

586 Assuming that the failure path remains essentially the same (e.g., cohesive in the  
587 adhesive layer), it is usually observed that the fracture resistance increases as the

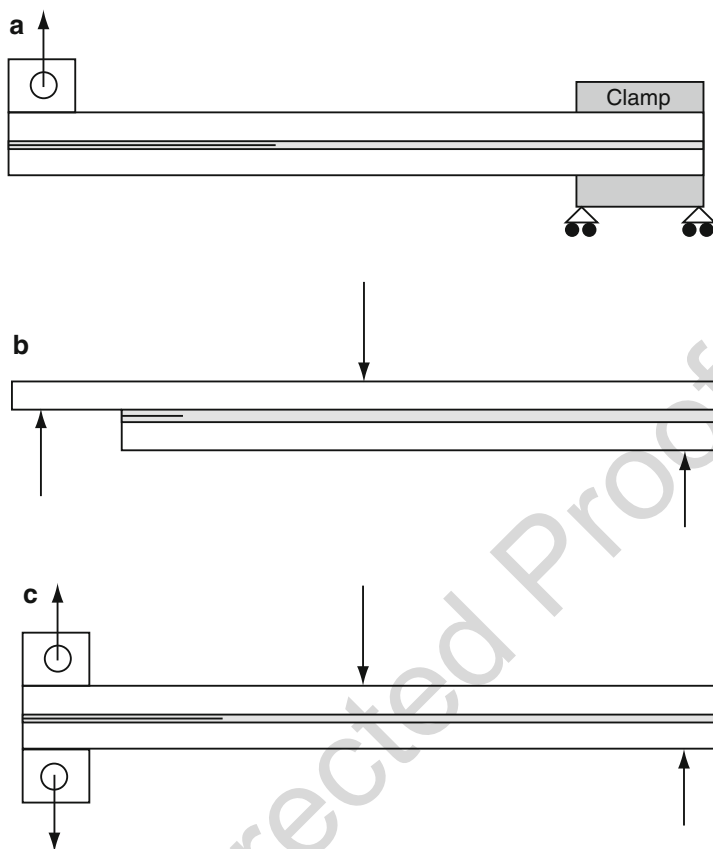


**Fig. 8** (a) The fixed-ratio mixed-mode (*FRMM*) test specimen. (b) The mixed-mode flexure (*MMF*) test specimen. (c) The mixed-mode bend (*MMB*) test specimen

percentage of mode II increases. This is consistent with the notion that  $G_{Ic}$  represents the lower bound value of fracture resistance and that additional mechanisms come into play as the mode II loading contribution is increased. Such mechanisms include the increased friction contribution, the increased elongation and distortion of the damage zone ahead of the crack tip, the increase in microcracking, and the ensuing shear failure of the ligands between such features should these be present. Many different failure criteria have been proposed to model mixed-mode fracture envelopes for adhesive joints and many of these criteria were initially developed for the delamination of composites. Reeder (1993) and Dillard (2010) have reviewed a number of these criteria. The criteria tend to be phenomenological in nature and reasonable modeling of the envelopes can often be achieved provided the failure path remains unchanged. Simple criteria developed include the linear, the bilinear, and the linear interaction criteria. More complex interaction criteria have also been developed. This is still an evolving research area.



### 20.3.5 Effects of Adhesive Layer Thickness

In all the fracture tests described above, the values of  $G_c$  determined can depend upon the thickness of the adhesive layer. The dependence of adhesive layer (or bondline) thickness,  $h_a$ , was discussed by Kinloch (1987) where the dependence of  $G_{Ic}$  values on  $h_a$  in TDCB joints bonded with epoxy adhesives was described. Such tests revealed that for a brittle adhesive, the values of  $G_{Ic}$  were insensitive to bondline thickness, but a strong dependence was observed for tougher adhesives, with values increasing to a maximum before reaching a plateau. The trends may be rationalized by a consideration of the plastic zone size,  $r_p$ , at the crack tip. Under plane stress conditions (as exist at the edges of the joint), the value of  $r_p$  is given by:

$$r_p = \frac{1}{2\pi} \cdot \frac{EG_c}{\sigma_y^2}, \quad (26)$$

where  $E$  is Young's modulus of the adhesive and  $\sigma_y$  its yield strength. Under plane strain conditions (as exist at the center of the joint), the value of  $r_p$  is given by:

$$r_p = \frac{1}{6\pi} \cdot \frac{EG_c}{\sigma_y^2}. \quad (27)$$

When the value of  $h_a$  is too small to allow for the full development of the plastic zone, then  $G_c$  is dependent upon  $h_a$ . Clearly, brittle adhesives (low  $G_c$ , high  $\sigma_y$  values) will have smaller values of  $r_p$  and will be less likely to show the dependence of  $G_c$  upon  $h_a$ . The ISO standard for mode I testing (ISO 2009) gives some recommendations for selection of values of  $h_a$ . First, the analysis has only been verified experimentally for values of  $h_a$  between 0.1 and 1.0 mm, so ideally bondlines should be selected within this range. Second, as the usual goal is for  $G_{Ic}$  to be independent of specimen geometry, then values of  $h_a > 2r_p$  should ideally be selected.

The dependence of  $G_{Ic}$  (and also  $G_{IIIc}$ ) upon bondline thickness was observed by Chai (1986, 1988) who noted that values of  $G_{Ic}$  and  $G_{IIIc}$  were also dependent upon bondline thickness for brittle adhesives. Adhesive layer thickness should therefore be considered carefully when designing adhesive-jointed structures and test coupons.

## 20.4 Peel Testing

### 20.4.1 Introduction to Peel Testing

The adhesive-joint fracture tests discussed above have been concerned with joints formed between substrates that deform in a linear-elastic manner during the loading of the joint such that the concepts of linear-elastic fracture mechanics apply. Such tests are used routinely to measure fracture energy,  $G_c$ . However, there is also a

requirement to be able to measure the performance of adhesive joints formed between substrates that may deform extensively during an adhesion test. Examples include the adhesion of flexible layers such as food packaging laminates, electronic components, and the structural bonding of relatively thin sheet metal in the automotive industry. In his forward to the special issue on peel in the *International Journal of Adhesion and Adhesives* (Moore 2008), Moore distinguished between two general types of peel test, namely, those that are dependent upon geometry and those that are geometry independent. Geometry-dependent peel tests are numerous and these typically measure the peel force per unit width of joint, commonly called the peel strength. Geometry-independent peel tests, on the other hand, measure a geometry-independent parameter such as fracture energy,  $G_c$  with units  $\text{J/m}^2$ . Using fracture mechanics and the concept of energy balance, significant progress has been made in recent years toward the goal of developing and refining geometry-independent peel tests (Kinloch et al. 1994; Kinloch and Williams 2002). At least in principle, a peel test can now be used to determine the adhesive fracture energy of a joint even when extensive plastic deformation of the peel arm(s) has occurred during the test.

#### 20.4.2 Geometry-Dependent Peel Tests

As discussed by Moore (Moore 2008), several peel test configurations have been developed over the years and many developments and modifications to these have been variously proposed in the literature. It is not the aim of the present chapter to review these techniques, but rather the aim here is to identify some of the main types of peel test that fall into this category and discuss their advantages and their limitations.

In the so-called fixed-arm peel tests, one substrate is fixed to a rigid base (the rigid substrate) and the other (the flexible substrate) is peeled by a test machine at a defined applied peel angle, which can be varied between tests. Figure 9a shows a schematic fixed-arm peel test. Standardized peel tests describe both  $90^\circ$  and  $180^\circ$

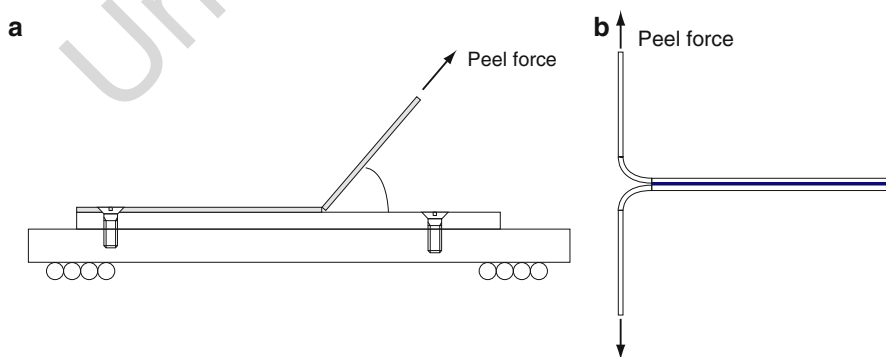


**Fig. 9** (a) The fixed-arm peel test arrangement and (b) the T-peel test arrangement

fixed-arm peel tests (BSI 1993a, b), but the peel angle can be varied typically from 45° to 180°. Peel tests are typically performed at a constant rate of peeling and the standards specify such details as the width, thickness, and width–thickness ratio of the substrates. The apparatus used to control the peel angle is also described in the various standards, for example, by attaching the peel arm to a cylinder mounted on bearings that is then rotated to create the peel. A floating roller and a climbing drum apparatus are specified in two tests that have been standardized by ASTM (2004a, 2006). The average peel force per unit width (the peel strength) is reported. For the peeling of two flexible substrates, the T-peel test is often adopted. In the T-peel test, the two flexible substrates are bonded over part of their length and the unbonded ends are peeled at 180° and the peel strength is determined as above. A T-peel test has been standardized (BSI 2005). It is common for the substrates in a T-peel test to take up an asymmetric profile when the failure path runs along one adhesive–substrate interface. The T-peel can then become a “Y-peel” as the local peel angle differs from the 180° peel angle applied. In such cases, the effective peel angle between the bonded portion of the joint and the load-line should be measured. For the peeling of two rigid substrates a fixture such as the floating roller peel test can be used. Such a fixture incorporates two rollers, and the peel arm is forced through the rollers at constant speed such that it slides on the roller and curves through a defined angle during peel. Again, the average peel force per unit width is measured and reported as the peel strength.

Clearly, while comparative measurements can be made using the above types of peel test, the results obtained will depend upon such factors as the mechanical properties of the peel arms, their thickness, and also upon such factors as the applied peel angle, and the effective “local” peel angle at the peel front. Also, in a study to evaluate these different types of peel test, Kawashita et al. (2005) demonstrated that in tests such as the floating roller peel test, frequently the peel arm does not conform to the roller geometry. This was identified using a modified and partially cutaway apparatus, which allowed the conformation to be evaluated. Such peel tests can be valuable to industry for the purposes of selecting a suitable adhesive for a given substrate material, for developing a surface pretreatment, or for investigating the effects of altering one test parameter (e.g., temperature, humidity or rate of peel). However, the results obtained in one peel test are rarely transferable to other geometries and have limited predictive capability. For this reason, much recent attention has been directed toward the development of geometry-independent peel tests, as is discussed in the next section.

### 20.4.3 Geometry-Independent Peel Tests

The peel strength determined in the above “geometry-dependent” peel tests is a measure of the total work done on the joint during the peeling process. Due to the plastic deformation of the peel arm(s), this total energy measure can be significantly greater than the energy required to drive a crack through the joint under linear-elastic conditions. Bearing this in mind, it is easy to see how peel test results can be

manipulated to achieve impressive numerical results by simply changing the substrate, for example, by changing from a high yield strength aluminum alloy to pure aluminum for the peel arm, significant increases in measured peel strength can be obtained for an otherwise identical joint. Recent research activity into peel testing (Kinloch and Williams 2002) has thus focused on the development of procedures (both test techniques and analysis schemes) to isolate the energy required to fracture the peel sample, termed the adhesive fracture energy,  $G_A$ , from the total input energy to the system, termed  $G$ . The underlying energy balance is:

$$G_A = G - G_p, \quad (28)$$

where  $G_p$  represents the plastic energy dissipated in the peel arm. In, for example, the 90° fixed-arm peel test for flexible to rigid peel arms, energy is dissipated by local plastic bending of the peel arm at the peel front. Then, as the section of the peel arm forced through a tight curvature at peel front subsequently straightens out, there is further, reversed plastic bending in the arm. In addition, there may be sufficient tension in the peel arm to exceed the yield strength of the substrate and hence there is additional tensile plastic energy dissipation in the joint. Thus, in the above energy balance,  $G$  is a measure of how difficult it is to peel one substrate from another in the joint whereas  $G_A$  is a measure of how well the substrates are stuck.

As described in Kawashita et al. (2006), the ESIS TC4 committee has developed a test protocol covering both the fixed-arm and the T-peel tests, together with an analysis to obtain the geometry-independent adhesive fracture energy,  $G_A$ , termed the adhesive fracture toughness in the ESIS TC4 protocol, but equivalent to the adhesive fracture energy,  $G_c$ . Because the tests require that the plastic energy dissipated in the peel arms be determined, it is also necessary to perform an additional tensile test on the peel arms. The tests developed accommodate situations where the adhesive layer thickness is negligible (e.g., when two polymer films are molded together as is common in packaging laminates) and also when the adhesive layer thickness is not negligible, that is,  $h_a > 0$ ; thus the deformation of the layers needs to be taken into consideration in the analysis. For this latter case, the tensile modulus of the adhesive material is required. This may be available from adhesive manufacturers' data sheets, otherwise a tensile test on the bulk adhesive will be needed.

In the fixed-arm peel test as shown schematically in Fig. 9, the substrates (which can be the same or different materials) are bonded along their length but excluding one section, typically 30 mm in length, which is left unbonded to allow for gripping in a test machine. The size of the test specimen and indeed the test jig to be used are not defined precisely in the ESIS protocol. The protocol permits applied peel angles in the range of 0–180° to be selected although in practice the fixed-arm peel tests are most commonly performed with an applied peel angle of 90°. The protocol additionally requires peel test to be performed at applied angles of 45° and 135°. During the development of the procedures and analysis, there was great interest in applying different peel angles to the joints, as although the total energy applied to the specimen,  $G$ , will be a strong function of applied peel angle, the adhesive fracture

toughness,  $G_A$ , should be independent of peel angle, as has indeed been shown to be the case in the round-robin tests coordinated by ESIS-TC4. Perhaps the most difficult experimental aspect of the fixed-arm peel test is ensuring that the fixed arm is (and remains) rigidly attached to the base. Also, the peel force is usually applied via the crosshead of a testing machine and the base should be fixed to a linear bearing trolley such that the specimen can slide with minimum friction during the peeling of the arm. If the fixed arm is attached to the base using an adhesive, it is important to ensure that this does not fail during the test. The fixed arms are commonly bolted to the free-sliding base. When bolts are used, it is necessary to accommodate the bolt holes in the fixed arm only at the peeling end of the joint, and through both the peel arm and fixed arm at the other end. When this is done, the second bolt is outside of the length of joint to be peeled in the test. It is also possible to use a wider fixed arm than peel arm, such that the extra width of the fixed-peel arm can be used to bolt down this arm to the sliding base.

The fixed-arm peel test is conducted at a rate of 10 mm/min when the applied angle is  $90^\circ$  and when other angles are used, then at speeds to give the same equivalent crack speed. The peel force is measured as a function of peel-arm displacement and an average force is determined over a minimum of 30 mm of peel fracture. If peel proceeds via a stick-slip mechanism, then average peel forces at initiation (cohesive fracture) and arrest (interfacial fracture) are determined separately. Figure 10 shows the steady-state peel force obtained in a fixed-arm peel test.

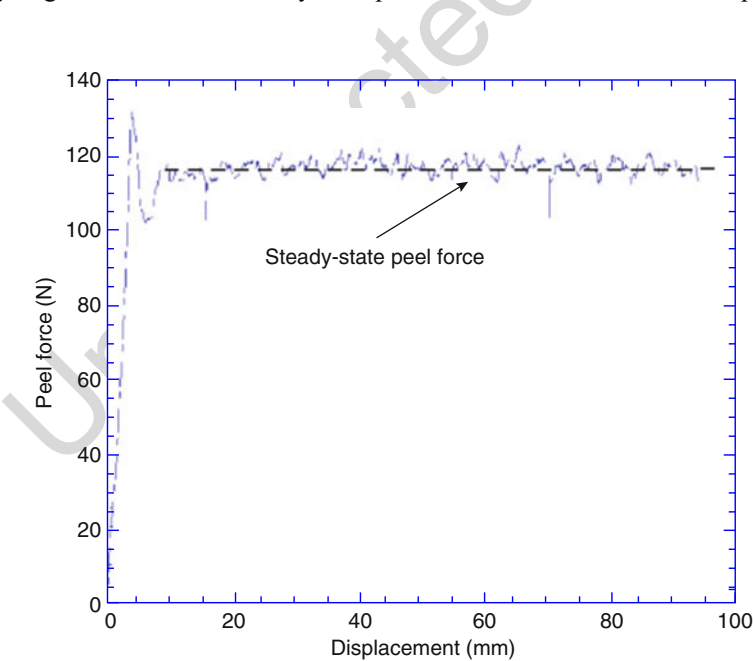


**Fig. 10** Peel force versus crosshead displacement obtained during fixed-arm peeling at 10 mm/min at an angle of  $90^\circ$ . The adhesive used was Bondmaster ESP110 and the peel arm was 0.1 mm thick aluminum

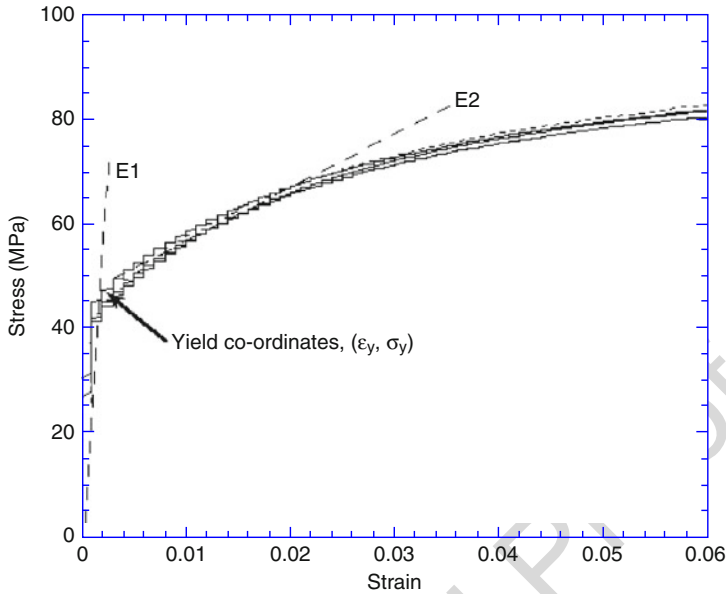


**Fig. 11** Stress–strain data obtained for an aluminum peel arm, showing the initial modulus  $E_1$ , the initial plastic modulus  $E_2$  used in the bilinear model, and the yield coordinates

In this test, an aluminum peel arm of thickness 0.5 mm has been bonded to a rigid aluminum alloy base using Bondmaster ESP110 epoxy adhesive. This was then peeled at an angle of  $90^\circ$  and at a rate of 10 mm/min.

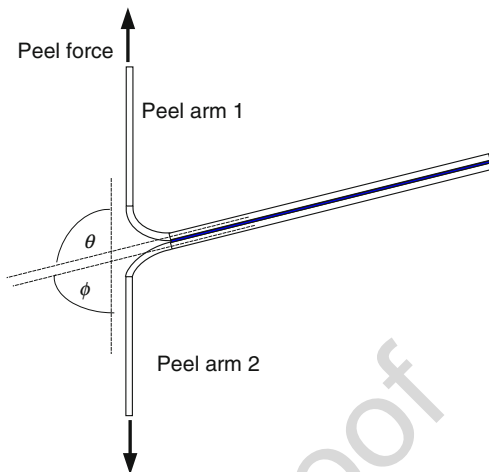
As mentioned above, in addition to the fixed-arm peel test, it is necessary to perform a tensile test on the peel arm. This is performed at the same test speed as used in the peel test. The stress–strain curve is determined. Five parameters are obtained from the tensile test, namely,  $E_1$ ,  $E_2$ ,  $\alpha(E_2/E_1)$ ,  $\epsilon_y$ , and  $\sigma_y$ . These are shown in Fig. 11. The elastic modulus ( $E_1$ ) is defined as the slope of the stress–strain curve at small deformations and before yielding has occurred. In order to define the plastic modulus ( $E_2$ ), it is suggested that the tensile specimen be allowed to continue extending for as long as possible.  $E_2$  is drawn to the slope of the initial plastic region. This straight line should be drawn approximately between the limits of  $\epsilon_y - 10\epsilon_y$ . The parameter  $\alpha$  is then given by the ratio of the two slopes,  $E_2/E_1$ . If the peel arm work hardens, a work hardening coefficient is determined from the power law:

$$\sigma = A\epsilon^N. \quad (29)$$

If the “work hardening” portion of the stress–strain curve exhibits a negative slope, then values of  $\alpha$  and  $E_2$  are set to zero (and not negative) (Moore and Williams 2007).

The plastic bending in the fixed-arm peel test can be modeled using large-displacement beam theory with modifications for plastic bending (Kinloch and Williams 2002). Much of the development of the correction procedures has focused on how the

**Fig. 12** T-peel schematic specimen showing asymmetric loading due to differing peel-arm stiffness



stress–strain behavior of the peel arm is treated. Indeed, solutions have been formulated for three cases: the various approaches investigated and adopted have been (1) the use of a bilinear model to fit the data, (2) the application of a power law, and (3) the digitization of the complete stress–strain curve. The digitization procedure provides the most accurate results but frequently the simple bilinear model of the stress–strain behavior is sufficient. The analysis of the test results is most conveniently performed using software developed at Imperial College called ICPeel. This software is freely available from the Imperial College Web site <http://www.imperial.ac.uk/meadhesion>.

Preparing T-peel test specimens is simpler than preparing fixed-arm peel specimens as there is no need to attach one substrate to a fixed base and no need for a linear bearing trolley to accommodate the specimen sliding. A typical T-peel test specimen is shown schematically in Fig. 12b. Two flexible substrates are bonded with a 30 mm disbond, as above. The substrates may or may not be of the same material. According to the protocol (Moore and Williams 2007), loading is performed at 10 mm/min. Figure 12 shows the peel angles that may be obtained in the T-peel test. If the loading remains symmetric in the test, then both the peel angles will be  $90^\circ$ . However, if the substrates are of different stiffness, or the crack runs to an interface such that the adhesive is all on one side, then the peel angles will be  $\varphi$  and  $\theta$  (rather than  $90^\circ$ ) as shown in Fig. 12. To account for the plastic work done on the substrates, a tensile test on the arms is again necessary. If the substrates are dissimilar, then tensile tests on each peel-arm material is required. The analysis of the resulting tensile test is as described above for the fixed-arm peel test.

The analysis of the T-peel test data is similar to that for the fixed-arm peel test, except that the peel arms are treated individually. Only one of the peel angles needs to be considered since  $\varphi = \pi - \theta$ . For the two peel arms individually:

$$G_1 = \frac{P}{b}(1 + \cos \phi) \text{ and } G_2 = \frac{P}{b}(1 - \cos \phi), \quad (30)$$

where subscripts 1 and 2 refer to the individual peel arms. Determining the adhesive fracture toughness,  $G_A$ , for the two peel arms individually then:

$$(G_A)_1 = G_1 - (G_P)_1 \quad \text{and} \quad (G_A)_2 = G_2 - (G_P)_2. \quad (31)$$

For the complete T-peel joint combining the individual contributions above leads to:

$$G_A = (G_A)_1 + (G_A)_2. \quad (32)$$

The main limitation of the peel tests described above is that the adhesive fracture toughness,  $G_A$ , is determined from the difference between two numbers, that is,  $G - G_P$ . When modern, structural adhesives are employed to bond the substrates, these two numbers may be large, and as a consequence, the repeatability of the  $G_A$  values determined may be poor. Recent research has investigated the application of various validity criteria for peel tests. One such criterion has been to limit the size of the plastic correction term,  $G_P$ , to a fixed percentage of  $G$ , for example, a limit of  $(G_P/G) < 80\%$  has been utilized. Another criterion proposed has been to limit the maximum strain in the peel arm.

## 20.5 Relationship Between $G_c$ (Bulk, Fracture, and Peel)

As discussed in Sect. 1, fracture tests on bulk adhesive specimens are frequently undertaken as part of the materials development process. Loading is necessarily in mode I in bulk tests as even if other loading modes are applied, the crack path will tend to deviate to run locally in mode I. Values of  $K_{Ic}$  or  $G_{Ic}$  are determined, and these relate to the toughness of the bulk adhesive. The tests are very sensitive to the initial notching conditions and the values are those associated with crack initiation (unless steady-state propagation is clearly observed in the CT specimens).

Fracture tests on adhesive joints are more complex, as the loading mode, the adhesive, the substrate, and the interface or interphase region all have an effect on the values of  $G_c$  determined. In addition, both initiation and steady-state propagation values of  $G_c$  are usually determined, allowing the resistance curve, that is, the plot of  $G_c$ , versus crack length to be drawn. Comparisons of  $G_c$  values between bulk and mode I adhesive-joint fracture tests can be drawn, but considerable care is required when making this comparison. For example, it is often observed that for the DCB or TDCB tests, provided the adhesive layer is sufficiently thick to avoid the effects discussed in Sect. 3.4 and provided the crack grows cohesively through the adhesive layer with no rising R-curve observed, the value of  $G_{Ic}$  from the joint is equivalent to the value of  $G_c$  obtained in the bulk test. Clearly, if the bondline thickness is insufficient to allow for the full development of the plastic zone or if a weak interface causes the crack failure path to deviate from running cohesively in the adhesive, then lower values of  $G_c$  may be measured in the joint than in the bulk. If the adhesive joint exhibits rising R-curve behavior, which may occur if additional energy absorbing



mechanisms develop as the cracks propagate, then in such cases only the initiation values of  $G_{Ic}$  from the joint may be comparable to the bulk values. Also, when comparing bulk and joint adhesive properties, the state of cure of the adhesive should be shown to be equivalent as the exact processing conditions are affected by factors such as the thermal inertia of the joint and potential exothermic reactions of the bulk. Measurement of the glass transition temperature of the cured adhesive in the bulk and joint can be compared using techniques such as differential scanning calorimetry.

Finally, peel tests are used routinely by industries to assess adhesion. In geometry-dependent peel tests,  $G$  is the total energy dissipation on peeling and is significantly affected by factors such as the material properties of the peel arm, its thickness, and the angle of peel. In broad terms, these tests measure how difficult it is to peel the arms. This value of  $G$  may be many times greater than the value of  $G_{Ic}$  determined using the DCB or TDCB test. The degree of adhesion is just one of several factors that influence this measure. In geometry-independent peel tests, the energy dissipated plastically in the peel arms is determined and taken away from the total energy dissipation  $G$  to yield the adhesive fracture toughness,  $G_A$ . It is the value of  $G_A$  that may be considered equivalent to  $G_{Ic}$ , provided that the failure paths in the peel test and in the adhesive joint are both cohesive, in the adhesive layer. It should be noted that in the fixed-arm peel test, failure paths often occur close to the adhesive-substrate interface and thus may, in principle, yield values of  $G_A$  that are lower than the values of  $G_{Ic}$  determined using DCB or TDCB specimens in which cohesive cracks run through the center of the adhesive layer. This difference may be insignificant for brittle adhesives where the plastic zone size is small, but may be larger for tough adhesives. T-peel tests are sometimes preferred for this reason, as similar failure paths can be observed to the LEFM tests.

---

## 20.6 Conclusions

This chapter has described and discussed the fracture tests commonly performed on both bulk adhesive specimens and on adhesive joints. Whenever possible, fracture mechanics approaches have been followed with the goal of determining geometry-independent toughness values. Fracture tests on bulk adhesives are commonly conducted as part of the materials development process. Key to obtaining valid fracture results in bulk tests is to ensure (1) the generation of sufficiently sharp initial notches and (2) the manufacture of sufficiently good quality test specimens that pass the linearity and size criteria, as imposed by the standard, and thus allow the plane strain fracture toughness of the adhesive to be measured. The fracture toughness values obtained in bulk tests (i.e.,  $K_{Ic}$  and  $G_{Ic}$ ) will not be influenced by “adhesive-joint” factors such as constraint or substrate effects, or the quality of interfacial adhesion achieved.

Fracture tests on adhesive joints are always more complex than tests on bulk adhesive specimens and a  $G$  rather than a  $K$  approach is invariably followed for their analysis. The adhesive is present as a thin layer, it may be constrained by the

presence of nearby substrates and the failure paths may be influenced by the poor adhesion with the substrate. Fracture tests on adhesive joints are commonly conducted in mode I (tensile opening mode), mode II (in-plane shear mode), and mixed-mode I/II (combinations of mode I and II). The key to success in all LEFM fracture mechanic tests is to ensure that the substrates do not deform plastically during loading. Plastic deformation of the substrates would violate the assumptions of LEFM and invalidate the results. In mode I, the DCB and TDCB test specimens are almost universally employed and these tests have been standardized. Either test may be used for the determination of  $G_{Ic}$ . The choice of which to use is likely to depend upon factors such as the toughness of the adhesive, the properties of the substrate material employed, and whether or not crack length measurement is possible. In mode II, the ELS, ENF, the 4-point loaded ENF, and the tapered ENF (TENF) test specimens have all been employed to measure  $G_{IIc}$  values in adhesive joints with various levels of success. There is currently no agreed test standard for the determination of  $G_{IIc}$  in adhesive joints, but efforts are underway in the ESIS-TC4 (a European Fracture Committee) to develop a mode II standard, based on the ELS test method. The situation for mixed-mode fracture is similar, with several test specimens having been proposed but none yet standardized for adhesive joints. Values of  $G_c$  obtained from fracture tests on adhesive joints can be sensitive to variations in bondline thickness, and to assess this possibility reference should be made to the size of the plastic zone in relation to the bondline thickness.

Peel testing of flexible substrates can be considered as a class of fracture test, albeit one accompanied by extensive plastic deformation of the peel arm(s). A multitude of peel tests have been proposed and typically these determine a value of the peel strength, that is, a measure of how difficult it is to peel the arms during the test. Peel tests are thus highly geometry dependent. Recent research has focused on test and analysis methods to obtain geometry-independent values, for example, adhesive fracture toughness – one measure of how well the substrates are bonded. The method requires additional information about the stress–strain characteristics of the peel arms and also of the adhesive layer, so that the energy dissipated in these can be determined and accounted for in the fracture toughness values determined.

Finally, a major goal of fracture mechanics has been to derive geometry-independent values of the fracture parameter  $G_c$ . Great progress has been made in this endeavor with the determination of  $G_{Ic}$  from standardized bulk and adhesive-joint tests and  $G_A$  from geometry-independent peel tests. However, great care is required with the interpretation of these fracture parameters.

---

## References

- ASTM (1990) ASTM D3433. Annual book of ASTM standards. Adhesives section 15, Philadelphia. 15.06
- ASTM (1999) ASTM D5045. Determination of the fracture toughness of polymers
- ASTM (2004a) Standard test method for floating roller peel resistance of adhesives. West Conshohocken, PA: ASTM International

- ASTM (2004b) Standard test method for mixed mode I-mode II interlaminar fracture toughness of unidirectional fiber reinforced polymer matrix composites. ASTM Stand D6671M:1–14
- ASTM (2006) Standard test method for climbing drum peel for adhesives. West Conshohocken, PA: ASTM International
- Baldan A (2004) Review: adhesively-bonded joints and repairs in metallic alloys, polymers and composite materials – adhesives, adhesion theory and surface pretreatment. *J Mater Sci* 39:1–49
- Berry JP (1960) Some kinetic considerations of the Griffith criterion of fracture-I; equations of motion at constant deformation. *J Mech Phys Solids* 8:207–216
- Bishopp JA (2005) Surface pretreatment for structural bonding. In: Cognard P (ed) *Handbook of adhesives and sealants*, vol 1. Elsevier, pp 163–214
- Blackman BRK (2008) Delamination in adhesively bonded joints, Chapter 22. In: Sridharan S (ed) *Delamination behaviour of composites*. Woodhead Publishing, Cambridge
- Blackman BRK, Dear JP et al (1991) The calculation of adhesive fracture energies from DCB test specimens. *J Mater Sci Lett* 10:253–256
- Blackman BRK, Hadavinia H et al (2003a) The calculation of adhesive fracture energies in mode I: revisiting the tapered double cantilever beam (TDCB) test. *Eng Fract Mech* 70(2):233–248
- Blackman BRK, Kinloch AJ et al (2003b) Measuring the mode I adhesive fracture energy,  $G_{IC}$ , of structural adhesive joints: the results of an International round-robin. *Int J Adhes Adhes* 23:293–305
- Blackman BRK, Kinloch AJ et al (2005) The determination of the mode II adhesive fracture energy,  $G_{IIC}$ , of structural adhesive joints: an effective crack length approach. *Eng Fract Mech* 72:877–897
- Brunner AJ, Murphy N et al (2009) Development of a standardised procedure for the characterisation of interlaminar delamination propagation in advanced composites under fatigue mode I loading conditions. *Eng Fract Mech* 76(18):2678–2689
- BSI (1993a) Peel test for a flexible bonded-to-rigid test specimen assembly. 90 degree peel, Adhesives. London: BSI
- BSI (1993b) Peel test for a flexible bonded-to-rigid test specimen assembly. 180 degree peel, Adhesives. London: BSI
- BSI (2001) Determination of the mode I adhesive fracture energy,  $G_{IC}$ , of structural adhesives using the double cantilever beam (DCB) and tapered double cantilever beam (TDCB) specimens. BS 7991
- BSI (2005) T-Peel test for flexible-to-flexible bonded assemblies, Adhesives. London: BSI
- BSI (2009) Structural adhesives. Guidelines for the surface preparation of metals and plastics prior to adhesive bonding. London: BSI, 35 pp
- Chai H (1986) Bond thickness effect in adhesive joints and its significance for mode I interlaminar fracture of composites. In: *Seventh conference on composite materials: testing and design* ASTM STP 893. American Society for Testing and Materials, Philadelphia
- Chai H (1988) Shear fracture. *Int J Fract* 37:137–159
- Davies P, Blackman BRK et al (2001) Mode II delamination. In: Moore DR, Pavan A, Williams JG (eds) *Fracture mechanics testing methods for polymers adhesives and composites*,ESIS publication 28. Elsevier, Amsterdam/London/New York, pp 307–334
- Dillard DA (2010) Improving adhesive joint design using fracture mechanics. In: Dillard DA (ed) *Advances in structural adhesive bonding*. Woodhead Publishing, Oxford/Cambridge/New Delhi, pp 350–388
- Dillard DA, Singh HK et al (2009) Observations of decreased fracture toughness for mixed mode fracture testing of adhesively bonded joints. *J Adhes Sci Technol* 23(10–11):1515–1530
- Edde FC, Verreman Y (1995) Nominally constant strain energy release rate specimen for the study of mode II fracture and fatigue in adhesively bonded joints. *Int J Adhes Adhes* 15:29–32
- Fernlund G, Spelt JK (1994) Mixed-mode fracture characterization of adhesive joints. *Compos Sci Technol* 50:441–449
- Hashemi S, Kinloch AJ et al (1990) The analysis of interlaminar fracture in uniaxial fibre-polymer composites. *Proc R Soc Lond A* 427:173–199
- ISO (2000) Standard test method for the determination of fracture toughness ( $G_c$  and  $K_{Ic}$ ) – a linear elastic fracture mechanics approach. ISO Standard ISO 13586

- ISO (2001) Standard test method for mode I interlaminar fracture toughness, GIC, of unidirectional fibre-reinforced polymer matrix composites. ISO 15024
- ISO (2009) Adhesives – determination of the mode I adhesive fracture energy GIC of structural adhesive joints using double cantilever beam and tapered double beam specimens. ISO Standard 25217
- Kawashita LF, Moore DR et al (2005) Comparison of peel tests for metal-polymer laminates for aerospace applications. *J Adhes* 81:561–586
- Kawashita LF, Moore DR et al (2006) Protocols for the measurement of adhesive fracture toughness by peel tests. *J Adhes* 82:973–995
- Kinloch AJ (1987) Adhesion and adhesives: science and technology. Chapman & Hall, London/New York
- Kinloch AJ, Williams JG (2002) The mechanics of peel tests. In: Pocius AV, Dillard DA (eds) *The mechanics of adhesion*, vol 1. Elsevier, Amsterdam, pp 273–302
- Kinloch AJ, Kodokian GKA et al (1992) The adhesion of thermoplastic fibre composites. *Philos Trans R Soc Lond A* 338:83–112
- Kinloch AJ, Lau CC et al (1994) The peeling of flexible laminates. *Int J Fract* 66:45–70
- Liechti KM, Freda T (1989) On the use of laminated beams for the deformation of pure and mixed mode fracture properties of structural adhesives. *J Adhes* 29:145–169
- Liu Z, Gibson RF et al (2002) The use of a modified mixed mode bending test for the characterisation of mixed mode fracture behaviour of adhesively bonded metal joints. *J Adhes* 78:223–241
- Martin RH, Davidson BD (1999) Mode II fracture toughness evaluation using four point bend, end notched flexure test. *Plast Rubber Compos* 28(8):401–406
- Molitor P, Barron V et al (2001) Surface treatment of titanium for adhesive bonding to polymer composites: a review. *Int J Adhes Adhes* 21:129–136
- Moore DR (2008) An introduction to the special issue on peel testing. *Int J Adhes Adhes* 28:153–157
- Moore DR, Williams JG (2007) A protocol for determination of the adhesive fracture toughness of flexible laminates by peel testing: fixed arm and T-peel methods. ESIS TC4 protocol
- O'Brien TK (1998) Composite interlaminar shear fracture toughness, GIIC: shear measurement or sheer myth? In: Bucinell RB (ed) *Composite materials: fatigue and fracture*, STP 1330, 7th vol. ASTM, West Conshohocken, pp 3–18
- Papini M, Furlund G et al (1994) Effect of crack growth mechanisms on the prediction of fracture load of adhesive joints. *Compos Sci Technol* 52:561–570
- Qiao P, Wang J et al (2003a) Analysis of tapered ENF specimen and characterization of bonded interface fracture under mode II loading. *Int J Solids Struct* 40:1865–1884
- Qiao P, Wang J et al (2003b) Tapered beam on elastic foundation model for compliance rate of change of TDCB specimen. *Eng Fract Mech* 70:339–353
- Reeder JR (1993) A bilinear failure criterion for mixed-mode delamination. In: Camponeschi ET (ed) *Composite materials: testing and design*, ASTM STP, vol 11. ASTM, Philadelphia, pp 303–322
- Ripling EJ, Mostovoy S et al (1964) Measuring fracture toughness of adhesive joints. *Mater Res Stand (ASTM Bull)* 4(3, March):129–134
- Swadener JG, Liechti KM et al (1999) Mixed mode fracture of automotive bonded joints. SAMPE-ACCE-DOE advanced composites conference, Detroit
- Williams JG (1988) On the calculation of energy release rates for cracked laminates. *Int J Fract* 36:101–119
- Williams JG (2001) Determination of KIC and GIC in polymers. In: Moore DR, Pavan A, Williams JG (eds) *Fracture mechanics testing methods for polymers, adhesives and composites*. Elsevier Science, Amsterdam

Luca Goglio

**Contents**

21.1	Introduction .....	556
21.2	Block Impact Tests .....	558
21.3	Impact Wedge Peel Tests .....	561
21.4	Hopkinson Bar Apparatus .....	563
21.5	Other Test Methods .....	574
21.5.1	Fracture Energy .....	574
21.5.2	Drop-Weight-Based Tests and Alternative Tests .....	577
21.6	Conductive Adhesives .....	585
21.7	Response to Environmental Conditions .....	588
21.8	Conclusions .....	589
	References .....	590

**Abstract**

Assessing the mechanical properties of adhesives and the joints strength requires specific tests. Indeed, since polymers are, in general, sensitive to the strain rate they undergo, different phenomena can be induced when a load is applied abruptly. Under such a condition, usually the adhesive tends to react to the deformation with higher stress and lesser ductility, which causes higher resisting loads but lower absorbed energy. This is why the common standard impact tests for adhesives, involving bonded blocks or strips, aim at measuring the energy required to break the bond.

However, since this result is not sufficient to characterize an adhesive, other types of tests have been introduced to obtain a deeper insight. Different types of specimens (samples of bulk adhesive, lap joint, butt joint, double cantilever beam) and test rigs (pendulum, falling weight, hydraulic actuator) have been

---

L. Goglio (✉)

Department of Mechanical and Aerospace Engineering, Politecnico di Torino, Torino, Italy

e-mail: [luca.goglio@polito.it](mailto:luca.goglio@polito.it)

adopted in many works to measure the properties of interest. The fracture energy, typical of fracture mechanics, requires ad hoc tests and processing to be measured in dynamic conditions. The Split-Hopkinson pressure bar, a special apparatus conceived to test materials at high strain rate, has been also applied with success to adhesives and joints. Also test rigs based on the falling weight schemes have been widely used. A special case is that of conductive adhesives, which are getting into use to replace soldering in electronic packaging: their capability to withstand the impact that a device can undergo in use must be assessed.

This chapter, mainly relying on the results available from the technical literature, presents a survey of various test methods, focusing on the related problems and achievements.

---

## 21.1 Introduction

In many of the applications in which adhesives are used, it is likely that they are exposed to loads applied abruptly. A first case is that of a bonded assembly included in a mechanism which, in its service, undergoes discontinuous loading. Examples are mechanisms which undergo intermitting contact, or machineries which exert a crushing action on a material (like mills), or devices conceived to absorb impacts regularly. A second case is that of structures which under normal service are not loaded impulsively but in special conditions (accidents of various types) can be subjected to impacts. This is especially true for automotive applications, in which the crashworthiness is of crucial importance, but it also applies to devices which accidentally can undergo impacts (for instance, due to misuse, fall, etc.). According to the case, the expectations are different: if the impacts are a normal service condition, they must be sustained repeatedly without damage; otherwise, if the impact is an exceptional case, the goal is to minimize its consequences, accepting that a certain level of damage (sometimes high) is unavoidable. It can be remarked that in the former case, the determination of the adhesive performance can be expressed in terms of force or stress, while in the latter case, the typical quantity involved is the absorbed energy.

Two typical issues arise about the behavior of an adhesive subjected to impact. The first one is whether an abrupt loading can cause brittle behavior in a material that under static or quasi-static conditions would not be brittle; this aspect is critical regarding the capability of absorbing energy. The second issue is assessing the influence of the loading rate on the adhesive response, i.e., the sensitivity of the adhesive properties to the strain rate.

It is clear that such issues, all concerning material response, need experimental results to be addressed. For this reason, ad hoc tests have been proposed and developed, also as international standards. The commonest is the block impact test, defined as an American Society for Testing and Materials (ASTM) standard – and subsequently also as European Standard (EN) and International Organization for Standardization (ISO) standard – in which an impact is applied, with a loading scheme similar to that of the Izod pendulum, to a block bonded to a base. Another

popular test, especially in the automotive industry, is the impact wedge peel test, originally developed by Ford and presently also defined as an ISO standard; in this case the bond between two sheet metal strips is broken by a wedge that goes through the joint. These two tests are described in the next two sections of this chapter.

In addition to these standard tests, a considerable amount of research on the impact of adhesives has been carried out and presented by many scientists over the last four decades. A special apparatus, developed for testing materials under high strain rate and applied also to adhesives, is the Hopkinson bar, described in a subsequent section. A selection of other special testing methods and the related modeling are described in a further section.

In many cases, apart from the rupture energy (which can be obtained directly with pendulum-like devices), the measurement carried out in impact testing is the force time history. The typical feature of the latter is its oscillating behavior – posing serious problems when analyzing the curve – which is justified by two arguments. The first explanation is based on the discontinuous nature of crack propagation: when the critical condition is attained, the crack grows, and this relieves the local stresses and makes the system more compliant; thus the load decreases; then, as the impactor advances further, the cycle restarts. The second explanation considers that the specimen receiving the impact starts to vibrate, independently of the damage that can occur. Moreover, the vibrational properties are not necessarily a feature of the specimen alone, since they often depend on the system formed by the specimen and the test rig (which comes into play with its deformability). Unfortunately, in many cases it is very difficult to distinguish one contribution from the other, especially when the recorded time history is the only information available. The operation of smoothing the recorded curve (e.g., by filtering the high-frequency content) implies the risk of losing some useful information; on the other hand, the raw data can be misleading, in the sense that purely dynamic effect can be taken as material properties (e.g., force peaks at breakage). Thus, the evaluation of impact measurements often requires careful judgment, to avoid erroneous interpretation and false results.

It is clearly impossible to recall in a short space all the experiences about impacts tests on adhesives reported in the literature and describe in detail the findings. The objective of the present review is to give general information about what is (and can be) done in this field regarding the experimental arrangements adopted, the types of results obtained, and the behaviors observed. Another broad and detailed state-of-the-art review on adhesives and joints under impact has been very recently presented by Machado et al. (2017). From these reviews, an interested reader could get an address to select the types of experiments and results that fit his/her need. Of course, examining the original literature is always recommended. Among the several contributions appeared in recent times, the special issue of the *Int. J. of Adhesion and Adhesives* on “Impact phenomena of adhesively bonded joints,” Sato and Goglio (2015), can be mentioned.

It can be also remarked that often the cited articles are not exclusively dedicated to experimental works, since they report also the numerical and/or analytical modeling of the specimen behavior. This is due both to the use of the experimental results

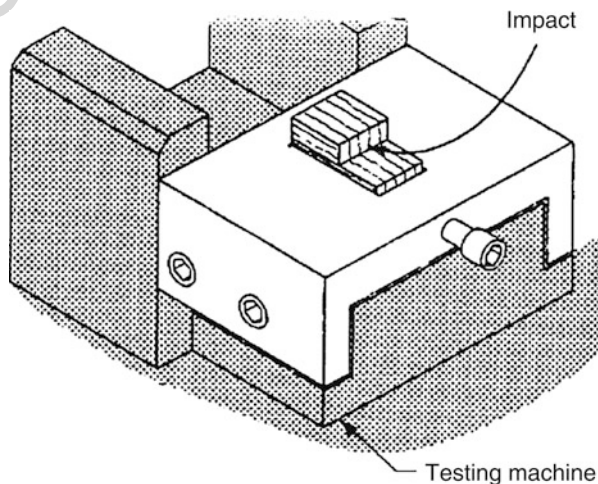
115 to validate the models and to the additional insight given by modeling to understand  
116 the stress and strain state during the tests.

## 117 21.2 Block Impact Tests

118 The basic principle on which this test, given by the ASTM D950 standard and by  
119 ISO 9653:1998 and EN ISO 9653:2000 as well, relies is to apply an impact loading  
120 condition, mainly in shear, by means of a test rig similar to that used for Izod  
121 resilience measurement. Figure 1 shows the experimental arrangement. An upper  
122 block (usually of steel) is bonded onto another larger block which, in turn, is fixed  
123 to the base of the test rig. The first block is struck by a hammer, in a direction parallel  
124 (at least at the beginning of the impact) to the bond surface. The energy required to  
125 fracture the sample is obtained from that lost by the pendulum, considering a  
126 correction for the kinetic energy of the projected parts. The reason for using this  
127 type of specimen, quite different from a real joint, is double. First, the block offers a  
128 large lateral face, which is easy to hit by means of the hammer. Secondly, the scheme  
129 aims at creating a condition of pure and constant shear in the adhesive layer.

130 A thorough analysis of this case has been carried out by Adams and Harris (1996)  
131 who, examining the features of this test, have analyzed in detail the contact condi-  
132 tions between hammer and side of the block. In an ideal situation, the impacting  
133 surfaces of the hammer and of the block should be perfectly parallel, giving a  
134 uniform load on the block. In practice, a certain degree of misalignment is unavoid-  
135 able. The authors, by means of finite element analyses, have compared (Fig. 2) the  
136 ideal case (I) with the limit cases in which – due to misalignment – the contact occurs  
137 at the upper edge of the block (case II) or near to the bond (case III). Their main  
138 findings are that, even in case of perfect alignment (Fig. 3, case I), the stresses in the

**Fig. 1** ASTM block impact test (From Bezemer et al. 1998, copyright Elsevier)





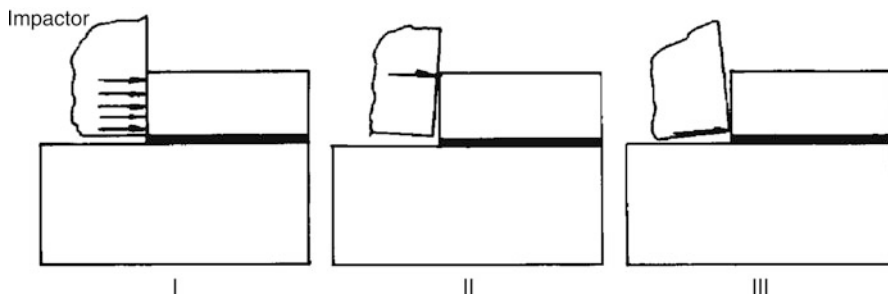


**Fig. 2** Possible modes of impact of the pendulum against the block: (I) perfectly parallel; (II) far from the bond; (III) close to the bond (From Adams and Harris 1996, copyright Elsevier)

adhesive are far from being constant: the shear stress peaks near to the bond end at the impacted side; also the peel stress is significant and peaks near to the bond end at the impacted side; then it decreases monotonically assuming negative sign at the opposite bond end. The non-constancy of the shear stress is generated by the “differential straining” mechanism due to the deformability of the block (see ► Chap. 24, “Analytical Approach”) that emphasizes the stress value at the end of the bond. The peel stress can be primarily regarded as a bending stress caused by the rotation of the impacted block, which – also in this case due to the deformability – is not linearly distributed.

In case of misalignment, the distribution of the shear and peel stress is strongly influenced, as shown in Fig. 3 (cases II and III), due to the changes of moment value and the compressive local deformation of the block (this effect can be regarded as a compression that “irradiates” from the contact point).

If the contact occurs far from the bond (case II), the bending moment is higher, and the peak of peel stress increases, while the local deformation of the block has little influence and the shear stress is not much affected. Conversely, if the contact occurs close to the bond (case III), the combination of low bending moment and compressive local deformation of the block causes a compressive peel stress in the adhesive close to the impacted bond end. At the same time, the local deformation of the block increases the differential straining at the same bond end, which causes a higher peak of shear stress.

Obviously, these features refer to the stress distribution at the beginning of the impact; then the situation evolves depending on the deformations (and damage) that take place. Thus, in global terms, the loading conditions and the strain energy are influenced, depending on the specific case; this aspect is important, since the elastic energy in the steel blocks can be even higher than the rupture energy of the adhesive.

From all these reasons, it comes out clearly that the block impact test is not suitable to give absolute figures about the energy absorption of an adhesive, due to the dependence of the results on the test rig and testing conditions. The only usefulness of the test is that of comparing the behavior of different types of adhesives, but also in this perspective the results must be considered carefully, keeping in mind the importance of the possible misalignments.

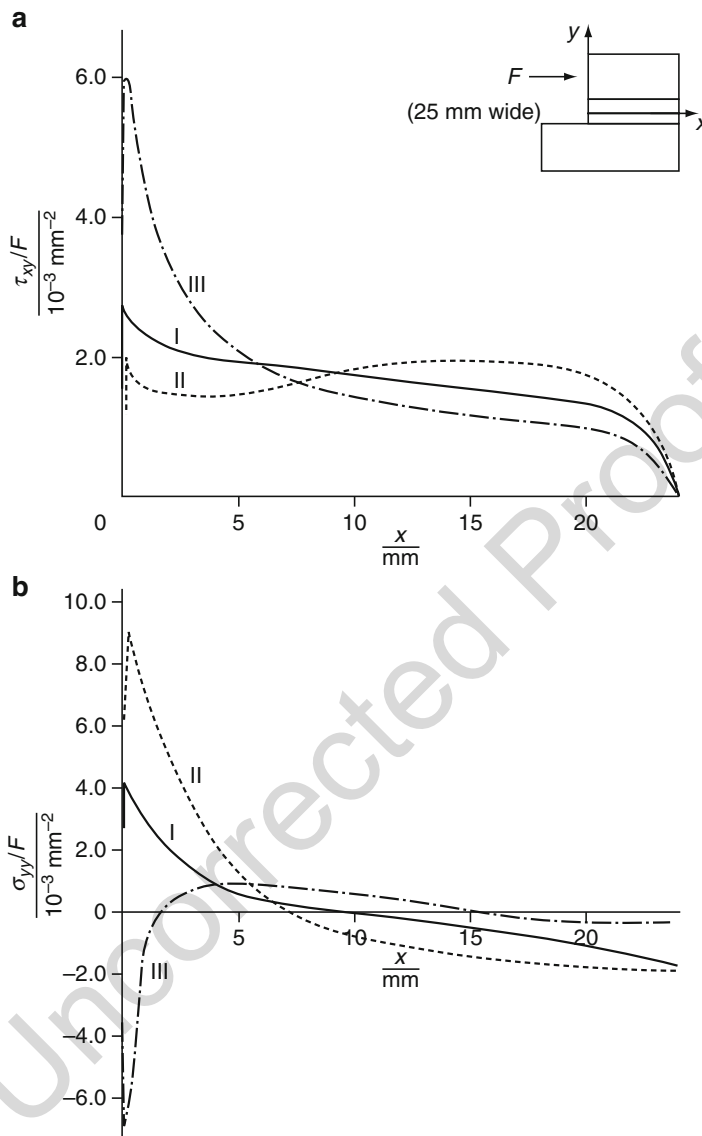


**Fig. 3** Stress distribution on the adhesive midplane of the impact block ASTM 250 for different loading cases: (a) shear stress; (b) peel stress (From Adams and Harris 1996, copyright Elsevier)

171 An alternative specimen for impact testing of adhesives, aiming at a stress  
 172 distribution mainly in shear and suitable for a speed higher than that reachable  
 173 with a pendulum, has been proposed by Bezemer et al. (1998). The specimen  
 174 in this case is formed by a ring bonded to a coaxial rod; the radial gap defines the  
 175 desired thickness of adhesive. In the test, the rod is hit axially – and pushed away

from the ring – by a projectile released from a drop tower or launched by an air gun, depending on the speed which is wanted; obviously, also static loading on a standard test machine is possible, especially for the sake of comparison. The contact force between projectile and rod is measured and recorded during the test; hence the displacement can be calculated by integration of the time history, and, in turn, also the energy can be obtained. The authors recognize that, though the motion of the rod with respect to the ring generates a tangential relative displacement, the strains and the stresses are not of pure shear; thus also a considerable normal stress is applied to the adhesive, in spite of the expectation. On the other hand, compared to the block impact, this solution still offers the advantages of a lesser sensitivity to misalignment and broader range of possible loading speed. However, this type of test is not widespread and has not reached the level of a standard.

### 21.3 Impact Wedge Peel Tests

Another objection against the block impact test is that the adherends involved (blocks) are thick and this does not reflect real applications, in which bonding is usually adopted to join thin parts. From this viewpoint, it appears more realistic to test a bond which joins two metal strips, highly deformable both elastically and plastically. This is just what is done with the “Impact wedge peel test,” foreseen by the standards ISO 11343:2003 and EN ISO 11343:2005. The specimen (Fig. 4) is made by two metal strips, formed and bonded together to obtain the shape of a Y. The strips are 90 mm long and 20 mm wide; their thickness can range between 0.6 and 1.7 mm. The bonding length is 30 mm, without any pre-cracking or crack initiator; the not bonded zones form the arms of the Y, which are clamped when the specimen is mounted on the test rig. Even if, to obtain the Y shape, the strips can be formed after bonding, it is recommendable to preform them, to avoid the risk of damaging the adhesive in the forming operation. The specimen is loaded by a wedge which is one side of a rectangular shackle and goes through the bond, thus separating the strips in peeling mode. The pull is applied to the shackle by means of a pendulum

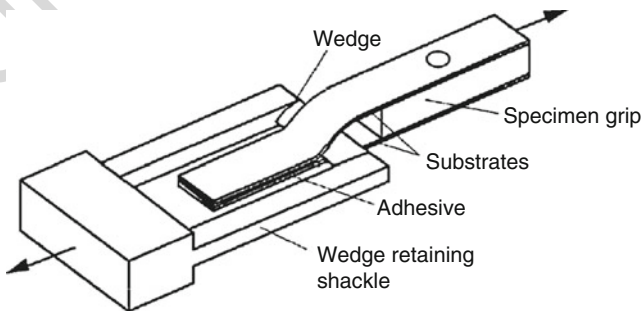


**Fig. 4** ISO 11343 wedge impact peel test specimen (From Blackman et al. 2000, copyright Kluwer)

or an actuator, with typical test speeds of 2 or 3 m/s depending on the material of the strips (lower value for steel, higher value for aluminum). During the test, the impact force is measured and recorded for subsequent processing.

A broad study of this test has been carried out by Blackman et al. (2000), who – on the basis of a series of tests carried out on several types of adhesives, at different speeds and temperatures, and using a high-speed hydraulic machine – have analyzed the effect of the specimen geometry and type of crack growth. The onset and the propagation of the rupture have been observed by means of high-speed photography. Furthermore, the authors have reviewed the methods proposed by the standard to extract the results and have applied a finite element model to reproduce the fracture of the specimen.

Two types of crack growth can be observed in this test, stable and unstable. In case of stable growth it has been observed that the crack tip runs ahead the wedge at approximately constant offset; thus the propagation speed is given by the wedge speed. The force time history exhibits initial peaks, due to dynamic effects originated by the sudden contact of the impactor with the specimen, and then a plateau appears and lasts for most of the test. Furthermore, the elevated plastic deformation of the metal strips that takes place involves a considerable amount of strain energy.

In case of unstable growth, typical at low temperature ( $-40\text{ }^{\circ}\text{C}$  in these experiments), or with a brittle adhesive, the crack runs rapidly through the whole bond, at a speed much higher than that of the wedge. The force time history after the initial peaks does not exhibit any plateau and oscillates close to zero. After the test, the strips appear almost undeformed, i.e., little plastic deformation takes place, and the measured energy is much lower than in the previous case.

According to the ISO standard, the average cleavage force can be calculated from the time history by considering the data between 25% and 90% of the time interval from the beginning to the end of the curve. The energy is given by the area under the curve between the same end points multiplied by the test speed. The reason for this assumption is to discard the data corresponding to the initial peaks and the “tail” of the curve. Blackman et al. (2000) remark that such procedure works well in case of stable crack growth, but it fails and can lead to false results in case of unstable growth, which does not exhibit any plateau.

An important aspect of the impact wedge peel test is that in case of stable crack growth; part of the energy is spent for deforming the metal strips (this aspect does not affect the unstable crack growth, which, however, is not suitable for the abovementioned reasons). Thus, also with this test, the measurement does not yield a property of the adhesive *in se* but of the assembly formed by adhesive and strips. Another factor that potentially affects the results is the friction between the wedge and the surfaces of the specimen during the fracturing process. However, the finite element simulations performed by Blackman et al. (2000) show that this aspect has minor importance, the leading factor being the adhesive fracture energy  $G_c$ . From the knowledge of the latter parameter, which can be measured with a fracture mechanics test such as the double cantilever beam, the time history of the impact wedge test can be reconstructed with finite element modeling.

## 21.4 Hopkinson Bar Apparatus

In addition to the limitations already mentioned, the two tests described in the previous sections present the further restriction that the strain rate attained in the adhesive cannot be much high, since it usually does not exceed  $10^2 \text{ s}^{-1}$ . When testing at higher strain rates is needed, the suitable equipment is the so-called Hopkinson bar, which in the last years has become probably the most used by the researchers of the field.

This name is due, historically, to the apparatus used at the beginning of the twentieth century by B. Hopkinson to study the pressure waves generated by explosions or projectiles. In the experiment, the explosion (or the projectile) attained one end of a long and thin bar suspended horizontally, creating a pressure pulse which propagated through the bar until the other end, where a short cylinder of the same diameter of the bar was provisionally attached by means of a grease film or magnetically. This cylinder, called time-piece, was projected by the pulse against a ballistic pendulum which gave the measure of the momentum contained in it; the momentum remained in the bar was measured by observing its oscillation. By varying the length of the time-piece, it was possible to assess the length of the pressure pulse.

The version of the apparatus used nowadays was introduced by Kolsky (1963), who added a second bar, from which the name “Split-Hopkinson pressure bar” comes from; the specimen of material to be tested is inserted between the two bars, as shown schematically in Fig. 5a. The projectile, usually fired by means of a pneumatic gun, impacts the first bar (incident bar), generating the incident pulse which, at the bar/specimen interface, is partially reflected and partially propagates in the specimen. From the specimen, the pulse is transmitted to the second bar

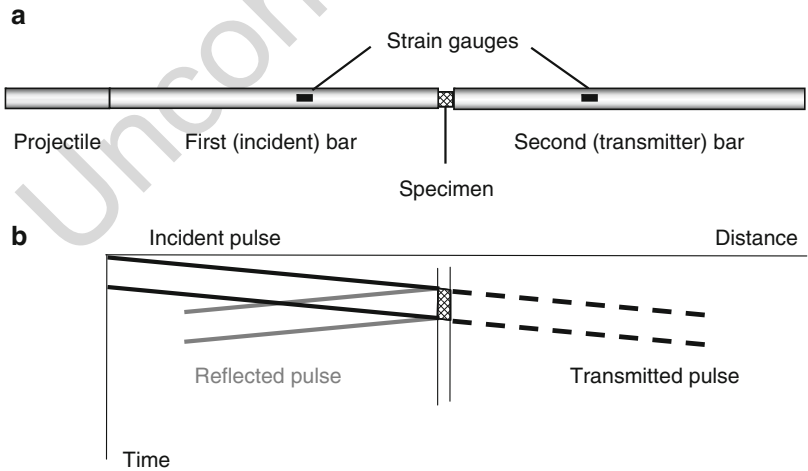


**Fig. 5** Schematics of the Split-Hopkinson pressure bar (a) and related Lagrangian diagram (b)

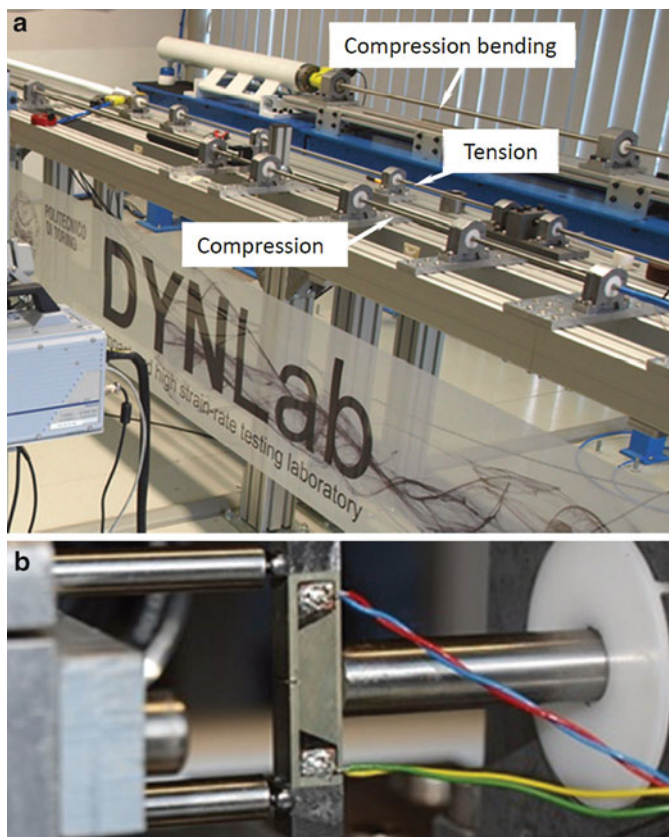


**Fig. 6** Split-Hopkinson pressure bar: (a) overall view of the rig including three bars for different test conditions; (b) detail of the bending fixture (Politecnico di Torino, DYNLAB)

(transmitter bar). The situation is described graphically by the so-called Lagrangian diagram presented in Fig. 5b. A concrete example of Split-Hopkinson pressure bar is shown in Fig. 6. The pulses are measured by means of strain gages placed on both incident and transmitter bar, thus their time history can be stored by means of a transient recorder, usually a digital oscilloscope or an acquisition board. From such measurements the stress ( $\sigma$ ), strain ( $\epsilon$ ), and strain rate ( $\dot{\epsilon}$ ) in the specimen can be obtained as

$$\sigma(t) = E_0 \frac{A_0}{A} \epsilon_{\text{tra}}(t) \quad (1)$$

$$\epsilon(t) = -2 \frac{c_0}{L} \int \epsilon_{\text{ref}}(t) dt \quad (2)$$

$$\dot{\epsilon}(t) = -2 \frac{c_0}{L} \epsilon_{\text{ref}}(t) \quad (3)$$

where, respectively,  $E_0$ ,  $A_0$ , and  $c_0$  are Young's modulus, cross section, and wave velocity of the bar,  $A$  and  $L$  are the cross section and the length of the specimen,  $\varepsilon_{tra}$  is the strain pulse transmitted in the second bar, and  $\varepsilon_{ref}$  is the strain pulse reflected in the first bar. Equations 1, 2, and 3 are based on the assumption that the specimen has reached equilibrium conditions; this requires that its length be smaller than the length of the pulse. Clearly, the measurement cannot be taken directly at the interface; thus the strain gages are placed at a distance from the end of each bar; this is potentially a source of error since the pulses during their travel (from the bar end to the gage) change in shape and assume a delay that must be evaluated.

As far as the adhesives are concerned, the Hopkinson bar has been applied to the characterization of materials and also butt or lap joints. The arrangement described above is suitable for testing in compression (that can be applied by simple contact); in case of tension, the system must be modified, usually by means of a threaded connection. Moreover, it is required to generate a tensile pulse in the bars, and this can be obtained in two ways. The first is to use a reverse loading system, so that the impact of the projectile applies tension to the first bar, as done by Yokoyama (2003) and also (actually to test polymers, but the case would apply also to adhesives) by Chen et al. (2002). The second and more popular solution is to generate, as usually, an initial compressive pulse that travels through both bars; the transmission of this pulse from the first to the second bar is given by a split ring, inserted between them, which prevents the specimen from being loaded in compression (Fig. 7). It is also possible to avoid the use of the split ring if the dimensions of the threaded parts of specimen and bars are accurately manufactured to obtain a precise fit of the ends of the bar (Fig. 8). When the compressive pulse reaches the end of the second bar, it is

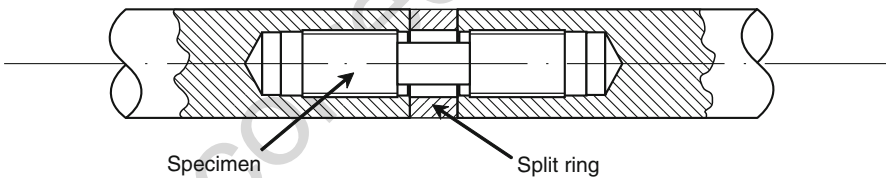


**Fig. 7** Use of threaded specimen and split ring to carry out tensile tests with the Hopkinson bar (From Goglio et al. 2008, copyright Elsevier)

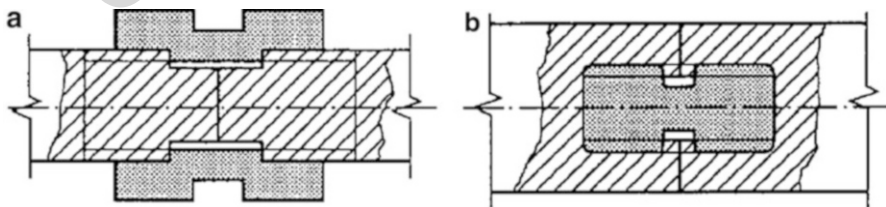


**Fig. 8** Use of threaded specimen without split ring to carry out tensile tests with the Hopkinson bar: (a) tubular specimen; (b) solid specimen (From Bragov and Lomunov 1995, copyright Elsevier)



reflected back as a tensile pulse which stresses the specimen, while the ring gives no contribution under tension.

Several studies based on the Hopkinson bar have been presented by Yokoyama and co-workers. In Yokoyama and Shimizu (1998), the shear strength of pin-and-collar specimens (ASTM D4562) bonded with cyanoacrylate has been studied with the Hopkinson bar and compared to the static case. Both steel and aluminum have been considered as adherend materials. Later, Yokoyama (2003) has tested under tension butt joints made with cyanoacrylate adhesive and two different types of adherends, namely, a bearing steel and a high-strength aluminum alloy. The impact tests have been carried out on a Hopkinson bar; other comparative tests at intermediate and low loading rates have been performed on a standard test machine. The experimental work is supported by a finite element analysis of the stress state in the joint. In both studies, the main findings are that the joint strength, expressed as peak force or stress, increases with the loading rate, while the deformation decreases. There is an optimum value of adhesive thickness (about 35  $\mu\text{m}$ ), for which the tensile strength is maximized; furthermore, the strength is influenced by the material of the adherends, steel, or aluminum. In the case of butt joints also the absorbed energy has been evaluated, by integrating the load-deformation curve. It has been noticed that the amount of energy is influenced by the material of the adherends; as in case of steel adherends, it decreases significantly with the loading rate.

Again, Yokoyama et al. (2012a, b) have studied with the Hopkinson bar the response of bulk specimens made of two different structural adhesives (epoxy and methacrylate) tested in compression. A tapered striker has been used to apply a nearly constant strain rate. Both adhesives have shown marked strain rate dependence, and it has been found that a modified Ramberg-Osgood model predicts well the stress-strain curve in loading, but not the strain softening after yielding and the unloading phase.

Recently, Yokoyama and Nakai (2015) have tested brim-and-crown butt joints, fabricated with aluminum alloy or pure titanium and joined by an epoxy. A Hopkinson apparatus modified by adopting a tubular output bar has been used. The experiments have shown that the tensile strength increases significantly with the loading rate and decreases under increasing adhesive thickness, for both adherend types.

Goglio et al. (2008) have tested a bicomponent epoxy under tension and compression, to assess the effect of the strain rate on the strength of this adhesive. Also, in this work both the Hopkinson bar and a hydraulic test machine have been employed, depending on the desired strain rate (from  $10^{-3}$  to  $3 \times 10^3 \text{ s}^{-1}$ ).

Under compression, the stress-strain curve of the adhesive exhibits an initial linear (elastic) rise, then a wide plateau, and again a rise with increasing slope. These features remain the same under any strain rate values, as it can be observed in Fig. 9: increasing the strain rate, the yield stress increases; thus the plateau is shifted upward and starts at larger strain. This observation has led to define a dynamic factor as  $k = \sigma_{\text{dynamic}}/\sigma_{\text{static}}$ , obtained by the ratio (averaged over the plateau) of the points on the curve at a chosen rate to the points on the static curve. The available data have been used to define prediction formulae for  $k$  as a function of the strain rate, based on



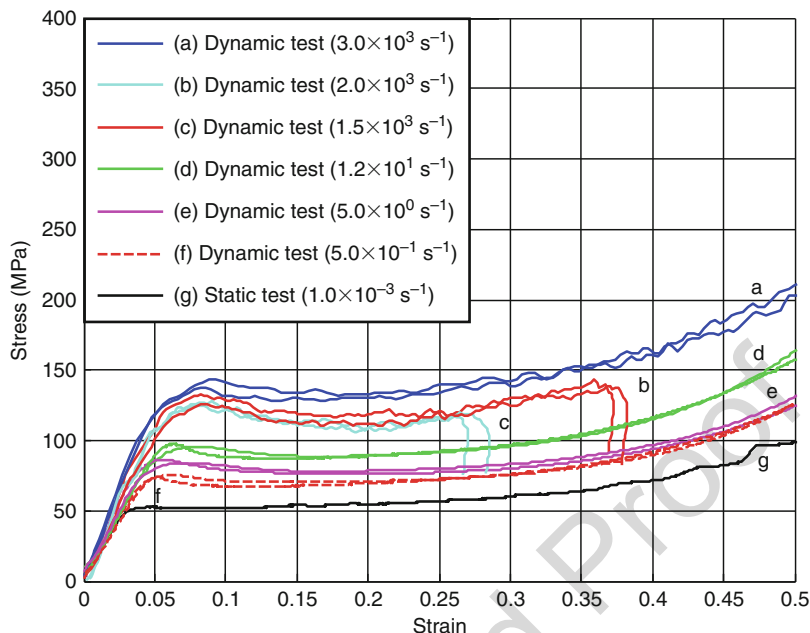


**Fig. 9** Dynamic stress-strain curves under compression at different strain rates, case of cold cured adhesive (From Goglio et al. 2008, copyright Elsevier)

a log-log fit as shown in Fig. 10. The two popular models, to account for the strain rate influence, of Cowper-Symonds and Johnson-Cook have been applied to this case. None of them can reproduce the experimental data over the whole range tested ( $10^{-3}$ - $10^3$   $s^{-1}$ ); thus they can be conveniently replaced by a poly-linear (in log-log scale) fit in the form  $k = A\dot{\epsilon}^n$ , where  $A$  and  $n$  are coefficients determined over each chosen range. From Fig. 10, it can be also appreciated that the  $k$  factor assumes, at the highest strain rate tested, values close to 3; this gives a measure of the elevated sensitivity of the adhesive to the strain rate.

Testing under tension at high strain rate presents particular problems. Apart from the abovementioned modifications to the apparatus required to apply positive stress, the measurement is hindered by the different response of the material. Indeed, the material usually behaves as brittle, and the specimen cracks soon after the stress-strain curve has reached its maximum. The only value that can be obtained is in practice the 0.2% (or other chosen percentage) proof stress. However, this value is also strongly dependent on the strain rate.

There are other specific problems, which affect testing with the Hopkinson bar, that deserve to be mentioned.

One concerns the first part of the stress-strain diagram, corresponding to the elastic behavior and, therefore, useful to evaluate the elastic modulus of the material. This part of the diagram corresponds to a time range of the test in which the equilibrium conditions still have not been achieved in the specimen, since as a

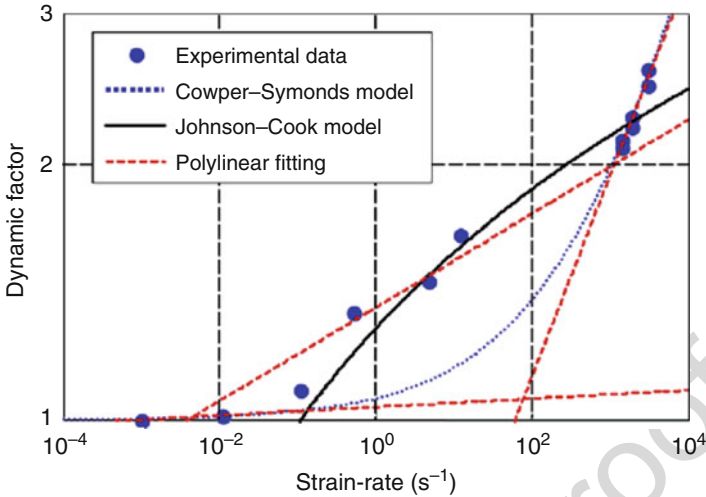


**Fig. 10** Dynamic factor  $k$  (case of cold cured adhesive): fitting of the experimental values with Cowper-Symonds, Johnson-Cook, and poly-linear models (From Goglio et al. 2008, copyright Elsevier)

practical rule it can be assumed that equilibrium is achieved after the waves have traveled back and forth more than three times along the specimen (Chen et al. 2002). Thus, the values of the elastic modulus can be affected by uncertainty and must be regarded with care.

A general survey – not specifically related to adhesives – of the problems concerning the measurements by means of the Hopkinson bar has been presented by Bragov and Lomunov (1995). Apart from presenting nonconventional applications of the Hopkinson bar (such as dynamic hardness and toughness testing), these authors discuss the problems of signal synchronization and strain rate constancy. The former problem is originated by the difficulty in recognizing the exact beginning of the three measured pulses (incident, reflected, transmitted), which in this paper is corrected by checking that the sum of the incident and reflected pulses equals the transmitted strain pulse. The latter problem is due to the fact that the strain rate, according to Eq. 3, is proportional to the reflected pulse, which decreases as the specimen hardens and its cross section increases during the test. The remedy is to modify the shape of the incident pulse, by means of a tapered projectile or an auxiliary specimen (pulse shaper) placed at the impacted end of the first bar: in this way the incident pulse assumes an increasing amplitude, while the reflected pulse tends to be constant.

Zhao and Gary (1996), presenting a study related to the measurement of small strains with the Hopkinson bar, have considered two important sources of error. The first is the dispersion (related to the difference between phase and group velocities of the waves), which the authors correct with a numerical procedure. The second is the determination of the time delay between the signals, for which an iterative procedure

is proposed. These authors also propose an identification technique to treat the data corresponding to the initial transient of the measurement, when the equilibrium in the specimen is not yet attained.

In a general perspective, not solely related to testing of adhesives, the problem of the dispersion has been considered by Tyas and Watson (2001). They have proposed to correct the measurement by means of two factors, termed  $M_1$  and  $M_2$ , one relating measured surface strain to average strain over the cross section and the other relating average axial strain to average axial stress (dynamic elastic modulus).

Another source of error is the effect of the nonuniform distribution of stress and strain over the cross section, related to radial inertia. This problem, considered again in general case by Forrestal et al. (2007), becomes important when the diameter of the bar is large and, therefore, the wave is no longer mono-dimensional. The corrections which are proposed are based on the theoretical solution for the wave propagation.

Sen et al. (2011) have carried out tests on single-lap joints of different overlap lengths; they have found that the (apparent) strength expressed as average stress decreases by increasing the overlap – in accordance to what is found also under static loading – and that the edges of the adhesive are subjected to the maximum strain. An important remark about this type of measurements is that, as stated previously, in Hopkinson bar testing, the stresses should be uniform throughout the length of the sample, which is more difficult to achieve in case of lap joints.

Similarly, Challita et al. (2011) have carried out quasi-static, intermediate, and high strain rate tests (the latter on a Hopkinson bar) on double-lap joints, using compression-shear and tensile-shear specimens. It has been found that the shear strength increases for increasing strain rate until  $10^3 \text{ s}^{-1}$  then decreases. Correction coefficients based on the previous work Challita and Othman (2010) have been used to estimate the maximum stress, accounting for the nonuniform distribution.

Testing with the Hopkinson bar has been applied also to nonconventional cases, to assess the material response in special conditions. For instance, Martinez et al. (1998) have studied the behavior of a confined adhesive, i.e., when it cannot freely expand laterally under compression. The interest for such case is related to the use of an adhesive to join, in an armored panel, the front ceramic layer to the metal backing plate. To this aim, the adhesive specimen in the Hopkinson bar tests has been surrounded by a confinement tube. The study, carried out on several types of adhesives, has evidenced an optimum value of the adhesive thickness in the armor, in order to ensure enough strength to contain the ceramic fragments and the minimum reflection of the pressure wave. A work by Adamvalli and Parameswaran (2008) has studied the influence of the temperature on the strength of single-lap joints, bonded with an epoxy adhesive, tested at different loading rates (Fig. 11). It has been found that, on the one hand, at the highest loading rate tested ( $4.7 \text{ MPa}/\mu\text{s}$ ), the strength is more than three times the corresponding static value; on the other hand, an increase of temperature from  $25^\circ\text{C}$  to  $100^\circ\text{C}$  reduces by 35% the strength.

Ravi Sankar et al. (2015) have used a Hopkinson bar to test lap joints with split-cylinder geometry, made with similar or dissimilar metals (steel, aluminum) joined by an epoxy. The results, supported by finite element modeling to assess the stress

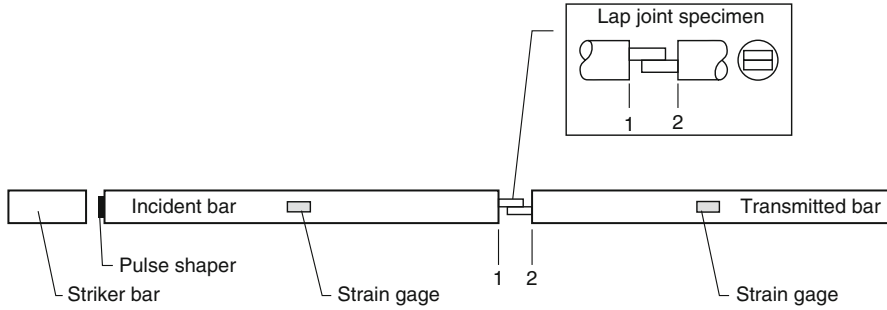


**Fig. 11** Setup of the Hopkinson bar for testing lap joints at high temperature (From Adamvalli and Parameswaran 2008, copyright Elsevier)

distribution, indicate that the strength is dictated by the less stiff adherend. A further interpretation by these authors is that the strength measured using the Hopkinson bar represents the volume averaged shear stress in the adhesive layer, as stated by Challita and Othman (2010).

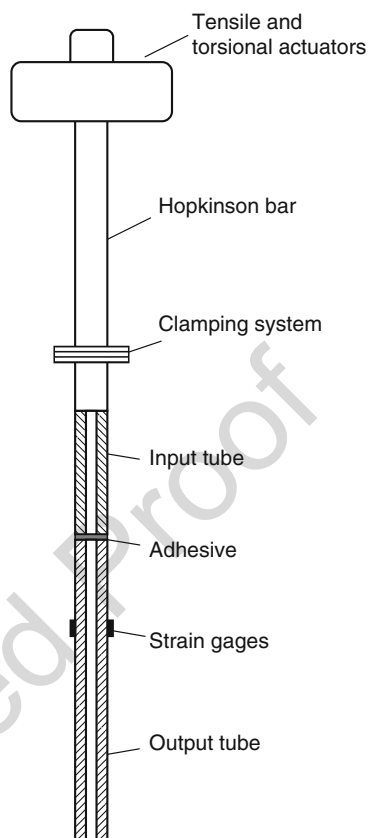
The method of the Hopkinson bar testing has also been applied to specimen types other than cylinders or lap joints.

Sato and Ikegami (1999) have measured the dynamic strength of an epoxy adhesive by testing butt joints of tubes subjected to shear and normal stress. Their equipment (Fig. 12) include a Hopkinson bar suspended vertically and loaded at the upper end by hydraulic actuators which apply, before the beginning of the test, a torsional and a tensile preload. Nearby the lower end, the bar is clamped by a mechanism that can be released rapidly. The specimen is formed by an upper short tube (load input tube), screwed at its upper end to the Hopkinson bar, and a long lower tube (load output tube), instrumented with strain gages. When the clamp is released, the elastic energy accumulated in the bar creates the waves that travel from one tube to the other, thus loading the adhesive layer. The reason for an elevated length of the output tube is to avoid that the back reflection of the waves at its lower end could interfere with the useful signals. The result is a chart, of the type shown in Fig. 13, reporting the failure conditions under different combinations of peel and shear stress. Also, cases of failure under static loading are reported in the diagram, for comparison with the dynamic case; it is evident that the stress values under impact are approximately double than the static ones. The authors have also tried to interpolate the experimental points with the popular Tresca and von Mises failure criteria, but the best fit (solid lines in the figure) is given by a polynomial in the form

$$\tau_d'^2 (\sigma_d - \sigma_d') + \sigma_d' \tau_d'^2 = 0 \quad (4)$$

where  $\sigma_d$  and  $\tau_d$  are the applied normal and shear stresses and  $\sigma_d'$  and  $\tau_d'$  are the strength values measured experimentally. This formula, although not supported by a theoretical background, has also the merit of predicting an increase of the bearable

**Fig. 12** Schematic of the modified Hopkinson bar used by Sato and Ikegami (1999) to test butt joints of tubes under tension and torsion



shear stress in case of negative (i.e., compressive) normal stress; this can be noticed by extrapolating to the left the curves in Fig. 13.

An evolution of the Hopkinson bar is the test rig presented by Kihara et al. (2003) to measure the shear strength of adhesive layers (Fig. 14). A prism of hexagonal cross section, screwed between bars 1 and 2, is bonded to a pair of plates which, in turn, are screwed to the additional bars 3. When the pulse, generated from top by the impact of the projectile 0 against bar 1, travels through the prism, it propagates also laterally to the bonds and the plates. The skew slit contained in each plate acts as a reflector which deviates most of the pulse toward bar 3. In addition to the strain gages placed on bar 1 and 2, as usually in the Hopkinson bar scheme, a rosette is applied on each lateral plate to measure the strains in a point close to the adhesive layers. A peculiar phenomenon noticed by the authors is that in case of low incident pulse (in bar 1), the adhesive withstands the shear stress and is fractured by the tensile normal stress generated by the reflection in the plate. Conversely, in case of high incident pulse, it is the shear stress (in combination with compressive stress) that causes the fracture of the adhesive. By means of this apparatus, the authors have

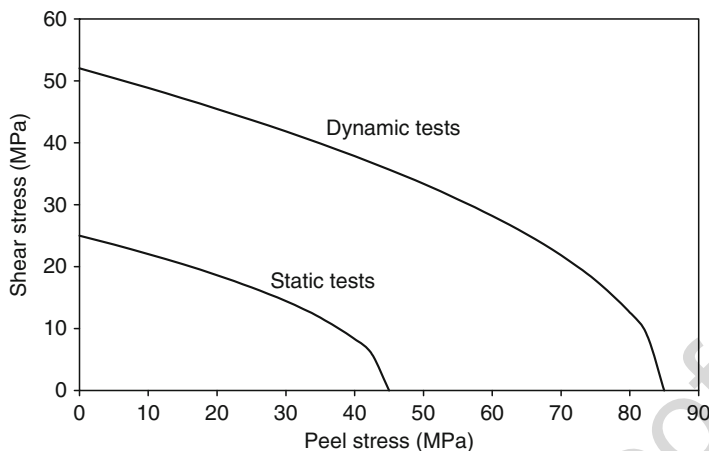


**Fig. 13** Limit curves for dynamic and static stress of tubular butt joints subjected to normal and shear stresses based on the results of Sato and Ikegami (1999)

obtained a value of shear strength comparable to that obtainable by cylindrical butt joints subjected to torsion.

Wang and Xu (2006) have performed tensile dynamic tests with the Hopkinson bar on convex-edge joints, shaped in such a way to eliminate the edge singularity in the interface of dissimilar materials, so obtaining a nearly uniform stress distribution and a more correct measurement of the strength. This specimen type is not exactly a bonded joint; however the findings can be useful to design a butt-bonded specimen.

Gilat et al. (2007) have studied the response of two epoxy resins, one untoughened and one toughened, in the strain rate range  $10^{-5}$ –700 1/s, under tensile and torsion loading. Tests at low and medium strain rates have been carried out on a hydraulic (biaxial) machine, those at high strain rates with a tensile or a torsional Hopkinson bar. The latter have been adapted by clamping, respectively, a force or a torque which is then released. A transition from ductile to brittle behavior has been noticed under tension under increasing strain rate; conversely, ductile behavior has been observed under torsional shear at any strain rate.

In a comprehensive work concerning the mechanical properties of the crash-optimized adhesive Betamate 1496 V, May et al. (2015) have used a modified Hopkinson apparatus in which no input bar is foreseen: the striker hits directly the specimen, and the force is measured by a film transducer attached to the end of the output bar. The deformation of the specimen is captured by means an electro-optical system based on a high-speed camera which keeps track of a pair of markers painted on the edges of the specimen.

Very recently, Neumayer et al. (2016) have used a Hopkinson bar to study the impact response of butt- and lap-shear joint specimens, measuring the strain in the adhesive by means of Digital Image Correlation (DIC), achieving a better accuracy than in traditional way. It has been noticed that DIC has given a 12.28 times higher

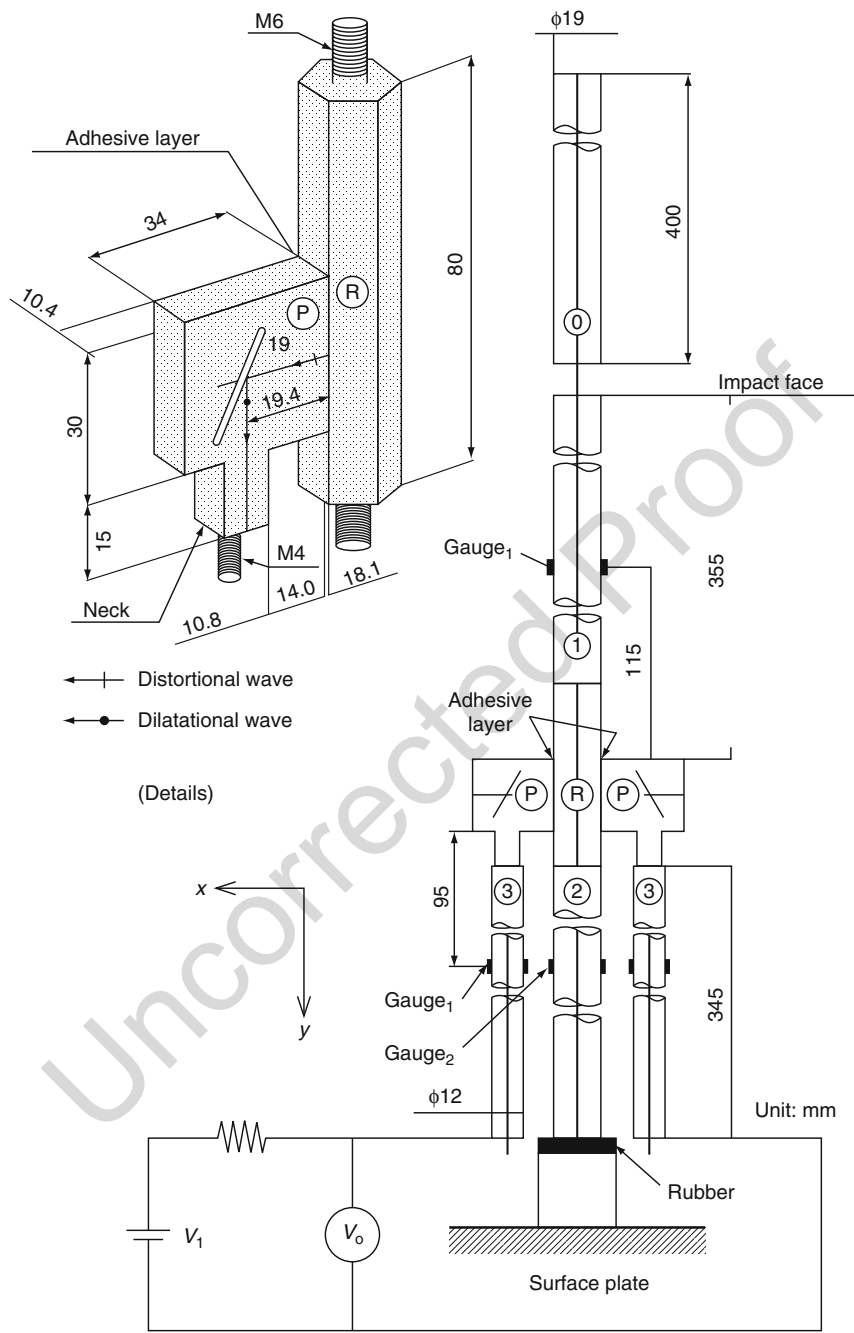


**Fig. 14** Test rig to measure the impact strength of adhesive layers (From Kihara et al. 2003, copyright Elsevier)

509 adhesive stiffness and a 1.83 times lower energy in case of butt joints (respectively,  
 510 6.13 and 1.29 times in case of lap-shear joints).

## 511 21.5 Other Test Methods

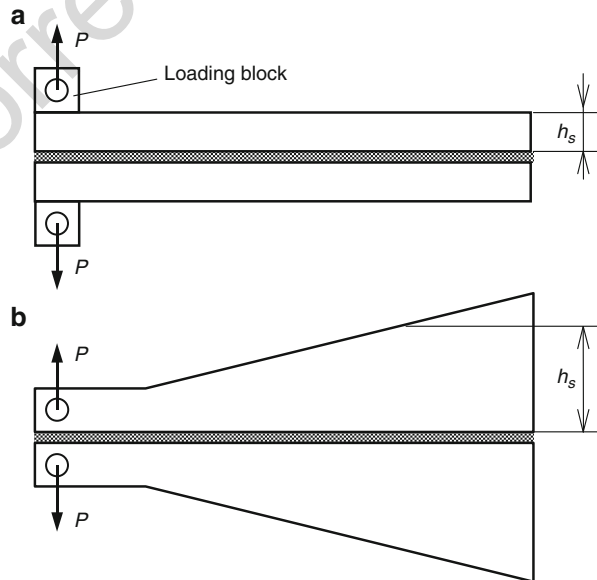
512 In addition to the test schemes described in the previous sections, some other methods  
 513 have been applied to test adhesives and joints under impact loading. Most of them are  
 514 based on schemes that reprise static cases, for the geometry of the specimens or the  
 515 loading system. The reason for this is not only to recover known cases but – most of  
 516 all – to evaluate easily the changes in the joint response induced by the loading rate.

### 517 21.5.1 Fracture Energy

518 Regarding the measurement of the adhesive fracture energy  $G_c$ , under impact (or, in  
 519 general, dynamic) conditions, the double cantilever beam test and the tapered double  
 520 cantilever beam test (Fig. 15) must be adapted to account for the effect induced by  
 521 the loading rate. Indeed, in statics the base for the measurement is the formula  
 522 (Williams 1984):

$$G_c = \frac{P_c^2}{2b} \frac{dC}{da} \quad (5)$$

**Fig. 15** Double cantilever beam specimen (a) and tapered double cantilever beam specimen (b)





where  $P_c$  is the critical load for crack propagation,  $b$  is the joint width,  $a$  is the crack length, and  $C$  is the specimen compliance, i.e., the displacement to force ratio ( $\delta/P$ ). In case of an impact test, the main problem which arises in evaluating the fracture energy is that (as already remarked previously) the force-displacement curve exhibits strong oscillations and, therefore, it is tricky to read from it the relevant information. To avoid this problem, expressions that do not directly make use of load values must be adopted, such as for the double cantilever beam specimen (Kinloch 1997):

$$G_c = \frac{3}{16} \frac{F}{N^2} \frac{\delta_c^2 h_s^3 E_s}{(a + \chi_1 h_s)^4} \quad (6)$$

where  $F$  and  $N$  are correction factors which, respectively, account for the large deflection of the beam and the stiffening effect of the loading block at the ends of the arms,  $\chi_1$  is another correction factor accounting for beam root rotation, and  $h_s$  and  $E_s$  are, respectively, the height of the beams and Young's modulus of the substrate material. The critical displacement for crack propagation  $\delta_c$  and the crack length  $a$  can be monitored by means of an optical system, as long as the test goes on. In the case of the tapered double cantilever beam specimen, the formula accounts also for the variable beam height.

A sophisticated analysis about the measurement of the fracture energy at high rate of loading has been presented by Blackman et al. (2009). These authors have used the double cantilever test and the tapered double cantilever test to evaluate the behavior of an epoxy adhesive, under loading conditions varying from quasi-static to 15 m/s. The experimental setup includes a hydraulic actuator to apply the load, a high-speed camera, and the suitable electronic devices for measuring, amplifying, processing, and storing the data (Fig. 16). Four different types of crack growth have been identified in this work, namely, (1) slow-rate stable, (2) slow-rate unstable, (3) fast-rate unstable, and (4) fast-rate stable. Here, "stable" is termed the case of steady propagation, while "unstable" is a discontinuous growth, showing sequences of arrest and propagation. It is interesting to notice that the unstable crack growth can occur at intermediate load rate in the tested range; the difference between slow rate and fast rate depends on whether the kinetic energy of the specimen arms is negligible or not with respect to the fracture energy of the adhesive. It is also remarkable that, at the highest load rate adopted in the tests, the crack growth is again stable; obviously in this case the dynamic effects (importance of the kinetic energy, uncertainty on the measured load) are important. For instance, in case of fast-rate loading and double cantilever beam specimen, the formula for the corrected fracture energy (i.e., accounting for the dynamic effects) is

$$G_{lc} = \frac{3}{4} \frac{Eh^3(V/2)^2 t^2}{(a + \Delta_I)^4} \frac{F}{N^2} - \frac{33}{140} \frac{Eh(V/2)^2}{c_L^2} \quad (7)$$

for type 3 crack growth and

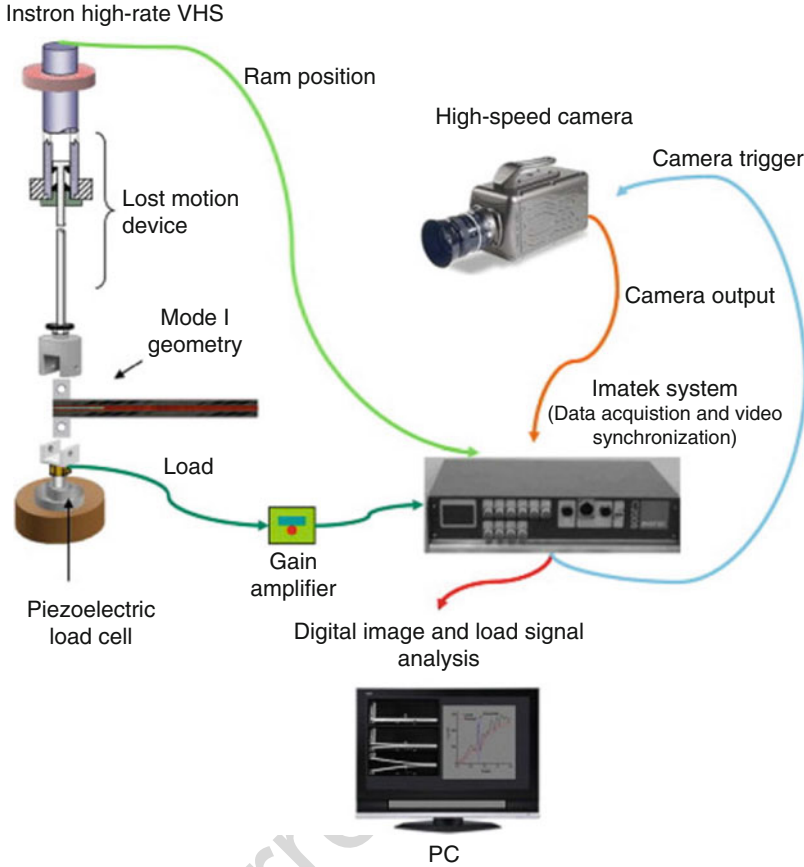


**Fig. 16** Experimental setup for high rate testing of adhesives under high rate of loading (From Blackman et al. 2009, copyright Elsevier)

$$G_{Ic} = \frac{3}{4} \frac{Eh^3(V/2)^2 t^2}{(a + \Delta_I)^4} \frac{F}{N^2} - \frac{111}{280} \frac{Eh(V/2)^2}{c_L^2} \quad (8)$$

for type 4 crack growth. In both Eqs. 7 and 8,  $E$  is Young's modulus of the substrate material,  $h$  is the height of the beam,  $V$  is the velocity applied by the actuator,  $t$  is the time,  $a$  is the crack length,  $\Delta_I$  is the correction factor for beam root rotation,  $F$  and  $N$  are – again as in Eq. 6 – the correction factors for large deflection of the beam and stiffening effect of the loading blocks, and  $c_L$  is the longitudinal wave speed in the substrate material. The first term in Eqs. 7 and 8, which can be obtained from Eq. 6, has the meaning of energy calculated as in static conditions, from which the second term, corresponding to the kinetic energy of the beams, is subtracted. Analogous formulae, of higher complexity due to the non-constancy of the beam section, are available for the tapered double cantilever beam specimen (see again Blackman et al. 2009).

### 21.5.2 Drop-Weight-Based Tests and Alternative Tests

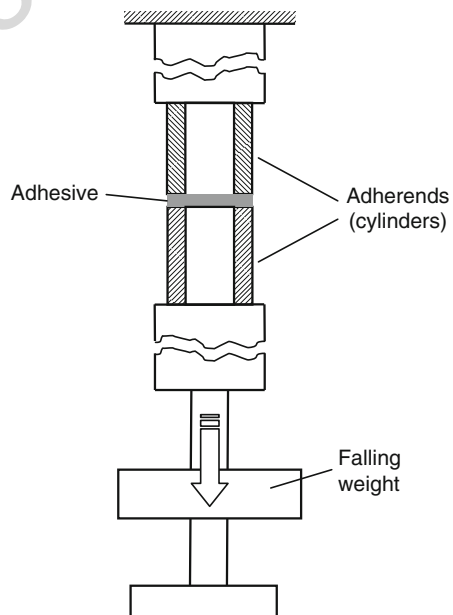
Also in the field of adhesive joining, drop-weight machines are probably the test rigs that have been used first to generate impact conditions.

Beevers and Ellis (1984) have carried out tests on joint specimens fabricated both from mild steel and aluminum coupons, bonded with a toughened epoxy. A drop-weight machine equipped with a strain-gage transducer has been used for impact testing. Compared to the static case, at 4 m/s impact, the steel joints have exhibited a significant increase in ultimate load, while only a small change has been observed for the aluminum joints. This is ascribed to the different strain rate response of the two materials.

Jordan (1988) has described the use of a special drop-weight testing machine, defined “instrumented guillotine.” Its peculiar features are the use of a counterweight to adjust the impact energy, from a maximum of 800 J to values lower than 100 J, and a striker of linear shape. The apparatus has been used to test sandwich-type specimens, comparing the impact behavior of epoxy- and acrylic-bonded joints with riveted or spot-welded ones.

Regarding the measurement of the impact strength in terms of force or stress, a first case is represented by the simple butt joint of hollow cylinders, loaded axially in tension. A thorough evaluation of it has been presented by Sawa et al. (2002, 2003). In these works, impact tests have been carried out on specimens made of two hollow steel cylinders bonded together (Sawa et al. 2002) and a hollow steel cylinder bonded to a hollow aluminum cylinder (Sawa et al. 2003); in both works the adhesive is an epoxy, and the outside and inside diameters of the cylinders are 15 and 5 mm, respectively. Figure 17 shows the experimental setup; it can be noticed

**Fig. 17** Schematics of the impact test on cylindrical butt joints used by Sawa et al. (2002) and Sawa et al. (2003)



that the load is applied by releasing, from a chosen height, a weight that hits the flange of the coaxial guide bar which, in turn, applies the tension to the lower cylinder. The measurements are taken by means of strain gages placed on the surface of the cylinders, close to the bond. The papers describe in detail the finite element elastoplastic modeling of the experiments, which aims at assessing the state of stress and strain in the adhesive; in particular, the peak stress occurs at the outside edge of the interface, its value decreases as the adhesive thickness increases (while the opposite trend occurs under static loading). When the specimens are formed by two steel cylinders, fracture always occurs at the lower adhesive/metal interface, which is reached first by the pulse arriving from bottom; in case of dissimilar adherends, fracture occurs at the adhesive/aluminum interface. The impact energy is higher in case of steel-aluminum specimens than in case of steel-steel, about 1.7 times if the lower cylinder is of aluminum, and about 1.5 times if the upper cylinder is of aluminum. Conversely, the opposite behavior is observed for the peak load, which is higher in case of steel-steel specimen.

Another notable case is the study of lap joints under different impact conditions. A reason in favor for this choice is that the single-lap joint is the commonest type of specimen used for static testing; thus it appears straightforward to test the same geometry under dynamic conditions, to evaluate the influence of the loading rate without introducing additional (and possibly misleading) effects due to a change of geometry.

Goglio and Rossetto (2008) have tested single-lap specimens using a modified instrumented Charpy pendulum (Fig. 18). The specimen is mounted on the hammer by means of a fixture that pulls its front half; the back half of the specimen is connected to a transverse tail. When, at the end of the fall, the hammer reaches its lowest position, the tail impacts a pair of stoppers fixed to the pendulum base, and

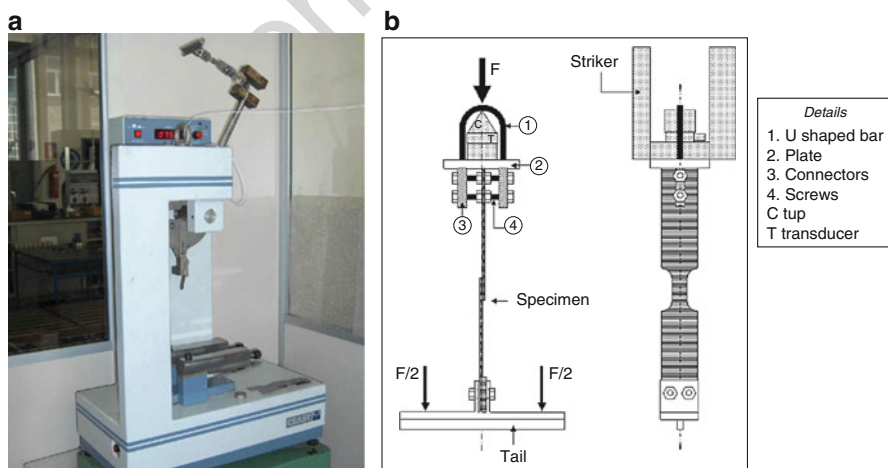


**Fig. 18** Charpy pendulum adapted to test lap joints: (a) overall view; (b) fixation of the specimen on the hammer (From Goglio and Rossetto 2008, copyright Elsevier)

this causes tension in the specimen. This scheme is opposite to that used in other works, such as by Harris and Adams (1985), in which the specimen is fixed at its back half to the pendulum base; the hammer during its fall hooks the front half specimen, thus applying the traction. The hammer is instrumented with a piezoelectric load cell, so that the force can be measured and recorded. The scheme reproduces, in dynamic conditions, the usual stress state of the single-lap joints, with shear and peel stresses concentrated at the overlap ends. It is worth noting that in this kind of test, although the hammer speed is moderate (some m/s), for adhesive layers of some tenths of mm the magnitude of the resulting shearing strain rate is  $10^3 \text{ s}^{-1}$ .

In the work by Goglio and Rossetto (2008), several combinations of bonded length (3, 8, 12.5 mm), adherend thickness (1.5, 3 mm), and adhesive thickness (0.5, 1 mm) have been tested, with the aim of producing failure under different blends of stress. In all cases the adherends were of mild steel, and the adhesive was a bicomponent epoxy; failure occurs in the adhesive, while the adherends remain undamaged. The main result is represented by the graph of Fig. 19 in which (with the same style as of Fig. 13) the maximum values of stress (calculated with a mono-dimensional model) corresponding to failure conditions are reported. Also the points corresponding to failure under static loading are plotted for comparison. The increase of stress values changing from static to impact conditions is evident; regarding the effect of the adhesive thickness, it must be remarked that the thinner layer, under the same speed applied by the pendulum, undergoes a higher strain rate.

A drawback of the use of a pendulum is that, due to the transfer of energy from the hammer to the specimen, the speed during the impact is not exactly constant (although the speed drop is usually limited). A solution to avoid this, used by Cayssials and Lataillade (1996), is to replace the pendulum with a heavy rotating

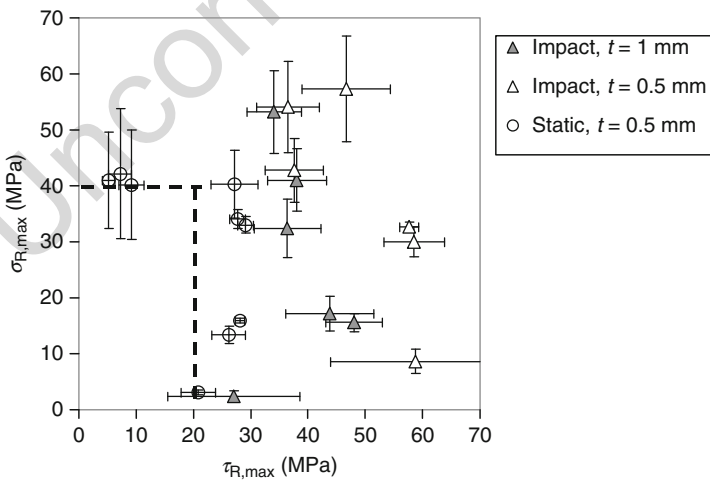


**Fig. 19** Failure locus described by normal and tangential maximum stresses; bars show  $\pm 1$  standard deviation (From Goglio and Rossetto 2008, copyright Elsevier)

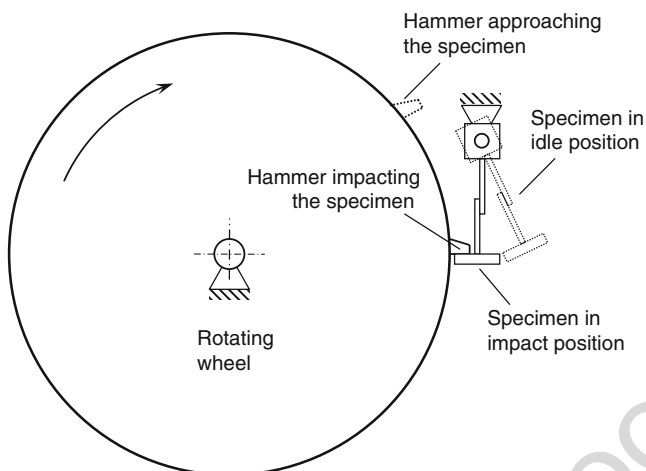


**Fig. 20** Schematic of the inertia wheel used by Cayssials and Lataillade (1996)

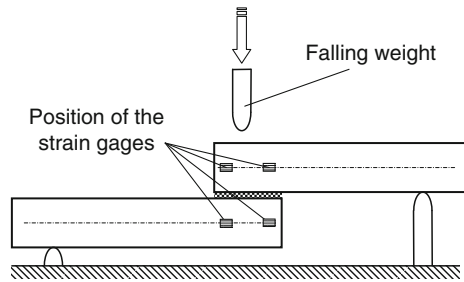
wheel, termed “inertia wheel,” schematized in Fig. 20. Once the wheel (driven by a motor) has reached the desired speed, the specimen is set in position and struck by a hammer fixed at the wheel periphery. Due to the high moment of inertia of the wheel, the reduction of speed is negligible. Also Marzi et al. (2015) have used a rotary device, to assess the dynamic strength of bonded T-peel specimens. Their work has especially aimed at evaluating the performance of a 3D optical systems designed to measure the deformations.

A further alternative to the drop-weight scheme is the use of the “quick crusher,” mounted on a standard tensile testing machine. With this device, the jaws are initially kept open, while the crosshead accelerates; then, they suddenly clamp the specimen, applying an impact load. Schiel et al. (2015) adopted it to assess the impact behavior of bonded joints between zinc-coated or painted sheet metal, typical of the automotive industry. They have found that, in joints fabricated with epoxy adhesives, the weak point is the metal-coating interface or the coating itself.

Another mode in which a lap joint can be impact loaded is out of plane bending. The reason of interest for this case is that, although bonded panels are designed and tested considering their service condition (which, usually, causes in plane loading), the capability of sustaining unexpected transverse impact loads must be assessed as well. For instance, in aerospace construction cases of interest are impacts with debris (in service) and fall of tools (during manufacturing or maintenance).

To validate a spring-mass model of a lap joint under three-point bending, Pang et al. (1995) have carried out low-velocity impact tests on joints of composite laminates, hit by the hemispherical impactor of a drop tower instrumented with semiconductor strain gages to measure the force. Two different overlap lengths and two different adherend thicknesses have been used in the experiments; also the drop height has been varied to obtain different velocities in the range 3.6–4.6 m/s approximately. In this way, the authors have measured the force time history in the

**Fig. 21** Schematic of the transverse impact tests carried out by Higuchi et al. (2002)



impacts and, in particular, the peak force, to correlate it with joint geometry and impact velocity.

Similar experiments have been carried out by Higuchi et al. (2002) to validate the finite element analysis of a single-lap joint. The specimens used in this work were mild steel plates bonded with an epoxy adhesive; strain gages have been applied (in longitudinal direction) on the mid thickness of the adherends to measure the local strain during the impact (see Fig. 21); the impact velocity was about 1 m/s. The goal of this work is to assess the stress distribution on the adherend-adhesive interface which is obtained from finite element results, since it is not possible to measure it directly (the model is validated by comparing its results in points at mid thickness of the adherends, where experimental measurements have been obtained with strain gages). The main findings concern the maximum principal stress  $\sigma_1$ , which attains its maximum near the edge of the interface of the adhesive with the upper (impacted) adherend. It has been noticed that, unlike the case of static loading, such principal stress increases for increasing adherend Young's modulus, overlap length, and adherend thickness; this is due to the fact that, increasing these parameters, the joint reacts with higher stiffness to the displacement imposed by the impactor. Conversely, increasing the adhesive thickness, the principal stress decreases, as it happens in the case of static loading.

Vaydia et al. (2006) have considered the case of bonded composite panels, again impact loaded in three-point bending. In this work, the specimens were epoxy-carbon strips manufactured from carbon fabric; three distinct types of adhesives were used, namely, two different bicomponent epoxies and a nanoclay-reinforced (7%) epoxy. The latter case is considered to test the strength of an adhesive composition suitable to improve its performance under harsh condition (moisture uptake), although such high nanoclay content is expected to reduce the mechanical properties. Impact is applied by the tip of a drop-weight machine, with the setup shown in Fig. 22; the velocity is in the range 1–2 m/s. An extensive finite element analysis was carried out to understand the response of the joint to this loading condition. Model results confirm that there is a strong stress concentration at the ends of the overlap; in particular the peel component has a negative peak at the end of the upper (i.e., impacted) adherend and a positive peak at the end of the unloaded adherend. This fact can be understood by means of a simple argument about the rigid body relative rotation of the two adherends induced by the impact. Also, the shear stress peaks at the ends of the overlap, but the intensity is lower. The examination of

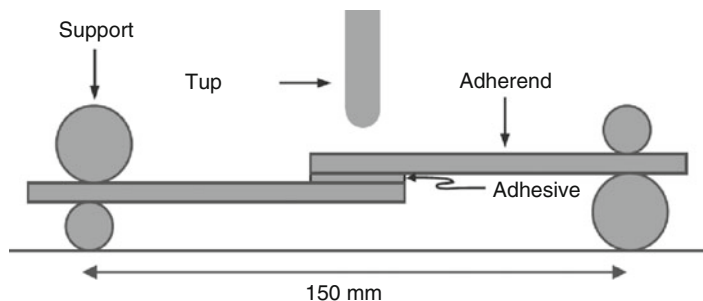


**Fig. 22** Schematic of the transverse impact testing of bonded composites (From Vaidya et al. 2006, copyright Elsevier)

the broken specimen suggests that the crack is initiated by the shear stress and then propagated by the dominant peel stress.

In addition to the strength of adhesives under impact, also the properties related to dynamic deformability are of interest. Sato and Ikegami (2000) have studied the cases of lap joints and scarf joints subjected to axial impact loads. Preliminarily, they have measured the attenuation of the axial strain waves in a special specimen of epoxy adhesive, manufactured (by molding the adhesive resin) as a cylinder of length 900 mm and diameter 20 mm. From these results, the complex compliance of the material was obtained and, in turn, used to identify the parameters of a five-element Voigt model of viscoelasticity. These material data have been introduced in the finite element simulation of the impact tests on the joints. The joints used in these tests were made by aluminum strips 4 mm thick – bonded with the abovementioned epoxy – and adopting three different kinds of geometry, namely, single lap (square ended), tapered, and scarf. The equipment used for carrying out the tests is shown in Fig. 23; the impact bar driven by the cam hits the upper end of the specimen applying the impact load. The main difference between the types of specimen is that in the lap joint, the offset of the adherend midplanes creates a bending moment, from which high stresses originate; in the tapered lap joint this effect is mitigated; for the scarf joint the adherends are aligned and the stresses propagate easily through the joint. The measurements confirm these remarks; in the tapered lap joints (overlap length 100 mm, taper length 50 mm), the peak stresses are reduced about 50% with respect to the single lap (overlap length 100 mm); in the case of scarf joint, the stresses are even much smaller and smoothly distributed, since the stress concentration is relieved.

A comparison of the effect of the strain rate on the mechanical response of a brittle and a ductile adhesive has been carried out by Sugaya et al. (2011), using a drop-weight machine in the tests at higher rates. These authors have found that for the brittle adhesive, the elastic modulus is insensitive to the strain rate, while under increasing strain rate, the tensile strength and the strain at failure increase (the latter remained anyhow small, as only the elastic range was extended). The effect of the strain rate on the ductile adhesive is to increase the tensile strength and to reduce the strain at failure.



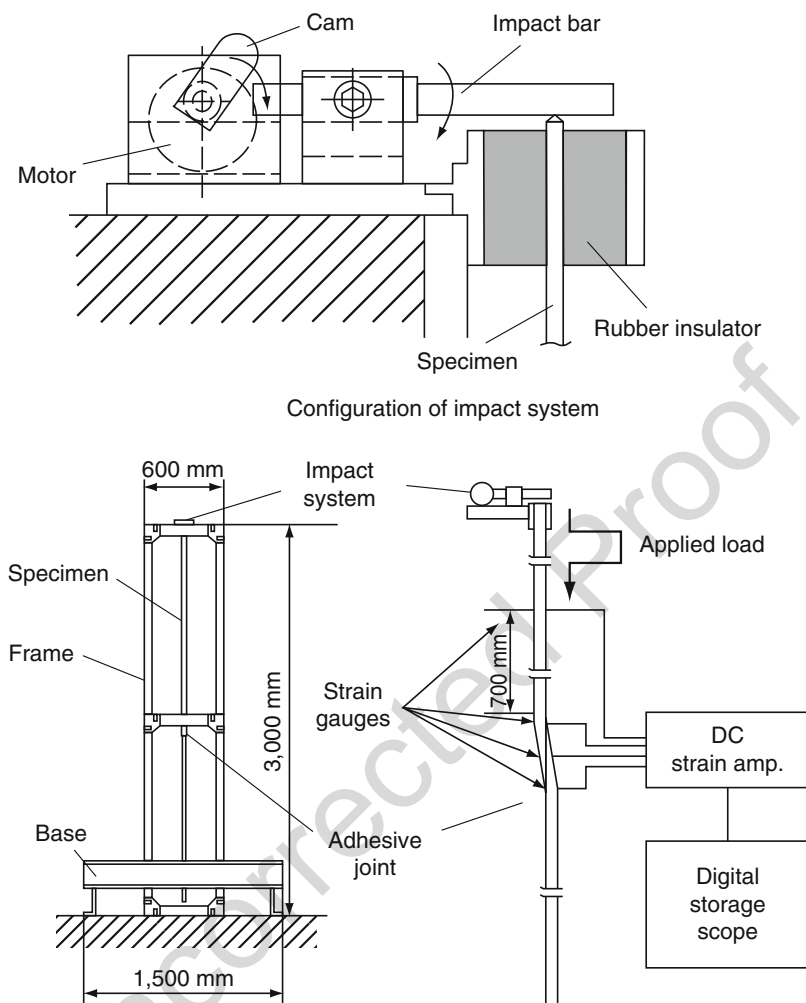


**Fig. 23** Experimental equipment for impact testing of lap and scarf joints (From Sato and Ikegami 2000, copyright Elsevier)

Liao and Sawa (2011) have studied the strength of steel shafts bonded in epoxy hollow cylinders and subjected to axial push-off loads. To support their finite element modeling, they have carried out experiments on a drop-weight machine, and the strains in the cylinder have been measured with strain gages. Good agreement has been found between calculated and measured results.

Al-Zubaidy et al. (2012) have tested experimentally the impact behavior of adhesive bonds between steel plates and CFRP sheets, mainly used for retrofitting existing steel structures. Double strap specimens with different numbers of CFRP layers, fabricated with an epoxy adhesive, have been subjected to impact loads up to

5 m/s applied by means of a drop-weight machine. The results have shown the existence of an effective bond length, above which a further increase in overlap does not increase the ultimate load. Compared to the static strength, the impact strength has increased at loading rate 3.5 m/s and decreased at higher rates.

Liao et al. (2013) have modeled single-lap adhesive joints with dissimilar adherends (aluminum-steel) subject to tensile impact and carried out experiments on a drop-weight machine. In the finite element calculations, the Cowper-Symonds model has been used to account for the strain rate dependence. Finite element and experimental results have agreed in showing that (unlike the case of static loading) under impact the failure starts at the interface of the stiffer adherend.

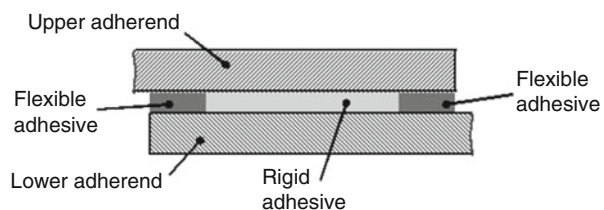
By investigating the behavior of a phenolic resin adhesive blended with rubber, using a pendulum-like testing machine, Adachi et al. (2015) have found an experimental validation of the principle of equivalence between strain rate and temperature. They advance that impact strength could be predicted by applying the principle.

Kadioglu and Adams (2015) have studied the behavior of a flexible viscoelastic tape for automotive application. Single-lap joints of high-strength steel have been tested on a pendulum equipped with a load cell and a laser for measuring the displacement. Compared to static response, an increase of more than twice in adhesive shear strength has been noticed at 1.4 m/s impact speed.

The impact behavior of a pressure-sensitive adhesive has been studied by Hayashida et al. (2015) using butt joint and double cantilever beam specimens and measuring the deformations by means of a high-speed camera. Transparent adherends have been used to observe cavitation and fibrillation, which are the phenomena controlling ductility for this adhesive. It has been noticed that under increasing strain rate, the strength of the butt joints increases, while the fracture energy of the double cantilever beam specimens decreases. This is ascribed to the fact that at high strain rate, the pressure-sensitive adhesive becomes brittle due to viscoelastic effects.

Silva et al. (2016) have studied joints for automotive use, fabricated by combining adhesives of different types, ductile or brittle, as sketched in Fig. 24. The ductile and soft adhesive is placed in the ends of the joint overlap, to smoothen the stress concentrations, while the brittle and hard adhesive is set in the middle of the joint. Impact tests carried out with a drop-weight machine have shown that such a design exploits the best of the two kinds of adhesives, in terms of ultimate load (as shown in Fig. 25) and energy.

**Fig. 24** Schematic of mixed adhesive joint



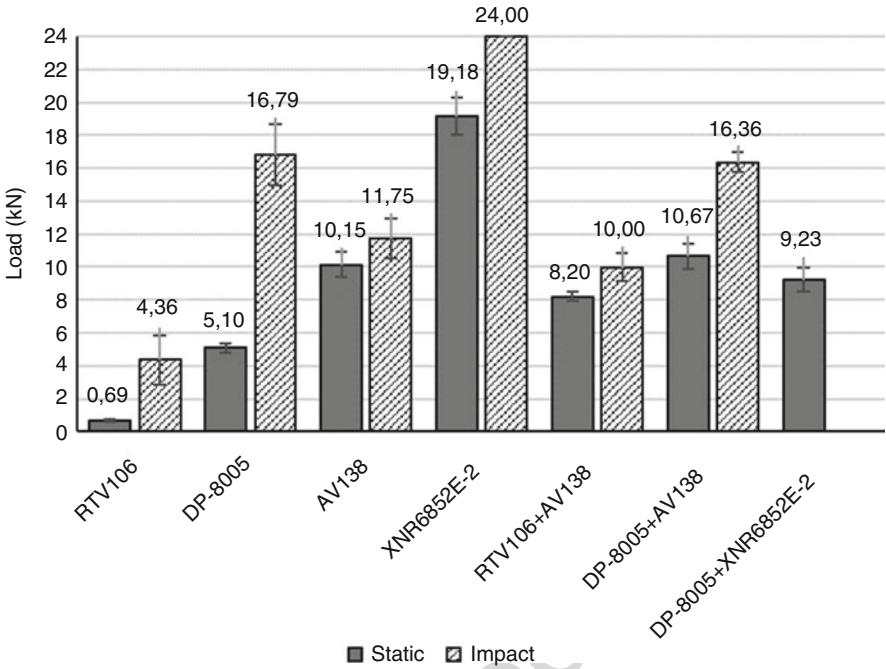


**Fig. 25** Average maximum load comparison between static and impact conditions (From Silva et al. 2016, copyright Latin American Journal of Solids and Structures)

## 21.6 Conductive Adhesives

A field of application that has received attention in the last two decades is the use of conductive adhesives to replace soldering in electronic applications. Such change can bring advantages mainly of ecological type, eliminating the dangerous substances that can be produced by the soldering process and the need for energy to melt the solder. An important advantage given by adhesive joining is that the pitch between neighboring contacts can be shorter compared to the case of soldering, and this is beneficial as far as miniaturization is concerned. Apart from the technological differences introduced by adopting a new technology, the main concerns related to the use of adhesives in this field are unstable contact resistance and impact strength.

Zwolinsky et al. (1996) have reported results obtained by a project of the National Center for Manufacturing Sciences (NCMS), carried out in the early 1990s to assess the suitability of 25 conductive adhesives available on the market at that time. In particular, regarding the assessment of the impact strength, experiments of two types were performed. In the first phase of the project, specimens made with a plastic leaded chip carrier (PLCC) bonded on a coupon were dropped repeatedly from two

different heights, respectively, 0.457 m (18 in.) and 0.914 m (36 in.), recording the number of drops needed to detach the PLCC for each height. In the second phase, drop tests were carried out in specimens formed by a board containing a collection of components, joined by bonding. Each specimen was subjected to three drops from the height of 0.914 m (36 in.). The presence of damage due to the impacts is noticed both by visual inspection and by measurement of the electrical resistance. The result of this series of tests was that the commercial adhesives used at that time were not capable to withstand the impact condition. The authors recommend evaluating the impact performance of an adhesive with a series of 6 drops from 1.52 m (60 in.), with a specimen formed by a bonded PLCC. This recommendation is one of the bases of the NCMS specification for solder replacement adhesives.

Another study of the impact performance of the conductive adhesives was carried out by Daoquiang and Wong (1999). To overcome the poor impact performance of the commercial conductive adhesives, these authors have proposed an adhesive of new formulation containing epoxy-modified polyurethane resin and bisphenol-F. The adopted impact test method is again the one proposed by NCMS and mentioned above (Fig. 26); the channel in which the specimen under test is dropped has the aim of avoiding rotation, thus forcing the part to impact the ground with a defined edge. In their work, these authors have also measured the internal damping of the adhesive, and they have noticed that the materials having high loss factor ( $\tan \delta$ ) are also the most capable to withstand the impacts.

It is evident that the abovementioned experiments obtain, as outcome, the simple result of failure or survival of the specimens. No insight is found about the stress state in the bonds; furthermore, the drop test assesses the strength of the bonded

**Fig. 26** Schematics of the NCMS drop test for bonded electronic components

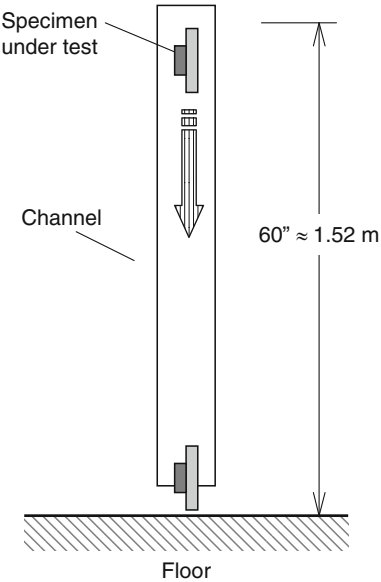
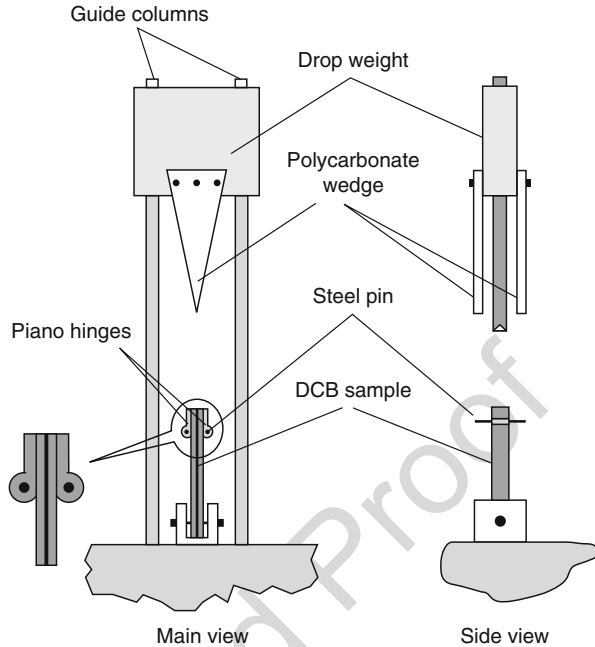


**Fig. 27** Falling wedge test arrangement for conductive adhesives (From Xu and Dillard 2003, copyright IEEE)



specimen, not of the adhesive itself. More recent works aim at studying the impact behavior of the bonded electronic parts with the methods of fracture mechanics or structural dynamics.

Wu et al. (2003) have tested surface mount joints in printed circuit boards, comparing the behavior of an isotropic conductive adhesive with a traditional lead-tin soldering alloy. Joint specimens have first undergone impact on a modified Hopkinson bar, specialized to create three-point bending conditions. Then, after the impact, the specimens (if not already failed) have been destructively tested under shear to assess their residual strength. It has been noticed that the residual shear strength of the joints decreases under increasing strain rate. Compared to the soldering alloy, the adhesive has exhibited lower strength, which nonetheless can be considered satisfactory for practical applications.

Xu and Dillard (2003) have studied the impact strength of conductive adhesives by means of a new impact test, termed falling wedge test (Fig. 27). Its principle is similar to that of the double cantilever beam: a pair (because of the symmetry of the specimen) of wedges fall along a drop tower and with its motion splits apart the two substrates of the bonded joint, mounted vertically on the base of the test rig. To avoid the typical problems related to impact load measurement (already recalled in this section), no load measurement is carried out directly. In the test rig the deformation of the sample is captured by means of a high-speed camera, so that the displacement of the end points and the deformed shape of each beam are obtained from the images. The fracture energy is calculated as

$$G_c = \frac{9\delta_0^2 EI}{4Ba^4} \quad (9)$$

where  $\delta_0$  is the opening displacement,  $E$  is Young's modulus of the substrate,  $I$  is the moment of inertia of the beam section,  $B$  is the beam width, and  $a$  is the crack length. It is easy to notice that Eq. 9 is a simplified version of Eq. 6, in which the correction factors are neglected. The specimens are coupons of printed circuit boards bonded in their central part (by means of a spacer); the adhesives are three different silver-filled epoxy adhesives, especially produced for this research. The tests have been carried out at several temperatures, between  $-70^\circ\text{C}$  and  $90^\circ\text{C}$ , at a fixed impact speed of about 1.6 m/s. It has been observed that the results are influenced by the temperature when the glass transition temperature ( $T_g$ ) of the adhesive is in the considered range; in particular a maximum of  $G_c$  has been noticed for a test temperature close to the  $T_g$  of the adhesive under consideration. These series of tests have confirmed the correlation between the loss factor of the material and the fracture energy.

Rao et al. (2004), reprising the case considered in a work mentioned above (Daoquiang and Wong 1999), have added the study of the first natural frequencies and mode shapes of an electronic packaging formed by a PLCC bonded to a coupon of printed board. From the theoretical viewpoint, an ideal impulse would excite all natural frequencies of the system. This study has considered the first ten natural frequencies, whose range of values, obtained with a finite element model, is extended up to 2 kHz approximately. The impact behavior of the adhesive is adequate if its damping is high enough to dissipate energy over the whole range. The authors have measured the loss factor of four different adhesives, in a frequency range from 0.1 to 3,000 Hz. Comparing these measurements with the results obtained from the drop tests, it has been once again observed that the capability of withstanding the impact is related to the internal damping.

A comprehensive state-of-the-art review on conductive adhesives has been presented by Irfan Mir and Kumar (2008), which considers the main related problems and, among these, the aspects regarding impact strength.

## 21.7 Response to Environmental Conditions

A quite peculiar case is that considered by Park and Kim (2010), who have tested single-lap joints between composite panels subjected to transverse impact of ice spheres, to reproduce the effect of hailstones against an aircraft or other structures exposed to the phenomenon. The experiments and the related finite element simulations have shown that damage occurs if the kinetic energy of the impactor exceeds a threshold. The most important failure mode is delamination, both for panels and joints; however, also adhesive failure can occur. Examination of the specimens has shown that the damage is mainly due to the stress concentration related to the joint. Thus, a joined assembly is more susceptible to this type of damage than a monolithic panel.

Zhang et al. (2015) have studied the response to the strain rate after hydrothermal exposure in an experimental study on joints made of metal adherends (steel, aluminum) bonded with a toughened epoxy. By comparing the response at several crosshead speeds with the quasi-static conditions, they have noticed that: loading rate and aging can be regarded as independent influencing factors (with negligible interaction); the ultimate load is increased by loading rate and decreased by the hydrothermal exposure. The effects of these two factors can be accounted for by means of a linear empirical formula, to predict the resulting strength.

---

## 21.8 Conclusions

This chapter has described the main tests used to assess the impact strength of adhesives and joints, considering both those foreseen by international standards and those appeared in research papers. The main types of test rigs used in the experiments are pendulum, falling weight and Hopkinson bar, or evolutions of these.

The major conclusions of this survey are the following:

1. Of the two standard test methods, the block impact (ASTM D950) is the easiest to carry out and does not require sophisticated equipment, but the only result it gives is the absorbed energy. Moreover, the specimen made of bonded blocks is far from the case of a typical joint, made of thin substrates; thus, this test can give (at best) only a comparison between different adhesive systems. The study by Adams and Harris (1996) has shown that even small errors of alignment can deeply modify the stress profile in the specimen; thus also the use of this test for comparison between adhesives is questionable.
2. The other test foreseen by a standard is the wedge peel impact (ISO EN 11343). Although in this case the arrangement is more representative of a real joint, the immediate answer given by the test rig is a property (energy) of the system formed by specimen and adhesive. Sophisticated data processing is required to extract further information and correlate the result of this test with the adhesive fracture energy  $G_c$ , as done by Blackman et al. (2000). These authors have also shown that in case of unstable crack growth, the ISO standard procedure to process the force time history can produce wrong results. They have also found that the effect of the friction between wedge and strips plays a minor role, compared to  $G_c$ .
3. When the mechanical properties of the adhesive at high loading rate (strain rate  $10^3 \text{ s}^{-1}$ ) are sought, the appropriate test rig is the Hopkinson bar. This apparatus is suitable to test specimens of adhesive under compression in straightforward manner; tests under tension can be carried out with modifications of the basic scheme. Also simple joints can be tested, by properly adapting the ends of the bars. In the last decade, this equipment has become more and more popular and adapted to tests specimens of various shapes (e.g., lap, pin-collar) under different loading conditions (e.g., tension, bending, shear).

4. In the research works presented in the literature, many test rigs are based on the falling weight scheme; alternatively, the impact is applied by a hydraulic ram. In most cases, the specimens are single-lap joints, impacted axially (i.e., in tension) or transversally (i.e., in bending). Usually, in this kind of tests, the impact force is measured by a load cell embedded in the impactor, and the time history is recorded electronically. The typical problem of this measurement is that what is actually measured depends also on the dynamic response of the system formed by specimen and test rig; thus the observed oscillation is not only due to the start and growth of the crack in the joint. For this reason, when the determination of fracture mechanics properties (usually  $G_c$ ) is sought, the use of force measurements is avoided, and the displacement is preferred instead.

As a final remark, it can be added that frequently the experimental studies on the behavior of adhesive or joints under impact are presented together with finite element simulations. This interaction between testing and modeling is, in this field, especially needed, since the possibility of direct measurement of the desired quantities is limited and hindered by the complications introduced by the dynamic response of the tested system.

## References

- Adachi T, Kataoka T, Higuchi M (2015) Predicting impact shear strength of phenolic resin adhesive blended with nitrile rubber. *Int J Adhes Adhes* 56:53–60
- Adams RD, Harris JA (1996) A critical assessment of the block impact test for measuring the impact strength of adhesive bonds. *Int J Adhes Adhes* 16:61–71
- Adamvalli M, Parameswaran V (2008) Dynamic strength of adhesive single lap joints at high temperature. *Int J Adhes Adhes* 28:321–327
- Al-Zubaidy H, Al-Mahaidi R, Zhao X-L (2012) Experimental investigation of bond characteristics between CFRP fabrics and steel plate joints under impact tensile loads. *Compos Struct* 94:510–518
- ASTM D950-03, Standard Test Method for Impact Strength of Adhesive Bonds. ASTM Int
- Beevers A, Ellis MD (1984) Impact behaviour of bonded mild steel lap joints. *Int J Adhes Adhes* 4:13–16
- Bezemer AA, Guyt CB, Vlot A (1998) New impact specimen for adhesives: optimization of high-speed-loaded adhesive joints. *Int J Adhes Adhes* 18:255–260
- Blackman BRK, Kinloch AJ, Taylor AC, Wang Y (2000) The impact wedge-peel performance of structural adhesives. *J Mater Sci* 35:1867–1884
- Blackman BRK, Kinloch AJ, Rodriguez Sanchez FS, Teo WS, Williams JG (2009) The fracture mechanics of adhesives under high rates of loading. *Eng Fract Mech* 79:2868–2889
- Bragov AM, Lomunov AK (1995) Methodological aspects of studying dynamic material properties using the Kolsky method. *Int J Impact Eng* 16:321–330
- Cayssials F, Lataillade JL (1996) Effect of the secondary transition on the behaviour of epoxy adhesive joints at high rates of loading. *J Adhesion* 58:281–298
- Challita G, Othman R (2010) Finite-element analysis of SHPB tests on double-lap adhesive joints. *Int J Adhes Adhes* 30:236–244
- Challita G, Othman R, Casari P, Khalil K (2011) Experimental investigation of the shear dynamic behavior of double-lap adhesively bonded joints on a wide range of strain rates. *Int J Adhes Adhes* 31:146–153



- Chen W, Lu F, Cheng M (2002) Tension and compression tests of two polymers under quasi-static and dynamic loading. *Polym Test* 21:113–121
- Daoqiang L, Wong CP (1999) High performance conductive adhesives. *IEEE Trans Electron Packag Manuf* 22:324–330
- Forrestal MJ, Wright TW, Chen W (2007) The effect of radial inertia on brittle samples during the split Hopkinson pressure bar test. *Int J Impact Eng* 34:405–411
- Gilat A, Goldberg RK, Roberts GD (2007) Strain rate sensitivity of epoxy resin in tensile and shear loading. *J Aerosp Eng* 20:75–89
- Goglio L, Rossetto M (2008) Impact rupture of structural adhesive joints under different stress combinations. *Int J Impact Eng* 35:635–643
- Goglio L, Peroni L, Peroni M, Rossetto M (2008) High strain-rate compression and tension behaviour of an epoxy bi-component adhesive. *Int J Adhes Adhes* 28:329–339
- Harris JA, Adams RD (1985) An assessment of the impact performance of bonded joints for use in high energy absorbing structures. *Proc Inst Mech Eng* 199:121–131
- Hayashida S, Sugaya T, Kuramoto S, Sato C, Mihara A, Onuma T (2015) Impact strength of joints bonded with high-strength pressure-sensitive adhesive. *Int J Adhes Adhes* 56:61–72
- Higuchi I, Sawa T, Suga H (2002) Three-dimensional finite element analysis of single-lap adhesive joints subjected to impact bending moments. *J Adhesion Sci Technol* 16:1327–1342
- ISO EN 11343 (2003) Adhesives – Determination of dynamic resistance to cleavage of high-strength adhesive bonds under impact conditions – Wedge impact method
- Jordan M (1988) The instrumented guillotine impact testing apparatus. *Int J Adhes Adhes* 8:39–46
- Kadioglu F, Adams RD (2015) Flexible adhesives for automotive application under impact loading. *Int J Adhes Adhes* 56:73–78
- Kihara K, Isono H, Yamabe H, Sugibayashi T (2003) A study and evaluation of the shear strength of adhesive layers subjected to impact loads. *Int J Adhes Adhes* 23:253–259
- Kinloch AJ (1997) Adhesives in engineering. *Proc Inst Mech Eng Part G* 211:307–335
- Kolsky H (1963) Stress waves in solids. Dover Publications, New York
- Liao L, Sawa T (2011) Finite element stress analysis and strength evaluation of epoxy-steel cylinders subjected to impact push-off loads. *Int J Adhes Adhes* 31:322–330
- Liao L, Sawa T, Huang C (2013) Experimental and FEM studies on mechanical properties of single-lap adhesive joint with dissimilar adherends subjected to impact tensile loadings. *Int J Adhes Adhes* 44:91–98
- Machado JJM, Marques EAS, Campilho RDSG, da Silva LFM (2017) Adhesives and adhesive joints under impact loadings: an overview. *J Adhesion*. <https://doi.org/10.1080/00218464.2017.1282349>
- Martínez MA, Chocron IS, Rodríguez J, Sánchez Gálvez V, Sastre LA (1998) Confined compression of elastic adhesives at high rates of strain. *Int J Adhes Adhes* 18:375–383
- Marzi S, Biel A, Hesebeck O (2015) 3D optical displacement measurements on dynamically loaded adhesively bonded T-peel specimens. *Int J Adhes Adhes* 56:41–45
- May M, Hesebeck O, Marzi S, Böhme W, Lienhard J, Kilchert S, Brede M, Hiermaier S (2015) Rate dependent behavior of crash-optimized adhesives – Experimental characterization, model development, and simulation. *Eng Fract Mech* 133:112–137
- Mir I, Kumar D (2008) Recent advances in isotropic conductive adhesives for electronics packaging applications. *Int J Adhes Adhes* 28:362–371
- Neumayer J, Kuhn P, Koerber H, Hinterhölzl R (2016) Experimental determination of the tensile and shear behaviour of adhesives under impact loading. *J Adhes* 92:503–516
- Pang SS, Yang C, Zhao Y (1995) Impact response of single-lap composite joints. *Compos Eng* 5:1011–1027
- Park H, Kim H (2010) Damage resistance of single lap adhesive composite joints by transverse ice impact. *Int J Impact Eng* 37:177–184
- Rao Y, Lu D, Wong CP (2004) A study of impact performance of conductive adhesives. *Int J Adhes Adhes* 24:449–453
- Ravi Sankar H, Adamvalli M, Kulkarni PP, Parameswaran V (2015) Dynamic strength of single lap joints with similar and dissimilar adherends. *Int J Adhes Adhes* 56:46–52
- Sato C, Goglio L (2015) Guest editorial. *Int J Adhes Adhes* 56:1–2

- 1020 Sato C, Ikegami K (1999) Strength of adhesively-bonded butt joints of tubes subjected to combined  
1021 high-rate loads. *J Adhes* 70:57–73
- 1022 Sato C, Ikegami K (2000) Dynamic deformation of lap joints and scarf joints under impact loads. *Int*  
1023 *J Adhes Adhes* 20:17–25
- 1024 Sawa T, Suzuki Y, Kido S (2002) FEM stress analysis and strength of adhesive butt joints of similar  
1025 hollow cylinders under static and impact tensile loadings. *J Adhes Sci Technol* 16:1449–1468
- 1026 Sawa T, Suzuki Y, Kido S (2003) Stress analysis and strength estimation of butt adhesive joints of  
1027 dissimilar hollow cylinders under impact tensile loadings. *J Adhes Sci Technol* 17:943–965
- 1028 Schiel M, Kreling S, Unger C, Fischer F, Dilger K (2015) Behavior of adhesively bonded coated  
1029 steel for automotive applications under impact loads. *Int J Adhes Adhes* 56:32–40
- 1030 Sen O, Tekalur SA, Jilek C (2011) The determination of dynamic strength of single lap joints using  
1031 the split Hopkinson pressure bar. *Int J Adhes Adhes* 31:541–549
- 1032 Silva MRG, Marques EAS, da Silva LFM (2016) Behaviour under impact of mixed adhesive joints  
1033 for the automotive industry. *Lat Am J Sol Struct* 13:835–853
- 1034 Sugaya T, Obuchi T, Sato C (2011) Influences of loading rates on stress-strain relations of cured  
1035 bulks of brittle and ductile adhesives. *J Sol Mech Mater Eng* 5:921–928
- 1036 Tyas A, Watson AJ (2001) An investigation of frequency domain dispersion correction of pressure  
1037 bar signals. *Int J Impact Eng* 25:87–101
- 1038 Vaidya UK, Gautam ARS, Hosur M, Dutta P (2006) Experimental-numerical studies of transverse  
1039 impact response of adhesively bonded lap joints in composite structures. *Int J Adhes Adhes*  
1040 26:184–198
- 1041 Wang P, Xu LR (2006) Convex interfacial joints with least stress singularities in dissimilar  
1042 materials. *Mech Mater* 38:1001–1011
- 1043 Williams JG (1984) *Fracture mechanics of polymers*. Ellis Horwood, Chichester
- 1044 Wu CML, Li RKY, Yeung LH (2003) Impact resistance of SM joints formed with ICA. *J Electron*  
1045 *Packag* 125:93–97
- 1046 Xu S, Dillard D (2003) Determining the impact resistance of electrically conductive adhesives using  
1047 a falling wedge test. *IEEE Trans Compon Packag Technol* 26:554–562
- 1048 Yokoyama T (2003) Experimental determination of impact tensile properties of adhesive butt joints  
1049 with the split Hopkinson bar. *J Strain Anal* 38:233–245
- 1050 Yokoyama T, Nakai K (2015) Determination of the impact tensile strength of structural adhesive  
1051 butt joints with a modified split Hopkinson pressure bar. *Int J Adhes Adhes* 56:13–23
- 1052 Yokoyama T, Shimizu H (1998) Evaluation of impact shear strength of adhesive joints with the split  
1053 Hopkinson bar. *JSME Int J Ser A* 41:503–509
- 1054 Yokoyama T, Nakai K, Mohd Yatim NH (2012a) High strain-rate compressive properties and  
1055 constitutive modeling of bulk structural adhesives. *J Adhes* 88:471–486
- 1056 Yokoyama T, Nakai K, Mohd Yatim NH (2012b) High strain-rate compressive behavior of bulk  
1057 structural adhesives: epoxy and methacrylate adhesives. *JSME Int J A-Solid M* 6:131–143
- 1058 Zhang F, Yang X, Xia Y, Zhou Q, Wang H-P, Yu T-X (2015) Experimental study of strain rate  
1059 effects on the strength of adhesively bonded joints after hygrothermal exposure. *Int J Adhes*  
1060 *Adhes* 56:3–12
- 1061 Zhao H, Gary G (1996) On the use of SHPB techniques to determine the behaviour of materials in  
1062 the range of small strains. *Int J Solids Struct* 33:3363–3375
- 1063 Zwolinski M, Hickman J, Rubin H, Zaks Y, McCarthy S, Hanlon T, Arrowsmith P, Chaudhuri A,  
1064 Hermansen R, Lau S, Napp D (1996) Electrically conductive adhesives for surface mount solder  
1065 replacement. *IEEE Trans Compon Packag Manuf Technol Part C* 19:241–250

David A. Dillard and Tetsuo Yamaguchi

**Contents**

22.1	Introduction .....	594
22.2	Blister Tests .....	594
22.3	Sealants and Elastomeric/Foam Adhesives .....	598
22.4	Indentation Tests .....	601
22.5	Scratch Tests .....	603
22.6	Tack .....	604
22.7	CTE, SFT, and Residual Stresses .....	607
22.8	Conclusions .....	609
	References .....	609

**Abstract**

This chapter gives a brief description of special mechanical tests for various types of materials and sample geometries, such as blister tests for membranes/adhesives/coatings, tensile tests and shear tests for sealants and foam adhesives, indentation and scratch tests for coatings, tack tests for pressure sensitive adhesives, and bimaterial curvature tests for characterizing residual stress, stress-free temperature, and coefficient of thermal expansion of adhesives bonded to substrates of interest. In addition, some applications of these tests are also described in this chapter.

D. A. Dillard (✉)

Biomedical Engineering and Mechanics Department, Virginia Polytechnic Institute and State University, Blacksburg, VA, USA

e-mail: [dillard@vt.edu](mailto:dillard@vt.edu)

T. Yamaguchi

Machine Elements and Design Engineering Laboratory, Department of Mechanical Engineering, School of Engineering, Kyushu University, Fukuoka, Japan

e-mail: [yamaguchi@rheo.t.u-tokyo.ac.jp](mailto:yamaguchi@rheo.t.u-tokyo.ac.jp); [yamaguchi@mech.kyushu-u.ac.jp](mailto:yamaguchi@mech.kyushu-u.ac.jp)

## 22.1 Introduction

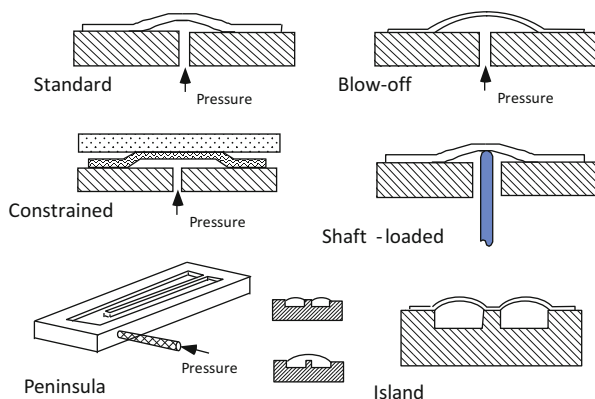
In addition to standard adhesion tests or failure tests, many of which are described in other chapters of this handbook, a wide range of special tests are also performed for specific purposes in industry or in scientific research. In this chapter, several of these special mechanical tests are reviewed, including blister tests for membrane/adhesive/coating, tensile tests and shear tests for sealants and elastomeric foam adhesives, indentation tests and scratch tests for characterizing coating adhesion.

## 22.2 Blister Tests

The blister test is a method to determine the fracture (adhesion) energy between a substrate and a flexible adherend, which could consist of a plate or membrane adhered to the substrate or could simply be an adhesive layer or coating. The blister test was first introduced by Dannenberg for characterizing paint adhesion (Dannenberg 1961; Maugis 1999), although the more familiar form was introduced by Williams (1969). Blister tests are typically loaded by pressurizing the cavity between the substrate and flexible adherend and monitoring the growth of the debond as a function of applied pressure and, in some cases, time. Blister tests can be advantageous for some systems, including when pressurization may mimic actual application conditions, when relevant environments can be used as the pressurization media, and to avoid the need for mechanically gripping for loading. A wide range of blister configurations has been proposed and used, including some which are illustrated in Fig. 1.

In the standard blister test, the flexible adherend is assumed to behave as a plate, with compliance based solely on plate bending. Assuming that the pressure-deflection relationship is linear, the fracture energy is easily obtained by determining the deflected shape at a given pressure using simple plate theory, resulting in:

**Fig. 1** Illustrations of several blister test configurations



$$\mathcal{G} = \frac{3p^2(1-\nu^2)a^4}{32Eh^3} \quad (1)$$

where  $\mathcal{G}$  is the applied strain energy release rate,  $p$  is the pressure,  $\nu$  is the Poisson's ratio of the plate,  $a$  is the radius of the debond,  $E$  is the modulus of the plate, and  $h$  is the thickness of the plate (Anderson et al. 1977). When the thickness of the flexible adherend is very large compared to the debond radius, the assumption of plate bending is no longer valid, and the solution approaches that of a penny-shaped crack between two bodies (Anderson et al. 1977). This results, for example, in

$$\mathcal{G} = \frac{3p^2a}{2\pi E} \quad (2)$$

for the the case of a semi-infinite, incompressible adherend bonded to a rigid substrate. On the other hand, when the thickness of the flexible adherend is very thin, the resistance to deflection comes not from plate bending but primarily from membrane stretching, resulting in the membrane blister specimen (Gent and Lewandowski 1987). The membrane deflection solution is inherently nonlinear and more involved, and becomes dependent on the residual stress present within the membrane.

For the membrane blister, the hole radius  $a_0$  (or in some cases, a larger debond initiated during fabrication) is given as the initial decohesion radius, and the membrane is inflated and effectively peeled off at the radius  $a$  ( $>a_0$ ). The relationship between the central deflection  $\delta$  and the pressure  $p$  of a circular membrane with no residual stress is given by (Hencky 1915)

$$\delta = C \left( \frac{pa^4}{Eh} \right)^{1/3} \quad (3)$$

where  $C$  is a constant dependent on the Poisson's ratio (e.g.  $C = 0.662$  for  $\nu = 0.3$  and  $C = 0.595$  for  $\nu = 0.5$ ). The energy release rate  $\mathcal{G}$  for this geometry is given by (Gent and Lewandowski 1987)

$$\mathcal{G} = \frac{5CD}{4} \left( \frac{p^4a^4}{Eh} \right)^{1/3} = \frac{5D}{4} p\delta \quad (4)$$

where  $D = 0.518$  for  $\nu = 0.3$  and  $0.519$  for  $\nu = 0.5$ . As pressure is gradually increased, debonding is expected to occur at a critical pressure  $p_c$  for a debonding energy of  $\mathcal{G}_c$

$$p_c = \left( \frac{4w}{5CD} \right)^{3/4} \frac{(Eh)^{1/4}}{a_0} \quad (5)$$

at a critical central deflection of

$$\delta_c = \left( \frac{4wC^3}{5DEh} \right)^{1/4} a_0 \quad (6)$$

In all of these test configurations, debonding can often be induced between the adherend and substrate by injecting a gas (for example, nitrogen) or a liquid (e.g. water) under pressure through a small hole in the substrate, as shown in Fig. 2. This membrane form of the blister test has certain advantages in that mechanical testing is sometimes possible even for thin films which are, in general, difficult to evaluate with other mechanical testing approaches due to the soft or delicate nature of the film. Fracture mechanics theory can be applied to evaluate the fracture energy, and with appropriate analysis, accurate measures of debond energy can be obtained. Another advantage is the fact that the test geometry is similar to that in actual usage for coatings or paint, i.e., the evaluation of the film is possible in a geometry relevant to actual applications.

While the blister test provides several advantages for the quantitative evaluation of the fracture energy, there are disadvantages. For example, in order to put holes to pressurize the film, fabrication processes of drilling or etching are often needed, and securing an appropriate initial configuration that results in desired delamination without tearing or bursting the membrane can be involved. In some cases, an auxiliary adherend can be adhered on top of the membrane to reinforce it, though this influences the resulting deformation and energy analysis. For complex hole structures, such as the island and peninsula blister tests, discussed later, the process of undercutting the membrane can be even more complex. In addition, the blister test is limited to sufficiently flexible films like polymer coatings. For hard films, brittle fracture of the film can occur prior to the delamination under the applied pressure. Again, for such cases, a backing or auxiliary adherend can be added to reinforce the fragile coating, however, often resulting in a successful means to evaluate adhesion.

In order to overcome such disadvantages, the blister test has been extended by several researchers. The inverted blister test (Fernando and Kinloch 1990; Jiang and Penn 1990; Fernando et al. 1993) has been developed to reduce the likelihood of cohesive failure or film bursting. Figure 3 schematically shows the inverted blister test. A sufficiently tough and flexible substrate of film geometry is delaminated from the coating or the adhesive adhered firmly onto the support plate, instead of delamination of the coated thin film from the substrate in the standard blister test. The island blister test (Allen and Senturia 1989), the peninsula blister test (Dillard and Bao 1991), and the constrained blister test (Chang et al. 1989) have been proposed. These tests are schematically shown in Fig. 1. In the island blister test, a small “inner island” induces larger driving force for the propagation of the delamination front than that on the periphery (the crack

**Fig. 2** Geometry of the membrane blister test. Fluid is injected through a small hole of radius  $a_0$  under a pressure  $p$  and the membrane of thickness  $h$  is deflected by  $\delta$  and peeled off at radius  $a$

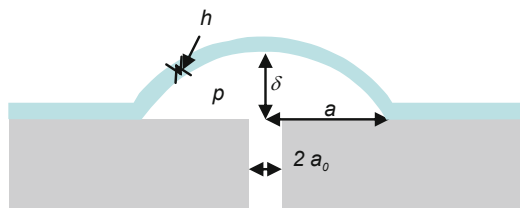
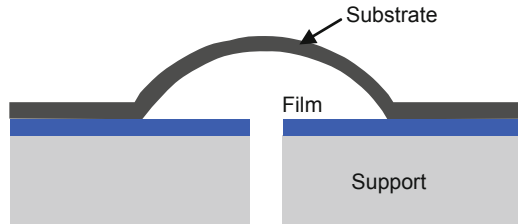


**Fig. 3** Geometry of the inverted blister test



initiation point for the standard blister test), which results in effective delamination at the interface between the film and the substrate island. The peninsula blister test is an extension of the the island blister test, developed to improve the stability in that it is a constant energy release rate specimen. Both tests tend to induce high values of applied energy release rate because of the very localized debonding fronts (Lai and Dillard 1994; Liechti and Shirani 1994; Lai and Dillard 1996; Xu et al. 2006). In the constrained blister test, a transparent rigid cover plate prevents the film from bursting while permitting observation of the delamination front (Chang et al. 1989; Lai and Dillard 1990a, b). Theoretical treatment of some of these tests can also be found in Williams (1997).

Although pressurization of circular or other confined cavities are popular for blister tests, mechanical loading has also been reported as with the shaft-loaded blister (Wan and Mai 1996) and is sometimes simpler to implement in the laboratory. Simple linear versions of blister tests are also popular. The central debonded region of a strip bonded along much of its length to a rigid substrate can be displaced from the substrate, inducing a peeling action. This configuration, known as the pull-off (Gent and Kaang 1986), strip blister (Liechti and Liang 1992), or V-peel (Wan 1999) test by various authors, is simple to perform and results in a particularly simple solution when the flexible adherend deformation is controlled by membrane stretching:

$$\mathcal{G} = \frac{3F\theta}{8b} \quad (7)$$

where  $F$  is the applied force,  $\theta$  is the peeling angle in radians, and  $b$  is the width of the strip. One advantage of this geometry is that the relatively shallow debonding angles reduce plastic bending in the adherends, often resulting in practical or measured peel energies that are closer to the actual debond energy (Kinloch et al. 1994; Moidu et al. 1995, 1998b; Kinloch and Williams 2002; Kinloch et al. 2006).

There are other variations of the blister test and the literature abounds with a range of solutions, so special care should be used for when applying the equations reported in the literature for various blister configurations. In particular, solutions often apply to either block-like (or semi-infinite), plate-like, or membrane-like behavior, as discussed above, so the relative thickness of the flexible substrate to the debond size is of critical importance. Transition regions have been considered by several

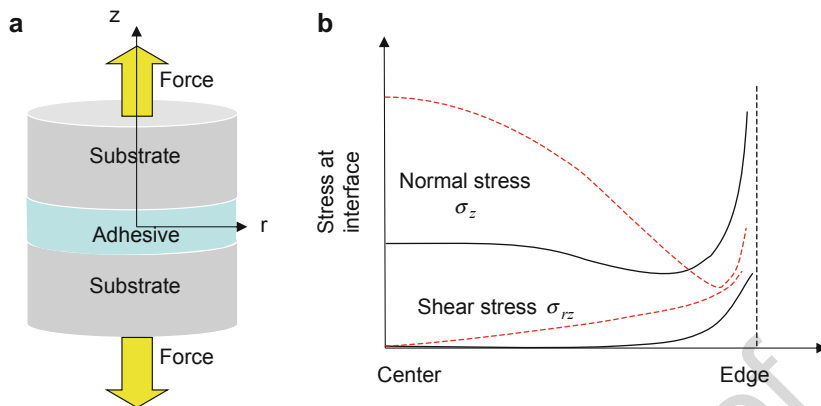
authors (Anderson et al. 1977; Wan and Lim 1998). The transition from plate bending to membrane stretching has received some attention and becomes important when deflections become relatively large (say on the order of the flexible adherend thickness (Wan and Lim 1998). Finally, the presence of residual stress within membrane-like adherends can significantly affect deflections and energy release rate (Dillard and Bao 1991; Wan et al. 2003). Such residual stresses often arise when processing the materials to make specimens, and must be considered and characterized to achieve meaningful experimental results.

## 22.3 Sealants and Elastomeric/Foam Adhesives

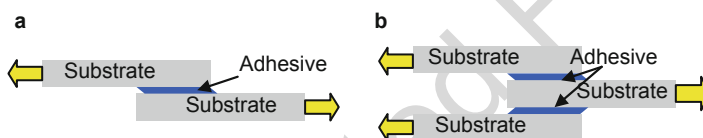
Sealants share many similarities with other adhesives, but are often distinguished by their ability to fill gaps and undergo large strains while maintaining a sealing function, forming a barrier or protective layer against water, air, and other intruding media. There are a number of unique challenges for sealant formulation, joint design, and long term durability, however (Klosowski and Wolf 2015). Elastomer adhesives and foam pressure sensitive adhesive tapes are other types of adhesives, but also are used in thick bondline form. Many of the test methods and analysis procedures covered elsewhere in adhesion texts (Anderson et al. 1977; Kinloch 1987; Adams et al. 1997; Pocius 1997; Dillard 2002) and this handbook can be adapted to evaluate these softer and often thicker material systems, though complications can arise and test method adaptations are often employed. Here, the tensile or butt joint test, shear test, tensile adhesion test, and peel test are briefly reviewed with relevance to such materials.

Figure 4a shows the geometry for the tensile butt joint test, also known as the poker-chip or button test. Two rigid cylinders are bonded end to end with the adhesive or sealant of interest, and the joint is tested by applying tensile forces to the cylinders, measuring the load at break and, in some cases, the load-displacement curves as well as. Alignment of these specimens can be problematic, as slight eccentricity or misalignment can significantly affect the stress state uniformity and the resulting rupture load (Anderson et al. 1988). Though the test method looks quite simple, special care is also required for the data analysis. In practice, the stress distribution at the adhesive-substrate interface is not uniform (see Fig. 4b), but depends on the elasticity (modulus and Poisson's ratio Normalized) of the cylinders and the adhesive, and also strongly depends on the aspect ratio (thickness/diameter), especially for elastomeric adhesives. A range of solutions can be found, depending on the material and geometric parameters (Lindsey 1967; Anderson et al. 1977; Adams et al. 1978; Shephard 2002). Because of the significant difference in modulus between the substrate and adhesive layer, large triaxial tensile stresses arise within the bond. Assuming the adherends may be considered rigid, the strain can range widely, falling between the bound imposed for highly confined, uniaxial strain conditions approached as the thickness to diameter ratio approaches zero, and the uniaxial stress solution (i.e. very large adhesive thickness to diameter ratio), as respectively given by





**Fig. 4** (a) Geometry of a specimen of tensile test for butt joint. (b) stress distribution at the interface between adhesive and substrate (*solid lines* for smaller Poisson's ratio adhesive, *dashes lines* for elastomeric adhesive)



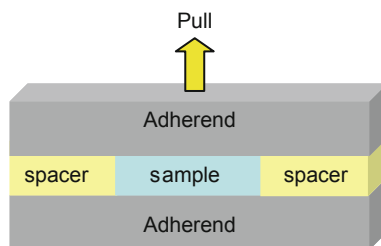
**Fig. 5** Geometry of a specimen of shear test for (a) the single-lap joint, and (b) the double-lap joint

$$\frac{(1 + \nu)(1 - 2\nu)}{(1 - \nu)} \frac{\sigma_x}{E} \leq \epsilon_x \leq \frac{\sigma_x}{E} \quad (8)$$

This shows that for highly constrained systems, Poisson's ratio also becomes very important, as small deviations from ideal elastomer ( $\nu = 1/2$ ) behavior can dramatically affect the resulting apparent stiffness of the joint (Lai et al. 1992). Specialized precision experimental methods to measure such Poisson's ratios or bulk moduli (Rightmire 1970; Yu et al. 2001; Dillard et al. 2008; Tizard et al. 2012; Motamed et al. 2014) may be needed for some modeling purposes of highly constrained elastomers.

Figure 5 illustrates two types of the shear tests, nominally used to measure the apparent shear strength (ASTM-D1002-99 1999; Packham 2005). In the single-lap joint, an adhesive is sandwiched between two plates and shearing is applied by tensile loading until failure occurs. Though this test has advantages in that the method is quite simple and typical of many joint configurations, complexities associated with load eccentricity, bending moments, and terminal regions result in non-uniform normal and shear stress states along the length of the bond (Goland and Reissner 1944; ASTM-D4896-95 2001), effects that are exaggerated by the larger bondline thickness of elastomeric material systems discussed in this section.

**Fig. 6** Geometry of a specimen of tensile adhesion test for sealants, elastomers, or foam adhesives



In order to reduce the rotation and peeling resulting from the eccentricity, the double lap joint has sometimes been advocated. The double-lap joint essentially consists of two single-lap joints, and although peeling is reduced by the symmetric configuration, it is not eliminated and can continue to dominate failure (Borgmeier and DeVries 2000).

Figure 6 is a schematic of the tensile adhesion test, where the adhesive is filled into the space between two adherends and two spacers. In the tensile adhesion test, after the spacers are removed from the specimen, the adhesive may be extended by external loading. When a given elongation (i.e., 25%, 100%, etc.) is reached, the specimen may be fixed for a period of time (ex. 24 hours) with spacers, and any resulting failure type (cohesive or adhesive) is recorded. Cyclic straining, including in the presence of environment, is a common means to load such specimens (ASTM-C719-14 2014) for durability assessment.

Finally, yet another common characterization method for many adhesives, including sealants, are a variety of peel tests. 180° peel tests are particularly common for sealant testing because of the very simple fixturing requirement, though 45°, 90°, and other angles are also used. Reinforcing wire or fabric is often embedded in the sealant to provide enough integrity to prevent peel arm rupture, and also to minimize peel arm straining, which can significantly affect the measured peel force and resulting debonding energy calculations. Stretching of the peel arm requires additional input work, which is typically accomplished through larger crosshead movement, albeit with smaller required forces (Lindley 1971). Although commonly tested at fixed displacement rates (ASTM-C794 2010), these tests can be loaded at a range of rates, temperatures, and humidities, for example, to assess long term performance through viscoelastic superposition methods. Dead loads can also be applied to obtain long-term failure rate information.

Elastomeric foam tapes produced by several manufacturers are finding applications in a wide range of non-structural and even semi-structural applications, including supporting road signs, facades, ceilings, and some load-bearing supports, as well as in the assembly of some transportation vehicles and trailers. Combining a relatively thick, highly dissipative and flexible layer with adequate adhesion offers opportunities for significant energy dissipation, potentially resulting in damage-tolerant solutions where design stress levels are relatively small. Some of these products can be used as alternatives to more traditional sealants, including for mounting windows in commercial buildings. Representative studies of such materials can be found in Townsend et al. (2011a, b, 2012).

## 22.4 Indentation Tests

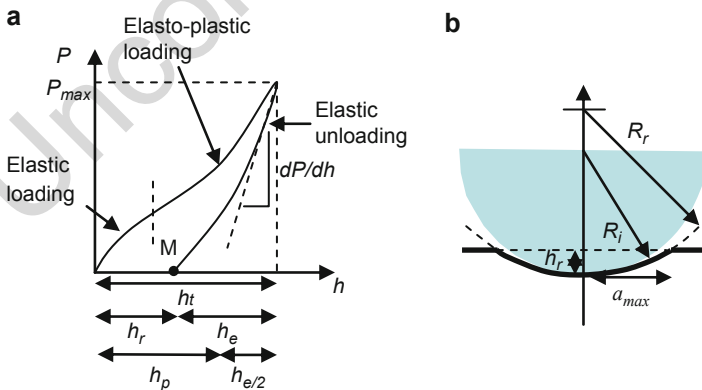
Indentation tests can be used to determine the **hardness** and the elastic modulus of a material (Tabor 2000), and in some cases, the interfacial fracture resistance of thin coatings (Ritter et al. 1989, 1992). Several tests are proposed using different types of indenters such as spherical, three-sided pyramidal, or four-sided Vickers, and the tests are performed not only on a macroscopic scale but also on a microscopic one; measurement of the hardness at very small scales is called nanoindentation. Advantages of the indentation test include that only a small sample is needed, minimal specimen preparation is required, and in some cases even portable equipment can be used to measure the mechanical properties of the material.

Figure 7 shows a schematic for an indentation test of a flat specimen with a spherical indenter. The depth of penetration of a rigid spherical indenter beneath the specimen is  $h_t$  at full load  $P_{\max}$ . When the load is removed, assuming no reverse plasticity, the unloading is elastic and at complete unloading, there is a residual impression of depth  $h_r$ . If the load  $P_{\max}$  is reapplied, then the reloading is elastic through a distance  $h_e = h_t - h_r$  according to the Hertz equation:

$$P = \frac{4}{3}E^*R^{1/2}h_e^{3/2} \quad (9)$$

where  $E^*$  is the composite elastic modulus

$$\frac{1}{E^*} = \frac{1 - \nu^2}{E} + \frac{1 - \nu'^2}{E'} \quad (10)$$



**Fig. 7** Load-Displacement curve for an elastic-plastic specimen loaded with a spherical indenter (radius  $R_i$ ) showing both loading and unloading response. Upon loading, there is an initial elastic response followed by elasto-plastic deformation. Upon unloading, the specimen shows elastic response and comes back to the residual displacement  $h_r$  with the residual impression of radius  $R_r$ .

where  $E$ ,  $E'$ ,  $\nu$  and  $\nu'$  correspond to Young's moduli and Poisson's ratio for the substrate and indenter, respectively and

$$\frac{1}{R} = \frac{1}{R_i} - \frac{1}{R_r} \quad (11)$$

with  $R_i$  and  $R_r$  being the indenter radius and the radius of residual impression, respectively.

Using these equations with the known indenter parameters ( $E^*$ ,  $\nu'$ , and  $R_i$ ) and measured radius of residual impression  $R_r$ , the elastic modulus of the material  $E$  can be determined. The hardness  $H$  can also be quantified by

$$H = \frac{P_{\max}}{\pi a_{\max}^2} \quad (12)$$

where  $a_{\max}$  is the contact radius at maximum load.

Microindentation tests are performed to measure the hardness and the elastic modulus of small specimens with low applied loads. One of the most difficult problems in the microindentation test is to determine the contact radius (Fischer-Cripps 2000). In this case, the contact radius is estimated by the following equation.

$$a_{\max} = \sqrt{2R_i h_p - h_p^2} \cong \sqrt{2R_i h_p} \quad (13)$$

where  $h_p = h_t - h_e/2$  is the the plastic depth, as defined in Fig. 7. Oliver and Pharr (1992) proposed a method to determine the plastic depth as

$$h_p = h_t - \frac{3}{4} \frac{P_{\max}}{dP/dh}. \quad (14)$$

the derivative  $dP/dh$  is calculated by the initial slope of the load-displacement curve at the unloading phase (see Fig. 7).

The use of indentation tests to measure coating adhesion has received wide attention, including for very thin coatings (Oliver and Pharr 2010). Delamination can result from a combination of shearing and tensile stresses developing across the interface. Indentation can induce high stresses across the interface in the vicinity of the interface, but also can induce a compressive in-plane residual stress within the coating, which can contribute to the debonding process through buckling-driven delamination (DeBoer and Gerberich 1996a, b; deBoer et al. 1997a). Overlayers or superlayers can also be added to provide additional stored energy to drive the delamination at the desired interface (Bagchi et al. 1994). A related test, the notched coating adhesion test (Chang et al. 1997; Dillard et al. 1999), involves indentation with a razor blade to sever the coating and induce local debonding, which can then be propagated by subsequent mechanical straining of the substrate. This test has also been used to assess structural adhesive durability as the diffusion times are much shorter for open-faced coatings rather than bonded adhesive joints (Chang et al. 1997;

Moidu et al. (1998a). Other experimental approaches are able to use residual stress alone to propagate debonding, both for tensile (Farris and Bauer 1988) and compressive coating stress states (Hutchinson et al. 2000). Comprehensive theoretical treatments of stresses and fracture of layered and coated systems can be found in Hutchinson and Suo (1992) and Freund and Suresh (2010).

## 22.5 Scratch Tests

The scratch test is a method to determine the adhesion strength of a coated layer, and many embodiments of this method have been proposed, including a number with commercially available instruments designed for this purpose. In the scratch test, as schematically shown in Fig. 8, an indenter or stylus is translated across a coated substrate, typically at a constant velocity under an applied normal force of increasing magnitude. Stresses are introduced at the interface between coating and substrate, and at a critical load, delamination of the coating occurs. Benjamin and Weaver (1963) performed a simple analysis for the scratch test by using the following equations.

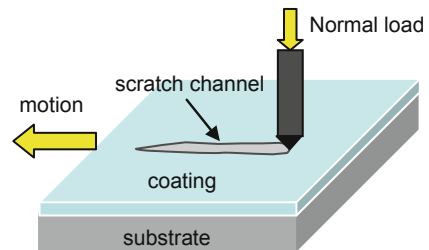
$$F = \frac{AH}{\sqrt{R^2 - H^2}} \quad (15)$$

and

$$A = \sqrt{\frac{W}{\pi H}} \quad (16)$$

where  $A$  is the radius of the contact circle,  $R$  is the radius of the stylus tip,  $W$  is the applied normal load,  $H$  is the indentation hardness of the substrate, and  $F$  is the lateral force. Though they tried to evaluate the coating adhesion by the normal load  $W$  and the lateral force  $F$  at which the the coating is removed from the substrate, there existed several difficulties such as, delamination of the coating before removal, thinning of the film instead of removal, complex elasto-plastic deformation of both coating and substrate, and so on. As with many other coating adhesion tests, real complications make the analysis difficult unless simplifying assumptions are appropriate. In order to improve the scratch test, more sophisticated apparati have been developed. The normal

**Fig. 8** Schematic of the scratch test, in which a coated substrate is moved to the left against a fixed stylus



load is not only controlled to determine the critical load  $W_c$  required to initiate delamination, also the optical microscopy for the monitoring the scratch process and acoustic spectroscopy for detecting acoustic emissions have been employed.

Microscratch and nanoscratch tests have been discussed widely, including in deBoer et al. (1997b). Sarin (1995) developed an alternate version of the scratch test, turning the experiment on its side and performing a micro-scratch test on the cross section of the sample, as shown in Fig. 9. After the edge of the cross section is precisely polished, the scratch test is carried out on a microscopic scale. As a result, the failure mode can be isolated and determined at the coating/substrate interface. In fact, for a titanium carbide (TiC) film coated onto a silicon nitride/titanium carbide (Si<sub>3</sub>N<sub>4</sub> + TiC) ceramic composite, he could generate a crack along the coating/substrate interface and thus obtained a delamination failure mode.

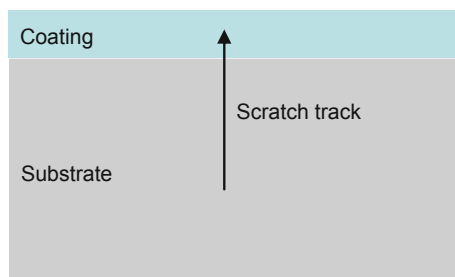
While the scratch test is advantageous for its simplicity in the geometry and ease of the sample preparation, there are several disadvantages. The test is often limited to hard, brittle coatings or nonlinear elasto-plastic deformation complications arise, where the failure mode of the scratch test is not well understood (Bull 2001). Furthermore, the test is very sensitive to the material and the surface geometry or topography of the stylus (Oroshnik and Croll 1978).

However, the scratch test is one of the most popular adhesion tests in both industry and academic research. This comes from the fact that this technique is applicable to the evaluation of a wide range of systems, and commercial equipment is available to perform a variety of functions, such as surface roughness measurement, the evaluation of mechanical properties of the coating, and so on. In particular, the scratch test appears useful for many situations involving hard and brittle coatings. For softer coating, though this test is difficult to extract a true delamination mode from, it is still useful as a complementary test of other techniques. For further information, refer to Lacombe (2006) and references therein.

## 22.6 Tack

Tack is surprisingly complex, with quantitative values often involving a combination of conforming, wetting, bonding, and removal phenomena. Based on the concept of quantifying the adhesion resulting after application of light and momentary pressure,

**Fig. 9** Scratch test using microindenter. The indenter is driven across the substrate and the adhesive on the cross section



tack is intended to measure the aggressiveness of a polymer surface. Tack is widely measured on pressure sensitive adhesives (PSA), but is also of interest in probing the degree of cure or consolidation as other adhesives move from their liquid application state to their solid use state, and for other applications involving adhesion development at interfaces. An underlying concern for tack measurements is that although the intention is to measure the ability of the adhesive to quickly wet and hold a substrate, tack tests inherently involve debonding. Thus, the bonding process is confounded by the debonding process that also occurs upon separation. This involves the creation of new surfaces as cavitation and fibrillation occur, as well as significant rheological dissipation as materials stretch, draw, and break.

Tack is measured by a number of different techniques, ranging from an individual's perception of the "thumb appeal" of an adhesive to sophisticated characterization of the loads and deformations and failure mechanisms involved in bonding and debonding process. Primary tack measurement techniques include probe tack tests, loop tack, quick stick, and rolling ball techniques. These techniques are illustrated schematically in Fig. 10.

The probe tack test involves bringing a probe of desired shape into contact with the adhesive with a prescribed force and duration, then withdrawing the probe at a fixed displacement rate. Some units involve a mechanically driven punch that rises to lift a weight to which a PSA tape has been affixed. The weight can be selected to provide the desired initial contact force and pressure. The probe then drops at a fixed rate, as a load cell records the force. More versatile test frames have also been used to apply controlled force application and probe removal to a wide range of specimens. Although peak values of removal force have typically been recorded and used in quantifying tack, additional information can be obtained from the load deformation trace, such as illustrated in Fig. 11. Other metrics that may be of interest include the area under the force removal curve, the amount of deformation at which the peak force occurs, or the deformation required to completely sever the bond. A range of probe configurations have been used, but flat cylindrical punches of several

**Fig. 10** Illustrations of several test methods used to characterize tack of pressure sensitive adhesives: (a) flat probe tack, (b) loop tack, and (c) rolling ball tack

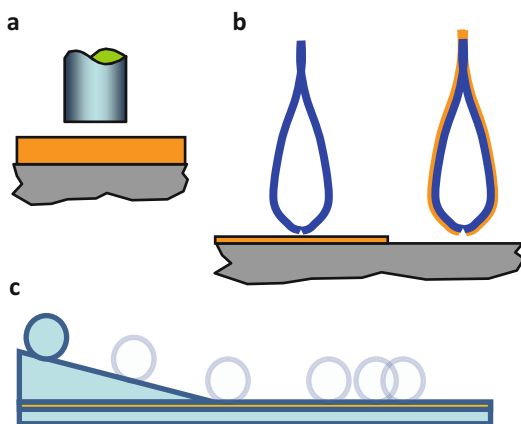
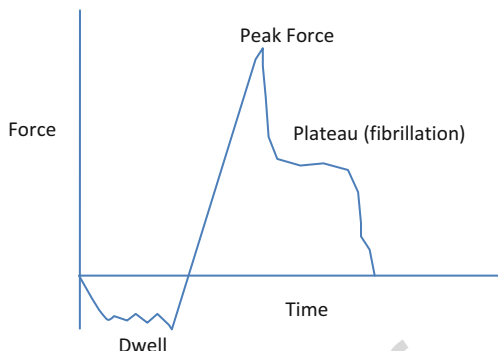


**Fig. 11** Illustration of force vs time trace for a probe tack test of a pressure sensitive adhesive as the probe is compressed to make contact, held for a fixed dwell time, then removed



millimeters in diameter are common, with rounded tips and other configurations used for certain applications.

Zosel (1998) has made wide use of these probe tack techniques characterize the tack of pressure sensitive adhesives as a function of substrate roughness, contact time, contact pressure, and other factors. His work has clearly shown that the drop in load from its initial peak is often due to the onset of internal cavitation within the adhesive layer. The onset of cavitation limits the peak force, but leads to fibrillation which dissipates significant amounts of energy, increasing the energy required to sever the bond. Creton and coworkers have developed sophisticated techniques for carefully aligning the contact, photographing the resulting failure modes, and relating this behavior to material properties (Lakrout et al. 1999). They have also shown that the rate-dependent peak force is related to the frequency-dependent modulus of the adhesive, with lower modulus adhesives exhibiting the onset of cavitation at lower applied loads (Gent and Wang 1991).

The rolling ball tack test involves rolling a ball down an incline and characterizing tack by the ability of the adhesive to arrest the forward motion of the rolling ball. In essence, the ball is placed a given height above a horizontal table supporting the adhesive layer; the potential energy of the ball is converted to kinetic energy as the ball rolls down an incline to the plane containing the adhesive layer, and this energy is then dissipated, primarily through viscoelastic processes, as the ball is brought to a stop. Assuming an ideal conversion of potential energy (the mass of the ball times its height above the plane) to kinetic energy, this energy is equivalent to the distance the ball travels on the adhesive layer times some average dissipative force. One caveat of the rolling ball test is that the rates of bonding and debonding can be significantly larger than encountered in most other tack tests, a fact that can significantly affect the perceived tack of rate-dependent viscoelastic materials.

Other tack tests common for PSAs include the loop tack and quick stick test. The loop tack test involves bringing a loop of adhesive tape, sticky side out, into contact with a rigid adherend of specified length. After contact with what are typically very small contact pressures when the backing is flexible, the crosshead is reversed and the loop is removed from the substrate. The initial portion of the test is similar to a



peel test at just over  $90^\circ$ , albeit one that is conducted without the bonding step normally used to prepare peel test specimens. As the debonds approach one another, the stiffness of the backing becomes more significant, and the loop tack begins looking and acting more like a probe test. Here, the backing stiffness again becomes important in that it controls the size of the contact that remains at final separation; thicker and stiffer backings lead to greater contact areas at final separation, resulting in larger peak force measurements. Some users report using the peak force when recording loop tack results, while others report using the plateau that results during the initial peeling process. These are clearly very different phenomena that are controlled by different mechanisms, again suggesting the complexity of performing and interpreting tack tests in general and loop tack tests in particular (Plaut and Ritchie 2004). The PSTC procedure known as the quick stick test is related to initial phase of the loop tack test. A tape is laid on a horizontal surface, without applying external mechanical pressure, and the strip is removed by pulling on one end. Again, this test resembles a  $90^\circ$  peel test.

---

## 22.7 CTE, SFT, and Residual Stresses

Residual stresses are of significant importance in many adhesive applications. In some applications, including for structural adhesive joints, the residual stresses induced within a bond can be larger than stresses induced by mechanical loading the joint experiences within its service life. Because residual stresses can represent locked-in stresses that are present at all times, their duration can become a factor in joint life. Also, because they can be ever present, residual stresses can make adhesive layers and coatings more susceptible to environmental damage, including environmental stress cracking (Dillard et al. 1995).

The coefficient of thermal expansion can be measured through several methods, the most direct being through linear or volumetric dilatometry. Thermal mechanical analyzers (TMA) are ideally suited for such measurements, as their components are made of very low expansion materials such as quartz. With precise temperature control, they are able to accurately measure linear dimensional changes as a function of temperature. They are often equipped to measure other properties such as softening temperature, etc. in addition to the coefficient of thermal expansion as a function of temperature.

While the coefficient of thermal expansion is nominally a property of the bulk adhesive, the residual stress, often the term of interest for design, is a property of a bonded joint or structure. One of the simplest means to measure the residual stress in an adhesive layer or coating is with the use of the bimaterial curvature technique. For several centuries, people have known that when two dissimilar beams are bonded together at the interface and subjected to a temperature change, a curvature will result. This curvature is a function of the relative moduli and thicknesses of the two beams or plates, the difference or mismatch in their CTEs, and the temperature change to which they are exposed. The resulting stresses are easily determined but

are quite nonuniform (Timoshenko 1925). A very significant simplification occurs when the thickness of one layer is significantly smaller than the other. For example, if a softer polymeric adhesive is applied as a thin coating on a stiffer substrate, the resulting curvature becomes a function of the residual stress within this coating layer. For appropriate geometries then, characterizing the curvature of bimaterial strips provides a direct measure of the residual stress experienced within the adhesive or coating layer. Dating back to the work of Stoney (1909):

$$\sigma = \frac{E_s t_s^2}{6(1 - \nu_s)h\rho} \quad (17)$$

where  $\sigma$  is the equal biaxial stress in the thin film,  $h$  is the thickness of the film,  $E_s$ ,  $t_s$ , and  $\nu_s$  are the modulus, thickness, and Poisson's ratio of the thick substrate, and  $\rho$  is the radius of curvature. Several improvements have been proposed to refine the equation to cover a broader range of specimen configurations (Freund et al. 1999; Yu et al. 2003). This can be applied to thermal, hygral (Li et al. 2012), or other swelling mechanisms as well. Such tests are easily performed in commercial dynamic mechanical analyzers (DMA), which boost excellent force and displacement resolution in a carefully controlled temperature chambers (Case et al. 2005). Figure 12 illustrates applications of this technique in which a bimaterial strip is cantilevered at one end and the deflection of the other end is measured. Knowing the geometry of the specimen and the moduli of substrate and adhesive layer, one can determine the difference in coefficient of thermal expansion between the substrate and adhesive as well as the stress-free temperature.

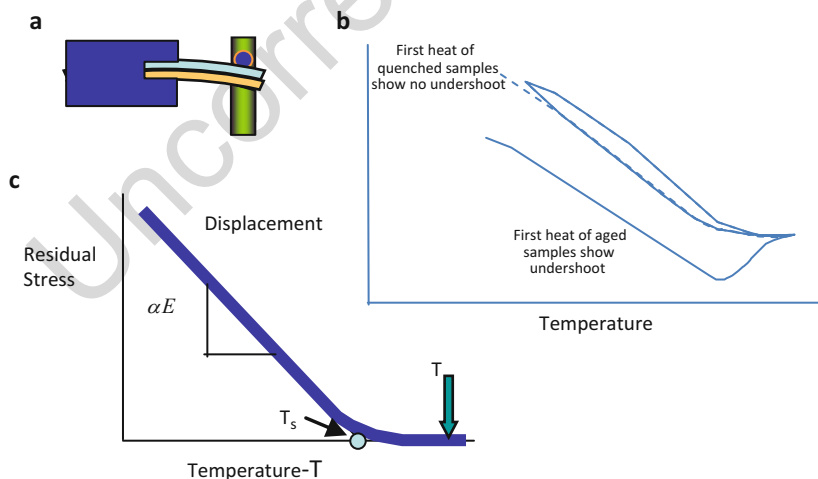


**Fig. 12** Illustration of bimaterial curvature technique to measure coefficient of thermal expansion and stress-free temperature of adhesive layer showing: (a) test sample, (b) representative deflection results, and (c) residual stress predictions

## 22.8 Conclusions

This chapter describes a few examples of the special tests to measure the mechanical properties of the membranes, films, adhesives, coating, sealants, and foam/elastomeric adhesives. The major conclusions are the following:

1. A wide range of blister tests have been developed and utilized to characterize adhesion, and in some cases, moduli and other properties of adhering membranes and adherends.
2. For mechanical tests of thick samples sandwiched between two substrates such as sealants, elastomeric or foam adhesives, shear tests and tensile adhesion tests have been commonly applied.
3. Indentation tests are performed to evaluate the elastic modulus and the hardness of the coating, and in some cases, interfacial fracture energies associated with coating adhesion.
4. In the scratch tests, a stylus is driven across a coated surface under a normal load. The critical load is determined by the first appearance of the failure. While the test can be applied for hard and brittle coating, quantitative evaluation for the soft and ductile coating is more complex.
5. Several tack tests, such as probe tack, loop tack, quick stick and rolling ball tack tests are used to evaluate the aggressiveness of a polymer surface.
6. The coefficient of thermal expansion (CTE) and the stress-free temperature (SFT) can be important in engineering design and are often measured to estimate residual stresses in adhesives.

## References

- Adams RD, Coppendale J, Peppiatt NA (1978) Stress analysis of axisymmetric butt joints loaded in torsion and tension. *J Strain Anal* 13(1):1–10
- Adams RD, Comyn J, Wake WC (1997) Structural adhesive joints in engineering. Chapman and Hall, London
- Allen MG, Senturia SD (1989) Application of the island blister test for thin-film adhesion measurement. *J Adhes* 29(1–4):219–231
- Anderson GP, Bennett SJ, DeVries KL (1977) Analysis and testing of adhesive bonds. Academic Press, New York
- Anderson GP, Chandapeta S, DeVries KL (1988). Effect on removing eccentricity from button tensile tests. Adhesively bonded joints: testing, analysis, and design. S. Johnson, ASTM. **STP-981**
- ASTM-C719-14 (2014) Standard test method for adhesion and cohesion of elastomeric joint sealants under cyclic movement (Hockman cycle). ASTM, West Conshohocken
- ASTM-C794 (2010). Standard test method for adhesion-in-peel of elastomeric joint sealants. ASTM, West Conshohocken, PA
- ASTM-D1002-99 (1999). Standard test method for apparent shear strength of single-lap-joint adhesively bonded metal specimens by tension loading (metal-to-metal). Annual book of ASTM standards. ASTM, West Conshohocken, 15.06: 42–45
- ASTM-D4896-95 (2001) Standard guide for use of adhesive-bonded single lap-joint specimen test results, Annual book of ASTM standards, vol 15.06. ASTM, West Conshohocken, pp 419–424

- 501 Bagchi A, Lucas GE, Suo Z, Evans AG (1994) New procedure for measuring the decohesion energy  
502 for thin ductile film on substrates. *J Mater Res* 9(7):1734–1741
- 503 Benjamin P, Weaver C (1963) Adhesion of metals to crystal faces. *R Soc Proc Ser A* 274  
504 (1357):267–273
- 505 Borgmeier PR and KL DeVries (2000). Interpreting adhesive joint tests. 2nd international sympo-  
506 sium on adhesive joints, Newark
- 507 Bull SJ (2001) Can the scratch adhesion test ever be quantitative? Adhesion measurement of films  
508 and coatings. K. L. Mittal. Utrecht, vol 2. VSP, p 107
- 509 Case SL, O'Brien EP, Ward TC (2005) Cure profiles, crosslink density, residual stresses, and  
510 adhesion in a model epoxy. *Polymer* 46(24):10831–10840
- 511 Chang YS, Lai YH, Dillard DA (1989) The constrained blister – a nearly constant strain-energy  
512 release rate test for adhesives. *J Adhes* 27(4):197–211
- 513 Chang T, Sproat EA, Lai YH, Shephard NE, Dillard DA (1997) A test method for accelerated  
514 humidity conditioning and estimation of adhesive bond durability. *J Adhes* 60(1–4):153–162
- 515 Dannenberg H (1961) Measurement of adhesion by a blister method. *J Appl Polym Sci* 5:125–134
- 516 DeBoer MP, Gerberich WW (1996a) Microwedge indentation of the thin film fine line. 1. Mechan-  
517 ics. *Acta Mater* 44(8):3169–3175
- 518 DeBoer MP, Gerberich WW (1996b) Microwedge indentation of the thin film fine line. 2. Experi-  
519 ment. *Acta Mater* 44(8):3177–3187
- 520 deBoer MP, Kriese M, Gerberich WW (1997a) Investigation of a new fracture mechanics specimen  
521 for thin film adhesion measurement. *J Mater Res* 12(10):2673–2685
- 522 deBoer MP, Nelson JC, Gerberich WW (1997b) Mechanics of interfacial crack propagation in  
523 microscratching. *Thin Films: Stresses Mech Properties Vi* 436:103–108
- 524 Dillard DA (2002) Fundamentals of stress transfer in bonded systems. In: Dillard DA, Pocius AV  
525 (eds) *Adhesion science and engineering I: the mechanics of adhesion*, vol 1. Elsevier, Amster-  
526 dam, pp 1–44
- 527 Dillard DA, Bao Y (1991) The peninsula blister test – a high and constant strain-energy release rate  
528 fracture specimen for adhesives. *J Adhes* 33(4):253–271
- 529 Dillard D, Parvatareddy H, Clifton AP (1995). Environmental stress cracking In high performance  
530 adhesives and composites. *Antec 95 – the plastics challenger: a revolution in education*,  
531 conference proceedings, Vols I-iii–Vol I: Processing; Vol Ii: Materials; Vol Iii: Special areas,  
532 pp 3971–3975
- 533 Dillard DA, Chen B, Chang TN, Lai YH (1999) Analysis of the notched coating adhesion test.  
534 *J Adhes* 69(1–2):99–120
- 535 Dillard DA, Mallick A, Ohanehi DC, Yu J-H, Lefebvre DR (2008) A high precision experimental  
536 method to determine Poisson's ratios of encapsulant gels. *J Electron Packag Trans ASME* **130**  
537 (Compendex):0310061–0310067
- 538 Farris RJ, Bauer CL (1988) A self-delamination method of measuring the surface-energy of  
539 adhesion of coatings. *J Adhes* 26(4):293–300
- 540 Fernando M, Kinloch AJ (1990) Use of the inverted-blister test to study the adhesion of photo-  
541 polymers. *Int J Adhes Adhes* 10(2):69–76
- 542 Fernando M, Kinloch AJ, Vallerschamp RE, Vanderlinde WB (1993) The use of the inverted-blister  
543 test to measure the adhesion of an Electrocoated paint layer adhering to a steel substrate (Vol  
544 12, Pg 875, 1993). *J Mater Sci Lett* 12(16):U1243–U1243
- 545 Fischer-Cripps AC (2000) A review of analysis methods for sub-micron indentation testing.  
546 *Vacuum* 58(4):569–585
- 547 Freund LB, Suresh S (2010) *Thin film materials: stress, defect formation and surface evolution*.  
548 Cambridge, Cambridge University Press
- 549 Freund LB, Floro JA, Chason E (1999) Extensions of the Stoney formula for substrate curvature to  
550 configurations with thin substrates or large deformations. *Appl Phys Lett* 74(14):1987–1989
- 551 Gent AN, Kaang S (1986) Pull-off forces for adhesive tapes. *J Appl Polym Sci* 32:4689–4700
- 552 Gent AN, Lewandowski LH (1987) Blow-off pressures for adhering layers. *J Appl Polym Sci*  
553 33(5):1567–1577
- 554 Gent AN, Wang C (1991) Fracture-mechanics and cavitation in rubber-like solids. *J Mater Sci*  
555 26(12):3392–3395

- 556 Goland M, Reissner E (1944) The stresses in cemented joints. *J Appl Mech* 11:A17–A27
- 557 Hencky H (1915) Über den spannungszustand in kreisrunden platten mit verschwindender  
558 biegesteifigkeit. *Zeitschrift für Mathematik und Physik* 63:311–317
- 559 Hutchinson JW, Suo Z (1992) Mixed-mode cracking in layered materials. *Adv Appl Mech*  
560 29(29):63–191
- 561 Hutchinson JW, He MY, Evans AG (2000) The influence of imperfections on the nucleation and  
562 propagation of buckling driven delaminations. *J Mech Phys Solids* 48(4):709–734
- 563 Jiang KR, Penn LS (1990) Use of the Blister test to study the adhesion of brittle materials.1. Test  
564 modification and validation. *J Adhes* 32(4):203–216
- 565 Kinloch AJ (1987) Adhesion and adhesives: science and technology. Chapman and Hall, London
- 566 Kinloch AJ, Williams JG (2002) The mechanics of peel tests. In: Dillard DA, Pocius AV (eds) *The*  
567 *mechanics of adhesion*, vol 1. Elsevier, Amsterdam, pp 273–302
- 568 Kinloch AJ, Lau CC, Williams JG (1994) The peeling of flexible laminates. *Int J Fract* 66(1):45–70
- 569 Kinloch AJ, Hadavinia H, Kawashita L, Moore DR, Williams JG (2006) A numerical analysis of the  
570 elastic-plastic peel test. *Engineering Fracture Mechanics* 73:2324–2335. (Copyright 2006, The  
571 Institution of Engineering and Technology)
- 572 Klosowski J, Wolf AT (2015) Sealants in construction. Boca Raton: CRC Press
- 573 Lacombe R (2006) Adhesion measurement methods: theory and practice. CRC Press, Boca Raton
- 574 Lai YH, Dillard DA (1990a) An elementary plate-theory prediction for strain-energy release rate of  
575 the constrained blister test. *J Adhes* 31(2–4):177–189
- 576 Lai YH, Dillard DA (1990b) Numerical-analysis of the constrained blister test. *J Adhes* 33(1–2):63–74
- 577 Lai YH, Dillard DA (1994) A study of the fracture efficiency parameter of blister tests for films and  
578 coatings. *J Adhes Sci Technol* 8(6):663–678
- 579 Lai YH, Dillard DA (1996) A comparison of energy release rates in different membrane blister and  
580 peel tests. *J Adhes* 56(1–4):59–78
- 581 Lai YH, Dillard DA, Thornton JS (1992) The effect of compressibility on the stress distributions in  
582 thin elastomeric blocks and annular bushings. *J Appl Mech-Trans Asme* 59(4):902–908
- 583 Lakrout H, Sergot P, Creton C (1999) Direct observation of cavitation and fibrillation in a probe tack  
584 experiment on model acrylic pressure-sensitive-adhesives. *J Adhes* 69(3–4):307–359
- 585 Li YQ, Dillard DA, Lai YH, Case SW, Ellis MW, Budinski MK, Gittleman CS (2012) Experimental  
586 measurement of stress and strain in Nafion membrane during hydration cycles. *J Electrochem*  
587 *Soc* 159(2):B173–B184
- 588 Liechti KM, Liang YM (1992) The interfacial fracture characteristics of Bimaterial and sandwich  
589 blister specimens. *Int J Fract* 55(2):95–114
- 590 Liechti KM, Shirani A (1994) Large-scale yielding in blister specimens. *Int J Fract* 67(1):21–36
- 591 Lindley, P. B. (1971). Ozone attack at a rubber- metal bond. *J Institution Rubber Industry* 5(6):  
592 243–248
- 593 Lindsey GH (1967) Triaxial Fracture Studies. *J Appl Phys* 38(12):4843–4852
- 594 Maugis D (1999) Contact, adhesion and rupture of elastic solids. Springer, Heidelberg
- 595 Moidu AK, Sinclair AN, Spelt JK (1995) Analysis of the peel test – prediction of adherend plastic  
596 dissipation and extraction of fracture energy in metal-to-metal adhesive joints. *J Test Eval*  
597 23(4):241–253
- 598 Moidu AK, Sinclair AN, Spelt JK (1998a) Adhesive joint durability assessed using open-faced peel  
599 specimens. *J Adhes* 65(1–4):239–257
- 600 Moidu AK, Sinclair AN, Spelt JK (1998b) On the determination of fracture energy using the peel  
601 test. *J Test Eval* 26(3):247–254
- 602 Motamed A, Bhasin A, Liechti KM (2014) Using the poker-chip test for determining the bulk  
603 modulus of asphalt binders. *Mech Time-Depend Mater* 18(1):197–215
- 604 Oliver WC, Pharr GM (1992) An improved technique for determining hardness and elastic modulus  
605 using load and displacement sensing indentation experiments. *J Mater Res* 7(6):1564–1583
- 606 Oliver WC, Pharr GM (2010) Nanoindentation in materials research: past, present, and future. *MRS*  
607 *Bull* 35(11):897–907
- 608 Oroshnik J, Croll WK (1978) Threshold adhesion failure. An approach to aluminum thin-film  
609 adhesion measurement using the stylus method. In: *Adhesion measurement of thin films, thick*  
610 *films and bulk coatings*, 2–4 Nov 1976. ASTM, Philadelphia

- Packham DE (ed) (2005) Handbook of adhesion. Wiley, Chichester
- Plaut RH, Ritchie JL (2004) Analytical solutions for peeling using beam-on-foundation model and cohesive zone. *J Adhes* 80(4):313–331
- Pocius AV (1997) Adhesion and adhesives technology: an introduction. Hanser, Munich
- Rightmire, G. K. (1970). Experimental method for determining Poisson's ratio of elastomers. *J of Lubrication Tech* 92 Ser F(3): 381–388
- Ritter JE, Lardner TJ, Rosenfeld L, Lin MR (1989) Measurement of adhesion of thin polymer-coatings by indentation. *J Appl Phys* 66(8):3626–3634
- Ritter JE, Sioui DR, Lardner TJ (1992) Indentation behavior of polymer-coatings on glass. *Polym Eng Sci* 32(18):1366–1371
- Sarin VK (1995) Micro-scratch Test for Adhesion Evaluation of Thin Films. In: Mittal KL (ed) Adhesion Measurement of Films and Coatings. VSP, Utrecht, p 175
- Shephard N (2002) Stresses and fracture of elastomeric bonds. In: Dillard DA, Pocius AV (eds) Adhesion science and engineering-I: the mechanics of adhesion, vol 1. Elsevier, Amsterdam
- Stoney GG (1909) The tension of metallic films deposited by electrolysis. *Proc R Soc A* 82:172–175
- Tabor D (2000) The hardness of metals. Oxford University Press, London
- Timoshenko SP (1925) Analysis of bi-metal thermostats. *J Opt Soc Am* 11:233–255
- Tizard GA, Dillard DA, Norris AW, Shephard N (2012) Development of a high precision method to characterize Poisson's ratios of Encapsulant gels using a flat disk configuration. *Exp Mech* 52(9):1397–1405
- Townsend BW, Ohanehi DC, Dillard DA, Austin SR, Salmon F, Gagnon DR (2011a) Characterizing acrylic foam pressure sensitive adhesive tapes for structural glazing applications-part I: DMA and ramp-to-fail results. *Int J Adhes Adhes* 31(7):639–649
- Townsend BW, Ohanehi DC, Dillard DA, Austin SR, Salmon F, Gagnon DR (2011b) Characterizing acrylic foam pressure sensitive adhesive tapes for structural glazing applications-part II: creep rupture results. *Int J Adhes Adhes* 31(7):650–659
- Townsend B, Ohanehi DC, Dillard DA, Austin SR, Salmon F, Gagnon DR (2012) Developing a simple damage model for the long-term durability of structural glazing adhesive subject to sustained wind loading. *J Archit Eng* 18(3):214–222
- Wan KT (1999) Fracture mechanics of a V-peel adhesion test – transition from a bending plate to a stretching membrane. *J Adhes* 70(3–4):197–207
- Wan KT, Lim SC (1998) The bending to stretching transition of a pressurized blister test. *Int J Fract* 92(4):L43–L47
- Wan KT, Mai YW (1996) Fracture mechanics of a shaft-loaded blister of thin flexible membrane on rigid substrate. *Int J Fract* 74(2):181–197
- Wan KT, Guo S, Dillard DA (2003) A theoretical and numerical study of a thin clamped circular film under an external load in the presence of a tensile residual stress. *Thin Solid Films* 425(1–2):150–162
- Williams ML (1969) Continuum interpretation for fracture and adhesion. *J Appl Polym Sci* 13(1):29–40
- Williams JG (1997) Energy release rates for the peeling of flexible membranes and the analysis of blister tests. *Int J Fract* 87(3):265–288
- Xu DW, Liechti KM, de Lumley-Woodyear TH (2006) Closed form nonlinear analysis of the peninsula blister test. *J Adhes* 82(8):831–866
- Yu JH, Dillard DA, Lefebvre DR (2001) Pressure and shear stress distributions of an elastomer constrained by a cylinder of finite length. *Int J Solids Struct* 38(38–39):6839–6849
- Yu JH, Guo S, Dillard DA (2003) Bimaterial curvature measurements for the CTE of adhesives: optimization, modeling, and stability. *J Adhes Sci Technol* 17(2):149–164
- Zosel A (1998) Effect of fibrillation on the tack of pressure sensitive adhesives. *Int J Adhes Adhes* 18(Compendex):265–271

Uncorrected Proof

Erol Sancaktar

## Contents

23.1	Introduction .....	616
23.2	Classical Models .....	616
23.2.1	General Deformation Theories .....	616
23.2.2	Rubber Elasticity .....	620
23.2.3	Viscoelasticity Considerations .....	625
23.2.4	Interrelationship Between the Tensile and Shear Properties .....	629
23.2.5	Time–Temperature Superposition .....	629
23.3	Advanced Models .....	631
23.3.1	Nonlinear Viscoelasticity .....	631
23.3.2	Empirical Description of Creep Behavior .....	632
23.3.3	Increases in Joint Strength Due to Rate-Dependent Viscoelastic Adhesive Behavior .....	633
23.3.4	Reductions in Stress Concentration Due to Viscoelastic Adhesive Behavior .....	636
23.3.5	Singularity Methods .....	636
23.3.6	Bulk Adhesive as Composite Material .....	637
23.3.7	The Concept of the Interphase .....	639
23.3.8	Damage Models .....	647
23.3.9	The Effects of Cure and Processing Conditions on the Mechanical Behavior .....	657
23.4	Prediction of Limit (Threshold) and Failure Stresses .....	659
23.5	Conclusion .....	660
References	.....	661

## Abstract

A complete approach to modeling adhesives and sealants needs to include considerations for: deformation theories and viscoelasticity with linearity and

E. Sancaktar (✉)

Department of Polymer Engineering, University of Akron, Akron, OH, USA

e-mail: [erol@uakron.edu](mailto:erol@uakron.edu)



nonlinearity considerations, rubber elasticity, singularity methods, bulk adhesive as composite material, damage models, the effects of cure and processing conditions on the mechanical behavior, and the concept of the “interphase.”

## 23.1 Introduction

Most adhesives are polymer-based materials and exhibit viscoelastic behavior. Some adhesives are elastomer materials and also exhibit full or partial rubberlike properties. The word “elastic” refers to the ability of a material to return to its original dimensions when unloaded, and the term “mer” refers to the polymeric molecular makeup in the word “elastomer.” In cases where brittle material behavior prevails, and especially, when inherent material flaws such as cracks, voids, and disbonds exist in such materials, the use of the methods of fracture mechanics are called for. For continuum behavior, however, the use of damage models is considered appropriate in order to be able to model the progression of distributed and non-catastrophic failures and/or irreversible changes in material’s microstructure, which are sometimes described as “elastic limit,” “yield,” “plastic flow,” “stress whitening,” and “strain hardening.” Many adhesive materials are composite materials due to the presence of secondary phases such as fillers and carriers. Consequently, accurate analysis and modeling of such composite adhesives require the use of the methods of composite materials.

A complete approach to modeling adhesives and sealants, therefore, needs to include considerations for deformation theories, viscoelasticity, bulk adhesive as composite material, damage models, and the effects of cure and processing conditions on the mechanical behavior.

## 23.2 Classical Models

### 23.2.1 General Deformation Theories

The deformation theory was first introduced by Hencky (1924), and can be described in the form:

$$\epsilon_{ij} = \left( \frac{\sigma_{kk}}{9K} \right) \delta_{ij} + \psi S_{ij}. \quad (1)$$

where  $S_{ij}$  is the deviatoric stress tensor. Equation 1 reduces to the elastic stress–strain relations when  $\psi = 1/2 G$ , where  $G$  is the elastic shear modulus. If the scalar function  $\psi$  is defined as

$$\psi = \left( \frac{1}{2G} \right) + \Omega \quad (2)$$

then Eq. 1 can be interpreted in the form

$$\epsilon_{ij} = \epsilon_{ij}^E + \epsilon_{ij}^V + \epsilon_{ij}^P \quad (3)$$

where

$$\epsilon_{ij} = \left( \frac{\sigma_{kk}}{9K} \right) \delta_{ij} + \left( \frac{S_{ij}}{2G} \right) + \Omega S_{ij} \quad (4)$$

and

$$\epsilon_{ij}^P = \Omega S_{ij} \quad (5)$$

with  $\Omega$  being a scalar function of the invariants of the stress tensor, and the superscripts E, V, and P representing elastic, viscoelastic, and plastic behaviors, respectively.

Consequently, the relation

$$\epsilon = \left( \frac{\sigma}{E} \right) + \Lambda \sigma \quad (6)$$

is obtained for uniaxial tension on the basis of Eqs. 4 and 5 with  $\Lambda = 2\Omega/3$ .

Ramberg and Osgood (1943) used a special form of Eq. 6 with  $\Lambda = K\sigma^{n-1}$  to result in:

$$\epsilon = \left( \frac{\sigma}{E} \right) + K\sigma^{n'} \quad (7)$$

where K and  $n'$  are material constants.

They reported that Eq. 7 could be used successfully to describe uniaxial tension and compression behavior of various metal alloys. Equation 7 was later modified by McLellan (1969) to accommodate strain rate effects. McLellan interpreted the terms E, K, and  $n'$  of Eq. 7 as material functions with the function E representing viscoelastic behavior and functions K and  $n'$  representing work-hardening characteristics. The terms E, K, and  $n'$  were all described as functions of the strain rate ( $d\epsilon/dt$ ) so that rigidity, stress, and plastic flow, respectively, were all affected by variations in the strain rate.

Renieri et al. (1976) used a bilinear form of rate-dependent Ramberg–Osgood equation to describe the stress–strain behavior of a thermosetting adhesive in the bulk tensile form. The bilinear behavior was obtained when  $\log \epsilon_p$  was plotted against  $\log \sigma$ , where  $\epsilon_p$  represents the second term on the right-hand side of Eq. 7. The model adhesive they used was an elastomer-modified epoxy adhesive with and without carrier cloth. They made several modifications on the form of the equation previously used by McLellan. First, the plastic strain  $\epsilon_p$  was assumed to be a function of the over-stress above the elastic limit stress (the development of over-stress approach will be presented subsequently) and second, the stress levels  $\sigma^*$  defining the intersection point

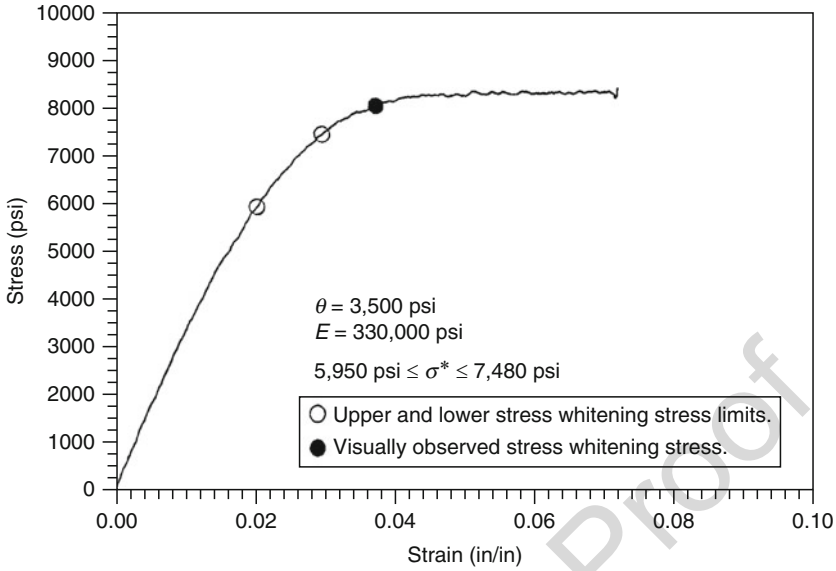


**Fig. 1** A stress–strain diagram identifying upper and lower stress-whitening stress limits,  $\sigma_U$  and  $\sigma_{L,0}$ , respectively, as well as the visually observed stress-whitening stress. The modulus of elasticity,  $E$ , and the elastic limit stress,  $\theta$  for the bulk adhesive tested are  $3.3 \times 10^5$  and  $3.5 \times 10^3$  psi (2276 and 24 MPa), respectively

for the bilinear behavior were found to occur slightly below the stress-whitening stress values. The equations they developed in this fashion are given as:

$$\epsilon = \frac{\sigma}{E}, \quad 0 < \sigma < \theta \quad (8.1)$$

$$\epsilon = \left(\frac{\sigma}{E}\right) + K_1[\sigma - \theta]^{n_1} \quad \theta < \sigma < \sigma^* \quad (8.2)$$

$$\epsilon = \left(\frac{\sigma}{E}\right) + K_2[\sigma - \theta]^{n_2} \quad \sigma^* < \sigma < Y \quad (8.3)$$

where  $\theta$  is the elastic limit stress (yield stress) in simple tension,  $Y$  is the maximum stress, and  $K_1$ ,  $K_2$ ,  $n_1$ , and  $n_2$  are strain rate–dependent material functions. Renieri et al. (1976) reported that the adhesive material properties were different before and after stress whitening due to changes in material behavior, and therefore bilinear equations of the form (Eq. 8) were needed to describe such behavior. Brinson et al. (1975) determined that for the adhesive with the carrier cloth the parameter  $n$ , Eq. 7, varied much less with strain rate in comparison to the adhesive without the carrier cloth. They concluded that the bilinear forms they proposed, Eq. 8, accurately predicted the rate-dependent behavior of their model adhesive.

Figures 1 and 2 show the application of the model described above to the stress–strain and stress-whitening behaviors of a bulk thermosetting epoxy film

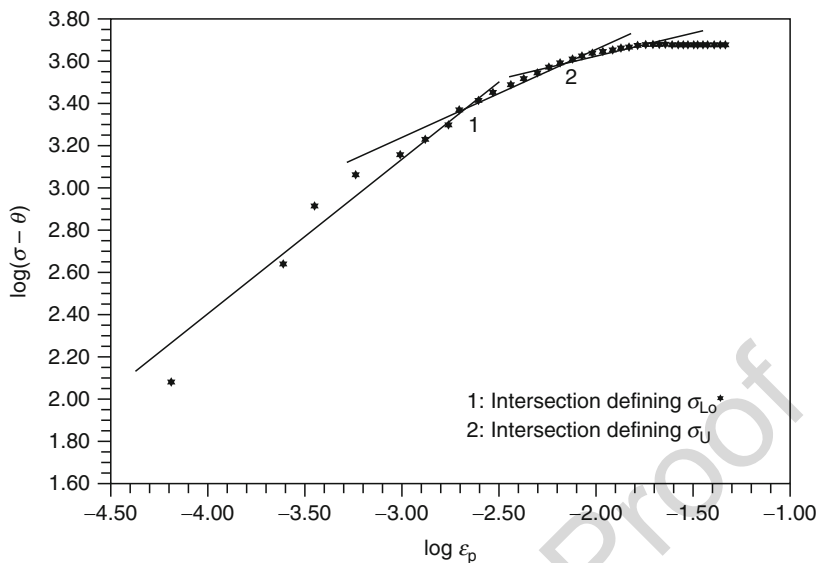


**Fig. 2** A dual bilinear fit stress–strain diagram identifying upper and lower stress-whitening stress limits,  $\sigma_U$  and  $\sigma_{Lo}^*$ , respectively, as well as the visually observed stress whitening stress. The modulus of elasticity,  $E$ , and the elastic limit stress,  $\theta$  for the bulk adhesive tested are  $3.3 \times 10^5$  and  $3.5 \times 10^3$  psi (2276 and 24 MPa), respectively

adhesive containing a nonwoven nylon mat, as obtained by Sancaktar and Beachtle (1993). In this application, two intersection points are identified by intersecting two pairs of bilinears, each of which containing a common slope line as part of the bilinear sets (Fig. 2). This procedure was called “dual bilinear fit” by Sancaktar and Beachtle (1993). These intersection points define upper and lower stress-whitening stress limits shown in Fig. 1.

Ramberg–Osgood-type equations were also used to describe shear behavior of structural adhesives. Zabora et al. (1971) used a rate-dependent form of the Ramberg–Osgood equation to describe the shear behavior of structural adhesives in the bonded form.

Simple power function–type relations may be utilized in an empirical fashion to describe nonlinear elastic behavior of structural adhesives in tensile and shear modes when their mechanical behavior is found to be relatively rate insensitive. For example, Sancaktar and Schenck (1985) used a power function relation given by

$$\tau = K\gamma^r \quad (9)$$

where  $\tau$  and  $\gamma$  are shear stress and strain, respectively, to represent the nonlinear elastic shear behavior of a thermoplastic polyimidesulfone adhesive in the bonded form. Sancaktar and Dembosky (1986) showed that when the stress–strain curve has a well-defined initial elastic region and a yield point,  $\tau_y$ , then a bimodal relation given by

$$\gamma = \frac{\tau}{G}, \quad \tau < \tau_y \quad (10.1)$$

$$\gamma = B\tau^m \quad \tau > \tau_y \quad (10.2)$$

can be utilized more appropriately.

### 23.2.2 Rubber Elasticity

Vulcanized rubber materials typically have more than 200% elongation in a tensile test and are capable of returning rapidly and forcibly to their original dimensions when load is removed. This elastic response is due to the three-dimensional cross-linked network molecular structure they have. An elastomer, on the other hand, typically has elongation rates of 100% or more and a significant amount of resilience. Resilience is represented by the area under the elastic portion of the stress-strain curve, and therefore refers to a material's ability to undergo elastic deformations.

#### Estimation of Rubber Material Properties

Tension in a stretched ideal rubber arises from the entropy contribution. The change in entropy between the stretched state (S) and unstretched state ( $S_0$ ) is related to the number of conformations in the corresponding states with the relation:

$$S - S_0 = k \left[ \ln \left( \frac{W}{W_0} \right) \right] \quad (11)$$

where  $k$  = the Boltzmann constant =  $1.3804 \times 10^{-16}$  dyn-cm/K, and  $W_0$  and  $W$  are the number of initial (unstretched) and the final (stretched, and reduced) possible conformational states, respectively. Evaluation of the number of possible conformational states leads to:

$$S - S_0 = - \left( \frac{1}{2} \right) N_0 k \left\{ \left( \frac{L}{L_0} \right)^2 + 2 \left( \frac{L_0}{L} \right) - 3 \right\} \quad (12)$$

where  $N_0$  = the number of network chains in sample of initial length and cross-sectional area  $L_0$  and  $A_0$ , respectively. In the stretched state, the length and the cross-sectional area become  $L$  and  $A$ , respectively.

In the rubbery state, the material is assumed to be incompressible, so that:

$$L_0 A_0 = LA \quad (\text{i.e., } V = \text{constant}). \quad (13)$$

For ideal rubber, force can be related to temperature,  $T$ , and the entropy differential with the relation:

$$F = -T \left( \frac{dS}{dL} \right)_T \quad (14)$$

144 Consequently, differentiation of Eq. 12 results in:

$$F = \left( \frac{N_0 k T}{L_0} \right) \left\{ \left( \frac{L}{L_0} \right) - \left( \frac{L_0}{L} \right)^2 \right\}. \quad (15)$$

145 Division of Eq. 15 by the instantaneous cross-sectional area (A) yields the true  
146 stress ( $\sigma_T$ ) equation for ideal rubber:

$$\sigma_T = \frac{F}{A} = nRT \left\{ \left( \frac{L}{L_0} \right)^2 - \left( \frac{L_0}{L} \right) \right\} \quad (16)$$

147 where  $n$  = the number of moles of network chains per unit volume (i.e.,  $\text{cm}^3$ ) =  $d/M_C$ ,  
148 where  $d$  = the density ( $\text{g}/\text{cm}^3$ ),  $M_C$  = the number average molecular weight between  
149 successive points of cross-linkage, and

$$n = N_0 / (A_0 L_0) N_{AV}. \quad (17)$$

150 Division of Eq. 15 by initial cross-sectional area ( $A_0$ ) yields the engineering stress  
151 ( $\sigma$ ) equation for ideal rubber:

$$\sigma = \frac{F}{A_0} = nRT \left\{ \left( \frac{L}{L_0} \right) - \left( \frac{L_0}{L} \right)^2 \right\}. \quad (18)$$

152  
153 If a cross-linked network is produced from originally linear rubber molecules by  
154 the addition of " $n_c$ " moles of tetrafunctional cross-linking agent per  $\text{cm}^3$  of rubber,  
155 then each cross-link originates four network chains, and each chain belongs to two  
156 cross-links. Consequently, there are  $2 n_c$  moles of network chains per  $\text{cm}^3$  in the  
157 cross-linked network, that is,  $2 n_c = n = d/M_C$ .

158 For any portion of the stress-strain curve, the isothermal Young's modulus (E) is  
159 defined as

$$E = L \left( \frac{d\sigma_T}{dL} \right)_T = \left( \frac{d\sigma_T}{e_T} \right)_T \quad (19)$$

160 and substitution in Eq. 16 results in:

$$E = nRT \left\{ 2 \left( \frac{L}{L_0} \right)^2 + \left( \frac{L_0}{L} \right) \right\}. \quad (20)$$

A remarkable aspect of Eq. 20 is that it gives Young's modulus as a function of extension (or strain) which conflicts with the customary definition for elastic modulus.

For small magnitudes of strains approximating the condition  $L = L_0$ , Eq. 20 yields:

$$E(\Delta L \sim 0) = 3nRT = \frac{3dRT}{M_C}. \quad (21)$$

### Constitutive Elastic Rubber Behavior

The incremental work,  $dW_1$ , done by the stress  $\sigma_1$  is

$$dW_1 = \sigma_1 L'_2 L'_3 (dL_1) \quad (22)$$

where  $(L'_i)$  are the new dimensions of a volumetric material element.

Therefore,

$$\frac{dW_1}{L_1 L_2 L_3} = \sigma_1 \lambda_2 \lambda_3 d\lambda_1 \quad (23)$$

where "extension ratio" or "stretch ratio":

$$\lambda = \frac{L}{L_0}. \quad (24)$$

Superposition of the contributions from  $\sigma_2$  and  $\sigma_3$  results in

$$\frac{dW}{V_0} = dU_0 = \sigma_1 \lambda_2 \lambda_3 d\lambda_1 + \sigma_2 \lambda_1 \lambda_3 d\lambda_2 + \sigma_3 \lambda_1 \lambda_2 d\lambda_3 \quad (25)$$

where  $V_0$  is the initial volume and  $U_0$  is the strain energy density.

Differentiation of the strain energy density results in:

$$\frac{dU_0}{d\lambda_1} = \sigma_1 \lambda_2 \lambda_3 \Rightarrow \sigma_1 = \left( \frac{1}{\lambda_2 \lambda_3} \right) \left( \frac{dU_0}{d\lambda_1} \right) \quad (26)$$

The stretch ratio invariants,  $(I'_1, I'_2, I'_3)$ , are defined as follows:

$$I'_1 = \lambda_{xx}^2 + \lambda_{yy}^2 + \lambda_{zz}^2 = \lambda_1^2 + \lambda_2^2 + \lambda_3^2 \quad (27)$$

$$\begin{aligned} I'_2 &= \lambda_{xx}^2 \lambda_{yy}^2 + \lambda_{yy}^2 \lambda_{zz}^2 + \lambda_{zz}^2 \lambda_{xx}^2 - \lambda_{xy}^4 - \lambda_{yz}^4 - \lambda_{zx}^4 \\ &= \lambda_1^2 \lambda_2^2 + \lambda_2^2 \lambda_3^2 + \lambda_3^2 \lambda_1^2 \end{aligned} \quad (28)$$

$$I'_3 = \lambda_{xx}^2 \lambda_{yy}^2 \lambda_{zz}^2 + 2\lambda_{xy}^2 \lambda_{yz}^2 \lambda_{zx}^2 - \lambda_{xx}^2 \lambda_{yz}^4 - \lambda_{yy}^2 \lambda_{zx}^4 - \lambda_{zz}^2 \lambda_{xy}^4 = \lambda_1^2 \lambda_2^2 \lambda_3^2 \quad (29)$$

The strain energy density,  $U_0$ , is a function of the stretch ratio invariants:

$$U_0 = U_0(I'_1, I'_2, I'). \quad (30)$$

For an incompressible material,

$$\frac{V}{V_0} = I'_3 = 1 \quad (31)$$

Substitution in Eq. 26 yields:

$$\begin{aligned} \sigma_1 &= \left( \frac{1}{\lambda_2 \lambda_3} \right) \left( \frac{dU_0}{d\lambda_1} \right) \\ &= \left( \frac{1}{\lambda_2 \lambda_3} \right) \left\{ \left[ \left( \frac{dU_0}{dI'_1} \right) \left( \frac{dI'_1}{d\lambda_1} \right) \right] + \left[ \left( \frac{dU_0}{dI'_2} \right) \left( \frac{dI'_2}{d\lambda_1} \right) \right] + \left[ \left( \frac{dU_0}{dI'_3} \right) \left( \frac{dI'_3}{d\lambda_1} \right) \right] \right\}. \end{aligned} \quad (32)$$

Noting that,  $(dI'_1/d\lambda_1 = d\lambda_1; dI'_2/d\lambda_1 = 2\lambda_1(\lambda_2^2 + \lambda_3^2), \text{ and } dI'_3/d\lambda_1 = 2\lambda_1\lambda_2^2\lambda_3^2,)$  substitution yields:

$$\sigma_1 = \left( \frac{2}{\lambda_1 \lambda_2 \lambda_3} \right) \left\{ \left( \frac{dU_0}{dI'_1} \right) \lambda_1^2 + \left( \frac{dU_0}{dI'_2} \right) \lambda_1^2 (\lambda_2^2 + \lambda_3^2) + \left( \frac{dU_0}{dI'_3} \right) \lambda_1^2 \lambda_2^2 \lambda_3^2 \right\}. \quad (33)$$

If the work–strain energy relation is used to determine, say,  $\sigma_1$ , the pressure must be added since for an incompressible solid, pressure,  $p$ , does not contribute to strain energy as there is no volume change. Therefore,

$$\sigma_1 = \left\{ \left( \frac{1}{\lambda_2 \lambda_3} \right) \left( \frac{dU_0}{d\lambda_1} \right) + p \right\}. \quad (34)$$

### Mooney–Rivlin Equations for Rubber Elasticity

With this model, the strain energy density function is assumed to be a linear function of  $(I'_1)$  and  $(I'_2)$ , that is,

$$U_0 = \left( \frac{\Phi}{2} \right) (I'_1 - 3) + \left( \frac{\Psi}{2} \right) (I'_2 - 3) \quad (35)$$

where  $\Phi$  and  $\Psi$  are material constants. Therefore,

$$\sigma_i = \lambda_i^2 \Phi - \left( \frac{\Psi}{\lambda_i^2} \right) + p. \quad (36)$$

A relation between the Mooney–Rivlin parameters,  $\Phi$  and  $\Psi$ , and the stretch components can be obtained as follows: Consider the first stress invariant,  $J_1$ ,



$$J_1 = \sigma_1 + \sigma_2 + \sigma_3$$

$$= \Phi(\lambda_1^2 + \lambda_2^2 + \lambda_3^2) - \Psi \left\{ \left( \frac{1}{\lambda_1^2} \right) + \left( \frac{1}{\lambda_2^2} \right) + \left( \frac{1}{\lambda_3^2} \right) \right\} + 3p \quad (37)$$

189 but  $J_1 = 3p \Rightarrow$

$$\Phi(\lambda_1^2 + \lambda_2^2 + \lambda_3^2) = \Psi \left\{ \left( \frac{1}{\lambda_1^2} \right) + \left( \frac{1}{\lambda_2^2} \right) + \left( \frac{1}{\lambda_3^2} \right) \right\}. \quad (38)$$

190  $\sigma_3$  is zero for the condition of plane stress, and therefore:

$$p = \left( \frac{\Psi}{\lambda_3^2} \right) - \lambda_3^2 \Phi. \quad (39)$$

191 For incompressible materials, the condition  $\lambda_1^2 \lambda_2^2 \lambda_3^2 = 1$  holds, resulting in  
192  $\lambda_3^2 = 1/\lambda_1^2 \lambda_2^2$  and

$$p = - \left( \frac{\Phi}{\lambda_1^2 \lambda_2^2} \right) + \lambda_1^2 \lambda_2^2 \Psi. \quad (40)$$

193 Substitution yields

$$\sigma_1 = \lambda_1^2 \Phi - \left( \frac{\Psi}{\lambda_1^2} \right) + \left\{ - \left( \frac{\Phi}{\lambda_1^2 \lambda_2^2} \right) + (\lambda_1^2 \lambda_2^2 \Psi) \right\}. \quad (41)$$

194 Therefore,

$$\sigma_1 = [\Phi + \Psi \lambda_2^2] \left\{ \lambda_1^2 - \left( \frac{1}{\lambda_1^2 \lambda_2^2} \right) \right\} \quad (42)$$

195 and

$$\sigma_2 = [\Phi + \Psi \lambda_1^2] \left\{ \lambda_2^2 - \left( \frac{1}{\lambda_1^2 \lambda_2^2} \right) \right\} \quad (43)$$

196 For a tensile (uniaxial) test, the conditions  $\sigma_2 = 0$  and  $\lambda_2 = \lambda_3$  are valid.  
197 Furthermore, if incompressible material behavior is assumed, the conditions  $\lambda_1 \lambda_2$   
198  $\lambda_3 = 1$  and  $\lambda_2 = \lambda_3 = 1/\sqrt{\lambda_1} = 1/\sqrt{\lambda_1}$  also become valid. Therefore,

$$\sigma_1 = \lambda_1^2 \left[ \Phi + \left( \frac{\Psi}{\lambda_1} \right) \right] \left[ 1 - \left( \frac{1}{\lambda_1^3} \right) \right]. \quad (44)$$

199 Typically, for many polymers, comparison of the Mooney–Rivlin parameters,  $\Phi$   
200 and  $\Psi$ , reveal the relationship:  $0 < \Psi < (0.2)\Phi$ .

For small strains, the relation  $\lambda = (1 + \epsilon)$  holds, and substitution in Eq. 44 results in:

$$\sigma_1 = ((1 + \epsilon_1)^2 \Phi - \left[ \frac{\Phi}{(1 + \epsilon_1)} \right] + \Psi(1 + \epsilon_1) - \left[ \frac{\Psi}{(1 + \epsilon_1)^2} \right]). \quad (45)$$

Simplification of Eq. 45 by approximation results in:

$$\sigma_1 \cong 3(\Phi + \Psi)\epsilon_1. \quad (46)$$

204

### 23.2.3 Viscoelasticity Considerations

#### Linear Viscoelasticity

The differential forms of the fundamental constitutive relations are given as:

$$P\{S_{kl}\} = 2Q\{\epsilon_{kl}\} \quad (47)$$

$$P'\{\sigma\} = Q'\{\epsilon\} - Q''\{AT\} \quad (48)$$

where A is the thermal expansion function, T is the temperature,  $S_{kl}$  and  $\epsilon_{kl}$  are stress and strain deviators, respectively, and the differential operators are defined as:

$$P = \sum_{i=0}^u a_i(x, t, T) \frac{\partial^i}{\partial t^i} \quad (49)$$

$$Q = \sum_{i=0}^v b_i(x, t, T) \frac{\partial^i}{\partial t^i} \quad (50)$$

$$P' = \sum_{i=0}^{u'} a'_i(x, t, T) \frac{\partial^i}{\partial t^i} \quad (51)$$

$$Q' = \sum_{i=0}^{v'} b'_i(x, t, T) \frac{\partial^i}{\partial t^i} \quad (52)$$

$$Q'' = \sum_{i=0}^{v''} b''_i(x, t, T) \frac{\partial^i}{\partial t^i} \quad (53)$$

$$Q''\{AT\} = \int_{T_0}^{T(x, t)} Q'''\{\alpha(T')\} dT \quad (54)$$

$$Q''' = \sum_{i=0}^{v'''} b'''_i(x, t, T) \frac{\partial^i}{\partial t^i} \quad (55)$$

In Eqs. 49 through 55, the terms  $(a_i, a'_i, b_i, b'_i, b''_i, \text{ and } b'''_i)$  are material properties and the integers  $u, u', v, v', v'', \text{ and } v'''$  reflect the complexity of the material behavior, and  $t$  represents time. In Eq. 54, the quantity  $\alpha$  represents the coefficient of thermal expansion.

The same constitutive relations can also be represented in integral equation form given by:

$$\sigma(x, t) = \int_{-\infty}^t E_V(x, t, t') \left[ \frac{\partial \epsilon(x, t')}{\partial t'} \right] dt' - \int_{-\infty}^t E_{VT}(x, t, t') \frac{\partial [AT(x, t')]}{\partial t'} dt' \quad (56)$$

and

$$S_{kl}(x, t) = 2 \int_{-\infty}^t E(x, t, t') \frac{\partial \epsilon_{kl}(x, t')}{\partial t'} dt' \quad (57)$$

where  $E_V$  and  $E_{VT}$  are the relaxation moduli as functions of time and time and temperature, respectively. As shown by Flügge (1975), the assumptions of elastic dilatational behavior or no volume change are frequently used in three-dimensional analyses of polymeric materials. As for distortion operations, however, any mechanical model (Maxwell, Kelvin, three-parameter solid, etc.) can be used.

## Linear Viscoelastic Mechanical Models in One-Dimension

### Kelvin Model

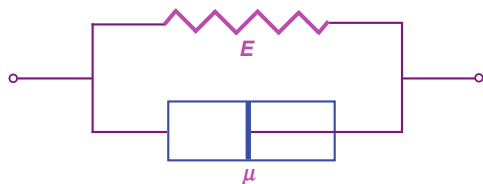
The Kelvin model (Fig. 3) exhibits solid-like behavior, because the behavior of the dashpot is restricted by the spring.

The constitutive equation for the Kelvin model is given by:

$$\left( \frac{d\epsilon}{dt} \right) + \left( \frac{E}{\mu} \right) \cdot \epsilon = \frac{\sigma}{\mu} \quad (58)$$

where  $\mu$  is the coefficient of viscosity in solid form.

**Fig. 3** The Kelvin model



229 The creep condition can be described with the application of the Heaviside step  
 230 function,  $H(t)$ :

$$\sigma(t) = \sigma_0 H(t) \quad 0 < t, \quad (59)$$

231 to result in the creep equation governing with the initial condition  $\epsilon_0 = 0$ , at  $t = 0$ :

$$\epsilon = \left(\frac{\sigma_0}{E}\right) \left\{1 - e^{-(E/\mu)t}\right\} \quad (60)$$

232 Therefore, the Kelvin model exhibits “delayed elasticity” with the creep strain  
 233 approaching its final value gradually (Fig. 4).

234 In order to understand the relaxation behavior predicted by the Kelvin model, it can  
 235 be assumed that the strain is fixed at  $t = t_1$  subsequent to a creep test, that is,  $\epsilon$   
 236  $(t_1) = \epsilon_1 = \text{const}$ . Therefore, the Kelvin model constitutive equation yields the relation:

$$\left(\frac{E}{\mu}\right) \cdot \epsilon = \frac{\sigma}{\mu} \quad (61)$$

237 which, with the condition  $d\epsilon/dt = 0$ , results in the relation:

$$\sigma = E \cdot \epsilon = \sigma_0 \left\{1 - e^{-(t_1/t_R)}\right\} < \sigma_0 \quad (62)$$

238 where  $t_R = (\mu/E)$  is the relaxation time. Therefore, when the strain is fixed, the stress  
 239 is immediately relaxed by a certain amount, and then remains at this value, that is,  
 240 relaxation is incomplete.

#### 241 Maxwell Model

242 The Maxwell model (Fig. 5) exhibits fluidlike behavior, due to the presence of the  
 243 fluid element, the dashpot, which is not restricted by the solid spring element.  
 244 Because of this reason, it is suitable for noncross-linked polymers.

**Fig. 4** Delayed elasticity with Kelvin model's creep behavior

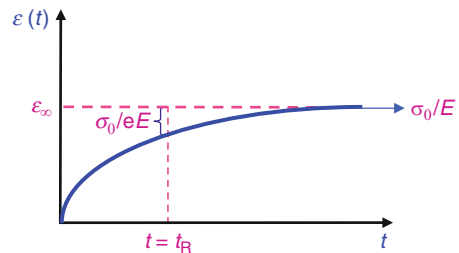
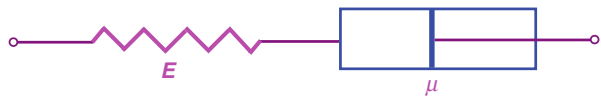


**Fig. 5** The Maxwell model



The constitutive equation for the Maxwell model is given by:

$$\left(\frac{d\epsilon}{dt}\right) = \frac{(d\sigma/dt)}{E} + \frac{\sigma}{\mu} \quad (63)$$

For the creep condition, Eq. 59, along with the initial condition,  $\epsilon_0 = \sigma_0/E$ , at  $t = 0$ , results in the governing equation for creep behavior:

$$\epsilon(t) = \left(\frac{\sigma_0}{\mu}\right)t + \left(\frac{\sigma_0}{E}\right). \quad (64)$$

This equation describes unbounded creep. It allows unlimited deformation under finite stress, which describes typical fluid property.

The creep recovery behavior of the Maxwell model shown in Fig. 6 reveals that just prior to releasing the load, the following relation is valid:

$$\epsilon(t) = \left(\frac{\sigma_0}{\mu}\right) \cdot t + \left(\frac{\sigma_0}{E}\right). \quad (65)$$

At the instant the stress is released, the strain will decrease by the amount,  $\sigma_0/E$ , (linear material). After this instantaneous change in strain, the spring (E) will not undergo any additional deformation.

For the relaxation condition, use of the relation:

$$\epsilon(t) = \epsilon_0 H(t) \quad 0 < t \quad (66)$$

along with the initial condition,  $\sigma(0) = \sigma_0$ , at  $t = 0$ , results in the governing equation for relaxation, which represents the stress behavior during a relaxation test:

$$\sigma(t) = \sigma_0 \cdot e^{-(t/t_R)}. \quad (67)$$

The limiting conditions for this relaxation behavior can be calculated as follows:  $t \rightarrow 0 \Rightarrow (\sigma(t) \rightarrow \sigma_0)$ , as well as the “elastic after effect”:  $t \rightarrow \infty \Rightarrow (\sigma(t) \rightarrow 0)$ .

Substitution of the Maxwell model relaxation time,  $t_R = (\mu/E)$ , into Eq. 67 results in:

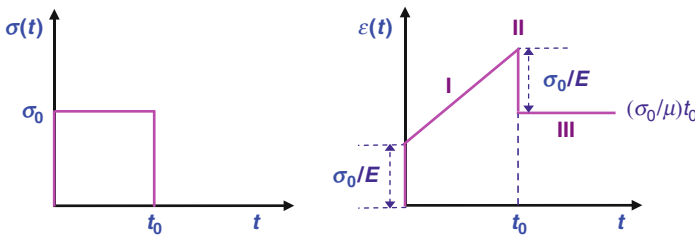


**Fig. 6** The creep recovery behavior of the Maxwell model

$$\sigma(t = t_R) = \frac{\sigma_0}{e} (e = \exp(1) = 2.72). \quad (68)$$

Note that by identifying the time it takes for the stress level to relax to the value,  $\sigma_0/e$ , it is possible to determine the (solid) material viscosity coefficient,  $\mu$ , if the Young's modulus,  $E$ , for the material is available.

### 23.2.4 Interrelationship Between the Tensile and Shear Properties

The constitutive equations proposed for characterization of solid polymer materials in the tensile mode can be reformulated for the case of pure shear. One approach is to replace tensile stress and strain variables by their shear counterparts.

It is usually desirable to run a simple bulk tensile test program and subsequently predict (calculate) shear properties from their tensile counterparts. This approach requires a clearly defined relationship between shear and tensile elastic limit and yield variables and material properties. The elastic limit and yield stress values can be related between tensile and shear conditions by using an appropriate failure criterion, such as maximum normal stress, maximum shear stress, and distortion energy criteria. A material parameter that needs to be converted in addition to the usual elastic properties is the viscosity coefficient. This can be done by using Tobolsky's (1960) assumption of equivalent relaxation times in shear and tension. Application of this assumption results in the relation:

$$\mu_S = \mu_T/2(1 + \nu) \quad (69)$$

where  $\mu_S$  and  $\mu_T$  refer to the viscosity coefficients in shear and tension, respectively, and  $\nu$  is Poisson's ratio. An application of this procedure for a linear viscoelastic (over-stress) model was shown by Sancaktar and Brinson (1980).

### 23.2.5 Time–Temperature Superposition

The time–temperature superposition principle (TTSP) is used to extend the creep and relaxation data obtained at higher temperatures to values at lower temperatures and longer times in the same strain and stress ranges. Provided that no structural changes occur in the material at high temperatures, TTSP can be used for amorphous and semicrystalline thermoplastics and thermosets for extrapolation purposes. In order to apply this principle, one should first construct a “master curve,” where the complete compliance–time or relaxation modulus–time behavior is plotted at a constant temperature. For the “master curve,” a reference temperature  $T_0$  is chosen. As shown by Ahlonis et al. (1972), the relation for the compliance observed at any time  $t$  and temperature  $T_0$  is given in terms of the experimentally observed compliance values at different temperatures  $T$  as:

$$D(T_0, t) = \left[ \frac{\rho(T)T}{\rho(T_0)T_0} \right] D(T, t/a_T) \quad (70)$$

where

$$D(t) = \frac{\epsilon(t)}{\sigma} \quad (71)$$

and  $\rho(T)$  is the temperature dependent density. An illustration of this procedure is shown in Fig. 7, where adjustments for any change in the material density are ignored.

A similar relation for the relaxation modulus is given as:

$$E(T_0, t) = \left[ \frac{\rho_0(T_0)T_0}{\rho(T)T} \right] E(T, a_T t) \quad (72)$$

where

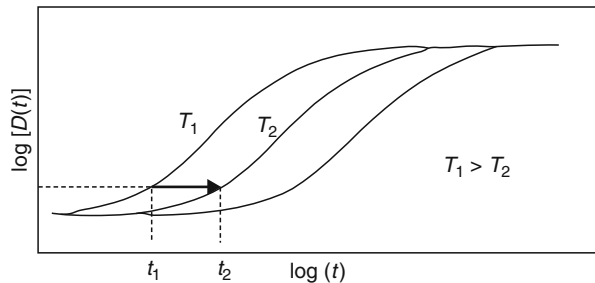
$$E(t) = \frac{\sigma(t)}{\epsilon}. \quad (73)$$

The term  $a_T$  is a time shift factor which can be obtained with the application of the Williams–Landel–Ferry (WLF) equation, reported by Ferry (1961).

For most polymeric materials, the polymer's glass transition temperature ( $T_g$ ) is chosen as the reference temperature for accurate results. Even though Ferry (1961) reports that the above equations have not been proven to be valid below the  $T_g$ , data showing its application for  $T < T_g$  is available in the literature. Examples of applications to structural adhesives in the bulk form were given by Renieri et al. (1976) and Keuner et al. (1982).

The application of the TTSP can be extended into the nonlinear viscoelastic region, as shown by Darlington and Turner (1978). Examples on the establishment of rate–temperature superposition based on WLF equation as applied to peeling problems have been given by Kaelble (1964, 1969), Hata et al. (1965), and Nonaker (1968). Nakao (1969) and Koizumi et al. (1970) report superposition based on Arrhenius' equation.

**Fig. 7** An illustration of time–temperature (t-T) superposition procedure for shifts in creep compliance,  $D(t)$ . Adjustments for any change in the material density are ignored



## 23.3 Advanced Models

### 23.3.1 Nonlinear Viscoelasticity

Equations 47, 48 and 56, 57 can also be used to describe nonlinear material behavior provided that  $a_i$ ,  $b_i$ , etc., and  $E$ ,  $E_V$  are functions of stresses, strains, their derivatives, and their invariants in addition to the functional variables shown.

On the basis of their observations on polymers, composites, and adhesives, Hiel et al. (1983), Rochefert and Brinson (1983), and Zhang et al. (1985) report that the extent of nonlinearity is dependent on both the stress level and the timescale. Constitutive relations having the form of Eqs. 56 and 57 are in agreement with this observation. Schapery (1966, 1969a, b) reports that stress- and strain-dependent material properties of nonlinear constitutive equations have a thermodynamic origin. For example, the one-dimensional constitutive relation

$$\epsilon = g_0 D(0) \sigma + g_1 \int_0^t \Delta D(\phi - \phi') \left[ \frac{d(g_2 \sigma)}{d\tau} \right] d\tau \quad (74)$$

includes the variables  $g_0$ ,  $g_1$ , and  $g_2$ , which reflect stress dependence of the Gibbs free energy. In Eq. 74,  $D(0)$  is the initial value of the linear viscoelastic creep compliance,  $\Delta D(\phi)$  is the transient component, and the quantities

$$\phi = \phi(t) = \int_0^t dt' / a_\sigma \quad (75)$$

and

$$\phi' = \phi(\tau) = \int_0^\tau dt' / a_\sigma \quad (76)$$

are reduced time parameters and depend on the shift function  $a_\sigma$ . “ $a_\sigma$ ” is a function of stress and change with entropy production and free energy changes (Peretz and Weitsman 1982).

An equation similar to Eq. 74 can be written with strain as the independent state variable. In this equation, the strain-dependent properties  $h_0$ ,  $h_1$ ,  $h_2$ , and  $a_\epsilon$  reflect the changes in the Helmholtz free energy.

In using nonlinear mechanical models, in addition to utilizing nonlinear elastic and shear thickening or thinning dashpot elements, a perturbation technique can also be used to incorporate nonlinear behavior. This is accomplished by adding small perturbation terms which are functions of the current level of elastic strain and strain rate to the elastic and viscous coefficients, respectively. This method was originally



proposed by Davis (1964) and later applied by Renieri et al. (1976) in material characterization of bulk adhesives.

Further discussions on nonlinear viscoelastic theory are given by Green and Adkins (1960) and Hilton (1975).

### 23.3.2 Empirical Description of Creep Behavior

The constitutive equations obtained with the use of mechanical models can be solved for the creep condition given by

$$\sigma(t) = \sigma_0 H(t) \quad (77)$$

with  $\sigma_0$  and  $H(t)$  describing the level of constant stress and the unit step function, respectively, to result in a creep equation. In some cases, however, empirical relations describing time-dependent strain functions are preferred over this method for practical reasons. Actual creep data can be fitted with such functions to yield accurate analysis in conjunction with equations of the form 56, 57, or 74.

A variety of mathematical forms have been proposed to describe the creep behavior of adhesives and polymers in an empirical fashion. The simplest procedure is called the log-log method based on the assumption that the logarithm of the secondary creep rate is linearly related to the logarithm of the stress level at which the creep occurs. This assumption results in a creep relation which is a linear function of time but nonlinear function of stress in the secondary range. An application of this method to polymeric materials was given by Sancaktar et al. (1987).

The creep relation which is most commonly used in the literature is the "power-law" compliance given by

$$D(t) = D_0 + D_1 t^{n''} \quad (78)$$

where  $D_0$  is the instantaneous compliance, and  $D_1$  and  $n''$  are material constants. Note that Eq. 78 allows time reduction by a stress-dependent shift factor to describe stress-enhanced creep. Equations of this form were used by researchers such as Weitsman (1981) and Ravi-Chandar and Knauss (1984) for viscoelastic stress analysis and fracture mechanics considerations (respectively) of adhesives and polymeric materials.

Various methods have been proposed to determine the parameters  $D_0$ ,  $D_1$ , and  $n''$  of Eq. 78. For example, Findley and Peterson (1958) subtract the instantaneous strain from the total strain and plot the transient strain on log-log paper. A comparison and discussion of different methods was given by Dillard and Hiel (1985).

As shown by Sancaktar (1991), Figs. 8 and 9 illustrate the variation of adhesive shear stress at the overlap edges of double lap joints as predicted by linear and nonlinear viscoelastic analyses. In Fig. 8, the linear analysis was performed using the Maxwell model with different relaxation times,  $t_R$ , and the nonlinear analysis was

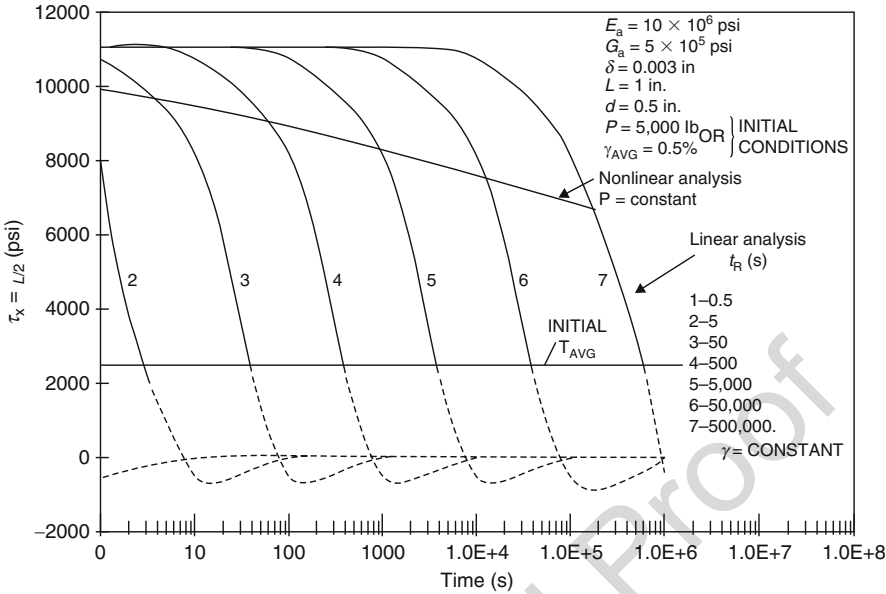


**Fig. 8** Variation of adhesive shear stress at the overlap edges of double lap joints as predicted by linear and nonlinear viscoelastic analyses. The linear analysis was performed using the Maxwell model with different relaxation times,  $t_R$ , and the nonlinear analysis was performed using Eq. 78 with a stress-dependent shift factor. The joint dimensions used in analysis are also shown with  $\delta$ ,  $L$ , and  $d$  representing adhesive thickness, overlap length, and the main plate thickness, respectively.  $E_s$  and  $G_a$  represent the Young's modulus for the substrate and the shear modulus for the adhesive, respectively

performed using Eq. 78 with a stress-dependent shift factor. Figure 9 illustrates the ability to obtain matching results between the two models by using the Maxwell model with variable relaxation time,  $t_R$ , as given by Sancaktar (1991).

Additional methods and discussions on constitutive equations for creep were given by Gittus (1975).

### 23.3.3 Increases in Joint Strength Due to Rate-Dependent Viscoelastic Adhesive Behavior

Due to their viscoelastic nature, most adhesives exhibit rate-dependent material behavior, which can be modeled, for example, by using mechanical model characterization.

In order to describe the rate dependence of limit stress and elastic limit strain for polymeric and adhesive materials in the bulk form, Renieri et al. (1976) and Sancaktar and Brinson (1980) utilized a semiempirical approach proposed by Ludwik (1909) in the form:

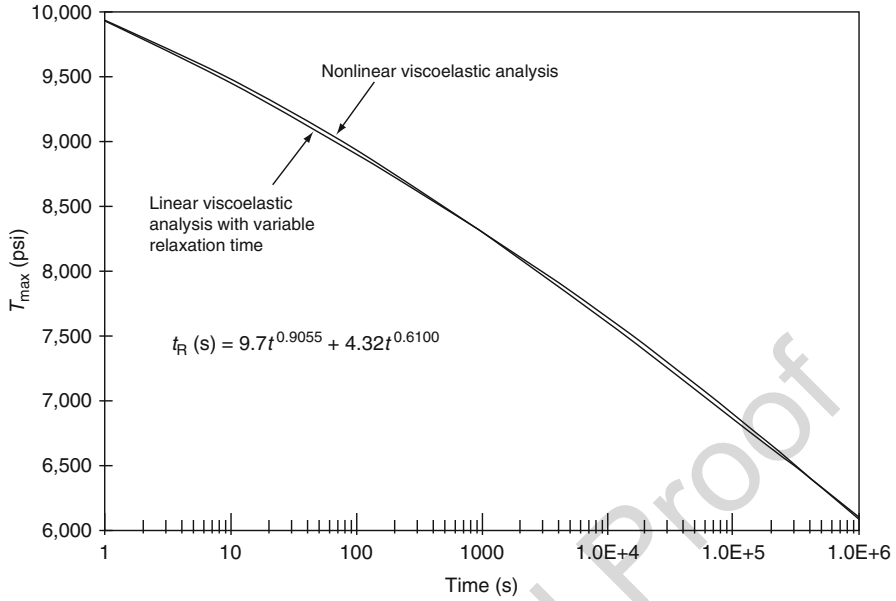


**Fig. 9** Variation of maximum adhesive shear stress in double lap joints based on nonlinear viscoelastic analysis, using Eq. 78 with a stress-dependent shift factor, and linear viscoelastic analysis, using the Maxwell model with variable relaxation time,  $t_R$

$$\tau_{ult} = \tau' + \tau'' \log \left[ \frac{(d\gamma/dt)}{(d\gamma'/dt)} \right] \quad (79)$$

where  $\tau_{ult}$  is the ultimate shear stress,  $d\gamma/dt$  is the initial elastic strain rate, and  $\tau'$ ,  $\tau''$ , and  $d\gamma'/dt$  are material constants.

Renieri et al. (1976) and Sancaktar and Brinson (1980) used the same form of Eq. 79 to describe the variation of elastic limit shear stress ( $\tau_{el}$ ) and strains ( $\gamma_{el}$ ) with initial elastic strain rates. These expressions may be written as:

$$\tau_{el} = \phi' + \phi'' \log \left[ \frac{(d\gamma/dt)}{(d\gamma'/dt)} \right] \quad (80)$$

and

$$\gamma_{el} = \zeta' + \zeta'' \log \left[ \frac{(d\gamma/dt)}{(d\gamma'/dt)} \right] \quad (81)$$

where  $\phi'$ ,  $\phi''$ ,  $\zeta'$ , and  $\zeta''$  are material constants. Sancaktar et al. (1984) and Sancaktar (1985) later showed applicability of Eqs. 79 through 81 for adhesives in the bonded form and also proposed superposition of temperature effects on these equations.

As reported by Ward and Hadley (1993), the theoretical basis of Eq. 79 can be found in the Eyring theorem, according to which the mechanical response of an adhesive is a

process that has to overcome a potential barrier, ( $\Delta E$ ). This barrier decreases not only with increasing stress but also with increasing temperature. Based on the Eyring theorem, the relationship between a limit stress, say  $\tau_{el}$ , and the strain rate can be written as:

$$\frac{d\gamma}{dt} = A \exp \left[ \frac{(\tau_{el} V - \Delta E)}{RT} \right] \quad (82)$$

where  $A$  is a pre-exponential factor,  $R$  is the gas constant, and  $V$  is the activation volume.

Equation 82 can be expressed in logarithmic form as:

$$\tau_{el} = \left\{ \frac{\Delta E}{V} \right\} + \frac{\{2.303RT \log[(d\gamma/dt)/A]\}}{V} \quad (83)$$

Sharon et al. (1989) applied Eq. 83 to describe rate- and temperature-dependent variation of four structural adhesives in the bulk form. They used the shift factor  $[\log(1/A)] \times 10^{-3}$  on the temperature ( $^{\circ}\text{C}$ ) to describe the effect of rate.

If the energy barrier term  $\Delta E/V$  of Eq. 83 is also affected by temperature, then one needs two shift factors in Eqs. 79 through 81 to describe rate-temperature effects on limit stress-strain equations:

$$\tau_{el} = \{a_{T1}\}\theta' + \left\{ \{a_{T2}\}\theta'' \log \left[ \frac{d\gamma/dt}{d\gamma'/dt} \right] \right\} \quad (84)$$

and

$$\gamma_{el} = \{b_{T1}\}\zeta' + \left\{ \{b_{T2}\}\zeta'' \log \left[ \frac{d\gamma/dt}{d\gamma'/dt} \right] \right\} \quad (85)$$

where  $a_{Ti}$  and  $b_{Ti}$  are shift factors as functions of temperature. Figure 10 illustrates an application of Eq. 84 by Sancaktar et al. (1984), showing the variation of elastic limit shear stress with initial elastic strain rate and environmental temperature for an epoxy adhesive film with polyester knit fabric carrier cloth. The adhesive was tested in the bonded lap shear mode.

In order to analyze the effects of rate and temperature on the interfacial strength of bonded joints, one can initially use a simple energy approach in the following manner: A critical energy level,  $W_c$ , is used to represent interfacial failure. In the presence of adhesive, substrate, and interphase (a distinct material layer between the substrate and the adhesive layer which transmits the rigid substrate's energy to the adhesive layer), the combined elastic energy can be written as:

$$V_a \left\{ \left( \frac{1}{2} \right) \epsilon_{\text{adhesive}}^2 E_{\text{adhesive}} \right\} + V_{ip} \left\{ \left( \frac{1}{2} \right) \epsilon_{\text{interphase}}^2 G_{\text{interphase}} \right\} + V_s \left\{ \left( \frac{1}{2} \right) \epsilon_{\text{substrate}}^2 E_{\text{substrate}} \right\} = W_c \quad (86)$$

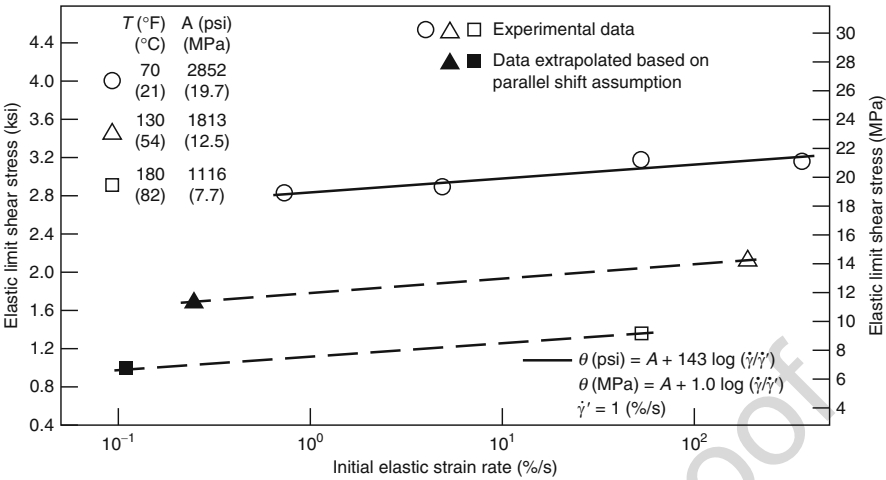


**Fig. 10** Variation of elastic limit shear stress with initial elastic strain rate and environmental temperature, and comparison with Ludwik’s equation for an epoxy adhesive film with polyester knit fabric carrier cloth. The adhesive was tested in the bonded lap shear mode

where  $V_a$ ,  $V_{ip}$ , and  $V_s$  represent volume fractions of the adhesive layer, interphase, and the substrate, respectively. If Eq. 86 is considered in conjunction with Eq. 85 to include rate–temperature effects, then it can be easily deduced that higher  $W_c$  levels are obtained at high rate and/or low temperature levels since the proportion of elastic strains increases with increasing elastic limit strains due to high rate and/or low temperature levels.

### 23.3.4 Reductions in Stress Concentration Due to Viscoelastic Adhesive Behavior

If the adhesive material exhibits viscoelastic behavior, then the high stress magnitudes observed at the overlap end region of bonded joints are expected to diminish in time due to the creep process. For example, Weitsman (1981) utilized the nonlinear viscoelastic “power-law” response, which describes a stress-enhanced creep process to illustrate time-dependent reductions in shear stress peaks along the adhesive layers of symmetric double lap joints. Sancaktar (1991) later illustrated the applicability of the correspondence principle to the same problem with the use of Maxwell chain to approximate the continuous change in the relaxation time and to coincide with the results calculated using nonlinear viscoelastic theory, as shown in Figs. 8 and 9.

### 23.3.5 Singularity Methods

Theoretically, geometrical singularities exist at sharp interface corners. The strength of such singularities depends on the local geometry, including the actual corner

radius, and the material properties. Barsoum (1989) considered the cases of elastic adhesive at a rigid corner, and nonlinearly hardening adhesive at a square rigid corner. He showed that for an elastic adhesive, the obtuse angle notch gives a much weaker singularity and, hence, a greater failure load.

Assuming linear elasticity, Groth (1988) proposed an exact solution for the adhesive stresses at an interface corner in the form of a power series:

$$\sigma_{ij} = \sum_{k=1}^{\infty} K_k H_{ij}^k(\phi) \zeta^{\lambda_k} + \text{Continuous part} \quad (87)$$

where  $\sigma_{ij}$  is the stress tensor,  $\zeta = r/h$  is a nondimensional radial distance from the singularity,  $(H_{ij}^k)$  are functions depending on the geometry angle  $\Phi$  of the corner,  $K_k$  constitutes generalized stress intensity factors, and  $\lambda_k$  defines the strength of singularities governed by the eigenvalues of the  $\lambda_k$  in the open interval  $\text{Re}(\lambda_k) < 1$ . Due to restrictions on finite strain energy at the singularity, values of  $\text{Re}(\lambda_k) \geq 1$  are not allowed. Obviously, based on Eq. 87, more than one singular term may influence the stress field close to an interface corner. Dempsey (1995) showed that in addition to the power-type singularities, that is,  $O(r^{-\lambda})$  as  $r \rightarrow 0$ , and  $\lambda$  representing the strength of singularity, power-logarithmic-type singularities, that is,  $O(r^{-\lambda} \ln r)$  as  $r \rightarrow 0$ , may occur for homogeneous boundary conditions of composite wedge problems.

Stress singularities at butt joint interface corners were discussed by Reedy and Guess (1995) and Sawa et al. (1995).

### 23.3.6 Bulk Adhesive as Composite Material

Since most adhesives contain secondary phase materials such as fillers and carrier cloth, they should be treated as composite materials in constitutive modeling. The interesting aspect in such treatment is the fact that such secondary phase constituents form adhesive bonds with the adhesive matrix in small scale. Consequently, localized non-catastrophic failures within the bulk adhesive consisting of interfacial separations are expected to cause constitutive behavior changes for the adhesive bulk. Such behavior can be properly described by using “damage mechanics models,” some of which will be described later in this chapter within the context of adhesive materials.

It is known that particle size, shape, and volume fraction all affect the mechanical behavior of filled polymers. For example, electrically and thermally conductive adhesives which usually contain dispersed metal particles of varying aspect ratios, but usually within the micron size range, require the methods of Eshelby (1959) for characterization. These types of adhesives sometimes require directional properties. Kerner (1956), Hashin and Shtrikman (1963), Budiansky (1965), and Hill (1965) provided methods for calculation of elastic moduli for isotropic materials filled with spherical particles. Methods for elastic moduli of unidirectional reinforced polymers

with infinitely long fibers were given by Hill (1964) and Chow and Hermans (1969). Bulk and shear moduli for disk- and needle-shaped inclusions were considered by Wu (1966) and Walpole (1969).

As reported by Ashton et al. (1969), Halpin and Tsai introduced approximate equations for square fiber reinforcement by reducing Hermans' (1967) solution using numerical solutions of elasticity theory. Equations for slender rigid inclusions at low concentrations were developed by Russel and Acrivos (1973). As for effective thermal expansion coefficient of filled polymers, the effects of filler geometry and constituent material properties have been studied by Kerner (1956).

Using the generalized approach of Eshelby, Chow (1978a) derived relations for the bulk modulus, transverse and longitudinal Young's moduli, and the two effective shear moduli,  $G_{12}$  and  $G_{13}$ , of the filled polymer containing aligned ellipsoidal particles at finite concentration. Chow (1978b) also derived relations for the linear and volumetric thermal expansion coefficients for filled polymers containing aligned ellipsoidal inclusions at finite concentration. He concluded that in such filled systems, the volumetric expansion varies only slightly with the aspect ratio of the ellipsoid, while longitudinal and transverse linear expansions show strong dependence on the particle shape. All the modulus calculations developed by Chow are based on the following assumptions: (1) The filler particles are well bonded to the matrix, and consequently, the isostrain condition at the particle/matrix interface can be used to develop the method. (2) The shapes of particles are uniform ellipsoids with the aspect ratio  $C_p$ , representing the ratio of the major to minor axes. (3) The particles are distributed with their corresponding axes aligned.

Wei (1995) and Sancaktar and Wei (1998) applied the elastic moduli and thermal expansion coefficient relations developed by Chow in describing the material behavior of electronically conductive (filled) adhesives in order to be able to determine, accurately, the thermal mismatch stresses which occur between the adhesive and the substrates in the bonded form. Both finite element analysis and closed form solutions were used for stress analysis.

The results given by Chow are consistent with the well-known rule of mixtures used in long fiber-reinforced composites. When the aspect ratio,  $C_p$ , of the particle is  $C_p > 50$ , the moduli are not a function of  $C_p$ . Therefore, for larger  $C_p$ , the composite's behavior is more like that of long fiber-reinforced composite. For intermediate aspect ratio cases, i.e.,  $1 < C_p < 50$ , Sancaktar and Wei (1998) proposed an approximation of Chow's elastic moduli formulas by utilizing the method used for randomly oriented short fibers in predicting the behavior of particle filled adhesives, so that the composite material can be treated as isotropic, as suggested by Agarwal and Broutman (1990).

As for the thermal expansion coefficient, the isotropy assumption was accomplished simply by using one-third of the volumetric thermal expansion coefficient, as suggested by Lipatov et al. (1991). It should be noted, however, that in special cases of conductive adhesive applications, directional conduction may be required, in which case the use of non-isotropic, directional material properties would be necessary.

The constitutive models cited above for predicting filled polymer behavior all assume perfect adhesive bond between the fillers and the polymer matrix. As such

filled polymers are loaded, however, failure of adhesive bonds is expected in proportion to the applied force and the duration of its application. This, in turn, is expected to result in changes in the constitutive properties of the filled polymer adhesive. Lipatov et al. (1991) reported a decrease in the modulus of elasticity of a filled elastomer at separation of filler particles from the binder and described it with the approximate formula

$$\frac{E_x}{E_f} = \exp^{-4.3(V_x)} \quad (88)$$

where  $E_f$  is the initial elastic modulus for the filled polymer with unbroken bonds,  $V_x$  is the volume fraction of unbonded filler, and  $E_x$  is the composite's elastic modulus when the fraction,  $V_x$ , of the filler particles are no longer bonded to the matrix.

Garton et al. (1989) discussed stiff polar molecular additives which interact strongly with the (thermoplastic or thermoset) matrix polymer adhesive, thus decreasing the composite free volume,  $f$ , as given by the equation

$$f = V_1 f_1 + V_2 f_2 + k V_1 V_2 \quad (89)$$

where  $V_1$  and  $V_2$  are the volume fractions of the polymer matrix and additive, respectively,  $f_1$  and  $f_2$  are the corresponding fractional free volumes, and  $k$  is an interaction parameter. The composite properties – bulk elastic modulus, bulk strength (to a lesser degree) – as well as bonded joints properties of strength and stiffness are reported by Garton et al. (1989) to increase with reductions in composite free volume.

In another study, Sancaktar and Kumar (2000) obtained increases in the lap joint strength by selectively rubber toughening the high stress concentration regions of the adhesive overlap. This novel approach to increase the lap joint strength by using functionally gradient adhesive introduced a method different from the traditional methods of either increasing the lap joint area or altering the joint geometry. For the different configurations of adhesive arrangements tried, the trends obtained in finite element analysis matched the trends obtained by tensile shear testing.

### 23.3.7 The Concept of the Interphase

There is strong interrelationship between the properties of the adhesive and the substrates in shaping the final joint behavior. A more accurate prediction of the joint behavior can be obtained by including a distinct “interphase” region in modeling the overall joint behavior. Earlier, in Sect. 3.3, the interphase was defined as “a distinct material layer between the substrate and the adhesive layer which transmits the rigid substrate's energy to the adhesive layer.” An early discussion of this concept was provided by Sharpe (1972). This concept becomes especially relevant as efficient methods for inducing mechanically distinct surface topography and chemically distinct interlayers emerge. The use of excimer pulse lasers for surface treatment



and topography inducement on metal adherends, shown by Sancaktar et al. (1995), cure and post-cure of interphase regions around carbon fibers embedded in epoxy matrix via resistive electric heating by the fiber, shown by Sancaktar and Ma (1992), microwave curing of carbon-epoxy composites, which produce “interfacial strengths higher than that achievable in thermally cured system,” as shown by Agrawal and Drzal (1989), and the production of a transcrystalline region in crystalline polymers upon solidifying when in contact with a substrate, as shown by Hata et al. (1994), all provide examples of current methods used to create distinct interphases. Another main reason for the presence of an interphase region is the chemical primer (sizing) applied to the adherend surfaces to improve adhesion. The diffusion of this sizing into the adhesive matrix can create a concentration gradient. There are other possible mechanisms which could lead to an interphase region. Some examples are: possible polymeric diffusion into the substrate during the adhesion process, selective adsorption of one or more of the components in the matrix before curing, and the presence of free volume differences between the bulk polymer and the polymer near the substrate–matrix boundary, possibly created by thermal stresses. Figure 11 shows different “interphases” between an epoxy-based, approximately 80% wt silver flake-filled electrically conductive adhesive and different substrates.

Adequate analysis and understanding of the interphase between an adherend and an adhesive is critical for the design of efficient bonded structures and composite materials. In adhesion science and technology circles, it is a well-accepted fact that the mechanical properties of the (polymeric) adhesive material are altered in regions close to the adherend due to the adhesion process. For example, Knollman and Hartog (1985) reported approximately 10% reduction in the adhesive bulk shear modulus, in an interphase region comprising approximately 20% of the bulk adhesive thickness. Consequently, a satisfactory mechanical analysis on the adherend–adhesive interaction should include a finite thickness interphase with its own material properties rather than assuming an interface with unknown properties or very high strength and negligible thickness. Modeling of the adhesive–adherend interphase becomes especially relevant

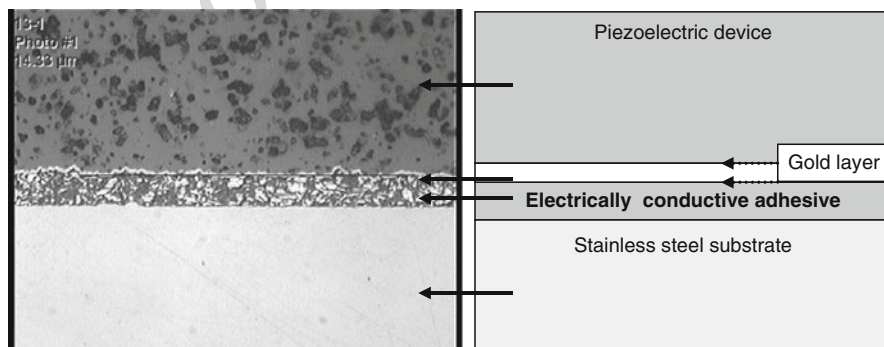


**Fig. 11** Illustration of “interphases” between an epoxy-based, approximately 80% wt silver flake-filled electrically conductive adhesive and stainless steel and piezoelectric substrates. The flake size is approximately 7  $\mu\text{m}$

in understanding and design of composite materials with “tailored” interphases which increase the toughness of the composite material. The adherend surfaces have distinct topographies, which result in a collection of miniature joints in micron, and even nanoscale when bonded adhesively. The methods of continuum mechanics can be applied to this collection of miniature joints by assuming continuous or a combination of continuous/discontinuous interphase zones.

Using the case of a carbon fiber embedded in epoxy matrix, Sancaktar and Zhang (1990) and Sancaktar et al. (1992) reported that nonlinear viscoelastic behavior of the matrix and the interphase may have a profound effect on the mechanism of stress transfer.

Sancaktar’s analytical model involves a cylindrical interphase surrounding an elastic fiber of finite length. The interphase region has nonlinear viscoelastic material properties. The region surrounding the interphase (which can be assumed to be the bulk of the adhesive matrix) is also assigned nonlinear viscoelastic properties, which are different from those of the interphase. The nonlinear viscoelastic material behavior of the interphase zone and the matrix is represented using a stress-enhanced creep. Different interphase diameter values and different material properties for the interphase and the matrix are used to determine their effects on the interfacial shear stress. Results of this analysis reveal that depending on the relative magnitudes of interphase and matrix viscoelastic material properties, it is possible to have stress reductions or increases along the fiber and, hence, the critical fiber length obtained will also vary accordingly, as illustrated in Fig. 12. This result reveals that not only the quality of adhesion but also the material properties of the bulk matrix and the interphase, all of which can be affected by cure conditions, can affect the critical fiber length, a concept introduced by Kelly and Tyson (1965) to gage the fiber–matrix interfacial strength.

The analytical and experimental results presented so far reveal the possibility for mutual reduction between rate, temperature, and interphase thickness, as shown by Sancaktar et al. (1992). The application of fiber sizing typically results in thicker interphases, and the cross-head rate,  $v$ , can be related to the shear strain rate,  $d\gamma/dt$ , and the interphase thickness,  $\delta$ , with the relation:

$$v = f\left(\frac{d\gamma}{dt}\right) \cdot g(\delta). \quad (90)$$

Therefore, based on classic shear lag analysis (also based on definition of shear strain), it can be shown that for a fixed strain rate (function) the effect of increased cross-head rate can be induced by increasing the interphase thickness (i.e., application of fiber sizing). Indeed, the experimental results reveal shorter fragment lengths for increased cross-head rate and/or presence of fiber sizing. Based on this premise, the following superposition relations can be written for the interfacial strength,  $\tau_c$ :

$$\tau_c(T, v, \delta) = \tau_c(T_0, a_T v, \delta) \quad (91)$$

$$\tau_c(T, v, \delta) = \tau_c(T_0, v, \delta/a_T) \quad (92)$$

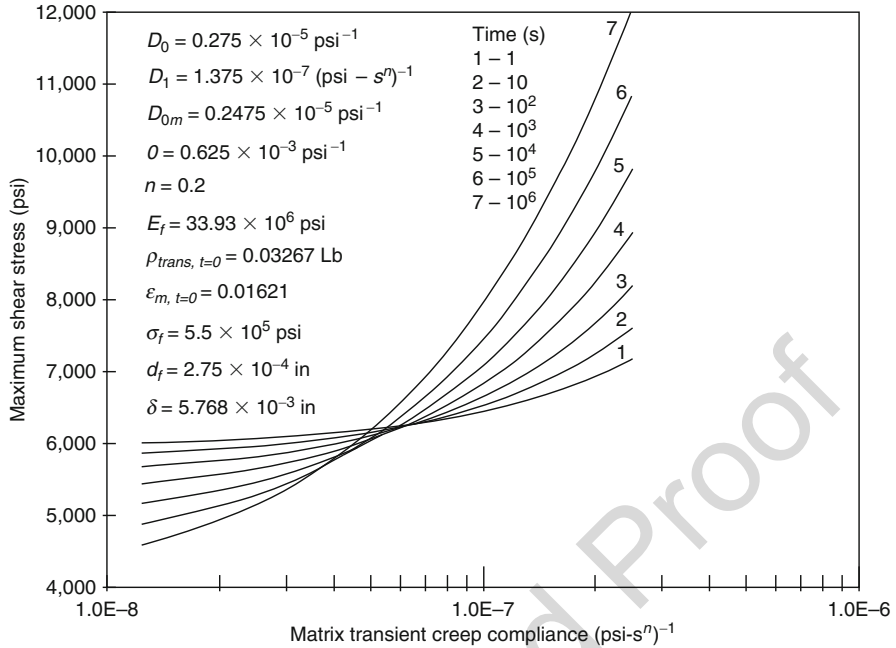


**Fig. 12** The variation of the maximum shear stress with time and matrix transient creep compliance based on a nonlinear viscoelastic stress analysis of a cylindrical interphase zone for maximum transferred load. The nonlinear analysis was performed using Eq. 78 with a stress-dependent shift factor.  $D_0$  and  $D_1$  are the interphase instantaneous and transient creep compliances,  $\delta$  is the interphase thickness, and the subscripts m and f indicate matrix and fiber, respectively

630 and,

$$\tau_c(T, v, \delta) = \tau_c(T_0, v/a_\delta, \delta_0) \quad (93)$$

631 where  $T$  is the temperature,  $T_0$  is a reference temperature, such as room temperature,  
 632  $\delta_0$  is an interphase thickness used as reference, and  $a_T$  and  $a_\delta$  are shift factors  
 633 reflecting the effects of changes in temperature and interphase thickness, respec-  
 634 tively, in comparison with reference values.

635 In order to represent the composite behavior of the adhesive/adherend interphase,  
 636 where the polymeric adhesive is mechanically interlocked to the surface projections  
 637 of a metal adherend, Sancaktar (1996) proposes a “smeared” modulus zone.  
 638 Although deformation within the bulk adhesive is likely viscoelastic, simple elastic  
 639 relationships probably suffice, to describe deformation within the topographic sur-  
 640 face region. Therefore, simple elastic relationships are used to relate strain gradient  
 641 within those regions to topography.

642 The equivalent elastic modulus,  $G_{IP}$ , for the mechanically interlocked interphase  
 643 is calculated by assuming an “isostress” condition for the interphase, illustrated in  
 644 Fig. 13. In other words, the adhesive and the adherend surface (projections) are  
 645 subjected to the same level of shear stress,  $\tau_{IP}$ , at the interphase, while the composite

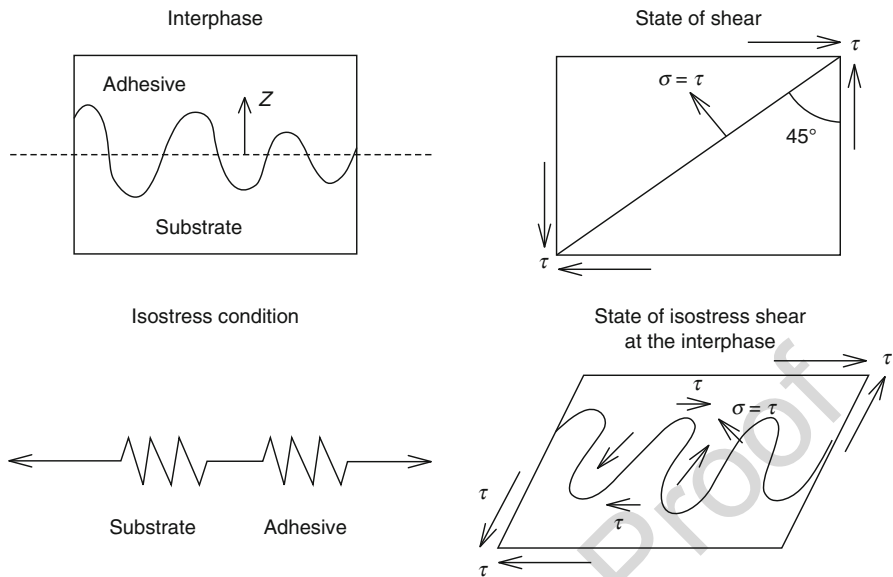


**Fig. 13** The state of isostress shear at the interphase

interfacial shear strain,  $\gamma_{IP}$ , is a volumetric weighted average of the adhesive and adherend strains, that is,

$$\gamma_{IP} = (V_{fA})(\gamma_A) + (V_{fS})(\gamma_S). \quad (94)$$

In Eq. 94,  $\gamma_A$  and  $\gamma_S$  are the adhesive and substrate shear strains at the interphase and  $V_{fA}$  and  $V_{fS}$  are the volume fractions of the adhesive and the substrate surface (projections) at the interphase. Assuming that the adhesive essentially fills the voids, the adhesive volume fraction can be equated to the sum of the void volume fractions of each lamina.

With the assumption that the deformations in both the adhesive and the adherend are elastic, the interphase shear modulus can be defined as:

$$G_{IP} = \tau_{IP} / \gamma_{IP}. \quad (95)$$

Using Eqs. 94 and 95 and Hooke's law to represent adhesive and adherend's material behavior, the following expression can be obtained for the interphase shear modulus:

$$G_{IP} = \frac{G_S G_A}{V_{fA} G_S + V_{fS} G_A} = \frac{G_S G_A}{V_{fS} (G_S - G_A) + G_A} \quad (96)$$

where  $G_A$  and  $G_S$  are the elastic moduli for the adhesive and the adherend, respectively.

Failure at the interphase is more likely with higher strain gradients,  $d\gamma_{IP}/dz$ . Of course, in the limit, a strain discontinuity defines failure based on mechanics principles. Based on this premise, a mathematical expression can be obtained to gage the possibility of failure using the shear moduli of the adhesive and the adherend along with the adhesive volume fraction,  $V_{fA}$ , at the interphase. For this purpose, differentiation of Eq. 95 along the interphase thickness direction (z-direction) results in

$$\frac{dG_{IP}}{dz} = -\tau_{IP}\gamma_{IP}^{-2} \left( \frac{d\gamma_{IP}}{dz} \right). \quad (97)$$

An equivalent expression can be obtained by differentiating Eq. 96 with respect to z:

$$\frac{dG_{IP}}{dz} = -\frac{G_S G_A (G_S - G_A)}{[V_{fA}(G_S - G_A) + G_A]^2} \left( \frac{dV_{fA}}{dz} \right). \quad (98)$$

An expression relating the shear strain gradient,  $d\gamma_{IP}/dz$  at the interphase to the volume fraction,  $V_{fA}$ , and the differential volume fraction  $dV_{fA}/dz$ , of the adherend voided during surface preparation can now be obtained by equating Eqs. 97 and 98. Both parameters are experimentally determinable, as discussed by Sancaktar (1996).

Interfaces usually constitute a weak link in the chain of load transfer in bonded joints. Also, the discontinuity of the material properties causes abrupt changes in stress distribution, as well as causing stress singularities at the edges of the interfaces. It is very desirable to optimize the substrate surface topography at the interfaces to maximize the load-bearing capacity of bonded joints and to improve their deformational characteristics.

During the second half of the twentieth century, a considerable amount of research work has been published related to the interface stress distributions focusing on flat surfaces between two different materials except when the effects of surface roughness were investigated. In general, stress distributions, stress concentrations, singularities, and surface roughness effects were studied. These studies, however, were not extended to the development of a general methodology to include surface topography effects for varying configurations which can be represented by different mathematical functions.

An investigation by Sancaktar and Narayan (1999) on adhesively bonded scarf joints revealed that the angle between the bonded interface and the loading direction had a significant influence on the stress distributions at the interface. Their analysis revealed that the distributions of stresses became more uniform along the adhesive layer when scarf angles varying from lap joint to butt joint in an increasing order of scarf angle were considered. The transverse and shear stress distributions were in a decreasing order for scarf angle increments of  $15^\circ$  between  $30^\circ$  and  $90^\circ$ , while a reverse trend was observed for the normal stress distributions. The peak normal stress was minimum for the  $30^\circ$  scarf joint; on the other hand, the magnitudes of transverse and shear stresses were minimum when a butt joint was used. Uniformly

distributed external shear loading on the joints led to higher stresses in lap joints, while 75° scarf joints had the lower values.

Sancaktar and Narayan (1999) stated that an attention to the type of stress (i.e., normal, transverse or shear) provided information relevant to the type of failure (i.e., brittle- or ductile-type failures). The authors also introduced newly defined design parameters: stress times substrate volume, stress divided by substrate volume, and stress (strain) gradients along and across the adhesive joint, as a general methodology to compare adhesive joints for design optimization.

In highly deformable adhesives, most of which are elastomeric in nature, such as those used in pressure sensitive tape and tack applications, a high amount of deformation results in cavitation of the material under dilatation. High dilatation may lead to cavitation in localized regions of the adhesive layer starting at a microscopic scale.

It is also desirable to know the magnitudes of shear and normal stresses individually since some adhesives are weak in shear loading (ductile adhesives) while others are weak in normal stress loading (brittle adhesives).

High levels of stresses result in crack propagation in brittle adhesives and cavitation induced failures in deformable adhesives. Furthermore, not only the magnitudes but also the gradients of stresses and strains become an important issue in optimizing the joint strength. Large strain gradients at adhesive–substrate interfaces may result in bond failure.

The magnitude of strain gradients depends on the volume fractions of the adhesive and substrate materials within the effective bond region defined by the geometry of the surface topography. The effect of bonded substrate volume, corresponding to the volume of substrate projections beyond a common baseline on the substrate, on the strain gradients across the adhesive layer can be found by relating the volume fraction gradients to the strain gradients. For this purpose, the composite behavior of the adhesive/adherend interphase, where the polymeric adhesive is mechanically interlocked into the surface projections of an adherend can be utilized to determine an equivalent composite modulus, as suggested by Sancaktar (1996) and discussed above.

Mechanical adhesion depends on surface topography, which can be considered a collection of many geometrical forms. Therefore, mechanical adhesion depends on the stress states of different adhesive joint geometries on the scale of the surface topography, which may include many lap, butt, and scarf joints in the “interphase” region. To address this issue, Ma et al. (2001) compared the stress distributions in adhesive joints as functions of varying geometrical interfaces described mathematically in polynomial or other functional forms, as well as the material properties of the adhesive and the adherend or two different substrates joined by an infinitesimally thin adhesive layer. For this purpose, a mathematical procedure was developed to utilize the complementary energy method, by minimization, in order to obtain an approximate analytical solution to the 3-D stress distributions in bonded interfaces of dissimilar materials. In order to incorporate the effects of surface topography, the interface was expressed as a general surface in Cartesian coordinates, that is,  $F(x, y, z) = 0$ , and the results verified by comparison with

Finite element analysis (FEA). Their methodology involved the following steps: (1) Choose the appropriate stress functions,  $\Phi_{mn}$ , to satisfy stress boundary conditions and utilize equilibrium conditions to relate the stress functions to the stress distribution functions. (2) Use stress interface boundary conditions to reduce the unknown variables in the stress distribution functions obtained. (3) Define a function ( $II$ ) as the sum of complementary energy ( $I$ ) and the penalty function  $\left( R \sum_{i=1 \dots 3}^{y=f(x,z)} (u_i^A - u_i^B)^2 \right) \cdot (R)$  is chosen such that it is the largest positive number which causes the total system complementary energy to change by only 0.1%. (4) Use the remaining unknown variables to minimize the function ( $II$ ) formed in step 3, using the Newton quadratic method, and solve all the unknown variables to obtain the complete stress distribution functions.

The continuity of displacements was enforced at the interface area, approximately, using the fundamental theorem for surface theory of differential geometry, described by Struik (1950), instead of directly using displacements. This way, the integrations of displacements were avoided, and the stress distributions could be calculated more accurately.

For example, for a flat interface (on  $x$ - $z$  plane), such as a butt joint, they utilized the following stress functions:

$$\Phi_{xx}^A = \left( z^2 - \frac{1}{4} \right)^2 \left( y - \frac{1}{2} \right)^2 f_1(x, y, z) \quad (99)$$

$$\Phi_{yy}^A = \left( z^2 - \frac{1}{4} \right)^2 \left( x^2 - \frac{1}{4} \right)^2 f_2(x, y, z) \quad (100)$$

$$\Phi_{zz}^A = \left( x^2 - \frac{1}{4} \right)^2 \left( y - \frac{1}{2} \right)^2 f_3(x, y, z) \quad (101)$$

$$\Phi_{xy}^A = \left( x^2 - \frac{1}{4} \right) \left( z^2 - \frac{1}{4} \right)^2 \left( y - \frac{1}{2} \right) f_4(x, y, z) \quad (102)$$

$$\Phi_{xz}^A = \left( x^2 - \frac{1}{4} \right) \left( z^2 - \frac{1}{4} \right) \left( y - \frac{1}{2} \right)^2 f_5(x, y, z) \quad (103)$$

$$\Phi_{yz}^A = \left( x^2 - \frac{1}{4} \right)^2 \left( z^2 - \frac{1}{4} \right) \left( y - \frac{1}{2} \right) f_6(x, y, z) \quad (104)$$

$$\Phi_{xx}^B = \left( z^2 - \frac{1}{4} \right)^2 \left( y + \frac{1}{2} \right)^2 f_7(x, y, z) \quad (105)$$

$$\Phi_{yy}^B = \left( z^2 - \frac{1}{4} \right)^2 \left( x^2 - \frac{1}{4} \right)^2 f_8(x, y, z) \quad (106)$$

$$\Phi_{zz}^B = \left(x^2 - \frac{1}{4}\right)^2 \left(y + \frac{1}{2}\right)^2 f_9(x, y, z) \quad (107)$$

$$\Phi_{xy}^B = \left(x^2 - \frac{1}{4}\right) \left(z^2 - \frac{1}{4}\right)^2 \left(y + \frac{1}{2}\right) f_{10}(x, y, z) \quad (108)$$

$$\Phi_{xz}^B = \left(x^2 - \frac{1}{4}\right) \left(z^2 - \frac{1}{4}\right) \left(y + \frac{1}{2}\right)^2 f_{11}(x, y, z) \quad (109)$$

$$\Phi_{zz}^B = \left(x^2 - \frac{1}{4}\right)^2 \left(z^2 - \frac{1}{4}\right) \left(y + \frac{1}{2}\right) f_{12}(x, y, z). \quad (110)$$

Functions ( $f_n(x, y, z)$ ) are of the type:

$$g_{n1} \sinh(x) \sinh(z) + g_{n2} \sinh(x) \cosh(z) + g_{n3} \cosh(x) \sinh(z) + g_{n4} \cosh(x) \cosh(z)$$

where ( $g_{ni}$ ) are polynomials of ( $h_{ni1} + h_{ni2}x + h_{ni3}z$ ), and ( $h_{ni1}$ ), ( $h_{ni2}$ ), and ( $h_{ni3}$ ) are polynomials of ( $a_{n1j} + \dots + a_{n1jm}y^{m-1}$ ). The selection of ( $\sinh x$ ), ( $\cosh x$ ), ( $\sinh z$ ), ( $\cosh z$ ), and  $y$  facilitated numerical calculations.

A typical distribution for the normal stress,  $\sigma_{yy}$ , common to both substrates A and B at the bonded interface of a three-dimensional flat interface between these substrates is shown in Fig. 14. This stress is calculated by the novel mathematical procedure based on differential geometry and the penalty function as described by Ma et al. (2001), and summarized above. Figure 15 shows the transverse stresses  $\sigma_{xx}$ , on substrates A and B at the bonded interface, illustrating the discontinuity of this stress across the interface, as sometimes called the “stress jump.” Again, these stresses are calculated by the novel mathematical procedure based on differential geometry and the penalty function as described by Ma et al. (2001), and summarized above.

### 23.3.8 Damage Models

The incremental theory of plasticity assumes that the strains depend on the entire history of loading. The total increments of deviatoric strain  $\Delta \epsilon_{ij}$  is composed of a viscoplastic component

$$\Delta \epsilon_{ij}^P = d\lambda S_{ij} \quad (111)$$

where  $d\lambda$  is a variable depending on the loading history, and an elastic component

$$d\epsilon_{ij}^E = \left( \frac{dS_{ij}/dt}{2G} \right) \quad (112)$$

so that



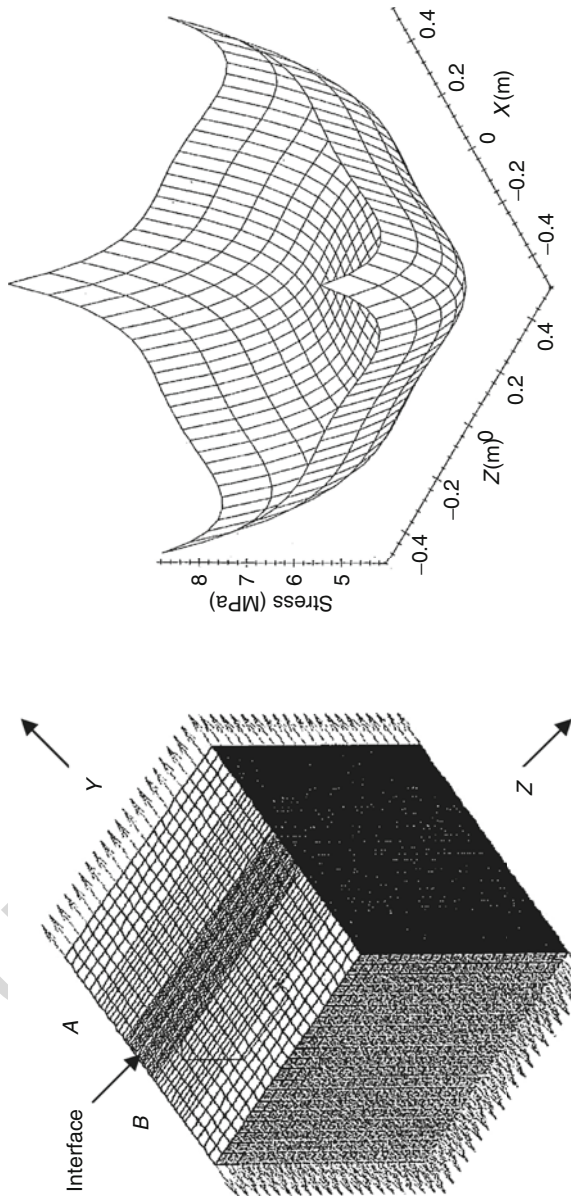


**Fig. 14** A three-dimensional flat interface between two substrates A and B, loaded as shown and analyzed by FEA with the mesh pattern shown (left). A typical distribution for the normal stress,  $\sigma_{yy}$ , common to both substrates A and B at the bonded interface is shown on the right, as calculated by a novel mathematical procedure based on differential geometry and the penalty function

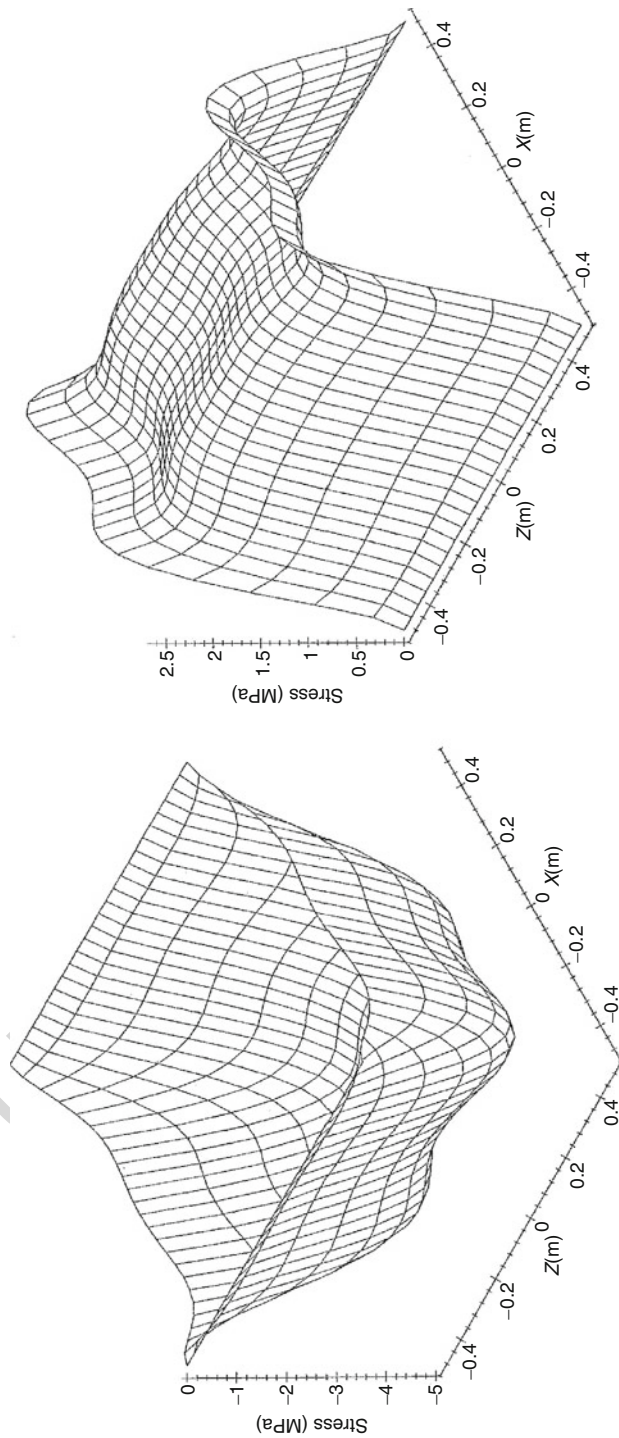


**Fig. 15** The transverse stresses  $\sigma_{xx}$  on substrates A (left) and B (right) at the bonded interface, illustrating the discontinuity of this stress across the interface, as sometimes called the “stress jump,” calculated by a novel mathematical procedure based on differential geometry and the penalty function

$$\frac{d\epsilon_{ij}}{dt} = \frac{d\epsilon_{ij}^E}{dt} + \frac{d\epsilon_{ij}^P}{dt}. \quad (113)$$

Obviously, a yield criterion is needed to determine the actual magnitudes of plastic strain increments. This theory was first proposed by Prandtl (1925) and Reuss (1930).

Several constitutive forms were proposed to describe the viscoplastic term of Eq. 113 by various researchers. Among these, Sokolovsky (1948) used the assumption that the viscoplastic component is a function of the over-stress above the yield point. On the basis of his experimental observations, Sokolovsky determined that the over-stress should be defined above the elastic limit, as a function  $F(\sigma - \theta)$ , so that

$$\epsilon = \frac{\sigma}{E}, \sigma \leq \theta. \quad (114.1)$$

$$\epsilon = \left(\frac{\sigma}{E}\right) + F \frac{(\sigma - \theta)}{E}, \sigma > \theta. \quad (114.2)$$

The over-stress idea can be incorporated into the viscoelastic mechanical models by means of adding sliding elements to describe yield or termination points. With such an application, equations containing viscosity terms are obtained in a form similar to (24.114). For example, Brinson et al. (1975), Renieri et al. (1976), Sancaktar and Brinson (1979, 1980), Sancaktar (1981), Sancaktar and Padgilwar (1982), Sancaktar et al. (1984), and Sancaktar and Schenck (1985) used the modified Bingham model developed by Brinson (1974) to describe the shear and tensile material behavior of structural adhesives in the bulk and bonded forms:

$$\sigma = E\epsilon \quad \sigma \leq \theta \quad (115.1)$$

$$\frac{d\epsilon}{dt} = \frac{d\sigma}{dt} + \frac{(\sigma - \theta)}{\mu} \theta < \sigma \leq Y \quad (115.2)$$

$$\sigma = Y \quad \sigma \geq Y. \quad (115.3)$$

The model describes linear elastic behavior below the elastic limit  $\theta$ , linear viscoelastic behavior between  $\theta$ , and the maximum stress  $Y$  and perfectly plastic behavior above  $Y$ . When the sliding element is activated at  $\sigma = \theta$ , the model becomes essentially a Maxwell element, as illustrated in Fig. 16.

A similar application was also reported first by Chase and Goldsmith (1974) and later by Sancaktar (1981), Sancaktar and Padgilwar (1982), Sancaktar et al. (1984), and Sancaktar and Schenck (1985), in modifying a three-parameter solid model with a sliding element to describe the mechanical behavior of polymeric materials and adhesives. Figure 17 shows stress-strain-strain rate behavior of LARC-3 carrier-cloth supported solid film adhesive and comparison with the Chase-Goldsmith

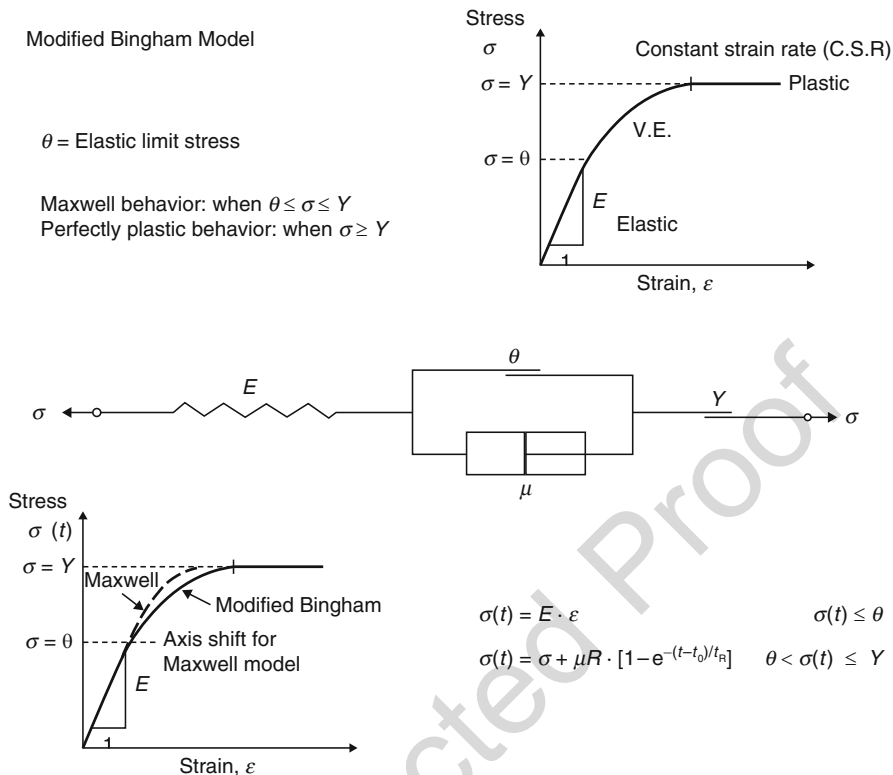


**Fig. 16** The modified Bingham model and its comparison with the Maxwell model.  $t_R = \mu/E$  = relaxation time and  $t_0$  is the time to reach elastic limit

model. LARC-3, a linear condensation polyimide adhesive, was made at NASA Langley Research Center by adding a 2:1 molar ratio of 3,3',4,4'-benzophenone tetracarboxylic dianhydride (BTDA) (0.010 mol)/pyromellitic dianhydride (PMDA) (0.005 mol) to 3,3'-diaminobenzophenone (DABP) (0.015 mol) in 429 of diglyme.

The Chase-Goldsmith model constitutive equations are given as (see Fig. 18):

$$\sigma = E\epsilon \leq \sigma_{\text{static}} \quad (116.1)$$

$$\frac{d\epsilon}{dt} = \left( \frac{(d\sigma/dt)}{E_1} \right) + \frac{(\sigma - \sigma_{\text{static}})}{\mu'} \sigma \geq \sigma_{\text{static}} \quad (116.2)$$

where

$$\sigma_{\text{static}} = \left[ \frac{E_1}{(E_1 + E_2)} \right] (Y + E_2\epsilon) \quad (117)$$

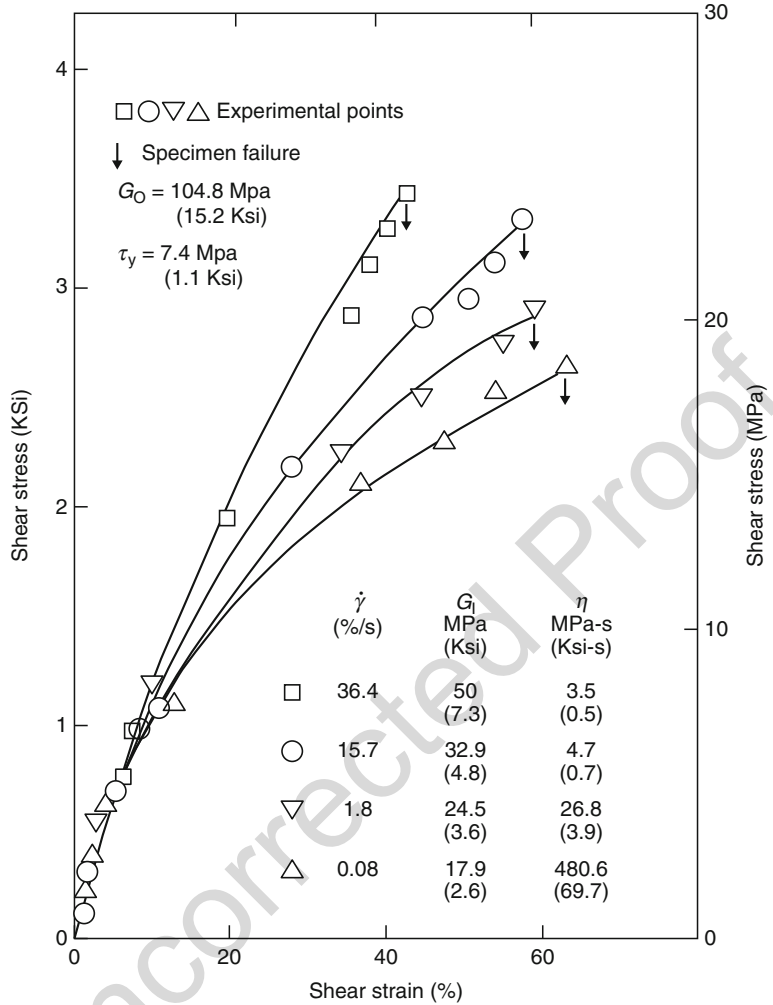


**Fig. 17** Stress–strain–strain rate behavior of LARC-3 adhesive bonded in symmetric-single lap configuration, and comparison with the Chase–Goldsmith model

813 and

$$\mu' = \left[ \frac{E_1}{(E_1 + E_2)} \right] \mu. \tag{118}$$

814

815 To obtain the constant strain rate relation, the above constitutive equation is  
816 solved using the condition,  $d \epsilon / dt = R = \text{constant}$ , to result in:

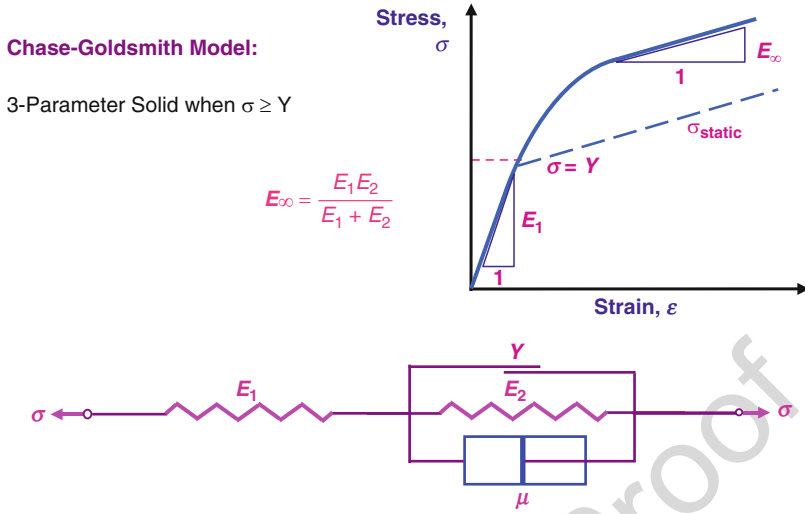


**Fig. 18** The Chase–Goldsmith model

$$\sigma = \left[ \frac{E_1}{(E_1 + E_2)} \right] \{ (Y + \mu' R + E_2 \epsilon (1 - \exp[-\alpha(\epsilon - \epsilon_Y)])) \} + \left\{ Y + \left[ \frac{E_1 E_2}{(E_1 + E_2)} \right] (\epsilon - \epsilon_Y) \right\} \exp[-\alpha(\epsilon - \epsilon_Y)] \quad (119)$$

where

$$\epsilon_Y = \frac{Y}{E_1} \quad (120)$$

$$\alpha = \frac{E_1}{\mu' R}. \quad (121)$$

Previous investigations by Sancaktar and Brinson (1979, 1980), Sancaktar (1981), and Sancaktar and Padgilwar (1982) on toughened structural adhesives with and without a carrier (Metlbond 1113 and 1113-2 solid film adhesives, respectively) showed that the bonded adhesive behavior was predominantly affected by the presence of inherent flaws and the ensuing fracture processes due to their presence. Figure 19 shows the variability of the shear stress–strain behavior in the symmetric-single lap joint form for similar specimens tested under monotonic loading. Prior to testing, a neutron radiography examination of the joints shown in Fig. 19 revealed that the variations in the stress-strain behavior were results of inherent flaws (voids) in the bond line, which constituted approximately 6–8% of the bond area. With brittle adhesives, the presence of inherent flaws may lead to fracture processes and catastrophic failures.

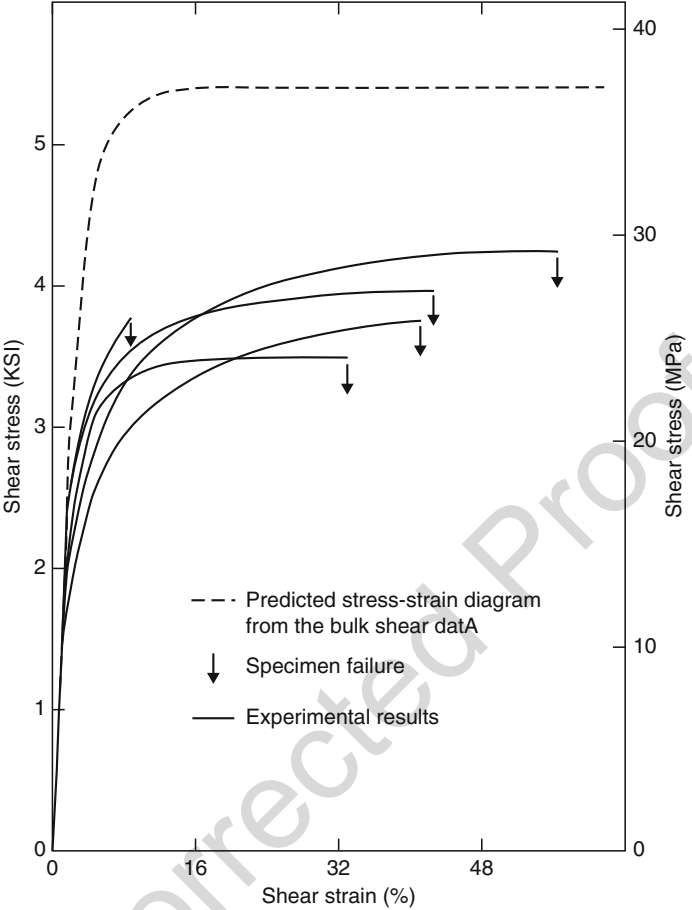


**Fig. 19** Symmetric single lap adhesive stress–strain response of Metlbond-1113 film adhesive with synthetic carrier cloth and containing inherent flaws prior to testing. The dashed line represents the stress–strain behavior predicted for the same testing rate based on the bulk adhesive data

An isothermal theory of separation in (thermoplastic or pressure sensitive) polymer-solid adhering systems based on drawing of filaments is given by Good and Gupta (1988).

Ganghoffer and Schultz (1996) stated that the influence of damage on the mechanical behavior is specified through the concept of strain equivalence. They propose that the constitutive law for the damaged material is given by that of the virgin material if the stress tensor  $\sigma$  is replaced by the effective stress tensor  $\sigma/(1 - d)$  with the term,  $d$ , representing the extent of damage between the virgin state,  $d = 0$  and complete failure,  $d = 1$ .

Another example of empirical damage modeling in joints bonded using silver flake-filled electrically conductive adhesives was given by Gomatam and

Sancaktar (2006a, b), who introduced a comprehensive fatigue life predictive model for single lap joints subjected to variable loading (2006b). For the purpose of formulating a fatigue life predictive model, a linear relationship is established first between the maximum cyclic load  $P_{\max}$  (or maximum principal stress,  $\sigma_{\max}$ , as suggested by Gomatam (2002), and Gomatam and Sancaktar (2004)) and the number of cycles  $N$ :

$$P_{\max} = C' + m'N \quad (122)$$

where  $(C')$  and  $(m')$  are the intercept and slope for this linear relation, respectively.

For the purpose of the analytical fatigue life predictive model, two separate analytical equations were proposed depending on the intensity (severe or moderate) of the load-ratio first applied, at a maximum cyclic load level. The total fatigue life,  $N_{\text{Total}}$ , under severe-to-moderate condition was predicted by the relation

$$N_{\text{Total}} = n_s + \frac{\Delta C}{m_M} - (C_s - P) \left( \frac{1}{m_s} - \frac{1}{m_M} \right) \left( 1 - \frac{n_s}{N_s} \right). \quad (123)$$

The total fatigue life under moderate-to-severe condition, on the other hand, was predicted by

$$N_{\text{Total}} = n_M + N_s \left( 1 - \frac{n_M}{N_M} \right). \quad (124)$$

The term  $\Delta C$ , in Eqs. 123 and 124, is defined as:

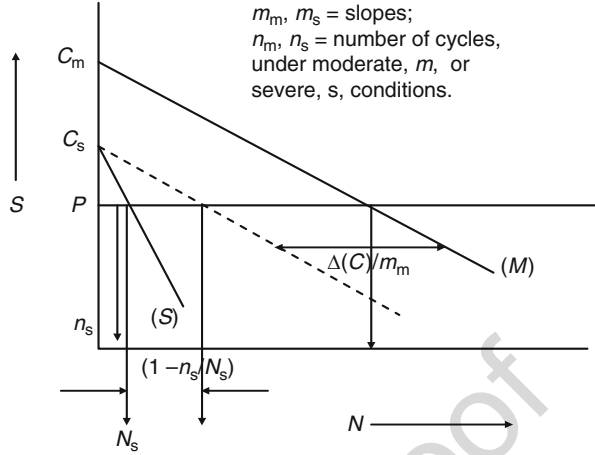
$$\Delta C = C_M - C_s, \quad (125)$$

where  $C_M$  and  $C_s$  are the intercepts, and  $m_M$  and  $m_s$  are the slopes for the linear relationships between the maximum cyclic load  $P_{\max}$  (or maximum principal stress,  $\sigma_{\max}$ ) and the number of cycles  $N$  under moderate and severe conditions, respectively.  $n_M$  and  $n_s$  are the number of cycles applied under moderate and severe conditions, respectively.

As illustrated in Fig. 20, in going from moderate-to-severe conditions, the predicted remaining life for the sample under the severe condition,  $N_s[1 - (n_M/N_M)]$ , is simply added to the number of cycles under moderate conditions ( $n_M$ ), based on experimental predictions without making any slope corrections, Eq. 124. In going from severe-to-moderate condition, however, a slope correction,  $[C_s - P] \{ (1/m_s) - (1/m_M) \} [1 - (n_s/N_s)]$ , is also made, in order to make the severe and moderate load–number of cycles ( $P$ – $N$ ) curves parallel, and shift the intercepts to add the remaining life,  $\Delta C/m_M$ , to that already used up under severe condition (i.e.,  $n_s$ ). These particular methodologies were chosen based on experimental observations. Utilizing the above equations, the total fatigue life of the joints subjected to varying loading conditions, namely, severe-to-moderate and moderate-to-severe were computed for a set of test cases, in addition to experimentally determined values, for the



**Fig. 20** Illustration of the cumulative fatigue damage model



purpose of model validation. Comparison between the experimental and predicted values validated the accuracy and efficiency of the proposed model.

In order to render the model usable with different stress components ( $\sigma_{xx}$ ,  $\sigma_{yy}$ ,  $\sigma_{zz}$ ,  $\tau_{xy}$ ,  $\tau_{yz}$ ,  $\tau_{xz}$ ) instead of the maximum cyclic load values, Gomatam (2002) utilized the maximum and minimum principal and von Mises stresses obtained from non-linear elastoplastic finite element analyses to calculate the ratios of peak stress values obtained at corresponding maximum load levels. These stresses were then compared to the intercept ratios obtained from the P–N curves at given environmental conditions. This comparison procedure revealed the maximum principal stress as the appropriate parameter to be used in the form of stress-number of cycles (S–N) curves, that is,

$$\sigma_{\max} = C + mN \quad (126)$$

where  $C$  and  $m$  are, respectively, the intercept and slope values based on maximum principal stress. The mathematical basis for the maximum principal stress to replace the maximum cyclic load in Eq. 122 was illustrated by performing fatigue tests under three different maximum load,  $P_{\max}$ , conditions, and considering the following relations:

$$\frac{C'_3}{C'_1} = \frac{C_3}{C_1}, \quad (127)$$

and

$$\frac{C'_2}{C'_1} = \frac{C_2}{C_1} \quad (128)$$

where  $(C'_1, C'_2, C'_3)$  relate to Eq. 122, and  $C_1, C_2, C_3$  relate to Eq. 125.

In order to account for environmental effects, such as elevated temperature and humidity, a superposition method was applied for fatigue life prediction by shifting the slopes and the intercepts between different environmental conditions. For this purpose, design charts were formulated based on experimental data. These design charts comprise two parts, one for shifting the slope and the other for shifting the intercept between different environmental conditions. Once the slopes and the intercepts are determined, Eqs. 122 and 125 would yield the fatigue life of the joint at the new environmental condition, as illustrated in Fig. 21 (Gomatam and Sancaktar 2006b).

The proposed model was also extended to bonded cases with varying stress states. For this purpose, a nonlinear elastoplastic finite element analysis (FEA) for ambient condition, and a nonlinear thermoelastoplastic FEA for elevated temperature conditions were performed using two different lap joint geometries and boundary conditions to represent two distinct states of stress. Utilizing the FEA results, relations between the stress components, slopes, and intercepts were established. The intercepts were found to be inversely proportional to the maximum stresses, and the slopes directly proportional to a shear stress component. Thus, by using these relations along with knowledge of the stress states for only two joint configurations, the slope and intercept for any other lap joint with unknown P–N ( $\sigma - N$ ) behavior could be computed, from which the fatigue life of the joint could be predicted.

### 23.3.9 The Effects of Cure and Processing Conditions on the Mechanical Behavior

Cure and processing conditions have strong effects on the resulting mechanical properties of structural adhesives in the bulk and bonded forms.

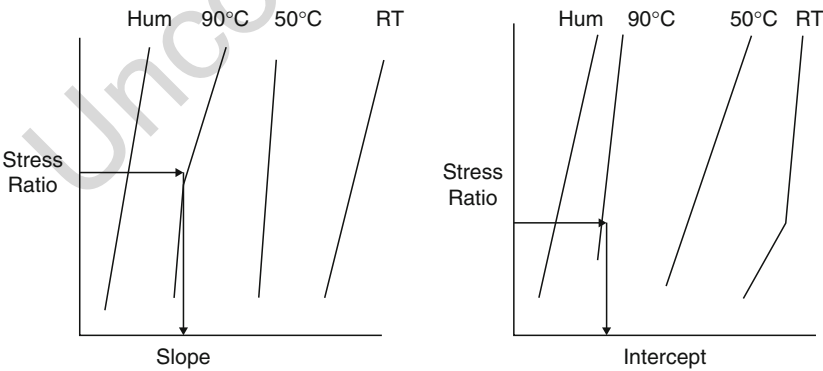


**Fig. 21** The shifting mechanism, shown by horizontal arrows, implemented for the purpose of predicting fatigue life of joints subject to a stress ratio ( $R$ ), and maximum cyclic load of  $P_{max}$ , from one test environment (28 °C, or 50 °C, or 90 °C) to another at the same stress ratio, and maximum cyclic load, RT indicates room temperature

Variation of various mechanical properties of an epoxy adhesive with or without a carrier cloth as functions of cure temperature, time, and cooldown conditions, and their effects on bulk tensile properties were studied by Sancaktar et al. (1983), Jozavi and Sancaktar (1989a, b, c), and Sancaktar (1995), with the work by Jozavi and Sancaktar (1989c) providing information on the effects of cure conditions on the relaxation behavior of bulk thermosetting adhesives. A comparison of the degree of cure with bulk strength was given by Jozavi and Sancaktar (1988). The effects of the cure parameters on the stress-whitening behavior were given by Jozavi and Sancaktar (1989a, b). The effects on the bonded joint behavior were discussed by Shaw and Tod (1989), Sancaktar and Ma (1992), and Turgut and Sancaktar (1992). In general, mechanical properties are improved with increases in cure temperature and time and with slow cooldown. Such increases, however, have an upper limit, and further increases in cure parameter magnitudes lead to deterioration in adhesive mechanical properties. Consequently, in general, the variation of mechanical properties are bell-shaped functions, showing an initial increase with decreasing slope followed by a decreasing trend, when plotted against the cure parameters.

Additional information on the effects of cure conditions were provided by Sinclair (1992).

In the case of particle-filled adhesive systems, such as electrically conductive adhesives, the viscosity,  $\mu$ , during processing and cure is a function of filler volume fraction,  $\Phi$ , shear rate,  $d\gamma/dt$ , and resin conversion level,  $\alpha$ . The development of viscosity from a chemorheological point of view is important as it relates to the wetting and diffusive characteristics of the adhesive during its cure. These characteristics ultimately determine the viability of the interphase and, therefore, the overall adhesive bond. A comprehensive model may be represented by combining the following models: the power law describing the shear rate effect (Wildemuth and Williams 1985), Castro-Macosko model describing the conversion effect (Castro et al. 1984), and Liu model describing the filler volume fraction effect (Liu 2000). Such a combined model takes the form:

$$\mu\left(\phi, \frac{d\gamma}{dt}, \alpha\right) = A \cdot (\phi_m - \phi)^{-2} \cdot \left(\frac{d\gamma}{dt}\right)^{C_0+C_1\cdot\alpha} \cdot \left[\frac{\alpha_{gel}}{(\alpha_{gel} - \alpha)}\right]^{D+E\cdot\alpha} \quad (129)$$

where  $A$ ,  $C_0$ ,  $C_1$ ,  $D$ , and  $E$  are model constants that can be determined by multivariable nonlinear regression analysis of isothermal data. The maximum filler volume fraction,  $\Phi_m$ , and conversion at gel point,  $\alpha_{gel}$ , values are usually known for typical thermosets.

Zhou and Sancaktar (2008) incorporated the isothermal temperature effects to obtain a general-form comprehensive model in the form:

$$\mu\left(T, \phi, \frac{d\gamma}{dt}, \alpha\right) = A \cdot \exp\left(\frac{B}{T}\right) \cdot (\phi_m - \phi)^{-2} \cdot \left(\frac{d\gamma}{dt}\right)^{C_0+C_1\cdot\alpha} \cdot \left[\frac{\alpha_{gel}}{(\alpha_{gel} - \alpha)}\right]^{D+E\cdot\alpha} \quad (130)$$

where  $B$  is the activation temperature and other coefficients are same as in Eq. 129.

In order to model realistic adhesive processing, usually with a broad temperature range, nonisothermal tests usually need to be undertaken. The comprehensive isothermal chemoviscosity model, based on Eq. 130, can then be extended to nonisothermal temperature cure cycle through nonlinear regression analysis of nonisothermal data.

In fact, nonisothermal temperature cure is a different process from isothermal cure. The reaction kinetics, total reaction order, and even the reaction energy for epoxy systems may not be constant and same, but process dependent. Therefore, modifications need to be made to reflect the effects of such a difference.

An improvement in the model predictability is expected by allowing parameters  $D$  and  $E$  in Eq. 130 to change with temperature during nonisothermal cure. Furthermore, both of these parameters also show some variation with the volume fraction ( $\Phi$ ) and shear rate ( $(d\gamma/dt)$ ). A modified comprehensive model was thus proposed as follows (Zhou and Sancaktar 2008):

$$\mu\left(T, \phi, \frac{d\gamma}{dt}, \alpha\right) = A \cdot \exp\left(\frac{B}{T}\right) \cdot (\phi_m - \phi)^{-2} \cdot \left(\frac{d\gamma}{dt}\right)^{C_0 + C_1 \cdot \alpha} \cdot \left[\frac{\alpha_{\text{gel}}}{(\alpha_{\text{gel}} - \alpha)}\right]^{D^* + E^* \cdot \alpha} \quad (131)$$

where

$$D^* = D_0 + D_1 \cdot \left(\frac{d\gamma}{dt}\right) + D_2 \cdot \phi + D_3 \cdot T \quad (132)$$

$$E^* = E_0 + E_1 \cdot \left(\frac{d\gamma}{dt}\right) + E_2 \cdot \phi + E_3 \cdot T \quad (133)$$

with  $D_i$  and  $E_i$  values to be determined by data fitting.

## 23.4 Prediction of Limit (Threshold) and Failure Stresses

In predicting limit (threshold) conditions, such as the elastic limit, yield, and failure conditions, classical failure criteria, such as the maximum normal stress criterion, maximum shear stress criterion and the distortion energy (von Mises) criterion can be employed.

If the yield strength,  $\sigma_y$ , of the material is the same under tensile and compressive conditions, that is,  $\sigma_{yc} = \sigma_{yt}$ , the von Mises failure criteria, which is based on (deviatoric) distortion energy considerations, provides accurate predictions of yield:

$$(\sigma_1 - \sigma_2)^2 + (\sigma_2 - \sigma_3)^2 + (\sigma_1 - \sigma_3)^2 = \text{constant} = 2\sigma_y^2. \quad (134)$$

The left-hand side of Eq. 134 is related to the second invariant,  $(J'_2)$  of the stress deviator tensor by the relation:

$$6J'_2 = (\sigma_1 - \sigma_2)^2 + (\sigma_2 - \sigma_3)^2 + (\sigma_1 - \sigma_3)^2 \quad (135)$$

If the condition,  $\sigma_{yc} > \sigma_{yt}$ , prevails, then the hydrostatic pressure,  $p$ , also affects the yield process. A given stress tensor,  $\sigma_{ij}$ , can be written as:

$$\sigma_{ij} = p + \sigma_{\text{deviatoric}},$$

and the hydrostatic pressure,  $p$ , is defined as:

$$p = (1/3)[\sigma_1 + \sigma_2 + \sigma_3] \quad (136)$$

Therefore, by using Eqs. 134–136, the von Mises yield criterion can be modified to the form:

$$\begin{aligned} 2(\sigma_{yc} - \sigma_{yt})[\sigma_1 + \sigma_2 + \sigma_3] + [(\sigma_1 - \sigma_2)^2 + (\sigma_2 - \sigma_3)^2 + (\sigma_1 - \sigma_3)^2] \\ = 2\sigma_{yc}\sigma_{yt}. \end{aligned} \quad (137)$$

Conditions resulting in the creation of free volume, such as crazing (stress whitening) and cavitation relate to the magnitude of the hydrostatic stress. Level of the critical (or crazing) strain,  $\epsilon_{CR}$  at such occurrences can be predicted using the relation:

$$\epsilon_{CR} = C + (D/p) \quad (138)$$

where  $C$  and  $D$  are temperature and rate-dependent material constants, and  $p$  is the hydrostatic stress.

## 23.5 Conclusion

Constitutive modeling of adhesives and sealants include considerations for deformation theories and viscoelasticity with linearity and nonlinearity considerations, rubber elasticity, singularity methods, bulk adhesive as composite material, damage models, and the effects of cure and processing conditions on the mechanical behavior. However, the concept of the “interphase” must always be kept in mind for accurate predictions in mechanical behavior of surfaces and joints bonded with adhesives and sealants. Interfaces may constitute a weak link in the chain of load transfer in bonded joints. Also, the discontinuity of the material properties causes abrupt changes in stress distribution, as well as causing stress singularities at the edges of the interfaces. In most engineering joints the adherend surfaces have distinct topographies, which result in a collection of miniature joints in micron, and even nanoscale when bonded adhesively. If the interphase is not considered as a

discrete collection of individual chemical bonds, the methods of continuum mechanics can still be applied to this collection of miniature joints by assuming continuous or a combination of continuous/discontinuous interphase zones. Thus, the displacement at the interphase need not be continuous at every location. The analysis of a miniature joint contributing to the overall adhesion in a macro joint can be performed in a fashion similar to that for the macro joint itself, which is usually studied with the employment of the methods of linear or nonlinear elasticity, viscoelasticity, plasticity, fracture, damage, and/or failure mechanics.

## References

- Agarwal BD, Broutman LJ (1990) Analysis and performance of fiber composites, 2nd edn. Wiley, New York, p 131
- Agrawal R, Drzal LT (1989) *J Adhes* 29:63
- Ahlonis JJ, MacKnight WJ, Shen M (1972) Introduction to polymer viscoelasticity. Wiley-Interscience, New York
- Ashton JE, Halpin JC, Petit PH (1969) Primer on composite materials. Analysis Technomic, Stamford, p 77
- Barsoum RS (1989) *J Adhes* 29:149
- Brinson HF (1974) In: Kausch H et al (eds) Deformation and fracture of high polymers. New York, Plenum
- Brinson HF, Renieri MP, Herakovich CT (1975) Fracture mechanics of composites. ASTM SPT 593:177
- Budiansky B (1965) *J Mech Phys Solids* 13:223
- Castro JM, Macosko CW, Perry SJ (1984) *Polym Commun* 25:82
- Chase KW, Goldsmith W (1974) *Exp Mech* 14:20
- Chow TS (1978a) *J Polym Sci Polym Phys Ed* 16:959
- Chow TS (1978b) *J Polym Sci Polym Phys Ed* 16:967
- Chow TS, Hermans JJ (1969) *J Compos Mater* 3:382
- Darlington MW, Turner S (1978) Creep of engineering materials. Mechanical Engineering, London
- Davis JL (1964) *J Polym Sci A* 2:1311
- Dempsey JP (1995) *J Adhes Sci Technol* 9:253
- Dillard DA, Hiel C (1985) Proceedings of the 1985 SEM spring conference on experimental mechanics, Las Vegas, p 142
- Eshelby JD (1959) *Proc R Soc Lond A* 252:561
- Ferry JD (1961) Viscoelastic properties of polymers. Wiley, New York
- Findley WN, Peterson DB (1958) *ASTM Proc* 58:841
- Flügge W (1975) Viscoelasticity, 2nd edn. Springer, Berlin
- Ganghoffer JF, Schultz J (1996) *J Adhes Sci Technol* 10:775
- Garton A, Haldankar GS, Mclean PD (1989) *J Adhes* 29:13
- Gittus J (1975) Creep, viscoelasticity and creep fracture in solids. Wiley, New York
- Gomatam RR (2002) Modeling fatigue behavior of electronically conductive adhesives. PhD dissertation, The University of Akron, Akron
- Gomatam RR, Sancaktar E (2004) *J Adhes Sci Technol* 18:1833
- Gomatam RR, Sancaktar E (2006a) *J Adhes Sci Technol* 20:69
- Gomatam RR, Sancaktar E (2006b) *J Adhes Sci Technol* 20:87
- Good RJ, Gupta RK (1988) *J Adhes* 26:13
- Green AE, Adkins JE (1960) Large elastic deformations and non-linear continuum mechanics. Oxford University Press, New York
- Groth HL (1988) *Int J Adhes Adhes* 8:107

- 1047 Hashin Z, Shtrikman S (1963) *J Mech Phys Solids* 11:127
- 1048 Hata T, Gams M, Kojimer K (1965) *Kobunshikagahn (Chem High Polym, Jpn)* 22:160
- 1049 Hata T, Ohsaka K, Yamada T, Nakamue K, Shibata N, Matsumoto T (1994) *J Adhes* 45:125
- 1050 Hencky HZ (1924) *Z Angew Math Mech* 4:323
- 1051 Hermans JJ (1967) *Proc R Acad Amst B70*:1
- 1052 Hiel C, Cardon AH, Brinson HF (1983) The nonlinear viscoelastic response of resin matrix composite laminates. Virginia Polytechnic Institute and State University report no. VPI-E-83-6
- 1053 Hill R (1964) *J Mech Phys Solids* 12:199
- 1054 Hill R (1965) *J Mech Phys Solids* 13:213
- 1055 Hilton HH (1975) In: Baer E (ed) *Engineering design for plastics*, Robert E. Krieger, Huntington, New York
- 1056 Jozavi H, Sancaktar E (1988) *J Adhes* 25:185
- 1057 Jozavi H, Sancaktar E (1989a) *J Adhes* 27:143
- 1058 Jozavi H, Sancaktar E (1989b) *J Adhes* 27:159
- 1059 Jozavi H, Sancaktar E (1989c) *J Adhes* 29:233
- 1060 Kaelble DH (1964) *J Colloid Sci* 19:413
- 1061 Kaelble DH (1969) *J Adhes* 1:102
- 1062 Kelly A, Tyson WR (1965) *Mech Phys Solids* 13:329
- 1063 Kerner EH (1956) *Proc Phys Soc B69*:808
- 1064 Keuner VH, Knauss WG, Chai H (1982) *Exp Mech* 22:75
- 1065 Knollman GC, Hartog JJ (1985) *J Adhes* 17:251
- 1066 Koizumi S, Fuhue N, Matsunaga T (1970) *Nihon Setchahu Kyohaishi. J Adhes Soc Jpn* 6:437
- 1067 Lipatov YS, Babich VF, Todosijchuk TT (1991) *J Adhes* 35:187
- 1068 Liu DM (2000) *J Mater Sci* 35:5503
- 1069 Ludwik PG (1909) *Elemente der technologischen mechanik*. Springer, Berlin, p 9
- 1070 Ma W, Gomatam R, Fong R, Sancaktar E (2001) *J Adhes Sci Technol* 15:1533
- 1071 McLellan DL (1969) *Appl Polym Symp* 12:137
- 1072 Nakao K (1969) Preprint, symposium on mechanisms of adhesive failure, Tokyo, p 47
- 1073 Nonaker Y (1968) *Nihon Setchahu Kyokaishi (J Adhes Soc Jpn)* 4:207
- 1074 Peretz D, Weitsman Y (1982) *J Rheol* 26:245
- 1075 Prandtl L (1925) *Proceedings of the 1st international congress on applied mechanics*, Technisch Boekhandel en Dructerrg, Delft, p 43
- 1076 Ramberg W, Osgood WR (1943) Description of stress-strain curves by three parameters. NACA TN 902, Washington, DC
- 1077 Ravi-Chandar K, Knauss WG (1984) *Int J Fract* 25:247
- 1078 Reedy ED Jr, Guess TR (1995) *J Adhes Sci Technol* 9:237
- 1079 Renieri MP, Herakovich CT, Brinson HF (1976) Rate and time dependent behavior of structural adhesives. Virginia Polytechnic Institute and State University, College of Engineering report no. VPI-E-76-7
- 1080 Reuss E (1930) *Z Angew Math Mech* 10:266
- 1081 Rochefert MA, Brinson HF (1983) Nonlinear viscoelastic characterization of structural adhesives. Virginia Polytechnic Institute and State University report no. VPI-E-83-26
- 1082 Russel WB, Acrivos A (1973) *Z Angew Math Phys* 24:581
- 1083 Sancaktar E (1981) *Intl J Adhes Adhes* 1:329
- 1084 Sancaktar E (1985) *Intl J Adhes Adhes* 5:66
- 1085 Sancaktar E (1991) *J Adhes* 34:211
- 1086 Sancaktar E (1995) *J Adhes Sci Technol* 9:119
- 1087 Sancaktar E (1996) *Appl Mech Rev* 49:S128
- 1088 Sancaktar E, Beachtle D (1993) *J Adhes* 42:65
- 1089 Sancaktar E, Brinson HF (1979) The viscoelastic shear behavior of a structural adhesive. Virginia Polytechnic Institute and State University, College of Engineering report no. VPI-E-79-14
- 1090 Sancaktar E, Brinson HF (1980) In: Lee LH (ed) *Adhesion and adsorption of polymers*. Polymer science and technology series, vol 12-A. Plenum, New York, p 279
- 1091

- 1100 Sancaktar E, Dembosky SK (1986) *J Adhes* 19:287
- 1101 Sancaktar E, Kumar S (2000) *J Adhes Sci Technol* 14:1265
- 1102 Sancaktar E, Ma W (1992) *J Adhes* 38:131
- 1103 Sancaktar E, Narayan K (1999) *J Adhes* 13:237
- 1104 Sancaktar E, Padgilwar S (1982) *J Mech Des* 104:643
- 1105 Sancaktar E, Schenck SC (1985) *Ind Eng Chem Prod Res Dev* 24:257
- 1106 Sancaktar E, Wei Y (1998) In: van Ooij WJ, Anderson H (eds) *Mittal Festschrift on adhesion science and technology*. VSP, Utrecht, p 509
- 1107
- 1108 Sancaktar E, Zhang P (1990) *Trans ASME J Mech Des* 112:605
- 1109 Sancaktar E, Jozavi H, Klein RM (1983) *J Adhes* 15:241
- 1110 Sancaktar E, Schenck SC, Padgilwar S (1984) *Ind Eng Chem Prod Res Dev* 23:426
- 1111 Sancaktar E, Jozavi H, El-Mahallawy AH, Cenci NA (1987) *Polym Test* 7:39
- 1112 Sancaktar E, Turgut A, Guo F (1992) *J Adhes* 38:91
- 1113 Sancaktar E, Babu SV, Zhang E, D'Couto GC, Lipshitz H (1995) *J Adhes* 50:103
- 1114 Sawa T, Temma K, Nishigaya T, Ishikawa H (1995) *J Adhes Sci Technol* 9:215
- 1115 Schapery RA (1966) *Proceedings of the 5th U.S. national congress of applied mechanics*, ASME, p 511
- 1116
- 1117 Schapery RA (1969a) Further development of a thermodynamic constitutive theory: stress formulation. Purdue University report no. 69-2
- 1118
- 1119 Schapery RA (1969b) *Polym Eng Sci* 9:295
- 1120 Sharon G, Dodiuk H, Kenig S (1989) *J Adhes* 31:21
- 1121 Sharpe LH (1972) *J Adhes* 4:51
- 1122 Shaw SJ, Tod DA (1989) *J Adhes* 28:231
- 1123 Sinclair JW (1992) *J Adhes* 38:219
- 1124 Sokolovsky VV (1948) *Prikl Matematiha I Mehhanika* 12:261
- 1125 Struik DJ (1950) *Classical differential geometry*. Addison-Wesley, New York
- 1126 Tobolsky AV (1960) *Properties and structure of polymers*. Wiley, New York
- 1127 Turgut A, Sancaktar E (1992) *J Adhes* 38:111
- 1128 Walpole LJ (1969) *J Mech Phys Solids* 17:235
- 1129 Ward IM, Hadley DW (1993) *Mechanical properties of solid polymers*. Wiley, New York, p 206
- 1130 Wei Y (1995) *Electronically conductive adhesives: conduction mechanisms, mechanical behavior and durability*. PhD dissertation, Clarkson University, Potsdam, New York
- 1131
- 1132 Weitsman Y (1981) *J Adhes* 11:279
- 1133 Wildemuth CR, Williams MC (1985) *Rheol Acta* 24(1):75
- 1134 Wu TT (1966) *Int J Solids Struct* 2:1
- 1135 Zabora RF, Clinton WW, Bell JE (1971) *Adhesive property phenomena and test techniques*. AFFDL-TR-71-68
- 1136
- 1137 Zhang MJ, Straight MR, Brinson HF (1985) *Proceedings of the 1985 SEM spring conference on experimental mechanics*, Las Vegas, p 205
- 1138
- 1139 Zhou J, Sancaktar E (2008) *Chemorheology of epoxy/nickel conductive adhesives during processing and cure*. *J Adhes Sci Technol* 22:957
- 1140



Liyong Tong and Quantian Luo

## Contents

24.1	Introduction .....	666
24.2	Classical Analytical Analysis of Single-Lap Joints .....	668
24.2.1	Adhesive Stress .....	668
24.2.2	Load Update and Bending Moment Factor .....	673
24.3	Other Analytical Solutions for Single-Lap Joints .....	674
24.3.1	Adhesive Stress with the Effects of Transverse Shear and Geometric Nonlinearity .....	674
24.3.2	Coupled Formulation for Load Update of Single-Lap Joints .....	677
24.3.3	Numerical Comparisons .....	679
24.3.4	Analytical Approach for Adhesive Joints with Material Nonlinearity .....	682
24.4	Analytical Approach of Other Lap Joints .....	685
24.4.1	Analytical Solutions of Symmetric Lap Joints Subjected to General Loadings .....	685
24.4.2	Analytical Solutions of Asymmetric and Unbalanced Joints .....	686
24.5	Failure Criteria Based on Continuum Mechanics .....	691
24.5.1	Shear and Peel Stresses of an Adhesive Joint with a Semi-infinite Length .....	691
24.5.2	Failure Prediction Using the Criteria Based on Continuum Mechanics .....	692
24.6	Failure Criteria Based on Fracture Mechanics .....	692
24.6.1	Failure Prediction Using Energy Release Rates .....	693
24.6.2	Analytical Solutions of Energy Release Rates for Cohesive Failure and Debonding .....	694
24.6.3	Failure Prediction Considering Plastic Deformation .....	697
24.7	Summary .....	698
References	.....	698

L. Tong (✉) · Q. Luo

School of Aerospace, Mechanical and Mechatronic Engineering, The University of Sydney, Sydney, NSW, Australia

e-mail: [liyong.tong@sydney.edu.au](mailto:liyong.tong@sydney.edu.au); [quantian.luo@sydney.edu.au](mailto:quantian.luo@sydney.edu.au)

### Abstract

This chapter presents analytical approach for determining stress and strength of adhesively bonded joints. Selected applications of adhesively bonded joints are discussed first, and then mathematical models for stress analysis of these joints are outlined. Various closed-form solutions for adhesive stresses and edge bending moment for balanced single-lap joints are presented and compared. The method for finding analytical solutions for asymmetric and unbalanced adhesive joints is also discussed. Explicit expressions for mode I and mode II energy release rates for cohesive failure and interfacial debonding are presented for asymmetric joints with a semi-infinite length subjected to general load combinations.

## 24.1 Introduction

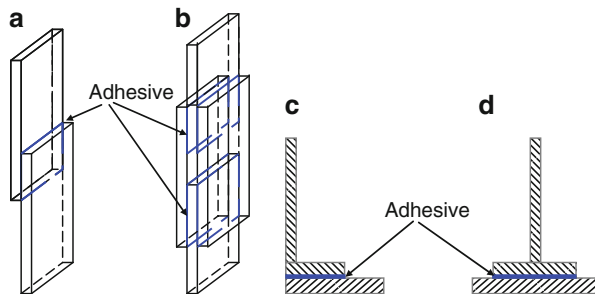
Adhesive bonding technology is increasingly being used in practical structures due to its load-transferring performance. It can be used to effectively join similar and dissimilar thin sheets of materials via forming superb load-bearing structural joints (Adams et al. 1997; Tong and Steven 1999). It can behave superior to mechanical fastening in joining composite parts due to relatively smooth stress distribution compared to highly localized stress concentration in mechanically fastened joints. It is finding wider applications in many industries. For example, in aerospace and automotive industries, it is used to connect thin-walled structural parts; in civil engineering, it is used to reinforce concrete structures by bonding composite materials; and in intelligent structural systems, it is used to bond functional materials to host structures.

Figure 1 depicts some of the typical joint configurations to join structural panel components.

When adhesive bonding is used to repair or strengthen structural defects, such as cracks and ballistic damage, single-sided, double-sided, scarf and step repair configurations, as shown in Fig. 2, are usually used.

Reinforced concrete (RC) beams with adhesively bonded fiber-reinforced polymer (FRP) as shown in Fig. 3a have also been widely used in civil engineering. In this case, the fiber-reinforced polymer plate plays the role of bridging the cracks in the concrete beams, thus slowing down or arresting the crack propagation. Figure 3b

**Fig. 1** Common joint configurations: (a) single-lap joint; (b) double-lap joint; (c) L-joint; (d) T-joint



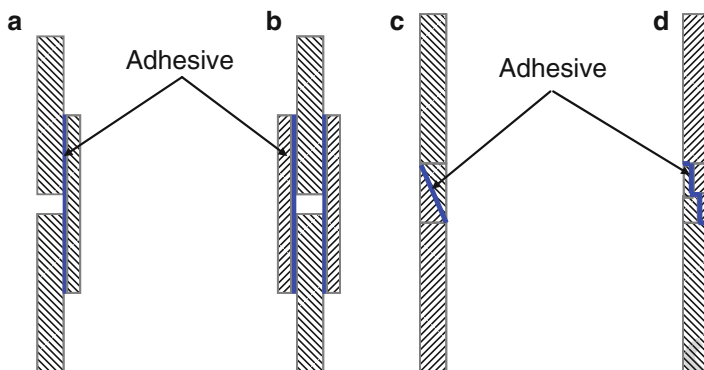


**Fig. 2** Composite repair configurations: (a) single-strap joint; (b) double-strap joint; (c) scarf joint; (d) step joint

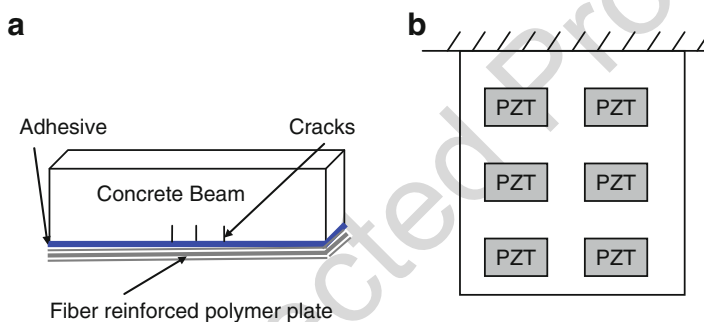


**Fig. 3** Adhesive bonding technology used in civil engineering and intelligent structure systems: (a) FRP-plated RC beam; (b) PZT smart plate

illustrates a piezoelectric (PZT) smart plate, in which PZT patches are adhesively bonded to the plate surface to control its structural performance.

Figures 1, 2, and 3 illustrate that lap-type adhesive joints are common configurations used in practical structures. Although lap-type joints have the features of two-dimensional (2D) geometry, their stress analysis usually involves three-dimensional (3D) stresses and strains; hence it is a 3D problem in nature. Numerical methods, such as finite element analysis (FEA) (see ► Chap. 25, “Numerical Approach: Finite Element Analysis”), have been used to solve 3D problems of adhesively bonded structures. However, simple and closed-form solutions are important in terms of identifying fundamental characteristics and key parameters. Analytical solutions can also be useful in preliminary design stage as they can offer in timely fashion, simple, quick, and meaningful answers. Therefore, considerable efforts have been devoted to the development of analytical approach for determining stress and strength of an adhesively bonded joint. Hence, this chapter focuses on presentation of basic mechanics models and analytical solutions for selected adhesively bonded joints.

In order to derive closed-form explicit solutions for adhesively bonded joints/structures, it is important to develop appropriate mechanics models that take into account fundamental characteristics and key parameters. It is a compromise between the including of selected physical behavior and likelihood of admissible explicit solutions, and this balance plays a vital role in the development of analytical solution methods.

A lap-type joint often consists of one or more adhesive layer(s) sandwiched between two or more beams/plates usually referred to as adherends. An adherend usually has a thickness smaller than the other in-plane dimension(s), and when the aspect ratio, that is, in-plane dimension-to-thickness ratio, is sufficiently large, it is reasonable to model the adherends as a beam or plate. As the theory for beam-like structures have been well established, adherends in most adhesively bonded structures can be simplified as beam- or plate-like structures. An adhesive layer typically has a thickness of a fraction of a millimeter, for example, a bondline thickness of approximately 0.2 mm is common in secondarily bonded aerospace or automobile structures. The stress state in the adhesive layer is rather complex in 3D or 2D nature when the adherends are modeled as plates or beams, respectively. However, in practice, an adhesive is very thin compared to an adherend; therefore, the adhesive layer is generally modeled by an infinite number of springs or an interface by assuming that the only adhesive normal (thickness direction) and shear stresses exist, and they remain constant across the bondline thickness and only vary along the bondline length. This approximation leads to a mechanics model (referred as 1D model) that permits analytical solutions for stresses in an adhesively bonded joint.

In this chapter, analytical models and solutions for adhesively bonded joints treated as beam-like structures are presented.

## 24.2 Classical Analytical Analysis of Single-Lap Joints

The simplest geometric configuration of adhesively bonded structures is probably the single-lap joint (SLJ), which has been widely used as a standard test specimen to calibrate adhesive properties and has been shown to be representative and challenging in identifying fundamental characteristics and key parameters in bonded lap joints.

### 24.2.1 Adhesive Stress

#### Average Shear Stress Model

This model treats the adherend as a rigid bar and the adhesive as continuous shear spring, which is based on the assumption that the adherends are so stiff that they do not deform and only the adhesive deforms as it is so soft, as shown in Fig. 4a. In this model, the adhesive shear stress uniformly distributes within the adhesive and is given by:

$$\tau = F/(2c) \quad (1)$$

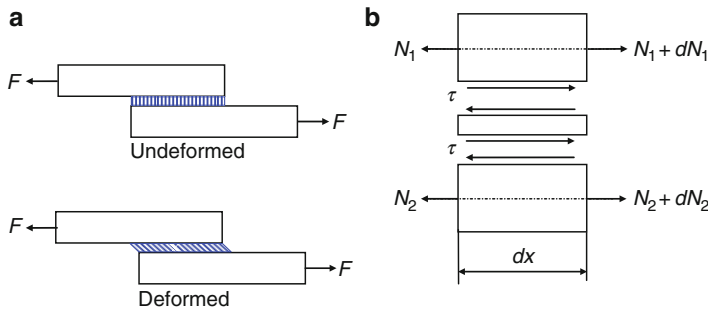


**Fig. 4** Stress analysis of the adhesive based on the one parameter elastic medium: (a) an average shear stress model; (b) free body diagrams of the shear lag model

where  $F$  is the applied tensile force per unit width and  $(2c)$  is the overlap length; the unit width of a beam has been assumed. In this chapter, the unit width and plane stress state are assumed for brevity. The results can be easily extended to plane strain state by changing the related parameters. Also, the composite adherends with the symmetric lay-ups are assumed. The results can be directly applied to joints with isotropic adherends.

### Shear Lag Model

Volkersen (1938) proposed a shear lag model, in which the adherend was modeled as a rod undergoing axial or longitudinal deformation only and the adhesive as a continuous shear spring. As shown in Fig. 4b, the equilibrium and constitutive equations for adherends 1 and 2 are:

$$\frac{dN_1}{dx} + \tau = 0; \frac{dN_2}{dx} - \tau = 0 \quad (2)$$

$$N_i = A_{di} \frac{du_i}{dx} \quad (i = 1, 2) \quad (3)$$

where  $A_d$  is the extensional stiffness and subscript  $i$  ( $i = 1, 2$ ) denotes adherend 1 and 2. The adhesive shear stress is defined as:

$$\tau = \frac{G_a}{t_a} (u_2 - u_1) \quad (4)$$

where  $G_a$  and  $t_a$  are the shear modulus and thickness of the adhesive.

The shear stress can be found by solving Eqs. 2, 3, and 4 and is given by:

$$\tau = \left( \frac{\beta_v F}{2} \right) \left[ \frac{\cosh \beta_v x}{\sinh \beta_v c} - \frac{(1 - \psi) \sinh \beta_v x}{(1 + \psi) \cosh \beta_v c} \right] \quad (5)$$

where  $\beta_v = \sqrt{\frac{(1 + \psi) G_a}{t_a A_{d1}}}$  and  $\psi = \frac{A_{d1}}{A_{d2}}$

This solution clearly shows that the shear stress is not uniform along the bondline length direction and peaks at the adhesive ends. The maximum shear stress occurs at one end and is given by:

$$\tau_{\max} = \left( \frac{\beta_v F}{2} \right) \left[ \frac{\cosh \beta_v c}{\sinh \beta_v c} - \frac{(1 - \psi) \sinh \beta_v c}{(1 + \psi) \cosh \beta_v c} \right] \text{ when } \psi \geq 1 \quad (6a)$$

OR

$$\tau_{\max} = \left( \frac{\beta_v F}{2} \right) \left[ \frac{\cosh \beta_v c}{\sinh \beta_v c} + \frac{(1 - \psi) \sinh \beta_v c}{(1 + \psi) \cosh \beta_v c} \right] \text{ when } \psi \leq 1 \quad (6b)$$

For a relatively long overlap, the maximum shear stress can be approximately written as:

$$\begin{aligned} \tau_{\max} &= \frac{\psi \beta_v F}{1 + \psi} \text{ when } A_{d1} \neq A_{d2} \\ \text{or : } \tau_{\max} &= \frac{1}{2} \beta_v F \text{ when } A_{d1} = A_{d2} \end{aligned} \quad (6c)$$

In Eq. 6c,  $\sinh \beta_v c \approx \cosh \beta_v c$  is assumed, which is sufficiently accurate in most adhesive joints used in engineering.

### Adhesive-Beam Model

Goland and Reissner (1944) proposed an adhesive-beam model for the single-lap joint shown in Fig. 5a, in which a two-parameter elastic medium and Euler beams are used to model the adhesive and adherends, respectively.

The free body diagrams of an infinitesimal element are shown in Fig. 6a, and the equilibrium equations of adherends 1 and 2 are:

$$\begin{cases} \frac{dN_1}{dx} + \tau = 0; & \frac{dQ_1}{dx} + \sigma = 0; & \frac{dM_1}{dx} + \frac{t_1}{2} \tau - Q_1 = 0 \\ \frac{dN_2}{dx} - \tau = 0; & \frac{dQ_2}{dx} - \sigma = 0; & \frac{dM_2}{dx} + \frac{t_2}{2} \tau - Q_2 = 0 \end{cases} \quad (7)$$

where  $t_1$  and  $t_2$  are the thicknesses of adherends 1 and 2,  $t_2 = t_1$  is for the balanced joints, and  $\tau$  and  $\sigma$  are the adhesive shear and peel stresses, defined by:

$$\tau = \frac{G_a}{t_a} \left[ (u_2 - u_1) + \left( \frac{t_1}{2} \frac{dw_1}{dx} + \frac{t_2}{2} \frac{dw_2}{dx} \right) \right]; \sigma = \frac{E_a}{t_a} (w_2 - w_1) \quad (8)$$

in which  $E_a$  is Young's modulus of the adhesive.

By using the Euler beam theory, Eqs. 7 and 8, the governing equations for adhesive stresses can be derived as:

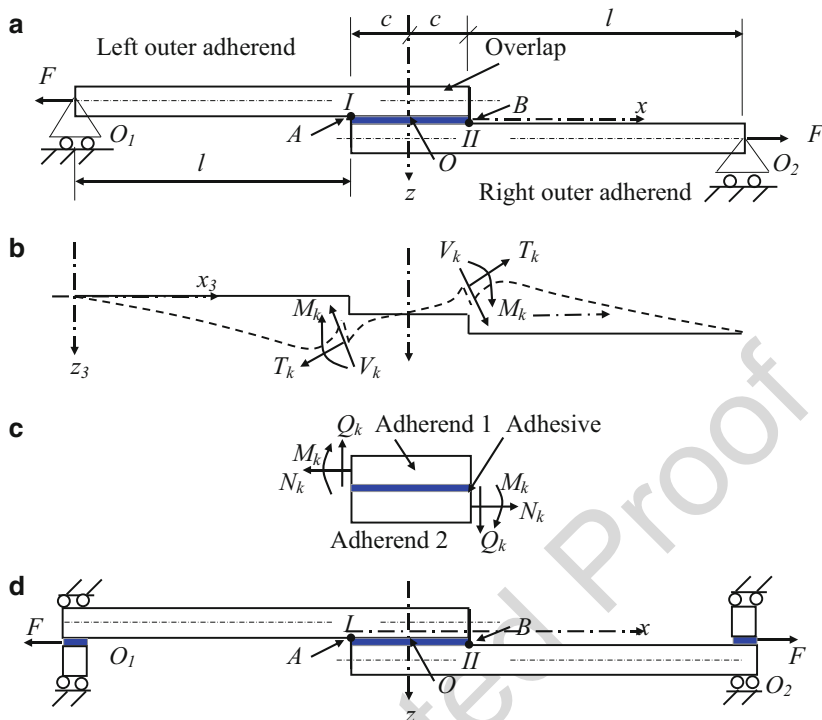


**Fig. 5** A single-lap joint: (a) configuration; (b) deformation and forces in cross sections *I* and *II* of the deformed single-lap joint; (c) forces at the overlap edges; (d) SLJ with alignment tabs

$$\frac{d^3 \tau}{dx^3} - \beta_c^2 \frac{d\tau}{dx} = 0; \frac{d^4 \sigma}{dx^4} + 4\beta_\sigma^4 \sigma = 0 \quad (9)$$

146 in which

$$\beta_c^2 = \alpha_a \beta_\tau^2; \beta_\tau = \sqrt{\frac{8G_a}{A_{d1}t_a}}; \beta_\sigma = \frac{\sqrt{2}}{2} \times \sqrt[4]{\frac{2E_a}{D_1 t_a}}; \alpha_a = \frac{1}{4}(1 + \alpha_k); \alpha_k = \frac{4A_{d1}t_1^2}{D_1} \quad (10)$$

147 where  $D_1$  is the bending stiffness of adherends 1 and 2 and  $\alpha_a$  and  $\alpha_k$  reflect the  
148 influences of composite lay-ups. For isotropic adherends,  $\alpha_a = 1$  and  $\alpha_k = 3$ .

149 Solving Eq. 9 with the boundary conditions shown in Fig. 5b, c yields:

$$\begin{cases} \tau = \frac{\beta_c(Ft_1 + 2\alpha_k M_k) \cosh \beta_c x}{8\alpha_a t_1 \sinh \beta_c c} + \frac{\alpha_k(Ft_1 - 2M_k)}{8\alpha_a t_1 c} \\ \sigma = B_{\sigma 1} \sinh \beta_\sigma x \sin \beta_\sigma c + B_{\sigma 4} \cosh \beta_\sigma x \cos \beta_\sigma c \end{cases} \quad (11)$$

150 where

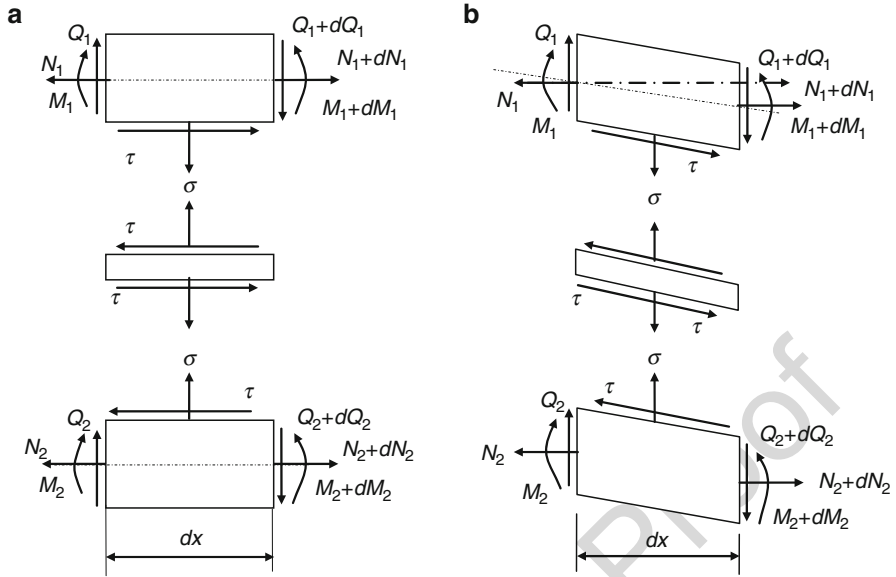


**Fig. 6** Stress analysis of the adhesive based on a two-parameter elastic medium: (a) free body diagrams of a **linear** overlap; (b) free body diagrams of a **nonlinear** overlap

$$\begin{cases} B_{\sigma 1} = \frac{2\beta_{\sigma}[M_k\beta_{\sigma}(\sinh \beta_{\sigma}c \cos \beta_{\sigma}c + \cosh \beta_{\sigma}c \sin \beta_{\sigma}c) + V_k \sinh \beta_{\sigma}c \sin \beta_{\sigma}c]}{\sinh 2\beta_{\sigma}c + \sin 2\beta_{\sigma}c} \\ B_{\sigma 4} = \frac{2\beta_{\sigma}[M_k\beta_{\sigma}(\sinh \beta_{\sigma}c \cos \beta_{\sigma}c - \cosh \beta_{\sigma}c \sin \beta_{\sigma}c) + V_k \cosh \beta_{\sigma}c \cos \beta_{\sigma}c]}{\sinh 2\beta_{\sigma}c + \sin 2\beta_{\sigma}c} \end{cases} \quad (12)$$

As  $\sinh \beta_{\sigma}c > 1$  and  $\sinh \beta_c c > 1$  in most cases, the maximum shear and peel stresses occur at the adhesive edges and can be simplified as:

$$\tau_{\max} = \frac{Ft_1(\beta_c c + \alpha_k) + 2\alpha_k M_k(\beta_c c - 1)}{8\alpha_a t_1 c}; \sigma_{\max} = \beta_{\sigma}^2 \left( M_k + \frac{V_k}{\beta_{\sigma}} \right) \quad (13)$$

It is noted that the stress analysis of Goland and Reissner (1944) is for adhesively bonded isotropic joints, and an extension to composite joints is presented here.

### Adhesive Models Based on Two-Dimensional Elastic Theory

When an adhesive layer is relatively thick, the above adhesive model of assuming constant shear and peel strains may not be effective. In fact, shear and peel strains are not constant, and the axial strain may not be ignored even if the adhesive is very thin (e.g.,  $<0.2$  mm) (Ojalvo and Eidinoff 1978; Luo and Tong 2004). In addition, the constant adhesive model does not satisfy the boundary condition of free shear stress at an adhesive end.



To capture stress variation through the adhesive thickness and free edge stress in the adhesive ends, models based on the 2D elastic theory have been used. Allman (1977) and then Chen and Cheng (1983) assumed linear variation of peel stress and constant shear stress across the adhesive thickness. Ojalvo and Eidinoff (1978) and then Carpenter (1980) adopted linear variation of shear stress and constant peel stress through the thickness. Luo and Tong (2004) chose linear and higher-order variations of shear, peel, and axial normal stresses across the adhesive thickness.

Adams and Mallick (1992) and then Zhao and Lu (2009) developed analytical models for the adhesively bonded joints using 2D elasticity, in which both adhesive and adherends are described as elastic media. Their models can be applied to joints with thick adhesive. Analytical solutions of adhesively bonded composite joints for this model are unavailable or too complicated.

When the adhesive is thin (e.g.,  $<0.3$  mm), the adhesive model with constant shear and peel stresses can be used to describe overall structural performance of adhesively bonded joints. Since the adhesive stresses are not constant across the thickness even for very thin adhesive, the adhesive shear and peel stresses should be deemed as an approximation to those in the adhesive midplane.

## 24.2.2 Load Update and Bending Moment Factor

Due to load eccentricity in the SLJ of Fig. 5a, large deflections must be considered, as shown in Fig. 5b. This means that the bending moment  $M_k$  and the shear force  $V_k$  at the overlap ends need to be updated with structural deformation. This geometric nonlinearity can be characterized by the bending moment factor or edge moment factor  $k$  and is defined as:

$$M_k = k \frac{(t_1 + t_a)}{2} F \quad (14)$$

It is noted that  $t_a$  is ignored in the definition of edge moment factor  $k$  in Goland and Reissner (1944). They presented the uncoupled formulation for determining the joint edge force update and adhesive stresses in Part I and Part III of their work. In Part I, the large deflections of both outer adherends and overlap were considered with the overlap being treated as an entire beam. Deflections of the left outer adherend and the overlap of the SLJ in Fig. 5 are:

$$w_3 = A \sinh \beta_k x_3 + \frac{(t_1 + t_a)x_3}{2(l+c)}; w_o = B \sinh \beta_o x_o + \frac{(t_1 + t_a)x_o}{2(l+c)} \quad (15)$$

in which

$$\beta_k = \sqrt{\frac{F}{D_1}}; \quad \beta_o = \sqrt{\frac{F}{D_o}} \quad (16)$$

where  $D_o$  is the bending stiffness of the entire overlap and  $A$  and  $B$  are the integration constants to be determined by the continuity conditions at intersection  $I$ . The joint edge forces  $M_k$  and  $V_k$  can be found by using  $M_k = -D_1 w_3''(l)$  and  $V_k = -D_1 w_3'''(l)$ . The edge moment factor is given by:

$$k = \frac{1}{1 + (\beta_k/\beta_o)\tanh \beta_o c \coth \beta_k l} \quad (17)$$

or :  $k = \frac{1}{1 + (\beta_k/\beta_o)\tanh \beta_o c}$  when  $\coth \beta_k l \approx 1$

## 24.3 Other Analytical Solutions for Single-Lap Joints

### 24.3.1 Adhesive Stress with the Effects of Transverse Shear and Geometric Nonlinearity

In the classical adhesive-beam model proposed by Goland and Reissner (1944), the equilibrium equations are derived from Fig. 6a by using the Euler beam to model the isotropic adherends. That is, the overlap geometric nonlinearity, transverse shear, and normal stiffness of the adherends are not modeled. In adhesively bonded composite structures, such as single-lap joints and single-sided patch repairs, geometric nonlinearity and transverse shear stiffness can significantly affect the adhesive stresses due to large deflection and relatively lower transverse stiffness of composites. Therefore, geometric nonlinearity and transverse stiffness should be considered.

When the geometric nonlinearity is considered, the associated free body diagrams are illustrated in Fig. 6b. To model transverse stiffness of the adherends, the Timoshenko or higher-order beam theory needs to be used to model the adherends (Srinivas 1975; Renton and Vinson 1975; Carpenter 1991; Yang and Pang 1993; Luo and Tong 2008; Yousefsani and Tahani 2013). In the analytical formulations conducted by Luo and Tong (2008), the following variables are introduced:

$$\begin{cases} 2u_s = u_2 + u_1; & 2w_s = w_2 - w_1; & 2\phi_s = \phi_2 - \phi_1 \\ 2u_a = u_2 - u_1; & 2w_a = w_2 + w_1; & 2\phi_a = \phi_2 + \phi_1 \\ 2N_s = N_2 + N_1; & 2Q_s = Q_2 - Q_1; & 2M_s = M_2 - M_1; & 2V_s = V_2 - V_1 \\ 2N_a = N_2 - N_1; & 2Q_a = Q_2 + Q_1; & 2M_a = M_2 + M_1; & 2V_a = V_2 + V_1 \end{cases} \quad (18)$$

where subscripts  $1$  and  $2$  indicate adherends 1 and 2; subscripts  $s$  and  $a$  denote the symmetric and anti-symmetric deformations; and the variables have the usual meanings used in Timoshenko beam theory.

The equilibrium equations derived by considering the geometric nonlinearity of Fig. 6b are (Luo and Tong 2007, 2008):

$$\begin{cases} \frac{dN_1}{dx} + \tau = 0; & \frac{dQ_1}{dx} + \sigma + \tau\phi_1 = 0; & \frac{dM_1}{dx} + \frac{t_1}{2}\tau - Q_1 = -N_1\phi_1 \\ \frac{dN_2}{dx} - \tau = 0; & \frac{dQ_2}{dx} - \sigma - \tau\phi_2 = 0; & \frac{dM_2}{dx} + \frac{t_1}{2}\tau - Q_2 = -N_2\phi_2 \end{cases} \quad (19)$$

219 When the Timoshenko beam is used to model the adherends, the adhesive shear  
220 and peel stresses can be expressed as:

$$\tau = \frac{2G_a}{t_a} \left( u_a + \frac{t_1}{2} \phi_a \right); \sigma = \frac{2E_a}{t_a} w_s \quad (20)$$

221 The governing equations taking into account the geometric nonlinearity of the  
222 overlap and the transverse shear stiffness of the adherends can be derived by using  
223 Eqs. 18, 19, and 20 and the constitutive equations of the Timoshenko beam, and they  
224 are given by (Luo and Tong 2008):

$$\begin{cases} \frac{d^3 u_a}{dx^3} - \frac{\beta_\tau^2}{4} \left( \frac{du_a}{dx} + \frac{t_1}{2} \frac{d^2 w_a}{dx^2} \right) = 0 \\ \frac{d^4 w_a}{dx^4} - \frac{\alpha_k \beta_\tau^2}{2t_1} \left( \frac{du_a}{dx} + \frac{t_1}{2} \frac{d^2 w_a}{dx^2} \right) - \frac{\beta_k^2}{2} \frac{d^2 w_a}{dx^2} = 0 \end{cases} \quad (21)$$

$$\frac{d^2 u_s}{dx^2} = 0; \frac{d^4 w_s}{dx^4} - 4\beta_{ng}^2 \frac{d^2 w_s}{dx^2} + 4\beta_{ng}^4 w_s = 0 \quad (22)$$

225 where

$$\beta_{ng}^2 = \left( \beta_g^2 + \frac{\beta_k^2}{8} \right); \beta_{ng}^4 = \left( \beta_\sigma^4 + \frac{\beta_k^2 \beta_g^2}{2} \right); \beta_g = \frac{1}{2} \times \sqrt{\frac{2E_a}{G_{k1} t_a}} \quad (23)$$

226 in which  $G_{k1}$  is the shear stiffness of adherends 1 and 2.

227 When the boundary conditions are prescribed, analytical solutions of Eqs. 21  
228 and 22 can be obtained. Luo and Tong (2008) derived the analytical solutions for  
229 given forces at overlap edges. For composite SLJs, the analytical solutions of  
230 Eq. 21 are:

$$\begin{cases} u_a = A_{a2} \cosh \beta_{a1} x + A_{a4} \cosh \beta_{a2} x + A_{a7} \\ w_a = B_{a1} \sinh \beta_{a1} x + B_{a3} \sinh \beta_{a2} x + B_{a6} x \end{cases} \quad (24)$$

231 where

$$\beta_{a1}, \beta_{a2} = \frac{1}{2} \left[ \beta_c^2 + \frac{\beta_k^2}{2} \pm \sqrt{\beta_c^4 + \left( 1 - \frac{1}{2\alpha_a} \right) \beta_c^2 \beta_k^2 + \frac{\beta_k^4}{4}} \right] \quad (25)$$

232 The analytical solutions of Eq. 22 for composite SLJs are:

$$\begin{cases} u_s = \frac{F}{2A_{d1}}x \\ w_s = \frac{B_{s1}^-}{B_{s2}^+} \sinh \beta_{s1}^- x \sin \beta_{s2}^- x + \frac{B_{s4}^-}{B_{s4}^+} \cosh \beta_{s1}^- x \cos \beta_{s2}^- x & \Delta < 0 \\ w_s = \frac{B_{s1}^+}{B_{s2}^+} \cosh \beta_{s1}^+ x + \frac{B_{s4}^+}{B_{s4}^+} \cosh \beta_{s2}^+ x & \Delta > 0 \end{cases} \quad (26)$$

233 where

$$\begin{cases} \Delta = \beta_{ng}^4 - \beta_{n\sigma}^4 \\ \beta_{s1}^- = \sqrt{\beta_{n\sigma}^2 + \beta_{ng}^2}; \quad \beta_{s2}^- = \sqrt{\beta_{n\sigma}^2 - \beta_{ng}^2} & \Delta < 0 \\ \beta_{s1}^+ = \sqrt{2} \sqrt{\beta_{ng}^2 + \sqrt{\beta_{ng}^4 - \beta_{n\sigma}^4}}; \beta_{s2}^+ = \sqrt{2} \sqrt{\beta_{ng}^2 - \sqrt{\beta_{ng}^4 - \beta_{n\sigma}^4}} & \Delta > 0 \end{cases} \quad (27)$$

234 It can be shown that, for the case of thick adherend, thin adhesive and low  
235 transverse shear stiffness of the adherends,  $\Delta > 0$ ; otherwise,  $\Delta < 0$ . In general,  
236  $\Delta < 0$  for isotropic adherends made of steel and aluminum, and  $\Delta > 0$  for composite  
237 adherends due to the lower transverse shear stiffness. As  $t_a \rightarrow 0$ ,  $\Delta > 0$ ; it becomes a  
238 problem of interface fracture or delamination (Luo and Tong 2009b, c).  $\Delta = 0$  is a  
239 special case, whose solutions can be obtained by letting  $\Delta \rightarrow 0$  in the solutions for  
240  $\Delta < 0$  or  $\Delta > 0$ .

241 By using Eqs. 20, 24, and 26, adhesive stresses can be directly obtained, and the  
242 details can be found in Luo and Tong (2008). In most cases,  $\beta_{a1}^2 \approx \beta_c^2 \gg \beta_{a2}^2$ ,  $\beta_g^2$   
243  $\gg \beta_k^2$ , and  $\beta_\sigma^2 \gg \beta_k^2$ . When these approximations are used, the analytical solutions  
244 can be simplified. The simplified adhesive stresses at the adhesive ends are:

$$\tau_{\max} = \frac{[2\alpha_k M_k + Ft_1(1 - r_k)]\beta_{a1}c \coth \beta_{a1}c}{8\alpha_a t_1 c} + \frac{\alpha_k (Ft_1 - 2M_k)\beta_{a2}c \coth \beta_{a2}c}{8\alpha_a t_1 c} \quad (28)$$

$$\sigma_{\max} = \begin{cases} \beta_\sigma^2 \left[ M_k + \left( \frac{\beta_{s1}^-}{\beta_\sigma^2} \right) V_k \right] & \Delta < 0 \\ \beta_\sigma^2 \left[ M_k + \left( \frac{\beta_{s1}^+ + \beta_{s2}^+}{2\beta_\sigma^2} \right) V_k \right] & \Delta > 0 \end{cases} \quad (29)$$

245 The adhesive stresses of a single-lap joint reach maximum at the edges, which are  
246 important in assessing the adhesive joint strength. The expressions of maximum  
247 adhesive stresses obtained using different analytical models are summarized in  
248 Table 1.

$$\text{where } r_k = \frac{\beta_k^2}{2\beta_c^2}$$

249  
250 It can be shown that when  $\beta_k \rightarrow 0$ , the maximum adhesive stresses in nonlinear  
251 analysis degenerate to those in linear analysis. It is noted that different strategies can  
252 be used to obtain analytical solutions of adhesively bonded composite joints with  
253 and without considering geometrical nonlinearity. When the linear overlap is  
254 assumed, it is handy to express the governing equations in terms of the adhesive

**Table 1** Comparisons of the maximum adhesive stresses

t.2	Adherend model	Maximum peel stress	Maximum shear stress
t.3	Average stress model		$F/(2c)$
t.4	Shear lag model		$\beta_s F/2$
t.5	Linear adhesive-Euler-beam model	$\beta_\sigma^2 \left( M_k + \frac{V_k}{\beta_\sigma} \right)$	$\frac{(2\alpha_k M_k + Ft_1)\beta_{a1}c}{8\alpha_a t_1 c} + \frac{\alpha_k(Ft_1 - 2M_k)}{8\alpha_a t_1 c}$
t.6	Nonlinear adhesive-Timoshenko-beam model	$\beta_\sigma^2 \left[ M_k + \left( \frac{\beta_{a1}^-}{\beta_\sigma^2} \right) V_k \right] \quad \Delta < 0$	$\frac{[2\alpha_k M_k + Ft_1(1 - r_k)]\beta_{a1}c \coth \beta_{a1}c}{8\alpha_a t_1 c}$
t.7		$\beta_\sigma^2 \left[ M_k + \left( \frac{\beta_{a1}^+ + \beta_{a2}^+}{2\beta_\sigma^2} \right) V_k \right] \quad \Delta > 0$	$+\frac{\alpha_k(Ft_1 - 2M_k)\beta_{a2}c \coth \beta_{a2}c}{8\alpha_a t_1 c}$

stresses. When geometrical nonlinearity is considered, it is convenient to write the governing equations in terms of the adherend displacements.

### 24.3.2 Coupled Formulation for Load Update of Single-Lap Joints

One distinctive and challenging feature of a single-lap joint is its eccentric load path, which leads to the geometric nonlinearity that requires the load update. Goland and Reissner (1944) conducted uncoupled formulation for the load update and the adhesive stresses, respectively. In their formulation, the overlap was treated as a homogeneous beam for determining load update.

#### Coupled Formulation with Adhesive Shear Deformation Effect But No Overlap Nonlinearity

Hart-Smith (1973) showed that the uncoupled formulation of Goland and Reissner (1944) is inconsistent with the force conditions of an individual adherend at the overlap ends. To overcome this deficiency and consider the influence of the adhesive deformation, Hart-Smith (1973) modeled each adherend of the overlap as an individual beam and derived the coupled formulation for load update and the adhesive shear stress. By using continuity conditions at intersection  $I$ , Hart-Smith (1973) obtained the edge moment factor and then simplified it as:

$$k = \frac{1}{1 + \beta_k c \coth \beta_k l + (\beta_k c)^2 / 6} \quad \text{or} \quad k = \frac{1}{1 + \beta_k c + (\beta_k c)^2 / 6} \quad \text{when } \coth \beta_k l \approx 1 \quad (30)$$

In this formulation (Hart-Smith 1973), the force conditions at intersections  $I$  and  $II$  are consistent; the influence of the adhesive shear strain is included, and the large deflections of the outer adherends are also modeled. However, the equilibrium equations in Eq. 7 and  $w_1 \approx (w_1 + w_2)/2$  are used in this formulation. It is noted that Eq. 7 does not model the overlap geometric nonlinearity, and hence the large deflection effect of the overlap is ignored. Because  $w_1 \approx (w_1 + w_2)/2$  is used, the effect of the adhesive peel strain on the edge moment factor is also neglected.

### Coupled Formulation with the Shear and Nonlinear Effects But No Peel Effect

Oplinger (1994) treated the adherends as individual beams and considered the influence of the overlap deflection. The governing equations with the coupling of the adhesive shear strain and the overlap large deflection were derived, and then analytical solutions for SLJs were found. The edge moment factor was derived as:

$$k = \frac{R_3 \left(1 + \frac{t_a}{t_1} + R^2 C_2\right) + 8R_4 \frac{T_{h21}}{T_{h22}} R \left[C_1 \left(1 + \frac{t_a}{t_1}\right) - C_2\right]}{\left(1 + \frac{t_a}{t_1}\right) \left[R_3 + 8R_4 \frac{T_{h21}}{T_{h22}} R C_1 + \sqrt{8} (1 + R^2 C_1) \frac{T_{h21}}{T_{h1}}\right]} \quad (31)$$

The parameter definitions in the above equation can be found in Oplinger (1994) and are not given here due to complexity. In Eq. 31, the overlap geometric nonlinearity and the adhesive shear, but not peel strain, are considered. In Eqs. 30 and 31, the adherends are modeled as Euler beams, and thus the transverse shear stiffness is not modeled.

### Fully Coupled Nonlinear Formulation

Luo and Tong (2007, 2008) proposed fully coupled nonlinear formulation for isotropic SLJs based on the Euler beam theory and then extended to composite SLJs based on the Timoshenko beam theory. The displacements in Eqs. 24 and 26 are derived by taking into account geometric nonlinearity of the overlap and transverse shear stiffness of the adherends. The displacements of the left outer adherend of Fig. 5 can be derived as:

$$u_3 = \frac{F}{A_{d1}} x_3 + u_{o1}; w_3 = -\frac{M_k \sinh \beta_k x_3}{F \sinh \beta_k l} + \frac{t_1 + t_a}{2(l + c)} x_3 \quad (32)$$

By using the continuity conditions at intersection  $I$ , unknowns  $M_k$ ,  $u_{o1}$ , and  $B_{a6}$  can be determined. The adherend displacements, adhesive stresses, and the updating forces at the overlap ends can be obtained simultaneously. The simplified edge moment factor is given by:

$$k = \frac{1 + (\beta_k c)^2 \left[ \frac{\beta_{a1} c f(\beta_{a2} c) - 1}{8\alpha_a \beta_{a1} c (1 + t_a/t_1)} \right]}{1 + (\beta_k c) \coth \beta_k l + (\beta_k c)^2 \left[ \alpha_{sM} + \frac{\beta_{a1} c f(\beta_{a2} c) + \alpha_k}{8\alpha_a \beta_{a1} c} \right]} \quad (33)$$

where

$$f(\beta_{a2} c) = \frac{\beta_{a2} c \coth \beta_{a2} c - 1}{(\beta_{a2} c)^2}; \alpha_{sM} = \frac{\beta_{s1}^-}{2\beta_{\sigma c}^2} (\Delta < 0) \text{ or} \quad (34)$$

$$\alpha_{sM} = \frac{\beta_{s1}^+ + \beta_{s2}^+}{4\beta_{\sigma c}^2} (\Delta > 0)$$

For the isotropic adherends,  $\alpha_a = 1$ ,  $\alpha_k = 3$ , and  $\beta_{a1} \approx \beta_c = \beta_\tau$ , Eq. 33 degenerates to that given in Luo and Tong (2007) for the isotropic SLJ. When the peel effect is neglected, Eq. 33 becomes:

$$k = \frac{1 + (\beta_k c)^2 \left[ \frac{\beta_{a1} c f(\beta_{a2} c) - 1}{8\alpha_a \beta_{a1} c (1 + t_a/t_1)} \right]}{1 + (\beta_k c) \coth \beta_k l + (\beta_k c)^2 \left[ \frac{\beta_{a1} c f(\beta_{a2} c) + \alpha_k}{8\alpha_a \beta_{a1} c} \right]} \quad (34a)$$

In this case, the model is equivalent to that proposed by Oplinger (1994). In experiment, alignment tabs are often used to reduce peeling effects as shown in Fig. 5d (Adams et al. 1997; Tong and Steven 1999). In this case, the edge moment factor is (Luo and Tong 2016):

$$k = \frac{\frac{1 + (\beta_k c)}{\sinh \beta_k l} + (\beta_k c)^2 \left[ \frac{\beta_{a1} c f(\beta_{a2} c) - 1}{8\alpha_a \beta_{a1} c (1 + t_c/t)} \right]}{1 + (\beta_k c) \coth \beta_k l + (\beta_k c)^2 \left[ \alpha_{sM} + \frac{\beta_{a1} c f(\beta_{a2} c) + \alpha_k}{8\alpha_a \beta_{a1} c} \right]} \quad (34b)$$

When  $F$  is large,  $\sinh(\beta_k l) \gg \beta_k c$ ; in this case,  $k$  calculated by Eq. 34b is almost the same as that by Eq. 33.

Equation 33 includes all geometric parameters and material properties of composite single-lap joints except for the transverse normal stiffness. A good correlation with geometrically nonlinear FEA results has been illustrated in Luo and Tong (2007, 2008). In some cases, the following equations may also be used to predict the edge moment factor (Luo and Tong 2007):

$$k = \frac{1}{1 + \beta_k c \coth \beta_k l} \text{ or } k = \frac{1}{1 + \beta_k c} \text{ when } \coth \beta_k l \approx 1 \quad (35)$$

Equation 35 is simple and applicable for SLJs with a short overlap. Zhao et al. (2010) derived the second formula of Eq. 35 by considering overlap rotation and ignoring the overlap deformation. They showed that it was suitable for SLJs with a stiff overlap.

### 24.3.3 Numerical Comparisons

Two examples of single-lap joints are used to illustrate the above formulations. One is an isotropic SLJ and the other is a composite SLJ. The data of the isotropic SLJ are  $E_1 = 70$  (GPa),  $\nu_1 = 0.34$ ,  $t_1 = 1.6$  (mm);  $E_a/E_1 = 0.008$ ,  $\nu_a = 0.4$ ; and  $c/t_1 = 32$  and  $l/c = 5$ . For the composite SLJ,  $t_1 = 1.6$  (mm),  $t_a = 0.2$  mm,  $c/t_1 = 32$ ,  $l/c = 1.25$ ; and  $E_a = 2.4$  (GPa),  $\nu_a = 0.4$ . The ply thickness of composite adherends is 0.2 mm, and the ply material properties are  $E_L = 138$  (GPa),  $E_T = 9.4$  (GPa),  $\nu_{LT} = 0.32$ ,

$G_{LT} = 6.7$  (GPa); and  $\nu_{23} = 0.32$ ,  $G_{23} = 3.56$  (GPa); and the lay-up is  $[90/0/90/0]_s$ . The numerical results are presented for the SLJs in plane strain.

**Edge Moment Factor**

The edge moment factors ( $k$ ) of the isotropic SLJ predicted by various analytical solutions are illustrated in Fig. 7. It is noted that  $\Delta < 0$  when the Timoshenko beam is used to model isotropic adherends of this SLJ. It has been shown that edge moment factor predicted by Eq. 33 correlates very well with that predicted by the geometrically nonlinear FE analyses (Luo and Tong 2007, 2008).

Figure 7 indicates that the edge moment factor predicted by the formulation of Goland and Reissner (1944) is significantly larger than that predicted by Eq. 33 (Luo and Tong 2007, 2008) with an increase of the applied force due to ignoring influence of the adhesive deformation; the edge moment factor calculated by Oplinger’s formulation (1994) is obviously larger than that of Eq. 33 owing to neglecting the peel effect. The edge moment factor calculated using Eqs. 35 or 30 (Hart-Smith 1973) is considerably lower than that of Eq. 33. Equation 35 was given in Luo and Tong (2007), and the second formula in Eq. 35 was also derived by Zhao et al. (2010). This equation can be directly extended to composite SLJs.

Figure 8 shows the edge moment factors of the composite SLJ calculated by using the theoretical formulations. It is noted  $\Delta > 0$  for this composite SLJ. It has also been illustrated that  $k$  calculated by Eq. 33 correlates well with that of the geometrically nonlinear FE analyses (Luo and Tong 2008) for the composite SLJs.

Oplinger’s formulation (1994) is not easy to be extended to the laminated adherends, and thus its results are not given in this figure. Since  $k$  for Eq. 34a is equivalent to that of Oplinger’s model, the peel effect can be observed by comparing

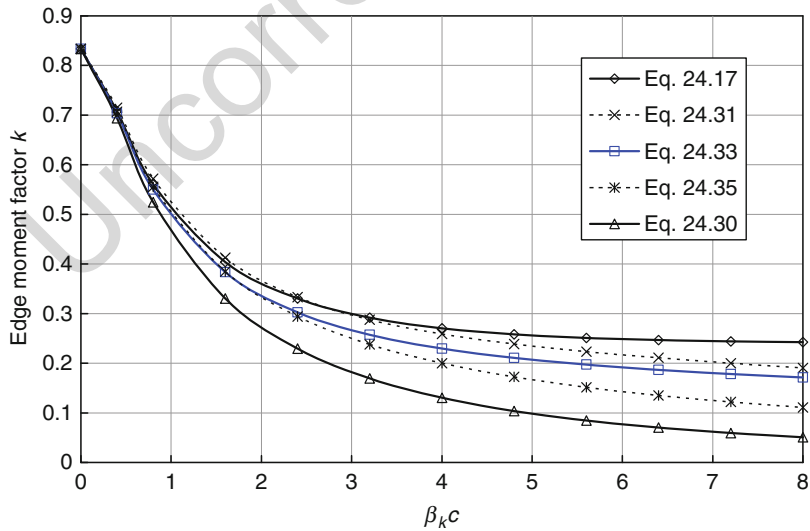


**Fig. 7** Edge moment factor of the isotropic SLJ predicted by the beam-adhesive models



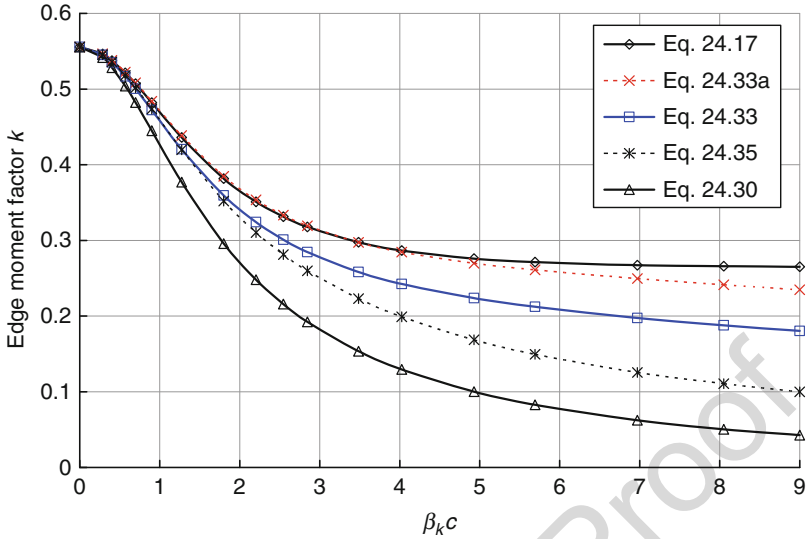


**Fig. 8** Edge moment factor of the composite SLJ predicted by the beam-adhesive models

$k$  for Eqs. 33 and 34a. It can be seen that the influence of adhesive peel strain on the edge moment factor is significant and should not be ignored.

### Adhesive Stresses

When the updating edge forces are determined, the relevant adhesive stresses can be calculated, and they are plotted in Figs. 9 and 10 for the composite SLJ.

Figures 9 and 10 illustrate distributions of the shear and peel stresses for the composite SLJ predicted by the linear adhesive-beam model based on the Euler beam theory and the nonlinear adhesive-beam model based on the Timoshenko beam theory, respectively.

In Figs. 9 and 10, the same edge moment factor at  $\beta_k c = 9$  calculated Eq. 33 is used for both models. Figure 9 shows that there are slight differences in values of shear stress predicted by the linear adhesive-beam model based on the Euler beam theory and the nonlinear adhesive-beam model based on the Timoshenko beam theory. However, there exist significant differences in the adhesive peel stress for the two models as shown in Fig. 10, including peak values and distribution patterns.

Harris and Adams (1984) investigated single-lap composite joints using a geometrically nonlinear finite element analysis (NFEA). They observed a small discrepancy in shear stress but large differences in the adhesive peel stress and the edge moment by comparing numerical results of Goland and Reissner (1944) with those of the NFEA. Figures 8, 9, and 10 confirm their observations through analytical solutions, as Luo and Tong (2008) illustrated that the edge moment factor, shear, and peel stresses predicted by the nonlinear adhesive-beam model based on the Timoshenko beam theory correlate well with those of the NFEA using commercial software NASTRAN.

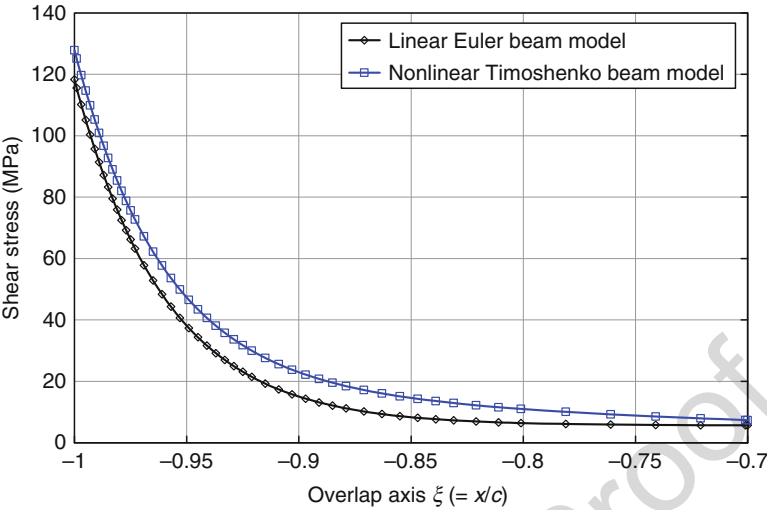


**Fig. 9** Shear stress predicted by the linear adhesive-beam model based on the Euler beam theory and the nonlinear adhesive-beam model based on the Timoshenko beam theory

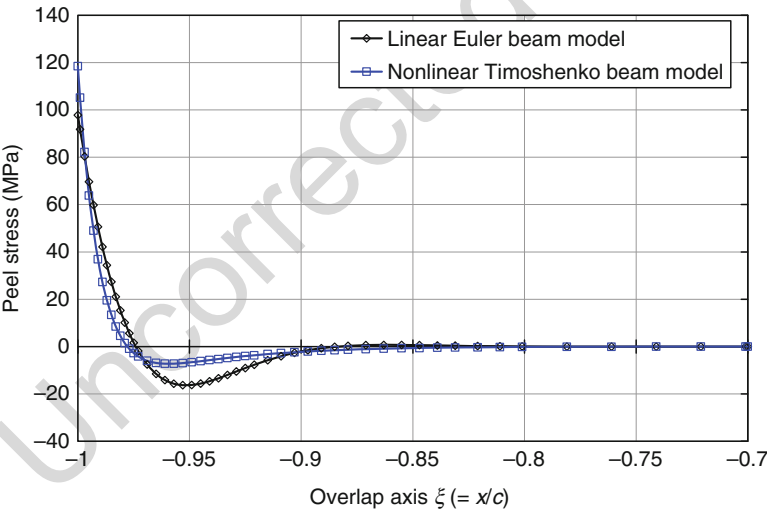


**Fig. 10** Peel stress predicted by the linear adhesive-beam model based on the Euler beam theory and the nonlinear adhesive-beam model based on the Timoshenko beam theory

**24.3.4 Analytical Approach for Adhesive Joints with Material Nonlinearity**

In design and strength analysis of adhesively bonded structures, nonlinear material properties need to be considered as soft or ductile adhesive materials can behave in

plastic regime. Owing to stress concentration and singular features, stresses near an edge of an adhesively bonded joint can reach beyond elastic limitation. Hence, material nonlinear analysis for adhesive joints is important. Analysis of material nonlinearity is usually required to be considered for all structural materials. However, due to low linear limitation of the ductile adhesive, stress–strain relationship of an adherend may still be within linear range when the adhesive is loaded beyond its linear limitation. Hence, only the adhesive material nonlinearity is considered here. For isotropic adherends that yield, Adams et al. (1997) have proposed a single design methodology (see ► Chap. 27, “Design Rules and Methods to Improve Joint Strength”).

Hart-Smith (1973) conducted material nonlinear analysis for SLJs using the linearly elastic and perfectly plastic model to describe the adhesive shear stress–strain relationship and the linear material property for the adhesive peel stress and adherends. In his analysis (Hart-Smith 1973), the adhesive layer is divided into elastic and plastic regions as shown in Fig. 11. Grant and Teig (1976) considered material nonlinearity of adhesive by dividing the adhesive into multiregions, in which the shear lag model was used. The obtained governing equations were then solved numerically.

Delale et al. (1981) used a strain energy function to define stress–strain relationships in conducting material nonlinear analysis for lap joints. Material nonlinear analysis of unbalanced lap joints subjected to general loadings was conducted by Bigwood and Crocombe (1990). In their analysis, the adherends were modeled as linearly elastic plates deforming in cylindrical bending, and plastic deformation theory was applied to the adhesive material. The stress–strain curve was described by using a continuous mathematical function. The adhesive yielding rule was assumed to obey the von Mises yield criterion. Bigwood and Crocombe (1990) derived a set of six simultaneous nonlinear differential equations in conjunction with the prescribed stress–strain function and then solved these nonlinear differential equations using finite difference method. The effect of the adhesive thickness on lap joint strength was also studied in Bigwood and Crocombe (1990).

Yang et al. (2004) developed an analytical model to predict the adhesive stress and strain distributions. In their analysis, the adherends were modeled as a laminated anisotropic plate, and the adhesive constitutive equation was described using the elastic–perfectly plastic constitutive relationship. The von Mises yield

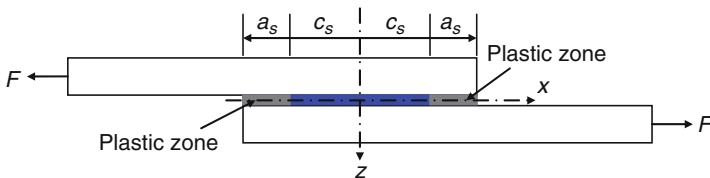


**Fig. 11** Elastoplastic analysis of shear lag joints

criterion was also applied to the adhesive plastic deformation. They derived and numerically solved coupled differential equations of SLJs. In this analysis (Yang et al. 2004), the material nonlinear FEA was conducted for numerical comparison, and cohesive failure was studied. Lee and Kim (2007) presented a closed-form analytical model for material nonlinear analysis of symmetric SLJs, in which the elastoplastic perfect material property for adhesive was considered. The analysis was conducted for independent shear and peel stresses in the adhesive.

As discussed in the above brief review, material nonlinear analysis of adhesively bonded structures is very complicated, and analytical solutions are not admissible in general. Here, we only present analytical solutions of symmetric SLJs in tension with the elasto-perfectly plastic adhesive material using the shear lag model to explain the analytical approach for adhesively bonded joints with material nonlinearity.

As shown in Fig. 11, the governing equations for elastic and plastic parts can be written as (Hart-Smith 1973; Grant and Teig 1976; Lee and Kim 2007):

$$\begin{cases} \frac{d^2\tau}{dx^2} = \beta_v^2\tau & -c_s \leq x \leq c_s \\ \frac{d^2\gamma}{dx^2} = \frac{2\tau_s}{A_{d1}t_a} & c_s \leq |x| \leq c \end{cases} \quad (36)$$

where  $c = c_s + a_s$  and  $\gamma$  is the adhesive shear strain and  $\tau_s$  is the adhesive yield stress. The analytical solution of the shear stress in  $|x| \leq c_s$  can be readily obtained:

$$\tau = \frac{\beta_v(F - 2a_s\tau_s)\cosh \beta_v x}{2\sinh \beta_v c_s} \quad (37)$$

When the maximum value of Eq. 37 is equal to  $\tau_s$ , the plastic deformation will occur in the adhesive edge. The critical force  $F$  is equal to  $(2\tau_s/\beta_v)$ . With an increase of applied load  $F$ , the plastic deformation will develop along the adhesive. The following equation can be obtained from Eq. 37 to determine the plastic zone length  $a_s$ :

$$2\tau_s \sinh \beta_v(c - a_s) = \beta_v(F - 2a_s\tau_s)\cosh \beta_v(c - a_s) \quad (38)$$

When the plastic zone is small,  $\sinh \beta_v(c - a_s) \approx \cosh \beta_v(c - a_s)$ . In this case, the plastic zone length  $a_s$  is approximately given by:

$$a_s = \frac{\beta_v F - 2\tau_s}{2\beta_v\tau_s} \quad (39)$$

When  $a_s$  is determined, the stress distribution can be obtained: when  $|x| \leq (c - a_s)$ , it is given by Eq. 37 and it is equal to  $\tau_s$  in  $(c - a_s) < |x| \leq c$ .

## 24.4 Analytical Approach of Other Lap Joints

### 24.4.1 Analytical Solutions of Symmetric Lap Joints Subjected to General Loadings

In Sects. 2 and 3, analytical solutions for single-lap joints are derived from the governing equations of Eqs. 9, 20, and 21 for the linear and nonlinear overlaps. The governing equations are also applicable to the other symmetric lap joints such as single-strap joints and cracked lap shear specimens.

#### Linear Overlap Based on the Euler Beam Theory

The general solutions of Eq. 9 are (Goland and Reissner 1944):

$$\begin{cases} \tau = A_1 \sinh \beta_c x + A_2 \cosh \beta_c x + A_3 \\ \sigma = (B_1 \sinh \beta_\sigma x + B_2 \cosh \beta_\sigma x) \sin \beta_\sigma x + (B_3 \sinh \beta_\sigma x + B_4 \cosh \beta_\sigma x) \cos \beta_\sigma x \end{cases} \quad (40)$$

where  $A_i$  and  $B_i$  ( $i = 1, 2, 3; j = 1, 2, 3, 4$ ) are integration constants determined by relevant boundary conditions. When the forces at both overlap edges are prescribed, the boundary conditions can be derived as:

$$\begin{cases} \int_{-c}^c \tau(x) dx = N_{II} - N_{III}; & \frac{d\tau(\mp c)}{dx} = \frac{\beta_\tau^2}{8I_1} [t_1(N_2 - N_1) - 2\alpha_k(M_2 + M_1)]_{x=\mp c} \\ \frac{d^2\sigma(\mp c)}{dx^2} = -2\beta_\sigma^4(M_2 - M_1)|_{x=\mp c}; & \frac{d^3\sigma(\mp c)}{dx^3} = -2\beta_\sigma^4(V_2 - V_1)|_{x=\mp c} \end{cases} \quad (41)$$

By substituting Eqs. 40 into 41, the integration constants can be determined. Delale et al. (1981) presented analytical solutions of lap joints under tension, bending, and transverse shear, respectively.

#### Nonlinear Overlap Based on the Timoshenko Beam Theory

The general solutions of Eqs. 20 and 21 are (Luo and Tong 2008):

$$\begin{cases} u_a = A_{a1} \sinh \beta_{a1} x + A_{a2} \cosh \beta_{a1} x + A_{a3} \sinh \beta_{a2} x + A_{a4} \cosh \beta_{a2} x + A_{a5} x^2 + A_{a6} x + A_{a7} \\ w_a = B_{a1} \sinh \beta_{a1} x + B_{a2} \cosh \beta_{a1} x + B_{a3} \sinh \beta_{a2} x + B_{a4} \cosh \beta_{a2} x + B_{a5} x^2 + B_{a6} x + B_{a7} \end{cases} \quad (42)$$

When  $\Delta < 0$ , the analytical solutions are given by:

$$\begin{cases} u_s = A_{s1} x + A_{s2} \\ w_s = (B_{s1}^- \sinh \beta_{s1}^- x + B_{s2}^- \cosh \beta_{s1}^- x) \sin \beta_{s2}^- x + (B_{s3}^- \sinh \beta_{s1}^- x + B_{s4}^- \cosh \beta_{s1}^- x) \cos \beta_{s2}^- x \end{cases} \quad (43a)$$

When  $\Delta > 0$ , the solutions are:

$$\begin{cases} u_s = A_{s1}x + A_{s2} \\ w_s = B_{s1}^+ \sinh \beta_{s1}^+ x + B_{s2}^+ \cosh \beta_{s1}^+ x + B_{s3}^+ \sinh \beta_{s2}^+ x + B_{s4}^+ \cosh \beta_{s2}^+ x \end{cases} \quad (43b)$$

where the integration constants  $A_{ai}$  and  $B_{ai}$  ( $i = 1, 2, \dots, 7$ ),  $A_{si}$ , and  $B_{sj}^-$  or  $B_{sj}^+$  ( $i = 1, 2$ ;  $j = 1, 2, 3, 4$ ) can be determined by associated boundary conditions. When the forces at both overlap edges are given, the solutions can be found in Sect. 2 of Luo and Tong (2008). For the symmetric single-strap and lap shear joints, the analytical solutions can be obtained directly from the formulations of Luo and Tong (2008).

For double-lap and double-strap joints, analytical analyses are attributed to those for asymmetric joints by using the variable transformation discussed in Luo and Tong (2002) for the host beam with the piezoelectric patches bonded on the top and bottom surfaces. The analysis for asymmetric joints will be presented in the next section.

#### 24.4.2 Analytical Solutions of Asymmetric and Unbalanced Joints

Analytical analysis of balanced single-lap joints gives us insight into the essences of stress analysis for adhesively bonded joints. It has been widely used for adhesive characterization and benchmarking numerical methods and experimental testing. In general, adherends are asymmetric and adhesive joints are unbalanced.

Analytical approaches for unbalanced adhesive joints based on the Euler beam theory have been developed by a number of researchers (Hart-Smith 1973; Delale et al. 1981; Bigwood and Crocombe 1989; Luo and Tong 2002; Shahin et al. 2008). Luo and Tong (2009b, c) modeled the adherends as Timoshenko beams. Since the analytical procedure for the Euler beam is similar to that for the Timoshenko beam, the formulations are presented here for the Timoshenko beam only.

Fully coupled nonlinear analytical solutions for asymmetric and unbalanced adhesive joints are very complicated. Nevertheless, when the updated loadings are given, linear analysis based on the Timoshenko beam theory can predict sufficiently accurate adhesive stresses except for the case of very large deflection.

When the linear adhesive-beam model based on the Timoshenko beam theory is used, the distributions of adhesive shear and peel stresses are almost the same as those of the nonlinear model, and the values of the shear stress is slightly lower than that of the nonlinear analysis. Therefore, the linear adhesive-beam model based on the Timoshenko beam for stress analysis of asymmetric and unbalanced joints may be sufficiently accurate for engineering applications.

#### Governing Equations of Asymmetric and Unbalanced Linear Joints

In this model of adhesively bonded joints with asymmetric and unbalanced adherends, the geometric nonlinearity is not included; the adherends are described

as the Timoshenko beam and a two-parameter elastic medium is used to model the adhesive. Also, the adhesive stresses should be deemed as those in the adhesive's midplane. It should be noted that the predicted shear stress may be slightly lower due to ignoring the geometric nonlinearity.

The equilibrium equations and adhesive stresses are shown in Eqs. 7 and 8, respectively. The constitutive equations for laminated adherends with asymmetric lay-ups are:

$$\begin{aligned} N_i &= A_{di} \frac{du_i}{dx} - B_i \frac{d\phi_i}{dx}; Q_i = G_{ki} \left( \frac{dw_i}{dx} - \phi_i \right); \\ M_i &= B_i \frac{du_i}{dx} - D_i \frac{d\phi_i}{dx} \quad (i = 1, 2) \end{aligned} \quad (44)$$

where  $B_i$  ( $i = 1, 2$ ) are the extension-bending coupling stiffness of the adherends. By substituting Eqs. 7 and 44 into Eq. 8, the governing equations in terms of shear and peel stresses can be derived as (Luo and Tong 2009b, c):

$$\begin{cases} \frac{d^3\tau}{dx^3} - k_1 \frac{d\tau}{dx} - k_2\sigma = 0 \\ \frac{d^4\sigma}{dx^4} - k_5 \frac{d^2\sigma}{dx^2} + k_4\sigma + k_3 \frac{d\tau}{dx} = 0 \end{cases} \quad (45)$$

where

$$\begin{aligned} k_1 &= k_\tau k_{1d}; k_2 = k_\tau k_{2d}; k_3 = k_\sigma k_{2d}; k_4 = k_\sigma k_{4d}; k_5 = k_\sigma k_{5d}; k_\tau = G_a/t_a; \\ k_\sigma &= E_a/t_a \end{aligned} \quad (46)$$

$$\begin{cases} k_{1d} = \frac{D_1}{\Delta_1} \left( 4\alpha_{a1} + \frac{t_1 B_1}{D_1} \right) + \frac{D_2}{\Delta_2} \left( 4\alpha_{a2} - \frac{t_2 B_2}{D_2} \right); & k_{4d} = \frac{A_{d1}}{\Delta_1} + \frac{A_{d2}}{\Delta_2} \\ k_{2d} = \frac{t_1}{2\Delta_1} \left( A_{d1} - \frac{2B_1}{t_1} \right) - \frac{t_2}{2\Delta_2} \left( A_{d2} + \frac{2B_2}{t_2} \right); & k_{5d} = \frac{1}{G_{k1}} + \frac{1}{G_{k2}} \end{cases} \quad (47)$$

$$\Delta_i = A_{di} D_i - B_i^2; \alpha_{ai} = \frac{1 + \alpha_{ki}}{4}; \alpha_{ki} = \frac{A_{di} t_i^2}{4D_i} \quad (i = 1, 2) \quad (48)$$

Equation 45 is a set of differential equations with coupled shear and peel stresses. In the above equations,  $k_{1d}$  and  $k_{4d}$  reflect the extension, bending, and extension-bending coupling effects of the adherends;  $k_{2d}$  indicates the unbalanced condition of the substrates that couples the shear and peel stresses; and  $k_{5d}$  denote the shear stiffness. The shear and peel stresses become decoupled when  $k_{2d} = 0$ , which is seen in the case of balanced joints with identical substrates. If  $k_{5d} = 0$ , Eq. 45 becomes the governing equations based on the Euler beam theory. When the shear and peel stresses are solved analytically from Eq. 45, forces and displacements can be derived from Eqs. 7 and 44, respectively.

### Boundary Conditions

The governing equations shown in Eq. 45 can be analytically solved without introducing any other assumption for the prescribed boundary conditions. When the forces at the adhesive joint ends *I* and *II* are given, the boundary conditions can be expressed as:

$$\begin{cases} x = -c : \frac{d\tau}{dx} = k_\tau H_{nl}; & \frac{d^2\sigma}{dx^2} - k_5\sigma = k_\sigma H_{ml}; & \frac{d^3\sigma}{dx^3} - k_5\frac{d\sigma}{dx} + k_3\tau = k_\sigma H_{ql} \\ x = c : \frac{d\tau}{dx} = k_\tau H_{nl}; & \frac{d^2\sigma}{dx^2} - k_5\sigma = k_\sigma H_{ml}; & \frac{d^3\sigma}{dx^3} - k_5\frac{d\sigma}{dx} + k_3\tau = k_\sigma H_{ql} \end{cases} \quad (49)$$

where

$$\begin{cases} H_{nj} = \left[ \left( \frac{D_2}{\Delta_2} + \frac{B_2 t_2}{2\Delta_2} \right) N_{j2} - \left( \frac{D_1}{\Delta_1} - \frac{B_1 t_1}{2\Delta_1} \right) N_{j1} \right] - \left[ \left( \frac{A_{d2} t_2}{2\Delta_2} + \frac{B_2}{\Delta_2} \right) M_{j2} + \left( \frac{A_{d1} t_1}{2\Delta_1} - \frac{B_1}{\Delta_1} \right) M_{j1} \right] \\ H_{mj} = - \left[ \left( \frac{A_{d2}}{\Delta_2} M_{j2} - \frac{A_{d1}}{\Delta_1} M_{j1} \right) - \left( \frac{B_2}{\Delta_2} N_{j2} - \frac{B_1}{\Delta_1} N_{j1} \right) \right] \\ H_{qj} = - \left( \frac{A_{d2}}{\Delta_2} Q_{j2} - \frac{A_{d1}}{\Delta_1} Q_{j1} \right) \quad (j = I, II) \end{cases} \quad (50)$$

where  $N_{jk}$ ,  $M_{jk}$ , and  $Q_{jk}$  ( $j = I, II$ ;  $k = 1, 2$ ) are the force components in adherends 1 and 2 at the joint ends *I* and *II*.

### Analytical Approaches

Analytical solutions of the governing equations with coupled shear and peel stresses were discussed in detail in Luo and Tong (2002) for piezoelectric smart beams, in which the Euler beam theory was used. Stress analysis for adhesively bonded composite joints is to solve Eq. 45 with boundary conditions in Eq. 49.

One method to solve this boundary value problem of the ordinary differential equations is elimination; it attempts to obtain the uncoupled equations with higher-order differentiations by eliminating the coupled terms (Humi and Miller 1988). In this method, the boundary conditions with the higher-order differentiations should also be derived. This technique has been used to solve the governing equations with the coupled shear and peel stresses for adhesive joints based on the Euler beam theory by Hart-Smith (1973), Delale et al. (1981), Bigwood and Crocombe (1989), and Shahin et al. (2008). In these formulations, the Euler beam is used to model the adherends. In the adhesive joint model of Delale et al. (1981), the adhesive axial deformation is also considered.

Alternatively, the coupled equations can be directly solved (Humi and Miller 1988). The solutions are then substituted into the governing equations to find the relationships of the integration constants, and the boundary conditions can be directly used. To solve Eqs. 45 and 49, the general solutions of Eq. 45 can be obtained analytically, and then the relationships of the integration constants are



derived by substituting the general solutions into the first or second equation of Eq. 45. The integration constants can be determined by these relationships and the boundary conditions of Eq. 49. This approach is simpler than the elimination method in general. Luo and Tong (2009b, c) used this method for a semi-infinite long bonded composite joint. Here, analytical solutions for the adhesive joint with a length of  $(2c)$  are introduced as follows.

### General Solutions

Substituting  $\tau = Ae^{\sqrt{k_\sigma}\beta_t x}$  and  $\sigma = Be^{\sqrt{k_\sigma}\beta_t x}$  into Eq. 45 yields (Luo and Tong 2009b, c):

$$\lambda^3 + a_1\lambda^2 + a_2\lambda + a_3 = 0 \quad \text{or } \beta_t = 0 \quad (51)$$

where

$$\begin{aligned} \lambda &= \beta_t^2; a_1 = -\left(\frac{k_\tau k_{1d}}{k_\sigma} + k_{5d}\right); a_2 = \frac{k_{4d}}{k_\sigma} + \frac{k_\tau k_{1d} k_{5d}}{k_\sigma}; a_3 \\ &= -\frac{k_\tau(k_{1d} k_{4d} - k_{2d}^2)}{k_\sigma^2} \end{aligned} \quad (52)$$

There are two different sets of solutions for Eq. 51, depending on:

$$\Delta = Q^3 - R^2 \quad \text{where } Q = \frac{a_1^2 - 3a_2}{9} \quad \text{and } R = \frac{2a_1^3 - 9a_1a_2 + 27a_3}{54} \quad (53)$$

where  $\Delta$  is a function of  $t_a$ ; it may be larger than, equal to, or less than zero. It has been shown that  $\Delta \geq 0$  as  $t_a \rightarrow 0$  (Luo and Tong 2009b). That is, when the adhesive layer is sufficiently thin,  $\Delta \geq 0$ ; and  $\Delta < 0$  when the adhesive is relatively thick.

Relying on the characteristic roots of the associated polynomial equation shown in Eq. 51, analytical solutions of Eq. 45 are given by (Luo and Tong 2009b, c):

$$\begin{cases} \tau = A_1 \sinh \beta_1 x + A_2 \cosh \beta_1 x + (A_3 \sinh \beta_2 x + A_4 \cosh \beta_2 x) \sin \beta_3 x \\ \quad + (A_5 \sinh \beta_2 x + A_6 \cosh \beta_2 x) \cos \beta_3 x + A_7 \\ \sigma = B_1 \sinh \beta_1 x + B_2 \cosh \beta_1 x + (B_3 \sinh \beta_2 x + B_4 \cosh \beta_2 x) \sin \beta_3 x \\ \quad + (B_5 \sinh \beta_2 x + B_6 \cosh \beta_2 x) \cos \beta_3 x + B_7 \end{cases} \quad (\Delta < 0) \quad (54)$$

or

$$\begin{cases} \tau = A_1 \sinh \beta_1 x + A_2 \cosh \beta_1 x + A_3 \sinh \beta_2 x + A_4 \cosh \beta_2 x \\ \quad + A_5 \sinh \beta_3 x + A_6 \cosh \beta_3 x + A_7 \\ \sigma = B_1 \sinh \beta_1 x + B_2 \cosh \beta_1 x + B_3 \sinh \beta_2 x + B_4 \cosh \beta_2 x \\ \quad + B_5 \sinh \beta_3 x + B_6 \cosh \beta_3 x + B_7 \end{cases} \quad (\Delta \geq 0) \quad (55)$$

where calculation of  $\beta_i$  ( $i = 1, 2, 3$ ) for Eqs. 54 and 55 can be found in Luo and Tong (2009a, b);  $A_i$  and  $B_i$  ( $i = 1, 2, \dots, 7$ ) are the integration constants.

### Determination of the Integration Constants

There are 14 integration constants in Eqs. 54 or 55. By eliminating shear stress in Eq. 45, a 6 order differential equation with respect to peel stress can be obtained, and thus  $B_7 = 0$ . The axial equilibrium equation of adherend 1 of the overlap is shown in Eq. 41. By substituting Eqs. 54 or 55 into the first or second equation in Eq. 45, six simple relationships of the integration constants can be derived. There are six independent equations in Eq. 49. Therefore, 13 independent equations can be used to determine the 13 integration constants without introducing additional assumptions.

Directly solving the 13 simultaneous algebraic equations is too complicated in the context of obtaining the closed-form solutions. By using the method in Luo and Tong (2002), two sets of three simultaneous equations with three unknowns can be obtained, respectively. Therefore, explicit analytical solutions can be derived. The details can be found in Luo and Tong (2002) and are not discussed further here due to the space limitation.

### Geometrically Nonlinear Analysis for Unbalanced Single-Lap Joint

Fully coupled nonlinear analysis for unbalanced SLJs was conducted by Li et al. (2015) with flexible interfaces being considered. Free body diagrams for the unbalanced SLJ are the same as those in Fig. 6b except that adherends 1 and 2 are not identical. By using the Timoshenko beam theory and the free body diagrams, the governing equations for the unbalanced SLJ with geometrical nonlinearity can be derived. The nonlinear terms in the governing equations were linearized by using following transformation (Jiang et al. 2016):

$$N_1 = \frac{A_{d1}P}{A_{d1} + A_{d2}}; N_2 = \frac{A_{d2}P}{A_{d1} + A_{d2}} \quad (56)$$

where  $A_{d1}$  and  $A_{d2}$  are the extensional stiffness of adherends 1 and 2;  $P = N_1 + N_2$ . The linearized coupling differential equations are (Jiang et al. 2016):

$$\begin{aligned} \frac{d^6 w_1}{dx^6} + a_{11} \frac{d^5 u_1}{dx^5} + a_{12} \frac{d^4 w_1}{dx^4} + a_{13} \frac{d^3 u_1}{dx^3} + a_{14} \frac{d^2 w_1}{dx^2} + a_{15} \frac{du_1}{dx} + a_{16} w_1 &= f(x) \\ \frac{d^4 w_1}{dx^4} + b_{13} \frac{d^3 u_1}{dx^3} + b_{14} \frac{d^2 w_1}{dx^2} + b_{15} \frac{du_1}{dx} + b_{16} w_1 &= g(x) \end{aligned} \quad (57)$$

By eliminating  $w_1$  from Eq. 57 or using the approach in Sect. 3.1, a 9 order ordinary differential equation can be obtained (Eq. 23 in Jiang et al. 2016). By letting  $\lambda = \beta_t^2$ , a 4 order of polynomial equation is derived, and thus the analytical solutions for unbalanced geometrically nonlinear SLJs can be derived. Edge moment factors  $k_1$  and  $k_2$  are defined as:

$$k_1 = \frac{2M_1^*}{P(t_1 + t_a)}; k_2 = \frac{2M_2^*}{P(t_1 + t_a)} \quad (58)$$

where  $M_1^*$  and  $M_2^*$  are the undated bending moments at edges I and II. Other parameters in Eqs. 56–58 can be found in Jiang et al. (2016).

## 24.5 Failure Criteria Based on Continuum Mechanics

Failure of adhesively bonded structures can occur in adherends, adhesive, and interface. In this chapter, only failures in an adhesive and at interface between the adherend and adhesive are considered, referring to cohesive failure and debonding or delamination.

The adhesive shear and peel stresses peak at adhesive edges, and the peak stresses increase to infinity with the adhesive thickness decreasing to zero. Therefore, the failure of the adhesive joint will be initiated from the adhesive edge generally. There are two types of failure criteria to assess adhesive joint strength, based on continuum mechanics and fracture mechanics, respectively.

The failure criteria based on continuum mechanics can be summarized as (Huang et al. 2002):

$$\text{Maximum stress criterion : } \sigma_{\max} < [\sigma] \text{ and } \tau_{\max} < [\tau] \quad (59a)$$

$$\text{Von Mises criterion : } (\sigma_{\text{von}})_{\max} < [\sigma] \quad (59b)$$

$$\text{Tsai-Wu criterion : } \left[ \frac{\sigma_{\max}}{[\sigma]} \right]^2 + \left[ \frac{\tau_{\max}}{[\tau]} \right]^2 < 1 \quad (59c)$$

where  $[\sigma]$  and  $[\tau]$  are allowable shear and peel stresses of the adhesive material calibrated by experimental testing;  $\sigma_{\text{von}}$  is the von Mises stress.

When the above criteria are used to assess strength of adhesive joints, the maximum stresses need to be determined. The adhesive stresses in symmetric lap joints are given in Sects. 2 and 3 of this chapter. The analytical approaches for asymmetric and unbalanced adhesive joints are discussed in Sect. 4, and their closed-form solutions are normally complicated. If the adhesive is thin and the overlap is long enough, e.g.,  $c > 20(t_1 + t_a + t_2)$ , the joint length may be approximately treated to be semi-infinite. In this case, the adhesive stresses can be found, and the analytical solutions are given in Luo and Tong (2009c).

### 24.5.1 Shear and Peel Stresses of an Adhesive Joint with a Semi-infinite Length

When the length of an adhesively bonded composite joint is semi-infinite, the shear and peel stresses can be expressed as (Luo and Tong 2009b, c):

$$\begin{cases} \tau = A_2 e^{-\beta_1 x} + e^{-\beta_2 x} (A_5 \sin \beta_3 x + A_6 \cos \beta_3 x) \\ \sigma = B_2 e^{-\beta_1 x} + e^{-\beta_2 x} (B_5 \sin \beta_3 x + B_6 \cos \beta_3 x) \end{cases} \quad \Delta < 0 \quad (60a)$$

$$\begin{cases} \tau = A_2 e^{-\beta_1 x} + A_4 e^{-\beta_2 x} + A_6 e^{-\beta_3 x} \\ \sigma = B_2 e^{-\beta_1 x} + B_4 e^{-\beta_2 x} + B_6 e^{-\beta_3 x} \end{cases} \quad \Delta > 0 \quad (60b)$$

By substituting Eqs. 60a or 60b into the first or second equation in Eq. 45, three relationships of the integration constants are obtained. By eliminating three unknowns from the three relationships and the three boundary conditions, a set of three-order algebraic equations can be derived for the coupled shear and peel stresses, which can be solved analytically. An explicit form of shear and peel stresses can be found, and the details are given in Luo and Tong (2009b, c).

## 24.5.2 Failure Prediction Using the Criteria Based on Continuum Mechanics

When the maximum stresses are determined and the allowable stresses are calibrated, failure criteria based on continuum mechanics can be used to predict adhesive joint failure. When the failure criteria in Eqs. 59a and 59b are used to predict joint failure, it is found (Adams 1989; Gleich et al. 2001; da Silva et al. 2006) that the failure trend for different adhesive thickness predicted by the adhesive-beam models proposed by Goland and Reissner (1944) is different from that of the experimental results. In theory, the maximum stresses increase with decreasing adhesive thickness. However, failure load decreases with increasing the adhesive thickness when it is relatively thick, such as  $t_a > 0.1$  mm.

It is believed that the peak stresses in the thicker adhesive allow yielding to spread, and the global yielding may develop before the maximum stress reaches the allowable value (Hart-Smith 1973; da Silva et al. 2009). When the global yielding occurs, the adhesive thickness effect on the failure load may be predicted by the material nonlinear analysis (see details in da Silva et al. 2009). Gleich et al. (2001) showed the partial agreement with this trend when the fracture mechanics approach was used. Due to complex and singular feature of stresses in the vicinity of an adhesive edge, failure criteria based on the damage zone model and fracture mechanics have been used to predict joint failure.

## 24.6 Failure Criteria Based on Fracture Mechanics

As the adhesive is normally thin in bonded structures, stress concentration occurs near adhesive edges. The adhesive edge stresses increase with a decrease in adhesive thickness. As the adhesive thickness approaches zero, the edge shear and peel stresses defined by Eqs. 8 or 10 will reach infinite. That is, stress singularity appears near the adhesive edges. The singular stress fields in a free edge of laminates and at interface of dissimilar materials have been widely studied.

Here, failure criteria based on energy release rates for adhesive joints will be discussed.

### 24.6.1 Failure Prediction Using Energy Release Rates

Failure criteria based on fracture energy release rates can be written as (Fernlund et al. 1994):

$$G_T < G_{Tc} \text{ at } \varphi = A \tan \sqrt{\frac{G_{II}}{G_I}} \text{ or } \left( \frac{G_I}{G_{Ic}} \right)^2 + \left( \frac{G_{II}}{G_{IIc}} \right)^2 < 1 \quad (61)$$

where  $G_I$ ,  $G_{II}$ , and  $G_T$  are mode I, mode II, and total energy release rates and  $G_{Ic}$ ,  $G_{IIc}$ , and  $G_{Tc}$  are their critical values, respectively;  $\varphi$  is the phase angle. The critical energy release rates  $G_{Ic}$ ,  $G_{IIc}$ , and  $G_{Tc}$  are measured by testing.  $G_I$  and  $G_{II}$  or  $G_T$  and  $\varphi$  can be analytically or numerically determined. Here, only the analytical solutions are discussed.

### Energy Release Rate and J-Integral

An adhesive joint subjected to general loadings is illustrated in Fig. 12. When the J-integral is calculated along the adhesive joint boundary, the total energy release rate is given by (Fernlund and Spelt 1991; Fernlund et al. 1994):

$$G_T = \frac{1}{2} \left( \frac{N_1^2}{A_{d1}} + \frac{N_2^2}{A_{d2}} + \frac{M_1^2}{D_1} + \frac{M_2^2}{D_2} + \frac{Q_1^2}{G_{k1}} + \frac{Q_2^2}{G_{k2}} - \frac{N_o^2}{A_{d0}} - \frac{M_o^2}{D_o} - \frac{Q_o^2}{G_{ko}} \right) - Q_1 \phi_1 - Q_2 \phi_2 + Q_o \phi_o \quad (62)$$

where  $A_{do}$ ,  $D_o$ , and  $G_{ko}$  are extensional, bending, and shear stiffnesses of an entire beam in the uncracked part. It is noted that, unlike stress intensity factor, stress singularity is not required for calculating energy release rates.

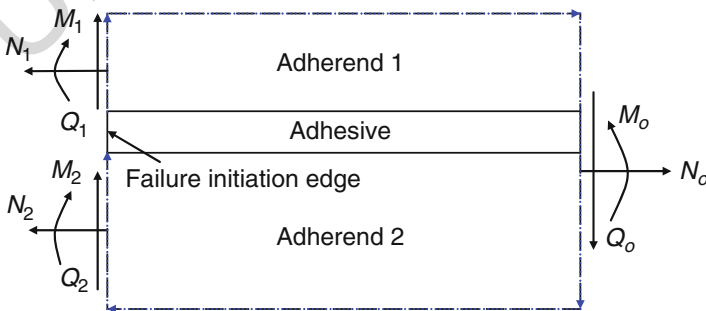


**Fig. 12** The J-integral and energy release rate of an adhesively bonded joint

### Mode Partition Method

The total energy release rate is not sufficient to predict structural strength as the critical total energy release rate depends on the phase angle. That is, fracture modes must be separated. Four methods of mode partition may be used for fracture of adhesive joints: (1) the local method based on the stress singular field (Hutchinson and Suo 1992), (2) the global method based on the beam theory (Williams 1988), (3) the method using the adhesive edge stresses based on the adhesive-beam model (Fernlund and Spelt 1991), and (4) the global-local method (Luo and Tong 2012; Harvey et al. 2014; Li et al. 2015).

When the adhesive edge stresses are utilized to calculate energy release rates of the adhesive joint in Fig. 12, they can be written as (Fernlund and Spelt 1991):

$$G_I = \int_0^{\varepsilon(0)} t_a \sigma d\varepsilon = \frac{1}{2k_\sigma} [\sigma(0)]^2; G_{II} = \int_0^{\gamma(0)} t_a \tau d\gamma = \frac{1}{2k_\tau} [\tau(0)]^2 \quad (63)$$

### Singular Feature of the Adhesive Edge Stresses

As energy release rates  $G_I$  and  $G_{II}$  are finite values, we have:

$$\lim_{t_a \rightarrow 0} \sigma(0) = \lim_{t_a \rightarrow 0} \sqrt{\frac{2E_a G_I}{t_a}} \rightarrow \infty; \lim_{t_a \rightarrow 0} \tau(0) = \lim_{t_a \rightarrow 0} \sqrt{\frac{2G_a G_{II}}{t_a}} \rightarrow \infty \quad (64)$$

When the local and global methods are used for mode partition, only the force components shown in Fig. 12 are required as input. When Eq. 63 is utilized to separate fracture modes, the adhesive stresses need to be determined firstly, which is normally complicated. In this chapter, simple formulations of energy release rates for adhesively bonded joints will be discussed.

## 24.6.2 Analytical Solutions of Energy Release Rates for Cohesive Failure and Debonding

### Energy Release Rates for Cohesive Failure of Adhesive Joints

For an adhesively bonded joint with a semi-infinite length subjected to general loadings, the adhesive shear and peel stresses are given in Eqs. 60a or 60b when the adherends are modeled as Timoshenko beams. The explicit expressions of the adhesive stresses and their maximum values are given in Luo and Tong (2009b, c). By using Eq. 63, the energy release rates for cohesive failure can be obtained.

### Energy Release Rates for Debonding or Delamination of Adhesive Joints

The interface stresses for a sufficiently thin adhesive layer are given in Eq. 60b. As the adhesive thickness approaches zero, energy release rates can be derived as (Luo and Tong 2009b, c):

$$G_I = \frac{k_{1d}}{2(k_{1d}k_{4d} - k_{2d}^2)} \left[ \frac{k_{2d}H_{nl}}{k_{1d}} + \left( H_{ml} + k_f \sqrt{\frac{k_{5d}}{k_{4d}} \left( 1 - \frac{k_{2d}^2}{k_{1d}k_{4d}} \right)} H_{ql} \right) \right]^2; \quad (65)$$

$$G_{II} = \frac{H_{ld}^2}{2k_{1d}}$$

where  $H_{nl}$ ,  $H_{ml}$ , and  $H_{ql}$  are given in Eq. 50, which are used to define the boundary conditions at the joint end  $I$ . When adherends 1 and 2 are symmetrically laminated,  $B_1 = B_2 = 0$ ; in this case, Eq. 61 can be expressed as:

$$\begin{cases} G_I = \frac{k_{1d}}{2(k_{1d}k_{4d} - k_{2d}^2)} \times \left\{ \frac{k_{2d}}{k_{1d}} \left[ \left( \frac{N_2}{A_{d2}} - \frac{N_1}{A_{d1}} \right) - \frac{1}{2} \left( \frac{t_2 M_2}{D_2} + \frac{t_1 M_1}{D_1} \right) \right] \right. \\ \left. - \left( \frac{M_2}{D_2} - \frac{M_1}{D_1} \right) - k_f \sqrt{\frac{k_{5d}}{k_{4d}} \left( 1 - \frac{k_{2d}^2}{k_{1d}k_{4d}} \right)} \left( \frac{Q_2}{D_2} - \frac{Q_1}{D_1} \right) \right\}^2 \\ G_{II} = \frac{1}{2k_{1d}} \left[ \left( \frac{N_2}{A_{d2}} - \frac{N_1}{A_{d1}} \right) - \frac{1}{2} \left( \frac{t_2 M_2}{D_2} + \frac{t_1 M_1}{D_1} \right) \right]^2 \end{cases} \quad (66)$$

in which  $N_k$ ,  $M_k$  and  $Q_k$  ( $k = 1, 2$ ) are the force components in adherends 1 and 2 at the joint ends  $I$  where the fracture is initiated as shown in Fig. 12.

In Eq. 66,  $k_f$  ( $1 \leq k_f \leq \sqrt{2}$ ) reflects the influence of interface deformation near the crack-tip. As  $t_a \rightarrow 0$ ,  $k_f \rightarrow 1$ ; and when  $\Delta = 0$ ,  $k_f = \sqrt{2}$ . When the Euler beam theory is used to model the adherends,  $k_{5d} = 0$ . Equation 66 is reduced to the energy release rates for debonding or delamination derived based on the Euler beam theory (Luo and Tong 2009a).

If  $B_1 = -B_2$  and  $k_{2d} = 0$ , the energy release rates can be simplified as:

$$\begin{cases} G_I = \frac{A_{d1}}{4(A_{d1}D_1 - B_1^2)} \left[ -(M_2 - M_1) - \frac{B_1}{A_{d1}}(N_2 + N_1) - k_f \sqrt{\frac{A_{d1}D_1 - B_1^2}{A_{d1}G_{k1}}} (Q_2 - Q_1) \right]^2 \\ G_{II} = \frac{A_{d1}D_1 - B_1^2}{16(4\alpha_{d1}D_1 + t_1B_1)} \left[ \frac{2D_1 - B_1t_1}{(A_{d1}D_1 - B_1^2)}(N_2 - N_1) - \frac{A_{d1}t_1 - 2B_1}{(A_{d1}D_1 - B_1^2)}(M_2 + M_1) \right]^2 \end{cases} \quad (67)$$

The energy release rate  $G_I$  ( $G_{II} = 0$ ) for a double cantilever beam with crack length  $a$  subjected to a pair of load  $P$  is:

$$G_I = \frac{A_{d1}(Pa)^2}{4(A_{d1}D_1 - B_1^2)} \left[ 1 + \frac{k_f}{a} \sqrt{\frac{A_{d1}D_1 - B_1^2}{A_{d1}G_{k1}}} \right]^2 \text{ or} \quad (68)$$

$$G_I = \frac{(Pa)^2}{D_1} \left( 1 + \frac{k_f}{a} \sqrt{\frac{D_1}{G_{k1}}} \right)^2 \text{ when } B_1 = 0$$

Energy release rates in Eq. 65 are derived on the basis of adhesive edge stress by letting the edge adhesive thickness approach zero. Similar results are obtained in Bruno et al. (2003) and Wang and Harvey (2012) based on the beam theory. That is, these formulations are global ones.

For an interface crack or debonding of an adhesive joint, local details (stress, force, or deformation) near a crack-tip should be taken into account. By using the beam theory and considering the local details, analytical formulations of the mode mixity ratios can be derived (Luo and Tong 2012; Harvey et al. 2014; Li et al. 2015). For the isotropic adherends, two simple formulations are given in (Luo and Tong 2012):

$$\frac{G_{II}}{G_I} = \frac{3(1-r^2)^2}{(2+r+2r^2)^2} \text{ when } M_1 = -M_2; N_1 = N_2 = Q_1 = Q_2 = 0 \quad (69)$$

$$\frac{G_I}{G_{II}} = \frac{3(1-r^2)^2}{(2+r+2r^2)^2} \text{ when } N_1 = -N_2; M_1 = M_2 = Q_1 = Q_2 = 0 \quad (70)$$

where  $r (=t_1/t_2)$  is the thickness ratio. The numerical studies in Harvey et al. (2014) and Li et al. (2015) show that Eqs. 69 and 70 are quite accurate when  $0.1 \leq r \leq 10$ .

## Numerical Comparison of Energy Release Rates for the Cracked Lap Shear Specimen

An ASTM Round Robin for calculating energy release rates of cracked lap shear specimens (CLS) was reported by Johnson (1986). In this work, the energy release rates were calculated by nine groups for the two ASTM CLS specimens with four different debonded lengths ( $a = 53.54, 57.35, 76.4$  and  $152.6$ ), one with symmetrical substrates (CLS-A:  $t_1 = t_2$ ) and the other with asymmetrical substrates (CLS-B:  $t_1 = 2 t_2$ ). The CLS-B specimen configurations are shown in Fig. 13. The material properties are  $E_1 = E_2 = 72.45$  GPa,  $\nu_1 = \nu_2 = 0.33$ ,  $E_a = 1.932$ , and  $\nu_a = 0.4$ . It is indicated that the total energy release rate and mode ratio  $G_I/G_{II}$  predicted by the geometrically nonlinear finite element analysis (NFEA) were lab-to-lab consistent with the observed experimental behaviors (Johnson 1986).

Fernlund et al. (1994) calculated the total energy release rate and mode ratio  $G_I/G_{II}$  for the CLS-A and CLS-B specimens using both local and global methods. The mode ratios for the CLS-A specimen predicted by both methods are almost the same as those of the NFEA, while the mode ratios for the CLS-B specimen predicted by both methods are considerably different from those of the NFEA.

For the CLS-B specimen, the force components at the adhesive edge can be calculated using the formulations in Tong and Luo (2008). The adhesive edge stresses are then calculated using Eq. 57. The total energy release rate and mode ratio  $G_I/G_{II}$  are then obtained by using Eq. 60a or 60b. The total energy release rate for the CLS-B specimen predicted by Eqs. 57 and 60 is almost the same as that of the NFEA (Tong and Luo 2008). The mode ratios predicted by theoretical formulations and the NFEA are illustrated in Fig. 13. In Fig. 13, NFEA-1, NFEA-2, and NFEA-3



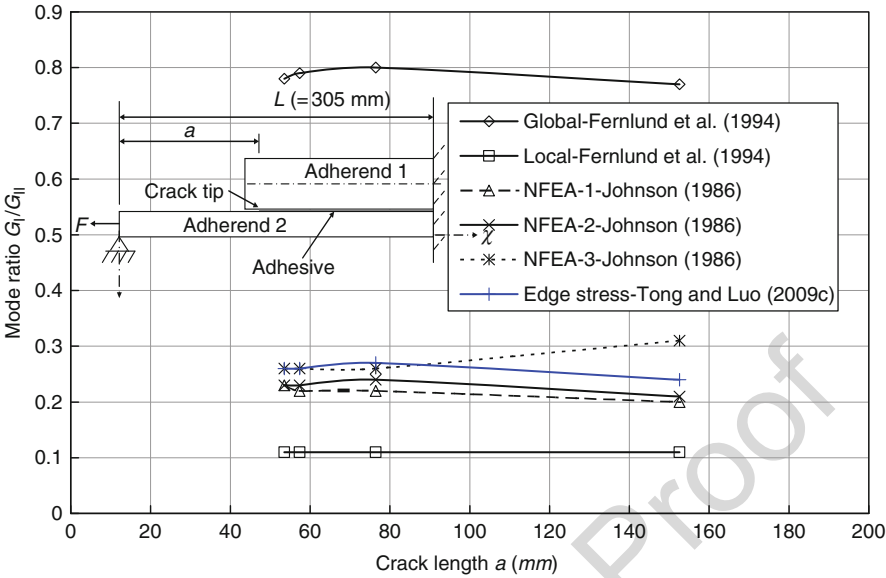


**Fig. 13** The mode ratios of the CLS-B specimen predicted by theoretical formulations and the geometrically-nonlinear finite element analyses

are referred to the NFEA results in Johnson (1986); the mode ratios predicted by using the local and global methods are taken from Fernlund et al. (1994); and the mode ratios calculated by the adhesive edge stresses are from Tong and Luo (2008).

It is noted that the coupling effect of interface shear and peel stresses are neglected in the global mode partition method in Williams (1988) and Fernlund et al. (1994). Since both local and global methods do not consider the adhesive layer, the mode ratios predicted by these methods are considerably different from that of the NFEA. The mode ratio predicted by the adhesive edge stresses based on the adhesive-beam model (Luo and Tong 2009b, c) correlates well with the NFEA given in Johnson (1986).

### 24.6.3 Failure Prediction Considering Plastic Deformation

Fracture mechanics-based criteria have shown promising agreement with the experimental results for brittle adhesives (Adams 1989; Fernlund et al. 1994; Tong 1996; Van Tooren 2004; Luo and Tong 2009c). The energy release rate criterion can be applied to cohesive failure and interface fracture. When it is used, energy release rate and its critical value for each mode should be calculated and measured. When fracture mechanics-based criteria are used, fracture envelopes are normally set up to assess crack initiation and propagation. For ductile adhesives, plastic deformation occurs before structural failure and the cohesive zone model has been widely used to

764 assess structural failure of adhesively bonded structures (Sheppard et al. 1998;  
765 Blackman et al. 2003; Liljedahl et al. 2006).

---

## 766 24.7 Summary

767 Analytical approaches for adhesively bonded structures are presented in this chapter.  
768 Stress analysis for adhesively bonded joints is conducted using the classical  
769 adhesive-beam model and the other adhesive-beam models. Closed-form solutions  
770 of symmetric joints are presented, and analytical procedures of asymmetric and  
771 unbalanced joints are discussed. Load update for single-lap joints is investigated in  
772 detail. Numerical results calculated using the classical and other formulations are  
773 illustrated and compared. It is shown that the nonlinear adhesive-beam model based  
774 on the Timoshenko beam theory provides enhanced results compared to the linear  
775 adhesive-beam model based on the Euler beam theory for adhesively bonded  
776 composite structures. Analytical solutions of energy release rates for cohesive failure  
777 and delamination are presented, and several failure criteria are reviewed and  
778 discussed.

779 **Acknowledgment** The authors are grateful for the support of the Australian Research Council via  
780 a Discovery Projects grant (DP140104408).

---

## 781 References

- 782 Adams RD (1989) Strength predictions for lap joints, especially with composite adherends: a  
783 review. *J Adhes* 30(1–4):219–242
- 784 Adams RD, Mallick V (1992) A method for the stress analysis of lap joints. *J Adhes* 38  
785 (3–4):199–217
- 786 Adams RD, Comyn J, Wake WC (1997) Structural adhesive joints in engineering. Chapman and  
787 Hall, London
- 788 Allman DJ (1977) A theory for the elastic stresses in adhesive bonded lap joints. *Q J Mech Appl*  
789 *Math* 30:415–436
- 790 Bigwood DA, Crocombe AD (1989) Elastic analysis and engineering design formulae for bonded  
791 joints. *Int J Adhes Adhes* 9(4):229–242
- 792 Bigwood DA, Crocombe AD (1990) Nonlinear adhesive bonded joint design analyses. *Int J Adhes*  
793 *Adhes* 10(1):31–41
- 794 Blackman BRK, Hadavinia H, Kinloch AJ, Williams JG (2003) The use of a cohesive zone model  
795 to study the fracture of fibre composites and adhesively-bonded joints. *Int J Fract* 119(1):25–46
- 796 Bruno D, Greco F, Lonetti P (2003) A coupled interface-multilayer approach for mixed mode  
797 delamination and contact analysis in laminated composites. *Int J Solids Struct* 40(26):7245–7268
- 798 Carpenter W (1980) Stresses in bonded connections using finite elements. *Int J Numer Methods*  
799 *Eng* 15(11):1659–1680
- 800 Carpenter WC (1991) A comparison of numerous lap joint theories for adhesively bonded joints.  
801 *J Adhes* 35(1):55–73
- 802 Chen D, Cheng S (1983) An analysis of adhesive-bonded single lap joints. *J Appl Mech* 50(1):109–115
- 803 Delale F, Erdogan F, Aydinoglu MN (1981) Stresses in adhesively bonded joints—a closed form  
804 solution. *J Compos Mater* 15:249–271

- 805 Fernlund G, Spelt JK (1991) Failure load prediction of structural adhesive joints, part 1: analytical  
806 method. *Int J Adhes Adhes* 11(4):213–220
- 807 Fernlund G, Papini M, McCommond D, Spelt JK (1994) Fracture load predictions for adhesive  
808 joints. *Compos Sci Technol* 51(4):587–600
- 809 Gleich DM, Van Tooren MJL, Beukers A (2001) Analysis and evaluation of bondline thickness  
810 effects on failure load in adhesively bonded structures. *J Adhes Sci Technol* 15(9):1091–1101
- 811 Goland M, Reissner E (1944) The stresses in cemented joints. *J Appl Mech* 11:A17–A27
- 812 Grant P, Teig IC (1976) Strength and stress analysis of bonded joints, British Aircraft Corporation  
813 Ltd. Military Aircraft Division, Report No SOR PJ 109
- 814 Harris JA, Adams RD (1984) Strength prediction of bonded single lap joints by non-linear finite  
815 element methods. *Int J Adhes Adhes* 4(2):65–78
- 816 Hart-Smith LJ (1973) Adhesive-bonded single-lap joints, NASA Langley research Center, NASA  
817 CR-112235
- 818 Harvey CM, Wood JD, Wang S, Watson A (2014) A novel method for the partition of mixed-mode  
819 fractures in 2D elastic laminated unidirectional composite beams. *Compos Struct* 116:589–594
- 820 Huang H, Yang CD, Tomblin JS, Harter P (2002) Stress and failure analyses of adhesive-bonded  
821 composite joints using ASTM D3165 specimens. *J Compos Technol Res* 24(2):93–104
- 822 Humi M, Miller W (1988) Second course in ordinary differential equations for scientists and  
823 engineers. Springer-Verlag, New York
- 824 Hutchinson JW, Suo Z (1992) Mixed mode cracking in layered materials. *Adv Appl Mech*  
825 29:63–191
- 826 Jiang Z, Wan S, Zhong Z, Li M (2016) Geometrically nonlinear analysis for unbalanced adhesively  
827 bonded single-lap joint based on flexible interface theory. *Arch Appl Mech* 86(7):1273–1294
- 828 Johnson WS (1986) Stress analysis of the cracked lap shear specimen—an ASTM round robin,  
829 NASA Technical Memorandum 89006
- 830 Lee J, Kim H (2007) Elasto-plastic analysis of adhesively bonded symmetric single lap joints under  
831 in-plane tension and edge moments. *J Adhes* 83(9):837–870
- 832 Li W, Cheng G, Wang D, Wu J (2015) A mixed mode partition method for delaminated beam  
833 structure. *Eng Fract Mech* 148:15–26
- 834 Liljedahl CDM, Crocombe AD, Wahab MA, Ashcroft IA (2006) Damage modelling of adhesively  
835 bonded joints. *Int J Fract* 141(1–2):147–161
- 836 Luo Q, Tong L (2002) Exact static solutions to piezoelectric smart beams including peel stresses—I:  
837 theoretical formulation. *Int J Solids Struct* 39(18):4677–4695
- 838 Luo Q, Tong L (2004) Linear and higher order displacement theories for adhesive bonded lap joints.  
839 *Int J Solids Struct* 41(22–23):6351–6381
- 840 Luo Q, Tong L (2007) Fully-coupled nonlinear analysis of single lap adhesive joints. *Int J Solids*  
841 *Struct* 44(7–8):2349–2370
- 842 Luo Q, Tong L (2008) Analytical solutions for adhesive composite joints considering large deflection  
843 and transverse shear deformation in adherends. *Int J Solids Struct* 45(22–23):5914–5935
- 844 Luo Q, Tong L (2009a) Calculation of energy release rates for cohesive and interlaminar delami-  
845 nation based on the classical beam-adhesive model. *J Compos Mater* 43(4):331–348
- 846 Luo Q, Tong L (2009b) Energy release rates for interlaminar delamination in laminates considering  
847 transverse shear effects. *Compos Struct* 89(2):235–244
- 848 Luo Q, Tong L (2009c) Fracture prediction of adhesively bonded structures using energy release  
849 rates. *J Adhes Sci Technol* 23(10):1415–1440
- 850 Luo Q, Tong L (2012) Analytic formulas of energy release rates for delamination using a  
851 global-local method. *Int J Solids Struct* 49(23–24):3335–3344
- 852 Luo Q, Tong L (2016) Solutions for clamped adhesively bonded single lap joint with movement of  
853 support end and its application to a carbon nanotube junction in tension. *J Adhes* 92(5):349–379
- 854 Ojalvo IU, Eidinoff HL (1978) Bond thickness upon stresses in single-lap adhesive joints. *AIAA J*  
855 16(3):204–211
- 856 Oplinger DW (1994) Effects of adherend deflection on single lap joints. *Int J Solids Struct*  
857 31(18):2565–2587

- 858 Renton WJ, Vinson (1975) The efficient design of adhesive bonded joints. *J Adhes* 7(3):175–193
- 859 Shahin K, Kember G, Taheri F (2008) An asymptotic solution for evaluation of stresses in balanced  
860 and unbalanced adhesively bonded joints. *Mech Adv Mater Struct* 15(2):88–103
- 861 Sheppard A, Kelly D, Tong LY (1998) A damage zone model for the failure analysis of adhesively  
862 bonded joints. *Int J Adhes Adhes* 18(6):385–400
- 863 da Silva LFM, Rodrigues TNSS, Figueiredo MAV, de Moura MFSF, Chousal JAG (2006) Effect of  
864 adhesive type and thickness on the lap shear strength. *J Adhes* 82(11):1091–1115
- 865 da Silva LFM, das Neves PJC, Adams RD, Spelt JK (2009) Analytical models of adhesively bonded  
866 joints-part II: comparative study. *Int J Adhes Adhes* 29(3):331–341
- 867 Srinivas S (1975) Analysis of bonded joints, NASA TN D-7855, Apr 1975
- 868 Tong L (1996) Bond strength for adhesive-bonded single-lap joints. *Acta Mech* 117(1–4):101–113
- 869 Tong L, Luo Q (2008) Chapter 2 Analysis of cracked lap shear (CLS) joints. In: da LFM S,  
870 Oechsner A (eds) *Modelling of adhesively bonded joints*. Springer, Heidelberg
- 871 Tong L, Steven GP (1999) *Analysis and design of structural bonded joints*. Kluwer Academic,  
872 Boston. 1999
- 873 Van Tooren MJL (2004) Experimental verification of a stress singularity model to predict the effect  
874 of bondline thickness on joint strength. *J Adhes Sci Technol.*, 2004 18(4):395–412
- 875 Volkersen O (1938) “Die Nietkraftverteilung in Zugbeanspruchten Nietverbindungen mit  
876 Konstanten Laschenquerschnitten” (The rivet load distribution in lap-joints with members of  
877 constant thickness subjected to tension). *Luftfahrtforschung* 15:41–47
- 878 Wang S, Harvey C (2012) A theory of one-dimensional fracture. *Compos Struct* 94(2):758–767
- 879 Williams JG (1988) On the calculation of energy release rates for cracked laminates. *Int J Fract*  
880 36(2):101–119
- 881 Yang C, Pang SS (1993) Stress–strain analysis of adhesive-bonded single-lap composite joints  
882 under cylindrical bending. *Compos Eng* 3(11):1051–1063
- 883 Yang CD, Huang H, Tomblin JS, Sun WJ (2004) Elastic-plastic model of adhesive-bonded single-  
884 lap composite joints. *J Compos Mater* 38(4):293–309
- 885 Yousefsani SA, Tahani M (2013) Analytical solutions for adhesively bonded composite single-lap  
886 joints under mechanical loadings using full layerwise theory. *Int J Adhes Adhes* 43:32–41
- 887 Zhao B, Lu ZH (2009) A two-dimensional approach of single-lap adhesive bonded joints. *Mech*  
888 *Adv Mater Struct* 16(2):130–159
- 889 Zhao X, Adams RD, da Silva LFM (2010) A new method for the determination of bending  
890 moments in single lap joints. *Int J Adhes Adhes* 30(2):63–71

# Numerical Approach: Finite Element Analysis

# 25

Ian A. Ashcroft and Aamir Mubashar

## Contents

25.1	Introduction .....	702
25.1.1	Brief History of the Finite Element Method .....	703
25.1.2	Recent Developments .....	704
25.1.3	Applications of Finite Element Analysis .....	707
25.1.4	Comparison with Other Methods .....	708
25.2	The Finite Element Method .....	708
25.2.1	Fundamentals of the Finite Element Method .....	709
25.2.2	Natural Coordinates .....	711
25.2.3	Isoparametric Elements and Numerical Integration .....	712
25.3	Nonlinear Finite Element Analysis .....	714
25.3.1	Sources of Nonlinearity .....	714
25.3.2	Solution Algorithms .....	715
25.4	Thermal Analysis .....	716
25.4.1	Introduction .....	716
25.4.2	Heat Conduction .....	716
25.5	Dynamic Analysis .....	718
25.5.1	Introduction .....	718
25.5.2	Free Vibration .....	719
25.5.3	Dynamic Response Analysis .....	720
25.6	Application of the Finite Element Method .....	720
25.6.1	Preprocessing .....	720
25.6.2	Processing .....	724
25.6.3	Post-processing .....	725

I. A. Ashcroft (✉)

Faculty of Engineering, University of Nottingham, Nottingham, UK

e-mail: [ian.ashcroft@nottingham.ac.uk](mailto:ian.ashcroft@nottingham.ac.uk)

A. Mubashar

Mechanical Engineering, Middle Eastern Technical University, Northern Cyprus Campus,  
Akara, Turkey

e-mail: [mubashar@metu.edu.tr](mailto:mubashar@metu.edu.tr)

© Springer International Publishing AG, part of Springer Nature 2018

L. F. M. da Silva et al. (eds.), *Handbook of Adhesion Technology*,

[https://doi.org/10.1007/978-3-319-55411-2\\_25](https://doi.org/10.1007/978-3-319-55411-2_25)

701

28	25.7	Application of FEA to Adhesive Joints .....	726
29	25.7.1	General Considerations .....	726
30	25.7.2	Stress Analysis .....	727
31	25.7.3	Failure Analysis .....	730
32	25.7.4	Advanced Analysis Methods .....	732
33	25.8	Summary and Conclusions .....	737
34		References .....	738

**Abstract**

Finite element analysis (FEA) is a widely used computer-based method of numerically solving a range of boundary problems. In the method, a continuum is subdivided into a number of well-defined elements that are joined at nodes, a process known as discretization. A continuous field parameter, such as displacement or temperature, is now characterized by its value at the nodes, with the values between the nodes determined from polynomial interpolation. The nodal values are determined by the solution of an array of simultaneous equations using computational matrix methods, and the accuracy of the results is dependent on the discretization, the accuracy of the assumed interpolation form, and the accuracy of the computation solution methods. The current popularity of the method is based on its ability to model many classes of problem regardless of geometry, boundary conditions, and loading. Modeling the behavior of adhesive joints is complicated by a number of factors, including the complex geometry, the complex material behavior, and the environmental sensitivity. FEA is currently the only technique that can comprehensively address the challenges of modeling bonded joints under realistic operating conditions. However, a reliable and robust method of using FEA to model failure in bonded joints is still to be developed.

**25.1 Introduction**

In its 50-year life, the finite element method (FEM) has progressed from a specialist technique of the aerospace stress analyst to a ubiquitous tool of advanced engineering analysis, widely taught in undergraduate programs and the foundation of a billion-dollar industry. It is based on two basic concepts. The first is the representation of a continuum as a number of simple, well-defined sub-elements with a finite number of degrees of freedom. The second is the solution of differential equations by the weak (or generalized) method through the application of numerical integration techniques. This reduces a potentially unsolvable differential equation to a series of simple, linear simultaneous equations, which can be solved through the application of matrix methods. The methods at the core of the finite element method were proposed in the nineteenth century, but it was only with the development of microprocessor computers that the solution of the large number of simultaneous equations required to represent complex problems became practical. The power of the method is in its simplicity and generality, being unbounded by geometry, loads, boundary conditions, or class of problem. However, it should be remembered that both the discretization process and

the numerical solution methods used in the finite element method involve errors, and, hence, the FEM will always present an approximate solution to a problem. In most cases, these errors can be minimized and are usually more than compensated for by the reduction in errors associated with simplifying a problem to a level that enables an exact solution to be determined. The mathematical basis of the FEM is now well established and its role as a practical engineering tool widely recognized. Further development, application, and usage of the method are envisaged in the foreseeable future.

Although numerous analytical methods for determining stresses in bonded joints have been proposed, they generally require significant simplification of geometry, boundary conditions, and material behavior; even then, the more advanced analyses are exceedingly complex, sometimes requiring numerical methods of solution. The application of FEM to bonded joints, with its capability of handling complex geometry, material behavior, and boundary conditions, as well as nonlinearity and multi-physics modeling, is potentially very attractive. However, a number of cautions should be observed. Firstly, the thickness of the adhesive layer with respect to other dimensions is usually small, raising problems of creating a suitable mesh with a reasonable number of elements, while avoiding excessive element distortion. Secondly, adhesive material behavior can be exceedingly complex and will vary considerably with environment, presenting problems in adopting a suitable material constitutive law. Thirdly, the interface between the adhesive and adherend is difficult to model accurately, and at certain points, theoretical singularities exist at the bi-material junction, presenting difficulties in applying standard failure criteria. These issues can all be addressed to some degree to provide effective analyses of bonded joints, and it is envisaged that further advances in these areas will be made and that the application of FEA to bonded joints will continue to increase. However, despite all the advantages, it should still be remembered that the FEM is an approximate technique, and the integrity of results is highly dependent on the skills of the analyst.

This chapter is subdivided into a number of sections. This section provides a general background to the development and application of the FEM. Section 2 provides the fundamentals of the method, and Sect. 3 discusses some of the practical aspects of finite element modeling. Section 4 discusses application of the FEM to adhesively bonded joints, and Sect. 5 provides conclusions from the chapter and indicates potential future developments in the application of FEA to bonded joints.

### 25.1.1 Brief History of the Finite Element Method

The finite element method is a numerical analysis procedure that provides an approximate solution to problems in various fields of engineering. It is based on the matrix methods of structural analysis of the 1920s and 1930s. Advances in the aerospace industry and the development of computers in the 1950s and 1960s saw further development and computerization of these methods. Interest in delta wings leads to the requirement for a two-dimensional (2D) element of arbitrary shape. In 1956, the stiffness of a general 2D triangular element was derived (Turner et al. 1956), and in 1959, the direct stiffness method as a general, computer-based method

of structural analysis was proposed (Turner 1959). This was the direct precursor of nearly all current commercial finite element analysis (FEA) methods.

The term finite element was introduced by Clough (1960), and the first widely used finite element program was written by Wilson in the early 1960s (Fish and Belytschko 2007). The applicability of the method to general field applications was described by Zienkiewicz and Cheung (1967), and by the end of the 1960s, finite element analysis (FEA) was being applied to a wide variety of boundary problems, such as heat transfer, fluid flow, dynamics, free and forced vibration, and electrical and magnetic fields. The mathematical foundations of the finite element method were laid down in the 1970s (Champion and Ensminger 1988). In the 1980s, generalized software packages designed to run on powerful computers were developed, and improved techniques for analyzing nonlinear problems were established.

The personal computer (PC) was introduced in the late 1970s, and by the 1990s, the PC became sufficiently powerful to be practical for FEA. Commercial FEA software for PCs was developed and became widely used. FEA is now used in practically all fields of engineering analysis and is the clearly favored technique for many industries, including aerospace, automotive, nuclear, electronics, and defense. Several software vendors offer extremely powerful, general purpose, finite element software which can solve a wide range of problems.

### 25.1.2 Recent Developments

Finite element modeling was once the domain of a few high-technology industries and academic communities. An increase in the sophistication of the method and a widening of the user base has been accompanied by a shift from in-house software codes to powerful, user-friendly commercial software. The market is now dominated by a relatively small number of general commercial software packages and a number of more specific codes satisfying niche markets. Most of the commercial packages are capable of user modification, such as the introduction of user-written elements or material constitutive models.

A recent trend in the commercially available software is the availability of multi-physics simulations. The finite element method can be applied to many classes of problems such as structural, heat transfer, material transport (such as diffusion), fluid mechanics, and electromagnetic. Multi-physics analysis is concerned with the coupling of different analysis classes, such as thermo-structural, fluid-chemical, electro-thermal, fluid-structural, hygro-thermo-structural, etc. In multi-physics modeling, the nature of the coupling must be considered. For example, in a fully coupled thermo-mechanical analysis, both the effect of the thermal field on the structural response and the effect of the structural response on the thermal field are represented. This is implemented by partitioning the structural and field analyses using common time integration. The thermal and structural analyses are then performed either concurrently or sequentially, and communication is achieved via a common data transfer file. For strongly coupled systems, data transfer should be on the iterative level, but for weakly coupled systems, an incremental data transfer is usually sufficient. There may also be



situations that a single software or type of analysis is not able to solve for all the physics inherent in certain complex structures and systems. Such situations include problems involving fluid and structural domain interaction, system-level rigid body dynamics with inclusion of flexible parts, or inclusion of hydraulic/pneumatic control in a finite element-based simulation. In such cases, multiple solvers can be linked together by using software that acts as controller for all the involved solvers. The control software facilitates the transfer of information between the solvers during the simulation process and also provides mapping between field variables. The information exchange between solvers is generally linear, where one solver completes a job and the results are provided to the next solver. Such a linkage enables optimization and design space exploration studies involving various fields that fully interact with each other. However, the computational requirements of running these studies are generally high as multiple iterations are required to find an optimized solution. The limitations of computational requirements have been mostly met by the use of high performance computing clusters (HPCs). HPCs provide a multi-node, multicore configuration where a master node schedules the jobs received from multiple users. Installation and maintenance of HPCs is a costly business, and many companies are now moving toward cloud computing. In cloud computing, Internet-based services may be used to access remote compute clusters for the solution of large finite element-based problems. The access to cloud-based computing resources can be requirement based, which may help in reducing the cost of an analysis. The current issues with the use of cloud computing are related to the availability of high-speed Internet and data security.

In a drive to make the finite element method more accessible to users of various levels of experience, packaging of complex finite element analysis in the form of apps is becoming increasingly popular. A few commercial finite element software (such as COMSOL) are now providing this as a built-in capability and providing server applications for deploying the apps across the enterprise. The advantage of this approach is that complex finite element analysis models, which take a considerable time, effort, and level of expertise to setup, are developed and validated by experts in the field. These validated finite element models are then packaged as apps, allowing predetermined parameters to be changed in a controlled fashion, thus enabling users less experienced in finite element theory to carry out various types of studies.

Another area of current development is in damage and failure modeling. It is impossible for a linear finite element analysis to predict failure in a structure. However, in nonlinear analysis, it is possible to implement a failure model, and increasingly complex failure models are now supplied as standard features of commercial FEA software. It should be noted, however, that even though the failure model may look complex, the method of implementation within FEA is usually fairly straightforward. In most cases, this involves utilization of the results from the various increments of a nonlinear analysis. These are processed via some failure model to determine whether failure or damage has occurred in any of the elements. The properties of the failed or damaged elements are then modified, usually by control of the element stiffness matrix, removal of elements, or affecting nodal connectivity/element interaction.

One of the simplest failure models is that based on plastic yielding. In this case, progressive yielding of the structure is modeled until a “limit state” or state of “global

yielding” is reached. Fracture mechanics principles can also be used within an FEA. This can be based on either the stress intensity factor or energy approaches. An extension to this approach is cohesive zone modeling (CZM), which also allows for damage of a material ahead of a crack. The CZM technique allows the modeling of damage and failure in ductile (Dugdale 1960; Barenblatt 1962) and quasi brittle (Hillerborg et al. 1976) materials. The technique uses a layer of cohesive elements to represent a potential crack path or interface. The virtual crack closure technique (VCCT) for the determination of strain energy release rate was proposed by Rybicki and Kanninen on 1977 but has only recently been implemented in major commercially available finite element software. Another method for modeling cracks in materials is the extended finite element method (XFEM). The XFEM uses enriched shape functions to represent a discontinuous displacement field (Mohammadi 2008). The main advantage of XFEM is that the crack may initiate at any point in the material and propagate based on loading conditions. No remeshing is required as the crack can grow within an element and need not follow element boundaries. In order to overcome the individual drawbacks of CZM and XFEM methods, when applied to the adhesive joints, a combination of the two methods has been used (e.g., Mubashar et al. 2014; Stuparu et al. 2016). In such adhesive joint models, the XFEM is used to simulate cohesive damage and failure within the adhesive layer, whereas CZM is used to represent interfacial damage and crack growth. This enables crack initiation and propagation that can transfer from a cohesive crack to an interfacial crack and vice versa. However, such highly nonlinear models suffer from non-convergence problems, and some form of viscous stabilization is generally used to obtain a converged solution. Neumayer et al. (2016) attempted to develop a cohesive element that is able to predict cohesive as well as interfacial failure in the adhesive layer. The advantage of such a formulation is that a single layer of cohesive elements would be able to correctly predict the type of failure in an adhesive joint. The reduction in the finite element model size comes from using structural elements such as beams or shell elements for adherends. The proposed finite element formulation was used to determine the strength of single lap adhesive joints where it provided good prediction of failure strength of the joint under cohesive failure. However, for interfacial failure, the strength of the adhesive joints was underestimated by the proposed cohesive element.

Another methodology to alleviate problems associated with continuum meshes during large deformation simulations is to use meshless methods. One such method is smoothed particle hydrodynamics (SPH), which is generally used for highly nonlinear solid mechanics problems. In this method, a material continuum is approximated by discretization involving particles rather than elements, which allows for large deformations and crack propagation along arbitrary paths. The SPH method is a particle-based representation of the partial differential equations of a continuum. The particles are not directly connected to each other but are affected by neighboring particles. This means that the value of field variable at a point also includes contributions from the neighboring elements, where the number of neighboring elements contributing to a particle is based on a kernel function. The value of a field variable is determined by an interpolation scheme. Displacement is the field variable in the case of a structural analysis, as in the finite element method. A few attempts have been made to apply this method to adhesive joints (e.g., Tsai et al. 2014; Mubashar and Ashcroft 2015).

Continuum damage mechanics-based models are now available and implemented in commercial finite element software. Damage may be regarded as the growth of microvoids or microcracks in a material (Lemaitre and Desmorat 2005). Continuum damage mechanics was introduced in the late 1950s (Kachanov 1958) and is able to predict the reduced load bearing capacity of a material before failure. Damage is related to the growth of microcracks and microvoids in a material. Damage in a material is generally defined by a damage variable that has constitutive equations for evolution. The damage variable may be defined such that it is based on some physical characteristic of the material or is a representation of the effects of damage, e.g., reduction in stiffness. Damage may be isotropic or anisotropic and has also been defined for fatigue and creep loading conditions. The damage model combined with a failure criterion can be used in conjunction with plasticity models, providing a complete definition of material behavior.

### 25.1.3 Applications of Finite Element Analysis

Owing to the general nature of the finite element method, it can be used to solve boundary value problems in many fields. The initial applications of the finite element method were in aircraft structures, but it is now widely applied to the solution of many other engineering problems. These include the stress and thermal analysis of components, crash analysis of vehicles and aircraft, seismic analysis of civil engineering structures, nuclear engineering, fluid flow analysis, soil structure interaction, steady-state and transient behavior of electronic devices, and electromagnetics. The use of composites is increasing in modern structures, such as aircrafts and automobiles, and FEA provides a convenient method to determine the performance and durability of composites. The fabrication of different types of composite lay-up can be explored at design stage to avoid problems during manufacturing. FEA can also be used in the optimization of structural components where automatic mesh generation makes the process highly automated. Full vehicle body noise and vibration analysis are performed to improve the performance of modern automobiles. Virtual crash testing of aircraft and drop testing of electronic devices such as mobile phones and laptops may now be conducted using commercially available FEA software. Applications in offshore structures include ship design and reliability studies of oil and gas equipment. Manufacturing industry is also taking advantage of the capabilities of finite element method where finite element method-based simulation models are used to develop better cutting tools, estimate the best machining conditions, predict residual stresses, and determine the shape of a part after forming processes.

A recent area of application is in biomedical engineering where FEA is used to determine the performance of implants such as heart valves and the expansion of stents during angioplasty. Prosthesis designs may be analyzed using FEA so they can be adapted to a particular patient. Other biomedical applications involve modeling of bone, biological soft tissues, blood flow, and blood vessels (Kojić et al. 2008). Some examples of finite element models, including a heart stent, chassis for multi-axle

vehicle, an adhesively bonded composite T-Joint, and two-dimensional orthogonal machining, are shown in Fig. 1.

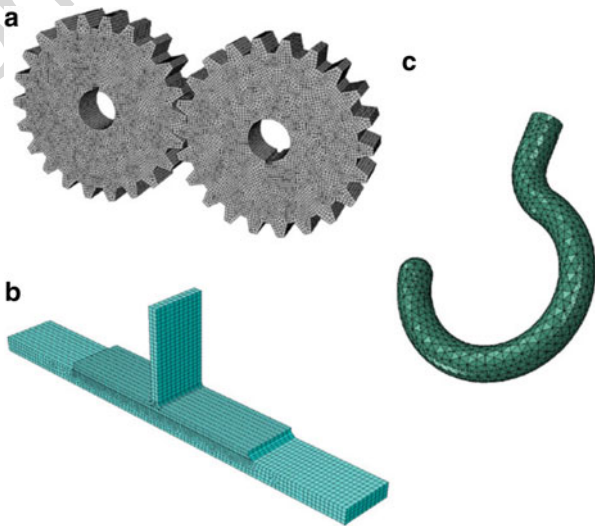
**25.1.4 Comparison with Other Methods**

Other analysis methods that use discretization include the finite difference method, the boundary element method, and the finite volume method. However, FEA is by far the most commonly used method in structural mechanics. The finite difference method approximates differential equations using difference equations. The method works well for two-dimensional problems but becomes cumbersome for regions with irregular boundaries (Segerlind 1984). Another difference between the finite element and finite difference methods is that in the finite difference method, the field variable is only computed at specific points, while in the finite element method, the variation of a field variable within a finite element is available from the assumed interpolation function (Hutton 2003). Thus the derivatives of a field variable can be directly determined in finite element method as opposed to the finite difference method where only data concerning the field variable is available. The boundary element method is also not general in terms of structural shapes (MacNeal 1994).

**25.2 The Finite Element Method**

This section provides a condensed view of the fundamentals of the finite element method, in which an attempt has been made to summarize the underlying theory behind the main classes of analysis that may usefully be used in analyzing

**Fig. 1** Examples of finite element models: (a) a heart stent, (b) chassis of a multi-axle vehicle, (c) composite T-joint, and (d) machining of material



adhesively bonded joints. One of the many textbooks on finite element analysis, such as Cook (1995) or Zienkiewicz and Taylor (2000), should be referred to for a more complete treatment of the subject.

### 25.2.1 Fundamentals of the Finite Element Method

In the finite element method (FEM), a continuous structure is considered as a number of smaller elements joined at nodes. Each node has a limited number of degrees of freedom (dof). Hence, the continuum is now represented by a finite number of dof and determined by the number of elements, the number of nodes per element, and the number of dof per node. Over each element, a field quantity, such as displacement in structural analysis, is interpolated, usually adopting a polynomial form, from values of the field quantity at the nodes. By joining the elements, the field quantity is interpolated over the whole structure by an array of polynomial expressions. A set of simultaneous equations is formulated in which the primary unknowns are the values of the field quantity at the nodes.

There are a number of variants of the finite element method depending on the formulation and solution of the problem. The most common variant is the stiffness method in which the displacement compatibility conditions are satisfied and the equations of equilibrium are solved to yield the unknown nodal displacements. The governing equation using matrix symbolism is of the following form:

$$[F] = [K][u] \quad (1)$$

where  $[u]$  is a vector of unknown values of the field quantity at the nodes,  $[K]$  is a matrix of known constants, and  $[F]$  is a vector of known loads. In stress analysis,  $[u]$  is the displacement vector,  $[F]$  is the vector of applied loads, and  $[K]$  is the stiffness matrix.

The most widely used methods in finite element formulation are the variational method and the method of weighted residuals. The variational approach involves the solution of a governing partial differentiation equation, such as the equilibrium equation in an elasticity problem, by determining the conditions that make some quantity (or functional) stationary (i.e., either maximum or minimum). In elasticity problems, the functional used is the total potential energy of the structure. First, an approximate form for the solution is assumed. This must be admissible, that is it must satisfy internal compatibility and essential boundary conditions. The stationary potential energy theorem is then used to determine the optimum value for the constants. This theorem states that for all admissible configurations of a conservative system, those that satisfy the equations of equilibrium make the potential energy stationary with respect to small admissible variations of displacement, i.e., equilibrium configurations are defined when

$$\frac{\partial \Pi_p}{\partial a_i} = 0 \quad (2)$$

339 where  $\Pi_p$  is potential and  $a_i$  is the  $i$ th dof.

$$\Pi_p = U + \Omega \quad (3)$$

340 where  $U$  is the strain energy and  $\Omega$  is the potential of the load system. The strain  
341 energy in a stressed body is given by

$$U = \frac{1}{2} \int \{\varepsilon\}^T [E] \{\varepsilon\} dV \quad (4)$$

342 where  $[E]$  is the elastic constant matrix, which defines the relationship between stress  
343  $\{\sigma\}$  and strain  $\{\varepsilon\}$ , i.e.,

$$\{\sigma\} = [E] \{\varepsilon\} \quad (5)$$

344 The potential of the load system is

$$\Omega = -\{u^e\}^T \{F^e\} \quad (6)$$

345 The total potential of the system is therefore

$$\Pi_p = U + \Omega = \frac{1}{2} \int \{\varepsilon\}^T [E] \{\varepsilon\} dV - \{u^e\}^T \{F^e\} \quad (7)$$

346 A shape function,  $[N]$ , is used to relate the vector of displacements in the element,  
347  $\{u\}$ , to the vector of nodal displacements,  $\{u^e\}$ .

$$\{u\} = [N] \{u^e\} \quad (8)$$

348 The strain vector can then be determined by partial differentiation of the dis-  
349 placement vector, giving

$$\{\varepsilon\} = \left\{ \frac{du}{dx} \right\} = \left[ \frac{dN}{dx} \right] \{u^e\} = [B] \{u^e\} \quad (9)$$

350 where  $[B]$  is the strain-displacement matrix. Substituting (9) into (7),

$$\Pi_p = \frac{\{u^e\}^T}{2} \int [B]^T [E] [B] dV \{u^e\} - \{u^e\}^T \{F^e\} \quad (10)$$

351 Applying the stationary potential energy theorem,

$$\frac{\partial \Pi_p}{\partial \{u^e\}} = 0 = \int [B]^T [E] [B] dV \{u^e\} - \{F^e\} \quad (11)$$

$$\{F^e\} = \int [B]^T [E] [B] dV \{u^e\} \quad (12)$$

and as  $\{F^e\} = [K^e]\{u^e\}$ :

$$[K^e] = \int [B]^T [E] [B] dV \quad (13)$$

Equation 13 can be solved by numerical integration for each element.

### 25.2.2 Natural Coordinates

It can be seen that integration of the  $[B]$  matrix is necessary for element formulation via the variational approach. A numerical integration method, such as Gauss quadrature, is used in which the real element shape is mapped onto an idealized element shape with well-defined boundaries and hence integration limits. This is achieved by transforming from the physical coordinate system (e.g.,  $xy$ ) to a natural coordinate system (e.g.,  $\xi\eta$ ) as shown in Fig. 2.

The shape functions can now be derived in terms of the natural coordinates. However, it is necessary to transform the variables to the physical coordinates in order to determine  $[B]$ . This can be achieved using the chain rule. For the 2D case in Fig. 2,

$$\frac{\partial N}{\partial \xi} = \left( \frac{\partial N}{\partial x} \right) \left( \frac{\partial x}{\partial \xi} \right) + \left( \frac{\partial N}{\partial y} \right) \left( \frac{\partial y}{\partial \xi} \right) \quad (14)$$

$$\frac{\partial N}{\partial \eta} = \left( \frac{\partial N}{\partial x} \right) \left( \frac{\partial x}{\partial \eta} \right) + \left( \frac{\partial N}{\partial y} \right) \left( \frac{\partial y}{\partial \eta} \right) \quad (15)$$

In matrix form, this can be rewritten as

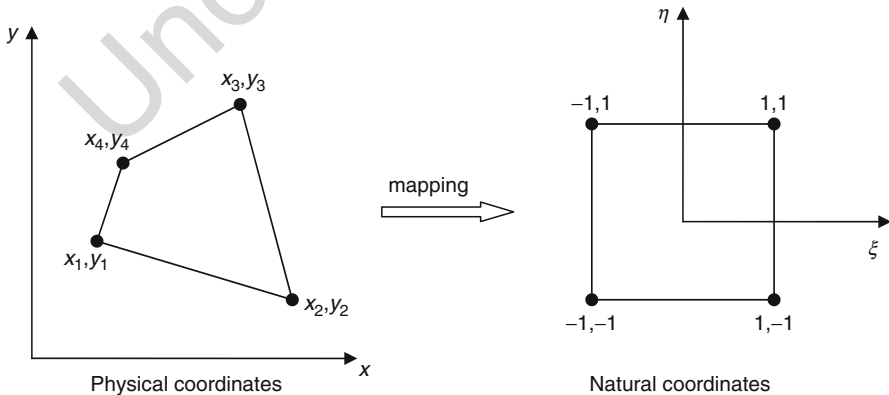


**Fig. 2** Transformation from physical to natural coordinates

$$\begin{bmatrix} \frac{\partial N}{\partial x} \\ \frac{\partial N}{\partial y} \end{bmatrix} = [J]^{-1} \begin{bmatrix} \frac{\partial N}{\partial \xi} \\ \frac{\partial N}{\partial \eta} \end{bmatrix} \quad (16)$$

where the Jacobian matrix  $[J]$  is given by

$$[J] = \begin{bmatrix} \frac{\partial x}{\partial \xi} & \frac{\partial y}{\partial \xi} \\ \frac{\partial x}{\partial \eta} & \frac{\partial y}{\partial \eta} \end{bmatrix} \quad (17)$$

The Jacobian can be regarded as the scale factor that relates the physical length with the reference length. Element distortion affects the Jacobian determinant and introduces errors into the numerical integration. Thus element distortion needs to be controlled to obtain acceptable integration results.

### 25.2.3 Isoparametric Elements and Numerical Integration

In isoparametric elements, the same interpolation functions are used to define the variation of the primary variable across the element and the shape of the element. In other words,  $[N]$  is used to determine the element shape from the nodal coordinates  $[x^e]$  (hence the term shape function, which takes on added significance for isoparametric elements) and to determine element displacement from nodal displacements.

$$x = [N][x^e]^T \quad (18)$$

$$u = [N][u^e]^T \quad (19)$$

In the case of quadratic or higher interpolations, this has the advantage that the distribution of the primary variable is represented more closely and also that the element sides can be curved. The element stiffness matrix requires the strain-displacement relationship to be known, e.g., for the one-dimensional case:

$$\varepsilon_x = \frac{du}{dx} = \left( \frac{d}{dx} [N] \right) \{u^e\} \quad (20)$$

where

$$\frac{d}{dx} = \frac{d\xi}{dx} \frac{d}{d\xi} \quad (21)$$



384 As  $[N]$  is expressed in terms of natural coordinates, the chain rule for differenti-  
 385 ation must be used. First, the Jacobian is calculated as

$$J = \frac{dx}{d\xi} = \frac{d}{d\xi}[N]\{x^e\} \quad (22)$$

386 And hence the  $[B]$  matrix is calculated as

$$[B] = \frac{1}{J} \frac{d}{d\xi}[N] \quad (23)$$

387 The stiffness matrix  $[k]$  is now obtained using

$$[k] = \int [B]^T [E] [B] dx = \int [B]^T [E] [B] J d\xi \quad (24)$$

388 The only issue left is that Eq. 24 cannot generally be solved algebraically. Instead  
 389 a numerical integration scheme (such as *Gauss Quadrature*) has to be used to  
 390 determine the stiffness matrix. An integral having arbitrary limits can be transformed  
 391 so that its limits are from  $-1$  to  $1$ , e.g.,

$$I = \int_{x_1}^{x_2} f(x) dx \quad (25)$$

392 can also be expressed as

$$I = \int_{-1}^1 \varphi(\xi) d\xi \quad (26)$$

393 and therefore, as in all isoparametric formulations in FEA, the integral can be  
 394 evaluated between the same limits  $-1$  and  $1$ . In general, the integral can be  
 395 computed by sampling from a number of points and multiplying by an appropriate  
 396 value or *weighting factor*  $W$ . This leads to the following generalization for *Gauss*  
 397 *quadrature*:

$$I = \int_{-1}^1 \varphi(\xi) d\xi \approx W_1 \varphi_1 + W_2 \varphi_2 + \dots + W_n \varphi_n \quad (27)$$

398 where  $n$  is the number of sampling (Gauss) points. As the number of gauss points  
 399 increases, more accurate integration results are obtained in general. On the other  
 400 hand, using too many Gauss points would require more computational resources,  
 401 and the results may not improve.

The element stiffness matrices are summed to form the global stiffness matrix, as given in Eq. 1, which will be a symmetrical square matrix with the order of the numbers of dof in the finite element model. Sophisticated computational techniques have been developed that enable the solution of these equations for large assemblages of elements, thereby, allowing complex structures to be modeled to a high degree of accuracy. Once all the nodal degrees of freedom have been determined, it is a relatively simple procedure to determine strains in the elements from Eq. 9 and then to calculate stresses using Eq. 5.

---

## 25.3 Nonlinear Finite Element Analysis

### 25.3.1 Sources of Nonlinearity

In a linear analysis, response is directly proportional to load. This is applicable if displacements and rotations are small, stress is directly proportional to strain, and loads maintain their original directions as the structure deforms. In a linear analysis, equilibrium reactions are written in terms of the original configuration, and displacements are obtained by solving a single set of equilibrium equations.

Nonlinearity typically arises because of material or geometric nonlinearities. Nonlinearity makes the problem more difficult because the geometry, support conditions, and material properties required for the equilibrium equations are not known until the solution is known. The solution cannot be obtained in a single step, and some sort of iterative solution must be used, together with a relevant convergence test. In a nonlinear analysis, the principle of superposition cannot be applied, and a separate analysis is required for each load case.

Geometric nonlinearity arises when deformations are large enough to significantly alter the way load is applied or resisted by the structure. Examples include follower loads, membrane stiffening, and snap-through effects. Finite element analysis of large deflection problems is carried out using the same elements as used in small deflection analysis, but extra attention must be paid to errors due to excessive element distortion. Nonlinear solution algorithms update the stiffness matrix in the solution process, ensuring equilibrium equations based on the deformed configuration are generated.

Contact nonlinearity may also be considered a form of geometric nonlinearity. Most real problems involve contacting bodies; however, in many cases, this is circumvented in FEA by the use of simplifying boundary conditions. However, in cases where the interaction of two or more bodies is of interest, a contact analysis must be set up. It should be noted that if contact is not set up, the two contacting bodies will simply pass through each other. Numerous methods of incorporating contact in FEA are available but most involve two main steps. The first is the detection of contact, and the second is the imposition of forces to prevent interpenetration of the contacting bodies. In order to detect penetration, it is usual to first identify the surfaces that are likely to make contact. As a nonlinear analysis

proceeds, checks are then made to assess contact. Once contact has been made, the penetration distance is calculated and appropriate forces applied to prevent interpenetration. From this analysis, the point of contact, contact force, deformed shape of contacting bodies, and contact stresses can all be calculated. The results may be influenced by the mesh in the contact region, the nonlinear controls, and the contact algorithms used.

Material nonlinearity may be hyperelastic or elastoplastic. The difference between the behavior of an elastic and elastoplastic material is seen on unloading as in the former case, the unloading path coincides with the loading path, whereas in the latter case, a different unloading path results in permanent deformation when the load has been removed. Elastoplastic behavior is characterized by a linear region up to the yield point, after which softening behavior is seen. Hyperelastic materials such as elastomers exhibit nonlinear elastic response for even large strains.

### 25.3.2 Solution Algorithms

Numerical methods are incapable of solving nonlinear equations explicitly, and the actual behavior must be approximated by a sequence of linear steps. Incremental and iterative methods are available to solve a system of nonlinear equations. In the incremental method, the response is approximated by dividing the solution into a number of linear increments and updating the stiffness at each increment. The incremental method may underestimate the nonlinear behavior, and a progressive divergence from the actual response may be observed. A better approximation would be obtained by decreasing the size of the increments, but for a controlled reduction in error, an iterative method is required.

Iterative methods utilize the secant stiffness, which is defined as  $F/u$ . One of the commonly used iterative techniques is the Newton-Raphson method. The first stage in this method is the same as the first increment in the incremental method. After the increment, as the stiffness as a function of displacement is known, the internal forces can be calculated from:

$$r = ku \quad (28)$$

where  $k$  is the secant stiffness at the end of increment. The difference between the applied force and the resisting force can then be calculated from:

$$e = F - r \quad (29)$$

This force imbalance can then be used to drive the displacement toward the correct value by using an equilibrium iteration method at constant load. The process can be repeated until a suitably small imbalance is attained.

The Newton-Raphson method may be computationally expensive in a multi-dof problem because a new global stiffness matrix is used in each iterative step.

In the modified Newton-Raphson method, the same global stiffness matrix is used in all the iterative steps within an increment. This method requires more iterations to achieve convergence, but each iteration is computed far more quickly.

Appropriate selection of convergence criteria is essential to obtain sufficient accuracy in a reasonable time. Convergence is also based on the solution algorithm. Convergence failure is usually defined when the convergence tolerance is not reached in a specified number of iterations. In this case, it is common to reduce the incremental load step.

## 25.4 Thermal Analysis

### 25.4.1 Introduction

Thermal analysis is primarily concerned with the calculation of temperature distribution in a body and the magnitude and direction of heat flow. There are many similarities between the formulation and solution of thermal and structural problems in FEA. The global FE equation for a steady-state thermal problem is

$$[K_T][T] = [Q] \quad (30)$$

where  $[K_T]$  is a matrix of material constants including thermal conductivity,  $[T]$  is a column matrix of nodal temperatures, and  $[Q]$  is a column matrix of thermal loads. Thermal finite elements are assembled in a similar way as structural finite elements. In contrast to stress analysis, however, thermal analysis is a scalar problem as temperature is nondirectional. Also, a thermal finite element node has only one degree of freedom, namely, temperature. In a thermal analysis, the temperature field (like the displacement field in structural analysis) is continuous, but the temperature gradients (like strains in structural analysis) are not continuous between elements, and higher mesh refinement is required in regions where temperature gradient changes rapidly.

### 25.4.2 Heat Conduction

Fourier heat conduction equation for an isotropic material:

$$f_x = -k \frac{\partial T}{\partial x} \quad \text{or} \quad q_x = -kA \frac{\partial T}{\partial x} \quad (31)$$

where  $f_x$  is heat flux per unit area ( $\text{Wm}^{-2}$ ),  $k$  is the thermal conductivity ( $\text{Wm}^{-1} \text{K}^{-1}$ ),  $q_x$  is the rate of heat flow (W), and  $A$  is the cross-sectional area ( $\text{m}^2$ ). The negative sign indicates that heat flows in the opposite direction to the increase in temperature. This can be extended to a general anisotropic case:

$$\begin{Bmatrix} f_x \\ f_y \\ f_z \end{Bmatrix} = - \begin{bmatrix} k_x & 0 & 0 \\ 0 & k_y & 0 \\ 0 & 0 & k_z \end{bmatrix} \begin{Bmatrix} \partial T / \partial x \\ \partial T / \partial y \\ \partial T / \partial z \end{Bmatrix} \quad \text{or} \quad \{f\} = -[D]\{T_{\partial}\} \quad (32)$$

If the energy balance in a differential element is considered,

$$- \left[ \frac{\partial}{\partial x} \quad \frac{\partial}{\partial y} \quad \frac{\partial}{\partial z} \right] \begin{Bmatrix} f_x \\ f_y \\ f_z \end{Bmatrix} + Q = c\rho \frac{\partial T}{\partial t} \quad (33)$$

where  $Q$  is the rate of internal heat generation per unit volume,  $c$  is the specific heat ( $\text{J kg}^{-1} \text{K}^{-1}$ ),  $\rho$  is the mass density ( $\text{kg m}^{-3}$ ), and  $t$  is time. From Eqs. 32 and 33, the common form of the governing partial differential equation for heat transfer can be obtained.

$$\frac{\partial}{\partial x} \left( k_x \frac{\partial T}{\partial x} \right) + \frac{\partial}{\partial y} \left( k_y \frac{\partial T}{\partial y} \right) + \frac{\partial}{\partial z} \left( k_z \frac{\partial T}{\partial z} \right) + Q = \rho c \frac{\partial T}{\partial t} \quad (34)$$

In a steady-state problem,  $\partial T / \partial t = 0$ . Therefore, for an isotropic material (where  $k_x = k_y = k_z$ ) under steady-state conditions, Eq. 34 reduces to

$$k \left( \frac{\partial^2 T}{\partial x^2} + \frac{\partial^2 T}{\partial y^2} + \frac{\partial^2 T}{\partial z^2} \right) + q_v = 0 \quad (35)$$

Many other problems are governed by an equation of the same form as Eq. 34, which is known as the quasi-harmonic equation. Table 1 lists different classes of problems governed by the quasi-harmonic equation.

When a steady-state condition does not exist, the temperature changes as a function of time. This is resisted by the thermal mass, which is dependent on the mass density and the specific heat of the material. In a transient thermal analysis, Eq. 30 is reformulated as

**Table 1** Classes of problem governed by the quasi-harmonic equation

Field problem	Unknown (T) (potential)	Material constant ( $K_T$ )	Load (Q)
Heat conduction	Temperature	Thermal conductivity	Internal heat generation
Diffusion	Moisture concentration	Diffusion coefficient	Moisture source
Seepage flow	Hydraulic head	Permeability	Storage
Electric conduction	Voltage	Electric conductivity	Internal current source
Electrostatics	Voltage	Permittivity	Charge density
Magnetostatics	Magnetic potential	Reluctivity	Current density
Elastic torsion	Stress function	1/shear modulus	Twice the rate of twist

$$[K_T]\{T\} + [C]\left\{\frac{dT}{dt}\right\} = \{Q(t)\} \quad (36)$$

[C] is the heat capacity matrix and is assembled from element heat capacity matrices.

$$[C] = \sum [C^e] \quad \text{where} \quad [C^e] = \int [N]^T [N] \rho c dV \quad (37)$$

In a transient analysis,  $\{T\}$  is required as a function of time when the initial temperatures are prescribed and  $\{Q(t)\}$  is a known function of time. This calculation is usually performed as a direct integration in time. At the  $n$ th instant of time, Eq. 36 is written in the form:

$$[K_T]\{T\}_n + [C]\left\{\frac{dT}{dt}\right\}_n = \{Q\}_n \quad (38)$$

Direct integration is then based on the formula:

$$[T]_{n+1} = [T]_n + \Delta t \left( (1 - \gamma) \left\{\frac{dT}{dt}\right\}_n + \gamma \left\{\frac{dT}{dt}\right\}_{n+1} \right) \quad (39)$$

where the time integration constant,  $\gamma$ , is chosen by the analyst.

## 25.5 Dynamic Analysis

### 25.5.1 Introduction

In dynamics problems, frequencies and modes of vibration and/or response to time-dependent forces are determined. This section provides an introduction to the way that a number of dynamic and vibration problems can be solved in a finite element package. These aspects are further developed in ► Chaps. 29, “Design for Impact Loads,” and ► 30, “Vibration Damping of Adhesively Bonded Joints.” The governing equation for structural dynamics in FEA is

$$[K][u] + [C][\dot{u}] + [M][\ddot{u}] = [F(t)] \quad (40)$$

where  $[K]$  is the stiffness matrix,  $[C]$  is the damping matrix, and  $[M]$  is the mass matrix.  $u$  is displacement and the load,  $F$ , is a function of time. It can be seen from this equation that the externally applied forces are resisted by the sum of three resisting forces. These are stiffness forces given by  $[K][u]$ , damping forces given by  $[C][\dot{u}]$ , and inertia forces given by  $[M][\ddot{u}]$ .

If there are no nonlinearities,  $[K]$ ,  $[C]$ , and  $[M]$  contain only constants, i.e., they are not functions of time or displacement. In general, a dynamic FEA analysis seeks to determine displacements, velocities, and accelerations as a function of time, given the load and material properties. In many cases, however, a dynamic analysis has the simpler goal of determining the frequencies and modes of vibration, and this is discussed in the next section.

## 25.5.2 Free Vibration

In free vibration, loads are either zero or constant. Constant massless loads affect natural frequencies only if they modify the stiffness of the structure. Loads associated with mass are included in  $[M]$ . All dof move in phase with each other at the same frequency. Motion can be described as displacements varying sinusoidally with time relative to a mean configuration  $[u_m]$  associated with any constant loads  $[F_c]$ . The mean configuration can be computed from a standard static analysis:

$$[u_m] = [K]^{-1}[F_c] \quad (41)$$

If  $[F_c]$  is zero, then the mean configuration is the unstressed shape. The displacement as a function of time can then be described by the following equation:

$$\{u\} = \{u_m\} + \{\bar{u}\} \sin \omega t \quad (42)$$

where  $\{\bar{u}\}$  is the vector of nodal displacement amplitudes in vibration. The governing equation for undamped free vibration can thus be derived:

$$\{\bar{u}\}([K] - \lambda[M]) = 0 \quad \text{where} \quad \lambda = \omega^2 \quad (43)$$

This is an eigenvalue problem and has the trivial solution  $\{\bar{u}\} = 0$  and nontrivial solutions equal to the number of dof. Each solution consists of an eigenvalue (in this case the square of the natural frequency of vibration,  $\omega_i^2$ ) and an associated eigenvector (in this case the mode of vibration  $\{\bar{u}\}_i$ ). The smallest nonzero value of  $\omega_i$  is the fundamental frequency of vibration. The physical interpretation of Eq. 43 is that the various vibration modes are different displacement configurations in which elastic loads are in balance with inertia loads. Unlike a static problem, no support is required to obtain a solution for an eigenvalue problem. An unsupported structure will undergo rigid body modes in which all strains and the natural frequency are zero.

Unless there is shock loading, only the lowest frequency modes are usually important in structural response, and only a selected number of solutions are generally specified by the user, regardless of the number of dof in the model. It should also be noted that lower modes will have more elements per wave and hence the discretization error will be less.

### 25.5.3 Dynamic Response Analysis

Dynamic response analysis is concerned with the response of a structure to an arbitrary time-dependent loading. For dynamic response analysis, Eq. 40 is written as

$$[K][u_n] + [C][\dot{u}_n] + [M][\ddot{u}_n] = [F(t)_n] \quad (44)$$

where  $[F_n]$  is the known time-dependent forcing function at the  $n$ th instant and the equation is solved for displacements, velocities, and accelerations corresponding to  $[F_n]$ .  $n = 1, 2, 3$ , etc. corresponds to times of  $t = 0$ ,  $t = \Delta t$ ,  $t = 2\Delta t$ , etc., where  $\Delta t$  is a time increment. After the response is calculated at instant  $n$ , the time is incremented by  $\Delta t$  and the response calculated at instant  $n + 1$ . Hence a plot of displacement, velocity, or acceleration as a function of time can be constructed.

Dynamic response analysis can be undertaken in FEA by using a modal method or by a direct integration method. The latter is so called because no transformation to a special form is required and the governing equation is solved by a step-by-step procedure in the time domain. Hence direct integration advances the solution from a known condition at time  $t$  to an unknown condition at time  $t + \Delta t$ . Two forms of direct integration are commonly encountered. In an explicit integration scheme, the solution at time  $t + \Delta t$  is obtained from a consideration of equilibrium at time  $t$ . This is most suitable for high-frequency response and shock loading in which many time increments are considered. In an implicit integration scheme, the solution at time  $t + \Delta t$  is obtained by considering equilibrium at time  $t + \Delta t$ . This is more computationally expensive as a stiffness matrix conversion is required at each time increment and is more suitable to low frequency and inertial problems.

## 25.6 Application of the Finite Element Method

The finite element modeling process has three main stages, which are termed preprocessing, processing, and post-processing.

### 25.6.1 Preprocessing

In the preprocessing stage, the geometric model is created, and material parameters, loads, boundary conditions, and analysis controls are defined. The geometric model is discretized by meshing with elements. This process results in a data file containing all the necessary information in a format required for the finite element processor. The preprocessing is increasingly being carried out by sophisticated graphical interfaces; however, the ability to create or modify the data files using text editors is usually retained. Many of the commercial graphical preprocessors are capable of preparing data files in a format suitable for a number of different processors.



A number of questions must be asked before modeling commences. The most important of these are probably: Is finite element modeling necessary? What information is required from the analysis and to what degree of accuracy? Finite element modeling can be an expensive activity, and if an effective analytical solution has already been derived for the problem, then this will almost inevitably be a cheaper option. Analytical models for adhesively bonded joints are discussed in ► [Chap. 24, “Analytical Approach.”](#) Experimental methods should also be considered. A clear understanding of what is required from the analysis, and to what degree of accuracy, is needed before the model can be properly planned. The finite element method is always an approximation, and one of the most important skills of the modeler is determining how to create the simplest model that provides the required answer to the required degree of accuracy. A good principle is to start with an oversimple model and to gradually refine this model until sufficient accuracy has been achieved. Some analytical or experimental validation of the simple model provides confidence in the modeling approach and can be used to justify further extension of the analysis. Once the nature of the problem has been understood and simplified to a form suitable for finite element analysis, the finite element model can be planned. Key decisions to be made at this stage are the type of analysis, the selection of element type(s), the meshing strategy, and the load and boundary condition simulation.

Most finite element packages have an element library of hundreds of different element types. These can be divided into three geometric types, namely, structural elements (e.g., bar, beam, shell elements), planar elements (e.g., plane stress, plane strain, and axisymmetric elements), and solid elements (e.g., brick, wedge, tetrahedron). A further subdivision is by the order of the element. Linear elements are only capable of modeling straight boundaries. Higher order elements (e.g., quadratic and cubic) are characterized by mid-element nodes and can provide a more accurate interpolation of field variation within the element. These elements are more computationally expensive, and a compromise between the number and order of elements should be considered. Isoparametric elements use the same parameters to define geometry and field variation and are capable of representing curved sides and surfaces, as discussed in Sect. 26.2.3.

Models can be constructed using a number of different types of elements as long as there is acceptable element connectivity. Particular attention must be paid to the dof at common nodes and interpolation functions along common edges and surfaces. The network of elements and nodes that discretize the model is called the mesh. Mesh density refers to the number of elements in a given region and is increased to give greater accuracy in critical locations. In noncritical regions and where there are low stress gradients, it is more efficient to use a low mesh density. Transition zones are used to provide a smooth transition from regions of high and low mesh density. Sharp changes in mesh density may result in excessive element distortion and should be avoided in critical areas. A careful choice of geometric entities will greatly simplify the mesh generation process.

The process of modifying the mesh to improve the accuracy of the solution is termed mesh refinement. Ideally, the results should converge to an exact solution as the mesh is refined. Mesh generation is often the most time-consuming activity for

the modeler, and care must be taken to ensure that the mesh contains enough elements to produce results of sufficient accuracy while avoiding an excessive number of elements that will result in large files and long process times. Efficient meshes become increasingly important in three-dimensional (3D) modeling and nonlinear analysis. In the early days, finite element meshes were created by manually editing an input text file, which was labor intensive and required detailed planning. Nowadays, meshes are usually created using semiautomatic methods via graphical interfaces. In semiautomatic methods, the user defines the boundary discretization, and computer algorithms are used to generate the mesh. Fully automatic methods are also available that can be used for self-adaptive mesh refinement. Examples of meshing a 3D bracket using different elements are shown in Fig. 3. Before applying the finite element mesh, the desired position for nodes at the boundaries of the bracket were specified, a process sometimes called seeding. The element type was then specified and an automatic meshing algorithm used to create the final mesh. Hexahedral meshes can generally be generated for regular shapes using automatic mesher, while tetrahedral meshes may have to be used for more complex shapes. Examples of meshes for single lap joints are shown in Fig. 4. The free mesh was generated using a medial axis mesher, and the structured mesh was generated by an advancing front mesher. It can be seen that the former is useful for meshing the complex geometry involved in modeling the adhesive spew fillet; however, the latter results in a more controlled mesh when the geometry is simpler.

In most structural applications, maximum stresses occur at a boundary. It is important, therefore, to ensure that the mesh conforms closely to the boundaries of the model. Finite element models are generally stiffer than the continuous structure. This can be minimized by ensuring that elements remain close to being square. In general, the performance of elements will deteriorate as they become distorted or reach high aspect ratios. Commercial software vendors generally provide indicators regarding the limits of operation of their element formulations and the means of checking for excessive distortion or element aspect ratios in the model.

An element will have both geometric and material properties. Spatially, an element is defined by its nodes; however, additional geometric input is usually

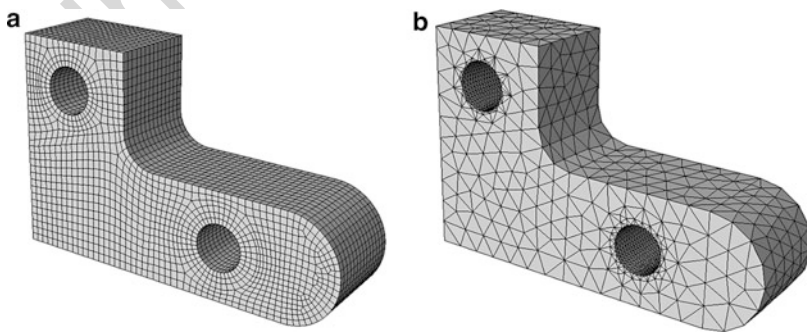


**Fig. 3** An example of the application of different elements to a problem. (a) Hexahedral element mesh, (b) tetrahedral element mesh

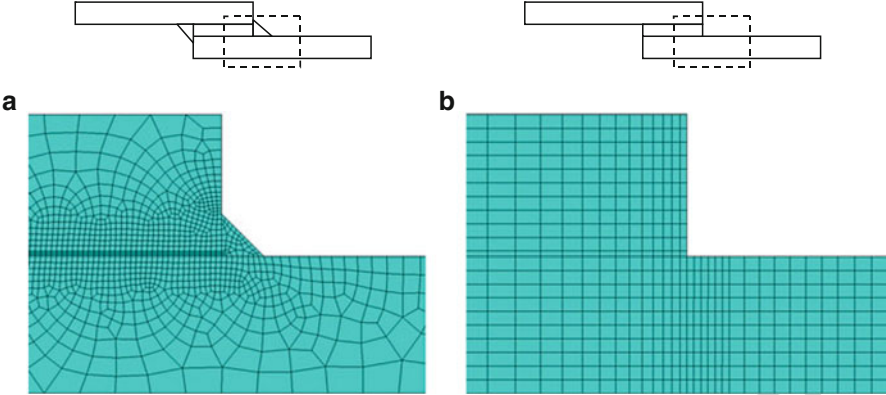


**Fig. 4** Examples of finite element meshes for a single lap joint based using different meshing algorithms. **(a)** a free mesh created using a medial axis mesher, **(b)** a structured mesh created using an advancing front mesher

required for line and surface elements. For structural analysis, the minimum material property is the modulus of elasticity. In most cases, Poisson’s ratio or shear modulus must also be specified. If an orthotropic material is used, then the orientation of the material must be specified as well as the elastic constants relative to each principal axis. If post-yield behavior is to be modeled, then an elastoplastic material model must be applied and the yield and hardening behavior defined. Constitutive adhesive and sealant models are discussed in more detail in ► [Chap. 23, “Constitutive Adhesive and Sealant Models.”](#) Additional material properties will also be required for dynamic or thermal analysis.

Various forms of symmetry are often present in a structure that can be used to reduce the size of the FEA model, thereby reducing modeling and processing time. Total reflective symmetry exists when a plane exists in the structure such that half the structure and loading on one side of the plane is the mirror image of the structure and loading on the other side of the plane. As each half of the model will behave in an identical manner, only half of the structure needs to be analyzed. The condition of symmetry is represented in the model by the application of boundary conditions along the plane of symmetry. Some structures may have more than one plane of symmetry in which case the size of the model can be further reduced. In the case of axisymmetrical structures, all planes intersecting a single axis are planes of symmetry, and in this case, a 3D structure can be accurately modeled with a 2D model. Other conditions such as geometric and/or loading antisymmetry can also be used to reduce the model size in some cases. A careful consideration of the mechanics of the problem should be used to apply the correct boundary conditions in these cases.

The simulation of boundary conditions and other forms of restraint requires an understanding of the mechanics of the problem. As with other elements of the modeling procedure, the selection of boundary conditions will involve some simplification of the problem, which must be justifiable. The choice of boundary conditions defines the extent of the model. In some cases, more than one

constraining condition should be analyzed to provide upper and lower boundary values for the analysis. An important consideration when applying constraints is to ensure that rigid body motion is prevented. If not, the system stiffness matrix will be singular, and a fatal error will occur in the processing stage. Constraint equations can be used to further define the boundary conditions. For example, constraint equations can be used to ensure that a certain plane remains plane under deformation, while it can otherwise translate or rotate in space. Similarly, a line can be constrained to remain straight under load.

In most software packages, loads can be applied to nodes, elements, or geometric features. However, in all cases, the loads will be converted into equivalent nodal loads for the analysis. If stresses close to the point of loading are not critical, then the high stress concentrations under a point load can be ignored, as according to Saint-Venant's Principle, this will not affect the stress distribution in other parts of the structure. If the area of loading is important, then attention must be paid to the method of load application to ensure that the nodal loading is representative of the actual loading. One method to reduce stress concentrations close to the loading point is to use additional elements to transfer the loads. However, if the actual point of contact is important, a contact analysis may be required. Another way to apply a load is by the specification of a prescribed displacement.

Once a finite element model is set up in the preprocessing stage, it is sent to a finite element processor, generally referred to as solver, for solution.

## 25.6.2 Processing

In the processing stage, the solver solves the problem and creates output files with the results of the analysis process such as nodal deflections, element stresses, etc. This normally involves the solution of many thousands of equations and can involve the creation of large temporary files. Processing is generally controlled by the software package. With most packages, the progress of the analysis can be monitored. This is particularly useful in nonlinear analysis as the analysis time tends to be longer and the user can observe progress toward convergence of the solution against a selected convergence criterion. Both implicit and explicit finite element schemes are available in commercial finite element solvers. Explicit methods are used for the solution of large deformations and short duration events such as crash, blast, or impact. Explicit methods are conditionally stable, while the implicit methods are unconditionally stable.

With the advent of multicore processors and HPCs, a solution can be solved using multiple processor cores. This decreases the time required to solve a problem by dividing the problem domain into several smaller domains and sending each smaller domain to a single processor core. However, in terms of solution time, all problems do not scale linearly when solved using multiple processor cores. The communication overhead due to data transfer between the solution domains may in fact increase the solution time in some cases. Extra software licenses are generally required for employing multiple cores for solution of a problem.

25.6.3 Post-processing

The output from the processor enables the user to analyze the results from the analysis in text and/or graphical form. This is termed post-processing. The user can view an analysis log giving details of the analysis process and search for status messages created by the software to indicate possible errors in the analysis. With the tendency toward larger models, sifting through large text files can be laborious, and it is now more common to view results in graphical mode. However, some output in text format is often required, and this can usually be controlled via the graphical interface.

Graphic postprocessors are capable of presenting results in many different formats. One of the most useful plots to look at initially is the deformed mesh. Any major errors should be obvious from the deformed shape. If the scale of the deformation is being assessed from this plot, the magnification factor must be set to 1. Contour plots can then be used to show the distribution of stresses, strains, displacements, or other parameters through the structure. The deformation of a single lap joint with aluminum adherends after application of a 6 kN load is shown in Fig. 5. Joint displacement is illustrated on the deformed shape in the form of a displacement contour plot. Results in various directions can usually be viewed as well as a number of calculated parameters such as principal and von Mises equivalent stresses and strain energy density. These should be viewed “unsmoothed” in the first instance in order to identify areas where further mesh refinement is required.

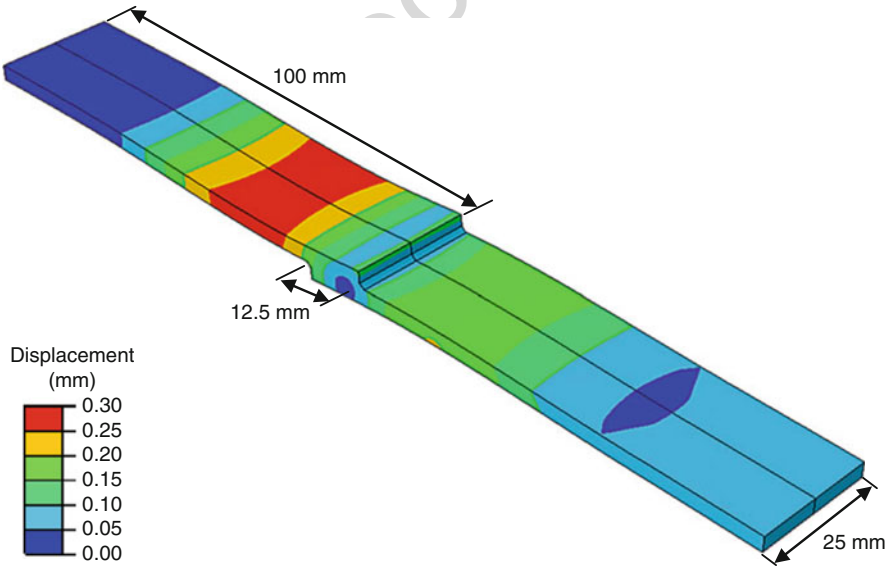


**Fig. 5** Displacement contours and deformation of a single lap joint with aluminum adherends after application of a 6 kN tensile load

The post-processing software may also be used to check the integrity of the model, e.g., by showing information on element distortion or negative pivot errors. Text output files should be searched for warnings and errors. Problems with memory allocation may also be identified here. Another useful check that can be made is to compare applied loads with reactions to ensure that equilibrium is maintained in the principal directions.

## 25.7 Application of FEA to Adhesive Joints

### 25.7.1 General Considerations

A number of analytical methods for the analysis of adhesive joints are available (Volkersen 1938; Goland and Reissner 1944; Demarkles 1955; Adams and Peppiatt 1973), but these methods are limited in their applicability by joint geometry and stress conditions. The analytical methods may provide a good overall measure of joint stress levels but are not able to provide detailed information in the regions of high stresses where failure initiation occurs. Analytical models are described in detail in ► Chap. 24, “Analytical Approach.” Finite element modeling has been successfully used to model adhesive joints of various configurations and enables a detailed analysis of the stress state developing in a joint under complex loading conditions. However, the nature and geometry of adhesive joints presents some unique challenges to finite element modeling. Theoretical stress singularities are present in many adhesive joint configurations, especially in joints with square or sharp edge adherends, as illustrated in Fig. 6.

Stress concentrations tend to exist at the ends of overlaps, and refined meshes are required in regions of high stress gradient. The thickness of the adhesive layer is usually small compared to the overall geometry of the joint; thus, a small element size is required in the adhesive layer as compared to the adherends. If the same element size is used throughout the joint, the problem becomes too cumbersome computationally, and a suitable mesh that transitions in size from the adhesive layer to the adherends is required. An example of mesh transition in a plate is shown in Fig. 7. The size of elements gradually increases from the region of fine mesh to the region of coarse mesh in the transition region. Such transitions enable accuracy to be retained in critical regions while reducing the overall number of elements in the model. However, it should be noted that there is usually element distortion in the transition regions that may affect accuracy.

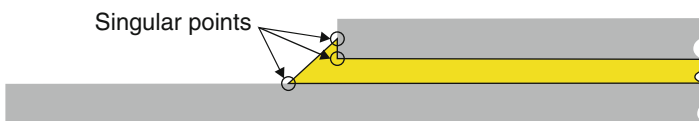


**Fig. 6** Points of theoretical stress singularity in adhesive joints

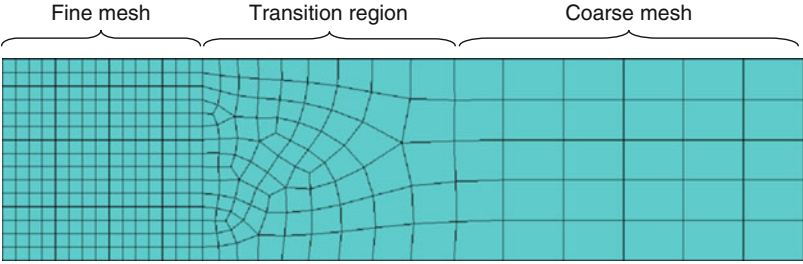


**Fig. 7** Transition mesh in a 2D plate



**Fig. 8** Rotation of overlap after application of load in a single lap joint

Adhesive and adherend may exhibit considerable plasticity before failure and thus require nonlinear material models. In single lap joints, rotation of adherends occurs during loading, as illustrated in Fig. 8, and geometrically nonlinear analysis is required to determine the correct stress state.

Adhesive fillets are formed at the ends of overlaps and need to be included in the analysis. Other factors that may need to be considered in the FEA include anisotropic behavior of adhesives and adherends and the synergetic effects of various factors such as temperature, moisture, stress, etc., which may lead to complex, non-intuitive behavior. Informed decisions regarding these factors are needed, while developing a finite element model and necessary modifications needs to be made to finite element models based on the required results, available time, and available computational resources. Adhesive joints are generally analyzed to determine stresses resulting from different types of loadings or to determine the residual strength of joints by carrying out a failure analysis.

### 25.7.2 Stress Analysis

This type of analysis is based on the study of stresses and strains in adhesive joints. By considering the stress state in single lap joints, which are commonly used in industry and have a simple geometry, it can be seen that a complex state of stress is present in adhesive joints. When loaded in tension, the shear stresses in the adhesive layer in single lap joints have a nonuniform distribution owing to the differential straining of the adherends. This shear lag effect, as shown in Fig. 9, causes maximum stresses at the ends of the overlap.

The second factor influencing the stress state in a single lap joint is the rotation of the adherends due to unsymmetric loading. Peel stresses are generated in the adhesive layer, which are maximum at the overlap edges. Thus, when the combined state of stress is considered for a single lap joint, the highest stresses occur at the





**Fig. 9** Shear lag effect in adhesive joint

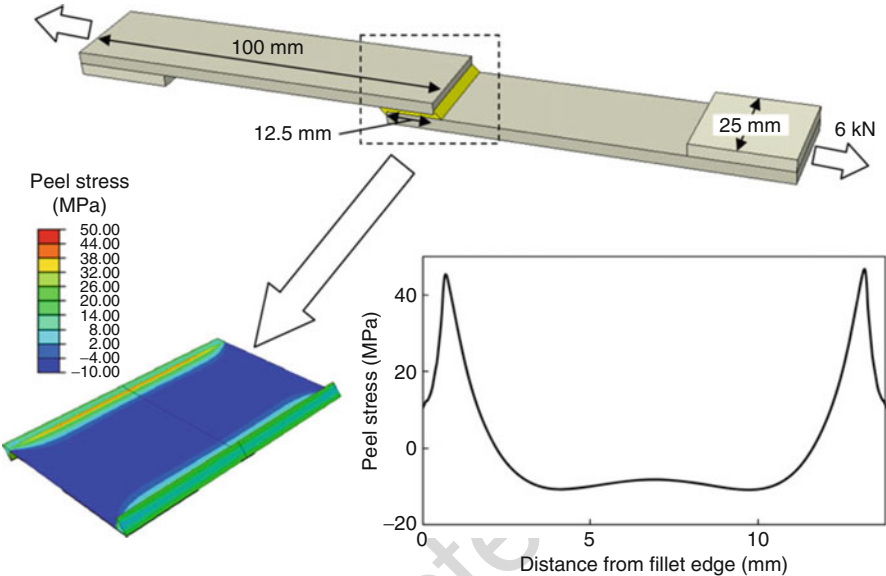


**Fig. 10** Contour plot of peel stresses in adhesive layer and plot of peel stress variation along the overlap length in the middle of the adhesive layer for an aluminum-epoxy single lap joint

overlap end regions. An example of the FEA-determined stress distribution in the adhesive layer of a single lap joint is shown in Fig. 10. The maximum peel stresses may be seen to occur at the overlap ends. Stress states in other types of joints may be more complex depending on joint geometry and loading.

Bulk tensile testing has shown that adhesives generally exhibit plasticity, and, hence, nonlinear material properties are required to model their behavior over the full load range. Nonlinear properties may also be required for adherends. Thus, a combination of elastoplastic material models may be used to predict the behavior of adhesive joints under load. The definition of the yield surface is important when using elastoplastic material models. The von Mises yield surface is commonly used for the analysis of metals, which assumes that the yield behavior is independent of hydrostatic stress. As a result, the yield surface is identical in tension and compression. However, the yield behavior of polymers has been shown to exhibit hydrostatic stress dependence (Ward and Sweeney 2004) as the yielding starts earlier in tension than in compression. Thus, a yield criterion which includes hydrostatic stress effects should be used to determine the yield surface. Various yield criteria with hydrostatic stress dependence such as Drucker-Prager, Mohr-Coulomb, and modified Drucker-Prager/cap plasticity model have been implemented in commercially available finite element software.



As most adhesives are polymeric materials, they may exhibit a time-dependent response to loading. Hence under certain conditions, a viscoelastic or viscoelastic-plastic material model may be required to determine the time-dependent response of the adhesive to loading. Constitutive models for adhesives are discussed in more detail in ► Chap. 23, “Constitutive Adhesive and Sealant Models.”

An analyst may use a suitable failure criterion with stress analysis to determine if the stresses or strains obtained from the finite element model are within permissible limits. Various failure criteria have been used, in combination with elastoplastic material models, to predict adhesive joint strength. These include maximum stress, maximum strain, plastic yielding, maximum principal stress or strain, and plastic energy density. An example of plastic strains developing in an adhesive joint can be seen in Fig. 11. The zone of plastic deformation initially appears in the middle of the adhesive layer and expands toward the edges of the joint as load increases, as indicated in the figure, before growing toward the overlap center.

Maximum stress- and strain-based failure criteria were used by Harris and Adams (1984) to predict the failure of single lap joints. A nonlinear finite element analysis with an elastoplastic material model for the adhesive and adherends was carried out. The selection of stress- or strain-based failure criterion was based on the results of uniaxial tensile test results. For an un-toughened adhesive, a brittle failure was observed and a maximum stress criterion was used, while for a toughened adhesive, failure was ductile and a maximum strain-based criterion was used. However, these

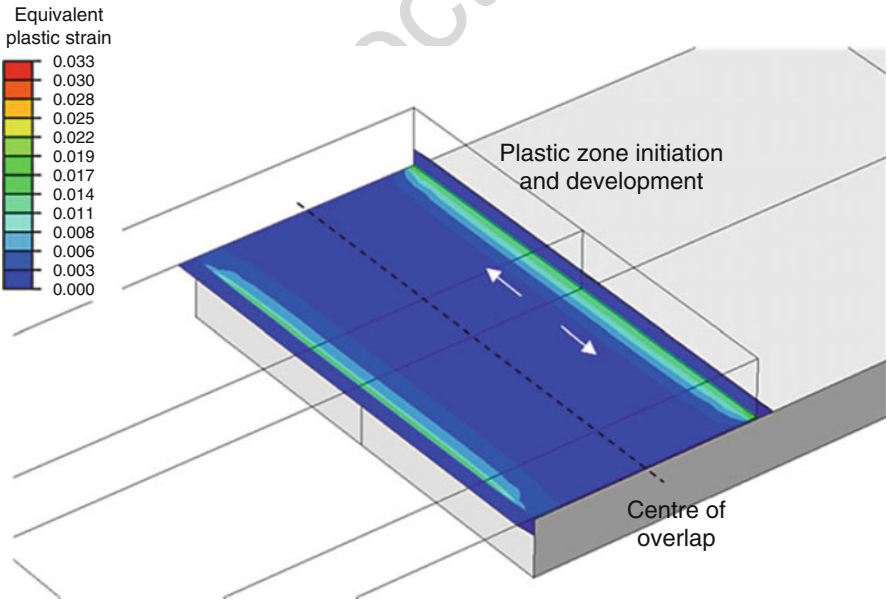


**Fig. 11** Equivalent plastic strain in adhesive layer of a single lap joint subjected to tensile loading using an elastoplastic material model

criteria are difficult to implement when highly localized stress concentrations or stress singularities exist in an adhesive joint.

In order to avoid the problems of localized stress effects in adhesive joint strength prediction, Crocombe (1989) used a global yielding criterion. Failure of the joint was defined when a path of adhesive along the overlap region started deforming plastically and no further increase in applied load was observed. This criterion was used to study failure in single lap, double lap, and shear test joints, and a good correlation between experimental and numerical results was reported. Failure in the adhesive layer was defined when the overall region of the adhesive layer became plastic and was not able to support any load. However, this type of failure criterion may not be applicable in joints where localized failure may occur. Dorn and Liu (1993) used an accumulative plastic strain-based criterion for single lap joint strength prediction. A critical region was identified, and the maximum accumulative effective plastic strain in the critical region was used as a parameter for strength prediction. Another approach is to use a hybrid method, for example, a global finite element model was used with a localized analytical solution for a circular crack which was proposed by Wahab et al. (2004).

The strength-based failure methods are relatively simple to use; however, they are sensitive to mesh refinement, and an overall mesh convergence study should be carried out to obtain reliable results. In the case of stress singularities, the selection of failure criteria, based on localized values, becomes difficult. Although the concept of selection of a failure parameter at a characteristic length from the singularity may be used; the selection of an appropriate characteristic length becomes important in this case. Alternatives are to average over an area or to define failure when a value is exceeded in all elements in a defined area. Wahab et al. (2001a) compared a wide range of strength of materials-based failure criteria using both the characteristic length and averaging methods.

### 25.7.3 Failure Analysis

Failure in an adhesive joint may occur in the adhesive layer, in the adherends, or at the interface of adhesive and adherend. Failure in the adhesive layer is generally referred to as cohesive failure, while failure in the region of the adherend-adhesive interface (or interphase) is known as interfacial failure. Both types of failures may be incorporated in a finite element model. Failure analysis differs from the stress analysis approach described above in that a suitable failure criterion is provided as part of the material definition in the finite element model. Both failure initiation and crack propagation may be included in a finite element model. In failure initiation models, a state variable is used to indicate if a material has failed; however, no change in material stiffness is considered. In models with crack propagation criteria, the elements satisfying the failure criteria are considered to have no stiffness and may be removed from the analysis. This is in contrast to stress analysis where the elements surpassing a failure criterion remain part of the analysis and continue to contribute to the overall stiffness of the material. Failure criteria may be based on stress or strain, fracture mechanics, or continuum damage models. Stress- and strain-

based failure criteria were discussed in the previous section, and continuum damage models are discussed in the next section.

Fracture mechanics methods assume there is an existing flaw or crack in the material, and that crack growth will occur when a selected fracture criterion is satisfied. Fracture mechanics considers that a crack may be loaded in three different ways: (i) Mode I where the load is applied normal to the crack plane, (ii) Mode II where the load acts to produce in-plan shear, and (iii) Mode III where load generates an out-of-plane shear. The fracture criterion may be energy based, such as the critical strain energy release rate,  $G_c$ , proposed by Griffith (1920), or stress based, such as the critical stress intensity factor,  $K_{Ic}$ , given by Irwin (1957). In recent years, the J-integral approach has been used to determine the strain energy release rate through the use of a path-independent integral around the crack tip. In linear elastic materials, J is equal to  $G$ ; in nonlinear elastic materials, J represents the nonlinear strain energy release rate. The energy-based fracture mechanics failure criteria dictate that failure will occur when the strain energy release rate equals a critical value, the fracture energy, which is ideally independent of the size and geometry of the structure. In the stress-based approach, the stress intensity factor can be computed at the crack tip and compared to the critical value of stress intensity factor, the fracture toughness. Most of the commercially available finite element software are able to determine strain energy release rate and stress intensity factors. For nonlinear materials, the J-integral may be used.

Wahab et al. (2001a) compared  $G$  and  $J$  as failure criteria for predicting fatigue threshold in bonded composite joints with various strength-based criteria. A principal stress-based criterion provided good threshold predictions for small plastic deformations. From the elastic and elastoplastic fracture parameters, the J-integral was shown to correlate well with the threshold load of different joints. In this work, the virtual crack closure technique (VCCT) was used to determine  $G$ . This is based on Irwin's crack closure integral method, which assumes that the energy absorbed upon crack growth is equal to the work required to close the crack. In an attempt to overcome the limitations of linear elastic fracture mechanics, Stein et al. (2015) presented a material model for brittle failure in adhesive lap joints, which is based on the concepts of finite fracture mechanics. The proposed material model is based on tensile strength and fracture toughness of adhesive in Mode I. A number of adhesive lap joint configurations were used for the validation of the proposed material model. The stress predictions of the proposed material model, when compared to a cohesive zone element-based finite element adhesive joint model, were promising. The cohesive zone elements are discussed in the next section.

One of the limitations of the fracture mechanics methods is that they require the existence of a pre-crack to determine the strain energy release rate (or other fracture mechanics parameter). Fracture mechanics approaches may require several finite element analyses to determine fracture energies at different crack lengths. Design of the mesh for fracture mechanics problems also requires special consideration. A "spider web" mesh configuration is generally favored in fracture mechanics problems. This consists of concentric circles, which are focused at the crack tip. At the crack tip, special elements may be used that are capable of representing the

theoretical singularity. These are generally known as crack tip or singularity elements. An example finite element mesh for fracture mechanics-based failure models is shown in Fig. 12.

**25.7.4 Advanced Analysis Methods**

Advanced analysis techniques include methods that cannot only predict failure but can also predict damage evolution in a material. A specimen is said to be damaged when a large number of microcracks are randomly scattered over a large part of the volume such that the volume partially loses the ability to transfer load and the fracture strength is reduced. A typical stress-strain diagram with damage is shown in Fig. 13. A material model with elastic and plastic material definitions would follow the “abcd” curve, while a damage- and failure-based model would follow the “abcd” curve where material stiffness starts to degrade after point “c” and complete failure occurs at point “d.”

A method of predicting failure based on the concepts of stress and fracture mechanics is the cohesive zone method. The cohesive zone model has been used increasingly in recent years to simulate crack initiation, propagation, and failure. The cohesive zone model allows multiple cracks to be modeled, and the direction of crack propagation need not be known in advance; however, cohesive zone elements need to be present at all possible crack paths. Cohesive zone models follow a traction-separation constitutive law to predict failure initiation, damage, and failure. Several shapes for the traction-separation law have been presented in the literature, with the bilinear, exponential, and trapezoidal shapes, as shown in Fig. 14, being the most commonly used for strength prediction.

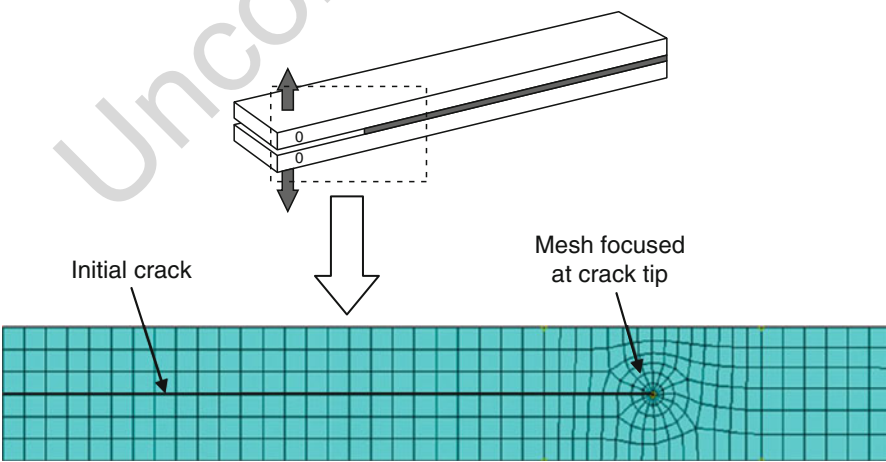


**Fig. 12** Finite element mesh for a fracture mechanics-based failure model

**Fig. 13** Typical uniaxial stress-strain response of a ductile material

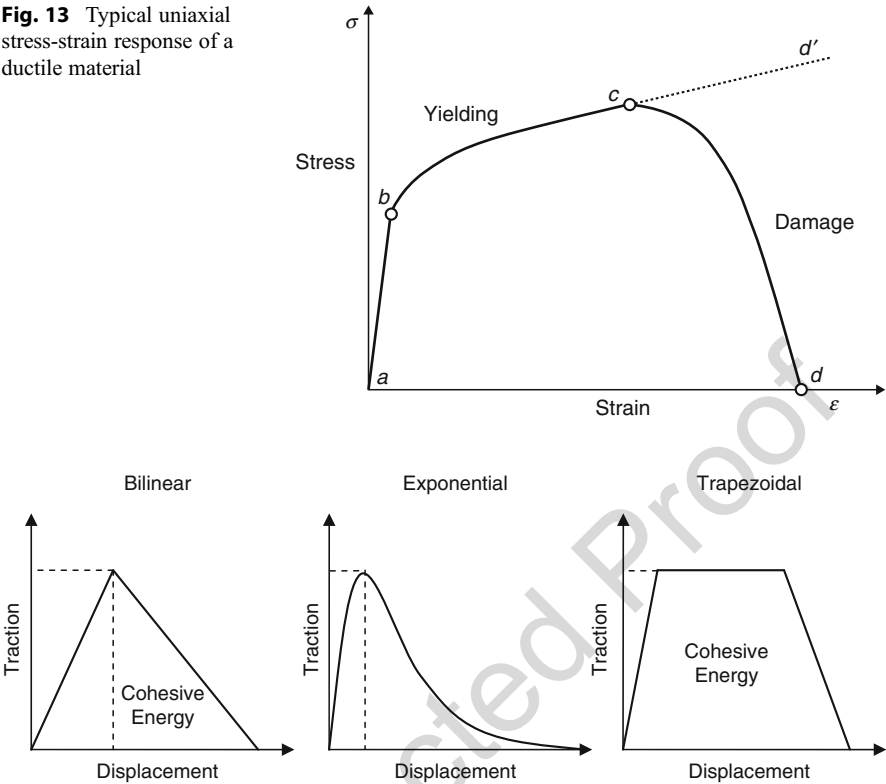


**Fig. 14** Different types of cohesive zone damage model

The shape of the traction-separation law is difficult to determine from experimental methods and is often assumed or simplified. The effect of the shape of traction-separation law is dependent on the nature of the problem including specimen geometry and material behavior. The shape of the traction-separation law also influences the numerical performance of the solution, and more convergence difficulties have been observed when using trapezoidal than bilinear traction-separation laws in a finite element analysis. Thus, the selection of cohesive zone law should be based on all the mentioned factors. Generally, a trapezoidal traction-separation curve is considered more suitable for ductile materials, while a bilinear cohesive zone law is commonly used for brittle and composite materials. In a bilinear traction-separation law, the initial response of the cohesive zone is elastic until reaching a critical traction. Once the critical traction is reached, stiffness degradation starts and continues until it reaches zero and failure occurs. The area under the traction-separation curve is equal to the fracture toughness of the material and is known as the cohesive energy,  $G_{coh}$ .

Several methods have been suggested for calibration of the traction-separation laws; however, a generally accepted method is still required. The method used by

Liljedahl et al. (2007) was to obtain the cohesive zone model parameters using a combination of experimental and numerical methods. A mixed mode flexure (MMF) specimen was tested to failure under three-point bending conditions. The experimental results, along with a fracture mechanics-based finite element model, were used to determine the fracture energy of the adhesive. The experimentally determined fracture energy was then used in a cohesive zone model and the optimum value of tripping traction determined by fitting to the MMF data. The cohesive zone model parameters obtained in this manner were then used to predict the damage and failure in single lap joints. The methodology provides a set of cohesive zone model parameters that are independent of joint geometry. Desai et al. (2016) used a J-integral-based approach where J-integral was determined from the experimental load-displacement curve of a DCB adhesive specimen and the parameters of the cohesive law were determined. The experiments were conducted at two loading rates and for different thicknesses of the adhesive layer. It was shown that the cohesive zone law parameters determined by this method were not unique for a particular type of adhesive and were sensitive to the loading rate and thickness of the adhesive layer. A few researchers have successfully used inverse methods to determine a unique set of cohesive law parameters (Azevedo et al. 2015; Desai et al. 2016). In this approach, the experimentally determined load-displacement curve and the load-displacement curve obtained from a cohesive zone-based finite element model are compared and the difference between the two curves is minimized by changing the values of the cohesive law parameters. Although this method can provide a unique set of parameters for the cohesive law, it is computationally expensive, as many simulation runs are needed to find the best fit of the experimental load-displacement curve.

One of the main limitations of the cohesive zone model is that cohesive elements should be present on the crack path. Although several layers of cohesive elements may be introduced in a structure, it is not feasible to introduce cohesive elements between every field element, even in a moderate size mesh. The method is suitable for interfacial failure or crack representation when the bulk material failure, based on micro-mechanics, does not affect fracture. An example of the use of cohesive zone elements in a single lap joint is shown in Fig. 15. A layer of cohesive elements is embedded at the experimentally observed crack path. After the application of a tensile load, the cohesive zone elements started to show damage, which is represented by a damage variable. The damage variable can have values between zero and one where zero indicates no damage and one represents fully damaged material.

Continuum damage models are able to predict damage and failure in a ductile material. A damage variable is used in continuum damage models to determine the degradation in material stiffness. The damage variables used are of two types; the first type can predict the value of damage but does not characterize the damage itself, such as damage equivalent stress. The second type of damage variable is linked to some physical definition of damage such as porosity or relative area of micro-cavities (Voyiadajis and Kattan 2005). This type of variable is based on macroscopic material properties, and its evolution is governed by a state equation. If several

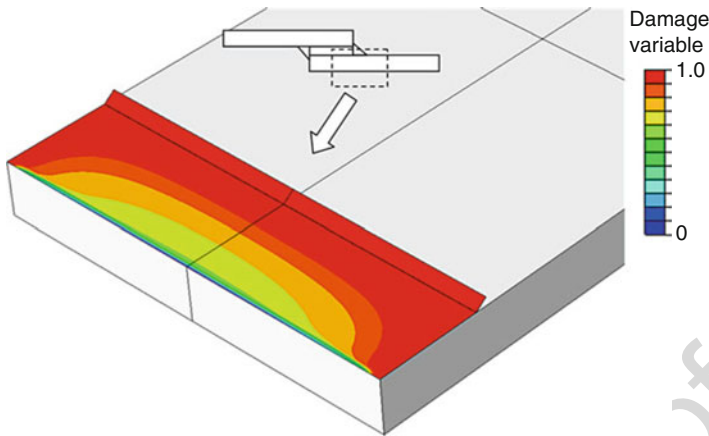


**Fig. 15** Adhesive layer of a single lap joint, modeled using cohesive zone elements, after application of tensile load. A damage variable with values between zero and one represents the amount of damage: zero meaning no damage and one meaning fully damaged

damage mechanisms occur in a material, each of them may be represented by an independent damage variable.

A general framework for damage models was provided by Lemaitre and Desmorat (2005). It consists of the definition of variables that define the state of corresponding material mechanisms, known as state variables. The damage model framework also includes the definition of state laws and definition of the laws of evolution of the state variables. The Gurson model is one of the models based upon a continuum damage framework that has been used to determine the strength of polymers. A comparison of continuum damage and fracture mechanics models for fatigue threshold prediction, when applied to composite double lap and lap strap joints, showed slightly better results with the continuum damage model (Abdel Wahab et al. 2001c).

Adhesively bonded joints are subjected to several environmental factors including temperature, moisture, and ultraviolet light, which affect their long-term performance. A finite element-based multi-physics analysis provides a convenient method for analyzing the effects of not only individual factors but also their combined effects on joints. Moisture is known to degrade the performance of adhesive joints over time, and the diffusion of moisture in adhesive joints has been determined using the finite element method (Abdel Wahab et al. 2001b). Coupled diffusion-stress FEA combined with the cohesive zone method has been used to predict the failure of bonded joints subjected to environmental aging (Loh et al. 2003; Liljedahl et al. 2007). The distribution of normalized moisture concentration in the adhesive layer of a single lap joint after moisture conditioning in water at 50 °C for 6 months is shown in Fig. 16. The joint has non-absorbing adherends, and moisture is only diffusing through the exposed adhesive surfaces. It can be seen that the center of the adhesive layer has very low moisture concentration. Recent advances in multi-



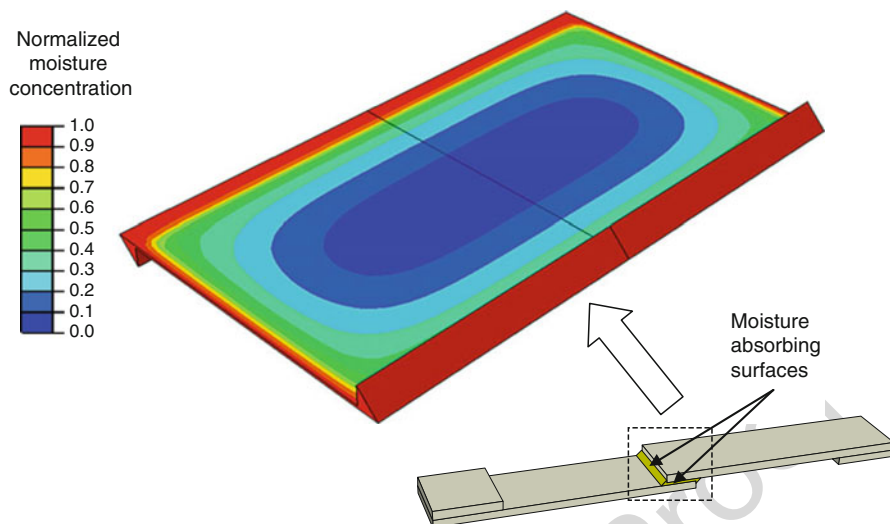


**Fig. 16** Normalized moisture concentration in the adhesive layer of a single lap joint when conditioned in water at 50 °C for 6 months

physics hygro-mechanical analysis are focused on developing methodologies that can predict the moisture distribution in an adhesive joint under varying humidity conditions (Mubashar et al. 2009) and thus enable the development of joint durability tools that can be used at the design stage to predict performance under realistic in-service conditions. This subject is further developed in ► [Chap. 31, “Effect of Water and Mechanical Stress on Durability.”](#)

Another important characteristic of adhesives is their time-dependent response to loads. Adhesives may exhibit viscoelastic or visco-plastic material behavior, such as creep and relaxation, resulting in time-dependent stresses and strains. In adhesives with a high glass transition temperature relative to the operating temperature, it may be acceptable to model the adhesive with a time-independent material model. However, as temperature, absorbed moisture, stress level, and time under load increase, there is an increased likelihood of errors in using such a model. Selection of a time-dependent material model will depend on a number of factors including the polymer type and the stress state. Adhesives generally show linear viscoelastic behavior at low stress conditions and a nonlinear viscoelastic or visco-plastic response at higher stresses. A number of commercially available FEA products have some form of standard linear solid viscoelasticity model implemented in the form of Prony series. Nonlinear viscoelastic material models are becoming available in commercial finite element software and can now be used without writing a user material subroutine. Adhesive models that include viscoelastic effects are discussed in ► [Chap. 24, “Analytical Approach.”](#) Constitutive adhesive and sealant models and creep are detailed in ► [Chap. 36, “Storage of Adhesives.”](#)

Finite element analysis may also be used to determine the response of adhesive joints under impact loading. Adhesives generally exhibit strain rate dependent



material properties under impact conditions. The solution of impact problems is difficult to obtain from closed form solutions, and the FEM is an excellent tool to solve such problems. Explicit finite element solvers can easily solve large deformation problems and dynamic events where inertia of the structure is of significant importance. ► Chap. 29, “Design for Impact Loads.” treats this subject.

---

## 25.8 Summary and Conclusions

The finite element method provides a powerful tool for solving problems that are difficult to solve using closed form solutions. Recent developments in the computer industry and the commercially available finite element codes have made it possible to apply the method to a vast number of application areas. Multi-physics problems can be solved to determine the effects of different physics. Another important development is the application of finite element analysis to damage and failure modeling. The method is general in nature and may be applied to complex geometries and loading conditions. The method is based on discretizing a domain then solving a set of equations to determine the response of the continuum. The method can be used to solve nonlinear problems which may involve material, geometric, or contact nonlinearity. In case of nonlinear problems, iterative methods are commonly used to solve the system equations. The finite element method has been developed for application in field problems such as thermal analysis where heat conduction, convection, and radiation problems may be solved. Another application of finite element method is in dynamic analysis. Dynamic problems such as free vibrations or full dynamic response of a system may be solved using commercially available finite element software.

Due to the complex behavior of adhesive joints and the effects of environmental factors on their performance, finite element analysis has been proven to be one of the best tools for adhesive joint design and analysis. The geometry and loading of adhesive joints may require special considerations in terms of model development and meshing. Nonlinear stress analysis methods have been successfully used to analyze the behavior of various types of adhesive joints under loading, and a number of stress- or strain-based criteria have been proposed to determine the residual strength of an adhesive joint. Failure analysis methods based on fracture mechanics concepts have also been applied to adhesive joints with varying degrees of success, and, more recently, the cohesive zone method has been successfully applied to predict damage and failure in adhesive joints of different types. Continuum damage models, which are capable of predicting damage as well as failure, have also seen some degree of success when applied to adhesive joints. The effects of environmental degradation, mainly those of moisture and temperature, may be included in multi-physics FEA to determine the durability of adhesive joints. The time-dependent viscoelastic behavior of adhesives may also be included in durability studies to determine the time-dependent response of adhesives to applied loads. Finally, the response of adhesive joints under impact loading may be studied using explicit finite element codes.

The rapid development in computing power and FEA codes, together with increased automation of the technique, will see the finite element method become more mainstream, becoming an important part of the design and analysis procedure. Highly complex problems can now be solved easily using high performance computing clusters, and as these high performance clusters become available for desktop systems, the complexity of problems being solved will continue to increase. At present, the specific complexities of analyzing adhesively bonded joints using FEA means that it is still mainly the domain of specialists. However, in the future, it is envisaged that routines enabling the nonspecialist to use the finite element method to accurately solve defined adhesive joint problems will become more widely available.

## References

- Abdel Wahab MM, Ashcroft IA et al (2001a) *Compos Part A* 32:59
- Abdel Wahab MM, Ashcroft IA et al (2001b) *J Adhes* 77:43
- Abdel Wahab MM, Ashcroft IA et al (2001c) *J Adhes Sci Technol* 15:763
- Adams RD, Peppiatt NA (1973) *J Strain Anal* 8:134
- Azevedo JCS, Campilho RDSG et al (2015) *Theor Appl Fract Mech* 80(Part B):143
- Barenblatt GI (1962) *Adv Appl Mech* 7:55
- Champion ER, Ensinger JM (1988) *Finite element analysis with personal computers*. Marcel Dekker, New York
- Clough RW (1960) Second ASCE conference on electronic computation, Pittsburgh
- Cook RD (1995) *Finite element modeling for stress analysis*. Wiley, New York
- Crocombe AD (1989) *Int J Adhes Adhes* 9:145
- Demarkles LR (1955) Tech Note 3413, Nat. Advisory Committee, Aeronautics, Washington, D.C
- Desai CK, Basu S et al (2016) *J Adhes* 92:819
- Dorn L, Liu W (1993) *Int J Adhes Adhes* 13:21
- Dugdale DS (1960) *J Mech Phys Solids* 8:100
- Fish J, Belytschko T (2007) *A first course in finite elements*. Wiley, Chichester
- Goland M, Reissner E (1944) *J Appl Mech Trans Am Soc Mech Eng* 66:A17
- Griffith AA (1920) *Philos Trans R Soc A* 221:163
- Harris JA, Adams RD (1984) *Int J Adhes Adhes* 4:65
- Hillerborg A, Mod  er M et al (1976) *Cem Concr Res* 6:773
- Hutton DV (2003) *Fundamentals of finite element analysis*. McGraw-Hill, New York
- Irwin GR (1957) *J Appl Mech* 24:361
- Kachanov LM (1958) *Izv Akad Nauk USSR Otd Tekh Nauk* 8:26
- Koji   M, Filipovi   N et al (2008) *Computer modeling in bioengineering: theoretical background, examples and software*. Wiley, Chichester/West Sussex
- Lemaire J, Desmorat R (2005) *Engineering damage mechanics: ductile, creep, fatigue and brittle failures*. Springer – Verlag, Berlin/Heidelberg
- Liljedahl CDM, Crocombe AD et al (2007) *Int J Adhes Adhes* 27:505
- Loh WK, Crocombe AD et al (2003) *J Adhesion* 79:1135
- MacNeal RH (1994) *Finite elements: their design and performance*. Marcel Dekker, New York
- Mohammadi S (2008) *Extended finite element method: for fracture analysis of structures*. Blackwell, Oxford
- Mubashar A, Ashcroft IA (2015) *J Adhes*. <https://doi.org/10.1080/00218464.2015.1081819>
- Mubashar A, Ashcroft IA et al (2009) *J Adhes* 85:711
- Mubashar A, Ashcroft IA et al (2014) *J Adhes* 90:682
- Neumayer J, Koerber H et al (2016) *Compos Struct* 146:75
- Rybicki EF, Kanninen MF (1977) *Eng Fract Mech* 9:931

- 1190 Segerlind LJ (1984) Applied finite element analysis. Wiley, New York  
1191 Stein N, Weißgraeber P et al (2015) Compos Struct 133:707  
1192 Stuparu F, Constantinescu DM et al (2016) J Adhes 92:535  
1193 Tsai CL, Guan YL et al (2014) Int J Adhes Adhes 51:67  
1194 Turner MJ (1959) Structural and materials panel paper, AGARD meeting, Aachen  
1195 Turner MJ, Clough RW et al (1956) J Aero Sci 23:805  
1196 Volkersen O (1938) Luftfahrtforschung 15:41  
1197 Voyiadjis GZ, Kattan PI (2005) Damage mechanics. Taylor & Francis, New York  
1198 Wahab MA, Ashcroft IA et al (2004) J Strain Analysis 39:173  
1199 Ward IM, Sweeney J (2004) An introduction to the mechanical properties of solid polymers. Wiley,  
1200 Chichester  
1201 Zienkiewicz OC, Cheung YK (1967) The finite element method in structural and continuum  
1202 mechanics. McGraw-Hill, London  
1203 Zienkiewicz OC, Taylor RL (2000) The finite element method, The basis, vol 1. Butterworth &  
1204 Heinemann, Oxford

Andreas Öchsner

## Contents

26.1	Introduction .....	742
26.2	Substructures .....	743
26.2.1	Introductory Example .....	743
26.2.2	General Case of Static Condensation .....	747
26.2.3	Static Condensation Applied to Substructures .....	748
26.3	Submodels .....	751
26.3.1	Introductory Example .....	751
26.3.2	Submodeling Based on Internal Forces .....	751
26.3.3	Submodeling Based on Enforced Displacement .....	754
26.4	Boundary Element Method .....	755
26.4.1	Introductory Example .....	755
26.4.2	General Comments .....	761
26.5	Finite Difference Method .....	763
26.5.1	Introductory Example .....	763
26.5.2	General Comments .....	768
26.6	Conclusion .....	770
	References .....	770

## Abstract

The aim of this chapter is to introduce special numerical techniques. The first part covers special finite element techniques which reduce the size of the computational models. In the case of the substructuring technique, internal nodes as parts of a finite element mesh can be condensed out so that they do not contribute to the size of the global stiffness matrix. A postcomputational step allows to determine the unknowns of the condensed nodes. In the case of the submodel technique, the

A. Öchsner (✉)

Faculty of Mechanical Engineering, Esslingen University of Applied Sciences, Esslingen, Baden-Württemberg, Germany

e-mail: [andreas.oechsner@gmail.com](mailto:andreas.oechsner@gmail.com)

results of a finite element computation based on a coarse mesh are used as input, i.e., boundary conditions, for a refined submodel. The second part of this chapter introduces alternative approximation methods to solve the partial differential equations which describe the problem. The boundary element method is characterized by the fact that the problem is shifted to the boundary of the domain and as a result, the dimensionality of the problem is reduced by one. In the case of the finite difference method, the differential equation and the boundary conditions are represented by finite difference equations. Both methods are introduced based on a simple one-dimensional problem in order to demonstrate the major idea of each method. Furthermore, advantages and disadvantages of each alternative approximation methods are given in the light of the classical finite element simulation. Whenever possible, examples of application of the techniques in the context of adhesive joints are given.

---

## 26.1 Introduction

The most spread engineering tool to simulate structural problems is the finite element method (FEM). This approximation method has attracted the attention of analysts largely due to its property of discretizing a continuous system into a series of finite elements, which can be associated with physical parts. The single elements are then assembled to obtain the complete system solution using given initial and boundary conditions. The assembly process uses appropriate balance equations at the nodes which are used to define the elements and serve also as connection points between the elements.

The existing literature on finite elements is by now very extensive and encompasses all types of common field problems such as structural mechanics, heat and mass transfer, fluid flow and acoustics, see the reviews (Mackerle 1995a, b), or the classical textbooks (Reddy 2006; Öchsner and Merkel 2013; Öchsner 2016).

As in the case of existing literature, there is a huge number of finite element codes ranging from simple academic programs such as FEAP (Robert L. Taylor) to commercially available general purpose programs. Some of the common commercial codes used in industry as well as in academia are NASTRAN (Richard H. MacNeal, Robert Schwendler), ANSYS (John Swanson), MARC (Pedro Marcal), ABAQUS (David Hibbitt), and ADINA (Klaus-Jürgen Bathe).

Nowadays, commercial finite element programs are quite powerful and user friendly codes which are available for all platforms of operating systems. Some commercial packages, such as ABAQUS or MARC (Javanbakht and Öchsner 2017), even allow to extend the functionality via user subroutines.

However, reliable results can only be obtained when the user of such commercial packages understands the problem, how to model it, the behavior of finite elements, the assumptions and limitations of the code, and when the analyst is able to check for errors at all stages. It is not necessary that the end-user understands in detail all procedures and routines, but incorrect results, which may cause serious damage such as production delay, redesign, or even collapse, can be avoided only by those who

understand the basic ideas and single steps of the FEM (cf. ► [Chap. 25, “Numerical Approach: Finite Element Analysis”](#)).

A practical limit of the finite element method can be reached if the system of equations contains so many unknowns that the used computer hardware (working memory) is no more able to handle the size of the matrix system. To overcome this problem, special finite element techniques, i.e., substructuring and sub-modelling, can be applied (Cook et al. 2002). These techniques are introduced in the first part of this chapter. Newer approaches to overcome the problem of limited computer hardware can be summarized under the expression of parallel computing where a computational task is partitioned and parallel processed on several computers.

On the other hand, the finite element method is only one of the classical approximations methods in engineering. The boundary element method (BEM) (Banerjee 1994) and the finite difference method (FDM) (Mitchell and Griffiths 1980) are alternative numerical approaches to solve problems described by partial differential equations. Despite the fact that the finite element method is the major engineering tool, each of the classical methods has its own advantages and disadvantages and may be depending on the specific problem more or less appropriate than the finite element method. A brief introduction of these classical approximation methods in the context of adhesion technology can be found in (da Silva and Campilho 2012).

A common feature from the theoretical foundation is that all these classical approximation methods can be derived based on the weighted residual method (Brebbia et al. 1984). The second part of this chapter introduces both alternative methods based on a one-dimensional problem in order to describe the main idea of the approach. Each subsection closes with some general comments on advantages and disadvantages of the alternative method and examples of applications in the context of adhesive joints. All the presented techniques and methods in this chapter are not very common in standard engineering practice. Thus, the major idea is to introduce the main concept of each technique based on simple examples and to bring the reader in a position where he can decide if it makes sense for him to look deeper in one of the mentioned techniques.

---

## 26.2 Substructures

### 26.2.1 Introductory Example

The idea of substructuring a large finite element model will be introduced in the following based on one-dimensional bar elements. This focus on one-dimensional elements reveals the advantage that the entire notation remains rather simple compared to the general three-dimensional approach whereas the steps are the same as in the general case. A tapered bar element (it should be noted here that in the case of a bar with constant axial stiffness  $EA$ , the finite element solution at the nodes is equal to the analytical solution) of length  $L$  with linearly changing cross sections from  $A_1$

to  $A_2$  between the two boundary nodes is considered in the following. In addition, the displacement field between the nodes should be linearly interpolated, i.e., the element is based on linear interpolation functions. For such an element, the elemental stiffness matrix is given by:

$$\mathbf{K}^e = \frac{E}{L} \times \frac{A_1 + A_2}{2} \begin{bmatrix} 1 & -1 \\ -1 & 1 \end{bmatrix}. \quad (1)$$

This finite element is used to compose a simple substructure as shown in Fig. 1 where two elements are used to model a part of a tapered bar.

The stiffness matrix given in Eq. (1) can be applied to these two elements to formulate the principal finite element equation for both elements as:

$$\frac{E_I}{L_I} \times \frac{A_1 + A_2}{2} \begin{bmatrix} 1 & -1 \\ -1 & 1 \end{bmatrix} \begin{bmatrix} u_1 \\ u_2 \end{bmatrix} \begin{bmatrix} F_1 \\ F_2 \end{bmatrix} \quad (\text{element I}), \quad (2)$$

$$\frac{E_{II}}{L_{II}} \times \frac{A_2 + A_3}{2} \begin{bmatrix} 1 & -1 \\ -1 & 1 \end{bmatrix} \begin{bmatrix} u_2 \\ u_3 \end{bmatrix} \begin{bmatrix} F_2 \\ F_3 \end{bmatrix} \quad (\text{element II}). \quad (3)$$

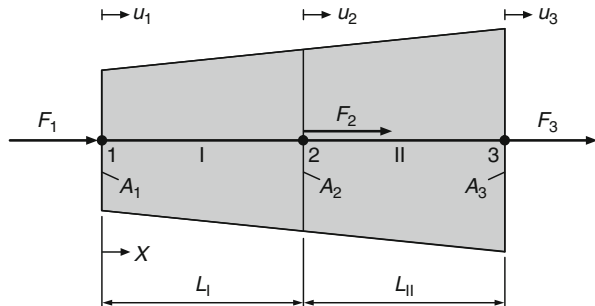
Assembling of these individual finite element equations gives the global finite element formulation in the general form  $\mathbf{Ku} = \mathbf{F}$  as:

$$\frac{E}{2L} \begin{bmatrix} (A_1 + A_2) & -(A_1 + A_2) & 0 \\ -(A_1 + A_2) & (A_1 + 2A_2 + A_3) & -(A_2 + A_3) \\ 0 & -(A_2 + A_3) & (A_2 + A_3) \end{bmatrix} \begin{bmatrix} u_1 \\ u_2 \\ u_3 \end{bmatrix} = \begin{bmatrix} F_1 \\ F_2 \\ F_3 \end{bmatrix}. \quad (4)$$

The last equation (4) constitutes a system of three linear independent equations for the three unknown nodal displacements  $u_1, \dots, u_3$ . The second equation of (4) can be rearranged to express the internal unknown  $u_2$  as a function of the boundary values  $u_1$  and  $u_3$  as:

$$u_2 = \frac{2L}{E} \frac{F_2}{A_1 + 2A_2 + A_3} + \frac{(A_1 + A_2)u_1}{A_1 + 2A_2 + A_3} + \frac{(A_2 + A_3)u_3}{A_1 + 2A_2 + A_3}. \quad (5)$$

**Fig. 1** Simple substructure consisting of two linear bar elements with linearly changing cross sections. Finite element nodes are numbered by Arabic numbers (1, 2, 3) and are symbolized by black circles (•). The finite elements themselves are numbered by Roman numbers (I, II)



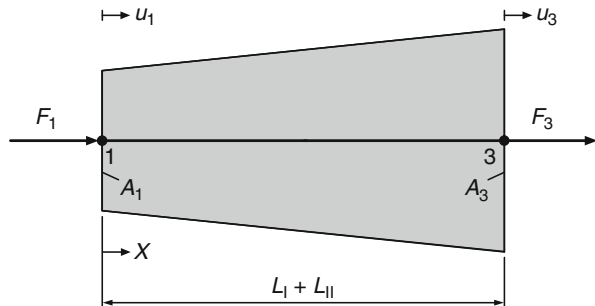
This relationship in the form  $u_2 = u_2(u_1, u_3)$  can be substituted back into the first and third equation of (4). After rearranging and collecting common expressions, the following  $2 \times 2$  system of equations remains for the nodal boundary values of the element shown in Fig. 2:

$$\frac{E}{2L} \frac{(A_1 + A_2)(A_2 + A_3)}{A_1 + 2A_2 + A_3} \begin{bmatrix} 1 & -1 \\ -1 & 1 \end{bmatrix} \begin{bmatrix} u_1 \\ u_2 \end{bmatrix} = \begin{bmatrix} F_1 + \frac{A_1 + A_2}{A_1 + 2A_2 + A_3} F_2 \\ F_3 + \frac{A_2 + A_3}{A_1 + 2A_2 + A_3} F_2 \end{bmatrix}. \quad (6)$$

The described process of partially solving a system of equations of a given substructure in such a way that only interconnecting or boundary nodes remain in the system is known in literature as *static condensation*. In the general approach, only such nodes are often condensed out where no boundary conditions are prescribed. As a consequence, the external force  $F_2$  in Eq. (6) can be set to zero in the following derivations. From a practical point of view, static condensation changes the order of which nodal unknowns are calculated. For the given example shown in Figs. 1 and 2, the nodal displacements  $u_1$  and  $u_3$  would be first calculated and then by substituting these results into Eq. (5), the internal nodal value  $u_2$  would be obtained. It should be noted here that static condensation does *not* introduce any further approximation into the finite element analysis. The attribute “static” is used to distinguish from a similar process in structural dynamics where the stiffness and mass matrix are reduced. However, the condensation introduced in the case of dynamics further approximates in the mass matrix. The effect of creating substructures and assembling them to solve a global system of equations will be illustrated in the following simple example shown in Fig. 3.

The shown tapered bar is discretized by four linear elements of linearly changing cross sections. The bar is fixed at the left-hand side and the right-hand end is subjected to a force boundary condition  $F$ . The two left- and right-hand elements, i.e., elements (I + II) and elements (III + IV), should be grouped to substructures and used to solve the problem. The classical solution procedure without substructures would consist of assembling the global stiffness matrix of all four elements which would result in the following  $5 \times 5$  stiffness matrix:

**Fig. 2** Superelement obtained from the substructure shown in Fig. 1





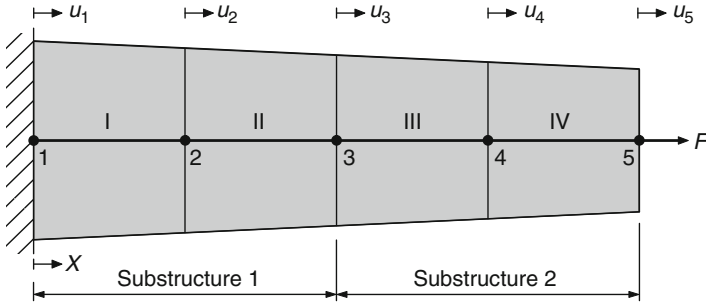


**Fig. 3** Tapered bar, discretized by four linear elements with linearly changing cross sections. Each element has the same length  $L$  and the same Young's modulus  $E$ . Finite element nodes are symbolized by black circles (•)

$$\frac{E}{2L} \begin{bmatrix} (A_1 + A_2) & -(A_1 + A_2) & 0 & 0 & 0 \\ -(A_1 + A_2) & (A_1 + 2A_2 + A_3) & -(A_2 + A_3) & 0 & 0 \\ 0 & -(A_2 + A_3) & (A_2 + 2A_3 + A_4) & -(A_3 + A_4) & 0 \\ 0 & 0 & -(A_3 + A_4) & (A_3 + 2A_4 + A_5) & -(A_4 + A_5) \\ 0 & 0 & 0 & -(A_4 + A_5) & (A_4 + A_5) \end{bmatrix} \quad (7)$$

Thus, the classical approach results in a  $5 \times 5$  global system of equations or after considering the boundary condition at the left-hand end, i.e., deleting the first row and column of the global system of equations, in a reduced  $4 \times 4$  system which must be solved. Using the approach based on substructures as indicated in Fig. 3, the following two superelements based on Eq. (6)

$$\underbrace{\frac{E}{2L} \frac{(A_1 + A_2)(A_2 + A_3)}{A_1 + 2A_2 + A_3}}_{\alpha_1} \begin{bmatrix} 1 & -1 \\ -1 & 1 \end{bmatrix} \begin{bmatrix} u_1 \\ u_2 \end{bmatrix} = \begin{bmatrix} \dots \\ 0 \end{bmatrix}, \quad (8)$$

$$\underbrace{\frac{E}{2L} \frac{(A_3 + A_4)(A_4 + A_5)}{A_3 + 2A_4 + A_5}}_{\alpha_2} \begin{bmatrix} 1 & -1 \\ -1 & 1 \end{bmatrix} \begin{bmatrix} u_3 \\ u_5 \end{bmatrix} = \begin{bmatrix} 0 \\ F \end{bmatrix}, \quad (9)$$

need to be assembled to the following global system of equations:

$$\frac{E}{2L} \begin{bmatrix} \alpha_1 & -\alpha_1 & 0 \\ -\alpha_1 & \alpha_1 + \alpha_2 & -\alpha_2 \\ 0 & -\alpha_2 & \alpha_2 \end{bmatrix} \begin{bmatrix} u_1 \\ u_2 \\ u_3 \end{bmatrix} = \begin{bmatrix} \dots \\ 0 \\ F \end{bmatrix}. \quad (10)$$

After introducing the boundary condition at the left-hand end, i.e.,  $u_1 = 0$ , only a  $2 \times 2$  system remains to be solved. Compared to the global system of equations in the classical approach, introduction of substructures reduces the demand on the computer storage space by 50% in the elaborated example. The final results for nodal displacements and stresses are shown in Fig. 4. Due to the linear interpolation

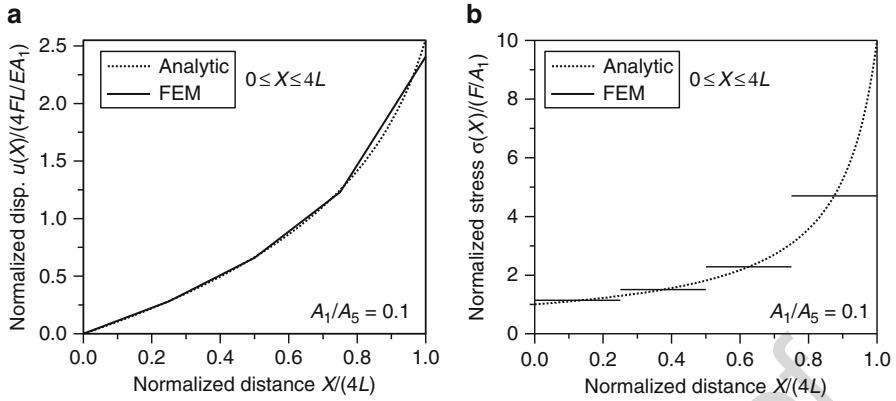


**Fig. 4** Comparison between finite element and analytical solution for the problem shown in Fig. 3: (a) normalized displacements; (b) normalized stresses

functions, the finite element solution gives a piecewise linear approximation of the deformation. Nevertheless, four elements give a quite good overall representation of the deformed shape for the given input data. Due to the linear shape functions of the applied elements, the strains and stresses are constant in each element and the finite element solution approximates the analytical solution only in an average sense. If higher accuracy for the stresses or strains is required, more elements or elements with higher order interpolation functions must be introduced.

## 26.2.2 General Case of Static Condensation

A more formal procedure for the static condensation introduced in the previous sections can be described as follows (Cook et al. 2002). Let equation  $\mathbf{K}^s \mathbf{u}^s = \mathbf{F}^s$  be the global system of equations for a given substructure. Then, this equation can be rearranged in the following manner:

$$\begin{bmatrix} \mathbf{K}_{bb} & \mathbf{K}_{bc} \\ \mathbf{K}_{cb} & \mathbf{K}_{cc} \end{bmatrix}^s \begin{bmatrix} \mathbf{u}_b \\ \mathbf{u}_c \end{bmatrix}^s = \begin{bmatrix} \mathbf{F}_b \\ \mathbf{F}_c \end{bmatrix}^s, \quad (11)$$

where  $\mathbf{u}_b$  are the unknowns to be retained and  $\mathbf{u}_c$  are the internal values which should be condensed. The unknowns to be retained are sometimes called super or master nodes while the internal nodes are sometimes denoted as slaves. The external loads  $\mathbf{F}$  are in the same way separated. Equation (11) can be solved by blockwise inversion of the stiffness matrix, i.e., inversion of a  $2 \times 2$  block matrix

$$\begin{bmatrix} \mathbf{A} & \mathbf{B} \\ \mathbf{C} & \mathbf{D} \end{bmatrix}^{-1} = \begin{bmatrix} (\mathbf{A} - \mathbf{B}\mathbf{D}^{-1}\mathbf{C})^{-1} & -(\mathbf{A} - \mathbf{B}\mathbf{D}^{-1}\mathbf{C})^{-1}\mathbf{B}\mathbf{D}^{-1} \\ -\mathbf{D}^{-1}\mathbf{C}(\mathbf{A} - \mathbf{B}\mathbf{D}^{-1}\mathbf{C})^{-1} & \mathbf{D}^{-1} + \mathbf{D}^{-1}\mathbf{C}(\mathbf{A} - \mathbf{B}\mathbf{D}^{-1}\mathbf{C})^{-1}\mathbf{B}\mathbf{D}^{-1} \end{bmatrix} \quad (12)$$

182 to obtain

$$F_b = \frac{u_b}{(K_{bb} - K_{bc}K_{cc}^{-1}K_{cb})^{-1}} + K_{bc}K_{cc}^{-1}F_c \quad (13)$$

183 and by introducing this expression in the second matrix equation of the solution of (11):

$$u_c = K_{cc}^{-1}(F_c - K_{cb}u_b). \quad (14)$$

184 This expression can be used for the calculation of  $u_c$ , when  $u_b$  is known.  
 185 Considering (14) in the first equation of (11) and rearranging, the following expres-  
 186 sion can be obtained

$$\underbrace{(K_{bb} - K_{bc}K_{cc}^{-1}K_{cb})}_{\text{condensed stiffness matrix}} u_b = \underbrace{F_b - K_{bc}K_{cc}^{-1}F_c}_{\text{condensed load vector}}, \quad (15)$$

187 or in compact form:

$$K_{\text{cond}}^s u_b = K_{\text{cond}}^s. \quad (16)$$

188

### 189 26.2.3 Static Condensation Applied to Substructures

190 In the following, a finite element mesh as shown in Fig. 5 which is subdivided in two  
 191 substructures A and B is considered, adapted from (Raghu 2009). The nodes at the  
 192 interface where substructure A is connected to B are collected in a group “i”. The  
 193 remaining nodes of substructures A are named “a” and the respective nodes remaining  
 194 for substructure B are called “b”. All external forces acting on nodes “a” are collected in  
 195 a vector  $F_a$ , the same for external forces acting on the group of nodes “i” or “b”.

196 The principal finite element equations  $K^s u^s = F^s$  for each substructure ( $s = A$   
 197  $\vee B$ ) can be arranged in the following way according to the distinction a-i and i-b:

$$\begin{bmatrix} K_{aa} & K_{ai} \\ K_{ia} & K_{ii}^A \end{bmatrix} \begin{bmatrix} u_a \\ u_i \end{bmatrix} = \begin{bmatrix} F_a \\ F_i \end{bmatrix}, \quad (17)$$

$$\begin{bmatrix} K_{ii}^B & K_{ib} \\ K_{bi} & K_{bb} \end{bmatrix} \begin{bmatrix} u_i \\ u_b \end{bmatrix} = \begin{bmatrix} F_i \\ F_b \end{bmatrix}. \quad (18)$$

198 These two equations can be assembled to the global finite element equation  
 199  $Ku = F$  to obtain

$$\left[ \begin{array}{cc|c} K_{aa} & K_{ai} & 0 \\ K_{ia} & K_{ii} & K_{ib} \\ \hline 0 & K_{bi} & K_{bb} \end{array} \right] \begin{bmatrix} u_a \\ u_i \\ u_b \end{bmatrix} = \begin{bmatrix} F_a \\ F_i \\ F_b \end{bmatrix}, \quad (19)$$

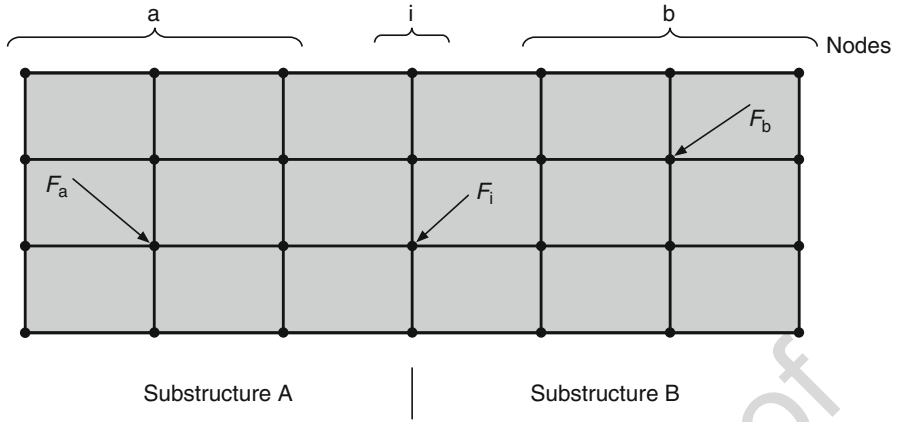


**Fig. 5** Finite element model subdivided into two substructures A and B. Nodes at the interface of both structures are collected in group “i,” the remaining nodes of substructure A are denoted by “a”, while the remaining nodes of substructure B are denoted by “b”. Finite element nodes are symbolized by *black circles* (•)

where  $\mathbf{K}_{ii} = \mathbf{K}_{ii}^A + \mathbf{K}_{ii}^B$ . Equation (19) can be now treated as Eq. (11) to calculate the condensed stiffness matrix and the condensed load vector as given in Eq. (15):

$$\mathbf{K}_{\text{cond}} = \begin{bmatrix} \mathbf{K}_{aa} & \mathbf{K}_{ai} \\ \mathbf{K}_{ia} & \mathbf{K}_{ii} \end{bmatrix} - \begin{bmatrix} \mathbf{0} \\ \mathbf{K}_{ib} \end{bmatrix} \mathbf{K}_{bb}^{-1} \begin{bmatrix} \mathbf{0} & \mathbf{K}_{bi} \end{bmatrix} \quad (20)$$

$$= \mathbf{K}^A + \mathbf{K}_{\text{cond}}^B. \quad (21)$$

$$\begin{aligned} \mathbf{F}_{\text{cond}} &= \begin{bmatrix} \mathbf{F}_a \\ \mathbf{F}_i \end{bmatrix} - \begin{bmatrix} \mathbf{0} \\ \mathbf{K}_{ib} \end{bmatrix} \mathbf{K}_{bb}^{-1} \mathbf{F}_b, \\ &= \begin{bmatrix} \mathbf{F}_a \\ \mathbf{0} \end{bmatrix} + \begin{bmatrix} \mathbf{0} \\ \mathbf{F}_i - \mathbf{K}_{ib} \mathbf{K}_{bb}^{-1} \mathbf{F}_b \end{bmatrix}, \end{aligned} \quad (22)$$

$$= \begin{bmatrix} \mathbf{F}_a \\ \mathbf{0} \end{bmatrix} + \mathbf{F}_{\text{cond}}^B. \quad (23)$$

Thus, the condensed global system of equations  $\mathbf{K}_{\text{cond}} \mathbf{u}_{\text{cond}} = \mathbf{F}_{\text{cond}}$  can be written in the following manner:

$$(\mathbf{K}^A + \mathbf{K}_{\text{cond}}^B) \begin{bmatrix} \mathbf{u}_a \\ \mathbf{u}_i \end{bmatrix} = \begin{bmatrix} \mathbf{F}_a \\ \mathbf{0} \end{bmatrix} + \mathbf{F}_{\text{cond}}^B. \quad (24)$$

A graphical representation of the condensed finite element model is shown in Fig. 6 where the nodes of group “b” are completely vanished. In addition, the equations for the condensed stiffness matrix and load vector of substructure B are

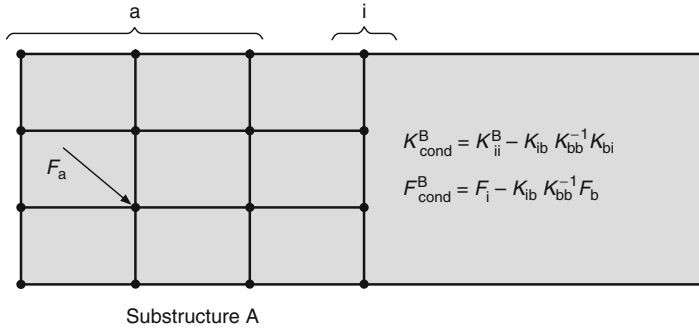


**Fig. 6** Finite element model after static condensation. Finite element nodes are symbolized by black circles (•)

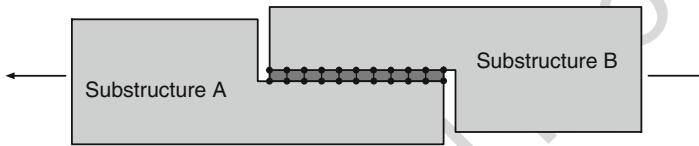


**Fig. 7** Single-step lap joint with adherends considered as substructures. Only the mesh of the adhesive layer is required at the first step of the computation. Finite element nodes are symbolized by black circles (•)

given which are required to calculate the condensed global system according to Eq. (24). Looking at these two equations, the important conclusion can be drawn that the condensed model of substructure B is independent of the stiffness of substructure A. Thus, any changes in substructure A will be considered correctly and the same result as calculated from the entire structure will be obtained.

The described procedure for connecting different substructures implies that the finite element mesh at the interface of the substructures is identical. However, there are more advanced techniques which allow the connection of substructures even when neither mesh pattern nor element types match along the interface (Knight et al. 1991; Zhao et al. 1999; Dohrmann et al. 2000; Gmür and Kauten 1993).

A typical example for the substructuring technique from the context of adhesive technology is shown in Fig. 7 (Groth 1986) where a single-stepped lap joint is modeled.

Both adherends were treated as substructures with the lower and upper adhesive interface nodes considered as the supernodes. Substructure A was condensed to the lower row of nodes while substructure B was condensed to the upper row of nodes. The only assumption in Groth (1986) was that the adherends behave linearly, i.e., that no material or geometrical nonlinearities are considered.

A more sophisticated approach to model a single-lap joint was introduced by Paroissien et al. (2013) who modeled the entire adhesive layer as a single four-node

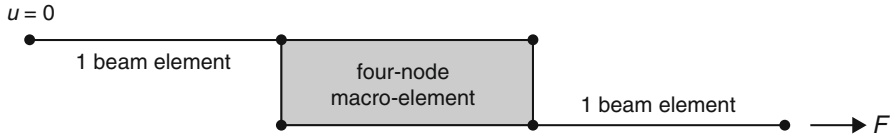


**Fig. 8** Modeling approach of a single-lap joint where the adhesive layer is represented by a single macro-element while the adherends are single beam elements. Finite element nodes are symbolized by black circles (•) (Adapted from Paroissien et al. 2013)

macroelement with elasto-plastic material behavior, see Fig. 8. The advantage of this simplified approach was seen in the extremely small finite element model, i.e., only based on six nodes, which allows the conduction of extensive parametric studies.

## 26.3 Submodels

### 26.3.1 Introductory Example

The same simple example as in Sect. 2.1 should be considered in the following. It is now assumed that the area of interest is near the left-hand boundary, i.e.,  $X \rightarrow 0$ , and that the coarse mesh shown in Fig. 9 does not provide the required accuracy in regards to the stresses.

To increase the accuracy without increasing the degrees of freedom in the global mesh, a first simulation can be based on the coarse mesh as shown in Fig. 9. The obtained results, i.e., the nodal displacement at node 2 can be used in a second step as displacement boundary condition for the submodel shown in Fig. 10. This submodel comprises the same domain as element I in the coarse mesh but is discretized by five finite elements of constant length  $L/5$ . A second simulation based on the submodel and the boundary condition resulting from the coarse mesh simulation gives a much better approximation of the stresses in the domain  $0 \leq X \leq L$ . For the given data set, the analytical solution for the normalized stress at the fixed support is equal to 1 while the result from the submodel gives only a deviation of 1.8%. However, the result based on the coarse mesh deviates by 14.3% in this area near the left-hand boundary (Fig. 11).

### 26.3.2 Submodeling Based on Internal Forces

To generalize the introductory example of Sect. 3.1, the finite element structure shown in Fig. 5 is again considered. However, only the isolated substructure A should be now considered and be subjected to the internal loads from substructure B to A which are acting on the interface nodes of group “i” (Raghu 2009). To this end, Eq. (24) can be rearranged to the following form:

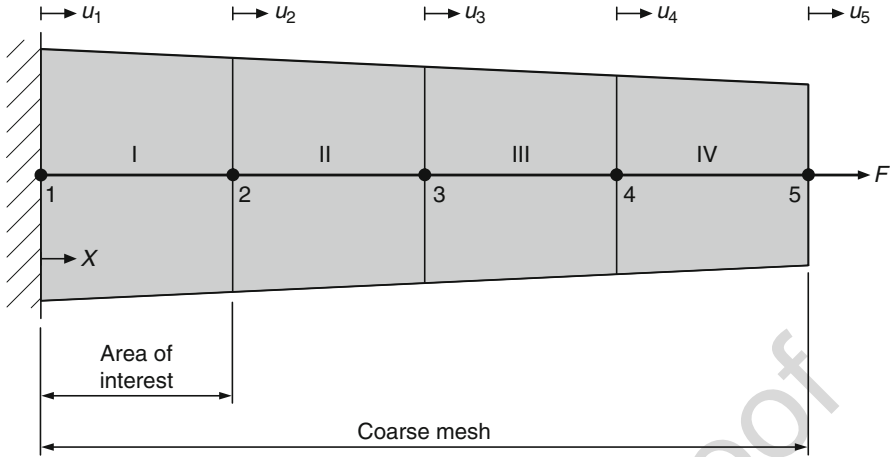
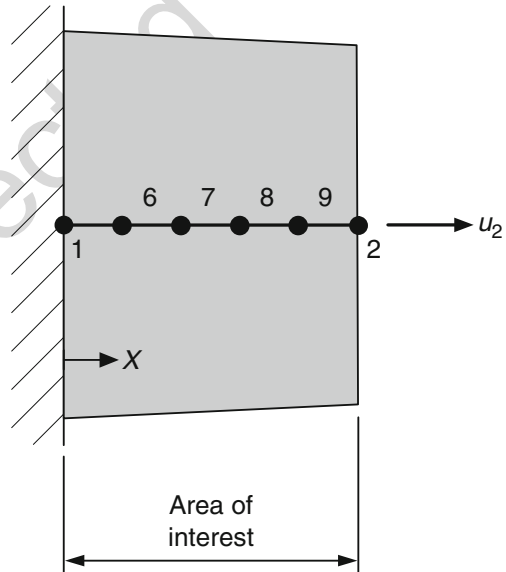


**Fig. 9** Tapered bar, discretized by four linear elements with linear changing cross sections. Each element has the same length  $L$  and the same Young's modulus  $E$ . High accuracy for the stresses is required near the left boundary. Finite element nodes are symbolized by *black circles* (•)

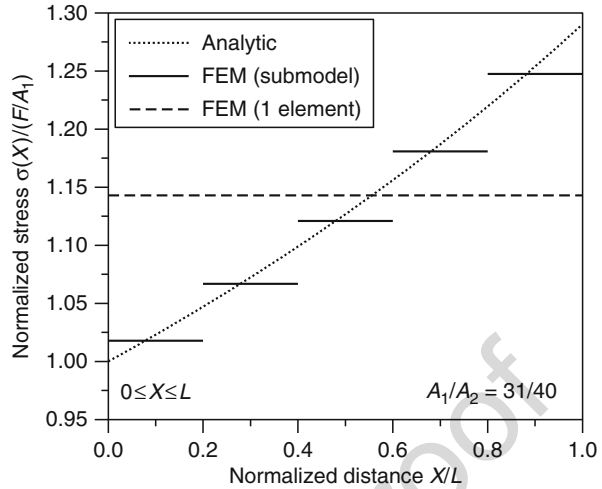
**Fig. 10** Submodel composed of five finite elements. Finite element nodes are symbolized by *black circles* (•)



$$\begin{bmatrix} K_{aa} & K_{ai} \\ K_{ia} & K_{ii}^A \end{bmatrix} \begin{bmatrix} u_a \\ u_i \end{bmatrix} = \begin{bmatrix} F_a \\ f_i \end{bmatrix} + \underbrace{\begin{bmatrix} -(K_{ii}^B - K_{ib}K_{bb}^{-1}K_{bi}^0)u_i - K_{ib}K_{bb}^{-1}F_b \end{bmatrix}}_{F_{BA}}, \quad (25)$$

255 where  $F_{BA}$  is the internal load vector from substructure B to A. It can be shown that  
 256 this force is composed of two parts. To this end, the principal finite element equation

**Fig. 11** Stress results for the submodel structure and comparison with the analytical solution and the stress obtained from the coarse mesh



for substructure B according to (18) must be solved for a given  $\mathbf{F}_B$  and the condition  $\mathbf{u}_i = \mathbf{0}$ . One way to solve this  $2 \times 2$  system of equations is to calculate the inverse  $(\mathbf{K}^B)^{-1}$  and to solve for the remaining unknowns, i.e.,  $\mathbf{F}_i$  and  $\mathbf{u}_b$ :

$$\mathbf{F}_i = \mathbf{K}_{bb}^{-1} \mathbf{K}_{ib} \mathbf{F}_b, \quad (26)$$

$$\mathbf{u}_b = \mathbf{K}_{bb}^{-1} \mathbf{F}_b. \quad (27)$$

It can be seen from the last equations that a part of the force  $\mathbf{F}_{BA}$  is the force over the interface when substructure B is constrained to zero at the interface ( $\mathbf{u}_i = \mathbf{0}$ ) and loaded with the external force vector  $\mathbf{F}_B$ . The second part of  $\mathbf{F}_{BA}$  can be obtained by considering Eq. (18) under a given prescribed displacement at the interface ( $\mathbf{u}_i \neq \mathbf{0}$ ) and the condition that no external force is acting on the nodes of group “b” ( $\mathbf{F}_b = \mathbf{0}$ ). Solving of the  $2 \times 2$  system for the remaining unknowns, i.e.,  $\mathbf{F}_i$  and  $\mathbf{u}_b$ , gives:

$$\mathbf{F}_i = (\mathbf{K}_{ii}^B - \mathbf{K}_{ib} \mathbf{K}_{bb}^{-1} \mathbf{K}_{bi}) \mathbf{u}_i, \quad (28)$$

$$\mathbf{u}_b = -\mathbf{K}_{bb}^{-1} \mathbf{K}_{bi} \mathbf{u}_i. \quad (29)$$

Thus, the second part of the force  $\mathbf{F}_{BA}$  is the force over the interface when substructure B is constrained with an enforced displacement at the interface ( $\mathbf{u}_i \neq \mathbf{0}$ ) and the condition no external force is acting on nodes “b”. This second part of the force  $\mathbf{F}_{BA}$  is indirectly dependent on stiffness changes of submodel A. As a result, a stiffness modification in structure A will change the displacement  $\mathbf{u}_i$  and this will change the internal force. Consequently, any stiffness changes in submodel A will lead to an inherent inaccuracy in the local analysis of submodel A if the internal force method is used. A graphical representation of the submodel A is given in Fig. 12 where in addition the internal force  $\mathbf{F}_{BA}$  is indicated.



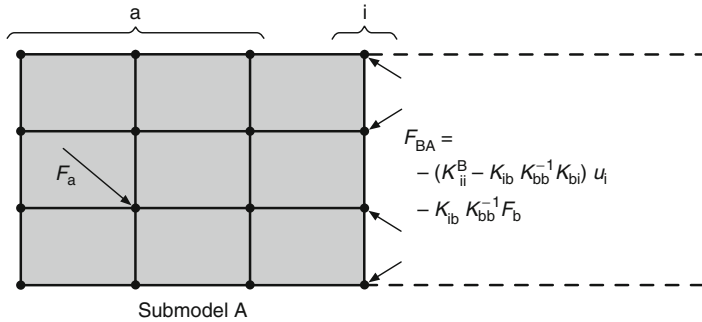


**Fig. 12** Internal force submodeling method for submodel A. Finite element nodes are symbolized by black circles (•)

### 26.3.3 Submodeling Based on Enforced Displacement

An alternative way of submodeling consists of analyzing submodel A alone by imposing a displacement at the interphase nodes “i”. This enforced displacement is normally obtained from a global analysis as shown in the introductory example of Sect. 3.1. Evaluating the principal finite element equation of substructure A according to Eq. (17) for a given displacement  $u$  gives the remaining primary unknown as:

$$u_a = K_{aa}^{-1} (F_a - K_{ai} u_i). \quad (30)$$

As can be seen from the last equation, the same conclusion as in the case of internal force submodeling method holds: Any stiffness change in submodel A will lead to an inherent inaccuracy in the local analysis of submodel A if the enforced displacement method is used. A graphical representation of the submodel A is given in Fig. 13 where in addition the external displacement  $u_i$  is indicated.

Because submodels normally consist of a refined mesh, it is required to interpolate the nodal displacements from the global mesh along the cut boundaries to all the nodes of the finer mesh along the cut boundaries.

A typical example of the submodeling technique is given in (Wang et al. 2009) where single-lap joints were experimentally and numerically investigated. A schematic sketch is shown in Fig. 14 where the global model and the submodel are shown. For the coarse mesh, the arc segment of the spew fillet was even omitted and only a rectangular shape was considered, cf. the dotted line in Fig. 14a. To give some idea on the mesh density, the coarse mesh in this investigation contained 13,000 elements while the submodel, which comprises a much smaller part of the entire structure, could be discretized with 12,000 elements in order to achieve high accuracy in this area.

An typical alternative example for the submodeling technique is given in (Wahab et al. 2004) where an adhesively bonded composite beam was investigated. There, a fine submodel was used which contains the details of a semicircular crack in the center of the adhesive layer.

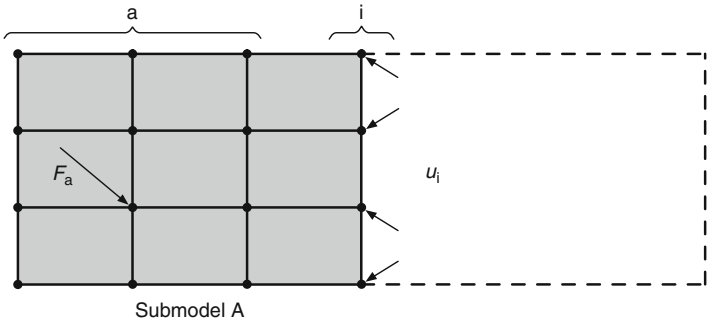


**Fig. 13** Enforced displacement submodeling method for submodel A. Finite element nodes are symbolized by black circles (•)

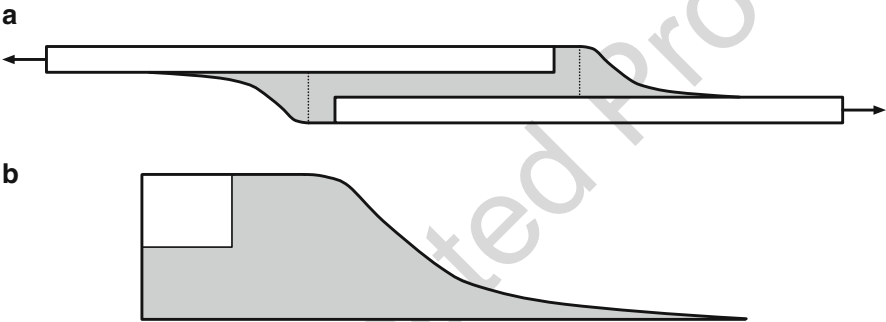


**Fig. 14** Schematic sketch of a single-lap joint with spew fillet (a) entire model to be discretized with a coarse mesh; (b) submodel to be discretized with a fine mesh

## 26.4 Boundary Element Method

### 26.4.1 Introductory Example

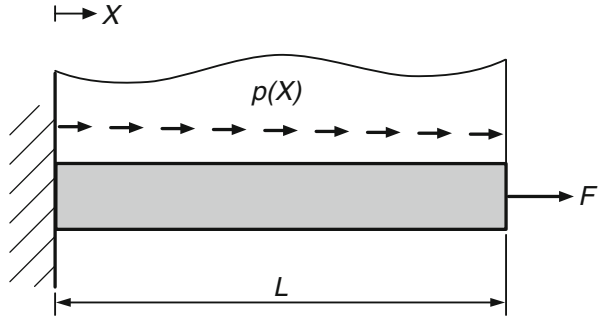
The mathematics involved in the derivation of the boundary element method is much more demanding than in the case of the finite element method. Thus, the major idea of the boundary method is introduced based on the loaded bar as shown in Fig. 15. The general approach can be found in the common textbooks (Banerjee 1994; Raamachandran 2000; Gaul et al. 2003; Beer et al. 2008).

The problem is described by the following partial differential equation

$$EA \frac{d^2 u}{dX^2} = -p(X) \tag{31}$$

and the boundary conditions

**Fig. 15** Bar loaded with a distributed load  $p(X)$  and an end load  $F$



$$u(X=0) = 0 \text{ and } \frac{du}{dX}(X=L) = \frac{F}{EA}. \quad (32)$$

In a more formal way, Eq. (31) can be written as

$$EA\mathcal{L}\{u\} = -p(X), \quad (33)$$

where the second-order differential operator is given by  $\mathcal{L} = \frac{d^2}{dX^2}$ . The partial differential equation describes the problem in each point of the domain and is therefore called the strong formulation or the initial statement. However, this partial differential equation can be only fulfilled in each point by the exact solution. Replacing the exact solution by an approximate solution results in a so-called residual  $R$ :

$$R = \frac{d^2u}{dX^2} + \frac{p(X)}{EA} \neq 0. \quad (34)$$

The principal idea of the weighted residual method is to multiply the residual with a so-called weighting function  $w$  and to request that the error vanishes over a certain region of the domain. This leads to the so-called inner product:

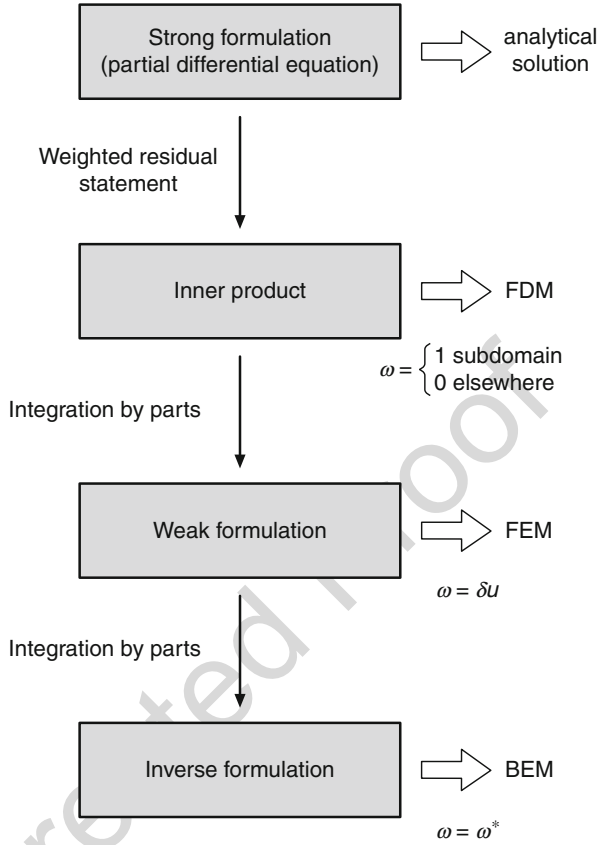
$$\int_0^L \left( \frac{d^2u}{dX^2} + \frac{p(X)}{EA} \right) w dX \stackrel{!}{=} 0. \quad (35)$$

Equation (35) can be integrated by parts in order to shift the differential operator from the field variable  $u$  to the weight function  $w$ . Depending on the order of integration and the choice of the weight function  $w$ , it is possible to derive based on the weighted residual method all the classical approximation methods, cf. Fig. 16 and (Brebbia et al. 1984; Zienkiewicz and Taylor 2000).

The first integration by parts of the derivative term in Eq. (35) yields

$$\int_0^L \frac{d^2u}{dX^2} dX = \left[ \frac{du}{dX} w \right]_0^L - \int_0^L \frac{du}{dX} \frac{dw}{dX} dX, \quad (36)$$

**Fig. 16** Classical approximation methods in the context of the weighted residual method



and the so-called weak form is obtained:

$$\int_0^L \frac{du}{dX} \frac{dw}{dX} dX = \int_0^L \frac{p(X)}{EA} w dX + \left[ \frac{du}{dX} w \right]_0^L. \quad (37)$$

The weak form is characterized by the fact that the order of derivative in the field variable and the weight function is the same. This statement is normally used to derive finite element formulations. Integration by parts of the first integral in the weak form according to Eq. (37) gives

$$\int_0^L \frac{du}{dX} \frac{dw}{dX} dX = \left[ u \frac{dw}{dX} \right]_0^L - \int_0^L u \frac{d^2 w}{dX^2} dX, \quad (38)$$

and the so-called inverse formulation is derived as:

$$\int_0^L u \frac{d^2 w}{dX^2} dX = - \int_0^L \frac{p(X)}{EA} w dX - \left[ \frac{du}{dX} w \right]_0^L + \left[ u \frac{dw}{dX} \right]_0^L. \quad (39)$$

The characteristic of the inverse formulation is that the differential operator  $\mathcal{L}$  is completely shifted to the weight function  $w$ . The next step is to choose a weight function  $w$ . In the scope of the boundary element method, the weight function is chosen to be a fundamental solution:  $w = w^*$  (Love 1944; Sokolnikoff 1956). This fundamental or Kelvin solution  $w^*$  is in the considered case the deformation which is observed at some point  $X$  of an infinite bar due to a unit force at some distant point  $\xi$  in the bar. Alternatively, it is that function which satisfies the differential equation with right-hand side zero at every point of an infinite bar except the force point at which the right-hand side is infinite. Applied to our problem, the fundamental solution is defined by:

$$\frac{d^2 w^*}{dX^2} = \delta(X - \xi), \quad (40)$$

where the Dirac delta function  $\delta(x, \xi)$  is defined in a simple manner as:

$$\delta(X - \xi) = \begin{cases} \infty & \text{for } X = \xi \\ 0 & \text{for } X \neq \xi \end{cases} \quad (41)$$

In the scope of the boundary element method, the selection or sifting property, i.e.,

$$\int_{x_1}^{x_2} f(X) \delta(X - \xi) dX = f(\xi), \quad (42)$$

is the main property which is used for the theoretical derivations. Equation (40) can be multiplied with the field variable  $u$  and integrated to obtain, under consideration of the selection property, the following statement:

$$\int_0^L \frac{d^2 w^*}{dX^2} u(X) dX = \int_0^L \delta(X, \xi) u(X) dX = u(\xi), \quad (43)$$

which leads with Eq. (39) to the so-called representation formula

$$u(\xi) = - \int_0^L \frac{p(X)}{EA} w^* dX - \left[ \frac{du}{dX} w^* \right]_0^L + \left[ u \frac{dw^*}{dX} \right]_0^L. \quad (44)$$

Last equation yields the value  $u(\xi)$  inside the domain, i.e., the bar, if the boundary solution is known.

In order to continue the derivation, the fundamental solution must be known. For the condition given in Eq. (40), the fundamental solution is given by:

$$w^* = \frac{1}{2} |X - \xi|. \quad (45)$$

However, it must be noted here that no fundamental solution can be obtained for some differential operators. The graphical representation of Eq. (45) is shown in Fig. 17 where it can be seen that the function has a kink at  $X = \xi$ . As a result, the first-order derivative shows a jump of magnitude 1, which corresponds to the introduced unit load  $F(\xi) = 1$ . The second-order derivative is everywhere zero except for the load point where the value converges infinity.

Furthermore, it can be seen from Eq. (45) that the displacement of the infinite bar is constraint to zero at the load point:  $w^*(X = \xi) = 0$ . The first-order derivative of Eq. (45) is given for  $X \neq \xi$  as (cf. Fig. 17b)

$$\frac{dw^*}{dX} = \frac{1}{2} \times \text{sgn}(X - \xi), \quad (46)$$

where “sgn” is the signum function defined as:

$$\text{sgn}(X - \xi) = \begin{cases} +1 & \text{for } X > \xi \\ 0 & \text{for } X = \xi \\ -1 & \text{for } X < \xi \end{cases} \quad (47)$$

As can be seen from Fig. 17, the second-order derivative of Eq. (45) is given by the Dirac delta function.

Inserting the fundamental solution (45) and boundary conditions into the representation formula (44) gives

$$u(\xi) = - \int_0^L \frac{p}{EA} w^* dX - \underbrace{\frac{du}{dX}}_{F_o/(EA)} w^* \Big|_L + \frac{du}{dX} w^* \Big|_0 + u \frac{dw^*}{dX} \Big|_L - \underbrace{u \frac{dw^*}{dX}}_0 \Big|_0 \quad (48)$$

or

$$u(\xi) = - \int_0^L \frac{p(X)}{EA} \frac{1}{2} |X - \xi| dX - \frac{F}{EA} \frac{1}{2} |L - \xi| + \left( \frac{du}{dX} \right)_0 \frac{1}{2} |\xi| + u_L \frac{1}{2}. \quad (49)$$

Last equation gives the displacement at any point  $\xi$  in the domain only in terms of boundary variables. The domain integral  $\left( \int_0^L \dots \right)$  does not contain any unknown and can therefore be regarded as a constant term. To obtain two equations for the unknown boundary values  $\left( \frac{du}{dX} \right)_0 = \left( \frac{du}{dX} \right)_{(X=0)}$  and  $u_L = u(X = L)$ , the load point

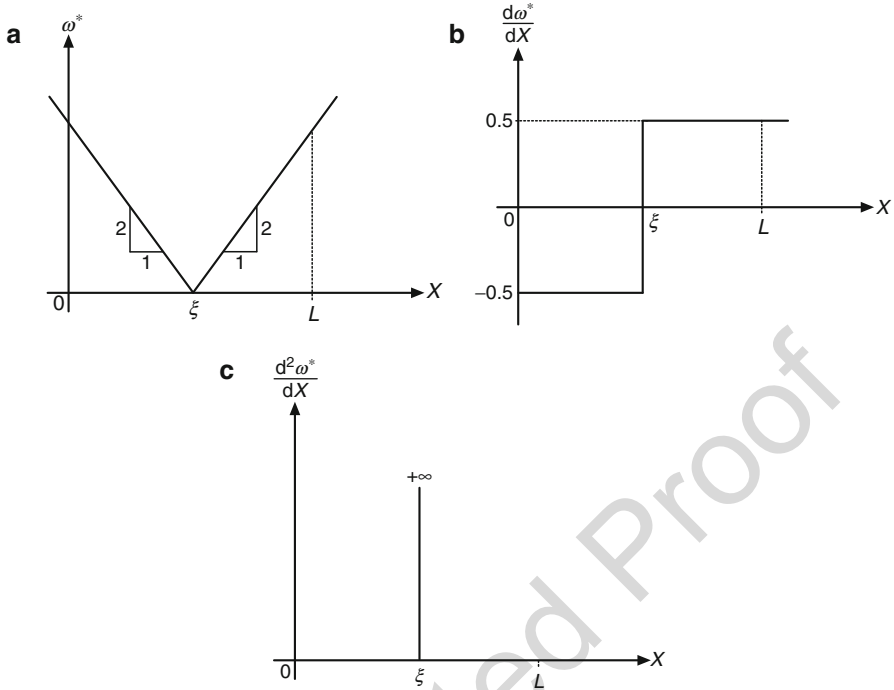


**Fig. 17** Fundamental solution for a bar subjected to a unit concentrated load at location  $X = \xi$ : (a) schematic sketch of  $w^*$ ; (b) first-order derivative; (c) second-order derivative

371 can be placed on the boundaries. With  $\xi = 0$  and  $\xi = L$ , the following two equations  
 372 are obtained:

$$\underbrace{u(\xi = 0)}_0 = - \int_0^L \frac{p(X)}{2EA} |X| dX - \frac{F_0 L}{2EA} + \frac{u_L}{2}, \quad (50)$$

$$u(\xi = L) = - \int_0^L \frac{p(X)}{2EA} |X - L| dX + \left( \frac{du}{dX} \right)_0 \frac{1}{2} |-L| + \frac{u_L}{2}. \quad (51)$$

373 This system of two equations can be solved to obtain the two unknowns. It is  
 374 assumed for simplicity that the distributed load is constant, i.e.,  $p(X) \rightarrow p_0$ , to obtain  
 375 the unknowns as:

$$u(X = L) = \frac{F_0 L}{EA} + \frac{p_0 L^2}{2EA}, \quad (52)$$

$$\left( \frac{du}{dX} \right) \Big|_{(X=0)} = \frac{F_0}{EA} + \frac{p_0 L}{EA}. \quad (53)$$

376 The last step is the calculation of the value  $u(\xi)$  inside the domain based on the  
 377 boundary values. Inserting the two calculated boundary values in Eq. (49) gives the  
 378 distribution of the displacement as:

$$u(\xi) = \frac{p_0}{EA} \left( L\xi - \frac{\xi^2}{2} \right) + \frac{F_0 \xi}{EA}, \quad (54)$$

379 which is equal to the analytical solution. However, this holds only for this simple  
 380 case and is not true in general since only approximate solutions are obtained.

### 26.4.2 General Comments

381 The major difference between the modeling of a problem with the finite element  
 382 method and the boundary element method is related to the discretization, cf. Fig. 18.  
 383 In the case of the finite element method, the entire domain must be discretized,  
 384 whereas the boundary element method requires only the discretization of the bound-  
 385 ary. In addition, a symmetry plane does not require a discretization. As a direct result,  
 386 the size of the obtained system of equations can be much lower than in finite element  
 387 approaches.

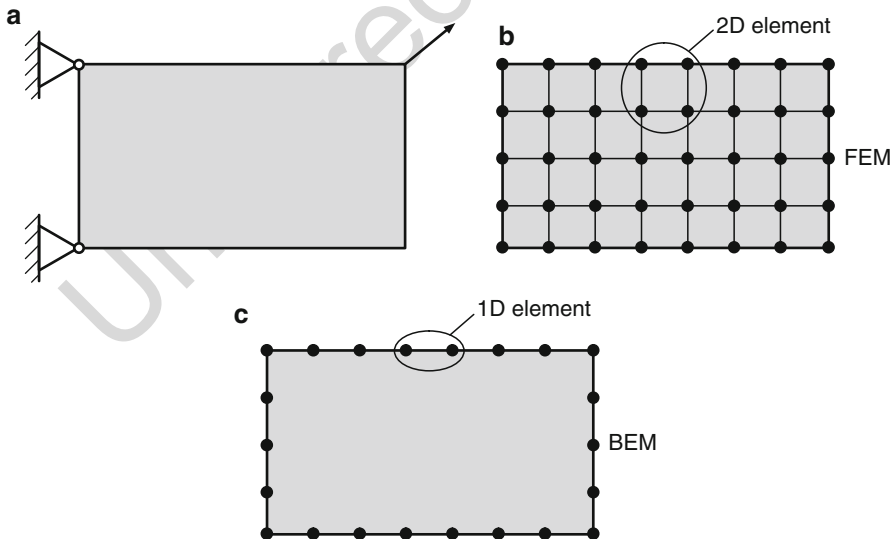


**Fig. 18** Comparison between the general FEM and BEM approach: (a) structural model; (b) finite element mesh; (c) boundary element mesh



Furthermore, changes in the geometry are much easier to incorporate if only the boundary must be subdivided by a mesh. Further advantages of the boundary element method are in the case of stress concentrations where the stresses are evaluated, for example, on the crack boundary and not at the integration points inside the element as in the case of the finite element method. Apart from this, the treatment of infinite and semi-infinite boundaries is much easier in the case of the boundary method. As in the case of the finite element method, there are practically no limitations concerning the geometry which can be modeled. However, there are several disadvantages which must be mentioned. First of all, the derivation of the method is highly mathematical and the theoretical foundation is still not incorporated in many engineering degree courses. The stiffness matrix in the case of the boundary element method might be much smaller compared to the finite element approach but the matrix is fully populated and many highly efficient equation solvers which take advantage of the band structure obtained with finite element approaches cannot be used. Domain integrals must be considered in the case of nonlinearities which requires at least some kind of coarse mesh inside the domain and the dimensionality is no longer reduced.

Typical applications of the boundary element method in the context of adhesion technology are commonly found for the modeling of cracks (fracture mechanics) and other types of stress singularities (Lee 1998), cf. the bibliography of Mackerle (1995a). The article by Vable and Maddi (2006) addresses the specific problems (i.e., numerical modeling considerations which limited the application of BEM in the past) related to bonded joints and boundary element simulation. In addition, numerical results of lap joints, cf. Fig. 19, with several spew angles were presented which demonstrate the potential of the boundary element method in analysis of bonded joints. In a similar way, (Gonçalves et al. 2014) analyzed single-lap joints by the BEM code BEASY to evaluate peak shear and peel stress distributions. In addition, the BEM results were compared to analytical and finite element solutions.

Another typical application of the boundary element method in the context of adhesion technology is the simulation of reinforcement or repair of damaged (e.g., cracked) panels by adhesively bonded patches. This repair technique is quite common in aerospace industry and several references cover this practical topic, see (Young and Rooke 1992; Wen et al. 2002, 2003; Lourenço et al. 2003; Pisa and Aliabadi 2015).

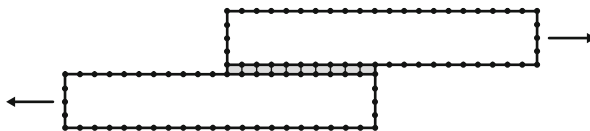


**Fig. 19** Lap joint simulated with the boundary element method. The location and the density of the boundary nodes (symbolized by black circles (•)) are only schematically indicated

## 26.5 Finite Difference Method

The first widely known approximation method for partial differential equations is the finite difference method (Southwell 1946; de G Allen 1955) which approximates the governing equations of a field problem using local expansions for the variables, generally truncated Taylor series. Comprehensive descriptions of the method can be found for example in (Forsythe and Wasow 1960; Collatz 1966; Mitchell and Griffiths 1980).

### 26.5.1 Introductory Example

To illustrate the major idea of the finite difference method, the solution of an end-loaded bar as shown in Fig. 20 will be considered. A good introduction to the application of the finite difference method to Bernoulli beams can be found, for example, in Bathe (1996).

The problem in Fig. 20 is described by the ordinary differential equation

$$EA \frac{d^2 u}{dX^2} = -p(X) \quad (55)$$

which is to be solved in the domain  $X \in [0, L]$  under the given boundary conditions

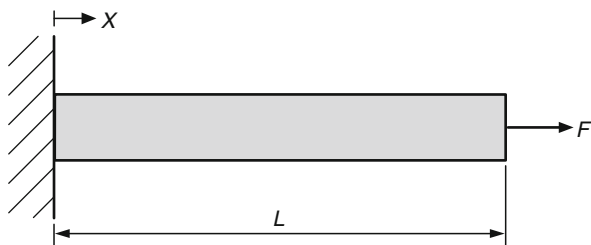
$$u(X=0) = 0, \quad (56)$$

$$F(X=L) = F. \quad (57)$$

The problem shown in Fig. 20 implies that the distributed load is zero ( $p(X) = 0$ ) in Eq. (55). As a first step to solve the differential equation, it is assumed that the numerical solution is to be determined only at a set of  $n$  points within the domain including the end, cf. Fig. 21.

These  $n$  nodes or grid points will be used to derive approximations to the derivatives of the function  $u(X)$ . To simplify the approach, these  $n$  nodes are equally spaced, at a distance equal to  $\Delta X$ . As in the case of the finite element method, high gradients would require a smaller node spacing in order to meet the requirements on the

**Fig. 20** Bar with constant axial stiffness  $EA$ , loaded at its tip with a single force  $F_0$



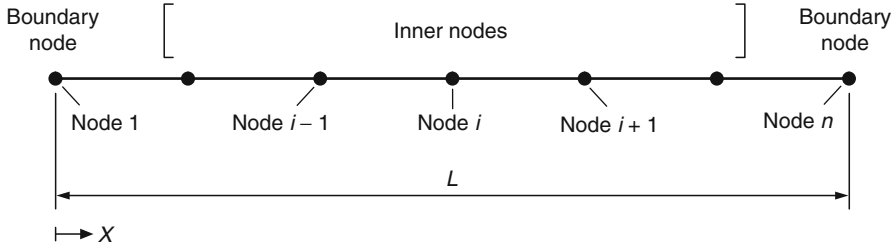


**Fig. 21** Finite difference model of a one-dimensional problem

accuracy of the approximate solution. However, the general idea of the finite difference method will be here introduced based on an equi-spaced division of the domain. A typical inner node of the domain is denoted in the following by  $i$  and the two neighboring nodes are called  $i - 1$  on the left-hand and  $i + 1$  on the right-hand side. For sufficient smooth functions  $u(X)$ , a Taylor's series expansion around node  $i$  gives:

$$u_{i+1} = u_i + \left(\frac{du}{dX}\right)_i \Delta X + \left(\frac{d^2u}{dX^2}\right)_i \frac{\Delta X^2}{2} + \cdots + \left(\frac{d^k u}{dX^k}\right)_i \frac{\Delta X^k}{k!}, \quad (58)$$

$$u_{i-1} = u_i - \left(\frac{du}{dX}\right)_i \Delta X + \left(\frac{d^2u}{dX^2}\right)_i \frac{\Delta X^2}{2} - \cdots + \left(\frac{d^k u}{dX^k}\right)_i \frac{\Delta X^k}{k!}. \quad (59)$$

The infinite series of Eqs. (58) and (59) are truncated for practical use after a certain number of terms. As a result of this approximation, the so-called truncation errors occurs. Summing up the expression of Eqs. (58) and (59) gives

$$u_{i+1} + u_{i-1} = 2u_i + \left(\frac{d^2u}{dX^2}\right)_i \Delta X^2 + \frac{1}{12} \left(\frac{d^4u}{dX^4}\right)_i \Delta X^4 + \cdots, \quad (60)$$

or rearranged for the second-order derivative:

$$\left(\frac{d^2u}{dX^2}\right)_i = \frac{u_{i+1} - 2u_i + u_{i-1}}{\Delta X^2} - \underbrace{\frac{1}{12} \left(\frac{d^4u}{dX^4}\right)_i \Delta X^2}_{O(\Delta X^2)} - \cdots. \quad (61)$$

The  $O$  in Eq. (61) reads “order of” and states if the second-order derivative of  $u(X)$  is approximated by the first expression on the right-hand side of Eq. (61), the truncation error is of order of  $\Delta X^2$ . This approximation is a second-order accurate approximation because of the truncated terms. In a similar way, other derivatives can be derived from Eqs. (58) and (59). Subtracting of Eqs. (58) from (59) gives

$$u_{i+1} - u_{i-1} = 2 \left(\frac{du}{dX}\right)_i \Delta X + \frac{1}{3} \left(\frac{d^3u}{dX^3}\right)_i \Delta X^3 + \cdots \quad (62)$$

459 or rearranged for the first-order derivative

$$\left(\frac{du}{dX}\right)_i = \frac{u_{i+1} - u_{i-1}}{2\Delta X} - \underbrace{\frac{1}{6} \left(\frac{d^3u}{dX^3}\right)_i \Delta X^2}_{o(\Delta X^2)} - \dots \quad (63)$$

460 This last approximation of the first-order derivative is called centered difference  
461 or centered Euler and the truncation error is of order  $\Delta X^2$ . Rearranging Eq. (58), i.e.,

$$u_{i+1} - u_i = \left(\frac{du}{dX}\right)_i \Delta X + \left(\frac{d^2u}{dX^2}\right)_i \frac{\Delta X^2}{2} + \dots, \quad (64)$$

462 or

$$\left(\frac{du}{dX}\right)_i = \frac{u_{i+1} - u_i}{\Delta X} - \underbrace{\left(\frac{d^2u}{dX^2}\right)_i \Delta X}_{o(\Delta X)} - \dots, \quad (65)$$

463 gives an expression for the forward difference or forward Euler approximation of the  
464 first-order derivative. In a similar way, Eq. (59) can be rearranged to obtain the  
465 backward difference or backward Euler approximation of the first-order derivative as:

$$\left(\frac{du}{dX}\right)_i = \frac{u_i - u_{i-1}}{\Delta X} + \underbrace{\left(\frac{+d^2u}{dX^2}\right)_i \Delta X}_{o(\Delta X)} - \dots \quad (66)$$

466 Further derivatives of  $u(X)$  can be obtained if  $u$  is evaluated at nodes  
467  $i + 2$ ,  $i - 2$ , etc. through a Taylor's series about the node  $i$ . Some common expres-  
468 sions for derivatives of different order are summarized in Table 1.

469 Returning to the problem shown in Fig. (20) and described by Eq. (55), a finite  
470 difference approximation of second-order accuracy for node  $i$  can be written as:

$$EA \left( \frac{u_{i+1} - 2u_i + u_{i-1}}{\Delta X^2} \right) = -p_i, \quad (67)$$

471 or as

$$\frac{EA}{\Delta X} (-u_{i-1} + 2u_i - u_{i+1}) = R_i, \quad (68)$$

472 where the equivalent nodal force  $R_i$  resulting from a distributed load  $p(X)$  is in  
473 general given for an *inner* node  $i$  as:  $R_i = \int_{-\Delta X/2}^{\Delta X/2} p(\tilde{x}) d\tilde{x}$ . In this integral, the local

t.1 **Table 1** Finite difference  
t.2 approximations for various  
t.3 differentiations, (Bathe  
t.4 1996)

Derivative	Finite difference approximation	Error
$\left(\frac{du}{dX}\right)_i$	$\frac{u_{i+1}-u_i}{\Delta X}$	$O(\Delta X)$
	$\frac{u_i-u_{i-1}}{\Delta X}$	$O(\Delta X)$
	$\frac{u_{i+1}-u_{i-1}}{2\Delta X}$	$O(\Delta X^2)$
$\left(\frac{d^2u}{dX^2}\right)_i$	$\frac{u_{i+1}-2u_i+u_{i-1}}{\Delta X^2}$	$O(\Delta X^2)$
$\left(\frac{d^3u}{dX^3}\right)_i$	$\frac{u_{i+2}-2u_{i+1}+2u_{i-1}-u_{i-2}}{2\Delta X^3}$	$O(\Delta X^2)$
$\left(\frac{d^4u}{dX^4}\right)_i$	$\frac{u_{i+2}-4u_{i+1}+6u_i-4u_{i-1}+u_{i-2}}{\Delta X^4}$	$O(\Delta X^2)$

474 coordinate  $x$  has its origin at the location of node  $i$ . In the case of the boundary nodes,  
475 the equivalent nodal loads must be calculated as  $R_1 = \int_0^{\Delta x/2} p(\tilde{x})d\tilde{x}$  in  $R_n = \int_{-\Delta x/2}^0$   
476  $p(\tilde{x})d\tilde{x}$  order to completely distribute the entire load  $p(X)$  to the nodes.

477 Returning to the example shown in Fig. 20 and assuming  $n = 5$  nodes, i.e., two  
478 boundary nodes and three inner nodes, the evaluation of the finite difference  
479 approximation at the inner nodes [2,4] gives:

node 2 :  $\frac{EA}{\Delta X}(-u_3 + 2u_2 - u_1) = 0,$  (69)

node 3 :  $\frac{EA}{\Delta X}(-u_4 + 2u_3 - u_2) = 0,$  (70)

node 4 :  $\frac{EA}{\Delta X}(-u_5 + 2u_4 - u_3) = 0.$  (71)

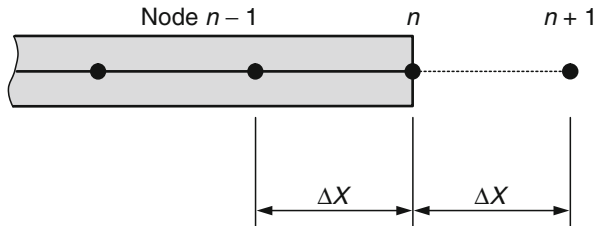
480 These three equations still contain five unknowns  $u_1, \dots, u_5$ , and it is required to  
481 introduce the boundary conditions in order to solve this system of equations. The given  
482 displacement  $u_1 = 0$  (Dirichlet or first-type boundary condition) can be easily intro-  
483 duced in Eq. (69) but the consideration of the force boundary condition (Neumann or  
484 second-type boundary condition) at the right-hand boundary requires more efforts.  
485 Considering the equilibrium condition (Fish and Belytschko 2007), i.e.,  $\frac{dN}{dX} = -p(X)$   
486 together with the integrated form of the differential equation (55) gives the following  
487 expression for the internal normal force  $N$  as a function of the derivative of  $u(X)$ :

$$EA\left(\frac{du(X)}{dX}\right)_i = N(X). \tag{72}$$

488 To evaluate the gradient in Eq. (72), the different formulations given in Table 1  
489 can be used. If the higher accurate centered difference scheme should be used, it is  
490 necessary to introduce a fictitious node outside the bar as shown in Fig. 22.

491 Then, the finite difference approximation for the boundary node 5 can be  
492 written as:

**Fig. 22** Fictitious finite difference node  $n + 1$  outside the bar



$$\text{node 5 : } \frac{EA}{\Delta X} (-u_6 + 2u_5 - u_4) = 0, \quad (73)$$

and the gradient at the boundary node together with the force equilibrium, i.e.,  
 $N_5 = F$ , reads as

$$\left( \frac{du(X)}{dX} \right)_5 = \frac{u_6 - u_4}{2\Delta X} = \frac{F}{EA}, \quad (74)$$

from which the expression for  $u_6$  can be obtained as:

$$u_6 = u_4 + \frac{2F\Delta X}{EA}. \quad (75)$$

This result can be introduced in Eq. (73) to receive the required expression to  
 substitute  $u_5$  in Eq. (71) by given values:

$$u_5 = u_4 + \frac{F\Delta X}{EA}. \quad (76)$$

Thus, the final system of equations under consideration of the boundary conditions is given as:

$$\frac{EA}{\Delta X} \begin{bmatrix} 2 & -1 & 0 \\ -1 & 2 & -1 \\ 0 & -1 & 1 \end{bmatrix} \begin{bmatrix} u_2 \\ u_3 \\ u_4 \end{bmatrix} = \begin{bmatrix} 0 \\ 0 \\ F \end{bmatrix}. \quad (77)$$

It should be mentioned here that the same result can be obtained in this case based  
 on the finite element method. Simplifying Eq. (7) for constant cross-sectional area, i.e.,

$$\frac{EA}{\Delta X} \begin{bmatrix} 1 & -1 & 0 & 0 & 0 \\ -1 & 2 & -1 & 0 & 0 \\ 0 & -1 & 2 & -1 & 0 \\ 0 & 0 & -1 & 2 & -1 \\ 0 & 0 & 0 & -1 & 1 \end{bmatrix} \begin{bmatrix} u_1 \\ u_2 \\ u_3 \\ u_4 \\ u_5 \end{bmatrix} = \begin{bmatrix} 0 \\ 0 \\ 0 \\ 0 \\ F \end{bmatrix}, \quad (78)$$

and consideration of the boundary condition, i.e.,  $u_1 = 0$ , and elimination of  $u_5$   
 gives the same expression as in Eq. (77).

## 26.5.2 General Comments

The difference between the modeling of a problem with the finite element and the finite difference method is related to the discretization, cf. Fig. 23. In the case of the finite element method, the domain must be discretized with elements (which are composed of nodes and boundaries and which may have a bad shape), whereas the finite difference method requires only the discretization based of grid points which are not joined to elements. As a direct consequence, results are in the case of the finite difference method only obtained at the grid points and not interpolated as in the case of the finite element method. If required, such an interpolation between the grid points must be additionally implemented.

The advantage of the finite difference method is the simple computer implementation of the procedures and thus, it is easy to write own codes and to implement or consider new features. The drawback can be the consideration of the boundary conditions for complex shaped geometries and the consideration of the symmetry of the stiffness matrix might be difficult. Thus, many applications of the finite difference method are restricted to simple geometries. To overcome these problems, the so-called finite difference energy method was developed (Bushnell et al. 1971) where the displacement derivatives in the total potential energy of a system are approximated by finite differences and the minimum condition of the potential energy is used to calculate the unknown displacements.

In engineering practice, the finite difference method is nowadays not widely used and only quite a few publications are available since commercial finite element packages offer a huge range of features and possibilities to incorporate arbitrary geometries and nonlinearities. Typical examples of the application of the finite difference method in the context of adhesive technology are shown in Fig. 24. Crocombe and Bigwood (1992) derived a new sandwich model which considers the nonlinear stress-strain response of both the adherends and the adhesive layer under arbitrary loads imposed on the ends of the sandwich element. This new sandwich model can be easily incorporated into a wide variety of common adhesive geometries, cf. Fig. 24a. To model the adhesive layer, a series of nonlinear shear and tensile springs was assumed under consideration of the von Mises yield criterion.

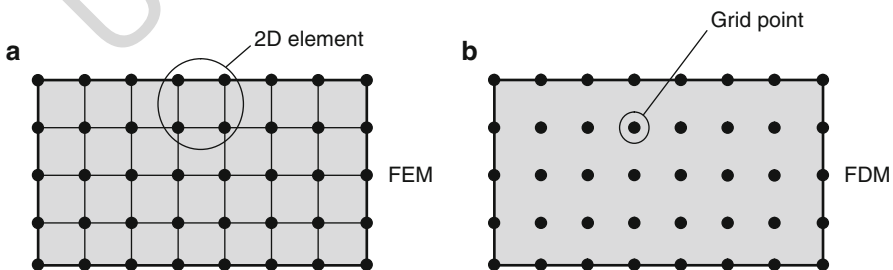


**Fig. 23** Comparison between the general FEM and FDM approach: (a) finite element mesh; (b) finite difference grid points. The structural model is shown in Fig. 18a

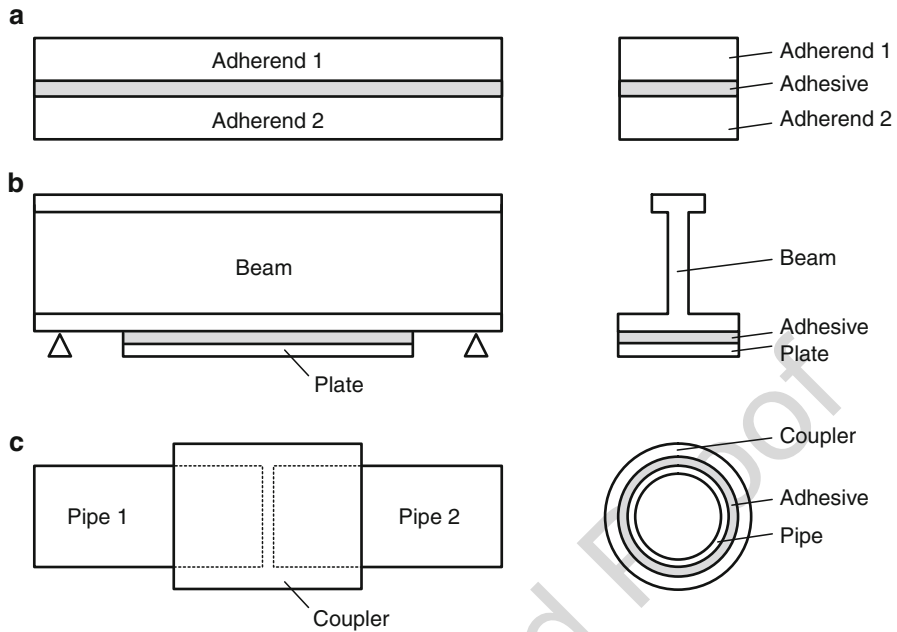


**Fig. 24** Examples of simple geometries for finite difference approach: (a) Sandwich model; (b) beam with strengthening plate; (c) pipe joint

The analytical derivations resulted in a set of six nonlinear first-order differential equations which were solved numerically using a finite-difference scheme. The model shown in Fig. 24a was extended by Wang et al. (2003) to include shear deformation of the adherends and then coupled to an existing analytical model for the detached adherend in a peel specimen. The major goal was to develop a reliable model of predicting adhesive failure in arbitrary joints to large-scale adherend yielding. As in the case of Crocombe and Bigwood (1992), a system of six nonlinear first-order differential equations was obtained and solved by the DBVPFD solver (*Double (Precision) Boundary Value Problem Finite Difference*) from the IMSL (*International Mathematical and Statistical Library*) Fortran library (IMSL Math/Library Manual 1997). A method for determining the elastic shear and peel stresses in an adhesive joint between a strengthening plate and a beam, cf. Fig. 24b, was developed by (Stratford and Cadei 2006) where the governing equations for shear and peel stresses were solved using a finite difference scheme with constant node spacing. The stresses in adhesively bonded composite tubular joints, cf. Fig. 24c, subjected to torsion were investigated by (Xu and Li 2010). Their analytical derivations resulted in a system of 18 second-order partial differential equations and 6 linear equations with 24 unknowns which were solved by a mathematical model based on the finite difference method.

In order to use a more realistic cohesive zone model which added the effects of normal stresses to a classical pure shear model, Carrara and Ferretti (2013) applied



**Table 2** Suggested applications of different approximation methods.

Method	Suggested application
Finite element method (FEM)	Any standard engineering problem; nonlinearities
Boundary element method (BEM)	Cracks; stress singularities; large stress gradients
Finite difference method (FDM)	Own code development and solution of new analytical derivations for simpler geometries

the finite difference method to solve a system of first-order nonlinear ordinary differential equations. The problem itself was related to fibre-reinforced polymer plates which were bonded on a concrete structure.

## 26.6 Conclusion

In the scope of this chapter, special numerical techniques were covered. First of all, techniques to reduce the size of a model in a computational finite element approach were presented. Substructuring and submodeling allow a significant reduction of the model size. However, it seems that the permanent increase of the performance of computer hardware pushes these techniques a bit to the background. Nevertheless, the presented methods are highly efficient and can dramatically reduce computational times and save resources. The second part of the chapter focused on alternative approximation methods. The boundary element and the finite difference method were introduced and advantages and disadvantages highlighted. The boundary method shows its advantages in the context of stress singularities while the finite difference method is easy to implement for simple geometries. Suggestions for the application of the different approximation methods are summarized in Table 2.

## References

Banerjee PK (1994) Boundary element methods in engineering. McGraw-Hill, London

Bathe KJ (1996) Finite element procedures. Prentice-Hall, Upper Saddle River

Beer G, Smith I, Duenser C (2008) The boundary element method with programming. Springer, Wien

Brebbia CA, Felles JCF, Wrobel JCF (1984) Boundary element techniques: theory and applications. Springer, Berlin

Bushnell D, Almroth BO, Brogan F (1971) Finite-difference energy method for nonlinear shell analysis. Comput Struct 1:361–387

Carrara P, Ferretti D (2013) A finite-difference model with mixed interface laws for shear tests of FRP plates bonded to concrete. Compos Part B Eng 54:329–342

Collatz L (1966) The numerical treatment of differential equations. Springer, Berlin

Cook RD, Malkus DS, Plesha ME, Witt RJ (2002) Concepts and applications of finite element analysis. Wiley, New York

- 586 Crocombe AD, Bigwood DA (1992) Development of a full elasto-plastic adhesive joint design  
587 analysis. *J Strain Anal Eng Des* 27(4):211–218
- 588 da Silva LFM, Campilho RDSG (2012) *Advances in numerical modelling of adhesive joints*.  
589 Springer, Heidelberg
- 590 de G Allen DN (1955) *Relaxation methods*. McGraw-Hill, New York
- 591 Dohrmann CR, Key SW, Heinstein MW (2000) A method for connecting dissimilar finite element  
592 meshes in two dimensions. *Int J Numer Meth Eng* 48:655–678
- 593 Fish J, Belytschko T (2007) *A first course in finite elements*. Wiley, Chichester
- 594 Forsythe GE, Wasow WR (1960) *Finite-difference methods for partial differential equations*. Wiley,  
595 New York
- 596 Gaul L, Kögl M, Wagner M (2003) *Boundary element methods for engineers and scientists*.  
597 Springer, Berlin
- 598 Gmür TC, Kauten RH (1993) Three-dimensional solid-to-beam transition elements for structural  
599 dynamics analysis. *Int J Numer Meth Eng* 36:1429–1444
- 600 Gonçalves DJS, Campilho RDSG, Silva LFMD, Fernandes JLM (2014) The use of the boundary  
601 element method in the analysis of single lap joints. *J Adhes* 90:50–64
- 602 Groth HL (1986) Calculation of stresses in bonded joints using the substructuring technique. *Int J*  
603 *Adhes Adhes* 6(1):31–35
- 604 IMSL Math/Library Manual (1997) Chapter 5: differential equations. Visual Numeric Inc, Houston
- 605 Javanbakht Z, Öchsner A (2017) Advanced finite element simulation with MSC Marc: application  
606 of user subroutines. Springer, Cham
- 607 Knight NF, Ransom JB, Griffin OH, Thompson DM (1991) Global/local methods research using a  
608 common structural analysis framework. *Finite Elem Anal Des* 9:91–112
- 609 Lee SS (1998) Boundary element analysis of the stress singularity at the interface corner of  
610 viscoelastic adhesive layers. *Int J Solids Struct* 35(13):1385–1394
- 611 Lourenço F, Aguirre IF, Albuquerque EL, Sollero P (2003) Boundary element analysis of panels  
612 reinforced by adhesive plates. In: Pesce CP (ed) *Proceedings of the 17th international congress*  
613 *of mechanical engineering – COBEM 2003*
- 614 Love AEH (1944) *A treatise on the mathematical theory of elasticity*. Dover Publications, Mineola
- 615 Mackerle J (1995a) Fastening and joining: finite element and boundary element analyses – a  
616 bibliography (1992–1994). *Finite Elem Anal Des* 20:205–215
- 617 Mackerle J (1995b) Some remarks on progress with finite elements. *Comput Struct* 55:1101–1106
- 618 Mitchell AR, Griffiths DF (1980) *The finite difference method in partial differential equations*.  
619 Wiley, New York
- 620 Öchsner A (2016) *Computational statics and dynamics: an introduction based on the finite element*  
621 *method*. Springer, Singapore
- 622 Öchsner A, Merkel M (2013) *One-dimensional finite elements: an introduction to the FE method*.  
623 Springer, Berlin
- 624 Paroissien E, Gaubert F, Veiga AD, Lachaud F (2013) Elasto-plastic analysis of bonded joints with  
625 macro-elements. *J Adhes Sci Technol* 27(13):1464–1498
- 626 Pisa CD, Aliabadi MH (2015) Boundary element analysis of stiffened panels with repair patches.  
627 *Eng Anal Bound Elem* 56:162–175
- 628 Raamachandran J (2000) *Boundary and finite elements – theory and problems*. Alpha Science  
629 International, Pangbourne
- 630 Raghu ES (2009) *Finite element modeling techniques in MSC.NASRAN and LS/DYNA*. Arup,  
631 London
- 632 Reddy JN (2006) *An introduction to the finite element method*. McGraw Hill, Singapore
- 633 Sokolnikoff I (1956) *Mathematical theory of elasticity*. McGraw-Hill, New York
- 634 Southwell RV (1946) *Relaxation methods in theoretical physics*. Clarendon Press, Oxford
- 635 Stratford T, Cadei J (2006) Elastic analysis of adhesion stresses for the design of a strengthening  
636 plate bonded to a beam. *Constr Build Mater* 20(1–2):34–45
- 637 Vable M, Maddi JR (2006) Boundary element analysis of adhesively bonded joints. *Int J Adhes*  
638 *Adhes* 26:133–144

- 639 Wahab MMA, Ashcroft IA, Crocombe AD (2004) A comparison of failure prediction methods for  
640 an adhesively bonded composite beam. *J Strain Anal* 39(2):173–185
- 641 Wang RX, Cuia J, Sinclair AN, Spelt JK (2003) Strength of adhesive joints with adherend yielding:  
642 I. Analytical model. *J Adhes* 79(1):23–48
- 643 Wang ZY, Wang L, Guo W, Deng H, Tong JW, Aymerich F (2009) An investigation on strain/stress  
644 distribution around the overlap end of laminated composite single-lap joints. *Compos Struct*  
645 89:589–595
- 646 Wen PH, Aliabadi MH, Young A (2002) Boundary element analysis of flat cracked panels with  
647 adhesively bonded patches. *Eng Fract Mech* 69:2129–2146
- 648 Wen PH, Aliabadi MH, Young A (2003) Boundary element analysis of curved cracked panels with  
649 adhesively bonded patches. *Int J Numer Methods Eng* 58:43–61
- 650 Xu W, Li G (2010) Finite difference three-dimensional solution of stresses in adhesively bonded  
651 composite tubular joint subjected to torsion. *Int J Adhes Adhes* 30:191–199
- 652 Young A, Rooke DP (1992) Analysis of patched and stiffened cracked panels using the boundary  
653 element method. *Int J Solids Struct* 29(17):2201–2216
- 654 Zhao C, Hobbs BE, Mühlhaus HB, Ord A (1999) A consistent point-searching algorithm for  
655 solution interpolation in unstructured meshes consisting of 4-node bilinear quadrilateral ele-  
656 ments. *Int J Numer Methods Eng* 45:1509–1526
- 657 Zienkiewicz OC, Taylor RL (2000) *The finite element method – volume 1: the basis*. Butterworth-  
658 Heinemann, Oxford

# Design Rules and Methods to Improve Joint Strength

# 27

Lucas Filipe Martins da Silva, E. A. S. Marques, and  
R. D. S. G. Campilho

## Contents

27.1	Introduction .....	774
27.2	Factors Affecting Joint Strength .....	778
27.2.1	Adhesive Properties .....	778
27.2.2	Adherend Properties .....	780
27.2.3	Adhesive Thickness .....	781
27.2.4	Overlap .....	784
27.2.5	Residual Stresses .....	786
27.3	Methods to Increase Joint Strength .....	787
27.3.1	Filletts .....	787
27.3.2	Adherend Rounding .....	788
27.3.3	Adherend Shaping .....	790
27.3.4	Other Geometric Solutions .....	792
27.4	Hybrid Joints .....	792
27.4.1	Mixed Adhesive Joints .....	794
27.4.2	Adhesive Joints with Functionally Graded Materials .....	795
27.4.3	Rivet-Bonded Joints .....	795
27.4.4	Bolted-Bonded Joints .....	796
27.4.5	Weld-Bonded Joints .....	796

---

L. F. M. da Silva (✉)

Department of Mechanical Engineering, Faculty of Engineering, University of Porto, Porto, Portugal

e-mail: [lucas@fe.up.pt](mailto:lucas@fe.up.pt)

E. A. S. Marques

Instituto de Ciência e Inovação em Engenharia Mecânica e Engenharia Industrial (INEGI), Porto, Portugal

e-mail: [emarques@fe.up.pt](mailto:emarques@fe.up.pt)

R. D. S. G. Campilho

Instituto Superior de Engenharia do Porto (ISEP), Instituto Politécnico do Porto, Porto, Portugal

e-mail: [raulcampilho@gmail.com](mailto:raulcampilho@gmail.com)

24	27.5	Repair Techniques .....	796
25	27.6	Configurations Recommended for Various Types of Joints .....	797
26	27.6.1	Butt Joints .....	797
27	27.6.2	Lap Joints .....	798
28	27.6.3	Strap Joints .....	799
29	27.6.4	Reinforcements .....	801
30	27.6.5	Cylindrical Joints .....	801
31	27.6.6	T Joints .....	803
32	27.6.7	Corner Joints .....	805
33	27.7	Conclusions .....	805
34		References .....	807

### Abstract

One of the main reasons for the increasing use of adhesive bonding is the fact that the stress distribution is more uniform than with other conventional methods of joining which enables to reduce weight. However, even in adhesive joints the stress distribution is not perfectly uniform and this leaves room for improvements. The major enemy of adhesive joints is peel or cleavage stresses. These should be reduced if strong joints are to be designed. In this chapter, the main factors influencing the joint strength are first discussed. The focus is on lap joints because these are the most common. Methods are then proposed to improve the joint strength by using fillets, adherend profiling, and other geometric solutions. Hybrid joining is also a possibility to improve the strength of adhesive joints, and adhesives may be used in conjunction with rivet or bolts, for example. Joints may be damaged in some way and it is important to discuss also methods to guarantee an efficient repair design. Finally, configurations are recommended for several types of joints such as butt joints, strap joints, cylindrical joints, and T joints. The main rule for all cases is to spread the load over a large area and reduce the peel stresses.

## 27.1 Introduction

Knowledge of the state of stresses inside the adhesive layer of an adhesively bonded joint is essential for joint strength prediction and joint design. There are two methods for the stress analysis of lap joints, namely analytical and numerical methods. Analytical methods using closed-form algebra employ classical linear theories in which some simplifications are used. The finite element (FE) method, on the other hand, is a well-established numerical technique which can handle complex structures and nonlinear material properties where classical methods generally fail to work. Although the closed-form solutions have their limitations, they are easy to use, especially for parametric studies. The FE method needs large computer power, especially if high accuracy is required, and experienced personnel. Consequently, the former is widely used for joint design and the latter for research or for complex geometries. There are many analytical models in the literature for obtaining stress and strain distributions. Many closed-form models are based on modified shear-lag

equations, as proposed originally by Volkersen (1938). Reviews of these closed-form theories and their assumptions can be found in da Silva et al. (2009a, b) and in ► Chap. 24, “Analytical Approach.” As the analytical equations become more complex (including factors such as stress variation through the adhesive thickness, plasticity, thermal effects, etc.), there is a greater requirement to use computing power to solve for the stresses. Hart-Smith (1973) had a great influence on the methods used for stress analysis of adhesive joints. Versions of this method have been prepared as Fortran programs and have been used extensively in the aerospace industry. Other analyses have been implemented in spreadsheets or as a program for personal computers (PCs). The software packages are there to assist in the design of efficient joints. A brief overview of commercial PC based analysis/design software packages is given in Table 1. The main features of each software package are identified. As shown in Table 1, the existing software packages are very specific and most of them only cover one or two joints geometries. For most of the softwares, the selection process is dependent on the previous experience of the designer, apart from those of da Silva et al. (2009c) and Dragoni et al. (2010).

The design philosophy associated to adhesive joints is radically different from that of other traditional methods of joining such as bolts or rivets. Therefore, it is not advised to take a joint initially designed for another type of joining method and modify it for adhesive bonding. The first point in design is to choose a suitable adhesive which will depend on the type of loading, the adherends to bond, and the environment (temperature and humidity). Adhesives, which are polymeric materials, are not as strong as the adherends they are joining such as metals or composites. However, when they are loaded over a large area such as in a single-lap joint, they can provide a high strength, sufficient to deform plastically the metal in some cases or to break the composite. That is why when designing an adhesive joint, the load must be spread over a large area and not concentrated in one point. Peel loads are the greatest enemy of the designer of bonded joints (Adams et al. 1997). The adhesive should be loaded in shear whenever possible and the peel and cleavage stresses should be avoided. However, there might be limitations in terms of manufacturing process, cost, consequences of failure, and desired final appearance that may complicate the designing process.

The strength of an adhesive joint in the absence of environmental factors is determined by the mechanical properties of the adhesive and adherends, the joint geometry, and the residual internal stresses. In effect, localized stresses are not always apparent and may occur as a result of differential thermal expansion of the adhesive and adherends. Another cause is shrinkage of adhesive during cure. These factors are all discussed and simple design guidelines are given. The joint strength can be improved by a number of techniques such as fillets, adherend shaping, and other geometric solutions. All these aspects are discussed in detail. Hybrid joints are increasingly being used for improving the strength of adhesive joints. Adhesive can be used in conjunction with a rivet, a bolt, or a spot weld. The advantages of such solutions are explained in this chapter. Repair techniques are also treated because joints may be damaged in some way and it is important to discuss methods to guarantee an efficient repair design. Finally, configurations are recommended for several types of joints such as butt joints, strap joints, cylindrical joints, and T joints.

t.1 **Table 1** Software packages available in the market (Adapted from National Physical Laboratory (2007))

t.2	Name	Supplier	Application	Features
t.3	BOLT	G.S. Springer Stanford University, USA	Design of pin-loaded holes in composites	Prediction of failure strength and failure mode
t.4				Three types of bolted joints: Joints with a single hole, joints with two identical holes in a row
t.5				Joints with two identical holes in tandem
t.6				Applicable to uniform tensile loads and symmetric laminates
t.7	BISEPSLOCO	AEA Technology, UK	Closed-form computer code for predicting stresses and strains in adhesively bonded single- lap joints	Tensile/shear/bending moment loading
t.8				Adhesive peel and shear stress predictions
t.9				Allowance for plasticity in adhesive layer
t.10				Thermal stress analysis
t.11	BISEPSTUG	AEA Technology, UK	Closed-form computer code for predicting stresses and strains in adhesively bonded coaxial joints	Stepped and profiled joints
t.12				Orthotropic adherends
t.13				Torsional and axial loading
t.14				Allowance for plasticity in adhesive layer
t.15	CoDA	National Physical Laboratory, UK	Preliminary design of composite beams and panels, and bolted joints	Thermal stress analysis
t.16				Synthesis of composite material properties (lamina and laminates for a range of fiber formats)
t.17				Parametric analyses
t.18				Panel and beam design
t.19	DLR	DLR- Mitteilung, Germany	Preliminary design of composite joints	Bonded and bolted double shear joints
t.20				Bearing, shear-out, pin shear, and bypass tensile failure prediction
t.21				Adhesively bonded and bolted joints
t.22				Linear-elastic and linear- elastic/plastic behavior
t.23	DLR	DLR- Mitteilung, Germany	Preliminary design of composite joints	Tension and shear loading
t.24				Symmetric and asymmetric lap joints
t.25				Bearing, shear-out, pin shear, and bypass tensile failure prediction (washers and bolt tightening)

(continued)

**t.26 Table 1** (continued)

t.27	Name	Supplier	Application	Features
t.28	FELOCO	AEA Technology, UK	Finite element module computer code for predicting stresses and strains in adhesively bonded lap shear joints	Stepped and profiled joints
t.29				Tensile/shear/bending moment/pressure loading
t.30				Linear and nonlinear analysis
t.31				Peel, shear, and longitudinal stress predictions in adhesive layer and adherends
t.32				Thermal stress analysis for adherend and adhesive
t.33	PAL	Permabond, UK	“Expert” system for adhesive selection	Joined systems include:
t.34				Lap and butt joints, sandwich structures, bushes/gears/bearings/shafts/pipes/threaded fittings
t.35				Elastic analysis
t.36				Creep/fatigue effects on joint stiffness (graphical)
t.37	RETCALC	Loctite, UK	Interactive windows-based software general purpose	Joint strength
t.38				Correction factors (temperature and fatigue)
t.39	ESDU	Engineering Science Data Unit, UK	Software for use in structural design	ESDU 78042 shear stresses in the adhesives in bonded joints. Single-step double-lap joints loaded in tension
t.40				ESDU 79016 inelastic shear stresses and strains in the adhesives bonding lap joints loaded in tension or shear (computer program)
t.41				ESDU 80011 elastic stresses in the adhesive in single-step double-lap bonded joints
t.42				ESDU 80039 elastic adhesive stresses in multistep lap joints loaded in tension (computer program)
t.43				ESDU 81022 guide to the use of data items in the design of bonded joints
t.44	Joint Designer (da Silva et al. 2009c)	Faculty of Engineering, University of Porto, Portugal	Closed-form computer code for predicting stresses and strength in adhesively bonded joints	Accessible to nonexperts
t.45				Lap joints
t.46				Adhesive peel and shear stress predictions
t.47				Joint strength prediction
t.48				Allowance for plasticity in adhesive layer and adherends
t.49				Orthotropic adherends
t.50				Thermal stress analysis

(continued)



**t.51 Table 1** (continued)

t.52	Name	Supplier	Application	Features
t.53	JointCalc (Dragoni et al. <a href="#">2010</a> )	Henkel AG, Germany	Closed-form computer code for predicting stresses and strength in adhesively bonded joints	Accessible to non-experts
t.54				Single- and double-lap joints, single- and double-strap joints, peel joints and cylindrical joints
t.55				Adhesive peel and shear stress predictions
t.56				Joint strength prediction

**27.2 Factors Affecting Joint Strength**

The major factors that affect the joint strength of lap joints are the material properties (adherends and adhesive) and the geometry (adherend and adhesive thickness, and overlap). Residual internal stresses due to thermal effects should also be taken into account. The stress distribution in adhesive joints is not uniform (see ► [Chaps. 24, “Analytical Approach”](#) and ► [25, “Numerical Approach: Finite Element Analysis”](#)), therefore, the average shear stress (i.e., load divided by the bonded area) can be much lower than the local maximum stress. Failure always occurs at the stress concentrations and it is fundamental to decrease these stress peaks if a joint strength improvement is required. There are general guidelines to increase the joint strength by minimizing the stress concentrations:

- Use an adhesive with a low modulus and ductile behavior
- Use similar adherends or if not possible balance the stiffness
- Use a thin adhesive layer
- Use a large bonded area

Each of these factors is discussed next and detailed design guidelines are given. The residual stresses caused by thermal effects are also discussed. Note that the joint strength can be further improved by using adhesive fillets, adherend tapers, and adhesive bands along the overlap or hybrid joints. These solutions are described in Sect. 3.

**27.2.1 Adhesive Properties**

It is very important to distinguish adhesive strength and joint strength. The joint strength may not increase if a stronger adhesive is used. The joint strength depends not only on the adhesive strength but also on its ductility and stiffness. Adhesives with high ductility and flexibility have generally a low strength. However, when used in a joint, their ability to distribute uniformly the stress along the overlap (low stiffness) and deform plastically

**Fig. 1** Effect of the adhesive modulus on the adhesive stress distribution along the overlap

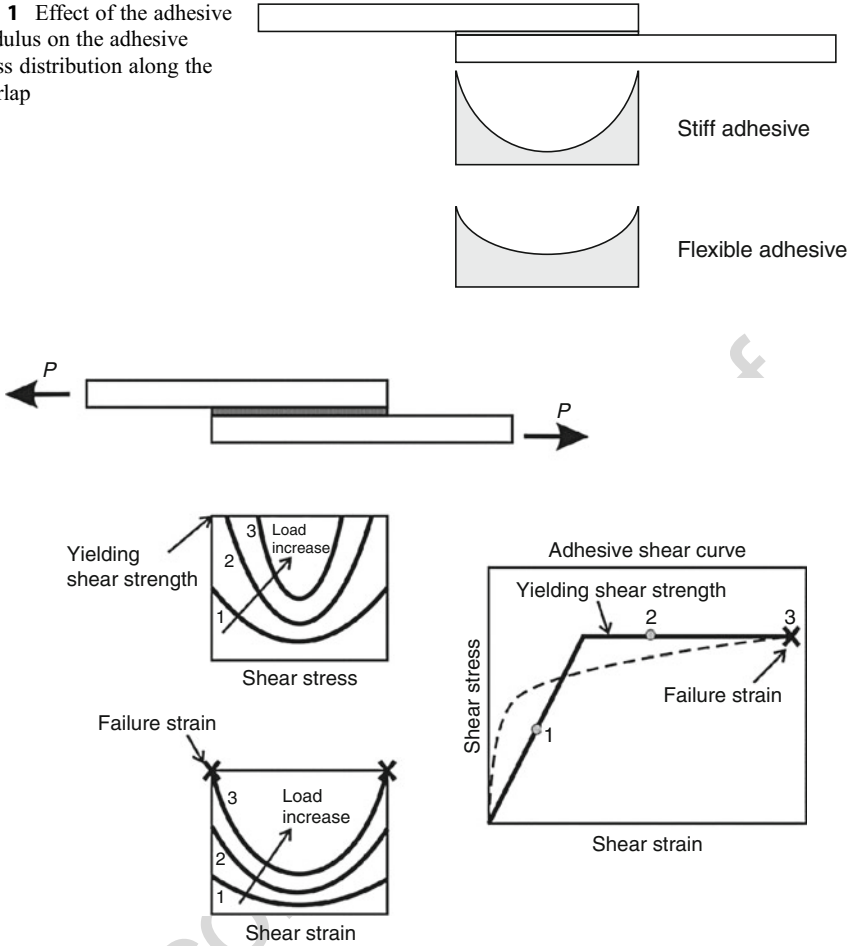
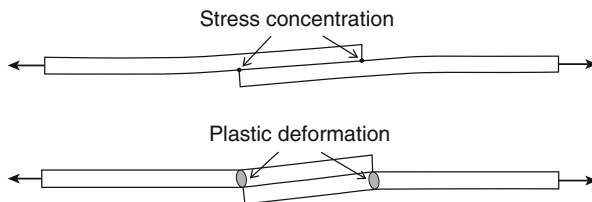


**Fig. 2** Effect of the adhesive ductility on the adhesive stress distribution along the overlap (Adapted from Hart-Smith (1973))

can give a joint strength much higher than with apparently strong but less ductile adhesives (da Silva et al. 2006). A low modulus adhesive gives a more uniform stress distribution compared to a stiff adhesive where there is a high stress concentration at the ends of the overlap (see Fig. 1). A ductile adhesive is able to redistribute the load and make use of the less stressed parts of the overlap, whereas a brittle adhesive concentrates the load at the ends of the overlap giving a low average shear stress (see Fig. 2). Adhesives are either strong, brittle, and stiff, or weak, ductile, and flexible. The ideal would be to have a strong, ductile, and flexible adhesive but this is very difficult to achieve, although the properties are independent. It is recommended to use ductile adhesives, but this also depends on the overlap, as will be seen in Sect. 2.4.

**Fig. 3** Adherend yielding in a single-lap joint



Ductile adhesives are also more resistant to crack propagation than brittle adhesives, giving a much higher toughness. The fatigue strength is generally lower for brittle adhesives. If the fatigue limit is measured in terms of a percentage of the static maximum joint strength, then the fatigue life of joints with ductile adhesives is considerably higher than that of joints with brittle adhesives. This is due to a more uniform stress distribution and also because of the higher damping energy associated to ductile adhesives. In the case of nonuniform loading such as peel, cleavage, or thermal internal stresses, a joint with a ductile adhesive will also give a better response.

### 27.2.2 Adherend Properties

Adherend properties also have a huge impact on the joint strength. The most important are the adherend modulus and its strength. The higher the adherend modulus, the lower will be its deformation at the ends of the overlap, where the load transfer takes place, and the lower will be the effect of the differential straining in the adhesive (Volkersen 1938). The adherend strength is also fundamental and can explain many joint failures. In the case of metallic adherends, the adherend yielding can cause a premature failure of the joint. As the load imposed on the joint increases, the stress imposed at the edge of the overlap increases. When the stress reaches the yield point of the steel, large plastic strains result, creating a plastic hinge as shown in Fig. 3. Although the stresses are limited, the strains associated with the stress in the plastic range are very large. As the maximum adhesive strain is limited, it therefore fails when the maximum adhesive strain is exceeded. In other words, it is the adherend yielding that controls failure.

In the case of composite laminate adherends, it is recommended to have the outer layers with a direction parallel to the loading direction to avoid intralaminar failure of these layers. In any case, the major problem is the low transverse strength (through the thickness) of composites that is of the same order or lower than the adhesive tensile strength. This is a major problem of adhesive joints with composites that tend to fail in an interlaminar manner due to the high peel stresses at the ends of the overlap, as shown in Fig. 4. If failure occurs in the composite, a failure criterion in the adhesive (maximum stress and maximum strain) overestimates the joint strength. Predictions based on the composite transverse stress at the interface compare very well with the experiments (da Silva et al. 2009b). One solution to decrease the peel stresses is by tapering the adherends, as will be discussed in Sect. 3.3.

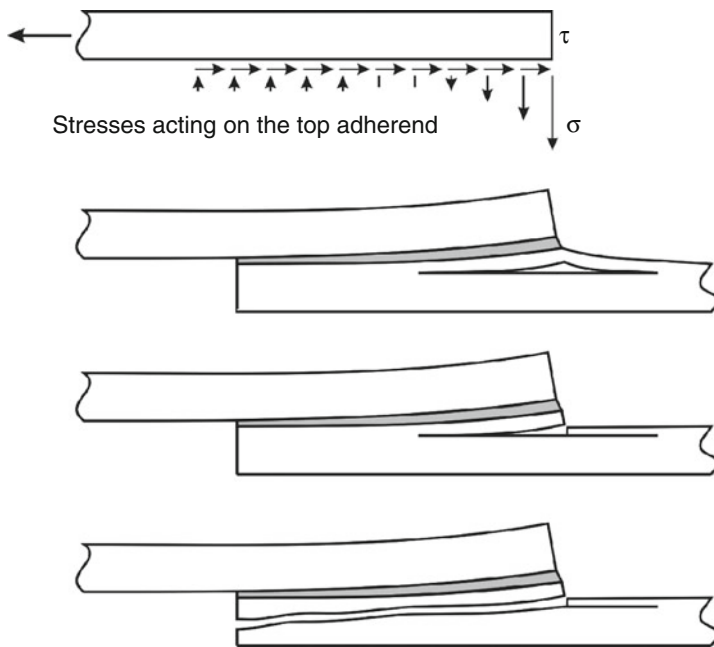


**Fig. 4** Interlaminar failure of the composite in adhesive joints (Adapted from Hart-Smith (1973))

The use of dissimilar adherends decreases the joint strength due to a nonuniform stress distribution (see Fig. 5b). To reduce this problem, the joint should be designed so that the longitudinal stiffness of the adherends to be bonded are equal, i.e.,  $E_1 t_1 = E_2 t_2$ , where  $E$  is the longitudinal modulus,  $t$  the thickness, and the subscripts (1, 2) refer to adherend 1 and adherend 2.

### 27.2.3 Adhesive Thickness

The effect of the bondline thickness on single-lap joints is well-documented in the literature. Most of the results are for typical structural adhesives and show that the lap-joint strength decreases as the bondline increases (da Silva et al. 2006; Adams and Peppiatt 1974). Experimental results show that for structural adhesives, the optimum joint strength is obtained with thin bondlines, in the range of 0.1–0.2 mm. However, the classical analytical models such as those of Volkersen (1938) or Goland and Reissner (1944) predict the opposite. There are many theories that attempt to explain this fact and this subject is still controversial. Adams and Peppiatt (1974) explained that an increase in the bondline thickness increases the probability of having internal imperfection in the joint (voids and microcracks), which will lead to premature failure of the joints. Crocombe (1989) shows that thicker single-lap joints (SLJs) have a lower strength, by considering the plasticity of the adhesive. An elastic analysis shows that the stress distribution

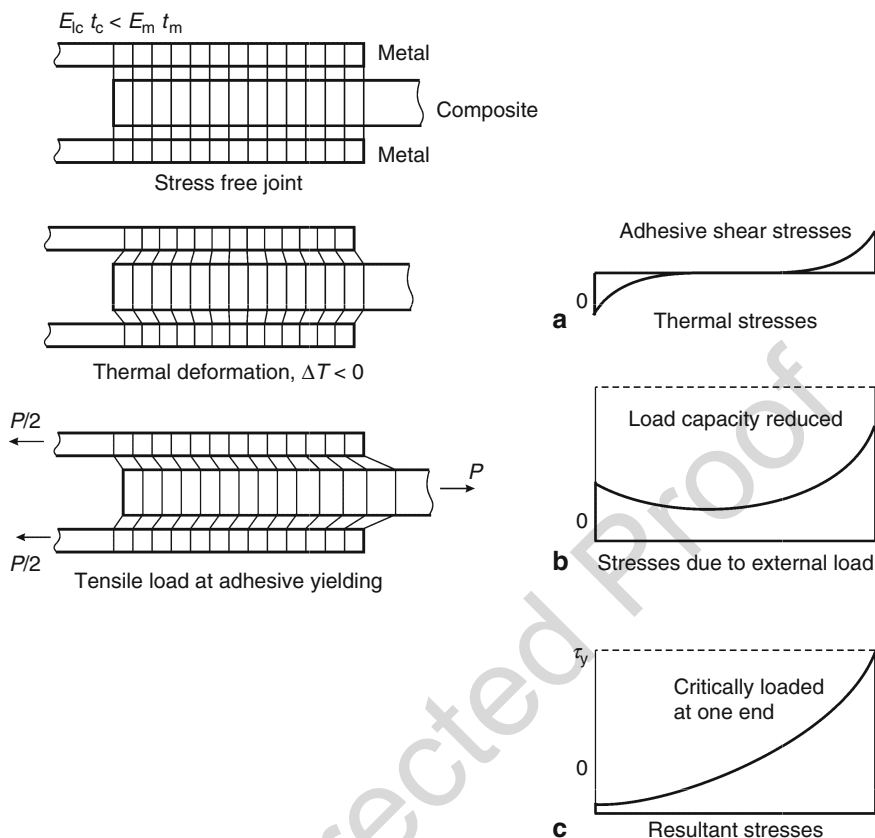


**Fig. 5** Adhesive shear stresses in a metal/composite double-lap joint for the case where the composite has a lower longitudinal stiffness than the metal ( $E_{lc} t_c < E_m t_m$ ) under a tensile load and a thermal load, at adhesive yielding ( $\tau_y$ ) (Adapted from Hart-Smith (1973))

of a thin bondline is more concentrated at the ends of the overlap than a thicker bondline which has a more uniform stress distribution. A thin bondline will therefore reach the yielding stress at a lower load than a thick bondline. However, when yielding does occur in a thicker joint, there is a less “elastic reserve” to sustain further loading, thus yielding spreads more quickly (see Fig. 6). Gleich et al. (2001) showed with a finite element analysis on single-lap joints that increases in the interface stresses (peel and shear) as the bondline gets thicker cause the failure load of a bonded joint to decrease with increasing bondline thickness. They found that for the low bondline thickness range, an optimum distribution of stresses along the joint interface exists for maximum joint strength. Grant et al. (2009a) found a reduction in joint strength with increasing the bondline thickness when testing SLJs for the automotive industry with an epoxy adhesive. The strength reduction was attributed to the higher bending moments for the lap

**Fig. 6** Stress distribution in a thick (*top*) and in a thin (*bottom*) adhesive layer

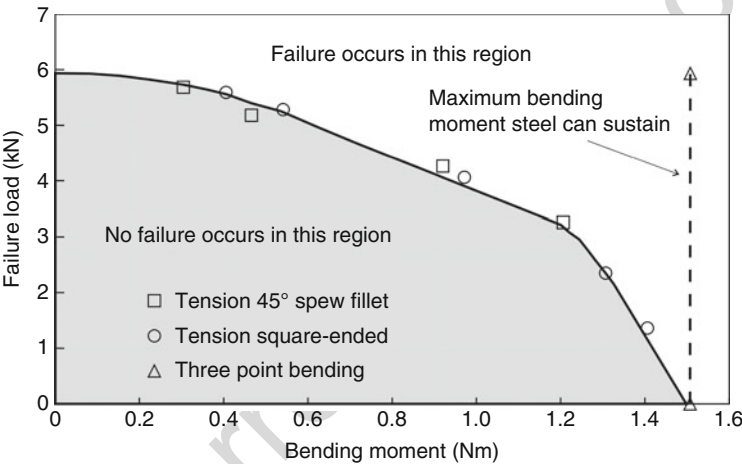
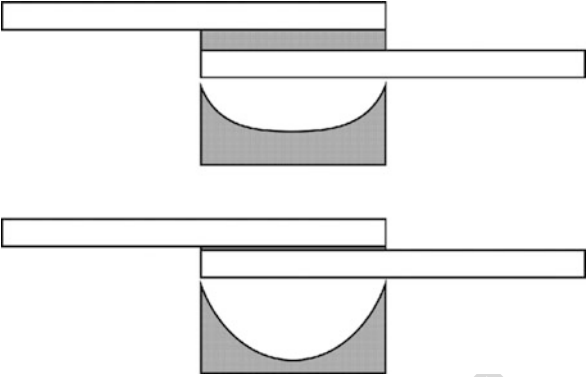


**Fig. 7** Failure envelope for lap joints produced from sheet steel and an epoxy adhesive

joints with thick bondlines due to the increase in the loading offset. Figure 7 shows the failure envelope obtained by Grant et al. (2009a) for single-lap joints under tension and three-point bending with mild steel where failure is dictated by the adherend yielding. It can be seen that there is a clear relationship between the bending moment at the edge of the overlap at failure, and the tensile failure load. This forms an envelope of failure, where any combination of load and bending moment outside the envelope means that failure occurs, and any combination inside means that the joint will not fail. The limits are defined by the relationship between bending moment and failure load that can be deduced from the adhesive/adherend combination, and the maximum bending moment that can be sustained by the adherend. Further studies (Grant et al. 2009b, c) show that this failure envelope is also applicable to other types of joints (T joints) and environments (temperature).

## 27.2.4 Overlap

Increasing the joint width increases the strength proportionally. However, the effect of the overlap length depends on the type of adhesive (i.e., ductile or brittle) and on the adherend yielding strength. Three cases should be considered: elastic adherends (e.g., high-strength steel) and ductile adhesive, elastic adherend and brittle adhesive and adherends that yield. For elastic adherends and ductile adhesives (more than 20% shear strain to failure), the joint strength is approximately proportional to the overlap. This is because ductile adhesives can deform plastically, redistribute the stress as the load increases, and make use of the whole overlap. In this case the failure criterion is the global yielding of the adhesive. For adhesives with intermediate ductility, the adhesive fails because the strain in the adhesive at the ends of the overlap reaches the adhesive shear strain to failure (see Fig. 8). For elastic adherends and brittle adhesives, the joint strength is not proportional to the overlap and a plateau is reached. This is because the stress is concentrated at the ends of the overlap and a longer overlap does not alter the stress distribution along the overlap. For adherends that yield, the failure is dictated by the adherend yielding and again a plateau is reached corresponding to the adherend yielding.

Adams et al. (1997) proposed a simple methodology for designing single-lap joints under tension, which is represented graphically in Fig. 9. The upper limit is given by the load corresponding to the total plastic deformation of the adhesive (global yielding) which is

$$P_{GY} = \tau_y \cdot b \cdot l \quad (1)$$

where  $P_{GY}$  is the failure load of the adhesive due to global yielding,  $\tau_y$  is the yield strength of the adhesive,  $b$  is the joint width, and  $l$  is the overlap length. A lower limit

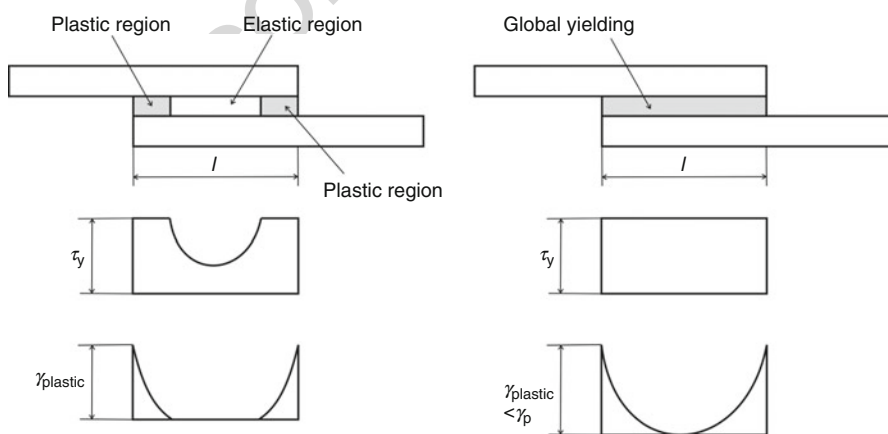
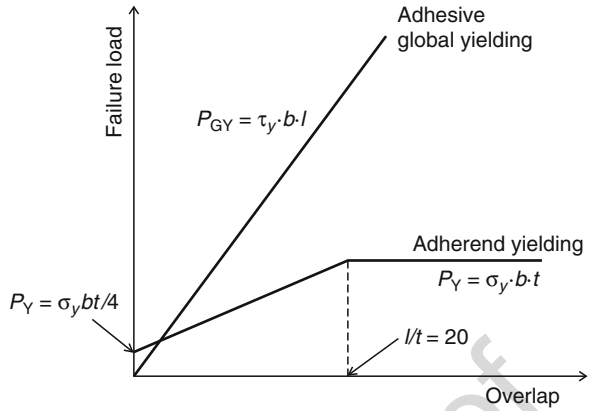


**Fig. 8** Failure due to adhesive shear strain (*left*) and due to global yielding (*right*).  $\tau_y$  is the yielding shear stress, and  $\gamma_p$  is the plastic shear strain at failure

**Fig. 9** Failure load vs. overlap length ( $P_{GY}$  is the failure load of the adhesive due to global yielding,  $\tau_y$  is the yield strength of the adhesive,  $b$  is the joint width,  $l$  is the overlap length,  $t$  is the adherend thickness,  $P_Y$  is the maximum load that can be carried which just creates adherend yield, and  $\sigma_y$  is the yield strength of the adherend)



is given when the adherends yield plastically. The direct tensile stress ( $\sigma_t$ ) acting in the adherend due to the applied load  $P$  is

$$\sigma_t = P/bt \quad (2)$$

where  $t$  is the adherend thickness. The stress at the inner adherend surface ( $\sigma_s$ ) due to the bending moment  $M$  is

$$\sigma_s = 6M/bt^2 \quad (3)$$

where ( $M = kPt/2$ ), according to Goland and Reissner (1944). The variable  $k$  is the bending moment factor which reduces (from unity) as the lap rotates under load. The stress acting in the adherend is the sum of the direct stress and the bending stress. Thus, the maximum load which can be carried which just creates adherend yield ( $P_Y$ ) is

$$P_Y = \sigma_y bt / (1 + 3k) \quad (4)$$

where  $\sigma_y$  is the yield strength of the adherend. For low loads and short overlaps,  $k$  is approximately 1. Therefore, for such a case,

$$P_Y = \sigma_y bt / 4 \quad (5)$$

However, for joints that are long compared to the adherend thickness, which is the case here ( $l = 15$  mm and  $t = 0.95$  mm), the value of  $k$  decreases and it is assumed that it tends to be zero. In this case, the whole of the cross section yields and

$$P_Y = \sigma_y \cdot bt \quad (6)$$

This criterion has been applied with successful results to thin bondlines and a conservative value has always been obtained (Adams et al. 1997). The prediction is



also conservative for thin bondlines (less than 1 mm) but overestimates the results of thicker bondlines (more than 1 mm). This could be explained by the fact that the model does not take into account strain hardening of the steel. For a more accurate solution, the bending moment factor  $k$  could be computed according to Hart-Smith's equation that takes into account the adhesive thickness (Hart-Smith 1973). Note, however, that Eq. (4) would now require a numerical solution because  $k$  also depends on the load applied  $P$ . Moreover, Hart-Smith's bending moment factor is inaccurate when the adherend deforms plastically.

For joints with ductile adhesives, the failure load is given by the load that causes adhesive global yielding along the overlap. This criterion works reasonably well provided the failure shear strain of the adhesive is more than 20%. However, for brittle adhesives, this methodology is not applicable (da Silva et al. 2008). For joints with a brittle adhesive, the Volkersen's model can be used (da Silva et al. 2009b) and the failure occurs when the maximum shear stress at the ends of the overlap exceeds the shear strength of the adhesive. Alternatively, the finite element method can be used.

## 27.2.5 Residual Stresses

One of the main advantages of using adhesive bonding is the possibility to bond dissimilar materials, such as carbon fiber-reinforced plastics (CFRP) to aluminum in many aeronautical applications. However, dissimilar adherends may have very different coefficients of thermal expansion (CTE). Thus, temperature changes may introduce thermal stresses in addition to the externally applied loads. The chemical process of adhesive curing as well as the thermal variations during cure can lead to shrinkage and may also introduce internal stresses. Deformations or even cracks can appear. It is important to consider thermal effects because these generally lead to a joint strength reduction, even though in some cases the opposite happens (da Silva et al. 2004). Several authors have found that the stresses caused by adhesive shrinkage have much less effect on the lap-joint strength than those generated by the adherend thermal mismatch. Thermal loads are especially important when bonding adherends with different CTEs (Hart-Smith 1973). For metal/composite joints for example, the metal tends to shrink as the temperature is decreased from the cure value (generally a high temperature) and this is partially resisted by the composite (lower CTE), thereby inducing residual bond stresses especially at the ends of the joint. One end has positive residual shear stresses and the other end has negative residual shear stresses (see Fig. 5a). The thermal stresses are beneficial at one end of the joint but have the reverse effect on the other side of the joint. The thermal load  $\Delta T$  is given by Eq. (7):

$$\Delta T = T_O - T_{SF} \quad (7)$$

where  $T_O$  is the operating temperature and  $T_{SF}$  is the stress-free temperature. It is reasonable to consider the stress-free temperature as the normal cure temperature of the adhesive for most cases.

## 27.3 Methods to Increase Joint Strength

### 27.3.1 Fillets

Various authors have shown that the inclusion of a spew fillet at the ends of the overlap reduces the stress concentrations in the adhesive and the substrate (Adams and Peppiatt 1974; Crocombe and Adams 1981; Adams et al. 1986; Adams and Harris 1987; Dorn and Liu 1993; Tsai and Morton 1995; Lang and Mallick 1998; da Silva and Adams 2007a). The load transfer and shear stress distribution of a single-lap joint with and without fillet are schematically represented in Fig. 10. It can be seen that there is a stress concentration at the ends of the overlap for the single-lap joint with a square end. Modification of the joint end geometry with a spew fillet spreads the load transfer over a larger area and gives a more uniform shear stress distribution. The fillet not only gives a smoother load transfer but also alters the stress intensity factors as shown in Fig. 11.

Adams and Peppiatt (1974) found that the inclusion of a 45° triangular spew fillet decreases the magnitude of the maximum principal stress by 40% when compared to a square end adhesive fillet. Adams and Harris (1987) tested aluminum/epoxy single-lap joints with and without fillet and found an increase of 54% in joint strength for the filleted joint. Adams et al. (1986) tested aluminum/CFRP single-lap joints and found that the joint with a fillet is nearly two times stronger than the joint without a fillet. Crocombe and Adams (1981) did similar work but included geometric (overlap length, adhesive thickness, and adherend thickness) and material (modulus ratio) parameters. The reduction in peel and shear stresses is greatest for a low modulus ratio (low adhesive modulus), a high adhesive thickness, and a low adherend thickness.

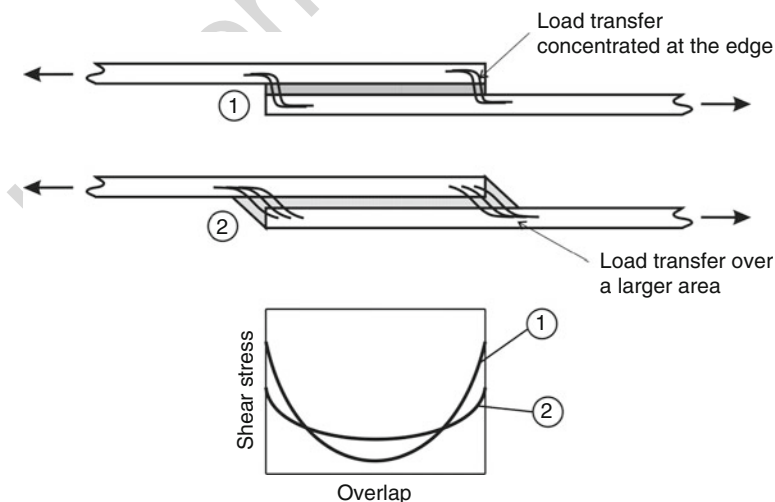


**Fig. 10** Load transfer and shear stress distribution in single-lap joints with and without fillet

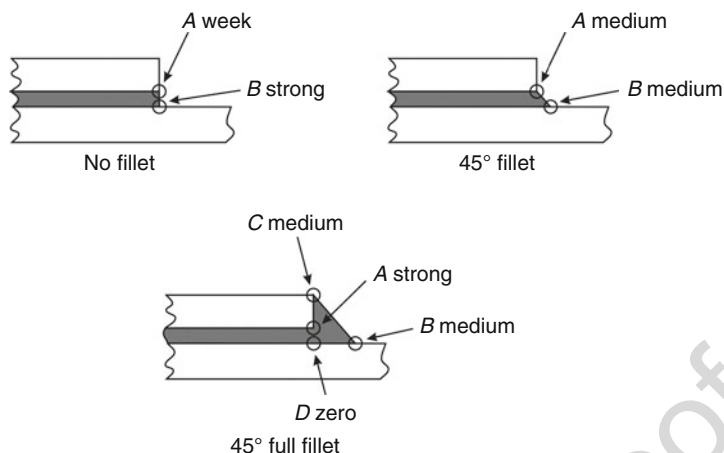


**Fig. 11** Stress intensity factors in adhesive lap joints with different spew fillet geometry

Dorn and Liu (1993) investigated the influence of the spew fillet in plastic/metal joints. The study included an FE analysis and experimental tests and they concluded that the spew fillet reduces the peak shear and peel adhesive stresses and decreases stress and strain concentrations in the adherends in the most critical regions. They also studied the influence of different adhesive and different metal adherends. A ductile adhesive and a more balanced joint (aluminum/plastic instead of steel/plastic) give a better stress distribution.

Tsai and Morton (1995) studied the influence of a triangular spew fillet in laminated composite single-lap joints. The FE analysis and the experimental tests (Moire interferometry) proved that the fillet helps to carry part of the load, thus reducing the shear and peel strains.

The above analyses are limited to triangular geometry. Lang and Mallick (1998) investigated several different geometries: full and half triangular, full and half rounded, full rounded with fillet, oval, and arc. They showed that shaping the spew to provide a smoother transition in joint geometry significantly reduces the stress concentrations. Full rounded with fillet and arc spew fillets give the highest percent reduction in maximum stresses whereas half-rounded fillet gives less. Furthermore, increasing the size of the spew also reduces the peak stress concentrations.

The spew fillet is not beneficial in all situations. In effect, the spew fillet tends to generate more thermal stresses than a square-end geometry when used at low temperatures (da Silva and Adams 2007a).

### 27.3.2 Adherend Rounding

Adhesive single-lap joints may have several singular (infinite) stresses. The stresses tend to infinite at crack tips and at bi-material junctions. Fracture mechanics can be

applied to treat the singular points at crack tips. As regards the bi-material singularities, there can be two or three, depending on the joint geometry (see Fig. 11). For both situations, there is an abrupt change in slope giving a sharp corner. The stress field in the vicinity of a sharp corner depends on the mesh used. A stress limit criterion will therefore lead to arbitrary results. The first FE analyses 40 years ago used coarse meshes due to computer memory limitations and therefore did not capture the infinite stress at singular points. The joint strength predictions obtained with stress or strain limit-based criteria compared well with the experimental results (Harris and Adams 1984). With computer power development, finer meshes can be used which led to a better stress distribution description but also to stresses that tend to infinite at singular points. The stress or strain limit failure criteria give, in this circumstance, more conservative predictions and are therefore very arguable.

Groth (1988) used a fracture mechanics approach without considering a pre-existing crack. He formulated a fracture criterion based on an equivalent generalized stress intensity factor similar to that in classical fracture mechanics. Comparing it to a critical value, joint fracture may be predicted. However, the critical stress intensity factor needs first to be tuned with an experimental test which makes this approach questionable.

Another approach for dealing with the singularity points is to use a cohesive zone model (CZM). This approach is associated to interface elements and enables to predict crack initiation and crack growth. It is a combination of a stress limit and fracture mechanics approach and relatively mesh insensitive. Many researchers are using this tool with accurate results (de Moura et al. 2006). However, the parameters associated to the CZM require previous experimental “tuning” and the user needs to know beforehand where the failure is likely to occur. This subject is discussed in detail in ► Chap. 25, “Numerical Approach: Finite Element Analysis.”

In practical joints the sharp corners are always slightly rounded during manufacture and the singular points will not necessarily exist. Adams and Harris (1987) studied the influence of the geometry of the corners. Using a simplified model, the effect of rounding on the local stress was investigated. Rounding the corner removes the singularity. Therefore, small local changes in geometry have a significant effect. They also performed an elastic-plastic analysis by calculating the plastic energy density. They found that the stress distribution is more uniform with a maximum some distance from the corner. The reason they give is that as the corner is approached, although the normal stress increases, the rigid adherend restrains the adhesive in the transverse direction. The net hydrostatic component is increased and yield is suppressed so that close to the corner there is a reduction in plastic energy density. It should be borne in mind that the effects are local: far away from the corner the stress distribution is unaffected. Apart from the simplified model, Adams and Harris (1987) tested three types of aluminum/rubber-toughened epoxy single-lap joints so that local changes at the end of the joint could be assessed. They found excellent agreement between the predicted joint strengths, with the modified models, and the experimental values. Zhao et al. (2011a, b) developed further the initial work of Adams and Harris (1987) and studied the cases illustrated in Fig. 12. They found that for joints bonded with brittle adhesives, the effect of adherend corner radius is

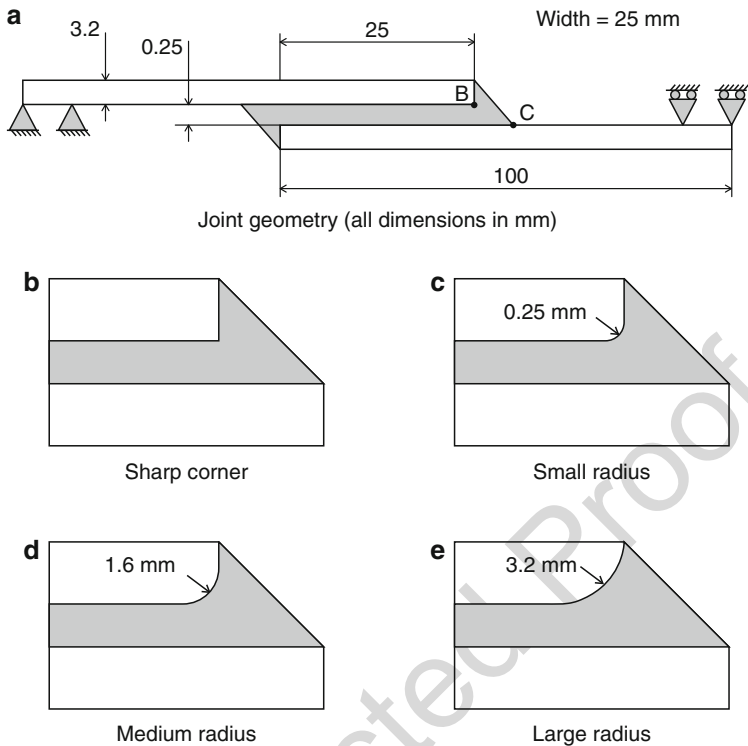


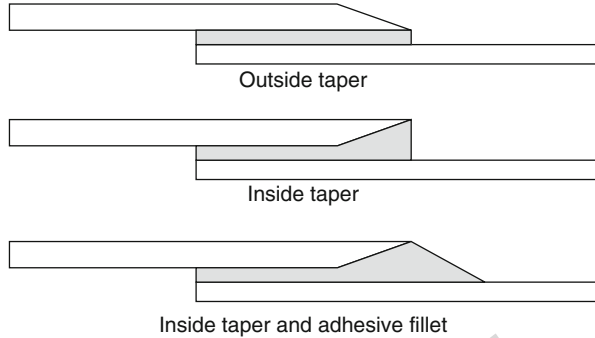
**Fig. 12** Aluminum/epoxy single-lap joints with different degrees of rounding

larger than that with ductile adhesives. For the brittle adhesive, the joint strength with large-radius adherend corners increases about 40% compared with that of sharp adherend corners. For large-radii adherend corners, a criterion based on continuum mechanics can be used to predict joint strength because there is no stress singularity. For joints with sharp and small adherend corners, a new criterion based on an average value around the singularity was proposed and demonstrated to be accurate for joint strength prediction with ductile adhesives.

### 27.3.3 Adherend Shaping

Adherend shaping is a powerful way to decrease the stress concentration at the ends of the overlap. Figure 13 presents typical geometries used for that purpose. Some analytical models were proposed to have a more uniform stress distribution along the overlap (Cherry and Harrison 1970). However, the FE method is more appropriate for the study of adherends shaping. The concentrated load transfer at the ends of the overlap can be more uniformly distributed if the local stiffness of the joint is reduced. This is particularly relevant for adhesive joints with composites due to the low

**Fig. 13** Adherend shaping



transverse strength of composites (see Sect. 2.2). Adams et al. (1986) addressed this problem. They studied various configurations of double-lap joints where the central adherend is CFRP and the outer adherends are made of steel. They found with FE and experiments that the inclusion of an internal taper and an external fillet can triple the joint strength. The same geometry was studied at low temperatures and it was found that the thermal stresses reduce substantially the joint strength (da Silva and Adams 2007a).

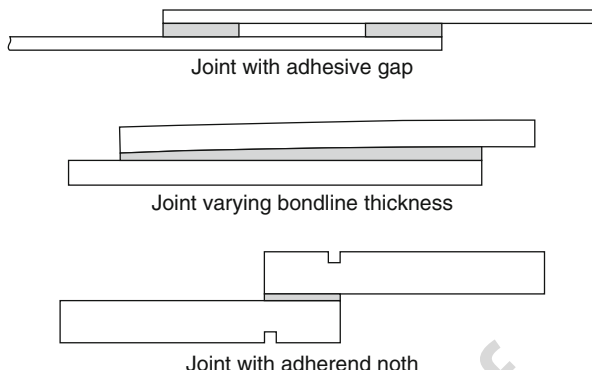
Hildebrand (1994) did similar work on SLJs between fiber-reinforced plastic and metal adherends. The optimization of the SLJs was done by modifying the geometry of the joint ends. Different shapes of adhesive fillet, reverse tapering of the adherend, rounding edges, and denting were applied in order to increase the joint strength. The results of the numerical predictions suggest that, with a careful joint-end design, the strength of the joints can be increased by 90–150%.

The use of internal tapers in adherends in order to minimize the maximum transverse stresses at the ends of bonded joints has also been studied by Rispler et al. (2000). An evolutionary structural optimization method (EVOLVE) was used to optimize the shape of adhesive fillets. EVOLVE consists of an iterative FE analysis and a progressive removal of elements in the adhesive which are low stressed.

Other examples of joint-end modifications for joint transverse stress reduction but using external tapers are those of Sancaktar and Nirantar (2003) and Kaye and Heller (2005). Kaye and Heller (2005) used numerical optimization techniques in order to optimize the shape of the adherends. This is especially relevant in the context of repairs using composite patches bonded to aluminum structures (see Sect. 3.5) due to the highly stressed edges.

Tapers (internal or external), or more complex adherend shaping, are excellent methods to reduce the peel stresses at the ends of the overlap and, therefore, to increase the joint strength. Internal tapers with a fillet seem to be the more efficient way to have a joint increase, especially with brittle adhesives and when composites are used. The FE method is a convenient technique for the determination of the optimum adherend geometry; however, the complexity of the geometry achieved is not always possible to realize in practice.

**Fig. 14** Various forms of geometric complexity



#### 27.3.4 Other Geometric Solutions

Other complex geometrical features such as voids in the bondline, surface roughness, notches in the adherend, etc. can be used to increase the joint strength. Again, the FE method should be used to find the optimum adherend geometry, bearing in mind that the complexity of the geometry might not be practical (see Fig. 14).

Nakagawa et al. (1999) studied the effect of voids in butt joints subjected to thermal stresses and found that stresses around defects in the center of the joint are more significant than those near the free surface of the adhesive. Lang and Mallick (1999) and de Moura et al. (2006) studied the influence of gaps in the adhesive and found that a gap in the middle of the overlap has little effect on joint strength. That is because the stress is more concentrated at the ends of the overlap. However, if a ductile adhesive that makes use of the whole overlap is used, then a joint strength improvement is expected.

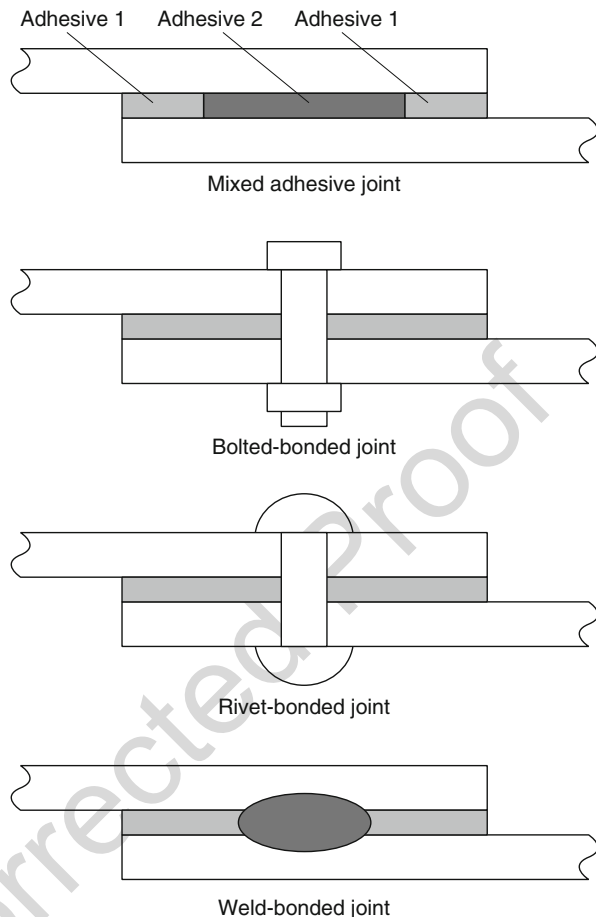
Kim (2003) proposed an analytical model supported by FE modeling to study the effect of variations of adhesive thickness along the overlap. The author showed that the variations found in practice have little effect on the adhesive stresses along the overlap.

Kwon and Lee (2000) studied the influence of surface roughness on the strength of tubular joints by modeling the stiffness of the interfacial layer between the adherends and the adhesive as a normal statistical distribution function of the surface roughness of the adherends. The authors found that the optimum surface roughness was dependent on the bond thickness and applied load.

Sancaktar and Simmons (2000) investigated the effect of adherend notching on the strength and deformation behavior of single-lap joints. The experimental results showed a 29% increase in joint strength with the introduction of the notches, which compared well with the FE analysis results.

### 27.4 Hybrid Joints

Joints combining different methods of joining are increasingly being used. The idea is to gather the advantages of the different techniques leaving out their problems. For example, the combination of friction stir welding with adhesive

**Fig. 15** Hybrid joints

bonding is able to overcome the inherent defects that occur when lap joints are  
 friction stir welded (Braga et al. 2016) and produce stronger joints. Another  
 possibility is to use more than one adhesive along the overlap or varying the  
 adhesive and/or adherend properties. All these cases have been grouped here  
 under a section called “hybrid joints” (see Fig. 15). It is important to note that  
 hybrid joints are especially well-suited for industrial applications, as they provide  
 immediate handling strength while the adhesive is not fully cured (da Silva et al.  
 2011c). Such joints are particularly difficult to simulate using analytical models for  
 obvious reasons, however, they can be tailor designed for a given application  
 (Moroni et al. 2010). The FE method is the preferred tool to investigate the  
 application of such techniques and find design guidelines. Campilho et al. (2012)  
 used finite element models to successfully optimize the geometry of hybrid spot-  
 welded/bonded single-lap joints, employing a CZM FE analysis.



#### 27.4.1 Mixed Adhesive Joints

Mixed modulus joints have been proposed in the past to improve the stress distribution and increase the joint strength of high modulus adhesives. The stiff, brittle adhesive should be in the middle of the overlap, while a low modulus adhesive is applied at the edges prone to stress concentrations. Sancaktar and Kumar (2000) used rubber particles to toughen the part of the adhesive located at the ends of the overlap and increase the joint strength. The concept was studied with the FE method and proved experimentally. Pires et al. (2003) also proved with an FE analysis and experimentally with two different adhesives that the mixed adhesive method gives an improvement in joint performance. Temiz (2006) used an FE analysis to study the influence of two adhesives in double-lap joints under bending and found that the technique decreases greatly the stresses at the ends of the overlap. Bouiadjra et al. (2007) used the mixed modulus technique for the repair of an aluminum structure with a composite patch. The use of a more flexible adhesive at the edge of the patch increases the strength performance of the repair. Das Neves et al. (2009a, b) have developed an analytical model that takes into account two adhesives along the overlap and permits to determine the best combination of adhesives and the optimum geometric factors (e.g., overlap) to have the maximum joint strength. The authors showed that the technique is more efficient for single-lap joints than for double-lap joints. More recently, da Silva and Lopes (2009) have studied single-lap adhesive joints maintaining the same brittle adhesive in the middle of the overlap and using three different ductile adhesives of increasing ductility at the ends of the overlap. A simple joint strength prediction is proposed for mixed adhesive joints. The mixed adhesive technique gives joint strength improvements in relation to a brittle adhesive alone in all cases. For a mixed adhesive joint to be stronger than the brittle adhesive and the ductile adhesive used individually, the load carried by the brittle adhesive must be higher than that carried by the ductile adhesive. Marques and da Silva (2008) studied mixed adhesive joints with an internal taper and a fillet. They show that the use of a taper and a fillet have little effect on the strength of mixed adhesive joints. The ductile adhesive at the ends of the overlap is sufficient to have an improved joint strength in relation to a brittle adhesive alone. The taper and the fillet are only useful when the brittle adhesive is used alone. One of the problems associated with the mixed adhesive technique is the adhesive proper separation. The best way to control the process is to use film adhesives. However, it is difficult to find compatible adhesives in the film form. This is a problem for the manufacturers to solve. Meanwhile, the physical separation of the paste or liquid adhesives can be achieved by using polymer wires or with the use of silicone strips even though a small portion of the load-bearing area is necessarily reduced.

The technique of using multi-modulus adhesives has been extended to solve the problem of adhesive joints that need to withstand low and high temperatures by da Silva and Adams (2007b, c). At high temperatures, a high temperature adhesive in the middle of the joint retains the strength and transfers the entire load while a low temperature adhesive is the load-bearing component at low temperatures, making the high temperature adhesive relatively lightly stressed. The authors studied various configurations with the FE method and proved experimentally that the concept works, especially with dissimilar adherends. The work of Marques et al. (2011)

expanded the use of this concept demonstrating its use for even higher temperatures, using ceramic and metal substrates.

## 27.4.2 Adhesive Joints with Functionally Graded Materials

The mixed adhesive joint technique can be considered a rough version of a functionally graded material. The ideal would be to have an adhesive functionally modified with properties that vary gradually along the overlap allowing a true uniform stress distribution along the overlap. One of the earlier works attempting to achieve this effect was performed by Sancaktar and Kumar (2000). Their work used rubber particles to modify locally the adhesive at the ends of the overlap but this technique does not create a truly gradually modified adhesive. Gannesh and Choo (2002) and Apalak and Gunes (2007) have used functionally graded adherends instead of functionally graded adhesives. Gannesh and Choo (2002) used a braided preform with continuously varying braid angle and the variation of the braid angle measured to realistically evaluate the performance of adherend modulus grading in a single-lap bonded joint. An increase of 20% joint strength was obtained due to a more uniform stress distribution. Apalak and Gunes (2007) studied the flexural behavior of an adhesively bonded single-lap joint with adherends composed of a functionally gradient layer between a pure ceramic ( $\text{Al}_2\text{O}_3$ ) layer and a pure metal (Ni) layer. The study is not supported with experimental results and the adhesive stress distribution was not hugely affected. The work of Carbas et al. (2014) was the first to achieve joint strength improvements with a gradually modified adhesive. The authors have employed induction heating to achieve a gradually modified cure of the adhesive in single-lap bonded joints, reducing stiffness at the ends of the overlap and increasing it in the central section, with good results. This is an area that is still being intensively studied and where modeling at different scales is essential.

## 27.4.3 Rivet-Bonded Joints

Liu and Sawa (2001) investigated, using a three-dimensional FE analysis, rivet-bonded joints and found that for thin substrates, bonded joints, riveted joints, adhesive joints, and rivet-bonded joints gave similar strengths while for thicker substrates the rivet-bonded joints were stronger. They proved this experimentally. Later, the same authors (Liu et al. 2004) proposed another technique similar to rivet-bonded joints: adhesive joints with adhesively bonded columns. Strength improvements are also obtained in this case. The advantage of this technique is that the appearance of the joint is maintained in relation to an adhesive joint. Grassi et al. (2006) studied through-thickness pins for restricting debond failure in joints. The pins were simulated by tractions acting on the fracture surfaces of the debond crack. Pirondi and Moroni (2009) found that the adhesive layer strongly increases the maximum load and the initial stiffness in comparison to a joint with a rivet alone. When failure of the adhesive occurs, the joint behaves as with only a rivet.

#### 27.4.4 Bolted-Bonded Joints

Chan and Vedhagiri (2001) studied the response of various configurations of single-lap joints, namely bonded, bolted, and bonded-bolted joints by three-dimensional FE method and the results were validated experimentally. The authors found that for the bonded-bolted joints, the bolts help to reduce the stresses at the edge of the overlap, especially after the initiation of failure. The same type of study was carried out by Lin and Jen (1999).

#### 27.4.5 Weld-Bonded Joints

Al-Samhann and Darwish (2003) demonstrated with the FE method that the stress peaks typical of adhesive joints can be reduced by the inclusion of a weld spot in the middle of the overlap. They studied later (Darwish and Al-Samhann 2004) the effect of adhesive modulus and thickness and concluded that for rational design of weld-bonded joints, adhesives of low Young's modulus are recommended with the largest possible bondline thickness. Darwish (2004) also investigated weld-bonded joints between dissimilar materials and found that the introduction of an adhesive layer resulted in an increased joint strength and a better stress distribution.

---

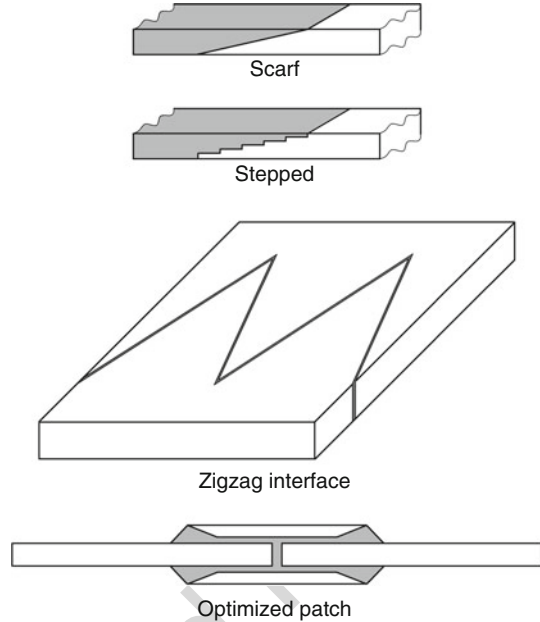
### 27.5 Repair Techniques

Adhesively bonded repairs are generally associated to complex geometries and the FE method has been extensively used for the design and optimization of the repair, especially with composites. The literature review of Odi and Friend (2002) about repair techniques illustrates clearly this point. Typical methods and geometries are presented in Fig. 16. Among the various techniques available, bonded scarf or stepped repairs are particularly attractive because a flush surface is maintained which permits a good aerodynamic behavior. Gunnion and Herszberg (2006) studied scarf repairs and carried out an FE analysis to assess the effect of various parameters. They found that the adhesive stress is not much influenced by mismatched adherend layups and that there is a huge reduction in peak stresses with the addition of an over-laminate. Campilho et al. (2007) studied scarf repairs of composites with a cohesive damage model and concluded that the strength of the repair increased exponentially with the scarf angle reduction.

Bahei-El-Din and Dvorak (2001) proposed new design concepts for the repair of thick composite laminates. The regular butt joint with a patch on both sides was modified by the inclusion of pointed inserts or a "zigzag" interface to increase the area of contact and improve the joint strength.

Soutis and Hu (1997) studied numerically and experimentally bonded composite patch repairs to repair cracked aircraft aluminum panels. The authors concluded that the bonded patch repair provides a considerable increase in the residual strength.

**Fig. 16** Repair techniques



Tong and Sun (2003) developed a pseudo-3D element to perform a simplified analysis of bonded repairs to curved structures. The analysis is supported by a full 3D FE analysis. The authors found that external patches are preferred when the shell is under an internal pressure, while internal patches are preferred when under an external pressure.

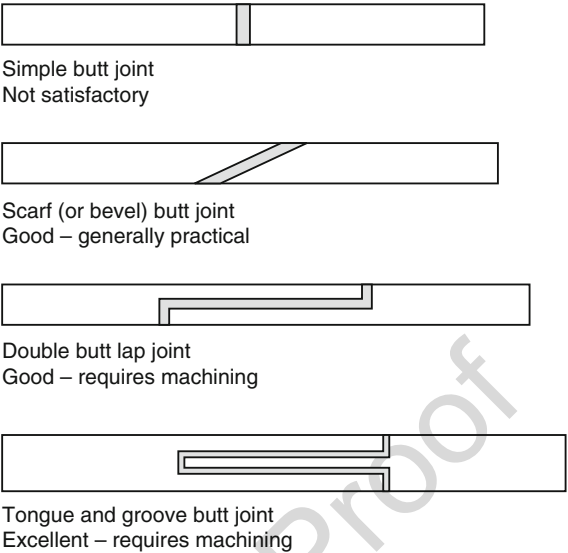
## 27.6 Configurations Recommended for Various Types of Joints

In an ideal joint, the adhesive must be loaded in shear and the load-bearing area must be as large as possible. These are two golden rules for the design engineer. However, this is not always possible to achieve for any type of joint such as a T joint, for example. Design guidelines are given next for butt joints, lap joints, cylindrical joints, corner joints and T joints.

### 27.6.1 Butt Joints

The simplest joint to manufacture is the butt joint. However, this type of joint does not resist bending loads because that puts the adhesive in cleavage. In the case of thick adherends, the joint strength can be improved by using the designs represented in Fig. 17. All the modifications presented in that figure reduce the cleavage stresses in the adhesives. The tongue-and-groove joints are particularly efficient because they

**Fig. 17** Butt joints (Adapted from Petrie (2000))

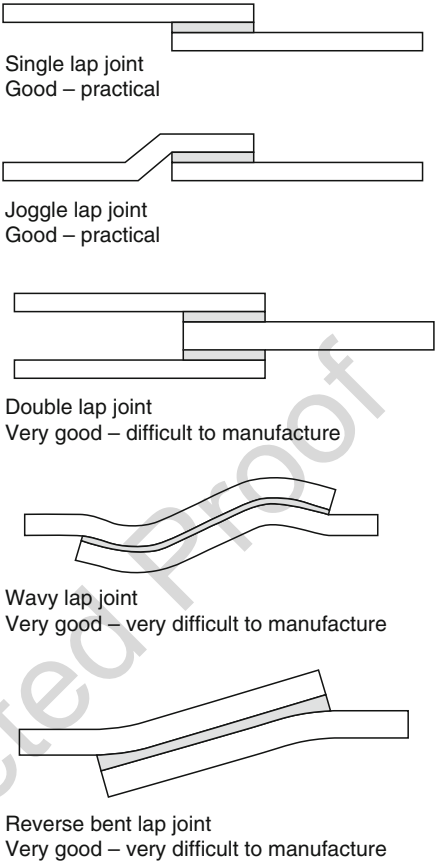


are self-aligned and act as reservoir for the adhesive. Nakagawa and Sawa (2001) studied scarf joints using photoelasticity and a 2D FE model. One of the conclusions is that under a static tensile load, an optimum scarf angle exists, where the stress singularity vanishes and the stress distributions become flat near the edge of the interface, but under thermal loads, the optimum scarf angle is not found. Dvorak et al. (2001) showed with an FE analysis and experimental results that adhesively bonded tongue-and-groove joints between steel and composite plates loaded are stronger than conventional strap joints.

**27.6.2 Lap Joints**

Lap joints are the most common type of joint because they are easy to manufacture and the adhesive is mostly loaded in shear. However, the load is not collinear, especially in single-lap joints, and this leads to peel stresses at the ends of the overlap (see ► Chap. 24, “Analytical Approach”). Some solutions have been proposed in Sect. 3 to decrease the peel stresses for single-lap joints. Another solution is to alter the lap joint as shown in Fig. 18. The joggle joint is the simplest solution to have load aligned if the adherend is easy to deform. The double-lap joint has a more balanced construction, which decreases drastically the bending moment. However, even with this type of joint, there are internal bending moments that cause peel stresses at the ends of the central adherend, as shown in Fig. 19. Other more recent solutions include the “wavy” joint and the “reverse bent” joint. Ávila and Bueno (2004) analyzed the “wavy” configuration. An FE analysis and experiments show that great strength improvements can be obtained with this technique.

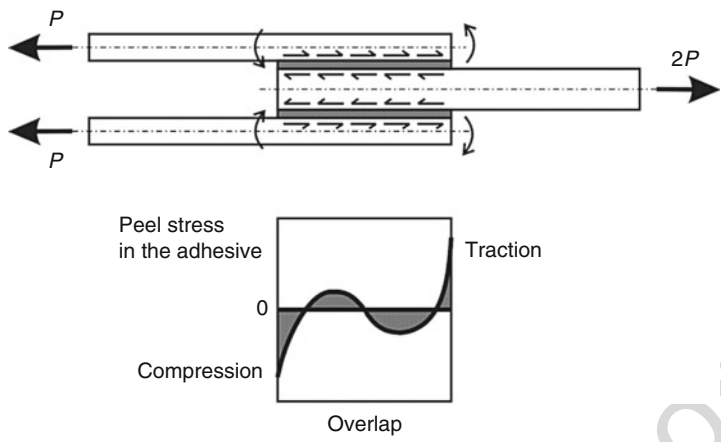
**Fig. 18** Lap joints



Fessel et al. (2007) also studied this type of joint as well as joints with bent substrates along the overlap. An FE analysis and experiments show great joint strength improvements. Sancaktar and Lawry (1980) also demonstrated with photoelastic experiments up to 71% increase in load-carrying capacity in single-lap joints with 15° prebent adherends.

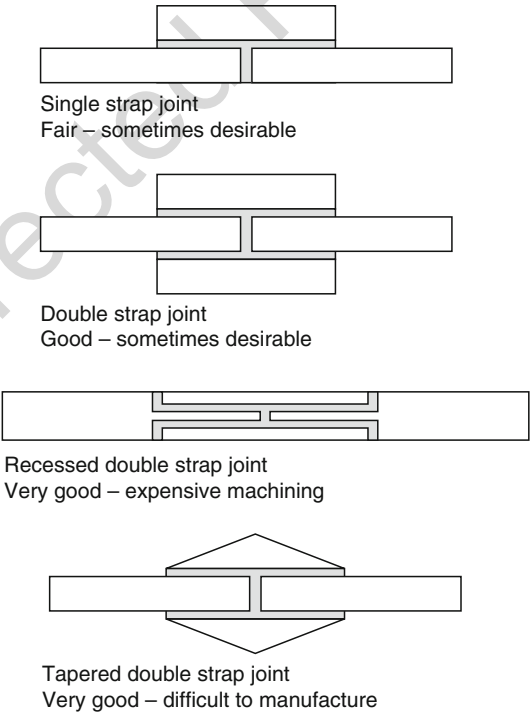
### 27.6.3 Strap Joints

Various configurations are presented in Fig. 20. As in the case of single-lap joints, the strap joint with only one strap is subjected to peeling stresses because the load is not collinear. The joint with two straps reduces the bending moment and is therefore stronger. The straps with a taper and the recessed joints are the most efficient but require a lot of machining. This type of joint is used in the context of repairs in the fuselage of aeronautical structures with patches made of aluminum or composite (Kaye and Heller 2005).



**Fig. 19** Peel stresses in the adhesive in a double-lap joint

**Fig. 20** Strap joints (Adapted from Petrie (2000))



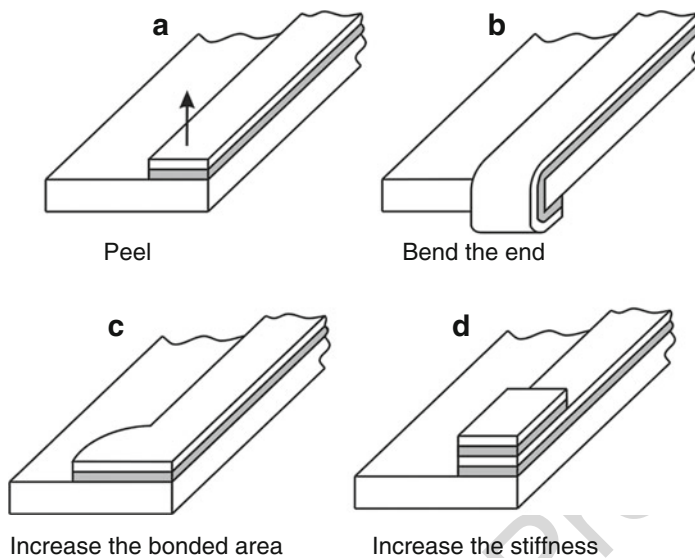


**Fig. 21** Methods to decrease the peel in adhesively bonded joints with a thin adherend and a rigid base (Adapted from Kohen (1954))

#### 27.6.4 Reinforcements

The loading of joints where a thin plate is bonded to a thick component leads generally to peel, as shown in Fig. 21a. Figure 21b–c present solutions to reduce the peel by increasing the resistant area. It is also common practice to bond reinforcements to the thin adherends in order to increase its rigidity. However, in this case, the bending loads can induce cleavage in the adhesive. In Fig. 22, some solutions are presented to reduce the cleavage of joints with reinforcements. The joint strength can be improved with increases in the bonded area, the flexibility of the edges, and the rigidity of the base.

#### 27.6.5 Cylindrical Joints

Adhesive bonding is very convenient to bond tubes. The loading can be axial or in torsion. In case of axial loading, there are stress concentrations at the ends of the overlap as in lap joints with plane adherends. In the case of torsion, there is only the effect of differential straining. In the case of axial loading, the square end can be substituted by a taper, as shown in Fig. 23. Figure 24 presents some cylindrical joints that are commonly used in bars and tubes. These solutions are advantageous in



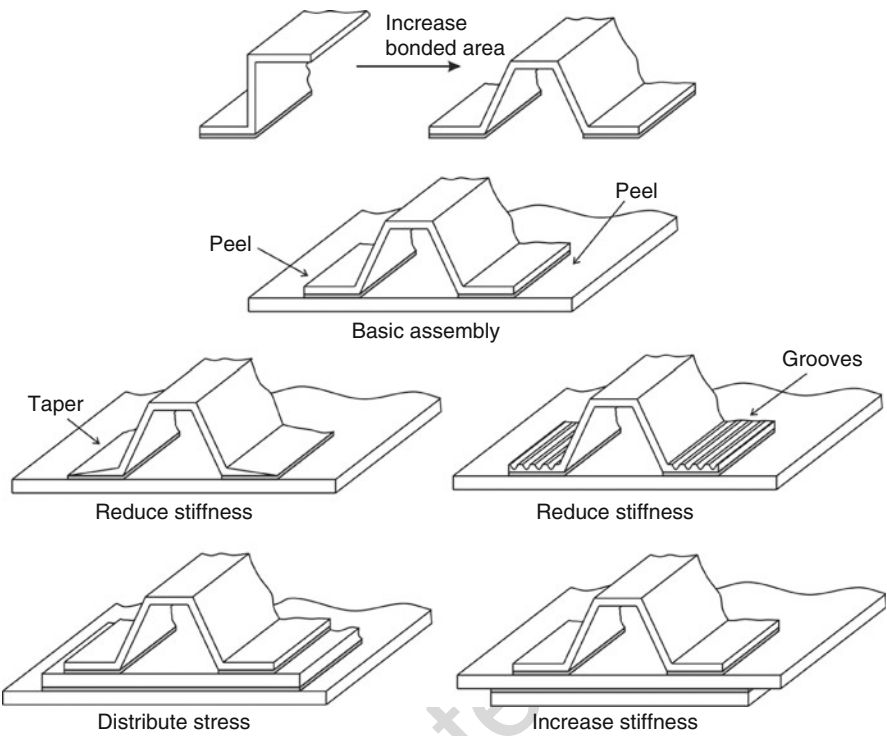


**Fig. 22** Solutions to decrease the cleavage in joints with a reinforcement (Adapted from Kohen (1954))

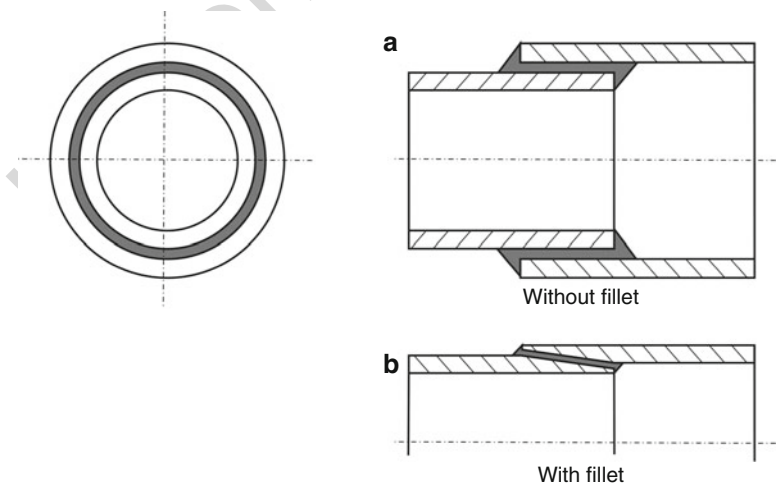
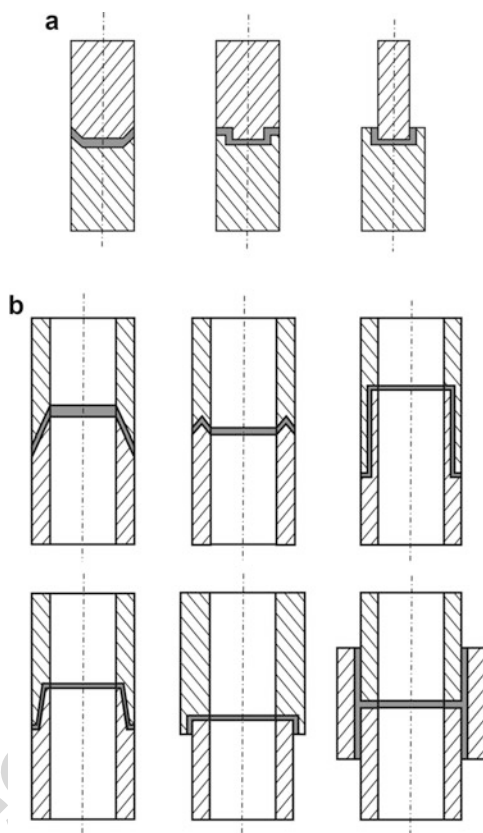


**Fig. 23** Tubular joint with square end (a) and with a taper (b)

**Fig. 24** Cylindrical joints with bars (**a**) and tubes (**b**) (Adapted from Petrie (2000))



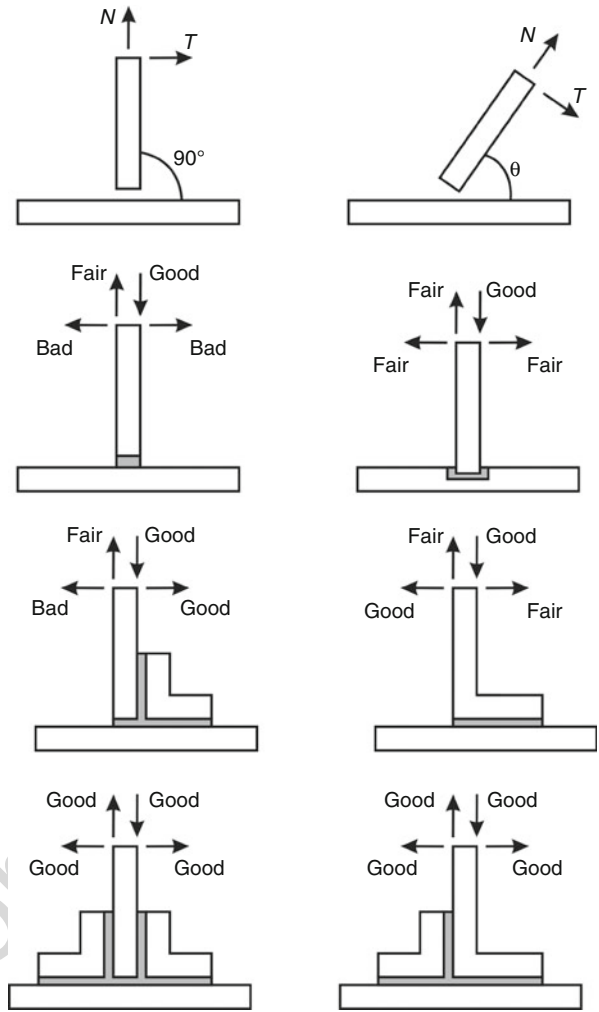
relation to the butt joints because a larger bonded area is obtained and the peel stresses are reduced. However, most of the solutions presented in Fig. 24 require heavy machining, which obviously renders the process expensive.

Several analytical models can be used to find the optimum design such as those of Lubkin and Reissner (1956) for tubular joints under axial loading and Adams and Peppiatt (1977) for torsion. Other loading modes have also been studied: internal and external pressure (Terekhova and Skoryi 1973) and asymmetric moments and forces (Kukovyakin and Skoryi 1972). Kim et al. (1992) studied various configurations of tubular joints (single overlap, double overlap, adherends tapering) and found with an FE analysis and experimentally that the double-lap configuration is the strongest joint.

## 27.6.6 T Joints

In T joints (see Fig. 25), two adherends are orientated perpendicularly ( $\theta = 90^\circ$ ). However, components with an orientation different from  $90^\circ$  are also included

**Fig. 25** T joints (Adapted from Adams et al. (1997))



in this type of joints. The loading can be in the plane of the plate ( $N$ ) or transverse to it ( $T$ ). The analysis of this type of joint is more difficult than lap joints or tubular joints and there are no analytical models for design purposes. Some configurations are presented in Fig. 25. The main objective of the proposed solutions is to minimize the peel loading and increase the shear loading. da Silva and Adams (2002) have shown experimentally that a strong base decreases the peel in the adhesive and enables to increase drastically the failure load in relation to a flexible base. Apalak (2002) studied the geometrical nonlinear response of T joints and obtained similar results. Design guidelines are given in terms of the length of the support, fillet, and other geometrical factors. Marcadon et al. (2006) studied T joint for marine applications and found that both the

overlap length and also the distance between the T plywood and the base have an influence on the tearing strength.

### 27.6.7 Corner Joints

Corner joints are similar to T joints. Figure 26 presents the solutions usually used to decrease the peeling stresses in the adhesive. These solutions are similar to those adopted for T joints. More elaborate constructions are presented in Fig. 27 proposed and tested by Keimel (1966). Apalak and Davies (1993) studied different types of corner joints using a linear FE analysis and proposed design guidelines based on the overall static stiffness and stress analysis. They found that in terms of stress and stiffness, the transverse loading ( $T$  in Fig. 26) is the most critical. The support length, the thickness, and length of the reinforcements increase the stiffness of the joint and decrease the peak stresses at the adhesive. Feih and Shercliff (2005) modeled simple corner joints with composites. Experimental testing showed an increase in joint strength of up to 100% by altering the fillet shape.

---

## 27.7 Conclusions

Simple design rules for single-lap joints were proposed as a function of the main variables that influence joint strength: adhesive and adherend properties, adhesive thickness, overlap, and residual stresses. The main rules are:

- Use an adhesive with a low modulus and high ductility
- Use similar adherends whenever possible
- Use a thin adhesive layer
- Use a large bonded area

Several methods to increase the joint strength were discussed for lap joints: fillets, adherend shaping, and other geometric solutions. The designer should always bear in mind that when designing an adhesive joint, the load must be spread over a large area and not concentrated in one point. Peel loads are the greatest enemy of the designer of bonded joints.

Adhesive in conjunction with other methods of joining were explained: rivet, bolt, and welding. The idea is to get a synergetic effect and combine the advantages of two methods. Mixed adhesive joints and functionally graded joints are also very promising techniques.

Various types of repairs are discussed in order to obtain the maximum strength recovery. The scarf joint is particularly efficient and aesthetically attractive.

Finally, configurations are recommended for various types of joints: butt joints, lap joints, reinforcements, T joints, and corner joints. The philosophy behind all the designs is to spread the load over a large area and decrease the peel stresses.

**Fig. 26** Corner joints  
(Adapted from Adams et al.  
(1997))

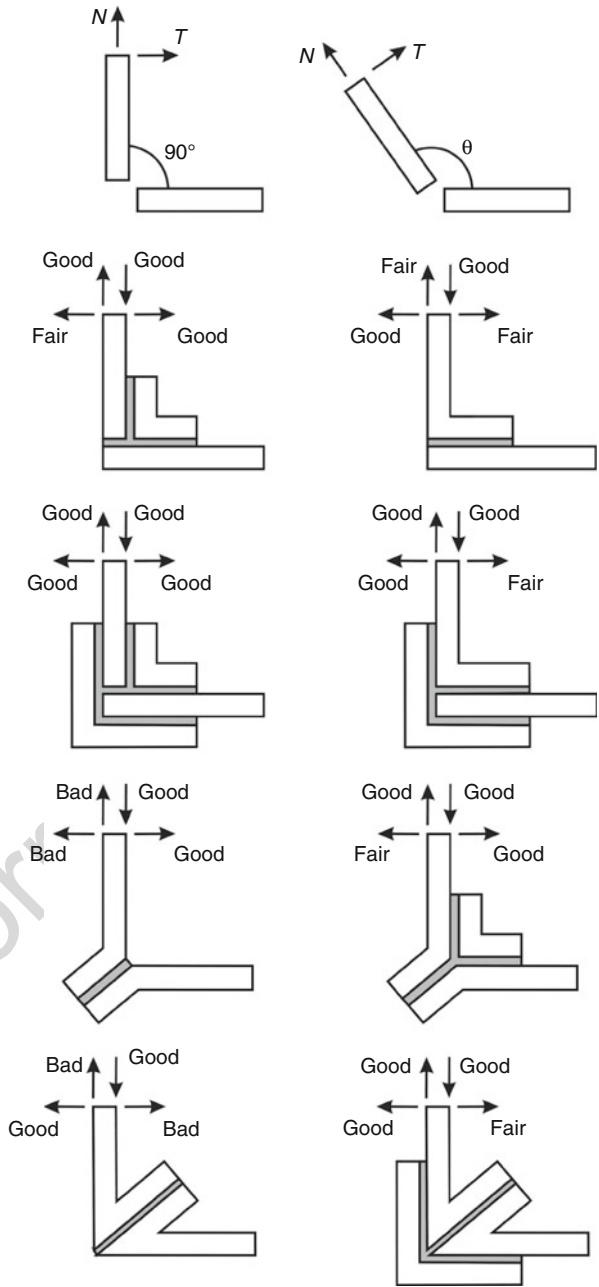
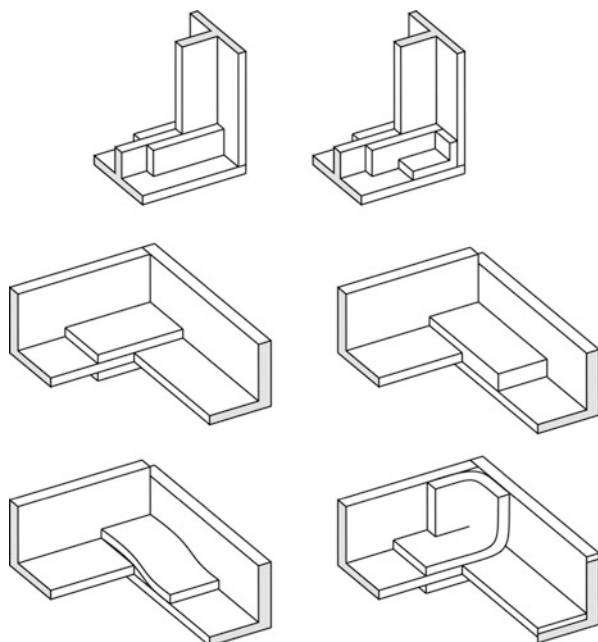


**Fig. 27** Corner joint constructions (Adapted from Keimel (1966))



## References

- Adams RD, Harris JA (1987) The influence of local geometry on the strength of adhesive joints. *Int J Adhes Adhes* 7:69
- Adams RD, Peppiatt NA (1974) Stress analysis of adhesive-bonded lap joints. *J Strain Anal* 9:185
- Adams RD, Peppiatt NA (1977) Stress analysis of adhesively-bonded tubular lap joints. *J Adhes* 9:1
- Adams RD, Atkins RW, Harris JA, Kinloch AJ (1986) Stress analysis and failure properties of carbon-fibre-reinforced-plastic/steel double-lap joints. *J Adhes* 20:29
- Adams RD, Comyn J, Wake WC (1997) *Structural adhesive joints in engineering*, 2nd edn. Chapman & Hall, London
- Al-Samhann A, Darwish SM (2003) Strength prediction of weld-bonded joints. *Int J Adhes Adhes* 23:23
- Apalak MK (2002) On the non-linear elastic stresses in an adhesively bonded T-joint with double support. *J Adhes Sci Technol* 16:459
- Apalak MK, Davies R (1993) Analysis and design of adhesively bonded corner joints. *Int J Adhes Adhes* 13:219
- Apalak MK, Gunes R (2007) Elastic flexural behaviour of an adhesively bonded single lap joint with functionally graded adherends. *Mater Design* 28:1597
- Ávila AF, Bueno PO (2004) Stress analysis on a wavy-lap bonded joint for composites. *Int J Adhes Adhes* 24:407
- Bahei-El-Din YA, Dvorak GJ (2001) New designs of adhesive joints for thick composite laminates. *Compos Sci Technol* 61:19
- Bouiadjra BB, Fekirini H, Belhouari M, Boutabout B, Serier B (2007) Fracture energy for repaired cracks with bonded composite patch having two adhesive bands in aircraft structures. *Comput Mater Sci* 40:20

- 755 Braga DFO, de Sousa LMC, da Silva LFM, Moreira PMGP (2016) Aluminium friction stir  
756 weldbonding joints. *J Adhes* 92:665
- 757 Campilho RDSG, de Moura MFSF, Domingues JJMS (2007) Stress and failure analyses of scarf  
758 repaired CFRP laminates using a cohesive damage model. *J Adhes Sci Technol* 21:855
- 759 Campilho RDSG, Pinto AMG, Banea MD, da Silva LFM (2012) Optimization study of hybrid spot-  
760 welded/bonded single-lap joints. *Int J Adhes Adhes* 37:86
- 761 Carbas RJC, Critchlow GW, da Silva LFM (2014) Adhesively bonded functionally graded joints by  
762 induction heating. *Int J Adhes Adhes* 48:110
- 763 Chan WS, Vedhagiri S (2001) Analysis of composite bonded/bolted joints used in repairing.  
764 *J Compos Mater* 35:1045
- 765 Cherry BW, Harrison NL (1970) The optimum profile for a lap joint. *J Adhes* 2:125
- 766 Crocombe AD (1989) Global yielding as a failure criterion for bonded joints. *Int J Adhes Adhes*  
767 9:145
- 768 Crocombe AD, Adams RD (1981) Influence of the spew fillet and other parameters on the stress  
769 distribution in the single lap joint. *J Adhes* 13:141
- 770 da Silva LFM, Adams RD (2002) The strength of adhesively bonded T-joints. *Int J Adhes Adhes*  
771 22:311
- 772 da Silva LFM, Adams RD (2007a) Techniques to reduce the peel stresses in adhesive joints with  
773 composites. *Int J Adhes Adhes* 27:227
- 774 da Silva LFM, Adams RD (2007b) Joint strength predictions for adhesive joints to be used over a  
775 wide temperature range. *Int J Adhes Adhes* 27:362
- 776 da Silva LFM, Adams RD (2007c) Adhesive joints at high and low temperatures using similar and  
777 dissimilar adherends and dual adhesives. *Int J Adhes Adhes* 27:216
- 778 da Silva LFM, Lopes MJCQ (2009) Joint strength optimization by the mixed adhesive technique.  
779 *Int J Adhes Adhes* 29:509
- 780 da Silva LFM, Adams RD, Gibbs M (2004) Manufacture of adhesive joints and bulk specimens  
781 with high-temperature adhesives. *Int J Adhes Adhes* 24:69
- 782 da Silva LFM, Rodrigues T, Figueiredo MAV, de Moura M, Chousal JAG (2006) Effect of adhesive  
783 type and thickness on the lap shear strength. *J Adhes* 82(11):1091
- 784 da Silva LFM, Critchlow GW, Figueiredo MAV (2008) Parametric study of adhesively bonded  
785 single lap joints by the Taguchi method. *J Adhes Sci Technol* 22(13):1477
- 786 da Silva LFM, das Neves PJC, Adams RD, Wang A, Spelt JK (2009a) Analytical models of  
787 adhesively bonded joints – part II: comparative study. *Int J Adhes Adhes* 29:331
- 788 da Silva LFM, das Neves PJC, Adams RD, Spelt JK (2009b) Analytical models of adhesively  
789 bonded joints – part I: literature survey. *Int J Adhes Adhes* 29:319
- 790 da Silva LFM, Lima RFT, Teixeira RMS (2009c) Development of a computer program for the  
791 design of adhesive joints. *J Adhes* 85:889
- 792 da Silva LFM, Pirondi A, Oschner A (2011) Hybrid adhesive joints, 1st edn. Springer, Heidelberg
- 793 Darwish SM (2004) Analysis of weld-bonded dissimilar materials. *Int J Adhes Adhes* 24:347
- 794 Darwish SM, Al-Samhann A (2004) Design rationale of weld-bonded joints. *Int J Adhes Adhes*  
795 24:367
- 796 das Neves PJC, da Silva LFM, Adams RD (2009a) Analysis of mixed adhesive bonded joints – part  
797 I: theoretical formulation. *J Adhes Sci Technol* 23:1
- 798 das Neves PJC, da Silva LFM, Adams RD (2009b) Analysis of mixed adhesive bonded joints – part  
799 II: parametric study. *J Adhes Sci Technol* 23:35
- 800 de Moura MFSF, Daniaud R, Magalhães AG (2006) Simulation of mechanical behaviour of  
801 composite bonded joints containing strip defects. *Int J Adhes Adhes* 26:464
- 802 Dorn L, Liu W (1993) The stress state and failure properties of adhesive-bonded plastic/metal  
803 joints. *Int J Adhes Adhes* 13:21
- 804 Dragoni E, Goglio L, Kleiner F (2010) Designing bonded joints by means of the JointCalc software.  
805 *Int J Adhes Adhes* 30:267
- 806 Dvorak GJ, Zhang J, Canyon O (2001) Adhesive tongue-and-groove joints for thick composite  
807 laminates. *Compos Sci Technol* 61:1123

- Feih S, Shercliff HR (2005) Adhesive and composite failure prediction of single-L joint structures under tensile loading. *Int J Adhes Adhes* 25:47
- Fessel G, Broughton JG, Fellows NA, Durodola JF, Hutchinson AR (2007) Evaluation of different lap-shear joint geometries for automotive applications. *Int J Adhes Adhes* 27:574
- Gannesh VK, Choo TS (2002) Modulus graded composite adherends for single-lap bonded joints. *J Compos Mater* 36:1757
- Gleich DM, van Tooren MJL, Beukers A (2001) Analysis and evaluation of bondline thickness effects on failure load in adhesively bonded structures. *J Adhes Sci Technol* 15:1091
- Goland M, Reissner E (1944) The stresses in cemented joints. *J Appl Mech* 66:A17
- Grant LDR, Adams RD, da Silva LFM (2009a) Experimental and numerical analysis of single lap joints for the automotive industry. *Int J Adhes Adhes* 29:405
- Grant LDR, Adams RD, da Silva LFM (2009b) Experimental and numerical analysis of T-peel for the automotive industry. *J Adhes Sci Technol* 23:317
- Grant LDR, Adams RD, da Silva LFM (2009c) Effect of the temperature on the strength of adhesively-bonded single lap and T joints for the automotive industry. *Int J Adhes Adhes* 29:535
- Grassi M, Cox B, Zhang X (2006) Simulation of pin-reinforced single-lap composite joints. *Compos Sci Technol* 66:1623
- Groth HL (1988) Stress singularities and fracture at interface corners in bonded joints. *Int J Adhes Adhes* 8:107
- Gunnion AJ, Herszberg I (2006) Parametric study of scarf joints in composite structures. *Compos Struct* 75:364
- Harris JA, Adams RD (1984) Strength prediction of bonded single lap joints by non-linear finite element methods. *Int J Adhes Adhes* 4:65
- Hart-Smith LJ (1973) Adhesive bonded double lap joints. NASA CR-112235
- Hildebrand M (1994) Non-linear analysis and optimization of adhesively bonded single lap joints between fibre-reinforced plastics and metals. *Int J Adhes Adhes* 14:261
- Kaye RH, Heller M (2002) Through-thickness shape optimisation of bonded repairs and lap-joints. *Int J Adhes Adhes* 22:7
- Kaye R, Heller M (2005) Through-thickness shape optimisation of typical double lap-joints including effects of differential thermal contraction during curing. *Int J Adhes Adhes* 25:227
- Keimel FA (1966) In: Bodnar MJ (ed) *Applied polymer symposium no 3*. Wiley, New York, p 27
- Kim H (2003) The influence of adhesive bondline thickness imperfections on stresses in composite joints. *J Adhes* 79:621
- Kim KS, Kim WT, Lee DG, Jun EJ (1992) Optimal tubular adhesive-bonded lap joint of the carbon fiber epoxy composite shaft. *Compos Struct* 21:163
- Kohen GW (1954) Design manual on adhesives. Machine Design, April
- Kukovyakin VM, Skoryi IA (1972) Estimating the strength of bonded cylindrical joints. *Russ Engng J* 52:40
- Kwon JW, Lee DG (2000) The effects of surface roughness and bond thickness on the fatigue life of adhesively bonded tubular single lap joints. *J Adhes Sci Technol* 14:1085
- Lang TP, Mallick PK (1998) Effect of spew geometry on stresses in single lap adhesive joints. *Int J Adhes Adhes* 18:167
- Lang TP, Mallick PK (1999) The effect of recessing on the stresses in adhesively bonded single-lap joints. *Int J Adhes Adhes* 19:257
- Lin W-H, Jen M-HR (1999) The strength of bolted and bonded single-lapped composite joints in tension. *J Compos Mater* 33:640
- Liu J, Sawa T (2001) Stress analysis and strength evaluation of single-lap adhesive joints combined with rivets under external bending moments. *J Adhes Sci Technol* 15:43
- Liu J, Liu J, Sawa T (2004) Strength and failure of bulky adhesive joints with adhesively-bonded columns. *J Adhes Sci Technol* 18:1613
- Lubkin JL, Reissner E (1956) Stress distribution and design data for adhesive lap joints between circular tubes. *ASME* 78:1213



- 861 Marcadon V, Nadot Y, Roy A, Gacougnolle JL (2006) Fatigue behaviour of T-joints for marine  
862 applications. *Int J Adhes Adhes* 26:481
- 863 Marques EAS, da Silva LFM (2008) Joint strength optimization of adhesively bonded patches.  
864 *J Adhes* 84:917
- 865 Marques EAS, Magalhães DNM, da Silva LFM (2011) Experimental study of silicone-epoxy dual  
866 adhesive joints for high temperature aerospace applications. *Materwiss Werksttech* 42:471
- 867 Moroni F, Pironi A, Kleiner F (2010) Experimental analysis and comparison of the strength of  
868 simple and hybrid structural joints. *Int J Adhes Adhes* 30:367
- 869 Nakagawa F, Sawa T (2001) Photoelastic thermal stress measurements in scarf adhesive joints  
870 under uniform temperature changes. *J Adhes Sci Technol* 15:119
- 871 Nakagawa F, Sawa T, Nakano Y, Katsuo M (1999) Two-dimensional finite element thermal stress  
872 analysis of adhesive butt joints containing some hole defects. *J Adhes Sci Technol* 13:309
- 873 National Physical Laboratory (2007) Design and testing of bounded and bolted joints. Queen's  
874 Printer, Scotland
- 875 Odi RA, Friend CM (2002) A comparative study of finite element models for the bonded repair of  
876 composite structures. *J Reinf Plast Comp* 21:311
- 877 Petrie EM (2000) Handbook of adhesives and sealants. McGraw-Hill, New York
- 878 Pires I, Quintino L, Durodola JF, Beevers A (2003) Performance of bi-adhesive bonded aluminium  
879 lap joints. *Int J Adhes Adhes* 23:215
- 880 Pironi A, Moroni F (2009) Clinch-bonded and rivet-bonded hybrid joints: application of damage  
881 models for simulation of forming and failure. *J Adhes Sci Technol* 23:1547
- 882 Rispler AR, Tong L, Steven GP, Wisnom MR (2000) Shape optimisation of adhesive fillets. *Int*  
883 *J Adhes Adhes* 20:221
- 884 Sancaktar E, Kumar S (2000) Selective use of rubber toughening to optimize lap-joint strength.  
885 *J Adhes Sci Technol* 14:1265
- 886 Sancaktar E, Lawry P (1980) A photoelastic study of stress distribution in adhesively bonded joints  
887 with prebent adherends. *J Adhes* 11:233
- 888 Sancaktar E, Nirantar P (2003) Increasing strength of single lap joints of metal adherends by taper  
889 minimization. *J Adhes Sci Technol* 17:655
- 890 Sancaktar E, Simmons SR (2000) Optimization of adhesively-bonded single lap joints by adherend  
891 notching. *J Adhes Sci Technol* 14:1363
- 892 Soutis C, Hu FZ (1997) Design and performance of bonded patch repairs of composite structures.  
893 *Proc Instn Mech Engrs Part G* 211:263
- 894 Temiz S (2006) Application of bi-adhesive in double-strap joints subjected to bending moment.  
895 *J Adhes Sci Technol* 20:1547
- 896 Terekhova LP, Skoryi IA (1973) Stresses in bonded joints of thin cylindrical shells. *Strength Mater*  
897 4:1271
- 898 Tong L, Sun X (2003) Nonlinear stress analysis for bonded patch to curved thin-walled structures.  
899 *Int J Adhes Adhes* 23:349
- 900 Tsai MY, Morton J (1995) The effect of a spew fillet on adhesive stress distributions in laminated  
901 composite single-lap joints. *Compos Struct* 32:123
- 902 Volkersen O (1938) Die nietkrafteerteilung in zubeanspruchten nietverbindungen mit konstanten  
903 loschonquerschnitten. *Luftfahrtforschung* 15:41–47
- 904 Zhao X, Adams RD, da Silva LFM (2011a) Single lap joints with rounded adherend corners: stress  
905 and strain analysis. *J Adhes Sci Tech* 25:819
- 906 Zhao X, Adams RD, da Silva LFM (2011b) Single lap joints with rounded adherend corners:  
907 experimental results and strength prediction. *J Adhes Sci Tech* 25:837

Gregory L. Anderson

## Contents

28.1	Introduction .....	812
28.2	Joint Types and Their Critical Dimensions .....	813
28.2.1	Butt Joints .....	814
28.2.2	Lap Joints .....	816
28.2.3	Corner or Angle Joints .....	818
28.2.4	Seam or Edge Joints .....	819
28.3	Critical Sealant Properties .....	820
28.3.1	Chemical Properties .....	820
28.3.2	Physical Properties .....	822
28.3.3	Mechanical Properties .....	823
28.3.4	Adhesion .....	825
28.4	Differential Movement Tolerances .....	826
28.5	Conclusions .....	828
	References .....	828

## Abstract

This chapter describes the many factors to go into the design of reliable sealant joints. Common causes of sealant joint failure are addressed. The various joint types are discussed and illustrated, and their critical dimensions and materials are described. Sealant properties critical to joint assembly, cure, function, reliability, and aging are discussed. These include chemical, physical, mechanical, and adhesion properties. Proper measurement of these properties is also presented. Finally, calculation of the differential movement of the substrates in a sealant joint, the accommodation of which is the primary mechanical requirement of a sealant joint, is discussed.

G. L. Anderson (✉)

R&D Laboratories, Propulsion Systems – Launch Systems Group, Orbital ATK, Corinne, UT, USA

e-mail: [greg.anderson@orbitalatk.com](mailto:greg.anderson@orbitalatk.com)

## 28.1 Introduction

The use of sealant joints is prevalent in building design and construction, aerospace, automotive, electronics, tank fabrication, and construction industries. There are two major purposes of sealants in joints: (1) the sealant fills space, creating a seal, and must maintain that seal throughout the useful life of the structure; and (2) the sealant provides a barrier to the transfer of fluids. Secondary functions of sealants can include electrical and/or thermal insulation, noise reduction, vibration dampening, surface smoothing, providing a protective coating, and providing protection from tampering. There is an important distinction to be made between an adhesive joint and a sealant joint. Whereas adhesive joints are designed to inhibit the movement of the substrates, sealant joints are designed to allow and accommodate the inservice movement of the substrates.

Proper design of sealant joints is critical to the reliability of the joints. The general types of sealant joints and the critical geometric parameters that must be considered in joint design will be discussed in detail. Because the proper selection of materials is absolutely critical to the reliability of sealant joints, the critical sealant properties will also be discussed.

When designing sealant joints, an understanding of the most common causes of sealant joint failure is important in order to eliminate as many of the causes as possible. The four most common causes of sealant joint failure are: poor adhesion of the sealant to the substrate, poor joint design, poor workmanship in creating the joint, and aging. Poor joint design will be eliminated through the proper selection of sealant material and joint critical geometric parameters discussed in later sections. Aging is a function of sealant material selection and the selection of other materials that go into a sealant joint. Chemical compatibility among the various materials is essential to the long life of a sealant joint and will be discussed in detail in Sect. 3.

Achieving adequate adhesion of the sealant to the substrates is normally accomplished by ensuring that there is nothing on the substrate surfaces to inhibit or preclude a strong bond. This not only means ensuring that the bond surfaces are dry and free from oil, other contaminants, or from release agents (especially important when bonding to concrete), it also means that the surface must be free from dust and loose, friable material at the substrate surface. Elimination of loose substrate material at the bond surface may require a fresh cut of masonry or concrete. Many primers applied to porous substrate bond surfaces reinforce the substrate and fix any remaining loose material strongly to the surface.

Excellent surface preparations for porous surfaces include blasting with oil-free compressed air, abrasive media, or high pressure water (dry time is a must in this case) and grinding or wire brushing followed by oil-free dry compressed air blasting. For nonporous substrates, solvent wiping with clean cloth following immediately by a clean cloth dry wipe is the preferred approach. Solvent wiping of porous substrates is not recommended, because the solvent can wash the contaminant into the porous substrate where it is free to diffuse back to the surface or interface over time.

In addition to substrate bond surface preparation, poor workmanship can also negatively affect mixing and insertion of the sealant into the joint. Thorough mixing is important for solvated or waterborne sealants and two-part sealants. Thorough mixing of the solvated and waterborne systems ensures even distribution of the sealant within the solution, and improper mixing can lead to less than adequate sealant remaining in the joint. Improper mixing of two-part systems will lead to the areas of uncured sealant that will not reliably perform as a fluid barrier. Insertion of the sealant needs to be done by forcing the sealant into the joint so that it fills the space and wets the substrate surfaces. In order for this to be accomplished well, the sealant must be forced to flow into the joint in advance of the applicator. Following application of the sealant, it is also good practice to tool the sealant, i.e., push the sealant into the joint using a convex-shaped screed. Tooling the surface further compresses the sealant against the substrate surfaces, creates an attractive smooth sealant surface, and creates a slight concavity to that surface which is beneficial from a structural design standpoint.

An additional note of caution is given at this point regarding the application of sealant at low temperature. At the temperatures lower than normal use temperature, the joint will be more open than normal. Care should be taken to tool the sealant surface sufficiently to avoid extrusion of the cured sealant from the joint at normal operational temperature. Also important is the fact that at lower temperatures, the sealant cure rate or solvent evaporation rate will be slower. This will likely require additional fixturing time to not disturb the joint prematurely. Finally, water-based sealant emulsions should always be kept above 5 °C to avoid freezing.

In addition to this text, there are several other references dealing with the design of sealant joints (Amstock 1973; Prane 1977; Panek and Cook 1984; Petrie 2007). Also, ASTM International has a written standard on the use of sealants in joints, standard C-1193.

---

## 28.2 Joint Types and Their Critical Dimensions

There are four main types of sealant joints with variations within each type. They are butt joints, lap joints, angle or corner joints, and seam or edge joints. The two most prevalent are butt and lap joints. Both are used for joining substrates parallel to one another. In selecting one over the other, one must consider access to the joint for sealant insertion. Because the butt joint is more accessible, inserting the sealant into a butt joint is generally easier to do. An exception to this is joining substrates in a factory where at least one substrate can be readily moved into place after applying sealant to the other substrate. In such factory-made sealant joints, accessibility is not an issue. For much of sealant joint assembly in the field, accessibility dictates the use of butt joint. Where practicable, however, the lap joint has better weather and environment protection of the sealant than the butt joint.

Each of the four joint types and their variations will now be discussed. The critical dimensions and supporting materials crucial to the joint design will also be discussed.

## 28.2.1 Butt Joints

Common butt joints are depicted in Fig. 1. In all its variations, the substrates of a butt joint are both parallel and aligned. The overriding design feature of the simple and complex butt joints is that there must be sufficient sealant in the joint to handle the joint elongation and contraction and the recovery of the sealant following the extremes of elongation and contraction. It is also extremely important to understand that even though the load on the sealant can be unidirectional in line with the substrates, the stress state in the sealant, especially at the interfaces of the sealant with the substrates, is highly complex.

Sealants are in general nearly incompressible. Thus, they will change their shapes to accommodate the joint expansion or contraction, but they will not change their volume. Because the sealant remains firmly fixed at the substrate bond interfaces, it is the center region of the sealant in a butt joint that deforms the most when the joint is loaded. Correspondingly, the stresses are the highest at the edges of the bond surfaces where the restriction of the deformation is the greatest, as depicted in Fig. 2. In fact, bondline stress is a function of the elongation of the sealant-free surface, increasing with increasing elongation. As can be seen in Fig. 2, deeper butt joints have significantly higher bondline stresses than shallow butt joints, because the increased volume of sealant requires increased sealant-free surface elongation in order to maintain a constant sealant volume.

Two other design considerations are pertinent to generalized width versus depth guidelines for reliable simple sealant butt joints. At very low depths, there is usually insufficient bond area of the sealant to the substrates to have reliable adhesion. On the other hand, at very large width-to-depth ratios, buckling of the sealant can occur when the joint contracts. This can cause the sealant to be extruded from the joint where abrasion of the sealant can occur, drastically reducing the sealant life. Extruded sealant can also be a safety hazard in some instances.

With these design considerations in mind, the following are standard guidelines for the preferred depth of the sealant as a function of the joint width:

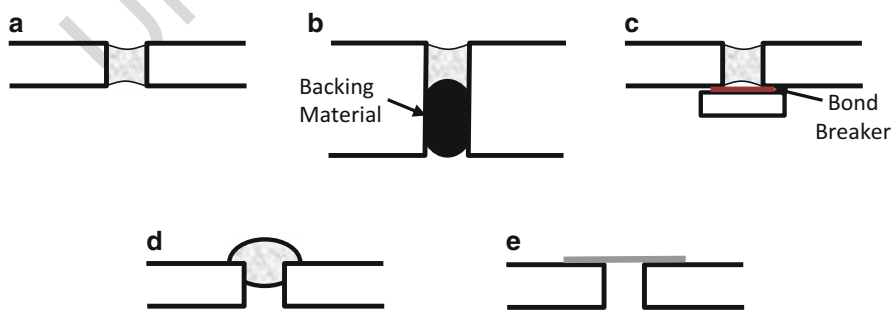


**Fig. 1** Butt joints: (a) simple thin-substrate butt joint, (b) simple thick-substrate butt joint, (c) compound butt joint, (d) sealant bead seal, and (e) sealant tape seal

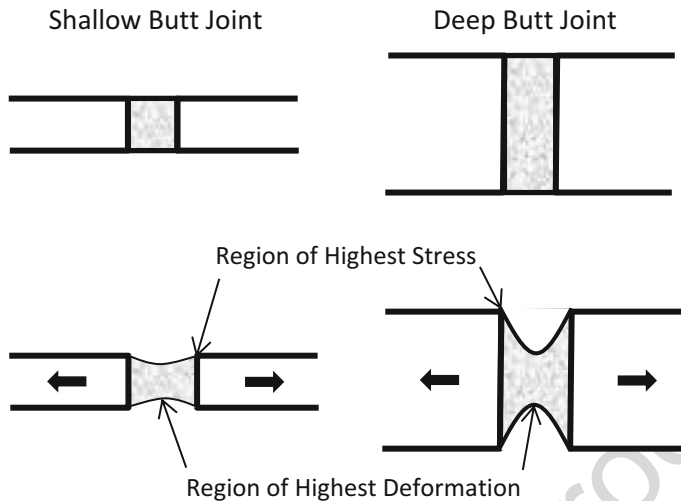


**Fig. 2** Sealant deformation in simple shallow and deep butt joints subjected to elongation

- For width less than or equal to 0.5 in (13 mm), the depth should be equal to the width, but not less than 0.25 in (6 mm)
- For width greater than 0.5 in (13 mm) and less than or equal to 1 in (26 mm), the depth should be 0.5 in (13 mm)
- For width greater than 1 in (26 mm), the depth should be half the width

There are other practical considerations regarding the maximum width desirable. Sealant slump from the joint can occur in shallow simple butt joint geometries. The tendency of the sealant to slump increases as the joint width increases. Also, some sealants either require moisture to cure or require solvent evaporation for the sealant to set. With these materials, increased time is required for sealant solidification to occur. This increases the tooling time and the overall manufacturing time.

In order to regulate the depth of the sealant fill, the butt joint gap must have a bottom. Having a bottom is also important from two practical standpoints: it ensures the sealant properly flows into the joint – forcing sealant to flow into the joint ahead of the applicator, and it forces the sealant to wet out the substrate bond surfaces for good adhesion. Creating a bottom in a simple butt joint is accomplished by inserting backing material (or backing rod) into the joint to the proper depth. Materials commonly used for this application are typically soft and resilient such as closed- or open-cell urethane foams, closed-cell butyl rubber or polystyrene foams, polyethylene rod or solid rods of neoprene, or butyl rubber. A desirable feature of the backing material is that it creates a water barrier as a secondary seal in case of sealant joint failure. Open-cell backing materials may be needed for many one-part sealant systems that require moisture exposure to initiate cure even though the open-cell structure does not provide a moisture barrier. Closed-cell backing materials have the added benefit that they hold their shape better, ensuring that they remain in place

during sealant insertion. A commonly used backing material good for most applications is closed-cell polyethylene foam rod, which provides a nonadhering surface for the sealant, doesn't slip after placement, and forms a moisture barrier. In order to keep the backing material from slipping, closed-cell foam rods should have a diameter 25–35% greater than the joint opening, and open-cell rods should have a diameter 40–50% greater than the joint opening.

There are two important chemical considerations in selecting a backing material. The selected material must be chemically compatible with both the substrate and sealant materials and the sealant carrier solvent in solvated sealant systems. There should also be a minimum amount of chemicals that can diffuse from the backing material over time in order to preclude staining of the sealant.

An issue with complex butt joints and simple butt joints containing backing material is termed three-sided adhesion. If the sealant is allowed to bond to the backing material or the bottom member (in the case of the complex joint), the sealant will be bonded on three sides. This allows sealant deformation on only one surface. Because of the incompressible nature of sealants, the elongation under joint extension subjected to the free surface of the sealant and the consequent bondline stress at the sealant-free surface corners is roughly doubled in comparison to sealant joints bonded on just the two sides. This will likely result in peeling of the sealant from the substrate surface, destroying the joint seal. In order to avoid this, the adhesion of the sealant to the backing material should be minimal. In the case of complex butt joints, bond breaker material (typically polyethylene or Teflon™ film or tape or a carefully applied chemical release agent) is applied to the surface of the bottom member of a complex joint that will contact the sealant. Teflon™ film is easily placed in position, but care must be taken to ensure that it stays in place during sealant insertion. Liquid release agents can be easily painted onto the appropriate surface. Aerosol release agents should be used with caution. While they are easily applied to the surface prior to securing the bottom member in place, application with the bottom member already in place requires careful masking of the bond surfaces of the two substrates. Use of bond breaker materials is especially critical in joints with large gap widths subjected to significant joint opening.

It is mechanically advantageous to create an hourglass shape in the sealant of a butt joint (see Fig. 1b) prior to sealant solidification. This will allow greater deformation at the center of the sealant during its operational life, transferring less stress to the bondline when the joint expands. The hourglass shape is achieved by using a rod-shaped backing material to produce a concave bottom surface and by tooling the exposed upper surface. Care should be taken to keep the tooling concavity to 1/8 in (3 mm) in order to preclude buckling of the sealant in the center when the joint contracts.

### 28.2.2 Lap Joints

Sealant is used in lap joints in two different ways. Sealant may be used between the two parallel off-set substrates forming a sandwich lap joint similar to adhesive in adhesive lap joints. A bead of sealant may also be used as a fillet or a sealant tape can

be applied that spans both substrates at the end of the joint to provide a fluid barrier. These variations of sealant use in lap joints are shown in Fig. 3.

For the sandwich lap joint, the substrates must be held in place during sealant cure or setting. This can be done with mechanical fasteners such as rivets or bolts. In the automotive industry, specially formulated sealants are used that allow spot welding through the sealant layer as a means of greatly increasing the manufacturing rate. In Fig. 3, rivets are shown as the fixturing mechanism. The elongation of the sealant-free surface in a sandwich lap joint can be easily calculated as shown in Fig. 4 (Thompson 1990). If the differential movement of the two substrates in termed  $M$ , and the thickness of the sealant is termed  $d$ , then the sealant-free surface length after the differential movement ( $d'$ ) is given by the following relationship:

$$d' = (M^2 + d^2)^{1/2}, \quad (1)$$

and the elongation of the sealant-free surface ( $e$ ) is:

$$e = (M^2 + d^2)^{1/2} - d. \quad (2)$$

This relationship shows the importance of the sealant layer thickness. By increasing the thickness, higher differential movement can be accommodated in a sealant with a given elongation capability or extensibility.

If one makes the simplifying assumption that the shape change in a butt joint can be neglected (valid only for small substrate movements), one can easily compare the free-surface elongations of sealant in a butt joint with that in a sandwich lap joint. For example, if the differential movement in the joints is 1/8 inch (3 mm) and the thickness of the sealant in a sandwich lap joint or width of the sealant in a butt joint is 1/4 inch (6 mm), the sealant-free surface elongation in the lap joint is 12 percent compared with

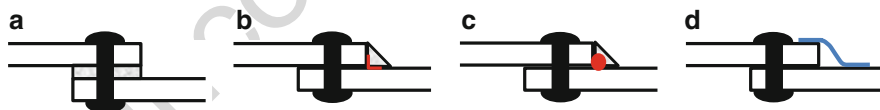
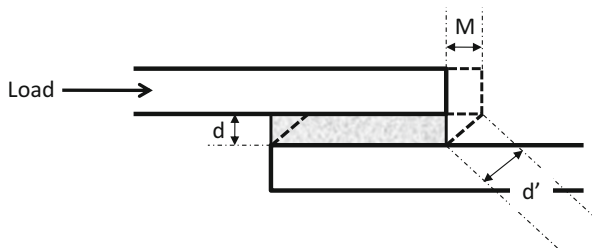


**Fig. 3** Lap joints: (a) sandwich, (b) sealant bead fillet with bond breaker, (c) sealant bead fillet with backing material, and (d) sealant tape fillet

**Fig. 4** Free sealant surface elongation ( $d'$ ) in a sandwich lap joint





50 percent for the butt joint. When one considers that the sealant shape change in the butt joint increases the free-surface elongation, the difference is even greater.

From this simple relationship, it is seen that the sealant-free surface elongation is always significantly less in the sandwich lap joint than that in the butt joint. Thus, from a mechanical perspective, the use of the lap joint is preferable. It is mainly the accessibility of the sealant in the butt joint that makes it preferable in main practical situations.

When using a sealant bead as the sealing fillet, the use of backing material or bond breaker can reduce the sealant bondline stresses, greatly enhancing the reliability of the joint. In order for sealant tapes to be effective, the tape must form a moisture or fluid barrier and resist chemical attack by the moisture or fluid. The bond of the pressure-sensitive adhesive used to bond the tape to the substrates is typically very sensitive to the surface condition of the substrate. Ensuring that these bond surfaces are clean, dry, and dust-free will usually ensure a good sealant tape bond and a subsequent seal. It is important to consider that sealant tape provides only a two-dimensional seal as opposed to the three-dimensional seal of a sealant bead fillet. Thus, a breach in the tape seal can allow fluid exposure to the entire joint length, whereas a bead fillet breach allows only local fluid exposure.

### 28.2.3 Corner or Angle Joints

When corners of structures need to be sealed, a designer has several options. These are shown in Fig. 5. If the thickness of the substrates is sufficient, it may be possible to use a butt joint with proper backing material. This is termed a simple angle or corner joint in Fig. 5. Although simple to make, there are usually better options from a structural point of view in cases where the sealant loading is significant. Applying a sealant bead fillet on the interior corner allows the substrates to support the sealant material, increasing performance of the joint. This type of joint is especially useful in

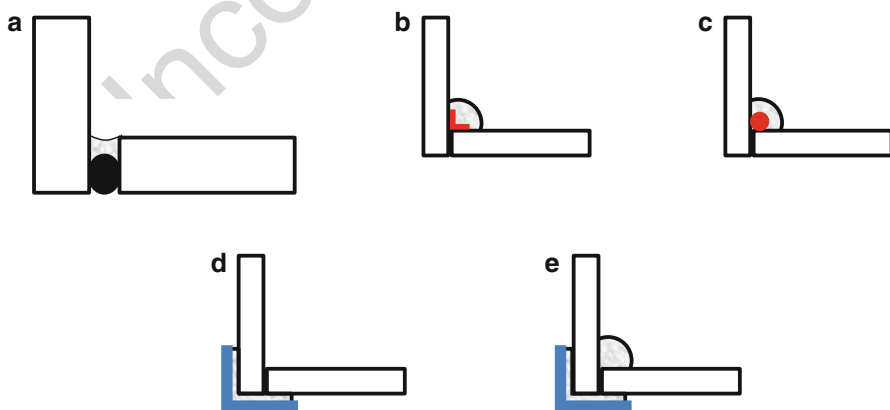


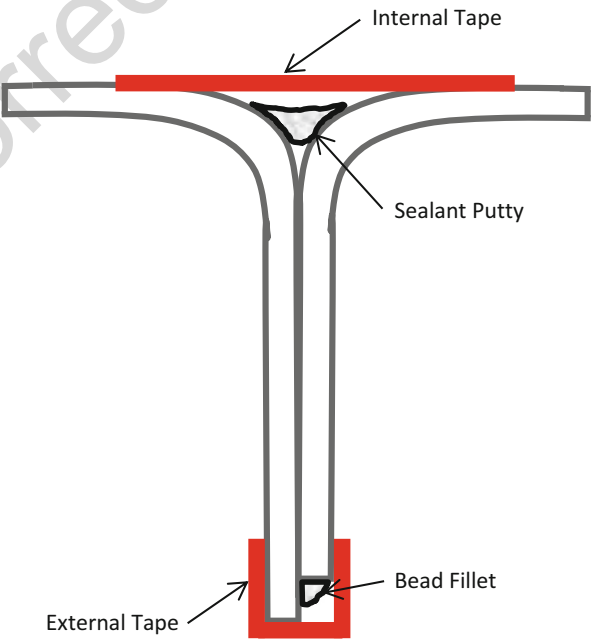
**Fig. 5** Corner or angle joints: (a) simple, (b) sealant bead with bond breaker, (c) sealant bead with backing material, (d) sandwich seal supported, and (e) bead seal supported

tank fabrication. By placing the sealant bead internal to the tank, the fluid pressure acts to augment the seal. Because the opposite is also the case, a designer should not use a sealant fillet on the outside of a tank. When using a sealant bead, proper use of bond breaker or backing rod materials reduce bondline stresses significantly. Supported corner joints can also be sealed with a sealant bead on the interior of the joint. By using the sealant in a sandwich configuration between the corner-forming substrates and the support, a lap-like sealant joint is formed. Although this joint geometry can be more labor-intensive to create, the structural benefits of a lap joint are inherent in this design geometry.

**28.2.4 Seam or Edge Joints**

The use of sealants and sealant tapes in seam or edge joints requires only that a seal be created and maintained. In this type of joint, there is no significant differential movement between the substrates. Figure 6 shows the four different methods available for sealing a seam. The most fail-safe method is pressing putty into the internal seam opening. As in the corner or angle joint, the internal fluid pressure will tend to enhance the seal in this type of joint. The other method for creating an internal seal is to apply a sealant tape that spans the two joined substrates. The use of sealant tape in this geometry carries with it the same limitations and required bond surface cleanliness as in the lap joint case.

**Fig. 6** Various uses of sealants in seam or edge joints



## 28.3 Critical Sealant Properties

There are many sealant properties that are critical to the design and assembly of reliable sealant joints. These critical properties include chemical, physical, and mechanical aspects of the sealant material.

### 28.3.1 Chemical Properties

Critical chemical properties of sealants include cure rate and its related properties of pot life, working life, tack-free time, depth of cure and skinning, cure shrinkage, chemical resistance, and weatherability. Chemical compatibility is also a major issue that must be addressed.

The rate of the cure reaction affects sealant use in different ways depending on the cure mechanism. For two-part sealants in which a curing agent is mixed into the sealant base, the rate of cure determines the allowable time between mixing and when the sealant must be inserted into the joint. Two different terms are used for this allowable time: pot life and working life. The pot life is typically determined from viscosity measurements and is often considered to be the time between the end of the mixing operation and the point at which the initial end-of-mix viscosity doubles in magnitude. Working life is typically determined by monitoring the ability of the sealant to be spread onto a substrate surface and wet that surface properly. Thus, the working life is a more subjective measurement than the pot life, but it is more representative of the actual use of the sealant.

The rate of cure for a one-part sealant material in which cure is initiated upon contact with moisture is important in determining the depth of cure. One-part sealants cure from the outer surface that is exposed to surface or environmental moisture, and the cure proceeds inward, toward the center of the sealant material. Curing beyond the outer surface depends on moisture diffusing into the sealant material. This diffusion process is slowed significantly or stopped completely when the sealant cures sufficient to create the desired “tight” moisture barrier. Because the sealant underneath the cured surface remains uncured due to the exclusion of water from the bulk of the sealant, the phenomenon is often called “skinning.” Once the sealant forms a cured skin, only the water molecules already within the sealant will be able to initiate further sealant cure. After consuming the available water molecules in additional sealant cure, no water is available to drive to cure to completion. In this way, the rate of reaction determines the maximum depth of cure by setting a limit to the amount of cure-initiating water that can diffuse into the sealant.

For solvated sealant formulations that require diffusion of the solvent or water to the surface of the sealant where it can evaporate, solidifying the sealant, diffusion, and evaporation rates are also important in determining the depth of sealant that can be fully solidified. Rapid loss of solvent or water at the sealant surface can create a skin not unlike that in the curing sealant system. In this case, the skin prohibits or significantly slows the further diffusion of solvent or water from the bulk of the sealant to the sealant surface where it can evaporate. This keeps the bulk of the sealant from solidifying, effectively creating an analogous depth of cure.

The tack-free time is that time necessary to cure or solidify the sealant to a sufficient degree that the surface is no longer sticky or tacky. This occurs near complete sealant surface cure or solidification. Tack-free time is especially important in sealant joints where physical appearance is important. Until the point where the surface is no longer tacky, the sealant surface must be kept dust free in order to preclude dust from sticking to the surface and ruining the appearance of the joint. The tack-free time is also often used as the time required before the joint has achieved sufficient handling strength to allow manufacturing or assembly with the sealant joint to continue.

Cure shrinkage is important to the structural capability of sealant joints. If cure shrinkage is excessive it may cause the sealant to pull away from the substrate surface, thus destroying the seal. In less dramatic fashion, cure shrinkage in joints where the seal is not broken creates stress and strain on the sealant that is additive to the thermal and structural loads that the sealant must accommodate to maintain the seal of the joint. Cure shrinkage in sealants that solidify through a chemical reaction is typically less than 10%. Shrinkage occurring in solvent-borne sealants can be greater than 10% as the sealant solidifies. It is in these sealants systems that shrinkage can be especially detrimental to the reliability of the joint seal.

The resistance of the sealant to chemical and environmental attack is the principal property that determines the ultimate life of most sealant joints. During the life of a sealant joint, the sealant may be subjected to hot and cold temperature extremes, thermal cycling, moisture, and UV and solar radiation. Many sealants are also exposed to chemicals such as petroleum-based fuel, alkali or acidic solutions or fumes, ozone, and salt water spray. Chemical and/or environmental exposure can cause sealants to soften, harden, contract, swell, embrittle, crack, craze, and dissolve or disintegrate. Such exposure can also inhibit sealant solidification or cause the sealant to debond from the substrate.

Solar radiation causes the most widespread damage of sealants used outdoors. The majority of this damage is in the form of breaking chemical bonds within the sealant polymer molecules. Water and water vapor can degrade sealants chemically by hydrolysis of the chemical bonds or physically by cyclical swelling and contracting of the sealant caused by moisture absorption and desorption (Wolf 2009).

In general, polysulfide sealants resist attack from fuels and water and have good chemical resistance. Polyurethane sealants are especially resistant to alkali exposure. Polyurethane, acrylic, and polychloroprene (neoprene) are all moisture-resistant. Polychloroprene and butyl rubber sealants both have good general chemical resistance. Silicones, although expensive, are often the sealant of choice, because they are strongly resistant to moisture and all chemicals. Silicones are also the most resistant sealants to UV and solar radiation.

Chemical compatibility among the various materials used in a sealant joint is also paramount to a long life for the joint. The sealant and substrates must not only be chemically compatible, but the choice of primer, bond breaker, and backing materials, where used, must take into consideration the chemical compatibility. The most typical offenders when it comes to chemical compatibility are plasticized sealants that contain species that are not chemically bound within the sealant and are free to diffuse into other surrounding materials (e.g., butyl rubber) and solvated sealants.

The cure reaction for many silicone sealants is initiated by acid added at low levels to the sealant formulation. Acids are chemically incompatible with concrete, marble, and limestone. When acid-containing silicone sealants are used in joints with these substrate materials, the acid reacts with the substrate bond surfaces creating salts at the bond interface. These salts destroy the sealant/substrate adhesion and cause debonding and loss of the seal. In order to use a silicone sealant with these substrates, a silicone formulated without acid is required. Another known chemical incompatibility is silicone and polychloroprene. Use of these two materials together in a sealant joint is to be avoided. Solvated sealant use in joints containing plastic or rubber materials should be undertaken only after chemical compatibility studies of the sealant with these materials are performed. Typical incompatibility will manifest itself over time by causing the sealant or substrate to soften, harden, crack, and/or craze. A standard test method for determining chemical compatibility is ASTM D-471.

### 28.3.2 Physical Properties

The important physical properties of sealants include the rheology, permeability, hardness, and thermal capability. They are distinct from the mechanical properties which are material responses to external loading.

Rheology refers to the fluid character of a material. There are two basic fluid forms of sealants: self-levelling and non-sag. Self-levelling sealants have sufficiently low viscosity to allow the sealant to flow and create a horizontal free surface. Non-sag sealants are typically thixotropic, or shear thinning. At high rates of shearing, these materials have low viscosity relative to their viscosity at low rates of shearing. Thus, a non-sag sealant will exhibit lower viscosity when being mixed – allowing thorough mixing, but will exhibit a high viscosity that allows the sealant to stay in place and hold its form once the mixing is completed and the material is inserted into the joint. There are two important standards relating to fluid sealant rheology. ASTM C-639 standardizes the differentiation between self-levelling and non-sag fluid sealant designations. The quantification or measurement of the degree of sag-resistance is covered in ASTM D-2202.

Some sealants have a very high viscosity under all conditions. These putty-like sealants are often called mastics. A formal definition of a mastic material is a fluid with a viscosity greater than 500,000 cP.

Permeability, a measure of the ease with which fluids can move through a solid material, is a critical characteristic of sealants. Because all sealants have low permeability, permeability is typically not a selection criterion in choosing among various sealant formulations. Measurement of permeability can be difficult, and there is no standardized method for measuring permeability that is specific to sealants. Therefore, the designer is usually left to using the permeability data available in the technical data sheets for specific sealant formulations.

The thermal capability of sealants can often be a crucial selection criterion. Both the temperature extremes that a sealant will experience over its lifetime and the daily and seasonal fluctuations of temperature can be important. For exterior sealant joints,

the joint may typically see 25 °C temperature differences within a day and upward of 50 °C temperature seasonally. External joints loaded primarily by the thermal expansion and contraction of the substrates will experience tension in the cold winter months and compression in the hot summer months.

The upper temperature limit is especially critical, because it is at higher temperatures that sealant materials soften and/or break down, leading to failure of the sealant joint. Determination of thermal capability of sealants is standardized in ASTM D-573. As a rule of thumb, acrylic and polysulfide sealants are generally good to 95 °C, while silicones can usually handle 200 °C. A special class of fluorosilicone sealants can operate to temperatures as high as 260 °C.

On the lower end of the temperature capability, the glass transition temperature can be important. When the temperature drops below the glass transition of the sealant, the sealant acts like an adhesive, rather than a sealant, restricting the movement of the substrates. Low temperatures also cause the sealant in butt joints to be loaded in tension due to thermal contraction of the substrates. When the temperature drops below the glass transition of the sealant, the tensile stress in the sealant, the bondlines, and the substrates increases tremendously. This can result in failure of any of the three.

Typical values for the glass transition temperature of acrylic and polyvinyl acetate sealants are in the range -15 °C to -20 °C. The glass transitions of neoprene and fluoro-polymer sealants range from -22 °C to -32 °C. Polysulfide and polyurethane sealants exhibit glass transitions at approximately -40 °C. Silicone sealants have the best low-temperature performance with glass transitions of approximately -65 °C.

Hardness is a very important property of a sealant. Changes in hardness over time reflect chemical changes internal to the sealant. Hardening can indicate that additional cure or solvent or plasticizer loss is occurring. Softening can be indicative of chemical or physical breakdown of the sealant. Due to these factors, measuring the hardness of the sealant over time is important to monitoring its useful life.

Hardness is inversely related to the flexibility of the sealant. Flexibility is, of course, crucial to a functioning sealant joint where substrate movement is accommodated. From this standpoint, low hardness is good. However, softer materials tend to have low resistance to abrasion and tearing. Depending on the requirements of a given sealant joint, the sealant selection may be preferential to softer or harder sealant formulations.

Because hardness is easy to measure and indicative of many performance capabilities, hardness is typically used as a quality conformance test. ASTM standards C-661 and D-2240 govern hardness measurements.

### 28.3.3 Mechanical Properties

Mechanical properties of sealants are those properties that define how sealants react to external loading. It is important to keep in mind that sealant materials are viscoelastic in nature; thus, many of these critical properties are rate and temperature dependent.

The tensile strength of a sealant is typically measured using a specimen commonly referred to as a dogbone. Tensile strength determination has been standardized in ASTM D-412. Also covered in this standard are determinations of the elongation capability of sealants and their modulus of elasticity. The elongation capability is the maximum extension a sealant will accommodate prior to rupture, and it is usually expressed as a percentage of the original length. Elongation is such a critical parameter for sealants that ASTM C-920 uses this property to classify different sealants. For example, a sealant that can elongate between 12.5% and 24% is termed a Class 12.5 sealant, while one that can elongate more than 25% is a Class 25 sealant. Measurement of the elongation is fairly simple. Sealants have such low stiffness that the crosshead displacement of the test device can be used for the elongation measurement without resorting to the use of extensometers or strain gages. Use of electromechanical extensometers or strain gages is not appropriate for sealants, because their use significantly affects the measured values. Laser or optical extensometers should be used when higher precision measurements are desired.

The technical term for stiffness is modulus of elasticity or Young's modulus. The modulus of elasticity is defined as the ratio of stress to strain. The stress is the load applied to the specimen divided by its cross-sectional area. The strain is the ratio of the extension or elongation of the specimen divided by its original length. It is the low modulus of elasticity of sealants combined with their high elongation capability that allows them to accommodate the differential movement of the substrates. In comparison with adhesives that are used in joints to restrict the substrate movement, the modulus of elasticity is typically one or two orders of magnitude smaller, and the elongation capability is 2–10 times greater.

The modulus of a sealant can change dramatically over time due to environmental or chemical exposure, additional cure, or solvent diffusion and evaporation from solvated sealants. Additional cure or solvent loss leads to increase in the modulus of the sealant over time. With increasing modulus, the ability of the sealant to accommodate the differential movement of the substrates is reduced. Environmental and chemical exposures of sealants tend to reduce the modulus over time. This would not typically be a problem, if all other properties remained the same. Unfortunately, they do not. The reduction in modulus is typically brought about by chemical degradation of the sealant, making the sealant more permeable and less able to maintain a seal. With enough degradation, the cohesive strength of the sealant and the adhesion of the sealant to the substrates will deteriorate.

The compressive strength of sealants is the maximum compressive stress a sealant can withstand without deteriorating. Although compressive strength is an important property, the tensile strength is generally lower and can be used as a conservative estimate of the compressive strength. For this reason, and also because failure of a sealant loaded in compression is much more difficult to determine than failure under tensile loading, there is no ASTM standard for determining the compressive strength of a sealant. To perform compressive strength testing, a short cylinder molded from sealant can be used. Care should be taken to keep the length-to-diameter ratio near one to avoid buckling of the cylinder during testing. Careful review of the load versus displacement data can reveal the failure load or the load at which the sealant starts to deteriorate.

Compression set is a term relating to the inability of many sealants to recover to their original dimensions following prolonged compressive loading. Compression set is not a favorable property, and it is very undesirable property in cases where the sealant joint is subjected to cyclic loading. Thus, fatigue resistance can be directly related to compression set. Compression set usually occurs in sealant formulations that cure slowly over time or that degrade over time due to environmental exposure. In general, oleoresinous caulking compounds and polybutene-based sealants are very susceptible to compression setting, while polysulfides, polyurethanes, and silicones are not. Acrylic, butyl rubber, and polychloroprene (neoprene) sealants can experience compression setting depending on the magnitude of the compressive load and the environmental conditions.

Tear and abrasion resistance are related properties. The measurement of both is standardized in ASTM D-624. As was stated earlier, harder materials, in general, exhibit greater resistance to both tearing and abrasion. Polyurethane sealants are particularly resistant to tearing and abrasion.

Stress relaxation is defined as the time-dependent relaxation of stress in a material subjected to a fixed displacement. Stress relaxation is observed in all viscoelastic materials and is directly related to creep. Creep is the time-dependent elongation of a material subjected to a fixed load. Excessive creep can result in failure of a material when the elongation due to creep exceeds the elongation capability of the material. The term for this type of failure is creep rupture. The magnitudes of creep and stress relaxation that a material will experience are inversely proportional to the crosslink density of the material. Creep rupture generally occurs in materials that do not crosslink or that have a very low-crosslink density. Stress relaxation testing can be performed using dogbone specimens subjected to a given elongation, typically between 20% and 80% of the elongation capability of the material.

### 28.3.4 Adhesion

The overriding consideration with respect to the adhesion of sealants is that the sealant and surface preparation should be selected to ensure that the adhesion strength exceeds the cohesive strength of the sealant. This can necessitate that extra care be used in the substrate bond surface preparation or that a primer be used, but ensuring that any failure that occurs will be cohesive in the sealant rather than adhesively to the substrate is a primary design consideration.

ASTM C-1135 can be used to determine the tensile adhesion strength of a sealant bond. Although there is no ASTM standard that specifically addresses the measurement of the adhesion or bond strength of sealants loaded in shear, the standards in place for adhesive bonds can be used (single-lap shear – ASTM D-1002; notched-lap shear – ASTM D-3165; and double-lap shear – ASTM D-3528). Much of the adhesion testing that is performed in the industry is testing to determine the effects of environmental and chemical exposure on sealant adhesion. This exposure can be either static or cyclic (Gutowski and Cerra 2009).



## 28.4 Differential Movement Tolerances

The ability of a sealant to accommodate the differential movement of the substrates in a sealant joint is the primary mechanical performance requirement of a sealant. There are many sources of this differential movement. In the use of sealants in building construction, the sources include changes in temperature that cause the substrates to expand or contract, changes in moisture content that can cause porous substrates such as concrete and masonry to swell or shrink, building loads including those induced by the settling of the building over the first two-to-three years, and environmental loads due to wind and earthquakes. Sealant joints should generally not be load-bearing in nature. To be so is counter to the primary mechanical purpose of the sealant joint, accommodating the differential movement. For this reason, the overall design of a building should limit vertical movement through the use of structural reinforcements and key and tongue-and-groove joints.

The differential movement caused by the various mechanisms is additive. Calculation of movement caused by building loads, building settling, and environmental loads are the providence of structural engineers and are beyond the scope of this chapter. Suffice it to say that these loads can be significant, and the input of a competent structural engineer in determining their magnitude is essential to the design of the sealant joints.

The calculations of differential movement caused by temperature changes, though straightforward, must consider all of the following aspects: ambient temperature and the temperature of the sealant material and substrates when the joint is assembled, any movement of the substrates during the processes of sealant insertion and cure, the joint geometry and material used, the substrate mechanical constraints that limit movement, any expected compression set that the sealant may experience, and the expected temperature extremes throughout the sealant joint lifetime.

The total joint movement due to temperature changes can be calculated from the following equation:

$$M_{total} = (T_{max} - T_{min}) \cdot \alpha_{substrate} \cdot l_{substrate} \quad (3)$$

In the equation,  $M_{total}$  is the total joint movement,  $T_{max}$  is the maximum temperature the joint will experience due to ambient heating and the absorption of radiant heat,  $T_{min}$  is the minimum temperature the joint will experience including wind chill,  $\alpha_{substrate}$  and  $l_{substrate}$  are the coefficient of thermal expansion and the unrestrained length of the substrates. Accounting for the absorption of radiant heat can be very important. A dark metal substrate that is in direct sunlight can have a temperature 40 °C higher than the ambient temperature, greatly increasing the joint movement.

For butt joints, this total joint movement should be broken down into movement that will expand or contract the sealant width. The movement creating joint expansion ( $M_{exp}$ ) is:

$$M_{exp} = (T_0 - T_{min}) \cdot \alpha_{substrate} \cdot l_{substrate}, \quad (4)$$

571 where  $T_0$  is the temperature of the substrates at the time of sealant insertion and cure.  
 572 The movement creating joint compression is:

$$M_{comp} = (T_{max} - T_0) \cdot \alpha_{substrate} \cdot l_{substrate} \quad (5)$$

573 The sealant in the joint must accommodate these movements considering the  
 574 actual joint width when the sealant is inserted and cured or set. The necessary joint  
 575 widths to accommodate joint expansion and contraction are easily calculated from  
 576 the elongation capabilities of the sealant in tensile and compression. These values are  
 577 standard information in the technical data sheets of sealants, often using the term  
 578 dynamic movement capability and expressed as a percentage. Where only one value  
 579 is given, it should be used for both tension and compression. Calculation of these  
 580 minimum widths is accomplished using the following relationships:

$$w_{exp} = (100 \cdot M_{exp}) / S_{ten}, \text{ and} \quad (6)$$

$$w_{comp} = (100 \cdot M_{comp}) / S_{comp}. \quad (7)$$

581 In these relationships,  $w$  is the minimum joint width expressed in mm,  $M$  is also in  
 582 mm and is calculated from the preceding equations, and  $S_{ten}$  and  $S_{comp}$  are the  
 583 elongation capabilities of the sealant, in tension and compression respectively, and  
 584 expressed in percent.

585 The movement due to moisture extremes in porous substrates can be calculated in  
 586 much the same way, once the coefficient of moisture expansion is determined for the  
 587 substrate. The movement due to moisture and any movement due to building and  
 588 environmental loads can be added to the thermally induced movement when they are  
 589 significant. The overall required joint width can then be calculated using the relation-  
 590 ships above, and the smaller of the two calculated joint width, with an appropriate  
 591 safety factor, is used for the minimum joint width. From a practical perspective, it is  
 592 important to remember the differences between the as-designed sealant joints and the  
 593 as-built sealant joints and the effects these differences may create. Both geometric  
 594 tolerances and the accuracy of substrate placement must be considered in the design  
 595 of the joints.

596 For lap joints, the differential movement can also be easily calculated. In these  
 597 joints it is the minimum thickness of the joint that must be calculated in the design of  
 598 the joint geometry. This is done by ensuring that the elongation of the sealant-free  
 599 surface does not exceed the elongation capability of the sealant. This is done by  
 600 setting the free surface elongation ( $e$  Eq. (1) discussed in Sect. 2.2) equal to the  
 601 sealant elongation capability and solving the equation for the minimum sealant  
 602 thickness ( $d_{min}$  in the following equation).

$$S_{ten} = (M_{exp}^2 + d_{min}^2)^{1/2} - d_{min} \quad (8)$$

$$S_{comp} = (M_{comp}^2 + d_{min}^2)^{1/2} - d_{min} \quad (9)$$

## 28.5 Conclusions

The proper use of sealants and design of sealant joints must entail consideration of the chemical, physical, and mechanical properties of the sealant and substrate materials and the joint geometry. There are four main sealant joint geometries: butt joints, lap joints, corner or angle joints, and seam or edge joints. Corner and seam joints typically have very limited or no mechanical requirements; they must simply create a lasting seal. The main mechanical requirement of butt and lap joints is to accommodate the differential movement of the substrates. This differential movement dictates the minimum width of butt joints and the minimum thickness of lap joints. The calculation of the substrate differential movement due to temperature and moisture extremes is straightforward, while the influence of external loading on this movement can be complex and will require the services of a structural engineer.

Butt joints are typically chosen over lap joints due to the accessibility of the sealant for repairs and replacement. The use of backing material and bond breaker is essential to creating reliable butt joints. Creating an hourglass shape in the cure or set sealant can greatly decrease the stresses a sealant bond is subjected to.

Most failures of sealant joints can be eliminated by careful selection of the sealant and proper preparation of the substrate bond surfaces. In selecting the sealant, consideration of the chemical, physical, and mechanical properties within the framework of the joint geometry is essential. For joints that require a large volume of sealant, solvated systems and curing systems that require moisture to initiate the cure should not be selected, because they will likely not completely solidify. Chemical compatibility of all materials that will be in contact in the assembled joint, sealant, primer, substrates, bond breaker, and backing material, and the fluids to which the sealant joint will be subjected is essential. Hardness, permeability, and thermal capability of the sealant are the principal physical properties that should be considered in the sealant selection. The mechanical properties of the sealant must match the end use of the sealant joint. Compression set and creep rupture are factors somewhat unique to some sealants that can dramatically reduce the lifetime of a sealant joint.

## References

- Amstock JS (1973) Sealants. In: Cagle CV (ed) Handbook of adhesive bonding. McGraw Hill, New York, pp 1–41
- Gutowski WS, Cerra AP (2009) Adhesion testing of sealants. In: Mittal KL, Pizzi A (eds) Handbook of sealant technology. CRC Press, Boca Raton, pp 191–222
- Panek JR, Cook JP (1984) Construction sealants and adhesives, 2nd edn. Wiley, New York
- Petrie EM (2007) Handbook of adhesives and sealants, 2nd edn. McGraw Hill, New York
- Prane JW (1977) Sealants and caulks. In: Skeist I (ed) Handbook of adhesives. Van Nostrand Reinhold, New York, pp 692–715
- Thompson JE (1990) Design considerations unique to sealants. In: Dostal CA (ed) Engineering materials handbook: adhesive and sealants, vol III, 3rd edn. ASM International, Cleveland
- Wolf AT (2009) Sealant durability and service life of sealant joints. In: Mittal KL, Pizzi A (eds) Handbook of sealant technology. CRC Press, Boca Raton, pp 143–190

Chiaki Sato

## Contents

29.1	Introduction .....	830
29.2	Stress Waves .....	831
29.3	Material Properties Under High Strain-Rate Conditions .....	832
29.3.1	Constitutive Relations of Metals .....	832
29.3.2	Constitutive Relations of Plastics .....	833
29.4	Stress Analysis of Adhesively Bonded Joints Subjected to Impact Loads .....	834
29.4.1	Theoretical Approach .....	834
29.4.2	Infinite Lap-Strap Joints .....	834
29.4.3	Single Lap Joints .....	839
29.4.4	Finite Element Analysis .....	840
29.5	Impact Strength Evaluation of Adhesively Bonded Joints .....	844
29.5.1	Failure Criteria for Adhesively Bonded Joints .....	844
29.6	Applications .....	847
29.6.1	Crash of Car Structures .....	847
29.7	Conclusions .....	849
References	.....	850

## Abstract

Design methods of adhesively bonded joints subjected to impact loading are discussed in this chapter. Methodologies to treat the dynamic responses of structures are shown. In these cases, it is necessary to analyze the stress distribution considering stress wave propagation because inertia effects of the structures are more significant than those in quasi static conditions. Constitutive relations of materials are discussed. The relations are highly dependent to the stress and strain rates. Thus, the dependence should be considered for the dynamic analysis of materials. Some examples of stress analysis are shown, where closed-form

C. Sato (✉)

Precision and Intelligence Laboratory, Tokyo Institute of Technology, Midori-ku, Yokohama, Japan  
e-mail: [csato@pi.titech.ac.jp](mailto:csato@pi.titech.ac.jp)

approaches and dynamic finite element analyses are explained. In addition, an actual application, a crash problem of car structures, is explained because adhesively bonded joints have been recently introduced to car structures and the design of the joints subjected to impact loads has become very important.

### 29.1 Introduction

In actual applications of adhesively bonded joints, there are many cases in which joints are subjected to impact loading. For instance, weldbonding joints, in which spot welding and adhesive bonding are combined, are widely used in the body structures of cars (see ► Chap. 46, “Automotive Industry”). Joints are subjected to impact loading when the cars are crashed in accidents. Adhesively bonded joints are also used in aircraft structures in these days, and impacts should be considered to design the airframe because bird-strike accidents may occur. Therefore, design for impact loads of adhesively bonded joints has become important, and a proper design method is required.

Other problems, in which impact occurs in a lower velocity range than those of car crash or bird strikes, has also become important. Dropping impact failure of mobile phones is one example. In mobile phones, there are several joints bonded with adhesives or pressure sensitive adhesives (PSAs). When a mobile phone drops and collides with the floor, an impact loading occurs and is applied to the structure, although the impact velocity and the maximum stress are relatively lower than in the case of higher velocity impacts. Thus, impact problems have a very wide range in impact velocity or loading rate, and methodologies depend on the type of loading rate.

Figure 1 shows the relation between types of impact, strain rates occurring in materials subjected to impacts, and typical experimental methods. Impact conditions can be categorized in three ranges: low velocity, medium velocity, and high velocity. In the low velocity range, problems cannot be treated as impact but as vibration. In the

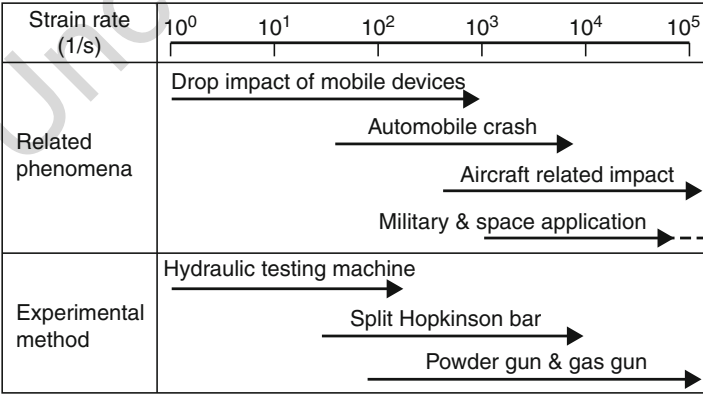


Fig. 1 Types of impact related phenomena, strain rates, and experimental methods

medium velocity range, stresses and strains propagate as waves in materials. In the high velocity range, a body collides with another body faster than the sound velocity of the bodies, and the sound velocity increases up to the impact velocity. The increase occurs due to the density and temperature increase by compression of the bodies. The stress waves higher than normal sound velocity are called “shock waves.” The above mentioned examples of cars, aircrafts, and mobile phones are included in the problems of medium velocity impacts that are mainly treated in this chapter.

The design process of adhesively bonded joints subjected to impact loading is basically the same as that to static loading. These processes include experimental investigations of material properties and failure criteria, stress analyses, and strength prediction by applying failure criteria to the analyzed stresses. The difference between impact and static cases is in the stress analysis considering stress wave propagations, the dependency of stress–strain relations, and the strength of materials. Experimental methods for impact phenomena are shown in ► Chap. 21, “Impact Tests.” In this chapter, the introduction of dynamic problems, stress analyses, and strength predictions are mainly discussed.

## 29.2 Stress Waves

Dynamic mechanics of materials is different from the static. In dynamic cases, inertia forces occurring in bodies should be considered. This is equivalent to solving the kinetic equation at each point in the bodies. In dynamic conditions, the stress value at a point changes with time, and the stress transmits in the solid. The stress variation in time and space domains is called “stress waves” (Goldsmith 2001).

The governing equations of stress waves propagating in three-dimensional space denoted with vector ( $\mathbf{x}$ ) are as follows:

$$\rho \frac{\partial^2 \varphi(\mathbf{x}, t)}{\partial t^2} = (\lambda + 2G) \nabla^2 \varphi(\mathbf{x}, t), \quad (1)$$

$$\rho \frac{\partial^2 \psi(\mathbf{x}, t)}{\partial t^2} = G \nabla^2 \psi(\mathbf{x}, t), \quad (2)$$

where ( $t$ ) is time, ( $\varphi(\mathbf{x}, t)$ ) is the field of dilatational waves, ( $\psi(\mathbf{x}, t)$ ) is the field of shear waves, ( $\rho$ ) indicates density of the solid, ( $\lambda$ ) and ( $G$ ) are the Lamé constant and the shear modulus of the solid, respectively, ( $\nabla$ ) and ( $\nabla^2$ ) are nabla and Laplacian operators. Since Eqs. 1 and 2 are wave equations, they can be expressed with velocities ( $c_1$ ) and ( $c_2$ ) as:

$$\frac{\partial^2 \varphi}{\partial t^2} = c_1^2 \nabla^2 \varphi, \quad (3)$$

$$\frac{\partial^2 \psi}{\partial t^2} = c_2^2 \nabla^2 \psi, \quad (4)$$

where  $(c_1)$  is  $(\sqrt{(\lambda + 2G)/\rho})$ , and  $(c_2)$  is  $(\sqrt{G/\rho})$ . In ordinary solids,  $(c_1)$  is greater than  $(c_2)$ . Therefore, dilatational waves can propagate faster than shear waves in the solids.

## 29.3 Material Properties Under High Strain-Rate Conditions

Constitutive relations (stress–strain relations) of materials are greatly dependent on stress and strain rates. Therefore, the dependency should be considered for precise simulation of impact phenomena. Constitutive relations and their loading-rate dependencies are shown in this section.

### 29.3.1 Constitutive Relations of Metals

Most metals show elasto-plastic behavior when they are loaded. They behave as linear elastic materials in low stress conditions, and plastic materials in high stress conditions over their yield points or proof stresses. The yield point is determined by yield criteria, and the plastic deformation over the yield point is described by flow rules. A flow rule in three-dimensional space can be obtained from the deformation and translation of the yield surface, which is expressed by work hardening of one-dimensional loading if the material is isotropic. Therefore, expression of work hardening is very important and can determine the flow rule. There are several models expressing work hardening, as shown in Fig. 2. Elastic and perfect plastic models are models for materials having no work hardening. The linear hardening model can describe a work hardening of constant rate with respect to plastic strain. As nonlinear models, power hardening model, Ludwik type hardening model, and Swift type hardening model are frequently used (Johnson and Mellor 1973).

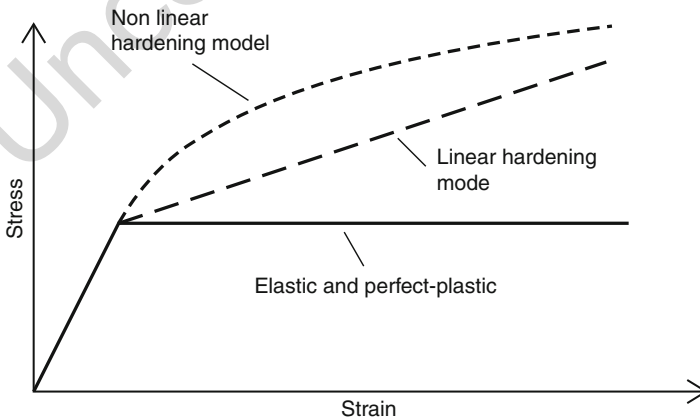


**Fig. 2** Stress strain curves with or without work hardening

In impact conditions, the loading rate is quite high, so that the plastic behavior of metals is much influenced. In order to describe the loading-rate dependency, several models have been presented. The Johnson–Cook model, shown in Eq. 5, is a model by which Ludwik type hardening and loading-rate dependency can be expressed (Johnson and Cook 1983).

$$\sigma = (\sigma_0 + B\epsilon^n) \left\{ 1 + C \ln \left( \frac{\dot{\epsilon}^p}{\dot{\epsilon}_0} \right) \right\} \left\{ 1 - \left( \frac{T - T_r}{T_m - T_r} \right)^m \right\} \quad (5)$$

where ( $\sigma$ ) and ( $\sigma_0$ ) are stress and yield stress, respectively, ( $\epsilon$ ) is stress, ( $\dot{\epsilon}_0$ ) is a standard strain rate, ( $\dot{\epsilon}^p$ ) is the rate of equivalent plastic strain, ( $T$ ) is the temperature of the material, ( $T_r$ ) is room temperature, and ( $T_m$ ) is the melting point of the material. Parameters ( $B$ ), ( $C$ ), ( $m$ ), and ( $n$ ) should be determined experimentally. This model is suitable for high-rate deformations or high velocity impacts in which the temperature of materials increases due to the collision and the material constants change (Mayer 1990). The Cowper–Symonds model can also express high-rate condition by means of increasing the yield point of a material subject to impact (Cowper and Symonds 1952). The model can be shown as follows:

$$\frac{\sigma_d}{\sigma_s} = 1 + \left( \frac{\dot{\epsilon}^p}{D} \right)^{\frac{1}{P}} \quad (6)$$

where, ( $\sigma_d$ ) is the dynamic yielding stress, ( $\sigma_s$ ) is the static yielding stress, ( $\dot{\epsilon}^p$ ) is the rate of equivalent plastic strain, and ( $D$ ) and ( $P$ ) are parameters determined experimentally. Both the Johnson–Cook model and the Cowper–Symonds model are widely used for impact analyses and are included in many packages of finite element methods (FEMs).

### 29.3.2 Constitutive Relations of Plastics

Plastics are in the glassy state and linear elastic at low temperatures. The nature of plastics changes to a viscoelastic state around the glass transition temperature ( $T_g$ ) and to rubbery state in temperature range higher than  $T_g$ . Thus, the constitutive relations change from linear elastic to rubber elastic via viscoelastic. Since high loading-rate conditions are equivalent to low temperature conditions in terms of the temperature time superposition principle, plastics tend to become brittle in high loading-rate conditions.

Plastics are very often used in temperature ranges lower than their  $T_g$ s, so that their constitutive relations used for analyses should be linear elastic. However, strictly speaking, their moduli have a weak dependency to loading rates. If the dependency is a problem for impact analyses, the variation of moduli should be compensated. For this purpose, viscoelastic models are sometimes used to express the loading rate dependency (Sato and Ikegami 2000).



The situation of adhesives is different from that of ordinary plastics because adhesives are often plasticized to increase their ductility and cannot be treated as simple linear elastic materials. In this case, elasto-plastic models should be applied. Goglio, Peroni et al. have investigated the constitutive relation of a ductile epoxy adhesive at high strain rates using the split Hopkinson bar method (Goglio et al. 2008). The adhesives showed large plastic deformation that was much better fitted with a poly-linear model than the Johnson–Cook model and the Cowper–Symonds model.

---

## **29.4 Stress Analysis of Adhesively Bonded Joints Subjected to Impact Loads**

### **29.4.1 Theoretical Approach**

A correct stress analysis is necessary to estimate the strength of adhesively bonded joints. Much research on the problem has been carried out since the first theory emerged: Volkersen's shear lag model (Volkersen 1938). Since the stress distribution in joints depends on dimensions, types of materials and particularly the configuration, suitable designs to reduce stress concentration has been pursued. Stress analysis using FEM has a history of over 30 years, and almost all joint configurations have been investigated already with the method. For instance, Adams and Peppiatt conducted FEM analysis of lap joints and compared them with the closed forms of Goland–Reissner model (Adams and Peppiatt 1974). Other research treated the joints considering the elasto-plastic or viscoelastic properties of adherends and adhesives. However, dynamic analyses of the joints are still rare because they are more difficult than the static ones. The difficulty is due to the fact that a dynamic analysis needs repeated calculations and consumes much of computer resources.

### **29.4.2 Infinite Lap-Strap Joints**

Sato expanded the Volkersen's model to a dynamic model considering the inertia force effect of the adherends and derived series solutions of the governing equations for infinite lap-strap joints, which had boundary conditions simpler than single lap joints (Sato 2009). For ordinary adhesively bonded joints, cured adhesive resins are lighter than adherend materials, and the adhesive thickness is very smaller than that of adherends. Therefore, the inertia force of the adhesive layer is negligible and is thus not considered in the model.

Figure 3 shows the load equilibrium and deformation compatibility for the dynamic Volkersen's model of a lap-strap joint having a half-infinite length. The joint configuration has only one discontinuity at the edge of the joint, and its boundary condition is easier to treat than other joint configurations such as finite length single lap joints because stress reflection occurs only at the edge.

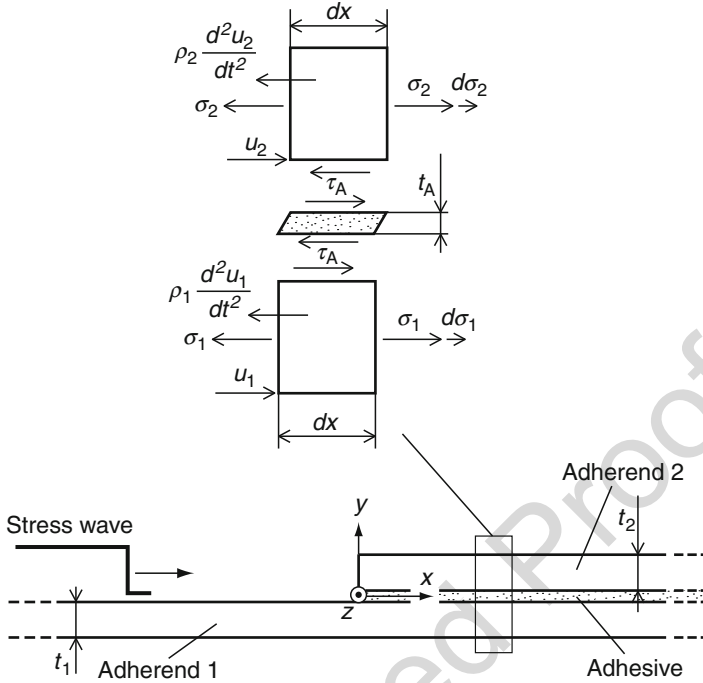


**Fig. 3** Equilibrium condition in infinite lap-joint (Sato 2009)

The force equilibrium of the half-infinite length lap-joint in the case of a dynamic condition can be determined considering the inertia forces  $(t_1 W \rho_1 \frac{\partial^2 u_1}{\partial t^2})$  and  $(t_2 W \rho_2 \frac{\partial^2 u_2}{\partial t^2})$  of the adherends as follows:

$$t_1 W \frac{\partial \sigma_1}{\partial x} + W \tau_A = t_1 W \rho_1 \frac{\partial^2 u_1}{\partial t^2}, \quad t_2 W \frac{\partial \sigma_2}{\partial x} - W \tau_A = t_2 W \rho_2 \frac{\partial^2 u_2}{\partial t^2}, \quad (7)$$

where  $(t_1)$ ,  $(t_2)$ ,  $(\rho_1)$ , and  $(\rho_2)$  are the thicknesses and densities of adherend 1 and adherend 2, respectively;  $(W)$  is the width of the joint; and  $(u_1)$ ,  $(u_2)$ ,  $(\sigma_1)$ , and  $(\sigma_2)$  denote the longitudinal displacements and normal stresses of adherends 1 and 2, respectively. Moreover,  $(\tau_A)$  is the shear stress of the adhesive layer, and  $(t)$  denotes the time since the beginning of loading. The normal strains of adherends 1 and 2 are denoted as  $(\epsilon_1)$  and  $(\epsilon_2)$ , respectively, and the shear strain (engineering strain) of the adhesive layer is denoted as  $(\gamma_A)$ . With  $(u_1)$  and  $(u_2)$ , the strains can be written as

$$\epsilon_1 = \frac{\partial u_1}{\partial x}, \quad \epsilon_2 = \frac{\partial u_2}{\partial x}, \quad \gamma_A = \frac{u_2 - u_1}{t_A}, \quad (8)$$

where  $(t_A)$  is the thickness of the adhesive layer.

The constitutive relations of the materials comprising the joint can be described as follows:

$$E_1 \epsilon_1 = \sigma_1, \quad E_2 \epsilon_2 = \sigma_2, \quad G_A \gamma_A = \tau_A, \quad (9)$$

where ( $E_1$ ) and ( $E_2$ ) are the Young's moduli of adherends 1 and 2, and ( $G_A$ ) is the shear modulus of the adhesive layer. Therefore, the governing equations of the dynamic Volkersen's model are given as follows:

$$\frac{\partial^2 u_1}{\partial x^2} + \frac{G_A}{E_1 t_1 t_A} (u_2 - u_1) = \frac{\rho_1}{E_1} \frac{\partial^2 u_1}{\partial t^2}, \quad \frac{\partial^2 u_2}{\partial x^2} - \frac{G_A}{E_2 t_2 t_A} (u_2 - u_1) = \frac{\rho_2}{E_2} \frac{\partial^2 u_2}{\partial t^2}. \quad (10)$$

When the thicknesses, moduli, and densities of the adherends are equal, they can be denoted by ( $t_s$ ), ( $E$ ), and ( $\rho$ ), and Eq. 10 can be written as

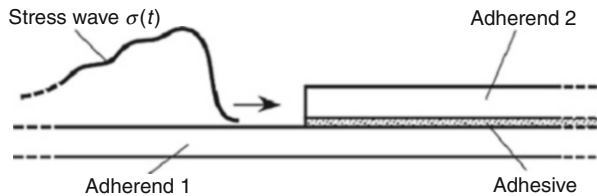
$$\frac{\partial^2 \tau_A}{\partial x^2} - \frac{2G_A}{E t_s t_A} \tau_A = \frac{\rho}{E} \frac{\partial^2 \tau_A}{\partial t^2}. \quad (11)$$

This equation is a simple modification of the governing equation of the Volkersen's model. It is obtained by adding the inertia force to the static equation. Although the governing equation of the static Volkersen's model is an ordinary differential equation, that for the dynamic Volkersen's model is a partial differential equation.

The boundary conditions for the model are defined as the situation in which a given stress wave transmits from adherend 1 into the joint, as shown in Fig. 4. If a strain gage is bonded on adherend 1 far from the joint end, the strain variation due to the stress wave propagation can be measured. In this case, the information of the progressive stress wave can be obtained, but have no information on the stress wave reflection occurring at the joint end.

The stress at the edge of adherend 2 is zero because this edge is a free surface. At the points of infinite distance ( $(x = \infty)$ ) in adherends 1 and 2, the displacements are zero because no stress wave reaches there within finite duration. When adherend 1 is virtually cut at the edge of the joint, the displacement of a virtual interface on the left part of adherend 1 can be expressed as the superposition of a displacement caused by the free-edge reflection of a progressive stress wave ( $\sigma_p(x - c_1 t)$ ) in adherend 1 and a displacement caused by a stress ( $\sigma_1(0, t)$ ) at ( $x = 0$ ). Note that ( $\sigma_p(x - c_1 t)$ ) is the stress distribution in the left part of adherend 1 due to a progressive wave. No stress wave reflection at the joint end is considered. In contrast, ( $\sigma_1(0, t)$ ) is the real stress

**Fig. 4** Boundary condition for infinite lap-strap joint (Sato 2009)



variation at the joint end. Therefore, all boundary conditions can be written as follows:

$$\begin{aligned} u_1(0, t) &= -2 \int_0^t c_1 \frac{\sigma_w(\xi)}{E_1} d\xi + \int_0^t c_1 \frac{\partial u_1(x, \xi)}{\partial x} \bigg|_{x=0} d\xi, \frac{\partial u_2(x, t)}{\partial x} \bigg|_{x=0} = 0, \\ u_1(\infty, t) &= 0, \quad u_2(\infty, t) = 0, \end{aligned} \quad (12)$$

where  $(\sigma_w(t) \equiv \sigma_p(0 - c_1 t))$  and  $(\xi)$  is a variable for the time integration. The function  $(\sigma_p())$  indicates the shape of a stress wave in the space domain  $(x)$ . In contrast,  $(\sigma_w())$  is a function in the time domain  $(t)$  and indicates the stress variation with respect to time caused by a stress wave propagation without reflection at  $(x = 0)$ . Therefore,  $(\sigma_w(t) \neq \sigma_1(0, t))$ .

Equations 11 and 12 are transformed into complex number domain  $(s)$  by the Laplace transform and are combined to the following equation:

$$H(0, s) = \frac{T_A(0, s)}{\Sigma_w(s)} = \frac{G_A c}{Et_A} \cdot \frac{4}{s + 3\sqrt{s^2 + 2c^2 k^2}}, \quad (13)$$

where  $(T_A(0, s))$  and  $(\Sigma_w(s))$  are the Laplace transforms of  $(\tau_A(0, t))$  and  $(\sigma_w(t))$ , respectively,  $(H(0, s))$  is the transfer function between  $(\Sigma_w(s))$  and  $(T_A(0, s))$ ,  $(k)$ , and  $(c)$  are given as follows:

$$k = \sqrt{\frac{G_A}{Et_s t_A}}, \quad c = \sqrt{\frac{E}{\rho}}. \quad (14)$$

This transfer function has enough information between the input stress waves and the stress fluctuation at the joint end that is the stress concentration point in the static case.

When a unit impulse stress wave is applied to the joint, the shear stress variation  $(\tau_{A \text{ imp}}(0, t))$  at the adhesive edge can be expressed as follows:

$$\tau_{A \text{ imp}}(0, t) = L^{-1}(H(0, s)) = \frac{G_A c}{Et_A} L^{-1} \left( \frac{4}{s + 3\sqrt{s^2 + 2c^2 k^2}} \right). \quad (15)$$

Here, a function  $(W(s))$  is defined as

$$W(s) \equiv \frac{4}{s + 3\sqrt{s^2 + a^2}} \wedge a = \sqrt{2}ck. \quad (16)$$

This function can be modified as

$$W(s) = \frac{4}{s} \sum_{n=0}^{\infty} \frac{(-1)^n}{3^{n+1}} \sum_{m=0}^{\infty} \frac{(-1)^m (n + 2m - 1)!!}{2^m \cdot m! \cdot (n - 1)!!} \left( \frac{\sqrt{2}ck}{s} \right)^{2m}. \quad (17)$$

233 The function  $(\Omega(\sqrt{2}ckt))$ , which is the inverse Laplace transform of  $(W(s))$ , can  
 234 be written as

$$\Omega(\xi) = \frac{4}{3} \sum_{m=0}^{\infty} \frac{(-1)^m}{2^m \cdot m!} \cdot \frac{\xi^{2m}}{(2m)!} \sum_{n=0}^{\infty} \left(-\frac{1}{3}\right)^n \frac{(n+2m-1)!!}{(n-1)!!}. \quad (18)$$

235 A function obtained by the inverse Laplace transform of the transfer function of a  
 236 dynamic system is equivalent to the impulse response of the system. Therefore, the  
 237 shear stress variation at the adhesive edge  $(\tau_{A \text{ imp}}(0, t))$  by a unit impulse stress wave  
 238 can be written as the following equation.

$$\begin{aligned} \tau_{A \text{ imp}}(0, t) &= L^{-1}(H(0, s)) = \frac{G_{AC}}{Et_A} L^{-1} \left( \frac{4}{s + 3\sqrt{s^2 + 2c^2k^2}} \right) \\ &= \frac{G_{AC}}{Et_A} \Omega(\sqrt{2}ckt). \end{aligned} \quad (19)$$

239 The indicial response  $(\tau_{A \text{ ind}}(0, t))$ , which is the response when a unit step stress  
 240 wave is applied to the joint, can be written as

$$\tau_{A \text{ ind}}(0, t) = \frac{G_{AC}}{Et_A} \int_0^t \Omega(\sqrt{2}ck\xi) d\xi = \sqrt{\frac{G_{AC}t_s}{2Et_A}} \int_0^{\sqrt{2}ckt} \Omega(\chi) d\chi. \quad (20)$$

241 The impulse response and the indicial response are shown in Fig. 5, where  $(\Omega())$  is  
 242 calculated approximately by the summation of terms in the series signified by the  
 243 symbols (m) and (n) up to 100.

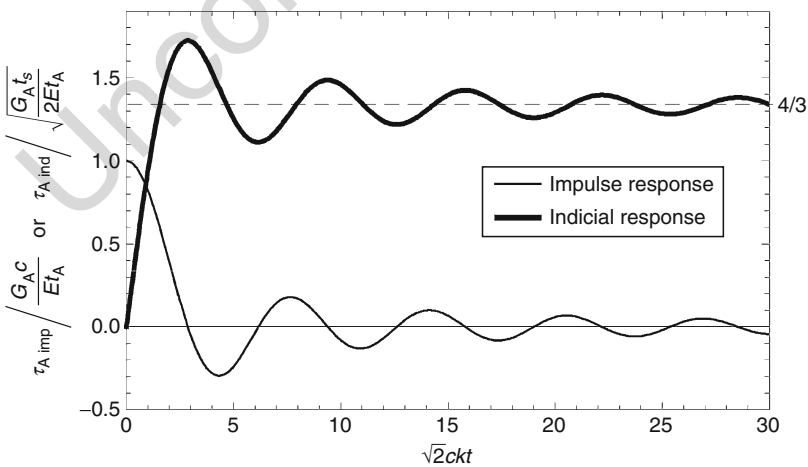


**Fig. 5** Impulse and indicial response of shear stress at the edge of adhesive layer (Sato 2009)

The shear stress variation ( $\tau_{A \text{ val}}(0, t)$ ) at the adhesive edge caused by a given applied stress wave ( $\sigma_w(t)$ ) can be calculated by using the convolution integration of its impulse responses as follows:

$$\begin{aligned}\tau_{A \text{ val}}(0, t) &= \int_0^t \tau_{A \text{ imp}}(0, t - \xi) \cdot \sigma_w(\xi) d\xi \\ &= \frac{G_{AC}}{Et_A} \int_0^t \Omega(\sqrt{2}ck(t - \xi)) \cdot \sigma_w(\xi) d\xi.\end{aligned}\quad (21)$$

In addition, ( $\tau_{A \text{ val}}(0, t)$ ) can also be expressed by a convolution integral of its indicial response and applied stress wave as follows:

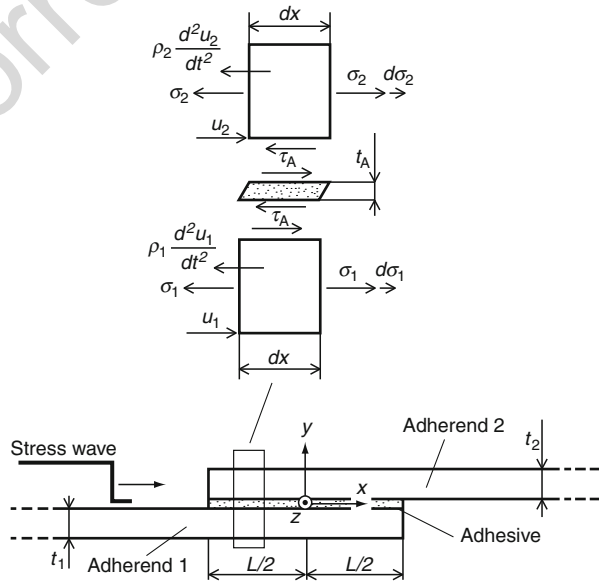
$$\tau_{A \text{ val}}(0, t) = \tau_{A \text{ ind}}(0, t) \sigma_w(0) + \int_0^t \tau_{A \text{ ind}}(0, t - \xi) \cdot \frac{d\sigma_w(\xi)}{d\xi} d\xi. \quad (22)$$

### 29.4.3 Single Lap Joints

Equation 10 can be also used to calculate the dynamic stress analysis of single lap joints. Unfortunately, boundary conditions for single lap joints are too difficult to be treated mathematically. Therefore, an example with a numerical solution is shown in this section.

The boundary conditions of a single lap joint shown in Fig. 6 can be written as:

**Fig. 6** Load balance in a single lap joint (Sato 2008)



$$\begin{aligned}
u_1|_{x=-\frac{L}{2}} &= -2 \int_0^t c_{s1} \frac{\sigma U(\lambda)}{E_1} d\lambda + \int_0^t c_{s1} \frac{\partial u_1(x, \lambda)}{\partial x} \bigg|_{x=-\frac{L}{2}} d\lambda, \frac{\partial u_2}{\partial x} \bigg|_{x=-\frac{L}{2}} = 0, \frac{\partial u_1}{\partial x} \bigg|_{x=\frac{L}{2}} = 0, \\
u_2|_{x=\frac{L}{2}} &= - \int_0^t c_{s2} \frac{\partial u_2(x, \lambda)}{\partial x} \bigg|_{x=\frac{L}{2}} d\lambda,
\end{aligned} \tag{23}$$

where ( $\sigma$ ) is the amplitude of stress wave, ( $U(t)$ ) is the unit step function, ( $c_{s1}$ ) and ( $c_{s2}$ ) are the longitudinal stress wave velocities of adherends 1 and 2, respectively, defined as ( $c_{s1} = \sqrt{E_1/\rho_1}$ ) and ( $c_{s2} = \sqrt{E_2/\rho_2}$ ).

Equations 10 can be transformed to discrete equations using the central difference for space and the backward difference for time shown as:

$$\begin{aligned}
&\frac{u_1(x_{n+1}, t_n)}{(\Delta x)^2} - \left( \frac{2}{(\Delta x)^2} + k_1 + \frac{c_{s1}}{(\Delta t)^2} \right) u_1(x_n, t_n) \\
&+ u_1(x_{n-1}, t_n)(\Delta x)^2 + k_1 u_2(x_n, t_n) = \frac{c_{s1}}{(\Delta t)^2} (-2u_1(x_n, t_{n-1}) + u_1(x_n, t_{n-2})) \\
&\frac{u_2(x_{n+1}, t_n)}{(\Delta x)^2} - \left( 2(\Delta x)^2 + k_2 + \frac{c_{s2}}{(\Delta t)^2} \right) u_2(x_n, t_n) \\
&+ u_2(x_{n-1}, t_n)(\Delta x)^2 + k_2 u_1(x_n, t_n) = \frac{c_{s2}}{(\Delta t)^2} (-2u_2(x_n, t_{n-1}) + u_2(x_n, t_{n-2}))
\end{aligned} \tag{24}$$

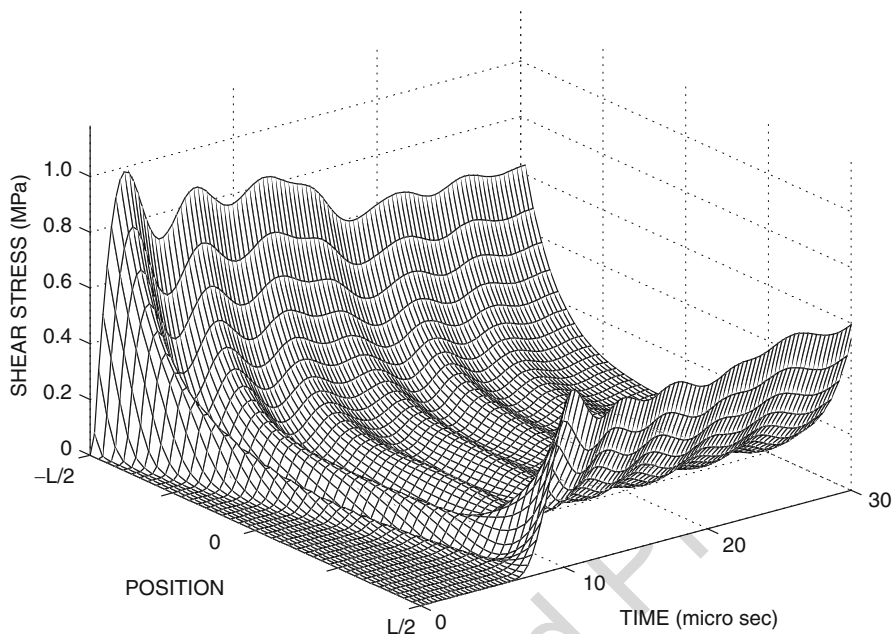
where ( $k_1 = G_A/(E_1 t_1 t_A)$ ) and ( $k_2 = G_A/(E_2 t_2 t_A)$ ). Stepwise time integration of Eq. 24 under the boundary condition shown in Eq. 23 gives displacement vectors ( $u_1$ ) and ( $u_2$ ) at each time step. Based on the results, distribution of shear stress ( $\tau_A$ ) can be calculated by the finite difference method.

Figure 7 shows a calculated result of shear stress distribution in the adhesive layer of a single lap joint subjected to a step load of 1 MPa in amplitude, using a MATLAB program (Sato 2008). Here, the single lap joint is 40 mm in lap length, 4 mm in thickness of the adherends, which are made of aluminum alloy having a tensile modulus of 72 GPa and the density of  $2.8 (\times) 10^3$  kg/m<sup>3</sup>. The thickness and the shear modulus of the adhesive layer are 0.1 mm and 1.0 GPa, respectively. It is shown in Fig. 7 that the stress near the load input side (Position =  $-L/2$ ) increases initially, and the stress at the opposite side (Position =  $L/2$ ) increases with a delay, which is due to the duration of stress wave propagation between the sides. At the load input side, there is stress oscillation, but it decays soon.

## 29.4.4 Finite Element Analysis

### Theoretical Background

The finite element method for solids is based on the principle of virtual work (Zienkiewicz 1971), and it is given by:



**Fig. 7** Shear stress distribution and variation along bondline of a single lap joint calculated based on the dynamic Volkersen's model (Sato 2008)

$$\int_V \sum_i \sum_j \sigma_{ij} \delta \epsilon_{ij} dV = \int_S \mathbf{q} \cdot \delta \mathbf{u} dS + \int_V \mathbf{b} \cdot \delta \mathbf{u} dV \quad (25)$$

where  $(\sigma_{ij})$  and  $(\delta \epsilon_{ij})$  indicate stress tensor and virtual variation of strain tensor, and  $(\mathbf{q})$ ,  $(\mathbf{b})$  and  $(\delta \mathbf{u})$  are surface force, body force applied to the solid and virtual displacement occurring in the solid, respectively. The subscripts (V) and (S) indicate total volume and total surface of the solid, respectively. Suffixes (i) and (j) denote the direction of (x), (y), and (z) axes. The principle of virtual work has the same meaning as the equilibrium equation which is one of the fundamental relations in solid mechanics. Note that the components of strain vector are not tensor strains, but engineering strains. Though stress and strain are tensor quantities, the vector notation is convenient to calculate virtual work. Equation 25 can be simplified by inner product of vector, and it is shown as follows:

$$\int_V \boldsymbol{\sigma} \cdot \delta \boldsymbol{\epsilon} dV = \int_S hf \mathbf{q} \cdot \delta \mathbf{u} dS + \int_V \mathbf{b} \cdot \delta \mathbf{u} dV. \quad (26)$$

A displacement vector  $(\mathbf{u})$  in a finite element is associated with the nodal displacement vector  $(hf\mathbf{a})$  of the element via the shape function matrix  $(hf\mathbf{N})$  of the element as follows:



$$\mathbf{u} = \mathbf{N}\mathbf{a}. \quad (27)$$

291 The strain vector ( $\boldsymbol{\epsilon}$ ) in the finite element is also associated with the nodal  
 292 displacement vector ( $\mathbf{a}$ ) via the strain–displacement relation matrix ( $\mathbf{B}$ ) of the  
 293 element as follows:

$$\boldsymbol{\epsilon} = \mathbf{B}\mathbf{a}. \quad (28)$$

294 Therefore, Eq. 26 can be approximated by the following:

$$\sum_V \boldsymbol{\sigma} \cdot \mathbf{B}\delta\mathbf{a}\Delta V = \sum_S \mathbf{q} \cdot \mathbf{N}\delta\mathbf{a}\Delta S + \sum_V \mathbf{b} \cdot \mathbf{N}\delta\mathbf{a}\Delta V. \quad (29)$$

295 Since Eq. 29 is an identical equation which is independent on ( $\delta\mathbf{a}$ ), the equation  
 296 can be modified as follows:

$$\sum_V \mathbf{B}^T \boldsymbol{\sigma} \Delta V = \sum_S \mathbf{N}^T \mathbf{q} \Delta S + \sum_V \mathbf{N}^T \mathbf{b} \Delta V. \quad (30)$$

297 When the constitutive relation of the solid is linear elastic, stress vector ( $\boldsymbol{\sigma}$ ) is  
 298 given by:

$$\boldsymbol{\sigma} = \mathbf{D}\boldsymbol{\epsilon} = \mathbf{D}\mathbf{B}\mathbf{a} \quad (31)$$

299 where ( $\mathbf{D}$ ) is local stiffness matrix. Equation 29 can be modified using matrix ( $\mathbf{D}$ ) and  
 300 is shown as follows:

$$\sum_V \mathbf{B}^T \mathbf{b}^f \mathbf{D} \mathbf{B} \mathbf{a} \Delta V = \sum_S \mathbf{b}^f \mathbf{N}^T \mathbf{b}^f \mathbf{q} \Delta S + \sum_V \mathbf{b}^f \mathbf{N}^T \mathbf{b}^f \mathbf{b} \Delta V. \quad (32)$$

301 The left term in Eq. 32 includes nodal displacement vector ( $\mathbf{a}$ ), and it can be  
 302 extracted from summation. Thus, the final form of the equation for the finite element  
 303 method is obtained:

$$\mathbf{K}\mathbf{a}' = \mathbf{F} + \mathbf{B} \quad (33)$$

304 where, ( $\mathbf{K} = \sum_V \mathbf{B}^T \mathbf{D} \mathbf{B} \Delta V$ ), ( $\mathbf{F} = \sum_S \mathbf{N}^T \mathbf{q} \Delta S$ ), ( $\mathbf{B} = \sum_V \mathbf{N}^T \mathbf{b} \Delta V$ ), and ( $\mathbf{a}'$ ) is the  
 305 total nodal displacement vector of whole the structure, and it is the sum of local  
 306 displacement vectors ( $\mathbf{a}$ ) defined in each element. Solving Eq. 33 gives ( $\mathbf{a}'$ ), and  
 307 then ( $\boldsymbol{\epsilon}$ ) is calculated using Eq. 28. The stress ( $\boldsymbol{\sigma}$ ) is obtained using Eq. 31.

308 For dynamic conditions, few modification of the static equation is necessary. That  
 309 can be done by adding the term of inertia force to the equation following  
 310 d'Alembert's principle. Equation 25 is modified to the following:

$$\int_V \sum_i \sum_j \sigma_{ij} \delta \epsilon_{ij} dV = \int_S \mathbf{q} \cdot \delta \mathbf{u} dS + \int_V \mathbf{b} \cdot \delta \mathbf{u} dV - \int_V \rho \ddot{\mathbf{u}}' \cdot \delta \mathbf{u} dV \quad (34)$$

311 where ( $\ddot{\mathbf{u}}'$ ) is acceleration vector. Therefore, Eq. 33 becomes:

$$\mathbf{K}\mathbf{a}' = \mathbf{F} + \mathbf{B} - \mathbf{M}\ddot{\mathbf{a}}' \quad (35)$$

where  $(\ddot{\mathbf{a}}')$  is total nodal acceleration vector of the structure, and  $(\mathbf{M} = \sum \rho \mathbf{N}^T \mathbf{N} \Delta V)$ . The symbol  $(\mathbf{M})$  is called the mass matrix.

For solving Eq. 35, explicit schemes for time integration are efficient and their use is increasing in many applications such as crash analysis of car bodies in the last two decades. The equation of explicit schemes is given by:

$$\ddot{\mathbf{a}}'_n = \mathbf{M}^{-1} (\mathbf{F}_n + \mathbf{B}_n - \mathbf{K}\mathbf{a}'_n). \quad (36)$$

To obtain  $(\mathbf{a}'_{n+1})$ , additional calculations have to be carried out using the central difference as follows:

$$\ddot{\mathbf{a}}'_{n+0.5} = \ddot{\mathbf{a}}'_{n-0.5} + \Delta t_n \ddot{\mathbf{a}}'_n \quad (37)$$

$$\mathbf{a}'_{n+1} = \mathbf{a}'_n + \Delta t_{n+0.5} \ddot{\mathbf{a}}'_{n+0.5'} \quad (38)$$

where  $(\Delta t_{n+0.5} - t_{n-0.5})$  and  $(\Delta t_n = \Delta t_{n+0.5} - t_{n-0.5})$ . As seen in Eq. 36, if a lumped weight matrix for  $(\mathbf{M})$  is used, inverse matrix calculation can be omitted. In addition, there is no need to store the entire matrix  $(\mathbf{K}^{-1})$  which includes many fill-ins or zeros after the forward elimination, and calculation of only  $(\mathbf{K}\mathbf{a}'_n)$  is a less memory consuming process. Because of such advantages, explicit schemes have recently become the only choice to treat huge-scale applications. As a matter of fact, crash analysis of whole car structures, which is one of the biggest calculation these days, can be completed using only a personal desk-top computer of high performance within few weeks. Many packages of explicit finite element analysis are commercially available now. The disadvantage of explicit scheme is the necessity of using a lumped matrix for  $(\mathbf{M})$ . Using a lumped matrix decreases the accuracy of results, and the use of high-order elements is also ineffective. Finer meshes are more suitable for explicit schemes than high-order elements.

### Examples of Dynamic Analysis for Adhesively Bonded Joints

Sawa et al. (1996) have conducted dynamic finite element analysis of adhesively bonded joints using an explicit solver: DYNA3D (Lawrence Livermore National Laboratory, Livermore, USA). The stress distribution and fluctuations of stresses in laminated plates subjected to perpendicular impacts were calculated, and it was found that a singular stress occurred at the edges of the interfaces and the stress increased with an increase of the ratio between the Young's moduli of the adherends and the adhesive. Higuchi et al. (2002a) conducted stress analysis of single lap joints subjected to impact bending moments and to impact tensile loads (Higuchi et al. 2002b). They found that the maximum principal stress in the joints increased as the Young's modulus of the adherends increased, although the phenomenon is opposite to static cases. They also investigated the influence of the Young's moduli of adherends on the stress distribution in a single lap joint

having different adherends (Sawa et al. 2003). Sawa et al. have also conducted several impact analyses of butt joints of hollow cylinders (Sawa et al. 2002) and verified the numerical results experimentally (Sawa et al. 2003). They also analyzed the case of impact bending moments applied to butt joints (Higuchi et al. 2003). The dynamic response of single lap joints subjected transverse impacts has been also studied by Yaidya et al. using LS-DYNA 3D (Vaidya et al. 2006).

## 29.5 Impact Strength Evaluation of Adhesively Bonded Joints

To predict the strength of adhesively bonded joints, strength criteria should be applied to the stress values obtained by analyses. Several types of strength criteria applicable to dynamic problems are explained below. In addition, an example of an actual application is also shown in that section.

### 29.5.1 Failure Criteria for Adhesively Bonded Joints

#### Stress–Strain Criteria

Stress–strain criteria are the most popular for strength evaluation of materials. They can be applied to strength predictions of adhesively bonded joints. If the stress or strain value at a point in a solid is greater than a particular threshold level, the solid is regarded to be broken. In the case of a linear elastic material, the stress–strain curve is perfectly linear, and the stress criterion is equivalent to the strain criterion. In contrast, stress criteria cannot be used for elastic perfect plastic materials because the proper threshold level of stress cannot be selected, and strain criteria are applied for this situation instead.

In a continuum, combined stress states are usual, and there are six components in each stress and strain. Strictly speaking, strength criteria should be functions of all the components. The simplest criterion for combined stress conditions are the maximum stress function shown in the following equation.

$$\max(\sigma_1, \sigma_2, \sigma_3) = \sigma_y, \quad (39)$$

where  $(\sigma_1)$ ,  $(\sigma_2)$ , and  $(\sigma_3)$  are principal stresses, and  $(\sigma_y)$  is the tensile strength of the material. This criterion can be used for brittle materials such as glass, ceramics, and hard plastics, including brittle epoxy adhesives.

If adhesives are ductile, strength criteria based on shear stress components are often used with analogies to metals. For example, the maximum shear stress criterion called the Tresca's criterion (Tresca 1869) or the maximum shear-strain energy criterion called the Mises' criterion (von Mises 1913) are well known, and they can be shown as follows:

(The maximum stress criterion)

$$\max\left(\left|\frac{\sigma_1 - \sigma_2}{2}\right|, \left|\frac{\sigma_2 - \sigma_3}{2}\right|, \left|\frac{\sigma_3 - \sigma_1}{2}\right|\right) = \tau_y \quad (40)$$

where  $(\tau_y)$  is the pure shear strength of the material.

(The maximum shear-strain energy criterion)

$$(\sigma_1 - \sigma_2)^2 + (\sigma_2 - \sigma_3)^2 + (\sigma_3 - \sigma_1)^2 = 2\sigma_Y^2 \quad (41)$$

where  $(\sigma_1)$ ,  $(\sigma_2)$ , and  $(\sigma_3)$  are principal stresses, and  $(\sigma_Y)$  is the pure tensile strength of the material. It is well known that plastic behaviors of metals are independent of hydrostatic pressures, and only deviation components of stress can affect yielding. The maximum stress criterion and the maximum shear-strain energy criterion are function of only the deviation components. In reality, the plastic behavior of ductile adhesives is slightly different from those of metals due to the generation of micro cracks or craze. Therefore, hydrostatic pressure can affect the plastic behavior of adhesives, but the effect is not so significant.

Since the strain rate is very high when impact loading is applied, ductile adhesives can become brittle and have a higher strength. Thus, the change should be introduced to the strength criterion to predict the proper strength. Highly ductile adhesives show the tendency of increasing the maximum stress without the loss of plastic deformation, thus becoming very brittle. For brittle adhesives, the maximum stress criterion may be applied increasing the strength parameters with respect to strain rates based on the impact tests. Sato and Ikegami, however, showed that the maximum shear-strain energy criterion is more suitable than the maximum stress criterion even for brittle adhesives (Sato and Ikegami 1999). In this case, parameters for the criterion such as  $(\sigma_Y)$  increased two times in the impact condition of about  $10^{11}$ – $10^{13}$  Pa/s in stress rate (see Chap. 21, “Impact Tests”).

### Stress Singularity Criterion

The disadvantage of stress–strain criterion is the presence of very high stresses in the adhesive layer at the ends of joints, which are often higher than the strength of the adhesive in bulk. The phenomenon is called “stress singularity,” and this occurs when elastic materials are assumed for adhesives and adherends, and joints have sharp edges at the ends. The stresses at singularity points can be infinite in elastic analyses. Such an infinite stress is not real because materials have a finite strength. However, it is sure that very sharp stress concentration must occur near the singularity points. An option for overcoming the problem is considering stress relaxation due to the inelastic behavior of adhesive layers. The other method is strength prediction using stress singularity parameters (Hattori et al. 1988). However, research on stress singularity of adhesive joints in dynamic conditions has been very few so far. Thus, further intensive studies are required.

### Fracture Mechanics and Cohesive Zone Model

At the tip of a crack in a solid, very sharp stress concentration occurs as well as stress singularity points. Thus, stress or strain criteria cannot be applied to these cases, and

fracture mechanics is used instead. Since almost all joints have no crack initially, the methodology of fracture mechanics cannot be applied directly to them. In contrast, fracture mechanics has an advantage because it can predict crack propagation. This aspect is useful to predict not only the initial failure, but also the final fracture of joints. The fatigue life of joints can also be treated by this method.

When fracture mechanics is applied to joint strength prediction, the presence of initial cracks should be assumed, and the stress distribution near the crack tip is analyzed. Then, based on the stress distributions obtained by the analysis, stress intensity factors or energy release rates should be calculated, although this process is not simple and easy. Another way is the virtual crack extension method (VCEM), by which the energy release rate can be calculated with small efforts (Parks 1977). Since cracks tend to propagate along the interface between adhesive layers and adherends, it is easy to apply VCEM to these problems. Therefore, to predict the strength of adhesively bonded joints, energy release rates are more used than stress intensity factors.

Applying fracture mechanics to impact problems has other difficulties. Local finer meshes, which are often used near stress concentration points in static finite element methods, are not suitable for dynamic calculation because the step of time integral depends on the smallest mesh size in the analytical model, and total calculation time increases drastically even if only one small mesh is used. Therefore, finite element analysis for fracture mechanics, which needs finer meshes near the crack tips for calculating the stress intensity factors, consumes time and computer resources.

A novel method called cohesive zone model (CZM) has been introduced for the calculations of fracture mechanics. This model has high applicability to dynamic calculations. In the method, adhesive layers or interfaces are modeled with springs having a particular load–displacement relation called “traction-separation law,” and the fracture mechanical characteristics are described by the model. A rule of CZM is that the area surrounded by the traction-separation curve should be equal to the fracture toughness (critical energy release rate) of the joint. The shape of traction-separation law is arbitrary. Proper shape should be selected among several types such as bilinear or trapezoidal curves shown in Fig. 8, so that the predicted strength can agree with experimental results.

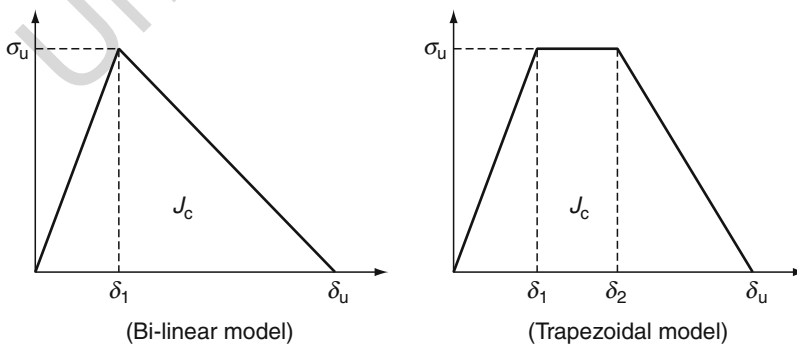


**Fig. 8** Types of traction-separation laws

The cohesive zone model has the advantage that initial crack and fine meshes are not necessary. In addition, CZM fits well explicit schemes. Thus, the method is suitable for dynamic analysis of adhesively bonded joints, and actual application has been started (see Sect. 6.1). The disadvantage of the model is the arbitrary selection of traction-separation law. Trial and error process is necessary to reach satisfactory results (see ► Chap. 25, “Numerical Approach: Finite Element Analysis” for more details on CZM).

## 29.6 Applications

Joint design considering impact loading is still rare in industries, but the number of cases has been gradually increasing over the last decade. Needs for impact analysis is recently increasing in several areas such as automotive and electronic industries. In addition, the progress of computers facilitates impact analyses. Small models can be analyzed with a desktop computer in these days. Several cases of joint design for impact loads are shown in the following sections.

### 29.6.1 Crash of Car Structures

Ordinary car structures comprised of steel panels, and they have been mainly joined by spot welding. Recently, a novel joining method called “weldbonding” has been applied to luxury cars. This is a combination method of spot welding and adhesive bonding to increase the torsional stiffness, fatigue life, and damping of the body. When a car built by “weldbonding” is crashed, the impact strength of joints bonded with the adhesive is very important because the joined steel panels should be largely deformed and absorb the kinetic energy. Early fracture of the joints leads to a smaller absorbed energy by the body. In addition, joint failure should be avoided in terms of product liability law. From these reasons, impact problems of adhesively bonded joints in car structures become important and are widely studied over the world.

Harris and Adams (1985) have examined the impact strength of lap-shear joints bonded with ductile adhesives. They also made open-ended cylinders of steel and aluminum alloy joined by spot welding and weldbonding with one of the ductile adhesives used for the lap-shear tests, and tested them under axial impact loading. The results indicated that the weldbonded joints had a small failure area and higher energy absorption than those joined only by spot welding.

Fay and Suthurst (1990) have been experimentally investigated the deformation and energy absorption of steel box beams joined by weldbonding. The results showed that the properties greatly depended on the configurations and spot intervals, although weldbonding is an effective method to absorb large kinetic energy. This research emphasized the necessity of a strength prediction method that can be applied to weldbonded joints. Recently, Belingardi et al. (2005) have investigated box-beams configurations suitable for impact loading. They prepared specimens of different configurations bonded with an adhesive and tested them using a drop-

weight testing machine. The integrity of specimens and their energy absorption highly depends on the configurations.

Nossek and Marzi (2009) have developed a CZM base method to predict the impact strength of adhesive joints for car structures. A trapezoidal traction-separation law was adopted. In this case, they expanded the CZM model from mode I condition to mode II and combined both stress conditions. In this study, the fracture toughness of adhesive joints was measured using tapered double cantilever beam (TDCB) specimens, and the strain-rate dependency of the adhesive was described by the Johnson–Cook model determined by impact tests of bulk adhesive. In addition, the impact test of a U-shape specimen bonded adhesively was carried out, as shown in Fig. 9 . The adhesively bonded part between the U-shape frame and the panel was partially separated in the experiment, and the deformation of the plate was well simulated by the finite element analysis based on their CZM method, as shown in Fig. 10 . Marzi et al. 2009a have measured the mode I fracture toughness of joints and investigated its stress-rate dependency using butt joint specimens and TDCB specimens. They presented a novel joint configuration called end-loaded shear joint (ELSJ) shown in Fig. 11 and measured mode

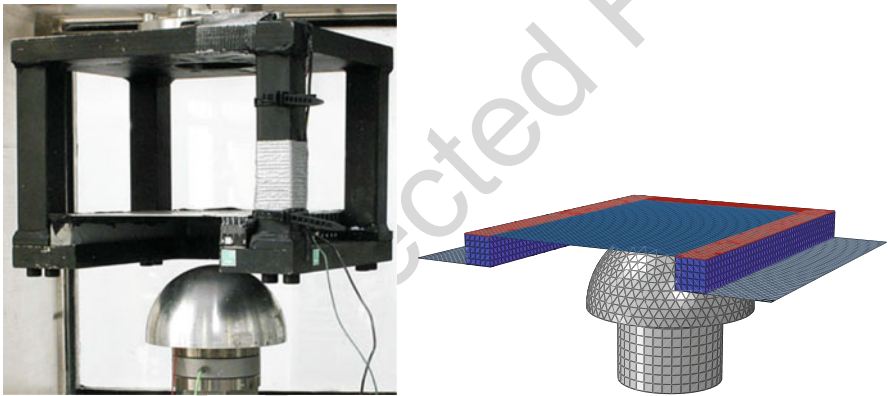


**Fig. 9** Experimental setup for impact test of U-shape specimen (Nossek and Marzi 2009)

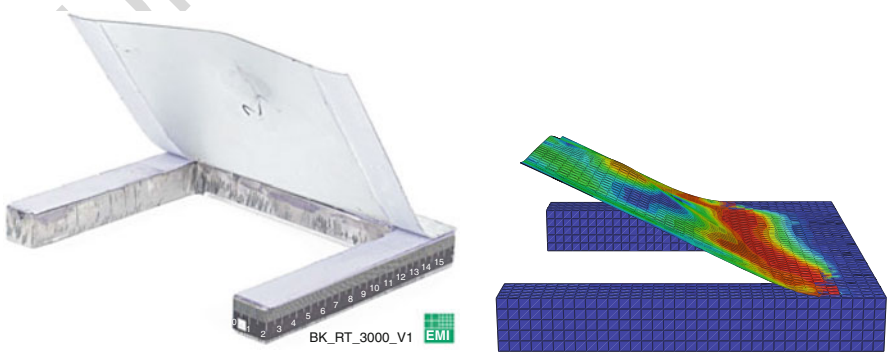


**Fig. 10** U-shape specimen after impact test and simulated result (Nossek and Marzi 2009)

II fracture toughness (Marzi et al. 2009b). These fracture toughnesses were applied to their mix-mode CZM criterion shown in Fig. 12, interpolating between the mode I and II traction-separation laws in the mixed-mode conditions, and a precise prediction method for adhesively bonded car structures was established. Marzi et al. applied the mixed-mode CZM criterion to the crash simulation of a floor pan model for cars bonded adhesively (Marzi et al. 2009c), and compared the prediction to experimental results (Marzi et al. 2008) shown in Fig. 13. The deformation of the floor pan specimen could be appropriately simulated by the finite element analysis based on the CZM model.

## 29.7 Conclusions

Research on the impact strength of adhesively bonded joints has been recently carried out very often. As mentioned above, the reason is due to the increase of demand from industries and the progress of computer technologies. The tendency seems to continue

**Fig. 11** Configuration of end-loaded shear joint (Marzi et al. 2009b)

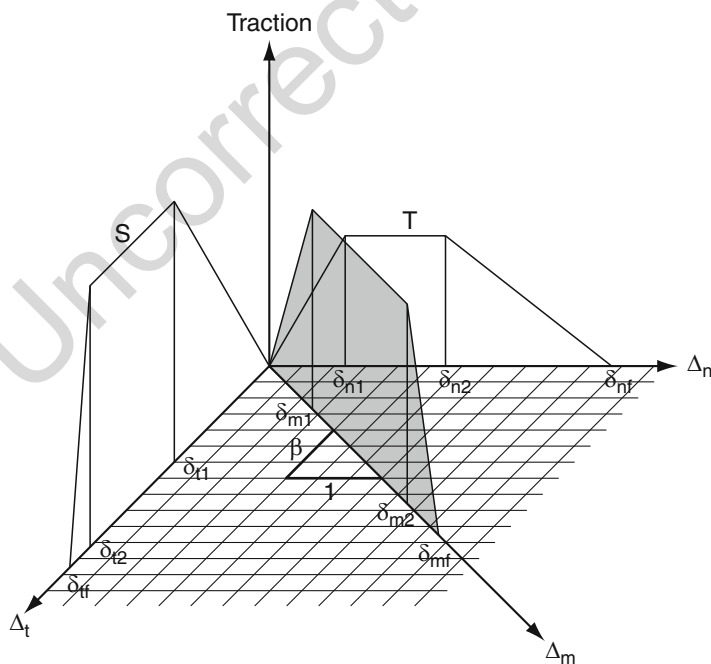
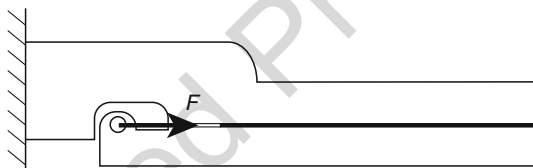


**Fig. 12** Traction-separation law for mixed-mode criterion (Marzi et al. 2009c)



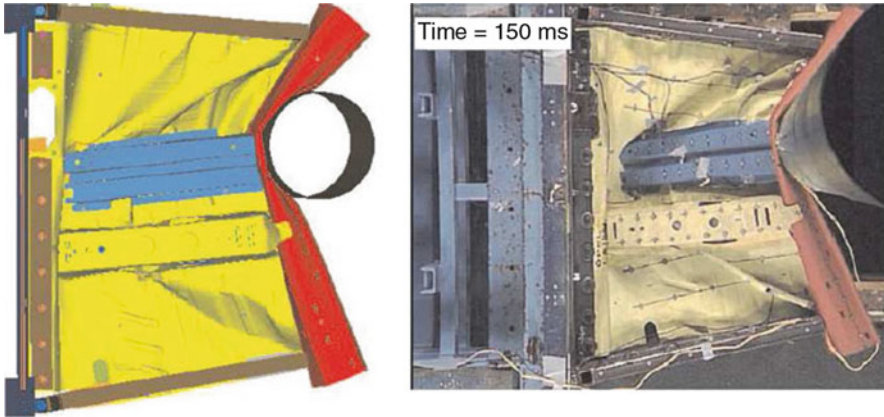


**Fig. 13** Deformation of floor pan specimen and simulated results (Marzi et al. 2009c)

in the near future. For the purpose, the integration of finite element analyses and strength criteria becomes important. Approaches using cohesive zone models are very promising for actual applications such as car structures because the approaches are suitable for finite element analyses based on explicit schemes. In contrast, closed-form approaches are necessary from an academic point of view and should be also taken for the impact problem of adhesively bonded joints to understand the nature of joint mechanics. Unfortunately, only few studies on the closed-form analyses have conducted already, so that more research should be done in the future.

There are many remaining topics on impact phenomena of adhesively bonded joints, which should be solved in the future. One of rising and promising research areas is impact problems of composite materials bonded adhesively. This analysis will be more important due to the increase of composite aircrafts, although it has difficulties of high impact velocity and the anisotropy of composite materials. In contrast, lower impact velocity will also become more important. Dropping impact problem of mobile phones has been analyzed (Akiba et al. 2006), but joining parts in the structure was not modeled. Even in low impact velocities, the modeling of adhesive joints is still a big problem and a material for research.

## References

- Adams RD, Peppiatt NA (1974) Stress analysis of adhesive-bonded lap joints. *J Strain Anal* 9:185
- Akiba H, Ohyama T et al (2006) Large scale drop impact analysis of mobile phone using ADVC on blue gene/L. *Proceedings of SC06, Tampa*, pp 1–26
- Belingardi G, Goglio L et al (2005) Impact behaviour of bonded built-up beams: experimental results. *Int J Adhes Adhes* 25:173
- Cowper GR, Symonds PS (1952) Brown Univ Div of Appl Math, Report 28
- Fay PA, Suthurst GD (1990) Redesign of adhesively bonded box beam sections for improved impact performance. *Int J Adhes Adhes* 10:128

- Goglio L, Peroni L et al (2008) High strain-rate compression and tension behaviour of an epoxy bi-component adhesive. *Int J Adhes Adhes* 28:329
- Goldsmith W (2001) *Impact, the theory and physical behaviour of colliding solids*. Dover, New York, p 25
- Harris JA, Adams RD (1985) An assessment of the impact performance of bonded joints for use in high energy absorbing structures. *Proc Inst Mech Eng* 199:121
- Hattori T, Sakata S et al (1988) A stress singularity parameter approach for evaluating adhesive strength. *JSME Int J Ser I* 31:718
- Higuchi I, Sawa T et al (2002a) Three-dimensional finite element analysis of single-lap adhesive joints subjected to impact bending moments. *J Adhes Sci Technol* 16:1327
- Higuchi I, Sawa T et al (2002b) Three-dimensional finite element analysis of single-lap adhesive joints under impact loads. *J Adhes Sci Technol* 16:1585
- Higuchi I, Sawa T et al (2003) Three-dimensional finite element analysis of stress response in adhesive butt joints subjected to impact bending moments. *J Adhes* 79:1017
- Johnson GR, Cook WH (1983) A constitutive model and data for metals subjected to large strains, high strain rates and high temperatures. In: *Proceedings of 7th symposium on ballistics* 541, The Hague, pp 541–547
- Johnson W, Mellor PB (1973) *Engineering plasticity*. Van Nostrand Reinhold 54, London
- Marzi S, Ramon-Villalonga L et al (2008) Usage of cohesive elements in crash analysis of large, bonded vehicle structures – experimental tests and simulation. In: *Proceedings of German LS-DYNA forum*, Bamberg, pp B.I.1–B.I.19
- Marzi S, Hesebeck O et al (2009a) A rate-dependent cohesive zone model for adhesively bonded joints loaded in mode I. *J Adhes Sci Technol* 23:881
- Marzi S, Hesebeck O et al (2009b) An end-loaded shear joint (ELSJ) specimen to measure the critical energy release rate in mode II of tough, structural adhesive joints. *J Adhes Sci Technol* 23:1883
- Marzi S, Hesebeck O et al (2009c) A rate-dependent, elasto-plastic cohesive zone mixed-mode model for crash analysis of adhesively bonded joints. In: *Proceedings of the 7th European LS-DYNA conference*, Salzburg
- Mayer MA (1990) *Dynamic behavior of materials*. Wiley, Hoboken, p 210
- Nossek M, Marzi S (2009) Cohesive zone modeling for adhesives. In: Hiermaier S (ed) *Predictive modeling of dynamic processes: a tribute to klaus thoma*. Springer, New York, pp 89–105
- Parks DM (1977) The virtual crack extension method for nonlinear material behavior. *Comput Methods Appl Mech Eng* 12:353
- Sato C (2008) Impact. In: da Silva LFM, Öchsner A (eds) *Modeling of adhesively bonded joints*. Springer, Berlin, p 279
- Sato C (2009) Dynamic stress responses at the edges of adhesive layers in lap strap joints of half-infinite length subjected to impact loads. *Int J Adhes Adhes* 29:670
- Sato C, Ikegami K (1999) Strength of adhesively-bonded butt joints of tubes subjected to combined high-rate loads. *J Adhes* 70:57
- Sato C, Ikegami K (2000) Dynamic deformation of lap joints and scarf joints under impact loads. *Int J Adhes Adhes* 20:17
- Sawa T, Senoo Y et al (1996) Interface stress response of laminated plates subjected to static and impact loads. *J Adhes* 59:1
- Sawa T, Higuchi I et al (2002) FEM stress analysis and strength of adhesive butt joints of similar hollow cylinders under static and impact tensile loadings. *J Adhes Sci Technol* 16:1449
- Sawa T, Suzuki Y et al (2003a) Stress analysis and strength estimation of butt adhesive joints of dissimilar hollow cylinders under impact tensile loadings. *J Adhes Sci Technol* 17:943
- Sawa T, Higuchi I et al (2003b) Three-dimensional finite element stress analysis of single-lap adhesive joints of dissimilar adherends subjected to impact tensile loads. *J Adhes Sci Technol* 17:2157
- Tresca HE (1869) *Memoire sur l'écoulement des corps solides*. Mém Présentés par divers savants 20:733

- 594 Vaidya UK, Gautam ARS et al (2006) Experimental–numerical studies of transverse impact  
595 response of adhesively bonded lap joints in composite structures. *Int J Adhes Adhes* 26:184  
596 Volkersen O (1938) Die nietkraftverteilung in zugbeanspruchten nietverbindungen mit konstanten  
597 laschen querschnitten. *Luftfahrtforschung* 15:41  
598 von Mises R (1913) *Mechanik der festen korper im plastisch deformablen zustand*. Göttingen Nachr  
599 Math Phys 1:582  
600 Zienkiewicz OC (1971) *The finite element method in engineering science*, 2nd edn. McGraw Hill,  
601 London, p 16

Uncorrected Proof

# Vibration Damping of Adhesively Bonded Joints

30

Robert D. Adams, Duncan G. A. Cooper, and Stuart Pearson

## Contents

30.1	Introduction	854
30.2	Damping Definitions	857
30.2.1	Specific Damping Capacity (SDC), $\psi$	857
30.2.2	Logarithmic Decrement, $\Delta$	858
30.2.3	Damping Ratio, $\zeta$	858
30.2.4	Loss Factor, $\eta$	859
30.3	Estimation of Damping Level in a Bonded Structure	859
30.3.1	Single-Lap Joint in Tension	860
30.3.2	Single-Lap Joint in Flexure	861
30.4	Experimental Evidence of Damping in Joints	864
30.4.1	Materials Used	864
30.4.2	Joint Manufacture	864
30.4.3	Vibration Test Apparatus	865
30.4.4	Temperature Testing of Joints	866
30.4.5	Results and Discussion	866
30.5	Perspective	871
30.6	Conclusions	873
Appendix		874
	Damping Measurement by the Free Decay Method	874
References		875

R. D. Adams (✉)

Department of Mechanical Engineering, University of Bristol, Bristol, UK

Department of Engineering Science, University of Oxford, Oxford, UK

e-mail: [r.d.adams@bristol.ac.uk](mailto:r.d.adams@bristol.ac.uk)

D. G. A. Cooper · S. Pearson

Department of Engineering Science, University of Oxford, Oxford, UK

e-mail: [Duncan.Cooper@Rolls-Royce.com](mailto:Duncan.Cooper@Rolls-Royce.com)

© Springer International Publishing AG, part of Springer Nature 2018

L. F. M. da Silva et al. (eds.), *Handbook of Adhesion Technology*,

[https://doi.org/10.1007/978-3-319-55411-2\\_30](https://doi.org/10.1007/978-3-319-55411-2_30)

853

**Abstract**

A study into the vibration characteristics of adhesively bonded single-lap joints has been carried out to investigate the effect of joint geometry and temperature variation on overall system damping. Concepts of vibration damping are introduced, and it is shown how to determine the damping of a system. The methodology of calculating the damping of even a simple bonded element in the form of a lap joint from material and geometric parameters is shown to be complex. The vibration damping of bonded joints has been extended into an experimental program using four different adhesives. These were AV119, a one-part epoxy; 9245, a structural bonding tape; 3532, a two-part polyurethane; and Hysol XEA 9359.3, a two-part structural adhesive. High-strength steel adherends were used to manufacture single-lap joints of varying overlap lengths. The specimens were vibrated flexurally and the damping values calculated using the free decay method. In this investigation, the damping of the adhesive layer dominates the damping of the specimens rather than the damping of the adherends. An optimum overlap ratio was found at approximately 0.25 in this study. The adhesives were tested under varying temperature conditions to illustrate the dominance of the glass transition temperature on the damping of the specimen.

It has been shown that the damping of a structure is unlikely to be improved by using adhesive bonding as a joining method.

**30.1 Introduction**

There are several reasons for controlling the vibration response of a structure. Health and safety may be adversely affected if people are subjected to excessive vibration and acoustic radiation from the vibrating surfaces. Also, equipment subject to external vibration may not perform as specified, or an item of vibrating equipment may cause adjacent machinery to perform in an unsatisfactory way. If resonant or near-resonant conditions occur in a structure, fatigue may cause cracks and eventual failure. The reduction of unwanted vibration, usually by damping, is an integral part of good engineering practice, and improvements are constantly sought. It is therefore important to understand the mechanics of damping and what factors, such as materials, temperature, frequency, and structural form, affect the amount of damping that might be expected from a structure.

Structural damping has become a very important property in many modern applications. For example, passenger comfort in vehicles often can be improved by increasing structural damping, while during the launch phase of a spacecraft, damping is essential to avoid damage to electronic components and other delicate parts. In the early days of the US space program, there were typically 90–100 failures on each satellite launched, 64% of these being due to vibration. By adding damping, resonant vibration amplitudes were halved, and there was a 20% overall performance improvement by reducing failure in electronic circuits. Current launch vehicles have to maintain satisfactory levels of damping. Where this is inherent within the structure, this is a bonus. Since most satellite

structures are made of composites which contain a lot of adhesive bonds, it is important to understand what levels of damping originate from what source. Structural damping is damping inherent to the bulk material from which the system is formed. It can also be present in joints or discontinuities and is caused by the presence of high local stresses. Damping can also be due to a variety of external effects, such as acoustic radiation. In its simplest case, vibration can be seen as steady state or freely decaying as shown in Fig. 1. If the excitation frequency coincides with a resonance frequency, then the amplitude of vibration can be magnified as shown in Fig. 2. If the damping is high, the transient decays more quickly, and the resonance amplitude is smaller. In practice, more complex situations exist in which there are several modes of vibration and hence several resonance frequencies. The excitation may not be sinusoidal as commonly depicted, but the same basic principles apply. The total energy dissipated by a structure in vibration is the sum of the energies lost in the structural material, the joints between members, and by radiation to the surroundings. Acoustic radiation may be high for thin

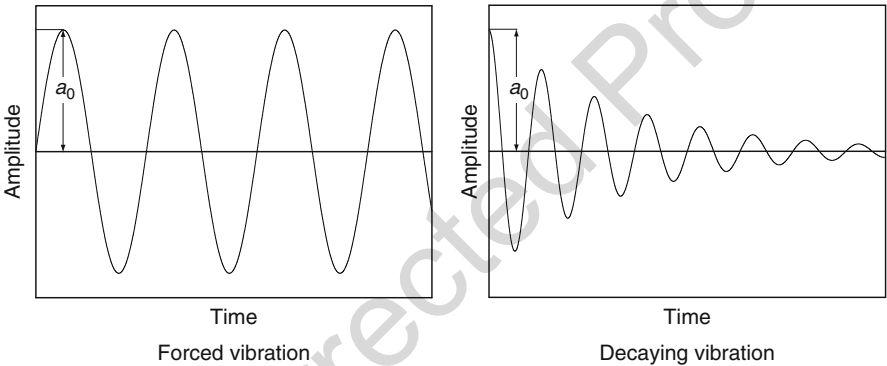
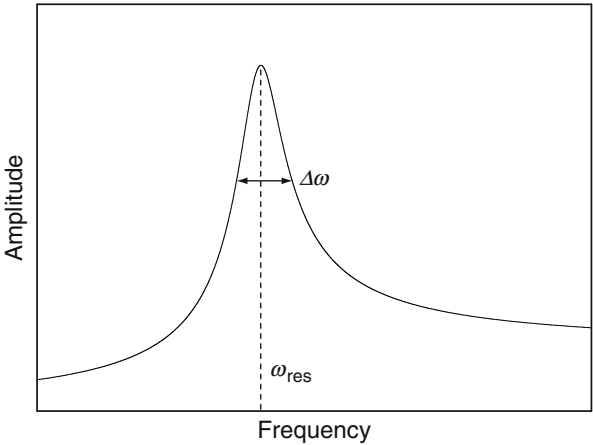


**Fig. 1** Forced vibration (steady state) and transient vibration

**Fig. 2** Illustrating the change of steady-state amplitude of vibration with the excitation frequency and the resonance frequency



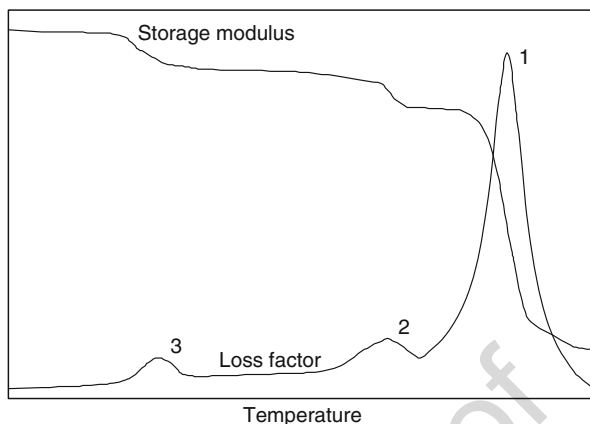
80 sheets of aluminum, composite, of honeycomb panels at ground level, but it will be  
81 much lower at high altitudes where the air pressure and density are low (Maheri et al.  
82 2008). Bolted and riveted joints usually allow some slip under load which results in  
83 energy loss by Coulomb friction. But if the joints are welded or brazed, there is no slip  
84 and so no energy dissipation. For many structures, it has been found necessary to add  
85 damping, often by using viscoelastic damping treatment in the form of a high damping  
86 polymer sandwiched between a thin metal film and the structure. Optimizing the  
87 parameters to achieve the optimum level of damping is quite complex, and the reader  
88 is referred to the books by Mead (1998) and Nashif et al. (1985) for a definitive  
89 explanation. From the successful use of these damping treatments, it might be expected  
90 that adhesively bonded joints, which are typically a sandwich of a polymeric layer  
91 between two metallic adherends, might also provide high damping.

92 The use of an adhesive with a high damping capacity can increase the damping of  
93 a bonded joint (Hildebrand and Vessonen 1997). However, high damping in an  
94 adhesive is usually associated with relatively low stiffness and strength. Hence, a  
95 balance between vibration amplitude and static strength and stiffness needs to be  
96 considered. An adhesive is a substance capable of usefully holding two surfaces  
97 together by surface attachment. An adhesive must have two fundamental character-  
98 istics. First, it must at some stage possess the properties of a fluid in order to  
99 thoroughly wet out the two surfaces to be bonded. Second, it must (when cured)  
100 have the properties of a solid to resist the tensile and shear forces that may be applied  
101 to separate the two surfaces. Adhesives are widely used in industry for joining  
102 surfaces as they offer a simple and strong form of joint, with better stress distribution  
103 and fatigue resistance than conventional joining methods (e.g., bolts, rivets, and  
104 welds). In motorcar body design and manufacture, there are considerable advantages  
105 in using adhesives in conjunction with weld bonding or sometimes in using adhe-  
106 sives alone. An adhesive offers a much reduced structural weight, with no loss of  
107 strength in terms of structural rigidity and impact performance, corrosion resistance,  
108 ease of joining dissimilar materials, and more flexibility in the design of body shape.

109 Adhesive bonding appears to provide attractive solutions for achieving joints  
110 with high damping. Tough structural adhesives (e.g., modified epoxies and poly-  
111 urethanes) have excellent strength and good damping properties due to their visco-  
112 elastic behavior. Multi-material structures usually contain a significant number of  
113 adhesively bonded joints, but the damping of such structures is not well understood.

114 Temperature is usually considered to be the single most important environmental  
115 factor affecting the properties of damping materials. The effect on damping is that three  
116 distinct regions can be observed. The first is the "glassy" region, where the material  
117 takes on extremely low values for the loss factor. The second region, the transition  
118 region, is characterized by having the loss factor achieve its maximum value. This  
119 temperature, at which the loss factor is a maximum, is known as the glass transition  
120 temperature ( $T_g$ ), which is the region where a polymer changes from a hard material to  
121 one that is softer or more rubbery. For cross-linked amorphous polymers such as resins,  
122 the cure or post-cure temperature governs  $T_g$ . Sometimes,  $T_g$  can be increased by  
123 raising the cure or post-cure temperature. Structural adhesives as a family of polymers  
124 are almost invariably used at temperatures below their  $T_g$  (Adams et al. 1997). The

**Fig. 3** Alpha (1), beta (2), and gamma (3) transitions in a typical polymer (From Adams and Singh 1995)



third region is the rubbery phase where the loss factor takes on a low value and varies slowly with temperature. Some low-stiffness rubbery adhesives are generally used above their  $T_g$ , which is typically about  $-50^\circ\text{C}$ . Most polymers have two or three regions in which the damping peaks, as shown schematically in Fig. 3.

The objective here is to understand the damping properties of joints bonded with various adhesives and to see how this might affect the overall damping of a structure. Some variables to be examined are the effects of adhesive properties, joint geometry, and temperature on the overall damping performance of a joint.

Finally, it must be remembered that damping is only of use in reducing vibration levels when the excitation frequency is at or near a resonance frequency.

## 30.2 Damping Definitions

Damping can be defined in a number of ways, and those commonly used are described as follows:

### 30.2.1 Specific Damping Capacity (SDC), $\psi$

This is defined as the ratio of energy dissipated per cycle ( $dW$ ) to the maximum elastic energy stored per cycle ( $W$ ), per unit volume as shown in Fig. 4. Thus,

$$\psi = dW/W \quad (1)$$

the ratio usually being expressed as a percentage. While the SDC is a material property, it also applies to structures in that  $dW$  represents the total energy dissipated, whether this is in the materials or by acoustic radiation, friction, etc., while  $W$  is the maximum vibratory stored energy in the structure. For this reason, it is a more useful and practical definition when assessing the overall damping of a structure (Lin et al. 1984).



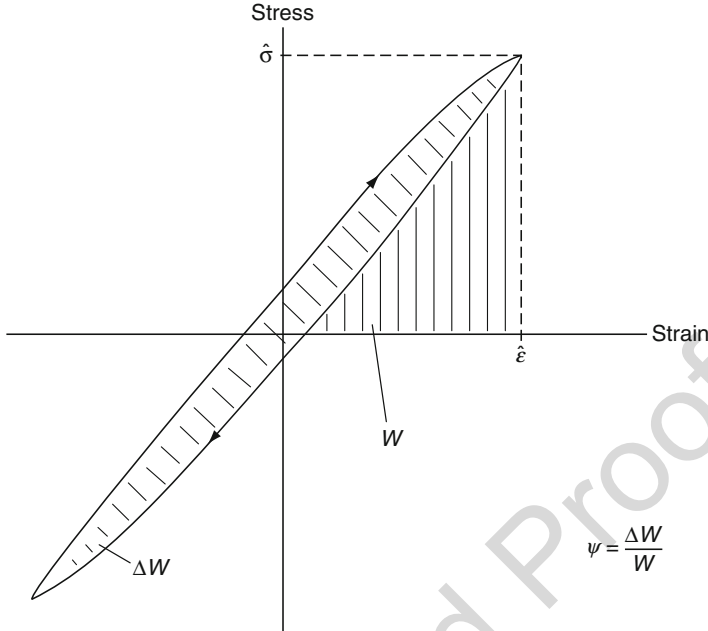


**Fig. 4** Definition of specific damping capacity (SDC)

### 30.2.2 Logarithmic Decrement, $\Delta$

The logarithmic decrement is found by measuring the rate of decay of a freely vibrating system at its resonance frequency once the excitation force has been removed. It can be found from a trace of vibration amplitude against time and relates the ratio of the  $n$ th to the  $n + N$ th cycle amplitudes by

$$\Delta = \frac{1}{N} \ln \frac{u_n}{u_{n+N}} \quad (2)$$

where  $u_n$  is the amplitude of the  $n$ th cycle and  $u_{n+N}$  is the amplitude of the  $n + N$ th cycle. A complete description of this method can be found in the Appendix.

### 30.2.3 Damping Ratio, $\zeta$

The damping ratio is the ratio of the actual damping in the system to the critical damping level for that same system. The system is said to be critically damped when  $\zeta = 1$ , overdamped when  $\zeta > 1$ , and underdamped when  $\zeta < 1$ .

### 30.2.4 Loss Factor, $\eta$

The loss factor is frequently used for damping in elastomers. The higher the loss factor, the higher the damping.

The equation below summarizes the relationship between each of these damping measurements:

$$\eta = \frac{\psi}{2\pi} = \frac{dW}{2\pi W} = \frac{1}{Q} = 2\zeta = \frac{\Delta}{\pi} = \tan \delta \quad (3)$$

where

- $\eta$ , loss factor
- $\psi$ , specific damping capacity
- $dW/W$ , ratio of dissipated energy and stored energy
- $Q$ , Q-factor
- $\zeta$ , damping ratio
- $\Delta$ , logarithmic decrement
- $\tan \delta$ , tangent of the phase angle

## 30.3 Estimation of Damping Level in a Bonded Structure

In a vibrating structure, the overall damping level for a particular mode of vibration will depend on the materials, the geometric form, and the mode of vibration. For most structures, it is unlikely that a single damping value exists which applies to all modes of vibration especially if (anisotropic) composite materials are used (Lin et al. 1984; Maheri et al. 2008). It is convenient to use the specific damping capacity (SDC), which was defined above, as the unit of damping. For a structure, we have

$$\text{SDC} = \text{Total energy dissipated} / \text{Maximum energy stored}$$

during a cycle of oscillation. For a vibrating bonded assembly, the stored energy will mainly be in the general structure with a small amount being stored in the adhesive. The question is how to calculate the energy dissipated and how to relate this to the total energy stored.

Most bonded joints will be used to connect thin metallic or composite sheets or panels, and the predominant mode of vibration will be in bending. This is a complex situation to analyze. The energy dissipation,  $dW_{\text{adhesive}}$ , in the adhesive is equal to the maximum energy stored in the adhesive (the energy stored per unit volume integrated over the volume) multiplied by the SDC,  $\psi$ , of the adhesive. Thus,

$$dW_{\text{adhesive}} = \int_{\text{volume}} \psi \tau^2 / 2G \quad (4)$$

where  $\tau$  is the shear stress and  $G$  is the shear modulus of the adhesive. The shear stress distribution in the adhesive layer is far from simple (Adams et al. 1997), whether the joint is loaded in tensile lap shear or in bending. If the shear stress is constant across the adhesive width,  $b$ , and thickness,  $t$ , and if, as with most polymers, the SDC is not a function of cyclic stress, then, for an overlap length  $l$

$$dW_{\text{adhesive}} = \frac{\psi_{\text{adhesive}} bt}{2G} \int_0^l \tau^2 dx \quad (5)$$

It would appear that the energy dissipated should be proportional to the adhesive thickness, so that thick joints might be best for high damping. However, it is known from mechanics that as the thickness of the adhesive layer is increased, the maximum shear stresses are reduced. For joint strength, that might be an advantage, but since the damping depends on the square of the shear stress, a reduction in shear stress, even though it is over a bigger volume, may not produce a significant increase in joint damping. Volkersen's shear lag theory (Adams et al. 1997) says that the peak shear stress at the joint end is inversely proportional to the square root of the adhesive thickness,  $t$ . A fourfold increase in  $t$  will reduce  $\tau$  by a half, and, since the energy stored is proportional to  $\tau^2$ , the dimension change will be largely canceled out as far as the energy dissipation is concerned. Of course, the reduced shear stress will be extended further into the overlap, thus increasing the volume integral, but the point being made here is that increasing the volume of the joint may not produce a corresponding increase in energy dissipation. In bending, the position is similar in that the energy dissipation is primarily at the ends of the overlap. For both tension and bending, increasing the overlap length has no influence on the energy dissipated in most cases.

The higher the shear modulus of the adhesive, the higher and more concentrated at the edge are the stresses. It might therefore be expected that the damping of a high modulus adhesive will be low in the joint form. But remember that the energy stored per unit volume is proportional to  $\tau^2/2G$ , and if a high value of  $G$  gives a high value of  $\tau$ , then the energy dissipated is greater. Since the energy dissipated is directly proportional to the energy stored, we have a complex situation and one which is not amenable to accurate solution by simple algebra. However, it is possible to give an indication of the trends by making some simplifying assumptions, and this is done below for the two examples given.

In the first example, a single-lap joint is loaded in cyclic tension, and in the other, a similar joint is loaded in free-free flexure. But it must be remembered that these are very much simplified examples. Probably the only satisfactory approach is to use a numerical solution.

### 30.3.1 Single-Lap Joint in Tension

Using the dimensions given in Fig. 5, and applying a load  $P$ , then the stress  $\sigma$  in the adherends is given by

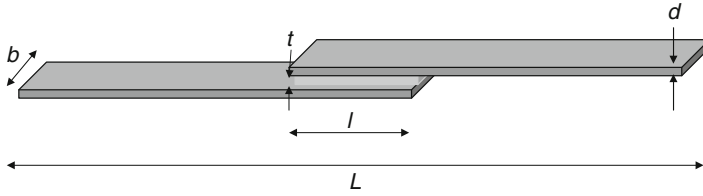


**Fig. 5** Lap joint dimensions. Overlap ratio is  $l/L$

$$\sigma = P/bd \quad (6)$$

Ignoring the overlap, the energy stored,  $W$ , is given by

$$W = \sigma^2 bd(L - l)/2E = (L - l)P^2/2Ebd \quad (7)$$

where  $E$  is Young's modulus of the adherends. In the adhesive layer, the shear stress,  $\tau$ , is usually not uniform (Adams et al. 1997), but we will in this case assume it to be the average shear stress given by

$$\tau = P/bl \quad (8)$$

and so the energy stored in the adhesive layer,  $W_{\text{adhesive}}$ , is

$$W_{\text{adhesive}} = P^2 t/2Gbl \quad (9)$$

The energy dissipated is then  $W_{\text{adhesive}} \psi_{\text{adhesive}}$ , and the overall SDC of the joint is the ratio of the energy dissipated in the adhesive layer to the total energy stored (from Eqs. 7 and 9, so

$$\psi_{\text{overall}} = \psi_{\text{adhesive}} t d E / l (L - l) G \quad (10)$$

Using some typical dimensions as  $t = 0.1$  mm,  $d = 1.6$  mm,  $l = 40$  mm, and  $L = 200$  mm and values of  $E = 200$  GPa (steel) and  $G = 40$  MPa (polyurethane), we have

$$\psi_{\text{overall}} = 0.125 \psi_{\text{adhesive}} \quad (11)$$

which indicates a lower level of damping than in the bulk polymeric adhesive.

### 30.3.2 Single-Lap Joint in Flexure

A vibrating beam is one of the simplest forms of system with distributed mass and stiffness. The motion is governed by a well-known (see Mead 1998; den Hartog 2008) fourth-order partial differential equation of the form

$$\frac{\partial^4 v}{\partial x^4} = \alpha^4 \frac{\partial^2 v}{\partial t^2}$$

(12)

where  $v$  is the displacement in the  $y$  (transverse) direction,  $x$  is the distance along the beam,  $t$  is time, and  $\alpha$  is a constant that incorporates the beam geometry and material properties.

The solution to this equation is of the form

$$v = (P \cos \alpha x + Q \sin \alpha x + R \cosh \alpha x + S \sinh \alpha x)(T \cos \omega t + U \sin \omega t)$$

(13)

where  $P$ ,  $Q$ ,  $R$ ,  $S$ ,  $T$ , and  $U$  are constants defined by the boundary conditions in space and time, and

$$\omega = 2\pi F$$

(14)

where  $F$  is the frequency of oscillation.

For a beam vibrating freely (no end restraints), the natural frequencies and the corresponding mode shapes can be defined. Figure 6 gives the mode shapes and the nodal positions for the first five modes of vibration. The constant  $B$  is used to define the natural frequency using the equation (den Hartog 2008)

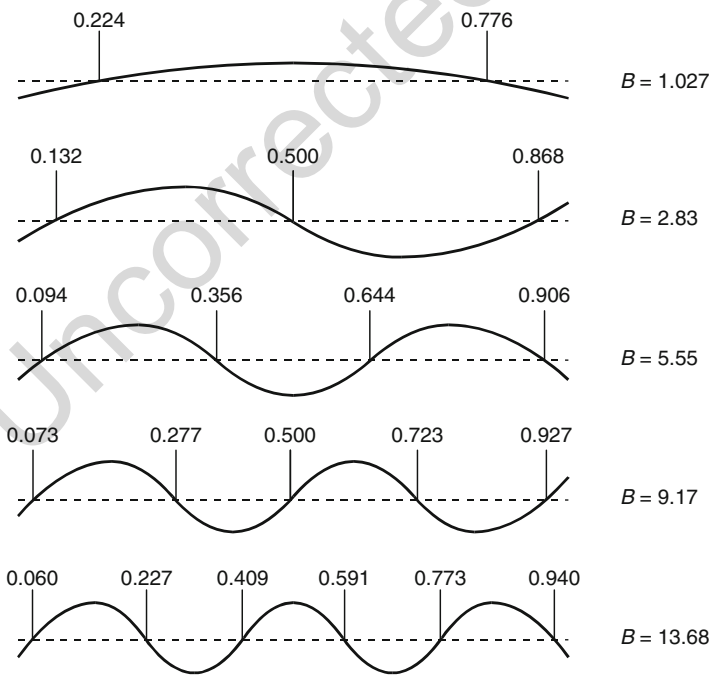


**Fig. 6** Mode shapes of a free-free beam with the nodal positions and B values shown

$$F(Hz) = \frac{B}{\ell^2} \sqrt{\frac{12 \sum EI}{m}} \quad (15)$$

where  $\ell$  is the length of the beam,  $\sum EI$  is the sum of the products of Young's modulus and the second moment of area for each layer about the neutral axis, and  $m$  is the mass per unit length. For a uniform beam:

$$\sum EI = E \frac{bd^3}{12} \quad (16)$$

where  $b$  is the width of the beam and  $d$  is the thickness. Also, for a uniform beam,  $m = \rho bd$  where  $\rho$  is the density. Thus

$$F(Hz) = \frac{Bdc}{\ell^2} \quad (17)$$

where  $c = \sqrt{E/\rho}$  = velocity of extensional waves in the beam.

The mode shapes shown in Fig. 6 are for a uniform beam. A lap joint has a thicker portion in the middle part of the beam, so it is necessary to use more complex mode shapes than the ones shown. For this reason, the following analysis is restricted to mode 1, and even this has to be simplified. It will therefore be assumed that there is a constant bending moment,  $M$ , carried over the overlap portion and that this bending moment decreases linearly from the edge of the lap to the free end of the beam.

For such a system, the shear stress in the adhesive peaks at the overlap edges and decreases to zero at the midpoint. For a soft adhesive such as a polyurethane, the shear stress,  $\tau$  varies linearly with distance  $x$  along the joint in the form

$$\tau = \tau_0 - kx \quad (18)$$

where  $\tau_0$  is the shear stress at one end of the joint and  $k$  is a constant such that  $\tau = -\tau_0$  at the other end. For an epoxy adhesive or for long joints, the shear stress distribution is nonlinear and peaks at the ends of the joint, but this is too complex to solve except numerically. Integrating through the volume as before for this linearly varying shear stress gives

$$W_{\text{adhesive}} = btl(\tau_0)^2/6G \quad (19)$$

For the free length of the adherend vibrating in flexure, the energy stored per unit length is  $M^2/2 EI$ , where  $I$  is the second moment of area. Letting the bending moment vary as

$$M = kx \quad (20)$$

and noting that  $M = 0$  at  $x = 0$  and  $M = M_0$  at the joint end ( $x = (L - l)/2$ ), the energy stored in bending in the adherends can be estimated to be

$$W_{\text{adherends}} = M_0^2(L - l)/6EI \quad (21)$$

Numerical analysis using an in-house program gives that for  $M_0 = 4 \text{ Nm}$ , the shear stress at the overlap ends,  $\tau_0$  is about 4 MPa. Inserting these values into the equations for energy stored gives

$$\psi_{\text{overall}} = 0.016\psi_{\text{adhesive}} \quad (22)$$

It can therefore be seen that the actual damping of the lap joint in bending is only about 1.6% of the damping of the polymeric adhesive for the parameters given above. Because of the interactions between the various parameters, this calculation should be regarded as giving an indication and cannot be extrapolated to other situations.

The above attempts at calculating the damping of adhesively bonded lap joints may look complex. Others have attempted the same but using even more complex analysis. The reader is referred to Mead (1998), He and Rao (1992a, b), and Saito and Tani (1984). The problem with these analyses is that they are far too difficult to use in most practical situations. Saito and Tani did, however, predict that there is an optimum overlap ratio (OR) of 0.2 for maximum damping.

## 30.4 Experimental Evidence of Damping in Joints

Because there is very little reliable data on damping in adhesively bonded lap joints, it has been necessary to use previously unpublished data from an in-house program at the University of Bristol by the author and his students.

### 30.4.1 Materials Used

Four different adhesives were tested, details of which can be found in Table 1. The adhesives were AV119, a one-part epoxy manufactured by Hexcel; 9245, a structural bonding tape (SBT) manufactured by 3M; 3532, a two-part polyurethane also manufactured by 3M; and Hysol XEA 9359.3, which is a two-component structural adhesive that exhibits high peel and high tensile lap shear strength.

In order to investigate the contribution of the adhesive damping in the specimen, a high-strength low-damping steel was used for the metallic parts of the lap joints (Adams 1972a, b).

### 30.4.2 Joint Manufacture

A simple lap joint consists of two sheets joined together with an overlap and is a very common joint design in industry. The joints were manufactured using an alignment jig that ensured a total joint length which could be manufactured of 200 mm with a

t.1
**Table 1** Data on adhesives

t.2	Adhesive name	AV119 araldite	3532 B/A structural adhesive	9245 structural bonding tape	Hysol XEA 9359.3
t.3	Manufacturer	Ciba polymers	3M	3M	Dexter
t.4	Type	One-part epoxy	Two-part, polyurethane	Tape	Two-part, epoxy
t.5	Working life	NA	5–15 min	3 months	NA
t.6	Cure	120 °C	Room temperature	140 °C	82 °C
t.7	Conditions	1 h	24 h	25 min	1 h
t.8	Post-cure	None	40 °C	None	None
t.9	Procedure		30 min		
t.10	Appearance	Opaque cream	Opaque brown	Light gray	Opaque green
t.11	Average shear modulus	~1,000 MPa	~40 MPa	~400 MPa	1,020 MPa

307 width of 25 mm. The total length of the specimens was kept constant, but the overlap
308 was varied by using different adherend lengths. A typical joint is shown in Fig. 5.

309 To ensure a good bond, careful procedures were followed for preparation of the
310 jig and bonding surfaces. The bonding surface of the adherend was first grit-blasted
311 before thorough cleaning with acetone. Both sides of the specimen were grit-blasted
312 to avoid bending of the adherends by releasing or introducing residual stresses. The
313 jig and spacers were also cleaned with acetone before spraying with a release agent.
314 This prevented problems with clamping following the cure process. Next, adhesives
315 were prepared and applied to the bonding surface as evenly as possible. The joints
316 were then cured under pressure in a hot press according to the manufacturer’s
317 specification. Once fully cured, the joints were cooled slowly to room temperature.

318
**30.4.3 Vibration Test Apparatus**

319 When measuring damping, it is important to ensure that it is only the damping of the
320 system under investigation (in this case a lap joint) that is measured and that other
321 sources of damping are eliminated as far as possible. To some extent, this is a matter of
322 judgment, but there are some obvious principles to follow. In particular, it is necessary
323 to eliminate extraneous sources of damping. Many authors use cantilevered speci-
324 mens that have unwanted damping in the clamp by micro-slippage. Others use
325 accelerometers to measure the motion; unfortunately, accelerometers deliver their
326 signals via leads that cause damping. It is essential to prove the apparatus by showing
327 that its inherent damping is an order of magnitude less than the specimen damping.
328 This is best done by testing a low-damping material such as a high-strength aluminum
329 alloy. One of the authors (RDA) has had a lot of experience in measuring damping in a
330 wide variety of materials and has designed suitable apparatus according to the task in



hand (see, e.g., Adams and Percival 1969; Adams and Fox 1972; Adams and Bacon 1973; Adams and Lloyd 1975; Guild and Adams 1981).

For lap joints, it is best to use flexural (bending) vibration as this is the most likely form of vibration such joints will be subject to. In the investigation reported here, a free-free beam method was used to study the damping behavior. To measure the damping properties of a material, it is necessary to vibrate the specimen at a known frequency and a known resonant mode of vibration. The apparatus uses permanent magnets attached to each end of the specimen and placed within the fields of flat coils. This apparatus is a modification by Adams and Singh (1995) of the Guild and Adams (1981) apparatus. A signal generator provided an output that was passed through a power amplifier to give an alternating current to one coil, exciting the beam into vibration. The motion of the second coil induces an output voltage proportional to its velocity. The damping of the system was calculated by the “free decay” method (described in the Appendix).

#### 30.4.4 Temperature Testing of Joints

The damping properties of some of the beams were measured within the temperature range 20–100 °C. Heating was undertaken in an oven with the heating rate kept constant and slow to ensure that, as far as practicable, the entire specimen was at the same temperature. Faster rates of heating would cause a temperature gradient to exist across the adhesive layer, producing unreliable data. At temperatures above the glass transition temperature of the adhesives, lap joints become unstable in bending, particularly for short overlaps.

#### 30.4.5 Results and Discussion

The SDC values of the adhesives studied, determined by both the free decay method and bandwidth at 20 °C, are shown in Fig. 7. For joints of the same overlap ratio (OR), defined as the ratio of the adhesive bond length to the total length of the joint (0.125), the 9245 and 3532 adhesives provide considerably (about 20 times) higher damping than the structural epoxy AV119. Even so, the epoxy adhesive increases the damping by about five times over that of the hard steel adherends alone. Similar epoxies give an SDC of about 10%, so the reduction factor is about 0.05. Measurements of the damping of the 9245 material give an SDC of about 300% (Kadioglu 2000). For the 9245 lap joints, the reduction factor is therefore about 0.03, which is of the same order as that for the epoxy adhesive.

However, Fig. 7 gives a simplistic and possibly misleading picture, and it will be shown below that changing the OR or the temperature can significantly alter this balance.

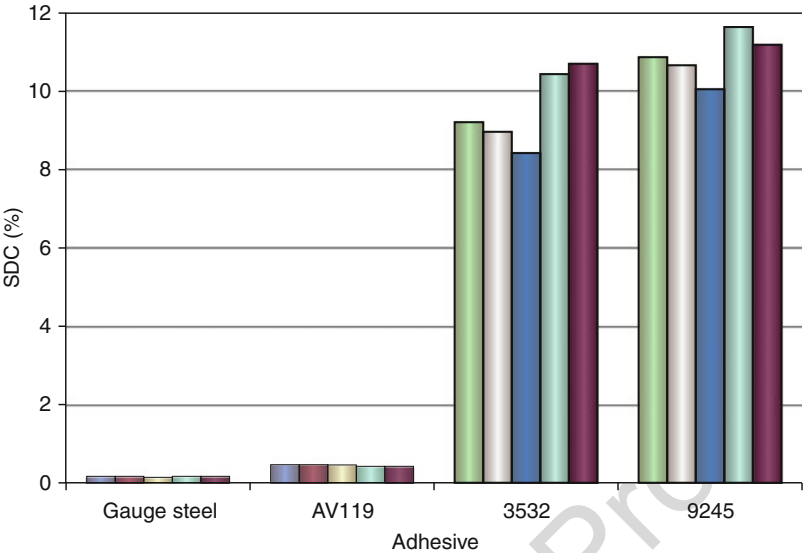


**Fig. 7** Specific damping capacity values for 25 mm overlap joints (OR is 0.125)

**Effect of Overlap Ratio**

The effect of OR on the damping capacity of various adhesively bonded joints is shown in Figs. 8 and 9. In the work reported here, the OR was varied from 0.1 to 1. A sandwich beam is one in which the overlap covers the entire length of the specimen, so the OR is 1. Compared to the damping capacity of a single gauge steel beam, it is reasonable to assume that the adhesive dominates the damping characteristics of a lap joint. It might therefore be expected that the optimum OR would be that of a sandwich beam ( $OR = 1$ ), as this type of joint contains the largest volume of adhesive. However this is not the case as can be seen in Figs. 8 and 9. It is clear there is an optimum OR of about 0.25 for the first mode of vibration.

Park (1996) experimentally concluded that the damping is maximized if a viscoelastic layer is located at the region of maximum displacement. All the tests investigated here were for the first mode of vibration. However, the region of maximum displacement is located at the ends of the specimen for a lap joint in flexural vibration. Peel forces are created by the offset of the loading across the overlap region. It would therefore appear a sensible conclusion that having these shear and peel stresses nearer the center of the beam can increase the damping capacity. It is clear that a balance exists between the damping effect provided by the volume of adhesive and the damping effect of the position of the shear and peel stresses. Note that the areas of greatest energy dissipation are at the edges of the adhesive bond, where local shear and peel stresses are a maximum for lap joints in the first mode of vibration. The results of this study show that an optimum OR is

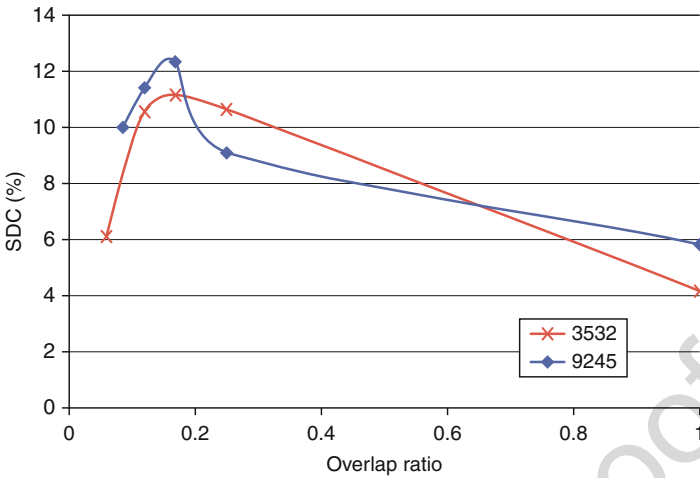


**Fig. 8** Variation of SDC with OR for 3532 and 9245 adhesives

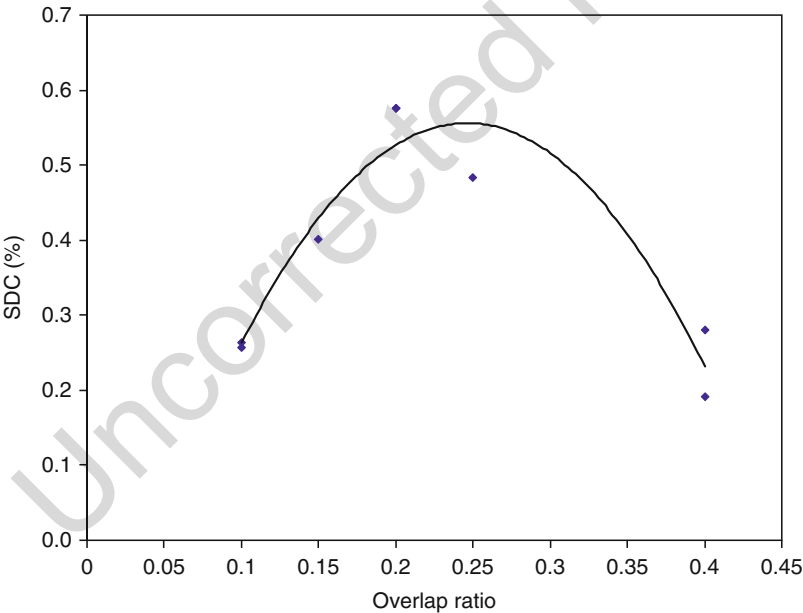


**Fig. 9** Variation of SDC with OR for AV119 joints

present at around 0.25. Saito and Tani (1984) showed theoretically that an optimum OR of about 0.2 exists for the first mode of vibration and that there should be an increase in natural frequency with OR. Their predictions are confirmed by the results shown in Fig. 9, but Park's prediction is contradicted.

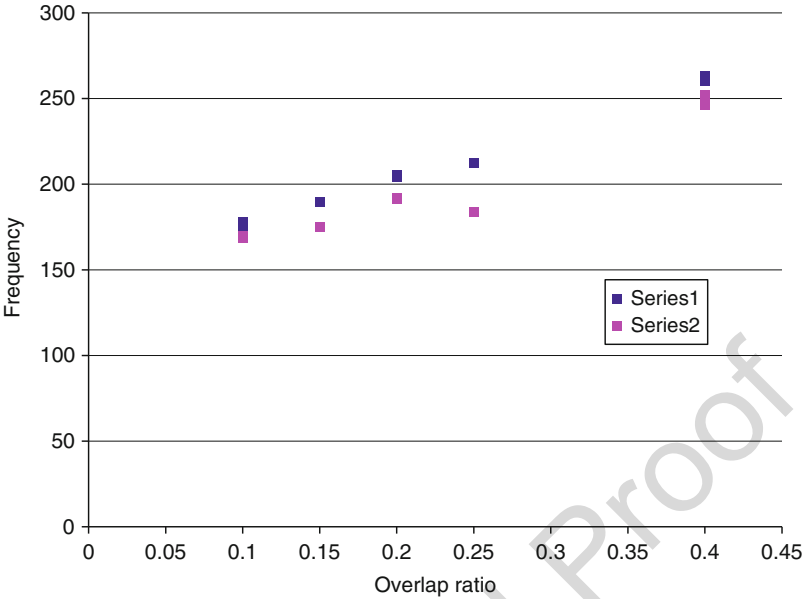


**Fig. 10** Variation of frequency (Hz) with OR for AV119 (series 1) and 9245 (series 2) single-lap joints in their first free-free mode of flexural vibration

Tests also showed an increase in natural frequency with OR as is demonstrated in Fig. 10. In vibrating systems, the resonant frequency is proportional to the square root of the ratio of the stiffness to the mass. Although a longer overlap increases the mass in proportion to the doubled thickness of the overlap, the bending stiffness of the overlap increases as the cube of this doubled thickness. Low-stiffness adhesives such as 9245 can shear in the adhesive thickness so these do not get the full (cubed) bending stiffness. The stiffer epoxy adhesive therefore shows a slightly stronger increase in frequency with OR, but the differences are small.

**Effect of Temperature**

Polymers are very susceptible to temperatures that leave metallic elements relatively unaffected. The reason for this is that the microstructural properties of polymeric materials result not from atomic interactions, as in metals, but from molecular interactions.

The results for AV119 and Hysol in the temperature range 20–90 °C are shown in Fig. 11. From the manufacturer’s data, AV119 is expected to have a Tg of around 120 °C, and the results demonstrate a smooth curve through the transition region with an expected peak around 120 °C. The other structural adhesive, Hysol, indicates the existence of a Tg at around 60 °C from the trend curve. Manufacturer’s data suggests a Tg of 85 °C.

It is important to note that structural adhesives as a family of polymers are usually used at temperatures below their Tg (Adams et al. 1997), except the rubbery

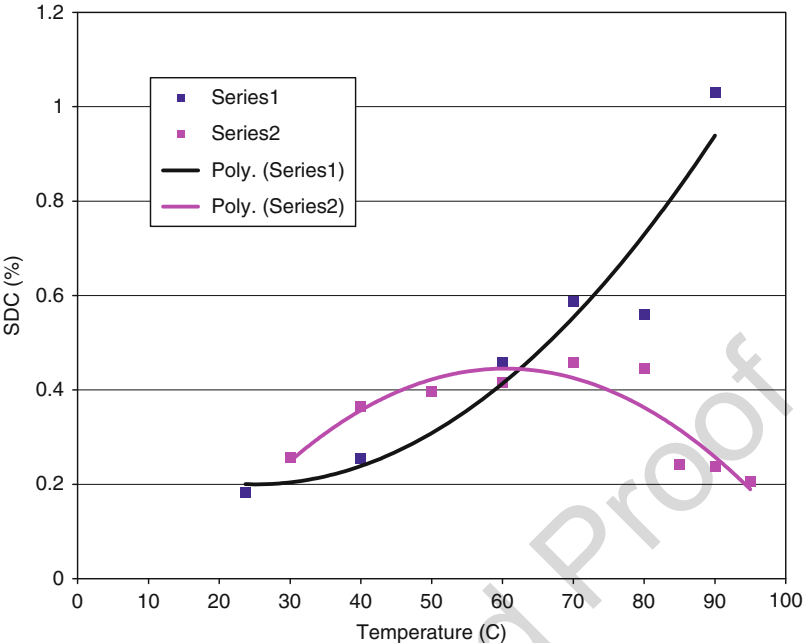


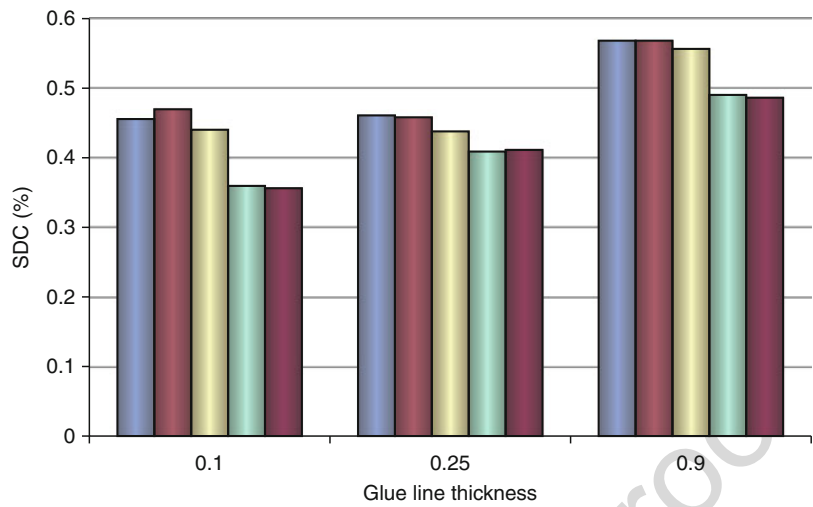
**Fig. 11** Variation of damping with temperature for two epoxy adhesives. Series 1 is AV119 and series 2 is Hysol 9359.3

adhesives such as 3532. It is unlikely, therefore, that temperature can be used as a device to enhance damping for structural adhesives.

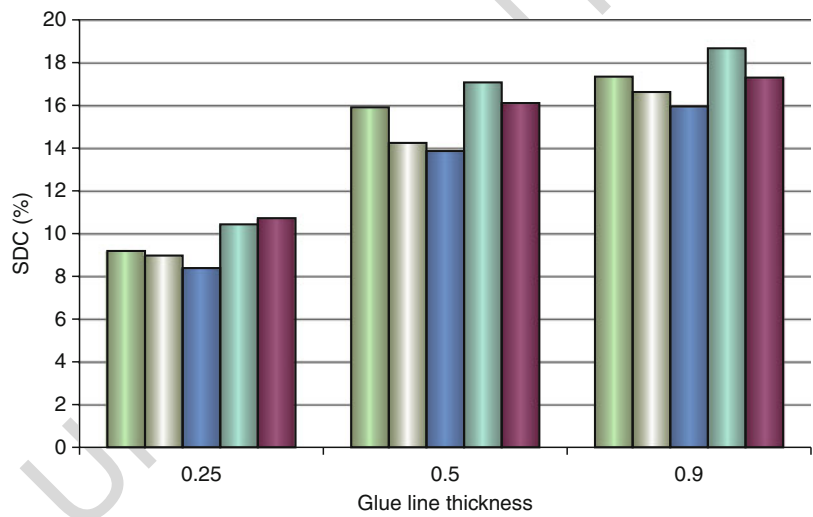
**Effect of Bondline Thickness**

Joints made using 3532 and AV119 both exhibited an increase in SDC with increase in glue line thickness. This trend is illustrated in Figs. 12 and 13. The trend is clearly more significant in the case of the 3532 joints, where quadrupling the glue line thickness leads to a doubling of measured SDC. For AV119 joints, only a small increase is observed. This is not unexpected, as it has already been established that the use of a stiff adhesive such as AV119 does not significantly increase the overall damping of the system. Therefore the act of increasing the amount of an adhesive that has negligible damping effect will itself also have a negligible effect.

Furthermore, the fact that increasing the glue line thickness of the AV119 by almost a factor of 10 results in only a negligible damping increase suggests that joint geometry is not the dominant factor in determining the effect of glue line thickness on damping. If it were, then we would expect similar rates of damping increase with joint thickness regardless of adhesive used. Instead it is the consequent increase in adhesive material present that plays the dominant role, and thus when an adhesive of low shear modulus is used, the observed damping increase is large, whereas when a stiff epoxy is used, there is very little effect.



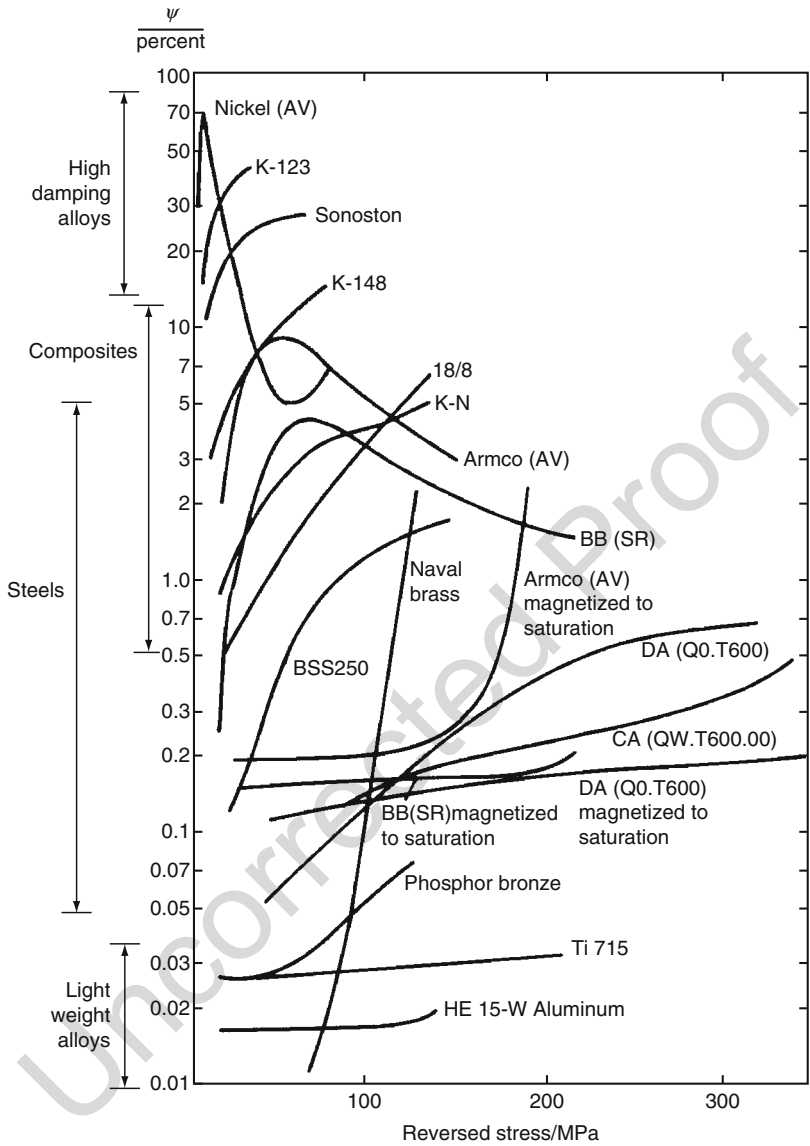
**Fig. 12** Variation of SDC (%) with bondline thickness (mm) for AV119 epoxy adhesive



**Fig. 13** Variation of SDC (%) with bondline thickness (mm) for 3532 polyurethane adhesive

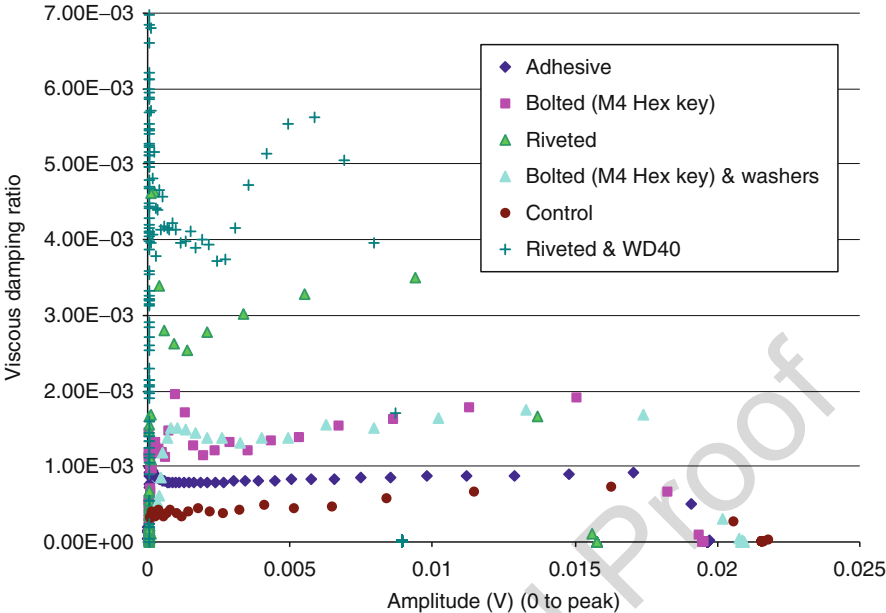
### 30.5 Perspective

Figure 14 shows how the damping of a wide range of composites and structural metals varies with cyclic stress. It can be seen that composites fall in the range 0.5–12% SDC which is toward the higher end of the range of structural metals.



**Fig. 14** SDC versus cyclic stress for a wide range of materials

The results for lap joints, made using low-damping steel substrates, are in the same range as structural composites. The structural epoxy AV119 is at the bottom of this range, and it is only the rubbery adhesives that show any significant damping. The overall contribution of the adhesively bonded joints to damping in a structure is therefore expected to be small or negligible and claims that



**Fig. 15** Variation of damping with amplitude for a variety of joining methods for a composite beam in flexural vibration. The control sample was brazed

bonded structures can provide high damping should be taken with a large grain of salt. The essential point is that the energy dissipated in the adhesive is in a very small volume, whereas the energy stored in the structure is very much higher, so the overall damping is small.

Figure 15 shows some results from Brearley et al. (2005) for a bonded beam structure which was vibrated in free-free flexure. The beam was made of two equal U-shaped sections joined by rivets, bolts, an adhesive, and by brazing. It is clear that the bonded beam had a damping level only just above that of the brazed beam, and it was much less than the beams which could rely on friction at their joints.

### 30.6 Conclusions

The general concept of vibration damping in vibrating structures and how it can be used to limit vibration amplitudes has been discussed. The various damping parameters have been defined, and their relationship is given. Equations that can be used to measure damping in steady-state vibration or under free decay have been presented.

Simple equations for calculating the damping of a lap joint in tension and bending have been developed, and it was predicted that the damping of the whole specimen would be much lower than that of the adhesive alone.



As there is very little experimental data available in the literature, the damping of a variety of adhesively bonded single-lap joints has been measured and presented by the authors. From the results collected, the following conclusions can be made:

1. An optimum OR of around 0.25 exists for adhesively bonded single-lap joints in flexural vibration.
2. Damping from adhesives in vibrating structures is small and much less than the adhesive alone. It should not be expected that adhesive bonding can be used to enhance the damping of a structure.

## Appendix

### Damping Measurement by the Free Decay Method

This is a relatively simple method of measuring the damping of a freely vibrating system. The logarithmic decrement (log dec.),  $\Delta$ , is measured from an amplitude-time graph and is based on measuring the rate of decay of the free vibrations. This method is only suitable for measuring low damping and free vibration.

During the experiment, readings are recorded by measuring the time taken for the amplitude of the waveform to decrease from  $A_1$  to  $A_2$  (Fig. 16).

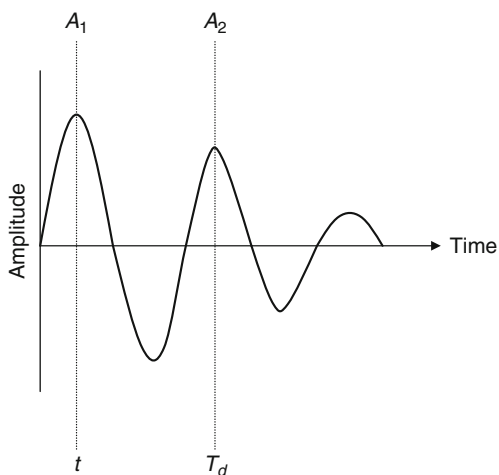
The relationship between log dec. and the damping ratio can be found by consideration of the equation for damped oscillation:

$$x = Ae^{-\zeta\omega t} \sin(\omega_d t + \theta)$$

$$A_1 = Ae^{-\zeta\omega t} \text{ and } A_2 = Ae^{-\zeta\omega(t+\tau_d)}$$

The log dec. is defined by

**Fig. 16** Variation of amplitude with time for a damped system



$$\Delta = \ln \frac{A_1}{A_2}$$

$$\Delta = \ln \frac{Ae^{-\zeta\omega t}}{Ae^{-\zeta\omega(t+\tau_d)}}$$

$$\Delta = \ln(e^{-\zeta\omega t + \zeta\omega(t+\tau_d)}) = \zeta\omega\tau_d$$

Noting that  $\tau_d = \frac{2\pi}{\omega_d} = \frac{2\pi}{\omega\sqrt{1-\zeta^2}}$

Therefore  $\Delta = \frac{2\pi\omega\zeta}{\omega\sqrt{1-\zeta^2}}$

And so if the damping ratio is small,  $\zeta \rightarrow 0$  and so

$$\Delta = 2\pi\zeta = \ln\left(\frac{A_1}{A_2}\right)$$

A more accurate result can be obtained by considering the decay over a number of peaks. The log dec. is then

$$\Delta = \frac{1}{N} \ln\left(\frac{A_1}{A_{N+1}}\right)$$

where  $N$  is the number of peaks calculated using the formula  $ft = N$ , where  $f$  is the frequency of oscillation, and  $t$  is the time taken for the amplitude to decay from  $A_1$  to  $A_2$ .

## References

- Adams RD (1972a) Damping of ferromagnetic materials at direct stress levels below the fatigue limit. *J Phys D Appl Phys* 5:1877–1889
- Adams RD (1972b) The damping characteristics of certain steels, cast irons and other metals. *J Sound Vib* 23:199–216
- Adams RD, Bacon DGC (1973) Measurement of the flexural damping capacity and dynamic Young's modulus of metals and reinforced plastics. *J Phys D Appl Phys* 6:27–41
- Adams RD, Fox MAO (1972) Measurement of the damping capacity and dynamic modulus of high-damping metals under direct cyclic stress. *J Phys D Appl Phys* 5:1274–1283
- Adams RD, Lloyd DH (1975) Apparatus for measuring the torsional modulus and damping of single carbon fibres. *J Phys E: Sci Instrum* 8:475–480
- Adams RD, Percival AL (1969) Measurement of the strain-dependent damping of metals in axial vibration. *J Phys D Appl Phys* 2:1693–1704
- Adams RD, Singh MM (1995) The effect of immersion in sea water on the dynamic properties of fibre-reinforced flexibilised epoxy composites. *Compos Struct* 31:119–127
- Adams RD, Comyn J, Wake WC (1997) *Structural adhesive joints in engineering*. Chapman & Hall, London
- Brearley T, Nehammer E, Rouse E, Vaughn D (2005) *An investigation into damping in structures*. Internal report. University of Bristol
- Den Hartog JP (2008) *Mechanical vibrations*. Maple Press, York
- Guild FJ, Adams RD (1981) A new technique for the measurement of the specific damping capacity of beams in flexure. *J Phys E Sci Instrum* 14:355–363

- 509 He S, Rao MD (1992a) Vibration analysis of adhesively bonded lap joint, part I: theory. *J Sound Vib*  
510 152:405–416
- 511 He S, Rao MD (1992b) Vibration analysis of adhesively bonded lap joint, part II: numerical  
512 solution. *J Sound Vib* 152:417–425
- 513 Hildebrand M, Vessonen I (1997) Experimental data on damping of adhesively bonded single-lap  
514 joints. VTT Manufacturing Technology, Finland
- 515 Kadioglu F (2000) Quasi-static and dynamic behaviour of a structural pressure sensitive adhesive.  
516 PhD thesis, University of Bristol, Bristol
- 517 Lin DX, Ni RG, Adams RD (1984) Prediction and measurement of the vibrational damping  
518 parameters of carbon and glass fibre-reinforced plastics plates. *J Compos Mater* 18:132–152
- 519 Maheri MR, Adams RD, Hugon J (2008) Vibration damping in sandwich panels. *J Mater Sci*  
520 43:6604–6618
- 521 Mead DJ (1998) *Passive vibration control*. Wiley, Chichester
- 522 Nashif AD, Jones DIG, Henderson JG (1985) *Vibration damping*. Wiley Interscience, New York
- 523 Park T-H (1996) Vibration and damping characteristics of a beam with a partially sandwiched  
524 viscoelastic layer. *J Adhes* 61:97–122
- 525 Saito H, Tani H (1984) Vibrations of bonded beams with a single-lap adhesive joint. *J Sound Vib*  
526 92:299–309

---

Lucas F. M. da Silva • Andreas Öchsner  
Robert D. Adams  
Editors

# Handbook of Adhesion Technology

Second Edition

Volume 2

With 919 Figures and 106 Tables



Springer

*Editors*

Lucas F. M. da Silva  
Department of Mechanical Engineering  
Faculty of Engineering  
University of Porto  
Porto, Portugal

Andreas Öchsner  
Faculty of Mechanical Engineering  
Esslingen University of Applied Sciences  
Esslingen, Baden-Württemberg, Germany

Robert D. Adams  
Department of Mechanical Engineering  
University of Bristol  
Bristol, UK  
Department of Engineering Science  
University of Oxford  
Oxford, UK

ISBN 978-3-319-55410-5      ISBN 978-3-319-55411-2 (eBook)  
ISBN 978-3-319-55412-9 (print and electronic bundle)  
<https://doi.org/10.1007/978-3-319-55411-2>

Library of Congress Control Number: 2018940005

1st edition: © Springer-Verlag Berlin Heidelberg 2011

© Springer International Publishing AG, part of Springer Nature 2018

This work is subject to copyright. All rights are reserved by the Publisher, whether the whole or part of the material is concerned, specifically the rights of translation, reprinting, reuse of illustrations, recitation, broadcasting, reproduction on microfilms or in any other physical way, and transmission or information storage and retrieval, electronic adaptation, computer software, or by similar or dissimilar methodology now known or hereafter developed.

The use of general descriptive names, registered names, trademarks, service marks, etc. in this publication does not imply, even in the absence of a specific statement, that such names are exempt from the relevant protective laws and regulations and therefore free for general use.

The publisher, the authors and the editors are safe to assume that the advice and information in this book are believed to be true and accurate at the date of publication. Neither the publisher nor the authors or the editors give a warranty, express or implied, with respect to the material contained herein or for any errors or omissions that may have been made. The publisher remains neutral with regard to jurisdictional claims in published maps and institutional affiliations.

Printed on acid-free paper

This Springer imprint is published by the registered company Springer International Publishing AG part of Springer Nature.

The registered company address is: Gewerbestrasse 11, 6330 Cham, Switzerland

The first edition of *Handbook of Adhesion Technology* has been very well accepted by the adhesion community with over 25,000 downloads per year. This was the main motivation for the preparation of this 2nd edition. Also, there has been a general increase of the scientific and industrial community in this technology, which justifies an update. There are more papers published every year, there are new journals related to the field, there are more national and international conferences, and there are more applications. A revolution is currently taking place in the transport industry where fuel is being replaced by electric power. This change means that lighter structures need to be manufactured with the use of light materials and more efficient joining methods such as adhesive bonding. But, the use of adhesive bonding is not limited to the transport industry, and there are several other applications described in this handbook such as the use of adhesives in medicine.

This 2nd edition of *Handbook of Adhesion Technology* is a complete revision of the 1st edition with an update of the methods that have been investigated recently, which are now fully accepted by the adhesion community. Themes that are now included in more detail include, for example, hybrid adhesives used for automotive applications, ecofriendly surface treatments, damage mechanics, joint durability prediction, functionally graded joints, adhesive selection for space applications, and, lastly, trends in bioadhesion. There is also a new chapter related to the application of adhesives in the oil industry. Besides these content changes, there has been a complete revision of all chapters in terms of text, figures, tables, and references for a more didactic character of this reference book.

The editors would like to thank the authors for their patience with the preparation of this handbook. Finally, the editors especially thank Dr. Christoph Baumann, Ms. Tina Shelton, and Ms. Monika Garg, Springer editors, who helped enormously toward the success of this handbook.

Department of Mechanical Engineering  
Faculty of Engineering  
University of Porto  
Porto, Portugal

Lucas F. M. da Silva

85 Department of Mechanical Engineering  
83 University of Bristol  
84 Bristol, UK

Robert D. Adams

88 Department of Engineering Science  
86 University of Oxford  
87 Oxford, UK

91 Faculty of Mechanical Engineering  
89 Esslingen University of Applied Sciences  
90 Germany

Andreas Öchsner

Uncorrected Proof

Adhesives have been used for thousands of years, but until 100 years ago, the vast majority was from natural products such as bones, skins, fish, milk, and plants. Since about 1900, adhesives based on synthetic polymers have been introduced, and today, there are many industrial uses of adhesives and sealants. It is difficult to imagine a product—in the home, in industry, in transportation, or anywhere else for that matter—that does not use adhesives or sealants in some manner.

Adhesion technology is nowadays a common approach to many joining situations. There are many books and several international journals dealing with this subject. However, when the end-user needs to apply this technology, he does not have the time or the resources to thoroughly study the various technologies related to adhesives and sealants. It is not practical to go through volumes of text and product information looking for the specific methods or processes to apply. However, such information should be close-by if the need arises. The *Handbook of Adhesion Technology* is intended to fill a gap between the necessarily simplified treatment of the student textbook and the full and thorough treatment of the research monograph and review article. The subject is treated very comprehensively and with the most up to date information so that the end-user has in a single book a proper guidance and fundamental knowledge required for many adhesive bonding or sealing applications.

The *Handbook of Adhesion Technology* is intended to be a book of reference in the field of adhesion. Essential information is provided for all those concerned with the adhesion phenomenon. Adhesion is a phenomenon of interest in diverse scientific disciplines and of importance in a wide range of technologies. Therefore, this handbook includes the background science (physics, chemistry, and materials science), engineering aspects of adhesion, and industry specific applications. It is arranged in a user-friendly format with ten main sections: theory of adhesion, surface treatments, adhesive and sealant materials, testing of adhesive properties, joint design, durability, manufacture, quality control, applications, and emerging areas. The sections contain each about five chapters written by internationally renowned authors who are authorities in their fields.

This Handbook is intended to be a reference for people needing a quick, but authoritative, description of topics in the field of adhesion and the use of adhesives and sealants. It is intended for scientists and engineers of many different backgrounds who need to have an understanding of various aspects of adhesion



technology. These will include those working in research or design, as well as others involved with marketing services. It is expected to be a valuable resource for both undergraduate and research students.

The editors would like to thank the authors for their patience with the preparation of this Handbook. Finally, the editors especially thank Christoph Baumann and Tina Shelton, Springer editors, who helped enormously toward the success of this Handbook.

Porto, Portugal  
Skudai, Johor, Malaysia  
Oxford, UK

Lucas F. M. da Silva  
Andreas Öchsner  
Robert D. Adams

---

# Contents

139

## 140 Volume 1

141	<b>1 Introduction to Adhesive Bonding Technology</b>	1
142	Lucas F. M. da Silva, Andreas Öchsner, and Robert D. Adams	
143	<b>Part I Theory of Adhesion</b>	<b>9</b>
144	<b>2 Theories of Fundamental Adhesion</b>	11
145	David E. Packham	
146	<b>3 Forces Involved in Adhesion</b>	43
147	Maurice Brogly	
148	<b>4 Wetting of Solids</b>	71
149	Martin E. R. Shanahan and Wulff Possart	
150	<b>5 Spreading of Liquids on Substrates</b>	101
151	Günter Reiter	
152	<b>6 Thermodynamics of Adhesion</b>	115
153	Wulff Possart and Martin E. R. Shanahan	
154	<b>Part II Surface Treatments</b>	<b>129</b>
155	<b>7 General Introduction to Surface Treatments</b>	131
156	Gary Critchlow	
157	<b>8 Surface Treatments of Selected Materials</b>	163
158	Guy D. Davis	
159	<b>9 Surface Characterization and Its Role in Adhesion Science and Technology</b>	197
160	John F. Watts	
161		

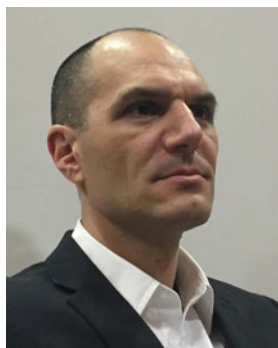
162	<b>10 Use of Surface Analysis Methods to Probe the Interfacial</b>	
163	<b>Chemistry of Adhesion</b> .....	227
164	John F. Watts	
165	<b>11 Organosilanes: Adhesion Promoters and Primers</b> .....	257
166	Marie-Laure Abel	
167	<b>Part III Adhesive and Sealant Materials</b> .....	<b>281</b>
168	<b>12 Classification of Adhesive and Sealant Materials</b> .....	283
169	Erol Sancaktar	
170	<b>13 Composition of Adhesives</b> .....	319
171	Hyun-Joong Kim, Dong-Hyuk Lim, Hyeon-Deuk Hwang, and	
172	Byoung-Ho Lee	
173	<b>14 Adhesive Families</b> .....	345
174	Eric Papon	
175	<b>15 Pressure-Sensitive Adhesives (PSAs)</b> .....	373
176	Charles W. Paul and Eric Silverberg	
177	<b>16 Selection of Adhesives</b> .....	409
178	Ewen J. C. Kellar	
179	<b>Part IV Testing of Adhesive Properties</b> .....	<b>431</b>
180	<b>17 Physical Properties</b> .....	433
181	David A. Dillard	
182	<b>18 Thermal Properties of Adhesives</b> .....	459
183	John Comyn	
184	<b>19 Failure Strength Tests</b> .....	489
185	Lucas F. M. da Silva, R. J. C. Carbas, and M. D. Banea	
186	<b>20 Fracture Tests</b> .....	523
187	Bamber R. K. Blackman	
188	<b>21 Impact Tests</b> .....	555
189	Luca Goglio	
190	<b>22 Special Tests</b> .....	593
191	David A. Dillard and Tetsuo Yamaguchi	
192	<b>Part V Joint Design</b> .....	<b>613</b>
193	<b>23 Constitutive Adhesive and Sealant Models</b> .....	615
194	Erol Sancaktar	

195	<b>24 Analytical Approach</b>	665
196	Liyong Tong and Quantian Luo	
197	<b>25 Numerical Approach: Finite Element Analysis</b>	701
198	Ian A. Ashcroft and Aamir Mubashar	
199	<b>26 Special Numerical Techniques to Joint Design</b>	741
200	Andreas Öchsner	
201	<b>27 Design Rules and Methods to Improve Joint Strength</b>	773
202	Lucas Filipe Martins da Silva, E. A. S. Marques, and R. D. S. G.	
203	Campilho	
204	<b>28 Design with Sealants</b>	811
205	Gregory L. Anderson	
206	<b>29 Design for Impact Loads</b>	829
207	Chiaki Sato	
208	<b>30 Vibration Damping of Adhesively Bonded Joints</b>	853
209	Robert D. Adams, Duncan G. A. Cooper, and Stuart Pearson	
210	<b>Volume 2</b>	
211	<b>Part VI Durability</b>	<b>877</b>
212	<b>31 Effect of Water and Mechanical Stress on Durability</b>	879
213	Ian A. Ashcroft, John Comyn, and Aamir Mubashar	
214	<b>32 Adhesives in Space Environment</b>	915
215	Sabine Dagrás, Julien Eck, Claire Tonon, and Denis Lavielle	
216	<b>33 Fatigue Load Conditions</b>	941
217	Ian A. Ashcroft	
218	<b>34 Creep Load Conditions</b>	975
219	Paul Ludwig Geiß and Melanie Schumann	
220	<b>35 Durability of Nonstructural Adhesives</b>	1009
221	James D. Palmer	
222	<b>Part VII Manufacture</b>	<b>1029</b>
223	<b>36 Storage of Adhesives</b>	1031
224	Hans K. Engeldinger and Cai R. Lim	
225	<b>37 Preparation for Bonding</b>	1051
226	Andreas Lutz	

227	<b>38 Equipment for Adhesive Bonding</b>	1091
228	Manfred Peschka	
229	<b>39 Environment and Safety</b>	1117
230	Ansgar van Halteren	
231	<b>Part VIII Quality Control</b>	<b>1127</b>
232	<b>40 Quality Control of Raw Materials</b>	1129
233	Kazutami Wakabayashi	
234	<b>41 Processing Quality Control</b>	1151
235	Kosuke Haraga	
236	<b>42 Nondestructive Testing</b>	1171
237	Robert D. Adams	
238	<b>43 Techniques for Post-fracture Analysis</b>	1195
239	R. Créac’hadeac	
240	<b>Part IX Applications</b>	<b>1233</b>
241	<b>44 Adhesively Bonded Joints in Aircraft Structures</b>	1235
242	L. John Hart-Smith	
243	<b>45 Aerospace Industry</b>	1285
244	Christian Désagulier, Patrick Pérès, and Guy Larnac	
245	<b>46 Automotive Industry</b>	1333
246	Klaus Dilger, Bernd Burchardt, and Michael Fraunhofer	
247	<b>47 Adhesive Bonding for Railway Application</b>	1367
248	Yasuaki Suzuki	
249	<b>48 Marine Industry</b>	1391
250	Peter Davies	
251	<b>49 Civil Construction</b>	1419
252	Stefan Böhm, Martin Kahlmeyer, Andreas Winkel, and Ilko Hartung	
253	<b>50 Electrical Industry</b>	1449
254	Kwang-Seok Kim, Jong-Woong Kim, and Seung-Boo Jung	
255	<b>51 Shoe Industry</b>	1483
256	José Miguel Martín-Martínez	
257	<b>52 Oil Industry</b>	1533
258	Silvio de Barros, Luiz C. M. Meniconi, Valber A. Perrut, and Carlos E.	
259	Reuther de Siqueira	

260	<b>Part X Emerging Areas</b> .....	<b>1557</b>
261	<b>53 Molecular Dynamics Simulation and Molecular Orbital</b>	
262	<b>Method</b> .....	<b>1559</b>
263	Ya-Pu Zhao, Feng-Chao Wang, and Mei Chi	
264	<b>54 Bioadhesives</b> .....	<b>1597</b>
265	Katharina Richter, Ingo Grunwald, and Janek von Byern	
266	<b>55 Biological Fibrillar Adhesives: Functional Principles and</b>	
267	<b>Biomimetic Applications</b> .....	<b>1641</b>
268	Stanislav N. Gorb and Lars Heepe	
269	<b>56 Adhesives with Nanoparticles</b> .....	<b>1677</b>
270	Ambrose C. Taylor	
271	<b>57 Adhesive Dentistry</b> .....	<b>1703</b>
272	John W. Nicholson	
273	<b>58 Adhesion in Medicine</b> .....	<b>1729</b>
274	Robin A. Chivers	
275	<b>59 Recycling and Environmental Aspects</b> .....	<b>1751</b>
276	Chiaki Sato	
277	<b>60 Adhesion Technology Recap: Current and Emerging Areas</b> .....	<b>1775</b>
278	Lucas F. M. da Silva, Andreas Öchsner, and Robert D. Adams	
279	<b>Index</b> .....	<b>1785</b>

## About the Editors



**Lucas F. M. da Silva** is currently Associate Professor with Aggregation at the Department of Mechanical Engineering of the Faculty of Engineering of the University of Porto and Director of the Integrated Master in Mechanical Engineering. He obtained his Ph.D. in bonding of composites from the University of Bristol (UK) in 2004. He leads the Adhesives Group, composed of post-docs, Ph.D. students, and M.Sc. students. He has published 206 ISI papers (174 as author and 32 as editor) and 23 books (9 as author and 14 as editor) mainly on adhesive joint mechanics. His papers were cited 4690 times and correspond to an h-index of 37 (SCOPUS, 06/02/2018).

One of his papers obtained the SAGE Best Paper Award 2010 and Donald Julius Groen Prize 2010 (both awards given by the Institution of Mechanical Engineers). He received in 2013 and 2018 the Award of Scientific Excellence by the Faculty of Engineering of the University of Porto.

He is editor-in-chief of *The Journal of Adhesion*, *Proceedings of the Institution of Mechanical Engineers, Part L: Journal of Materials: Design and Applications*, and *University of Porto Journal of Engineering*. He is also co-editor of two Springer book series (*Advanced Structured Materials* and *Springer Briefs in Engineering: Computational Mechanics*). He is member of the editorial board of *International Journal of Adhesion and Adhesives* and *Journal of Adhesion Science and Technology*. He is reviewer of 60 ISI journals.

He organizes international conferences on adhesive bonding (*Structural Adhesive Bonding* every odd year and *Industrial Applications of Adhesive Bonding* every even year) and materials (*Materials Design and*

Applications every even year), and founded the Portuguese Adhesion Society that belongs to European Adhesion Societies Group (EURADH).

He has seven pending patents. He developed a software for designing adhesive joints available online (*jointdesigner*). He is consultant of several international companies (e.g., Alstom, Nagase Chemtex, John Deere).



**Andreas Öchsner** is Full Professor for lightweight design and structural simulation at the Esslingen University of Applied Sciences, Germany. Having obtained a Diploma Degree (Dipl.-Ing.) in Aeronautical Engineering at the University of Stuttgart (1997), Germany, he spent the time from 1997 to 2003 at the University of Erlangen-Nuremberg as a research and teaching assistant to obtain his Doctor of Engineering Sciences (Dr.-Ing.). From 2003 to 2006, he worked as Assistant Professor in the Department of Mechanical Engineering and Head of the Cellular Metals Group affiliated with the University of Aveiro, Portugal. He spent 7 years (2007–2013) as a Full Professor at the Department of Applied Mechanics, Technical University of Malaysia, where he was also Head of the Advanced Materials and Structure Lab. From 2014 to 2017, he was a Full Professor at the School of Engineering, Griffith University, Australia, and Leader of the Mechanical Engineering Program (Head of Discipline and Program Director). His research interests are related to experimental and computational mechanics, cellular metals and thin structures and interphases. He has published over 450 scientific publications, comprising 13 research monographs, 23 book chapters, and four teaching books on finite element methods. He obtained more than 3000 citations in Google Scholar. He is the general Chairman of 12 international conferences on computational and experimental engineering (ACE-X series) and 14 international conferences in the area of heat and mass transfer (DSL series). His editorial work comprises posts as editor-in-chief of the international journal *Continuum Mechanics and Thermodynamics* (Springer), editor-in-chief of the Springer book series on Advanced Structured Materials, and editor of *SpringerBriefs in Applied Sciences and Technology: Computational Mechanics*.



His research activities were recognized in 2010 by the award of a higher doctorate degree (D.Sc.) by the University of Newcastle, Australia.



**Robert D. Adams** got his first degree, in Mechanical Engineering, from Imperial College, London, in 1962, and his Ph.D. from Cambridge University in 1967 and an Sc.D. in 2017. He was awarded a D.Sc. (Eng) from London University in 1986. Most of his academic career (1967–2005) was at Bristol University where he was made Full Professor in 1986. He was Head of the Department of Mechanical Engineering from 1994 to 1998 and Graduate Dean from 1998 to 2004. In 1991, he was awarded the Visiting Foreign Franqui Chair and Medal at the Free University of Brussels (VUB). He is now an Emeritus Professor of Applied Mechanics at the University of Bristol and a Visiting Professor at the Universities of Oxford and Oxford Brookes. He has published and edited several books and published about 200 papers in international refereed journals.

In 2011, he was awarded the R.L. Patrick Fellowship of the US Adhesion Society. He is active in organizing conferences and publishing and was a founder member of EURADH and WCARP, the main European and World series on Adhesion. He has been joint editor-in-chief of the *International Journal of Adhesion and Adhesives* since 1999. His main research area is on adhesively bonded joints, and he pioneered the application of finite element analysis for determining the stresses, strains, and strength of such joints. In addition to his adhesives research, he has also worked extensively on vibration properties in composites and developed low-velocity impact tests for nondestructively testing composites and sandwich structures.

- 393 **Marie-Laure Abel** Faculty of Engineering and Physical Sciences (A1), University  
394 of Surrey, Guildford, Surrey, UK
- 395 **Robert D. Adams** Department of Mechanical Engineering, University of Bristol,  
396 Bristol, UK
- 397 Department of Engineering Science, University of Oxford, Oxford, UK
- 398 **Gregory L. Anderson** R&D Laboratories, Propulsion Systems – Launch Systems  
399 Group, Orbital ATK, Corinne, UT, USA
- 400 **Ian A. Ashcroft** Faculty of Engineering, University of Nottingham, Nottingham,  
401 UK
- 402 **M. D. Banea** CEFET/RJ – Federal Center of Technological Education in Rio de  
403 Janeiro, Rio de Janeiro, Brazil
- 404 **Bamber R. K. Blackman** Department of Mechanical Engineering, Imperial  
405 College London, South Kensington Campus, London, UK
- 406 **Stefan Böhm** Department for Cutting and Joining Manufacturing Processes, Uni-  
407 versity of Kassel, Institute for Production Technologies and Logistics, Kassel,  
408 Germany
- 409 **Maurice Brogly** ENSCMu – LPIM – Equipe Chimie et Physico-Chimie des  
410 Polymères, Université de Haute Alsace, Mulhouse, France
- 411 **Bernd Burchardt** Weiningen Zürich, Switzerland
- 412 **R. D. S. G. Campilho** Instituto Superior de Engenharia do Porto (ISEP), Instituto  
413 Politécnico do Porto, Porto, Portugal
- 414 **R. J. C. Carbas** Institute of Science and Innovation in Mechanical and Industrial  
415 Engineering (INEGI), Faculty of Engineering, University of Porto, Porto, Portugal
- 416 **Mei Chi** State Key Laboratory of Nonlinear Mechanics (LNM), Institute of  
417 Mechanics, Chinese Academy of Sciences, Beijing, China
- 418 **Robin A. Chivers** York, North Yorkshire, UK

- 419 **John Comyn** Materials Department, Loughborough University, Leicestershire, UK
- 420 **R. Créac'hcadec** ENSTA Bretagne, Institut de Recherche Dupuy de Lôme, FRE  
421 CNRS 3744, Brest, France
- 422 Assemblages Multi-Matériaux, Institut de Recherche Dupuy De Lôme, Brest, France
- 423 **Duncan G. A. Cooper** Department of Mechanical Engineering, University of  
424 Bristol, Bristol, UK
- 425 **Gary Critchlow** Department of Materials, Loughborough University, Loughbor-  
426 ough, Leicestershire, UK
- 427 **Lucas F. M. da Silva** Department of Mechanical Engineering, Faculty of Engi-  
428 neering, University of Porto, Porto, Portugal
- 429 **Sabine Dagrás** Airbus Defence and Space, Toulouse, France
- 430 **Peter Davies** Materials and Structures Group, Marine Structures Laboratory, Brest  
431 Centre, IFREMER, (French Ocean Research Institute), Plouzané, France
- 432 **Guy D. Davis** ElectraWatch, Inc., Linthicum Heights, MD, USA
- 433 **Silvio de Barros** Department of Mechanical Engineering, Federal Center of Tech-  
434 nological Education in Rio de Janeiro – CEFET/RJ, Rio de Janeiro, RJ, Brazil
- 435 **Carlos E. Reuther de Siqueira** Department of Offshore Engineering, Petróleo  
436 Brasileiro S.A. – PETROBRAS, Rio de Janeiro, RJ, Brazil
- 437 **Christian Désagulier** ArianeGroup, Les Mureaux, France
- 438 **Klaus Dilger** Institute of Welding and Joining, TU Braunschweig, Braunschweig,  
439 Germany
- 440 **David A. Dillard** Biomedical Engineering and Mechanics Department, Virginia  
441 Polytechnic Institute and State University, Blacksburg, VA, USA
- 442 **Julien Eck** Airbus Defence and Space, Toulouse, France
- 443 **Hans K. Engeldinger** Product Development HAF Tapes, tesa SE, Norderstedt,  
444 Germany
- 445 **Michael Frauenhofer** Audi AG, Ingolstadt, Germany
- 446 **Paul Ludwig Geiß** Faculty of Mechanical and Process Engineering, Workgroup  
447 Materials and Surface Technologies (AWOK), University of Kaiserslautern, Kai-  
448 serslautern, Germany
- 449 **Luca Goglio** Department of Mechanical and Aerospace Engineering, Politecnico di  
450 Torino, Torino, Italy
- 451 **Stanislav N. Gorb** Department of Functional Morphology and Biomechanics,  
452 Zoological Institute at the University of Kiel, Kiel, Germany

- 453 **Ingo Grunwald** Department of Adhesive Bonding Technology and Surfaces,  
454 Adhesives and Polymer Chemistry, Fraunhofer Institute for Manufacturing Technol-  
455 ogy and Advanced Materials (IFAM), Bremen, Germany
- 456 **Kosuke Haraga** Tapes and Adhesives Department, Electronic Materials Division,  
457 Electronic Materials Business Unit, Denki Kagaku Kogyo Kabushiki Kaisha, Chuo-  
458 ku, Tokyo, Japan
- 459 **L. John Hart-Smith** Boeing Company, Long Beach, CA, USA
- 460 **Ilko Hartung** Dr. Kornder Anlagen- und Messtechnik GmbH & Co. KG,  
461 Bergheim, Germany
- 462 **Lars Heepe** Department of Functional Morphology and Biomechanics, Zoological  
463 Institute at the University of Kiel, Kiel, Germany
- 464 **Hyeon-Deuk Hwang** Laboratory of Adhesion & Bio-Composites, Program in  
465 Environmental Materials Science, Seoul National University, Seoul, Republic of  
466 Korea
- 467 **Seung-Boo Jung** School of Advanced Materials Science & Engineering,  
468 Sungkyunkwan University, Suwon, Gyeonggi-do, Republic of Korea
- 469 **Martin Kahlmeyer** Department for Cutting and Joining Manufacturing Processes,  
470 University of Kassel, Institute for Production Technologies and Logistics, Kassel,  
471 Germany
- 472 **Ewen J. C. Kellar** TWI Ltd. (The Welding Institute), Cambridge, Cambridgeshire,  
473 UK
- 474 **Hyun-Joong Kim** Laboratory of Adhesion & Bio-Composites, Program in Envi-  
475 ronmental Materials Science, Seoul National University, Seoul, Republic of Korea
- 476 **Jong-Woong Kim** School of Advanced Materials Engineering, Chonbuk National  
477 University, Jeonju, Jeollabuk-do, Republic of Korea
- 478 **Kwang-Seok Kim** Carbon & Light Materials Application Group, Korea Institute of  
479 Industrial Technology, Jeonju, Jeollabuk-do, Republic of Korea
- 480 **Guy Larnac** ArianeGroup, Saint Médard en Jalles, France
- 481 **Denis Lavielle** Airbus Defence and Space, Toulouse, France
- 482 **Byoung-Ho Lee** Laboratory of Adhesion & Bio-Composites, Program in Environ-  
483 mental Materials Science, Seoul National University, Seoul, Republic of Korea
- 484 **Cai R. Lim** Research & Development, tesa SE Hamburg, Norderstedt, Germany
- 485 **Dong-Hyuk Lim** Laboratory of Adhesion & Bio-Composites, Program in Envi-  
486 ronmental Materials Science, Seoul National University, Seoul, Republic of Korea
- 487 **Quantian Luo** School of Aerospace, Mechanical and Mechatronic Engineering,  
488 The University of Sydney, Sydney, NSW, Australia

- 489 **Andreas Lutz** Automotive, Dow Europe GmbH, R&D Automotive Systems,  
490 Horgen, Switzerland
- 491 **E. A. S. Marques** Instituto de Ciência e Inovação em Engenharia Mecânica e  
492 Engenharia Industrial (INEGI), Porto, Portugal
- 493 **José Miguel Martín-Martínez** Adhesion and Adhesives Laboratory, University of  
494 Alicante, Alicante, Spain
- 495 **Luiz C. M. Meniconi** Research and Development Center, CENPES, Petróleo  
496 Brasileiro S.A. – PETROBRAS, Rio de Janeiro, RJ, Brazil
- 497 **Aamir Mubashar** Mechanical Engineering, Middle Eastern Technical University,  
498 Northern Cyprus Campus, Akara, Turkey
- 499 **John W. Nicholson** Bluefield Centre for Biomaterials, London, UK  
500 Dental Physical Sciences, Institute of Dentistry, Queen Mary University of London,  
501 London, UK
- 502 **Andreas Öchsner** Faculty of Mechanical Engineering, Esslingen University of  
503 Applied Sciences, Esslingen, Baden-Württemberg, Germany
- 504 **David E. Packham** Materials Research Centre, University of Bath, Bath, UK
- 505 **James D. Palmer** Staffordshire, UK
- 506 **Eric Papon** Laboratoire des Polymères Organiques – UMR CNRS 5629, Univer-  
507 sity of Bordeaux, Pessac, France
- 508 **Charles W. Paul** Henkel Adhesives, Bridgewater, NJ, USA
- 509 **Stuart Pearson** Department of Mechanical Engineering, University of Bristol,  
510 Bristol, UK
- 511 **Patrick Pérès** ArianeGroup, Saint Médard en Jalles, France
- 512 **Valber A. Perrut** Research and Development Center, CENPES, Petróleo Brasileiro  
513 S.A. – PETROBRAS, Rio de Janeiro, RJ, Brazil
- 514 Metallurgical and Materials Engineering Department, Federal University of Rio de  
515 Janeiro, Rio de Janeiro, Brazil
- 516 **Manfred Peschka** Fraunhofer Institute, Bremen, Germany
- 517 **Wulff Possart** Lehrstuhl Adhäsion und Interphasen in Polymeren, Universität des  
518 Saarlandes, Saarbrücken, Germany
- 519 **Günter Reiter** Physikalisches Institut, Fakultät für Mathematik und Physik,  
520 Albert-Ludwigs Universität Freiburg, Freiburg, Germany
- 521 **Katharina Richter** Department of Adhesive Bonding Technology and Surfaces,  
522 Adhesives and Polymer Chemistry, Fraunhofer Institute for Manufacturing Technol-  
523 ogy and Advanced Materials (IFAM), Bremen, Germany

- 524 **Erol Sancaktar** Department of Polymer Engineering, University of Akron, Akron,  
525 OH, USA
- 526 **Chiaki Sato** Precision and Intelligence Laboratory, Tokyo Institute of Technology,  
527 Midori-ku, Yokohama, Japan
- 528 **Melanie Schumann** Faculty of Mechanical and Process Engineering, Workgroup  
529 Materials and Surface Technologies (AWOK), University of Kaiserslautern, Kai-  
530 serslautern, Germany
- 531 **Martin E. R. Shanahan** Institut de Mécanique et d'Ingénierie-Bordeaux (I2M),  
532 CNRS UMR 5295, Université de Bordeaux, Talence, France
- 533 **Eric Silverberg** Henkel Adhesives, Bridgewater, NJ, USA
- 534 **Yasuaki Suzuki** Suzuki Adhesion Institute of Technology, Ichinomiya, Aichi,  
535 Japan
- 536 **Ambrose C. Taylor** Department of Mechanical Engineering, Imperial College  
537 London, London, UK
- 538 **Liyong Tong** School of Aerospace, Mechanical and Mechatronic Engineering, The  
539 University of Sydney, Sydney, NSW, Australia
- 540 **Claire Tonon** Airbus Defence and Space, Toulouse, France
- 541 **Ansgar van Halteren** Industrieverband Klebstoffe e.V. RWI-Haus, Düsseldorf,  
542 Germany
- 543 **Janek von Byern** Austrian Cluster for Tissue Regeneration, Ludwig Boltzmann  
544 Institute for Experimental and Clinical Traumatology, Vienna, Austria
- 545 Faculty of Life Science, Core Facility Cell Imaging and Ultrastructure Research,  
546 University of Vienna, Vienna, Austria
- 547 **Kazutami Wakabayashi** APS Research Co Ltd, Osaka, Japan
- 548 **Feng-Chao Wang** State Key Laboratory of Nonlinear Mechanics (LNM), Institute  
549 of Mechanics, Chinese Academy of Sciences, Beijing, China
- 550 **John F. Watts** The Surface Analysis Laboratory, Faculty of Engineering and  
551 Physical Sciences, University of Surrey, Guildford, Surrey, UK
- 552 **Andreas Winkel** Department for Cutting and Joining Manufacturing Processes,  
553 University of Kassel, Institute for Production Technologies and Logistics, Kassel,  
554 Germany
- 555 **Tetsuo Yamaguchi** Machine Elements and Design Engineering Laboratory,  
556 Department of Mechanical Engineering, School of Engineering, Kyushu University,  
557 Fukuoka, Japan
- 558 **Ya-Pu Zhao** State Key Laboratory of Nonlinear Mechanics (LNM), Institute of  
559 Mechanics, Chinese Academy of Sciences, Beijing, China

Uncorrected Proof

# Effect of Water and Mechanical Stress on Durability

# 31

Ian A. Ashcroft, John Comyn, and Aamir Mubashar

## Contents

31.1	Introduction .....	880
31.2	Behavior of Structural Joints to Metals in Wet Surroundings .....	881
31.2.1	Effect of Humidity .....	881
31.2.2	Surface Treatment .....	886
31.2.3	Natural and Accelerated Aging .....	887
31.2.4	Stress .....	888
31.3	Water and Adhesives .....	890
31.3.1	Water Diffusion into Adhesive Bondline .....	890
31.3.2	Water and Adhesive Interfaces .....	892
31.4	Modeling the Effects of Moisture and Stress on Bonded Joints .....	893
31.4.1	Introduction .....	893
31.4.2	Diffusion of Moisture in Bonded Joints .....	895
31.5	Summary and Conclusions .....	912
31.6	Further Information .....	913
	References .....	913

## Abstract

Adhesive joints with structural adhesives are weakened significantly in air at high humidity, and the rate of decline is controlled by water diffusion into the

I. A. Ashcroft (✉)

Faculty of Engineering, University of Nottingham, Nottingham, UK

e-mail: [ian.ashcroft@nottingham.ac.uk](mailto:ian.ashcroft@nottingham.ac.uk)

J. Comyn

Materials Department, Loughborough University, Leicestershire, UK

e-mail: [j.comyn@lboro.ac.uk](mailto:j.comyn@lboro.ac.uk)

A. Mubashar

Mechanical Engineering, Middle Eastern Technical University, Northern Cyprus Campus, Akara, Turkey

e-mail: [mubashar@metu.edu.tr](mailto:mubashar@metu.edu.tr)



adhesive. There appears, however, to be a critical relative humidity, and only if this is exceeded are joints significantly weakened; evidence is that this is about 65%. The most harmful effect of water is potentially at the interface between the adhesive and adherend; however, surface treatment of metallic adherends can much improve water durability. Accelerated aging using elevated temperatures and humidities can provide information on the environmental resistance of different systems but does not easily correlate to aging in natural conditions. The entry of water into the adhesive layer can conform to the simple Fickian model, which just depends on two parameters (diffusion coefficient and solubility coefficient), but in some cases it is non-Fickian. Current state-of-the-art environmental degradation modeling of bonded joints involves multi-physics finite element analysis combined with progressive damage modeling. Essentially, this involves three main steps. The first step is modeling moisture transport through the joint in order to determine the moisture concentration distribution in the joint as a function of time. The second step involves evaluation of the transient mechanical-hygrothermal stress-strain state resulting from the combined effects of hygrothermal effects and applied loads. The final step involves incorporation of damage processes in order to model the progressive failure of the joint and hence enable the residual strength or lifetime of a joint to be predicted.

---

### 31.1 Introduction

Water, either as liquid or vapor, attacks all adhesive joints, and this is a major problem which limits the use of adhesives. Water is a problem because of its ubiquity and its high polarity. Water enters adhesives and alters their properties, but a potentially greater problem is attack by water on the adhesive interface. There are two main challenges in addressing the problems caused by the interactions between water and adhesive joints. The first is to reduce the deleterious effects of moisture on the joints, and the second is to develop an accurate method of predicting the effects of environment on the long-term in-service performance of joints. Both of these challenges have been the subject of extensive research, resulting in major advances in recent years, although there is still scope for further improvements. With structural adhesive joints to metals, it is now well established that loss of joint strength can be minimized by selection of a suitable pretreatment. It has recently been demonstrated that multi-physics finite element modeling combined with a suitable progressive failure criterion is an effective and powerful method of predicting the effects of environmental aging on bonded joints.

This chapter first discusses the effect that absorbed water has on the strength of adhesively bonded joints. The influence of adherend surface treatment, applied stress, and adhesive type on the environmental degradation of bonded joints is demonstrated. Methods of modeling the environmental degradation of adhesively bonded joints using coupled hygro-mechanical finite element (FE) analysis are then described.

**31.2 Behavior of Structural Joints to Metals in Wet Surroundings**

**31.2.1 Effect of Humidity**

There are many cases in the literature of adhesive joints with metallic adherends and rigid adhesives being weakened by exposure to wet surroundings, and a common feature is the shape of the plot of joint strength against time. Joint strength falls most rapidly at the beginning and eventually slows down to a very low or zero rate. Although the shapes of curves are similar, there are variations in the initial rates of strength loss and in the fraction of strength which is lost.

Experiments by Brewis et al. (1980a, b, c, 1981, 1987) exposed joints with aluminum adherends and a range of structural adhesives at 50 °C and 100% relative humidity (r.h.), and control specimens were either stored in the laboratory or at 50 °C and 50% r.h. The patterns which emerged are fairly typical, and they are illustrated in Fig. 1. It can be seen that on exposure to air at 100% r.h. and 50 °C, joint strengths initially fall, typically by 40–60%, but then tend to level out. In contrast little or no weakening is seen when joints are aged at 50% r.h. and 50 °C.

When joints exposed at 100% r.h. for 5,000 h are then stored for a further 5,000 h at 50% r.h., a significant part of the strength is recovered. This is shown by the triangular point and dotted line in Fig. 1. This indicates that the mechanism responsible for the decrease in joint strength at high humidity is at least partly reversible, which is demonstrated even more clearly in Fig. 2a. This figure shows the results from testing single-lap joints made from 7,075 aluminum alloy which had been

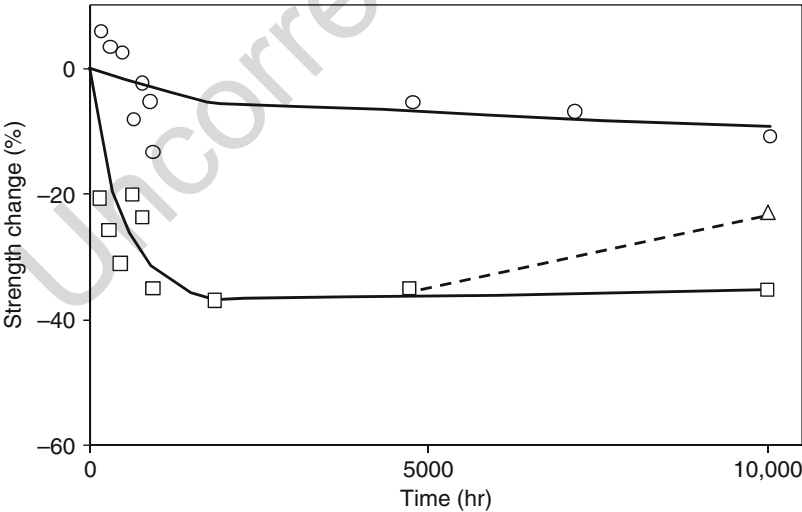
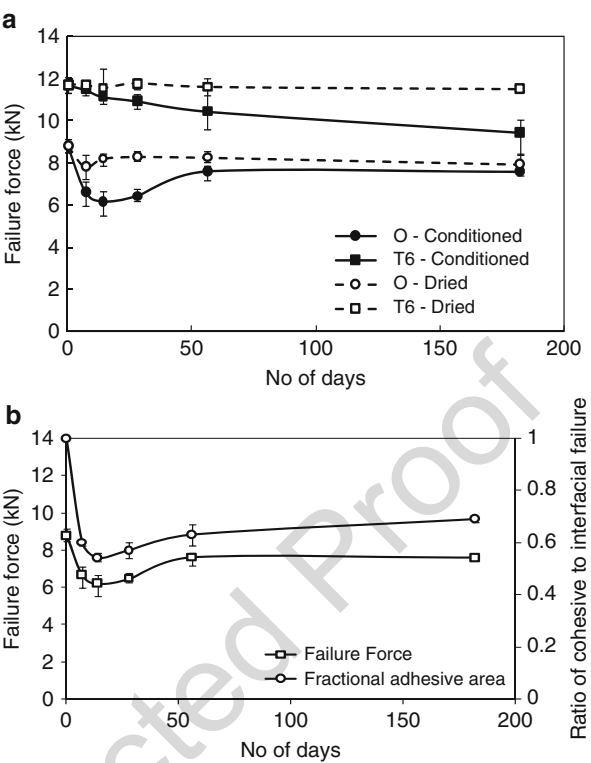


**Fig. 1** Strength of joints in aluminum alloy bonded with a nitrile-phenolic adhesive on exposure to wet air at 50 °C. ○ 50% r.h. □ 100%r.h. Δ Joints which have been exposed at 100%r.h. for 5000 h and then stored for a further 5000 h at 50% r.h (After Comyn et al. (1987). Crown copyright)

**Fig. 2** Effect of conditioning in deionized water at 50 °C on 7075 aluminum alloy/FM73 adhesive (Cytec Engineered Materials Ltd.) single lap joints. **(a)** Comparison of annealed (O) and heat treated (T3) adherends and recovery on drying. **(b)** Correlation between failure force and percentage of apparent interfacial failure (After Mubashar et al. (2009a))



anodized using the AC DC process described in Sect. 2.2 (Mubashar et al. 2009b). As well as demonstrating almost complete recovery of initial strength on drying, this figure also shows that adherend strength has a significant effect on joint behavior. The T6 heat-treated alloy exhibits a steady decline in strength with aging time, whereas the untreated alloy shows an initial steep decline in strength on aging, which then recovers. The main difference between the heat-treated and untreated alloys is that the yield strength is significantly lower in the latter, resulting in yielding of the adherend at the ends of the overlap when dry joints are tested. This results in greater rotation of the joint and higher peel stresses in the adhesive at the ends of the overlap. After short periods of exposure to moisture, the adhesive is significantly plasticized in the area of highest stress at the ends of the overlap, but most of the adhesive still has low moisture content, and hence overall joint behavior is little changed. On longer-term exposure, the adhesive becomes increasingly plasticized, reducing joint rotation and the magnitude of peel stresses.

It was also seen in the work of Comyn et al. (1987) that the use of a primer with a nitrile phenolic adhesive produced a marked improvement on dry and humid aged strengths and that the amount of failure at the adhesive-metal interface increased with time of exposure at 100% r.h. The latter observation is further illustrated in Fig. 2b, which shows a correlation between the joint strength and the proportion of apparent interfacial failure, as determined from digital image analysis of the fracture

surfaces. Surface analysis technique showed that what appeared to be interfacial failure from optical analysis of the fracture surfaces was actually failure in the primer close to the oxide layer. This explains why the loss in strength is largely reversible, as true interfacial failure involving thermodynamic displacement of the adhesive by water, as described in Sect. 4, would be irreversible.

Although joints are weakened by exposure to air of high humidity (e.g., 80–100% r.h.), it has been frequently observed that joints can withstand exposure at lower humidities (e.g., 50% r.h. or less) for long periods without weakening. In experiments on epoxide adhesives, Brewis et al. (1980a, c, 1981) found no significant weakening of joints after exposure for 10,000 h at about 45% r.h. and 20 °C. Figure 3 shows that joints with a range of adhesives (Ashcroft et al. 2001) are not significantly weakened on exposure to a natural hot/dry climate for up to 6 years. Here the average temperature was 25 °C and the average r.h. 55%. The adhesive symbols used in the legend of the figure are explained in Table 1.

Such information led to the proposal from Gledhill et al. (1980) that there must be a critical concentration of water in the adhesive, and corresponding relative humidity in the surroundings, which demarcates conditions under which weakening will occur, from those under which it will not. In a joint which is absorbing water, there may be an outer zone where the critical water concentration is exceeded, and this zone can be regarded as a crack in the bondline which can be dealt with by fracture mechanics. The hypothesis was tested by testing butt joints bonded with an

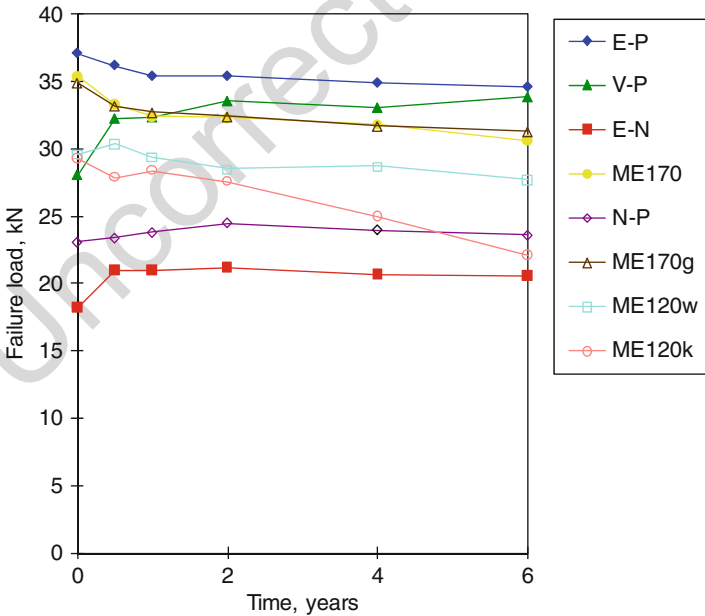
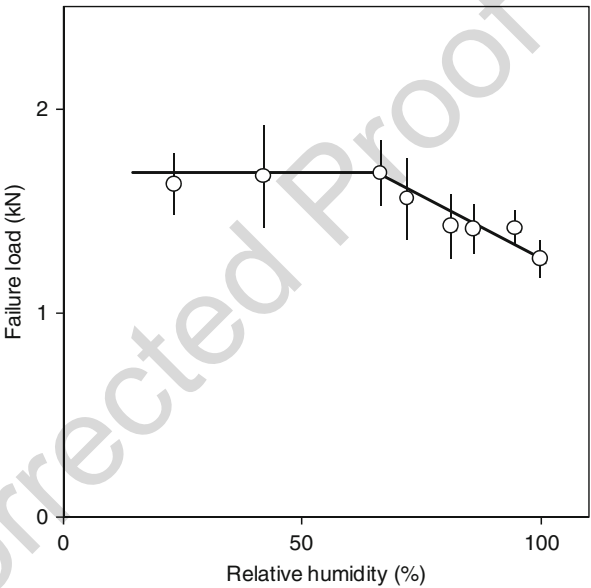


**Fig. 3** Strength of unstressed double lap joints on exposure to a hot/dry climate for up to 6 years (After Ashcroft et al. (2001). Crown copyright)

**Table 1** Description of symbols used in Figs. 3 and 9 (From Ashcroft et al. (2001))

Symbol	Adhesive type	Cure temp.	Description
E-P	Epoxy-polyamide	170 °C	Unsupported film, high temp.
V-P	Vinyl-phenolic	150 °C	Nylon supported film
E-N	Epoxy-novalac	170 °C	Supported film, high temp.
ME170	Modified epoxy	170 °C	Unsupported film, high temp.
ME170g	Modified-epoxy	170 °C	Glass beads, high temp.
N-P	Nitrile-phenolic	177 °C	Unsupported film, high peel
ME120w	Modified-epoxy	120 °C	Film, woven nylon carrier
ME120k	Modified epoxy	120 °C	Film, knitted nylon carrier

**Fig. 4** Dependence of joint strength upon relative humidity, after 10,080 h exposure (After Brewis et al. (1990))



epoxide immersed in water at 20, 40, 60, and 90 °C and also in air at 20 °C and 55% r.h. All the water-immersed joints became weaker, and it could be shown using the fracture mechanics approach that the strengths of the joints could be correlated if the critical concentration of water in the adhesive was 1.35%.

Brewis et al. (1990) attempted to locate the critical conditions for some aluminum joints bonded with an epoxide adhesive. Surface preparation of the aluminum alloy adherends was by sandblasting; this was chosen because of the poor durability of sandblasted joints, a factor which was thought would give rapid results, which would be particularly sensitive to changes in relative humidity. Joints stored for up to 1,008 h did not weaken with increasing r.h. A slight weakening was evident after 2,016 h, and this became greater after 5,040 and 10,080 h. After 10,080 h, the locus had a kink at 65% r.h. (Fig. 4). This corresponds to a critical water concentration of water in the adhesive of 1.45%, a value which is very similar to that of Gledhill et al. (1980).

Micro- and nanoparticles are commonly added to adhesives as reinforcements to improve the strength of the adhesive joint under mechanical and environmental loads. These particles may act as sites for water absorption in the adhesive layer. Barbosa et al. (2015) used natural cork microparticles to improve the toughness of a brittle epoxy adhesive. The adhesive was mixed with 1% cork, and moisture absorption and desorption were experimentally observed at room temperature and 50 °C in water. No appreciable difference between the moisture diffusion rates was observed for the adhesive samples with and without cork microparticles. However, less variation in mechanical properties of the adhesive with cork microparticles were observed when compared to the original adhesive sample. Most of the mechanical strength of both types of adhesive samples recovered after drying the moisture-conditioned specimens. Sadigh and Ali (2016) mixed reduced graphene oxide (RGO) particles in an epoxy-based adhesive, Araldite 2011, to improve the strength of unconditioned and moisture-affected adhesive butt joints. The addition of RGO nanoparticles improved the strength of unconditioned adhesive joints by 22% when 0.5 wt. % fraction particles were added. However, the addition of nanoparticles changed the failure mode of the adhesive butt joints to interfacial failure from a cohesive failure. The joints were then conditioned in distilled and seawater for 30 days, after which the adhesive layer was saturated. The strength of the adhesive butt joints with 0.5 wt. % RGO decreased by 10% and 40% from the exposure to distilled water and seawater, respectively. In comparison, the strength of the conditioned adhesive butt joints without RGO nanoparticles decreased by 16% and 36% after conditioning in distilled and seawater, respectively. Thus a major improvement in the joint strength in conditioned adhesive butt joints was not seen with the addition of RGO nanoparticles.

Under combined hygrothermal loading, adhesive joints with dissimilar adherends have shown large decreases in strength. Korta et al. (2015) experimentally and numerically investigated adhesive joints between dissimilar material adherends, including carbon fiber composite, aluminum, and steel. The adhesive joints were subjected to hygrothermal cycling testing according to automotive industry standards. It was found that the joints debonded under the applied hygrothermal cyclic loads without the application of mechanical loads. The major reason for debonding was found to be the difference in the coefficient of thermal expansion of the dissimilar adherends. It has been observed that the moisture uptake of some composites may be decreased by increasing the amount of reinforcing fibers. This was observed during the durability study of FRP/steel adhesive joints (Heshmati et al. 2016). Moisture conditioning of the adhesive, CFRP, and GFRP specimens was performed for up to a year at 20 °C and 45 °C in water and at 45 °C, 95% r.h. It was reported that the maximum moisture uptake of GFRP composite material decreased by 40% by increasing the fiber volume from 46% to 62%. The change in the overall stiffness of the adhesive joint was found to be negligible owing to the insignificant effect of moisture on longitudinal properties of unidirectional composites. Low permeability adherends were also considered a reason for an insignificant loss of stiffness of the adhesive joints.

### 31.2.2 Surface Treatment

Surface treatment of metals is the most effective way of optimizing the resistance of joints to water. A graphic illustration of the effect of surface treatment on the wet durability of adhesive joints to aluminum was given by Butt and Cotter (1976), and their data are shown in Fig. 5. The surface treatments employed were etching in chromic-sulfuric acid, alkaline etching, solvent degreasing, and phosphoric acid anodizing. Before exposure the different treatments gave identical joint strengths, but exposure at 43 °C and 97% r.h. produced differences. Here the degreased adherends performed worst, and those etched in chromic-sulfuric acid did best. In this case phosphoric acid anodization gave a poor performance, but this is unusual.

The surface pretreatment of aluminum alloys for adhesive bonding has been reviewed by Critchlow and Brewis (1996). The literature in the period 1976–1991 on the wet durability of aluminum joints bonded with epoxide adhesives has been reviewed by Armstrong (1997). Critchlow and Brewis (1995) have also reviewed surface treatments for the titanium alloy Ti-6Al-4V.

One of the most effective pretreatments for bonding aluminum is chromic acid anodizing (CAA); however, there are health and safety concerns and environmental issues with the use of hexavalent chromium in this process, which is also highly complex and time-consuming. This has led to extensive research into alternative procedures. One of the most promising alternatives is the “AC DC” method proposed by Critchlow et al. (2006) (see ► Chap. 7, “General Introduction to Surface Treatments”). This is a mixed sulfuric-phosphoric acid anodization in which there is an initial AC anodizing stage which cleans the surface and produces an open porous oxide structure, suitable for bonding, as shown in Fig. 6a. This is followed by a DC

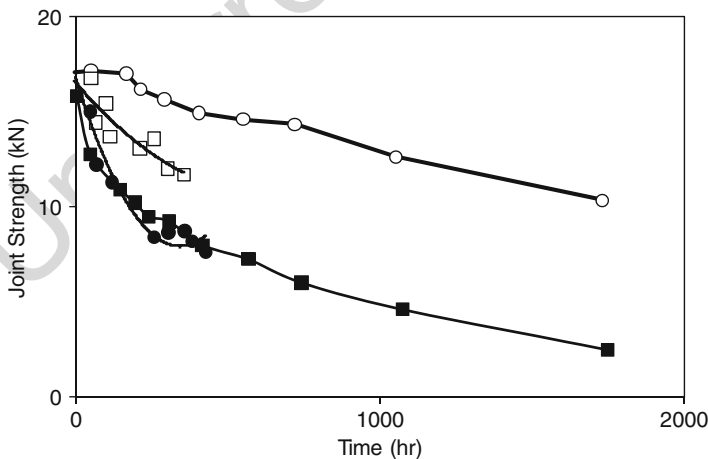


**Fig. 5** Effect of high humidity (97% r.h. at 43 °C) on the strength of aluminum joints bonded with an epoxide polyamide adhesive (After Butt and Cotter (1976)). Surface treatments are ○ chromic-sulfuric acid etch, □ alkaline etch (commercial formulation), ■ solvent degrease, and ● phosphoric acid anodize

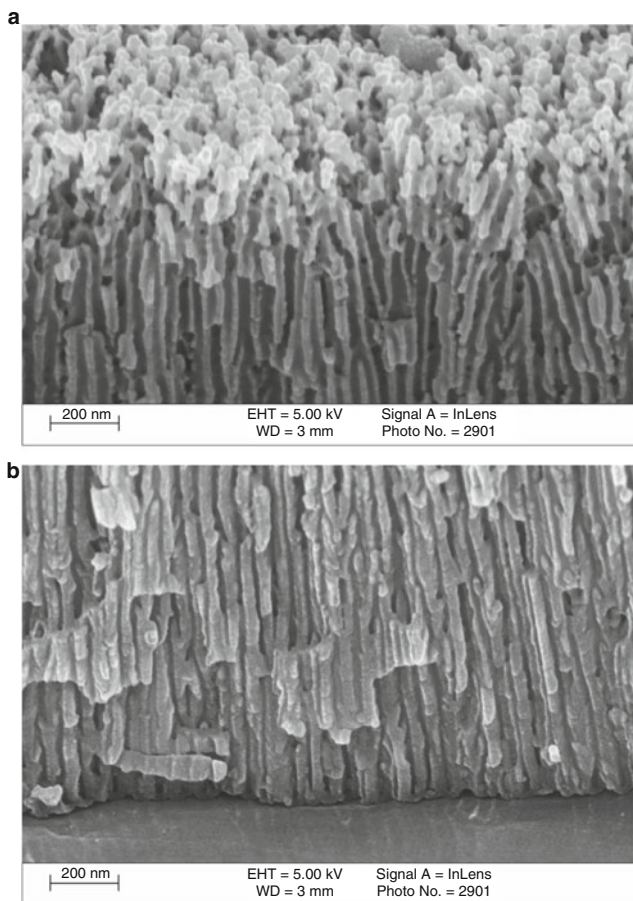


**Fig. 6** Cross section through “AC DC” engineered oxide layer showing “crumpet” structure with (a) open structure at the surface for wetting and bonding and (b) dense structure at metal interface for corrosion protection (After Mubashar et al. (2009a))

anodizing stage which produces a thick compact film for corrosion protection, as shown in Fig. 6b. The complete cross section of the oxide layer somewhat resembles that of a crumpet. The complete process takes approximately 15 min, compared with approximately 95 min for the commercial CAA process and has been shown to result in comparable performance under a range of conditions, as illustrated by Fig. 7.

### 31.2.3 Natural and Accelerated Aging

A comparison of aging joints in natural and laboratory conditions has been undertaken by Ashcroft et al. (2001); they commented that their data are probably unique. The aluminum adherends were etched in chromic acid and bonded with a total of eight



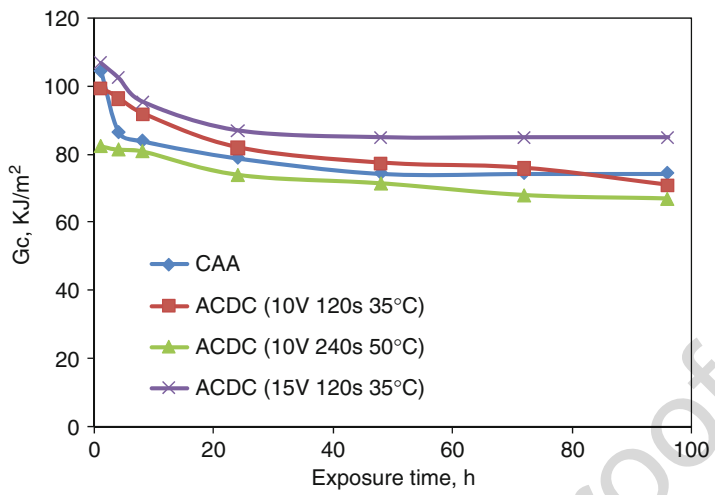


**Fig. 7** Comparison of wedge test results for CAA and AC DC pretreated aluminum/epoxy joints conditioned at 50 °C in deionized water. Legend refers to different parameters used in the AC DC process

**Table 2** Natural weathers used by Ashcroft et al. (2001)

	Climate	Location	Average conditions		
			Temperature	r.h.	Monthly rainfall
	Hot/wet	Australia	23 °C	85%	297 mm
	Hot/dry	Australia	25 °C	55%	39 mm
	Temperate	UK	10 °C	78%	49 mm

epoxide or phenolic adhesives, which were exposed to the natural weathers shown in Table 2. Laboratory aging was at 20 °C and 60% r.h. or at 35 °C and 85% r.h.

The mode of failure was predominantly cohesive, but the amount of interfacial failure increased with both natural and laboratory aging. This was often accompanied by metallic corrosion, particularly in hot/wet conditions.

A conclusion was that there is no simple method of determining the long-term durability from accelerated tests and that excessive temperatures and humidities will trigger degradation mechanisms which are not representative. In general, accelerated tests tend to overestimate the reduction of joint strength.

### 31.2.4 Stress

Joints tend to weaken more rapidly if they are stressed during exposure. Davis and Fay (1993) reported the time to failure for joints, both stressed and unstressed, with mild steel and zinc-coated steel adherends. Results for zinc-nickel-coated steels are

shown in Fig. 8 showing that all unstressed joints survived for 2.5 years and that survival of the others decreases with increasing stress.

Fay and Maddison (1990) measured times to failure at 100% r.h. and 42–48 °C for joints in steel with a number of surface treatments and bonded with a toughened epoxide adhesive. Their results showed that failure was hastened by increasing stress and that time to failure can be much increased by selection of an appropriate surface treatment.

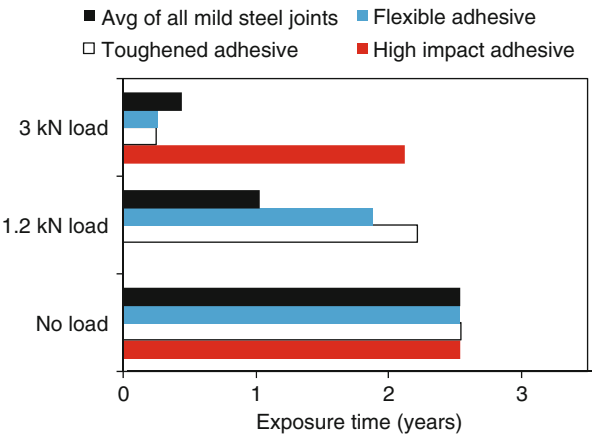
Parker (1988) described durability of stressed and unstressed joints in clad aluminum alloy BS 2L73 exposed to hot/wet, hot/dry, and temperate climates for up to 8 years. A variety of surface treatments were used. Joints were stressed to either 10% or 20% of their dry strength. Failure was hastened by increasing stress. At 20% stress the order of effectiveness of surface treatments was phosphoric acid anodize > chromic acid anodize > chromic acid etch.

The effect of cyclic stresses on the durability of aluminum-epoxide joints has been observed by Briskham and Smith (2000), using a range of surface treatments. Joints were immersed in water at 55 °C with average stress levels of approximately 0.15 or 1.2 MPa and a frequency of 2 Hz. The best-performing treatment was phosphoric acid anodization and treatment with an aminosilane coupling agent was the poorest, which perhaps was not expected as this performed better than all the other methods with unstressed joints. Joints with phosphoric acid anodization consistently failed in a cohesive manner, while all the other methods showed some interfacial failure.

Reference has been made above to work by Ashcroft et al. (2001) on aging joints in natural and laboratory conditions. Their program included exposing stressed joints, and their results for joints in a natural hot/wet climate after 6 years are shown in Fig. 9 (see Table 1 for further description of the adhesives used in this study). It can be seen that all stressed joints with the epoxy polyamide (E-P) and one of the modified epoxy (ME120k) adhesives are reduced to zero strength, while most of the others maintain a significant fraction of their strength.

The effect of moisture under various types of loading is another area that has been explored. Fernandes et al. (2016) experimentally observed the effect of moisture under mode I and mode II loading of composite-bonded double cantilever and

**Fig. 8** Average failure times of the zinc-nickel coated steel joints



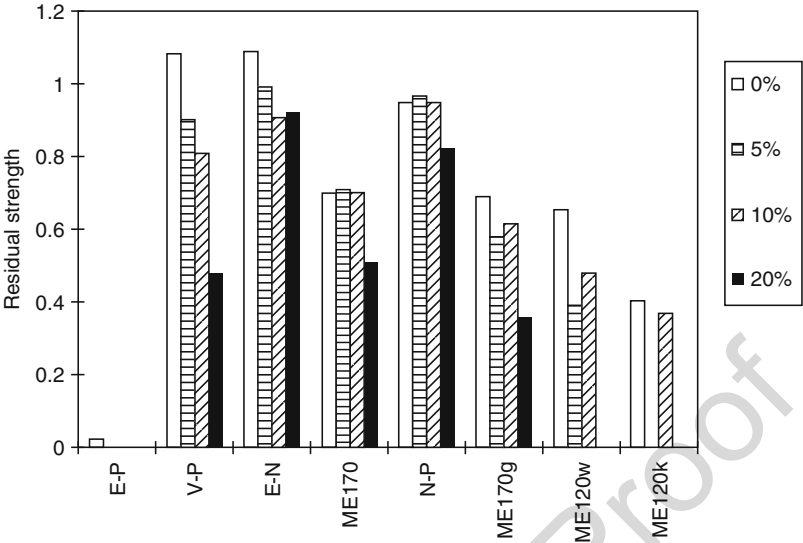


**Fig. 9** Effect of stress on double lap joints exposed to hot/wet climate for 6 years (After Ashcroft et al. (2001). Crown copyright)

end-notched flexure adhesive joints. The joints were conditioned at 55%, 75% r.h., and in water, and fracture energies for the two modes, i.e., mode I and II, were determined. A reduction in fracture energy under both modes of fracture was observed. However, a sharp decrease in fracture energy was observed between 75% r.h. and water than between 55% and 75% r.h. Krishnan et al. (2016) conditioned glass fiber composite pipes by placing them in water at 80 °C for 1,500 h. The pipes were then tested by applying cyclic loads. Five stress conditions were applied ranging from completely axial stress to fully hoop stress. By using the first ply failure as the failure criterion of the pipes, failure envelopes were developed under the selected loading conditions. It was observed that the failure mode of the composite pipes changed as the stress loading conditions were changed. The three types of failure observed included matrix cracking, local leakage failure, and weepage failure.

### 31.3 Water and Adhesives

#### 31.3.1 Water Diffusion into Adhesive Bondline

All adhesives absorb water, and water uptake data for a number of structural adhesives are collected in Table 3. Such data are obtained by measuring the weight of water absorbed by an immersed film and include the diffusion coefficient  $D$  and the weight absorbed at equilibrium  $M_E$ . This means that adhesive layers in joints will absorb water and its vapor and transmit it to the interface. This cannot be prevented by sealing the edges with a paint or lacquer, as these also absorb water. The data can

t.1 **Table 3** Water uptake properties of structural adhesives

t.2	Adhesive	Temperature (°C)	D (10 <sup>-12</sup> m <sup>2</sup> s <sup>-1</sup> )	M <sub>E</sub> (%)
t.3	Nitrile-phenolic <sup>a</sup>	25	3.3	1.5
t.4		50	4.7	4.5
t.5	Vinyl-phenolic <sup>a</sup>	25	1.8	3.5
t.6		50	2.3	8.6
t.7	FM1000 epoxide-polamide <sup>b</sup>	1	0.075	(20.4)
t.8		25	1.1	(15.8)
t.9		50	3.2	(15.5)
t.10	Acrylic adhesives toughened with <sup>c</sup>			
t.11	Chlorosulfonated polyethylene	23	0.64	0.73
t.12		37	1.2	0.82
t.13		47	0.94	3.27
t.14	Nitrile rubber	23	0.19	1.72
t.15		37	0.28	2.99
t.16		47	0.66	3.89
t.17	Epoxides, DGEBA with hardener <sup>d</sup>			
t.18	Di(1-aminopropylethoxyether)	25	0.13	5.0
t.19		45	0.46	4.7
t.20	Triethylene tetramine	25	0.16	3.8
t.21		45	0.32	3.4
t.22	1,3-Diaminobenzene	25	0.19	2.3
t.23		45	0.97	3.1
t.24	Diaminodiphenylmethane	25	0.0099	4.1
t.25		45	0.006	1.6

t.26 Bracketted values of M<sub>E</sub> are not true equilibrium values, but maximum uptake observed in systems that then lost weight

<sup>a</sup>Brewis et al. (1987)

<sup>b</sup>Brewis et al. (1980c)

<sup>c</sup>Bianchi et al. (1990)

<sup>d</sup>Brewis et al. (1980a)

283 be used to calculate the rate at which water will enter joints and water concentration  
284 profiles within them (Comyn 1983). This is discussed in more detail in Sect. 4.2.

285 The rate of the initial fall in strength of exposed joints is controlled by the rate of  
286 water diffusion in the bondline. This is demonstrated in Fig. 10 where joint strengths  
287 are compared with the amount of water to have entered a joint. Although the scales  
288 of the two ordinates have been adjusted to give a best fit, there is nevertheless an  
289 excellent comparison between the points, which are for measured joint strengths, and  
290 the line which is the calculated water level.

291 Parker (1988) has shown a linear relationship between joint strength and the  
292 square root of exposure time to humid conditions, for some titanium alloy joints  
293 bonded with a modified epoxide adhesive, demonstrating that the decline in strength  
294 is controlled by the diffusion of water. Some joints had been exposed for 11 years.

**Fig. 10** Comparison of joint strength (*experimental points*) with calculated water uptake (*line*) by joints bonded with DGEBA-DAPEE epoxide adhesive (After Brewis et al. (1980b))

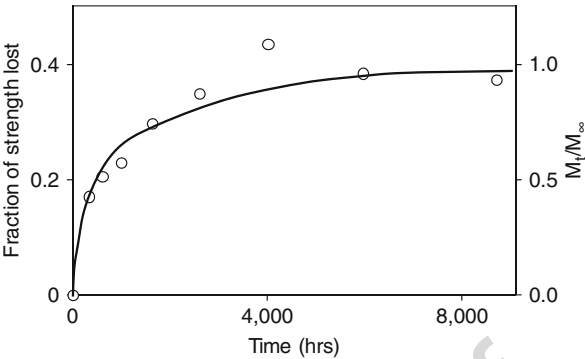


**Table 4** Values of work of adhesion for various interfaces in dry air and in water

Interface	Work of adhesion ( $\text{mJm}^{-2}$ )		Interfacial debonding in water
	Air	Water	
Epoxide/steel	291	−255	Yes
Epoxide/aluminum	232	−137	Yes
Epoxide/silica	178	−57	Yes
Epoxide/CFRP	88–90	22–44	No

The diffusion of water in structural adhesives obeys the Arrhenius equation, which means that the rate of diffusion increases strongly with temperature. The expected consequence of this is that joints will weaken more rapidly as the temperature rises. This was shown to be the case by Gledhill and Kinloch (1974) and Gledhill et al. (1980). Here butt joints in mild steel, prepared by degreasing and grit blasting, were bonded with an epoxide adhesive and immersed in water.

### 31.3.2 Water and Adhesive Interfaces

Water in a joint may attack the adhesive by causing it to swell, craze, crack, or hydrolyze, but it is its role in attacking the interface which is potentially the most important in bringing about weakening (Comyn 1983).

Thermodynamic work of adhesion is the minimum amount of work that must be done to separate an adhesive-substrate interface (see ► Chap. 6, “Thermodynamics of Adhesion”). If this has a positive value, the interface is stable. A negative value indicates an unstable bond, and this is the case for adhesive-metal interfaces in water. Some data are shown in Table 4. This is because metal oxides have very high surface free energies, water has extreme properties, and in particular is the high value of the polar component of surface free energy, which is approximately  $51 \text{ mJ m}^{-2}$ .

Kinloch (1983) has compared work of adhesion of adhesive interfaces in air and in water with their tendency to debond interfacially in an unstressed condition. Some data are shown in Table 4. The fact that interfacial debonding only occurs when the

thermodynamic work of adhesion is negative is evidence of the validity of thermodynamics in predicting the durability of adhesive bonds. Because metals have high-energy oxide surfaces, the work of adhesion in the presence of water will be negative, i.e., water may displace the adhesive from the substrate. However, it should be remembered that thermodynamic work of adhesion is only of relevance when the mechanism of bonding is entirely by physical adsorption. Further, work of adhesion can only be related to joint strengths when failure is at the interface and, as discussed in Sect. 2.1 in a joint with an effective surface pretreatment apparent interfacial on closer inspection which may in fact be in the adhesive or primer close to the interface. This is significant as the effect of water where this type of failure has been seen has been shown to be largely reversible, whereas thermodynamic displacement of the adhesive by water is irreversible.

Chemical bonds across the interface would confer strength and resist the thermodynamic displacement of the adhesive by water. These may be ionic attractions for adhesives on metals and covalent bonds with silane coupling agents. Mechanisms of adhesion have been reviewed by Comyn (2005).

---

## **31.4 Modeling the Effects of Moisture and Stress on Bonded Joints**

### **31.4.1 Introduction**

It is generally agreed that the most common cause of environmental degradation in bonded joints involves the absorption of moisture into the joint. This has a number of effects that must be incorporated into any mechanistically based mechanical model of the joint to be used for modeling the effects of environmental aging. The most important of these are:

- (i) Plasticization of the adhesive (and adherend in some cases), which will affect mechanical properties, the internal stress distribution, and potentially the failure criterion
- (ii) Hygroscopic expansion of the adhesive, which will affect residual stresses in the joint
- (iii) Weakening of the interface (or interphase) by various mechanisms, which will potentially affect the failure criterion

In order to be able to predict the effects cited above, it is first necessary to be able to quantify moisture transport through the joint. The absorbed moisture will cause swelling as well as degradation of the constituent parts and the interface region.

This will affect the stresses in the joint and the residual strength. Once both moisture transport and the subsequent degradation processes have been successfully modeled, there is still the critical issue of predicting the residual strength. Traditionally, strength of materials or fracture mechanics methods have been used to predict the failure of bonded joints. However, both of these approaches have limitations, and neither approach can model the evolving initiation and propagation of damage that is

a characteristic of failure in many environmentally degraded joints. Owing to these limitations, progressive damage models are being increasingly used to model the behavior of advanced materials such as structural adhesives.

This section discusses the steps involved in current state-of-the-art environmental degradation modeling of bonded joints. Essentially, this involves three main steps.

The first step is modeling moisture transport through the joint in order to determine the moisture concentration distribution through the joint as a function of time. The second step involves evaluation of the transient mechanical-hygrothermal stress-strain state resulting from the combined effects of hygrothermal effects and applied loads. The final step involves incorporation of damage processes in order to model the progressive failure of the joint and hence enable the residual strength or lifetime of a joint to be predicted. These steps are illustrated in Fig. 11 which shows a general framework for explicitly modeling the effects of environment on the mechanical performance of bonded joints.

There are two main challenges to developing an accurate predictive method along these lines: firstly, accurate modeling of the various effects of aging on the mechanical model, and secondly, incorporating a failure model that accurately represents not just the final failure load but the complete cycle of damage initiation and propagation leading to failure. These issues will be discussed in the following sections.

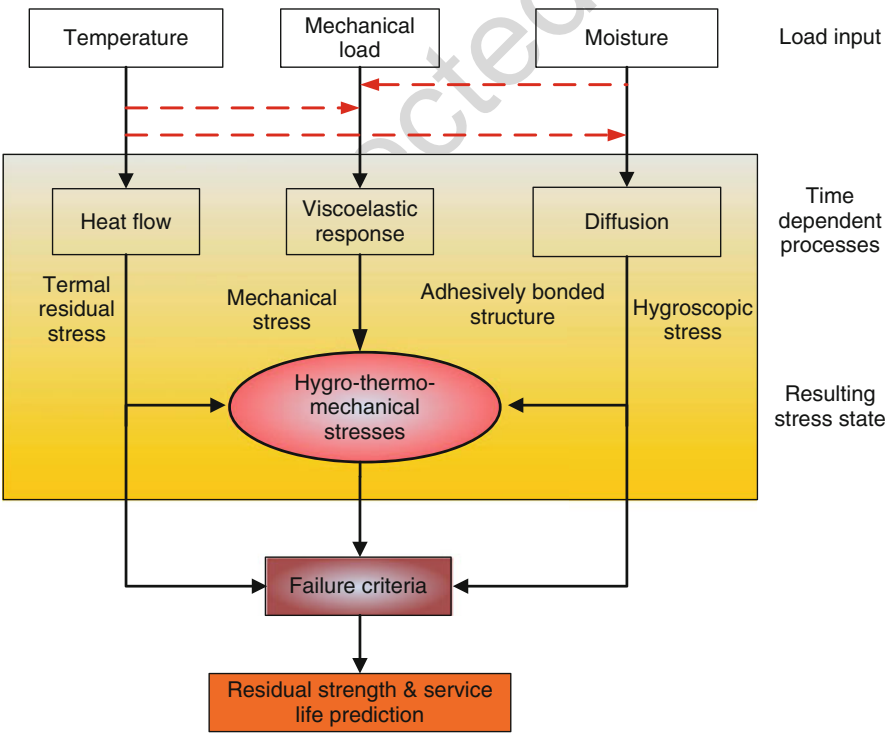


**Fig. 11** Framework for modeling the environmental aging of adhesively bonded joint

### 31.4.2 Diffusion of Moisture in Bonded Joints

In order to understand and model the effect of absorbed moisture on adhesives, we need to investigate moisture transport mechanisms and how they can be represented mathematically. Mass (or molecular) diffusion describes the transport of molecules from a region of higher concentration to one of lower concentration. This is a stochastic process, driven by the random motion of the molecules. This results in a time-dependent mixing of material, with eventual complete mixing as equilibrium is reached. Mass diffusion is analogous to other types of diffusion, such as heat diffusion, which describes conduction of heat in a solid material, and hence similar mathematical representations can be made.

#### Modeling Diffusion

It has been suggested by Crank (1975) that the kinetics of sorption of moisture in polymers is governed by two limiting cases. Case I (Fickian or diffusion controlled), in which moisture transport is a stochastic process driven by the presence of a concentration gradient, predominates in systems where the penetrant has little hygroelastic effect on the polymer or the rate of diffusion is much less than that of relaxation. In Case I diffusion, the weight uptake is initially linear with respect to the square root of time, i.e., if the amount sorbed at time  $t$  is  $Kt^n$ , then  $n$  is equal to 0.5.

In Case II (relaxation controlled) diffusion is more rapid than relaxation, consequently, there is a discontinuity in concentration between the swollen and unswollen polymer. Initially the discontinuity advances into the polymer with a constant velocity resulting in linear initial uptake of penetrant with respect to time, i.e., if the amount absorbed at time  $t$  is  $Kt^n$ , then  $n$  is equal to 1. In many cases, both the mechanisms described above are present to varying degrees, resulting in anomalous uptake, i.e.,  $n$  is between 0.5 and 1. Various different forms of anomalous uptake have been identified, as described by Crank (1975).

#### Fickian Diffusion

In this case diffusion can be presented in a quantitative manner by adapting the mathematical equations of heat conduction derived by Fourier in 1822, as shown by Fick in 1855. The mathematical theory of diffusion is based on the hypothesis that the rate of transfer of a diffusing substance through a unit area of a section is proportional to the concentration gradient measured normal to the section. This hypothesis is presented mathematically by Eq. 1, which is usually referred to as Fick's first law (Crank 1975):

$$F = -D \frac{\partial c}{\partial x} \quad (1)$$

where  $F$  is the flux or rate of transfer per unit area,  $c$  is the concentration of diffusing substance,  $x$  is the space coordinate measured normal to the section, and  $D$  is the diffusion coefficient. The negative sign in Eq. 1 is due to the fact that diffusion occurs in the direction opposite to that of increasing concentration.



411 Considering the transport of moisture through an element in which concentration  
 412 increases, there must be a proportional decrease in flux across the distance of  
 413 the element in order to conserve mass. This is expressed mathematically by  
 414 Fick's second law, which is shown in Eq. 2 for one-dimensional diffusion:

$$\frac{\partial c}{\partial t} = -\frac{\partial F}{\partial x} = \frac{\partial}{\partial x} \left( D \frac{\partial c}{\partial x} \right) = D \frac{\partial^2 c}{\partial x^2} \quad (2)$$

415 Equation 2 can easily be extended to two or three dimensions. Many classes of  
 416 problem are governed by an equation of a similar form to Fick's second law, e.g., the  
 417 governing equation for heat transfer is given by

$$\frac{\partial}{\partial x} \left( k_x \frac{\partial T}{\partial x} \right) + \frac{\partial}{\partial y} \left( k_y \frac{\partial T}{\partial y} \right) + \frac{\partial}{\partial z} \left( k_z \frac{\partial T}{\partial z} \right) + Q = \rho c \frac{\partial T}{\partial t} \quad (3)$$

418 where  $T$  is temperature,  $k_i$  is conductivity in the  $i$  direction,  $Q$  is rate of internal  
 419 heat generation,  $c$  is specific capacity, and  $\rho$  is density. This form of equation is  
 420 sometimes called the quasi-harmonic equation; other classes of problem  
 421 governed by this equation include electrical conduction and magnetostatics. All  
 422 problems governed by the quasi-harmonic equation can be solved by finite  
 423 element analysis programs with general field solvers. These solvers are often  
 424 presented in terms of thermal analysis in commercial finite element software;  
 425 however, they can also be used for other classes of problem by using the analogy  
 426 of the controlling equation.

427 Equation 2 can be solved using standard techniques for solving differential  
 428 equations for cases with simple boundary conditions, e.g., where  $D$  is assumed to  
 429 be constant or has a defined variation with concentration. For example, the solution  
 430 to Eq. 2, for the case of a plane, semi-infinite sheet (i.e., 1D diffusion) where the  
 431 region  $x$  ( $-l < x < l$ ) is initially at uniform concentration  $C_o$ , the surfaces are  
 432 maintained at a constant concentration  $C_1$  and temperature, and  $D$  is constant, is  
 433 given by Eq. 4:

$$\frac{C - C_o}{C_1 - C_o} = 1 - \frac{4}{\pi} \sum_{n=0}^{\infty} \frac{(-1)^n}{2n+1} e^{\left[ \frac{-D(2n+1)^2 \pi^2 t}{4l^2} \right]} \cos \frac{(2n+1)\pi x}{2l} \quad (4)$$

434 Similar solutions can be found for two- or three-dimensional diffusion; however,  
 435 these require the summation of the terms of multiple infinite series to obtain  
 436 convergence. A simpler method is to solve as the product of the 1D solutions. For  
 437 example, in two dimensions, the total concentration can be calculation from the  
 438 concentration in the  $x$  and  $y$  directions using Eq. 5:

$$1 - \frac{c}{c_0} = \left( 1 - \frac{c_x}{c_0} \right) \left( 1 - \frac{c_y}{c_0} \right) \quad (5)$$

Equation 4 can be integrated with respect to  $x$  to determine the total mass of water absorbed at time  $t$ . If  $M_t$  indicates the mass of the total amount of penetrant absorbed at time  $t$  and  $M_\infty$  is the mass at saturation, then

$$\frac{M_t}{M_\infty} = 1 - \sum_{n=0}^{\infty} \frac{8}{(2n+1)^2 \pi^2} e^{\left[ \frac{-D(2n+1)^2 \pi^2 t}{4l^2} \right]} \quad (6)$$

At low concentrations, Eq. 6 can be simplified to Eq. 7:

$$\frac{M_t}{M_\infty} = \frac{4}{l} \left[ \frac{Dt}{\pi} \right]^{1/2} \quad (7)$$

Equations 6 and 7 are used with experimental mass uptake data to determine  $D$ . This can then be used in Eq. 4 to predict concentration variation through a joint as a function of time.

### Non-Fickian Diffusion

In some cases, the Fickian model does not accurately represent moisture uptake in adhesives. This is illustrated in Fig. 12a which shows the uptake plot for an epoxide immersed in water at 50 °C. The experimental data appears to indicate Fickian diffusion; however, the best fit of the Fickian diffusion equation to the data indicates equilibrium is reached more slowly than predicted by Fickian diffusion. This type of behavior is sometimes termed pseudo-Fickian behavior. In general, anomalous behavior is seen at high temperatures and humidity.

Many models have been suggested to describe anomalous (non-Fickian) uptake, and a number of the more relevant to structural adhesives will be discussed. Diffusion-relaxation models are concerned with moisture transport when both Case I and Case II mechanisms are present. Berens and Hopfenberg (1978) assumed

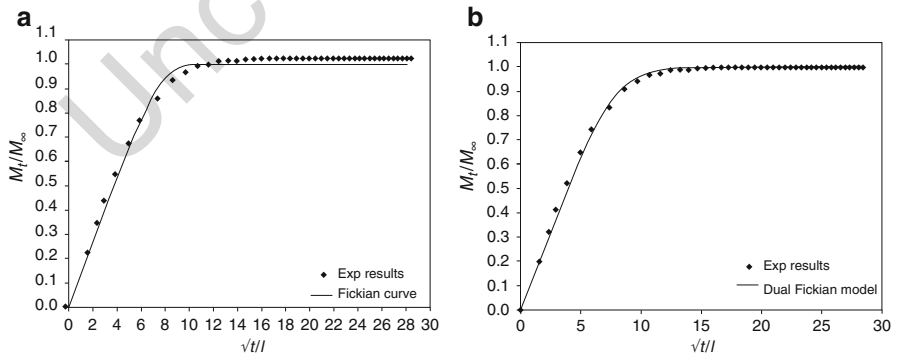


**Fig. 12** Moisture uptake in an epoxide demonstrating (a) non-Fickian uptake and (b) improved curve fitting with dual-Fickian model

that the net penetrant uptake could be empirically separated into two parts, a Fickian diffusion-controlled uptake and a polymer relaxation-controlled uptake. The equation for mass uptake using Berens and Hopfenberg's model is shown below:

$$M_t = M_{D\infty} \left[ 1 - \sum_{n=0}^{\infty} \frac{8}{(2n+1)^2 \pi^2} e^{\left[ \frac{-D(2n+1)^2 \pi^2 t}{4l^2} \right]} \right] + \sum_i M_{R\infty,i} [1 - e^{-\Omega_i t}] \quad (8)$$

where  $M_t$  is the total mass at time  $t$  and  $M_{D\infty}$  is the equilibrium amount of sorption in the unrelaxed polymer.  $M_{R\infty,i}$  and  $\Omega_i$  are the equilibrium sorption owing to the relaxation process and the relaxation rate constant, respectively, for the  $i$ th relaxation process. Berens and Hopfenberg (1978) showed that in general, only one or two relaxation terms are required to provide a good fit to the experimental data.

Dual-sorption models are based on the premise that while some penetrant molecules diffuse normally in the polymer matrix, others will be affected by polymer-penetrant interactions or micro-void filling. Carter and Kibler (1978) addressed this problem in terms of the probability that a water molecule may react with a polymer molecule. Their model is based on the theory that moisture in a polymer network can be either bound or free. The probability that a free water molecule becomes bound is  $\gamma$ , and the probability that a bound water molecule is emitted from the bound site and becomes mobile is  $\beta$ . When  $\gamma$  and  $\beta$  are small

$$\frac{M_t}{M_{\infty}} = 1 - \frac{\gamma}{\gamma + \beta} e^{-\beta t} - \frac{8\beta}{\pi^2(\gamma + \beta)} \sum_0^{\infty} \frac{1}{(2n+1)^2} e^{-K(2n+1)^2 t} \quad (9)$$

where  $K = \pi^2 D/l^2$ .

Loh et al. (2005) proposed a dual-uptake model based on the summation of two Fickian diffusion models. Physically this can be interpreted as two different uptake processes operating in parallel, both of which are adequately described by Fickian diffusion. This model was seen to accurately represent anomalous moisture transport in an epoxy-based material exposed to different levels of humidity. Both of the Fickian diffusion models are based on Eq. 4, with separate diffusion coefficients ( $D_1$  and  $D_2$ ) and saturation levels ( $M_{1\infty}$  and  $M_{2\infty}$ ), respectively. It can be seen in Fig. 12b that these models provide similar, good fits to the anomalous moisture uptake of the epoxy. It also has the advantage of the other anomalous models that it can be easily incorporated into a finite element analysis.

In some cases, a pseudo-equilibrium stage is reached in the moisture uptake, which is then followed by a secondary uptake process. This is illustrated in Fig. 13a. This type of behavior indicates that the absorbed moisture has triggered an additional moisture uptake mechanism. For example, differential hygroscopic expansion may lead to cracking and moisture uptake by capillary action. In order to model the moisture uptake shown in Fig. 13a, Mubashar et al. (2009a) proposed a dual Fickian model with a Heaviside step function. This model was termed the "delayed" dual Fickian model, where the secondary uptake is modeled by a power law. The mass uptake by a delayed dual Fickian model is, hence, given by

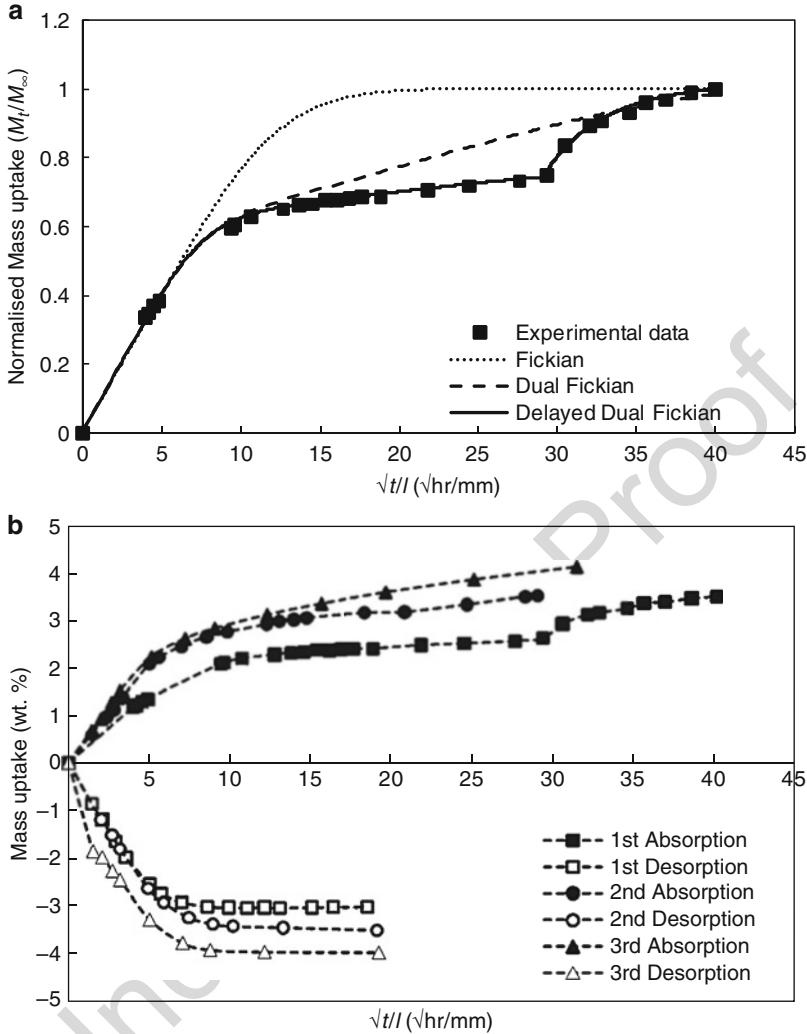


**Fig. 13** Moisture uptake in FM73 at 50 °C in deionized water showing (a) secondary uptake and (b) effects of cyclic uptake (After Mubashar et al. (2009b))

$$\begin{aligned}
 M_t = & \left( 1 - \frac{8}{\pi^2} \sum_{n=0}^{\infty} \frac{1}{(2n+1)^2} e^{\frac{-D_1(2n+1)^2 \pi^2 t}{4l^2}} \right) \times M_{1\infty} \\
 & + \left( 1 - \frac{8}{\pi^2} \sum_{n=0}^{\infty} \frac{1}{(2n+1)^2} e^{\frac{-D_2(2n+1)^2 \pi^2 t}{4l^2}} \right) \times M_{2\infty} + \Phi(t - t_1)(at^b + c)
 \end{aligned} \quad (10)$$

where  $\Phi$  is the Heaviside step function,  $t_1$  is the start time of secondary uptake as determined experimentally, and  $a$  and  $b$  are the power law constants determined by

curve fitting. It can be seen in Fig. 13a that this provides an excellent fit to data with a secondary uptake curve.

Another consideration in modeling the uptake of moisture by adhesives is that the uptake behavior can be different in absorption and desorption and can change with number of sorption cycles. This is illustrated in Fig. 13b. It can be seen that the rate of moisture absorption and the equilibrium moisture content increase from the first to second absorption cycle, although there is little difference between the second and third absorption cycles. Desorption is faster than absorption and more closely resembles Fickian diffusion. Mubashar et al. (2009a) proposed a method of incorporating the moisture history effects illustrated in Fig. 13b in a finite element-based predictive methodology.

The equilibrium moisture content in an adhesive is dependent on the relative humidity. Henry's law states that at constant temperature, the amount of a given gas dissolved in a given type and volume of liquid is directly proportional to the partial pressure of that gas in equilibrium with that liquid. This can be extended to molecular diffusion of a fluid in a polymer as the equilibrium quantity of a diluent within a polymer,  $c_d$ , is proportional to the environmental activity of the diluent,  $a_d$ :

$$c_d = ka_d \quad (11)$$

where  $k$  is Henry's law constant and, in the case of moisture absorption, the activity that relates to relative humidity as activity is  $p/p_0$  and relative humidity is  $(p/p_0) \times 100$ . The symbols  $p$  and  $p_0$  represent the vapor pressure and saturated vapor pressure of water, respectively. Henry's law does not allow for polymer-penetrant chemical interaction and is generally only applicable at low concentrations or in systems in which the penetrant and polymer have little affinity for each other.

An improvement on Henry's law is the Flory-Huggins model, which takes into account the large difference in size between the polymer and penetrant molecules and interactions between the two:

$$\ln a_d = \ln V_d + \left(1 - \frac{v_d}{v_p}\right)V_p + \chi_d V_p^2 \quad (12)$$

where the subscripts "d" and "p" refer to the diluent and polymer, respectively,  $V$  is volume fraction,  $v$  is molar volume, and  $\chi_d$  is a polymer-penetrant interaction term. As the molar volume of the polymer is generally much greater than that of the penetrant, Eq. 12 can be simplified to

$$\ln a_d = \ln V_d + V_p + \chi_d V_p^2 \quad (13)$$

Figure 14a shows the relationship between relative humidity and equilibrium moisture concentration for an epoxide. It can be seen for this material that the relationship between equilibrium moisture content and relative humidity is poorly described by Henry's law but is described satisfactorily by the Flory-Huggins equation.

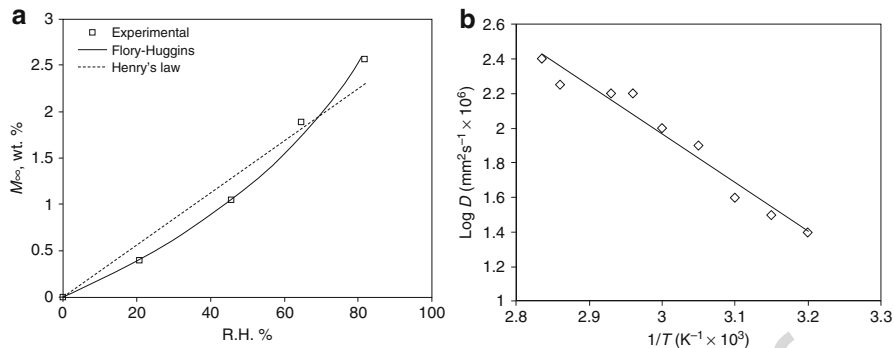


**Fig. 14** Moisture uptake in epoxide demonstrating (a) effect of relative humidity on equilibrium moisture content and (b) effect of temperature on diffusion coefficient

As noted in Sect. 3.1, the rate of diffusion increases with temperature, and it has been proposed that the diffusion coefficient of water in adhesives is related to temperature by the Arrhenius relationship in Eq. 14:

$$D = D_0 \exp\left(-\frac{E}{RT}\right) \quad (14)$$

where  $D$  is the diffusion constant at temperature,  $T$ ,  $D_0$  is a constant,  $E$  is the activation energy for diffusion, and  $R$  is the gas constant. Figure 14b shows that this relationship can be used to satisfactorily model the effect of temperature on the diffusion coefficient of an epoxy adhesive. It has also been seen experimentally that applied stress also increases the diffusion rate as the intermolecular distance increases; however, this is usually regarded as a secondary effect.

Once an appropriate diffusion model has been identified and the model parameters determined through experimentation, the moisture concentration within the adhesive on exposure to a particular environment can be predicted. For simple geometries and boundary conditions, analytical models can be used, whereas for more complex cases, the finite element method can be used. This is discussed in more detail by Abdel Wahab et al. (2001). An example of the predicted moisture concentration in an aluminum-epoxy single-lap joint conditioned at 50 °C/95% r.h. can be seen in Fig. 15. In this case, the moisture concentration was predicted using the finite element method and a dual Fickian model. The results from 2D plane strain and 3D finite element models were compared in order to evaluate the errors associated with a 2D simplification of the joint. In the 3D model, moisture can diffuse into the joint from the ends of the overlap and the sides of the joints, whereas in the 2D model, the latter diffusion path is not modeled and, hence, can be related to a joint with a very long diffusion path in the out-of-plane direction compared with the in-plane diffusion path. Figure 15a shows the variation in the moisture concentration across the width of the overlap and the center of the overlap. The 2D model underpredicts the moisture concentration at the edges; however, a reasonable

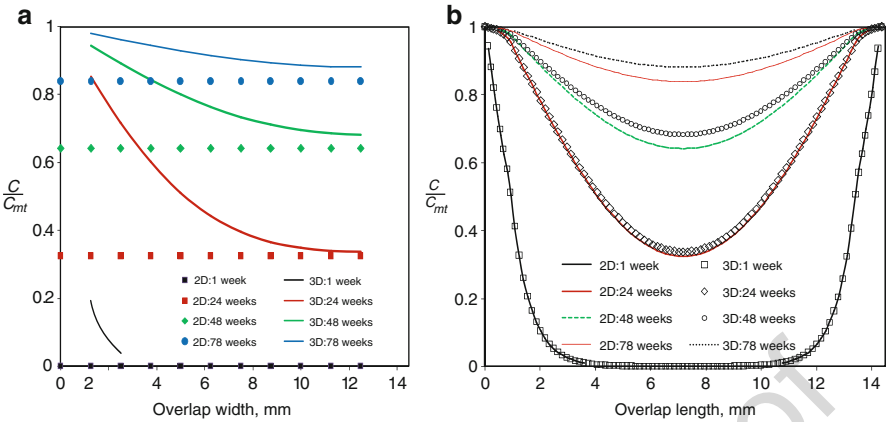


**Fig. 15** Predicted moisture concentration in an aluminum-epoxy single lap joint conditioned at 50 °C/95% r.h. Moisture distribution across (a) the joint width at the center of the overlap and (b) the overlap at the middle of the joint width (Jumbo 2007)

prediction of the moisture concentration at the center of the width is obtained. This is because the overlap length of the single-lap joint was 12.5 mm compared with a joint width 25 mm. The variation in concentration along the overlap in the middle of the joint width is shown in Fig. 15b. It can be seen that the difference between the 2D and 3D models increases at longer conditioning times as the moisture diffusing from the sides of the samples begins to make a more significant contribution to the total moisture concentration in the middle of the joint width. It can also be seen in this figure that even at 50 °C and a joint with a shortest diffusion distance of only 6.25 mm, the joint has still not reached saturation after 78 weeks of conditioning. This gives some indication of the time scales involved in reaching equilibrium in industrial joints under temperate service conditions.

### Modeling Stress and Strain

The first step in mechanical modeling is to determine the mechanical properties, which in a polymeric adhesive will be dependent on the temperature and the moisture concentration. Figure 16 shows the effect of absorbed moisture on stress-strain plots obtained from tensile testing bulk samples of a modified epoxy adhesive. It can be seen in Fig. 16a that at 22 °C, absorbed moisture has a relatively small effect on the modulus but a larger effect on the ultimate tensile strength (UTS) and failure strain. Comparing the dry plot with the plot with 1.8 weight % of absorbed moisture, it can be seen that the absorbed moisture has resulted in a slightly lower modulus, a reduction in UTS of approximately 20%, and an increase in strain to failure of over 100%. The plastic strain energy density at failure has also increased significantly. Whether the absorbed moisture is detrimental to performance will, hence, depend on the failure criterion used. Increasing the moisture to 2.3% sees a further extension of the trends seen with 1.8% absorbed moisture, whereas increasing the moisture to 4.1% results in a strain to failure of a similar value to the dry tested samples. Hence,

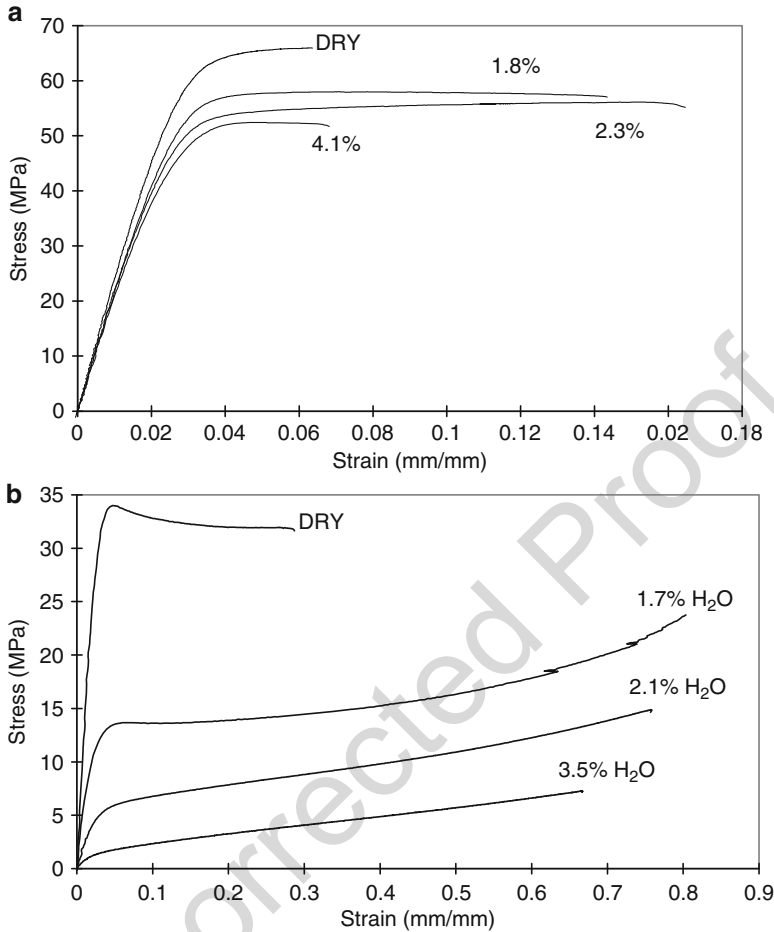


**Fig. 16** Effect of absorbed moisture on the bulk mechanical properties of a modified epoxy adhesive at (a) 22 °C (b) 90 °C

at high levels of moisture uptake, it can be seen that mechanical performance is reduced according to stress-, strain-, or energy-based failure criteria.

The effect of moisture on stress-strain plots for samples tested at 90 °C can be seen in Fig. 16b. Firstly, it is worth comparing the dry stress-strain plots at the two temperatures in Fig. 16a, b where it can be seen that increasing temperature has a similar effect to the absorbed moisture, i.e., reduction in modulus and UTS and an increase in strain to failure and plastic strain energy density at failure. However, comparing Fig. 16a, b for the samples with absorbed moisture shows that the effect of moisture is far more drastic. This can be explained by looking at the effect of moisture on the glass transition temperature ( $T_g$ ). Figure 17a shows the results from differential thermomechanical analysis (DTMA) of the modified epoxy adhesive used to generate the stress-strain plots shown in Fig. 16. It can be seen that as



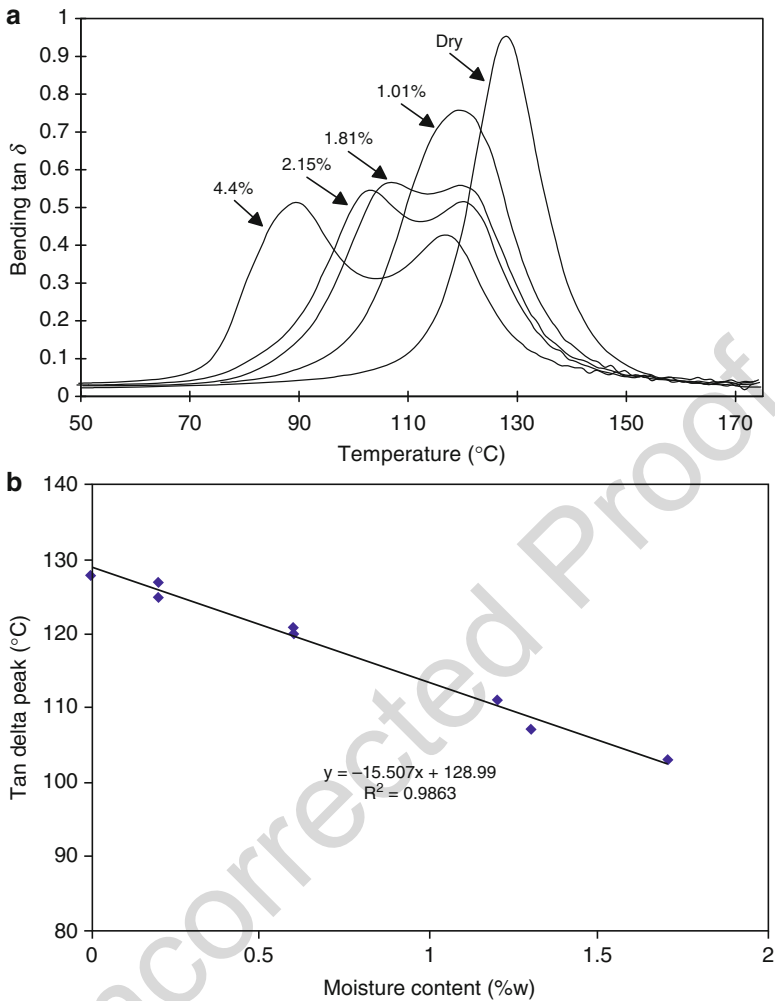


**Fig. 17** (a) Results from DTMA testing of a modified epoxy adhesive, (b) relationship between  $\tan \delta$  peak and moisture concentration

moisture is absorbed, the  $\tan \delta$  peak broadens, eventually resolving to two distinct peaks. This can be attributed to the fact that as temperature increases in the DTMA test, moisture desorbs from the sample, resulting in a variation in moisture concentration through the sample. The first peak therefore represents the saturated material and the higher temperature peaks the partially dried material. The temperature of the first  $\tan \delta$  peak is assumed to represent the  $T_g$  of the saturated material and is plotted against the saturated moisture concentration in Fig. 17b. This figure shows that there is an approximately linear relationship between the temperature of the first  $\tan \delta$  peak (and hence  $T_g$ ) and the moisture concentration, with the slope indicating a decrease

in  $T_g$  of approximately 15 °C with each weight % of moisture absorbed. It can be seen from the figure that the dry  $T_g$  of the adhesive is approximately 130 °C but that with 3% absorbed moisture, this will have reduced to approximately 85 °C. This explains the drastic effect of moisture on the mechanical properties of the adhesive at 90 °C shown in Fig. 16b.

The results discussed above illustrate that the mechanical properties of an adhesive are highly dependent on moisture concentration, and similar trends have been observed by others investigating different adhesive systems, e.g., Viana et al. (2016a). This relationship, together with an appropriate diffusion model, can be used to predict the distribution of mechanical properties within an adhesive layer as moisture is absorbed. The next step is to model the effect of the absorbed moisture on the mechanical performance of the joint, normally through an examination of the stress distribution in the adhesive layer. Stresses can be broadly categorized as either mechanical stresses or residual stresses.

In a bonded joint, three main sources of residual stresses can be identified. These are changes in temperature, leading to thermal stresses; changes in moisture content, leading to hygroscopic stresses; and changes due to chemical reactions, leading to curing stresses. The curing stresses in typical adhesively bonded joints are small compared with the thermal and hygroscopic stresses and in any case can be incorporated into analysis of the thermal stresses once the stress-free temperature has been determined. In bonded joints there may be significant residual thermal stresses from the curing operation followed by modification of these stresses as moisture is absorbed. The combined stresses are termed hygrothermal stresses. These residual stresses are generally modeled in a similar way. In fact, it is more accurate to refer to this effect as residual strains as this is what is induced by the temperature and the moisture. The stresses are only generated when these strains are not allowed to develop fully by applied constraints. Residual thermal,  $\varepsilon_{th}$ , and hygroscopic,  $\varepsilon_{hy}$ , strains are determined from

$$\varepsilon_{th} = \alpha_{th}(\Delta T) \quad (15)$$

and

$$\varepsilon_{hy} = \alpha_{hy}(\Delta c) \quad (16)$$

where  $\alpha_{th}$  and  $\alpha_{hy}$  are experimentally determined coefficients of linear expansion. If only one form of residual strain is being modeled, then it is possible to use the thermal strain capability that almost all FE codes have. If both forms are to be modeled, then some FE codes (such as Abaqus) have user routines where coefficients of expansion can be defined or strains from a previous analysis can be used as initial conditions for a subsequent analysis. In both cases it will be necessary to run coupled analyses, where the output from one analysis (thermal or moisture) forms the input to another (stress). In addition to these forms of residual stress, it will also be necessary to model the change in adhesive material response (plasticization) caused by the absorbed moisture and any changes in temperature, as discussed

above. This is most easily achieved by utilizing the field-dependent material property facility that many FE codes have. In these, adhesive material properties such as modulus and yield stress or the constants relating to a viscoelastic constitutive model can be defined as a function of a field variable, such as temperature or moisture.

The steps in modeling the combined effects of thermal residual stresses on cooling from the cure temperature, hygrothermal stresses from conditioning in a high-humidity environment, and hygro-thermo-mechanical stresses from mechanically loading the environmentally aged joint are shown in Fig. 18. The option of allowing for relaxation of stresses through creep of the adhesive is also indicated in the figure. Figure 19 illustrates the hygro-thermo-mechanical evolution of von Mises equivalent stress in an aluminum-epoxy single-lap joint conditioned at 50 °C/95% r.h. The line plots indicate the levels of stress at each stage after cure, as illustrated in the hygro-thermo-mechanical analysis framework (Fig. 18). At 20 °C (dry) a fairly uniform thermal stress of approximately 25 MPa is seen, which increases slightly at the edges of the overlap. An increase in temperature to 50 °C reduces the stress to approximately 13 MPa in most areas along the overlap length. The stresses are further reduced to about 7 MPa after saturation with moisture, with the distribution retaining a similar shape after saturation. On cooling down to 20 °C after saturation, the stress level increases to about 10 MPa. The application of a 5 kN tensile load on the joint increases the stress in every area along the profile and results in a more nonuniform distribution, owing to the differential straining of the adherends and rotation of the overlap area under the applied load. It should be noted that the failure load for this joint is approximately 20 kN, as will be discussed in the next section.

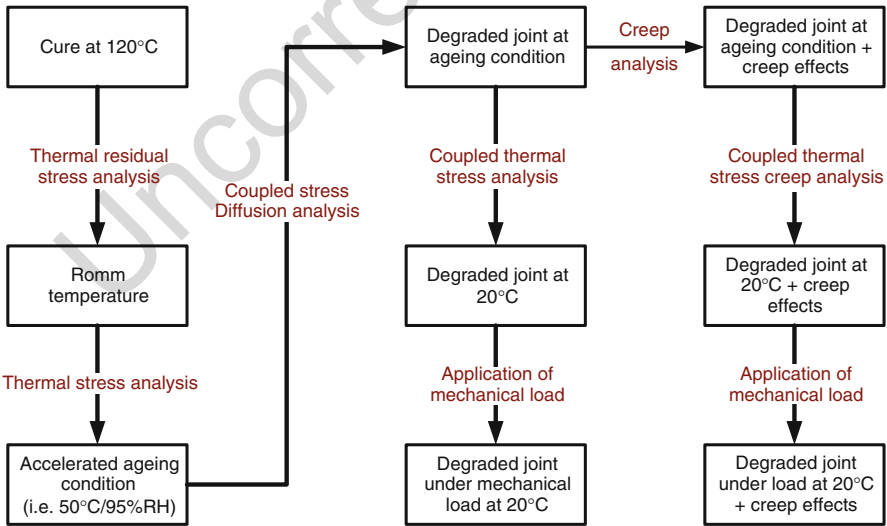


**Fig. 18** Overall methodology for predicting the effect of environment on bonded joints including residual stress effects (Jumbo 2007)

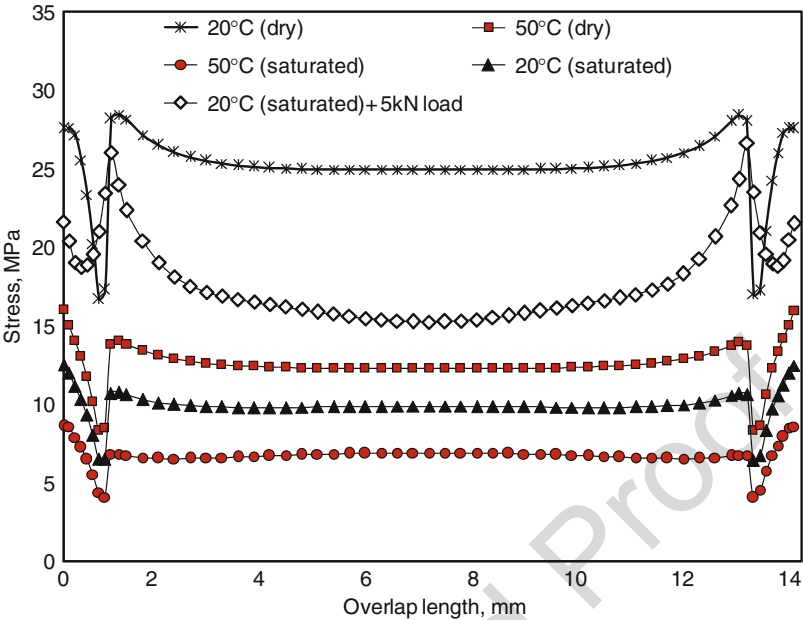


**Fig. 19** Equivalent von Mises stress along the middle of the joint overlap in an aluminum-epoxy single lap joint conditioned at 50 °C/95% r.h (Jumbo 2007)

Han et al. (2014) developed a finite element model with full-field coupling of moisture, temperature, and stress fields where a stress-dependent diffusion coefficient was used. The effects of creep were introduced into the model via a time-hardening power law creep model, and the effects of thermal and hygroscopic expansion were also incorporated. The moisture, temperature, and stress fields were related using field variables and providing experimental data in a tabular form. Results of the finite element model showed good correlation with the experimental results obtained for a single-lap joint. Such finite element models are an attempt to improve the fidelity of the adhesive joint modeling and incorporate the synergetic effects of various factors by using multi-physics-based finite element formulations.

**Modeling Damage and Failure**

In order to predict failure, a suitable failure criterion needs to be applied to the mechanical model of the joint. The simplest form of failure analysis is to define failure when a suitable failure criterion has exceeded a permissible limit, e.g., when the equivalent von Mises stress has exceeded the yield stress of the material. However, this type of analysis is problematic when one has theoretical stress singularities, such as in adhesive joints, as the definition of failure becomes mesh dependent. Also, there is no indication of how the part eventually fails or what is the maximum load sustained. In order to predict this, progressive damage modeling is

required. Two different forms of progressive damage modeling have generally been used with adhesive joints: cohesive zone modeling (CZM), where the failure is localized along a plane (Loh et al. 2003; Liljedahl et al. 2007; Mubashar et al. 2011), and continuum damage modeling (CDM), where the failure can occur throughout the material (Hua et al. 2007). Potential sites for damage modeling include the adhesive, the interface, and the adherend. The CZM approach is more directly applicable to interfacial failure and certain forms of adherend failure, while the CDM is more relevant to failure in the adhesive. This subject is discussed in detail in ► Chap. 25, “Numerical Approach: Finite Element Analysis.”

Jumbo (2007) used both CZM and CDM, together with the procedure illustrated by Fig. 18, to predict the effect of environmental aging on the mechanical performance of a number of different types of bonded joint including the double-lap joint (DLJ) shown in Fig. 20a. A typical finite element mesh used in his analysis is shown in Fig. 20b. In the cohesive zone modeling, a bilinear cohesive material model was used, as illustrated in Fig. 21. The bilinear traction-separation law is given by

$$t_e = \frac{2G_c v_e}{v_m v_c} \quad \text{if } 0 \leq v_e \leq v_c \quad (17)$$

$$t_e = \frac{2G_c}{v_m} \left( \frac{v_m - v_e}{v_m - v_c} \right) \quad \text{if } v_c \leq v_e \leq v_m; \quad (18)$$

$$t_e = 0 \quad \text{if } v_e > v_m \quad (19)$$

It can be seen that the effective traction ( $t_e$ ) is a function of the effective opening displacement ( $v_e$ ) and is reversible until the critical effective opening displacement ( $v_c$ ) has been reached. The other parameters that define the failure behavior are the area under the traction-separation curve, which corresponds to the strain energy release rate ( $G_c$ ) and the maximum effective opening displacement ( $v_m$ ). The values for the moisture-dependent cohesive zone law parameters were derived from experimental work done by Liljedahl et al. (2005, 2007) using mixed mode flexure (MMF) tests, the moisture-dependent mechanical properties of the adhesive, and calibrated values using the load displacement plots from aluminum/adhesive FM73 (Cytac Engineered Materials Ltd.) single-lap joints. Moisture-dependent mechanical properties were also used for the carbon fiber-reinforced polymer (CFRP) adherend, together with a moisture-dependent Tsai-Wu failure criterion, although failure in the CFRP did not occur in the models, in agreement with the experiments.

The predicted effect of 50 °C, 95% r.h. conditioning of the joint shown in Fig. 20 using the CZM discussed above is illustrated in Fig. 22. In Fig. 22a it can be seen that the failure load is predicted to decrease with conditioning time. A comparison of the predicted failure load with that measured experimentally can be seen in Fig. 22b. For exposure times up to 12 weeks, the CZM predictions show good agreement with the experimental failure loads. At 26 weeks, the failure load is underestimated and is within the large experimental error at 52 weeks. It is unknown whether the

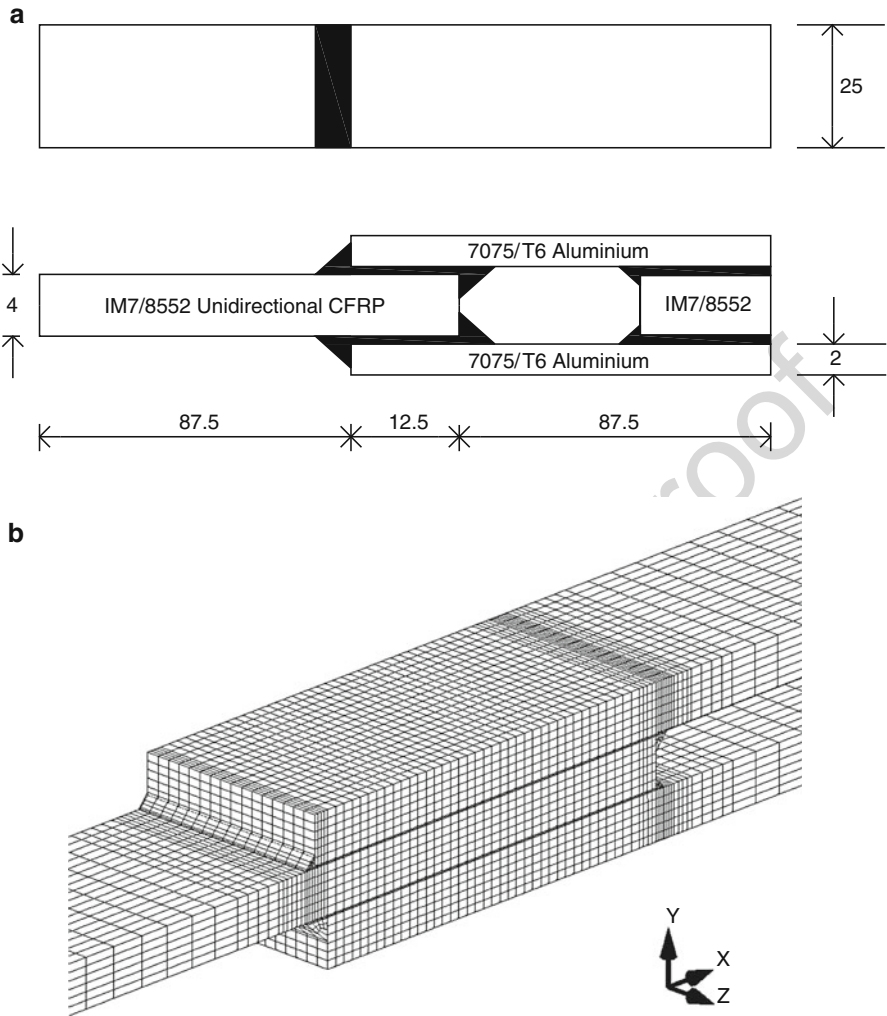


**Fig. 20** (a) Dimensions of CFRP/Al double lap joint (b) typical FE mesh (Jumbo 2007)

experimental increase in strength at 26 weeks and subsequent decrease at 52 weeks are “real” effects or experimental scatter. The latter is more likely; in which case the predictions are probably as good as can be expected. Liu et al. (2016) used a similar approach for modeling the adhesive joint strength degradation in double-lap shear joints with carbon/epoxy composite adherends. The bilinear traction-separation law was degraded for the moisture-conditioned adhesive joints. Different degradation factors were used for the adhesive layer and the adhesive-adherend interface, where the interfacial layer was degraded using an extra factor. The degradation factors were determined using Eq. 20.:

**Fig. 21** Bilinear cohesive zone model

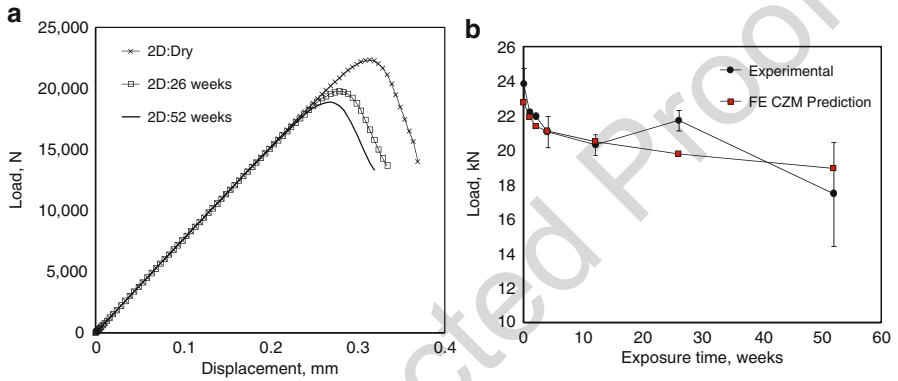
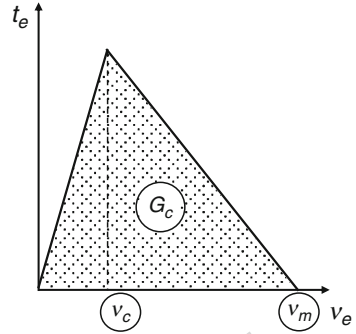


**Fig. 22** Effect of aging at 50 °C, 95% r.h. on (a) the load-displacement and (b) the failure load of a CFRP/Al/epoxy DLJ using CZM (Jumbo 2007)

$$T_H = T_0 \sqrt{\frac{\sigma_H}{\sigma}} f \quad (20)$$

where  $T_H$  and  $T_0$  are critical tractions with and without moisture absorption and  $\sigma_H$  and  $\sigma$  are ultimate tensile strengths of the adhesive with and without moisture absorption.  $f$  is the degrading factor used for the interface.

Jumbo (2007) also used the Gurson-Tvergaard-Needleman (GTN) CDM to predict failure in the same joints (see ► Chap. 23, “Constitutive Adhesive and Sealant Models”). This model was proposed by Gurson (1977) to model damage in elastic-plastic materials incorporating void formation, growth, and coalescence, leading to crack formation and failure, and was later extended by Needleman and Tvergaard (1984). This model is potentially applicable to damage prediction in rubber-toughened polymers, as the rubber particles are sites for cavity nucleation. The yield condition is defined as

$$F = \left( \frac{\bar{\sigma}}{\sigma_y} \right)^2 + 2q_1 f^* \cosh \left( \frac{q_2 \sigma_{kk}}{2\sigma_y} \right) - \left[ 1 + (q_1 f^*)^2 \right] = 0 \quad (21)$$

where  $\bar{\sigma}$  is the equivalent stress,  $\sigma_y$  is the yield stress of the matrix material, and  $\sigma_{kk}$  is the hydrostatic stress. The parameters  $q_1$  and  $q_2$  were introduced by Tvergaard to account for the effect of void interactions on the stress distribution between cavities but are usually derived from finite element calibration of experimental curves. Damage evolution is measured by the void volume fraction  $f$  which increases due to void nucleation and growth. Void nucleation is controlled by a normal distribution of stress or plastic strain, and the modified model replaces the void volume fraction  $f$  with the modified void volume fraction  $f^*$ . A rapid decrease in the load-carrying capacity of the material if void coalescence occurs is linked to  $f^*$ , such that

$$f^* = f \quad \text{if } f \leq f_c \quad (22)$$

where

$$f^* = f_c + \left( \frac{f_u^* - f_c}{f_F - f_c} \right) (f - f_c) \quad (23)$$

where  $f_c$  is the critical void volume fraction and  $f_F$  is the void volume at failure, and for most metals,  $f_u^* = 1/q_1$ . The existing value of the void volume fraction changes due to the growth of existing voids and the nucleation of new voids and is characterized by

$$\dot{f} = \dot{f}_{\text{growth}} + \dot{f}_{\text{nucleation}} \quad (24)$$

The growth of voids is given by

$$\dot{f}_{\text{growth}} = (1 - f) \dot{\varepsilon}_{kk}^p \quad (25)$$

For modeling purposes, plastic strain-controlled nucleation of void has been used and is given by

$$\dot{f}_{\text{nucleation}} = \frac{f_N}{S\sqrt{2\pi}} \exp \left[ -\frac{1}{2} \left( \frac{\varepsilon_m^p - \varepsilon_n}{S} \right)^2 \right] \dot{\varepsilon}_m^p \quad (26)$$

where  $f_N$  is the void volume fraction of forming particles,  $\varepsilon_n$  is the mean strain at which void nucleation occurs,  $S$  is the standard deviation,  $\sigma_n$  is the mean stress for void nucleation, and  $\sum = \bar{\sigma} + \frac{1}{3}\sigma_{kk}$ . When the material reaches 90% of the void volume fraction at failure,  $f_F$ , the material is considered to have failed, with the stiffness and of the failed element reduced to zero.

The property requirements for the model are

- Young's modulus and Poisson's ratio
- Moisture-dependent effective shear-hardening curves  $\sigma_o(\varepsilon_o^p)$ . The initial, critical, and failure volume fractions ( $f$ ,  $f_c$ , and  $f_F$ )



- The void interaction parameters,  $q_1$  and  $q_2$
- The volume fraction of nucleating particles  $f_N$
- The standard deviation and mean strain for void nucleation ( $S$  and  $\epsilon_n$ )

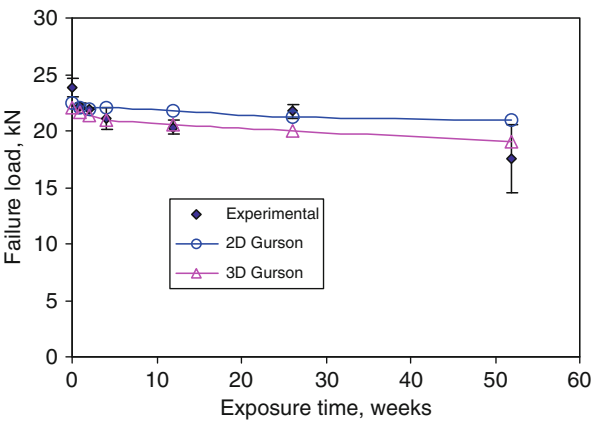
The direct experimental determination of some of these constants is difficult, leading to their determination by an iterative process using FE analysis. Hence, in Jumbo (2007), some of the model parameters were determined from experimental data and others by calibrations from FE analysis of a representative joint. The results are shown in Fig. 23. It can be seen that the 2D model slightly overpredicts the failure load but that a good agreement is seen with the experimental data with the 3D model. Comparing Figs. 22b and 23, it can be seen that the 3D Gurson model agrees well with the CZM.

### 31.5 Summary and Conclusions

It is often seen that the strength of adhesive joints decreases on aging in natural environments. This is usually because of the effect of environmental moisture, which is absorbed by polymeric adhesives and affects both the mechanical behavior of the adhesive and the interface between the adhesive and adherend. These effects are usually increased by increasing temperature or the application of stress. The effect on the interface is potentially the most damaging; however, this can usually be mitigated by the application of a suitable surface treatment prior to bonding. In this case it is often seen that the effects of absorbed moisture are largely reversible.

The effect of environment on adhesive joints is commonly investigated experimentally through accelerated aging tests in which joints are exposed to high temperature and humidity. This can provide a useful comparison of different systems but cannot be used to predict the performance of joints under actual service conditions. Currently, the best method of predicting the effect of environmental aging on the strength of bonded joints is through coupled hygro-mechanical finite element

**Fig. 23** Effect of aging at 50 °C, 95% r.h. on the failure load of a CFRP/Al/epoxy DLJ predicted using the Gurson CDM (Jumbo 2007)



analysis. The first stage in this method is to determine the moisture distribution in the joint as a function of time from a diffusion analysis. This is used to determine the spatial distribution of mechanical properties and the applied hygroscopic strain. A mechanical analysis is then used to determine the stresses in the joint as a function of aging time, and an appropriate failure criterion can be used to predict the residual strength of the joint as a function of aging time. This method is now well developed and has been validated for simple joints; however, further development and validation are required. It would also be useful to develop a software tool based on this method for the nonspecialist designer.

---

## 31.6 Further Information

The most comprehensive treatment of wet durability is Kinloch (1983). In this, Minford (1983) has compared wet durabilities of joints with phenolic and epoxide-based adhesives. Joints in aluminum have been reviewed by Brewis (1983), and Mahoon (1983) has dealt with titanium and Brockmann (1983) with steel. Reviews which have provided updates are those by Critchlow and Brewis (1995, 1996) which, respectively, deal with the surface treatment of titanium and aluminum and that by Armstrong (1997). A comprehensive comparison of accelerated aging and natural aging has been made by Ashcroft et al. (2001). Modeling the environmentally induced degradation of adhesively bonded joints has been reviewed by Crocombe et al. (2008). The effects of temperature and moisture on adhesives and adhesive joints have recently been reviewed by Viana et al. (2016b).

---

## References

- Abdel Wahab MM, Ashcroft IA et al (2001) *J Adhes* 77:43  
Armstrong KB (1997) *Int J Adhes Adhes* 17:89  
Ashcroft IA, Digby RP et al (2001) *J Adhes* 75:175  
Barbosa AQ, da Silva LFM et al (2015) *J Adhes Sci Technol* 29:1714  
Berens AR, Hopfenberg HB (1978) *Polymer* 19:489  
Brewis DM (1983) In: Kinloch AJ (ed) *Durability of structural adhesives*. Applied Science Publishers, London, p 215. Chapter 5  
Brewis DM, Comyn J et al (1980a) *Polymer* 21:1477  
Brewis DM, Comyn J et al (1980b) *Int J Adhes Adhes* 1:35  
Brewis DM, Comyn J et al (1980c) *Polymer* 21:134  
Brewis DM, Comyn J et al (1981) *Poly Engg Sci* 21:797  
Brewis DM, Comyn J et al (1987) *Int J Adhes Adhes* 7:30  
Brewis DM, Comyn J et al (1990) *Int J Adhes Adhes* 10:247  
Briskham P, Smith G (2000) *Int J Adhes Adhes* 20:33  
Brockmann W (1983) In: Kinloch AJ (ed) *Durability of structural adhesives*. Applied Science Publishers, London, p 281. Chapter 7  
Butt RI, Cotter JL (1976) *J Adhes* 8:11  
Carter FG, Kibler KG (1978) *J Compos Mater* 12:118  
Comyn J (1983) In: Kinloch AJ (ed) *Durability of structural adhesives*. Applied Science Publishers, London, p 85. Chapter 3

- Comyn J (2005) In: Adams RD (ed) *Adhesive bonding: science, technology and applications*. Woodhead Publishing Ltd., Cambridge, UK, p 123. Chapter 6
- Comyn J, Brewis DM et al (1987) *J Adhes* 21:59
- Crank J (1975) *The mathematics of diffusion*. Oxford Science Publications, Oxford
- Critchlow GW, Brewis DM (1995) *Int J Adhes Adhes* 15:161
- Critchlow GW, Brewis DM (1996) *Int J Adhes Adhes* 16:255
- Critchlow GW, Ashcroft IA et al (2006) *Anodising aluminium alloy*, United Kingdom: Patent No GB 3421959A
- Crocombe AD, Ashcroft IA et al (2008) In: da Silva LFM, Ochsner A (eds) *Modelling of adhesively bonded joints*. Springer, Berlin, p 225. Chapter 8
- Davis RE, Fay PA (1993) *Int J Adhes Adhes* 13:97
- Fay PA, Maddison A (1990) *Int J Adhes Adhes* 10:179
- Fernandes RL, de Moura MFSF et al (2016) *Int J Adhes Adhes* 68:30
- Gledhill RA, Kinloch AJ (1974) *J Adhes* 6:315
- Gledhill RA, Kinloch AJ et al (1980) *J Adhes* 11:3
- Gurson AL (1977) *J Eng Mater Technol. Trans ASME* 99:2
- Han X, Crocombe AD et al (2014) *J Adhes* 90:420
- Heshmati M, Haghani R et al (2016) *Compos Part B* 92:447
- Hua Y, Crocombe AD et al (2007) *J Adhes Sci Technol* 21:179
- Jumbo FS (2007) *Modelling residual stresses and environmental degradation in adhesively bonded joints*. PhD thesis, Loughborough University, Loughborough
- Kinloch AJ (ed) (1983) *Durability of structural adhesives*. Applied Science Publishers, London
- Korta J, Mlyniec A et al (2015) *Compos Part B* 79:621
- Krishnan P, Abdul Majid MS et al (2016) *Compos Struct* 148:1
- Liljedahl CDM, Crocombe AD et al (2005) *J Adhes Sci Technol* 19:525
- Liljedahl CDM, Crocombe AD et al (2007) *Int J Adhes Adhes* 27:505
- Liu S, Cheng X et al (2016) *Compos Part B* 91:431
- Loh WK, Crocombe AD et al (2003) *J Adhes* 79:1135
- Loh WK, Crocombe AD et al (2005) *Int J Adhes Adhes* 25:1
- Mahoon A (1983) In: Kinloch AJ (ed) *Durability of structural adhesives*. Applied Science Publishers, London, p 255. Chapter 6
- Minford JD (1983) In: Kinloch AJ (ed) *Durability of structural adhesives*. Applied Science Publishers, London, p 135. Chapter 4
- Mubashar A, Ashcroft IA et al (2009a) *J Adhes* 85:711
- Mubashar A, Ashcroft IA et al (2009b) *Int J Adhes Adhes* 29:751
- Mubashar A, Ashcroft IA et al (2011) *Eng Fract Mech* 78:2746
- Needleman A, Tvergaard V (1984) *J Mech Phys Solids* 32:461
- Parker BM (1988) *J Adhes* 26:131
- Sadigh S, Ali M (2016) *J Fail Anal Prev* 16:1134
- Viana G, Costa M et al (2016a) *J Adhes* 93:95
- Viana G, Costa M et al (2016b) *Proc I Mech E Part L* 0:1

Sabine Dagrás, Julien Eck, Claire Tonon, and Denis Lavielle

## Contents

32.1	Introduction .....	916
32.2	Adhesives Used in Space Programs .....	917
32.3	Environment Specification .....	920
32.4	Testing .....	923
32.4.1	Adhesives Testing Methodology .....	923
32.4.2	Test Facilities .....	924
32.5	Impact of Space Environment on Adhesives .....	929
32.5.1	Degradation Mechanisms .....	929
32.5.2	Irradiation Effects .....	932
32.6	Conclusion .....	938
	References .....	939

## Abstract

Adhesives are widely used on a spacecraft for several reasons. They allow a significant mass reduction and, using an adhesive allows. The combination of several properties (as the mechanical fixation and some electrical function). One of their main drawbacks is that they are organics and thus they react with space environment.

Among all the components of the space environment which could lead to material degradations, the three most important are the energetic charged particles (protons and electrons particles with different fluxes and energies), the electromagnetic radiation from the direct solar flux (and most specifically in the Ultra Violet wave length) and the Atomic Oxygen (ATOX) coming from the photo-dissociation of the oxygen molecules of the atmosphere by the solar

S. Dagrás (✉) · J. Eck · C. Tonon · D. Lavielle  
Airbus Defence and Space, Toulouse, France  
e-mail: [sabine.dagras@airbus.com](mailto:sabine.dagras@airbus.com); [julien.eck@airbus.com](mailto:julien.eck@airbus.com); [claire.tonon@airbus.com](mailto:claire.tonon@airbus.com);  
[denis.lavielle@airbus.com](mailto:denis.lavielle@airbus.com)

electromagnetic radiation. These factors lead to physicochemical degradation of the adhesives, which can affect their functional properties.

All the adhesives used in spacecraft have to be validated on ground before launch and their behavior in space environment must be evaluated. Test facilities are developed to simulate charged particles, UV, and ATOX constraints. Even if it is not possible to be 100% representative of the in-orbit conditions, tests, methodologies and specifications exist to correctly evaluate the degradation and to take into account the adhesives end of life properties, in the spacecraft design.

Atoms and molecules along the charged particles trajectory can be either excited or ionized. The primary effects are generally deformation, embrittlement, and discoloration, which impact the mechanical integrity of the adhesive. The modification of mechanical properties is generally the result of the competition between chain scissions and crosslinking in the macromolecular chains.

The main UV effect on adhesives is generally a degradation of their optical properties (e.g., solar cell cover glass). Indeed, during the interaction of a photon with an atom or a molecule of the material, the photon can either be absorbed or diffused with possible loss of energy. These photochemical effects may result in a change of color of the material, leading to an increase of solar absorptance.

Atomic Oxygen might also have detrimental effects on adhesives, mainly erosion of surfaces and oxidation.

---

## 32.1 Introduction

Spacecrafts and space systems in general significantly evolved till the first systems launch into orbit in the years 1960. The missions evolved and it is now required to have more and more power and function accessible for the telecommunication spacecraft as for the earth observation or scientific missions.

These missions' new developments and needs lead to a significant increase of the spacecraft sizes and masses. Due to launchers constraints, it is now required to optimize as much as possible the satellites design and all the parts and equipments are reduced and accommodated to limit their mass. Taking into account these constraints, it is not possible any more to have spacecraft mainly composed of metallic materials which strongly behave in the specific space environment. Polymers and composite materials used in space systems were thus more and more developed and current satellites hold various organic materials for various applications. Among all these organic materials, the adhesives are widely used including for external applications on the satellites and can thus be fully exposed to space environment.

In parallel of this mass reduction objective, space missions' durations are extended and satellites shall now withstand more than 15 years in orbit without degradation of their functionality. The reliability of all the satellites parts have to be demonstrated on ground before launch. Among all the parameters to be evaluated, the behavior of organic materials (including adhesives) to space environment is a driver in the spacecraft design. Indeed, the materials in orbit are submitted to various



**Fig. 1** Illustration of the satellites evolution. First spacecraft in orbit, Sputnik (*left*) and a recent telecommunication spacecraft (*right*)

constraints such as radiations of charged particles, ultraviolet, Atomic Oxygen... (Fig. 1).

The following chapter address the behavior of adhesives in space environment and is thus composed as follows.

In the first part of this chapter, a description of the typical uses and needs related to adhesives on spacecraft is given. Then, the specificities of the space environment are explained. Once in orbit, the adhesives have to withstand constraints as particles radiations, UV, and Atomic Oxygen (ATOX) that are not present on Earth.

Depending on the mission, the location and the adhesive use on the spacecraft, these constraints can vary a lot.

Before spacecraft launch, the adhesives have to be validated and tested on ground with conditions as representative as possible of the space environment. In this chapter, the testing methodologies are detailed.

Finally, the impact of this space environment on adhesives and the associated degradations are developed. The degradation mechanisms and the effects of the irradiation on the adhesive macroscopic properties are presented.

---

## 32.2 Adhesives Used in Space Programs

Adhesives are widely used in space applications for many different applications. This material family combines several properties which are really important for space programs:

- They allow durable bonding of dissimilar materials (e.g., polymer/metal, composite/metal, etc.)
- They allow significant mass reduction for mechanical fixation compared to traditional screws or rivets. This mass reduction is generally a driver for a domain where each gram avoided is important.
- Some adhesive families allow a use in an extended temperature range, which can be of high interest for external areas of the spacecraft. On spacecraft solar

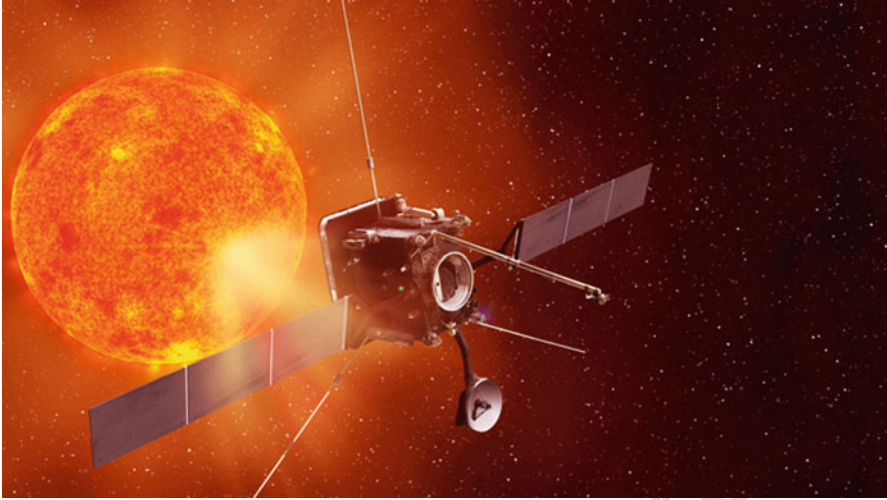


**Fig. 2** Adhesives used for space applications should have low-outgassing levels. They shall withstand space environment harsh constraints: extreme temperatures, high vacuum, UV and radiation environment, and/or Atomic Oxygen

arrays, temperature excursions can reach  $-180\text{ }^{\circ}\text{C}/+180\text{ }^{\circ}\text{C}$  as illustrated in Fig. 2.

- The combination of several properties (mechanical fixation and electrical grounding as an example) is finally an advantage for spacecraft's design optimization.

The main use of adhesives on a space instrument or a spacecraft is the mechanical fixation. Adhesives shall withstand important loads due to the spacecraft launch (vibration and acoustics constraints). Once in-orbit, the most significant mechanical loads are shocks due to deployment of subassemblies (e.g., solar arrays, antennas). Another critical parameter is the large variation of materials thermal expansions which can be observed due to the important temperature ranges (typically between  $-180\text{ }^{\circ}\text{C}/+180\text{ }^{\circ}\text{C}$  for external appendices). This might induce thermomechanical deformations.

Therefore, impact of space environment on mechanical properties is mandatory to assess the acceptability for the use of adhesives on spacecraft structures. The mechanical design of structural adhesive joints is driven by mechanical loads during on-ground tests and launch. The ageing during operational in-orbit lifetime is driven by thermomechanical loads, as no vibration loads comparable to the launch loads exist.

In addition to its mechanical function, an adhesive could also be used for its electrical or thermal properties. Indeed, adhesives loaded with conductive fillers allow the grounding of most of the spacecraft parts. On the contrary, adhesives could



**Fig. 3** Examples of adhesive use on spacecrafts: bonded stand-off for MLI (multilayers insulation) blankets mechanical installation on spacecraft structure (*left*), optical surface reflectors bonded on spacecraft structure for thermal control purpose (*middle*), electronic PCB proceeds through “touch up” after completing frame bonding, which uses a new automated adhesive dispensing process (NASA.gov image) (*right*)

be also be used as varnish or conformal coating for electrical insulation purposes (see Fig. 3). When applied for the bonding of thermal active parts, as heatpipes, thermal conductivity of the adhesive is a driver to guarantee the thermal efficiency of the component onto the structure. The same advantage is foreseen in electronic assembly, as the ability of thermally conductive adhesives helps dissipating heat as more and more power dissipating components are mounted on PCB.

Finally, the optical properties of some adhesives are used on space systems. The most relevant example consists in transparent adhesives used for the bonding of the solar cells cover glasses. The evolution of the transmission properties of the adhesive (yellowing due to interaction between adhesive and radiations and UV) is a driver in the solar arrays design and sizing.

Even if adhesives are advantageous for some applications, they also present drawbacks for space applications. As they are organic products, their properties are modified during the spacecraft in-orbit life, due to exposure to space environment (and more specifically radiation and UV). Moreover, the adhesives are submitted to vacuum once in orbit and their volatile components outgas. This can be a major constraint for missions where the outgassed components could lead to the molecular contamination of the instruments optics, degrade their optical properties, and reduce the instruments performance.

Therefore, the validation on ground of adhesive behavior to such constraints is performed through dedicated and specific test campaigns.

Several adhesive chemical families are used in spaces programs. Among all of them, the most used are the epoxies for their mechanical properties, silicones for their good behavior to thermal environment, acrylics (generally used as tapes), and polyurethanes.

As space industry represents a relatively reduced commercial amount compared to other industrial sectors, it is not possible to develop specific adhesives for each application. Most of the adhesives used on a spacecraft are therefore commercial products nevertheless, for some really specific applications, developments are performed to cover a dedicated mission and the adhesive formulation can be adapted to be more resistant to space environment.



### 32.3 Environment Specification

The space environment represents a harsh medium for all spacecraft. Proper assessment of the potential effects is an essential part of the engineering process leading to the qualification of any element of the spacecraft (Space weather effect catalogue). As defined in ECSS Standard (ECSS-Q-ST-10-04C), the natural space environment of a given item corresponds of environmental conditions defined by the external physical world for the given mission.

The main components of the space environment that can lead to material degradations are:

- Meteoroids and debris
- Galactic cosmic rays (GCR)
- Solar energetic particles (SEP)
- Photons, from the  $\gamma$  rays to the radio frequency
- The solar wind
- Atomic Oxygen

Whereas debris and micrometeorites can induce instantaneously damages in the materials, the remaining constraints can be assimilated as ageing factors. In that latter cases, the cumulative effect of these constraints lead to progressive degradation of the materials all along the mission duration. In this chapter, we will focus on the effects of UV, particle radiations, and Atomic Oxygen (ATOX).

A spacecraft receives electromagnetic radiation originating from the direct solar flux. The solar spectrum can be divided as follows in several parts depending on the wavelength range considered:

- Soft X-rays or XUV (0.1 nm–10 nm)
- Extreme ultraviolet or EUV (10 nm–121 nm)
- Ultraviolet or UV (100 nm–400 nm)
- Visible or VIS (380 nm–760 nm)
- Infrared or IR (0.70  $\mu$ m–1 mm)

In general, for material testing, the spectrum used for solar simulation is limited to the UV region because, although this band is responsible for only 1% of the total solar irradiance, it is assumed that the major degradation of the materials is due to these photons.

The second type of radiation leading to potential degradation of the materials is particle radiation. Energetic charged particles are encountered in interplanetary space and in the magnetospheres of moons or planets. There are different types of particles, coming from different origins. The main ones are:

- The cosmic rays, entering the solar system from the interstellar medium and composed of protons, electrons, and fully ionized nuclei. Their energy remains in the GeV to TeV range.

- 187 – The solar energetic particles, originating from Sun flaring or from shock waves  
188 associated with coronal mass ejections, consist of protons, electrons, and heavy  
189 ions with energies from a few tens of keV to GeV ranges.
- 190 – The solar wind, which is part of the Sun's outer atmosphere expanding outwards  
191 and composed mainly of protons, electrons, alphas with an energy range between  
192 few eV and few keV.

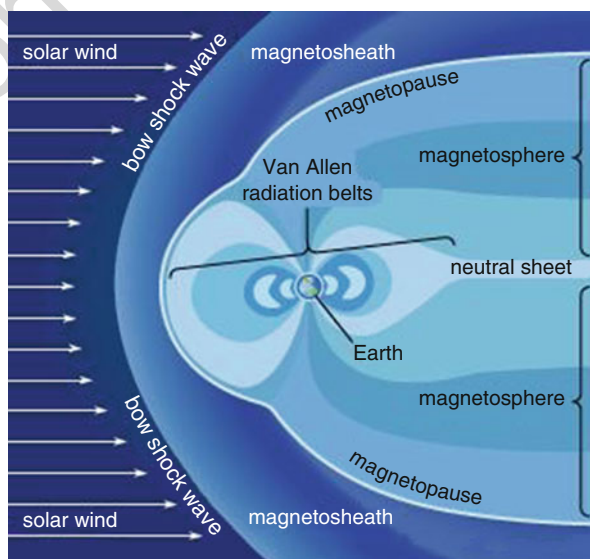
193 Although the energy of the cosmic rays and the solar energetic particles are much  
194 higher than the ones of the solar wind or of the particles within the radiation belts,  
195 their flux are relatively low and thus their contribution to the material degradation is  
196 negligible. Conversely, this type of radiation (cosmic rays and solar energetic  
197 particles) are a major concern for electrical components as it can induce so called  
198 single event that could lead to their dysfunction or their destruction.

199 Geomagnetic fields of the planets or the moons influence the energetic particles  
200 and can also induce specific radiation environments. The particles coming from the  
201 interplanetary medium are trapped in the magnetic field and then accelerated along  
202 the field lines depending on their polarization. Thus, radiations belts are created  
203 around the planets or moons.

204 Around the Earth, these radiation belts are also called Van Allen belts. They are  
205 composed of an inner and an outer belt and extend from typically 100 up to  
206 65,000 km. These belts are mainly constituted of protons (with energies up to  
207 hundreds of MeV) and electrons (energies up to few MeV) coming from the  
208 solar wind.

209 As illustrated in Figs. 4 and 5, depending on its orbit (Low-Earth Orbit, Medium-  
210 Earth Orbit, Geostationary-Earth Orbit), the satellite will be submitted to different  
211 particles flux and energies with the Van Allen belts.

**Fig. 4** Radiation belts  
illustration (<https://www.britannica.com/science/Van-Allen-radiation-belt>)



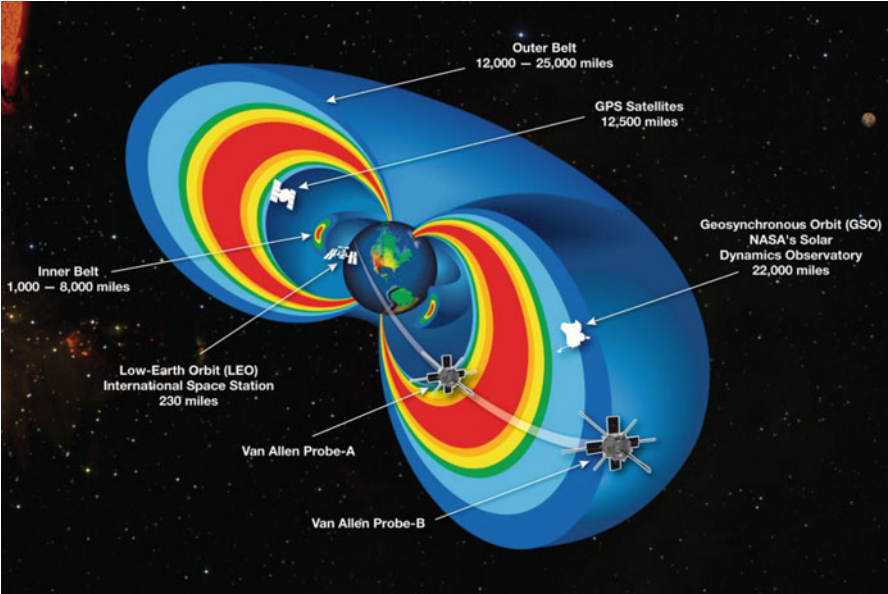


**Fig. 5** Space radiations belts for the satellites different orbits ([https://www.nasa.gov/mission\\_pages/sunearth/news/gallery/20130228-radiationbelts.html](https://www.nasa.gov/mission_pages/sunearth/news/gallery/20130228-radiationbelts.html))

Whereas the LEO missions, characterized by a spacecraft altitude below typically 1000 km, are located below the inner belt and are submitted to relatively low particle radiations, GPS or GEO missions are inside the outer belt and submitted to higher particle fluxes, leading to significant dose levels compared to LEO ones. Additionally, in the outer belt, the fluxes of low-energy particles are higher than in the inner belt, leading to an increase of the deposited dose within the external materials, directly exposed to space environment.

In the case of interplanetary missions, specific radiation environments shall also be considered. As an example, in the case of Jovian missions, during the cruising phase between the planets, the spacecraft will be mostly submitted to solar wind but also to radiations belts of Jupiter or its moons (Ganymede, Europa, etc.), characterized by important fluxes of highly energetic electrons.

Missions towards the Sun are also exposed to very specific environments. The probes are exposed to very high flux of solar wind particles together with high temperatures, leading to potential synergistic effects.

Another component of the space environment able to induce degradation of the materials is Atomic Oxygen. These atoms are generated during the photo-dissociation of the oxygen molecules of the atmosphere by the solar electromagnetic radiation (mainly short wavelengths,  $\lambda < 243$  nm), leading to the breaking of the diatomic bonds (NASA-HDBK-6024). These atoms are very reactive and can interact with the spacecraft materials through oxidation mechanisms.

Atomic Oxygen is present around Earth but can also be produced in other planetary environments, such as the Mars orbital environment, where oxygen is present.

## 32.4 Testing

### 32.4.1 Adhesives Testing Methodology

As a general rule, any technology used on a spacecraft has to be qualified with regards to functional and environmental constraints.

For adhesives, this rule is also applicable. Therefore, for each adhesive application, a test plan is set up to finalize the different functional and environmental stresses that need to be verified on ground to validate further space application.

The main applications for adhesives in space are either structural (up to a certain extent for general purpose adhesives) or electrical for grounding adhesives or optical (to bond glasses or transparent materials) as already mentioned in ► Chap. 4, “Wetting of Solids.”

Due to the stringent space environment, many environmental stresses are to be considered both before launch (long-term storage) and after launch for the mission (vacuum, radiation, temperature cycling, etc.). All these stresses are mission dependent and are analyzed on a case by case basis even if general guidelines are driven by ECSS standards (ECSS-Q-ST-70-06C).

The adhesives qualifications generally consist in two levels:

- A test campaign on samples. Samples are processed in order to evaluate the adhesive properties evolution before and after accelerated ageing.
- An overall validation at equipment and system level. Specific tests campaign could be performed on new development on spacecraft to qualify the bonding against vibrations and mechanical constraints representative of the launch campaign. (e.g., vibration, shock, etc.). This addition of some other stresses can reveal any potential weak points in adhesive use.

In all cases, functional studies (mechanical, thermal, electrical, etc.) are performed to determine the limits of the tests to be performed on test samples to validate the mission profile.

However, in terms of risk mitigation, the major part of the qualification is performed at sample level.

The general principle of the test campaign on adhesive samples is described in Fig. 6. The test flow-chart is composed of different branches:

- One set of reference samples (not experiencing any stress)
- Several sets of stressed samples that combine conditions to simulate the mission profile

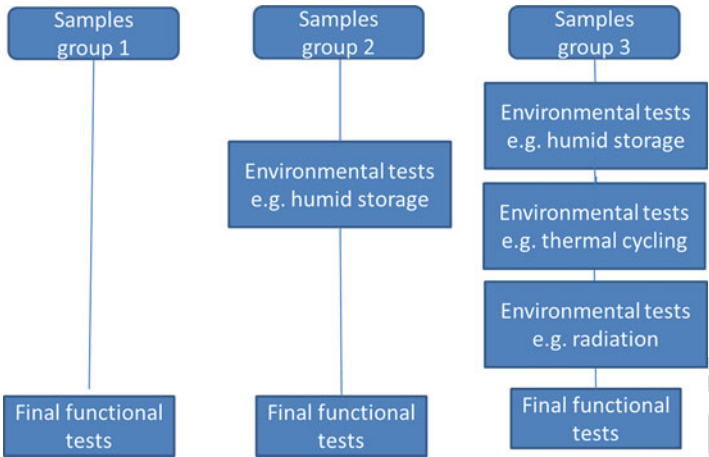


**Fig. 6** Test campaign typical flow chart at adhesive samples level

A typical example of such a test program is represented in Fig. 6 where the central branch simulates storage conditions and the right branch cumulated storage and mission profile.

At the end of the program, both reference samples and stressed samples are functionally tested and final values are compared to reference ones.

The characterization tests are defined to be representative of the relevant properties. Mechanical tests as shear test or peeling can be performed if the adhesive is used for parts fixation. Electrical or optical measurements could also be done.

In function of the need, functional tests could be performed which aim to validate the macroscopic use of the adhesive. More detailed characterizations tests could be performed to understand the degradation phenomena which occurred in the material (DSC, RMN, etc.).

Generally, the test plan includes a success criteria based on an acceptable functional change before and after submission to environmental tests (typically 20% decrease for a mechanical strength decrease).

Among all the constraints seen by an adhesive on a spacecraft, the specific behavior to radiations, ATOX and UV has to be analyzed and validated by tests on ground.

**32.4.2 Test Facilities**

**Radiations**

For the specific radiation validation, as mentioned in Sect. 5, the best approach is to simulate as close as possible on ground the expected radiation mission constraint.

For particle radiation, particle accelerators (protons, electrons) are generally used to irradiate the samples. Parameters like particles, flux, vacuum conditions (to remove potential oxygen related bleaching) are key parameters to consider.

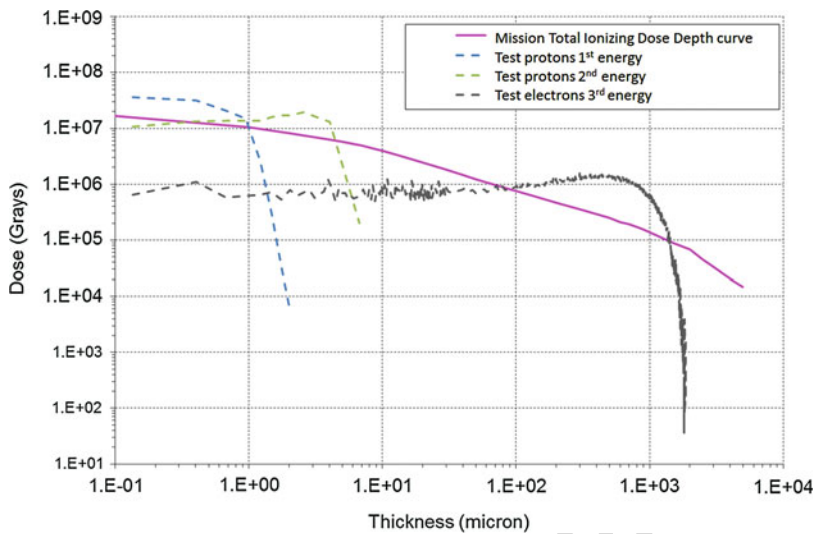


**Fig. 7** Example of calculated real total ionizing dose (TID) depth curve and ground irradiation dose profiles

Also, when characterizing materials in space, it is important to simulate the total ionizing dose profile expected in the material.

This dose is expressed in Grays or in rads (1 Gray = 100 rads): 1 Gray corresponds to the absorption of 1 Joule per kg of matter.

As explained in Sect. 5, in space, the resulting dose profile is due to a combination of different particles (nature, energy, and flux). It is not possible to reproduce on ground the exact combination but an appropriate choice of several particles with dedicated energies allows approaching the flight conditions as illustrated in Fig. 7.

In low-earth orbit missions, the spacecraft external dose is generally quite low, in the range of  $5 \times 10^5$  Gy on surface materials (typical order of magnitude). However, for geostationary missions, surface dose as high as  $1 \times 10^9$  Gy can be obtained and dose in the range of a few MGy can be achieved below a small shielding.

In adhesives directly exposed to external environment, the dose level decreases quickly when penetrating within the materials.

The use of Co60 (Cobalt 60 – gamma rays) exposure leads (due to gamma photons/matter interaction) to flat dose profile energy deposition. In that case, as the dose deposited within the material thickness is homogeneous, it is not possible to reproduce a dose profile and a dose level is applied, leading to an under/overexposure of the tested sample depending on the set parameters.

For bulk materials (and low radiation levels), Co60 exposure might be used provided it is representative of the expected in orbit conditions (heavily shielded material with typical aluminum shielding thickness higher than 5 mm, and dose contribution mainly related to Bremsstrahlung effect).

To simulate the dose profile on ground, particles accelerators like Van de Graaff are generally used with energies lying from a few tens of keV to a few MeV for

protons and few hundreds of keV to a few MeV (typically 3 to 5) for electrons. Ion implanters can also be used for low energy protons (up to a few hundred keV).

Generally, homogeneous irradiation surfaces are of the order of 50 mm × 50 mm up to 200 mm × 200 mm.

Fluxes used in the radiation tests are limited to a typical range of  $1 \times 10^{12}$  particles/cm<sup>2</sup>/s. When the flux is too high, a temperature increase can occur on the samples and change drastically the radiation behavior with regards to future mission conditions. This phenomenon is particularly true for organic materials as this temperature increase lead to the overrun of the glass transition. Generally, fluxes in orbit are a few orders of magnitude lower and radiation exposure last up to 15 years instead of a few hours or days for on-ground simulation.

Therefore, fluxes shall be a compromise between representativeness and test duration.

On some accelerators, secondary vacuum conditions are achievable or use of flowing Nitrogen gas is also acceptable (leading to absence of oxygen). For low energy protons (up to a few hundred keV), irradiations under secondary vacuum conditions are mandatory to avoid any interaction of particles with air molecules.

## UV

In general, the spectrum used for solar simulation is limited to the UV region, because it is assumed that the major degradation is due to these photons (ECSS-Q-ST-70-06C)].

For UV irradiation, one constraint is to simulate as close as possible the external atmosphere solar spectrum. Indeed, for organic materials like adhesives, specific wavelength, specific to extra-atmospheric solar spectrum could have a specific effect on materials degradation (low wavelength and high energy).

Xe-based lamp can generally be used in this case. The xenon lamp spectrum differs from all solar spectra because of the intense line output in the 800–1100 nm region. The use of specific filters allows the reduction of the mismatch and provides the closest spectral match to solar spectra.

Another constraint is to limit the acceleration factor. If not controlled, temperature as high as 200 °C can be reached quickly (especially under vacuum) at samples level and lead to thermal degradation not representative of real in orbit degradation.

Finally, vacuum conditions during exposure are important to make sure that no specific gas absorption will occur (decreasing the spectrum part at low end) and allowing oxygen residues interaction with material surface.

To do a space simulation in a reasonable time, it is required to accelerate the irradiations as fast as possible without modifying the degradation mechanisms which could induce wrong results. This problem is that of the reciprocity principle of equivalent sun hours (ESH). When using a nonfiltered Xenon light source, an acceleration factor limitation to 3 is recommended (ASTM E512) in order to limit the thermal charge on the materials.

In order to apply a higher acceleration factor, Xenon sources with specific filters can be used. These filters allow the removal of the visible and infrared part of the spectrum (see Fig. 8). Thus samples are only exposed to UV radiations leading to a thermal charge reduction by a factor of 10 (see Fig. 9).

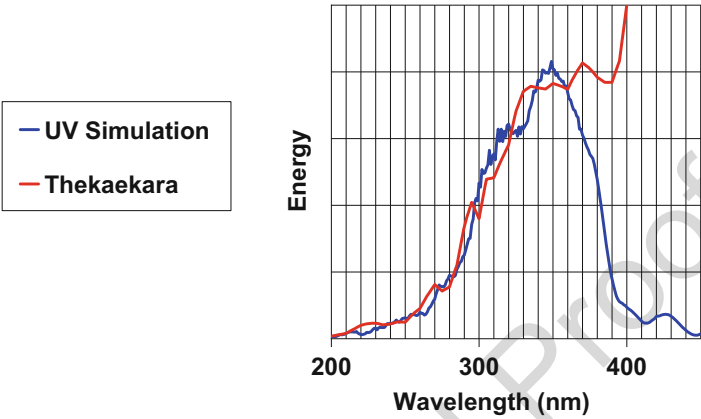


**Fig. 8** Example of one UV simulation compared to Thekaekara spectrum

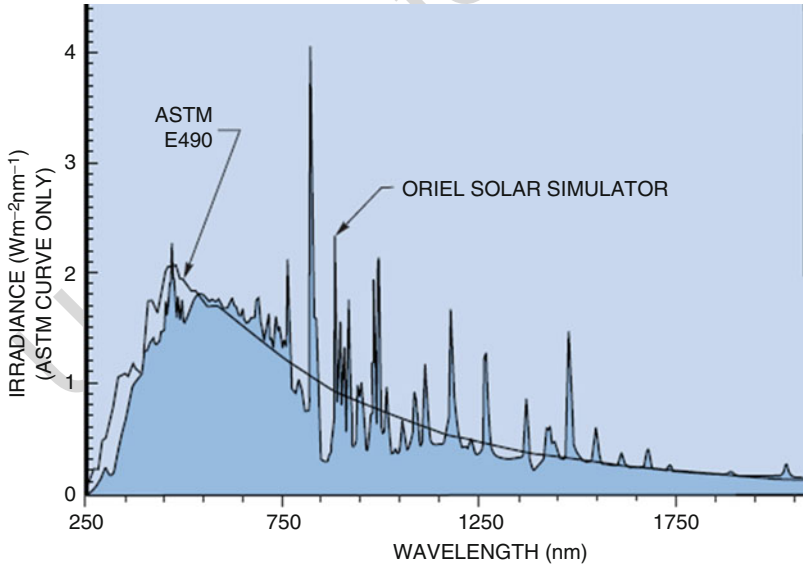


**Fig. 9** Typical output spectral distribution of AM 0 Simulators normalized to the ASTM E490 standard spectrum by matching total power density from 250–2500 nm (<https://www.newport.com/n/solar-simulator-spectral-irradiance-data>)



### Degradation Estimation

The solar constant is defined in (ECSS-Q-ST-10-04C) as the radiation that falls on a unit area of surface normal to the line from the Sun, per unit time, outside the atmosphere, at one astronomical unit (1 AU = average Earth-Sun distance).

In the case of ultraviolet radiations, it is estimated that the degradation is a function of the solar illumination in the UV (wavelengths typically between 200 and 400 nm), expressed in  $\text{W.m}^{-2}$ . This illumination is also usually expressed in space technology by the number of equivalent sun hours (ESH), which, for GEO environment, is equal to the UV part of the solar spectrum integrated over 1 h:

$$1 \text{ ESH} = 108 \times 3600 = 3.888.10^5 \text{ J.m}^{-2} \quad (1)$$

where  $108 \text{ W.m}^{-2}$  represent the integrated flux on the UV range of the solar spectrum.

### Equation 1: Definition of an ESH (Equivalent Sun Hours)

As an example, over 1 year (8760 h), GEO satellite materials, depending on their location on the spacecraft, can be exposed up to 2500 ESH per year.

Note that simulation tests in laboratory specify that the tested material will have to be irradiated with the same number of UV ESH and the same spectral distribution as the material in the specified mission conditions. It has to be noticed that the solar spectral distribution is very difficult to completely reproduce in laboratory. The difference can conduct to bad interpretation of the importance and/or nature of the degradation.

### ATOX

The Atomic Oxygen Simulators that are used around the world, depending on the energy of the Atomic Oxygen fluxes, can be divided into thermal and hyperthermal. The basic physical processes used for those sources are supersonic expansion, laser detonation, ion neutralization, electron-simulated desorption, and photo-dissociation (Kleiman et al. 2003).

One of the most representative technologies for materials testing applications was shown to be the laser-sustained discharge sources, where lasers are used to produce a high-temperature plasma that is subsequently expanded in a free jet or supersonic nozzle to produce a high-velocity neutral beam. Such sources have been demonstrated to produce beams of the desired velocity of  $8 \text{ km.s}^{-1}$  at flux levels of  $1017\text{--}1018 \text{ cm.s}^{-2}$ , i.e., exhibited both the appropriate energy for LEO simulation and high flux required for accelerated testing.

The cost and limited availability of materials test time in these high-quality LEO environment simulators has generated considerable interest in the use of thermal energy oxygen atoms produced by plasma asher for materials testing (Banks et al. 2013). This type of facility can be operated easily at low cost. However, the main drawback is the lack of representativeness with major differences in terms of variations in species, energies, thermal and radiation exposures, all of which may result in different reactions and erosion rates.

However, due to the variety and complexity of the differences between the LEO Atomic Oxygen environment and ground laboratory simulations, differences exist which have not allowed the development of a simple relationship or proportionality between the LEO and ground laboratory erosion yields. Two of the most significant differences between most ground laboratory and LEO environments are the energy and directionality of the Atomic Oxygen.

### Specific Test Facilities

Some laboratories have developed for decades a specific test facility that combines particle irradiation (electrons/protons) and UV irradiation under secondary vacuum. In addition, in-situ measurements like thermo-optical measurements can be performed before re-exposure of the samples to ambient atmosphere.

Typical exposure areas are here again around 50 mm × 50 mm up to 200 mm × 200 mm. Cooling systems (coupled to sample back surface to limit temperature increase) are used for sample temperature regulation.

Acceleration factors in the range of 10–50 are generally proposed and exposure of a few years in orbit can be simulated in a few days or weeks.

In terms of acceleration, it is important to note that the acceleration factors for UV and particle irradiation, even if tested in the same facility, are about different values. However, the same rule applies to not overstress the samples by a too high acceleration factor leading to too high temperature increase of the samples that would generate appearance of nonrepresentative ageing mechanisms.

---

## 32.5 Impact of Space Environment on Adhesives

### 32.5.1 Degradation Mechanisms

In the case of polymers, radiation effects have been extensively studied (Makhliis 1975; Paillous 1993). The difference must be done between charged particles (electrons, protons, heavy ions), which energy (from 1 keV to several MeV) is sufficient to excite and ionize molecules and UV photons but is insufficient to ionize them (excepted for far UV).

Indeed, ionization occurs when the incident energy of the particle is sufficient to overcome the binding energy of electrons in atoms or molecules, thus creating ions. On another hand, excitation occurs when the incident energy is not sufficient to ionize molecules but can create excited intermediate electronic states (triplets, singulets, color centers), by the excitation of the molecule and the transfer of an electron from a fundamental state to an excited state.

This can be summarized for a molecule AB by:

– Excitation  $AB \rightarrow AB^*$

– Ionization  $AB \rightarrow AB^+ + e^-$

We present here both effects of ultraviolet and charged particles, as these components of space environment contribute to the degradation of adhesives.

The effect of Atomic Oxygen (ATOX) are also presented.

An important point to be considered is the thickness of the degraded zone for each parameter.

In the case of ultraviolet radiations, the effect depends on the absorption of the material:

- For low absorbent materials in the considered wavelengths, the degradation can apply at high thickness,
- For high absorbent materials, the damage will be limited to more superficial effects.

The difficulty to evaluate the degraded zone is that the degradation generally appears as a change of the absorption properties of the material, the material becoming more absorbent. The consequence is a limitation of the degraded thickness as the irradiation persists.

In the case of charged particles, electrons and protons have to be distinguished, as their stopping power in matter is different. Depth penetration in matter, and thus degraded thickness, is far more important for electrons than for protons: a few microns for protons to compare with several hundred of microns to millimeters for electrons.

In this section, the degradation of the polymer matrices due to radiations is mainly considered. Nevertheless, as a function of the specific use of the adhesive, the degradation of the loads can also be important.

## Ultraviolet

During the interaction of a photon with an atom or a molecule of the material, the photon can either be absorbed or diffused with possible loss of energy. In space environment, the solar electromagnetic spectrum covers wavelengths from  $10^{-4}$  to  $10^4$   $\mu\text{m}$ , with a spectral distribution close to a black body at 5762 K. The total energetic flux (called the solar constant) is  $1366 \text{ W.m}^{-2}$  (ASTM E490). However, the degradation of materials is mainly due to the ultraviolet radiation, with wavelengths lower than 0.4  $\mu\text{m}$ . The energetic flux in this range is  $118 \text{ W.m}^{-2}$ .

Two phenomena can be distinguished, depending on the wavelength:

- $0.2 < \lambda < 0.4 \text{ } \mu\text{m}$ : the energy of ultraviolet photons is between 3.1 eV at 0.4  $\mu\text{m}$  and 6.2 eV at 0.2  $\mu\text{m}$ . This energy is not sufficient to ionize molecules but can generate excitation.
- $\lambda < 0.2 \text{ } \mu\text{m}$ : the energy of the photons is sufficient to ionize molecules, leading for example to scissions or crosslinking in polymer chains.

These photochemical effects may result in a change of color of the material, increase of solar absorptance and/or loss of mechanical properties.

**Charged Particles**

The energy of charged particles in space environment is usually between 1 keV and several MeV. Atoms and molecules along their trajectory can be either excited or ionized.

In the case of an ionization, the secondary electron, liberated during the primary interaction between the charged particle and the matter, can have sufficient energy to leave the site of the primary interaction and produce new excitations and ionizations along its trajectory, before being thermalized and absorbed at a few hundred angstroms from the primary interaction site (see Fig. 10). The reactions held on the track of the secondary electron are often grouped and form clusters, responsible for the chemical modification of the material.

If the secondary electron is not sufficiently energetic, it can be recaptured by the parent ion to form an excited molecule or a free radical. A free radical can recombine with the material to form the initial material or can diffuse around the interaction site, leading to the formation of new chemical products. This can be particularly important for contamination aspects. Indeed, the materials outgassing is controlled on space programs as it can degrade the nearest instruments (such as telescope) properties.

Consequently, if we consider that the nature of the created species only depends on the interaction with secondary electrons, then, it is independent of the nature of the radiation. On the contrary, the spatial distribution of the created species will depend on the radiation. In the case of protons, the primary track is linear and the defects are distributed in dense clusters very close to the track. In the case of

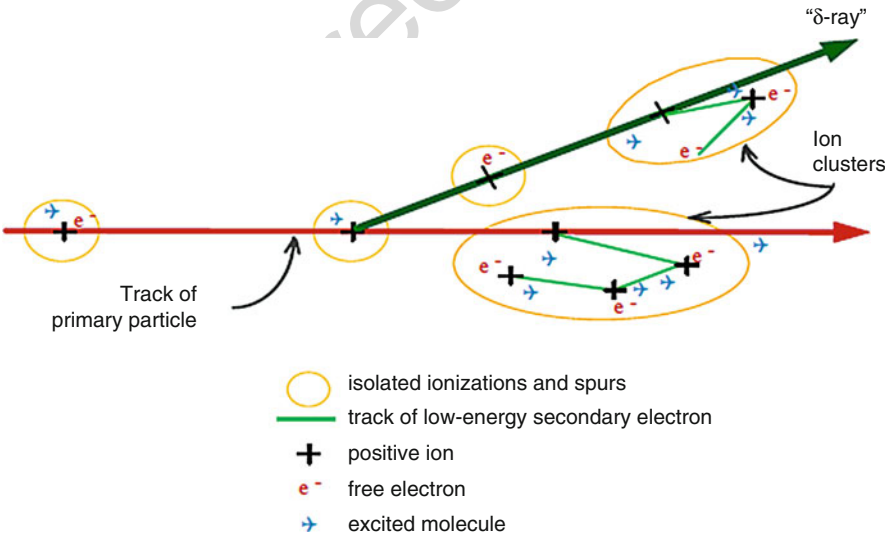


**Fig. 10** Distribution of ions and excited molecules along the trajectory of a rapid electron (Clegg and Collyer 1991)

electrons, the effects will be more dispersed because of the scattering of the particles in matter. Moreover, the difference of mass between electrons and protons induces different stopping powers and penetration depths in matter.

In the case of charged particles, it is generally estimated in a first approximation that the degradation is a function of the quantity of reactional intermediates (excited molecules, free radicals, etc.), then a function of the dose of energy which is absorbed in the material.

## ATOX

Atomic Oxygen can react with polymers, carbon, and many metals to form oxygen bonds with atoms on the exposed surface. For most polymers, hydrogen abstraction, oxygen addition, or oxygen insertion can occur. With continued Atomic Oxygen exposure, all oxygen interaction pathways eventually lead to volatile oxidation products. This results in gradual erosion of hydrocarbon or halocarbon material. Silicone materials, a family of commonly used spacecraft materials, are an exception to polymeric materials that erode away with Atomic Oxygen exposure. With Atomic Oxygen exposure, oxidation reactions cause the surface of silicones to oxidize and volatilize their hydrocarbon content and convert to a hardened silica-based surface layer, which is resistant to Atomic Oxygen erosion.

ATOX effects can be important on space materials and it is thus important to know it. However, this will not be discussed in details as adhesives are generally shielded from direct exposure to Atomic Oxygen, and they are not affected by this space environment factor.

## 32.5.2 Irradiation Effects

### Mechanical Properties

Change in mechanical properties is particularly critical in the case of polymers. Both UV and particles can damage polymers.

The primary effects are generally deformation, embrittlement, and discoloration, which impact the mechanical integrity and the thermal equilibrium of the material. These effects are determined by measurement of changes in lap shear strength, tensile strength, peel test or fatigue tests following irradiation.

The modification of mechanical properties is the result of the competition between chain scissions and crosslinking in the macromolecular chains. Scissions are ruptures in the macromolecular chain and lead to a diminution of the elastic and the resistance limits and an increase of the elongation capability. On another hand, crosslinking consists in the formation of new transversal bonds in the macromolecular chain: the polymer becomes two- or three-dimensional. This contributes to an increase of the resistance limit but a diminution of flexibility, the polymer becoming more fragile. The crosslinking is illustrated on silicone rubbers through several studies (Zhang et al. 2006; Jochem et al. 2013). After 200 keV proton irradiation up to a fluence of  $10^{15}$  p<sup>+</sup>/cm<sup>2</sup> or 400 keV electron irradiation up to a fluence of  $3.10^{15}$  e<sup>-</sup>/cm<sup>2</sup>, the network densifies, which leads to an increase of the glass

**Fig. 11** Cracks in an epoxy adhesive foil after irradiation

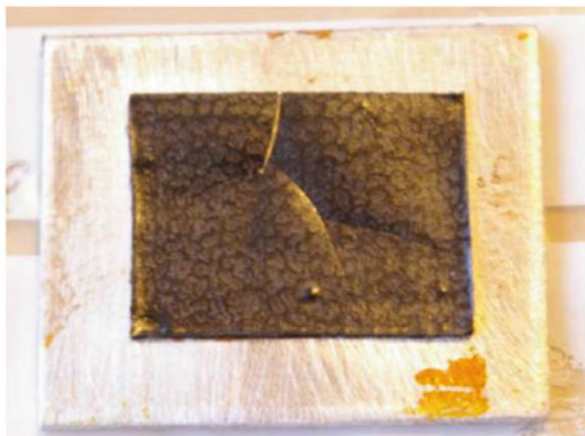
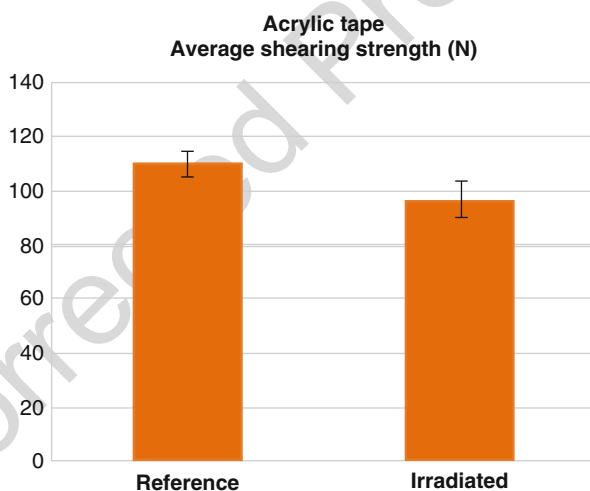


**Fig. 12** Illustration of the mechanical properties degradation (shear strength) on an acrylic adhesive before and after electrons irradiation



transition temperature of a few degrees, an increase in tensile strength and an increase of the modulus. All these changes reflect the increase of the macromolecular chain rigidity after irradiation. Even if protons penetrate less than electrons, the effects of the irradiation are similar and can be detected on the bulk material properties (see Figs. 11 and 12).

At higher doses, the competition between crosslinking and chain scission is in favor of the second one, resulting in a degradation of the polymer. As the crosslinks density decreases, the tensile strength also decreases and surface cracks are initiated as a result of the backbone chain length reduction (Fig. 13).

Few studies are available on epoxies used as adhesives, as they are generally protected from direct environment exposure and they are known to be very resistant to radiation from a mechanical point of view. When epoxies are used as a matrix for

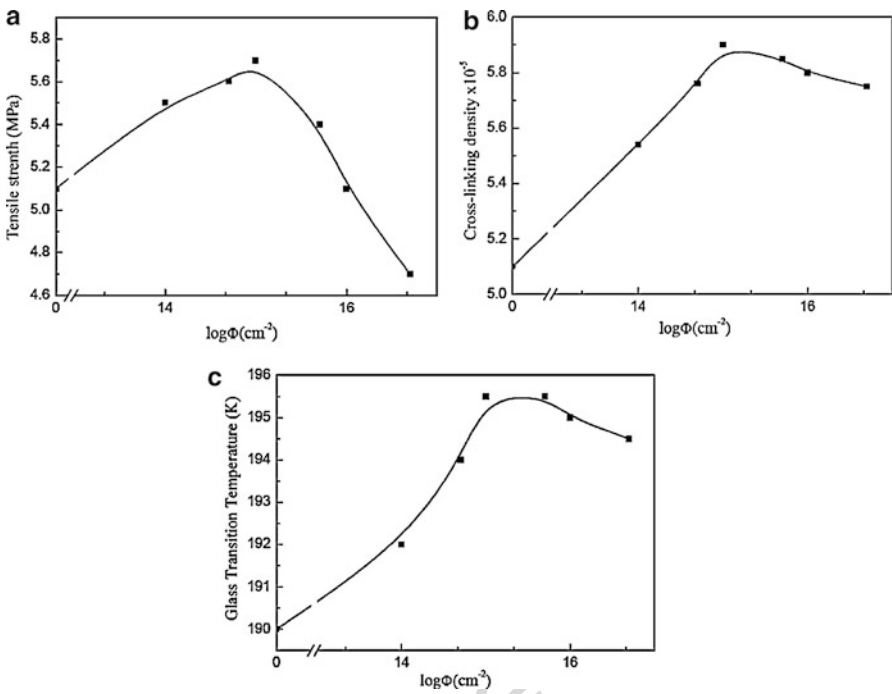


**Fig. 13** Evolution of properties of a silicone rubber versus proton irradiation fluence: tensile strength (*left*), crosslinking density (*middle*), glass transition temperature (*right*) (Zhang et al. 2006)

composites in structural applications, plasticization of the polymers at elevated temperatures increases residual deformations in the material structure, while at low temperatures, embrittlement of the polymer, repeated from cycle to cycle, multiplies the effect of microcracking and changes of the composite's properties. Depending on the delta-CTE between the matrix and the fiber, the additional microcracking due to radiation degradation may be of second order compared to the effect of thermal cycling only as described in Fig. 14 (Paillous and Pailler 1994).

**Optical and Thermo-Optical Properties**

The macroscopic effect of the degradation of polymers is a change of color of the material, which is coming from the chemical reactions in organic molecules (bond breakage or crosslinking).

It is known that UV radiation can darken optical adhesives and coatings. In this regard, silicones are superior to epoxies. An example is given in Fig. 15 (Fisher et al. 2013). The UV irradiation of several silicone adhesives used for bonding solar cells on panels show a coloration of the glue, which is favored by the creation of crosslinks.

Charged particles may also lead to discoloration of adhesives. Depending on the particles energy, the effect can be observed in the bulk material (Fig. 16).

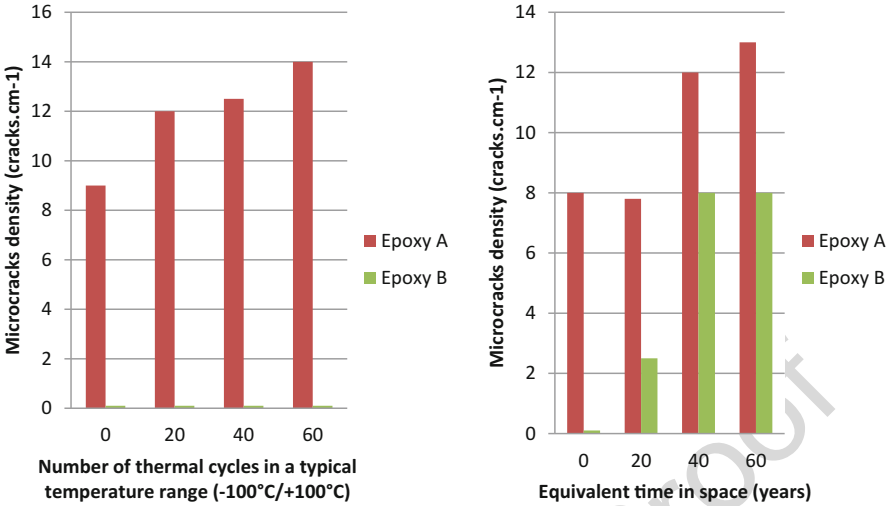


**Fig. 14** Example of typical microcracking evolution: effect of thermal cycling (*left*) and effect of a combined thermal cycling and GEO-simulated environment (*right*) on two different epoxy adhesives. In this example, the Epoxy A is affected by thermal cycling and radiations while the Epoxy B is only affected by radiative environment

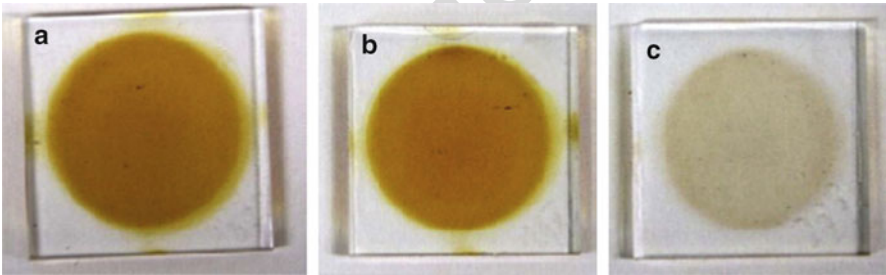


**Fig. 15** Silicone glues used for the assembly of solar cells: Picture of sandwiched samples (coverglass/glue/coverglass) after UV exposure under vacuum using the ESTEC SUV facility, (a) Elastasil S 690, (b) Elastosil S 695, (c) Dow Coming DC 93-500 (Fisher et al. 2013)

An increase of the solar absorptivity can also be observed for polymer adhesive tapes, which can be critical if they are used for satellite thermal control purposes where specific optical properties are needed. Generally, this change is mainly attributed to the polymer substrate, with a slight contribution of the adhesive. As for example, the comparison between 3 M™ 92 (kapton®/silicone) and Permaccel P-224 (kapton®/acrylic) after combined UV and charged particles irradiation shows a slightly higher degradation of the silicone tape, due to the difference in the absorption properties of the adhesive (Marco et al. 2009) (see Fig. 17).



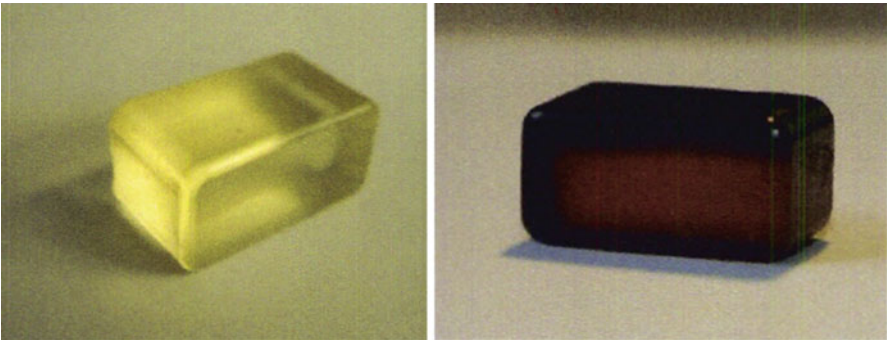
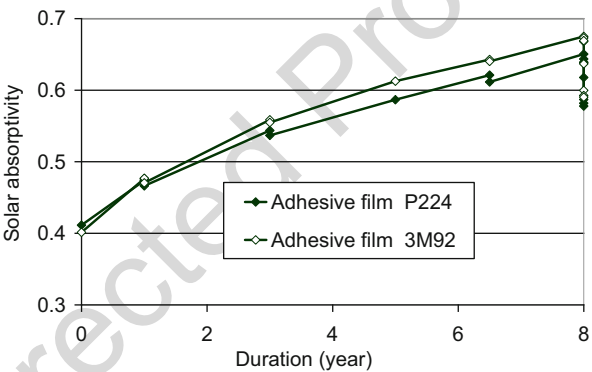


**Fig. 16** Silicone bulk adhesive evidence of color change before and after charged particles irradiation (strong darkening)

**Fig. 17** Solar absorptivity evolution of adhesive tapes after the simulation of 8 years in geostationary environment (Marco et al. 2009). 3 M™ 92 (kapton®/silicone) and Permadel P-224 (kapton®/ acrylic)

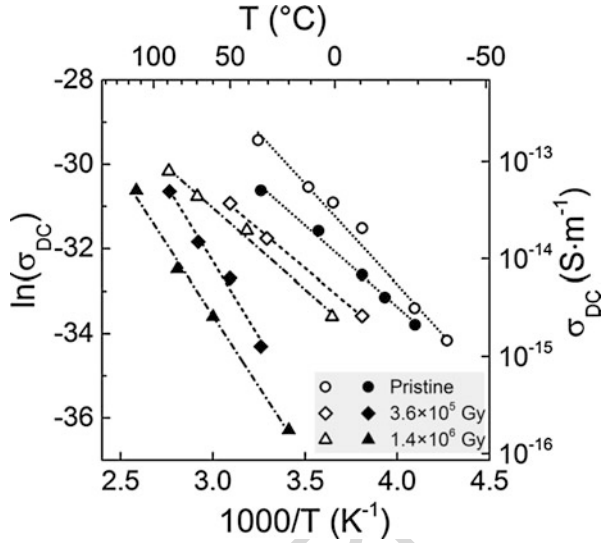


**Electrical Properties**

Changes in the electric conductivity have already been observed on materials after irradiation. This phenomenon results from the interaction of the charged particles of the space environment with materials and is very complex. It depends on the initial electrical conductivity (in surface and in volume), the secondary emission, and the photoemission of the material. In some cases, the accumulation of charges at the surface of the material can be followed by electric discharges and electromagnetic emission, which alters the material locally and can affect the good functioning of electronic equipments.

Epoxy adhesives have generally a good behavior with respect to radiation environment. The irradiation at high-radiation doses has however an effect on the bulk conductivity of epoxies. On Scotch-Weld™ DP490, a decrease of the bulk conductivity can be observed from  $10^{-14} \Omega^{-1} \cdot m^{-1}$  for epoxy pristine samples to  $2 \cdot 10^{-15} \Omega^{-1} \cdot m^{-1}$  after 400 keV electrons irradiation (up to  $10^6$  Gray) (Siegel and Stewart 1969). Indeed, at such dose level, high energy radiation can induce physicochemical ageing which tends to lower ionic transport and therefore the overall bulk conductivity.

**Fig. 18** Arrhenius plot of  $\sigma_{DC}$  as measured by surface potential decay method on irradiated silicone samples: without fillers (open symbols  $\circ, \square, \Delta$ ) and with fillers (filled symbols  $\bullet, \blacksquare, \blacktriangle$ ). Corresponding values of temperature and  $\sigma_{DC}$  are displayed on the upper x-axis and right-hand y-axis, respectively. Arrhenius fits of data are represented by dashed lines (Lewandowski et al. 2016)



Silicone adhesives irradiated in similar conditions (400 keV electrons, up to  $1.4 \cdot 10^6$  Gray) also reveals a decrease in the electrical conductivity (Lewandowski et al. 2016). The behavior of the adhesive is affected by the presence of the inorganic fillers in the formulation, which contribute to enhance the degradation (Fig. 18). A suggested mechanism is the crosslinking in the silicone network and at filler-matrix interfaces. The densification of  $\text{SiO}_3$  crosslinks in the polymer network after irradiation leads to an increase in resistivity. On another hand, if the polymer is charged with inorganic fillers, the  $\text{SiO}_4$  crosslinks generated at filler-matrix interface become the most restrictive barrier to the charge transport, so that the increase of resistivity is higher for charged adhesive than for the neat one.

**Outgassing**

Once in space environment, adhesives are under vacuum, so they exhibit outgassing of volatile and sometimes condensable components, which can become contaminants for critical surfaces. Irradiation can affect the outgassing, as the degradation of the polymer leads to gas generation. Indeed, gas yields are good indicators of radiation resistance and can help in understanding degradation mechanisms.

VUV radiation and protons can increase the outgassing rate of adhesive materials. A study dedicated to the vacuum UV photolysis of a polydimethylsiloxane (PDMS) polymer has indicated the breakdown of the  $\text{Si-CH}_3$  bond as the most probable reaction occurring and resulting in the formation of methane and hydrogen as volatile split-off compounds (Roggero 2015).

Another problem is the liberation of contaminant species when scissions of chains occur. These sources of contamination can affect all the spacecraft and have to be taken into account in contamination studies.



**Fig. 19** Bubbles creation on an acrylic transfer tape due to irradiation (before irradiation on *left*/ after irradiation on *right*).

In the case of very high dose rates, volatile species created during irradiation might not have time to diffuse out of the material. The internal constraints generated by the gas accumulation can then lead to unexpected phenomena.

Figure 19 presents an example of acrylic adhesive degradation after exposure to particles irradiation with a high flux. Outgassing phenomena is highlighted as bubbles are visible below the tape.

## 32.6 Conclusion

Various properties of the adhesives are used on satellites. Indeed, they can be used for optical, thermal, electrical reasons in addition to their more common fixation use. To fulfill all these functions, several materials families are applied as silicones, epoxies, acrylics, or polyurethanes.

In function of their location on a spacecraft and depending on the mission, they can be submitted to different constraints and, among all of them, the specific space environment constraints (charged particles, UV, or Atomic Oxygen). It is important to know and to understand the physicochemical degradations in the adhesive materials due to this environment to evaluate the EOL (end of life) properties and to be able to correctly design the satellites parts.

It is not possible to reproduce the exact space environment on ground; nevertheless, specific test facilities were developed to be able to test as representatively as possible the different materials (including adhesives) and to characterize their degradation. As an example, some of the facilities enable to cumulate UV and different charged particles irradiation under vacuum.

Various effects of space environment can be observed on adhesives in function of the constraint type. The reaction of a material to charged particles, UV and Atomic Oxygen are different and several properties can be affected.

The photochemical effect induced by the interaction of a photon with the material while submitted to UV irradiation may result in a change of color of the adhesive and/or loss of mechanical properties.

While submitted to charged particles irradiation (protons or electrons), the adhesives atoms and molecules can be either excited or ionized. The result consists generally in a first step in a cross linking of the macromolecules and finally in a chain scission while submitted to an increasing ionization dose level. The overall mechanical properties of the adhesives are generally impacted with an increase of the adhesive stiffness associated to an additional brittleness.

Atomic Oxygen can also react with polymers and, for the sensitive materials, a surface erosion is generally the main effect.

Adhesives are used on spacecraft for various applications. Depending on the satellite mission, the use and location of the adhesive, the undergone environment can be very different, leading to various material degradations mechanisms.

In the future, two different ways forward for adhesives on the space industry could be considered:

- Specific developments and formulation of adhesives used on scientific programs for dedicated applications (functionalization of the adhesives). These specific developments would take into account the behavior of the organic compound with regards to space constraints.
- Using more commercial adhesives not specifically developed to withstand the space constraints (charged particles, Atomic Oxygen, or UV). In this case, there will not have specific developments but an adaptation of the spacecraft design to take into account the adhesive limitations and its degradation due to the environment.

In both cases, it is important to know and to understand the behavior of adhesives in space environment and the physicochemical phenomenon associated. The tests performed on ground in dedicated facilities and the R&D studies on this really specific domain are thus a major point in the future of space programs.

---

## References

- ASTM E-490 Standard. Solar constant and zero air mass solar spectral irradiance tables
- ASTM E512 Standard. Practice for combined simulated space environment testing of thermal control materials with electromagnetic and particulate radiation. American Society for Testing and Materials, Philadelphia
- ASTM.E.490A Standard. Solar constant and zero air mass solar spectral irradiance tables
- Roggero A (2015) Analyse du vieillissement d'un adhésif silicone en environnement spatial: influence sur le comportement électrique », CIRIMAT/ONERA. PhD thesis
- Banks BA, Dill GC, Loftus RJ, de Groh KK, Miller SK (2013) Comparison of hyperthermal ground laboratory atomic oxygen erosion yields with those in low earth orbit. NASA/TM—2013-216613
- Clegg DW, Collyer AA (1991) Irradiation effects on polymers. Elsevier Applied Science, London/New York
- ECSS-Q-ST-10-04C (2008) Space engineering: critical item control
- ECSS-Q-ST-70-06C (2008) Space product assurance: particle and UV radiation testing for space materials

- Fisher HR et al (2013) Degradation mechanism of silicone glues under UV irradiation and options for designing materials with increased stability. *Polym Degrad Stab* 98:720–726
- Fornes E et al (1981) The effects of electron and gamma radiation on epoxy based materials. 3rd annual technical review, Nov 16–19
- <https://www.britannica.com/science/Van-Allen-radiation-belt>
- [https://www.nasa.gov/mission\\_pages/sunearth/news/gallery/20130228-radiationbelts.html](https://www.nasa.gov/mission_pages/sunearth/news/gallery/20130228-radiationbelts.html)
- <https://www.newport.com/n/solar-simulator-spectral-irradiance-data>. Newport light sources. Technical note: “solar simulator spectral irradiance data”
- Jochem H et al (2013) Effects of 400 keV electrons flux on two space grade silicone rubbers. *Mater Chem Phys* 141:189–194
- Kleiman J, Iskanderova Z, Gudimenko Y, Horodetsky S (2003) Atomic oxygen beam sources: a critical overview. Proceedings of the 9th international symposium on materials in a space environment, Noordwijk, 16–20 June 2003
- Lewandowski S et al (2016) Particle flux effects on physicochemical polymer degradations. *J Spacecr Rocket* 53(6):1146–1151. <https://doi.org/10.2514/1.A33500>
- Makhlis FA (1975) Radiation physics and chemistry of polymers. *J Chem Educ* 53(2):138. <https://doi.org/10.1021/ed053pA138.1>
- Marco J, Remaury S, Tonon C (2009) Eight years GEO ground testing of thermal control coatings. ISMSE 11 – unpublished
- NASA-HDBK-6024 (2014) Spacecraft polymers atomic oxygen durability handbook
- Paillous A (1993) Radiation damage to surface and structure materials. In: The behavior of systems in the space environment, pp 383–405. [https://doi.org/10.1007/978-94-011-2048-7\\_17](https://doi.org/10.1007/978-94-011-2048-7_17)
- Paillous A, Pailler C (1994) Degradation of multiply polymer-matrix composites induced by space environment. *Composites* 25(4):287–295
- Siegel S, Stewart T (1969) Vacuum-ultraviolet photolysis of polydimethylsiloxane. Gas yields and energy transfer. *J Phys Chem* 73:823–828
- “Space weather effect catalogue” ESTEC/Contract No.14069/99/NL/SB; ESA Space Weather Study (ESWS); WP 310 Range of space weather and effects (ESWS-FMI-RP-0001)
- Tavlet M, Hominal L (1997) Shear tests on adhesive for magnet collars for the LHC. *Cryogenics* 38(1998):47–50
- Tonon C (2000) PhD thesis, ENSAE
- Van de Voorde M, Restat C (1972) Selection guide to organic materials for nuclear engineering. CERN technical report, pp 72–77
- Zhang L et al (2006) Effect of 200 keV proton irradiation on the properties of methyl silicone rubber. *Radiat Phys Chem* 75:350–355

Ian A. Ashcroft

## Contents

33.1	Introduction .....	942
33.2	General Considerations .....	943
33.2.1	Fatigue Loading .....	943
33.2.2	Fatigue Initiation and Propagation .....	945
33.2.3	Fatigue Testing .....	946
33.3	Factors Affecting Fatigue Behavior .....	947
33.3.1	Load Factors .....	947
33.3.2	Environmental Factors .....	948
33.4	Prediction Methods .....	950
33.4.1	Total-Life Methods .....	950
33.4.2	Phenomenological Methods .....	955
33.4.3	Fracture Mechanics Methods .....	959
33.4.4	Damage Mechanics Methods .....	964
33.5	Creep-Fatigue .....	966
33.6	Impact Fatigue .....	970
33.7	Conclusion .....	971
	References .....	972

## Abstract

Fatigue involves the failure of materials under cyclic loading, where the maximum load can be significantly lower than that required to cause static failure. Polymeric adhesives, as with most materials, are susceptible to fatigue failure, and hence, fatigue should be accounted for when designing bonded structures subjected to cyclic loading. Adhesive joints have potentially good fatigue resistance compared with other joining methods; however, they are also susceptible to accelerated fatigue failure due to the combined actions of fatigue with

I. A. Ashcroft (✉)

Faculty of Engineering, University of Nottingham, Nottingham, UK

e-mail: [ian.ashcroft@nottingham.ac.uk](mailto:ian.ashcroft@nottingham.ac.uk)

environmental ageing and/or viscoelastic creep. In this chapter, the effect of the environment and various fatigue loading parameters on the fatigue behavior of adhesively bonded joints is discussed before describing the main methods of characterizing and predicting fatigue. Traditionally, fatigue behavior has been characterized through the use of experimentally derived stress–life plots, and fracture mechanics-based progressive crack growth methods have also been widely discussed. In more recent years, damage mechanics-based progressive modeling methods have been proposed that have the advantage of predicting both initiation and crack progression phases of fatigue and have also been shown to be readily adapted to the prediction of variable amplitude fatigue and combined fatigue–environmental ageing. The chapter finishes with descriptions of two special cases of fatigue: creep-fatigue and impact fatigue, which have been shown to be extremely detrimental to the fatigue life of bonded joints under certain conditions.

---

### 33.1 Introduction

In engineering, fatigue relates to the failure of a structure under cyclic loading, generally, at a significantly lower load than that required for quasistatic failure. Some form of fatigue loading is present in most engineering structures, for example, aircraft, ships, cars, buildings, and bridges, and is also seen in many nonengineering applications, such as sports equipment, furniture, and even human parts, such as knees and elbows. Fatigue is a particularly dangerous phenomenon as it can result in sudden, catastrophic failure after many years, or decades, of safe service. This is because a long period can be spent in the initiation phase of fatigue damage, in which there are little or no outward signs of damage. Damage can accelerate unstably once a critical degree of damage has been attained, leading to rapid failure of the structure. Fatigue damage can be initiated or accelerated by many factors, such as accidental impact, overloading, corrosion, surface damage, and abrasion.

The ubiquitous nature and potentially disastrous effect of fatigue in engineering structures means that in applications where cyclic loading is significant, the designer must attempt to design against fatigue failure. Unfortunately, the stochastic nature of fatigue damage means it is difficult to predict accurately. This difficulty is compounded by the fact that the in-service loading and environment of many engineering components, which can significantly affect the fatigue process, are seldom known to a great degree of accuracy. Hence, it is generally difficult to design against fatigue failure without resorting to large safety factors, and hence incurring the large structural inefficiencies associated with overdesign, with subsequent cost and performance consequences. An alternative to designing against fatigue failure is to monitor parts for fatigue damage at prescribed intervals and remove them from service before damage reaches a critical point. This is a useful and efficient method of preventing fatigue failure where crack growth is stable and can be easily monitored. However, in some cases, such as is often the case with adhesive joints, monitoring fatigue damage is difficult, for example, if the damage initiation is in an

inaccessible location or the critical crack size before rapid fracture is small. In this case, an alternative strategy is required to combat fatigue, such as automatic replacement of parts after the design life or a “safe fail” design.

One of the benefits of bonded joints is that stresses are more uniformly distributed than in riveted or bolted joints. However, stress concentrations will, of course, still exist in bonded joints, as discussed in detail in ► Chaps. 24, “Analytical Approach,” and ► 25, “Numerical Approach: Finite Element Analysis.” Another potential advantage is that the bonding process does not explicitly weaken the adherends as the high temperatures and phase transformations involved in welding and the hole drilling required for rivets and bolts can. Although, it should be noted that there are likely to be stress concentrations in the adherend in the joint area which may initiate adherend fatigue failure, such as is seen in aluminum adherend single-lap joints at high cycles and in the delamination of composite adherends. In general, adhesively bonded joints perform well in fatigue compared with bolted and welded joints; however, a number of potential problems for adhesive joints subjected to fatigue should also be recognized. Both the adhesive and the interfacial region between adhesive and adherend are potentially sensitive to the environment and this will affect the fatigue resistance of the joint. Adhesives can also be susceptible to creep under certain conditions, and combined with fatigue this can lead to accelerated failure. In a bonded joint, failure can occur in the adhesive, in the adherend, or in the interfacial region between the two, and the relative fatigue resistance of the various components is dependent on many factors, such as geometry, environment, and loading, and may vary as damage progresses. This complex failure process means that it can be difficult to accurately predict fatigue failure in adhesively bonded joints under real service conditions.

Section 2 discusses some of the main factors when considering fatigue, with particular reference to issues applicable to bonded joint. Section 3 discusses how various loading parameters and environmental conditions affect the fatigue behavior of bonded joints. Section 4 presents the main methods of characterizing and predicting the response of bonded joints to fatigue loading. Finally, there are sections on the special cases of creep-fatigue and impact fatigue (Sects. 5 and 6), before the final summary and conclusion.

---

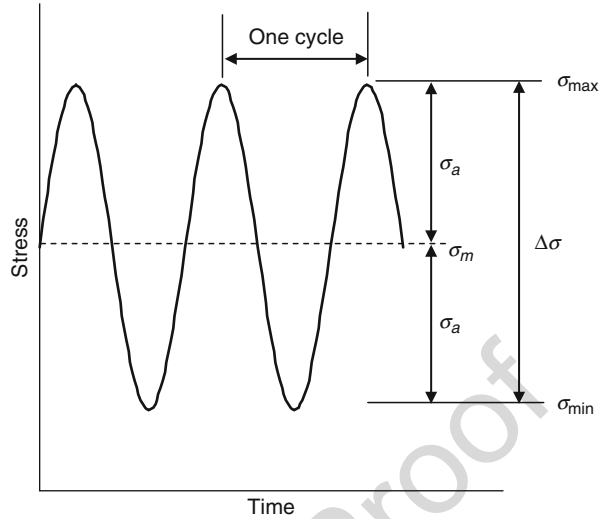
## 33.2 General Considerations

### 33.2.1 Fatigue Loading

In fatigue, the load varies with time, and the load spectrum is usually characterized in terms of peaks and troughs in the varying load. A fatigue cycle is defined as the time between adjacent peaks, and the fatigue frequency is the number of cycles in a unit time, for example, Hz (cycles per second). A fatigue spectrum can be characterized in terms of the applied load or displacement for simple samples, but in more complex structures, it is often more useful to consider the cyclic stress (or some other



**Fig. 1** Constant amplitude, constant frequency, stress-controlled, sinusoidal waveform

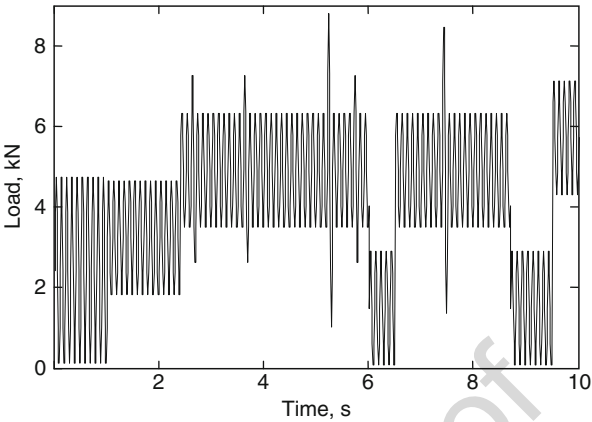


parameter that can be related to failure, such as strain or strain energy release rate) in areas of possible fatigue failure.

It is common in laboratory experiments to represent fatigue as a constant amplitude, sinusoidal waveform, as illustrated in Fig. 1. This is termed constant amplitude fatigue (CAF) and the waveform may be defined by the frequency and two stress parameters, such as the maximum stress ( $\sigma_{\max}$ ) and the stress amplitude ( $\sigma_a$ ). Other parameters defined in Fig. 1 are the mean stress ( $\sigma_m$ ), the minimum stress ( $\sigma_{\min}$ ), and the stress range ( $\Delta\sigma$ ). In most engineering applications, however, it is likely that frequency, amplitude, mean, and waveform will vary with time. This is called variable amplitude fatigue (VAF). The first step in analyzing components subjected to VAF is the characterization of fatigue spectra experienced by the component in service. It is possible to characterize the in-service load spectra through simulation or experimentation. In some cases, a typical spectrum may be repeated throughout the structure's life and will be similar for each structure manufactured, for example, the takeoff and landing sequences of a commercial passenger aircraft or the run-up sequence of power generation equipment. However, for many applications, e.g., private cars, the spectra can vary considerably from unit to unit. In this case, a "worst-case scenario" or statistical approach may have to be taken.

Once the in-service load spectrum has been generated, it can be used in simulations and/or testing. In order to accelerate a fatigue test program, it is generally preferable to reduce the spectrum. In metals, where the materials may be rate insensitive over a large range, an easy method of accelerating tests is to compress the spectrum by testing at high frequency, although any time-dependent effects, such as corrosion or creep, will not be accurately represented in such a test. Hence, when devising accelerated service simulation tests for adhesive joints, care must be taken

**Fig. 2** Example of a load-controlled, variable amplitude waveform



when introducing acceleration techniques that any influential time-dependent or load sequencing effects are retained in the spectrum. Another way of reducing the spectrum is to remove cycles from the spectrum that do not contribute to the fatigue damage. Figure 2 shows a reduced fatigue spectrum used to represent the fatigue loading on an aircraft wing. It can be seen that this is a load-controlled fatigue spectrum that includes changes in the load amplitude and mean, but maintains a constant frequency.

### 33.2.2 Fatigue Initiation and Propagation

The fatigue life of a structure is often divided into initiation and propagation phases. In adhesively bonded joints, the differentiation between these two phases, and even if there really are two such phases, remains a contentious issue. At the predictive modeling level, a distinction can be made between how a propagating crack is analyzed and how the number of cycles before a macrocrack has formed can be predicted, and this can pragmatically be used to differentiate between the initiation and propagation phases.

Fatigue initiation in adhesives is a complex and little-understood process. Commercial adhesives are multicomponent materials, with filler particles, carrier mats, and toughening particles typically added, and failure may involve many mechanisms, including matrix microcracking (initiation, growth, and coalescence), filler particle fracture or debonding, cavitation of rubber toughening particles, and debonding of carrier mat fibers. An additional difficulty in characterizing the fatigue initiation process in bonded joints is that initial damage tends to be internal. This makes nondestructive characterization difficult, whereas with destructive characterization methods, it is difficult to avoid sectioning artifacts. In most cases, a purely mechanistic definition of the initiation and propagation phases is not achievable, and a more pragmatic approach must be taken. In terms of in-service inspection,

initiation may be linked to the detectability of flaws, the end of the initiation life being indicated by the first detection of a crack using whatever technique is being deployed. For the stress analyst, a useful differentiation is to treat the fatigue damage as an initiation phase until a sufficient crack has formed that further growth can be predicted using fracture mechanics. In finite element-based damage mechanics, the initiation phase can be defined as the period before complete damage of an element.

Mechanistically, there is also a blurring between the definitions of “damage” and “cracking” in a bonded joint. For example, a region considered as damaged rather than cracked will often contain microcracking, and in a cracked joint, only an idealized version of the main macrocrack is usually considered, whereas this will almost certainly be accompanied by other types of damage in a process zone ahead and around the main crack. In finite element modeling, damage is often represented by reducing the material properties (the continuum damage mechanics approach), usually stiffness, of an element. Cracking is usually modeled by detaching elements at nodes, after which fracture mechanics methods can be used to model crack propagation. In cohesive zone modeling, both damage and crack growth are represented by using specialized elements to join adjacent continuum elements. This is discussed in detail in ► [Chap. 25, “Numerical Approach: Finite Element Analysis.”](#)

### 33.2.3 Fatigue Testing

Mechanical testing of bonded joints can range from inexpensive coupon tests through the testing of structural elements to the testing of full prototypes, which may be extremely expensive. In all cases, however, fatigue testing will be considerably lengthier and more costly than quasistatic testing.

Coupon tests can fulfil a number of roles. Single material tests may be used to generate material property data, while joints can be tested to compare material systems or joint geometries, evaluate performance over a range of loading and environmental conditions, generate design data, or provide validation data for predictive models. Coupon samples used in the fatigue testing of bonded joints are similar to those used in quasistatic testing, as discussed in ► [Chaps. 19, “Failure Strength Tests,”](#) and ► [20, “Fracture Tests.”](#) Simple lap joints, such as single- and double-lap joints, are generally used to generate stress–life ( $S$ – $N$ ) curves, and standard fracture mechanics tests, such as the double cantilever beam, are used to generate fatigue crack growth curves. The fatigue testing of adhesive lap joints is covered by the standards BS EN ISO 9664:1995 and ASTM D3166-99. In the former, it recommends that at least four samples should be tested at three different stress amplitude values for a given stress mean, such that failure occurs between  $10^4$  and  $10^6$  cycles. This standard also advises on statistical analysis of the data. In general, fatigue data exhibits greater scatter than quasistatic data and this needs to be taken into account when using safety factors with fatigue data. Further advice on the application of statistics to fatigue data can be found in BS 3518-5:1966.

### 33.3 Factors Affecting Fatigue Behavior

#### 33.3.1 Load Factors

Load factors that will affect the fatigue behavior of adhesively bonded joints include the amplitude, mean, and minimum stresses and frequency. In common with most materials, fatigue life in a bonded joint will tend to decrease if the stress amplitude or the mean stress increases. The maximum stress is also important. If this is greater than the yield stress, then low cycle fatigue (LCF) will occur, greatly reducing the fatigue life. In some cases, a critical stress, called an endurance limit, may exist, below which fatigue failure will not occur. As adhesives tend to be viscoelastic or viscoplastic in nature, then a nonzero mean stress can lead to progressive creep of the joint over time. This is exacerbated at low frequencies, where time under load may become as significant as number of cycles in defining failure. At high frequencies, hysteretic heating may lead to premature failure or the high strain rates involved may induce brittle fracture. High strain rates are also seen in impact fatigue, in addition to dynamic effects, which, as discussed in Sect. 6, can be extremely detrimental to adhesives. Most bonded joints are designed for tensile loading, and if the joint is subjected to accidental compressive loading, then buckling may occur, from which high peel forces will arise, leading to rapid fracture.

In variable amplitude fatigue, load interaction effects have been observed to both accelerate and retard the rate of fatigue damage, in different materials. Fatigue crack growth rate retardation is probably the more commonly reported phenomenon. For example, it is generally reported that overloads retard fatigue crack propagation in ductile metals. Proposed mechanisms to account for this phenomenon include the effect of compressive residual stresses in the vicinity of the crack tip, crack tip closure effects, and crack tip blunting. Although neglecting such beneficial effects by using a noninteractive lifetime predictive methodology can remove the opportunity to achieve a lighter structure, at least, the design errs on the side of safety. However, if the load interactions cause crack growth acceleration, the structure under investigation can fail much earlier than predicted using CAF data and a noninteractive prediction methodology. Although most published work indicates retardation behavior after an overload, there is also work in the literature reporting crack growth acceleration for both metals and composites. These studies report several different mechanisms accounting for the acceleration behavior. For example, Nisitani and Nakamura (1982) studied the crack growth behavior of steel specimens tested under a spectrum composed of a very small number of overloads and a very large number of cycles below or near the fatigue limit. They observed that the application of a linear cumulative damage rule resulted in extremely nonconservative predictions of fatigue life. A possible explanation was that although understress cycles cannot initiate a crack, they can potentially contribute to the fatigue damage created by overloads. Farrow (1989) found that the fatigue life of composite laminates subjected to small block loading was shorter than that for laminates subjected to large block loadings when the blocks had different mean stress levels. He called this phenomenon the “cycle mix effect.” Schaff and

Davidson (1997a, b) reviewed the study made by Farrow and developed a strength-based wearout model. They suggested that the cycle mix effect occurred during the transition from one CAF stage to another having a higher mean stress value, although they did not discuss the mechanisms behind the strength degradation during this transition. Erpolat et al. (2004a) observed a similar crack acceleration effect when VAF testing bonded CFRP double-lap joints.

**33.3.2 Environmental Factors**

It is well known that adhesives and adhesion can be adversely affected by factors in the natural environment effects, and that this is a topic of considerable complexity (see ► Chap. 31, “Effect of Water and Mechanical Stress on Durability”). When environmental effects are combined with fatigue testing, we have an added complexity, owing to the introduction of coupled time-dependent effects. The main effects of environmental exposure can be classified as those affecting the adhesive, those affecting the adherend, and those affecting the interface (or interphase) between the two. In terms of the adhesive, an increase in temperature or the absorption of moisture generally results in plasticization of the adhesive, with an accompanying reduction in modulus and failure load. However, strain to failure and fracture toughness may increase. This can affect fatigue initiation and propagation in a number of ways. The plasticization will tend to reduce stress concentrations, although stresses may now be significant over a larger area; hence, the resistance to brittle fatigue failure may increase, but the resistance to creep-fatigue may decrease. These effects will become more significant close to the glass transition temperature ( $T_g$ ), and similarity can be seen between the effects of absorbed moisture, increased temperature, and decreased test rate (or frequency). Some of these issues are illustrated by the results shown in Table 1 (data from Ashcroft et al. 2001a, b). This table shows the fatigue limits for bonded CFRP lap-strap and double-lap joints. In the case of the lap-strap joints, it can be seen that temperature has little effect on

**Table 1** Effect of environment on the fatigue limit for bonded CFRP-epoxy lap-strap and double-lap joints (Data from Ashcroft et al. 2001a, b)

Sample	Preconditioning	Test conditions	Fatigue limit (kN)
Lap-strap joint	Vacuum desiccator	−50 °C/ambient	14
		22 °C/ambient	15
		90 °C/ambient	14
		90 °C/97% RH	7
	45 °C/85% RH	22 °C/95% RH	15
		90 °C/ambient	5
		90 °C/97% RH	5
Double-lap joint	Vacuum desiccator	−50 °C/ambient	10
		22 °C/ambient	10
		90 °C/ambient	3.3

the fatigue threshold of those sample stored and tested in nominally dry conditions. However, samples tested in hot-wet conditions experience a significant reduction in the fatigue threshold. Samples were also conditioned under high humidity conditions until saturation. Samples subsequently tested wet at 22 °C had no change in the fatigue threshold compared to those tested dry, whereas samples tested at 90 °C, whether wet or dry, experienced a large reduction in the fatigue threshold. Interpretation of these results is complicated by the fact that complex mixed mode failure paths were observed. In order to explain these results, the effect of temperature and moisture on the mechanical behavior of the adhesive must be considered. The stress to failure and modulus of the adhesive decreases as the temperature increases, but the strain to failure and total strain energy density at failure increases. The competing effects of these different trends conspire to maintain the fatigue limit at a relatively constant value between 22 °C and 90 °C when stored and tested dry. Differential thermomechanical analysis (DTMA) was carried out on samples saturated to different moisture levels, and it was seen that for every 1% of moisture absorbed, the glass transition point of the adhesive decreased by approximately 15 °C. As the  $T_g$  of this adhesive is approximately 130 °C, the saturated adhesive tested at 22 °C would not be expected to behave markedly differently from those tested dry at 22 °C and 90 °C. However, the saturated sample tested at 90 °C is in the glass transition temperature range as the adhesive is capable of absorbing 3–4% of moisture. It is clearly less capable of resisting stress under these conditions, and hence the fatigue limit is greatly reduced. If the lap-strap results are now compared with the results from testing double-lap joint manufactured using the same materials, it can be seen in Table 1 that whereas the lap-strap joints are relatively temperature insensitive over the test range when dry, the double-lap joints experience a large decrease in fatigue resistance as temperature is increased from 22 °C to 90 °C. This can be attributed to creep-enhanced failure at the higher temperature in the double-lap joint, which experiences accumulated creep because the joint remains under a tensile load throughout the fatigue testing. This phenomenon is prevented in the case of the lap-strap joints because the CFRP strap adherend spanning the loading points remains elastic. The combined effects of fatigue and creep are discussed further in Sect. 5.

Moisture can also affect the interface between the adhesive and adherend, and this can significantly affect the fatigue behavior of a bonded joint. For example, Little (1999) carried out fatigue tests on aluminum single-lap joints bonded with the same adhesive as that in the experiments discussed above. He found that with chromic acid-etched (CAE) adherends, there was little difference in the fatigue threshold of those samples tested dry and those tested immersed in distilled water at 28 °C. However, samples with grit-blasted and degreased (GBD) adherends exhibited a significantly lower fatigue threshold when tested wet, and the locus of failure changed from cohesive failure in the adhesive to failure in the interfacial region. Datla et al. (2011a) also investigated the combined effects of temperature and humidity on the fatigue behavior of adhesive joints with pretreated aluminum adherends. In their case, an asymmetric double cantilever beam was used and it was found that for their system, the joint degradation was mainly influenced by

elevated temperature at high crack growth rates and elevated moisture at low crack growth rates. They also investigated the effect of a cyclic ageing environment for this joint, with intermittent salt spray on these joints (Datla et al. 2011b) and found superior fatigue performance compared with joints subjected to constant humidity ageing. They attributed this to salt water environment causing lower water concentrations in the adhesive. For further reading on this subject, Costa et al. (2017) have recently reviewed the published literature regarding the effect of environmental conditions and ageing on fatigue performance.

### 33.4 Prediction Methods

The ability to predict the fatigue behavior of bonded joints is potentially useful for a number of reasons. Firstly, it can be used to support the design of bonded structures, to ensure that fatigue failure is not likely to occur in service, and to aid in the design of efficient fatigue-resistant joints, resulting in safer, cheaper, and higher performance structures. Analytical or computational predictive modeling can help in these objectives; however, the current state of confidence in such modeling means that in most cases, it must be accompanied by a complementary testing program. Modeling can also be helpful in developing and understanding of the mechanisms involved in fatigue failure. This can be achieved through comparing the results from carefully designed experimental tests with the predicted results from progressive damage models. Finally, predictive modeling can be used to support the in-service monitoring and re-lifeing of structures.

The main goals in the modeling of fatigue are to predict the time (or number of cycles) for a certain event to occur (such as macrocrack formation, critical extent of damage, or complete failure) or to predict the rate of change of a fatigue-related parameter, such as crack length or “damage.” The various methods of doing this are presented in this section, and the approach used is to introduce and describe each of the main methods that have been used to date, together with one or two examples of their application to bonded joints.

#### 33.4.1 Total-Life Methods

In the total-life approach, the number of cycles to failure ( $N_f$ ) is plotted as a function of a load-related variable, such as stress or strain amplitude. Where the loading is low enough that the deformation is predominantly elastic, a stress variable ( $S$ ) is usually chosen and the resultant plot is termed an  $S$ – $N$  curve, or Wöhler plot, and this is known as the stress–life approach. Under these conditions, a long fatigue life is often seen, and hence this is sometimes termed “high cycle fatigue” (HCF). The  $S$ – $N$  data is either plotted as a log-linear or a log-log plot and a characteristic equation can be obtained by empirical curve fitting. The constants in the curve-fitted equations are dependent on many factors, including material, geometry, surface condition, environment, and mean stress. Caution should be exercised when trying to apply  $S$ – $N$



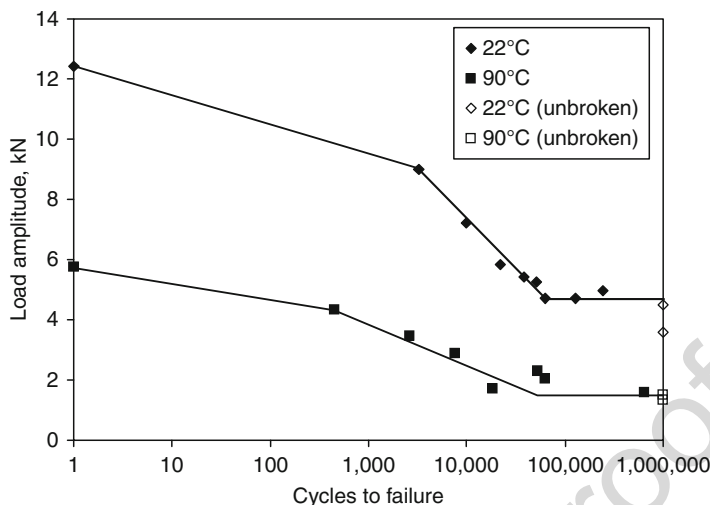


**Fig. 3** Load-life curve for CFRP-epoxy double-lap joints (Data from Ashcroft et al. 2001b)

data beyond the samples and conditions used to generate the data. The standard stress-life method gives no indication of the progression of damage, although in some cases, the onset of cracking is indicated on the plot in addition to the complete failure, hence allowing the initiation and propagation phases to be differentiated. The above factors mean that the  $S-N$  curve is of rather limited use in predicting fatigue behavior; however, it is still useful as a design tool and in fatigue modeling as a source of validation data. A further limitation in the application of  $S-N$  curves to fatigue prediction in bonded joints is that there is no unique relation between the easily determined average shear stress in the adhesive layer and the maximum stress. For this reason, load rather than stress is often used in total-life plots for bonded joints and these are known as  $L-N$  curves. A typical  $L-N$  curve for epoxy-bonded CFRP double-lap joints is shown in Fig. 3. It can be seen that the  $L-N$  curve can be divided into a number of different regions: a low cycle fatigue (LCF) region below approximately 1000 cycles, a high cycle fatigue (HCF) region between approximately 1000 and 100,000 cycles, and an endurance limit region above approximately 100,000 cycles.

Fatigue life depends not only on the load amplitude but also on the mean load as either increasing the mean or increasing the amplitude tends to result in a reduction of the fatigue life. This is illustrated in Fig. 4a, which shows results from fatigue testing steel-epoxy single-lap joints at different load amplitudes and  $R$ -ratios (maximum load/minimum load), where an increasing value of  $R$  indicates an increasing mean for a given load range. It can be seen that either increasing the mean or increasing the amplitude results in a reduction of the fatigue life. The relationship between amplitude and mean on the fatigue life can be illustrated in a constant-life diagram in which combinations of mean and amplitude are plotted for a given fatigue life. A constant-life diagram plotted from the data in Fig. 4a is shown in Fig. 4b. This



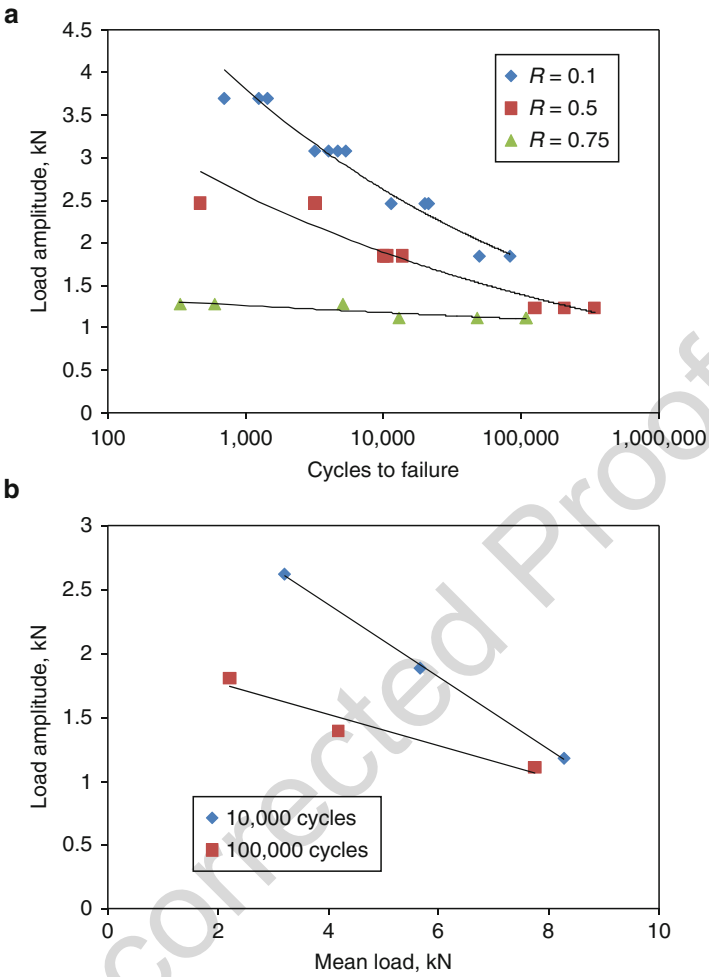


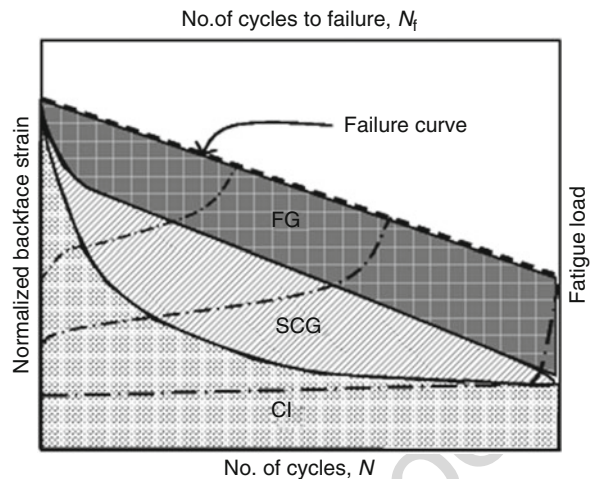
**Fig. 4** (a) Effect of  $R$ -ratio on fatigue life. (b) Constant-life diagram (Data from Crocombe and Richardson 1999)

relationship can be represented by the Goodman (linear) or Gerber (parabolic) relationships (Dowling 1999). It can be seen that in this case, a linear relationship provides a reasonable fit to the experimental data.

In some cases, efforts have been made to differentiate between the initiation and propagation phases in the  $S-N$  behavior of bonded joints. Shenoy et al. (2009a) used a combination of back-face strain measurements and sectioning of partially fatigued joints to measure damage and crack growth as a function of number of fatigue cycles.

It was seen from the sectioned joints that there could be extensive internal damage in the joint without external signs of cracking; therefore, determination of an initiation phase from external observations alone is likely to lead to an

**Fig. 5** Enhanced load–life curve for adhesively bonded single-lap joints, showing regions of crack initiation (CI), stable crack growth (SCG), and fast crack growth (FG). The broken lines show back-face strain as a function of number of cycles (Shenoy et al. 2009a)



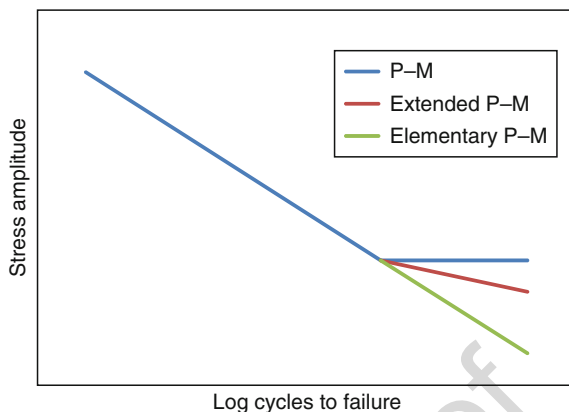
overestimation of the percentage of the fatigue life sent in initiation. Shenoy et al. (2009a) identified three regions in the fatigue life of an aluminum/epoxy single-lap joint, as illustrated in Fig. 5. An initiation period (CI) in which damage starts to accumulate, but a macrocrack has not yet formed, a stable crack growth (SCG) region in which a macrocrack has formed and is growing slowly, and a fast crack growth region (FCG), which leads to rapid failure of the joint. It was seen that the percentage of life spent in each region varied with the fatigue load. At low loads, the fatigue life was dominated by crack initiation, whereas crack growth dominated at high loads. The broken lines in Fig. 5 show how the back-face strain signal varies as a function of fatigue cycles. This can be used to characterize the different phases of crack growth, in particular a rapid change in the back-face strain is seen when the fatigue failure enters the fast crack growth region.

The  $S$ – $N$  (or  $L$ – $N$ ) curve is only directly applicable to constant amplitude fatigue, whereas in most practical applications for structural joints a variable amplitude fatigue spectrum is more likely. A simple method of using  $S$ – $N$  data to predict variable amplitude fatigue is that proposed by Palmgren (1924) and further developed by Miner (1945). The Palmgren–Miner (P–M) rule can be represented by

$$\sum \frac{n_i}{N_{fi}} = C \quad (1)$$

where  $n_i$  is the number of cycles in a constant amplitude block,  $N_{fi}$  is the number of cycles to failure at the stress amplitude for that particular block and can be obtained from the  $S$ – $N$  curve, and  $C$  is the Miner's sum and is ideally assumed to equal 1. Using Eq. (1), the fatigue life of a sample in variable amplitude fatigue can be predicted from an  $S$ – $N$  curve obtained from constant amplitude fatigue testing of similar samples. However, there are a number of serious limitations to this method, primarily, the assumptions that damage accumulation is linear, that there is no damage below the fatigue threshold, and that there are no load history effects.

**Fig. 6** Comparison of P–M, extended P–M, and elementary P–M methods of predicting variable amplitude fatigue cycles to failure



Modifications to the P–M rule have been suggested to address some of the deficiencies; for instance, the extended and elementary P–M rules shown in Fig. 6 have been proposed to allow cycles below the fatigue threshold to contribute to the damage sum. Modifications to account for nonlinear damage accumulation and interaction effects have also been suggested; however, any improvements are at the expense of increased complexity and/or increased testing requirements, and the basic flaw in the method, i.e., that it bears no relation to the actual progression of damage in the sample, is still not addressed. Erpolat et al. (2004a) used the P–M law and the extended P–M law, in which cycles below the endurance limit also contribute to damage accumulation, to predict failure in an epoxy-CFRP double-lap joint subjected to a variable amplitude (VA) fatigue spectrum. The resulting Miner's sum was significantly less than 1, varying between 0.04 and 0.3, and decreased with increasing load. This indicates that load sequencing is causing damage acceleration, i.e., that the P–M rule is nonconservative in this case.

Some materials exhibit a stress level below which fatigue failure will not occur, known as the fatigue or fatigue limit. In this case, it may be possible to use the data from one sample to predict the fatigue limit for a different geometry or loading condition. A useful method is to experimentally determine the fatigue limit using a calibration sample and to then calculate the value of a suitable failure parameter at the fatigue limit. The fatigue limit can then be predicted for different geometries for failure in the same material by determining the load at which the fatigue limit value of the chosen failure parameter is reached in the new geometry. This is a potentially attractive method as the fatigue threshold value of the chosen failure criterion can be determined from an inexpensive test and then used to predict the fatigue limit for joints that would be expensive to test experimentally. However, in practice, there are the same difficulties as those in the prediction of the quasistatic failure load of adhesive joints, i.e., selection of an appropriate and robust failure criterion, dealing with the theoretical stress singularities, scaling issues and differences in the stress conditions in the simple test and application joints. Abdel Wahab et al. (2001a) predicted the fatigue threshold in CFRP-epoxy lap joints using a variety of stress- and strain-based failure criteria, taking the value of stress and strain at a distance of

0.04 mm from the singularity to avoid mesh sensitivity. They also used the plastic zone size as a failure criterion.

Under high stress amplitudes, plastic deformation occurs and the fatigue life is considerably shortened. This is known as “low cycle fatigue” (LCF). Coffin (1954) and Manson (1954) proposed that  $N_f$  could be related to the plastic strain amplitude,  $\Delta\epsilon_p/2$ , in the LCF region.

$$\frac{\Delta\epsilon_p}{2} = B(N_f)^\beta \quad (2)$$

where  $B$  and  $\beta$  are material constants. The strain–life approach is more difficult to implement than the stress–life method as plastic strain is difficult to measure, particularly for nonhomogenous material systems such as bonded joints. Also, structural joints tend to be used in HCF applications, and hence the strain–life method has seen little application to adhesively bonded joints. Abdel Wahab et al. (2010a, b) proposed a low cycle fatigue damage law based on continuum damage mechanics and applied this to bulk adhesive samples and single-lap joints.

### 33.4.2 Phenomenological Methods

In the phenomenological approach, fatigue damage is characterized as a function of a measurable parameter, most commonly the residual strength or stiffness after fatigue damage. The reduction in stiffness with fatigue damage, known as stiffness wearout, has the advantage that it can be measured nondestructively; however, it is not directly linked to a failure criterion and may not be very sensitive to the early stages of damage. The strength wearout method provides a useful characterization of the degradation of residual strength, but requires extensive destructive testing. In the strength wearout method, the joint’s strength is initially equal to the static strength,  $S_u$ , but decreases to  $S_R(n)$  as damage accumulates through the application of  $n$  fatigue cycles. This degradation can be represented by:

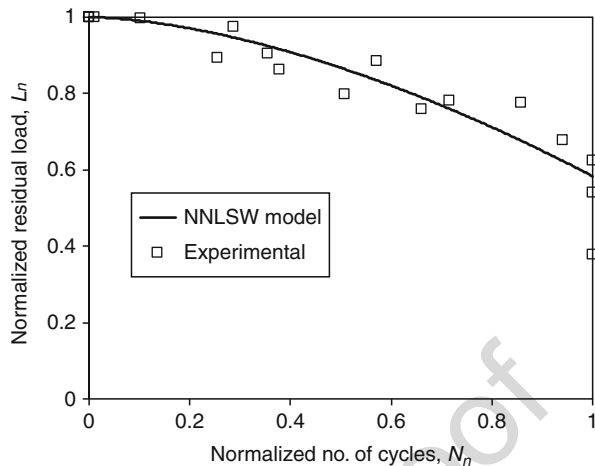
$$S_R(n) = S_u - f(S_u, S_{\max}, R)n^\kappa \quad (3)$$

where  $\kappa$  is a strength degradation parameter,  $S_{\max}$  is the maximum stress, and  $R$  is the ratio of minimum to maximum stress (i.e.,  $R = S_{\min}/S_{\max}$ ). Failure occurs when the residual strength equals the maximum stress of the spectrum, i.e., when  $S_R(N_f) = S_{\max}$ .

Shenoy et al. (2009b) proposed a modified version of this equation that they termed the normalized nonlinear strength wearout model (NNLSWM), which is given by:

$$L_n = 1 - \frac{(L_u - L_{\max})}{L_u} (N_n)^\eta \quad (4)$$

**Fig. 7** The normalized nonlinear strength wearout model applied to aluminum-epoxy single-lap joints tested at different loads (Shenoy et al. 2009b)



where  $\eta$  is a constant and the normalized residual failure load,  $L_n$ , is:

$$L_n = \frac{L_R(n)}{L_u}$$

and the normalized cycles to failure,  $N_n$ , is:

$$N_n = \frac{n}{N_f}$$

where  $L_R(n)$  is the quasistatic failure load after  $n$  fatigue cycles and  $L_u$  is the quasistatic failure load prior to fatigue loading. Figure 7 shows this model applied to aluminum alloy-epoxy single-lap joints tested at three different fatigue loads. It can be seen that the model fits all the data reasonable well, thus providing a simple method of predicting the residual strength in a joint under any combination of constant fatigue load and number of cycles. However, if the fatigue load varies, modifications to this approach may be required, as discussed in the next section.

Schaff and Davidson (1997a, b) used the strength wearout method to predict the residual strength degradation of a composite material subjected to a variable amplitude loading spectrum. However, they noted a crack acceleration effect in the transition from one constant amplitude (CA) block to another, the cycle mix effect, and proposed a cycle mix factor, CM, to account for this. Erpolat et al. (2004a) proposed a modified form of Schaff and Davidson's cycle mix equation to model the degradation of CFRP-epoxy double-lap joints subjected to a variable amplitude fatigue spectrum. They showed that this model represented the fatigue life of bonded joints under variable amplitude fatigue more accurately than Palmgren–Miner's law. Shenoy et al. (2009c) proposed various further modifications to this approach, which they applied to aluminum alloy-epoxy single-lap joints subjected to various forms of VAF. The application of the cycle mix factor to predict strength wearout and cycles

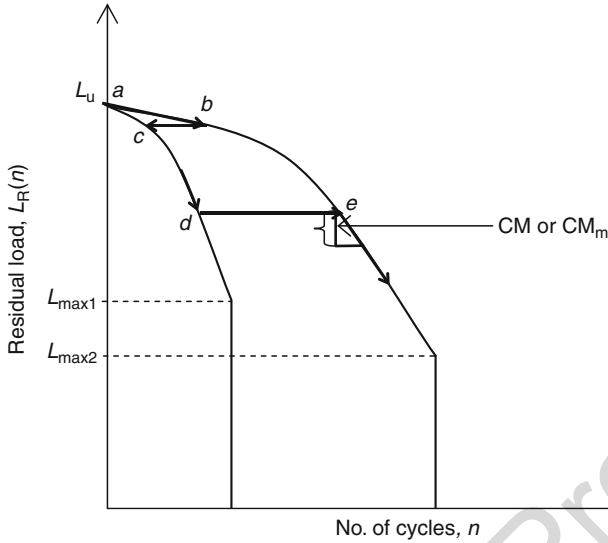


**Fig. 8** Illustration of the nonlinear strength wearout with cycle mix factor approach to predict variable amplitude fatigue

to failure for VAF is illustrated in Fig. 8. The figure shows two strength wearout curves, showing the reduction in the residual load for constant amplitude fatigue with maximum fatigue loads of  $L_{max1}$  and  $L_{max2}$ . Both of these curves can be represented by a nonlinear strength wearout equation, such as Eq. (4). If a variable amplitude fatigue spectrum commences with a maximum fatigue load of  $L_{max2}$ , then the decrease in the residual load with fatigue cycles initially follows path  $a-b$ . If at point  $b$  the maximum fatigue load increases to  $L_{max1}$ , there is a horizontal jump to the strength wearout curve for the higher load and the residual load starts to decrease more quickly, following curve  $c-d$ . At point  $d$ , the maximum load is decreased to  $L_{max2}$ , and we have another horizontal jump to the relevant strength wearout curve. However, at point  $e$ , the cycle mix factor is also applied, which has the effect of an immediate reduction in the residual load by an amount CM (or  $CM_m$ ). Shenoy et al. (2009c) proposed two cycle mix factors. The first was the cycle-independent cycle mix factor used by Erpolat et al. (2004a) given in Eq. (5).

$$CM = \alpha \left[ (\Delta L_{mn})^{\beta L_{max}} (\Delta L_{max,1} / \Delta L_{mn,1})^{\gamma} \right] \quad (5)$$

$\Delta L_{mn}$  and  $\Delta L_{max}$  are the mean and maximum load changes during the transition from one mean load to the other,  $\alpha$  and  $\beta$  are experimentally determined parameters, and  $\gamma$  was assumed to be unity in this case. The second was termed the modified cycle mix factor (MCM) approach. This was developed after observing that a better fit to the experimental data could be made if the cycle mix factor was greater in the

low cycle regime than in the high cycle regime. As it had already been noted that with these joints the fatigue life was propagation dominated in the low cycle regime and initiation dominated in the high cycle regime, the desired effect was achieved by making the cycle mix factor dependent on the extent of damage in the sample, as shown in Eq. (6).

$$CM_m = \left( \frac{\zeta}{OL} + \alpha \right) \left[ (\Delta L_{mn})^{\beta L_{max}} (\Delta L_{max} / \Delta L_{mn})^y \right] \quad (6)$$

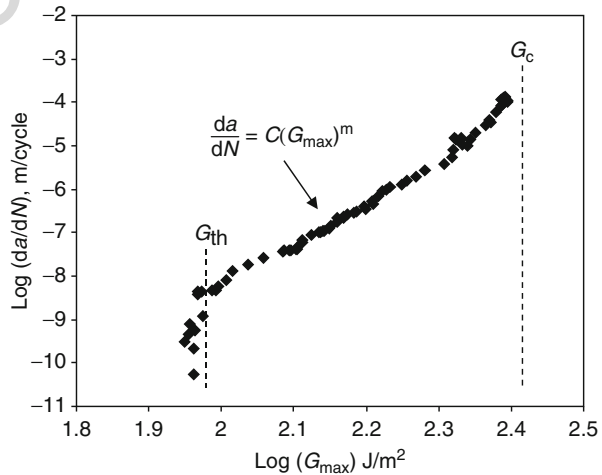
where OL is the overlap length and  $\zeta$  is a damage parameter. In Shenoy et al. (2009c),  $\zeta$  was determined by fitting a power law curve to experimental plots of damage/crack growth against number of cycles. Hence,  $\zeta$  was defined as:

$$\zeta = m_1 (n)^{m_2} \quad (7)$$

where  $m_1$  and  $m_2$  are experimentally determined constants.

It can be seen in Fig. 9 that the cycle mix parameter was applied when the fatigue loading became less severe, i.e., after the jump from  $d$  to  $e$ , but not when the fatigue loading became more severe, i.e., following the jump from  $b$  to  $c$ . This is consistent with Gomatam and Sancaktar (2006) who observed damage acceleration when “moderate” loading conditions followed “severe” loading conditions, but not when the order was reversed. It is also consistent with the mechanistic argument put forward by Ashcroft (2004) who attributed crack growth accelerations seen in adhesives subjected to intermittent overloads to the damage caused by the overloads to the adhesive ahead of the crack tip. It was proposed that this damage reduced the fatigue resistance of the adhesive and resulted in accelerated crack growth for the cycles of lower amplitude following an overload.

**Fig. 9** Experimental fatigue crack growth curve for a CFRP-epoxy double cantilever beam (Data from Ashcroft and Shaw 2002)



As with strength degradation, stiffness degradation rate can be considered as a power function of the number of load cycles. Although stiffness degradation has the advantage that it can be measured nondestructively, it does not give a direct indication of the residual strength of a fatigued structure. However, if this link can be made, then stiffness degradation can be a useful method of in-service structural integrity monitoring.

### 33.4.3 Fracture Mechanics Methods

The fracture mechanics approach deals predominantly with the crack propagation phase; hence, it is assumed that crack initiation occurs during the early stages of the fatigue cycling or that there is a preexisting crack. The rate of fatigue crack growth,  $da/dN$ , is then correlated with an appropriate fracture mechanics parameter, such as Griffith's (1921) strain energy release rate,  $G$ , or Irwin's (1958) stress intensity factor,  $K$ . Paris et al. (1961) proposed that  $da/dN$  was a power function of the stress intensity factor range,  $\Delta K (=K_{\max} - K_{\min})$ , i.e.:

$$\frac{da}{dN} = C \Delta K^m \quad (8)$$

where  $C$  and  $m$  are empirical constants, dependent on factors such as the material, the fatigue frequency, the  $R$ -ratio, and environment. Although  $K$  is the most widely used fracture mechanics parameter in the fracture analysis of metals, it is more difficult to apply to bonded joints, where the constraint effects of the substrates on the adhesive layer complicates characterization of the stress field around the crack tip. Therefore,  $G$  is often used as the governing fracture parameter for adhesives if linear elastic fracture mechanics (LEFM) is applicable (i.e., localized plasticity). If an elastoplastic fracture mechanics (EPFM) parameter is required, owing to more widespread plasticity, then the J-integral ( $J$ ) is generally used (Rice 1968). If creep is significant, then a time-dependent fracture mechanics parameter, such as  $C^*$  or  $C_t$ , should be considered, as discussed in Sect. 5.

A plot of the experimentally measured crack growth rate against the calculated  $G_{\max}$  or  $\Delta G$  often exhibits three regions, as illustrated in Fig. 9, which shows the fatigue crack growth curve for a CFRP-epoxy double cantilever beam (DCB). Region I is defined by the threshold strain energy release rate,  $G_{th}$ , in which crack growth is slow enough to be deemed negligible. Region II is described by a power law equation similar to Eq. (6) and is, hence, sometimes referred to as the Paris Region. In Region III, there is unstable fast crack growth as  $G_{\max}$  approaches the critical strain energy release rate,  $G_c$ .

In a general form, the relationship between the fatigue crack propagation rate and a relevant fracture parameter,  $\Gamma$ , can be represented by:

$$\frac{da}{dN} = f(\Gamma) \quad (9)$$



The number of cycles to failure can be determined from:

$$N_f = \left( \int_{a_0}^{a_f} \frac{da}{f(F)} \right) \quad (10)$$

where  $a_0$  is the initial crack length and  $a_f$  is the final crack length. Equation (10) can be solved using numerical crack growth integration (NCGI). A simple method of predicting VA fatigue from a CA FCG curve is to perform numerical crack growth integration. In this method, the crack size,  $a$ , and corresponding fracture parameter, such as strain energy release rate range,  $\Delta G$ , is assumed to be constant throughout a CA stage. The crack growth rate per cycle,  $da/dN$ , for this stage can be obtained using an appropriate correlation, such as the Paris law. Multiplication of this rate by the number of cycles in the stage,  $n$ , gives the overall crack growth during the stage,  $\Delta a$ . This is used to find the crack size for the subsequent stage ( $a_{i+1} = a_i + \Delta a_i$ ) and the procedure is repeated until  $G_{\max}$  exceeds the fracture energy,  $G_c$ , or until  $\Delta G$  becomes equal to  $\Delta G_{th}$ . This algorithm is summarized below.

Repeat

$$a_{i+1} = a_i + n_i \cdot \frac{da}{dN}(\Delta G_i(R_i, a_i, \dots)) \quad (11)$$

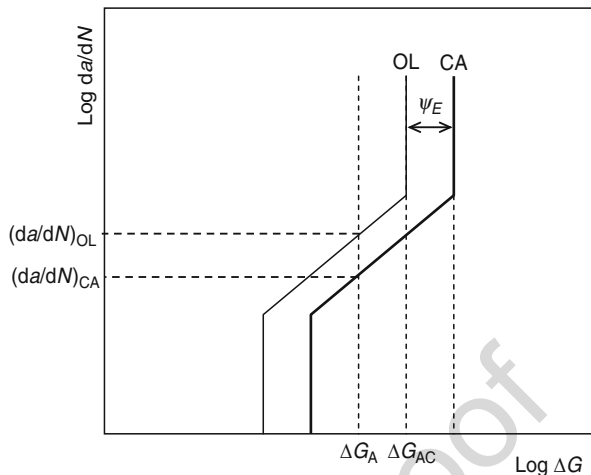
Until  $G_{\max, i+1} \geq G_c$  { $G$  increasing with  $a$ } or

Until  $\Delta G_{\max, i+1} \leq \Delta G_{th}$  { $G$  decreasing with  $a$ }

Abdel Wahab et al. (2004) proposed a general method of predicting fatigue crack growth and failure in bonded lap joints incorporating NCGI and finite element analysis (FEA). The crack growth law was determined from tests using a DCB sample and this was used to predict the fatigue crack growth, and hence the fatigue life, of single- and double-lap joints manufactured from the same materials.

The numerical integration technique can easily be adapted to the prediction of fatigue crack growth in variable amplitude (VA) fatigue. Erpolat et al. (2004b) applied the NCGI technique for the prediction of crack growth in CFRP/epoxy DCB joints subjected to periodic overloads. This tended to underestimate the experimentally measured crack growth, indicating a crack growth acceleration mechanism, and an unstable, rapid crack growth period was also seen when high initial values of  $G_{\max}$  were applied. This behavior was attributed to the generation of increased damage in the process zone ahead of the crack tip when the overloads were applied, and Ashcroft (2004) proposed a fracture mechanics-based model that could predict this behavior. It was assumed that under constant amplitude conditions, FCG can be represented by  $\Delta G_{th}$ ,  $G_c$ , and the two Paris constants,  $C$  and  $m$ , as represented by CA in Fig. 10. It can be seen that if a CA fatigue load with a strain energy release rate range of  $\Delta G_A$  is applied, then the resulting crack growth rate will be  $(da/dN)_{CA}$ . In most cases,  $\Delta G_A$  will be calculated assuming undamaged material ahead of the crack tip, and this is likely to be adequate for predictive purposes. However, the crack resistance and hence  $(da/dN)_{CA}$  will be associated with the damage zone

**Fig. 10** The damage shift method of predicting fatigue crack growth under variable amplitude (Ashcroft 2004)

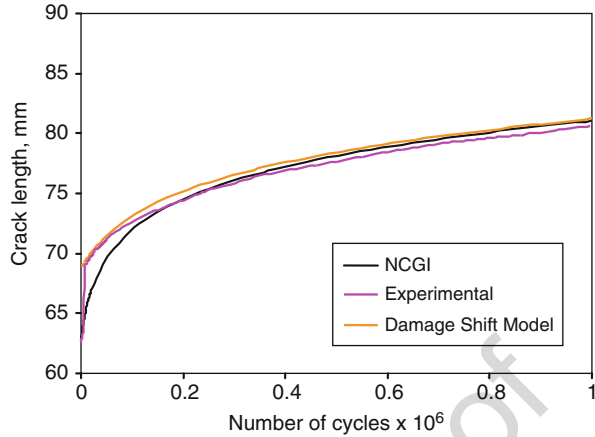


created by the CA fatigue loading. If an overload is superimposed onto the CA spectrum, then the damage ahead of the crack zone will increase and the resistance to crack propagation will decrease. It is proposed that this increased damage can be represented by a lateral shift in the FCG curve. The FCG curve associated with this increased damage is represented by curve OL in Fig. 10. It can be seen that the value of  $da/dN$  at  $\Delta G_A$  has increased to  $(da/dN)_{OL}$ , i.e., that there is a crack acceleration effect, which is represented by a “damage shift” parameter,  $\psi_E$ , which can be easily determined for a given spectrum through a simple experimental test program. Theoretically, all that is needed to determine  $\psi_E$  is the crack growth rates under CA and VA fatigue for a single value of  $\Delta G_A$ .

If  $\Delta G_A$  is increased, a critical point will eventually be reached at which  $G_{max}$  of the overloads is equal to the value of  $G_c$  for the shifted FCG curve, OL. This point is shown as  $\Delta G_{AC}$  in Fig. 10. Unstable or quasistatic fracture then occurs. If  $G$  increases with crack length, then this will lead to catastrophic failure of the joint. However, if  $G$  decreases with  $a$ , as when testing DCB samples in displacement control, then the crack will eventually stop if the  $G$  arrest ( $G_{arr}$ ) value is reached before the joint has completely fractured. The value of  $\Delta G_A$  associated with the crack arrest point ( $\Delta G_{arr}$ ) will now be much smaller, and hence crack growth will be greatly reduced. This is consistent with the experimental crack growth behavior shown in Fig. 11, where there is a rapid increase in crack length after approximately 5000 fatigue cycles, after which there is a period of lower crack growth rate than that predicted by NCGI. It can be seen in Fig. 11 that the damage shift model is capable of predicting both the initial crack jump and the subsequent reduction in the crack growth rate.

The fatigue crack growth approach will only predict the correct fatigue life if it is dominated by the fatigue propagation phase. However, if the initiation phase is significant, then this approach will underestimate the fatigue life and a method of predicting the number of cycles before the macrocrack forms is required. This can be done empirically in a similar fashion to the stress–life approach, with the number of

**Fig. 11** Fatigue crack growth for CFRP-epoxy DCB subjected to overloads



cycles to fatigue initiation,  $N_i$ , being plotted as a function of a suitable stress (or other) parameter rather than cycles to total failure,  $N_f$  (Shenoy et al. 2009a). An alternative approach, suggested by Levebvre and Dillard (1999), is to use a stress singularity parameter as the fatigue initiation criterion. They showed that under certain conditions, the singular stress,  $\sigma_{kl}$ , in an adhesive lap joint could be represented by:

$$\sigma_{kl} = \frac{Q_{kl}}{x^\lambda} \quad (12)$$

where  $Q_{kl}$  is a generalized stress intensity factor, dependent on load, and  $\lambda$  is an eigenvalue that can be related to the order of the singularity. It was proposed that  $N_i$  could be defined in terms of  $\Delta Q$  (or  $Q_{\max}$ ) and  $\lambda$  in a 3D failure map. This approach has been combined with a fracture mechanics approach by Quaresimin and Ricotta (2006) to obtain a predictive method explicitly modeling both the initiation and propagation phases. An alternative to this is to use one of the damage mechanics methods described in Sect. 4.4.

Adhesives and polymer composites tend to exhibit fast fracture, and hence it may be preferable to design for a service life with no crack growth, using  $G_{th}$  as the design criteria. Abdel Wahab et al. (2001a) investigated this approach for bonded lap-strap joints. Elastic ( $G$ ) and elastoplastic ( $J$ ) fracture parameters, crack placement, and initial crack size were investigated. This approach has also been extended to samples subjected to environmental ageing by incorporating the method with a semicoupled transient hygro-mechanical finite element analysis (Ashcroft et al. 2003). Ashcroft and Shaw (2002) used  $G_{th}$  from testing DCB joints to predict the  $10^6$  cycle endurance limit in lap-strap and double-lap joints at different temperatures. The predictions were reasonable, apart from the double-lap joint tested at  $90^\circ\text{C}$ , which failed at a far lower load than predicted. This was attributed to accumulative creep in the double-lap joint, which could be seen in plots of displacement against cycles at constant load amplitude.

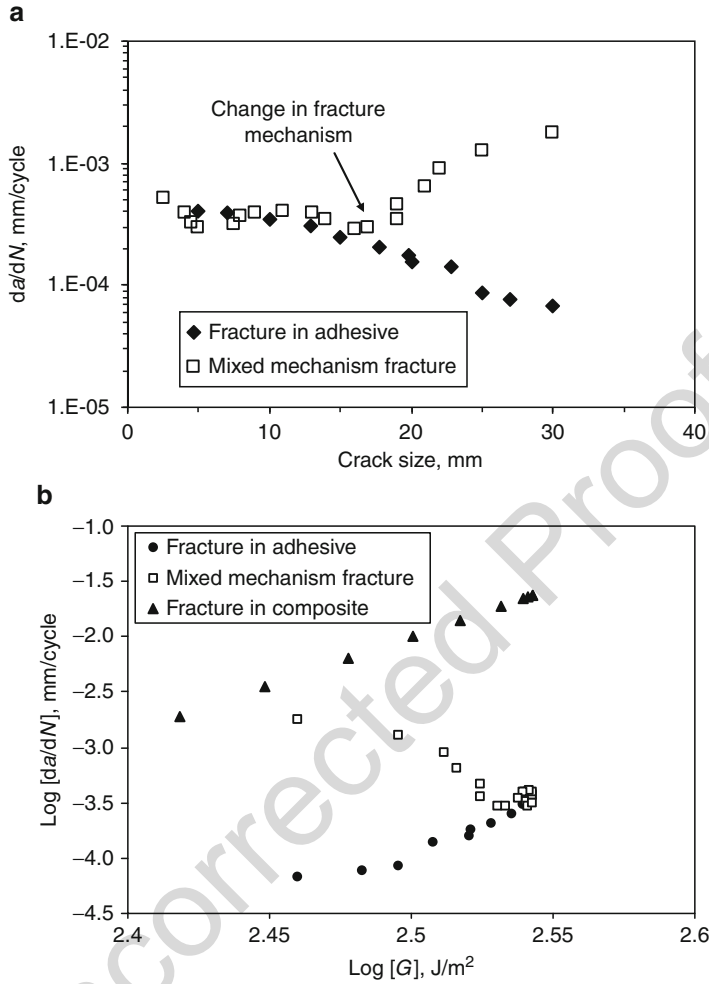


**Fig. 12** (a) Fatigue crack growth rate as a function of crack length for fracture in the adhesive and a mixed mechanism fracture. (b) Fatigue crack growth plots for fracture in the adhesive layer in the composite and a mixed mechanism fracture

It is quite common in adhesively bonded joints to have more than one failure mechanism, for example, cohesive failure in the adhesive, failure at the interface, interlaminar failure, or matrix failure in composite substrates, occurring in the fatigue life of a joint. This will affect the fatigue crack growth, as illustrated in Fig. 12a. If the various mechanisms occur sequentially, then failure criteria for the joint can also be applied sequentially in a fatigue lifetime predictive methodology. However, if more than one mechanism is occurring at one time, anomalous fatigue crack growth can occur. This is illustrated in Fig. 12b for the case of a CFRP-epoxy lap-strap joint in which fracture is initially in the adhesive before developing into a

mixed mechanism failure with an increasing proportion of failure in the composite adherend. It can be seen that in the mechanism fracture, the fatigue crack growth exhibits anomalous behavior as the crack growth rate decreases as strain energy release rate increases, which is not represented by a Paris-type crack growth law. Ashcroft et al. (2010) proposed a mixed mechanism fracture model of the following form:

$$\left(\frac{da}{dn}\right)_m = f \left[ A_a, \left(\frac{da}{dn}\right)_a, A_c \left(\frac{da}{dn}\right)_c \right] \quad (13)$$

where  $A$  indicates area fraction of failure mode, as seen in the fracture surface, and the subscripts m, a, and c represent mixed, adhesive, and composite, respectively. The simplest form of this law is a simple additive one, i.e.:

$$\left(\frac{da}{dn}\right)_m = A_a \left(\frac{da}{dn}\right)_a + A_c \left(\frac{da}{dn}\right)_c \quad (14)$$

Equation (14) assumes there is a proportional relationship between the area fraction of a particular failure mode and its effect on the mixed FCG rate; however, this is not necessarily the case. It may be the case that one of the fracture mechanisms has a disproportionate effect on the mixed FCG rate. A simple way to accommodate this is to substitute the actual area fraction,  $A_i$ , in Eq. (14) with an effective area fraction,  $A'_i$ , as illustrated in Eq. (15)

$$\left(\frac{da}{dn}\right)_m = A'_a \left(\frac{da}{dn}\right)_a + A'_c \left(\frac{da}{dn}\right)_c \quad (15)$$

A method of mapping the actual area fraction to the effective area fraction is required, and Ashcroft et al. (2010) illustrated how power laws and polynomial relationships could be used for this purpose. It was shown that the proposed model was capable of predicting the anomalous fatigue crack growth behavior shown in Fig. 12.

### 33.4.4 Damage Mechanics Methods

The fracture mechanics methods have the limitation that the initiation phase is not accounted for and that damage is through a single planar crack propagating through undamaged material, which may not physically represent the real behavior very well. The damage mechanics approach addresses some of these problems by allowing progressive degradation and failure to be modeled, thus representing both initiation and propagation phases. Continuum damage mechanics (CDM) requires a damage variable,  $D$ , to be defined as a measure of the severity of the material damage, where  $D$  is equal to 0 for undamaged material and 1 for fully damaged material. Abdel Wahab et al. (2001b) developed the following fatigue damage equation:

$$D = 1 - \left[ 1 - A(\beta + m + 1) \Delta \sigma_{\text{eq}}^{\beta+m} R_v^{\beta/2} N \right]^{\frac{1}{\beta+m+1}} \quad (16)$$

where  $\Delta \sigma_{\text{eq}}$  is the von Mises stress range,  $R_v$  is the triaxiality function (which is the square of the ratio of the damage equivalent stress to the von Mises equivalent stress),  $m$  is the power constant in the Ramberg–Osgood equation, and  $A$  and  $\beta$  are experimentally determined damage parameters. The number of cycles to failure ( $N_f$ ) can be determined from Eq. (16) using the condition at the fully damaged state,  $D = 1$  at  $N = N_f$ , giving:

$$N_f = \frac{\Delta \sigma_{\text{eq}}^{-\beta-m} R_v^{-\frac{\beta}{2}}}{A(\beta + m + 1)} \quad (17)$$

Abdel Wahab et al. (2001b) found that the approach described above compared favorably with the fracture mechanics approach when applied to the constant amplitude fatigue of CFRP-epoxy double-lap joints. Abdel Wahab et al. (2010a) later extended this approach to the low cycle fatigue of bulk adhesive where damage evolution curves were derived assuming isotropic damage and a stress triaxiality function equal to one that agreed well with experimental measurements. In further work, Abdel Wahab et al. (2010b) applied the approach to single-lap joints which required determination of the triaxiality function to account for the multiaxial stress state in the joint, and it was seen that this value varied along the adhesive layer. The dependency of the triaxiality function on the joint type was further investigated by Abdel Wahab et al. (2011a, b).

Although the CDM approach described above enabled the progressive degradation of the adhesive layer to be characterized, it did not allow the initiation and propagation phases of fatigue to be explicitly modeled. Shenoy et al. (2010a) used a damage mechanics-based approach to progressively model the initiation and evolution of damage in an adhesive joint, leading to crack formation and growth. In this approach, the damage rate  $dD/dN$  was assumed to be a power law function of the localized equivalent plastic strain range,  $\Delta \epsilon_p$ , i.e.:

$$\frac{dD}{dN} = C_D (\Delta \epsilon_p)^{m_D} D \quad (18)$$

where  $C_D$  and  $m_D$  are experimentally derived constants. The fatigue damage law was implemented in a finite element model. In each element, the rate of damage was determined from the finite element analysis using Eq. (18), and the element properties degraded as:

$$E = E_0(1 - D)$$

$$\sigma_{yp} = \sigma_{yp0}(1 - D) \quad (19)$$

$$\beta = \beta_0(1 - D)$$

where  $E_0$ ,  $\sigma_{yp0}$ , and  $\beta_0$  are Young's modulus, yield stress, and plastic surface modifier constant for the Parabolic Mohr–Coulomb model, respectively, and  $D = 1$  represents a fully damaged element, which was used to define the macrocrack length. The fatigue life was broken into a number of steps with a specified number of cycles,  $\Delta N$ , and at each step, the increased damage determined using Shenoy et al. (2010a):

$$D_{i+1} = D_i + \frac{dD}{dN} dN \quad (20)$$

showed that this method could be used to predict total-life plots, the fatigue initiation life, fatigue crack growth curves, and strength and stiffness wearout plots and could also be extended to variable amplitude fatigue (Shenoy et al. 2010b). Walander et al. (2014) experimentally studied Mode-I fatigue crack growth in rubber and polyurethane-based adhesives using a double-cantilever beam specimen. A damage growth law of a similar form to Eq. (20) related damage evolution with three material parameters:  $\alpha$ ,  $\beta$ , and  $\sigma_{th}$ , which were determined from the experimental data. Good correlation between the experimental data and the proposed damage law for fatigue was reported.

A similar approach was proposed by Khoramishad et al. (2010a) in which the rate of damage was related to the maximum principal strain,  $\epsilon_{max}$ , rather than the equivalent strain and a threshold strain,  $\epsilon_{th}$ , was used rather than a plastic strain in order to define a strain below which fatigue damage does not occur.

$$\frac{dD}{dN} = \begin{cases} C \times (\epsilon_{max} - \epsilon_{th})^b, & \epsilon_{max} > \epsilon_{th} \\ 0, & \epsilon_{max} \leq \epsilon_{th} \end{cases} \quad (21)$$

where  $C$  and  $b$  are experimentally determined material damage constants. In this case, the damage initiation and fracture was modeled using a bilinear cohesive zone model (as described in ► Chap. 25, “Numerical Approach: Finite Element Analysis”) and the damage variable was used to degrade the parameters of the cohesive model as illustrated in Fig. 13. This method was later extended to incorporate the effect of varying load ratio (Khoramishad et al. 2010b), variable amplitude fatigue (Khoramishad et al. 2011), and the effect of moisture degradation (Katnam et al. 2011).

Pirondi and Moroni (2010) also proposed a method of predicting fatigue crack growth using cohesive zone elements within a finite element analysis. In this case, the damage rate was related to the strain energy release rate. Oinen and Marquis (2011) presented a damage model for the shear decohesion of combined clamped and adhesively bonded (i.e., hybrid) joints that incorporated a linear-exponential cohesive zone model and a frictional contact model to account for a combined slip and decohesion response to loading.

### 33.5 Creep-Fatigue

Evidence of creep in the fatigue testing of bonded lap joints has been observed by a number of authors. It was seen in Sect. 4.3 that application of a standard fracture mechanics method can significantly overpredict the fatigue life if there is

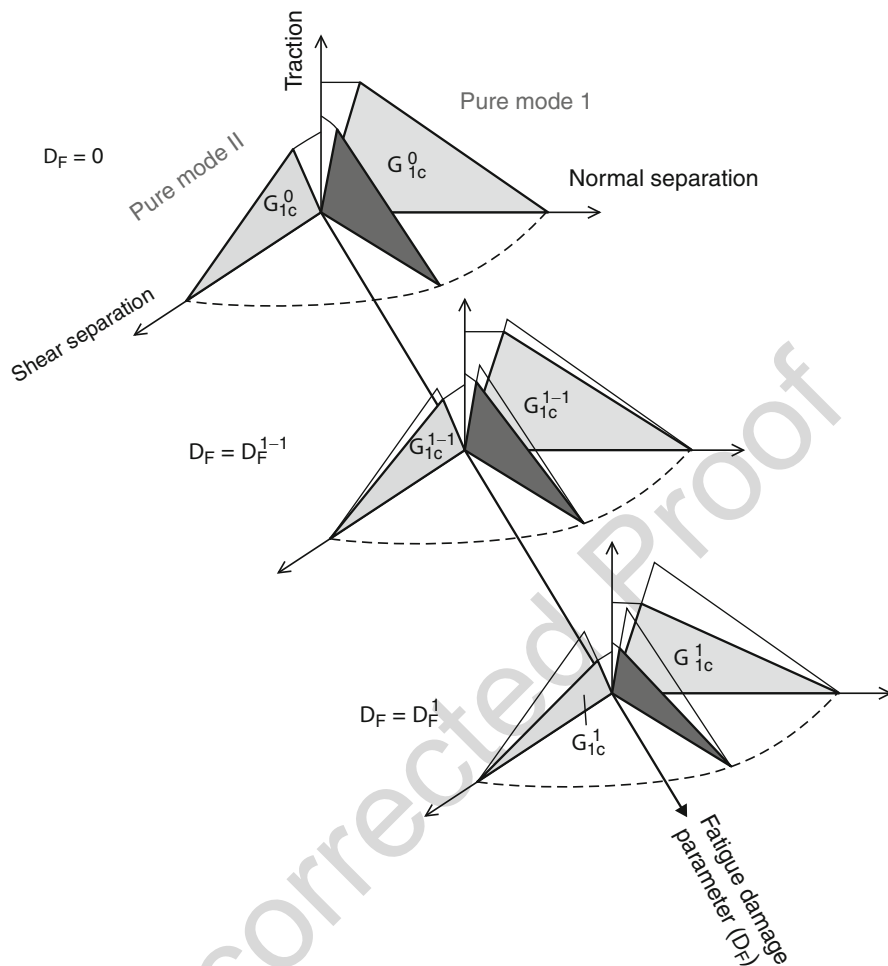
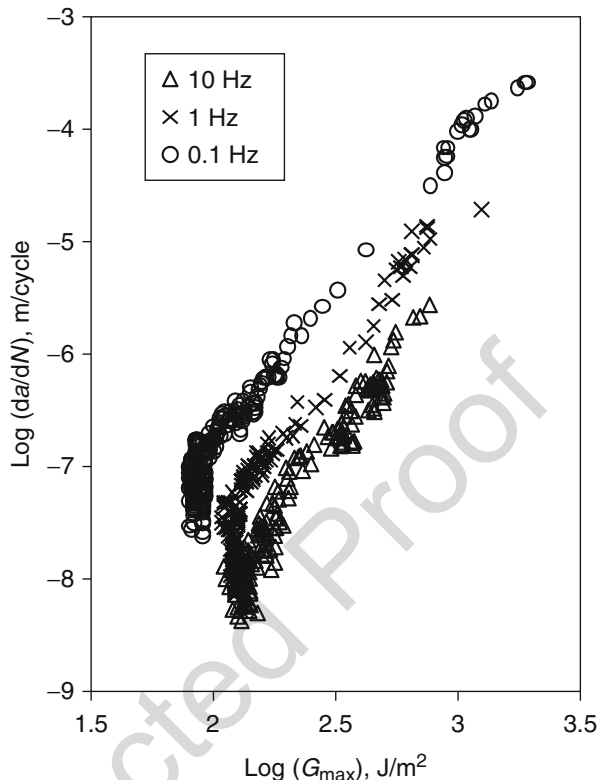


**Fig. 13** Degradation of cohesive zone model parameters with increasing fatigue damage (Khoramishad et al. 2010a)

significant accumulated creep. This is not surprising as polymeric adhesives will exhibit some degree of viscoelastic or viscoplastic behavior over a part of their operating range. The importance of the creep contribution to fatigue failure will depend on a number of factors such as the nature of the adhesive, the ambient temperature and humidity, the joint geometry, the mean fatigue load, and the frequency. Fatigue crack growth in such circumstances may still be adequately represented by LEFM or EPFM parameters; however, different fatigue crack growth curves will be required for different frequencies and temperatures, as shown in Fig. 14. However, if creep is significant, then fatigue crack growth may be better represented by a time-dependent fracture mechanics (TDFM)



**Fig. 14** The effect of test frequency on fatigue crack growth plots for steel-epoxy DCB samples (Al-Ghamdi et al. 2003)



parameter. Landes and Begley (1976) proposed a TDFM parameter analogous to Rice's J-integral that they called  $C^*$  and defined it as follows:

$$C^* = \int_{\Gamma} W^* dy - T_i \left\{ \partial \frac{\dot{u}}{\partial x} \right\} ds \quad (22)$$

where

$$W^* = \int_0^{\dot{\epsilon}_{ij}} \sigma_{ij} d\dot{\epsilon}_{ij} \quad (23)$$

$\Gamma$  is a line contour taken counter clockwise from the lower crack surface to the upper crack surface,  $W^*$  is the strain energy rate density associated with the stress  $\sigma_{ij}$  and strain rate  $\dot{\epsilon}_{ij}$ ,  $T_i$  is the traction vector defined by the outward normal  $n$  along  $\Gamma$ ,  $\dot{u}_i$  is the displacement rate vector, and  $s$  is the arc length along the contour.  $C^*$  is valid

only for extensive steady-state creep condition, and Saxena (1986) proposed an alternative parameter,  $C_t$ , that was suitable for characterizing creep crack growth from small scale to extensive creep conditions. This was defined as:

$$C_t = -\frac{1}{B} \partial U_t^* \left( \frac{a, t, \dot{V}_c}{\partial a} \right) \quad (24)$$

where  $B$  is sample width,  $a$  is crack length,  $t$  is time,  $U_t^*$  is an instantaneous stress–power parameter, and  $\dot{V}_c$  is the load line deflection rate.

In cyclic loading,  $C_t$  will vary with the applied load, and an average value of  $C_t$ ,  $C_{t(ave)}$ , may be used to characterize the fatigue-creep crack growth. Al-Ghamdi et al. (2004) proposed three methods of predicting creep-fatigue crack growth in bonded joints. In the first method, an appropriate fracture mechanics parameter is selected and plotted against the fatigue crack growth rate (FCGR =  $da/dN$ ) or the creep crack growth rate (CCGR =  $da/dt$ ). A suitable crack growth law is fitted to the experimental data and crack growth law constants are determined at different temperatures and frequencies. Empirical interpolation can then be used to determine crack growth law constants at unknown temperatures and frequencies. This method can also be used to predict crack growth under conditions of varying frequency, load, and temperature.

The second method was called the *dominant damage approach* and assumes that fatigue and creep are independent mechanisms and that crack growth is determined by whichever is dominant. In this case, crack growth should be predominantly either cycle or time dependent. For example, if creep is the dominant damage mechanism, then plots of  $da/dt$  against a suitable TDFM should be independent of frequency and can be used to predict the fatigue life in terms of time under load rather than number of cycles.

The third method was termed the *crack growth partitioning approach* in which it is assumed that crack growth can be partitioned into separate cycle-dependent (fatigue) and time-dependent (creep) components, both of which contribute the total crack, as represented by the following equation:

$$\frac{da}{dN} = \left( \frac{da}{dN} \right)_{\text{fatigue}} + \frac{1}{f} \left( \frac{da}{dt} \right)_{\text{creep}} \quad (26)$$

Al-Ghamdi et al. (2004) proposed the following form of Eq. (26):

$$\frac{da}{dN} = D(G_{\max})^n + \frac{mC_{t(ave)}^q}{f} \quad (27)$$

where the fatigue crack growth constants  $D$  and  $n$  are determined from high-frequency tests, and the creep crack growth constants  $m$  and  $q$  are determined from constant load crack growth tests. Under some conditions, this method still underpredicts the crack growth, in which case a creep-fatigue interaction term may be added:

$$\frac{da}{dN} = D(G_{\max})^n + \frac{mC_{t(ave)}^q}{f} + CF_{\text{int.}} \quad (28)$$

where  $CF_{\text{int.}} = R_f^p R_c^y C_{fc}$  and  $R_f$  and  $R_c$  are scaling factors for the cyclic and time-dependent components, respectively.

$$R_f = \frac{(da/dN)}{(da/dN) + (da/dt)/f}$$

$$R_c = \frac{(da/dt)/f}{(da/dN) + (da/dt)/f}$$

and  $p$ ,  $y$ , and  $C_{fc}$  are empirical constants.

### 33.6 Impact Fatigue

There is increasing interest in the effects of repetitive low-velocity impacts produced in components and structures by vibrating loads. This type of loading is known as impact fatigue. Typical plots of normalized force as a function of time from the impact fatigue testing of a bonded single-lap joint are shown in Fig. 15. It can be seen that the duration of the main peak is approximately 2 ms and that subsequent peaks are of significantly smaller magnitude. It can also be seen that the maximum force,  $F_{\max}$ , and the load time for the first peak,  $T_F$ , decrease with the number of cycles, which is indicative of progressive fatigue damage in the adhesive. As the force is not constant in an impact fatigue test, it is useful to define a mean maximum force  $\bar{F}_{\max}$  as:

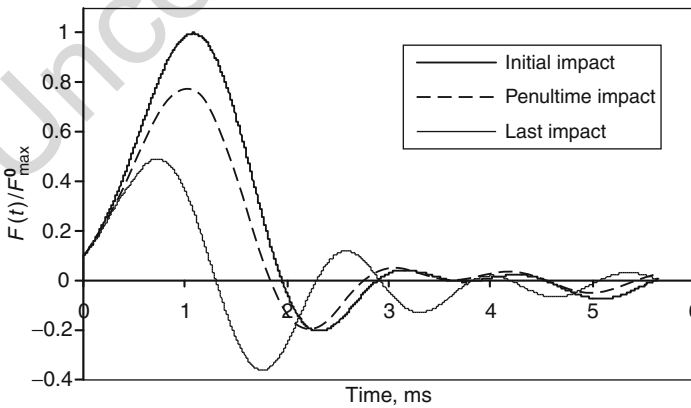


**Fig. 15** Variation in force and strain with time in a typical impact in the impact fatigue testing of a bonded lap joint (Casas-Rodriguez et al. 2007)

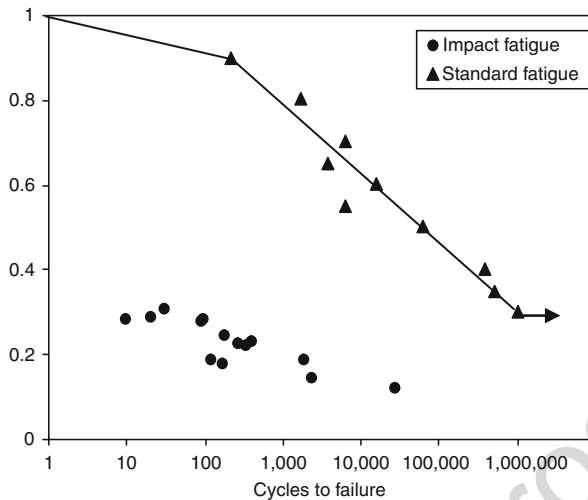


**Fig. 16**  $F$ - $N$  diagrams for aluminum-epoxy single-lap joints in impact and standard fatigue (Casas-Rodriguez et al. 2007)

$$\bar{F}_{\max} = \frac{1}{N_f} \sum_{i=1}^{N_f} F_i^{\max} \quad (29)$$

In Fig. 16, the normalized mean maximum force is plotted against the logarithm of cycle to failure and it can be seen that an approximately linear relationship is observed, with cycles to failure increasing as the force decreases, as expected. A plot for similar single-lap joints, manufactured with the same materials and processes, tested in standard fatigue with a constant force amplitude, sinusoidal waveform can also be seen in Fig. 16. It can be seen from this that the impact fatigue appears to be significantly more damaging than the standard fatigue. Casas-Rodriguez et al. (2008) also compared damage and crack growth in CFRP-epoxy lap-strap joints in standard and impact fatigue and found that the accumulated energy associated with damage in impact fatigue was significantly lower than that associated with similar damage in standard fatigue. It was also seen that the fracture surfaces, and hence, the fracture mechanisms, were quite different for the two types of loading. Ashcroft et al. (2011) also investigated the impact fatigue of notched bulk adhesive samples, developing an impact fatigue growth law based on the dynamic strain energy release rate.

### 33.7 Conclusion

It can be seen that a number of techniques have been used to model fatigue in bonded joints. Although most methods have limitations, all are useful in understanding and/or characterizing the fatigue response of bonded joints, and it is expected that further

developments will continue in all the methods described. For instance, the traditional load–life approach is useful in characterizing global fatigue behavior, but is of little use in fatigue life prediction and provides no useful information on damage progression in the joint. However, combined with monitoring techniques, such as back-face strain or embedded sensors, and FEA, the method could potentially form the basis of an extremely powerful in-service damage monitoring technique for industry.

The fracture mechanics approach is potentially a more flexible tool than the stress–life approach as it allows the progression of cracking to failure to be modeled and can be transferred to different sample geometries. Problems with the traditional fracture mechanics approach include: selection of initial crack size and crack path, selection of appropriate failure criteria, load history, and creep effects. Also the fracture mechanics approach does not accurately represent the accumulation and progression of damage observed experimentally in many cases. However, recent modifications to the standard fracture mechanics method have seen many of these limitations tackled.

In future developments, it is expected that fatigue studies of bonded joints will continue to increase our knowledge of how fatigue damage forms and progresses in bonded joints and this will feed into the models being developed. In addition to further developments and extension to the approaches described above, it is expected that an area for huge potential advances is in the incorporation of increasingly sophisticated damage growth laws into finite element analysis models to develop a more mechanistically accurate representation of fatigue in bonded joint than is currently available. It is also hoped that many of the techniques described above will reach sufficient maturity to form the basis of useful tools for industry, both in the initial design and in-service monitoring of bonded joints in structural applications subjected to cyclic loading.

## References

- Abdel Wahab MM, Ashcroft IA, Crocombe AD, Hughes DJ, Shaw SJ (2001a) *Compos Part A* 32:59
- Abdel Wahab MM, Ashcroft IA, Crocombe AD, Hughes DJ, Shaw SJ (2001b) *J Adhes Sci Technol* 15:763
- Abdel Wahab MM, Ashcroft IA, Crocombe AD, Smith PA (2004) *Compos Part A* 35:213
- Abdel Wahab MM, Hilmy I, Ashcroft IA, Crocombe AD (2010a) *J Adhes Sci Technol* 24:305
- Abdel Wahab MM, Hilmy I, Ashcroft IA, Crocombe AD (2010b) *J Adhes Sci Technol* 24:325
- Abdel Wahab MM, Hilmy I, Ashcroft IA, Crocombe AD (2011a) *J Adhes Sci Technol* 25:903
- Abdel Wahab MM, Hilmy I, Ashcroft IA, Crocombe AD (2011b) *J Adhes Sci Technol* 25:925
- Al-Ghamdi AH, Ashcroft IA, Crocombe AD, Abdel Wahab MM (2003) *J Adhes* 79:1161
- Al-Ghamdi AH, Ashcroft IA, Crocombe AD, Abdel-Wahab MM (2004) *Proceedings of the 7th international conference on structural adhesives in engineering*. IOM Communications, London, pp 22–25
- Ashcroft IA (2004) *J Strain Anal* 39:707
- Ashcroft IA, Shaw SJ (2002) *Int J Adhes Adhes* 22:151
- Ashcroft IA, Abdel Wahab MM, Crocombe AD, Hughes DJ, Shaw SJ (2001a) *Compos Part A* 32:45
- Ashcroft IA, Abdel-Wahab MM, Crocombe AD, Hughes DJ, Shaw SJ (2001b) *J Adhes* 75:61
- Ashcroft IA, Abdel-Wahab MM, Crocombe AD (2003) *Mech Adv Mater Struct* 10:227

- 896 Ashcroft IA, Casas-Rodriguez JP, Silberschmidt VV (2010) *J Adhes* 86:522
- 897 Ashcroft IA, Silberschmidt VV, Echard B, Casas-Rodriguez JP (2011) *Shock Vib* 18:157
- 898 Casas-Rodriguez JP, Ashcroft IA, Silberschmidt VV (2007) *J Sound Vib* 308:467
- 899 Casas-Rodriguez JP, Ashcroft IA, Silberschmidt VV (2008) *Comp Sci Technol* 68:2663
- 900 Coffin LF (1954) *Trans Am Soc Mech Eng* 76:931
- 901 Costa M, Viana G, da Silva LFM, Campilho RDSG (2017) *J Adhes* 93:127
- 902 Crocombe AD, Richardson G (1999) *Int J Adhes Adhes* 19:19
- 903 Datla NV, Ulicny J, Carlson B, Papini M, Spelt JK (2011a) *Eng Fract Mech* 78:1125
- 904 Datla NV, Ulicny J, Carlson B, Papini M, Spelt JK (2011b) *Int J Adhes Adhes* 31:88
- 905 Dowling NE (1999) *Mechanical behaviour of materials*. Prentice Hall, New Jersey, pp
- 906 390–392
- 907 Erpolat S, Ashcroft IA, Crocombe AD, Abdel Wahab MM (2004a) *Int J Fatigue* 26:1189
- 908 Erpolat S, Ashcroft IA, Crocombe AD, Abdel Wahab MM (2004b) *Comp A* 35:1175
- 909 Farrow IR (1989) Damage accumulation and degradation of composite laminates under
- 910 aircraft service loading: Assessment and prediction, Vol. I & II. PhD thesis, Cranfield Institute
- 911 of Technology
- 912 Gomatam R, Sancaktar E (2006) *J Adhes Sci Technol* 20:69
- 913 Griffith AA (1921) *Phil Trans R Soc A* 221:163
- 914 Irwin GR (1958) Fracture. In: Flugge S (ed) *Handbuch der physik VI*. Springer, Berlin, pp 551–590
- 915 Katnam KK, Crocombe AD, Sugiman H, Khoramishad H, Ashcroft IA (2011) *Int J Dam Mech*
- 916 20:1217
- 917 Khoramishad H, Crocombe AD, Katnam K, Ashcroft IA (2010a) *Int J Fatigue* 32:1146
- 918 Khoramishad H, Crocombe AD, Katnam K, Ashcroft IA (2010b) *Int J Adhes Adhes* 32:1278
- 919 Khoramishad H, Crocombe AD, Katnam K, Ashcroft IA (2011) *Eng Fract Mech* 78:3212
- 920 Landes JD, Begley JA (1976) *Mechanics of crack growth*, ASTM STP 590. American Society for
- 921 Testing and Materials, Philadelphia, pp 128–148
- 922 Levebvre DR, Dillard DA (1999) *J Adhes* 70:119
- 923 Little MSG (1999) Durability of structural adhesive joints. Ph.D. thesis, London, Imperial College
- 924 of Science, Technology and Medicine
- 925 Manson SS (1954) Behaviour of materials under conditions of thermal stress. In: National Advisory
- 926 Commission on aeronautics. Report 1170. Lewis Flight Propulsion Laboratory, Cleveland,
- 927 pp 317–350
- 928 Miner MA (1945) *J Appl Mech* 12:64
- 929 Nisitani H, Nakamura K (1982) *Trans Jpn Soc Mech Eng* 48:990
- 930 Oinen A, Marquis G (2011) *Eng Fract Mech* 78:163
- 931 Palmgren A (1924) *Z Ver Dtsch Ing* 68:339
- 932 Paris PC, Gomez MP, Anderson WE (1961) *Trend Eng* 13:9
- 933 Pirondi A, Moroni F (2010) *J Adhes* 86:501
- 934 Quaresimin M, Ricotta M (2006) *Comp Sci Technol* 66:647
- 935 Rice JR (1968) *J Appl Mech* 35:379
- 936 Saxena A (1986) In: Underwood JH et al (eds) *Fracture mechanics: seventeenth volume*, ASTM
- 937 STP 905. American Society for Testing and Materials, Philadelphia, pp 185–201
- 938 Schaff JR, Davidson BD (1997a) *J Comp Mater* 31:128
- 939 Schaff JR, Davidson BD (1997b) *J Comp Mater* 31:158
- 940 Shenoy V, Ashcroft IA, Critchlow GW, Crocombe AD, Abdel Wahab MM (2009a) *Int J Adhes*
- 941 *Adhes* 29:361
- 942 Shenoy V, Ashcroft IA, Critchlow GW, Crocombe AD, Abdel Wahab MM (2009b) *Int J Fatigue*
- 943 31:820
- 944 Shenoy V, Ashcroft IA, Critchlow GW, Crocombe AD, Abdel Wahab MM (2009c) *Int J Adhes*
- 945 *Adhes* 29:639
- 946 Shenoy V, Ashcroft IA, Critchlow GW, Crocombe AD (2010a) *Int J Fatigue* 32:1278
- 947 Shenoy V, Ashcroft IA, Critchlow GW, Crocombe AD (2010b) *Eng Fract Mech* 77:1073
- 948 Walander T, Eklind A, Carlberger T, Stigh U (2014) *Proc Math Sci* 3:829

Paul Ludwig Geiß and Melanie Schumann

## Contents

34.1	Introduction .....	976
34.2	Viscoelastic Models .....	977
34.2.1	Creep Under Static Stress Conditions (Retardation) .....	979
34.2.2	Creep Under Static Strain Conditions (Relaxation) .....	982
34.2.3	Generalized Models .....	985
34.3	Superposition Principles .....	986
34.3.1	Boltzmann Superposition Principle .....	986
34.3.2	Correspondence Principle .....	987
34.3.3	Time-Temperature Superposition Principle .....	988
34.4	Experimental Testing .....	989
34.4.1	Accessing Creep Properties of Adhesives by Rheometric Test Procedures .....	989
34.4.2	Retardation Test Methods with Adhesively Bonded Joints .....	991
34.4.3	Relaxation Test Methods with Adhesively Bonded Joints .....	1000
34.4.4	Relation of Stress Relaxation and Static Load Creep .....	1003
34.5	Predictive Methods .....	1005
34.6	Conclusions .....	1005
References	.....	1006

## Abstract

Polymer-based adhesives that have been especially designed to feature a high degree of toughness, flexibility, or even deliberately viscoelastic properties exhibit a pronounced time-dependent stress-strain behavior under static mechanical load conditions. Therefore, a suitable mechanical approach to describe and experimentally access phenomena related to creep in polymers and adhesives

P. L. Geiß (✉) · M. Schumann

Faculty of Mechanical and Process Engineering, Workgroup Materials and Surface Technologies (AWOK), University of Kaiserslautern, Kaiserslautern, Germany

e-mail: [geiss@mv.uni-kl.de](mailto:geiss@mv.uni-kl.de); [schumann@mv.uni-kl.de](mailto:schumann@mv.uni-kl.de)

needs to consider elastic as well as viscous material properties. Creep occurs at load levels below the yield strength, and particularly, creep of viscoelastic materials by definition is assigned to reversible deformation being able to recover after unloading. In technical practice, the term creep is often being used to describe arbitrary time-dependent strain including viscous and elastic-viscous behavior. The concept of generating mechanical substitute models dates back to the late eighteenth century. The Maxwell model, for example, represents a serial connection of a spring-(elastic) and a dashpot-(viscous) element. Other viscoelastic models are discussed in terms of their creep (retardation) strain and relaxation stress response to a corresponding stress or strain input in the generalized form of a step-unit function. The resulting constitutive laws for stress-strain-time relationship under static stress or strain conditions can be applied in the limits of linear elasticity where the Boltzmann superposition principle and the correspondence principle are valid. The options for experimentally accessing creep and relaxation phenomena range from standardized procedures to advanced test methods, which are discussed in the context of experimental data. Applying the theoretical background of the standard models for viscoelasticity to the experimental results can improve the reliability of predictive methods intending to extrapolate results from short-term experiments to a long-term timescale.

---

## 34.1 Introduction

In the seventeenth century, the British physicist Robert Hooke (Purrington 2009) defined the basic relation between stress and strain as “*Ut tensio, sic vis.*,” meaning extension is proportional to force. This so-called Hooke’s law is valid for many inorganic materials in the linear elastic region, where force-induced deformations are reversible and the material will completely return to its initial shape after removing the force without any delay or residual plastic deformations.

In the linear elastic region, constitutive material models are able to correlate strain to stress without the need to consider the history of stress and strain events a specific object or assembly has been subjected to previously. If an elastoplastic material is subjected to mechanical stress, it will also respond with instantaneous elastic deformation but above the yield strength deform plastically at a deformation rate governed by the process of deformation. Again, the behavior is not considered to be time dependent.

In most crystalline or amorphous inorganic materials, strong metallic bonds or ionic bonds are responsible for a dense structure and high level of rigidity. After exceeding the linear elastic stress-strain area, in metal alloys plastic deformation is related to the generation and movement of dislocations in the crystalline structure such as edge dislocations, screw dislocations, and sliding along grain boundaries. Amorphous inorganic glassy materials generally exhibit brittle fracture properties on a short-term timescale but are known to also deform plastically and time dependently under long-term static load conditions or at elevated temperatures. Metals and alloys also respond to elevated temperatures with a reduction of the linear elastic



deformation threshold generally referred to as the yield strength, especially once the temperature approaches or has exceeded the recrystallization temperature.

The mechanisms of plastic deformation and creep under static load conditions in organic polymer materials such as adhesives are somehow different from that and need to be considered when using structural adhesive bonds in the presence of so-called dead loads which frequently may occur due to the mere influence of gravity of the mass of a certain structure.

In 1921, Hermann Staudinger (Priesner 1983) postulated that polymers consist of chain-like macromolecules with typically carbon-carbon bonds as the repeating unit responsible for creating the backbone of a polymer chain. The average molecular weight, its statistical distribution, the presence of secondary bonds between adjacent chains, the degree of entanglement, and crosslinking by side chains are the dominant parameters influencing the mechanical properties of polymer materials.

Depending on the degree of geometric order, polymer materials may also develop crystallinity by self-organized alignment of chains or segments into stacks and on a superordinated level into spherulites. Examples of semicrystalline polymer materials include isotactic or syndiotactic polypropylene. Most adhesive polymer materials, however, show little or no macroscopic level of crystallinity. Plastic deformation in polymers can either take place by the creation of voids (crazing), by the rotation between chain segments, or by sliding between adjacent polymer chains. While crazing can be considered as a specific type of cracking on a micro- and nanoscopic size level, segment rotation and chain sliding are reversible physical phenomenon.

Micro-Brownian movement is related to a change in conformation without dislocating the center of gravity of the polymer chain, while strain by macro-Brownian is characterized by a local movement of the center of gravity of a polymer chain under the effect of, e.g., mechanical stress. As with the mechanisms of creep described above for inorganic crystalline or amorphous materials, the inelastic deformation of polymers is strongly related to the temperature, since in addition to mechanical stress, temperature serves as a source of activation energy to stimulate rotation and related Brownian movement on a nanoscopic level. In the range of the glass transition area, the ability of chain segments to rotate is strongly promoted with increasing temperature. Above the so-called glassy state of a polymer, the linear elastic properties diminish, and the relation between stress and strain can no longer be approximated by Hooke's law with adequate accuracy. This is the reason why several viscoelastic models have been subsequently developed, to provide means of describing, analyzing, and predicting the mechanical behavior of materials exhibiting an elastic and viscous time- and temperature-dependent stress-strain relationship.

---

## 34.2 Viscoelastic Models

The term viscoelasticity combines viscous and elastic stress-strain flow characteristics. If material behavior is dominated by viscous flow, it is generally referred to as a fluid, whereas if the elastic properties dominate the mechanical properties of a material, it is considered to be solid. Most adhesives are applied in a liquid or

112 pasty condition to allow wetting and promote spreading and then are required to  
 113 phase change into a solid. In the liquid state, rheology provides the methods to  
 114 differentiate between elastic and viscous flow characteristics, while dynamic  
 115 mechanical analysis of cured adhesive polymers uses similar principles to access  
 116 elastic and viscous parameters of the stress-strain response.

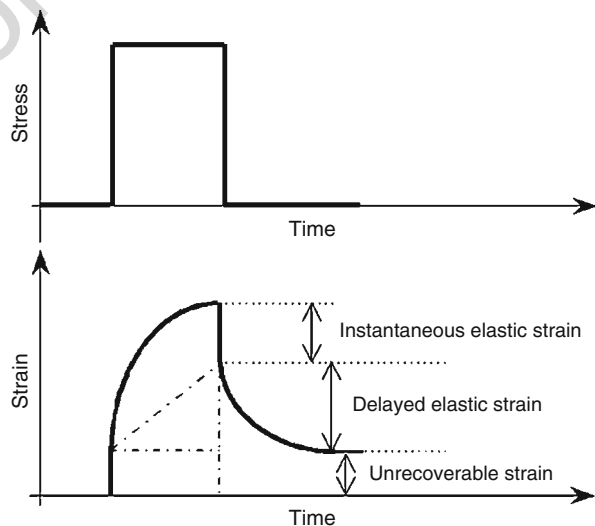
117 If no stress threshold is required to initiate viscous flow, the behavior is called  
 118 viscoelastic; if a certain stress threshold (yield strength) needs to be overcome before  
 119 the beginning of time-dependent viscous flow, the behavior is addressed as viscoplastic.

120 When subjected to constant stress for a certain period of time, three basic parts of  
 121 strain response may typically be observed. Immediately after applying a certain  
 122 amount of stress, instantaneous elastic strain takes place followed by delayed elastic  
 123 strain. Delayed elastic strain will completely recover after removing stress. It is often  
 124 referred to as primary creep. Following delayed elastic strain, viscous flow can often  
 125 be observed for polymer adhesive materials with low crosslinking density. Strain  
 126 caused by viscous flow leads to permanent deformation and is generally referred to  
 127 as non-recoverable strain or secondary creep. Figure 1 illustrates schematically the  
 128 strain response of such a material to a limited period of stress. The level of  
 129 instantaneous elastic strain upon loading corresponds to the instantaneous strain  
 130 recovery after removing the load.



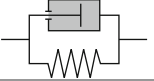
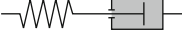
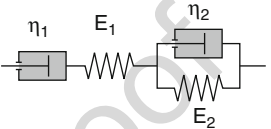
131 The aim of viscoelastic models is to use a combination of mechanical elastic and  
 132 viscous standard elements to generate a comprehensive mechanical substitute sys-  
 133 tem showing more or less simplified viscoelastic properties and thus to provide  
 134 parameters for building constitutive equations suitable for the prediction of visco-  
 135 elastic behavior and the characterization of viscoelastic materials.

136 James Clerk Maxwell (Niven 2003) proposed in 1867 a simplified mechanical  
 137 model consisting of a viscous dashpot in a serial connection to an elastic spring to  
 138 describe viscoelastic material properties.

**Fig. 1** Schematic strain response of viscoelastic materials to a period of stress



**Table 1** Comparison of various viscoelastic models and related differential equations,  $\sigma$ : stress parameter,  $\epsilon$ : strain parameter,  $E$ : elastic parameter,  $\eta$ : viscous parameter,  $\lambda$ : relaxation time

t.2	HOOKE-spring element (linear elasticity) $\sigma = E_0 \cdot \epsilon$	
t.3	NEWTON-fluid (linear viscosity) $\sigma = \eta_0 \cdot \dot{\epsilon}$	
t.4	KELVIN-VOIGT-solid $\sigma = E_0 \cdot \epsilon + \eta_0 \cdot \dot{\epsilon}$	
t.5	MAXWELL-fluid $\sigma + \lambda_0 \cdot \dot{\sigma} = \eta_0 \cdot \dot{\epsilon}$ ( $\lambda_0 = \eta_0/E_0$ )	
t.6	BURGERS-fluid (four parameter model) $\sigma + \left(\frac{\eta_1}{E_1} + \frac{\eta_2}{E_2} + \frac{\eta_2}{E_2}\right) \cdot \dot{\sigma} + \left(\frac{\eta_1 \cdot \eta_2}{E_1 \cdot E_2}\right) \cdot \ddot{\sigma} = \eta_1 \cdot \dot{\epsilon} + \left(\frac{\eta_1 \cdot \eta_2}{E_2}\right) \cdot \ddot{\epsilon}$	

The spring element is considered to behave according to Hooke's law in a linear elastic manner, while the mechanical behavior of the dashpot equates linear viscous flow of a Newtonian fluid. The following models of, e.g., Lord Kelvin and Woldemar Voigt (Thomson 1875) suggested a parallel connection of a dashpot and a spring element, while the Burgers model (Burgers 1935) named after the Dutch physicist Johannes Martinus Burgers consists of a Maxwell element and a Kelvin-Voigt element in series. Further generalized Maxwell or Kelvin-Voigt models connected an arbitrary or even infinite number of single elements to generate a spectral distribution of relaxation and retardation properties. Table 1 gives an overview of the most commonly used mechanical models for viscoelasticity and their corresponding differential equations.

**34.2.1 Creep Under Static Stress Conditions (Retardation)**

The time-dependent increase in strain of viscoelastic polymers under static stress conditions is generally referred to as creep or retardation. To describe creep behavior of adhesive joints under static stress conditions using viscoelastic models, it is assumed that a specimen be subjected at a certain time  $t = 0$  to a defined constant level of tensile stress  $\sigma = \sigma_0$  or shear stress  $\tau = \tau_0$ .

The stress-strain history then provides the boundary conditions for solving the differential equation in the following way:

$$\begin{aligned} \epsilon &= 0 \text{ for } t < 0 \\ \sigma &= 0 \text{ for } t < 0 \\ \sigma &= \sigma_0 = \text{constant for } t \geq 0 \end{aligned} \tag{1}$$

### Creep Response of the Maxwell Model

The single spring element of the Maxwell fluid (Niven 2003) does not exhibit any time-related strain behavior, and the response to stress  $\sigma_0$  at  $t = 0$  can be expressed as

$$\varepsilon(t)_{\text{spring}} = \frac{\sigma_0}{E} \quad (2)$$

The parameter  $E$  represents the elastic constant of the spring element.

The time-dependent strain of the dashpot element due to viscous flow under constant stress can be described as follows:

$$\varepsilon(t)_{\text{dashpot}} = \frac{\sigma_0}{\eta} \cdot t \quad (3)$$

with  $\eta$  being a parameter related to the Newtonian viscous flow behavior of the dashpot element and the stress response of this dashpot being proportional to the strain rate. The overall time-dependent strain of the Maxwell fluid thus can be calculated as

$$\varepsilon(t) = \frac{\sigma_0}{\eta} \cdot t + \frac{\sigma_0}{E} \quad (4)$$

Dividing the viscous parameter  $\eta$  with a dimension unit of Pa·s by  $E$  with a dimension unit of Pa provides the parameter  $\lambda$  generally referred to as the relaxation time. The time-dependent retardation strain response of the Maxwell model can then be expressed as

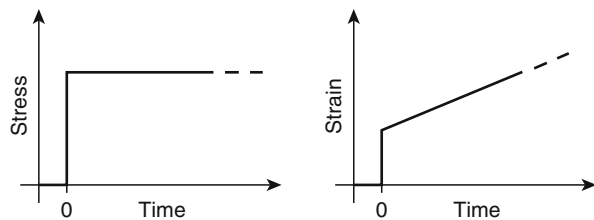
$$\varepsilon(t) = \frac{\sigma_0}{\eta} \cdot t + \frac{\sigma_0}{E} = \frac{\sigma_0}{E} \cdot \left(1 + \frac{t}{\lambda}\right) = \sigma_0 \cdot F(t) \quad \text{with } \lambda = \eta/E \quad (5)$$

The term  $F(t)$  generally is referred to as the creep function. After a certain time of creep corresponding to  $\lambda$  has passed, the ratio  $t/\lambda$  equals 1, and the viscous strain matches the initial elastic strain.

The right side of Fig. 2 illustrates the resulting strain response for the schematic stress history indicated on the left side of Fig. 2.

The Maxwell model allows the approximation of elastic and creep strain under static stress as a function of time by assigning elastic compliance leading to instant

**Fig. 2** Stress history and corresponding creep response for viscoelastic materials according to the Maxwell spring and dashpot model



elastic strain to the spring part of the model. The flow due to creep is represented by the linear slope related to the single dashpot element with linear viscous flow properties.

In practice, viscoelastic adhesive polymers do not show a discontinuous sharp bend but rather a smooth transition from the initial elastic strain to steady-state creep. A further refinement of the viscoelastic model is therefore needed to create a model converging with actually observed viscoelastic behavior.

### Creep Response of the Kelvin-Voigt Model

The Kelvin-Voigt model (Thomson 1875) addresses this issue by using a parallel connection of a spring and a dashpot. The boundary condition for solving the corresponding differential equation is that spring and dashpot at all times share the same level of strain:

$$\varepsilon_{(\text{Spring})} = \varepsilon_{(\text{Dashpot})} \quad (6)$$

The applied stress is shared by both the spring and the dashpot element:

$$\sigma_0 = \sigma_{(\text{Spring})} + \sigma_{(\text{Dashpot})} \quad (7)$$

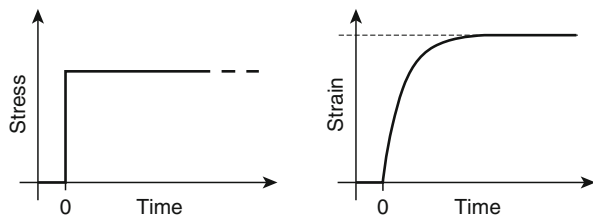
The solution of the differential equation for the time-dependent creep response under these boundary conditions can be expressed as

$$\varepsilon(t) = \frac{\sigma_0}{E} \cdot \left(1 - e^{-t/\lambda}\right) = \sigma_0 \cdot F(t) \quad (8)$$

where again the ratio  $\lambda = \eta/E$  is the relaxation time and  $F(t)$  is the creep function of the Kelvin-Voigt model. When a period of time with a duration of  $\lambda$  has passed, the exponent  $t/\lambda$  equals 1 and the factor  $e^{-1}$  attains a value of  $\approx 0.37$ . Accordingly, creep strain at relaxation time has reached  $\approx 63\%$  of the infinite ultimate value for this specific viscoelastic model. Figure 3 illustrates the schematic time-dependent creep response of the Kelvin-Voigt model for a similar load history like in Fig. 2.

Compared to the previously discussed Maxwell model and actual experimental data, the advantage of the Kelvin-Voigt model is that the strain exponentially approaches an ultimate strain limit without any discontinuities. Steady-state long-term creep and initial elastic strain, however, are not represented in the overall strain response according to the Kelvin-Voigt model.

**Fig. 3** Schematic creep response to a stress step function for viscoelastic materials according to the Kelvin-Voigt model



### Creep Response of the Burgers Model

The combination of both the Kelvin-Voigt and the Maxwell model in the Burgers model (Burgers 1935) leads to an even more realistic approach. The solution of the corresponding differential equation can be obtained by simply adding the Kelvin-Voigt and Maxwell shares of the time-dependent strain response.

$$\begin{aligned}\varepsilon(t) &= \sigma_0 \cdot \left( \frac{1}{E_1} + \frac{1}{\eta_1} \cdot t + \frac{1}{E_2} \left( 1 - e^{-\frac{t E_2}{\eta_2}} \right) \right) \\ &= \sigma_0 \cdot \left( \frac{1}{E_1} + \frac{1}{E_1 \cdot \lambda_1} \cdot t + \frac{1}{E_2} \left( 1 - e^{-\frac{t}{\lambda_2}} \right) \right) = \sigma_0 \cdot F(t)\end{aligned}\quad (9)$$

with the relaxation times  $\lambda_1 = \eta_1/E_1$  and  $\lambda_2 = \eta_2/E_2$  and  $F(t)$  being the creep function of the Burgers model. The assignment of the individual spring and dashpot elements according to this model has been shown in Table 1.

The schematic strain retardation response of the Burgers model to a step-function stress input is illustrated in Fig. 4.

The creep response according to the Burgers model in Fig. 4 covers all elementary aspects of time-dependent viscoelastic behavior including instantaneous elastic strain, secondary steady-state creep in the long-term area, and a delayed elastic strain transition behavior that can be, e.g., fitted to experimental data according to the choice of the  $\eta_1$ ,  $E_1$ ,  $\eta_2$ , and  $E_2$  parameters.

Increasing the number of interconnected spring and dashpot elements in building viscoelastic models will increase the degrees of freedom in fitting the models to experimental data and for generalized models based on an infinite number of single elements will match the continuum mechanics approach of solid and fluid dynamics.

The challenge in selecting an appropriate viscoelastic model for a specific area of practical application is to obtain the simplest relation but still to achieve the desired level of accuracy.

### 34.2.2 Creep Under Static Strain Conditions (Relaxation)

If a bonded assembly is subjected to a defined strain condition like a joint in a confined construction, creep-related phenomena in the adhesive polymer would lead

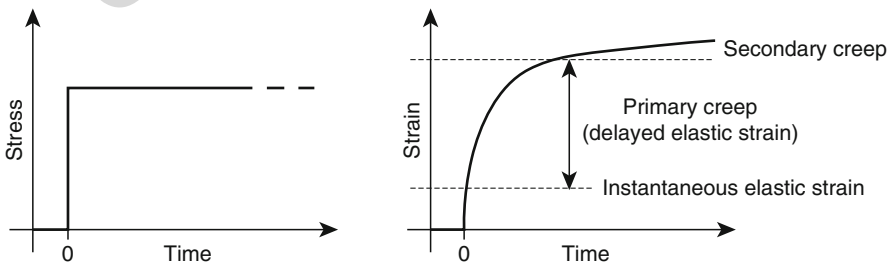


**Fig. 4** Creep response for viscoelastic materials according to the Burgers model

to a time-dependent reduction of stress. This process is generally referred to as relaxation.

In describing relaxation behavior of adhesive joints using viscoelastic models, it is assumed that a specimen is subjected at a certain time  $t = 0$  to a defined constant level of strain  $\varepsilon = \varepsilon_0$  in tensile load conditions or  $\tan \gamma = \tan \gamma_0$  in the case of shear-loaded joints.

The strain-stress history again provides the boundary conditions for the differential equation as follows:

$$\begin{aligned} \varepsilon &= 0 \text{ for } t < 0 \\ \sigma &= 0 \text{ for } t < 0 \\ \varepsilon &= \varepsilon_0 = \text{constant for } t \geq 0 \end{aligned} \quad (10)$$

### Relaxation of the Maxwell Model

Relaxation of the simple Maxwell fluid model will decrease the initial level of stress caused by the elasticity of the spring element by viscous elongation of the dashpot until all stress has been completely relieved. The solution of the first-order linear differential equation in the case of  $\varepsilon = \varepsilon_0 = \text{const}$  describes the time-dependent relaxation of stress for the Maxwell model as follows:

$$\sigma(t) = E \cdot \varepsilon_0 \cdot \left( e^{-\frac{t}{\lambda}} \right) = \varepsilon_0 \cdot R(t) \quad (11)$$

with  $E$  being a parameter representing the elastic constant of the spring element,  $\lambda = \eta/E$  being the relaxation time, and  $R(t)$  being the relaxation function of the Maxwell model. The characteristic time-dependent stress relaxation response of the Maxwell model to a step-function strain input is illustrated in Fig. 5.

### Relaxation of the Kelvin-Voigt Model

Since the Kelvin-Voigt model consists of a parallel connection of spring and dashpot, the initial level of stress depends on the viscosity  $\eta$  assigned to the dashpot and the strain rate when applying initial strain at  $t = 0$ .

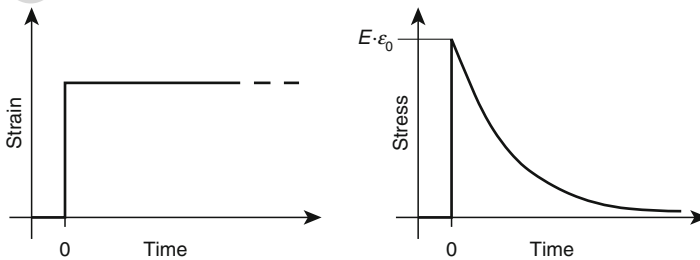


**Fig. 5** Relaxation of stress according to the simple Maxwell model

The stress response to a step-function type of strain signal as indicated on the left side of Fig. 5 would jump to an infinite level. Therefore, this model is not able to give a reasonable approximation of relaxation phenomenon under these preconditions.

### Relaxation of the Burgers Model

The extension to the four-parameter Burgers model provides again a more detailed description of relaxation in viscoelastic polymer materials. The initial differential equation and the assignments of parameters are as follows:

$$\sigma + \left( \frac{\eta_1}{E_1} + \frac{\eta_1}{E_2} + \frac{\eta_2}{E_2} \right) \cdot \dot{\sigma} + \left( \frac{\eta_1 \cdot \eta_2}{E_1 \cdot E_2} \right) \cdot \ddot{\sigma} = \eta_1 \cdot \dot{\varepsilon} + \left( \frac{\eta_1 \cdot \eta_2}{E_2} \right) \cdot \ddot{\varepsilon} \quad (12)$$

The initial stress upon application of a constant strain is governed by the Maxwell spring element  $E_1$ , and relaxation on a long-term timescale is dominated by the Maxwell dashpot  $\eta_1$ , while the Kelvin-Voigt section with  $E_2$  and  $\eta_2$  governs the delayed elastic relaxation. Solving the differential equation by Laplace transformation is, e.g., comprehensively described in Betten (2008).

Another possibility to work with the parameters if the viscoelastic Burgers models in evaluating and predicting relaxation phenomena is by using a recursive definition of the relaxation function  $\sigma(t)$ . Therefore, the total period of time to be considered is first divided into  $n_t$  incremental steps, and the calculation of strain for each consecutive step is based on the value of the preceding one.

Starting at  $t = 0$ , again assuming a strain-stress sequence according to a strain step function for relaxation experiments with

$$\begin{aligned} \varepsilon &= 0 \text{ for } t < 0 \\ \sigma &= 0 \text{ for } t < 0 \\ \varepsilon &= \varepsilon_0 = \text{constant for } t \geq 0 \end{aligned} \quad (13)$$

both dashpots  $\eta_1$  and  $\eta_2$  will give a rigid response to an instantaneous strain input  $\varepsilon_0$ . In consequence, the total initial strain of the Burgers model in the first incremental step is governed by the spring element  $E_1$  and can be calculated as

$$\sigma(n_t = 1) = E_1 \cdot \varepsilon_0 \quad (14)$$

During the next incremental step,  $\sigma(n_t = 1)$  will cause the dashpot  $\eta_1$  to expand to a strain of

$$\varepsilon_{\eta_1}(n_t = 2) = \frac{\sigma(n_t = 1)}{\eta_1} \cdot \Delta t \quad (15)$$

During this step, no load has been transferred to the second spring element  $E_2$ , and the increase of strain in dashpot  $\eta_2$  can be approximated in the same manner:

$$\varepsilon_{\eta_2}(n_t = 2) = \frac{\sigma(n_t = 1)}{\eta_2} \cdot \Delta t \quad (16)$$



278 The total viscous strain  $\varepsilon_{\eta 1}(n_t = 2) + \varepsilon_{\eta 2}(n_t = 2)$  will reduce the elongation of  
 279 the  $E_1$  spring element to a value of  $\varepsilon_0 - (\varepsilon_{\eta 1}(n_t = 2) + \varepsilon_{\eta 2}(n_t = 2))$  and reduce the  
 280 overall stress in the next step to

$$\sigma(n_t = 2) = E_1 \cdot (\varepsilon_0 - \varepsilon_{\eta 1}(n_t = 2) - \varepsilon_{\eta 2}(n_t = 2)) \quad (17)$$

281 The last incremental effect to be considered according to this recursive model is  
 282 that the strain in dashpot  $\eta_2$  has transferred a part of the load to the spring element  $E_2$ .  
 283 For the calculation of the next step, this spring element carries the load

$$\sigma_{E2}(n_t = 3) = E_2 \cdot \varepsilon_{\eta 2}(n_t = 2) \quad (18)$$

284 The stress causing dashpot  $\eta_2$  to further expand is reduced accordingly to

$$\sigma_{\eta 2}(n_t = 3) = \sigma(n_t = 2) - E_2 \cdot \varepsilon_{\eta 2}(n_t = 2) \quad (19)$$

285 The resulting increase in strain of dashpot  $\eta_2$  for the next step will then be

$$\varepsilon_{\eta 2}(n_t = 3) = \frac{\sigma(n_t = 2) - E_2 \cdot \varepsilon_{\eta 2}(n_t = 2)}{\eta_2} \cdot \Delta t \quad (20)$$

286 Following the third increment, the calculation is repetitive, and the accuracy  
 287 depends on the choice of the number of increments  $\Delta t$  in relation to the total time  
 288 span to be considered. The recursive definition can easily be implemented into  
 289 computer-based spreadsheet calculation tools and be extended to other spring-  
 290 dashpot combinations if desired.

### 291 34.2.3 Generalized Models

292 The greater the number of connected spring and dashpot elements in a viscoelastic  
 293 model, the better a fitting to the material behavior of a specific polymer can be  
 294 accomplished. In the generalized Maxwell model, a spring and dashpot are  
 295 connected to an arbitrary number of Maxwell elements in parallel. In the generalized  
 296 Kelvin-Voigt model, a Maxwell element is connected to an arbitrary number of  
 297 Kelvin-Voigt elements in series.

298 The notional transition from a finite number of elements to an infinite number  
 299 (i.e., a spectrum) of elements leads to models where  $\Gamma(\lambda)$  expresses the probability  
 300 density of relaxation times in the generalized Maxwell model. The relaxation  
 301 function of the generalized Maxwell spectrum then is

$$R(t) = \int_0^{\infty} \Gamma(\lambda) \cdot e^{(-t/\lambda)} d\lambda \quad (21)$$

In a similar way, for an infinite number of elements in the generalized Kelvin-Voigt model,  $f(\lambda)$  may be used to express the probability density of retardation times, and the creep function  $F(t)$  for the spectrum in the case of the generalized Kelvin-Voigt model can be written as

$$F(t) = \int_0^{\infty} f(\lambda) \cdot (1 - e^{(-t/\lambda)}) d\lambda \quad (22)$$

The functions  $\Gamma(\lambda)$  and  $f(\lambda)$  characterize the retardation and respectively the relaxation spectra and thus represent the distribution of retardation and relaxation time values in a specific material. Further details are given in Haddad (1995) and de With (2006).

### 34.3 Superposition Principles

Describing and predicting viscoelastic properties of polymer materials or adhesively bonded joints on the basis of analytical mathematical equations is only justified in the limits of linear viscoelasticity. Linear viscoelasticity is typically limited to strain levels below 0.5%. Furthermore, linear viscoelastic behavior is associated to the Boltzmann superposition principle, the correspondence principle, and the principle of time-temperature superposition.

#### 34.3.1 Boltzmann Superposition Principle

According to the Boltzmann superposition principle, the time-dependent strain caused by two individual stress incidents  $\sigma_1(t)$  and  $\sigma_2(t)$  can be calculated as  $\varepsilon_1(t) + \varepsilon_2(t)$  if  $\sigma_1(t)$  would cause  $\varepsilon_1(t)$  and  $\sigma_2(t)$  would cause  $\varepsilon_2(t)$ . In consequence, according to the Boltzmann superposition principle in the linear viscoelastic range, strain responses from subsequent stress histories may simply be summarized if according to the criterion of proportionality at any instant of time, the strain response behaves proportional to the stress level:

$$f[c \cdot \sigma(t)] = c \cdot f[\sigma(t)] (c = \text{constant}) \quad (23)$$

The criterion of superposition of input histories can be expressed accordingly as

$$f[\sigma_1(t_1), \sigma_2(t_2), \dots, \sigma_n(t_n)] = f[\sigma_1(t_1)] + f[\sigma_2(t_2)] + \dots + f[\sigma_n(t_n)] \quad (24)$$

Figure 6 illustrates how the Boltzmann superposition principle will affect the total creep strain in a step-loaded creep experiment.

When at a time  $t_1$  the initial stress  $\sigma_1$  is applied, then the time-dependent strain  $\varepsilon_1(t)$  is induced in

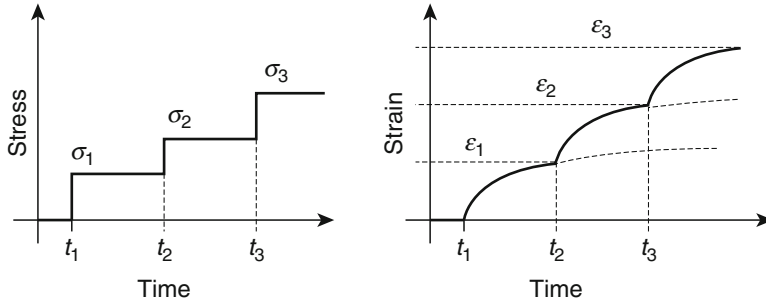


**Fig. 6** Effect of the Boltzmann superposition principle on creep strain in a step-loading creep experiment

$$\varepsilon_1(t) = \sigma_1 \cdot J(t) \quad (25)$$

According to linear viscoelasticity, the compliance  $J(t)$  is independent of stress, i.e.,  $J(t)$  is the same for different stress levels at a particular time. Once the following stress increment  $\sigma_2 - \sigma_1$  is applied at time  $t_2$ , the additional strain increase due to stress increment  $\sigma_2 - \sigma_1$  is

$$\varepsilon_2(t) = (\sigma_2 - \sigma_1) \cdot J(t - t_2) \quad (26)$$

In a similar way, the additional strain increase due to  $\sigma_3 - \sigma_2$  can be calculated as

$$\varepsilon_3(t) = (\sigma_3 - \sigma_2) \cdot (t - t_3) \quad (27)$$

### 34.3.2 Correspondence Principle

The correspondence principle following the Boltzmann superposition principle allows the conversion of the common mechanical relationships of linear elasticity theory into linear viscoelasticity simply by replacing  $\sigma$  by time-dependent  $\sigma(t)$  and  $\varepsilon$  by time-dependent  $\varepsilon(t)$ . Young's modulus  $E$  is accordingly transformed to the creep modulus  $E_C(t) = \sigma/\varepsilon(t)$  or the creep compliance  $J(t) = \varepsilon(t)/\sigma$ , respectively, and the relaxation modulus  $E_R(t) = \sigma(t)/\varepsilon$ . These time-dependent parameters can be determined from tensile creep and relaxation experiments. In compression or shear mode, the corresponding parameters of moduli are calculated in a similar manner.

In linear viscoelasticity, the creep function and the relaxation function are inter-related, and each would permit the derivation of the viscoelastic constitutive relation under the condition that the principle of time invariance can be applied, meaning that the material is influenced only by  $\sigma(t)$  and  $\varepsilon(t)$  and no other influencing variables are being effective. In summary, in the idealized case of the isothermal linear viscoelasticity under the conditions of static stress or strain, the linear viscoelastic behavior of a material may adequately be described by the creep function  $F(t)$ , the relaxation function  $R(t)$ , the retardation spectrum, or the relaxation spectrum.

### 34.3.3 Time-Temperature Superposition Principle

The time-temperature superposition principle is based on the assumption that in the linear viscoelastic region, the different mechanical parameters exhibit similar temperature dependence. Under this precondition, an increase in temperature will cause a similar change in mechanical properties as an increase in time for the time-dependent mechanical viscoelastic parameters. In the case of a cyclic mechanical stress or strain excitation of a viscoelastic material, an increase of temperature will have a similar effect as a reduction of frequency according to the principle of time-temperature superposition. The principle of time-temperature superposition therefore is commonly applied on, e.g., data obtained by dynamic mechanical thermal analysis. The dynamic mechanical thermal analysis (DMTA) provides an effective method for measuring transitions due to morphological or chemical changes, or both, in a polymer as it is heated/cooled through a specified temperature range. For the dynamic mechanical thermal analysis (e.g., according to ASTM D 4065), a specimen of known geometry is subjected to a mechanical oscillation either at fixed or natural resonant frequencies. Elastic (storage) and viscous (loss) moduli of the specimen are then measured at varying temperatures and frequencies. Plots of the elastic modulus ( $E'$ ,  $G'$ ) related to the spring properties in the viscoelastic behavior or the loss modulus ( $E''$ ,  $G''$ ) related to the viscous dashpot properties are indicative of the viscoelastic characteristics of the specimen. The ratio  $E''/E'$  or  $G''/G'$  is defined as the loss factor  $\tan \delta$  which provides a measure of the mechanical damping due to inner friction of a viscoelastic polymer material. Rapid changes in viscoelastic properties in a particular range of temperatures, times, or frequencies are generally referred to as transition regions. Dynamic mechanical testing provides a method for determining elastic and loss moduli as a function of temperature, frequency or time, or both. A plot of the elastic modulus and loss modulus of material versus temperature provides a fingerprint of elastic and viscous properties as a function of temperature or frequency.

Experimental data obtained during such a dynamic mechanical analysis at different temperatures and frequencies can be converted using a shift function  $a = f(T)$  with  $T$  being the temperature, to merge temperature-dependent data into a master curve. This master curve then, e.g., represents the mechanical properties for a chosen temperature  $T_0$  at time or frequency levels beyond the range that had been experimentally applied in collecting the underlying data. The shift function was originally published by Williams, Landel, and Ferry (Ferry 1970) and proved to be applicable for most elastic and amorphous polymers and in its general form is fitted to give best conformity of the master curve by two parameters  $C_1$  and  $C_2$ :

$$\log a_T = \frac{C_1 \cdot (T - T_0)}{C_2 + T - T_0} \quad (28)$$

If the glass transition temperature  $T_G$  is chosen as  $T_0$ , for many polymer material parameters,  $C_1 = 17.44$  and  $C_2 = 51.6$  K have provided a good approximation.

This method can also be applied to the extrapolation of time- and temperature-dependent creep behavior. Experimental creep curves first need to be obtained at a series of different temperatures over a specific time period, followed by the values of compliance plotted on a logarithmic timescale. After one creep curve at a chosen temperature is defined as reference, creep curves at other temperatures are then shifted one by one along the log timescale until they superimpose to a single curve in the ideal case. Curves above the reference temperature are shifted to the right, and those below are shifted to the left. This procedure can be applied to predict long-term creep compliance on the basis of short-term tests at different temperature levels in the range of linear viscoelasticity.

In practice, polymers and adhesive joints are often being used under service conditions exceeding the limitations of linear viscoelasticity. Indications for non-linear viscoelastic properties include the observation that creep compliance changes for different stress levels and that the mechanical behavior not only depends on the summarized history of previous mechanical incidents but also from the sequence in which they have been applied. In this case, the simplified constitutive equations of linear viscoelasticity will fail in describing time-dependent mechanical properties. Further reference to nonlinear viscoelasticity is given in Haddad (1995) and Brinson and Brinson (2008).

---

## 34.4 Experimental Testing

### 34.4.1 Accessing Creep Properties of Adhesives by Rheometric Test Procedures

The term “rheology” was first introduced by Bingham and Crawford in 1948 (Scott Blair 1969). Rheology today provides a large range of experimental procedures to study the flow of fluids and the plastic deformation of soft solids.

Most scientific rheometric instruments are designed to apply a constant or oscillating torque to a sample located in a precisely adjusted and thermally controlled gap between test plates which may carry a flat or conical surface. The parallel plate (or plate-plate) geometry has the advantage of being able to take preformed sample discs which can be especially useful when working with film or tape adhesives. The main disadvantage of parallel plates is due to the fact that the shear rate varies across the radius of the sample. In most cases, an average value for the shear rate is displayed in the test results. The cone to plate geometry is designed to maintain a uniform shear rate by narrowing the shear gap toward the center of the sample.

Rheological tests are especially useful to experimentally determine the limits of linear viscoelasticity of an adhesive bulk sample, to investigate its zero-shear viscosity as a measure for creep under long-term loading, and to obtain a data basis for the calculation of relaxation time spectra.

**Limits of Linear Viscoelasticity (LVE)**

In a strain sweep under dynamic oscillation, increasing levels of strain are applied at a certain frequency. According to ASTM D 7175, the departure of the linear viscoelastic region is defined as the point at which the elastic modulus  $G'$  deviates by more than 10% from a constant (plateau) value. It should be considered that the choice of test frequency has an impact on the limit of LVE with higher frequencies causing a shift of the LVE limit to lower strain values. Figure 7 illustrates the oscillatory strain-sweep results for a hot melt adhesive in plate-plate geometry with a diameter of 25 mm at 70 °C and a test frequency of 0.1 Hz obtained with a Bohlin Gemini 150 rheometer. Departure from linear behavior occurs in this case at about 30% of deformation.

Reference on creep in relation to the rheology of pressure-sensitive adhesives is given in ► Chap. 15, “Pressure-Sensitive Adhesives (PSAs)” by C.W. Paul.

**Zero-Shear Viscosity**

At sufficiently low shear rates, creep-sensitive adhesives exhibit a so-called zero-shear viscosity (ZSV). Creep-sensitive adhesives include non-crosslinked hot melt adhesives or non-crosslinked pressure-sensitive adhesives. This parameter is indicative for the bulk adhesive’s resistance to permanent deformation under long-term loading.

Zero-shear viscosity (ZSV) may be derived for such materials from rheological creep tests under constant shear stress. The zero-shear viscosity is determined as the “steady-state viscosity” at sufficiently low levels of shear stress in the linear

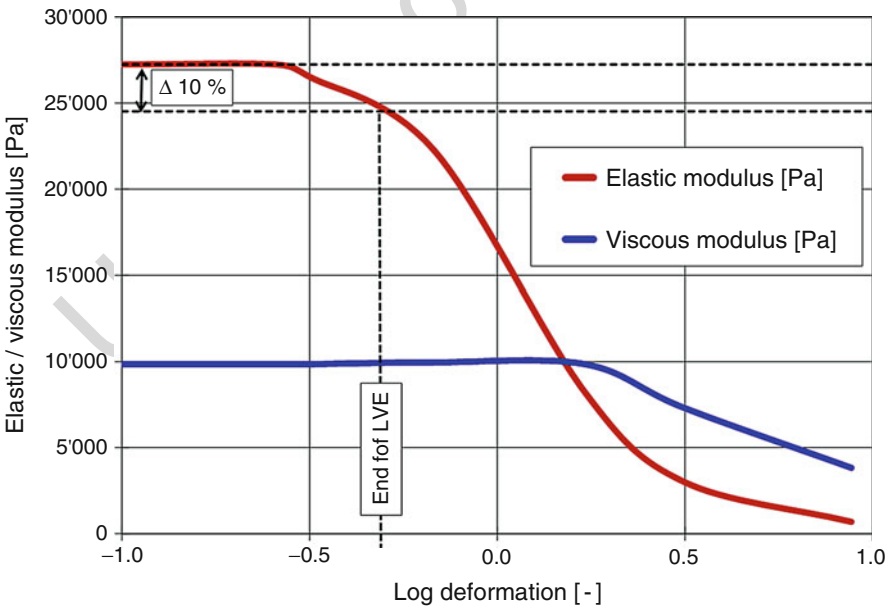


**Fig. 7** Identification of the limit of linear viscoelasticity from an oscillatory strain-sweep test

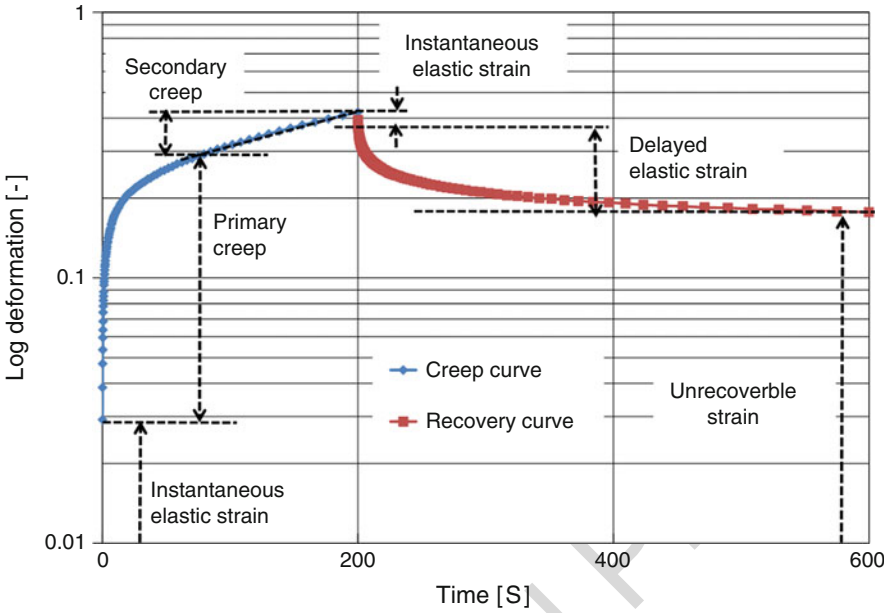


**Fig. 8** Identification of secondary creep in a rheometric creep test

viscoelastic region, where strain curves should be independent of the level of stress. The steady-state viscosity criterion relates to the change in strain as a function of time and may be included in the experimental parameters of most rheometric instruments to facilitate the selection of a sufficient timescale. As the adhesive acquires secondary creep, the slope of the strain vs time diagram represents the zero-shear viscosity, and the differential of the slope approaches 1.00. Most rheometer software gives readout of the slope as the test progresses and can be set to automatically accept the data when this steady-state criterion is attained. Using state-of-the-art software tools for non-linear regression analysis, the viscoelastic parameters and relaxation time corresponding to a preselected model according to Table 1 may be fitted to the experimental data of rheometric creep/creep recovery tests. Figure 8 illustrates the time-dependent strain of a hot melt adhesive in a rotation-mode experiment under a constant stress of 1000 Pa, in plate-plate geometry with a diameter of 25 mm and a temperature of 70 °C. In this specific case, the zero-shear viscosity in the region of secondary creep converges to a level of approximately 1 MPas.

### 34.4.2 Retardation Test Methods with Adhesively Bonded Joints

Due to the polymer nature of most structural engineering adhesives, their viscoelastic deformation behavior is strongly time and temperature dependent and associated to creep (retardation) under static or so-called “dead-load” condition.

There are several standards dealing with creep and long-term mechanical properties.

ISO 899 Part 1 “Plastics – Determination of creep behaviour” specifies a method for determining the tensile creep of plastics in the form of standard bulk test specimens like specified in ISO 527. The method is suitable for use with rigid and semirigid and filled plastic materials and can be applied to the testing of adhesive bulk specimen in the form of dumb-bell-shaped test specimens molded directly or machined from molded sheets. The method is intended to provide data for engineering design and research and development purposes. Acquiring data for engineering-design purposes requires the use of extensometers like video extensometers allowing a precise measuring of the gauge length of the specimen during the test. A multi-sample tensile creep tester with video extensometer is displayed in Fig. 9.

Tensile creep properties strongly depend on the preparation procedure, the dimensions of the specimen, and the test environment. The thermal history of the test specimen has also shown to have a significant effect on creep behavior. Consequently, when exact comparative results are required, these factors must be carefully controlled.



**Fig. 9** Multi-sample tensile creep tester with video extensometer



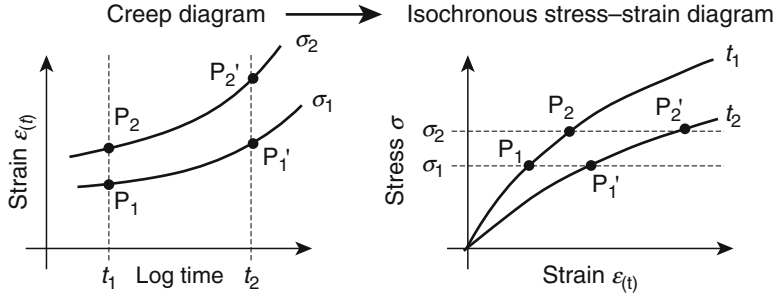


**Fig. 10** Conversion of creep data into isochronous stress-strain diagrams

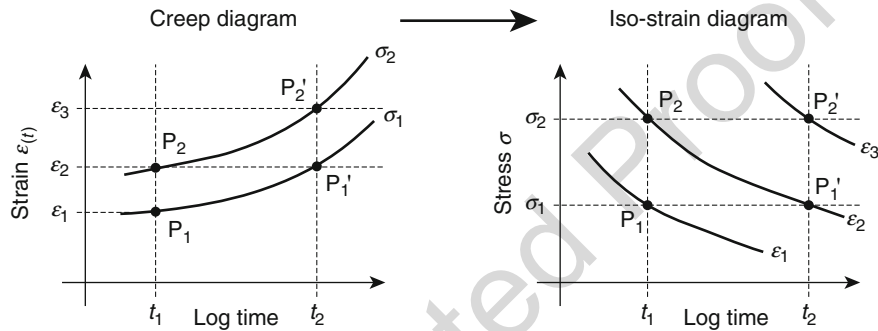


**Fig. 11** Conversion of creep data into iso-strain diagrams

In determining creep properties, a series of specimens are subjected to static loads at different levels, and their increase in strain over time is measured. Data may be either presented directly as creep strain on a logarithmic timescale, as creep modulus  $E_C(t) = \sigma/\varepsilon(t)$ , or as isochronous stress-strain diagrams where the relation between stress on the axis of ordinates over strain on the axis of abscissa is presented for different time levels. The schematic approach to converting creep data into an isochronous stress-strain diagram is illustrated in Fig. 10.

Other ways to present creep data include compilation to stress-time diagrams with continuous lines indicating time-dependent strain limits. Therefore, this way of plotting creep data is frequently referred to as an iso-strain diagram. The schematic approach for converting creep data into an iso-strain diagram is illustrated in Fig. 11.

A third alternative way of presenting the time-dependent stress-strain relationship due to creep under static load conditions is to plot the creep modulus  $E_C(t)$  on a logarithmic timescale. Provided that the materials creep is linear viscoelastic, data at different stress levels should cause similar time-dependent values of creep modulus. The schematic approach for converting creep data into a creep modulus versus time diagram is illustrated in Fig. 12.

Since the long-term behavior of bonded joints is strongly influenced by the adhesive-surface interaction at the interface, a prediction of creep and relaxation

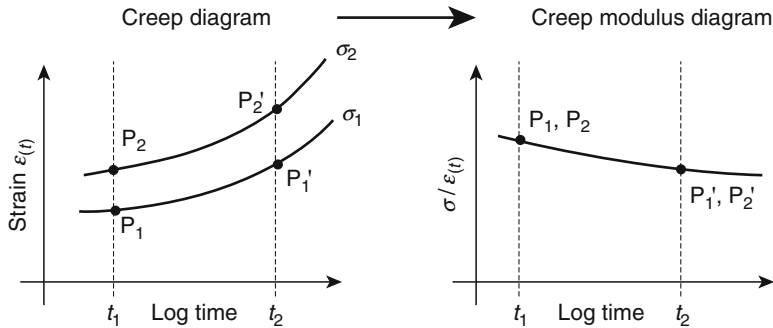


**Fig. 12** Conversion of creep data into creep modulus versus time diagrams

for adhesives cannot only be founded on data obtained from adhesive bulk specimen in tensile mode but should consider shear load conditions and geometric bond line size effects close to practice adhesive joint assemblies.

The standard ISO 15109 “Adhesives – Determination of the time to rupture of bonded joints under static load” is focused on time to rupture of bonded lap shear specimens under a specific static load. No time-dependent shear strain is recorded according to this standard. Initial stress levels are chosen as a percentage of the ultimate tensile lap shear strength in quasi-static experiments in accordance with ISO 4587. The results are expressed as a graph of stress versus time to failure including remarks on the type of failure pattern for each specimen.

A more sophisticated procedure is described in ASTM D 1780 “Standard Practice for Conducting Creep Tests of Metal-to-Metal Adhesives.” This standard covers the determination of the amount of creep of metal-to-metal adhesive bonds due to the combined effects of temperature, tensile shear stress, and time. The primary intention of this test procedure using single lap shear specimens is to provide basic data for the choice of safe working stresses for applications in which the allowable deformation within the service life of the structure is the criterion of failure. The standard is intended to be used with standard testing machines in combination with extensometers allowing to measure shear strain close to the bond line of the employed lap shear specimen.

For the purpose of conducting creep experiments with adhesively bonded joints under natural or accelerated aging conditions, several spring loaded creep test instruments have been suggested. Since constant-stress creep tests are desirable, the usual common practice would be using constant dead weight load tests with gravity causing the predefined level of load. Creep tests made by means of spring loading or fixtures, which involve deflection or strain measurements for the application of load, are generally considered to be unsatisfactory because the creep strain of the specimen will cause a reduction of stress due to, e.g., contraction of a tensile spring. However, if the total deformation or extension in the adhesive is large, corrections can be used to compensate for the decrease in stress because of the extension in the adhesive. Spring-loaded units have the advantage of reduced weight

compared to creep testers applying the required creep load directly by means of masses. Commercial creep test instruments overcome the problem of bulky load weights by using cantilevers to amplify the load to the desired stress level during the creep experiment. Special care needs to be taken to eliminate friction in the cantilever movement since this is likely to tamper the test results.

Spring-loaded instruments for conducting creep tests on single lap shear specimens in tensile or compressive mode are described, e.g., in ASTM D 2294 “Standard Test Method for Creep Properties of Adhesives in Shear by Tension Loading (Metal-to-Metal)” or ASTM D 2293 “Standard Test Method for Creep Properties of Adhesives in Shear by Compression Loading (Metal-to-Metal).” In ASTM D 2294, the tension creep test apparatus consists of a hollow loading chamber, a solid extension rod with provisions for attachment of test specimens, and a spring. A testing machine is required to apply the static load, and a microscope is being suggested to measure the amount of creep shear strain. According to ASTM D 2293, the load conditions are adjusted in a less accurate manner by compressing a spring between two bushings to the desired load by tightening a nut. The applied load can be estimated by deflecting the spring of a given measured amount as predetermined from a calibration curve.

The standard ASTM D 4680 “Standard Test Method for Creep and Time to Failure of Adhesives in Static Shear by Compression Loading (Wood-to-Wood)” also applies a compressive force to shear specimens to monitor the creep properties of wood adhesives in lap shear geometry.

Since creep is considered as a key weakness of pressure-sensitive adhesives, various specific test methods and standards have been developed to evaluate the creep resistance of pressure-sensitive adhesives like in the European Standard EN 1943 (“Self-adhesive tapes. Measurement of static shear adhesion”), FINAT (Federation Internationale des Fabricants et Transformateurs d’Adhesives et Thermo-collants sur Papier et autres Supports), test method FTM 8 (Resistance to shear from a standard surface), or Pressure-Sensitive Tape Councils test method PSTC 107 (Harmonized International Standard for Shear Adhesion of Pressure-Sensitive Tape) by either monitoring the time- and load-dependent displacement of an adhesive specimen under shear load or simply recording the time to failure. The result of the so-called SAFT-test (“Shear Adhesion Failure Temperature”) indicates the temperature at which a sample has failed that has been subjected to an environment with steadily rising temperature under static shear load.

Figure 13 represents the typical course of a creep experiment using single lap shear specimen bonded with a viscoelastic acrylic adhesive under tensile load. The curve progression can be divided into three phases of creep. At the end of phase I, instantaneous elastic strain and delayed elastic strain are completed, and the creep progress in phase II is dominated by secondary creep. At the end of phase II, creep accelerates leading to failure of the specimen at the end of phase III.

Failure can either occur due to cohesive fracture of the adhesive, due to interfacial sliding, or due to adhesive debonding at or close to the adhesive substrate interface.

A set of creep experiments at different load levels can be used to build creep-strength-time curves indicating at which time- and load-related limits a failure under

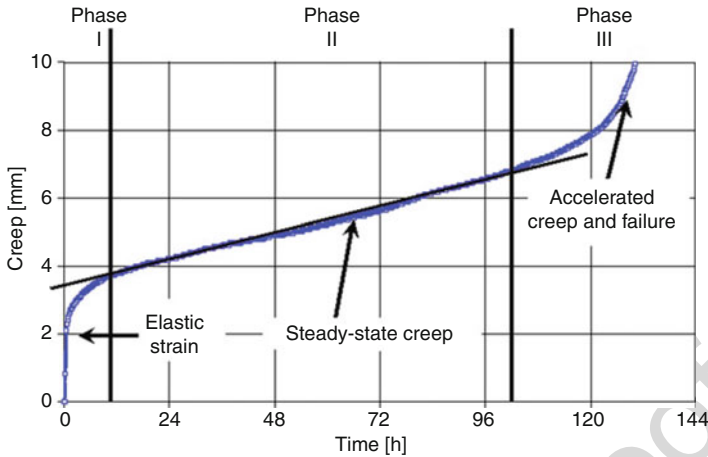


**Fig. 13** Typical course of a creep experiment for single lap shear specimen with a viscoelastic acrylic adhesive (Geiß 1998)

static load condition is to be expected for a certain adhesive-substrate combination. The construction of a so-called “creep rupture envelope” by connecting the points of the onset of the tertiary creep stage is shown in Fig. 14.

The creep rupture envelope in Fig. 14 was obtained at a temperature of 60 °C. Creep rupture envelopes for the same type of adhesive joint at different temperatures may show different characteristics if, e.g., the failure mode is changed by the influence of heat.

The empirical prediction of long-term behavior from such technical test methods may often not lead to the desired level of certainty since the failure of specimens under static shear loads may involve random fracture mechanisms which cause a wide scattering of the results in terms of time to failure. In addition to this, the failure of viscoelastic adhesives in creep experiments often occurs when high strain values far beyond the limits of linear viscoelasticity have been reached which are not tolerable in most technical applications and therefore do often not contribute satisfactory to the application-related long-term predictability.

Excessive shear strain should generally be avoided in adhesive joints because cohesive failure is likely to occur once shear deformation leads to a buildup of tensile stress at the end of the overlap bond area. In practice, it has been found that strain in assemblies with rubbery moisture curing one-component polyurethane adhesives should be limited to values of shear strain  $\tan \gamma$  below 0.5. Specific viscoelastic pressure-sensitive tapes may even tolerate shear strains of  $\tan \gamma$  up to 2. The maximum tolerable strain of structural adhesive joints using adhesives with a highly crosslinking density, however, is typically more than one order of magnitude lower than that.

Due to the significance of limiting shear strain, creep data can be presented as iso-strain curves. This can be accomplished by taking stress-strain data from creep experiments at different stress levels and converting them to iso-strain lines (Fig. 15).

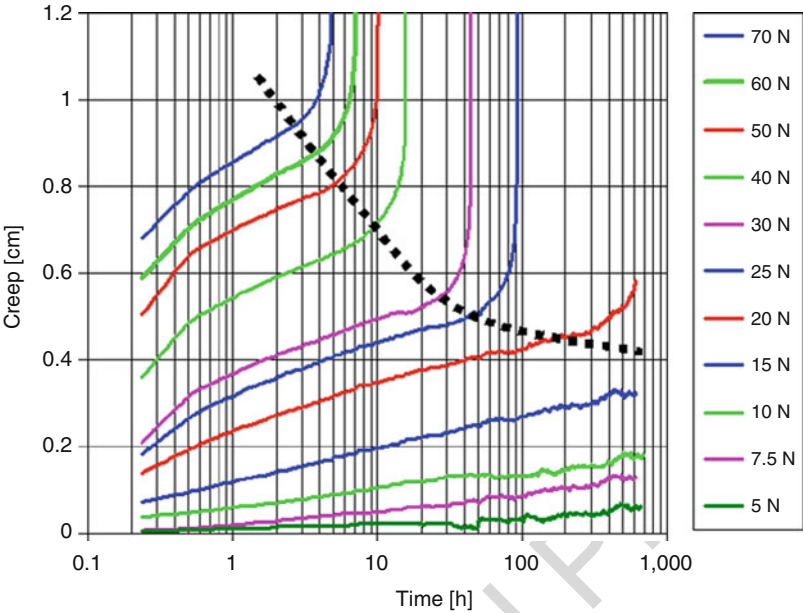


**Fig. 14** Creep-strength-time diagram based on a set of creep experiments at different levels of static load at a temperature of 60 °C (Geiß 1998)

The presentation of creep data in the manner according to Fig. 15 allows to easily read stress limits if a certain allowable application-related strain level due to creep must not be exceeded within a given timeframe. Other ways to present creep data include isochronous stress-strain diagrams (Fig. 10) or creep modulus-time diagrams (Fig. 12).

Attempts to project results from short-term creep tests to a longer timescale often fail because the increase of shear strain during a static load creep experiment will lead to a change of the state of stress in the adhesive joint and will eventually cause an excessive amount of superimposed tensile stress near the end of the overlap area. Therefore, the dotted lines in Fig. 15 merely represent a “guide to the eye” projection rather than a mathematically confirmed extrapolation.

The problem of changing the state of stress in a static long-term experiment is less in relaxation tests compared to creep tests. Since the strain in relaxation tests is to be maintained at a constant level throughout the test time, a better accessibility to a mathematically based extrapolation may often be achieved. Section “4.3” will further address this matter.

Beyond collecting empirical creep data for specific adhesives or adhesive joints, it is in some cases desirable to derive viscoelastic parameters in relation to the previously discussed mechanical substitute models of viscoelasticity from the test results. The challenge hereby is to distinctively separate instantaneous elastic and delayed elastic strain (primary creep) from non-recoverable strain (secondary creep) and to determine whether the principles of linear viscoelasticity may or may not be applied.

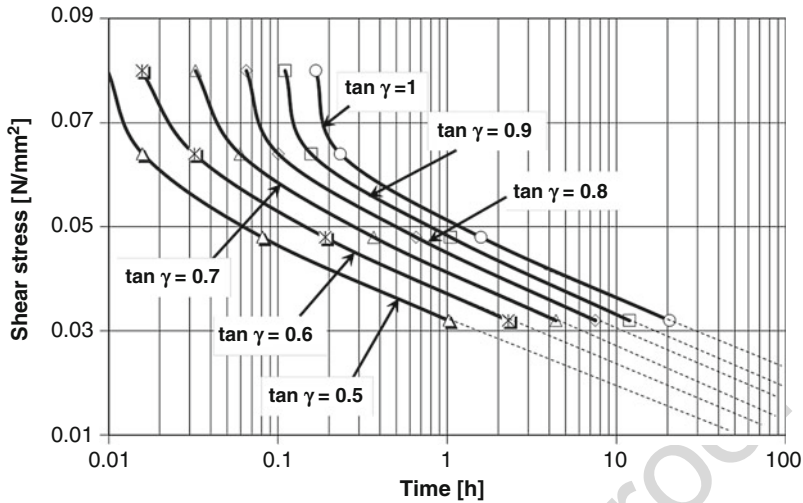


**Fig. 15** Load-dependent time to reach different deformation limits indicated by iso-strain curves derived from static load creep experiments in lap shear specimens with a viscoelastic acrylic adhesive (Geiß and Vogt 2007)

A good method to reduce the amount of test specimens needed to collect creep data on different stress levels is to take advantage of the so-called step-loading experiments. In an experiment with step loading, the stress is again and again increased after a certain period of time. The viscoelastic response in consequent load steps in Fig. 16 should be similar if the Boltzmann superposition principle can be applied and the material is behaving according to linear viscoelasticity.

In the experiment illustrated in Fig. 16, the first step (caused by a load of 32 N) has led to an initial deformation of the sample of a bit less than 4 mm. During the following load steps with a repeated stress growth of 125% of the preceding load, the additional creep response decreases with higher total strain values, and also the slope at the end of each step decreases, although the total stress becomes larger. This indicates that the viscoelastic parameters of the specific material at these levels of creep change due to a strain hardening type of behavior, and the creep response does not represent linear viscoelastic properties.

In some cases, it may be useful to dissent from the method of creep experiments under a constant static load and to subject the adhesive joint to a sequence of periodical static load events. The additional information obtained in this manner is the creep and the creep recovery behavior of an adhesive joint with viscoelastic properties (Fig. 17). The test in this case was carried out using single lap shear specimens and a time controlled mechanical lifting device to apply and remove a balanced weight causing a periodically repeating history of static load inputs.

**Fig. 16** Creep response of an acrylic viscoelastic adhesive in a step-loading experiment (Geiß 1998)

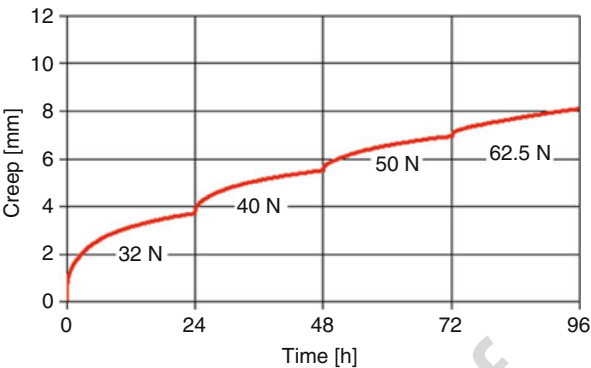
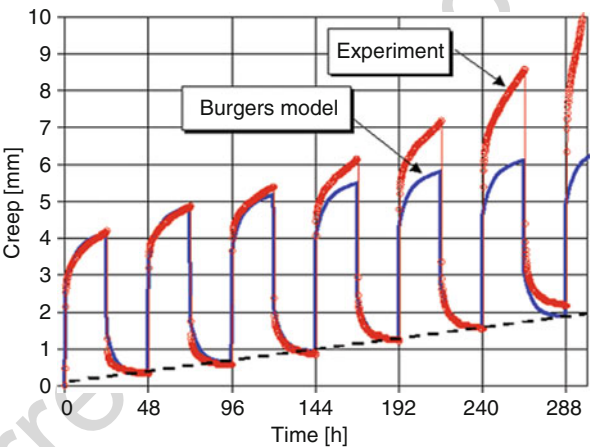


**Fig. 17** Creep and creep recovery of a lap shear specimen bonded with an adhesive based on a SIS block copolymer formulation (Geiß 1998)



The line connected by data points in Fig. 17 represents the experimental data, while the continuous curve relates to the numerically simulated behavior based on the four parameter Burgers model for viscoelasticity. The load history consists of repeatedly loading for 24 h followed by 24 h of recovery.

The steadily increasing residual strain after recovery gives a clear indication of the viscous dashpot properties  $\eta_1$  in the Maxwell section of the Burgers model. The  $E_1$  spring properties can easily be fitted according to the repeating elastic strain in the creep and creep recovery sequence. The parameters  $\eta_2$  and  $E_2$  in the Kelvin-Voigt part of the Burgers model could be adjusted to adequately fit the experimental data during the first two cycles.

In this specific test, an early indication of damage accumulation could already be observed in the third cycle by a deviation of the experimental data from the predicted behavior based on the Burgers parameters. In the following cycles, this deviation increased steadily, leading to the failure of the specimen during the seventh load cycle.



This example was intended to illustrate how a combination of experiment and simulation based on simple viscoelastic models can contribute to generate added value from creep experiments without expanding their complexity.

A recurring challenge in designing creep experiments is the choice of the load levels and width of their distribution. Quasi-static lap shear tests at low strain rates indicate the short-term load capacity of the joint. As a rule of thumb, the higher the strain rate dependency of the modulus and fracture strength of an adhesive is, the lower the static load as a percentage of the ultimate fracture strength should be chosen if no other application-related considerations govern the level of static load to be used in a specific experiment. Structural adhesives may have a static load-bearing capacity in the range of 70% to even 90% of their short-term strength. Creep resistance of pressure-sensitive adhesives may be limited to 20% of their short-term strength or even less.

To overcome the risk of investing efforts in creep experiments resulting in strain levels beyond the area of relevancy for a certain application, relaxation test methods may provide an effective alternative test procedure.

#### 34.4.3 Relaxation Test Methods with Adhesively Bonded Joints

In the engineering process of bonded structures, the limits for maximum tolerable deformations in a structure to maintain its functionality and appearance are often important for the design of the adhesive joint. The shear strain of adhesive joints is generally expressed as  $\tan \gamma = s/d$ , where  $s$  is the displacement of the adherends and  $d$  is the thickness of the adhesive layer. Once the admissible  $\tan \gamma$  deflection is established, relaxation tests may provide an effective method to determine the related static load capacity of an adhesive or adhesive joint or the required size of the bond area to support a given load under such limitations.

While creep experiments apply a constant load to the sample and follow the increase of strain over time, the relaxation method applies a fixed strain to the specimen at the beginning of the test and records the decrease in stress over time caused by relaxation of the adhesive polymer. The basic difference in creep (retardation) testing versus relaxation testing is illustrated in Fig. 18.

To obtain accurate relaxation data, the elastic behavior of the test instrument needs to be taken into account. The elastic compliance of a fixed test frame would generally influence the designated level of constant strain if the stress and the associated load of the test frame decrease during the course of the experiment. The following experimental relaxation data in Fig. 19 were therefore obtained in single overlap shear relaxation tests using a testing machine with noncontact video extensometry and closed-loop control to apply the initial strain at a predefined constant strain rate and then keep the true shear strain in the bond area on a precisely constant level throughout the test.

On the left side of Fig. 19, data have been plotted on a logarithmic timescale with linear ordinate units. Conversion to a double logarithmic scale on the right side of Fig. 19 leads to a linearization of the relaxation characteristic, which allows a better



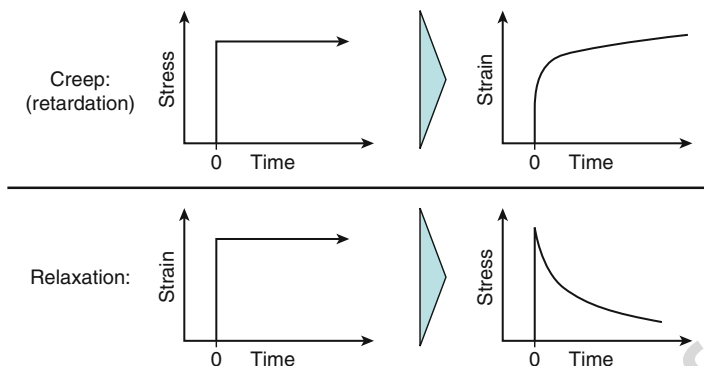


**Fig. 18** Comparison of input and response in creep (retardation) and relaxation tests

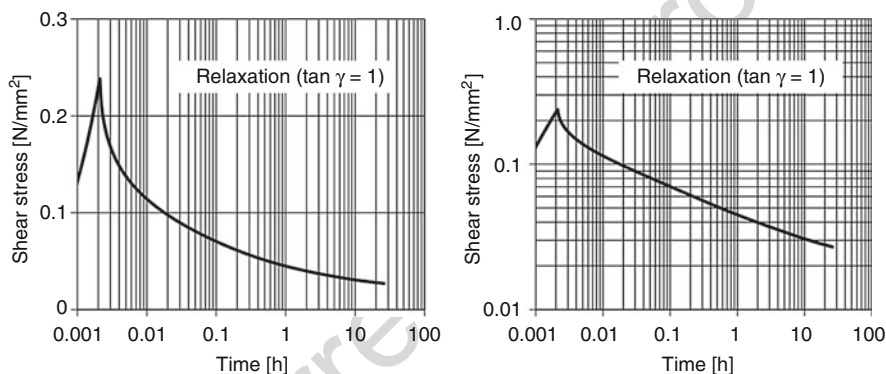


**Fig. 19** Relaxation of shear-loaded adhesive joints with a viscoelastic acrylic adhesive, *left*: linear ordinate, *right*: logarithmic ordinate

projection and extrapolation of relaxation on a prolonged timescale. The relaxation data in Fig. 20 have been acquired in a similar manner starting from different shear strain levels  $\tan \gamma$ .

In the range of the applied strain values between  $\tan \gamma = 0.5$  and  $\tan \gamma = 1$ , a good linear conformity at times of relaxation beyond 1 h can be observed. Linearity in this case means that the decrease in shear stress as a function of time can be approximated by the following equation:

$$y(t) = b \cdot t^{(-1/a)} \quad (29)$$

On a double logarithmic scale, the equation transforms to

$$y(t) = (-1/a)t + b \quad (30)$$

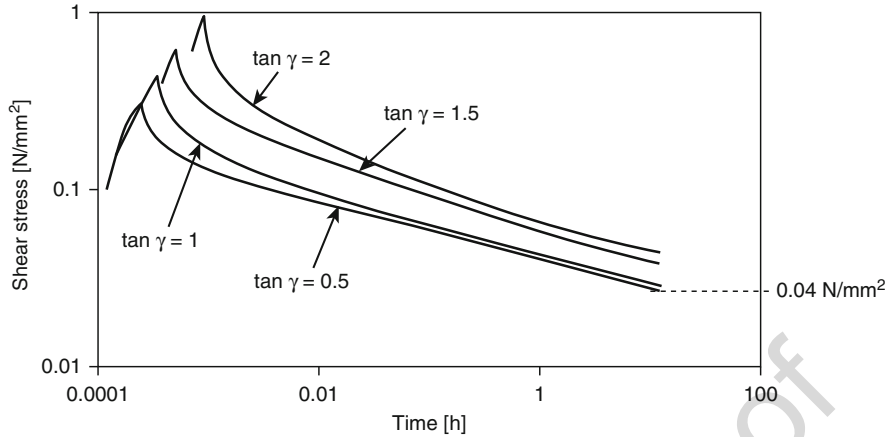


**Fig. 20** Relaxation of shear-loaded adhesive joints from different strain levels with a viscoelastic acrylic adhesive

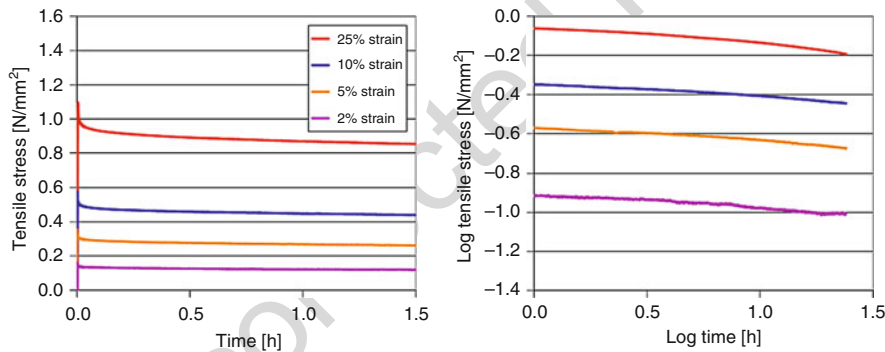


**Fig. 21** Relaxation behavior of an elastoplastic adhesive on a double logarithmic scale (Geiß and Vogt 2007)

If the creep behavior of an adhesive or adhesive joint meets this criterion, the  $-1/a$  and  $b$  parameters can easily be retrieved by linear regression. The factor  $b$  is proportional to the initial load applied to the specimen (elastic properties of the adhesive), and the slope parameter  $a$  relates to the relaxation properties of the adhesive.

The data in Fig. 21 have been obtained in relaxation experiments using bulk specimen of elastoplastic adhesives at initial strain levels ranging from 2% to 25%.

Similar to the shear stress relaxation of the adhesive joints in Fig. 20, the relaxation behavior in the long-term timescale in Fig. 21 exhibits a sufficient degree

**Table 2** Parameters obtained by linear regression of the relaxation curves in Fig. 21

Initial strain [%]	Linear regression parameters	
	$-1/a$	$\log b$
2	-0.0736	-0.9046
5	-0.0709	-0.5653
10	-0.0684	-0.3413
25	-0.0909	-0.0482

of linearity in the double logarithmic representation of the experimental data. The parameters obtained by linear regression are listed in Table 2.

It was found that in this case the parameter ( $-1/a$ ) relating to relaxation neither depended on the initial strain values up to 10% nor on the corresponding initial stresses from which the relaxation tests started. The initial stress levels calculated from the  $\log b$  parameter were in this case in good agreement with the actual measured stress values at the beginning of the relaxation experiments.

#### 34.4.4 Relation of Stress Relaxation and Static Load Creep

Taking into account the transferability of creep and relaxation results, the following considerations may be useful in predicting static load limits of adhesives or adhesive joints.

The experimental data of time-dependent stress from relaxation tests can be converted and applied to estimate maximum load values under creep conditions. This can be done considering the assumption that the declined value of shear stress after a specific time in the relaxation experiment will cause less deformation when this residual level of stress is constantly applied in a corresponding creep experiment.

To approve this concept experimentally, single overlap shear specimens were subjected to stress relaxation at room temperature after imposing an initial strain of  $\tan \gamma = 1$ . During relaxation, time-dependent stress values were determined for 0.5, 2, 8, and 16 h (Fig. 22).

The results of four corresponding creep experiments applying the time-dependent load values from Fig. 22 indicate that the predicted strain limit of  $\tan \gamma = 1$  was not exceeded in either one of the creep tests and the congruence between relaxation and creep becomes better in the long-term scale (Fig. 23).

All of the above conclusions have been drawn for isothermal conditions without considering a thermal fluctuation under creep conditions but which in practice represent the usual case during the service life of structural adhesive joints. Considering temperature effects in creep-dependent lifetime prediction can follow a worst-case scenario in which either the definition of the load-dependent fracture envelope or the test for compliance with predefined strain limits is carried out at the maximum

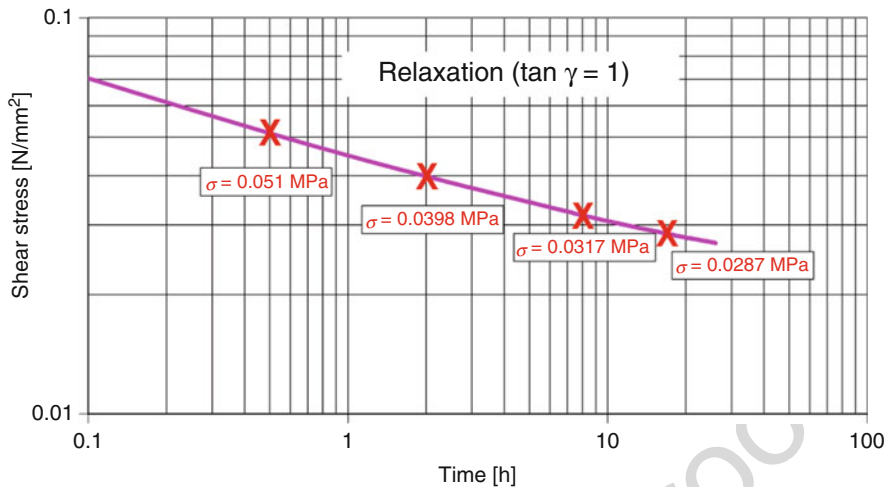


**Fig. 22** Relaxation data for aluminum lap shear specimens bonded with a viscoelastic acrylic adhesive (Geiß and Vogt 2005)

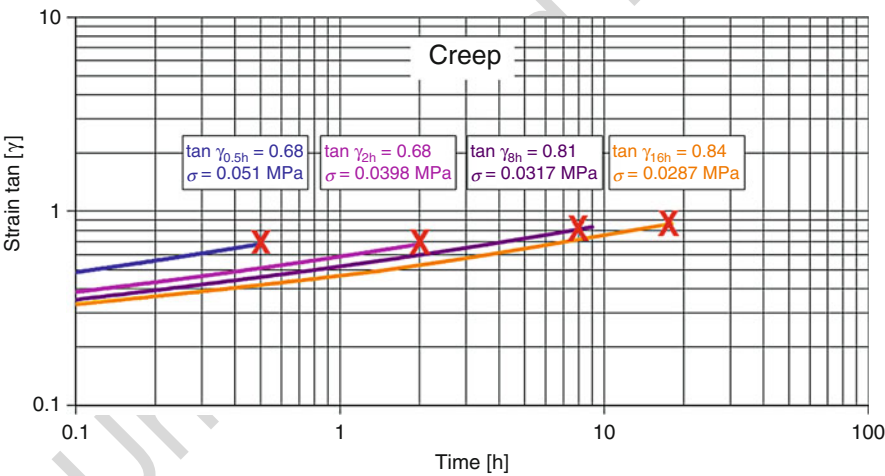


**Fig. 23** Results of creep experiments under static stress at ambient temperature corresponding to load values extracted from Fig. 22 (Geiß and Vogt 2005)

temperature to be expected during service life. This conservative approach is likely to lead to excessive contingency reserves.

Alternatively, extended effort must be taken to collect creep data in the above described manner at different temperatures relevant for a specific application and to then estimate total levels of creep under in service conditions based on the probability of different temperature exposures during service life using predictive numerical methods.

## 34.5 Predictive Methods

Long-term life prediction for adhesives and adhesive joints based on short-term laboratory tests remains a demanding challenge. Testing is generally carried out with the intention of simulating and often accelerating time-dependent effects that may happen to a joint during its lifetime under less severe conditions. Extrapolation methods generally intend to establish correlations involving temperature, time to rupture, and stress so that the least possible number of accelerated tests may be used to derive a sufficient lifetime prediction.

The basic starting point for building a descriptive creep function in correlation to experimental data for the purpose of extrapolation is the following equation:

$$\varepsilon(t) = F(\sigma, t, T) = f(\sigma) \cdot g(t) \cdot h(T) \quad (31)$$

Besides the level of stress, both time and temperature need to be explicitly included in the representation since both parameters significantly affect the creep response. The functions  $f(\sigma)$ ,  $g(t)$ , and  $h(T)$  are introduced on the basis of the assumption of superposition of the effects of stress, temperature, and time. While the viscoelastic models discussed in Sect. 2 may provide a starting point for establishing the function to describe the time- and stress-dependent part of the creep function, the time-temperature superposition equation of Williams, Landel, and Ferry (Sect. 2) should be considered for building time- and temperature-related descriptive empirical creep functions for the purpose of extrapolating and predicting creep behavior of a certain adhesive material or an adhesive joint. Due to the large bandwidth of adhesive mechanical polymer properties, no further generalized recommendation for a valid procedure can be given at this point.

It must further be pointed out that such predictive methods based on numerical evaluation can only be applied under the premise that no mechanisms of aging, being either independent or related to the presence of mechanical load, are superimposing the long-term behavior and thus the durability. Common detrimental environmental influences on the static load-bearing capacity of adhesive joints include an increase of compliance and reduction of the glass transition temperature due to absorption of humidity or water or swelling under the influence of other media. Other aging effects may include corrosive attack starting at the bondline, debonding at or close to the interface between adhesive and substrate, or chemical aging of the adhesive polymer under the influence of temperature, oxygen, or ultraviolet or other ionizing radiation. Further reference on aging of adhesively bonded joints is given in ► Chaps. 31, “Effect of Water and Mechanical Stress on Durability,” and ► “Effect of Radiation and Vacuum.”

## 34.6 Conclusions

The enhanced plasticity and toughness of modern adhesives has become an important property in applications where dissipation of energy in the case of impact, the ability to compensate thermal movement, or the reduction of vibration leads to added

value and improved service performance. Viscoelastic behavior can theoretically be predicted and analyzed by means of mechanical models including combinations of elastic and viscous elements to simulate the time-dependent viscoelastic stress-strain response to mechanical loads.

Due to the increased use of elastomer adhesives, there has been a strong need to develop experimental techniques leading to reliable engineering data in less time which generate materials data that can be implemented into modern design tools such as finite element simulation and used to predict the durability of adhesive joints under specific service conditions.

Creep experiments under constant load conditions are quite familiar and have been described in various international standards because they require rather little experimental equipment. The amount of material-specific data, which can be retrieved from such tests, is, however, limited, and the validity of long-term extrapolation remains often questionable.

Relaxation tests require a higher level of instrumental accuracy but may provide a better pathway in acquiring material-specific data from smaller number of individual tests and specimens. Since adhesive technical data sheets generally lack information on creep and relaxation properties, the design of structural adhesive joints to be used under static creep load conditions will require a significant effort and time for the acquisition and evaluation of experimental creep or relaxation data. Predictive numerical methods to extrapolate experimental creep data or to provide a lifetime prediction in terms of creep rupture probability need to consider time- and stress-related factors as well as the strong temperature dependency of creep-related phenomena. On the basis of the creep and relaxation functions derived from viscoelastic models in combination with shift factors based on the principle of time-temperature superposition, an adequate modeling of time- and temperature-dependent long-term stress-strain behavior becomes feasible.

Extrapolation of short-term data can only be made if it is known that the material is not subject to superimposed time-dependent changes in properties which may lead to a reduced load-bearing capacity and damage after a stable period. Extrapolation generally should not exceed more than 1 logarithmic unit of time beyond experimental data without adequate justification and in no case beyond 1.5 units as, e.g., recommended in the EOTA (European Organization for Technical Approvals) Guidance Document 003 "Assessment of working life of products" which is relevant for products of the building and construction industry.

---

## References

- Betten J (2008) Creep mechanics, 3rd edn. Springer, Heidelberg, pp 237–248
- Brinson HF, Brinson LC (2008) Polymer engineering science and viscoelasticity, an introduction. Springer, New York
- Burgers JM (1935) First report on viscosity and plasticity. Committee for the study of viscosity. Academy of Sciences, Amsterdam
- de With G (2006) Structure, deformation, and integrity of materials, volume II: plasticity, viscoelasticity, and fracture. Wiley-VCH, Weinheim, pp 569–645

- 846 Ferry JD (1970) Viscoelastic properties of polymers, 2nd edn. Wiley-Interscience, New York
- 847 Geiß PL (1998) Verarbeitungskonzepte und Belastungskriterien für Haftklebstoffe. Dissertation,  
848 University of Kaiserslautern. Hinterwaldner Verlag, Munich
- 849 Geiß PL, Vogt D (2005) Assessment and prediction of mechanical long-term properties of adhesives  
850 with high plasticity. *J Adhes Sci Technol* 19:1291–1303
- 851 Geiß PL, Vogt D (2007) Durability of pressure sensitive adhesive joints. In: Proceedings of the 30rd  
852 pressure sensitive tape council tech conference (PSTC)
- 853 Haddad YM (1995) Viscoelasticity of engineering materials. Chapman & Hall, London
- 854 Niven WD (ed) (2003) The scientific papers of James Clerk Maxwell, vol 2. Dover Publications,  
855 New York
- 856 Priesner C (ed) (1983) H. Staudinger, H. Mark und K. H. Meyer: Thesen zur Größe und Struktur der  
857 Makromoleküle. Wiley-VCH, New York
- 858 Purrington RD (2009) The first professional scientist: Robert Hooke and the Royal Society of  
859 London. Birkhäuser, Basel
- 860 Scott Blair GW (1969) Rheology – a brief historical survey. *J Texture Stud* 1:14–18
- 861 Thomson W Baron 1st Kelvin (1875) Elasticity, 9th edn. Encyclopaedia Britannica, London

James D. Palmer

**Contents**

35.1	Introduction .....	1010
35.2	Durability Considerations .....	1011
35.2.1	Joint Design .....	1011
35.2.2	Choice of Substrates and Adhesive Selection .....	1012
35.2.3	Plasticizer Content of Substrates .....	1012
35.2.4	Surface Preparation and Primer Selection .....	1013
35.2.5	Methods of Application and Assembly .....	1014
35.3	Methods for Estimating and Evaluating Durability .....	1015
35.3.1	Elevated Temperature and UV Radiation .....	1016
35.3.2	Antioxidants and Stabilizers .....	1018
35.3.3	Water, Humidity, and Saline Solutions .....	1021
35.3.4	Stress and Fatigue .....	1022
35.3.5	Assessment by Combinations of Factors .....	1023
35.4	Durability and the Construction Products Regulation .....	1025
35.4.1	Sustainability .....	1026
35.5	Conclusions .....	1027
	References .....	1027

**Abstract**

In all bonded assemblies, the durability of the adhesive or sealant joint is important to the integrity of the article concerned. The considerations of joint design, adhesive, sealant and substrate selection, surface preparation, and primer selection along with methods of application including mixing procedures, application techniques, and joint assembly are all reviewed. Methods of evaluation of durability and test regimes including exposure to elevated and reduced temperatures, UV radiation, moisture, saline solutions, stress, and fatigue, both

J. D. Palmer (✉)  
Staffordshire, UK  
e-mail: [jpalmerconsultancy@googlemail.com](mailto:jpalmerconsultancy@googlemail.com)



individually and combined in cycles, are considered. The relevance and application of these test condition to specific situations are discussed, including the role of antioxidants and cross-linking additives to improve durability. Reference is made to the corresponding standards according to the major standard organizations, such as the International Standards Organization (ISO), the European Committee for Standardization (CEN), and the British Standards Institute (BSI), and also to European directives and regulations and national legislation.

## 35.1 Introduction

A review of the literature shows that the majority of the published research relates to the study of the durability of structural adhesives and that there is little published specifically on the durability of nonstructural adhesives; however, the mechanisms and factors that lead to the failure of nonstructural adhesive bonds are the same as those for structural adhesives and are presented in detail elsewhere in this book. This chapter, therefore, illustrates the principle factors affecting durability, the available methods for estimating and evaluating durability, and the options for improving the performance of bonded materials utilizing examples from the world of adhesive and sealant applications. In conclusion, the importance of durability in the realm of building and construction is discussed in relation to the forthcoming EC Construction Products Regulation.

Structural adhesives are defined as adhesives that can resist substantial loads and that are responsible for the strength and stiffness of the structure (Adams et al. 1997) and are generally rated by their shear strength. Nonstructural adhesives then are lower strength materials and tend to be rated by their peel strength (Petrie 2007). However, this is a generalization that can be misleading as in both cases the adhesive is responsible for the structural integrity of the bond, if not necessarily the entire structure.

Durability is the ability to maintain the required performance over a given or long time, under the influence of the potential degradation factors, including temperature, humidity, water, UV radiation, abrasion, chemical attack, biological attack, corrosion, weathering, frost, freeze-thaw, and fatigue. Durability is, therefore, dependent on the intended use of the product and its service conditions, and the assessment of durability can relate to the bonded assembly as a whole or to its performance characteristics. In either case, the underlying assumption is that the performance will be maintained at an acceptable level, in relation to its initial performance, throughout its working life (EC Guidance Paper F 2004).

A large number of standard test methods and specifications have therefore been developed to define adhesive and sealant applications and performance requirements including durability. Many of these are application or market specific and designed around the intended use and service conditions, ranging from specifications for wall covering adhesives (BS 3046: 1981) to test methods for determination of adhesion and cohesion properties of sealants after exposure to heat water and artificial light through glass (BS EN ISO 11431: 2002).

## 35.2 Durability Considerations

Whenever an adhesive joint is made as part of a product or device, there is always concern about the joint durability whether this is in a box of breakfast cereal, the sole of a shoe, or an external panel of a motor car. The consequences of joint failure can, therefore, range from nuisance to endangering lives.

As already stated, the durability or permanence of a bonded assembly is dependent on the intended use and service conditions to which the bond will be exposed. However, the joint design, choice of substrates, adhesive selection, substrate preparation, and primer selection, where appropriate, plus the method of application and assembly all have significant impact on the service life of adhesively bonded materials. Most or all of these considerations are interdependent, for example, the joint design and substrates chosen will limit the range of suitable adhesives that can be employed. In a similar way, the durability of a sealed joint is only as good as the adhesion of the sealant (and primer) to the surfaces forming the joint. Primers and/or sealants will adhere to surfaces only if those surfaces are properly prepared. A very large proportion of all sealant joint failures result from poor or inadequate surface preparation.

### 35.2.1 Joint Design

Many factors need to be considered when designing a bonded assembly, which will utilize adhesive or sealant. They include the purpose of the joint and the stresses likely to be encountered, the substrates to be joined and their physical properties, such as coefficient(s) of linear expansion, the type of materials forming the joint, maximum and minimum temperatures predicted for the components and their heat capacity and conductivity, and any other external influences such as exposure to chemical attack (e.g., water, acids, solvents, etc.), physical movement from vibration, etc.

Joint geometry is a prime consideration, and bonded joints need to be designed so that loading stresses will be directed along the lines of the greatest strength of the adhesive or sealant. In general, joints may be subject to tensile, compressive, shear, or peel stresses, often in combination, and adhesives and sealants are strongest in shear, compression, and tension and perform less effectively under peel or cleavage loadings. Sufficient adhesive surface or bonded area must also be provided between the adherends to enable the transfer of forces via the bonded joint. In general adhesive joints are relatively low in cross-sectional area compared to sealant joints, and an additional consideration in sealant joint design is the designed movement accommodation required of the sealant. During their service life, sealants are subjected to mechanical stresses due to movement, and for a given amount of movement, wide joints will place less induced stress on the sealant than narrow joints, with implications for their durability. For example, consider a 5 mm movement in a joint:

10 mm wide bead – the movement is  $5/10 \times 100\% = 50\%$ .

20 mm wide bead – the movement is  $5/20 \times 100\% = 25\%$ .

### 35.2.2 Choice of Substrates and Adhesive Selection

In contrast to other traditional mechanical joining methods such as riveting, welding, and screwing, adhesive bonding has little or no adverse effect on the material characteristics of the surfaces to be joined. However, in general, in the area of nonstructural adhesives, designers do not consider that materials have to be bonded, paying more attention to appearance and other aesthetic properties, and consequently the service life of bonded assemblies can be severely limited by the choice of substrate. Materials that contain plasticizers, or processing oils, for example, or have a mismatch in their coefficient of thermal expansion can result in bond strength deterioration with many adhesive types in relatively short timescales. Plasticizers are a common source of nonstructural bond failures and are discussed in more detail below.

Formulators have developed many adhesive and sealants to suit most substrate types and properties, and adhesive selection is most commonly carried out by first considering the substrates to be bonded. Most manufacturers of adhesives and sealants publish guides of this type, and many can be found on the Internet to assist designers.

The choice of an adhesive or sealant for a specific situation will be governed by consideration of several key parameters in relation to the manufacturing process to be employed: the setting time required, the initial performance requirements, the durability and ultimate performance requirements, the total product and process costs, and the associated health, safety, and environmental hazards associated with the product use. Additionally, sealants are most often selected on the basis of the intended joint movement accommodation requirement.

The selection of adhesive is critical to fulfilling the design requirements in many applications, but in many industries, the adhesive component of the finished product represents a small percentage of the overall cost; however, its importance in terms of quality and durability of the finished products assumes much greater proportions. This is particularly the case in the manufacture of inflatable lifesaving equipment, such as life rafts and jackets. Solvent-borne polychloroprene adhesives are commonly used to bond rubberized fabrics in the manufacture of these items, and, for obvious reasons, all possible measures are utilized to ensure the durability of the bond. While the water resistance and general durability of correctly formulated polychloroprene adhesives are relatively good, the addition of isocyanate prepolymers, as part of the application process, to these systems is commonly employed to produce further cross-linking and enhanced longevity.

### 35.2.3 Plasticizer Content of Substrates

Many plastic polymers contain plasticizers to make them softer and more flexible as determined by the finished product requirement for a specific application. Plasticizers are generally high boiling point organic liquids with molecular weights in the 400+ region, which have a degree of compatibility with the polymer concerned. In

polyvinyl chloride, for example, the most commonly used plasticizers are the phthalate esters, such as dioctyl, dinonyl, and didecyl phthalate and their iso isomers. In the most flexible materials, commonly made from plastisols, where the polymer is dispersed in plasticizer and then heated to melt the polymer into the plasticizer, forming a homogeneous liquid, which forms a solid on cooling in a molding process, the plasticizer content can be in the order of 50% by weight. Since plasticizers are not bound chemically to the polymer and are held by relatively weak intermolecular forces, most are capable of migrating to the interface, where they can come into contact with the adhesive or sealant layers. Plasticizers also have an affinity for most adhesive polymers and can migrate across this interface resulting in softening of the adhesive or sealant and consequent reduction in physical properties and, in the worst case, cohesive adhesive failure. This migration of plasticizer into adhesive or sealant will also cause change in the physical properties of the plastic substrate itself such as dimensional changes and even surface stress cracking.

One application area where this is of particular relevance is the adhesive bonding of floor and wall covering materials, and the relative resistance of adhesive systems to plasticizer migration can be determined utilizing the standard method described in EN 1903: (2008), “Adhesives – Test method for adhesives for plastic or rubber floor coverings or wall coverings – Determination of dimensional changes after accelerated aging.” This method gives a measure of the suitability of a plastic or rubber floor or wall covering/adhesive combination by monitoring dimensional changes during defined conditioning sequences when bonded to a specific substrate. The floor or wall covering test pieces, with dimensions of  $(250 \pm 5) \text{ mm} \times (250 \pm 5) \text{ mm}$  or  $(300 \pm 5) \text{ mm} \times (300 \pm 5) \text{ mm}$ , are first preconditioned for 6 h at  $80 \text{ }^\circ\text{C} \pm 2 \text{ }^\circ\text{C}$  before measuring their dimensions and are then bonded to uncoated fiber cement panels using the test adhesives and dimensions measured again. The test assemblies are then stored at  $50 \text{ }^\circ\text{C}$  for a 13 day period each followed by 24 h conditioning at room temperature prior to measuring the dimensions again. The interpretation being that the more cycles to which the test pieces are exposed, without significant dimensional change, the more durable the adhesive and floor or wall covering combination will be in service.

### 35.2.4 Surface Preparation and Primer Selection

Correct surface preparation is critical to achieving optimum bond strength and joint reliability. Cleaners, such as surfactants and solvents, are used to ensure that surfaces to be bonded are clean and free from dust and other loose materials, grease, oils, and other impurities that may affect the adhesion and ultimate bond strength.

Pretreatments are also used to enhance bonding performance including mechanical treatments such as grinding and blasting to produce a rough surface texture and effectively increase the bonded area; physical treatments such as corona discharge, flame, or plasma treatments to improve bonding performance by increasing surface energies; and primers or adhesion promoters.

Primers and adhesion promoters are normally low-viscosity solutions of either isocyanate prepolymers or organosilanes, which function by surface penetration into and chemical adhesion to the substrate(s) and chemical adhesion to the subsequently applied adhesive or sealant, increasing bonding performance and durability. Again, formulators have developed ranges of primers to suit most adhesive or sealant and substrate combinations, and selection guides are widely available.

### **35.2.5 Methods of Application and Assembly**

Automated methods for preparation, adhesive application, and bond assembly give the best reproducibility and best control of durability; however, such automation is frequently not possible. Manufacturers' recommendations in data sheets and on containers should always be followed and particular attention paid to storage conditions, mixing procedures, adhesive or sealant application, and joint assembly.

#### **Storage Conditions**

Storage temperature extremes can cause problems, which limit the effectiveness and shorten the service life of adhesives and sealants. Temperatures below zero can irreparably damage emulsion adhesives and sealants causing agglomeration or coagulation of the polymer emulsion. Many modern products are made freeze-thaw stable by the addition of chemicals such as glycols, but generally prolonged storage at low temperatures is inadvisable. Conversely, high storage temperatures can lead to premature polymerization of reactive adhesives severely impeding bonding performance. High humidity can also have adverse effects; for example, adhesives supplied in powder form require adequate protection from moisture vapor during storage to prevent premature curing or agglomeration making use and application difficult.

#### **Mixing Procedures**

Adequate mixing of multicomponent adhesives and sealants requires particular attention. Unless supplied in pre-weighed kit form, the correct proportioning of components is essential, and the duration and intensity of mixing with the correct type of mixer should be utilized to produce a homogeneous mix that is not overheated and with minimal unintentional air entrainment. However, excessive shear during mixing can damage some types of emulsion adhesives and sealants.

#### **Application**

In all adhesive and sealant applications, the aim is to apply a uniform layer of material of the appropriate thickness across the entire area to be joined to achieve the optimum performance. In many manual or semiautomatic applications, this is achieved by using spacers or jigs to control product thickness. Pressure-fed application equipment is also often utilized to ensure a consistent flow of product.

## Joint Assembly

Once the adhesive or sealant has been applied to the substrate or substrates, the joint should be assembled within the allowable “open” or “assembly” time, that is, between the minimum and maximum recommended times. With solvent-borne contact adhesives, for example, sufficient time for solvent evaporation must be allowed to prevent solvent entrapment, which can lead to premature failure, especially when bonding impermeable substrates. The maximum open time with hot-melt adhesives, which set on cooling, can be very short and should be closely monitored.

Ambient conditions can also affect the bond formation process. For example, high relative humidity can lead to condensation of moisture on the exposed drying surface of a solvent-based adhesive, as the heat of evaporation of the solvent causes the temperature of the adhesive film to drop below the dew point of the surrounding atmosphere. Such a film of moisture will impede the coalescence of the two films of a contact adhesive.

## Workmanship

Quality of workmanship is obviously a key factor in the durability of bonded assemblies, and standard test methods are written in such a way to try to minimize any variability in laboratory evaluations. However, laboratory conditions cannot accurately reflect the actual application methods and conditions employed, and there have been some attempts to study the influence of workmanship on durability. One such study by Zhao and Zhang (1997) looked at the influence of workmanship on the bonding of ceramic tiles to external walls. In this study, they looked at three variables, tile setting pressure, adhesive inner cavity, and adhesive open time, and measured their effects on tile bonding or pull-off strength. Not surprisingly, their results indicated that the influences of these variables are significant and that when some or all of these factors appear simultaneously, the combined effect is cumulative in the reduction of pull-off strength.

---

## 35.3 Methods for Estimating and Evaluating Durability

Having taken into account the above considerations and completed the selection process, it is always desirable to know that the bonded assembly will meet the durability expectations of the product, that is, be “fit for purpose.” For this reason, adhesive selection is often made on the basis of past experience or “heritage data,” and a proven track record is recognized as a suitable method for demonstrating fitness for purpose. For example, the approved document in support of Regulation 7 of the UK Building Regulations – workmanship and materials – lists “past experience” as one of the ways of demonstrating fitness for the purpose of a material.

However, such historical data is frequently not available, and other methods of assessment need to be employed. Durability tests that measure an adhesive or sealant’s performance retention during exposure to the main elements of its service

environment have, therefore, been developed, and this is usually measured in some accelerated manner because natural processes are too time-consuming to allow qualification in an appropriate timescale.

At this point, it is worth noting that accelerated and natural aging tests do not always produce the same results. Ashcroft et al. (2001) undertook a comparison of aging joints in natural and laboratory conditions, with aluminum adherends, bonded with structural adhesives. A conclusion of their work was that there was no simple method of determining the long-term durability from accelerated tests and that excessive temperature and humidity will trigger degradation mechanisms, which are not representative. In general, accelerated aging tests tend to overestimate the reduction of joint strength. The published standard (ISO 9142 2003), Adhesives – Guide to the selection of standard laboratory aging conditions for testing bonded joints, which describes laboratory aging conditions under which adhesive joints may be exposed to various environmental influences, climatic or chemical, for the purpose of assessing the effects of such influences on certain properties, recognizes these limitations, warning in the introductory abstract that “The results obtained using the procedures described in this international standard are not necessarily applicable to the determination of the service life of a bonded assembly because there is no direct relation between the test results and the behavior of a bonded assembly over a period of time under service conditions. However, for certain specific applications, experience with the procedures may enable a correlation to be established.”

Obviously, the purpose of an accelerated aging test is to cause a more rapid deterioration of the bonded assembly, and by paying due consideration to the actual service conditions, the accelerated aging conditions can be selected to recreate as closely as possible the failure mechanisms that would be seen in those actual service conditions. The accelerated aging conditions usually selected involve some environmental factors, which the bonded assembly might encounter, such as elevated temperature, UV radiation, high humidity, water immersion, exposure to aqueous salt solutions in spray form, and/or combinations of these, which may be in periodic cycles, as well as other predictable service factors such as stress and fatigue, where normal service loads can be applied in combination with the environmental accelerating factors above, or extreme loads, beyond normal service, to induce premature degradation.

### 35.3.1 Elevated Temperature and UV Radiation

Perhaps the simplest durability evaluation is the exposure of hot-melt adhesives to elevated temperature for prolonged periods with their durability assessed by their color stability; the longer the period of exposure before significant discoloration occurs, the more durable the adhesive. While this test gives an indication of the ability of the adhesive to withstand long periods in the melt tank at or above the application temperature, it also gives an indication of the durability of the adhesive in

service. Discoloration of the adhesive can be particularly significant with light-colored substrates.

All polymers containing hydrogen undergo oxidation by a free radical chain mechanism; however, the rate at which oxidation occurs varies with the chemical structure of the polymer. Polymers that are commonly used in adhesive formulations differ considerably in their sensitivity to oxidation. Acrylates, for example, are highly resistant to oxidation and do not generally require antioxidants at ambient temperatures, whereas unsaturated elastomers are highly susceptible to oxidative decomposition and require a relatively high concentration of antioxidants for protection. Both heat and light accelerate the oxidation of polymers, both increase the rate of reaction, but heat also increases the rate of inward diffusion of oxygen and the loss of antioxidants and stabilizers from the adhesive or sealant by volatilization. Mechanical deformation of the end product during service (“fatigue”) also accelerates the oxidation of adhesives and sealants. Oxidation of the polymeric components results in a deterioration of the physical properties, which can ultimately lead to bond failures, and the addition of antioxidants and stabilizers to improve durability is normally necessary.

The deleterious effects of oxidation on polymer properties results from the breakdown of very unstable hydroperoxides in the polymer chain in the presence of light. This in turn leads to chain scission (molecular weight reduction) and the production of new free radicals which accelerate the oxidation process (Scott 1998).

Elevated temperature-accelerated aging techniques rely on the dependence of the rate of reaction on temperature as expressed in the Arrhenius equation, where the rate constant  $k$  of a reaction and the absolute temperature  $T$  are related using the gas constant  $R$ :

$$k = A \exp(-Ea/RT) \quad (1)$$

In its original form, the pre-exponential factor  $A$  and the activation energy  $Ea$  are considered to be temperature independent (IUPAC Compendium of Chemical Terminology 2nd Edition 1997).

Elevated temperature is often used to estimate the in-can stability of adhesives and sealant formulations. This is usually applied by a simple “rule of thumb” that says the reaction rate of the degradation mechanisms involved doubles for every 10 °C increase in temperature, and therefore 1 week storage at 50 °C approximates to 8 weeks at room temperature (20 °C). Application of this rule will likely be conservative in the prediction of shelf life and must be verified by real-time validation testing conducted at room temperature for the targeted shelf life.

One example of in-can stability testing is given in ISO 15908 (2002), Adhesives for thermoplastic piping systems – Test method for the determination of thermal stability of adhesives, where samples of the adhesives in their relevant packaging, a minimum three test pieces for each packaging and adhesive variant, are stored at room temperature (23 °C ± 2 °C and 50% relative humidity) and at elevated temperature (for 1 month at 50 °C ± 2 °C followed by 24 h at 23 °C ± 2 °C and 50% relative humidity). After this period, the adhesive viscosities are measured and



their performances determined by measurement of the shear strength of bonded relevant plastic pipe systems. A stable viscosity and maintenance of bonding performance is assumed to indicate in-can stability; however, the standard method also recognizes that actual shelf life (in-can stability) can only be verified by tests conducted at actual storage conditions for the targeted shelf life period.

### 35.3.2 Antioxidants and Stabilizers

Antioxidants and stabilizers are added to most polymer systems to improve durability. Antioxidants fall into two major categories, primary and secondary, (Petrie 2004) and within primary antioxidants, there are two main chemical types, hindered phenolics and aromatic amines. Primary antioxidants function by donating their reactive hydrogen to the peroxy free radicals so that the propagation of subsequent free radicals does not occur.

The most widely used antioxidants for polymer protection are phenolics. These products generally resist staining or discoloration. However, they may form quinoid structures upon oxidation, which lead to yellowing. Phenolic antioxidants include simple phenolics, bisphenolics, polyphenolics, and thiobisphenolics. Hindered phenolics, such as butylated hydroxytoluene (BHT), high molecular weight phenolics, and thiobisphenolics, are the most popular of the primary antioxidants. They are suitable as long-term stabilizers in almost all cases.

BHT has long been the workhorse of the antioxidant industry, and it possesses US Food and Drug Administration (FDA) approval for food contact. However, BHT is a relatively volatile material that is gradually being replaced by higher molecular weight antioxidants that resist migration. Thiobisphenolics can also act as peroxide decomposers (secondary antioxidants) at temperatures above 100 °C. Therefore, they are often found in higher-temperature applications.

Amines, normally arylamines, may be more effective than phenolics, but most are staining and discoloring and lack FDA approval for use in contact with food. Amines are commonly used in the rubber industry, but they also find uses in applications such as wire and cable formulations and in polyurethane polyols.

Secondary antioxidants are used in conjunction with primary antioxidants to provide added stability to the polymer. They function by decomposing any hydroperoxides to form nonreactive products. Typical secondary antioxidant compounds contain sulfur or phosphorous. The more popular secondary antioxidants are thioesters (thiodipropionic acid derivatives and polythiodipropionates) and organophosphites.

Organophosphites provide color stability but have a hygroscopic tendency. Hydrolysis of phosphites can ultimately lead to the formation of phosphoric acid, which can corrode processing equipment. Tris-nonylphenyl phosphite (TNPP) is the most commonly used organophosphite followed by tris(2,4-di-tert-butylphenyl) phosphite. Thioesters have high heat stability but have an inherent odor, which can be transferred to the host polymer.

The by-products of polymer degradation can also have a damaging effect on the durability of adhesive and sealant bonds necessitating the addition of specific stabilizers. For example, polychloroprene polymers can decompose by dehydrochlorination, liberating hydrochloric acid, which can attack the adhesive or sealant and the substrates. The addition of metal oxides, such as zinc oxide or magnesium oxide, which act as acid acceptors helps to overcome this problem.

### Pressure-Sensitive Adhesives

The use of pressure-sensitive adhesives (PSAs) in modern manufacturing has developed significantly in recent years. No longer are PSAs limited to temporary attachment applications, such as packaging tapes, but are increasingly being used in more sophisticated applications such as mobile telephones for the bonding of keypad switch assemblies. Pressure-sensitive applications have also been expanded to include a wide range of temperatures, ranging now from  $-40^{\circ}\text{C}$  to  $+120^{\circ}\text{C}$ . For example, airline baggage tag labels need to perform in low and high temperatures, often over a time period of a few hours. Some tapes intended for the construction or automotive markets need to perform at even higher-temperature extremes. So prediction of durability and service life has assumed greater significance to formulators of this type of adhesive.

PSAs are usually characterized by their three common properties of tack, peel resistance, and shear resistance, which can be determined by standard laboratory test procedures. Each of these properties is affected by temperature change. Indeed, as already noted, most adhesives exhibit different properties when subjected to temperature, and in the case of PSAs, the bond is almost always thermoplastic, softening at elevated temperature and becoming more brittle at lower temperatures. As the temperature increases, the adhesive mass softens and “wets” the substrate more rapidly and completely, and the tack and peel properties increase. At some point, however, the adhesive has softened to the point that its cohesive strength is less than the substrate adhesion, and the adhesive mass splits, failing cohesively, that is, the locus of failure has changed from adhesion to cohesive within the adhesive. As the temperature continues to increase, the adhesive mass continues to soften, and the tack and peel values continue to go down.

In testing shear resistance, one always looks for cohesive failure. As the temperature increases, shear resistance goes down as the adhesive mass softens. This reduction in shear resistance will be fairly slow and steady, to the point where the mass is so soft that it will not support a load for any appreciable time.

It is important, therefore, that adhesives be evaluated for performance over a wide temperature range and bearing in mind the difference between application temperature and end-use temperature. The application temperature, at which the adhesive is applied to a surface and is expected to achieve a bond, is, generally, limited to the lower end and a narrower band of the temperature range, whereas the end-use temperature, at which the adhesive must perform adequately once the bond is made, is usually at the extreme ends, both high and low, of the temperature scale.

In standard laboratory tests, the limits of application temperature are determined by placing the test samples and substrates at the selected temperature and allowing

439 them to equilibrate. Sample bonds are made at this temperature, and the laminated  
440 samples are allowed to reside for a specific period, after which performance prop-  
441 erties are measured at that temperature. The limits of end-use temperature can be  
442 determined by making the sample bonds at a temperature within the application  
443 temperature range and allowing the bond to build for a specified time at this  
444 temperature. After this residence period, the samples are placed at the test temper-  
445 ature for a period of time to achieve equilibrium and then the performance properties  
446 determined at that temperature. These test conditions are achieved by the use of  
447 environmental chambers, freezers, or ovens.

448 Alternative indications for durability of PSAs in specific applications can be  
449 obtained from modifications to these methods for determining performance prop-  
450 erties, and the two most commonly used tests are the peel adhesion failure time (PAFT)  
451 and shear adhesion failure temperature (SAFT).

452 The PAFT is determined using 25 mm strips of adhesive coated onto standard  
453 polyester film and bonded to standard stainless steel panels. The bonded assemblies  
454 are placed in a suitable enclosure to maintain the required test temperature and a  
455 weight (usually either 500 or 1,000 g) attached to the polyester film such that the  
456 assembly will peel in a 180° configuration. The time for the bond to fail at the test  
457 temperature is recorded, often using a suitable automatic recording device. Similarly,  
458 the SAFT is determined using a square adhesive contact area of 25 mm<sup>2</sup> applied on  
459 to a standard polyester film and bonded to standard stainless steel panels and then  
460 placed in an oven starting at 25 °C. A 500 g weight is applied, and the temperature is  
461 raised by 5 °C every 10 min and the point at which the sample fails is recorded.  
462 Alternatively, if appropriate, the actual substrates intended for the application  
463 concerned can be utilized to make the tests more meaningful to the end use.

464 Accelerated aging tests are also employed to estimate the durability of PSAs.  
465 While there is no standard set of aging conditions, 70 °C, the standard aging  
466 condition for rubbers, on which most original PSAs were based, is commonly  
467 used; however, other test temperatures may be used depending on the temperature  
468 sensitivity of the components to be bonded. Unapplied samples, meaning that the  
469 samples are aged with the release liner in place, after which the liner is removed and  
470 the samples are applied to the test surface to determine performance properties, will  
471 give an indication of the “shelf life” to end use, whereas applied samples, meaning  
472 that the samples are applied to the test surface for the aging period before the  
473 determination of performance properties, will give an indication of the service life  
474 of the product after it is bonded to a substrate.

475 While pressure-sensitive adhesive performance at various temperatures can be  
476 determined by practical tests, as described above, it is also possible to predict the  
477 temperature performance of pressure-sensitive adhesives. The polymers used in  
478 pressure-sensitive adhesives will have a variety of glass transition temperatures  
479 (T<sub>g</sub>), and for a pressure-sensitive adhesive to be effective, the formulated mass  
480 must have a T<sub>g</sub> of between 50 and 70 °C below the temperature at which the  
481 adhesive is to be used. At the same time, however, the T<sub>g</sub> cannot be so low that  
482 the adhesive mass is so soft that it fails cohesively even at room temperature. A  
483 variety of analytical techniques used to determine the T<sub>g</sub> of the adhesive mass

include differential scanning calorimetry (DSC), differential thermal analysis (DTA), and dynamic mechanical analysis (DMA). Of these, the most commonly used method is DMA. DMA will measure the bulk properties of the adhesive mass, which will include the base polymer and any additives in it. It does not take into consideration any interfacial relationships between the adhesive and the surfaces to which it is bonded.

DMA can determine the storage modulus ( $G'$ ) and loss modulus ( $G''$ ) of the adhesive mass by sweeping through a range of frequencies and temperatures. Dividing  $G''$  by  $G'$  yields the property called tan delta, and plotting tan delta against temperature will give peaks that relate to the  $T_g$  of the adhesive mass. The type of information developed by DMA and other thermal analytical techniques can, therefore, be used to formulate adhesives that will perform well at ambient conditions and at temperature extremes. However, final practical evaluations of the adhesive formulation, the substrates to be used in the application and the temperature ranges to be seen in the application, must be undertaken.

### 35.3.3 Water, Humidity, and Saline Solutions

Moisture ingress during service is thought to be responsible for many examples of premature joint failure. Accelerated aging tests are, therefore, commonly carried out by exposing joints or structures to either water immersion or water vapor. Moisture ingress in joints can occur either by bulk diffusion through permeable substrates or the adhesive or by wicking across an interface or through cracks or voids in the adhesive. Once present, water molecules can cause a modification in the adhesive mechanical properties, for example, by plasticization or by a reduction in the glass transition temperature. Alternatively, it is proposed that interfacial bonds can be disrupted or modification of the adherend surface can result, for example, by hydration of a metal.

The rate of water ingress by diffusion through the adhesive is principally determined by its diffusion coefficient. An increase in temperature will rapidly increase the rate of water uptake in line with Fickian diffusion models as the diffusion coefficient will increase significantly with temperature. Such a hot-wet environment is generally regarded as a very aggressive form of accelerated aging (Critchlow 2005).

The installation of exterior artificial sports surfaces is one application where water resistance is required. Adhesives are used in this process to bond seaming tape to artificial grass or other carpet materials at the joints between adjacent lengths of carpet, and there are performance specifications for these bonded assemblies set by the national or international sports governing bodies, such as rugby, football, or tennis. The durability of these installations is assessed in the laboratory by accelerated aging of test bonds of the substrates involved using elevated temperature and water immersion as described in EN 13744 (2004). Test joints are immersed in a water bath maintained at 70 °C for 336 h (14 days) before the physical properties of tensile and peel strength are determined by the standard method described in EN

12228 (2002) and compared with the properties determined with un-aged joints. In this example, the durability requirements are deemed to be satisfied if the minimum performance requirements are exceeded before and after accelerated aging. In other applications, a maximum allowable percentage deterioration in physical properties will constitute the specification requirement.

Adhesives for ceramic tiles are specified by the standard EN 12004 (2007) (Adhesives for tiles – Requirements, evaluation of conformity, classification, and designation) and include performance requirements for cementitious, dispersion, and reaction resin adhesive types for all internal and/or external walls and floor and ceiling applications. Annex ZA, of this standard, sets out the requirements, which address the provisions of the Construction Products Directive (see Sect. 4 below) and include assessments of durability. Compliance with these requirements confers a presumption of fitness for purpose for the applications and form part of a CE mark. In these cases, durability is assessed by elevated temperature and/or water immersion accelerated aging or freeze-thaw cycling of test specimens and then determining tensile or shear adhesion strength against minimum requirements.

Saline solutions are also commonly employed by immersion or spray to mimic sea, coastal, or road conditions. Initially developed to evaluate the corrosion resistance of coatings for metals, the salt spray test can be used to evaluate the durability of adhesive- and sealant-bonded assemblies. The apparatus for testing consists of a closed testing chamber, where a salted solution, most commonly a solution of sodium chloride, is sprayed by means of a nozzle. This produces a corroding environment in the chamber, and thus, pieces in it are attacked under this severe corroding atmosphere. Testing periods can range from a few hours (e.g., 8 or 24 h) to more than a month before the determination of physical properties for comparison with their initial values. Chamber construction, testing procedure, and testing parameters are standardized under national and international standards, which describe the necessary information to carry out the test and give the testing parameters such as temperature, air pressure of the sprayed solution, preparation of the spraying solution, concentration, pH, etc.

Salt spray testing is popular because it is cheap, quick, well standardized, and reasonably repeatable. There is, however, only a weak correlation between the duration in salt spray test and the expected life in service, since the corrosive processes involved are very complicated and can be influenced by many external factors. Nevertheless, salt spray test is widely used in the automotive, construction, and aerospace industries.

### 35.3.4 Stress and Fatigue

Stress- or fatigue-induced degradation of adhesive- and sealant-bonded assemblies in nonstructural applications is often characterized by cyclic loading of a test assembly. Polymeric materials, including adhesives and sealants, are viscoelastic in nature, and their responses in such tests tend to be time and frequency dependent. Higher frequencies often induce localized heat, resulting in temperature changes that

can dramatically affect the results, and slow frequencies can also result in poorer performance than expected due to creep rupture. Therefore, care is needed when specifying the temperature and frequency of testing regimes (Dillard 2005).

The lower-frequency “creep” or “creep-rupture” tests are time dependent. In these tests, joints are subjected to a nominally constant load. The tests may proceed for a chosen time period or may be continued until complete rupture occurs. For example, the durability of thermoplastic adhesives for nonstructural wood applications is classified in European standards EN 204 (2001) and EN 205 (2003) according to their ability to withstand various water treatments and relatively rapidly applied loads. However, an additional characteristic that can be specified is resistance to static load, which can be determined using the method described in EN 14256 (2007). This method is used to determine the ability of a test piece bonded with a thermoplastic adhesive, to support a given load for up to 21 days without fracture or excessive distortion, and specifies a mean survival time of 14 days.

### 35.3.5 Assessment by Combinations of Factors

Some durability evaluations use a combination of these elements of accelerated aging. For example, an indication of the durability of adhesives used for bonding thermoplastic pressure pipe systems is given in EN 14814 (2007), Adhesives for thermoplastic piping systems for fluids under pressure – Specifications, which references the test method given in ISO 9311-3, where test pipe assemblies incorporating adhesively bonded joints are subjected to internal hydrostatic pressures up to 3.2 times the nominal maximum operating pressure for 1,000 h without leaking. Passing this test regime is a requirement of the initial type tests to demonstrate compliance with the specification but is also expected to give an indication of the “in-service” performance of the system.

### Insulating Glass Units

Lowe et al. (1994) studied the water durability of insulating glass units manufactured with polysulfide sealants by accelerated aging of glass to sealant adhesive joints at 95% relative humidity in an environmental chamber set at 60 °C for up to 14 months. Among their conclusions were that the glass to sealant joints were weakened by this test regime; that the sealants absorbed large amounts of water, which attacks at the interface between the glass and sealant; and that the amount of interfacial failure increases with exposure. Studies such as this, in conjunction with those undertaken by sealant and raw material manufacturers, have been instrumental in the development of the standard for insulating glass units (double glazed units) EN 1279 (a standard in six parts published between 2002 and 2008) which describes how to assess durability by accelerated aging of test double glazed units. The function of the polymer sealant utilized to seal the edges of the insulating glass units is to hold the unit together and prevent the penetration of moisture into the unit and escape of insulating gases placed between the panes. Durability is evaluated by exposure to temperature and humidity cycles, which attempt to replicate the actual in-service

exposure conditions of glazing units in buildings, that is, elevated temperature combined with high humidity, along with low-temperature cycles, and interspersed with periods of longer duration with exposure to high humidity. The efficiency of the seal is then determined by measuring the amount of moisture that has penetrated into the unit, by gravimetric analysis of the desiccant, which is contained within the hollow aluminum spacer bar that forms the gap between the panes in the construction of the unit.

The rate of escape of insulating gas (usually argon or sulfur hexafluoride) through the sealant is also determined using gas chromatography by containing the test unit in a rig and sweeping the annular space around the unit with air into the chromatograph. The standard specifies maximum penetration levels and rates for both test regimes.

Nonstructural sealants for use in construction works are classified by their performance characteristics as determined according to ISO 11600. Sealant manufacturers, who adopt this classification scheme, use designations, which indicate the sealants end use (either general construction, type F, or glazing, type G), its movement accommodation capability (in the range 7.5–25%), its modulus (defined as high or low), and its elasticity or plasticity, totaling 11 sealant classes, with all these performance characteristics determined using specified test methods. This classification system is a helpful aid to specifiers who can match their design requirements to the sealant performance characteristics. Within Europe, this classification system is to be augmented with the affixation of a CE mark to indicate suitability for purpose and the performance requirements, including durability, for building applications defined in new standards currently being developed (FprEN 15651 parts 1 to 5: 2009). The durability clause in these new standards indicate that the sealant performance determined by classification to the appropriate ISO 11600 specification will indicate suitable durability of the sealant after aging. It also notes that nonstructural sealants are easy to use, ready to use, and easy to remove when any unavoidable or unexpected degradation arises.

## Electronics

There are numerous applications for adhesives in electronics manufacturing industries, some bringing additional property requirements for adhesive formulators, particularly those of conductivity and heat and stress dissipation. Licari and Swanson (2005) give a complete exposition on the subject.

To exhibit electrical conductivity, the adhesives typically employed, such as epoxy resins, need to be filled with electrically conductive particles, for example, metal powder like silver, because they are inherently insulators. The selection of an electrically conductive (or insulating) adhesive, therefore, is most often based on the adhesives' conductivity or resistivity and its ability to retain those properties for the expected service life of the electronic equipment. Accelerated aging tests have been developed by industry that can give indications of durability and also be used for qualification of adhesives. Typical regimes involve heat aging for 1,000 h at 150 °C, combined with any or all of the following: moisture exposure, thermal cycling, vibration, and thermal or mechanical shock, with the

performance expectation that bond strengths and electrical properties will be maintained throughout.

One major cause of failure in this field is large mismatch in the coefficient of thermal expansion of the substrates concerned, especially when bonded with high modulus adhesives, and so adhesives have been formulated from more elastomeric resins, which can effectively dissipate the stresses induced in these situations and can be demonstrated by the accelerated test cycles described above.

---

## **35.4 Durability and the Construction Products Regulation**

The largest commercial market for adhesives and sealants is their use in building and construction. The Construction Products Directive (89/106/EEC) (CPD) is currently undergoing review and will be remade as the Construction Products Regulation (CPR) probably coming into force in 2012 or 2013. European regulations, unlike directives, are translated directly into law in the member states without the need for national statutes and instruments (and the potential for differing national interpretations). Thus, the basic work requirements (formerly essential requirements in the CPD) of the CPR will become compulsory in all member states.

The CPD (and CPR) recognize that member states have provisions, including requirements, not only to building safety but also to health, durability, energy economy, protection of the environment, and other aspects important in the public interest. The articles of the Regulation require that these basic work requirements are satisfied during an economically reasonable working life, where the working life is the period of time during which the performance will be maintained at a level compatible with the fulfillment of the basic work requirements and an economically reasonable working life presumes that all relevant aspects are taken into account, such as costs of design, construction, and use; costs arising from hindrance of use; risks and consequences of failure of the works during its working life and costs of insurance covering these risks; planned partial renewal; costs of inspections, maintenance, care, and repair; costs of operation and administration; disposal; and environmental aspects.

For adhesive and sealant materials, their durability in service, in relation to these basic requirements, is connected with the characteristics of the products, and the mandates issued by the European Commission for the development of harmonized technical specifications (harmonized European Norms – hEN), that is, standards and, for certain products, European Technical Approvals (ETAs), also include durability aspects.

As a passport for a product to be marketed and used in the single market without the need for any other additional requirements, a CE mark may be affixed when it can be demonstrated that all the provisions of the CPR including these basic work requirements have been satisfied. Thus, standards and technical specifications must include provisions for the assessment of durability. A main route to this assessment involves the performance testing of a product to determine the variation in its characteristics under a given action or cycle of actions. However, the standard and



specification writers are required to strike a balance between the cost of testing and the additional information that can result from such tests.

For products that are covered by hENs, the specific durability assessment requirements are stated in Annex ZA of the standard, and the results of that durability assessment form part of the aforementioned CE mark.

### 35.4.1 Sustainability

The increasing concerns about the impact of the activities of man on the environment have brought new challenges to adhesive and sealant manufacturers as customers have begun to specify requirements relating to the sustainable consumption and production of the earth's resources. Such considerations relate not only to the raw materials used to manufacture the adhesive and sealant products but also to the end of life options, including recycling possibilities, of the products and articles made with them and their ultimate destination and impact on the environment. In order to minimize all these impacts, full life cycle analysis techniques are employed to identify where improvements can be made. As adhesives and sealants are most commonly employed to join dissimilar materials, so the ability to de-bond assemblies to facilitate recycling activities has become an additional consideration for the formulator and a new area for research workers and adds another new dimension to considerations of durability in-service, with the now required coexistence of durable, yet dismantle-able properties.

The dismantling and recycling of electrical appliances have received much publicity in the western world, particularly in relation to the exposure of workers in the developing world to the toxic chemicals, which are contained within them and are of relatively high value for recycling purposes. However, the promotion of waste recycling in the construction industry particularly in the west is becoming increasingly important, because of the dwindling availability of landfill sites. The building materials currently used in the market utilize a wide range of components from metals to inorganic and organic substances often to improve their strength, function, or aesthetic appearance, but their separation is often difficult to achieve, and combined materials cannot be recycled or reused. Obviously, in any manufacturing sector, if adhesively bonded joints can be made to separate easily by some method, the recycling of such combined materials becomes much easier, and new technologies have been developed in an attempt to satisfy this requirement. One of these technologies recognizes that hydrogen bonding and intermolecular forces are the main forces that join adherends and a method that extends intermolecular distance will facilitate bond dismantling. This is achieved by incorporating thermally expansive particles into the adhesive or sealant, such that when they are expanded by heating, typically above 100 °C, the intermolecular distance is extended by the expansive forces, bond strength is reduced, and the materials are separated. Ishikawa et al. (2005) conducted a study on these types of adhesive for use in the construction industry. They examined the durability of the bonded assemblies by accelerated aging tests at 60 °C and found that there is no deterioration in bonding performance

and that joints could be easily separated by heating between 150 and 180 °C. From these studies, they were able to conclude that durability and dismantle ability were able to coexist in the systems tested.

---

## 35.5 Conclusions

This chapter describes and discusses the main factors affecting the durability of nonstructural adhesives and sealants, and the methods used for their estimation, and their applicability to actual service life prediction. The major conclusions that can be drawn are the following:

1. Appropriate adhesive and sealant selection, which takes into account the properties of the materials to be joined and the expected service conditions and service life, is essential to ensure the durability of bonded assemblies, and much advice and assistance is available from manufacturers.
2. Standard test procedures have been developed to assist this selection process and predict durability in the absence of “heritage” data to establish suitability for purpose. However, these standard test methods rely on acceleration techniques to produce deterioration of properties in reduced timescales, which may induce mechanisms and pathways that are not present under “normal” service conditions. So these tests need to be supported by determinations conducted under “normal” service conditions.
3. Durability and its estimation are becoming increasingly important in all industrial manufacturing sectors for the calculation of economic service life of products including their human health and environmental impacts and cost of maintenance. This is particularly relevant in the construction industry.

---

## References

- Adams RD, Comyn J, Wake WC (1997) Structural adhesive joints in engineering, 2nd edn. Chapman & Hall, London
- Approved Document to support Regulation 7 – Material and workmanship (1999) (H.M.S.O)
- Ashcroft IA, Digby RP, Shaw SJ (2001) *J Adhes* 75:175
- BASA (1999) Guide to the ISO 11600 classification of sealants for building construction
- BASA (2008) Industry guide to the professional application of construction sealants on site
- BS 3046 (1981) Specification for adhesives for hanging flexible wallcoverings
- BS EN ISO 11431 (2002) Building construction. Jointing products. Determination of adhesion/cohesion properties of sealants after exposure to heat, water and artificial light through glass
- Critchlow GW (2005) In: Packham DE (ed) Handbook of adhesion, 2nd edn. Chichester, Wiley
- Dillard DA (2005) In: Packham DE (ed) Handbook of adhesion, 2nd edn. Chichester, Wiley
- EN 12004 (2007) Adhesives for tiles. Requirements, evaluation of conformity, classification and designation
- EN 12228 (2002) Surfaces for sports areas – determination of joint strength of synthetic surfaces

- 776 EN 1279 parts 1 to 6 (2002 to 2008) Glass in building. Insulating glass units  
777 EN 13744 (2004) Surfaces for sports areas – procedure for accelerated aging by immersion in hot  
778 water  
779 EN 14256 (2007) Adhesives for non-structural wood applications – test method and requirements  
780 for resistance to static load  
781 EN 14814 (2007) Adhesives for thermoplastic piping systems for fluids under pressure.  
782 Specifications  
783 EN 1903 (2008) Adhesives – test method for adhesives for plastic or rubber floor coverings or wall  
784 coverings – determination of dimensional changes after accelerated ageing  
785 EN 204 (2001) Classification of thermoplastic wood adhesives for non-structural applications  
786 EN 205 (2003) Adhesives. Wood adhesives for non-structural applications. Determination of tensile  
787 shear strength of lap joints  
788 European Commission, Guidance Paper F (2004) Durability and the construction products directive  
789 FprEN 15651 parts 1 to 5 (2009) Sealants for non-structural use in joints in buildings and pedestrian  
790 walkways  
791 Ishikawa H, Seto K, Shimotsuma S, Kishi N, Sato C (2005) *Int J Adhes Adhes* 25:193  
792 ISO 11600 (2003) Building construction. Jointing products. Classification and requirements for  
793 sealants  
794 ISO 15908 (2002) Adhesives for thermoplastic piping systems. Test method for the determination  
795 of thermal stability of adhesives  
796 ISO 9142 (2003) Adhesives – guide to the selection of standard laboratory ageing conditions for  
797 testing bonded joints  
798 IUPAC (1997) *Compendium of chemical terminology*, 2nd edn  
799 Licari JJ, Swanson DW (2005) *Adhesive technology for electronic applications*. William Andrew,  
800 Norwich  
801 Lowe GB, Lee TCP, Comyn J, Huddersman K (1994) *Int J Adhes Adhes* 14:85  
802 Petrie EM (2004) Antioxidants for adhesives – web publication by SpecialChem  
803 Petrie EM (ed) (2007) *Handbook of adhesives and sealants*, 2nd edn. New York, McGraw-Hill  
804 Scott G (1998) Stabilisation of adhesives against environmental peroxidation – Society for Adhe-  
805 sion and Adhesives. One day meeting on ‘Stability of Adhesives’  
806 Zhao ZY, Zhang WL (1997) *Int J Adhes Adhes* 17:47

Uncorrected Proof

Hans K. Engeldinger and Cai R. Lim

**Contents**

36.1	Introduction .....	1032
36.1.1	Basics of Adhesive Storage .....	1032
36.1.2	Classification of Adhesives Based on Storage Criterion .....	1033
36.2	Storage at Room Temperature .....	1034
36.2.1	Solvent-Based Adhesives .....	1035
36.2.2	Water-Based Dispersion Adhesive .....	1037
36.2.3	Hot-Melt Adhesive .....	1038
36.2.4	Reactive Adhesives .....	1040
36.3	Storage at Low Temperatures .....	1043
36.3.1	Basics of Adhesive Storage at Low Temperatures .....	1043
36.3.2	Temperature and Reactivity: The Arrhenius Equation .....	1046
36.3.3	Storage Between Freezing Point and Room Temperature .....	1048
36.3.4	Storage Below Freezing Point .....	1048
36.4	Conclusion .....	1049
	References .....	1049

**Abstract**

A chapter on adhesive storage should be closely aligned with the current market practice. As such, a major part of this chapter focuses on the shelf life and safety aspect of adhesives. The adhesive shelf life is dependent on the adhesive system and the storage conditions, in particular, the temperature. For a stronger emphasis on the effect of temperature on adhesive shelf life, this chapter is subdivided into *Storage at Room Temperature* and *Storage at Low Temperature*.

H. K. Engeldinger (✉)

Product Development HAF Tapes, tesa SE, Norderstedt, Germany

e-mail: [jkengeldinger@gmail.com](mailto:jkengeldinger@gmail.com)

C. R. Lim

Research &amp; Development, tesa SE Hamburg, Norderstedt, Germany

e-mail: [CaiRong.Lim@tesa.com](mailto:CaiRong.Lim@tesa.com)

Due to the flammability and possible health hazards of solvent-based adhesives and majority of the chemically reactive adhesives, their storage usually requires special safety measures.

Adhesive manufacturers are required to provide information on the shelf life and storage conditions in the product technical data sheet, as well as a description of the possible hazards in the safety data sheet (Material Safety Data Sheet, MSDS), e.g., in the event of a fire.

Due to the wide range of adhesive systems available, it is not possible to devise a standard storage guideline applicable to all adhesives. In this chapter, adhesives are divided into four categories: solvent-based, water-based, hot-melt, and reactive adhesives. For some adhesives, their physical characteristics should also be considered (e.g., liquid or solid in the form of powder, granules, or film). Considering the variety of adhesive systems, it is necessary to provide a short introduction on the adhesive to indicate the type of packaging and storage conditions needed and its potential hazards.

Similarly, in cases where the adhesive shelf life may be extended through storage at low temperatures, it should also be indicated on the packaging, although this applies to limited adhesive systems and applications. In order to explain the quantitative effect of low temperatures on adhesive storage, a brief subtopic on activation energy and temperature-dependent chemical reaction (Arrhenius equation) is provided.

---

## **36.1 Introduction**

### **36.1.1 Basics of Adhesive Storage**

The proper storage of an adhesive is a prerequisite to maintain the adhesive properties for the adhesion process and, beyond that, for the final bond performance (bonding strength, heat resistance, and other specific properties). The significance of the appropriate storage conditions is usually presented in the quality assurance documentation of the adhesive. Essentially, the adhesive is guaranteed by the manufacturer throughout the shelf life under the storage conditions specified in the product technical data sheet. The optimization of the adhesive shelf life normally commences with the adhesive development, with storage stability tests integral to the design specifications.

As a rule, manufacturers are required to inform customers of the adhesive shelf life under the recommended conditions in the product information. Within this period, the specified adhesive properties should be guaranteed for delivery as well as for the final bond performance after appropriate processing steps. The manufacturing date, shelf life, and suitable storage temperature of the adhesive should also be indicated on the packaging. While many products can be stored at room temperature, some may require low temperatures for a prolonged shelf life. The aspect of storage at low temperatures will be addressed separately.

Besides complying with international and national laws and regulations, institutional measures to ensure environmental protection and occupational health and safety must also be adhered to during adhesive storage. They are applicable throughout the supply chain, from production to delivery by the adhesive manufacturer, to distribution by the agent if necessary, and, finally, to the end user after processing. In the European standard, EN 12701 (European Standard 2001) titled “Determination of words and phrases relating to the product life of structural adhesives and related materials,” definitions and requirements applicable to structural adhesives with storage life limited by possible change of properties are clearly specified.

The compliance with safety procedures constitutes another notable aspect of adhesive storage. A series of adhesives are classified as hazardous materials due to the presence of highly flammable solvents or components presenting health hazards such as cyanoacrylates or acrylates containing high monomer contents. In addition, hardeners of reactive adhesives such as isocyanates, amines, or peroxides should be considered. An important reference is the REACH (Registration, Evaluation, Authorization and Restriction of Chemicals -EC 1907/2006) regulation, implemented by the European Parliament in 2007 to ensure that manufacturers take the responsibility to manage risks from chemicals and to provide safety information on the chemicals.

It is also an international practice to include exposure controls and other measures in the safety data sheet, so as to ensure the safety of personnel handling of the adhesives. The manufacturers are responsible for compiling the necessary documents and are required to provide them to customers at all times.

Special provisions and measures regarding the storage facilities of adhesives are established according to building and environmental regulations. Among them, fire control, which includes firefighting equipment, evacuation plan, and fire engine access route, is an important point for consideration. At the same time, attention should be accorded to the prevention of water pollution which may be caused by the leaching of hazardous materials into groundwater.

This chapter mainly covers the aspect of adhesive storage, according to the industrial standard. The storage of adhesives in households or offices, usually in small quantities (e.g., in tubes), is mostly subjected to other conditions and regulations.

### 36.1.2 Classification of Adhesives Based on Storage Criterion

Due to the existence of different adhesive systems and the potential hazards associated with each system, there are different types of packaging as well as storage conditions and shelf life. Adhesives can be classified according to specific criterion and properties. In the literature, one can find various classifications based on the assembly process, delivery form, adhesion mechanism, or application. Within the same adhesive group, the adhesives can be further categorized based on their physical states or characteristics: liquid, paste, or solid (through viscosity measurements and rheological characterization) or solvent based, water based, or those

without volatile content (through solid content measurements). Another classification can be made based on the adhesion mechanism: physically dried adhesives from solution, solidified hot-melt adhesive, or chemically cross-linked single- and two-component reactive adhesives.

This chapter attempts to classify the different adhesives based on a few key points concerning storage. Based on storage criterion, adhesives can be classified into four main groups: solvent-based, water-based, hot-melt, and reactive adhesives. These groups mainly differ in their shelf life and potential hazards. Nonetheless, within such classifications, overlaps are possible. For instance, there are reactive hot-melt adhesives and reactive solvent-based adhesives.

Other considerations include the delivery form and packaging, which differentiate solid adhesives from liquid adhesives. Liquid adhesives are usually stored in sealed packaging, containers, barrels, or tanks at room temperature between 18 °C and 25 °C. Homogeneous products can be stored for a year or more due to the limited physical or chemical changes within the system. For nonhomogeneous products, due to the possible sedimentation of fillers or segregation of different phases during storage, stirring is usually necessary to return the system to its original state before use. Any premature chemical reactions caused by inappropriate storage conditions (e.g., higher temperature or longer duration) are irreversible, and they usually render the adhesives ineffective or unusable.

Solid adhesives such as hot melts are relatively easier to handle during packaging and storage, whether they are in the form of blocks, in crushed form as granules, in powdered form in cartons or sacks, or in the form of rolled sheets.

During the storage of reactive adhesives, the influence of humidity is another important consideration besides temperature, especially for moisture-sensitive bonding agents such as cyanoacrylates or single-component polyurethanes, which harden upon contact with moisture, like hardeners of reactive adhesives. Among special reactive adhesives are those which react under anaerobic conditions or in UV light and require storage under oxygen-rich or dark conditions, respectively. The packaging of such adhesives should also be adequate to prevent any undesired chemical reactions before use.

Reactive adhesives which are particularly sensitive require storage in a conditioned environment, with regulated temperature and humidity. To achieve fast adhesion during mass production, highly reactive adhesives containing catalysts are often required. However, they are not suitable for room temperature storage. Instead, low temperatures are required. Special measures of low-temperature storage and the affected adhesive groups will be addressed in Sect. 3.

---

## 36.2 Storage at Room Temperature

The term “room temperature” is sometimes misused. It was meant to define the temperature in a conditioned room, usually enclosed, such as an office or a work area, e.g., laboratory. The temperature range may vary according to the location, e.g., as narrow as 20–23 °C in a measurement laboratory or as wide as 18–25 °C in rooms



where temperature sensitivity is not as crucial, such as storage hall for general goods. Unless specified, room temperature mentioned in this chapter refers to a temperature range of 18–25 °C.

Additionally, it is a basic condition in adhesive storage to keep the adhesive in its original sealed packaging before use, as far as possible, even if humidity does not always appear to influence the adhesive shelf life.

## 36.2.1 Solvent-Based Adhesives

### Solvent-Based Adhesive Group

This class of adhesives consists of solutions of polymers, resins, and, where applicable, other additives in organic solvents. They have low to moderate viscosities and solid contents ranging from 15% to 40% in weight, which correspond to solvent contents ranging from 60% to 85% in weight. They are applied as PSA or contact adhesives.

The base polymer should be soluble in common solvents. The rate of dissolution is dependent on the polarities of both the base polymer and the solvent and the molecular weight of the polymer. Predominantly, acrylate, polyvinyl acetate, natural or synthetic rubber, polychloroprene, polyurethane, polyvinylpyrrolidone, or polyvinylchloride (PVC) constitute the base polymer for such adhesives. Nonetheless, solutions combining phenolic resins and rubber are also used.

Common solvents used are those which are easily available and cost effective. They should have a good solubility but low toxicity. Therefore, the use of chlorinated solvents such as dichloromethane or trichloroethylene has been effectively banned in the EU since December 2010 despite their good solubility, as they may be carcinogenic or pose health risks (e.g., optic neuropathy).

In general, the following solvents are used: petroleum naphtha 60/95, petroleum naphtha 80/110, ethyl acetate, acetone (dimethyl ketone), butanone (methyl ethyl ketone), toluene (methylbenzene), ethanol, isopropanol, or sometimes tetrahydrofuran, which is a suitable solvent for PVC. For adhesive storage, key data of the corresponding solvents such as boiling point, flash point, and the rate of evaporation are necessary. Table 1 shows a summary of these data for the solvents mentioned above. (Flash point refers to the lowest temperature at which a volatile liquid can vaporize to form an ignitable mixture in air.)

The rate of evaporation is a ratio of the time required to evaporate a measured amount of liquid to that of a reference liquid (ethyl ether).

### Storage and Shelf Life

Storage vessels of solvent-based adhesives which include jerry cans, drums, and containers with capacities of up to 30, 200, and 1,000 L, respectively, are made of metals such as aluminum or steel. Drums either have a sealable lid or are sealed but equipped with a faucet outlet. Sealed drums should only be stored upright. Otherwise, the drum lid may be easily damaged on contact with adhesives, especially those containing aggressive solvents, causing the contents to leak. Plastic vessels are

**Table 1** Properties of solvents used in solvent-based adhesives

Solvent	Boiling point (°C) at 1,010 mBar	Flash point (°C) according to DIN EN 22719	Rate of evaporation ethyl ether = 1
Acetone	56	−19	2.1
Butanone	80	−1	6
Ethanol	78	+12	62
Ethyl acetate	77	−4	2.9
Isopropanol	82	+12	11
Tetrahydrofuran	66	−17	2.3
Toluene	111	−6	6

not suitable as storage containers for solvent-based adhesives, as solvents may diffuse through the container walls – unless they are protected by a barrier coating. Solvent-based adhesives are generally stable during storage, as they hardly undergo alterations as homogeneous solutions in sealed vessels. Hence, they usually have a recommended shelf life of up to 2 years. However, for some, the viscosity may change gradually with time. Though uncommon, some solvent-based adhesives may contain fillers or reactive components, which affect the storage stability through phase separation or cross-linking.

**Hazard Potential**

Solvent-based adhesives are classified as hazardous goods, as they contain a significant portion of highly flammable solvents. Thus, it is essential to comply with laws and regulations concerning fire prevention and firefighting.

Adhesive containers should be labeled with the appropriate hazard symbols. In storage facilities, no ignition sources should be present or allowed to come into contact with solvents or their fumes, and the generation of sparks should be avoided. Additionally, it is necessary for all electrical equipment to be explosion proof and all containers should be earthed. It is also mandatory for personnel to be equipped with safety shoes having conductive soles to minimize the accumulation of static electricity. Similarly, production equipment or vehicles should not generate any sparks.

The maximum quantity of solvent-based adhesives allowed in a storage room is limited (to 10,000 L in Germany). In an “active storage,” where the containers with adhesives would be opened or siphoned, an exhaust system must be installed to minimize the accumulation of solvent fumes. Secondary containment is often necessary to prevent the adhesives from entering the earth or groundwater in the event of a spill as shown in Fig. 1.

Further information on this aspect may be obtained from national or international regulations such as REACH (the new European law concerning chemicals) or specialized contributions from corporate entities such as *Fundamentals of Hazardous Materials by Denios, Germany* *Fundamentals of Hazardous Materials* (2009/2010).



**Fig. 1** Storage of flammable solvents and solvent-based adhesives in a protective storage chamber (Photo: Denios)

## **36.2.2 Water-Based Dispersion Adhesive**

### **Water-Based Adhesive Group**

Water-based dispersion adhesives consist of oligomers dispersed in water with surfactants as dispersing agents and stabilizers. Before dispersions, natural rubber latex and casein were used to manufacture such adhesives. Currently, polyvinyl acetate (PVAc) and polyacrylate serve as synthetic base polymers for water-based PSA, while polychloroprene and thermoplastic polyurethane serve the same purpose for water-based contact adhesives.

Compared to solvent-based adhesives, water-based dispersion adhesives have several advantages: environmentally friendly and nonflammable. In addition, a larger quantity of the adhesive can be dispersed in water without a significant increase in the viscosity. Thus, a solid content of 40–70% in weight is common, and this is almost twice of that compared to solvent-based adhesives.

### **Storage and Shelf Life**

Water-based dispersion adhesives are mostly stored in plastic containers. Smaller containers with capacities of up to 30 L are made of polyethylene (PE), while larger containers which come in 100-L vessels or up to 800-L containers are made of polypropylene (PP). To ensure stability, the container thickness should be

proportional to its size. In fact, such containers are often made of glass fiber-reinforced polypropylene. Larger containers can also be stabilized using metal casings or cages.

However, one drawback of water-based dispersion adhesives is the limited storage stability due to various influencing factors. In particular, they must be protected from frost, as freezing usually causes irreversible damage to the dispersions.

Furthermore, the stability of such dispersions is pH dependent. In fact, many of them (except PVAc dispersions) coagulate in neutral or acidic conditions, leading to the failure of the adhesive system. This can be avoided by the addition of neutralizing agents such as ammonium hydroxide or alkali hydroxides with pH values in the range of 9–10.

Water-based dispersion adhesives also face the problem of possible contamination through microbial attacks, especially when industrial water or mains water is used during their production. During microbial attacks, dispersions undergo partial coagulation, resulting in brownish discoloration and a strong odor. With that, the adhesive becomes unusable. Thus, a microbiological analysis is necessary to determine the bacteria count before storage.

With that in mind, most manufacturers of water-based dispersion adhesives recommend storage durations of 6–12 months at 5–25 °C.

### **Hazard Potential**

As water-based dispersion adhesives do not pose any health hazards and are non-flammable, there is no critical concern associated with their storage. Despite so, precautions relating to the concerned chemicals and information provided in the safety data sheets should be taken note of, in the event of a spill. Contact with the skin and splashes into the eye should also be avoided, like most chemicals. Upon contact with chemicals such as ammonia, some dispersion adhesives emit an odor. For environmental concerns, contaminants such as alkaline or acidic materials should not be discharged into the groundwater.

## **36.2.3 Hot-Melt Adhesive**

### **Hot-Melt Adhesive Group**

Hot-melt adhesives range from viscous to solid forms in storage at room temperature. To allow proper application during the adhesion process, they have to be melted at elevated temperatures. Following that, they solidify on cooling to form strong bonds between the substrates. Polymers such as ethylene-vinyl acetate, polyamide, and polyester constitute the base polymers of harder hot-melt adhesives with higher melting points, while the softer ones consist of polyacrylates, styrene-butadiene copolymers, or thermoplastic polyurethane. However, as such polymers exhibit lower adhesion and tack properties, they are usually used in combination with tackifiers. While the soft and viscous hot-melt adhesives exhibit better tack than solid ones, the solid hot-melt adhesives provide a stronger bonding.

There are different delivery forms available: soft hot-melt adhesives are preferably packed into compact blocks or cartons, while highly viscous hot-melt granules are usually powdered with fine mineral powder such as talcum or silica to inhibit the

clumping of the granules. This allows them to remain fit for storage. In contrast, as solid hot-melt adhesives do not form clumps easily, they are available in the form of powder, granules, or to some extent, sticks. Hot-melt adhesives also exist as films on release paper, wound into rolls. Such films can be pre-cut into sheets, which are used immediately for mass productions, instead of being stored for later use.

### Storage and Shelf Life

During manufacture, hot-melt adhesives are mostly filled in their molten state at high temperatures, after which they solidify upon cooling. They are available in compact forms in 200-L vessels or in cartons, which are coated with release agents, and are finally delivered as blocks. Pressure vessels are often used as special storage containers as they are suitable for adhesive storage under pressure, after the heating and melting of the adhesives. Many of these adhesives undergo crystallization during cooling after manufacture. However, this does not impact the adhesion properties, as crystallization is reversed during the subsequent heating process before bonding. Such reversible behavior is characteristic for thermoplastic materials.

Powdered and granulated hot-melt adhesives are usually prepared by crushing the solid form and then preferably packed and stored in 25-kg paper sacks. As hot-melt adhesives are sensitive to moisture, the paper sacks should be coated with polyethylene (PE) to prevent deterioration by the diffusion of moisture through the paper sacks. Polyamide is not used as a moisture barrier because it can absorb up to 3% weight of water during extended storage. Polyester is also not an option due to similar reason, though it has a lower moisture absorption capacity. The larger the surface area of the particle or smaller the particle size, the faster is the rate of absorption. During subsequent heating between 150 °C and 180 °C, the presence of moisture in the adhesive leads to the formation of bubbles or foam in the adhesive joint, which reduces the adhesive stability and leads to quality problems.

During production of hot-melt films, hot-melt adhesives undergo heat extrusion and cooling on release-coated paper or film. When soluble polymers such as thermoplastic polyurethane are used, the solution can be coated onto the release paper, dried, and converted into a larger roll, before it is slit into smaller rolls. A large roll may measure 250 µm in thickness (with release paper), 2000 m in length, 2 m in width, and weigh up to 1 t. Hot-melt adhesives tend to flow under high pressure loads even at room temperature. Thus, large rolls should only be stored for a short period of time on a flat support or upright manner, otherwise deformation would occur. For longer storage durations, the problem may be avoided by fixing the roll on a rotating rack, which allows it to slowly rotate continuously, as shown in Fig. 2.

For adhesive tapes with liner, regardless of the size of the rolls, humidity should be taken into consideration. At a high humidity, the paper within the liner absorbs moisture from the environment despite the silicon interface, especially after drying. When this occurs, the paper tends to swell. This affects the structure of the paper, which may then be transferred to the adhesive film. However, this concerns only the outermost layers of the roll. This effect can be avoided either by air-tight packing of individual rolls or the conditioning of the entire storage room to a temperature of 20–23 °C and a humidity which is lower than 50%.



**Fig. 2** Rotating racks for adhesive jumbo rolls in a temperature-regulated storage hall (Photo: tesa Werk Offenburg)

In general, by adhering to the moisture-related measures, hot-melt adhesives can be stored unchanged for a long period of time. The recommended shelf life of hot-melt adhesives ranges from 18 to 24 months, provided they are stored at 10–25 °C, under dry conditions.

### **Hazard Potential**

Since most hot-melt adhesives do not contain volatile components, they are not highly flammable and do not pose any health hazard during normal handling. As such, they are also used in packaging for grocery. Unlike the rest, no special measures are required for an incident-free storage.

## **36.2.4 Reactive Adhesives**

### **Reactive Adhesive Group**

Reactive adhesives comprise all adhesives which undergo a chemical reaction during the adhesion process and in doing so, solidify. Single-component systems can react chemically in the presence of external influences such as heat, UV light, moisture, or anaerobic conditions. On the other hand, two-component systems usually react through the mixing of reactive components, e.g., resins and catalysts, at room

temperature without external influences. During storage and before processing, reactive adhesives often exist in forms ranging from liquid to paste.

The most important types of two-component adhesives are moisture-sensitive polyurethane, comprising polyol resin and isocyanate catalyst, and heat-sensitive epoxy, comprising bisphenol-A or bisphenol-F resins and polyamide catalyst. Both single- and two-component adhesive systems are available in the market. Single-component reactive adhesives, which include cyanoacrylate and silicone, are also widely known, with the latter often being used as a sealant.

A particular adhesive group used for heat-resistant bonding is the single-component reactive adhesive, formulated as a combination of phenolic resin and nitrile rubber, in the form of heat-activated films (HAF). These contain latent hardeners for the phenolic resins, which are activated at temperatures above 120 °C. The advantages include clean and precise handling.

UV-sensitive and anaerobic-sensitive adhesives also belong to the reactive adhesive systems, which should be stored under chilled conditions.

### **Storage and Shelf Life of Two-Component Reactive Adhesives**

Resins and hardeners of two-component adhesives should be stored in separate metal drums, jerry cans, vessels, or larger containers. The quantity of each component to be stored is determined according to their mixing ratio. Polyurethanes and epoxy resins differ in the type of chemical reactions they undergo during the hardening process. On top of that, both systems are used in combination with different hardeners and have different storage requirements.

Polyurethanes are traditionally produced from the reaction of isocyanates and polyols.

Isocyanates (e.g., methylene diphenyl diisocyanate [MDI]), the most commonly used hardeners for polyurethanes have low viscosities and undergo crystallization in chilled conditions below 15 °C. At temperatures above 40 °C, isocyanates undergo a chemical reaction (i.e., dimerization), which increases their viscosities. In addition, upon exposure to moisture, they react with water molecules to produce polyurea and carbon dioxide gas, which results in outgassing and the formation of a layer of film. To prevent such occurrence, isocyanates must be stored at temperatures in the range of 20–35 °C and in the absence of moisture. Under these conditions, the shelf life is approximately 6 months.

Polyols, unlike isocyanates, are generally chemically stable. However, in many instances, they contain additives such as catalysts, fillers, and pigments for special applications. During storage, mineral fillers may sediment at different rates depending on their densities and the viscosity of the bulk solution. In such situations, the material should be stirred immediately before use to ensure homogeneity. However, this should be done without generating entrapped air in the mixture. Hence, it is essential to notify the user with a “Stir before use” label on the container.

Epoxy resins comprise bisphenol diglycidyl ethers. Having moderate to high viscosities, they are mostly delivered in jerry cans or vessels. While pure epoxy resins tend to crystallize upon storage for longer durations, this phenomenon can be reduced by

mixing bisphenol-A with bisphenol-F. Often, such adhesives are also loaded with fillers. Hence, they should be monitored for any sedimentation during storage.

Hardeners are mostly polyether amines or similar amine composites. They have moderate to high viscosities and a typical amine smell.

The storage of resins and hardeners in sealed containers is less critical compared to that of polyurethanes, as every component is chemically consistent. Thus, they can be stored for 12 months at temperatures between 20 °C and 25 °C.

### **Storage and Shelf Life of Single-Component Reactive Adhesives**

Single-component polyurethanes consist of prepolymers, a fraction of which is pre-reacted polyurethanes with terminal isocyanate groups. Due to their moisture sensitivity, they have to be stored away from moisture or possible contact with water, preferably in metal containers. They require similar storage conditions as MDI hardeners, although in the reduced forms, they are less reactive. In the absence of moisture, the viscosity increases during storage. As such, manufacturers usually recommend a shelf life of 3–6 months at 20–25 °C.

Single-component epoxy resins contain dicyandiamide as latent hardeners, which are activated at high temperatures – usually above 150 °C. As such, they belong to the class of heat-activated adhesives. They are available in viscous or paste forms, and those of even higher viscosities are available as films on release paper.

Apart from hardeners, some adhesives in this category also contain an additional activator, with which a faster rate of reaction can be achieved. This effectively shortens the duration needed for the adhesion process or lowers the activation temperature. However, this also leads to reduced storage stability of the adhesive.

Heat-activated films (HAF) can be stored for 12–18 months under dry conditions at room temperature, depending on the type of phenolic resins present in the system. For special applications, such as in the electronic industry, clean room environment and subsequent dust-proof packaging and storage are necessary.

Cyanoacrylate belongs to the single-component reactive adhesives. Due to its fast-acting characteristic, it is commonly known as “superglue.” In the presence of water, it undergoes rapid polymerization, causing the adhesive to set. Thus, it must be stored in leak-proof containers, completely protected from moisture or water during its storage. Otherwise, it may react prematurely and become unusable. This is guaranteed by the manufacturers through the use of suitable packaging, usually in small quantities from 5 g to 5 kg. When stored in their original packaging in dry conditions at 20–23 °C, the shelf life ranges from 6 to 12 months.

Anaerobic adhesives are derived from dimethacrylate esters and are often low in viscosities. They react only in the absence of oxygen and when in contact with a metal surface at the same time. In order to prevent premature polymerization, these adhesives should be packed in a way which allows them to be in constant contact with oxygen. Having a diffusion-resistant packaging can also ensure that oxygen does not diffuse out of the packaging during storage. They are mainly used as bolt adhesives or for the sealing and securing of mechanical devices. These adhesives should be stored in a cool environment. For instance, they can be stored at 5 °C in their original sealed packaging for 1 year.



UV-sensitive adhesives are based on acrylate-modified epoxy resins, polyurethanes, and, among others, polymers. They are single-component reactive adhesives, which undergo rapid polymerization upon irradiation with UV light with wavelengths ranging from 400 to 500 nm. These adhesives should be stored in small opaque containers of up to 50 mL in volume. They can be stored in their original containers for 6 months at 10–25 °C.

### **Hazard Potential**

Due to their reactivity, reactive adhesives and hardeners have to be stored according to special regulatory requirements. The containers of such materials should be labeled with the appropriate warning symbols and possible hazards associated with the content, as indicated in the safety data sheets. Nonetheless, under normal storage in their original packaging, they are not expected to pose any hazards.

Nonetheless, mandatory precautions to contain a spill due to leaking or damaged packaging are necessary. Such precautions include secondary containment (e.g., trays) and spill kits or absorbents at accessible locations to soak up hazardous liquids for subsequent disposal. Personnel handling spilled adhesives should also be equipped with personal protective equipment (PPE) such as coats or gowns, gloves, safety goggles, and respiratory apparatus. In general, any contact with reactive adhesives should be avoided. While cyanoacrylates bond to the skin in seconds, epoxy resins and polyurethanes can trigger allergies. Other hazardous adhesive raw materials include hardeners used in the manufacture of polyurethanes. One example is methylene diphenyl diisocyanate (MDI), which poses health risks due to occupational exposure such as respiratory tract irritation and sensitization.

A more critical situation would be that of a fire. Suitable extinguishing agents or fire extinguishers should be available to combat fires which are small enough. Beyond that, larger fires may lead to uncontrollable chemical reactions with the accumulation of toxic by-products. For instance, single-component epoxy resins may trigger strong exothermic reactions with promoters at temperatures above 120 °C. In the presence of more than 1 kg of the materials, such exothermic reactions can hardly be extinguished. As a result, the surrounding may be heated up to temperatures of 500 °C or higher. Thus, in the event of a fire, the fire response team must be immediately summoned. The team should also be informed of the materials involved and provided with their safety data sheets.

---

## **36.3 Storage at Low Temperatures**

### **36.3.1 Basics of Adhesive Storage at Low Temperatures**

The main reason for adhesive storage under cool or cold conditions is to extend the adhesive shelf life. For some adhesives, storage at low temperature is absolutely necessary, while for some, it is recommended where longer storage durations are necessary. However, there are also some adhesives which can be damaged when stored under cold conditions.

For adhesives requiring storage at low temperatures, the same conditions should also apply during transportation from manufacturers to the customers. In the event that the adhesives are exported out of cold or temperate climates to warmer ones, insulated containers are essential.

To achieve the desired cooling, filled adhesive containers are stored in cooling chambers or freezers. In doing so, the cooling capacity of the adhesive should be balanced with the cooling efficiency and the temperature of the cooling system. As liquid adhesives are cooled, physical effects such as an increase in viscosity may occur through a reduction in the rate of filler sedimentation. Further cooling may even halt the sedimentation of the fillers. At the same time, solute components may crystallize out of the adhesive. Most importantly, cooling retards the chemical cross-linking reactions, thereby enhancing the adhesive shelf life.

The cooling of adhesives for storage followed by reconditioning to room temperature before use usually incurs additional costs, and for larger adhesive quantities, this may be a very time-consuming process. The tempering of full containers or vessels may take up to a few days depending on the temperature difference within the contents, especially when the bulk material is not stirred. Large rolls of reactive adhesive films, requiring storage at low temperatures, have similar behaviors. In practice, the conditioning of cooled adhesives before handling may take longer than expected, as the application of heat has to be conducted with caution. Overheating may lead to unwanted outcomes such as premature cross-linking in reactive adhesives or elevated vapor pressures, which present a flash fire hazard in the presence of solvent-based adhesives. Another effect is the condensation of water vapor on the cooled packaging, as the adhesives are brought into warm conditions. If the adhesives are applied too fast before conditioning, the condensed water droplets may lead to defective bonding between the adhesives and the substrates. These points should be taken into consideration during a good logistic practice.

The need for storage at low temperatures only concerns a small group of the commonly available adhesives in the market. In Sect. 1.2, adhesives are categorized into four groups: solvent-based, water-based, hot-melt, and reactive adhesives. In this section, key points of storage at low temperatures will be addressed based on these categories.

Most adhesives requiring cool or cold storage conditions are reactive adhesives, many of which are single-component adhesives. For some, cross-linking reactions begin even at room temperature, thus compromising the adhesive shelf life. Apart from fluid adhesives, this problem also concerns reactive adhesive films and pre-pregs (pre-impregnated sheets).

Unlike reactive adhesives, solvent-based adhesives seldom require such storage conditions as the reaction rates of reactive components, such as polyurethanes, epoxies, and phenolic resins, can be distinctly lowered by dilution with solvents. Thus, storage at low temperatures is only occasionally recommended for solvent-based adhesives. For normal storage in storage halls with higher ambient conditions, the temperature should be conditioned to a level not beyond the upper limit of room temperature, i.e., 25 °C (with the exception of up to 30 °C, depending on the solvent) through cooling.

Hot-melt adhesives do not require storage at low temperatures, because being pure thermoplastic materials, they are neither chemically reactive nor do they undergo physical changes at room temperature. Furthermore, they do not emit solvent vapors or other gases during their storage. Thus, at room temperature, these adhesives remain unchanged and can be stored for extended periods of time.

In contrast to reactive adhesives, water-based dispersion adhesives generally cannot withstand such storage conditions and must be protected from low temperatures. In such dispersions, water acts as the carrier medium, in which the adhesive components are dispersed as microspheres. Thus, when water freezes at 0 °C, phase separation occurs. As the water crystallizes and the adhesive components separate from the liquid medium and condense, the adhesive coagulates, as shown in Fig. 3a, b. When this

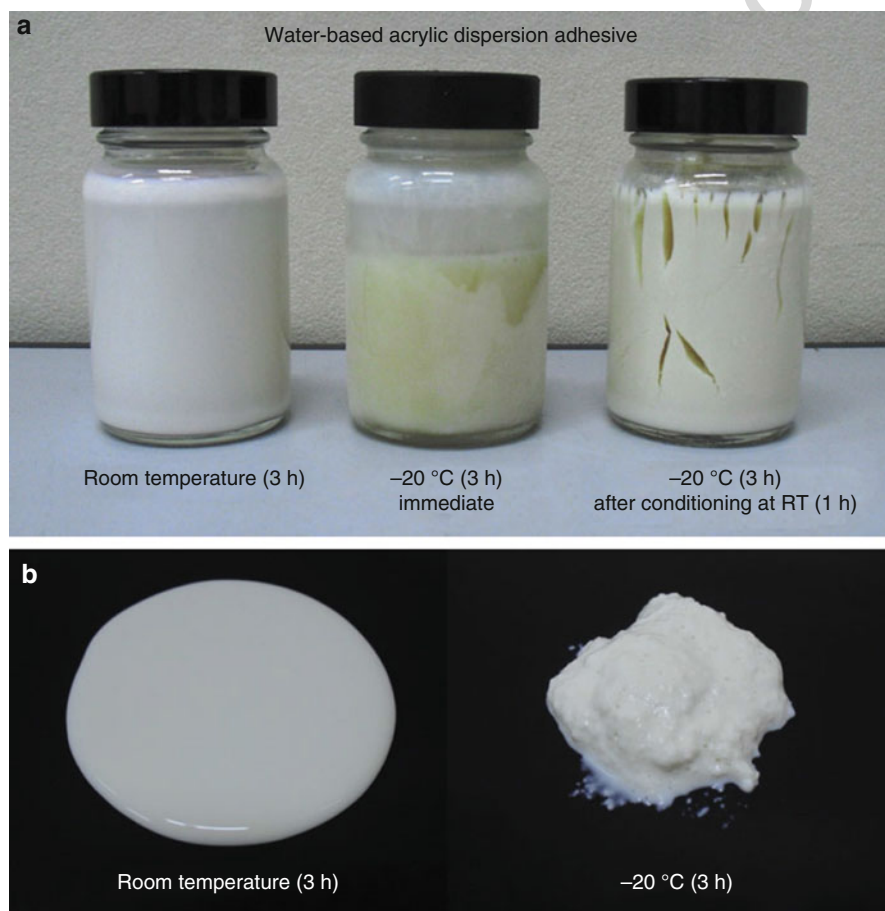


**Fig. 3** (a) Effect of cold storage on a water-based acrylic dispersion adhesive, (b) coagulation of water-based acrylic dispersion adhesive due to cold storage

happens, the adhesive becomes unusable. Hence, water-based dispersion adhesives are mostly stored at room temperature. Nonetheless, some manufacturers recommend storage temperatures between 5 and 25 °C to inhibit microbial attacks.

### 36.3.2 Temperature and Reactivity: The Arrhenius Equation

The shelf life of reactive adhesives can be extended by reducing their reactivity (i.e., rate of collision of reacting molecules per unit time). This can be achieved by increasing the free path of the molecules, through the dilution of the adhesive. However, for the dilution to be effective for this purpose, a reduction of the solid content by approximately 30–40% is necessary. Hence, in practice, dilution is only used as a means to reduce the adhesive viscosity. A more effective way to reduce the reactivity would be to decrease the mobility of the reacting molecules through cooling.

The Arrhenius equation describes the dependence of the chemical rate constant on the absolute temperature as follows:

$$k = A \cdot e^{\frac{-E_A}{RT}}, \quad (1)$$

where

$k$  is the rate constant of the reaction.

$A$  is the pre-exponent to indicate the number of molecular collisions per unit time.

$E_A$  is the activation energy of the reaction (J mol<sup>-1</sup>).

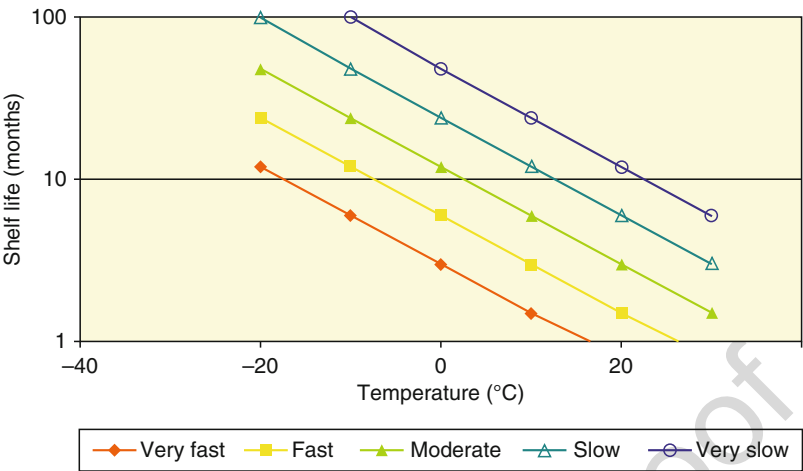
$R$  is the gas constant, with a value of 8.314 (J mol<sup>-1</sup> K<sup>-1</sup>).

$T$  is the absolute temperature (K<sup>-1</sup>).

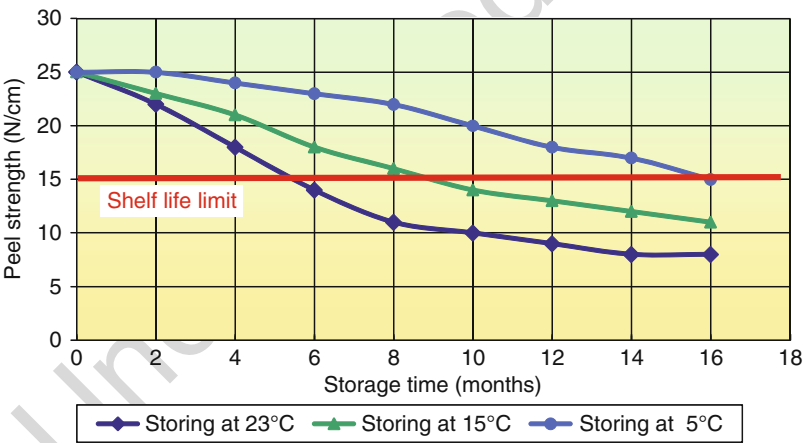
Most chemical reactions have similar dependence on temperature: the reaction rate doubles with every 10 °C increase in temperature and halves with every 10 °C drop in temperature. In practice, this could translate, for instance, to an adhesive having a shelf life twice as long when stored at a temperature of 10 °C instead of 20 °C. Figure 4 shows the relationship between the temperature and the shelf life of an adhesive, with different reaction rate constants.

Figure 5 shows the influence of storage time and temperature of a one-component reactive adhesive on the peel strength of bonded electronic composites, from which the corresponding storage shelf life was deduced. In this example, a heat-activated adhesive (epoxy resin/dicyandiamide) was used for bonding polyimide film to stiff printed circuit material. Before its use, the adhesive was stored over a long period of time at 23 °C, 15 °C, and 5 °C. The specified peel strength for the application was 15 N cm<sup>-1</sup> (L-peel test according IPC-TM-650 2.4.9). The peel strength was measured at an interval of 2 months. Based on the specified peel strength of 15 N cm<sup>-1</sup>, the corresponding shelf life at each storage temperature was recorded, as shown in Table 2.

In general, the trend observed fulfills the law of Arrhenius.



**Fig. 4** Reactive adhesives: shelf life as a function of temperature, with different reaction rate constants



**Fig. 5** Reactive adhesives: influence of storage time and temperature on peel strength

**Table 2** Effect of storage temperature of reactive adhesive on shelf life

Storage temperature	Shelf life
23 °C	5.5 months
15 °C	9 months
5 °C	16 months

t.1  
t.2  
t.3  
t.4

**36.3.3 Storage Between Freezing Point and Room Temperature**

A temperature range between freezing point and room temperature is adequate to accommodate the majority of the adhesives which require storage at low temperatures. This can be described as “storage under cool conditions” in contrast to storage under 0 °C, which is described as “storage under cold conditions.” Some manufacturers or suppliers provide only general storage instructions such as “cool and dry” or “cool and frost-free” instead of the exact storage temperature and duration, while some provide only a temperature range. The wide variety of adhesive types adds yet another dimension to the storage temperature. The following list (Table 3) shows a selection of some of the typical adhesive groups with the appropriate storage conditions.

**36.3.4 Storage Below Freezing Point**

Adhesives which require storage below freezing point are usually stored at temperatures between −20 °C and −25 °C. Such conditions are generally necessary for reactive adhesives, due to two main reasons as follows.

First, for normal reactive single-component adhesives, they are usually stored in large quantities after manufacture for a significant period of time, before they are filled into smaller quantities and delivered to the market. Hence, to eliminate any undesired chemical reactions during storage, low storage temperatures are essential. This group of adhesives includes cyanoacrylates and UV-sensitive epoxy resins. When stored at −20 °C, in dark conditions, they have a minimum shelf life of approximately 2 years.

Second, highly reactive single-component adhesives, such as catalyzed epoxy resins in the form of films, are viable at room temperature for only a few days. However, at −20 °C, they can be stored for approximately 6 months.

This category of adhesives also includes prepregs, which are used in the aviation industry for the construction of aircraft, e.g., to bond the molded parts together. Prepregs are made of woven glass fibers, or more recently carbon fibers, which have been soaked in and pre-reacted with a mixture of epoxy resins and hardeners. They usually undergo temporary storage at −20 °C and are conditioned to room temperature before use, where they are assembled with the substrates and cured. Apart from epoxy resins, phenolic resins can also be used as raw materials for prepregs.

**Table 3** Storage of different types of adhesives

Water-based dispersion adhesives	5–25 °C (Cooling chamber/room temperature)
Cyanoacrylate adhesives	5–15 °C (Cooling chamber/fridge)
Single-component adhesives polyurethane	15–25 °C (Cooling chamber/room temperature)
Methyl methacrylate adhesives	0–5 °C (Cooling chamber/fridge)
Phenolbutyral adhesive films	5–10 °C (Cooling chamber)
Phenolic resin/rubber adhesive films	5–15 °C (Cooling chamber)
UV-sensitive epoxy adhesives	5–15 °C (Fridge, dark)

## 36.4 Conclusion

In summary, this chapter has shown that, while the compliance to recommended measures during adhesive storage is absolutely necessary, it is usually manageable. The different types of storage and the corresponding shelf lives for different groups of adhesives and composites have also been addressed. In addition, the need to consider the potential hazards of the adhesives or their components during storage and transport is highlighted.

Generally, external influences on the adhesive characteristics during storage, such as temperature, humidity, and other physical effects, are controllable. Where necessary, measures such as suitable packaging and containers, as well as the conditioning of the storage halls, should be implemented.

On top of that, adhesive storage should also be taken into consideration in the development of new adhesives. Therefore, new adhesives should not only be tested against their applications but also their storability and shelf lives, before they are launched in the market. While such tests usually constitute the most time-consuming step during the design process, shortening the time taken for this step during the development phase could potentially result in customer claims later on.

It is a common practice to subject new products or bound parts to accelerated aging in order to simulate storage over long periods of time. This can be achieved through oven storage or environmental cycling tests for a defined period such as 6 weeks. Such tests are often helpful, except when there are other influencing factors apart from temperature and humidity. In such circumstances, it is difficult to establish the exact storage stability.

During storage, any unintended chemical reactions within the adhesives can also lead to problems during or after processing. Hence, new raw materials should be evaluated for potentially undesired chemical reactions to avoid disappointment when such problems arise during the storage of the end products.

Such measures also apply when changes to the adhesive contents are required, for instance, when replacements of hazardous raw materials with environmental-friendly substitutes are called for. In particular, there is an increasing drive toward the use of halogen-free adhesives in the electronic and automotive industries. In general, any change in adhesive formulations would require a series of testing for the storage stability, besides the standard property test profiles.

Currently, another challenge is the desire of many industries to have an adhesive with a shorter wetting-out time for the adhesion process and, yet, better adhesion properties. This would require a highly reactive adhesive, which normally requires storage at low temperatures to guarantee a reasonably long shelf life.

---

## References

- European Standard (2001) DIN EN 12701
- Fundamentals of Hazardous Materials (2009/2010) Denios, Germany

Andreas Lutz

**Contents**

37.1	Introduction .....	1053
37.2	Training and Education .....	1055
37.3	Health and Safety Aspects .....	1055
37.3.1	Preventive Measures While Storing the Adhesive .....	1056
37.3.2	Preventive Measures While Working with the Adhesive .....	1056
37.3.3	Preventive Measures While Processing .....	1057
37.4	Mixing of Adhesives .....	1058
37.4.1	Vacuum Mixing .....	1060
37.4.2	Continuous and Batch Process .....	1060
37.4.3	Vertical and Horizontal Mixing .....	1061
37.4.4	Kneader .....	1062
37.4.5	Agitator Design .....	1062
37.4.6	Centrifugal Mixing .....	1064
37.5	Adhesive Storage .....	1065
37.5.1	Storage Condition .....	1066
37.5.2	Packaging Size .....	1068
37.5.3	Packaging Material .....	1068
37.6	Dispensing of Adhesives .....	1069
37.6.1	Single-Component Dispensing .....	1069
37.6.2	Two-Component Dispensing .....	1069
37.6.3	Hot Melt Dispensing .....	1072
37.6.4	Higher-Volume Dispensing .....	1072
37.7	Mixing and Metering of the Adhesives Before the Application .....	1074
37.7.1	Low- to Medium-Volume Application .....	1074
37.7.2	Medium- to Large-Volume Application .....	1077
37.8	Transferring the Product .....	1077
37.9	Substrate Preparation .....	1081
37.9.1	Preparation of Steel Substrates .....	1082
37.9.2	Preparation of Aluminum Substrates .....	1083

A. Lutz (✉)

Automotive, Dow Europe GmbH, R&amp;D Automotive Systems, Horgen, Switzerland

e-mail: [alutz@dow.com](mailto:alutz@dow.com)



33	37.9.3 Preparation of Magnesium Substrates .....	1084
34	37.9.4 Preparation of Low-Energy Substrates .....	1086
35	37.10 Quality Control .....	1087
36	37.11 Conclusion .....	1088
37	References .....	1089

## Abstract

Adhesives are used today with increasing volumes in many applications in different industries and are supplied to the end customers in various forms. Very common are liquid adhesives, pastes, mastics, as well as adhesive films or tapes. Less common are powder systems for coating purposes. Adhesives are used where more conventional mechanical or thermal joining technologies can't be used because the joint area is not accessible (e.g., for a spot welding or riveting gun), entire areas need to be bonded (tile or carpet bonding), or if improved mechanical joint performance is required. Improved mechanical performance could be increased joint stiffness, longtime durability, or corrosion resistance under environmental exposure.

Bonding with adhesives is not a simple operation, and a lot of preparation work is necessary before the adhesive can be applied to the designated bonding area (Shields J, Adhesives handbook. Butterworths, London, 1985). A chain of preparation processes is required. It starts with the mixing of the adhesive and its storage before the transfer to the customer. At the customer, the adhesives need to be transferred to the operation area. The substrates to which the adhesive will be applied have to be well prepared. The final process step includes the dispensing of the adhesive to the substrate and the joining of the parts which are intended to be bonded. Some adhesive formulations require an accurate metering of different components. Some, sensitive adhesive operations require a monitoring of the application, e.g., by vision systems, to guarantee the correctness of the application. Each of the steps is important and contributes equally to the quality of the final adhesive application. See below the summary of the different process preparation steps:

1. Adhesive mixing at the supplier
2. Packaging of the adhesive at the supplier
3. Adhesive storage at the supplier or the customer
4. Transferring the adhesive from the storage to the application area
5. Substrate preparation
6. Metering and dispensing the adhesive
7. Quality control

Depending for which application, in which industry, and by which end customers adhesives are used, different application techniques and dispensing and metering devices are chosen.

For smaller bonding operations like sealing work at construction sites, repair work at car garages, or to fix tiles to a floor, adhesives are typically manually applied out of smaller containers like cartridges. If adhesives are used in a larger scale, like at an automotive line, for example, for metal bonding reasons or to bond windows to the frame of a car, a robot application is used, which pumps the adhesive out of drums and transfers it to a dozer and a gun for the final application. The adhesive itself can be applied in different ways like as a simple bead, sprayed, extruded, or by air assistance, called swirling. Which technique is used depends on factors like the application, the rheological property of the adhesive, and the application temperature. Therefore, the rheological properties of the adhesive formulation need to be tailored to the application. Lower viscous adhesives can be applied by spraying or extrusion beside the simple bead application. Higher viscous adhesives are often limited to bead application, or the application temperature needs to be significantly increased to be applicable by other methods.

This chapter will discuss in further detail each item of the process chain: the storage of adhesives, the transfer to the application area, the different metering and dispensing technologies, the used mixing equipments, the substrate preparation, and the quality control. Proposals are made regarding people education and how to create a safe working environment.

---

## 37.1 Introduction

Adhesives are used for many applications in a lot of different industries like in automotive (Symietz and Lutz 2007), marine, packaging, or building and construction (see Part I, Applications).

Typical applications examples are:

- Bonding of car bodies
- Bonding of structural parts in airplanes (National Research Council 1976)
- Applying foils on new cars for protecting during transport
- Lamination of composites like GFC (glass fiber composites)
- Coating of cans, tubes, or pipes
- Chemical-resistant flooring
- Labeling in the food or packaging industry
- Packaging of food or pharmaceuticals

Adhesives are used to bond various different substrates such as metal, glass, wood, or plastic among many others (Houwink 1967). The appropriate adhesive and its chemistry have to be chosen in dependence of the application and the substrate which is bonded. A wide range of different chemistries are used to formulate adhesives. The chemical nature of the adhesive defines its field of application.

Most adhesives which are used in the industry today are using epoxy, polyurethane, acrylic, and silicone or rubber chemistry.

One- or two-part adhesives are dominantly applied, although there are multiple-component adhesive systems in use as well. One-part adhesives are commonly supplied with an inhibited curing system which can be activated, e.g., by heat or by UV radiation. Two-part adhesives are supplied with separate components, one is the resin component and the other the hardener component. The latter contains reactive chemicals, which enable cross-linking and polymer building of the resin part through a chemical reaction of different functional groups.

The hardening of the adhesives happens either through a chemical reaction as described above or through simply physically binding to the surface. The chemical reaction in case of a one-part adhesive depends on the chemical nature of the adhesive (Habenicht 1990). So do polyurethane- or silicone-based adhesives cure in the presence of moisture, whereas cyan-acrylic-based adhesives are inhibited by the presence of oxygen and cure under nonaerobic conditions. Other adhesives like epoxy one-part adhesives cure with heat. Two-part adhesives contain, beside the resin part, a hardener part which consists of reactive molecules or polymers which react together with the resin part. Typical examples are epoxy- or acrylic-based adhesive formulations.

In the following a summary of properties for some representative adhesive systems is given:

- Epoxies adhere very well to a lot of different substrates like steel (Symietz and Lutz 5/2008), aluminum, stone, or wood. They offer a high bonding strength, are resistant to chemicals, and show a good heat resistance. Epoxies are used to fill gaps and larger volumes and are applied in thinner layers. They can be formulated in different viscosities, low or high, and with different filler levels. Epoxies typically cure with heat or can be formulated as two-component products which cure in the presence of a separate hardener component.
- Polyurethanes are polymers which are very flexible and tough and which show a very good performance under peel loading and good adhesion to nonpolar substrates like plastic or rubber, as well as to paints and ceramics. They mostly cure with humidity which can cause curing issues in case of extreme humidity conditions.
- Acrylics can be cured in different ways like with peroxides or with UV light. The curing is much faster than the curing of epoxy or of polyurethane adhesives. Acrylics are used to fill gaps and to bond plastic or metal parts. They offer a good environmental and heat stability and show a good performance under peel and shear loading. It needs to be considered that acrylics can be incompatible with some metals which are used in dispensing equipments. Acrylics can be formulated to pressure-sensitive adhesives which adhere to surfaces simply by applying some pressure during the application.

Adhesives are used in applications where other joining methods cannot be used or because they offer unique performance features like a high strength combined with

high flexibility and superior durability (Lees (1997)). It is therefore very important to prepare the adhesive bonding as accurate as possible to take the best advantage of this bonding technology.

---

## 37.2 Training and Education

Many people may think that bonding by using adhesives just requires applying the adhesive to the bonding area and it will stick. But the use of adhesives for bonding purposes requires a well-defined process including steps like:

- The correct choice of the adhesive
- Correct handling of the adhesive
- Correct mixing and metering
- Preparation of the surface where the adhesive is applied to
- Quality checks to guarantee the constant quality of the bond
- Use of curing sources for one-component adhesives like ovens or radiation sources

All this requires a certain level of know-how, not only of the chemist or engineer but also of the worker who is daily working with the adhesive. In addition, the suppliers of the substrates like the metal or plastic suppliers or the suppliers of the lubricants need a fundamental understanding about the adhesives, the necessary preparation prior to the application, and about the application itself.

Training is required for all the people who are involved in the application of the adhesive. The workers who are daily dealing with the adhesive have to be instructed before using the adhesives and regularly trained as well.

There are institutes at universities who are offering a certified education in adhesive technology and their application.



A good educational background prevents from making mistakes in the preparation of the adhesive and the substrate, helps to choose the right adhesive solution, and helps to apply it correctly. Education is further discussed in ► Chap. 41, “Processing Quality Control.”

---

## 37.3 Health and Safety Aspects

Adhesives are a blend of different chemicals and therefore potentially hazardous to the environment and the user. The information about the risk can be found on the labels and the material safety data sheets. According to their risk and health, ranking precautions have to be taken to create a safe working environment. Health and safety aspects are further developed in ► Chap. 39, “Environment and Safety.”

Figure 1 below shows what typically can be found on labels and in material safety data sheets and what will change in the near future.

New GHS/CLP Regulation (future)	CHIP Regulations actually being used in Europe
Applies to both the supply/use and transportation of chemicals	Applises only to supply and use of chemicals
Aligning supply with transport regulation	Supply labeling and transport labeling are different
GHS - Pictograms wiht a white background and red border 	Orange Hazard Symbols 
Term "Mixture"	Term "Preparation"
Term "hazardous"	Term "dangerous"
H-Phrases / Statements	Risk (R) phrases with the code numbers, e.g. R43
P-Phrases / Statements (5 types)	Safety (S) phrases with the code numbers; e.g. S24, S37

**Fig. 1** Change from old CHIP (Chemicals Hazard Information and Packaging) to new GHS (Globally Harmonized System of Classification and Labeling of Chemicals) regulation

**37.3.1 Preventive Measures While Storing the Adhesive**

Adhesives are filled in different packaging forms and sizes. Used commonly for smaller volumes are cartridges, bottles, or tubes and for bigger volumes pails or drums.

Generally all containers should be stored in a dry and cool place, preferably below 25 °C. Some reactive or solvent-containing adhesives would require cooler storage, preferably temperatures below 10 °C or even below 0 °C. If not, the adhesive viscosity could increase during storage, which could negatively influence its application characteristics, physical properties like adhesion, or even mechanical properties like joint durability. For some adhesive systems, like water-containing products, too low storage temperatures on the other side could lead to crystallization.

The adhesive containers ideally should be stored in dependence of their used chemistry. The same chemistry should be stored together; for example, epoxy adhesives should be stored separately from acrylic adhesives. The adhesive containers should be stored above collecting trays to prevent pollution in case of a leakage or spill. Depending on their hazardous potential, adhesives need to be stored in special places:

- Flammable material should be stored in rooms which are especially fire resistant and explosion protected.
- Adhesives which have a strong odor should be stored in a room with special ventilation.

**37.3.2 Preventive Measures While Working with the Adhesive**

An adequate personal protection should be used if working with adhesives. The safety data sheet has to be consulted to obtain detailed information about the

precautions which have to be taken if working with the specific adhesive. The given shelf lives should be respected or the adhesive supplier consulted if any adhesive is applied beyond the shelf life.

The personal protection should at least consist of:

- Protecting glasses or goggles
- Long-sleeved lab coats
- Gloves

Gloves should be changed regularly and the used ones should be disposed. The material the gloves are made of should prevent the penetration of the adhesive through the glove to the skin. Latex gloves, for example, are not recommended to be used if working with epoxy adhesives. In this case nitrile gloves should be chosen. The lab coat should be regularly and professionally cleaned. The thickness of the coat should be thick enough to prevent the adhesive from migrating through the woven to the skin. Respiration masks might be used for solvent-containing adhesives, adhesives with strong odor, or if special substrate preparations are needed, which require the use of wet chemistry.

Adhesives are chemical blends using different organic polymers. Some examples of special preventive measures, which are recommended to be taken in dependence of the chemistry of the adhesive, are listed below:

- Some adhesives, like epoxy-, rubber- or acrylic resin-based formulations, are skin sensitizing and require the use of special gloves.
- Acrylic-based adhesives and hardener compounds of two-part formulations can have a strong odor and would require working under proper ventilation.
- Solvent-containing adhesives contain flammable solvents and must be kept away from any heating source, would require working under proper ventilation, or for some instances would require the use of respiration masks.

### 37.3.3 Preventive Measures While Processing

Adhesives can be applied automatically by pumping the material out of a pail or drum and transfer it through hoses and possibly a dozer to the nozzle. The adhesive is applied from the nozzle to the substrate. Certain pressures and temperatures are applied to guarantee a good flow of the adhesive from the pail or drum over the dozer to the nozzle.

The following precautions are recommended to be taken during processing of the adhesive:

- Avoid an overheating of the adhesive which could lead to an increase of the viscosity and eventually can block the hoses or the dozer.
- Shield the equipment properly because it is under pressure.

- Switch of the heat and pressure after longer breaks like overnight or over the weekend.
- Use heated follower plates in case the adhesive viscosity is that high that it cannot be applied at ambient temperatures. Do not use heated pail or drum jackets.
- Work on specially sealed floors or use collection trays to be prepared in case of a spill.

On the other hand, larger amounts of adhesives are commonly manually applied like in case of applying chemical-resistant floor protections or for tile as well as carpet bonding. In such cases, special masks should be worn in addition to the other recommended equipments to protect against the odor of the adhesive or against evaporation of a solvent.

After the application of the adhesive, other operations can be additionally applied like spot welding in case of joining doors for cars or grinding of parts after the repair of cars. In such cases, special precautions need to be taken in addition like:

- Installing a proper ventilation if thermal joining methods are applied through the adhesive
- Wearing dust masks during the grinding operation
- Wearing any other protective equipments like long-sleeved lab coats or any eye protection like goggles

---

## 37.4 Mixing of Adhesives

Adhesives consist of different raw materials. Organic monomers and polymers usually are the main part of a formulation and mostly contribute to the adhesives' mechanical and physical performance. In addition to the organic part of a formulation, other raw materials like inorganic mineral fillers or solvents are used. For reactive adhesives, curing agents and accelerators are added to the formulation to cross-link the organic part of the formulation, for example, at ambient or higher temperatures or in the presence of humidity, heat, or UV light.

In single-component adhesives, all the raw materials are added in one component. In two-part adhesives, the formulation is separated into two components. One part, usually called part A, contains the organic resins, and the other part, called part B, contains the hardener and accelerator.

Adhesives are mixed at the supplier and filled in either smaller container sizes like cartridges or in bigger sizes like pails and drums. For some applications the adhesive bulk and other components like the hardener part or solvents are mixed at the end user just before the application.

The correct mixing of the adhesive is a precondition to achieve a good homogeneity of the mixture and to obtain the best mechanical performance of the bond. There are many different kinds of mixers and stirring elements available on the market. Which kind of mixer is adequate depends on chemical nature of the adhesive, the viscosity of the adhesive, and its sensitivity to external factors like

humidity or oxygen. It is proposed to investigate together with the equipment supplier which equipment suits best for the intended application.

Mixers which are used in the laboratory or the ones which are used for manufacturing could be very similar in their design. There is not much principal difference with regard to the different elements a mixer consists of.

A mixer typically consists of a vessel in which the mixing happens. For laboratory purposes it can be a disposable small container like a simple metal can. The vessel can be surrounded by a heated jacket to allow heating or cooling during the mixing operation. A gear drives the stirring elements. There are many different stirring elements on the market. Which one is chosen depends on many different factors like what kind of adhesive is formulated, how high the viscosity is, or how shear sensitive the formulation is. Ideally, the mixer is connected to a vacuum pump and can be flushed with inert media like nitrogen. In addition, the entire equipment can contain a discharge valve, a vapor filter, and a control panel. A window to watch the mixing is recommended and commonly used. For easy access for maintenance and inspection reasons, the mixer usually is equipped with a lifting column. Figure 2 shows a lab planetary mixer like it is used to formulate smaller quantities of higher viscous adhesives.

**Fig. 2** Lab mixer with lift and planetary agitators, used to formulate adhesive samples of about 400 g





Different mixing methods are described in this section. ► Chapter 38, “Equipment for Adhesive Bonding,” also describes the mixing of adhesives but focuses on the equipment itself.

### 37.4.1 Vacuum Mixing

Vacuum mixing is defined as such: mixing in a closed system under an internal pressure which is significantly lower than atmospheric pressure.

Mixing under vacuum has an important influence on the adhesive’s end performance. It helps to reduce the porosity of a cured adhesive and therefore helps to maximize properties like strength and durability (Angos 2007). But, for some formulations like those which are based on cyan-acrylics, the presence of oxygen can be necessary for the stability of the product.

Mixing in many cases happens under vacuum for the following additional reasons:

- Deaeration to obtain a void-free product
- Obtain an oxygen-free product, to prevent a decomposition in the presence of oxygen in case of sensitive formulation ingredients
- To prevent a possible chemical reactions or a microbiological growth
- Prevent contact of the mixture with water, in case of ingredients which can react in the presence of water
- Dewatering or evaporating solvents of heat-sensitive formulations
- To more easily change the physical state from, for example, a paste to a dry powder or from a slurry to a paste
- For dosing of light powders or pastes into the formulation
- Acceleration of mixing through, e.g., better and faster wetting of powders
- Better dispersion of smaller-volume ingredients
- A lower-density material is obtained, and therefore smaller volumes need to be handled

Because of all the listed benefits it offers, vacuum mixing is mostly used for the mixing of adhesives at the adhesive supplier.

### 37.4.2 Continuous and Batch Process

The mixing equipment can be divided into continuous types and batch types. In a laboratory, batch-type equipments are dominantly used. Although in an adhesive production both types are in operation, the batch-type equipment is more commonly used. A lot of adhesives like epoxy-based adhesives are mixed in a batch-type procedure.

Batch systems can be either stationary or transportable, whereas continuous systems are stationary only. The dosing of the raw materials happens sequentially and

contributes significantly to the overall batch time. The raw material can be added either manually or automatically. Automatic dosing is used if the adhesives are produced on a regular base, the same raw materials are used, and the volumes are high.

A continuous system is a fully automatic operation. The raw materials are added once and not sequentially like if using the batch process. The most important unit of this system is the metering unit. It must be carefully calibrated and regularly inspected.

A batch system is the most precise operation, because each ingredient is added separately and is accurately balanced.

### 37.4.3 Vertical and Horizontal Mixing

In theory the mixing of the adhesive can be done vertically, horizontally or centrifugally. The mixing speed can be varied and adjusted to the product properties. The size of the vessel depends on the volume which will be mixed. It can vary from a few hundred grams for laboratory purposes to about 50–500 kg for upscaling purposes or to about 800 l to about 30,000 l for manufacturing.

In vertical mixers the rotor is installed in a 90° angle to the bottom of the vessel, and for horizontal mixers, the rotor is parallel to the ground. The cylindrical vessel form is used for horizontal mixers. In case of vertical mixers, it can have a conical or a cylindrical form.

Vertical mixers are very frequently used for laboratory purposes, because they are somehow easier to operate and require less space. For the manufacturing of bigger volumes, the choice of the mixer type depends on items like how the raw materials like to be charged and the final product likes to be discharged, and it depends on the available floor space. Figure 3a shows a planetary mixer head and butterfly agitators,



**Fig. 3** Head and agitators of a planetary mixer which are used in production (a) and in a laboratory (b) to mix adhesive formulations. Butterfly agitators are used for the manufacturing mixer and finger blade agitators for the laboratory mixer. The production mixer has a volume capacity of about 1 t and the laboratory mixer of about 10 kg

and Fig. 3b shows a pilot mixer. Both are used to mix adhesive formulations of higher viscosities.

#### 37.4.4 Kneader

For very high viscous materials, kneaders are preferably used. They usually contain a kind of sigma blades, which are able to cut materials like solid rubbers apart and can knead them effectively. An extrusion screw is discharging the material out of the vessel.

Figure 4 shows a kneader which is used in a laboratory for mixing of very viscous adhesives like rubber- or polyurethane-based adhesive formulations.

#### 37.4.5 Agitator Design

The design of the agitator should be in line with the required mixing function and the expected result of the mixing. For making simple blends, dispersions, or for making adhesives, a different agitator design will be chosen. Adhesive formulations can differ a lot with regard to their viscosity and flow behavior. Depending on the used type of polymers, their molecular weight, and depending on the used fillers, as well as on the ratio of organic polymer to mineral filler, the viscosity can vary from very low to very high. The flow behavior of low viscous materials is totally different from the flow characteristics of higher viscous products (Alhofen 2005).

Important factors for the decision of which agitator would suit best are:

- The viscosity of the mixture
- The shear rate which needs to be applied
- The nature of the ingredients (e.g., shear sensitive or not)
- The heat stability of the adhesive formulation

**Fig. 4** Laboratory kneader

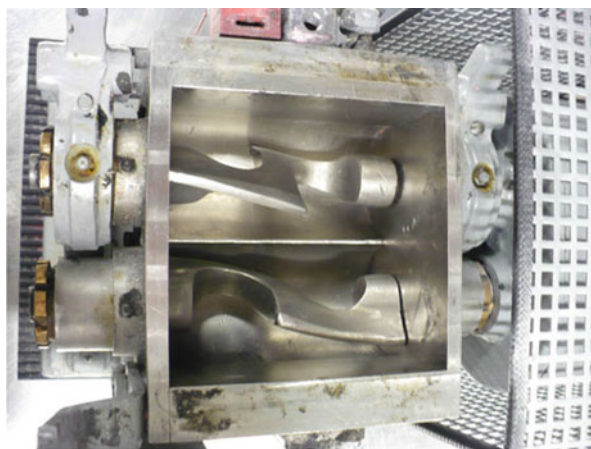
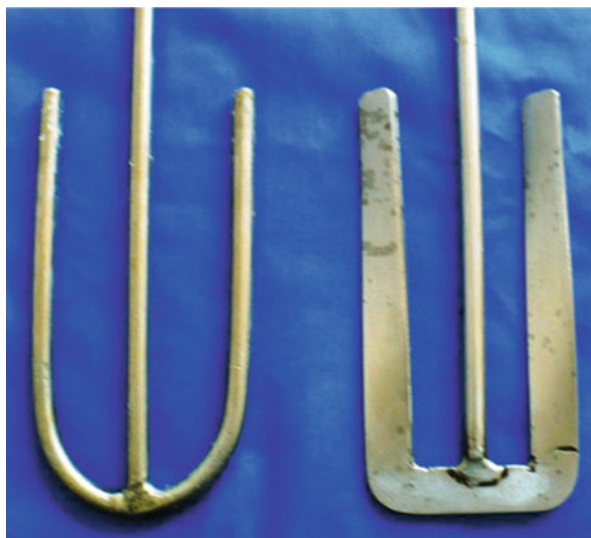


**Fig. 5** Two anchor agitators with different shapes



For very low viscous formulations, a simple anchor stirrer can be chosen. Figure 5 shows two anchor agitators, which only differ in their shape.

However, most adhesive formulations require, because of their higher viscosity, agitators which offer a higher shear and flow.

The following needs to be considered:

- Higher viscous materials do not flow easily and need a special stirring equipment which possibly rotates and travels through each point of the vessel.
- The agitator should offer a good heat transfer in the mixture, especially for higher viscous materials, to avoid local overheating.
- The agitator gear needs to cope with the high load of a high viscous material.

There exist many different agitator designs which are suitable to mix higher viscosities. Some of them are described in more detail below.

Stationary high-shear agitators are used for materials with medium to high viscosities and for materials which flow well:

- High-speed dispersers are used if medium shear and a higher flow is required.
- Rotor-stator mixers can be used alternatively but offer a higher shear and a lower flow.

Figure 6 shows a photo of a high-speed disperser.

These systems are able to mix even higher viscosities if combined with an anchor blade in addition. Such systems are available as dual- or triple-shaft mixers. The slower-moving anchor removes the material from the vessel wall and the bottom and transports it to the high-shear agitator. Obviously, triple-shaft systems are able to

**Fig. 6** High-speed disperser



412 handle even higher viscosities than dual-shaft systems. Because of the slow-moving  
413 anchor, the system is limited to well-flowing mixtures.

414 In case of planetary agitators, the blades are moving through the material and each  
415 agitator can move on its own axis. Such planetary agitators are suitable for higher  
416 viscous and not easily flowing materials. Double planetary mixers are typically used  
417 for mixing of materials like adhesives, sealants, dental pastes, composites, foams,  
418 plastisols, or metal slurries. A scraping blade is commonly used in addition to  
419 remove the material from the vessel wall during mixing. Planetary agitators are  
420 most efficient at high viscosities because the shear rate in the paste increases  
421 proportionally with the increasing material viscosity.

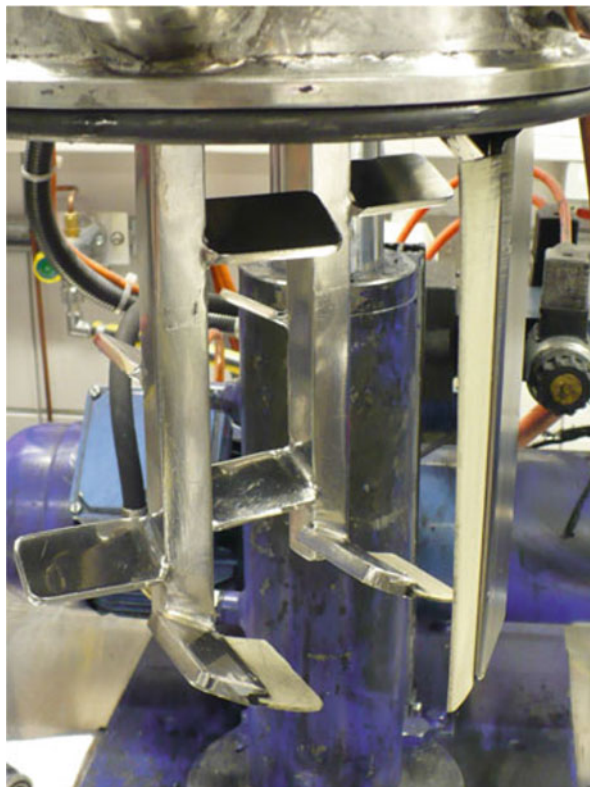
422 Different blades can be used. Typical agitator designs are finger blades, older  
423 rectangular-shaped blades, and newer HV blades. The latter are able to even mix formu-  
424 lations of highest viscosities, which usually are mixed by using a kneader or an extruder.

425 Figure 7 shows a photo of finger blade agitators used in a planetary laboratory  
426 mixer.

#### 427 **37.4.6 Centrifugal Mixing**

428 Centrifugal mixing is used for high-speed mixing and was originally developed for  
429 dental materials. Disposal cups are used for the mixing of the adhesives. The cup and

**Fig. 7** Finger blade agitators which are used in a planetary laboratory mixer, including a scraper blade



a mixing arm are rotating in opposite directions at high-speed rates of up to 3,000 rounds per minute. Figure 8 shows the mixing chamber and the mixing cup of a speed mixer which is used in the laboratory for the development of adhesives. The biggest advantage over vertical or horizontal mixing is the required mixing time. It varies from a few seconds to a few minutes only. On the other hand, the volume which can be handled is limited which is a clear disadvantage over the other mixing technologies. It varies, depending on the speed mixer model, from a few hundred grams to about 3 kg. Speed mixing is mainly used for lab screening purposes in combination with a design of experiments. Many different cup dimensions are available. Direct mixing in convenient cartridges or syringes is possible.

### 37.5 Adhesive Storage

The manufactured adhesive can be stored in different packaging forms, like for smaller quantities in cartridges, tubes, or bottles and for bigger scales in pails or drums. Adhesive films are systems which consist of an adhesive dry film applied to a paper, a glass fiber, or an aluminum foil and are usually stored in boxes.



**Fig. 8** Mixing chamber of a speed mixer including a mixing cup



A correct storage is very important to conserve the adhesive properties until the material is supplied to the end user and to avoid any loss of performance, change in rheological properties, or to avoid a possible decomposition of the material through an inappropriate storage. Adhesive storage is treated in more detail in ► [Chap. 36, “Storage of Adhesives.”](#)

### 37.5.1 Storage Condition

The applied storage conditions depend on the adhesive formulation, specifically the chemical nature of the resins, and in case of reactive adhesives, it additionally depends on which curing and accelerator system is used.

Generally, the filled adhesive should be stored in a safe environment, not exposed to heat, to humidity, or, for light-sensitive adhesives, not exposed to light. Good ventilation should be given. The specific storage conditions are commonly written on the labels and can be read in the material data sheets.

Two- or multiple-part formulations have a significantly longer shelf life than one-component adhesives with integrated curing agent and accelerator (Lutz and Brändli 3/2010). The shelf life of one-component adhesives strongly depends on the chemical nature of the formulation and on the acceleration system. Multiple-part adhesives have a shelf life of about 6–24 months and single part of about 3–12 months only. The shelf life can be prolonged by a time factor of about 2–4 for one-part adhesives, through storage in a refrigerator below 10 °C or by freezing below 0 °C. Excluded from cooled storage are products which are known to show phenomena during storage, like phase separation, crystallization, or sedimentation of ingredients of the formulation.

Some examples of adhesive formulations which require special storage conditions are given below:

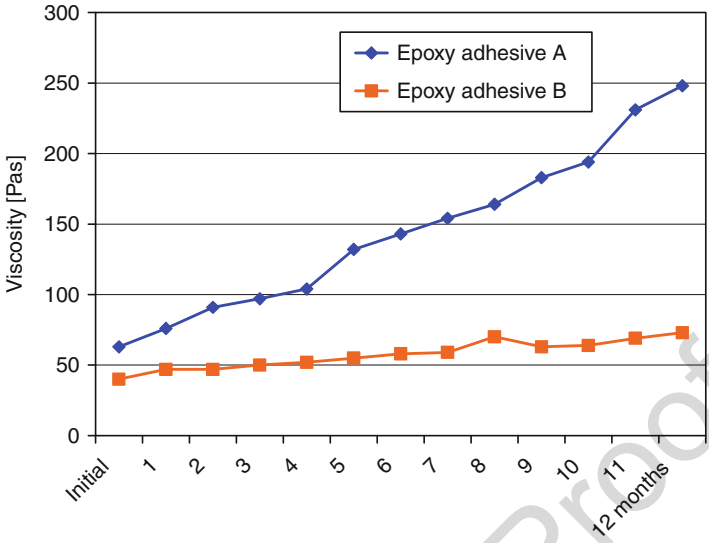


**Fig. 9** Shelf life of two epoxy adhesive formulations. Formulation B is significantly more stable than formulation A

- Reactive one-part adhesives, which can increase in viscosity over time depending on temperature, should be stored under air conditioning or in a cooled warehouse. Examples are accelerated one-part epoxy or rubber-based adhesives.
- Some adhesive formulations may tend to crystallize during storage and would require a storage above a certain temperature.
- Adhesives which cure with humidity like polyurethane or silicone adhesives should be stored in a dry environment.
- UV light-curable epoxy or acrylic adhesives should be stored out of light.
- Because of their strong odor, acrylic adhesives should be stored in a room with good ventilation.

Figure 9 shows the viscosity stability over time at 23 °C storage for two one-part epoxy adhesive formulations. Adhesive B increases only very little in viscosity over time and therefore is significantly more stable than adhesive A. Adhesive A would need to be stored in a cooled area, like in a fridge or an air-conditioned warehouse.

Figure 10 shows the decrease of the lap-shear strength of shear specimens which are bonded with one-part epoxy adhesives and stored under 80% relative humidity at 23 °C before being cured. Adhesive B shows a much better resistance to water absorption than adhesive A. If using adhesive A for bonding, the joint should be cured quickly, at least before about 1 week after the application of the adhesive. Adhesive B could stay uncured for about 6–8 weeks.



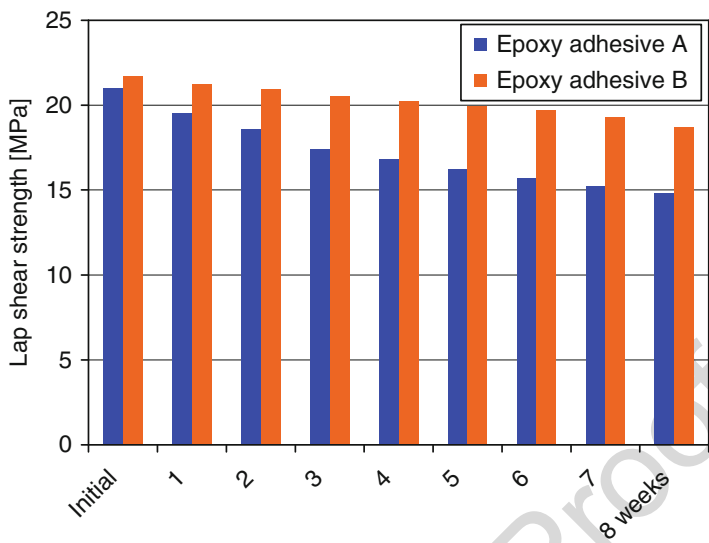


**Fig. 10** Decrease of lap-shear strength of humidity-exposed lap-shear specimen

**37.5.2 Packaging Size**

The size of the container should be chosen based on the adhesive consumption. If only small volumes are used, small packaging sizes like cartridges, bottles, or tubes should be chosen. Adhesives have a specific shelf life, and the use of bigger packaging sizes for small-volume applications would inevitably lead to disposing significant amounts of adhesive. If large amounts of adhesives are consumed, the application typically is done out of pails or drums using pumps which transfer the adhesive through hoses from the drum to the nozzle where the adhesive is applied to the bonding area.

**37.5.3 Packaging Material**

Depending on the chemical nature of the adhesive or of the hardener compound in case of two-part systems, the material used for the container, for example, cartridges, can be different. Corrosive materials, for example, the hardener compound of a two-part epoxy system, should not be stored in metal containers. Cartridges or bottles made out of plastic are mostly used. Humidity-sensitive adhesives like polyurethane adhesives should be stored in containers which show a low diffusion rate of water. Aluminum cartridges or especially, e.g., metal-coated plastic containers are preferred in this case over simple plastic ones. Special plastic bags which contain, for example, an aluminum liner are recommended to be used for pails or

drums. The plastic inliner prevents on one hand the contamination of the drum or pail with adhesive, which saves cleaning costs, and on the other hand limits the water diffusion into the material. The adhesives should be shipped in a package which is sealed in a way that no material could leak in case of a damage of the container.

## 37.6 Dispensing of Adhesives

Adhesives can be applied in a lot of different ways to the bonding area. The used methods for dispensing depend on which kind of adhesives is applied, whether one- or two-part adhesives are used, and how much adhesive needs to be applied. In this section, dispensing methods are described.

### 37.6.1 Single-Component Dispensing

For most of the manual operations, the use of smaller packaging sizes like cartridges, bottles, tubes, or even syringes are fully sufficient.

For cartridges, there is a broad range of different sizes, and they are made out of different materials like plastic or aluminum. The adhesive is statically applied through a nozzle by using a handgun. Different sizes and shapes of nozzles exist for simple bead application or for the extrusion of the adhesive. Different handguns are available: manual operated ones as well as pneumatically or electrically operated handguns. Which handgun suits depends on how much pressure can be applied for the application. Applying too high pressures could damage the cartridge which could result in a leakage. The viscosity of the material determines the amount of pressure which needs to be applied. High viscous materials can be applied by using a heated gun, or the cartridge can be stored in a cartridge oven before the application.

For bottles, there are special bottle dispensers in use like simple hand pumps or volumetric dispenser. Adhesive dispenser controllers are used to offer a high accuracy to meet customer requirements for multivalve dosing or coating or spray operations. Figure 11 below shows typical dispensing equipment for one- and two-part adhesive formulations. It contains a cartridge gun, cartridges, and a nozzle.

### 37.6.2 Two-Component Dispensing

Two-component adhesives are commonly filled in dual cartridges. Depending on the mixing ratio, the sizes for each of the two cartridges are different. Typical mixing ratios are 1:1, 2:1, 4:1, or even 10:1. Special handguns have to be used. There is a new system for two-part applications which is a kind of mono-cartridge including two separate chambers. The benefit is that normal handguns can be used. The nozzle used for applying two-part adhesives is a cylindrical tube, which contains the mixing

**Fig. 11** Cartridge gun, plastic nozzle, aluminum cartridge for dispensing of one-component adhesives and mono-cartridge for dosing two-part adhesives

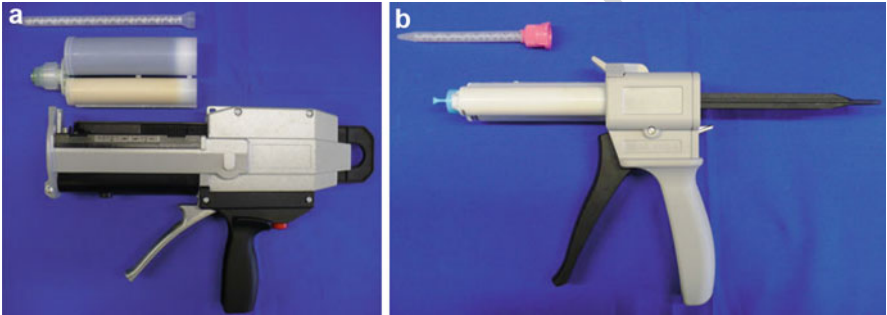


**Fig. 12** Typical cartridge guns and statically mixers for dispensing of two-part adhesives. Bigger (a) and smaller (b) packaging size

elements. The elements are stationary parts that force the materials to combine as they travel through the length of the mixer. The length of the nozzle and amount of mixing elements vary, and the adequate type is typically recommended by the adhesive supplier. Special guns which can dynamically mix the two components in a special mixing chamber are also used, before applying it through the nozzle. Such dynamic mixing is preferably used for high viscous two-part adhesive formulations like some polyurethane adhesives used for car windscreen bonding or for structural bonding in trim shop.

Figure 12 shows two typical handguns, a bigger- and a smaller-size one, which are commonly used for applying two-part adhesives. Figure 13 shows two different cartridge systems, which are used to store two-part adhesives. One is a mono-cartridge with two separate chambers in one cartridge; the other is a double-cartridge

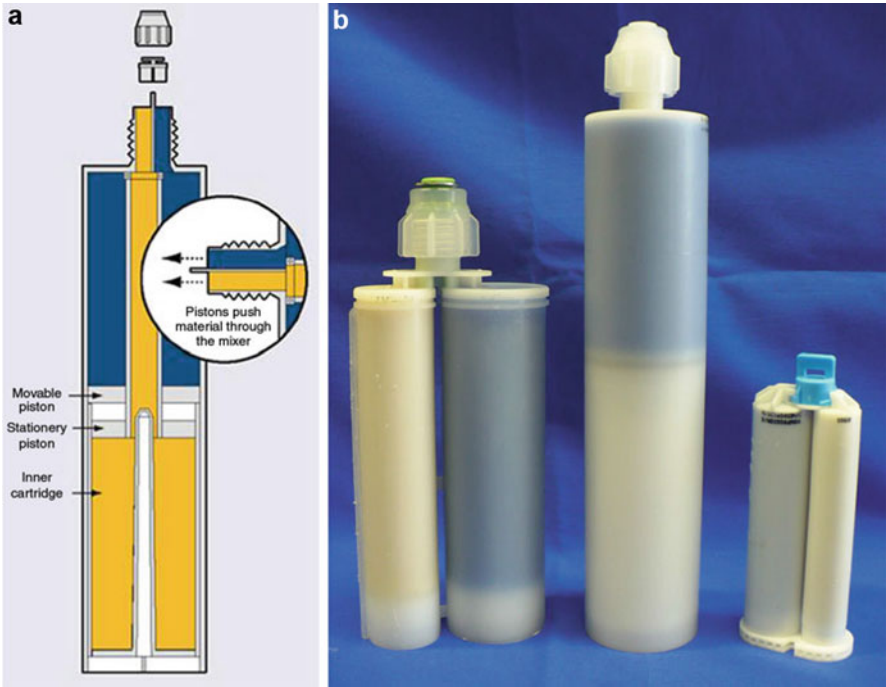


**Fig. 13** Mono-cartridge TAHM™ system as supplied by Nordson with two chambers (a) and double Mixpac cartridge systems as supplied by Sulzer for applying two-part adhesive formulations: 2:1 mixing ratio, 215 ml and 15 ml volume (b)

**Fig. 14** Different kinds of static mixers



system with two separate cartridges for components A and B. Figures 14 and 15 show different kind of static mixers as well as different mixing elements. Figure 16 shows a dynamic mixing element used for mixing of two-part formulations.

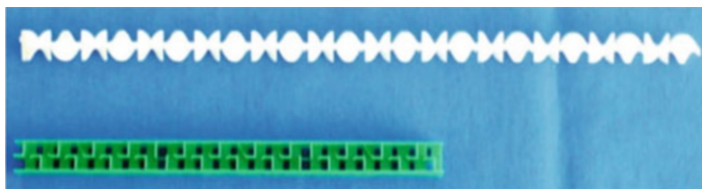


**Fig. 15** Different mixing elements, as supplied by Sulzer Mixpac and used for static mixing of two-part adhesive products

**Fig. 16** Dynamic mixing element for mixing two-part formulations



### 37.6.3 Hot Melt Dispensing

Hot melt adhesives are very high viscous formulations and can only be applied at high temperatures. Special heated handguns (glue guns) can be used, or the cartridges can be heated in a special cartridge oven to lower the material's viscosity before the application (Satriana 1974). Figure 17 shows a cartridge oven and a heated cartridge gun.

### 37.6.4 Higher-Volume Dispensing

For higher-volume applications or continuous operations like applications at car manufacturers or in the building and construction industry, the adhesive is applied out of pails or drums. Typical pails contain about 25–50 l of material and drums about 200 l. It is recommended to use plastic liners to avoid a pollution of the drum or pail. In this case the drum or pail can be reused and just the plastic bag needs to be disposed. Figure 18 shows a typically used pail with a plastic liner. Some of the inliner may contain an aluminum foil which prevents water penetration through the inliner to the bulk adhesive. Such systems are applied in case of water-sensitive materials like polyurethane-based adhesives.

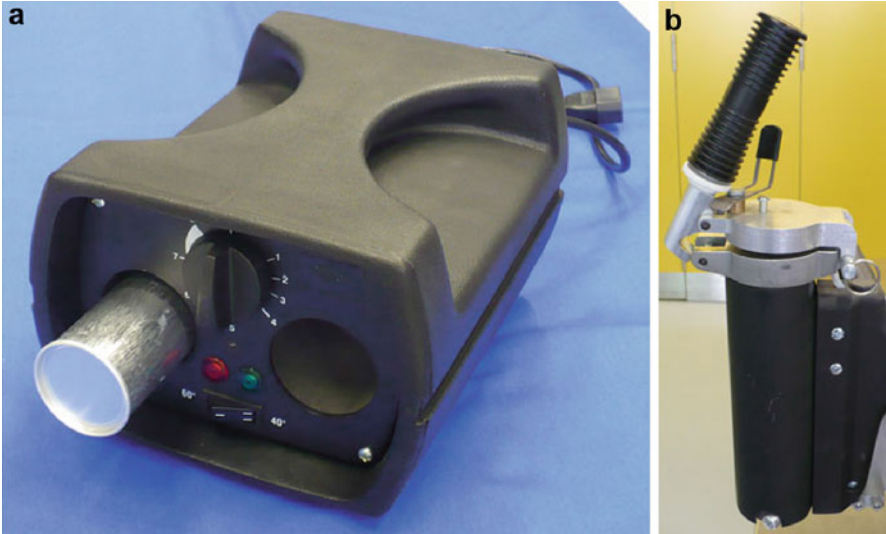


**Fig. 17** Cartridge oven (a) and heated gun (b)

**Fig. 18** Pail and inliner for adhesive storage



## **37.7 Mixing and Metering of the Adhesives Before the Application**

One-part adhesive formulations do not require a special mixing process prior to the application, but two- or multiple-part adhesives need to be mixed before the application of the adhesive.

Mistakes in mixing definitely have a negative effect on the quality of the bond. For example, if not applying the correct ratio of A to B component, this can give low initial strength values and bad results with regard to the longtime durability of the bond. There are several mixing and dispensing options, and each offers advantages and disadvantages.

### **37.7.1 Low- to Medium-Volume Application**

Most suppliers supply their multiple-component systems in prepacked forms like in cartridges. No metering is necessary in this case.

For adequate automatic mixing, there are mixing devices for application out of dual cartridges like handguns or automatic guns and static or dynamic mixers. Static mixers like described above are by far mostly used.

The following points are crucial for a good mixing of two-component adhesive systems:

- The rheological properties of both components A and B should be adjusted in a way that both components mix well.
- The length of the static mixer and the number of mixing elements should be defined depending on the formulation.
- Before applying the static mixer, both components A and B need to be equally balanced.
- The first few grams of material after mixing should be disposed.
- Regularly change the static mixer and dispose the old one.

Possible application issues are:

- The adhesive can cure at the cartridge nozzle, and this could result in a leak at the cartridge plunger.
- The application itself is limited to low viscosities; high viscous materials are difficult to dispense by using handguns.
- If using automatic guns in combination with a high viscous material, the high pressure during the application can damage the cartridge plunger, and this can result in a leakage of the adhesive.

Figure 19 shows the content of a typical two-part adhesive set which is used for the repair of parts of a car. It shows which different kinds of guns can be used and



**Fig. 19** Typical two-part adhesive set for manual applications

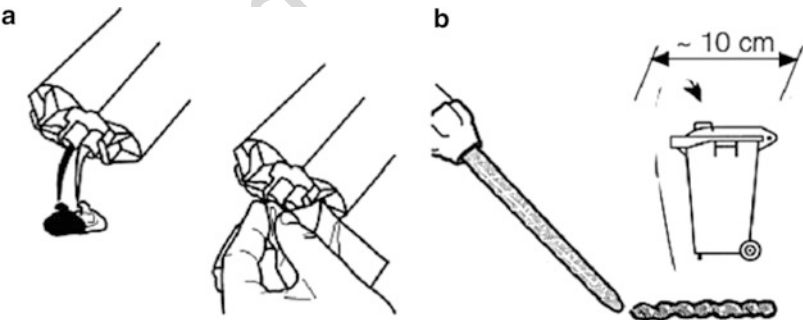
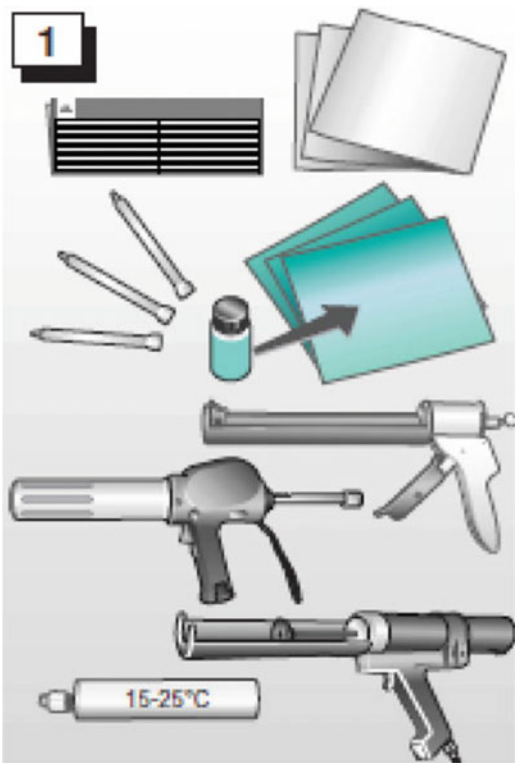


**Fig. 20** Balancing components A and B before applying the static mixer (a). Dispose the first few grams of material (b)

contain, beside the adhesive cartridge, a bottle of activator and cloths to apply it and to wipe it off the substrate.

Figure 20 below shows two important preparation steps before the application of a two-part material. Figure 20a shows the balancing of both components before



**Fig. 21** Application of a two-part epoxy adhesive used for the body repair of cars



**Fig. 22** Adhesive bond line after salt spray testing



617 putting the static mixer on, and Fig. 20b shows the disposal of the first grams of  
618 material before the adhesive is applied to the substrate.

619 Figure 21 shows a typical bonding operation performed in garages for the repair of  
620 car bodies (Lutz 6/2009). The adhesive, in this case, is manually applied by using a  
621 cartridge gun and a static mixer, which are described above. The adhesive used for this  
622 application is a structural two-part epoxy adhesive, applied with a mixing ratio of 2:1.

623 Figure 22 shows an adhesively bonded joint after 480 h of salt spray testing. The  
624 bonded surface shows no trace of corrosion compared to the surrounding area and

**Fig. 23** Spot-weld sealed by using a two-part adhesive



demonstrates the corrosion resistance and sealing potential of the applied adhesive. Figure 23 shows the use of mixed joining technologies, spot welding, and adhesive bonding. In this case, adhesives not only offer strength but also seal the spot-weld against possible galvanic corrosion.

### 37.7.2 Medium- to Large-Volume Application

For medium- to large-adhesive applications, metering and mixing dispense systems are used for applying adhesives like epoxy, polyurethane, polyester, or silicone formulations. Such systems offer an accurate measure, mixing and dispensing for two-part adhesives, and an accurate dispensing for one-part products. There are different models in use like reciprocation or rotary dispensing units.

The following metering principles are used:

- Positive rod displacement
- Piston displacement
- Double-action piston metering
- Piston cup metering
- Dual reciprocating piston metering
- Gear metering

The metering system which is used depends on the kind of adhesive and the application.

## 37.8 Transferring the Product

The transferring of the adhesives out of drums and pails is commonly done by using a follower plate combined with a pulping or gear pump. The product is further transferred through pipes and possibly a dozer to a nozzle which applies the adhesive to the area to bond. Gear pumps can have certain disadvantages like:

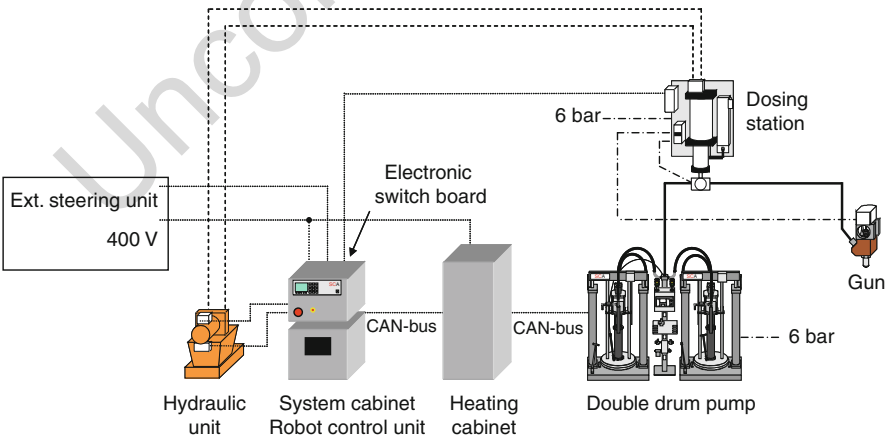
- Bringing shear stress into the adhesive, which could negatively influence the rheological properties of the material
- Because high-shear stress brings heat into an adhesive mixture, the viscosity of a reactive adhesive can increase considerably through a starting polymerization, and, as a result, pipes and dozers can be blocked

Depending on the adhesive’s viscosity, the material has to be heated to offer a good material flow. For this purpose the follower plate and each section of the application equipment can be heated. The heat should be switched off in case of longer breaks. Heated drums or pail jackets are not recommended to be used because if the temperature is not carefully controlled, too much heat can be transferred into the material which eventually can lead to a burning of the material as a result of an exothermic reaction.

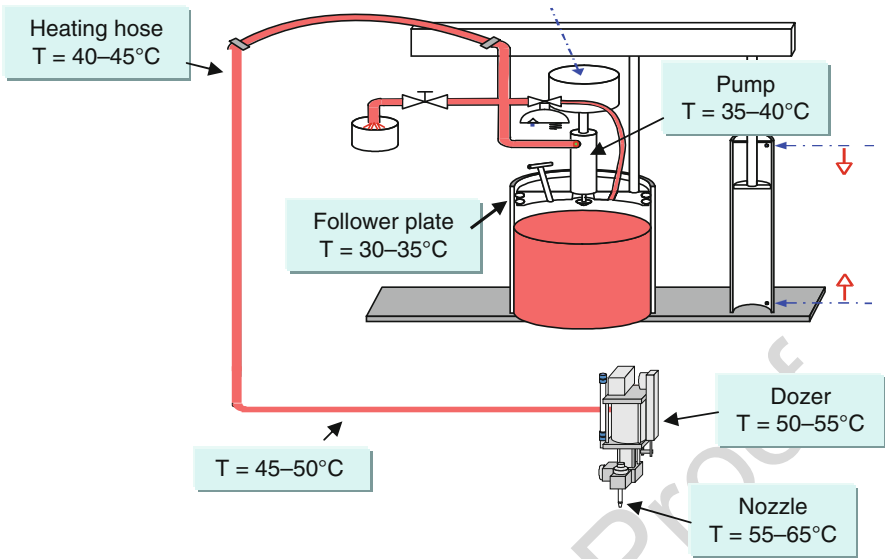
In simple application equipments, the adhesive flows through a pipe to a gun and is manually applied. More sophisticated equipments use a dozer which controls the applied volume and the pressure and applies the adhesive very accurately through a nozzle. If temperature is required for a good material flow, ideally a temperature gradient, with a gradually increasing temperature from the follower plate over the dozer to the nozzle, is applied. The dozer can vary in volume and in pressure which can be used. The amount of necessary pressure depends on the rheological adhesive properties and on the application. Ideally, first in-first out dozer is used to avoid an adhesive plaque building in the dozer through an increase of the adhesive’s viscosity over time, which eventually can block the dozer after a certain time of operation.

Figure 24 shows a heated application equipment which is commonly used to apply one-part adhesives, like in the automotive industry for car body bonding.

Figure 25 shows the flow of the material from the pumping of the material out of the pail or drum, over the material transfer in the hoses to the dozer and the final



**Fig. 24** Application equipment as supplied by SCA Schucker and which is used to apply one-part adhesives



**Fig. 25** Material flow and applied heat per section

**Fig. 26** Gun system to apply one-part adhesives



transfer to the nozzle. If heating is required, the temperature is gradually increased as shown.

Figure 26 shows a dozer and gun system which is used to apply one-part adhesives. The dozer controls the applied adhesive volume, and the gun finally

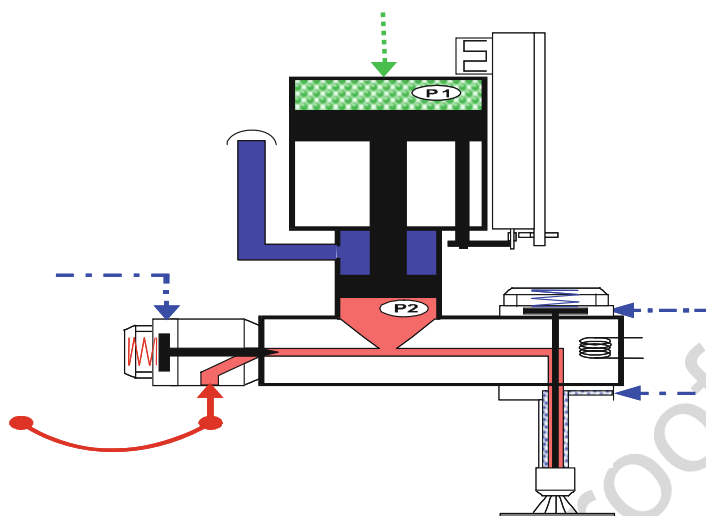


**Fig. 27** Hydraulic dosing station

applies the adhesive to the bonding area. Hydraulic, pneumatic, or electronic dosing systems are in use. Hydraulic and electronic dozers are preferred over pneumatic systems because more pressure can be applied and the application can be run faster. Electronic systems have an advantage over hydraulic systems because they do not require space for an aggregate.

Figure 27 shows a hydraulic dosing station. In blue, incoming material into the dozer and in red material which is transferred out of the dozer and to the nozzle.

The application out of the nozzle to the bonding area can happen in different forms. It depends on the applied pressure and the dimension of the nozzle. Since the application part is discussed in more detail in ► [Chap. 38, “Equipment for Adhesive Bonding,”](#) only a few automatic application methods are briefly described hereunder.

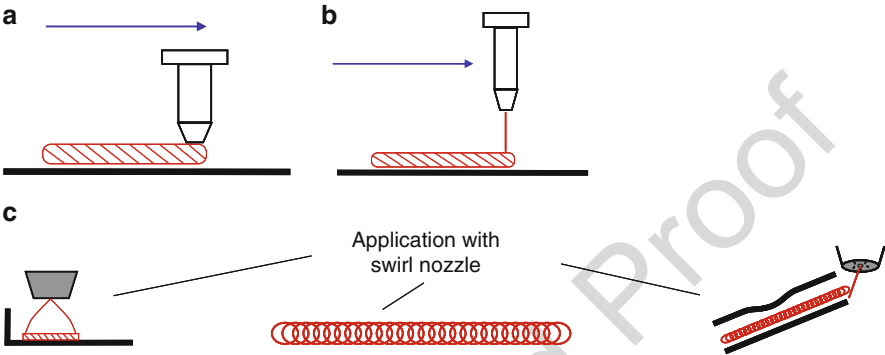
There are some application methods which are frequently used in the industry: bead, swirl, spray, jet-spray application, or extrusion. Which one is used depends on the application and on the rheological properties of the material. Higher viscous materials are not easy to spray but applicable as a bead or by extrusion. Lower viscous materials are applicable faster by using methods like jet spraying or swirling, which are commonly used in the application of structural adhesives to bond car bodies.

Table 1 summarizes the applied conditions for each application technology. The adhesive can be applied much faster, if using the air-assisted swirl or the jet-spray method compared to a simple bead application which saves a significant amount of process time. The swirl technique is limited with regard to the applicable volume, which is less compared to the applied volume of other technologies. Because the application is assisted by air, entrapped air can lead to the occurrence of bubbles at the bond surface after the curing of the adhesive.

The nozzle diameters and the applied dozer pressures differ a lot in dependence of the used technology. In particular the smaller nozzle diameters which are used for the

**Table 1** Application parameters for different application techniques

Application type	Nozzle diameter	Pressure	Distance to surface	Application speed
Bead	1–3 mm	10–20 bar	About the diameter of the bead: 2–5 mm	150–300 mm/s
Swirl	0.8–1.2 mm	10–120 bar	20–40 mm	200–600 mm/s
Jet spray	0.5–0.8 mm	100–200 bar	5–20 mm	300–600 mm/s



**Fig. 28** Different application technologies: bead application (a), jet-spray application (b), and swirl application (c)

jet-spray application can cause issues with blocked nozzles, if the fillers which are used for the adhesive formulation are not below a certain particle diameter or if they tend to form agglomerates.

Figure 28 shows the principles of the discussed application technologies.

### 37.9 Substrate Preparation

The preparation of the substrate before the application of the adhesive is very important for the quality of the bond and the performance of the bond during operation (Metals Handbook 1982). A good preparation is a guaranty for a maximum bonding strength, best fatigue durability, and best resistance to environmental factors like the exposure of the bond to humidity, heat, UV light, and salt.

The required surface preparation depends on which substrate will be bonded and which kind of adhesive is applied. Some metals, for example, have oxide layers like aluminum, magnesium, or titanium. In this case, the surface preparation focuses on stabilizing the oxide layer.

Depending on the chemistry of the adhesive, the adhesion to different substrates and the tolerance for surface contamination are different. Epoxy- and acrylic-based adhesives bond well to a variety of different surfaces like metals, aluminum, or composites and tolerate some degree of surface contamination like oil if cured by

heat. They are not adhering well to low-energy surfaces like plastic. Two-part epoxy formulations need a cleaning of the surface to remove any contamination. Special two-part acrylic-epoxy hybrid adhesives are able to bond even on oily polar surfaces like metals. Newly developed purely epoxy-based two-component adhesives have been developed which are capable to absorb surface oils. But there is a time limitation after which the adhesive needs to be subjected to heat to facilitate the oil absorption into the adhesive. The application of heat at temperatures typically above 100 °C and below 140 °C should be done after several hours. Some uniquely catalyzed acrylic two-part formulations bond well to nonpolar surfaces like plastic.

Polyurethane-based adhesives adhere well to coated or painted surfaces like on ceramic-coated glass, electro-coated or painted metal, or to plasma-treated low-energy surfaces. Usually a primer or an activator is applied to the surface before adding the adhesive.

This section gives a brief overview of the substrate preparation and is treated in more detail in ► [Chap. 8, “Surface Treatments of Selected Materials.”](#)

### 37.9.1 Preparation of Steel Substrates

Beside stainless steel, most adhesives, especially epoxy- and acrylic-based ones, bond well to steel surfaces. The steel substrates can differ in strength, surface topography, and their composition.

The preparation for bonding is different whether one-part heat-curing adhesives or two-part formulations are used. In the case of one-part epoxy adhesives, the surface just needs to be cleaned from any contamination like dust. Oil is tolerated in an amount lower than about 3 g/m<sup>2</sup>. Higher viscous oils like dry lubes are tolerated up to about 2 g/m<sup>2</sup>. In case of applying two-part formulations, with the exception of acrylic-epoxy hybrids, oil and any other contaminations need to be carefully removed.

For a better long-term durability of the bond, for example, a better resistance against galvanic corrosion, a coating of the steel surface is recommended. This coating is usually a zinc coating (galvanized steel), either hot-dipped zinc or electro-galvanized zinc coating, and is used in many industries like in the automotive industry. The quality of the zinc layer has to be high to offer a good durability and corrosion resistance of the adhesive bond. The achievable mechanical strength values are high and often even higher than the strength values for the non-coated steel. An insufficient quality of the zinc layer often results in a delaminating of the zinc layer under loading of the bond. The adhesion, especially of the e-coat, the filler, and the paint, can be further optimized by applying crystals, like zinc and iron phosphates, to the metal surface. This treatment, called phosphating, is often used, for example, in the automotive industry.

In addition to the above-described metal coating, organic methods can be used like epoxy coating, e-coating, or the application of paint. In this case, the achievable bond strength values strongly relate to the quality of the coating and are generally

lower than the strength values for the non-coated steel. Not all adhesives adhere well to painted surfaces, and their adhesion has to be tested in advance (Dettner 1991).

### 37.9.2 Preparation of Aluminum Substrates

Aluminum substrates are available in different alloys and surface topographies as sheet panels or casting parts. To prevent the aluminum oxide layer from undefined growth, a special surface treatment of the aluminum is necessary.

The cleaning of the surface can be done thermally, chemically, or electrochemically. It is necessary for the following reasons:

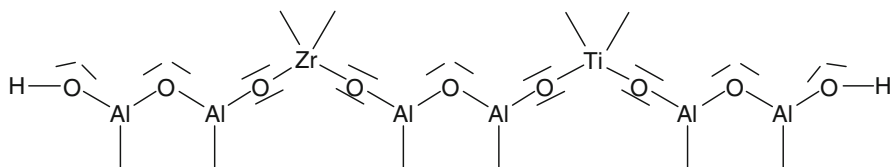
- Remove oil and surface contamination.
- Remove aluminum fines.
- Remove surface enrichments of trace elements.
- Remove the not perfect natural oxide layer.

Thermal cleaning is done by coil annealing in a furnace. The chemical cleaning can be done by immersion of the coil into an acidic or alkaline solution. Alternatively, the solution can be sprayed on the coil. The electrochemical cleaning is done in sulfuric or phosphoric solutions.

In addition to the cleaning of the surface, a chemical conversion treatment or an anodizing process can be applied which offers more homogenous surface properties. The oxide layer is stabilized, and the adhesion of the adhesive, the primer, or the paint is improved. Anodizing is commonly used to prepare aluminum for bonding in the aerospace industry.

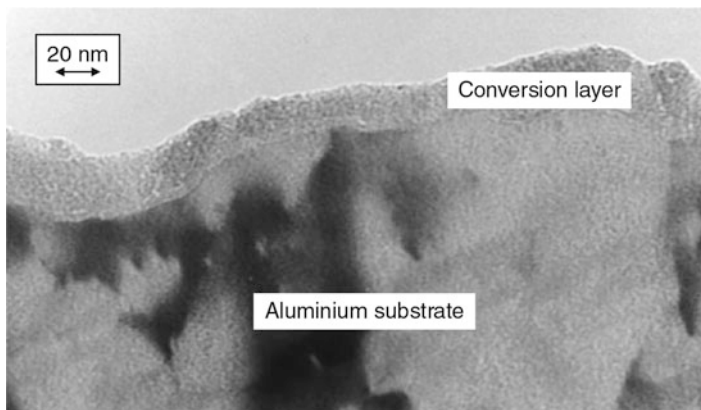
The chemical conversion of the aluminum surface happens in the presence of titanium and fluoride ions in a sulfuric solution. Some treatments use zirconium ions together with titanium ions. The sulfuric acid and the fluoride ions are pickling the surface, and the metal salts are responsible for the passivation of the surface. The titanium and zirconium ions react with the aluminum oxide on the surface and form a mixed oxide layer. Like the cleaning process, it can be applied by an immersion or by a spray process. Figure 29 shows the simplified chemical formula for the mixed oxide layer.

Figure 30 shows a microscope picture of a cut image of an aluminum sample which has been prepared using titanium and zirconium surface treatment.



**Fig. 29** Simplified chemical formula of the mixed oxide layer





**Fig. 30** Cut image of an aluminum sample passivated by using titanium and zirconium surface treatment

### 37.9.3 Preparation of Magnesium Substrates

Chromate conversion coatings are effective treatments for magnesium and are applied before the adhesive bonding or the paint, but the chemistry used is harmful and restricted by regulations. The alternatives to the chromate treatment and the treatment process for magnesium are discussed below in further detail (Skar and Albright (2002)).

Generally the pretreatment of magnesium includes the following steps:

1. Treatment of the magnesium cast: e.g., machining, deburring, or grinding.
2. Rinse with water (omitted in case of a no-rinse process).
3. Cleaning with alkaline solution.
4. Rinse with water.
5. Optional: activation by acidic pickling.
6. Applying the conversion coating.
7. Rinse with water (omitted in case of a no-rinse process).
8. Rinse with deionized water.
9. Drying at 90–105 °C.
10. Applying the adhesive or the paint.

After the machining and the deburring, the die cast part is cleaned by using an alkaline solution. In some cases there can be an etching or pickling step applied before the conversion treatment. The conversion coating can be applied like for aluminum by immersion into a bath or by spraying.

The cleaning of magnesium casts happens in an alkaline solution. In the case of magnesium, there is an optimum pH range of about 10–11 in which the etching rate shows the highest value. Below or above that range, the etching is less effective because of a lower etching rate. For aluminum, the etching rate increases with an increasing pH.

The acidic pickling can be done by using acidic solutions of different acids like sulfuric acid, phosphoric acid, hydrofluoric acid, nitric acid, or chromic acid. The etching depth can vary from a few micrometers only to about 50 μm. The etching rate depends on which acid is used; it is high for sulfuric acid and low for nitric acid.

In the case of chromate treatment, the magnesium oxide on the surface reacts together with chromate ions to form a chemical complex and establishes a defined surface film of magnesium and chromium chromate.

As alternative to a chromate treatment (Gehmecker 1994), other chemical coatings can be chosen like:

- Similar to aluminum treatment: titanium and zirconium fluorides
- Phosphate or phosphate-permanganate solutions
- Solutions containing vanadate, manganate, and molybdate

The chromate treatment alternatives offer a similar good adhesion of the adhesive if, in addition, a cleaning and pickling process is used. If pickling is not done, the chromate treatment offers the best adhesion performance. A proposed combination is using a cleaner with a pH of about 9–11 and an acidic pickling. The alternative treatments are missing the self-healing and inhibiting effect of the chromate layer, which offers an additional corrosion protection. An exception is the mixed metal treatment. The performance of the different treatments was tested by performing accelerated corrosion tests. The loss in bonding strength was by far lower than the loss of strength of not treated lap-shear specimen. Table 2 lists some commercially available conversion treatments for magnesium.

Beside the chemical treatment, anodizing is an effective treatment method too. The magnesium part is the anode in an electrochemical cell and dissolves into magnesium ions. Together with electrolyte, a defined oxide and hydroxide layer is

**Table 2** Commercially available chromate-free conversion treatments

Supplier	Treatment	Type
AHC Oberflächentechnik GmbH	MagPass™	Vanadate, molybdate, and manganate solution
Chemetall GmbH	Gardobond (TM)X4707	Titanium-zirconium hexafluorides
	Gardobond (TM)X4740	Zirconium hexafluorides
Henkel	Alodine(TM) 5200	Titanium and/or zirconium oxyfluoro compounds with polymer additions
	Alodine(TM) 4850	Same as above
	Alodine(TM) 400	Same as above
	Alodine(TM) 160	Zirconium fluorides and magnesium oxides

845 formed on the magnesium surface. If phosphates, fluorides, silicates, or chromates  
846 are present in the electrolyte, they will be incorporated into the surface layer.

#### 847 **37.9.4 Preparation of Low-Energy Substrates**

848 Plastics can be either thermoset or thermoplastic materials. Examples for thermoset  
849 materials are polymerized epoxy, polyester, or phenolic resins, which do not melt  
850 after being cross-linked. Thermoplastics are materials like polyolefins, for example,  
851 polyethylene or polypropylene, polycarbonates, polyamides (e.g., nylon), or acrylo-  
852 nitrile butadiene styrene (ABS). Thermoplastic materials are increasingly used in  
853 industries like in automotive for reasons like weight saving. Thermoplastic materials  
854 like polyethylene or polypropylene exhibit low surface energies and are by far less  
855 polar than other substrates like steel or aluminum. Polar functions like oxides or  
856 hydroxides are missing at the surface. For good adhesion of low-energy surfaces, a  
857 good surface preparation is necessary to offer a good initial and also durable  
858 adhesion (Korane 2000).

859 For the following reasons, a surface preparation is strongly recommended:

- 860 • Removal of possible contaminations like release agents or oils
- 861 • Increase the surface energy of the substrates, by adding more polarity to the  
862 surface
- 863 • Adding texturing to the surface, to increase the available bonding surface

864 The preparation of plastic parts can be done by different methods (Bienak 2009).  
865 Those methods are summarized below in more detail.

866 Cleaning of the surface can be done by using solvents or special pastes which  
867 remove possible contaminations like oils or release agents.

868 The surface can be abraded to remove contaminations but also to offer a  
869 textured surface, which increases the bonding area. Different abrasion methods  
870 can be used.

871 A flame treatment oxidizes the surface and creates polar oxide groups on the  
872 surface. The surface energy is increased and the adhesion improved. Figure 31  
873 shows the plasma treatment of a polypropylene surface. Plasma is generally gener-  
874 ated by adding energy into a gas, so that it becomes ionized. It can be used for the  
875 cleaning of the surface but also can create polar groups on plastic substrates similar  
876 to flame treatment. Low-pressure or atmospheric pressure plasma is generated by  
877 applying a high voltage. The plasma contains free electrons, which are accelerated  
878 and create ions from the gas. In contact with any kind of surface, the energy of the  
879 plasma is transferred and causes reactions on the surface in a way that radicals are  
880 formed on the substrate surface. Those radicals can react with oxygen or different  
881 gases, like nitrogen or argon, and form functional groups on the surface. Polar  
882 functional groups like carbonyl, carboxyl, or hydroxyl are formed. The surface can  
883 be additionally activated through the cleavage of carbon bonds by UV radiation.

**Fig. 31** Atmospheric plasma treatment of a polypropylene surface (Source Plasmatreat GmbH, Germany)



Corona treatment uses a high-frequency discharge at about 15–25 kHz. The energy transfer to the substrate is high in this particular case due to oscillating electrons between the electrodes.

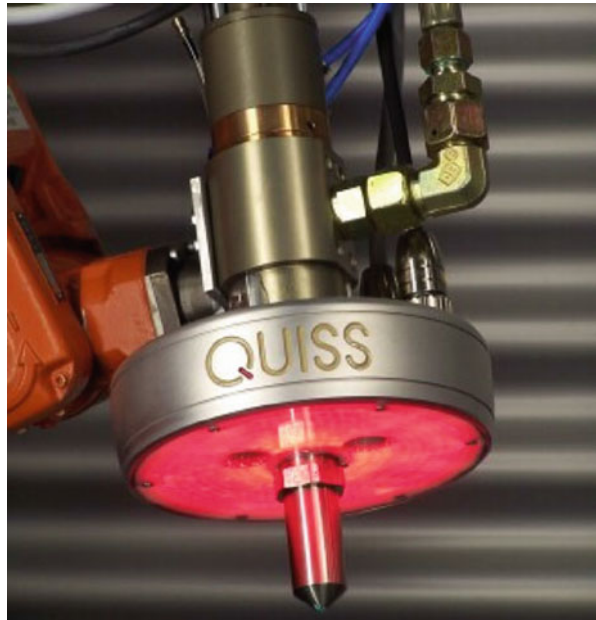
## 37.10 Quality Control

The quality of the bond needs to be audited in order to guarantee its performance. This is very important because adhesives are applied today in critical areas where a long lifetime of the bond is required. The application itself can be controlled by accurate metering and dispensing and by using dosing systems. The right equipment makes certain that the correct amount and mixing ratio are used and that the adhesive is applied exactly there, where it should be applied. In case of any incorrect dosing, the system will stop the application and will give a warning. The application can be controlled further by using vision systems, which are monitoring the application and control the positioning of the adhesive and any inconsistency within the adhesive bead. Such systems are, for example, in use in the automotive industry to control sensitive adhesive applications in the body shop.

Figure 32 shows a vision system which is installed directly at the application nozzle and controls the bead structure as well as the positioning of the bead on the metal sheet. Any failure, like bead disruptions, will be corrected in a second application step. Similar systems are used, for example, in the packaging industry to control the application of the glue to corrugated paper.

Another, but deconstructive, method is the control of the bond by dismantling the part and by visible inspection of the bond. This part's audit can be done regularly like once a day, a week, or a month depending on the importance of the application. Car bodies or parts of a body, which are using adhesive bonding in addition to older methods like spot welding, are regularly put apart for inspection purposes.

**Fig. 32** Vision systems as supplied by QUISS GmbH to the automotive industry



Quality control is discussed in more detail in ► [Chap. 41, “Processing Quality Control.”](#)

### 37.11 Conclusion

Adhesives are widely used in many industries for various different applications like in the automotive industry for bonding entire car bodies, or in the packaging industry for attaching labels, or for various applications in households. Many more examples could be listed. The adhesive bonding technology offers a lot of advantages over other more conventional joining methods.

Because one finds so many examples where the performance of the final product relies much on the performance of the adhesive bond, like in glued car bodies, the process of preparation before the application of the adhesives contributes a lot to the final quality of the bond.

Failure in mixing or in metering, as well as in dispensing, can result in a disastrous performance of the adhesive bond during usage. Each step of the described process chain needs a careful preparation and execution. The people who are working either in the developing or in the manufacturing stage of the adhesive bonding process or are applying the adhesives should be trained how to correctly use the material and how to prepare the substrates to achieve the best initial and long-term bonding performance. The precautions which should be taken to work safely should be well understood.

## References

- Alhofen B (2005) Get into the thick things. [www.chemicalprocessing.com](http://www.chemicalprocessing.com)
- Angos C (2007) Vacuum mixing. [www.processingmagazine.com](http://www.processingmagazine.com)
- Bienak D (2009) Preparing polymeric substrates for bonding. [www.reinforcedplastics.com](http://www.reinforcedplastics.com)
- Dettner HW (1991) Pocket dictionary for metal surface treatment. Leuze Verlag, D-7968 Saulgau
- Gehmecker H (1994) Chrome free pre-treatment of magnesium parts. In: 51st world conference on magnesium
- Habenicht G (1990) Kleben. Springer-Verlag Berlin Heidelberg
- Houwink R (1967) Adhesion and Adhesives, Elsevier Science & Technology, Oxford, United Kingdom
- Korane KJ (2000) Guidelines for bonding plastics, machine design. <http://www.machinedesign.com/adhesives/guidelines-bonding-plastics>
- Lees WA (1997) Adhesives in engineering design. Springer GmbH, Berlin
- Lutz A (2009) Crash-resistant two-component adhesives for repairs, adhesion adhesives & sealants. Adhäsion Kleben & Dichten, Springer Fachmedien Wiesbaden
- Lutz A, Brändli C (2010) Optimal haftend, temperaturstabil und länger lagerfähig, adhesion adhesives & sealants. Adhäsion Kleben & Dichten, Springer Fachmedien Wiesbaden
- Metals handbook (1982) 9th edn, vol 5, Surface cleaning, finishing and coating, ASM
- National Research Council (1976) Structural adhesives with emphasis on aerospace applications. Dekker. Adhesion and Adhesives, Elsevier Science & Technology, Oxford, United Kingdom
- Satriana J (1974) Hot melt adhesives: manufacture and applications. Noyes Data Corporation. Adhesion and Adhesives, Elsevier Science & Technology, Oxford, United Kingdom
- Skar JI Albright D (2002) Emerging trends in corrosion protection of magnesium die castings. Magnesium Technology., Springer, Cham pp. 585–591
- Symietz D, Lutz A (2007) Structural bonding in automotive manufacturing. Verlag moderne Industrie Verlag Moderne Industrie, Die Bibliothek der Technik, D-80992, Munich, Germany
- Symietz D, Lutz A (5/2008) Strukturkleben von hochfestem Stahl, leightweightdesign. Vieweg +Teubner Verlag, Germany

Manfred Peschka

**Contents**

38.1	Introduction .....	1092
38.2	Manual Processing .....	1092
38.3	General Design of a Metering and Mixing Machine .....	1093
38.4	Components Required for the Machine-Processing of Adhesives .....	1094
38.4.1	Drum Presses (RAM) .....	1095
38.4.2	Pressure Containers .....	1095
38.4.3	Pumps .....	1095
38.4.4	Valves .....	1099
38.4.5	Mixing Devices .....	1102
38.5	Computational Fluid Dynamics (CFD) as a Tool for the Further Development of Metering Components .....	1104
38.6	Automation and Robotics .....	1106
38.6.1	Prerequisites for Automating Adhesive Application .....	1106
38.6.2	Parameters Affecting Accuracy and Methods of Compensation .....	1106
38.6.3	Dosing Accuracy (Dynamic Behavior of a Two-Component Metering and Mixing Machine) .....	1108
38.7	Interface Between the Robot Control and Metering Control .....	1113
38.7.1	Accelerated Curing .....	1113
38.7.2	UV-Radiation .....	1113
38.7.3	Induction .....	1114
38.8	Conclusions .....	1115
	References .....	1116

**Abstract**

This chapter describes the equipment required for manual adhesive bonding processes. For some readers, the comments about equipment may seem trivial,

M. Peschka (✉)  
Fraunhofer Institute, Bremen, Germany  
e-mail: [manfred.peschka@purenum.de](mailto:manfred.peschka@purenum.de)

but they are important as nonobservance of these points can in practice lead to flawed bonded joints.

The individual components which make up mixing and dosing systems have been described and their special features outlined in an attempt to quantify the hitherto qualitative descriptions that have prevailed in the literature.

Thereafter, some basics of automation and robotics are outlined with a special excursion on the topic parameters affecting accuracy. Terminal opportunities of accelerated curing are explained using the examples of UV radiation and inductive heating.

---

## 38.1 Introduction

The equipment required for manual adhesive bonding processes will first of all be described. For some readers the comments about equipment may seem trivial, but they are important. This is because nonobservance of these points can in practice lead to flawed bonded joints.

The individual components which make up mixing and dosing systems will then be described and their special features outlined. This is an attempt to quantify the hitherto qualitative descriptions that have prevailed in the literature.

Thereafter some basics of automation and robotics are outlined with a special excursion on the topic parameters affecting accuracy.

Finally the opportunities of accelerated curing are explained using the examples of UV radiation and inductive heating.

---

## 38.2 Manual Processing

The properties of a bonded joint are created during a production process. Chemical reactions convert the starting materials (monomers, prepolymers) into a cured adhesive film. The adhesion to the substrates and the cohesion can, however, easily be inadvertently influenced. This is the reason why a bonding process must be strictly carried out in accordance with prespecified conditions. In practice, the individual workers are a significant variable, and this is a further reason why industrial bonding processes are being increasingly automated. The manual processing of adhesive systems therefore puts very high requirements on the persons undertaking the work and on their understanding of adhesive bonding processes.

Not least for this reason, a group of experts under leadership of Fraunhofer IFAM developed a series of training courses for training personnel in all aspects of adhesive bonding. These courses have been accredited Europewide and successfully running for more than 10 years. Three course levels are offered, reflecting the differing responsibilities of the relevant personnel:



- European Adhesive Bonder (course duration: 1 week)
- European Adhesive Specialist (course duration: 3 × 1 week)
- European Adhesive Engineer (course duration: 8 × 1 week)

The courses conclude with an examination before an independent examination committee. Successful completion of a course ensures the participants are able to effectively apply adhesive bonding technology in their work area. All persons who are involved in adhesive bonding technology are highly recommended to take the relevant training courses.

In order to be able to keep the workplace clean, it is sensible to work on a base mat made of strong paper or foil. This can be disposed of after completing the work, meaning that a clean workplace is once again available for the next bonding task.

Before starting the actual bonding work, all the required auxiliary processing materials including cleaning agents should be gathered together. In order to weigh out the components of a two-component adhesive, a suitable balance must be used. The resolution of the balance must be an order of magnitude higher than the required accuracy of the weighing. It must be ensured that the balance is horizontally positioned.

Beakers that are used for mixing components must have smooth edges and be resistant to the adhesives and cleaning agents. Experience has shown that Polypropylene beakers are ideal. Spatulas made of high-grade steel are particularly good for mixing. When mixing, ensure that material on the edge and base of the beaker is constantly included in the mixing process. A mixture is homogenous when it has a uniform color and there are no streaks.

Cartridge guns are suitable for applying one-component adhesives. These guns can be mechanically or pneumatically operated. Similar cartridge guns are available for processing 2-C adhesives which are packaged in special twin cartridges. In combination with static mixers, this means that possible faults due to an incorrect mixing ratio and inhomogeneous mixing are avoided.

The following equipment is required to monitor the ambient conditions and time:

Thermometer  
Hygrometer  
Laboratory clock

---

### 38.3 General Design of a Metering and Mixing Machine

The machine-processing of adhesives involves a number of different tasks:

- Maintaining a stock of adhesive (or the components).
- Removal of the adhesive (or components) from a storage container.
- Transporting the adhesive (or the components).

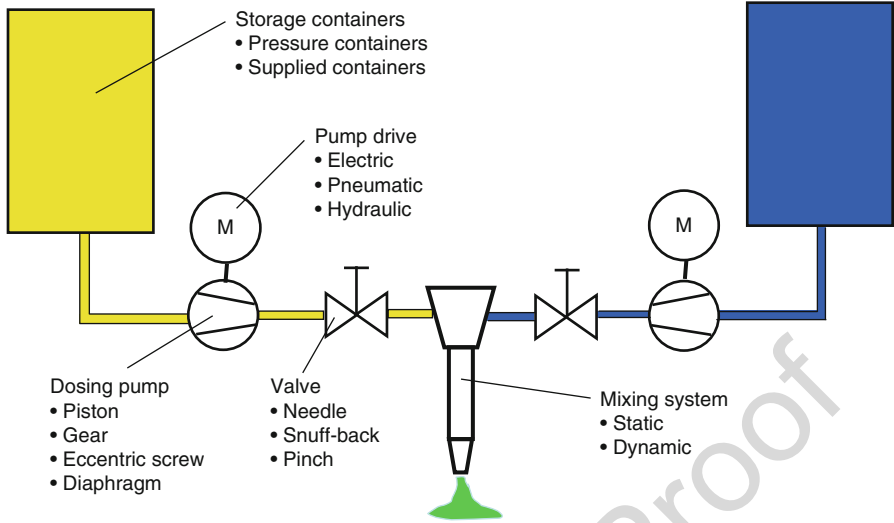


**Fig. 1** 2-C dosing system (schematic representation)

- Dosing the adhesive (or the components).
- Mixing the adhesive – if the adhesive consists of several components.
- Applying the adhesive.

The word “dosing” here has different meanings. Sometimes it refers to the measuring out of quantities of the two components to get the correct mixing ratio, other times it refers to the measuring out of the total quantity of adhesive to be applied. To avoid ambiguity, a proposal is made here: Dosing will be used to refer to the measuring out of the components (2-C) prior to mixing. Applying is used to refer to the application of the correct amount of adhesive to the substrate.

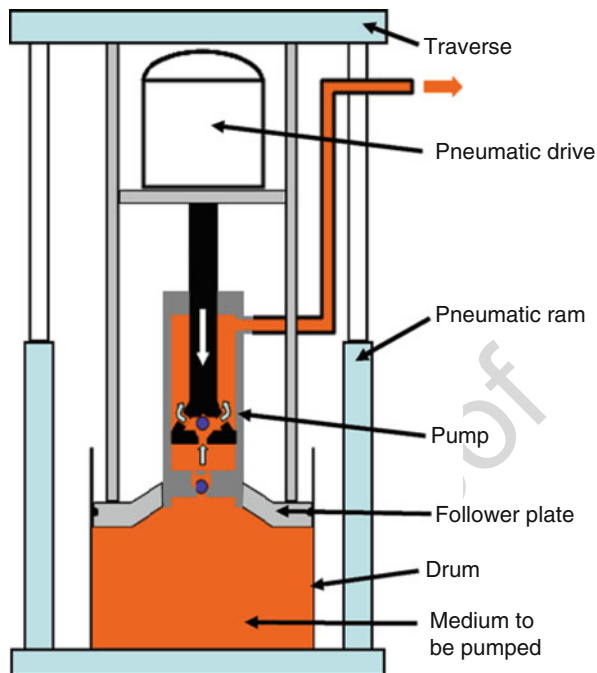
The simplest conceivable machine dosing system consists of a storage container under a defined pressure. When an opening is released, the adhesive flows, and the flow rate depends on the viscosity of the adhesive and the geometry of the opening (diameter and length). This type of application system is often used for micro-production, whereby defined pressure impulses are passed to a cartridge using a pressure/time controlled unit.

Additional components such as pumps and valves are necessary when applying larger volumes of adhesive. The following figure shows the schematic representation of a dosing and mixing system (Fig. 1).

### 38.4 Components Required for the Machine-Processing of Adhesives

This section attempts to specify the features of the various machine components. In some cases, however, the indicated ranges are exceeded.

**Fig. 2** Fundamental structure of a RAM



#### 38.4.1 Drum Presses (RAM)

The adhesive is compressed using a drum follower plate. Via a telescope frame, pressure can be exerted on the surface of the adhesive by the follower plate, so that the adhesive flows into the center to the pump.

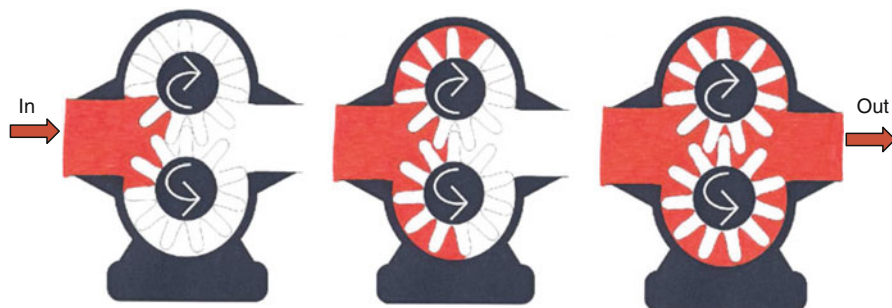
The plate is pressed against the surface of the adhesive. In the car manufacturing industry, and indeed anywhere where uninterrupted production must be guaranteed, the feed containers are present in duplicate. When a storage container becomes empty, the second container is automatically brought into operation. Whilst the production continues, the empty container can be changed (Fig. 2).

#### 38.4.2 Pressure Containers

These can also act as intermediate containers to allow uninterrupted operation of the plant. If equipped with a riser pressure, containers cover the original barrel ensuring a contamination-free operation. They are not suitable for all viscosities.

#### 38.4.3 Pumps

Pumps are required for transporting the adhesives or their components over large distances (= feed pumps) and for exact volumetric dosing (= dosing pumps). In this section, the key features of different types of pumps will be outlined.



- There must always be pressure on the inlet side(!), *not* self-priming
- Virtually pulsation-free adhesive metering
- Permanent metering
- Use of filler-containing adhesives possible (Mohs' hardness < 5!)
- Operating pressure up to max. 100 bar
- Metering output proportional to the drive speed
- Heatable systems available
- Viscosities: low( $\approx 10_1$  mPas) to high ( $\approx 10^5$  mPas)
- Slip increases with duration of use, not detectable from outside

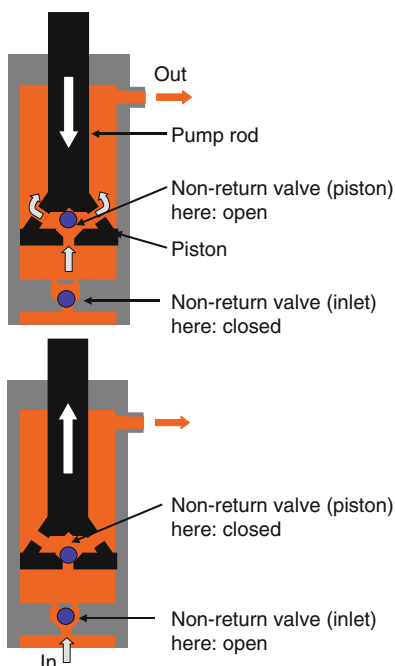
**Fig. 3** Gear pump – design, function, and characteristics

### 143 Gear Pumps

144 This type of pump is also used in many other technical areas. It transports a fluid by  
 145 creating defined partial volumes between the sled wall and one tooth respectively of  
 146 the two gear wheels. The rotation of the gears carries these partial volumes from the  
 147 intake side to the discharge side. Gear pumps are used as both feed pumps and  
 148 dosing pumps. They are usually driven by an electric motor. As the speed of an  
 149 electric drive can be very easily controlled, very precise dosing is possible using gear  
 150 pumps. The features are summarized in Fig. 3.

### 151 Double Acting Piston Pumps

152 These pumps are often used for processing highly viscous adhesives. The design of a  
 153 twin piston pump is schematically shown in Fig. 4. The special feature of a twin  
 154 piston pump is that it transports materials in both movement directions. This is  
 155 achieved due to the fact that the two chambers, which are separated by the piston, are  
 156 kept in phase with each other by a nonreturn valve, and the cross-section of the lower  
 157 chamber is twice as large as the cross-section of the upper chamber. When the pump  
 158 is at the bottom dead center, both nonreturn valves close (= piston valve and foot  
 159 valve). If the piston now moves upwards, the foot valve opens and the lower  
 160 chamber is filled. Simultaneously, the adhesive in the upper chamber is transported  
 161 via the outlet into the connected pipe system. After reaching the top dead center and  
 162 reversal of movement of the piston, the piston valve opens and the foot valve closes.



- Self-priming
- Slight pressure lost on movement reversal (ca. 5–10%)
- Permanent metering
- Abrasive filler-containing adhesives can be processed (Mohs' hardness >5)
- Operating pressure up to 400 bar
- Metering proportional to the speed of the piston
- Heatable systems available
- Viscosity range: ca.  $10^1$ – $10^6$  mPas
- Wear cannot be detected from outside in every case

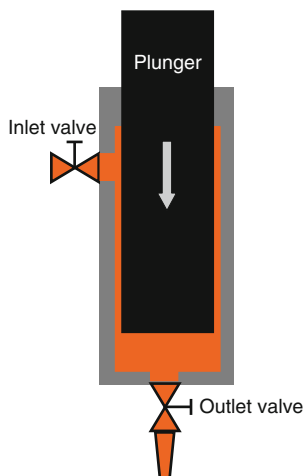
**Fig. 4** Double acting piston pump – design, function, and characteristics

The upwards movement of the piston forces the volume of adhesive from the lower chamber into the upper chamber. As the cross-section of the upper chamber is only half that of the lower chamber, not only the upper chamber is filled but the excess adhesive is transported via the outlet into the pipe system. At the moment of reversal of movement at the dead centers of the piston pump, there are short periods of lower pressure at the outlet, which is due to the switching time of the nonreturn valves.

These pumps are used as both feed pumps and dosing pumps. The drive system in most cases is pneumatic. Hydraulic drive systems are used when there are very demanding requirements. When used as a dosing pump, it must be remembered that the fleeting low pressure at the points of reversal is accompanied by a decrease in the applied quantity. The accuracy of gear pumps cannot be achieved.

### Single Acting Piston Pumps

These pumps are used as very accurate dosing pumps for high viscosity and/or abrasive adhesives (adhesives with abrasive fillers). The design and operation are explained in Fig. 5. When the inlet valve opens, the pump is filled due to the pressure to which the material is exposed. On reaching the top dead center, the inlet valve closes and the piston is moved until the desired dosing pressure is reached. The opening of the outlet valve starts the application process, which must be completed before the bottom dead center is reached. Before starting the next application process, the pump has to be filled again. The drive is pneumatic when the accuracy



- Self-priming
- Pulsation-free metering
- Limited metering volume
- Abrasive filler-containing adhesives can be processed (Mohs' hardness >5)
- Operating pressure up to 400 bar
- Metering proportional to the speed of the plunger
- Heatable systems available
- Viscosity range: ca.  $10^1$ – $10^6$  mPas
- Wear can be detected from outside

**Fig. 5** Single acting piston pump – design, function, and characteristics

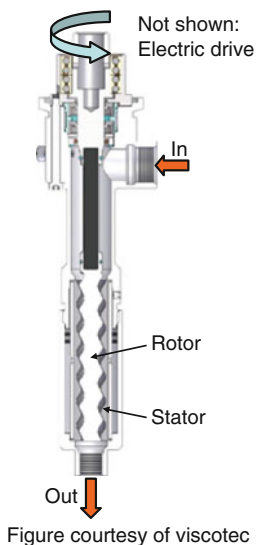
requirements are low. For higher accuracy applications, hydraulic or electric drives are used. Since about 2005, electric drive systems, with a three-phase servo motor and a recirculating ball screw, have rapidly driven hydraulic drives out of the marketplace. Their advantages are their cleanliness (no droplets of hydraulic oil!) and favorable cost. Electric drives are available as standard modules. Single action piston pumps are the standard for chassis production (body in white).

### Eccentric Screw Pumps

These pumps are widely used for dispensing a wide variety of chemical and food media. They have been used for applying adhesives since the start of the third century AD. The design and operation are explained in Fig. 6. The advantage of these pumps is that they can be operated without valves. Defined partial volumes form between the rotor and stator, and these are transported along the axis of the rotor by rotation. At the end of the adhesive application, a short reversal of the rotor promotes breaking of the adhesive thread. These pumps are driven by electric motors. When operating these pumps, special attention must be paid to a number of points:

- If possible, the first filling of the pump should be undertaken manually. Dry running of the rotor destroys the stator.
- When cleaning the pump, ensure that the solvent being used for the cleaning is compatible with the material from which the stator is made. Depending on the application, the manufacturers provide stators made of different elastomers.

The simple mechanical design and the relatively small pressure loss when pumping highly viscous adhesives mean that these pumps are particularly attractive for highly integrated production lines.



- Self priming
- Pulsation-free metering
- Permanent metering
- Abrasive filler-containing adhesives can be processed (Mohs' hardness >5)
- Operating pressure up to 100 bar
- Metering proportional to the drive speed
- Viscosity range: ca.  $10^1$ – $10^6$  mPas
- Wear can not be detected from outside

**Fig. 6** Eccentric screw pump – design, function, and characteristics

## Other Types of Pumps

In addition to the pump types which have been mentioned, other pumps are also used for transporting and dosing adhesives for special areas of application. Only brief mention of these pumps is therefore appropriate here.

Diaphragm pumps are mainly used as feed pumps for low-viscosity and medium-viscosity adhesives. In these pumps, the pump chamber is defined by a diaphragm. The fluid is transported via two nonreturn valves, which act as input and output valves, and the oscillating motion of the diaphragm.

Peristaltic pumps are usually used for process engineering applications. These pumps are occasionally used in cases where small amounts of low-viscosity adhesives have to be applied. The flexible tube is pinched by cams or rollers and the adhesive therein becomes trapped ("occluded"). Due to the rotation of the cams or rollers, the adhesive is transported from the inlet to the outlet of the pump. The benefit of peristaltic pumps is that the actual pump mechanism does not come into contact with the medium being pumped.

### 38.4.4 Valves

Valves are used to control the flow of an adhesive in a pipe system. They are present as inlet and outlet valves on pumps. Application valves are often the last component of the adhesive delivery section.

#### Needle valves

This type of valve is by far the most common type of valve in use. A circular valve seat is closed by a suitable valve needle (Fig. 7). By movement of the valve needle in

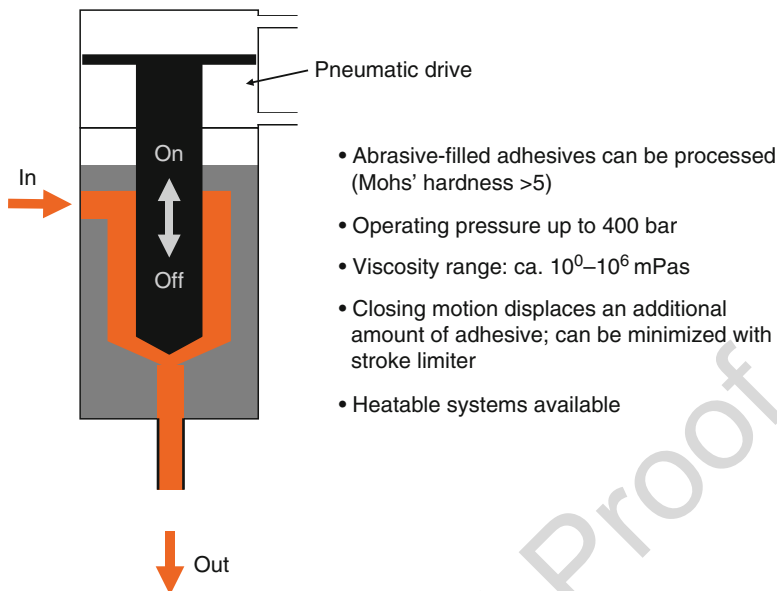


**Fig. 7** Needle valve – design, function, and characteristics

the direction of the longitudinal axis, the cross-section of the valve seat is opened and the adhesive is able to flow. The drive for the opening and closing movement can be pneumatic, pneumatic/spring force, hydraulic, or electromagnetic. Depending on the nature of the adhesive being processed (viscosity, fillers) and the boundary conditions for the process (pressure, temperature), there is a wide choice of cross-sectional area and materials (elastomers or hard metal) for the valve seat.

### Snuff-Back Valve

The kinematics of the opening and closing motion of a snuff-back valve is precisely the reverse of that of a needle seat valve (Fig. 8). To open the valve the piston is moved forward and this opens the valve cross-section. To close the valve, the piston is retracted until the free cross-section of the valve seat is closed. This generates a slight vacuum in the outlet needle, allowing effective thread break of the adhesive at the end of the application. The sealing of the valve on the outer surface of a cylinder is more technically demanding than sealing a needle seat. The pressure region in which absolute sealing can be guaranteed is therefore limited. In industrial practice this type of valve is only used in a few very special applications.

### Pinch Valve

Pinch valves are used for low-viscosity adhesives which are processed in the pressure range up to 10 bar (Fig. 9). The tube cross-section is pinched in such a way by a pneumatically driven lever that the flow of adhesive is stopped. The



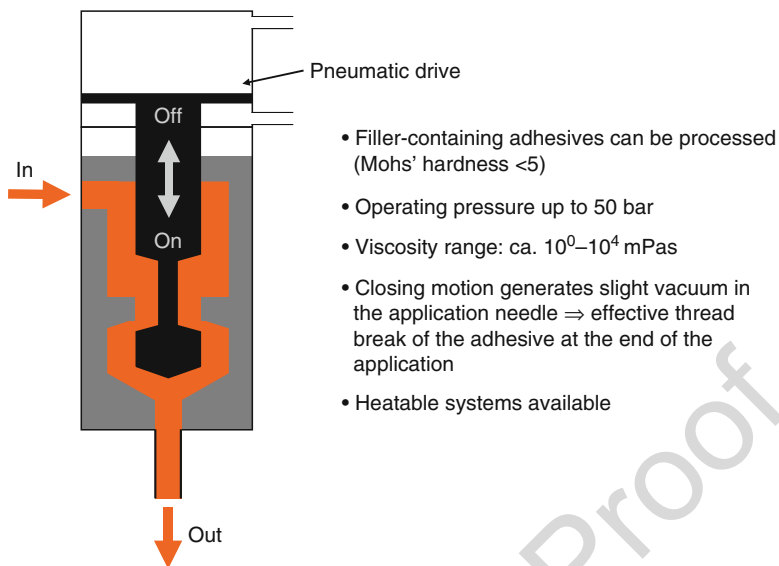


**Fig. 8** Snuff-back valve – design, function, and characteristics

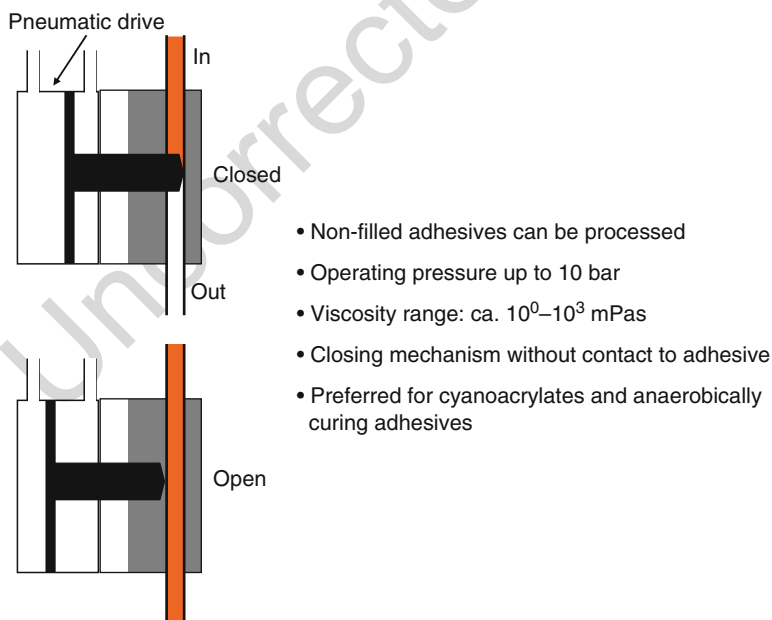


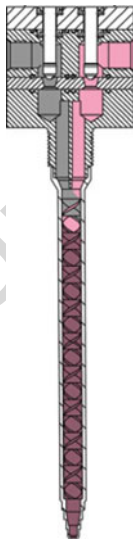
**Fig. 9** Pinch valve – design, function, and characteristics

248 advantage is that the actual valve mechanism does not come into contact with the  
 249 adhesive. This type of valve is preferred for processing anaerobically curing adhe-  
 250 sives and cyanoacrylates.

### 251 38.4.5 Mixing Devices

#### 252 Static Mixing Devices

253 A static mixer consists of a smooth-walled tube which contains an arrangement  
 254 of elements for customized routing of the flow (Fig. 10). The name indicates that  
 255 the individual elements of the mixer do not move but are static in the mixing  
 256 tube. The energy required for the mixing is extracted from the flow energy. The  
 257 most familiar type of static mixer is the Kenics mixer which was developed back  
 258 in the 1970s. Right-handed and left-handed mixing elements split the flow of  
 259 adhesive and ensure a doubling of the number of layers at each mixing element.  
 260 The number of layers is given by  $2^n$ , where  $n$  is the number of mixing elements.  
 261 At the end of the mixing tube, layers can no longer be detected, namely, the  
 262 mixture is homogenous. There are a large number of different designs (number  
 263 of mixing elements and diameter of the mixing tube) for different mixing tasks.  
 264 When commissioning a new dosing and mixing plant, an important task is to  
 265 determine which mixer gives satisfactory results. The smallest possible mixer  
 266 which gives a homogenous mixture is chosen here, in order to minimize the



- Fixed mixing elements in the tube => “static” mixer
- Mixing energy is removed from the flow
- Alternating clockwise and anticlockwise mixing elements split the flow of adhesive into layers until it is homogenous
- Number of layers:  $2^n$  ( $n$  –number of mixing elements)
- For poorly miscible adhesive components, the process of introducing the two components into the mixer has increased importance
- Favorable-cost mixer, maintenance-free
- Cannot be adjusted
- Many variants and sizes for adapting to the mixing task
- Mixing ratio range: ca 100:100 ... 100:3
- Viscosity differences of the components up to ca. 10

Figure courtesy of Nordson EFD

**Fig. 10** Static mixing device – design, function, and characteristics

volume of waste. Static mixers are normally not rinsed and are discarded at the end of a production run.

It is claimed in the literature that static mixers can only be used for mixing ratios of the order of 1:1 and for components having similar viscosities. In practice, this has long been disproved. Adhesives with mixing ratios of 10:1 and with a similarly large difference in the viscosities of the components have been successfully mixed, demonstrating the effectiveness of static mixers.

### Dynamic Mixing Devices

A dynamic mixer automates the process of manual mixing in a beaker (Fig. 11). The adhesive components are introduced into the mixing chamber in the correct mixing ratio. An externally driven mixing element mixes the two components until they are homogenous at the outlet nozzle. The name indicates that a moving (rotating) mixing element is used for the mixing process. The energy required for mixing is supplied from outside. Depending on the operating conditions, this leads to a temperature increase in the adhesive and a concomitant decrease in the pot life. There is a vast array of different sizes and designs available for different applications. When starting up the system, the speed of the mixing element is increased until the components are homogeneously mixed. A further increase in the speed does not improve the homogeneity of the mixture. Moreover, the increased energy input unnecessarily shortens the pot life. A dynamic mixer must also be rinsed at intervals during the ongoing production, in order to prevent closing of the outlet opening. This produces

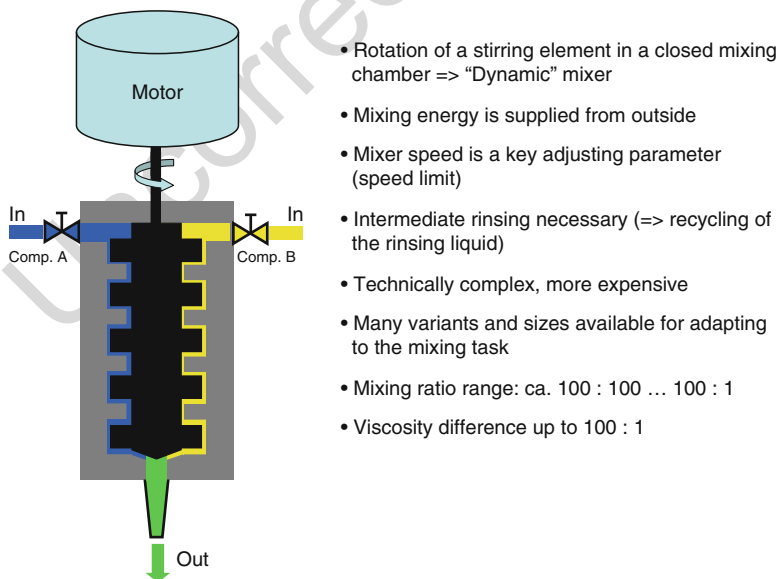


**Fig. 11** Dynamic mixing device – design, function, and characteristics

hazardous waste which must be disposed of accordingly. The limits on the mixing ratio which can be processed and the viscosity differences between the adhesive components are broader than for static mixers.

---

## **38.5 Computational Fluid Dynamics (CFD) as a Tool for the Further Development of Metering Components**

Starting in the 1960s, industrial adhesive bonding technology began to switch over from purely manual processing to machine processing. The current state of technology today has largely developed in an empirical way. Dosing technology and the adhesives themselves have largely developed during the past 50 years. On reflection it is clear that:

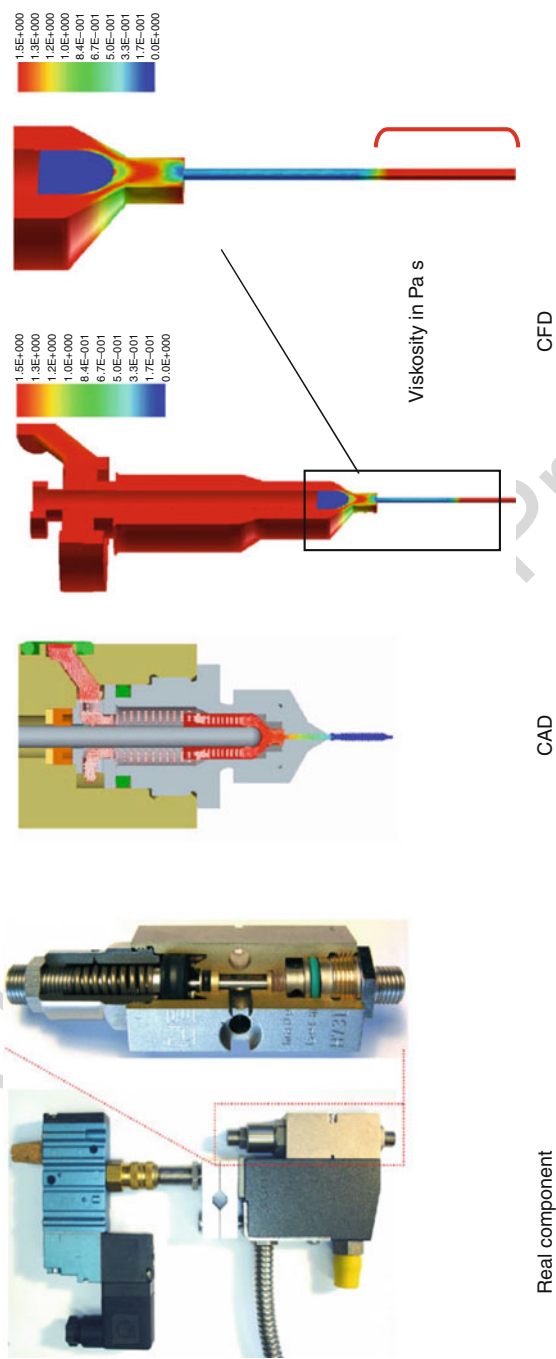
- The complexity of adhesives has continuously increased. The formulations are composed of an increasing number of individual substances, and this is placing ever high requirements on the dosing technology.
- It is also evident that industrial processes are becoming shorter, with an increased degree of automation.

Both these trends will probably continue in the future, meaning that an understanding of the interplay between the adhesives and the processing machinery is absolutely vital. The challenges involved here can no longer be solved using empirical approaches. Accurate analysis of the flow conditions inside dosing machinery and customization of the rheological properties for special plant components will determine whether a system (adhesive plus processing plant) can be operated in an effective way.

One tool that can help solve these challenges is to employ Computational Fluid Dynamics simulation. This gives an insight into the inside of dosing and mixing plants. The processes involved can be studied in quasi slow motion and this provides valuable information about the various flow anomalies which are constantly observed in practice.

The underlying Finite Volume Method divides the system geometry into small (linked) partial volumes of the same magnitude analogue to the well-known finite elements in CAD (Computer Aided Design). The differential equations that describe the flow are converted in this way into difference equations (integrals to be summed). These can then be solved as a linear equation system using a high-performance Solver. If this calculation is repeated for each time step, the result is a description of the time-dependent transient flow.

Figure 12 shows, by way of example, the inside of a needle valve which is commonly used as an application valve for hot melts. As the flow channel is rotation-symmetric, it suffices to consider half the cross-section in order to describe the flow.



Figures courtesy of UES AG

Fig. 12 Needle valve – cross section and visualization of the flow

## **38.6 Automation and Robotics**

### **38.6.1 Prerequisites for Automating Adhesive Application**

When an adhesive is manually processed and manually applied, there is a control system with closed loop between the dosing and mixing plant on the one hand and the worker on the other hand. The speed with which the worker moves the application nozzle across the workpiece determines, together with the machine settings, the cross-section of the applied adhesive bead. Small machine deviations are recognized by the worker automatically and are unconsciously corrected. This control system with closed loop is absent if the application of the adhesive is also automated. An automatic moving system solely travels a programmed distance at a programmed speed. Inaccuracies of the dosing and mixing plant are not automatically corrected. The moving system does not recognize these errors. In order for the desired results to be achieved with automatic application, a number of measures must therefore be taken:

- The accuracy of the dosing and mixing plant must be adapted to the requirements of the automatic application (in most cases the accuracy must be increased).
- The control system of the dosing plant must contain control loops that allow monitoring of the dosing and mixing processes, so that the control system recognizes deviations from the set value and can identify these as errors.
- The control systems of the dosing and mixing plant and the robotic system must communicate with each other via an interface.

A further consideration is what variant is most suitable for the planned production:

1. The robot moves the adhesive nozzle across a stationary component.
2. The robot moves the component across a stationary nozzle.

In the second case, the robot can also join the component after the adhesive application. It must be noted that this type of production has longer cycle times than application with a moving nozzle. Certainly, the number of robots and handling robots is lower. This is ultimately a question of economics, which should be clarified at an early stage of the project.

### **38.6.2 Parameters Affecting Accuracy and Methods of Compensation**

In order to discuss the factors which affect the dosing accuracy assume that a pneumatically driven piston dosing pump is being used. The free cross-sections of the piston dosing pump and pneumatic motor define the transmission ratio. For example a transmission ratio of 20:1, setting the air pressure at the inlet of the

pneumatic motor to 2 bar gives a material pressure in the piston dosing pump of 40 bar. This material pressure is constant in the whole system, including the downstream pipe system. If the outlet valve is now opened, there is a pressure drop across the pipe system, which to a first approximation can be calculated according to the Bernoulli's principle. For simplicity here it is assumed that the adhesive is a Newtonian fluid and that there is laminar flow. According to Bernoulli, the pressure drop for laminar tubular flow is given by:

$$\Delta p = \frac{128 \cdot l \cdot \eta \cdot Q}{\pi \cdot d^4}$$

where:

$\eta$  = viscosity of the fluid

$Q$  = volume flow rate

$l$  = length of the tube

$d$  = diameter of the tube

The viscosity is the only variable here. The viscosity in turn depends on the temperature. Independent by of the absolute viscosities of the different adhesives, the temperature-dependent change is ca. 5% per degree Celsius. For the dosing plant under consideration with a pneumatically driven piston dosing pump, this means that fluctuations in the adhesive temperature directly cause fluctuations in the discharge rate. A temperature change of 1 °C leads to a ca. 5% change in the applied amount of adhesive.

For a pneumatic drive, automatic adjustment of the compressed air supply to the accuracy demanded by a specific application requires disproportionately high complexity. In practice, a pneumatic piston dosing pump does not possess such temperature compensation. This type of plant is only used with a robot in situations where fluctuations of the application rate are not a criterion for exclusion.

For hydraulic dosing plants, the dosing pressure can be controlled very precisely via a servo valve in the hydraulic system. If the adhesive temperature is measured and if the hydraulic pressure, and hence the dosing pressure, is adapted to the measured values, then good temperature compensation for the temperature-dependent flow properties of the adhesive can be achieved.

Rotatory dosing pumps such as gear pumps or eccentric screw pumps which are electrically driven do not have the aforementioned drawbacks. The control occurs internally in the drive system. The pump size (in ccm/revolution), the transmission ratio and the individually determined slip-factor allow exact correlation between the speed of the drive and the resulting volume flow. The internal control loop of the electrical drive adjusts the set value. The control loop usually consists of an incremental counter, which monitors the speed within the work cycle (2–5 ms). If a difference between the actual increment and the set increment is recorded (contouring error), the power uptake of the motor is adjusted with the aim of no longer having a difference at the end of the next cycle (cycle time). Factors such as viscosity changes in the adhesive result in altered power uptake by the drive.

The pressure in the plant is not specified, rather it independently sets itself based on the resistance to flow.

A widely used means to improve the accuracy of dosing plants is to minimize the length of pipe between the dosing plant and the application valve. In the extreme case that means dosing plants having an application valve flanged onto its outlet. This design describes the current state of technology for manufacturing automobile bodies (body in white).

### **38.6.3 Dosing Accuracy (Dynamic Behavior of a Two-Component Metering and Mixing Machine)**

The processing of two-component (2-C) adhesives requires synchronous flow of the two components. The spotlight here generally falls on the accuracy of the dosing unit. The dosing unit is, however, only one part of a total system in which the adhesive components and their flow behavior play a major role.

The dosing process is an intermittent process. Features of this process are that the adhesive components undergo an abrupt change from a state of non-flow to a state of flow at the start of the dosing, and vice-versa at the end of the dosing process. Consistent and synchronous dosing is only possible if the two components of the adhesive have identical pressures at the point where they flow together in the processing plant. Only then will there be an even flow of the components and compliance with the prescribed mixing ratio. If this condition is not met, one of the two components will be over-dosed.

The point at which the two components flow together is not accessible experimentally. Up until now, no statements have been able to be made about how synchronous the two components flow, in particular at the start of the dosing process. It is known from the literature (Sauer 1989) that the period of time from the start of the dosing to the moment of establishment of a steady state of flow is the order of a second.

A second is a short time. However, when one considers the typical application rates of up to 400 mm/s currently used or highly dynamic processes with application times of just a few seconds then that one second becomes very significant. For this reason, detailed information is desired about the interactions between an electrically-driven – and hence high-precision – adhesive processing unit and nonlinear fluids (adhesive components), in particular at the start of the dosing.

The main difficulty in trying to evaluate the quality of the dosing unit (quality = accuracy with which the prescribed mixing ratio is complied with over the duration of the dosing process) is the lack of accessibility to take measurements. In practice the dosed components flow into a mixer at whose outlet the mixing ratio cannot be measured. Therefore the dosing unit has to be separated from the mixer. By a special designed nozzle, access to the outlet can be gained (see Fig. 13).

The specially designed nozzle allows separate application of the two components and also allows the pressures in the line system of the dosing unit to be set the same, as is the case for operation with a directly flanged mixing unit. This so ensures there



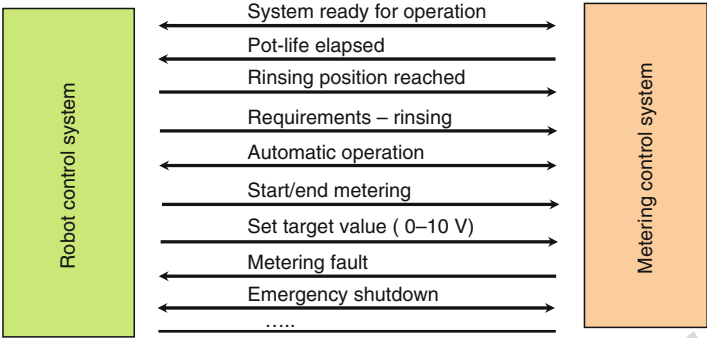


**Fig. 13** Schematic representation of the experimental access to the interface between the dosing unit and mixer

is no falsification due to different pressures between the start of the operation and taking measurements.

The measurements themselves were performed contactless using a laser scanner (see schematic representation in Fig. 14). As part of the studies to determine the suitability of the measuring equipment, the effects of various parameters were evaluated:

- Shadow;
- Undercut of the applied bead;
- Color of the adhesive components (possibly require a modified exposure time)

These preliminary studies used a cured 1-C adhesive to determine the accuracy of the measuring method using an analytical microscope. Following the contactless measurements, thin discs were taken from the adhesive bead to accurately examine the cross-section under the microscope. This showed up the following deviations:

- Effect of shadow: Not measurable
- Effect of the undercut: +0.82% ... +1.15%
- Effect of the color: –1.55% ... –2.64% (see also Fig. 15)

The effect of the undercut on the mixing ratio measurement will be smaller in practice than the individually measured values because the deviations for the two components are of the same order of magnitude and so cancel each other out. Only for mixing ratios far from 1:1 would there be an effect on the overall result, and even this would be less than 1%.

Depending on the color of the adhesive bead, its cross-section is underestimated to a differing extent. Considering, however, the practically common combination of black and white (having deviations of –2.36% and –2.64%, respectively), these



**Fig. 14** Schematic representation of the measuring method (Source: Mikro-Epsilon)

deviations cancel each other out. To achieve good measurement results with minimal scatter, different exposure times must, however, be chosen for these two colors. As such, this color combination represents a challenge because in order to determine the mixing ratio both beads (black and white) must be measured simultaneously. A compromise must be found here for the exposure time.

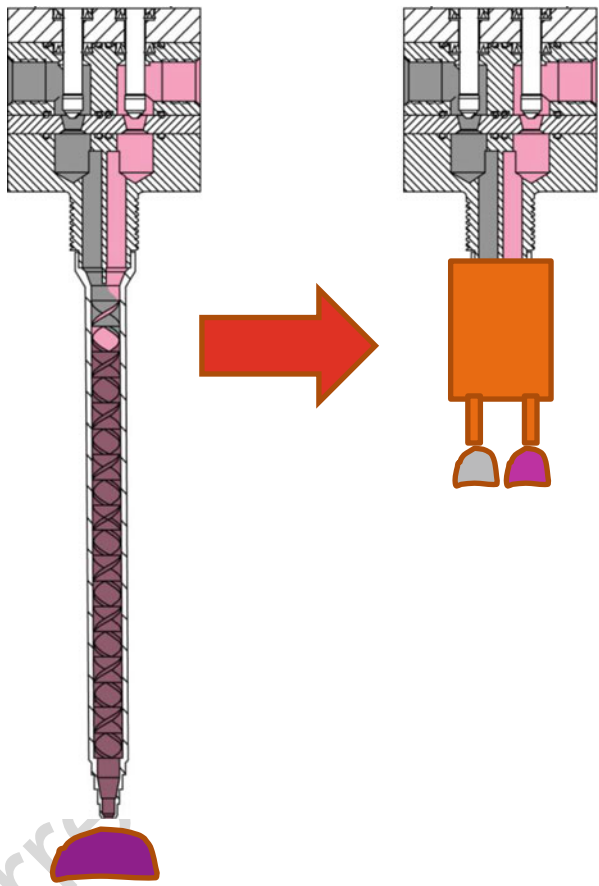
### Measurement of the Mixing Ratio

Figure 16 below shows the experimental set-up. The equipment was firmly secured on a coordinate table. The application base was moved at a constant speed below the special nozzle.

Figure 17 shows an example signal plot, with time resolution of the dynamic behavior of the two individual components compared with the machine operation.

It can be seen that after 0.1 s, the metering machine achieves steady state. There is a difference in time (delay) of 0.4 s until the components are applied. A small difference in time (delay) between the onsets of dosing of the two components is without significance. It also can be seen that a modification of the diameters of

**Fig. 15** Effect of the color of the adhesive beads on the measurement results



**Fig. 16** Schematic representation of the dosing unit for time-resolved measurement of the mixing ratio (*left*) and taking actual measurements (*right*)

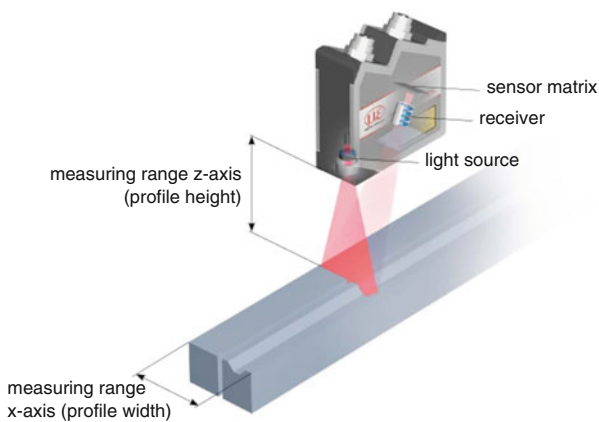




**Fig. 17** Example signal plot for adhesive flow (mixing ratio 2:1) compared with dosing pump motor operation

internal piping (3.5 mm vs. 4.5 mm) in this case has no influence on components flow. After ca. 0.35 s, a steady state of flow is established for component B. Steady state of flow (component A) is established after ca. 0.9 s. This means that the prescribed mixed ratio is established ca. 0.9 s after the start of application and ca. 1.3 s after start of dosing.

A very interesting aspect can be seen as well: While preparing the test the calibration of the metering pumps was not performed properly. This led to an improper function of pump A delivering ca. 20% less than required. Without the new measuring method this mistake would not be able to detect!

Further detailed measurements using different adhesives have resulted in the following findings:

- The non-steady state at the start of the dosing (= a state in which the mixing ratio lies outside the range prescribed by the adhesive manufacturer) can last up to 1.3 s.
- The duration of the non-steady state is largely determined by the differing flow behavior of the two adhesive components.

The overall system can be optimized by having detailed knowledge of that system, which comprises the processing units and adhesive components. The differing flow behavior of the adhesive components can be compensated by controlling the dosing unit. The signal plot provides accurate data about the required delay of the dosing pumps in order to guarantee synchronous dosing of the two components. The acceleration rates to achieve the prescribed mixing ratio were realized by altering the acceleration of the drive motors such that there was equivalent acceleration of the two components.

The new measuring method has a number of different uses:

- Verification of a dosing rate agreed between an equipment manufacturer and user
- Identification of the causes of production faults
- Development of customized dosing technology and specific adaptation of an overall system

**38.7 Interface Between the Robot Control and Metering Control**

An interface allows communication between the control systems of the mixing and dosing plant and the robot. The exchange of signals replaces the person-machine control loop for manual application. In addition to general signals such as “emergency-stop” or “automatic operation,” individual signals adapted for specific task are exchanged. An example is shown in Fig. 18. The directions of the arrows indicate the directions of the signals. For example, the signal “ready for operation” is sent in one direction: from the dosing plant control system to the robot control system. For the robot control system this means that only when this signal is received can the automatic process be started. The “emergency-stop” signal is sent in both directions. If the emergency-stop button on the dosing control is pressed, not only must the dosing plant stop immediately but also the robot. An analogous situation arises when the emergency-stop button is pressed on the robot control.

**38.7.1 Accelerated Curing**

A demand of the industrial practice is that the time for curing an adhesive should be as short as possible. But often different requirements of the complete process anticipate the use of a quick curing adhesive. For this reason, methods were developed enabling the user to handle the adhesive as long as needed and to cure within seconds or minutes after having joint the adherends.

**38.7.2 UV-Radiation**

The intensity of electromagnetic radiation increases with decreasing wavelength. High-energy, short-wave radiation in the UVA and UVB regions can excite electrons

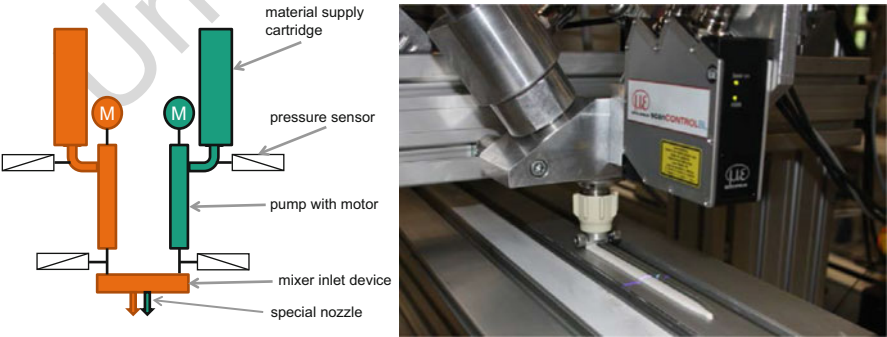


**Fig. 18** Example of an interface

in the outer shells of atoms and hence result in rapid chemical reactions. This mechanism is utilized for curing specially formulated adhesives. At least one of the two substrates must be permeable for the radiation. Note that materials which are transparent to the human eye are not necessarily permeable for UV radiation.

Curing can take place in three different ways:

*Via radicals:* UV acrylates cure via a radical reaction within seconds. The reaction is inhibited by oxygen. This means that adhesive which emanates from the joint forms a sticky surface. To avoid this, the curing can be carried out under a protective gas atmosphere. The UV absorption normally takes place in the wavelength region between 320 and 450 nm.

*Via cations:* UV epoxides cure rapidly via a cationic reaction (ca. 30–90 s). Oxygen does not inhibit the reaction. Adhesive which emanates from the joint forms a dry surface. The UV absorption is usually in the wavelength region between 320 and 450 nm.

*Dual cure:* A combination of UV curing and another curing mechanism (anaerobic, thermal, moisture-activated) is able to cure the adhesive film at points which are not accessible to the UV radiation (“shadow curing”). The UV absorption normally takes place in the wavelength region between 320 and 450 nm.

UV radiation is invisible to the human eye but can irritate and damage the eyes. There is a risk of blindness and also skin irritation (sunburn). In addition to UV radiation, UV emitters also emit a large amount of visible light. The resulting brightness can also lead to eye damage if emitters are not properly used. For this reason, UV emitters which are incorporated into industrial plants must be shielded such that no UV radiation is emitted externally. Despite this protection, safety glasses must be worn at all times when working with UV emitters. During operation, most industrial UV emitters produce a small amount of ozone. This must be removed by suitable extraction, to avoid any danger to personnel working with the equipment.

The complex measures required for UV protection were the impulse for the development of rapidly curing adhesives which do not require UV radiation. Initiators are now available which absorb in the visible region (400–560 nm). Adhesives formulated with these initiators cure under the influence of special blue light emitters.

### 38.7.3 Induction

Induction is a process in which heat is induced in electrically conducting workpieces. When a low-frequency alternating current flows through a coil (= inductor), an alternating magnetic field is produced. This induces eddy currents in ferromagnetic materials and produces magnetic hysteresis losses. The heat is generated in the component itself. The effectiveness, the transferrable energy, and the comparatively accurate temperature control are major advantages over other heating methods.

For adhesive bonding, the induction is used for indirect heating of the adhesive. The inductor must be adapted to the shape and desired temperature profile. Likewise,

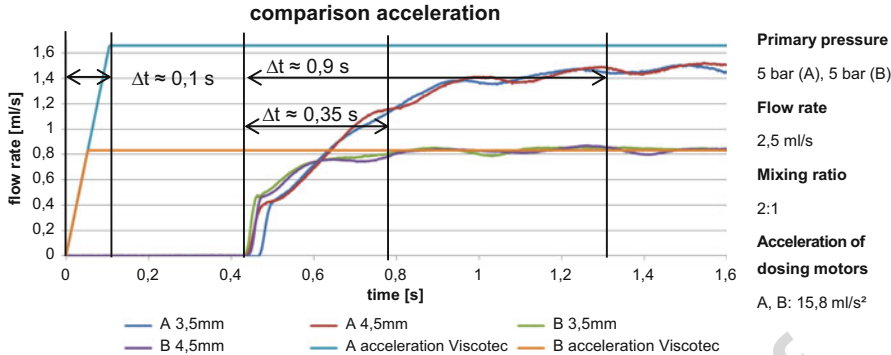


**Fig. 19** Saw blade with adhesively bonded cutting elements through induction heating

the frequency has to be adapted to the size and conductivity of the component. The reproducibility of the heating depends on the uniformity of thickness of the adhesive film, which in turn depends on the allowable variation of a component, and requires precise control of the temperature in the sensitive region for adhesive curing.

A saw blade is shown in the Fig. 19. This is used for sawing materials such as marble and granite. It consists of a steel body with sintered diamond cutting segments which are normally brazed onto the saw body. The temperatures which arise during this process cause internal stress in the saw body. After production, the saw body has considerable unevenness and it has to be straightened.

If the cutting segments are bonded rather than brazed, the joints are subjected to a maximum temperature of only 200 °C. There is much lower internal stress in the saw body and no straightening is required after production. The engineering properties, namely, the cutting performance and wear performance are equivalent for the two manufacturing methods.

### 38.8 Conclusions

A large array of auxiliary equipment is available for processing adhesives, regardless of whether that is carried out manually or automatically. To describe all such equipment in detail here would require far more space than is available in this chapter. It has therefore been attempted to describe particular pieces of equipment, such as pumps, which are widely used, covering how they function, areas of use, and also quantitative aspects. It can be stated in summary that the machine processing and the automatic application of adhesives is a highly developed technical discipline.

**Acknowledgments** The presented findings were made within ZeDeMAB. Project 18155 N ZeDeMAB (project term: 01.05.2014 – 30.04.2016) of the Forschungsvereinigung Schweißen und verwandte Verfahren e.V. of the DVS, Aachener Straße 172, 40223 Düsseldorf, was funded via the AiF under the CORNET program of the Federal Ministry of Economics and Technology following a decision by the German Parliament. We are most grateful for this financial support.

## References

- With the exception of articles in a few technical journals, little has been published about industrial adhesive bonding technology. Anyone wishing to acquire a deeper understanding of this topic is recommended to refer to the two books listed below
- Cognard P (ed) (2006) Adhesive and sealants, handbook of adhesives and sealants, vol 2. Elsevier, Amsterdam
- Endlich W (1998) Kleb- und Dichtstoffe in der modernen Technik; ein Praxishandbuch der Kleb- und Dichtstoffanwendung. Vulkan-Verlag, Essen
- Sauer J (1989) Neue Aspekte der Qualitätssicherung bei der Herstellung von Klebeverbindungen mit zweikomponentigen Klebstoffen. Heinrich Vogel Fachzeitschrift GmbH, Aachen



Ansgar van Halteren

## Contents

39.1	Introduction .....	1118
39.2	Health Protection .....	1118
39.2.1	Work Protection .....	1119
39.2.2	Consumer Protection .....	1119
39.2.3	Health Risks .....	1119
39.2.4	Health Protection When Using Adhesives: Examples of Toxicological Assessment .....	1120
39.2.5	Adhesive Selection .....	1123
39.3	Environmental Protection .....	1123
39.3.1	Air .....	1124
39.3.2	Water .....	1124
39.3.3	Soil .....	1124
39.3.4	Examples of Assessing the Environmental Impact of Adhesives .....	1125
39.4	Conclusion .....	1125
	References .....	1126

## Abstract

The handling of adhesives in a responsible way throughout their lifecycle, namely from their manufacture via the usage stage right through to recycling and disposal, is a generally recognized principle. The development and manufacture of adhesives is carried out following the principle of Responsible Care® and the subsequent rules for sustainable development defined by the International Council of Chemical Associations. This specifically means that health protection and environmental compatibility considerations are taken into account when developing and manufacturing new adhesives. This has consequences for the composition of the adhesives, the product design, the recommendations for

A. van Halteren (✉)  
 Industrieverband Klebstoffe e.V. RWI-Haus, Düsseldorf, Germany  
 e-mail: [ansgar.v.halteren@klebstoffe.com](mailto:ansgar.v.halteren@klebstoffe.com)

application of adhesives, and the purpose of use and for the recycling of bonded products after they have been used. This chapter deals with the different aspects of consumer, work, and environmental protection, including health and safety information, related to the use of adhesives in industrial and private areas.

## 39.1 Introduction

The handling of raw materials and products in a responsible way throughout their lifecycle, namely from their manufacture via the usage stage right through to recycling and disposal, is nowadays a generally recognized principle. For many years now, the development and manufacture of adhesives has been carried out following the principle of Responsible Care<sup>®</sup> and the subsequent rules for sustainable development as defined by the International Council of Chemical Associations (Fig. 1) (ICCA 2008). This specifically means that health protection and environmental compatibility considerations are taken into account when developing and manufacturing new adhesives. This has consequences for the composition of the adhesives, the product design, the recommendations for application of the adhesive and the purpose of use, and for the recycling of bonded products after they have been used.

## 39.2 Health Protection

The aim of health protection is to protect people against hazards and exposure. “Work protection” is used to describe protection in commercial and industrial work environments while “consumer protection” refers to private users.

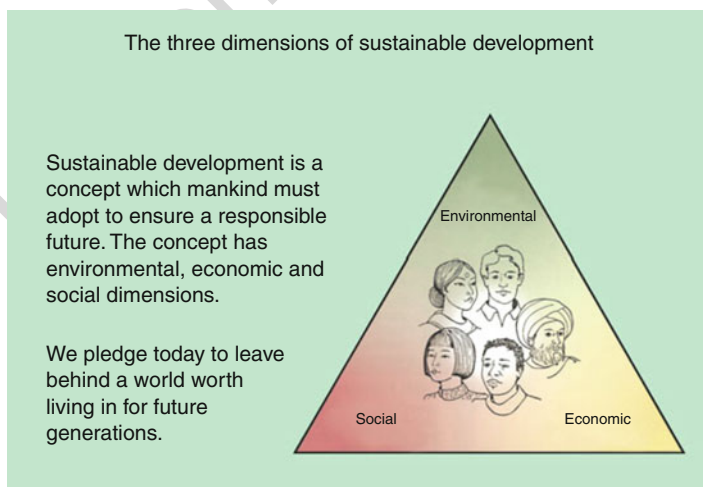


**Fig. 1** ©Industrieverband Klebstoffe e.V., Düsseldorf, Germany

### 39.2.1 Work Protection

Industrial and commercial users of adhesives require special protection because they work on a daily basis with adhesives, often for many hours a day. In addition to hazards associated with the physical properties of adhesives such as flammability, explosiveness, and burns when using hot melts, it is in particular chemical effects such as toxicity, skin irritation, acid burns, and allergies that have to be avoided. This is achieved by equipping the workplace (workplace guidelines) with air replenishment systems and local extractors, personal protection equipment such as work clothing, gloves, and safety glasses and by ensuring that hygiene regulations are adhered to, for example, thorough washing of the skin before breaks and at the end of work and refraining from eating, drinking, and smoking in the workplace. Safety officers monitor compliance with these safety measures. Personnel who work with adhesives undergo regular training on matters relating to work safety and environmental protection. If special risks are involved, then personnel undergo regular medical examinations.

### 39.2.2 Consumer Protection

Although in a professional work environment possible hazards can be efficiently managed using suitable protective measures, even in situations where there is long-term use, the situation is different for private individuals using adhesives at home where no special protective measures are taken. Different requirements are hence put on these adhesives. This is also so because private users, unlike industrial users, generally have no knowledge of the properties and potential hazards of products. That is why only relatively few of all the known types of adhesives are available to private users, and even then only small amounts are made available in the form of tubes, cartridges, and tins. On the other hand, private users do not use adhesives every day, but rather only occasionally, and even then only in limited quantities and for limited periods of time. As such, the protective measures described for industrial users are generally neither possible nor necessary. It is nevertheless essential that the safety information given on the small packages is observed, as well as basic principles of work hygiene.

### 39.2.3 Health Risks

The area of toxicology is concerned with issues relating to the effects of chemical compounds and mixtures of chemicals. Assessing the health risk is a multistep process. The first step is sound assessment of possible undesirable properties of substances based on recorded data. In the second step, the quantities of material involved and the nature and degree of any possible contact are determined. It is then investigated whether an undesired effect of a material can be caused as a result of this contact. There is no health risk for people if there is no contact with the undesired

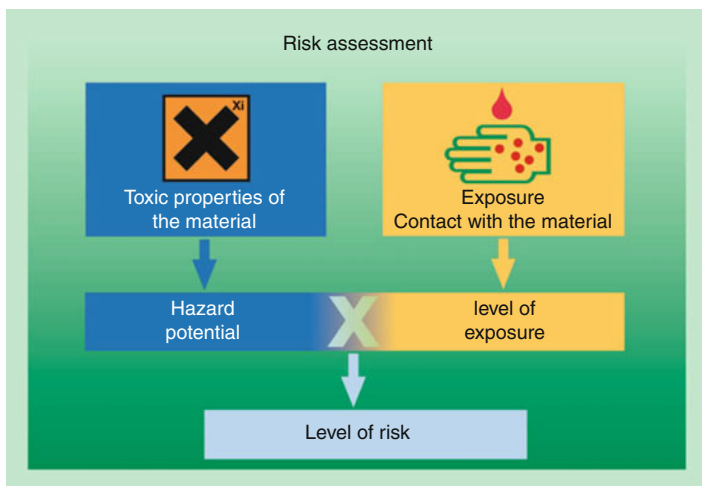


**Fig. 2** ©Industrieverband Klebstoffe e.V., Düsseldorf, Germany

material. The risk assessment determines whether and to what extent there is a health risk to people as a result of the relevant hazard potential of the substance and the nature and degree of exposure (Fig. 2). Although the exposure can for example be reduced by automated processing (e.g., robots) or by taking suitable protective measures (e.g., gloves, extraction of vapors, safety glasses, etc.), the hazard potential is a fundamental property of a substance or formulation (mixture of substances). The hazard potential generally decreases when the fraction of hazardous material present is lower. Small amounts of a hazardous substance can often be present without the product having to be accordingly labeled. The physicochemical properties of the substance, the nature and degree of exposure, and the ability of the substance to get into the body determine the relevant amount and the resulting dose that can be taken up by the body. In general, there is no undesired effect below a certain dose. The dose level determines whether and to what degree a substance can harm a person's health. The risk to human health is determined from the hazard potential of the substance and the exposure (opportunity for contact).

#### 39.2.4 Health Protection When Using Adhesives: Examples of Toxicological Assessment

Of the many different types of adhesives, those discussed below are those that are also commonly used in the household:

##### Physically Hardening Adhesives

The active components are mainly solid polymers and resins. For application these must be converted to a liquid form. This can either be carried out by users by means

of heating (hot melts) or can be carried out by adhesive manufacturers by dissolving the components in organic solvents or dispersing the components in water. The dry, fully aired adhesive is generally unreactive and biologically inert. There is hence usually no health hazard. In contrast, there is a potential health hazard from auxiliary components, such as organic solvents, that are present in some of these adhesives. These can make up as much as 80% of the weight of the adhesive product.

### **Hot Melts**

These adhesives contain largely polymers and resins and only small amounts of auxiliary materials. There is virtually never a health hazard. When applying these adhesives manually, there is the risk of burns and users must protect themselves against this. During heating, small amounts of auxiliary materials, contaminants, and cleavage products can be liberated, but these are insignificant when small amounts of adhesive are being processed. In an industrial or commercial environment, an extraction system is recommended due to the larger quantities being used and the longer working times with the adhesives.

### **Solvent Containing Adhesives (e.g., Contact Adhesives)**

In these adhesives, the polymers and resins are dissolved in organic solvents. The hazard potential is determined by the nature of the solvent (e.g., flammability, irritation potential). Due to the high volatility of the solvents, exposure by inhalation of the vapors is the biggest problem. For most solvents, the maximum concentration at the workplace and limiting factors are laid down (workplace limit value). Due to the small amounts of adhesive used by private users, these limit values are generally not reached or are only exceeded for a very short time.

### **Dispersion Adhesives (e.g., PVAc – Polyvinylacetate/Wood Adhesives)**

In the adhesives, the organic solvents are replaced by water and suitable polymers are dispersed in the water. There are hence no potential health hazards from organic solvents. However, water-based adhesives are sensitive to attack by microorganisms (e.g., mold formation). For that reason, dispersion adhesives contain small amounts of preservatives for protection purposes. The potential health hazard is the triggering of allergic skin reactions, for example, allergic reactions triggered by natural polymers such as natural rubber and non-modified colophony resins. The risk of sensitization in nonallergic people is generally extremely low due to the very small amounts of preservatives in the adhesives. Skin contact is here the exposure issue. Depending on the mode of application, skin contact may be unavoidable, as, for example, when using wallpaper pastes. However, here the concentration of preservatives is reduced as a result of mixing with water. As even wearing protective gloves for a long time can lead to skin irritation (e.g., caused by constant sweating), it is worth considering whether the very low risk of direct skin contact causing an allergic reaction justifies wearing protective gloves.

### **Pressure Sensitive Adhesives**

Private users only come into contact with these adhesives in the form of self-adhesive articles such as labels, adhesive tape, etc. As such, these adhesives represent no hazard to private users in practice. Such articles are manufactured industrially using adhesives in the form of solutions, but mostly using dispersions and melts.

### **Chemically Curing Adhesives**

The chemically reactive monomers/oligomers and hardeners and cross-linking agents determine the potential health hazard of these products. Once fully cured, the adhesive polymers are in general nonhazardous. Exposure and risk considerations hence only apply for the time period up until the adhesives have fully cured.

### **Cyanoacrylate Adhesives (Superglues)**

This group of adhesives reacts with water from the surroundings or water on the substrate. As private individuals only usually use small drops when applying the adhesive, the potential health hazard here is that if there is contact with the eyes or splashes of adhesive enter the eye then undesired bonding can take place (can gradually be dissolved using a soap solution). When being used industrially and commercially, possible irritation caused by the cyanoacrylate monomer, thermal effects, and the rapid polymerization reaction have to be taken into consideration. Increasing the humidity prevents irritation of the respiratory tract. Therefore, cyanoacrylate adhesives must be specifically labeled. When carrying out major bonding tasks, not only is it recommended to adjust the humidity of the air but also to wear safety glasses and protective gloves.

### **Silicone Adhesives**

Silicones react with water. Depending on the type of silicone, this reaction releases either acetic acid or alcohols. The acetic acid can be clearly sensed by the nose before any irritation begins. In general, the slowly released amounts are so small that they present no health risk, especially in the case of private users. Old formulations of neutral silicones that release butanone oxime must be labeled, but they are only used nowadays for special applications.

### **Epoxy Resin Adhesives**

Epoxy resins are widely used by hobbyists and in home do-it-yourself applications because of their good bonding properties, for example, for bonding glass, ceramics, or metals. This is particularly so because the supplied twin-nozzle container allows even the smallest quantities to be dispensed and then mixed. Liquid epoxies resins, and also cross-linking agents, irritate the skin and eyes and cause skin hypersensitivity. As such, hobbyists should avoid epoxy resin adhesives contacting the skin. For the industrial application of epoxy resins, safety glasses and suitable gloves must be worn. Epoxy resins having a molecular weight up to 700 are irritating to eyes and skin and they bear the potential risk of causing skin hypersensitivity. Therefore, epoxy resin systems must be labeled accordingly.

### 39.2.5 Adhesive Selection

For the private use of adhesives, there are no legal requirements. The selection of an adhesive is left largely to the experience of users and the recommendations of manufacturers. For commercial users, and in particular for industry, the selection of a suitable adhesive system for a particular application must be based on the technical requirements and the potential health hazard. In a situation where two adhesives are equally suitable, the one providing the lower potential health hazard must be chosen. If using an adhesive that does represent a potential health hazard is unavoidable for technical reasons, the exposure must be limited by taking suitable measures, which may even include automating the process, such that a risk to health is prevented. Safe working with adhesives is guaranteed by observing this regulation and the other regulations described in this section. Adhesive manufacturers provide support here by providing information in the form of technical data sheets and safety data sheets. If necessary, users should contact the adhesive manufacturers directly. As is clear from the iterations in this section, adhesive manufacturers make considerable efforts to protect the health of both private and professional users of their products. It must be mentioned here that from a quantity point of view, only a small number of adhesives have to be classified as hazardous formulations.

Private users complying with the safety instructions given on containers and industrial workers complying with relevant company regulations in their production facilities serve to protect people in accordance with the motto: “prevention is better than cure.”

## 39.3 Environmental Protection

Environmental issues have gained increasing importance over recent decades. The following is an example of a positive contribution to the environment: The car manufacturing industry uses up to 40 kg of adhesive sealants in each vehicle. The main objective of this is to save energy in the form of fuel by means of so-called “lightweight design,” whereby less weight has to be moved over the lifetime of the car and so resources are saved (e.g., 3-l car). On the other hand, the adhesives in this same example could burden the environment if there are residues left over from the application and any cleaning. At the end of the lifecycle of the car, the adhesive that was used must not adversely affect the recycling process and must be disposed of in accordance with regulations. In order to determine the effects on the environment, an environmental assessment is carried out. The expected concentration in the environment is calculated using a model. Simultaneously, the concentration at which no harm is expected to environmental organisms is determined. The calculation models and determination methods are laid down in international standards (European Chemicals Bureau 2003; European Chemicals Agency 2008). An adverse effect on or harm to the environment can be excluded with certainty if the Predicted Environmental Concentration (PEC) is less than the predicted concentration for which no

harm to environmental organisms occurs (Predicted No-Effect Concentration – PNEC), taking into account safety factors.

### 39.3.1 Air

The emission of organic solvents is detrimental to air quality. As such, considerable efforts have been made by the adhesives industry over many years to switch to low-solvent adhesives and where possible to solvent-free adhesive systems. There has been considerable success, and this has also been beneficial for health protection. Today, adhesive bonding is only responsible for less than 3% of all the solvent emissions in Europe. The few large-scale industrial applications operate with solvent-recovery systems. One typical example for a significant reduction of the use of solvent-based adhesives is the construction industry: While, for example, in Germany in 1985 the fraction of solvent-containing adhesives was still about 50%, it is in 2010 less than 10% with a still decreasing tendency. Dispersion adhesives and reactive systems have largely replaced these solvent-containing adhesives (Adhesion KLEBEN and DICHTEN 2010).

### 39.3.2 Water

With dispersion adhesives there is a particular risk of contaminating surface waters. Organic polymers and pre-polymers, although not easy to biodegrade, can be removed in biological treatment plants with the excess sludge. The use of these adhesives in handicraft work, in the home, and for DIY work normally results in only relatively small amounts of adhesive ending up in large amounts of wastewater (communal treatment works). As polymers usually have low toxicity for water organisms and due to the very low concentrations of adhesives in the wastewater, an adverse effect on the treatment plant and adjacent surface waters (outfall) is not expected in this case. In industry, residual adhesive and rinse water must be disposed of in accordance with waste legislation.

### 39.3.3 Soil

When used by private individuals, liquid adhesive residues are usually collected in the hazardous waste collection boxes, but are also often disposed of with the rest of the household waste. The amounts involved here are, however, small. For industrial and commercial users, disposal must be carried out in accordance with the so-called waste code numbers (to be found on the safety data sheets), which determine how the waste is disposed. Adhesive residues are normally disposed of as landfill or incinerated. Regarding the latter, specific contamination of the air by the incineration plants is not expected. The energy used in the manufacture of the adhesives can be partially recovered here.



### 39.3.4 Examples of Assessing the Environmental Impact of Adhesives

#### Production and Industrial Use of Adhesives

In industry, residues of cured adhesives and also non-cross-linked and liquid adhesives occur as waste. The former, as solid materials are either directly passed on as waste for disposal, or are preferably passed on for recycling. In the least favorable environmental scenario, they are disposed of as landfill. They are, however, usually recycled, either via composting or for energy recovery via incineration. Depending on how they have been treated, liquid adhesives are discharged with the wastewater and are either directly passed to a treatment plant or, if necessary, passed to a treatment plant after undergoing a specific pretreatment. There they are biodegraded or removed.

#### Do-It-Yourself/Private Use of Adhesives

Adhesives used in private household/Do-It-Yourself have to be considered in different groups:

- Solid adhesive waste from the home such as hardened paper or wood glue is usually disposed of with the rest of the household waste.
- Water is usually used to remove water-soluble, hardened adhesives in the home, for example, for removing wallpaper paste. This adhesive-containing water is disposed of with the household wastewater via the water treatment plant. The adhesive components, for example, cellulose derivatives, which are dissolved to varying extents, can easily be eliminated under real environmental conditions, meaning that only very small amounts enter the outfall (river). When composting is used for recycling, cellulose decomposes slowly but thoroughly – as known for plant materials.
- Adhesives used in the home, for example, roofing adhesives, or around the home, for example, for the car, are exposed to processes that can wash out the adhesive, for example, rain. This means that a small amount of adhesive ends up in drain water and then directly enters surface waters.

Considering all the adhesives that are in use, the expected environmental concentration (PEC) is determined. The most unfavorable scenario is assumed in order to ensure that all conceivable possibilities have been taken into account (Fig. 3).

## 39.4 Conclusion

Adhesives as a whole do not represent a major environmental problem. Nevertheless, cured and nonrecyclable residues, as well as excess adhesive from applications are waste materials. These materials not only have to be disposed of, but also represent an unnecessary use of materials and resources. The principle of recyclable design, made possible by having detachable bonded joints, will be important in the future. Besides

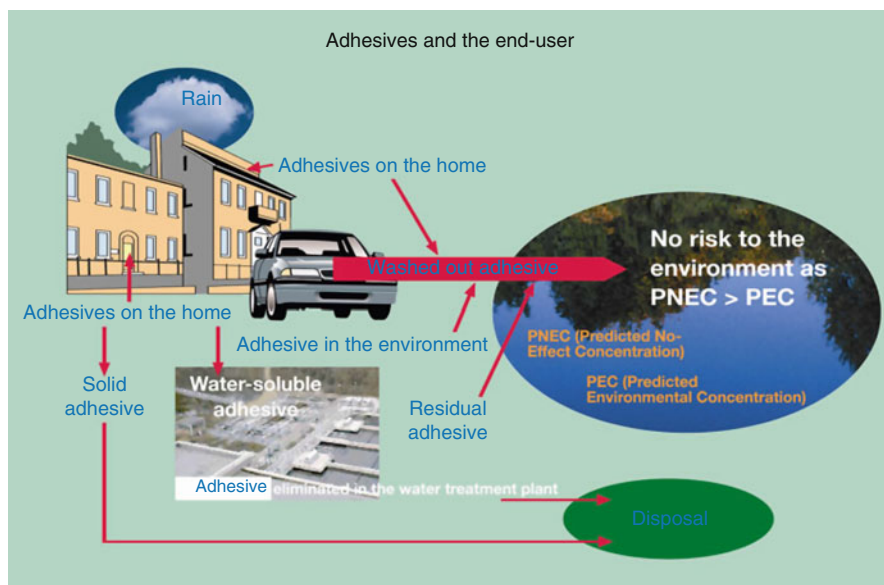


**Fig. 3** ©Industrieverband Klebstoffe e.V., Düsseldorf, Germany

technologies for separating bonded materials, a further challenge of bonding technology will be resource-friendly optimization of production and application processes. It will be necessary to incorporate non-removable adhesive into future recycling processes. This will mean that the adhesive to be used for manufacturing a component will have to be customized to the recycling process at the end of the component's lifetime.

## References

- Adhesion KLEBEN and DICHTEN (2010) Industrieverband Klebstoffe, Handbuch Klebtechnik 2010/2011, Wiesbaden
- ECB – European Chemicals Bureau (2003) Technical guidance document on risk assessment of chemical substances following European regulations and directives. European Communities, Ispra, Apr 2003
- ECHA – European Chemicals Agency (2008) Guidance on information requirements and chemical safety assessment, Helsinki, May 2008
- ICCA – International Council of Chemical Associations (2008) ICCA Responsible Care Report 2008, Brussels

Uncorrected Proof

Kazutami Wakabayashi

## Contents

40.1	Introduction .....	1130
40.2	Types and Roles of Raw Materials for Adhesives .....	1130
40.2.1	Main Components .....	1131
40.2.2	Solvents .....	1133
40.2.3	Tackifiers .....	1133
40.2.4	Plasticizers .....	1134
40.2.5	Fillers .....	1134
40.2.6	Thickeners .....	1134
40.2.7	Pigments .....	1134
40.2.8	Other Important Components .....	1134
40.2.9	Functional Components .....	1135
40.2.10	Functional Fillers .....	1138
40.3	Quality Control Procedures for Raw Materials .....	1139
40.3.1	Acceptance of Raw Materials .....	1139
40.3.2	Inspection for Acceptance .....	1140
40.3.3	Quality Control of Raw Materials in Storage .....	1143
40.3.4	Inspection for Shipment .....	1143
40.4	Material Standards .....	1145
40.4.1	Main Components .....	1146
40.4.2	Solvents .....	1146
40.4.3	Tackifiers .....	1146
40.4.4	Plasticizers .....	1147
40.4.5	Fillers .....	1147
40.4.6	Thickening Agents .....	1148
40.4.7	Pigments .....	1148
40.4.8	Other Raw Materials .....	1148
40.5	Conclusion .....	1149
	References .....	1150

K. Wakabayashi (✉)  
 APS Research Co Ltd, Osaka, Japan  
 e-mail: [k.wakabayashi.aps@jcom.home.ne.jp](mailto:k.wakabayashi.aps@jcom.home.ne.jp)

## Abstract

Since raw materials for adhesives influence the performance of final adhesive products, the selection, storage, handling, and testing of the raw materials are very important. In this chapter, types of raw materials including basic resins, hardeners, fillers, and functional additives for adhesives are firstly described. In addition, the roles of the materials are also shown. Practices for the quality control of the raw materials consisting of acceptance inspections and testing are also explained. Other tests conducted when adhesive products are shipped are explained too. These tests should be carried out following test standards. The standards for testing raw materials, and standards for materials are also mentioned in this chapter.

## 40.1 Introduction

Quality control of products can be done considering only four elements called “4M.” Adhesives are not an exception to that concept. 4M is the abbreviation of “Materials,” “Method,” “Machine,” and “Man.” Managing the four elements, the quality of products can be ensured. Another word, “5M,” which includes “Management” is sometimes used instead of 4M (Ozawa 1987).

What is the definition of “Management” in terms of quality control? Generally speaking, it can be defined as the actual conducts to carry out the whole cycle of “Plan,” “Do,” “Check,” and “Action” (PDCA) for all items. The PDCA cycle is called the Shewhart cycle or Deming cycle (Deming 2000). Note that the management of raw materials is the most important to control the quality of adhesives.

Commercial products of adhesive are varied and the number of raw materials involved in them is almost infinite. The reason to employ so many raw materials is that adhesives need special compositions to meet the different demands or conditions such as adherends, applications, conditions of use, environments, and laws such as regulation concerning the registration, evaluation, authorization, and restriction of chemicals (REACH). Figures 1 and 2 show the main composition of adhesives commercially available. Since adhesives are varied, the raw materials also vary to a great extent. In this chapter, the description is concentrated in synthesized organic adhesives which are commercially available and widely used, because this reduces the number of combinations.

## 40.2 Types and Roles of Raw Materials for Adhesives

An ordinary process of adhesion is performed as shown in Fig. 3 (see Part G). The first step of the process is application of adhesives. Every adhesive must be liquid just before the application. The liquefaction can provide fluidity to the adhesive and help it to enter the micro structure of an adherend surface. The phenomenon is called “wetting.” Methods to induce the liquefaction are as follows:

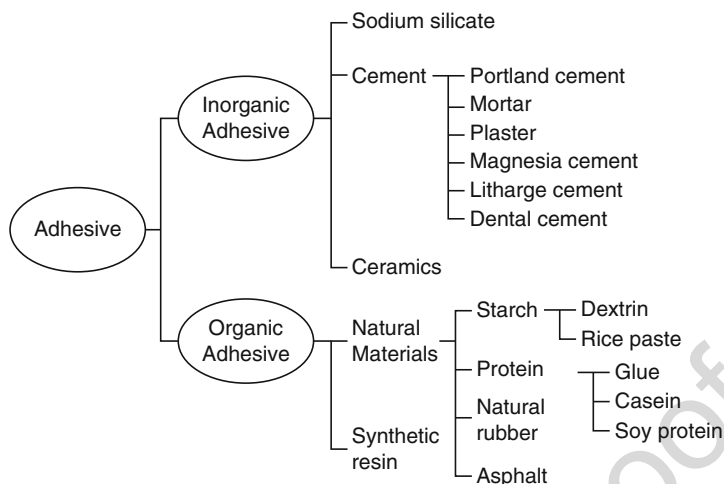


**Fig. 1** Classification of adhesives by categories of materials

1. Use of solvents such as water or organic solvents
2. Dispersion of micro particles in water, i.e., emulsion adhesives or latex dispersion adhesives
3. Heating, i.e., hot-melt adhesives
4. Use of liquid monomers or oligomers that can be polymerized

Water, solvents, surface-active agents, liquid monomers, or oligomers are the key components for liquefaction of adhesives. The performance of adhesives depends on the mechanical properties of the cured bulk adhesive. To emphasize the performance, many kinds of additives are blended to an adhesive, i.e., tackifiers, plasticizers, antioxidants (age inhibitors), curing agents (vulcanizing agents), adhesion promoters, and fillers. Adhesives consisting of mono component are very rare.

Functional adhesives have to have functions such as flameproofness or conductivity besides the intrinsic function to bond adherends together. Flame retardants or conductive fillers are used for the purpose. They are also the components of the adhesives. More information on composition of adhesives is given in ► [Chap. 13, "Composition of Adhesives."](#)

## 40.2.1 Main Components

The main components of adhesives are polymeric materials such as elastomers or synthetic polymers. The main component type for a certain adhesive is decided by the designer considering the type of adherends and use conditions. Control items to

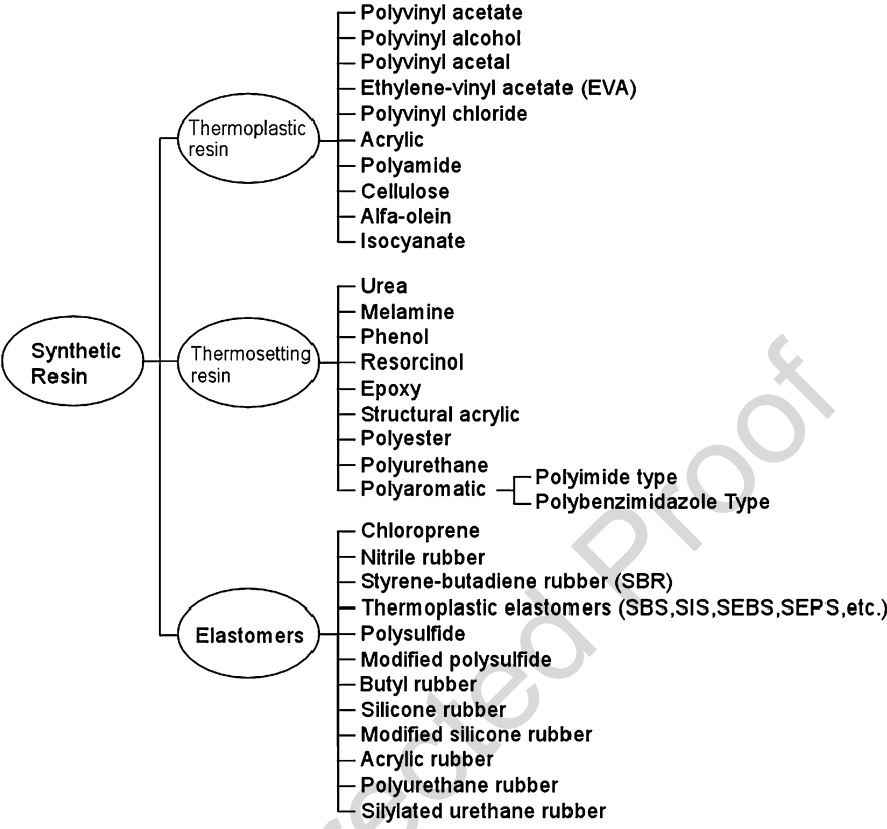
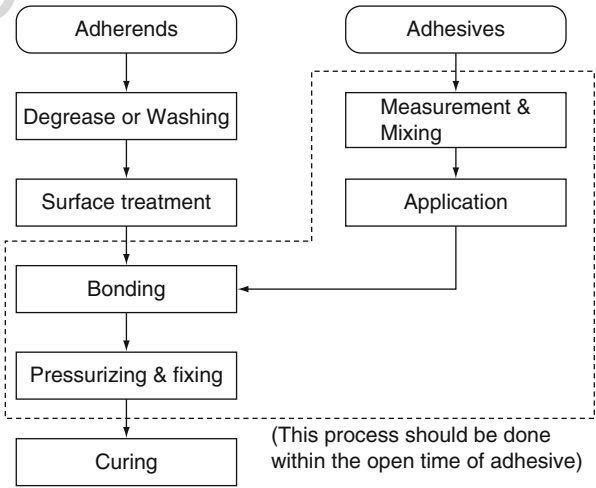


**Fig. 2** Classification of synthetic resins for adhesives

**Fig. 3** Adhesive and adherend preparation in bonding processes



be considered is as follows: solubility parameters, average molecular weights, Mooney viscosity, crystallinity, and existence or nonexistence of functional groups. Materials that can be used as main components of elastomer adhesives are polychloroprene rubbers, nitrile rubbers (butadiene-acrylonitrile copolymer), SBR (styrene-butadiene copolymer), thermoplastic elastomers (SBS, SIS, SEBS, SEPS etc.), butyl rubbers, acrylic rubbers, silicone rubbers, polysulfides, modified polysulfides, modified silicone rubbers, and silyl urethanes.

Materials that can be used as main components of thermoplastic adhesives are vinyl acetate, polyvinyl alcohol, polyvinyl acetal, ethylene-vinyl acetate copolymer (EVA), vinyl chloride, acrylic resin, polyamide, cellulose, alfa-olefin resin, and waterborne isocyanate resin.

Materials that can be used as main components of thermosetting adhesives are urea resin, melamine resin, phenolic resin, resorcinol resin, epoxy resin, structural acrylic resin, polyester, polyurethane, polyimide, polybenzimidazole, etc.

## 40.2.2 Solvents

The role of solvents is to reduce the viscosity of adhesives and to improve fluidity. That can provide the adhesives wettability to create an intimate contact with the surface of adherends. Solvents must be able to dissolve the components of adhesives. Solubility parameter is an index to show the soliditvity of solvents. A solvent can dissolve a high amount of materials whose solubility parameters are close to that of the solvent. Water, alcohols, aromatic hydrocarbons (e.g., toluene and xylene), ketones (e.g., methyl ethyl ketone and cyclohexanone), acetate esters (e.g., ethyl acetate and butyl acetate), n-hexane, cyclohexane, methylene chloride are used due to their solubility, dehydration rate, noncombustibility, and workability. To meet the demands concerning environmental issues, the use of some solvents such as toluene, xylene, ethylbenzene, and styrene is restricted by laws such as the air pollution control law legislated by Ministry of the Environment in Japan (The Ministry of the Environment 1996).

## 40.2.3 Tackifiers

A tackifier is a component to provide initial tackiness to adhesives. The compatibility of the tackifier to the main components is very important to increase the tackiness without degradation of the adhesive mixture. For that purpose, natural resins such as rosin and dammar, modified rosins such as coumarone-indene resin, polymerized rosin, hydrogenated rosin and rosin ester, and polyterpene resin are used. Recently, alkylphenol resins, terpene phenol resins, and xylene resins are out of use because of their hazardous nature inducing sick building syndrome.



#### 40.2.4 Plasticizers

Plasticizers can give flexibility to resins and are often used for vinyl resins. For instance, phthalic esters such as dioctylphthalate (DOP) and dibutyl phthalate (DBP), aliphatic diprotic acid esters, glycol esters, resin acid esters, and phosphoric esters are used as plasticizers. The use of phthalic esters has been decreasing because of environmental regulations.

#### 40.2.5 Fillers

The purposes to mix fillers with adhesives are (1) viscosity control, (2) suppression of resin invasion into porous adherends, and (3) strengthen the cured adhesive layer. Commonly used materials for fillers are minerals such as calcium carbonate, clay, talc, and diatom earth. Cellulose powders and recycled rubber powders are also used for the purpose.

#### 40.2.6 Thickeners

Thickeners are water-soluble polymers used for increasing the viscosity of emulsion, dispersion, and latex adhesives. Typical materials for thickeners are casein, methylcellulose, carboxymethyl cellulose, polyvinyl alcohol, and sodium polyacrylate.

#### 40.2.7 Pigments

Pigments such as titanium white, carbon black, and organic colors are used for coloring adhesives. Mixing of pigments in adhesives can make them less noticeable. In addition, the method has another function in which adhesives mixed with pigments can be visualized by color. Pigments must not react with the other components of an adhesive. Preservation stability of the mixture has to be checked experimentally.

#### 40.2.8 Other Important Components

Antiseptic agents, antiaging agents, antifoam agents, adhesion promoters (e.g., aminosilane coupling agents, alkyltitanate, etc.), or fragrances can be applied to adhesives as necessary.

## 40.2.9 Functional Components

Recent adhesives may include new types of components that can be used as main components or modifiers.

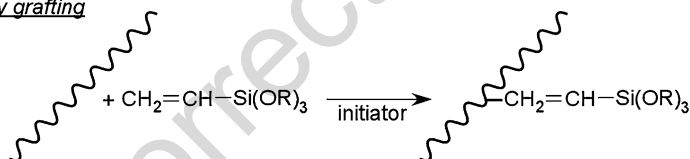
### Silane Coupling Agents

It is widely known that aminosilane coupling agents can be added to adhesives to improve their adhesion strength. Aminosilane coupling agents have organic groups and alkoxy groups that can modify the main resin components of adhesives. Alkoxy groups have compatibility with inorganic materials. They also condense with each other and produce cross-linked structures, which leads to desirable properties such as resistance to climate, acid tolerance, heat resistance, resistance to solvent attack, etc. Aminosilane coupling agents have recently been introduced to many types of resins or elastomers. Special coupling agents suitable for particular materials have also been developed. The methods to apply aminosilane coupling agents to resin or elastomers are as follows (Yanagisawa 2007):

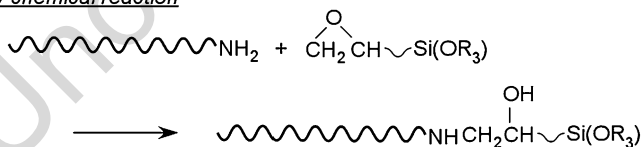
1. Graft reaction
2. Chemical reaction
3. Copolymerization

These methods are shown in Fig. 4.

#### By grafting



#### By chemical reaction



#### By copolymerization

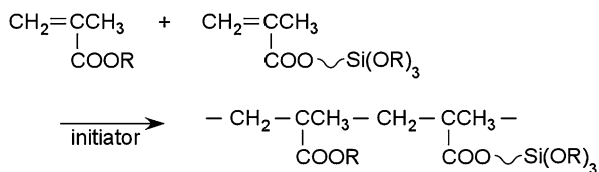


**Fig. 4** Methods to introduce silane coupling agents to molecules

## Functional Acrylic Materials

Oxazoline acrylic polymers have an oxazoline group, which is a kind of cyclic imino ether, as side chains. Ethylenimine acrylic polymers are modified with ethylenimine. Both materials have been used as main components of acrylic adhesives (Noda 2005). Oxazoline acrylic polymers can be applied to paints, coats, adhesives or pressure-sensitive adhesives (PSAs), and textile treating agents as water-base cross-linkers. Applications of oxazoline acrylic polymers are as follows:

1. Water-base cross-linkers: Although carboxyl groups in water-base resins are neutralized by amines or ammonia, oxazoline groups do not react with carboxyl groups and are stable in liquid conditions. When the water-base resin dehydrates, neutralizing agents are evaporated, and the carboxyl groups start to react with the oxazoline groups.
2. Primers for plastics: Oxazoline acrylic polymers have good adhesion compatibility to plastics. The reason seems to be the presence of polarity, affinity, and interaction caused by oxazoline groups that are a kind of cyclic imino ethers. The carboxyl groups in the polymer react with the oxazoline groups and they can also give the polymers good adhesion to plastics.
3. Film laminating adhesives: Although EVA emulsion is often used for film lamination as adhesives, the bonding strength to polyvinyl chloride (PVC) and polyolefin films is not high. The defect can be corrected adding oxazoline acrylic polymers to EVA emulsions having carboxyl groups.

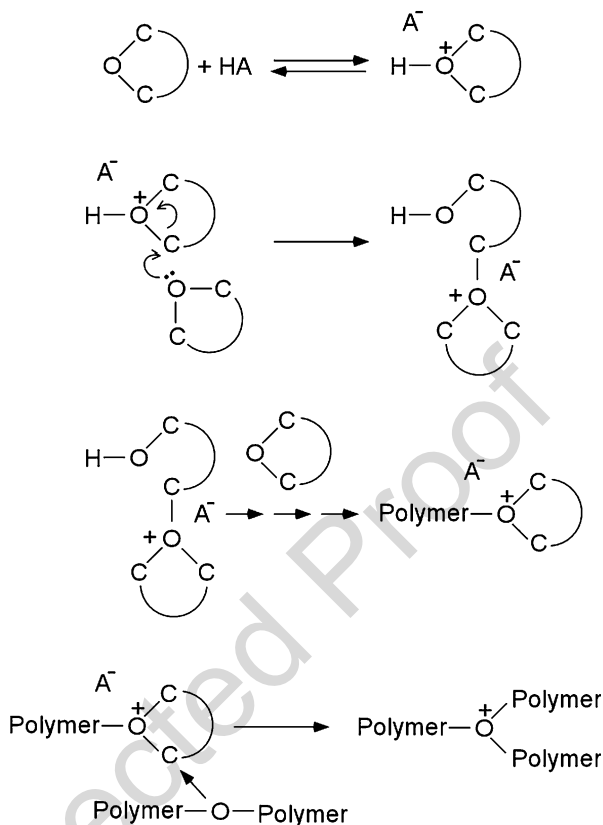
Ethylenimine acrylic polymers have high bond strength to many types of materials because ethylenimine groups are very reactive. The reactions caused by ethylenimine groups can be categorized as (a) polymerization by ring-opening ionic polymerization, (b) introduction of primary amine group in side-chain of acrylic polymers by ring-opening addition of ethylenimine groups to carboxyl groups, and (c) aziridinyl reaction (modification with preservation of aziridinyl groups). The good reactivity of ethylenimine acrylic polymers enables them to be cross-linkers for water-base polymers having carboxyl groups. When the polymers are used as a part of two-part cross-linking systems, use of a double-headed gun is necessary.

## Oxetane Polymers

Oxetane polymers are polymers having oxetane rings that are a kind of four-membered cyclic ether. The ring has high strain and basicity, and the polymer can cause cation ring-opening polymerization, as shown in Fig. 5. The characteristic of oxetane polymers are as follows (Sasaki and Crivello 1992; Crivello and Sasaki 1993a, b; Sasaki et al. 1995; Sasaki 2000):

1. The result of the Ames test is negative even in the condition of low molecular weight monomers.
2. Quick curing to mix to epoxy materials.
3. Relatively high molecular weight of generated polymers.
4. Diversity of synthesis methods because of oxetane ring stability under alkali conditions.
5. Volume shrinkage due to curing is not large and almost equal to epoxy resins.

**Fig. 5** Cationic ring-opening polymerization of cyclic ethers



Such characteristics are suitable for using the material for modifiers of UV curing epoxy adhesives applied to electronic parts.

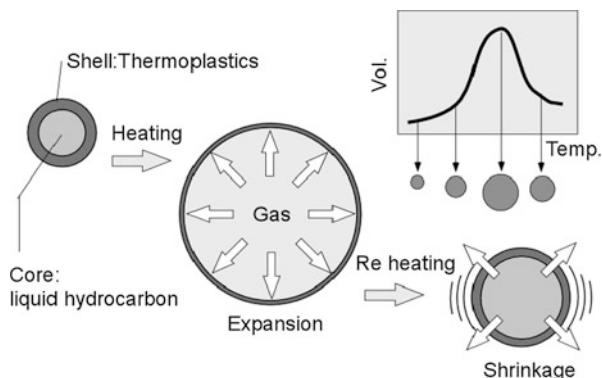
### Amorphous Polyalphaolefin

Amorphous polyalphaolefins are olefin polymers that are in amorphous condition and have relatively low molecular weights. They are synthesized by copolymerization of propylene alone, propylene and ethylene, or butane-1.

The characteristics of amorphous polyalphaolefins are as follows:

1. Good adhesion compatibility for polyolefins such as polyethylene (PE) and polypropylene (PP).
2. They can be used alone as hot-melt adhesives.
3. Mixture with EVA hot-melt adhesives may be sprayed to adherends.
4. They can be mixed with large amounts of mineral fillers.
5. They can be mixed in asphalt with a good dispersion.
6. Safe and harmless (compatible with the standard: US Food and Drug Administration (FDA) 21CFR.175.105).

**Fig. 6** Deformation mechanism of thermally expandable microcapsules (TEMs)



These characteristics lead to applications such as hot-melt adhesives, modifiers for hot-melt adhesives, modifiers for resins or elastomers, modifiers to prevent corrosion for waxes, and modifiers for asphalts.

### Thermally Expandable Microcapsules

Thermally expandable microcapsules (TEMs) are micro spheres of 10–40  $\mu\text{m}$  in diameter, having thermoplastic shells filled with liquid hydrocarbon of low boiling points. As their temperature rise, the inner pressure increases and the shell is softened. That leads to huge expansion of the sphere up to 20–40 times in volume, as shown in Fig. 6. The TEMs can be applied to dismantlable adhesives, thermally expandable adhesives, or sealants.

### Core-Shell Rubber

Core-shell rubbers have been developed to improve the ductility of epoxy resins without heat resistance reduction. Core-shell technology is a kind of capsulation process in which hydrophobic core resins can be covered with hydrophilic shell resins. There are many combinations of core and shell materials and wide varieties of dimensions, 40–500 nm in diameter, for instance. A method to pre-react liquid carboxylated nitrile butadiene rubber (C-NBR) and an epoxy resin and mix the product into the epoxy resin has been used for long time and it is a typical approach to design structural adhesives recently. Mixture of core-shell rubber is much more effective than those by the C-NBR method.

## 40.2.10 Functional Fillers

### Carbon Nanotubes

Carbon nanotubes are hollow carbon structures as a graphite sheet wound cylindrically. Their diameter is few  $\text{\AA}$  to 100 nm. Since the aspect ratio is very large, the material has a fibrous form. Carbon nanotubes having one graphite layer are called SWCNT (Single-Walled Carbon Nanotube). Other carbon nanotubes are called

MWCT (Multiwalled Carbon Nanotube) (Iijima 1991; Saito 2003; Fan et al. 1999; Nakayama 2002; Akita et al. 2001).

The characteristics of carbon nanotubes are as follows:

1. Chemical stability
2. High electric and thermal conductivity
3. High mechanical properties
4. High electron emission property

The carbon nanotubes are very promising to apply for adhesives as fillers to emphasize the strength and electric or thermal conductivity. Mixing of carbon nanotubes is not easy because of their strong cohesive attraction. Dispersion technology has to be established to obtain good characteristics.

### **Fine Calcium Carbonate**

Fine calcium carbonates, coated with aminosilane coupling agents, have been developed. Their diameter is about 20 nm. The material is promising as fillers to reinforce structural adhesives or elastomer adhesives (Tutui 2006).

### **Micro Balloons**

Micro balloons are convenient to reduce the weight of adhesives because the density of the balloons is very low. Typical micro balloons are 5–300  $\mu\text{m}$  in diameter, and 0.7  $\text{g}/\text{cm}^3$  in density. They have hollow structures comprising of silica (60–65 wt%), alumina (27–33 wt%), and ferric oxide (less than 4 wt%) (Tozaki 2006). The mixture should be carried out so that the micro balloons could not be broken. Since the macro balloons are difficult to be dispersed into resins, they are mixed with solvents and dispersed. After the mixture, the solvents are extracted by evaporation.

---

## **40.3 Quality Control Procedures for Raw Materials**

### **40.3.1 Acceptance of Raw Materials**

Acceptance inspections are necessary when raw materials are received. The name, type, and quantity of a material should be verified. The delivery conditions of raw materials, for instance, chilled transport, are also important in some cases and should be checked. After the acceptance inspections, there are several inspection tests to check the quality of the materials, which should fit the requirements. When these tests are carried out by suppliers of materials, users should check the specification documents indicating the test results. Recently, suppliers tend to contract for these tests. However, tests by users are still important to make sure the quality of their products. Capabilities of users to conduct tests are indispensable to decide the types and sequences of tests, which should be discussed and agreed with the suppliers testing the materials. Types of inspection tests are explained in the following section. Specification documents often include information for workers' health protection

295 such as material safety data sheet (MSDS), which should be always available to the  
296 worker.

297 When a raw material is accepted, the storage term of the material starts. Thus, the  
298 inventory list of a warehouse should be updated. Stored raw materials should be used  
299 “first in, first out.” Too long storage term than the shelf life of a material is  
300 prohibited. On the package of each material, tag labels indicating necessary infor-  
301 mation such as receiving date should be stuck. Inventory managements are important  
302 not only for the performance proof of materials and final products, but also for  
303 accounting managements and chemical material managements for acting in accord-  
304 dance with pollutant release and transfer register (PRTR), which is linked to raw  
305 material purchase, production, and shipping of final products. Nowadays, the  
306 updating of inventory lists can be automatically done with that of the PRTR database  
307 using computers.

### 308 **40.3.2 Inspection for Acceptance**

309 In inspection tests for receiving raw materials, the following properties should be  
310 investigated: chemical equivalent, impurity content rate, molar weight, viscosity,  
311 specific weight (density), color, transparency, conductivity, permittivity, etc. Among  
312 these properties, chemical equivalent, impurity content rate, molar weight, and  
313 viscosity are important.

#### 314 **Chemical Equivalent**

315 For raw materials of reactive adhesives, the chemical equivalent values are very  
316 important to specify the reactivity, and often tested. Epoxy equivalents for epoxy  
317 resins, and functional group equivalents for hardeners are experimentally deter-  
318 mined. Methods to measure the epoxy equivalents are described by industrial  
319 standards as follows: International organization for standardization (ISO) 3001,  
320 Japan industrial standards (JIS) K 7236, and American society for testing and  
321 materials (ASTM) D 1652. For instance, JIS K 7236 indicates the methods using  
322 titration. In this process, an epoxy sample is solved with chloroform, mixed with  
323 acetic acid, tetraethylammonium bromide, and crystal violet solution. The epoxy  
324 sample solution is finally titrated with perchloric acid–acetic acid solution. If auto-  
325 matic titrators can be used, the epoxy sample solution is titrated with perchloric  
326 acid–acetic acid solution by the machines. Functional group equivalents for hard-  
327 eners should also be measured because these are important parameters for adhesive  
328 curing.

#### 329 **Impurity Content Rates**

330 Adhesives for electronic applications are sensitive to impurities. For instance,  
331 inclusion of conductive particles often induces problems of insulation breakdown.  
332 Chlorine inclusion can cause corrosion of metal parts such as electrodes made of  
333 oxygen-free copper foils on flexible circuit boards that can react with chlorine in  
334 adhesives for bonding the foils and the boards, yield dendrites, and lead to insulation

breakdown. Since the phenomena occur at very low density of chlorine, the content rates should be checked by standards such as ISO 21627 and JIS K 7243.

### Molecular Weight

Since main components of adhesives are usually monomers of low molecular weight, the performance of the adhesives is not influenced by the variation of the molecular weight. Thus, it is not important to measure the molecular weights of the components. In contrast, for pressure-sensitive adhesives (PSAs), raw materials such as rubbers and tackifiers have relatively higher molecular weight than those of adhesives, and the variations lead to deviations of the final performances. Therefore, the molecular weights of the raw materials for PSAs are often measured by experimental methods such as end group determination, colligative property measurements, light scattering, ultracentrifugation, viscosity measurements, and gel permeation chromatography (GPC). These methods should be selected properly for objective materials.

### Viscosity

Viscosities of raw materials are very important because they can influence not only the properties of final adhesive products, but also the production process. Methods for measuring viscosities of liquid raw materials are included in the following standards: ISO 2555, ISO 3219, JIS K 7117, and ASTM D1084.

Viscosities of liquids can be described as:

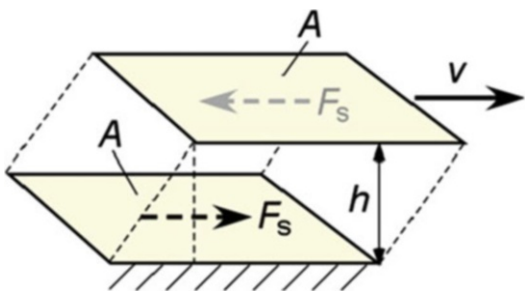
$$\tau = \mu \dot{\gamma} \quad (1)$$

where,  $\tau$ ,  $\mu$ , and  $\dot{\gamma}$  signify shear stress, viscosity, and shear strain rate, respectively. Consider the situation shown in Fig. 7, in which there are two parallel plates of area  $A$  with a separation distance of  $h$ , where the plates translate in relation to each other with a velocity  $v$ . The shearing force  $F_s$  is given by the following equation.

$$F_s = \mu A \frac{v}{h} \quad (2)$$

Although the international system of units (SI unit) for viscosity is Pa·s, cps is also used often for raw materials of adhesives and PSAs. For viscous liquids, Brookfield-

**Fig. 7** Relation between shear force and shearing velocity in viscous fluid





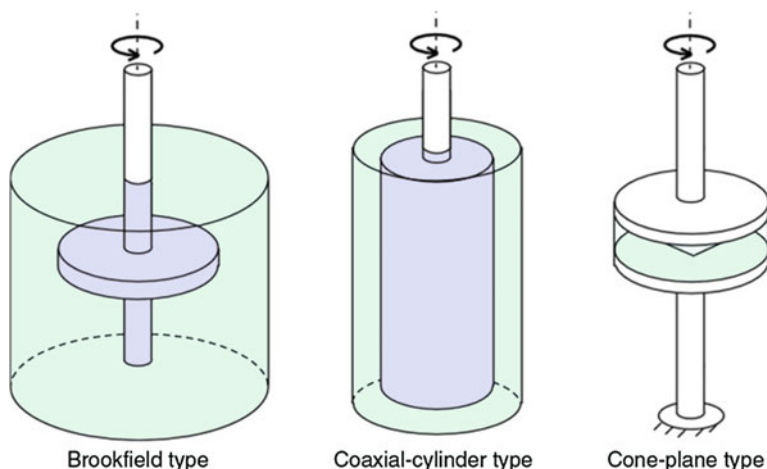


**Fig. 8** Types of viscometers for a viscous fluid

type viscometers or coaxial-cylinder-type viscometers, shown in Fig. 8, are usually used. For higher viscous materials, cone-plane-type viscometers (Fig. 8), Mooney viscometer, and rheometers are used. For example, a Brookfield-type viscometer has a spindle rotating in the liquid with a constant rotational velocity, and the resultant torque is measured. The viscosity of the liquid can be calculated from the torque and calibration results of standard viscous materials commercially available.

For elastomers and rubbers, Mooney viscometers are used, which are documented in standards ISO 289 and JIS K 6300. Brookfield-type viscometers can also be used for elastomers. Elastomers should be dissolved in a solvent in content of 10–20 wt% before measuring with Brookfield-type viscometer.

### **Density (Specific Weight)**

Densities and specific weights are basic material properties and should be measured to check errors of adhesive production. The measurement methods of specific weights are defined by standards ISO1183, JIS K7112, and ASTM D792. Densities are basically equivalent to specific weights, and the selection depends on the nature of the material. Densities are suitable for liquids, and specific weights are for solids. The density of a liquid can be measured with pycnometers or specific gravity cups, whose inner volumes are known. The density is calculated dividing the mass of the liquid by the volume.

Since volumes of solids are quite difficult to measure, specific weights are appropriate for solids (ISO 3675, JIS-K2249). Specific gravity balances are usually used for the measurements. The weights in air and water of a solid are measured using balances. The difference between the weights in air and water is equivalent to the buoyancy indicating the volume of the solid. Dividing the weight of the solid by the buoyancy yields the specific weight. The density of the solid can be calculated multiplying the specific weight and the density of water. The method has a problem

that it cannot be applied to water-soluble materials. In this case, volumes of the materials should be measured by different methods.

For liquids such as solvents, areometers can be used. They are convenient because specific weights of liquids can be measured in the containers.

### 40.3.3 Quality Control of Raw Materials in Storage

Circumstance controls are very important for raw materials in storage. The most influential condition on material degradation is temperature. Air conditioners for warehouses, refrigerators, and freezers should be appropriately selected for the required temperature conditions of raw materials, and used. Although humidity and ultraviolet irradiation are lesser influential than temperature, protection methods have to be taken not only in storage, but also in processing of adhesive products.

For adhesive production, particular amounts of raw materials are extracted by pumps from the containers such as metallic barrels, and transferred to reaction vessels. Some materials such as isocyanate resins are very sensitive to humidity, and solidify when the containers are kept open. For the materials, time limits of opening containers should be specified and kept by workers. Consuming up materials soon after the containers are opened is a good idea. Therefore, proper plans for the production of adhesives can contribute to the quality control of raw materials.

Adhesives for electronic applications are nowadays processed in clean rooms. If containers for raw materials are dirty and contaminated, the cleanliness of the clean rooms may decrease. Therefore, the containers should be stored in clean conditions in order to prevent them from contaminations. More information on storage is given in ► Chap. 36, "Storage of Adhesives."

Education of raw material managers is another point of importance. No manager is the worst. Irresponsible managers are almost the same as no manager. In these situations, the performance of raw materials cannot be proved, and possibilities of defective products increase. Indispensable rules such as keeping materials in proper conditions of storage, and making overdue materials unusable are obeyed strictly by the managers. Disposals of overdue materials may occur due to production plans. Even in the cases, managers must not be blamed.

### 40.3.4 Inspection for Shipment

When adhesives are shipped after the processing, users of raw materials become supplier of products. Inspection should be done to the adhesive products to prove the performances. Specification sheets should be issued for users if required. Sampling tests of industrial adhesives are rare unlike household adhesives. Tests of each production lot are usual.

Inspection tests before shipments of adhesive products are as follows: adhesion strength, tackiness, hardness, viscosity, density, volume shrinkage, thermal expansion, shelf life, pot life, gelation time, water resistance, chemical resistance, weather

resistance, flame retardance, electric conductivity, color, optical properties, amount of volatile organic compounds (VOC) emergence, etc. Some of these tests are the same as those tests for acceptance. Before shipment, strength tests of joints are very important for adhesives in terms of performance proof (see ► Chap. 19, “Failure Strength Tests”). In contrast, for PSAs, tackiness is important (see ► Chap. 15, “Pressure-Sensitive Adhesives (PSAs)”). Other important properties that should be tested are shown below.

### **Shelf Life**

Shelf life is a term during which adhesive can be stored without undesirable physical and chemical changes. The term depends on the storing condition of the adhesive. Thus, the shelf life of an adhesive should be indicated with the storage condition such as temperature, humidity, and light. Since some adhesives are sensitive to oxygen or humidity, the shelf lives of the adhesives should be stored with unopened container during a term, then the viscosities or joint strengths are experimentally measured. The procedure is denoted in test standards such as ASTM D 1337 (see ► Chap. 18, “Thermal Properties of Adhesives”).

### **Pot Life (Working Life)**

Pot life (working life) is the time length in which an adhesive can be applied and used to join after the adhesive comes to an applicable condition. For instance, two-part epoxy adhesives gradually cure and harden after the mixing of the parts, and become too stiff to be applied after their pot lives, decreasing the bond strength. For moisture curable adhesives, the pot lives start when the adhesives are extracted from the containers. Pot lives are determined measuring the viscosities or joint strengths of adhesives with respect to time. The procedures are denoted in some standards, i.e., ISO10364, JIS K 6870, and ASTM D 1338 (see ► Chap. 18, “Thermal Properties of Adhesives”).

### **Curing Shrinkage**

Reactive adhesives such as epoxy and acrylic resins may induce shrinkage stresses that reduce often the bonding strengths. Therefore, the volume shrinkage should be measured by standards such as JIS K6911, in which adhesives are cured in a mold and the dimension of the adhesive is measured to calculate the shrinkage ratio.

### **Curing Rate**

Curing rate is important information for users of adhesives. However, ordinary adhesives cure gradually and sometimes reach to the final strength within a few days. Hence, the time to the final strength is less important than the time when de-molding or handling of the joints can be possible, because the total time of bonding processes highly depends on the de-molding or handling time. In contrast, a too short curing time, which is equivalent to a short pot life, spoils the workability. Therefore, curing rates are very important and should be measured using many specimens such as lap shear joints with respect to time.

### Strength and Hardness

Although the strength of the adhesive in bulk is not so important to be often measured, sometimes it is necessary to verify the specification. For the strength test of adhesives in bulk, dog bone specimens for tension or rectangular specimens for bending are used. In contrast, hardness of adhesives in bulk can be used as an index of curing condition, and is measured in terms of quality control. Hardness measurements include scratch tests and indentation tests, and the latter, such as the Shore test, is often utilized for adhesives in bulk. A Shore hardness tester has a small diamond half sphere equipped at the tip of a hammer, and the hammer hits the surface of a specimen. Hardness is calculated from the height of the hammer rebounding after the collision. A too soft adhesive implies under-cure or mixture of air bubbles, and a too hard adhesive means over curing.

### Glass Transition Temperature

Glass transition temperature ( $T_g$ ) is an important parameter for the quality control of adhesive formulation. The temperature is also related to the maximum usable temperature of adhesives. Adhesives are softened and become viscoelastic around the  $T_g$ . The  $T_g$  of an adhesive can be measured with differential scanning calorimetry (DSC), thermo mechanical analyzer (TMA), and dynamic mechanical analyzer (DMA). The  $T_g$  is calculated from the absorbed or emitted energy measured with DSC, deformation with TMA, and fluctuation of viscoelastic parameters with DMA, although the values from the methods are slightly different. Therefore, the definition of  $T_g$  is quite ambiguous. There is another similar temperature called softening point measured by penetration or bending tests using TMA. This is very close to  $T_g$  in value (see ► Chap. 18, “Thermal Properties of Adhesives”).

### Other Properties

Nowadays, additional functions become important and the performance should be tested. For instance, since the use of Pb solder is nowadays prohibited by the restriction of the use of certain hazardous substances in electrical and electronic equipment (RoHS), conductive adhesives are used instead. For the adhesives, electric conductivity and shear resistance are vital, and their tests, besides other conventional tests, should be conducted. Thus, some adhesives developed in the future may have novel functions that conventional adhesives do not have, and new test methods and standards should be required to check the functions. From the environmental point of view, measurements of volatile organic compound (VOC) emergence and dismantlability of adhesives will become more important in the future (see chapter 58).

---

## 40.4 Material Standards

Since qualities of raw materials influence considerably the performances of adhesive products, the materials should be tested appropriately by test standards depending on the types of materials. The material standards are discussed below.

#### 40.4.1 Main Components

The main components of adhesives are polymers such as elastomers and synthetic resins, and monomers and oligomers for reactive adhesives. As shown in Sect. 3.2, properties that should be tested are chemical equivalent, molecular weight, viscosity, etc. In addition, solubility parameters, crystallinity, and presence of functional groups are also indispensable check points for the design of adhesives.

1. Solubility parameters: Solubility parameters are values indicating the solubility of plastic materials. Materials having similar solubility parameters can be dissolved and adhere to each other very well. Therefore, the value is very convenient to select the main component of an adhesive applied to a particular material. Solubility parameters of ordinary plastic materials may be shown in handbooks (e.g., Handbook of Adhesives edited by Skeist (1990)). Suppliers should be asked about solubility parameters of special plastics.
2. Crystallinity and presence of functional groups: Ordinary polymers except amorphous polymers have crystalline parts. Crystallinity of polymers affects the properties. Polymers of high crystallinity have high cohesive attraction. In contrast, low crystallinity leads to good contact to the adherend surfaces. Therefore, attention should be paid to the crystallinity of polymers used for adhesives. For instance, polychloroprene rubber has several types of low, medium, and high crystallinity, which are shown in the technical data provided by the suppliers. Type selection should be done carefully to design adhesives. The presence of functional groups (e.g., hydroxyl, carboxyl, amino, and epoxy groups) is also important to design adhesives, and the information is also indicated in technical data.

#### 40.4.2 Solvents

Properties that should be controlled for solvents are molecular weight, specific weight (density), boiling temperature, ignition temperature, aqueous solubility, initial boiling point, dry point, sulfur content, bromine index, residue on evaporation, moisture content, etc. Each solvent has a material standard (Table 1) and the properties are controlled by the suppliers.

#### 40.4.3 Tackifiers

Properties controlled for tackifiers are molecular weight, specific weight (density), melting temperature, softening temperature, aqueous solubility, solvent solubility, melt viscosity, burning point, etc. Molecular weights of tackifiers are measured by vapor pressure osmometry (VPO) methods. Melting temperatures and softening temperatures are measured by the method shown in a standard JIS K 2207. The Cleveland method is widely used to measure the burning point of tackifiers.

t.1 **Table 1** Material standard for solvents

t.2	Solvent	ISO	JIS
t.3	n-Hexane (very pure)		JIS K0504
t.4	Mineral spirit		JIS K2201
t.5	Toluene, xylene	ISO 5272,5280	JIS K2435
t.6	Industrial methylated alcohol		JIS K1505
t.7	Isopropanol		JIS K1522
t.8	Methyl cellosolve		JIS K 8895
t.9	Ethyl acetate	ISO 1836	JIS K 1513
t.10	n-Butyl acetate	ISO 1836	JIS K 1514
t.11	Isobutyl acetate		JIS K 8377
t.12	Acetone	ISO1090	JIS K 1503
t.13	Methyl ethyl ketone		JIS K 1524
t.14	Methyl isobutyl ketone	ISO 1245	
t.15	Trichloroethylene	ISO 2212	JIS K 1508
t.16	Perchloroethylene	ISO 2213	JIS K 1521
t.17	1,1,1-Trichloroethane		JIS K 1600

t.18 *ISO* International Organization for Standardization, *JIS* Japan Industrial Standardst.1 **Table 2** Material standard for tackifiers

t.2	Solvent	ISO	JIS
t.3	Dibutyl phthalate (DBP)		JIS K6752
t.4	Diocetyl phthalate (DOP)		JIS K6753
t.5	Di-isodecyl phthalate (DIDP)	ISO 2520, 21, 22	JIS K6750
t.6	Tritolyl phosphate (TCP)		JIS K6752

t.7 *ISO* International Organization for Standardization, *JIS* Japan Industrial Standards543 **40.4.4 Plasticizers**

544 Properties controlled for plasticizers are molecular weight, specific weight, oxidation  
 545 degree, ester number, refraction index, loss on heating, oxidation degree after  
 546 heating, boiling temperature, melting temperature, viscosity, etc. Material standards  
 547 for plasticizers are shown in Table 2.

548 **40.4.5 Fillers**

549 Important characteristics for fillers are low density, uniform dispersibility, workabil-  
 550 ity of cured bulk including fillers, minimum decrease of properties of cured bulk  
 551 (e.g., mechanical properties, resistance for water, chemicals heat, and weather) by  
 552 inclusion of fillers, large maximum content, low cost, etc. Controlled properties are  
 553 average grain size, specific surface area, pH, etc. Since the suppliers usually provide  
 554 experimental reliable data, the users do not test again by themselves.

#### 40.4.6 Thickening Agents

Casein, which is a type of protein included in milk, is used as a thickening agent for adhesives. There are three types of casein: acid casein, lactic casein, and rennet casein, depending on the production process. Acid casein is used for latex adhesives as thickening agents. Since casein is basically insoluble in water, alkali water solutions (e.g., with ammonia, potassium hydrate, sodium hydrate, borax, etc.) are used after water immersion to swell. Quality check of casein is conducted to measure the viscosity of water solution of 1–2%.

Methylcellulose, carboxymethyl cellulose, polyvinyl alcohol, sodium polyacrylic, and polyacrylamide copolymer are also used for thickening agents. The qualities of methylcellulose and carboxymethyl cellulose are checked measuring the viscosity of water solution of 2–5%. For polyvinyl alcohol, viscosity (4% at 20 °C), saponification number, and polymerization degree are indexes of the quality.

#### 40.4.7 Pigments

Color pigments are often mixed in adhesives. Since there are many types of pigments, which can affect the performance of adhesives, thorough discussion between users and suppliers of pigments is indispensable. Standards for pigments are shown in Table 3.

#### 40.4.8 Other Raw Materials

Other raw materials such as antiseptic agent, antiaging agent, antioxidizing agent, antifoam agent, and adhesion promoter are also mixed to adhesives. Tests by users of these materials are very rare. Specifications provided by suppliers should be checked and usable conditions should be kept.

**Table 3** Material standard for pigments

Solvent	ISO	JIS
Titanium oxide (titanium white)	ISO 591	JIS K 5116
Zinc oxide (zinc flower)		JIS K 5102
Carbon black		JIS K 5107
Ferric oxide (colcothar)	ISO 1248	JIS K 5109
First yellow G (Arylide yellow G)		JIS K 5217
Phthalocyanine blue		JIS K 5241

ISO International Organization for Standardization, JIS Japan Industrial Standards

## 40.5 Conclusion

The performance of adhesives depends on the quality of raw materials used for the adhesives. Therefore, it is easy to understand that the quality control of the raw materials is very important. As adhesive manufacturers design and provide adhesives which meet the demand of the market, raw material makers should provide appropriate products to adhesive makers, understanding and considering their needs.

To keep the quality of raw materials, the specifications of materials and their testing methods should be determined and agreed by adhesive makers and raw material makers. Standards of materials and testing methods can be used to decide the specifications. All the purchase and shipping of raw materials should be done following the specifications. For instance, inspection of raw materials are carried out based on their specifications before shipping by raw materials makers, and specification sheets of each product lot are issued. For recent novel raw materials, such as functional fillers for conductivity or flame retardancy, new standards should be established.

Since testing methods are varied, selection of necessary and sufficient tests is important in terms of efficiency and economy. Storage condition of raw materials is also very important to proof the performance of final products. Temperature and humidity of storages or warehouses should be within the range shown in the specification of materials. No material over the shelf life can be used to produce adhesives. First-in first-out sequence is a good manner to manage the inventory of raw materials. Education for workers who treat raw materials is also an effective investment to maintain high quality of adhesive products.

Raw materials for adhesives have to be selected to meet the demands such as high performances, additional functions, and durability including environmental resistance. Traditional techniques to realize the desirable performance is to blend raw materials. Other methods, which have been introduced recently, are as follows:

1. Polymer alloying: This can be applied not only to mutually compatible materials, but also to noncompatible ones using compatibilizing agents.
2. Copolymerization, graft polymerization: They can combine immiscible materials, which leads to hybrid effects and synergies.
3. Pre-reaction: This can introduce sea-island structures in cured adhesive, and useful to reinforce adhesive layers. The technique has been applied to structural adhesives already.
4. IPN (inter penetrate network) structures: Developing of molecular chains penetrating each other can improve the resistance of cured bulk materials due to the stress relaxation. For instance, elastic adhesives have IPN structures comprising an epoxy backbone and modified silicone molecular chains.
5. Nanotechnology: This can be applied to surface modification.
6. Microcapsules. This can be used to realize novel functions such as dismantlability.



These methods are very promising to establish new materials for futures adhesion technology.

The other important requirement for ensuring the quality of raw materials is frequent and close communication between material providers and users. Information-sharing between providers and users is very crucial and indispensable for total quality control of adhesive products.

---

## References

- Akita S et al (2001) *Appl Phys Lett* 79:1691  
Crivello JV, Sasaki H (1993a) *J Macromol Sci Pure Appl Chem* A30:173  
Crivello JV, Sasaki H (1993b) *J Macromol Sci Pure Appl Chem* A30:189  
Deming WE (2000) *Out of the crisis*. The MIT Press, Cambridge (reprinted version) 88  
Fan S et al (1999) *Science* 283:512  
Iijima S (1991) *Nature* 354:56  
Nakayama Y (2002) *Ultramicroscopy* 91:49  
Noda N (2005) *Adhes Technol Jpn* 25:29  
Ozawa M (1987) *TQC and management*, Japan Standards Association, p 116  
Saito Y (2003) *J Nanosci Nanotechnol* 3:39  
Sasaki H (2000) *J Photopolym Sci Technol* 13:119  
Sasaki H, Crivello JV (1992) *J Macromol Sci Pure Appl Chem* A29:915  
Sasaki H, Rudzinski JM et al (1995) *J Polym Sci A* 33:1807  
Skeist I (1990) *Handbook of adhesives*, 3rd edn. Springer, New York, p 13  
The Ministry of the Environment (1996) Government of Japan, Air pollution control law No. 32  
Tozaki I (2006) *Adhes Technol Jpn* 26:52  
Tutui S (2006) *Adhes Technol Jpn* 26:25  
Yanagisawa S (2007) *Adhes Technol Jpn* 27:26

Kosuke Haraga

**Contents**

41.1	Introduction .....	1152
41.2	Mathematical Background .....	1153
41.3	Basic Requirements for Highly Durable Adhesion .....	1155
41.4	Important Points for Adhesion Process Control .....	1158
41.4.1	Dimension Allowance of Parts Bonded Adhesively .....	1158
41.5	Management and Preparation of the Bonding Surface .....	1161
41.5.1	Wettability Measurement of the Bonding Surface .....	1161
41.5.2	Surface Treatment to Improve Adhesion Adequateness .....	1161
41.5.3	Primer Coating .....	1162
41.5.4	Pot Life of Adhesives .....	1162
41.5.5	Verification of Adhesive Spreading and Curing After the Bonding Process .....	1163
41.5.6	Inspection .....	1164
41.5.7	Process Design .....	1165
41.6	Additional Efforts to Ease Process Quality Control .....	1165
41.6.1	Reduction of Operator's Tasks .....	1165
41.6.2	Foolproof .....	1165
41.6.3	Use of Adhesives with an Easy Process Control .....	1166
41.7	Education and Training .....	1168
41.7.1	Operator's Education and Qualification .....	1168
41.7.2	Thorough Exchange of the Information About Process Changeovers .....	1168
41.8	Conclusion .....	1168
References	.....	1169

---

K. Haraga (✉)

Tapes and Adhesives Department, Electronic Materials Division, Electronic Materials Business  
Unit, Denki Kagaku Kogyo Kabushiki Kaisha, Chuo-ku, Tokyo, Japan  
e-mail: [kosuke-haraga@denka.co.jp](mailto:kosuke-haraga@denka.co.jp)

## Abstract

The processing quality control of adhesively bonded joints in actual production lines is discussed in this chapter. To improve the yield ratio of products, a scientific approach based on both probabilistic design and statistical treatment is indispensable. In addition, control of environmental conditions and materials is also very important. For the purpose, a realistic trial-and-error approach should be done to meet any demands or to solve problems occurring in the production. Investigation of reasons decreasing joint strength is another key point that should be done. The strength decrease occurs often due to mechanical or chemical mismatch of adherends and adhesives. The surface treatment of adherends is important too. Inspection, which can be carried out easily, is desirable in actual production lines.

Process design should be done appropriately to improve the efficiency and the economy of the lines and to increase the yield ratio of products. Parallel processes should be avoided if sequential processes can be adopted. Reduction of operator's tasks is another important issue. The concept of foolproof should be introduced in the process design.

Proper adhesive selection is vitally important, not only for good strength but also for increasing operation efficiency. New types of adhesives have been available to meet the demands to control the process easily. The education and training of operators are also an essential issue. Operators should learn standard procedures to perform their work appropriately. The necessary information should be exchanged properly.

## 41.1 Introduction

It is quite difficult to check visually the adequateness of adhesion bonding after the joining process. Therefore, design of bonded joints, process optimization, and its control are very important. In this chapter, some important aspects are discussed to obtain practically good adhesion in the fabrication lines of products having adhesively bonded joints. The quality control in adhesives production is not treated here. This aspect is, for example, treated in Petrie (2007).

The quality control of adhesively bonded joints in fabrication lines includes control of adhesion processes, appropriate design of joints to ease the process control, and education and direction for works to conduct the manufacturing. Many efforts have been made to improve the quality stabilities (Petrie 2007; Espie 1995; Roberts 1990; DeFrayne 1983; Bandaruk 1962). Due to the invention of new types of adhesives such as acrylics whose strengths are less sensitive to processing conditions than those of conventional adhesives, the quality control can be done more easily and precisely in these days than the previous as shown by Haraga et al. (2009).

Statistical approach is essential to control the quality of adhesively bonded joints in products. Both probabilistic designs of the joints and precision enhancement in each process to increase the yield ratio of useable joints are important. Statistical

approaches, in which the average and standard deviation of joint strengths are obtained and used for joint design or predicting the expected strength range, have been performed in several investigations (Straalen et al. 1998; Stroud et al. 2001; Hadj-Ahmed et al. 2001; Gorbatkina Yu and Ivanova-Mumjieva 2001; Seo and Lim 2005; Vallee et al. 2005a, b, 2006; Arenas et al. 2010). The idea can be applied to actual production processes in industries. Additionally, particular practical methods to improve the yield ratio of usable joints in each stage should be established.

## 41.2 Mathematical Background

Statistical methods are indispensable for ensuring the reliability of adhesively bonded joints. The mathematical background of statistical methods is very briefly explained in this section. See other textbooks (e.g., Montgomery 2008) for more details.

Imagine the case in which there are many samples having their own attributions. For instance, adhesively bonded specimens can be regarded as the samples, and they have strengths as the attributions. The attributions can be often treated with numerical values. A graph, in which the number of samples within a particular range of the numerical value is plotted, as shown in Fig. 1, is called histogram. In this figure, the abscissa axis denotes the range of strength, and the axis of ordinate signifies the number of samples. The summation of the histogram is obviously equal to the total number of the samples.

It is empirically known that a histogram becomes a type of symmetrical shape as shown in Fig. 1 if the sample number is large enough and its attributions are random events such as strength of materials or dimensions of machined parts, for example. If the axis of ordinate is normalized with the total sample number and the attribution range is minimized, the histogram reaches asymptotically a curve called normal distribution or Gaussian distribution as shown in Fig. 2 that is plotted with the function as follows:

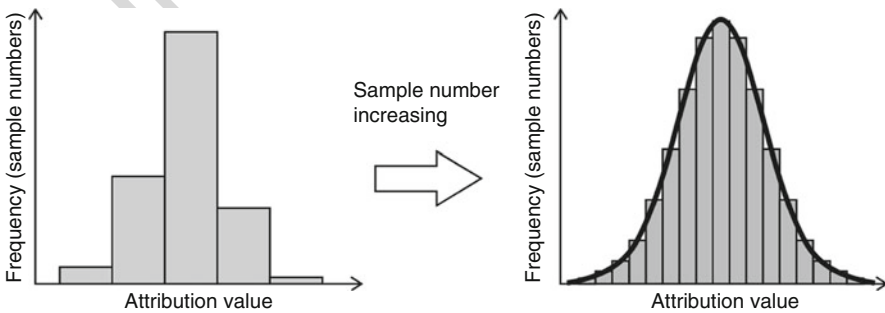


**Fig. 1** A schematic illustration of histogram and the shape change with respect to sample members' increase

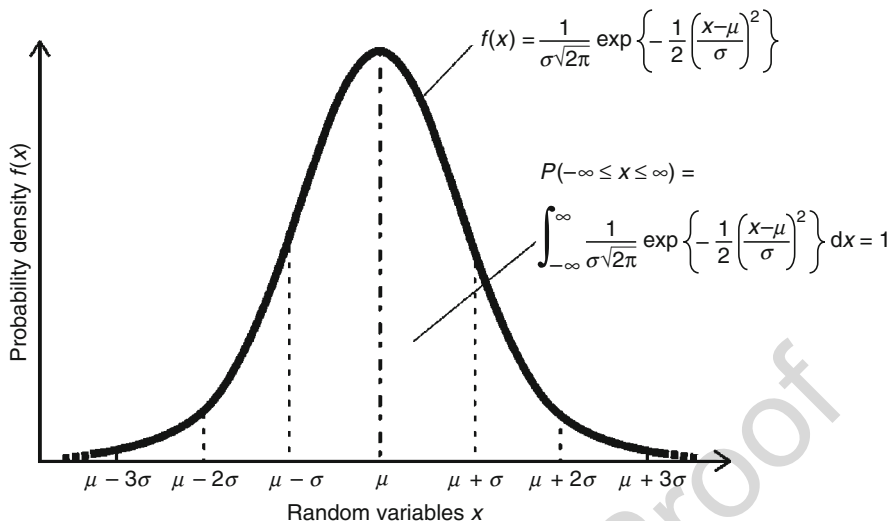


**Fig. 2** A schematic illustration of normal distribution

$$f(x) = \frac{1}{\sigma\sqrt{2\pi}} \exp\left\{-\frac{1}{2}\left(\frac{x-\mu}{\sigma}\right)^2\right\} \quad (1)$$

where  $x$ ,  $\mu$ , and  $\sigma$  denote attribution values, average values, and standard deviations of the sample population that can be defined by the following Eqs. 2 and 3:

$$\mu = \frac{1}{n} \sum_{i=1}^n x_i \quad (2)$$

$$\sigma = \sqrt{\frac{1}{n} \sum_{i=1}^n (x_i - \mu)^2} \quad (3)$$

The abscissa axis of normal distribution curves is called random variables, and its ordinate signifies probabilistic density that is equivalent to the existence probability of samples per unit range of the abscissa axis. The existence probability of samples within a particular range ( $a \leq x \leq b$ ) can be calculated with the following Eq. 4. The integration of existence probability through the whole range is obviously equal to 1:

$$P(a \leq x \leq b) = \int_a^b f(x) dx = \int_a^b \frac{1}{\sigma\sqrt{2\pi}} \exp\left\{-\frac{1}{2}\left(\frac{x-\mu}{\sigma}\right)^2\right\} dx \quad (4)$$

The existence probability of samples within a symmetrical range of  $\pm k$  from the average  $\mu$ , which is denoted as  $P(\mu - k \leq x \leq \mu + k)$ , can be also calculated with the following Eq. 5:

$$P(\mu - k \leq x \leq \mu + k) = \int_{\mu-k}^{\mu+k} \frac{1}{\sigma\sqrt{2\pi}} \exp\left\{-\frac{1}{2}\left(\frac{x-\mu}{\sigma}\right)^2\right\} dx \quad (5)$$

For instance,  $P(\mu - k \leq x \leq \mu + \infty) = \frac{1}{2}\{1 + P(\mu - k \leq x \leq \mu + k)\}$ , and  $P(\mu - 3\sigma \leq x \leq \mu + 3\sigma) = 0.9973$ . Therefore, 99.73% of samples exist within the range of  $\mu \pm 3\sigma$ . Imagine a situation where the average strength of joint specimens is 20 MPa and the standard deviation is 3 MPa. In this case, 68.26% of the specimens are within the strength range of 17–23 MPa, 95.45% are within 14–26 MPa, and 99.73% are within 11–29 MPa, respectively. In the final case, the ratio of the samples out of the range ( $\mu \pm 3\sigma$ ) is very small because it is 0.27%.

When the reliability of adhesively bonded joints should be considered, joints too weak in strength are out of use. However, too strong joints are not problems. Therefore,  $P(\mu - k \leq x \leq \mu + \infty)$  is more crucial than  $P(\mu - k \leq x \leq \mu + k)$ . The relations between them can be shown as follows:

$$P(\mu - k \leq x \leq \mu + \infty) = \frac{1}{2}\{1 + P(\mu - k \leq x \leq \mu + k)\} \quad (6)$$

Some problems happen when the statistical methods derived above are actually applied to the reliability evaluation of products. At first, all products cannot be inspected. The most usual method is sampling inspection. Thus, it is necessary to predict the average and standard deviation of a population from a small number of samples inspected. This process is called “statistical estimation.” For instance, strength tests of adhesively bonded specimens are adapted to this process because relatively small number of specimens such as five or ten are usually used in order to “estimate” the statistical properties of a large population. The process has been investigated very much. Unfortunately, the method is not versatile because obtaining precise information from few specimens is difficult. Enough number of samples is necessary for determining the precise statistical properties.

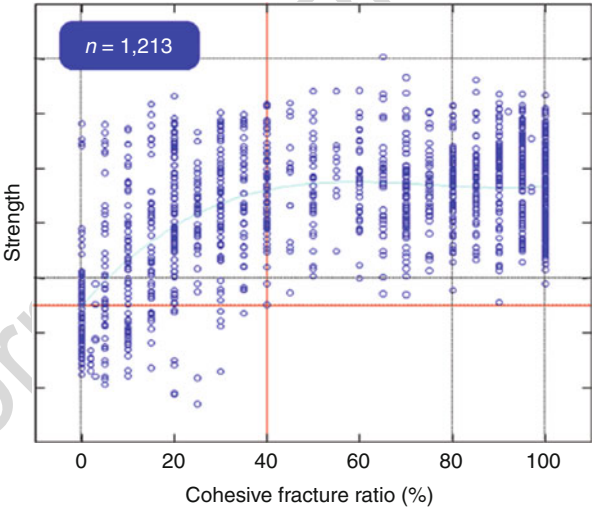
### 41.3 Basic Requirements for Highly Durable Adhesion

Highly durable adhesion has to include such capabilities as high strength, low strength scatter, and high resistance to environmental and loading conditions. To realize a highly durable adhesion, an indispensable requirement is cohesive fracture, by which fracture occurs not along the interfaces between the adhesive layer and the adherends but only in the adhesive layer. Table 1 shows the experimental results of acoustic emission (AE) measurement in the case of tensile tests using lap-shear specimens (Haraga 2008). The percentage of the ultimate load corresponding to the first AE occurrence and the total number of AE counts up to fracture are shown. This result implies that interfacial fractures happen at a lower stress than that of cohesive fractures because AE occurs in the case of interfacial fractures much earlier than in

t.1 **Table 1** Percentage of the ultimate load corresponding to the first occurrence of acoustic emission (AE) and total counts of AE until the fracture for different failure conditions (interfacial fracture or cohesive fracture) in adhesively bonded joints

t.2	Fracture condition	Sample no.	Percentage of ultimate load corresponding to the first AE count	Total AE counts until fracture
t.3	Interfacial fracture	1	7%	25
t.4		2	8%	17
t.5		3	31%	117
t.6		Average	15%	53
t.7	Cohesive fracture	1	51%	19
t.8		2	76%	11
t.9		3	100%	1
t.10		Average	76%	10

**Fig. 3** A typical relation between joint strength and cohesive fracture ratio (cohesive fracture area/total adhesion area (C/T)) where the total number of experiments (n) is 1213



140 the case of a cohesive fracture. Since cyclic loads or heating cycles tend to cause  
141 stress concentrations around the edges of interfaces due to the loads applied and the  
142 thermal stresses, they cause interfacial fracture with a low strength and the joints fail  
143 under relatively low loads and short cycles (Haraga 1992).

144 A typical relation between cohesive fracture ratio (cohesive fracture area/total  
145 adhesion area (C/T)) and joint strengths is shown in Fig. 3. In this case, the total  
146 number of experiments (n) is 1213. There is a threshold in joint strength around 40%  
147 of the C/T. Below a C/T of 40%, the number of weak joints increases. Weak joints are

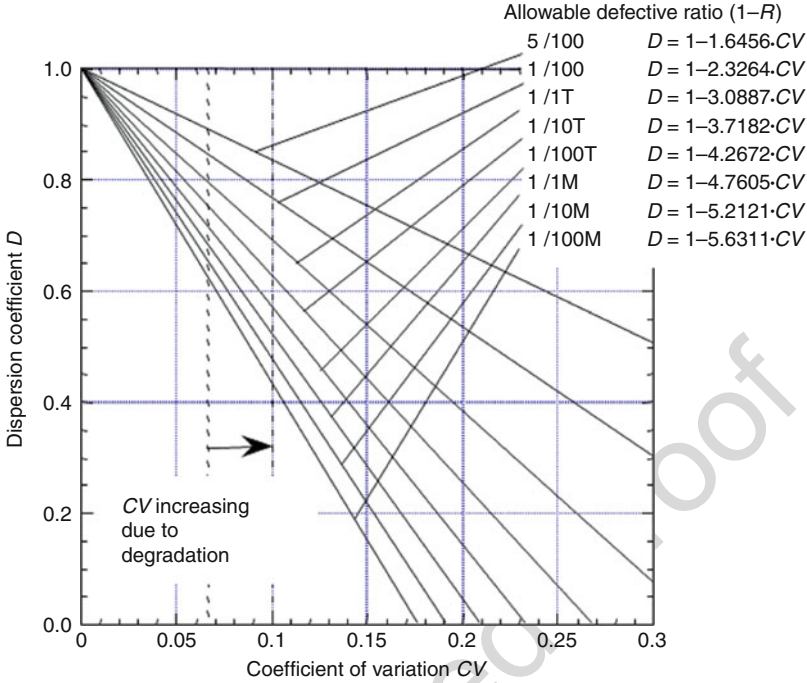


**Fig. 4** Relation between the coefficient of variation CV, the dispersion coefficient D, and the allowable defective ratio (1-R) in strengths of adhesively bonded joints

very rare for a C/T over 40%. A highly durable adhesion can be realized if the C/T of a joint is over 40% just after its production process.

The other index of adhesion durability is the coefficient of variation (CV) that is defined as the standard deviation divided by the average strength. Adhesively bonded joints show a fairly good correlation between the CV and the C/T. A low CV under 0.15 is necessary, and 0.10 is desirable for highly durable adhesion. Interfacial fracture increases the CV. A large CV condition over 0.2 gives unreliable joints and should be avoided (Haraga 2008).

Figure 4 shows the CV and the dispersion coefficient (D) in a case of adhesive joints (Haraga 1992; Teramoto et al. 1993; Nakajima et al. 1997). D is defined as a factor that is multiplied with average joint strength, and this product gives the maximum strength of defectives as shown in Fig. 5, where R is yield ratio of useable joints and 1-R is allowable defective ratio. For instance, when 1-R is 1/100,000 and CV is 0.15, D can be determined as 0.36 with Fig. 4. This case indicates the condition of a sample having a strength lower than 36% of the average joint strength among 100,000 samples. If CV is 0.2 and 1-R is 1/100,000, D becomes 0.15, and this case is obviously not a reliable design. A basic and important rule about reliable design of adhesively bonded joints is the management of C/T under 40% and CV under 0.15.



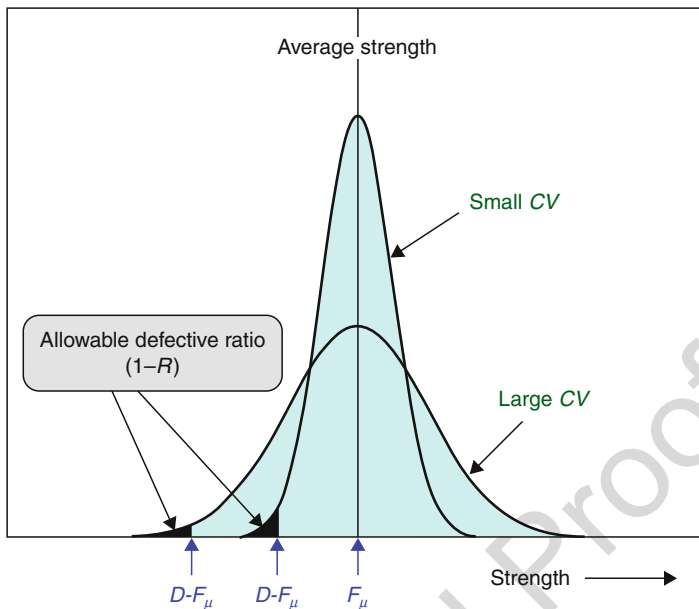


**Fig. 5** A schematic illustration of the relation between the average bonding strength  $F_\mu$ , the allowable defective ratio  $1-R$ , and the dispersion coefficient  $D$

## 41.4 Important Points for Adhesion Process Control

### 41.4.1 Dimension Allowance of Parts Bonded Adhesively

#### Substrate Deformation

A serious error in the adhesion process is to ignore the dimension allowance of the substrate. Some members are often machined beyond their specified dimension allowance indicated in the design drawing. As shown in Fig. 6, a required flat surface Fig. 6a can be deformed as Fig. 6b or c. The hat cross-sectional member shown in Fig. 7a can be finished in the cross section as Fig. 7b or c due to bad bending forming or can be spring-backed as Fig. 7d or e. Such deformations cause strength deviation due to nonuniform adhesive thickness or bad adhesive spreading or defective goods due to the tilt of the bonded parts.

#### Applied Pressure to Parts in the Bonding Process

Pressure has to be applied to parts during the curing process of adhesives. In this process, excess pressure applied to the members shown in Fig. 7a can induce undesirable deformation as shown in Fig. 7b. Conversely, in the case of Fig. 7c, the member can deform by excess pressure and take the shape shown in Fig. 7a. The deflected members shown in Fig. 7c, d are flattened by pressurization. In such cases, a spring-back force is induced when the applied pressure is released after the

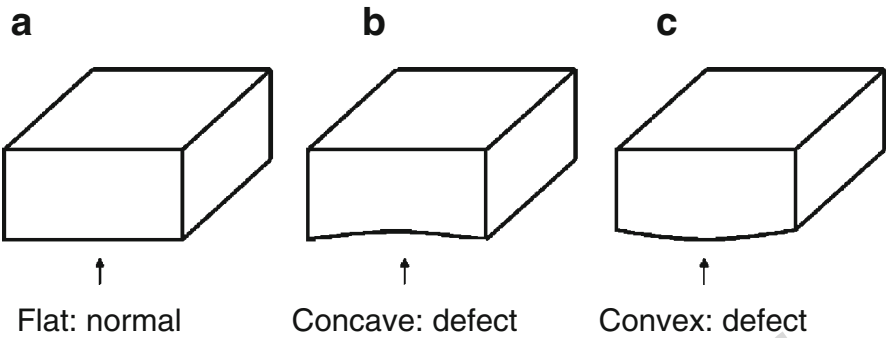


**Fig. 6** Undesirable shape of the bonding surface due to machining

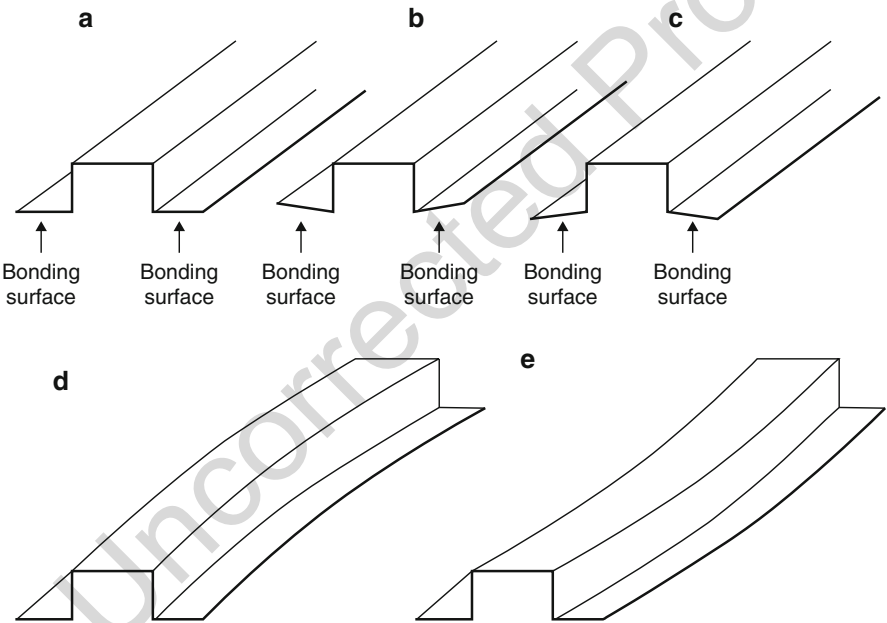


**Fig. 7** Undesirable deformation of hat members due to plastic forming (**a**) no deformation, (**b**) concave deformation in the flange, (**c**) convex deformation in the flange, (**d**) convex deflection, and (**e**) concave deflection

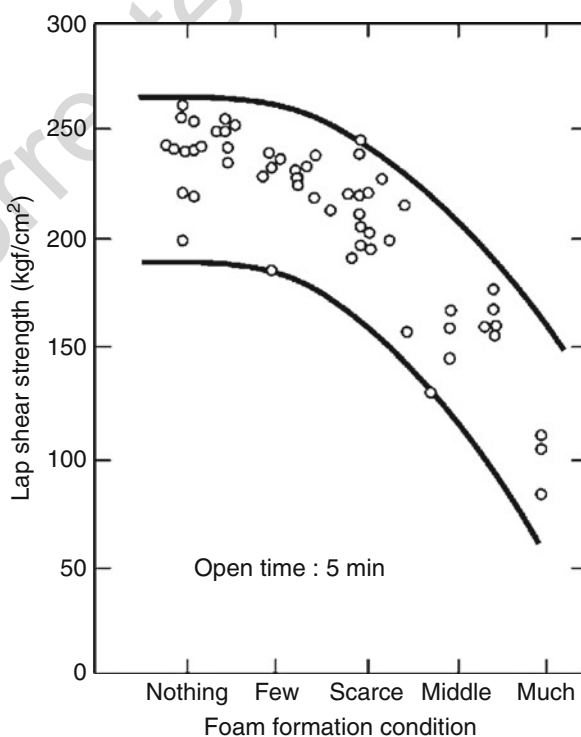
184 bonding process because residual stress occurs due to the permanent deformation.  
185 The spring-back forces act as creep loads to adhesive joints. Creep rupture often  
186 happens not only in the case of weak adhesives such as pressure-sensitive adhesives  
187 at ambient temperature but also in the case of strong adhesives if they are subjected  
188 to high temperatures during a paint-baking process, for instance.

### Environmental Condition Control

Temperature and humidity have to be controlled appropriately during the cure reaction of adhesives. In summer, ambient curing adhesives need a quick operation in bonding process because their gelation time is short. In winter, since gelation time is longer, the time of pressure application is also longer. To avoid the variance of operation and keep the sequence constant, temperature control using air conditioners is highly recommended. Humidity control is also very important, especially when using humidity-cured adhesives or sealants, such as instantaneous adhesives or silicone adhesives. Sometimes, humidity is not “desirable” but rather “indispensable,” and it is necessary to increase humidity when it is very low. On the contrary, in the case of two-part urethane adhesives, the strength decreases due to the foam formation in the adhesive layer, which tends to happen especially in hot-wet conditions, if the operation time from adhesive application to bonding is long, as shown in Fig. 8. Therefore, dehumidification is recommended in such cases. In addition, since polyol components in urethane adhesives tend to absorb water very much, seal-up of adhesive container is also very important.

Dew condensation on the surface of substrates before bonding is another problem. The dews can corrode the surface before bonding and inhibit adhesive tack. Just

**Fig. 8** Strength variation of joints bonded with a two-part ambient curing urethane adhesive with respect to the foam formation conditions, where open time is the time from adhesive application to lapping adherends, in which the substrates are kept in ambient condition



after the start of room heating in winter, cold members may cause dews on their surfaces. Therefore, humidity control is also necessary in this situation.

### 41.5 Management and Preparation of the Bonding Surface

#### 41.5.1 Wettability Measurement of the Bonding Surface

The surface condition of substrates before bonding depends on the production lot, the shelf condition, and the storage period. Even if the surface is degreased with solvents or chemicals before bonding, it is not necessarily suitable for adhesion. As a method to evaluate the adhesion adequateness easily, wettability tests can be applied using standard liquids commercially available. It is reasonable to measure the wettability of substrates by random inspection once in each morning and afternoon or every time the production lot changes. Experimentally proved minimum value of wettability for proper adhesion is 36–38 mN/m, where the wettability is denoted as surface tension. The use of parts having poor wettability is never accepted. Action to improve the wettability has to be carried out.

#### 41.5.2 Surface Treatment to Improve Adhesion Adequateness

It is frequent that low wettability surfaces influence badly the production line of the goods. It is desirable to introduce surface treatment processes to low wettability materials such as thermoplastics. For instance, short wavelength UV irradiation with low-pressure mercury lamps and ambient pressure plasma irradiation are popular for the purpose. Even short-term irradiation can improve the wettability of surface very much and the bond strength increases, as shown in Fig. 9.

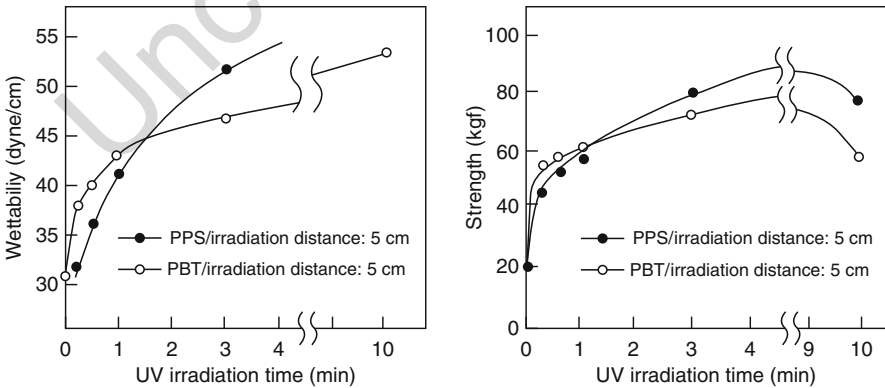


**Fig. 9** Variations of wettability and strength of polyphenylene sulfide (PPS) and polybutylene terephthalate (PBT) with respect to UV irradiation

**41.5.3 Primer Coating**

To improve adhesion strength, primer coating can be applied on the surface of members. Generally speaking, a thin primer layer is advantageous in adhesion compatibility rather than a thick layer, as shown in Fig. 10. Thicker primer layers decrease bond strength. However, too thin primer layers lead to a problem of spreading defect. Applying primer coating properly with a spray or brush is quite difficult and leads to considerable variation in bond strength. Therefore, the use of low-density solution primers is recommended because a light amount of primer is left on the surface even though an excess of solution is applied.

**41.5.4 Pot Life of Adhesives**

Quick-curing adhesives have short pot lives, which are often shorter than the total time of the bonding process including adhesive mixture, application, joining, and pressurization. Therefore, when the total time is too long, the joint strength decreases, as shown in Fig. 11. Bonding time control is very important in such cases. The control can be done, for instance, using a timer having a ring or light signal capability. The timer has to be turned on when adhesive mixing starts. Operators should finish their work by the ring or light signals indicating the end of time tolerance.

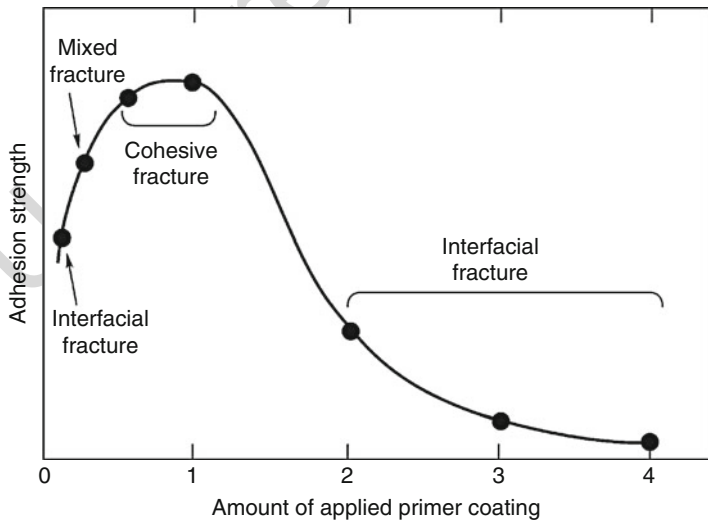


**Fig. 10** Relation between adhesion strength and applied amount of primer coating

**Fig. 11** A typical strength variation of lap-shear joints bonded with a two-part ambient curing modified acrylic adhesive with respect to time from the mixture to the application of the adhesive

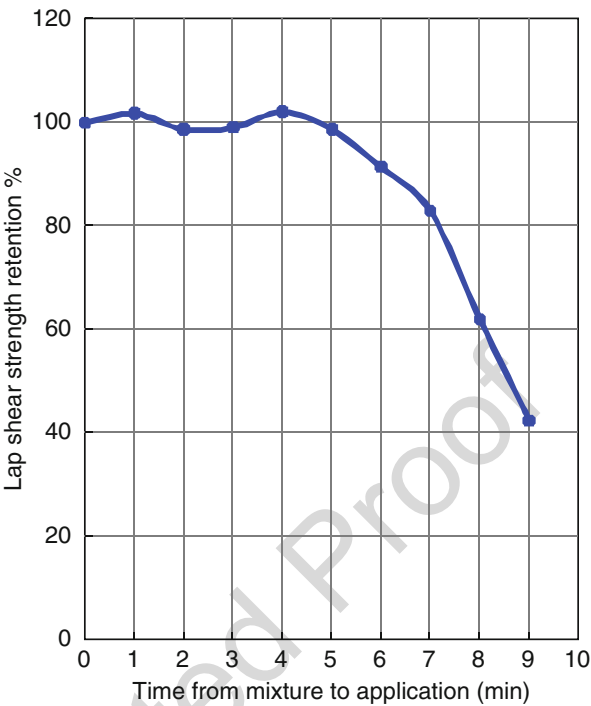
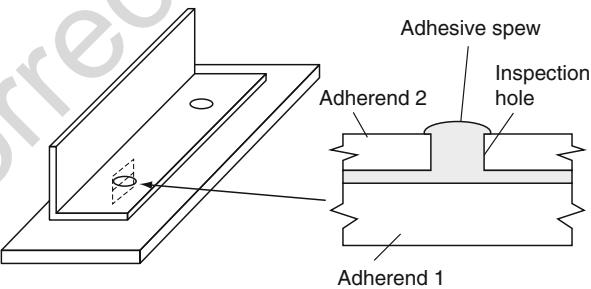


**Fig. 12** Verification of adhesive spreading and curing using inspection holes



**41.5.5 Verification of Adhesive Spreading and Curing After the Bonding Process**

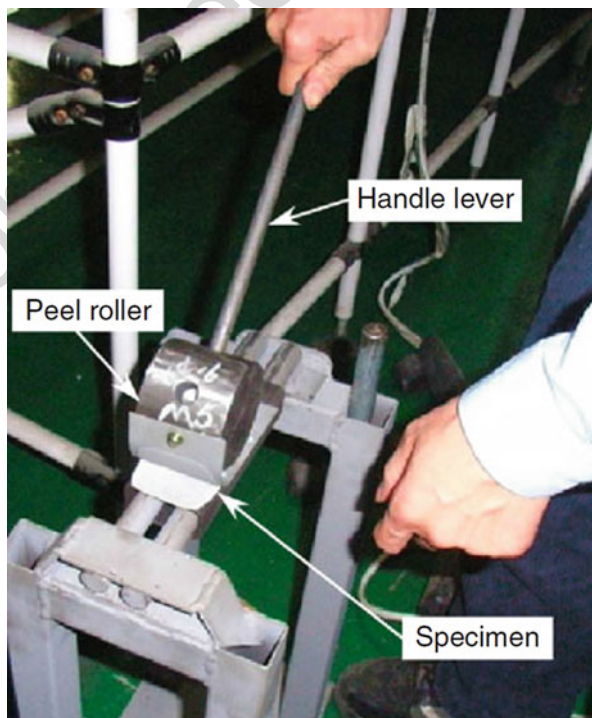
It is often requested but not easy to verify the spreading and curing conditions of adhesives in joints after the bonding process. An usual method is to check the amount of spew and its hardness. Another one, which is more sophisticated, is the inspection hole method shown in Fig. 12. In this method, a hole is machined in one adherend to confirm the amount of adhesive and its curing condition. If

enough amount of adhesive is applied and is spread properly along the surface, a spew can be found from the hole, and the curing condition of the adhesive can be checked by pushing the spew. This method is available even when side spews do not form.

#### 41.5.6 Inspection

The performance of structures bonded adhesively is assessed with strength tests of samples selected randomly or dummy samples. If testing machines are not available in factories, alternative test methods that should be easy to carry out are necessary. Unfortunately, such cases are not rare because testing machines are expensive. Figure 13 shows an example: a simple peel test using a manual testing machine of reasonable price, consisting of a roller and a lever (Haraga et al. 2009). The curing situation of adhesive and the C/T are used as the criterion of the test, and C/T should be greater than 40% to pass the inspection. When testing machines are available, the strength of samples can be used as the criterion.

**Fig. 13** Manual testing machine consisting of a peel roller and a handle lever for peel tests of specimens



### 41.5.7 Process Design

#### Optimum Process Layout of Automatic Devices and Manual Operation

Although a fully automatic bonding process including adhesive application and joining of adherends is possible, it is hard to check visually the mixture condition, the applied amount of adhesive, and its application patterns. Imaging technologies are, of course, possible to use recently. However, there are several problems in terms of cost and accuracy so far. A combined process of automation and manual work is very efficient for such situations. For instance, adherend joining can remain a manual operation to check the adhesive condition mentioned above, which is helpful to avoid defects.

#### Adoption of a Sequential Process

An advantage of manual operation is the availability of a sequential process from adhesive mixture to pressurization. This whole process can be carried out continuously by one person. On the other hand, a parallel process is dangerous because the pot life of the adhesive applied to many queuing parts can be attained if the production line stops before the joining process. Since automation needs a parallel process, a waiting system for the adhesive application, which is activated when the following processes consume too much time, has to be installed.

---

## 41.6 Additional Efforts to Ease Process Quality Control

### 41.6.1 Reduction of Operator's Tasks

The quality of products depends not only on the process control but also on the operator's attentiveness. Therefore, the reduction of operator's tasks is very important. Too excess loads are not acceptable. The process should be designed to ease manual works. Refinement of product design is also effective to reduce difficulties in adhesive joining.

### 41.6.2 Foolproof

Mistakes done by operators are another problem. For instance, the adhesive bonding of different parts having similar configurations can cause mistakes. Errors about bonded sides, positions, or alignment of parts must be avoided too. For such cases, it is a good idea to make bumps and dimples (or holes) to facilitate the joining, as shown in Fig. 14. To control the position and the pattern of the combination, side matching, directional alignment, and positioning of parts can be conducted easily.



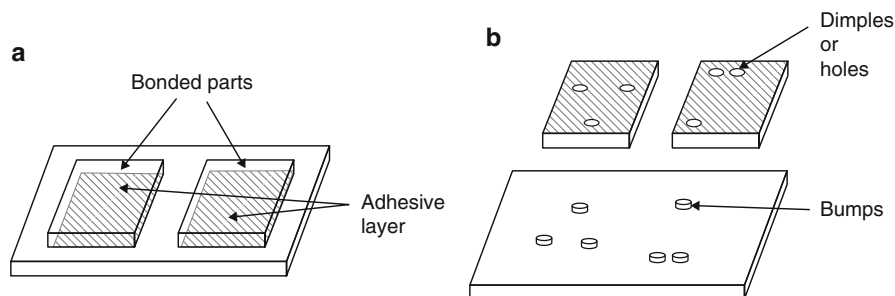


**Fig. 14** Foolproof method to prevent operators' mistakes of bonding sides, positions, or alignment of parts using bumps or dimples (or holes); (a) without this method, (b) with this method

### 41.6.3 Use of Adhesives with an Easy Process Control

#### Use of Oil Accommodating Adhesives

Surface cleaning of adherends is vitally important for good adhesion, and it influences the performance of the joints. Recently, oil-accommodating adhesives, which can be used directly for oily surface, are available. Two-part acrylic adhesives (SGA) and some types of one-part thermosetting adhesives have this capability. Surface cleaning processes can be omitted, and scattering of bond strength can be reduced using this type of adhesives.

The use of oil-accommodating adhesives has the advantage that steel parts can be stored in oiled condition and degreased before bonding is no longer necessary. The oil prohibits the stains on the surface of the steel parts that can reduce the bond strength. The whole process is also simplified very much.

#### Use of Adhesives Tolerant to Wide-Range Mixture Ratios

Two-part ambient-setting acrylic adhesives (SGA) have wider permissible ranges in terms of mixture ratio than two-part epoxy adhesives, as shown in Fig. 15 (Denki Kagaku Kogyo Co., Ltd 2009). Even if the mixture varies, or the adhesive parts are applied individually on each surface, the bonding strength is not so much influenced because of radical polymerization. The use of adhesives insensitive to mixture ratio is convenient to simplify the control of the mixture process.

#### Use of Visually Checkable Adhesives

Mixture ratios of two-part adhesives can be visualized to assign the proper colors to the adhesive parts, as shown in Fig. 15. In actual production lines, sample color tables are helpful for operators to check the mixture ratio.

Innovative adhesives, whose color can be changed with respect to cure progress, are recently available. Figure 16 shows the color change of a two-part ambient-setting acrylic adhesive: NS700 series (Denki Kagaku Kogyo Co., Ltd., Japan) (Tomioka 2010). The colors of the two parts of the adhesive are white and black before mixing. The adhesive becomes green after mixing the two parts. The color

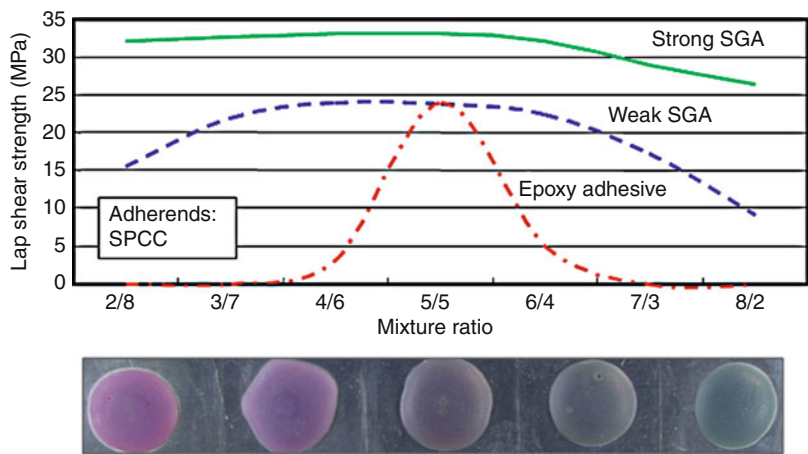
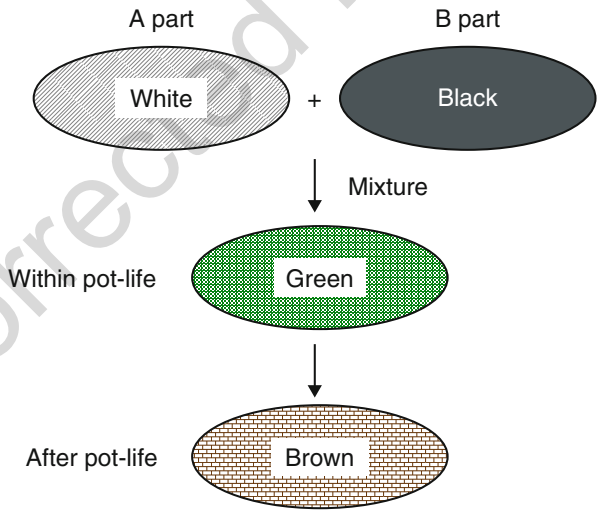


**Fig. 15** Relation between mixture ratio of adhesive parts, lap-shear strength, and variation of adhesive colors (SGA second-generation acrylic adhesive, SPCC cold rolled steel sheet)

**Fig. 16** Colors change depending on the polymerization time in the case of a two-part ambient curing modified acrylic adhesive: NS700 series (Denki Kagaku Kogyo Co., Ltd., Japan)



changes to brown when gelatification starts and to dark brown after full curing. It is possible for operators to check visually the mixture and the curing conditions of adhesives with this method.

### Use of Adhesives Including Spacers

The adhesives shown in Figs. 15 and 16 include plastic fillers as spacers to keep the bond-line thickness constant. The use of such adhesives is very helpful to control the thickness without particular attentiveness.

## **41.7 Education and Training**

### **41.7.1 Operator's Education and Qualification**

Appropriate education for operators is indispensable for a work of good quality in adhesion processes. At first, a process manual book has to be written. Apparatus, materials including adhesives and solvents, procedures, and inspection methods have to be indicated comprehensibly using pictures or photos. Not only the standard working methods and conditions but also the maximum and minimum values of permissible allowance for each condition must be indicated in the procedure description. Determination criteria to pass the inspection should be indicated with specific samples. Prohibited actions have to be indicated explicitly.

Lectures and training for operators should be given using the process manual book. The reason for minimum and maximum criteria must be explained appropriately so that operators can understand them entirely, and there should be no "black box" in the processes.

For operators providing adhesion works at vitally important sites, theory, practice, and examinations are mandatory. The operators passing the examinations can be approved as qualified operators. Only the qualified operators have to be appointed to carry out adhesion processes at important sites.

### **41.7.2 Thorough Exchange of the Information About Process Changeovers**

Processing procedures, methods, and conditions must not be altered by each operator. If any processes shown in the manual book need to be changed to improve the performance, the operator has to inform the manager in advance. The suggestion must be investigated by the manager with the process designer. If the suggestion is worth to be employed, the process can be changed after the authorization of the process and the revision of the process manual book. This rule is indispensable, and all operators must be obligated to comply it.

## **41.8 Conclusion**

For the processing quality control of adhesively bonded joints, scientific approach based on both probabilistic design and statistical treatments is necessary. For decreasing the ratio of defective joints, the coefficient of variation (CV) of the samples should be kept small. The cohesive fracture ratio (C/T) of fractured joint surfaces is vitally important to keep CV small. Since the cohesive fracture ratio decreases often due to mechanical or chemical mismatch of adherends and adhesives, the surface treatment of adherends is important.

Process design should be done appropriately to improve the efficiency and the economy of the lines and to increase the yield ratio of products. The use of sequential

processes, reduction of operator's tasks, and foolproof for workers are also very important and should be introduced in the production process.

The condition of adherend members, adhesives, and process environments are changing continuously with time. Care should be taken to the change and establish flexible adhesion processes and procedures that can meet the change. Therefore, adhesion process should have high adaptivity to the conditional change. The process design should be done as such. The methods shown in this chapter are just typical examples, and other particular efforts must be necessary for each practical process. Reexamination of actual processes in terms of increasing the yield ratio of products having adhesively bonded joints is also essential.

The education and training of operators are effective investments to avoid making defectives and stopping the production line. Inspection of goods is not only the final barrier of shipping defective products but also the first stage of quality control actions.

---

## References

- Arenas JM, Narbon JJ et al (2010) *Int J Adhes Adhes* 160:165  
Bandaruk W (1962) *J Appl Polym Sci* 217:220  
DeFrayne GO (1983) Adhesive specification and quality control. In: Schneberger GL (ed) *Adhesives in manufacturing*. Marcel Dekker, New York  
Denki Kagaku Kogyo Co., Ltd. (2009) *HARDLOC brochure*  
Espie AW (1995) *Int J Adhes Adhes* 81:85  
Gorbatkina Yu A, Ivanova-Mumjieva VG (2001) *Int J Adhes Adhes* 41:48  
Hadj-Ahmed R, Foret G, Ehrlicher A (2001) *Mech Mater* 77:84  
Haraga K (1992) *Adhes Technol* 28:33  
Haraga K (2008) *Kagaku Kogyo* 271:277  
Haraga K, Ganryu Y et al (2009) *Mitsubishi Denki Giho* 19:23  
Montgomery DC (2008) *Introduction to statistical quality control*, 6th edn. Wiley, Hoboken  
Nakajima Y, Taguchi K et al (1997) *Eng Mats* 87:104  
Petrie EM (2007) *Handbook of adhesives and sealants*. McGraw-Hill, New York, pp 203–226  
Roberts RW (1990) *Processing quality control*. In: *Adhesives and sealants*, vol 3. Engineered material handbook. ASM International, pp 735–742  
Seo DW, Lim JK (2005) *Compos Sci Technol* 1421:1427  
Straalen IJJ, Wardenier J et al (1998) *Int J Adhes Adhes* 41:49  
Stroud WJ, Krishnamurthy T et al (2001) *AIAA2001–1238* 1:12  
Teramoto K, Okajima T et al (1993) *J Adhes Soc Jpn* 37:44  
Tomioka T (2010) *Nikkei Monozukuri* 59:67  
Vallee T, Correia JR et al (2005a) *Compos Sci Technol* 331:340  
Vallee T, Riberio J et al (2005b) *Proc Int Symp Bond Behav FRP Struc* 149:155  
Vallee T, Correia JR et al (2006) *Compos Sci Technol* 1915:1930

Robert D. Adams

## Contents

42.1	Introduction .....	1172
42.2	The Nature of Defects in a Joint .....	1175
42.3	Tests Carried Out Before Bonding .....	1178
42.4	Testing After Bonding and During Service .....	1180
42.4.1	Ultrasonics (Pulsed) .....	1180
42.4.2	Sonic and Ultrasonic Vibrations .....	1184
42.4.3	Spectroscopic Methods .....	1186
42.4.4	Other Acoustic Methods .....	1187
42.4.5	Acoustic Emission .....	1188
42.4.6	Thermal Methods .....	1188
42.4.7	Optical Holography .....	1190
42.4.8	Visual .....	1190
42.5	Future Developments .....	1190
42.6	Conclusions .....	1191
References	.....	1191

## Abstract

The objective of any system of nondestructively examining an adhesive joint is to obtain a direct correlation between the strength of the joint (howsoever defined) and some mechanical, physical, or chemical parameter which can readily be measured without causing damage to the joint. Faults may be defined as anything which could adversely affect the short- or long-term strength of a joint. There are two basic areas for examination in properly made joints, the *cohesive* strength of

R. D. Adams (✉)

Department of Mechanical Engineering, University of Bristol, Bristol, UK

Department of Engineering Science, University of Oxford, Oxford, UK

e-mail: [r.d.adams@bristol.ac.uk](mailto:r.d.adams@bristol.ac.uk)

the polymeric adhesive and the *adhesive* strength of the bond between the polymer and the substrate. In addition, voids, disbonds, and porosities create an additional issue for inspection.

During the production phase, and also in service with critical structures, it is essential to use nondestructive tests to assess the quality and fitness for purpose of the product. The nondestructive test will not measure strength directly but will measure a parameter which can be correlated to strength. It is, therefore, essential that a suitable nondestructive test is chosen and that its results are correctly interpreted. Typical defects found in adhesive joints are described and an indication given of their significance. The limits and likely success of current physical nondestructive tests will be described and future trends outlined.

It is shown that a variety of techniques are available for disbond detection, ultrasonics, and different types of bond tester being the most commonly used. These techniques are very time-consuming, especially if large bond areas are to be tested. Monitoring interfacial properties is much more difficult, and there is currently no reliable test after the joint is made although there are some indications of a possible way forward using high-powered lasers.

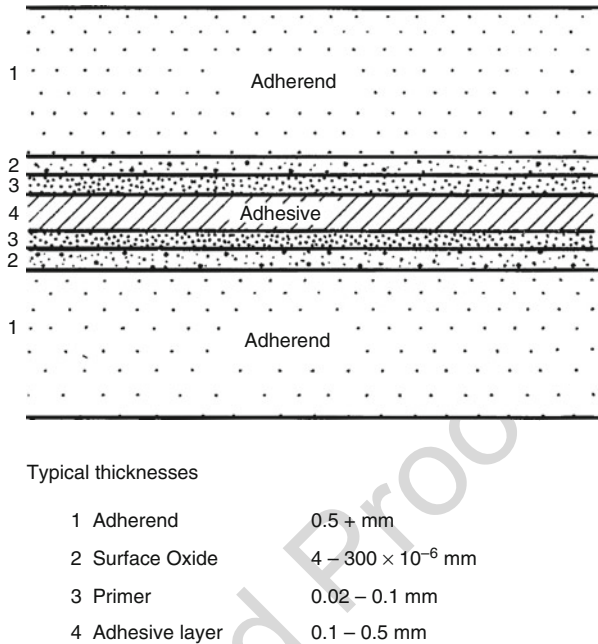
---

## 42.1 Introduction

Adhesive bonding offers the designer many advantages, especially in being able to join dissimilar materials without bolts, rivets, etc. (Adams et al. 1997). However, despite its potential advantages, the use of adhesive bonding in safety critical structures has been limited by a lack of adequate nondestructive testing (NDT) procedures: Without such procedures, the reliability of a structure cannot be guaranteed. When using advanced composites, adhesive bonding is often preferred because these materials have low transverse tensile and local bearing strength. The problem comes when it is found to be necessary to define how strong the joint is. While there are certain situations when it is possible to be reasonably confident of the initial strength of a joint if it has been carefully made by a well-established process and there is a record of previous destructive tests, this cannot be guaranteed for the lifetime of the joint. If we add to this the possibility of joints being made incorrectly, we quickly come to the conclusion that there is a need for a technology to determine the strength of a joint without breaking it. This is called nondestructive testing, evaluation, or inspection, usually abbreviated to NDT, NDE, or NDI. Such testing will usually be performed after manufacture or at stages during manufacture. However, in more stringent applications, inspection during service may also be required.

Ideally, a nondestructive test would predict the strength of the bonded joint and its susceptibility to environmental attack. This is very difficult to achieve, partly because a direct measurement of strength cannot be nondestructive, so it is necessary to correlate strength with other properties, such as bond area, interfacial stiffness, etc. Also, the stress distribution in a typical adhesive joint is far from uniform, and so the strength is much more sensitive to the integrity of some areas of the joint than to

**Fig. 1** A simplified schematic diagram showing the various layers in an adhesive joint



others. Measuring bond area, stiffness, and so on will not necessarily give good correlations with strength. Changes in these properties do, however, give an indication that a joint may be defective.

In order to understand the nondestructive evaluation of the strength of an adhesive joint, we need to understand the mechanics, physics, and chemistry which are involved in the production and stressing of such a joint. The details of these factors are given elsewhere in this book, so only a brief description will be given here. A bonded joint generally consists of two adherends or substrates, connected by an adhesive layer. However, it is vital to understand that there are also two surfaces and that adjacent to these is an interphase region such that the adhesive properties do not change abruptly to those of the adherend. These different zones are shown schematically in Fig. 1. The most commonly used form of adhesively bonded joint is in tensile lap shear, as shown schematically in Fig. 2. Many theories have been used to analyze the stresses in bonded joints (see ► [Chaps. 24, “Analytical Approach,”](#) and ► [26, “Numerical Approach: Finite Element Analysis”](#) in this book), but the essence is shown in Figs. 3 and 4. Here, it can be seen that the shear and peel (transverse tensile) stresses are a maximum at the joint ends, while the middle of the joint generally has low stresses. Failure is therefore going to begin at these joint ends and then propagate toward the interior of the joint until total failure occurs. Another important class of adhesively bonded components is in repair patches, particularly for aircraft. It is often cost-effective and convenient to apply a patch rather than to replace an aircraft component, particularly if the need to repair is remote from the source of the component (Pyles 2003; Baker et al. 2009). Since the repair is often

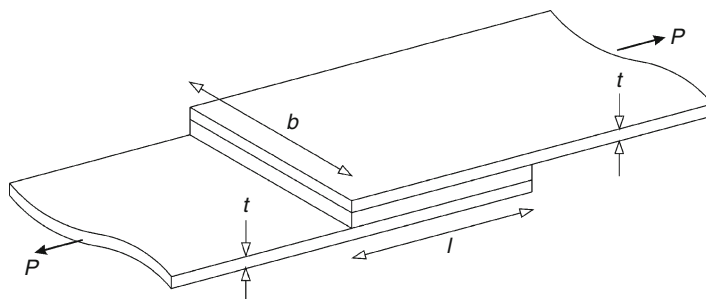


**Fig. 2** Schematic diagram of a single-lap joint bonding adherends of thickness  $t$  and width  $b$  with an overlap  $l$

**Fig. 3** Variation of shear stress with distance along the overlap according to Volkersen's theory

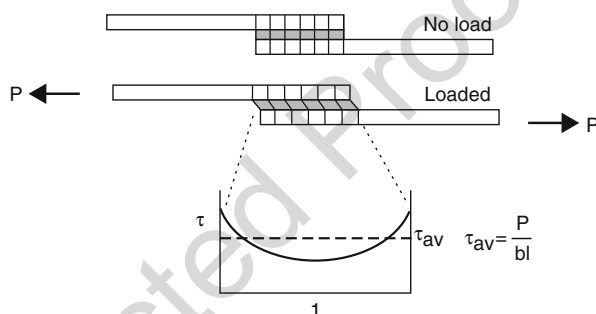
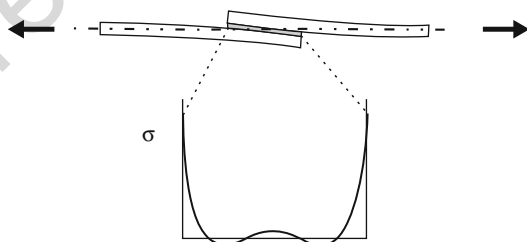


**Fig. 4** Variation of transverse tensile stress (peel) with distance along the overlap according to Goland and Reissner's theory



made in non-factory conditions, it is important to be able to carry out some form of nondestructive inspection before releasing the vehicle back into service.

There exists a wide variety of nondestructive testing techniques for interrogating structures. These range from well-known methods such as ultrasonics and X-rays to a variety of specialist methods such as shearography, tapping, and thermal. However, it must be stressed that many of the techniques used with metallic structures are quite unsuitable for use with bonded joints. Various authors have reviewed the literature on nondestructive testing of bonded joints. The reader is referred to Hagemaijer (1985), Guyott et al. (1986), Adams et al. (1987), the special edition of NDT International which was edited by Adams and Cawley (1988), and recently by



Cawley (2005). Crane and Dillingham (2008) have provided an excellent review of adhesive bonding with composite materials.

The objective of this chapter is to describe the mechanics and physics of the main NDE methods for adhesively bonded joints and to indicate what is possible and not possible.

## 42.2 The Nature of Defects in a Joint

It is instructive at this stage to examine the types of defect which may occur in bonded structures. First, let us consider lap joints in which the bonded area is a few square centimeters or more. Figure 5 illustrates many of the possible defects.

*Porosity* is caused by volatiles and entrained air in the adhesive. The voids may also be due to products of the chemical reaction[s] involved in curing the adhesive. Porosity is therefore present in most bond lines to some extent. *Adhesive cracks* are due to problems with curing (cure and/or thermal shrinkage) or to large applied stresses, either one-off or repeated (fatigue). Local areas of *poor cure* are due to incorrect mixing of the adhesive system. Larger areas, possibly extending through the whole bond line, are either due to incorrect mixing, incorrect formulation, or insufficient thermal exposure. Sometimes, poor cure is self-correcting with time in that the chemical reaction continues, albeit slowly. Voids are often due to air becoming trapped by the pattern of laying the adhesive or to insufficient adhesive being applied. Voids can also be caused by relative movement of the adherends

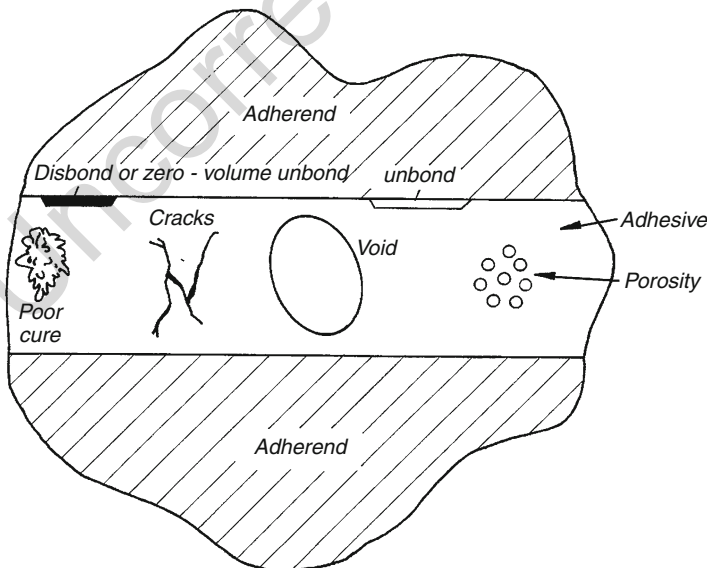


**Fig. 5** An illustration of the various defects which might be present in an adhesive bond line



**Fig. 6** Void in adhesive bond line most probably caused by moving the joint before the adhesive had reached a sufficient state of cure

during the curing process. Large voids cannot be caused by volatiles, unless something is very wrong with the adhesive system. Figure 6 shows what can happen in a tubular joint when the adherends are moved before the adhesive has reached a stage in its cure cycle when it has hardened sufficiently. The voids offer a path for the ingress of water or other fluids and fatigue crack initiation (see ► [Chap. 33, “Fatigue Load Conditions”](#) in this book). *Surface unbonds* are an alternative form of void, often caused when adhesive is applied to one adherend only and unevenly. The most dangerous form of these can occur where the adhesive and adherend are in contact, but there is no significant bond strength between them. Such defects may be caused by poor surface preparation, failure to remove the manufacturer’s backing film completely, a loose substrate, and so on. Such bonds are called *zero-volume unbonds* or *kissing bonds*. While the latter term is commonly used today, it implies there is a bond, whereas, in fact, there may be no bond at all, or only a very weak one. Jeenjitkaew et al. (2010) and Marty et al. (2004) have given an excellent description of the causes and morphology of kissing bonds. Galy et al. (2017) and Jeenjitkaew and Guild (2017) feature among various authors who have tried to make realistic kissing bonds and then to devise methods to test them. *The main problem is to be able to make these joints so that they are representative of true structures. Only then can the process of testing them move forward.*

The presence of defects in lap joints is more indicative of poor joint manufacture than of impending failure, especially for short-term loading. Over the long term, defects may allow faster ingress of water or aggressive substances or provide sites for fatigue crack nucleation. It still, therefore, remains necessary to look for these defects. Karachalios et al. (2013) have shown that the strength of lap joints may or may not be affected significantly by large voids in the interior of a lap joint. This is because fracture initiation in the adhesive occurs due to the failure strains in many

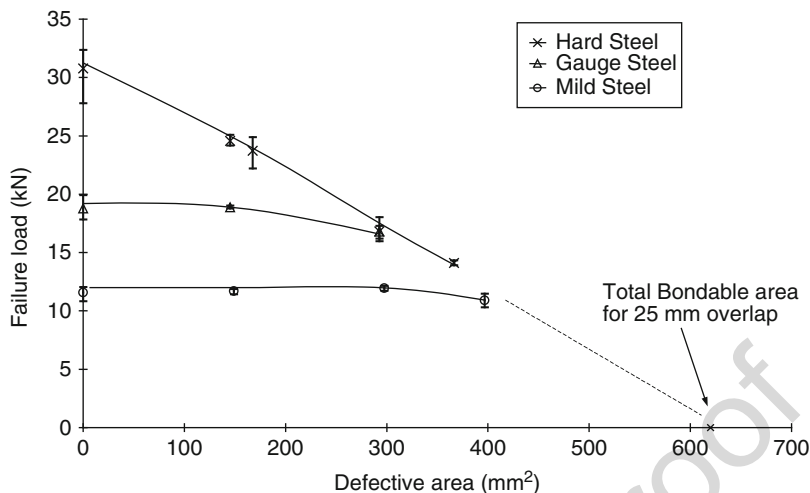


**Fig. 7** Variation of failure load with defective area for single-lap joints bonded with AV119 adhesive showing how the lap-shear strength is a function of adherend type and remaining bond area (From Karachalios et al. 2013)

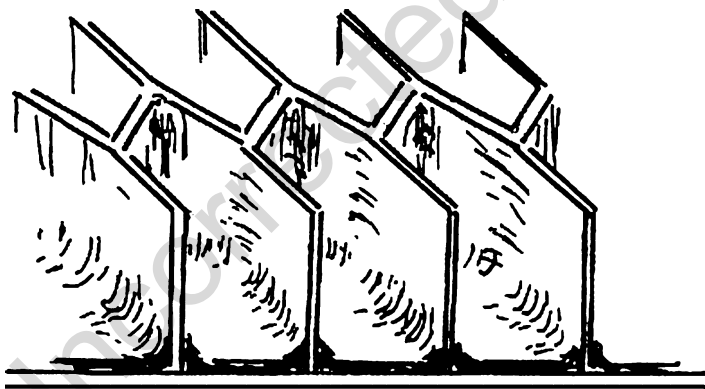
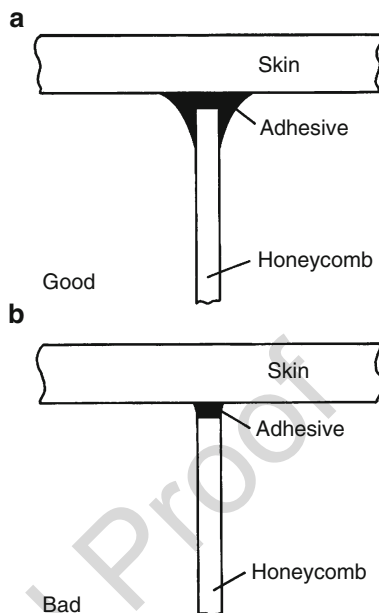


**Fig. 8** A sketch of honeycomb bonded to a skin and showing the fillet (From Adams et al. 1997)

adhesives being much less than the yield strains of structural steel or aluminum. However, if high-strength alloys are used with modern rubber-toughened epoxies, the lap joint strength is more or less proportional to the bonded area. This is shown in Fig. 7.

The other major form of joint used with structural adhesives is the T joint used in bonding honeycomb to the skins as shown in Fig. 8. The skin and core are bonded by a large number of these lightly stressed joints. It is essential that the adhesive forms a generous fillet, as shown in Fig. 9a, and not the apparently more economical but weaker joint shown in Fig. 9b. Some years ago, the author tried to stiffen an

**Fig. 9** Good and bad bonds between honeycomb and skin  
(From Adams et al. 1997)



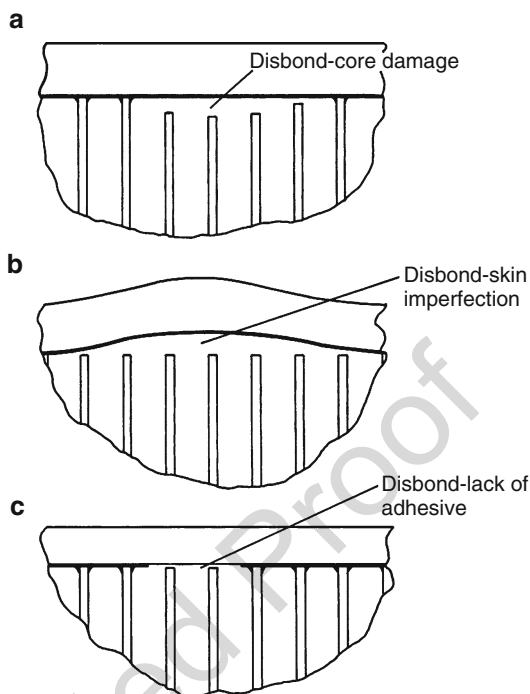
aluminum alloy honeycomb core by filling with a polyurethane foam. This was then scraped down to the level of the honeycomb and the bond made. Unfortunately, the foam prevented the formation of the fillet, and the joint failed at a low load. With bonded honeycomb structure, the major defects consist of a lack of attachment between the core and the skin. This may be due to several causes such as locally crushed honeycomb (Fig. 10a), skin defects (Fig. 10b), or lack of adhesive (Fig. 10c). In themselves, none of these defects may reduce the short-term joint strength. However, as for the lap joint, they may show poor preparation and may provide sites for fatigue crack propagation.

## 42.3 Tests Carried Out Before Bonding

In order to make a successful adhesive joint, it is vitally important that the surfaces to be bonded should be properly prepared. Usually, this means clean, chemically active, and sufficiently strong. We therefore need surface inspection tests to ensure that the surfaces do not contain excessive amounts of water vapor, hydrocarbons, or other contaminants. Today, there exist many powerful laboratory tools for assessing surface properties. However, these are rarely used in manufacturing environments since they are slow and expensive.

A simple test involves the wettability of the surface, by measuring the contact angle. A full discussion of surface preparation and wettability is given in Part B in this book. If the surface is clean, it is readily wetted, and a drop of water will spread

**Fig. 10** Possible defects with honeycomb core and skin system (From Adams et al. 1997)



over a large area. However, if it is contaminated, the water will remain as droplets. A useful procedure with carbon-reinforced or glass fiber-reinforced plastics is to abrade the surface with a fine “wet and dry” carborundum paper until a thin film of water can be spread over it. A more quantifiable test involves measuring the spread of a liquid drop of constant volume through a transparent gauge placed over the drop or by looking at the “contact angle” between the drop and the surface. Commercial products are also available which will indicate the suitability of the surface for bonding by showing as colored. These self-indicating primers also contain substances to enhance the bond between the surface and the adhesive. The main problem is the uncertain life expectancy and stability of these primers.

The Fokker Contamination Tester, described by Bijlmer (1978), uses an oscillating probe to measure the electron emission energy. This varies greatly with the degree of surface contamination and can even be used to detect residues from alkaline cleaning operations.

None of these methods is totally satisfactory, and the best means of ensuring that a “good” surface exists prior to bonding is carefully to control the processes leading to its preparation, having previously established “good practice.” Maintaining good control over the manufacturing process will increase the probability of achieving a defect-free joint, and this is particularly important in the case of adhesive strength for which no satisfactory nondestructive testing method currently exists (Schliekelmann 1972; Kim and Sutliff 1978).

Crane and Dillingham (2008) claim that the tape peel test (in which a PSA tape is pressed on to a surface and then peeled off) offers an approach that is potentially inexpensive which could be implemented in a fast-paced production environment. Unfortunately, there is insufficient data at this time on the wide range of possible contaminants and the possible levels of concentration for this approach to be applied without further testing. However, it does offer an approach to providing the NDE engineer an important tool to access the adhesion potential of a composite surface before the consolidation of a component.

## 42.4 Testing After Bonding and During Service

By far the majority of nondestructive testing (NDT) techniques associated with adhesive bonds are applied after the joint has been made and are usually carried out at the manufacturing location or during service. Most techniques are void detectors, and, although it is claimed that the cohesive strength of the adhesive is being assessed, this is unlikely to be the case.

### 42.4.1 Ultrasonics (Pulsed)

The monitoring of ultrasonic echoes forms one of the most widely used methods of nondestructive testing for bonded joints and composites. The method is commonly used for the detection of disbands, voids, and porosity.

An incident pulse of ultrasound will be reflected and transmitted (assuming normal incidence and hence no refraction) at each interface of the joint. The amplitudes of the reflected ( $R$ ) and transmitted ( $T$ ) pulses for a unit amplitude incident signal are dependent on the acoustic impedances of the materials on either side of the interface and are given by

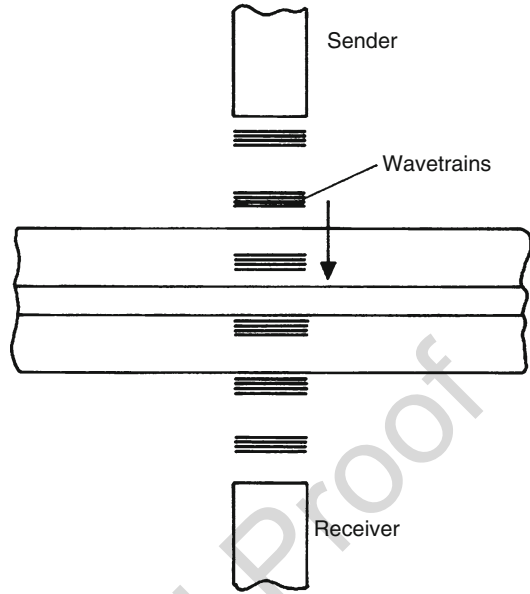
$$R = \frac{Z_2 - Z_1}{Z_1 + Z_2} \quad (1)$$

$$T = \frac{2Z_2}{Z_1 + Z_2} \quad (2)$$

where  $Z$  is the acoustic impedance given by  $\rho c$ ,  $\rho$  is the density, and  $c$  is the speed of sound in the material under examination. Subscripts 1 and 2 denote the materials on the incident and remote sides of the interface, respectively.

If a defect is assumed to contain air or any other low-density substance, it will have a very low acoustic impedance relative to the adhesive or adherend. A pulse incident at the defect is almost totally reflected, leaving negligible energy to be transmitted through the defect. Measurement of the reflected or transmitted energy may therefore be used to indicate the presence of a defect. The simple ray model of a pulse of ultrasound being specularly reflected at a defect is valid when the defect

**Fig. 11** Schematic of ultrasonic pulse in through-transmission mode (From Adams et al. 1997)

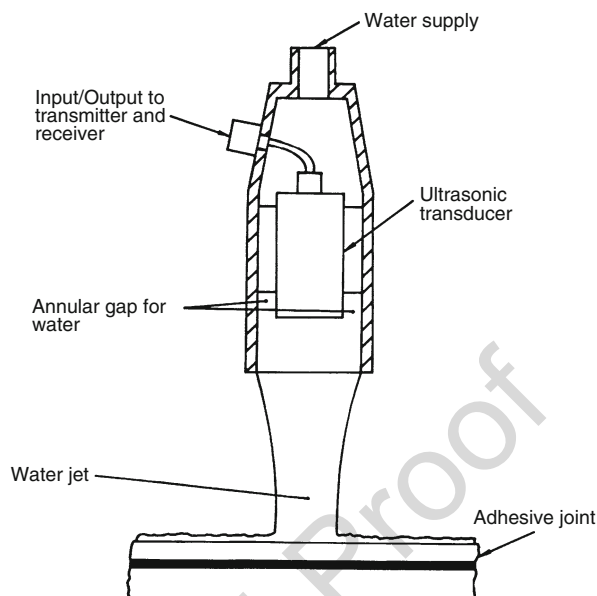


diameter is about one wavelength or larger. Porosity typically comprises pores which are orders of magnitude smaller than the wavelength. Therefore, porosity does not give simple specular reflection but scatters energy in all directions, thus attenuating the propagating pulse.

Various techniques based on ultrasonics are used in connection with adhesive joints. Essentially, a small piezoelectric crystal is pulsed repetitively, causing it to radiate high-frequency sound waves at the natural frequency of the crystal. Normally, these brief wave trains (about five cycles long, at 1–20 MHz and repeated say 1,000 times/s) traverse the joint and can be detected, either by using the same crystal or by using a separate receiver (Fig. 11). By interrogating the change which has taken place in the wave train, it is possible to deduce various characteristics of the structure through which it has traveled. The probes have to be correctly aligned and care must be taken so that the pulse will not be reflected or diffracted by curvatures in the surface. If the adhesive contains imperfections such as roughness, cracks, or porosities, the waves will be scattered, and less will be detected by the receiver. If there is a void, the wave can be partially or totally reflected, again reducing what is transmitted. Fine detail can be revealed, if at all, only by using focused or otherwise concentrated “beams” and intelligent analysis.

In ultrasonic inspection, there are two basic techniques which are commonly used, through transmission and pulse echo. The *through-transmission* technique monitors the amplitude of an ultrasonic pulse transmitted through the joint. The amplitude can be reduced effectively to zero when a disbond larger than the beam width is present, smaller amplitude reductions being seen in the case of porosities, microcrackings, disbonds, and voids whose plan area is smaller than the beam width.

**Fig. 12** Water-jet probe  
(From Guyott et al. 1986)

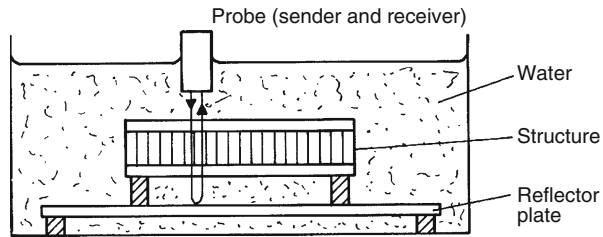


The technique uses separate transmitting and receiving transducers, positioned on either side of the structure to be tested. Alignment of one transducer with the other is vitally important and can present difficulties when large components are tested. Alignment of the transducer axis perpendicular to the surface to be tested, however, is not as critical as with other techniques. Through transmission is often used for the production inspection of large structures such as aircraft fuselage and wing sections, coupling generally being achieved with water jets, such as shown schematically in Fig. 12. The method is also particularly suited to the inspection of honeycomb structures. Using a pulse-echo technique (see below), only the bonding of the top face to the core can be tested reliably, whereas using through transmission, both top and bottom bonds between skins and core can be inspected in a single test. However, through transmission is not generally suitable for in-service inspection since access to both sides of the structure is often difficult or impossible and the attenuation and reflections even in “good” structure can be sufficiently large to render the technique of little value. Also, while it gives an indication that a defect exists, no information about its depth within the structure can be obtained. The *pulse-echo* technique generally uses a single transducer as both the transmitter and receiver. Provided the ultrasonic pulses generated by the transducer are short enough, the individual echoes from each interface can be resolved, their position and amplitude being used to detect the presence of a defect. A large fraction of the pulse will be reflected at a defect owing to its large reflection coefficient; echoes from features behind the defect will also be reduced or disappear.

It is also possible to use a single transducer in a “double through-transmission” configuration. This is achieved by placing a reflector plate beneath the structure in an immersion tank as shown in Fig. 13 and monitoring the echo from the reflector plate.



**Fig. 13** Water bath used for ultrasonic C-scan inspection  
(From Adams et al. 1997)



As in through transmission, this signal is almost completely attenuated by disbands larger than the beam, smaller amplitude reductions being produced by voids, porosities, and smaller disbands. In all pulse-echo testings, alignment of the transducer axis perpendicular to the surface of the structure or reflector plate is important if the reflected signal is to be received back at the transducer. Sometimes, a second receiver probe is used instead of the reflector, the two probes being linked by a yoke. This is often necessary with honeycomb structures since the returning signal is very weak and is swamped by the much more powerful reflected signals. The probe is traversed automatically over the structure, and the amplitude of the signal associated with transmission through the structure is indicated on an *X-Y* or similar recorder. The *X* and *Y* coordinates correspond to the position on the surface, while some other parameter, such as gray scales or false color, is used to indicate quality. Because of the inconvenience of immersing the whole component or specimen, special water-jet probes can be used on large (aerospace) structures. Again, probe alignment is a serious problem.

Good coupling between the transducers and the structure is essential and can be achieved by pressing them together with a film of glycerine or some similar coupling agent between them. Liquid couplants have the disadvantage of affecting the surface if this is in any way absorbent. Alternatives include laser-induced and monitored ultrasonics (Monchalín 1993) and air-coupled probes (Farlow and Hayward 1994; Schindel and Hutchins 1995). Other non-contacting ultrasonic transducers include electromagnetic acoustic transducers (EMATs) (Thompson 1990). Another method is to use a rubber wheel (Drinkwater and Cawley 1994) which can be rolled over the surface. The mechanical characteristics of the rubber are carefully chosen for maximum impedance matching and minimum attenuation.

Several methods of displaying ultrasonic reflections are available, the most common being *A*- and *C*-scans. The simplest presentation is an *A*-scan which shows the amplitude of the signal as a function of time (or distance, if a value for the velocity of sound in the medium is known), as shown in Figs. 14 and 15. In manual testing, an *A*-scan is obtained at each test point and is interpreted by the operator.

If the amplitude of the through-transmitted signal (or of a particular echo in pulse-echo testing) is monitored at each point on the surface of the test piece, a *C*-scan can be produced. Measurements at each point are taken using a scanning mechanism, which produces a plan of the defect positions but gives no information on their depth. The example of Fig. 16 shows a *C*-scan of an adhesive joint sample roughly 100 mm square that had been subjected to environmental attack. Large edge

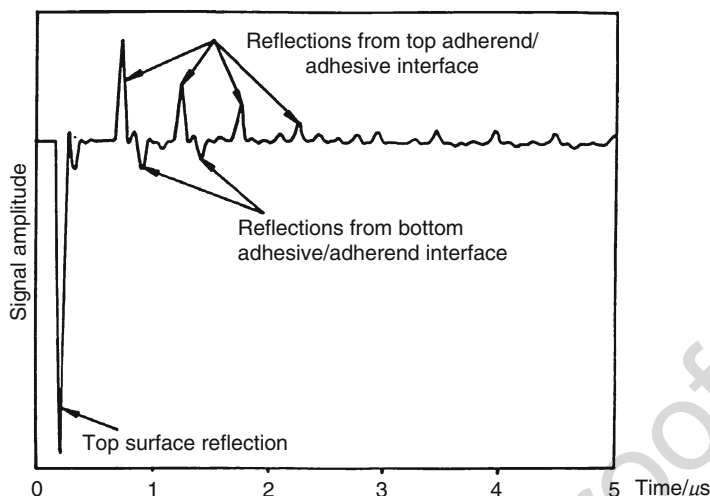


**Fig. 14** Schematic of A-scan from a good joint (From Guyott et al. 1986)

disbonds can clearly be seen, together with groups of small disbonds remote from the edges. Corrosion of the aluminum on one side of the sample that was unbonded is also evident. The automatic scanning mechanisms required to produce *C*-scans usually employ immersion or water-jet coupling, whereas *A*-scan devices often use the contact technique. Portable scanning frames to facilitate *C*-scans on site are also available commercially.

Other ultrasonic techniques which show promise are oblique incidence waves (Pilarski et al. 1990) and Lamb waves (Bork and Challis 1995). Rose and coworkers (1995, 1996; Puthillath and Rose 2010; Rose and Ditri 1992) have used guided ultrasonic waves to detect defects in adhesively bonded joints. Gowini and Moussa (2016) used surface acoustic waves to investigate the change in surface acoustic wave (SAW) phase velocity due to the change in adhesion of a thin film using an aluminum nitride (AlN)/silicon (Si) SAW sensor. They showed that as the adhesion of the film weakens on the surface of the AlN/Si SAW sensor, the velocity dispersion profiles fluctuate since as the adhesion of the layer improves the stress transmitted increases and the wave is more confined in the film layer. Gauthier et al. (2017) Used Lamb waves and showed that modes could be very sensitive to the nature of the interface, that is to say to the level of adhesion, if properly selected.

#### 42.4.2 Sonic and Ultrasonic Vibrations

In the through-thickness direction, an adhesively bonded joint can be regarded as an oscillating system. In its simplest form, the system consists of two masses separated by a spring [the adhesive]. Any variation from a given standard might be thought to indicate the presence of a defect. Unfortunately, the system is more complex than

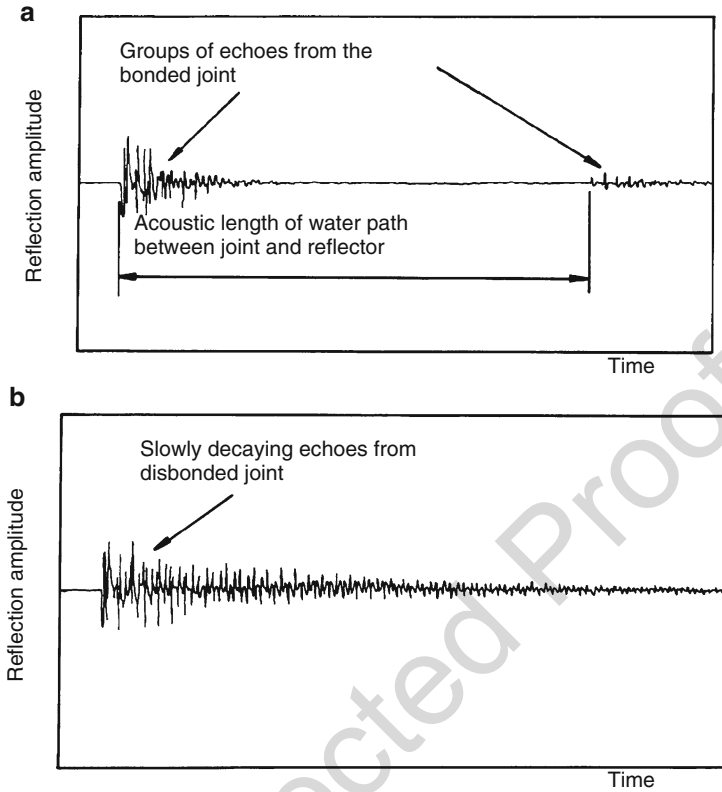


**Fig. 15** A-scans from (a) good and (b) disbonded joints (From Guyott et al. 1986)

this. For instance, a reduced stiffness of the adhesive layer might be due to porosity, non-optimum cure, cracks, or simply a thicker layer than usual. On the other hand, if the joint was in a panel which was consistently produced by using a film adhesive to control the bond-line thickness, then any variation in frequency would indicate a defect of some sort, although it would not be easy to ascertain of what kind.

Sonic vibration techniques, using frequencies of 1–30 kHz, measure the local stiffness of the structure. Disbonds reduce the local stiffness as measured perpendicular to the surface. Usually, only disbonds or voids can be found, the minimum detectable size depending on the size and depth of the defect. Although the detectable defect size is larger than that obtained using ultrasonic techniques, the tests are often more convenient since they do not require a couplant between the transducer and the test structure.

Commercially available mechanical impedance measuring instruments generally take measurements at a single preset frequency. The impedance is highest over good areas and lowest over disbonded areas. The test becomes unreliable when the structure itself becomes more flexible as the impedance of a defective zone can be higher or lower than that of a good zone, depending on the frequency (Cawley 1984,

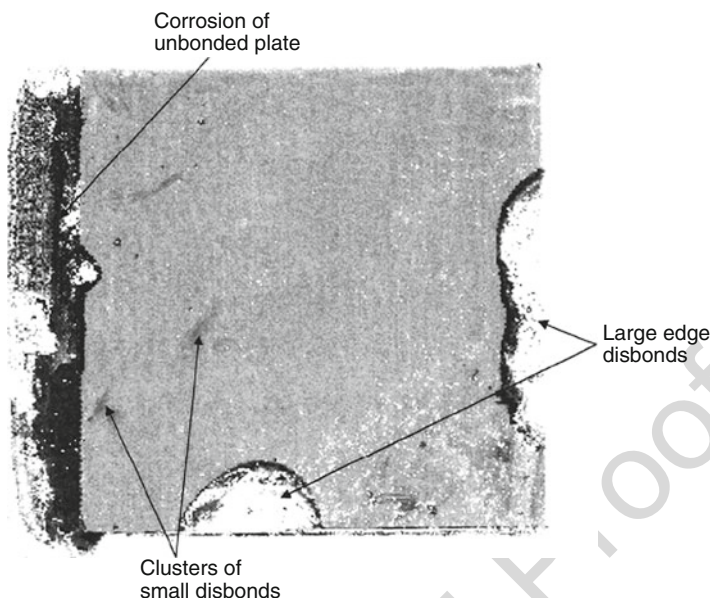


**Fig. 16** C-scan of joint after environmental attack showing large edge disbonds and smaller disbonds remote from edges (From Vine et al. 2001)

1988). One advantage of this type of test is that, instead of using a couplant, a dry point contact is used between the transducer and structure. This dry contact has a finite stiffness (Lange and Teumin 1971) which must be kept as high as possible, to maximize the sensitivity of the technique.

A different principle is used in ultrasonic resonance testing. Here, thickness vibrations are induced in the adherend/adhesive/adherend sandwich in which the two adherends are considered to act as rigid masses, while the adhesive is an almost massless spring. If the type and thickness of the metal sheets are constant, then the resonant frequency is a function of the thickness and bulk modulus of the adhesive.

By injecting short pulses of broadband ultrasound (0.5–15 MHz) into a bonded panel and using modern digital techniques to obtain a frequency spectrum in “real time” of the structural response, it is possible to observe differences between good and bad structures. Lloyd and Brown (1978) showed that certain phenomena, such as water absorption, can be readily detected by this method.

A general preview of vibration techniques for testing composites and adhesives is given by Cawley and Adams (1987).

#### 42.4.3 Spectroscopic Methods

Ultrasonic spectroscopy or the measurement of the through-thickness vibration characteristics of an adhesive joint can be used for the nondestructive testing of

the cohesive properties of the adhesive layer (Cawley and Hodson 1988). The modulus of the adhesive can be determined from measurement of the through-thickness natural frequencies if the thickness of the adhesive layer is known. The Fokker Bond Test Mk II (Schliekelmann 1975), which uses a spectroscopic measurement, is the only commercially available instrument which claims to indicate the cohesive properties of the adhesive in a joint. Frequency and amplitude changes in the first two modes of through-thickness vibration of a system comprising the transducer and the joint are measured. These parameters depend on both the adherend and the bond-line thicknesses as well as the material properties. The range of frequencies over which the instrument operates is typically between 0.3 and 1.0 MHz. Small voids and disbonds at different depths in a multilayer joint can be detected reliably. However, prediction of the cohesive strength of the adhesive is questionable (Guyott et al. 1987) since the frequency shifts, resulting from a change in cohesive properties or bond-line thicknesses, are small and of a similar magnitude to each other. Thus, to obtain a true measure of the cohesive properties with this instrument, the bond-line thickness must be kept constant (or be measured separately). Roth and Giurgiutiu (2017) used piezoelectric wafer active sensors which were permanently bonded to the aircraft structure. Electromechanical impedance spectroscopy, a local vibration method, was used to detect disbonds from the changes in the mechanical impedance of the structure surrounding the disbond. The main problem with this method is the need to bond the sensors in a sufficient number of places to provide a realistic NDE method.

#### 42.4.4 Other Acoustic Methods

Tapping the structure with a hammer or coin is one of the oldest methods of nondestructive inspection. This is essentially a subjective method, and there has been considerable uncertainty about the physical principles involved. When a structure is struck with a hammer or coin, the impact depends on the local impedance of the structure and the hammer used. The local change in structural stiffness produced by a defect changes the nature of the impact. This is indicated by the force-time history of the impact on the structure which can be measured by incorporating a force transducer in the hammer. Impacts on good and disbanded areas of an adhesively bonded structure are shown in Fig. 17. Characteristically, the impact on the sound structure has a higher peak force and a shorter duration than that on the damaged area. Thus, a measure of either peak force or duration can be used to locate defects. Since the method uses only measurements of impact force, no transducers need to be attached to the structure, thus avoiding the coupling and alignment problems which arise with ultrasonic techniques (Cawley and Adams 1988, 1989). The sensitivity and reliability can be increased by further processing the force-time histories such as by taking Fourier transforms of the signal to present the data in the frequency domain (force vs. frequency). Hart-Smith and Thrall (1985) recommend the coin-tap test since it is unable to find flaws that are so small that they can be ignored anyway!

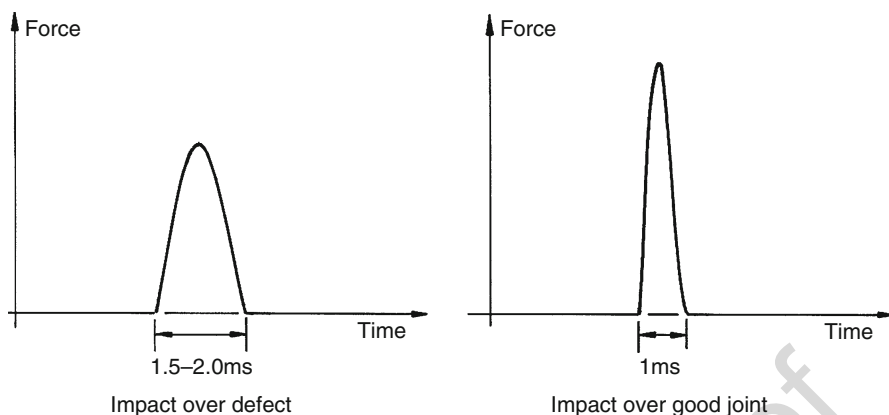


**Fig. 17** Tapping with an instrumented hammer over a good and a disbonded joint

#### 42.4.5 Acoustic Emission

Application of stress to a material will eventually lead to microscopic fracture or slip (Curtis 1982). This is usually associated with a local release of energy which propagates as a stress wave. The wave has a high-frequency content and is referred to as “acoustic emission” [or stress wave emission] which can be detected either by a high-frequency microphone or by a piezoelectric transducer. Unfortunately, it is necessary to stress the joint to a high proportion of its failing load in order to generate sufficient emissions, and there is doubt whether this is practical in most cases. It is therefore not recommended for general use although there are occasions where it may be effective.

#### 42.4.6 Thermal Methods

By heating one surface of a bonded sandwich structure and observing the temperature rise of the opposite face, areas of debond, which resist the transfer of heat, show as cool areas. Alternatively, if the heated face is scanned, debonds will show as hot areas.

The temperature rise on the heated surface is governed by the amount of energy deposited and the speed of application, combined with the thermal properties of the surface material. If the thermal pulse is short enough, the ensuing diffusion process is totally controlled by the material itself. The contrast observed at either surface due to the presence of defects depends on the defect size, its depth from the observed surface, the initial surface temperature rise, and the thermal properties of the material. While these parameters change from one specimen to another, the testing technique is always to record the temperature variation of either surface directly after the thermal transient has been applied. Temperature differences caused by the presence of defects may be seen over timescales ranging from sub-millisecond to

several seconds, depending on the material properties and thickness. The useful information is often obtained within 500 ms, so it is necessary to use a system which can acquire many sequential images in this time window.

The equipment required to perform transient thermography falls into two categories: the transient heat source and the thermal imaging/analysis system. The heat pulse must have a sufficiently fast rise time to provide a rapid temperature rise since it is the steepness of the temperature gradient which provides the contrast between defective and non-defective areas. In materials of high thermal diffusivity [the ratio of thermal conductivity to mass density] such as metals and carbon composites, this rapid temperature rise can conveniently be provided by discharging several kilojoules of energy from a bank of capacitors through xenon flashtubes which are directed at the area of interest. For poor thermal conductors such as glass fiber composites, the rate of heating produced by hot-air blowers is frequently adequate. Temperature sensing is normally done with a scanning infrared camera. Heat pulses or moving heat sources were used by Reynolds (1988). Temperature-sensitive paints of liquid crystals and thermoluminescent coatings can also be used. High-power lasers can be used, but care must be taken to avoid causing damage to the surface.

Major improvements in thermal imaging equipment have been made in recent years. Early work on the method used a thermal imaging camera whose output was recorded on a video tape, the analysis being performed on the recorded image using slow-motion replay and freeze-frame facilities. (The technique was once called pulse video thermography (Hobbs et al. 1991).) Now the images are stored digitally, and automatic processing routines are available (Shepard 1997).

In general, the sensitivity of the method is reduced as the depth of the defect from the surface monitored by the thermal imaging camera is increased. The sensitivity is best expressed as the defect diameter/depth ratio required for the defect to be detectable. This sensitivity is material specific and must be determined experimentally using specially fabricated test plates containing flat-bottomed holes of different diameters and depths. Typical values of the ratio of minimum detectable defect diameter to defect depth are 2–4 for metals (Hobbs et al. 1994). The performance in carbon fiber composite may be somewhat poorer than this because the composite has higher conductivity in the plane of the fibers than in the through-thickness direction. The heat therefore tends to diffuse parallel to the surface, rather than through the thickness, and so is less affected by the presence of disbands or delaminations that run parallel to the surface. However, there is a wide variety of sensitivities reported in the literature on carbon fiber composites (Hobbs et al. 1994). In general, the best results are obtained if the maximum possible amount of energy is deposited on the surface of the structure, though care must be taken to avoid thermal damage.

Conventional X-ray techniques are of little use on metal-to-metal bonded joints since the polymeric adhesive is much less dense than the adherends. Metallic fillers (Segal and Kenig 1989) can be used to enhance the contrast and show tapering or voids. However, the density of fiber-reinforced plastics adherends is of a similar order to the adhesive and so X-rays can be used, by choosing a suitable energy and flux. For honeycomb-cored panels, X-rays are used for checking the position of the



core and whether it has been locally crushed or otherwise damaged and to monitor the position of water ingress.

A thermal neutron source can also be used (Michaloudaki et al. 2005) since neutrons are absorbed or scattered by hydrogenous materials such as hydrocarbons. Unfortunately, such sources are typically nuclear reactors and accelerators, and so are neither cheap nor readily available!

Tighe et al. (2016) interrogated carbon fiber-reinforced plastic (CFRP) single-lap joints to compare the detection of different defect types using pulsed phase thermography (PPT). A PTFE insert, of the type widely used to simulate defects in composite materials, was added to the bond line of the joint. Liquid layer kissing defects were simulated using silicon grease. PPT clearly identified the PTFE insert but not the silicon grease contamination. PPT identified the silicon grease defect when the joint was loaded, probably because loading opens the defect and produces a gap that provides sufficient thermal contrast for detection.

#### 42.4.7 Optical Holography

By using holographic interferometry, it is possible to measure surface displacements to less than 0.5  $\mu\text{m}$ . Load is applied to a structure by vibration, vacuum cup, pressure, or heat. Defects show as local perturbations in the holographic interferogram (Rao et al. 1990). The technique has found application with sandwich structures but not lap or similar joints.

#### 42.4.8 Visual

Hart-Smith and Thrall (1985) recommend a visual inspection of the adhesive fillet and suggest it is the most effective of all inspection techniques for bonded joints. The state of the fillet is a good indication of the state of the adhesive at the end of the joint. A porous fillet indicates too high a heat-up rate or the presence of moisture in the joint. A lack of fillet indicates a lack of pressure and may indicate internal voids. Just as the water-break test is an indicator of the adherend surface, the contact angle of the cured adhesive at the end of the fillet, formed when the adhesive was liquid, indicates if surface contamination is present.

---

### 42.5 Future Developments

The major problem with nondestructively assessing the strength of adhesively bonded joints remains the so-called kissing bond, in which there is continuity, but little or no strength. Many years ago, the author tried to generate a high-intensity tensile stress pulse which would fracture a kissing bond. Using mechanical impact, it proved impossible to achieve a sufficiently short-duration pulse which could be reflected as a tensile pulse in a thin adhesive joint. Gupta and coworkers (1990;



Gupta and Yuan 1993; Yuan and Gupta 1993, 1998) used high-intensity lasers to create tensile shock waves which could fracture weak bonds between a coating and a substrate. Bossi and coworkers at Boeing (Bossi et al. 2002, 2004, 2009, 2011) also tried to generate high-intensity, short-duration stress pulses to fracture these kissing bonds in adhesively bonded joints. After experimenting with flash electron beams, they settled on high-intensity lasers which gave pulses of a few hundred nanosecond duration. With joints made using carbon fiber-reinforced plastic (CFRP) adherends, they were able to distinguish bond quality on surfaces created with different peel ply preparations such as polyester and nylon fabric and surfaces prepared with contamination using a silicone release agent. When examined with conventional ultrasonics, these joints appeared to be identical. The technique developed by Bossi et al. is to use a laser-induced pulse to fracture a weak kissing bond and then to use conventional ultrasonics to detect this fracture. They have developed the technique for application to real aircraft structures. Monchalin 2007 has also worked on this method. The problem is to fracture a weak bond while not fracturing an otherwise good bond and to leave it in such a state so that it can be seen using conventional ultrasonics. The technique is interesting and seems to offer a way forward.

---

## 42.6 Conclusions

The types of defect encountered in adhesive joints and the nondestructive testing techniques available to detect them have been reviewed. Several techniques are available for disbond detection, the most commonly used being ultrasonics and different types of bond tester. These techniques are very time-consuming if large bond areas are to be tested; so there is increasing interest in rapid scanning methods such as transient thermography. The detection of poor cohesive properties is more difficult but can be achieved with ultrasonic or dielectric measurements. Monitoring interfacial properties is much more difficult, and there is currently no reliable test after the joint has been made. The high-intensity laser method is the only possible technique at the moment, but this needs a lot of development before it might become commercially acceptable.

Finally, we still need to correlate measurable defects with actual strength in the way in which joints are used, that is, in the tensile lap-shear mode where the main stresses are at the joint ends. Since the middle of the joint is relatively lowly loaded, detection of voids in the middle may indicate poor production and a possible leakage path, but it may not necessarily indicate a weak joint.

---

## References

- Adams R, Cawley P, Guyott CCH (1987) Nondestructive inspection of adhesively-bonded joints. *J Adhes* 21:279–290
- Adams RD, Comyn J, Wake WC (1997) *Structural adhesive joints in engineering*, 2nd edn. Chapman & Hall, London, 359 pp

- Baker A, Rajic N, Davis C (2009) Towards a practical structural health monitoring technology for patched cracks in aircraft structure. *Compos Part A* 40:1340–1352
- Bijlmmr PA (1978) In: Allen KW (ed) *Adhesion*, 2nd edn. London, Applied Science Publishers, 45 p
- Bork U, Challis R (1995) NDE of the adhesive fillet size in a T-peel joint using ultrasonic lamb waves and a linear network for data discrimination. *Meas Sci Technol* 6:72–84
- Bossi R, Housen K, Shepherd W (2002) Using shock loads to measure bonded joint strength. *Mater Eval* 60:1333–1338
- Bossi R, Housen K, Shepherd W (2004) Application of stress waves to bond inspection. In: SAMPE proceedings, Long Beach
- Bossi R, Housen K, Shepherd W, Sokol D (2009) Laser bond testing. *Mater Eval* 67:819–827
- Bossi R, Lahrman D, Sokol D, Walters C (2011) Laser bond inspection for adhesive bond strength. In: SAMPE proceedings, Long Beach
- Cawley P (1984) The impedance method of nondestructive inspection. *NDT Int* 17:59–65
- Cawley P (1988) The sensitivity of the mechanical impedance method of NDT. *NDT Int* 20:209–215
- Cawley P (2005) Nondestructive testing. In: *Adhesive bonding: science, technology and applications*. Woodhead, Cambridge, UK
- Cawley P, Adams RD (1987) Vibration techniques. In: Summerscales J (ed) *Nondestructive testing of fibre-reinforced plastics*. Elsevier Applied Science, London, pp 151–200
- Cawley P, Adams RD (1988) The mechanics of the coin-tap method of nondestructive testing. *J Sound Vib* 122:299–316
- Cawley P, Adams RD (1989) The sensitivity of the coin-tap method of non-destructive testing. *Mater Eval* 47:558–563
- Cawley P, Hodson MJ (1988) The NDT of adhesive joints using ultrasonic spectroscopy. In: Thompson DO, Chimenti DE (eds) *Review of progress in QNDE 8B*. Plenum Press, New York, pp 1377–1384
- Crane RL, Dillingham G (2008) Composite bonding. *J Mater Sci* 43(20):6682–6694
- Curtis GJ (1982) Nondestructive testing of adhesively-bonded structures with acoustic methods, ultrasonic testing – non conventional testing techniques. Wiley, Chichester
- Drinkwater BW, Cawley P (1994) An ultrasonic wheel probe alternative to liquid coupling. *Brit J NDT* 36:430–433
- Farlow R, Hayward G (1994) Real-time ultrasonic techniques suitable for implementing non-contact NDT systems employing piezoceramic composite transducers. *Brit J NDT* 36:926–935
- Galy ME, Moysan J, El Mahi A, Ylla N, Massacret N (2017) Controlled reduced-strength epoxy-aluminium joints validated by ultrasonic and mechanical measurements. *Int J Adhes Adhes* 72:139–146
- Gauthier C, El Kettani ME, Galy J, Pedoi M, Leduc D, Izbicki J-L (2017) Lamb waves characterization of adhesion levels in aluminum/epoxy bi-layers with different cohesive and adhesive properties. *Int J Adhes Adhes* 74:15–20
- Gowini MEL, Moussa WA (2016) Investigating the change in surface acoustic wave velocity due to the change in adhesion of a SU-8 thin film using a SU-8/AIN/Si SAW sensor. *Int J Adhes Adhes* 68:102–114
- Gupta V, Yuan J (1993) Measurement of interface strength by the modified laser spallation technique, II applications to metal/ceramic interfaces. *J Appl Phys* 74:2397–2404
- Gupta V, Argon AS, Cornie JA, Parks DM (1990) Measurement of interface strength by laserpulse-induced spallation. *Mater Sci Eng A* 126:105–117
- Guyott CCH, Cawley P, Adams RD (1986) The non-destructive testing of adhesively bonded structure: a review. *J Adhes* 20:129–159
- Guyott CCH, Cawley P, Adams RD (1987) Use of the Fokker bond tester on joints with varying adhesive thickness. *Proc IMechE* 201(B1):41–49
- Hagemaijer DJ (1985) *Adhesive bonding of aluminium alloys*. Marcel Dekker, New York

- Hart-Smith LJ, Thrall EW (1985) Adhesive bonding of aluminium alloys. Marcel Dekker, New York, pp 241–335
- Hobbs CP, Kenway-Jackson D, Milne JM (1991) Quantitative measurement of thermal parameters over large areas using pulse video thermography *proc SPIE*, vol 1467. Thermosense XIII, Orlando, pp 264–277
- Hobbs CP, Kenway-Jackson D, Judd MD (1994) Proceedings of the international symposium on advanced materials for lightweight structures. ESTEC, Noordwijk, (ESA-WPP-070)
- Jeenjitkaew C, Guild FJ (2017) The analysis of kissing bonds in adhesive joints. *Int J Adhes Adhes* 75:101–107
- Jeenjitkaew C, Luklinska Z, Guild FJ (2010) Morphology and surface chemistry of kissing bonds in adhesive joints produced by surface contamination. *Int J Adhes Adhes* 30:643–653
- Karachalios EF, Adams RD, da Silva LFM (2013) The strength of single lap joints with artificial defects. *Int J Adhes Adhes* 45:69–76
- Kim DM, Sutliff E (1978) The contact potential difference (CPD) measurement method for prebond nondestructive surface inspection. *SAMPE Q* 9:59–63
- Lange YV, Teumin II (1971) Dynamic flexibility of dry point contact. *Sov J NDT* 7:157–165
- Lloyd EA, Brown AF (1978) In: Allen KW (ed) Adhesion, 2nd edn. London, Applied Science Publishers, 133 pp
- Marty NP, Desai N, Andersson J (2004) NDT of kissing bond in aeronautical structures. In: Proceedings of the 16th world conference for NDT, Montreal
- Michaloudaki M, Lehmann E, Kostas D (2005) Neutron imaging as a tool for the non-destructive evaluation of adhesive joints in aluminium. *Int J Adhes Adhes* 25:257–267
- Monchalain J-P (1993) Progress towards the application of laser ultrasonics in industry. In: Thompson DO, Chimenti DE (eds) Review of progress in QNDE 12. Plenum Press, New York, pp 495–506
- Monchalain J-P (2007) Laser-ultrasonics: principles and industrial applications, Chapter 4. In: Chen CH (ed) Ultrasonic and advanced methods for nondestructive testing and material characterization. World Scientific, Singapore, pp 79–115
- Pilarski A, Rose JL, Balasubramian K (1990) The angular and frequency characteristics of reflectivity from a solid layer embedded between two solids with imperfect boundary conditions. *J Acoust Soc Am* 87:532–542
- Puthillath P, Rose JL (2010) Ultrasonic guided wave inspection of a titanium repair patch bonded to an aluminum aircraft skin. *Int J Adhes Adhes* 30:566–573
- Pyles R (2003) Aging aircraft: USAF workload and material consumption life cycle patterns. RAND, Pittsburgh
- Rao MV, Samuel R, Ramesh K (1990) Dual vacuum stressing technique for holographic NDT of honeycomb sandwich panels. *NDT Int* 23:267–270
- Reynolds WN (1988) Inspection of laminates and adhesive bonds by pulse-video thermography. *NDT Int* 21:229–232
- Rose JL, Ditre JJ (1992) Pulse-echo and through transmission lamb wave techniques for adhesive bond inspection. *Br J Nondestr Test* 34:591–594
- Rose JL, Rajana KM, Hansch MKT (1995) Ultrasonic guided waves for NDE of adhesively bonded structures. *J Adhes* 50:71–82
- Rose JL, Rajana KM, Barshinger JM (1996) Guided waves for composite patch repair of aging aircraft. In: Thompson DO, Chimenti DE (eds) Review of progress in QNDE. Plenum Press, New York, pp 1291–1298
- Roth W, Giurgiutiu V (2017) Structural health monitoring of an adhesive disbond through electro-mechanical impedance spectroscopy. *Int J Adhes Adhes* 73:109–117
- Schindel DW, Hutchins DA (1995) Applications of micromachined capacitance transducers in air-coupled ultrasonics and nondestructive evaluation. *IEEE Trans Ultrason Ferroelectr* 42:51–58
- Schliekelmann RJ (1972) The nondestructive testing of adhesively bonded metal-to metal joints. *Nondestruct Test* 5:79–86

- Schliekelmann RJ (1975) Nondestructive testing of bonded joints – recent developments in testing systems. *Nondestruct Test* 8:100–103
- Segal E, Kenig S (1989) Acceptance criteria for NDE of adhesively bonded structures. *Mater Eval* 47:921–927
- Shepard SM (1997) Introduction to active thermography for non-destructive evaluation. *Anti Corros Methods Mater* 44:236–239
- Thompson RB (1990) Physical principles of measurements with EMAT transducers. In: Mason WP, Thurston RN (eds) *Physical acoustics*, vol XIX. Academic, New York, pp 157–200
- Tighe RC, Dulieu-Barton JM, Quinn S (2016) Identification of kissing defects in adhesive bonds using infrared thermography. *Int J Adhes Adhes* 64:168–178
- Vine K, Cawley P, Kinloch AJ (2001) The correlation of non-destructive measurements and toughness changes in adhesive joints during environmental attack. *J Adhes* 77:125–161
- Yu A, Gupta V (1998) Measurement of in situ fiber/matrix interface strength in graphite/epoxy composites. *Compos Sci Technol* 58:1827–1837
- Yuan J, Gupta V (1993) Measurement of interface strength by the modified laser spallation technique. I. Experiment and simulation of the spallation process. *J Appl Phys* 74:2388–2397

R. Créac'hcadec

**Contents**

43.1	Introduction .....	1196
43.1.1	Structural Bonding, a Plural Science .....	1196
43.1.2	The Need for a Plural Science to Solve the Equation of Bonding .....	1197
43.1.3	Interactions Between These Areas .....	1198
43.1.4	What About the Role of Interfaces .....	1199
43.1.5	The Importance of Multi-scale and Multi-physics Observations .....	1200
43.1.6	The Importance of Observation on the Understanding of the Physics of Failure .....	1200
43.2	The Difficulty of Identifying an Adhesive or Cohesive Failure .....	1202
43.2.1	Presentation of the Different Modes of Failure .....	1202
43.2.2	Subjectivity of the Analysis .....	1202
43.2.3	A Multitude of Experimental Setups to Try to Understand the Failure of Bonded Assemblies .....	1204
43.3	Macroscopic and Mesoscopic Optical Observations .....	1204
43.3.1	Failure Surfaces .....	1204
43.3.2	The Importance of Local Geometry on Adhesive Joint Failure .....	1207
43.4	Microscopic Optical Observations .....	1209
43.4.1	One-Dimension Roughness .....	1209
43.4.2	Scanning Electron Microscopy .....	1210
43.4.3	Nanoindentation .....	1212
43.4.4	Atomic Force Microscopy .....	1212
43.4.5	Confocal Microscopy .....	1213
43.4.6	X-Ray Microtomography .....	1214
43.5	Physicochemical Analysis .....	1215
43.5.1	Scanning Electron Microscopy with Energy-Dispersive X-Ray Spectroscopy .....	1215
43.5.2	Scanning Electron Microscopy with Raman Spectroscopy .....	1216
43.5.3	X-Ray Photoelectron Spectroscopy .....	1218

R. Créac'hcadec (✉)

ENSTA Bretagne, Institut de Recherche Dupuy de Lôme, FRE CNRS 3744, Brest, France

Assemblages Multi-Matériaux, Institut de Recherche Dupuy De Lôme, Brest, France

e-mail: [romain.creac'hcadec@ensta-bretagne.fr](mailto:romain.creac'hcadec@ensta-bretagne.fr); [Romain.Creac'hcadec@ensta-bretagne.fr](mailto:Romain.Creac'hcadec@ensta-bretagne.fr)

32	43.5.4	Differential Scanning Calorimetry .....	1219
33	43.5.5	Thermogravimetric Analysis .....	1223
34	43.5.6	Attenuated Total Reflectance-Fourier Transform Infrared (ATR-FTIR)	
35		Spectroscopy Technique .....	1223
36	43.6	Mechanical Observations .....	1224
37	43.6.1	3D Digital Image Correlation .....	1224
38	43.6.2	Digital Volume Correlation .....	1226
39	43.6.3	Ultrasonic Testing .....	1228
40	43.7	Conclusions .....	1228
41		References .....	1229

## Abstract

Fracture observation is one of the key ways to understand the behavior of bonded assemblies. The plural science of bonded assemblies includes three main areas such as polymer sciences, physical chemistry of surfaces and interfaces, and mechanics. Solving the equation of adhesion needs intersection of all these aspects. Moreover, this multi-physics science is also a multi-scale one. Understanding surface fracture deals with all these aspects. This chapter presents three types of measurement systems: microscopy, compositional analysis/material identification, and mechanical observations. A table sums up an exhaustive list of the major observation devices and precise references of works that use these types of methods. Then, the main methods are detailed with macroscopic and mesoscopic observations, microscopic observation, physicochemical analysis, and mechanical observations.

## 43.1 Introduction

One can wonder why people are so interested on the failure mode of bonded assemblies. One reason is probably the need for manufacturers and users in various industrial fields to trust in this technology of multi-material assemblies. Users are very often interested in having cohesive failures in the adhesive, mainly for a reason that is not so objective. The idea is linked to the need to have predictable failures. So, cohesive failure means that physical phenomena happen in the “material” of the adhesive. It seems to be easier to predict it than with the contribution of the interfaces. However, sometimes these failures occur at the interface with interesting strength, etc. So, how can we understand these fractures?

### 43.1.1 Structural Bonding, a Plural Science

By definition, a bonded structure is composed of two substrates connected together by a bonding agent called the adhesive. This bond defines two interfaces connecting each other the substrates to the adhesive. The assembly made of the adhesive and the

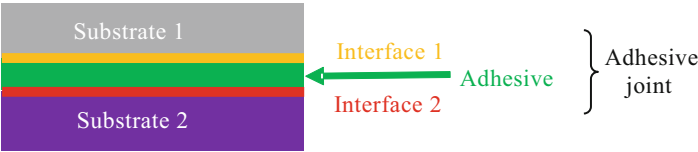
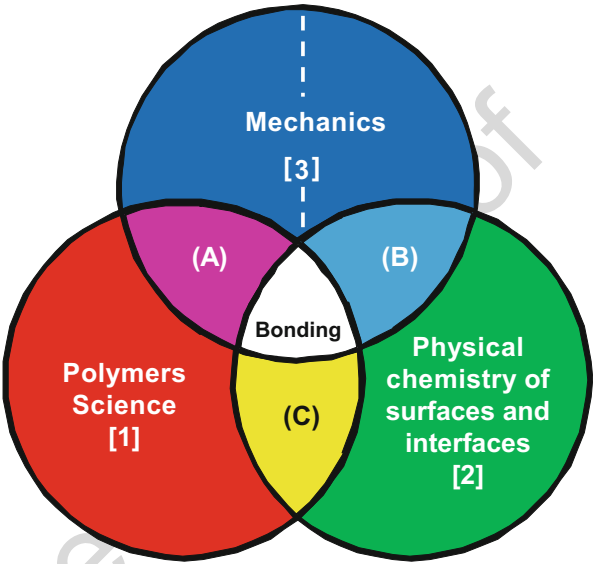


**Fig. 1** Structure of an adhesive joint made of two interfaces and the adhesive

**Fig. 2** Structural bonding, a plural science



two interfaces constitutes an adhesive joint. Figure 1 presents a very schematic view of this structure. The analysis of this structure, therefore, requires understanding the behavior of each constituent: adhesive, interfaces, and substrates. Each of these elements, by its essence, contributes to influencing the response of such a structure subjected to mechanical loading.

### 43.1.2 The Need for a Plural Science to Solve the Equation of Bonding

Structural bonding is a plural science. Representing it, in a schematic way, is not easy as the domains linked to structural bonding interpenetrate. Figure 2 presents the problem to solve for finding an acceptable solution for the behavior of a bonded structure. The solution is defined in the center (in white). This area is the overlap of three strong scientific domains: the science of polymers (1), the physico-chemistry of surfaces and interfaces (2), and mechanics (3). Understanding and being able to predict the behavior of a bonded structure mean being able to cover and interact with

these three areas. This plurality makes difficult, but nevertheless very interesting, the problematic of structural bonding.

### **Area of Polymers Science (1)**

Adhesives are for the most part polymers. Polymers constitute a class of materials in their own. Because these materials possess dissipative processes, they are very useful for bonded assemblies. They are generally characterized by high breakage energies.

### **Area of Physico-chemistry of Surfaces and Interfaces (2)**

The notion of interface defines the boundaries of a domain. Indeed, the field of application of the “science of polymers” is limited because of the presence of the two substrates. These polymer/substrate boundaries provide an interface that needs to be understood. An adhesive is not only a polymer, but it is also a material with an adhesive capacity. Understanding of the phenomena of adhesion requires analysis on several scales. Several concepts from the molecular scale up to the macroscopic scale are thus studied. Total adhesion is generally analyzed by decomposition into mechanical adhesion, physical adhesion, and chemical adhesion. Mechanical adhesion incorporates the notions of wetting, mechanical anchoring, and diffusion/interdiffusion. Physical adhesion is concerned with the different forces that interact at short and long distances (van der Waals, electrostatics, etc.). Finally, chemical adhesion is concerned with covalent bonds. Numerous references highlight the complexity of these phenomena and theories on adhesion.

### **Area of Mechanics (3)**

The last domain proposed to solve the equation of bonding is mechanics. The problems proposed by the industry must meet a specification. This document specifies under which conditions and under which constraints the bonded assembly must resist: durability, environment, stress rates, temperatures, fracture loads, etc. The difficulty of this field is, therefore, to be able to propose means of characterization and prediction of the mechanical strength of the assembly.

## **43.1.3 Interactions Between These Areas**

The solution of the structural bonding problem requires a very wide range of skills which are difficult to dissociate from one to another. Thus, in order to show these interactions, Fig. 2 defines three subdomains marked “A, B, and C,” highlighting these interactions between the “science of polymers,” the “physico-chemistry of surfaces and interfaces,” and “mechanics.” The intersection of these interactions constitutes an approach for solving the problem of structural bonding. Initially, several decades ago, these interactions were weak. Today, these areas are increasingly interacting. The best marker of this evolution is the organization of congresses around adhesive bonding which often revolve around two parallel sessions, one physico-chemistry and the other rather mechanical.



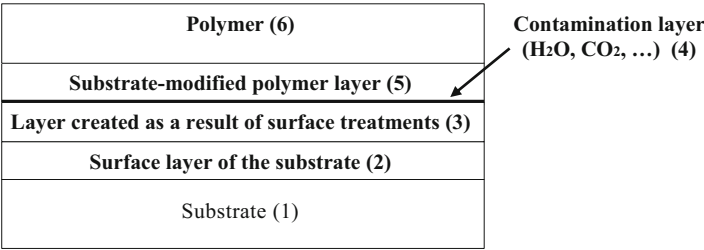


**Fig. 3** Representation of a polymer-metal interphase (Coulaud 2007)

**43.1.4 What About the Role of Interfaces**

The analysis of the failure modes of bonded assemblies differs from the “classical” analyses of materials by the eternal question, what is the role of the interfaces?

**Example of Structure: Polymer/Metal Interface**

The interphase is a geometric boundary that defines the transition between the adhesive and the polymer. This zone is characterized by numerous physical, chemical, and mechanical phenomena. Figure 3 presents a sectional view of this bonding zone (Coulaud 2007). The structure is characterized by numerous layers from the substrate (1) to the polymer (6): the surface layer of the substrate (2), a layer resulting from surface treatments (3), a contamination layer (H<sub>2</sub>O, CO<sub>2</sub>, etc.), and a layer of polymer modified by the substrate (5). This structure is specific to the nature of the materials used (substrate and polymer) as well as to the manufacturing process. It is therefore necessary to question its influence on the macroscopic behavior observed.

**Example of a Macroscopic Behavior**

Figure 4 shows the influence of interfaces on the macroscopic behavior of adhesives (Arnaud 2014). For Hysol<sup>®</sup>-EA9309.3NA adhesive, modified Arcan shear tests were performed. Two treatments were compared. The first is an unclogged sulfur anodizing treatment. The second treatment comprises corundum abrasion 220 followed by an anti-stick treatment. The same curing cycle was applied to the adhesive. For treatment A, the maximum load reached is close to 16 kN, and the maximum displacement at break is approximately 0.3 mm. The observed behavior is nonlinear and identical for the three tests performed. For the specimen with anti-adhesion, the nonlinear behavior followed is the same. For the second, load and displacement at failure are considerably lower. Moreover, for the three tests carried out, the displacements at break (visible with the green, blue, and brown dots) are dispersed. Given the plasticity of the adhesive, the fracture loads are similar. For all six tests, the failure is adhesive. This example clearly highlights the contribution of interfaces to the response of a bonded joint. Figure 4b shows the multilayer structure of an adhesive joint: the adhesive, the two interfaces, and the substrates. Vallat (2013) symbolizes the contribution of this structure as a chain composed of five

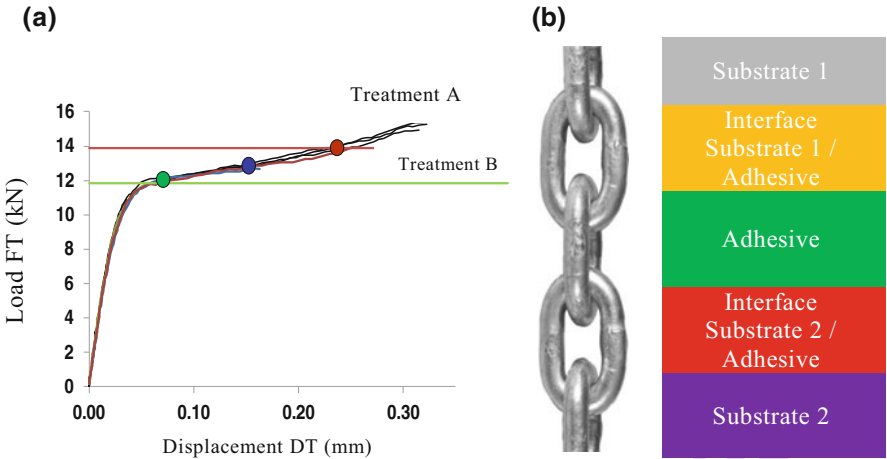


**Fig. 4** Macroscopic role of interfaces on the behavior of an adhesive in an assembly: (a) demonstration of the influence of surface treatment on modified Arcan shear tests (Arnaud 2014) and (b) multilayer structure of a bonded joint (Vallat 2013)

links. Each link is an important element. It is the failure of one of these links, placed in series, which generates the failure of the whole assembly.

### 43.1.5 The Importance of Multi-scale and Multi-physics Observations

As a consequence of the structure of bonded assemblies itself, to understand fracture, it is necessary to use multi-scale and multi-physics observations. In this chapter, most of these methods are presented.

### 43.1.6 The Importance of Observation on the Understanding of the Physics of Failure

#### Structural Adhesives Are Sources of Defects

The manufacturing process generates intrinsic defects during the production of the bonding. Adams characterizes these defects (see ► Chap. 42, “Nondestructive Testing”). Figure 5 presents the various defects observed. They may be bound to the surface preparation with areas having adhesion defects, with or without kiss bonding. These defects can be related to macroscopic porosities: absence of adhesive or to microscopic porosities. They can also be linked to the polymerization process: cross-linking defects, cracks generated during shrinkage, and cross-linking gradient. As a consequence, the modes of failure are a manifestation of different physics which can be observed in the fracture surfaces.

**Fig. 5** Various defects which might be present in an adhesive bond line (Adams see ► Chap. 42, “Nondestructive Testing”)

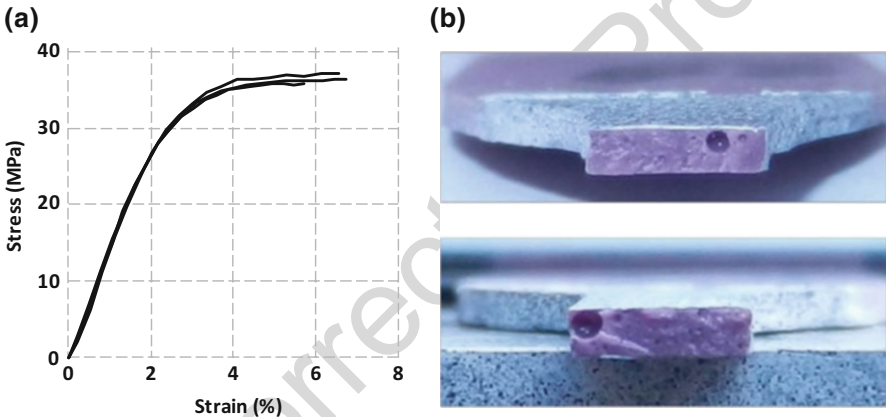
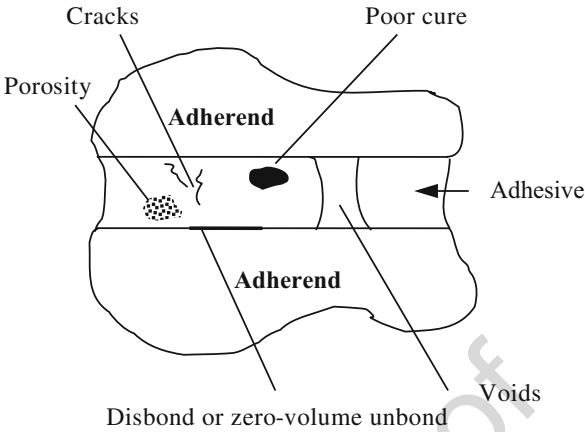


**Fig. 6** Tensile tests on bulk samples: (a) Dog-bone samples, (b) Air bubbles in the section (Arnaud 2014)

### Example of an Application: Dog-Bone Tensile Specimen

Dog-bone tensile specimens are classical tests to characterize the mechanical properties: Young’s modulus and Poisson’s ratio. Arnaud et al. (2015) carried out these tests. Figure 6 presents the stress-strain curves. A linear behavior is firstly observed and then a nonlinear one. Tests were performed with a crosshead speed of 0.5 mm/min. Though special care was considered to manufacture the specimens, all the fractures occurred near a porosity observed in Fig. 6b. This is a very simple example, but it highlights the need to well understand physics to explain the behavior observed. This analysis starts with the observation of the fracture surface. This chapter is dedicated to the different means to observe fracture in adhesive bonds. The main message that must be understood by the reader is the fact that observation setups are closely related to the comprehension of the physics observed.

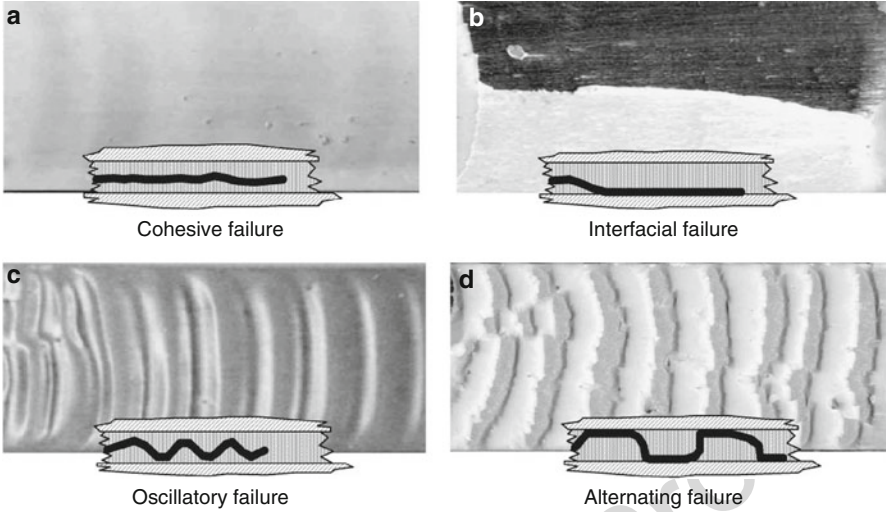


**Fig. 7** Different locus of failure and crack trajectories observed in mode I testing of adhesively bonded double cantilever beam (DCB) specimens. (a) Cohesive failure, (b) Interfacial failure, (c) Oscillatory failure, (d) Alternating failure. (Chen and Dillard 2001)

## 43.2 The Difficulty of Identifying an Adhesive or Cohesive Failure

### 43.2.1 Presentation of the Different Modes of Failure

Chen et Dillard (2001) presented in their work different kinds of failures for adhesively bonded assemblies. Four types can be distinguished (Fig. 7): failure in the adhesive, also called cohesive failure or failure at the interface between the adhesive and the substrate. These modes are commonly observed and very easy to determine. Two types of failure called oscillatory and alternating failures also exist as described in Fig. 7c, d.

### 43.2.2 Subjectivity of the Analysis

Figure 8 presents two specimens after failure. The test considered was a modified Thick-Adherend Shear Test that applied shear loadings to these interfaces (Cognard et al. 2011a). Two surface treatments were used: mechanical preparation with abrasion followed by acetone degrease and chemical treatment. With the first surface treatment, the failure is fully adhesive. With the second one, the failure is mainly cohesive (around 90% cohesive). Therefore, determining the role of the interface on the strength at failure seems to be quite easy. Figure 9 shows failure

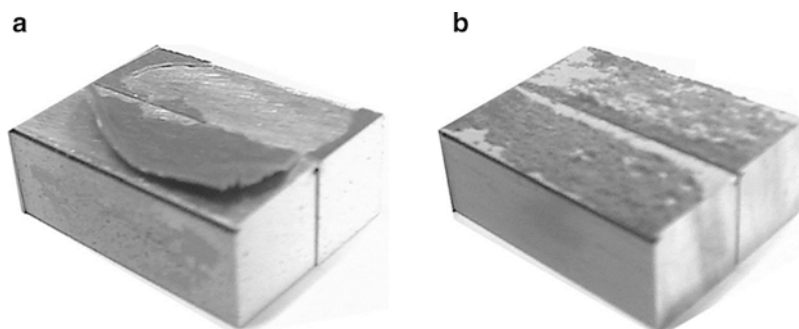


**Fig. 8** Influence of the surface preparation on the failure mode for an epoxy adhesive: (a) results with a mechanical preparation and (b) results with a chemical one (Cognard et al. 2011a)

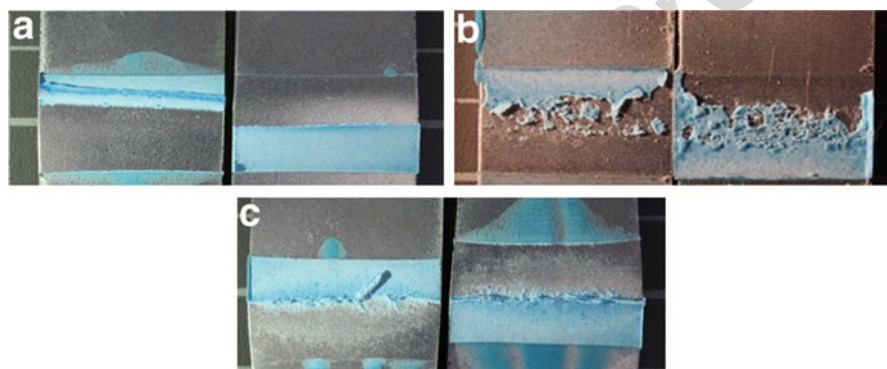


**Fig. 9** Failures in single-lap joints with steel substrates: (a) fully adhesive failure, (b) 50% cohesive failure, (c) mixed mode adhesive-cohesive failure (Legendre et al. 2016)

surfaces for single-lap shear tests with hard steel sheet metal substrates with a zinc coating (Legendre et al. 2016). The failure is adhesive (Fig. 9a) and mixed-mode adhesive/cohesive in Fig. 9b. The main question that can be asked is about the surface described in Fig. 9c. How is the cohesive failure defined? If there are blue areas on both sides of the joint, it is easy to determine a cohesive failure. However, looking close to the interface, a “white” zone can be observed: a close adhesive failure zone. It seems that in this zone the interface transmitted the kinematic deformation of the substrate to the adhesive and after that broke. Research is still under way to determine whether this area can be defined as cohesive or not. It depends today on the country and on the industrial field where it is considered. One element in discussion is the fact that it is possible to predict or not a reliable strength at failure with this type of fracture surface.

### 43.2.3 A Multitude of Experimental Setups to Try to Understand the Failure of Bonded Assemblies

The purpose of this chapter is not to give a detailed and exhaustive list of methods of analysis but to propose multi-scale and multi-physical analysis methods to analyze the failure of bonded assemblies. Thus, the following table gives a non-exhaustive list of characterization setups used in the three domains of bonded assemblies described above. Three types of analyses can be considered despite some recovery.

- Microscopy techniques are used to mainly observe at different scales surfaces and adhesives from the millimeter (macroscopic observation) to the nanometer. These observations were in the past realized in two dimensions. Nowadays the third dimension can be more easily considered thanks to confocal microscopy or X-ray micro-tomography systems.
- The second domain is used to analyze the composition and the identification of the material. These ones are mainly physicochemical analysis based on thermal and spectroscopy applications.
- The third domain is based on the comprehension of the deformation of the bonded assemblies to understand fracture. It is mainly linked to kinematic observations in order to define the localization of the mechanical failure process.

Table 1 presents these three domains. References of recent works are listed for each analysis. Only certain methods are described later in this chapter more precisely.

## 43.3 Macroscopic and Mesoscopic Optical Observations

### 43.3.1 Failure Surfaces

#### Within the Adhesive

The load path influences the failure mode within the adhesive. Créac'hcadec et al. (2014) characterized the behavior of a thick flexible adhesive (Sikaflex-265) under different monotonic tensile/compression-shear loads, using a modified Arcan fixture, which was designed to limit stress concentrations in order to define an experimental methodology enabling structural adhesives to be characterized up to failure. The results allow defining the load and displacement envelopes characterizing the adhesive to failure under multiaxial loading conditions.

For the different tests, cohesive failures were observed around the median plane of the adhesive (Fig. 10). These fracture surfaces underline the good quality of the cohesion between Sikaflex<sup>®</sup>-265 and ABS substrates using Sika<sup>®</sup>Primer-206 G+P. It seems that a specific fracture pattern characterizes each test configuration. The load direction seems to determine the topography of the fracture pattern. For tensile tests, fracture surfaces are smooth and have a fault in the center of the surface as well

t.1 **Table 1** Different experimental devices to observe failures in bonded assemblies

t.2	Acronym	Name explanation	References
t.3	Microscopy		
t.4	AFM	Atomic force microscope	Critchlow 96
t.5		Confocal microscopy	Aguiar et al. (2012), Beuguel et al. (2017), and Hase et al. (2014)
t.6	FIB	Focused ion beam	Pecnik et al. (2015)
t.7	FFM	Friction force microscopy	–
t.8	OP	Optical profilometer	–
t.9	SAM	Scanning acoustic microscopy	Oehler et al. (2012)
t.10	SEM	Scanning electron microscope	Aguiar et al. (2012) and Hase et al. (2014)
t.11	STM	Scanning tunneling microscopy	–
t.12	TEM/ STEM	Transmission electron microscopy/ scanning transmission electron microscopy	Mine et al. (2017) and Liu (2013)
t.13	XRM	X-ray micro-tomography	Bele et al. (2017), Bouterf et al. (2017), and Liu (2013)
t.14	Compositional analysis and material identification		
t.15	Thermal analysis		
t.16	DSC	Differential scanning calorimetry	Devaux et al. (2015)
t.17	DTA	Differential thermal analysis	Devaux et al. (2015)
t.18	TGA	Thermogravimetric analysis	–
t.19	Spectroscopy		
t.20	AES	Auger electron spectroscopy	Comyn (1992) and Critchlow et al. (2006)
t.21	EBSD	Electron backscatter diffraction	Haddadi et Tsivoulas (2016) and Koseki et al. (2016)
t.22	EDS/ EDX	Energy-dispersive X-ray spectroscopy	Cardell et Guerra (2016)
t.23	FTIR	Fourier transform infrared spectroscopy	Gorassini et al. (2016), Zięba-Palus et al. (2016), and Zhao et al. (2016)
t.24	GC-MS	Gas chromatography mass spectrometry	Zięba-Palus et al. (2016)
t.25	GD- OES/MS	Glow discharge-optical emission spectrometry/mass spectrometry	Heikkilä et al. (2016)
t.26	ICP- OES/MS	Inductively coupled plasma-optical emission spectrometry/mass spectroscopy	Gazulla et al. (2017)
t.27	IGA	Instrumental gas analysis	Vera et al. (2012)
t.28	LA-ICP- MS	Laser ablation-inductively coupled plasma-mass spectrometry	Uerlings et al. (2016)
t.29	LC-MS	Liquid chromatography-mass spectrometry	Cacho et al. (2016)
t.30	LEXES	Low-energy electron-induced X-ray emission spectrometry	Charbonnier et al. (1986)
t.31	NMR	Nuclear magnetic resonance spectroscopy	Böhm et al. (2016)

(continued)



**t.32 Table 1** (continued)

t.33	Acronym	Name explanation	References
t.34	Raman	Raman spectroscopy	Cardell et Guerra (2016), Davies et al. (2009), and Zhao et al. (2016)
t.35	RBS	Rutherford backscattering spectrometry	–
t.36	TOF-SIMS	Time-of-flight secondary ion mass spectrometry	Kadiyala et al. (2016)
t.37	TXRF	Total-reflection X-ray fluorescence spectroscopy	Kanrar et al. (2014)
t.38	XPS/ESCA	X-ray photoelectron spectroscopy/ electron spectroscopy for chemical analysis	Choudhury et Jones (2006) and Kadiyala et al. (2016)
t.39	XRD	X-ray diffraction	Tsunekawa et al. (2011)
t.40	XRF	X-ray fluorescence	Aldrich-Smith et al. (2005) and Procaccini et al. (2011)
t.41	XRR	X-ray reflectivity	Yeom et al. (2016)
t.42	Mechanical observations		
t.43	AT	Acoustic emission testing	Croccolo et Cuppini (2009) and Magalhães et de Moura (2005)
t.44	2D/3D –DIC	Two- or three-dimensional digital image correlation	Créac’hcadec et al. (2008), Créac’hcadec et al. (2015), and Maurice (2012)
t.45	DVC	Digital volume correlation	Bele et al. (2017) and Bouterf et al. (2017)
t.46		Nanoindentation	Davies et al. (2009) and Pecnik et al. (2015)
t.47		Ultrasonic measurement	Ghiassi et al. (2014)

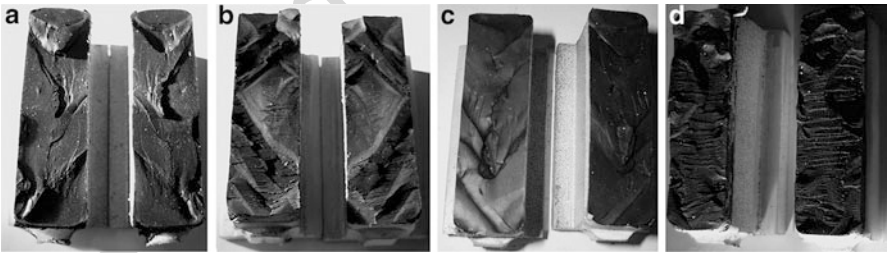


**Fig. 10** Fracture patterns of the adhesive in bonded assemblies for tensile/compression-shear tests: (a) tensile test, (b) shear test, (c) traction-shear test, (d) compression-shear test (Créac’hcadec et al. 2014)

as a V-shaped line at one of the ends of the sample (Fig. 10a). The analysis of the patterns represented in Fig. 10b shows clearly rhombus shapes. Small streaks are also observed associated with a failure at different levels in the adhesive thickness when loaded under shear. Under tensile-shear loads (Fig.10c), the failure mode is quite similar to the case of tensile loadings; the tensile part of the load seems to govern the failure mode. Moreover the tangential displacement at failure is lower



under tensile-shear loads than under shear loads. Fracture patterns under compression-shear (Fig. 10d) show a rough surface where streaks are more pronounced and denser than during the shear loading situation. The fracture path is not straight and very irregular as the adhesive has been ripped out locally associated with the compression part of the load.

### Adhesive/Cohesive Mixed-Mode Failure Surface

The load path also affects the type of failure, i.e., adhesive failure close to the interface or cohesive failure in the adhesive. Arnaud et al. (2015) made similar modified Arcan tests for a bicomponent epoxy adhesive. The main part of the work was to identify the influence of the water aging of bonded assemblies. The fracture surfaces shown in Fig. 11 present the initial mode of failure without aging. They observed that in tension, the failure was mainly cohesive for the unaged state. Then, it became partially cohesive during aging. But at the last aging time, it was again fully cohesive. This evolution seems to indicate that the interface was slightly affected by humid aging in tension. However, it was not clear enough to conclude on a real interfacial degradation. In the other loading directions, the failure is mainly adhesive and does not reveal any evolution during aging (Fig. 11b–d).

## 43.3.2 The Importance of Local Geometry on Adhesive Joint Failure

One way to understand fracture surface is to know where the fracture initiated. A lot of works were made to understand the contribution of the free edges of bonded assemblies. These zones are mainly the reasons of failure in adhesive joints. Karachalios et al. (2013) explained the failure process of single-lap shear tests with the localization of damage initiation at the extremity of the substrate in the middle of the test specimen. The failure process then develops on each side of bonded joint to finally reach to interface (Fig. 12a). This analysis was obtained thanks to the fracture surface observed (Fig. 12b). This study was carried out with ductile substrates and adhesives.

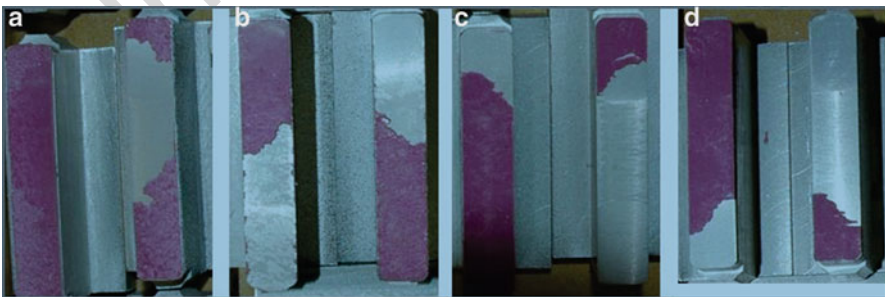


**Fig. 11** Fracture profiles of the modified Arcan test during seawater aging; results are presented for the initial fracture surfaces (Arnaud et al. 2015): (a) tensile test, (b) shear test, (c) traction-shear test, (d) compression-shear test

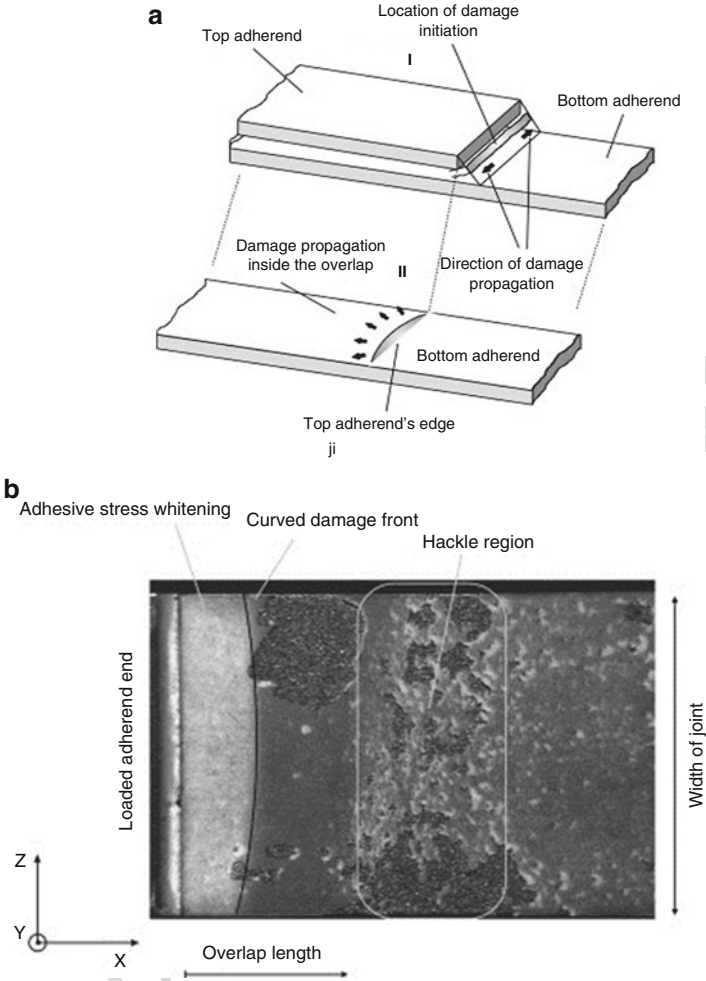


**Fig. 12** Failure mechanism in single-lap shear test: (a) Description of failure mechanisms for ductile adhesives, (b) failure pattern of a 60 mm overlap with AV 119 adhesive (Karachalios et al. 2013)

Understanding the contribution of the free edge is very important. To analyze these geometries, finite element methods are very useful and used. Cognard et al. (2011b) analyzed the influence of some geometrical parameters on the stress concentrations in the case of the single-lap joints (Fig. 13). The stress concentrations can contribute to fracture initiation in the adhesive joints and thus can lead to an incorrect analysis of the adhesive behavior. Therefore, understanding the stress distribution in an adhesive joint can lead to improvements in adhesively bonded assemblies. This study was accomplished using finite element simulations under elastic assumption using refined meshes and using a pressure-dependent model, which accurately describe the elastic limit of the adhesive. It has been shown that geometries used

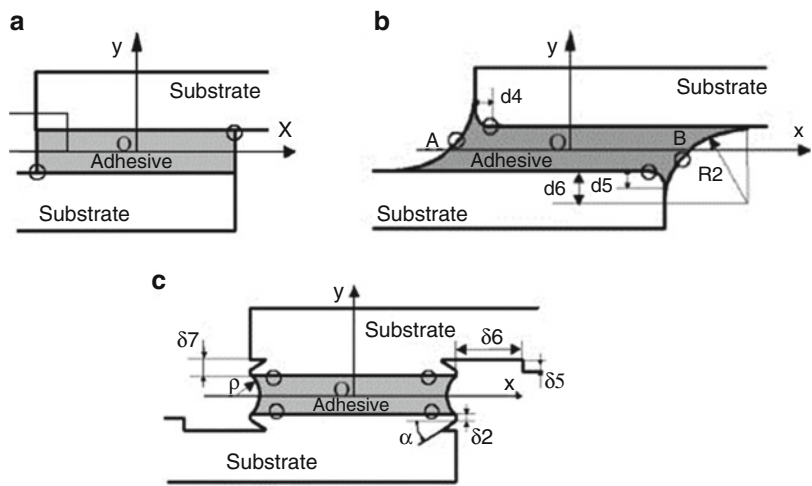


**Fig. 13** Influence of local geometry on the strength at failure (“o” zone of maximal equivalent stress in the adhesive under elastic assumption): (a) straight geometry, (b) geometry with a chamfer, (c) geometry with beaks (Cognard et al. 2011b)

in various studies in order to reduce the influence of edge effects can generate quite large stress gradients close to the adhesive-free edges.

Specific geometries can significantly limit the influence of edge effects .The use of substrates with beaks and a cleaning of the free edges of the adhesive allow a large reduction in the stress state close to the free edges of the adhesive and thus allow an optimization of the maximum transmitted load in single-lap joints. The numerical results underline that the overlap length and the adhesive thickness also have an influence on the stress distribution in the joint. Moreover, it has been shown that significant evolution of the stress can exist throughout the thickness of the adhesive; therefore, simplified methods that roughly analyze the average stress state through the joint can overestimate the maximal transmitted load of single lap joints. Thus, refined analyses of the stress distribution in the adhesive are necessary to obtain precise design of adhesively bonded assemblies. To sum up, it is necessary to take special care to the local geometry: the principle proposed (Fig 14a) and how it is manufactured (Fig. 14b–d).

### 43.4 Microscopic Optical Observations

#### 43.4.1 One-Dimension Roughness

Mechanical adhesion is mainly explained by the surface topology. Thanks to a rugosimeter Arnaud (2014) determined the parameters of a one-dimension roughness, parameters which favor in particular the mechanical attachment, in order to be able to reuse them during future coating applications. Thus samples of aluminum

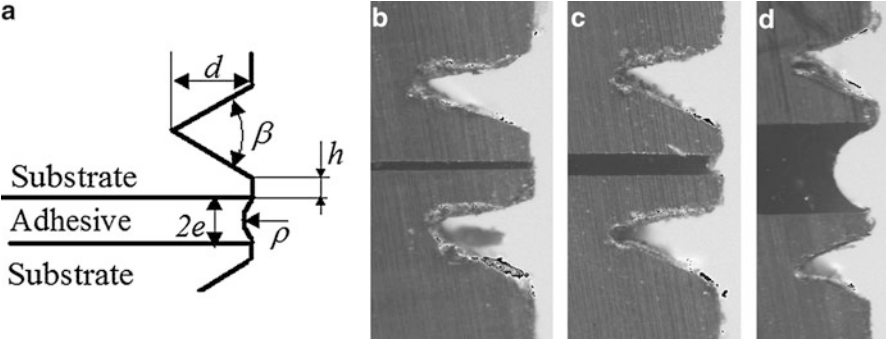


**Fig. 14** Geometry of the free edge of modified Arcan test specimen to reduce the edge effects with beaks: (a) definition of the local geometry (Cognard 2008), (b) cross view for an adhesive thickness of  $2e = 0.1$  mm, (c) cross view for an adhesive thickness of  $2e = 0.2$  mm, (d) cross view for an adhesive thickness of  $2e = 1$  mm (Cognard et al. 2010)

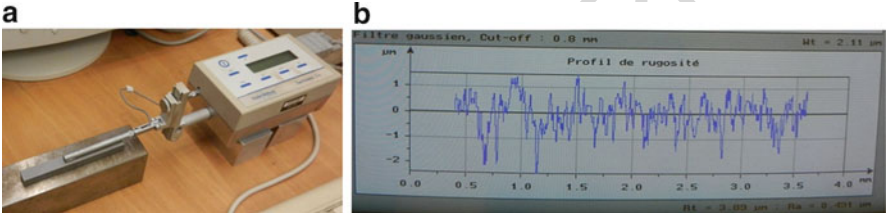


**Fig. 15** Analysis of a substrate with a rugosimeter: (a) measuring device and (b) roughness profile generated after passing the rugosimeter along a line (Arnaud 2014)

2017 were studied, in the form of bars of 10 mm thickness and surface  
10 × 100 mm<sup>2</sup>. A roughness profile was obtained by passing the roughness tester  
on a straight line of the substrate (Fig. 15b). For better precision, it was necessary to  
measure several lines. The results are given in Table 2. The mean gap, defined as the  
arithmetic mean of the absolute values of the distances between peaks and troughs,  
noted Ra, and the total gap, defined as the most important distance between the  
highest peak and the deepest trough, noted Rt, measured were, respectively,  
0.455 µm and 3.46 µm. These two parameters are the most influential in terms of  
roughness.

### 43.4.2 Scanning Electron Microscopy

The scanning electron microscope is a tool able to observe surfaces from 10 to  
0.1 µm. Figure 16a presents an example of a scanning electron microscope (SEM)  
study of an Arcan aluminum-adhesive-aluminum-modified assembly. An overall  
view of the adhesive shows the presence of fillers or porosities in the adhesive.

t.1 **Table 2** Roughness parameters for an untreated substrate (Arnaud 2014)

t.2	Line	L1	L2	L3	L4	L5	L6	Mean value	Standard deviation
t.3	Ra (μm)	0.489	0.546	0.491	0.395	0.427	0.383	0.455	0.064
t.4	Rt (μm)	3.86	3.99	3.89	2.8	2.65	3.54	3.46	0.587

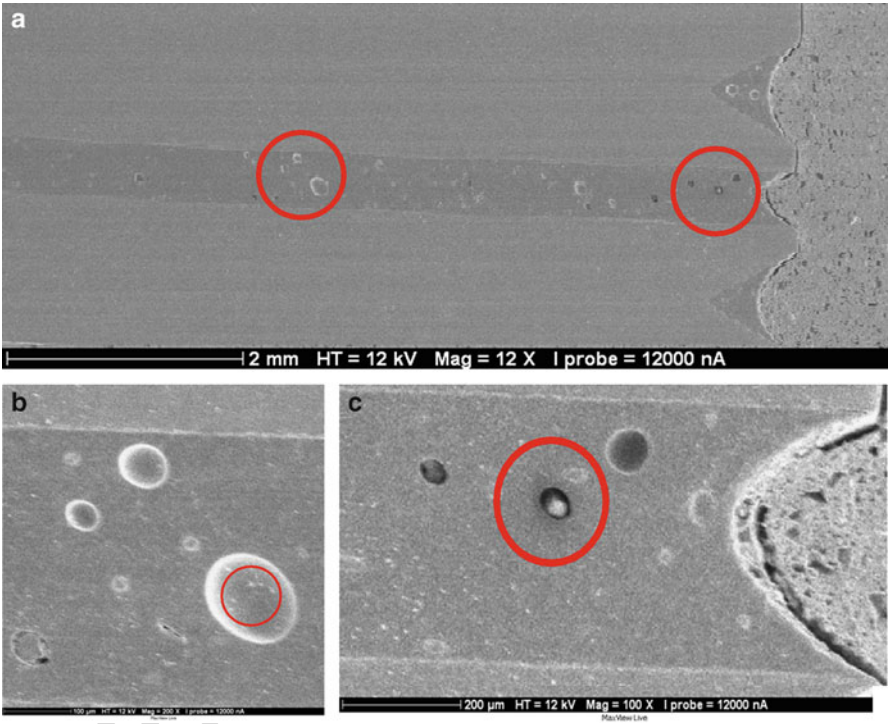
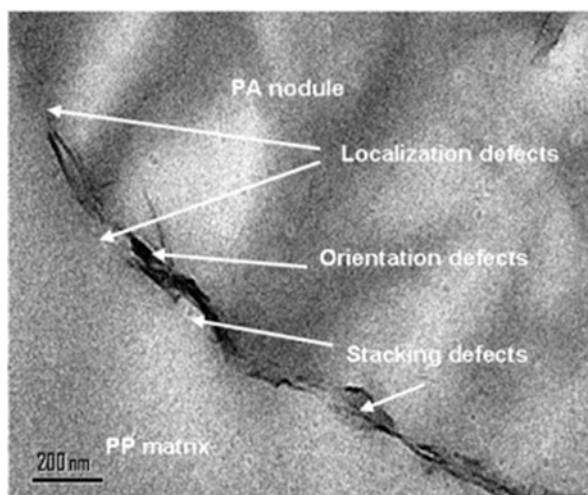


**Fig. 16** Scanning electron microscopy of an aluminum-epoxy-bonded assembly: (a) overview, (b), (c) zooms of some details (Arnaud 2014)

329 Two different patterns are distinguished, surrounded in Fig. 16a. A zoom is made on  
330 these details in Fig. 16b, c. Thanks to these observations, we are able to confirm the  
331 presence of charges in the adhesive and to measure them. The diameter of these  
332 beads announced by the supplier is 0.13 mm, which seems consistent with the  
333 observations of microscopy. Scanning electron microscopy is generally completed  
334 with addition measurement systems like energy-dispersive X-ray spectroscopy; one  
335 would be able to distinguish a void from a sphere, for example. A list of these  
336 systems is detailed in Table 1.

**Fig. 17** TEM micrograph of the interphase: evidence of structural defects (Beuguel et al. 2017)



More detailed information can be obtained. This is the case of the work of Beuguel et al. (2017). They observed decohesion between a polypropylene matrix and a polyamide nodule. Figure 17 was obtained with a higher resolution thanks to a transmission electron microscope.

#### 43.4.3 Nanoindentation

The discontinuity between two elements, the substrate and the adhesive or the matrix and the nodules, is a source of questions. Mechanicians are very interested in having local information on the mechanical properties. Is it an interface? Is it an interphase? What happens in this discontinuity? The use of nanoindentation provides local variations in the Young's modulus. The principle is based on a load applied very locally thanks to a pyramid. The process of indentation is measured with a load-displacement curve. The posttreatment gives then the reaction of the material indented. Davies et al. (2009) used this technique trying to approach a variation of the Young's modulus between an aluminum substrate and an epoxy adhesive along the geometric interface. In Fig. 18b zero defines the origin of this interface. For a positive abscissa, the values are defined for the adhesive. For a negative abscissa, this is the substrate that is measured. Several measurements were made for three adhesive thicknesses: 0.33 mm, 0.65 mm, and 1.23 mm. They conclude that if an interaction between the substrate and the adhesive exists for the materials considered, this zone is very thin around two microns of thickness.

#### 43.4.4 Atomic Force Microscopy

The atomic force microscopy is able to provide information up to 10 nm. The measurement principle is based on the flexion of a beam which is moved over a



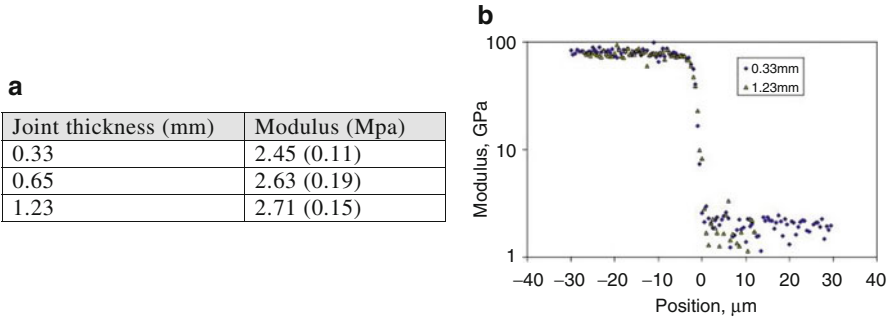


**Fig. 18** Nanoindentation of an epoxy adhesive: **(a)** measured Young’s modulus values, mean (standard deviation) of 10 values for each sample, measured at mid-thickness by nanoindentation; **(b)** across aluminum/adhesive interface, two joint thicknesses (Davies et al. 2009)

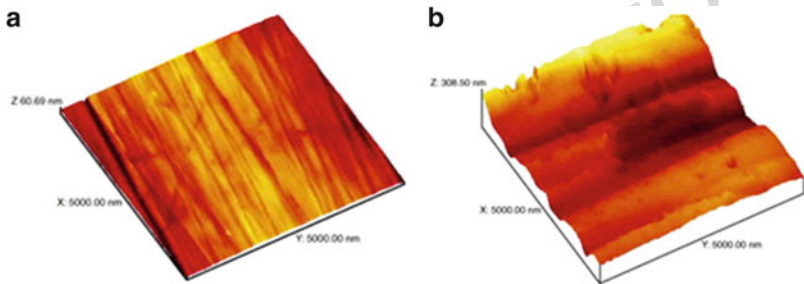


**Fig. 19** AFM measurements (Critchlow et al. 2006): **(a)** AFM image of hand-polished nickel tooling ( $5 \times 5 \mu\text{m}$  area). Vertical scale 60 nm; **(b)** AFM image of abraded nickel tooling, vertical scale approximately 0.3  $\mu\text{m}$

surface. The interaction between the tips of the beam induces a deflection of the beam which is measured. This interaction permits to define the topology of the measured surface. This is the first mean to use AFM. The second principle is based on the recording of the load necessary to deflect the beam. Thanks to this load measured, it is possible to obtain a map defining the local mechanical properties of the surface. The measurement process is quite long but gives a lot of information for small surfaces. Figure 19 gives results coming from the work of Critchlow et al. (2006). They analyzed the difference between hand-polished and abraded surfaces.

#### 43.4.5 Confocal Microscopy

The confocal microscope is an optical microscope able to measure information on a surface with a small depth of field. As a consequence, the volume studied has a maximal depth of 350–400  $\mu\text{m}$ . To observe structures through this volume, the

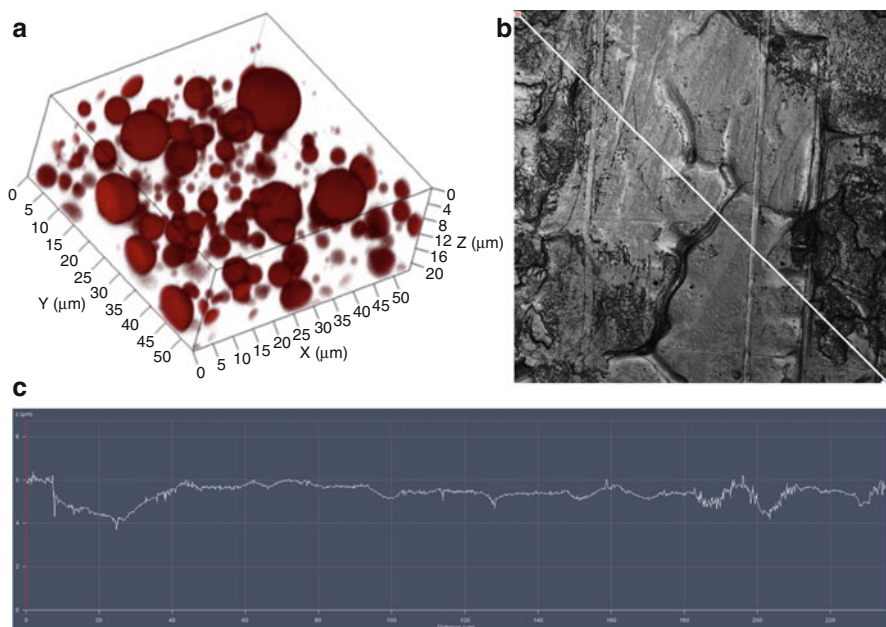


**Fig. 20** Confocal microscopy: (a) confocal micrograph of PP/PA6 blend: 3D observation of nodular morphology (Beuguel et al. 2017), (b) 3D measures of a zinc coating (Legendre et al. 2016), c roughness profile obtained along the *white cross line* (b)

material should be translucent. Beuguel et al. (2017) used this technique to observe the nodular morphology of a PP/PA6. Figure 20a defines the volume studied. The nodules are in red. It is possible to observe the variation of their dimensions, their distribution in a 3D space. Legendre et al. (2016) also used this technique to have a 3D topology of a steel sheet surface with a zinc coating. As previously shown in this chapter for the one-dimension roughness, it is possible to extract from this geometry the profile of the surface along a line (Fig. 20b, c).

#### 43.4.6 X-Ray Microtomography

In recent years, the development of measurement techniques has evolved toward three dimensions. The microtomography principle is based on the X-ray method. A specimen is lighted with an X-ray source. The image obtained is recorded thanks to a two-dimension screen placed behind the specimen. To obtain the third dimension, the specimen is placed on a rotary vertical axis. Between each measurement, a step of rotation is imposed. All these steps describe a complete turn. The whole images are then post-treated to build a three-dimension volume. Maurice (2012) used this technique to measure the voids in an aeronautical adhesive film. In this industrial field, the process imposes to use a pressure chamber, i.e., an autoclave, to reduce



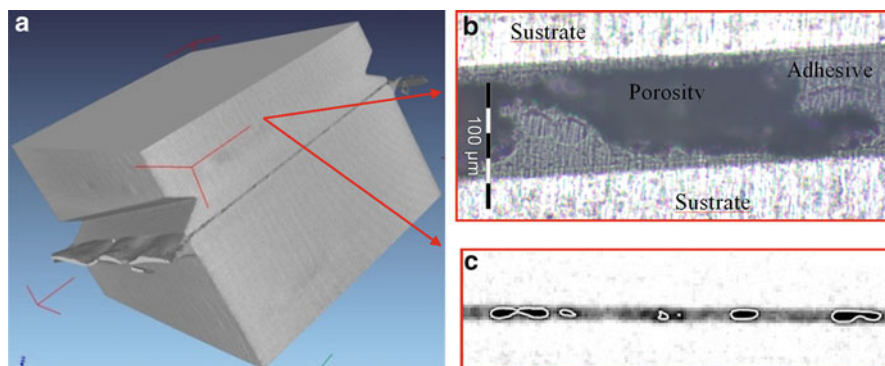


**Fig. 21** Microtomography analysis of an aeronautical adhesive: (a) 3D tomography measurement, (b) SEM cross view, (c) measurement of porosity by microtomography (Maurice 2012)

porosity in the assembly. It is slightly dependent on the pressure and temperature cycles. Figure 21 presents these results. Large voids were observed. The size of these defects is relatively important: their height is similar in scale to the adhesive thickness, and their length can be two or three times larger. Microtomography observation, performed on a sample of about 10 mm height, width, and length, confirmed this observation, and numerical post-processing of the results using myVGL™ software enables the void ratio to be measured as, at least, 20% in volume.

## 43.5 Physicochemical Analysis

### 43.5.1 Scanning Electron Microscopy with Energy-Dispersive X-Ray Spectroscopy

To understand X-ray spectroscopy, it is firstly necessary to understand the term spectroscopy. It can be defined as an experimental study to decompose in a succession of elementary data a complex and physical phenomenon. The set of these elementary data is called the spectrum. The data can be an energy, a wavelength, a frequency, etc.

An energy-dispersive X-ray spectroscopy gives information about the chemical composition of the analyzed material. The impact of the electron beam on the sample produces X-rays which are characteristic of the elements present on the sample. Figure 22 shows an analysis of the particles described in red in Fig. 16. The lines of the spectrum are specific for an atom. Figure 22 defines lines for carbon (C), oxygen (O), aluminum (Al), silicon (Si), and gold (Au). Carbon (C) and oxygen (O) are detectable. They correspond to the polymer material detected by the EDX beam behind the bead. The fillers are therefore glass beads, and very little porosity is detectable. The gold comes from the coating made before the analysis to make the samples conductive (Arnaud 2014).

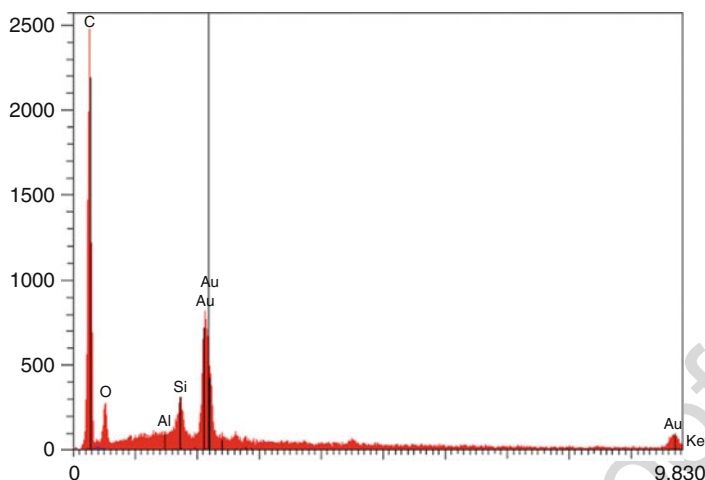


**Fig. 22** EDX analysis of two particles in an adhesive joint in red (Fig. 16) (Arnaud 2014)

The EDX spectroscopy is often coupled with a SEM in order to have the distribution of the atom in a representative surface. Arnaud (2014) studied with this method a coating based on molybdenum disulfide  $\text{MoS}_2$  (Fig. 23). Sulfur and molybdenum are present in good atomic mass ratio (Fig. 23c). In addition to the aluminum 2017, alloy made of aluminum and copper, there are elements of silicon, magnesium, oxygen, and carbon which must constitute the remainder of the coating. The EDX analysis in Fig. 23 confirms that sulfur (e) and molybdenum (f) are located in the same places and are very complementary to aluminum (d), constituting the majority of the coating. The position of the silicon appears to be an inclusion or pollution. The random position of the other species, carbon (b), oxygen (c), and magnesium (d) suggests their presence in the coating at lower amounts, which is confirmed by the percentages by mass.

In this context, it is necessary to make an important remark about fracture analysis. Pollution of the broken specimen must be fought. Particular attention should be given to samples just after their failure. Thanks to the progress of the analysis methods and the increase of their sensitivity, it is now possible to observe and detect very little particles. These particles can come from the test specimen but also from a contamination of the environment. In order not to be orientated in a wrong way, no pollution of the test samples must be satisfied.

### 43.5.2 Scanning Electron Microscopy with Raman Spectroscopy

When a well-known monochromatic ray light is applied to a material, the reflected signal is out of phase due to an exchange of energy between the ray light and the environment. This effect is called the Raman effect. The spectroscopy analysis of the reflected light gives information on the material itself. It is then possible to identify

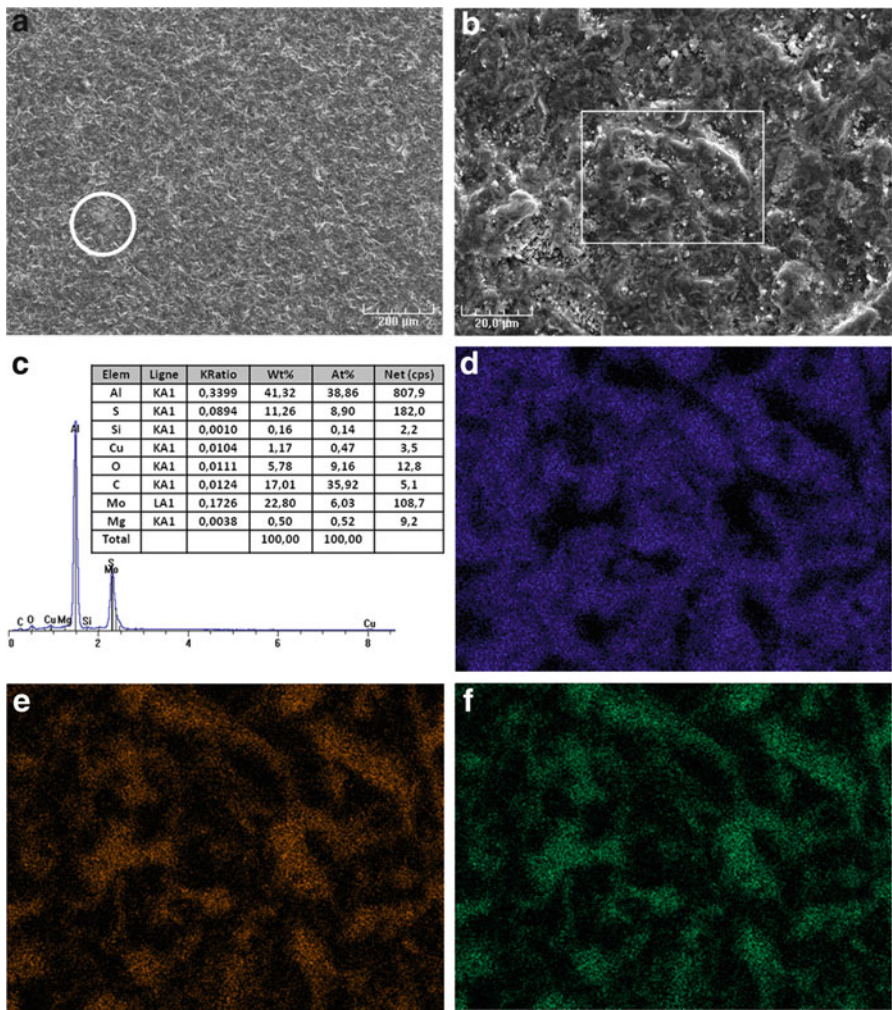
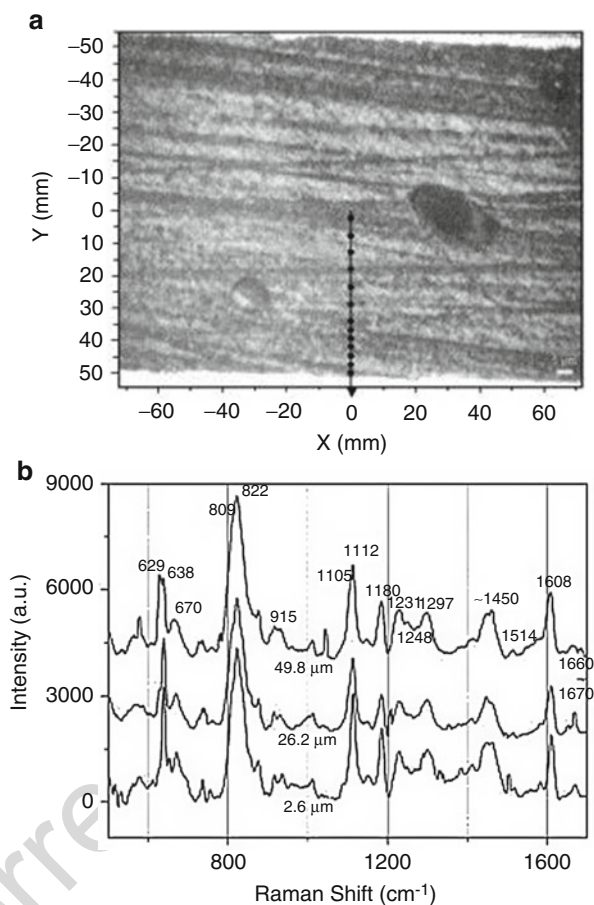


**Fig. 23** SEM observations of an aluminum 2017 substrate treated with a molybdenum disulfide coating: (a) zoom  $\times 100$ , (b) zoom  $\times 1,000$ , (c) EDX study of the composition of the zone with zoom  $\times 1,000$ , (d) aluminum, (e) sulfur, (f) molybdenum (Arnaud 2014)

molecules, chemical bonds, their proportions, and their structure. The method used by Raman analysis produces better spatial resolution than the attenuated total reflectance-Fourier transform infrared (ATR-FTIR) spectroscopy technique and makes it possible to analyze smaller samples.

Davies et al. (2009) tried to identify modification of the interface between an epoxy adhesive and an aluminum substrate. Across the interface (Fig. 24a), they observed local spectra (Fig. 24b). These spectra allow local variations in molecular species to be detected. Analysis of these results in terms of molecular groups is

**Fig. 24** (a) Optical view of the cross section analyzed by Raman scattering (100× objective lens in *white* light). Substrates (*white*) at *top* and *bottom* of photo. Each *black circle* corresponds to a Raman spectrum recorded, in the adhesive, (b) three Raman spectra along the cross section (Davies et al. 2009)



446 complicated, as this was a formulated commercial adhesive. The spectra (Fig. 24b)  
 447 point out the chemical bonds: C=C, C-O, C-H, CH-OH, and C<sub>6</sub>H<sub>6</sub>-H. Each Raman  
 448 shift is representative of a chemical bond. The analysis was completed in their work  
 449 with other analysis methods. It was the crossing of all the method used that can  
 450 propose scientific structured results. More information can be found in their work  
 451 (Davies et al.).

### 452 43.5.3 X-Ray Photoelectron Spectroscopy

453 Whereas X-ray Raman spectroscopy applies monochromatic ray light on a surface,  
 454 photoelectron spectroscopy applies an X-ray. The depth impacted by the X-ray  
 455 radiation is up to 5 nm. It enables to analyze the chemical composition and the  
 456 chemical bonds of the surface. For example, Kadiyala et al. (2016) analyzed joint

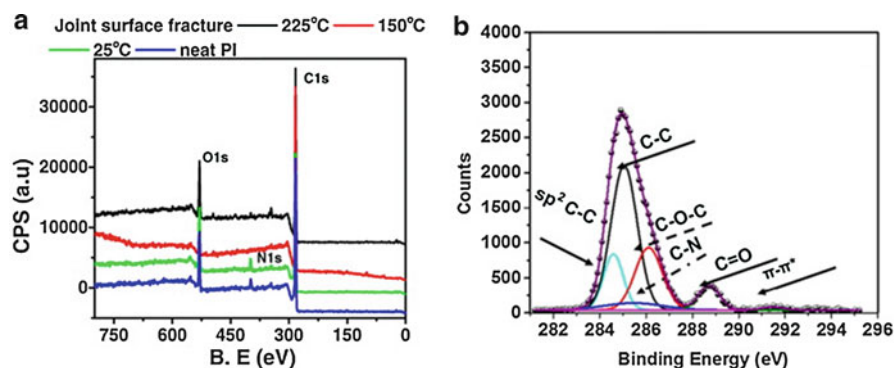


**Fig. 25** (a) XPS survey of neat and fractured joint surfaces of PI; (b) The C1s core-level XPS spectra for joint surfaces fractured at 25 °C (Kadiyala et al. 2016)

interface fractures of a thermoplastic semicrystalline polyimide for different temperatures: 25 °C, 150 °C, and 225 °C. As Fig. 25b points out, the type of chemical bonds and their quantities can be identified.

#### 43.5.4 Differential Scanning Calorimetry

The curing process of an adhesive is analyzed by solving the energy equation (Devaux et al. 2015):

$$\rho C_p \frac{\partial T}{\partial t} = \nabla(\lambda \nabla T) + \phi_r, \quad \text{with } \phi_r = \rho \Delta H_r \frac{\partial \alpha}{\partial t}$$

where  $\rho$  is the density of the adhesive,  $C_p$  the specific heat,  $\lambda$  the conductivity of the adhesive,  $T$  the temperature,  $H_r$  the total heat of the polymerization reaction, and  $\alpha$  the degree of cure.  $\phi_r$  is the heat flux produced by the polymerization reaction.

Two main phenomena are involved during adhesive curing: polymerization and cross-linking. There is a competition between these two events during the curing process. For a bicomponent epoxy adhesive, the uncured resin is mixed with a hardener according to a ratio recommended by the manufacturer in order to initiate the curing process. The chemical reaction within the mixture proceeds, and polymer chains cross-link to each other. As a result, molecular weight increases, causing an increase in viscosity. The cross-linking is an exothermic reaction; thus, the formation of the polymer network generates heat which results in a temperature increase. The molecular weight continues to increase until the gel time. It is the time for which the adhesive transforms from a liquid phase to a solid phase. This transition is also called the gel point. From this point, the molecular weight increases until forming a fully cross-linked polymer network. As a consequence, it is necessary to have reliable



information on the curing process. The differential scanning calorimetry can provide such information.

### Kinetic Analysis

As an example, Devaux et al. (2015) studied Hysol EA-9321 adhesive from Henkel, a two-component thixotropic, solvent-free epoxy-based resin. The adhesive is prepared using a mixing ratio of 2:1 by weight of the respective constituents (resin and hardener). According to the manufacturer's data sheets, a specimen cured during 1 h at 82 °C is completely cured (curing degree  $\alpha = 1$ ), and the glass transition temperature of specimens cured during 5–7 days at 25 °C is 88 °C.

The heat released during the cure reaction was detected by using a heat-flux differential scanning calorimeter connected to a thermal analyzer. This calorimeter is made of two steel pans. One of these is empty, and the other one contains sample weighting between 5 and 10 mg.

At first, dynamic and isothermal scans were carried to determine kinetic parameters of each one. Then, both kinds of scans were conducted to simulate few steps curing cycles.

Dynamic scans were carried out in the temperature range of 25–200 °C at constant heating rates of 5, 10, 15, and 20 °C/min. Isothermal scans were run at temperatures ranging from 25 to 100 °C. Equilibrium at the target isothermal temperature was reached in the sample holder with a rate of 20 °C/min. This rate was chosen sufficiently fast to prevent the reaction between resin and hardener before the start of isothermal scan. Coupled scans were made in the same way as previously, i.e., a dynamic scan was conducted until the required isothermal temperature, and then a second dynamic scan was conducted until the second required isothermal temperature.

For each scan, a second heating run on the same sample under the same conditions was carried in order to define the baseline along which the curve heat flow versus time is integrated.

The DSC curves in dynamic analysis are shown in Fig. 26. The shape of the exotherm was heating dependent. The value of the total heat released was determined by integrating heat flow versus time under the exotherm along a straight baseline. This heat of reaction,  $\Delta H_T$ , was independent of the heating rate (Table 3).

Figure 27 shows the heat flow released versus time for isothermal scans. The maximum heat flow is reached faster for high curing temperatures, due to the acceleration of the reaction between resin and hardener. Table 4 presents the heat of reaction released during isothermal scanning.  $\Delta H_{ISO}$  is calculated by integrating the area under the heat flow versus time curves along a straight baseline, defined as previously.

The curing degree,  $\alpha$ , is based on isothermal and dynamic scans and is calculated as  $\Delta H_t / \Delta H_T$ ;  $\Delta H_t$  is the heat of reaction released during isothermal scan at time  $t$  and  $\Delta H_T$  the total enthalpy of reaction calculated during dynamic scans. In this way, intermediate curing states of the adhesive as a function of time over isothermal temperatures were determined.

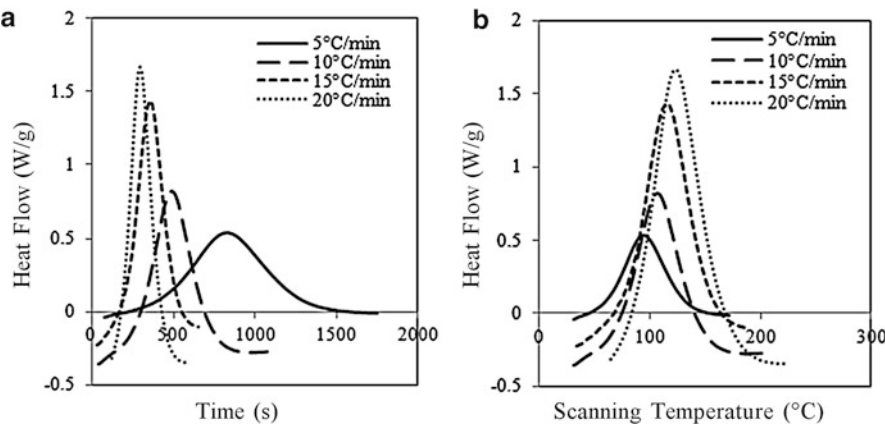
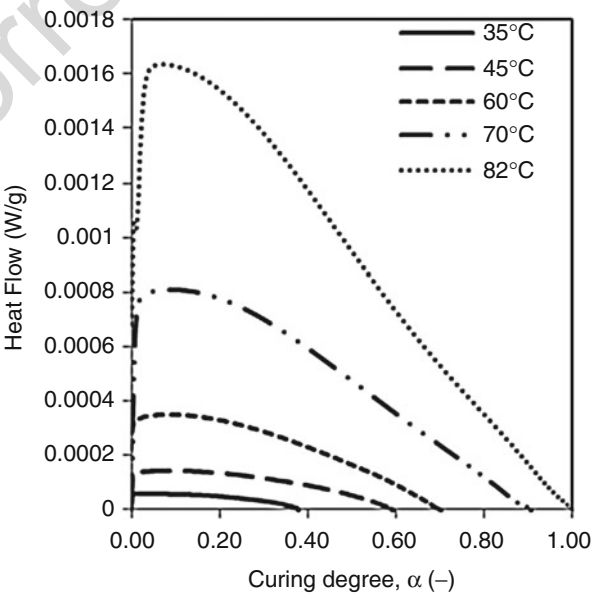


**Fig. 26** Dynamic scanning: heat flow at different heating rates as function of (a) time and (b) temperature (Devaux et al. 2015)

t.1 **Table 3** Total heat of reaction at different heating rates (Devaux et al. 2015)

t.3	Parameter	dT/dt (°C/min)			
		5	10	15	20
t.4	$\Delta H_T$ (J/g)	334.1	351.03	326.66	353.1

**Fig. 27** Heat flow at different isothermal temperatures (Devaux et al. 2015)



t.1 **Table 4** Isothermal scanning results (Devaux et al. 2015)

t.2	Parameter	T <sub>cure</sub> (°C)				
		35	45	60	70	82
t.4	ΔH <sub>ISO</sub> (J/g)	130.73	202.07	240.03	310.03	341.18
t.5	α (-)	0.38	0.59	0.70	0.91	1.0
t.6	t	4 h25	3 h33	2 h40	1 h30	46 min

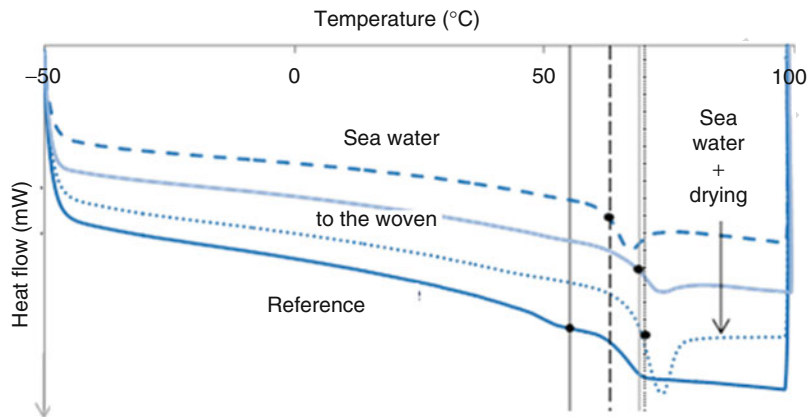


**Fig. 28** DSC results: influence of the accelerated aging on an epoxy adhesive (Arnaud 2014)

**Analysis of the Glass Transition Temperature (Tg)**

The evolution of Tg provides information on the physical phenomena affecting the polymer studied. Thus, Arnaud (2014) studied the evolution of an accelerating aging under temperature and seawater absorption. Figure 28 presents the evolution of the heat flow versus temperature for a rate of 10 °C/min. Four types of specimens were tested. The reference submitted to a cold curing cycle. The Tg measured was 55 °C defined by the inflection point on Fig. 28 (“reference curve”). A second specimen was cold cured and post-cured at 40 °C during 1 month. Tg increased to 71 °C (Fig. 28; “to the woven” curve). It was fully cured like the study presented by Devaux et al. (2015). The third curve defines a cold-cured adhesive and aged in seawater at a temperature of 40 °C (Fig. 28; “seawater” curve). The Tg obtained increased to 63 °C indicating the post-cured of the adhesive during aging. A fourth specimen was cold cured aged in seawater at a temperature of 40 °C and dried in an oven at 40 °C during 1 month (Fig. 28; “seawater + drying” curve). The Tg obtained was 70 °C. This specimen points out the reversible phenomenon of the seawater aging. The evolution of the Tg measured by DSC gives information on the physical phenomena.



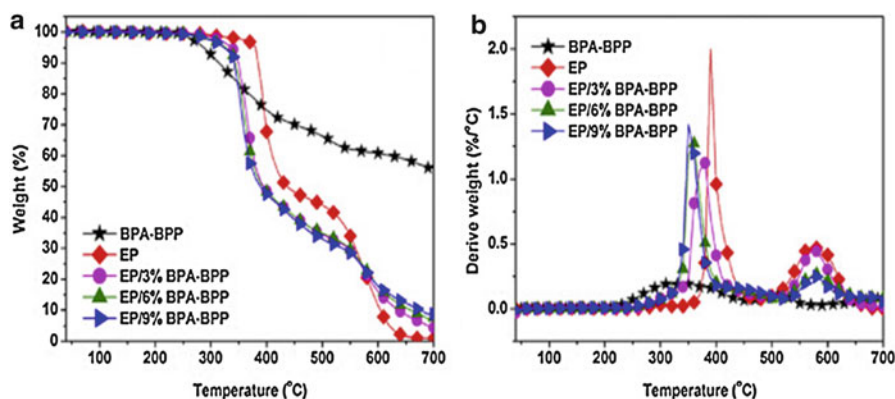


**Fig. 29** TGA analysis (Zhao et al. 2016)

### 43.5.5 Thermogravimetric Analysis

The thermogravimetric analysis consists on measuring with precision the weight of a specimen submitted to a thermal loading under a controlled atmosphere with air, azote, oxygen, etc. The measured variations transcribe the chemical reactions that occurred. The principle is similar to a measured combustion. At the end, residues are generally analyzed to quantify nonorganic charges. To explain this method, it is possible to quote the work made by Zhao et al. (2016). They analyzed with thermogravimetric analysis the composition of an adhesive made of two components: epoxy and a flame retardant named bisphenol-A bridged penta(anilino) cyclotriphosphazene (BPA-BPP). The results are plotted in Fig. 29. The evolution of weight was described regarding the temperature under nitrogen atmosphere. Different compositions were studied, starting with the BPA-BPP and the epoxy themselves. The weight of BPA-BPP started to decrease around 250 °C. At 700 °C, the residual weight was 60%. It means that there were residual nonorganic components. For the epoxy analysis, two main variations occurred (Fig. 29b) around 400 °C and 600 °C. Each peak corresponds to a chemical reaction. Then they studied the mixture.

### 43.5.6 Attenuated Total Reflectance-Fourier Transform Infrared (ATR-FTIR) Spectroscopy Technique

As the previous spectroscopies presented before, the attenuated total reflectance-Fourier transform infrared (ATR-FTIR) spectroscopy technique is based on the infrared light on the material. The returned signal is then measured. The difference is linked to the properties of the material. Each peak measured is specific to a chemical bond. It is also possible to define their quantities. Gorassini et al. (2016)

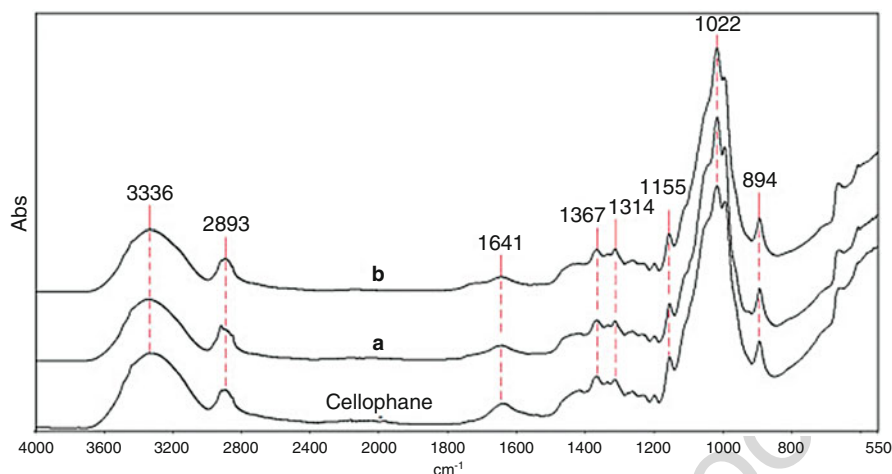


**Fig. 30** ATR-FTIR spectra of cellophane, backing side of unaged (a) and artificially aged (b) tape C (Gorassini et al. 2016)

studied the composition of an old pressure-sensitive adhesive, used to assemble pages in very old books, in order to recover and understand the initial chemical properties of the adhesive and their modifications due to aging. Three adhesive were tested: a cellophane available in literature and a commercial adhesive unaged and aged. They confirmed that the adhesive used was mainly made of cellulose acetate (Fig. 30).

## 43.6 Mechanical Observations

The following points are not often defined as a “post-fracture analysis” because these measurements are generally carried out in the laboratory during an instrumented test. However, it is very important for mechanical engineers to establish the relation between the loads applied, the deformations of the bonded assemblies, and their fracture surfaces. As the experimental methods need posttreatment after the test, they can be defined as “post-fracture analysis.” Moreover, these methods can bring a lot of information to understand the fracture of adhesives.

### 43.6.1 3D Digital Image Correlation

3D digital image correlation systems are able to measure the displacement of a surface in three dimensions (Cognard et al. 2005; Créac'hcadec et al. 2008; Maurice 2012). It is made of a pair of cameras and a lighting system that take pictures at a defined time rate. The frames are then recording with different signals like the tensile

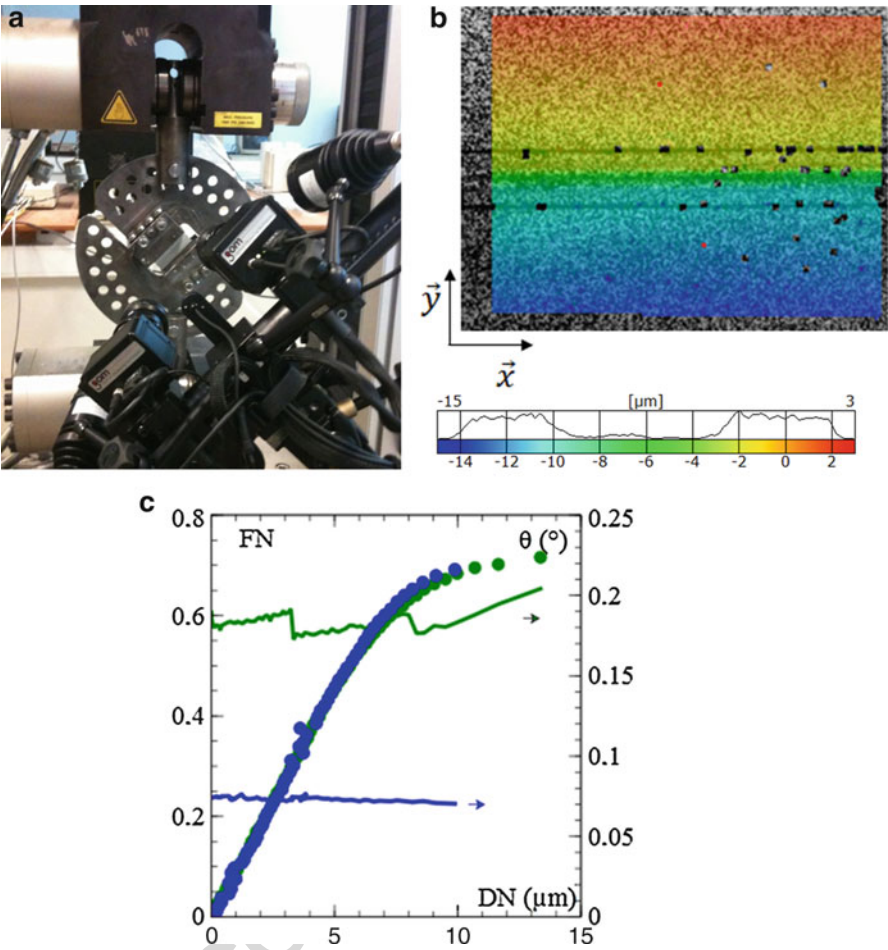


**Fig. 31** 3D digital image correlation system: (a) Modified Arcan experimental device, (b) image recorded and post-analyzed with the relative displacement of both sides of the adhesive joint in the out of plane y-direction DN, (c) tensile load, relative displacement DN curve (Maurice 2012).

load of the test machine. Figure 31 presents an example of a modified Arcan test measured with this type of system. Figure 31b presents a post-treated frame with the adhesive joint area analyzed composed of the adhesive and two aluminum substrates. The correlation system provides a kinematic field for the entire picture. Here the relative displacement of both sides of the adhesive in the y-direction is plotted. The resolution of this system is around 1/100 pixels. It depends on the scale factor to convert it in millimeters. As a result, Fig. 31c plots a load-displacement curve in blue. It is then possible to develop law behavior to explain such observations (Cr  ac  hadeac 2008). Most of all, Maurice (2012) improved the posttreatment

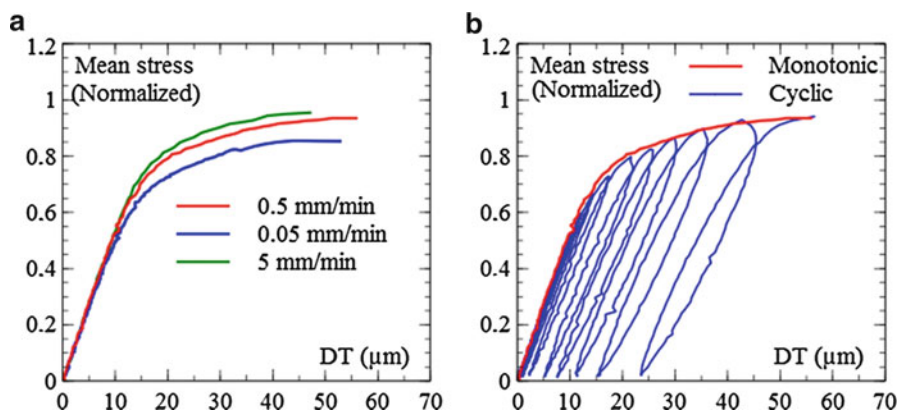


**Fig. 32** Influence of strain rate and behavior under cyclic loads of bonded assembly under shear loads: (a) strain rate effect and (b) behavior under cyclic loads (Maurice 2012)

method to explain the cleavage along the x-direction that can be observed if the alignment of the Arcan device is not well done. This technique is very interesting to understand the type of fracture. It is then possible to measure different phenomenon behaviors of the adhesive joints, like strain rate effect or cyclic behaviors (Fig. 32). For fatigue test, an improvement is necessary to have real-time measurements (Créac'hacdec et al. 2015). This method is very interesting and can be used for local measurements. Davies et al. (2009) pointed out the linear evolution of the shear strain for a thick epoxy adhesive. No specific behavior close to the interface was observed (Fig. 33).

### 43.6.2 Digital Volume Correlation

The digital image correlation gives information on the surface of an observed specimen. The next question is then what happens in the material. That's the reason why digital volume correlation is developing a lot. The principle is similar to the microtomography principle described before. However, a 3D reconstruction is made for each step of loading like the 3D image correlation system. It is then possible to have in three dimensions the evolution of the strains versus loading path. Boufert et al. (2017) studied the microstructure of a core and observed with a resolution of 12 μm. The volume is defined in Fig. 34a. They applied a load thanks to the indentation sphere (Fig. 34b). They post-treated their recorded frame and were able to plot a stress field (Fig. 34c). This method is very useful to have information in the assembly. This is not very developed in the adhesive field, but in the coming years, it will probably bring to the adhesion community very important data.

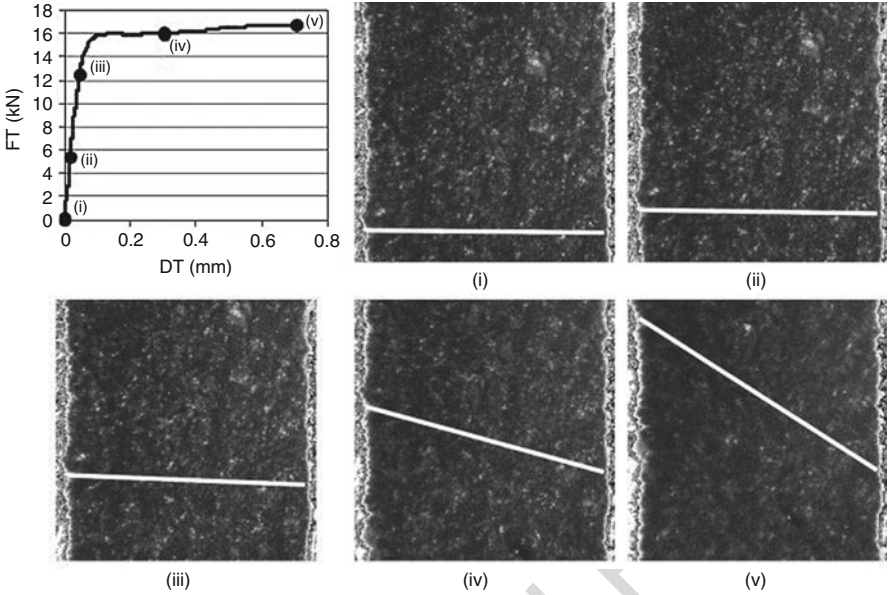


**Fig. 33** 2D digital image correlation for a pure shear deformation of a thick epoxy adhesive joint (Davies et al. 2009)

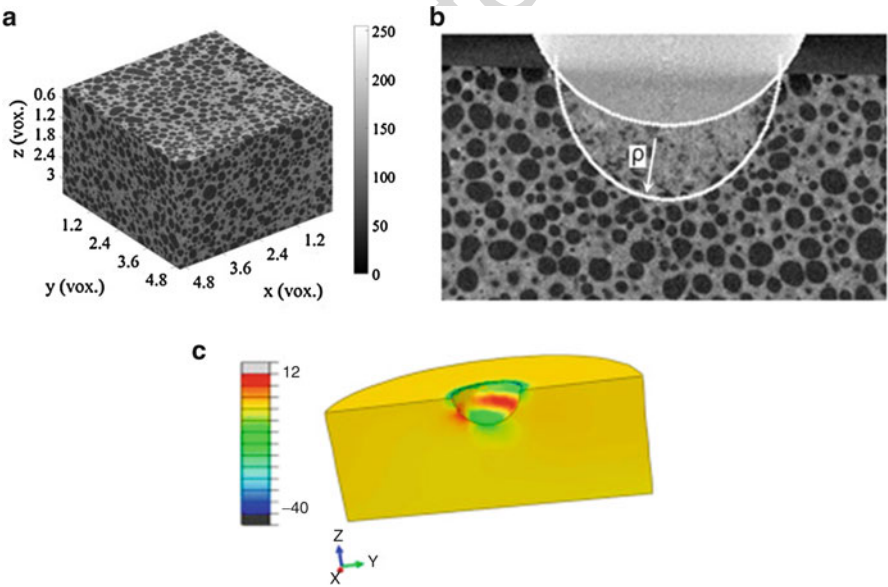


**Fig. 34** Digital volume correlation: (a) 3D rendering of the microstructure of the core material studied herein and observed at a resolution of  $12\text{ }\mu\text{m}$ . The size of the volume is  $4.8 \times 4.8 \times 3.2\text{ mm}^3$ ; (b) section of the microstructure with the indenter (in white) that applied the load, (c) stress field extracted from the DVC measurements (Bouterf et al. 2017)



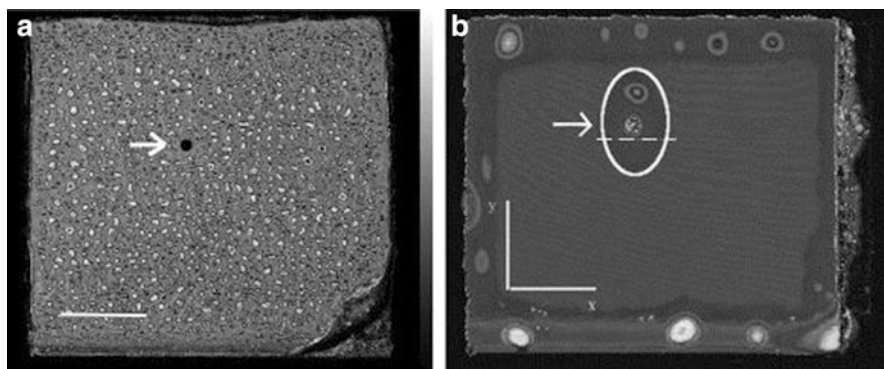


**Fig. 35** Ultrasonic images (C-scans) of a sample in immersion in Harrison solution: (a) without clear coat after 331 h (b) with clear coat after 315 h of immersion in Harrison solution. *White scale bars: 5 mm. The arrows mark the initial defects (holes of 0.5 mm diameter)* (Oehler et al. 2012)

### 43.6.3 Ultrasonic Testing

Nondestructive tests are very interesting to bring information on adhesion. This is the case for ultrasonic tests. The principle is described in the chapter dedicated to NDT methods (see ► Chap. 42, “Nondestructive Testing”). An ultrasonic wave is generated to a surface. The return signal is measured. The difference is linked to the material itself. Oehler et al. (2012) worked on decohesion of an interface subjected to an immersion in Harrison solution. A hole with a diameter of 0.5 mm was made in the coating. A good coating and a bad one were tested. Decohesion was observed with ultrasonic scans (Fig. 35) for the clear coat.

This method was used by Maurice (2012) for composite single-lap shear tests (Fig. 36). Tests were performed with a tensile testing machine. The test was stopped at different load levels. Ultrasonic measurements were performed at each step of loading. The overlap was observed. At the corner, a fracture initiated linked to the edge effects and then propagated to the center. This is particularly visible in Fig. 36b. After this propagation, the fracture of the whole specimen occurred.

## 43.7 Conclusions

Solving the equation of adhesion needs information coming from multi-physics and multi-scale analysis.

1. Fracture analyses are a huge source of information. This information comes from various supports: microscopy, compositional analysis/material identifications, and mechanical observations.
2. Each means of analysis should not be taken separately. It is the intersection of these different types of analysis that constructs the failure understanding.

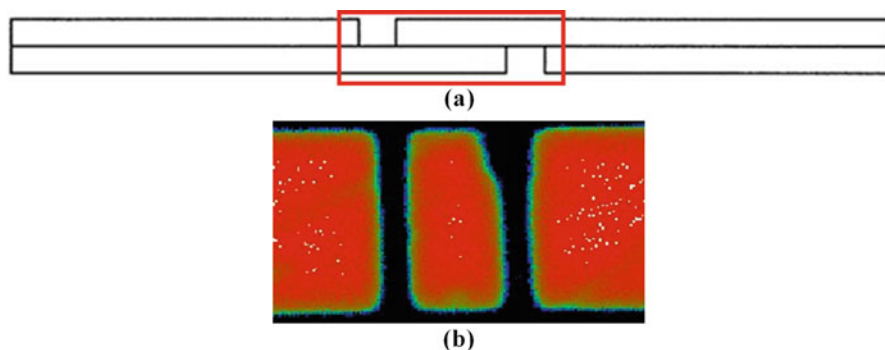


**Fig. 36** US scan for a composite single-lap shear test sample: (a) geometry of the specimen, (b) example of US scans obtained at different loads for different specimens; the scale goes from 0.3 (red) to 4 dB (blue) of signal loss (Maurice 2012)

3. In this chapter, the mainly experimental devices are presented, but this list is not exhaustive.
4. The development of measurement methods is increasing with precision and sensitivity. The today's means are certainly not those of tomorrow's ones.
5. Having a good picture or a good spectrum needs good operators to prepare the sample, not to pollute them, to master the observation device, etc.
6. Moreover, good pictures are not synonymous of good interpretations. To have a good explanation, it is necessary to have a long experience, especially in these observation techniques. The failure comprehension is then the intersection of specialists of each domain area.
7. Scientists or industrials that work on adhesion should be able to interact with all these domains. This is not so simple due to the initial training of each one.

**Acknowledgements** This work was realized using different results coming from PhD theses I had the pleasure to supervise. So I really want to thank N. Arnaud, O. Devaux, J. Legendre, J. Maurice, for the work they performed. I also want to thanks the different research collaborators (industrials and academic) for their help and their financial support. I also want to thank Philippe Elies and Gérard Sinquin (Université de Bretagne Occidentale) for the measurements they performed in the Pimm-DRX technology platform: Imaging, Microscopy and x-ray diffraction.

## References

- Aguiar TR, Andre CB, Arrais CAG, Bedran-Russo AK, Giannini M (2012) Micromorphology of resin–dentin interfaces using self-adhesive and conventional resin cements: a confocal laser and scanning electron microscope analysis. *Int J Adhes Adhes* 38:69–74. <https://doi.org/10.1016/j.ijadhadh.2012.05.009>
- Aldrich-Smith G, Jennett N, Housden J (2005) Adhesion of thin coatings – the VAMAS (TWA 22-2) interlaboratory exercise. *Surf Coat Technol* 197:336–344. <https://doi.org/10.1016/j.surfcoat.2004.07.113>

- Arnaud N (2014) Analyse de l'effet du vieillissement en milieu humide sur le comportement mécanique d'adhésifs en assemblages sous sollicitations multiaxiales. Université de Bretagne Occidentale, Brest
- Arnaud N, Créac'hcadec R, Cognard JY, Davies P, Gac PYL (2015) Analysis of the moisture effect on the mechanical behaviour of an adhesively bonded joint under proportional multi-axial loads. *J Adhes Sci Technol* 29:2355–2380. <https://doi.org/10.1080/01694243.2015.1067018>
- Bele E, Goel A, Pickering EG, Borstnar G, Katsamenis OL, Pierron F, Danas K, Deshpande VS (2017) Deformation mechanisms of idealised ceramets under multi-axial loading. *J Mech Phys Solids*. <https://doi.org/10.1016/j.jmps.2017.01.002>
- Beuguel Q, Ville J, Crepin-Leblond J, Mederic P, Aubry T (2017) Influence of clay mineral structure and polyamide polarity on the structural and morphological properties of clay polypropylene/polyamide nanocomposites. *Appl Clay Sci* 135:253–259. <https://doi.org/10.1016/j.clay.2016.09.034>
- Böhm R, Hauptmann M, Pizzi A, Friedrich C, Laborie M-P (2016) The chemical, kinetic and mechanical characterization of tannin-based adhesives with different crosslinking systems. *Int J Adhes Adhes* 68:1–8. <https://doi.org/10.1016/j.ijadhadh.2016.01.006>
- Bouterf A, Adrien J, Maire E, Brajer X, Hild F, Roux S (2017) Identification of the crushing behavior of brittle foam: from indentation to oedometric tests. *J Mech Phys Solids* 98:181–200. <https://doi.org/10.1016/j.jmps.2016.09.011>
- Cacho JJ, Campillo N, Viñas P, Hernández-Córdoba M (2016) Dispersive liquid-liquid micro-extraction for the determination of nitrophenols in soils by microvial insert large volume injection-gas chromatography–mass spectrometry. *J Chromatogr A* 1456:27–33. <https://doi.org/10.1016/j.chroma.2016.05.098>
- Cardell C, Guerra I (2016) An overview of emerging hyphenated SEM-EDX and Raman spectroscopy systems: applications in life, environmental and materials sciences. *TrAC Trends Anal Chem* 77:156–166. <https://doi.org/10.1016/j.trac.2015.12.001>
- Charbonnier M, Romand M, Roche A, Gaillard F (1986) Adhesive bonding of aerospace materials – surface characterization of metallic adherends. *Int J Adhes Adhes* 6:199–206. [https://doi.org/10.1016/0143-7496\(86\)90006-0](https://doi.org/10.1016/0143-7496(86)90006-0)
- Chen B, Dillard DA (2001) The effect of the T-stress on crack path selection in adhesively bonded joints. *Int J Adhes Adhes* 21:357–368. [https://doi.org/10.1016/S0143-7496\(01\)00011-2](https://doi.org/10.1016/S0143-7496(01)00011-2)
- Choudhury T, Jones FR (2006) The interaction of silanes with amorphous silicon oxide surfaces. *Int J Adhes Adhes Silane Coupling Agents* 26:79–87. <https://doi.org/10.1016/j.ijadhadh.2005.03.007>
- Cognard JY (2008) Numerical analysis of edge effects in adhesively-bonded assemblies application to the determination of the adhesive behaviour. *Comput Struct* 86:1704–1717. <https://doi.org/10.1016/j.compstruc.2008.02.003>
- Cognard JY, Davies P, Gineste B, Sohier L (2005) Development of an improved adhesive test method for composite assembly design. *Compos Sci Technol, JNC13-AMAC-Strasbourg* 65:359–368. <https://doi.org/10.1016/j.compscitech.2004.09.008>
- Cognard JY, Créac'hcadec R, Sohier L, Leguillon D (2010) Influence of adhesive thickness on the behaviour of bonded assemblies under shear loadings using a modified TAST fixture. *Int J Adhes Adhes Spec Issue Joint Des* 30:257–266. <https://doi.org/10.1016/j.ijadhadh.2009.11.003>
- Cognard JY, Bourgeois M, Créac'hcadec R, Sohier L (2011a) Comparative study of the results of various experimental tests used for the analysis of the mechanical behaviour of an adhesive in a bonded joint. *J Adhes Sci Technol* 25:2857–2879. <https://doi.org/10.1163/016942411X569345>
- Cognard JY, Créac'hcadec R, Maurice J (2011b) Numerical analysis of the stress distribution in single-lap shear tests under elastic assumption – application to the optimisation of the mechanical behaviour. *Int J Adhes Adhes* 31:715–724. <https://doi.org/10.1016/j.ijadhadh.2011.07.001>
- Comyn J (1992) Practical surface analysis, 2nd edition: Volume 1: Auger and X-ray photoelectron spectroscopy Edited by: D. Briggs and M.P. Seah John Wiley & Sons, 1990, 657 + xiv pp. *Int J Adhes Adhes* 12:124. [https://doi.org/10.1016/0143-7496\(92\)90036-U](https://doi.org/10.1016/0143-7496(92)90036-U)
- Coulaud M (2007) Rôle des interfaces et interphases dans les assemblages collés. PhD thesis, Institut National des Sciences Appliquées de Lyon, Lyon



- Créac'hcadec R, Cognard JY, Heuzé T (2008) On modeling the non-linear behaviour of thin adhesive films in bonded assemblies with interface elements. *J Adhes Sci Technol* 22:1541–1563
- Créac'hcadec R, Jamin G, Cognard JY, Jousset P (2014) Experimental analysis of the mechanical behaviour of a thick flexible adhesive under tensile/compression-shear loads. *Int J Adhes Adhes* 48:258–267. <https://doi.org/10.1016/j.ijadhadh.2013.09.040>
- Créac'hcadec R, Sohier L, Cellard C, Gineste B (2015) A stress concentration-free bonded arcane tensile compression shear test specimen for the evaluation of adhesive mechanical response. *Int J Adhes Adhes* 61:81–92. <https://doi.org/10.1016/j.ijadhadh.2015.05.003>
- Critchlow GW, Litchfield RE, Sutherland I, Grandy DB, Wilson S (2006) A review and comparative study of release coatings for optimised adhesion in resin transfer moulding applications. *Int J Adhes Adhes* 26:577–599. <https://doi.org/10.1016/j.ijadhadh.2005.09.003>
- Croccolo D, Cuppini R (2009) Adhesive defect density estimation applying the acoustic emission technique. *Int J Adhes Adhes* 29:234–239. <https://doi.org/10.1016/j.ijadhadh.2008.06.001>
- Davies P, Sohier L, Cognard J-Y, Bourmaud A, Choqueuse D, Rinnert E, Créac'hcadec R (2009) Influence of adhesive bond line thickness on joint strength. *Int J Adhes Adhes* 29:724–736. <https://doi.org/10.1016/j.ijadhadh.2009.03.002>
- Devaux O, Créac'hcadec R, Cognard JY, Mathis K, Lavelle F (2015) FE simulation of the curing behavior of the epoxy adhesive Hysol EA-9321. *Int J Adhes Adhes* 60:31–46. <https://doi.org/10.1016/j.ijadhadh.2015.03.005>
- Gazulla MF, Rodrigo M, Orduña M, Ventura MJ, Andreu C (2017) High precision measurement of silicon in naphthas by ICP-OES using isooctane as diluent. *Talanta* 164:563–569. <https://doi.org/10.1016/j.talanta.2016.12.023>
- Ghiassi B, Verstrynge E, Lourenço PB, Oliveira DV (2014) Characterization of debonding in FRP-strengthened masonry using the acoustic emission technique. *Eng Struct* 66:24–34. <https://doi.org/10.1016/j.engstruct.2014.01.050>
- Gorassini A, Adami G, Calvini P, Giacomello A (2016) ATR-FTIR characterization of old pressure sensitive adhesive tapes in historic papers. *J Cult Herit* 21:775–785. <https://doi.org/10.1016/j.culher.2016.03.005>
- Haddadi F, Tsivoulas D (2016) Grain structure, texture and mechanical property evolution of automotive aluminium sheet during high power ultrasonic welding. *Mater Charact* 118:340–351. <https://doi.org/10.1016/j.matchar.2016.06.004>
- Hase A, Wada M, Mishina H (2014) Scanning electron microscope observation study for identification of wear mechanism using acoustic emission technique. *Tribol Int* 72:51–57. <https://doi.org/10.1016/j.triboint.2013.12.006>
- Heikkilä I, Eggertson C, Randelius M, Caddeo-Johansson S, Chasoglou D (2016) First experiences on characterization of surface oxide films in powder particles by Glow Discharge Optical Emission Spectroscopy (GD-OES). *Metal Powder Report* 71:261–264. <https://doi.org/10.1016/j.mprp.2016.03.005>
- Kadiyala AK, Sharma M, Bijwe J (2016) Exploration of thermoplastic polyimide as high temperature adhesive and understanding the interfacial chemistry using XPS, ToF-SIMS and Raman spectroscopy. *Mater Des* 109:622–633. <https://doi.org/10.1016/j.matdes.2016.07.108>
- Kanrar B, Sanyal K, Misra NL, Aggarwal SK (2014) Improvements in energy dispersive X-ray fluorescence detection limits with thin specimens deposited on thin transparent adhesive tape supports. *Spectrochim Acta B At Spectrosc* 101:130–133. <https://doi.org/10.1016/j.sab.2014.07.018>
- Karachalios EF, Adams RD, da Silva LFM (2013) Single lap joints loaded in tension with high strength steel adherends. *Int J Adhes Adhes* 43:81–95. <https://doi.org/10.1016/j.ijadhadh.2013.01.016>
- Koseki S, Inoue K, Usuki H (2016) Damage of physical vapor deposition coatings of cutting tools during alloy 718 turning. *Precis Eng* 44:41–54. <https://doi.org/10.1016/j.precisioneng.2015.09.012>
- Legendre J, Jacquet D, Créac'hcadec R (2016) The role of steel plasticity on the failure pattern of single lap joints. Presented at the Euradh 2016 and Adhesion '16, 11th European Adhesion Conference and 13th International Triennial Conference on the science and Technology of Adhesion and Adhesives, Glasgow
- Liu Y (2013) “Tri-3D” electron microscopy tomography by FIB, SEM and TEM: application to polymer nanocomposites (PhD thesis). INSA de Lyon

- Magalhães AG, de Moura MFSF (2005) Application of acoustic emission to study creep behaviour of composite bonded lap shear joints. *NDT & E International* 38:45–52. <https://doi.org/10.1016/j.ndteint.2004.06.005>
- Maurice J (2012) Characterization and modeling of the 3D elastic plastic behavior of structural adhesives films for aeronautical applications. PhD thesis, Université de Bretagne Occidentale, Brest
- Mine A, De Munck J, Van Ende A, Poitevin A, Matsumoto M, Yoshida Y, Kuboki T, Van Landuyt KL, Yatani H, Van Meerbeek B (2017) Limited interaction of a self-adhesive flowable composite with dentin/enamel characterized by TEM. *Dent Mater* 33:209–217. <https://doi.org/10.1016/j.dental.2016.11.010>
- Oehler H, Alig I, Lellinger D, Bargmann M (2012) Failure modes in organic coatings studied by scanning acoustic microscopy. *Prog Org Coat Coat Sci Int* 2011 74:719–725. <https://doi.org/10.1016/j.porgcoat.2011.09.017>
- Pecnik CM, Courty D, Muff D, Spolenak R (2015) Fracture toughness of esthetic dental coating systems by nanoindentation and FIB sectional analysis. *J Mech Behav Biomed Mater* 47:1–11. <https://doi.org/10.1016/j.jmbbm.2015.03.006>
- Procaccini R, Ceré S, Pellice S (2011) Development and thermal evolution of silver clusters in hybrid organic–inorganic sol–gel coatings. *Surf Coat Technol* 205:5464–5469. <https://doi.org/10.1016/j.surfcoat.2011.06.018>
- Tsunekawa S, Aoki Y, Habazaki H (2011) Two-step plasma electrolytic oxidation of Ti–15V–3Al–3Cr–3Sn for wear-resistant and adhesive coating. *Surf Coat Technol* 205:4732–4740. <https://doi.org/10.1016/j.surfcoat.2011.04.060>
- Uerlings R, Matusch A, Weiskirchen R (2016) Reconstruction of laser ablation inductively coupled plasma mass spectrometry (LA-ICP-MS) spatial distribution images in Microsoft excel 2007. *Int J Mass Spectrom* 395:27–35. <https://doi.org/10.1016/j.ijms.2015.11.010>
- Vallat MF (2013) Tests d'adhésion et pertinence des mesures, 17ème Journées d'Etudes sur l'Adhésion. JADH13, Aussois
- Vera P, Ulliaque B, Canellas E, Escudero A, Nerin C (2012) Identification and quantification of odorous compounds from adhesives used in food packaging materials by headspace solid phase extraction and headspace solid phase microextraction coupled to gas chromatography–olfactometry–mass spectrometry. *Anal Chim Acta* 745:53–63. <https://doi.org/10.1016/j.aca.2012.07.045>
- Yeom B, Jeong A, Lee J, Char K (2016) Enhancement of fracture toughness in organic/inorganic hybrid nanolaminates with ultrathin adhesive layers. *Polymer* 91:187–193. <https://doi.org/10.1016/j.polymer.2016.03.078>
- Zhao B, Liang W-J, Wang J-S, Li F, Liu Y-Q (2016) Synthesis of a novel bridged-cyclotriphosphazene flame retardant and its application in epoxy resin. *Polym Degrad Stab* 133:162–173. <https://doi.org/10.1016/j.polymdegradstab.2016.08.013>
- Zięba-Palus J, Nowińska S, Kowalski R (2016) Application of infrared spectroscopy and pyrolysis gas chromatography for characterisation of adhesive tapes. *J Mol Struct Mol Mater Biol Mol Syst Nanostruct A Collect Contrib Presented XIIIth Int Conf Mol Spectrosc* 1126:232–239. <https://doi.org/10.1016/j.molstruc.2015.11.050>

Uncorrected Proof

L. John Hart-Smith

## Contents

44.1	Introduction .....	1236
44.2	Adhesive Characteristics Required for Design and Analysis .....	1238
44.3	Surface Preparation .....	1243
44.4	Design of Adhesively Bonded Joints .....	1248
44.5	Additional Considerations for the Design and Analysis of Adhesively Bonded Joints in Fiber-Polymer Composite Structures .....	1253
44.6	Design Features Ensuring Durability of Bonded Joints .....	1256
44.7	Load Redistribution Around Flaws and Porosity .....	1260
44.8	Effects of Thermal Mismatch Between Adherends on Strength of Bonded Joints .....	1264
44.9	Inspection, Testing, and Quality Control .....	1265
44.10	Concerns About the Misplaced Emphasis of the Quality-Control Inspections for Bonded and Composite Structures .....	1271
44.11	Bonded Repairs .....	1276
44.12	Other Industry-Specific Factors .....	1277
44.13	Examples of Use of Adhesive Bonding in Aircraft Structures .....	1278
44.14	Conclusion .....	1281
	References .....	1282

## Abstract

This chapter focuses on experience with adhesively bonded joints in aircraft structures. It covers their analysis (emphasizing the inherent nonuniformity of adhesive bond stresses), their design, some common pitfalls in past and current practices (the worst of which is the continued myth that adhesive bond load transfer is distributed uniformly over the bond area, so that all that is needed to

L. J. Hart-Smith (✉)

Boeing Company, Long Beach, CA, USA

e-mail: [leonard.john.hart\\_smith@verizon.net](mailto:leonard.john.hart_smith@verizon.net); [john.hart-smith@bigpond.com](mailto:john.hart-smith@bigpond.com); [john.hart-smith@virginbroadband.com.au](mailto:john.hart-smith@virginbroadband.com.au)

make stronger joints is more bond area), and the critical need for ensuring that the glue is stuck (not by after-the-fact monitoring, which is all but impossible and therefore unreliable, but by proper specifications and quality control during manufacture). It covers the load redistribution around defects and damage, showing that not all damage causes an immediate loss of strength (even though repairs may be necessary to protect against subsequent environmental degradation). It emphasizes a little-appreciated point that the adhesive bond, itself, must never be designed to be the weak link in the chain of strength, so that it cannot act as an instantly catastrophic fuse; the weak link must be in an adherend outside the joint for bonded designs to be reliable. This chapter also includes a discussion of the choice of appropriate bonding tool concept and the great benefits from sometimes using nontraditional tools. The key issue is shown to be that the governing tolerance is not that for the parts, or the tool, but for the thickness of the bond line. The real critical tolerance is on the order of 0.025 mm (0.001 in.), not  $\pm 0.4$ –0.8 mm (0.016–0.032 in.). This requires a far more thorough coordination between design of the parts and the bond tool than has customarily been applied in the past. It is made abundantly clear that tighter and tighter tolerances on the parts and tools are not the way to go. One must rely on a drape-to-fit manufacturing philosophy, the benefits from which are shown to be enormous. The issue of inspection is discussed because a failure to understand what can work and what needs to be checked has led to far reaching adverse consequences. Misplaced faith in after-the-fact inspections is shown to have replaced the proper emphasis on proper process control during manufacture. It is shown to be impossible to restore 100% of bonded-joint strength after it has been manufactured incorrectly (or manufactured “correctly” in accordance with process specifications that simply do not work). And the futile search for the Holy Grail of being able to monitor degradation of bond strength during service has led to a ban on using this technology, in some instances, even when there is no other alternative approach that works. This chapter concludes with examples of the successful widespread application of adhesively bonded joints in aircraft primary structure.

---

## 44.1 Introduction

There are two basic classes of adhesive bonding in aeronautical structures. One is structural bonding, with epoxy, phenolic, or acrylic adhesives, that transfers load between members. The second is sealants that protect against corrosion at interfaces. The stiffnesses of these classes of polymers differ greatly, but the two basic needs are remarkably similar. The first is that the adhesive or sealant will stay stuck for the life of the structure, in all service and storage environments, while the second is that the adhesive will not fail even when the surrounding structure has been broken.

Given that the mechanical properties of these polymers are orders of magnitude lower than those of the adherends they bond together, this second requirement may seem difficult to achieve. Nevertheless, it has been possible by distributing the load

transfer as a shear load over a sufficiently large area and the use of sufficient steps for bonded joints between thick highly loaded adherends. The key is to protect the adhesive from direct or induced peel loads while using the shear capability of the adhesive to transfer the loads. This requires efficient joint designs, which are easily established for thin structures but which become progressively more complicated for thicker structures. The details of the joints are described here and in other chapters in the volume.

Ensuring that the adhesive or sealant is stuck properly in the first place, and that it continues to adhere for the life of the structure, is actually the more challenging of the two needs because it is so misunderstood by far too many of those involved in this industry and others. The science of adhesion is vital to the success of bonded joints, but its importance is largely unrecognized today. The greatest difficulty in this regard is that success is completely dependent on correct surface preparation and processing, which cannot be verified by any of the standard nondestructive post-inspections. Worse, while the correct techniques are known, many of the process specifications of past, and even current, applications of adhesive bonding violate these requirements. They continue to be used because the inappropriate methods do not always result in instantaneous separations between the components, so not everyone involved acknowledges that there is a problem. This doubt is reinforced because most of the inspection methods can detect only physical gaps between the members, not whether or not they are actually bonded together. The procurement system makes it difficult for military services to allocate costs that would be incurred to update repair manuals for products that are long out of production but still in service. There is also a concern, in a litigious society, that any change in specifications would cast doubt on the integrity of every part made under the older procedures, regardless of whether or not such concerns could be justified. Sadly, the consequence of not implementing improvements promptly has been a reluctance to apply the technology as widely as it ought to be because of the bad reputation created by every group of in-service failures.

The bonding processes themselves are actually remarkably tolerant of quite wide deviations from nominal requirements, but when the specifications are inappropriate, or simply not followed, the consequences are very widespread. Worse, defects in mechanically fastened structures tend to be local, and 100% of the design strength can be restored by drilling out and replacing defective fasteners or even a few discrete parts. But processing errors in bonded and composite structures, once made, create situations in which no repair short of complete disassembly and remanufacture can restore 100% of the design strength and durability. It is not possible to inspect quality into bonded and composite structures afterward; they need to be made correctly in the first place. The cultural changes needed to ensure this are actually the greatest of all the obstacles to the more widespread use of bonded structures. Conversely, the durability of those bonded structures that were made appropriately is legendary, in regard to both fatigue and corrosion. The incentives for widespread use of bonded aerospace structures remain tremendous.

This chapter is presented from the perspective of what actually happens, rather than what should happen, in the hope that it will encourage improvements to be

made throughout the industry and regulatory authorities. Without these, it is unlikely that the full benefits of this technology will ever be attained because of the bad image created by the occasional lapses in quality and highly publicized consequences. Even so, it should be noted that, with the only exception of the well-known Aloha 737 incident in 1988, the kind of surface preparation and processing problems described here have resulted only in additional costs, which have inhibited the application of this technology, rather than created circumstances that made safety a concern. The contents of this chapter focus on what over 30 years of experience has been identified as the key issues that need to be understood in creating reliable bonded structures – issues that are rarely even mentioned in standard treatises on the subject, such as why it is imperative to not design to nominal loads but to ensure that the bonded joints will never be the weak link in the structure.

This chapter addresses the following topics: Adhesive Characteristics Needed for Design and Analysis; Surface Preparation; Design of Adhesively Bonded Joints; Additional Considerations for the Design and Analysis of Adhesively Bonded Joints in Fiber–Polymer Composite Structures; Design Features Ensuring Durability of Bonded Joints; Load Redistribution Around Flaws and Porosity; Effects of Thermal Mismatch Between Adherends on Strength of Bonded Joints; Inspection, Testing, and Quality Control; Concerns About the Misplaced Emphasis of the Quality-Control Inspections for Bonded and Composite Structures; Bonded Repairs; Other Industry-Specific Factors; and Examples of Use of Adhesive Bonding in Aircraft Structures.

---

## 44.2 Adhesive Characteristics Required for Design and Analysis

At the macro level, at which most bonded-joint analyses are made, the mechanical data needed are complete stress–strain curves in shear for a range in temperatures covering the operating environment. Typical structural adhesives are stronger and more brittle at low temperatures and weaker and more ductile at high temperatures than at room temperature, as shown in Fig. 1.

Despite these great differences in bulk individual mechanical properties, the strength of structural joints (in which the adhesive strains are far from uniform) is far less sensitive to the test temperature than that of short-overlap test coupons (in which the adhesive strains are close to uniform, which is why they are used to generate the stress–strain curves). (This is explained in more detail below, in terms of elastic–plastic adhesive models (Hart-Smith 1973a, 1974).)

The nonlinear behavior shown in Fig. 1 is not the result of plastic deformation akin to that for ductile metals. It can best be understood in the context of the strain invariants that eventually resulted in the development of the strain-invariant failure theory (SIFT) failure model for fiber–polymer composites. This had its foundation in earlier such analyses developed by Gosse (see Gosse and Christensen 2001) for the failure of homogeneous polymers, including adhesives constrained between much stiffer adherends. There are only two possible failure mechanisms available for any solid homogeneous material. One is dilatation which, in the context of adhesively

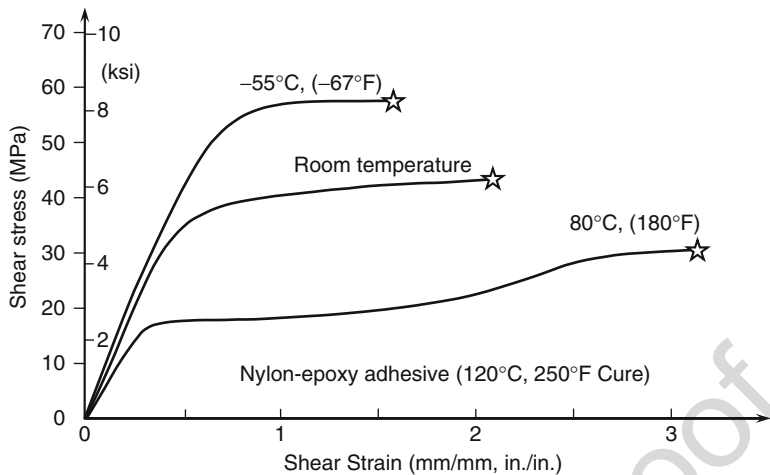


**Fig. 1** Adhesive stress–strain curves in shear, as a function of temperature

bonded joints, is associated with the induced peel stresses at the ends of the bonded overlap. The other is distortion, which is the dominant behavior of the adhesive layer away from the ends. According to the SIFT model, there is absolutely no interaction between these two mechanisms, which is why it is permissible to prepare separate analysis methods for shear-load transfer in bonded joints and for premature failures by peel. Peel failures represent a failure of the adhesive layer to utilize its full shear-transfer capability.

The value of the first strain invariant, the sum of three orthogonal strain components,

$$J_1 = \epsilon_1 + \epsilon_2 + \epsilon_3, \quad (1)$$

cannot be measured on any pure (neat) adhesive test coupon because failure by distortion according to the other (von Mises shear strain) invariant,

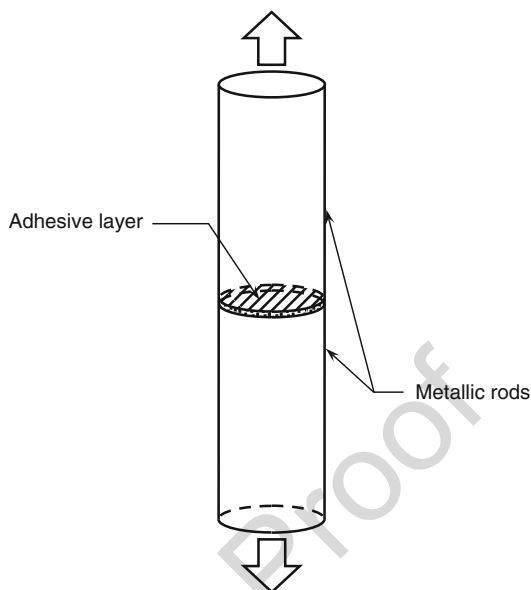
$$\gamma_{VMcrit} = \sqrt{\frac{1}{2} [(\epsilon'_1 - \epsilon'_2)^2 + (\epsilon'_2 - \epsilon'_3)^2 + (\epsilon'_3 - \epsilon'_1)^2]}, \quad (2)$$

(where the prime denotes principal values) occurs before the dilatational limit had been reached. Failure of polymers by dilatation (increase in volume) occurs only in a constrained environment, as between two circular rods bonded at their ends and pulled apart, as shown in Fig. 2 (or between the adherends in bonded joints). Transverse constraints, perpendicular to the load, are needed to prevent the natural Poisson contractions which, if they occurred, would decrease the dilatational strains in the adhesive.

The strain-invariant polymer failure model (SIFT) permits the superposition of separate analyses for shear and induced peel loads. There is no interaction between



**Fig. 2** Butt-jointed test coupon to measure  $J_1$  strain invariant for adhesives



the two failure mechanisms. While the need for this has been minimized through sound design practice (gentle tapering of the ends of the adherends to minimize the induced peel stresses, as explained later), the new model puts this technique on a secure scientific foundation and also accommodates any applied transverse shear loads.

At the microlevel, initial damage in bonded joints is defined by whichever of the two strain invariants reaches its critical value first. At the ends of the overlap in a badly designed bonded joint or test coupon, the dilatational  $J_1$  failure mechanism would always occur first. There are no significant peel stresses in the interior of the joint, so the distortional invariant will be exceeded first. The visual consequences of this failure may seem to be one of dilatation because the first indication is the formation of a series of hackles formed at roughly  $45^\circ$  from the adherends being bonded together, as shown in Fig. 3. (Exactly the same model applies for in-plane-shear failures in the matrix between parallel fibers in composite laminates.) These are, in reality, failures by distortion, which result in tensile fractures perpendicular to the highest principal stress.

Once hackles start to form, the adhesive layer is no longer a continuum but a series of parallel ligaments being bent elastically. There is no precise model for progressive damage to adhesive layers as more and more shear strain is applied, but a constant-stress model has served as a very useful model. This is explained in Fig. 4, based on the notion that damage starts at the knee in the stress-strain curve and that there should be some limit on how much can be tolerated, like the 2% offset definition of design ultimate load for mechanically fastened joints in ductile members. The tail end of the stress-strain curve is reserved for load redistribution around bond flaws and damage, as discussed later. It is recommended here that the knee in

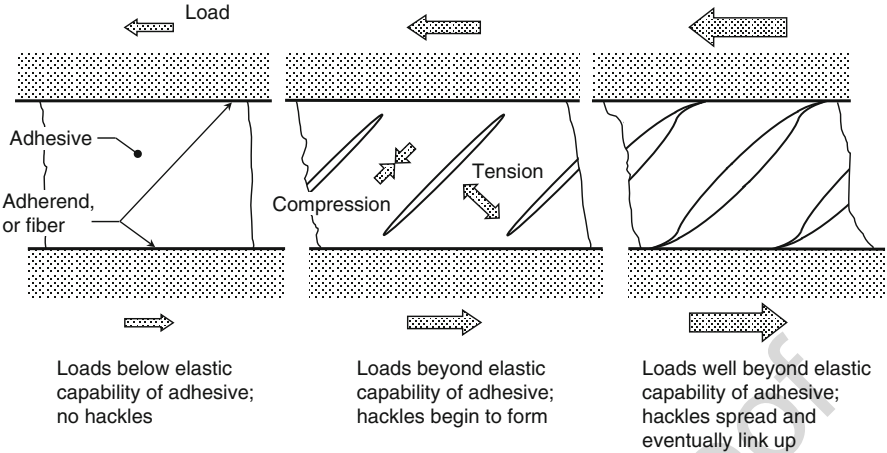
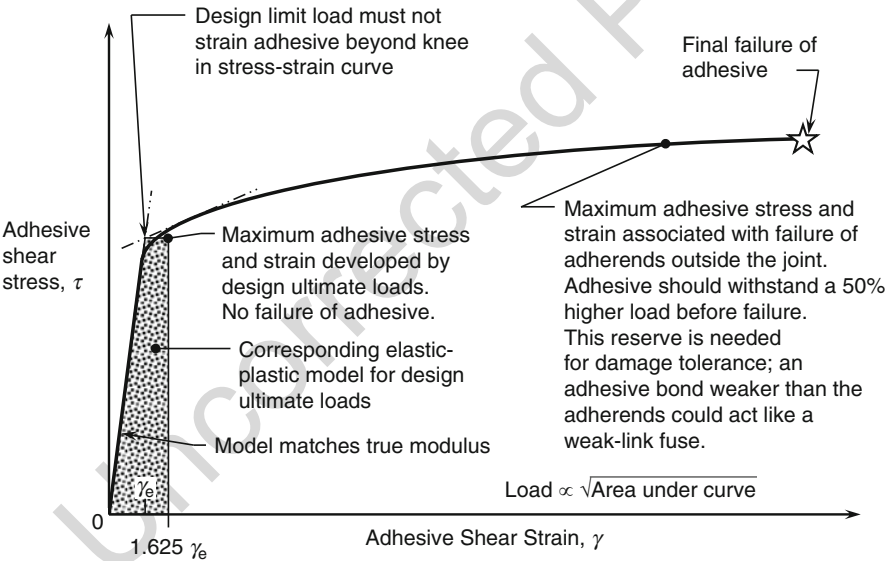


Fig. 3 Formation of hackles in adhesively bonded joints



Note that design process must account for nonlinear adhesive behavior, but a precise stress-strain curve is not mandatory. An approximation, based on a similar adhesive, will usually suffice.

Fig. 4 Relations between knee in stress–strain curve and design limit and ultimate loads

the stress–strain curve be defined to be the design limit load, for each environment (but it should be acknowledged that the bonded structures and composite repair facility for the Royal Australian Air Force, in Amberley, Queensland, have successfully set the design limit strain at twice that value). What is now clear is that the

original notion (Hart-Smith 1973a, 1974) of designing to ultimate design load at the very end of the stress–strain curve is no longer appropriate.

In the event that the adhesive is so brittle, in a particular environment, that there is insufficient “nonlinear” behavior to satisfy the conditions described in Fig. 4, design ultimate strength is established at the end of the short stress–strain curve in shear, and design limit load is then set at two thirds of that load. These conditions are more frequently encountered in deep space than in atmospheric flight conditions. Brittle adhesives are used on aircraft primarily in high-temperature applications as in the vicinity of engines. In such environments, even brittle adhesives are quite ductile.

The stress–strain curves of adhesive layers under a close-to-uniform state of deformation, as in Fig. 1, are customarily measured on a thick-adherend test coupon using very sensitive displacement extensometers, developed by Krieger (1988), as shown in Fig. 5. Each aluminum adherend is typically 9.5 mm (0.375 in.) or 12.7 mm (0.5 in.) thick to enforce a close-to-uniform shear strain in the adhesive.

Most adhesives are still characterized by the average shear stress measured on standard lap-shear test coupons (ASTM D-1002) in a variety of environments. This can be misleading in the context of joint design since this so-called adhesive shear strength varies with the adherend material, their thickness usually 1.3 mm (0.063 in.), and with the length of the overlap, as described by Hart-Smith (1993). Such coupons should never be used for anything other than quality-control tests, for which their complex mixture of variable shear and peel stresses makes them very useful.

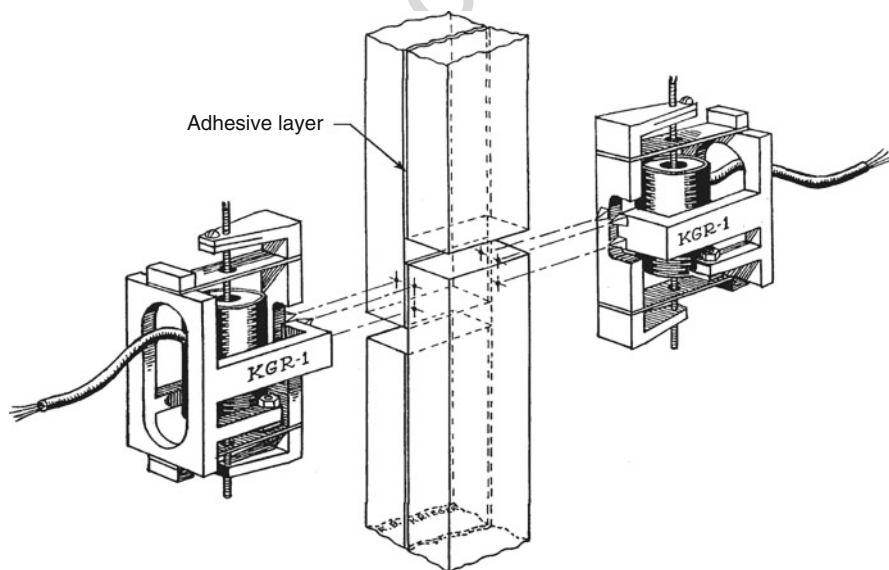


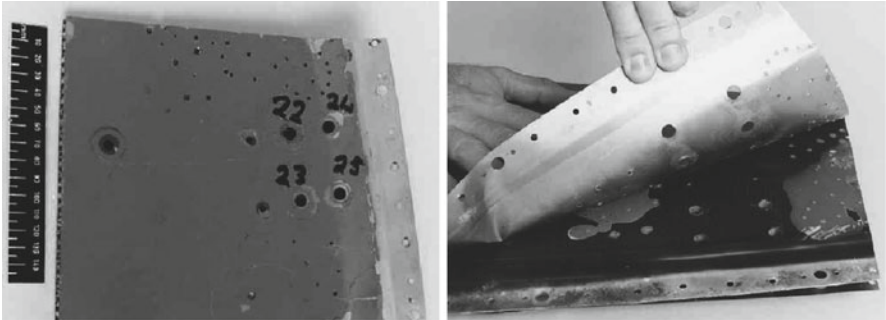
**Fig. 5** Thick-adherend adhesive test coupon and instrumentation (Printed with permission of American Cyanamid Corporation)

Some researchers have also measured what they perceive to be fracture mechanics properties under up to three modes, the first being crack opening and the second shear, thinking that these properties could form the basis of bonded-joint design. The author has yet to see any successful joint designed using these properties and will not discuss them further. No such value can be related to the long overlap needed to ensure the minimum shear strain in the middle of the overlap, where the adhesive is not critical and is low enough to prevent the accumulation of creep damage to the bond line. Worse, if the bonded joint is critical under peel-stress (Mode I) loads at the ends of the overlap, it should be redesigned to make the adherends thinner there, so that the crack-opening mode is no longer critical. It makes little sense to accurately establish the low strength of a badly designed bonded joint when it is so simple to modify the design to achieve a far higher strength, for which the adhesive is not critical in peel – one in which the merits of the adhesive's shear strength are allowed to dominate.

---

### 44.3 Surface Preparation

Proper preparation of surfaces to be bonded is the most critical step in creating durable bonded joints. This is best known for bonded aluminum structures because of the publicity given to the USAF-funded Primary Adhesively Bonded Structures Technology (PABST)-bonded fuselage demonstrator, performed at the Douglas Aircraft Company in Long Beach, California, in response to almost 10 years of widespread in-service disbonds associated with the first generation of 180 °C (250 °F)-cured epoxy adhesives in combination with etched, rather than anodized, surfaces. All earlier bonded aircraft structures (done mainly by de Havillands in England and Fokker in Holland) had been trouble-free because they used phenolic adhesives over chromic acid-anodized surfaces. In the 1940s and 1950s, the pioneers in this field, such as de Bruyne (1957) and Schliekelmann (1983), had studied potential durability issues very thoroughly before they undertook production bonding. Unfortunately, their diligence created the illusion that no bonded structures would ever have durability problems, so when others later changed materials and processes for bonding to simplify the manufacturing of bonded structures, they omitted to conduct the same kind of thorough durability testing and relied on short-term static tests alone, with disastrous consequences. Whole fleets of aircraft built to US bonding specifications during the late 1960s and early 1970s had all their bonded structures remanufactured. Some tried to do only local repairs, to no avail, as indicated by Hart-Smith and Davis (1996), in which it was shown that nearly half of all bonded repairs were to the same structures that had already been repaired for the same global processing errors. The disbonds would not occur until water was absorbed into the adhesive layer, which took time, but was inevitable. Local repairs are useful for impact damage to a properly bonded structure, in which none of the surrounding structure is likely to disbond, but they are unsuitable for global processing errors, as shown in Fig. 6.



Exterior and internal views of the same bonded honeycomb panel, after a second failure (Large Dark gray Area), showing innumerable small holes drilled to inject resin after the first failure, to make it impossible to detect those disbonds, and the shiny resin-free inner skin surface to which the injected adhesive (two irregular light gray areas) had clearly never bonded.

**Fig. 6** The futility of local bonded repairs to global interfacial failures

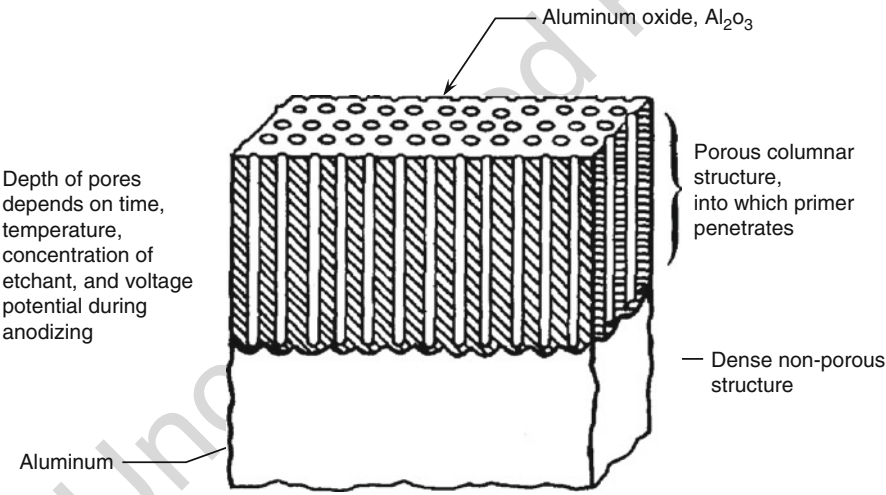


**Fig. 7** Representation of pores in anodized aluminum surface prepared for bonding (Thrall Jr. and Shannon (1985), Chap. 4; Marceau, Boeing)

270 All of this should have come to an end in the middle of the 1970s when  
271 phosphoric acid anodizing and optimized etch processes were established, particu-  
272 larly since Bethune at Boeing developed the simple wedge-crack test, ASTM  
273 D-3762 (Marceau et al. 1977), that made it easy to distinguish between properly  
274 and improperly prepared bonding surfaces. The properly prepared surfaces had a  
275 stable oxide coating, with many pores that the primer could penetrate, as shown in  
276 Fig. 7.

It should be noted that, while the test procedure is very reliable, it is rendered ineffective if the “permissible” extent of interfacial disbond growth during the 1 h-long test is set so high that it fails to reject unacceptable surface treatments. The tests reported by Thrall Jr. and Shannon (1985) show that the limit should have been set at no greater than 3.2 mm (0.125 in.), which is consistent with the very large number of PABST tests that never showed more than 1.6 mm (0.063 in.) of growth. Yet the limit set for the ASTM standard was 19 mm (0.75 in.) which, according to the tests reported by Thrall Jr. and Shannon (1985), would result in more than 95% of all of their bonded structures having been “acceptable,” no matter how bad they actually were.

It is also worth noting that a key element of the PABST bonding processes was the use of a phenolic-based primer, BR-127. And it is particularly significant that the first generation of 180 °C (250 °F)-cured epoxy adhesives that absorbed water so fast, and were associated with the many earlier in-service bond failures, were later found to perform just as reliably on the improved surface treatments as the second generation of such adhesives that were far more resistant to water absorption.

Sadly, even 20 years later, the author was to see local repairs being made to large engine cowls using the same obsolete surface preparations as had caused the failures that were being repaired. When he pointed out the inevitability of further failures to the rest of the panel, in the not too distant future, it was explained to him that the use of the better newer materials and processes in the repairs would violate the aircraft’s type certificate. It was illegal to not repair it in any way other than to make it conform to the original structure when it was built! This attitude was not confined to commercial aircraft. Repairs to helicopter blades continued to be made using paste adhesives over sandpaper-abraded aluminum surfaces. In this case, the explanation provided was that the model concerned had been out of production for over 20 years, so there was no mechanism to update the technical orders governing its maintenance and repair. In these cases, and many others, the futility of the obsolete repairs was well understood, even by those performing them. Is it not time to put an end to such practices? Surely the interests of aviation are better served by reliable surface treatments for bonding than by perpetuating other techniques that are known to be unreliable. Interestingly, the same organization that provided the service data cited by Hart-Smith and Davis (1996) has since found that they suffered not a single failure on 3,000 bonded composite patches they applied over grit-blasted/silane aluminum surfaces. The financial incentives to mandating the use of only reliable surface treatments are well established.

Other metal alloys, such as steel and titanium, also need appropriate surface treatments for bonded applications. The surface treatments for various metals are described in other chapters.

For bonded and co-bonded fibrous composite structures, the need for proper surface treatment is far less known. The absence of reliable after-the-fact inspection techniques that besets metal bonding is exacerbated by the failure to include any durability tests as part of the quality assurance program for the production of bonded composite structures. Just as with the adhesive bonding of metallic structures, the lap-shear test coupon alone has been found to be insufficient to ensure the durability

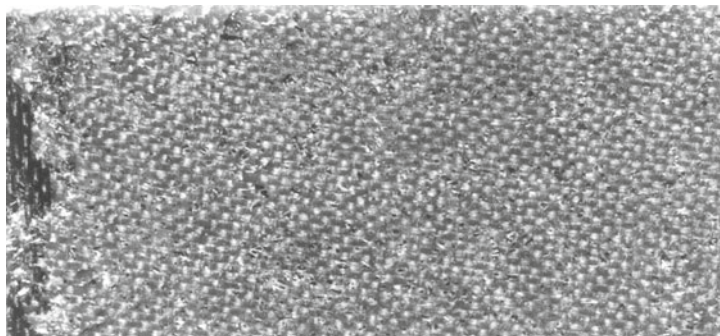
of any bonded joints. At best it can ensure only that the adhesive was cured properly (adequately cross-linked) – not that the adhesive is actually stuck. The reason for this inexcusable omission would seem to be that corrosion has been seen in conjunction with the failed bonded aluminum structures and that fiber–polymer composites cannot corrode. Whatever the cause, the need for the surfaces being bonded to have a higher energy level (be more active) than the surface of the adhesive is just as great for bonding polymers as for bonding metal alloys. Most of the surface treatments for composite surfaces to be bonded ensure precisely the opposite – that the surface will be totally inert. Some peel plies have even been coated with a silicone release agent to ensure that the peel plies can be stripped off without the slightest damage to the underlying substrate (Hart-Smith et al. 1996). This is not to imply that the problems with bonded composite aeronautical structures are as widespread as they were with bonded metallic structures. Rather, the problem is one of not knowing because there is no way of finding out before the parts separate in service. Worse, since there is no mandated durability test for bonded composite structures equivalent to the wedge-crack test, at the time of manufacture, such structures continue to be produced with no means of ensuring that they will not fall apart at some later date.

Of all the specified surface treatments for bonded composite joints, only low-pressure grit blasting has an unblemished service record. The reason why it has not been standardized on is inexplicable since none of the other techniques can be applied for bonded repairs, so there is no way of any manufacturer or operator avoiding having to master this technique. One cannot put a peel ply back on a structure and peel it off a second time.

Another critical issue with bonding of composite structures is pre-bond moisture, which can exist in a multiplicity of forms, each with its own distinct adverse consequences. Moisture absorbed in cured laminates and driven to the surface by the heat of the bond cycle prevents any adhesion from occurring without creating detectable symptoms. Such water lowers the energy level of the substrate, as described by Mahoney (1988), and can lead to the condition illustrated in Fig. 8, in which a complete area failed to bond but was not detected. Figure 8 shows a perfect replica of the original peel ply, known to be free of silicone, on both sides of the adhesive layer. There was no sign of adhesion at all. Yet this and many similar panels had passed all quality-control lap-shear test coupons and 100% ultrasonic inspection at the time of manufacture. It is known that these parts had been cured many months before they were bonded in another part of the country; they were not dried in an oven before bonding. Clearly, they should have been.

Moisture absorbed by the adhesive before it is cured has the effect of creating a weak porous bond. Moisture condensed on the surface of uncured adhesive films taken out of the freezer and unwrapped before it had thawed out also collects at the interface and prevents the glue from sticking. Sometimes, even when the need to properly dry laminates before bonding has been recognized and specified, it has not always been enforced at the facilities of remote suppliers. Yet the need to do so continues to be demonstrated conclusively, along with the benefits from doing so, as reported by Myhre et al. (1982).





10X

Note clear imprint at left of *other* peel ply in skin underneath adhesive layer, to which the adhesive also failed to bond.

**Fig. 8** Peel ply imprint *left* by failure of adhesive to bond to a composite surface

Peel plies continue to be the most frequently specified surface preparations for bonding fiber-polymer composites. But they are not always reliable. Worse, there have been cases in which silicone was transferred from bagging film used in consolidation cycles. There is a tendency to underrate the importance of the so-called consumable products, like bagging film, breather, peel plies, etc., which are stripped off cured or staged parts and discarded after the cure. Some specifications even leave the selection of these materials entirely up to suppliers, with no restrictions. That is wrong! All surfaces that come in contact with the final composite part in both its uncured and cured states need to be controlled just as tightly as the prepreg itself. After all, most of them are cured together in an intimate contact. It is a standard practice to isolate tool-preparation rooms in which release agents are applied from any bonding or composite clean room. Workers there wear clean white gloves. Every article that comes in contact with uncured adhesives or composite materials, or surfaces to be bonded, needs to be treated as a potential source of contamination or a nonbond, no matter how insignificant the article seems to be. Not all procedures are as strict as this, but the loopholes in the paperwork need to be closed. There is one specific polyester peel ply that several organizations within Boeing prefer that is made on dedicated machines to eliminate contamination. This is the only peel ply permitted to be used for the 777 horizontal and vertical tails and on all subsequent production. Even so, the most stringent of tests are required to ensure the absence of silicone on each roll before it is allowed into the factory. Their prior experiences and current research sponsored by the Federal Aviation Administration (FAA) (see Bardis 2001) both confirmed the need for such care. The author would still prefer to also see the universal acceptance of something equivalent to the wedge-crack test for metal bonding – a sustained peel load in a hostile (hot/wet) environment to confirm the absence of all other mechanisms for creating inert bonding surfaces, as well. Any such lapse in quality will affect the entire structure. It is not difficult to detect the conditions that lead to global processing errors before they



occur, provided that one looks, and nothing can be done about them if they are not detected until after the part is built.

#### 44.4 Design of Adhesively Bonded Joints

The design and analysis procedures cited in this chapter were developed by the author under three government-sponsored R&D contracts over a period of years. The first was for NASA Langley during the period 1970–1973 (Hart-Smith 1973b, c, d, e), in which the elastic–plastic adhesive model was introduced and the first of the A4E series of Fortran computer codes was derived. The second increment of work was for the USAF at WPAFB, during and following the PABST bonded fuselage contract, from 1976 to 1983. Three new computer codes, A4EI, A4EJ, and A4EK, were produced and the effects of flaws and variable bond layers were covered (Hart-Smith 1982a, b, 1984a, b). There were many publications from the first two contracts. The third, also for the USAF, concerned bonded composite patches over cracks and corrosion damage in metallic structures, from 1997 to 2003 (Hart-Smith 2001). Not all of the analyses from the most recent contract have yet appeared in print.

The design of double-lap and single-lap bonded joints between nominally uniformly thick adherends is straightforward. The design of the 100% full-load transfer bonded joints with no fail-safe rivets for the pressurized PABST bonded fuselage, Thrall Jr. and Shannon (1985), was reduced to a single table of overlap versus skin thickness, supplemented by a requirement to gently taper the ends of the overlaps locally for the thicker skins to prevent premature-induced peel failures. It is crucial to note that the overlaps are universal in the sense that they are independent of the magnitude of any applied loads. This enables the design of the bonded joints to be completed before the internal loads in a structure have been established. The key to this design method is explained in Fig. 9, for double-lap joints, in which the overlap is established as the sum of the elastic trough needed to ensure that the minimum adhesive shear stress is so low as to prevent creep from occurring there under even sustained loads and the “plastic” load-transfer zones needed to transmit the full strength of the adherends outside the joint.

As first presented, this method is conservative in the sense that no credit is taken for the small increment of load transferred through the elastic trough. When designing patches in confined areas, the width of the plastic zones could be reduced by a length  $2/\lambda$  to compensate for this effect. All of the tests during the PABST program to validate the method were at the slightly longer overlaps.

Figure 10 presents the actual sizes used for the PABST fuselage, as a function of basic skin thickness.

The splice plates should be made half as thick as the skins, for maximum theoretical efficiency, to make each end of the bonded overlap equally efficient. However, early tests of such joints showed a propensity for fatigue failures in the splice plate, where the skins butted together, rather than in the skins, which had a nominally equal stress. Consequently, the splice plates were made one gauge thicker. The overlaps in this table can be approximated by a simple design rule, that the

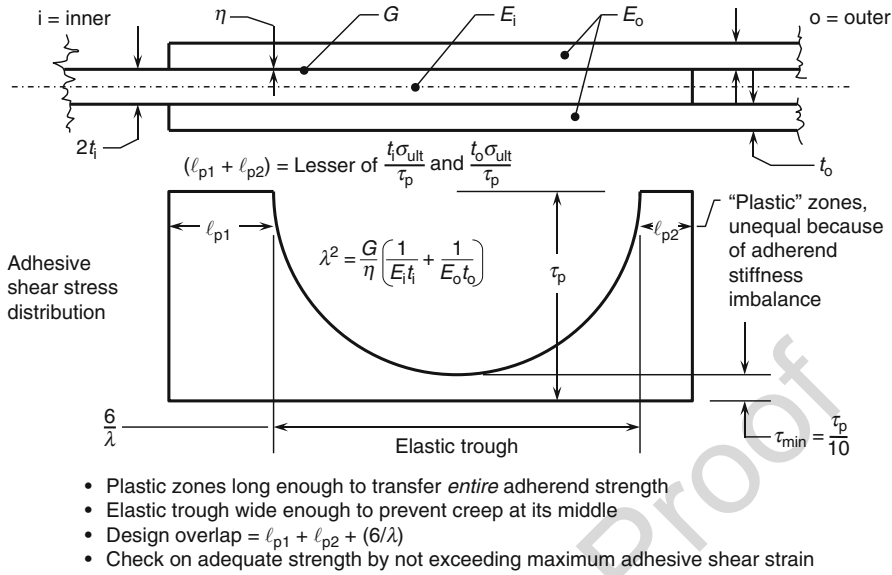


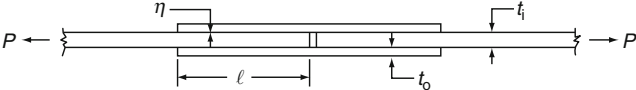
Fig. 9 Design procedure for double-lap bonded joints

Central sheet thickness $t_i$ (in.)	0.040	0.050	0.063	0.071	0.080	0.090	0.100	0.125
Splice sheet thickness $t_o$ (in.)	0.025	0.032	0.040	0.040	0.050	0.050	0.063	0.071
Recommended overlap <sup>1</sup> $\ell$ (in.)	1.21	1.42	1.68	1.84	2.01	2.20	2.39	2.84
Strength of 2024-T3 aluminum (lb/in.)	2600	3250	4095	4615	5200	5850	6500	8125
Potential ultimate bond strength (lb/in.) <sup>2,3</sup>	7699	8562	9628	10,504	10,888	11,865	12,151	13,910

<sup>1</sup>Based on 160°F or 140°F/100% RH properties needing longest overlap. Values apply for tensile or compressive in-plane loading. For in-plane shear loading, slightly different lengths apply.

<sup>2</sup>Based on -50°F properties giving lowest joint strength and assuming taper of outer splice straps thicker than 0.050 in. Strength values corrected for adherend stiffness imbalance.

<sup>3</sup>For nominal adhesive thickness  $\eta = 0.005$  in. For other thicknesses, modify strengths in ratio  $\sqrt{\eta/0.005}$ .



(Unit Conversion Factors: 1.0 in. = 25.4 mm, 1,000 lb/in. = 175 kN/mm)

Fig. 10 Standard design overlaps for double-lap bonded joints between aluminum adherends

overlap be 30 times the thickness of the central adherend (skin). If there is a substantial stiffness imbalance between the adherends, the load transfer through the bond will be intensified at one end, with respect to the other, resulting in decreased shear strengths.

Figure 10 includes a comparison between the theoretical bond strengths if the adhesive was strained to the very end of the stress-strain curve in shear and the strength of the 2024-T3 skins. For the thinnest skins, the bond has three times the strength of the skins, while for the thickest skins in the table, the ratio has fallen to about 1.5:1. This is why, for still thicker skins, it would be necessary to resort to splice designs with one or more steps in the overlap, to restore the margin in the bond strength. The need for this excess strength is described in a later section of load redistribution around flaws and defects. It should be noted, however, that the bond will fail by creep if an applied load sufficient to yield the aluminum adherends is maintained indefinitely. The higher bond lengths can be achieved only for loads that are quickly applied and removed.

The information in Fig. 10 needed to be supplemented only by the design modifications in Fig. 11, whereby the ends of the overlap of the thicker adherends were tapered down to a maximum tip thickness of 0.75 mm (0.030 in.), to minimize induced peel stresses in the adhesive. (The corresponding tip thickness for fiber-polymer composite adherends is only 0.50 mm [0.020 in.] because of interlaminar weaknesses.) If this local tapering was omitted for the thicker adherends, the adhesive would fail under induced peel stresses long before its shear strength could be attained.

The design of single-lap bonded joints is even simpler because the most critical location for any long-overlap bonded joint is in the adherends at one or both ends of

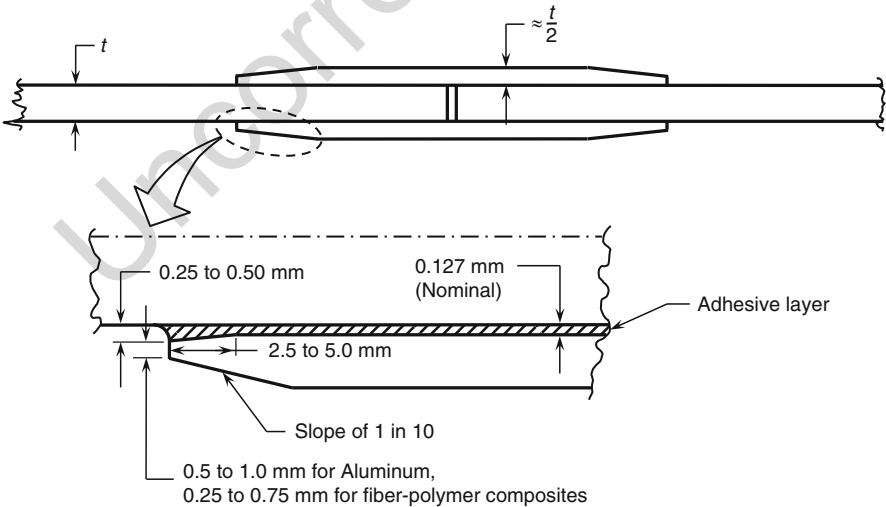


**Fig. 11** Tapering at ends of bonded overlap, to restrict induced peel stresses

the adherends, as the result of combined membrane and bending stresses. These are minimized by increasing the overlap, as explained by Hart-Smith (1973c, 1978). Analyses for the PABST bonded fuselage established a design overlap-to-thickness ratio of 80:1. (This can be reduced to 60:1 for single-lap joints that are stabilized against bending of the adherends, as by being part of a sandwich panel.) Tapering of the ends of the overlap to alleviate induced peel stresses is still necessary using the proportions shown in Fig. 11. The bending moment at one end of the overlap is intensified greatly whenever one adherend is stiffer (thicker) than the other. It is not possible to make single-lap or single-strap (flush) bonded joints with a strength greater than the adherends outside the bonded overlap, so they tend to be used only for thinner more lightly loaded structures.

The analyses referred above are essentially exact but can be applied only to bonded joints between adherends of uniform thickness. A new approximate method was developed during the composite repair of aircraft structure (CRAS) R&D contract that covers tapered adherends as well. The method, explained by Hart-Smith (2001/2002), relies on the knowledge that the adhesive stresses will be extremely low everywhere except in the immediate vicinity of changes to or interruptions in the thickness of the adherends. It starts with a closed-form analysis in which it is assumed that all the members are fused rigidly together over the entire overlap. The load sharing between the overlapped members can also account for residual stresses caused by thermal dissimilarities between adherends, as between composite patches and cracked metallic structures and between bonded titanium stepped plates at the ends and sides and the composite skins to which they are bonded. This level of analysis will predict local spikes of instantaneous load transfer at every discontinuity in load path. The second step in the analysis, also by closed form, distributes those spikes as plastic load-transfer zones of finite width, assuming locally uniform adherend thicknesses that match the real local thicknesses. If the plastic zone needed to transfer each load spike is less than the characteristic length  $1/\lambda$  defining the elastic load-transfer length, where  $\lambda$  is the exponent of the elastic stress distribution (see Fig. 9), the load spike is replaced by an elastic load distribution with an integral matching the calculated spike. This simple method was shown to be exactly equivalent to the precise solutions in the event that the adherends really were of uniform thickness.

Bonded joints between thicker adherends than covered by Fig. 10 need stepped-lap joint designs, as in Fig. 12, for the higher loads associated with thicker members.

Instead of an increment of load transferred at each end of the bonded overlap, there is an increment of load transferred at each end of each step in such a joint. The addition of more steps requires an increase in the bonded area, but it is important to note that an increase in bond area without any increase in the number of steps is ineffective, as explained in Fig. 13. For bonded composite joints, the strength is predicted to keep increasing all the way to a single ply per step.

Each step in a stepped-lap bonded joint is characterized by exactly the same governing differential equations as govern simple overlaps between uniformly thick adherends.

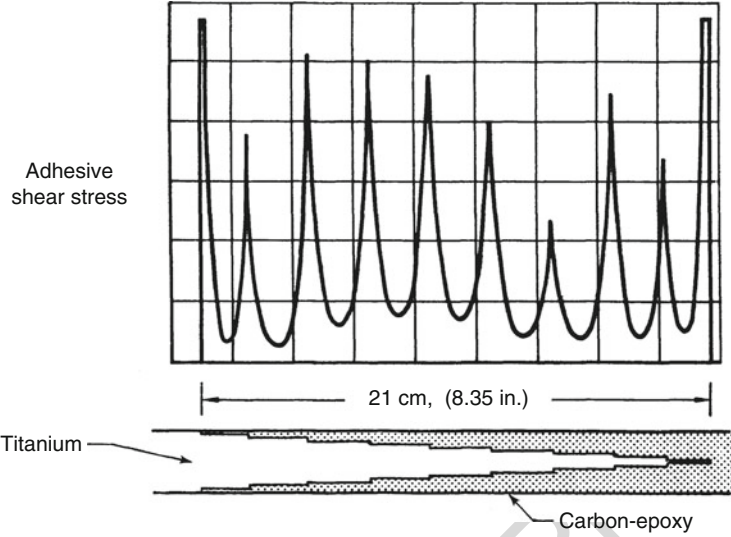
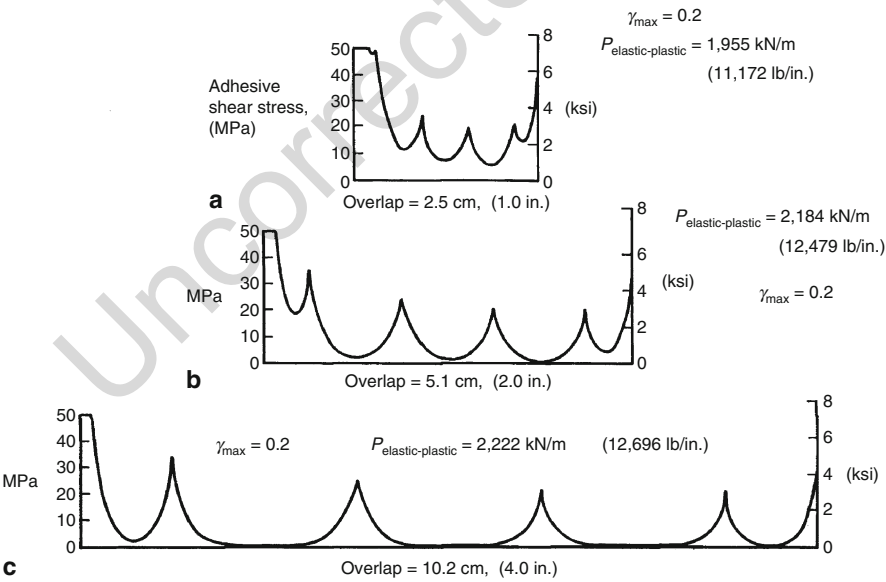


**Fig. 12** Stepped-lap bonded joints for thicker adherends (AIAA Astronautics and Aeronautics)



Note: All cross sections identical and all step lengths proportional

**Fig. 13** Insensitivity of joint strength to bond area without an increase in the number of steps

There have, for decades, now, been reliable analytical tools available for the design and analysis of adhesively bonded joints. Even so, there is still far too much reliance on the oversimplified model whereby the bond strength is assumed to be the product of some fictitious uniform adhesive “allowable” shear stress and the bond area. If more joint strength was needed, all one had to do, according to this procedure, was to increase the bonded area. Bonded joints do not obey such rules. Such a formula is valid today only in the context of short-overlap test coupons in which the goal is to create as closely as possible a uniform state of stress and strain in the adhesive. In the context of structural bonded joints, such a model ceased to be applicable by the end of the First World War, when airframes stopped being made from wood and fabric. That was the last time that the glue was stronger than the materials being bonded together, so that almost any design would work if the scarf angle was low enough.

The most reliable of the mechanics-based bonded-joint models are of closed form because of the locally very high stress and strain gradients, and the need for iteration to cover material nonlinearities makes finite-element solutions difficult. The finite-element models need to be converged with respect to grid size because accuracy of such analyses is not guaranteed. This problem has been exacerbated in the realm of fiber–polymer composites by the patently false simplifying assumption that the fiber and resin constituents can be homogenized into a single “equivalent” anisotropic solid. A by-product of this error is the myth of singularities at the edges of composite panels, at every change in fiber direction, which has spawned a whole field of study. The singularities vanish the instant that the notion of zero-thickness interfaces is discarded. Yet some researchers have devoted their entire career to the study of such mathematically created conditions that do not exist in physical reality. One needs to be very careful in interpreting finite-element analyses of bonded joints. Conversely, it was only through the use of properly converged finite-element models of discrete fibers in a block of resin that Gosse (1999, private communication) was able to finally validate his concept of dilatation as the primary failure mechanism for constrained polymers in bonded joints and composite laminates. There were no singularities, and the correct answer was unchanged when the mesh size was doubled or halved.

---

#### **44.5 Additional Considerations for the Design and Analysis of Adhesively Bonded Joints in Fiber–Polymer Composite Structures**

When boron–epoxy and carbon–epoxy composites were first introduced into aerospace structures, the only form of prepreg available was unidirectional tape. This imposed on the design of stepped-lap bonded joints some restrictions that were covered by empirical design rules. Those people involved in designing such joints, at that time, all knew not to put a layer of 90° fibers adjacent to the metal step plate and designed their laminate lay-up sequence and step heights accordingly. Consequently,

interlaminar failures in the composite could be avoided and the failure forced into through-the-thickness breaking of either the composite or metallic adherends. This was meant to occur outside the bonded overlap, but it was rapidly learned from test that the thin end step of the (usually) titanium step plate would fatigue off if that step was too long. This meant that, as far as the adhesive was concerned, it was necessary only to show that it had an integrated shear strength greater than the strength of the weaker adherend. Peel stresses were eliminated automatically because the end step in the composite was always too thin to allow them to develop to a significant level. So the A4EG and later A4EI stepped-lap bonded-joint analysis codes made no provision for interlaminar failures in the composite adherends.

Later, when carbon-fiber reinforcement was made available in the form of woven fabrics, it slowly became apparent that laminates could fail interlaminarly adjacent to, but not in, the adhesive layer. In retrospect, it probably took too long for the causes to sink in. Half of the surface of a woven fabric is covered by tows of  $90^\circ$  fibers. The application of a transverse shear force would cause cracks to run up through those bundles until they were arrested by the first  $0^\circ$  fibers they encountered, as explained in Fig. 14.

If these initial cracks progressed any further, it would be in the form of delaminations parallel to the adhesive layer, as shown.

These two codes could not provide such a check since there were no places to enter the interlaminar strengths. Initially, that would not have mattered since there was no way to measure the interlaminar shear strength of an all- $90^\circ$  laminate, either, so there was no reference data to compare against. The standard shear stress test coupon was for an all- $0^\circ$  laminate, although tests were also run on  $0/90^\circ$  cloth laminates and those containing  $\pm 45^\circ$  layers. But these were not standard properties and were not catalogued at the time. When the need for these data did become apparent, the McDonnell Aircraft Company engineers performed a very large

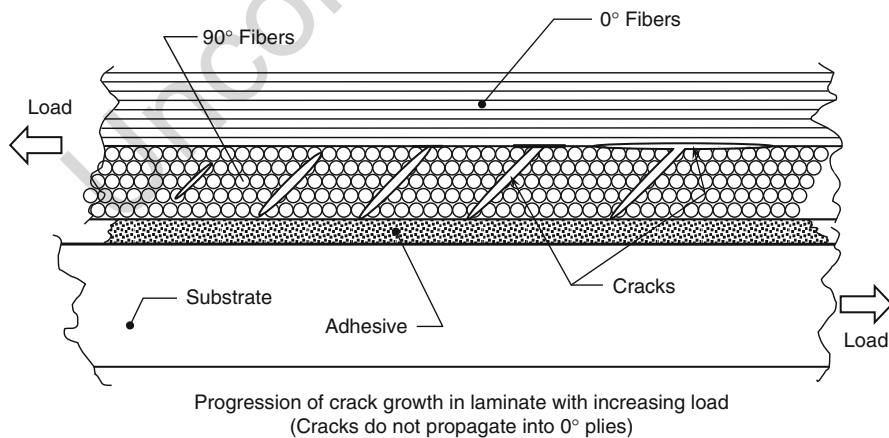


**Fig. 14** Interlaminar cracking through bundles of  $90^\circ$ . Fibers adjacent to a bond line acted on by a  $0^\circ$  load

number of tests on uniform adherends, not stepped-lap joints, to characterize the interlaminar failures as a function of laminate fiber pattern and adherend thickness. They then proceeded to use the A4EI code in reverse to establish fake adhesive properties which would match the measured interlaminar failure strengths using tables to document the adhesive “properties” to be used. This worked, but it was complicated badly by the presence of induced peel stresses at the ends of the overlap that caused their own set of interlaminar failures. These were governed by a different power law in regard to the adherend thickness from that governing the shear-load transfer, as explained earlier.

Eventually, the author realized that what was needed was a revision to the A4EI codes to allow separate checks to be made for adhesive shear failures and interlaminar shear failures using two sets of properties that did not need to be fiddled. There also needed to be a peel-stress cutoff because the codes were being improperly used to analyze uniformly thick adherends as well as stepped-lap joints. The peel failures, if they occurred, would do so in the manner of Fig. 15; they would always precede the shear failures, undercutting it, unless they were excluded by the use of thin adherend tip thicknesses.

The coding for the interlaminar shear effect has been completed, but not yet distributed. However, that for premature peel failures has not been. The author still feels that the correct response to induced peel failures is to reduce the adherend tip thickness, rather than accepting an unnecessary decrease in shear-load transfer capability. Also, until recently, the theory with which to analyze the shear and peel failures in the resin was not available. Some people believed that there had to be an interaction between the shear and peel stresses. With the advent of the SIFT failure model (Hart-Smith 2010) for fiber–polymer composites, it is now possible to analyze the stresses and strains in the resin, including those from residual thermal stresses resulting from curing the laminate at a temperature much higher than its operating temperature. It is now clear that the distortion and dilatation failures in the resin are separate and unrelated, so there is no interaction between shear and peel. The SIFT model characterizes strength in terms of two characteristic invariants for each

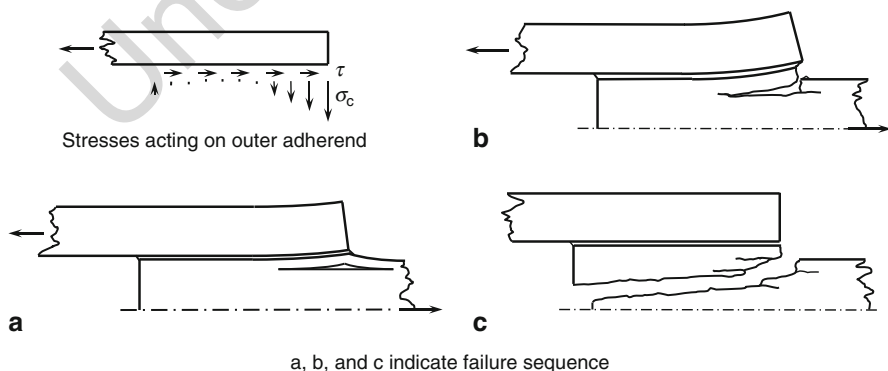


**Fig. 15** Induced peel-stress failures in composite laminates with excessive tip thicknesses



constituent (fibers and resin), so it also overcomes the problem of measuring the reference strengths to be inserted into the code for checking against. These invariants do not vary with the nature of the loads, so a test under one set of loads can be converted into a strength under all other sets of loads (unless there is a change in failure mode or in the constituent that is failing). There is now hope for a greatly improved analysis capability of the strength of both stepped and uniform bonded joints.

Unfortunately, more work remains to be done. The original codes were written in Fortran IV; the author is not fluent in the later versions, and there has been no funding available to pay someone who is. Even so, the author knows of one organization where his revised listing of the code enabled them to get an operational version accounting for the shear effects. But they have yet to master the SIFT model, so they must still rely on the McDonnell empirical test data for the reference properties. Finite-element modeling techniques, using ply-by-ply models for the laminates, have been able to characterize the effect of the fiber direction adjacent to the bond on the load-transfer distribution; very little goes through the softer 90° layers. Unfortunately, they are even weaker than they are softer, so the problem of premature failure remains. Accounting for nonlinear adhesive behavior is not easy with finite elements, either.

Even though the analysis codes associated with these extensions of the A4EI codes are not widely available yet, it is considered important to explain these additional phenomena, for which the understanding is complete. Without this explanation, there will continue to be confusion over measured test failures that the old theory cannot explain which brings with it a level of conservatism in design so severe as to unnecessarily restrict the use of bonded composite structures.

---

## 44.6 Design Features Ensuring Durability of Bonded Joints

Durability in bonded joints requires both that the bonded interfaces are stable (the glue stays stuck) and that the adhesive is not failed by the combination of mechanical loads and residual thermal stresses caused by dissimilar adherends. The first issue has nothing to do with the geometry of any bonded joint, although joints fail faster under peel-dominated loads than under shear loads. There are two limits associated with durability that are influenced by the geometry of the joint. The first of these is the peak shear and peel stresses at the ends of each overlap. This is obvious and well understood. The other is to limit the strain level near the middle of the overlap, even in the most severe environment. This is the little understood requirement represented by setting the minimum stress level at or less than 10% of the maximum, which defines the overlap needed to prevent any creep from accumulating. The need for such a requirement was exposed by some of the early fatigue tests on the PABST program. Quite misleading conclusions, both positive and negative, could be drawn from durability tests on short-overlap coupons, as explained by Thrall Jr. and Shannon (1985).

The key to the success of these designs was the acknowledgment that the adhesives' shear stresses were, and should be, highly nonuniform. There are enormous differences between the way adhesives behave, under what appear to be the same external loads, in short-overlap test coupons and long-overlap structural joints, as explained in Fig. 16.

Tests on short-overlap coupons cannot be relied upon to differentiate between adhesives (and surface treatments) that will endure in service and those that will (or have) not. At best, they can make comparisons between slightly different adhesives in the same class. It is almost impossible to prove in the short term that a bonded joint will last 30 years or more in service. Any test under representative load conditions would have to last at least 30 years to indicate a satisfactory result. If the load intensities were increased or the test environment aggravated, to ensure a test result in a short time, there would be no way of knowing what the corresponding service life would be under realistic conditions. And the best adhesive systems would last for 30 years under realistic loads even when tested in artificially severe environments, unless the structural elements wore out first. The only saving grace is that the surface treatments associated with premature in-service interfacial failures could be accelerated and made to fail rapidly under adverse conditions. In other words, the inferior systems could be identified rapidly, but the best systems could be identified only by not appearing on the list of unacceptable systems.

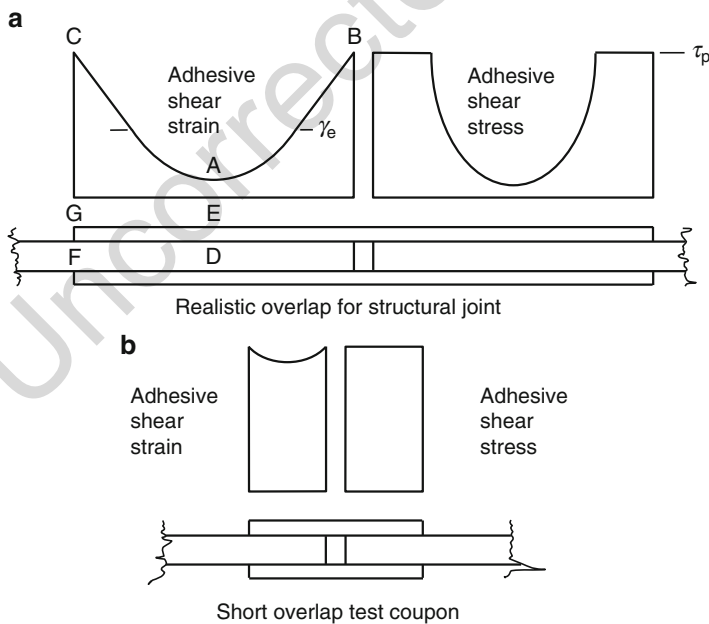


**Fig. 16** Differences between short-overlap test coupons and long-overlap bonded joints. (a) Realistic overlap for structural joint. (b) Short-overlap test coupon

The reason why properly designed bonded joints do not suffer from mechanical fatigue failures is that the most critical conditions are not developed where the adhesive is protected by the adherends. This can be understood by characterizing the minimum and maximum adhesive shear strains firstly as a function of bonded overlap and secondly as a function of adherend thickness, accounting for the effect of the environment in each case. This is illustrated in Fig. 17, for room temperature.

The reason why short overlaps should not be used for structural joints is that even the smallest loads can result in the critical conditions being developed at the ends of the overlap, under sustained load, or by an accumulation of incremental loads, because there is no restraint on the minimum shear strain developed in the middle of the overlap. Once the overlap has exceeded a critical value, proportional to the thickness of the adherends, there is such a constraint on the minimum shear strain, at the middle of the overlap, that simultaneously imposes a limit on the peak shear strain at the ends of the overlap, through compatibility of deformations. No matter how long the loads are applied, the peak shear strain at the ends cannot grow indefinitely. Testing during the PABST program showed that creep did accumulate steadily at the ends of the overlap as long as the load remained. However, it recovered during periods of unloading, every time, with exactly the same shear strain at the end of 8 h into the 5th load cycle as the 14th, for example. There is no counterpart to this behavior possible for short-overlap test coupons, in which such creep occurs but accumulates cycle by cycle instead of recovering. For still longer

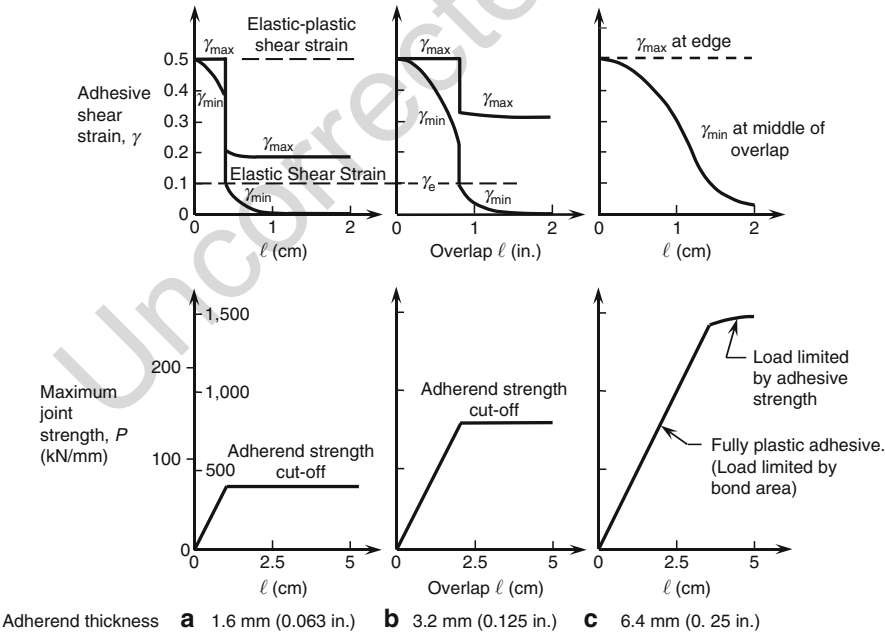


**Fig. 17** Effects of adherend overlap and thickness on maximum and minimum shear strains at room temperature

overlaps, the minimum adhesive shear strain decreases asymptotically toward zero, but the peak values remain constant, since the load that can be applied to the bond is limited by the strength of the adherends. So, provided that the design overlap is long enough to extend to the far side of the transition between short- and long-overlap behavior, for the most critical of the environments, any further increases are of no benefit (apart from the provision of a reasonable assembly tolerance).

The influence of the environments on the design overlaps is shown in Figs. 18 and 19 for the hot/wet and cold environments. It is usually found that the upper service temperature limit sets the design overlap because then the adhesive is at its softest and weakest, while the lowest temperature establishes the limiting joint strength because that is the condition of least strain energy, but not by much, as noted in Fig. 1.

Figures 17, 18, and 19 also show that, for the thinnest adherends, there is a deep precipice on the peak shear strain when crossing the critical overlap and that the

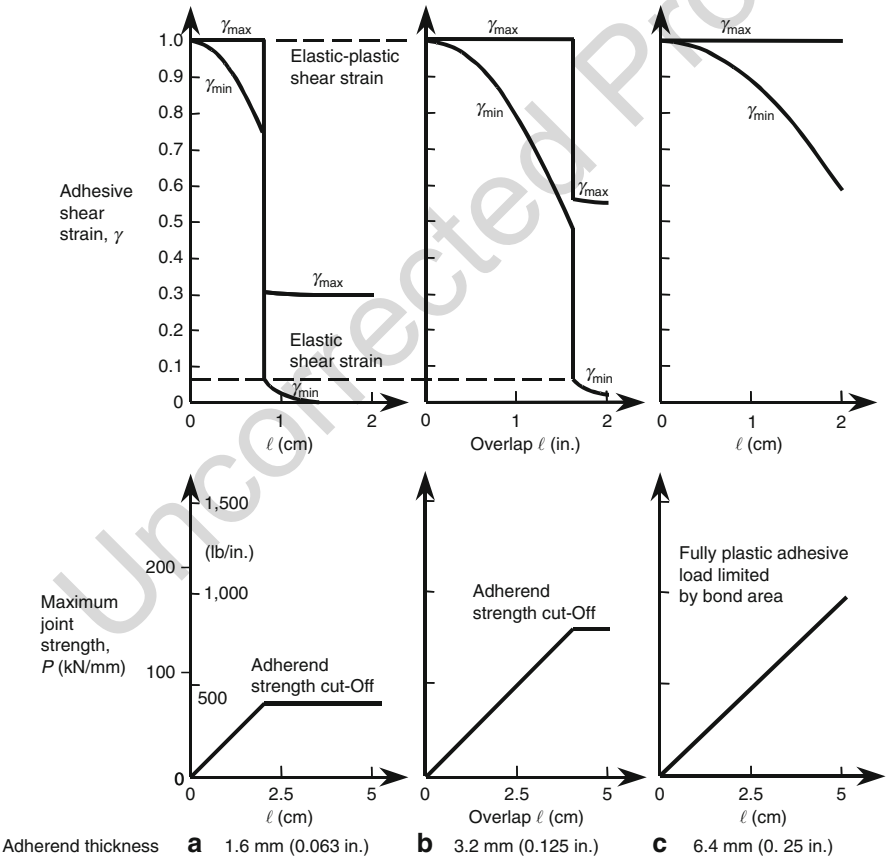


**Fig. 18** Effects of adherend overlap and thickness on maximum and minimum shear strains, at maximum service temperature

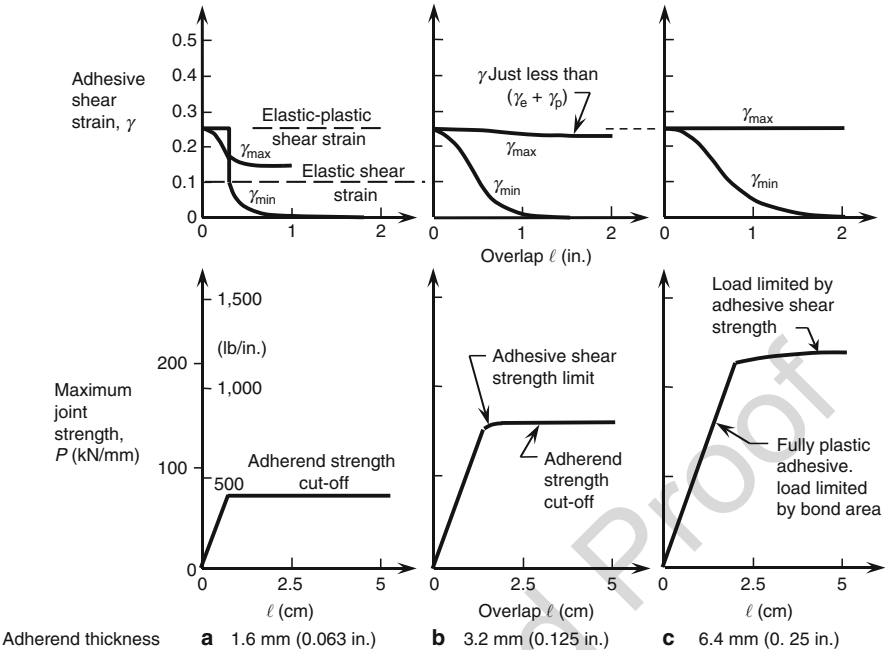


**Fig. 19** Effects of adherend overlap and thickness on maximum and minimum shear strains, at minimum service temperature

precipice decreases with increasing adherend thickness. There was absolutely no precipice left for 6.35 mm (0.25 in.) thick adherends, indicating that the whole concept of preventing bond failures by limiting the peak adhesive shear strain would no longer prevail, even though the minimum adhesive shear strain could be made low enough. The key to success is that both limits on adhesive strain have to be present. This is why stepped-lap joints are necessary for thicker adherends. But with that design feature to limit the strains in the adhesive, the joints have proved to be just as durable as for the simpler joints used for thinner adherends. The stepped-lap titanium-to-carbon/epoxy-bonded joints at the wing roots on the F/A-18 aircraft are a testament to this, at load intensities of almost 5.25 kN/mm (30,000 lb/in.).

## 44.7 Load Redistribution Around Flaws and Porosity

One of the most remarkable characteristics of well-designed bonded joints, as defined earlier, is their tremendous tolerance for quite large local defects. Provided that the surface treatment and processing were correct, the damage would not spread. (On the other hand, quite the opposite was true in the case of global processing errors, for which it was only a matter of time for absorbed moisture to attack the interfaces on poorly bonded metallic structures. The mechanism for spreading initial failures on

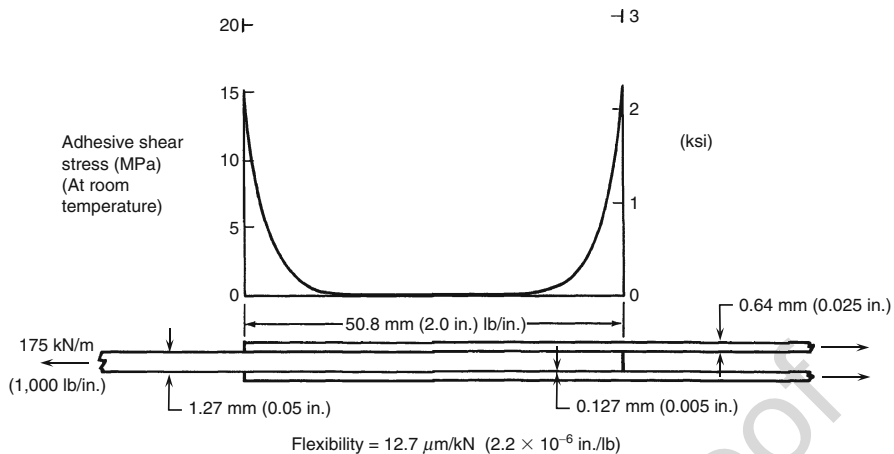


**Fig. 20** Adhesive shear stress distribution for bonded joint with no defects

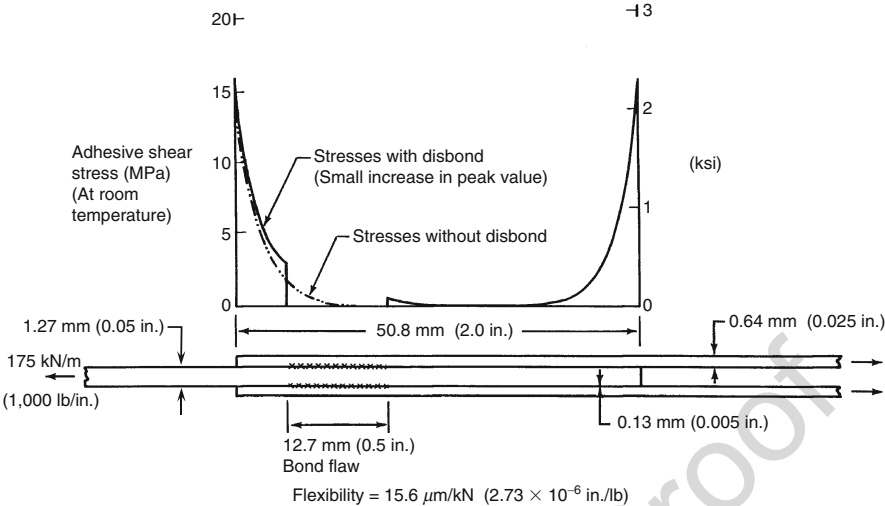
improperly bonded composite structures is not clear, but the result was just as inevitable.) The same state of nonuniform stress and strain that ensures the durability of properly designed bonded joints is responsible for the ability to tolerate local flaws with no loss of overall strength. It is self-evident that, if the adhesive layer ever was uniformly critically strained, there could be no tolerance to even the slightest flaw.

Figure 20 shows the calculated adhesive shear stress distribution, at room temperature, for a bonded splice on the side of the pressurized PABST fuselage. What is remarkable is that, even at the 1.3-P proof pressure condition of 175.13 N/mm (1,000 lb/in.), the adhesive was not even strained beyond its elastic capability at the ends of the overlap. (The lightly loaded elastic trough appears to be unnecessarily long, but it is actually sized by the hot/wet environment, not by any room-temperature event.)

If it is now supposed that there is a half inch disbond one quarter of an inch from the edge of the 2 in. overlap per side, the adhesive stresses would be modified slightly, as shown in Fig. 21.

The increment of load that used to be transferred through the now defective area is now shared by extra loads in the immediate vicinity of each side of the defect – without affecting the peak stress at the ends of the overlap. This is indicative of a robust capacity of properly designed bonded joints to tolerate large local defects, provided that one can rely on the remainder of the bonded area remaining stuck. (This capacity is lost whenever the adjacent bonded areas are also on the point of failing.)

If it is further supposed that the same defect, or damage, had occurred right at the edge of the overlap, the redistributed adhesive stresses would be as shown in Fig. 22. Again, remarkably, the value of the peak adhesive stress would not be affected. It would simply be moved to the edge of the defect, where load transfer again becomes possible. This kind of defect would need to be sealed to prevent the intrusion of water, which would freeze and expand at high altitude, thereby spreading the initial damage or defect, under what is known as the freeze/thaw cycle. However, the same size defect in Fig. 21 would best be recorded but otherwise left alone. Any attempt to repair it



**Fig. 21** Load redistribution due to local bond flaw near the edge of the overlap

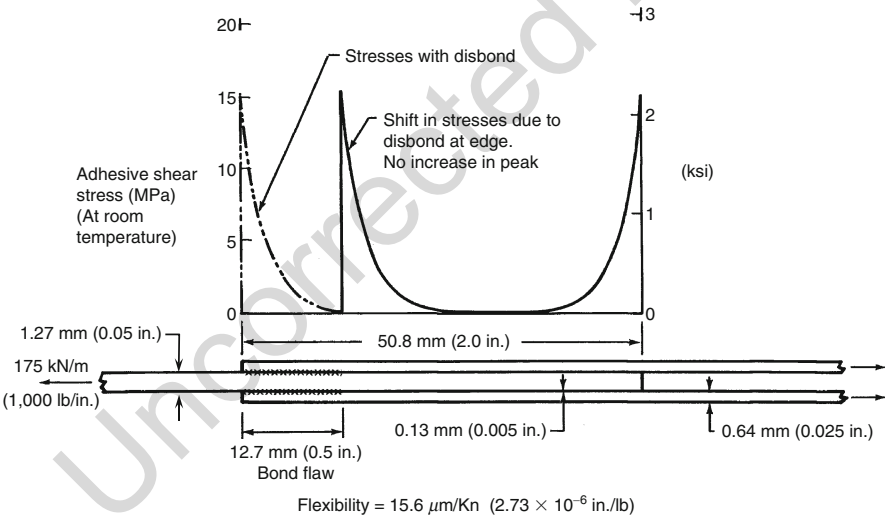


**Fig. 22** Load redistribution due to local bond flaw at the edge of the overlap

would break the environmental protection, by cutting through the primer and exposing bare untreated metal on the edge of any hole that might be drilled to enable resin to be injected to fill the gap and make the discrepancy undetectable in future. All that would be accomplished is to decrease the remaining life, without any increase in joint strength. If the surfaces have been prepared properly, most local damage will not spread. If they were not prepared properly, local repairs are pointless, since the adjacent bonded areas will soon need to be repaired themselves, as noted earlier.

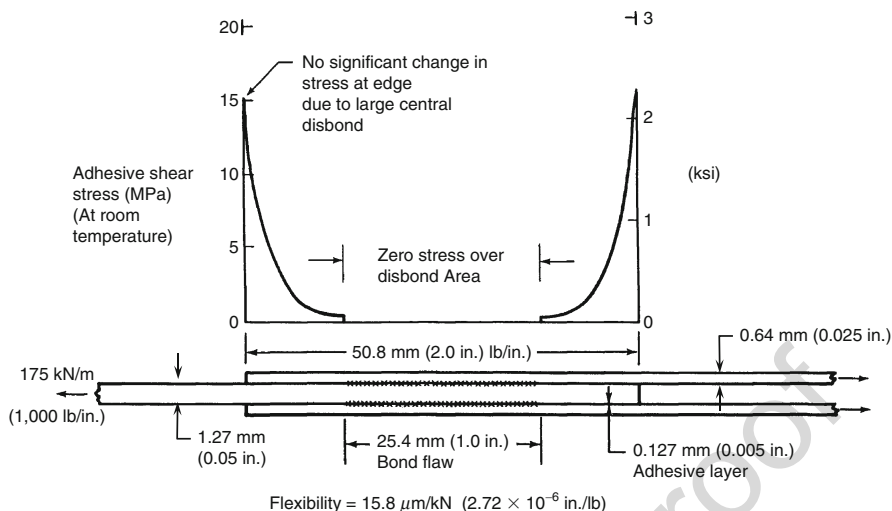


**Fig. 23** Load redistribution due to local porosity in a bonded overlap

If the defect was created in the form of a trapped bubble in the middle of the overlap, as in Fig. 23, when the edges of the overlap were pinched off and there were too few small vent holes in the splice plates (this omission is really usually only a problem with large-area doublers), there would be a large area of porosity where the gap between the adherends was too great for the adhesive layer to fill. The natural occurrence of porosity is discussed by Hart-Smith (1982b). Obviously, since there was no load being transferred there anyway, the presence of such occasional areas of porosity may be considered unimportant, unless it were to cause a misfit with adjacent stiffeners (which is a problem with larger-area bonded doublers with no vent holes). It should also be noted that it is impractical to fill every little bubble in the area of porosity and that, even if this were possible, the gap between adherends could not be reduced and the locally thick bond layer could never pick up its designated increment of load anyway. The thicker bond layer necessarily associated with porosity, unless it occurred everywhere as the result of pre-bond moisture in the uncured adhesive film, ensures that the porous area will not fail, even if it occurred in an area of high nominal shear stress. What most porosity does is to transfer extra load to any adjacent thinner regions in the adhesive bond layer.

Figures 20, 21, 22, and 23 are typical of local flaws in and damage to thin bonded structures. They are usually innocuous and should not be repaired, except when it is necessary to seal exposed edges to prevent the ingress of moisture. This is because of the large excess of strength of the bond over the adherends. For thicker structures, this excess strength is diminished, and flaws and damages can become more significant, as explained by Hart-Smith (1982a).

The preceding examples refer to one-dimensional situations. When bond flaws are assessed in two dimensions, the need for the bond to always be stronger than the adherends becomes abundantly clear. If the adherends are stronger than a properly



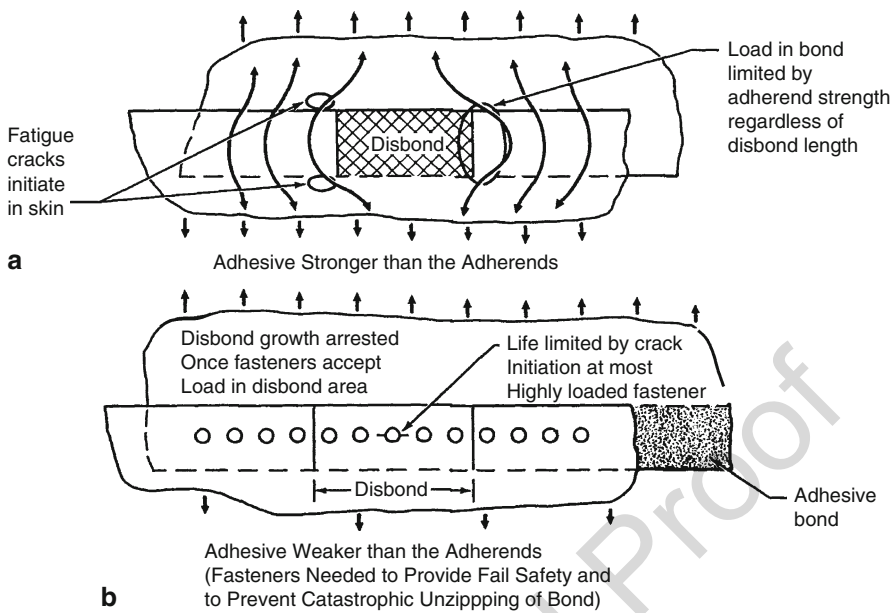


**Fig. 24** Two-dimensional load redistribution around a large flaw in a bonded overlap: (a) adhesive stronger than the adherends; (b) adhesive weaker than the adherends

processed bonded joint with no defects, any large defect or damage acquires the characteristics of a through crack in metallic skins, as explained in Fig. 24.

Provided that the bond outside the defective or damaged area is stronger than the adherends, the initial damage cannot possibly spread. Instead, the diverted load will either initiate fatigue cracks in the skin, just outside the damage, or delaminations in composite laminates, at the same locations. In either event, there will be a long interval in which the damage can be detected before it becomes critical. Without such protection from what appears to be merely excess strength in a one-dimensional assessment, large bond flaws would behave like cracks in metallic structures, even if all of the surface treatment and processing had been the best in the world. This is why it is always necessary to design bonded joints so that they can never become the weak link in the load path.

#### 44.8 Effects of Thermal Mismatch Between Adherends on Strength of Bonded Joints

When thermally dissimilar materials are bonded together, residual thermal stresses are developed that usually detract the remaining strength available for transmitting mechanical loads. These phenomena occur whenever titanium edge members are bonded around the edges of composite panels to permit the use of mechanical fasteners during final assembly of the structure or to permit disassembly in service

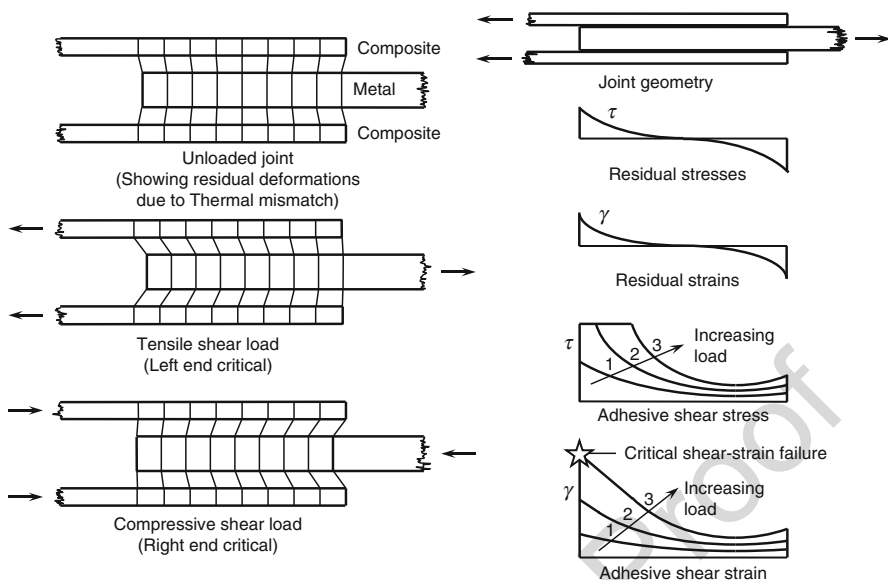


**Fig. 25** Effects of adherend thermal mismatch on adhesively bonded joints

for inspections and repairs. These thermal stresses are roughly proportional to the difference in temperature between the curing and operational temperatures. Their analysis is explained by Hart-Smith (1978) and illustrated in Fig. 25.

The key issue is that, whereas the shear stresses and strains in the adhesive that are caused by mechanical loads have the same sign at each end of the overlap, the shear stresses and strains caused by adherend thermal mismatch have opposite signs from end to end. Consequently, the thermal effects weaken bonded structures below the strength that would be expected if such considerations had been omitted from analyses. Also, the critical end of the joint can change between tensile and compressive lap-shear loads. The issue is complicated by the fact that some of the thermal strains can creep out of short-overlap test coupons, but they cannot be ignored in long-overlap joints. These effects are more pronounced on thicker structure than on thinner adherends and, in extreme cases, can cause bonded joints between thermally dissimilar materials to actually self-destruct during cooldown after curing at elevated temperatures. The problems are significant for aircraft structures and can be the critical load cases for most space structures. For this reason, acrylic adhesives are used more on space structures than on aircraft structures, for which epoxy adhesives dominate.

## 44.9 Inspection, Testing, and Quality Control

Inspection of bonded and composite structures is one of the most contentious issues associated with these two technologies. A few years ago, the author was told by USAF colleagues of a PhD thesis at WPAFB in which it was estimated that

inspection accounted for over one third of the life-cycle cost of composite structures in their fleet, while the material cost was less than 2% of that total. In spite of the willingness to spend so much money on inspections, mostly in service, the inability to guarantee the quality of such structures after they have been built is a great impediment to their more widespread use. One is forced to conclude that the inspection programs in place have not provided good value for money, as is explained in the next section. In fact, the service record of these structures is far better than this image suggests. The only problems of any significance have been those associated with failure to detect the use of inappropriate processing at the time of initial manufacture. One post-manufacture inspection method can reliably assess whether or not the glue is still stuck at any time during the service life of the structure. This is the bonded pull tabs described by Hart-Smith (1995) and illustrated in Fig. 26. If the surface has deteriorated, the tab will easily be pulled off the surface if a drop of water is applied in conjunction with the peel load. This is known to work on metal-bond structures, per the tests run during the PABST program. It has yet to be applied widely on composite structures, possibly out of concern to damage the underlying structure if the bond were not defective. However, the one manufacturer who did so as part of the process of evaluating and solving a problem reported that it worked just fine.

The inherent inadequacies of some of the expensive standard inspections for bonded and composite structures are described later after describing the various kinds of defects. It is first necessary to differentiate between mechanically induced damage, which is relatively easy to detect, and weaknesses created by inappropriate processing, which can be found reliably at the time of manufacture only by a combination of shear and peel test coupons. This condition cannot be detected by standard ultrasonic inspections because, initially, there is no gap to be found. However, if the defects are not detected until much later, it is necessary to examine the fracture surface to confirm that the failure was interfacial (for a processing error) and, therefore, that it could potentially extend over the entire bonded area. Impact

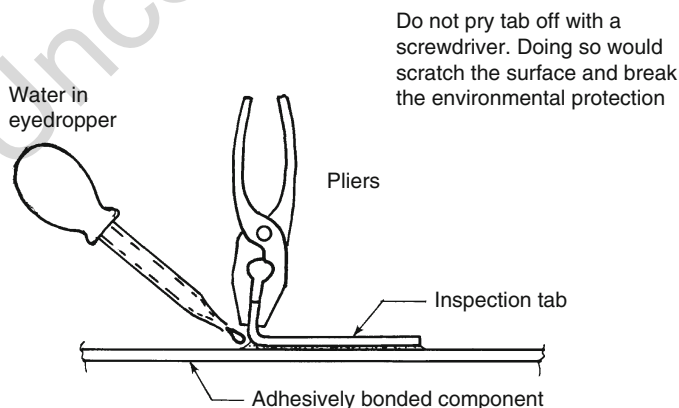


**Fig. 26** Use of bonded tabs to assess bond strength at any stage in the life of bonded structures

damage tends to be far more localized, and it is unlikely to spread because it takes far more force to break bonds cohesively. Such failures are characterized by a rough fractured adhesive surface on both adherends. Discrepancies found by ultrasonic inspections at the time of initial manufacture fall into a different category. These are misfits that cause voids and porosity in bonded joints. That is the one valuable contribution that these expensive and time-consuming inspections can make. However, there is an even quicker and far more reliable technique for securing the same information. At SAAB, instead of discarding the bleeder pack after the parts are made, it is part of the inspection process for the fuselage panels of the SAAB 340 and SAAB 2000 aircrafts (Hart-Smith and Strindberg 1995, 1997). The local absence of any squeeze out, or any local excessive squeeze out, is an unambiguous indication of where the detail parts did not fit together properly, as explained in Fig. 27. (The need for such bleeder packs, which were not needed for the bonded wing panels, arose because of the use of standard rigid external bonding tools.)

Such local defects are usually structurally insignificant, as explained earlier, but, once detected, cause inordinate inspection costs during service to prove that they have not grown, even though extensive service history indicates that they will not if the processing had been reliable.

However, if such discrepancies are repetitive, considerable future costs can be eliminated by modifying the bonding tool or the individual parts so that such misfits are eliminated from future production, as explained by Hart-Smith and Strindberg (1997). While it may seem contrary to intuitive thinking, by anyone who has not read and understood Deming's books on Total Quality Management, defect-free bonded

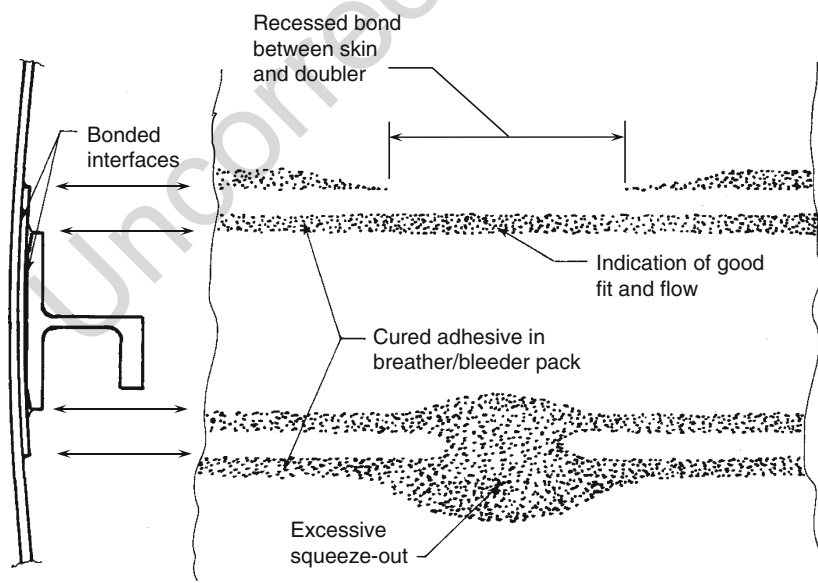


**Fig. 27** Use of bleeder pack to indicate the location of any misfitting detail parts

and composite structures really are the least expensive to make. The absence of defects is the path to even more reductions in inspection costs since, after ten consecutive defect-free assemblies have been made, it is permitted to switch to a sampling inspection plan instead of having to inspect 100% of every assembly. In the same vein, there are two positions on whether or not it is necessary to attach traveler coupons to every single part being anodized or if it is sufficient to validate the temperatures, chemical concentrations, voltages, and the like, in the tank farm only at the beginning and end of each shift. The only additional information that traveler coupons on every detail part can provide is assurance that the electrical connections needed for anodizing have been attached correctly. But that detail can also be verified by visual inspection and is sometimes nullified by stringing all coupons in a single patch together to save time in testing them, instead of attaching them to parts one at a time in such a way that they could be anodized only by current that first flowed through the part it was validating. The issue is clouded by the need to measure both voltage and current flow to ensure complete anodizing and not merely the use of polarized light inspections to detect anodizing. This method has failed repeatedly to detect under-anodizing, as noted during the PABST program. This condition has been created by undetected corrosion in the electrical circuit that reduced current flow, even though the correct voltage was maintained, and by too low temperature in the tank farm. In other words, all that the use of 100% traveler coupons ensures, beyond what validating the tank farm twice a shift can do, could have been ensured by diligent visual inspections during the processing. It would seem that, if these 100% inspections were detecting discrepancies not found by the twice-a-shift inspections, the processing specifications were not being followed carefully enough. The author would suggest that the extra tests should be superfluous if there is a stable fully trained workforce in the bond shop but that they serve as a useful insurance policy if there is so much labor turnover that additional training ought to be occurring. These shear and peel coupon tests are neither expensive nor time-consuming. However, it should always be remembered that increments of the inspection budget once dissipated on unnecessary tests will not be available at some future date to resolve some unanticipated real problem. Inspection dollars are most valuable when they are solving problems or confirming their absence, rather than in buying off discrepant parts as is – without causing the discrepancies to be eliminated from subsequent parts.

Once reliable process specifications have been established, their application for metal bonding is customarily validated by two tests on coupons referred to as traveler coupons that are processed with the part. One of these tests is the lap-shear coupon (ASTM D-1002), tested at room temperature, and the other some form of peel test in a hot/wet (hostile) environment. Common peel tests are the wedge-crack test (ASTM D-3762 with a far more stringent requirement on the absence of interfacial failures than in this specification) and the climbing-drum peel test (ASTM D-1781). As noted earlier in this chapter, the first test ensures only that the resin in the adhesive has been exposed to the correct thermal profile, while the second ensures durability in service. Both tests are needed. The parts processed with the coupons are primed within the strict limits on exposure after the

915 etching, anodizing, and rinsing have been completed. (In the auto-industry, the  
916 priming is often an electro-dip process at the end of the other surface treatments,  
917 but the lower volume of production and greater size of the parts have not favored this  
918 approach for aerospace. It would help if it had, since the need for such critical control  
919 of the primer thickness being sprayed on might then be avoided. But that appears to  
920 be a development for the future.) The bare surfaces will deteriorate with time if not  
921 primed promptly but can safely be stored after priming. They are then left on hold  
922 until the traveler coupon tests have been completed, typically in an hour, and not  
923 released to the assembly area until the coupon tests have been satisfied. The surfaces  
924 of the actual parts have to be reprocessed if the coupons fail the test. This delay is  
925 avoided when the tank farm is validated only twice per shift, rather than for each tank  
926 load of parts. But the saving must be weighed against the risk of far greater recovery  
927 costs if parts have been bonded together before some discrepancy is discovered.

928 In the case of bonded composite parts, the standard process inspections are  
929 incomplete, in the sense that only lap-shear coupons are mandated. There is rarely  
930 any use of a peel test to ensure that the adhesive is stuck properly. In the author's  
931 opinion, based on years of observation of manufacturing and in-service experience,  
932 there ought to be because there is no other way of discontinuing the use of surface  
933 treatments that have been found to be inadequate. This issue is discussed by Hart-  
934 Smith (2003).

935 It is vital to understand that each kind of test evaluates only one factor. The  
936 shear test cannot assess durability, and the peel test cannot ensure complete cross-  
937 linking of the resin. Perhaps the worst violation of this principle is the use of  
938 ultrasonic inspections to overrule failure to pass the coupon tests for parts that are  
939 deemed too expensive to scrap. There are never any written specifications allowing  
940 this, but there are also no written instructions prohibiting material review boards  
941 from making such decisions. Fortunately, since the introduction of phosphoric acid  
942 bonding and phenolic-based adhesive primers, the processes have become more  
943 robust than the testing techniques, and such decisions have not created a safety  
944 problem.

945 There is a similar confusion with bonded composite structures, related to a  
946 widespread failure to understand that process-verification coupons cannot do so if  
947 the requirements are set so low that even badly processed parts can exceed the  
948 requirements. It is therefore often necessary that the coupons *not* have the same fiber  
949 pattern as any individual part. Only an all-0° lap-shear coupon can impart enough  
950 load to fail a properly processed adhesive layer. Failure outside the bonded overlap  
951 in a far weaker quasi-isotropic laminate tells nothing whatever about the strength of  
952 the adhesive layer or whether or not it had been fully cured. So the use of such fiber  
953 patterns as bonded-joint test coupons is always inappropriate, no matter what the  
954 design of the structure is. Similarly, all-0° peel test coupons are needed to evaluate  
955 durability because it is so easy to divert any interlaminar crack through any layer of  
956 90° fibers. Sadly, not only is there yet any agreement on the need for durability tests  
957 of bonded composite joints, there is not even a universal recognition of the need for  
958 the composite coupons that are used to be strong enough to pass only when a full-  
959 strength bond has been created.

Ultrasonic inspections can, at best, tell only that no impact damage has occurred that was of sufficient magnitude to create internal delaminations and that the parts did or did not fit together properly when they were first bonded together. However, there are some far more reliable and far less expensive visual inspections that can ensure proper fit – and reveal a lot about the processing too! This is explained in Fig. 28, taken from Hart-Smith (1995). The fillet cannot achieve the preferred shape if the adhesive was not heated up correctly to make it flow; it cannot wet a contaminated surface; and it cannot even form if the parts are too far apart. The shape of the fillet is an invaluable reliable indicator of a good bonded joint, and such an inspection is both rapid and inexpensive. The total absence of any fillet indicates a gap just as reliably as any ultrasonic inspection. Indeed, it is necessary to seal any edges where there is no fillet before attempting to use ultrasonic inspections because liquid that could ingress through an open edge could mask the extent of such gap from any ultrasonic inspection, which relies on gaps to create signals of discrepancies. A porous spew for an epoxy adhesive would indicate the presence of pre-bond moisture but would be expected for a phenolic adhesive. (Despite their excellent service record, phenolic adhesives tend not to be used much in aeronautical structures today because of the higher pressures needed than for curing epoxy adhesives.)

To summarize the salient points about inspections and quality control for bonded structures, it is vital that appropriate processes be specified – and followed. Verifying this requires both shear and peel tests in a hot/wet environment for metal bonding and bonded composite structures. Ultrasonic inspections can be relied upon to find only in-service impact damage, not progressive degradation. However, ultrasonic inspections at the time of manufacture can identify gaps and misfits and point the way to major cost savings by eliminating such discrepancies from future parts, even if they were structurally insignificant. Any defect, once detected, incurs enormous subsequent inspection costs to prove that it has not grown. It is far less expensive to make parts with no defects than to buy them off as is. Although it is usually not

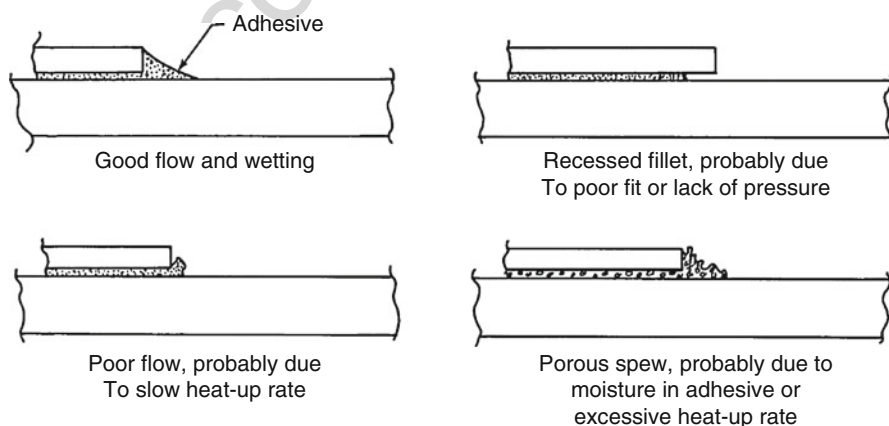


**Fig. 28** Importance of visual inspections of bonded structures

mentioned in any specifications, visual inspections can be incredibly valuable, even if they do not eliminate the need for all other tests.

---

#### **44.10 Concerns About the Misplaced Emphasis of the Quality-Control Inspections for Bonded and Composite Structures**

Just as the primary purpose for the structural analysis of aeronautical structures should be to make the structures better than if the analyses had not been performed, the primary purpose of inspections should be to make the structures better than if the inspections had not been performed. Unfortunately, because analysis and inspection seem to be done too late in the construction process, both fail to achieve their best potential. Indeed, the primary emphasis seems to be to respond to regulations that the structures must merely be shown to be safe. In both cases, the products would be even safer if those tasks were performed much earlier.

The current illogical emphasis on after-the-fact ultrasonic inspections would appear to have its origin in practices developed for the assembly of rivetted metallic aircraft many decades ago. Instead of step-by-step inspections during manufacture, reliance was placed on thorough after-the-fact inspections. Most mistakes could be corrected by drilling out and replacing a few badly driven rivets. This would restore the structure to 100% of its design strength, with no loss of safety or reduction in fatigue life. It may or may not have been the least expensive approach to inspection, but at least, in that context, it was reliable. Fixing any problems as they were created would have been far less expensive (in the author's opinion, based on his experiences and observations), but if there were no defects to find, the intermediate inspections were perceived as a waste of money and repeated interruptions to the assembly schedule. The problem with adhesively bonded and fiber-polymer composite structures is that after-the-fact repairs are usually incapable of restoring 100% of the loss of strength caused by the defects, particularly in components with large loads in them. In short, it is not possible to inspect quality into such parts after they have been made and assembled. The only way to ensure high quality in bonded and composite structures is by appropriate process control, before and during the manufacture and assembly of the parts. Sadly, many of the approved process standards and inspections fail to do so reliably. Worse, many of the approved repairs merely conceal the existence of the damage from further inspections without any increase in strength. The author must conclude that many of the inspections that are performed are done merely because it is possible to do so, rather than as part of a rational quality assurance program. This problem is exacerbated by the absence of what are perceived as critical after-the-fact inspection capabilities. But that excuse misses the fundamental point – belated repairs to bonded structures are inherently incapable of restoring 100% of the design strength. And, with bonded metal structures, these same after-the-fact repairs break the environmental protection that was created during bonding and thereby decrease the service life of the structure.

The purpose of this section is to draw attention to some of these issues, in the hope that their exposure will encourage improvements. It should be noted at the



outset that this is not a matter of simply spending more money doing the same things more thoroughly. There is widespread irrefutable evidence that improved quality during manufacture greatly decreases the cost of making and inspecting the parts. If there are no defects to be found, there are no costs incurred by fixing them and no interruptions to the flow of manufacturing through Material Review Board (MRB) activities. The focus here will be on bonded structures, but many of the same considerations apply to composite structures, too.

It is first necessary to distinguish between the two possible mechanisms of failure of bonded joints. The first, which has proved to be by far the most troublesome, is adhesion failures in which the adhesive was never stuck to the adherends, even if there was no gap between the parts to be detected by ultrasonic inspection. This is an interfacial failure that has not degraded the adhesive itself but totally destroyed its capability to transmit load. The second is cohesive failure within the glue line, which results from impact damage. Such damage tends to spread extremely slowly, if at all, because in a properly designed bonded joint, the undamaged joint itself is never the weak link, as explained earlier. The adherends will fail before such damage can be spread. With interfacial failures, however, there is no need for a load to cause the nonbond to spread. There is a third kind of defect, porosity, that occurs during assembly when the parts do not fit together properly or when the bonding tool prevents them from fitting together. The importance of interface control is explained by Hart-Smith (1997). Whereas there is a standard tolerance on the parts on the order of  $\pm 0.75$  mm (0.03 in.), the tolerance on a glue line that is nominally  $\pm 0.125$  mm (0.005 in.) thick is only  $\pm 0.025$  mm (0.001 in.). This is impossible to satisfy unless the parts being bonded are able to drape to fit, as with skin/doubler combinations. If the gap between the parts is more than about 0.25–0.50 mm (0.010–0.020 in.), the adhesive will flow out of the gap if it is cured by high temperature. Only paste adhesives can be used to fill gaps between parts, and they tend to have lower environmental durability than high-temperature-cured film adhesives. More critically, they take far longer to cure, requiring that the parts be left in assembly jigs for far longer. Worse, since paste adhesives start to cure as soon as they are mixed, this imposes severe limitations on the permissible lay-up time. But the problem with misfitting parts does not end with the creation of porosity or voids. Gaps between parts to be bonded together are not uniform over the entire bond area. Consequently, there are adjacent areas of ultrathin bonds, which are very stiff and attract all the load transfer, and excessively thick bonds, which shed the load they should have been transferring to adjacent thinner bonds, as explained in Fig. 29.

This nonuniformity in load transfer is in addition to the nonuniformities discussed earlier whereby most of the load is transferred immediately adjacent to the ends of each bonded overlap. What the variable bond-line thickness causes that is totally overlooked when one thinks of a uniform adhesive shear stress throughout the entire bond area (which is still a popular model in spite of the evidence) is that, once the thicker bond areas have been established, whether by porosity or voids, even if it were possible to fill the cavity with adhesive, let alone ensure that it adhered, the thick bond regions would not transfer load anyway. This false perception has even worse consequences. The believers in the concept of a uniform adhesive shear stress

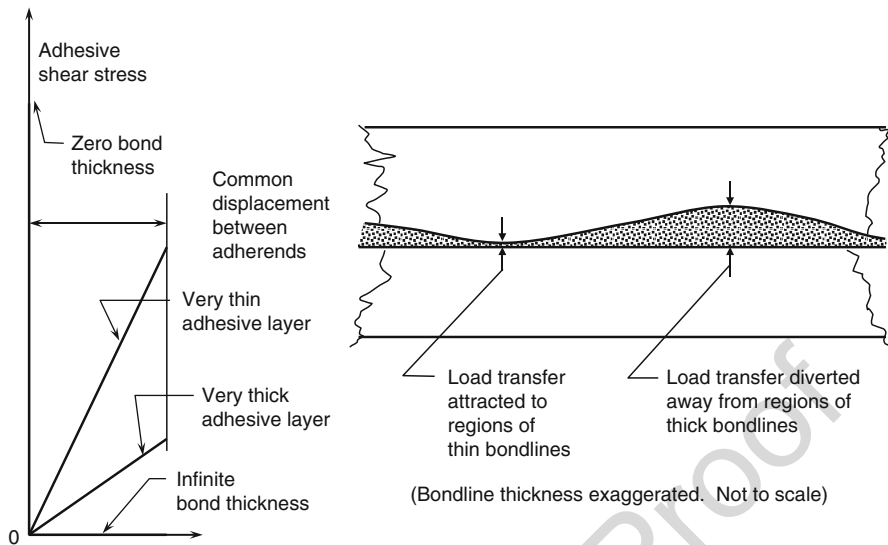


**Fig. 29** Load-transfer redistribution caused by variable bond-line thickness

1075 throughout the bonded area consequently believe that increasing the bond area  
 1076 increases the joint strength. The reality, as explained earlier, is that the strength  
 1077 increases with bond area only until a plateau in strength is attained. Further increases  
 1078 in bond area are futile; only the addition of more steps can increase the shear strength  
 1079 of the joint.

1080 The *only* way to deal with this potential problem of unanticipated variation in  
 1081 shear transfer is to ensure that it never occurs by properly coordinating the design of  
 1082 the structure and the bonding tool(s) before the parts are bonded together. When this  
 1083 has not been done, it is standard practice to identify and locate any thicker gaps and  
 1084 to insert additional adhesive, so that no voids or porosity are created. It is then quite  
 1085 wrongly believed that this must be a “good” bond because ultrasonic inspections  
 1086 cannot identify any defects.

1087 In a similar vein, it should be obvious that, if the adherend surfaces are not  
 1088 processed appropriately, there is no way to make the glue stick other than to  
 1089 disassemble the parts and start all over again. But, if there are no gaps between the  
 1090 parts, the inability of the standard ultrasonic inspections to detect any of the defects  
 1091 that they are assumed to be capable of detecting results in the bonds being accepted  
 1092 when they should not have been. There has, for decades, been a lot of effort devoted  
 1093 to detecting the so-called kissing bonds. But even if such a method were established,  
 1094 discovering the problem at the end of manufacturing leaves absolutely no possibility  
 1095 of restoring the strength of the bonds to anywhere near their design capacity or,  
 1096 sometimes, even to achieving any increase in strength. At most, such “repairs”  
 1097 would simply conceal the existence of the zero-strength bonds. Worse, such defects  
 1098 would be global, not local the way porosity tends to be.

1099 The only bonds that are capable of being restored are cohesive failures from  
1100 impact damage, which is usually found visually, provided that the repair is  
1101 performed before contaminants have entered the cavity.

1102 With very few exceptions, adhesively bonded structures have demonstrated  
1103 excellent durability in service. The problem is that processing errors, whether they  
1104 were caused by inappropriate approved processing specifications whereby the pro-  
1105 cess was being diligently but unknowingly done wrong or by undetected lapses in  
1106 process control with processes that would have worked if they had been done right,  
1107 have tended to involve hundreds or thousands of parts that needed to be fixed. Even  
1108 so, the author knows of only one fatality to which a poor bond contributed – and,  
1109 even then, that contribution was the result of an inappropriate choice of adhesive, not  
1110 to a lapse in quality control or inspections at the time of manufacture. (Even then,  
1111 there were many missed opportunities to prevent the final failure long before it  
1112 happened; the nonbonds were merely the trigger that started the process, not the  
1113 ultimate cause.) The problem with the interfacial failures has been one of cost to  
1114 rebuild those structures, not safety. Most bonded structures have been in secondary  
1115 structures. But, because of the few fleet-wide problems that have occurred, there has  
1116 been a reluctance by most aircraft manufacturers to apply adhesive bonding as  
1117 widely as it should have been, based on its technical merits. This reluctance has  
1118 been compounded by the erroneous belief that doing so required better inspection  
1119 techniques rather than better process control. It has been intensified by the observa-  
1120 tion that the most reliable manufacturers of bonded aircraft structures had a stable  
1121 workforce, so that the skills built up could be maintained. This is contrary to the hire-  
1122 and-fire mentality in other countries in which the existence of special skills is  
1123 denied to support the prevailing business plans.

1124 Much of the porosity generated in large-area bonds could have been prevented by  
1125 proper venting during cure. This can be achieved by a grid of small holes in doublers  
1126 to overcome the tendency to pinch off the edges and trap any air inside. This was  
1127 standard practice for the bonded fuselage panels on the SAAB 340 and SAAB 2000  
1128 commuter aircraft. The wings of the same aircraft were bonded in a special nonrigid  
1129 bonding tool that totally eliminated all bond defects, resulting in far better bonded  
1130 structures at a far lower price. This is described by Hart-Smith and Strindberg  
1131 (1997). In this case, the vents were achieved by having loose fasteners in the  
1132 determinate assembly holes used to keep the skin, doublers, and stiffeners located  
1133 properly. This technique permitted a complete visual inspection of the parts inside  
1134 the vacuum bag to ensure that they all fitted together properly before the parts were  
1135 bonded together because the creation of short escape paths for any trapped air or  
1136 volatiles eliminated the need for bulky bleeder packs which, in many other applica-  
1137 tions, did more harm than good because the associated bridging prevented the  
1138 application of pressure in some areas. Because pressures are uniform inside auto-  
1139 claves, there is no mechanism to displace the air in voids, only to compress it.

1140 This reluctance to apply bonded structures more widely has had one beneficial  
1141 result, in the author's opinion. Apart from the titanium-to-composite stepped-lap  
1142 bonded joints used on the wings of the F/A-18 aircraft and on the tails of many  
1143 military aircraft, there have been relatively few applications of bonded structures

where the local loads have been of high intensity. This is a good thing, in the sense that bonded joints should never be allowed to become the weak link in the structure. Unfortunately, this need usually is not even acknowledged, let alone understood. This is easy to achieve when only thin or laminated components are bonded together. Rivetted joints are more appropriate for higher load intensities since the multiplicity of discrete fasteners retards the spread of any damage. A bonded design in which the adhesive is the weak link, even if the processes are all performed correctly, is tantamount to a weak-link fuse over the whole area, with the potential for damage to spread rapidly once started, as was explained earlier. In addition, there is not yet enough acceptance of what is needed to manufacture thick bonded structures. (Fokker was smart enough to use bonded laminated wing skins on the F-28 aircraft so that no single bond line was heavily loaded, even though the total load intensity in the skin was substantial.) This is most evident in the widespread failure to understand how to deal with induced peel stresses when the ends of the bonded overlaps are too thick. This problem does not arise with stepped-lap joints or laminated structures with the ends of the overlaps staggered, because the outermost end steps where the peel stresses would develop are always thin, which is consistent with Fig. 12. But these high-load bonded joints achieved their reliability because of their complexity, which comes at a higher cost.

In the absence of a proper understanding of induced peel stresses, it has become fashionable to believe that a fracture mechanics analysis of the peel stresses is what is needed. The author believes that this approach has arisen because the standard shear-transfer analyses can be applied to adherends of any thickness and contains no interaction with peel stresses to cause a reduction in the predicted shear strength of the bonded joint. This, in turn, has arisen because, prior to the recent development of the SIFT model for predicting the strength of fiber-polymer composite laminates (Hart-Smith 2010), it had not been appreciated that there was no interaction. Also, the SIFT model does not require the assumed existence of a preexisting crack at the end of the bond line. The two cohesive failure mechanisms for the adhesive really are governed by independent criteria, both of which must be satisfied. The two mechanisms are governed by different power laws related to the adherend thickness, as noted earlier. It is not clear to the author how fracture mechanics methods developed for cracks in homogeneous materials can ever be related to the peel failure of adhesively bonded metallic structures or to delaminations in distinctly heterogeneous fiber-polymer composites; the calculations seem to him to have all the feel of fitting an analysis to test data by use of adjustable parameters that cannot be measured directly. Nevertheless, it is now common for such analyses to be carried out as part of the certification process. But, the author is unaware of any use of such output to improve the design of bonded structures. They seem to be accepted as an unavoidable burden. Indeed, in some cases, these analyses have caused the rejection of what experience has taught the author to bonded joints that were not critical in peel. Regardless of their technical merits, or otherwise, a valid peel-stress analysis which identifies that a bonded joint is critical under induced peel stresses is an unambiguous warning that the design is unsatisfactory because the peel-stress failures will undercut the potential shear strength of the joint. The most appropriate

response to the results of such an analysis is to reduce the thickness of the adherends where the peel-stress failures are predicted to occur, at the edges of the overlap, until further analysis shows that peel stresses are no longer critical. This can always be done in such a way as to maintain the joint shear strength. Indeed, it can actually enhance the shear strength by eliminating the pinch-off that can occur at the ends of uniformly thick adherends. At this stage, the peel stresses would no longer govern, so even a crude analysis would suffice. The problem with now being capable of performing an analysis for peel stresses has led to a failure to employ the good design practices that were developed during the time it was not possible to perform any such analysis. The author's concerns about the use of fracture mechanics as an analysis tool for bonded joints is exacerbated by its inherent incapability of establishing what the overlap should be because this is governed by the minimum shear stress in the middle of the overlap where there is absolutely no possibility of a preexisting crack that would allow fracture mechanics to be employed and where, even if there were, it would never show up as being critical in a fracture mechanics analysis because the bond stresses are almost zero there.

In the same vein, overly complicated co-cured composite parts with embedded wrinkles in the fibers are often "passed" by ultrasonic inspections that detect no voids in the structure. Wrinkles in the fibers, which cause a far greater loss of measured strength than typical levels of porosity in parts that are rejected, do not count as defects because of the widespread acceptance of the myth that fiber-polymer composites are homogeneous. Sometimes, the complexity of co-cured parts is so great that detectable voids are created. But, no matter what is done after that point, it is impossible to straighten out the fibers to restore the strength of the laminates. In other words, the inspection comes far too late to permit the structures to be restored to their design strength, and, in some cases, there is not even an acknowledgment that there is a problem with the parts.

The author would recommend that it is time to totally rethink the quality assurance programs for bonded and composite structures. It is known, from experience, which currently approved processes should be banned, and it is known what needs to be done to ensure low-cost defect-free parts by proper coordination of the parts and the bonding tools and by adherence to reliable processes. It is necessary to stop relying, instead, on the approach of pretending to inspect quality into the parts and assemblies after they have been bonded together because, by that stage, any defects that have occurred will ensure that the parts can never be restored to 100% of their design strength.

---

## 44.11 Bonded Repairs

Bonded repairs should be looked upon as joints that are made at some time after initial manufacture. They need to be made under the same rules and procedures, but it is obviously not possible to repeat the very same surface treatments for bonded metal structures or even for composite structures if a peel ply had been used. In both cases, low-pressure grit blasting has proved to be the most reliable surface treatment

for repairs. This is often followed by the application of a silane coupling agent when composite patches are bonded over cracks in metallic structures. Such patches have been found to be both very reliable and effective (Baker and Jones 1987); they have most often been used when there is no other alternative but to scrap the part because rivetted repairs are sometimes impossible or ineffective (not stiff enough to restrain a crack from any further growth).

As noted earlier, local bonded repairs to bonded metallic structures that were made according to inappropriate specifications are an exercise in futility since the remainder of the structure is also about to disbond. Such structures need to be totally remanufactured in accordance with better processes even when the specific repair manual states otherwise. The most critical issue about the repair of damaged or disbanded composite structures is the difficulty of thoroughly drying the laminates before the repair is executed. Absorbed water takes a very long time to remove from both face sheets and honeycomb cores. This causes such parts to be out of service for a long time.

---

## 44.12 Other Industry-Specific Factors

A little publicized fact about adhesive layers is that they act as electrical insulators. Today's jet transports made from aluminum protect the passengers and crew because they are contained in a complete Faraday cage. There are a number of adverse consequences if that cage is interrupted by insulators between the individual metallic skin panels. The most obvious is that lightning strikes will cause far more damage if there is no continuous conductive path between the strike zone and discharge point. Indeed, simulated lightning-strike tests during the PABST program showed extensive local burning of the adhesive layers at the bonded joint between adjacent skin panels. This is why composite aircraft need special conductive coatings to compensate for the poor conductivity of even carbon fibers and for the periodic total interruptions through bonded joints. A lesser-known issue is that the establishment of even small potential differences between the panels on aluminum aircraft caused by the overzealous application of sealant to prevent corrosion can interfere with some of the small voltages involved in transistorized communication systems. The possible interferences with these systems that are responsible for the powering off of electronic devices during takeoff and landing are of concern. It is therefore important that the individual panels that make up the exterior skin of aircraft, and presumably rockets and missiles also, are grounded together with sufficient connections. The notion of an all-bonded structure is really a myth. Some minimum number of tight-fitting dry rivets is needed to provide electrical connections. These are easily located in the many low-stress areas in bonded joints without causing any fatigue problems. A rivet hole in the middle of a bonded overlap, where the stress level is only half that of the surrounding skins, has a fatigue life some 20 times longer than in a rivetted joint between the skins. Once this need for some holes is acknowledged, it makes sense to use such holes for determinate assembly, to minimize the need for most of the traditional costly assembly tools, and to simplify bagging by eliminating the need

for holding fixtures. This concept was used on the bonding tools to both simplify and improve the manufacture of the bonded stiffened wing skins used on the SAAB 340, as discussed by Hart-Smith and Strindberg (1997). There needs to be a balance between coating every fastener and every faying surface with sealant to prevent corrosion and the need for electrical continuity. Perhaps the cost savings from determinate assembly may provide the encouragement to include the necessary connections to create a true Faraday cage on aerospace structures.

Another issue about bonded aircraft structures is that the surfaces created by anodizing and etching to enhance the adhesion of adhesive primers are more prone to corrosion than normal rolled or machined aluminum surfaces. It is therefore necessary to be very careful, particularly in bilge areas and around galleys, to create and maintain reliable corrosion protection. The polymers used in adhesives tend not to degrade with time and environmental exposure, but some do absorb water and other chemicals. Even so, the primary concern has been for the durability of the interfaces.

---

#### 44.13 Examples of Use of Adhesive Bonding in Aircraft Structures

---

Some aircraft manufacturers have made far more extensive use of adhesive bonding than others. De Havillands (now absorbed into BAe) and Fokker were the pioneers in using adhesive bonding in primary aircraft structures. The Fokker F-27 Friendship and F-28 Fellowship aircraft are renowned for their successful widespread use of adhesive bonding. SAAB and Cessna used primary structural bonding widely after the PABST program had validated the second successful generation of materials and processes. However, other major airframers have restricted the use of adhesive bonding to mainly secondary structures, primarily because of the failures created by the pre-PABST bonding processes and surface treatments developed in the USA. The most significant difference between the two levels of application would appear to be the stability in the labor force, for a variety of reasons. It is not the result of technical ignorance of what is needed to make bonding work, or of the benefits it can create.

Figure 30 shows the extensive application of adhesive bonding to the aluminum airframe of the SAAB 340 aircraft. This aircraft has an incredible structural efficiency and durability, which could not have been achieved with conventional rivetted structures.

Cessna made even more extensive application of bonding to the fuselage of the Citation III jet aircraft and used the same technology to make wings on other aircraft with far fewer fuel leaks than on conventional rivetted wing boxes. Figure 31 shows a typical frame/longeron intersection point on the Citation III fuselage skin, showing how not only the waffle doubler and longerons are bonded to the skin but the outer half of the frame is, too. What is significant about this design is that both stiffener flanges are continuous where they contact the skin; there is no weakness associated with the traditional mousehole in the frames to allow longerons to pass through.



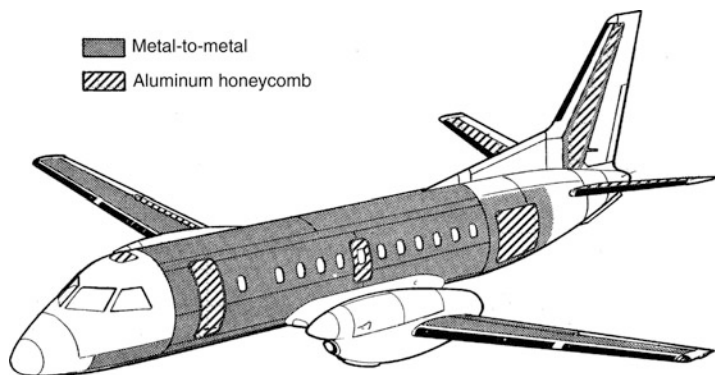


**Fig. 30** Application of adhesive bonding to SAAB 340 fuselage, wings, and tail

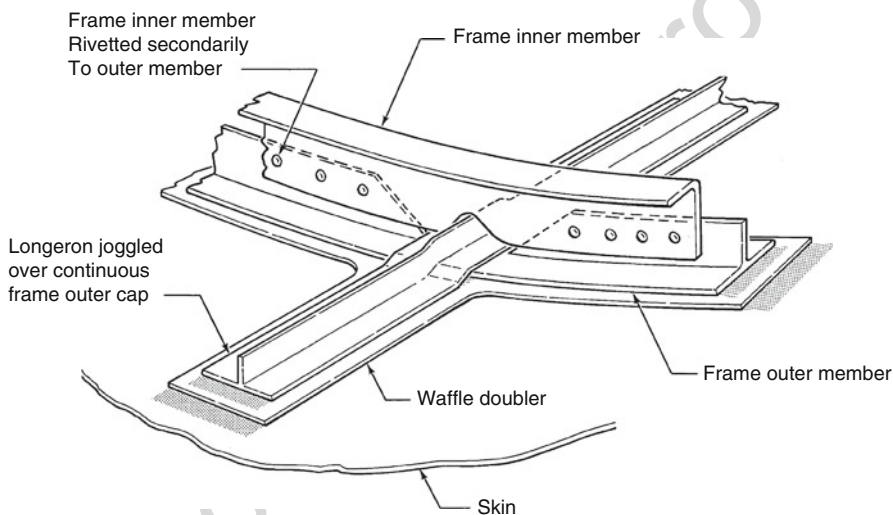


**Fig. 31** Cessna Citation III bonded frame/longeron intersection

1314 The secondary structures, control surfaces, and fixed panels on the Boeing  
 1315 747 made extensive use of metal bonding, mainly with honeycomb. Many of these  
 1316 components have been replaced by composite structures on later models, but most of  
 1317 these components should still be classified as bonded structures. For example, the  
 1318 777 composite tails (see Fig. 32) are made by co-bonding pre-cured stiffeners to  
 1319 green skins. These are classified as primary structures, surpassing in both size and  
 1320 load intensities the earlier NASA-funded flight demonstration programs on the  
 1321 737 and DC-10. All current-production Airbus aircraft have primary composite  
 1322 structures in their horizontal and vertical tails. Today, virtually all modern transport  
 1323 aircraft have composite control surfaces, wing-root fillets, and various other second-  
 1324 ary structures.



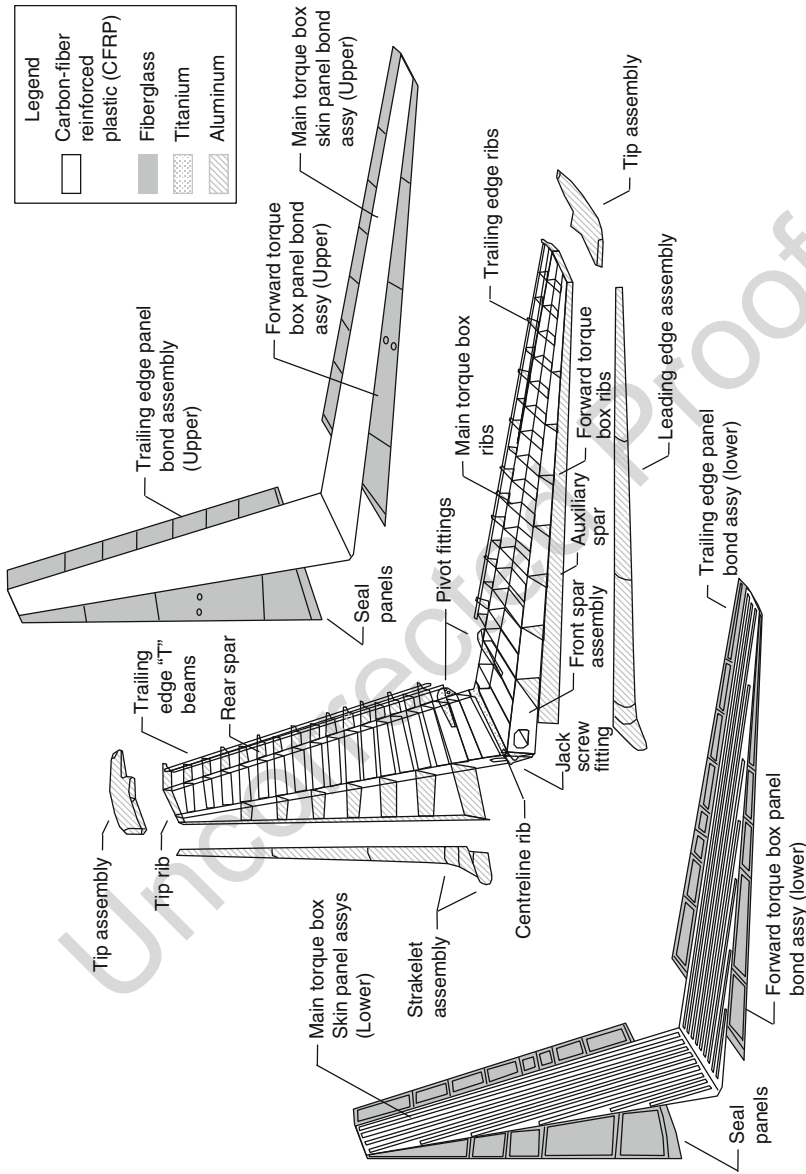


**Fig. 32** Co-bonded composite primary structure on Boeing 777 tail

Military aircraft have made much more use of primary composite structures than on commercial transport aircraft, but most new general aviation aircraft since the resurgence of this industry a decade ago have made even more extensive use of composites, co-cured and bonded, in their primary structures. Their smaller size favors this method of manufacture.

Adhesive bonding has a tremendous advantage over co-curing of composites for high production rates. Co-cured structures require the use of the largest tools for a greater time than bonding together of simple details, many of which can be cured in a single autoclave cycle. This was recognized by the team that developed the Lear Fan all-composite executive transport aircraft over 20 years ago. It was planned for a production rate of one aircraft a day. The tooling costs would have been unaffordable if the design had been based on large integrally stiffened assemblies. This issue is still important today. The minimum-cost prototype development program is often a co-cured design because the effects of production rate are not considered. Once the structural tests have been completed, the option of less expensive more dispersed production is lost, and high production costs are often locked in place. It would make more sense not to minimize the cost of the prototypes in isolation but to build prototypes of the lowest-production-cost design instead.

---

#### 44.14 Conclusion

This chapter has focused on adhesively bonded joints in aircraft structures, emphasizing why and how they work, when they are superior to mechanically fastened joints, some examples of great successes, and an explanation (with cures) for less than successful applications. There is more coverage of experience with bonded joints than the science that enabled them to work. Those details are found in much greater depth in other chapters in this book. However, there is also some discussion of devoutly held beliefs about bonded joints that are so wrong that they have inhibited the more widespread use of bonding because of unwarranted concerns about durability and monitoring degradation. Despite having been able to characterize the nonuniform transfer of load through bonded joints for decades, the most widely taught method simply, and quite erroneously, assumes that the load distribution is uniform to “simplify” design and analysis. Inspections have not been used wisely since so many of them are applied at the wrong time in the life of the product. Sadly, the most valuable inspections, visual, are downgraded as being too primitive to use because they rely on skill, a variable human factor, ignoring the fact that most of the instruments used can never find some of the most critical information that is sought. There is a tendency to conduct an inspection for reasons more related to the existence of an instrument that is supposed to be able to detect some defect rather than that there is any real need, or likely benefit, from the inspection. Worse, the most critical source of bond failure – the failure to adhere in the first place – is often not acknowledged as the most critical (because any such error will have global impact). Instead, there is too much focus on inspections for local damage, which the adhesive

is often able to tolerate with no loss in strength by rearranging the load-transfer distribution. The reason for the misplaced emphasis is merely that it is possible to detect that kind of discrepancy. The hope is that, by exposing these issues, and how to address them, there will be a greater willingness in the future to use bonding where it really is the best approach – and to not knowingly take shortcuts (even if they are “approved”) that give it a bad name because the impact is so widespread. The confirmed success stories about adhesive bonding in aircraft structures are substantial and have been for decades; they just need better publicizing to neutralize the bad press from the failure cases, none of which can reasonably be blamed on ignorance. The author concludes with the following suggestion to encourage the more widespread use of bonded aeronautical structures. Waiting until someone devises a reliable after-the-fact inspection method for bonded structures before accepting the advantages of bonded structures, where they make sense, is going to take an extremely long time if it is ever accomplished. And, in any case, as explained earlier, such a technique could not enable the design joint strengths to ever be restored; it is too late to try to inspect quality into a part after it has been built. Some aircraft manufacturers have already demonstrated that carefully following appropriate processes is both feasible and reliable. The service record of properly bonded aircraft structures is exemplary. There is no need to wait for an additional safety net, for which no need has yet been found, to justify less diligence during the manufacturing processes before committing this proven technology to production.

**Acknowledgments** Parts of this chapter have earlier been published as “Aerospace Industry Applications of Adhesive Bonding” (Adhesive Bonding, edited by R. D. Adams, Woodhead Publishing Ltd., Cambridge, 2005, pp. 489–527) (Reproduced with permission from Woodhead).

## References

- Baker AA, Jones R (eds) (1987) Bonded repairs of aircraft structures. Martinus Nijhoff, Dordrecht, pp 77–106
- Bardis J (2001) Effects of surface preparation on long-term durability of composite adhesive bonds. In: Proceedings of MIL-HDBK-17 meeting, Santa Barbara, 16 Oct 2001
- de Bruyne NA (1957) Fundamentals of adhesion. In: Bonded aircraft structures. A collection of papers given in 1957 at a conference in Cambridge, England, Bonded Structures, Duxford, pp 1–9
- Gosse JH, Christensen S (2001) Strain invariant failure criteria for polymers in composite materials. AIAA paper AIAA-2001-1184, presented to 42nd AIAA/ASME/ASCE/AHS/ASC structures, structural dynamics, and materials conference, Seattle, 16–19 Apr 2001
- Hart-Smith LJ (1973a, 1974) Analysis and design of advanced composite bonded joints. NASA Langley contract report NASA CR-2218, January 1973; reprinted, complete, Aug 1974
- Hart-Smith LJ (1973b) Adhesive-bonded double-lap joints. NASA Langley contract report NASA CR-112235, Jan 1973
- Hart-Smith LJ (1973c) Adhesive-bonded single-lap joints. NASA Langley contract report NASA CR-112236, Jan 1973
- Hart-Smith LJ (1973d) Adhesive-bonded scarf and stepped-lap joints. NASA Langley contract report NASA CR-112237, Jan 1973

- 1410 Hart-Smith LJ (1973e) Non-classical adhesive-bonded joints in practical aerospace construction.  
1411 NASA Langley contract report NASA CR-112238, Jan 1973
- 1412 Hart-Smith LJ (1978) Adhesive-bonded joints for composites – phenomenological considerations.  
1413 Douglas Paper 6707, presented to Technology conferences, associates conference on advanced  
1414 composites technology, El Segundo, 14–16 March 1978; in Proceedings, pp 163–180; reprinted  
1415 as designing adhesive bonds. *Adhes Age* 21:32–37, Oct 1978
- 1416 Hart-Smith LJ (1982a) Design methodology for bonded-bolted composite joints. USAF contract  
1417 report AFWAL-TR-81-3154, 2 vols, Feb 1982
- 1418 Hart-Smith LJ (1982b) Adhesive layer thickness and porosity criteria for bonded joints. USAF  
1419 contract report AFWAL-TR-82-4172, Dec 1982
- 1420 Hart-Smith LJ (1984a) Effects of flaws and porosity on strength of adhesive-bonded joints. Douglas  
1421 paper 7388, presented to 29th National SAMPE symposium and exhibition, Reno, 3–5 Apr  
1422 1984; in Proceedings, pp 840–852
- 1423 Hart-Smith, LJ (1984b) Bonded-bolted composite joints. Douglas paper 7398, presented to AIAA/  
1424 ASME/ASCE/AHS 25th structures, structural dynamics and materials conference, Palm  
1425 Springs, 14–16 May 1984; published in *J Aircraft* 22, 993–1000 (1985)
- 1426 Hart-Smith LJ (1993) The bonded lap-shear test coupon – useful for quality assurance, but  
1427 dangerously misleading for design data. McDonnell Douglas paper MDC 92K0922, presented  
1428 to 38th international SAMPE symposium & exhibition, Anaheim, 10–13 May 1993; in Pro-  
1429 ceedings, pp 239–246
- 1430 Hart-Smith LJ (1995) Reliable nondestructive inspection of adhesively bonded metallic structures  
1431 without using any instruments. McDonnell Douglas paper MDC 94K0091, presented to 40th  
1432 international SAMPE symposium and exhibition, Anaheim, 8–11 May 1995; in Proceedings, pp  
1433 1124–1133
- 1434 Hart-Smith LJ (1997) Interface control – the secret to making DFMA<sup>®</sup> succeed. McDonnell  
1435 Douglas paper No. MDC 96K0132, presented at SAE aerospace manufacturing technology  
1436 conference & exposition, Seattle, 2–5 June 1997, and published in Proceedings, pp 1–10, SAE  
1437 Paper No. 972191
- 1438 Hart-Smith LJ (2001) Explanation of delamination of bonded patches under compressive loads, using  
1439 new simple bonded joint analyses. Presented to 3rd quarterly CRAS review, in conjunction with  
1440 Fifth Joint DoD/FAA/NASA conference on aging aircraft, Kissimmee, 10–13 Sept 2001
- 1441 Hart-Smith LJ (2001/2002) A demonstration of the versatility of rose's closed-form analyses for  
1442 bonded crack patching. Boeing paper MDC 00K0104, presented to 46th international SAMPE  
1443 symposium and exhibition, Long Beach, 6–10 May 2001; in Proceedings, 2002: a materials and  
1444 processes Odyssey, pp 1118–1134
- 1445 Hart-Smith LJ (2003) Is it really more important that paint stays stuck on the outside of an aircraft  
1446 than that glue stays stuck on the inside? Boeing paper PWMD02-0209, presented to 26th  
1447 Annual meeting of the adhesion society, Myrtle Beach, 23–26 Feb 2003
- 1448 Hart-Smith LJ (2010) Application of the strain invariant failure theory (SIFT) to metals and fibre-  
1449 polymer composites. *Philos Mag* 90(31):4263–4331
- 1450 Hart-Smith LJ (n.d.) The Goland and Reissner bonded lap joint analysis revisited yet again – but  
1451 this time essentially validated. Boeing paper MDC 00K0036, to be published
- 1452 Hart-Smith LJ, Davis MJ (1996) An object lesson in false economies – the consequences of not  
1453 updating repair procedures for older adhesively bonded panels. McDonnell Douglas paper  
1454 MDC 95K0074, presented to 41st International SAMPE symposium and exhibition, Anaheim,  
1455 22–25 March 1996; in Proceedings, pp 279–290
- 1456 Hart-Smith LJ, Strindberg G (1995) Developments in adhesively bonding the wings of the SAAB  
1457 340 and 2000 aircraft. McDonnell Douglas paper MDC 94K0098, presented to 2nd PICAST &  
1458 6th Australian aeronautical conference, Melbourne, 20–23 March 1995; abridged version in  
1459 Proceedings 2:545–550
- 1460 Hart-Smith LJ, Strindberg G (1997) Developments in adhesively bonding the wings of the SAAB  
1461 340 and 2000 aircraft. McDonnell Douglas Paper MDC 94K0098, full paper published in *Proc*  
1462 *Inst Mech Eng, Part G J Aerosp Eng* 211:133–156

- 1463 Hart-Smith LJ, Redmond G, Davis MJ (1996) The curse of the nylon peel ply. McDonnell Douglas  
1464 paper MDC 95K0072, presented to 41st International SAMPE symposium and exhibition,  
1465 Anaheim, 25–28 March 1996; in Proceedings, pp 303–317
- 1466 Krieger RB Jr (1988) Stress analysis concepts for adhesive bonding of aircraft primary structure. In:  
1467 Johnson WS (ed) Adhesively bonded joints: testing, analysis and design, ASTM STP 981.  
1468 American Society for Testing and Materials, Philadelphia, pp 264–275
- 1469 Mahoney CL (1988) Fundamental factors influencing the performance of structural adhesives.  
1470 Internal Report, Dexter adhesives & structural materials division. The Dexter Corporation, 1988
- 1471 Marceau JA, Moji Y, McMillan JC (1977) A wedge test for evaluating adhesive bonded surface  
1472 durability. *Adhes Age* 1977:28–34
- 1473 Myhre SH, Labor JD, Aker SC (1982) Moisture problems in advanced composite structural repair.  
1474 *Composites* 13(3):289–297
- 1475 Schliekelmann RJ (1983) Adhesive bonding and composites. In: Hayashi T, Kawata K, Umekawa S  
1476 (eds) Progress in science and engineering of composites, vol 1. Fourth international conference  
1477 on composite materials, North-Holland, pp 63–78
- 1478 Thrall EW Jr, Shannon RW (eds) (1985) Adhesive bonding of aluminum alloys. Marcel Dekker,  
1479 New York, pp 241–321

Christian Désagulier, Patrick Pérès, and Guy Larnac

**Contents**

45.1	Introduction .....	1286
45.2	Specific Requirements .....	1288
45.2.1	Launchers .....	1288
45.2.2	Spacecrafts .....	1289
45.2.3	Where Are the Adhesive Bonds? .....	1291
45.2.4	Which Adhesives for What? .....	1294
45.2.5	What Are the Adhesive Selection Drivers? .....	1301
45.2.6	And the Adhesive Tapes? .....	1301
45.3	Material and Process Characterization .....	1302
45.3.1	Structural Bonding or Not? .....	1302
45.3.2	What Specific Properties Do Space Applications Call for? .....	1302
45.4	Surface Preparation .....	1314
45.4.1	The Case of Composites .....	1314
45.4.2	The Two-Part Epoxy Adhesive .....	1315
45.4.3	The Metallic Parts .....	1316
45.4.4	Aluminum Alloys .....	1317
45.4.5	Titanium Alloys .....	1318
45.5	Nondestructive Inspection .....	1318
45.6	Strength, Failure, and Durability .....	1325
45.6.1	Sandwich Structure Bonding Construction .....	1325
45.6.2	Monolithic Room Temperature Bonding .....	1326
45.6.3	A Commercial Bonding Case .....	1327

C. Désagulier (✉)

ArianeGroup, Les Mureaux, France

e-mail: [christian.desagulier@airbusafran-launchers.com](mailto:christian.desagulier@airbusafran-launchers.com); [CHRISTIAN.DESAGULIER@astrium.eads.net](mailto:CHRISTIAN.DESAGULIER@astrium.eads.net)

P. Pérès · G. Larnac

ArianeGroup, Saint Médard en Jalles, France

e-mail: [patrick.peres@airbusafran-launchers.com](mailto:patrick.peres@airbusafran-launchers.com); [guy.larnac@airbusafran-launchers.com](mailto:guy.larnac@airbusafran-launchers.com)

26 45.7 Conclusions ..... 1329

27 45.7.1 By Way of Summary ..... 1329

28 45.7.2 And Finally ..... 1330

29 References ..... 1330

**Abstract**

30 This chapter aims to introduce some of the specific bonding-related issues that

31 face those responsible for bonding operations in space applications. We have to

32 consider two cases: structures for launchers and structures for satellite where the

33 environment in terms of load is different. In the case of launchers, extremely high

34 mechanical loads over a short time occur, and for satellites, there is the gravity

35 magnified by about 20, followed by exposure to extremely high temperatures

36 over a very long period, with the observation and telecom satellites under zero

37 gravity.

38

39 To design for such broad specifications and to select materials, such as

40 adhesives, it is just the first in a series of challenges.

41 To perform tests on Earth reproducing space-like environments while subject

42 to terrestrial gravity is the second and not the least significant.

43 This chapter is intended to be an introduction to the issues which have to be

44 considered together in the case of spatial bonding from the bottom, on Earth,

45 upward, to space.

**45.1 Introduction**

46

47 At the beginning of the space conquest in the 1960s, the structural parts of launchers

48 and satellites were mainly made of metal. Here and there, lighter aluminum foil or

49 fiber glass-reinforced plastic composite parts replaced metal as the satellites grew in

50 mass and volume in parallel to the launchers. The word “composite” began to be

51 used to designate structures built up using several different types of materials from

52 various origins (metallic or organic). One found, on one hand, the monolithic

53 composite parts, which refers to the organic stacking of woven glass fabric at various

54 angles, pre-impregnated with resin and cured under pressure. On the other hand, one

55 found mainly 100% metallic, light plane structures made with aluminum foil skins

56 bonded with an organic film to honeycomb core material. At the very beginning,

57 based on conventional design reflexes, the metallic and organic parts were mechan-

58 ically fitted together, and those first composite parts were reserved for no structural

59 parts. This was also due to a lack of experimental feedback, i.e., of confidence, in the

60 behavior of such polymeric parts in a spatial environment.

61 For assembly, the mature aeronautical industry used nut/bolt and rivet systems

62 after drilling, which came from the general mechanical industry. If saving mass

63 was obviously an issue in aircraft, it was even more critical in spacecraft. Before

64 escaping the grips of gravity, the energy required for launching is directly dictated

65 by the weight, and the amount of energy is borne by the launcher. It was the space

industry that applied the aeronautical principles, as far as the arrival in the scene of composite materials was concerned. At the beginning of the 1970s, the epoxy resin associated with glass and boron fibers brought improved specific strength (strength divided by density), enabling the introduction of composite monolithic structural parts instead of metallic ones. Finally, carbon fibers arrived in the 1980s and with them, their assembly at the stage of primary structural parts, in monolithic truss structures or sandwich panels, as parts of the bodywork of satellites. At present, aircraft manufacturers are developing processes capable of one-shot 5-m-diameter-wide, 20-m-long main structural parts. They use several processes like automatic tow of carbon fiber placement, 3D mixed carbon/aramid woven fabric, out-of-autoclave curing, and unidirectional or fabric, pre-impregnated with resin. Dry fibers preformed and consolidated after resin injection or with infusion process are also in production line. In conclusion, priority is given to innovation to make as much headway as possible to reduce the weight of planes, to switch the more numerous parts in gray aluminum to black ones. An Airbus A300–600 was 5% composite material in 1970; this proportion is ten times higher in Airbus A350 XWB today.

The same trend can be seen in the launcher industry. The composite rate increased from 15% in Ariane 5 launcher to up to 63% in the new launcher Ariane 6 and even more in A6 with four booster versions where the level of composite reaches 63%.

Thanks to the adhesive bond technology, 40% cost savings in production were achieved in aeronautics in comparison with riveting where the weight has been divided by 2.5 for some parts.

Bonding in spacecraft dates back to the same era as composite materials, with composites including, on one hand, the previously mentioned fibers reinforced with plastic, like fiber glass, carbon, aramid reinforced with epoxy, phenolic, and thermoplastic resin and, on the other hand, lighter metal alloys, mainly such as aluminum and titanium. Even more so than aircrafts, spacecrafts were the ideal candidates for composite material application and especially carbon fiber-reinforced plastic (CFRP), characterized by high specific stiffness and specific strength, i.e., the ratio values of the Young's modulus and strength to failure divided by the density. These specific mechanical properties associated with a low coefficient of thermal expansion (CTE) result in a light, highly loaded, dimensionally stable structure. For a designer, composite design generates potentially sizeable weight savings, keeping in mind that for space injection by a launcher, "mass is money."

Since the nut/bolt and rivet systems after drilling are dedicated to joining metal, bonding is mandatory for assembling composite parts, and the rules of designing and justifying holes are well known with metal. Because of its anisotropic behavior, designing and justifying a hole in a composite part is much more complex. In principle, local reinforcement is generally performed. The lay-up sequence is also optimized. Drilling composites is not a safe operation as delamination can occur.

Since adhesives with thermo-structural resistance became available, bonding was implemented in aircrafts, more largely in helicopters than in airplanes, such as filling agents for rooms and load-wide spreading agents between the bolted or riveted metal parts.



Let us be reminded that in the 1960s, two phenomena appeared with metallic structures assembled with adhesive bonds:

- Adhesive bond corrosion. It was the degradation of the oxide layer on the metal junction due to hydrolysis of the polymer of the adhesive.
- Sandwich structure corrosion. This phenomenon was generated by the confined atmosphere in the cell with the presence of humidity and corrosive gas coming from the polymerization residues.

Solutions have been founded with:

- Hydrophobic adhesives
- Deposition of anticorrosion primer based on chromate and suppression of plating aluminum
- Improvement of the stability of the oxide layer with chromate or phosphorus anodic conversion (protection of honeycomb cells)

The protection against atmospheric corrosion was also one of the first applications of the bonding agents between metallic parts, as wet barriers. With the arrival of composites, the issue of assembling composite and metal parts together was brought sharply into focus. If the resin formulators went a significant way to meeting requirements (mechanical, thermal), dedicated metal surface preparation prior to bonding had to be developed, most of the metals being subjected to surface corrosion with the production of brittle oxides, especially aluminum alloy. Prior to functional application, to bond, particular attention is paid to the behavior of adhesives in a space environment, that is to say, the vacuum, the thermal cycling, and the radiations. Most of the time, adhesives exhibit very different behavior according to the materials with which they have been brought into contact in the space environment against temperature; here, one is referring to the possible damage under thermo-mechanical fatigue.

There is now a choice of composite material made from various compositions, fibers, resins, and adhesives, capable of dealing with the space environment provided that the preliminary selection fills such stringent specifications.

---

## 45.2 Specific Requirements

Adhesive bonds in the launcher and the spacecraft have an eminent place in the aerospace industry.

### 45.2.1 Launchers

Launchers are built in several stages and assembled together. Each stage is separated from the launcher at different altitudes in order to release weight when propellant is

fully used. Depending on the architecture, solid or liquid propulsion or a mixture of both systems, the launcher has to be protected against the high temperature met on the surface of the structures.

After 141 s of flight, the launcher Ariane 5 reaches an altitude of around 67 km at about 2,000 m/s!

Ariane 5 is considered as a “powered launcher” due to its two solid boosters. The initial thrust delivered by the two boosters and the cryogenic engine Vulcain 2 is around 13,000 kN (90% coming from the boosters).

The most demanding mechanical load occurs in the launch phase mainly during booster combustion with a very high acceleration (more than 20 g). Even if the propulsion phase with solid propulsion lasts around 2 min, a lot of vibration over a broad range of frequencies and heavy acoustic environment (150 db) are generated. Therefore, a damping solution is searched and adhesive bonds with damping materials are used.

When cryogenic propellants are used for liquid propulsion, cryogenic insulation is needed to limit propellant evaporation ( $-253^{\circ}\text{C}$  for LH2 and  $-183^{\circ}\text{C}$  for LOX) and ice formation.

## 45.2.2 Spacecrafts

To illustrate the challenge when using bonding in spacecraft, here are some figures that will need to be dealt with.

One must distinguish three phases which is the specificity of this task.

In the first phase, lasting several months, one needs to deal with the integration of the satellite at the launch pad. Care has to be taken to avoid any risk of contamination and damage. As soon as the satellites are covered and protected by fairing, the atmosphere inside the fairing (temperature and humidity) is permanently controlled until the launch.

The second phase lasts few minutes, starting from the ignition of the launcher up to the orbital injection of the payload (telecom, Earth, and deep space observation satellites, transportation vehicle for International Space).

The most demanding mechanical load occurs in this phase during booster combustion with 20–30 g acceleration, 30 Hz/8,000 Hz vibration, and 150 dB, 5 Hz/120 Hz acoustical environment. The payload must be qualified to sustain these severe conditions. The separation of the stage from pyrotechnic system generates an energetic shock which could damage some sensitive equipment of the satellite (especially scientific satellites).

This is followed by the orbital phase, of a very long duration, 15 years or more of orbital life for telecom satellites.

The main environmental conditions with which compliance is required are temperature, thermal cycling, outgassing vacuum, radiation, and electrostatic drain (see Fig. 1).

Here, one has to distinguish the spacecrafts dedicated to work in low Earth orbit (LEO) from those in geosynchronous Earth orbit (GEO).

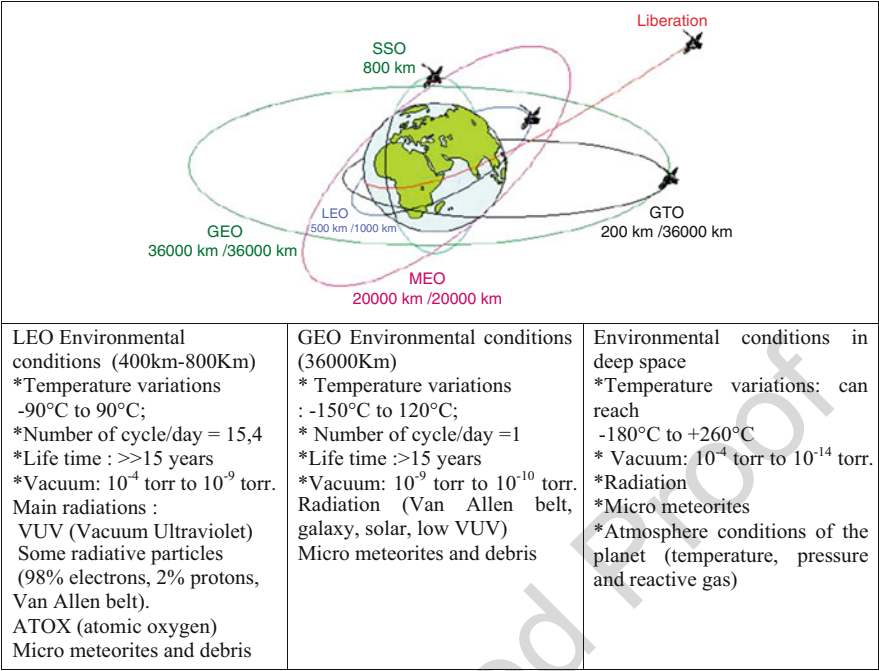


**Fig. 1** Overview of the environment conditions met by satellites in space

For the LEO applications, further issues regarding the external surface exposed to space are to be taken into consideration like atomic oxygen flux (ATOX) combined with solar ultraviolet radiation (UV), ions' radiation, and various high-energy photonic exposure like gamma rays and micrometeoroids and dust collisions.

The GEO satellites are mostly telecom orbits. In this case, the external equipment is subjected to a thermal environment depending on the Sun exposure, under a secondary vacuum for 15 years. The main source of radiation to consider is from the ultraviolet. Thermal cycling and radiation exposure met during long missions are the main mechanisms responsible of the aging of the structures.

The space telescopes, due to their high thermal stability requirements, are confined in chambers. The Herschel and Planck telescopes built under the responsibility of Thales Alenia Space operate between 1.2 and 1.8 billion kilometers (L2 Lagrange point). The Herschel SiC mirror, the highest ever placed into orbit, and the composite Planck mirror, designed and manufactured by Airbus Satellites, operate at -250 °C.

As one can see, there are two families of constraints with which the bonding will have to deal successively: the constraints due to the launch, mainly static and dynamic, over a short period of time, and the constraints due to the space environment over a long period of time, mainly thermomechanical. Aging due to the thermal-mechanical stresses, mismatches between adhesive and adherents, metallic or composite, especially in extreme temperature variations, is the prime concern compared to mechanical fatigue.

If the spacecraft is manned, flammability in microgravity conditions, offgassing, and toxicity are added requirements as for simple aircrafts.

45.2.3 Where Are the Adhesive Bonds?

Launchers

Structural adhesive bonds are defined as any rupture of the adhesive bond will cause significant damage of the mechanical part and hence the loss of the mission.

Thermal protections and thermal insulations are bonded to the structural parts which are made of metal or composite materials (see Fig. 2).

External thermal protections of the stages are used depending on the design of the launcher and the aerothermal conditions. Because of their low thermal conductivity, structures made of composite materials must be protected against high thermal flux met during the flight.

Thermal protection is required when the launcher is powered with solid boosters. Compared to liquid propulsion, solid propellant cannot be used to cool down the hottest part of the nozzle. The thermal protection is achieved with ablative materials

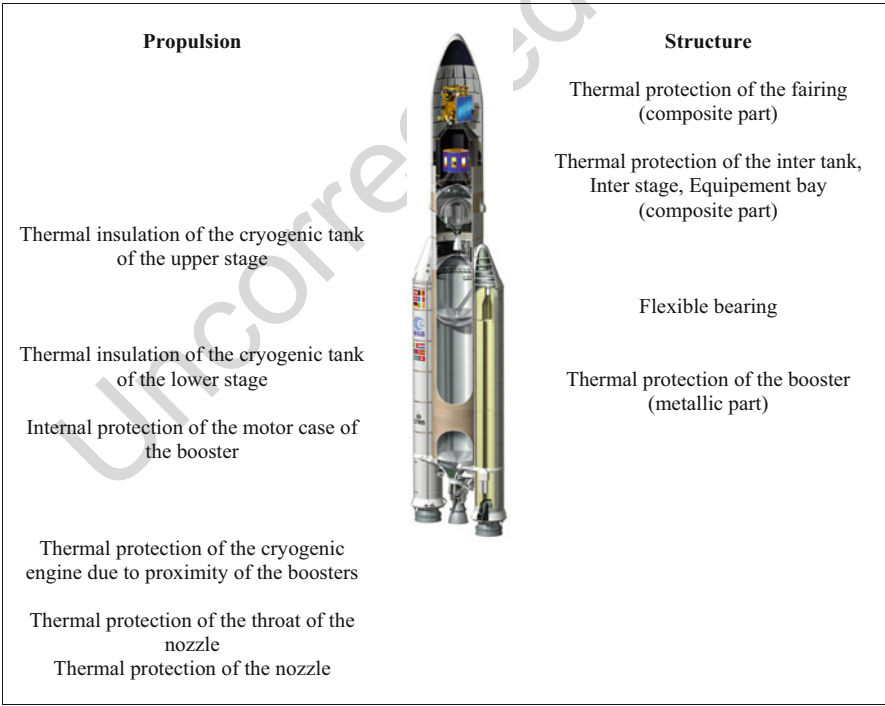


**Fig. 2** Ariane 5 launcher artist's view – main thermal protection and structural bonding locations (ASL)

which are bonded onto the structural parts. For all these cases, thermal protection systems do not sustain general mechanical loads but only thermal loads.

The design of adhesive bonds must take into account thermal gradients and thermal expansion mismatches with the structural part which is in general metallic.

A detailed description of the nozzle design allows to see the complexity of this part due to various material properties mixing composite (carbon/carbon, carbon/phenolic resin, glass/phenolic), elastomers, and metals (see Fig. 3).

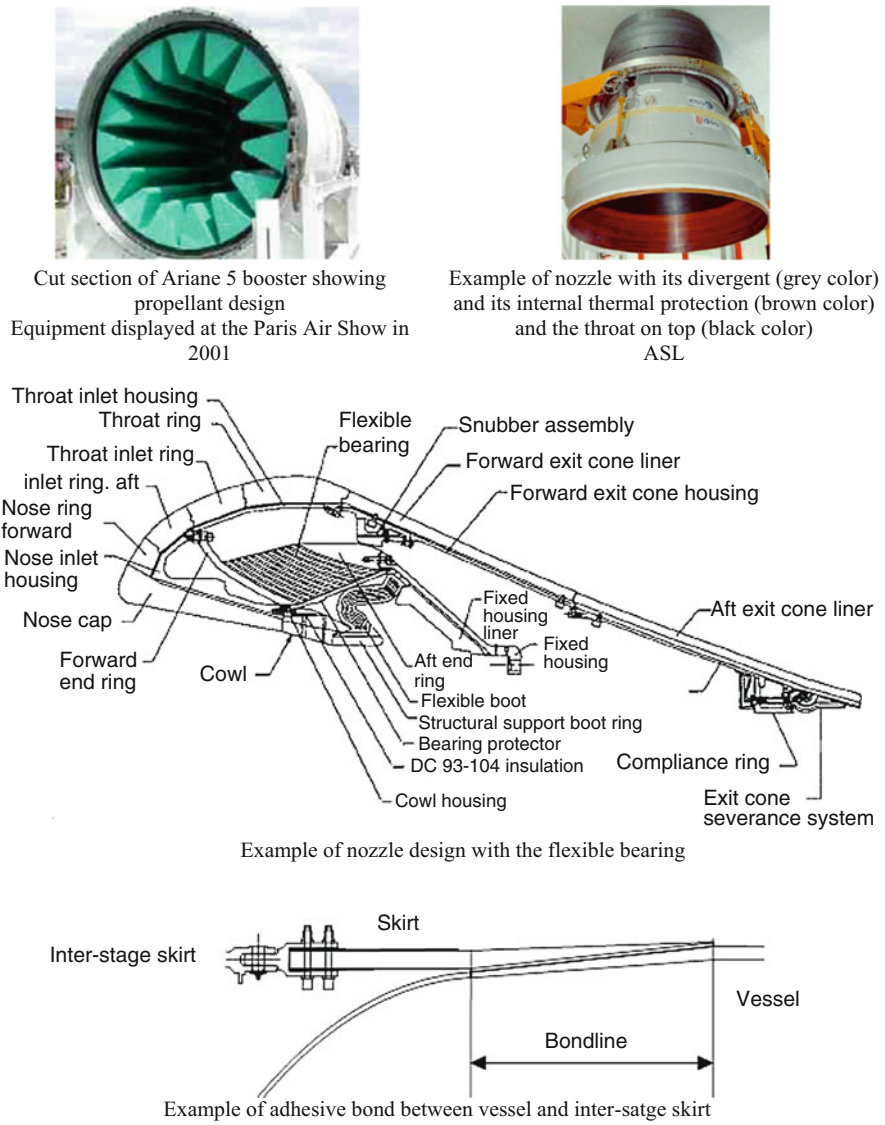


**Fig. 3** Examples of adhesive joint solutions for solid rocket motor

Pushed by the constant need of reducing the upper stage weight in order to launch more payloads, engineers use composite materials and, as much they can, adhesive bonds.

The first example is the sandwich structure used for the upper part of Ariane 5 launcher. The sandwich is made of two composite skins glued on an aluminum honeycomb core. This structure provides the best compromise lightweight/rigidity, and it is one of the best solutions to cope with buckling requirement which is very critical for slim structures.

Adhesive bond solutions can be chosen to assemble two composite panels and to make a junction between an aluminum ring and a composite structure. An alternative solution of designing composite structures to be buckling resistant is to reinforce the structural part with bonded stiffeners (Collier et al. 2010) as used in aircraft fuselage (see Fig. 4).

A good example of an optimized structure which uses adhesive bonds is the composite structure used in Ariane 5 to launch two heavy satellites (dual launch); named SYLDA (see Fig. 5). SYLDA is manufactured by Airbus Safran Launchers (ASL).

**Satellite**

Satellite design is mainly governed by minimization of the weight of its skeleton structure for the benefice of telecom equipment or scientific devices. Two other stringent requirements are taken into account by satellite designers, the management of thermal exchange and the electrical “exchange.” The satellite is built with a central tube from which platforms for equipment, antenna reflectors, and solar panels are attached. The propulsion requires a high pressure tank located inside the central tube.

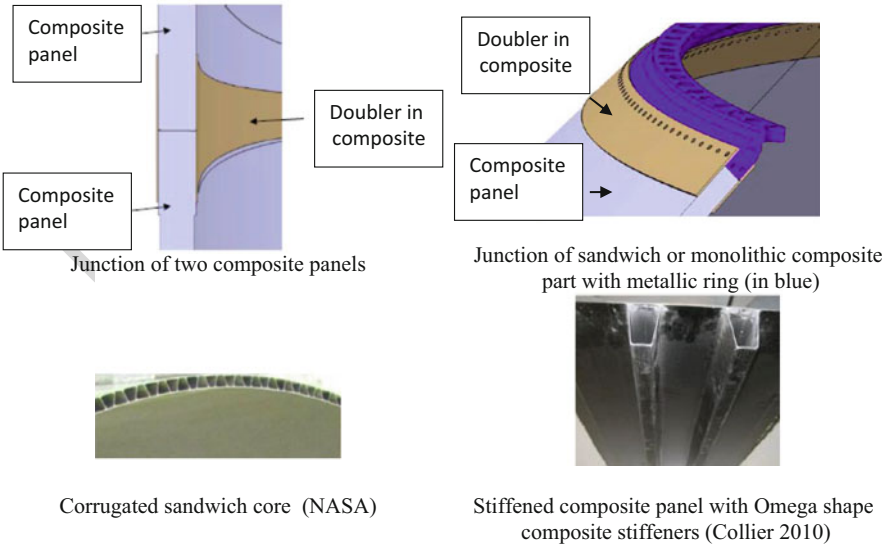


**Fig. 4** Examples of adhesive bonds for structural parts of launcher

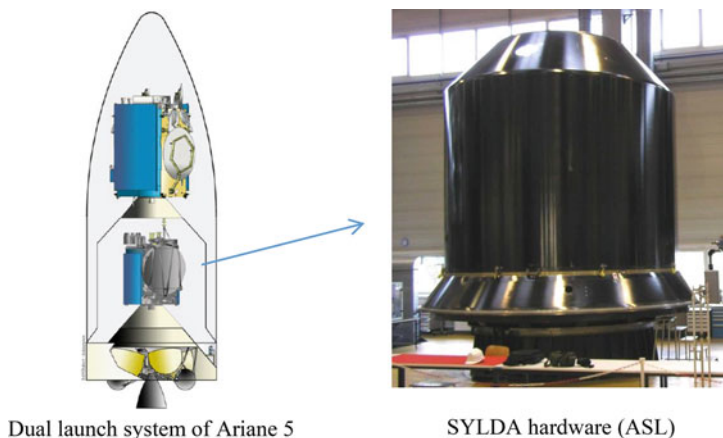


**Fig. 5** View of SYLDA structure (height, 4.6–6.4 m) made in sandwich with carbon fiber-reinforced plastic designed with adhesive bonds

All these structures are made of composite materials which provide lightness, stiffness, and thermal stability. Metal or ceramic parts are glued on composite materials (see Fig. 6). Junctions with bolts are used for assembling electronic equipment and mechanisms of jettisoning with constraints (dismounting requirements).

The central tube is actually the vertebral column made of sandwich using high performance carbon fiber.

The equipment platform made of a sandwich structure is linked to the tube via struts also made in composite. The parts are bonded with bolts via metallic interfaces. When the strut is designed with metallic straps, an adhesive bond with a composite part is used.

The design of reflectors is driven by high thermal stability requirements. These requirements can be fulfilled by using composite materials with specific carbon fiber and lay-up sequences. All the parts are stuck together (see Fig. 6).

Solar panels are made of composite frames where all the solar cells are glued on it.

Mirrors or optical systems can be glued on their stands. Very large mirrors like Herschel's mirror (diameter of 3.5 m) made of silicon carbide cannot be manufactured in one piece. The retained solution was not to use glue to assemble the eight petals but brazing because of its better resistance to dynamic loads during the launch and radiation in its space life.

#### 45.2.4 Which Adhesives for What?

For the most part, adhesives are formulated in order to offer behavioral properties related to those of the composite and metal substrates, regarding the fluctuating and extreme stresses flowing between the adherend and the adhesive, both having to work together.



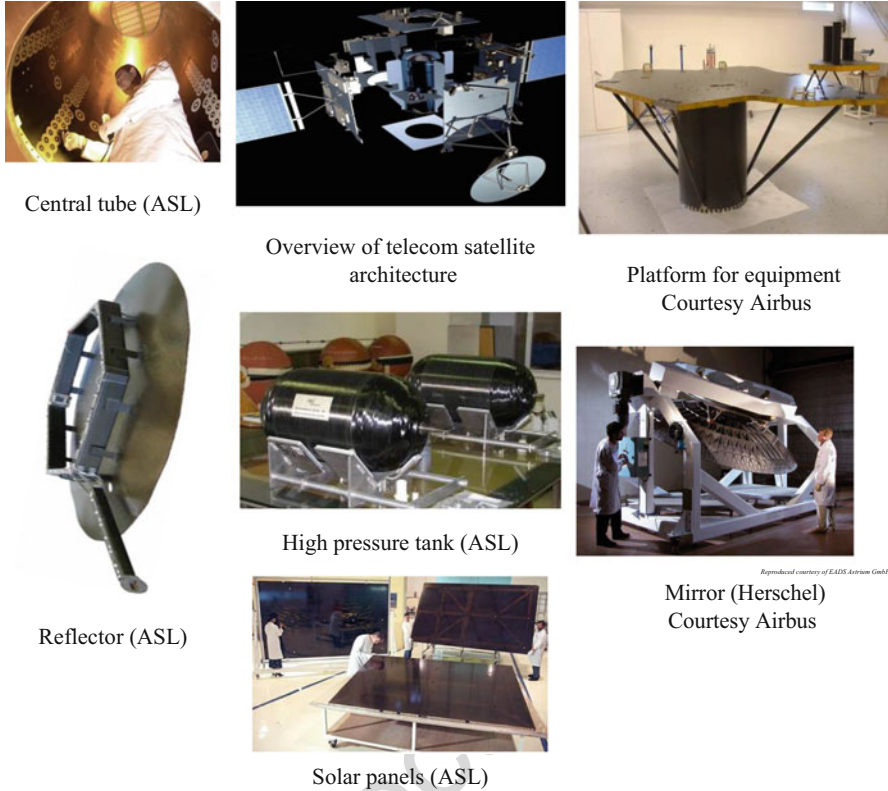


**Fig. 6** Satellite exploded view – various cases of structural bonding on all the parts displayed

## General Design for Launchers

The structures using composites such as interstage, intertank, equipment bay, and fairing are submitted to static, dynamic (vibration, acoustic, shock), and thermal loads. Pushed by the competition with metallic solutions, designers try to use as much as possible aeronautics composite materials. The aeronautical industry uses pre-impregnated epoxy resins. Because of their limited temperature resistance, composite parts submitted to thermal aerodynamic fluxes are protected. One of the solutions is to glue thermal protection panels with silicone or epoxy-based adhesives (see Fig. 7a). But this efficient method is expensive and a projection process is preferred (see Fig. 7b). However, all the thermal protection cannot be sprayed.

The spray process can be easily automatized with robot assistance and does not need adhesive since only a surface preparation or a primer is required.

The same approach is followed with the thermal insulation of the cryogenic tanks (see Fig. 7c). Cryogenic insulation could be done by gluing foam panels on the aluminum alloy tank or by spraying the foam.

Manufacturing of composite sandwich structures can be done with a two-step process. Preliminary cured skins are glued with a honeycomb core. In order to reduce





a) Thermal protection of interstage with cork panel

Courtesy of Airbus Defence and Space Systems  
Spain



b) Example of sprayed thermal protection (ASL)



c) Ariane 5 cryogenic tank –thermal insulation bonding (CRYOSPACE image)

**Fig. 7** Example of thermal protection of the structural parts of the launcher

cost, the structure can be done in one step usually called co-curing process. In this case the skins are cured together with the core with or without an epoxy adhesive film in between.

Again when composite structures are made with a skin reinforced with stiffeners, both solutions are also used depending on the complexity of the part. In case of co-curing process, stiffeners made of resin pre-impregnated carbon fiber are pre-shaped, sometimes semi-cured and laid down on the mold. The second step consists in making the skin with same process of pre-impregnated deposition. At the end, both skins and stiffeners are cured together. In general an epoxy adhesive film is used.

The transmission of the loads between composite structures is generally done with an aluminum interface. The rationale comes from the separation requirements of the different structures of the launcher during its flight. The junction of the metallic interface with the composite could be done with two composite or aluminum splices bolted or glued together.

Because of the toroidal moments generated at the interface of each stage, designers are reluctant to use adhesive joint solutions to transmit the loads. The

performance of adhesion is driven by shear, and peeling effects due to bending must be avoided.

In some cases, adhesive solutions are selected as illustrated by SYLDA design (see Fig. 5). Drilling holes in composite structures leads systematically to local reinforcement of the structure, and when weight optimization is searched, adhesive bonding is one of the solutions especially for the structures located in the upper part of the launcher close to the satellites where the ratio weight/performance is 1/1.

Solid propulsion uses a lot of adhesive bonds:

- The first case is one of the most critical interfaces between propellant and internal thermal protection. Both are complex materials and the mechanisms of adhesion are not simple to solve. This interface called liner is generally formulated by the manufacturer of the propellant who has also a great knowledge of the composition of the thermal insulation, generally an elastomer (EPDM, NBR, etc.)-based material reinforced with fillers and sometimes with chopped fibers.
- The second one is the interface between the protection and the vessel which can be metallic (e.g., steel for Ariane 5) or composite (e.g., Vega). Specific adhesives are also required to be compatible with the elastomer and epoxy resin used in the composite. Adhesives formulated with phenolic resins are generally efficient.
- The third one concerns the composite motor case design. The composite vessel is bonded to the composite skirts via a compliant material, the role of which is to adapt the deformation mismatch of the two structures (mainly hoop strain of the vessel and the longitudinal strain of the skirt). The junction of the composite structures with the compliant material is done with an epoxy adhesive. The nozzle design requires proofed adhesive joints because of the harsh thermal environment. All the pieces such as the throat made on carbon-carbon composite and the divergent made of carbon and or glass fiber-reinforced phenolic resin are glued to metallic parts. Epoxy-based adhesives are generally used.

The last example can be illustrated by the flexible bearing. This a laminate made with elastomer reinforced with sheets of metal or composite. All the elements are glued together.

Flexible bearings are used for the steering nozzle. This concept can be also used for the load transmission from the booster to the cryogenic tank (A5 concept) with a specific function of filtering vibration and then participating in the payload comfort.

One can summarize that launchers which are designed with composite structures use adhesive solutions when no alternative solution is available as seen for the motor case with its nozzle for solid propulsion or when significant advantage in weight reduction is gained compared to bolted or riveted solutions.

Adhesives such as epoxy, phenolic, and silicone-based products are usually provided by different suppliers (3M, SOLVAY, STRUCTIL, HUNSTMAN, LORD, DOW, etc.). Some adhesives could need a specific formulation to meet the required thermomechanical performance or to be adapted to specific processes. This last point is crucial because adhesive suppliers are reluctant to develop specific adhesives for a narrow or niche market (complex formulation and low volume).

## General Design Purposes for Satellites

Satellite designers use a lot of solutions based on adhesive bonds. Adhesive bonds allow:

- To save weight
- To easily assemble tiny pieces
- To not degrade composite structures
- To improve vibration damping
- To cope with tightness requirement
- To avoid electrochemical coupling effect
- To link different types of materials which have significant different thermal expansion coefficients

Sandwich structures are manufactured with standard processes or with co-curing process in the same manner than sandwich structures for launchers. But we can highlight that high modulus (polyacrylonitrile based) or very high modulus (pitch based) carbon fibers are preferred to increase the rigidity and the thermal stability. For electrical constraints, aluminum skin is used to manufacture sandwich panels.

The central tube of more than 5 m height can have more than 100 interfaces. A lot of internal (propellant tanks junction) and external (communication modules webs, Earth panel) metallic inserts (aluminum, titanium, invar, etc.) are glued with epoxy-based adhesives (see Fig. 8a, b).

Aluminum inserts, frames, and titanium telecom reflector parts are bonded by bicomponent epoxy adhesives that cure at room temperature (see Fig. 8c, d).

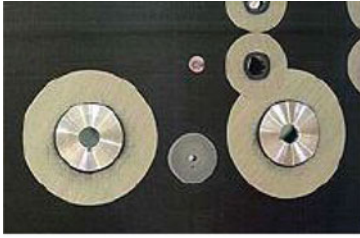
Control of heat exchanges inside the satellite is crucial to provide thermal stability of the optical instruments and electronic devices. The internal temperature is around 25 °C, and the external temperature can vary from –100 to 100 °C depending on the mission, the orbit. The conditions of the environment with respect to the orbits are reported in Fig. 1.

Heat exchanges with the environment being only by solar radiation, the structure of the satellite is protected with solutions providing the appropriate thermo-optical properties (multilayer insulation system, paintings, etc.). Optical surface reflectors are small pieces glued on the surface exposed to solar radiation.

The list of adhesives which can sustain the harsh environment met in space is limited, and silicone-based adhesives are often selected because of their stability at high temperature (up to +250 °C) and are easy to handle. For instance, solar panels are glued on the substrate with a silicone-based adhesive.

But silicone is not selected to stick mirror because of contaminant risk.

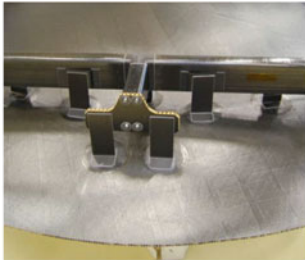
Reentry vehicles are designed with a front shield able to sustain the high aerothermal fluxes met during the high speed flight in the atmosphere of the planet (Mars, Venus, Saturn's satellite Titan, etc.). Ablative thermal protection is usually used and the tiles are glued on the structural part. Epoxy adhesives and room temperature vulcanized adhesives are commonly used. For instance, a space-grade silicone-based adhesive has been used with success for various spacecrafts



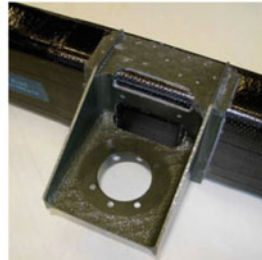
a) Aluminum insert embedded in sandwich panel (ASL)



b) Wedges glued on sandwich panel (Courtesy Airbus Satellite)



c) Rear reflector face bonded to composite monolithic backing structure (ASL)



d) Titanium alloy ASL reflector antenna fitting after surface treatment and bonding

**Fig. 8** Example of assemblies with adhesive bonds

developed by Airbus Safran Launchers such as Beagle and ExoMars for Mars exploration and Huygens for Titan exploration (see Fig. 9). The same adhesive was used for bonding and also for sealing the junction lines between panels or tiles.

This adhesive choice is driven by a complex dynamic distribution of the thermal flux with regard to the time against the deviation of the thermal insulation properties.

The choice of room temperature vulcanized silicone has more to do with the thermal resistance of that particular adhesive family than shear strength. In such an application, a minimum of 0.5-MPa-out-of-plane resistance is currently specified. In applications at such high temperatures, the choice of a silicone adhesive combines the mechanical resistance with a thermal insulation. No toughening properties are required since there is no creeping against the mechanical load.

Engineers in charge of the selection of adhesives must be aware of the contaminant risk which is a major source of satellite failure:

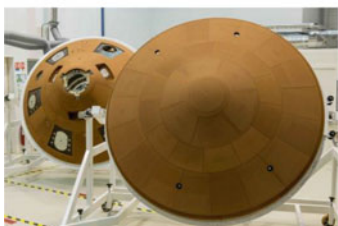
- Weakening of the performance of the optical system
- Damage of the electronic equipment due to electrostatic discharges
- Weakening of the electrical production of the solar panels
- Modification of the thermo-optical properties (emissivity, absorption, etc.)



Bonding of cork tile on Beagle 2 front shield  
(ASL)



Beagle 2 heat shield assembly  
(ASL)



Exo Mars front shield  
(ASL)



Huygens front shield  
2.7 m in diameter, 60 half-angle conic  
spherical tiles  
(ASL)

**Fig. 9** Examples of reentry vehicle design with ablative front shield

413 On can summarize that different types of adhesives are used depending on the  
414 following applications:

- 415 – Load transmission
- 416 – Thermal continuity
- 417 – Electrical continuity
- 418 – Optical compatibility

419 For long mission in space, organic materials must be protected against the  
420 radiation. This is the reason why an aluminized blanket covered the thermal shield  
421 of Huygens during the 7-year journey through the solar system via Venus, Earth, and  
422 Jupiter up to Saturn and during the 22 days of ballistic phase between the jettisoning  
423 of the Cassini orbiter. Cassini spacecraft was launched from Earth on October  
424 15, 1997; Huygens landed on Titan on January 14, 2005.

425 Keep in mind that while anything can be bonded with anything else, there is no  
426 universal adhesive despite the slogan for space applications: the main driver is the  
427 temperature of the joint. This means a selection of adhesive which is compatible of  
428 the thermal expansion mismatch between the adherends.

429 Films or pastes are selected according to the environmental specifications to  
430 which they are subjected, as already said (mechanical and thermal), with respect to  
431 the design of the parts and the implementation of the bonding assemblies. For  
432 instance, the dimension of the part, especially if the parts are at the scale of the

launcher, 5.4 m in diameter, can dictate the process, i.e., the choice of a room temperature adhesive, for economic reasons (there is always an economical aspect in bonding to be taken into account): this prevents investing in an autoclave which a hot temperature adhesive would require. But this investment can appear as mandatory for technical reasons; one can understand that for the most parts, the higher the curing temperature, the higher the thermal resistance.

### 45.2.5 What Are the Adhesive Selection Drivers?

As one has seen, adhesives for space applications are designed to withstand loads of mechanical origins during launch and from thermal origin in orbit, while the fitted parts have to deal with different thermomechanical loads.

Bonding is a dedicated process to assemble dissimilar components and requires a rigorous approach to selection according to its properties, not only chemical but also physical, such as viscosity, in order to deliver the controlled thickness of the joint during implementation and restrain the creeping during polymerization. Aside from that, the bonding line control means to point out, at least in practice for a two-component room temperature (RT) paste, (1) the ratio of the mixing, (2) its homogeneity, (3) the pot life of the mixing at RT, (4) the pressure for full intimacy during the hardening, and (5) the minimum waiting time for hardening before handling, all these precautions observed and carried out under regulated temperature and hygroscopic conditions. To give a preliminary example, it is not rare that one has to bond a low CTE titanium part to a high CTE two-part epoxy adhesive. The issue that the design office and the material and process experts have to deal with is to guarantee a cohesive failure at the predicted margin level.

### 45.2.6 And the Adhesive Tapes?

The space industry makes extensive use of adhesive tapes. The major formulator companies propose such space-grade tapes as Kapton, Tedlar, and Teflon, polyester or foam coated with various very high bonding capabilities, sensitive to pressure. Kapton tape is the most appreciated with respect to the high temperature resistance of Kapton, intensively used as dielectric insulator of solar cell panels. The Kapton tape is associated with acrylic or fully reticulated silicone adhesives: outgassing is the driving factor for the choice of the adhesive part of the tape, the unwanted event being the bubbling between the tape and the adherends under vacuum. Acrylic foam is also widely used in association with Velcro fastening. The Velcro fasteners, nylon based and easy to manage, were bonded 10 years ago with space-grade silicone (Dow Corning 93500). Its high release properties led to implement the silicone at the end of all epoxy bondings. Occasionally, with respect to the manufacturing flow chart, this was time consuming and required a mandatory dedicated location to insulate the silicone adhesive implementation from other adhesive families, in space and in time. Since Velcro coated with self-adhesive very high bonding acrylic

472 foam is available, it can be easily implemented at anytime and anywhere according  
473 to the breakdown of the integration process by simply pressing it on by hand.

---

## 474 **45.3 Material and Process Characterization**

### 475 **45.3.1 Structural Bonding or Not?**

476 Roughly, two kinds of bonding can be identified:

- 477 – Structural bonding where high mechanical and thermal loads are required,  
478 designed by the strength of cohesive failure of the adhesive or the adherends
- 479 – Bonding subjected to loads where the properties of the adhesive far exceed the  
480 requirements of the adherend assembly whatever the strength to failure, in the  
481 adherends and in the adhesive

482 Whatever the definition might be, for space applications, the loads taken into  
483 account for the design are those calculated, increased by the margin factor for the  
484 considered application, and the cohesive failure mode (in the adhesive or in the  
485 adherends) will be the mode expected.

486 As a result, one will admit that bonding shall be referred to as “structural”  
487 when the bonded joint is designed with respect to the safety policy margins,  
488 the higher the residual allowance, the better the design. In other words, it  
489 means that, most of the time, the adhesive joint should have high thermo-  
490 mechanical properties often approaching the ultimate ones in the interests of  
491 optimization, i.e., mass saving, the higher residual allowance being not far  
492 from the ultimate.

493 Considering metal to metal bonding (aluminum alloy, titanium alloy, stain-  
494 less steel, Invar), composite to metal (carbon, glass, aramid fiber-reinforced  
495 resin, epoxy or cyanate based), and composite to composite, the adhesion level  
496 will depend on the ability of the adhesive and the surface adherend preparation  
497 to sustain the combination of various mode stresses (3D static, dynamic) with  
498 loads displayed in peeling, cantilever, and pull-out configurations, rarely  
499 according to a pure shear strength to which the adhesives are dedicated: there  
500 lies the challenge.

### 501 **45.3.2 What Specific Properties Do Space Applications Call for?**

502 Before implementation in space equipment, adhesives are subjected to extensive  
503 characterization, from the elementary state according to standard tests and in context  
504 through representative working configurations, in terms of geometry and adherends,  
505 for validation and finally tested at the real scale for qualification, all properties  
506 having to comply with the specifications according to the predicted space environ-  
507 ment enhanced by security margin company policy.

Selection and validation of adhesives are based on their intrinsic properties which must be compatible with engineering and manufacturing process requirements (ECSS-Q-70-71A rev 1). Therefore, the following parameters are generally determined:

- Pot life ASTM D-2471
- Viscosity (key parameter for processing which is sensitive to environmental conditions: temperature, humidity); ASTM D 1824
- Thixotropy (property required when adhesive deposition is handmade)
- Gel time (determination of time of adhesive processing before it reaches solid state, interaction with tooling and pressure application)
- Degree of curing (compatibility with the manufacturing process of the hardware, sensitivity to stoichiometric deviation in case of combining multiparts)

The key properties of adhesives for space environment are:

- Glass transition temperature (T<sub>g</sub>): ASTM D-3418
- Outgassing

This test expresses collected volatile condensed matter (% CVCM), total mass loss (% TML), and recovered mass loss (% RML) according to ECSS Q-70-02A. This test is performed in vacuum with or without thermal cycling. ECSS-Q-70-20A specifies 100 cycles. The temperature range covers the application conditions. It could be more than  $-150$  to  $+150$  °C. The adhesive for space qualification does have an amount of RML and TML less than 1% and a CVCM less than 0.1%. These acceptance limits are submitted for derogation depending on the absolute quantity of adhesive implemented:

- Thermal coefficient of expansion (CTE): ASTM D-696
- Moisture ingress: ASTM D-1151 and D-570

It is well known that a plasticization phenomenon occurs in epoxy polymers which affects the overall characteristics such as T<sub>g</sub>.

General mechanical properties of the adhesive (Young's modulus, shear modulus, elongation at break) are obtained by performing:

- Tensile tests (dog bone sample ASTM D-628, EN ISO 527-2 -butt joint; ASTM D2095)
- Shear test (thick adherent shear test ISO 11003-2; double lap joint ASTM D-3528)

Single-lap shear tests (ASTM D-1002, ASTM D-3165, ISO 4557) are very often used because test samples are easy to manufacture and to test.



However, it is well known that stress field in a lap joint is rather complicated and that relationship between failure and true bond strength between adhesive and substrate cannot be determined with confidence. This test is generally used for quality control acceptance of adhesives:

– Shore D Hardness (ASTM D-2240)

In general, the validation of the adhesive is based on several test samples with a minimum of five tests for each type of test, and some of the tests are done for three batches of adhesive to cover the variability of the product.

The validation phase of the adhesive is also linked to the final application. Shear tests are, for instance, tested at different temperatures and for different conditions of curing.

Moreover two additional tests are sometimes performed.

The Arcan test allows combining tension/shear and compression/shear modes. This test is well appropriated to validate failure criteria of the adhesive and to identify plasticity. Due to the complex behavior of the adhesive, this test must be accompanied with simulation being able to take into account plasticity phenomena. Plastic yield behavior depends on both the deviatoric (von Mises) and the hydrostatic pressure. This model allows describing the difference observed when the adhesive is in tension or in compression. Such criterion proposed by Raghava et al. (1973) is rather effective to predict quite well biaxial test results.

More sophisticated models such as those proposed by Drucker and Prager (1952) and Prager (1995) are not yet fully used by design offices. They prefer to deal with conservatism approaches based on experimental test campaigns.

To justify damage tolerance initiated by a lack of adhesive or the presence of porosity, the energy of crack propagation in mode I ( $G_{IC}$ ) is also characterized. Double cantilever beam test (ASTM D-3433, ISO 2009) is the most common test to measure  $G_{IC}$ . This test is not easy to master due to the strong influence of the boundary conditions. Such test can be performed with composite adherends. Best results are obtained with unidirectional composite adherends; otherwise, damage generally occurs between the first and the second ply inside the laminate. In space applications, high modulus carbon fibers are often used to improve the ratio stiffness/density enabling a better performance in buckling. However, due to the lower adhesion properties with epoxy resin compared to composite made with high resistance carbon fiber, the performance in adhesion with very high modulus carbon fiber is often less.

Fracture test on bulk adhesive coupons is not a common test because it is not always possible to manufacture such coupons without microporosity and introducing machining defects.

Other characteristics are determined depending on the application. It could be:

– Electrical resistance:

Composite materials and adhesive joints are not good thermal and electrical conductive materials compared to aluminum alloys. This is one of the drawbacks of composite materials.

Thermal conductivity	Aluminum alloy 150 W/m.°C
	Epoxy resin (0.18–0.20 W/m.°C)
	CFRP 54 W/m.°C in the fiber direction, 1 W/m.°C in the transverse direction
Electrical resistivity	Aluminum alloy: 4.6–4.8 μohm.cm
	Epoxy resin: 1E21–6E21 μohm.cm
	CFRP: 97,100–287,000 μohm.cm in the fiber direction and 210,000–1.58E6 μohm.cm in the transverse direction

Research programs have been launched to improve these properties by adding carbon nanotube fillers. If increasing electrical conductivity has been obtained at laboratory scale, no industrial application has come out.

The solution used by designers to guarantee the continuity of the electric conductivity is to fix metal braids with conductive glue enriched with silver fillers:

- Thermal cycling ECSS-Q70-04
- Offgassing of toxic materials: ECSS-Q70-29
- Flammability: ECSS-Q70-21
- Particle and UV radiation: ECSS-Q70-06

The verification of the adhesive bond is based on several tests performed on samples which have to be representative of conditions applied on the real part. This is the key issue because the statistical analysis of the main nonconformances of adhesive bonds is generated by wrong cleaning or bad surface preparation (particulate and molecular contaminations) and poor adhesive processing (insufficient training of the operator, bad monitoring of the curing process, etc.).

**Tests for Adherence Verification**

The objective of these tests is to verify the adherence level (load or energy to separate the bodies linked together) in different environments met during the whole life of the parts. Several tests generally recommended by space agencies are used by the space industry. ESA publishes numerous ECSS documents elaborated with the industry and laboratories in Europe.

Peel and shear tests are commonly performed and cleavage as well. For sandwich structures, flatwise tensile tests (ASTM C-6297) and edgewise compression tests (ASTM C 364) are usually performed.

For thermal protection glued on the surface (metal or composite), flatwise tensile tests or peeling tests are performed (see Fig. 10).

The adherence verification is based on a test matrix which must be compliant to the justification requirements.

Peeling tests (ASTM D-1781, D-1876, D-3167, D-3933, ISO4578) are very often used at the beginning of the development giving a first qualitative estimation of the adherence. Illustration of a good or a bad adhesion based on the load curve and failure mode is given in Fig. 11. But care must be taken with peeling test definition

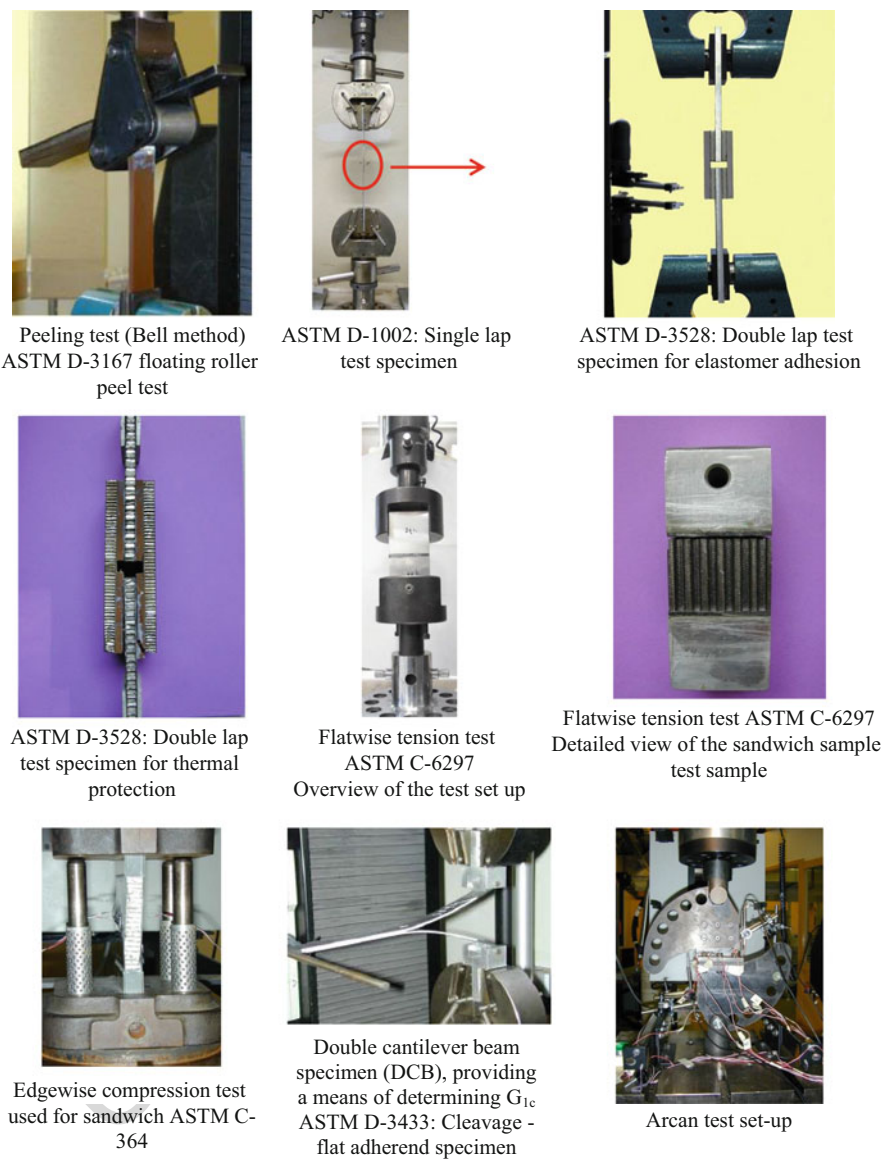
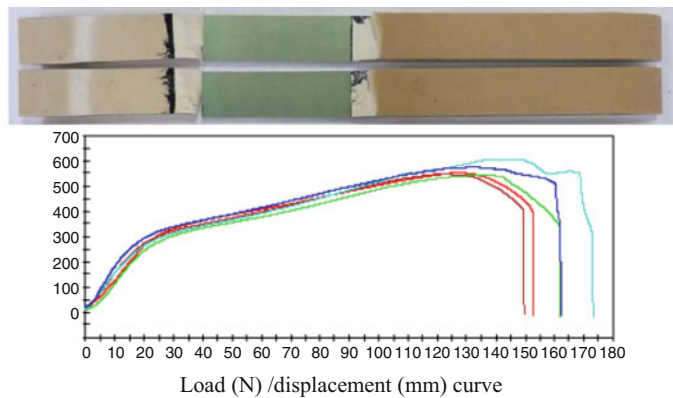


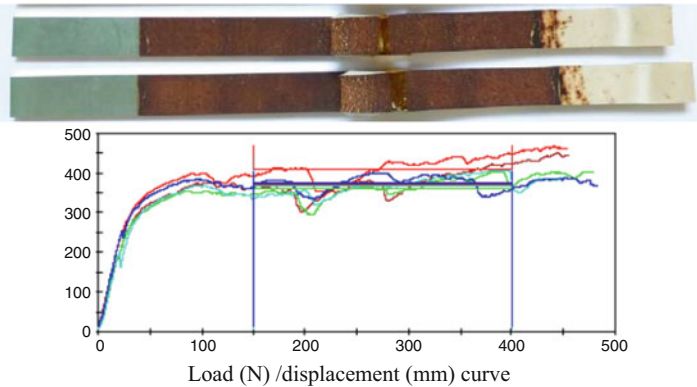
**Fig. 10** Examples of main tests used for adherence measurement

especially when it concerns adherence with elastomers. The peeling test is a geometry-dependent test.

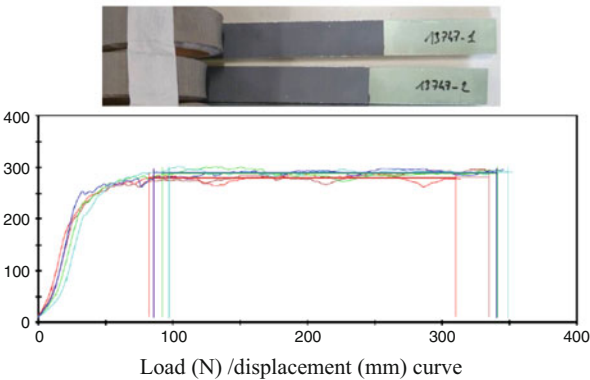
This is the reason why the verification of the adherence is much more reliable when determined with double shear tests and flatwise tensile tests for which cohesive failure is required for both.



Example of good adhesion (rupture of the elastomer without peeling)



Example of good adhesion (rupture inside the adhesive)



Example of bad adhesion (rupture in between the adhesive and the elastomer)

**Fig. 11** Illustration of different peeling behaviors of adherence between metal and elastomer

The environmental effects are taken into account, and the main difficulty is to find out the right method to accelerate aging when performed on ground which is representative of the real life in space environment.

### On Ground

Moisture ingress combined with temperature and mechanical loads is the main contributor of adhesive performance reduction. It is important to highlight that water is not an active factor of aging but rather than a powerful actor to reveal and to enhance defects at the interface or the interphase of adhesive joints.

If accelerated aging is generally performed, natural aging is sometimes considered for specific cases. Aging cycles combining temperature and moisture are determined via Arrhenius's law. Care must be taken to choose adhesives from which moisture ingress is reversible (Fickian diffusion) in order to avoid any damage of the molecular chains, especially at the interface with the adherends.

The effects of moisture ingress are threefold:

- Plasticization of the adhesive and adherends in some cases. This affects the mechanical properties ( $T_g$ , for instance) and modifies internal stress distributions in the joint.
- Hygroscopic expansion which could affect the stress field in the adhesive.
- Weakening the interface/interphase.

The wedge test (ASTM D-3762, ISO 15107) is an effective test to determine the bondline durability as a function of the adherend surface preparation whether it is metal or composite. This test allows discriminating tough adhesives with the environment effect from brittle ones. Though adhesives enable the crack generated by the wedge to grow slowly and stop, for brittle adhesives the crack grows faster running out of the specimen length. The stability of the crack is time dependent with respect to the environment, usually the combination of temperature and humidity (see Fig. 12).

Durability tests performed by Popineau (2015) on composite/aluminum adhesive joint have revealed the mode of failure changed during aging. Cohesive rupture observed in the adhesive in the initial state became adhesive with a rupture at the interface adhesive/aluminum. This test shows that care has to be taken with hybrid joints where the mechanism of osmotic pressure can be responsible for the performance reduction of the adhesive joint.

### In Space

For satellite design, the following environmental factors are systematically taken into account:

- Vacuum (outgassing)
- Thermal cycling
- Electromagnetic radiation (UV, X, g)
- Particles (electron, proton)

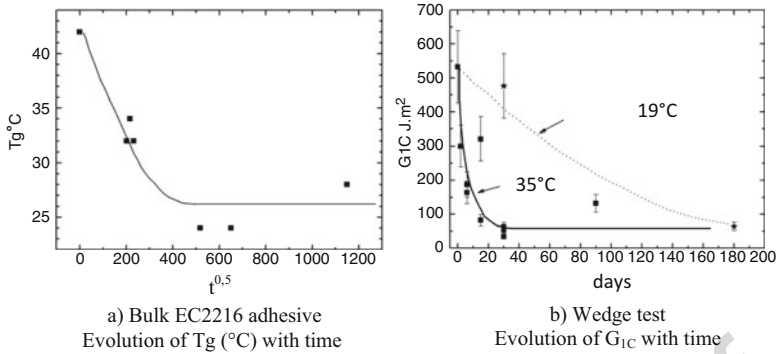


**Fig. 12** Effect of moisture with time (a) Tg evolution with EC2216 adhesive when immersed in water at 35 °C, (b) evolution of energy release rate  $G_{IC}$  of composite/aluminum joints immersed in water at 19 °C and 35 °C (Popineau 2015)

- 672 – Atomic oxygen
- 673 – Micrometeorites

674 For manned spacecraft, two additional tests are required:  
675 Offgassing represents the substances liberated by materials in microgravity that  
676 are harmful to the crew. Offgassing has to be avoided (ECSS-Q-70-29).  
677 The flammability test measures the capability with which a material is set on fire  
678 (ECSS-Q-70-21, ISO 22538 1-4 dealing with oxygen safety).  
679 For satellites, the main problems to overcome are linked to:

680 (a) Thermal cycling in vacuum

681 The most critical properties (mainly shear properties) are evaluated before and  
682 after thermal cycling according to the aging test agreed upon in the space industry.  
683 ESA specifies standard aging of 100 cycles under  $10^{-5}$  torr vacuum, between  $-100$   
684 and  $+100$  °C with a heating and cooling rate of  $10$  °C/min with a 5 min dwell (ECSS  
685 Q 70 04 A). It is not rare that 2,000 cycles are implemented. The thermal cycling is  
686 subjected to deviations with respect to the particular operational needs. For infor-  
687 mation, this thermal cycling is to bring closer the LEO external equipment typically  
688 subjected to a  $[-90$  °C,  $+90$  °C] temperature range, under  $[10^{-4}$  torr,  $10^{-9}$  torr]  
689 vacuum range, with 16 cycles/day and that of the GEO is exposed to a  $[-150$  °C,  
690  $+120$  °C] temperature range, under  $[10^{-9}$  torr,  $10^{-10}$  torr] vacuum range, with  
691 1 cycle/day. These figures depend on the spacecraft mission, the location of the  
692 equipment on the spacecraft regarding its exposure to the Earth and the Sun, and the  
693 properties of the materials in relation to their thermal balance. So, if the properties of  
694 the materials, i.e., the adhesives, are assessed after thermal cycling, the equipment at  
695 its final stage of manufacturing is also thermally cycled under vacuum. For instance,  
696 the telecom antenna reflectors in GEO are qualified in the  $[-180$  °C,  $+180$  °C]  
697 thermal domain, requirements due to a stabilization of the composite on Earth at the

end of manufacturing (monolithic composite stress relieving, completion of the chemical conversion of the resins and adhesives, complete degassing of all the materials and assemblies).

For the cases of telecom reflectors, the final thermal cycling aims to guarantee a misshaping variation under operational temperatures compliant with the focus control of the radio-frequency signal against the temperature directly exposed to the Sun or completely shadowed by the Earth, ranging with the seasons. In this respect, the thermal load cases for distortion analysis are assessed in order to highlight the most severe cases with respect to the maximum and minimum temperatures on the different parts of the reflector shell. With respect to this, the various cases below are distinguished:

- EQBOL, equinox period at the beginning of reflector's life
- SSEOL, summer solstice at the end of reflector's life
- EQEOL, equinox period at the end of reflector's life
- WSEOL, winter solstice at the end of reflector's life
- OSRBOL, optical surface reflector reflection at the beginning of reflector's life

Depending upon the telecom mission, an EQBOL may correspond to the shell cold case and the maximum gradient, and the OSRBOL may correspond to the shell hot case.

It is impossible to reproduce the space environment for ground testing of space system elements because of the variety and complexity of the environments which can generate more or less degradation of the material.

The reliability of the test results depends on simulating the critical effects of the space environments for a particular mission (ISO 15856 Simulation guidelines for radiation exposure of nonmetallic materials).

Since the International Space Station is available for such experiments, a lot are mounted on board. Among other programs from the USA and Japan, the European Technology Exposure Facility (EuTEF) was mounted outside the station for carrying out experiments that required exposure to space environment for monitoring degradation dynamics in low Earth orbit and acquiring information in terms of contamination, atomic oxygen, ultraviolet and X-ray radiation, micrometeoroids, and debris (see Fig. 13). These international experiments, where the results are shared by the scientific community, increase knowledge and guide the development of new materials (like nanomaterial-based materials). If new materials are to be qualified in real conditions right from the outset, the qualification of large functional parts is not for the near future, and space equipment is still really only declared good for qualification when they start to work well.

(a) The generation of contaminants has a strong effect on:

- Modification of heat exchange by modifying thermal optical (emissivity)
- Thermal and physical properties (influence on thermal coefficient of expansion which could affect thermal stability of the structure)



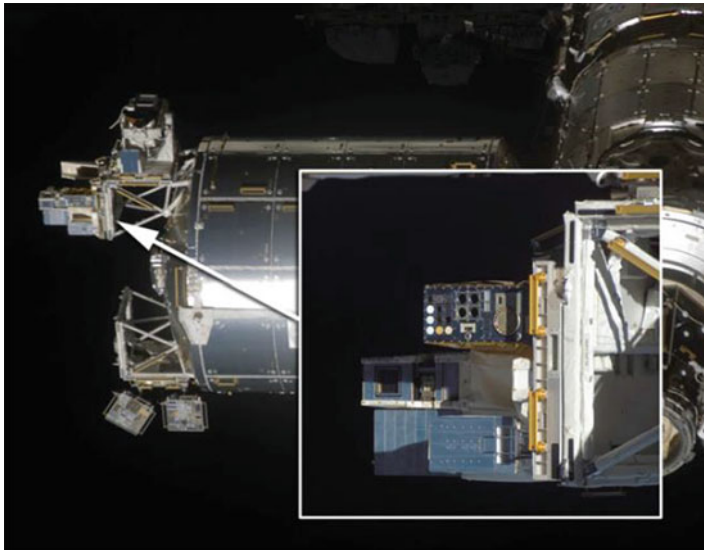


**Fig. 13** European Technology Exposure Facility (EuTEF) mounted on the International Space Station (NASA images)

- Electrical perturbation of the electronic devices (dielectric discharge, perturbation of the measures, etc.)

It is well known that polymers are sensitive to radiation, particles, and atomic oxygen generating micro-cracks, surface modification, and production of contaminants. The effects are limited to the surface with varying penetration depth (few microns for protons, several millimeters for electrons). Ceramic fibers are less sensitive, and composites made with carbon fiber are not much sensitive to ultraviolet radiation. For long-term exposure, composite structures are overwrapped with a protective film. Concerning outgassing which generates contaminants, resins less sensitive to moisture are selected such as the new generation of epoxy resins displaying moisture uptake less than 1% or even less, but for specific missions, cyanate resins with moisture uptake less than 0.2% are selected.

The atomic oxygen test is only performed for materials which operate at low Earth orbits.

For structural applications, the adhesive is usually protected by the adherends. The evolution of the adhesive properties with UV and particle radiations concerns those used for the optical devices or system glued on the surface for thermal control, for instance.

### Tests on Technology Coupons

The process validation of adhesive joints is carried out through demonstrators where the different bonded parts are manufactured to scale 1 and the bonding



implementation defined: surface preparation, adhesive conditioning, film implementation or multipart mixing, tooling assembly under pressure, curing parameters, temperature- and moisture-regulated conditions for room temperature adhesive (typically  $22 \pm 3$  °C,  $50 \pm 10\%$  moisture content), autoclave curing cycle (120 °C or 180 °C in the case of co-bonding process), and inspections before and after bonding. All these methodological steps are to ensure an effective and homogeneous adhesion.

The adherence verification of the adhesive joint is not limited to simple shear or peel tests, but to more complex tests which are representative of the real design, the real manufacturing processes and of course the real surface preparation are needed to reproduce load configurations.

These tests are generally well instrumented in order to validate numerical simulations (see Fig. 14).

Tensile and shear are generally performed for the inserts. Web, wedge, or cleat junctions are tested in tensile, shear, and bending.

Then, comes the qualification of the equipment for delivery to the customer, bonding included, according to the dynamic, acoustic, thermal loads, under nitrogen and vacuum atmosphere, with safety margins.



Reduced scale structure loaded in tension to validate the performance of adhesive skirt / vessel junction (ASL)



Out-of-plane strength to failure test on elementary bonded cleats (ASL)



Bending test on elementary adhesive bond (ASL)

**Fig. 14** Examples of technology test sample able to load adhesive joints in representative conditions

Damage tolerance justification is generally done at subscale level or even with coupons. For adhesive bonds, this consists in including the bondline, defects which are mainly representative of lack of adhesive and of process variation.

**Part Qualification**

The qualification of structures is carried out via scale-one tests generally in static conditions at ambient temperature (in some cases with temperature) with a numerical justification for margin of safety (see Fig. 15). The qualification model is loaded up to rupture.

In the framework of qualification with proto-flight model (approach quite often used for satellites and rather seldom for launchers), the limit load is applied, and the structure must be healthy without any damage at the end of the test campaign. One hundred percent of the structure is then controlled with nondestructive inspection.

**In Production Phase**

Structural adhesive joints are 100% controlled. This could be via nondestructive inspections or via proof tests. In some cases, such as adhesive bonds of thermal



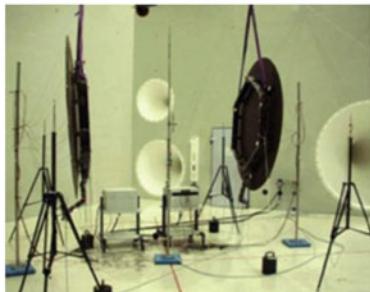
Static test on scale-one motor case to test the adhesive vessel/skirt joint (ASL)



Thermal cycling with or without vacuum of the reflector (ASL)



Dynamic tests of an antenna reflector (ASL)



Acoustic test of an antenna reflector (ASL)

**Fig. 15** Illustration of some tests performed on scale-one structures for qualification

protection, the health of the bond is determined by the control of the parameters which monitor the manufacturing process.

For satellites the acceptance of adhesive bonds is in fact done via series of tests performed on the scale-one part.

The health of adhesive bonds is controlled after thermal cycling tests and dynamic or static tests. For some brittle parts like antenna reflectors, acoustic tests are also performed.

---

## **45.4 Surface Preparation**

### **45.4.1 The Case of Composites**

When faced with a bonding case, there is a motto which should not be forgotten: “The Devil is in the details.” Among all the details, surface preparation is the decisive one. The aim of such a preparation is to remove anti-adhesive contaminants like grease or release agent residues which are in the air of the workshop (aliphatic hydrocarbon) and to promote a chemical–physical roughness deemed favorable to adhesion. Composite preparation is realized by sanding (silicon carbide paper, alumina oxide fabric, grade 240 up to 1,000) and wiping with solvents (acetone, ethanol, isopropanol), now often substituted by wiping with alternative liquids without volatile organic components according to the new REACH (Registration, Evaluation, Authorization and restriction of CHemicals, the new health and safety and environmental regulations enacted by the European Union) regulations. All these operations are performed with disposable talc-free gloves if carried out by hand or via an automated process in the case of extensive surface preparation. It should be stressed that surface preparation by hand depends on the skill of the operator. This is a major issue concerning bonding in the workshop. An alternative solution is to cure composites with a peel ply covering the surface to be glued. Peel ply is removed (tear-off) from the surface before gluing. This solution is very cost-effective and efficient. The main drawback is the risk of leaving on the surface undesirable products (small pieces not detectable and pollution), since the operation is done manually.

Among the reliable surface preparations which can be automated and which are taken into consideration to contribute to the improvement of quality assurance, without material drawbacks, are the low pressure plasma to break organic molecular bonds, laser, and blasting methods. All these automated processes are from now progressively introduced in spacecraft equipment manufacture since they are growing in size.

The automated inspection of the surface preparation also remains an issue.

Several research initiatives have been done investigating several techniques. Among them, a recent program has been carried in the framework of European project called ENCOMB (extended NDT for composite bonding – FP7 – third call). The most representative contaminants met in the workshop have been studied, among them hydraulic fluid, release agent (pollution generated by release film),

834 and moisture (see Table 1). The most pertinent techniques proposed by the labora-  
835 tories involved in the consortium were tested.

836 Automated infrared spectroscopy probe surface analyses are a promising  
837 approach, but aerosol wetting technique (AWT) is more mature and applicable in  
838 the workshop.

839 Up to now, the surface inspection (the adhesiveness through the surface energy  
840 displayed by the chemical–mechanical activation) is checked by the classic and  
841 simple so-called water break test or water drop test: after wetting with an aerosol on  
842 the surface of the composite which has just been prepared for adhesive application,  
843 low surface energy deemed unfavorable for bonding shall translate as separate  
844 droplets of water, whereas high surface energy meaning good surface preparation  
845 shall translate as a continuous film (the reader shall note that the words employed are  
846 qualitative and not quantitative, and verbs are to be understood in the conditional:  
847 because bonding is an art before being a science). This test is not so simple, as it  
848 requires more visual analysis performed by an inspector who can only rely on his  
849 memory (see Fig. 16). Currently, within the framework of a European research  
850 program, Airbus Company is conducting extensive industrial bonding studies.  
851 Among those, a robust and reliable surface monitoring method based on the manned  
852 model has been developed: after spraying water droplets at the range of about  
853 0.1–0.3 mm, the wetting is characterized by the mean droplet size and their distri-  
854 bution. The image is recorded by a camera and analyzed by software. A hot air gun  
855 then dries the surface of the composite, if needed.

856 THz/GHz reflectometry is very sensitive to moisture but this emergent technique  
857 is not yet used in space industry.

858
45.4.2 The Two-Part Epoxy Adhesive

859 It is not necessary to put the importance of the surface preparation and its sensitivity  
860 under the spotlight, especially for composite surfaces. For economic reasons, manual  
861 sanding is still often the way for (1) removing dust and surface decontamination  
862 (aliphatic hydrocarbon, release agent residue contaminants) and (2) chemical

t.1
**Table 1** Main methods investigated in ENCOMB project to detect defects

Method	HF	RA	MO
Laser-induced breakdown spectroscopy	+	+	
X-ray fluorescence spectroscopy	+		
Infrared spectroscopy	+	+	+
Laser scanning vibrometry	+	+	+
THz/GHz reflectometry	+	+	+
Aerosol wetting technique (AWT)	+	+	
Optical stimulated electron emission	+	+	+

t.10
+ Possible detection

*HF* hydraulic fluid/water contamination of CFRP, *RA* release agent (silicone-based) contamination on CFRP surfaces, *MO* moisture uptake in CFRP

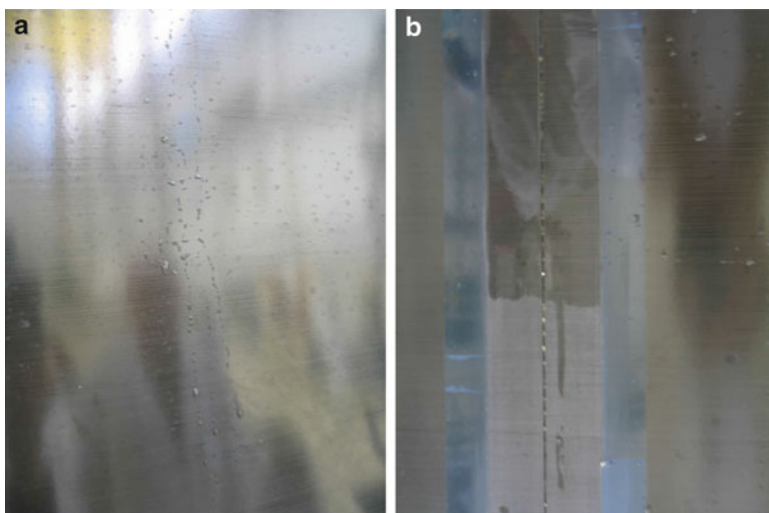


**Fig. 16** Wetting tests on a composite part (discontinuous droplets on (a) side, continuous water film on (b))

activation (electron peeling, micro roughness generation), and everybody knows how sensitive epoxy adhesives are to deviations in the surface composition. These operations will be entrusted to skilled workers.

In the case of two-part room temperature adhesives, the adhesive is applied on the facing sides of the adherends after manual or automated mixing during the open time period of the mixture (45–90 min), and afterward, pressure tools are placed on the assembly for delivering the pressure required for bonding (between 200 and 1,000 hPa).

An illustration is given of a bonding process after such a preparation in the case of the Ariane 5 satellite adaptor (see Fig. 17).

### 45.4.3 The Metallic Parts

The metallic parts on spacecraft are mainly made of aluminum and titanium alloys because they are lightweight. Prior to structural bonding, they are subjected to proven surface standard treatments from the aeronautical sector. Due to the short open time period for bonding after the surface treatment (8–24 h), the metallic parts are often coated with organic primers to postpone their ability to bond and to procure or increase their resistance against corrosion if at risk (atmospheric, galvanic).

The application of a primer raises the same issues as the adhesive, a primer being an adhesive coating, but in this case, two interfaces are to be held in place, the first one between the metal and the primer and the second one between the primer and the adhesive.

In all the cases, because of the great variety of compositions of metal parts, combined with the extensive number of hardening and annealing treatments, there is



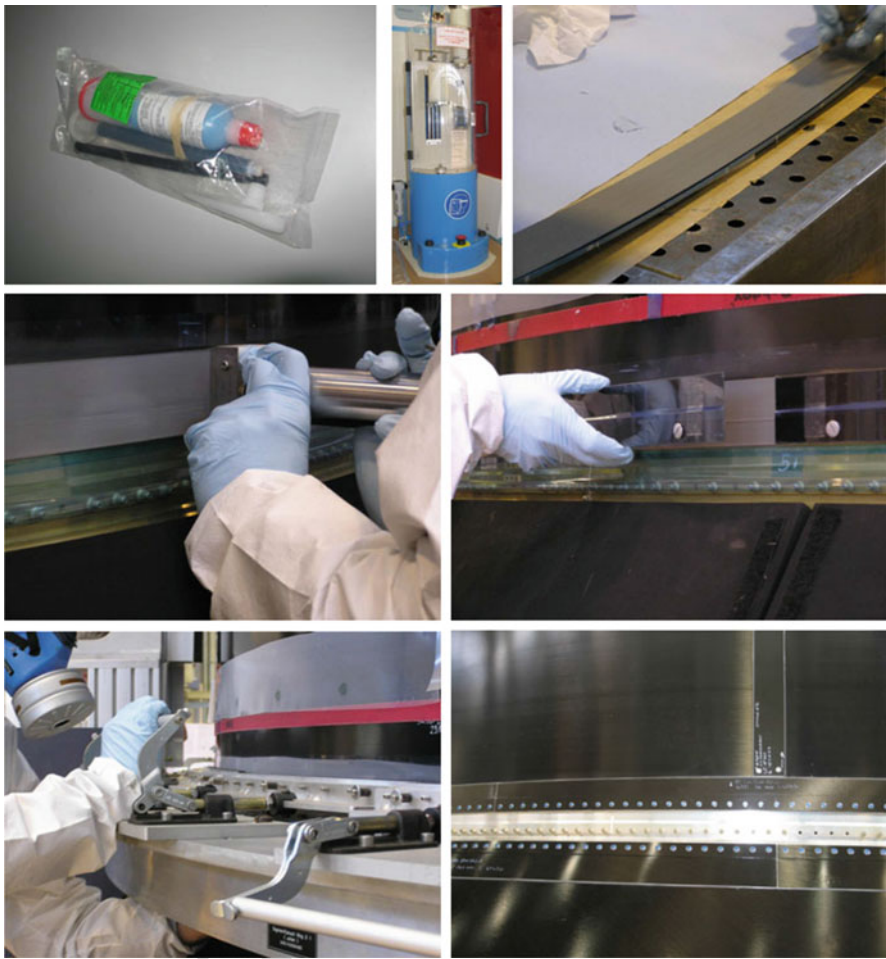


**Fig. 17** Room temperature bonding sequence for composite assembly (from *top* to *bottom*, from *left* to *right*: two-part adhesive tube, mixing device, bond deposit on monolithic composite part, on sandwich part, docking of the two part, pressurization, assembly achieved ready for inspection (ASL))

not “a” standard treatment by alloy family but various possibilities, even if aluminum alloys have historical feedback from experience. However, preliminary tests should be conducted to determine the performance of the bonding in the case in hand.

#### 45.4.4 Aluminum Alloys

The surface preparation of aluminum before fitting, such as painting and bonding, is mandatory because aluminum alloys offer high sensitivity to superficial oxidation with the natural and instantaneous appearance of a brittle aluminum hydroxide coating.

This phenomenon which can be compared to what happened with a highly sensitive photographic film upon exposure to the light is more or less pronounced, depending on the ambient atmospheric conditions, i.e., the temperature and the moisture level. With respect to bonding, the challenge was in producing a compatible and suitable surface for the application of the adhesive prior to bonding operations. The idea was to chemically favor the growth of a stable and hard thin coating of aluminum hydroxide. As a result, two main different pretreatments are used, the first one in the USA based on phosphoric acid anodizing and the second one in Europe, consisting in a sulfochromic acid etching by a chromic acid anodizing (ASTM D-2651-01). For structural bonding, it has been demonstrated that the optimum values are achieved when the anodizing is partially sealed, despite a loss of corrosion protection. See also Part B – Surface treatments for more details on this subject.

Alternate surface preparations are now introduced due to the new REACH regulations prohibiting implementation of listed chemical elements without enhanced health and safety protection and the release into the environment without significant recycling, in particular for the cancer-inducing hexavalent chromium. The chromium substitution was deployed a few years ago in the automotive industry, and the aeronautical industry can benefit from the studies performed following such substitution. Some alternate formulation packs are proposed mainly based on  $\text{Cr}^{3+}$  solutions, and they have been compared via extensive tests with regard to all the requirements for aluminum applications on aircraft. The space industry in turn benefits from these advances, where it appears that there is not only one alternate chemical solution but several, depending on the specific application. For structural bonding cases, the complicated ones are not necessarily the best. Green surface pretreatment qualifications are still in progress.

These alternative Cr6 free solutions are in their final step of qualification and are progressively introduced in surface treatment supply chain. There are new axes of research in order to evaluate new treatment generation totally exempt of heavy metals.

#### 45.4.5 Titanium Alloys

The surface pretreatment for titanium is the well-known nitric hydrofluoric acid etching by a sodium bifluoric solution (ASTM D-2651-01). Some proprietary deviations from this basic treatment are taken by manufacturers. For example, hold release mechanism brackets in titanium alloy (Ti6Al4V) are used for mounting on antenna reflectors as parts of pyrotechnic mechanisms in order to deploy the reflectors in orbit before entering in operation.

---

### 45.5 Nondestructive Inspection

In space industry, high quality of the structures is required because no failure is allowed. The demonstration of the high level of reliability of the structures must be proved either by demonstrating that the process is well mastered (well-known

operation done by certified operators) or by the demonstration of the health of the structure. The second issue can be assessed by performing proof tests or by performing nondestructive controls. In fact, a combination of these three methods is carried out.

If a large panel of techniques is now available based on standard physical principles (perturbation of electromagnetic wave motion, mechanical wave motion, heat wave motion) to control the health of metallic and composite structures, the determination of the health of adhesive bonds is still a challenge. The main sources of difficulties come from:

- No direct access to the joint and the recorded signal can be disturbed by the heterogeneity and anisotropy of the adherends which are also different in nature (composite/metal).
- Complexity of the shape of the piece.
- Contactless method is sometimes needed to avoid any contamination.

If a design to cost approach is followed by designers, design to control is also to be considered to avoid further trouble in nondestructive investigation. This could be illustrated with a simple example showing the detection of local debonding in titanium/CFRP composite joints with pulse-echo ultrasonic mode (see Fig. 18). Control via the titanium adherend is the worse method which could be imposed by the design (no access to the composite part).

In some cases, when overlap of the reflected signals occurs, the diagnosis can be improved, thanks to the numerical simulation of the wave propagation. Simulation can improve the reliability of the diagnosis but also to replace the numerous and costly test samples being manufactured with defects. One can refer to CIVA software able to simulate control with X-ray technique, eddy current, and ultrasounds. Such tool is able to establish the probability of detection curves by simulation.

The main nondestructive methods used in the aerospace industry are:

- Ultrasounds
- Infrared thermography

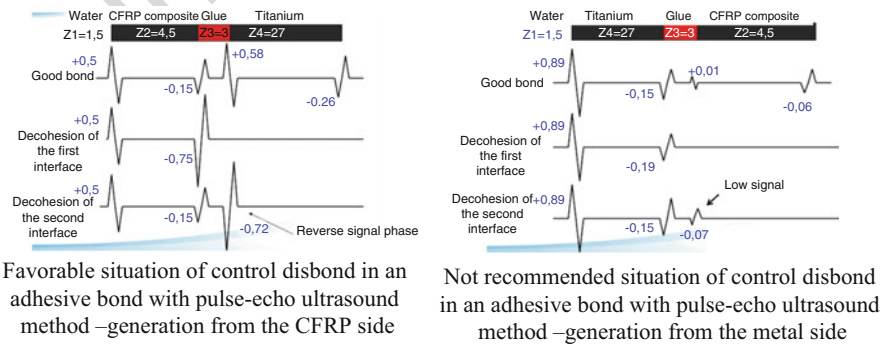


**Fig. 18** Illustration of potential difficulty in defects detection in a hybrid adhesive joint



- 959 – Shearography (interference of coherent electromagnetic waves)
- 960 – X-ray

961 All these methods are able to detect debonding between the adhesive and the  
962 adherends or a lack of adhesive (see Fig. 19). Ultrasound techniques are able to do  
963 more with the detection of porosity and cracks or even a lack of curing of the  
964 adhesive.

965 The defects that can be detected with the infrared response (IR) of the bonded  
966 equipment subjected to heating are lack of adhesive, bubbles, and discontinuities  
967 between the adhesive and the adherends (meaning, for instance, discontinuous  
968 adhesive distribution at the interfaces), air blade between skins to honeycomb  
969 core, or composite to composite or composite to metal bubbles in the joint.

970 The numerous literature sources reviewed recently by Ehrhart et al. (2010) clearly  
971 show no nondestructive industrial methods are available to discriminate a “structural  
972 bond” from a “kissing bond,” even if efforts are continuously done at research level.

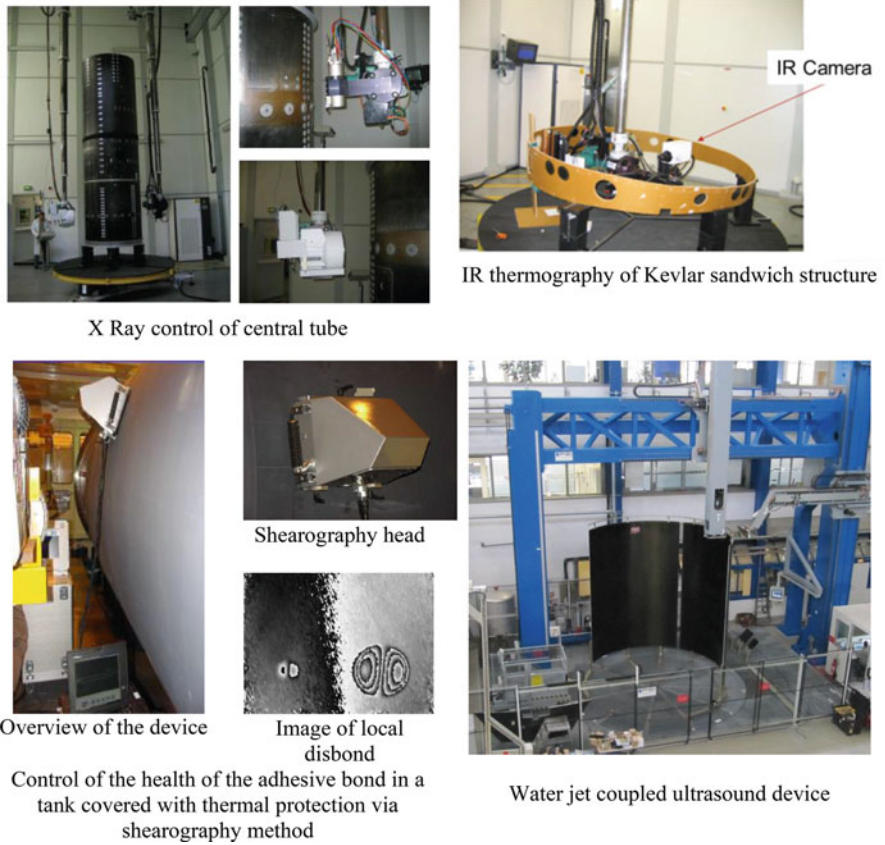


**Fig. 19** Illustration of the principal nondestructive techniques used at ASL

This is the reason why adhesive bond technology is not used so much for high-loaded structures in aeronautic because of the cost to demonstrate robustness and reliability of the adhesive joints. See also ► [Chap. 42, “Nondestructive Testing”](#) for more details on nondestructive testing.

Two principal definitions of kissing bond are met in literature:

- (a) Two surfaces in contact but not bonded
- (b) Smooth bond consisting of two surfaces separated by a thin layer of liquid such as contamination

Finally, kissing bond reflects the cases where the two parts are in intimate contact but with a weak adhesion force.

According to the Ehrhart et al. (2010), ultrasonic alternative methods (US spectroscopy, nonlinear US, guided waves, oblique incidence, shear wave resonance, etc.) as well as laser proof tests (LASAT, LBI, laser ultrasonic) and other methods like shearography and active thermography have high potential for the measurements of adhesive bond strength, thanks to the new generation of sensors which are more sensitive (mK for IR thermography and few nanometer for shearography).

The shearography technique consists of generating a small deformation on the surface of the structure and measuring the out-of-plane deformation (mechanical loading with low depression). This technique is similar to a proof test but performed at low stresses. This fulfilled technique is very relevant to control the health of the adhesion of the thermal protection. This solution is cost-effective, thanks to an automation control with robot.

Recent researches in the detection kissing bonds have been initiated with ultrasound-guided wave pushed by aerospace industry needs. One of the potential solutions is to generate specific guided waves able to capture information provided by the interface/interphase which has in principle a different rigidity than the bulk adhesive. Castaings (2014) and his coworkers have deeply investigated this route, and significant improvements have been achieved, thanks to advanced computation tools which enable better understanding of wave propagation (see Fig. 20). Validation of the models has also been improved with experimental measures based on 3D laser velocimetry. The expected results are not possible without the development of appropriated sensors providing the generation of the desired guided wave at the right range of frequencies and the right level of power.

The research has started with the detection of defects in single-lap shear test samples with no dispersive materials (aluminum plates).

SH0 guided wave mode was generated and detected via Electro Magnetic Acoustic Transducers (EMAT) in 3-mm-thick aluminum plates with a 50 mm overlap in single-lap shear tests (see Fig. 21). Three samples were investigated, each with the aluminum/adhesive interfaces prepared differently (with or without sanded aluminum surfaces) applied, the third was polluted using an oily agent, and the last one the adhesive was a thin glass-epoxy self-supported film. Signals transmitted past the various lap joints revealed good signal-to-noise ratios, good uniformity in the

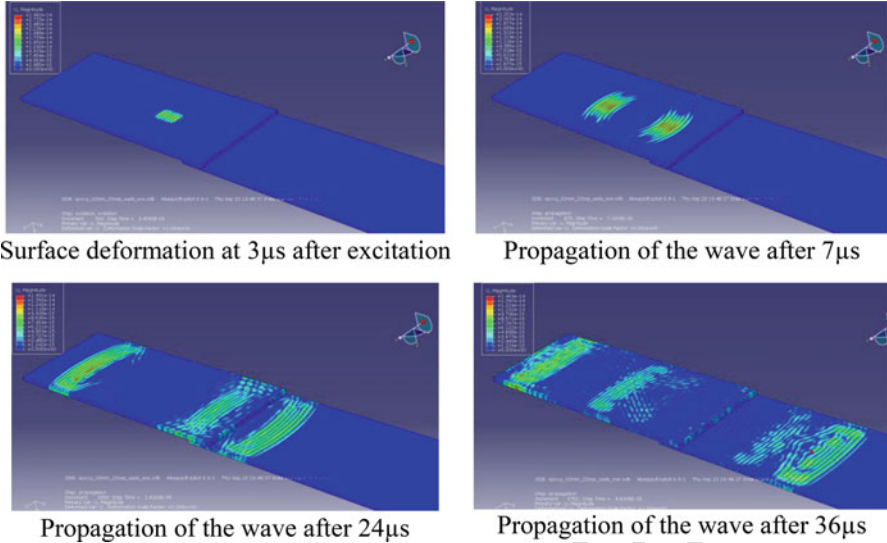


**Fig. 20** Simulation of SH0 wave propagation in single-lap shear test samples: ABAQUS computation

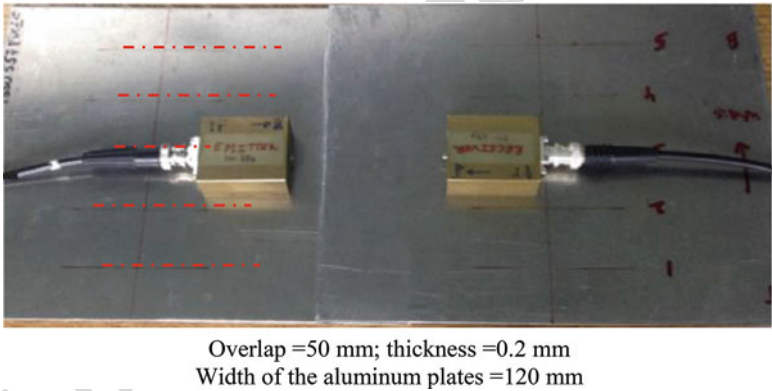


**Fig. 21** EMAT sensors in pulse and catch configuration over the bondline in single-lap shear samples (*dot red line*, different positions of EMAT sensors)

1016 adhesive bonds, and high sensitivity of the investigated transmitted SH0 mode to the  
1017 adhesion quality.

1018 This academic study has shown a good reproducibility of the signals measured for  
1019 five positions of the sensors in the width. Thanks to EMAT sensors development, the  
1020 signals are different with respect to the type of defects. But the shape and the  
1021 amplitudes of the signals are not easy to analyze without the help of simulation  
1022 where the main blocking point is still the quantification of the ultrasound properties  
1023 of the interfaces (see Fig. 22).

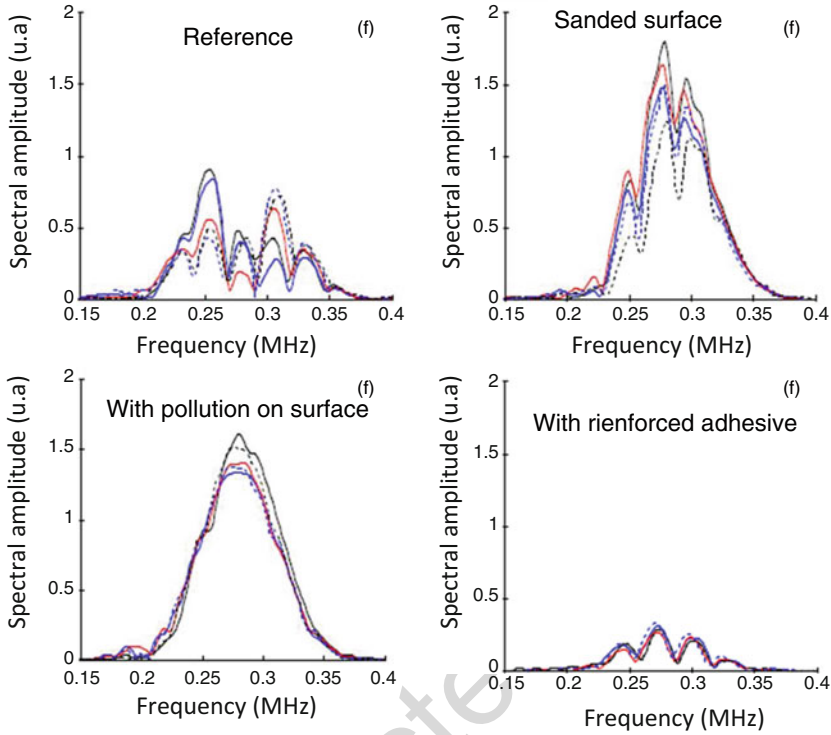


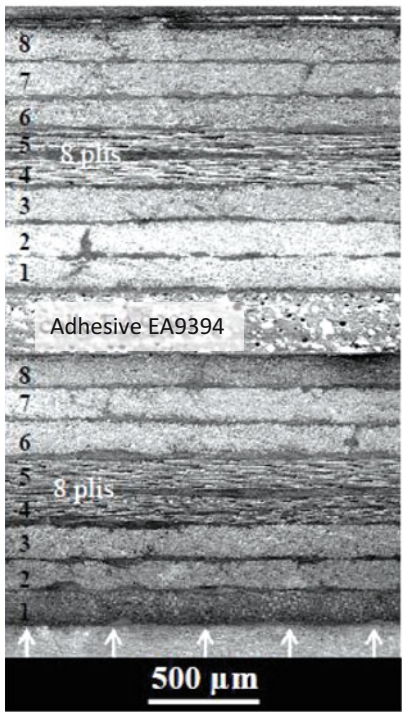
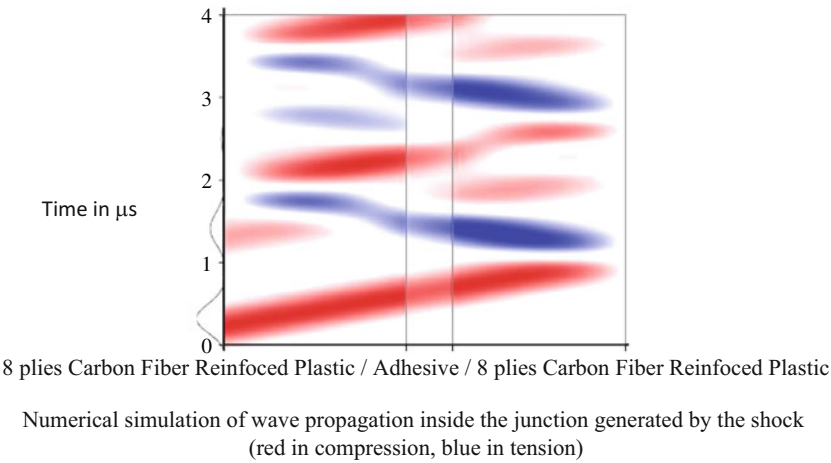
**Fig. 22** Evolution of SH0 guided wave signals generated with EMAT 250 KHz sensors; reproducibility of five measures (Castaings 2014)

The same study has been done with quasi-isotropic composite materials as adherends. Even if the signals are repeatable, they cannot discriminate the defects with the same accuracy. Therefore, new development of sensors and more sophisticated data processing tool in relation with simulation are needed for composite materials.

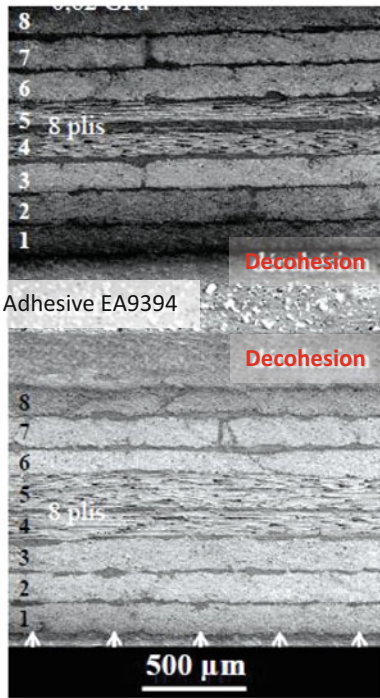
Other authors investigated nonlinear ultrasounds (Yan et al. 2009). It is assumed that when a large amplitude ultrasonic wave propagates through the kissing bond region, the system will behave nonlinearly, and so detection and quantification may be possible. They showed that an imperfectly bonded specimen exhibited much higher nonlinearity than that of a perfectly bonded specimen. These experiments are still performed with academic samples made with metallic adherends.

Laser shock adhesion test (LASAT) is a new promising technique. Considered as proof test, the thermoelastic excitation produced by the multiple pulse laser induces an ultrasonic surface and bulk wave propagation in the material. The combination of the incident and reflected wave can create tension stresses inside the material enough to test interface/interphase adhesion and to detect weak bond (see Fig. 23).

The main target is to find out the appropriated laser shock parameters which strongly depend on the adhesive bond definition to position the maximum traction stresses at the interface (Pertion et al. 2010; Gay 2011).



Shock generating 0.46 GPa pressure  
No decohesion



Shock generating 0.62 GPa pressure  
Decohesion of the two interfaces

**Fig. 23** Micrographic observations of adhesive joints of two eight plies laminate adherends after laser shock (Gay 2011)



All the difficulties hinge on mastering the stress field in terms of intensity and location. Too much energy provided by the laser can damage the surface of the material especially for composite materials. Therefore, the determination of the conditions which guarantees the relevance of the proof test of adhesive bonds must be done with a good understanding of the phenomena, the development of accurate numerical simulation validated by accurate measures, thanks to real-time diagnostics with laser Doppler velocimetry of the free surface and transverse shadowgraphy. Even if some devices are now commercialized (mobile laser bond inspection (LBI) system), LASAT it not yet used in production line.

The diagram of wave propagation shows in this case the maximal tensile stress is located nearby the opposite site of the laser impact and the adhesive joint is less loaded in tension (see Fig. 23). In this case, the resistance of the interphase between adhesive and composite is lower than the interlayers and intra layers of the composite.

---

## 45.6 Strength, Failure, and Durability

Due to the fact that it is impossible to reproduce representative tests on Earth and that all is based on the reliability of the prediction, it is agreed in the space industry that the durability of the equipment shall be guaranteed by a policy of high safety margins: the margin given by the chemical behavior at high temperature (at the molecular scale) up to the mechanical properties at room temperature (at the macroscopic scale). It is also agreed that the equipment is qualified in simulation facilities according to conventional aging.

This attitude is essentially due to the specificity of composite materials, where the stresses are endured first by the interfaces, at the resin-to-matrix/fiber interface, at the resin pre-impregnated inter-ply, and finally at the bonding interfaces.

Companies are increasingly investing in automatic lay-up, heating-up, and line manufacturing devices to render the implementation of composites more reliable and robust despite the fact that the production rate of space industry does not justify by itself.

To illustrate a commercial bonding case, two generic bonding cases are presented below: a sandwich construction with an adhesive film cured at high temperature and then the room temperature bonding of two composite parts.

### 45.6.1 Sandwich Structure Bonding Construction

As a result, the compression resistance along the plane and the pull out-of-plane resistance, always as a function of temperature, are the drivers for sandwich structures. The selection of the adhesive film need to comply with all the thermo-mechanical needs at the elementary level, the outgassing space requirements, and

last but not least, the adhesive needs to satisfy the manufacturing process chart from the industrial point of view, technically (120 °C class for typical sandwich curing assembly, 180 °C class co-curing of the skins to honeycomb core, light areal weight supported or unsupported) and economically. A good film adhesive choice shall be a choice, where the compression load withstanding shall depend only on the composition of the skin (aluminum alloy, aramid, glass, or carbon high resistance or high modulus fibers), the thickness of the skin (in terms of space equipment, the count unit is 0.1 mm), and the honeycomb core definition (cell diameter often from 2 to 6 mm and density from 16 to 50 kg/m<sup>3</sup> varying with the foil thickness of the honeycomb core). From a technological point of view, the compression resistance need shall be guaranteed by a minimum pull-out resistance, bearing in mind that there is no pure compression load but a combination of various angular loads supposed to contribute to the failure strength.

To predict the behavior and prevent durability issues, as mentioned here above, the sandwich structure is fully characterized after numerous thermal cycles under inert gassing (to prevent nonrepresentative oxidation effects on Earth) such as nitrogen or helium (depending on the range of temperature (see Fig. 1).

The expansion characteristics (coefficient of thermal expansion, coefficient of moisture expansion) and the thermal properties (through-the-thickness conductivity and the calorific capacity) are checked in addition to the mechanical properties. In most cases, a 1 MPa pull-out strength associated with a cohesive failure in the honeycomb or in the composite skins is often considered as acceptable for satellite sandwich parts.

With such a result, a value of 300 MPa compressive strength associated with a Young's modulus of 150 GPa delivered by the implementation of ultra-high modulus carbon fiber is displayed by satellite composite sandwich structural parts designed and experimented.

Regarding the sandwich failure mode when subjected to a compressive load, the various failure modes have been set out in the ESA Handbook (ESA PSS 03 203). The failure modes generally observed are (1) facing failure which is the adequate mode rendering correct equilibrium of the spreading of the stress flux provided that the failure load complies with the predicted value, (2) intracellular buckling when the flexural behavior of the skins regarding the cell size induces such behavior according to a certain critical level of loading, and (3) outward face wrinkling when the secondary out-of-plane vector component of the main compressive strength is higher than the flat tensile resistance of the skins to honeycomb.

## 45.6.2 Monolithic Room Temperature Bonding

In most cases, a two-part room temperature adhesive with a tensile lap shear of 20 MPa at room temperature and 10 MPa at 120 °C shall be appropriate for bonding composite to composite and composite to metal on spacecraft. The choice of the adhesive shall be considered as appropriate when the failure is cohesive instead of adhesive, either in the bonded line, when the shear strength of the adhesive is lower than the shear strength of the adherends (metal or composite), or within the

1121 composite thickness, when the inter laminar cohesion (the ability of the resin-to-fiber  
1122 interfaces to withstand the loads) is lower than the adhesive cohesion. One specific  
1123 attention is required when characterizing this type of adhesive. Due to the cold  
1124 curing mechanism, the kinematic is slow, and time/temperature equivalence should  
1125 be used with a lot of precautions in order to determine the appropriate mechanical  
1126 performance of the assembly in real conditions.

1127 **45.6.3 A Commercial Bonding Case**

1128 The case of applying bonding in real life is illustrated by the case of a radio-frequency  
1129 antenna reflector. This reflector is dedicated to telecom satellite broadband service such  
1130 as television, Internet, and wireless access networking services in the Ku band  
1131 (12–18 GHz). This reflector belongs to the category of the high-throughput satellite  
1132 (HTS), meaning, in order to designate any satellite (Ku band or Ka band, 20–40 GHz), it  
1133 uses very small spot beams in order to obtain multiple orders of additional throughput  
1134 compared to classic fixed satellite service. This can be achieved according to a multi-  
1135 source antenna principle or shaped antenna principle according to the multi-beam signal  
1136 monitoring. Airbus Safran Launchers designs and manufactures both (see Fig. 24).

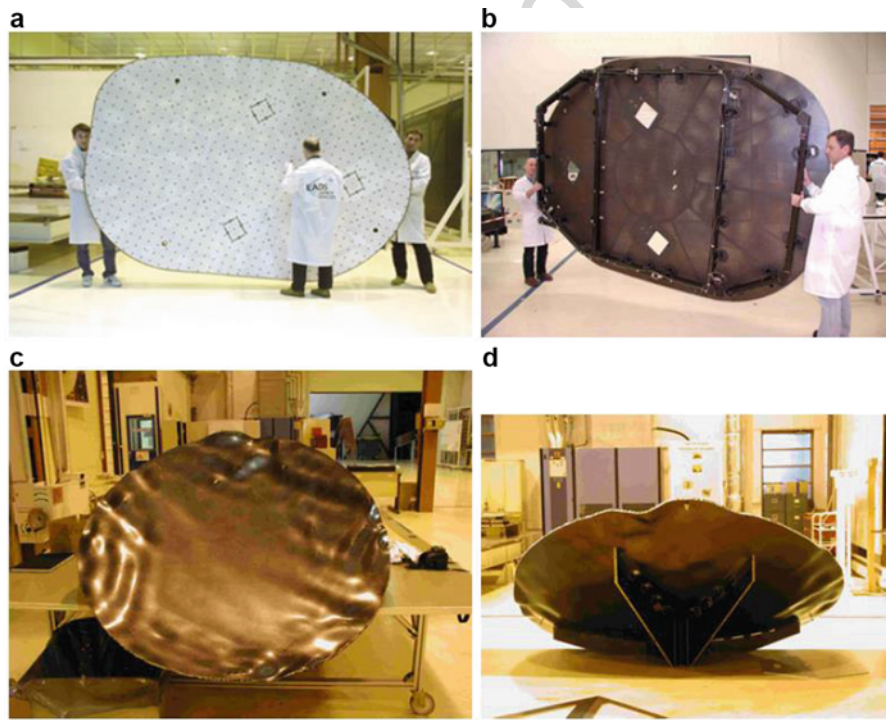


**Fig. 24** Multisource antenna reflector  $2.8 \times 3.5$  m (a, b) and multi-spot 1.6-m-diameter antenna reflector (c, d) – ASL



The backing structure is structurally bonded to the reflector shell of the Airbus Safran Launchers Ku-band reflector named ULR (for ultralight reflector): 2.2 m diameter CFRP sandwich shell and monolithic backing structure and titanium and Invar fittings for a total mass of  $10 \text{ kg} \pm 1 \text{ kg/m}^2$ . This reflector concept has been mounted on telecom satellites since the beginning of the third millennium.

The working environment is the following: (1) to withstand the dynamic and acoustic launching loads with a sine vibration environment of 10 g/out-of-plane axis and 15 g/in-plane axis, 7.90 g is reached on a shell equivalent to 1,000 N pulling out, a dynamic stress time of 1/2 h, and a few minutes acoustic stress time up to 150 dB, (2) to withstand the geostationary orbital thermal loads  $[-50^\circ\text{C}, +50^\circ\text{C}]$  up to jettisoning of the launcher fairing, and (3) to withstand a thermal stress time of 15 years.

First, the joints are tested at the elementary level and the loading cases predicted and margined according to out-of-plane, peeling, and cantilever directions after space-like aging thermal cycling. These tests will validate the design of the adherends and the industrial manufacturing process for the implementation of adhesives. Therefore, the mechanical tests demonstrate the ability of the bonded fitting to withstand the margined predicted loads. Then, it is necessary to validate the design at the margin loads. This is done through mechanical tests operated on representative artificially aged samples (preliminarily space aged by thermal cycling): static pull-out-of-plane test and cantilever for peeling tests.

The industrial step consists in using optimized tools to reproduce the elementary bonding conditions which have been established to provide the required properties. The more optimized (reliable and faster) it is, the cheaper it will be – the ever-present obsession at all stages of industrial productions, space industry included.

The cleats are bonded with an array of tools for ensuring a stress-free assembly after the surface preparation (sanding/ethanol wiping), the adhesive being applied in situ with a tube mixing device, with the dedicated static pressure application during hardening.

With the cure time over, an ultrasonic inspection is carried out for bubble detection in the joint. Repair is required if the defect exceeds the specification (filling of the bubble or debonding and replacement of the cleat).

Once the backing structure is bonded to the shell, the qualification tests are carried out to check that the equipment can withstand the launching loads and the thermo-mechanical behavior as predicted.

First, the reflector undergoes thermal cycles within the extreme temperatures under vacuum to reveal possible weakness at the bonding interfaces, before shaking through the acoustic test performed in a chamber reproducing the launcher conditions. Finally, the reflector is shaken according to the dynamic spectrum of the launcher.

At the qualification stage, the reflector being designed to work in all the launching cases, the dynamical and acoustical vibration spectra are maximized in order to cover the spectra of all the launchers existing (Ariane, Proton, Delta, Longue Marche).

A final ultrasonic check performed after thermal cycling will sign off the qualification for delivery to the customer.

There is no room for error in space, no return ticket, and the possibility of repair is unusual; the Hubble telescope in low Earth orbit still remains an exception.

In summary, the qualification tests performed on each flight model include thermal cycling and thermal stress distortion measurement, dynamic and acoustic tests representative of the launch margin load, and ultrasonic inspection after tests on each cleat junction for the structural bonding parts. Each reflector antenna, i.e., equipment, is considered as a prototype model where all the qualification tests are performed before launching.

---

## 45.7 Conclusions

### 45.7.1 By Way of Summary

The assemblies are key issues for mastering the cost of space structures as well as performance. A non-careful mastering of the quality of the process and non-appropriate design can lead to a dramatic impact in late assembly phase or during the in-life service of the product. The challenge is to design and manufacture, while ensuring optimal thermomechanical returns over mass investment keeping in mind the minimization of the production cost.

As surface bonding has been preferred to local fastening for spreading the loads with the result of optimizing the design to mass, the challenge then consists in the selection, for a joint where the resistance is governed like the cogs in a clock by the specific behavior of two adherends, the glue on one hand and the working environment on the other.

The design office associated with the material and processes experts deals everyday with these inputs for succeeding the correlation between the predicted margined level and the real level withstood, sign of an optimal combination and trust in structural bonding.

### Launchers

Upper-stage structures are made in composite materials and the load transfer between stages is still done via bolted solutions. Few parts are designed with adhesive bonds. The adhesive bond solution is only proposed when mass optimization is the main driver. Apart from sandwich manufacturing which is now obtained via co-curing process, the main drawbacks of the adhesive bond solution are linked to the low confidence of the designer regarding kissing bond detection not yet solved and the qualification cost. The main applications of adhesive bonds are met in thermal protection of structural parts, thermal protection for cryogenic vessel, thermal protection of the stages, and thermal protection of the solid rocket motor. The success of the adhesive solution is based on stringent manufacturing process requests to perform a lot of controls of raw materials and process parameters and last but not least to have skill and qualified operators. Rigorous procedures established in close collaboration between designers, material and process specialists, and manufacturing specialists are the key to successfully mastering adhesive bonds.

1222 The major difficulty encountered by material specialist concerns adhesion with  
1223 elastomers where the mechanisms of adhesion with metals and composites are  
1224 complex to master.

## 1225 **Satellites**

1226 Adhesive bonds in satellite design are the mandatory technology for fastening parts  
1227 enabling the optimization of the structures. Each gram of structural material saved is  
1228 a gram of propellant added and, consequently, satellite lifetime extended (remember  
1229 that for satellites “the lighter it is, the more profitable it is”).

1230 The selection of adhesives is based on the mission of the satellite governed by the  
1231 constraints of space environment (orbit around planet and deep space trip). If  
1232 moisture ingress (outgassing constraints) and thermal cycling are the key parameters,  
1233 radiation resistance is required for limited applications. In principle, adhesive joints  
1234 are not directly exposed to the aggressive space environment.

## 1235 **45.7.2 And Finally**

1236 “It is not the glue which makes the gluing” (Max Ernst) but preparation, inspection,  
1237 and deep control of the process. The adhesive shall determine the maximum loading  
1238 allowable for the bonding assembly, but structural bonding shall occur when the  
1239 adherend surfaces have been suitably adapted after the dedicated preparations to  
1240 provide conditions of interphase formations (this slight mixed layer on an atomistic  
1241 scale between the adherends and the adhesive). The cohesive failure mode is the only  
1242 mode which provides reliable prediction since one knows the separate properties of  
1243 the adherends and the adhesive on the whole. If somebody had to summarize the  
1244 particularities of bonding for space applications, he would formulate the following  
1245 equation: space bonding = high mechanical loads (launcher and satellite) over a  
1246 short time + high thermal loads (satellite only) over a long time, and it is the  
1247 challenge with which one is faced.

1248 The feedback from experiments in bonding is crucial because, apart from every-  
1249 thing one does know, there is everything one never knows, which is huge. Some-  
1250 times, it hinders technological breakthroughs having to balance the cost with risk  
1251 reduction up to almost zero, with the financial issues, the reduction of manufacturing  
1252 costs, and added payload mass.

---

## 1253 **References**

- 1254 Castaings M (2014) SH ultrasonic guided waves for the evaluation of interfacial adhesion. *Ultra-*  
1255 *sonics* 54:1760–1775
- 1256 Collier C, Ainsworth J, Yarrington P, Lucking R (2010) Ares V interstage composite panel concept  
1257 and ring frame spacing trade studies. 51st AIAA/ASME/ASCE/AHS/ASC structures, structural  
1258 dynamics, and materials conference, Orlando
- 1259 Drucker DC, Prager W (1952) Soil mechanics and plastic analysis or limit design. *Q Appl Math* 10  
1260 (2):157–165

- 1261 ECSS-Q-70-71A rev 1, Space product assurance. Data for selection of space materials and  
1262 processes
- 1263 Ehrhart B, Valeske B, Muller C-E, Bockenheimer C (2010) Methods for the quality assessment of  
1264 adhesive bonded CFRP structures –a Résumé. 2nd international symposium on NDT in  
1265 aerospace
- 1266 ESA PSS 03 203 Structural materials handbook
- 1267 Gay E (2011) Comportement de composites sous choc induit par laser: Développement de l'essai  
1268 d'adhérence par choc des assemblages de composites collés, PhD thesis
- 1269 Pertion M, Blouin A, Monchalain J-P (2010) Adhesive bond testing of carbon – epoxy composites by  
1270 laser shockwave. J Phys D Appl Phys 44(3):034012
- 1271 Popineau S (2015) Durabilité en Milieu Humide d'Assemblages Structuraux collés type Alumin-  
1272 ium/Composite. PhD thesis
- 1273 Prager W (1995) The theory of plasticity: a survey of recent achievement. Proceedings of the  
1274 institution for mechanical engineers
- 1275 Raghava R, Caddel RM, Yeh GS (1973) The macroscopic yield behavior of polymers. J Mat Sci  
1276 8:225–232
- 1277 Yan D, Drinkwater BW, Neild SA (2009) Measurements of the ultrasonic nonlinearity of kissing  
1278 bond in adhesive joints. NDT E Int 42:459–466

Klaus Dilger, Bernd Burchardt, and Michael Frauenhofer

**Contents**

46.1	Introduction .....	1334
46.2	General .....	1334
46.2.1	Press Shop .....	1336
46.2.2	Body Shop .....	1336
46.2.3	Paint Shop .....	1336
46.2.4	Trim Assembly .....	1336
46.2.5	Power Train .....	1337
46.3	Specific Requirements .....	1337
46.3.1	Adhesively Bonded Sheets in the Press Shop .....	1337
46.3.2	Adhesives in the Body Shop .....	1338
46.3.3	Adhesives in the Paint Shop .....	1344
46.3.4	Adhesives in the Assembly Line/Trim Shop .....	1344
46.3.5	Adhesives in the Power Train .....	1346
46.4	Other Specific Requirements .....	1347
46.5	Surface Preparation .....	1348
46.6	Strength and Durability .....	1349
46.7	Durability .....	1354
46.8	Type of Failure .....	1363
46.9	Quality Control .....	1364
46.10	Repair and Recycling .....	1365
46.11	Conclusions .....	1365
References	.....	1366

K. Dilger (✉)

Institute of Welding and Joining, TU Braunschweig, Braunschweig, Germany

e-mail: [k.dilger@tu-bs.de](mailto:k.dilger@tu-bs.de)

B. Burchardt

Weiningen Zürich, Switzerland

e-mail: [burchardt.bernd@ch.sika.com](mailto:burchardt.bernd@ch.sika.com)

M. Frauenhofer

Audi AG, Ingolstadt, Germany

e-mail: [michael.frauenhofer@audi.de](mailto:michael.frauenhofer@audi.de)

## Abstract

Modern cars contain about 15 kg of adhesive (IVK 2017). Adhesives are used to avoid corrosion, to stiffen the car body, to obtain a better crash performance, to join different materials that are not weldable, and for sealing purposes. Adhesives are used in powertrain and car body applications. In the car body, up to 200 m of structural adhesives are applied. The trend toward a new lightweight design leads to the necessity to join different materials in a material mix. Here, the use of high strength steels, light metals, and fiber-reinforced plastics has expanded extremely in the last years. In terms of adhesive bond, one has to deal with different surfaces and thermal expansion. Additionally, the adhesive has to act as an electrical insulation to prevent the joint from forming contact corrosion. In this chapter, typical applications for automobiles are shown. Additionally, suitable adhesive properties and surface treatments are discussed.

## 46.1 Introduction

Adhesive bonding of automobiles started with sealing applications like the substitution of the windscreen gasket by a bonding seam of a rubber elastic adhesive or gap filling with an adhesive to prevent corrosion. The sealing adhesives led to a stiffening of the car body because the bonded windows could act as a shear field and the adhesively bonded joints were stiffer than spot welded flanges due to the complete connection. To further improve the stiffness, an increasing number of adhesives with a high modulus was used. Since these adhesives were not suitable to improve the behavior of the joint in a crash situation, they could not be used as a real structural element, which would enable to reduce the number of spot welds. The third generation of adhesives with enhanced crash properties finally offers the opportunity to use adhesive bonding as a real structural joining alternative in an automobile construction. We can generally distinguish between applications in the automobile body and the power train. Regarding bonding in the car body, you have to take into account that the body has to be painted, meaning that the adhesives have to be applied before or after certain painting processes. This is of high importance in terms of the selection of the suitable adhesive. In Fig. 1a, typical bondings on raw metal in the car body are shown. Fig. 1b gives examples of bondings on painted panels.

Regarding the strength of the adhesive bonds, one can distinguish between high strength and high stiff bonds and bonds with lower strength and a higher flexibility. To produce high strength joints, often epoxy adhesives are used with a low bondline thickness of about 0.2 mm. Windows are bonded with a highly elastic polyurethane adhesive with a bondline thickness of more than 2 mm (Fig. 2).

## 46.2 General

The process chain in an automobile production can be separated in the production of the **car body** and the components, respectively **the powertrain**. The stages of the body production are the **press shop**, the **body shop**, and the **paint shop**. The final



**Fig. 1** (a,b) Typical bondings in a modern automobile

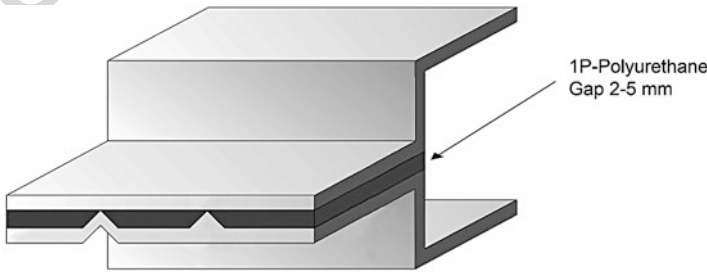


**Fig. 2** Typical semistructural and structural bondlines

production step to finish the automobile is the **trim assembly**. While in the press shop besides of a possible use of bonded blanks no adhesives are used, adhesives are applied in the three other areas mentioned and have to undergo the following process steps.

#### **46.2.1 Press Shop**

Classically, sheets made of steel – uncoated or zinc coated – and aluminum alloys are cut and cold formed in a deep drawing process. To prevent the metals from corrosion and to facilitate the pressing process, the blanks have an oily surface. A modern approach is the use of a warm forming process where the deformation and the hardening of the steel (e.g., 22MnB5) is performed at the same time. Therefore, the sheets have to be heated to a temperature of about 850 °C, which could cause the formation of a thick oxide layer. To prevent the parts from this oxidation, a special coating is used, which has to be taken into account for the subsequent joining procedure.

#### **46.2.2 Body Shop**

The formed parts are brought together to assemblies in the body shop. Here, almost every joining technique is used. The standard method used for joining of steel is spot welding, whereas for light metals mechanical joining like clinching and riveting is commonly used. Independent of the material used and of the joining technique, the application of adhesives is necessary or beneficial to prevent the parts from corrosion. Adhesive bonding is used in steel and aluminum bodies to stiffen the parts and to improve the crash behavior. In a mix material design, the use of adhesives is essential to avoid the contact corrosion that could result from the contact of materials that have a different electrochemical potential. The adhesives applied in the body shop will be cured in the oven, which is needed to cure the electro-coated paint. Therefore, during all of the processes performed in the body shop, the adhesive is liquid and the handling strength has to be obtained by an additional joining technology.

#### **46.2.3 Paint Shop**

Before the paint is applied, different pretreatments like cleaning and phosphating are executed. The paint is applied in different layers. It starts with the application of the electrolytic cathaphoretic paint and the curing of that layer during about 30 min at a temperature of 180 °C. Afterward, more paint layers are applied and cured at temperatures from 110 °C to 150 °C. The resulting layer structure is shown in Fig. 3.

#### **46.2.4 Trim Assembly**

In the trim assembly, the windows and different panels and other optical elements are bonded to the painted body. Thus, the paint layer becomes part of the structure, which



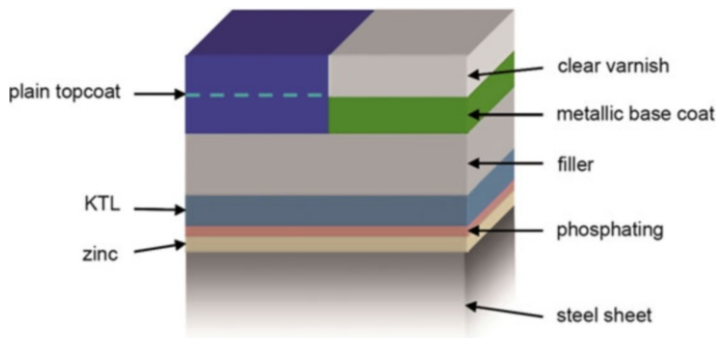


**Fig. 3** Different layers of paint due to the current painting process of a car body

has to be taken into account if there is a demand for a higher strength. Additionally, the chemical base of the paint, the color, and the painting process are of a high importance in terms of the resulting properties. Because of the heat sensibility of the applied materials and the assembly process, only cold curing adhesives can be applied.

## 46.2.5 Power Train

In the power train, adhesives are used for shaft-to-hub connections, for sealing purposes and as a thread lock. Special demands for the adhesives used result from the high temperatures and the contact with fuels and lubricants.

## 46.3 Specific Requirements

### 46.3.1 Adhesively Bonded Sheets in the Press Shop

To reduce weight, metal sheets with a varying thickness are used for forming parts. In this case, the wrought products are made of sheets with different thicknesses by welding or differential rolling. Hence, to produce the so-called tailored blanks, different sheets are welded together in general by laser beam welding before they are formed in the pressing process. This is very common for linear and nonlinear joints. A new possibility to improve stiffness and corrosion resistance is the use of so-called bonded blanks where two sheets are bonded together prior to the pressing process. In this context, it is important that the adhesive has a sufficient green strength to ensure the right position of the blanks during the pressing process, but nevertheless there is enough plasticity to avoid the formation of cracks in the adhesive layer during the deformation process. One possibility to achieve this behavior is the use of an adhesive with two hardening procedures. The green strength results from a viscosity increase due to the cooling of the hot applied adhesive, and the final strength is formed by crosslinking due to the chemical reaction after the

pressing process that takes place in a furnace at 180 °C (Wisner et al. 2014). An example of a part made from bonded blanks is shown in Fig. 4.

**46.3.2 Adhesives in the Body Shop**

Adhesives are typically used in the body shop for structural flange bonding spot weld bonding, clinch bonding, etc. in a so-called hybrid process. Here, the adhesive is applied on one sheet and after joining of the parts the additional joining technique takes place. Further applications are hem flange bonding and antifleutter bonding.

Adhesives used in the car body structure have very specific and demanding requirements:

1. They need adhesion on oiled bare, electrogalvanized, or hot-dip galvanized steel and on aluminum metal sheets.
2. They undergo the complete pretreatment process for the electro coat including the heat curing in the EC oven. The adhesives are designed to cure under these conditions.
3. A temperature resistance of 200 °C over half an hour is needed, but due to the variety of production processes between the different manufacturers and even between different plants up to 220 °C is specified, or at the lower end under low bake conditions 160 °C for 15 min. Therefore, the curing properties of adhesives have to be adapted to the specific process conditions of the individual production line.
4. In certain cases, parts with uncured adhesive are stored or shipped. Under these conditions adhesives may absorb moisture from the atmosphere and when curing at 180 °C the absorbed moisture will cause bubbles, thus reducing the strength of the adhesive.

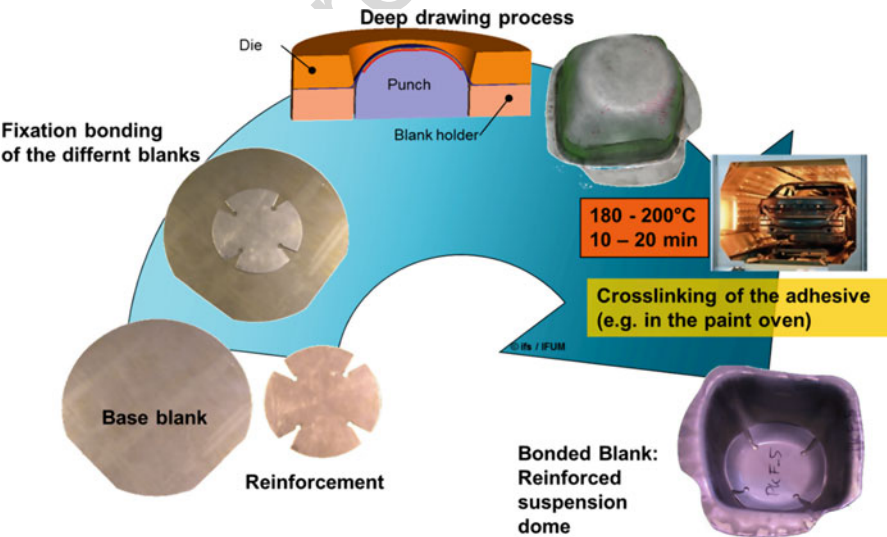


**Fig. 4** Bonded blank technology (Wisner et al. 2015)

5. Adhesives must be applied in a liquid stage to achieve a proper wetting, and thus they usually do not withstand the conditions of the pretreatment baths. Therefore, a precuring or pregelation is often required. Due to separate handling, this is easier for the bolt-on parts like doors and hoods since adhesives used for them are often cured in a separate prebaking oven or by induction curing. The newest generation of structural adhesives does not need such a precuring any more.
6. Since all body shop adhesives are applied directly on the metal surface, corrosion resistance is crucial. And it is even more demanding than the corrosion resistance of coatings, since there is no specific pretreatment, and the structural adhesives replacing welding operations must withstand much higher loads than a coating. Regarding the corrosion tests, every car company has its own test requirements, because they have individual longtime records with their specific test conditions. But in general, they have the following requirements in common: the combination of salt spray, high humidity, and temperature change. These conditions give usually similar results depending upon the time and the number of cycles.

### Structural Flange Bonding (Hybrid joining)

Typical configurations of the use of different joining technologies at one flange in a hybrid joining process are shown in Fig. 5.

To build up the structure of the car body, welding is the standard technology to join metals and especially spot welding is used for all steel cars. In the last 30 years, the requirements for car design have changed due to the pressure of lower fuel consumption and higher safety for the occupants, which revealed the limits of the spot welding technology in terms of durability, crash resistance, and production speed in connection with thinner high strength metal sheets or in a more obvious case, with aluminum substrates.

To overcome the drawbacks of spot welding, other joining technologies have been evaluated including riveting, self-piercing riveting, clinching, and bonding.

The structural adhesives marketed for the automotive industry at the beginning of 1990 were rather brittle and not really resistant under high-impact conditions. Consequently, the adhesives industry developed the new generation of high-performance structural adhesives in this decade.

These combine the strength of standard epoxy adhesives with higher deformability before break. These are often formulated as warm-melt adhesives

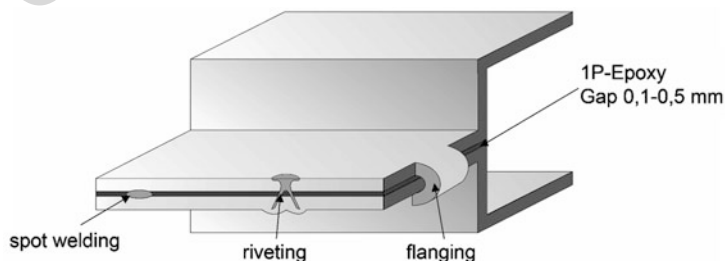


**Fig. 5** Hybrid joining of a flange in a car body

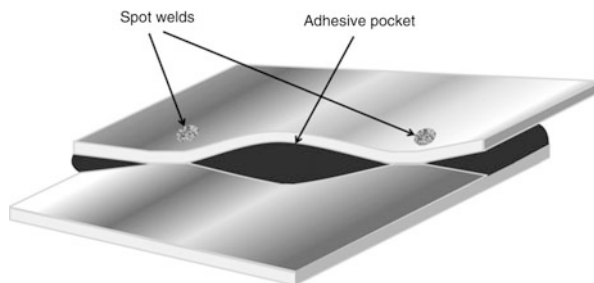
and applied at temperatures up to 60–80 °C, and after cooling, they get highly viscous enough to withstand the pretreatment operations. But these warm-melt properties have to be well balanced, because if the viscosity of the adhesive is too high after cooling, spot welding will lead to pocket formation as demonstrated in Fig. 6.

The welding will need more electrical and pressure power since a thicker layer of adhesive acts as an insulator. Usually, this is addressed as squeezability, which means the property of the adhesive to flow under a small pressure when the metal sheets are put together. The challenge for the adhesive formulator is to balance a low viscosity at the application temperature of 80 °C with a rather high viscosity at room temperature to achieve a good washout resistance and at the same time a good squeezability (Stepanski 2010).

Another critical point is linked with the reactivity of the adhesive. It needs heated pumps and tubes for the application at temperatures between 50 °C and 80 °C. But due to the inherent reactivity of such one-component adhesives, there will be a slow increase of its viscosity over time. The flow in the tubes will then be reduced and when increasing the temperature to keep the constant flow, the viscosity increase continues and the tubes will be blocked. This is important in cases where the consumption of the adhesive is rather low or the tubes are long. Therefore, not only the design of the adhesive is important, but also when planning the application equipment, it should be clear that the adhesive in the tubes should regularly not stay for a longer period at elevated temperature. Since this is specific to the adhesive and the equipment of the production line, it has to be evaluated in detail by the responsible engineers for every single application. For all adhesives application, it is recommended to use heated pipes since this guarantees a rather constant application viscosity.

The need to reduce the weight of a car leads to the use of alternative materials that have to be joined with a similar material or a different material in a so-called hybrid construction. Here, traditional joining and welding processes are often not suitable due to different reasons. One is the difference in between the thermal expansion coefficients of the materials, another is the electric potential of the material. Adhesives are suitable for bonding of almost any material and reduce the mentioned problems, thus increasing the use of adhesives in automobiles significantly in the last 10 years. In Fig. 7, the material mix in a modern car structure is shown.

**Fig. 6** Pocket formation when welding through a highly viscous adhesive



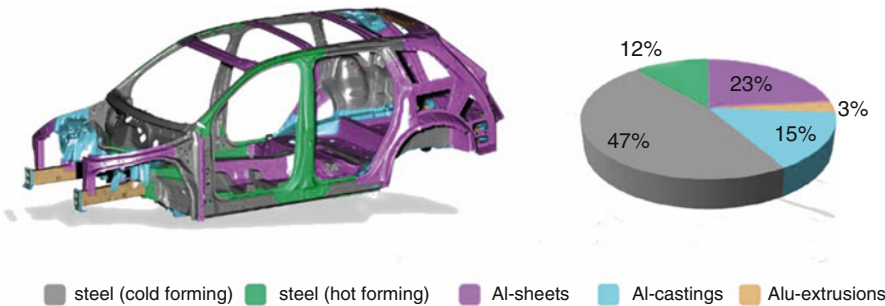


**Fig. 7** Material distribution in the Audi Q7 (Audi)

Here it is necessary to compensate the different elongations of the parts due to the different thermal expansion (CTE-Mismatch) by a thick and elastic adhesive layer. However, such an adhesive layer can reduce the stiffness of the part significantly so that adhesives with a middle modulus of 10–100 MPa are developed.

**Hem Flange Bonding**

Bonding of hem flanges has now been practiced for more than 30 years. At the beginning, the reason was more corrosion protection than the increase in stiffness. Meanwhile, the hem flange bonding contributes to the structural stiffness of hoods. And it is an important element for the resistance of the doors against side impact. The adhesive prevents the inner door panel with the reinforcement bar to slip out of the hem flange upon impact.

Regarding application, the hem flange bonding needs very specific processes. To fulfill the strength and corrosion requirements, the flange should preferably be filled completely. But in this case, the hemming tools and also the parts will soon become soiled, which would then require an additional manual cleaning step. Therefore, the application is carried out on the inner side of the outer panel to avoid the adhesive to be squeezed out. There is another difficulty. The high pressure of the hemming tools press the gap to almost zero, but the metal bounces back due to its elastic properties thus creating voids. Some adhesives use small glass bubbles as a filler in order to keep a gap of 0.3 mm, which reduces the number of voids.

In addition, the doors are seam sealed to achieve a proper corrosion protection. But when the air is entrapped in the hemming area, bubbles will be formed in the hem flange sealant on curing, while reducing the visual quality of the sealing bead. And if not sealed, the hem flange has a high risk for corrosion because of these voids. This problem has not been solved yet to the satisfaction of the engineers. A possible solution is the application of the seam sealer onto the hot hem flange when using induction heating, but then the cycle time will get too long, which means additional expensive tools. The different steps of hem flange bonding are shown in Fig. 8.

**Antiflutter Bonding**

A third important application is antiflutter bonding. To avoid rattling noises, the gap between the outer panel and the inside structural metal sheet of a hood must be filled

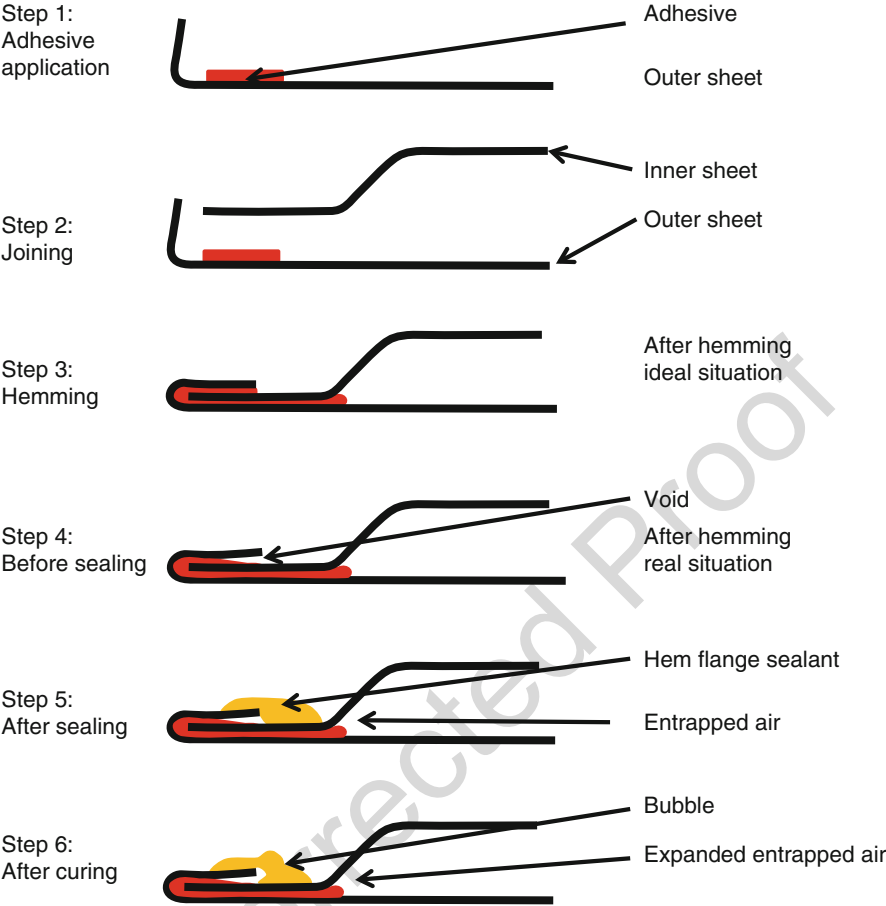


**Fig. 8** Main process steps of hem flange bonding

with a suitable material. This often is soft rubber foam to avoid any surface marking, but in this case no increase in stiffness is possible. With the push toward lightweight design, the gauge of the outer metal panels has become thinner and thinner. And when using a “semi-structural” adhesive, the stability of such a hood can be increased. This is also a structural adhesive because it contributes to the stiffness of the hood, but due to the requirements regarding surface quality with no marking on the outside panel, a balance between strength, modulus, and elongation must be found. If the adhesive becomes too strong, there will be an unacceptable surface marking (read-through) on top of the bonded area, and if the E-modulus of the adhesive is too low, there is no stiffening effect. The best solution would be a high modulus adhesive with no read-through. Unfortunately this “read-through” is caused only to 10% by the shrinkage due to the chemical reaction of the adhesive itself, the other 90% is due to the physical shrinking from 180 °C to room temperature.

The surface marking (Fig. 9) can go in both directions, but due to the thermal shrinkage of the adhesive, in most cases it is indentation.

In the phase of the heating-up in the oven, there are differences of up to 60 °C between the inner and outer metal sheet and when the adhesive cures at this stage, surface marking after cooling can be observed. Tests with a two-component adhesive curing at room temperature showed that with cold curing the marking was significantly reduced. Unfortunately, it is very difficult to get adhesion on oily metal sheets using two-component adhesives.

Figure 10 shows typical applications at a front hood. There is a hem flange area either around the whole perimeter or only in the front and the back, and on the side of a spot-welded area but with the same structural hem flange adhesive. The reinforcement bars of the inner panel are bonded with thick adhesive layers (usually around 3–5 mm thickness). In areas where higher pressure onto the outside panel is expected when closing the front hood by hand, a larger area is supported. To apply the adhesive on such a larger area, the multidot application is preferred. This has the

**Fig. 9** Surface marking by antifiutter bonding

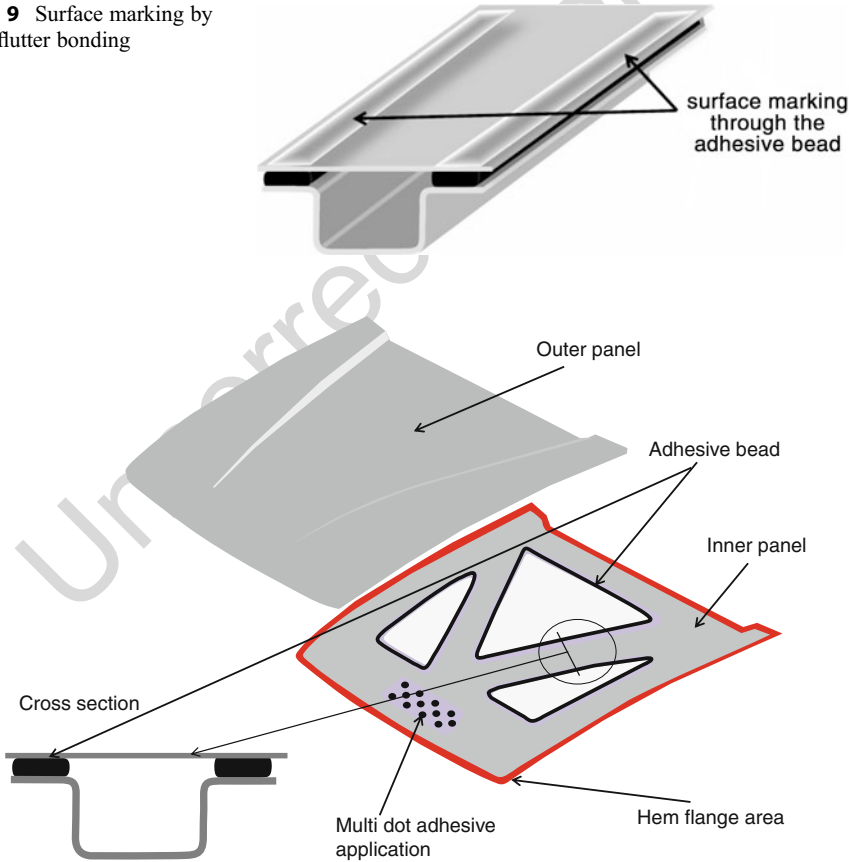


**Fig. 10** Antifiutter bonding applications

advantage that there are gaps between the dots, and the electrocoat can flow into these gaps and provide the necessary corrosion protection.

Adhesives used in a car have to work at temperatures between  $-40\text{ }^{\circ}\text{C}$  and  $105\text{ }^{\circ}\text{C}$ . More demanding than the temperature is the resistance toward humidity because hot and humid conditions can reduce the strength of adhesives significantly depending on formulation and chemistry.

There is also a differentiation between inside and outside parts. Outside parts have not only to pass high temperature and high humidity tests but also the corrosion test cycles like the VDA 621-415. Inside parts are exposed to higher temperatures (in some areas up to  $120\text{ }^{\circ}\text{C}$ ) than outside parts but are not exposed to a corrosive environment (Table 1).

**46.3.3 Adhesives in the Paint Shop**

In the paint shop, there are only some minor applications of antiflutter bonding and seam sealing with materials which need similar properties like adhesives in terms of good weathering resistance and good adhesion. These sealants are polyvinylchloride plastisols in most of the cases, as they are used for underbody coating and do not provide high strength. In this case, the adhesion occurs on a coated surface, which offers more opportunities in the formulation and no issues regarding corrosion. Since the paints are cured in the paint ovens, their heat can also be used to cure the sealants. Temperatures are typically between  $140\text{ }^{\circ}\text{C}$  and  $160\text{ }^{\circ}\text{C}$  with the tendency to baking at lower temperatures. Since the paint process follows the body shop operations, all body shop adhesives have to withstand the baking conditions of the paint. There are efforts to move all non-paint operations out of the paint shop, thus bonding in the paint shop will be the exception.

**46.3.4 Adhesives in the Assembly Line/Trim Shop**

The largest variety of adhesives is used for all the parts assembled in the trim shop. Since many parts are produced at suppliers or subsuppliers and are installed in the car either by screws, bolts, or clips, there are only a few applications performed directly at the assembly line. This is also due to the fact that adhesives need a specific process for curing or hardening, which in most cases do not fit into the required short

**Table 1** Test conditions of VDA 621-415 corrosion test cycle (Available from VDA website [www.VDA.de/en/publikationen](http://www.VDA.de/en/publikationen))

One cycle		
Day	Duration	Condition
1	24 h	Salt spray DIN 50021 SS
2–5	4 × 24 h	DIN 50017 KFW
6–7	2 × 24 h	23 °C, 50% relative humidity

This cycle of 7 days is run ten times. The overall duration is 10 weeks



cycle time of often less than 1 min. Most bonded parts are preassembled and built into the car as finished parts. Adhesive bonding of these separately built-on parts is not within the scope of this chapter.

The most important structural bonding in the final assembly is the installation of the windows. Even if the adhesive for this purpose must be flexible enough to prevent a breakage of the glasses due to high stresses through deformation, the resulting increase in torsion stiffness (a high quality property of a car) depends on the car design in the range of 50–80% with almost no additional cost and no increase in weight. Therefore, direct glazing has replaced the rubber gaskets in almost all car production lines and has become an important element for the torsion stiffness of the car. This installation principle of direct glazing can also be transferred to the installation of other panels like a separate lightweight roof made of aluminum or carbon fiber composite.

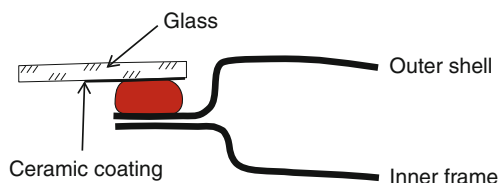
The most important application at the assembly line is the bonding of the glasses. Figure 11 shows a typical cross section of a frame with the adhesive bead. Usually, a triangular bead with a height of 8–10 mm and a width at the base of 10 mm is applied onto the glass which is then installed into the car. This is necessary to cope with the tolerances of the frame and the glass.

The use of 1-C polyurethane adhesives is state of the art. Standard grades are applied at room temperature and need fixation for at least 1 h to get sufficient strength to hold the window in place. Warm-melt windshield adhesives are applied at temperatures between 60 °C and 80 °C and on cooling they build up sufficient initial strength to hold the windows in place during curing with no additional fixations. The adhesives are fully cured after 3–7 days depending on the climate conditions.

The warm-melt properties must be balanced very thoroughly. If the adhesive is setting too fast, it does not wet the surface enough and there will be disbonding under torsion stress. To increase the slow curing speed in cold and dry atmospheres, two component systems are available, which are either real 2C systems or 1C adhesives accelerated with water paste. These are used when the bonded structure has to bear load at a very early stage.

An important detail is the conductivity of the windshield adhesives. If such adhesives were formulated with higher amounts of carbon black as filler, the direct contact of such an adhesive with aluminum would lead to severe and fast contact corrosion and would destroy the aluminum in the case that the isolation through the paint is damaged. Also, if a radio antenna is integrated into the glass (e.g., a rear window), the impedance of the adhesive will play an important role for the quality of radio reception.

**Fig. 11** Cross-section of windshield bonding



When windshield adhesives are directly exposed to sunlight, the thin adhesion layer directly on the glass will be destroyed by UV-radiation. Therefore, a UV protection is a must. In the beginning of windshield bonding, this was achieved by a black primer, but under severe UV-radiation, even this rather stable UV-blocking primer was destroyed over time. With the application of a screen-printed ceramic frit (see Fig. 11) to the bonding area of the glass, the necessary high-quality UV protection could be achieved. More than 30 years of success in windshield bonding has proven the reliability and durability of this technology.

The replacement of windshields must be possible, too. At the beginning, this was an important criterion against the introduction of direct glazing. But with specifically designed cutting knives or with high strength steel wires, the removal for repair purposes was possible in a short time. To facilitate the repair, a minimum thickness of the adhesive layer must be guaranteed, preferably more than 3 mm.

The success of windshield bonding encouraged the designers to bond other panels onto the frame. In particular, the roof is in study, because saving weight on top with an aluminum or carbon fiber composite roof, will lower the point of gravity and improve the road handling. An overview on elastic bonding can be found in the booklet of Burchardt et al. (1998) and Cognard (2006).

For the fixation of model names and door trims as well as rubber gaskets, pressure sensitive adhesive tapes are commonly used. Such pressure sensitive adhesives (PSA) are highly sensitive to stress. The parts should be attached in a completely stress-free state and with a defined pressure. After the application, the adhesive continues to wet the surface and to build up the final adhesion. Brockmann (Brockmann and Grüner 2003) investigated the creep behavior of such tapes and he found out that under load the tape may creep over its whole overlap length and is still bonding with the same shear and peel strength as in the unloaded stage.

**Besides the areas described above, adhesives are used for different purposes in the engine and the gearbox. These applications are described below.**

### **46.3.5 Adhesives in the Power Train**

In the power train, adhesives are used for shaft-to-hub connections, for sealing purposes, and as a thread lock.

For shaft-to-hub connections mainly anaerobic acrylates are used. In most cases, the adhesive bond is supported by a shrinking of the hub to the shaft. By this hybrid joining process, both a high axial strength and a high torque can be achieved. A secondary effect of the shrinking is residual stresses in the parts, which can lead to a reduction of the fatigue strength. Especially for rigid materials like sinter metal this can cause problems; therefore that the shrinkage should be reduced and the adhesive part of the strength should be increased [17, 18] Lit.-Stellen ergänzen.

To produce these bonded shrink fits, the hub should not be heated up to more than 200 °C to avoid damage of the adhesive and the shaft should not be cooled to avoid condensed water.

Figure 12 gives an overview about the shrink fit process to produce a gear-shaft connection.

Thread locks are made by either anaerobic or microencapsulated adhesives. These adhesives have a defined initial breakaway torque.

Silicones are often used for As gaskets formed at a place in the power train. To enhance the curing time, there are UV-curing products on the market. It is important that – because of the bad paint adhesion on silicone-contaminated surfaces – silicones are only used for power train applications and it has to be ensured that no contamination of body parts is possible.

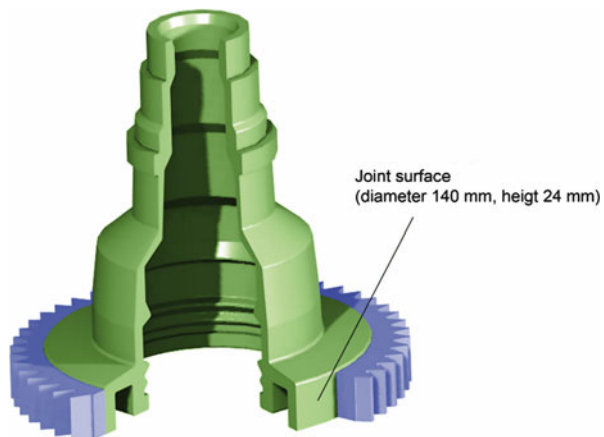
## 46.4 Other Specific Requirements

Adhesives used in a car body need a temperature resistance of at least 105 °C and must resist high humidity conditions as well as temperature change between –40 °C and +80 °C. Such adhesives are often tested under the so-called cataplasma condition, that is, 70 °C in a water saturated atmosphere. Each car manufacturer has its own test regime but they rely on the combination of high humidity and temperature. In addition, the UV resistance of the system must be checked either with exposure to sunlight in areas like Florida or in test chambers with UV-lamps in combination with heat and/or moisture. The interpretation of such artificial weathering needs experience, since the extrapolation for the real-life weathering cannot be done automatically.

On top of technical requirements additional properties are requested. One is low fogging of small ingredients or plasticizers in the adhesive and another is low odor, since customers became more sensitive toward the smell of adhesives.

For outside application, fuel resistance, resistance to cleaning agents, and washing fluid for the windshield and headlights are required in addition to water and corrosion resistance.

**Fig. 12** Bonded shrink fit



## 46.5 Surface Preparation

The right surface preparation is the key to successful adhesive bonding. Therefore, it is at first sight surprising that bonding in the body shop with the highest strength requirements occurs on oily surfaces. But to be sure, these systems have been tested extremely thoroughly and only those combinations of adhesives, oils, and metal surfaces are allowed to use which have passed all test. And then, it is up to the quality control system over the whole value chain from the suppliers of adhesives, oils, and metals to the stamping plant to make sure that all process steps are well under control. And all changes have to be communicated before implementation.

The fact that body shop adhesives are cured at temperatures about 180 °C helps the adhesive to absorb the oil and get in direct contact to the surface with good wetting. The weakest area of the surface is the thin oxide layer which is on all metal surfaces.

The phosphatation process which creates a good adhesion layer for the paint cannot be used since the adhesives are applied at an earlier stage during the assembly of the metal parts.

In the future, precoated metal sheets could probably be used, but then the spot weld bonding would be no more possible. In addition, one has to keep in mind that the adhesive strength on such coatings is lower than that of high strength structural adhesives. Even the adhesion quality of a hot dip galvanized steel coating has to be tested since with some structural adhesive the zinc layer debonds from the metal surface.

In case of aluminum, a pretreatment is necessary to achieve a long-term-corrosion-resistant adhesion. Whereas in the aerospace industry, anodizing processes are state of the art, automotive industry has been looking for more cost-effective solutions. A Cr (VI) passivation provided the best results and is now used as benchmark for new chrome-free pretreatments necessary due to the environmental impact of chrome. The best and most cost-efficient results are reached with a passivation of the aluminum in a coil coating process. But this implies that the lubricants needed for the drawing of the aluminum sheets is compatible with the adhesive. Otherwise a separate washing process of the stamped parts would be necessary which is not really economic. A new article from Rechner et al. (2010) discusses different surface pretreatments.

In addition to solvent cleaning, new methods with laser, CO<sub>2</sub>, and plasma treatment are available. A short overview has been written by Schulz (2010) (See also Part B).

As the oven for the EC coat can be used for curing, almost all body shop adhesives are one component systems. The heat curing helps to absorb the oil thus providing the necessary adhesion.

In contrast to such one component systems, it is very difficult to get adhesion on oily surfaces with 2-C adhesives. Due to the immediate start of the curing after mixing of the two components, the time to replace the oil on the surface is too short in comparison with the curing speed, because the monomer or prepolymer components of the adhesive resin and hardener react faster with each other than they are able to wet the surface. Only with very long open time adhesives there is some chance to get adhesion. Significant efforts are made to use 2-C adhesives for

bonding of hoods to reduce the thickness of the outer sheet without surface marking.

Also a challenge is the adhesion on painted surfaces. This has been intensively tested with the introduction of direct glazing. Since there are so many different paint surfaces due to the chemistry, process conditions, and requirements for the paints, there are three different approaches to achieve good adhesion for the windshield adhesive:

1. Bond on the surface of the filler or directly on the EC coat. This requires a cover tape applied before the coating of the paint. The masking tape must be then removable without any residues on the surface even after several bake cycles. And in addition, the paint must stick on the tape and should not chip when removed. The masking is an additional process with additional costs. The EC coat provides the highest adhesion strength with values in the range of 15 MPa.
2. The use of a primer to prepare the paint surface for the windshield bonding. This is a commonly used process. It is mostly a manual operation with the risk of contamination of other areas with the primer. But with specific formulated primers it is possible to achieve adhesion on all paint surfaces.
3. Bond directly on the top coat. This requires a thorough testing of all paint surfaces and a specific formulated adhesive adapted to that paint type. It means more quality control tests during production. But also in this case it is necessary to mask those car bodies which undergo a repainting process, because additional paint layers usually have less adhesion than the first one, which would create a weak interphase for the bonding system.
4. In general, the adhesion within the paint layers determines the strength of bonding on paint. High modulus windshield adhesive can build up stronger bonds than the paint which leads then to adhesive failure within the paint layer instead of failure within the adhesive itself. This applies also for other parts like, for example, a roof made of aluminum or carbon fiber composite installed at the assembly line.

---

## 46.6 Strength and Durability

Strength and durability is not inherent to an adhesive but it must always be seen in the context of the whole design of the bonded joint, the substrates, the expected permanent maximum and cyclic loads in combination with environmental influences like climate, radiation, and oxidation.

Figure 13 shows a relation between strength and deformation for the world of adhesives. It visualizes in which strength range different adhesive types usually work, even if there may be exceptions. And it helps to think about the balance between strength and deformation.

The range of strength of structural adhesives used in automotive production is marked at one end by windshield adhesives with rather low modulus and high elongation and at the other end by very high strength epoxy adhesives. The top end of adhesives for automotive bodies are crash-supportive epoxy-hybrid adhesives

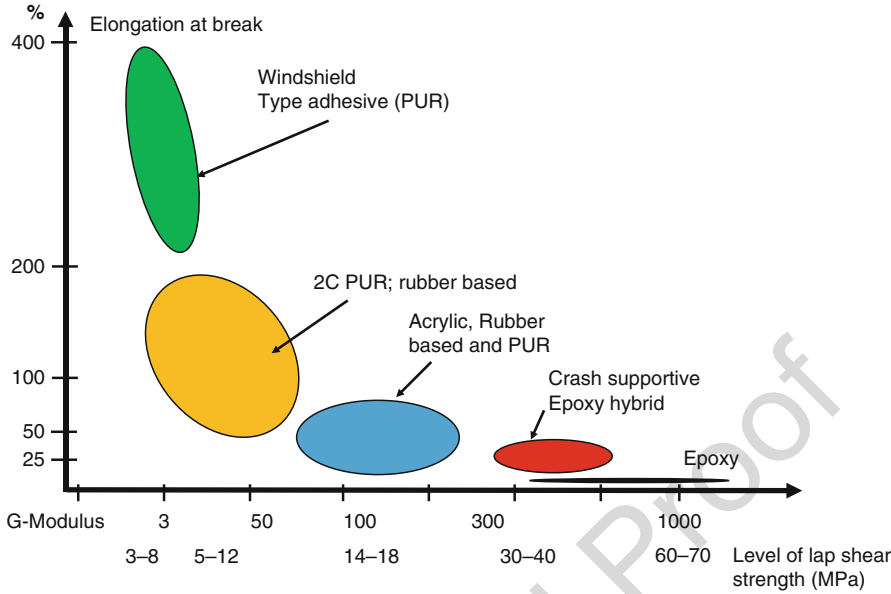


**Fig. 13** Landscape of adhesives for structural automotive applications (PUR polyurethane)

which have a somewhat lower G-modulus than very high strength epoxies, but significantly higher elongation. In between, there is a large area where the mechanical properties of the adhesives can be varied. In automotive applications, this broad range can be covered with 1- and 2-C polyurethanes, rubber- or acrylic-based adhesives, and epoxies or modified epoxies. There are also PVC- or acrylic-plastisol type products, but these provide due to their thermoplastic properties no real structural strength. The right approach for engineers is to define first the required mechanical properties of the adhesive for given substrate combinations with respect to the expected mechanical loads and then select the adhesive with the corresponding profile. This differs from the standard approach where the adhesive with the highest strength is selected for structural applications without really taking into account other important adhesive properties and the mechanical behavior of the substrates themselves.

When designing bonded joints, the right bonding area and overlap length is the key element for a successful bonding to guarantee the required load transfer with respect to the given mechanical properties of the substrates.

For example, when bonding metal to glass, a too strong adhesive in combination with a large bonding area or length will lead to glass breakage when exposed to very low temperatures. Or a too strong adhesive for the bonding of glass fiber or carbon fiber composites will lead to the delamination of the matrix resin from the fiber thus not providing the desired bond strength. By reducing the modulus of the adhesive and increasing the bonded area, the required load can be transferred without such delamination.

It is important to know that adhesives need a certain area to be able to transfer the desired load. Adhesives with very high modulus and low elongation at break are limited when enlarging the bonding area since they have no uniform stress distribution within the bond line. By increasing the bonding area, adhesives with lower modulus and higher elongation at break can transfer even higher loads than hard and brittle high strength adhesives and are in addition more tolerant toward impact stress.

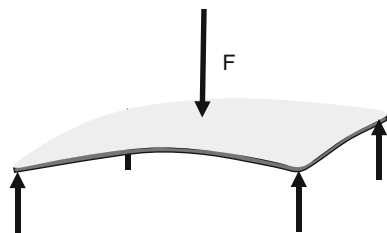
What is the real strength required for structural bonding? This central question cannot be answered in a simple way. The most important property is not the lap shear strength but the G-modulus or E-modulus, which can be used in calculations for the stiffness of a bonded structure. The bonding of a sun roof lid gives an idea about this effect. In this example, the lid is bent as shown in Fig. 14 with a force of up to 500 N, and depending on the modulus of the antifleutter and hem flange adhesive, the deformation is measured and calculated.

The calculation made by Deimel (1993) of the deformation depends on the modulus shows that the bending could be reduced from 7.8 to 4.8 mm at the given bending force of 500 N (Fig. 15). The maximum allowed bending was 5.8 mm. This is of real importance since at a car speed of more than 200 km/h the air would deform the lid too much and blow it away. The real bending measured with adhesives with 0 MPa (a deformable rubber), 5 MPa (a windshield adhesive), 20 MPa (a modified polyurethane (PUR) adhesive), and 100 MPa (a flexibilized 2C epoxy adhesive) showed a rather good correlation with the calculation. The stiffness increase was slightly higher than calculated which can be explained by the fact that the modulus was measured as secant modulus at one-third of the maximum shear strength. And in reality, at very low deformation, the modulus is higher. This example shows that for structural antifleutter bonding, a modulus of 50 to maximum 100 MPa will be enough to get the necessary stiffening effect. With a modulus of 1,000 MPa or more, the risk of surface marking will be much higher especially when using thinner metal sheets. And be aware that high strength steel sheets will not have less surface marking because it is the E-modulus of the steel which determines this property and not the yield strength.

In this real case, the requirement from the design was the necessity of a very thin lid to save space overhead. Plastisol-based antifleutter material did not provide the required stiffness, and when using a very strong epoxy adhesive to get the maximum increase in stiffness, surface marking occurred. The solution was a modified PUR-adhesive with a G-modulus of 50 MPa limiting the bending to 5.2 mm but with no surface marking.

The key to design bonded joints is the knowledge of E-modulus or G-modulus. These values can be used to calculate and predict the strength of a bonded joint. In

**Fig. 14** Bending of sun roof lid



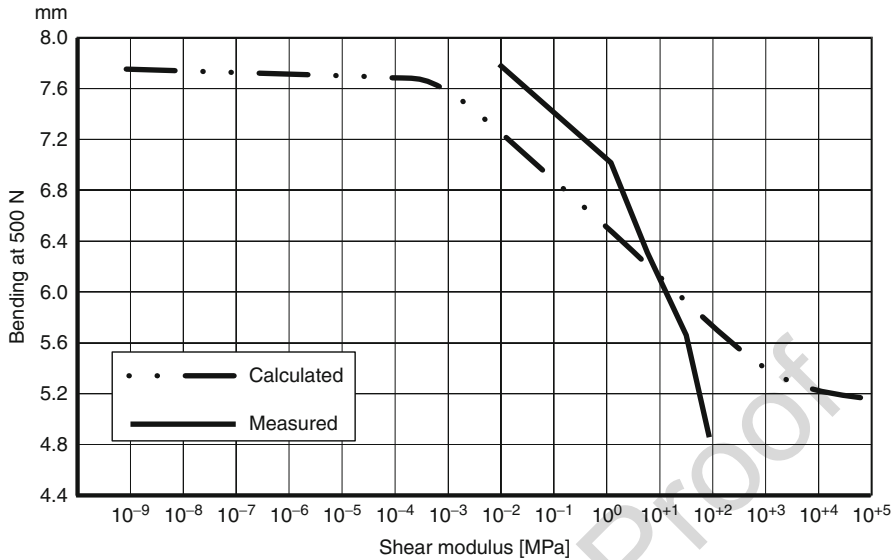


**Fig. 15** Stiffness of sun roof lid depending on shear modulus

contrast, the value of the lap shear strength of a joint is of no use since this depends on the specific properties of the substrate and the geometry of the samples and thus not inherent to the adhesive properties. A good overview of the design and calculation principles of bonded structural joints can be found in a series of articles by Schlimmer (Bornemann and Schlimmer 2004a, b; Bieker and Schlimmer 2004). Design of joints with structural adhesives and sealants is also treated in ► Chaps. 27, “Design Rules and Methods to Improve Joint Strength,” and ► 28, “Design with Sealants,” respectively.

A short example of a calculation is used to demonstrate this effect. When bonding a lap shear sample made from mild steel with yield strength of 280 MPa, a metal gauge of 1 mm, and a bonded area of 300 mm<sup>2</sup> (12 × 25 mm<sup>2</sup>), the force to reach the yield strength is 1 mm × 25 mm × 280 MPa or 7,000 N. The lap shear strength of the adhesive will be calculated with 23.3 MPa. Due to the small increase of the strength of the steel on yield, in practice not more than 25 MPa can be expected. And there will be no adhesive providing more than 25 MPa, even if the inherent strength of an adhesive may be much higher.

The other example will be a lap shear joint sample with 1 mm steel and an adhesive with 5 MPa lap shear strength (e.g., a windshield adhesive). In this case, when the bonding area is 1,800 mm<sup>2</sup>, which corresponds with an overlap length of 72 mm, there is also a failure in the steel.

The lap shear strength is a measure which depends on the sample design whereas the G-modulus is an inherent adhesive property. The benefit of a lap shear test is a simple specimen for quality control of the combination of adhesive, adhesion, and surface quality.



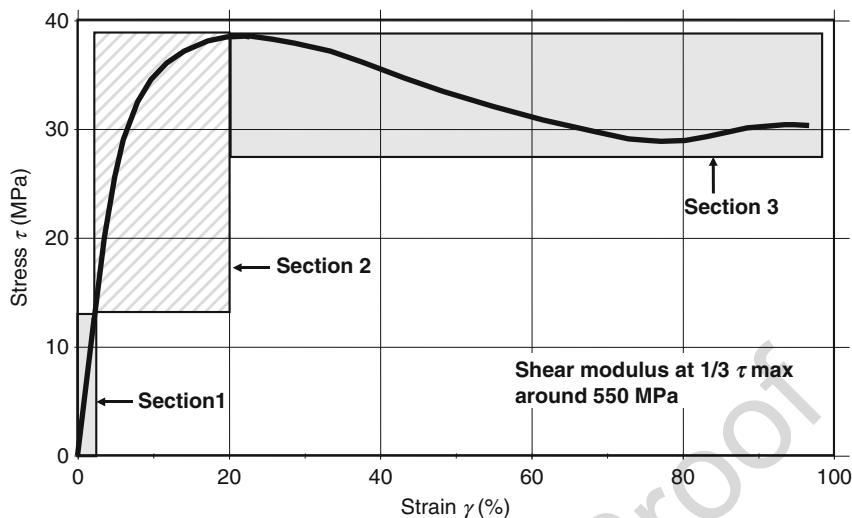
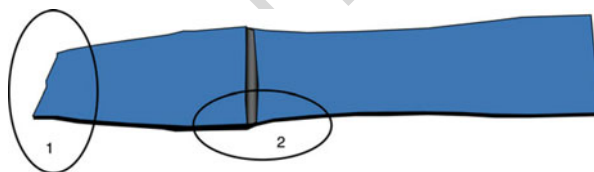


**Fig. 16** Stress–strain diagram of a crash-suitable adhesive

**Fig. 17** Failure of a lap shear sample with a crash-suitable adhesive



The diagram in Fig. 16 shows three sections. Section 1 is the area where the adhesive shows almost linear behavior and the strength and the deformation of the bond can be predicted and calculated for the lifetime.

Section 2 is an area where the adhesive shows resistance against short time high load without damage. And it can be seen that the maximum load in this section is almost in the range of 40 MPa, which is far above the strength level of the steel in the calculated example above. Sections 1 and 2 are typical for high strength structural adhesive, also for the brittle types. Section 3 shows the additional benefit of a crash-suitable adhesive because such adhesives start to deform significantly without break absorbing enough energy to keep the parts together. Figure 17 shows that these adhesives really work with a broken lap shear sample which proves the calculation above. Two areas are remarkable in Fig. 17. In area 1, the metal broke after it exceeded its tensile strength, and in area 2, very high stress concentration occurred due to the metal deformation. At failure, it was observed that at the edge in area 2 the adhesive started to crack but due to the built-in nanoscale crack stoppers it did not break. Such adhesives are designed that during curing phase separation occurs and phase of elastomeric nanoparticles is built, which act as crack stopper published by Burchardt et al. (2009).

Such a property is crucial in case of a sudden overload through an impact. In particular, hard and brittle adhesives with very high strength (higher than 1,000 MPa

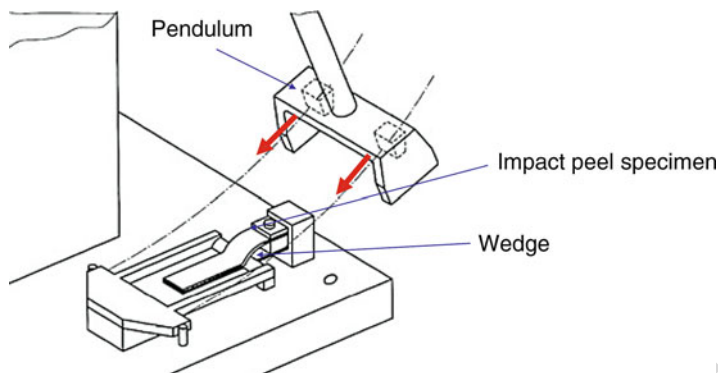


**Fig. 18** Impact peel test (crash) – ISO 11 343

**Fig. 19** Impact peel test specimen



G-modulus) fail under such loads very fast and these are not recommended for automotive applications where impact resistance is needed. The impact performance is tested with an impact peel tester shown in Fig. 18, where a weight on a pendulum drives a wedge through the specimen and the forces are recorded.

The test specimen is a wedge sample as illustrated in Fig. 19.

The diagram of an impact peel test in Fig. 20 shows the difference of a crash-suitable adhesive in contrast with a very good structural automotive adhesive.

The first peak of the curves is the initial peel resistance and the jagged curve gives the average value of the impact peel strength. Whereas the standard structural adhesive ends after 15 ms with an average peel force of 400 N, the crash-suitable one withstands for almost 20 ms providing a peel force of 900 N. The area under the curve is a measure of the energy absorption of the adhesives itself. Of course, the small amount of adhesive in a bonded structure is not absorbing the crash energy. It is the structure which is held together by such a high-performance adhesive thus providing better results than a spot welded part.

More information on impact is given in ► Chaps. 21, “Impact Tests,” and ► 29, “Design for Impact Loads.”

## 46.7 Durability

A key question of bonded joints is the durability since adhesives are not metals and their performance is more dependent on temperature and environmental influences. And an engineer has the responsibility for the function of the structure over the

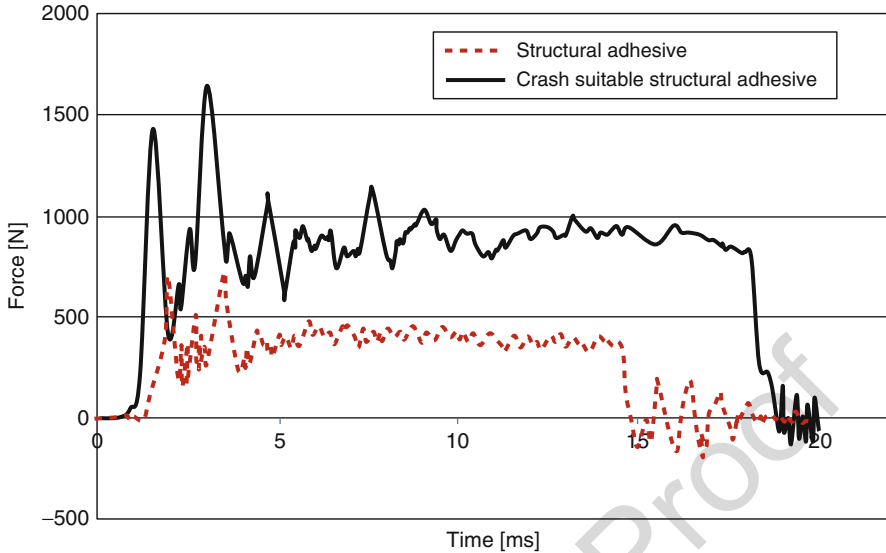


**Fig. 20** Diagram of an impact peel test

designed lifetime even under harsh environmental conditions. How can the durability of an adhesive be evaluated?

The durability of adhesive bonding is determined by four elements:

1. Durability of the substrates
2. Durability of the adhesive itself
3. Durability of the boundary layer
4. Durability of the bonded system

The durability of the substrates and the bulk adhesives can be tested separately with shouldered test samples. These tests give an indication if the bulk material can provide the required performance.

Testing of the adhesion within the boundary layer needs more effort. Metal adhesion in automotive industry always means adhesion on the oxide layer. This layer is attacked by moisture in combination with oxygen which leads to disbonding over a certain period of time. All surface preparations and specific ingredients of the adhesives have the goal to slow down this deterioration of the oxide interphase as well as possible. This is usually tested by cycles like the VDA test. And it can be seen that under these conditions, the oxide layer will be destroyed over time. In order to have a correlation of this effect in comparison with real-life corrosion results, every car manufacturer has its own cycles.

An important contribution for a durable adhesive is the exclusion of moisture. This does not mean that the adhesive layer cannot get wet, but it must be able to dry up again and in cases where moisture may remain longer, it is recommended to protect the adhesive with a sealant, especially in the lower areas of the car. This is

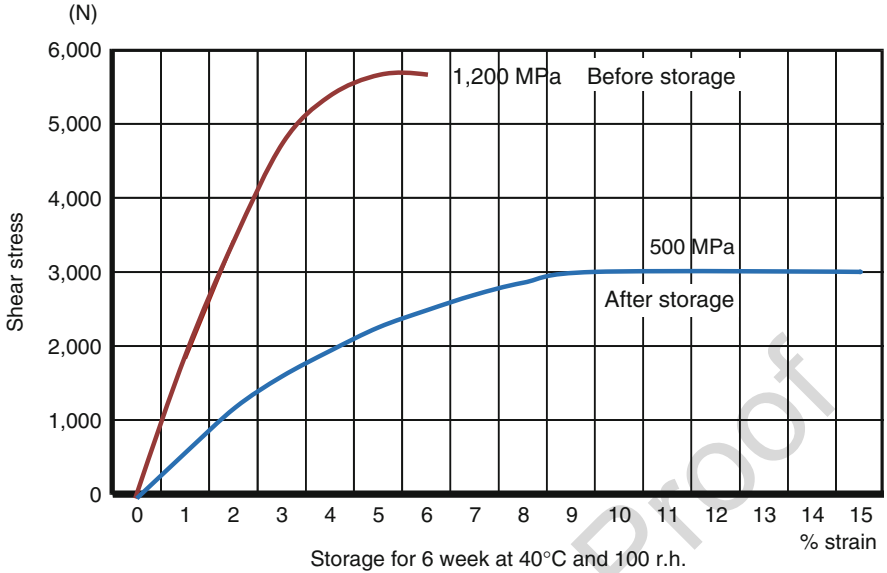


**Fig. 21** Decrease in shear modulus of an epoxy adhesive after humidity storage

anyway a good solution, since the corrosion starts from the cut edges of the metal sheets which are not really protected by the adhesive squeezed out in an uncontrolled way. To simulate the effect of humidity on the adhesive, the samples should be conditioned in a humidity chamber (for example, according to DIN 50017) before testing, because the saturation of the adhesive with moisture will lead to a plasticizing effect and reduce the strength and modulus of the adhesive but reflect better the reality (see Fig. 21).

Figure 21 shows the decrease of the modulus of a standard epoxy adhesive after storage at high humidity. Of course, this effect is dependent on the formulation of the adhesive, but all adhesives are affected by humidity to a certain degree. This effect cannot be detected with simple lap shear samples because the lap shear strength is almost unchanged (see calculation above). There is sometimes even a slightly higher lap shear strength observed since the plasticizing effect of the humidity reduces the brittleness of the adhesive and the failure occurs at slightly higher forces.

The durability for a bonded system can be tested by applying cyclic loads on either simple lap shear specimens, more sophisticated H-specimens or on the whole bonded structure (e.g., the whole car body). It is recommended to run a corrosion test or at least a high humidity test upfront ( Fig. 22).

Since adhesives are plastic materials, they may creep under high loads and therefore the expected static load is a determining factor for the durability. Compared to lap shear strength or tensile strength measured with shouldered test bars, the resistance toward static load is significantly lower. It is recommended to use only in the range of 3% to a maximum 10% of the maximum lap shear strength for the calculation of the sustainable permanent static loads for the use phase.

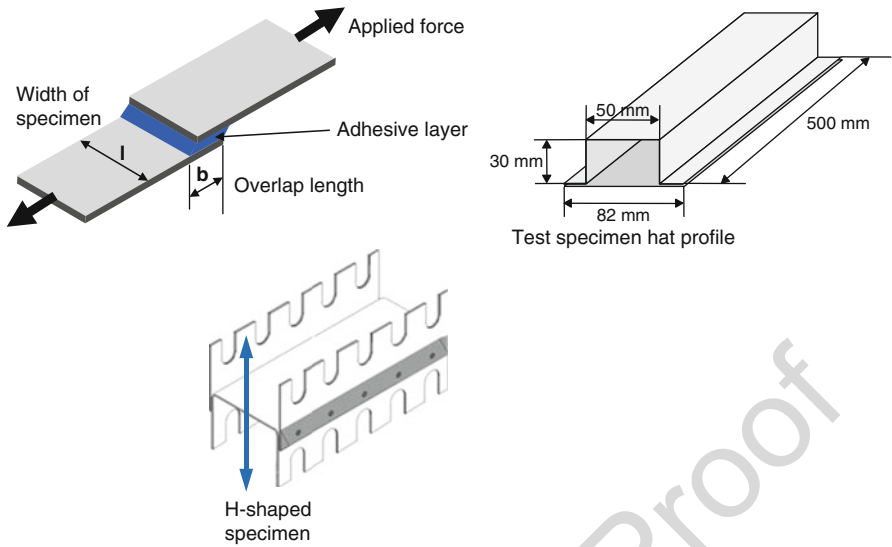


**Fig. 22** Test specimen for durability

Under dynamic stress, adhesives can withstand much higher loads (up to 30% of the maximum load).

When measuring fatigue, the strength level of a windshield adhesive after more than 20 million cycles is in the range of 0.2–0.3 MPa, which is in the range of 3–5% of its initial lap shear strength (Fig. 23). When tested under the corresponding static load, nearly the same result occurs, but it is not clear if this correlation is valid for all adhesives.

For windshield bonding, an additional durability issue is the resistance to UV radiation. The directly exposed bonding zone of the adhesive is destroyed by UV radiation if not protected by a screen print on the glass with sufficient UV absorption or with other methods of masking. Using only a black primer is not sufficient to guarantee a durable adhesion for the predicted lifetime. The UV transmission must stay below a value of less than 0.2%. Inspection at cars after 8–10 years lifetime in various environments built in 1987 and 1988 have shown that there was reduced adhesion in areas where the UV transmission was higher, because at that time the quality of the screen print on the glass was not on the level of today. Nevertheless, the windshields were still bonded to the frame without leakage which shows the robustness of this technology. Even after more than 30 years of use, polyurethane windshield adhesives show no relevant decrease in strength and do not lose their mechanical properties significantly. A precondition for a durable adhesion is, as with the body shop adhesives, the exclusion of permanent moisture.

The combination of bonding with other joining methods like spot welding, riveting, or clinching called hybrid bonding or hybrid joining gives additional benefits. The punctual joining methods provide immediate fixation and they also take away the static load from the adhesive which gives superior dynamic fatigue strength due to an even stress distribution, especially in combination with very thin metal sheets. Hybrid bonding

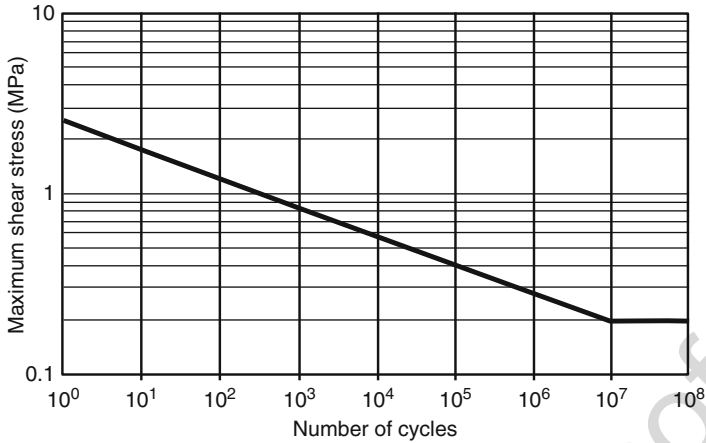


**Fig. 23** Fatigue curve of a windshield adhesive

will allow lightweight design by using thinner metal sheet made from very high strength steel without reducing strength and durability. Due to the material savings, the additional process cost will not be higher since the number of welded spots or rivets can be significantly reduced and the application speed of an adhesive is higher than that of spot welding. Therefore, the overall number of robots in a real production would be the same. The weight increase by the additional adhesive is in the range of a maximum of 2 kg for a whole car body, but the weight savings can be in the range of 20%. Thus, the savings in material for steel compensates the cost for the adhesive.

The Wöhler-diagram in Fig. 24 demonstrates the difference in durability of different adhesive types. The 1C epoxy starts with the highest strength level but after ten million cycles, the remaining strength is lower than that of a polyurethane toughened epoxy which has a lower initial strength but due to its reduced crack sensitivity, a higher durability. The rubber-based adhesive and the 2C epoxy adhesive have a similar behavior. These tests were run with aluminum AlMg5Mn single lap shear samples and a surface treatment with Ti/Zr. The overlap length was 12.5 mm and the size of the metal plates 110 × 48 × 1.5 mm. The adhesives were conditioned with a 480 h salt spray test according to DIN 50021 before testing. Spot-welded samples would have already failed at the initial load level of all these adhesives.

Real-life experience from cars shows that spot weld bonded areas provide a much better corrosion resistance than spot welded areas alone because the adhesive fills the joint preventing the intrusion of moisture.

When bonding metal sheets with the typical thickness for automotive use in the range between 0.6 and 1.5 mm, bonded samples can typically bear higher loads during more cycles.

The diagram in Fig. 25 illustrates this case. Spot weld bonded H-samples (see Fig. 22) start the fatigue test at a stress level of around 60 kN and end after six million cycles at around 30 kN, which is the starting level of the Metal Active Gas (MAG)-welded sample.

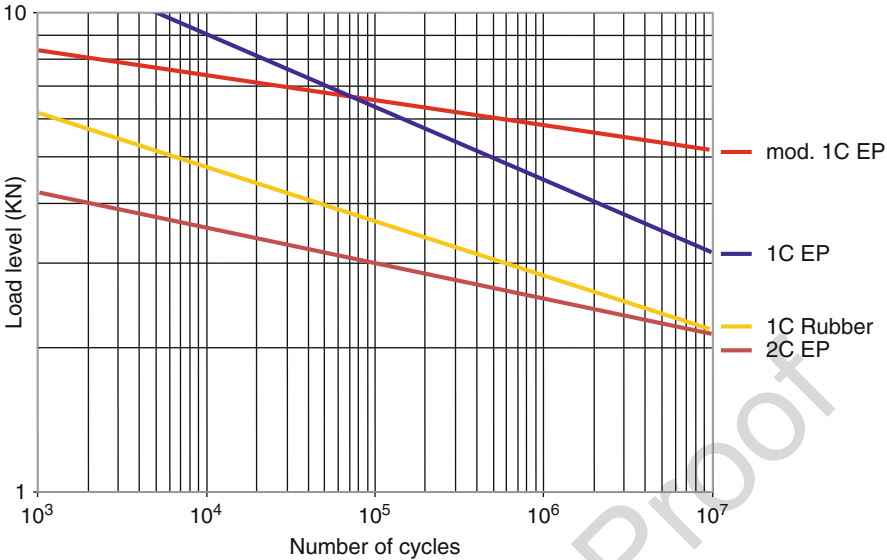


**Fig. 24** Fatigue strength after 480 h salt spray test (EP epoxy)

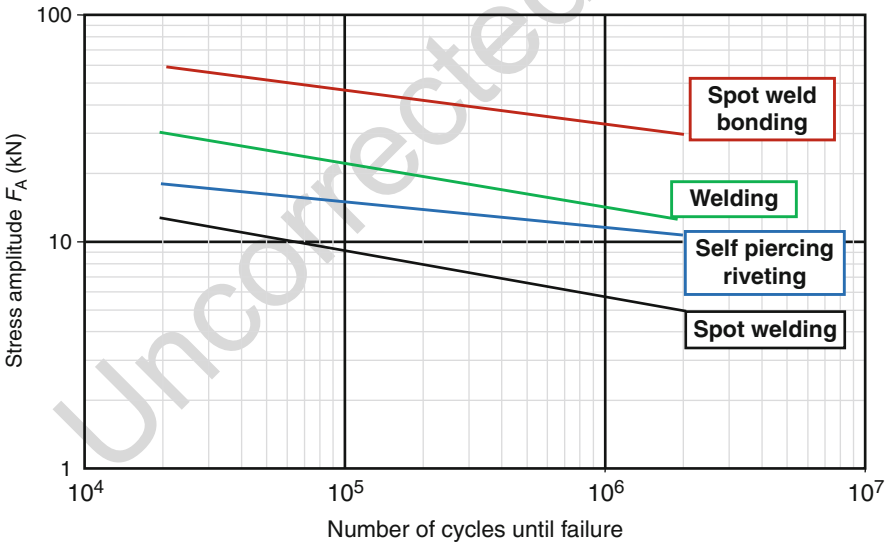


**Fig. 25** Fatigue strength with different joining methods

Spot-welded single lap shear samples under the same conditions show a much lower force level at the end of the test. Since the performance of punctual fixations like rivets or spot welds is more sensitive to the thickness of the metal sheets, adhesive bonding exhibits even more advantage with thinner metals. Since this is a double

logarithmic diagram, the difference in the load level of spot welding and bonding is 6–32. Therefore, with such hybrid bonding, the bond strength under fatigue is determined by the adhesive bonding alone. Premium car producers like AUDI, BMW, Mercedes, and even VW use bonding in combination with high strength steel. For example, the newest AUDI A 1 reports a bond length of 60 m (ATZ extra 2010).

Whereas Fig. 17 shows the influence of adhesive properties on the durability, the diagram in Fig. 26 gives a comparison between the effect of adhesive bonding on steel and aluminum.

In this case, the samples are hat profiles preconditioned at 70 °C and 92% RH for 240 h and the distance of the spot welds is 50 mm.

The load is expressed in the torsion moment, and it can be seen that a spot-welded aluminum profile with 2 mm thickness gives the worst results, even if it ends up at nearly the same level as the spot welded steel with 1 mm thickness. Comparing the result of 1 mm spot-weld bonded steel with 1.2 mm spot-weld bonded aluminum, the aluminum shows already a better durability.

What is also obvious is how much improvement can be seen between the spot-welded 2.0 mm aluminum and the 2.0 mm spot-weld bonded aluminum. The distance between the spot welds is 50 mm which is longer than the usual 30 mm. With shorter distances between the spot welds, the results for the spot-welded samples would be better but will not reach the level of bonded samples.

This is not only observed with these test specimens, but it was also proven in the comparison of real spot weld bonded cars, as shown in Fig. 27.

Depending on the design of the car, the increase in static torsion stiffness is for steel cars between 15% and 25%. The 38% are a case where due to the longer spot-weld distance and the weaker structure the improvement was significantly higher. Car 3 was a convertible with additional stiffening bars at the bottom; therefore, the improvement was lower. But what was rather unexpected were the results obtained for cars 5 and 6. Car 5 was a conventional steel car with a high structural stiffness,

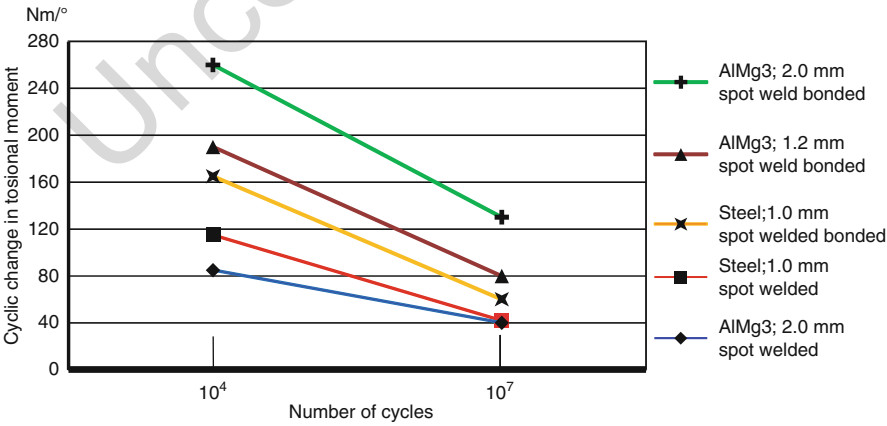


**Fig. 26** Fatigue strength: comparison of spot welded and bonded aluminum and steel



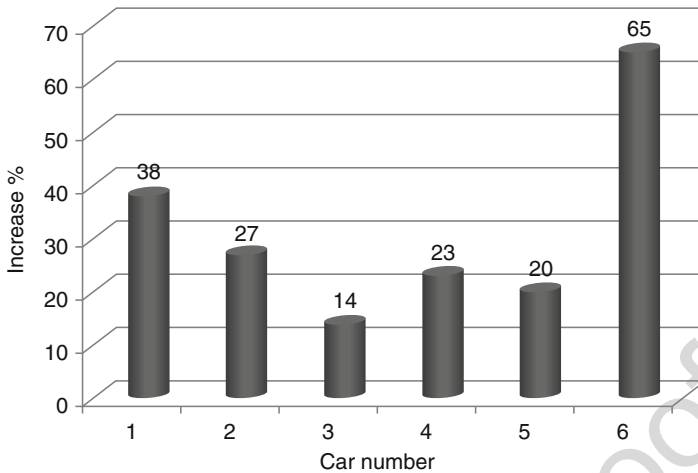


**Fig. 27** Stiffness increase of spot weld bonded cars measured before and after curing of the adhesive

and the improvement through bonding was with 20% in the expected range. The car 6 was the same design but made from aluminum. And since it was an experimental car, the aluminum sheets were stamped in the same tools like the steel sheets, which means the increase of the metal thickness for aluminum versus steel was in the range between 0.1 mm and 0.2 mm. But the increase in stiffness was 65%, which is much higher than with steel car and confirms the results of the hat profiles. And the weight for the car body in aluminum was 55% lower than for the same steel car. This concept is realized in the current Jaguar XJ.

As already mentioned, the lap shear strength of an adhesive is not very relevant to the strength of a bonded joint because when enlarging the bonded area, the force can also be transferred with adhesives of lower strength, but remember the G-modulus, which is important for the stiffness of the structure.

In the diagram in Fig. 28, the strength of spot welded and spot-weld bonded lap shear samples with 45 mm width and 16 mm overlap plus one spot weld is shown. It shows that strength level is only determined by adhesive bonding. After the failure of the bond, the spot weld can still bear the additional load as was shown in the research report from Hahn and his group (Hahn and Wißling 2007).

The calculated lap shear strength of the bond based on this diagram is about 11.1 MPa. One spot weld accounts for 3,500 N, and with a spot weld distance of 30 mm such a welded flange with a length of 1,000 mm, for example, would provide failure load of 116.6 kN. Assuming a lap shear strength for the adhesive of 11 MPa and an overlap of 12 mm for the bonded area, the corresponding failure load of the bonded flange with a length of 1,000 mm will be 132 kN. According to this calculation, a lap shear strength of 10 MPa is sufficient for bonding thin steel sheets in comparison with spot welding. The crack resistance of an adhesive is more important than its maximum strength.

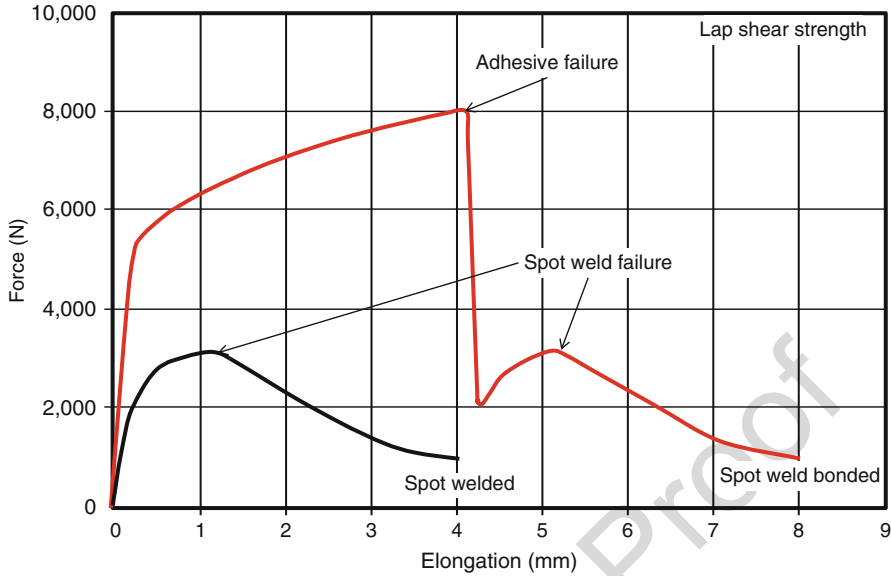


**Fig. 28** Failure diagram of bonded and spot weld bonded lap shear sample

And for the stiffness, only the G-modulus is important and with the rather thin adhesive layers of 0.3–0.5 mm in a spot-weld bonded flange, there will be no significant difference between an adhesive with 100 and 1,000 MPa G-modulus in the overall torsion stiffness of the car body.

The diagram also shows the benefit of the hybrid joining since the failure of the spot weld occurs at higher elongation.

Another important property for durability is the glass transition temperature, abbreviated as  $T_g$ . Since adhesives are organic polymers, their properties are much more temperature dependent than metals. And a measure for the temperature stability is the  $T_g$ . In Fig. 29, the dynamic mechanical analysis (DMA) of a crash-suitable epoxy adhesive is shown with a  $T_g$  of about 90–100 °C depending on how the  $T_g$  is determined. Usually for body shop adhesives, the  $T_g$  should be above 80 °C to avoid a strong change in the modulus of the adhesive because the modulus changes about a factor of 100 between 60 °C and 120 °C (see diagram in Fig. 22). There are two different ways to determine the  $T_g$ . One is the intersection point of the two tangents at 85 °C and the other is the point of inflection of the storage modulus curve at 100 °C. Since the  $T_g$  is not an exact temperature, it is better to look at the storage modulus curve to see the real difference in modulus below and above  $T_g$ .

On the other hand, a low  $T_g$  (below –50 °C) does not mean that the adhesive does not fulfill the requirements. Typical windshield adhesives always work at temperatures above their  $T_g$ , as it is shown in Fig. 30. But the decrease in the modulus for this type of adhesive in the working range of –40 °C to +100 °C is from 20 to 2, which is only about the factor of 10 lower.

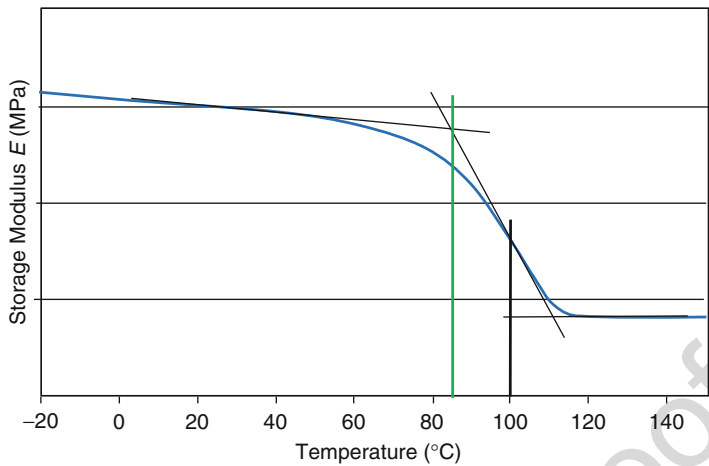


**Fig. 29** Determination of the  $T_g$  with DMA analysis of a structural adhesive

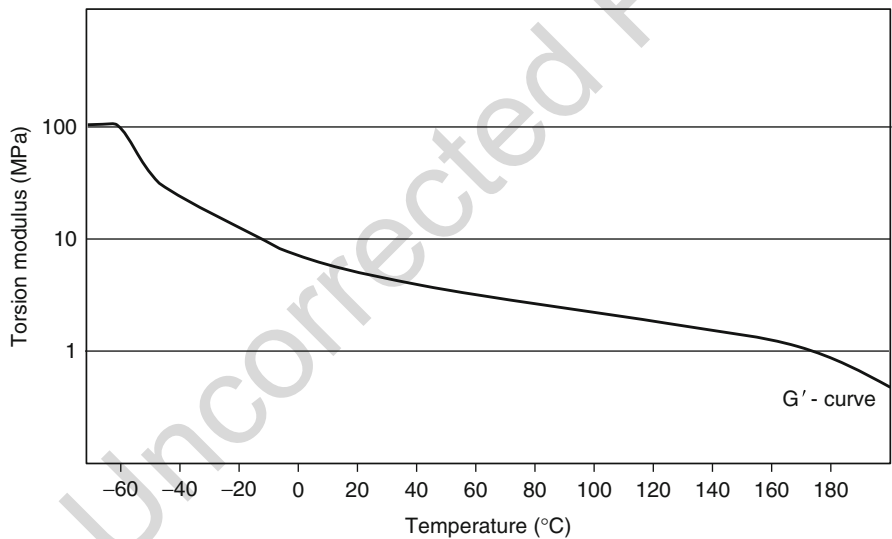


**Fig. 30** Torsion modulus over temperature of a 1C PUR adhesive

More information on the durability of adhesive joints is given in Part F.

### 46.8 Type of Failure

The same failures as in other bonding applications apply to adhesive bonding in automotive. They are:

796 Failure of one of the substrates  
797 Failure of the adhesive  
798 Adhesion failure

799 When designing a bonded joint, the goal is to achieve at least a break within the  
800 adhesive. This guarantees that the adhesion is higher than the cohesion and the  
801 adhesive is fully utilized. If failure in one of the substrate occurs, the bonding fulfills  
802 the requirements. Such failures can be much better predicted due to the inherent  
803 material properties of the substrates or the adhesive.

804 But in reality, failure occurs in most cases within the adhesion zone. This is the  
805 main reason that engineers have some doubts to use adhesives in structural  
806 applications.

807 When bonding metal substrates, it is the deterioration or corrosion of the oxide  
808 layer which destroys the adhesion zone. With plastic substrates, effects like plasti-  
809 cizer migration or residues of release agents are often reasons for failure, whereas  
810 moisture plays a less important role.

811 In real cars, bonded structures show overall an even better durability than spot  
812 welds since the overlap of the metal sheets is much better protected against  
813 corrosion.

814 When bonding plastic parts like Sheet Moulding Compound (SMC) or even  
815 carbon fiber composites, moisture will have the same plasticizing effect on the  
816 matrix resin as on the adhesive.

---

## 817 46.9 Quality Control

818 As mentioned in the introduction, adhesives are process materials. This is similar to a  
819 welding process. For these processes, it is very difficult to control the quality of a  
820 bonded joint in a nondestructive way. Therefore, it is crucial to control the process  
821 parameters of each production step, to check the properties of the adhesive with the  
822 real substrates and it is necessary to control the surface conditions of the substrates  
823 itself. And even with nondestructive testing methods, it is not possible to check the  
824 quality and durability of the adhesion itself. This can only be done with thorough  
825 adhesion tests upfront with original substrates and original process conditions.

826 Therefore, the way to a durable bond goes along with a survey of all relevant  
827 process parameters. If this is guaranteed, bonded joints have the same life expect-  
828 tancy as other parts of the car body structure.

829 It is recommended to run separate lap shear samples along the whole process  
830 which can then be tested separately to have a continuous process survey. But this  
831 does not differ from the quality control system of the paint process.

832 The quality of a bonding process depends to a high degree on the quality of the  
833 personnel. Therefore, a similar level of education is needed as for the welding  
834 specialists. The Institut für Angewandte Materialforschung (IFAM) in Bremen offers  
835 education courses for three different levels of expertise and everyone who wants to  
836 use structural adhesive bonding. See Part H for more information on Quality control.

---

## 46.10 Repair and Recycling

It is true the repair of bonded joints is different from that of bolt-on parts. But in comparison with riveted, spot welded, or welded structures, the removal of bonded parts may be even easier. When repairing bonded metal structures, the removal of a damaged part is done by mechanical abrasion or with hammer and chisel. The adhesive is then removed by abrasion like it is done with painted surfaces. More challenging in the repair case is to bond a new part on the old structure. It is not possible to use the same adhesive as in the production line since the process conditions are different. In this case, 2-C high strength adhesives with improved impact resistance can be used as published by Lutz (2009). And to process these adhesives correctly, well-educated personnel is required.

Windshield adhesive can be removed either with a steel wire or with specific cutting tools. This is nowadays a standard procedure in repair shop and it can even be done within 1 h on the road.

In this context, it is important that the bonding area is designed in a way that enough space for the cutting tools ore wire is available. There is no need to remove the old adhesive layer completely. It is recommended to bond on a maximum 1 mm thick layer of the old windshield adhesive after the proper surface preparation with a primer which gives additional corrosion protection when the paint layer suffered damage when removing the windshield.

With the idea of recycling, adhesively bonded parts are under pressure since the common perception is that such parts cannot be separated again. And it is true if dissimilar materials are bonded together the separation of the different substrates needs more effort. There are activities to develop adhesive which disbond on command, but it is almost impossible to have durable adhesion under all relevant conditions and in addition an easy disbonding, for example, under high temperatures or by chemical reaction. See Chap. 58.

For bonded metal parts, this is in the recycling case not a real issue since the amount of adhesive in a car body structure is with about 2 kg lower than the weight of the paint. When shredding the metal parts, adhesives as plastic materials can be separated in the same way as the paint and other plastic residues.

---

## 46.11 Conclusions

Adhesive bonding for structural applications has become an important joining technology in the production of cars. It is for decades a well-established method to join doors and hoods and install glasses. And with a new generation of impact-suitable structural adhesives, premium cars have introduced hybrid joining to build lighter cars with increased impact performance. This chapter may help to exploit the full potential and the benefit of adhesive bonding in combination with other joining methods for cars. In particular, the engineers of premium cars in Germany have already started to trust such a technology and use it to a larger extent. It takes time for

the implementation because the full benefit can only be achieved when the car body is designed for this technology.

The main obstacles are the lack of education and experience of the design engineers who have to implement adhesive bonding.

---

## References

- ATZ extra (2010) Presentation of the new AUDI A:1
- Bieker C, Schlimmer M (2004) Berechnung und Auslegung von Klebverbindungen (Teil 3). Adhäsion, Kleben & Dichten 7:38–42
- Bornemann J, Schlimmer M (2004a) Berechnung und Auslegung von Klebverbindungen (Teil 1) Adhäsion. Kleben & Dichten 5:30–33
- Bornemann J, Schlimmer M (2004b) Berechnung und Auslegung von Klebverbindungen (Teil 2) Adhäsion. Kleben & Dichten 6:40–42
- Brockmann W, Grüner KJ (2003) Betrachtung zum Kriechverhalten von Haftklebstoffen, 17. Internationales symposium Swissbonding, Rapperswil
- Burchardt B, Diggelmann K, Koch S, Lanzendörfer B (1998) Elastic bonding. Verlag Moderne Industrie, Landsberg
- Burchardt B, Schulenburg JO, Linnenbrink M (2009) New building blocks for lightweight structures. Adhesion, Adhesives & Sealants 10:22–27
- Cognard P (2006) Handbook of adhesives and sealants, vol 2, General knowledge, application techniques, new curing techniques. Elsevier, New York
- Deimel A (1993) Fachhochschule München, Einfluss der Klebstoffsteifigkeit auf das Verformungsverhalten geklebter Fahrzeugkomponenten, Diploma work
- Hahn O, Wißling M (2007) Methodenentwicklung zur Berechnung von höherfesten Stahlklebverbindungen des Fahrzeugbaus unter Crashbelastung. Abschlussbericht Forschungsvereinigung Stahlanwendung e.V, Düsseldorf
- Industrieverband Klebstoffe IKV 2017: [www.klebstoffe.com/die-welt-des-klebens/anwendungsbiete/fahrzeugbau.html](http://www.klebstoffe.com/die-welt-des-klebens/anwendungsbiete/fahrzeugbau.html)
- Lutz A (2009) Crash resistant two-component adhesives for repairs “As good as new”. Adhesion extra Adhesives & Sealants 10:28–29
- Rechner R, Jansen I, Beyer E (2010) Laser- und Plasmaverfahren im wirtschaftlichen Vergleich. Adhäsion, Kleben & Dichten 1–2:36–43
- Schulz D (2010) Gut gereinigt ist halb geklebt. Adhäsion, Kleben & Dichten 7–8:18–22
- Stepanski H (2010) Punktschweißkleben im Automobilbau. Adhäsion, Kleben & Dichten 5:30–35, 6:35–41
- Wisner G, Stammen E, Dilger K, Spiekermeier A, Halanesh M, Hübner S, Behrens B-A (2015) Kleben und Umformen von Stahlblechen in Bonded-Blank-Technik für den Automobil-Rohbau. In: DVS-Berichte Band 315 (2015). DVS Media GmbH, Düsseldorf, S, pp 171–177
- Wisner G, Stammen E, Fischer F, Dilger K, Zillessen A, Brodel M. (2014) Accelerated adhesive bonding of wood panels for prefab houses. In: Martínez JMM (ed) EURADH 2014 10th European adhesive conference – proceedings. 22.04. – 25.04.2014, Alicante/Spain 2014. pp 307–310, 2014, ISBN. 978-84-616-8627-8

Yasuaki Suzuki

**Contents**

47.1	Introduction .....	1368
47.2	Adhesive Bonding Application for Current Rolling Stock .....	1368
47.2.1	Railcar Structures and Their Fabrication .....	1368
47.2.2	Application of Adhesives in Rolling Stock .....	1370
47.2.3	Use of Sealants .....	1377
47.2.4	Pressure-Sensitive Adhesives .....	1378
47.3	Application of Adhesives for Prototype Railcars in Japan .....	1380
47.4	Application of Structural Adhesive for Rolling Stock over the World .....	1383
47.4.1	Britain (Seeds 1984) .....	1383
47.4.2	France .....	1387
47.4.3	Germany .....	1388
47.4.4	Switzerland .....	1389
47.4.5	Indonesia .....	1389
47.5	Conclusion .....	1390
	References .....	1390

**Abstract**

Adhesion is an indispensable joining technology for railway industries. Adhesives are used for the fabrication of almost all rolling stocks. In the steel main structure of conventional rolling stocks, adhesives are applied for bonding decorated aluminum sheets of wall and ceiling to frames, bonding of floor covering to floor plate, and fixing heat insulating material to the inside of carbody. Large amount of sealants is also used even in the conventional rolling stocks. Recent high-speed trains have modern light-weight structures consisting of aluminum hollow extrusions, sandwich panels, or carbon fiber reinforced plastics. For the structures, adhesion plays an important role as a structural joining method. Even for conventional rolling

Y. Suzuki (✉)

Suzuki Adhesion Institute of Technology, Ichinomiya, Aichi, Japan

e-mail: [yasuzuki-1@nifty.com](mailto:yasuzuki-1@nifty.com)

stocks, the use of adhesives is increasing. For instance, weldbonding is nowadays experimentally applied to the aluminum body structures. Moreover, adhesive is used to smooth the outsides of each carbody and between the outersurfaces of carbody and window. As a result, aerodynamic noises inside and outside the train and energy consumption are considerably reduced.

Maglev trains will be increasingly use in the future, and the use of adhesives will expand due to the demand of reducing weight and energy consumption. In this chapter, the cases in Japan are mainly explained. World-wide cases are shown in Sect. 4.

---

## 47.1 Introduction

Railways have progressed with three important missions such as high speed, safety, and mass transportation. In particular, a high speed rail system called “Shinkansen,” which means new railway trunk line, has been developed in Japan over the last four decades and has significantly contributed to the development of Japan. Nowadays, the network is prolonged to many subsidiary regions including Hokkaido island through an undersea tunnel even though it is far from the main island of Japan.

In addition, Chuo Shinkansen as a detour of Tokaido Shinkansen that utilizes the Superconducting Maglev will be constructed (Central Japan Railway 2009a).

Rolling stock, which means railcars of broad sense, consumes the smallest energy per person-distance among all the transportation systems. It is about half that of buses and one-sixth of that of cars (Kamiura et al. 2000). In addition, since the power source is mainly electric, the consumption of fossil fuel by rail systems is relatively small. Therefore, we might say that trains are the most environmentally friendly transportation system.

Recently, high speed, passenger comfort, safety, and being environmentally friendly are indispensable for railway systems, and they lead to the importance of weight saving, high strength, high rigidity, noise insulation, vibration damping, thermal insulation, incombustibility, and recyclability. In addition, as the service life and model-change intervals of railcars are shortened, the cost reduction has also become an important factor (Miyamoto 1998). To meet such vast demands, introducing multimaterial structures, in which different materials are joined together and used respecting their own characteristics, is a good solution. The most promising method to join the multimaterial structures of trains is adhesion.

---

## 47.2 Adhesive Bonding Application for Current Rolling Stock

### 47.2.1 Railcar Structures and Their Fabrication

The main structure of railcars is called the “body structure.” It consists of six panels: side constructions, roof construction, end constructions, and an underframe. Stainless steel and aluminum alloy are increasingly used instead of carbon steel for weight



reduction and easy maintenance as the main structure. They are mainly fabricated by welding. By eliminating the thickness increment for corrosion, stainless steel body structure can be lighter than carbon steel body.

For stainless steel body structures, panels are joined using spot welding on a frame joined by welding. Figure 1 shows an example of the body structure of 205 series electric railcar for commuting made of stainless steel (Matsuzawa 1986). As shown in this figure, corrugated stainless steel plate are spot welded on an underframe.

Aluminum alloy cars are fabricated with another method. Large-scale extrusions are used in order to reduce the total length of welding and they are joined by metal inert gas (MIG) or laser welding technique. For instance, E2 series and 700 series Shinkansen cars have a double-skin structure consisting of large-scale aluminum hollow extrusions welded continuously along the longitudinal direction, as shown in Fig. 2 (Abiko and Kobayashi 1998). This method can use automatic processes because there are very few columns or beams and that contributes greatly for cost reduction. Recently, another novel method called Friction Stir Welding, whose thermal input to joints is smaller than the conventional welding methods, has been gradually adopted for new types of aluminum cars instead of MIG welding in order to reduce the thermal deformation and enhance the fabrication accuracy.

In the body structures, modules such as heat insulating materials, floor deck, floor covering (made of non-rigid polyvinyl chloride (PVC), polyolefin, or rubber), inside panels (made of decorated aluminum sheet with melamine resin, aluminum panels pasted non-rigid PVC film, or fiber reinforced plastics (FRP)), windows (made of glass or polycarbonate), interior parts such as seats, lighting equipments, air conditioning equipments, and wiring and piping are equipped. In addition, hard wiring

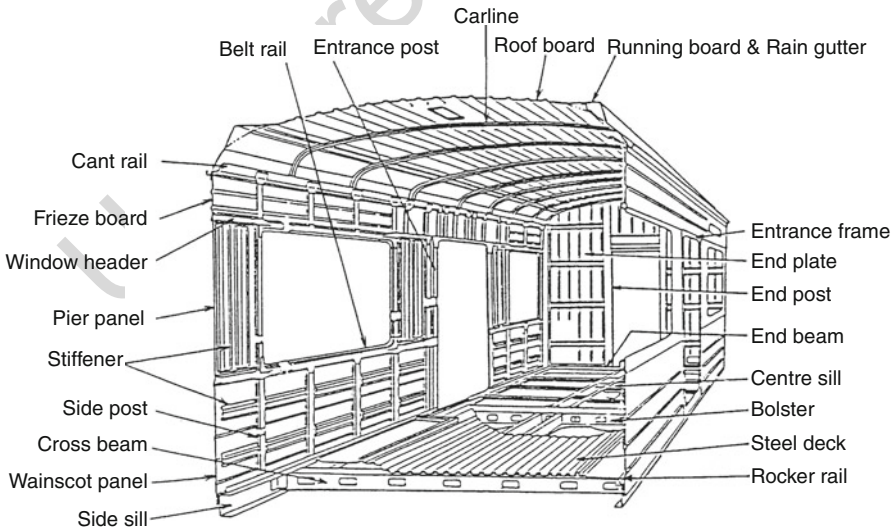


**Fig. 1** Body structure of 205 series electric railcar for commuting made of stainless steel (Matsuzawa 1986)

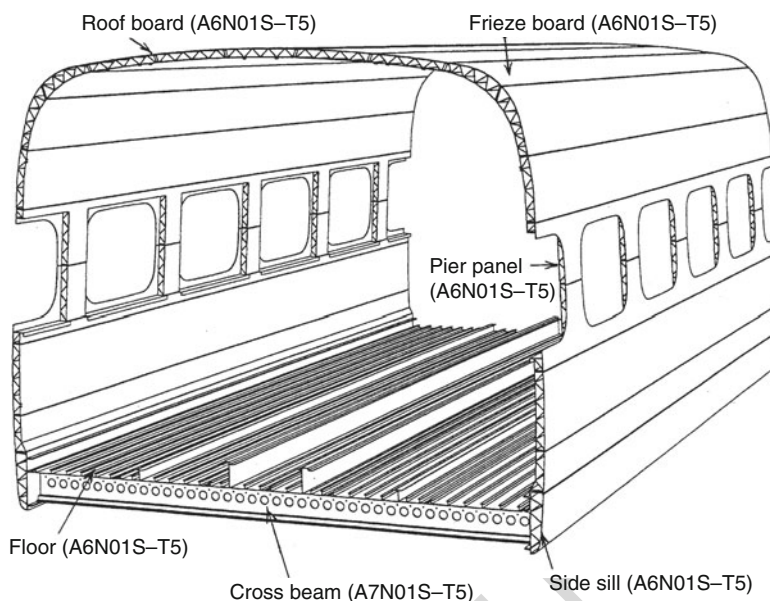


**Fig. 2** Body structure of 700 series Shinkansen made of large-scale aluminum hollow extrusions (Abiko and Kobayashi 1998)

and heavy equipments such as transformers or compressors are placed under the floor, that is, the complete sequence of rolling stock fabrication.

### 47.2.2 Application of Adhesives in Rolling Stock

In current rolling stock, adhesives are mainly utilized to join interior equipments. Table 1 summarizes typical adhesive applications for rolling stock use (Suzuki 2006, 2009). Figure 3 shows the share ratio of adhesive types and purposes in the cases of suburban electric cars and Shinkansen cars (Suzuki 2006, 2009).

The main applications of adhesives are:

#### 1. Ceiling board and air ducts

The ceiling board of cars has a sandwich structure consisting of decorated aluminum surface plates with melamine and incombustible lightweight board cores bonded with two part epoxy adhesives, as shown in Fig. 4 (Suzuki 2007). The space between the ceiling board and the roof sheet is used as air conditioner ducts in the case of electric railcar for commuting, as shown in Fig. 5 (Suzuki 2007).

#### 2. Partition panel

The partition of Shinkansen cars has a sandwich structure made of similar materials as the ceiling mentioned above. The bonding of the sandwich panels is performed with two part epoxy adhesives too.

t.1 **Table 1** Use of adhesives in present rolling stock (Suzuki 2006, 2007)

t.2	Position	Adherends	Adhesives	Application
t.3	Roof	Electric insulated roof sheet/roof sheet	Nitrile rubber	Spray
t.4	Ceiling board	Decorated sheet with melamine resin (Al)/incombustible lightweight board/Al or FRP panel	Epoxy	Spatula
t.5	Air duct	Air duct plate(Al)/polychloroprene sponge or soft polyurethane foam	Polychloroprene rubber	Paint brush or spray
t.6	Partition panel	Decorated sheet with melamine or PVC resin (Al)/incombustible lightweight board/plate (Al)	Epoxy	Spatula
t.7	Heat insulating material	Oxidized acrylic fiber or carbon fiber/outside plate (steel, SUS, Al)	Nitrile rubber	Spray
t.8	Decorated wall sheet	Spacing plate (incombustible hardboard, rigid PVC)/frame (steel, SUS, Al) Spacing plate (incombustible hardboard, Rigid PVC)/decorated sheet with melamine or PVC resin (Al)	Nitrile rubber Nitrile rubber	Paint brush Paint brush
t.9	Entrance	Liner under threshold plate (rigid PVC)/side sill	Nitrile rubber	Paint brush
t.10	Floor	Resilient floor covering (nonrigid PVC)/floor plate(Al) Resilient floor covering (nonrigid PVC)/floor compound material (epoxy resin) Resilient floor covering (nonrigid PVC)/floor coating (polyurethane resin) Resilient floor covering (polyolefin resin)/floor plate(Al) floor plate(Al)/Al honeycomb/floor plate (Al) (sandwich panel)	Nitrile rubber Nitrile rubber Polyurethane Polyurethane Film type epoxy	Spray Spray Spray Spray Hot-press
t.11	Door	Plate(SUS)/paper or Al honeycomb/ decorated plate (Al) Plate (SUS)/paper or Al honeycomb/plate (SUS) Plate (Al)/paper or Al honeycomb/plate (Al)	Epoxy Epoxy Epoxy	Spatula Spatula Spatula
t.12	Seat	Decorated side plate (Al)/extrusion (Al) Seat frame (Steel, Al)/soft polyurethane foam	SGA Polychloroprene rubber	Gun Paint brush
t.13	Inspection lid	Decorated sheet with melamine resin (Al)/extrusion (Al) Incombustible lightweight board/plate (Al)	SGA SGA	Gun Gun
t.14	Parts inside of the car	Keeping box of cassette tape for announcement on the train (PMMA/PMMA) Magazine rack in the first class car (PMMA/PMMA) Circuit-breaker cover (PMMA/PMMA)	Methylene dichloride (solvent bonding)	Syringe

(continued)

t.15 **Table 1** (continued)

t.16	Position	Adherends	Adhesives	Application
t.17	PVC pipe	Joint part of rigid PVC pipe	PVC	Paint brush
t.18	Etc.	Metal/metal Rubber/metal	SGA Chloroprene rubber	Gun Paint brush

t.19 *Al* aluminum, *SUS* stainless steel, *PVC* polyvinyl chloride, *SGA* second generation acrylic adhesive, *PMMA* polymethylmethacrylate

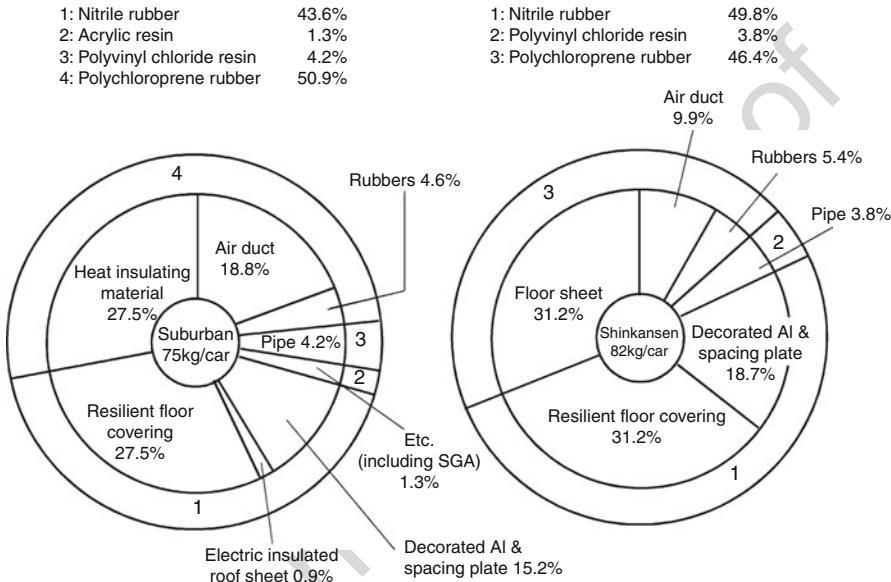


**Fig. 3** Share ratio of adhesive types and purposes for suburban electric car and Shinkansen car (Suzuki 2006, 2009)

- 109 3. Ceiling of decks and inspection lid
- 110 The ceiling of decks and inspection lid for Shinkansen and limited express cars
- 111 are made of aluminum corrugated panels (Fig. 6) bonded with an epoxy adhesive
- 112 (Sugano 1992). Limited express is a special train faster than ordinary expresses in
- 113 Japan.
- 114 4. Heat insulating material
- 115 Heat insulating material (thickness:30–50 mm) is usually installed between
- 116 painted side plates and roof sheets because the temperature of the outside plates
- 117 can rise up to 80 °C and drop below –30 °C. Typical materials for heat insulating
- 118 are oxidized acrylic fibers or carbon fibers. They are bonded on the back of
- 119 outside plates with heat resistant nitrile rubber adhesives. In some cases, 20-mm-
- 120 thick heat insulating material is bonded on the back of decorated inside walls.

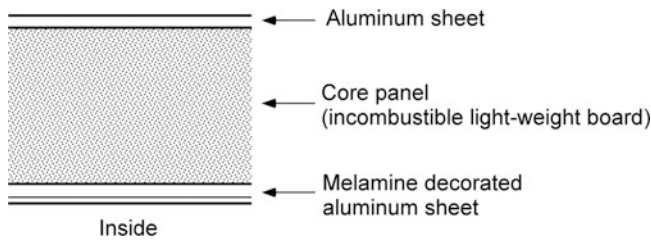


**Fig. 4** Sandwich structure for ceiling and duct board (Suzuki 2007)

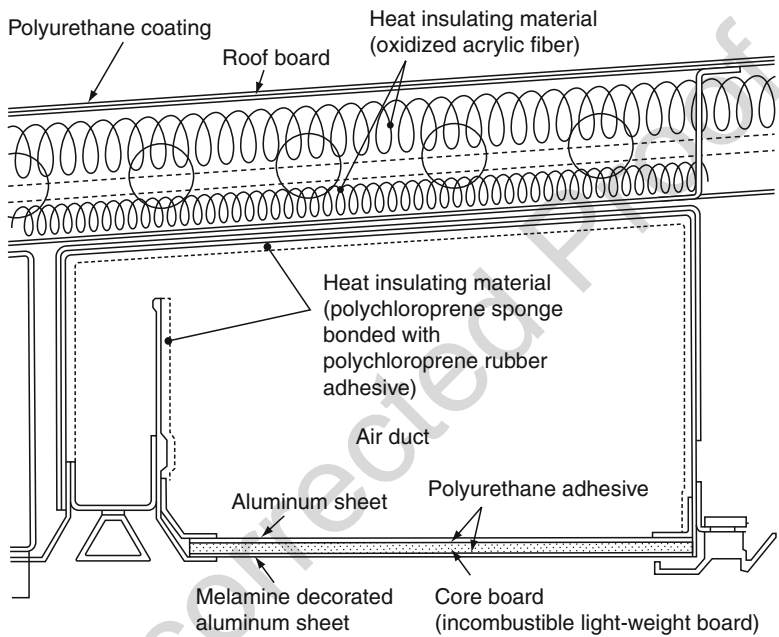


**Fig. 5** Air duct between the ceiling board and the roof board (commuting electric car) (Suzuki 2007)

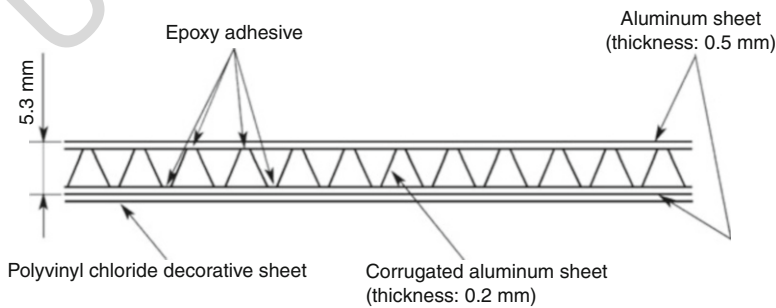


**Fig. 6** Sandwich panel for door deck ceiling and inspection lid (Sugano 1992)

5. Inside wall decorating sheets

Inside walls, which are made of aluminum sheets decorated with melamine resin or non-rigid PVC sheets, are joined to the frame using adhesives or screws. In almost all cases, a spacing plate made of flame retardant hardboard or rigid PVC is inserted between the inside walls and the frames to adjust their flatness and to prevent generation of creaky noise. The spacing plate is bonded on frames and the back of walls with nitrile rubber adhesives.

Decorated aluminum sheets with PVC are used for Shinkansen and limited express cars. Aluminum sheets are joined to the frame using adhesives or screws, and a primer is applied on the surface. Nonrigid PVC sheets having a pressure-sensitive adhesive layer are bonded on the surface.

6. Floor plate and floor covering

Typical floor structures of cars are shown in Fig. 7 (Suzuki 2007). The case of 700 series Shinkansen car is shown in Fig. 7a. A heat insulating material made of oxidized acrylic fibers is installed on the aluminum extrusions. Floor plates of aluminum-aluminum honeycomb sandwich structure bonded with a film type epoxy adhesive are screwed on it. Floor covering made of nonrigid PVC is bonded with a nitrile rubber adhesive.

Floor structures of limited express type, suburban, for commuting, non-governmental railroad, and subway electric railcars are shown in Fig. 7b. In them, floor compound material made of epoxy resin and light weight aggregate

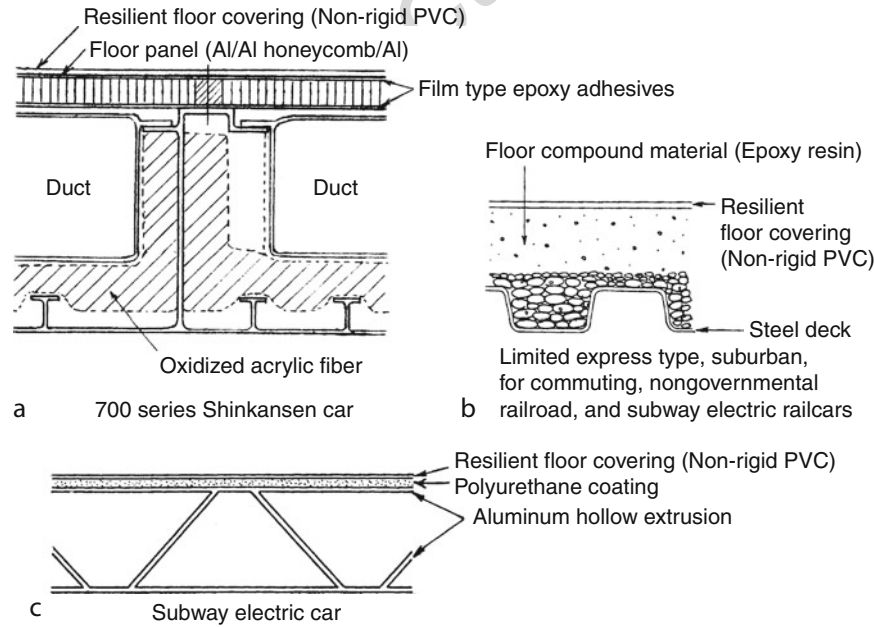


Fig. 7 Typical floor structures of railcars (Suzuki 2007)



is plastered and cured on steel deck, and PVC floor coverings are bonded on the surface of it with nitrile adhesives.

Floor structures of subway electric cars made of aluminum are shown in Fig. 7c. PVC floor coverings are bonded with a two-component polyurethane adhesive on polyurethane-coated floor plate of aluminum hollow extrusions.

#### 7. Cover-all hood

As shown in Fig. 8, N700 series Shinkansen cars adopt cover-all hoods between cars to reduce external noise and running resistance (Central Japan Railway 2009b). They consist of soft elastic materials bonded adhesively and have led to energy savings as well as reduction of noise outside and inside the car.

#### 8. Other items

Door panels have a sandwich structure consisting of aluminum or stainless steel surface plates and aluminum or paper honeycomb core bonded with two part epoxy adhesives. On inspection lids, switchboard covers, and seat side panels, decorated aluminum sheets with melamine resin are bonded with second-generation acrylic adhesives (SGAs) to aluminum frames or stiffeners. Figure 9 shows the cross section of a railcar with adhesively bonded parts (Suzuki 2007).

#### 9. Carbon fiber reinforced plastic (CFRP) bogie (Nishimura 2014)

Figure 10 shows a bogie that adopted CFRP leaf springs developed by Kawasaki Heavy Industries Co. (Nishimura 2014). In this bogie, CFRP is adopted as the main structure of the bogie frame, and as shown in Fig. 11, the CFRP frame is provided with a suspension function so that the primary suspension is unnecessary.

This CFRP spring has a three-layer structure of CFRP/GFRP/CFRP using adhesive, and the upper and lower CFRP layers are designed to support the bending load and the intermediate layer GFRP supports the shear load (Nishimura 2014).

Since the CFRP springs have structures that only ride on axles, those have the feature that it is easy to absorb the irregularity of the railway, and it reduces the wheel load loss by half. This bogie has been proved to fulfill all requirements of

**Fig. 8** Cover-all hood used in N700 series Shinkansen car (Central Japan Railway 2009b)



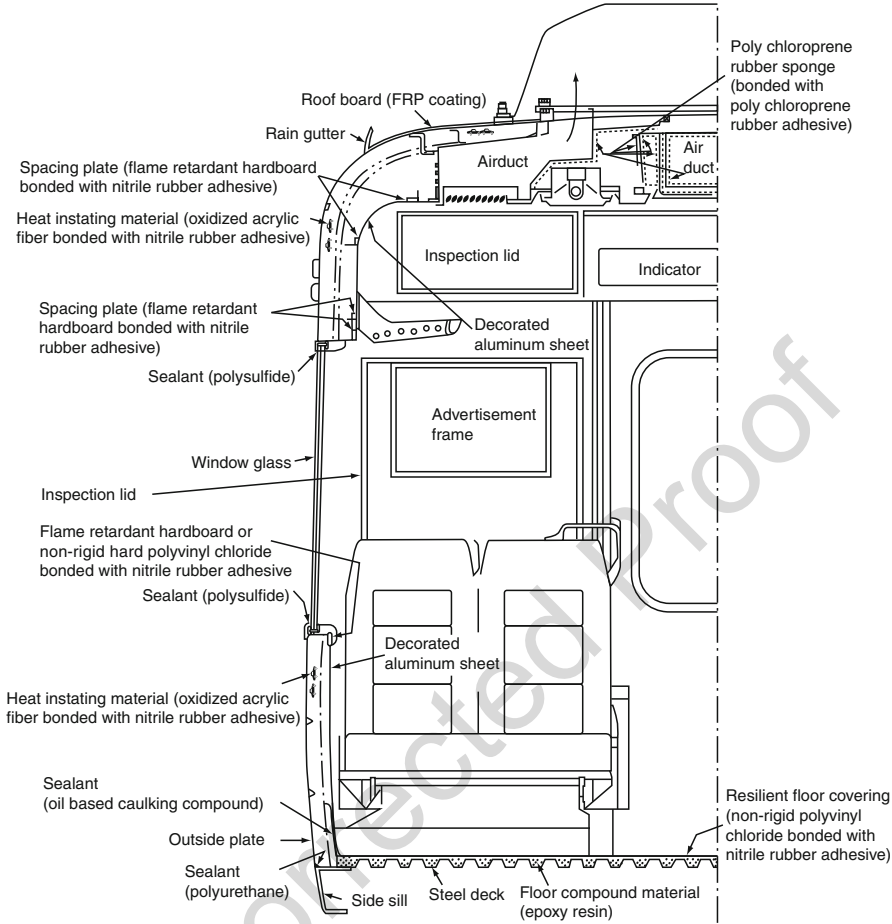


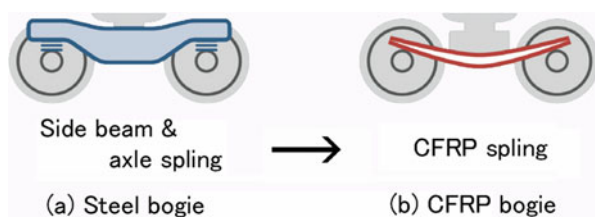
**Fig. 9** Adhesive bonded or sealant filled parts in cross section of a railcar for private railways (Suzuki 2007)

**Fig. 10** Carbon fiber reinforced plastic (CFRP) bogie (Nishimura 2014)





**Fig. 11** CFRP spring which serves two functions of side beam and axial spring (Nishimura 2014)



regulation 49 CFR 213.333 on traveling safety of rolling stock by the Federal Department of Transportation of the United States of America.

The mass per one CFRP spring is about 50 kg, and the weight reduction of about 450 kg is achieved by one bogie (about 900 kg per one car). This bogie was first adopted as a 6000 type train of Kumamotodentetsu Co. in 2014 and was adopted as a 7200 series suburban type DC train in Shikoku Railway Company in 2016.

### 47.2.3 Use of Sealants

Sealants are widely used in railcar structures. Sealants can protect the structure and equipment from corrosion, increase the service life, and keep the airtightness of railcars in air-conditioning. For high-speed trains such as Shinkansen, airtightness is important because the outer pressure of the trains varies when they enter or exit from a tunnel. The same phenomenon can also occur when trains cross each other. In these cases, airtightness can keep passengers comfortable.

Table 2 shows examples of sealant application for railcar structures (Suzuki 2007). Figure 12 also shows some sealant applications (Japan Association of Rolling Stock 2005, 2006). Figure 13 shows the ratio of sealant types used in the structures of stainless cars for private railway and Shinkansen (Suzuki 2007). In Japan, there were a national railway owned by the government and private railways owned by companies previously. The national railway has been privatized and separated to JR companies, so that JRs are not national railways anymore and are included in the category of “private railways” in definition. However, JRs are not called “private railways” due to the convention. The word “private” indicates the railways except JRs and municipal transportations in Japan.

Generally, silicone sealants have good electric insulation, weather resistance, and good bonding strength. However, they also have disadvantages such as getting dirty due to contamination and low paint adhesion. Therefore, silicone sealants are applied to roof, equipments under the floor or around pipeworks. Since modified silicone sealants can be painted, they are applied to exteriors as waterproof or decorative sealants. Polyurethane sealants have a very good weather resistance and are, therefore, used for waterproof purposes. Although polysulfide sealants are two-part type and need primers, their water and weather resistance are good enough to apply to join and seal glass to metals. Nondrying type oil-based caulking compounds have good insulation and environmental resistance, but their bond strength is not high.

t.1 **Table 2** Use of sealants in present rolling stock (Suzuki 2007)

t.2	Position	Applied parts	Sealant
t.3	Body structure	Headlight mount End surroundings Entrance post and outside plate surroundings Outside plate seam (stainless car) Entrance threshold plate Bodyside door pocket Outside plate hem – side sill Headlight – outside plate (aluminum car)	Modified silicone Modified silicone Modified silicone Modified silicone Polyurethane Polyurethane Polyurethane Silicone
t.4	Roof top	Pantograph base Ventilator base Rain gutter (steel) – outside plate Up and down footstep	Polyurethane, silicone Silicone Polyurethane Polyurethane
t.5	Window & door	Side window unit, end window unit, and cab front window unit Train destination indicator window Sliding door window and hinged door window (outside) Sliding door window and hinged door window (inside) Polycarbonate window – outside plate (Series 100 Shinkansen passenger’s room)	Polysulfide, modified polysulfide Polysulfide, modified polysulfide Polysulfide, modified polysulfide Polysulfide Polyurethane Silicone
t.6	Interior	Hatten Center pin cover Air duct insulator watertight treatment	Polyurethane, oil-based caulking compound Polyurethane Butyl rubber
t.7	Equipment	Piping inside room End treatment of electric cable pipe Outlet port of equipment Riser pipe on floor Canon plug Water pipe fitting	Oil-based caulking compound Oil-based caulking compound Oil-based caulking compound Oil-based caulking compound, silicone Oil-based caulking compound, silicone Modified silicone, silicone

t.8 All the sealants are applied with caulking guns

204 Therefore, they are not suitable for air tight applications, but for equipments under  
205 the floor or around pipeworks. Joining detachable parts is one of the oil-based  
206 caulking compound applications.

207 **47.2.4 Pressure-Sensitive Adhesives**

208 Typical applications of pressure-sensitive adhesives (PSAs) are shown in Table 3  
209 and mentioned before (Suzuki 2007).

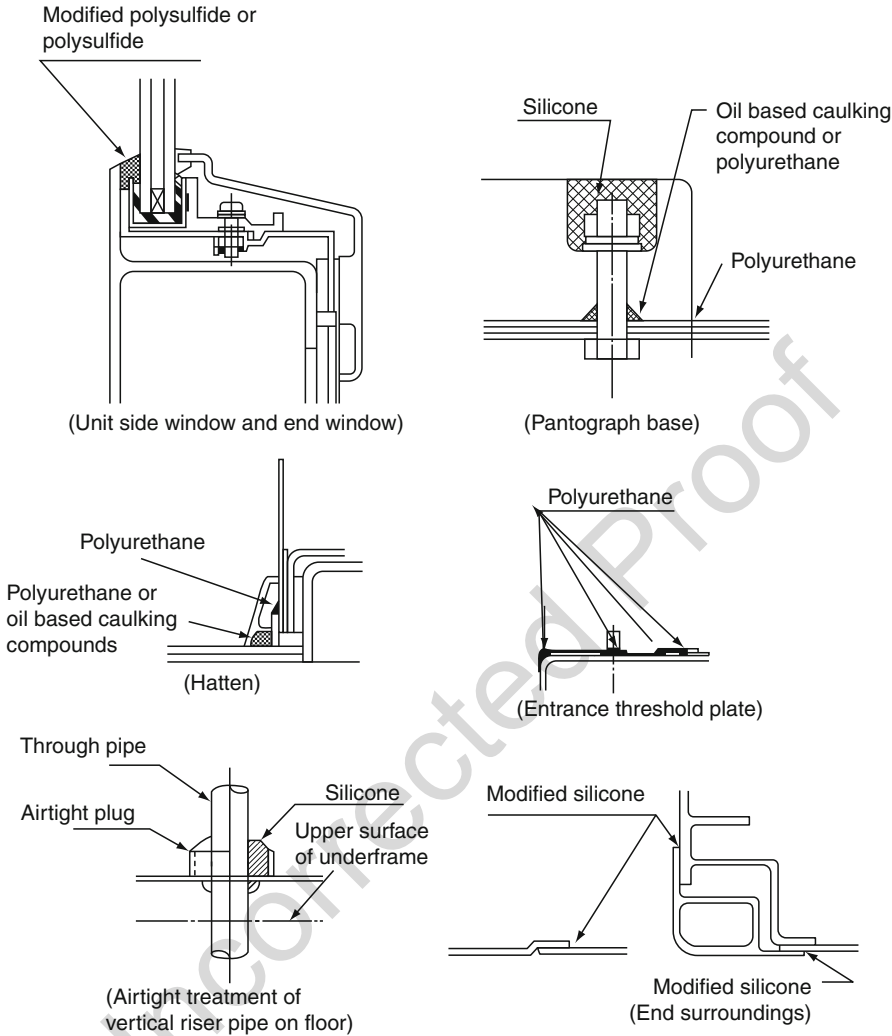


**Fig. 12** Sealant application in railcar structures (Japan Association of Rolling Stock 2005, 2006)

1. Bonding Decorating Aluminum Sheets to Spacing Plates  
As mentioned in Sect. 2.2 (5), when decorating aluminum sheets are bonded to spacing plates, double-side-coated PSA tapes are used in some cases. Nitrile rubber adhesives must be applied to the surface of the spacing plate and dried in advance.
2. Aluminum Panels Covered with Nonrigid PVC Film  
As mentioned before, Shinkansen and limited express type electric railcars have aluminum panels covered with nonrigid PVC film bonded with PSA. The panels are made with a press.
3. Name Plates  
Name plates are bonded to the structure using both double-side PSA tapes and rivets.

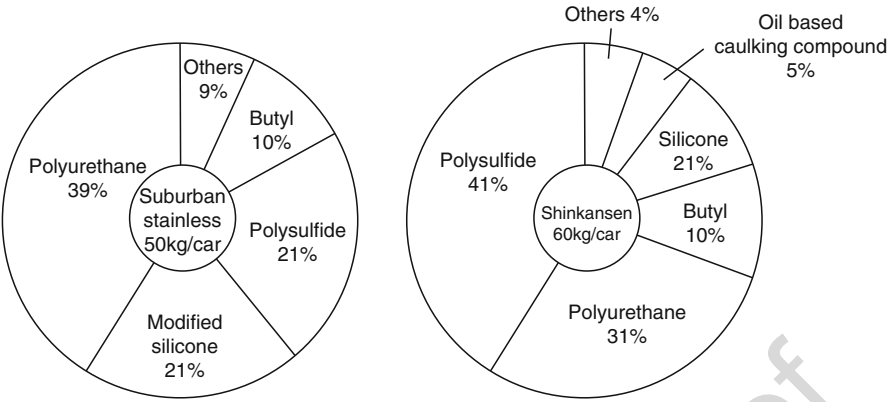


**Fig. 13** Ratio of sealant types used in the structures of suburban stainless cars and Shinkansen cars (Suzuki 2007)

**Table 3** Use of pressure-sensitive adhesives (PSAs) in present rolling stock (Suzuki 2007)

Position	Adherends	Supply
Decorated wall sheet	Spacing plate (incombustible hardboard, rigid PVC)/decorated aluminum plate Nonrigid polyvinyl chloride film/Al plate	Double-side PSA-coated tape Acrylic PSA(back side)
Name plate	Name plate/Outside skin, inner decorated plate, polyvinyl chloride films having PSA	Double-side PSA-coated tape
Discriminating strip	Color strip (Nonrigid polyvinyl chloride)/outside plate (Al, SUS)	Double-side acrylic PSA-coated tape

Al aluminum, SUS stainless steel, PSA pressure sensitive adhesive

4. Discriminating Strips (color strips)

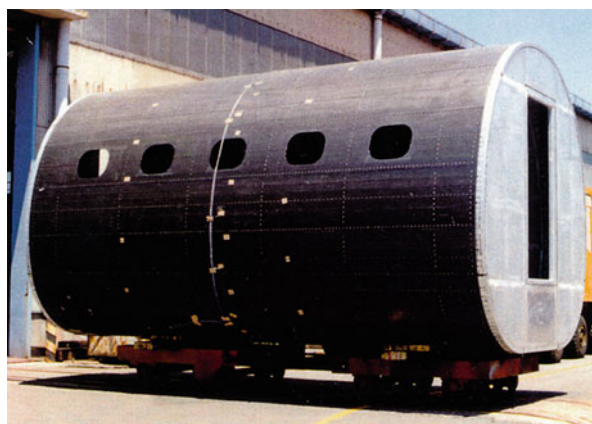
In stainless cars and aluminum cars, discriminating colored PVC strips, which have PSA on one side, are pasted along the outer surface of their bodies in the longitudinal direction.

**47.3 Application of Adhesives for Prototype Railcars in Japan**

1. CFRP Body Structure

Weight saving is a very important issue, even for trains. Sophisticated lightweight materials have recently been introduced in railcar body structures. Phenol resin-based carbon fiber reinforced plastics (flame resisting CFRP), for instance, have been applied to a prototype structure shown in Fig. 14a (the outside) and (b) (the inside) (Suzuki and Sato 1993). The structure is 6 m in length and was made by Railway Technical Research Institute, Nippon Sharyo, Ltd., and Toray Industries Co., Ltd. in cooperation, using CFRP plates. The structure is made from curved outside CFRP plates and stiffeners as a unit by the pultrusion technique. The

**Fig. 14** A prototype carbon fiber reinforced plastic (CFRP) body structure for high speed trains using panels molded by pultrusion method (Suzuki and Sato 1993)



(a) Outside of CFRP body structure



(b) Inside of CFRP body structure

300-mm-width CFRP panels were joined to aluminum alloy frames with Huckbolts<sup>®</sup> (Alcoa co.) and a two-part room temperature setting epoxy adhesive. According to the results of strength tests and a finite element analysis, the structure has equal strength and stiffness as structures made only of aluminum alloy.

## 2. CFRP Roof Construction

A prototype body construction of Shinkansen was experimentally produced by Tokyu Sharyo Corporation. This had a roof construction consisting of four blocks made of phenol resin-based CFRP, as shown in Fig. 15 (Matsuoka and Aso 1992). Each block had different structures which were compared in terms of strength and weight. Block 1 and 2 had CFRP carlines and purlines crossed in a grid and bonded to a CFRP skin. The frames and skin of block 2 were thicker than those of block 1. In block 3, the structure had a sandwich panel (30 mm thick) of CFRP skins and a polyurethane foam core between carline without purline. Block 4 consisted of only a sandwich structure (50 mm thick) of CFRP skins (1 mm thick) and paper honeycomb core filled with a phenolic foam without frames. The

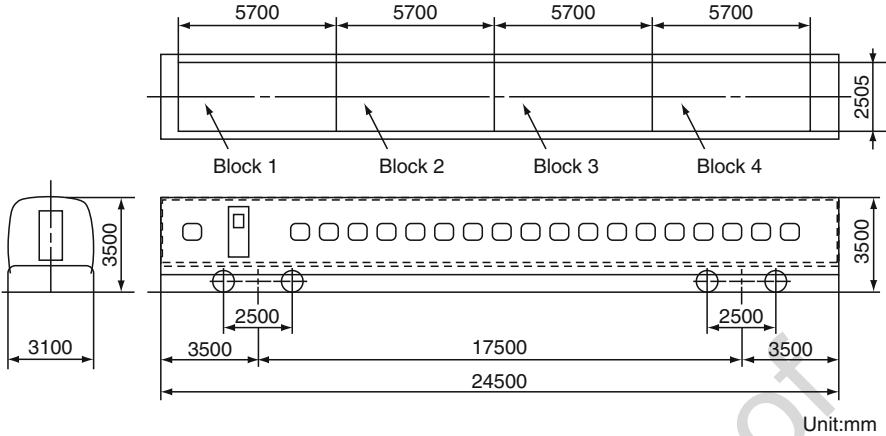


**Fig. 15** Carbon fiber reinforced plastic (CFRP) roof construction divided into four blocks (Matsuoka and Aso 1992 and Matsuoka 1992)

structure of block 4 was most effective to reduce the weight because ceiling boards and heat insulating materials could be omitted and air ducts were simplified due to adoption of curved sandwich structures.

The aluminum rims were bonded to the edges of each block using a heat setting epoxy adhesive. A double lap joint in which CFRP side was double with 80 mm lap length was used.

The aluminum rims of block were welded to the other of it's and aluminum side and end constructions, as shown in Fig. 16 (Matsuoka 1992). Due to the use of this structure, the weight (4.3 t) of body structure was lighter than its of the present Shinkansen. The stiffness and airtightness of this prototype body structure were satisfied usefulness.

3. Weldbonding Structures (Sasaki 1995)

East Japan Railway Company (JR-East) constructed a prototype train: TRY-Z, which consisted of carbodies of three different type structures. A front car was made of thin-wall aluminum hollow extrusions welded continuously. The other front car had a monocoque sandwich structure in which aluminum honeycomb and plates were brazed. The middle car had a skeleton body structure of aluminum alloy joined by a combined method of spot welding and adhesion by a heat setting adhesive. This method is called "weldbonding."

4. Body Structure for Maglev Trains

Japan Air Lines has developed a type of normal conduction maglev trains called High Speed Surface Transport (HSST), in which several types of sandwich panels were used as shown in Table 4 (Japan Alminium Association 1990).

5. CFRP Bogie Frame

A CFRP bogie frame shown in Fig. 17 was experimentally made by Railway Technical Research Institute. The side beams of the frame have four webs made by dry hand lay-up of carbon prepregs (Wako et al. 1992). The vertical webs had

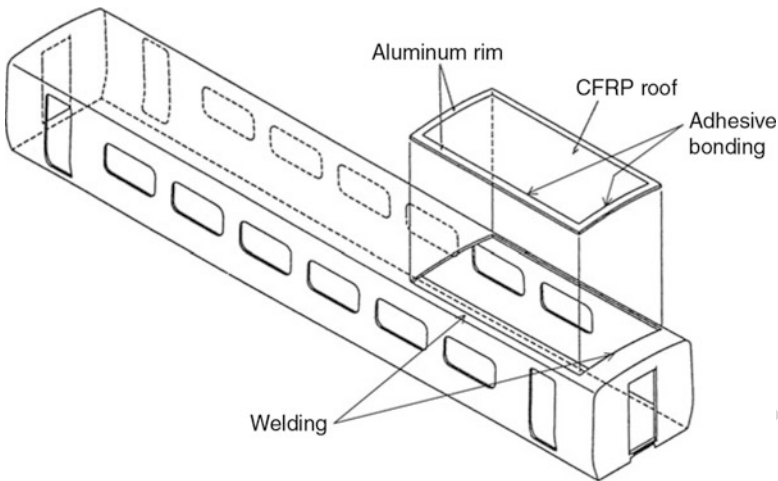


**Fig. 16**    Joining method of a carbon fiber reinforced plastic (CFRP) roof block to the main structure (Matsuoka and Aso 1992; Matsuoka 1992)

t.1    **Table 4**    Adhesively bonded sandwich structures used in prototype HSST car (Japan Alminium Association 1990)

t.2	Prototype car	Position	Composition of sandwich structure
t.3	HSST-03	Floor board Ceiling board Side ceiling board Side sliding door	CFRP/Nomex <sup>®</sup> honeycomb/CFRP GFRP/Paper honeycomb/GFRP GFRP/Al honeycomb/GFRP Al/Al honeycomb/Al
t.4	HSST-04	Floor board	Stainless steel/plywood/stainless steel
t.5	HSST-05	Floor board	Al/Al honeycomb/Al

276    an U shape for a large bonding area. The horizontal webs of flat shape were  
277    bonded on the bonding area of the vertical webs and to the honeycomb cores with  
278    a heat setting adhesive (121 °C). The cross beams of the frame were CFRP pipes  
279    made by filament winding. The tip of the cross beam were inserted to the side  
280    beam and joined with a room temperature setting adhesive.

281    **47.4    Application of Structural Adhesive for Rolling Stock over**

282    **the World**

283    **47.4.1    Britain (Seeds 1984)**

284    **Present Use**

285    A large amount of adhesives is used in the construction of railcars, including solvent-  
286    based, anaerobic, and cyanoacrylate products, but these do not form structural  
287    adhesives. The uses of structural adhesives have been divided into three categories.



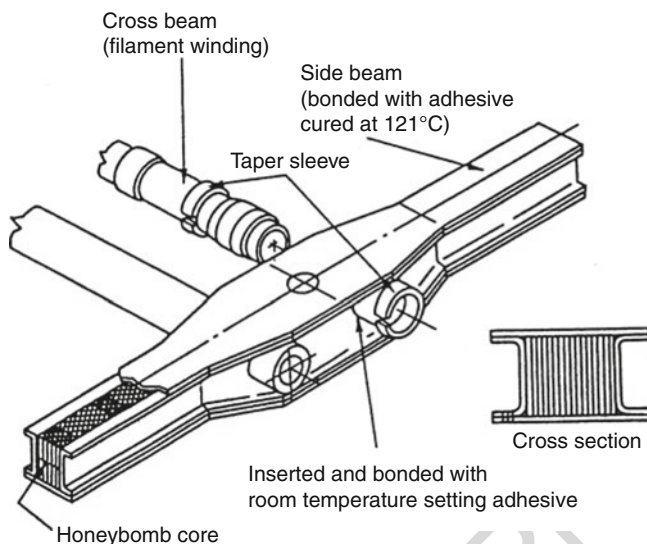


**Fig. 17** Carbon fiber reinforced plastic (CFRP) bogie frame fabricated with adhesives (Wako et al. 1992)

### 1. Simple Fastening

In this group, the normal operating stresses are quite low although high loads may occasionally have to be borne. An example of this type is the use of a two-part epoxy adhesive to bond steel kicking-strips to the base of the aluminum sliding door.

### 2. Sandwich Panel Construction

This represents a major use of structural adhesives in the industry, and a wide range of internal trim panels are produced in this way by bonding melamine to plywood or aluminum.

### 3. Structural Bonding

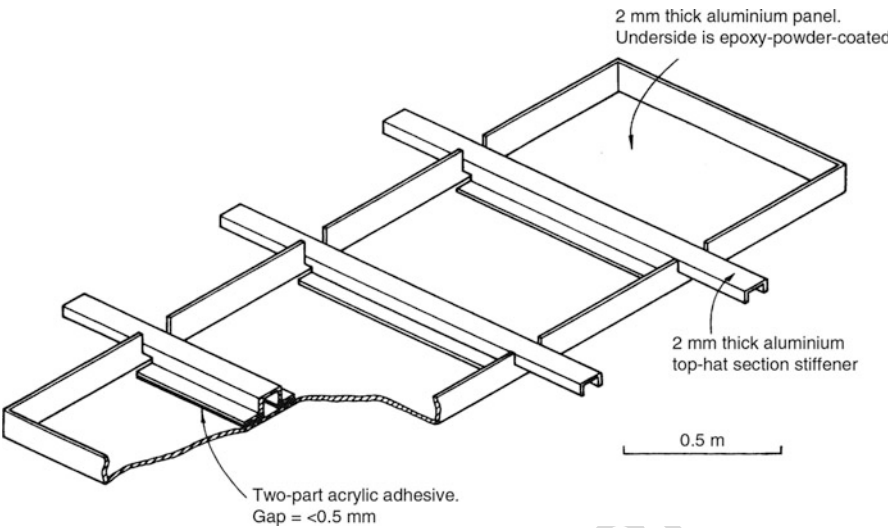
Two particular examples are worth noting. The first is the bonding of steel stiffening strips with acrylic adhesive to the rear surface of glass fiber reinforced plastic (GFRP) window-surround panels to prevent flexing and to provide additional stiffness under impact. The second example is the bonding of aluminum skin and honeycomb structure to make the sliding doors which are situated on the outside of the latest suburban coaches (passenger railcars without power unit).

## Development Work

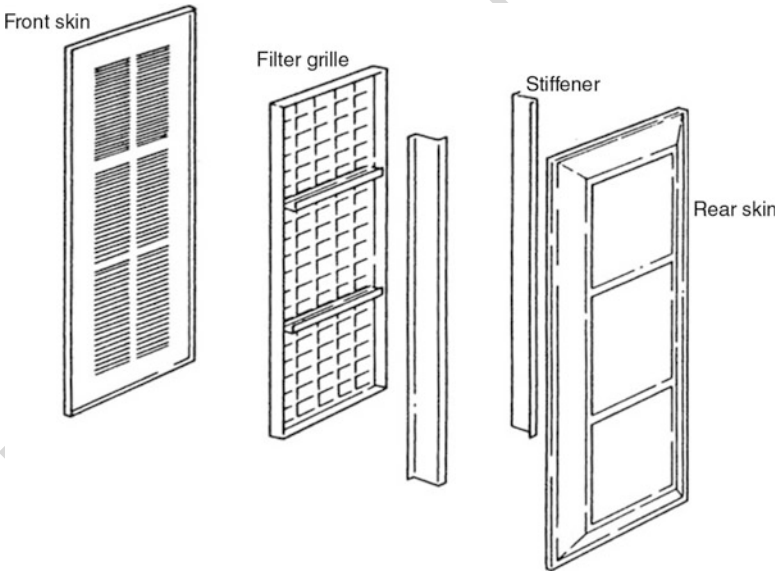
### 1. Aluminum Ceiling Panel

Figure 18 shows the design of the aluminum ceiling panel intended for use on the latest inter-city coaches (Seeds 1984). The requirement is to fasten the top-hat stiffeners to the upper side of the panel without damaging the epoxy-paint finish on the underside. Two-part separate application acrylic adhesive met the requirements of the joint and a light abrasion plus a solvent wipe gave adequate preparation.





**Fig. 18** Aluminum ceiling panel bonded adhesively (Seeds 1984)



**Fig. 19** Bodyside (filter) door components of Class 58 locomotive (Seeds 1984)

2. Class 58 Locomotive Bodyside Door

The locomotive door is presently made by spot-welding a number of pressed components, as shown in Fig. 19 (Seeds 1984). The use of structural adhesive bonding has several important advantages. The surface finish can be greatly improved by eliminating the spot-weld blemishes; dimension variation in the

components can be absorbed by using a gap-filling adhesive, and therefore a smoother finish could be obtained; and finally, adhesive bonding can provide a faster process for a capital outlay of less than that for spot-welding.

Under impact conditions, joints using this steel bonded with conventional toughened epoxy and acrylic adhesives fail preferentially at the zinc/steel interface, and this leads to an unacceptable impact performance. By testing a wide range of adhesives, it was found that the shear modulus had to be less than 100 MPa to enable the adhesive in the joint to deform sufficiently under impact to prevent the over-stressing of the interface.

As an environmental durability test, measurement of lap-shear strength after exposure to 95% RH at 40 °C was carried out. The only adhesive which met all of the requirements was a two-part acrylic adhesive. That adhesive also had the desired cure characteristics (work life 5 min, de-jig time 30 min).

### 3. Coach Bodyside

The present method for constructing the coach bodyside on suburban railcars uses a spot welding process. The panel consists of 2-mm IZ steel<sup>®</sup> (zinc-coated steel) skin and top-hat section stiffeners, and Fig. 20 shows the panel components arranged horizontally on the spot-welding jig (Seeds 1984).

The advantages of doing this would be two-fold: firstly, the process could be made several times faster for a capital outlay lower than that for the present spot-welding equipment and secondly the resulting surface finish would be considerably better than the spot-welded panels, thereby saving most of the time presently taken to prepare the bodyside for painting.

Adhesive joints should be sufficiently strong and stiff for the structure to operate in 20–40 years. The determination of strength and stiffness requirements has been



**Fig. 20** The arrangement of the bodyside module components of suburban coach on the assembly jig (Seeds 1984)

tackled in two distinct ways: first, by the use of structural models of vehicles (e.g., Finite Element Method) and second, by direct comparison with spot-welds at both the joint and structural level.

Experiments indicate that in shear (the principal stress in the bodyside panel) the adhesive joints can be twice as strong as the equivalent spot-weld joint, but joint stiffness has been shown to be approximately similar.

Using toughened single-part epoxy adhesives which can be cured at 120 °C, prototype equipment, able to produce full-size bonded panels in a 2- to 3-h cycle time, will permit at least a twofold increase in production rate compared with the spot-welding process.

Several full-scale bonded panels have been prepared, and the results have proved successful in demonstrating the capabilities of structural adhesives. Assembly and service trials will be conducted within the next 15 months.

#### 47.4.2 France

Société Nationale des Chemins de fer Français (SNCF) made a full-scale prototype composite structure of Train à Grande Vitesse (TGV) double-decker trains whose maximum speed is 350 km/h (Cléon 1994). It comprises sandwich structures of glass fiber and carbon fiber reinforced epoxy resin skins and honeycomb or foam cores bonded adhesively. A half tube of the structure was integrally formed by a vacuum suction method at 120 °C. A pair of the half tubes was joined together along the longitudinal midlines at the top and bottom using adhesives, as shown in Fig. 21. The weight saving of the structure led to noise reduction, dynamic stress decrease in the lower structure, and energy saving due to the decrease of its distance for acceleration and reduction of speed.

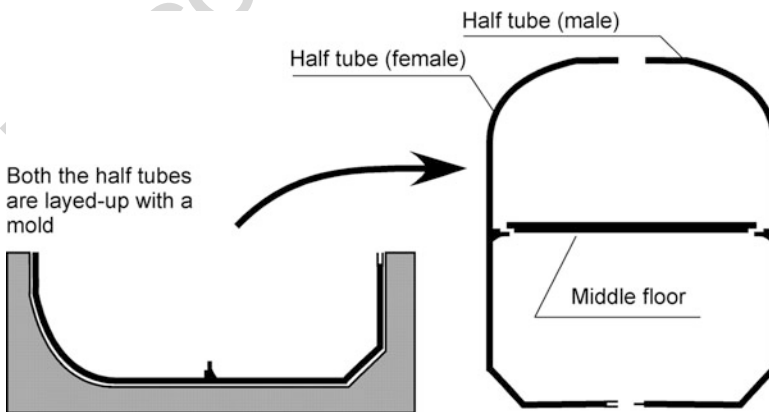


**Fig. 21** Fabrication of Train à Grande Vitesse (TGV) double-decker prototype consisting of composite materials (Cléon 1994)

47.4.3 Germany

German high speed train: Intercity-Express (ICE) has viewing windows and blind windows, whose cross sections are shown in Fig. 22 (Rahn et al. 1991). Since these windows are bonded to the body panel making the outer surfaces of the body smooth, the aerodynamic drag of the train is minimized. The window structure is also effective to improve the airtightness and water vapor impermeability of the car. The window glasses are bonded adhesively into aluminum frames. This method is called “direct glazing.” The complete window units are screwed into the coach body, and the joint between adjacent windows and between window and coach body is plugged with an elastic filling material. This principle has already been applied to the center trailers of the ICE with very good results. The windows were subjected to a long series of fatigue tests in various environmental conditions and passed comfortably.

Such flat surfaces are very effective to reduce the running noise in the ICE train because almost all the noise is only due to aerodynamic noise at speed of 300 km/h.

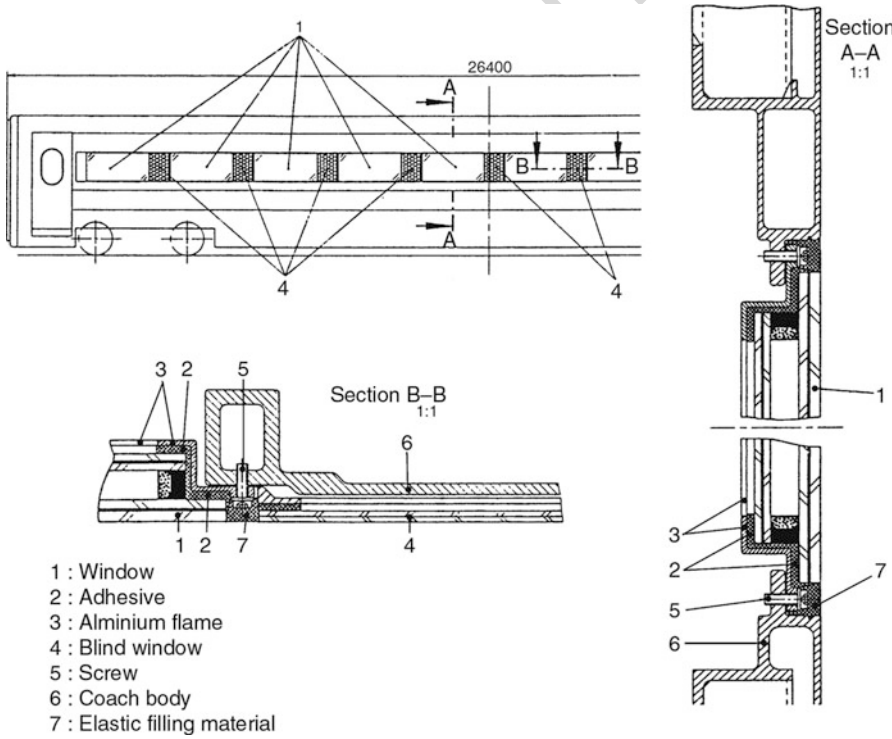


Fig. 22 Cross section of Intercity-Express (ICE) trailer car windows (Rahn et al. 1991)

#### 47.4.4 Switzerland

In Switzerland, Schindler Waggon AG made a 1:2.5 scaled prototype of train cars shown in Fig. 23 (Romagna et al. 1997). The structure was fabricated by the wet filament winding method of knitted multi-axial glass fabric tape onto rigid foam cores supported by ring-shaped frames that were made by the filament winding method too. Local reinforcements, heat insulating material, wiring and air ducts, frames for door and window openings, and in situ wound ring frame were integrated into the body structure, which had enough strength, stiffness, and surface flatness. Therefore, the structure was advantageous in terms of costs and productivities.

#### 47.4.5 Indonesia

Prototype railcars consisting of multimaterials were fabricated in the Jabotabek project. For instance, the frames were mild steel, the roof construction were painted mild steel sheets, the front end construction was FRP, and the rear end construction and the side construction were stainless steel. The side constructions were bonded to the frames with a two-part room temperature setting epoxy adhesive using positioning jigs. The cars have been in service for already 4 years.

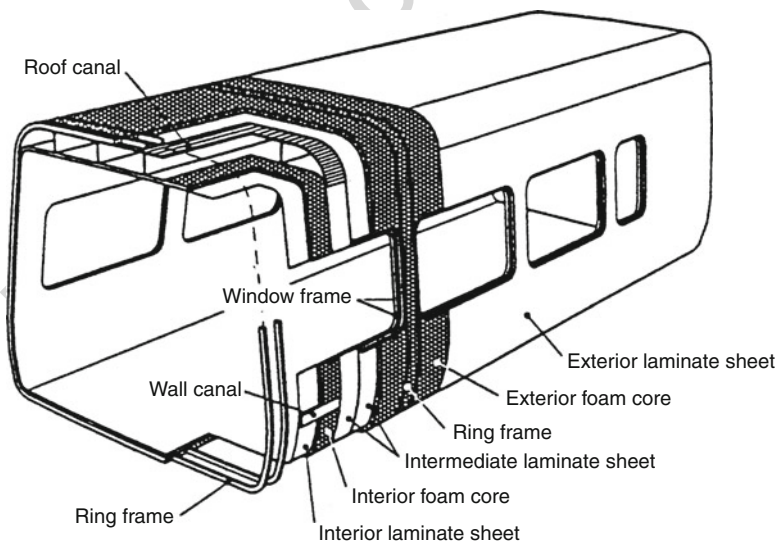


**Fig. 23** Novel construction concept for the filament wound, highly integrated carriage body of passenger coaches (Romagna et al. 1996)

## 47.5 Conclusion

To meet the demands of faster speed, weight saving, noise reduction, cost reducing in terms of production and maintenance, joining methods in train structures are increasingly diversified as well as the materials. Adhesion is a joining method having advantages such as low stress concentration, high stiffness, and large damping, so that the use of adhesion will expand in train applications as research proceeds.

## References

- Abiko Y, Kobayashi G (1998) Rolling stock & technology 1:22 (in Japanese)
- Central Japan Railway (2009a) Central Japan Railway Company data book 2009, pp 24–25
- Central Japan Railway (2009b) Central Japan Railway Company environmental report 2009, p 6
- Cléon LM (1994) Proceedings of the World Congress on railway research 2:673 (in French)
- Japan Aluminium Association (1990) Research report of aluminium alloy and lightweight of rolling stock -Research on lightweight of rolling stock as high speed transportation, pp 42–53 (in Japanese)
- Japan Association of Rolling Stock (2005) Industries standard JRIS R 0206-1; rolling stock-guidelines for rigging design-Part 1:underfloor installations (in Japanese)
- Japan Association of Rolling Stock (2006) Industries standard JRIS R 0144:rolling stock-designing guidelines for sealing material (in Japanese)
- Kamiura M, Sunaga M et al (2000) Tetsudo Kougaku, Morikita Shuppan. p 213 (in Japanese)
- Matsuoka S (1992) Denkisha no kagaku, 45(12):30–34 (in Japanese)
- Matsuoka S, Aso K (1992) Tokyu car technical review 42:6–19 (in Japanese)
- Matsuzawa H (1986) Introduction for passenger car engineering, Railway System Research, p 106 (in Japanese)
- Miyamoto M (1998) Kougyouzairyou, 46(3):108 (in Japanese)
- Nishimura T (2014), Tetsudosharyokogyo (Journal of Japan Association of Rolling Stock Industries), 470:21–24
- Rahn T, Hochbruck H et al (1991) ICE Hightech on rails. Hestra-Verlag, p 116
- Romagna J, Anderegg K et al (1996) Proceedings of 17th International European Chapter of SAMPE Conference, 57
- Sasaki K (1995) Rolling stock & technology, 8:13 (in Japanese)
- Seeds A (1984) Int J Adhes Adhes 4:17
- Sugano T (1992) Nikkei New Materials, July 13:8 (in Japanese)
- Suzuki Y (2006) Fundamental and application of structural adhesive bonding edited by Miyairi H, CMC, p 343 (in Japanese)
- Suzuki Y (2007) “Adhesion handbook ver.4” edited by The Adhesion Society of Japan, Nikkan Kogyo Sinbun, p 1011 (in Japanese)
- Suzuki Y (2009) A textbook of adhesion technology for men aiming a professional edited by The Adhesion Society of Japan, Nikkan Kogyo Sinbun, pp 179–187 (in Japanese)
- Suzuki Y, Sato K (1993) RRR, 6:9 (in Japanese)
- Wako K, Umezawa Y, Tokuda A (1992) RTRI report, 6(10):19 (in Japanese)

Peter Davies

## Contents

48.1	Introduction .....	1392
48.2	Specific Requirements .....	1392
48.2.1	Certification .....	1392
48.2.2	Manufacturing Conditions .....	1395
48.2.3	The Marine Environment .....	1404
48.3	Surface Preparation .....	1404
48.3.1	Composite Substrates .....	1405
48.3.2	Metallic Substrates .....	1406
48.4	Mechanical Behavior .....	1407
48.4.1	Type of Adhesive .....	1407
48.4.2	Substrates .....	1409
48.4.3	Interface .....	1409
48.5	Durability in a Marine Environment .....	1410
48.5.1	Degradation Mechanisms .....	1410
48.5.2	Predicting Marine Aging Effects .....	1411
48.5.3	Testing to Simulate the Marine Environment .....	1412
48.6	Quality Control .....	1413
48.7	Repair and Recycling .....	1413
48.8	Conclusions .....	1414
	References .....	1415

## Abstract

This chapter describes the use of adhesive bonding to assemble structures in the marine industry. The marine environment is extremely aggressive, and this has resulted in the widespread use of fiber-reinforced composite materials. Adhesive

P. Davies (✉)

Materials and Structures Group, Marine Structures Laboratory, Brest Centre, IFREMER,  
(French Ocean Research Institute), Plouzané, France

e-mail: [peter.davies@ifremer.fr](mailto:peter.davies@ifremer.fr)

bonding is a lightweight and corrosion-resistant means of joining these materials. The main emphasis of this chapter will therefore be on the assembly of composites, though some examples of metal bonding will also be discussed. Three industrial applications are used to illustrate the use of adhesive bonding: small pleasure boats, high performance racing yachts, and bonded structures in the offshore industry. Each has specific design requirements, and there is no single marine adhesive suitable for all structures, but the requirement for long-term durability in a seawater environment is common to all these applications.

---

## 48.1 Introduction

The marine industry encompasses a wide range of structures, from small boats to offshore oil platforms. It covers small boatyards, large production line-based boat assembly plants, naval shipyards, and a host of subcontracting companies providing services from design through to offshore platform repair. Many of these use large quantities of adhesives and sealants, and it is not possible to provide a description of all of them. In this chapter, the role of adhesive bonding in the marine industry will be described through three examples of application areas: small pleasure boats, high performance racing yachts, and bonded structures for the offshore oil and gas industry. The materials involved are mostly fiber-reinforced composites, as these are the materials which are most frequently assembled by adhesive bonding in this industry. They range from low cost glass mat or woven roving-reinforced polyester, widely used in pleasure boats, to high performance carbon fiber-reinforced epoxy and honeycomb sandwich for racing yachts.

---

## 48.2 Specific Requirements

In this section, we will first present the particularities of adhesive bonding for this industry. There are a number of specific marine requirements, resulting from regulatory requirements, the way marine structures are assembled, and the environment they meet in service. Thus, when considering adhesive bonding of structures for marine applications, in comparison with other industrial applications, the following points need particular attention:

- Certification
- Manufacturing conditions
- The marine environment

### 48.2.1 Certification

All marine structures require certification by classification societies (Bureau Veritas, Lloyds, Det Norske Veritas (DNV), Germanischer Lloyds, American Bureau of



Shipping (ABS), etc.), so in order to obtain approval, it is necessary to take account of their requirements from the design stage. In addition to extensive recommendations, developed to ensure structural integrity, several of these societies also have requirements for the adhesive materials to be used in assembly. These are intended to ensure conformity with specified requirements, by subjecting test samples to physical, chemical, environmental, or operational stresses in a recognized laboratory. Many adhesive suppliers indicate certification authority approval for marine use in their product data sheets. Table 1 shows typical requirements. It is important to note that these tests are performed on adhesively bonded joints, usually in the form of lap shear specimens, and not bulk adhesives. The approval is therefore specified for particular substrates and includes their surface preparation and the joint manufacturing procedure.

Taking the DNV guidelines (DNV 2009) as an example, the approval procedure is based on the requirements of the DNV guidelines for classification of high speed, light craft, and naval surface craft (DNV 1991). The adhesive supplier indicates a “manufacturer’s specified minimum value” (msmv) for lap shear strength and cleavage strength. Standard tests are then performed to check these and obtain a reference value. The marine durability of approved adhesives is then taken into account by stipulating a percentage of mechanical strength retention after weathering under load. Specimens are weathered under different conditions, as shown in Table 2, and tests are performed on the aged specimens in order to determine property retention.

Here, the weathering condition involves loading according to ASTM D2919 (test method for determining durability of adhesive joints stressed in shear by tensile loading) to a constant stress and weathering according to ASTM D1183 (resistance of adhesives to cyclic laboratory aging conditions). The latter includes a cycle for exterior marine exposure:

**Table 1** Typical requirements for approval of marine adhesives

Tests type	Condition	Requirement
Lap shear testing	Control (room temperature)	Manufacturer’s values achieved
	Elevated temperatures	
	Cold temperatures	
Cleavage peel testing	Control (room temperature)	Manufacturer’s value achieved
	Elevated temperatures	
	Cold temperatures	
Fatigue testing	ASTM D3166	Target value achieved (e.g., 10 <sup>7</sup> cycles)
Immersion tests	Water	Minimum % retention achieved
	Fuel	
Glass transition temperature	ASTM E1356 (calorimetry)	Above minimum value (e.g., 70 °C for military ships)

t.1 **Table 2** Marine durability conditions for adhesive-type approval (DNV 2009)

t.2	Test	Aging condition	Requirement
t.3	Lap shear	Loaded to msmv and weathered (ASTM D1183) 28 days	Mean >90% reference
t.4	ASTM D1002 or D3163	56 days	Mean-2 standard deviations >95% 28-day value
t.5	Cleavage fracture	Loaded to msmv and weathered (ASTM D1183) 28 days	Mean >90% reference
t.6	ASTM D3433	56 days	Mean >95% 28-day value

- 90 – 48 h at 71 °C and <10% humidity
- 91 – 48 h at 23 °C immersed in artificial seawater
- 92 – 8 h at –57 °C, 100% humidity
- 93 – 64 h at 23 °C, immersed in artificial seawater

94 This 7-day cycle is to be repeated four and eight times for the 28- and 56-day  
 95 exposures. Adhesive approval thus requires considerable testing, based on proce-  
 96 dures designed to ensure long-term durability based on accelerated aging. Prediction  
 97 of long-term behavior will be discussed further below.

98 For small boats (up to 24 m long), design and scantling rules have been assembled  
 99 in a recent set of ISO (International Standards Organization) documents. Part 6 of  
 100 this set is entitled “Small Craft-Hull construction and Scantlings – Structural  
 101 arrangements and details” (ISO12215-6 2008) and includes a section on bonding.  
 102 Bonded stiffener, bulkhead, and deck-hull assemblies are considered, Fig. 1.

103 An Annex to this ISO document provides a design criterion for adhesive bonding. In  
 104 order to determine the bonded area, a simplified approach based on shear loading is  
 105 proposed. Shear stresses should be limited to 20% of the nominal bond shear strength,  
 106 i.e., a safety factor of 5. This factor is intended to account for both stress concentrations  
 107 in real joints and the viscoelastic (time and temperature dependent) nature of adhesives.  
 108 Shear data values, to be used if test values are not available, are provided, Table 3.

109 There are few guidelines for the use of adhesively bonded assemblies offshore as  
 110 currently such structures are mainly welded steel. However, UKOOA (United  
 111 Kingdom Offshore Operators Association) proposed a set of guidelines for the use  
 112 of glass-reinforced plastic (GRP) pipework offshore, Part 4 of which includes  
 113 sections on installation and assembly (UKOOA 1994). For adhesively bonded  
 114 assemblies, a quality program is proposed, which requires the recording of key  
 115 values, namely:

- 116 – Temperature and relative humidity
- 117 – Connection identification number
- 118 – Curing temperature and time
- 119 – Signature of pipe fitter and inspector

120 Formal training is required for pipe fitters, and each field bond shall be inspected  
 121 by an approved inspector.

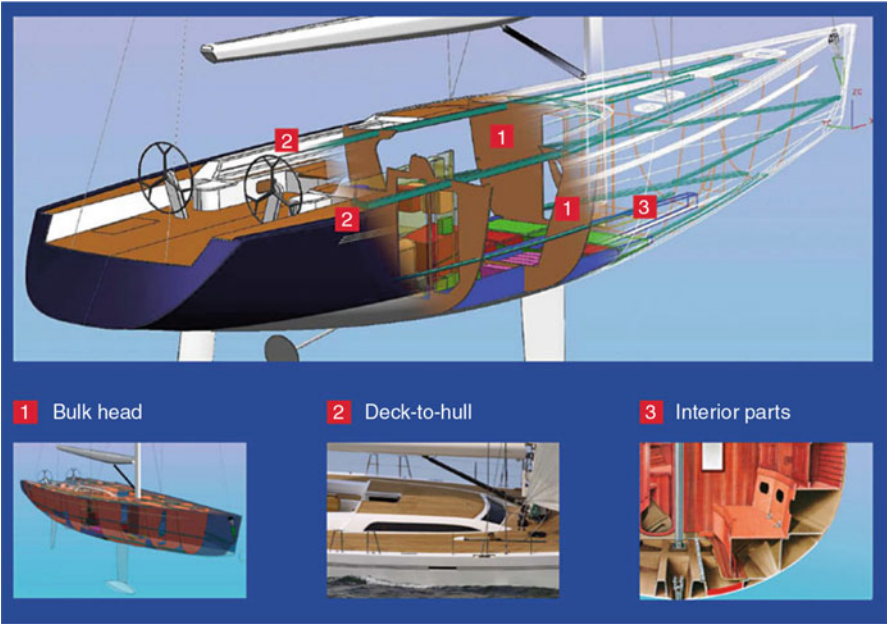


**Fig. 1** Types of bonded marine assembly used in small boats (Figure Bostik)

**Table 3** Nominal and design shear stresses in adhesively bonded joint (ISO12215-6 2008)

	Adhesive	Nominal bond shear strength, MPa	Design shear stress in bonded joint, MPa
t.1	Cold-cured epoxy	27	5.4
t.2	Epoxy-type paste	40	8
t.3	Polyester or vinylester resin or paste	15	3

**48.2.2 Manufacturing Conditions**

In this section, various examples of adhesively bonded marine structures will be presented, in order to illustrate the type of joints used in the marine industry and show how they are manufactured.

**Pleasure Boats**

The manufacture of small boats is largely manual, and over 90% of boats smaller than 6 m long are manufactured from GRP. Hand lay-up is the principal fabrication method. However, closed mold techniques such as infusion and resin transfer molding are becoming more popular as legislation on volatile emissions becomes more strict. There are two types of bonded joint of particular importance, internal bulkheads and deck to hull joints. Adhesive bonding is increasingly being used to fix

internal structures, such as bulkheads, to the hull structure, Fig. 2. Adhesive is placed on the hull and the bulkheads are then assembled using locating jigs to maintain them in position. The bulkheads may be plywood or sandwich materials, and the traditional way of fixing them to the hull was by placing strips of fabric impregnated by resin using hand lamination (known as overlamination). This is a time-consuming operation so adhesive bonding is progressively replacing it. Methacrylate adhesives are being used today for this operation as they offer reasonable properties and simple surface preparation. The properties of marine adhesives are described in more detail later in this chapter.

Figure 3 shows an example of a marine plywood bulkhead in a small motorboat. This bulkhead/hull joint was instrumented as part of a study performed to determine the loads seen by adhesive joints in service (Bauer et al. 2004).

**Fig. 2** Placing adhesive before bonding internal motor boat structure (Photo Plexus)



**Fig. 3** Adhesively bonded marine plywood bulkhead in 6 m motor boat



Hull stiffeners may also be either overlaminated or bonded (e.g., Junhou and Sheno [1996](#)). In many small production boats, a multi-stiffener molding is produced, and bonded to the hull in one shot, rather than bonding individual stiffeners. A recent study on stiffeners for military vessels within the EUCLID RTP 3.21 project (McGeorge and Weitzenbock [2004](#)) described the design and fabrication of bonded pultruded sections to stiffen large superstructure panels (Davies et al. [2004](#)). This allowed cost savings compared to the traditional overlaminated assembly method, but infusion of the structure with the stiffeners in a single piece may prove more cost-effective.

A second operation, once the internal structure is in place, is deck to hull assembly, Fig. 4. This joint between deck and hull is critical to the structural integrity of the vessel and may be highly loaded in a motor boat. The sealant properties of flexible adhesives such as polyurethanes are used to provide a water tight bond, which may be 10 mm thick in places. Locating pins are used to align the two parts.

**Fig. 4** Hull to deck assembly using a polyurethane adhesive. (a) Adhesive placement, (b) guide pin to ensure alignment (Photos Sika), (Sika [2009](#))





Adhesive bonding is again used as an alternative to laminating with GRP, as it is faster (and hence cheaper) and more energy absorbent. Few published studies have reported on the mechanical integrity of such assemblies, but a recent study (Diez de Ulzurrun et al. 2007) evaluated different adhesive systems for this type of assembly. Mono-component and bicomponent polyurethanes and methacrylate adhesives, with different joint thicknesses from 2 to 10 mm, were tested between glass-reinforced polyester substrates. The different adhesives showed more or less ductile behavior, and the optimal adhesive changed according to the parameter considered (failure load, strain to failure, load transfer between substrates). This underlines the difficulty in optimizing the performance of such a complex joint even when the joint design is fixed. Gap-filling ability may be as important as mechanical properties in allowing lower dimensional tolerances for the two components. The aesthetic appearance of the finished joint is also very important, and there are various designs which allow the joint to be hidden, such as external profiles or rails, Fig. 5.

For both these applications, bulkhead and deck to hull assemblies, large quantities of adhesive must be applied, so adhesives must be formulated to allow sufficient working time before cure starts. Adhesives are also used in finishing operations. For example, the deck surface in large yachts is made of wooden strips adhesively bonded to the composite molding, Fig. 6. The operation involves the adhesive bonding of wooden strips, often in the form of prefabricated planking with a plywood backing and a higher quality wood surface such as teak, to the clean, primed deck. Waterproof polyurethane adhesives, with good gap-filling properties, are widely used. In a second operation known as deck caulking, the joints between the strips are filled (similar to the traditional caulking of seams between timber planks with tarred rope to waterproof sailing ship hulls). Primers are necessary to ensure a good bond to wood.

Another pleasure boat application is bonding of windows. Bonding of glass or transparent polymer (polycarbonate or acrylic) panels to the vessel superstructure, using flexible, moisture curing polyurethane adhesives, provides a waterproof connection and contributes to structural rigidity (Sika 2009). UV resistance is

**Fig. 5** Finished deck-hull bond on a small motorboat, joint hidden by elastomer profile





**Fig. 6** Deck manufacture (Photos Bostik)

particularly important for this application, and surface preparation is critical. Light abrasion is used followed by cleaning and priming before adhesive application. The adhesive thickness is calculated to minimize shear deformation and depends on the window dimensions. Deformation is the ratio of movement to thickness, so larger windows require thicker bond lines for a given deformation. Below 1 m a minimum thickness of around 3 mm is typical.

### Racing Yachts

For larger racing vessels, the materials are closer to aerospace sandwich materials, with carbon fiber-reinforced epoxy composite skins on honeycomb or foam cores widely used. In these boats, there are two types of adhesive bond. The first is within the sandwich material itself. The sandwich is manufactured by bonding the core to the skins with two layers of adhesive. This may involve multiple curing steps. For example, a first external skin is laid up and cured, the core is then bonded to this with a film adhesive and cured, and finally the second adhesive layer and second inner skin are laid up and cured. The adhesives are generally epoxy films, which wet the honeycomb and form a meniscus, Fig. 7a. This is a delicate operation; the integrity of the facing/core bond is critical to obtaining required sandwich properties. Defects may be introduced, Fig. 7b, and post-bonding nondestructive control is not simple. Some recent papers (Okada and Kortschot 2002; Ural et al. 2003) have examined the influence of interface parameters on mechanical performance. It was shown that resin fillets absorb energy so their size determines interface fracture energy. By controlling the cure conditions, it is possible to optimize this.

The second level of adhesive assembly in this application is at the structural level. Figure 8 shows a 60-ft-long (18 m) racing yacht, for which both bi-component-toughened methacrylate and epoxy paste adhesives are used to assemble the internal honeycomb sandwich structures.

The hulls of an ocean racing multihull are even larger, they may be over 30 m long. In most cases they are produced in two sections, which must then be joined together, Fig. 9. This is a very long bond line and requires great care. The substrates are abraded and degreased before bonding. A combination of adhesive bonding and

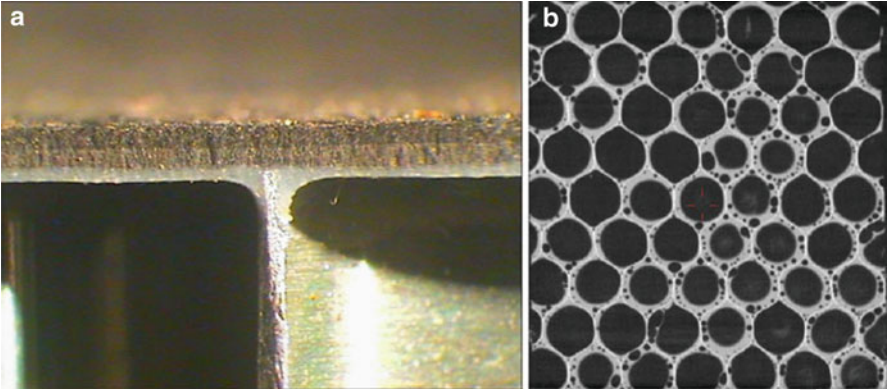


**Fig. 7** Sandwich structure. Adhesive film bonding of facing to core. (a) Meniscus on core, (b) X-ray tomography view of defects in adhesive at bonded interface (Davies et al. 2010)



**Fig. 8** Sixty-foot racing yacht (Photo Huntsman)

overlamination is used, and the entire structure is heated with a vacuum applied. For this application a high performance epoxy adhesive paste is used.

Finally, another critical application is in mast structures. In the latest racing multihulls, these may be over 40 m long and are again produced by bonding two





**Fig. 9** Racing trimaran central hull halves during assembly

half shell moldings together, though in this case an autoclave is used when one is available.

For both small boats and racing yachts, the adhesive bond line thickness is rather variable; it is not possible to maintain tight composite tolerances with this type of hand lay-up or oven manufacture, so adhesive thickness can reach several millimeters. This is much thicker than for aerospace structures, produced using film adhesives with carrier fabric in autoclaves, for which a typical bond line thickness is less than 0.2 mm. The consequences of this larger bond line thickness may be significant, resulting in:

- Defects in the adhesive
- Variable cure conditions
- Local stress concentrations

It is not straightforward to quantify the influence of bond line thickness, and the range of thicknesses of interest for marine structures has received less attention than the aerospace range. Published data from a range of different tests tend to suggest a drop in properties of epoxy and methacrylate adhesives (for the particular adhesives and conditions tested) as thickness increases (e.g., Tamblin et al. 2001; Jarry and Shenoï 2006; Davies et al. 2009). However, as tests are not easy to analyze and manufacturing and curing conditions vary between structures, it is not easy to predict the local effects and stress concentrations which will dominate joint performance, so appropriate testing is essential.

### Offshore Structures

There are few applications of adhesive bonding in the offshore industry, but this situation is evolving, and there is considerable potential for new applications. For

example, Cowling (1997) listed seven areas in which adhesive bonding could be used, in order of increasing load-bearing:

- Attachment of safety and equipment notices
- Small metal pipe support brackets (frequently retrofitted)
- Low pressure piping (for corrosion resistance)
- Stanchions and bracket supports
- Modification of deck plating
- Partition bulkhead support frames
- Plate to frame connections in accommodation and process plant areas

Some adhesive assemblies are currently used on offshore oil platforms to join tube sections in cooling and firewater pipework systems. These are filament wound glass/epoxy composite tubes produced in lengths of a few meters and assembled as required, using flanges or “tulip” joints. Assembly of the latter is shown in Fig. 10; a male tapered end is bonded inside a matched female end with an epoxy adhesive and cured with a heated mat. Such pipes are subjected to both internal pressure and axial loading (Knox et al. 2000).

A second offshore industry application which involves large quantities of adhesive for polymer/metal bonding is in the assembly of thermal insulation to flow lines (Pattee and Kopp 2000; Hansen and Rydin 2002). A thick polymer coating, which may be epoxy, polyurethane, or polypropylene, is chosen for its thermal properties. It is often filled with hollow glass spheres to make a syntactic foam to improve its thermal insulation. This coating is bonded to the steel tube which conveys the oil from the subsea wells to the platform, Fig. 11a. There may be hundreds of meters of such flow lines in a large offshore field, and maintaining the temperature of the fluid is critical if pipeline blockage is to be avoided. The insulation is bonded to the tubes in the factory. The steel is first coated with an FBE (fusion-bonded epoxy) coating. This is a corrosion protection, applied in powder form then heated to melt and cover the surface and cure. The insulation layer is then applied, and the tubes are then transported offshore, typically 12 m in lengths. Assembly of these tubes, into a

**Fig. 10** Assembly of pipework using taper/taper bonded joints (Photo Ameron)



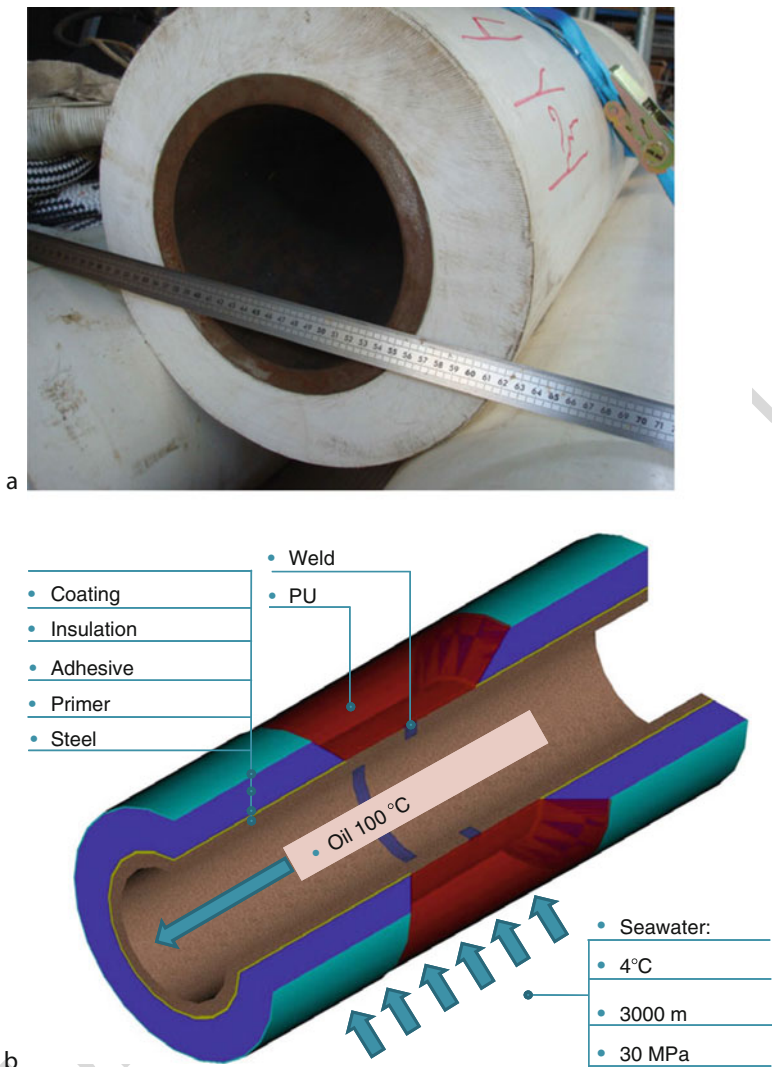


**Fig. 11** (a) Section showing thermal insulation on steel flow line. (b) Field joint, liquid polyurethane

continuous flow line hundreds of meters long, is performed by welding at sea just prior to installation. The region close to the welds is a critical zone. In order to weld this area, there is initially no insulation, so a “field joint” is made after welding. There are various solutions, but filling the gap with a polyurethane is a popular method, Fig. 11b. This is a very demanding application; the material must adhere to the steel tube and to the insulation, polymerize very rapidly, and show good thermal and wet aging properties.

There is also currently interest in adhesives to assemble and repair steel structures on offshore platforms, where welding is not allowed for safety reasons. Robust procedures are needed, capable of ensuring a good bond in a humid environment with a simple surface preparation such as grit blasting (Bordes 2009). Repairs are discussed in a later section.

### 48.2.3 The Marine Environment

The marine environment involves a combination of high relative humidity and/or immersion in seawater, temperatures from  $-30$  to  $70$  °C ( $0$ – $35$  °C in water), and exposure to sunlight. Although the vast majority of seawater has a salinity of between  $3.1\%$  and  $3.8\%$ , seawater is not uniformly saline throughout the world. Where mixing occurs with fresh water at river mouths or near melting glaciers, seawater can be substantially less saline. The pH of seawater is alkaline, usually in the range  $7.5$ – $8.5$ .

Mechanical loads on marine structures can be extremely varied. They may be quasi-static, due to hydrostatic pressure as a result of immersion at constant depth, for example, cyclic, due to waves and currents, or dynamic, due to wind gusts, wave slamming loads, or water hammer in pipework. Finally, assemblies placed in shallow seawater for a few weeks will be colonized by biological fouling, so antifouling paints are widely employed. These must be compatible with the adhesives used.

Polymers may be sensitive to all these environmental factors and particularly to water and temperature. In addition, the influence of different parameters such as mechanical loading and water diffusion is known to be coupled, mechanical loads accelerate water ingress, and water affects the stresses developed in a joint. Adhesive formulation for marine applications is therefore critical, but, as will be discussed in more detail below, it is not yet possible to fully predict long-term marine performance of adhesive assemblies. Appropriate testing is therefore again essential to guarantee satisfactory performance.

## 48.3 Surface Preparation

There is a vast literature on surface preparation for adhesive bonding, and readers will find detailed discussions both elsewhere in this volume and in various reference books (Kinloch 1987; Adams 2005; Weitzenbock 2012). Here only some aspects specific to marine applications and the marine environment will be discussed. Modern boat structures are generally composite, mainly for cost reasons though the ability to produce complex design features and the good corrosion resistance of these materials are also important. Adhesive bonding is similar to the technology used to assemble fibers in a composite, and it has been readily adopted in boatyards. When all-metallic structures are to be assembled, then welding is still the preferred route, but adhesive bonding may be needed in hybrid joints such as those involving steel and composites. For example, in some large military vessels such as the French La Fayette-class frigates, composite superstructures are attached to metallic hulls

323 (LeLan et al. 1992; Mouritz et al. 2001; Boyd et al. 2004). Such joints require care to  
324 avoid corrosion, and surface preparation is critical (Cao and Grenestedt 2004).

### 325 48.3.1 Composite Substrates

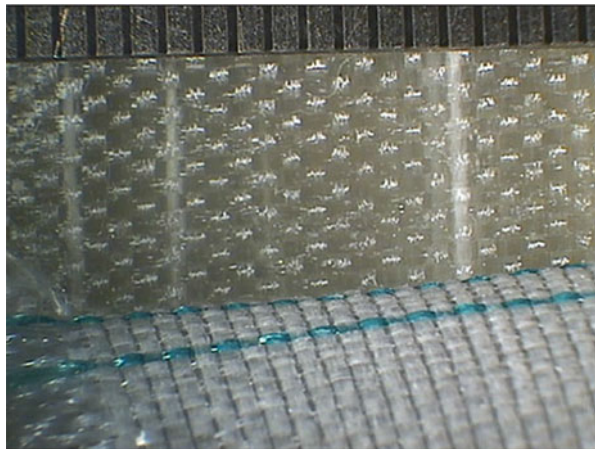
326 Polymer matrix composite surface preparation before adhesive bonding consists of  
327 between two and five steps

- 328 (i) Cleaning/degreasing
- 329 (ii) Surface abrasion
- 330 (iii) Application of a surface activator
- 331 (iv) Application of a primer
- 332 (v) Application of the adhesive

333 In most cases in boatyards, only steps (ii) and (v) are used, but for many marine  
334 applications, “peel plies” are used to protect the surface of molded parts before  
335 bonding. These are fine polyester or nylon fabric layers, which are placed over the  
336 region to be bonded, Fig. 12. The peel ply is peeled off just before the adhesive is  
337 applied, to reveal a clean, rough surface.

338 Unfortunately, in order to remove them easily, peel plies are often coated with  
339 lubricants or other low surface energy products, which can be transferred to the  
340 surface and interfere with the bonding process. It is therefore essential to run  
341 preliminary tests for a new substrate/peel ply/adhesive combination in order to  
342 ensure compatibility. Figure 13 shows an example of results from a study of marine  
343 composites assembled by overlamination with and without peel plies (Davies et al.  
344 2005). The delamination resistance of a continuously laminated 16 woven glass fiber  
345 ply-reinforced polyester composite is compared with that of composites for which  
346 fabrication was stopped after half the layers were molded. One of these was

**Fig. 12** Peel ply (lower)  
during removal from glass  
fiber-reinforced composite  
surface. Scale in millimeters



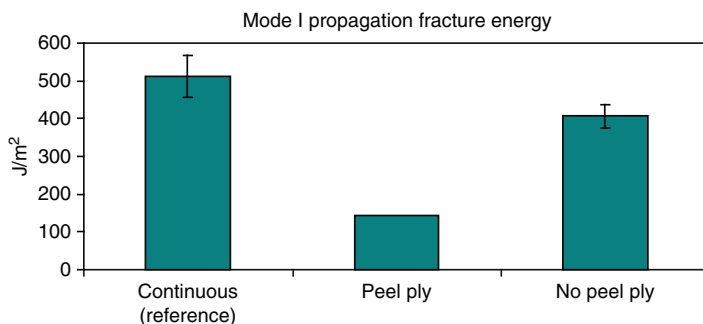


**Fig. 13** Example of influence of peel ply on delamination resistance of woven glass-reinforced polyester

protected with a peel ply, the other was not. One week later the fabrication was continued, the remaining eight layers were laid up either onto the surface after peel ply removal or onto the unprotected surface. Delamination resistance to propagation of a mid-thickness crack was then measured on DCB (double cantilever beam) specimens. In this case, not using a peel ply provided significantly better results than when a peel ply was used, even though peel plies are sold specifically to allow manufacturers to avoid additional surface preparation. This is one example, in other cases peel plies do fulfill their function, but various problems in the aerospace industry have led to great concern over peel ply surface preparation (Hart-Smith 2002).

In some military boatyards, a sacrificial mat layer is added during manufacture when secondary bonding is required. This can then be removed by grinding, ensuring that a new surface is exposed before bonding.

### 48.3.2 Metallic Substrates

Preparation of metallic surfaces, in most cases steel or aluminum, for bonding generally includes a combination of a mechanical treatment, such as grit blasting, with a chemical cleaning procedure (Hashim 1999). It should be emphasized that the choice of surface preparation in an industrial application may be governed by practical considerations (availability of equipment used for other operations such as painting, e.g., or cost) and may not be the optimal choice based on laboratory tests. A recent study suggests that the limiting factor in steel bonding on military vessels may be the strength of the anticorrosion primer paint which is used to coat the steel substrates (Speth et al. 2010).

It is well known that aluminum alloys require special treatments in order to develop good durability, but the toxicity of the favored chromic acid anodization has led to development of alternative treatments (Armstrong 1997; Critchlow et al. 2006). Figure 14 shows a schematic set of results which illustrate the influence of this type of preparation. Short-term strength is similar with and without a chemical treatment, but long-term durability is seriously affected if the treatment is not



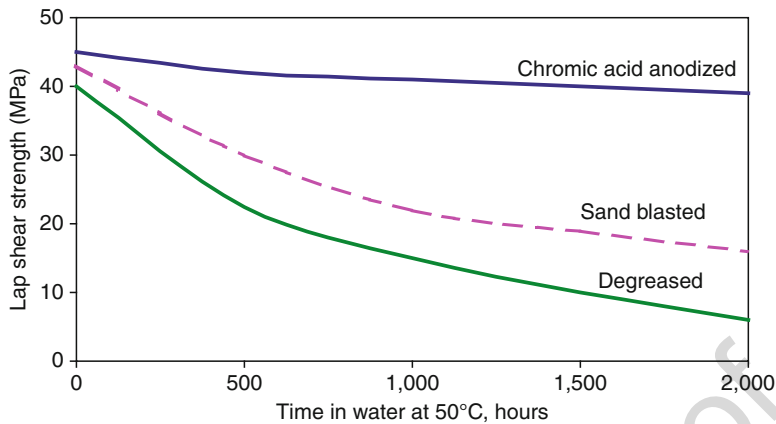


**Fig. 14** Schematic illustration of the influence of surface preparation on aluminum single-lap shear bond durability in water, monocomposant epoxy adhesive

performed. Titanium alloys are also sometimes used in critical marine applications, and Golaz et al. (2013) showed that a combined surface treatment of sanding, degreasing, and chemical etching showed the best durability in salt water.

## 48.4 Mechanical Behavior

The mechanical behavior of adhesively bonded composite joints depends on the type of adhesive, the properties of the substrates, particularly in the through-thickness direction, and the care taken to guarantee the interface between the two.

### 48.4.1 Type of Adhesive

The reader will have noted from the discussion of applications above that there are three types of adhesive widely used in the marine industry. These are polyurethanes (PU), methacrylates (MA), and epoxies (EP). Each generic type includes a very large range of grades, with their advantages and disadvantages, and there is some overlap between them. Figure 15 shows examples of the tensile stress-strain properties of each. The PU is a room temperature cure low stiffness high ductility grade, of the type widely used for composite pleasure boat deck-hull assembly. The methacrylate is an intermediate solution, again with a room temperature cure. The epoxy system is a two-component paste adhesive, a high performance structural adhesive widely used in marine applications, cured for 4 h at 50 °C.

There are clearly very significant differences between these products, in terms of stiffness, strength, and ductility. Each is formulated for a specific type of assembly. As noted above, the mechanical behavior is only one element to be considered in

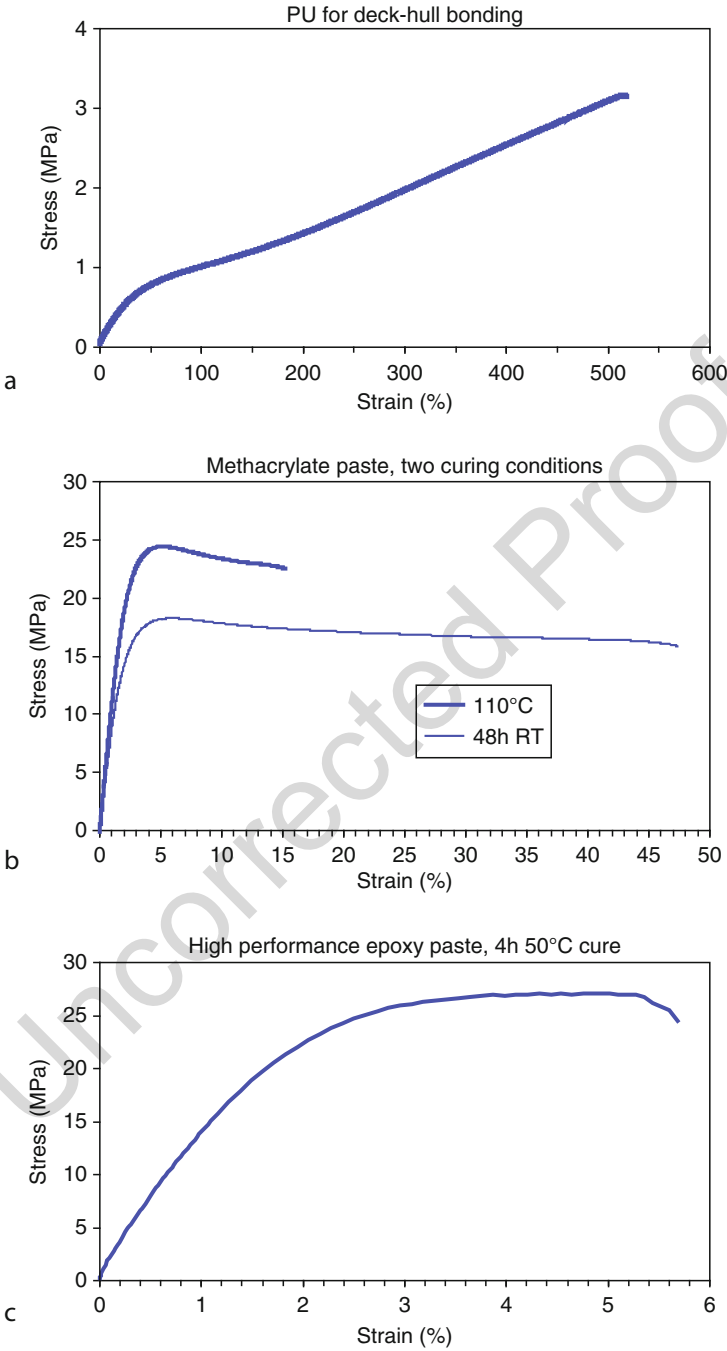


**Fig. 15** Typical marine adhesive tensile stress-strain plots, (a) PU, (b) methacrylate (48 h room temperature and 24 h RT then 2 h 110 °C curing), (c) epoxy (12 h RT, 4 h 50 °C cure)



material choice. For a boatbuilder, gap filling or sufficient viscosity to allow bonding onto vertical surfaces may be as or more important, while for an offshore flow line thermal properties may be critical. In addition to a range of “standard” commercial products, adhesive suppliers will therefore formulate special products designed specifically for an end user’s requirements.

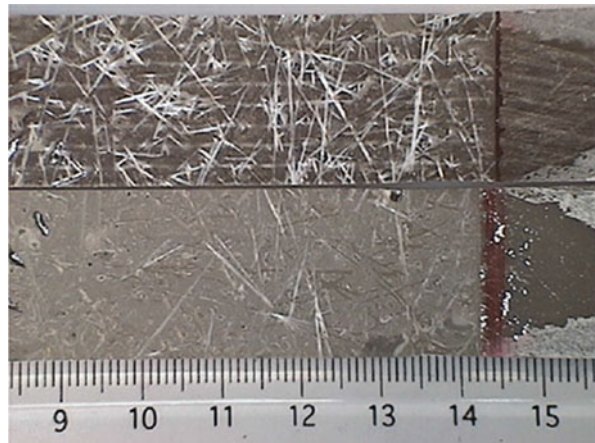
#### 48.4.2 Substrates

If the adhesive is correctly chosen and a suitable surface preparation has been applied, then the resulting joint strength is limited by the through-thickness properties of the composite substrate. The majority of the GRP used for small boats is based on unsaturated polyester resins reinforced by woven glass and/or chopped strand mat. The weakest link tends to be the glass mat reinforced layer. The fracture energy of this layer may be significantly lower than that of a woven fiber-reinforced composite, so there is no point in applying very high performance adhesives to assemble these materials. This is illustrated by Fig. 16 below, which shows the fracture surface of an adhesively bonded marine composite assembly involving an epoxy adhesive and two glass rovimat (alternate layers of woven roving and random glass mat) reinforced vinylester substrates. Failure under mode I (opening) loading occurs by crack propagation in the mat layer.

#### 48.4.3 Interface

There are many factors influencing the mechanical strength of an adhesive/composite interface in a marine structure. The tests available to characterize such interfaces are relatively limited, and few studies have addressed this specific problem. Wedge tests can provide information, and a test originally proposed by Boeing (ASTM

**Fig. 16** Fracture surfaces of joint after crack propagation under mode I (opening) loading. *Upper* substrate shows mat over woven composite, *lower* substrate shows mat over epoxy adhesive. Starter crack (film insert) at *right* of photo



D3762) is often used to evaluate qualitatively the influence of environments on interface behavior in metal assemblies (Popineau and Shanahan 2006; Adams et al. 2009). This involves pushing a wedge between two adhesively bonded metallic adherends and measuring the influence of the environment on crack propagation in the stressed specimen.

---

## 48.5 Durability in a Marine Environment

### 48.5.1 Degradation Mechanisms

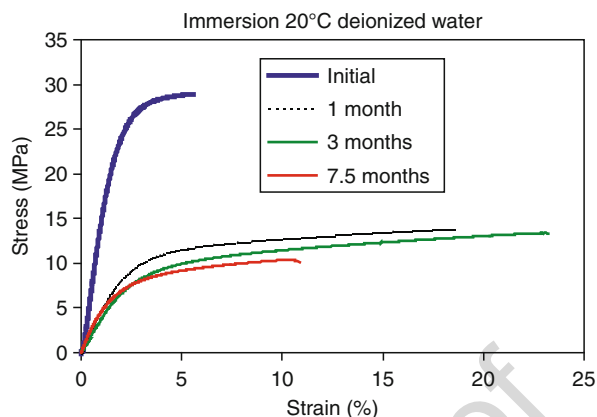
The entry of water into an adhesive will affect its physical and mechanical properties. Changes may be reversible (swelling, plasticization) or permanent (leaching out of additives or even hydrolysis involving chain breakage). The kinetics of these changes will depend on the exact adhesive formulation and on the environmental conditions, particularly temperature. While it is not possible today to predict with accuracy the extent of degradation of adhesives, there is much empirical data available on mechanical properties. This is a subject which has been studied extensively (see, e.g., Kinloch 1983; Bowditch 1996; Xiao and Shanahan 1997), but as there are many parameters needed to characterize an assembly completely, it is not a simple task to apply data from one to another. The very large number of adhesives on the market does not simplify this task; a major adhesive supplier may have a dozen standards in their marine catalogues, plus many more “special” formulations.

One of the conclusions of an HSE (UK Health and Safety Executive) report on the use of adhesive bonding in the offshore industry published in 1997 was that “long term durability under severe service conditions is uncertain due to a shortage of design data at present” (Cowling 1997). There has been work to remedy this since then, but for many potential users, this is still one of the reasons invoked to avoid adhesive bonding. It is important to underline certain points which put this problem in perspective. First, water ingress into a well-bonded joint is not instantaneous. A recent study (Bordes 2009) on diffusion into a 1.5-mm-thick fully immersed bulk epoxy adhesives in natural seawater at 20 °C indicated that even in this case, which is much more severe than the case of a joint between metallic adherends, the material was not saturated after 18 months. Using the diffusion rates for bulk adhesives, it is possible to estimate the time necessary to saturate even a small adhesively bonded steel joint, and this may take several years, particularly for an underwater assembly in water at 10–20 °C.

Second, the initial effect of water is very often to plasticize the adhesive, causing stiffness to drop but strain to failure to increase, Fig. 17. Subsequent degradation (after 7.5 months in this case) results in lower strain to failure.

Adhesives are designed to work in shear, and under shear loads, the strain to failure of modern structural adhesives can be very large (Cognard et al. 2005). This means that the influence of stress concentrations at joint edges may be reduced by water, though this effect must be considered relative to the local adhesive strength which may also be reduced. This initial effect is reversible, and subsequent drying

**Fig. 17** Influence of water on adhesive tensile properties, epoxy 1 h 80 °C cure



will enable initial properties to be recovered. Nevertheless, after long periods of immersion, permanent damage of the adhesive may occur, and accelerated testing is needed to establish when this will start.

Third, bonded areas may be very large, plates 250 mm square were studied in a recent offshore project, and even after several years in service, only a small edge region will be affected by water ingress. Thus, in practice, the main concern is not usually the adhesive itself but the adhesive/substrate region, which may provide a privileged path for water entry and debonding. Provided the integrity of this interface is ensured by an appropriate surface treatment and primer, then long-term durability can be achieved (Sargent 2005).

Finally, it should be noted that failures of adhesive joints in service are rare if recommended surface preparation and curing procedures have been followed.

## 48.5.2 Predicting Marine Aging Effects

With the rapid increase in numerical computing power, there have been attempts to formalize the different environmental contributions in order to provide a procedure to predict assembly durability (Crocombe 1997; Loh et al. 2002; Bordes et al. 2009). Figure 18 shows a simple scheme. This is based on an initial identification of diffusion coefficients and mechanical parameters. The relationships between water content and properties such as tensile modulus, tensile strength, and interfacial fracture energy are then established. A coupled numerical model for the joint of interest is then constructed. This allows local water content to be defined and resulting changes in adhesive and interface properties to be predicted. At present, there are various factors which prevent this rather simplified approach from providing accurate lifetime predictions, notably the viscoelastic nature of most adhesives, the difficulty in defining reliable tests to characterize interface strength, and the need to include the role of substrate corrosion. Nevertheless, it is probable that in the medium-term future, such approaches will provide a more rigorous basis to guarantee long-term performance of adhesive joints.

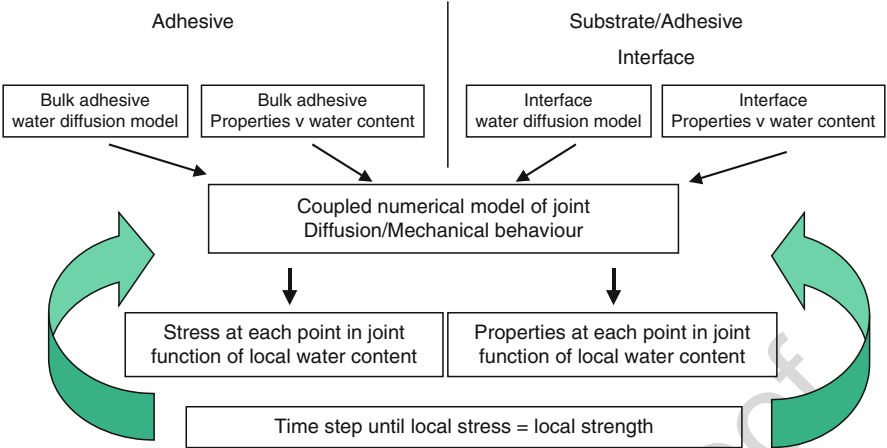


**Fig. 18** Simplified representation of a tool to predict the lifetime of an adhesively bonded marine assembly

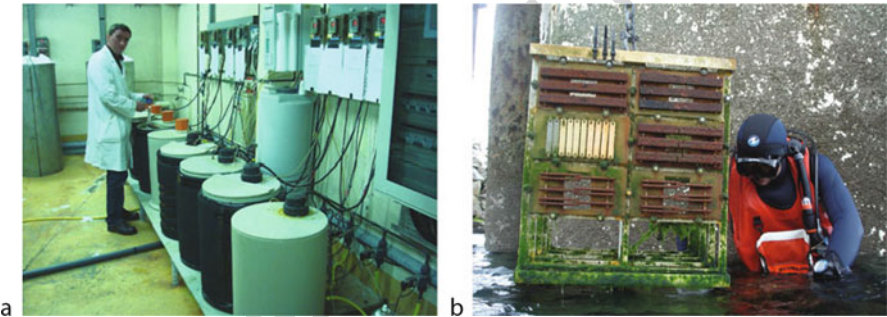


**Fig. 19** Marine aging of test samples. (a) Laboratory seawater aging test facility, and (b) removal of samples by divers after aging in tidal zone at sea

### 48.5.3 Testing to Simulate the Marine Environment

Given the difficulties in predicting long-term behavior, today most estimations of durability are based on aging tests. This is reflected in the marine adhesive-type approval tests described previously, which specify a percentage strength retention after short accelerated aging tests. Figure 19 shows facilities for seawater immersion testing. In the laboratory, Fig. 19a, this consists of a set of 60 l seawater tanks maintained at different temperatures (up to 90 °C). Natural seawater is used, pumped from the sea, and renewed continuously. This is essential, as many polymers release additives during aging which can rapidly change the composition of the water in closed aging tanks and affect the degradation kinetics. Tests at elevated temperatures are used to accelerate the degradation mechanisms; an Arrhenius plot is then used to

extrapolate to longer times at lower immersion temperatures. This is a very pragmatic approach, and interpretation of the results requires some caution. Adhesives are complex polymer formulations, and raising temperature may affect certain additives disproportionately. For this reason, longer tests are also performed at sea, Fig. 19b, so that the validity of extrapolations can be checked by tests under more realistic conditions.

## 48.6 Quality Control

Quality control of adhesively bonded joints is complex. There are two issues. First, is it possible to detect the presence or absence of adhesive, and second, if the adhesive is present, will it transmit loads between the two substrates? Detecting the absence of adhesive in a joint is possible using techniques such as tapping, frequently used in boatyards, or ultrasonic C-scan. The latter can detect areas without adhesive even when 10-mm-thick steel plates are bonded. Determining whether the adhesive will fulfill its function of transferring load between the substrates is more difficult and requires some form of mechanical loading to be applied. Thus, proof loading cycles are commonly applied to test pipework systems. A complementary approach advocated in the 1997 Health and Safety Executive (HSE) report was that as inspection of adhesively bonded connections is inherently difficult, quality assurance should be built into the bonding process and post-bonding coupon testing (Cowling 1997). Thus, operator certification may be required by certification societies for critical joints. In recent years there has been some progress in instrumentation of bond lines, and this may allow in situ monitoring in the future. For example, implanted optical fibers can be used to detect moisture in epoxy adhesives (Karalekas et al. 2009; Mieloszyk and Ostachowicz 2017).

## 48.7 Repair and Recycling

Repair of composite boat structures is routine, and many boatyards have extensive experience (e.g., Biddick 2005). These repairs are usually made by hand lay-up of materials similar to the original materials and generally use scarf or chamfered joints. There is some debate over the scarf angles to use, which can vary from 6:1 up to 16:1 or more (Pfund 2007). The certification societies provide general guidelines and favor at least a 16:1 ratio which requires more material removal, usually by grinding. Germanischer Lloyd provides an expression for minimum scarf ratio (chamfer length  $l_s$ /chamfer thickness  $t_s$ ) (Germanischer Lloyd 2006):

$$\sigma_{\text{mat}}/\tau = (l_s/t_s) \cdot x$$

with  $\sigma_{\text{mat}}$  the material tensile strength,  $\tau$  the allowable shear stress (9 MPa for a shop repair, 7 MPa for a field repair), and  $x$  a factor depending on the type of repair,

1 for hand lay-up and up to 1.15 if vacuum cure is used. Ductile resins (vinylesters or epoxies) with elongation to break of at least 2.5% are recommended.

Composite patches may also be used to repair metallic structures, and recent studies have indicated the potential of such repairs for naval and offshore structures (e.g., Bowditch et al. 2004; Turton et al. 2005). These may be applied using infusion or preimpregnated materials or adhesively bonded and can be applied to repair fatigue cracks and corrosion damage or for reinforcement purposes. Advantages over metallic repair are:

- Avoid hot working
- Conform to complex surface geometry
- Reduced costs
- Rapid application
- Lightweight (easy to transport and handle)

A recent study to investigate composite repair of offshore riser tubes has been described by Alexander and Ochoa (2010). Prefabricated carbon/epoxy half shells were adhesively bonded to steel tubes and proved satisfactory during testing under internal pressure and tensile and flexural loads. There is also considerable interest in composite repair of subsea pipelines, Lieu and Green (2016) provided an overview recently, and an ISO document exists (2013).

Recycling and end-of-life management of marine structures are topical issues. Adhesively bonded joints assembled using thermosetting adhesives are, like welding, not easy to disassemble, and alternative thermoplastic adhesives may become more popular. There are also some bio-sourced adhesives available, but to date their properties, particularly after immersion, are considerably lower than those of conventional adhesives. It should be noted that the quantities of adhesives used in marine structures such as boats are significantly smaller than the amounts of composites, and the recycling of the latter is currently the main priority.

---

## 48.8 Conclusions

Adhesive bonding is very widely employed to assemble and repair marine structures. New markets are appearing, the renewable marine energy sector (offshore wind, wave, and tidal energy) will require adhesives for structures such as turbine blades, and long-term durability in a marine environment will remain a key issue for these applications. This chapter has presented some current applications, and it is clear that considerable experience is already available to guide future projects. Certification societies are making efforts to provide a framework for marine use of adhesives which is closer to that of the aircraft industry, and this should result in improved joint quality. In parallel, several academic groups have recognized the importance of durability and are developing numerical tools to aid the designer and end user in predicting the lifetime of adhesive joints.



**Fig. 20** Data recorder adhesively bonded to Galapagos sea lion (Photo Huntsman) using modified epoxy adhesive



Challenges remain, and very specific marine bonding problems have been addressed. Figure 20 shows one example, in which time-depth recorders are attached to Galapagos sea lions in order to study their behavior. The adhesive has to withstand the heavy impact of 100 kg sea lions rolling, scratching, hitting rocks, as well as the salt water of the Pacific Ocean and the strong sun radiation. A modified epoxy adhesive was used successfully, enabling unique results to be obtained. These indicated that these sea lions dive to more than 500 m depths.

## References

- Adams RD (ed) (2005) Adhesive bonding: science, technology and applications. Woodhead Publishing Limited, Cambridge
- Adams RD, Cowap JW, Farquharson G, Margary GM, Vaughn D (2009) The relative merits of the Boeing wedge test and the double cantilever beam test for assessing the durability of adhesively bonded joints, with particular reference to the use of fracture mechanics. *Int J Adhes Adhes* 29 (6):609–620
- Alexander C, Ochoa OO (2010) Extending onshore pipeline repair to offshore steel risers with carbon-fiber reinforced composites. *Compos Struct* 92(2):499–507
- Armstrong KB (1997) Long-term durability in water of aluminium alloy adhesive joints bonded with epoxy adhesives. *Int J Adhes Adhes* 17(2):89–105
- Bauer P, Roy A, Casari P, Choqueuse D, Davies P (2004) Structural mechanical testing of a full-size adhesively bonded motorboat. *J Eng Mar Environ* 218(M4):259–266
- Biddick K (2005) Structural repairs. *Prof Boatbuilder* 97:174–191

- Bordes M (2009) PhD thesis. Aging of adhesive joints in a marine environment for offshore applications. INSA, Lyon. (in French)
- Bordes M, Davies P, Cognard J-Y, Sohier L, Sauvant-Moynot V, Galy J (2009) Prediction of long term strength of adhesively bonded steel/epoxy joints in sea water. *Int J Adhes Adhes* 29 (6):595–608
- Bowditch MR (1996) The durability of adhesive joints in the presence of water. *Int J Adhes Adhes* 16:73–79
- Bowditch MR, Harper TI, Lane JA (2004) Feasibility study to compare steel and adhesive/composite-based emergency repair methods for damaged hulls. HSE report 293
- Boyd SW, Blake JIR, Shenoi RA, Kapadia A (2004) Integrity of hybrid steel-to-composite joints for marine applications. *J Eng Mar Environ* 218(M4):235–246
- Cao J, Grenestedt JL (2004) Design and testing of joints for composite sandwich/steel hybrid ship hulls. *Compos Part A Appl Sci Manuf* 35:1091–1105
- Cognard JY, Davies P, Gineste B, Sohier L (2005) Development of an improved adhesive test method for composite assembly design. *Compos Sci Technol* 65:359–368
- Cowling MJ (1997) A review of adhesive bonding for offshore structures. HSE report, OTO 96 030
- Critchlow GW, Yendall KA, Bahrani D, Quinn A, Andrews F (2006) Strategies for the replacement of chromic acid anodising for the structural bonding of aluminium alloys. *Int J Adhes Adhes* 26:419–453
- Croccombe AD (1997) Durability modelling concepts and tools for the cohesive environmental degradation of bonded structures. *Int J Adhes Adhes* 17:229–238
- Davies P, Choqueuse D, Bigourdan B, Gauthier C, Joannic R, Parneix P, L’Hostis J (2004) Design, manufacture and testing of stiffened panels for marine structures using adhesively bonded pultruded sections. *J Eng Mar Environ* 218(M4):227–234
- Davies P, Baley C, Loaec H, Grohens Y (2005) Interlaminar tests for marine applications. Evaluation of the influence of peel plies and fabrication delays. *Appl Compos Mater* 12(5):293–307
- Davies P, Sohier L, Cognard JY, Bourmaud A, Choqueuse D, Rinnert E, Créac’hadeac R (2009) Influence of adhesive bond line thickness on joint strength. *Int J Adhes Adhes* 29:724–736
- Davies P, Choqueuse D, Bourbouze G (2010) Micro-tomography to study high performance sandwich structures. *J Sandw Struct Mater*. On-line doi:[10.1177/1099636209344273](https://doi.org/10.1177/1099636209344273)
- Diez de Ulzurrun I, López F, Herreros MA, Suárez JC (2007) Tests of deck-to-hull adhesive joints in GFRP boats. *Eng Fail Anal* 14(2):310–320
- DNV (1991) Guidelines for classification of high speed, light craft and naval surface craft
- DNV (Det Norske Veritas) (2009) Standard for certification, no. 2.9, type approval programme no. 1–501.12, adhesives
- Germanischer Lloyd (2006) Rules and guidelines, materials and welding, part 2 non-metallic materials, section 3, repair of components, part 2
- Golaz B, Michaud V, Lavanchy S, Manson JE (2013) Design and durability of titanium adhesive joints for marine applications. *Int J Adhes Adhes* 45:150–157
- Hansen AB, Rydin C (2002) Development and qualification of novel thermal insulation systems for deepwater flow lines and risers based on polypropylene. OTC 12141. Houston
- Hart-Smith LJ (2002) Adhesive bonding of composite structures – progress to date and some remaining challenges. *J Comp Tech Res* 24(3):133–153
- Hashim SA (1999) Adhesive bonding of thick steel adherends for marine structures. *Mar Struct* 12 (6):405–423
- ISO 12215-6 (2008) International standards organisation. Part 6 “Small Craft-Hull construction and scantlings – structural arrangements and details”
- ISO/CD 24817 (2013) Composite repair for pipework and vessels – qualification and design, installation, testing and inspection
- Jarry E, Shenoi RA (2006) Performance of butt strap joints for marine applications. *Int J Adhes Adhes* 26:162–176



- Junhou P, Shenoi RA (1996) Examination of key aspects defining the performance characteristics of out-of-plane joints in FRP marine structures. *Compos A: Appl Sci Manuf* 27(2):89–103
- Karalekas D, Cugnoni J, Botsis J (2009) Monitoring of hygrothermal ageing effects in an epoxy resin using FBG sensor: a methodological study. *Compos Sci Technol* 69:507–514
- Kinloch AJ (1983) *Durability of structural adhesives*. Applied Science Publishers, London
- Kinloch AJ (1987) *Adhesion and adhesives: science and technology*. Chapman & Hall, London
- Knox EM, Cowling MJ, Hashim SA (2000) Fatigue performance of adhesively bonded connections in GRE pipes. *Int J Fatigue* 22(6):513–519
- Lieu SC, Green MA (2016) Testing and history of composite repair systems for subsea pipe repair, OTC 26373. OTC Asia, Kuala Lumpur
- Loh WK, Crocombe AD, Abdel Wahab MM, Ashcroft IA (2002) Environmental degradation of the interfacial fracture energy in an adhesively bonded joint. *Eng Fract Mech* 69:2113–2128
- McGeorge D, Weitzenböck J (2004) Adhesive bonding. *Spec Ed J Eng Mar Environ* 218(M4):i–ii
- Mieloszyk M, Ostachowicz W (2017) Moisture contamination detection in adhesive bond using embedded FBG sensors. *Mech Syst Signal Process* 84:1–14
- Mouritz AP, Gellert E, Burchill P, Challis K (2001) Review of advanced composite structures for naval ships and submarines. *Compos Struct* 53(1):21–41
- Okada R, Kortschot MT (2002) The role of the resin fillet in the delamination of honeycomb sandwich structures. *Compos Sci Technol* 62(14):1811–1819
- LeLan JY, Parneix P, Gueguen PL (1992) Composite material superstructures. *Proceedings of 3rd Ifremer conference on nautical construction with composites*. IFREMER publication 15, pp 399–411
- Pattee FM, Kopp F (2000) Impact of electrically heated systems on the operation of deepwater subsea oil flow lines. OTC11894, Houston
- Pfund B (2007) Which ply first? *Prof Boatbuilder* 107:70–81
- Popineau S, Shanahan MER (2006) Simple model to estimate adhesion of structural bonding during humid ageing. *Int J Adhes Adhes* 26(5):363–370
- Sargent JP (2005) Durability studies for aerospace applications using peel and wedge tests. *Int J Adhes Adhes* 25(3):247–256
- Sika Marine Application guide (2009) 3rd edn. <http://www.sikaconstruction.com/ipd-mag-0.0.pdf>. Access Dec
- Speth DR, Yang YP, Ritter GW (2010) Qualification of adhesives for marine composite-to-steel applications. *Int J Adhes Adhes* 30(2):55–62
- Tamblin JS, Yang C, Harter P (June 2001) Investigation of thick bond line adhesive joints. DOT/FAA/AR-01/33
- Turton TJ, Dalziel-Job J, Livingstone F (2005) Oil platforms, destroyers and frigates – case studies of QinetiQ's marine composite patch repairs. *Compos Part A* 36:1066–1072
- UKOOA (1994) Specifications and recommendations for the use of GRP piping offshore. Part 4, Fabrication and installation
- Ural A, Zehnder AT, Ingraffea AR (2003) Fracture mechanics approach to face sheet delamination in honeycomb: measurement of energy release rate of the adhesive bond. *Eng Fract Mech* 70(1):93–103
- Weitzenböck JR (ed) (2012) *Adhesives in marine engineering*. Woodhead Publishing, Cambridge
- Xiao GZ, Shanahan MER (1997) Water absorption and desorption in an epoxy resin with degradation. *J Polym Sci B* 35:2659

Stefan Böhm, Martin Kahlmeyer, Andreas Winkel, and Ilko Hartung

## Contents

49.1	Introduction .....	1420
49.2	Concrete Construction .....	1420
49.2.1	Introduction .....	1420
49.2.2	Concrete as Substrate Material for Adhesive Bonding .....	1421
49.2.3	Applications .....	1422
49.3	Glass Construction .....	1432
49.3.1	Introduction .....	1432
49.3.2	Glass as Substrate Material for Adhesive Bonding .....	1432
49.3.3	Applications .....	1433
49.4	Timber Construction .....	1437
49.4.1	Introduction .....	1437
49.4.2	Timber as Substrate Material for Adhesive Bonding .....	1437
49.4.3	Applications .....	1439
49.5	Steel Construction .....	1441
49.5.1	Introduction .....	1441
49.5.2	Steel as Substrate Material for Adhesive Bonding .....	1441
49.5.3	Applications .....	1442
49.6	Conclusions and Outlook .....	1443
References	.....	1444

## Abstract

Adhesive bonding in the construction sector has a long tradition that dates back to the Nabataean and Babylonian ages. However, contemporary fastening technology

S. Böhm (✉) · M. Kahlmeyer · A. Winkel

Department for Cutting and Joining Manufacturing Processes, University of Kassel, Institute for Production Technologies and Logistics, Kassel, Germany

e-mail: [s.boehm@uni-kassel.de](mailto:s.boehm@uni-kassel.de); [m.kahlmeyer@uni-kassel.de](mailto:m.kahlmeyer@uni-kassel.de); [a.winkel@uni-kassel.de](mailto:a.winkel@uni-kassel.de)

I. Hartung

Dr. Kornder Anlagen- und Messtechnik GmbH & Co. KG, Bergheim, Germany

e-mail: [ihartung@dr-kornder.de](mailto:ihartung@dr-kornder.de)

must fulfill criteria other than simple wall and brick building. Topics like freedom in design, energy efficiency, repair, and lightweight construction are continuously addressed. In particular, bonding of dissimilar materials requires the improvement of joining technologies, and thus adhesion technology is equally evolving.

This chapter aims to introduce applications of adhesive bonding in civil construction. For this purpose, four fields of application (concrete construction, glass construction, timber construction, and steel construction) are considered with regard to already established and novel joining techniques. Particularities of the individual substrate materials are described as well as commonly used and suitable adhesive systems and the specific requirements of their applications.

---

## 49.1 Introduction

Today's engineers are faced with a wide variety of constructive and design-related tasks which require a great understanding of joining processes and material combinations.

Adhesive bonding has been employed for centuries. However, modern adhesive technology in civil construction is still a niche application, especially compared to other industrial sectors like the automotive industry. The field of civil construction is still cautious with this innovative joining technique and also has been historically very conservative.

One reason for this fact may be found in the Codex Hammurabi, a comprehensive set of Babylonian rules, which dates back to about 1750 BC. In that time, the builder had to compensate the owner's loss in case of damage. He was even sentenced to death if the owner of the house was killed because of a collapse of the building.

Above all, the main reason for the restrained use is the high demands on the predictability of the long-term behavior of the connections. Compared to other bonding methods such as welding or screwing, predictions for adhesive joints are more complex. Moreover, the manufacturing of adhesive bonds is a sensitive process, whereby the control on the construction site is just possible to a very limited extent. Thus, merely technically mature and proven methods are used, and new techniques must first prove their reliability.

However, adhesives have proven their efficiency and among others are established nowadays in the fastening and strengthening technology with concrete as substrate, in structural glazing, in timber construction, and to a small extent in steel construction.

---

## 49.2 Concrete Construction

### 49.2.1 Introduction

The development of concrete and mortar dates back to around 6500 BC when the Nabataeans used concrete-like materials in northern Jordan. The Babylonians used pitch or lime as mortar for constructions of baked bricks.

A forerunner to modern concrete and mortar is *opus caementicium* (Roman concrete). The Romans used volcanic ash (natural pozzolans) as a component of the mixture, which enabled underwater curing, and, more importantly, made long-lasting structures possible, which stand the test of time (e.g., the dome of the Pantheon in Rome, completed around AD 125).

Actually, any mortar or concrete, as it is used today, is an adhesive. Binders that exclusively harden under air are referred to as non-hydraulic, whereas lime and especially cement are hydraulic binders since these require water for their setting process.

Concrete is widely used in civil construction for buildings, bridges, road surfaces, and further components which have to meet the demands of long-term durability in combination with high compressive strength. The versatility of concrete is based upon the fact that both a prefabrication of cast components as well as direct processing on the construction site is possible. As long as prefabricated parts are utilized, quality control can be integrated into the general production process of standard industrial fabrication. However, the manufacturing of security-relevant parts or bonds directly on construction site is difficult to supervise, and hence high requirements regarding quality assurance and strict guidelines are necessary. Nevertheless, adhesive bonding of structures to concrete components is successfully carried out in the fields of anchoring systems and strengthening.

## 49.2.2 Concrete as Substrate Material for Adhesive Bonding

Concrete is one of the most durable materials and is commonly employed in civil engineering. However, the adhesion between newly hardened and old concrete is very poor. It can be improved though by surface roughening and latex emulsions or epoxy resins serving as an intermediate layer on which the repair mortar or concrete is applied (Mailvaganam 1997).

In general, special requirements must be placed on adhesives when bonding to concrete. A sufficient adhesion of epoxy resins to dry concrete is achieved if the surface is clean and slightly roughened, e.g., by means of sandblasting or a needle hammer, so that the cement skin is removed and the grain is partially exposed. For economic reasons, bonding cannot be limited to dry summer weather, and thus adhesives must also stick to wet concrete. Furthermore, the curing has to be ensured even in cold, damp weather. Due to the concrete's porosity and its vulnerable surface, reagents such as acids, salts, and water may harm the concrete or the bond. The influence of the corrosive media is especially severe when alternating cycles of wetting and drying or freezing and thawing occur. Coatings (based on silicones, epoxy resins, urethanes, bitumes, oil-based paints, acrylics, styrene butadienes, chlorinated rubber, vinylesters, polyesters, or linseed oil) can decrease the extent of deterioration because of a reduced water absorption and chloride ion penetration.

The alkalinity ( $\text{pH} = 12$ ) of concrete may also pose a problem for the adhesive's polymeric structure and the long-term behavior of the adhesion. If a quick repair of

components is required, acrylates prove beneficial instead of epoxy resins since the curing of the former is fast and even readily achieved at low temperatures. Nevertheless, the alkaline concrete demands the use of special acrylic systems that are insensitive to alkaline hydrolysis.

It is advisable to verify the properties of the adhesive bond by means of preliminary tests that are suited to the specific application and its requirements (Zilch and Mühlbauer 2007; Krelaus et al. 2008).

### 49.2.3 Applications

#### Tiles and Floors

##### Tiles

Besides the use of reactive resins or dispersion adhesives, in 90% of the respective applications, ceramic tiles are laid with *cement-based systems*. These are provided as dry mortar blends; thus, they have to be mixed with water and other liquid additives prior to application to ensure hydraulic setting. The final product is water resistant. Cement-based mortars contain cement binder as the main part, quartz sand or powdered limestone as filler, and special additives such as defoamers, wetting agents, and thickeners.

Although these mortars harden rapidly, in most cases the process is finished not before 24 h (Grimm 2013). In recent years, fast-curing adhesive mortars based on special cements have been developed to take the need for short-term construction into account. Tiles fastened by these adhesive mortars may already be grouted just hours after the laying of the tiles (Geiß 2006).

For the application of mortars on “moving” grounds, special blends have been developed which contain polymeric components, e.g., ethylene-vinyl acetate copolymer, or waterborne latex dispersions that are admixed to the basic mortar. Besides the increase of adhesion, these mortars dampen vibrations and take up stresses more effectively than systems without elastic inclusions.

*Reaction resin tile adhesives* set by a chemical curing process and are usually based on polyurethane or epoxy. The filled resin and the unfilled curing agent are mixed at the construction site prior to use. Since these adhesives are highly developed products, they are used far more often in professional construction than in do-it-yourself applications (Grimm 2013). For instance, they are utilized in highly loaded areas, for industrial flooring, for wet or otherwise chemically contaminated outdoor terraces, and for tiling cantilevered balconies which are submitted to high-temperature changes (Geiß 2006).

*Dispersion tile adhesives* are based on finely dispersed polymeric particles in water (e.g., styrene acrylate dispersions). Therefore, they can be directly applied at the construction site without the need of further mixing or adding other components. Because these systems are set physically by evaporation, hardening takes more time compared to chemically reactive adhesives. Furthermore, these systems are not

suitable for outdoor applications since they are, in most cases, frost sensitive. However, for renovation work, for the installation of skirtings, borders or similar, dispersion-based adhesives are particularly convenient.

## Flooring

For bonding parquet, the following types of adhesives are mainly used:

- Dispersion parquet adhesives
- Solvent-based resin flooring adhesives
- Reactive resin flooring adhesives

Although waterborne dispersions, for instance, on the basis of polyvinyl acetate, are the most environmental friendly adhesives for parquet on the market, their use may be critical because excessive swelling of the timber may lead to parquet distortion. Apart from timber-based floor covers, other materials, e.g., linoleum, rubber, cork, and polyvinyl chloride, are almost exclusively fixed with dispersion-based adhesives.

Solvent-based flooring adhesives possess excellent processing characteristics. The amount of parquet swelling is reduced due to the absence of water. Therefore, despite their relative high concentration of volatile organic compounds (20–25%), they are still the most used systems in the market with a share of approximately 65–70%. Common solvents are acetates, alcohols, or ketones like acetone or mixtures thereof in which a thermoplastic resin like polyvinyl acetate is dissolved. Also, mineral fillers such as chalk are admixed. Furthermore, solvent-based contact adhesives are used predominantly for bonding flooring to shape-giving substrates like stairs or skirting boards because of their higher initial adhesion in processing (Geiß 2006).

Bright timber like maple and beech which is highly sensible to swelling even requires the application of both water- and solvent-free adhesives, that is, reactive polyurethane and epoxy-based systems.

## Pavement Marking Tapes

Pressure-sensitive adhesives (PSA) are applied for the installation of pavement marking tapes onto the driving surface. A typical tape consists of a waffle-like rubber support layer, equipped with a polyurethane coating and attached ceramic particles. This combination achieves a high flexibility with a good visibility/reflective power and an optimum tire grip (see Fig. 1). The PSA is located on the bottom side of the rubber. For a good adhesion, the application of a primer after a thorough cleaning of the road surface might be necessary depending on the surface type (concrete, asphalt, bitumen). As a function of the field of application, several types of marking tapes are available, e.g., systems that outlive a perennial stress by traffic as well as tapes which are only temporarily used for building site markings (3M 2013, 2016).

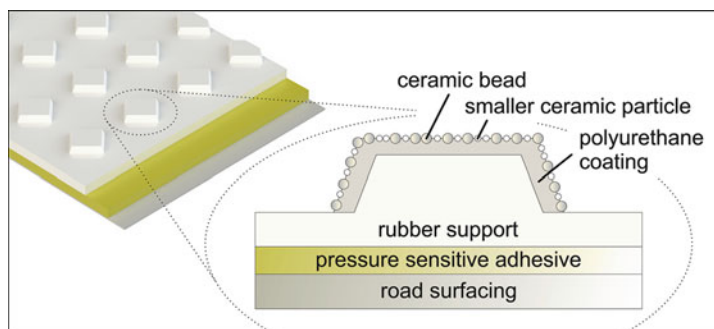


**Fig. 1** Schematic structure of a pavement marking tape (Source: tff)

## Fastening Technology

Fastening in the construction industry is often achieved with anchors in masonry or hardened concrete. Besides systems that feature fixation by mechanical interlock (deformation-controlled anchors, torque-controlled anchors, undercut anchors), bonded anchors effectively transmit forces from the body into cracked or non-cracked concrete by a hardened binder (Carroll 2014; Götz et al. 2010).

The binder consists of synthetic resin, cement, or even of a mixture of both. The operating principle of bonded anchors is based on a material closure; the hardened resin fills the gap between the anchor or threaded rod and the borehole wall and transfers external loads.

The bond strength largely depends on the nature and extent of the hole cleanliness (Geiß 2006). Although recently bonded anchors have been developed which require virtually no hole cleaning, systems generally show significantly reduced bond strengths, when a certain amount of drilling dust remains at the borehole wall. Thus, special care must be taken in cleaning the drill hole. This is especially the case when the anchor rod is inserted only by hammering without a turning motion. The latter removes adhered drilling dust from the borehole wall more effectively and ensures a better distribution and inclusion of dust within the mortar or adhesive. For a complete dust removal, most often a sequence of repeated blowing out of the bore dust and cleaning of hole wall with a brush is carried out.

Expansion forces do not occur before prestressing and loading of the anchor. During the setting, no spreading forces are generated. Since bonded anchors create much lower expansion forces as compared to metal expansion anchors, the former are more suitable for components with small thicknesses and fixtures with a low edge distance (Geiß 2006).

To evaluate the expectable structural strength of these systems, a destructive pullout test is commonly performed. However, the long-term behavior is in general not well understood. This clearly shows that the development of *in situ* nondestructive monitoring methods for structural components is of utmost importance (Rizzo et al. 2010).

Chemically bonded anchors are prone to different failure modes (Rizzo et al. 2010):

**Fig. 2** Partly destroyed glass capsule for bonding anchors. The small glass tube contains the curing agent (Source: tff)



- 216 (a) Failure of the anchor material
- 217 (b) Concrete cone failure
- 218 (c) Bond failure of the interphase (anchor/resin or resin/concrete)
- 219 (d) Combination of failure modes (b) and (c)

220 Bonded anchors can be subdivided into four categories (Carroll 2014; Götz et al.  
221 2010):

- 222 • Capsule-type systems
- 223 • Prepacked injection-type systems
- 224 • Post-installed rebar connections
- 225 • Expansion anchors

### 226 Capsule-Type Systems

227 Capsule-type bonded anchors make use of reactive polymeric resins which are  
228 encapsulated in soft-skin walls (plastic foil bags) or glass vials. In these containers,  
229 the resin and curing agents are separated from each other and thus cannot react prior  
230 to cartridge destruction (see Fig. 2).

231 Since styrene-containing resins are classified as hazardous to health and environ-  
232 ment in many countries, styrene-free systems are increasingly available (Geiß 2006).  
233 Most often, the resin is based on vinylester or unsaturated polyester, which is cured  
234 with dibenzoyl peroxide. Additional components are fillers (quartz), catalysts, and  
235 stabilizers.

236 Prepacked capsules ensure an optimal mixing ratio and therefore enable, assum-  
237 ing homogeneous mixing, a thorough curing of the resin. The cartridge size and  
238 hence the amount of resin are adapted to the required borehole diameter and the hole  
239 depth which directly relate to the dimension of the anchor itself. Since the gap  
240 between the anchor rod and the borehole wall has to be filled completely, dimension  
241 tolerances of the drill holes also have to be considered.

242 For fixation, the glass vial or foil bag is inserted into the borehole. Subsequently,  
243 the reservoir is destroyed by the anchor stud. A chisel at the stud end can support  
244 effective mixing of the components. The accomplishable load capacity is generally



lower for systems which make solely use of opening the cartridges by striking without any additional rotatory motion because of insufficient mixing of the components.

Compared to glass cartridges, foil bags have the advantage of a lower damage sensitivity during transport and handling. Furthermore, in overhead applications, foil bags prove beneficial as they remain in the borehole without the need of further fixation.

### **Prepacked Injection-Type Systems**

Injection systems are provided either in cartridges or as bulk material. Bulk material components have to be properly mixed in stoichiometric amounts before filling the cavity. In cartridges, resin and hardener are stored in separate chambers that are side by side (shuttle) or coaxial (cartridge inside cartridge) (Carroll 2014). The adhesive is blended in a static mixer prior to injection. The amount of resin injected is dependent on the drill hole depth. After filling, the anchor bar is pushed into the cavity. Leaking resin at the well mouth indicates a complete filling of the drill hole.

Although their curing via a polyaddition generally takes much longer compared to radical polymerization systems, epoxy resins are widely used in civil engineering to anchor both threaded rods and reinforcing bars in hardened concrete. In addition, they are advantageous for larger hole tolerances and anchorage lengths (Geiß 2006). Common applications include bridge widening, structure-mounted signs, luminaries and light poles, concrete repair and rehabilitation, and tunnel finishing. Other adhesives applied are vinylester systems and unsaturated polyesters. The curing cycles of the injected resins are commonly chemically prolonged to ensure sufficient processing times for hole filling and the subsequent setting of the anchor rod.

### **Post-installed Rebar Connection**

Rebars (Carroll 2014) are commonly used for the reinforcement of concrete. Anchors can be divided into two groups: cast-in-place and post-installed. A typical cast-in-place anchor consists of a rebar which is set before the concrete is placed. The rebar may require a protective coating to avoid corrosion and is finally fixed by the hardening of the surrounding concrete.

Instead, a post-installed rebar is set in a borehole filled with resin in order to facilitate the concrete reinforcement. This system features higher limit stress as compared to the cast-in-place anchors and is often used for starter bars.

### **Expansion Anchor**

Concrete is highly prone to cracking. This is due to shrinkage during hardening and because of loading in the tensile zone of the material. As the building component is loaded and unloaded, these cracks open and close (Rizzo et al. 2010). Bonded anchors as described above (e.g., for setting at the bottom side of a dynamically loaded ceiling) are not suitable for load transmission with predominant tensile amplitude in cracked concrete. Thus, expansion anchors have to be applied which generate spreading forces (form closure) by means of cones. The setting of the anchor rod is the same as in conventional bonded anchors (hitting and turning the rod

into a cylindrical hole). Due to a tension load induced into the fastening element, the adhesive bond between the anchor rod and the adhesive partly dissolves and the cones are pushed into the mortar. The resulting expansion forces and therefore the cottering between the mortar shell and the borehole wall are essential for the transition of tensile forces into the ground (Geiß 2006).

## Structural Reinforcement

Nowadays, civil building engineers are increasingly faced with the challenge of strengthening existing buildings and thus ensuring the durability or even increasing it because of altered circumstances. The reasons are (Bergmeister 2001):

- Changing the purpose of the building (e.g., due to higher loads or damage)
- Rebuilding and thus change in the supporting structure
- Reduction of structural safety due to concrete and steel corrosion
- Reduction of bending by a stiffness increase
- Design errors

The so-called surface-bonded reinforcement is a readily available method that strengthens concrete structures quickly, economically, and usually without further intervention in the building (Gao et al. 2004; Ferrier et al. 2001; Oehlers 2001; Wu et al. 2005; Dutta et al. 2001; Meier 1994; Meier and Munger 1995). For this method, steel and carbon fiber-reinforced polymers (CFRP) are commonly applied. Methods of attachment range from solely adhesive bonding to hybrid jointing techniques, e.g., adhesive bonding in combination with bolting.

This external reinforcement increases the flexural stiffness and load-carrying capacity of the previously deficient beams, provided that the attachment method enables a reliable transfer of stress between the concrete surface and the reinforcement element.

Thus, special attention must be paid to the interaction of concrete and adhesive which can only be achieved by clean (oil-free) and dry substrates. Besides wet-chemical methods (degreasing, primer treatment), mechanical methods are widely used for adhesion enhancement. For joining concrete and/or steel, sandblasting and grinding have proven beneficial. These methods effectively remove loose particles and contaminations, that is, oxide layers on metals and the weak top layer of cement stones (laitance) that is generated during the hardening of the fresh concrete (Hollaway 2008). In addition, these methods beneficially modify the surface texture and thus increase the bond strength. Sandblasting is carried out by a transportable sandblasting unit, whereas grinding is often conducted by using special grinding attachments on drilling machines.

The ability to built up adhesion to wet surfaces only plays a subordinate role because the application of the bonded reinforcement is usually done on the underside of the component and is therefore protected from rain. However, reliable curing at high humidity levels and low temperature is a prerequisite for this application. Epoxy resins have proven extremely effective. Furthermore, the process of carbonation and the chloride exposure must not be harmful to a great extent during the lifespan.

### Strengthening by Steel

A large number of techniques currently exist for strengthening of concrete structures and enhancing the flexural strength like external post-tensioning systems or the attachment of plates to the tension site of concrete beams (McKenna and Erki 1994; Shayan et al. 2003).

The latter method was first established in Paris, France, in 1964 where due to a static calculation error, a bridge had to be reinforced. In the late 1960s, engineers at Swiss Laboratories for Materials Testing and Research (EMPA) in cooperation with construction firms began to post-strengthen structures by means of bonded steel plates, based on the work of L'Hermite and Bresson. Comprehensive research effort was also conducted to establish an appropriate design basis. In Germany, similar work was carried out at the University of Braunschweig – Institute of Technology (Meier 1994).

Corrosion at the steel-epoxy interface can adversely affect bond durability with premature failure/collapse being the result (Karbhari et al. 1997; Keller and Gürtler 2006). A high degree of adhesion between steel and concrete is accomplished by compressed air jets or sandblasting to remove rust from the metal to prepare a suitable surface for coatings and bonds. Afterward, the lamellae are coated with a primer for corrosion protection which enhances the long-term efficiency of the strengthening capability (Brunner 1996; Kleist 1998).

Considerable effort has been conducted to understand the method of surface-bonded reinforcements, and engineers have also reported on the results of field implementation ranging from use in apartments to that in arched and prestressed bridge decks. Although extensively used in Europe for over a decade, this method suffers from a number of disadvantages ranging from difficulty in placement to concerns related to overall durability. Steel plates are heavy and hence hard to handle during erection and may be limited in length due to weight and size restrictions where utility lines and other obstructions exist. At the minimum, jacks, extensive scaffolding, and winches or cranes are needed for buildup. The length restriction necessitates the use of joints that need special attention since on-site welding is not possible due to the destructive effect of heat from the welding process on the adhesive. In addition, corrosion of the steel plates or at the steel-resin interface still plays a major role despite protective actions like sealings. Due to water seepage through concrete and resin, a reduction in failure load may occur. Furthermore, if the steel is loaded in compression, a detachment of the bonded sheet might occur at or near a cap beam. Beyond that, the steel enhances the overall self-weight of the buildings, and the structure gauge might be affected negatively. Due to the high weight, stripping of the steel plates can be executed not less than 24 h after the joining process.

Therefore, over the past years, strengthening by CFRP evolved which does not feature such drawbacks (Hollaway 2008).

### Strengthening by CFRP

CFRP as externally bonded reinforcement elements are increasingly used in the rehabilitation of deteriorating and deficient concrete structures (Stahlton 2011). The

method was first applied in 1991, when the Ibach Bridge near Lucerne was supported by bonded CFRP strips (Meier and Munger 1995). This technique was also employed at the town hall in Gossau SG and at an office building in Flims, Switzerland. The roof of the garage which had been insufficiently designed showed cracks and had to be rehabilitated. By bonding CFRP plates, the building could be quickly and safely reconditioned.

The strengthening procedure based on CFRP is dependent on the particular purpose and can be divided into four execution methods (Grunewald 2012; Zilch 2013; StoCretec 2016):

- (a) Adhesive bonding of CFRP plates/lamellae onto concrete
- (b) Adhesive bonding of CFRP strips into slots within concrete
- (c) Laminating of carbon fiber layings directly onto concrete
- (d) Pretensioned CFRP lamellae

A CFRP surface preparation may consist of a solvent treatment for removing adhesion-lowering substances, but usually, CFRP plates are sanded prior to their application to ensure sufficient adhesion. Water condensation on the CFRP should be avoided as a durable bond cannot be guaranteed under damp circumstances.

Since the respective composite element is bonded directly onto the concrete substrate, the efficiency of the rehabilitation scheme depends on the combined effect of the entire system with emphasis on the integrity and durability of the bond between CFRP and concrete. Premature debonding or loss of force transfer of the CFRP reinforcement due to degradation of bond strength can result in failure of the strengthened structural component, even at lower load levels than the strengthening can theoretically resist. The performance characteristics of the substrate, CFRP, adhesives, as well as the interfaces are all prone to deterioration by environmental exposure. Hence, there is a need to assess its effect on these materials and on the bond itself.

The use of CFRP techniques does not require closure of traffic lanes or a major disturbance of existing traffic patterns since extensive scaffolding, barriers, and heavy equipment are unnecessary. Strengthening by CFRP can be achieved in very close quarters and in areas where access is limited. This not only increases the ease of retrofit but also results in lower overall systems cost. It must be kept in mind that although the material cost attributed to composites is higher than that of steel, it is the total systems cost, which includes equipment, time, and detour costs, that needs to be considered when comparing the application of both reinforcement materials.

### **Adhesive Bonding of CFRP Plates/Lamellae onto Concrete**

The method of bonding CFRP onto concrete is especially suited for flexural strength enhancement of even concrete or round structures with a large diameter. A crosswise sheet bonding enables a biaxial strengthening (see Fig. 3). In addition, the level of shear force can be increased by application of CFRP angle elements.

**Fig. 3** Ceiling strengthened with CFRP plates (Source: Stahlton AG)



CFRP plates possess a high specific stiffness and strength ratios, outstanding fatigue behavior, and a negligible thermal expansion and are corrosion resistant. Furthermore, in comparison to steel, they are lighter and hence easier to handle. Thus, they can simply be positioned at the concrete substrate on the construction site without the need of extensive scaffolding and jacks. In addition, support is obsolete during the curing process of the epoxy resin since the initial adhesion strength is sufficient for holding the CFRP in position. Special care must be taken to attach the CFRP strips rapidly to the substrate without bulges occurring.

Due to the low rigidity of the lamellae with a thickness of 1–1.5 mm, they are often delivered as coils (Hollaway 2008; StoCretec 2016). The material is supplied in different dimensions and can be easily cut into necessary proportions on the construction site.

### **Adhesive Bonding of CFRP Strips into Slots Within Concrete**

Prior to bonding, slots with a width of 3–6 mm and a depth of 15–30 mm are milled into the concrete substrate. The recess is filled with epoxy resin and the preformed strips are pressed into the mold. Afterward, excessive adhesive is removed (see Fig. 4). The free ends of the rods may require further anchoring (Hollaway 2008).

The method highly increases the load capacity and bending strength of the construction to a high extent. The procedure is especially suited for systems where combined shear forces and moments occur and in areas with high stress gradients. Since the strips line up precisely with the surface level, they are effectively protected against mechanical damage (Mihala 2008). A further benefit is the visual appearance of the strengthening structure. Besides the advantages cited above, the procedure is also suitable for crack width limitation. In general, large cracks diminish the durability of structures. However, injection of reactive resins into cracks is not ideal for components where crack motion due to repetitive strain or variable forces can occur. The integration of glued CFRP into slots is a promising alternative for solving this issue (Meier 1994).

**Fig. 4** Strengthened concrete structure achieved by bonding CFRP strips into slots  
(Source: StoCretec GmbH)



**Fig. 5** Strengthening of a column by a direct laminating approach (Source: StoCretec GmbH)



#### Laminating of Carbon Fiber Layings Directly onto Concrete

Carbon fibers can also be attached on-site using a wet lay-up technique. Because the strengthening effect is dependent on the fiber orientation, the procedure is especially versatile and can easily be adapted to the conditions on the construction site for reinforcing different building structures.

The bonded layings enhance the flexural strength when laminated on flat substrates or result in high transversal forces when applied to the outside of concrete beams (Corradi et al. 2007). The procedure is often utilized for round elements, e.g., supporting pillars (see Fig. 5).

The laminating resin is applied onto the concrete surface; an impregnation of the latter with a primer is optional. A surface treatment is not required (Hollaway 2008). Afterward, the layings are deposited, followed by a second resin impregnation and a final coating which meets the required visual appearance.



### **Pretensioned CFRP Lamellae**

In critical areas which are particularly susceptible to tensile stresses, a high degree of reinforcement can be achieved by introducing compressive forces into the basic structure. An enhancement in this way is conducted, for example, by prestressing systems (Suter and Jungo 2001; Berset et al. 2002). These comprise an anchor fixed to the concrete substrate, which holds a CFRP lamella and a connected stress head in place. Alternatively, the CFRP is directly glued onto the steel end anchorage which in turn is fixed with screws and dowels. The lamella is tensioned hydraulically or with means of a manually adjustable tensioning head and is afterward fixed in the tensioned position. The prestressing force is introduced into the concrete exclusively through the anchors at the lamella ends. Adhesive bonding of lamellae to the concrete surface is not necessary to achieve a reinforcing effect. However, often the CFRP is glued to the substrate for protective purposes (Berset et al. 2002).

---

## **49.3 Glass Construction**

### **49.3.1 Introduction**

Glass, being a versatile construction material, possesses a high compressive strength and modulus besides its excellent long term durability. However, its brittleness and the high notch sensitivity exhibit major challenges when connecting glasses for construction applications. Nonetheless, direct contact between glasses and other hard materials like metals must be prevented. Thus, intermediate layers are necessary.

For this reason, adhesive bonding is predestined as a joining technique, allowing a homogeneous stress distribution over a large area and avoiding penetration of the glass by mechanical fasteners and clamping devices, which leads to reduced local stress peaks. Traditionally, glass in buildings is mainly used for windows as separating feature, but laminated safety glass (LSG) can also act as a load-carrying support element for large-size glazing. Recently, structural glass elements, such as beams, columns, and floors, are realized despite an absence of technical standards and/or practical recommendations as reference for design and construction (Biolzi et al. 2010; Haldimann et al. 2008).

However, due to rapidly advancing research and development in construction with glass, more highly transparent building envelopes and other structural elements are to be expected in the future (Weller and Schadow 2007).

### **49.3.2 Glass as Substrate Material for Adhesive Bonding**

Silicate glass is used almost exclusively in the construction sector. The most common is soda-lime silicate glass, which consists mainly of quartz sand, lime, and soda. The liquid state consists of  $\text{SiO}_2$  (about 70%),  $\text{CaO}$  and  $\text{MgO}$  (about 12%),

and  $\text{Na}_2\text{O}$  (about 15%). During the solidification, silicon oxides form a network of  $\text{SiO}_4$  tetrahedra into which the alkalis are embedded (Wörner and Freitag 2012).

Glass possesses a theoretical strength in the range of 1–100 GPa; the real (tensile bending) strength of annealed float glass is limited to 20–110 MPa. This mismatch results from small defects in the glass surface, which especially may be caused by cutting and grinding processes at the edge of a pane. A common method for increasing the strength of glass is prestressing by thermal treatment, leading to an inhomogeneous stress distribution across the section. Depending on the prestress level, several categories can be differentiated. Annealed float glass exhibits reduced internal prestresses; it breaks into large shards at relatively low forces. Heat-strengthened glass features medium tensile and compressive stresses, whereas fully tempered glass shows a more extensive crack branching because of increased energy release (Louter 2007).

The surface energy of glass in the solid state is in the range of 300–500 mJ/m<sup>2</sup>. Hence, the thermodynamic prerequisite for sufficient wetting with organic adhesives is theoretically given. Nevertheless, the hydrophilic surface of glass absorbs water from the environment, which results in a thin water layer. In particular, in the case of glasses with high alkali content, hydrolysis and the formation of  $\text{SiOH}$  groups on the surface lead to a reduction in surface energy, so that no ideal, purely oxidic surface is to be expected. Moreover, it must be taken into account that other corrosive media (neutral, alkaline, and acidic) also affect the surface characteristics. Also, the relatively low thermal expansion coefficient of  $5\text{--}10 \cdot 10^{-6} \text{ K}^{-1}$  must be taken into consideration, because this may cause stresses in the adhesive bond, e.g., for structural glazing facades, where large metallic and glass substrates are joined (Habenicht 2009). Pretreatments for achieving long-term stable bonding of glass are the application of silane coupling agents by wet-chemical processes, flame pyrolytic deposition of silicate layers (Pyrosil<sup>®</sup>), activation of the surface with atmospheric pressure plasma, and layer deposition by plasma polymerization (Wagner 2009).

### 49.3.3 Applications

#### Laminated Glasses

Laminated glass is a composite material consisting of one or more sheets of glass or synthetic polymers like acrylic glass joined together with one or more interlayers, simultaneously acting as adhesive and separator. Laminated safety glass (LSG) meets special safety requirements according to EN ISO 12543. To avoid a shattering into sharp pieces and to enhance the mechanical properties, LSG combines the unique characteristics of glass with the benefits of a tough but highly elastic organic material (Keller and Mortelmans 1999; Haldimann et al. 2008). For many structural applications, it is required to guarantee residual carrying capacity and to avoid dropping out after breakage. For this reason, LSG often consists of two or more prestressed glasses with an interlayer of polyvinyl butyral (PVB) or ethylene-vinyl acetate (EVA). The mechanical behavior of the composite is influenced by the



thickness of the glasses as well as the thickness and condition of the interlayer (Headley 2014; Jalham and Alsaed 2011; Biolzi et al. 2010). Moreover, the adhesion between the organic interlayer and the glass is relevant for the performance. A high adhesion of the polymeric foil ensures that glass fragments stick to the foil even after break, whereas a low adhesion improves the impact resistance because the interlayer retains its mobility and can be pulled from between the glass panes (Keller and Mortelmans 1999). For the production of LSG, a prelamination is carried out by heated pressure rollers, and subsequently the final product is formed in an autoclave at higher temperatures for expelling air pockets and, in case of thermoset EVA foils, for cross-linking (Headley 2014; Jalham and Alsaed 2011).

## Glass Facades

Structural glazing is a term used for several methods of attaching a curtain wall of glass to a support structure. Common technologies of attachment are spider fittings, clamps, structural silicone adhesives, as well as structural adhesive tapes. Built in 1903, the Margarete Steiff Toy Factory in Giengen, Germany, featured one of the earliest examples of glazed curtain walls in Europe and the first double-skin facade ever built. One major field of adhesive bonding in the construction industry is structural sealant glazing, especially structural silicone glazing (SSG), a technique for bonding glass to the frame of a building by silicone adhesives, which mainly must withstand live loads, such as wind, and in some cases the self-weight of the panel (dead load). By the late 1960s, the total vision system was developed, where glass panes were structurally bonded to glass mullions by silicones. In 1983, the construction of the 37-story-high Park Avenue Tower in New York City laid the foundation for SSG facades. The transparent architectural design, enabled by the use of a medium-modulus silicone, became so popular that today SSG is one of the most versatile forms of curtain wall construction in the commercial facade business and enhances the artistic appeal of buildings (see Fig. 6) (Klosowski and Wolf 2016; White et al. 2010; Giesecke 2007).

To support dead loads and to resist live loads while being able to compensate different thermal elongations, medium-modulus adhesives with elastomeric properties, low creep behavior, and high durable adhesion are required. Because the interface between structural adhesives and glasses is usually directly exposed to sunlight, the adhesive must resist UV light at least for an expected service life of 30–50 years. Besides, in particular for protective, safety, and security glazing systems, the joint must withstand high load rates (hurricane, bomb blast, earthquake) over a short impact time. For many structural glazing applications, silicones are predestined because of their special properties caused by their different chemical backbone compared to other, purely organic-based adhesives. They display a very low glass transition temperature ( $T_g$ ) owing to the flexibility of their siloxane polymer backbone. The time-temperature superposition principle implies that a low  $T_g$  stands for a high flexibility of the polymer chains at high temperatures within very short time scales. Thus, the theory predicts particularly good performance for silicone adhesives when submitted to sudden load conditions. Moreover, they remain highly elastic and allow a tension equalization over a large temperature

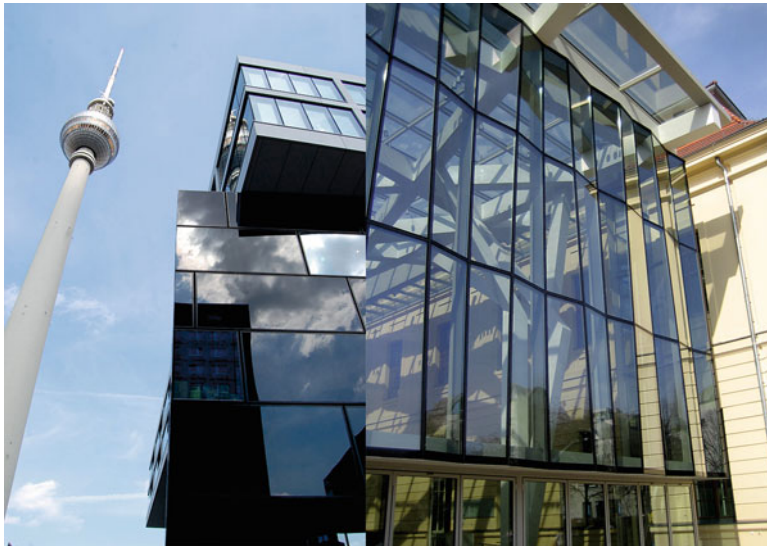


**Fig. 6** Examples of structural sealant glazing constructions (*left* adhesively bonded all-glass facade edge of the Alea 101 office building, Berlin; *right* hybrid glass facade with inserted mechanically fastened toggle spacers and bonded glass panes of the Jewish Museum Berlin) (Source: Verrotec GmbH)

range, are nearly inert to chemicals, and exhibit excellent resistance to moisture and weathering. These properties mark silicones as perfect adhesives for long durable bonds (Giesecke 2007; White et al. 2010).

Commonly, structural loads are transferred from the panel to the framing via a linear structural adhesive fixation along the panel's perimeter. The number of adhesive bonds per panel leads to the division into two- or four-sided SSG structures. Two-sided SSG are either vertically or horizontally bonded to the substructure on mutually opposing panel edges. Four-sided SSG is achieved by applying adhesive in all four edges of each pane. Because in case of two-sided bonding two edges are captured by conventional glazing channels, the functional reliability is higher compared to the four-sided variants. Nevertheless, the importance of the sealant is obvious in both versions. Besides the number of adhesive joints, the construction of SSG facades is different in regard to the dead load support and mechanical restrains. The guideline for European technical approval for structural sealant glazing (ETAG 002) differentiates four basic types of SSG construction (cf. Table 1). National regulations lay down the need for restraint systems for various applications (Kłosowski and Wolf 2016).

Moreover, it is important to ensure a reproducible bonding process. Ideally, the production of structurally glazed curtain wall modules, especially four-sided variants, should be carried out as factory production to guarantee a controlled environment with proper surface preparation and quality assurance programs. But, especially in case of maintenance or repair, the structural bonding operation must

**Table 1** Basic types of SSG (ETAG 002)

Type	Mechanical dead load support	Mechanical safety retention device
I	Yes	Yes
II	Yes	No
III	No	Yes
IV	No	No

be executed on the construction site, and temporary mechanical fasteners may be required to firmly hold the panes in place until a sufficient cross-linking density is reached.

Besides linear bond lines, technologies have been developed that allow adhesive point fixations of curtain wall elements near the corners. These point-fixing elements can lead to frameless and visually appealing glass facades (Dow Corning 2011). In case of LSG panes, the fastening can be achieved by bonding on the outer glass surface. Alternatively, the outer glass layer of the pane can be penetrated by the point holder and the joint is thus glued to an inner layer of the LSG pane.

While in SSG a metallic substructure forms the building to which the facade elements are glued, glass can also act as a structural element itself. In Amsterdam, the entrance of a Chanel store was designed by replacing the old brickwork by glass bricks and door and window frames. For the realization of this facade, more than 7.000 handmade glass elements were joined by a tension equalizing UV-curing adhesive (Delo 2016).

**Other Glass Construction Elements**

Further construction elements made of glass are divided into overhead glazing, accessible glazing, as well as railings and balustrades. Flexible adhesives such as silicones with limited strength but high elasticity are not always suitable for these applications. Even though SSG necessitates the use of elastic adhesives, structural silicones are neither stiff nor strong enough and unsuitable for small adherend surfaces in many applications. Although annealed glass is a relatively flat product, heat treating causes roller wave distortions, so that assembly tolerances must be taken into account for the selection of the adhesive. For tolerances of more than 1 mm, it is recommended to use epoxy-based systems with sufficient gap-filling properties, whereas the use of contact adhesives such as acrylic-based systems is possible for smaller spacings. Especially for transparent substrates like glasses, UV-curing acrylics, as used for the previously described Crystal House in Amsterdam, should also be considered. Nevertheless, for many applications, the limited absorption of deformation and compensation of thermal elongations of these rigid systems must be considered already in the design phase (Haldimann et al. 2008).

Due to the brittleness and unpredictable failure behavior, glass is considered as a structurally unsafe material. To reduce the risk of a spontaneous failure of load-bearing structures, research was carried out to obtain ductile failure behavior by the combination of glass with other materials like CFRP, stainless steel, concrete, or

even timber. Moreover, the exclusive use of adhesives to obtain a ductile fracture behavior was examined. Glass beams, composed of multiple overlapping glass segments being adhesively bonded by acrylic adhesives, lead to transparent construction elements with a ductile failure behavior (Louter 2007).

The potential of glass elements in construction engineering can be seen on a record-breaking construction in China. A 430 m long suspension bridge in the Chinese province Hunan, opened in summer 2016, consisting of a structural glass deck and banisters with side hanging stay cables. With a width of 6 m, the bridge spans a canyon between two cliffs and hovers over a vertical drop of 300 m. The bridge consists of 99 panes of three-layer safety glass (Yiin 2016).

---

## 49.4 Timber Construction

### 49.4.1 Introduction

Timber from well-managed forests is one of the most sustainable and oldest materials used in the construction industry. The key advantages of timber are the very high strength-to-weight ratio, the ability to transfer tension and compression forces, and its suitability as a flexural member. The excellent durability, performance, and insulating properties against heat and sound make timber a versatile working material. It can be easily shaped and connected by screws, nails, bolts, and dowels. Furthermore, there have been significant advances in adhesive technology.

Connections achieved by adhesive bonding can result in a better appearance, are often stiffer, and require less timber. Examples of structural timber connections include finger joints, scarf joints, glued gusset joints, and splice joints, which can reach better mechanical properties compared to butt or lap joints (see Fig. 7) (Porteous and Kermani 2012; Serrano 2000).

In case of thermosetting adhesives, the joints perform better than mechanical connectors with regard to fire resistance. The main disadvantages of adhesively bonded timber parts are the necessity of quality control during manufacture and the risk of degradation in conditions of fluctuating moisture content, especially in case of joints between dissimilar materials. However, the developments in adhesive technology have led to an increase of glued joints for structural timber construction as well as for engineered wood products (EWP) (Porteous and Kermani 2012).

### 49.4.2 Timber as Substrate Material for Adhesive Bonding

Due to the fibrous and porous structure of almost all types of timber, the adhesion of wood-based materials is predominantly caused by form closure. In addition, intermediate molecular binding forces between the polar wood surface and adhesives can support the strength of the joint. In some cases, even covalent bonds form, for instance, in the reaction of isocyanate or epoxy containing adhesives and hydroxyl groups of the cellulose molecules. Besides this, the polarity of wood results in

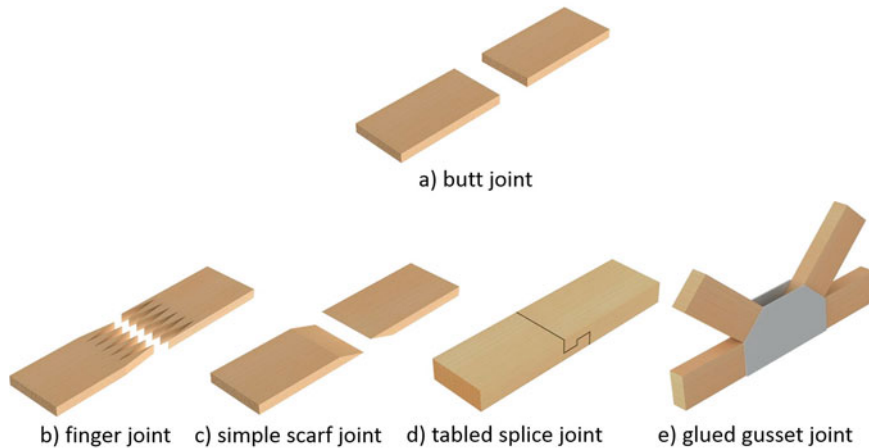


**Fig. 7** Examples of structural timber connections which can be realized by adhesive bonding (Source: tff)

hygroscopy that must be taken into account since the presence of water influences the setting process of many adhesives as well as the performance of both adhesive and adherent (Habenicht 2009; Custódio et al. 2009).

Although adhesive bonding of wood does not pose much of a problem, an adequate surface pretreatment is appropriate for:

- Reproducing long-term durable bonds
- Establishing a close fit between the adherents
- Creating freshly cut or planned surfaces free of irregularities and contaminants
- Enabling a sufficient wetting and penetration by the adhesive

Immediately after surface preparation, the surface undergoes an inactivation process by external contamination (airborne chemical contaminants, oxidation, and pyrolysis), as well as self-contamination, that is the migration of hydrophobic wood extractives to the surface leading to a reduction of surface energy. To achieve optimal adhesion conditions, the inactivation process of a prepared surface must be taken into account. For this reason, for an appropriate bond the bonding process should be carried out immediately after cutting and activation (Custódio et al. 2009).

Especially in case of timber constructions, adhesives should be selected with regard to the expected exposures. It is required that adhesives are resistant against relevant chemicals, temperatures, and microorganisms and insects that may influence the adhesive bond. The resistance to humidity is of greatest importance (Rug and Mönck 2015). Phenolic and aminoplastic polycondensation adhesives for load-bearing timber structures can be divided into two categories with regard to the expected climatic exposure conditions (Porteous and Kermani 2012).

- I. Suitable for indoor and outdoor applications – adhesives should withstand full outdoor exposure and temperatures up to 50 °C.
  - II. Primary suitable for indoor applications – adhesives may not be able to withstand prolonged exposure to weather or temperatures above 50 °C.
- Suitable structural wood adhesives recommended for several service environments are listed in Table 2.

49.4.3 Applications

Engineered Wood Products

In order to add value to the raw material and to overcome the limitations of sawn timber, several EWP have been developed which often involve the use of adhesive joints. As a natural product, wood is a material with a strong anisotropic behavior and an inhomogeneous, porous structure. It mainly consists of cellulose fibers, hemicellulose, and lignin. Characteristics are the large property variation in the processed state, such as swelling and shrinkage due to moisture absorption and release, leading to the development of EWP (Habenicht 2009). Many of these products use the same approach: cutting solid wood into small pieces (sheets, laminations, or even fibers) and joining them to gain a more homogeneous material (Serrano 2000). Glued laminated timber (glulam) is an example of an EWP, which consists of dried thin planks of wood with parallel grain to the longitudinal axis in each layer. Durable and moisture-resistant structural adhesives are used for their interlaminar bonding. Glulam laminate is commonly used for columns, trusses, bridges, portal frames, post, and beam systems (Porteous and Kermani 2012). Further EWP products like laminated lumber, plywood, and particleboards and their applications are described in the literature.

Glued-In Rods

Glued-in rods (GiR) are an effective way for both constructing new and strengthening existing timber structures. Most applications have used GiR reinforcements with

Table 2 Adhesives for structural timber engineering (Levy 2012)

Primary service environment	Main types of adhesives
Fully exterior use	(Phenol)-resorcinol-formaldehyde
(Withstands long-term water and drying)	Emulsion polymer/isocyanate
	Melamine-formaldehyde
Semi-exterior use	Melamine-urea formaldehyde
(Withstands short-term water soaking)	Isocyanate
	Epoxy
Interior use	Urea-formaldehyde
(Withstands short-time high humidity)	Casein



metal bars for repair, strengthening of solid timber beams and for joining concrete slabs and floor beams. Requirements like limited weight or resistance to corrosion can be fulfilled by the use of pultruded fiber-reinforced plastic (FRP) rods instead. To realize GiR, a hole with defined diameter is drilled into a wood block (usually softwood or glulam). After cleaning the hole, e.g., by compressed air, a certain amount of adhesive is filled in followed by the insertion of the rod. Different variants of GiR were developed to enhance the quality control of this process and to allow a better performance (Steiger et al. 2015).

A large number of adhesives have already been investigated for this application. Epoxy-based systems have been able to achieve high adhesion on both the metal rod and the wood surface. They showed excellent pullout strengths, so in the end the wood itself became the weakest link. Other commonly used adhesives are phenol-resorcinol adhesives and polyurethanes. Besides shrinkage during initial hardening, gap-filling qualities, viscosity, moisture, temperature-dependent properties like creeping as well as loads and geometrical conditions must be considered during the selection process for optimum GiR applications (Steiger et al. 2015).

### Reinforcement of Timber Structures

For strengthening and repair of timber structures, the use of FRP has been shown to be an effective and economical method as compared to traditional techniques. The selection of adhesives has to be undertaken with great care. Five categories of adhesives for FRP reinforcement of timber are available: epoxies, polyurethanes, polyesters, phenolic resins, and aminoplastics. Similar to GiR, two-part, cold-curing epoxy adhesives are particularly appropriate, not least because of their good gap-filling properties and their low curing shrinkage. External reinforcements utilize almost exclusively plane products whereas internal reinforcement use pultruded rods and plates. These are inserted into timber slots or grooves (Schober et al. 2015).

Four different applications of reinforced timber structures can be divided. Beam-end reinforcements are commonly used variants for repair and support of wood structures only at the edges. Therefore, holes or grooves are inserted into locally prepared beams followed by the insertion of adhesives and reinforcement elements like FRP. Furthermore, a tension reinforcement perpendicular to the grain can be useful to increase or maintain the load-carrying capacity of structures. Since notches, holes, curved beams, and beams with variable height result in high tensile stresses perpendicular to the grain, which is an unsuitable load type for wood as an anisotropic material, FRP reinforcement with defined fiber orientation can be used to enhance the performance locally. Other variants for structural elements, loaded by shearing or bending, can also be enhanced by FRP, either internally or externally. In some cases, a prestressing of FRP elements can be beneficial on the tension side of beams, which presents the most effective utilization of FRP reinforcement (Schober et al. 2015; Triantafillou and Deskovic 1992).

## 49.5 Steel Construction

### 49.5.1 Introduction

Adhesive-bonded steel joints are nowadays not only used in automotive and airplane industry (Pasternak and Mainz 2006). However, although adhesive bonding has significant benefits in comparison to other joining techniques, constructions in civil engineering which are completely made of steel (or metal in general) are not commonly achieved by the use of adhesion technology. Usually, these connections are established by welds, screws, bolts, or rivets.

One main reason for this fact is that adhesive bonding processes are often lacking in order to ensure the process reliability and long-term stability of the bonds.

In the classical steel body, forces are absorbed by individual beams and struts. However, this local load concentration is unfavorable for glued joints (Geiß et al. 2012; Geiß 2008). This situation could be remedied by a modified design. Yet, there is a lack of experience in adhesive construction. In addition, dimensional tolerances of the components are unavoidable in construction. Gap thicknesses of several millimeters to centimeters are generally difficult to compensate by adhesives if at all (KIT 2016a). More often, adhesives are applied for joining steel with other materials, such as glass in the structural-facings sector. In this case, mostly silicone-based adhesives, urethanes, and epoxy resins are used.

### 49.5.2 Steel as Substrate Material for Adhesive Bonding

Since the surface energy of steel is sufficiently high, gluing to steel is generally not an issue. In order to produce long-term resistant, high-strength adhesive bonds, grinding or sandblasting is necessary when layers like rust or scale adhere to the surface which does not have sufficient adhesion to the base material. Due to production processes before the bonding and the necessity of corrosion protection, steel surfaces are usually oiled. Several adhesives are capable of achieving good bonds even at high levels of oiling ( $>3 \text{ g/m}^2$ ), such as, for example, acrylates or some epoxy resins. As a rule, however, these surface contaminations have to be removed prior to bonding (Henning and Moeller 2011).

Special attention must be paid to the type of steel used. Stainless steels are passivated by their chromium content in such a way that the reactivity toward corrosive media is reduced. Due to this passivation, the strength of intermolecular bonds between the adhesive and the steel necessary to achieve a good adhesion may also be reduced (Habenicht 2009). However, this statement has not been demonstrated in general (Geiß et al. 2012), and the bond strength needs to be evaluated for any combination of adhesive and steel grades.

The bonding to galvanized steels can be problematic in that the zinc layer has a different adhesion to the steel substrate, depending on the type of deposition



(hot-dip or electrolytic galvanizing). Furthermore, the adhesive strength is influenced by the different orientations of larger zinc crystallites, as a heterogeneous stress distribution is thereby generated within the adhesive layer (Habenicht 2009).

Today, in steel construction, polyesters, vinylesters, acrylates, epoxy resins, polyurethanes, or hybrid systems are employed (Dilger 2011). Especially the polymerizing systems (acrylates, esters) prove beneficial, since these readily cure at low temperatures and are more insensitive to mixing errors (Feldmann et al. 2006).

Structural thermosetting adhesives, which have been successfully used in car body shops for several years like one-component epoxy-based systems, are not suitable for many steel structure applications because of the required high curing temperatures (between 175 °C and 190 °C) and the resulting difficulties on construction site.

### 49.5.3 Applications

As mentioned above, gluing in steel construction (as in the construction industry in general) only has a very limited range of use, even though in the past initial attempts have been made to increase its application. Therefore, the examples listed here are rather of an academic nature or part of basic research and are not routinely used in steel construction.

#### Bridge Building

In 1955, a bridge based on hybrid bonding technology (adhesive bonding backed up with screws) was raised over a side channel of the river Lippe in Marl, Germany (Brockmann and Neeb 2001). In this case, rods were adhesively bonded with the lower and upper belt with a polyester-phenolic resin via a flange connection.

Besides other examples (Brockmann and Neeb 2001; Piekarczyk and Grec 2012), further developments at the time were scarce due to the limited properties of the adhesives and experiences compared to contemporary joining techniques. However, even today, gluing in bridge construction remains a niche application. This is mainly due to the progressive development of welding technology with regard to the realization of complex structures. In addition, statements about the long-term stability of adhesive bonds under environmental influences can only be made inadequately.

A common method for strengthening decks in ship construction is the application of sandwich structures where an elastomeric adhesive fills the gap between two steel sheets. These steel-polymer-steel structures (SPS) possess a promising torsion rigidity. Furthermore, the elastic core is able to relieve stress peaks. Feldmann et al. were investigating such laminates for the post-strengthening of road bridges (Feldmann et al. 2006). They achieved a reduced cover plate bending and thus a higher load capacity.

### **Metal Framework Facades**

Recent glass facades demand a highly stiff supporting structure with a maximum bearing capacity which effectively takes up the occurring loads (e.g., wind loads) but which at the same time makes light-flooded architectural design and construction possible (Pasternak and Mainz 2007). Mullion and transom facades which use profiles with a rectangular hollow cross section are a suitable construction variant for this kind of task. However, an additional strengthening in terms of an increased load-bearing capacity and improved stiffness can be achieved by glued-in steel sheets. The effectiveness of this method could be evaluated by means of a four-point bending test at the Brandenburg Technical University (Pasternak and Mainz 2007).

Especially for industrial halls, facades made of trapezoidal profiles are employed which in general are attached to the support structure by means of nails, rivets, or screws. However, the fastening methods possess several disadvantages like the possibility of rust formation or the local occurrence of dents (Pasternak and Mainz 2007). Thus, Pasternak and Mainz developed a fastening method that makes use of a hook profile adhesively bonded to the trapezoidal sheets. They determined the optimal construction parameters in terms of normal stresses in dependence of hook length or type of the adhesive system used.

### **Hybrid Bonding**

As already mentioned, adhesives are often not able to compensate larger bonding gaps in the range of several millimeters to centimeters. However, these gaps are unavoidable due to high tolerances in building construction. Scientists at the Karlsruhe Institute of Technology have developed a method that can solve this discrepancy (KIT 2016a, b). For this purpose, inorganic granules are adhered to the steel surface with an organic structural adhesive. The steel surface is simultaneously sealed by the adhesive and protected against corrosion. The components thus treated are subsequently connected by means of a grouting mortar.

---

## **49.6 Conclusions and Outlook**

In structural engineering, two connection techniques are currently employed. On the one hand, mechanical fixing elements are used. These transfer forces only locally and, in addition, may partially damage the adherends. On the other hand, welding is a widely spread joining technology that results in stiff and resilient structures. However, welding is only suitable for certain material combinations. Thus, many novel design concepts cannot be realized.

Adhesive technology leads to a high material utilization and freedom of design and is therefore nowadays already established in some sectors of the construction industry. This includes not only maintenance and repair but also the realization of novel building structures.

Since concrete itself can be referred to as an (inorganic) adhesive, in concrete construction all processes are basically bonding processes. In addition, the use of organic systems can be beneficial for further applications, e.g., for anchor systems and reinforcement elements.

The glass industry best illustrates the high potential of adhesive bonds. SSG facades play an increasing role due to their excellent design possibilities. The development of suitable silicones and acrylic systems as well as special types of glass (prestressed glasses, laminated glasses) are likely to lead to further construction projects that will benefit from the advantages of glued joints.

In timber construction, the use of adhesives is also quite common. By the use of adhesion technology, new material combinations could be achieved, which feature many advantages. In addition adhesives are employed for structural bonding as well as for reinforcement applications.

In steel construction, adhesive bonding is less common. Nevertheless, several research projects demonstrate its benefits even in this sector. This results not least from the vast diversity of materials and the resultant difficulty of joining by well-established techniques.

Even if adhesive bonding is already established in many areas of construction, its potential is not yet fully exploited. The reasons for this are the relatively low level of trust in this technology, the lack of knowledge in the use of adhesives, as well as the limited process control. Future developments should address these current deficits in order to successfully expand the application of adhesive technology in the civil construction sector.

---

## References

- 3M (2013) 3M stamark pavement marking tape, series 380. 3M Traffic Safety and Security Division, St. Paul. <http://multimedia.3m.com/mws/media/8492770/3m-stamark-pavement-marking-tape-series-380-flyer.pdf?fn=380.pdf>. Accessed 16 Nov 2016
- 3M (2016) Verlegeanleitung für 3M Stamark Dauermarkierungsfolien auf Betondecken. 3M Deutschland GmbH, Neuss. [http://multimedia.3m.com/mws/media/3450620/verlegeanleitung-beton-plus-programm.pdf?fn=PM\\_%2028\\_ESD\\_IB\\_DE.pdf](http://multimedia.3m.com/mws/media/3450620/verlegeanleitung-beton-plus-programm.pdf?fn=PM_%2028_ESD_IB_DE.pdf). Accessed 16 Nov 2016
- Bergmeister K (2001) Kleben im Betonbau – Theoretische Grundlagen und Bemessungsvorschläge. Beton Stahlbetonbau 96(10):625–633
- Berset T, Schwegler G, Trausch L (2002) Verstärkung einer Autobahnbrücke mit vorgespannten CFK-Lamellen tec21 128(22):27–29
- Biolzi L, Cattaneo S, Rosati G (2010) Progressive damage and fracture of laminated glass beams. Constr Build Mater 24(4):577–584
- Brockmann W, Neeb T (2001) Stand der Klebtechnik im Stahlbau. Stahlbau 70(2):106–115
- Brunner R (1996) Kleben im Baubereich. Seminar Modernes Kleben, Trends aus Industrie und Forschung, EMPA Dübendorf, 1996. EMPA, Dübendorf, pp 70–79
- Caroll B (2014) Selecting and specifying the most effective anchor type. Eng J Dublin. <http://www.engineersjournal.ie/2014/10/28/selecting-specifying-effective-anchor-type/>. Accessed 14 Nov 2016
- Coming D (2011) Structural Glazing Handbuch. Dow Corning GmbH, Wiesbaden. <http://www.dowcorning.com/content/publishedlit/62-0979-03.pdf>. Accessed 22 Nov 2016

- Corradi M, Grazini A, Borri A (2007) Confinement of brick masonry columns with CFRP materials. *Compos Sci Technol* 67(9):1772–1783
- Custódio J, Broughton J et al (2009) A review of factors influencing the durability of structural bonded timber joints. *Int J Adhes Adhes* 29(2):173–185
- Delo (2016) So schön kann das Kleben sein. *adhäsion KLEBEN & DICHTEN* 60(10):51–52
- Dilger K (2011) Kleben. In: Henning F, Moeller E (eds) *Handbuch Leichtbau – Methoden, Werkstoffe, Fertigung*, 1st edn. Carl Hanser, München
- Dutta PK, Mosallam A, Vargas J, Mikhael D (2001) A fast method for field evaluation of concrete/FRP adhesive bonding in extreme temperatures. In: Repecka L, Saremi FF (eds) *SAMPE symposium and exhibition*. Taylor & Francis, Long Beach, pp 451–462
- Feldmann M, Völling B, Geßler A et al (2006) Kleben im Stahlbau. *Stahlbau* 75(10):834–846
- Ferrier E, Lagarde G, Hamelin P (2001) Concrete beams reinforced by fibre-reinforced plastics: the effect of temperature on the adhesive layer. *Compos Sci Technol* 61:425–431
- Gao B, Kim J, Leung CKY (2004) Experimental study on RC beams with FRP strips bonded with rubber modified resins. *Compos Sci Technol* 64(16):2557–2564
- Geiß PL (2006) Klebtechnik übernimmt tragende Rolle im Bauwesen. *adhäsion KLEBEN & DICHTEN* 50(1/2):14–18
- Geiß PL (2008) Geklebte Bauwerke. *Blickpunkt Kleben* 6
- Geiß PL, Fritzsche C, Kleiner F, Peschka M, Rauscher M, Schmale HC, Vogt, D, Zanotti A, Weber C, Boldt F, Wibbeke, M (2012) Merkblatt 382 – Kleben von Stahl und Edelstahl Rostfrei. Stahl-Informations-Zentrum, Informationsstelle Edelstahl Rostfrei
- Giesecke A (2007) Strukturverglasung – Fusion von Form und Funktion. *adhäsion KLEBEN & DICHTEN* 51(7/8):24–27
- Götz B, Böhme C, Borgmeier R, Burger K, Grote L, Hettich U, Modersohn WJP, Peisl C, Schmitt P, Schneider S, Wendt A, Bisping H, Heinicke F (2010) Technisches Merkblatt – Verankerungen mit Verbunddübelssystemen. Bundesverband Bausysteme e.V, Koblenz. [http://bv-bausysteme.de/tl\\_files/bv-bausysteme/downloads/FV%20Duebel-%20und%20Befestigungstechnik/duebel\\_merkblatt\\_verbundsysteme\\_0810\\_36s\\_web.pdf](http://bv-bausysteme.de/tl_files/bv-bausysteme/downloads/FV%20Duebel-%20und%20Befestigungstechnik/duebel_merkblatt_verbundsysteme_0810_36s_web.pdf). Accessed 2 Nov 2016
- Grimm R (2013) Durchblick: Welche sind die wichtigsten Fliesenkleber? Verlagshaus Wohlfahrt GmbH, Duisburg. <http://www.baustoffwissen.de/wissen-baustoffe/baustoffknowhow/grundlagen/bauchemie/durchblick-welche-sind-die-wichtigsten-fliesenkleber/>. Accessed 5 Nov 2016
- Grunewald D (2012) Verstärkung von Betonbauteilen mit geklebter Bewehrung – Auswirkung auf die Baupraxis. *Beton Stahlbetonbau* 107:A29–A30
- Habenicht G (2009) *Kleben – Grundlagen, Technologien, Anwendungen*. Springer, Berlin
- Haldimann M, Luible A, Overend M (2008) Structural use of glass – structural engineering documents 10. International Ass. for Bridge and Structural Engineering, Zürich
- Headley M (2014) EVA finds popularity among decorative fabricators. *ME USGlass* 49(4). [http://industry.glass.com/USGlass/2014/April/NewsAnalysis\\_Trends.htm](http://industry.glass.com/USGlass/2014/April/NewsAnalysis_Trends.htm). Accessed 13 Nov 2016
- Hollaway LC (2008) Advanced fibre polymer composite structural systems used in bridge engineering. *ICE Man Bridge Eng*. <https://doi.org/10.1680/mobe.34525.0503>
- Henning F, Moeller E (2011) *Handbuch Leichtbau – Methoden, Werkstoffe, Fertigung*. Hanser, München
- Jalham IS, Alsaed O (2011) The effect of glass plate thickness and thickness of the bonding interlayer on the mechanical behavior of laminated glass. *New J Glass Ceram* 1:40–48
- Karbhari VM, Engineer M, Eckel DA II (1997) On the durability of composite rehabilitation schemes for concrete: use of a peel test. *J Mater Sci* 32:147–156
- Keller T, Gürtler H (2006) Design of hybrid bridge girders with adhesively bonded and compositely acting FRP deck. *Compos Struct* 74:202–212
- Keller U, Mortelmans, H (1999) Adhesion in laminated safety glass – what makes it work? *Glass processing days*. 13–16 June, Tampere, pp 353–356
- KIT (2016a) Hybride Klebverbindung. Karlsruhe Institute of Technology, Karlsruhe. <https://www.kit-technology.de/de/technologieangebote/details/591/>. Accessed 7 Nov 2016

- KIT (2016b) Connection between two joining partners and method for establishing said connection. WO 2016/091377 A1
- Kleist A (1998) Verstärkung von Stahlbeton mit CFK-Lamellen. Tiefbau Ingenieurbau Straßenbau 40:35–41
- Klosowski J, Wolf AT (2016) Sealants in construction, 2nd edn. CRC Press, Boca Raton
- Krelaus R, Freisinger S, Schmidt M (2008) Adhesive bonding of structural members at the Gaertnerplatz Bridge in Kassel. In: Fehling E, Schmidt M, Stürwald S (eds) Ultra high performance concrete (UHPC). Kassel University Press, Kassel, pp 597–604
- Levy SM (2012) Construction calculations manual. Elsevier, Amsterdam
- Louter C (2007) Adhesively bonded reinforced glass beams. Heron 52(1/2):31–58
- Mailvaganam NP (1997) Construction technology update no. 11 – effective use of bonding agents. Institute for Research in Construction, National Research Council of Canada
- McKenna JK, Erki MA (1994) Strengthening of reinforced concrete flexural members using externally applied steel plates and fibre composite sheets – a survey. Can J Civ Eng 21(1):16–24
- Meier U (1994) Rehabilitation of structures with the CFRP sheet bonding technique – advancing with composites. In: Crivelli-Visconti I (ed) Advancing with composites, Materials and technologies, vol 1. Woodhead Publishing, Cambridge
- Meier U, Münger F (1995) Repair of structures through external bonding of thin carbon fiber sheets. IABSE Rep 73(1/2):1167–1172
- Mihala R (2008) Bauwerkverstärkung mit eingeschlitzten CFK-Lamellen in Beton. Zement + Beton 1:4–5
- Oehlers DJ (2001) Development of design rules for retrofitting by adhesive bonding or bolting either FRP or steel plates to RC beams or slabs in bridges and buildings. Composites A 32(9):1345–1355
- Pasternak H, Meinz J (2006) Versuche zu geklebten Verstärkungen im Stahlhochbau. Bauingenieur 81:212–217
- Pasternak H, Meinz J (2007) Kleben im Stahlbau – zwei Beispiele aus dem Fassadenbau. Bauingenieur 82:115–124
- Piekarczyk M, Grec R (2012) Application of adhesive bonding in steel and aluminium structures. Arch Civ Eng 58(3):309–329
- Porteous J, Kermani A (2012) Structural timber design to Eurocode 5. Wiley-Blackwell, Oxford
- Rizzo P, Spada A, Degala S et al (2010) Acoustic emission monitoring of chemically bonded anchors. J Nondestruct Eval 29(1):49–61
- Rug W, Mönck W (2015) Holzbau – Bemessung und Konstruktion. Beuth, Berlin
- Schober KU, Harte AM, Kliner R, Jockwer R, Xu Q, Chen JF (2015) FRP reinforcement of timber structures. In: Harte A, Rietsch P (eds) Reinforcement of timber structures – a state-of-the-art report. Shaker, Aachen
- Serrano E (2000) Adhesive joints in timber engineering – modelling and testing of fracture properties. KFS, Lund
- Shayan A, Sanjayan JG, Swamy N (2003) Evaluation of an epoxy-based steel plating system for strengthening bridge decks. Int J Mat Prod Tech 19(3/4):284–294
- Stahlton (2011) Verstärkung von Tragkonstruktionen. Stahlton AG, Hinwil. <http://www.stahlton-bautechnik.ch/images/stories/produkte/verstaerkung/Bewehrungen005.pdf>. Accessed 14 Nov 2016
- Steiger R, Serrano E, Stepinac M, Rajčić V, O'Neill C, McPolin D, Widmann R (2015) Reinforcement with glued-in rods. In: Harte A, Rietsch P (eds) Reinforcement of timber structures – a state-of-the-art report. Shaker, Aachen
- StoCretec (2016) Tragwerksverstärkung, Höhere Belastbarkeit für Stahlbetonbauwerke. StoCretec GmbH, Kriftel. [http://stocretec.de/media/documents/download\\_broschuere/0\\_bi\\_os/140080\\_DE-Broschuere\\_Betoninstandsetzung-Tragwerksverstaerkung\\_2013htm.pdf](http://stocretec.de/media/documents/download_broschuere/0_bi_os/140080_DE-Broschuere_Betoninstandsetzung-Tragwerksverstaerkung_2013htm.pdf). Accessed 21 Nov 2016
- Suter R, Jungo D (2001) Vorgespannte CFK-Lamellen zur Verstärkung von Bauwerken. Beton Stahlbetonbau 96(5):350–358

- 1033 Triantafyllou T, Deskovic N (1992) Prestressed FRP sheets as external reinforcement of wood  
1034 members. *J Struct Eng* 118(5):1270–1284
- 1035 Wagner A (2009) Alterungsbeständigkeit strukturell geklebter Stahl- und Glasverbunde.  
1036 Technische Universität Kaiserslautern
- 1037 Weller B, Schadow T (2007) Forschung und Entwicklung im Konstruktiven Glasbau. *Stahlbau* 76  
1038 (3):162–166
- 1039 White C, Tan K, Wolf A, Carbary L (2010) Advances in structural silicone adhesives. In: Dillard  
1040 DA (ed) *Advances in structural adhesive bonding*, 1st edn. CRC Press, Boca Raton
- 1041 Wörner JD, Freitag C (2012) Glasbau. In: Zilch K, Diederichs CJ, Katzenbach R, Beckmann KJ  
1042 (eds) *Handbuch für Bauingenieure – Technik, Organisation und Wirtschaftlichkeit*, 2nd edn.  
1043 Springer, Berlin
- 1044 Wu Z, Yuan H, Kojima Y et al (2005) Experimental and analytical studies on peeling and spalling  
1045 resistance of unidirectional FRP sheets bonded to concrete. *Compos Sci Technol* 65  
1046 (7/8):1088–1097
- 1047 Yiin W (2016) Tourists test the safety of 984-foot-high Chinese glass bridge – with sledgehammers.  
1048 The Washington Post, Washington, DC. [https://www.washingtonpost.com/news/morning-mix/  
1049 wp/2016/06/28/tourists-test-the-safety-of-a-chinese-glass-bridge-by-trying-to-break-it-with-  
1050 sledgehammers](https://www.washingtonpost.com/news/morning-mix/wp/2016/06/28/tourists-test-the-safety-of-a-chinese-glass-bridge-by-trying-to-break-it-with-sledgehammers). Accessed 15 Nov 2016
- 1051 Zilch K (2013) Verstärken von Betonbauwerken mit CFK. 1. DAfStb-Jahrestagung, Deutscher  
1052 Ausschuss für Stahlbeton e.V., Berlin. [http://www.dafstb.de/application/Jahrestagungen/zilch.  
1053 pdf](http://www.dafstb.de/application/Jahrestagungen/zilch.pdf). Accessed 21 Nov 2016
- 1054 Zilch K, Mühlbauer C (2007) Zum Fügen von Ultra-Hochfestem Beton (UHPC) durch Verkleben –  
1055 Grundlegende Untersuchungen. In: *Bauen mit innovativen Werkstoffen*, VDI-Berichte 1970,  
1056 VDI-Verlag, Düsseldorf, pp 37–46

Kwang-Seok Kim, Jong-Woong Kim, and Seung-Boo Jung

**Contents**

50.1	Introduction .....	1450
50.2	Classification of Electrically Conductive Adhesives .....	1453
50.2.1	Isotropic Conductive Adhesives .....	1454
50.2.2	Anisotropic Conductive Adhesives .....	1456
50.2.3	Non-conductive Adhesives .....	1459
50.3	Conductive Filler Materials for ECAs .....	1459
50.3.1	Hybrid Metallic Fillers .....	1460
50.3.2	Carbon-Based Nanomaterials .....	1461
50.3.3	Hybrid Nonmetallic Fillers (Conductive Polymers and PEDOT:PSS) .....	1463
50.4	Specific Requirements .....	1464
50.4.1	Electrical Conductivity .....	1464
50.4.2	Thermomechanical Properties .....	1469
50.5	Reliability .....	1471
50.5.1	Test Vehicle Design .....	1472
50.5.2	Storage Test in Harsh Environments .....	1474
50.5.3	Mechanical Reliability .....	1478
50.6	Conclusions .....	1479
References	.....	1480

---

K.-S. KimCarbon & Light Materials Application Group, Korea Institute of Industrial Technology, Jeonju,  
Jeollabuk-do, Republic of Koreae-mail: [ore21@kitech.re.kr](mailto:ore21@kitech.re.kr)

J.-W. Kim

School of Advanced Materials Engineering, Chonbuk National University, Jeonju, Jeollabuk-do,  
Republic of Koreae-mail: [wyjd78@gmail.com](mailto:wyjd78@gmail.com)

S.-B. Jung (✉)

School of Advanced Materials Science & Engineering, Sungkyunkwan University, Suwon,  
Gyeonggi-do, Republic of Koreae-mail: [sbjung@skku.edu](mailto:sbjung@skku.edu)



## Abstract

Electrically conductive adhesives (ECAs) are used for the joining of electrical and electronic components in the electrical industry. ECAs are composites consisting of a polymeric matrix and electrically conductive fillers. The mechanical properties are provided by the polymeric matrix, while the electrical conductivity is supplied by the conductive fillers. Typically, there are three types of conductive adhesives, viz., isotropic, anisotropic, and non-conductive adhesives. These adhesives are classified according to their conductivity, which is controlled by the conductive filler content in the polymer matrix. For their application in the electrical industry, there are two main specific requirements for these adhesives, i.e., electrical conductivity and thermomechanical properties. In this chapter, the mechanism underlying the electrical conduction in adhesive joints is derived, while the thermal and mechanical parameters that should be measured are introduced. Some recent advances related to the improvement of ECAs are also addressed. In terms of the evaluation of the reliability of adhesives in electronics, the basic test procedures, including several specific test methods and analysis techniques, are explained. Recommendations are also given to select a suitable test method.

## 50.1 Introduction

Conventionally, the joining of components in the electrical and electronic industries was mainly achieved by employing metallic materials, such as low melting point Sn-Pb solders. Sn-Pb solders are generally used to join similar or dissimilar metallic materials, such as Cu to Cu or Cu to Ni, etc., which are used as interconnect materials in electrical/electronic systems. When using Sn-Pb solders for joining, Sn plays the major role in the joining process, while Pb is included to lower the melting temperature and increase the ductility, thereby enhancing the thermomechanical reliability, preventing whisker formation, and decreasing the thickness of the inter-metallic compound layers which could be formed between the solder and other metallic materials.

Although Sn-Pb solder alloys provide a low melting point and good mechanical reliability, the toxicity and environmental incompatibility of the lead contained therein are forcing changes in the world market for electronic products which will dramatically reduce and possibly even eliminate their use altogether. As a consequence, the industry is changing its primary interconnect technology from Pb-based solder alloys to Pb-free alloys and electrically conductive adhesives (ECAs) (Liu and Lin 2005; Kim et al. 2005; Yin et al. 2006; Zhang et al. 2006; Plumbridge 2004). Although various Pb-free solders have already been developed, most current commercial Pb-free solders, such as Sn-Ag and Sn-Ag-Cu, have higher melting temperatures than that of Sn-37Pb solder, which raises the soldering temperature and, thus, reduces the integrity, reliability, and functionality of the printed circuit boards, components, and other attachments. On the other hand, ECAs generally have a lower processing temperature, which minimizes the thermal damage of the



packaging components, as well as many other distinct advantages that solder alloys cannot offer. They are flexible, capable of fine pitch interconnections, environmentally friendly, and cheaper to manufacture (Kim et al. 2008a).

The first employment of ECAs in the electrical and electronic industries was realized in the early 1970s for attaching semiconductor chips and other passive devices onto ceramic substrates in the fabrication of hybrid microcircuits. Epoxy technology pioneered the use of isotropic conductive adhesives for die attach applications in 1966. These early adhesives were filled with gold and silver powders and flakes which provided electrical and thermal pathways for the bonded devices (Lau 1995). However, those rare metal fillers must be reduced to allow their application in ECAs from the aspect of cost. Researchers are recently focusing on high aspect ratio and highly conductive fillers such as metallic nanowires and carbon-based nanomaterials instead of excess weight loading of rare metal fillers.

Nowadays, ECAs are mainly employed in advanced electronic packaging technologies, such as chips on flex (COFs), chips on glass (COGs), and flip chip attachment on printed circuit boards (PCBs). Figure 1 shows schematic images of these electronic packages. Before proceeding to the discussion on the concept and applications of ECAs, a brief introduction to electronic components and packaging technologies is helpful.

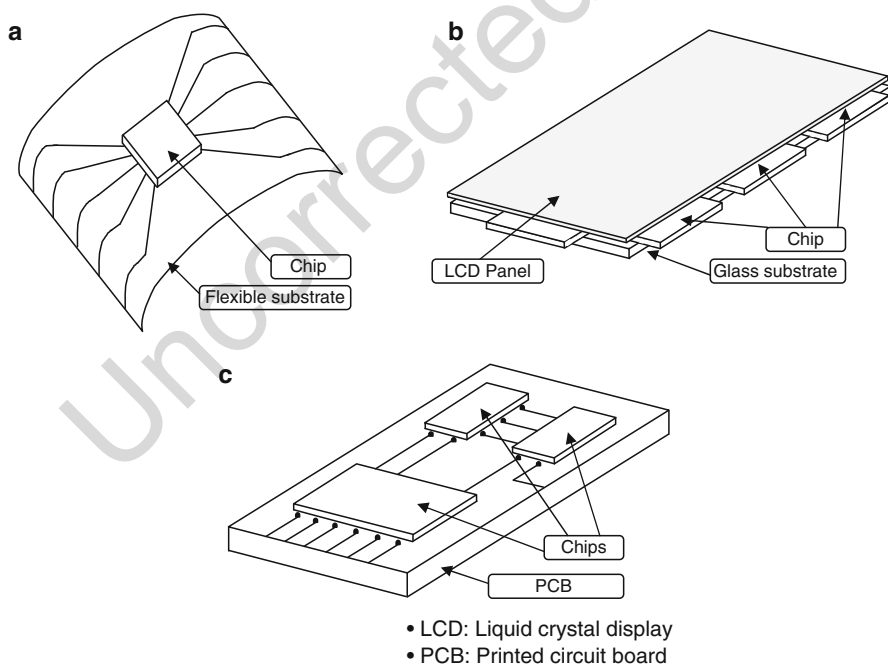


**Fig. 1** Schematic description of various electronic packages with adhesives: (a) chip on flexible substrate, (b) chip on glass substrate, (c) chip on rigid board

The technical developments realized in the industry in the last two decades of the twentieth century were enabled by the enormous progress made in microelectronic and semiconductor technology, due to the miniaturization of integrated circuits (ICs). Reducing the circuit dimensions reduces the transmission distances and increases the achievable speed of operation, and, in this way, the performance of the chips could be enhanced dramatically. The chips in the circuit communicate with each other through an input/output (I/O) system of interconnects, and these delicate chips and their embedded circuitry are dependent on the package for support and protection. At this time, the major functions of the electronic package are to provide a path for the electrical current that powers the circuits on the chip, distribute the signals onto and off of the silicon chip, or remove the heat generated by the circuit and support and protect the chip from hostile environments.

In the microelectronic packaging industry, flip chip technology, which was introduced for ceramic substrates by IBM in 1962, provides the highest packaging density and performance and the lowest packaging profile. Flip chip technology involves the connection of a chip to a substrate with the active face of the chip facing toward the substrate. Generally, flip chip technology can provide a cost-effective packaging method in various applications, such as telecommunication, computers, display products, and automobiles. The interconnection in flip chip packages that was firstly suggested by IBM was achieved by solder bonding. Flip chip interconnects formed by solder bonding are called solder-bumped flip chip interconnects, and they consist of essentially three basic elements. These include the chip, the solder bump, and the substrate. An underfill is often used to improve the reliability of the interconnect system. Figure 2 shows a brief schematic diagram showing the flip chip packaging structure with a ball grid array bonding. Each of these elements and the processes used to assemble them together affect the performance and cost of the interconnect system. Therefore, the performance and cost must be compared on the

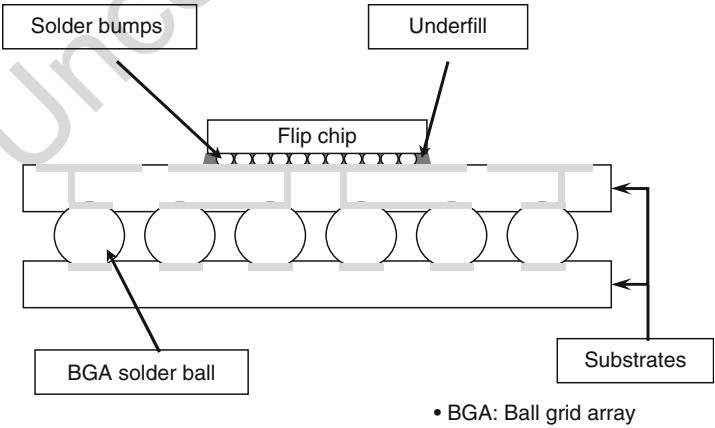


**Fig. 2** Package structure for flip chip ball grid array

basis of the interconnect system as a whole, and not merely on the basis of any single element of the interconnect assembly.

Eutectic Sn-Pb alloys are widely used as interconnects in solder-bumped flip chip packages. However, as indicated above, there are increasing concerns about the use of Sn-Pb alloy solders, because Pb, a major component in the solder, has long been recognized as a health threat to human beings. With the phasing out of Pb-bearing solders, various ECAs have been identified as environmentally friendly alternatives to Sn-Pb solders in flip chip applications. There are three leading ECA flip chip methodologies: isotropic conductive adhesives (ICAs), anisotropic conductive adhesives (ACAs), and non-conductive adhesives (NCAs). ICAs consist of an insulating adhesive polymer matrix with a high loading of conductive particles. The conduction mechanism is based on the percolation theory of electrical conduction afforded by the physical contact of the conductive particles. ACAs are similar to ICAs, except that they have a lower conductive filler content and thus provide unidirectional conductivity in the vertical or z-direction (perpendicular to the plane of the substrate). This means that the controlled conductive filler loading provides a higher resistance interconnect through the thickness of the adhesive than those of the ICA or solder-bumped interconnects. NCAs, on the other hand, do not consist of conductive particles but rather maintain a pure mechanical contact between the bumps and pads due to the application of a compressive force, and it is this that ensures the electrical connectivity between them. Nowadays, NCAs are being considered as an alternative to ACAs, because they can achieve a finer pitch of input/outputs (I/Os) due to the absence of any dispersion of conductive particles between I/Os and their better electrical performances. However, some issues concerning their performance and long-term reliability have recently been raised, so that a technical review of each material is essential. Figure 3 provides a comparison of the three ECA technologies, and a more detailed description of them will be provided in the next chapter.

---

## 50.2 Classification of Electrically Conductive Adhesives

Adhesives are basically organic materials containing a small amount of additive materials such as conductive or dielectric materials. The organic materials in adhesives can be separated into two different types depending on their structure and thermal behavior: thermoplastics and duromers (Aschenbrenner et al. 1997; Habenicht 1990). While thermoplastics are hot melting and can be plasticized and reshaped at temperatures above their glass transition temperature ( $T_g$ ), duromers are thermosetting and can be modeled during the curing process only (Aschenbrenner et al. 1997). Today, most adhesives are thermosetting ones based on epoxy resins, which provide high heat resistance and excellent adhesion to a variety of substrates. However, they are not thermally reversible and cannot be dissolved in common organic solvents, because they are cross-linked after bonding. In addition, thermosetting adhesives provide a low interconnection resistance, because they are easy to exclude between the bonding electrodes during the bonding process. There are various kinds of conductive particles that can be used to endow the adhesives with

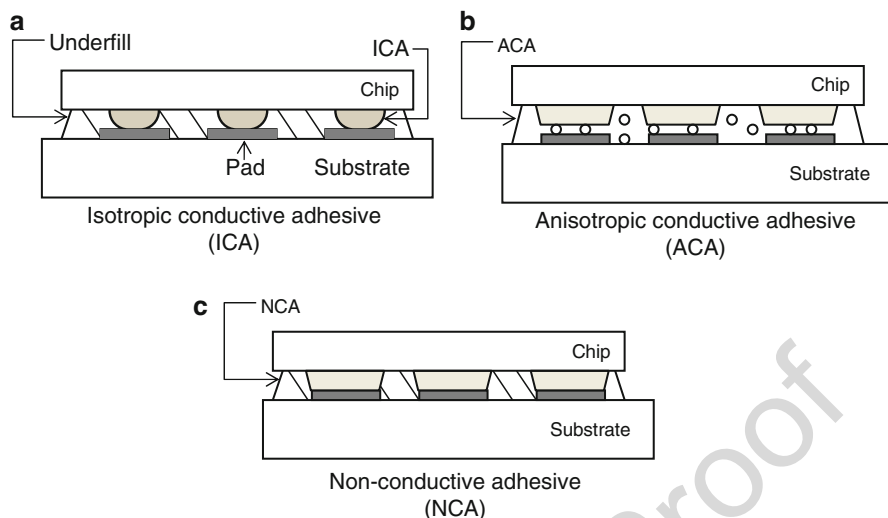


**Fig. 3** Schematic descriptions of three ECA technologies: (a) isotropic conductive adhesive (ICA), (b) anisotropic conductive adhesive (ACA), (c) non-conductive adhesive (NCA)

electrical conductivity. Ag is by far the most common conductive material for ECAs, but most of the recent ACAs employ polymer particles coated with various metals. Polymer particles are more elastic and, therefore, have the potential to compensate for the strains within the adhesive interlayer induced by thermal expansion (Aschenbrenner et al. 1997). Here, we will briefly introduce the various adhesives, starting with ICAs.

## 50.2.1 Isotropic Conductive Adhesives

ICAs are generally fabricated using adhesive and metallic conductive fillers that impart the desired adhesive and electrical properties, respectively. Typically, silver flakes and powders are utilized, because of their high electrical conductivity, chemical stability, and low cost. Processed Ag fillers must have suitable properties in order to fabricate compatible ICAs. For example, several micron-sized Ag flakes with a loading of 25–30% by volume in ICAs can give good conductive and adhesive properties (Markley et al. 1999). The particle size, particle size distribution, and other important characteristics can be controlled by the manufacturer by manipulating the various processing conditions, e.g., the lubricant concentration used during the formation of the neutral Ag particles. Only slight variations in the concentration of the lubricant, such as oleic acid, can cause significant changes in the application properties, such as the adhesive conductivity and stability (Markley et al. 1999). Therefore, it is important to understand how Ag fillers impact the properties of ICAs.

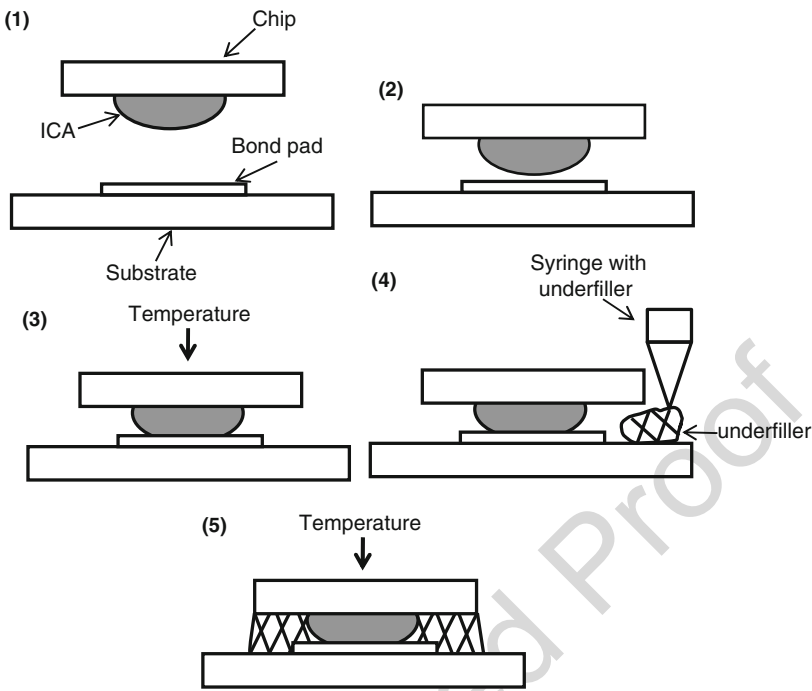


**Fig. 4** Bonding and packaging procedure with ICAs

The general form of ICAs is a viscous paste statistically filled with a sufficient content of metal flakes to provide conductivity in all directions (up to 30 vol.%). The conductivity between the particles is based on their touching each other. The process flow can be divided into five steps, as shown in Fig. 4 (Aschenbrenner et al. 1997):

- Application of the isotropic conductive paste (ICP) precisely onto the points to be electrically connected
- Alignment of the bumps to the electrodes on the substrate
- Bonding the chip by curing the adhesive typically at over 150 °C for several minutes
- Applying an underfill material to compensate for the thermal mismatch
- Curing of the underfill material

Generally, the electrical conductivity of ICAs increases with increasing filler content, which means that they are transformed from an insulator to a conductor. This can be explained by percolation theory. Percolation theory was developed to mathematically deal with disordered media, in which the disorder is defined by a random variation in the degree of connectivity (Zallen 1983). The main concept of the percolation theory is the existence of a percolation threshold, which is a critical

filler concentration at which the resistivity drops dramatically. At the percolation threshold, it is believed that all of the conductive filler particles come into contact with each other and form a three-dimensional network. The resistivity decreases only slightly as the filler concentration is further increased (Lau et al. 2003). Figure 5 schematically describes the decrease in the resistivity with increasing filler content based on percolation theory.

The ICAs used in flip chip technologies serve not only to provide electrical continuity but also to support the mechanical load experienced during chip operation. Therefore, the mechanical strength of ICA joints has been another major reliability concern in electronic assembly technology. The electrical conductivity is proportional to the filler content; however, a too high filler concentration can deteriorate the mechanical integrity. The electrical continuity is achieved by the contact of the metal fillers, but the mechanical integrity is provided by the curing of the polymer resin. Therefore, the challenge in an ICA formulation is to use as much conductive filler as possible to achieve high electrical conductivity without affecting the mechanical properties adversely (Lau et al. 2003).

## 50.2.2 Anisotropic Conductive Adhesives

From the viewpoint of their conduction and mechanical joining, ACAs are similar to ICAs, except that they have lower concentrations of conductive particles. This lower concentration provides unidirectional conductivity in the vertical or z-direction (perpendicular to the plane of the substrate), which is why they are called anisotropic conductive adhesives. In the same way, ACA materials are prepared by dispersing electrically conductive particles in an adhesive matrix at a concentration far below the percolation threshold. The concentration of particles is controlled, so that sufficient particles are present to ensure reliable electrical conductivity between the assembled parts in the z-direction, while insufficient particles are present to achieve percolation conduction in the X-Y plane (Kim

**Fig. 5** Resistivity with volume fraction of a conductive filler according to the percolation theory

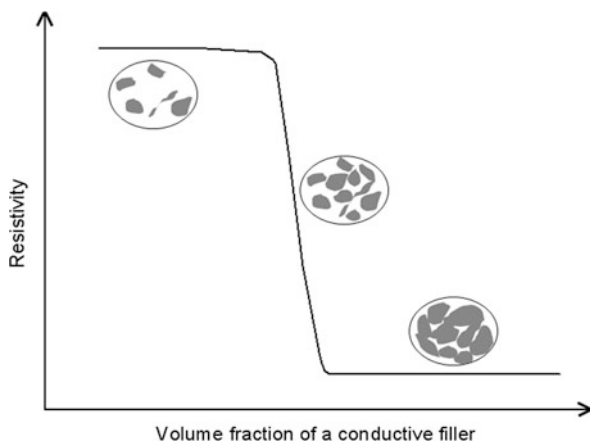


**Fig. 6** Schematic description of flip chip structure with ACA

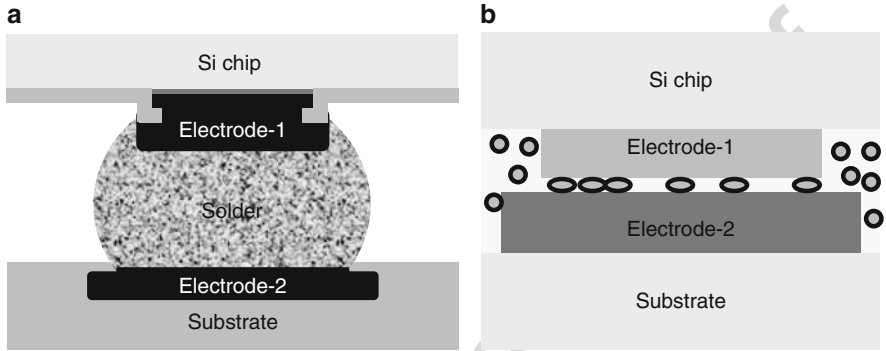
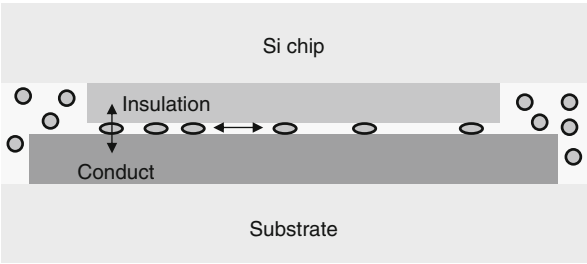


**Fig. 7** Structure comparison between solder and ACA joints: (a) flip chip with solder bumps, (b) flip chip with ACAs

et al. 2008b). Figure 6 shows a schematic description of an ACA interconnect, showing the electrical conductivity in the joint. The volume loading of conductive filler in ACAs is 5–20 vol.%, which is much lower than that of ICAs. This low volume loading is insufficient for interparticle contact and prevents conductivity in the X-Y plane of the adhesives. The Z-axis adhesive, in film or paste form, is interposed between the surfaces to be connected (Li and Wong 2006). However, the controlled conductive filler loading still provides a higher resistance interconnect through the thickness of the adhesive than that of the solder-bumped interconnect. A comparison between the solder-bumped and ACA joint structures is shown in Fig. 7.

From Fig. 7, it can also be seen that the area of the pad used for joining with the solder should be much larger than that used for ACAs. When we employ solder for the interconnect, the smallest pitch, which means the distance between the center point of a solder bump and that of the next one, is more than 50  $\mu\text{m}$ , but it can be decreased to less than 30  $\mu\text{m}$  by using ACAs. This limitation of solders based on ECAs is mainly caused by the difficulty involved in the bumping technology of solder, e.g., the screen printing of the solder paste, the evaporation of the solder materials, and the electroplating process. Using these processes, aligning the mask opening before the deposition of the solder is essential and requires high accuracy, so

the extent to which the pitch and joining area can be reduced is limited. However, ultrafine pitch interconnections can be achieved when employing ACAs for joining. The fine pitch capability of ACAs is limited by the particle size of the conductive filler, which is only a few microns or a few nanometers in diameter. Therefore, a finer pitch is easily achieved these days by using smaller particles.

Heat and pressure are simultaneously applied to this stack-up until the particles bridge the two conductor surfaces. ACAs utilize both a thermosetting polymer and a thermoplastic polymer for their adhesive matrix. The thermosetting type is hardened by the thermally initiated chemical reaction during heating, while the thermoplastic matrix is hardened by cooling after heating. Many recently commercialized ACAs employ a thermosetting polymer based on epoxy resin, which provides a high heat resistance and excellent adhesion to a variety of substrates, although they are not thermally reversible and cannot be dissolved in common organic solvents, because they are cross-linked after bonding. In addition, thermosetting adhesives provide a low interconnection resistance, because they are easy to exclude between the bonding electrodes during the bonding process. The main advantage of thermoplastic adhesives is the relative ease with which the interconnection can be disassembled for repair operations, because they are rigid materials at temperatures below the  $T_g$  of the polymer, but exhibit flow characteristics above their  $T_g$  (Li and Wong 2006). Conductive fillers are generally metal microparticles or polymer cores coated with some high conductivity metals. Their basic particle shape is spherical. Ag is the most frequently used material for metal particles, due to its moderate cost, high electrical conductivity, high current-carrying capacity, and low chemical reactivity. Au is another widely employed filler material, but its cost prohibits large volume applications. An alternative to these noble metal fillers is polymer particles coated with conductive metals, such as Au, Ag, and Cu. The size of the polymer cores generally ranges from 1 to 5  $\mu\text{m}$ , and they are coated with a Cu, Ni, or Au layer a few nanometers in thickness. Polymers generally have viscoplastic properties, so that they allow the external compressive stresses applied to the package to be easily released. Figure 8 shows the two different deformation behaviors of the particles when external forces are applied to the ACA joint. However, most importantly, they are much cheaper to make than metal-only fillers, so that they are the most commonly used conductive fillers in industry.

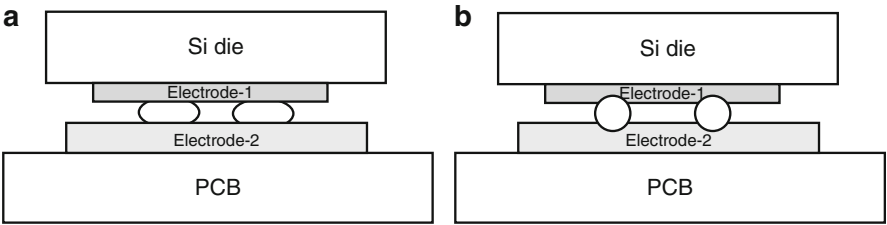


**Fig. 8** Schematic description of two deformation behaviors in ACA joints: (a) soft conductive fillers, (b) rigid conductive fillers



50.2.3 Non-conductive Adhesives

In contrast to ICAs and ACAs, NCAs do not consist of conductive particles but rather maintain a pure mechanical contact between the bumps and pads due to the application of a compressive force, and it is this that ensures the electrical connectivity between them. The quality of the electrical contact depends solely on the magnitude of the mechanical contact pressure. A high mechanical contact pressure is critical in providing a low electrical connection resistance, which is induced by the cross-linking shrinkage and thermal strain during the curing and cooling processes. The formation of contact spots depends on the surface roughness of the contact partners. Bringing the two surfaces close to each other enables a small number of contact spots to form, which allows the electric current to flow. When the parts are pressed together during the sealing process, the number and area of these single contact spots are increased according to the macroscopic elasticity or flexibility of the parts and the microhardness and plasticity of the surfaces, respectively (Li and Wong 2006). Nowadays, NCAs are being considered as an alternative to ACAs, because they can achieve a finer pitch of input/outputs (I/Os), due to the absence of any dispersion of conductive particles between the I/Os and better electrical properties. NCA joints avoid short-circuiting and are not limited by the particle size or percolation phenomena, leading to a reduction of the connector pitch. Another important advantage of NCAs is their cost-effectiveness, which is achieved by the exclusion of conductive fillers. Figure 9 compares the shape of ACA and NCA joints enlarging electrical contact area.

50.3 Conductive Filler Materials for ECAs

The conductive filler in the conventional ECAs is metallic particles or flakes. These filler materials have some critical limitations in terms of lower electrical conductivity and inferior impact performance induced by unstable network formation of particle fillers. Considering these challenges of traditional filler materials, there are three

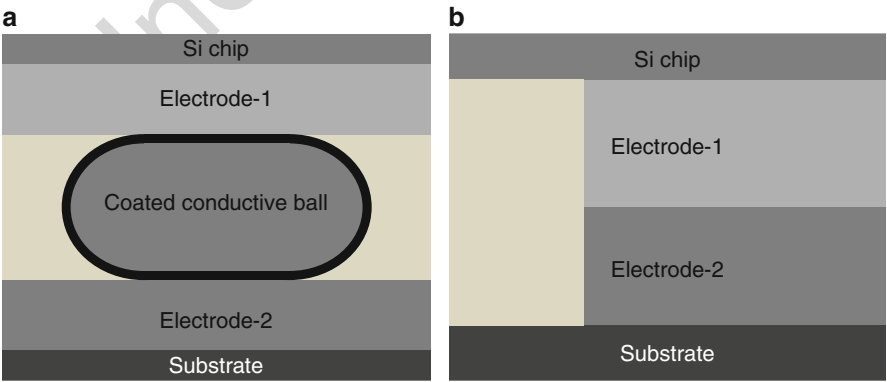


Fig. 9 Comparison of contact areas between ACA and NCA joints: (a) ACA joint, (b) NCA joint

major approaches to enhance the electrical conductivity of ECAs, which include (i) hybrid metallic fillers, (ii) carbon-based nanomaterials, and (iii) hybrid nonmetallic fillers: conductive polymers and poly(3,4-ethylenedioxythiophene)-poly(styrenesulfonate) (PEDOT:PSS).

### 50.3.1 Hybrid Metallic Fillers

Metallic fillers are widely used in the field of printed electronics due to their high conductivity and excellent compatibility with metal electrodes. Printed components using ink or paste with the metallic fillers have been used in fabrications of various applications such as flexible radio frequency identification (RFID) tags, flexible heaters, and organic light-emitting diodes. In general, printed components are thermally treated in high temperature in order to decrease contact resistance formed among metal fillers or induce interparticle necking by atomic interdiffusion. Recently, highly conductive interconnects can also be established via some other technical approaches, e.g., plasma, microwave, and intense pulsed light (IPL) treatment, instead of thermal heating (Kim et al. 2013, 2015; Song et al. 2015). Figure 10 shows a schematic of IPL sintering and its commercial system which provide the selective sintering at lower temperatures within several microseconds.

Hybrid metallic fillers mean the incorporation of one-dimensional metallic nanowires into metal particle or flake fillers to improve electrical conductivity through an increase of metallurgical connections between each individual metallic filler. The metallic nanowires prefer to establish conductive networks rather than metallic particle or flake fillers because one-dimensional metallic structures are capable of forming a continuous network at lower loading level of the filler than spherical or platelet fillers (Grujicic et al. 2004). In particular, at lower temperatures, sintering process is controlled by surface diffusion due to mass flow to minimized Gibbs free energy (Mayo 1996), resulting in weak contacts between conventional metallic fillers. Since the

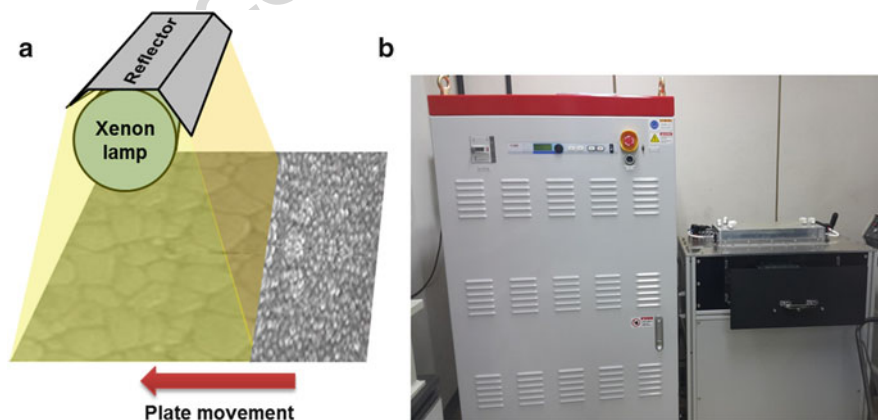


**Fig. 10** (a) A schematic of IPL sintering and (b) its system (PSFL-4021-PC, [www.pstek.co.kr](http://www.pstek.co.kr))

metallic nanowires are also likely to sinter at a low temperature, the large longitudinal size of nanowires makes it easy for fillers contacted weakly to sinter each other and bond. As shown in Fig. 11, the increased number of conductive pathways and the better quality of conductive linkage are obtained by mixing metallic nanowires with metal particles or flakes. Since the nanowires act as bridges among the spherical metal fillers, electrical conductivity of ECAs is dramatically improved (Chen et al. 2007).

The dimension of metal fillers in ECAs critically determines their electrical conductivity. As explained above, the conventional filler is metal particles (0 dimensional), and different dimensional fillers such as nanowires and nanorods (1 dimensional) are regarded as promising conductive fillers, since they can provide electrical percolation at relatively low concentrations (Wu et al. 2007). Figure 12 shows the examples of different dimensional silver fillers.

Chen et al. reported the incorporation of silver nanowires into ECAs (Chen et al. 2010). It was found that the electrical conductivity of the system composed with silver nanowires and nanoparticles is higher than that with either one of the two co-fillers (Chen et al. 2010). Zhang et al. reported the sintering characteristics of ECAs filled with surface-modified silver nanowires (Zhang et al. 2011). The sintering of silver nanowires can form high electrical conductivity of the ECAs although the high temperature of heat treatment is not suitable for most epoxy adhesives (Zhang et al. 2011). Yang et al. described a novel formulation method for a high-performance ECA which consisted of silver nanorods, nanoparticles, and modified epoxy matrix (Yang et al. 2012). The ECA film was able to achieve low resistivity of  $3\text{--}4 \times 10^{-5} \Omega \text{ cm}$ .

### 50.3.2 Carbon-Based Nanomaterials

To meet the requirements for high-performance electronic devices, ECAs are required to achieve high electrical conductivity at lower filler contents. Recently,

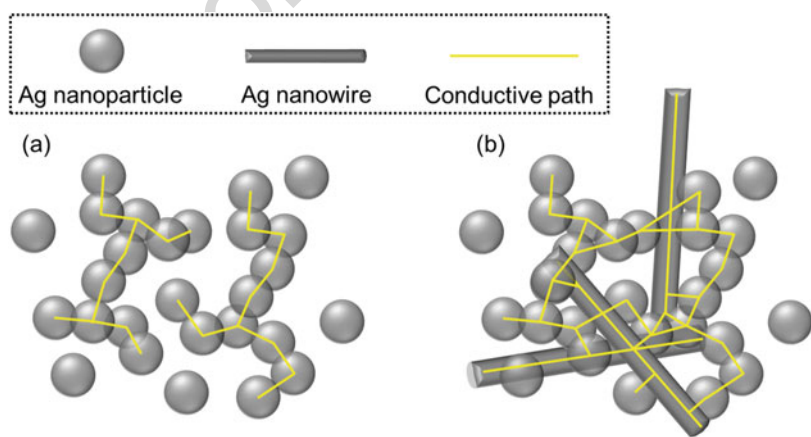


**Fig. 11** Illustration of conductive paths for ECAs filled with (a) silver nanoparticles and (b) silver nanowires

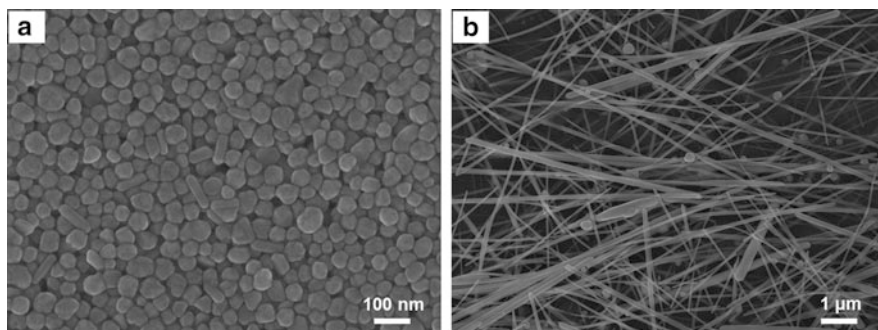


**Fig. 12** Field-emission scanning electron microscope images of (a) silver nanoparticles and (b) silver nanowires

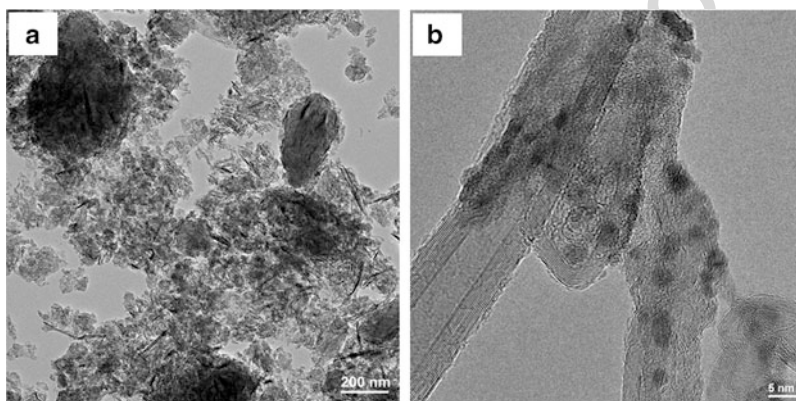


**Fig. 13** Transmission electron microscopy images of (a) the graphene flakes and (b) multi-walled carbon nanotubes

many efforts have been devoted to obtaining high conductivity of ECAs with low silver loading by introducing the carbon-based nanomaterials such as carbon nanotubes (CNTs) and graphene into the conventional formulation of ECAs. Figure 13 shows examples of representative carbon-based nanomaterials.

CNTs are one of the ideal reinforcing carbon-based nanomaterials for enhancement of polymer composites because of their intrinsic marvelous physical, electrical, and thermal properties. Addition of CNTs can improve the mechanical properties as well as the electrical conductivity. However, the introduction of CNTs into ECAs has significant challenges in processing, dispersion control, and their high cost (Yim et al. 2016). Graphene is also one of the promising conductive fillers which can provide more stable electrical networks for ECAs' application. It is confirmed that graphene is much more effective than other carbon-based filler materials. However, the agglomeration problem of carbon-based filler materials including CNTs and

graphene leads to other problems such as increase in viscosity and poor dispersion, which cause the outstanding properties to be suppressed, resulting in the ECAs with minimal performance improvement (Amoli et al. 2015). To overcome these problems, (1) surface modification of graphene using organic materials (to exfoliate graphene in which the interaction occurs via either covalent bonding or via  $\pi$ - $\pi$  stacking) (Kim et al. 2012) and (2) surface decoration of graphene with inorganic nanoparticles (incorporation of silver nanoparticle-decorated graphene to reduce the tunneling resistance) (Amoli et al. 2015) have been suggested.

### 50.3.3 Hybrid Nonmetallic Fillers (Conductive Polymers and PEDOT:PSS)

This approach to improve the electrical conductivity of ECAs is mixing with conventional ECAs with conductive polymers such as polypyrrole (PPy) (Mir and Kumar 2010), polyaniline (PANI) (Desvergne et al. 2011), and polypoly (3,4-ethylenedioxythiophene)-poly(styrenesulfonate) (PEDOT:PSS) (Chueh et al. 2015). The electrical conductivity of conductive polymers are determined by the loading, dispersion, and geometry (shape and diameter) of conductive fillers, degree of resin curing, and cross-link density, and so forth (Lilei et al. 1999; Kim and Shi 2001; Lee et al. 2005). Chemical structures of the representative electrically conductive polymers are shown in Fig. 14.

PPy is one of the promising conductive polymers for ECAs due to ease of synthesis, stability, and low cost (Mir and Kumar 2010). PPy has been modified with other polymers to form composites and improve its processing properties which

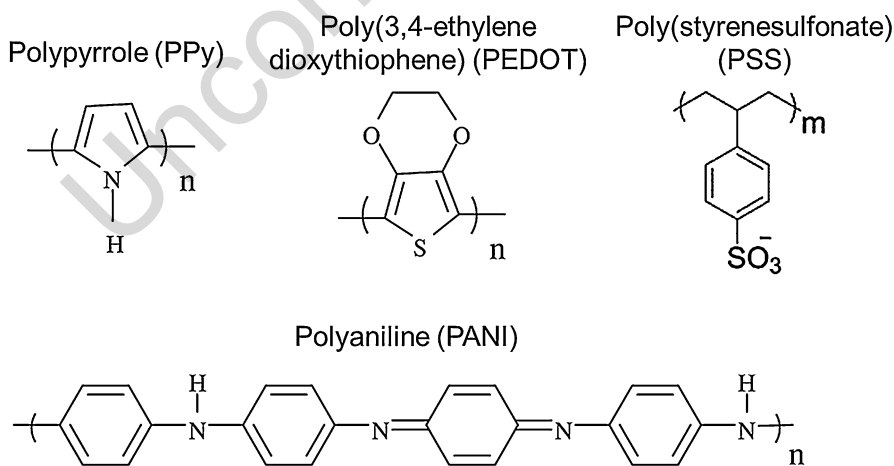


**Fig. 14** Schematic of the representative electrically conductive polymers: PPy, PEDOT, PSS, and PANI

enable to provide better electrical performance such as smooth percolation curves. Mir et al. reported the composite manufactured by blending PPy with epoxy was utilized as ICAs, and their electrical conductivity, impact properties, and thermal and morphological characteristics were demonstrated with various concentrations of PPy in the epoxy matrix (Mir and Kumar 2010).

PANI is also a suitable conductive polymer for improving the properties of the conventional ECAs owing to its high polymerization yield, good environmental stability combined with moderate electrical conductivity, and low cost. Mir et al. presented the composite of PANI in an epoxy/anhydride matrix, which is suitable as ICAs with enhanced impact properties and conductivity (Mir and Kumar 2010). Gumfekar et al. reported the reduced percolation threshold and enhanced conductivity of the silver-PANI-epoxy system via improved dispersion of silver fillers (Gumfekar et al. 2011).

PEDOT:PSS has recently been studied and is emerging as a major attraction for next commercial ECAs. Chueh et al. reported ECAs comprising of the silver-plated graphite powder, PEDOT:PSS, and organic additives improved the electrical conductivity by at least two orders of magnitude compared with those filled with graphite powders only (Chueh et al. 2015).

---

## 50.4 Specific Requirements

There are at least three important requirements for the application of conductive adhesives in the electrical industry. The first one is the electrical resistance. Because of the typical low electrical conductivity of the polymer materials, a high electrical conductivity or low resistivity is definitely the most important factor for the conductive adhesive. Secondly, we should carefully consider the thermal properties of the adhesive. The bonding process with the adhesives is optimized by their thermal properties, e.g., their  $T_g$  and curing behavior. Finally, we would like to discuss in this chapter the thermomechanical properties of the adhesives. The thermomechanical properties determine the long-term reliability of the adhesive interconnect, so it is necessary to review how the thermomechanical properties can be measured and the results analyzed.

### 50.4.1 Electrical Conductivity

When two metallic conductive pads are electrically interconnected by an adhesive, there is a large difference in their electrical conductivity in comparison with solder-bumped interconnects. The solder-bumped joint is based on the melting of the solder and chemical reaction between the solder and metallic pad. In this case, some chemical compounds such as intermetallic compound layers form at the interface, which makes it possible to fill the interface without any large gap remaining.



Therefore, the electrical resistance of the solder joint largely depends on the bulk resistance of the constituent components, e.g., the metal pad used for bonding, intermetallic compounds, and solder. However, in the case of adhesive interconnects, the joining process is essentially based on the mere physical contact between the pad and pad or pad and conductive fillers included in the electrically conductive adhesives. When two conductors are connected by a mere physical contact, the interfacial resistance, i.e., the contact resistance, is much larger than the bulk resistance when a current is flowing through the joint pathway. Therefore, the calculation or exact measurement of the contact resistance is a key point to evaluate the electrical conductivity of each adhesive interconnect. There are three main types of electrically conductive adhesive interconnects, all of which include bulk resistance and contact resistance components. Here, we will discuss the electrical conductivity of the adhesive joint with a simple derivation of the total resistance of the ACA interconnect.

When a spherical particle meets a metallic pad, there are three separate contributions to the resistance: the intrinsic conductive resistance of each particle, the constriction resistance at the contacts, and the tunneling resistance at the contacts (Holm 1979; Ruschau et al. 1992). Therefore, the connection resistance through the conductive particles,  $R_c$ , is expressed by

$$R_C = R_i + R_{CR} + R_f \quad (1)$$

where  $R_i$  is the intrinsic resistance of an individual particle,  $R_{CR}$  is the constriction resistance caused by the bending of the current flow paths, and  $R_f$  is the tunneling or film resistance associated with any insulating film which may be covering each metallic surface. At the point of contact between the conducting particles and the metallic bumps or pads, the majority of the current will flow through the areas of metal-to-metal contact. Thus, the current is constricted to flow through these areas, and the resistance will therefore be higher than if the current were passing directly through a straight path with no constriction. The resistance increase caused by this structure is called the constriction resistance. Some examples of insulating films in which tunneling behavior is observed are oxidation layers, residues of resin in the adhesives, and contaminants on the metal films. The electrical conduction must then proceed across these gaps, which represent electrical potential barriers to conduction. Therefore, tunneling is needed to allow conduction between the electrodes. Tunneling is a process by which electrons on one side of the barrier jump to the other side without any energy input, in which case the resistance increase caused by the potential barriers is called the tunneling resistance.

Among the contributions to the connection resistance described above, the intrinsic resistance of an individual conductive particle can be estimated with respect to its deformation. Since the metal-coated conductive particles are deformed plastically during the bonding process of an ACF, the numerical model for the calculation of the connection resistance should consider the plastic deformation of the conductive particles. Yim and Paik (1998) derived the connection resistance of an ACF joint

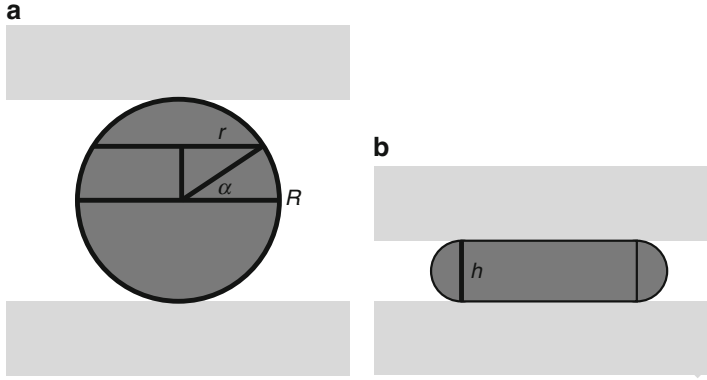


**Fig. 15** Deformation model of the conductive particle: (a) before deformation and (b) after deformation

from Holm's electrical contact theory, and the derived model described the connection resistance of the ACF in terms of the sample geometry, particle size, applied pressure, and the intrinsic properties of the conductive particles. However, this model is valid only for the elastic deformation of the conductive particles; therefore, it cannot reflect their plastic deformation. For a more exact prediction of the connection resistance, the plastic deformation of the conductive particles should be considered. Maattanen (2003) derived the connection resistance of metal-coated polymer particles using the degree of deformation during the bonding process of an ACF. He described the degree of deformation as

$$\text{Degree of deformation} = 1 - \left( \frac{h}{2R} \right) \quad (2)$$

where  $h$  is the distance between the electrodes and  $R$  is the radius of the undeformed conductive particles which are shown in Fig. 15. The area of the spherical cap forms the metal contact area, and, therefore, the metal contact area,  $A$ , and the length of the conductor,  $l$ , are given as

$$A = 2\pi R^2 \left( 1 - \frac{h}{2R} \right) \quad (3)$$

$$l = \frac{\pi h}{2} \quad (4)$$

However, since the current would flow only through the thin metal layer of the conductive particles, the average area of the metal film should be calculated. The average area can be derived as follows:



$$\begin{aligned}
\left(\frac{1}{A}\right) &= \frac{\int_0^{\pi h/4} \frac{dS}{2\pi t R \cos \alpha}}{\int_0^{\pi h/4R} dS} \\
&= \frac{\int_0^{\pi h/4R} \frac{d\alpha}{2\pi t R \cos \alpha}}{\int_0^{\pi h/4R} d\alpha} \\
&= \frac{4R}{\pi h} \frac{1}{2\pi t R} \int_0^{\pi h/4R} \frac{d\alpha}{\cos \alpha} \\
&= \frac{2}{\pi^2 h t} \int_0^{\pi h/4R} \left[ \ln \tan \left( \frac{\pi}{4} + \frac{\alpha}{2} \right) \right] \\
&= \frac{2}{\pi^2 h t} \ln \tan \left[ \frac{\pi}{4} \left( 1 + \frac{h}{2R} \right) \right]
\end{aligned} \tag{5}$$

476

477 where  $r = R \cos(\alpha)$ ,  $S = R\alpha$ ,  $dS = R d\alpha$ , and  $t$  is the thickness of the metal layer on  
 478 the particle. For  $\alpha$ , see Fig. 15.

479 Since there is spherical symmetry, an approximation can be made, and the  
 480 problem is solved using Ohm's law, and the formula for the intrinsic resistance of  
 481 the deformed particle,  $R_i$ , is written as follows:

$$R_i = \rho \frac{l}{A} = \rho \frac{\pi h}{2} \left( \frac{1}{A} \right) = \frac{\rho}{\pi t} \ln \tan \left[ \frac{\pi}{4} \left( 1 + \frac{h}{2R} \right) \right] \tag{6}$$

482 where  $\rho$  is the resistivity of the metal coating.

483 In electrical interconnects made using ACAs, electrical conduction is provided by  
 484 the conducting particles trapped within the interconnection area. At the point of  
 485 contact between the conducting particles and the metallic bumps or pads, the  
 486 majority of the current will flow through the areas of metal-to-metal contact. Thus,  
 487 the current is constricted to flow through these areas, and the resistance will,  
 488 therefore, be higher than if the current were passing directly along a straight path  
 489 with no constriction. This resistance is called the constriction resistance. According  
 490 to Holm (1979), the constriction resistance,  $R_{CR}$ , can be written as

$$R_{CR} = \frac{(\rho_1 + \rho_2)}{2d} \tag{7}$$

491 where  $\rho_1$  and  $\rho_2$  are the intrinsic resistivities of the conductive particles and  
 492 substrate, respectively, and  $d$  is the diameter of the metal contact area. Looking  
 493 closer at the diameter of the contact area in different compression situations, it  
 494 is possible to derive a formula for it in the case of metal-coated polymer  
 495 particles. The area is a spherical cap of the conductive particle where the size  
 496 is a variable depending on the degree of deformation. The formula for the metal  
 497 contact area is

$$\pi \left( \frac{d}{2} \right)^2 = 2\pi R^2 \left( 1 - \frac{h}{2R} \right) \quad (8)$$

Therefore,

$$d = R \sqrt{8 \left( 1 - \frac{h}{2R} \right)} \quad (9)$$

Substituting Eq. 9 into (7) yields

$$R_{CR} = \frac{(\rho_1 + \rho_2)}{2R \sqrt{8 \left( 1 - \frac{h}{2R} \right)}} \quad (10)$$

For contacting materials that form metal-to-metal contacts and that do not oxidize, the tunneling resistance,  $R_f$ , is zero. This oxidation problem is considered a special case, and, therefore, we can neglect the oxidation term in this simple derivation. Finally, according to the schematic of an ACF interconnection, the connection resistance,  $R_c$ , considering the plastic deformation of a metal-coated polymer sphere is described by

$$R_c = R_{CR-1} + R_{CR-2} + R_i = \frac{(\rho_1 + \rho_2)}{2R \sqrt{8 \left( 1 - \frac{h}{2R} \right)}} + \frac{(\rho_1 + \rho_3)}{2R \sqrt{8 \left( 1 - \frac{h}{2R} \right)}} + \frac{\rho_1}{\pi t} \ln \tan \left[ \frac{\pi}{4} \left( 1 + \frac{h}{2R} \right) \right] \quad (11)$$

where  $R_{CR-1}$  and  $R_{CR-2}$  are the constriction resistances generated between the conductive particle and the two electrodes,  $\rho_1$  is the resistivity of the conductive particles, and  $\rho_2$  and  $\rho_3$  are the resistivities of the electrodes.

Using this derivation, the connection resistance of the ACA interconnect can be easily calculated by the simple investigation of the physical shape of the connected pathway. This derivation is based solely on the physical contact of the two unmelted metals, so it could be applied to the other two types of adhesives, i.e., ICAs and NCAs. In the case of ICAs, the shape of the current flowing path is more complex, which means that the contact resistance might also be more complex than that in the ACA case. However, the resistance components of an ICA interconnect are completely identical to those of an ACA interconnect, so the derivation and calculation of the components are also easy to perform. In the case of an NCA, there are no conductive fillers and, therefore,  $R_{CR}$  and  $R_i$  can be excluded from the derivation. This means that the connection resistance for an NCA joint consists only of  $R_f$ , so that the resistance should also be lower than that of an ACA joint.

In summary, the electrical conductivity of adhesive joints is dominated by the physical contact between the two unmelted conductive materials, and, therefore, the

resistance of the joint seems to be nearly equal to the contact resistance. Among the various adhesives, ACAs are considered to be the least conductive materials, and the resistance is controlled by the joint structure and constituent materials.

## 50.4.2 Thermomechanical Properties

According to various previous studies concerning the bonding process for the joining of adhesive electronic components, it was reported that the electrical properties of the ACF flip chip package are highly affected by the bonding temperature and pressure. Especially, the contact resistance of the adhesive joints is highly correlated with the deformation of the metal bump or conductive fillers induced by the pressure applied during the bonding process. This is because if the conductive fillers are too spread out between adjacent bumps or pads, due to too much pressure being applied, they may end up contacting each other, creating the same effect as short-circuiting; whereas if the bonding pressure is too low, the particles may not be able to make contact between the connecting bumps and pads. After the complete bonding process, the adhesive joints are established by the compressive forces generated by the shrinkage stress in the adhesive matrix. The shrinkage stresses originate from the thermomechanical properties of the adhesives, such as the thermal shrinkage and thermal stiffness generated during or after the thermal reaction (Kwon and Paik 2004; Yu et al. 2013). This shrinkage stress, influenced by the thermal shrinkage and buildup stiffness, is responsible for the contact integrity in an adhesive joint, and, therefore, the evaluation of the shrinkage behavior is very important for the optimization of the bonding process. Generally, the shrinkage stress is generated by the curing reaction of the adhesives, which means that the thermal and thermomechanical behavior of the adhesives during heating and cooling should be evaluated before the application of the adhesives in electronics.

The first parameter we should examine is the degree of curing of the adhesives containing  $T_g$  and the reaction ratio during heating and cooling. Kwon and Paik (2004) described the evaluation of the degree of curing of an ACF joint with a differential scanning calorimeter (DSC). They defined the term, degree of curing, as follows:

$$\text{Degree of cure} = \frac{\Delta H(\text{uncured adhesives}) - \Delta H(\text{heated adhesives})}{\Delta H(\text{uncured adhesives})} \times 100 \quad (12)$$

Figures 16 and 17 present an example of the DSC measurement curves for an ACF and NCF. From Fig. 16, we can obtain the  $T_g$  information of the ACF and NCF employed, while the degree of curing is calculated using Fig. 17. Generally, for electronic applications, faster curing with a lower  $T_g$  is favorable for various reasons, such as the impact of a high temperature on other nearby components, the deviation of the process temperature from the conventional reflow profile for solder joining, and the manufacturing efficiency. Especially, from the viewpoint of the impact on nearby components, the  $T_g$  of the adhesive is highly correlated with its applicable

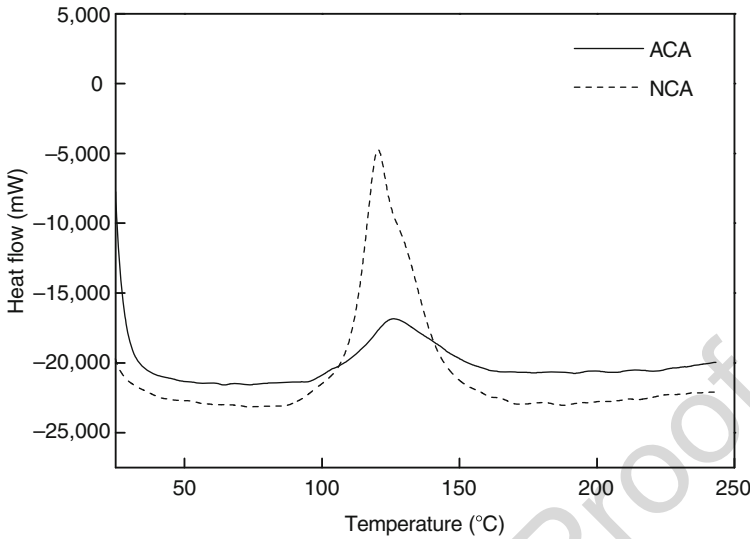


**Fig. 16** Comparison of heat flow with temperature between ACF and NCF

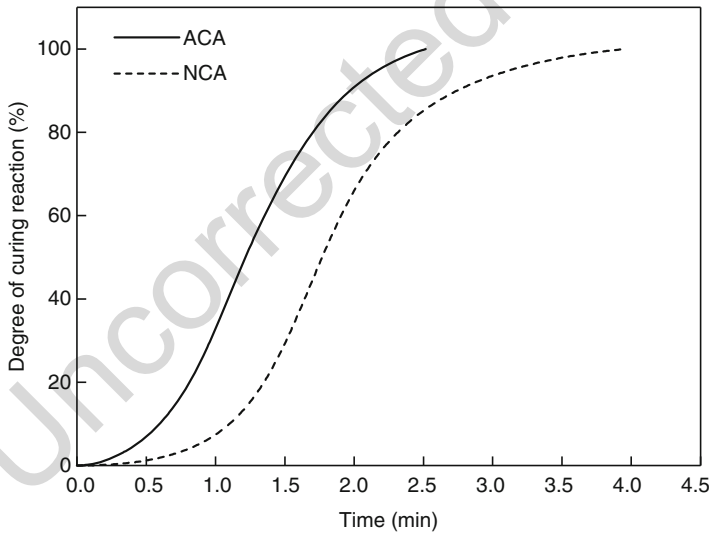


**Fig. 17** Comparison of curing degree with time between ACF and NCF

561 areas in electronics. That is, the bonding temperature is determined by the thermal  
562 stability of the nearby components, e.g., the substrate. For example, in display  
563 applications, a glass panel is used as a substrate, which means that the bonding  
564 temperature can be as high as 400 °C. However, polymer-based plastic substrates are  
565 typically used in printed circuit board (PCB) applications, where the bonding

temperature must be less than the  $T_g$  of the substrate, which is generally less than 200 °C. Therefore, adhesives with a lower  $T_g$  would be more favorable due to their wider range of applications.

As shown in Fig. 17, the degree of curing might also be different between adhesives consisting of different materials. The degree of curing determines the bonding time for adhesive joining, so that the manufacturing efficiency is highly related to this factor. For flip chip joining with adhesives, a chip with numerous metal bumps should be aligned on a substrate, e.g., glass, printed circuit board (PCB), or flexible polyimide-based one. After aligning the chip, a certain bonding force is applied to the chip to generate a compressive force in the adhesive area. At this time, the temperature is raised to that required for curing, which is typically 30–50 °C higher than the  $T_g$ . At this stage, the adhesive resin starts to undergo the curing reaction, which increases its viscosity and modulus, due to the development of a cross-linking structure. Both the bonding force and temperature are continuously applied in order for the adhesive to be fully cured. After the adhesive resin is fully cured, the bonding force is removed, and the assembly is cooled to room temperature. During the cooling process, shrinkage stress can develop, due to the thermal shrinkage and buildup of stiffness of the ACFs. Although the external bonding force is removed after the bonding process, the electrical conduction of the ACF joint is mechanically maintained by the compressive force due to the thermal shrinkage of the ACF (Kwon and Paik 2004). Referring to Fig. 17, it can be seen that a shorter time for full curing is favorable for the efficient joining of electronic components.

Next, we should examine the thermomechanical properties through the measurement of the coefficient of thermal expansion (CTE) of the adhesives. The CTE values can be obtained by the measurement of the length deformation with temperature (Noh et al. 2008). The length deformation can be measured by using a thermomechanical analyzer (TMA). Generally, the smaller the length deformation with temperature, the higher the CTE value. It is anticipated that the CTE value of an adhesive will determine the thermomechanical reliability of the electronic interconnect with the adhesive, that is, the similarity of the CTE values of the adhesive and the substrate and other nearby components is favorable for its long-term reliability. If the CTE of the adhesive is significantly different from those of the nearby components, the resulting mismatch of the CTE values may give rise to certain kinds of reliability problems, such as the thermomechanical fatigue cracking of the material, delamination of a layer, and unstable electrical contact between the metals. Therefore, for the design of a new adhesive material, the CTE values of its constituent materials should be carefully considered, and reliability testing with a fully fabricated sample or a computer simulation is essential to verify its acceptability for the application.

---

## 50.5 Reliability

The short-term quality and long-term reliability are always the most important considerations to determine the value of materials. Typically, it is considered that the best method of evaluating the reliability of an electronic component is an actual

application (Lau 1995). However, this is not always practical, especially during process development and optimization. Therefore, the reliability behavior of an interconnection is characterized by performing accelerated environmental tests, such as temperature cycling, thermal shock, high and low temperature storage, and high temperature and humidity testing. According to some previous studies, the main degradation mechanisms include the oxidation of the metal surfaces in the joint, stress concentration at a certain area during temperature fluctuations, and so on (Li and Wong 2006). Here, we will review the various reliability testing methods for adhesive interconnects, beginning with an introduction to test vehicle design for adhesive interconnects.

### 50.5.1 Test Vehicle Design

Basically, the test vehicle for the accelerated testing should resemble the real components or interconnect systems. That is, the test vehicle design must be such that it can be processed using all the technologies of interest. In addition, the ability to change the wafer layout, such that the user has flexibility in selecting an appropriate chip size for the application, is sometimes desirable to evaluate its technological capability (Lau 1995). Adhesives are used to join various systems in electronic manufacturing, e.g., Si die bonding to rigid printed circuit board (flip chip application), Si die bonding to flexible substrate (COF, chip on flexible substrate), Si die bonding to glass substrate (COG, chip on glass), rigid printed circuit board to flexible substrate, and so on. Therefore, proper test vehicle design is possible only after the consideration of the real application of the adhesives developed. After considering the application, the materials used for the chip, substrate, metal bump for joining, the number of bumps on a die, pitch of bump array, and bump array specification can be easily determined in the case where the target application is definite. Then, we should design conductive metal circuits of the test vehicle, in order to measure the total resistance of the circuits or a single bump interconnect.

Figure 18 shows an example of the test vehicle used for the reliability testing of the adhesives. As can be seen in the figure, the test vehicle is fabricated by joining an Si die to a flexible substrate that is typically made from polyimide. An adhesive film, ACF, was used for the joining process. This design is called the COF, and it is widely used in the manufacture of display modules such as liquid crystal displays (LCDs). Enlarged views of the test circuits are shown in Fig. 19. In the design of conductive circuits for electrical evaluation, it is important that we measure or calculate the resistance of only the adhesive interconnects, which consist of a metal bump on a die, adhesive, and metal pad on a substrate, excluding the resistance of any conductive traces on the Si die or substrate. This is possible if we apply the four-point electrical resistance measurement system with a proper design using the so-called Kelvin structure.

Figure 20 shows a schematic description of the Kelvin structure for the selective electrical characterization. This structure contains four metal bumps and pads for adhesive joining. The traces used as the voltage sense and current sense can be interchanged. The principle of operation of this structure is fully described in the

**Fig. 18** Test vehicle sample for reliability testing of adhesive interconnects

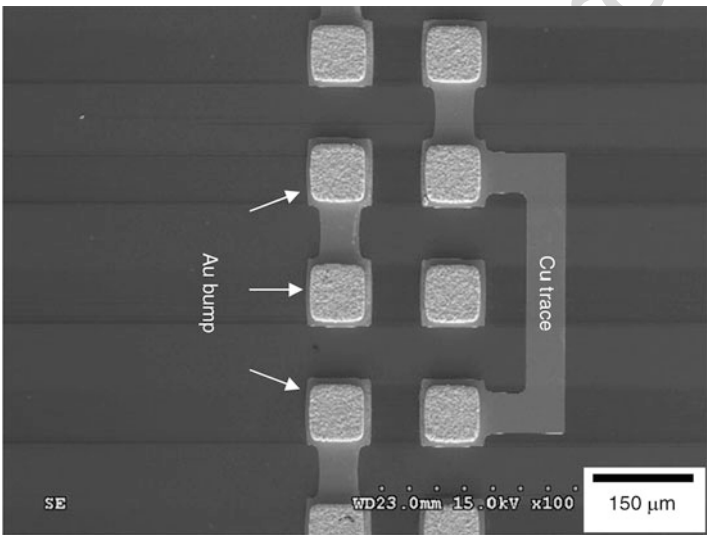
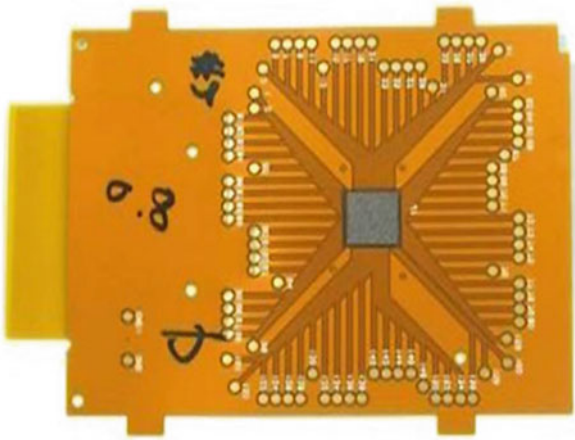


**Fig. 19** Scanning electron microscope image for surface of flip chip test vehicle

literature (Lau 1995) and is briefly introduced here as follows. Let us assume that the current flows through trace A, through bump 1, over the trace on the die, down bump 2, and out of trace B. It should be noted that traces C and D have no current flowing through them. Furthermore, trace C and bump 3 are at the same potential as the bottom of bump 2. Also, trace D and bump 4 are at the same potential as the top of bump 2. Therefore, any potential difference measured across traces C and D would represent the potential drop across bump 2. Given the current flowing through bump 2 and the measured potential difference across traces C and D, the bump resistance may be readily estimated.

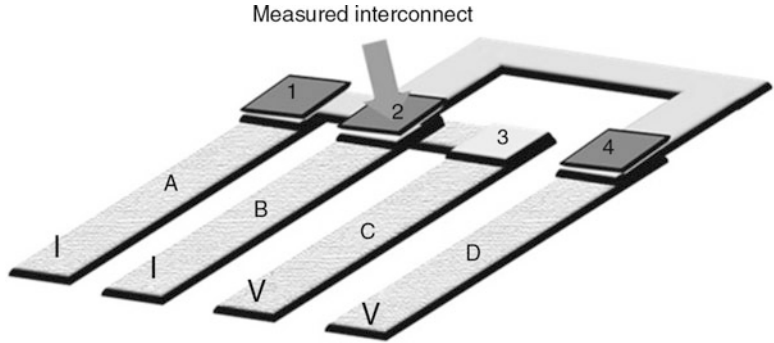


**Fig. 20** Schematic description of four-point measurement for Kelvin structure design

**50.5.2 Storage Test in Harsh Environments**

The past few years have witnessed explosive growth in the research and development efforts devoted to the improvement of adhesive joint reliability for mobile electronics. In the evaluation of the reliability, it is emphasized that the following must be noted in order to obtain a full understanding of the adhesive technology. To investigate the reliability of adhesives in an electronic component, the stability of the connection resistance of a single interconnect in the specific electrical system under environmental stress should be evaluated. Therefore, the design and fabrication of the test vehicle are essential prerequisites. Then, the environmental conditions to use for the reliability testing should be selected. Various testing methods are generally selected for the evaluation of adhesive interconnects, ranging from the reflow test to the pressure cooker test (PCT). Here, we will review the various environmental test methods and their failure analysis techniques.

The reflow test is typically conducted to evaluate the thermal stability of adhesive interconnects. Reflow is the process of melting and cooling of the solder placed on a substrate for joining various component electrodes to metal pads. Today, adhesive interconnection technology is also applied to join ICs to a PCB, and, therefore, these kinds of products are packaged with adhesive technologies together with the conventional reflow process. In these soldering processes, the package needs to be heated up to above 200 °C, which is much higher than the final bonding temperature of the adhesive interconnection. Therefore, the development of adhesives which can withstand multiple solder reflows was a major milestone in the process of its acceptance within the semiconductor packaging industry (Kim et al. 2008a). Figure 21 shows a reflow machine for soldering, and Fig. 22 shows a typical temperature profile for the reflow of Sn-based Pb-free solders.

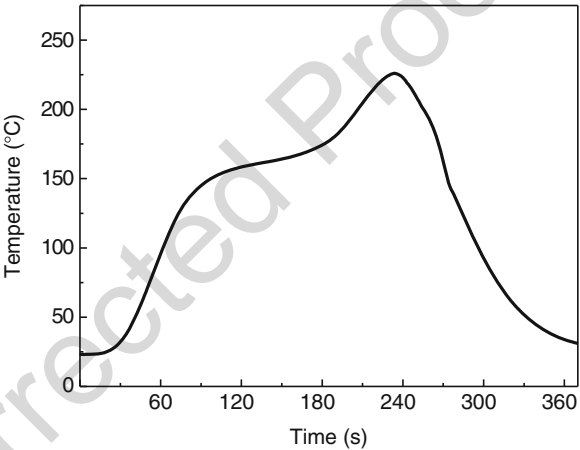
Thermal shock and temperature cycling tests are typically employed to evaluate the ability of the adhesive interconnect to resist the temperature variation during the operation of the electrical system. The adhesives in an electronic package serve as a mechanical mechanism for resisting the thermal deformation induced by the CTE mismatch between the upper chip and lower substrate. The thermally induced





**Fig. 21** Reflow machine (RF-430-N2, Japan Pulse Laboratory Ltd. Co., Japan)

**Fig. 22** Reflow temperature profile for Sn-based Pb-free solders



fatigue cracking through a constituent material and the delamination of the adhesive from the attached area, resulting from the mismatch in the CTE of the chip and substrate, are the major wear-out failure modes in adhesive joints. The thermal fatigue process involves microcrack initiation and coalescence followed by crack propagation. Figure 23 shows an example of a catastrophic failure mode of adhesive interconnect after thermal shock testing. The thermal shock test is an accelerated test form of the temperature cycling test. The thermal shock test controls only the highest and lowest temperatures in the testing zones, and then moves the position of the test samples from the first zone to the other, which means that the samples experience a very abrupt temperature variation during the testing. Meanwhile, the temperature cycling test controls the total temperature profile, so that the test samples can experience milder temperature variations. The detailed test methods for the test of electronic components are provided by the Joint Electron Device Engineering Council (JEDEC) standards. Figure 24 shows an example of a thermal shock testing chamber.

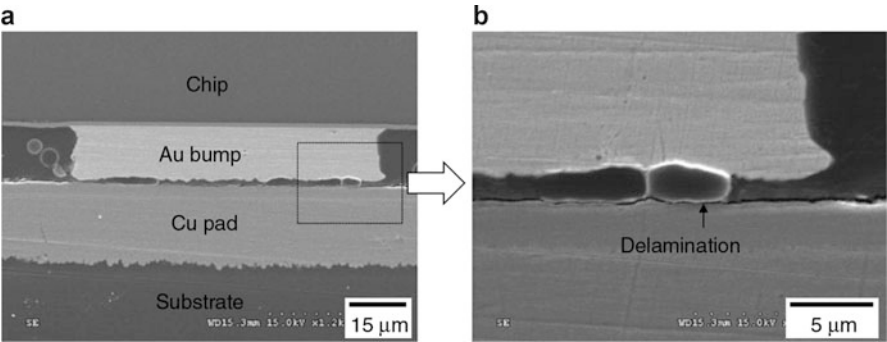


**Fig. 23** Failure mode for ACA interconnect after thermal shock testing

**Fig. 24** Thermal shock testing chamber (TSA-101S, Espec, Japan)



The high and low temperature storage test is also typically used to evaluate the ability of the adhesives to resist a harsh environment. In this case, the temperature variation is not included in the testing profile, so the test evaluates the effects of a fixed environmental temperature on the stability of the electrical system. Conventionally, this test was widely conducted to investigate the effects of a certain

temperature on the growth behavior of an intermetallic compound layer, which is a reaction layer formed between a solder and a metal substrate during a reflow process. However, it is also employed to evaluate the impact of long-term storage at a rigorously stabilized temperature on the electrical quality of the adhesive interconnect. The high temperature and humidity test is considered to be one of the most important test methods for the evaluation of adhesive joints, because of their high absorption of humidity. When a sample with an adhesive joint is placed in an environment having high humidity, the swelling of the polymeric conductive fillers in the ACA and z-directional expansion of the adhesive matrix occur. Figure 25 shows this behavior for the example of an ACA joint before and after the high temperature and humidity test (85 °C and 85% relative humidity for 500 h). After the test, no significant defects such as delamination or cracking of the adhesive matrix were evident, but initially the deformed conductive particles swelled upward due to the release of the residual z-directional shrinkage stress and the expansion of the polymeric cores of the conductive particles and adhesive matrix. After the joining process with the adhesives at room temperature, the z-directional stress in the adhesive areas was mainly compressive stress, but it decreased with increasing temperature and humidity. A small compressive stress induces the swelling of the polymer particles and adhesive matrix layer, and ultimately electric disconnection may occur in the worst case. The swollen conductive particles decrease the contact area, and, thus, the electrical connection resistance should increase during the testing.

For the failure analysis of the test samples after the harsh environmental tests, various analysis tools are employed, e.g., scanning electron microscopy (SEM) with a cross-sectional analyzing technique; X-ray microscopy; A-, B-, and C-mode scanning acoustic microscopy (A-SAM, B-SAM, and C-SAM, respectively); and

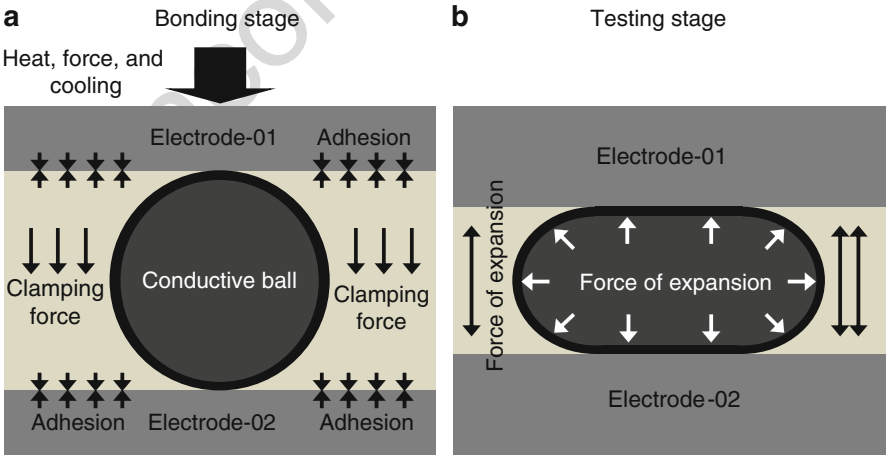


**Fig. 25** Schematics of stress field around the conductive particle: (a) after bonding, (b) during testing at high temperature and humidity

tomographic acoustic microimaging (TAMI), to analyze the failure samples. The continuous measurement of the electrical resistance should consequently be conducted during all of the environmental tests mentioned above.

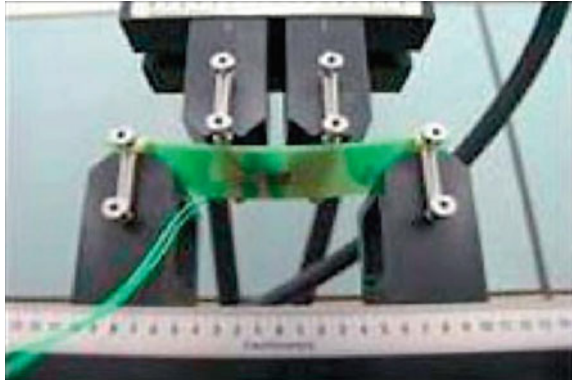
### 50.5.3 Mechanical Reliability

The adhesives used in the electronic industry serve not only to provide electronic continuity but also to support the mechanical load experienced during service. Therefore, the mechanical stability of the adhesive joints has been one of the major reliability concerns in electronic assembly technology. The mechanical peeling and shear test of the adhesive joints are typically performed to characterize the bonding strength at the adhesive-substrate interface. These two methods are very simple to implement. That is, the test procedure consists of the detachment of a component bonded with an adhesive on a substrate. During the detachment process, mechanical stress such as shearing or peeling is applied to the component, while the loading applied to a stress sensor is recorded for the characterization of the mechanical stability.

Owing to the increasing demand for portable electronic devices, which are affected by low-frequency and random vibrations, the reliability of electronic packages subjected to repetitive mechanical loads has recently become an important issue in the electronic industry (Noh et al. 2009). In this case, assembly warpage has been recognized as an important factor for determining the package reliability, as it can lead to IC failure, due to the delamination of a layer and cracking through a specific material in the subsequent process caused by dimensional instability and non-coplanarity. In particular, the cyclic bending reliability testing of various packages under different test conditions is widely conducted at the board or system level (Noh et al. 2009). The three-point or four-point bending test is one of the most frequently employed test methods, due to its suitability for testing large package samples under similar loading conditions (bending moments) within the inner load span. Here, we will review the four-point bending test for the evaluation of the mechanical reliability of adhesive joints.

Figure 26 shows a four-point bending tester used for testing a sample with an ACF. The tip of each support consists of a roller to ensure line contact with the test board, as shown in the figure. In this case, the in situ electrical resistance should also be measured, in order to identify the failure of the package during bending testing. The bottom supports are fixed, while the top supports move downward repetitively with the displacement profile prescribed by the sinusoidal movement of the actuator. The top and bottom support spans are fixed at a certain distance apart. For the measurement of the electrical resistance, a current is flowed through the metal circuits and adhesive joints. An event detector is generally used to determine when the overall electrical resistance exceeds a specific value. The experiments are typically performed at room temperature, but could also be done at higher ones. The bending fatigue test can be conducted using the load-control or displacement-control method.

**Fig. 26** Four-point bending tester for adhesive joint



## 50.6 Conclusions

This chapter describes the adhesive technologies used in the electrical industry with an introduction to the conduction mechanisms in adhesive joints, the specific requirements for the application of adhesives in electronics, and reliability evaluation methods. We will summarize this chapter with the following conclusions:

1. There are three types of electrically conductive adhesives typically used in the electrical industry, e.g., isotropic conductive, anisotropic conductive, and non-conductive adhesives.
2. Isotropic conductive adhesives have a large amount of conductive fillers (25–30 vol.%) with the electrical conductivity provided by the contact between the conductive fillers.
3. Anisotropic conductive adhesives are similar to isotropic conductive adhesives, except that they have a lower conductive filler content (5–20 vol.%) and thus provide unidirectional conductivity in the vertical or z-direction (perpendicular to the plane of the substrate).
4. Non-conductive adhesives have no conductive fillers but rather maintain a pure mechanical contact between the bumps and pads, due to the application of a compressive force, and it is this that ensures the electrical connectivity between them.
5. Considering the drawbacks of conductive filler materials in conventional ECAs, there are three major approaches to enhance the electrical conductivity and thermomechanical properties, which include (i) hybrid metallic fillers, (ii) carbon-based nanomaterials, and (iii) hybrid nonmetallic fillers: conductive polymers and PEDOT:PSS.
6. The conductivity of electrically conductive adhesives is described by percolation theory, which explains that the resistivity of an adhesive drops dramatically at a certain vol.% of conductive fillers.

7. The connection resistance at the interface between the adhesives and metal bumps is composed of three resistance components, i.e., the intrinsic resistance of the constituent materials, constriction resistance, and tunneling resistance.
8. Shrinkage stress is generated by the curing reaction of the adhesives, which means that the thermal and thermomechanical behavior of the adhesives during the bonding process should be evaluated before their use in electronics.
9. For the reliability testing of adhesives in electronics, a test vehicle for accelerated testing should be fabricated, which resembles the real components or interconnect systems. This means that the design of the test vehicle must be such that it can be processed using all of the technologies of interest.
10. Various testing methods are employed to evaluate the reliability of adhesives in electronics, such as temperature cycling, thermal shock, high and low temperature storage, and high temperature and humidity testing.
11. The mechanical peeling and shear tests of the adhesive joints are typically performed to characterize the bonding strength at the adhesive-substrate interface.

---

## References

- Amoli BM, Trinidad J, Hu A, Zhou YN et al (2015) Highly electrically conductive adhesives using silver nanoparticle(Ag NP)-decorated graphene: the effect of NPs sintering on the electrical conductivity improvement. *J Mater Sci: Mater Electron* 26:590–600
- Aschenbrenner R et al (1997) Adhesive flip chip bonding on flexible substrates. In: *Proceedings of 1st IEEE international symposium on polymeric electronics packaging*, IEEE, p 86
- Chen C, Wang L, Li R et al (2007) Effect of silver nanowires on electrical conductance of system composed of silver particles. *J Mater Sci* 42:3172–3176
- Chen D, Qiao X, Qiu X et al (2010) Effect of silver nanostructures on the resistivity of electrically conductive adhesives composed of silver flakes. *J Mater Sci: Mater Electron* 21:486–490
- Chueh TC, Hu CH, Yen SC (2015) Electrically conductive adhesives with low Ag content prepared by Ag self-activated plating and PEDOT:PSS. *J Electrochem Soc* 162:D56–D61
- Desvergne S, Gasse A, Pron A (2011) Electrical characterization of polyaniline-based adhesive blends. *J Appl Polym Sci* 120:1965–1973
- Grujčić M, Cao G, Roy WN (2004) A computational analysis of the percolation threshold and the electrical conductivity of carbon nanotubes filled polymeric materials. *J Mater Sci* 39:4441–4449
- Gumfekar SP et al (2011) Silver-polyaniline-epoxy electrical conductivity adhesives – a percolation threshold analysis. In: *IEEE 13th electronics packaging technology conference*, IEEE, p 180
- Habenicht G (1990) *Kleben*. Springer-Verlag, Berlin
- Holm R (1979) *Electric contacts*. Springer-Verlag, Berlin
- Kim HK, Shi FG (2001) Electrical reliability of electrically conductive adhesive joints: dependence on curing condition and current density. *Microelectron J* 32:315–321
- Kim JW, Kim DG, Hong WS et al (2005) Evaluation of solder joint reliability in flip-chip packages during accelerated testing. *J Electron Mater* 34:1550–1557
- Kim JW, Kim DG, Lee YC et al (2008a) Analysis of failure mechanism in anisotropic conductive and non-conductive film interconnections. *IEEE Trans Compon Packag Tech* 31:65–73

- Kim JW, Lee YC, Jung SB (2008b) Reliability of conductive adhesives as a Pb-free alternative in flip-chip application. *J Electron Mater* 37:9–16
- Kim J, Yim BS, Kim JM, Kim J (2012) The effects of functionalized graphene nanosheets on the thermal and mechanical properties of epoxy composites for anisotropic conductive adhesives (ACAs). *Microelectron Reliab* 52:595–602
- Kim KS, Bang JO, Choa YH et al (2013) The characteristics of Cu nanopaste sintered by atmospheric-pressure plasma. *Microelectron Eng* 107:121–124
- Kim KS, Park BG, Jung KH et al (2015) Microwave sintering of silver nanoink for radio frequency applications. *J Nanosci Nanotechnol* 15:2333–2337
- Kwon WS, Paik KW (2004) Fundamental understanding of ACF conduction establishment with emphasis on the thermal and mechanical analysis. *Int J Adhes Adhes* 24:135–142
- Lau JH (1995) Flip chip technologies. McGraw-Hill, New York
- Lau JH, Wong CP, Lee NC, Lee SWR (2003) Electronics manufacturing with lead-free, halogen-free & conductive-adhesive materials. McGraw-Hill, New York
- Lee HH, Chou KS, Shih ZW (2005) Effect of nano-sized silver particles on the resistivity of polymeric conductive adhesives. *Int J Adh Adh* 25:437–441
- Li Y, Wong CP (2006) Recent advances of conductive adhesives as a lead-free alternative in electronic packaging: materials, processing, reliability and applications. *Mater Sci Eng R* 51:1–35
- Lilei Y, Zonghe L, Johan L et al (1999) Effect of Ag particle size on electrical conductivity of isotropically conductive adhesives. In: *IEEE transactions on electronics packaging manufacturing*, IEEE, p 299
- Liu YH, Lin KL (2005) Damages and microstructural variation of high-lead and eutectic SnPb composite flip chip solder bumps induced by electromigration. *J Mater Res* 20:2184–2193
- Maattanen J (2003) Contact resistance of metal-coated polymer particles used in anisotropically conductive adhesives. *Solder Surf Mount Tech* 15:12–15
- Markley DL, Tong QK, Magliocca DJ et al (1999) Characterization of silver flakes utilized for isotropic conductive adhesives. In: *Proceedings of international symposium on advanced packaging materials*, IEEE, p 16
- Mayo MJ (1996) Processing of nanocrystalline ceramics from ultrafine particles. *Int Mater Rev* 41:85–115
- Mir IM, Kumar D (2010) Development of polypyrrole/epoxy composites as isotropically conductive adhesives. *J Adhes* 86:447–462
- Noh BI, Lee BY, Jung SB (2008) Thermal fatigue performance of Sn-Ag-Cu chip-scale package with underfill. *Mater Sci Eng A* 483–484:464–468
- Noh BI, Yoon JW, Kim JW et al (2009) Reliability of Au bump flip chip packages with adhesive materials using four-point bending test. *Int J Adhes Adhes* 29:650–655
- Plumbridge WJ (2004) Long term mechanical reliability with lead-free solders. *Solder Surf Mt Tech* 16:13–20
- Ruschau GR, Yoshikawa S, Newnham RE (1992) Resistivities of conductive composites. *J Appl Phys* 72:953–959
- Song CH, Ok KH, Lee CJ et al (2015) Intense-pulsed-light irradiation of Ag nanowire-based transparent electrodes for use in flexible organic light emitting diodes. *Org Electron* 17:208–215
- Wu H, Wu X, Ge M et al (2007) Properties investigation on isotropical conductive adhesives filled with silver coated carbon nanotubes. *Comps Sci Technol* 67:1182–1186
- Yang X, He W, Wang S et al (2012) Preparation and properties of a novel electrically conductive adhesive using a composite of silver nanorods silver nanoparticles and modified epoxy resin. *J Mater Sci: Mater Electron* 23:108–114
- Yim MJ, Paik KW (1998) Design and understanding of anisotropic conductive films (ACF's) for LCD packaging. *IEEE T Comp Pack Manu Tech* 21:226–224
- Yim BS, Kim K, Kim J et al (2016) Influence of functionalized graphene on the electrical, mechanical, and thermal properties of solderable isotropic conductive adhesives. *J Mater Sci: Mater Electron* 27:4516–4525

- 903 Yin CY, Lu H, Bailey C et al (2006) Analyzing the performance of flexible substrates for lead-free  
904 applications. In: Proceedings of 7th international conference on thermal, mechanical and  
905 multiphysics simulation and experiments in micro-electronics and micro-systems, IEEE, p 1  
906 Yu H, Adams RD, da Silva LFM (2013) Development of a dilatometer and measurement of the  
907 shrinkage behaviour of adhesives during the cure process. *Int J Adhes Adhes* 47:26–34  
908 Zallen R (1983) *The physics of amorphous solids*. Wiley, New York  
909 Zhang YL, Shi DXQ, Zhou W (2006) Reliability study of underfill/chip interface under accelerated  
910 temperature cycling (ATC) loading. *Microelectron Reliab* 46:409–420  
911 Zhang ZX, Chen XY, Xiao F (2011) The sintering behavior of electrically conductive adhesives  
912 filled with surface modified silver nanowires. *J Adhes Sci Technol* 25:1465–1480



José Miguel Martín-Martínez

**Contents**

51.1	Introduction .....	1484
51.2	Overview of the Shoe Bonding Process .....	1486
51.3	Surface Preparation of Upper and Sole Materials for Bonding .....	1487
51.3.1	Upper Materials .....	1488
51.3.2	Sole Materials .....	1490
51.3.3	Adhesives in Upper-to-Sole Bonding .....	1502
51.3.4	Polyurethane Adhesives .....	1503
51.3.5	Polychloroprene Adhesives .....	1517
51.4	Testing of Adhesive Joints in Shoe Bonding .....	1523
51.5	Conclusions .....	1526
	References .....	1527

**Abstract**

This chapter constitutes one of the very few reviews in the existing literature on shoe bonding, and it gives an updated overview of the upper-to-sole bonding by using adhesives. The surface preparation of rubber soles and the formulations of the solvent-borne and waterborne polyurethane and polychloroprene adhesives are described in more detail. The preparation of the adhesive joints and the specific adhesion tests in shoe bonding are also revised. Finally, the most recent developments dealing with shoe bonding are described.

J. M. Martín-Martínez (✉)

Adhesion and Adhesives Laboratory, University of Alicante, Alicante, Spain

e-mail: [jm.martin@ua.es](mailto:jm.martin@ua.es)

## 51.1 Introduction

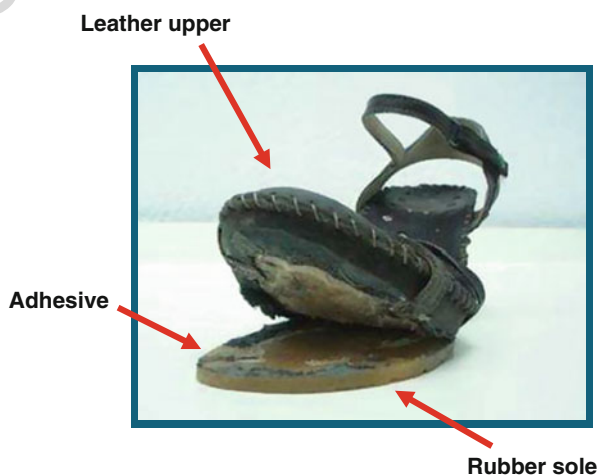
The attachment of the upper to the sole by means of adhesives in shoe manufacturing is one of the most exigent bonding technologies. Several different types of materials are used in shoe manufacturing most of them varying in nature and composition from year to year because of fashion requirements. Furthermore, the geometrical shape and the design of the upper and the sole change often in male and female shoes, and several models and kinds of shoes can be manufactured (casual shoes, sport shoes, boots, safety shoes, sanitary and orthopedic shoes). For each shoe, bonding must be specifically designed, and this situation happens twice a year (spring and fall seasons in shoe industry). This is one of the reasons for the difficulty in establishing unified methodologies for shoe bonding as there is no time for shoe manufacturers to react once debonding appears, i.e., the upper and the sole separate during use (Fig. 1).

Another particular feature in shoe industry is the lack of quality control of the materials and the adhesives used for bonding. Shoe manufacturers have extensive knowledge on the technology of making shoes, but their knowledge on bonding comes mainly from the experience and the advice of the adhesive manufacturers. Certainly, the bonding of the shoe parts is more of an art than a technology, and the shoe manufacturers are always worried and even scared when they have to attach the upper to the sole in the new models of shoes in the season. In fact, it is a common practice in several famous shoe brands to sew the upper to the sole simply because they do not trust in the quality of the adhesive bonding!

The above given arguments justify the writing of a review on the bonding of shoe industry based mainly on the experience of the author in the field acquired during more than 25 years.

The bonding with adhesives has been introduced in the footwear industry as an alternative to sewing or the use of nails, staples, or tacks to bond several parts of the

**Fig. 1** Upper-to-sole detachment in a shoe



shoes, the most critical part being the upper-to-sole bonding. The introduction of adhesive technology in shoe manufacturing provided several advantages: (i) More flexible and homogeneous joints were obtained; (ii) the stresses during use were similarly distributed all along the joints; (iii) improved aesthetic properties were obtained, and new design and fashion shoes were possible; and (iv) automation was feasible. However, as a limitation, the bonding with adhesives in shoe industry needs a severe control of all steps involved in the formation of the joints to avoid adhesion problems, mainly the separation of the sole from the upper. Although several parts of a shoe are bonded with adhesives (mounting, heel covering, box toe bonding, sticking of the soft lining, lift attachment, shank and cushion bonding, etc.), this chapter will be devoted only to the upper-to-sole attachment because it is the most critical bonding operation in shoe manufacturing.

Depending on the type of shoe, different bonding performance is required. Due to fashion issues, the bonding of the casual and the free-time shoes is relatively low exigent as the requested durability is not too high (3 years maximum). However, the sport shoes are extremely exigent in bonding as low weight, high performance under impact and flexural stresses, high comfort, and high durability are mandatory requirements. Safety shoes are the most exigent in terms of bonding because they have to work in the presence of solvents, high or low temperature, high-impact resistance, and all these should last for a long time.

There are not many reviews in the existing literature dealing with the adhesive bonding in shoe industry. Some Spanish books (Diputación de Alicante 1974; Amat-Amer 1999) devoted to shoe industry include some basic technical chapters dealing with the use of the adhesives for bonding operation, but they have not been translated to English. In the 1960s and 1970s, the Prüf- und Forschungsinstitut Pirmasens (PFI) in Pirmasens (Germany) (Fisher and Meuser 1964; Fisher 1971) and the Shoe Allied Trade Research Association (SATRA) in Kettering (England) (Pettit and Carter 1973) published excellent reports dealing with several specific aspects of the adhesive joints in shoe industry. More extensive literature dealing with the solvent- and waterborne polyurethane adhesives used in shoe industry has been published (some to be cited are Pettit and Carter 1973; Schollenberger 1977; Dollhausen 1985; Kozakiewicz 1991; Sultan Nasar et al. 1998; Frisch 2002), but minor attention has been paid to polychloroprene adhesives (some to be cited are Whitehouse 1986; Kelly and McDonald 1963; Harrington 1990; Guggenberger 1990; Lyons and Christell 1997; Martín-Martínez 2002). On the other hand, the surface preparation procedures of the upper and sole materials for shoe bonding have been widely considered in the literature (some to be cited are Oldfield and Symes 1983; Extrand and Gent 1987; Hace et al. 1990; Fernández-García et al. 1991; Lawson et al. 1996; Cepeda-Jiménez et al. 2002).

Most of the books devoted to footwear consider only a chapter devoted to adhesives or surface preparation of materials before bond formation, but rarely both aspects are described in the existing literature, and the understanding of the complex nature of the bonding process in shoe manufacturing is almost absent. A previous chapter written by the author dealing with shoe bonding was published in 2005 (Adams 2005), and the present chapter is an update of that chapter in which the

most recent scientific contributions have been addressed. Recently, a review dealing with the use of adhesives in the footwear industry has been published (Paiva et al. 2016). Obviously, the reader will find some similarities between the two chapters written by the author, but as a comprehensive updated view on shoe bonding is given, the reading of this chapter will certainly compensate for it.

This chapter is divided into four sections. The first section provides an overview of the bonding in the shoe industry. Conventional surface preparation of different sole and upper materials is described in section two, with special attention to the chlorination of rubber soles by using organic solvent solutions of trichloroisocyanuric acid. Both solvent-borne and waterborne polyurethane and polychloroprene adhesives are described in detail in section three with special reference to their formulations. Finally, the testing, the quality control, and the durability of the adhesive joints in shoe bonding are considered in section four.

## 51.2 Overview of the Shoe Bonding Process

Although each shoe may be constituted by materials of different nature with different shapes and the adhesives commonly used are polyurethane or polychloroprene adhesives, to produce an adequate bonding, the different operations/steps given in Fig. 2 must be followed.

The first operation consists in the surface preparation of the materials to be bonded (upper and sole). Irrespective of the inherent difficulty of bonding these materials, solvent cleaning and roughening are generally carried out. For difficult-to-bond materials, more aggressive chemical surface treatments and/or primer application are mandatory. Once the materials are ready for bonding, the adhesive is

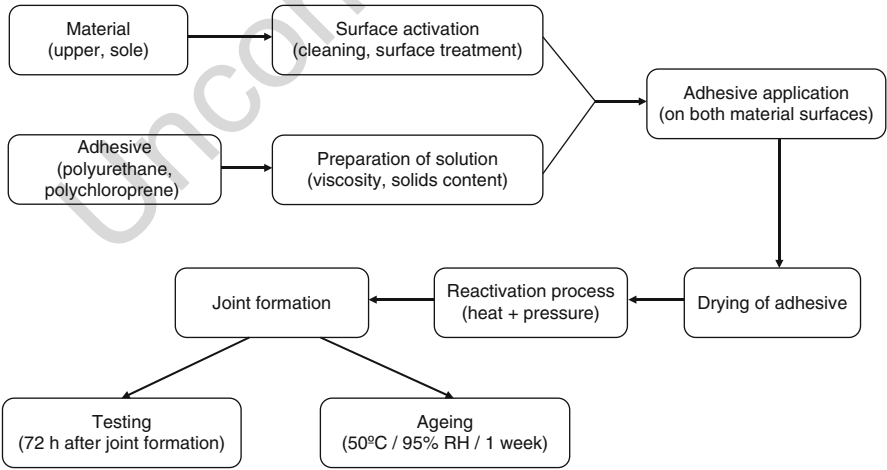


**Fig. 2** Schematic overview of the bonding process in shoe manufacturing (upper-to-sole attachment)

prepared by adjusting its viscosity and by adding isocyanate hardener, mainly for improving the durability of the adhesive joints. The application of the adhesive is a critical step to reach good bonding as the method of application (brush, roller, etc.), and the amount of adhesive determine the success of the joint; the adhesive is usually applied to both materials to be bonded, and, therefore, contact adhesives are used (reactive polyurethane hot melts are an exception because of they are applied on the sole only). The next step in the joint formation consists in the evaporation of the most solvent of the adhesive on the surfaces to be bonded, and because of the absence of tack, reactivation (i.e., sudden heating with infrared or halogen lamps) of the adhesive layers is carried out followed by immediate joining of the melted adhesive films applied on the two materials to be bonded followed by the application of pressure for a given time. Finally, the joints are cooling down before placing the shoe in the box.

Interestingly, green adhesion is a critical issue for shoe manufacturers. It is a general practice to place the thumb nail at the shoe front and try to separate the adhesive joint. If the joint resists the press of the thumb nail, the joint is considered acceptable. If it is not the case, sewing is a common practice!

In terms of the mechanisms of adhesion (see ► [Chap. 2, “Theories of Fundamental Adhesion”](#)) involved in upper-to-sole bonding, mechanical interlocking is important. Considering that most of the upper materials are porous and the adhesives used in shoe bonding are applied as liquids, an acceptable penetration of the adhesive into the upper is expected, and then the mechanical adhesion is generally favored. However, because several synthetic sole materials are nonporous and have in general a relatively low surface energy, both mechanical (e.g., roughening) and chemical (e.g., halogenation) surface preparations are necessary, and enhanced chemical adhesion is required. Therefore, the main mechanisms of adhesion involved in shoe bonding are mechanical interlocking and chemical. Furthermore, in the bonding of some rubber soles, the weak boundary layers produced by surface contaminants and/or by migration of antiadherend moieties to the interface during joint formation must be removed before joint formation.

In the following sections, the materials and their surface preparation prior to be bonded, the adhesives used, and the manufacture and testing of the upper-to-sole joints will be separately discussed. Each section will consider an overview of the current state of the art in shoe industry, and future trends will be highlighted too.

---

### 51.3 Surface Preparation of Upper and Sole Materials for Bonding

Depending on fashion, each year different materials have been and are currently used in the manufacturing of shoes, including the rubber soles (vulcanized styrene–butadiene rubber (SBR), thermoplastic rubber, ethylene propylene diene monomer (M-class) rubber (EPDM)) and different polymeric materials (leather; polyurethanes; ethylene–vinyl acetate copolymers, EVA; polyvinyl chloride, PVC; polyethylene, *Phylon*). In order to produce adequate adhesive joints, the surface

preparation of those materials is required (see part related to Surface Treatments). Surface preparation procedures for these materials must be quickly developed, and the validity of these treatments is generally too short because of fashion constrictions. Several procedures have been established to optimize the upper-to-sole bonding; the most of them are based in the use of organic solvents. Due to environmental and health issues, the solvents should be removed from the surface preparation procedure, and several environmental-friendly procedures for the surface preparation of different materials have been proposed.

Most of the upper and sole materials used in shoe industry cannot be directly joined by using the current adhesives (polyurethane and polychloroprene adhesives) due to their intrinsic low surface energy, the presence of contaminants and release agents, and antiadherend moieties on the surface. Therefore, the surface preparation of upper and sole must remove contaminants and weak boundary layers, and roughness and chemical functionalities able to produce adequate bond strength should be created.

A review on the formulation and characteristics of the main materials used in shoe manufacturing (except adhesives) was published by Guidetti et al. 1992. To the author's best knowledge, no additional reviews on the subject have been published later.

In this section, a short review of the main materials used in shoe bonding as well as their current surface preparation procedures will be considered. In the last part of this section, the current and alternative surface treatments for upper and sole materials are described.

### 51.3.1 Upper Materials

#### Leather

Full-chrome, semi-chrome, and vegetable-tanned leathers are still the main source and most common upper material in shoe manufacturing. In general, the porous nature of the leather facilitates its bonding with adhesives in solution, mainly solvent-borne polychloroprene adhesives. To obtain good adhesion, the weak grain layer of the leather must be removed by using rotating wire brushes (roughening) to expose the corium (the part of the leather with higher cohesion of the collagen fibers) to the adhesive (SATRA 1963). In general, deeper roughening of upper leather produces a stronger bond than light roughening. Furthermore, two consecutive adhesive layers are generally applied on the roughened leather. First, a low-viscosity adhesive solution (incorrectly called *primer*) is applied to fill the pore entrances of the corium fibers and to facilitate the wettability of the leather surface. At least 5 min later (or alternatively when the adhesive layer becomes dried), a second high-viscosity adhesive solution of the same nature than the previous one is applied; diffusion of the polymer chains between the two adhesive layers is produced, and a homogeneous adhesive layer with high cohesion is created on the upper leather surface.

The main issues that make difficult the bonding of upper leather are the existence of finishing on the surface to be bonded and the presence of high grease content. Deep or slight scouring or roughening is sufficient to remove the finishing and the weak grain leather. However, in thin leathers (such as buffalo or calf leathers), mild surface scouring followed by application of a primer is necessary to avoid leather tearing; the primer must increase the cohesion of the collagen fibers, and also it has to be compatible with the adhesive. Several primers for thin leathers have been proposed (Ferrandiz-Gómez et al. 1994), but they generally require the application of moderate temperature for being effective. Furthermore, different low-viscosity reactive solvent-based polyurethane primers containing about 10 wt% free isocyanate groups have been developed for improving the adhesion of difficult-to-bond leather (Vélez-Pagés 2003).

Depending on the amount (more than 11 wt% is critical) and type of grease (mainly unsaturated fatty acids) in the leather, poor adhesive bond can be produced. The fat may diffuse through to the surface of the polyurethane adhesive film (possibly while the adhesive still wet, with the solvent acting as the vehicle) and interfere with its subsequent coalescence with the adhesive or the sole. When polychloroprene adhesive is used, the reaction of the fatty acids with some components in the adhesive formulation (zinc oxide, magnesium oxide) forms insoluble metal soaps (salts of fatty acids) at the interface that impart antiadherent properties. Polyurethane adhesives are more tolerant to greasy leather than polychloroprene adhesives. The roughening of the leather is always necessary, and the addition of 5 wt% isocyanate hardener to the adhesive just before application helps to reach good adhesive joints.

Solvent-borne polychloroprene adhesives are excellent for bonding leather because of their high wettability and permanent tack (heat activation is not needed). However, these adhesives have poor performance with most of the rubber soles and with several synthetic upper materials. In these cases, polyurethane adhesives provide better performance.

### Synthetic Upper Materials

Several synthetic upper materials such as canvas, textiles, nylon, PVC on woven or nonwoven, and poromerics are used in shoe manufacturing. As for leather, most of these materials need roughening (to remove finishing) and/or solvent wiping, followed by application of two consecutive adhesive layers, to produce good adhesive joints.

*PVC uppers* may cause lack of adhesion due to the migration of plasticizer into any material with which the PVC comes in contact. Light roughening is necessary, or alternatively methyl ethyl ketone (MEK) wiping can be applied followed by the application of polyurethane adhesive containing 5 wt% isocyanate hardener. Alternatively, the application of a primer based on nitrile rubber followed by application of two-component polychloroprene adhesive may perform adequately. *PVC-coated fabrics* may have acrylic or urethane coatings on top. Acrylic coatings are readily soluble by MEK wiping, whereas the urethane coatings need tetrahydrofuran wiping.



*Polyurethane-coated fabrics* can be bonded by using polyurethane adhesives. Mild scouring using a fine rotary wire brush must be used to completely remove the coating before applying the adhesive.

*Poromerics* (nonwoven fabric supporting a microporous urethane layer) also need to be roughened with extreme care. When nylon, polyester, or cellulose interlayers are present, the application of isocyanate-based primers promotes the adhesion.

*Nylon fabric* uppers show serious adhesion problems. The best bonding is obtained by mild roughening followed by applying 2 wt% isocyanate-based primer; the application of two-component polyurethane adhesive is also necessary.

### 51.3.2 Sole Materials

Several kinds of sole materials are currently used in shoe manufacturing, the rubber soles are the most common. Few soles are made of natural products, such as leather or cork. The *leather soles* are not difficult to bond because they are porous and easily wetted by adhesive solutions. A primer is required to produce good bond with solvent-borne polychloroprene adhesives. The use of polyurethane adhesives is also feasible but not so effective, and there is the need of the previous application of low-viscosity polyurethane primer to which 2.5 wt% isocyanate hardener must be added. On the other hand, the *cork soles* are widely used for sandals, and they are joined with polychloroprene adhesives. In some cases, a thin EVA midsole is attached to the cork to improve its abrasion resistance and comfortability by using two-component polychloroprene adhesive (Martin 1971).

#### Rubber Sole Materials

Rubber soles are by far the most common in shoe industry. Vulcanized or unvulcanized (thermoplastic) rubber soles are generally used. In general, the bonding is produced with one- or two-component polyurethane adhesives, and a surface treatment is always required to produce good adhesive joints.

#### Thermoplastic Rubber (TR) Soles

Styrene-butadiene-styrene (SBS) block copolymers are adequate raw materials to produce *thermoplastic rubber (TR) soles*. SBS block copolymers contain butadiene domains – soft and elastic – and styrene domains – hard and tough. Because the styrene domains act as virtual cross-linking in the SBS structure, the vulcanization is not necessary to provide dimensional stability. The TR soles generally contain polystyrene (to impart hardness), plasticizers, fillers, and antioxidants, and processing oils can also be added. The TR soles have low surface energy, so a surface modification is needed to reach proper adhesion to polyurethane adhesive. Special adhesives for the TR soles have been developed to avoid surface preparation, but they have poor creep resistance.

Due to their softness, the TR soles cannot be roughened. The TR soles tend to swell by application of adequate solvents, and the mechanical interlocking of the adhesive is favored; however, vigorous rubbing must be avoided to maintain the mechanical integrity of the sole. Chemical treatments are necessary to improve the



adhesion of the TR to polyurethane adhesive, mainly cyclization (treatment with sulfuric acid) and halogenation.

The TR can be treated with concentrated sulfuric acid to yield a cyclized layer on the surface (Cepeda-Jiménez et al. 2001). This layer is quite brittle, and when it is flexed and stretched, microcracks are developed which help in the subsequent bonding by favoring the mechanical interlocking of the polyurethane adhesive with the TR. The thickness of the cyclized layer depends on the length of the treatment with sulfuric acid. On the other hand, the treatment with sulfuric acid mainly produces the creation of highly conjugated C–C bonds and the sulfonation of the butadiene units of the TR material. The immersion of TR for less than 1 min, the neutralization with ammonium hydroxide (it extracts the hydrogen from the sulfonic acid and leaves stabilized  $\text{SO}_3^- \text{NH}_4^+$  ion pair), and the high concentration of the sulfuric acid (95 wt%) are essential to produce an adequate surface treatment. The treatment with  $\text{H}_2\text{SO}_4$  increases the T-peel strength of surface-treated TR/polyurethane adhesive joints (Fig. 3). On the other hand, the styrene content in the TR determines the effectiveness of the treatment with sulfuric acid. The lower is the styrene content in the TR, the more noticeable are the modifications produced on the surface. Furthermore, the styrene content in the TR affects the extent but not the nature of the surface modifications produced by treatment with sulfuric acid.

Halogenation is the most common surface treatment for TR. The use of the chlorination surface treatment in improving the adhesion of several types and formulations of rubbers has been extensively demonstrated, and it is cheap and easy to apply. Furthermore, the chlorination surface treatment removes contaminants and antiadherend moieties from the rubber surface and imparts improved durability and aging resistance to the upper-to-sole joints, and the treated surfaces remain

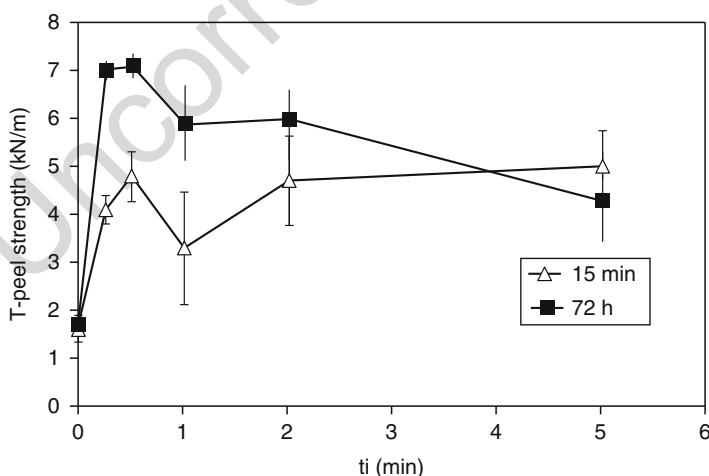


**Fig. 3** T-peel strength values (15 min and 72 h after joint formation) of sulfuric acid-treated TR rubber/polyurethane adhesive joints as a function of the immersion time (Cepeda-Jiménez et al. 2001)

**Fig. 4** Chemical structures of DCI (sodium dichloroisocyanurate) and TCI (trichloroisocyanuric acid)

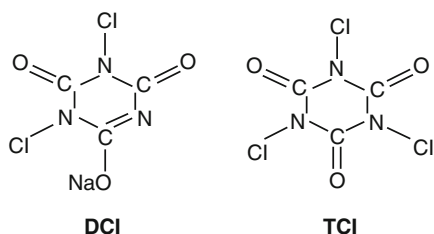
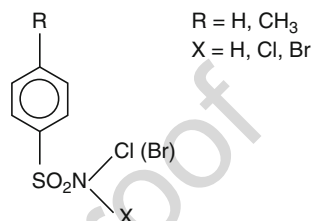


**Fig. 5** Chemical structure of chloramine T



reactive with the polyurethane adhesive for at least 3 months after surface preparation. Immersion in aqueous chlorine or in sodium hypochlorite aqueous solution is a very effective surface preparation for TR soles although fast evolution of chlorine is produced. Therefore, the organic chlorine donors for the treatment of the TR have been proposed alternatively for allowing moderate evolution of chlorinated species during surface treatment. The most commonly used chlorinating agent is an organic solvent (ketone or ester) solution of trichloroisocyanuric acid (TCI) – 1,3,5-trichloro-1,3,5-triazin-2,4,6-trione – (Fig. 4) which is very cheap and common (it is generally used as chlorinating agent in swimming pools). The organic solvent in the TCI solutions determines the degree of rubber wetting, and furthermore, the actual chlorinating species are produced by reaction of the TCI with the organic solvent. The use of the TCI solutions is quite satisfactory for the TR surface preparation although it should be applied with a soft brush and left to dry during moderate time to avoid degradation of the TR surface by the solvent (Carter 1971).

For avoiding the use of organic solvents in the chlorination agents, *acidified sodium hypochlorite aqueous solutions* containing 1-octyl-2-pyrrolidone as wetting agent have been successfully used for the treatment of the TR soles (Cepeda-Jiménez et al. 2003a). The treatment is restricted to about 1  $\mu\text{m}$  depth surface of the TR, and the enhanced adhesion is due to the improved wettability and the creation of chlorine moieties on the rubber surface. Furthermore, *aqueous solutions of sodium dichloroisocyanurate* (DCI) (Fig. 4) have been used to increase the adhesion of the TR soles (Cepeda-Jiménez et al. 2002). The chemical structure of DCI is somewhat similar to that of TCI, and relatively concentrated DCI water solutions are necessary to obtain good peel strength values. On the other hand, successful surface chlorination treatment of the TR has been obtained by using aqueous *N-chloro-p-toluenesulfonamide solutions* (obtained by acidifying chloramine T solutions) (Cepeda-Jiménez et al. 2003a) – Fig. 5. The actual chlorinating species is  $\text{SO}_2\text{-C}_6\text{H}_4\text{-NCl-Cl}$ . The surface treatment is carried out by immersion of the TR in

the aqueous chlorinating solution at 20–80 °C for about 1 min. The effectiveness of this treatment was ascribed to the introduction of chlorine and oxygen moieties on the rubber surface.

*Electrochemical treatments* have also been successfully proposed to improve the adhesion of the TR (Brewis et al. 1997). The treatment consists in the immersion of the TR in an electrochemical cell of silver nitrate in 3.25 M nitric acid. After treatment, the rubbers have to be washed with nitric acid and then with bidistilled deionized water until neutral pH is reached.

Several environmental-friendly surface preparations of the TR sole materials by means of radiations have been more recently proposed. These treatments are clean (no chemical or reaction by-products are produced) and fast, and furthermore online bonding at shoe factory can be produced, so the future trend in the surface modification of the rubber soles will be likely directed to the industrial application of those treatments. Corona discharge, low-pressure radio-frequency (RF) gas plasma, and ultraviolet (UV) enriched in ozone – UV-ozone – treatments have been successfully used at laboratory scale to improve the adhesion of several TR sole materials.

*Corona discharge* has been used to improve the adhesion of the TR to polyurethane adhesives (Romero-Sánchez et al. 2003a). Although the treatment with corona discharge improved the wettability of the TR due to the formation of polar moieties on the surface, and surface cleaning and removal of contaminants (mainly demolding silicone moieties) were produced, the peel strength values moderately increased.

*Low-pressure RF gas plasma* has been shown effective to enhance the adhesion of the TR to different polyurethane adhesives (Ortiz-Magán et al. 2001). Different gases (oxygen, nitrogen, and oxygen–nitrogen mixtures) were used to generate the RF plasma. The treatment produced the partial removal of hydrocarbon moieties from the TR surface, and the formation of oxygen moieties and surface roughness was also produced. On the other hand, the treatment of SBS rubber with low-pressure RF plasma in CCl<sub>4</sub> has also been proposed for improving its adhesion to polyurethane adhesive, and a drastic increase in the peel strength was observed after only a few seconds of treatment which was ascribed to the chemical bonding between the carbon–oxygen moiety species on the SBS surface and the isocyanate groups of the polyurethane adhesive (Tyczkowski et al. 2009). Water molecules strongly attached to the SBS surface were also found, and they reduced the adhesion by partial blocking of the functional groups against the action of isocyanates. On the other hand, because no correlation between the peel strength and the surface free energy was observed, the thermodynamic adhesion was unimportant, and the dominant role of the chemical adhesion was confirmed.

The surface treatment of the TR with *UV–ozone* produced with low-pressure mercury vapor lamp enriched in 175 nm wavelength has been shown to successfully increase its adhesion to polyurethane adhesive (Romero-Sánchez et al. 2003b). The UV–ozone treatment produced important surface modifications (improved wettability, roughness) incorporating oxygen and nitrogen moieties at the TR surface. The peel strength values increased after UV–ozone treatment of the TR, in a greater extent by increasing the treatment time (Fig. 6). More recently, several SBS rubbers

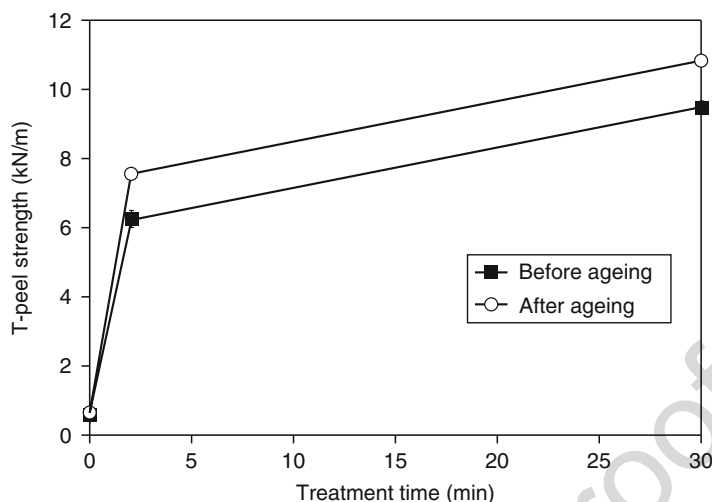


**Fig. 6** T-peel strength values of UV-ozone treated TR/polyurethane adhesive joints as a function of the UV treatment time (Romero-Sánchez et al. 2003)

containing different amounts of calcium carbonate and/or silica fillers were surface treated with UV-ozone to improve their adhesion to polyurethane adhesive (Romero-Sánchez and Martín-Martínez 2008). The nature and content of fillers determined the extent of surface modification and adhesion of SBS rubber treated with UV-ozone. The UV-ozone treatment improved the wettability of all rubber surfaces, and chemical (oxidation) and morphological modifications (roughness, ablation, surface melting) were produced. The increase of the UV-ozone treatment to 30 min led to surface cleaning due to ablation and/or melting of the most external rubber layers, and also incorporation of more oxidized moieties was produced. As a consequence of these surface modifications, the UV-ozone treatment increased the adhesive strength in all joints made with polyurethane adhesive, more noticeably in the joints made with the SBS rubbers containing silica filler. On the other hand, although the chemical modifications were produced earlier in unfilled rubber for short time of treatment with UV-ozone, they were more noticeable in silica-filled rubbers with low silica content for extended length of treatment. However, the oxidation process seemed to be inhibited for the SBS rubbers containing calcium carbonate filler.

### Vulcanized NR and SBR Soles

Although natural rubber (*crepe*) and nitrile rubber soles (common in the manufacturing of safety shoes due to its chemical inertness) are used, *sulfur-vulcanized natural rubbers* and *styrene-butadiene rubbers (SBR)* are the most common sole materials. The vulcanization system contains sulfur and activators (*N*-cyclohexyl-2-benzothiazole sulfenamide, dibenzothiazyl disulfide, hexamethylenetetramine, zinc oxide), and fillers (silica and/or carbon black, calcium carbonate) are added to control hardness and abrasion resistance. Antioxidants (zinc stearate, phenolic

antioxidant) and antiozonant (microcrystalline paraffin wax) are also necessary to avoid degradation processes and early aging. In general, vulcanization is carried out in a metal mold placed in hot plate press at about 180 °C for allowing the reaction of the zinc oxide and the stearic acid to produce zinc stearate, which is combined with hexamethylenetetramine to form an unstable complex. After vulcanization, the contact with moisture or different solvents apparently causes the breakdown of this complex with the appearance of the zinc stearate that migrates to the vulcanized NR or SBR sole which acts as an antiadherend material to polyurethane adhesive (Pettit and Carter 1964). On the other hand, during cooling after vulcanization, the paraffin wax migrates to the rubber surface also producing adhesion problems.

The causes of poor adhesion in vulcanized NR and SBR soles are quite diverse. Over-vulcanized external rubber layer is too stiff to support peel strength stresses. The presence of silicone release agents may reduce the bond strength of the vulcanized SBR sole joints. The presence of antiadherend moieties on their surfaces, their low surface energy, and the migration of low-molecular moieties (antiozonant wax, processing oils) to the interface once the adhesive joint is produced are other causes for the poor adhesion in vulcanized NR and SBR. The paraffin wax and zinc stearate are concentrated in a layer covering the vulcanized rubber surface with a thickness of about 2.0 µm. The factors favoring or inhibiting the migration of antiozonant wax to the vulcanized NR and SBR surfaces have not been fully understood. The temperature is one key factor that determines the migration of the antiozonant paraffin wax to the rubber surface. The antiozonant migration with the temperature in vulcanized rubber has been recently studied (Torregrosa-Coque et al. 2012) by heating at 40–90 °C for 15 h in an oven. The heating of vulcanized SBR at different temperatures caused a partial removal of paraffin wax from the surface, and at a temperature close to the paraffin wax melting point, the crystals of paraffin wax on the vulcanized SBR surface were melted, causing a decrease in the thickness of the paraffin wax film on the surface. Furthermore, the migration of zinc stearate to the paraffin wax layer on the vulcanized SBR surface occurred by heating at 90 °C, and even after heating at 90 °C, a thin film of paraffin wax always remained on the vulcanized SBR surface.

Time is another key factor that determines the migration of the antiozonant paraffin wax to the rubber surface causing the formation of a weak boundary layer of nonrubber contaminants which is deleterious for adhesion of rubber to polyurethane adhesives (Torregrosa-Coque et al. 2011a). Figure 7 shows the ATR-IR spectra of polyurethane coating on MEK surface cleaned vulcanized SBR just after application and after 2 weeks. The increase of the time favored the migration of paraffin wax which is noticed by the appearance of the methylene bands in the ATR-IR spectra of the vulcanized SBR at 2848, 2915, and 2950 cm<sup>-1</sup> on the polyurethane coating.

One of the key steps in the manufacturing of rubber/adhesive joints is reactivation, i.e., sudden heating of the thin adhesive layers on the substrates to be joined under infrared (IR) radiation to 80–90 °C for a few seconds to allow diffusion of the polymeric chains under pressure. This reactivation may cause the migration of low-molecular-weight additives to the rubber surface causing a lack of adhesion. The influence of the reactivation temperature (40–90 °C) on the surface properties of sulfur-vulcanized styrene–butadiene rubber on the extent of the diffusion of the

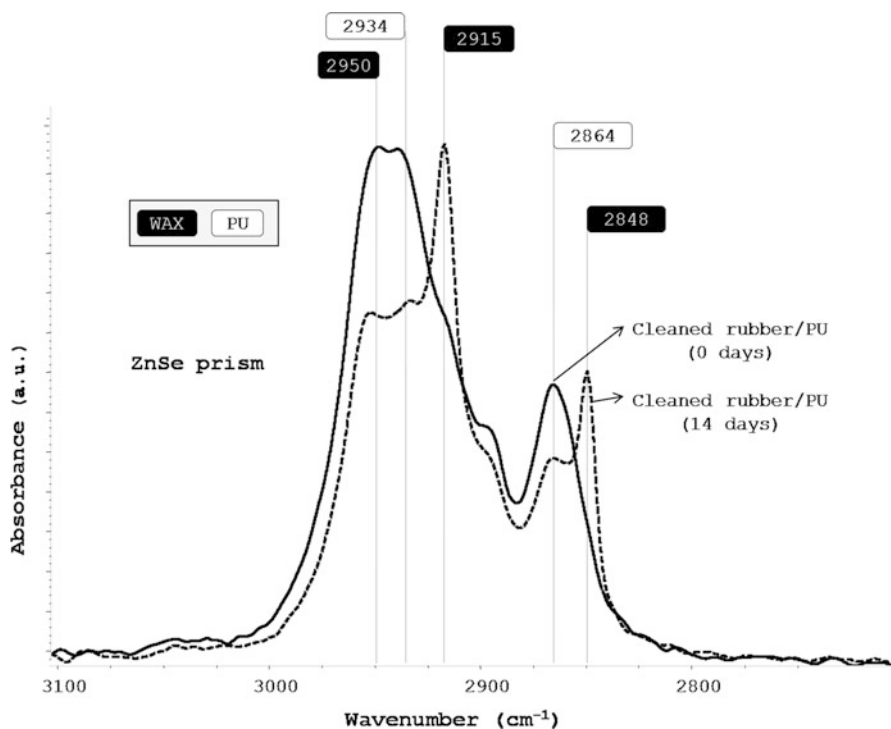


**Fig. 7** ATR-IR spectra obtained with ZnSe prism of polyurethane coating on MEK surface cleaned vulcanized SBR for different time after polyurethane coating deposition. 3100–2700  $\text{cm}^{-1}$  region (Torregrosa-Coque et al. 2011b)

paraffin wax and zinc stearate to the rubber surface has been studied (Torregrosa-Coque et al. 2011a). The reactivation of the rubber at different temperatures produced changes in the morphology and thickness of the paraffin wax layer on the surface. By increasing the reactivation temperature, a partial removal of paraffin wax was produced, and the thickness of the paraffin wax film on the rubber surface was reduced. On the other hand, the increase in the reactivation temperature increased the surface area of the melted paraffin wax layer that prevented migration from the rubber bulk, but a critical reactivation temperature at 90–100 °C existed at which the migration of zinc stearate to the paraffin wax layer on the rubber surface was favored. Furthermore, it has been demonstrated that the paraffin wax migrated from the vulcanized rubber bulk to the polyurethane–rubber interface, and, then, it diffused across the polyurethane coating and migrated later to the polyurethane coating surface (Torregrosa-Coque et al. 2011b). On the other hand, the extent of migration of the paraffin wax depended on the time after polyurethane adhesive deposition, and the faster migration was produced 1 h after applying the polyurethane adhesive.

The application of surface treatments to NR and SBR soles should produce improved wettability; creation of polar moieties able to react with the polyurethane adhesive, cracks, and heterogeneities should be formed to facilitate the mechanical

interlocking with the adhesive; and an efficient removal of antiadherend moieties (zinc stearate, paraffin wax, processing oils) has to be reached. Several types of surface preparation involving solvent wiping, mechanical and chemical treatments, and primers have been proposed to improve the adhesion of vulcanized NR and SBR soles. Chlorination with solutions of trichloroisocyanuric acid (TCI) in different organic solvents is by far the most common surface preparation for vulcanized NR and SBR.

Roughening of the SBR soles removes the over-vulcanized layer and surface contaminants (oils, molding release agents, antiadherend moieties, etc.) and creates roughness. After roughening, residues of the treatment must be removed by solvent wiping and/or the application of pressurized air. Although the removal of weak layers and the creation of surface heterogeneities may produce improved adhesion of the vulcanized NR and SBR soles, an additional chemical treatment is mandatory for achieving sufficient adhesive strength.

The soles can be chemically treated with concentrated sulfuric acid to improve their adhesion to polyurethane (Cepeda-Jiménez et al. 2000). This treatment is not restricted to the surface but also produces a bulk modification of the rubber because a decrease in the tensile strength and the elongation at break are caused. If the SBR contains paraffin wax, the treatment with sulfuric acid promotes its migration to the surface, and solvent wiping with petroleum ether is mandatory for obtaining good adhesion.

Several chlorinating agents have been used for SBR sole bonding. Acidified sodium hypochlorite aqueous solutions have been used successfully (Table 1), and the mechanism of chlorination has been established (Vukov 1984) that consists in the formation of  $\text{H}_2\text{ClO}^+$  species which produces the evolution of chlorine; then, the chlorine reacts with the double  $\text{C}=\text{C}$  bond of the rubber producing chlorinated hydrocarbon moieties on the surface and some cross-linking.

The most commonly used chlorinating agent in the chemical treatment of the SBR sole is ethyl acetate or MEK (butan-2-one) solution of trichloroisocyanuric acid (TCI). The organic solvent in the TCI solution determines the degree of rubber wetting, and the actual chlorinating species are  $\alpha$ -chloro ketones in TCI/MEK solutions, whereas acid chlorides are the reactive moieties in TCI/ethyl acetate solutions (Pastor-Blas et al. 2000). The reaction of these chlorinating species with the double  $\text{C}=\text{C}$  bonds of the rubber produces  $\text{C}-\text{Cl}$  species, and the reaction is not restricted to the surface, but it is penetrating about 100  $\mu\text{m}$  depth. On the other hand,

**Table 1** T-peel strength values (kN/m) of surface-chlorinated rubber/polyurethane adhesive/leather joints

Rubber	As-received	NaClO + HCl
SBR 1	1.8 (A)	5.6 (R)
SBR 2	0.2 (A)	14.0 (R)
SBR 3	0.9 (A)	7.8 (R)

A: Adhesion failure between the rubber and the adhesive  
R: Cohesive rupture of the rubber



the improved adhesion of the SBR soles treated with TCI solutions is due to the contribution of several mechanisms of adhesion: mechanical adhesion (cracks and pits are produced on the surface), chemical adhesion (chlorinated hydrocarbon, C=O moieties), removal of weak boundary layers (zinc stearate, paraffin wax), and thermodynamic adhesion (a decrease in contact angle is produced, i.e., improved wettability) (see ► Chap. 6, “Thermodynamics of Adhesion”). Furthermore, unreacted solid prismatic TCI crystals deposit during the application of the chlorination treatment on the SBR surface which can be dissolved in contact with the organic solvent in the polyurethane adhesive facilitating the creation of in situ reactive species.

The effectiveness of the chlorination treatment of the SBR soles with TCI solutions strongly depends on several experimental variables of the treatment (Martín-Martínez 2008). The most relevant ones are the application procedure of the TCI solution (brushing providing the best performance), the time between the application of the TCI solution and the polyurethane adhesive (a minimum of 10 min is necessary), the TCI concentration in the solution (less than 3 wt% TCI is recommended), and the roughening or solvent wiping before chlorination (more extensive treatment is produced).

The active chlorine content of the ethyl acetate solutions containing 3 wt% TCI determined the extent of the surface treatment of vulcanized SBR. The active chlorine concentration in the TCI solutions was not the only parameter determining the adhesion of vulcanized SBR, as the highest adhesive strength was not achieved by treating the rubber with the TCI solution with higher active chlorine content (García-Martín et al. 2010). Furthermore, the chlorine concentration in the TCI solutions was not stable in the course of time; the increase in time between TCI solutions preparation and SBR treatment allowed an increase in adhesive strength, the highest value corresponded to the joint produced with the vulcanized SBR treated with the TCI solution prepared for 60 days.

The influence of the temperature on the effectiveness of the chlorination treatment of vulcanized SBR with TCI solutions in organic solvents has been addressed. Vulcanized SBR was treated with 1 and 2 wt% TCI solutions in ethyl acetate and then thermally treated at 23 °C, 50 °C, or 65 °C for different time (Yin et al. 2012). Although this study was not intended for shoe industry, the results obtained revealed that the increase of the chlorination temperature up to 50 °C was very effective for SBR surface modification by TCI, leading to enhanced surface wettability, creation of chlorinated hydrocarbon moieties, and increased shear strength (from 2.0 to 9.7 MPa). However, later study (Yañez-Pacios et al. 2013) has shown that the application of temperature during chlorination of high antiozonant content vulcanized NR with TCI solutions in MEK did not increase the adhesion strength of the upper-to-sole joints. However, changes in wettability, surface chemistry, and roughness of the rubber were produced, all being irrelevant for improving adhesion likely due to the migration of antiozonants to the polyurethane adhesive-vulcanized NR interface with time after joint formation.

Due to organic solvent restrictions in the industry, aqueous chlorinating solutions have been tested as an alternative to TCI solutions in ethyl acetate or MEK. Aqueous



solutions of sodium dichloroisocyanurate (DCI) have been recently demonstrated to increase the adhesion of vulcanized SBR soles (Cepeda-Jiménez et al. 2002). The surface treatment with aqueous DCI solutions creates C–Cl moieties, removes antiadherend moieties from the SBR surface, and creates roughness. The use of a low DCI concentration in water is sufficient to obtain good peel strength values in SBR/waterborne polyurethane joints. Furthermore, vulcanized NR has been treated with aqueous sodium hypochlorite solution for various chlorination times up to 30 min (Radabutra et al. 2009). The degree of chlorination increased with the chlorination time up to 10 min then leveled off, but the roughness and stiffness increased gradually with chlorination time. The maximum peel strength was found at 1 min of chlorination time and decreased afterward because of the increase in the surface stiffness that acted as weak boundary layer.

As for TR, successful treatments of vulcanized NR and SBR soles with aqueous *N*-chloro-*p*-toluenesulfonamide solutions and electrochemical treatments have been reported at laboratory scale. Similarly, the treatment of SBR sole with oxidant inorganic salts (acidified potassium dichromate, potassium permanganate, Fenton's reactive) has been shown to be partially successful (Brewis and Dahm 2003).

*Primers* have also been used to improve the adhesion of SBR soles. Due to its high reactivity, isocyanate wipe has been proposed, but the most common treatment uses organic acid solutions. Solutions of lactic acid applied with stiff-bristled brush and with a scrubbing action are adequate to remove metal soap contamination (i.e., zinc stearate) on the surface of SBR sole and even replace roughening (Carter 1969). Solutions of different carboxylic acids (fumaric acid, maleic acid, acrylic acid, succinic acid, malonic acid) in ethanol have also been used as primers of SBR sole (Pastor-Sempere et al. 1995). The nature of the carboxylic acid determines the rate of diffusion into the polyurethane adhesive and the extent of rubber-adhesive interfacial interaction. Finally, mixtures of TCI and fumaric acid solutions have been tested in improving the adhesion of difficult-to-bond SBR sole, but it was demonstrated that the effectiveness of this treatment was mainly due to chlorination by TCI (Romero-Sánchez and Martín-Martínez 2003).

Treatment with supercritical fluids was also tested to remove zinc stearate and waxes from vulcanized SBR soles (Garelik-Rosen S, Torregrosa-Maciá R, Martín-Martínez JM (2003), unpublished results). The relative effectiveness of this treatment was ascribed to the dissolution of antiadherend moieties by penetration of the fluid into the rubber surface.

An alternative to water-based treatment is the use of low-pressure RF gas plasmas in the enhancement of the adhesion of vulcanized rubbers. The treatment in oxygen plasma for 1 min is enough to noticeably increase the adhesion of vulcanized SBR sole to polyurethane adhesive (Pastor-Blas et al. 1998). Later, three different configurations (direct, etching, and secondary downstream) of low-pressure RF oxygen plasmas for length of treatment between 1 and 10 min were used to modify the surface of vulcanized SBR (Torregrosa-Coque and Martín-Martínez 2011c). The direct oxygen plasma was the most aggressive treatment and the secondary downstream plasma the less one, and the oxygen plasma treatment caused surface oxidation and ablation on the SBR surface, as well as an increase of the temperature

that also determined the extent of paraffin wax migration which was produced for at least 24 h after oxygen plasma treatment; as a consequence, poor adhesion to polyurethane adhesive was obtained, due to the creation of a weak boundary layer of paraffin wax at the rubber–polyurethane interface.

Vulcanized ethylene propylene diene polymethylene (EPDM) rubber surface was treated with low-pressure RF argon–oxygen plasma to improve adhesion with compounded natural rubber (NR) during co-vulcanization (Basaka et al. 2011). The plasma treatment changed both surface composition (formation of C–O and C=O functional groups) and roughness of EPDM rubber, and consequently increased peel strength was obtained. In a different study, vulcanized NR containing intentionally noticeable excess of processing oils in its formulation was treated with argon–oxygen (Ar–O<sub>2</sub>) (2:1, vol/vol) low-pressure plasma for achieving a satisfactory level of adhesion to waterborne polyurethane adhesive (Cantos-Delegido and Martín-Martínez 2015). The effectiveness of the Ar–O<sub>2</sub> low-pressure plasma treatment depended on both the configuration of the plasma chamber shelves and the treatment time, the direct configuration provided the most effective surface modification of the vulcanized NR. However, even important surface modifications were produced by Ar–O<sub>2</sub> low-pressure plasma treatment, adhesion was not improved due to the creation of weak boundary layer at the polyurethane–rubber interface after joint formation. Heating at 80 °C for 12 h prior to Ar–O<sub>2</sub> low-pressure plasma treatment enhanced the extent of the surface modifications, and improved adhesion was obtained for treatment times higher than 600 s.

*Atmospheric plasma torch treatment* of vulcanized NR with different excess of paraffin wax and processing oils was carried out for improving adhesion to waterborne polyurethane adhesive (Kotrade et al. 2011). Similar chemical modifications (new C=O and C–N functional groups) and roughness were produced by plasma torch treatment in all rubbers, and the best results were obtained at a rubber surface nozzle of the plasma torch distance of 5 mm and a platform speed of 1 m/min. However, although the rubber surfaces were effectively modified by plasma torch, the adhesion to waterborne polyurethane adhesive was not improved. In a different study (Moreno-Couramjou et al. 2009), vulcanized NR was treated by atmospheric dielectric barrier discharges to improve its adhesion to silicone adhesive. The atmospheric plasma treatment with the use of allyl alcohol improved noticeably the adhesion by a factor of 10 due to the preferential formation of C–O bonds.

More recently the treatment with UV radiation combined with ozone (UV–ozone) in improving the adhesion of difficult-to-bond vulcanized NR (it contained an excess of processing oils) to waterborne polyurethane adhesive in footwear has been carried out (Moyano and Martín-Martínez 2014). Both the length of the treatment and the distance between the UV radiation source to the rubber surface were varied, and the effects of the treatment on the surface chemistry, wettability and surface energy, and topography of the rubber were analyzed. The treatment of the vulcanized rubber with UV–ozone removed hydrocarbon moieties and zinc stearate from the surface, surface oxidation (C–O, C=O, and COO- groups formation) occurred, and improved wettability and increased surface energy (mainly due to the polar component) were obtained. The UV–ozone surface treatment also caused heating of the surface and

increased the adhesion of the vulcanized rubber to waterborne polyurethane adhesive; the highest adhesion was obtained in the joints made with UV–ozone-treated rubber for 3 and 6 min at a UV radiation source–rubber surface distance of 5 cm.

### Polymeric Soles

Ethylene–vinyl acetate (EVA) block copolymer soles are common in sport and casual shoes due to their low density and easy coloring. EVA soles are difficult to bond with the polyurethane and polychloroprene adhesives commonly used in shoe industry, mainly due to their low surface energy. The higher the vinyl acetate content, the less difficult to bond the EVA sole is. The lightweight microcellular EVA soles can usually be adequately bonded after scouring using polyurethane and polychloroprene adhesives. The injection-molded EVA soles are more difficult to bond although roughening followed by application of two-component polychloroprene adhesive can give moderate bond strength (Martínez-García et al. 2003a). Corona discharge has been shown to be useful to improve the peel strength of injection-molded EVA soles containing 12 and 20 wt% vinyl acetate/polychloroprene adhesive joints. The improvement is ascribed to the creation of C=O and R-COO<sup>−</sup> moieties. Treatment with sulfuric acid also provided improved adhesion of injection-molded EVAs with vinyl acetate contents between 9 and 20 wt%, because this treatment produces sulfonation and creation of oxygen moieties on EVA surface (Martínez-García et al. 2003b). Oxygen and other gases low-pressure plasmas are very effective in improving the peel strength of joints produced with EVA soles with different vinyl acetate contents and two-component polyurethane adhesive (Cepeda-Jiménez et al. 2003b). The treatment is more effective with non-oxidizing plasmas, giving rise to a high roughness. Finally, the treatment with UV–ozone has been developed to enhance the bond strength between EVA sole and polyurethane adhesive (Landete-Ruiz and Martín-Martínez 2005). The surface modifications produced by UV–ozone treatment of two ethylene–vinyl acetate (EVA) copolymers containing 12 (EVA12) and 20 wt% (EVA20) vinyl acetate have been studied (Landete-Ruiz and Martín-Martínez 2015). The treatment with UV–ozone improved the wettability of both EVAs due to the creation of new carbon–oxygen moieties, and the extent of these modifications increased with increasing the time of treatment; the modifications produced in EVA20 were produced for shorter lengths of treatment. The UV–ozone treatment also created roughness and heterogeneities, and whereas roughness formation prevailed on the UV–ozone-treated EVA12, important ablation was dominant on the treated EVA20. T-peel strength values in joints made with polychloroprene adhesive increased. Short length of UV–ozone treatment (1 min) produced higher T-peel strength in joints made with EVA20, whereas higher T-peel strength values in joints made with EVA12 were obtained after treatment for 5–7.5 min in which a cohesive failure into a weak boundary layer on the treated EVA surface was found. Finally, the aging resistance of the treated EVA/polychloroprene adhesive joints was good, and the surface modifications on the UV–ozone-treated EVAs lasted for 24 h after treatment at least.

Ethylene–vinyl acetate (EVA) copolymers intended for sport sole manufacturing may contain noticeable amounts of low-density polyethylene (LDPE) – *Phylon*-type

soles – for improving abrasion resistance and decreasing cost; however, the EVA–PE blend had low polarity and showed poor adhesion. Good results have been obtained by applying extensive organic solvent wiping, followed by application of an UV-activated primer and by using two-component polyurethane adhesive. More recently, an effective environmental-friendly and fast surface treatment based on UV–ozone has been used to increase the wettability, polarity, roughness, and adhesion of EVA–PE material to leather with waterborne polyurethane adhesive (Jofre-Reche and Martín-Martínez 2013). The more extended length of treatment and the shorter UV source–substrate distance increased the wettability and created new carbonyl groups mainly, and the amounts of hydroxyl and carboxylic groups were increased. The UV–ozone treatment produced ablation and etching of the EVA–PE material surface, mainly in the vinyl acetate of the EVA; this topography was also caused by heating during UV–ozone treatment. For low length of UV treatment or high UV source–material distance, the modifications of the EVA–PE material were mainly produced in the ethylene causing the selective removal of vinyl acetate, whereas more aggressive conditions produced strong oxidation in the EVA–PE material. Finally, adhesive strength was noticeably increased in the UV–ozone-treated EVA–PE/polyurethane adhesive joints, and a cohesive failure in the leather was obtained.

Only polyurethane adhesives should be used to bond *PVC soles*. The adhesion problems of PVC derive from the presence of plasticizers and stabilizers (stearate type) able to migrate to the surface impeding the contact with the adhesive (creation of weak boundary layers). A solvent wiping on the PVC surface is usually effective in improving adhesion, and solvents such as MEK are adequate. On the other hand, treatment with 10 wt% aqueous solutions of sodium hydroxide has been successfully applied to increase the adhesion performance of plasticized PVC soles (Abbott et al. 2003).

*Polyurethane soles* usually contain silicone mold release agents which prevent adhesion. To remove them, mild roughening following by solvent wiping is necessary. The application of an isocyanate primer is very useful before polyurethane adhesive is applied. Solvent-free treatments have been proposed for polyurethane soles, mainly cryoblasting (Abbott et al. 2003). Cryoblasting consists in the bombardment of the PVC soles with particles of solid carbon dioxide at pressures about 0.4 MN/m<sup>2</sup>. The impact of the solid particles successfully removed mold release agents from the polyurethane surface improving their adhesion to polyurethane adhesive.

### 51.3.3 Adhesives in Upper-to-Sole Bonding

Contact adhesives based in one- and two-component polychloroprene (*neoprene*) and mainly polyurethane adhesives are the most commonly used in shoe industry to bond upper to sole (see ► Chaps. 14, “Adhesive Families,” and ► “Sealant Families”). These adhesives are bonded by autoadhesion which implies the application of the adhesive to both surfaces to be joined; diffusion of polymer chains must be achieved across the interface between the two adhesive films on the substrates to be

joined to produce intimate adhesion at molecular level. To achieve an optimum diffusion of the polymer chains, both high wettability and adequate viscosity and rheology of the adhesive should be achieved.

In the past, polychloroprene adhesives were more extensively used in upper-to-sole bonding, but nowadays polyurethane adhesives are preferred. Polychloroprene adhesives have better tack and improved wettability than polyurethane adhesives, but the polychloroprene adhesives are not compatible with the surface-treated rubber soles and cannot be used to joint PVC soles. Therefore, polyurethane adhesives show higher versatility on broader range of substrates and also have lower oxidative degradation in time. However, they require always the surface preparation of the materials to be bonded.

### 51.3.4 Polyurethane Adhesives

In 1960s, the solvent-borne polyurethane adhesives replaced the polychloroprene adhesives in the bonding of PVC soles for sport shoes. Today, the use of solvent-borne polyurethane adhesives is in decline due to environmental regulations and safety issues. Shoe industry was initially reluctant to the use of waterborne polyurethanes due to higher cost and reduced green strength. However, the use of waterborne polyurethanes is more common nowadays because their solid content is high and small amount of adhesive is needed to produce a similar joint than with solvent-borne adhesives. On the other hand, during the last decade, solvent-free polyurethane adhesives have been tested in shoe bonding. Although these adhesives have been widely used and effectively tested in the automotive industry, the advent in the shoe manufacturing is not as successful, likely because different machinery and bonding concepts need to be implanted. Shoe industry is, in general, quite reluctant to change bonding technologies, particularly when it implies a cost increase!

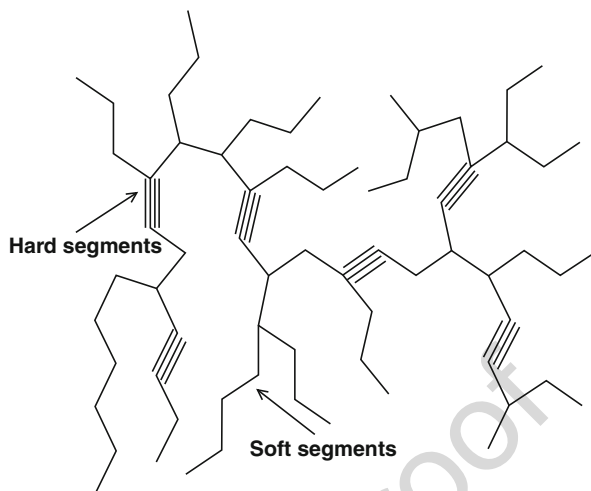
In this section, the solvent-borne, the waterborne, and the solvent-free polyurethane adhesives will be considered separately.

#### Solvent-borne Polyurethane Adhesives

Elastomeric thermoplastic polyurethanes are the main components in solvent solution adhesives for shoe industry. These polyurethanes are generally prepared in the form of pellets or chips by reacting an isocyanate (such as MDI – 4,4'-diphenylmethane diisocyanate), a long-chain diol (polyester or  $\epsilon$ -caprolactone type), and a chain extender (glycol) to produce a linear polymer with negligible chain branching and relatively low-molecular-weight ( $M_w = 200.000\text{--}350.000$  Da). The isocyanate to hydroxyl equivalent ratio (NCO/OH ratio) is usually kept near 1, thus producing a polymer with terminal hydroxyl groups which are able to form hydrogen bonds with the urethane moieties.

From a polymer physics point of view, the configuration of the elastomeric polyurethanes corresponds to a segmented structure (block copolymer of  $(AB)_n$  type) consisting of *soft* and *hard* segments (Fig. 8). Typically the *soft* segments are

**Fig. 8** Scheme of the segmented structure of thermoplastic polyurethane



composed of a rubbery polymer (mainly the polyol), the glass transition temperature ( $T_g$ ) which is located well below ambient temperature. The *hard* segments are generally produced by the reaction of the isocyanate and the short chain glycol (chain extender) and have a rigid and crystalline structure. The nonpolar low-melting *soft* segments are incompatible with the polar high-melting *hard* segments. As a result, phase separation (segregation) occurs in the polymer network.

Typical elastomeric polyurethanes used as adhesives in upper-to-sole bonding have a relatively low content of hard segments, and their properties are mainly determined by the soft segments. Therefore, these polyurethanes will be elastic in the range of temperature between the glass transition temperature (generally located between  $-30$  and  $-40$  °C) and the softening temperature of the elastomeric domains ( $50$ – $80$  °C). The low melting point permits the elastomeric polyurethane to be softened at relatively low temperature, with sufficient thermoplasticity (i.e., loss of cohesion at moderate temperature) and surface tack to ensure correct bond.

Solvent-borne polyurethane adhesives are generally prepared by dissolving the solid elastomeric polyurethane pellets or chips in a solvent mixture. Because polyurethanes have a linear molecular structure, the solid polymer does not need mastication prior to dissolving. The solubility of the elastomeric polyurethanes in ketone solvents is mainly governed by the degree of crystallinity in the polyester soft segments. The crystallinity can be varied by selecting the reactants and by controlling the molecular weight of the polyester. Generally, the elastomeric polyurethanes with low crystallization rates have long open times but poor peel strength and heat resistance. Those polyurethanes with high rates of crystallization have short open times but high peel strength and improved heat resistance. For this reason, mixtures of low and high crystallization rate polyurethanes are used to balance the open time and adhesion of the solvent-borne adhesives.

The solvents determine the viscosity and solubility of the elastomeric polyurethane, its storage stability, its wetting properties, and its evaporation rate when



applied on a substrate. The most common solvents are aromatic (toluene, xylene), tetrahydrofuran, dioxane, cyclohexanone, esters (ethyl acetate, butyl acetate), and ketones (acetone, methyl ethyl ketone). Commonly, two or more solvents are employed, a low-boiling and a high-boiling solvent. The low-boiling solvent assures rapid flash-off of the majority of the solvent after applying the adhesive solution on the substrate. The higher-boiling solvent helps to control the crystallization kinetics of the soft segments, thereby helping to extend the open time of the adhesive. In fact, once crystallization of the soft segments occurs, the open time expires. Other function of the high-boiling solvent is to keep the viscosity of the adhesive low (this is the reason for being called diluents), allowing the adhesive solution to wet the substrate by facilitating the polyurethane to penetrate the substrate surface, thus improving the mechanical interlocking. On the other hand, the addition of toluene avoids gel formation of the adhesive solutions during storage.

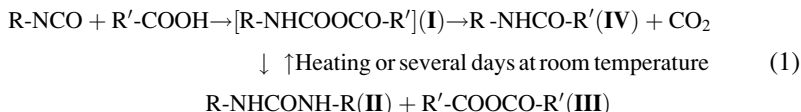
The formulation of the solvent-borne polyurethane adhesives may include several additives such as tack and heat resistance modifiers, plasticizers, fillers, tackifiers, antihydrolysis agents, and cross-linkers. Carboxylic acid as an adhesion promoter can also be added. A typical formulation of a solvent-borne polyurethane adhesive contains less than 20 wt% solid content only.

The spotting tack and/or the heat resistance of the elastomeric polyurethane adhesives may be extended by adding resins (alkyl phenolic, epoxide, terpene phenolic, coumarone) or polymers (low-crystallizing polyurethane, acrylic, nitrile rubber, chlorinated rubber, acetyl cellulose) (Penczek and Nachtkamp 1987) having low miscibility with the polyurethane. To improve adhesion together with heat resistance, reactive alkyl phenolic resins, chlorinated rubber, or other chlorine-containing polymers can be added.

The main additives used in the formulation of solvent-borne polyurethane adhesives are described in more detail below.

**Tackifiers.** One of the limitations of the elastomeric polyurethane adhesives is the lack of high immediate (green) adhesion to rubbers and polymers. One way to increase the green strength of the elastomeric polyurethanes is the addition of tackifiers mainly rosins or hydrocarbon resins (Arán-Aís et al. 2002). Addition of rosin as internal tackifier (i.e., incorporated during the synthesis of the polyurethane) favors the miscibility between the tackifier and the polyurethane. The hard segment content of the elastomeric polyurethanes containing rosin is higher than in regular polyurethanes because two kinds of hard segments are produced, urethane and urea–amide (this is produced by reaction of the isocyanate groups with the carboxylic acid of the rosin). Addition of rosin increases the molecular weight of the polyurethane and retards its kinetic of crystallization, and the immediate adhesion to vulcanized SBR sole is also increased.

A model system (phenyl isocyanate and acetic acid) has been studied to understand the reaction between the isocyanate group and the rosin (Irusta-Maritxalar ML, Fernández-Berridi MJ (2002), personal communication). The expected by-products of the reaction of the isocyanate and the carboxylic acid moieties are given in Eq. 1:



An unstable intermediate carbo-anhydride is formed (compound **I**), which under heating decomposes to produce urea (compound **II**) and anhydride (compound **III**) derivatives. These two compounds react by heating or by standing several days at room temperate to produce an amide compound (compound **IV**).

**Fillers.** Fillers should be highly dispersible in solution and should not settle down during the storage period of the adhesive. Whiting, talc, barite, calcium carbonate, attapulgit, and quartz flour have been suggested as fillers to lower the cost of the solvent-borne polyurethane adhesive, improve joint filling, and reduce the loss of adhesive during setting. In general, the fillers are incorporated during the preparation of the adhesive solutions by adding a small amount of solvent under high stirring speed for a short time, followed by addition of the other ingredients of the adhesive and all solvent under lower stirring rate and longer time (Maciá-Agulló et al. 1992).

*Pyrogenic (fumed) silicas* are the most common fillers of the polyurethane adhesives in shoe industry. When bonding highly porous materials (leather, textiles), fumed silicas are added to prevent undesirable penetration of the adhesive. The addition of the fumed silica adjusts the viscosity and rheology (thixotropy, pseudoplasticity) for application of the polyurethane adhesive solutions. The rheological properties of the polyurethanes containing fumed silica are due to the creation of hydrogen bonds between the silanol groups on the fumed silica particles and the urethane and carbonyl groups of the polymer, which increase the mechanical and rheological properties of the adhesives (Jauregui-Beloqui et al. 1999; Vega-Baudrit et al. 2009; Bahattab et al. 2011, 2012; Donate-Robles et al. 2014). Consequently, the cohesion properties of the polyurethane are increased, and improved initial peel strength is obtained, in a greater extent by increasing the amount of fumed silica (Bahattab et al. 2012). Several parameters of the fumed silica determine its performance as rheological additive of solvent-borne polyurethane adhesives. Low particle size and degree of agglomeration, specific surface areas between 200 and 300 m<sup>2</sup>/g, and the hydrophilic nature of fumed silicas increase the rheological, mechanical, and adhesion properties of the solvent-borne polyurethane adhesives (Pérez-Limiñana et al. 2003; Bahattab et al. 2011).

*Calcium carbonate* fillers have also been added to solvent-borne polyurethane adhesives for improving their mechanical properties and initial adhesion (Donate-Robles and Martín-Martínez 2011a, b). The addition of precipitated calcium carbonate (PCC) filler produced a moderate increase in the rheological and viscoelastic properties of the polyurethane due to the poor dispersion of filler and the weak interactions between the PCC nanoparticles and the polymer chains. Furthermore, the first glass transition temperature of the polyurethane decreased by adding PCC filler and the crystallinity of the soft segments as well, because of the disruption of the degree of phase separation in the polyurethane. The initial adhesive strength in

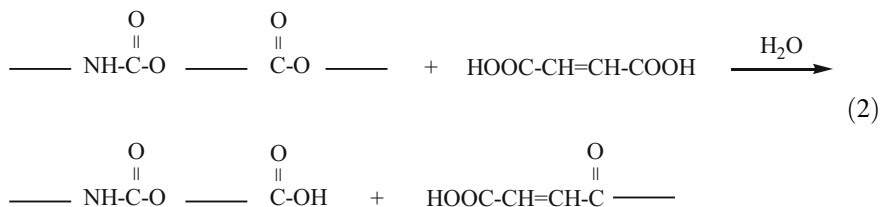


PVC/polyurethane adhesive/PVC joints increased noticeably by adding PCC filler; the greater the amount of filler, the greater the initial adhesive strength, and the highest final adhesive strength (72 h after joint formation) was obtained in the joint produced with the solvent-borne polyurethane adhesive containing 10 wt% PCC. The thermoplastic polyurethane–calcium carbonate interactions have been studied by using flow microcalorimetry and diffuse reflectance Fourier transform infrared spectroscopy (Donate-Robles et al. 2014). Three calcium carbonates (coated and uncoated precipitated calcium carbonate and natural ultramicrosized uncoated calcium carbonate) were added to solvent-borne polyurethane adhesives, and stronger polyurethane–filler interaction was shown in the uncoated precipitated calcium carbonate due to the fact that more of the surface was available for interaction. In fact, the polyurethane strongly adsorbed onto untreated calcium carbonate via the ester groups, and the stearate treatment of calcium carbonate greatly reduced the strength of interaction with the polyurethane due to blockage of the surface adsorption sites.

Nanometric *carbon black* (CB) filler has been added to solvent-borne polyurethane adhesives for improving adhesion. The CB and the polyurethane pellets were adequately dispersed in methyl ethyl ketone matrix, and an increase in the number and size of the carbon black aggregates in the polyurethane matrix was obtained by increasing the carbon black loading (Alvarez-García and Martín-Martínez 2015). The addition of the carbon black improved the rheological and viscoelastic properties of the adhesive, and the addition of higher amounts of CB changed the viscoelastic behavior of the polyurethane which became mainly elastic. On the other hand, the addition of CB loadings up to 12 wt% increased the thermal stability of the polyurethanes and increased their elongation at break without noticeable reduction in tensile strength. However, the polyurethane adsorbs less carbon black than fumed silica and calcium carbonate due to less accessible surface groups due to the presence of relatively important amount of micropores (Donate-Robles et al. 2014).

*Carboxylic acids.* It has been shown that improved adhesion can be obtained in joints produced with solvent-borne polyurethane adhesives containing small amount of different carboxylic acids. These carboxylic acids can be aliphatic or aromatic, can be unsaturated or saturated, may contain one or more carboxylic acid functionalities, and have hydroxyl, carbonyl, or halogen groups. Fumaric and maleic acids are the most common carboxylic acids added to the solvent-borne polyurethane adhesives for the joining of vulcanized SBR sole.

The effectiveness of the carboxylic acid as adhesion promoter is governed by its compatibility with the polyurethane and the solubility in the organic solvent selected to dissolve the polyurethane. It has been established (Pastor-Sempere et al. 1995) that the mechanism by which adhesion of SBR is increased is due to the carboxylic acid migration to the polyurethane adhesive surface once the adhesive joint is formed, removing zinc stearate and paraffin wax from the rubber surface. On the other hand, the carboxylic acid reacts with the polyurethane in the presence of a tiny amount of water which results in chain cleavage and disruption of polyurethane crystallinity (Eq. 2).



The addition of carboxylic acid decreases the molecular weight, tensile strength, and glass transition temperature of the polyurethane more markedly upon increasing the time after the adhesive is prepared and more noticeably for high amounts of carboxylic acid. As a consequence, lower viscosity of the polyurethane adhesive solutions and smaller peel strength values are obtained. The increased amount of the carboxylic acid in the solvent-borne polyurethane adhesive enhances its bond strength to SBR until a maximum value is reached. On the other hand, the nature of the polyurethane determines the degree of effectiveness of the carboxylic acid on adhesion of vulcanized rubber.

**Cross-linkers.** Polyisocyanates with functionality greater than two (such as p, p'', p''' – triisocyanate triphenylmethane, thiophosphoric acid tris(p-isocyanatophenyl) ester) can be added to improve specific adhesion and heat resistance of the polyurethane adhesives (especially those with slower crystallization rate). Most of them have 20–30 wt% solids and 5.4–7 wt% free NCO, and the most common solvent is ethyl acetate. About 5–10 wt% polyisocyanate is generally added in the adhesive solution just before application on the substrate, and it acts as cross-linking agent. Since all isocyanates react with the residual hydroxyl groups on the polyurethane, in solution they yield adhesive systems with a limited pot life (1–2 h to several days). The addition of the polyisocyanate improves the spotting tack and the heat activation of the freshly dried adhesive films, but after several days they lose their capacity to be reactivated.

In finished bonds, the elastomeric polyurethanes show a relatively low cross-link density and then are exposed to outstanding hydrolytic degradation under high humidity and temperature that can lead to a partial or complete loss of strength during shoe use. The hydrolytic degradation of the polyurethane can be inhibited by adding 2–4 wt% carbodiimide to the adhesive solution because the carbodiimide forms acyl ureas by reaction of the carboxyl groups arising from the hydrolytic degradation of the polyurethane (Dollhausen 1988).

### Waterborne Polyurethane Adhesives

Organic solvents are, in general, volatile, flammable, and toxic, in some degree. Further, organic solvent may react with other airborne contaminants contributing to smog formation and workplace exposure. Although solvent recovery systems and afterburners can be effectively attached to ventilation equipments, many shoe factories are switching to the use of waterborne adhesives.

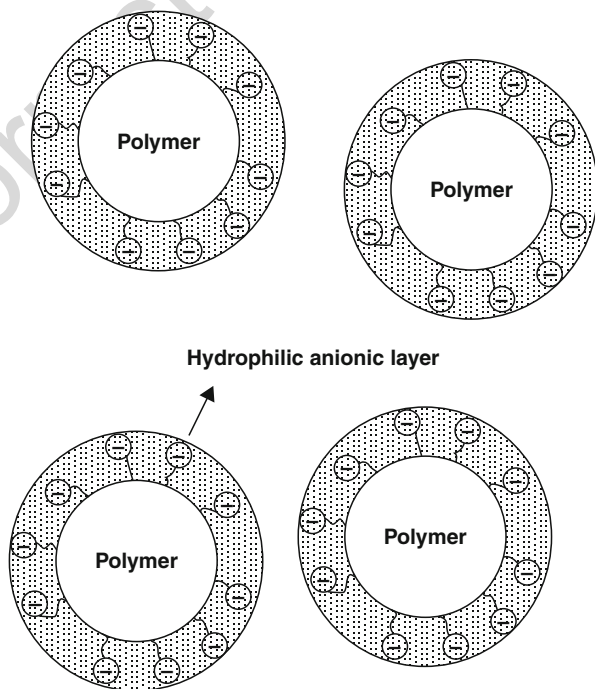
Waterborne polyurethane adhesives are an environmental-friendly alternative to the solvent-borne polyurethane adhesives. Those are the more logical choice to replace the solvent-borne adhesives because they can be processed on the same

machines, their performance in many applications is just as good as that of solvent systems, and they can be used economically despite their higher raw material and processing costs. However, the use of the waterborne polyurethane adhesives needs some minor changes in the current existing technology, essentially the additional heat required to remove water before joint formation. Furthermore, the waterborne polyurethane adhesives show additional limitations: (i) lack of tackiness at room temperature (heat activation is needed), (ii) poor wettability of some substrates (particularly greased leather), and (iii) polyurethane dispersions are thermodynamically unstable, and therefore they show relatively poor storage stability (dispersion collapses in the presence of metallic contaminants, at low temperature (generally below 5 °C), or by applying high stresses).

The polyurethane dispersions are constituted by urethane polymer particles wholly dispersed in water. The dispersion of the polymeric particles is feasible because of the presence of ionic hydrophilic groups chemically bonded to the main polymer chains which are oriented to the surface of the particles (Fig. 9). These dispersions are based on crystalline, hydrophobic polyester polyols (such as hexamethylene polyadipate), and aliphatic isocyanates (such as  $H_{12}$ MDI – methylene bis(cyclohexyl isocyanate) – or IPDI, isophorone diisocyanate).

There are several routes to produce polyurethane dispersions, the two most common are the so-called acetone and prepolymer methods. In the *acetone method*, the polyol, the anionic internal emulsifiers (such as dimethylolpropionic acid or

**Fig. 9** Scheme of the structure of waterborne polyurethane adhesive



diethylamine sodium sulfonate), and the isocyanate are reacted to obtain a prepolymer with hydrophilic groups (García-Pacios et al. 2010). The prepolymer is dissolved in acetone for decreasing viscosity, and the ionic groups are neutralized by addition of an amine (trimethylamine is generally used to neutralize the carboxylic acid moieties). The chain extension of the prepolymer is carried out by addition of or diol; both hydrazine and ethylene diamine are commonly used as chain extenders because of their faster reaction with isocyanates than with water. Then, water is added for obtaining the polyurethane micelles by phase inversion, and the acetone is removed by distillation at reduced pressure. In the *prepolymer method*, two basic steps are needed in order to produce a waterborne polyurethane dispersion: a prepolymer step and a chain extension step. The prepolymer obtained by reacting the polyol and the aliphatic isocyanate is modified through an internal emulsifier containing hydrophilic groups, thereby eliminating the use of external emulsifiers. The prepolymer containing the internal emulsifier is reacted with a tertiary amine (such as triethylamine) to increase the length of the polymer chain and increase the molecular weight of the polyurethane. The amine reacts with the pendant carboxylic acid groups, forming a salt that under adequate stirring allows the dispersion of the prepolymer in water. The chain extension step takes place in the water phase. The waterborne polyurethane dispersions obtained by the acetone and the prepolymer methods contain high-molecular-weight polyurethane chains, and they have polyurethane and polyurea linkages.

The method for preparing the waterborne polyurethane dispersions determines their properties, and it has been scarcely studied. In general, the acetone method produces more homogeneous anionic dispersions and well-controlled polyurethane structure. It has been shown that the method of synthesis determined the mean particle size, the crystallinity, and the viscosity of the waterborne polyurethane dispersions (Barni and Levi 2003). In later study it has been shown that the acetone method produced dispersions with narrower particle size distributions and higher crystallinity than the prepolymer method, and the adhesive strength was similar in the joints made with waterborne polyurethane dispersions prepared with both methods (Pérez-Limiñana et al. 2006).

The waterborne polyurethane dispersions generally have a pH between 6 and 9 and higher solid content (35–50 wt%) and lower viscosities (about 100 mPa.s) than the solvent-borne polyurethane adhesives. They are high-molecular-weight linear polyester ureas or urethanes constituted by small rounded spherical particles of about 0.1–0.2  $\mu\text{m}$  diameter.

The adhesive characteristics of the waterborne polyurethanes are mainly defined by the melting point and the crystallization kinetics of the polymer backbone. It is highly desirable to activate the adhesive at room temperature, but most of the waterborne polyurethane adhesives have melting point above 55 °C and need reactivation. The crystallization kinetics defines the open time of the adhesive. On the other hand, unlike solvent-borne adhesives, the viscosity of waterborne polyurethane adhesives is not dependent on the molar mass of the polymer but on the solids content, average particle size of the dispersion, and the existence of additives in the formulation.

The adhesion properties of the waterborne polyurethane adhesives are greatly determined by the polymer, and the formulations are generally simple including only small amounts of a thickener and an emulsifier. When formulating the waterborne polyurethane adhesives, the application conditions (heat activation, contact bond time, pressure) and substrate type must be taken into account. Because the properties of the waterborne polyurethane adhesives are mainly determined by the structure of the polyurethane, several studies analyzing the influence of different raw materials and the experimental variables of the synthesis procedure have been published. It has been concluded that the content of ionic groups, the hard-to-soft segment ratio, the nature and molecular weight of the polyol, the nature of the chain extender, the degree of neutralization of the prepolymer, and the nature of the counterion determined the properties of the waterborne polyurethane dispersions (Kim and Lee 1996; Jang et al. 2002).

Several studies have considered the influence of the *hard-to-soft segments or NCO/OH ratio* on the properties of the waterborne polyurethane dispersions. Most studies have shown that the increase in the NCO/OH ratio increased the mean particle size and enhanced the viscoelastic properties of the polyurethane dispersions (Pérez-Limiñana et al. 2007; García-Pacios et al. 2010; Vicent and Natarajan 2014). The variation of the viscosity of the waterborne polyurethane dispersion with the NCO/OH ratio is controversial. García-Pacios et al. (2011a) found that the increase in the NCO/OH ratio in waterborne polyurethane dispersions prepared with polycarbonate diol decreased the mean particle size and increased the Brookfield viscosity of the dispersions; however, the opposite trend was described previously (Madbouly et al. 2005). On the other hand, the increase in the NCO/OH ratio increases the urea and urethane hard-segment content in the polyurethane, and, therefore, the mechanical properties (i.e., Young's modulus and tensile strength) and the glass transition temperature increased by increasing the NCO/OH ratio of the waterborne polyurethane dispersion. On the other hand, the NCO/OH ratio affected the T-peel strength and single-lap shear adhesive strength of the waterborne polyurethane adhesives, and a maximum value is obtained for an NCO/OH ratio of 1.5 (García-Pacios et al. 2011a).

The influence of the nature, the structure, and the amount of the *diisocyanate* on the properties of waterborne polyurethane adhesives has been extensively studied. The cycloaliphatic diisocyanates (methylene bis(cyclohexyl isocyanate) – H<sub>12</sub>MDI – isophorone diisocyanate, IPDI) are the most commonly used because of the controlled reactivity during prepolymer formation. It has been shown that the waterborne polyurethane dispersions prepared with IPDI had lower mean particle size but lower mechanical properties than the ones prepared with H<sub>12</sub>MDI (Kim et al. 1994). Aromatic diisocyanates such as MDI and TDI have been used for preparing waterborne polyurethane dispersions, and they showed higher thermal and mechanical properties than the ones prepared with cycloaliphatic diisocyanates (Yang et al. 1999). Mixtures of aliphatic and aromatic diisocyanates have been used for preparing waterborne polyurethane dispersions, and the mechanical properties and adhesive strength were higher in the polyurethane made with MDI and lower with the one prepared with H<sub>12</sub>MDI (Rahman et al. 2014). However, after accelerated aging in

1070 salt water, the mechanical strength and adhesive strength were better in the poly-  
1071 urethanes prepared with mixture of H<sub>12</sub>MDI and MDI diisocyanate.

1072 The nature (diol, diamine), chain length, and amount of the *chain extender*  
1073 determined the properties of the waterborne polyurethane dispersions. The diol  
1074 chain extender produced polyurethanes with high degree of phase separation, higher  
1075 crystallinity, and good adhesive strength; this later is higher by increasing the chain  
1076 length of the diol (Orgilés-Calpena et al. 2016a). On the other hand, the diamine  
1077 chain extenders produced polyurea-urethanes that show lower crystallinity, lower  
1078 degree of phase separation, and lower peel strength than the ones prepared with diol  
1079 chain extenders (Rahman 2013).

1080 With respect to other raw materials, the *polyol* determines in greater extent the  
1081 properties of the waterborne polyurethane adhesives. The increase in the molecular  
1082 weight of the polyol (i.e., soft segments) produces dispersions with lower mean particle  
1083 size and increased toughness and elongation at break (Mumtaz et al. 2013), but both the  
1084 hardness and tensile strength decrease (Wang et al. 2015). On the other hand, the peel  
1085 strength decreases by increasing the molecular weight of the polyol (García-Pacios  
1086 et al. 2013a). The nature of the polyol (polyester, polyether, polycarbonate diol,  
1087 polycaprolactone) determines the degree of phase separation in the polyurethane and  
1088 affects noticeably the properties of the waterborne polyurethane dispersions. Because  
1089 of the existence of carbonate groups, the use of polycarbonate diol produces lower  
1090 degree of phase separation and increased shear adhesion with respect to the use of  
1091 polyester and polyether (García-Pacios et al. 2013b). More recently the polyols derived  
1092 from natural oils have been used for the synthesis of waterborne polyurethane disper-  
1093 sions (Yang et al. 2014; Hu et al. 2015). The waterborne polyurethane dispersions  
1094 prepared with natural dimer fatty acid-based polyester polyols exhibited excellent  
1095 water resistance, outstanding hydrolytic resistance and superior thermal stability than  
1096 the ones prepared with nonnatural-derived polyester polyols (Liu et al. 2011).

1097 The properties of the waterborne dispersions are also affected by the nature and  
1098 amount of the *ionic groups*. The increase in the content of dimethyl propionic acid  
1099 (DMPA) decreases the mean particle size and increases the viscosity of the water-  
1100 borne polyurethane dispersions (Huang and Chen 2007). Increased DMPA amounts  
1101 result in the higher hard-segment contents and the increase in the mechanical  
1102 properties of the polyurethanes (Cakić et al. 2013). Furthermore, the increase of  
1103 the DMPA content decreased the adhesion of the polyurethane dispersions (Rahman  
1104 and Kim 2006).

1105 The influence of the *solids content* on the properties of the polyurethane disper-  
1106 sions has been studied, and contradictory findings with respect to their influence on  
1107 the mean particle size have been found. It has been stated that the increase of the solids  
1108 content caused an increase in the mean particle size that was related to the decrease in  
1109 the viscosity of the polyurethane dispersions (Lee and Kim 2009). Another study  
1110 concluded that the mean particle size of the polyurethane dispersion decreased by  
1111 increasing its solids content, and an increase in the viscosity was found, and this was  
1112 related to the decreased particle-particle interactions and the higher degree of phase  
1113 separation (García-Pacios et al. 2011b). On the other hand, the increase in the solids  
1114 content does not affect the peel strength and decreases the single-lap shear strength of



the waterborne polyurethane dispersions (García-Pacios et al. 2011b). A recent study analyzed the structure and properties of high solids content waterborne polyurethane dispersions synthesized by combining ionic and nonionic monomers (Lijie et al. 2015). The adequate combination of the molecular weight of the polyether and the amount of DMPA improved the stability of the dispersion and increased the solids content of the polyurethane dispersion up to 52 wt%. Additionally, the glass transition temperature of the soft segments and the crystallinity of the polyurethane decreased, although the mechanical properties were improved.

*Thickeners* (polyvinyl alcohol, polyurethanes, polyacrylates, cellulose derivatives) are added to increase the low viscosity of the waterborne polyurethane adhesives and to avoid excessive penetration in porous substrates (Orgilés-Calpena et al. 2009a). The mechanism of thickening of the waterborne polyurethane adhesives by adding urethane-based thickener has been analyzed by confocal laser microscopy (Fig. 10). The addition of the thickener produces an entanglement in the polyurethane adhesive (seen as denser and whiter images in Fig. 10) which can be ascribed to the existence of interactions between the urethane-based thickener and the polyurethane. Several interactions take part in the thickening mechanism of the polyurethane adhesive dispersions by adding urethane-based thickener: (i) interactions between the terminal hydrophobic groups of the thickener with the polyurethane micelles, (ii) interactions by ionic adsorption of the polyester chains of the thickener with the ionic groups on the surface of the polyurethane particles, and (iii) interactions by hydrogen bonds between the urethane groups of the polyurethane dispersion and the urethane-based thickener (Orgilés-Calpena et al. 2009a, b). Figure 11 shows a schematic diagram of the thickening mechanism of waterborne polyurethane adhesive containing urethane-based thickener in which the formation of 3D micelle network is seen. On the other hand, the hard-to-soft segment ratios and the

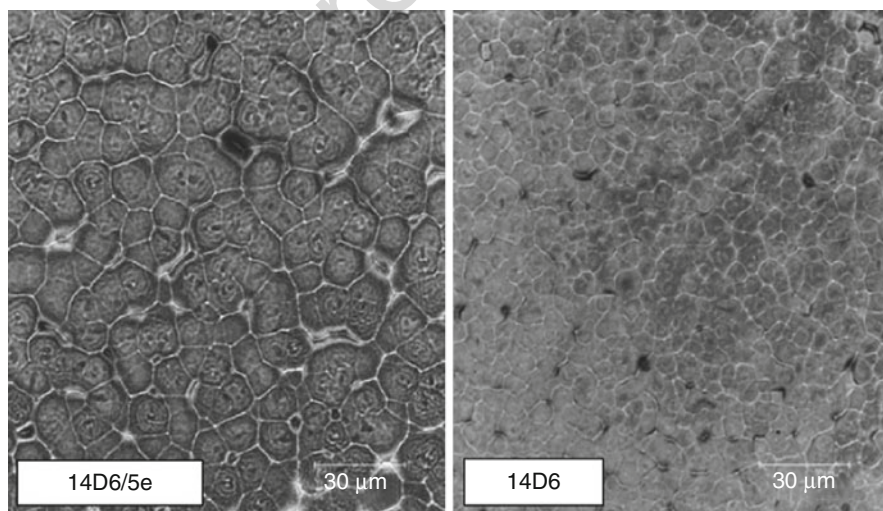


**Fig. 10** Micrographs of confocal laser microscopy corresponding to the waterborne polyurethane adhesives without (14D6) and with (14D6/5e) 5 wt% urethane-based thickener

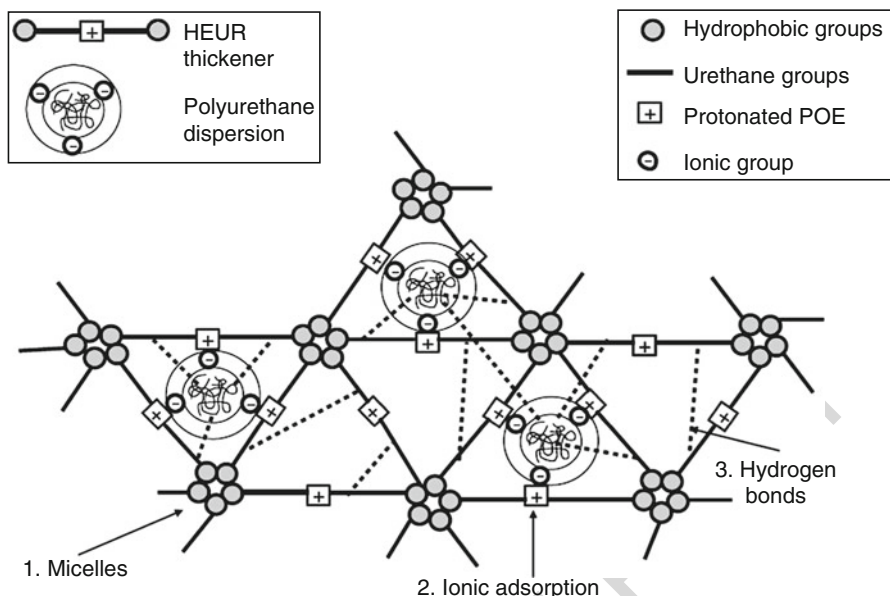


**Fig. 11** Thickening mechanism of waterborne polyurethane adhesive containing urethane-based thickener through the formation of 3D micelle network (Orgilés-Calpena et al. 2009b)

content of ionic groups determine the properties of the waterborne polyurethane adhesives. Thus, the addition of 5 wt% urethane-based thickener markedly increases the viscosity of the waterborne polyurethane adhesive more noticeably by decreasing the hard-to-soft segments ratio and by increasing the ionic group contents (Orgilés-Calpena et al. 2009a). On the other hand, as the hard-segment content of the thickened polyurethane adhesive decreases, the kinetics of crystallization is favored as a result of stronger polyurethane-thickener interactions.

*Emulsifiers* (surface active agents) assist to stabilize the pH of the waterborne polyurethane dispersion and to decrease its surface tension to obtain improved wettability. The emulsifiers are always oriented on the interface between the polymer particles and the aqueous phase. Small amounts must be added to avoid loss in bonding characteristics.

On the other hand, to achieve particular performance, dispersions of several polymers (vinyl acetate, acrylic ester) and resins (hydrocarbon resin, rosin esters) can be added to waterborne polyurethane adhesives. Special attention must be paid to the compatibility with the polyurethane to avoid dispersion collapse. In general, fillers are not added to waterborne polyurethane adhesives although dispersions of silicas can be added for adjusting the viscosity and the rheology.

To produce adequate bond, the waterborne adhesive solution is applied to the two substrates to be joined, and the water is evaporated at room temperature for about 30 min or by heating with hot air or infrared lamps at 50–60 °C for a few minutes. When the water comes out, the polyurethane viscosity rises, and a continuous film is formed



on the substrates. Then, the dry films are heat activated, and the melting of the crystalline soft segment is produced imparting tackiness to the films. The heat activation process of the waterborne polyurethanes is affected very strongly by the substrates to be bonded and by the process parameters such as temperature, pressure, and contact bond time. Increasing the adhesive film temperature, raising the pressure, and extending the time of contact have all similar effect, i.e., an increase of the actual contact area is produced, and better bond is obtained. After heat activation, the decrystallized polyurethane film is an amorphous viscoelastic melt with good flow properties. The decrease in viscosity after heat reactivation allows the adhesive film to wet the substrate, and the joining to the adhesive film on a second substrate under pressure is produced. Once the adhesive joint is formed, the bulk viscosity and the modulus of the adhesive increase, initially by cooling and afterward by the recrystallization of the polyurethane.

If an isocyanate is added as *cross-linker* of the waterborne polyurethane adhesive, the bond formation occurs much slower than with only the polyurethane, but a further increase in viscosity with time is obtained. The cross-linking reaction does not initially bring any increase in the peel adhesive strength at room temperature but increases the heat resistance of the bond. The most common cross-linkers are polyisocyanates (adequately modified with surface active agents to become emulsifiable in water), although azyridines, polycarbodiimides, and epoxies can also be used. The cross-linker is normally added to the dispersion and stirred in before application on the substrates. Once the cross-linker is added, the drying off of the water is important because the reaction with water reduces its effectiveness. Depending on the formulation, the adhesives can be applied over a period of 4–10 h without affecting the adhesion properties. The isocyanate cross-linker generally takes several days before the cross-linking reaction is completed. Unlike solvent-borne adhesives, the pot life of the adhesive dispersions is not associated with an increase in viscosity.

In general, the durability of the polyurethane adhesives is acceptable although they are water sensitive, particularly the polyether-based polyurethane. Protection against water degradation can be reduced by adding carbodiimides and/or polyisocyanates during curing.

The bond strength of the waterborne polyurethane adhesives is particularly dependent on the substrate. Good results are obtained with surface-chlorinated vulcanized rubbers and PVC, but adhesion to TR may be poor or variable (Abbott 1992). Adhesion to leather is sometimes insufficient, and roughening must be always carried out; adhesion to greasy or waterproof leathers and unroughened polyurethane coatings may also be difficult.

### **Solvent-free Polyurethane Adhesives**

Currently, the waterborne adhesives are being introduced into the shoe industry. Their performance is quite similar to that of the solvent-borne adhesives, so it can be estimated that for several years, they will be used in shoe industry. However, the future seems to be directed through the use of moisture-curing hot-melt urethane and thermoplastic urethane adhesives as they are 100% solids systems and evaporation of solvents is not necessary. Although the hot-melt urethanes could replace

waterborne adhesives, this could take longer to occur because of the vastly different equipment requirements and the change in the bonding concept by the shoe manufacturers.

Some literature has been published dealing with *moisture-reactive hot-melt polyurethane adhesives* (Frisch 2002). Most moisture-curing hot-melt adhesives are obtained by reacting a crystallizable polyol such as poly(hexamethylene adipate) and monomeric MDI (NCO/OH ratios = 1.5–2.2). A catalyst such as dimorpholinediethyl ether is also necessary. The polyester polyol plays a key role because the open time, the viscosity, and the glass transition temperature can be adequately tailored. A mixture of hydroxyl-terminated polyesters having different characteristics allows control of the adhesion and hardening time of the adhesive. Recently, reactive polyurethane hot-melt adhesives containing polycarbonate polyols derived from CO<sub>2</sub> and 4,4'-diphenylmethane diisocyanate (MDI) have been developed from improving the T-peel strength of leather/polyurethane adhesive/vulcanized SBR joints, and they show good green and final strength before and after high temperature/humidity aging and hydrolysis tests (Orgilés-Calpena et al. 2016a, b).

The moisture-curing hot-melt adhesives must be stored in nitrogen-sealed containers, and moisture must be fully excluded. These adhesives are crystalline solids at room temperature, and for application, heating is necessary (about 125 °C) to become low-viscosity liquids, and they are only applied on one of the substrates to be joined; the second substrate is immediately joined with minimal pressure. Simultaneously to the application of the adhesive, water can be sprayed onto the adhesives/materials in the amount necessary for facilitating the curing process. Although after cooling down the crystallinity is reached, about 24 h is necessary to develop the strength of a structural adhesive. Initial strength can be improved by adding polyester, thermoplastics, or polymerized acrylates. Addition of ketone–formaldehyde and terpene phenolic resins also increases adhesive performance. Limitations of these adhesives derive from the special equipments necessary for application and from the substrate nature (not all substrates can be bonded). However, some pre-reacted hot-melt adhesive types are liquids and may be applied by hand, by spraying, or even better by nozzles.

When the polyurethane hot-melt adhesive comes into contact with moisture, the irreversible curing of the adhesive is initiated. First, the water adds to the isocyanate group producing unstable carbamic acid, which in turn is transformed into a primary amine group. These amine groups generate linear urea bridges by reaction with additional isocyanate; a three-dimensional network is produced by cross-linking with more isocyanate groups, providing the structural bonding in moisture-cured hot-melt polyurethane adhesives.

The *thermoplastic polyurethane adhesives* are another future alternative for bonding in shoe industry. These adhesives have good holding strength after crystallization, but their cost is higher than the majority of the adhesives used in shoe industry. Most thermoplastic polyurethane adhesives are based in fast crystallization polyesters. They are prepared using a NCO/OH ratio near 2, and they have linear structure. They consist in two components (polyol and isocyanate) which have to be mixed at about 60 °C in the presence of a catalyst such as dibutyltin dilaurate; after reaction, the

1251 resulting polymer is pelletized and packed in nitrogen- and moisture-free atmosphere  
1252 containers. Application temperatures are higher than 170 °C, and to produce bonding  
1253 the same procedure as for moisture-cured hot-melt urethane is used.

### 1254 51.3.5 Polychloroprene Adhesives

1255 Although polychloroprene adhesives (more often called *neoprene* adhesives because  
1256 of the trade name given by Du Pont to the first commercial product) were extensively  
1257 used in the past in the sole-to-upper bonding, nowadays they have been practically  
1258 substituted by polyurethane adhesives. Therefore, there is no sense in providing an  
1259 extensive description of the polychloroprene adhesives in this chapter which the  
1260 prime aim is to provide an actual overview. A detailed description of the poly-  
1261 chloroprene adhesives for shoe bonding can be found in Chap. 14 of the book  
1262 entitled “Adhesive Bonding. Science, Technology and Applications” (Adams  
1263 2005). Therefore, in this chapter, the main features of these adhesives will be only  
1264 considered, and the reader can refer to that chapter for more detailed information.

1265 Solvent-borne polychloroprene adhesives are less used in shoe industry because  
1266 of the presence of aromatic organic solvents in their formulation which are currently  
1267 unacceptable. However, the most recent developed waterborne polychloroprene  
1268 adhesives can compete with waterborne polyurethane adhesives because of their  
1269 good performance in the upper-to-sole bonding. Furthermore, they are extremely  
1270 useful as nonpermanent adhesives in several mounting operations (previously to the  
1271 sole-to-upper attachment) involving porous substrates in the shoe manufacturing.

### 1272 Solvent-Borne Polychloroprene Adhesives

1273 Polychloroprene adhesives are contact adhesives (see ► Chap. 14, “Adhesive Fam-  
1274 ilies”). The diffusion process in polychloroprene rubber adhesives is mainly affected  
1275 by the solvent mixture of the adhesive (which determines the degree of uncoiling of  
1276 rubber chains) and by the ingredients in the formulation (mainly the amount and  
1277 nature of tackifier). The chemical nature and molecular weight of the poly-  
1278 chloroprene greatly determine its adhesive properties. The polychloroprene  
1279 adhesives show high peel strength; high green strength and noticeable resistance to  
1280 moisture, chemicals, and oils; excellent aging properties; and excellent temperature  
1281 resistance. These characteristics are important in shoe industry.

1282 Polychloroprene elastomers are produced by free radical emulsion polymeriza-  
1283 tion of 2-chloro-1,3-butadiene monomer. The emulsion polymerization of chloro-  
1284 prene involves the dispersing of monomer droplets in an aqueous phase by means of  
1285 suitable surface active agents, generally at a pH of 10–12. Polymerization is initiated  
1286 by addition of free radical catalyst at 20–50 °C. To obtain a high conversion in the  
1287 polymerization reaction and processable polymer, the addition of sulfur, thiuram  
1288 disulfide, or mercaptans is necessary (Whitehouse 1986).

1289 The crystallinity in the polychloroprene is essential in sole-to-upper bonding in  
1290 shoe industry. Crystallinity is produced by noticeable *trans*-1,4 addition (more than  
1291 90%) during polymerization. As a result of crystallization, the cohesive strength of

the polychloroprene is much greater than that of the amorphous polymer. Crystallization is reversible under temperature or dynamic stresses. Thus, for a temperature higher than 50 °C, uncured polychloroprene adhesives lose their crystallinity, and upon cooling the film recrystallizes, and cohesive strength is regained. The increase in the crystallinity improves the modulus, hardness, and cohesive strength of the polychloroprene adhesives but decreases their flexibility.

A typical composition of solvent-borne polychloroprene adhesive for upper-to-sole attachment is given in Table 2.

The role of the different components in solvent-borne polychloroprene adhesive is described below in more detail.

The sulfur-modified *polychloroprenes* with little or no branching are the most commonly used in shoe adhesives as they are soluble in aromatic solvents, and for difficult-to-bond substrates, methacrylic graft polymers show better performance. The polymer type influences several properties of the solvent-borne polychloroprene adhesives, mainly the molecular weight and the rate of crystallization. The increase in the molecular weight of the polychloroprene imparts higher solution viscosity, adhesive strength, and heat resistance. On the other hand, the increase in the crystallization rate of the polychloroprene improves the rate of development of the bond strength and the ultimate strength at high temperature, but a reduction in open time (*tack*) is obtained. However, the tack can be varied by changing the pressure during joint formation and by an adequate selection of the solvent; the lower the volatility of the solvent, the longer is the open time of the solvent-borne polychloroprene adhesive.

*Metal oxides* provide several functions in solvent-borne polychloroprene adhesives. The main function of the metal oxides in the polychloroprene adhesive formulations is acting as acid acceptor. Upon aging, small amounts of hydrochloric acid are released which may cause discoloration and substrate degradation. Magnesium oxide (4 phr) and zinc oxide (5 phr) act synergically in the stabilization of the solvent-borne polychloroprene adhesives against dehydrochlorination. On the other hand, the magnesium oxide retards scorch during mill processing of the polychloroprene adhesives and also reacts in solution with the *t*-butyl phenolic resin to produce an infusible resinate (a small amount of water is also necessary) which provides improved heat resistance. Furthermore, the zinc oxide produces a room temperature cure of the solvent-borne polychloroprene adhesives, giving increased strength and improved aging resistance.

**Table 2** Typical composition of a solvent-borne polychloroprene adhesive. *phr* means parts per hundred parts of rubber

Polychloroprene	100 phr
Tackifying resin	30 phr
Magnesium oxide	4 phr
Zinc oxide	5 phr
Water	1 phr
Antioxidant	2 phr
Solvent mixture	500 phr

1327 Addition of *resins* to solvent-borne polychloroprene adhesives serves to improve  
 1328 its specific adhesion, increases tack retention, and increases hot cohesive strength.  
 1329 *Para-tertiary* butyl phenolic resins are the most common, and amounts between  
 1330 35 and 50 phr are generally added. In general, the tack decreases by increasing the  
 1331 phenolic resin content in the polychloroprene adhesive, and bond strength reaches a  
 1332 maximum at about 40 phr, decreasing for higher amounts of phenolic resin.

1333 Solutions of polychloroprene adhesives containing metal oxides and *t*-butyl  
 1334 phenolic resin may show phasing (e.g., clear upper layer and flocculated lower  
 1335 layer of metal oxides) on standing upon days or months. To recover the full utility  
 1336 of the metal oxides, agitation before use is sufficient. Phasing is ascribed to the wide  
 1337 molecular weight distribution of the *t*-butyl phenolic resins.

1338 Terpene phenolic resins can also be added to solvent-borne polychloroprene  
 1339 adhesives to increase open tack time and to provide a softer glue line than the  
 1340 *t*-butyl phenolic resins. To provide adequate hot-bond strength, these resins are  
 1341 used in combination with a polyisocyanate-curing agent.

1342 An *antioxidant* (about 2 phr) should be added to the polychloroprene adhesives to  
 1343 avoid oxidative degradation and acid tendering of the substrates. Derivatives of  
 1344 diphenylamine (octylated diphenylamine, styrenated diphenylamine) provide good  
 1345 performance, but staining is produced. To avoid staining, hindered phenols or  
 1346 bisphenols can be added.

1347 *Solvent* affects the adhesive viscosity, the bond strength development, the open  
 1348 time, and the ultimate strength of the polychloroprene adhesives. Blends of three  
 1349 solvents (aromatic, aliphatic, oxygenate – e.g., ketones, esters) are generally added.  
 1350 Typical solvent blends for polychloroprene adhesives are given in Table 3. The open  
 1351 tack time of the solvent-borne polychloroprene adhesives partially depends on the  
 1352 evaporation rate of the solvent blend. If a solvent evaporates slowly, the solvent-  
 1353 borne polychloroprene adhesive will retain tack longer, whereas if the solvent  
 1354 evaporates quickly, the cohesive strength will develop more rapidly.

t.1 **Table 3** Influence of the solvent on the viscosity and the tack of polychloroprene adhesives.  
 Formulation: 100 phr polychloroprene elastomer; 4 phr MgO; 5 phr ZnO; 2 phr hindered phenolic  
 antioxidant; 500 phr solvent mixture (Whitehouse 1986)

t.2	Solvent	Mixing ratio	Solution viscosity 20 °C (mPa.s)	Tack time (min)
t.3	Toluene	–	4460	35
t.4	Toluene/n-hexane/MEK	35/5/15	3500	25
t.5	n-Hexane/MEK	55/45	1520	15
t.6	Cyclohexane/acetone	80/20	3700	18
t.7	MEK/acetone	75/25	2100	15
t.8	Toluene/n-hexane/ethyl acetate	34/33/33	3600	30
t.9	Toluene/MEK/acetone	34/33/33	3400	22
t.10	n-Hexane/acetone	50/50	1140	7
t.11	Dichloromethane	–	4670	30
t.12	1,1,1-Trichloroethane	–	4600	38

*Isocyanates* can be added to solvent-borne polychloroprene adhesive solutions as two-part adhesive systems. The reaction of the isocyanate with polychloroprene that leads to improved heat resistance property has not been fully explained as there are no active hydrogen atoms in the polychloroprene to allow reaction with isocyanate group. The two-part adhesive system is less effective with rubber substrates containing high styrene content and with butadiene–styrene block (thermoplastic rubber) copolymers. To improve the specific adhesion to those materials, addition of poly- $\alpha$ -methylstyrene resin to solvent-borne polychloroprene adhesives is quite effective (Tanno and Shibuya 1967).

**Waterborne Polychloroprene Adhesives**

In recent years, the use of solvent-borne polychloroprene adhesives has been seriously restricted, and waterborne adhesives have been developed. Polychloroprene latex differs from its solid elastomer counterpart (used in solvent-borne polychloroprene adhesive) in that it is a gel polymer (e.g., insoluble in organic solvents). Latex systems derive their bond strength characteristics from the gel structure rather than crystallinity as in solvent solution systems. Higher gel content leads to the same properties than polymers with higher crystallinity (Lyons and Christell 1997). Polymers with higher gel content exhibit higher cohesive strength, modulus, and heat resistance, but tack, open time, and elongation at break are reduced.

The initial formulations of the polychloroprene latex adhesives contain essentially the same components than the solvent-borne adhesives, except that water-based ingredients have to be used, surfactant, thickener and antifoaming agent must be added, and the compounding is particularly exigent. A typical composition of initial waterborne polychloroprene adhesive is given in Table 4.

In the last years, more simple and efficient formulations of waterborne polychloroprene adhesives for shoe industry have been developed (Kueker et al. 2016). The typical formulation of the current waterborne polychloroprene adhesives is given in Table 5 and consists in polychloroprene, acrylic or silica sol dispersion, zinc oxide, surfactant, antifoaming agent, and antioxidant. The preparation of these waterborne polychloroprene adhesives starts with the addition of the antioxidant to the polychloroprene dispersion, followed by slow addition of zinc oxide and the final incorporation of the acrylic or silica sol dispersion.

The final adhesive strengths obtained with the current waterborne polychloroprene adhesives are due to the cross-linking between the polychloroprene

**Table 4** Typical composition of the initial waterborne polychloroprene adhesive formulation

Polychloroprene dispersion	100 phr
Surfactant	As required
Antifoam	As required
Tackifying resin	50 phr
Thickener	As required
Zinc oxide	5 phr
Antioxidant	2 phr

**Table 5** Typical composition of the current waterborne polychloroprene adhesive formulation

Polychloroprene dispersion	100 phr
Surfactant	As required
Antifoam	As required
Silica sol dispersion	10 phr
Zinc oxide	1 phr
Antioxidant	2 phr

t.1  
t.2  
t.3  
t.4  
t.5  
t.6

1389 and the silica or acrylic micelles, and similar adhesive strengths to the ones obtained  
1390 with solvent-borne adhesives are obtained, although the open time is generally  
1391 longer. The use of silica sol dispersions with low mean particle size (i.e., about  
1392 5 nm) improves more the initial adhesive strength or wet bonding to leather than the  
1393 use of silica sol dispersions with higher mean particle size, and the increase in  
1394 the amount of silica causes softening and a decrease in the mechanical properties  
1395 of the polychloroprene. Finally, the heat resistance of the polychloroprene adhesives  
1396 can be noticeably increased by using hydroxylated polychloroprene dispersion due  
1397 to the hydrogen bond formation with the silica sol particles; in fact when this  
1398 hydroxylated polychloroprene dispersion is used, there is no need of adding poly-  
1399 isocyanate cross-linker for increasing the aging resistance, and this is even better  
1400 than by using solvent-borne polychloroprene adhesives (Kueker et al. 2016).

1401 Recently, the magnetic conditioning for 3 h of aqueous-based polychloroprene  
1402 contact adhesive has been proposed for increasing its adhesion (Souza et al. 2016).  
1403 To promote adhesion, a nanometric zinc oxide, carbon dioxide as catalyst, hydrox-  
1404 ylamine, and a magnetic conditioning process before the application of the adhesive  
1405 were carried out. The magnetic conditioning was performed in magnetic cell com-  
1406 prising of containers for circulation of the adhesive, two submerged centrifugal  
1407 hoses for transfer of the adhesive, a set of magnets iron–boron–neodymium with  
1408 magnetic field of 2120 gauss, gaussmeter, and agitators. Noticeable increase in shear  
1409 adhesion was obtained.

1410 The *polychloroprene latex* determines the initial tack and open time, the bond  
1411 strength and the hot-bond strength, the application properties, and the adhesives  
1412 viscosity. Because most of the latexes have low viscosities, most of the waterborne  
1413 polychloroprene rubber adhesives are sprayable. Thickeners such as fumed silicas  
1414 can be added to some formulations for increasing viscosity and thixotropy.

1415 Grafting of methyl methacrylate (MMA) onto polychloroprene rubber latex  
1416 (CRL) has been carried out by emulsion polymerization using a redox initiator,  
1417 and the surface diffusion-controlled process model was proposed to describe the  
1418 grafting mechanism (Zhang et al. 2012). The graft copolymer was blended with  
1419 tackifier and filler for waterborne contact adhesive applications, and the 180° peel  
1420 strength to canvas to other decoration materials showed similar performance than  
1421 solvent-based contact adhesive and superior to the one obtained with poly-  
1422 chloroprene and polymethyl methacrylate.

1423 Based on the synergistic effect of polychloroprene latex and styrene–acrylate  
1424 emulsion, waterborne contact adhesive containing 40 wt% styrene–acrylate emulsion



1425 and 1.25 wt% boric acid has been developed (Zhang et al. 2009). The blend had a good  
1426 shelf stability, its set time was 5 min, its tensile strength was reasonable, and it had very  
1427 high elongation at break. The performance of the waterborne contact adhesives was  
1428 found to be comparable to the solvent-based contact adhesives because they offered  
1429 good wetting ability to substrate, high initial tack was obtained, it possessed excellent  
1430 crystallization ability, and it enhanced the cohesive strength of the adhesive.

1431 Although noncompounded polychloroprene latex has good mechanical and stor-  
1432 age stability, *surfactants* are added commonly for stabilization. They function by  
1433 strengthening the interfacial film by maintaining or increasing the degree of solva-  
1434 tion or by increasing the charge density on the latex particle. More precisely,  
1435 surfactants are added to improve storage stability, substrate wetting, and attain  
1436 improved freeze resistance. However, incorporation of surfactants has an adverse  
1437 effect on cohesive properties and should be kept to a minimum. Water resistance and  
1438 tack may also be affected. Excessive stabilization of the adhesive mixture may  
1439 negatively affect coagulation (which is desirable in the wet bonding process).  
1440 Anionic emulsifiers (alkali salts of long-chain fatty acids and alkyl/aryl sulfonic  
1441 acids) or nonionic emulsifiers (condensation products of long-chain alcohols, phe-  
1442 nols, or fatty acids with ethylene oxide) can be used.

1443 Zinc oxide is the most effective *metal oxide* and plays three main functions:  
1444 (i) promote cure; (ii) improve aging, heat, and weathering resistance; and (iii) acid  
1445 acceptor. In general, 2–5 phr zinc oxide is added in latex formulations.

1446 *Resins* influence the adhesion, open time, tack, and heat resistance of the water-  
1447 borne polychloroprene adhesives. In some formulations, 30–60 phr is added, and  
1448 attention should be paid to the pH and compatibility with the surfactant. The glass  
1449 transition temperature, the softening point, the polarity, and the compatibility of the  
1450 resin with the polymer determine the adhesive properties. Thus, the hot-bond perfor-  
1451 mance is generally proportional to the softening point of the resin. *t*-Butyl phenolic  
1452 resins cannot be used in waterborne polychloroprene adhesives because of colloidal  
1453 incompatibility. Instead, terpene phenolic resins can be added to polychloroprene  
1454 latex without great reduction in hot strength as the resin content is increased; however,  
1455 the contact ability is reduced, and an adhesion failure is obtained, even at the 50 phr  
1456 level. Furthermore, the terpene phenolic resins have relatively poor tack but impart  
1457 good resistance to elevated temperatures to the polychloroprene latexes and require  
1458 either heat activation or pressure to achieve adequate bond strength. Rosin ester resin  
1459 emulsions are also effective in latex adhesives as they extend the tack life of the  
1460 polychloroprene latexes, but they do not have the reinforcing characteristics of the  
1461 terpene phenolic or alkyl phenolic resins. Hence, the cohesive strength and heat  
1462 resistance are sacrificed to obtain surface tack.

1463 New nitrogen-containing compounds have been proposed as highly efficient  
1464 *adhesion promoters* for adhesive compositions based on polychloroprene (Keibal  
1465 et al. 2011). On the other hand, similar *antioxidants* than for solvent-borne poly-  
1466 chloroprene adhesives can be used in the formulation of waterborne polychloroprene  
1467 adhesives.

1468 Addition of *thickeners* increases the viscosity of the polychloroprene latex adhe-  
1469 sives. Amounts up to 1 wt% of polyacrylates, methyl cellulose, alginates, and



polyurethane thickeners can be used. Particular attention should be paid to fluctuations in pH when thickener is added in the formulations. For low pH (7–10) formulations, fumed silica or some silicates can be used.

*Curing agents* have little effect on the performance of latexes with the highest gel content, but they are sometimes used with low-gel polymers to improve hot-bond strength while maintaining good contactability. Suitable curing agents are thiocarbonylides either alone or in combination with diphenylguanidine, zinc dibutyldithiocarbamate, and hexamethylenetetramine. Two-part systems have been developed using more active materials such as aqueous suspension isocyanates and hexamethoxy melamine. These agents produce a cross-linking reaction at room temperature and give fast bond development but exhibit a finite pot life. The most common use of the curing agents is with carboxylic latices. Isocyanates and melamines can be used, but zinc oxide is the most common curing agent. Zinc oxide cross-links carboxylated latices and improves bond strength by ionomer formation (Cuervo and Maldonado 1984). Carboxylated polychloroprene reacts slowly with zinc oxide in dispersed form, causing a gradual increase in adhesive gel content that can lead to restricted adhesive shelf life. Resin acid sites compete with the polymer acid sites for  $\text{Zn}^{II}$ ; the more resin acid sites, the more stable the adhesive is.

---

## 51.4 Testing of Adhesive Joints in Shoe Bonding

In order to produce an optimum adhesive bonding of upper to sole, apart from the adequate surface preparation of the sole and upper materials and the adequate choice of the adhesive, the procedure to produce the joint should be carefully controlled and optimized. To achieve adequate adhesion of upper to sole, the following issues should be considered.

1. Selection of the upper and sole materials. In general, formulators of upper and sole materials do not consider that they have to be bonded, but they pay more attention to match the hardness and mechanical properties and aesthetic of the materials. Furthermore, depending on fashion, different difficult-to-bond materials are used to produce shoes which make problematic to standardize bonding. In general, the formulation of the shoe materials must elude the presence of additives able to decrease the adhesion to polyurethane or polychloroprene adhesives (plasticizers, excessive amounts of processing oils, inadequate selection of antioxidants, and antioxidants), and especially the use of too greased leather upper must be avoided. On the other hand, the formulations must be repetitive, and first-class raw materials must be used. As a general rule, the use of adequately formulated uppers and soles avoid more than 90% of the bonding problems in shoe industry.
2. Selection of the adhesive. The adhesive must be selected considering the performance required for each joint. Adhesive must properly wet the upper and sole surfaces, and in this aspect, solvent-borne adhesives are excellent. One of the problems in the use of waterborne adhesives is their poor wettability, although an

adequate formulation may solve quite satisfactorily this limitation. In the selection of an adhesive, the following aspects should be particularly considered: nature and formulation of the materials to be bonded; stresses produced during shoe use; environment of use (solvents, acid, or alkali media), only for safety shoes; adhesive application restrictions (viscosity, rheological properties); specific requirements of the adhesive (pot life, working scheme in the shoe factory); and safety regulations.

3. Design of the joint. Fashion dictates the shape and geometry of the shoes. Sometimes, the shoes become difficult to bond because of high heels or heterogeneous shapes of soles. In general, the shoe designers do not pay attention to the bonding.

4. Adequate bonding operation. Several cases of poor adhesion in shoe bonding arise from a deficient operation. As a summary, the following aspects must be properly obeyed to assure an adequate upper-to-sole bonding:

- Surface treatments of upper and sole. The way to produce the surface preparation and the instruments used are critical. Furthermore, proper surface preparation for each upper and sole must be selected.
- Adhesive application. A thin film of adhesive (about 100  $\mu\text{m}$  thick) is applied to each of the two substrates to be bonded, and the solvent is removed by natural or forced evaporation. A heavier coat of adhesive is more likely to result in a cohesive failure in the substrate. The application procedure (brush, doctor knife, spray gum, roller, coater) and the amount of adhesive must be carefully controlled. The choice of the adhesive application devices depends mainly on the type and size of the materials to be bonded as well as on the rheological properties of the adhesive. Furthermore, the viscosity of the adhesive must be controlled, and the operation times (evaporation rate of organic solvents or water, open time, shelf life) must be strictly obeyed.
- Adhesive film drying. Controlled drying of the shoe bottom cements is preferable to natural drying. Removed excess water or organic solvent from an adhesive film is not entirely governed by the process of evaporation but also by the speed of absorption into the substrate. Porous substrates (such as leather) absorb water or organic solvents without detrimental effect on bond strength, whereas nonporous substrates need the complete solvent removal to produce adequate adhesion. Furthermore, a force drying may produce skin formation on the surface of the coating (especially if heavier adhesive coating is applied) leading to poor coalescence of the adhesive. A slight trace of organic solvent in the cement film on the upper at sole attaching is beneficial in giving complete coalescence. When necessary, although very fast drying can be achieved by radiant heat, the use of IR radiation and hot air is a more convenient method, and both provide more uniform heating.
- Bond formation. The components with the dry adhesive film are placed for 10–30 s in a “flash heater” – hot air or IR radiation can also be used – where a radiant heat source raises suddenly the temperature of the adhesive film above the crystalline melting of the polyurethane (heat activation or reactivation process). Recommended reactivation temperature for polyurethane adhesives

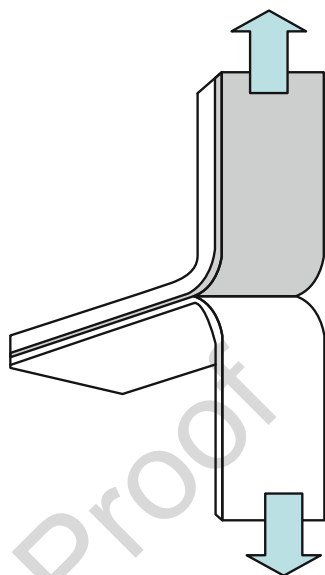
ranges between 45 and 85 °C, depending on the substrates and the adhesive characteristics. An insufficient reactivation temperature causes non-coalescence of the adhesive, and an excessive reactivation temperature decreases creep because the substrate is too hot and the adhesive is still soft when sole and upper are attached (SATRA 1963). In some particular cases, the reactivation temperatures of the adhesives higher than 100 °C are recommended to produce good performance. While still in their amorphous state, the adhesive films are brought together under pressure (typically 35–200 kPa) for 10–30 s (*stuck-on* process). The time interval after the heat activation process during which the films adhere is known as the “spotting tack.” Both the applied pressure and the pressing time of the upper to the sole must be adequately selected for each joint.

- Crystallization or curing of the adhesive. After bond formation, the adhesive joint needs time to gain sufficient cohesion. Time can vary, although in general a minimum of 24 h is required for crystallization, being 72 h the optimum. For waterborne adhesives, the curing time may be longer.

T-peel (see ► Chap. 20, “Fracture Tests”) and creep (see ► Chap. 34, “Creep Load Conditions”) tests are the most commonly used to establish the adhesion performance in shoe bonding. The peel test serves to determine the bonding properties of upper to sole in shoe industry. Peeling rate, material thickness, and size of test samples must be optimized. Standard T-peel tests require two rectangular test pieces of 150 mm long, 30 mm width, and 3 mm thick that are stuck together to cover it other to a length of at least 50 mm (Fig. 12). Standard peel rate is 100 mm/min. The joints are stored for 72 h in standard atmosphere (23 °C and 50% relative humidity) before carrying out the separation tests. Both the peel resistance and the way in which the separation occurs help to assess the bond. A minimum of five replicates, preferably ten, for each joint must be tested and averaged. Bond strength should be expressed as kN/m, although very often N/mm is used in the shoe industry. The loci of failure of the joints are generally expressed using the following capital letters:

- A: Adhesion failure (detachment of the adhesive film from one of the materials)
- C: Cohesive failure in the adhesive (separation within the adhesive film without detachment from the material)
- N: Non-coalescence failure (failure of the two adhesive films without detachment from the material)
- S: Surface cohesive failure of the material (breakdown of a substrate of low structural strength at its surface)
- M: Cohesive failure of one of the substrates

Under the influence of force and when heated, the adhesive layers of footwear material bonds suffer plastic flow. The creep test at constant temperature serves to assess the behavior of shoe material bonds when heated under the influence of a

**Fig. 12** T-peel test sample

constant peeling force over a fixed time. Weight between 0.5 and 2.5 kg can be fixed on the lower holders outside a heating oven where the test pieces can be heated at 50–70 °C. The unbounded ends of five test pieces are bent apart carefully and inserted in the holders. Temperature is generally raised to 60 °C after a warm-up period of 1 h. The test pieces are loaded with the chosen weight constantly for 10 min. Then, the heating oven is opened, and the separations of the bonds are marked.

Moisture and temperature are the main agents able to degrade the shoe joints. Therefore, adequate *aging tests* have been developed to assure adequate performance. In general, addition of polyisocyanate hardener increases the durability and retards aging in most of the upper-to-sole adhesive joints. Several tests have been proposed to establish the aging resistance of upper-to-sole bonds. The most common aging tests involve the immersion in hot water, the exposition of the joints to 50 °C and 95% relative humidity for 1 week, freeze-thaw cycles, and/or UV light. Generally, after aging T-peel tests are carried out to determine durability.

## 51.5 Conclusions

This review considered the current state of the art of the main issues involved in the bonding process of upper to sole in footwear manufacturing. The main innovations in the surface treatments of soles of different materials and the waterborne adhesives were addressed.

**Acknowledgment** The chapter was not possible without the help of several people who work in my laboratory. The financial support from the Spanish Research Agency (CICYT, MCYT, MICINN), the Generalitat Valencia (Conselleria de Educaci3n, Cultura y Deporte, Conselleria de

1619 Industria), and the University of Alicante is greatly appreciated. Last but not least, my deep  
1620 recognition and gratitude to Antonia Armentia-Agüero (Toñi) for her love and for her help in  
1621 several figure designs.

## References

- 1623 Abbott SG (1992) Solvent-free adhesives for sole attaching. SATRA Bull 109
- 1624 Abbott SG, Brewis DM, Manley NE, Mathieson I, Oliver NE (2003) Solvent-free bonding of shoe-  
1625 soling materials. *Int J Adhes Adhes* 23:225
- 1626 Adams RD (ed) (2005) Adhesive bonding: science, technology and applications. Woodhead  
1627 Publishing, Cambridge. Chapter 18
- 1628 Alvarez-García S, Martín-Martínez JM (2015) Effect of the carbon black content on the thermal,  
1629 rheological and mechanical properties of thermoplastic polyurethanes. *J Adhes Sci Technol*  
1630 29(11):1136
- 1631 Amat-Amer JM (1999) Tecnología del Calzado, 3rd Diputación de Alicante, Elda, pp 133–146.  
1632 Chapters 15 and 16
- 1633 Arán-Aís F, Torró-Palau AM, Orgilés-Barceló AC, Martín-Martínez JM (2002) Characterization of  
1634 thermoplastic polyurethane adhesives with different hard/soft segment ratio containing rosin  
1635 resin as an internal tackifier. *J Adhes Sci Technol* 16:1431
- 1636 Bahattab MA, Donate-Robles J, García-Pacios V, Martín-Martínez JM (2011) Characterization of  
1637 polyurethane adhesives containing nanosilicas of different particle size. *Int J Adhes Adhes*  
1638 31:97
- 1639 Bahattab MA, García-Pacios V, Donate-Robles J, Martín-Martínez JM (2012) Comparative prop-  
1640 erties of hydrophilic and hydrophobic fumed silica filled two-component polyurethane adhe-  
1641 sives. *J Adhes Sci Technol* 26:303
- 1642 Barni A, Levi M (2003) Aqueous polyurethane dispersions: a comparative study of polymerization  
1643 processes. *J Appl Polym Sci* 88(3):716
- 1644 Basaka GC, Bandyopadhyay A, Neogic S, Bhowmick AK (2011) Surface modification of argon/  
1645 oxygen plasma treated vulcanized ethylene propylene diene polymethylene surfaces for  
1646 improved adhesion with natural rubber. *Appl Surf Sci* 257:2891
- 1647 Brewis DM, Dahm RH (2003) Mechanistic studies of pretreatments for elastomers. In: *Proceedings*  
1648 *of Swiss Bonding 2003*, Zurich, p 69
- 1649 Brewis DM, Dahm RH, Mathieson I (1997) A new general method of pretreating polymers. *J Mater*  
1650 *Sci Lett* 16(2):93
- 1651 Cakić SM, Špirková M, Ristić IS, B-Simendić JK, M-Cincović M, Poręba R (2013) The waterborne  
1652 polyurethane dispersions based on polycarbonate diol: effect of ionic content. *Mater Chem Phys*  
1653 138(1):277
- 1654 Cantos-Delegido B, Martín-Martínez JM (2015) Treatment with Ar-O<sub>2</sub> low-pressure plasma of  
1655 vulcanized rubber sole containing noticeable amount of processing oils for improving adhesion  
1656 to upper in shoe industry. *J Adhes Sci Technol* 29(13):1301
- 1657 Carter AR (1969) Lacsol: problems and a new use. SATRA Bull 13(14):222
- 1658 Carter AR (1971) Halogenation of thermoplastic rubbers. SATRA Bull 14(13):202
- 1659 Cepeda-Jiménez CM, Pastor-Blas MM, Ferrándiz-Gómez TP, Martín-Martínez JM (2000) Surface  
1660 characterization of vulcanized rubber treated with sulfuric acid and its adhesion to polyurethane  
1661 adhesive. *J Adhes* 73:135
- 1662 Cepeda-Jiménez CM, Pastor-Blas MM, Ferrándiz-Gómez TP, Martín-Martínez JM (2001) Influence  
1663 of the styrene content of thermoplastic styrene-butadiene rubbers in the effectiveness of the  
1664 treatment with sulfuric acid. *Int J Adhes Adhes* 21:161
- 1665 Cepeda-Jiménez CM, Pastor-Blas MM, Martín-Martínez JM, Gottschalk P (2002) A new water-  
1666 based chemical treatment based on sodium dichloroisocyanurate (DCI) for rubber soles in  
1667 footwear industry. *J Adhes Sci Technol* 16(3):257

- 1668 Cepeda-Jiménez CM, Pastor-Blas MM, Martín-Martínez JM, Gottschalk P (2003a) Treatment of  
1669 thermoplastic rubber with bleach as an alternative halogenation treatment in the footwear  
1670 industry. *J Adhes* 79(3):207
- 1671 Cepeda-Jiménez CM, Torregrosa-Maciá R, Martín-Martínez JM (2003b) Surface modifications of EVA  
1672 copolymers by using RF oxidizing and non-oxidizing plasmas. *Surf Coat Technol* 174–175:94
- 1673 Cuervo CR, Maldonado AJ (1984) Solution adhesives based on graft polymers of neoprene and  
1674 methyl methacrylate. *Du Pont Elastomers Bull*
- 1675 Diputación de Alicante (1974) Estudio sobre control de calidad en la industria del calzado.  
1676 Diputación de Alicante, Alicante, pp 53–115. Chapter III
- 1677 Dollhausen M (1985) Polyurethane adhesives. In: Oertel G (ed) *Polyurethane handbook*. Hanser,  
1678 Munich, pp 548–562. Chapter 11
- 1679 Dollhausen M (1988) Polyurethane adhesives based on Baycoll, Desmocoll and Desmodur, Tech-  
1680 nical report. Bayer AG, Leverkusen
- 1681 Donate-Robles J, Martín-Martínez JM (2011a) Comparative properties of thermoplastic polyure-  
1682thane adhesive filled with natural or precipitated calcium carbonate. *Macromol Symp* 301:63
- 1683 Donate-Robles J, Martín-Martínez JM (2011b) Addition of precipitated calcium carbonate filler to  
1684 thermoplastic polyurethane adhesives. *Int J Adhes Adhes* 31:795
- 1685 Donate-Robles J, Liauw CW, Martín-Martínez JM (2014) Flow micro-calorimetry and FTIR  
1686 spectroscopy study of interfacial interactions in uncoated and coated calcium carbonate filled  
1687 polyurethane adhesives. *Macromol Symp* 338:72
- 1688 Extrand CW, Gent AN (1987) Contact angle and spectroscopic studies of chlorinated and  
1689 unchlorinated natural rubber surfaces. *Rubber Chem Technol* 61:688
- 1690 Fernández-García JC, Orgilés-Barceló AC, Martín-Martínez JM (1991) Halogenation of styrene-  
1691 butadiene rubber to improve its adhesion to polyurethane. *J Adhes Sci Technol* 5:1065
- 1692 Ferrándiz-Gómez T, Almela M, Martín-Martínez JM, Maldonado F, Orgilés-Barceló AC (1994)  
1693 Effect of surface modification of leather on its joint strength with polyvinyl chloride. *J Adhes Sci*  
1694 *Technol* 8:1043
- 1695 Fisher W (1971) Einheitliche Prüfmethode für Klebstoffe der Schuhindustrie. *Adhäsion* 15(1):372
- 1696 Fisher W, Meuser H (1964) Mindestvoraussetzungen für die Prüfung von Schuklebstoffen. *Shuh-*  
1697 *Tech* 55(9):1039
- 1698 Frisch KC Jr (2002) Chemistry and technology of polyurethane adhesives. In: Chaudhury M,  
1699 Pocius AV (eds) *Adhesion science and engineering. surface chemistry and applications*, vol 2.  
1700 Elsevier, Amsterdam, pp 776–801. Chapter 16
- 1701 García-Martín C, Andreu-Gómez V, Martín-Martínez JM (2010) Surface modification of vulca-  
1702nized styrene-butadiene rubber with trichloroisocyanuric acid solutions of different active  
1703 chlorine contents. *Int J Adhes Adhes* 30:550
- 1704 García-Pacios V, Costa V, Colera M, Martín-Martínez JM (2010) Affect of polydispersity on the  
1705 properties of waterborne polyurethane dispersions based on polycarbonate polyol. *Int J Adhes*  
1706 *Adhes* 30:456
- 1707 García-Pacios V, Colera M, Costa V, Martín-Martínez JM (2011a) Waterborne polyurethane dispersions  
1708 obtained with polycarbonate of hexanediol intended for use as coatings. *Prog Org Coat* 71:136
- 1709 García-Pacios V, Iwata Y, Colera M, Martín-Martínez JM (2011b) Influence of the solids content on  
1710 the properties of waterborne polyurethane dispersions obtained with polycarbonate of hexa-  
1711 nediol. *Int J Adhes Adhes* 31(8):787
- 1712 García-Pacios V, Colera M, Iwata Y, Martín-Martínez JM (2013a) Incidence of the polyol nature in  
1713 waterborne polyurethane dispersions on their performance as coatings on stainless steel. *Prog*  
1714 *Org Coat* 76(12):1726
- 1715 García-Pacios V, Jofre-Reche JA, Costa V, Colera M, Martín Martínez JM (2013b) Coatings  
1716 prepared from waterborne polyurethane dispersions obtained with polycarbonates of  
1717 1,6-hexanediol of different molecular weights. *Prog Org Coat* 76(10):1484
- 1718 Guggenberger SK (1990) Neoprene (polychloroprene)-based solvent and latex adhesives. In: Skeist  
1719 I (ed) *Handbook of adhesives*, 3rd edn. Van Nostrand Reinhold, New York, pp 284–306.  
1720 Chapter 15

- 1721 Guidetti G, Sacchetti G, Tribelhorn U (1992) In: Gum WF, Riese W, Ulrich H (eds) Footwear, in  
1722 reaction polymers. Hanser, Munich, p 649. Chapter IV-H
- 1723 Hace D, Kovacevic V, Manoglovic D, Smit I (1990) The investigation of structural and morpho-  
1724 logical changes after the chlorination of rubber surfaces. *Angew Makromol Chem* 176:161
- 1725 Harrington WF (1990) Elastomeric adhesives. In: Engineered materials handbook. Adhesives and  
1726 sealants, 3. ASM International, Washington, DC, pp 143–150
- 1727 Hu S, Luo X, Li Y (2015) Production of polyols and waterborne polyurethane dispersions from  
1728 biodiesel-derived crude glycerol. *J Appl Polym Sci* 132(6):41425
- 1729 Huang SM, Chen TK (2007) Effects of ion group content and polyol molecular weight  
1730 on physical properties of HTPB-based waterborne poly(urethane-urea)s. *J Appl Polym Sci*  
1731 105(6):3794
- 1732 Jang JY, Jhon YK, Cheong IW, Kim JH (2002) Effect of process variables on molecular weight and  
1733 mechanical properties of water-based polyurethane dispersion. *Colloids Surf A: Physicochem*  
1734 *Eng Asp* 196(2–3):135
- 1735 Jaúregui-Beloqui B, Fernández-García JC, Orgilés-Barceló AC, Mahiques-Bujanda MM, Martín-  
1736 Martínez JM (1999) Rheological properties of thermoplastic polyurethane adhesive solutions  
1737 containing fumed silicas of different surface areas. *Int J Adhes Adhes* 19:321
- 1738 Jofre-Reche JA, Martín-Martínez JM (2013) Selective surface oxidation of ethylene-vinyl acetate  
1739 and ethylene polymer blend by UV-ozone treatment. *Int J Adhes Adhes* 43:42
- 1740 Keibal NA, Bondarenko SN, Kablov VF (2011) Modification of adhesive compositions based on  
1741 polychloroprene with element-containing adhesion promoters. *Polym Sci Ser D* 4(4):267
- 1742 Kelly DJ, McDonald JW (1963) Solution compatibility of neoprene with elastomers and resins. *Du*  
1743 *Pont Elastomers Bull*
- 1744 Kim BK, Lee JC (1996) Waterborne polyurethanes and their properties. *J Polym Sci A: Polym*  
1745 *Chem* 34(6):1095
- 1746 Kim BK, Kim TK, Jeong HM (1994) Aqueous dispersion of polyurethane anionomers from  
1747  $H_{12}$ MDI/IPDI, PCL, BD, and DMPA. *J Appl Polym Sci* 53(3):371
- 1748 Kotrade Ph, Jofre-Reche JA, Martín-Martínez JM (2011) Surface modification of natural vulcanized  
1749 rubbers containing excess of antiadherent moieties. In: Proceedings of adhesion 2011, London
- 1750 Kozakiewicz J (1991) Polyurethanes and isocyanates containing hydrophilic groups as potential  
1751 components of water-borne adhesives. In: Allen KW (ed) *Adhesion 15*. Elsevier, London, pp  
1752 80–101. Chapter 6
- 1753 Kueker P, Jeske W, Melchior M (2016) Modern waterborne contact adhesives: 1k application  
1754 property level. In: Proceedings of FEICA 2016 conference, Vienna. Paper 16-BOS-05-2
- 1755 Landete-Ruiz MD, Martín-Martínez JM (2005) Surface modification of EVA copolymer by UV  
1756 treatment. *Int J Adhes Adhes* 25:139
- 1757 Landete-Ruiz MD, Martín-Martínez JM (2015) Improvement of adhesion and paint ability of EVA  
1758 copolymers with different vinyl acetate contents by treatment with UV-ozone. *Int J Adhes*  
1759 *Adhes* 58:34
- 1760 Lawson DF, Kim KJ, Fritz TL (1996) Chemical modification of rubber surfaces: XPS survey of the  
1761 reactions of trichloroisocyanuric acid at the surfaces of vulcanized elastomers. *Rubber Chem*  
1762 *Technol* 69:245
- 1763 Lee SK, Kim BK (2009) High solid and high stability waterborne polyurethane via ionic groups in  
1764 soft segments and chain termini. *J Colloid Interface Sci* 336(1):208
- 1765 Lijie H, Yongtao D, Zhiliang Z, Zhongsheng S, Zhihua S (2015) Synergistic effect of anionic and  
1766 nonionic monomers on the synthesis of high solid content waterborne polyurethane. *Colloids*  
1767 *Surf A Physicochem Eng Asp* 467(20):46
- 1768 Liu X, Xu K, Liu H, Cai H, Su J, Fu Z, Guo Y, Chen M (2011) Preparation and properties of  
1769 waterborne polyurethanes with natural dimer fatty acids based polyester polyol as soft segment.  
1770 *Prog Org Coat* 72(4):612
- 1771 Lyons D, Christell LA (1997) Waterborne polychloroprene adhesives. *Adhes Sealants Ind* 46
- 1772 Maciá-Agulló TG, Fernández-García JC, Pastor-Sempere N, Orgilés-Barceló AC, Martín-Martínez  
1773 JM (1992) Addition of silica to polyurethane adhesives. *J Adhes* 38:31

- Madbouly SA, Otaigbe JU, Nanda AK, Wicks DA (2005) Rheological behavior of aqueous polyurethane dispersions: effects of solid content, degree of neutralization, chain extension, and temperature. *Macromolecules* 38(9):4014
- Martin D (1971) Cork sandals. Weaknesses to guard against. *SATRA Bull* 14(13):195
- Martínez-García A, Sánchez-Reche A, Martín-Martínez JM (2003a) Surface modifications on EVA treated with sulfuric acid. *J Adhes* 79(6):525
- Martínez-García A, Sánchez-Reche A, Gisbert-Soler S, Cepeda-Jiménez CM, Torregrosa-Maciá R, Martín-Martínez JM (2003b) Treatment of EVA with corona discharge to improve its adhesion to polychloroprene adhesive. *J Adhes Sci Technol* 17(1):47
- Martín-Martínez JM (2002) Rubber base adhesives. In: Chaudhury M, Pocius AV (eds) *Adhesion science and engineering. surfaces chemistry and applications*, vol 2. Elsevier, Amsterdam, pp 573–675. Chapter 13
- Martín-Martínez JM (2008) Improving adhesion of rubber. In: Bhowmick AK (ed) *Current topics in elastomers research*. CRC Press, Boca Raton, pp 761–773
- Moreno-Couranjou M, Choquet P, Guillot J, Migeon HN (2009) Surface modification of natural vulcanized rubbers by atmospheric dielectric barrier discharges plasma treatments. *Plasma Process Polym* 6:S397
- Moyano MA, Martín-Martínez JM (2014) Surface treatment with UV-ozone to improve adhesion of vulcanized rubber formulated with an excess of processing oil. *Int J Adhes Adhes* 55:106
- Mumtaz F, Zuber M, Zia KM, Jamil T, Hussain R (2013) Synthesis and properties of aqueous polyurethane dispersions: influence of molecular weight of polyethylene glycol. *Korean J Chem Eng* 30(12):2259
- Oldfield D, Symes TEF (1983) Surface modification of elastomers for bonding. *J Adhes* 16:77
- Orgilés-Calpena E, Arán-Ais F, Torró-Palau AM, Orgilés-Barceló C, Martín-Martínez JM (2009a) Addition of different amounts of a urethane-based thickener to waterborne polyurethane adhesive. *Int J Adhes Adhes* 29:309
- Orgilés-Calpena E, Arán-Ais F, Torró-Palau AM, Orgilés-Barceló C, Martín-Martínez JM (2009b) Influence of the chemical structure of urethane-based thickeners on the properties of waterborne polyurethane adhesives. *J Adhes* 85:665
- Orgilés-Calpena E, Arán-Ais F, Torró-Palau AM, Orgilés-Barceló C, Martín-Martínez JM (2009c) Effect of annealing on the properties of waterborne polyurethane adhesive containing urethane-based thickener. *Int J Adhes Adhes* 29:774
- Orgilés-Calpena E, Arán-Ais F, Torró-Palau AM, Orgilés-Barceló C, Martín-Martínez JM (2009d) Addition of urethane-based thickener to waterborne polyurethane adhesives having different NCO/OH ratios and ionic groups contents. *J Adhes Sci Technol* 23:1953
- Orgilés-Calpena E, Arán-Ais F, Torró-Palau AM, Orgilés-Barceló C (2016a) Influence of the chain extender nature on adhesives properties or polyurethane dispersions. *J Dispers Sci Technol* 33(1):147
- Orgilés-Calpena E, Arán-Ais F, Torró-Palau AM, Orgilés-Barceló C (2016b) Novel polyurethane reactive hot melt adhesives based on polycarbonate polyols derived from CO<sub>2</sub> for the footwear industry. *Int J Adhes Adhes* 70:218
- Ortiz-Magán AB, Pastor-Blas MM, Ferrándiz-Gómez TP, Morant-Zacarés C, Martín-Martínez JM (2001) Surface modifications produced by N<sub>2</sub> and O<sub>2</sub> RF-plasma treatment on a synthetic vulcanised rubber. *Plasmas Polym* 6(1,2):81
- Paiva RMM, Marques EAS, da Silva LFM, António CAC, Arán-Ais F (2016) Adhesives in the footwear industry. *Proc IMechE Part L: J Mater: Des Appl* 230(2):357
- Pastor-Blas MM, Martín-Martínez JM, Dillard JG (1998) Surface characterization of synthetic vulcanized rubber treated with oxygen plasma. *Surf Interf Anal* 26:385
- Pastor-Blas MM, Ferrándiz-Gómez TP, Martín-Martínez JM (2000) Chlorination of vulcanized styrene-butadiene rubber using solutions of trichloroisocyanuric acid in different solvents. *J Adhes Sci Technol* 14:561
- Pastor-Sempere N, Fernández-García JC, Orgilés-Barceló AC, Torregrosa-Maciá R, Martín-Martínez JM (1995) Fumaric acid as a promoter of adhesion in vulcanized synthetic rubbers. *J Adhes* 50:25



- 1827 Penczek P, Nachtkamp K (1987) Resins used in adhesives. In: Frisch K, Reegen S (eds) *Advances*  
1828 *in urethane science and technology*, vol 4. Technomic, Las Vegas, p 121
- 1829 Pérez-Limiñana MA, Torró-Palau AM, Orgilés-Barceló AC, Martín-Martínez JM (2003) Modifi-  
1830 cation of the rheological properties of polyurethanes by adding fumed silica: influence of the  
1831 preparation procedure. *Macromol Symp* 194:161
- 1832 Pérez-Limiñana MA, Arán-Ais F, Torró-Palau AM, Orgilés-Barceló C, Martín-Martínez JM (2006)  
1833 Structure and properties of waterborne polyurethane adhesives obtained by different methods.  
1834 *J Adhes Sci Technol* 20(6):519
- 1835 Pérez-Limiñana MA, Arán-Ais F, Torró-Palau AM, Orgilés-Barceló C, Martín-Martínez JM (2007)  
1836 Influence of the hard-to-soft segment ratio on the adhesion of water-borne polyurethane  
1837 adhesive. *J Adhes Sci Technol* 21(8):755
- 1838 Pettit D, Carter AR (1964) Adhesion of translucent rubber soling. *SATRA Bull* 11(2):17
- 1839 Pettit D, Carter AR (1973) Behaviour of urethane adhesives on rubber surfaces. *J Adhes* 5:333
- 1840 Radabutra S, Thanawan S, Amornsakchai T (2009) Chlorination and characterization of natural  
1841 rubber and its adhesion to nitrile rubber. *Eur Polym J* 45:2017
- 1842 Rahman MM (2013) Synthesis and properties of waterborne polyurethane adhesives: effect of chain  
1843 extender of ethylene diamine, butanediol, and fluoro-butanediol. *J Adhes Sci Technol* 27(23):2592
- 1844 Rahman MM, Kim H (2006) Synthesis and characterization of waterborne polyurethane adhesives  
1845 containing different amount of ionic group (I). *J Appl Polym Sci* 102(6):5684
- 1846 Rahman MM, Lee I, Chun H, Kim H, Park H (2014) Properties of waterborne polyurethane-  
1847 fluorinated marine coatings: the effect of different types of diisocyanates and tetra-  
1848 fluorobutanediol chain extender content. *J Appl Polym Sci* 131:39905
- 1849 Romero-Sánchez MD, Martín-Martínez JM (2003) Treatment of vulcanised styrene-butadiene  
1850 rubber (SBR) with mixtures of trichloroisocyanuric acid and fumaric acid. *J Adhes* 79:1111
- 1851 Romero-Sánchez MD, Pastor-Blas MM, Martín-Martínez JM (2003a) Treatment of a styrene-  
1852 butadiene-styrene rubber with corona discharge to improve the adhesion to polyurethane  
1853 adhesive. *Int J Adhes Adhes* 23(1):49
- 1854 Romero-Sánchez MD, Pastor-Blas MM, Martín-Martínez JM, Walzak MJ (2003b) UV treatment of  
1855 synthetic styrene-butadiene-styrene rubber. *J Adhes Sci Technol* 17(1):25
- 1856 Romero-Sánchez MD, Martín-Martínez JM (2008) UV-ozone surface treatment of SBS rubbers  
1857 containing fillers: influence of the filler nature on the extent of surface modification and  
1858 adhesion. *J Adhes Sci Technol* 22(2):147
- 1859 SATRA-Preparation of leather uppers (1963) *SATRA Bull* 10(17):229
- 1860 Schollenberger CS (1977) Polyurethane and isocyanate-based adhesives. In: Skeist I (ed) *Handbook*  
1861 *of adhesives*, 3rd edn. Van Nostrand Reinhold, New York
- 1862 Souza EMM, da Costa W, Silva LGA, Wiebeck H (2016) Behavior of adhesion forces of the  
1863 aqueous-based polychloroprene adhesive magnetically conditioned. *J Adhes Sci Technol*  
1864 30(15):1689
- 1865 Sultan Nasar A, Srinivasan G, Mohan R, Radhakrishnan G (1998) Polyurethane solvent-based  
1866 adhesives for footwear applications. *J Adhes* 68:21
- 1867 Tanno T, Shibuya L (1967) Special behaviour of para tertiary phenol dialcohol in polychloroprene  
1868 adhesives. *Adhesives and Sealant Council Meeting*
- 1869 Torregrosa-Coque R, Martín-Martínez JM (2011) Influence of the configuration of the plasma  
1870 chamber on the surface modification of synthetic vulcanized rubber treated with low-pressure  
1871 oxygen RF plasma. *Plasma Process Polym* 8:1080
- 1872 Torregrosa-Coque R, Alvarez-García S, Martín-Martínez JM (2011a) Effect of temperature on the  
1873 extent of migration of low molecular weight moieties to rubber surface. *Int J Adhes Adhes*  
1874 31(1):20
- 1875 Torregrosa-Coque R, Alvarez-García S, Martín-Martínez JM (2011b) Migration of low molecular  
1876 weight moiety at rubber-polyurethane interface: an ATR-IR study. *Int J Adhes Adhes* 31:389
- 1877 Torregrosa-Coque R, Alvarez-García S, Martín-Martínez JM (2012) Migration of paraffin wax to  
1878 sulphur vulcanized styrene-butadiene rubber (SBR) surface: effect of temperature. *J Adhes Sci*  
1879 *Technol* 26(6):813

- 1880 Tyczkowski J, Krawczyk I, Wozniak B, Martín Martínez JM (2009) Low-pressure plasma chlori-  
1881 nation of styrene-butadiene block copolymer for improved adhesion to polyurethane adhesives.  
1882 Eur Polym J 45:1825
- 1883 Vega-Baudrit J, Sibaja-Ballester M, Nuñez S, Martín-Martínez JM (2009) Study of the relationship  
1884 between nanoparticles of silica and thermoplastic polymer (TPU) in nanocomposites. J Nano-  
1885 tech Prog Int (JONPI) 1:24
- 1886 Vélez-Pagés T (2003) Modificación de un serraje sin lijar por aplicación de un agente imprimante  
1887 monocomponente para mejorar su adhesión a adhesivos de poliuretano. Master thesis, Univer-  
1888 sity of Alicante
- 1889 Vicent BJ, Natarajan B (2014) Waterborne polyurethane from polycaprolactone and tetra-  
1890 methylxylene diisocyanate: synthesis by varying NCO/OH ratio and its characterization as  
1891 wood coatings. Open J Org Polym Mater 4(1):37
- 1892 Vukov R (1984) Halogenation of butyl rubber – a model compound approach. Rubber Chem  
1893 Technol 57(2):275
- 1894 Wang H, Zhou Y, He M, Dai Z (2015) Effects of soft segments on the waterproof of anionic  
1895 waterborne polyurethane. Colloid Polym Sci 293(3):875
- 1896 Whitehouse RS (1986) Contact adhesives. In: Wake WC (ed) Synthetic adhesives and sealants.  
1897 Wiley, Chichester, pp 1–29. Chapter 1
- 1898 Yañez-Pacios A, Antoniac I, Martín-Martínez JM (2013) Surface modification and adhesion of  
1899 vulcanized rubber containing an excess of paraffin wax treated with 2 wt% trichloroisocyanuric  
1900 acid solution at different temperature. In: Proceeding of 36th adhesion society conference,  
1901 Daytona Beach. Soft adhesives I -paper 1
- 1902 Yang C, Yang H, Wen T, Wu M, Chang J (1999) Mixture design approaches to IPDI-H6XDI-XDI  
1903 ternary diisocyanate-based waterborne polyurethanes. Polymer 40(4):871
- 1904 Yang Z, Zhu Y, Peng F, Fu C (2014) Preparation and application of undecylenate based diol for  
1905 bio-based waterborne polyurethane dispersion. Adv Mater Res 955–959:88
- 1906 Yin L, Zhou H, Quan Y, Fang J, Chen Q (2012) Prompt modification of styrene-butadiene rubber  
1907 surface with trichloroisocyanuric acid by increasing chlorination temperature. J Appl Polym Sci  
1908 124:661
- 1909 Zhang K, Shen H, Zhang X, Lan R, Chen H (2009) Preparation and properties of a waterborne  
1910 contact adhesive based on polychloroprene latex and styrene-acrylate emulsion blend. J Adhes  
1911 Sci Technol 23(1):163
- 1912 Zhang K, Huang C, Shen H, Chen H (2012) Modification of polychloroprene rubber latex by  
1913 grafting polymerization and its application as a waterborne contact adhesive. J Adhes 88(2):119

Silvio de Barros, Luiz C. M. Meniconi, Valber A. Perrut, and  
Carlos E. Reuther de Siqueira

## Contents

52.1	Introduction .....	1534
52.2	Standards and Recommended Practices .....	1537
52.2.1	ISO 24817:2015: Petroleum, Petrochemical and Natural Gas Industries – Composite Repairs for Pipework – Qualification and Design, Installation, Testing and Inspection .....	1538
52.2.2	API 653: Tank Inspection, Repair, Alteration, and Reconstruction .....	1540
52.2.3	ASME PCC-2–2015: Repair of Pressure Equipment and Piping .....	1541
52.3	Actual Applications .....	1541
52.3.1	FRP Pipe Connections .....	1542
52.3.2	Repair of Steel Pipes .....	1542
52.3.3	Ship Hull and Naval Structures .....	1543

S. de Barros (✉)

Department of Mechanical Engineering, Federal Center of Technological Education in Rio de Janeiro – CEFET/RJ, Rio de Janeiro, RJ, Brazil  
e-mail: [silvio.debarros@gmail.com](mailto:silvio.debarros@gmail.com)

L. C. M. Meniconi

Research and Development Center, CENPES, Petróleo Brasileiro S.A. – PETROBRAS, Rio de Janeiro, RJ, Brazil  
e-mail: [luiz.meniconi@gmail.com](mailto:luiz.meniconi@gmail.com)

V. A. Perrut

Research and Development Center, CENPES, Petróleo Brasileiro S.A. – PETROBRAS, Rio de Janeiro, RJ, Brazil

Metallurgical and Materials Engineering Department, Federal University of Rio de Janeiro, Rio de Janeiro, Brazil

e-mail: [vperrut@petrobras.com.br](mailto:vperrut@petrobras.com.br)

C. E. Reuther de Siqueira

Department of Offshore Engineering, Petróleo Brasileiro S.A. – PETROBRAS, Rio de Janeiro, RJ, Brazil

e-mail: [reuther@petrobras.com.br](mailto:reuther@petrobras.com.br)

16	52.3.4	Metallic Storage Tanks .....	1548
17	52.3.5	Pipe Saddles .....	1551
18	52.3.6	Coamings .....	1552
19	52.4	Conclusion .....	1553
20		References .....	1554

Abstract

There has been an increase in using adhesives in the oil industry in the last years. The main advantage of using adhesive bonding is to avoid the fire risk concerning the traditional weld process. Adhesives also feature protection against corrosion which is a main concern in offshore installations. Different from other industrial applications, where adhesive bonding is used to manufacture new structures or some parts of them, the oil industry mainly uses adhesives to repair pipelines, pipework, and offshore structures. This chapter shows that the use of composites has become a real alternative to structural repairs in situ as these materials become more and more reliable. The chapter also brings a summary of the most applied standards and the best practices recommended to perform bonded repair in offshore units. Finally, some examples of actual applications of adhesives are presented.

52.1 Introduction

There has been an increase in the use of structural adhesives in the oil and gas industry recently. These materials have some inherent performance advantages over other types of joining, mainly welding. They avoid hot work process, which is one of the main advantages in some areas of the oil and gas industry. They also feature protection against corrosion, and the assembly process is faster compared to other types of joining.

In oil installations, process plants, or ship platforms, some maintenance repairs are required during their operating life. Corroded pipes or sidewalls of ships and semisubmersible platforms are some examples. Usually the offshore production units must be sent to shipyards in order to perform repairs of metallic structures. Sometimes it is possible to stop the production for maintenance, but even in these cases an apparatus for inerting of tanks is needed for welding. It results in high direct and indirect costs. The use of composite repairs is an alternative to structural repairs in situ, avoiding the fire risk concerning the traditional weld process. Beyond the security issue, economical aspects should be considered. When welding is carried out in FPSO (floating, production, storage, and offloading) units, not only the tank to be repaired must be emptied but also the other surrounding tanks. It means that the storage capacity of the unit is compromised during the welding process. The reduction in storage capacity of the vessel leads to the reduction in the production of the unit causing financial losses. On the other hand, the use of composite patch repairs kept the reduction in storage capacity of the vessel to a minimum while the repair took place (Turton et al. 2005).

In what concerns corroded pipelines, adhesively bonded composite systems are also seen to be more economical than other repair alternatives. Duell et al. (2008) state that in this case, the use of composite repairs can be one fourth less expensive than welded steel sleeve repairs and three fourths less expensive than the complete replacement of the damaged segment.

Adhesively bonded composite repairs can be considered an effective repair for mechanical damage, such as dent on the longitudinal weld, by increasing the fatigue life of the defective pipe. In most applications, the use a primer adhesive is recommended. But sometimes the lamination resin is at the same time responsible for the adhesion between the repaired metallic substrate and the composite. Depending on the surface conditions, it can be necessary to use a resin as a filler to provide a smooth surface. Thickened resins are often used to fill corroded areas before applying the first layer of the composite material (Rohem et al. 2016).

Many commercial carbon fiber repair systems use epoxy resins (Alnaser and Keller 2015). An epoxy-based primer can also be applied to prevent galvanic corrosion and increase adhesion. The carbon fiber fabric is normally wetted with the epoxy resin, and the wetted fabric is wrapped by the hand around the pipe (Goertzen and Kessler 2007).

When using glass fiber fabric, some authors reported that a vinyl ester resin was found to provide an attractive combination of on-site processability, metal-composite bond toughness, and overall resistance to corrosion (Mablesen et al. 2000). Originally developed to be applied to onshore pipelines, glass fiber composite repairs were gradually proposed to be used in offshore pipelines such as risers. The complex combined loads acting on risers are one of main concerns, since it is completely different from onshore pipelines where the main load is internal pressure (Alexander and Ochoa 2010).

Some examples that show the viability of the use of bonded composite repairs to the two most widely encountered damage scenarios in floating offshore units, fatigue cracking and thickness loss due to corrosion, can be found in the literature. McGeorge et al. (2009) have demonstrated that these repairs can be applied for full-scale trials even under severe sea conditions.

In situ, submerged repairs of damaged piping using composites face several challenges. According to Dhanalakshmi et al. (1997), the primary challenge is the curing and material property development of composite systems that are based on liquid resins that wet out reinforcement and then are applied while submerged. The choice of the appropriate materials to be used is not the only issue. The entire repair operation must be carefully studied, and logistics issues, including the use of divers and the application of repairs to moving structures, must be considered (Mally et al. 2013).

Da Costa Mattos et al. (2014) report the use of a polyurethane pre-impregnated bidirectional glass fiber composite applied to repair corroded pipelines (Fig. 1). According to them, the water-activated polyurethane resin reduces composite preparation time by 50% and is fully cured after 2 h at 24 °C.

Different from other industrial applications, where adhesive bonding is used to manufacture new structures or some parts of them, the oil industry mainly uses adhesives to repair pipelines, pipework, and offshore structures. In most of those

**Fig. 1** Polyurethane pre-impregnated repair



**Fig. 2** Pipeline repair  
(courtesy of TEAM/  
FURMANITE) <https://twitter.com/furmanite/status/723008415182798848>



situations, field conditions are very difficult needing much skill to accomplish the repair operation (Fig. 2). The use of sophisticated surface preparation methods before applying the adhesive is so laborious that the repair becomes too expensive.

Mechanical surface preparation methods are more indicated rather than chemical modification of the surface. Abrasive methods are commonly applied to obtain a specific surface roughness (De Barros et al. 2015). Traditional abrasive wear and erosive wear, such as sandpapering and sandblasting, are still used, but they have been replaced by new methods. The bristle blasting system MBX (Monti Tools Inc., Houston, USA) has been widely used because it can be easily taken to field situations (De Barros et al. 2016). This system uses high-carbon steel wire bristles as shown in Fig. 3.

A new abrasive method is the use of different kinds of Sponge Media™ (Sponge-Jet Inc., Newton, USA). These composite abrasives incorporate micro-abrasive particles within high-performance synthetic sponge (Fig. 4). The main advantage, compared to sandblasting, for instance, is that the synthetic sponge can capture most of the contaminant particles resulting from the blasting operation.

**Fig. 3** MBX system**Fig. 4** Sponge-Jet system

This chapter is structured in three sections. After this introduction showing not only the advantages but also the challengers involving the use of adhesives in oil and gas industry, the next section brings a summary of the most applied standards and the best practices recommended to perform bonded repair in offshore units. The chapter ends with six examples to illustrate actual applications that have been proposed for adhesives in field situations.

---

## 52.2 Standards and Recommended Practices

In offshore structures, an important document, approved by classification societies, is “Design, Fabrication, Operation and Qualification of Bonded Repair of Steel Structures” – DNVGL-RP-C301 from DNV GL (Det Norske Veritas – Germanischer Lloyd). This Recommended Practice (RP) is based upon a project guideline developed within the Joint Industry Project (JIP) “Qualification of Adhesive Bonding in Structural Repair of FPSO’s” sponsored by ConocoPhillips, Norsk

Hydro, Petrobras, Petronas, Shell, and Statoil. The main focus of this document was placed on FPSOs and similar ship-like floating structures, but it can be also equally applicable to the repair of other types of offshore units.

The main objectives of this document are to:

- Provide an international RP of repairs practices for floating units using composite adhesive patches
- Serve as a technical reference document in contractual matters
- Reflect the state-of-the-art and consensus on accepted industry practice and server as a RP for composite adhesive patch repair design, analysis, application, and maintenance

Section 7 of this RP describes materials and bonding agents and points out special considerations for adhesive composite patches on steel substrates.

In what concerns composite repairs, a complementary document is the DNVGL-OS-C501 – Composite Components. It contains more information on the use of adhesives in composite laminated joints.

A list of important standards is summarized following.

#### **52.2.1 ISO 24817:2015: Petroleum, Petrochemical and Natural Gas Industries – Composite Repairs for Pipework – Qualification and Design, Installation, Testing and Inspection**

The objective of this standard is to ensure that pipework, pipelines, tanks, and vessels repaired using composite systems that are qualified, designed, installed, and inspected using this standard will meet the specified performance requirements. Repair systems are designed for use within the petroleum, petrochemical, and natural gas industries and also within utility service applications. The main users of this standard will be plant and equipment owners of the pipework and vessels, design contractors, suppliers contracted to provide the repair system, certifying authorities, installation, maintenance, and inspection contractors.

The qualification, design, installation, testing, and inspection procedures for composite repair systems in this standard cover situations involving the repair of damage commonly encountered in oil, gas, utility pipework systems, and vessels. The procedures are also applicable to the repair of pipelines, caissons, and storage tanks with appropriate consideration.

Procedures described in this standard cover the repair of metallic and GRP pipework, pipework components, and pipelines originally designed in accordance with a variety of standards, including ISO 15649, ISO 13623, ISO 14692, ASME B31.1, ASME B31.3, ASME B31.4, ASME B31.8, and BS 8010.

This standard is not a defect assessment standard. Within this standard, no statements are made regarding whether a specific defect is acceptable or unacceptable for repair. The standard assumes that a defect assessment has already been performed to, for example, ASME B31G or API RP 579. The starting point



for this standard is that a decision has been taken to repair a given defect with a composite repair system and the output from the defect assessment, e.g., MAWP (maximum allowed work pressure) or minimum remaining wall thickness is used as input for the repair design. The main concern of this standard is with the subsequent activities of repair qualification, design, installation, and inspection.

Repair systems are applied to restore structural integrity. The following repair situations are addressed:

- External corrosion, where the defect is or is not through wall. In this case, the application of a repair system will usually arrest further deterioration.
- External damage such as dents, gouges, and fretting (at supports).
- Internal corrosion, erosion, where the defect is or is not through wall. In this case, corrosion and/or erosion can continue after application of a repair system, and therefore the design of the repair system shall take this into account, i.e., the size of the defect at the end of the required design life of the repair should be taken as the size of the defect when designing the repair.
- Crack-like defects, where the defect is or is not through wall. It is a requirement that the length of the crack is known and will not increase during the lifetime of the repair. For through-wall cracks, the crack should be modeled as a type B defect (through-wall defect), either a circumferential or axial slot (depending on the crack orientation). For non-through-wall cracks, the crack should be modeled as type A defect (non-through-wall defect).
- Strengthening and/or stiffening in local areas.

Services that are covered within the scope of this standard include those normally found in an oil and gas production or processing installation. These include the following:

- Utility fluid, diesel, seawater, and air
- Chemicals (liquids)
- Production fluids, including liquid hydrocarbons, gaseous hydrocarbons, and gas condensates

The upper temperature limit is defined in this standard for different class of repairs in a detailed table. The lower temperature limit is dependent on the type of repair laminate being used. This limit is determined by the design requirements presented in detailed in a table of this standard.

The upper pressure limit is a function of defect type (internal, external, or through wall), defect dimensions (depth and extent), pipe diameter, design temperature, and repair design lifetime. Therefore, a unique number cannot be quoted, but rather the limit is derived for a given set of conditions by calculations in accordance with this standard using the qualification test data. The lower pressure limit, e.g., vacuum conditions, is determined by the design requirements based on external loads. All equations for thickness design are described on this standard.

The composite materials constituting the repair laminate considered within this standard are typically those with aramid (AFRP), carbon (CFRP), glass (GRP), or polyester (or similar material) fiber reinforcement in a polyester, vinyl ester, epoxy, or polyurethane polymer matrix. Other fiber and matrix types are also permissible once qualified.

The pipework and vessel substrates considered within the standard include carbon steel, 6 moly steel, stainless steel, duplex steel, super duplex steel, GRP, cupifer, aluminum, galvanized steel, and titanium. Careful consideration is required before repair of GRP lines because the damage in the pipe may be more extensive than is visible on the surface and may affect a longer length of the pipe than is immediately obvious; advice of the GRP pipe manufacture and repair system supplier shall be sought before a repair is installed.

### **52.2.2 API 653: Tank Inspection, Repair, Alteration, and Reconstruction**

This standard covers steel storage tanks built to API 650 and its predecessor API 12C. It provides minimum requirements for maintaining the integrity of such tanks after they have been placed in service and addresses inspection, repair, alteration, relocation, and reconstruction.

The scope is limited to the tank foundation, bottom, shell, structure, roof, attached appurtenances, and nozzles to the face of the first flange, first threaded joint, or first welding-end connection. Many of the design, welding, examination, and material requirements of API 650 can be applied in the maintenance inspection, rating, repair, and alteration of in-service tanks. In the case of apparent conflicts between the requirements of this standard and API 650 or its predecessor API 12C, this standard shall govern for tanks that have been placed in service.

This standard employs the principles of API 650; however, storage tank owner/operators, based on consideration of specific construction and operating details, may apply this standard to any steel tank constructed in accordance with a tank specification.

This standard is intended for use by organizations that maintain or have access to engineering and inspection personnel technically trained and experienced in tank design, fabrication, repair, construction, and inspection.

This standard does not contain rules or guidelines to cover all the varied conditions which may occur in an existing tank. When design and construction details are not given, and are not available in the as-built standard, details that will provide a level of integrity equal to the level provided by the current edition of API 650 must be used.

This standard recognizes Fitness-for-Service assessment concepts for evaluating in-service degradation of pressure-containing components. API 579-1/ASME FFS-1, Fitness-for-Service, provides detailed assessment procedures or acceptance criteria for specific types of degradation referenced in this standard. When this standard does not provide specific evaluation procedures or acceptance criteria for

a specific type of degradation or when this standard explicitly allows the use of Fitness-for-Service criteria, API 579-1/ASME FFS-1 may be used to evaluate the various types of degradation or test requirements addressed in this standard.

### **52.2.3 ASME PCC-2–2015: Repair of Pressure Equipment and Piping**

This standard provides methods for repair of equipment and piping within the scope of ASME Pressure Technology Codes and Standards after they have been placed in service. These repair methods include relevant design, fabrication, examination, and testing practices and may be temporary or permanent, depending on the circumstances. The methods provided in this standard address the repair of components when repair is deemed necessary based on appropriate inspection and flaw assessment. These inspection and flaw evaluation methods are not covered in this standard, but are covered in other post-construction codes and standards.

This document is divided into five parts:

Part 1 covers the scope, organization, and intent and is applicable to all articles in this standard and also provides guidance for the applicability of repair methods listed in this standard.

Part 2 covers repair methods and techniques that include the use of welding, brazing, soldering, or other methods involving metal deposit.

Part 3 covers mechanical repairs, with or without sealant, such as bolted clamps or fixtures, and includes all repair methods not covered in Part 2 or Part 4.

Part 4 covers repairs using nonmetallic means, such as nonmetallic liners and wraps, and bonding (e.g., joining by epoxy), including bonding of metallic components.

Part 5 covers examination and testing methods and techniques.

This standard provides technical information, procedures, and recommendations for repair methods that were determined by consensus to be recognized and generally accepted good engineering practice. Where equipment repair is subject to jurisdictional regulation, jurisdictional approvals may be required.

---

## **52.3 Actual Applications**

Steel and fiber-reinforced plastic (FRP) are commonly used materials in the oil industry. Sometimes there is a need to join them using adhesive bonding. There are three kinds of situations where adhesives have been used, and their application depends on the substrates to be joined – FRP/FRP joint, FRP/steel joint, or steel/steel joint:

### **FRP/FRP joints**

- FRP pipe connections
- Nonmetallic pipe saddle supports

### FRP/steel joint

- Repair of steel pipes
- Repair of naval structures
- Repair of storage tanks

### Steel/steel joint

- Metallic pipe saddle support

In what follows, some examples of actual applications of adhesives are presented considering these three types of substrate material combination.

## 52.3.1 FRP Pipe Connections

Two joining systems are normally adopted for the assembly of offshore production plant pipework, namely, socket/spigot and laminated joints, as displayed in Fig. 5. The first one is easier to apply in the field and has a self-aligning design but depends on good workmanship to provide a safe and sound connection. If the adhesive joint surfaces are badly cleaned or the adhesive itself is not properly prepared, the joint will have a high probability of failure in service.

The laminated type, on the other hand, is considered to be more reliable as it can be made as thick and long as required, to provide the necessary reinforcement. As several layers of reinforcing cloth and resin are applied from inside out, its final resistance is less variable. In the end, the choice between one type and another is much dependent on the contractor design philosophy.

## 52.3.2 Repair of Steel Pipes

Composite sleeve repair systems, now of widespread use in the market, were originally developed for the reinforcement of corroded pipelines and continue to gain wider acceptance in the pipeline industry for repairing a range of pipeline anomalies (Meniconi et al. 2002). Figure 6 presents the visual aspect of steel pipes before and after the application of the composite repair.

ISO/TS 24817 (2015) and ASME PCC-2 are the codes that cover all aspects of the technology, encompassing material qualification, repair design, installation, testing, and inspection. The documents allow reinforcement of a defected metallic pipe due to presence of general wall thinning, local wall thinning, pitting, gouges, blisters, laminations, cracks, and through-wall penetration. The defects can be located at the external or internal side of the pipe wall. Concerning the last case, the effectiveness of the repair is time-dependent, according to the evolution of the defect. The kinds of services covered are those normally found on hydrocarbon processing plants, like utility fluids, seawater, air, chemicals, production fluids, and

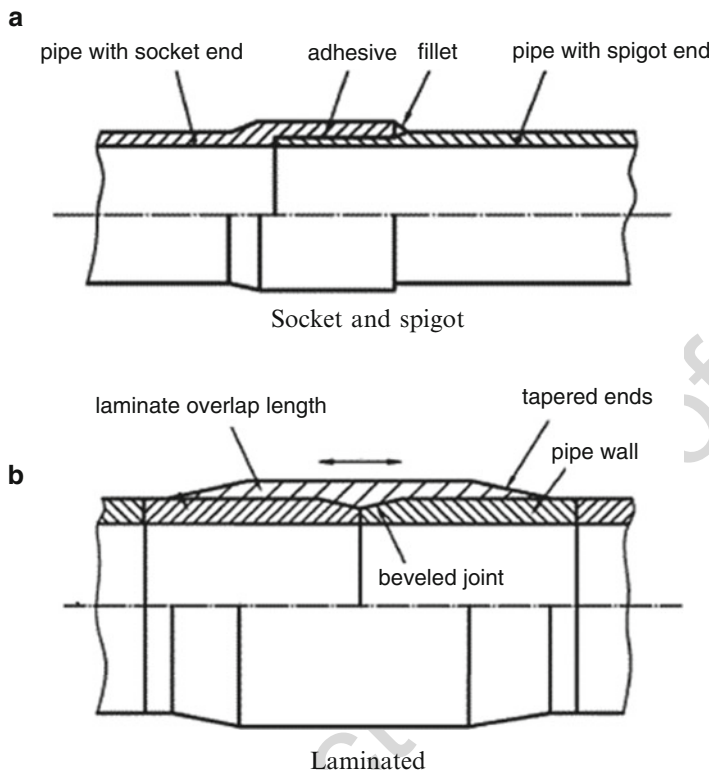


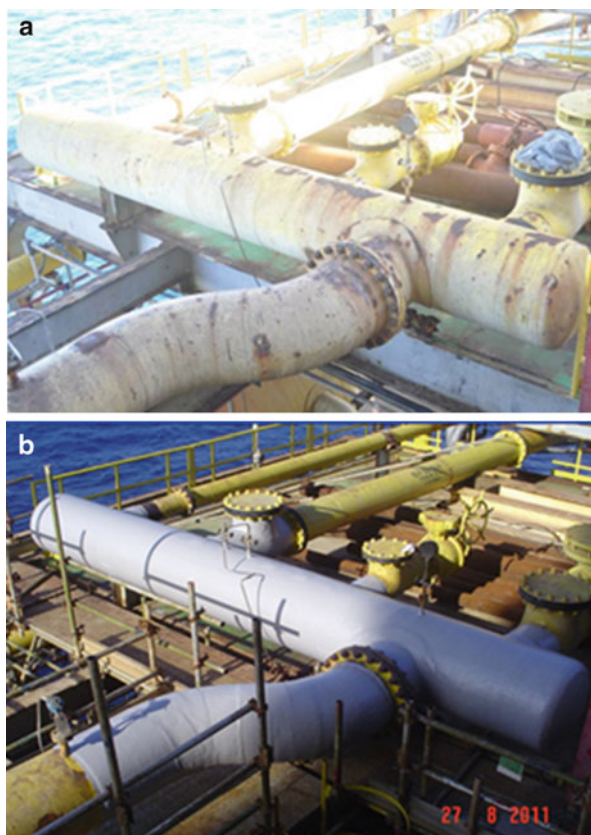
**Fig. 5** Two basic types of FRP pipe connections. (a) Socket and spigot. (b) Laminated

liquid and gaseous hydrocarbons. The composite materials most commonly used for the repair laminates are glass or carbon fibers for reinforcement and vinyl ester or epoxy resins for matrix. The upper limits for pressures and temperatures are obtained from qualification tests. The ISO document establishes three classes of repairs. The higher the class, the more demanding is the application and the information required, concerning material data, design capability, surface preparation, and degradation with time. In relation to lifetime, repairs are classified as short term (2 years), medium term (10 years), or long term (20 years).

### 52.3.3 Ship Hull and Naval Structures

Offshore production structures like floating, production, storage, and offloading (FPSO) vessels are designed to remain in station for 25 years or more. This is a major deviation from the traditional ship maintenance scheme, which involves dry docking every 5 years or so, for overhaul maintenance. Due to this scenario, in place

**Fig. 6** Steel pipes before (a) and after (b) the application of the composite repair



repair techniques are an excellent option to restore structural integrity without the need of interrupting production.

Composite patch repairs are one of those techniques, because no hot work is involved, turning the operation intrinsically safe. Many successful application cases of this technique are reported (Grabovac and Whittaker 2009). Figure 7 shows the first composite repair applied to the metallic hull of a ship platform operating in offshore Brazil.

The repair procedure based on reliability design method, as proposed by DNVGL-RP-C301, provides repair solutions that assure a minimum safety level in relation to a given limit state. For a specific repair, there is a need to identify all the possible failure modes that can cause bad performance in relation to its functional requirements. Examples of composite repair failure modes are debonding, matrix cracking, delamination, fiber rupture, fluid permeation, etc. Examples of functional requirements are load-bearing capacity, level of stiffness, fluid tightness, chemical inertness, erosion resistance, fire survival, etc. The concept of risk adopted is the

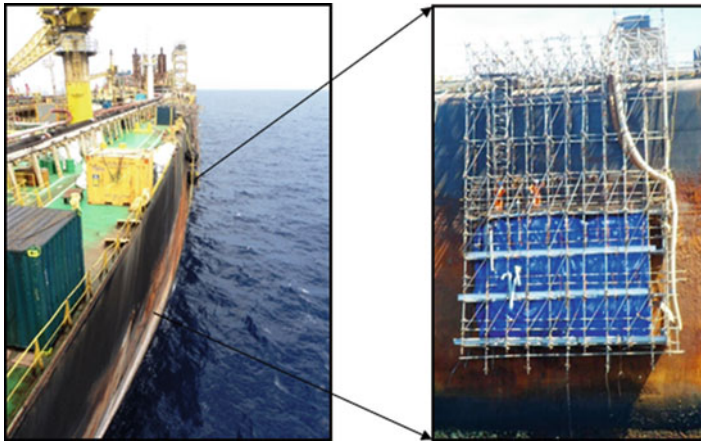


**Fig. 7** Composite repair applied to a ship hull

usual combination of probability and consequence of failure. Statistical methods are applied to guarantee a minimum reliability, corresponding to a probability of failure of  $10^{-3}$  once the repair is completed.

Composite bonded repairs are separated in four reliability repair classes with different levels of effort and optimization:

- Class 0 – Emergency repairs, done empirically without integrity and efficiency qualification by any code or standard.
- Class I – Noncritical repairs qualified by reliable estimates based on short-term and small-scale tests. Repair efficiency is evaluated by standard statistical methods.
- Class II – Noncritical repairs qualified by accelerated time degradation tests together with long-term behavior simulation models. The reliability level is higher than that of class I repairs. Classes I and II are the ones considered by the design document.
- Class III – Repairs qualified by long-term degradation tests, designed to assure the desired reliability level along the whole life of the structure. Given the little experience accumulated so far with composite bonded repairs, class III is not covered by DNVGL-RP-C301, yet.

The design equations criteria are formulated in terms of load and resistance characteristic values, affected both by partial safety factors, which take into account the random nature of design input data. Basically, the design process aims to satisfy the following inequality:

$$\gamma_F \cdot \gamma_{Sd} \cdot S_k \leq \frac{R_K}{\gamma_M \cdot \gamma_{Rd}} \quad (1)$$

where  $S_k$  is the characteristic effect of the load applied to the repaired structure that can lead to the failure mode under analysis. It is multiplied by partial load factors  $\gamma_F$ , associated to the variability of loading, and  $\gamma_{Sd}$  related to the uncertainties of the adopted model of structural behavior. Similarly,  $R_k$  is the characteristic structural resistance, divided by the partial resistance factors  $\gamma_M$ , referred to time and sampling variations of material strength and  $\gamma_{Rd}$ , concerning geometric aspects and fabrication processes. When dealing with the static capacity of the adhesive layer between the metallic substrate and the composite patch, the equation criterion above is written as:

$$J \leq \frac{R_{II}}{\gamma_M} \quad (2)$$

The load  $J$ , expressed as the energy per unit area of resulting adhesive debonding introduced by mechanical factored load combination, needs to be smaller than or at most equal to the mode II toughness of the interface,  $R_{II}$ , divided by the partial material factor  $\gamma_M$ , obtained from the Recommended Practice.

For the first applications of DNVGL-RP-C301, only class I repairs were considered. This class of repair is qualified by small-scale, short-term tests which results are statistically treated to make sure that the necessary repair capacity is achieved within design lifetime. This generally implies that larger partial safety factors are adopted, to account for aging effects. A minimum reliability level of  $10^{-3}$  is achieved when all the requirements are fulfilled.

The first scenario chosen for the application of composite repairs was the reposition of metallic thickness loss due to corrosion, given its simpler nature. Nevertheless, this kind of repair is classified as structural, because it attracts mechanical loading once deployed. The repair is also two-dimensional in nature, making it easier to design and qualify. It can be applied whenever there is sufficient lateral area to transfer the load from the metallic substrate to the composite patch repair, via shear stresses in the adhesive layer. Furthermore, it is a type of remedial action with great demand from an aging production platform fleet.

The two-dimensional repair qualified is rated “simple” according to the design document because it can be calculated by means of a basic theoretical model, since it fulfilled four requisites:

- The lamination directions coincide with those of the main loading.
- The overlap length  $L$  is long enough to provide regions in the bondline at the borders of the repair where the shear stresses at the adhesive were equal to zero, according to Fig. 8.

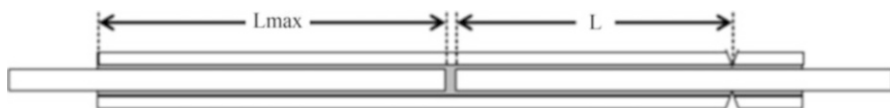


**Fig. 8** Modified double-strap specimen where notches are used to obtain the desired overlap length



This is achieved when the following expression holds:

$$L > 2 \frac{F}{w \cdot \tau_p} \text{ or } L > 2 \cdot e_m \tag{3}$$

where  $F$  is the repair failure load, estimated from simple models, and  $w$  is the composite patch width. The parameter  $\tau_p$  is the adhesive critical plastic shear stress and  $e_m$  is the maximum adhesive layer overlap effective length, obtained from double-lap shear tests (Meniconi et al. 2010).

Shorter overlap lengths can be accepted if:

- It is demonstrated that the minimum shear stress in the adhesive is smaller than 10% of the interface critical plastic shear stress.
- Bending stresses are limited, resulting in reduced adhesive peel stresses. Adhesives normally display limited strength against this kind of loading.
- Adhesive critical plastic shear stress is smaller than the out-of-plane shear strength of the repair laminate, estimated in a conservative way. This implies a failure mode by debonding of the adhesive layer rather than by delamination of the composite repair laminate.

For the bondline, there are two distinct failure modes that need to be considered. The most fundamental one is debonding propagating from the center at the discontinuity in steel. This corresponds to the case where a cracked steel plate is repaired. The other one is debonding propagating from the edges of a patch repair, but in general this only occurs after failure in steel by yielding had already developed thus showing that bondline fracture toughness is not the governing factor for the capacity of the repaired plate.

Common practice is to provide repair border edge thickness tapering widths of 10–20 times the total laminate thickness, which are generally enough to efficiently reduce the out-of-plane stresses that would trigger debonding from there. The thickness reduction at the boundaries of composite patch repairs also helps to protect them from lateral impacts and other contact damage. Table 1 lists the functional requirements proposed for a patch repair designed for metallic plating thickness loss reposition.

Some demonstration repairs already performed in the field showed that the design methodology proposed by DNVGL-RP-C301 proved feasible, at least for the

**Table 1** Functional requirements to be achieved by a thickness reposition patch repair

Functional requirements	Comments
Strength	Restore steel plating strength
Stiffness	Restore steel plating stiffness
Corrosion resistance	Not to be degraded by exposition to ambient
Temperature resistance	Material properties still acceptable at 60°C
Electric insulation	To prevent the formation of a galvanic pair

simpler case of restoration of steel thickness loss greater than the maximum allowable by the classification society of the offshore platform. Even though ambient conditions are generally far from ideal, it was possible to provide enough cleanliness, illumination, temperature, and humidity to make manual lamination work feasible. The importance of adequate surface preparation should never be underestimated.

It is strongly advised to pay special attention in planning surface preparation and execution of the first sealing layer of the repair. The previous cleaning and drying of the repair area are also important. Grit blasting is essential to get the necessary surface profile. Polymer-coated grit helped in performing a clean operation, but conventional grit will also suffice, if one considers that normally the areas to be repaired are not too extensive. The volume of dust to be aspirated afterward will not be excessive. It must be assured that the initial tasks – surface preparation, cleaning, and sealing – are performed sequentially without any delay, given the need of a dry, rust-free surface to obtain good adhesion between the patch repair and the metallic substrate. This is the optimal situation, but it demands good logistics to move and replace quickly the equipment and personnel involved in those tasks. It should be remembered that the repair location can be situated in a remote and difficult-to-access part of the platform.

Inspections executed afterward confirmed that the repairs already performed remain intact. More inspections will occur along the years, to make sure this situation continues. As this is a new development, only repair performance during the entire platform operational lifetime in real operational conditions will assure that the proposed solution works (Meniconi et al. 2014).

#### 52.3.4 Metallic Storage Tanks

Metallic storage tanks are cylindrical structures which hold oil and their derivatives and are very important to the supply chain in the oil industry. These tanks are made of thin steel plates welded together, and the large-capacity ones often are of the floating roof type. During operation, corrosion wall thickness loss frequently occurs at the inner metallic surface of the tank shell in contact with the roof seal, where rainwater tends to accumulate. The thickness loss can happen in wide areas, as the roof position changes during operation. Figure 9 shows defects found inside steel tank plating, characterized by general wall loss due to corrosion.

This corrosion mechanism may lead to a value less than acceptable minimum corroded wall thickness according to API 579 and can affect the structural integrity of the tank. In this case, welding repair is the most commonly used to restore integrity. This repair technique is quite complex and expensive, and hot working is necessary. Special care is needed to prevent severe deformation of the slender tank wall as it is heated during the welding process. In this context, composite repair seems to be an excellent alternative as this technology is very simple, fast, and cost-effective. The repair is accomplished by applying layers of carbon or glass fiber, at the outer surface of the tank wall, opposite to the corroded area. This is to avoid



**Fig. 9** Defects found in steel tank: inside view (*left*) and corroded surface detail (*right*)



**Fig. 10** Repairing a storage tank: repair overview (*left*) and repair application (*right*)

interference with the correct operation of the floating roof. An example of a repair in a storage tank can be seen in Fig. 10.

Differently from pipelines, there is no specific code to cover the repair of storage tanks by composite materials. Due to this factor, a design methodology for composite repairs of corroded storage tanks was proposed that considers the requirements of API 653, ISO/TS 24817 and DNVGL-RP-C301.

Two main factors turn composite repairs very suitable for this application. Firstly, the wide tank surface provides an extensive area to transfer loading from the steel plates to the composite laminates by means of shear stress in the adhesive layer between the two materials. Secondly, the steel tank wall plating is in a state of plane stress, mainly unidirectional, adequately resisted by composite laminates, which shows high stiffness and strength in lamination plane and fiber direction. Moreover, the materials, equipment, and workmanship involved are quite similar to those needed for painting operations, very common in this industrial environment.

The properties of the adhesive interface already mentioned, the critical plastic shear stress  $\tau_p$  and the maximum effective overlap length  $e_m$ , define a limit in steel thickness loss that can be reinstated by a patch repair. Figure 11 illustrates this

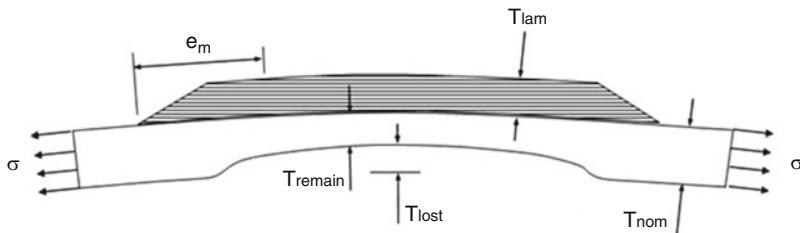


**Fig. 11** Schematic description of a patch repair, with relevant parameters

principle, by means of a segment of tank shell with unitary height. There is a corrosion thickness loss at the inside surface of the shell, remediated by a composite laminate reinforcement at the corresponding outside surface.

The local circumferential stress at the non-corroded plating away from the defected area is  $\sigma$ . The composite laminate thickness  $T_{lam}$  is readily obtained as the main design drive is to reinstate the stiffness loss caused by corrosion:

$$E_{lam} \cdot T_{lam} = E_{steel} \cdot T_{lost} \Rightarrow T_{lam} = \frac{E_{steel} \cdot T_{lost}}{E_{lam}} \quad (4)$$

The laminate elastic modulus  $E_{lam}$  (as well as all other composite properties) are referred to the circumferential direction of the tank wall. Once the circumferential stress is transferred from the metallic wall to the composite laminate through shear stresses at the adhesive interface, the highest unitary load  $f_p$  that can be transmitted is given by:

$$f_p = \tau_p \cdot e_m = \sigma_{lam} \cdot T_{lam} \quad (5)$$

The equilibrium of resultant forces implies that:

$$\begin{aligned} \sigma \cdot T_{nom} &= \sigma_{remain} \cdot T_{remain} + \sigma_{lam} \cdot T_{lam} \\ \sigma \cdot T_{nom} &= \sigma_{remain} \cdot (T_{nom} - T_{lost}) + \tau_p \cdot e_m \end{aligned}$$

so

$$\sigma_{remain} \cdot T_{lost} = T_{nom} \cdot (\sigma_{remain} - \sigma) + \tau_p \cdot e_m \quad (6)$$

The formulation above considers linear elastic behavior. Since the elastic modulus of the laminate is usually smaller than that of steel, the laminate thickness turns considerably greater than the steel thickness loss. Knowing composite laminates typical elastic moduli, high-strength carbon fiber is applied instead of fiberglass, to keep laminate thickness feasible to be applied in practice. As high-strength carbon is the chosen repair material, once the stiffness replacement criterion is fulfilled, the composite laminate circumferential stress  $\sigma_{lam}$  results low when compared with the corresponding strength. For this reason, it is possible to allow the stress acting on the

remaining steel wall,  $\sigma_{\text{remain}}$ , to reach steel yield strength  $S_y$ . The design code for atmospheric storage tanks limits the average circumferential stress at the shell,  $\sigma$ , to a typical value of  $0.75 S_y$ , during hydrostatic test. Considering this limit, the expression for the maximum steel thickness loss prone to be replaced by a patch repair then reads:

$$T_{\text{lost}} = 0.25 T_{\text{nom}} + \tau_p \cdot e_m / S_y \quad (7)$$

Typical figures are nominal steel plating thicknesses of 19 mm (at the level corrosion normally occurs), critical adhesive plastic shear stresses ( $\tau_p$ ) of 10 MPa, maximum effective overlap lengths  $e_m$  of 90 mm, and steel yield stresses of 250 MPa. In conclusion, up to 8.3 mm of steel thickness loss can be replaced by a composite patch repair laminate. This limit covers most corrosion cases that happen in practice. The major elastic modulus of the laminate is of the order of 100 GPa, compared with a modulus of 210 GPa for steel, so its thickness would be around 17 mm, roughly double the steel thickness lost. The average longitudinal stress at the composite laminate turns to be about 50 MPa, one sixth of its ultimate tensile limit of 300 MPa. The low stresses (and strains) at the laminate are important contributions for a long operational life of the repair and, moreover, of the adhesive interface.

### 52.3.5 Pipe Saddles

A pipe saddle is a structure used to support the pipe by transmitting the load or forces to the adjacent structure. It avoids direct contact between the pipe and the support, reducing stress concentration. Some of them are designed to allow longitudinal movement due to thermal expansion and contraction of pipe and are also designed to prevent damage to pipe thermal insulation. Figure 12 shows examples of adhesively bonding saddles with different substrates.

Carbon steel is the main material used for manufacturing the saddles. Stainless steel is another material that can be found. Saddles are installed just below the pipe mainly by welding, and this process can lead to some problems related to corrosion and metallurgical defects. These areas are susceptible to higher corrosion rates because of crevice and galvanic effects, and historically inspecting them has involved costly and time-consuming operations to lift the pipe or to cut the supports.

Corrosion under support is a well-known issue within all oil and gas assets around the world. The external corrosion forms itself between the pipe support and flow line and tends to be nonuniform and unpredictable. The corrosion is often caused by movement of the pipe on the support which damages the protective coating on the pipe. This leaves the exposed metal free to corrosion attack from the environment in an area where it cannot be detected and in most cases not even protected. The general problem with corrosion under pipe supports is that it is very hard to inspect the remaining wall thickness. In many cases the pipe would have to be lifted to understand the real impact of the corrosion attack. This is of course very labor intensive, risky, and expensive as the plant operations would have to be shut down.

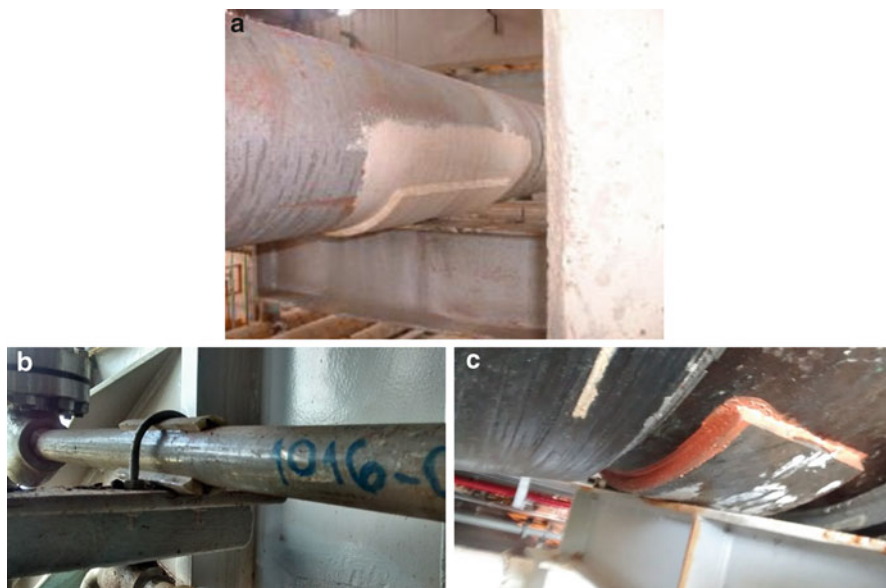


**Fig. 12** Pipe saddles: (a) steel pipe and steel saddle (b) steel pipe and FRP saddle (c) FRP pipe and FRP saddle

Alternatively, pipe saddle can be glued onto the pipe surface instead of welding. In addition, it is possible to use pipe saddles made of nonmetallic materials as FRP. They provide many advantages to the system: to prevent from further corrosion on support area, to avoid galvanic effect, to not require hot work to install, and to be faster and easier to install compared to welding. It is important to mention that the adhesive must be thoroughly applied to avoid crevice corrosion caused by trapped water (Fig. 13).

### 52.3.6 Coamings

Coaming is a raised metal border around a ship's deck or an equipment, designed to avoid oil leaking or chemical fluids into the sea. Welding is the main process used to place coamings over the metallic surface (Fig. 14).

The installation of these structures demands lots of time, workmanship, and logistic to perform welding. Furthermore, hot work can damage surround and internal paintings, which makes necessary to repaint these affected areas. This activity can be very complex, especially for internal surfaces where it might be required to install scaffolding inside the oil tank, for instance.

When installed at the beginning of the assembly process, these coamings create a physical barrier making it difficult for technicians, equipment, and assembly devices to move over the platform, which is still in the test and integration phase.





**Fig. 13** Adhesive application: over pipe surface (*left*) and the saddle (*right*)



**Fig. 14** Coaming: around an equipment (*left*) and detail of welded coaming (*right*)

In this context, the possibility of using alternative technologies, such as adhesive bonding, to the traditional method (welding), arises, allowing to increase productivity and to prevent rework in the painting process.

## 52.4 Conclusion

In this chapter, it was shown that the application of adhesives in many different situations in the oil industry has increased in the last years. The use of composites has become a real alternative to structural repairs as these materials become more and more reliable. In this sense, the development of adhesive bonding methods has become inexorable. On the other hand, it was shown that field conditions do not allow the use of sophisticated process to perform the adhesive bonding. It makes necessary to adjust the surface preparations methods to these unfavorable situations, for instance.

The chapter also brings a summary of the most applied standards and the best practices recommended to perform bonded repair in offshore units. Besides, some examples of actual applications of adhesives are presented. In what concerns the materials to be bonded, the three main situations where the adhesives have been used

in oil industry are presented, namely, FRP/FRP joint, FRP/steel joint, and steel/steel joint.

Despite of all the challengers involving the use of adhesives in field situations, the advantages of applying this technique are pushing engineers and researchers to propose the necessary solutions. There is no doubt that adhesive bonding is becoming essential as a safe joint technique in oil industry.

## References

- Alexander C, Ochoa OO (2010) Extending onshore pipeline repair to offshore steel risers with carbon–fiber reinforced composites. *Compos Struct* 92(2):499–507. ISSN 0263-8223, <http://dx.doi.org/10.1016/j.compstruct.2009.08.034>
- Alnaser IA, Keller MW (2015) Comparison of coupon and full-scale determination of energy release rate for bonded composite repairs of pressure equipment. *Eng Fract Mech* 146:31–40. ISSN 0013-7944, <http://dx.doi.org/10.1016/j.engfracmech.2015.07.023>. (<http://www.sciencedirect.com/science/article/pii/S0013794415003902>)
- API 579-1/ASME FFS-1 Fitness-For-Service (n.d.)
- API 653 (n.d.) Tank Inspection, repair, alteration, and reconstruction
- ASME PCC-2–2015 (n.d.) Repair of pressure equipment and piping
- da Costa Mattos HS, Reis JML, Paim LM, da Silva ML, Amorim FC, Perrut VA (2014) Analysis of a glass fibre reinforced polyurethane composite repair system for corroded pipelines at elevated temperatures. *Compos Struct* 114:117–123. ISSN 0263-8223, <http://dx.doi.org/10.1016/j.compstruct.2014.04.015>. (<http://www.sciencedirect.com/science/article/pii/S0263822314001822>)
- De Barros S, Kenedi PP, Ferreira SM, Budhe S, Bernardino AJ, Souza LFG (2015) Influence of mechanical surface treatment on fatigue life of bonded joints. *J Adhes.* <https://doi.org/10.1080/00218464.2015.1122531>. <http://dx.doi.org/10.1080/00218464.2015.1122531>
- De Barros S, Banea MD, Budhe S, de Siqueira CER, Lobão BSP, Souza LFG (2016) Experimental analysis of metal-composite repair of floating offshore units (FPSO). *J Adhes.* <https://doi.org/10.1080/00218464.2016.1177514>. <http://dx.doi.org/10.1080/00218464.2016.1177514>
- Design, fabrication, operation and qualification of bonded repair of steel structures – DNVGL-RP-C301 from DNV GL (Det Norske Veritas – Germanischer Lloyd) (n.d.)
- Dhanalakshmi M, Maruthan K, Jayakrishnan P, Rengaswamy NS (1997) Coatings for underwater and wet surface application. *Anti-Corros Methods Mater* 44(6):393–399
- DNVGL-OS-C501 – Composite Components (n.d.)
- Duell JM, Wilson JM, Kessler MR (2008) Analysis of a carbon composite overwrap pipeline repair system. *Int J Press Vessel Pip* 85(11):782–788. ISSN 0308-0161, <http://dx.doi.org/10.1016/j.ijpvp.2008.08.001>. (<http://www.sciencedirect.com/science/article/pii/S0308016108001026>)
- Goertzen WK, Kessler MR (2007) Dynamic mechanical analysis of carbon/epoxy composites for structural pipeline repair. *Compos Part B* 38(1, 1):–9. ISSN 1359-8368, <http://dx.doi.org/10.1016/j.compositesb.2006.06.002>. (<http://www.sciencedirect.com/science/article/pii/S1359836806000825>)
- Grabovac I, Whittaker D (2009) Application of bonded composites in the repair of ships structures – a 15-year service experience. *Compos A: Appl Sci Manuf* 40(9):1381–1398. ISSN 1359-835X, <http://dx.doi.org/10.1016/j.compositesa.2008.11.006>. (<http://www.sciencedirect.com/science/article/pii/S1359835X08002984>)
- ISO 24817: 2015 – Petroleum, petrochemical and natural gas industries – composite repairs for pipework – qualification and design, installation, testing and inspection (2015)
- Mableson AR, Dunn KR, Dodds N, Gibson AG (2000) Refurbishment of steel tubular pipes using composite materials. *Plast Rubber Compos* 29:10,558–10,565. <https://doi.org/10.1179/146580100101540770>



- Mally TS, Johnston AL, Chann M, Walker RH, Keller MW (2013) Performance of a carbon-fiber/epoxy composite for the underwater repair of pressure equipment. *Compos Struct* 100:542–547. ISSN 0263-8223, <http://dx.doi.org/10.1016/j.compstruct.2012.12.015>
- McGeorge D, Echtermeyer AT, Leong KH, Melve B, Robinson M, Fischer KP (2009) Repair of floating offshore units using bonded fibre composite materials. *Compos A: Appl Sci Manuf* 40 (9):1364–1380. ISSN 1359-835X, <http://dx.doi.org/10.1016/j.compositesa.2009.01.015>. (<http://www.sciencedirect.com/science/article/pii/S1359835X09000153>)
- Meniconi LM, Freire JF, Vieira RD, Diniz JC (2002) Stress analysis of pipelines with composite repairs. ASME. International pipeline conference, 4th international pipeline conference, pp 2031–2037. <https://doi.org/10.1115/IPC2002-27372>
- Meniconi LCM, Porciuncula IN, McGeorge D, Pedersen A (2010) Structural repair at a production platform by means of a composite material patch. *Offshore Technol Conf*. <https://doi.org/10.4043/20657-MS>
- Meniconi et al (2014) Experimental fatigue and aging evaluation of the composite patch repair of a metallic ship hull. *Appl Adhes Sci* 2:27. 10.1186/s40563-014-0027-8
- Rohem NRF, Pacheco LJ, Budhe S, Banea MD, Sampaio EM, de Barros S (2016) Development and qualification of a new polymeric matrix laminated composite for pipe repair. *Compos Struct* 152 (15):737–745. ISSN 0263-8223, <http://dx.doi.org/10.1016/j.compstruct.2016.05.091>. (<http://www.sciencedirect.com/science/article/pii/S0263822316307140>)
- Turton TJ, Dalzel-Job J, Livingstone F (2005) Oil platforms, destroyers and frigates – case studies of QinetiQ's marine composite patch repairs. *Compos A: Appl Sci Manuf* 36(8):1066–1072. ISSN 1359-835X, <http://dx.doi.org/10.1016/j.compositesa.2004.11.006>. (<http://www.sciencedirect.com/science/article/pii/S1359835X04002702>)

Uncorrected Proof

# Molecular Dynamics Simulation and Molecular Orbital Method

53

Ya-Pu Zhao, Feng-Chao Wang, and Mei Chi

## Contents

53.1	Introduction .....	1560
53.2	Molecular Dynamics Simulation .....	1561
53.2.1	Basic Theory .....	1562
53.2.2	Force Fields .....	1562
53.2.3	Boundary Conditions .....	1564
53.2.4	Energy Minimization .....	1566
53.2.5	Integrators .....	1567
53.2.6	Analysis of the MD Results .....	1568
53.2.7	Water Models Used in MD Simulations .....	1570
53.2.8	Examples of MD Implements .....	1571
53.3	Molecular Orbital Method .....	1576
53.3.1	Introduction .....	1576
53.3.2	Density Functional Theory .....	1578
53.3.3	Examples of DFT Calculations .....	1582
53.4	Hybrid Quantum Mechanics/Molecular Mechanics (QM/MM) Methods .....	1585
53.4.1	Basic Theory .....	1586
53.4.2	QM/MM Boundary Treatments .....	1588
53.4.3	Examples of QM/MM Simulations .....	1588
53.5	Ab Initio Molecular Dynamics (AIMD) .....	1590
53.6	Conclusion .....	1592
	References .....	1593

## Abstract

Computer simulations have provided a powerful technique in understanding the fundamental physics and mechanics of adhesion. In this chapter, various

Y.-P. Zhao (✉) · F.-C. Wang · M. Chi

State Key Laboratory of Nonlinear Mechanics (LNM), Institute of Mechanics, Chinese Academy of Sciences, Beijing, China

e-mail: [yzhao@imech.ac.cn](mailto:yzhao@imech.ac.cn); [wangfc@lnm.imech.ac.cn](mailto:wangfc@lnm.imech.ac.cn); [wangfc@ustc.edu.cn](mailto:wangfc@ustc.edu.cn);  
[chim@lnm.imech.ac.cn](mailto:chim@lnm.imech.ac.cn)

simulation methods pertaining to adhesion technology are introduced, such as the molecular dynamics simulations, the quantum mechanics calculations, the molecular orbital method, the density functional theory, and the molecular mechanics simulations. Besides, some combined methods such as the hybrid quantum mechanics/molecular mechanics simulations, ab initio molecular dynamics, and the density-functional-based tight-binding method are reviewed. General features and routines of these methods as well as the basic theory are described. The advantages and disadvantages of these methods are compared and discussed. Each method has the distinctive advantage and is suitable for specific condition. Some examples are proposed to give the direct perception when investigating adhesion issues using various simulation methods. All these instances are expected to be helpful to readers when performing the corresponding simulations and analyzing of the results.

### 53.1 Introduction

As hierarchical, multiscale, and complex properties in nature, as shown in Fig. 1, adhesion is an interdisciplinary subject, which undergoes vast experimental, numerical, and theoretical investigations from microscopic to macroscopic levels. As an example, adhesion in micro- and nano-electromechanical systems (MEMS/NEMS) is one of the outstanding issues in this field including the micromechanical process

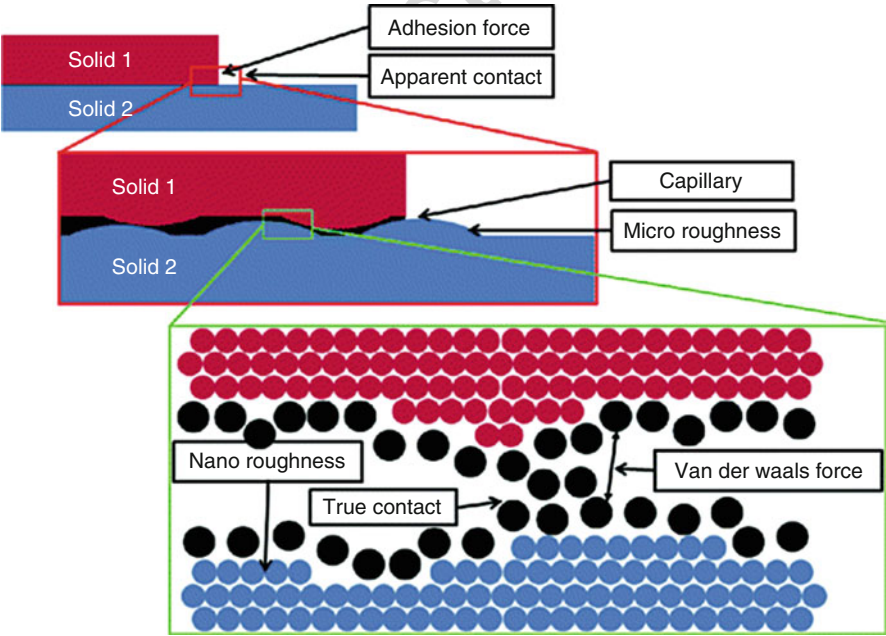


**Fig. 1** Hierarchical and multiscale nature of adhesion

of making and breaking of adhesion contact; the coupling of physical interactions; the trans-scale (nano–micro–macro) mechanisms of adhesion contact, adhesion hysteresis; and the new effective ways of adhesion control (Zhao et al. 2003).

Computer simulations including quantum mechanics (QM) calculations and molecular dynamics (MD) simulations have provided a powerful technique in understanding the fundamental physics of micro- and nanoscale adhesion (Shi et al. 2005; Yin et al. 2005; Chi and Zhao 2009; Yuan et al. 2009). QM method has been proven accurate and provided fundamental understanding for a wide variety of phenomena, including the energy levels of atoms, the band structure of lattice, and the chemical reaction of the materials. The key rule of the QM is to establish the Hamiltonians of the system and to solve the many-body Schrödinger equation (Leach 2001). QM method has the advantage over MD simulations that it includes the effects of charge transfer, polarization, and bond breaking and forming from the beginning. However, the QM computation is always expensive. So QM simulation is employed for the investigation of the chemical reaction in which a few number of atoms are needed, while MD simulation is well suited for the investigation of the dynamics process and time-dependent properties for relatively large systems (Allen and Tildesley 1989). Besides, the molecular mechanics (MM) simulation method is used to study the conformational transformation of the system. Due to some drawbacks of classical MD, *ab initio* MD (AIMD) is proposed to describe the molecular system dynamic behavior directly from the electronic structure. The development of the hybrid quantum mechanics/molecular mechanics (QM/MM) algorithm (Field et al. 1990) is guided by the general idea that an electronically important region of the system is treated with QM and the remainder admits a classical description, which combines both merits of QM and MM. The QM/MM method is a powerful and effective tool to investigate the adhesion issues such as the polymer interaction with metals. The density-functional-based tight-binding (DFTB) method is also one of the combined simulation methods which integrates the density functional theory (DFT) and the tight binding (TB) method. It should be noted that any one of the aforementioned methods has both advantages and disadvantages. One should pay extra attention when choosing a method before performing simulations.

---

## 53.2 Molecular Dynamics Simulation

Molecular dynamics (MD) is a computer simulation technique with which one can obtain the time evolution of a system of interacting particles (atoms, molecules, coarse-grained particles, granular materials, etc.). It was first introduced to study the interactions of hard spheres by Alder and Wainwright in the late 1950s (Alder and Wainwright 1959). With the rapid developments of the computer technology, MD simulations have become a powerful technique and are widely used in the study of proteins and biomolecules, as well as in materials science. This method is now routinely used to investigate the structure, dynamics, and thermodynamics of

biological molecules and their complexes addressing a variety of issues including tribology and adhesion (Bharat 2004).

### 53.2.1 Basic Theory

The basic idea of the MD simulations is to generate the atomic trajectories of a system of  $N$  particles by numerical integration, of a set of Newton's equations of motion for all particles in the system

$$m_i \frac{\partial^2 \vec{r}_i}{\partial t^2} = \vec{F}_i \quad (1)$$

where  $F_i$  is the force exerted on particle  $i$ ,  $m_i$  is the mass of particle  $i$ , and  $r_i$  is its current position. The force can be derived from the gradient of the potential energy

$$\vec{F}_i = - \frac{\partial U(\vec{r}_1, \vec{r}_2, \dots, \vec{r}_N)}{\partial \vec{r}_i} \quad (2)$$

in which  $U(\vec{r}_1, \vec{r}_2, \dots, \vec{r}_N)$  is the empirical interaction potential, depending on the position of the  $N$  particles. Given certain boundary conditions, as well as an initial set of positions and velocities, which are referenced as the initial condition, the equations of motions for a specific interatomic potential can be solved and then the information including atomic positions and velocities generated. One may have an interest in the conversion of this microscopic information to macroscopic observables such as pressure, energy, temperature, etc., which requires statistical mechanics. In contrast with the Monte Carlo method, MD is a deterministic technique: The subsequent time evolution is in principle completely determined. Two basic assumptions of the MD simulations are: (i) The motions of all the particles obey the classical Newton's laws of motion, and (ii) the interactions between any pair of the particles satisfy the superposition theorem.

To summarize, the highly simplified description of the MD simulation algorithm is illustrated in Fig. 2.

### 53.2.2 Force Fields

In a MD simulation, a force field which includes the functional form and parameter sets needs to be specified in order to describe the interaction between atoms and molecules, which is also called the potential energy of a system of particles. Force field functions and parameter sets are derived from both experimental work and high-level quantum mechanical calculations. Most force fields are empirical and consist of a summation of bonded forces associated with chemical bonds, bond angles, bond dihedrals, out-of-plane bending, and nonbonded forces associated with

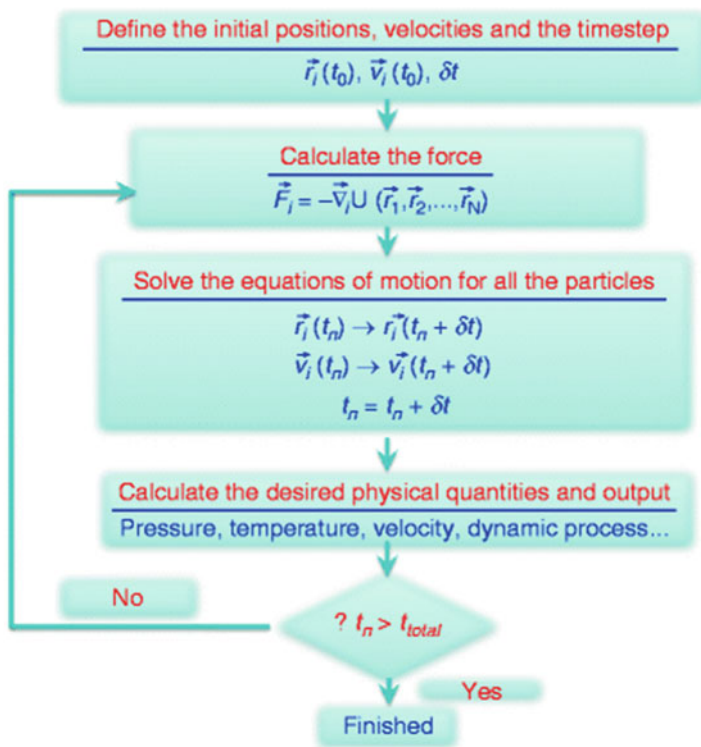


**Fig. 2** Simplified flowchart of a standard MD simulation

119 van der Waals forces and the Coulomb forces. The most commonly used functional  
120 forms are

$$U = U_{\text{nobond}} + U_{\text{bond}} + U_{\text{angle}} + U_{\text{dihedral}} + U_{\text{improper}} + U_{\text{elec}} \quad (3)$$

121 Van der Waals interaction can be expressed as the best well-known  
122 Lennard–Jones (LJ) 12–6 function (Jones 1924),

$$U_{\text{nobond}} = 4\varepsilon \left[ \left( \frac{\sigma}{r} \right)^{12} - \left( \frac{\sigma}{r} \right)^6 \right] \quad (4)$$

123 where  $\varepsilon$  is the depth of the potential well,  $\sigma$  is the distance at which the interatom  
124 potential is zero, and  $r$  is the distance between atoms. In a MD simulation, the  
125 truncation schemes are always adopted. Here, we introduce the simplest one in  
126 which the potential is discontinuous at  $r = r_c$

$$U_{\text{nobond}}(r) = \begin{cases} U_{\text{nobond}}(r) - U_{\text{nobond}}(r_c), & r < r_c \\ 0 & r \geq r_c \end{cases} \quad (5)$$

127 The interaction between pairs of bonded atoms has the form of

$$U_{\text{bond}} = k_b(r - r_0)^2 \quad (6)$$

128 where  $k_b$  is the stiffness of the bond with the usual 1/2 factor included and  $r_0$  is the  
129 equilibrium bond distance. The interaction of valence angles in the molecule can be  
130 written as

$$U_{\text{angle}} = k_a(\theta - \theta_0)^2 \quad (7)$$

131 where  $k_a$  is the stiffness of the bond angle with the usual 1/2 factor included and  $\theta$   
132 and  $\theta_0$  are the bond angle and its reference value, respectively.

133 The dihedral interaction, also referred to as torsional terms, can be written as

$$U_{\text{dihedral}} = k_d[1 + \cos(n\phi - \gamma)] \quad (8)$$

134 in which  $\phi$  is the dihedral angle,  $\gamma$  acts as an equilibrium angle,  $k_d$  is the force  
135 constant, and  $n$  is the multiplicity which gives the number of minimum points in the  
136 function as the bond is rotated through 360°. The improper torsion is used to  
137 describe the out-of-plane bending term. It can be modeled using the form of

$$U_{\text{improper}} = k_i(\psi - \psi_0)^2 \quad (9)$$

138 in which  $k_i$  is the improper torsion force constant and  $\psi$  and  $\psi_0$  are the improper  
139 torsion angle and its reference value, respectively.

140 The coulombic pairwise interaction is given by

$$U_{\text{elec}} = \frac{Cq_iq_j}{r} \quad (10)$$

141 where  $C$  is an energy conversion constant and  $q_i$  and  $q_j$  are the charges on the two  
142 atoms.

143 The abovementioned potentials can be classified into the empirical ones, which may  
144 not be sufficiently accurate to reproduce the dynamics of molecular systems in some  
145 cases. There are also a wide variety of semiempirical potentials, known as TB poten-  
146 tials, which use QM matrix representation whose elements are obtained through  
147 empirical formulae. For more accurate cases, ab initio QM methods are used to calculate  
148 the potential energy of the system on the fly, which is the combination of first principles  
149 electronic structure methods with MD based on Newton's equations of motion.

### 150 53.2.3 Boundary Conditions

151 There are two major types of boundary conditions: isolated boundary condition and  
152 periodic boundary condition (PBC). PBC enables a simulation to be performed using



a relatively small number of particles in such a way that the particles behave as if it was infinite in size and there were no edge effects. All the particles are expected to experience forces as though they were in a bulk solution. When using PBC, particles are enclosed in a box, and one can imagine that this box is replicated to infinity by rigid translation in all the Cartesian directions, completely filling the space. In a two-dimensional (2D) example, each simulation box is surrounded by 8 mirror images, while in 3D the mirror image number would be 26. The concept of 2D PBC is illustrated in Fig. 3. The shaded box (marked as “E”) represents the system being simulated, while the surrounding boxes are the copies in every detail. Even the velocities (indicated by the arrows) and the forces are exactly the same. When a particle leaves the simulation cell, it is replaced by another with exactly the same velocity, entering from the opposite cell face. So the number of particles in the cell is conserved. Furthermore, no particle feels any surface force, as these are now completely removed.

Forces on the primary particles are calculated from particles within the same box as well as in the image box. In Fig. 3,  $R_{\text{cut}}$  is the cutoff radius that is normally applied when calculating the force between two particles. As one can see, a particle may

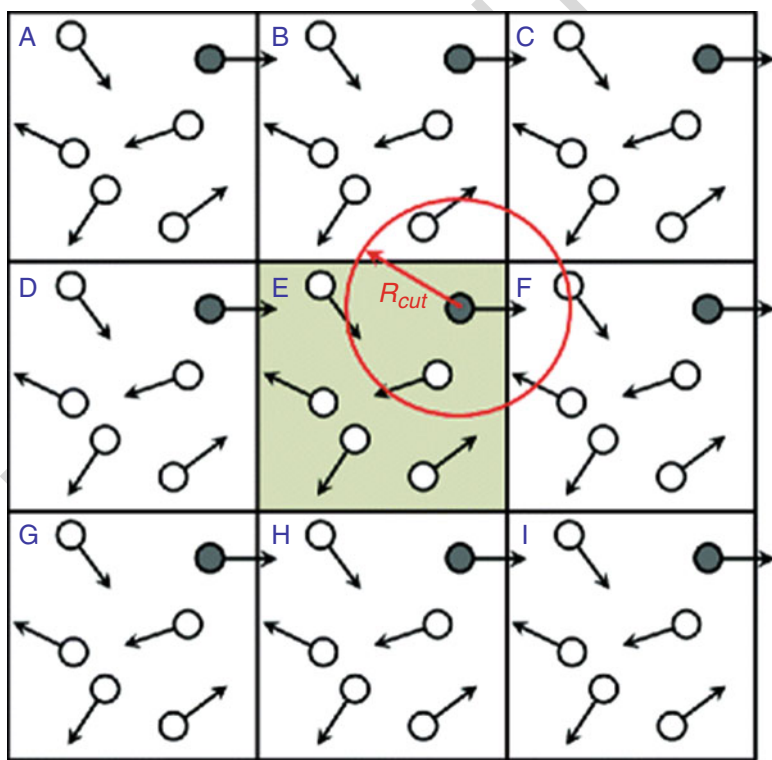


**Fig. 3** Illustration of 2D periodic boundary conditions. The shaded box E represents the system being simulated and the other ones are the images of E

interact with one in the neighboring cell (which is an image of one of the particles in the simulation cell) because it is within the cutoff radius. It ignores the equivalent particle in the simulation cell because it is too far away. In other cases the interaction comes from a particle in the simulation cell itself. Thus the interaction that is calculated is always with the closest image. This is known as the minimum image convention. These operating conditions greatly simplify the set up of a MD program and are commonly used. Of course, the size of the simulation box must also be large enough. If the simulation box is too small, a particle may interact with its own image in a neighboring box, which produces highly unphysical dynamics. The cutoff should be chosen such that a particle in the primary box does not see its image in the surrounding boxes. A practical suggestion is that one must always make sure that the box size is at least two times  $R_{\text{cut}}$  along all the directions where PBCs are effective.

There are boundaries existing inherently in some cases, where PBC cannot be used in computer simulations. Simulations which require no periodic boundaries are best suited to in vacuo simulations, such as the conformational study of an isolated polymer molecule. When simulating surfaces, it is particularly useful to apply the slab boundary conditions in which boundaries are periodic only in X and Y. The periodic cell in the XY plane can be any parallelogram. The origin of the X and Y atomic coordinates lies on an axis perpendicular to the center of the parallelogram. The origin of the Z coordinate is where the user specifies it, but it is recommended at or near the surface. The correct treatment of boundary conditions and boundary effects is crucial in MD simulations since it enables macroscopic properties to be calculated from MD simulations, which use relatively small numbers of particles (Leach 2001).

#### 53.2.4 Energy Minimization

In MM simulations, energy minimization (also called energy optimization or geometry optimization) methods are used to compute the equilibrium configuration of biomolecules, liquids, and solids. Moreover, MD simulations focusing on adhesion always deal with complex molecules or systems, in which the added hydrogens and broken hydrogen bond network in water would lead to quite large forces and structure distortion if the MD simulations were started immediately. To remove these forces, it is often preferable to carry out a short energy minimization on the conformation before MD simulations. Energy minimization is usually performed by gradient optimization; atoms are moved so as to reduce the net forces on them. The minimized structure has small forces on each atom and therefore serves as an excellent starting point for MD simulations. At that point, the configuration will hopefully be in local potential energy minimum. This can be done with two representative methods which involve the steepest descent algorithm and the conjugate gradient algorithm. In a steepest descent algorithm, at each iteration, the search direction is set to the downhill direction corresponding to the force vector (negative gradient of energy), while in a conjugate gradient algorithm, the force gradient is

combined at each iteration with the previous iteration information to compute a new search direction perpendicular (conjugate) to the previous search direction. Typically, steepest descent method will not converge as quickly as the conjugate gradient method, but may be more robust in some situations.

### 53.2.5 Integrators

MD simulation implement involves solving a system of three N second-order differential equations. Due to the complicated nature of this function, there is no analytical solution to the equations of motion, and they must be solved numerically. A standard method for solution of ordinary differential equations such as Eq. 1 is the finite difference approach. Given the initial conditions and the boundary conditions, one can solve the equations step by step. The time interval  $\delta t$  is always chosen to be one or several femtoseconds, which should be significantly smaller than the typical time taken for a molecule to travel its own length. Many different algorithms fall into the general finite difference pattern, such as Verlet, leapfrog, velocity Verlet, Beeman, and predictor–corrector algorithms. When choosing an algorithm to use, the following criteria should be considered: The algorithm should conserve energy and momentum. It should be computationally efficient and it should permit a long time step for integration. To illustrate the principles of the method, the velocity Verlet algorithm is selected, and its technical details which affect the choice in practice are discussed.

The velocity Verlet algorithm starts with the position  $r(t)$  and the velocity  $v(t)$  at time  $t$  and is carried out by repeating these instructions:

1. Calculate  $a(t)$ ,

$$a(t) = \frac{\partial^2 r(t)}{\partial t^2} \quad (11)$$

2. Calculate the position of the particle for the following time step,

$$r(t + \delta t) = r(t) + \delta t \cdot v(t) + \frac{1}{2} \delta t^2 \cdot a(t) \quad (12)$$

3. Calculate velocities at mid-step using

$$v\left(t + \frac{1}{2} \delta t\right) = v(t) + \frac{1}{2} \delta t \cdot a(t) \quad (13)$$

4. Calculate  $a(t + \delta t)$

$$a(t + \delta t) = \frac{\partial^2 r(t + \delta t)}{\partial t^2} \quad (14)$$

## 238 5. Complete the velocity move using

$$v(t + \delta t) = v\left(t + \frac{1}{2}\delta t\right) + \frac{1}{2}\delta t \cdot a(t + \delta t) \quad (15)$$

239 The velocity Verlet algorithm provides both the atomic positions and velocities at  
 240 the same instant of time and for this reason may be regarded as the most complete  
 241 form of Verlet algorithm. The advantage of this algorithm is that it requires less  
 242 computer memory, because only one set of positions, forces, and velocities need to  
 243 be carried at any one time. This convenience is not apparent in the original equations.  
 244 Besides, this algorithm conserves energy well even with relatively long time steps  
 245 and is numerically stable as well as simple to program.

## 246 53.2.6 Analysis of the MD Results

247 MD simulations provide the means to solve the equations of motion of the particles  
 248 and output the desired physical quantities in the term of some microscopic informa-  
 249 tion. In a MD simulation, one often wishes to explore the macroscopic properties of a  
 250 system through the microscopic information. These conversions are performed on  
 251 the basis of the statistical mechanics, which provide the rigorous mathematical  
 252 expressions that relate macroscopic properties to the distribution and motion of the  
 253 atoms and molecules of the N-body system. With MD simulations, one can study  
 254 both thermodynamic properties and the time-dependent properties. Some quantities  
 255 that are routinely calculated from a MD simulation include temperature, pressure,  
 256 energy, the radial distribution function, the mean square displacement, the time  
 257 correlation function, and so on (Allen and Tildesley 1989; Rapaport 2004).

258 The temperature of the system in MD simulations is calculated by

$$T = E_k / \left(\frac{d}{2} N k_B\right) \quad (16)$$

259 where  $E_k$  is the total kinetic energy of all the  $N$  particles,  $k_B$  is the Boltzmann  
 260 constant, and  $d = 2$  or  $3$  is the dimensionality of the simulation. The kinetic energy  
 261 of the system is obtained simply by the summation over all the particles,

$$E_k = \sum_{i=1}^N \frac{1}{2} m_i v_i^2, \quad (17)$$

262 where  $m_i$  and  $v_i$  are the mass and velocity of the  $i$ th particle, respectively. The radial  
 263 distribution function describes how the atomic density varies as a function of the  
 264 distance from one particular atom. It provides a particularly effective way of  
 265 describing the average structure of disordered molecular systems such as liquids.  
 266 The mathematical formula of the radial distribution function,  $g(r)$ , is

$$g(r) = \frac{n(r)}{4\pi\rho r^2\Delta r}, \quad (18)$$

in which  $n(r)$  is the mean number of atoms in a shell of width  $\Delta r$  at distance  $r$  and  $\rho$  is the mean atom density. The method needs not be restricted to one atom. All the atoms in the system can be treated in this way, leading to an improved determination of the radial distribution function as an average over many atoms.

The mean square displacement is a measure of the average distance a molecule travels. It is defined as

$$msd(t) = \left\langle [r_i(t) - r_i(0)]^2 \right\rangle, \quad (19)$$

where  $\langle \dots \rangle$  denotes here averaging over all the atoms and  $r_i(t) - r_i(0)$  is the distance traveled by atom  $i$  over some time interval of length  $t$ . The slope of the mean squared displacement versus time is proportional to the diffusion coefficient  $D$  of the diffusing atoms, which is given by the following Einstein relation,

$$D = \lim_{t \rightarrow \infty} \frac{1}{2dt} \left\langle [r_i(t) - r_i(0)]^2 \right\rangle, \quad (20)$$

where  $d$  has the same meaning as in Eq. 16. From a MD simulation, time-dependent properties such as correlation functions can also be calculated. A time correlation function is defined as

$$C(t) = \langle A(0)A(t) \rangle, \quad (21)$$

where  $\langle \dots \rangle$  represents an ensemble average and  $A$  is the dynamic variable of interest. Many other properties can be calculated based on the integral of this correlation function, such as diffusion coefficient  $D$ , the shear viscosity  $\eta$ , and the thermal conductivity  $\lambda$ . The corresponding computing formulas are listed as follows (Rapaport 2004):

$$D = \frac{1}{dN} \int_0^\infty \left\langle \sum_{i=1}^N v_i(0)v_i(t) \right\rangle dt, \quad (22)$$

in which  $d$  has the same meaning as in Eq. 16.

$$\eta = \frac{V}{3k_B T} \int_0^\infty \left\langle \sum_{x < y} p_{xy}(0)p_{xy}(t) \right\rangle dt, \quad (23)$$

where  $p_{xy}$  is the component of the pressure tensor (the negative of which is known as the stress tensor),  $V$  is the volume of the simulation box, and  $T$  is the temperature of the system.

$$\lambda = \frac{V}{3T^2} \int_0^\infty \langle S(0)S(t) \rangle dt, \quad (24)$$

where

$$S = \frac{1}{V} \left[ \sum_i e_i v_i + \frac{1}{2} \sum_{i \neq j} r_{ij} (f_{ij} \cdot v_i) \right], \quad (25)$$

and the instantaneous excess energy of the  $i$ th atom is

$$e_i = \frac{1}{2} m_i v_i^2 + \frac{1}{2} \sum_{i \neq j} u(r_{ij}) - \langle e \rangle. \quad (26)$$

In order to get the surface energy, for example, the surface energy of nanofilm, one should calculate the energy of nanofilm with PBC and the slab boundary conditions, respectively.

Then the surface energy can be expressed as

$$\gamma = \frac{E_{\text{pbc}} - E_{\text{slab}}}{2A}, \quad (27)$$

in which  $E_{\text{pbc}}$  is the total energy of the nanofilm with PBC, while  $E_{\text{slab}}$  is that with slab boundary conditions.

When carrying out a MD simulation, coordinates of the system can be obtained, which is called the trajectory of the system. It can be displayed graphically and also used for the analysis. To visualize (and analyze) the snapshots from MD simulations, one can use a variety of visualization programs including VMD (Humphrey et al. 1996) and AtomEye (Li 2003). At present there are several high-quality MD codes, which have been widely used by researchers. Some of them are open-source codes, such as LAMMPS (Plimpton 1995), GROMACS (Berendsen et al. 1995; Lindahl et al. 2001), and NAMD (Nelson et al. 1996; Kale et al. 1999). The last two show extra attention on the simulations of biomolecules. Besides, CHARMM (Brooks et al. 1983) and AMBER (Pearlman et al. 1995) are not free but are standard and extremely powerful codes in biology.

For more details of the MD simulations, there are numerous excellent books available on this subject (Allen and Tildesley 1989; Leach 2001; Rapaport 2004).

### 53.2.7 Water Models Used in MD Simulations

When dealing with adhesion issues of biomolecules surrounded by water, the solvent environment always has a significant influence on the properties of the biomolecules. Different types of the water models are illustrated in Fig. 4.

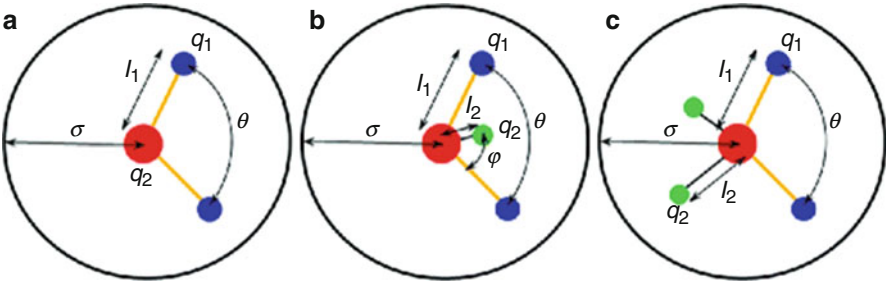


**Fig. 4** Illustration of three types of water model. The red, blue, and green balls represent O and H atoms and the massless charge, respectively

**Table 1** Parameters for water molecular models

Model	Type	$\sigma$ (Å)	$\epsilon$ kJ mol <sup>-1</sup>	$l_1$ (Å)	$l_2$ (Å)	$q_1$ (e)	$q_2$ (e)	$\theta^\circ$	$\phi^\circ$
SPC	A	3.166	0.650	1.0000	—	+0.410	-0.8200	109.47	—
SPC/E	A	3.166	0.650	1.0000	—	+0.4238	-0.8476	109.47	—
TIP3P	A	3.15061	0.6364	0.9572	—	+0.4170	-0.8340	104.52	—
TIP4P	B	3.15365	0.6480	0.9572	0.15	+0.5200	-1.0400	104.52	52.26
TIP5P	C	3.12000	0.6694	0.9572	0.70	+0.2410	-0.2410	104.52	109.47

The parameters of five representative and commonly used water models in MD simulations are listed in Table 1. SPC is the short term for “simple point charge,” and SPC/E denotes the extended simple point charge model with charges on the oxygen and hydrogen modified to improve the classical SPC water model; the SPC/E model results in a better density and diffusion constant than the SPC model. “TIP” in “TIPnP” stands for transferable intermolecular potential, while “nP” means there are n points used in the corresponding water model.

### 53.2.8 Examples of MD Implements

Barnacle cement is an underwater adhesive that is used for permanent settlement. Its main components are insoluble protein complexes. In the following simulations, 36-KD protein which has 38 amino acids and Mrcp-100K protein with 28 amino acids were chosen to study the adhesion properties of the barnacle cement (Yin et al. 2005). Energy minimization was performed first at the temperature of absolute zero in order to avoid improper structure of proteins. Then, the temperature of the system was increased to 300 K by giving every atom a prime velocity according to Boltzmann distribution, and the system was then thermally equilibrated for a short period of time. All the MD simulations were performed using GROMACS version

333 3.1. For the proteins, the standard GROMACS amino acid residue topology and  
334 parameters based on the GROMOS-96 force field (Lindahl et al. 2001) were used.  
335 The SHAKE algorithm (Ryckaert et al. 1977) was used to fix hydrogen bonds during  
336 the simulation. Leapfrog algorithm was employed to integrate the Newton's equa-  
337 tions of motion for all the atoms, with a time step of 1 fs. The temperatures of the  
338 system were always controlled at 300 K, where the weak coupling Berendsen  
339 scheme was used to control the temperature.

340 In this simulation, the proteins were stretched in a water solvent modeled by  
341 TIP3P water molecules (Jorgensen et al. 1983). The dimension of the simulation box  
342 was  $40 \times 40 \times 200$  Å with the PBC applied in all the three directions. The proteins  
343 were stretched at a velocity of 0.01 Å/ps.

344 It was found that there are mainly two regimes of protein deformation: fluctuation  
345 regime and extension regime. In the fluctuation regime, resistance to stretching is  
346 mostly due to the hydrogen bonds, while in the extension regime, the main resistance  
347 force is due to bonded interaction. Moreover, the hydrogen bonds in proteins play an  
348 important role in the adhesive ability of the protein. In Fig. 5, the stretching force  
349 becomes bigger when more hydrogen bonds are breaking and almost every peak of  
350 the force curve corresponds to a trough of the hydrogen bond number curve  
351 (indicated by the arrows). For proteins, the average energy needed to break or  
352 form a hydrogen bond is about 15–30 kJ/mol. It can also be found that the total  
353 energy of the Mrp-100K protein decreases with the increasing hydrogen bond  
354 number. All of this information shows that in fluctuation regime, hydrogen bonds  
355 are more significant than many other interactions, such as entropic force, van der  
356 Waals force, and so on. With this background knowledge, the efforts directed toward  
357 more detailed understanding of the properties of this adhesive and molecular biology  
358 studies would significantly contribute to progress in the basic field and potential  
359 applications such as biofouling prevention (Khandeparker and Anil 2007).

360 Since the barnacle is a saltwater organism, 36-KD protein stretching in seawater  
361 was also simulated.  $\text{Na}^+$  and  $\text{Cl}^-$  ions were also added to the water box with a  
362 concentration of about 17% to simulate the neutral seawater system. Figure 6 shows  
363 that the stretching force of 36-KD protein in seawater is larger than that in water. The  
364 more structural stability of 36-KD protein in seawater is due to two reasons. First, the  
365 electrostatic interaction between proteins and ions in seawater makes the structure  
366 more stable. Second, 36-KD protein forms more hydrogen bonds in seawater in  
367 fluctuation regime (there are 27 hydrogen bonds in seawater while only 19 hydrogen  
368 bonds in water).

369 Another example of MD simulations was performed to study adhesion and  
370 peeling of a short fragment of single-stranded DNA (ssDNA) molecule from a  
371 graphene surface (Shi et al. 2005). A short homogeneous ssDNA oligonucleotide  
372 containing 8 adenine bases in the B-helix form was placed on top of 3 graphene  
373 layers each containing 928 carbon atoms, with an average separation of about 7 Å.  
374 After energy minimization, the system was equilibrated at 300 K for 400 ps. In order  
375 to simulate the process of peeling ssDNA from graphene, a dummy atom was linked  
376 to one end of the ssDNA with a constraint force constant of 8 kcal/mol/Å<sup>2</sup>. Then the  
377 dummy atom was pulled at different peeling angles under a constant pulling velocity,



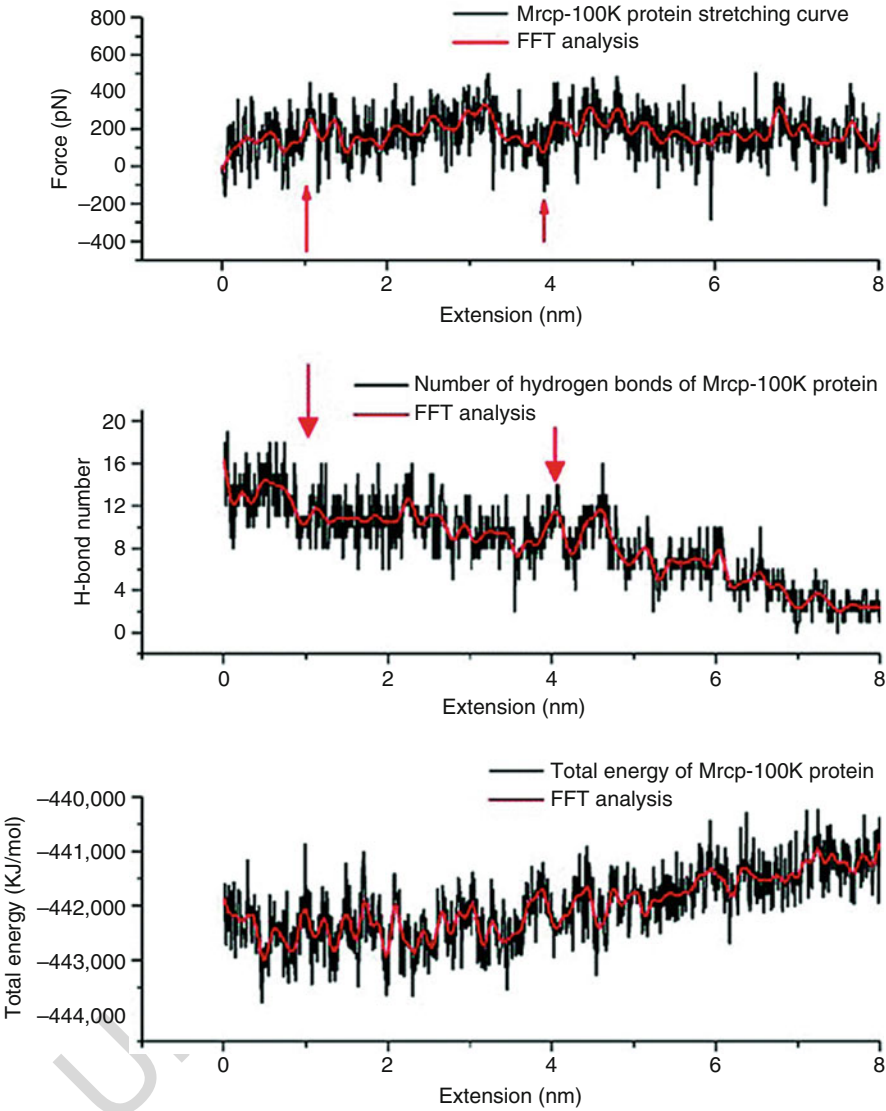


**Fig. 5** The variation of hydrogen bonds, strain (stretching), and total energy (stretching) (Reprinted from Materials Science and Engineering A, 409, Yin J and Zhao YP, Molecular Dynamics Simulation of Barnacle Cement, 160–166, Copyright (2005), with permission from Elsevier)

with the graphene fixed. All these simulations were performed using the code CHARMM (Brooks et al. 1983). Figure 7 depicts several snapshots of ssDNA peeled away from graphene under a constant velocity of 0.1 Å/ps and at a peeling angle of 90°.

**Fig. 6** 36-KD protein stretching in different solutions (Reprinted from Materials Science and Engineering A, 409, Yin J and Zhao YP, Molecular Dynamics Simulation of Barnacle Cement, 160–166, Copyright (2005), with permission from Elsevier)

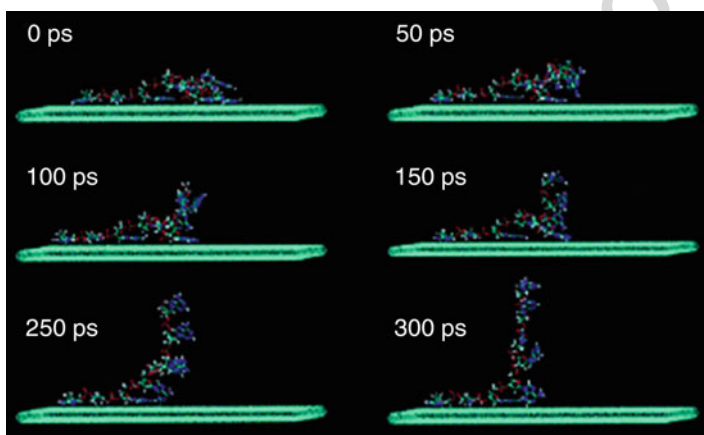
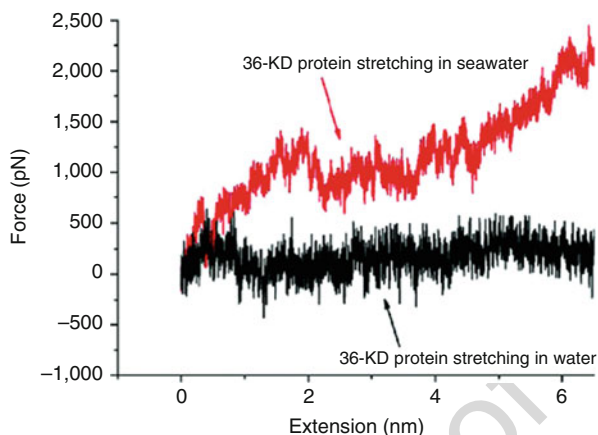


**Fig. 7** Steered MD simulation snapshots of peeling ssDNA from graphene at a peeling angle of 90° (With kind permission from Springer Science+Business Media: Shi et al. (2005), Fig. 3)

During the simulation, the pulling force was calculated and was represented in Fig. 8, which indicated that the pulling force reaches a local maximum value when a tightly attached DNA base is pulled off the surface and is relaxed before the next tightly attached base is to be pulled off. The peel-off force can be calculated from the global maximum of the force profile. Simulations of the peeling process under various pulling rates (from 0.01 to 0.4 Å/ps) and peeling angles (75°, 90°, 120°, and 135°) were also performed, with the calculated peel-off forces summarized in Fig. 9.

The black line in Fig. 9 shows the prediction of the critical peel-off forces using the homogeneous peeling model (Kendall 1975),

$$F(1 - \cos \theta) + F\varepsilon - \int_0^\varepsilon g(\varepsilon)d\varepsilon = \Delta\gamma \quad (28)$$

**Fig. 8** The pulling force exerted on one end of an adsorbed ssDNA as a function of simulating time. To eliminate excessive thermal noise, the pulling force is smoothed with a Gaussian filter of half width 4 ps (white line) (With kind permission from Springer Science +Business Media: Shi et al. (2005), Fig. 4)

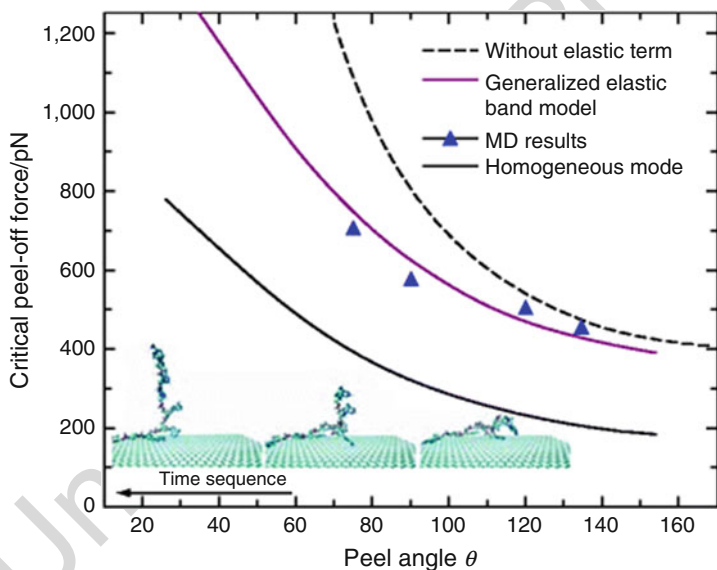
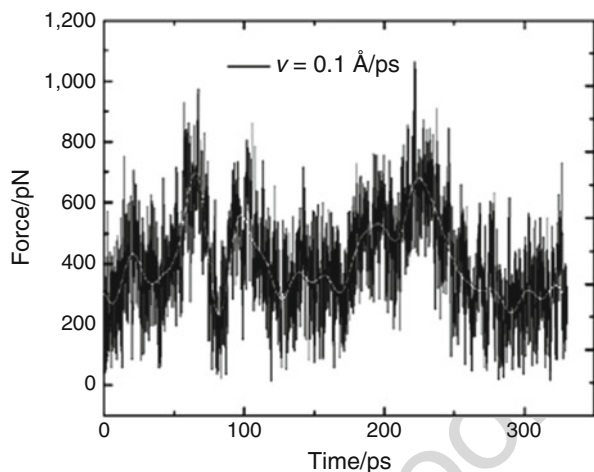


**Fig. 9** The critical peel-off forces of ssDNA oligonucleotide on graphene as a function of the peeling angle. The blue closed triangles are the results of direct MD simulations at peeling angles of 75°, 90°, 120°, and 135°, respectively (With kind permission from Springer Science+Business Media: Shi et al. (2005), Fig. 8)

where  $F$  is the peeling force at a peeling angle  $\theta$  from a substrate,  $g(\varepsilon)$  is used to describe the elasticity of the polymer,  $\varepsilon$  is the elastic strain along the length of the chain, and  $\Delta\gamma$  denotes the work of adhesion between the chain and the substrate. Considering the work of adhesion between ssDNA and substrate is not constant, the homogeneous peeling model can be modified as

$$F(1 - \cos \theta) + F\varepsilon - \int_0^\varepsilon g(\varepsilon) d\varepsilon = \Delta\gamma' \left( 1 - \left| \sin \frac{\pi}{l} x \right| \right) \quad (29)$$

where the constant work of adhesion is replaced by a sinusoidal function with  $l$  being the period of modulation of adhesion energy and  $x$  denoting the position along the chain. Equation 29 is the generalized elastic band model, and the corresponding results are illustrated as the red line in Fig. 9, which are in good agreement with the MD results. The simulations and models demonstrated that, for the same adhesion energy, the critical peel-off forces also depend on the peeling angle.

## 53.3 Molecular Orbital Method

### 53.3.1 Introduction

Molecular orbital (MO) theory is a method for determining molecular structure in which electrons are not assigned to individual bonds between atoms, but are treated as moving under the influence of the nuclei in the whole molecule (Daintith 2004). In this theory, each molecule has a set of MOs, in which it is assumed that each MO wave function  $\psi_i$  can be written as a summation of the following form (Pople and Beveridge 1970):

$$\psi_i = \sum_{\mu=1}^K c_{\mu i} \phi_{\mu}, \quad (30)$$

where  $\psi_i$  is a (spatial) MO,  $\phi_{\mu}$  is one of  $K$  atomic orbitals, and  $c_{\mu i}$  is the coefficient. This method is called the linear combination of atomic orbitals (LCAO) approximation and is widely used in computational chemistry.

MOs are often divided into bonding, antibonding, and nonbonding orbitals. In a bonding orbital, the electrons have a higher probability of being between nuclei than elsewhere. Electrons in the antibonding orbital tend to spend more time elsewhere than between the nuclei, while electrons in nonbonding orbital prefer to be in deep orbitals (nearly atomic orbitals) associated almost entirely with one nucleus.

In the MO theory, three necessary conditions must be satisfied when atomic orbitals combine together to form MOs:

1. The combining atomic orbitals must have the same symmetry about the molecular axis.
2. The combining atomic orbitals must be able to overlap to the maximum extent to form MOs, since the greater is the extent of overlap between the combining atomic orbitals, the greater will be the electron density in the region between the nuclei of the combining atoms and hence the stronger the bond between them.
3. The combining atomic orbitals must have the same or almost the same energy.

The first one is the most important, which decides whether these atomic orbitals can form MOs or not. The other two just affect the combination efficiency.

For diamagnetic species, MO method starts by assigning electrons in pairs to spatial functions  $\psi_1, \psi_2, \dots, \psi_n$ , which are then used in the construction of a many-electron wave function as a single determinant (Roothaan 1951; Pople and Beveridge 1970; Hehre 1976)

$$\Psi(1, 2, \dots, 2n) = \frac{1}{2^n} \times \begin{vmatrix} \psi_1(1)\alpha(1) & \psi_1(1)\beta(1) \cdots & \psi_n(1)\beta(1) \\ \psi_1(2)\alpha(2) & \cdots & \\ \vdots & & \\ \psi_1(2n)\alpha(2n) & \psi_1(2n)\beta(2n) \cdots & \psi_n(2n)\beta(2n) \end{vmatrix}, \quad (31)$$

where  $\alpha$  and  $\beta$  are spin functions. The MOs  $\psi_i$  are chosen so as to minimize the total energy of the system, that is, the expectation value of the many-electron Hamiltonian  $H$ ,

$$E = \int \dots \int \Psi(1, 2, \dots, 2n) H \Psi(1, 2, \dots, 2n) d\tau_1 d\tau_2 \dots d\tau_{2n}, \quad (32)$$

is in practice written in terms of a linear combination of nuclear centered atomic functions, as shown in Eq. 30. The coefficients,  $c_{\mu i}$ , in Eq. 30 are obtained at by solution of the Roothaan equations

$$\sum_{\nu} (F_{\mu\nu} - \varepsilon_i S_{\mu\nu}) c_{\mu i} = 0, \quad (33)$$

where  $S_{\mu\nu}$  is an overlap integral

$$S_{\mu\nu} = \int \varphi_{\mu}(1) \varphi_{\nu}(1) d\tau_1, \quad (34)$$

$\varepsilon_i$  is the one-electron energy associated with  $\psi_i$ , and  $F_{\mu\nu}$  is an element of the Fock matrix

$$F_{\mu\nu} = H_{\mu\nu} + \sum_{\lambda} \sum_{\sigma} P_{\lambda\sigma} [(\mu\nu|\lambda\sigma)(\mu\lambda|\nu\sigma)]. \quad (35)$$

Here  $H_{\mu\nu}$  is the element

$$H_{\mu\nu} = \int \varphi_{\mu}(1) \left[ -\frac{1}{2} \nabla^2 \right] \varphi_{\nu}(1) d\tau_1 + \sum_A^{\text{nuclei}} \int \varphi_{\mu}(1) \left[ \frac{1}{r_{1A}} \right] \varphi_{\nu}(1) d\tau_1. \quad (36)$$

which describes the motion of a single electron in a field of bare nuclei, and  $(\mu\nu|\lambda\sigma)$  is a two-electron integral

$$(\mu\nu|\lambda\sigma) = \iint \varphi_\mu(1)\varphi_\nu(1) \left[ \frac{1}{r_{12}} \right] \varphi_\lambda(2)\varphi_\sigma(2) d\tau_1 d\tau_2. \quad (37)$$

445 The one-electron density matrix,  $P$ , is given by

$$P_{\lambda\sigma} = 2 \sum_i c_{\lambda i} c_{\sigma i}, \quad (38)$$

446 where the summation is over the manifold of occupied MOs. Note that the  
 447 Roothaan equations are not readily amenable to solution in closed form. This is  
 448 simply because the quantity sought (the  $c_{\mu i}$ ) appears, disguised as  $P_{\lambda\sigma}$ , in their  
 449 formulation.

### 450 53.3.2 Density Functional Theory

451 The two basic methods in QM calculations are MO theory and density functional  
 452 theory (DFT). These two methods, often contrasting, but mostly cooperating, are  
 453 different approaches to tackling the electronic problems. MO method is always  
 454 adopted by the chemists who think that the MO is expressed as LCAO. The DFT  
 455 method is always used to treat infinite periodic systems by the physicists.

456 DFT is founded on the Hohenberg–Kohn (H–K) theorems (Hohenberg and Kohn  
 457 1964), which comes in two parts. The first one states that the ground state properties  
 458 of a many-electron system are uniquely functional of the ground state electron  
 459 density which depends on only three spatial coordinates. This implies that all  
 460 properties of the system are completely determined given only the ground state  
 461 density.

#### 462 The Hohenberg–Kohn Theorem

463 The second part of the H–K theorem states that the total energy of the ground state of  
 464 a many-electron system in an external potential  $V_{\text{ext}}(\vec{r})$  is a unique functional of the  
 465 electron density

$$E[n] = F[n] + \int n(\vec{r}) V_{\text{ext}}(\vec{r}) d\vec{r}. \quad (39)$$

466 This functional has its minimum (i.e., the ground state energy  $E_0$ ) for the ground  
 467 state electron density  $n_0(\vec{r})$

$$E_0 = E[n_0(\vec{r})] = \min_{n(\vec{r})} E[n]. \quad (40)$$

468 The functional  $F[n]$  is a universal function, independent of the external potential  
 469  $V_{\text{ext}}(\vec{r})$  and the same for all systems.

470 Levy gave a particularly simple proof of the Hohenberg–Kohn theorem (Levy  
471 1979): A functional  $O$  is defined as

$$O[n(\vec{r})] = \min_{|\Psi\rangle \rightarrow n(\vec{r})} \langle \Psi | \hat{O} | \Psi \rangle, \quad (41)$$

472 where the expectation value is found by searching over all wavefunctions,  $\Psi$ , giving  
473 the density  $n(\vec{r})$  and selecting the wave function which minimizes the expectation  
474 value of  $\hat{O}$ .

475  $F[n(\vec{r})]$  is defined by

$$F[n(\vec{r})] = \min_{|\Psi\rangle \rightarrow n(\vec{r})} \langle \Psi | \hat{F} | \Psi \rangle, \quad (42)$$

476 so

$$\hat{F} = \sum_i -\frac{1}{2} \nabla_i^2 + \frac{1}{2} \sum_{i \neq j} \frac{1}{|\vec{r}_i - \vec{r}_j|}. \quad (43)$$

477 Considering an  $N$ -electron ground state wavefunction  $\Psi_0$  which yields a density  
478  $n(\vec{r})$  and minimizes  $\langle \Psi | \hat{F} | \Psi \rangle$ , then from the definition of the functional  $E$

$$E[n(\vec{r})] = F[n(\vec{r})] + \int n(\vec{r}) V_{\text{ext}}(\vec{r}) d\vec{r} = \langle \Psi | \hat{F} + V_{\text{ext}} | \Psi \rangle. \quad (44)$$

479 The Hamiltonian is given by  $\hat{F} + V_{\text{ext}}$ , and so  $E[n(\vec{r})]$  must obey the variational  
480 principle,

$$E[n(\vec{r})] \geq E_o. \quad (45)$$

481 This completes the first part of the proof, which places a lower bound on  $E[n(\vec{r})]$ .

482 From the definition of  $F[n(\vec{r})]$  in Eq. 42, the following is obtained

$$F[n_0(\vec{r})] \leq \langle \Psi_0 | \hat{F} | \Psi_0 \rangle, \quad (46)$$

483 since  $\Psi_0$  is a trial wave function yielding  $n_0(\vec{r})$ . Combining  $\int n(\vec{r}) V_{\text{ext}}(\vec{r}) d\vec{r}$   
484 with the above equation gives

$$E[n_0(\vec{r})] \leq E_o, \quad (47)$$

485 which in combination with Eq. 46 yields the key result

$$E\left[n_0\left(\vec{r}\right)\right]=E_o. \quad (48)$$

### 486 The Kohn–Sham (KS) Equations

487 Kohn and Sham derived a coupled set of differential equations enabling the ground  
488 state density  $n_0\left(\vec{r}\right)$  to be found. The variational problems of minimizing the energy  
489 functional  $E\left[n\left(\vec{r}\right)\right]$  can be solved by applying the Lagrangian method of  
490 undetermined multipliers (Hohenberg and Kohn 1964). First, one considers an  
491 energy functional that does not explicitly have an electron–electron interaction  
492 energy term,

$$E_s\left[n\left(\vec{r}\right)\right]=\left\langle\Psi_s\left[n\left(\vec{r}\right)\right]\left|\hat{T}_s+\hat{V}_s\right|\Psi_s\left[n\left(\vec{r}\right)\right]\right\rangle, \quad (49)$$

493 where  $\hat{T}_s$  is defined as the kinetic energy of a non-interacting electron gas and  $\hat{V}_s$  is  
494 an external effective potential in which the non-interacting electrons are moving.  
495 Obviously,  $n_s\left(\vec{r}\right)\stackrel{\text{def}}{=}n\left(\vec{r}\right)$  if  $\hat{V}_s$  is chosen to be

$$\hat{V}_s=\hat{V}+\hat{U}+\left(\hat{T}-\hat{T}_s\right). \quad (50)$$

496 Thus, to find the ground state energy,  $E_0$ , and the ground state density,  $n_0$ , the  
497 one-electron Schrödinger equation,

$$\left[-\frac{\hbar^2}{2m}\nabla^2+V_s\left(\vec{r}\right)\right]\phi_i\left(\vec{r}\right)=\varepsilon_i\phi_i\left(\vec{r}\right), \quad (51)$$

498 should be solved self-consistently with

$$n(r)\stackrel{\text{def}}{=}n_s\left(\vec{r}\right)=\sum_i^N\left|\phi_i\left(\vec{r}\right)\right|^2. \quad (52)$$

499 The effective single-particle potential can be written in more detail as

$$V_s\left(\vec{r}\right)=V\left(\vec{r}\right)+\int\frac{e^2n_s\left(\vec{r}'\right)}{\left|\vec{r}-\vec{r}'\right|}d^3r'+V_{xc}\left[n_s\left(\vec{r}\right)\right], \quad (53)$$

500 where the second term is the so-called Hartree term describing the electron–electron  
501 Coulomb repulsion, while the final term  $V_{xc}$  is an implicit definition of the  
502 exchange–correlation potential. Here,  $V_{xc}$  includes all the many-particle interactions,  
503 which is given formally by the functional derivative  $V_{xc}\left(\vec{r}\right)=\frac{\delta E_{xc}\left[n\left(\vec{r}\right)\right]}{\delta n\left(\vec{r}\right)}$ .



Since the Hartree term and  $V_{xc}$  depend upon the density  $n(\vec{r})$ , which depends on the  $\phi_i$ , which in turn depends on  $V_s$ , the problem of solving the KS equation has to be done in a self-consistent (i.e., iterative) way. Usually, one starts with an initial guess for  $n(\vec{r})$ , then calculates the corresponding  $V_s$ , and solves the KS equations for  $\phi_i$ . Then, one calculates a new density and starts again. This procedure is then repeated until the input and output densities satisfy the accuracy.

### Exchange–Correlation Functionals

To solve Kohn–Sham equations, the exchange–correlation energy  $E_{xc}[n]$  must be known. However, because of the many-body effects,  $E_{xc}[n]$  cannot be derived exactly. Therefore, certain approximations are required for  $E_{xc}[n]$ . In physics, the most widely used approximation has been the local-density approximation (LDA), where the functional depends only on the density at the coordinate where the functional is evaluated,

$$E_{xc}[n] = \int \varepsilon_{xc}(n) n(\vec{r}) d^3r, \quad (54)$$

where  $\varepsilon_{xc}(n)$  is the exchange–correlation energy per particle of a uniform electron gas of density  $n$ . LDA has yielded valuable quantitative or at least semiquantitative results, especially for equilibrium structures of molecules and solids. The local spin-density approximation (LSDA) is a straightforward generalization of the LDA to include electron spin

$$E_{xc}[n_{\uparrow}, n_{\downarrow}] = \int \varepsilon_{xc}(n_{\uparrow}, n_{\downarrow}) n(\vec{r}) d^3r. \quad (55)$$

Highly accurate formulae for the exchange–correlation energy density  $\varepsilon_{xc}(n_{\uparrow}, n_{\downarrow})$  have been constructed from quantum Monte Carlo simulations of a free electron model (Perdew et al. 2005). Generalized gradient approximations (GGA) have yielded substantial improvements over the LDA for binding energies of molecules and solids as well as for barrier heights of chemical reactions. GGA are still local but also take into account the gradient of the density at the same coordinate

$$E_{xc}[n_{\uparrow}, n_{\downarrow}] = \int \varepsilon_{xc}(n_{\uparrow}, n_{\downarrow}, \vec{\nabla} n_{\uparrow}, \vec{\nabla} n_{\downarrow}) n(\vec{r}) d^3r. \quad (56)$$

Potentially more accurate than the GGA functionals are the so-called hybrid functionals, which have the generic form

$$E_{xc}[n_{\uparrow}, n_{\downarrow}] = \gamma E_x^{\text{exact}}[n(\vec{r})] + \int \varepsilon'_{xc}(n_{\uparrow}, n_{\downarrow}, \vec{\nabla} n_{\uparrow}, \vec{\nabla} n_{\downarrow}) n(\vec{r}) d^3r, \quad (57)$$

where  $E_x^{\text{exact}}$  is the exact exchange energy evaluated with KS orbitals and  $\gamma$  is a constant between 0 and 1.

### 53.3.3 Examples of DFT Calculations

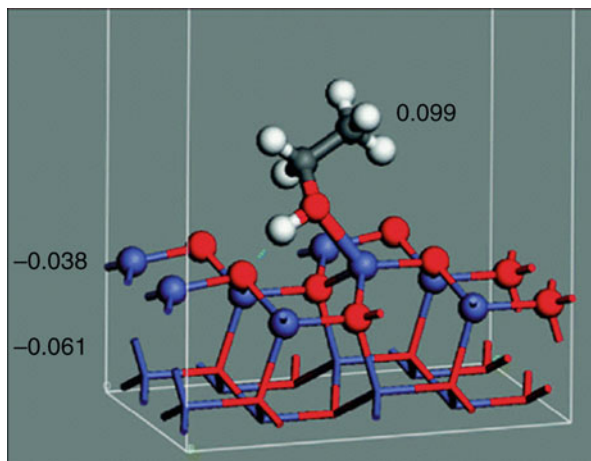
Gas sensors based on metal oxide–semiconductor materials as well as metal-doped graphene have attracted considerable attention during the past decade. Zinc oxide (ZnO), tin dioxide ( $\text{SnO}_2$ ), and Al-doped graphene have been chosen as sensing materials because of their excellent characteristics such as low cost, high sensitivity, rapid response, and fast recovery. Here two examples are given to show the general routine of DFT calculations and the analysis of the results.

DFT calculations were employed to explore the gas-sensing mechanisms of zinc oxide (ZnO) with surface reconstruction taken into consideration (Yuan et al. 2009). Mix-terminated  $(10\bar{1}0)$  ZnO surfaces were examined. Simulations of the adsorption process of various gases, that is,  $\text{H}_2$ ,  $\text{NH}_3$ , CO, and ethanol ( $\text{C}_2\text{H}_5\text{OH}$ ) gases, on the ZnO  $(10\bar{1}0)$  surface, were carried out. All the ab initio calculations were performed using DFT implemented in the DMol<sup>3</sup> program (Delley 2000, 2002). The widely used GGA with the exchange–correlation functional parameterized by Perdew and Wang (PW91) was adopted, calculating with restricted spin. Compared with LDA, GGA will not lead to a strong bonding of molecules. So if the calculated molecules are adsorbed on the ZnO surface, they will definitely bind in a real system. However, GGA overestimates binding distance and underestimates binding energy consequently.

A plane-wave basis set with an orbital cutoff distance of 3.9 Å was used. All-electron calculations and a double numerical basis set with polarization functions (DNP) were employed. Wave function integration in reciprocal space was performed via fine grid sampling of k points with a separation of  $0.02 \text{ Å}^{-1}$ . For the calculation of the density of states (DOS), a  $5 \times 8 \times 3$  Monkhorst–Pack grid was used. Charge transfer was calculated based on the Mulliken population analysis (MPA) (Mulliken 1955).

The ethanol ( $\text{C}_2\text{H}_5\text{OH}$ ) molecule adsorption on the ZnO surface is shown in Fig. 10. When an ethanol molecule approaches the ZnO surface, electronic

**Fig. 10** Optimized configuration of the ethanol molecule on the ZnO surface. Blue line represents hydrogen bond between H and O atoms (Reprinted with permission from Yuan et al. (2009). Copyright 2009 American Chemical Society)



560 interactions among nuclei and electrons disturb the initial configuration, inducing  
561 adsorption of the gas molecule on the ZnO surface. After the surface reconstruction  
562 induced by adsorption, energy-level splitting is found (Fig. 11a). Band structure is  
563 deflexed because of charge transfer (Fig. 11b).

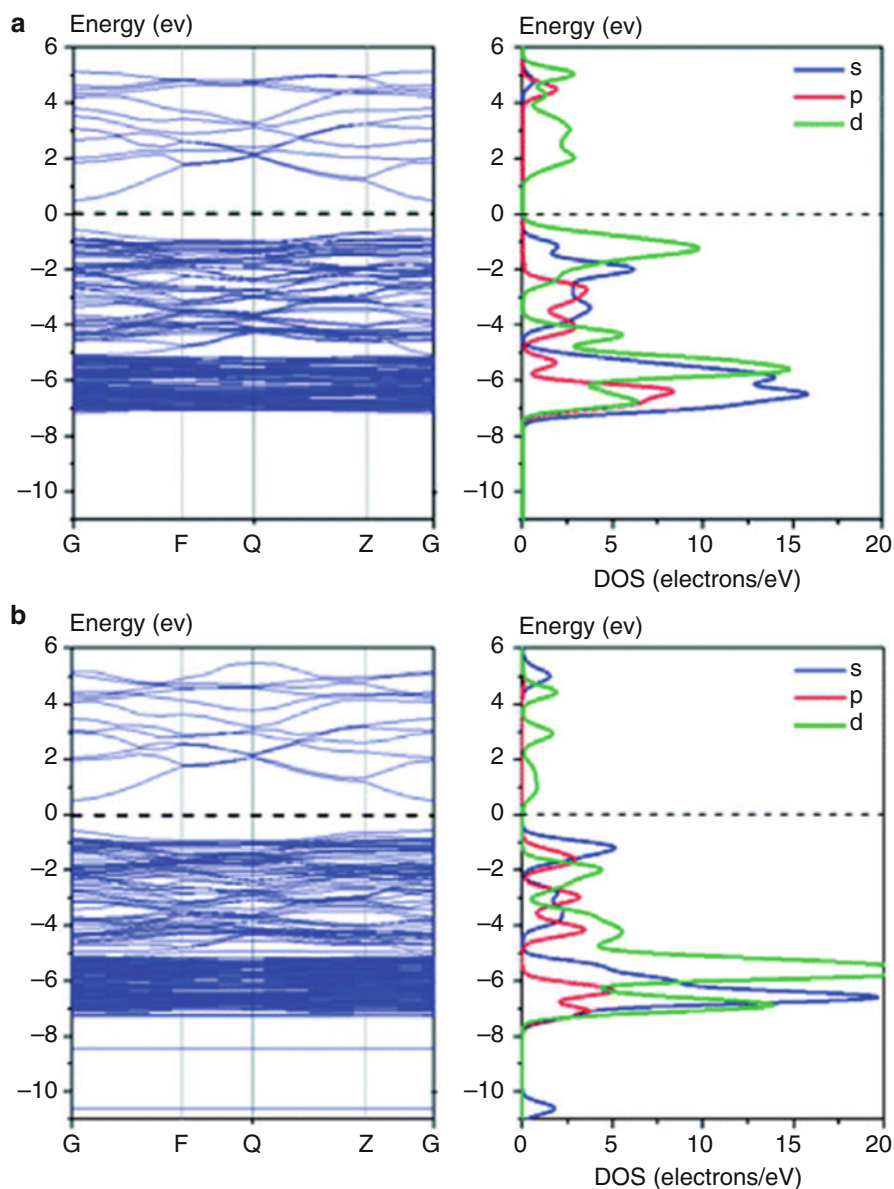


**Fig. 11** Band structure and PDOS of the (a) reconstructed and (b) ethanol-molecule-adsorbed ZnO surface (Reprinted with permission from Yuan et al. (2009). Copyright 2009 American Chemical Society)

Based on these calculations, two gas-sensing mechanisms were proposed and revealed that both surface reconstruction and charge transfer result in a change of electronic conductance of ZnO. When the gas molecule is adsorbed upon the surface, the electronic conductance of the gas sensor changes because of the joint effect of these two mechanisms. These results show good accordance with existing experiments and could help in understanding the sensing mechanism of ZnO-based gas sensors.

To search for a high sensitivity sensor for formaldehyde ( $\text{H}_2\text{CO}$ ), the adsorptions of  $\text{H}_2\text{CO}$  on the intrinsic and Al-doped graphene were investigated using DFT calculations (Chi and Zhao 2009). Structure optimizations as well as the corresponding total energy calculations were performed based on the GGA function with the Perdew–Burke–Ernzerhof (PBE) correction (Perdew et al. 1996). The DFT semicore pseudopotential (DSPP) core treatment (Delley 2002) was implemented for relativistic effects, which replaces core electrons by a single effective potential. To ensure that the results of the calculations are comparable, identical conditions were employed for the isolated  $\text{H}_2\text{CO}$  molecule, the graphene substrate, and also the adsorbed graphene system. The k-point was set to  $6 \times 6 \times 1$  for all slabs, which brought out the convergence criterion of  $10^{-5}$  a.u. on energy and electron density and that of maximum force of  $0.002 \text{ Ha}/\text{\AA}$ . Self-consistent field procedure was carried out with a convergence criterion of  $10^{-6}$  a.u. on energy and electron density. All DFT calculations were performed using DMol<sup>3</sup> code (Delley 1990, 2000).

In these calculations, the PBCs were applied to the supercells. A vacuum width of  $16 \text{ \AA}$  above was constructed, which ensured that the Z-axis of the periodic supercell (perpendicular to the graphene layer) was large enough so that there was no interaction between graphene sheets of adjacent supercells. Optimized configurations of intrinsic graphene and Al-doped graphene are illustrated in Fig. 12. The binding energy of the adsorbed systems is defined as

$$E_b = E_{\text{total}} - (E_{\text{sheet}} + E_{\text{H}_2\text{CO}}), \quad (58)$$

where the  $E_{\text{total}}$ ,  $E_{\text{sheet}}$ , and  $E_{\text{H}_2\text{CO}}$  denote the total energy of intrinsic or Al-doped graphene adsorbed system, isolated graphene or Al-doped graphene, and a  $\text{H}_2\text{CO}$  molecule, respectively. A negative  $E_b$  corresponds to a stable adsorption structure.

To investigate the changes of electronic structures in graphene caused by the adsorption of  $\text{H}_2\text{CO}$  molecule, electron density difference  $\Delta\rho$  is calculated, which illustrates how the charge density changes during this adsorption process.  $\Delta\rho$  is defined as

$$\Delta\rho = \rho_{\text{total}} - (\rho_{\text{sheet}} + \rho_{\text{H}_2\text{CO}}), \quad (59)$$

in which  $\rho_{\text{total}}$ ,  $\rho_{\text{sheet}}$ , and  $\rho_{\text{H}_2\text{CO}}$  denote electron density of the intrinsic or Al-doped graphene adsorbed system, graphene or Al-doped graphene, and a  $\text{H}_2\text{CO}$  molecule for the adsorbed system, respectively. The electronic density differences of energy

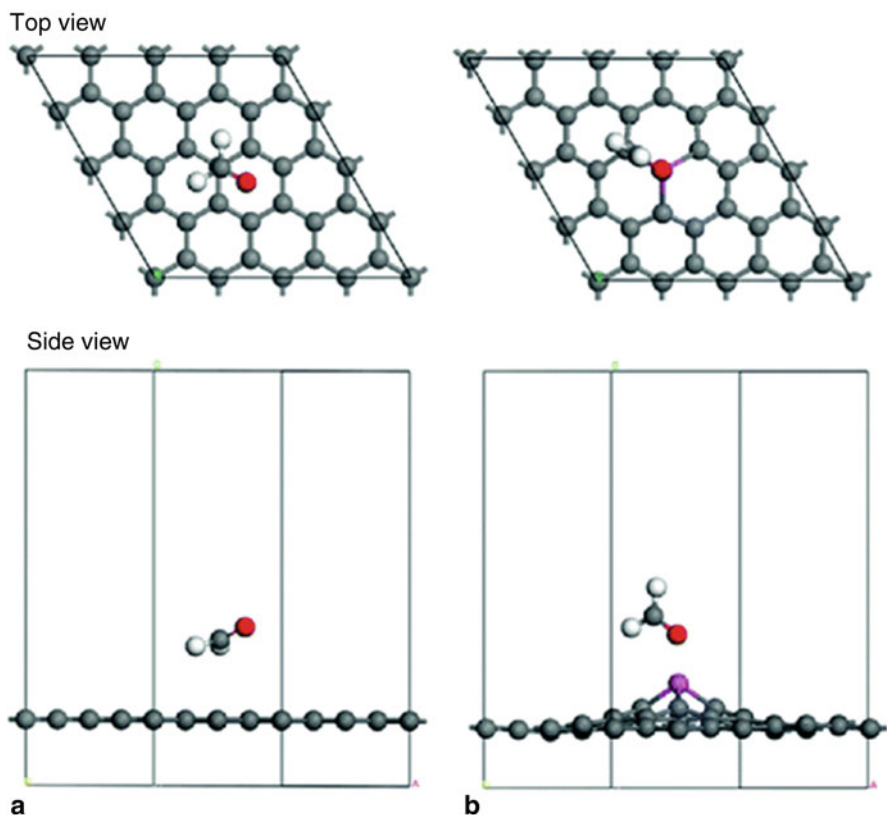


**Fig. 12** Optimized most stable configurations of (a) intrinsic graphene and (b) Al-doped graphene (Reprinted from Chi and Zhao (2009), Copyright (2009), with permission from Elsevier)

favorable intrinsic and Al-doped graphene with H<sub>2</sub>CO adsorptions are shown in Fig. 13. The net electron transfer from the Al-doped graphene to H<sub>2</sub>CO is four times more than that in the intrinsic grapheme, which indicates that the Al-doped graphene can be used as a novel sensor for the detection of H<sub>2</sub>CO molecules.

### 53.4 Hybrid Quantum Mechanics/Molecular Mechanics (QM/MM) Methods

As stated above, MD simulations and QM calculations show enormous capacity in handling problems in adhesion. However, in many cases, current force fields used in MD as well as MM simulations are not sufficiently accurate to reproduce the dynamics of molecular systems. At the same time, QM methods cannot deal with large systems because the simulations will be time-consuming or even become impossible. The simulation techniques have been expanded to combine the strength

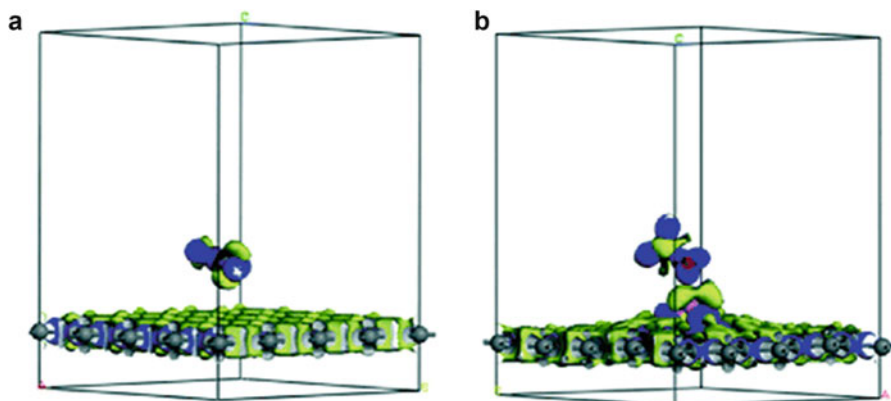


**Fig. 13** The electronic density difference isosurfaces for (a) H<sub>2</sub>CO–graphene system and (b) H<sub>2</sub>CO–Al-doped adsorbed systems with energy preferred configuration (graphene systems). The blue region shows the electron accumulation, while the yellow region shows the electron loss (Reprinted from Chi and Zhao (2009), Copyright (2009), with permission from Elsevier)

of both MM simulations and QM calculations, which is called the hybrid quantum mechanics/molecular mechanics (QM/MM) approach.

### 53.4.1 Basic Theory

The basic strategy for the QM/MM method lies in the hybrid potential in which a classical MM potential is combined with a QM one (Field et al. 1990). The energy of the system,  $E$ , is calculated by solving the Schrödinger equation with an effective Hamiltonian,  $H_{\text{eff}}$ , for the mixed quantum mechanical and classical mechanical system

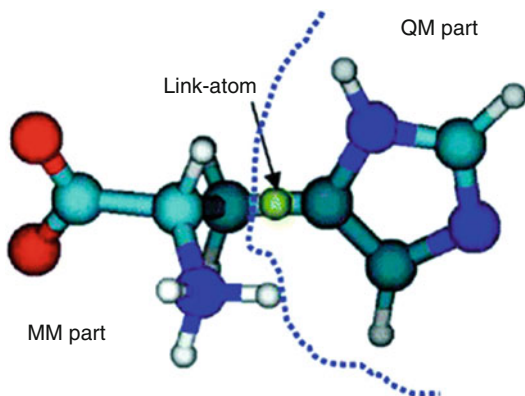
$$H_{\text{eff}}\psi(r, R_{\text{QM}}, R_{\text{MM}}) = E(R_{\text{QM}}, R_{\text{MM}})\psi(r, R_{\text{QM}}, R_{\text{MM}}), \quad (60)$$

where  $\psi$  is the electronic wave function of the quantum system,  $r$  is for the coordinates of the electrons,  $R_{\text{QM}}$  is the position of the quantum mechanical nuclei, and  $R_{\text{MM}}$  is for the molecular mechanical nuclei. The wave function,  $\psi$ , depends directly on  $r$ ,  $R_{\text{QM}}$ , and  $R_{\text{MM}}$ . The effective Hamiltonian for the mixed quantum and classical system is divided into three terms (Lyne et al. 1999)

$$H_{\text{eff}} = H_{\text{QM}} + H_{\text{MM}} + H_{\text{QM/MM}}, \quad (61)$$

where  $H_{\text{QM}}$  is the contribution from complete QM section (see QM in Fig. 14),  $H_{\text{MM}}$  is from the pure MM section (see MM in Fig. 14), and  $H_{\text{QM/MM}}$  is the interaction between the QM and MM portions of the system. Similarly, the total energy of the system calculated by solving the Schrödinger equation can likewise be divided into three component parts

**Fig. 14** An example of how to partition a molecule into QM and MM regions. The figure shows a histidine molecule, in which all the atoms in the imidazole ring are taken as QM atoms, while the remaining atoms are treated as MM atoms (Reprinted from Yang and Zhao (2006), Copyright (2006), with permission from Elsevier)



$$E_{\text{eff}} = E_{\text{QM}} + E_{\text{MM}} + E_{\text{QM/MM}}. \quad (62)$$

However, the pure MM term can be removed from the integral because it is independent of the electronic positions. So another way to express the total energy of the system is as the expectation value of  $H_{\text{eff}}$

$$E_{\text{eff}} = \langle \psi | H_{\text{QM}} + H_{\text{QM/MM}} | \psi \rangle + E_{\text{MM}}, \quad (63)$$

where  $H_{\text{QM}}$  is the Hamiltonian that can be obtained by either semiempirical, Hartree–Fock, or DFT.  $E_{\text{MM}}$  is an energy calculated based on a classical force field.  $H_{\text{QM/MM}}$  is the key term which involves combinations of the interaction of the MM atom “cores” with the electron cloud of the QM atoms, the repulsion between the MM and QM atomic cores, as well as the LJ term. The form of  $H_{\text{QM/MM}}$  is

$$H_{\text{QM/MM}} = - \sum_{iM} \frac{q_M}{|r_{iM}|} + \sum_A \frac{q_M Z_A}{|R_{AM}|} + \sum_{AM} 4\epsilon_{AM} \left( \frac{R_{\text{min},AM}^{12}}{R_{AM}^{12}} - 2 \frac{R_{\text{min},AM}^6}{R_{AM}^6} \right) \quad (64)$$

where  $q_M$  is the atomic point charge on the MM atom,  $r_{iM}$  is the QM electron to MM atom distance,  $Z_A$  is the core charge of QM atom  $A$ ,  $R_{AM}$  is the QM atom  $A$  to MM atom  $M$  distance, and  $\epsilon_{AM}$  and  $R_{\text{min},AM}$  are the LJ parameters for QM atoms  $A$  interacting with MM atom  $M$ . The critical term that allows the QM region to “see” the MM environment is the first term in the right side of Eq. 64 where the summation is over all interactions between MM atoms and QM electrons. The second term in Eq. 64 represents the core electron interaction between MM and QM atoms and is incorporated into the QM Hamiltonian explicitly. The van der Waals interaction between QM part and MM part is described by the third term in Eq. 64. As the integrated molecular orbital/molecular mechanics (IMOMM) method (Maseras and Morokuma 1995) is taken, the introduction of new parameters is avoided and the number of geometry variables is reduced as much as possible.



### 53.4.2 QM/MM Boundary Treatments

An important aspect of the formation of a hybrid potential is how to handle the covalent bonds between atoms that are described with different potentials, that is, the bonds existing at the interface of the QM and MM regions. Several methods have been proposed to deal with this problem, including the simple link-atom method (Field et al. 1990), the sophisticated hybrid-orbital technique (Ferre et al. 2002), and the pseudo-bond approach (Zhang et al. 1999).

In many situations, it is necessary to split a molecule between QM and MM regions, which means that there are covalent bonds between QM and MM atoms. These cleavage bonds must be treated in some way because the presence of broken bonds and unpaired electrons at the boundary of the QM region dramatically changes the electronic structure of the QM subsystem. As long as the QM and MM atoms are in different molecules, no such problem arises.

Here, the classical link-atom method was introduced as a typical example. The link atoms as shown in Fig. 14 are treated exactly like QM hydrogen atoms in the QM/MM scheme, and they are invisible to the MM atoms because no interactions between the link atoms and the MM atoms are calculated. Each bond that crosses the boundary between the two regions must be defined. The link atom should be placed along the bond between the QM and MM atoms. The exact distance does not matter since the position of the link atoms is optimized in subsequent calculations. For the IMOMM scheme, the introduction of link atom is modified to study organometallic reactions by subtracting the classical MM interactions with the real QM system.

### 53.4.3 Examples of QM/MM Simulations

The hybrid QM/MM method is employed to simulate the His-tagged peptide adsorption to ionized region of nickel surface. "His-tags" are used in nanomechanical systems and biosensors due to their functional side chains. Noji et al. exploited the high affinity of polyhistidine-tagged  $\beta$ -subunits for Ni-nitrilotriacetate (NTA) to immobilize an F1-ATPase  $\alpha 3 \beta 3 \gamma$  subcomplex on a solid surface as shown in Fig. 15 (Noji et al. 1997). His-tags were used by Montemagno et al. (Montemagno and Bachand 1999) to attach a biomolecular motor, F1-ATPase, to metal substrates, and they have tested the binding strength of a 6 $\times$ His-tagged synthetic peptide attached to Au-, Cu-, and Ni-coated coverslips.

The 6 $\times$ His-tagged synthetic peptide attachment to the ionized region in Ni substrate was studied with the peptide chelating with Ni ion considered (Yang and Zhao 2006). GAMESS (Schmidt et al. 1993) and TINKER (Ponder and Richards 1987) were employed for the QM/MM calculation of the His-tagged peptide chelating with Ni ion. GAMESS/TINKER can perform the IMOMM scheme (Maseras and Morokuma 1995), which spearheads the entry of hybrid QM/MM approaches in computational transition metal chemistry. In the QM/MM calculation, the imidazoles on the side chain of the peptide and the metal ion with several neighboring water molecules are treated as a QM part calculated by "GAMESS," and the remaining



**Fig. 15** Immobilization of F1-ATPase  $\alpha_3\beta_3\gamma$  subcomplex on solid surface by polyhistidine interaction with Ni-NTA (Noji et al. 1997) (Reprinted from Yang and Zhao (2006), Copyright (2006), with permission from Elsevier)

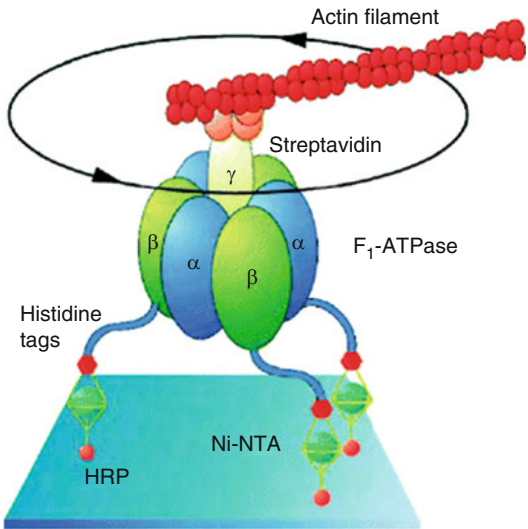


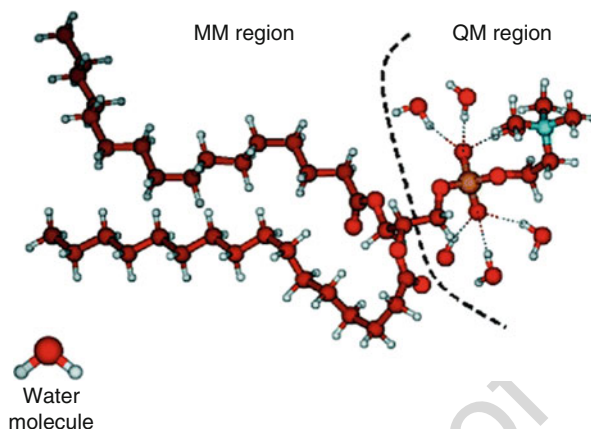
**Table 2** Binding energy and structural data for the optimized chelate structures

	$\Delta E$	$D_{(N-Ni)}$	$D_{(C1-L)}$	$D_{(C1-C2)}$	$D_{(Ni-O)}$	$\angle(N-Ni-N)$
Two His-tags chelate with $Ni^{2+}$						
HF(6-31+G**)/MM	-231.626	2.056	1.081	1.347	1.962	86.43
B3LYP(6-31+G**)/MM	-247.913	2.065	1.083	1.350	1.969	89.62
Four His-tags chelate with $Ni^{2+}$						
HF(6-31+G**)/MM	-314.077	2.083	1.072	1.341	1.973	93.38
B3LYP(6-31+G**)/MM	-326.062	2.090	1.075	1.342	1.976	93.40
Six His-tags chelate with $Ni^{2+}$						
HF(6-31+G**)/MM	-382.331	2.092	1.071	1.345	-	91.60
B3LYP(6-31+G**)/MM	-399.462	2.095	1.076	1.348	-	92.02
Experiment	-	2.112	-	1.355	2.065	93.50

atoms are treated as a MM part calculated by “TINKER.” The IMOMM method is used to deal with the QM part with the transitional metal.

All the geometry parameters and the binding energy are listed in Table 2. The QM/MM simulation results show that the 6×His-tagged peptide can form the most stable structure with high binding energy which is also confirmed experimentally. And the optimized structure data are obtained satisfactorily. The results obtained for the peptide-Ni chelate complexes also show that the present QM/MM approach is reasonable and effective. Such delicate properties as conformational changes and binding energy are modeled in the QM/MM calculations. It is shown that the QM/MM method can be used to probe aspects of metal chelate complexes from both fundamental and practical aspects.

**Fig. 16** The partition of DPPC and hydrated water molecules into QM and MM regions (Reprinted from Yin and Zhao (2009), Copyright (2009), with permission from Elsevier)



D is the distance,  $\angle$  is the angle (donor atom- $\text{Ni}^{2+}$ -donor atom), and L represents the link atom. All distances are in Angstrom, and energy in kJ/mol. Experimental data comes from references (Arici et al. 2002; Petrenko et al. 2004). “Reprinted from Materials Science and Engineering A, 423, Yang ZY and Zhao YP, QM/MM and classical molecular dynamics simulation of His-tagged peptide immobilization on nickel surface, 84–91, Copyright (2006), with permission from Elsevier”

In another example, the hybrid QM/MM method is applied to study the hydration phenomena of dipalmitoylphosphatidylcholine (DPPC) headgroup (Yin and Zhao 2009). In geometry optimization, the headgroup and its bound water molecules are treated at QM level of theory and the hydrocarbon chain with MM method (Fig. 16). All the geometry optimizations were carried out using the hybrid QM/MM method without any constraints, and hydrogen atoms were used as link atoms. First the hybrid QM/MM method was demonstrated to be both accurate and efficient enough to describe the conformations of DPPC headgroup. Then, both monohydration and polyhydration phenomena were investigated. In monohydration, different water association sites were studied. Both the hydration energy and the quantum properties of DPPC and water molecules were calculated at the DFT level of theory after geometry optimization. The binding force of monohydration was estimated by using the scan method. In polyhydration, more extended conformations were found and hydration energies in different polyhydration styles were estimated.

## 53.5 Ab Initio Molecular Dynamics (AIMD)

Classical MD is based on the established force fields or predefined interatomic potential. It is a powerful tool to serve problems of adhesion. The heart of any molecular dynamics scheme is the question of how to describe the interatomic interactions which always adopt some suitable functional forms to approximate the two-body, short-range or long-range interactions. The parameters used in the functions are always fitted by the experimental data or the ab initio simulation in some given condition.

Payne et al. listed some drawbacks of traditional MD in a review paper (Payne et al. 1992). Due to these reasons, AIMD has been established to describe the molecular system behavior directly from the electronic structure. In this way, the electronic system always keeps in the ground state and the dynamical behaviors of the system are all in the Born–Oppenheimer (BO) surface which is always called BOMD. Car and Parrinello introduced a new scheme (Car and Parrinello 1985) for AIMD that can perform finite temperature simulations and also did not involve electronic self-consistency at every MD step. Car–Parrinello molecular dynamics (CPMD) was the first to show that AIMD was possible. Some work has been performed using CPMD (Zang et al. 2009). The codes have been also utilized a lot in adsorption research. Mischler et al. used the CPMD to simulate the water adsorption on amorphous silica surfaces and the reaction of the water and the silicon (Mischler et al. 2005). The simulation procedures reveal that CPMD can perform a reaction dynamically.

CPMD has combined first principles electronic structure methods with MD based on Newton’s equations of motion. Ground state electronic structures were described according to DFT in plane-wave pseudopotential framework.

In CPMD, considering the parameters  $\{\psi_i\}$ ,  $\{R_I\}$ ,  $\{\alpha_\nu\}$  in energy function,

$$E[\{\psi_i\}, \{R_I\}, \{\alpha_\nu\}] = \sum_i \int_{\Omega} d^3r \psi_i^*(r) [-(\hbar^2/2m)\nabla^2] \psi_i(r) + U[n(r), \{R_I\}, \{\alpha_\nu\}], \quad (65)$$

are supposed to be time dependent, the dynamical Lagrangian,

$$L = \sum_i \frac{1}{2} \mu \int_{\Omega} d^3r |\dot{\psi}_i|^2 + \sum_I \frac{1}{2} M_I \dot{R}_I^2 + \sum_\nu \frac{1}{2} \mu_\nu \dot{\alpha}_\nu^2 - E[\{\psi_i\}, \{R_I\}, \{\alpha_\nu\}], \quad (66)$$

was introduced, where the  $\{\psi_i\}$  are subject to the holonomic constraints:

$$\sum_i \int_{\Omega} d^3r \psi_i^*(r, t) \psi_j(r, t) = \delta_{ij}. \quad (67)$$

In Eqs. 65 and 66,  $\{\psi_i\}$  are orbitals for electrons,  $\{R_I\}$  indicate the nuclear coordinates,  $\{\alpha_\nu\}$  are all the possible external constraints imposed on the system,  $\psi_i^*(r)$  is the complex conjugate of wave function  $\psi_i(r)$ ,  $\hbar$  is the reduced Planck constant,  $m$  is the mass of electron, and  $n(r) = \sum_i |\psi_i(r)|^2$  is the electron density; the dot indicates time derivative,  $M_I$  are the physical ionic masses, and  $\mu, \mu_\nu$  are arbitrary parameters of appropriate units. Then, the equations of motion can be written as:

$$\mu \ddot{\psi}_i(r, t) = - \frac{\delta E}{\delta \psi_i^*(r, t)} + \sum_k \Lambda_{ik} \psi_k(r, t), \quad (68)$$

$$M_I \ddot{R}_I = -\nabla_{R_I} E, \quad (69)$$

$$\mu_v \ddot{\alpha}_v = -\left(\frac{\partial E}{\partial \alpha_v}\right), \quad (70)$$

where  $\Lambda_{ik}$  are Lagrangian multipliers introduced in order to satisfy the constraints in Eq. 67. Then the equation of kinetic energy

$$K = \sum_i \frac{1}{2} \mu \int_{\Omega} d^3 r |\dot{\psi}_i|^2 + \sum_I \frac{1}{2} M_I \dot{R}_I^2 + \sum_v \frac{1}{2} \mu_v \dot{\alpha}_v^2, \quad (71)$$

is obtained (Car and Parrinello 1985). In fact,  $\mu, \mu_v$  have the dimensions of the mass which are called “fictitious mass.” In this scheme, the wave functions are treated as “particles” in which “mass” are  $\mu$ . When a suitable  $\mu$  is selected, the thickness of the BO surface can be controlled and the simulations are still close to the exact BO surface. So, the ground state wave function obtained by the initial configuration of the nuclei will stay close to its ground state during time evolution. Based on the technique mentioned, CPMD extends MD beyond the usual pair-potential approximation. In addition, it also extends the application of DFT to much larger systems.

Apart from the aforementioned combined simulation methods, the density-functional-based tight-binding (DFTB) method has been developed. DFTB is an accurate semiempirical method explicitly derived from Kohn–Sham DFT by making an expansion of the total energy functional around a reference charge density, which has been shown to be capable of producing reliable molecular structures and energy at a significantly reduced computational cost.

## 53.6 Conclusion

In this chapter, various simulation methods involving the adhesion technology have been reviewed, such as the MD simulations, the QM calculations, the MO method, the DFT calculations, the hybrid QM/MM simulations, the AIMD simulations, and the DFTB method. For each method, the basic theory and the general routine were described. Several representative examples of applications in the investigations of adhesion properties are given. Any one of the aforementioned methods has both advantages and disadvantages. Brief comparisons are listed in Table 3. To make a choice of the simulation method depends on the desired properties that one intends to obtain, while the computational capabilities should also be taken into account (as shown in Fig. 17).

Computer simulation forms a bridge between the molecules and the continuum mechanics of adhesion due to its multiscale, hierarchical, and complex nature (Kendall 2001). It is possible to speculate that the combined simulation methods with more efficiency and flexibility are still required and will lead the future directions of the simulation methodology in this fascinating field.

t.1 **Table 3** Brief comparisons of some simulation methods

t.2		Merits	Drawbacks
t.3	DFT	High accuracy; more details (electronic states, charge distribution, molecule orbits)	Limited to static states of small systems; slow and expensive
t.4	MD/MM	Available for large systems; fast and cheap	Disable in chemical reaction (bond breaking/forming); empirical potentials are used which lead to low accuracy
t.5	Hybrid QM/MM	Combined DFT with MM, extended the simulation system	Interactions between the QM region and MM region are difficult to describe
t.6	AIMD/CPMD	Combined MD with DFT; a balance between the time and precision	Limited to dynamic process of small systems
t.7	DFTB	Combined DFT with TB; works well for homonuclear system	Low accuracy for some heterogeneous system

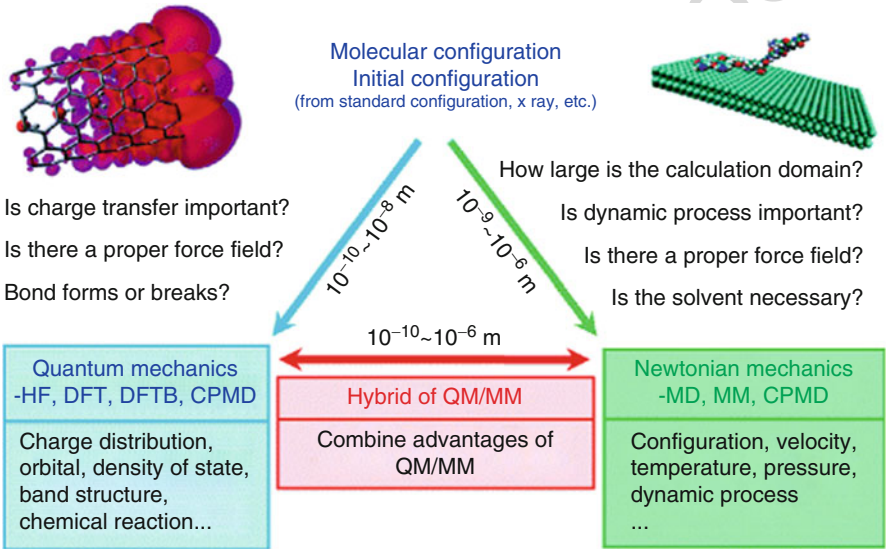


Fig. 17 Choices for the simulation methods

791 **Acknowledgments** Part of the work presented in this chapter was jointly supported by the  
792 National High-tech R&D Program of China (863 Program, Grant No. 2007AA021803), National  
793 Basic Research Program of China (973 Program, Grant No. 2007CB310500), and National Natural  
794 Science Foundation of China (NSFC, Grant Nos. 10772180, 60936001, and 11072244).

795 **References**

796 Alder BJ, Wainwright TE (1959) Studies in molecular dynamics. I. General method. J Chem Phys  
797 31(2):459  
798 Allen MP, Tildesley DJ (1989) Computer simulation of liquids. Oxford University Press, Oxford

- 799 Arici C, Ercan F, Atakol O, Basgut O (2002) Crystal structure of [N,N'-bis(3,5-dinitrosalicylidene-  
800 1,3-propanediaminato)bis(3,4-dimethylpyridine)]nickel(II)dioxane solvate. *Anal Sci* 18(3):375
- 801 Berendsen HJC, Vanderspoel D, Vandrunen R (1995) GROMACS: a message-passing parallel  
802 molecular dynamics implementation. *Comput Phys Commun* 91(1–3):43
- 803 Bharat B (2004) Springer handbook of nanotechnology. Springer, Berlin
- 804 Brooks BR, Bruccoleri RE, Olafson BD, States DJ, Swaminathan S, Karplus M (1983) CHARMM:  
805 a program for macromolecular energy, minimization, and dynamics calculations. *J Comput*  
806 *Chem* 4(2):187
- 807 Car R, Parrinello M (1985) Unified approach for molecular dynamics and density-functional theory.  
808 *Phys Rev Lett* 55(22):2471
- 809 Chi M, Zhao YP (2009) Adsorption of formaldehyde molecule on the intrinsic and Al-doped  
810 graphene: a first principle study. *Comput Mater Sci* 46(4):1085
- 811 Daintith J (2004) Oxford dictionary of chemistry. Oxford University Press, Oxford
- 812 Delley B (1990) An all-electron numerical method for solving the local density functional for  
813 polyatomic molecules. *J Chem Phys* 92(1):508
- 814 Delley B (2000) From molecules to solids with the DMol<sup>3</sup> approach. *J Chem Phys* 113(18):7756
- 815 Delley B (2002) Hardness conserving semilocal pseudopotentials. *Phys Rev B* 66(15):155125
- 816 Ferre N, Assfeld X, Rivail JL (2002) Specific force field parameters determination for the hybrid ab  
817 initio QM/MM LSCF method. *J Comput Chem* 23(6):610
- 818 Field MJ, Bash PA, Karplus M (1990) A combined quantum mechanical and molecular mechanical  
819 potential for molecular dynamics simulations. *J Comput Chem* 11(6):700
- 820 Hehre WJ (1976) Ab initio molecular orbital theory. *Acc Chem Res* 9(11):399
- 821 Hohenberg P, Kohn W (1964) Inhomogeneous electron gas. *Phys Rev B* 136(3):864
- 822 Humphrey W, Dalke A, Schulten K (1996) VMD: visual molecular dynamics. *J Mol Graph*  
823 14(1):33
- 824 Jones JE (1924) On the determination of molecular fields. II. From the equation of state of a gas.  
825 *Proc R Soc A* 106(738):463
- 826 Jorgensen WL, Chandrasekhar J, Madura JD, Impey RW, Klein ML (1983) Comparison of simple  
827 potential functions for simulating liquid water. *J Chem Phys* 79(2):926
- 828 Kale L, Skeel R, Bhandarkar M, Brunner R, Guroy A, Krawetz N, Phillips J, Shinozaki A,  
829 Varadarajan K, Schulten K (1999) NAMD2: greater scalability for parallel molecular dynamics.  
830 *J Comput Phys* 151(1):283
- 831 Kendall K (1975) Thin-film peeling-the elastic term. *J Phys D Appl Phys* 8(13):1449
- 832 Kendall K (2001) Molecular adhesion and its applications. Kluwer/Plenum, New York
- 833 Khandeparker L, Anil AC (2007) Underwater adhesion: the barnacle way. *Int J Adhes Adhes*  
834 27(2):165
- 835 Leach AR (2001) Molecular modelling: principles and applications. Pearson Education, New York
- 836 Levy M (1979) Universal variational functionals of electron densities, first-order density matrices,  
837 and natural spin-orbitals and solution of the v-representability problem. *Proc Natl Acad Sci U S*  
838 *A* 76(12):6062
- 839 Li J (2003) AtomEye: an efficient atomistic configuration viewer. *Model Simul Mater Sci Eng*  
840 11(2):173
- 841 Lindahl E, Hess B, van der Spoel D (2001) GROMACS 3.0: a package for molecular simulation and  
842 trajectory analysis. *J Mol Model* 7(8):306
- 843 Lyne PD, Hodoscek M, Karplus M (1999) A hybrid QM-MM potential employing Hartree-Fock or  
844 density functional methods in the quantum region. *J Phys Chem A* 103(18):3462
- 845 Maseras F, Morokuma K (1995) IMOMM: a new integrated ab initio + molecular mechanics  
846 geometry optimization scheme of equilibrium structures and transition states. *J Comput Chem*  
847 16(9):1170
- 848 Mischler C, Horbach J, Kob W, Binder K (2005) Water adsorption on amorphous silica surfaces: a  
849 Car-Parrinello simulation study. *J Phys Condens Matter* 17(26):4005
- 850 Montemagno C, Bachand G (1999) Constructing nanomechanical devices powered by biomolec-  
851 ular motors. *Nanotechnology* 10(3):225

- Mulliken RS (1955) Electronic population analysis on LCAO-MO molecular wave functions. I *J Chem Phys* 23(10):1833
- Nelson MT, Humphrey W, Gursoy A, Dalke A, Kale LV, Skeel RD, Schulten K (1996) NAMD: a parallel, object oriented molecular dynamics program. *Int J Supercomputer Appl High Perform Comput* 10(4):251
- Noji H, Yasuda R, Yoshida M, Kinosita K (1997) Direct observation of the rotation of F-1-ATPase. *Nature* 386(6622):299
- Payne MC, Teter MP, Allan DC, Arias TA, Joannopoulos JD (1992) Iterative minimization techniques for ab initio total-energy calculations: molecular dynamics and conjugate gradients. *Rev Mod Phys* 64(4):1045
- Pearlman DA, Case DA, Caldwell JW, Ross WS, Cheatham TE, Debolt S, Ferguson D, Seibel G, Kollman P (1995) AMBER, a package of computer programs for applying molecular mechanics, normal mode analysis, molecular dynamics and free energy calculations to simulate the structural and energetic properties of molecules. *Comput Phys Commun* 91(1–3):1
- Perdew JP, Burke K, Ernzerhof M (1996) Generalized gradient approximation made simple. *Phys Rev Lett* 77(18):3865
- Perdew JP, Ruzsinszky A, Tao JM, Staroverov VN, Scuseria GE, Csonka GI (2005) Prescription for the design and selection of density functional approximations: more constraint satisfaction with fewer fits. *J Chem Phys* 123(6):062201
- Petrenko PA, Gdaniec M, Simonov YA, Stavila VG, Gulea AP (2004) Crystal structure of monoprotonated Ni(II) nitrilotriacetate tetrahydrate. *Russ J Coord Chem* 30(7):813
- Plimpton S (1995) Fast parallel algorithms for short-range molecular dynamics. *J Comput Phys* 117(1):1
- Ponder JW, Richards FM (1987) An efficient newton-like method for molecular mechanics energy minimization of large molecules. *J Comput Chem* 8(7):1016
- Pople JA, Beveridge DL (1970) Approximate molecular orbital theory. McGraw Hill, New York
- Rapaport DC (2004) The art of molecular dynamics simulation. Cambridge University Press, Cambridge
- Roothaan CCJ (1951) New developments in molecular orbital theory. *Rev Mod Phys* 23(2):69
- Ryckaert JP, Cicciotti G, Berendsen HJC (1977) Numerical integration of the cartesian equations of motion of a system with constraints: molecular dynamics of n-alkanes. *J Comput Phys* 23(3):327
- Schmidt MW, Baldridge KK, Boatz JA, Elbert ST, Gordon MS, Jensen JH, Koseki S, Matsunaga N, Nguyen KA, Su SJ, Windus TL, Dupuis M, Montgomery JA (1993) General atomic and molecular electronic structure system. *J Comput Chem* 14(11):1347
- Shi XH, Kong Y, Zhao YP, Gao HJ (2005) Molecular dynamics simulation of peeling a DNA molecule on substrate. *Acta Mech Sin* 21(3):249
- Yang ZY, Zhao YP (2006) QM/MM and classical molecular dynamics simulation of His-tagged peptide immobilization on nickel surface. *Mater Sci Eng A* 423(1–2):84
- Yin J, Zhao YP (2009) Hybrid QM/MM simulation of the hydration phenomena of dipalmitoylphosphatidylcholine headgroup. *J Colloid Interface Sci* 329(2):410
- Yin J, Zhao YP, Zhu RZ (2005) Molecular dynamics simulation of barnacle cement. *Mater Sci Eng A* 409(1–2):160
- Yuan QZ, Zhao YP, Li LM, Wang TH (2009) Ab initio study of ZnO based gas sensing mechanisms: surface reconstruction and charge transfer. *J Phys Chem C* 113(15):6107
- Zang JL, Yuan QZ, Wang FC, Zhao YP (2009) A comparative study of Young's modulus of single-walled carbon nanotube by CPMD, MD, and first principle simulations. *Comput Mater Sci* 46(3):621
- Zhang YK, Lee TS, Yang WT (1999) A pseudobond approach to combining quantum mechanical and molecular mechanical methods. *J Chem Phys* 110(1):46
- Zhao YP, Wang LS, Yu TX (2003) Mechanics of adhesion in MEMS-a review. *J Adhes Sci Technol* 17(4):519

Katharina Richter, Ingo Grunwald, and Janek von Byern

## Contents

54.1	Introduction .....	1598
54.2	Natural Adhesives .....	1599
54.2.1	Natural Resins .....	1600
54.2.2	Natural Rubber .....	1601
54.2.3	Natural Polyesters .....	1602
54.2.4	Carbohydrates .....	1603
54.2.5	Protein-Based Adhesives .....	1606
54.2.6	Polyphenol-Based Adhesives .....	1608
54.3	Biological Adhesives .....	1611
54.3.1	Predation .....	1626
54.3.2	Defense .....	1627
54.3.3	Construction .....	1628
54.3.4	Attachment .....	1629
54.3.5	Locomotion .....	1630
54.4	Bioinspired Applications .....	1630
54.4.1	Antifouling .....	1631
54.4.2	Biomimetic Adhesives .....	1631
54.5	Challenges and Opportunities .....	1634
54.6	Conclusion .....	1635
References	.....	1636

K. Richter (✉) · I. Grunwald (✉)

Department of Adhesive Bonding Technology and Surfaces, Adhesives and Polymer Chemistry,  
Fraunhofer Institute for Manufacturing Technology and Advanced Materials (IFAM), Bremen,  
Germany

e-mail: [katharina.richter@ifam.fraunhofer.de](mailto:katharina.richter@ifam.fraunhofer.de); [ingo.grunwald@ifam.fraunhofer.de](mailto:ingo.grunwald@ifam.fraunhofer.de)

J. von Byern

Austrian Cluster for Tissue Regeneration, Ludwig Boltzmann Institute for Experimental and  
Clinical Traumatology, Vienna, Austria

Faculty of Life Science, Core Facility Cell Imaging and Ultrastructure Research, University of  
Vienna, Vienna, Austria

e-mail: [Janek.von.Byern@univie.ac.at](mailto:Janek.von.Byern@univie.ac.at)



## Abstract

Bioadhesion is a versatile tool used by many organisms for a variety of purposes. It has roles to play in construction, predation, defense, and attachment and covers different concepts based on biochemical and mechanical principles. The specific request on the bond combined with millions of years of evolution results in diverse inspirations for medical and technical applications. This requires knowledge of the adhesives themselves in terms of composition, structural design, and interaction with surfaces. This chapter gives an overview about natural adhesives and biological adhesives leading to bioinspired applications. The terminology used in this chapter is based on the adhesive's origin and usage and the underlying concept: while natural adhesives are composed of bio-based raw materials for artificial applications, biological adhesives are expressed by natural organisms for versatile purposes. The latter in particular can lead to bioinspired applications that are not restricted to adhesion, including concepts to avoid adhesion as in terms of antifouling. Both kinds of adhesive, i.e., natural and biological, are relevant for biocompatible adhesives. This characteristic is mandatory for applications as in cosmetics, food, or medicine. In view of their interaction with vital tissues and their medical eligibility, a brief digression into biomimetic adhesives is given.

## 54.1 Introduction

Bioadhesives are defined as natural polymers that act as adhesives. The compositions of bioadhesives are mostly complex and can contain proteins, carbohydrates, or lipids alone or complex mixtures with varying proportions. The first documented use of natural adhesives was 200,000 years ago by Neanderthals. They used tar from birch bark to join blades of rock with a shaft. Adhesives like wet lime, resins from trees, collagen, or semiliquid balsams were also used by the Egyptians, the Greeks, and the Romans for applications in marquetry, ceramics, and wood materials thousands of years ago. These adhesives had a natural origin in common. During the industrial revolution, the bioadhesives were replaced by synthetic ones. Nowadays the bioadhesive saga has reached a turning point, and new generations such as bioinspired and biomimetic adhesives are becoming more and more advanced (Mathias et al. 2016).

On the one hand, the increased focus on resource efficiency which is borne out from, among others, ecological needs is a major concern. Therefore natural adhesives are of particular interest. On the other hand, there is the challenging request of adhesion under harsh conditions like wet surfaces, which is excellently solved by marine organisms, many bacteria, and fungi. According to Aristotle, "If there is a better solution, nature has probably found it," and bioadhesives do indeed often provide inspiration and address needs like sustainability.

Adhesive materials and structures are used by many plants, animals, and microbes to attach themselves to inert substrates or to living tissue (Smith and Callow 2006; von Byern and Grunwald 2010; Smith 2016). Therefore, as for many technical applications, nature stands at parity for high-performance adhesion.

Among diverse purposes and complex raw materials, bioadhesives also serve solution approaches. The underlying principal mechanisms of adhesion are various. The octopus suction pad and the feet of geckos and flies, cases in which adhesion is achieved by physical means, are examples which show that biological adhesives do not necessarily have to involve complex biopolymers. Often the functional principles are worth investigating, and it is better to imitate these mechanisms than to attempt complete composition. Usually limited resources and high performance meet the technical requirements perfectly. There are three outstanding characteristics in connection with biological adhesion that are hardly reached by synthetic solutions: (i) bonding and debonding on demand, (ii) adhesion under wet conditions, and (iii) adherence to multiple substrates. The principle mechanisms of biological adhesion were classified into basically physical (interlocking, snap connection, staples, spreading device, suction, friction, capillary effects) and chemical (dry and wet adhesion). Sometimes different adhesion concepts are combined like interlocking, chemical interactions, as well as viscosity and capillarity forces (Schwotzer et al. 2012). Exemplary cases in particular for the chemical ones are reviewed in Sect. 3.

## 54.2 Natural Adhesives

Synthetic adhesives are required by industries in huge quantities for bonding nearly all kinds of substrates ranging from metal to human tissue. For many of these formulations, the environmental, health, and economic aspects are a matter of concern. There is an urgent need to substitute the majority of critical components deemed environmentally unsafe (Meyer-Rochow et al. 2015) such as phenol-formaldehyde or poly(vinyl acetate) (PVA) by biopolymers that are defined as high molecular mass compounds produced by living organism (Patachia and Croitoru 2016). Another objective is to avoid residual toxic chemicals such as volatile organic compounds (VOCs), epichlorohydrin, or methylene diphenyl diisocyanate (MDI). Beyond their composition, it is their end-of-life fate that has moved into focus (Erren et al. 2013). A global analysis of all mass-produced plastics ever manufactured revealed an estimated 8,300 million metric tons (Mt) of virgin plastics have been produced until 2017 of that less than 10% has been or can be recycled (Geyer et al. 2017). This scrutiny of the end-of-life management has also helped moving the focus to demands for recycling and degradation. The United States Environmental Protection Agency (US EPA) has already addressed these concerns, aiming to diminish the use of non-bioplastics in their pollution prevention program during the Obama administration (Gross and Kalra 2002). Despite the varying quality from batch to batch, adhesives originating from bioresources are commercially attractive, because of their numerous advantages like biodegradability, less toxicity, and natural biocompatibility. Today 15% of the adhesives are made out of renewable resources. The green content will increase in the next years by intensifying the use of second-generation biomass, which goes beyond the biofuel production used to synthesize biochemicals. There is a strong research and development focus to develop and commercialize the bioadhesive market. For adhesives

and sealants, the market is being driven by a rising trend in various end user segments to use eco-friendly or green adhesives. The projected goal is to reach about 1.24 billion US dollars in 2017 (<http://www.smithersapex.com/market-reports/green-adhesives-sealants-industrial-applications>). The bio-based adhesive market size accounts for roughly 1–2% of the overall demand. Using novel feedstock such as vegetable oil polyamides, polyisoprenes, soybean polyols, or epoxies could lead to a paradigm shift and change the product matrix of natural adhesives significantly (<http://www.adhesivesmag.com/articles/94808-auto-packaging-construction-lead-adhesives-and-sealants-market-growth>).

Placed into eight “families,” natural adhesives can be distinguished on the basis of their structure: nucleic acids, polyesters, polyisoprenoids, polyoxoesters, polyphenols, polysaccharides, polythioesters, and proteins (Kumar Patel et al. 2013). In the following sections, the most important species of natural adhesives are organized by source: starting with natural vegetable resins (rosin, terpene resins); followed by polyisoprenoids (natural rubber), natural polyesters (vegetable oil, shellac), carbohydrates (starch and dextrans, cellulose “derivatives,” gums, and exopolysaccharides), and proteins (collagen, blood, and vegetable proteins); and closing with polyphenols (lignin, bitumen). For an excursus to natural cross-linkers (e.g., genipin from *Gardenia spec.*) or bio-based epoxy curing agents, the reader is directed to Sung et al. (1998) and Shibata (2013).

## 54.2.1 Natural Resins

Numerous plants use exudates for repair or healing issues in case of injuries. These natural resins are from the chemical point of view related to terpenes and etheric oils. They are amorphous and consist of complex mixtures (phenols, resin acids, resin alcohols, unsaturated resins, resin esters). Natural resins are considered as green raw material, but due to their structure, they are hardly biodegradable. Of particular importance are resin sources of pine trees. Their isoprenoid terpene rosin and terpene resins are valuable additives to provide tack and peel to the adhesive mixture. Their multiple properties offer versatile applications that range from the usage in the preparation of thermoplastics like polyesters (Karak 2016) to uses within the formulation, e.g., of pressure-sensitive adhesives. Their individual chemical structures make significant differences in terms of their compatibility with the formulation. For instance, terpene resin derivatives from pines are tolerated by styrene-butadiene rubber but not d-limonene. In sum, natural resins offer a high potential for adjusting adhesives within the bio-based toolbox.

### Rosin

One of the oldest raw materials in the adhesion industry is rosin. It is used directly or converted to resin esters. Rosin is obtained from conifers and naturally synthesized as a defense compound. By distillation nonvolatile terpene components get separated from the fresh liquid resin. The semitransparent and colored solid has a piney odor and is brittle at ambient conditions. It consists out of abietic acid, an unsaturated

monobasic acid, and additional organic acids. Three classes of rosins can be distinguished: (i) gum rosin (pine gum), the secreted oleoresin from wounds in the living pine tree; (ii) wood rosin, resinous extract from the pine wood stump that was left after harvesting of the tree in the ground for about 10 years to enrich the heartwood in resin; and (iii) tall oil rosin (TOR), a distillate of tall oil (liquid rosin) named after the Swedish word for pine oil “tallolja.” Tall oil is a by-product from Kraft pulping (sulfate process) when pulping coniferous trees. The yellow blackish liquid composed of fatty acids (palmitic, oleic, and linoleic) and rosin acids (mainly abietic) results in TOR with reduced rosin content by fractional distillation. If the rosin content is too high, the material is brittle. In this case additives like beeswax or powdered biochar improve the adhesive strength. In formulations with traditional linseed oil and sand, it is used as gap filler in constructions. Due to its improvement of gloss, hardening, or antifouling properties, rosin-modified alkyd resins or rosin derivatives are used in paints and surface coatings (Karak 2016).

### Terpene Resins

Terpene resins are derivatives from turpentine ( $\alpha$ -pinene,  $\beta$ -pinene, 3-carene) or can be obtained from citrus plants (d-limonene). Three major structural classes can be distinguished: styrenated terpene resins, terpene-phenol resins, and polyterpene resins. Terpene resins can be obtained from terpenes by cationic polymerization. The oldest reference for terpene resins goes back to 1789, when turpentine was treated with sulfuric acid. Terpene resins are used in a wide variety of formulations, e.g., coating compositions or adhesive tapes (Adhesives & Sealants, Industry News 2017: Materials and Chemicals Overview, <http://www.adhesivesmag.com/articles/95737-materials-and-chemicals-overview>). To impart the tack in solvent-based or hot melt adhesives, terpene resins from monoterpenes are used in additive manufacturing (NPCS Board of Consultants and Engineers 2017). Terpene resins are supplied in solution or in solid forms, the latter available in a wide range of molecular weights and softening points (Adhesives & Sealants, Industry News 2017: Materials and Chemicals Overview, <http://www.adhesivesmag.com/articles/95737-materials-and-chemicals-overview>).

## 54.2.2 Natural Rubber

Natural rubber adhesive is based on cis-1,4-isoprenoid units. It belongs to the earliest substances used to bind materials. Because of its capacity to become elastic when heated, it is one of the most popular adhesives on the market and is typically used in bonding organic and porous materials like leather, paper, fabrics, as well as other rubber products. The adhesive is based on natural rubber, an extract from latex, which is the milk of the rubber tree, *Hevea brasiliensis*. The milk is composed out of 60–75% water, 25–35% rubber, 1.5–2.5% resins, 1.5–2% proteins, and 0.5–1% minerals. Eight types of basic natural rubber are recognized: ribbed smoked sheets, pale crepes, estate brown crepes, compo crepes, thin brown crepes (remills), thick brown crepes (ambers),

flat bark crepes, and pure smoked blanket crepes. The definition of these grades is described in the so-called Green Book (Cohen et al. 2008).

Natural rubber mixed with resin gives a sticky material, the adhesive. The unique chemical structure is responsible for its outstanding properties: high initial tack, excellent flexibility and tack retention. The cohesion is caused by the long entangled polymer chains of rubber and gives a highly elastic but brittle adhesive at low temperatures. By vulcanization, the addition of sulfur which acts as a cross-linker, the stability in terms of temperatures can be improved. The low strength due to the limited cohesion and adhesion at temperatures above 70 °C and the softening make it unsuitable for structural applications. Another disadvantage is the poor resistance to ultra violet radiation, ozone, organic solvents and oxidizing agents.

A well-known application is that for self-sealing envelopes. Also used in masking and cloth tapes, the compound found applications beyond those in packaging.

### 54.2.3 Natural Polyesters

Beeswax and vegetable oils belong to natural esters. While beeswax serves as appropriate softener within adhesive formulations but has no initial tack, the vegetable oils expose more suitable structures prerequisite to act as components in adhesives (Türünc et al. 2015). Vegetable oils are fatty acids or triglyceride esters from the seeds of plants (Karak 2016). The fatty acids, which are components of the triglycerides, can be saturated or unsaturated. Double bonds of unsaturated fatty acids are accessible for oxidation reactions, e.g., by cleavage or epoxidation. The modified oil gives access to dicarboxylic acids or epoxidized oils, respectively, which present appropriate reactive groups for formulations like pressure-sensitive adhesives (PSA) (Köckritz and Martin 2008; Li and Li 2014; Wu et al. 2015). Other than oxidation of double bonds, oleochemistry also uses hydrolysis to gain free fatty acids and glycerol or transesterification reaction to get fatty acid methyl esters (Türünc et al. 2015). Vegetable oil derivatives are preferably used for the polyester syntheses that have long-term durability and good adhesion. Advantages of triglycerides are their abilities to create three-dimensional networks and in case of ricinoleic acids from ricinolein (castor-oil-plant) an additional hydroxyl group, which serves as a natural polyol for polyurethanes.

### Shellac

Lacca in tabulis, lac, or shellac, also wrongly referred to as gummi lacca, is the general term for the refined form of lac, a natural polyester resin secreted by tiny scale insects. These phytophagous insects (*Kerria lacca*, *Laccifer lacca*, *Laccifer chinensis*) insert their mouthpart into the barks of specific trees. The insects secrete a sticky lac after transforming the ingested sap into a polyester resin. Therefore it is the only natural resin of economic interest with an animal origin. Shellac is neither a biopolymer nor a monomer; it's on a low level pre-polymerized. For refining issues to get shellac from the seed lac, three processes (bleaching, melting, and solvent extraction) are used. The resulting products vary in terms of characteristics like color

and properties. Depending on the refining method, four types of shellac are distinguished: bleached shellac (regular bleached shellac), bleached dewaxed shellac (refined bleached shellac), wax-containing shellac (orange shellac), and dewaxed shellac (dewaxed orange shellac) (Sankaranarayanan 1989).

Orange shellac and bleached shellac have molecular weights of 1006 g/mol and 949 g/mol, respectively, and the empirical formula for the average shellac molecule is  $C_{60}H_{90}O_{15}$ . Even with this relatively low molecular weight, shellac has excellent film-forming properties, good adhesion to a variety of surfaces, high gloss and surface hardness, good insulation qualities (sealing out moisture), abrasion resistance, and excellent UV stability that prevents darkening, and moreover it is nontoxic. An alcoholic (ethanol or methanol) solution results in good durability. Its solubility in water in the presence of alkalis makes it attractive for cosmetic purposes like hair spray and drug delivery. It consists of a complex mixture of aliphatic and alicyclic acids (jalaric acid, schellolic acid, and aleuritic acid, also butolic and kerrolic acids). Beyond its usage as a colorant, brush-on, wood finish, and food glaze, shellac has historically been used as an adhesive for wooden layers on the hulls of boats (Penning 1996; Specht et al. 1998; Buch et al. 2009). Shellac is one of just a few known bio-based duroplastics (Türk 2014).

#### 54.2.4 Carbohydrates

For many decades carbohydrates (monomeric, oligomeric, polymeric, and gum sugars) have been used as adhesives. Sugar and flour glue as well as corn starch glue are often used as homemade glues. The formulation is simple and the adhesive is versatile. These carbohydrates are chemically saccharides and appear in all organisms, namely, bacteria (xanthan gum and dextran), fungi (schizophyllan and scleroglucan), plants, and animals. Typically plants and animals often use the polymeric form (polysaccharides) as storage compounds (e.g., starch and glycogen), which can have adhesive properties. But polysaccharides are also used for cellular communication (glycosaminoglycans) or as structural biopolymers like chitin, alginate, chondroitin sulfate, or cellulose. Polysaccharides are eligible for adhesion because of the high density of polar functional groups and the high molecular weight leading to specific secondary structures (helical, sheet, or spiral conformation) due to noncovalent interactions. The degree of a carbohydrate's polymerization is highly dependent on origin, pretreatment, and measurement technology. The adhesion to substrates with high surface energy like wood or metals is favored by the polarity, while the cohesion benefits from conformational features. Both, adhesion and cohesion, benefit from the structural variability and can be enhanced by modifications of the functional groups (e.g., carboxylates or hydroxyl). Beyond the well-documented vegetable polysaccharide derivatives, chitosan with its origin in the exoskeleton (the most abundant polysaccharide after cellulose) of marine invertebrates and microbial exopolysaccharides show high potential for adhesives, especially for wood applications. In order to reduce the content of unwanted synthetically toxic components in commercial adhesive applications, one approach is to partly



substitute them with polysaccharides. Hence, numerous adhesives made of polysaccharides as a co-component have been developed. They are known as intermediate (bio)adhesives (Kumar Patel et al. 2013; Karak 2016).

Carbohydrate-based epoxy resins also moved into a tighter focus as a potential alternative with improved physical properties and more efficient curing than petroleum-based epoxy resins. Based on recent studies, covetable epoxy resins may also be designed coming from furan or isosorbides. Furanyl building blocks prepared from pentose, hexose, or polysaccharides could replace petroleum-based phenyl building blocks in thermoset resins, while epoxidized isosorbide has already been shown to be a suitable and favored substitute of bisphenol A. Beyond the suitability of furan derivatives in epoxy-based resins, carbohydrate derivatives are under investigation as epoxy curing agents (Baroncini et al. 2016).

### Cellulose Derivatives

Cellulosic adhesives are solvent-based thermoplastics. As polyhydroxyl alcohol with access to esterification and etherification reaction, esters and ether derivatives as well as polyblends of cellulose and cellulose graft copolymers provide a wide range of adhesive applications. Cellulose nitrate was the first inorganic ester derivative, and it is still one of the most important adhesives. It advanced to a famous “household” cement as it combines features like transparency, flexibility, and water indelibility with a wide range of solubility. Cellulose acetate butyrate is an ester that can be directly used in hot melt adhesives and is utilized in safety glass manufacture. Another ester, cellulose caprate, is used as hot and liquefied optical cement for the manufacture of compound lenses due to its good resistance against UV radiation and the possession of a refractive index near that of glass. Etherification of cellulose can open up the structure to enable solubility in water. The innate adhesive properties of cellulose ethers have been used as thickeners in adhesive formulations. They are of considerable industrial importance as their usage includes plywood adhesives, wallpaper and library pastes, latex adhesives, paper and textiles, and ceramic adhesives. Especially carboxymethylcellulose (CMC) is popular, because of its properties (nonstaining wallpaper adhesive, ease of slip/non-spoiling, high adhesive efficiency, and ease of makeup). Hence, CMC is appreciated in the ceramic industry due to its ability to act as a binder and to suspend materials during various stages of manufacture (Hon 1989).

For applications in adhesive technology, the polymeric degree and structure of cellulose derivatives, which has a direct impact on the solubility and swelling behavior, have to be considered in the preparation of suitable derivatives. In general the principle is valid: the higher the molecular weight, the higher its bond strength. For cellulosic adhesives, processing the adhesive becomes more difficult for increased molecular weights.

Cellulose is never met in pure form. It is a linear homopolysaccharide made up of glucose molecules. Due to its long linear structure, cellulose can achieve a degree of crystallinity of 60–80% depending on its age: the older the higher the crystallinity. Compared with starch and chitin, it has been revealed that even minor structural differences in the direction of the glycosidic bond (alpha or beta) decide if the

conformation is linear or helical and therefore if it is soluble in aquatic media (Türk 2014). These characteristics are of major interest in terms of water resistance and biodegradation. In sum depending on the modification, cellulose may be available as soft as well as tough solvent-based formulations or as hot melts. It adheres very well to porous materials and exhibits substantial resistance to fouling and oil.

### **Starch and Dextrins**

In the predynastic period, Egyptians treasured the practical use of starch when cementing it together with strips of papyrus. They boiled wheat flour with dilute vinegar to obtain an adhesive. Adhesives made from starch and dextrins are almost solely water based and used mainly in the paper and packaging industry. Especially the increasing sector of cardboard and corrugated board production suggests a rising demand. Also as bookbinder adhesive, it occupies a considerable niche market. Starch is a mixture of linear amylose and branched amylopectin. In contrast to the linear cellulose, starch forms a helix due to its alpha-glycosidic bond, which results in fundamental material differences. The previously mentioned isosorbide is a derivative prepared from starch. Dextrin, too, is processed starch by heat and acid to hydrolyze the polysaccharide in smaller fragments. These fragments undergo a repolymerization and result in a highly branched polymer with good solubility. Dextrins are classified by their solid contents and with respective increases in their molecular weights as canary dextrins, white dextrins, and British gums, the latter possessing the strongest adhesive of these three types. To improve the water resistance of waterborne bio-based starch adhesives is a challenging task. The dry strength of such adhesives is fairly high, but exposure to high moisture causes a significant decrease in “wet strength” (Kumar Patel et al. 2013). Treatments with phenolic compounds like caffeic acid and chitosan indicated promising results. Also a system based on modified starch and chitosan limited the water solubility of the starch adhesive (Karak 2016).

### **Potential of Blends, Gum Dispersions, and Exopolysaccharides**

In the context of intermediate or complete bio-based adhesives, different attempts have led to successes by blends of (i) corn starch with tannins, as substitute for phenol in the resin to get closer to formaldehyde-free wood adhesive, (ii) vinyl acetate grafted onto starch and combined with silica nanoparticles to improve water resistance and physical properties of the binding, (iii) and phenol-formaldehyde with fermented biomass, a co-product from ethanol production, comprising glycocalyx, adherent bacterial cells, and fibers (Kumar Patel et al. 2013). Blends of xylan derivatives with dispersing agents as poly(vinyl alcohol) or poly(vinyl amine) and addition of cross-linkers gave a potential wood adhesive as well.

Gums are exudates that are sweated out as a result of injuries to plant parts (e.g., bark) and solidify in air. Gums consist of hydrophilic and hydrophobic heteropolysaccharides with colloidal properties. Gums are suspension and emulsion stabilizing compounds as they inhibit crystallization. For this reason, they are used in hairsprays or in foods such as ice cream and jellies. Common gums are gum arabic, gum tragacanth (spermicidal gels), gum ghatti (enhanced oil recovery, explosive



additive, and wax emulsifier), gum karaya (denture adhesive cream due to high wet adhesive strength), and guar rubber (explosive additive, “fracfluid” additive).

Gum dispersions are heat resistant and possess an intrinsic tack. They are used in plaster adhesives, pressure-sensitive tape and dentures, paper adhesives, pharmaceutical tablet binders, and label pastes. Locust bean gum additionally exhibits excellent water resistance. The binding is comparable to D2 wood adhesive like poly(vinylacetate). Also comparable to this standard were some candidates of investigated microbial polysaccharides in a study of bacterial derived wood adhesives, except for xanthan (which was also successfully tested for wood applications in a different study); candidates included among others photo-curable dextran urethanes, exopolysaccharides from periphytic marine bacteria and from *Bacillus megaterium*, and pullulan (Karak 2016).

### 54.2.5 Protein-Based Adhesives

Three thousand five hundred years and most likely even longer ago, proteins from milk, egg white, and blood were intuitively used as binders and additives in construction materials. Proteins consist of amino acids which differ in their residues. Depending on their composition, they can be tailored for different purposes ranging from catalysis (enzymes), structuring (collagens), transport (ionic channels, hemoglobins), communication (hormones), protection (immunoglobulins), fixation of nitrogen (nodule bacteria), and movement (actin). Gluten (Latin *glūten* for glue) from wheat is a combination of gliadin (56%, responsible for viscosity due to its low molecular weight) and glutenin (44%, quaternary structures with molecular weights >1000 kDa), in sum an elastic storage protein with exceptional adhesive characteristics. It is the main component beyond water in seitan (meat substitute). Gluten is chiefly used in the baking industry but also in the paper industry, and furthermore as an additive in concrete and mortar, and in adhesives. A protein that obtained significant interest is casein, maintained from milk by lowering the pH; it was already used as paint in caves to bind pigments. It is also known as thermoset, namely, galalith, when cured with formaldehyde. The water resistance of casein paints can be achieved by adding chalk milk to it. Because of the food competition and its high price, casein was replaced widely. Still, it is used even today in the food sector for printing casein inks on sausage casings or for labeling bottles. Indoor paintings and paints in kindergartens are also often casein based (Türk 2014). Casein fibers have most comfortable, excellent water transportation, air permeability, and long-lasting antibacterial effects and have received valid international certifications for ecological textiles. These characteristics are attractive for the fashion sector, but in medical applications they were considered cytotoxic.

As a plethora of interesting, proteinaceous structures exists and corresponding unique properties have been identified, the areas of applications as adhesives have rapidly become extremely complex, as the following review focused on just the three major classics beyond casein shows. Treatment of the marine adhesive proteins is postponed and covered in the section polyphenol-based and bioinspired adhesives.

### **Fibrous Proteins (Collagen, Animal Glues, and Fish Glue)**

Collagen, keratin (wool), silk, and elastin are common fibrous proteins. As structuring molecules some of them are constructed hierarchically just like cellulose. Without pretreatment they can be used as reinforcing agents. Collagen is a by-product from leather manufacturing and is used in foods, pharmaceutical products, and medical devices (wound dressing and tissue engineering). In particular medical applications promise a substantial added value.

Animal glues are obtained by boiling bones (bone glue), skin (hide glue) or swim bladders, and skin and bones from fish (isinglass or fish glue). Cartilage glue, on the other hand, is not based on the same compound as other animal glues, but is made up of chondrin, a protein-carbohydrate complex, with less adhesive power (chondroitin sulfate glue). Boiling of the gelatine leads to a water-soluble substance that consists mainly of partially unfolded collagen, whose composition is similar to that of gelatine. All animal glues are high-polymer proteins and derivatives of collagen that form colloids (NPCS Board of Consultants and Engineers 2017).

Degradation, e.g., by hydrolysis and heating of collagen (mainly type I), results in gelatine, which was already used by the ancient Egyptians as an adhesive. Gelatine is able to swell and to absorb water due to a high content of polar residues (about 65%). It is amphiphilic, which makes it suitable as an additive to stabilize foams (Türk 2014). The sum of excellent properties inaugurates versatile niche applications as, for example, in stucco work as a gypsum additive (delaying hardening and increasing strength), in gas masks as an antifogging additive, in compostable candles on graves, and in gum blends as a smoothener and as barrier adhesive. Currently the price for gelatine is relatively low compared to that of synthetic or plant proteins.

### **Proteins in Tissue Engineering**

Substrates involved in surgeries are challenging substrates that require advanced adhesives and need to obey certain natural concepts: fibrinogen and fibrin are proteins present in blood plasma (see chapters in von Byern and Grunwald 2010) and so is albumin, which is inter alia located in the blood. Both and furthermore collagen possess remarkable properties and excellent biocompatibility. Therefore they are used as medical adhesives with FDA approval (albumin limited to surgical repair of acute thoracic aortic dissections). Albumins are globular proteins with amphiphilic character and a high content of the sulfur containing amino acid cysteine. They have polar domains exposed to the outer site, while the lipophilic ones are directed to the inner sphere. This structural feature enables them to function as transporters of water-insoluble compounds. Albumin-based adhesives are usually cross-linked with glutaraldehyde or similar organic compounds and reach an initial tack in about 30 s. Their bonding strength becomes maximal within a few minutes and ranges between 10 and 40 kPa (Bochynska et al. 2016). Fibrin and fibrinogen belong to the blood clotting system. In combination with thrombin, calcium ions, and factor XIII, they are the most commonly used bio-based tissue adhesives, although their bonding strength (approx. 0.01 MPa) is one order of magnitude lower than gelatine-resorcinol-formalin adhesives (approx. 0.1 MPa) (see chapters in von Byern and Grunwald 2010). Collagen and gelatine, a water-soluble derived form of collagen,

became integral parts of the surgeon's toolbox as well: its applications are established in tissue reconstruction, e.g., after drastic damage from combustion, owing to the high potential as a surgical sealant. The substrate can be enzymatically cross-linked by transglutaminase and gels in less than 5 min with bonding strengths about 15–45 kPa. Gelatine is considered biodegradable, non-immunogenic, and biocompatible. It usually needs a cross-linking agent as well as a polymeric additive (e.g., alginate based), with additional functional groups available for cross-links to achieve sufficient mechanical strengths. But it can also be designed as a two-component adhesive such as photochemically induced cross-linking of oxidized urethane dextran and gelatine (Mathias et al. 2016).

### **Vegetable Proteins**

Vegetable proteins like those of soybeans, maize, peas, or wheat gluten, as described above, are in principle all suitable for adhesion applications. As raw materials of by-products, they bear potential for sustainable substitutes, e.g., in wood adhesives. In contrast to casein, they benefit from mild hydrolysis (enzymatical or chemical) or physical treatment to alter their molecular structure by unfolding into a suitable conformation for adhesional processing. Due to its comparatively low costs and good adhesion characteristics, soy protein has established itself as a binder for fillers and pigments in (paper) coatings. Thus, it gives paper a glossy white surface. It was already used in the USA until the beginning of the last century as a low-budget (0.02 dollar/pound; Weakley and Mehlretter 1965) adhesive composed of soy protein, a nonvolatile starch dialdehyde, and lyophilized blood. Just cross-linked soy proteins are not suitable as pure material; they need to be blended with plasticizers because of their brittleness. Also the water content has a considerable impact on the material properties. Up to now just 0.5% of soy protein is used in industrial applications (Türk 2014).

Nevertheless, strength and water resistance of vegetable proteins are still far removed from commercial adhesives. Their potential, however, can be increased by blending them with poly(vinyl acetate) or poly(vinyl alcohol) but also with other proteins as described for the American low-budget formulation with blood and casein (Mathias et al. 2016).

### **54.2.6 Polyphenol-Based Adhesives**

Polyphenols are natural compounds found in animals and plants. These bulky molecules comprise an aromatic p-system and hydroxyl groups in phenolic groups like catechols. It is assumed that the catechol functionality is responsible for adhesive and cross-linking characteristics. In plywood industry the most common adhesives are phenol based and cross-linked by formaldehyde (phenol-formaldehyde). It stands out with excellent weather and water resistance. Based on the structural similarity, several attempts have been made to replace phenol by lignin derivatives. Lignin is composed out of p-coumaryl alcohols, coniferyl, and sinapyl. These three phenylpropanoid monomers give an amorphous polyphenol linked via a multitude of interunit bonds. Lignin is linked covalently to hemicellulose. It serves

as a waterproof and antimicrobial binder for cellulose fibers in wood and is a highly valuable by-product of the lignocellulosic bio-refinery and pulping industry. The latter is less suitable as the lignin coming from the bio-refinery for the use as adhesion. Lignin coming from the bio-refinery has fewer methyl groups and that enhances reactivity. Therefore the lignocellulosic residues have a high content of reactive lignin with access to condensation reactions with phenol and formaldehyde in alkaline conditions. Lignin can replace phenol up to 50% in the formulation (plywood based of such a formulation reached the outdoor grade pursuant to the Chinese National Standard) (Mathias et al. 2016). Homogeneous and constant batches of lignin can also be obtained directly starting from different biomass sources by environmentally friendly enzymatic processes. These enzymes involving laccases, tyrosinases, and lipoxigenases transform lignin into a reactive biopolymer that can be used, e.g., as prepolymers, in adhesives or coatings. A life cycle assessment explored the environmental sustainability of the production. Laccase-modified and reduced lignin-soy protein adhesives yielded more than half of the strength of a common polyurethane adhesive (Mathias et al. 2016).

Adhesives from marine sessile organisms are well designed for hydrated surroundings. Several mechanisms are responsible for this performance, depending on the purpose of shorter- or longer-lasting adhesions. In many adhesives key compounds in the composition could be identified such as the amino acid lysine, in case of the sperm cells from goby fish (Mathias et al. 2016), hydroxyproline, or 3,4-dihydroxyphenylalanine (DOPA). The marine bacterium *Alteromonas colwelliana* uses L-DOPA, tyrosine, and related quinones beyond exopolysaccharides for moisture-resistant adhesion just like some higher organisms like mussels do. DOPA is very versatile in its reactions that are depicted in Fig. 1. It can act as cross-linker or as initial adherent as well. Due to these abilities to adhere in wet conditions and to build up stable networks, these glues gave inspiration for biomedical applications and other technical uses (see Sect. 4.2).

DOPA is just one representative phenolic compound. Tannins, lignin, urushi, and cashew nut shell liquid (CNSL) are further examples. The shell of cashew nuts contains about 20% of CNSL, which is composed of an allergenic phenolic lipid, mainly anacardic acid (71–82%) and also cardol (4–20%), cardanol (1–9%), and 2-methylcardol (1–4%). Anacardic acid is a potent skin irritant, similar to the allergenic oil urushiol (toxin of ivy). The extraction process causes decarboxylation of the anacardic acid leading to cardanol (Maiorana et al. 2015). The structural increments are related to the properties of the resins, made up of phenolic compounds: (i) hydroxyl groups are responsible for good adhesion and proper reactivity at moderate temperatures; (ii) a long aliphatic side chain gives resistance to water, good anticorrosive properties, low viscosity, long open/application time, and flexibility; and (iii) the aromatic ring ensures excellent chemical resistance.

The oldest adhesive used by mankind, birch tar, is also considered to be a polyphenolic representative. Another well-known tar is bitumen, whose use was documented at the site of Umm el Tlell and Hummal (Syria). It dates back to about 70,000 years to the Middle Paleolithic (Boëda et al. 2008). Even though it cannot be considered as actually renewable, it is a natural petroleum tar, consisting of

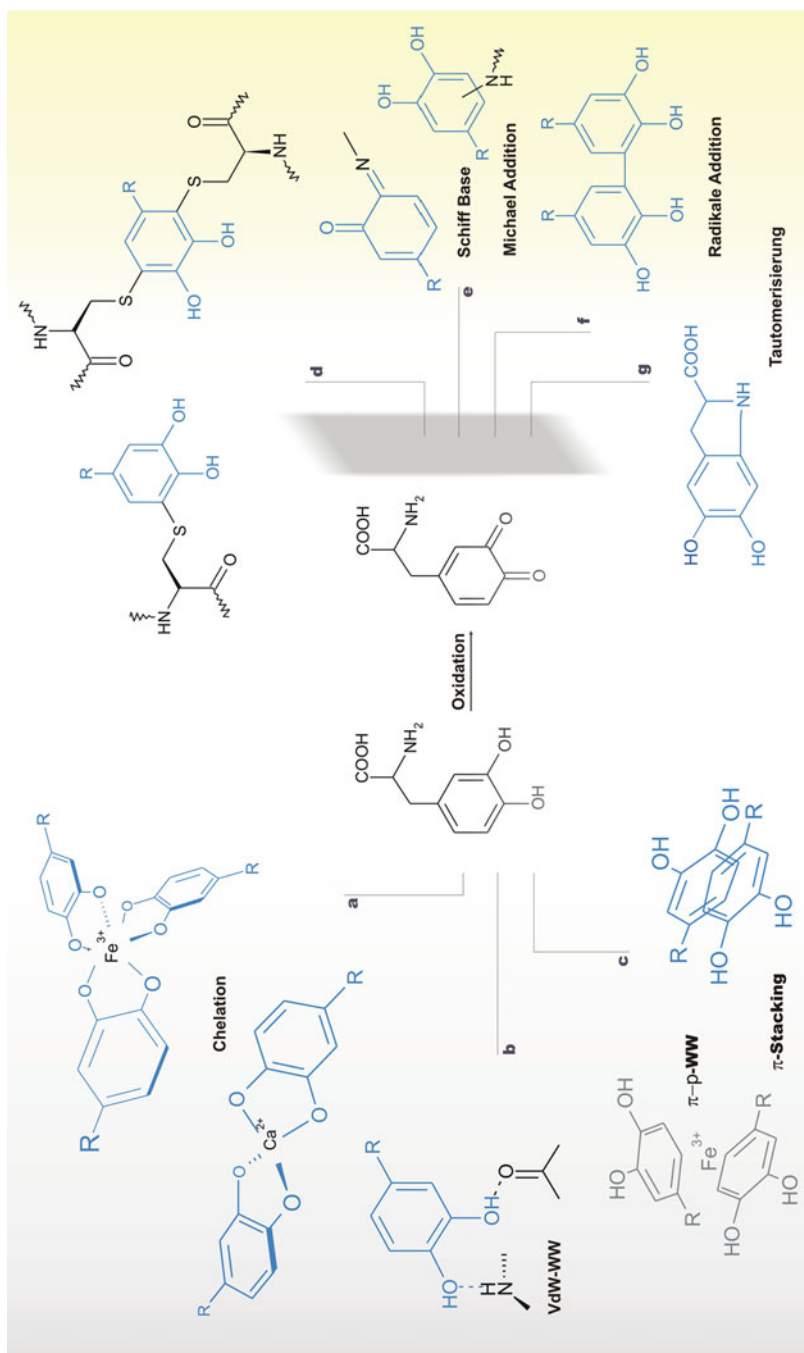


**Fig. 1** Catechols can act as chelating ligands and complex metal ions (a), the hydroxy group is capable of interacting by hydrogen bonding (b), the phenol can use its  $\pi$ -system for interactions with  $p$ -Orbitals and  $\pi$ -Orbitals (c). Quinones can form covalent bonds by reactions with thiols (d); form Schiff bases and undergo a

macromolecular chains that become solid by entanglement without any cross-linking, a natural hot melt. Resins (see Sects. 2.1 and 2.3.1) and tars have widespread uses as adhesives. Bitumen is available in liquid form, as water emulsion or in solvents, and also in solid form like hot melts. Additives like proteins or thixotroping agents are used in bitumen formulations to adjust their viscosity, tack, and mechanical strength. The tack can be improved by an addition of ionomeric elastomers and flexibility benefits from rubber latex in the formulation. Cigarette butts encapsulated with bitumen are used in construction and combine recycling with improving the mechanical properties of asphalt concrete by reducing thermal conductivity. This reduces the feared Urban Heat Island effect and also hot spots on roads caused by sunlight (Mohajerani et al. 2017).

### 54.3 Biological Adhesives

Bioadhesives from bacteria, plants, and animals have proven their efficacy for 500 million years and become adapted to suit the needs and requirements of the organisms producing them. However, still very little is known about the composition, production, secretion, and mechanical properties of the vast majority of these systems. Generally speaking, biological adhesion tends to be based on two principles:

- (i) Attachment via mechanical systems and interfacial forces, i.e., by van der Waals forces or capillary interactions as seen in geckos, flies, beetles, tree frogs, and ivy or by reduced-pressure systems as given in cephalopod suckers (see ► Chap. 55, “Biological Fibrillar Adhesives: Functional Principles and Biomimetic Applications”). Among these systems, hairy and smooth toe pads have been studied most extensively, and the structures present on the feet of gecko and tree frog species have become model systems with successful prototypes and applications.
- (ii) Usage of chemical bonds based on, e.g., proteins or other macromolecules. These secretions are released through specialized glands and serve not only for solitary attachment and locomotion as for mechanical system but also for other purposes such as construction or defense.

Around 100 marine and terrestrial organisms are known to secrete adhesives (see Graham 2005; Hennebert et al. 2015; von Byern et al. 2018 and contributions in Smith and Callow 2006; von Byern and Grunwald 2010; Smith 2016), but of these only a few organisms have already been characterized in detail or implemented into functional prototypes (see Tables 1, 2, 3, 4, 5). However, as even closely related

**Fig. 1** (continued) kind of Michael reaction (e) or by radical addition forming a aryl-aryl-coupling (f). The DOPA-quinon can also tautomerise to a melanin precursor (g) Image from Rischka et al. (2010) and republished with permission

**Table 1** Compilation of organisms using biological adhesives mainly for predation (no claim is made to completeness)

Bioadhesive main function	Phylum (zool)/order (bot)	Genus	Glue production	Chemical composition	Bonding properties	Major references
Predation	Ericales, Nepenthes, Lamiales	Carnivore plants ( <i>Drosera</i> , <i>Byblis</i> , <i>Pinguicula</i> )	Glue droplet on stalked gland, situated on the leaves	4% aqueous solution of single polysaccharide and chemical elements (Ca, Mg, K, Na)	Viscoelastic ( $10^2$ N/s/m <sup>2</sup> ), hygroscopic, bonding lost <70% rH	See contribution in von Byern and Grunwald (2010)
	Ctenophora	Comb jelly ( <i>Pleurobrachia</i> )	Conical cell with spiral filament (colloblast) in tentacles, projected against predators	Histochemical confirmation of basic proteins (pK <sub>S</sub> ≈ 8) and sugars	Not determined (n.d.)	von Byern et al. (2017b)
	Onychophora	Velvet worm ( <i>Principapillatus</i> , <i>Euperipatoides</i> )	Slime gland ducts in body cavity, glue ejected through slime papillae at the head	84–90% water, 55% protein (8–1300 kDa, major protein Et <sub>p1</sub> = 250, 350 kDa), major amino acids Gly (27 mol%) and Pro (13 mol%), 1.3% sugar (mannose, galactose), lipids, no toxin	n.d.	von Byern et al. (2017b) and von Byern et al. (2017a)
	Mollusca	Worm snail ( <i>Vermetus</i> , <i>Dendropoma</i> )	Sticky mucus net, produced by modified pedal gland system	Mucopolysaccharides and glycosylated proteins, toxic components	n.d.	Klöppel et al. (2013)
	Arthropoda	Orb-weaver spider ( <i>Leucage</i> , <i>Araneus</i> )	Glue droplets on viscid silk capture thread, produced by aggregate glands at abdominal spinneret	Proteins (>65 kDa), major amino acids Gly (22 mol%) and Pro (16 mol%), sugars (N-acetylglucosamine), lipids, choline, GABAmide, isethionate, elements (KNO <sub>3</sub> , H <sub>2</sub> PO <sub>4</sub> <sup>-</sup> , Na, Cl, Ca)	Resistant to UV irradiation, temperature (18–30°), high humidity range (20–90%), tensile strength 5–32 μN/mm	Graham (2005) and Sahni et al. (2014)



t.8	Fungus gnat larvae ( <i>Arachnocampa, Keroplatus</i> )	Glue droplets released through the mouth and attached to silk threads	Water (99%), proteins (58–62 kDa), chemical elements (P, S, K, Ca), free fatty acids, no sugars	Hygroscopic, bonding lost <80% rH, low bonding strength	von Byern et al. (2017b), Eberhard (1980), and Yeargan (1994)
t.9	Spitting spider ( <i>Scytodes</i> ) Bola spider ( <i>Mastophora</i> )	<i>Scytodes</i> : glue and toxin produced in cephalothorax (prosoma) and ejected through chelicera (mouth area) along a silk thread. <i>Mastophora</i> : silk thread with adhesive droplets produced from spinnerets, bola swung against prey (attracted by pheromones)	<i>Scytodes</i> : presumably small (3.5–7.0 kDa) glycine-rich and diglutamine-/dityrosine-containing peptides, high amount of toxins <i>Mastophora</i> : n.d.	<i>Scytodes</i> : contraction and shortening during hardening (force 0.1–0.3 mN) <i>Mastophora</i> : low viscosity liquid. Mass of folded threads within the sticky ball	
t.10	Harvestmen ( <i>Mitostoma</i> )	Pedipalps with clavated setae, secreting glue droplet	Triglycerides, oleic fatty acids, high water content	Pull-off force 7μN, dehydration, no solubility in 70% ethanol	See contribution in Smith (2016)
t.11	Rove beetles ( <i>Stenus</i> )	Glands located in the head, sticky labium catapulted toward prey	Proteins, sugars, and lipids	n.d.	See contribution in von Byern and Grunwald (2010) and Koerner et al. (2012)



**Table 2** Compilation of organisms using biological adhesives mainly for defense (no claim is made to completeness)

Bioadhesive main function	Phylum (zool)/ order (bot)	Genus	Glue production	Chemical composition	Bonding properties	Major references
t.1 t.2 Defense	Mollusca	Slug ( <i>Arion</i> ) and snails ( <i>Cornu</i> )	<i>Arion</i> , dorsal foot glands <i>Cornu</i> , defensive foamlike secretion, released through mantle cavity	<i>Arion</i> , matrilin- and lectin-like proteins, interpenetrating a sulfated polysaccharide network, chemical elements (Ca and Mg) <i>Cornu</i> , proteins (30, 50 and >120 kDa) (unpubl.), other molecules and elements not characterized yet	n.d.	See Wilks et al. (2015) and contribution in Smith (2016)
t.4	Echinodermata	Sea cucumber ( <i>Holothuria</i> , <i>Actinopyga</i> )	Sticky Cuvierian tubules, released through cloacal orifice. Glands located in the tubules	60% protein (17–220 kDa), major amino acids Gly (12–30 mol%) and Glx (9–16 mol%) depending on the species, 40% neutral sugar, toxin holothurin	Excreted tubules elongate 20x to original length, sticks within 10 s. Tensile strength >135 kPa	See contributions in von Byern and Grunwald (2010), Smith (2016), and Graham (2005)
t.5	Arthropoda	Chilopoda ( <i>Henia</i> , <i>Geophilus</i> )	Sternal glands (multicomponent system) located on the ventral body side	Two major proteins (12 and 130 kDa), some species additionally contain hydrogen cyanide (HCN); species-specific pH range	Hardening in the moment of release	von Byern et al. (2017b)
t.6		Termites ( <i>Tenuirotritermes</i> , <i>Nasutitermes</i> )	Gland in the head capsule ejects the glue through a modified pore (named fontanelar gun)	<i>Tenuirotritermes</i> resin composed of 62% $\alpha$ -pinene, 27% myrcene, and 11% limonene; some species also contain toxins and pheromones	Hardening within 10 s	Nutting et al. (1974) and contribution in von Byern and Grunwald (2010)

t.7	Chordata	Salamander ( <i>Ambystoma</i> , <i>Plethodon</i> )	Milky secretion from dorsal and ventral skin glands (two-component system)	70% water, 78% protein (15–120 kDa), 0.41% sugar (mannose, $\alpha$ -L- fucose, N-acetyl-D- glucosamine), lipids, chemical elements (Na, Cl, K, S); some species secrete distasteful substances with its glue	Hardening within seconds, tensile strength >1.7 MPa (unpubl.), hydrophobic in cured stage	von Byern et al. (2017b) and von Byern et al. (2017a)
t.8		Burrowing ground frog ( <i>Nothaden</i> )	One dorsal skin gland (granular gland)	85–90% water, 55–60% protein (13–500 kDa, dominant Nb-1R), major amino acids Gly (16 mol %) and Pro (9 mol%), 0.75 % sugar	Tensile strength >70 kPa (within 24 h), shear stress >2800 kPa (cured 1 week on wood)	See contributions in von Byern and Grunwald (2010), Smith (2016), and Graham (2005)
t.9		Hagfish ( <i>Eptareteus</i> , <i>Myxine</i> )	Lateral slime glands (two-component system), secreting proteinaceous threads and mucin vesicles	99.9% water, 0.002% thread (proteins) and 0.0015% mucin (acidic sulfated glycoproteins), chemical elements (Na, Cl, K)	Elastic and coherent soft hydrogel, high extensibility. No adhesiveness	von Byern et al. (2017b)

**Table 3** Compilation of organisms using biological adhesives mainly for construction (no claim is made to completeness)

t.1	t.2	Phylum (zool.)/ order (bot.)	Genus	Glue production	Chemical composition	Bonding properties	Major references
t.1	t.2	Arthropoda	Eusocial wasp ( <i>Polistes, Vespa</i> )	Salivary secretion used as binder for organic material to build papery nest. The number of glands varies between species	Species dependent: presumably mostly proteinaceous (>73%, siliklike) and insoluble polysaccharides, major amino acids (Ala, Ser, Gly), chemical elements as K, S, Zn, Fe	Water resistant, light weight (thickness 43 µm), tensile strength (0.25–1.02 MN/m <sup>2</sup> )	McGovern et al. (1988), Singer et al. (1992), and Cole et al. (2001)
t.1	t.2	Arthropoda	Honeybee ( <i>Apis</i> )	Wax glands (three cell types) located ventrally on the 4–7 abdominal segment	Mixtures of wax esters, hydrocarbons, free fatty acids, and alcohols	Mechanical manipulation at 35 °C, melting point at 62–64 °C, fragile at low temperature, not adhesive	Tulloch (1970) and Hepburn et al. (1991)
t.1	t.2	Arthropoda	Huntsman spider ( <i>Cebrennus, Leucorchestris</i> )	Sticky silk threads secreted from the abdominal spinneret to line and stabilize the burrow in the desert sand	n.d.	n.d.	Foelix et al. (2016) and Henschel (2017)
t.1	t.2	Arthropoda	Caddisfly larvae ( <i>Hesperophylax</i> )	Salivary gland secretions (silk and glue coat) as binder for organic/inorganic material constructions Silk as double fiber with 5 µm diameter, core (<100 nm), coating >0.5 µm thick	Silk core: H- and L-fibroin (>350 and 25 kDa); major amino acids Pro, Glu, Cal, Lys; chemical element as Ca Glue coat: neutral and acid glycoproteins, heme peroxidase	Stress 4.5 MPa (pH dependent), elongation up to 120%, recovery biphasic and Ca <sup>2+</sup> dependent	See contribution in Smith (2016)

t.7	Annelida	Sandcastle worm ( <i>Phragmatopoma</i> ) Tube worm ( <i>Sabella</i> )	Four distinct secretory cell types in the building organ release the cement to stick sand grains toward a tube	Proteins rich in DOPA, major amino acids Ser (29 mol%), Gly (26 mol%), Ala (10 mol%)	Tensile strength >2.4 MPa	See contributions in Graham (2005), Smith (2016), Graham (2005), and von Byern et al. (2017a)
t.8	Chordata	Swiftlet ( <i>Collocalia</i> )	Salivary secretions used as binder or solitary for bird nest building	Two glycoproteins, sialic acid-rich O-glycosylproteins		Oda et al. (1998)
t.9		African lungfish ( <i>Protopterus</i> )	Three types of goblet cells, which differ morphologically and histochemically Skin secretions form a protective outer cocoon against dry periods in the soil	Positive staining for sugars (PAS)	n.d.	Kitzan and Sweeny (1968) and Greenwood (1986)
t.10		Stickleback fish ( <i>Gasterosteus</i> )	Nest construction with organic material. Glue produced in the kidney, stored in the urinary bladder	Protein (Spiggin, 203 kDa), major amino acid Cys (8 mol%)	Highly elastic thread, silklike appearance	Van Iersel (1953) and Jakobsson et al. (1999)

**Table 4** Compilation of organisms using biological adhesives mainly for attachment (no claim is made to completeness)

Bioadhesive main function	Phylum (zool)/ order (bot)/ kingdom	Genus	Glue production	Chemical composition	Bonding properties	Major references
t.1 t.2 t.3	Bacteria	<i>Pseudomonas</i> , <i>Caulobacter</i>	Extracellular matrix, synthesized by three different mechanisms: ABC transporter, Wzx/Wzy dependent, synthase dependent. Attachment via fimbria/pilus	Adhesin (i.e., FimH) and exopolysaccharides as mannose, N-acetylglactosamine, rhamnose, etc.	Binding partly effected by acidic pH (4–5), adhesion µN range	See contribution in Smith (2016)
t.4	Fungi	Yeast ( <i>Candida</i> )	Depending on function (substrate or spore bonding), i.e., appressorium, hyphodium, conidia, epithelial cells	Species-specific macromolecules (EapI, 110 kDa protein, 90 kDa mannoprotein, etc.), mucilaginous matrix (containing mycosporine- alanine, cutinase, esterase, etc.), sugars (i.e., mannose, galactose)	Appressorium turgor pressure up to 8 MPa and force of 17 µN	See contribution in Smith (2016)
t.5	Ochrophyta	Diatom ( <i>Toxarium</i> )	Glue secreted through slit in the silica cell wall (termed raphe)	Protein (single >220 kDa), major amino acids (Gly 22 mol%, Asx 14 mol%, His 11 mol%), sulfate, chemical elements as Ca, Mg, sugars (mannose, xylose, etc.)	0.8 nN, self- healing properties	See contribution in Smith (2016)

t.6	Malvales Santalales	Flowering plant ( <i>Tilia</i> ) Mistletoe ( <i>Viscum</i> )	Pollen: 1. Pollenkitt produced by anther tapetum 2. Viscid thread is part of the ectexine	Pollenkitt: lipids, carotenoids, protein Viscid thread: polymer bases on sporopollenin Viscin: polysaccharide only	Viscid threads are flexible but not elastic threads	See contribution in von Byern and Grunwald (2010)
t.7	Asparagales	Orchid ( <i>Catasetum</i> )	Viscid disc, attachment of pollinarium to pollinator. Temporary attachment	Glycoprotein including sucrose, glucose, fructose	n.d.	Schlee and Ebel (1983)
t.8	Alismatales	Arrowhead vine ( <i>Syngonium</i> )	Aerial root hair, permanent attachment to all types of substrata	Proteins and polysaccharides	n.d.	Yang and Deng (2017)
t.9	Apiales	English ivy ( <i>Hedera</i> )		Arabinogalactan proteins, pectic polysaccharides, chemical element (Ca)	Combination of physical contact, chemical secretion, and shape modification. Tensile strength, 3.4 MPa (single root hair)	Melzer et al. (2010) and Huang et al. (2016)
t.10	Ulvales	Sea lettuce ( <i>Ulva</i> )	Vesicles with adhesive content in free-swimming zoospore	Protein (110 kDa), glycan moieties	Vesicle discharge and curing within 1 min, $\text{Ca}^{2+}$ - involvement	See contribution in Smith and Callow (2006)
t.11	Laminariales	Giant kelp ( <i>Macrocystis</i> , <i>Durvillaea</i> )	Vesicles (physodes) released from fertilized zygote for permanent attachment	Phlorotannin with phloroglucinol monomer. > 150 compounds with MW from 126 Da to 650 kDa, cross-linked Ca alginates	Tissue adaptation, thallus breakage, shear stress > 0.3 MPa	See contributions in Stevens et al. (2002), Smith and Callow (2006), and Graham (2005)

(continued)

t.12 **Table 4** (continued)

Bioadhesive main function	Phylum (zool)/ order (bot)/ kingdom	Genus	Glue production	Chemical composition	Bonding properties	Major references
t.13	Porifera	Demosponge ( <i>Lubomirskia</i> )	Baso-pinacocyte secreting spongins for permanent attachment. Chitin glands not determined yet	(a) Spongins (collagen-like protein) (b) Chitin (close to $\alpha$ -chitin)	n.d.	Evans (1977) and Ehrlich et al. (2013)
t.14	Cnidaria	Freshwater polyp ( <i>Hydra</i> ) Beadlet anemone ( <i>Actinia</i> )	Gland cells at the basal disc part of the peduncle for temporary bonding	<i>Hydra</i> : proteins (presumably glycosylated), protein characterization in progress <i>Actinia</i> : 96% water, 24% protein (12–200 kDa), 8% carbohydrate, 1% lipid, 67% chemical elements (Cl, Na, Mg), equinotoxins	Muscle-mediated detachment	Stabili et al. (2015) and Rodrigues et al. (2016)
t.15	Mollusca	Mussel ( <i>Mytilus</i> )	Byssus threads with distal adhesive plaque, originated from glands in the foot organ. Permanent bonding but mobility given by thread breakage and re-anchorage	6 foot proteins (115, 42–47, 5–7, 79, 9.5, 11.6 kDa) with different amounts of DOPA, collagenous core	Mussel plaque tensile strength >0.85 MPa (with seasonal variation), plaque area varies to surface energy	See contributions in von Byern and Grunwald (2010), Smith (2016), and Graham (2005)
t.16	Violet sea snail ( <i>Janthina</i> )	Violet sea snail ( <i>Janthina</i> )	Anterior part of the foot (propodium), mucus used as float, >12 cm long, >2 cm width	n.d.	Quick curing. Enclosure of gas to a foamlike buoy. Clear glue color	Laursen (1953)

t.18		Cephalopoda ( <i>Nautilus</i> , <i>Idiosepius</i> )	Adhesive glands on digital tentacle ( <i>Nautilus</i> ), dorsal mantle ( <i>Idiosepius</i> ), other body regions. Temporary attachment	Histochemical confirmation of acidic (1.0–2.5) and basic proteins (pH $\approx$ 8.0) and sugars	Weak bonding, fast release, for some species a mechanical detachment is assumed	See contribution in von Byern and Grunwald (2010)
t.19	Platyhelminthes	Flatworm ( <i>Macrostomum</i> )	Adhesive organ at the tail. Duo-gland system (one gland for attachment, other for release). Temporary attachment	Proteins (characterization in progress) and carbohydrates (PNA lectin); transcriptome	n.d.	Lengerer et al. (2016) and Lengerer et al. (2017)
t.20		Ectoparasite ( <i>Entobdella</i> )	Anterior adhesive pad with two gland types, with rod- or spheroid-like content	Protein, lack of sugars, lipids, and L-DOPA, similarities in amino acid composition to sea star, limpets, and barnacles	Cement-like glue, resistant to shear force from water current, temporary bonding	Kear and Evans- Gowing (1998) and Hamwood et al. (2002)
t.21	Arthropoda	Ticks ( <i>Dermacentor</i> , <i>Amblyomma</i> )	Salivary gland. Used as temporary attachment in the skin as a dowel	Two proteins (RIM36, 64P), major amino acids Gly, Pro, Tyr. Proteins similarity to keratin, collagen, glutenins. Protein 64 P homology to <i>Phragmatopoma</i> (see Sect. 3.3)	Glue with quick- hardening core and slow-hardening cortex, high bonding strength	Kemp et al. (1982), Graham (2005), and Hennebert et al. (2015) Johannes
t.22		Acom barnacle ( <i>Balanus</i> , <i>Megabalanus</i> )	Unicellular gland type in the body secrete cement for permanent bonding	84–90% protein (majors from 16–110 kDa), 1% sugar, major amino acids Ser (9–11 mol%), Leu 8–9 mol%), Pro (8 mol%)	Tensile strength >2 MPa (cyprid larva and adult)	See contributions in Smith (2016), Graham (2005), and von Byern et al. (2017a)

(continued)



t.23 **Table 4** (continued)

t.24	Bioadhesive main function	Phylum (zool)/ order (bot)/ kingdom	Genus	Glue production	Chemical composition	Bonding properties	Major references
t.25			Goose barnacle ( <i>Lepas</i> , <i>Doxima</i> )	Unicellular gland type in the stalk. Cement used as attachment and by <i>Doxima</i> also as buoy	<i>Doxima</i> : 92% water, 84% protein (60–85 kDa), major amino acids Ser (6–9 mol%), Gly and Ala (10 mol%), Leu (8–10 mol %), 1.5% sugars	Gas volume 19%, hardness 2.5 kPa, tensile strength 0.2 MPa	Zheden et al. (2015) and von Byern et al. (2017a)
t.26			Stoneflies ( <i>Dinocras</i> ) Fruit fly ( <i>Drosophila</i> ) Sphecoid wasps ( <i>Liris</i> )	Egg anchorage on substratum or prey: <i>Dinocras</i> : follicle cells with ovaries <i>Drosophila</i> : abdominal gland <i>Liris</i> : tubiform Dufour gland on the abdomen	<i>Dinocras</i> and <i>Drosophila</i> : protein, polysaccharide <i>Liris</i> : proteins (14–200 kDa, straight-chain hydrocarbons as pentadecane, (Z)-8-heptadecane	n.d.	See contribution in von Byern and Grunwald (2010)
t.27		Chaetognatha	Arrow worm ( <i>Spadella</i> )	Some species bear adhesive structures (appear as long rigid fingerlike processes) ventrally in the tail area. Temporary attachment	n.d.	n.d.	Michel (1984)

**Table 5** Compilation of organisms using biological adhesives mainly for locomotion (no claim is made to completeness)

Bioadhesive main function	Phylum (zool)/ order (bot)	Genus	Glue production	Chemical composition	Bonding properties	Major references
t.1 t.2 t.3 Locomotion	Ochrophyta	Diatoms ( <i>Craspedostauros</i> , <i>Pinnularia</i> )	Glue secreted through slit in the silica cell wall (termed raphe), gliding effected through actin filament	Extracellular polymeric substances (EPS) containing mostly sugars (mannose, glucose, galactose). Major amino acids (Gly 18 mol%, Ser 22 mol%, Thr 12 mol%)	Gliding speed >25 $\mu\text{m/s}$ , thickness >150 nm	Poulsen et al. (2014) and see contribution in Smith (2016)
t.4	Porifera	Demosponge ( <i>Tethya</i> )	Filamentous podia with three distinct gland types, formation of adhesive discs and central fiber	Mucopolysaccharides (not specified)	Movement up to 5–8 cm/week. Bonding to hard substrata	Fishelson (1981)
t.5	Mollusca	Gastropods ( <i>Cornu</i> , <i>Patella</i> )	Mucus released by numerous glands in the pedal sole (ventral body side)	Species-specific: protein (25–50%, mostly pH 1–4, 20–220 kDa); major amino acid Gly (13 mol %); sugar (i.e., mannose, fucose) composition; elements (Cl, K, Ca, S); saturated fatty acids as myristic, palmitic, and stearic acids; water content >93% (in limpets)	Tensile strength >518 kPa	See contributions in Smith (2016), Graham (2005), and Graham (2005)

(continued)

**t.6** Table 5 (continued)

t.7	Bioadhesive main function	Phylum (zool)/ order (bot)	Genus	Glue production	Chemical composition	Bonding properties	Major references
t.8				Two types of secretory cells (one adhesive, one de-adhesive) in the tube foot Detachment enzymes ensure the glue breakage for foot release			
t.9		Echinodermata	Sea star ( <i>Asterias</i> )  Sea urchin ( <i>Paracentrotus</i> )		21% protein (one major protein Sfp1), major amino acid Gly (10 mol%), 8% sugar  6,4% protein (inter alia nectin and cohesive proteins), 2.5% lipid, 1.2% sugar, large inorganic fraction (45.5%)	Tensile strength >198 kPa  Reversible adhesion through release of proteases and glycosylases, glue remains as footprint, tensile strength 340 kPa	See contributions in Smith (2016) and Graham (2005)  Lebesgue et al. (2016) and contributions in Smith (2016) and Graham (2005)



**Fig. 2** Biological adhesives used for different purposes such as for protection (1 barnacles), locomotion (2 starfish), defense (3 sea cucumber), and attachment (4 mussels)

species can differ with regard to gland morphology and/or adhesive composition and the secretions have become optimized for different purposes or environments, there are still a huge number of species whose adhesive secretions have not been investigated yet.

Biological adhesives are not exclusively used for settlement, but often also fulfill other purposes in connection with defense, predation, locomotion (Fig. 2), or nest construction and are superbly adapted morphologically, chemically, and physically to the needs and requirements of the organisms that produce them. Different from man-made synthetic systems, biological adhesion works over a wide range of temperatures, in different environments (aquatic, terrestrial, subterranean, arid), and under changing physicochemical conditions. Bonding can occur irrespective of texture or biological interference within milliseconds to all sorts of surfaces, be they natural, synthetic, biological, hard, or soft and with irregular or of complex substratum chemistry. Some organisms form permanent bonds for predation, attachment, or constructions; others use temporary adhesives to enable a holdfast on demand or for locomotion.

This diversity of organisms and variety of adhesive systems as well as the low amounts of secretion available make bioadhesion research challenging, but with access to advanced technological approaches, considerable progress in its characterization has already been made.

In particular most animal-based biological adhesives have been found to be typically polymers, formed by proteins and polysaccharides, which provide robust cohesion strength between the molecules and strong interaction with the contact area. In most animal glues, a high protein content is present (up to 90%), and technical progress has been made in some species, reaching full-length sequences of key proteins involved (Hennebert et al. 2015).

For many other biological adhesives listed in the tables below, a rough estimation of protein number, molecular mass (i.e., 4–650 kDa), and major amino acid residues (in particular serine, glycine, proline, and/or leucine) are available. Difficulties still appear in view of the carbohydrate characterization, as many adhesives contain a relatively low sugar fraction (<3% dry weight) (von Byern et al. 2017). For a few species, glycosidic protein bonds have been characterized in detail (Hennebert et al. 2015), and for most of the others, information on their sugar residues through lectin affinity tests is available. To the best of our knowledge, to date lipids have only rarely been characterized in adhesive secretions (e.g., permanent adhesive of barnacle larvae; Gohad et al. 2014). There is also some information available on the presence of chemical elements such as calcium, zinc, and iron. These kinds of ions serve as cross-linker and stiffen the protein-polysaccharide complex. Rare amino acids such as L-DOPA (L-3,4-dihydroxyphenylalanine) is prominent in the literature being the best characterized key compound in marine adhesive proteins but has been confirmed only in a few marine species (*Mytilus*, *Phragmatopoma*, *Sabella*). Beyond bioadhesion, L-DOPA also plays an important role in insect cuticle sclerotization and mechanical stability of cephalopod beak and polychaete jaws (Miserez et al. 2008).

Despite these technical obstacles, the natural biodiversity is clearly a blessing from a bio-prospecting perspective, providing countless opportunities to identify commonalities and functional principles, thereby developing a better understanding of adhesive mechanisms, evolutionary origins, and adaptations to specific environments and tasks. The key to unlock bioadhesion principles lies in comparative analyses with innovative research approaches based on intellectual and technical exchange as given by EU network projects such as COST Actions TD0906 and CA15216.

### 54.3.1 Predation

For prey capture through passive trap mechanisms, the glue is initially secreted externally and then attached as droplets or coating on silk threads (e.g., orb-weaver spider *Araneus* and fungus gnat larva *Arachnocampa*), a mucus web (worm snail *Vermetus*), tentacles (comb jelly *Pleurobrachia*), leaves (carnivorous plants *Drosera* and *Pinguicula*), or other prey capture devices. These traps are mostly exposed for days to weeks to varying habitat conditions (UV radiation, humidity, temperature, salinity, wind, rain) but still exhibit a bonding ability at prey contact. To minimize prey escape, the glue-containing parts are closely arranged to increase the number of contact points and to ensure that the tangling prey is rapidly entrapped by the sticky secretion. Observation in *Pleurobrachia* indicates that the animals could discard too

large prey items (von Byern et al. 2018) and also for *Arachnocampa* a defined breaking mechanism is discussed (von Byern et al. 2018). Orb-weaver spiders are known to cope with large prey items by forming high tensile silk threads (up to 0.5 GPa for the viscid silk) (Gosline et al. 1999). Gluing traps in animals/plants are not reused; instead new threads/leaves are formed and exposed. In carnivore plants like *Drosera* and *Pinguicula*, the prey is lured by glistening droplets and optic or odor signals (see respective contribution in von Byern and Grunwald 2010), while the cave-dwelling *Arachnocampa* attracts the prey by a specific light organ (Meyer-Rochow 2007). Also in view of their chemical compositions, the different biological adhesives vary strongly, being often highly adapted to specific habitat conditions and prey (or predator) type as recently shown for *Arachnocampa* (von Byern et al. 2018).

A few arachnid species as *Mitostoma* are known to actively capture prey by means of adhesives. While *Mitostoma* directly attaches the prey with its pedipalps, *Scytodes* and *Principapillatus* expel its secretion from a certain distance (up to 2 cm in *Scytodes* or 4 cm in *Principapillatus*) and within milliseconds onto the prey. Both use canalized structures in the head region (slime papillae, chelicerae) to build up a certain pressure and to control the flow direction (von Byern et al. 2018). Up to two separate jets are used, which run a zigzag pattern over the prey and substratum. Immediately after its release, the glue hardens and partly shrinks to tightly entangle the prey. The predators are able to control the glue amount and use more spit, if the prey is still struggling. While in *Scytodes* the glue is released with silk threads, in *Principapillatus* the ejected glue appears as translucent threads but does not contain silk. It remains questionable if the *Scytodes* glue is toxic itself, but it is known that the trapped prey is paralyzed by injecting toxin afterward. The glue of *Principapillatus* lacks a toxin, so instead digestive saliva is released with a bite to immobilize the prey. In addition to the prey capture, *Principapillatus* also uses its glue for defense against predators.

### 54.3.2 Defense

Besides, also other species are known to use adhesives as defense. However, while being very effective against the predators, it yet remains unclear for most of these species how they avoid being trapped by its own sticky secretion. Most of these secretions are located in particular epithelial glands (i.e., dorsally in the slug *Arion subfuscus* and burrowing ground frog *Notaden*, ventrally in chilopods as *Henia* or specific body regions in salamanders as *Plethodon*) (von Byern and Grunwald 2010; Smith 2016) to ensure a fast release onto the body surface.

Sea cucumber as *Holothuria* in contrast expels sticky threads (named Cuvierian tubules) when stressed by a predator (see respective contribution in von Byern and Grunwald 2010; Smith 2016). Termite soldiers as *Tenuirostritermes* fire their secretion in large distance (>3 cm), while spitting spiders and onychophorans (see paragraph in Sect. 3.1) use an oscillating behavior toward the predator or prey. Helicid snails as *Cornu* not only retract in their shell to protect themselves from predators but also secrete a foamlike slimy secretion through the shell opening. The

defensive glue of the American slug *Arion subfuscus* is formed by the matrilin-like proteins, heparan sulfate-like polysaccharides, and metal ions and currently used as template for medical sealant (Li et al. 2017).

Although the secretion of the hagfishes as *Eptatretus* is not adhesive (von Byern et al. 2018), the mucus they release from lateral skin glands strongly swells and clogs the gills and mouths of the predators. In general, the most defensive secretions are released during contact with the pesterer and dispersed over its body and in particular mouth only a few fires directly toward the predator. Exposure to air causes in *Henia*, *Tenuirostritermes*, and *Plethodon* an immediate hardening of the glue (von Byern et al. 2018), while the adhesives of *Arion*, *Cornu*, and *Eptatretus* remain viscoelastic for a certain time (von Byern et al. 2018; Smith 2016). The Cuvierian tubules in *Holothuria* in contrast remain sticky and form a large web, entangling the predator. In many defensive secretions (sea cucumber, salamander, chilopoda, termites), also toxic, distasteful, or noisomely components could be determined, serving to distract the predator additionally (see respective contribution in von Byern and Grunwald 2010; Smith 2016 von Byern et al. 2018 as well as Nutting et al. 1974), while other bioadhesives (e.g., *Notaden*, *Plethodon*) confirm its biocompatibility in cell culture and medical tests (see Sect. 4.2).

### 54.3.3 Construction

Biological adhesion and mucus are mainly used as binders for constructions incorporating inorganic/organic materials; a few species also use the secretions for other functions. Annelids as the sandcastle worm *Phragmatopoma* and the tube worm *Sabella* build permanent tubes, in which they reside (see respective contributions in Smith 2016). As given for mussels (see below), also these annelids use the amino acid L-DOPA as binder to stick the sand grains together and by this form strong and stable tubes (up to 40 cm) (Smith 2016). As the animals lift themselves from the soil with increasing tube length and thereby lose the possibility to uptake new construction material from the ground, suspended sand grains are collected, selected, and used for tube repair and partial increase.

In relation to sabellids, other animals form with their secretions temporary architectures. Stickleback fish as *Gasterosteus* build in the spring a tunnellike nest of plant origin for breeding. The threadlike glue is secreted from the kidney and dispersed by the fins on the nest material (Van Iersel 1953). Caddisfly larvae and hunting spiders combine silk and adhesives to form stabile cases/burrows; however, differences are given in the production site. The hunting spider *Cebrennus* releases the sticky silk threads from its abdominal spinneret to line and stabilize the burrow in the desert sand (Foelix et al. 2016). The caddisfly larva instead secretes its silk and glue from the salivary glands and uses all kinds of inorganic and organic material to build portable or substrate-bonded cases; some species even design multilevel cases. Most caddisflies are not as selective as the sabellids (see above) in view of its construction material and case design; some species use all types of material and design their bizarre-looking cases.



Salivary liquid and organic material is also used by social wasps as *Polybia* and birds (i.e., *Delichon*) as nest-cementing substance (Oda et al. 1998). Although the nest constructions may not appear as stable as the caddisfly case, the papery constructions of wasps are quite long-lasting (even after the inhabitant leave) and have very good stability and even water-resistant properties (McGovern et al. 1988). Besides its binder function, adhesives are also solitary used for constructions. Swiftlets build with their concentrated salivary breeding nests (also known as Edible bird's nests), while the African lungfish *Protopterus* (Greenwood 1986) form with its mucus protective cocoons to survive dry periods. The waxlike secretion of honeybees provides not only the basis for the honeycombs in nature but is also commonly used in cosmetics, food, and pharmaceutical industry. Besides bee wax, also other secretions as fish slime (Antony 1954, see Sect. 2) and the *Phragmatopoma* adhesives are known to have a high potential for medical applications, e.g., in the field of fetal membrane defect sites (Mann et al. 2012; Papanna et al. 2015) and spina bifida repair (Papanna et al. 2016) (see Sect. 4.2).

#### 54.3.4 Attachment

The usage of adhesives as a support for surface bonding is surely the most common purpose, used by bacteria, plants, and animals. Especially aquatic organisms use such secretions to withstand currents and avoid drifting. Some seal themselves or their eggs permanently to the substratum or biological surfaces (i.e., *Ulva*, *Macrocyctis*, *Lubomirskia*, *Mytilus*, *Balanus*, *Lepas*) and developed cement-like binders with high adhesive strength (up to 2 MPa), adapted to the strong hydrodynamic forces typical of the intertidal regions. Others like *Hydra*, *Nautilus*, *Idiosepius*, *Macrostomum*, *Entobdella*, and *Spadella* adhere only temporarily, "on demand." Detachment is presumably achieved mechanically through muscle contractions or body movements except for the case of *Macrostomum*, where a second gland type (so-called duo-gland system) secretes a detachment enzyme. *Janthina* and *Dosima* release a foamlike glue, enabling them to float on the water and in the water flea *Simocephalus* (Meyer-Rochow 1979); suction in combination with an adhesive may be employed for temporary attachments.

Terrestrial and in particular epiphytic plants (*Syngonium*, *Hedera*) use adhesives for attachment; furthermore a large number of flowers use pollenkitt or viscid threads for pollen binding and transport (*Catasetum*, *Tilia*, *Viscum*). Many insects as *Dinocras*, *Drosophila*, and *Liris* in particular use glues for egg anchorage; animals itself in particular use mechanical tools (see ► Chap. 55, "Biological Fibrillar Adhesives: Functional Principles and Biomimetic Applications") for attachment and bonding. Ectoparasites as *Entobdella* or ticks (*Dermacentor* or *Amblyomma*) secure themselves in the host tissue with an adhesive called cement. The cement portion is secreted after insertion of the mouthparts and solidifies almost immediately to tightly anchorage the animal in the tissue during the feeding phase (Kemp et al. 1982). The secretion of the second portion takes up to several days. After



753 feeding, ticks detach from the cement cones, which remain attached in or on the  
754 host's skin (Kemp et al. 1982; Suppan et al. 2017).

### 755 54.3.5 Locomotion

756 Also the here listed animals use glue or mucus to bond temporary to the substratum  
757 as given for temporary bonding species (see Sect. 3.4). However, the glue is  
758 synthesized and released mostly through structures, specialized for locomotion,  
759 i.e., the podia of *Tethya*, the gastropod pedal sole, or the tube foot of sea stars and  
760 sea urchins. Best known are surely the gastropods, which produce a highly effective,  
761 hydrogel-like mucus, enabling the animals to cross any smooth, sharp (razor blades),  
762 and even extreme superhydrophobic, anti-adhesive surfaces as poly-  
763 tetrafluoroethylene (PTFE, commonly known as Teflon) (Shirtcliffe et al. 2012).  
764 The mucus acts as glue, allowing the animals to adhere and push themselves forward  
765 mechanically by means of wavelike movements of the sole (Miller 1974). In  
766 contrast, *Paracentrotus* and *Asterias* likewise use a duo-gland system as *Macro-*  
767 *stomum* (see Sect. 3.4), in which one gland produces the glue and another secretes  
768 enzymes to break the bonding and enable movement. In particular the viscous  
769 gastropod mucus and its bonding ability on any surface make this secretion inter-  
770 esting not only for new bioinspired wound sealants (Li et al. 2017) but also to  
771 design anti-adhesive surfaces for medical implants and superhydrophobic paints  
772 (see Sect. 4.1).

---

## 773 54.4 Bioinspired Applications

774 Despite the diversity and superiority of biological adhesives (biocompatible, biode-  
775 gradable, lack of heavy metals, or absence of volatile organic compounds), synthetic  
776 adhesives in particular (e.g., phenol/resorcinol/urea-formaldehyde) dominate today's  
777 adhesive market and are used as ingredients in many sealants, furniture products, and  
778 cosmetics.

779 Although many synthetic adhesives offer necessary features for specific applica-  
780 tions such as for wood manufacturing or in microelectronics, as well in dentistry, their  
781 performance is far from optimal and they can have unacceptable properties with  
782 respect to their suitability as an essential biomedical tool (harmful, toxic, not biode-  
783 gradable, low adhesive strength, microbial contamination). Technological advances  
784 in the area of superior bioinspired materials have been made with scientific progress  
785 in biological adhesion, e.g., the ability to produce key elements like L-DOPA  
786 recombinants. Such key components enabled the development of tissue adhesive  
787 like Cell-TakTM (USA), the first example (year 1986, TM-No. 73604754) of a  
788 marine-derived sealant, based on mussel adhesive proteins only; other biomimetic  
789 analogues are currently in the research focus. As a result of our increased understand-  
790 ing of the interrelationships between biological adhesives and underlying mecha-  
791 nisms or similar boundary conditions, it is increasingly possible to transform this into

biomimetic solutions. In contrast to the desired copies in the field of bonding according to biological models, these perfectly adapted organisms cause extensive economic loss due to their adhesive powers. For this reason, the progress made in the course of clarifying adhesive phenomena also serves not least to prevent fouling.

#### 54.4.1 Antifouling

Bacterial biofilms are prevalent and possess benefits and damage at once. They cause problems, e.g., by inducing biocorrosion and biofouling in drinking water supplies, and they are liable for impaired safety in surgery and wound healing. But they are also used for waste water treatments (van der Kooij and Van der Wielen 2014). In contrast to nonadherent bacteria, these microorganisms use biofilms as matrices for cooperation and to establish synergistic interactions like preventing the washaway of enzymes and nutrients or in order to survive in hostile environments. Biofilm formation allows them to withstand periods of starvation by quorum sensing. Consequently the vast majority of microorganisms exist in nature in the form of biofilms. They adhere mostly on wet solid surfaces. Within the process of biofilm formation, several steps are distinguished, whereby the first two are interesting in terms of bioadhesion: (1) adsorption to the substrate by cell adhesion (this initial step can last from a few minutes to one hour of exposure and is based on proteins) and (2) formation of extracellular polymeric substances (EPS) composed of polysaccharides to achieve irreversible attachment by polymer bridging (Vandevivere and Kirchman 1993). A well-known example for bacteria attached to teeth and aggregated in a self-made hydrated polymeric matrix is dental plaque.

Micro- and macrofouling (Fig. 3) are causes of considerable economic damage. A 5% increase in biofouling has been shown to increase ship fuel consumption by 17%, with a 14% increase in greenhouse gas CO<sub>2</sub>, NO<sub>x</sub>, and SO<sub>2</sub> emissions. Biofouling of marine energy turbines is regarded as the primary and most persistent source of failure among these devices. Control of biofouling for aquaculture and fishery operations can account for up to 15% of total annual operating costs. Beyond that is biofouling of sensors a significant barrier to technology advancement due to the impact on data quality (Chapman et al. 2014). Consequently, preventive measures are a challenge for material science. To avoid biofouling is *inter alia* the purpose for the findings on the principles of action of biological adhesives. Different approaches ranging from the use of “confusing surfaces” – to prevent (micro) organisms from adaption – like dendrimer-based coatings to antimicrobial concepts or surface modifications with baretin have proven their potential. Also surface topology mimicking the skin of a shark has been shown to be effective.

#### 54.4.2 Biomimetic Adhesives

Today plenty of commercial adhesive agents are biomimetic. The most prominent representative is the gecko tape. The production of such kinds of adhesives is



**Fig. 3** Macrofouling caused by tough adherent organism, e.g., mussels and barnacles on different surfaces under harsh conditions (salinity, marine current)

estimated to account for 25 billion m<sup>2</sup> (Schwotzer et al. 2012). But for medical issues the market is attractive as well, as the modern surgery is affected by two major factors: cost containment and an aging population (Spotnitz and Burks 2008). Stopping bleedings or sealing and reconnecting tissues after surgical procedures are challenging subjects. The bonding technology emerged as a convenient alternative for wound closure instead of sutures and other tissue applications (Annabi et al. 2015). Recently the slime of slugs (genus *Arion*) was successfully used as an adhesive and sealant for a porcine heart (Li et al. 2017). Many biomimetic tissue adhesives are based on secretions from marine organism, e.g., mussels and algae, but also from terrestrial organism like snails and frogs. Their performance in aquatic conditions is acceptable but requires polymeric additives to adjust the three-dimensional network.

These glues received much attention during the last few years and ended up in mimetics of natural structures like DOPA-containing co-polypeptides and DOPA-functionalized poloxamers or catechol-modified alginate hydrogels (Lee et al. 2013; Bochynska et al. 2016). Red and brown algae also use a mechanism based upon phenolic compounds. Under hydrated conditions their secretions are able to adhere to hydrophilic as well as hydrophobic surfaces. An enzyme (vanadate-peroxidase) induces the cross-link between the polyphenol and the extracellular carbohydrate fibers and causes adhesion to the surface. Hence carbohydrate-based adhesives are worth imitating. Thus, an alginate-polyphenol hybrid adhesive, mimicking *Fucus serratus*, showed higher adhesion to Teflon<sup>TM</sup> than to glass (Kumar Patel et al. 2013).

As promising candidate the Australian frog *Notaden* was also identified as it exhibited five times stronger adhesive strength than fibrin glue on sheep meniscus tissue (Graham et al. 2005).

Various types of medical adhesives are in use as hemostats to form a barrier and stop bleeding (protein and polysaccharide based) or as sealants in order to establish an impervious barrier to gas and many body liquids (fibrin sealant, polyethylene glycol, albumin, and glutaraldehyde) or as adhesives to connect tissue or medical devices (cyanoacrylates, albumin, glutaraldehyde, and fibrin sealant) (Spotnitz and Burks 2008; Ferguson et al. 2010). This classification refers to their function in surgical context. With respect to the former sections, a division could also be used to summarize the medical adhesives according to the compounds' origins:

- (i) Natural or biological adhesives (protein based, sprayable foams or dry fibrin sealants, collagen, gelatine; polysaccharide based, chitosan, alginates, dextran, chondroitin sulfate glue)
- (ii) Synthetic and semisynthetic adhesives (albumin and glutaraldehyde, cyanoacrylates, polyurethanes, polyvinyl alcohol, polyethylene glycols, dendrimers)
- (iii) Biomimetic adhesives (mussel, sandcastle worm, frog, slug)

The development of high-performance adhesives for use with living tissue as shown in Fig. 4 keeps the surgical toolbox expanding (Spotnitz and Burks 2008). More insight is given in ► Chap. 58, "Adhesion in Medicine."

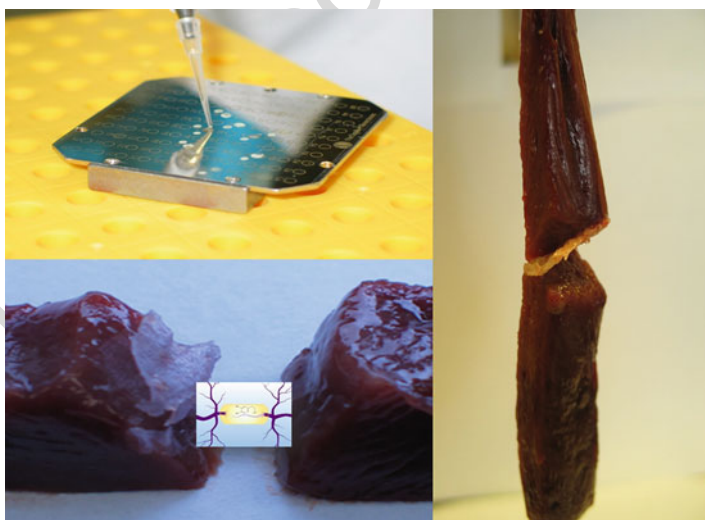


**Fig. 4** Investigation and characterization of biological adhesives by MALDI-TOF MS, application of a biomimetic adhesive to soft tissue and testing the joints (Images from Ingo Grunwald, Fraunhofer Institute for Manufacturing Technology and Advanced Materials (IFAM), Bremen, Germany, and reproduced with his permission)

## 54.5 Challenges and Opportunities

Each of the reviewed bioadhesives has advantages and drawbacks. In terms of *bacterial adhesion*, approaches for a forensic usage are in discussion. Considering that everyone's microbiome is highly individual like DNA is, the microbial fingerprint is a valuable hint in criminal investigations. But depending on the kind of test and recognition of the microbiome, this approach can be risky: in case of sequencing the genetic material, the latter can be manipulated by malicious software encoded into the physical nucleic acid strand. The resulting data can corrupt gene-sequencing software and take control of the underlying computer-aided analysis (<https://www.wired.com/story/malware-dna-hack/>). Adhesion at this minor scale in crime context as well as with regard to antifouling efforts reveals its high potential. So does the use of some algae and their adhesion to surfaces triggered by certain wavelengths of the light. Based on such knowledge, adhesion could be prevented by manipulations involving intelligent materials, for instance, modified materials in bioreactors.

Referring to carbohydrates chitosan displays impressive potential as fully bio-based adhesive (5 MPa shear strength on pine wood) (Kumar Patel et al. 2013). Microbial polysaccharides blended with surfactants showed trendsetting results as well. However, as with sugars, there is an increasing tendency to abandon starch solutions in choosing binders for clay and pigments. Preferable would be combinations of synthetic latexes with casein or vegetable proteins instead of starch dispersions.

Coming to proteins, many investigations in terms of constructional applications have indicated potential: gluten as a substituent (25%) in phenol-formaldehyde resin masses for use in particleboard production (medium-density fiberboard, MDF) did not affect the mechanical performance. As gluten is a by-product from the glucose syrup production, the costs (about 300 euros/t referred to protein desiccant) are more than one sixth less than urea-formaldehyde resins (363 euros/t) (Türk 2014). Assuming that the cost of such binders contributes about 25% to the production costs, a substitution might be more economic, even if more process time is required. Native proteins are mostly insoluble due to their tertiary or quaternary structures. Processing like degradation or reduction can impart the solubility for its use in adhesive formulations. In general proteinaceous adhesives combine biodegradability more favorably and are much more water resistant compared with carbohydrate-based adhesives. Except for chitosan "bio-based" mostly have a positive impact to any life cycle assessment as a substitute to petrochemical compounds, and they show just a few or no emissions.

Complete substitution of synthetic components to compete with commercial adhesives still needs to be realized. Intermediate bio-based adhesives are therefore just a compromise.

The construction and building sector remains as one of the most significant markets for adhesives. Their uses of adhesives range from flooring to structural purposes or building envelopes.

The family of medical adhesives represents another relevant market. Although "classical" medical adhesives and those specific for medical as well as dental devices

are rather heterogeneous, they can be grouped into one family. The global market for medical adhesives and sealants is estimated to reach over 15 billion US dollars in the year 2022 ([http://www.strategyr.com/MarketResearch/Medical\\_Adhesives\\_and\\_Sealants\\_Market\\_Trends.asp](http://www.strategyr.com/MarketResearch/Medical_Adhesives_and_Sealants_Market_Trends.asp)). Driven by an aging population, increasing surgical operational interventions, the rise in healthcare needs, and new treatment methods like the preferences for minimal invasive methods or the use of new tissue scaffold applications, the CAGR (compound annual growth rate) in the area of medical adhesives will reach top values of about 10% until 2021, with even higher values expected for the Asia-Pacific area ([http://www.strategyr.com/MarketResearch/Medical\\_Adhesives\\_and\\_Sealants\\_Market\\_Trends.asp](http://www.strategyr.com/MarketResearch/Medical_Adhesives_and_Sealants_Market_Trends.asp)).

The consciousness of the benefits involved by using bioadhesives in multiple areas (e.g., health, environmental, ethical) is evolving. Bioadhesives are popular; six billion US dollars have been estimated for the global market in 2019. It is possible to increase the sustainability of industrial processes while maintaining or increasing the competitiveness of enterprises. As long as the legislatures are aware of the need to go ahead with the development of bioadhesives and the technologies of second-generation biofuels, the development of bioadhesives will lead to products that can cope with commercial adhesives. Last but not least, the requirements for reducing the emissions of volatile organic compounds (VOCs) and the requirement for recyclable materials push the development of bioadhesives (Mathias et al. 2016).

The classical medical adhesives are normally grouped into (depending on the classification system) hemostats which stop bleedings, sealants which seal leakages (gas and nonclotting liquids), or adhesives that “glue” two tissues together.

This segment of classical medical adhesives alone will have a market size of about three billion US dollars in 2021 (markets) – indicating a highly attractive field of application for medtech companies today and in the future. The market is dominated by the USA and Europe, but emerging markets like those of South America and Asia offer quite significant growth opportunities. The growth rate is observed and checked, for instance, by the process of regulatory affairs (the USA with the FDA, Europe with CE marking) for the certification of new medical adhesives. At least in the EU, the process of the approval of medical devices like adhesives will be tightened due to new regulations. Regardless of this situation, the medical adhesive market and the research associated with it are expected to have a bright future.

---

## 54.6 Conclusion

Biological and microbiological adhesives have an enormous potential for industrial applications. The most prominent ones are constructional, packaging, and medical applications. Sustainable packaging will prevail. There is, however, also a need for manipulating and adapting biological adhesion for healthcare or food safety issues. On account of their impressively efficient and precise way to adhere to industrially challenging substrates, these materials need to be studied and the conditions under which initial adhesion occurs want to be understood. Thus, any activity furthering



insights into the principles of these compounds is significant, reflecting, for instance, the current worth of the stem cell industry 3.5 million pounds in the UK alone (Waugh et al. 2016).

Developing biocompatible adhesives with strong adhesive properties for medical applications is highly desirable, but the delicate balance between adhesive performance and biocompatibility is crucial and part of the legal and technical requirements. Although “tissue adhesives are far from ideal” (Li et al. 2017), there are many promising approaches under investigation (Balcioglu et al. 2016; Li et al. 2017).

Nearly all of the reviewed adhesive classes are important subjects of research to develop alternatives for petroleum-based materials, and the quest exists to develop bioinspired solutions and to achieve tailored adhesives for specific tasks including the prevention of fouling. As carbohydrates and vegetable proteins can be obtained from waste streams of renewable resources and may be produced in great abundance, they do not have to compete with food production and can be considered as a sustainable option. Nature is a prime candidate for inspiration and provides raw materials for applications in adhesives. Bioadhesives can be converted into a variety of useful adhesive products with a promising future, even if natural variations in quality are weaknesses. The interdisciplinary approach with inputs from chemistry, physics, bionics, biology, and engineering offers a wide range of possibilities. Thus, outstanding adhesive performance in nature can be elucidated on a molecular level and translated into technical concepts. Mechanical discrepancies can be bridged with hybrid materials from biological concepts in combination with synthetic components. Looking just at the largest market for adhesives (construction), a fast-growing market (packaging), and the exclusive market (medical adhesives), the future prospects for bioadhesives are positive. This trend is clearly evidenced by the increase in relevant publications covering the field over the last few years (Babu et al. 2013).

---

## References

- Annabi N et al (2015) Elastic sealants for surgical applications. *Eur J Pharm Biopharm* 95 (Pt A):27–39
- Antony AC (1954) Use of fish slime in structural engineering. *J Bombay Nat Hist Soc* 50 (3&4):682–683
- Babu RP, O'Connor K, Seeram R (2013) Current progress on bio-based polymers and their future trends. *Prog Biomater* 2:8
- Balcioglu S et al (2016) Design of xylose-based semisynthetic polyurethane tissue adhesives with enhanced bioactivity properties. *ACS Appl Mater Interfaces* 8(7):4456–4466
- Baroncini EA et al (2016) Recent advances in bio-based epoxy resins and bio-based epoxy curing agents. *J Appl Polym Sci* 133(45):44103
- Bochynska AI et al (2016) Tissue adhesives for meniscus tear repair: an overview of current advances and prospects for future clinical solutions. *J Mater Sci Mater Med* 27(5):85\_1–85\_18
- Boëda E et al (2008) New evidence for significant use of bitumen in Middle Palaeolithic technical systems at Umm el Tlel (Syria) around 70,000 BP. *Paléorient* 34(2):67–83
- Buch K et al (2009) Investigation of various shellac grades: additional analysis for identity. *Drug Dev Ind Pharm* 35(6):694–703
- Chapman J et al (2014) Bioinspired synthetic macroalgae: examples from nature for antifouling applications. *Int Biodeterior Biodegrad* 86A:6–13

- Cohen ER et al (2008) Quantities, units and symbols in physical chemistry. IUPAC/RSC Publishing, Cambridge
- Cole MR, Hansell MH, Seath CJ (2001) A quantitative study of the physical properties of nest paper in three species of Vespine wasps (*Hymenoptera, Vespidae*). *Insect Soc* 48:33–39
- Eberhard WG (1980) The natural history and behavior of the bolas spider *Mastophora dizzydeani* sp. n. (Araneidae). *Psyche J Entomol* 87(3–4):143–169
- Ehrlich H et al (2013) First report on chitinous holdfast in sponges (Porifera). *Proc R Soc B Biol Sci* 280(1762):20130339\_1–20130339\_9
- Erren TC et al (2013) Oceans of plastics: possible risks of cancer in marine wildlife and humans. In: Allodi S, Nazari EM (eds) Exploring themes on aquatic toxicology. Research Signpost, Trivandrum
- Evans CW (1977) The ultrastructure of larvae from the marine sponge *Halichondria moorei* Bergquist (Porifera, Demospongiae). *Cah Biol Mar* 13:427–433
- Ferguson J, Nürnberger S, Redl H (2010) Fibrin: the very first biomimetic glue – still a great tool. In: von Byern J, Grunwald I (eds) Biological adhesive systems: from nature to technical and medical application, 1st edn. Springer, Wien/New York
- Fishelson L (1981) Observation of the moving colonies of the genus *Tethya* (Desmospongia, Porifera) I. Behaviour and cytology. *Zoomorphology* 98:89–99
- Foelix RF et al (2016) Über den Bau der Wohnröhre bei wüstenlebenden Spinnen. *Arachne* 21(1):4–17
- Geyer R, Jambeck JR, Law KL (2017) Production, use, and fate of all plastics ever made. *Sci Adv* 3(7):e1700782\_1–e1700782\_5
- Gohad NV et al (2014) Synergistic roles for lipids and proteins in the permanent adhesive of barnacle larvae. *Nat Commun* 5:4414\_1–4414\_9
- Gosline JM et al (1999) The mechanical design of spider silks: from fibroin sequence to mechanical function. *J Exp Biol* 202(Pt 23):3295–3303
- Graham LD (2005) Biological adhesives from nature. In: Bowlin GL, Wnek G (eds) Encyclopedia of biomaterials and biomedical engineering. Taylor & Francis, Oxon
- Graham LD et al (2005) Characterization of a protein-based adhesive elastomer secreted by the Australian frog *Notaden bennetti*. *Biomacromolecules* 6(6):3300–3312
- Greenwood PH (1986) The natural history of African lungfishes. *J Morphol* 190(Suppl. 1):163–179
- Gross RA, Kalra B (2002) Biodegradable polymers for the environment. *Science* 297(5582):803–807
- Hamwood TE et al (2002) Preliminary characterization and extraction of anterior adhesive secretion in monogenean (platyhelminth) parasites. *Folia Parasitol* 49:39–49
- Hennebert E et al (2015) Experimental strategies for the identification and characterization of adhesive proteins in animals: a review. *Interface Focus* 5(1):20140064
- Henschel JR (2017) The biology of *Leucorchestris arenicola* (Araneae: Heteropodidae), a burrowing spider of the Namib dunes. In: Seely MK (ed) Namib ecology: 25 years of Namib research, Transvaal museum monograph, vol 7. Transvaal Museum, Pretoria
- Hepburn HR et al (1991) Synthesis and secretion of beeswax in hexabees. *Apidologie* 22:21–36
- Hon DNS (1989) Cellulosic adhesives. In: Hemingway RW, Conner AH (eds) Adhesives from renewable resources, ACS symposium series, vol 385. American Chemical Society, Washington, DC
- Huang Y et al (2016) Nanospherical arabinogalactan proteins are a key component of the high-strength adhesive secreted by English ivy. *Proc Natl Acad Sci U S A* 113(23):E3193–E3202
- Jakobsson S et al (1999) An 11-ketotestosterone induced kidney-secreted protein: the nest building glue from male three-spined stickleback, *Gasterosteus aculeatus*. *Fish Physiol Biochem* 20:79–85
- Karak N (2016) Biopolymers for paints and surface coatings. In: Pacheco-Torgal F, Ivanov V, Karak N, Jonkers H (eds) Biopolymers and biotech admixtures for eco-efficient construction materials, Woodhead publishing series in civil and structural engineering, vol 63. Elsevier, Amsterdam
- Kearn GC, Evans-Gowing R (1998) Attachment and detachment of the anterior adhesive pads of the monogenean (platyhelminth) parasite *Entobdella soleae* from the skin of the common sole (*Solea solea*). *Int J Parasitol* 28(10):1583–1593



- 1058 Kemp DH, Stone BF, Binnington KC (1982) Tick attachment and feeding: role of the mouthparts,  
1059 feeding apparatus, salivary gland secretions and the host response. In: Obenchain F, Galun R  
1060 (eds) Physiology of ticks. Pergamon Press, Oxford
- 1061 Kitzan SM, Sweeny PR (1968) A light and electron microscope study of the structure of *Pro-*  
1062 *topterus annectens* epidermis. I: mucus production. Can J Zool 46:767–772
- 1063 Klöppel A et al (2013) Detection of bioactive compounds in the mucus nets of *Dendropoma*  
1064 *maxima*, Sowerby 1825 (Prosobranch Gastropod Vermetidae, Mollusca). J Mar Biol  
1065 2013:1–9
- 1066 Köckritz A, Martin A (2008) Oxidation of unsaturated fatty acid and vegetable oils. Eur J Lipid Sci  
1067 Technol 110(9):812–824
- 1068 Koerner L, Gorb SN, Betz O (2012) Functional morphology and adhesive performance of the stick-  
1069 capture apparatus of the rove beetles *Stenus* spp. (Coleoptera, Staphylinidae). Zoology 115(2):  
1070 117–127
- 1071 Kumar Patel A, Mathias JD, Michaud P (2013) Polysaccharides as adhesives: a critical review. Rev  
1072 Adhes Adhes 1(3):312–345
- 1073 Laursen D (1953) The genus *Ianthina*. Dana-Report 38:1–40
- 1074 Lebesgue N et al (2016) Deciphering the molecular mechanisms underlying sea urchin reversible  
1075 adhesion: a quantitative proteomics approach. J Proteome 138:61–71
- 1076 Lee C et al (2013) Bioinspired, calcium-free alginate hydrogels with tunable physical and mechan-  
1077 ical properties and improved biocompatibility. Biomacromolecules 14(6):2004–2013
- 1078 Lengerer B et al (2016) Adhesive organ regeneration in *Macrostomum lignano*. BMC Dev Biol  
1079 16(20):1–16
- 1080 Lengerer B et al (2017) Organ specific gene expression in the regenerating tail of *Macrostomum*  
1081 *lignano*. Dev Biol. <https://doi.org/10.1016/j.ydbio.2017.07.021>
- 1082 Li A, Li K (2014) Pressure-sensitive adhesives based on epoxidized soybean oil and dicarboxylic  
1083 acids. ACS Sustain Chem Eng 2(8):2090–2096
- 1084 Li J et al (2017) Tough adhesives for diverse wet surfaces. Science 357(6349):378–381
- 1085 Maiorana A et al (2015) Bio-based epoxy resin toughening with cashew nut shell liquid-derived  
1086 resin. Green Mater 3(3):80–92
- 1087 Mann LK et al (2012) Fetal membrane patch and biomimetic adhesive coacervates as a sealant for  
1088 fetoscopic defects. Acta Biomater 8(6):2160–2165
- 1089 Mathias JD, Grédiac M, Michaud P (2016) Bio-based adhesives. In: Pacheco-Torgal F, Ivanov V,  
1090 Karak N, Jonkers H (eds) Biopolymers and biotech admixtures for eco-efficient construction  
1091 materials, Woodhead publishing series in civil and structural engineering, vol 63. Elsevier,  
1092 Amsterdam
- 1093 McGovern JN, Jeanne RL, Effland MJ (1988) The nature of wasp nest paper. TAPPI J 71(12):  
1094 133–139
- 1095 Melzer B et al (2010) The attachment strategy of English ivy: a complex mechanism acting on  
1096 several hierarchical levels. J R Soc Interface 7:1383–1389
- 1097 Meyer-Rochow VB (1979) The attachment mechanism of the waterflea *Simocephalus*. Microscopy  
1098 33: 551–553 & 558
- 1099 Meyer-Rochow VB (2007) Glowworms: a review of *Arachnocampa* spp. and kin. Luminescence  
1100 22:251–265
- 1101 Meyer-Rochow VB et al (2015) Commentary: Plastic ocean and the cancer connection: 7 questions  
1102 and answers. Environ Res 142:575–578
- 1103 Michel HB (1984) Chaetognaths of the Caribbean Sea and adjacent areas, NOAA technical report  
1104 NMFS, vol 15. NOAA/National Marine Fisheries Service, Seattle
- 1105 Miller SL (1974) Adaptive design of locomotion and foot form in prosobranch gastropods. J Exp  
1106 Mar Biol Ecol 14(2):99–156
- 1107 Miserez A et al (2008) The transition from stiff to compliant materials in squid beaks. Science  
1108 319:1816–1819
- 1109 Mohajerani A et al (2017) Physico-mechanical properties of asphalt concrete incorporated with  
1110 encapsulated cigarette butts. Constr Build Mater 153:69–80

- 1111 NPSC Board of Consultants & Engineers (2017) The complete book on adhesives, glues & resins  
1112 technology (with process & formulations). Asia Pacific Business Press Inc, Delhi
- 1113 Nutting WL, Blum MS, Fales HM (1974) Behaviour of the North American termite *Tenuiros-*  
1114 *tritermes tenuirostris*, with special reference to the soldier frontal gland secretion, its chemical  
1115 composition and use in defense. *Psyche* 84(1):167–177
- 1116 Oda M et al (1998) Study on food components: the structure of N-linked asialo carbohydrate from  
1117 the edible bird's nest built by *Collocalia fuciphaga*. *J Agric Food Chem* 46:3047–3053
- 1118 Papanna R et al (2015) Cryopreserved human amniotic membrane and a bioinspired underwater  
1119 adhesive to seal and promote healing of iatrogenic fetal membrane defect sites. *Placenta* 36  
1120 (8):888–894
- 1121 Papanna R et al (2016) Cryopreserved human umbilical cord patch for in-utero spina bifida repair.  
1122 *Ultrasound Obstet Gynecol* 47(2):168–176
- 1123 Patachia S, Croitoru C (2016) Biopolymers for wood preservation. In: Pacheco-Torgal F, Ivanov V,  
1124 Karak N, Jonkers H (eds) Biopolymers and biotech admixtures for eco-efficient construction  
1125 materials, Woodhead publishing series in civil and structural engineering, vol 63. Elsevier,  
1126 Amsterdam
- 1127 Penning M (1996) Aqueous shellac solutions for controlled release coatings. In: Karsa DR,  
1128 Stephenson RA (eds) Chemical aspects of drug delivery systems. The Royal Society of  
1129 Chemistry, Cambridge
- 1130 Poulsen N et al (2014) Isolation and biochemical characterization of underwater adhesives from  
1131 diatoms. *Biofouling* 30(4):513–23
- 1132 Rischka K et al (2010) Bio-inspired polyphenolic adhesives for medical and technical applications.  
1133 In: von Byern J, Grunwald I (eds) Biological adhesive systems: from nature to technical and  
1134 medical application, 1st edn. Springer, Wien/New York
- 1135 Rodrigues M et al (2016) Profiling of adhesive-related genes in the freshwater cnidarian *Hydra*  
1136 *magnipapillata* by transcriptomics and proteomics. *Biofouling* 32(9):1115–1129
- 1137 Sahni V et al (2014) Prey capture adhesives produced by orb-weaving spiders. In: Asakura T, Miller  
1138 T (eds) Biotechnology of silk. Springer, Dordrecht
- 1139 Sankaranarayanan Y (1989) Adhesives & Shellac. Shellac Export Promotion Council, Calcutta
- 1140 Schlee D, Ebel F (1983) Note on the chemical nature of the adhesive of viscid discs in *Catasetum*  
1141 *fimbriatum* Lindl. (Orchidaceae). *Am J Bot* 70(6):872–876
- 1142 Schwotzer W et al (2012) Biologische und biomimetische Klebstoffe (Teil 2) – Praxistauglichkeit  
1143 und Trends. *Adhäsion* 10:38–43
- 1144 Shibata M (2013) Bio-based epoxy resin/clay nanocomposites. In: Mittal V (ed) Thermoset nano-  
1145 composites. Wiley-VCH Verlag, Weinheim
- 1146 Shirtcliffe NJ, McHale G, Newton MI (2012) Wet adhesion and adhesive locomotion of snails on  
1147 anti-adhesive non-wetting surfaces. *PLoS One* 7(5), e36983. <https://doi.org/10.1371/journal.pone.0036983>
- 1148 Singer TL, Espélie KE, Himmelsbach DS (1992) Ultrastructural and chemical examination of paper  
1149 and pedicel from laboratory and field nests of the social wasp *Polistes metricus* say. *J Chem Ecol*  
1150 18(1):77–86
- 1151 Smith AM (2016) Biological adhesives. Springer, Cham
- 1152 Smith AM, Callow JA (2006) Biological adhesives. Springer, Heidelberg
- 1153 Specht F et al (1998) The application of shellac acidic polymer for enteric coating. *Pharm Technol*  
1154 10:20–28
- 1155 Spotnitz WD, Burks S (2008) Hemostats, sealants, and adhesives: components of the surgical  
1156 toolbox. *Transfusion* 48(7):1502–1516
- 1157 Stabili L et al (2015) The mucus of *Actinia equina* (Anthozoa, Cnidaria): an unexplored resource  
1158 for potential applicative purposes. *Mar Drugs* 13(8):5276–5296
- 1159 Stevens CL, Hurd CL, Smith MJ (2002) Field measurement of the dynamics of the bull kelp  
1160 *Durvillaea antarctica* (Chamisso) Heriot. *J Exp Mar Biol Ecol* 269:147–171
- 1161 Sung HW et al (1998) Feasibility study of a natural crosslinking reagent for biological tissue  
1162 fixation. *J Biomed Mater Res* 42(4):560–567

- 1164 Suppan J et al (2017) Tick attachment cement – reviewing the mysteries of a biological skin plug  
1165 system. Biol Rev. <https://doi.org/10.1111/brv.12384>
- 1166 Tulloch AP (1970) The composition of beeswax and other waxes secreted by insects. Lipids 5(2):  
1167 247–258
- 1168 Türk O (2014) Stoffliche Nutzung nachwachsender Rohstoffe. Grundlagen – Werkstoffe –  
1169 Anwendungen. Springer, Wiesbaden
- 1170 Türünc O et al (2015) From plant oils to plant foils: straightforward functionalization and  
1171 crosslinking of natural plant oils with triazolinediones. Eur Polym J 65:286–297
- 1172 van der Kooij D, Van der Wielen PWJJ (2014) Microbial growth in drinking-water supplies:  
1173 problems, causes, control and research needs. IWA Publishing, London
- 1174 Van Iersel JJA (1953) An analysis of the parental behaviour of the male three-spined stickleback  
1175 (*Gasterosteus aculeatus* L.). E. J. Brill, Leiden
- 1176 Vandevivere P, Kirchman DL (1993) Attachment stimulates exopolysaccharide synthesis by a  
1177 bacterium. Appl Environ Microbiol 59(10):3280–3286
- 1178 von Byern J, Grunwald I (2010) Biological adhesive systems: from nature to technical and medical  
1179 application. Springer, Wien/NewYork
- 1180 von Byern J et al (2017) Chemical characterization of the adhesive secretions of the salamander  
1181 *Plethodon shermani* (Caudata, Plethodontidae). Sci Rep 7(1):6647\_1–6647\_13
- 1182 von Byern J et al (2018) Examples of bioadhesives for defence and predation. In: Gorb SN, Gorb  
1183 EV (eds) Functional surfaces in biology III: diversity of the physical phenomena. Biologically-  
1184 inspired systems, vol 10. Springer International Publishing AG, p XV, 268
- 1185 Waugh DG et al (2016) Surface treatments to modulate bioadhesion: a critical review. Rev Adhes  
1186 Adhes 4(1):69–103
- 1187 Weakley FB, Mehlretter CL (1965) Low cost protein glue for southern pine plywood. For Prod J  
1188 15(1):8–12
- 1189 Wilks AM et al (2015) Double-network gels and the toughness of terrestrial slug glue. J Exp Biol  
1190 218(Pt 19):3128–3137
- 1191 Wu Y, Li A, Li K (2015) Pressure sensitive adhesives based on oleic acid. J Am Oil Chem Soc  
1192 92(1):111–120
- 1193 Yang X, Deng W (2017) Morphological and structural characterization of the attachment system in  
1194 aerial roots of *Syngonium podophyllum*. Planta 245(3):507–521
- 1195 Yeargan KV (1994) Biology of bolas spiders. Annu Rev Entomol 39:81–99
- 1196 Zheden V et al (2015) Mechanical properties of the cement of the stalked barnacle *Dosima*  
1197 *fascicularis* (Cirripedia, Crustacea). Interface Focus 5(1):20140049

# Biological Fibrillar Adhesives: Functional Principles and Biomimetic Applications

55

Stanislav N. Gorb and Lars Heepe

## Contents

55.1	Introduction .....	1642
55.2	Dynamic Adhesion for Locomotion .....	1644
55.3	Pad Structure .....	1645
55.4	Nature of Attractive Forces .....	1646
55.5	Multiple Contacts .....	1649
55.6	Contact Shape .....	1651
55.7	Slope and Hierarchy .....	1655
55.8	Adhesion Control .....	1657
55.9	Environmental Conditions Affecting Animal Adhesion .....	1662
55.10	Biomimetic Implications .....	1664
55.11	Conclusions .....	1669
	References .....	1671

## Abstract

Specific mechanisms of adhesion found in nature are discussed in the previous chapter (► Chap. 54, “Bioadhesives”). One of the most discussed biological systems in the last decade are the so-called fibrillar adhesives of insects, spiders, and geckos. These systems are adapted for dynamic adhesion of animals during locomotion and, therefore, have some extraordinary properties, such as (1) directionality, (2) preload by shear, (3) quick detachment by peeling, (4) low dependence on the substrate chemistry, (5) reduced ability to contamination and self-cleaning, and (6) the absence or strong reduction of self-adhesion. In the present chapter, we review functional principles of such biological systems in various animal groups with an emphasis on insects and discuss their biomimetic potential.

S. N. Gorb (✉) · L. Heepe

Department of Functional Morphology and Biomechanics, Zoological Institute at the University of Kiel, Kiel, Germany

e-mail: [sgorb@zoologie.uni-kiel.de](mailto:sgorb@zoologie.uni-kiel.de); [lheepe@zoologie.uni-kiel.de](mailto:lheepe@zoologie.uni-kiel.de)

The data on ultrastructure and mechanics of materials of adhesive pads, movements during contact formation and breakage, the role of the fluid in the contact between the pad and substrate are presented here. The main goal is to demonstrate how a comparative experimental approach in studies of biological systems aids in the development of novel adhesive materials and systems. The microstructured adhesive systems, inspired by studies of biological systems of insects, spiders, and geckos, are also shortly reviewed.

## 55.1 Introduction

Representatives of several animal groups, such as insects, arachnids, tree frogs, and lizards, are able to attach to and walk on smooth vertical surfaces and even on the ceiling (reviews by Gorb 2001; Scherge and Gorb 2001; Autumn 2006; Wolff and Gorb 2016). This ability is due to highly specialized attachment devices located at different parts of their legs. Biomimetic transfer of such systems into industrial applications is a very challenging task, and several working groups of materials scientists worldwide are currently attempting to reach this goal by applying various approaches of microfabrication and surface science in general. However, biological systems are far too complex for copying them exactly. That is why intensive structural and experimental comparative studies are required to find out which structural and mechanical features of real biological systems are essential for biomimetics. In order to understand functional principles of animal attachment devices, it is not enough to have information about external morphology of the structures. An integrative approach is necessary to combine data on ultrastructure and mechanical properties of materials, arrangement of muscles, joint design, movements during contact formation and breakage (motor control), sensorics, forces and their directionality, contact mechanics at micro- and nanoscale, potential substrates (surface profile and surface energy), and the presence and properties of the fluid in the contact between the pad and the substrate (chemical composition, viscosity, transporting system).

Two important questions have to be answered in order to select the right biological prototype for particular technological requirements. The first question is which product has to be developed, and the second one is which biological system possesses the ability we are going to mimic. Normally, the first and most important requirement from the industry of adhesives is that the new material has to be as sticky as possible. If this is the only requirement, one has to select a prototype among animals and plants using glue-like systems for permanent or long-term adhesion to the substrate (for review, see Gorb 2009 and this book ► Chap. 54, “Bioadhesives”). However, if the requirement for the new material is its ability to allow multiple adhesive cycles, for example, in robotic applications for robot locomotion on smooth walls and the ceiling, with the ability (1) to build and break the contact as fast as possible, (2) to attach to unpredictable surfaces, (3) to have lifetime of millions of attachment-detachment cycles, and (4) to not attach to itself, then we definitely have to search for prototypes among locomotory attachment devices of animals.

To understand principles, at which biological systems operate, detailed studies on ultrastructure, material properties, force range, and motion pattern during locomotion are necessary. Such studies became possible during the last years, because of new developments (1) in microscopical visualization techniques (atomic force microscopy, freezing and environmental scanning electron microscopy), (2) in the characterization of mechanical properties of biological materials and structures in situ and in vivo (measurements of stiffness, hardness, adhesion, friction) at local and global scales, and (3) in computer simulations.

In general, there are two different working strategies that aid in extracting structural and mechanical features of biological objects for further development of bioinspired systems. The first strategy deals with a careful detailed characterization of one particular biological system defined as a model object (one of the most prominent examples for fibrillar adhesives is the gecko toe). The second strategy is focused on a comparative study of a large variety of biological objects, which possess similar functional systems that appeared independently in the course of biological evolution. In our opinion, the second approach is more promising for biomimetics, because structural similarities, which evolved independently in different lineages of organisms, may indicate some kind of “optimal” solution for this type of system. Moreover, a comparative approach aids in extracting essential features and abandoning less important ones for designing artificial prototypes. Although different, these two approaches are complementary and help in the course of the biomimetic process.

Figure 1 provides a summary and categorization of essential features that contribute to the so-called gecko effect. In this chapter, along with this categorization,

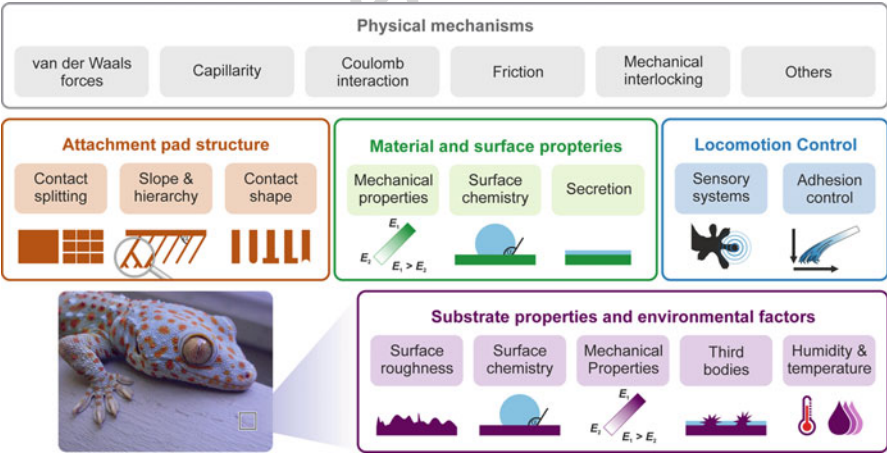


**Fig. 1** Summary and categorization of essential features that contribute to the so-called gecko effect: physical mechanisms, attachment pad structure, material and surface properties, and locomotion control. Various substrate properties and environmental factors may influence the adhesive performance of climbing animals (Adapted from Heepe and Gorb 2014. Photo copyright by Alex Mortillaro)

we report on our 15-year-long experience in studies of locomotory attachment devices in various animal groups with an emphasis on insects. The main goal is to demonstrate how a comparative experimental biological approach can aid in understanding biological attachment systems and derive design rules for the development of novel adhesive materials and systems.

## 55.2 Dynamic Adhesion for Locomotion

The adhesive contact between the leg and the substrate is mostly important for a rather short period of time of the stance phase and must be released during the swing phase (Fig. 2). These phases repeat infinitely in step cycles during locomotion. Therefore, adhesive structures of animal legs must fulfill several tasks, sometimes opposite to each other and reversibly executed in repeated step cycles (Gladun et al. 2009). (1) The sticky surface of the leg must be ready to immediately build adhesive contact with the substrate. The contact formation must be fast and established with minimal load on the ceiling. (2) Adhesion of few legs must be strong enough to hold the animal on the inclined and even on the overhanging substrate (reliability). (3) At the same time, adhesion must be low enough to allow smooth and quick detachment of the swinging leg. In other words, adhesion must be reversible. (4) The adhesive surface of the pad must be sticky enough to generate sufficient adhesive force to the substrate, but it should be secured from adhering to itself, to prevent disability of the adhesive surface for the next step cycle.

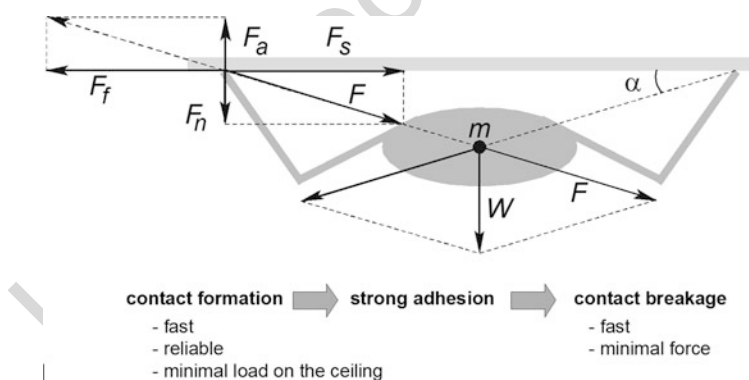


**Fig. 2** Ceiling situation. If the mass  $m$  of the animal is in the center of gravity, then its weight is  $W = m g$ , the angle of the ground reaction is  $\alpha$ , the normal pull-off force component is  $F_n$ , and the shear force component is  $F_s$ . Thus, the weight of the animal walking on the ceiling should be counterbalanced by two forces: friction ( $F_f$ ), which prevents leg sliding along the substrate, and adhesion ( $F_a$ ), which prevents leg separation from the substrate. In order to walk on the ceiling, it is not sufficient just to generate strong adhesive bond between the leg and substrate. Two additional problems have to be solved: (1) contact formation must be fast, reliable, and performed with the minimal load on the ceiling and (2) contact must be released in the fast manner and with the minimum of the applied load (From Gladun et al. 2009)



### 55.3 Pad Structure

To date, both the morphological and ultrastructural bases of the ability of animals to dynamically adhere to vertical surfaces have been studied in detail only in representatives of selected taxa, including insects (reviews by Gorb 2001, 2005; Federle 2006), arachnids (Homann 1957; Kesel et al. 2003; Niederegger and Gorb 2006; Wolff and Gorb 2016), tree frogs (Barnes 2006; Smith et al. 2006), and lizards (Hiller 1968; Autumn 2000, 2002; Huber, 1995a, b). In their evolution, animals have developed two distinctly different mechanisms to attach themselves to a variety of substrates: smooth pads and fibrillar (hairy, setose) pads. Due to the flexibility of the material of the attachment pads or fine surface outgrowths, both mechanisms can maximize the possible contact area with a wide range of substrate profiles (Gorb and Beutel 2001; Gorb 2005).

Interestingly, in different lineages, both types of attachment pads can be found. For example, within insects, such groups as orthopterans, hymenopterans, and thysanopterans bear smooth pads, whereas dipterans, coleopterans, and dermapterans possess mainly fibrillar pads. Within arachnids, representatives of Solifugae have smooth pads, whereas Araneae are characterized by fibrillar ones. Among reptiles, Gekkonidae and Anolinae have fibrillar pads, and some skinks have smooth ones. Additionally, these highly specialized structures are not restricted to one particular area of the leg. For example, in insects, they may be located on claws, derivatives of the pretarsus, tarsal apex, tarsomeres, or tibia. Recent phylogenetic analyses of hexapods based on the pad characters, processed together with characters of other organ systems, aided in resolving the question of the attachment pad evolution in hexapods and showed that these structures have evolved several times, independently (Gorb and Beutel 2001; Beutel and Gorb 2001, 2006).

Fibrillar systems always contain cuticle protuberances on their surfaces (Fig. 3). Protuberances on the fibrillar pads of Coleoptera, Dermaptera, and Diptera belong to different types. Representatives of the first two lineages have socketed setae originating each from two different cells. Setae range in their length from a few micrometers to several millimeters. Dipteran outgrowths are acanthae: single sclerotized protuberances originating from a single cell (Richards and Richards 1979). Structural features of adhesive outgrowths have been previously reported, for example, for flies, the acanthae are hollow inside (Bauchhenss 1979), and some of them contain pores under the terminal plate (Gorb 1998). These pores, presumably, deliver an adhesive secretion directly in the contact area. Pore canals at the base of the shaft may additionally transport secretions to the surface. In beetles, the setal bases are embedded in rubberlike material, which provides flexibility to the supporting material and helps the seta to adapt to various surface profiles.

Gecko setae are multibranching, hierarchical structures of 80–100  $\mu\text{m}$  in length (Ruibal and Ernst 1965; Stork 1983; Schleich and Kastle 1986; Roll 1995; Huber et al. 2005a; Rizzo et al. 2006). In anole lizards, setae are smaller and unbranched (ca. 20  $\mu\text{m}$  long) (Ruibal and Ernst 1965; Stork 1983; Rizzo et al. 2006). The gecko setae are not hollow inside. They are formed by proteinaceous fibrils held together by a matrix and surrounded by a proteinaceous sheath. Ordered protein constituent in these structures exhibits a diffraction pattern characteristic of  $\beta$ -keratin. Raman microscopy



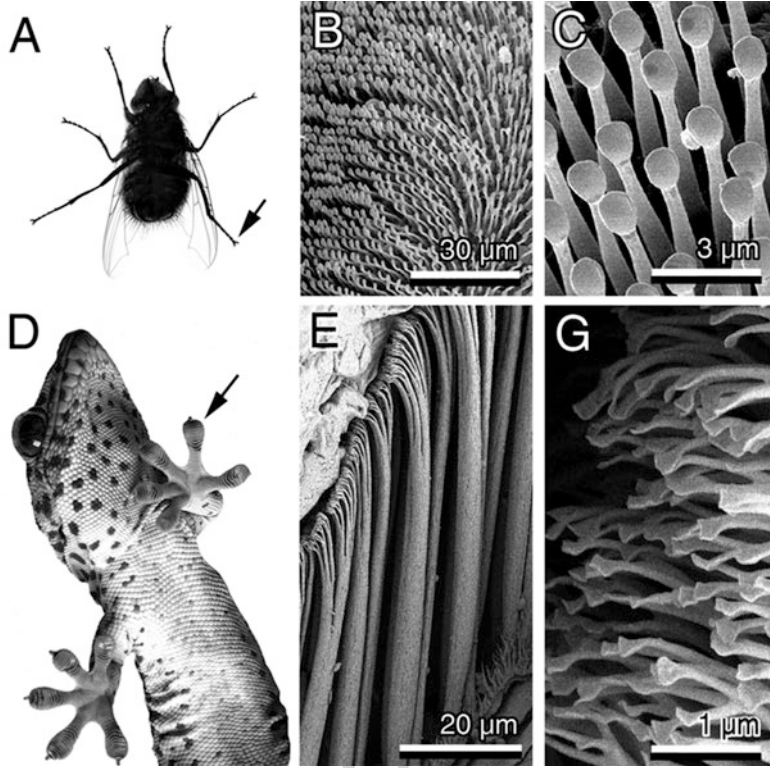


**Fig. 3** Wet fibrillar adhesive system of the fly (a–c) and dry fibrillar adhesive system of gecko (d–g). (b, c, e, g) Scanning electron microscopy images of adhesive setae. Both systems are similar according to the contact mechanics but differ in relative contribution of different physical forces to the overall adhesion. Insect mainly employ wetting phenomena, whereas gecko system is dominated by intermolecular van der Waals forces

of individual setae, however, shows the presence of additional protein constituents, some of which may be identified as  $\alpha$ -keratins (Rizzo et al. 2006). In anoles, setae emerge from the oberhautchen layer of the epidermal shedding complex into the cells of the clear layer, which act as templates for their growth (Alibardi 1997). The clear layer cells template the formation of spatular terminal elements. This means that setae are fully formed prior to shedding of the external epidermis during the shedding cycle.

### 55.4 Nature of Attractive Forces

There are two different adhesive mechanisms in fibrillar systems: a wet one, primarily based on capillarity, and a dry one, primarily based on intermolecular van der Waals interactions. Wet adhesive systems (insects) generate a thin fluid layer in the contact between single hairs and substrate, whereas dry ones (spiders, geckos)

do not. Pad fluids have been previously reported from fibrillar pads of reduviid bugs (Edwards and Tarkanian 1970), flies (Bauchhenss 1979; Walker et al. 1985), coccinellid (Ishii 1987; Kosaki and Yamaoka 1996), and chrysomelid (Eisner and Aneshansley 2000) beetles. The pad secretion contains nonvolatile, lipid-like substances that can be observed in footprints stained with Sudan Black. Microscopy data combined with gas chromatography and mass spectrometry showed that secretion of smooth pads of ants and locusts is an emulsion containing water-soluble and lipid-soluble fractions (Federle et al. 2002; Vötsch et al. 2002). For fibrillar pads, two chemically different secretion compositions were reported. Tarsal secretions of beetles were mainly lipid based (Geiselhardt et al. 2009, 2010; Betz 2010) with a small water fraction, whereas in flies it is assumed to be a mainly water-based microemulsion (Gorb 2001) with low lipid content. Footprints of secretion in flies, visualized by cryo-SEM, indicate as well an emulsion-like composition (Fig. 4). Detailed fluid evaporation measurements in beetles *Coccinella septempunctata* and flies *Calliphora vicina* by atomic force microscopy supported these observations (Langer et al. 2004; Peisker and Gorb 2012). In flies, a larger volatile fraction was observed, if compared to beetles (Peisker and Gorb 2012). This result is also reflected in the corresponding viscosities of tarsal secretions in flies and beetles. For flies (*C. vicina*) a viscosity of approximately 11 mPa·s was measured by microrheological technique, whereas for beetles (*C. septempunctata*) it was two times higher, and a viscosity of approximately 22 mPa·s was found (Fig. 5) (Peisker et al. 2014). Both secretions showed a Newtonian behavior.

In wet fibrillar systems, numerous experiments showed that the main contribution of attractive forces to the overall adhesion is due to capillarity. When hairy pads of the bug *Rhodnius prolixus* were treated with organic solvents, attachment was impaired (Edwards and Tarkanian 1970). Experiments with freely walking beetles strongly suggested that cohesive forces, surface tension, and molecular adhesion, mediated by the pad secretion, may be involved in the mechanism of attachment (Stork 1980a). Multiple local force-volume measurements, carried out on individual terminal plates of the setae of the fly *C. vicina* by application of atomic force microscopy (Langer et al. 2004), showed that adhesion strongly decreases as the volume of the secretion decreases, indicating that a layer of pad secretion covering the terminal plates is crucial for the generation of strong attractive force. These data provide direct evidence that, beside van der Waals forces, also attractive capillary forces, mediated by the pad secretion, contribute to the fly's attachment mechanism (Langer et al. 2004). Similarly, for beetles, traction force experiments on nanoporous plant (Gorb and Gorb 2002) and nanoporous artificial surfaces (Gorb et al. 2010), capable of adsorbing tarsal secretions, showed strong minimization of attachment ability.

In the hairy attachment system of gekkonid lizards, van der Waals interactions are responsible for the generation of attractive forces (Hiller 1968; Autumn et al. 2000, 2002). Experiments, in which the force-displacement curves were determined for individual spatulae by atomic force microscopy, showed that these smallest elements of the gecko's attachment devices generate forces of about 10 nN. An estimate of adhesion energy ( $\gamma$ ) from Kendall's classical peeling theory (Kendall 1975), which describes the force required to peel a tape of certain width (200 nm for

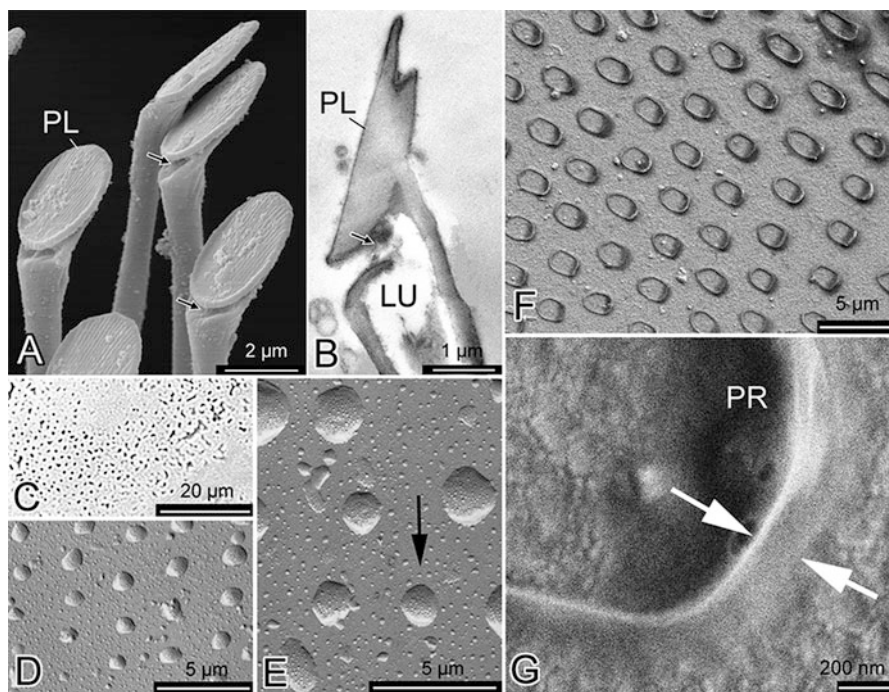


**Fig. 4** Fluid in wet fibrillar systems. (a, b) Tenent setae of the syrphid fly *Episyrphus balteatus* bearing lumen (LU) filled with the fluid and pores (black arrows) under platelike terminal contact elements (PL). (c) Pattern of microdroplets left by the fly *Calliphora vicina* on the glass surface, as viewed in phase contrast light microscope. (d, e) Same droplets frozen and further replicated with carbon-platinum coating technique and visualized in transmission electron microscope (black arrow indicates direction of coating). Please note pattern of nanodrops on the surface of major droplets. (f, g) Menisci formed around single terminal contact elements of the setae of the fly *C. vicina*. Fly leg was frozen in contact with smooth glass, carefully removed, and the fluid residues are viewed in cryo-SEM ((a, b) From Gorb 1998. c–e From Gorb 2001. (f, g) From Gorb 2007))

gecko spatula) from a rigid substrate in perpendicular direction, gives  $\gamma = 50 \text{ mJ}\cdot\text{m}^{-2}$  (Huber et al. 2005a). This value corresponds well to the range expected for adhesion by intermolecular forces ( $10\text{--}100 \text{ mJ}\cdot\text{m}^{-2}$ ; Israelachvili 1992). Using this value of adhesion energy, we may estimate the order of the theoretical force a gecko can produce, assuming all spatulae readily make intimate contact with the substrate and peel off simultaneously. Assuming an effective total peeling line, which is the sum of widths of all spatulae, of 1.8 km for the tokay gecko (Varenberg et al. 2010) and a peeling angle of  $30^\circ$ , shown to be the critical angle of detachment for gecko setae (Autumn et al. 2000), we obtain a maximum force of order 700 N or correspondingly a maximum supported weight of order 70 kg. This large value indicates that only small portions of spatulae are needed in contact with the substrate at each single step. While these estimates show that van der Waals forces can account for the measured adhesion, we cannot unambiguously exclude contributions from capillary forces (Huber et al. 2005b).

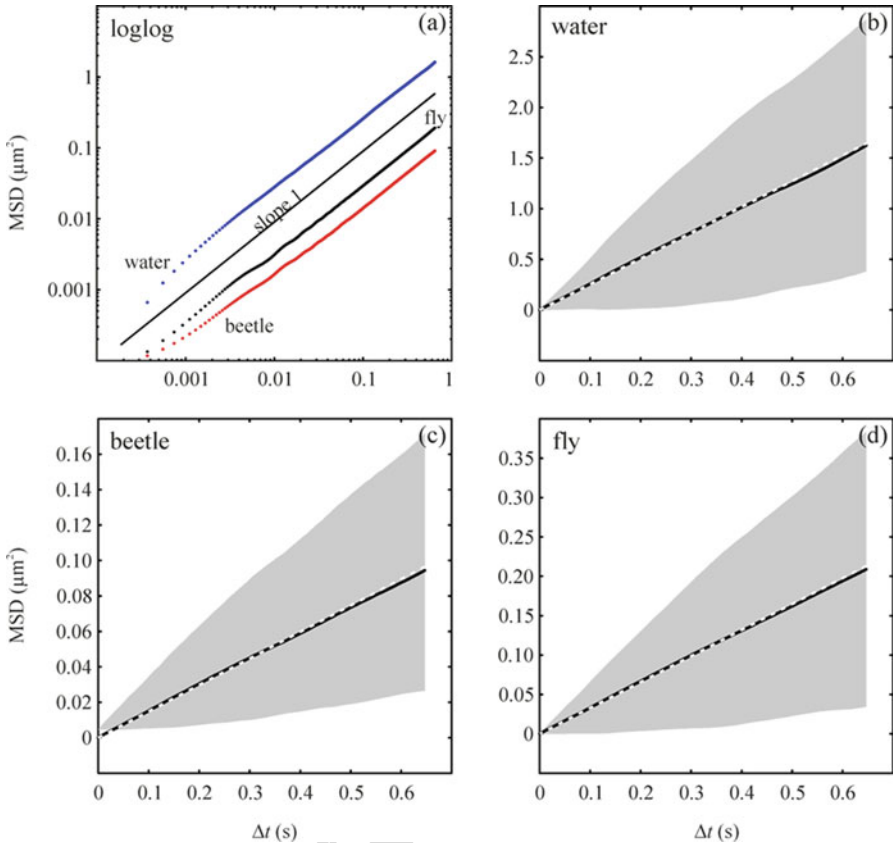


**Fig. 5** Plots of the mean square displacement (MSD) over the lag time for different fluids (Adapted from Peisker et al. 2014). **(a)** Dependence of the MSD on lag time (see *black line* with slope 1) for water (*blue dots*), the fly fluid (*black dots*), and the beetle fluid (*red dots*). The linear relationship in the log-log scale indicates purely viscous (Newtonian) properties of all fluids studied. For the fly and the beetle, all measurements were averaged. Representative MSDs for **(b)** water, **(c)** beetle fluid, and **(d)** fly fluid. *Black solid lines* are the MSD data points; the *gray-shaded area* is the standard deviation in each MSD data point; the *white-dashed lines* are linear fits to the data

### 55.5 Multiple Contacts

Based on the studies of different animal groups, an interesting correlation between the setal density and animal weight was found: the heavier the animal, the smaller and more densely packed are the terminal contact elements (Scherge and Gorb 2001) (Fig. 6). Using contact mechanics theories, this scaling effect was explained by applying the principle of contact splitting to the Johnson–Kendall–Roberts (JKR) contact theory (Johnson et al. 1971), according to which splitting up the contact into finer subcontacts increases adhesion on any substrate profile (Arzt et al. 2003). This

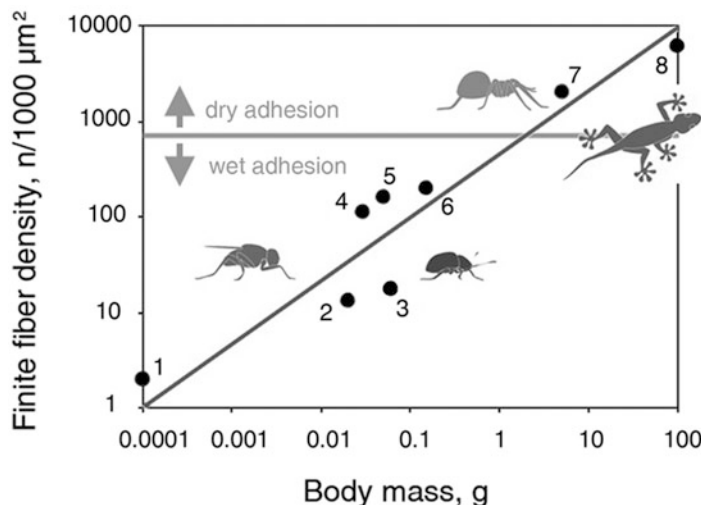


**Fig. 6** Dependence of the contact density of terminal contacts on the body mass in fibrillar pad systems in representatives from diverse animal groups: 1, 2, 4, 5, flies; 3, beetle; 6, bug; 7, spider; 8, gekkonid lizards (Adapted from Scherge and Gorb 2001). The systems, located above *solid horizontal line*, preferably rely on van der Waals forces (*dry adhesion*), whereas other ones mostly rely on capillary and viscose forces (*wet adhesion*)

relationship holds because animals cannot increase the area of the attachment devices proportionally to the body weight due to the different scaling rules for mass and surface area. Therefore, the increase of the attachment strength in hairy systems is realized by increasing the number of single contact points, i.e., by increasing the hair density. It has been shown later that this trend is different within each single lineage of organisms (Peattie and Full 2007). However, a closer look at the terminal contact elements in biological hairy adhesive systems involved in locomotion revealed that they are predominately spatula shaped (Gorb and Varenberg 2007) and cardinally differ from flat-punch- or hemisphere-ended structures (Fig. 7). Therefore, the application of the contact splitting principle to Kendall's peeling model (Kendall 1975) also provides a proper explanation of multiple contact geometry with spatula-like terminal elements. It demonstrates that an animal's attachment ability grows with an overall length of the peeling line, which is the sum of widths of all thin-film elements participating in contact (Fig. 8). This robust principle is found to manifest itself across eight orders of magnitude in an overall peeling line ranging from 64 μm for a little red spider mite to 1.8 km for a tokay gecko, generalizing the critical role of spatulate terminal elements in biological fibrillar adhesion (Varenberg et al. 2010).

Furthermore, other advantages of such hairy adhesive systems have been proposed. For example, in a smooth, continuous adhesive contact, once a crack is initiated at the adhesive interface, the crack may easily propagate over the entire contact area until complete detachment occurs. By contrast, in a fibrillar system, the crack leads initially to the detachment of one seta, and the elastically stored energy in



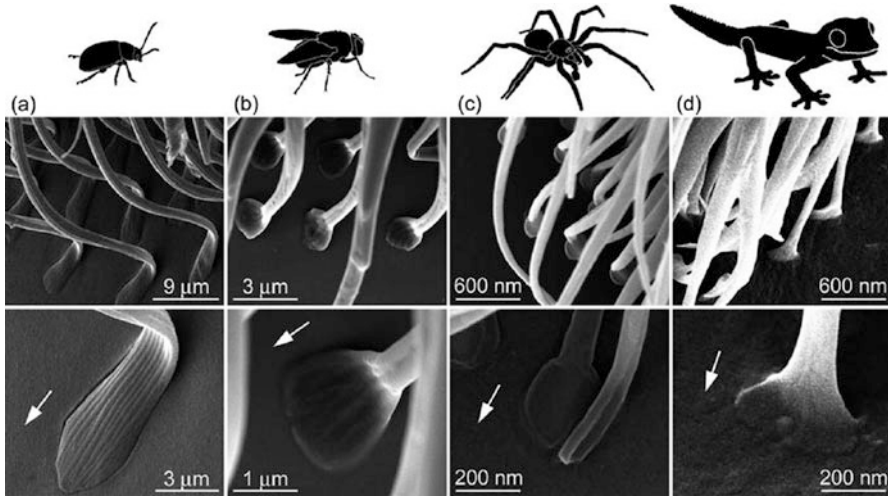


**Fig. 7** Cryo-SEM images of spatula-shaped thin-film terminal elements while in contact with smooth glass, in hairy attachment pads found in animals of evolutionary remote lineages. **(a)** Beetle (*Gastrophysa viridula*). **(b)** Fly (*Calliphora vicina*). **(c)** Spider (*Cupiennius salei*). **(d)** Tokay gecko (*Gekko gecko*). Arrows point in distal direction (From Varenberg et al. 2010)

the seta is released and can no longer contribute to the propagation of the crack (Jagota and Bennison 2002; Hui et al. 2004; Chung and Chaudhury 2005; Tang and Hui 2005). This principle is known as crack trapping. Thus, the crack has to be reinitiated at each individual subcontact. In addition, fibrillar systems adapt better to uneven and rough surfaces (Persson 2003; Persson and Gorb 2003; Kim and Bhushan 2007; Filippov et al. 2011). Because each seta is virtually independent of other neighboring setae, a seta can contact the asperities and valleys of a rough surface without being mechanically influenced by neighboring setae (Fig. 9a). In contrast, in a smooth system, the region around the contact with a surface asperity can be prevented from forming contact (Fig. 9b). Moreover, the effective stiffness of a fibrillar adhesive system is strongly reduced compared with the stiffness of the bulk material of setae. Therefore, the fibrillar system is more compliant to rough surfaces (Persson 2003). Since these effects are based on fundamental physical principles and mostly related to the geometry of the structure, they must also hold for artificial surfaces with similar geometry.

## 55.6 Contact Shape

Real biological adhesive contacts display a variety of shapes and only rarely resemble a hemisphere (Fig. 10). The influence of various contact shapes on the pull-off force for single contacts, as well as their scaling potential in contact arrays, was previously theoretically estimated (Spolenak et al. 2005) and experimentally

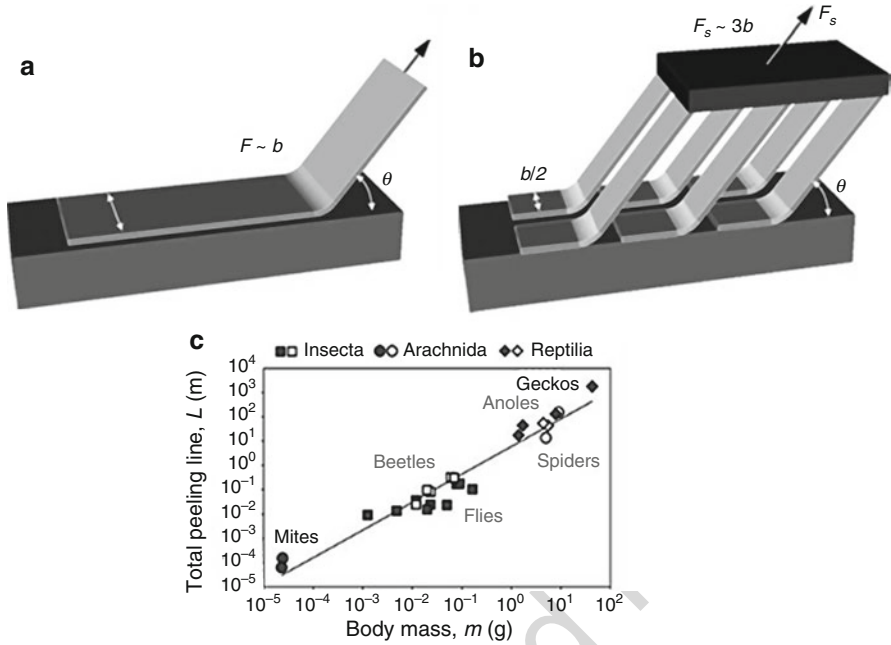


**Fig. 8** Graphical representation of the effect of adhesion enhancement by increasing the peeling line length. **(a)** A single piece of elastic film peeling from a rigid substrate. Peeling force  $F$  is proportional to the film width  $b$  (at constant peel angle  $\theta$  for given pair of materials). **(b)** A series of elastic films covering the same contact area as in **(a)**. Peeling force  $F_s$  is threefold the value  $F$  in **(a)** due to an overall growth of the peeling line length calculated as a sum of individual film widths. **(c)** Total peeling line (the sum of widths of all terminal elements) in fibrillar attachment systems of different animals as a function of their body mass (From Varenberg et al. 2010)

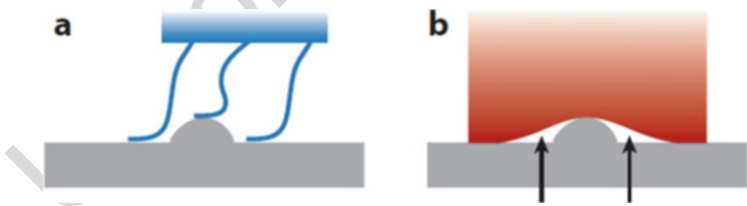


**Fig. 9** **(a)** Fibrillar and **(b)** smooth adhesive systems making contact with a rigid substrate with an asperity. Whereas in a fibrillar system, individual fibers can deform and follow surface irregularities without affecting neighboring setae **(a)**, in smooth elastic pads, regions around the asperity can be prevented from forming contact (arrows; **b**) (From Heepe and Gorb 2014)

demonstrated for artificial fibrillar adhesive systems (del Campo et al. 2007). It was concluded that non-spherical shapes, such as toroid, should lead to better attachment. In insects, spiders, and geckos, as shown in Fig. 7, the topmost hierarchical level of a seta that is responsible for the formation of intimate contact with the substrate

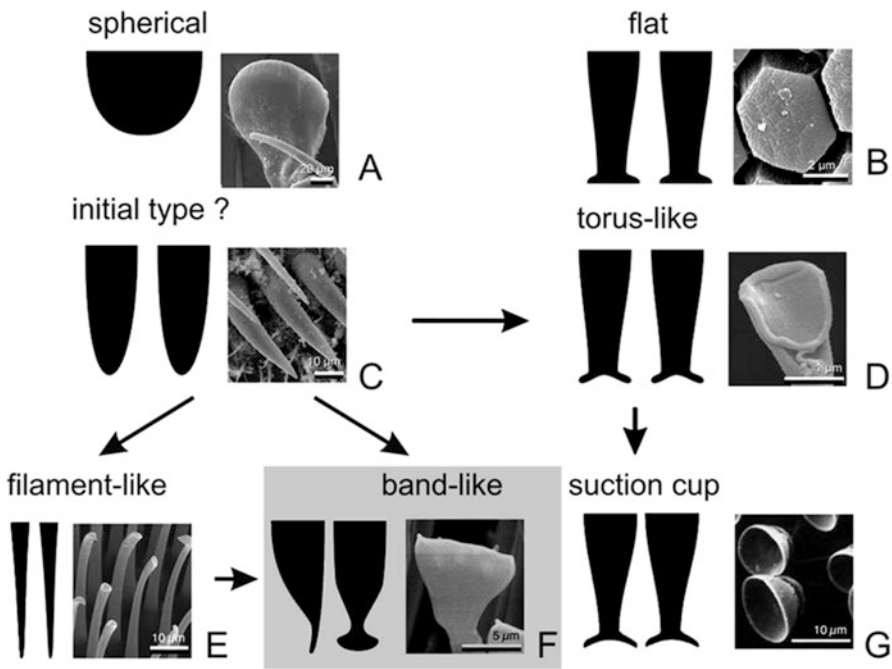


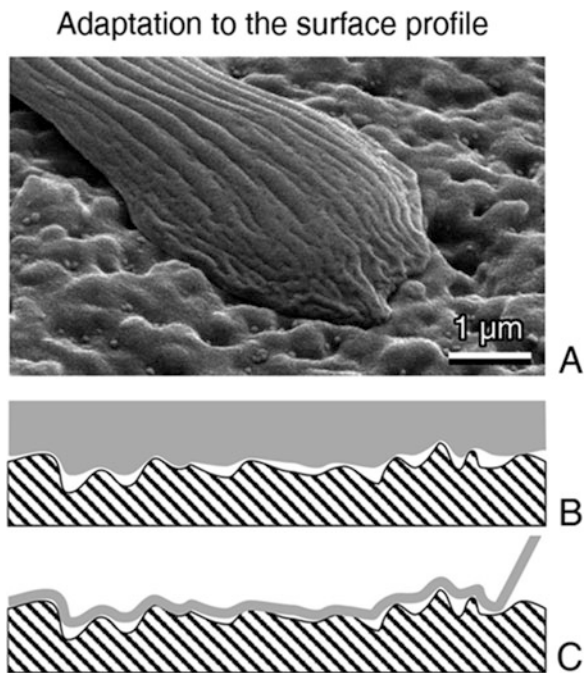
**Fig. 10** Shapes of attachment devices in nature and their hypothetical evolutionary pathways (shown as arrows). (a) Bug *Pyrhocoris apterus*, smooth pulvillus. (b) Grasshopper *Tettigonia viridissima*, surface of the attachment pad. (c) Fly *Myathropa florea*, unspecialized hairs on the leg. (d) Fly *Calliphora vicina*, seta of the pulvilli. (e) Ladybird beetle *Harmonia axyridis*, seta of the second tarsal segment. (f) Beetle *Chrysolina fastuosa*, seta of the second tarsal segment. (g) Male diving beetle *Dytiscus marginalis*, suction cups on the vertical side of the foreleg tarsi (Adapted from Spolenak et al. 2005). Band-like (tape-like, spatula-like) terminal contact elements (highlighted in gray) are most often observed in biological fibrillar adhesive systems capable of ceiling locomotion

resembles thin film-like or spatulae (Stork 1980b; Gorb 1998, 2000; Persson and Gorb 2003; Spolenak et al. 2005). Additionally, spatulae bear a gradient of thickness from the base to the tip of the spatula (fly, Gorb 1998; gecko, Persson and Gorb 2003; beetle, Eimüller et al. 2008) and a gradient in width as they become wider toward its free end. This geometrical property of setal tips can be observed in many animal species (Figs. 3 and 7). In contact, spatulae are aligned and orientated to the distal direction of the pad.

Several hypotheses have been previously proposed to explain the functional importance of such a contact geometry: (1) enhancement of adaptability to the rough substrate (Persson and Gorb 2003), (2) contact formation by shear force rather than by normal load (Autumn et al. 2000), (3) increase of total peeling line due to using an array of multiple spatulae (Varenberg et al. 2010), and (4) contact breakage by peeling off (Gao et al. 2005).



**Fig. 11** The role of the spatula-like terminal contact elements at the tips of adhesive setae in the adaptation to the surface profile (a–c) and in the increasing of the total peeling line. (a) Contact of the spatula of the beetle *Gastrophysa viridula* with the microrough surface. (b–c) Thick elastic material requires additional load to form adhesive contact (b), whereas adhesion interaction pulls the elastic thin film (even made of stiff material) into complete contact with the rough substrate surface (Adapted from Persson and Gorb 2003)



It appeared that the role of highly flexible terminal spatula elements as compliant contacting surfaces is critical (Persson and Gorb 2003). Since the effective elastic modulus of thin plates is very small, even for relatively stiff materials such as keratin or arthropod cuticle, this geometry is of fundamental importance for adhesion on rough substrates (Persson and Gorb 2003), due to the low deformation energy stored in the material during intimate contact formation (Fig. 11).

For adhesion activation, it is well known that the application of a normal load can enhance adhesion (Popov 2010). However, for hairy attachment systems, the adhesion force always remains smaller than the initially applied normal force. This would potentially be not enough to enable walking on the ceiling. Another possibility to activate or enhance adhesion forces is the application of a shear force. We have previously shown that an applied shear force to a particular direction of the spider's spatulated setae results in an increase of real contact area (Niederegger and Gorb 2006; Filippov et al. 2011). Also, flies employ shear movements during contact formation by their attachment devices (Niederegger and Gorb 2003). Previous authors revealed strong shear dependence of measured pull-off force in the gecko attachment system and even called this effect by the somewhat misleading term *frictional adhesion* (Autumn et al. 2000, 2006), which can be simply explained by Kendall's peeling model (Kendall 1975), when the tape is loaded/peeled off at very shallow angles to the substrate. In contrast, by peeling the tape off at very high angles, a very strong reduction in the adhesive force is obtained, which allows for a simple, quick, and energy-efficient detachment mechanism.

## 55.7 Slope and Hierarchy

The observed pull-off force of an adhesive structure may be defined by the difference between attractive forces arising due to, e.g., van der Waals or capillary interaction and the contact reaction forces, arising due to elastic deformation of the adhesive structure during contact deformation (Varenberg et al. 2011). In order to increase the pull-off force, either the attractive interactions have to increase, or the contact reaction forces have to decrease. The attractive forces, e.g., due to van der Waals interactions, reach a natural upper limit as soon as the adhesive structure and the contacting substrate form an intimate contact. In order to form intimate contact, especially to rough surfaces, adhesive structures have to be as soft as possible to enhance real contact area. This in turn, however, would increase the elastic deformations and thus the contact reaction force which would lead to a lower pull-off force. In light of the above, it is clear that there must be a trade-off for the adhesive structure between being soft enough, in order to form an intimate contact, and being stiff enough, to allow for the generation of a sufficiently high pull-off force. Solutions for this problem are either (a) in a hierarchical fibrillar design of the adhesive pad (Fig. 3d–f), (b) in a gradient material in nonhierarchical fibrillar structures (Fig. 12), or (c) in the tilted orientation of hairs relatively to the substrate (Fig. 13). In case of the gecko (see above), the complex hierarchical architecture of the adhesive pad made of relatively stiff  $\beta$ -keratin allows for a relatively low effective modulus (Persson 2003) while simultaneously avoiding setal condensation.

In geckos, there is a higher number of structural levels made of relatively stiff  $\beta$ -keratin (see above): lamella (the first lowermost level), seta (the second one), branching pattern of setulae (third and sometimes fourth level(s)), and spatulae (the uppermost one). Since many natural surfaces (stones, soil, tree bark, plants) have fractal roughness with several overlapping wavelengths, it is not enough to have adhesive pads optimized for one a particular wavelength of roughness. In order to optimize adhesion on a wide range of natural surfaces, biological fibrillar adhesives employed several hierarchical levels, each responsible for contact formation optimization for a particular range of wavelengths. In general, biological adhesive systems represent a kind of mirror structure of the natural fractal world.

Recently, numerous models were developed, in order to explain the role of the hierarchy in the functioning of biological adhesive pads (e.g., Kim and Bhushan 2007; Schargott 2009). While the hierarchical beam model with vertical beams shows the possibility of reducing the effective elastic modulus, the tilted beams are the key to obtaining very soft systems, even when the material employed has a high elastic modulus. In the model combining hierarchy and tilting, elastic and adhesive properties are furthermore enhanced (Schargott 2009). It is shown that when interacting with a rough stochastic surface, the attachment properties are improved with each additional hierarchical layer (Kim and Bhushan 2007; Schargott 2009).

Animals with fewer hierarchical levels have evolved different strategies for the same purpose. In the seven-spotted ladybird beetle (*Coccinella septempunctata*), a material gradient of tanned chitin at the setal base and the rubberlike resilin at the

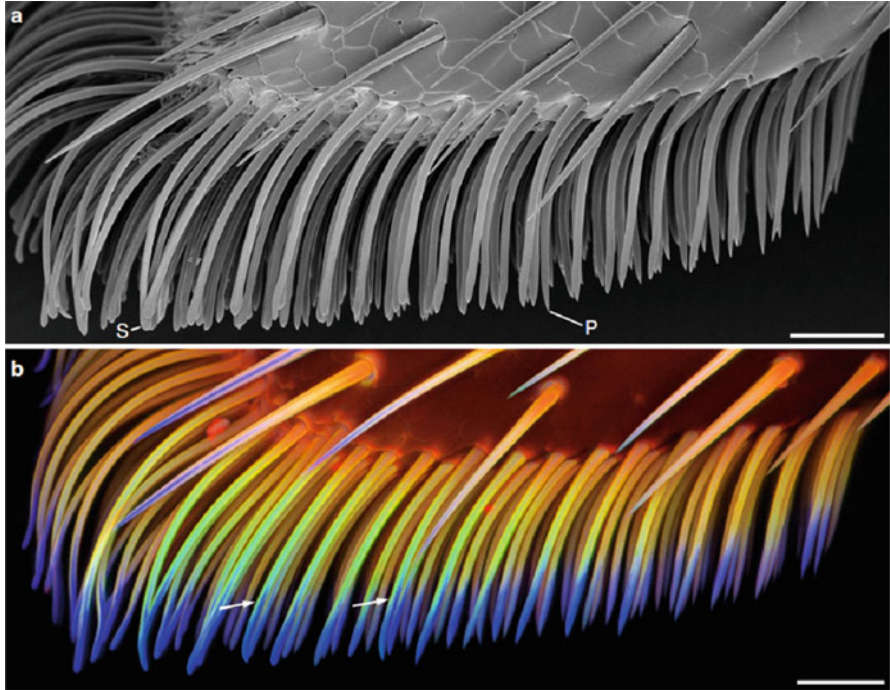


**Fig. 12** Morphology and material composition of adhesive tarsal setae. Ventral part of the second adhesive pad of a foreleg of a female *Coccinella septempunctata*, lateral view. (a) Scanning electron micrograph. (b) CLSM maximum intensity projection showing an overlay of the four different autofluorescences indicating the material composition. The *arrows* indicate the dorsoventral material gradient in exemplary setae. *S* exemplary spatula-like seta, *P* exemplary seta with a pointed tip. Scale bars, 25  $\mu$ m (From Peisker et al. 2013)

setal tip were recently found (Fig. 12; Peisker et al. 2013). Such a gradient in material properties similarly allows for an efficient adaptation to rough surfaces, due to the soft setal tip, while, at the same time, providing sufficient mechanical stability, due to stiffer base, to prevent clusterization and low contact reaction forces.

Tilted geometry of hairs is responsible for the bending mode of their deformation in contact rather than for the buckling one. It is clear that hairs are much stiffer in buckling than in bending. That is why tilted hair arrays have a much lower structural modulus of elasticity than a non-tilted one, and the adaptability to the surface profile of the tilted array is much higher. In addition, bending as a failure mode leads to lesser material fatigue than the buckling mode.

Additionally, asymmetrical shape of a single contact element in combination with the proper movements may provide the way to switchable adhesives, when contacts formed by fibers are activated and when the structure is sheared in the direction of the slope. The contact can be broken by peeling at high angles, when fibers are sheared in an opposite direction.

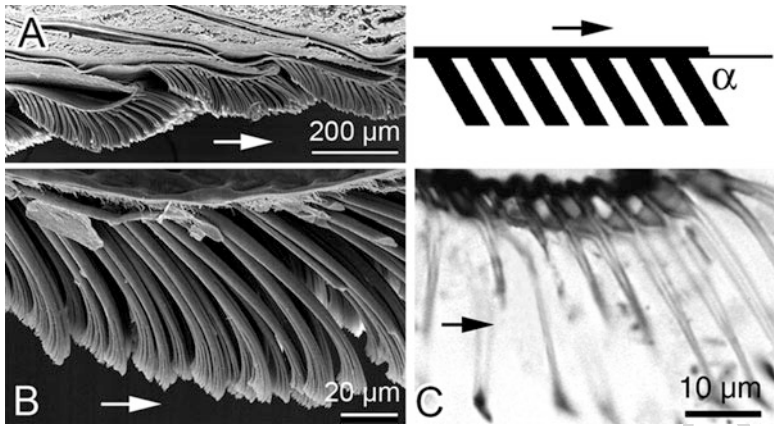


**Fig. 13** Slope angle of adhesive setae in the tokay gecko *Gekko gekko* (a, b) (SEM) and in the fly *Calliphora vicina* (c) (semithin section, light microscopy). Arrows indicate distal direction of the pad (From Gorb 2011)

### 55.8 Adhesion Control

Animal locomotion involves simultaneous peeling of many spatulae, at the level of adhesive pads (Fig. 7), at the level of contralateral legs (Fig. 14a, b), and sometimes also at the level of contralateral toe pads within one foot (Fig. 14c). Thus, in climbing animals, the situation is more complex than in Kendall's classical peeling model and resembles a hierarchical multiple peeling configuration (Pugno and Gorb 2009; Pugno 2011; Heepe et al. 2017a). On the macroscale, however, the peeling configuration of climbing animals may be reduced, for simplicity, to the peeling of two elastic tapes loaded at a common hinge (Fig. 14d). This double-peeling configuration has interesting adhesive properties, if compared to the classical single peeling. It exhibits a self-stabilized optimum peeling angle with a maximum in peeling force, i.e., the optimum configuration is reached irrespective of the initial peeling angle configuration of the system. Below the optimum angle, there is no delamination (peeling) but pure elastic deformation of the system. Above the optimum angle, stable delamination is observed. Figure 15 shows experimental results of the double-peeling configuration using an elastic adhesive tape (Heepe et al. 2017a).

When an animal is adhering to the ceiling, its legs tarsomeres are oriented toward the center of the body mass (Fig. 16a). In this orientation, setae are recruited by bending to their tilted direction, and spatulae are set under shear load. Under these conditions, setae are activated to their adhesive state. If five of the six insect legs are ablated, the animal is not able to adhere to the ceiling anymore, even if the average adhesive force of the single leg (measured for all six legs acting in concert and then normalized by the number of legs) should be sufficient to resist the body weight on the ceiling. However, with two intact legs, an animal can perfectly stay on the ceiling

**Fig. 14** (a) A beetle *Gastrophysa viridula* in contact with a glass ceiling (lateral view from behind). The arrow indicates weight force  $W$  acting at the center of mass. (b) Fly *Calliphora vicina* in contact with a glass ceiling (view from above through the glass ceiling). Arrows indicate contralateral leg movement. (c) Foot of a gecko *Gekko gecko* in contact with a glass ceiling (view from above through the glass ceiling). Arrows indicate contralateral toe pad movement. (d) Simplified mechanical model of the ceiling situation (lateral view from behind, similar to (a)). Two elastic tapes are in contact with a rigid ceiling and having a common hinge, where a load  $F$  is applied. The tapes make angles with respect to the substrate of  $\alpha_1$  and  $\alpha_2$  (From Heepe et al. 2017)

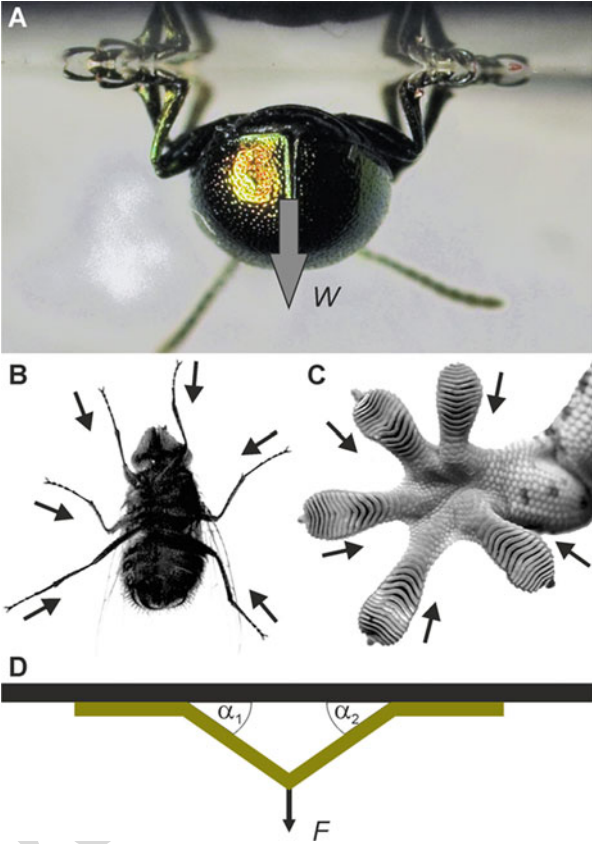


(Fig. 16b). With three remaining intact legs on one body side, an animal can reorient one leg to the other body side and stay on the ceiling (Fig. 16c). In the latter two cases, the adhesive system can be activated by shear force.

In light of the above results, the explanation of this phenomenon is rather simple. The situation of the single leg in contact can be simulated by a piece of sticky tape adhering to the ceiling and holding a certain mass. The peeling angle in such geometry would tend to be  $90^\circ$ , which according to Kendall's model (Kendall 1975) generates a rather low peeling force. When two or multiple tapes are combined, the peeling angle will be generally lower than  $90^\circ$ , due to the self-stabilization effect of such geometry.

High-speed video recordings of a fly foot attaching to the substrate show that the pulvilli are pressed down to the surface and also pulled towards the body. Through this movement, the claws become spread apart (Fig. 17a, b). During such an action, setae and their spatulae will be activated, and the maximal force will be reached. In order to detach, four different movements may occur (Fig. 17c–f) (Niederegger et al. 2001;



**Fig. 15** (a) Schematic of the experimental setup. Principal double-peeling configuration: the tape (dark gray) is in contact with glass substrates (light gray) and loaded with a force  $F$  at the hinge in the middle of the tape. The tape makes initial peeling angles with the substrate of  $\alpha_0$ . (b) Experimental results (open circles) of the double-peeling configuration using elastic adhesive tape. Experiments were started at initial peeling angles  $0^\circ$  and  $90^\circ$  as indicated by the arrows (Adapted from Heepe et al. 2017a)

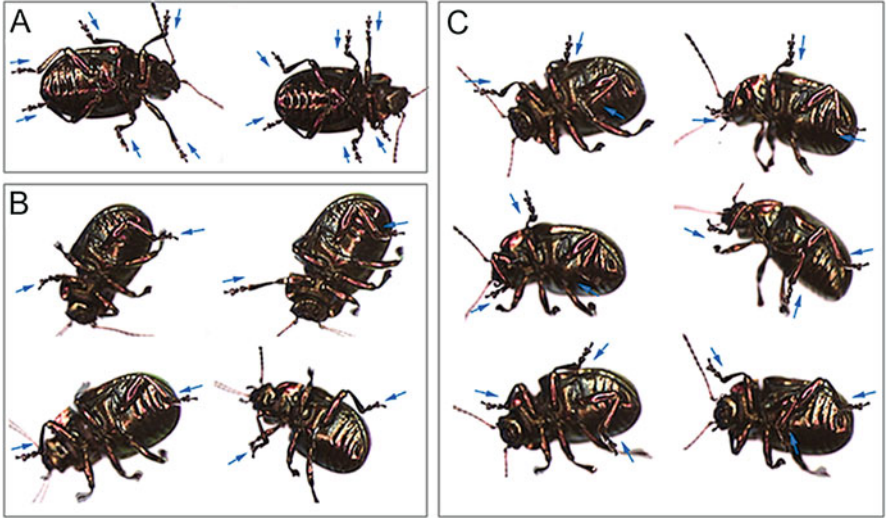
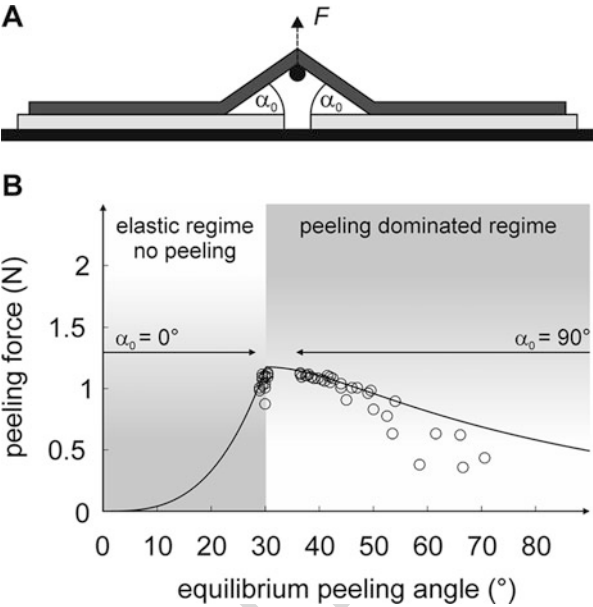


**Fig. 16** (a–c) Posture of the chrysomelid beetle *Chrysolina fastuosa* on the ceiling. (a) Intact beetles. (b) Two-legged beetles (four legs are removed). Arrows indicate orientation of leg tarsomeres. (c) Three-legged beetles (three legs on one body side are removed). Please note rearrangement of leg positions, in order to generate shear toward center of the body mass (arrows) (From Gorb 2011)

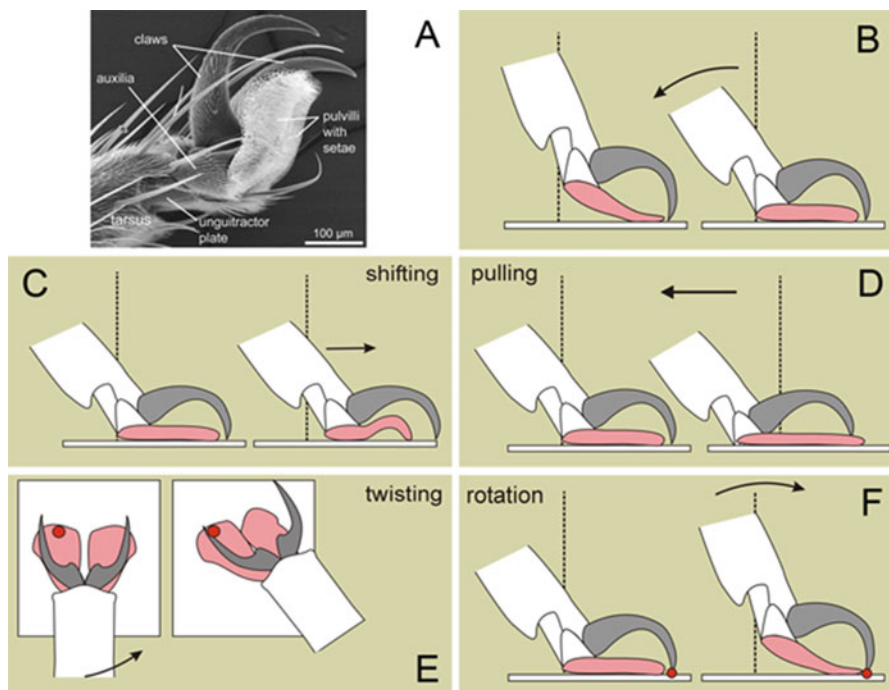


**Fig. 17** Attachment and detachment movements of the fly adhesive organs (diagrams are based on the high-speed video recordings under binocular microscope). (a) Side view of attachment organs (pulvilli) in the fly *Calliphora vicina* (SEM). (b) Movement at attachment. (c–f) Movements at detachment by using shifting (c), pulling (d), twisting (e), and rotation (f) (From Niederegger et al. 2001; Niederegger and Gorb 2003)

Niederegger and Gorb 2003). (1) In *shifting* (or *local peeling*), the foot is shortly moved forward. This compresses the pulvilli, which in turn leads to a smaller contact area and thus to a reduction of attachment forces. Additionally, peeling occurred at the level of the spatulae. (2) In *twisting*, the leg is turned by up to 90° and pulled backward. This bends the setae and eventually detaches them from the surface. (3) In *rotation* (or *global peeling*), the foot is lifted from its back to the front, which causes the claws to be passively pressed to the surface. With this force, the adhesion is interrupted by peeling at the level of the whole pad. (4) In *pulling*, the foot is simply pulled backward until the attachment devices detach from the surface. This type of detachment possibly requires quite strong force, but it happens in some behavioral situations, especially when the insect is stressed. In geckos, attachment is activated by proximodistal rolling out of the toe, whereas detachment is provided by distoproximal peeling of it (Gao et al. 2005).

Observations of the gait pattern in flies walking on a horizontal surface revealed that three opposing legs were in the swing phase (moving), whereas the other three legs remained in the stance phase (motionless) (Fig. 18a). Does the gait pattern of the fly change on the wall and ceiling? Using high-speed camera video recordings of

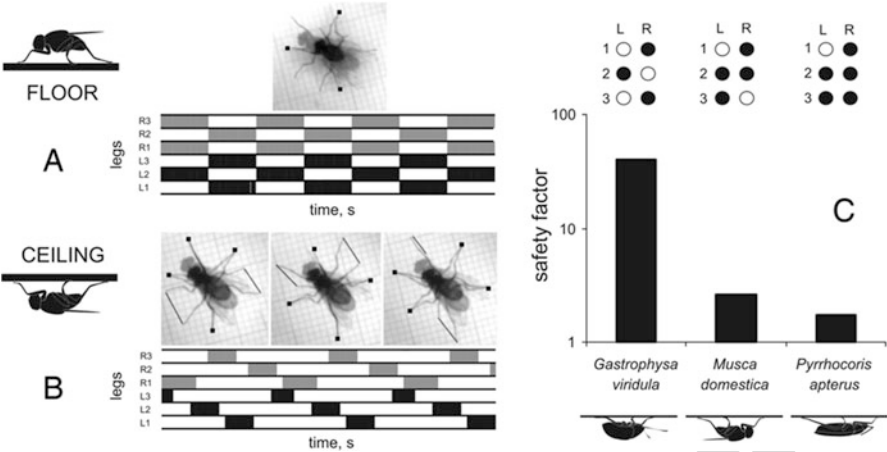


**Fig. 18** Gait patterns of insects on glass ceiling. (a, b) Gait diagram of the house fly, *Musca domestica*, on the floor (a) and ceiling (b) (From Niederegger et al. 2001; Gorb 2001, 2005). (c) Relationship between the safety factor (attachment force divided by the body weight) and the gait pattern on the ceiling in different insects. *Insets* show feet (black dots) that are typically in contact during the walk on smooth ceiling (From Gorb 2011)

flies walking on a vertical surface, it was shown that their gait pattern is not different from the pattern on a horizontal surface. However, the fly walking on the ceiling moved only two legs at once and four remained in the stance phase (Niederegger et al. 2001; Gorb 2001, 2005) (Fig. 18b). This result led us to assume that the gait pattern may contribute to the fly’s ability to adhere dynamically on the ceiling, in providing an optimal relationship between the body weight and the supporting contact area.

Experiments with insect species that have different safety factors (attachment force divided by the body weight) show that insects with a safety factor above 10 can employ tripod gait similar to one observed during locomotion on the floor. Insects with a safety factor in the range of 4–5 change their gait compared to that reported above for the fly. Insects with a safety factor lower than 3 change their gait to that, where only one leg is in the swing phase and the other five remain in the stance phase (Fig. 18c). These results show that dynamical adhesion in insects may also strongly rely on a multiple peeling configuration, especially in ceiling locomotion.

Thus, it is plausible to assume that biological adhesive systems try to actively use changes in their configuration of their tape-like contact geometry, to control and/or maintain adhesion. To securely stay on the ceiling, animals tend to keep their macroscopic peeling angle below the optimum. In this regime, no peeling occurs. Interestingly, in flies clinging to a glass ceiling, it was observed that their feet were in constant slow motion toward the body center of mass (Wigglesworth 1987), potentially due to the tarsal secretions produced in insect adhesive systems (Gorb 2001). After a certain sliding motion of the feet, they were quickly extended and reattached, thereby maintaining a position with a low macroscopic peeling angle. Quick and



easy detachment may be achieved by a simple active change of the macroscopic peeling angle above the optimum one by, e.g., proximodistal peeling in the case of flies (Niederegger et al. 2002) and distoproximal peeling or digital hyperextension in the case of geckos (Russel 1975). This may be possible, since their available contact area is restricted to the pad area and, thus, only a short peeling distance is necessary before complete detachment of a pad or a foot occurs.

## 55.9 Environmental Conditions Affecting Animal Adhesion

All natural surfaces have surface roughness on many different length scales (Persson 2014) which may strongly reduce attachment of animals (e.g., Gorb 2001; Gorb and Gorb 2002; Peressadko and Gorb 2004b; Huber et al. 2007; Voigt et al. 2008; Wolff and Gorb 2012). The influence of surface roughness on insect attachment has been proven experimentally in several studies (Gorb 2001; Peressadko and Gorb 2004b; Voigt et al. 2008; Bullock and Federle 2011). There seems to be a common trend that insects generate much higher forces on either smooth or rough surfaces with an asperity size exceeding  $3.0\text{ }\mu\text{m}$  than on those with the roughness ranging from  $0.3$  to  $3.0\text{ }\mu\text{m}$  (Fig. 19). This effect has been explained by the specific geometry of spatula-like terminal elements of insect tenent setae that are able to generate sufficient contact, if the surface irregularities are sufficiently large. Worst attachment has been observed on substrates with a roughness of  $0.3$  and  $1.0\text{ }\mu\text{m}$  (Fig. 19). In this case, the spatula-like terminal elements cannot follow the surface profiles with these small asperities, and thus, the area of real contact between these substrates and the tips of insect setae is very small. Since adhesion force depends on the area of real contact, insects were not able to attach successfully to surfaces with such a microroughness.

Interesting examples of natural anti-adhesive surfaces are well known from many plants, which are covered with microscopic wax crystals of different shapes, chemistry, and mechanical properties. To explain the anti-adhesive properties of these plant substrates, four hypotheses were previously proposed (Gorb and Gorb 2002). (i) Wax crystals cause microroughness, which considerably decreases the real contact area between the substrate and setal tips of adhesive pads (*roughness hypothesis*); see above. (ii) Wax crystals are easily detachable structures that contaminate pads (*contamination hypothesis*). (iii) Structured wax coverage may absorb the fluid from the setal surface (*fluid absorption hypothesis*). (iv) Insect pad secretion may dissolve wax crystals (*wax-dissolving hypothesis*). This would result in the appearance of a thick layer of fluid, making the substrate slippery. Recently, only the first three hypotheses were tested.

Contamination of insect pads by plant wax crystals has been demonstrated for several insects and in a series of plant species (e.g., Gaume et al. 2004; Gorb and Gorb 2006). It has been found that plants differ essentially in their contaminating effects on insect pads (Gorb and Gorb 2006). The degree of contamination depends on the micromorphology of waxes (Borodich et al. 2010). The analysis of the relationship between the contamination ability and geometrical parameters of wax

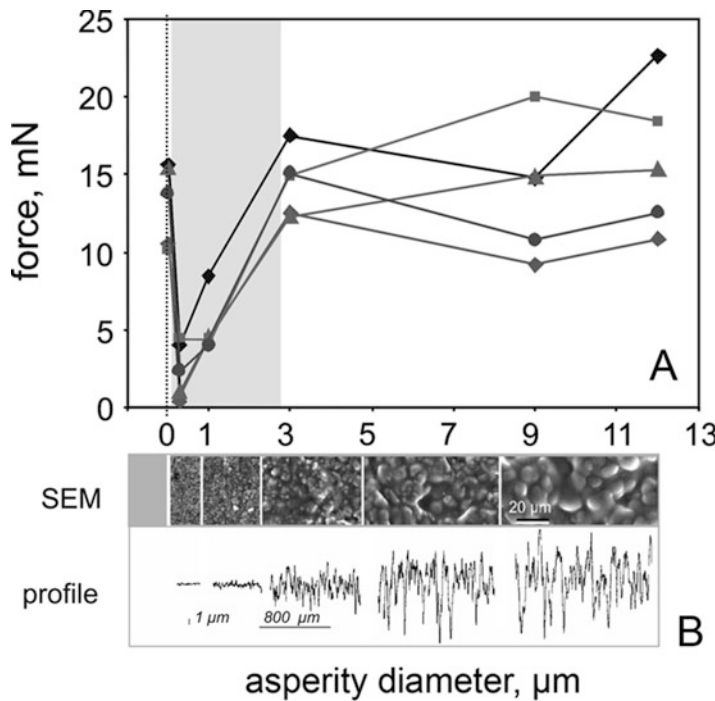


**Fig. 19** Role of the substrate roughness (asperity diameter) in the attachment of biological fibrillar adhesives. (a) Attachment forces of chrysomelid beetles *Gastrophysa viridula* measured on the horizontal surface of the drum of the centrifugal force tester on substrates with different roughness. (b) Surface of the substrate in SEM and measured with the profilometer (From Peressadko and Gorb 2004b)

crystals has shown that the contamination is related to both the largest dimension and the aspect ratio of crystals (Borodich et al. 2010).

The fluid absorption hypothesis was recently tested in an experimental study, where nanoporous substrates with the same pore diameter but different porosity (area of voids in a material surface, normalized over the total area) were used (Gorb et al. 2010). According to this hypothesis, absorption of the insect pad fluid by the porous substrate results in a reduction in the fluid thickness between the terminal plates of the insect pads and the substrate, and this leads to a reduction of capillary interaction in the contact area. Traction force experiments performed on tethered ladybird beetles walking on different porous substrates showed that forces were significantly reduced. The reduction in insect attachment on nanoporous surfaces may be explained by possible absorption of the secretion fluid from insect adhesive pads by porous media and/or the effect of surface roughness. The wax-dissolving hypothesis has not been experimentally tested yet.

A rather long-standing question in animal attachment is which substrate property is most important for the attachment ability: surface roughness or surface chemistry? Since the surface chemistry (here in terms of surface energy) affects the strength of

either van der Waals or capillary interaction, substrates with low surface energy are expected to reduce the overall attachment ability. In a recent experiment, traction forces of ladybird beetles *Coccinella septempunctata* were systematically measured on eight types of substrates, each with different chemical and topographical properties (England et al. 2016). The results clearly showed that surface roughness rather than surface chemistry essentially affected insect adhesion. Surface chemistry had no significant effect on the attachment ability of the beetles (England et al. 2016).

So far, however, the attachment ability of insects and also that of spiders and geckos has been tested on rigid substrates only, whereas the natural habitats of climbing animals may provide a variety of substrate stiffness ranging from rigid rock surfaces to soft, biofilm-covered substrates. Friction force measurements, using a centrifugal force tester, with male and female beetles *Coccinella septempunctata* on smooth silicone elastomer substrates with different stiffness between 2 and 0.3 MPa revealed an overall decrease in attachment ability if compared to a rigid substrate (Heepe et al. 2017b). Within the range of measured stiffness, female's attachment ability was not affected, whereas male's decreased with decreasing stiffness. This sexual dimorphism in attachment ability is explained by the presence of a specialized, discoidal seta type in males, which is not present in females (Heepe et al. 2017b). Substrate properties are not the only environmental factors shown to influence animal adhesion. Also the ambient humidity affects the attachment ability, as it was shown in the dry adhesive pads of geckos (Huber et al. 2005a; Niewiarowski et al. 2008; Puthoff et al. 2010; Prowse et al. 2011) and spiders (Wolff and Gorb 2011) as well as in the wet adhesive pads of beetles (Heepe et al. 2016). In all animals, reduced attachment ability was observed for very low and very high relative humidities, whereas maximum attachment ability was found for intermediate humidities (Heepe et al. 2016). This is particularly interesting since both types of adhesive systems (wet and dry) are supposed to be based on different physical interactions (capillarity versus van der Waals forces).

---

## 55.10 Biomimetic Implications

As mentioned above, fibrillar adhesive systems appeared several times in animal evolution and at least three times independently even in insect evolution. This fact may indicate that design principles of biological fibrillar adhesives must have an advantage for adhesion enhancement not only in biological systems but also in artificial surfaces having similar geometry. Geometrical effects discussed above, such as multiple individual contacts, high aspect ratio of single contact structures, peeling spatula-like tips of single contact elements, are responsible not only for generation of a strong pull-off force in such devices but also for other interesting features, such as adhesion reversibility, contamination reduction, etc. (Fig. 20). The physical background of these effects were intensively discussed theoretically in several publications (for early original work, see, e.g., Jagota and Bennison 2002; Arzt et al. 2003; Persson 2003; Persson and Gorb 2003; Chung and Chaudhury 2005; Gao et al. 2005; and for current reviews, Federle 2006; Autumn 2007;

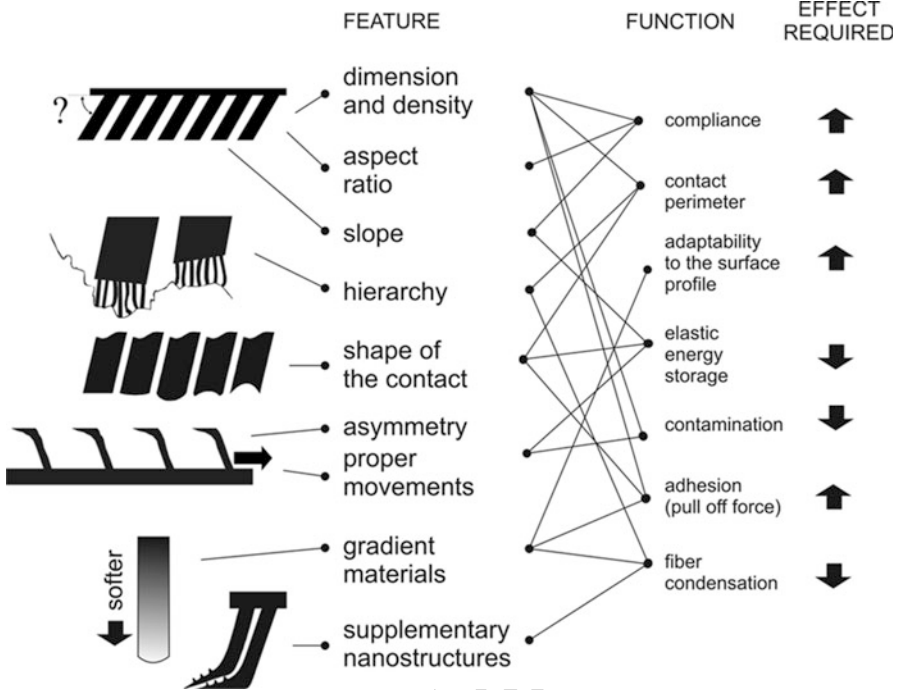


**Fig. 20** Some functional principles (*FEATURE*) at which biological reversible and biological adhesive systems operate. In the middle of the diagram, the functions (*FUNCTION*) and their relationship to the features are depicted. The resulting effect that is required for optimization is shown at the right-hand side (*arrows* indicate enhancement/reduction of the function). Simultaneous implementation of all these features in one artificial system is desirable but hardly possible. However, one principle or a combination of few of them can be implemented depending on particular requirements for material or system (From Gorb et al. 2007b)

Kampermann et al. 2010; Gorb 2011; Jagota and Hui 2011). For fibrillar biological systems, the following key functional properties can be defined (Autumn et al. 2007; Creton and Gorb 2007).

1. *Anisotropic attachment*: Attachment force variable depending on the setal-spatula orientation with respect to the substrate, normal load, and parallel drag.
2. *High adhesion coefficient*: Ratio of preload to pull-off force, which represents the strength of adhesion as a function of the compressive load.
3. *Low detachment force*: Animals detach their feet in a few milliseconds by different kinds of movement, which lead to peeling of adhesive structures at different levels.
4. *Universality of adhesion*: Van der Waals-based interaction and oil-based capillary interaction with the substrate depend basically on geometry of features (fibrillar shape, spatulae, fluid thickness, etc.) and are less dependent on the substrate chemistry.

5. *Self-cleaning*: The feet of geckos are resistant to the contamination by particles corresponding in size to typical environmental dirt particles (diameter 5–100  $\mu\text{m}$ ). In insects, secreted fluid may additionally contribute to rinsing of dirt particles. Biological fibrillar adhesive systems possess an anti-contaminating property.
6. *Anti-self-adhesion*: Hierarchical fibrillar structure avoids the self-adhesion of individual structural elements.
7. *Nonsticky default state*: Most of the fibrillar structures with an exception of mushroom-shaped setae are nonsticky by default, because only a very small contact fraction is possible without deforming the setal array.

Based on the inspiration from biology and using contact theory as a guideline, artificial surfaces were developed with enhanced pull-off forces in contact with the flat surface, if compared to the flat control. These materials have been produced using various micro- and nanofabrication techniques ranging from laser technology and carbon nanotube packaging to various lithography techniques (for early original work, see, e.g., Geim et al. 2003; Sitti and Fearing 2003; Peressadko and Gorb 2004a; Northen and Turner 2005; Yurdumakan et al. 2005; and for current reviews, e.g., Greiner et al. 2009; Sameoto and Menon 2010; Kwak et al. 2011) (Fig. 21). Independently on the pull-off forces achieved by the surface patterning, these materials are strongly limited in the patterned area. Usually, the overall patterned area was in the best case restricted to few square centimeters, which makes their use for industrial applications rather difficult. Also most bioinspired fibrillar adhesives are just based on the fibers with flat punches at their tips or in most elaborate cases sloped punches (Autumn et al. 2007), without implementation of proper terminal elements in the form of spatula or mushroom, as we know them from the majority of biological systems including insects, spiders, and geckos. So far, the best results of mimicking fibrillar adhesive systems have been achieved with mushroomlike surface microstructures (for early original work, see, e.g., Daltorio et al. 2005; Kim and Sitti 2006; Gorb et al. 2007a; Davies et al. 2009; for a current review, see Heepe and Gorb 2014). Some of these developments may be produced in large-scale industrial processes in the form of square meters large foils (Gottlieb Binder and Co 2017) (Fig. 22). Interestingly, such microstructures can be found in attachment pads of male beetles from the family Chrysomelidae. Although both sexes possess adhesive hairs on their tarsi, only males bear hairs with such extreme specialization for adhesion on the smooth surface and most likely to attach to female's covering wings during pairing (Stork 1980b; Voigt et al. 2008). It has been previously reported that males of the Colorado potato beetle *Leptinotarsa decemlineata* generate such a strong adhesion on the smooth clean glass that they are not able to break off the contact and that is why they have a hard time walking on this surface (Pelletier and Smilowitz 1987). The hairs responsible for this effect have broad flattened tips and narrowed flexible region below the tips. These features, as well as distribution patterns of pillars, were implemented in the design of the patterned polymer structure described here.

The adhesive properties of the industrial micropatterned adhesive foil were characterized using a variety of measurement techniques and compared with those

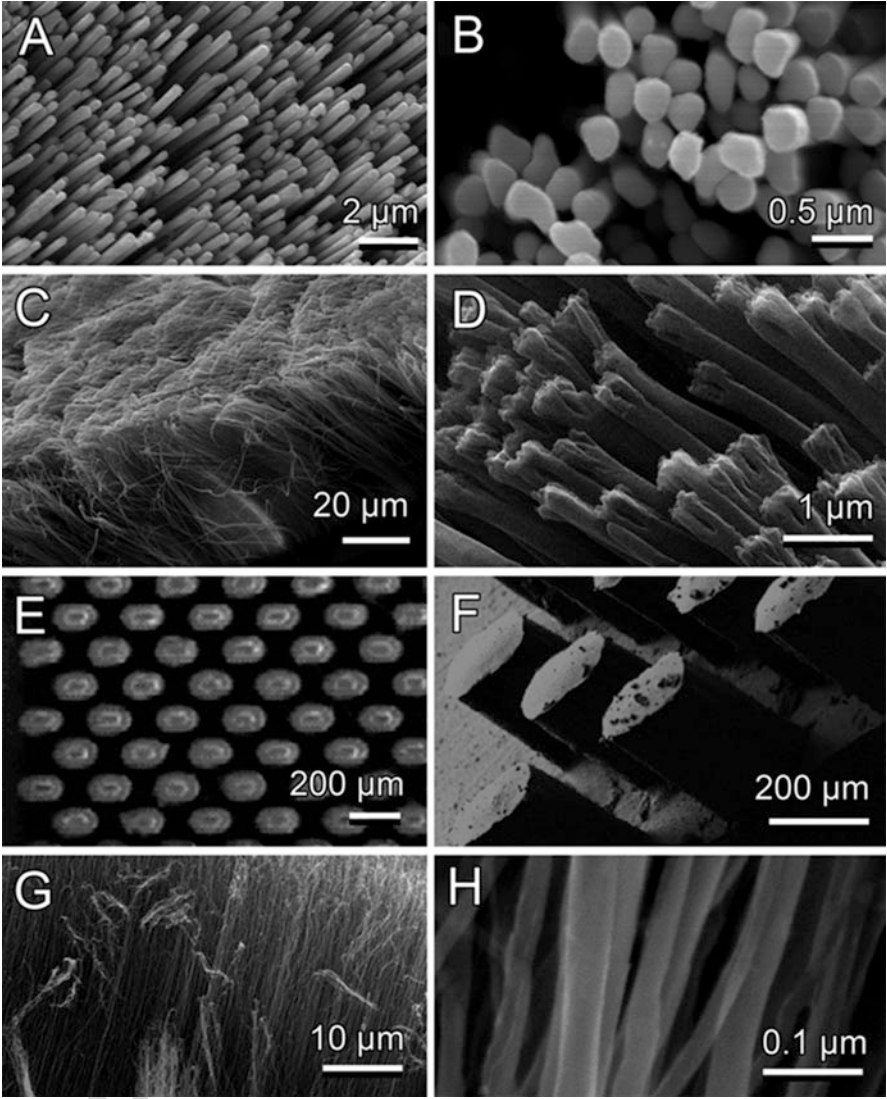


**Fig. 21** Bioinspired fibrillar adhesives of different dimensions. (a, b) Metallic nanowhiskers. (c, d) Hierarchically branching fiber arrays made of epoxy resin. (e, f) Silicone molds of laser-patterned metal surface. (g, h) Carbon nanotubes. (a–d, g, h) Original micrographs ((a–d, g, h) From Gorb 2010. (e, f) From Peressadko and Gorb 2004a)

of the flat foil made of the same polymer (Daltorio et al. 2005; Gorb et al. 2007a; Varenberg and Gorb 2008a, b, c; Heepe et al. 2011, 2012, 2013, 2014a, b, 2017a; Kovalev et al. 2012; Kizilkan et al. 2013, 2017; Kasem and Varenberg 2013; Denning et al. 2014; Breckwoldt et al. 2015). The foil with the microstructure pattern demonstrates considerably higher pull-off force per unit real contact area and per



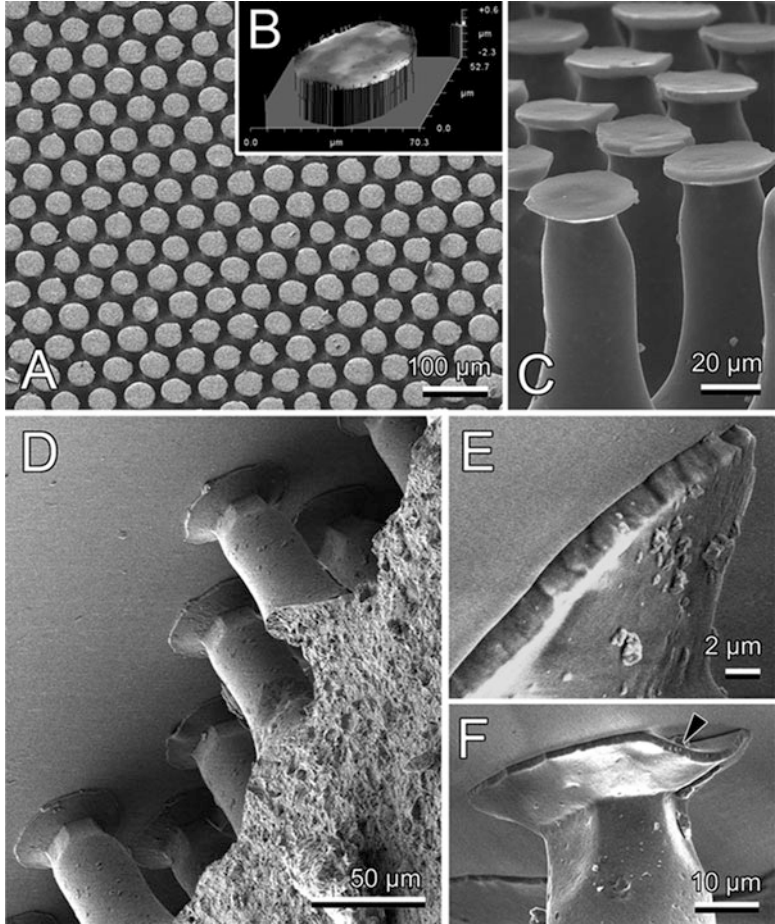


**Fig. 22** Patterned insect-inspired polivinylsiloxane surface. (a) Single structures are distributed on the surface according to the hexagonal pattern, in order to reach the highest packaging degree of single pillars (above aspect, SEM image). (b) White light interferometer image of a single pillar head demonstrates almost flat shape of the contacting surface. (c) Side aspect of the pillar array. (d–f) Behavior of structured PVS surfaces in contact with the glass surface (SEM images). Black arrowhead shows a dust particle in contact (From Gorb et al. 2007b)

unit apparent contact area as well. It is also less sensitive to contamination by dust particles, and after being contaminated and washed with soap and water, the adhesive properties can be completely recovered. The foil represents an industrial dry adhesive based on the combination of several principles previously found in biological attachment devices of insects, spiders, and geckos.

This material is a promising candidate for the application in dynamical adhesive systems, such as robot soles adapted for locomotion. Robots that could climb smooth and complex inclined terrains, like insects and lizards, would have many

applications such as exploration, inspection, or cleaning. Walking machines usually use suckers to hold onto vertical surfaces and under a surface. A primary disadvantage of this attachment principle is large energy consumption for vacuum maintenance. The novel biologically inspired materials may enable future robots to walk on smooth surfaces regardless of the direction of gravity. Mini-Whegs™, a small robot (120 g) that uses four-wheel legs for locomotion, was recently converted to a wall-walking robot with compliant, adhesive feet (Daltorio et al. 2005). The robot is capable of ascending vertical smooth glass surfaces using a micropatterned adhesive (Fig. 23a). A new version of this robot (about 22 g) is even able to transverse from the floor to the ceiling without detaching from the substrate (Fig. 23b). Another demonstration of adhesion capability of such material is shown in Fig. 23c, d. A PMMA plate, 20 × 20 cm, covered by the foil is sufficient to support the weight of a man attached to the glass ceiling (Fig. 23c). Using custom-built gloves for hands and feet, the material, in principle, allows climbing a vertical glass wall (Fig. 23d).

Bioinspired fibrillar materials can be additionally applied to the design of micro-gripper mechanisms with the ability to reversibly adhere and to adapt to a variety of surface profiles and for any kind of reversible adhesive tapes.

---

## 55.11 Conclusions

1. Real biological attachment systems usually rely on the combination of different functional principles based on elaborate micro- and nanostructures.
2. Attachment systems in biology can be subdivided according to their structure and basic physical forces responsible for enhancement of contact forces.
3. Reversible attachment devices used for locomotion may be hairy and smooth. Hairy systems consist of fine microstructures, whereas smooth systems are composed of materials with unusual inner structure. Due to the flexibility of the material of the attachment pads or fine surface structures, both mechanisms can maximize the possible contact area with a wide range of substrate profiles.
4. Recent phylogenetic analyses have shown that similar functional solutions for attachment have evolved several times independently in the evolutionary history of animals (e.g., geckos, anoles, spiders, beetles, flies, etc.).
5. In hairy systems, the density of single contact elements usually increases with increasing body weight of the animal group. From the scaling analysis, it has been previously suggested that animal lineages relying on dry adhesion (lizards, spiders) possess a much higher density of terminal contact elements compared to systems using the wet adhesive mechanism (insects).
6. Lizards' and spiders' attachment systems are mainly based on van der Waals forces, but also wetting phenomena caused by water absorbed on the surface have an effect on the attachment ability. In insects, mainly attractive capillary and viscous forces mediated by the pad secretion are the basic physical mechanism in their adhesion.



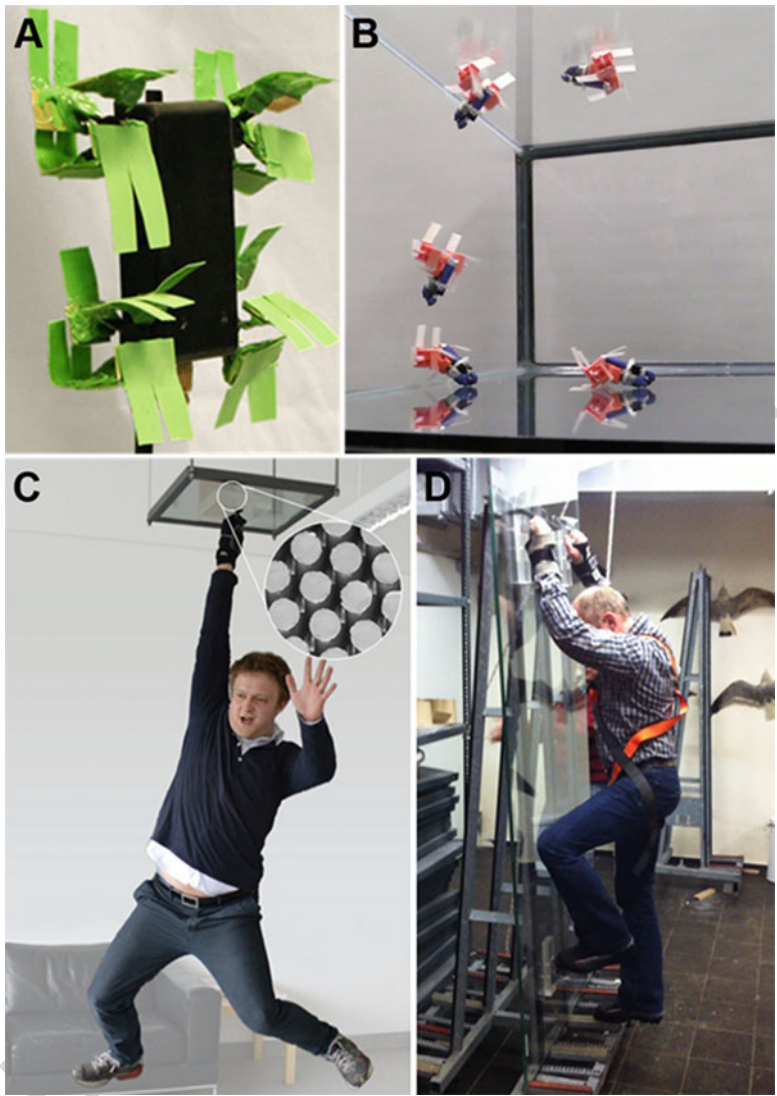


**Fig. 23** (a) Mini-Whegs™ on vertical glass with a microstructured adhesive tape (From Daltorio et al. 2005). (b) Inverted Mini-Whegs demonstrating internal transitions from floor to wall to ceiling (From Breckwoldt et al. 2015). (c) Photograph of a man attached to the glass ceiling by a 20 × 20 cm PMMA plate covered by microstructured adhesive tape (see SEM image in the *inset*) (original). (d) Photograph of a man attached to a vertical glass wall by custom-built gloves for hands and feet covered with the microstructured adhesive tape (original)

7. The effective elastic modulus of the fiber arrays is very small, which is of fundamental importance for proper contact formation and adhesion on smooth and rough substrates.

8. Hierarchical organization of surface features in attachment pads may enhance adaptability to real surfaces, which often have fractal roughness.
9. Asymmetrical shape of single contact element (tilted position relative to the support) in combination with proper movements may provide a way to switchable adhesives.
10. Hairy pads show a clearly cut minimum of adhesion at certain ranges of substrate roughness. Such a critical range of roughness depends on the relationship between the diameter of single contact elements of the pad and the length scale of the roughness.
11. During their evolution, plants have developed structures to prevent adhesion of insects. To explain anti-adhesive properties of plants, structured with crystalline waxes, four hypotheses were proposed: (1) roughness hypothesis, (2) contamination hypothesis, (3) wax-dissolving hypothesis, and (4) fluid absorption hypothesis.
12. Since many functional effects found in biological systems are based on fundamental physical principles which are mostly related to the geometry of the structure, they must hold also for artificial surfaces with similar geometry.

---

## References

- Alibardi L (1997) Ultrastructural and autoradiographic analysis of setae development in the embryonic pad lamellae of the lizard *Anolis lineatopus*. *Ann Sci Nat Zool Biol Anim* 18:51
- Arzt E, Gorb SN, Spolenak R (2003) From micro to nano contacts in biological attachment devices. *Proc Natl Acad Sci U S A* 100:10603
- Autumn K, Liang YA, Hsieh ST, Zesch W, Chan WP, Kenny TW, Fearing R (2000) Adhesion force measurements on single gecko setae. *Nature* 405:681
- Autumn K, Sitti M, Liang YA, Peattie AM, Hansen M (2002) Evidence for van der Waals adhesion in gecko setae. *Proc Natl Acad Sci U S A* 99:12252
- Autumn K, Dittmore A, Santos D, Spenko M, Cutkosky M (2006) Frictional adhesion: a new angle on gecko attachment. *J Exp Biol* 209:3569
- Autumn K, Gravish N, Wilkinson M, Santos D, Spenko M, Cutkosky M (2007) Frictional adhesion of natural and synthetic gecko setal arrays. In: *Proceedings of 30th annual meeting adhesion society, Inc, The Adhesion Society, Blacksburg, VA*
- Barnes WJP (2006) Whole animal measurements of shear and adhesive forces in adult tree frogs: insights into underlying mechanisms of adhesion obtained from studying the effects of size and scale. *J Comp Physiol A* 192:1179
- Bauchhens E (1979) Die Pulvillen von *Calliphora erythrocephala* (Diptera, Brachycera) als Adhäsionsorgane. *Zoomorphologie* 93:99
- Betz O (2010) Adhesive exocrine glands in insects: morphology, ultrastructure, and adhesive secretion. In: Byern J, Grunwald I (eds) *Biological adhesive systems. From nature to technical and medical application*. Springer, Vienna, pp 111–152
- Beutel RG, Gorb SN (2001) Ultrastructure of attachment specializations of hexapods (Arthropoda): evolutionary patterns inferred from a revised ordinal phylogeny. *J Zool Syst Evol Res* 39:177
- Beutel RG, Gorb SN (2006) A revised interpretation of the evolution of attachment structures in Hexapoda with special emphasis on Mantophasmatodea. *Arthrop Syst Phylogeny* 64(1):3–25
- Borodich FM, Gorb EV, Gorb SN (2010) Fracture behaviour of plant epicuticular wax crystals and its role in preventing insect attachment: a theoretical approach. *Appl Phys A Mater Sci Process* 100:63

- Breckwoldt WA, Daltorio K, Heepe L, Horschler AD, Gorb SN, Quinn R (2015) Walking inverted on ceilings with wheel-legs and micro-structured adhesives. In: Intelligent robots and systems (IROS), IEEE/RSJ international conference on. IEEE, Hamburg, Germany, pp 3308–3313
- Bullock JMR, Federle W (2011) The effect of surface roughness on claw and adhesive hair performance in the dock beetle *Gastrophysa viridula*. *Insect Sci* 18:298
- del Campo A, Greiner C, Arzt E (2007) Contact shape controls adhesion of bioinspired fibrillar surfaces. *Langmuir* 23:10235
- Chung JY, Chaudhury MK (2005) Roles of discontinuities in bio-inspired adhesive pads. *J R Soc Interface* 2:55
- Creton C, Gorb SN (2007) Sticky feet: from animals to materials. *MRS Bull* 32:466
- Daltorio KA, Gorb SN, Peressadko A, Horschler AD, Ritzmann RE, Quinn RD (2005) A robot that climbs walls using micro-structured polymer feet. In: Proceedings of international conference on climbing and walking robots CLAWAR, London, UK, pp 131–138
- Davies J, Haq S, Hawke T, Sargent JP (2009) A practical approach to the development of a synthetic Gecko tape. *Int J Adhes Adhes* 29:380
- Dening K, Heepe L, Afferrante L, Carbone G, Gorb SN (2014) Adhesion control by inflation: implications from biology to artificial attachment device. *Appl Phys A Mater Sci Process* 116:567
- Edwards JS, Tarkanian M (1970) The adhesive pads of Heteroptera: a re-examination. *Proc Roy Ent Soc Lond A* 45:1
- Eimüller T, Guttman P, Gorb SN (2008) Terminal contact elements of insect attachment devices studied by transmission X-ray microscopy. *J Exp Biol* 211:1958
- Eisner T, Aneshansley DJ (2000) Defense by foot adhesion in a beetle (*Hemisphaerota cyanea*). *Proc Natl Acad Sci U S A* 97:6568
- England MW, Sato T, Yagihashi M, Hozumi A, Gorb SN, Gorb EV (2016) Surface roughness rather than surface chemistry essentially affects insect adhesion. *Beistein J Nanotechnol* 7:1471
- Federle W (2006) Why are so many adhesive pads hairy? *J Exp Biol* 209:2611
- Federle W, Riehle M, Curtis ASG, Full RJ (2002) An integrative study of insect adhesion: Mechanics and wet adhesion of pretarsal pads in ants. *Integr Comp Biol* 42:1100
- Filippov AE, Popov VL, Gorb SN (2011) Shear induced adhesion: Contact mechanics of biological spatula-like attachment devices. *J Thero Biol* 276:126
- Gao H, Wang X, Yao H, Gorb SN, Arzt E (2005) Mechanics of hierarchical adhesion structures of geckos. *Mech Mater* 37:275
- Gaume L, Perret P, Gorb E, Gorb S, Labat J-J, Rowe N (2004) How do plant waxes cause flies to slide? Experimental tests of wax-based trapping mechanisms in three pitfall carnivorous plants. *Arth Struct Dev* 33:103
- Geim AK, Dubonos SV, Grigorieva IV, Novoselov KS, Zhukov AA (2003) Microfabricated adhesive mimicking gecko foot-hair. *Nat Mater* 2:461
- Geiselhardt SF, Geiselhardt S, Peschke K (2009) Comparison of tarsal and cuticular chemistry in the leaf beetle *Gastrophysa viridula* (Coleoptera: Chrysomelidae) and an evaluation of solid-phase microextraction and solvent extraction techniques. *Chemoeology* 19:185
- Geiselhardt SF, Federle W, Prüm B, Geiselhardt S, Lamm S, Peschke K (2010) Impact of chemical manipulation of tarsal liquids on attachment in the Colorado potato beetle, *Leptinotarsa decemlineata*. *J Insect Physiol* 56:398
- Gladun D, Gorb SN, Frantsevich LI (2009) Alternative tasks of the insect arolium with special reference to hymenoptera. In: Gorb SN (ed) Functional surfaces in biology – adhesion related phenomena, vol 2. Springer, Dordrecht/Heidelberg/London/New York, pp 67–103
- Gorb SN (1998) The design of the fly adhesive pad: distal tenent setae are adapted to the delivery of an adhesive secretion. *Proc Roy Soc Lond B* 265:747
- Gorb SN (2000) Biological microtribology: anisotropy in frictional forces of orthopteran attachment pads reflects the ultrastructure of a highly deformable material. *Proc Roy Soc Lond B* 267:1239

- Gorb SN (2001) Attachment devices of insect cuticle. Springer, New York
- Gorb SN (2005) Uncovering insect stickiness: structure and properties of hairy attachment devices. *Amer Ent* 51:31
- Gorb SN (2007) Smooth Attachment Devices in Insects: Functional Morphology and Biomechanics. *Adv In Insect Phys* 34:81
- Gorb SN (2009) Adhesion in nature. In: Brockmann W, Geiß PL, Klingen J, Schröder B (eds) *Adhesive bonding – materials, applications and technology*. Wiley-VCH, Weinheim, pp 346–356
- Gorb SN (2010) Biological and biologically inspired attachment systems. In: Bhushan B (ed) *Springer handbook of nanotechnology*. Springer Verlag, Berlin, pp 1525–1551
- Gorb SN (2011) Biological fibrillar adhesives: functional principles and biomimetic applications. In: da Silva LFM, Öchsner A, Adams RD (eds) *Handbook of adhesion technology*, pp 1409–1436. [https://doi.org/10.1007/978-3-642-01169-6\\_54](https://doi.org/10.1007/978-3-642-01169-6_54)
- Gorb SN, Beutel RG (2001) Evolution of locomotory attachment pads of hexapods. *Naturwissenschaften* 88:530
- Gorb EV, Gorb SN (2002) Attachment ability of the beetle *Chrysolina fastuosa* on various plant surfaces. *Entomol Exp Appl* 105:13
- Gorb EV, Gorb SN (2006) Do plant waxes make insect attachment structures dirty? Experimental evidence for the contamination hypothesis. In: Herrel A, Speck T, Rowe N (eds) *Ecology and biomechanics: a mechanical approach to the ecology of animals and plants*. Taylor & Francis, Boca Raton, pp 147–162
- Gorb SN, Varenberg M (2007) Mushroom-shaped geometry of contact elements in biological adhesive systems. *J Adhes Sci Technol* 21:1175
- Gorb SN, Varenberg M, Peressadko A, Tuma J (2007a) Biomimetic mushroom-shaped fibrillar adhesive microstructure. *J R Soc Interface* 4:271
- Gorb SN, Sinha M, Peressadko A, Daltorio KA, Quinn RD (2007b) Insects did it first: a micro-patterned adhesive tape for robotic applications. *Bioinspir Biomim* 2:S117
- Gorb EV, Hosoda N, Miksch C, Gorb SN (2010) Slippery pores: anti-adhesive effect of nanoporous substrates on the beetle attachment system. *J R Soc Interface* 7:1571
- Gottlieb Binder GmbH & Co KG (2017) <http://www.binder.de/en/products/geckonanoplast/>
- Greiner C, Arzt E, del Campo A (2009) Hierarchical Gecko - Like Adhesives. *Adv Mater* 21:479
- Heepe L, Gorb SN (2014) Biologically inspired mushroom-shaped adhesive microstructures. *Annu Rev Mater Res* 44:173
- Heepe L, Varenberg M, Itovich Y, Gorb SN (2011) Suction component in adhesion of mushroom-shaped microstructure. *J R Soc Interface* 8:585
- Heepe L, Kovalev AE, Varenberg M, Tuma J, Gorb SN (2012) First mushroom-shaped adhesive microstructure: A review. *Thero Appl Mech Lett* 2:014008
- Heepe L, Kovalev AE, Filippov AE, Gorb SN (2013) Adhesion failure at 180 000 frames per second: direct observation of the detachment process of a mushroom-shaped adhesive. *Phys Rev Lett* 111:104301
- Heepe L, Carbone G, Pierro E, Kovalev AE, Gorb SN (2014a) Adhesion tilt-tolerance in bio-inspired mushroom-shaped adhesive microstructure. *Appl Phys Lett* 104:011906
- Heepe L, Kovalev AE, Gorb SN (2014b) Direct observation of microcavitation in underwater adhesion of mushroom-shaped adhesive microstructure. *Beilstein J Nanotechnol* 5:903
- Heepe L, Wolff JO, Gorb SN (2016) Influence of ambient humidity on the attachment ability of ladybird beetles (*Coccinella septempunctata*). *Beilstein J Nanotechnol* 7:1332
- Heepe L, Raguseo S, Gorb SN (2017a) An experimental study of double-peeling mechanism inspired by biological adhesive systems. *Appl Phys A Mater Sci Process* 123:124
- Heepe L, Petersen DS, Tölle L, Wolff JO, Gorb SN (2017b) Sexual dimorphism in the attachment ability of the ladybird beetle *Coccinella septempunctata* on soft substrates. *Appl Phys A Mater Sci Process* 123:34
- Hiller U (1968) Untersuchungen zum Feinbau und zur Funktion der Haftborsten von Reptilien. *Z Morphol Tiere* 62:307

- Homann H (1957) Haften Spinnen an einer Wasserhaut? *Naturwissenschaften* 44:318
- Huber G, Gorb SN, Spolenak R, Arzt E (2005a) Resolving the nanoscale adhesion of individual gecko spatulae by atomic force microscopy. *Biol Lett* 1:2
- Huber G, Mantz H, Spolenak R, Mecke K, Jacobs K, Gorb SN, Arzt E (2005b) Evidence for capillarity contributions to gecko adhesion from single spatula nanomechanical measurements. *Proc Natl Acad Sci U S A* 102:16293
- Hui CY, Glassmaker NJ, Tang T, Jagota A (2004) Design of biomimetic fibrillar interfaces: 2. Mechanics of enhanced adhesion. *J R Soc Interface* 1:35
- Ishii S (1987) Adhesion of a Leaf Feeding Ladybird *Epilachna vigintioctomaculata* (Coleoptera: Coccinellidae) on a Virtically Smooth Surface. *Appl Entomol Zool* 22:222
- Israelachvili JN (1992) Intermolecular and surface forces: With Applications to Colloidal and Biological Systems, 2nd edn. Academic, London
- Jagota A, Bennison SJ (2002) Mechanics of adhesion through a fibrillar microstructure. *Integr Comp Biol* 42:1140
- Jagota A, Hui C-Y (2011) Adhesion, friction, and compliance of bio-mimetic and bio-inspired structured interfaces. *Mater Sci Eng R Rep* 72:253
- Johnson KL, Kendall K, Roberts AD (1971) Surface energy and the contact of elastic solids. *Proc R Soc Lond A* 324:301
- Kampermann M, Kroner E, del Campo A, McMeeking RM, Arzt E (2010) Functional Adhesive Surfaces with “Gecko” Effect: The Concept of Contact Splitting. *Adv Eng Mater* 12:335
- Kasem H, Varenberg M (2013) Effect of counterface roughness on adhesion of mushroom-shaped microstructure. *J R Soc Interface* 10:20130620
- Kendall K (1975) Thin-film peeling-the elastic term. *J Phys D Appl Phys* 8:1449
- Kesel AB, Martin A, Seidl T (2003) Adhesion measurements on the attachment devices of the jumping spider *Evarcha arcuata*. *J Exp Biol* 206:2733
- Kim TW, Bhushan B (2007) Adhesion analysis of multi-level hierarchical attachment system contacting with a rough surface. *J Adhes Sci Technol* 21:1
- Kim S, Sitti M (2006) Biologically inspired polymer microfibers with spatulate tips as repeatable fibrillar adhesives. *Appl Phys Lett* 89:26911
- Kizilkan E, Heepe L, Gorb SN (2013) Underwater adhesion of mushroom-shaped adhesive microstructure: an air-entrapment effect. In: *Biological and Biomimetic Adhesives: Challenges and Opportunities*. RCS, Cambridge, pp 65–71
- Kizilkan E, Struaben J, Staubitz A, Gorb SN (2017) Bioinspired photocontrollable microstructured transport device. *Sci Robotics* 2:eak9454
- Kosaki A, Yamaoka R (1996) Chemical composition of footprints and cuticula lipids of three species of lady beetles. *Jpn J Appl Entomol Zool* 40:47
- Kovalev AE, Varenberg M, Gorb SN (2012) Wet versus dry adhesion of biomimetic mushroom-shaped microstructures. *Soft Matter* 8:7560
- Kwak MK, Pang C, Jeong HE, Kim HN, Yoon H, Jung HS, Suh KY (2011) Towards the next level of bioinspired dry adhesives: new designs and applications. *Adv Funct Mater* 21:3606
- Langer MG, Ruppertsberg JP, Gorb SN (2004) Adhesion forces measured at the level of a terminal plate of the fly's seta. *Proc R Soc Lond B* 271:2209
- Murphy MP, Aksak B, Sitti M (2007) Adhesion and anisotropic friction enhancements of angled heterogeneous micro-fiber arrays with spherical and spatula tips. *J Adhes Sci Tech* 21:1281
- Niederegger S, Gorb SN (2003) Tarsal movements in flies during leg attachment and detachment on a smooth substrate. *J Insect Physiol* 49:611
- Niederegger S, Gorb SN (2006) Friction and adhesion in the tarsal and metatarsal scopulae of spiders. *J Comp Physiol A* 192:1223
- Niederegger S, Gorb SN, Vötsch W (2001) Fly walking: a compromise between attachment and motion? In: *Wisser A, Nachtigall W (eds) Technische Biologie und Bionik. 5. Bionik – Kongress, Dessau 2000*. Gustav Fisher Verlag, Stuttgart/Jena/Lübeck/Ulm, pp 327–330
- Niewiarowski PH, Lopez S, Ge L, Hagan E, Dhinojwala A (2008) Sticky gecko feet: the role of temperature and humidity. *PLoS One* 3:e2192

- 876 Northen MT, Turner KL (2005) A batch fabricated biomimetic dry adhesive. *Nanotechnology*  
877 16:1159
- 878 Peattie AM, Full RJ (2007) Phylogenetic analysis of the scaling of wet and dry biological fibrillar  
879 adhesives. *Proc Natl Acad Sci U S A* 104:18595
- 880 Peisker H, Gorb SN (2012) Evaporation dynamics of tarsal liquid footprints in flies (*Calliphora*  
881 *vicina*) and beetles (*Coccinella septempunctata*). *J Exp Biol* 215:1266
- 882 Peisker H, Michels J, Gorb SN (2013) Evidence for a material gradient in the adhesive tarsal setae of  
883 the ladybird beetle *Coccinella septempunctata*. *Nat Commun* 4:1661
- 884 Peisker H, Heepe L, Kovalev AE, Gorb SN (2014) Comparative study of the fluid viscosity in tarsal  
885 hairy attachment systems of flies and beetles. *J R Soc Interface* 11:20140752
- 886 Pelletier Y, Smilowitz Z (1987) Specialized tarsal hairs on adult male Colorado potato beetles,  
887 *Leptinotarsa decemlineata* (Say), hamper its locomotion on smooth surfaces. *Can Entomol*  
888 119:1139
- 889 Peressadko A, Gorb SN (2004a) When less is more: experimental evidence for tenacity enhance-  
890 ment by division of contact area. *J Adhes* 80:247
- 891 Peressadko A, Gorb SN (2004b) Surface profile and friction force generated by insects. In:  
892 Fortschritt-Berichte VDI, Boblan I, Bannasch R (eds) Surface profile and friction force gener-  
893 ated by insects, vol 249[15]. VDI Verlag, Düsseldorf, pp 257–263
- 894 Persson BNJ (2003) On the mechanism of adhesion in biological systems. *J Chem Phys* 118:7614
- 895 Persson BNJ (2014) On the fractal dimension of rough surfaces. *Tribol Lett* 54:99
- 896 Persson BNJ, Gorb SN (2003) The effect of surface roughness on the adhesion of elastic plates with  
897 application to biological systems. *J Chem Phys* 119:11437
- 898 Popov VL (2010) Contact mechanics and friction: physical principles and applications. Springer-  
899 Verlag, Berlin
- 900 Prowse MS, Wilkinson M, Puthoff JB, Mayer G, Autumn K (2011) Effects of humidity on the  
901 mechanical properties of gecko setae. *Acta Biomater* 7:733
- 902 Pugno NM (2011) The theory of multiple peeling. *Int J Fract* 171:185
- 903 Pugno NM, Gorb SN (2009) Functional mechanism of biological adhesive systems described by  
904 multiple peeling approach. In: Proceedings of the 12th international conference on fracture, July  
905 1217, Ottawa
- 906 Puthoff JB, Prowse MS, Wilkinson M, Autumn K (2010) Changes in materials properties explain  
907 the effects of humidity on gecko adhesion. *J Exp Biol* 213:3699
- 908 Richards AG, Richards PA (1979) The cuticular protuberances of insects. *Int J Insect Morphol*  
909 *Embryol* 8:143
- 910 Rizzo NW, Gardner KH, Walls D, Keiper-Hrynko JNM, Ganzke TS, Hallahan DL (2006) Charac-  
911 terization of the structure and composition of gecko adhesive setae. *J R Soc Interface* 3:441
- 912 Röhl B (1995) Epidermal fine structure of the toe tips of *Sphaerodactylus cinereus* (Reptilia,  
913 Gekkonidae). *J Zool* 235:289
- 914 Ruibal R, Ernst V (1965) The structure of the digital setae of lizards. *J Morphol* 117:271
- 915 Russell AP (1975) A contribution to the functional analysis of the foot of the Tokay, *Gekko gekko*  
916 (Reptilia: Gekkonidae). *J Zool (Lond)* 176:437
- 917 Sameoto D, Menon C (2010) Recent advances in the fabrication and adhesion testing of biomimetic  
918 dry adhesives. *Smart Mater Struct* 19:103001
- 919 Schargott M (2009) A mechanical model of biomimetic adhesive pads with tilted and hierarchical  
920 structures. *Bioinspir Biomim* 4(026002):9
- 921 Scherge M, Gorb SN (2001) Biological micro- and nanotribology: nature's solutions. Springer,  
922 Berlin
- 923 Schleich HH, Kastle W (1986) Ultrastrukturen an Gecko-Zehen (reptilia: sauria: gekkonidae).  
924 *Amphibia-Reptilia* 7:141
- 925 Sitti M, Fearing RS (2003) Synthetic gecko foot-hair micro/nano-structures as dry adhesives. *J*  
926 *Adhes Sci Technol* 17:1055
- 927 Smith JM, Barnes WJP, Downie JR, Ruxton GD (2006) Structural correlates of increased adhesive  
928 efficiency with adult size in the toe pads of hylid tree frogs. *J Comp Physiol A* 192:1193

- Spolenak R, Gorb SN, Gao H, Arzt E (2005) Effects of contact shape on the scaling of biological attachments. *Proc R Soc Lond A* 461:305
- Stork NE (1980a) Experimental analysis of adhesion of *Chrysolina polita* (Chrysomelidae: Coleoptera) on a variety of surfaces. *J Exp Biol* 88:91
- Stork NE (1980b) A scanning electron microscope study of tarsal adhesive setae in the Coleoptera. *Zool J Linnean Soc* 68:173
- Stork NE (1983) A comparison of the adhesive setae on the feet of lizards and arthropods. *J Nat Hist* 17:829
- Tang T, Hui CY (2005) Can a fibrillar interface be stronger and tougher than a non-fibrillar one? *J R Soc Interface* 2:505
- Varenberg M, Gorb SN (2008a) A beetle-inspired solution for underwater adhesion. *J R Soc Interface* 5:383
- Varenberg M, Gorb SN (2008b) Close-up of mushroom-shaped fibrillar adhesive microstructure: contact element behaviour. *J R Soc Interface* 5:785
- Varenberg M, Gorb SN (2008c) Shearing of fibrillar adhesive microstructure: friction and shear-related changes in pull-off force. *J R Soc Interface* 4:721
- Varenberg M, Pugno NM, Gorb SN (2010) Spatulate structures in biological fibrillar adhesion. *Soft Matter* 6:3269
- Varenberg M, Murarash B, Kligermann Y, Gorb SN (2011) Geometry-controlled adhesion: revisiting the contact splitting hypothesis. *Appl Phys A Mater Sci Process* 103:933
- Voigt D, Schuppert JM, Dattinger S, Gorb SN (2008) Sexual dimorphism in the attachment ability of the Colorado potato beetle *Leptinotarsa decemlineata* (Coleoptera: Chrysomelidae) to rough substrates. *J Insect Physiol* 54:765
- Vötsch W, Nicholson G, Müller R, Stierhof Y-D, Gorb SN, Schwarz U (2002) Chemical composition of the attachment pad secretion of the locust *Locusta migratoria*. *Insect Biochem Mol Biol* 32:1605
- Walker G, Yulf AB, Ratcliffe J (1985) The adhesive organ of the blowfly, *Calliphora vomitoria*: a functional approach (Diptera: Calliphoridae). *J Zool (Lond)* 205:297
- Wigglesworth VB (1987) How does a fly cling to the under surface of a glass sheet? *J Exp Biol* 129:373
- Wolff JO, Gorb SN (2011) The influence of humidity on the attachment ability of the spider *Philodromus dispar* (Araneae, Philodromidae). *Proc R Soc London, Ser B* 279:139
- Wolff JO, Gorb SN (2012) Surface roughness effects on attachment ability of the spider *Philodromus dispar* (Araneae, Philodromidae). *J Exp Biol* 215:179
- Wolff JO, Gorb SN (2016) Attachment structures and adhesive secretions in arachnids. Springer, Berlin
- Yurdumakan B, Ravavikar NR, Ajayan PM, Dhinojwala A (2005) Synthetic gecko foot-hairs from multiwalled carbon nanotubes. *Chem Commun* 16041421:3799

Ambrose C. Taylor

## Contents

56.1	Introduction .....	1678
56.1.1	Nanotechnology .....	1678
56.1.2	Nanoparticle Reinforcement .....	1679
56.2	Nanoparticles .....	1680
56.2.1	Nanoparticles Definition .....	1680
56.2.2	Equi-Axed Nanoparticles .....	1680
56.2.3	Nanotubes and Nanofibers .....	1681
56.2.4	Plate-like Nanoparticles .....	1683
56.2.5	Other Nanoparticles .....	1683
56.3	Manufacturing Using Nanoparticles .....	1684
56.3.1	Dispersion .....	1684
56.3.2	Mixing .....	1685
56.3.3	Sonication .....	1686
56.3.4	Alignment .....	1686
56.4	Properties of Nanoparticle-Modified Polymers .....	1687
56.4.1	Mechanical Properties .....	1687
56.4.2	Functional Properties .....	1688
56.4.3	Electrical Properties .....	1690
56.4.4	Fracture Toughness .....	1691
56.4.5	Fatigue Performance .....	1694
56.4.6	Peel and Lap-Shear Performance .....	1696
56.5	Conclusions .....	1696
References	.....	1697

A. C. Taylor (✉)

Department of Mechanical Engineering, Imperial College London, London, UK

e-mail: [a.c.taylor@imperial.ac.uk](mailto:a.c.taylor@imperial.ac.uk)



## Abstract

The increased commercial availability and the reduced prices of nanoparticles are leading to their incorporation in polymers and structural adhesives. This chapter outlines the principal types of nanoparticles, and the methods that may be used to disperse the particles in a polymer matrix. It discusses how nanoparticles can alter the mechanical properties (e.g., stiffness), electrical properties (e.g., conductivity), functional properties (e.g., permeability, glass transition temperature), and fracture performance of thermoset polymers. The effect of nanoparticles on joint performance is also discussed.

## 56.1 Introduction

### 56.1.1 Nanotechnology

It can be argued that nanotechnology is not new, as the use of nanoparticles to alter the properties of materials is not a recent development. For example, the late Roman (fourth century AD) Lycurgus cup is on display in London at the British Museum. This cup is made of cut glass, and looks green in reflected light, but appears red when light is shone through it. This effect is due to the light being scattered by the colloidal dispersion of gold and silver nanoparticles, which are about 70 nm in diameter, in the glass. Another example is carbon black, as used currently in millions of car tires and printer cartridges per year, which is composed of particles of size 20 nm and above. However, this material was first produced 3,500 years ago in China as lamp black.

Nanotechnology has become a hot topic in science and engineering in recent years. One of the definitive points in the history of nanotechnology came in a lecture by Richard Feynman, in 1959, entitled “There Is Plenty of Room at the Bottom” (Feynman 1959). In this lecture, Feynman highlighted the potential of working at a micro- or nanoscale, and discussed the problem of manipulating and controlling things on a small scale. He issued a challenge to scientists (and engineers) to work at very small scales, and this challenge is now being taken up.

So what is nanotechnology? Nanotechnology could be defined as the combination of existing technologies with the ability to observe and manipulate at the nanometer ( $10^{-9}$  m) scale (Hay and Shaw 2001; Harper 2003). The question is then, why is there so much interest in nanotechnology now? It is linked to (a) the expanding ability to synthesize nanometer-scale materials, and (b) the availability of the tools that enable the imaging of structures at this scale. Thus, it is now possible to characterize how nanoparticles are dispersed and start to understand why the observed effects occur, something that was not possible for the Romans. As the limits of the nanoscale, say at scales of less than 20 nm, are approached then different effects, such as quantum effects, become more significant.

A major concern with the use of nanoparticles is their potential toxicity. Care must be taken not to repeat the health problems caused by exposure to asbestos. Stories of potential catastrophe such as Michael Crichton’s book “Prey” and Prince Charles’ “grey goo” speech have not helped the perception of nanoparticles and nanotechnology

(Radford 2003). Hence, manufacturers are approaching this new technology cautiously. Studies are underway to assess the health effects and some results have been published (e.g., Lam et al. 2004; Warheit et al. 2004; Brown et al. 2007), but as yet there is no real agreement on the real dangers to health due to inhaling nanoparticles. It must be borne in mind that the nanoparticles in cured adhesives are not free in the atmosphere, but are bound into a matrix. Recent studies indicate that even during fracture of a nanoparticle-modified epoxy material, only a few nanoparticles are released into the atmosphere. In contrast, nanoparticles are produced in large quantities by the combustion of fossil fuels, and millions of tonnes of nano- and submicron-particles are already in use by various industries including in paints and toiletries.

### 56.1.2 Nanoparticle Reinforcement

Five basic characteristics of particulate fillers were defined by Rotheron and Hancock (1995). These remain true whether the particles are micro- or nanoparticles:

1. What properties are being sought?
2. What deleterious changes may also occur and can they be tolerated?
3. How easy is the filler to handle and how might it affect processing?
4. Are any special additives needed?
5. What is the true cost of using the filler, is it justifiable and are there more cost-effective alternatives?

Rotheron and Hancock (1995) observed that it is widely assumed that fillers are cheap and that polymers are expensive. Conversely, for nanoparticles it is widely assumed that nanoparticles are expensive and that polymers are cheap. This is not necessarily the case. As the nanoparticle manufacturing industry expands, nanoparticles are increasingly available in large (i.e., tonne) quantities. The prices of expensive nanoparticles such as carbon nanotubes are also being reduced. The price of nanoparticles varies greatly with the type, as well as with the purity of the material. For example, silica nanoparticles supplied dispersed as a masterbatch in epoxy cost about \$20/kg (Nanoresins 2008), and core-shell rubber nanoparticles similarly dispersed cost approximately \$12/kg (Kaneka 2008). Nanoclays can cost as little as \$7/kg (SigmaAldrich 2008). However, a kilogram of carbon nanotubes cost between \$400 and \$98,000 in Autumn 2009 (CheapTubes 2009).

Nanoparticles are, by definition, very small. It must be noted that the interparticle distance for nanoparticle-modified polymers is also very small, especially at high volume fractions. These factors may affect the interaction between a particle and its neighbors, or between a particle and the polymer surrounding it, or may affect the structure of the polymer itself. Hence, the properties of a particle-modified polymer may vary depending whether nanoparticles or microparticles are used.

The addition of nanoparticles can be simply a marketing tool, as the performance benefit that they provide could often be obtained using conventional fillers at a much lower cost. However, some very successful applications that rely on the small size

of nanoparticles have been shown, for example, the addition of ceramic nanoparticles to transparent coatings gives improved scratch resistance without loss of transparency. Nanoparticles have also been used in sporting goods, for example, carbon nanotubes in tennis racket or bicycle frames, and ski poles that use a glass fiber composite with silica nanoparticles.

## **56.2 Nanoparticles**

### **56.2.1 Nanoparticles Definition**

The common definition of a nanoparticle is that it has at least one dimension in the nanometer range. Indeed, the term “nano” has virtually replaced “submicron,” even when the latter is more appropriate. A search of the scientific literature published in the last 5 years yields more than 60,000 articles per year that mention “nano,” but less than 3,000 papers per year that mention “submicro” (of which almost a third mention “nano” as well). Nanoparticles are characterized by a large surface area to volume ratio. They can be made from a wide range of materials – metallic (e.g., gold, silver), ceramic (e.g., silica, alumina, layered silicates, silicon carbide), or organic (e.g., carbon black, rubber particles, graphene, carbon nanotubes, and nanofibers). Due to the small size of nanoparticles, the numbers present in nanoparticle-modified materials are enormous. For example, there are approximately  $10^{17}$  individual particles in 1 kg of 20 nm silica nanoparticles.

As many nanoparticles are smaller than the wavelength of light (about 400–700 nm), they appear translucent when added to a translucent polymer. A consequence of this is that they are too small to be seen using optical microscopy, but can be imaged by high-magnification techniques, such as transmission electron microscopy (TEM), atomic force microscopy (AFM), and field emission gun scanning electron microscopy (FEGSEM). The structure of nanoparticles can also be characterized using X-ray diffraction or other techniques (Wang 2001). Because the particles are so small, it is not normally possible to measure their mechanical properties, and hence these are assumed to be the same as for the bulk material, or equal to those of a similar material. For many applications, such as the prediction of the mechanical properties of nanoparticle-modified materials, this appears to be a reasonable assumption.

As with micron-sized fillers, the particle shape and aspect ratio are important in determining the properties of nanoparticle-modified materials, such as stiffness, flow characteristics, tensile strength, etc. The aggregation and dispersion of the particles are also important, and may also affect the properties. Nanoparticles can be classified by their shape, as equi-axed (e.g., spherical), rod-like, and plate-like. These classes will be discussed in turn.

### **56.2.2 Equi-Axed Nanoparticles**

Most equi-axed nanoparticles are spherical, but irregular particles are also available. The common particles are metallic (e.g., gold, silver), ceramic (e.g., silica, alumina,

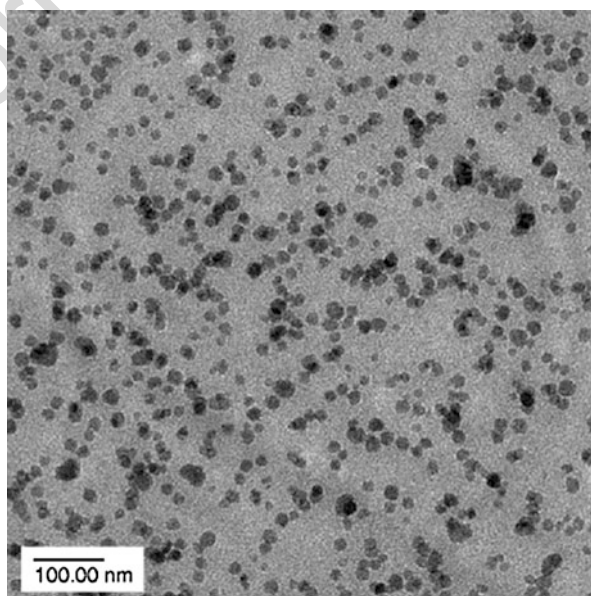
titania), or organic (e.g., rubber particles, fullerenes). The ceramic particles are typically prepared by sol-gel or flame-spraying methods; silica and alumina are commonly used with adhesives, see Fig. 1. Rubber particles are typically core-shell particles, with a soft core and a hard shell of a polymer such as poly(methyl methacrylate).

### 56.2.3 Nanotubes and Nanofibers

The rod-like nanoparticles that are commonly discussed in the scientific literature are carbon nanotubes. Carbon nanofibers (CNFs), which have a larger diameter, are also available. They are cheaper and are available in much larger quantities than carbon nanotubes. Ceramic nanotubes (e.g., zirconia, tungsten disulfide) or whiskers (e.g., silicon nitride, silicon carbide, alumina) can also be used.

Carbon nanotubes were first reported by Iijima (1991; Iijima and Ichihashi 1993), and are effectively sheets of graphite rolled into tubes. They are produced by chemical vapor deposition (CVD), electric arc, or laser ablation processes (Harris 1999, 2009). These techniques produce nanotubes with different lengths, straightness, purities, and degrees of entanglement. Hence, the nanotubes require purification to remove the amorphous carbon that is also produced, typically by heating them in a mixture of nitric and sulfuric acid (Gojny et al. 2003). CVD is becoming the most popular method for producing relatively large quantities of nanotubes relatively cheaply. In this technique, the nanotubes are grown on a ceramic substrate,

**Fig. 1** Transmission electron micrograph of silica nanoparticles in epoxy (Courtesy S. Sprenger)



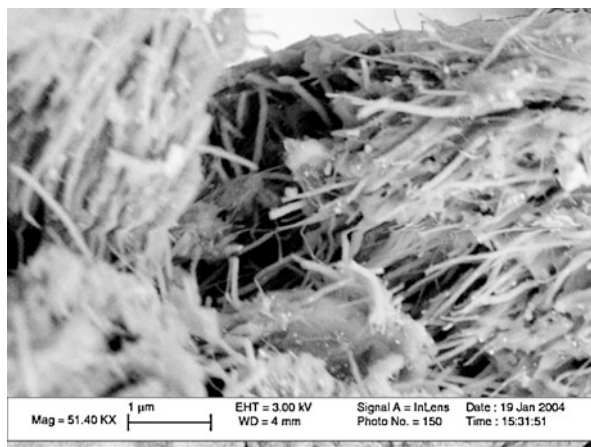
rather like the bristles of a brush. The length of the nanotubes can be controlled, and they have a relatively low degree of entanglement.

There are two principal types of carbon nanotubes. Firstly, single-walled nanotubes (SWNTs) have a single graphene layer rolled into a tube typically 1–2 nm in diameter, with hemispherical end caps (Iijima and Ichihashi 1993; Tjong 2006). Secondly, multiwalled nanotubes (MWNTs) are comprised of a number of coaxial graphene tubes, each with an end cap. The outer diameter of a MWNT is typically 3–10 nm. Under tension, only the outer layer of a MWNT carries the load as the van der Waals forces between the layers are too weak to transfer stress to the inner layers (Lau et al. 2004). Variants such as double-walled nanotubes (DWNTs) are also available. The length of nanotubes varies significantly, but they can be as long as several millimeters (Chakrabarti et al. 2006). Hence, nanotubes can possess very large aspect ratios. Their modulus has been measured to be up to 1 TPa, with strengths of up to 150 MPa (Demczyk et al. 2002), although they are rather flexible normal to their axis (Saito et al. 1998). However, it is difficult to adhere the tubes to a matrix, and hence surface treatments are used to activate the surface, which can weaken the tubes. The electrical properties of nanotubes vary from metallic to semiconducting depending on their chirality.

Vapor-grown carbon nanofibers do not have such a high aspect ratio as carbon nanotubes, and have more defects. However, they are significantly cheaper and available in much larger quantities. The nanofibers are typically 50–200 nm in diameter and 30–100  $\mu\text{m}$  long (Green et al. 2006; Zhou et al. 2007), as shown in Fig. 2.

Ceramic whiskers have been produced for many years, as reported by Gordon (1978), though their use in epoxies seems to be limited. However, aluminum borate whiskers have been combined with thermoset polymer matrices by Liang and coworkers (Liang and Hu 2004; Tang et al. 2007). Ceramic nanotubes have been produced by coating carbon nanotubes with silicon carbide (Morisada et al. 2007). Silicon carbide nanofibers, which can be about 40 nm in diameter with lengths of up to several hundred microns, have also been produced (Zhu et al. 2002; Bechelany et al. 2007).

**Fig. 2** Scanning electron micrograph of carbon nanofibers in an epoxy matrix, showing fractured surface (Courtesy J. H. Lee)



## 56.2.4 Plate-like Nanoparticles

A range of plate-like nanoparticles have been used with polymer matrices, including layered silicate nanoclays (e.g., montmorillonite), graphite, and  $\alpha$ -zirconium phosphate. Generally, these particles are comprised of stacks of platelets that are intercalated or exfoliated by the polymer during processing. The resulting morphology is typically described as “particulate” (or “conventional”), “intercalated” or “exfoliated,” as identified by wide-angle X-ray scattering (WAXS). These microstructures are shown schematically in Fig. 3 for a nanoclay-modified polymer. In an intercalated microstructure, polymer chains enter the galleries between the platelets and increase the measured spacing (Schadler 2003). For an exfoliated nanocomposite, the platelets are pushed further apart, and the spacing becomes too large to measure using WAXS. Note that an exfoliated structure may be described as “ordered” or “disordered,” as shown in Fig. 3, but the fully disordered exfoliated structure is relatively rare. For a particulate structure, the particles remain unchanged.

Nanoclays (e.g., montmorillonite, hectorite) are layered silicates with a structure of stacked platelets similar to that of mica. The platelet thickness is approximately 1 nm and the lateral dimensions of the plates can vary from 30 nm to tens of microns. Hence, the platelets have a high aspect ratio. The layers have a regular van der Waals gap in-between them, called the “interlayer” or the “gallery” (Alexandre and Dubois 2000). These nanoclays are hydrophilic, and hence are typically surface-treated using long chain alkylammonium compounds to make them organophilic. The stacks of platelets can be readily delaminated by organic molecules to form an intercalated or exfoliated structure.

Natural graphite has also been used. A combination of chemical and thermal treatments can generate exfoliated graphite platelets with a thickness of 20–100 nm. Here, the graphite is intercalated by an acid treatment, followed by exfoliation by a thermal shock at a temperature of around 600 °C. The platelet diameter is in the order of 10  $\mu\text{m}$ , and hence these platelets have a high aspect ratio (Yasmin and Daniel 2004; Yasmin et al. 2006b).

## 56.2.5 Other Nanoparticles

Carbon black is mostly an aciniform (grape-like cluster) particulate, which is produced by the incomplete combustion of oil. The current worldwide production

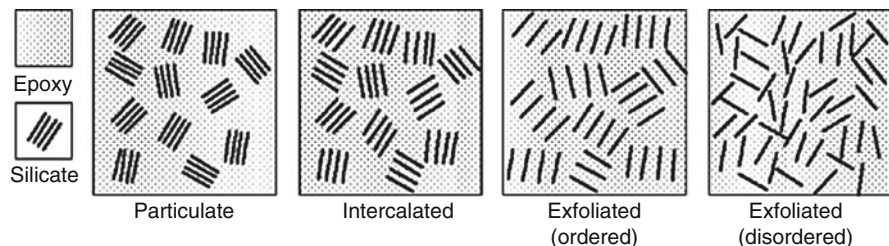


**Fig. 3** Microstructures of nanoclay-modified polymers



is 8.1 million tonnes per year. It is very common as a pigment in inks and toners, and as a functional filler in tires and rubber products (ICBA 2008).

## 56.3 Manufacturing Using Nanoparticles

### 56.3.1 Dispersion

To obtain the best properties from a nanoparticle-modified polymer, it is considered that the nanoparticles should be well dispersed, and each particle should be properly wetted by the polymer. If agglomerates are formed instead, these can act as defects resulting in a reduction in performance rather than any enhancement. This is a major challenge when preparing adhesive formulations.

Dispersing nanoparticles is difficult due to their high surface area and incompatibility with the matrix polymer. Generally, a surface treatment or compatibilizer is required, and once agglomeration occurs it is very difficult to break up the agglomerates. Hence, particles that are supplied pre-dispersed in a resin (e.g., Nanopox from Nanoresins, or the MX range of core-shell particles from Kaneka) are popular with formulators. However, there is no guarantee that this good initial dispersion will remain after subsequent processing. For example, the addition of a liquid rubber, which phase-separates during curing, to some systems can cause the nanoparticles to agglomerate (Mohammed 2007; Hsieh et al. 2010). Although it is normally assumed that good dispersion is required, small agglomerates do not necessarily adversely affect the performance of such systems.

Assessing the quality of the dispersion of nanoparticles is difficult, as the techniques that can identify particles at the nanoscale such as AFM and TEM involve lengthy specimen preparation. Only a very small volume of the sample can be studied using these techniques, and hence the results may not be representative of the material as a whole. Alternatively, X-ray diffraction can be used, as this technique can analyze a larger volume. However, the data do not characterize how well the particles are dispersed. It is normally suggested that dispersion should be assessed at three size scales – (a) optically, (b) by scanning electron microscopy, and (c) by transmission electron microscopy. If the results from all three techniques indicate a good dispersion of nanoparticles, then it is fairly safe to assume that this is the case. Many authors agree that using optical microscopy is useful to investigate the dispersion of nanoparticles as it highlights the presence of agglomerates (e.g., Hackman and Hollaway 2006; Brooker et al. 2008), although individual nanoparticles will not be visible. Quantitative methods to assess dispersion, using the gray scale of images or by a quadrat method, are being developed (Brooker et al. 2010).

It should be noted that even small volume fractions of nanoparticles involve huge numbers of nanoparticles and very small interparticle distances. Shaffer and Kinloch (2004) point out that one major difficulty with small diameter nanotubes is that they become increasingly difficult to wet. By trivial estimation, even a 1 vol% loading of single-walled nanotubes ensures that all of the polymer molecules are within one

radius of gyration (say 5 nm) of a nanotube. This result implies that complete wetting of high loading fractions of single-walled nanotubes will be difficult, at least by conventional means, and that even more modest concentrations may be brittle and hard to process due to the constraint of the matrix (Shaffer and Kinloch 2004).

The chemical functionalization of the nanoparticles' surface can help improve dispersion, as it can reduce agglomeration, and can also improve the bonding between the particle and the matrix (Gojny et al. 2003; Kathi and Rhee 2008).

### 56.3.2 Mixing

If nanoparticles are supplied well dispersed in a polymer, then simple mixing is often enough to blend the particles into an adhesive formulation (e.g., Kinloch et al. 2005). Low-shear mixing is also sufficient for well-compatibilized systems, as the thermodynamics of these materials can ensure a good dispersion. However, if nanoparticles are supplied as an untreated powder they will generally be agglomerated, and these agglomerates must be broken down during processing. Low-shear mixing alone will not break up these agglomerates. High-power dispersion methods, such as high-shear mixing and sonication, are the easiest methods to improve the dispersion of nanoparticles in polymers (Xie et al. 2005).

In a multicomponent system such as a structural adhesive, the polymer component into which the nanoparticles are introduced does not generally cause a noticeable difference in the final morphology (Hackman and Hollaway 2006; Brooker et al. 2008). However, the morphology may be dependent on the cure time and temperature; plus the temperature, time, and shear rate used for mixing.

For carbon nanotubes, Fiedler et al. (2006) report that the size and shape of the impeller and the mixing speed control the dispersion. Intensive stirring of MWNTs in epoxy resin can achieve a relatively good dispersion. However, reagglomeration occurs due to frictional contacts and elastic interlocking mechanisms (Schmid and Klingenberg 2000). SWNTs have a greater tendency to reagglomerate than MWNTs, and hence higher shear forces are required to achieve a reasonable dispersion.

High-shear mixing can be achieved using a range of techniques. Hackman and Hollaway (2006) compared low-shear mixing to the use of a grinding media mill, filled with 2 mm diameter glass beads. Green et al. (2006) compared low-shear mixing to high-shear mixing generated by extrusion of a nanoparticle-modified epoxy resin through a small orifice. In both cases, the high-shear method gave better dispersion. Glass beads have been shown to break down agglomerated nanoclay particles to form a uniform material. However, although neither work evaluated the dispersion at the nanometer-scale using microscopy, differences could be seen at the microscale (Hackman and Hollaway 2006).

A three-roll mill (or calender) has been used by Yasmin et al. to disperse nanoclay in epoxy (Yasmin et al. 2003; Yasmin et al. 2006a), and by Gojny et al. to disperse nanotubes in epoxy (Gojny et al. 2004). This method is commonly used to disperse microparticles in polymers (Fiedler et al. 2006). As it is not a continuous process, the material was collected and fed back into the mill after each pass. The authors



assumed that the dispersion was achieved (a) by the shear forces generated between the dispersing of the particles as smaller tactoids, and (b) by the combined shear and diffusion processes facilitating the separation and penetration of polymer between the clay platelets (Yasmin et al. 2003; Yasmin et al. 2006a). This process requires a relatively viscous material, and hence is suitable for higher loadings of nanoparticles. According to Fiedler et al. (2006), a major advantage of this method is that it allows the efficient manufacturing of larger quantities of nanocomposites, as the nanoparticle-modified polymer requires only minutes of processing. By comparison, low-shear methods may require processing times of hours.

### 56.3.3 Sonication

Sonication uses an ultrasonic bath or probe to apply sound energy to a liquid that contains particles. Many authors combine sonication and mixing, especially when using probe sonicators as the power is directed into only a small volume, and the low-shear forces do not generally ensure that all of the polymer passes through this volume. The combination of probe sonication with high-speed mixing has been reported to be a relatively successful way to disperse nanoparticles. This technique has been used with nanoclays in epoxy resin (Zunjarrao et al. 2006) and in polyimide (Gintert et al. 2007). It has also been used with carbon nanotubes in epoxy (Sandler et al. 1999).

The very localized introduction of energy from probe sonication leads to a considerable amount of damage, including buckling, bending, dislocations, and rupture of carbon nanotubes (Lu et al. 1996; Fiedler et al. 2006). It will also cause local heating of the sample, and hence if sonication is undertaken with a curing agent or initiator present it may be necessary to cool the sample to prevent premature curing (Lu et al. 1996). The use of an ultrasonic bath reduces the energy density and alleviates some of these problems, but the time taken to achieve a reasonable dispersion is much greater (Brooker et al. 2008).

The processing time can affect the size of nanoclay agglomerates (Lam et al. 2005). However, the d-spacing (the distance between the nanoclay platelets) was unaffected by the sonication time, and hence exfoliation of the nanoclay could not be achieved using sonication. Gintert et al. (2007) also found that sonication was an important step in breaking up nanoclay agglomerates.

### 56.3.4 Alignment

The properties of composites are generally improved by the alignment of the fibers, although this does produce an anisotropic material. It is also possible to align nanoparticles. This is generally achieved by physical means, for example, by application of a force, cutting, extrusion, or drawing (e.g., Ajayan et al. 1994; Baik et al. 2005). Alignment can also be achieved using the application of magnetic or electric fields, with carbon nanotubes (e.g., Chen et al. 2001; Martin et al. 2005),

and with layered silicates (e.g., Koerner et al. 2005). For more information on the alignment of carbon nanotubes, and their dispersion, see the review by Xie et al. (2005).

## 56.4 Properties of Nanoparticle-Modified Polymers

### 56.4.1 Mechanical Properties

The addition of high modulus particles increases the modulus of a polymeric material, independent of the particle size; although the stiffening effect may be higher for particles with larger aspect ratios. There are many theoretical models available to predict the modulus of particle-modified polymers, such as the Halpin-Tsai and Mori-Tanaka models (e.g., Ahmed and Jones 1990). These models have been shown to broadly apply for nanoparticle-modified polymers (e.g., Kinloch and Taylor 2006), see Fig. 4, though more accurate predictions can be obtained by finite element modeling (Sheng et al. 2004). The true aspect ratio of the particles, the degree of their alignment, and some idea of the strength of adhesion between the particle and the polymer matrix, are required for accurate predictions. However, the elastic properties of nanoparticles cannot generally be measured, and hence are almost unknown. This includes nanoclays such as montmorillonite (Vanorio et al. 2003). This absence of modulus data is because the small particle size makes it impossible to perform reliable measurements. Hence, most authors assume that the

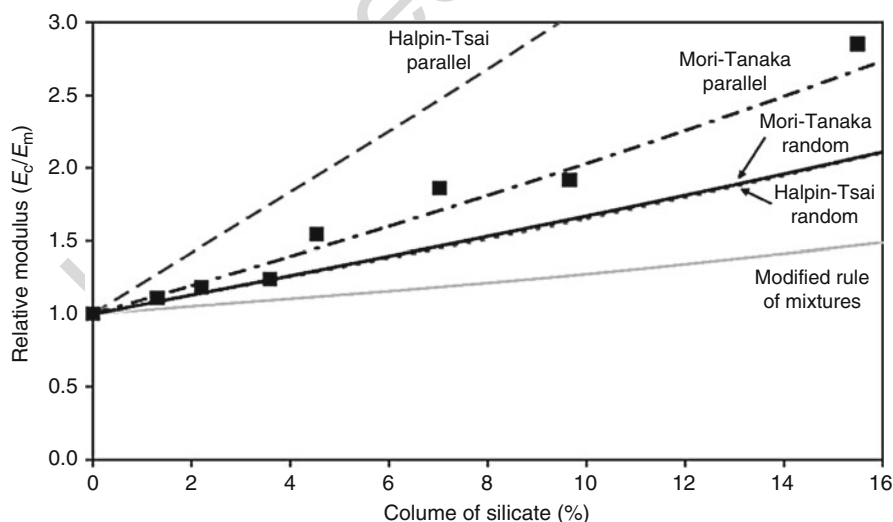


**Fig. 4** Relative modulus (composite modulus divided by matrix modulus) of epoxy polymer modified with nanoclay. Experimental data are shown as points, predictions using various theoretical models are shown as lines (Adapted from Kinloch and Taylor 2006)

properties (e.g., modulus, density) of the nanoparticles are equal to those of the bulk material, or of a similar material.

Examples of the stiffening effect that may be obtained using nanoparticles include the addition of 3% carbon nanofibers (CNF) to an amine-cured epoxy polymer (Zhou et al. 2007), which gave a 19% increase in modulus when added. This was accompanied by an increase in the tensile strength and a reduction in the strain to failure. These changes are typical of nanoparticle-modified epoxies. Generally, the stiffness is increased; the strain to failure and the tensile strength may be increased or remain the same. However, when small diameter particles are used, for example, 20 nm diameter silica nanoparticles, then the tensile strength remains unchanged. By comparison, the addition of hard microparticles tends to reduce both the strain to failure and the tensile strength.

**56.4.2 Functional Properties**

The high aspect ratio and low permeability of plate-like nanoparticles should provide good barrier properties when the particles are aligned and incorporated into thin films, by creating a tortuous path for diffusion (Hackman and Hollaway 2006; Sorrentino et al. 2006). Numerical predictions show that the permeability reduction is governed by the product  $a \cdot V_f$ , where  $a$  is the platelet aspect ratio and  $V_f$  is the volume fraction (Gusev and Lusti 2001). Epoxy films that were highly filled with nanoclay have been shown to have low oxygen permeability, up to three orders of magnitude lower than that of the unmodified epoxy (Triantafyllidis et al. 2006), see Table 1. The rate of diffusion of acetone into epoxy is also reduced by the addition of nanoclay (Chen and Curliss 2001), although these data did not reach saturation and so it is not possible to compare the equilibrium uptakes.

The fire resistance of nanoparticle-modified polymers has been studied, but most work has concentrated on thermoplastics. This has generally shown that the addition of nanoclays, and nanotubes, can improve the fire resistance (e.g., Gilman 1999; Gilman et al. 2000b; Beyer 2002). A significant amount of work has been performed using various thermoset polymers modified with nanoclays, including epoxy, vinyl ester, cyanate ester, and polyimide (e.g., Gilman et al. 1999a; Gilman et al. 1999b;

**Table 1** Oxygen permeability data for films of epoxy and nanoclay-modified epoxy (Adapted from Triantafyllidis et al. 2006)

Clay film composition	Clay film thickness (mm)	Epoxy-clay film thickness (mm)	O <sub>2</sub> permeability (cm <sup>3</sup> ml/m <sup>2</sup> day)
Epoxy	–	0.20	98.9
Epoxy-montmorillonite	0.060	0.11	≤0.1
Epoxy-montmorillonite	0.035	0.10	0.97
Epoxy-fluoroectorite	0.065	0.14	1.2

Gilman et al. 2000a). Tests using cone calorimetry showed that the addition of 10% of silicate reduced the peak heat release rate by up to 50%, and increased the mass of char residue formed. However, the onset time was also often reduced, probably due to presence of the surface treatment.

The thermal degradation behavior of nanoclay-modified epoxy has been studied, and is closely linked to the fire performance. Nanoclay has little effect on this behavior, and may even reduce the temperature at which degradation starts due to the relative instability of the surface treatment (Brnardic et al. 2008). The addition of carbon nanofibers to an amine-cured epoxy polymer had no effect on the decomposition temperature of epoxy (Zhou et al. 2007), but single-walled nanotubes have been shown to degrade the thermal stability (Puglia et al. 2003).

The effect on the glass transition temperature,  $T_g$ , of the addition of nanoparticles is dependent on the type of nanoparticles used and the interaction between the particles and the polymer (Becker and Simon 2006). The  $T_g$  can shift to a higher temperature than that of the unmodified polymer (e.g., Messersmith and Giannelis 1994; Kinloch and Taylor 2006; Bugnicourt et al. 2007). This may be due to a high interaction between the particles and the polymer, which may also locally change the properties of the polymer network. For example, the  $T_g$  of a polyurethane (PU) adhesive was increased from 32 °C to 62 °C by the addition of 5% of functionalized nanoclay (Dodiuk et al. 2006). Where polymer chains are intercalated between silicate platelets, then the silicate may constrain the polymer, hence increasing  $T_g$  (Kinloch and Taylor 2006). Bugnicourt et al. (2007) reported that  $T_g$  increased from 161 °C to 180 °C for an amine-cured epoxy modified with silica nanoparticles. They also noted that the poorer the dispersion, the lower the impact of the addition of silica on the magnitude of the  $\tan \delta$  peak and  $T_g$ . However, other tests showed no effect of the addition of silica nanoparticles (Bugnicourt et al. 2007; Johnsen et al. 2007; Hsieh et al. 2010). Reductions in the glass transition temperature have also been reported (e.g., Kornmann 1999). These reductions may be due to the surface treatment degrading during curing (Wang et al. 2000), or by enhanced free volume in the interphase between the particle and the matrix.

Carbon nanotubes have been shown to increase the rate of the curing reaction of epoxies (Yin et al. 1993; Puglia et al. 2003). This effect arises from the surface chemistry of the nanotubes (Shaffer and Sandler 2006). However, barium titanate nanoparticles did not affect the curing behavior of epoxy cured using diamino diphenyl methane (DDM) (Chandradass and Bae 2008).

The use of nanoparticles with a diameter less than that of the wavelength of light allows transparent particle-modified materials to be produced. In practice, the particles do reduce the optical transparency compared to the unmodified matrix due to differences in the respective refractive indices. For example, the light transmittance of epoxy modified with 25 nm diameter silica particles was greater than that for epoxy modified with particles of 540–1,520 nm (Naganuma and Kagawa 2002). However, using the smaller particles does give transmittance of 80–90% of the unmodified matrix value.

It is reported that the addition of nanoclays to epoxy will also reduce the coefficient of thermal expansion (CTE) of the epoxy polymer, as the CTE of the

ceramic particles is less than that of the polymer (Wang et al. 2000). For example, the CTE of epoxy below  $T_g$  can be reduced from 77 to 63  $\mu\text{m}/\text{m}^\circ\text{C}$  by the addition of 3% of nanoclay (Chen and Curliss 2001). However, the addition of nanotubes has been shown to have no significant effect on the CTE (Salinas-Ruiz 2009).

### 56.4.3 Electrical Properties

Alternating current (AC) impedance spectroscopy has been used to measure the conductivity of an amine-cured epoxy modified with multiwalled carbon nanotubes (MWNTs) (Sandler et al. 2003). The conductivity increased as a function of the MWNT weight fraction, see Fig. 5. There was an increase in conductivity of about two orders of magnitude, from  $10^{-9}$  to  $10^{-7}$  S/m, when 0.001 wt% of nanotubes was added. There was a further increase to above  $10^{-3}$  S/m for loading fractions of greater than 0.005 wt%. This increase in conductivity suggests that an infinite network of percolated nanotubes starts forming above 0.001 wt%. The authors also state that comparison with the direct current (DC) conductivity of the composites gave identical results. A similar transition in conductivity occurs for carbon black, but more than 1 wt% of carbon black is required (Sandler et al. 1999; Sandler et al. 2003), see Fig. 5.

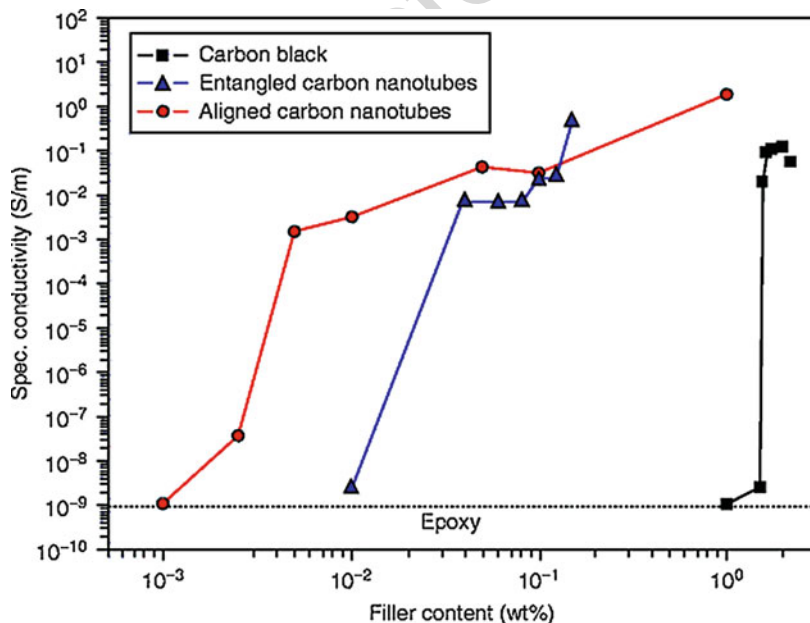


**Fig. 5** Conductivity versus filler content for aligned multi-walled carbon nanotubes, entangled nanotubes, and carbon black particles in epoxy (Courtesy M. Shaffer)

The addition of layered silicates to epoxy resin improves the surface discharge endurance of the polymer, considerably increasing the time before electrical breakdown occurs (Montanari et al. 2005). The addition of nonconducting silica or alumina nanoparticles will reduce the conductivity of the polymer (Cao et al. 2004). Layered silicates have been shown to increase the electrical breakdown strength and breakdown time (Imai et al. 2006), see Fig. 6. This indicates that these materials may have potential applications for electrical insulation materials.

The thermal conductivity of epoxy modified with carbon nanotubes has been investigated (Gojny et al. 2006). The authors reported that the thermal conductivity increased slightly with nanotube content, although the changes are very small compared to the changes in electrical conductivity.

#### 56.4.4 Fracture Toughness

It is well established that microparticles can increase the fracture toughness of thermoset polymers in mode I loading (e.g., Moloney et al. 1983; Kinloch and Taylor 2002). Indeed, this is the basis of most structural adhesives, which have a rubber or thermoplastic particulate toughening phase, often combined with co-tougheners. These particles may be preformed, or may be formed by phase-separation of an initially soluble polymer during curing. Inorganic particles such as glass or mica also provide a toughening effect, though the increases in toughness are generally lower than for rubber-toughening. In addition, hybrid formulations that combine rubber and glass particles have been shown to give high toughness.

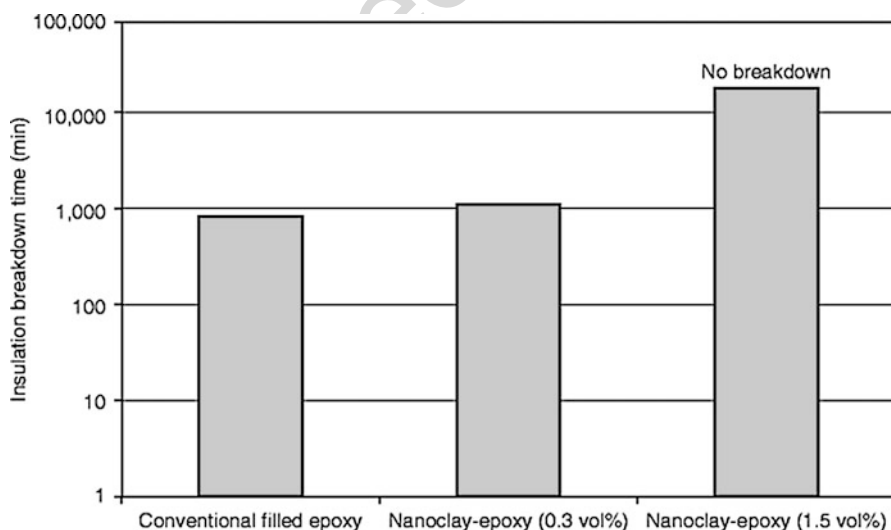


**Fig. 6** Insulation breakdown time for conventionally filled (50 vol% silica microparticles) epoxy, and this epoxy with added nanoclay under constant AC voltage (10 kV, 1 kHz) (Adapted from Imai et al. 2006)

The addition of nanoclay particles to epoxy has been shown to increase the toughness. The fracture energy of vinyl ester/epoxy systems containing 5 wt% nanoclay was increased more than two times compared to the unmodified polymer (Karger-Kocsis et al. 2003). There was no significant effect of the type of the surface treatment used on the nanoclay. Increasing the amount of nanoclay above 5 wt% reduced both the fracture toughness and fracture energy. Kinloch and Taylor compared the toughening effect due to the addition of layered silicate nanoparticles (nanoclays) with that due to similar microparticles, in this case mica (Kinloch and Taylor 2003, 2006). They reported higher fracture toughness values for the mica microparticles than for the nanoclays, see Fig. 7. They also showed that the fracture toughness was dependent on the weight fraction of nanoclay, with maximum toughness being achieved at between 1 and 5 wt% of nanoclay. The fracture toughness was also dependent on type of nanoclay used, and hence on the surface treatment and the resulting morphology. The addition of layered silicates does not always increase, and may reduce the fracture toughness, for example, with thermoset acrylic systems (Tarrant 2004).

Spherical nanoparticles have also been used to toughen epoxies. Ragosta et al. increased the fracture toughness,  $K_{IC}$ , of tetrafunctional epoxy cured with 4,4-diaminodiphenyl sulfone (DDS) from 0.5 to 1.2 MPa<sup>1/2</sup> using 10 wt% of silica particles (Ragosta et al. 2005). The particles were between 10 and 15 nm in diameter. It has also been shown that the addition of 13 nm diameter alumina particles increased the fracture toughness of epoxy, cured using a cycloaliphatic amine, from 0.5 to 1.2 MPa<sup>1/2</sup> using 11 vol% of alumina (Wetzel et al. 2006). Similarly, the addition of 11 vol% of 300 nm diameter titania particles increased  $K_{IC}$  to 0.85 MPa<sup>1/2</sup>.

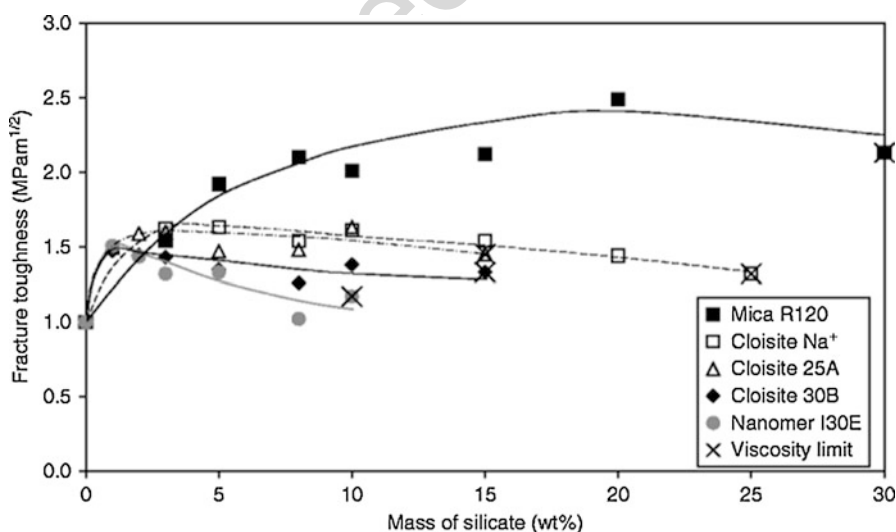


**Fig. 7** Fracture toughness of unmodified epoxy, mica microparticle- and nanoclay-modified epoxy versus content of layered silicate. Note “viscosity limit” indicates maximum silicate content before particle-modified resin becomes too viscous to cast (Adapted from Kinloch and Taylor 2006)



The addition of silica nanoparticles increased the fracture toughness of an anhydride-cured epoxy from 0.59 to 1.42 MPam<sup>1/2</sup> when 20 wt% of nanoparticles were added (Kinloch et al. 2005). These toughness values are equivalent to fracture energy,  $G_C$ , values of 100 and 460 J/m<sup>2</sup> respectively, see Fig. 8. In addition, 4 wt% of silica nanoparticles was sufficient to almost triple the fracture energy of the unmodified epoxy, to 290 J/m<sup>2</sup>. The toughening mechanisms involved have been discussed by Johnsen et al. (2007). Zhang et al. (2006) and Rosso et al. (2006) also reported toughness increases due to the addition of similarly sized silica nanoparticles.

The toughening mechanisms of silica nanoparticle-modified epoxy have been identified as plastic shear-yielding, and debonding of the polymer from the nanoparticles, followed by plastic void-growth of the epoxy (Hsieh et al. 2010). The toughening mechanisms of crack pinning, crack deflection, and immobilized polymer around the particles have all been discounted (Johnsen et al. 2007).

Micron-sized rubber particles toughen polymers by cavitating, hence relieving the constraint in the plastic zone at the crack tip. The matrix is then able to deform, absorbing energy by dilation and shear banding, thus giving an increased toughness. However, nanometer-sized rubber particles are thought not to cavitate, because the triaxial stresses required for cavitation are too high. Theoretical models predict that there is a minimum size below which rubber particles will not cavitate (Lazzeri and Bucknall 1993; Dompas and Groeninckx 1994). This diameter is predicted to be approximately 50 nm (Kody and Lesser 1999). This lack of cavitation of small rubber particles has been observed experimentally. For example, no cavitation was observed with carboxyl-terminated butadiene-acrylonitrile (CTBN) rubber particles,

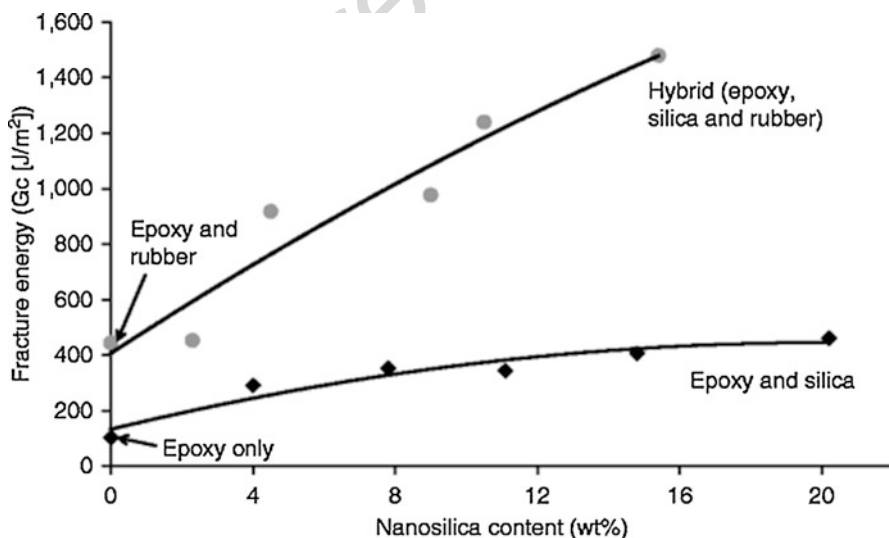


**Fig. 8** Fracture energy versus content of silica nanoparticles in epoxy and rubber-toughened (9% CTBN) epoxy (Adapted from Kinloch et al. 2005)



which were 200 nm in diameter, but cavitation was seen with micron-sized CTBN particles (Chen and Jan 1992).

However, cavitation was observed using 200 nm diameter core-shell latex particles comprised of a methacrylated butadiene-styrene copolymer (MBS) with a poly (methyl methacrylate) (PMMA) shell in a piperidine-cured epoxy polymer (Azimi et al. 1996b). Nano-sized core-shell rubber particles have also been reported to increase toughness (Liang and Pearson 2009). Liang and Pearson showed that the addition of 100 nm core-shell particles increased the fracture toughness of a piperidine-cured epoxy to  $3.1 \text{ MPam}^{1/2}$ . Although no toughness was reported for the unmodified epoxy, similarly cured material has a fracture toughness of between 0.9 and  $1.2 \text{ MPam}^{1/2}$  (Oba 1999; Kawaguchi and Pearson 2003). In earlier work, the toughening effect of 200 nm MBS core-shell particles were compared to 1, 10, and 100  $\mu\text{m}$  diameter CTBN particles (Pearson and Yee 1991). The fracture toughness was very dependent on particle size, and small particles are more efficient in producing a toughening effect than large particles.

The largest increases in toughness have been reported for so-called hybrid materials, which combine rubber and nanoparticle-modification of the epoxy. For example, the addition of silica nanoparticles to a rubber-toughened epoxy, using 9 wt% of CTBN, increased the toughness from 1.11 to  $2.19 \text{ MPam}^{1/2}$  when 15 wt% of nanoparticles were added (Kinloch et al. 2005). These toughness values are equivalent to fracture energy,  $G_C$ , values of 440 and  $1,480 \text{ J/m}^2$ , respectively, see Fig. 8. Synergistic increases in fracture toughness (Liang and Pearson 2009), and in impact strength (Zeng et al. 2007) have also been reported. Synergistic toughening has previously been reported for rubber-toughened epoxy with micron-sized glass beads (e.g., Kinloch et al. 1985; Azimi et al. 1996a). Increases in toughness have also been observed when nanoclay is added to rubber-modified epoxy, but there is not such a strong synergistic effect in this case (Liu et al. 2004).

#### 56.4.5 Fatigue Performance

Nanoparticles have been shown to improve the fatigue performance of thermoset polymers. Wetzel et al. (2006) measured the fatigue crack propagation (FCP) rate,  $da/dN$ , versus the stress-intensity factor range, and showed that this relationship follows the classic Paris-Erdogan law. These fatigue curves are shifted toward higher stress-intensity values as the nanoparticle content rises. At the same time, the gradient decreases. They reported that the gain in FCP resistance of alumina-modified epoxy nanocomposites (10 vol%) is comparable to the reinforcement achieved by rubber particles in epoxy, as was demonstrated using small amounts of rubber (5–10 phr CTBN) (Karger-Kocsis and Friedrich 1992), and is similar to that using 15–20 vol% of glass microspheres (Sautereau et al. 1995). In contrast to such traditional modifiers, the authors point out that the benefits conferred by nanoparticles are neither at the expense of modulus nor of strength.

Silica nanoparticles have been shown to significantly improve the cyclic-fatigue behavior of an anhydride-cured epoxy polymer, increasing the range of applied

stress-intensity factor at threshold,  $\Delta K_{th}$ , see Fig. 9 (Blackman et al. 2007). The nanoparticles also increased the fracture toughness,  $K_{IC}$ . The fatigue data followed the modified Paris law. Similarly, the addition of 200 nm diameter rubber particles increases fracture toughness and improves fatigue resistance (Azimi et al. 1996b). The fatigue data followed the classic Paris-Erdogan law. The use of 200 nm MBS particles in place of 1.5  $\mu m$  CTBN particles resulted in about one order of magnitude improvement in fatigue resistance. A synergistic effect between CTBN rubber particles and silica nanoparticles has also been shown in fatigue, with the maximum increase in the fatigue threshold value being recorded using 9 wt% of rubber and 9 wt% of silica (Sohn Lee 2009).

The addition of carbon nanofibers (CNF) to an amine-cured epoxy polymer significantly increased the number of cycles to failure, as measured using fatigue stress versus number of cycles to failure (S-N) curves (Zhou et al. 2007). The fatigue life went through a maximum at 2 wt% CNF, although only two specimens were used for each combination of stress level and CNF loading.

A reduction in crack growth rate per cycle has also been shown for an epoxy system with the addition of up to 0.5 wt% of carbon nanotubes (Zhang et al. 2007). The authors attributed this effect to pullout of the nanotubes that bridge across the crack opening.

Though there are data available that show how nanoparticles can change the fatigue performance of adhesives, there are no data that quantify the durability (i.e., the resistance to an environment such as water) of these materials when used as adhesives. However, it is likely that nanoparticle-modified adhesives will perform as conventionally filled adhesives.

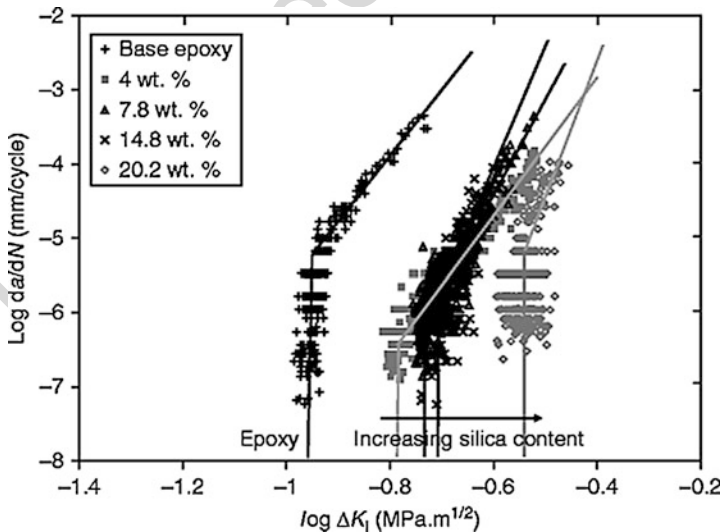


**Fig. 9** Logarithmic crack growth rate per cycle,  $d a/d N$ , versus logarithmic range of applied stress-intensity factor from cyclic-fatigue tests for unmodified epoxy and silica nanoparticle-modified epoxy (Courtesy J. Sohn Lee)

## 56.4.6 Peel and Lap-Shear Performance

The modification of a polyurethane (PU) adhesive using nanoclays was tested by Dodiuk et al. (2006), using adhesive joints made with aluminum-alloy adherends. The incorporation of functionalized nanoclays into PU improved the lap-shear strength by up to 195%. The functionalized nanoclays also gave higher peel strength than the unmodified PU. Increases of up to 40% were measured, but one of the nanoclays gave almost no change in the peel strength.

The lap-shear strength of carbon-fiber composites bonded using an epoxy adhesive was increased by 45% with the addition of 5% of MWNT (Hsiao et al. 2003). However, the locus of failure was also altered – from interfacial for the control specimens to cohesive for the nanotube-modified materials.

Climbing drum peel and lap-shear tests were performed using aluminum-alloy substrates, with a model rubber-toughened epoxy film adhesive (Gilbert et al. 2003). The adhesive was modified with 5 or 10 wt% of either 50 nm diameter alumina nanoparticles or alumina nanofibers with a diameter of 2–4 nm and an aspect ratio ranging from tens to hundreds. Both of the nano-modifiers increased the peel and shear strength. However, the more successful modification was the addition of 5% of alumina nanoparticles, which increased the peel strength of the adhesive by 50%, and the lap-shear strength by 15%.

The lap-shear and 180° peel test performance of very soft acrylic adhesives modified with nanoclay or silica nanoparticles were improved by the addition of nanoparticles (Patel et al. 2006). The addition of 6 wt% of nanoclay or 50 wt% of silica increased the peel force by about 40%.

Sprenger and coworkers used a room-temperature curing rubber-toughened epoxy adhesive with a  $T_g$  of 70 °C (Kinloch et al. 2003; Sprenger et al. 2003, 2004). The addition of only 4 wt% of 20 nm diameter silica nanoparticles doubled the fracture energy, from 1,200 to 2,300 J/m<sup>2</sup>. The addition of the nanoparticles also increased both the lap-shear and peel strength, as shown in Fig. 10.

## 56.5 Conclusions

Nanoparticle-modified polymers are being extensively researched, and a great deal of work has been done to produce nanoparticles. These nanoparticles are now commercially available in kilogram or tonne quantities, and at reasonable prices (\$10s per kilogram). Hence, nanotechnology and nanoparticles are beginning to be applied in commercial products. It is anticipated that nanoparticles will be increasingly used in structural adhesives. Their application will continue to expand as their availability increases, and hence as their cost decreases.

The dispersion of nanoparticles in polymer matrices can be difficult, and agglomerates can remain even after aggressive processing. These may have a significant detrimental effect on the properties of the material. For this reason, pre-dispersed nanoparticles, available as a masterbatch in a polymer, are attractive. However, these

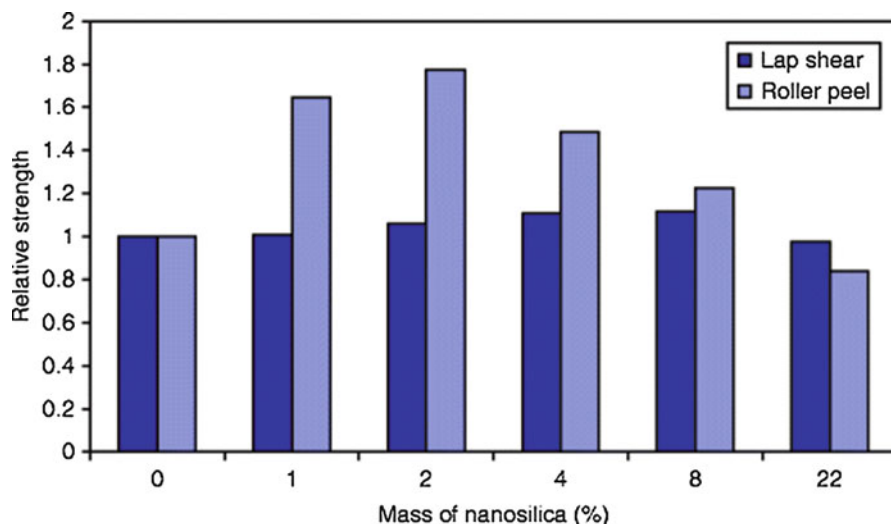


**Fig. 10** Lap-shear and roller peel strength for hybrid (nanosilica and rubber-modified) epoxy (Adapted from Kinloch et al. 2003)

particles can agglomerate during processing or curing, so there is no guarantee that a good dispersion will be obtained in the final material.

Nanoparticles have been shown to improve the structural and functional properties of thermoset polymers. However, in many cases similar increases can be obtained using micron-sized particles, especially for structural properties. High aspect ratio particles, such as carbon nanotubes or nanoclay, can give significant improvements in functional properties. Examples include electrical percolation at very low particle volume fractions and increases in barrier properties.

It is perhaps the synergistic effect of combining nanoparticles with existing technology based on micron-sized particles that is the most exciting area at present. For example, the fracture toughness and peel performance of adhesive joints can be improved by combining silica nanoparticles and rubber microparticles. Hierarchical materials like these, and patterned arrays of nanoparticles, appear to be the future developments in this field.

## References

- Ahmed S, Jones FR (1990) A review of particulate reinforcement theories for polymer composites. *J Mater Sci* 25:4933
- Ajayan PM, Stephan O et al (1994) Aligned carbon nanotube arrays formed by cutting a polymer resin-nanotube composite. *Science* 265:1212
- Alexandre M, Dubois P (2000) Polymer-layered silicate nanocomposites: preparation, properties and uses of a new class of materials. *Mater Sci Eng R* 28:1
- Azimi HR, Pearson RA et al (1996a) Fatigue of hybrid epoxy composites: Epoxies containing rubber and hollow glass spheres. *Polym Eng Sci* 36:2352

- 657 Azimi HR, Pearson RA et al (1996b) Fatigue of rubber-modified epoxies: effect of particle size and  
658 volume fraction. *J Mater Sci* 31:3777
- 659 Baik Y, Lee S et al (2005) Unidirectional alignment of carbon nano-sized fiber using drawing  
660 process. *J Mater Sci* 40:6037
- 661 Bechelany M, Brioude A et al (2007) Large-scale preparation of faceted Si<sub>3</sub>N<sub>4</sub> nanorods from beta-  
662 SiC nanowires. *Nanotechnology* 18:335305
- 663 Becker O, Simon GP (2006) Epoxy nanocomposites based on layered silicates and other nano-  
664 structured fillers. In: Mai YW, Yu ZZ (eds) *Polymer nanocomposites*. Woodhead, Cambridge, p  
665 594
- 666 Beyer G (2002) Carbon nanotubes as flame retardants for polymers. *Fire Mater* 26:291
- 667 Blackman BRK, Kinloch AJ et al (2007) The fracture and fatigue behaviour of nano-modified  
668 epoxy polymers. *J Mater Sci* 42:7049
- 669 Brnardic I, Macan J et al (2008) Thermal degradation kinetics of epoxy/organically modified  
670 montmorillonite nanocomposites. *J Appl Polym Sci* 107:1932
- 671 Brooker RD, Blackman BRK et al (2008) Nano-reinforcement of epoxy/thermoplastic blends. In:  
672 31st annual meeting of the adhesion society, Austin, USA, Adhesion Society, Blacksburg, USA
- 673 Brooker RD, Kinloch AJ et al (2010) The morphology and fracture properties of thermoplastic-  
674 toughened epoxy polymers. *J Adhes* 86:726
- 675 Brown DM, Kinloch IA et al (2007) An in vitro study of the potential of carbon nanotubes and  
676 nanofibres to induce inflammatory mediators and frustrated phagocytosis. *Carbon* 45:1743
- 677 Bugnicourt E, Galy J et al (2007) Effect of sub-micron silica fillers on the mechanical performances  
678 of epoxy-based composites. *Polymer* 48:1596
- 679 Cao Y, Irwin PC et al (2004) The future of nanodielectrics in the electrical power industry. *IEEE*  
680 *Trans Dielectric Electrical Insul* 11:797
- 681 Chakrabarti S, Nagasaka T et al (2006) Growth of super long aligned brush-like carbon nanotubes.  
682 *Jpn J Appl Phys Expr Lett* 45:L720
- 683 Chandradass J, Bae D-S (2008) Preparation and properties of barium titanate nanopowder/epoxy  
684 composites. *Mater Manuf Process* 23:116
- 685 CheapTubes (2009.) <http://www.cheaptubes.com>. Retrieved 4 Nov 2009
- 686 Chen C, Curliss D (2001) Resin matrix composites: organoclay-aerospace epoxy nanocomposites,  
687 Part II. *SAMPE J* 37:11
- 688 Chen TK, Jan YH (1992) Fracture mechanism of toughened epoxy-resin with bimodal rubber-  
689 particle size distribution. *J Mater Sci* 27:111
- 690 Chen XQ, Saito T et al (2001) Aligning single-wall carbon nanotubes with an alternating-current  
691 electric field. *Appl Phys Lett* 78:3714
- 692 Demczyk BG, Wang YM et al (2002) Direct mechanical measurement of the tensile strength and  
693 elastic modulus of multiwalled carbon nanotubes. *Mater Sci Eng A* 334:173
- 694 Dodiuk H, Belinski I et al (2006) Polyurethane adhesives containing functionalized nanoclays.  
695 *J Adhes Sci Technol* 20:1345
- 696 Dompas D, Groeninckx G (1994) Toughening behavior of rubber-modified thermoplastic polymers  
697 involving very small rubber particles. 1. A criterion for internal rubber cavitation. *Polymer*  
698 35:4743
- 699 Feynman RP (1959) .There's plenty of room at the bottom – an invitation to enter a new field of  
700 physics <http://www.zyvex.com/nanotech/feynman.html>. Accessed 9 Apr 2008
- 701 Fiedler B, Gojny FH et al (2006) Fundamental aspects of nano-reinforced composites. *Compos Sci*  
702 *Technol* 66:3115
- 703 Gilbert EN, Hayes BS et al (2003) Nano-alumina modified epoxy based film adhesives. *Polym Eng*  
704 *Sci* 43:1096
- 705 Gilman JW (1999) Flammability and thermal stability studies of polymer layered-silicate (clay)  
706 nanocomposites. *Appl Clay Sci* 15:31
- 707 Gilman JW, Harris RH et al (1999b) Cyanate ester clay nanocomposites: synthesis and flammability  
708 studies. In: *Evolving and revolutionary technologies for the new millennium 44th international*  
709 *SAMPE symposium/exhibition*, Long beach, CA, USA, Society for the Advancement of  
710 *Material and Process Engineering (SAMPE)*

- Gilman JW, Kashiwagi T et al (1999a) Flammability studies of polymer layered silicate nanocomposites: polyolefin, epoxy and vinyl ester resins. In: Ak-Malaika S, Golovoy A et al (eds) Chemistry and technology of polymer additives. Blackwell Science, Malden, p 249
- Gilman JW, Harris RH et al (2000b) Phenolic cyanate ester nanocomposites: effect of ammonium ion structure on flammability and nano-dispersion. In: Spring meeting, division of polymeric materials: science and engineering, American Chemical Society, San Francisco, USA, American Chemical Society
- Gilman JW, Jackson CL et al (2000a) Flammability properties of polymer-layered-silicate nanocomposites. polypropylene and polystyrene. Nanocomposites Chem Mater 12:1866
- Gintert MJ, Jana SC et al (2007) A novel strategy for nanoclay exfoliation in thermoset polyimide nanocomposite systems. Polymer 48:4166
- Gojny FH, Nastalczyk J et al (2003) Surface modified multi-walled carbon nanotubes in CNT/epoxy-composites. Chem Phys Lett 370:820
- Gojny FH, Wichmann MHG et al (2004) Carbon nanotube-reinforced epoxy-composites: enhanced stiffness and fracture toughness at low nanotube content. Compos Sci Technol 64:2363
- Gojny FH, Wichmann MHG et al (2006) Evaluation and identification of electrical and thermal conduction mechanisms in carbon nanotube/epoxy composites. Polymer 47:2036
- Gordon JE (1978) The new science of strong materials or why you don't fall through the floor. Penguin, Harmondsworth
- Green K, Dean D et al (2006) Aligned carbon nanofiber/epoxy nanocomposites. Polym Mater Sci Eng 94:53
- Gusev AA, Lusti HR (2001) Rational design of nanocomposites for barrier applications. Adv Mater 13:1641
- Hackman I, Hollaway L (2006) Epoxy-layered silicate nanocomposites in civil engineering. Composites Pt A 37:1161
- Harper T (2003) What is nanotechnology? Nanotechnology 14:U5
- Harris PJF (1999) Carbon nanotubes and related structures: new materials for the twenty-first century. Cambridge University Press, Cambridge
- Harris PJF (2009) Carbon nanotube science: synthesis, properties and applications. Cambridge University Press, Cambridge
- Hay J, Shaw S (2001) Into the Labyrinth. Chem Br 2001:34
- Hsiao K-T, Alms J et al (2003) Use of epoxy/multiwalled carbon nanotubes as adhesives to join graphite fibre reinforced polymer composites. Nanotechnology 14:791
- Hsieh TH, Kinloch AJ et al (2010) The toughness of epoxy polymers and fibre composites modified with rubber microparticles and silica nanoparticles. J Mater Sci 45:1193
- ICBA (2008) .International Carbon Black Association, <http://www.carbon-black.org>. Retrieved 9 Apr 2008
- Iijima S (1991) Helical microtubules of graphitic carbon. Nature 354:56
- Iijima S, Ichihashi T (1993) Single-shell carbon nanotubes of 1-nm diameter. Nature 363:603
- Imai T, Sawa F et al (2006) Effects of nano- and micro-filler mixture on electrical insulation properties of epoxy based composites. IEEE Trans Dielectric Electrical Insul 13:319
- Johnsen BB, Kinloch AJ et al (2007) Toughening mechanisms of nanoparticle-modified epoxy polymers. Polymer 48:530
- Kaneka (2008.) <http://www.kaneka.com>. Retrieved 9 Apr 2008
- Karger-Kocsis J, Friedrich K (1992) Fatigue crack-propagation and related failure in modified, anhydride-cured epoxy-resins. Colloid Polym Sci 270:549
- Karger-Kocsis J, Gryshchuk O et al (2003) Interpenetrating vinyl ester/epoxy resins modified with organophilic layered silicates. Compos Sci Technol 63:2045
- Kathi J, Rhee K (2008) Surface modification of multi-walled carbon nanotubes using 3-aminopropyltriethoxysilane. J Mater Sci 43:33
- Kawaguchi T, Pearson RA (2003) The effect of particle-matrix adhesion on the mechanical behavior of glass filled epoxies. Part 2. A study on fracture toughness. Polymer 44:4239
- Kinloch AJ, Lee JH et al (2003) Toughening structural adhesives via nano- and micro-phase inclusions. J Adhes 79:867



- Kinloch AJ, Maxwell DL et al (1985) The fracture of hybrid-particulate composites. *J Mater Sci* 20:4169
- Kinloch AJ, Mohammed RD et al (2005) The effect of silica nano particles and rubber particles on the toughness of multiphase thermosetting epoxy polymers. *J Mater Sci* 40:5083
- Kinloch AJ, Taylor AC (2002) The toughening of cyanate-ester polymers. Part I: physical modification using particles, fibres and woven-mats. *J Mater Sci* 37:433
- Kinloch AJ, Taylor AC (2003) Mechanical and fracture properties of epoxy/inorganic micro- and nano-composites. *J Mater Sci Lett* 22:1439
- Kinloch AJ, Taylor AC (2006) The mechanical properties and fracture behaviour of epoxy-inorganic micro- and nano-composites. *J Mater Sci* 41:3271
- Kody RS, Lesser AJ (1999) Yield behavior and energy absorbing characteristics of rubber-modified epoxies subjected to biaxial stress states. *Polym Compos* 20:250
- Koerner H, Hampton E et al (2005) Generating triaxial reinforced epoxy/montmorillonite nano-composites with uniaxial magnetic fields. *Chem Mater* 17:1990
- Kormmann X (1999) Synthesis and characterisation of thermoset-clay nanocomposites. Licentiate thesis, materials and manufacturing engineering department, University of Lulea, Lulea, Sweden
- Lam C-W, James JT et al (2004) Pulmonary toxicity of single-wall carbon nanotubes in mice 7 and 90 days after intratracheal instillation. *Toxicol Sci* 77:126
- Lam C-K, Lau K-T et al (2005) Effect of ultrasound sonication in nanoclay clusters of nanoclay/epoxy composites. *Mater Lett* 59:1369
- Lau K-T, Gu C et al (2004) Stretching process of single- and multi-walled carbon nanotubes for nanocomposite applications. *Carbon* 42:426
- Lazzeri A, Bucknall CB (1993) Dilatational bands in rubber-toughened polymers. *J Mater Sci* 28:6799
- Liang G, Hu X (2004) Preparation and performance of aluminum borate whisker-reinforced epoxy composites. I. Effect of whiskers on processing, reactivity, and mechanical properties. *J Appl Polym Sci* 92:1950–1954
- Liang YL, Pearson RA (2009) Toughening mechanisms in epoxy-silica nanocomposites (ESNs). *Polymer* 50:4895
- Liu WP, Hoa SV et al (2004) Morphology and performance of epoxy nanocomposites modified with organoclay and rubber. *Polym Eng Sci* 44:1178
- Lu KL, Lago RM et al (1996) Mechanical damage of carbon nanotubes by ultrasound. *Carbon* 34:814
- Martin CA, Sandler JKW et al (2005) Electric field-induced aligned multi-wall carbon nanotube networks in epoxy composites. *Polymer* 46:877
- Messersmith PB, Giannelis EP (1994) Synthesis and characterisation of layered silicate-epoxy nanocomposites. *Chem Mater* 6:1719
- Mohammed RD (2007) Material properties and fracture mechanisms of epoxy nano-composites. PhD thesis, mechanical engineering. Imperial college of science, technology and medicine, London
- Moloney AC, Kausch HH et al (1983) The fracture of particulate-filled epoxide resins. *J Mater Sci* 19:1125
- Montanari GC, Ciani F et al (2005) Electric strength, space charge and surface discharge characterization of nanostructured epoxy-silicate insulating materials. In: 2005 International symposium on electrical insulating materials, vols 1–3, Tokyo, Institute of Electrical Engineers, Japan
- Morisada Y, Miyamoto Y et al (2007) Mechanical properties of SiC composites incorporating SiC-coated multi-walled carbon nanotubes. *Int J Refract Met Hard Mater* 25:322
- Naganuma T, Kagawa Y (2002) Effect of particle size on the optically transparent nano meter-order glass particle-dispersed epoxy matrix composites. *Compos Sci Technol* 62:1187
- Nanoresins (2008.) <http://www.nanoresins.com>. Retrieved 9 Apr 2008
- Oba T (1999) The fatigue behaviour of toughened epoxy polymers. PhD thesis, mechanical engineering. Imperial college of science, technology and medicine, London

- Patel S, Bandyopadhyay A et al (2006) Synthesis and properties of nanocomposite adhesives. *J Adhes Sci Technol* 20:371
- Pearson RA, Yee AF (1991) Influence of particle-size and particle-size distribution on toughening mechanisms in rubber-modified epoxies. *J Mater Sci* 26:3828
- Puglia D, Valentini L et al (2003) Analysis of the cure reaction of carbon nanotubes/epoxy resin composites through thermal analysis and Raman spectroscopy. *J Appl Polym Sci* 88:452
- Radford T (2003) Brave new world or miniature menace? Why Charles fears grey goo nightmare. *The Guardian*, London, Issued 29 April 2003
- Ragosta G, Abbate M et al (2005) Epoxy-silica particulate nanocomposites: chemical interactions, reinforcement and fracture toughness. *Polymer* 46:10506
- Rosso P, Ye L et al (2006) A toughened epoxy resin by silica nanoparticle reinforcement. *J Appl Polym Sci* 100:1849
- Rothon RN, Hancock M (1995) General principles guiding selection and use of particulate materials. In: Rothon RN (ed) *Particulate-filled polymer composites*. Longman Scientific and Technical, Harlow, p 1
- Saito R, Dresselhaus G et al (1998) Physical properties of carbon nanotubes. Imperial College, London
- Salinas-Ruiz MDM (2009) Development of a rubber toughened epoxy adhesive loaded with carbon nanotubes, for aluminium – polymer bonds. PhD thesis, School of applied science, Cranfield University
- Sandler J, Shaffer MSP et al (1999) Development of a dispersion process for carbon nanotubes in an epoxy matrix and the resulting electrical properties. *Polymer* 40:5967
- Sandler JKW, Kirk JE et al (2003) Ultra-low electrical percolation threshold in carbon-nanotube-epoxy composites. *Polymer* 44:5893
- Sautereau H, Maazouz A et al (1995) Fatigue behavior of glass bead filled epoxy. *J Mater Sci* 30:1715
- Schadler LS (2003) Polymer-based and polymer-filled nanocomposites. In: Ajayan PM, Schadler LS et al (eds) *Nanocomposite science and technology*. Wiley-VCH, Weinheim, p 380
- Schmid CF, Klingenberg DJ (2000) Mechanical flocculation in flowing fiber suspensions. *Phys Rev Lett* 84:290
- Shaffer MSP, Kinloch IA (2004) Prospects for nanotube and nanofibre composites. *Compos Sci Technol* 64:2281
- Shaffer MSP, Sandler JKW (2006) Carbon nanotube/nanofibre polymer composites. In: Advani SG (ed) *Processing and properties of nanocomposites*. World Scientific, Singapore
- Sheng N, Boyce MC et al (2004) Multiscale micromechanical modeling of polymer/clay nanocomposites and the effective clay particle. *Polymer* 45:487
- Sigma Aldrich (2008.) <http://www.sigmaaldrich.com> Retrieved 9 Apr 2008
- Sohn Lee J (2009) The fatigue behaviour of nano-modified epoxy adhesives. PhD thesis, Department of mechanical engineering, Imperial college London, London
- Sorrentino A, Gorrasi G et al (2006) Barrier properties of polymer/clay nanocomposites. In: Mai YW, Yu ZZ (eds) *Polymer nanocomposites*. Woodhead, Cambridge, p 594
- Sprenger S, Eger C et al (2003) Nanoadhesives: toughness and high strength. *Adhaesion, Kleben and Dichten* 2003:24
- Sprenger S, Eger C et al (2004). Nano-modified ambient temperature curing epoxy adhesives. *Adhaesion, Kleben and Dichten* 2004:1
- Tang Y, Liang G et al (2007) Performance of aluminum borate whisker reinforced cyanate ester resin. *J Appl Polym Sci* 106:4131
- Tarrant AE (2004) Thermoset-acrylic/layered-silicate nanocomposites: synthesis and structure-property relationships. Imperial College London Thesis, London
- Tjong SC (2006) Structural and mechanical properties of polymer nanocomposites. *Mater Sci Eng R* 53:73
- Triantafyllidis KS, LeBaron PC et al (2006) Epoxy-clay fabric film composites with unprecedented oxygen-barrier properties. *Chem Mater* 18:4393



- 871 Vanorio T, Prasad M et al (2003) Elastic properties of dry clay mineral aggregates, suspensions and  
872 sandstones. *Geophys J Int* 155:319
- 873 Wang ZL (ed) (2001) Characterization of nanophase materials. Wiley-VCH, Weinheim
- 874 Wang Z, Massam J et al (2000) Epoxy-clay nanocomposites. In: Pinnavaia TJ, Beall GW (eds)  
875 Polymer-clay nanocomposites. Wiley, Chichester
- 876 Warheit DB, Laurence BR et al (2004) Comparative pulmonary toxicity assessment of single-wall  
877 carbon nanotubes in rats. *Toxicol Sci* 77:117
- 878 Wetzel B, Rosso P et al (2006) Epoxy nanocomposites – fracture and toughening mechanisms. *Eng*  
879 *Fract Mech* 73:2375
- 880 Xie X-L, Mai Y-W et al (2005) Dispersion and alignment of carbon nanotubes in polymer matrix:  
881 A review. *Mater Sci Eng R* 49:89
- 882 Yasmin A, Daniel IM (2004) Mechanical and thermal properties of graphite platelet/epoxy com-  
883 posites. *Polymer* 45:8211
- 884 Yasmin A, Abot JL et al (2003) Processing of clay/epoxy nanocomposites by shear mixing. *Scr*  
885 *Mater* 49:81
- 886 Yasmin A, Luo JJ et al (2006a) Mechanical and thermal behavior of clay/epoxy nanocomposites.  
887 *Compos Sci Technol* 66:2415
- 888 Yasmin A, Luo JJ et al (2006b) Processing of expanded graphite reinforced polymer nano-  
889 composites. *Compos Sci Technol* 66:1182
- 890 Yin M, Koutsky JA et al (1993) Characterization of carbon microfibers as reinforcement for epoxy  
891 resins. *Chem Mater* 5:1024
- 892 Zeng MF, Sun XD et al (2007) Effects of SiO<sub>2</sub> nanoparticles on the performance of carboxyl-  
893 randomized liquid butadiene-acrylonitrile rubber modified epoxy nanocomposites. *J Appl*  
894 *Polym Sci* 106:1347
- 895 Zhang H, Zhang Z et al (2006) Property improvements of in situ epoxy nanocomposites with  
896 reduced interparticle distance at high nanosilica content. *Acta Mater* 54:1833
- 897 Zhang W, Picu RC et al (2007) Suppression of fatigue crack growth in carbon nanotube composites.  
898 *Appl Phys Lett* 91:193109
- 899 Zhou Y, Pervin F et al (2007) Effect vapor grown carbon nanofiber on thermal and mechanical  
900 properties of epoxy. *J Mater Sci* 42:7544
- 901 Zhu YQ, Kroto HW et al (2002) A systematic study of ceramic nanostructures generated by arc  
902 discharge. *Chem Phys Lett* 365:457
- 903 Zunjarrao S, Sriraman R et al (2006) Effect of processing parameters and clay volume fraction on  
904 the mechanical properties of epoxy-clay nanocomposites. *J Mater Sci* 41:2219

John W. Nicholson

**Contents**

57.1	Introduction .....	1704
57.2	Surfaces for Bonding .....	1706
57.3	Surface Pretreatment .....	1708
57.4	Bonding Agents .....	1710
57.5	Evaluation of Bonding Agents .....	1713
57.6	Leakage and Bonding Agents .....	1713
57.7	Composite Resins .....	1714
57.8	Durability of Bonded Composite Resin Restorations .....	1715
57.9	Biocompatibility of Bonding Agents .....	1716
57.10	Adhesive Dental Restorative Materials .....	1717
57.11	Bonding of Glass-Ionomer Cements .....	1720
57.12	ART Technique .....	1723
57.13	Glass-Ionomer Fissure Sealants .....	1723
57.14	Bonding in Orthodontics .....	1724
57.15	Conclusions .....	1725
	References .....	1726

**Abstract**

The present chapter describes the adhesive techniques and materials that are widely used in modern clinical dentistry. There are two types of tooth-colored restorative material available to the dentist, the so-called composite resins and the glass-ionomer cements. There are, though, variations on these basic types, as explained in the chapter. In addition, there is the zinc polycarboxylate cement, which was the first adhesive dental restorative material to be developed, and it retains a niche in modern clinical practice.

J. W. Nicholson (✉)

Bluefield Centre for Biomaterials, London, UK

Dental Physical Sciences, Institute of Dentistry, Queen Mary University of London, London, UK

e-mail: [john.nicholson@bluefieldcentre.co.uk](mailto:john.nicholson@bluefieldcentre.co.uk); [jwnicholson01@gmail.com](mailto:jwnicholson01@gmail.com)

Composite resins do not themselves possess any adhesive properties, but need to be used in conjunction with separate adhesive substances known as bonding agents. Over recent years, the technology of these materials has developed rapidly and a wide variety of systems are currently available to the clinician. Bonding agents have been characterized by “generation,” and currently seventh generation bonding systems are available. However, a more useful classification is based on the number of steps involved in using them, and this is described in detail.

Bonding agents are applied to the tooth surface following cavity preparation, a process that involves the formation of a layer of deranged dentin known as the “smear layer.” Modern bonding agents may be either “etch-and-rinse,” in which case the smear layer is removed, or “self-etching,” where the smear layer becomes incorporated into the bonding layer. Whichever approach is used, the result is a treated surface to which the composite resin is applied. Testing of such systems is typically in shear mode, and they have been reported to give high shear bond strengths, even though they involve only a very thin layer between a hydrophilic substrate and a hydrophobic repair material.

Glass-ionomers, by contrast, are themselves hydrophilic and inherently adhesive to the tooth surface. It therefore requires only slight pretreatment, typically conditioning with 10% aqueous polyacrylic acid. Glass-ionomers rapidly form durable adhesive bonds to the tooth surface through the development of an ion-exchange layer at the interface. This ability to bond is exploited in both the Atraumatic Restorative Treatment (ART) technique and in bonding of orthodontic brackets, both of which are described in detail in the chapter.

---

## 57.1 Introduction

Dentistry is concerned with the preservation, repair, and replacement of teeth. In its contemporary form, it makes increasing use of adhesive materials and techniques. One example is the placement of adhesive materials to fill fissures of newly erupted teeth as a preventive procedure. Without this treatment, decay-inducing bacteria might otherwise lodge in these fissures, and cause caries to develop (Mount and Hume 2005). Other options in restorative dentistry include repair of teeth damaged by caries or trauma with the tooth-colored materials known as composite resins. Use of these materials involves bonding to the tooth by means of bespoke adhesive systems. Alternatively, teeth damaged by caries can be repaired with the other tooth-colored option, the glass-ionomer cement. These materials are inherently adhesive to both the dentin and enamel of the tooth, which in some applications is an advantage (Mount 2002).

Replacement of missing teeth using bridges typically employs bonding agents and surface pretreatment procedures (Roulet and Vanherle 2004). Tooth-realigning techniques used in the dental specialty known as orthodontics employ brackets and wires to force the teeth into more satisfactory positions. Adhesive materials can be used to hold these brackets in place. Aesthetic procedures, such as the placement of

ceramic veneers to improve the appearance of the incisors, also typically employ adhesives and surface pretreatments (Mount and Hume 2005).

From these comments it is apparent that adhesion and adhesives play important roles in modern dentistry. Current research covers many facets of the adhesion process, including surface pretreatment, formulation of adhesives, durability of bonded structures, and clinical effects of bonding agents and adhesive materials (Roulet and Vanherle 2004; Breschi et al. 2008). The deployment of these substances in the mouth is not entirely straightforward. The mouth is a biological structure, and as such is composed of both hard and soft tissues. The chemicals used as adhesives may have adverse effects, particularly on the soft tissue of the gingiva (gum) and pulp (living cells and blood vessels within the tooth). A theme of the current research is the biocompatibility of adhesive materials in the mouth.

Tooth repairs are required to be capable of surviving for a considerable time, typically of the order of 10–15 years. The long-term effects of foreign materials and their possible degradation products need to be considered in selecting repair materials and planning treatments involving their deployment.

There are many factors driving the changes to increased use of adhesive techniques in dentistry (Roulet and Vanherle 2004). First, there have been many years of research and development activity directed toward the fabrication of esthetic repair materials, both polymer- and ceramic-based. Second, there is an increasing patient demand for esthetic (i.e., tooth-colored) repairs. This is part of a wider trend toward improved dental esthetics that has seen a rise in the developed world of cosmetic dentistry as a branch of the profession and the increasing use of bleaching techniques to make the teeth whiter. This is associated with looking younger and also compensates for the ravages of strongly colored dietary components, such as coffee and red wine.

A third factor contributing to the increase in importance of adhesion in dentistry is that patients are retaining their natural teeth for longer. Whereas earlier generations were prepared to accept some tooth loss and even complete edentulousness as a consequence of ageing, the current generation is less tolerant of these possibilities. There has been a dramatic fall in the incidence of tooth decay in the past 40 years, a phenomenon which is multifactorial, but is closely allied to the increased use of fluoride for preventive purposes. Preventive measures include fluoridation of drinking water, the supply of fluoridated toothpastes, and the application of fluoridated gels by dental professionals (Nicholson and Czarnecka 2008a). As a result, patients retain many of their teeth well into old age, and having done so, are then unwilling to accept radical treatment options, such as extraction or even highly invasive repair with silver-tin amalgam. Increasing levels of affluence, too, make such patients willing to pay for demanding clinical procedures and more expensive materials, which means those based on adhesive techniques and materials.

Finally, the major advances in understanding of bond formation and durability to the tooth surface has enhanced the ability of the scientific community to develop reliable and long-lasting bonding agents. The dental literature reflects this, containing as it does many hundreds, possibly thousands, of scientific articles on the topic of bonding and adhesion. These range from fundamental studies of bonding

mechanisms and surface pretreatments to clinical studies of longevity of repairs and failure mechanisms.

One indication of the importance of this subject is that a specialist journal, the *Journal of Adhesive Dentistry*, was launched in 1999. However this is not the only forum for discussion of research on this topic, and other journals, such as *Journal of Dental Research*, *Dental Materials* and *Journal of Dentistry* also carry numerous research articles every year on adhesive dentistry.

The current chapter aims to cover the subject of adhesive dentistry as comprehensively as possible. Beginning with a consideration of the surfaces to which bonding takes place, it goes on to consider the nature of the main groups of esthetic dental repair materials (the composite resins and the glass-ionomer cements) and how their adhesion is brought about and their durability maximized. There is considerable focus both on fundamental understanding of the mechanism of adhesion and on the clinical outcomes that can be achieved using these materials. Finally, other clinical applications that rely on adhesion are described. These are (i) orthodontic bracket fixation, (ii) fissure sealing, and (iii) the so-called Atraumatic Restorative Treatment technique (ART). The latter is an important development in clinical dentistry, particularly aimed at Third World countries, which is possible only with adhesive materials and which marks an innovative approach within dentistry.

---

## 57.2 Surfaces for Bonding

Unlike adhesive bonding in most areas of technology, in dentistry adhesion involves a living substrate. This is more variable than most surfaces to which adhesive materials are typically applied. To understand the significance of this, the nature of the substrates that are encountered in dentistry must be considered, which means beginning with a consideration of the anatomy of the tooth.

The tooth consists essentially of two types of tissue, the enamel and the dentin. Their compositions are shown in Table 2. From this it can be seen that the mineral phase of the enamel far exceeds that of the dentin, resulting in the enamel being much the harder and more brittle of the two tissues.

Enamel and dentin are joined by a distinctive dentino-enamel junction (DEJ). This zone has important mechanical properties, uniting as it does a thin and highly brittle layer (enamel) with a tougher, more compliant underlying structure (dentin). Among the important properties of the DEJ is that it does not allow cracks to cross from the enamel to the dentin. This feature maintains the integrity of the whole tooth, so that even if small cracks appear in the enamel, they do not propagate through the dentin and damage the whole tooth.

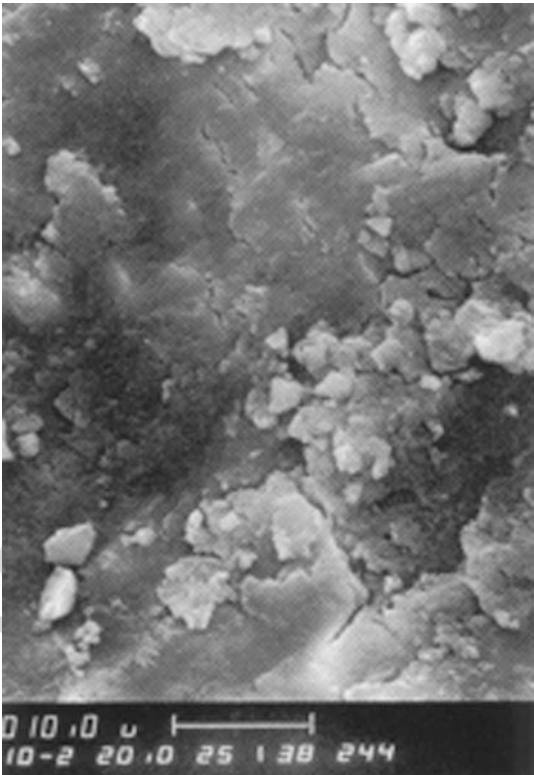
The mineral phase of the tooth is predominantly hydroxyapatite, which is a calcium phosphate mineral of nominal composition  $\text{Ca}_{10}(\text{PO}_4)_6(\text{OH})_2$  and has a Ca:P ratio of 1.67:1. Naturally occurring hydroxyapatite, such as that in teeth and also in bones, tends to be a slightly different composition from this idealized formula. It is typically calcium deficient and has a small proportion of its phosphate groups replaced by carbonates (Table 1). This natural mineral, though, is still very

**Table 1** Composition of tooth

	Enamel	Dentin
Inorganic phase (mainly hydroxyapatite)	94–96%	70%
Organic phase (mainly collagen)	4–5%	20%
Water	1%	10%
Ca:P ratio	1.64	1.56

t.1  
t.2  
t.3  
t.4  
t.5

**Fig. 1** SEM of smear layer formed by slow-speed cavity preparation, magnification  $\times 1000$  (Mount 1994)



hard and the details of its composition make little or no difference to its mechanical properties.

In order to carry out the various processes involved in dental repair, the tooth generally has to be cut with some sort of instrument. This is usually a rotary bur of the so-called dental drill. The cutting process results in the formation of a layer known as the smear layer on the surface of the tooth (Fig. 1). The smear layer is thin, typically 1–2  $\mu\text{m}$  deep, and is very tenacious. It consists of mineral phase embedded in denatured collagen, and is essentially material with a less ordered structure than uncut enamel or dentin.

The detailed composition, morphology, roughness, and tenacity of the smear layer vary according to the precise details of the cutting process (Ogata et al.

2001). Despite this, the smear layer may be left in place and act as the surface to which bonding is carried out. Dental adhesives need to be able to penetrate this layer, and possibly interact with it, to form a layer capable of being retained for many years. Bond strengths and durability are known to vary according to how this smear layer is created (Koibuchi et al. 2001), and the differences in its properties that result from the different ways it may be formed are responsible for the variations in clinical performance of dental bonding agents.

During the formation of the smear layer, cutting debris is usually forced down into the tubules of the dentin. This debris results in the formation of so-called “smear plugs” and they have the effect of reducing the permeability of the dentin, and also of reducing the total surface area available for bonding (Koibuchi et al. 2001). The reduction in permeability may be an advantage, however, as it stops fluid being forced up the dentinal tubules. This, in turn, protects the bond formed by an adhesive placed onto the cut surface.

The surface treatment that follows cutting may attempt to modify or remove the smear layer, in order to ensure that a uniform and reliable surface is left behind. It may also remove the smear plugs, thus opening the tubules and allowing the bonding agent to penetrate the tooth surface. This may not be desirable, since it may lead to postoperative sensitivity and discomfort in the patient. There is considerable debate amongst dental practitioners as to which is the best way to carry out tooth preparation, and these varying views show that, in the field of adhesive dentistry, maximizing the bond strength is not the only consideration.

---

### 57.3 Surface Pretreatment

The earliest dental restorative materials, gold foil and silver amalgam, have no adhesive properties whatsoever. They needed to be held in place by enlarging the cavity caused by the tooth decay, and forming undercuts. This is still the method used for retaining silver amalgam fillings, gold foil having passed into disuse many years ago. This approach of removing sound, healthy tooth tissue is widely recognized in the dental profession as a major disadvantage of silver amalgams (Mount and Hume 2005).

The first critical step in developing adhesion in dentistry occurred in 1955, when Buonocore reported the acid-etch process for pretreatment of enamel (Buonocore 1955). This employed solutions of phosphoric acid at 37% concentration, and when enamel surfaces were pretreated in this way, microscopic surface irregularities were created, and polymeric filling materials were able to flow into them before hardening. Once these materials had hardened, there was an interlocking effect that strongly united the filling material with the tooth. Shear bond strengths of the order of 20–25 MPa were obtained, which were enough for the resulting bonded filling to withstand the forces of biting and chewing, and to show very good retention rates.

At the time that this work was carried out, the existence of the smear layer was not known. It was obvious, however, that the acid-etch process was critical to successful bonding and that it involved the development of a surface to which bonding could

occur. The concentration of the phosphoric acid was critical, too. The apparently arbitrary concentration of 37% lies halfway between 25%, which was too dilute to be effective, and 50%, which is so concentrated that it removes too much tooth material, and does not result in the formation of a satisfactory interlock bond.

Acid etching owes part of its success to the nature of the enamel. Enamel contains very little protein or water and can therefore be dried without causing the structure to collapse. Clinically, the procedure leads to the observation of a chalky appearance to the enamel, which can be taken as an indication that etching has been successful and the surface is ready to receive the bonding layer.

Bonding to dentin has proved much more challenging. Dentin is wetter than enamel and contains protein in the form of collagen fibers. Acid etching as developed by Buonocore is much less successful when applied to dentin than to enamel, and shear bond strengths are much lower, typically lying in the region 5–10 MPa. This is because etching with 37% phosphoric acid changes the nature of the dentin surface, and it ceases to be a hard, mineralized tissue. Instead, removal of the mineral phase by the acid leaves behind a soft, collagen-rich surface structure, which collapses when dried with air. Unlike etched enamel, the resulting mat of collagen fibers forms only weak bonds with organic monomers, which is why the resulting shear bond strengths are low.

In order to form satisfactory bonds to dentin, it is important to replace the mineral component by monomer (generally termed “resin” by researchers in this field). This resin infiltration needs to take place immediately after removal of the mineral phase, or even possibly at the same time as the mineral phase is being removed, so that the collagen fibers do not collapse. This leads to the formation of an artificial structure consisting of resin-impregnated collagen fibers, which is known as the *hybrid layer* (Nakabayashi et al. 1982; Wang and Spencer 2003). The hybrid layer is strong, and is also sufficiently hydrophobic to allow the polymer-based composite resins to bond to it. Its depth varies with length of the infiltration step, and lies between 2.1 and 4.1  $\mu\text{m}$  (Nakabayashi and Saimi 1996).

In addition to hybrid layer formation, pretreatment of the surface may remove the smear layer and, more important, the smear plugs, thus opening up the tubules of the dentine. Uncured monomer (resin) is then able to flow into these open tubules and form rigid tags on polymerization. This provides an additional mechanism of retention. However, studies have shown that it is the formation of the hybrid layer that makes the biggest contribution to the bond strengths and that even resin systems that are too viscous to flow into the tubules and form resin tags are capable of generating high strength adhesive bonds (Nicholson 2000).

Pretreatment of the cut dentine surface was, for many years, carried out using weak organic acids, such as citric acid or ethylene diamine tetra-acetic acid (EDTA). This was recommended partly on the grounds of the proximity of the pulp. More recently, however, phosphoric acid has been used to etch the surface of dentin, so that similar pretreatments are now recommended for both types of tooth tissue (Nicholson 2000). This was originally called “total etch,” but is now more generally termed “etch-and-rinse” in order to emphasise that the treated surface must be rinsed before placing any further layer on it. In using this approach it is important to ensure



that the dentin is intact, and that there is no exposure of the pulp, and also that very short exposure times are used for phosphoric acid on dentin.

When the etch-and-rinse technique is used, it is important not to dry the tooth surface with air, in order to avoid the collapse of the collagen phase. This was originally known as the “wet” bonding technique, and was developed in the 1990s (Kanca 1996). It was important in simplifying the overall bonding process, and paved the way for the introduction of “etch-and-rinse” bonding agents, now considered one of the two important classes of bonding agent. These are typically based on organic solvents which are hydrophilic enough to interact with a surface containing reasonable amounts of water, such as acetone or ethanol (Tay et al. 1998). They can also dissolve the necessary organic monomers which form the resin layer in the surface of the cut tooth.

The question of how to prepare the tooth surface in order to obtain bonds that are strong and durable remains the subject of research, and there is evidence that the most effective technique varies with the type of bonding agent used. There is also the need to have reliable ways of determining success in bonding (Carvalho et al. 2012). Laboratory data on bond strength gives some information on possible clinical outcomes for bonded restorations, but the correlation is still uncertain. One problem is that laboratory studies typically use non-cariou tooth surfaces, and these differ significantly in their structure and morphology from surfaces affected by caries (Manolea et al. 2016).

Several studies of etching strategies on bond strength and durability have appeared in recent years. Etching remains popular and is also successful with enamel as the substrate using both etch-and-rinse and universal bonding agents (Takamizawa et al. 2016; Antoniazzi et al. 2016). With dentin, recent studies have suggested that dry-bonded etch-and-rinse systems can give strong bonds on both carious and non-cariou dentin, at least over a period of a year *in vitro* (Lenzi et al. 2016). Pre-etching has also been shown to improve the penetration of universal bonding agents into dentin, though this does not lead to improvements in bond strength (Wagner et al. 2014).

These recent laboratory findings have not received clinical endorsement. Generally clinical reports suggest that survival rates for bonded composite restorations are good, as described later in this chapter. However the state of the adhesive bond over time in clinical service is not known. It has been suggested that this subject should be given attention and that teeth repaired with composite resin then extracted for periodontal reasons could be examined carefully to determine the state of the bond, and in this way identify the characteristics of successful bonding agents (Carvalho et al. 2012).

---

## 57.4 Bonding Agents

Bonding agent is the term generally used in the field of adhesive dentistry to describe the substances applied to the surface of the tooth for use as an adhesive. Bonding agents are usually applied to the tooth surface by painting or dabbing them on using a

small brush. Manufacturers have formulated them mainly for application to dentin, and have used a variety of components. Details of formulations are generally not disclosed as they are proprietary, but it is known that the monomer 2-hydroxyethyl methacrylate (HEMA) is widely used in these blended materials. Other monomers known to be used include glutaraldehyde and mono- and dimethacrylates. As we have seen, acetone or ethanol, and also water may be employed as solvents for these systems.

The earliest systems consisted of three components, namely, (1) conditioning agent to fully or partially remove the smear layer, (2) primer for pretreating the dentin surface, and (3) bonding agent that was applied immediately before resin filling. Results with these systems were good, and have not so far been surpassed by any other systems. In clinical use, though, the use of such complicated systems was time consuming and not easy to tolerate by the patient, and so alternatives have been sought.

Modern formulations may combine primer and adhesive components in a single blend, in order to reduce the number of steps involved in the bonding process and to simplify the procedure for clinicians. Despite the widespread use of this approach, some sort of separate acid-etch process is required as the first step of bonding. This may be as a separate etching step, as in the etch-and-rinse approach, or as a combined etching/priming step using self-etching primers.

Etch-and-rinse adhesives are recommended for use with wet-bonding approach, to maintain the integrity of the collagen fibrils. Liquid bonding agent can be rubbed into the dentin surface as an alternative to brushing (Zander-Grande et al. 2011) in order to ensure good infiltration of the bonding agent into the tooth surface and to maintain adequate moisture content.

Self-etching primers are formulated differently from etch-and-rinse systems, and are acidic (Tay and Pashley 2001). They both etch and prime the surface in a single step without the need to rinse away the products of etching. Eliminating the rinse step has the advantage of reducing the technique sensitivity of the bonding process. This is because there is less chance of the clinician making mistakes during what is a very sensitive procedure.

Self-etching formulations are acidic because they contain acid-functional monomers, such as maleic acid. As a result of their acidity, these self-etching primers incorporate the components of the smear layer, a feature that cannot be avoided, as there is no rinse step to wash away the acid treated smear layer. However, this may not be desirable and there is evidence that retention of the smear layer components compromises the bond strength of these primers (Pashley and Carvalho 1997).

The acidity of self-etching primers varies depending on their composition, and these formulations may be classified as either weak or strong (Van Meerbeek et al. 2001). The mild self-etch primers have a pH of around 2, and dissolve the dentine surface only partially. A significant amount of mineral phase remains in the resulting hybrid layer and is bonded by carboxylate or phosphate groups from the acid-functional monomers in the primer formulation. These have been shown to give good clinical outcomes over periods of time of up to eight years (Peumans et al. 2010). By contrast, the strong self-etch primers have a pH as applied of around 1 or

below. This gives them a more aggressive interaction with the smear layer and causes them to generate a bonded surface that closely resembles the surface produced by the etch-and-rinse approach.

As well as etch-and-rinse and self-etch bonding agents, there are some brands available that can be used in either mode and are described as “universal” (Sezinando 2014). The most extensively reported universal bonding agent is Scotchbond™ Universal Adhesive (3 M Oral Care) and this material has been found to give equivalent micro-tensile bond strengths in both etch-and-rinse and self-etch modes (Hanabusa et al. 2012, Munoz et al. 2013). The moisture content of the dentin substrate did not affect bond strengths, probably because the liquid bonding agent itself contains a high proportion of water (D’Hoore et al. 2001). Clinical outcomes with this bonding agent have also been shown to be good (Perdigao et al. 2014).

Within the field of adhesive dentistry, bonding agents have been classified by generation (Dunn 2003). This classification considers that Buonocore’s original approach led to the first generation bonding agent (Buonocore 1955) and that the most recent type is the seventh generation bonding agent. This is a single-layer, one-component self-etching system. More helpfully, bonding agents have recently been classified by number of steps involved (Nicholson and Czarnecka 2016). Since this is based on a fundamental aspect of their use, it is considered more helpful than classification by generations, and is shown in Table 2.

Detailed information on the composition of the various components of bonding agents is not available, due to considerations of commercial confidentiality. However, the various formulations are generally made up of appropriate blends of monomers that vary in how hydrophilic or hydrophobic they are. Resulting films tend to allow some passage of dentinal fluid through them (Tay and Pashley 2003) and there is some evidence that this may assist hydrolytic degradation in service. Unfortunately, little data is available on the long-term clinical durability of these

**Table 2** Classification of modern bonding agents for dentistry (Nicholson and Czarnecka 2016)

Number of steps	Number of bottles	Type	Description	Comments
4	3	Etch-and-rinse	Etch, rinse, apply primer, then bonding agent	Complicated to use but results in the highest reliable bond strengths.
3	2	Etch-and-rinse	Etch, rinse, then apply prime & bond in one step	Agent for priming and bonding is in a single bottle. Gives reasonable bond strengths.
2	2	Self-etch	Apply self-etching primer, then bonding agent	Self-etching primer incorporates smear layer.
1	1	Self-etch	A single formulation comprising blended self-etching primer and bonding agent	Easiest to use. Gives acceptable bond strengths.

bonding agents, and most publications deal with short-term bond strengths, so the extent to which this interaction with dentinal fluid promotes degradation not clear.

Bonding studies have typically reported data for shear bond strengths, though there have also been a number of studies using tensile bond strengths. Values reported vary somewhat, as has been shown, depending on the nature of the particular bonding agent. Reported results typically lie in the range 15–25 MPa for shear bond strengths (Al-Ehaideb and Mohammed 2000; El Kalla and Garcia-Godoy 1998; May et al. 1997), though higher values have been reported. Tensile bond strengths, by contrast, typically lie around 10 MPa (May et al. 1997).

---

## 57.5 Evaluation of Bonding Agents

Clinical trials are the most appropriate tests of the effectiveness of bonding agents. However, they are time consuming and in vitro laboratory tests are more often used instead. Such tests are typically carried out on human teeth that have been extracted for orthodontic reasons or on bovine teeth, and shear bond strength and micro-tensile bond strengths are widely used as indicators of bonding effectiveness.

Results from these experiments need to be evaluated with care. For one thing, given the complex nature of the surface pretreatment processes, bond strength values are not simply material properties. Rather, they reflect a complex interaction between the strength of the composite resin bonded with the bonding agent, the nature of the bonding agent, the stress rate, and the sample size and its overall geometry (De Munk et al. 2005). Despite the need for caution in interpreting these results, useful information can be obtained from this type of test. For example, information on durability and on the effect of thermal cycling is best obtained from such tests.

---

## 57.6 Leakage and Bonding Agents

A clinical issue with bonding agents is the extent to which they have the ability to create a complete seal at the interface with the tooth. This is important to prevent exposure of the dentin to fluids from the mouth. Such exposure may lead to further decay beneath the restoration and may ultimately damage the pulp. Larger voids may allow bacteria to migrate into the space and this may also lead to further decay and associated damage.

The most widely studied of the types of leakage is known as microleakage. It is defined as the clinically undetectable passage of bacteria or fluids between a cavity wall and the restorative material (Kidd 1976). All of the bonding agents currently available for clinical use seem able to prevent this phenomenon and to seal the restorative margins fully.

Microleakage has conventionally been studied in vitro using dye penetration techniques, in which an organic dye dissolved in water is used to highlight the path of any imperfections through the interface between the tooth and the bonding agent/composite resin. This is a broadly satisfactory approach, although there can be

problems with it, as leakage may occur through the dentin rather than through the interface.

Even where there are no gaps capable of admitting a dye solution between the bonding agent and the substrate, some leakage of dentinal fluid has been found to occur (Sano et al. 1995; Tay and Pashley 2003). It is known as nano-leakage and is detectable with  $\text{Ag}^+$  ions in solution, typically as silver nitrate. Silver ions are much smaller than the dye molecules, and they will pass across an interface that is able to exclude dye solutions. Since its discovery as a phenomenon, nano-leakage has been widely studied in bonding agents and shown to take place through regions of enhanced permeability within the matrix of the composite resin.

Any voids associated with nano-leakage are too small to admit bacteria and so it is doubtful if they are in themselves sources of further tooth decay or other immediate clinical problems. However, they may well act as sites of hydrolytic degradation of the bonding agent and may thus grow to the point at which bacteria and their metabolic products may be admitted. This then leads to potential damage to the underlying tooth tissue.

---

## 57.7 Composite Resins

The materials which are retained in place using the bonding agents described in the preceding sections are the dental composite resins. Although all types of aesthetic dental repair materials are composites as defined in materials science, within dentistry the term is restricted to a particular group of materials (Nicholson 2000). These are based on relatively high molar mass monomers, such as bisGMA, an adduct of bisphenol A and glycidyl methacrylate, or urethane dimethacrylate (UDMA). In formulating composite resins for clinical use, these macromonomers may be diluted with other less viscous components, such as ethylene glycol dimethacrylate, and filled with an unreactive filler, such as silica or a barium silicate glass. Stress transfer between matrix and filler is aided by the use of a coupling agent, typically  $\gamma$ -methacroyloxy propyl trimethoxy silane.

Modern composite resins are cured by application of visible light at 470 nm, which activates a photo-sensitive initiator such as camphorquinone. The camphorquinone readily dissociates to form free radicals when exposed to visible light, and these bring about a cure reaction, converting the highly viscous paste to a hard, durable solid material. Typical material properties of these materials are shown in Table 3.

The advantage of composite resins is that they are esthetic (i.e., tooth-colored), and they are also durable. Reports of durability suggest that they are capable of surviving between 7 and 10 years in most patients, though this varies with the general state of oral hygiene of the patient.

Composite resins have an important disadvantage, though, and that is that, because they set by an addition polymerization mechanism, they are prone to shrink on setting. This may cause problems of leakage around the restoration, and also movement of the cusps of the tooth where bonding is particularly strong. These

**Table 3** Properties of composite resins (from McCabe and Walls 2008)

Property	Typical components/values
Main monomer	bisGMA or UDMA
Filler	50–78 wt% glass or quartz
Compressive strength	260–300 MPa
Tensile strength	40–50 MPa
Flexural strength	80–150 MPa
Modulus of elasticity	6–14 GPa

t.1  
t.2  
t.3  
t.4  
t.5  
t.6  
t.7

problems are minimized in clinical use by curing the composite resin in increments, gradually building up a full restoration layer by layer.

Within the family of composite resins are the polyacid-modified composite resins, so-called *compomers* (Nicholson 2006). These include components similar to those of glass-ionomer cements, that is, an acid-leachable glass as part of the filler phase, and a small proportion of acid-functional monomer. After setting by addition polymerization, these materials are able to draw in small amounts of moisture in the mouth, and this promotes a secondary acid–base reaction within the matrix. Studies suggest that this is of little practical benefit, though it does help liberate fluoride from the reactive glass filler, and thus allow these materials to release a small amount of fluoride steadily over prolonged periods of time. Like the conventional composite resins, polyacid-modified composites are used in conjunction with bonding agents in order for them to be retained adhesively within the tooth.

### 57.8 Durability of Bonded Composite Resin Restorations

The durability of bonds formed by bonding agents to enamel and dentin is critical to the clinical success of bonded composite restorations. Many studies have concentrated on short-term results only, typically as short as 24 h, and have neglected the fact that these bonds change with time. This is caused by a variety of factors (Breschi et al. 2008).

The first factor to be taken into account in considering bond durability is the ageing of the hybrid layer. This arises for a variety of reasons. There are natural variations in the temperature in the mouth, due to the consumption of hot and cold foods and beverages, and these affect the properties of the bond over time. The bond may also be affected by the consumption of acid foodstuffs, because these affect the hybrid layer by attacking the unprotected collagen fibers chemically. Lastly, the resin itself may undergo degradation *in situ*, resulting in loss of bond strength. Such degradation is typically hydrolytic in character and occurs due to uptake of water by the bonding layer, followed by reaction of the water with ester groups in the resin. Eventually, this leads to loss of portions of bonding agent, and an opening of the bonding layer to further infiltration and hydrolytic degradation.

Since many formulations of bonding agents combine hydrophilic or even ionic monomers with hydrophobic components, cured bonding agents may admit water

fairly easily. Indeed, they may behave as semipermeable membranes, forming distinct water channels within them in response to the ingress of the surrounding saliva. Water movement through bonding agents can be driven by osmotic pressure gradients arising because there are inorganic ions and hydrophilic monomers present, and in extreme cases this may result in the formation of water blisters over the adhesive layer (Breschi et al. 2008).

There is evidence that the new and simpler adhesives are less predictable in their long-term performance than the more established multi-step systems. Various suggestions have been made for improving their performance, of which the most practical appear to be (a) use of a hydrophobic coating and (b) application with extended cure time. This latter step improves the degree of polymerization and reduces the permeability of the bonding layer. It is thus a straightforward way of improving the long-term performance of modern adhesives.

---

## 57.9 Biocompatibility of Bonding Agents

Biocompatibility is defined as “the ability to perform with an appropriate host response in a specific location” (Williams 1987). Its study is complex and beyond the scope of this chapter, but it needs to be considered briefly in the context of the use of bonding agents in clinical dentistry. The tissues involved range in sensitivity from the completely inert (enamel) to the extremely delicate (the pulp), and their response to the range of types of chemical involved in bonding, including acids, monomers, and solvents, varies widely.

An important feature controlling the biocompatibility of bonding agents is the permeability of the dentin and also its thickness. This will determine whether or not monomers diffuse all the way through to the pulp and whether they arrive at sufficiently high concentrations to cause damage.

Of particular concern in these studies has been the presence of 2 hydroxethyl methacrylate (HEMA). This has been shown experimentally to be able to diffuse through the pulp chamber when released from a bonding agent placed beneath a composite resin (Hamid and Hume 1997). Thickness made a difference to the rate of diffusion, but even relatively thick layers of dentin (i.e., in the range 3.4–3.6 mm) were not sufficient to eliminate it completely. Another finding of significance was that diffusion of HEMA was much more rapid in teeth that had been severely affected by caries. In other words, the reason that tooth repair is needed clinically, caries, turns out to be responsible for affecting dentin permeability adversely, and opens the way for potentially harmful monomers to reach the pulp.

HEMA and other monomers used in bonding agents have been shown to be cytotoxic (Hume and Gerzina 1996). They inhibit cell proliferation and decrease mitochondrial activity significantly. The latter means that energy transduction processes in the living cells are affected adversely.

In a fully healthy tooth, pulp fibroblast cells differentiate into odontoblasts, and these cells contribute to the development of the tooth. Low concentrations of bonding agent monomers have been shown to affect this development. A variety



of processes can be affected at levels well below toxic concentration, including expression of collagen 1, osteonectin, and dental sialoprotein. This, in turn, affects the formation of mineral structures within the tooth (Bouillaguet et al. 2000).

Overall, it is clear that dentin bonding agents show significant levels of cytotoxicity to the cells of the pulp. Clinically, though, there has been little concern about this finding and no reported adverse effects in vivo. Reports of sensitivity, discomfort, or even complete death of the pulp have been notably absent from the clinical literature. It seems that biological testing in vitro may have exaggerated the extent to which bonding agents pose a threat.

Release of only small quantities of monomer may mean that only very small amounts reach the pulp itself under clinical conditions. Also, there is fluid circulation within the living pulp, and this may wash away diffusing monomers and potentially reduce the concentrations to below those needed for major cytotoxic damage to occur. Current clinical opinion is strongly supportive of the use of bonding agents in dentistry, despite the volume of data on their possible adverse biological effects.

---

## 57.10 Adhesive Dental Restorative Materials

In this section, the three naturally dental restorative materials will be considered. These are the zinc polycarboxylate cement and the glass-ionomer cements. The latter come in two broad groups, the conventional and the resin-modified glass-ionomers. In all three cases, they are placed as viscous pastes, pressed into place by the dentist to ensure that any surface irregularities are filled, and allowed to cure. They then harden and are finished by shaping them to the structure of the natural tooth with various carving tools. These materials will each be considered in turn.

Zinc polycarboxylate was the first of the adhesive dental restorative materials to be described. It was invented by Smith (1968) who reported that it was fabricated from aqueous polyacrylic acid and deactivated zinc oxide, and that it had excellent adhesion to both dentin and enamel. It was also found to have other desirable properties. For example, it set rapidly with minimal shrinkage, it was bland toward the soft tissues of the mouth, and it was almost completely insoluble in saliva (Smith 1968). Zinc polycarboxylate cement can thus be considered a major development in the field of adhesive dentistry. Typical properties of zinc polycarboxylate cement are shown in Table 4.

Sometime after its introduction to the dental profession, formulations of zinc polycarboxylate were made available in which the finely divided zinc oxide is combined with a dried powder of polyacrylic acid. The mixture is activated by the addition of an appropriate amount of water, and the whole mass sets rapidly to a solid, hard mass that is indistinguishable from formulations prepared from solutions of pre-dissolved polyacrylic acid. Set cements are opaque, due to the presence in them of considerable amounts of unreacted zinc oxide powder, which acts as a reinforcing filler.

Zinc polycarboxylate cements rapidly found use in clinical restorative dentistry. Applications included cavity lining, luting of crowns, and adhesion of orthodontic



t.1	<b>Table 4</b> Properties of zinc polycarboxylate cement	Property	Typical components/values
t.2		Liquid	40–50% polyacrylic acid
t.3		Powder: liquid ratio	2.5–3:1
t.4		Setting time	2.4–4 min
t.5		Compressive strength	80–100 MPa

564 brackets (see Sect. 14). They remain in use for these applications, but have been  
565 displaced to an extent by glass-ionomer cements.

566 The zinc oxide powder for these cements is modified, partly by mixing with small  
567 quantities of magnesium oxide, and partly by heat treatment at temperatures of  
568 between 1100 °C and 1200 °C. This reduces the reactivity toward polyacrylic acid  
569 so that the cement does not set too rapidly. Heat treatment causes a slight yellowing  
570 of the zinc oxide, due to the loss of a very small proportion of the oxygen. The  
571 resulting material is very slightly non-stoichiometric, with a formula corresponding  
572 to  $\text{ZnO}_{(1-x)}$ , where  $x$  is 70 ppm or less (Greenwood and Earnshaw 1984).

573 The bonding strengths of zinc polycarboxylates have been found to be adequate  
574 but not outstanding. Tensile bond strength values of the order of 4–6.5 MPa have  
575 been found for them to enamel in in vitro studies (Brantley and Eliades 2001).  
576 Tensile bond strengths to dentin are lower, suggesting that bonding takes place  
577 primarily to the mineral phase. Actual bond strengths may be higher than these  
578 reported figures, because failure is typically clearly cohesive within the cement,  
579 rather than adhesive in nature.

580 Studies have shown that bond strength varies with thickness of zinc poly-  
581 carboxylate cement. One study showed that the adhesive layer thickness was  
582 maximum at 205  $\mu\text{m}$  (Akinmade and Nicholson 1995) when bonding stainless  
583 steel strips together and determining bond strength in shear. Values ranged from  
584 2.5 to 4 MPa.

585 Zinc polycarboxylate cements not only form adequate bonds to enamel and  
586 dentin, they will also bond to base metals used in dentistry, and also to gold.  
587 However, there is almost no adhesive bond formed on the surface of porcelain  
588 (McCabe and Walls 2008).

589 The next adhesive repair material to become available to the dental profession  
590 was the glass-ionomer cement, which was first described by Wilson and Kent in  
591 1972 (Wilson and Kent 1972). These materials are now used in clinical dentistry  
592 for a variety of aspects of the repair of teeth damaged by dental decay. Depending  
593 on how they are formulated, they may be used as liners and bases or as full  
594 restorations, and they may also be formulated for other clinical uses, as shown in  
595 Table 5. They are esthetic in that they match the natural color of the tooth and,  
596 like the zinc polycarboxylate cement, they are able to bond directly to the surface  
597 of the tooth. They have the additional feature of being able to release small  
598 amounts of fluoride. This is generally considered beneficial preventing further  
599 decay of the repaired tooth, though this point has not been confirmed by clinical  
600 studies.

**Table 5** Typical properties of conventional glass-ionomer cements

Property	Typical components/values
Liquid	40–50% polyacrylic acid
Powder: liquid ratio	3:1
Setting time	2–4 min
Compressive strength	150–220 MPa

t.1  
t.2  
t.3  
t.4  
t.5

Glass-ionomers are usually made from polyacrylic acid, although acrylic acid/maleic acid copolymer is used in some brands as an alternative. Typically, an aqueous solution of this polymer is mixed with a special ion-leachable glass of complex composition. The glass is basic, and consists of an alumino-silicate structure augmented with phosphate and also containing fluoride species, such as  $\text{CaF}_2$  or cryolite,  $\text{Na}_3\text{AlF}_6$ . Setting occurs by neutralization, and involves the polymeric acid molecules being cross-linked with multivalent counter-ions ( $\text{Ca}^{2+}$ ,  $\text{Sr}^{2+}$ ,  $\text{Al}^{3+}$ ) after they have been leached from the glass. As indicated, the glasses are complex and often contain two phases, either completely or partially separated. The setting reaction is, therefore, also complicated and involves not only the formation of ionically cross-linked polymer chains but also hydration processes, the details of which are not yet clear. There is also evidence that an inorganic network forming species from the glass, consisting of phosphate moieties, contributes to the strengthening processes that occur in the cement matrix.

Whatever the detail of the setting reactions, they take place fairly rapidly so that typically after about 5 min the cement hardens and can then be finished by the dentist. Subsequently, some slow reactions take place that bring about maturation. This maturation causes gradual increases in translucency and compressive strength and takes place over several weeks following the initial hardening. The final product is a rigid material that has a porcelain-like appearance.

As well as the original glass-ionomer cement described above, there is another variation known as the resin-modified glass-ionomer cement (RMGIC). Like the conventional glass-ionomer, RMGIC contains a basic ion-leachable glass powder, and also a water-soluble polymeric acid. However, this type of material also contains water-soluble organic monomer, usually 2-hydroxyethyl methacrylate (HEMA). An initiator system is also required to bring about additional polymerization of the HEMA (Mitra 1991a).

In most RMGICs the initiator system is photosensitive, and most RMGICs are light cured. Initiators used are sensitive to blue light of wavelength 470 nm, which is the main light emitted by conventional dental curing lamps.

Some brands of RMGIC contain modified polymers. Typically, these are based on poly (acrylic acid) but contain a minority of branches that are terminated in vinyl groups. These undergo copolymerization with the HEMA on irradiation, which means that the final material contains organic as well as ionic cross-links when cured. Typical properties are given in Table 6.

Like conventional glass-ionomers, RMGICs form strong adhesive bonds to enamel and dentine (Mitra 1991b) and also release fluoride. The presence of

**Table 6** Typical properties of resin-modified glass-ionomer cement

Property	Typical components/values
Liquid	40–50% polyacrylic acid, plus 2-hydroxyethyl methacrylate (HEMA)
Powder:liquid ratio	3:1
Setting time	30 s (on application of curing lamp)
Compressive strength	150–180 MPa

HEMA causes the set RMGIC to have some hydrogel character, which means they are capable of swelling in water. In saliva, any such swelling occurs only slightly, if at all, so this does not pose any clinical problems.

RMGICs were originally developed for use as liners and bases in dentistry (Wilson 1990), but have since been formulated for use as complete restoratives. They can also be used for core build-up and for luting, though for the latter application, they are not photocured. Rather, they are cured with a two-part initiator that forms free radicals on mixing, so that they are able to set in the dark. They are widely used, and are reported to be reliable materials capable of giving good results in service. They have been particularly used in pediatric dentistry as alternatives to amalgam.

Based on observations from HEMA-based dental bonding agents, the presence of HEMA has been suggested to compromise the biocompatibility of RMGICs (Nicholson and Czarnecka 2008b). HEMA is released from RMGICs especially in the first 24 h. As already mentioned, it is able to diffuse through the dentin and affect the pulp, to which it has been shown to exhibit cytotoxicity. It may also have systemic effects on dental personnel, including contact dermatitis (Geukins and Goossens 2001) and sensitization (Katsumo et al. 1996). Safety precautions have been recommended for dental personnel using these materials, mainly to ensure good ventilation of the work place and to avoid breathing HEMA vapor from the unset RMGIC.

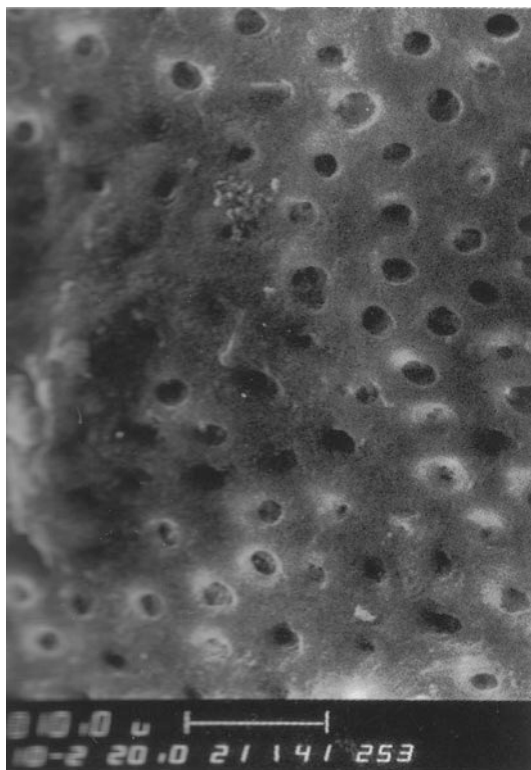
### 57.11 Bonding of Glass-Ionomer Cements

Glass-ionomers of all types are able to form adhesive bonds to the surface of the tooth. In order to do so under clinical conditions, the newly cut enamel and/or dentin surfaces are generally treated with a dilute solution of polyacrylic acid, typically at 10% concentration. This is a much milder treatment than that used with current bonding agents for composite resins and is more akin to pretreatments used with third generation bonding agents.

Conditioning with polyacrylic acid results in removal of the smear layer and of the smear plugs, and opens up the dentinal tubules (Fig. 2). It does not, however, lead to loss of much, if any, intact tooth mineral from the surface.

The glass-ionomer cement is then applied and allowed to cure. For conventional glass-ionomers, this occurs simply through the acid–base setting reaction already described; for RMGICs, it is generally brought about by exposure to a curing lamp.

**Fig. 2** SEM of dentin conditioned with 10–15 s application of 10% aqueous polyacrylic acid, magnification  $\times 900$  (Mount 1994)



Restorations of RMGIC are often completed in increments, to offset the polymerization shrinkage, as is the case for composite resins.

There have been many published studies of the bond strength of freshly placed glass-ionomers to tooth surfaces. Results obtained are generally relatively low, typically in the range 3–7 MPa when tested in shear. However, this has been shown, in reality, to be a measure of the tensile strength of the glass-ionomer, rather than the shear strength of the bond, as failure tends to be cohesive in nature (Mount 1991). Measured shear bond strengths for RMGICs tend to be slightly higher than for conventional glass-ionomers, a reflection of their higher tensile strengths (Mitra 1991b).

Despite the relatively low shear bond strengths, durability of glass-ionomer cements in clinical service is good. Studies have shown that survival rates may exceed those of bonded composite resins (Burgess et al. 1994), though there are problems about undertaking comparisons with the most recently developed materials and systems, since survival data and information on durability take several years to obtain.

Studies of marginal leakage with glass-ionomers, both conventional and resin modified, have given variable results. It is therefore not possible to draw conclusions about whether conventional or resin-modified glass-ionomers perform better in this

regard. However, it is possible to say that both types may exhibit marginal leakage and that neither is completely reliable in sealing enamel margins. Conversely there have been no satisfactory reports of the development of secondary caries below glass-ionomer restorations, which suggests that even if they leak they are sufficiently anticariogenic to prevent further tooth decay. This anticariogenic character may be attributed to the fluoride release in situ.

Glass-ionomers have been found to show distinct interactions with the tooth surface over the longer term. In an important paper, Ngo et al. (1997) showed that there was a pronounced zone formed at the interface between glass-ionomer cements and the tooth (Fig. 3). This study involved low-temperature Scanning Electron Microscopy examination of freshly extracted teeth that had been filled with a strontium-based conventional glass-ionomer and allowed to mature for 4 days. The interaction zone that formed within this time was not only clearly visible, but shown in subsequent studies to contain both calcium and strontium. Since there was originally no calcium in the cement and little or no strontium in the surface of the dentin, this result can only mean that there has been some sort of chemical reaction between the cement and the dentin to create this structure. Furthermore, it shows that adhesion of glass-ionomer cements involves an ion-exchange process.

Developments in tooth-colored restorative materials have caused some confusion within the dental profession. First, resin-modified glass-ionomers were launched and their composition, in terms of monomer and light-activated initiator, gave them some similarities with composite resins. Soon afterward, the compomers became available. They had a modest but distinct acid-base character which was responsible for maturation reactions within the material. This group of composites thus had some clear glass-ionomer character. The situation was clarified in a paper published in the mid-1990s (McLean et al. 1994), and a system of nomenclature was proposed that has subsequently been widely adopted.

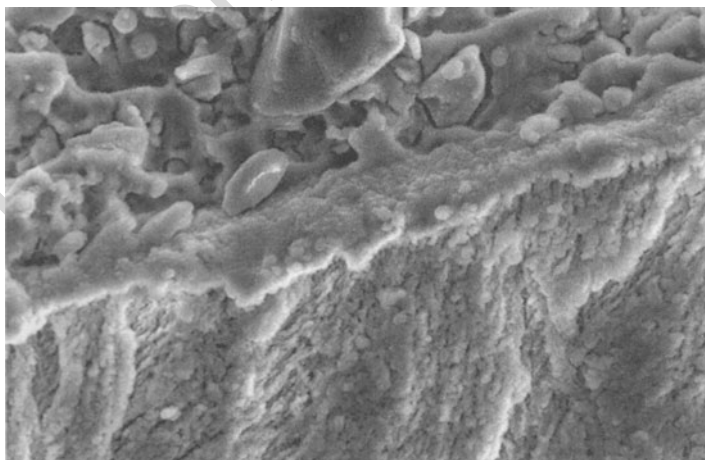


**Fig. 3** Low temperature SEM of interaction zone between glass-ionomer cement (*top*) and dentin (*beneath*), magnification  $\times 4317$  (Ngo et al. 1997)

Recently, this field has been reviewed (Mount et al. 2009) and the conclusion drawn that recent research shows it is the mechanism of bonding that is the most important distinction between the tooth-colored restorative materials. The ion-exchange mechanism can only occur in materials with a substantial acid-base setting mechanism, and this only occurs with glass-ionomer cements. No amount of modification can make systems that are fundamentally hydrophobic, and which set exclusive by polymerization, that is, composite resins, capable of undergoing ion-exchange bonding. These materials will always need bespoke and discrete bonding agents, of the type previously described.

---

## 57.12 ART Technique

The clinical technique known as Atraumatic Restorative Treatment (ART) has been developed since the mid-1980s in response to dental clinical needs in Third World countries. It is an important application of adhesive dental materials, specifically conventional glass-ionomer cements, and would not be possible without this type of adhesive material (Frencken et al. 2004). ART involves the removal of carious tooth tissue with hand instruments rather than conventional dental drills. These hand-held instruments take the form of spoon-shaped excavators, and come in graded sizes.

Following excavation of the soft carious matter, the cavity is cleaned and filled with freshly mixed glass-ionomer cement. Associated pits and fissures within the tooth are filled at the same time. This technique does not require electricity or clean water, so is particularly suitable for settings in the developing world where these facilities are either absent or unreliable.

Adhesive materials are essential for this technique because the tooth can only be excavated to remove soft matter, not drilled to extend the cavities with undercuts. This sort of mechanical retention is required by silver amalgam fillings, and cannot be deployed in regions where the drill cannot be used. The hand-operated excavators used in ART are not capable of removing undamaged enamel or dentin, so cannot be used to prepare undercut cavities.

Clinical reports covering 25 years experience have shown that ART is an effective treatment in a variety of countries of the world (Frencken et al. 2012). Modern conventional glass-ionomer cements for use with this technique have been formulated with optimized particle size and size-distribution glass powders, and they are found to perform very well in patients. Long survival times are being recorded, with almost no problems of debonding in clinical service.

---

## 57.13 Glass-Ionomer Fissure Sealants

Fissure sealing is a preventive technique carried out on newly erupted teeth. Deep fissures in such teeth may act as sites into which plaque and pellicle may become occluded, and it cannot be removed from these sites by brushing. Left undisturbed, this is likely to result in the development of caries.

So-called sealing of these fissures involves minor clinical procedures. First, the plaque and the pellicle are removed using a dental bur, after which the fissure is widened slightly but only within the enamel. To complete the process, some sort of filling material is placed in the newly opened fissure.

For some time, the material of choice was considered to be an unfilled resin, essentially a low viscosity blend of the type of monomers used in conventional composite resins. Such fissure sealants have good retention, which is obviously highly desirable.

However, there is beginning to be a shift in clinical opinion that favors glass-ionomers for this application. Initial results with these materials were not promising, for a variety of reasons. Their early bond strengths are lower than those of resin systems, and they had inferior wear resistance. This meant that they appeared to be lost fairly rapidly. Careful study shows, though, that this does not mean that the treated teeth are no longer protected. Teeth treated in this way do not develop caries and protection may last for at least 6 years (Pardi et al. 2003). This surprising result occurs for two reasons.

First, glass-ionomer fissure sealants release fluoride in amounts that are protective to the surrounding tooth tissue. Second, not all of a glass-ionomer sealant is actually lost. Deep within the fissures, glass-ionomer sealants are retained and not only retained, but also transformed over time. Changes which occur include increasing translucency, improvement in smoothness and in hardness, and elevation in the calcium and phosphate ion concentrations in the surface layer. These alterations take of the order of 2–3 years to develop and seem to be akin to the development of artificial enamel (Van Duinen et al. 2004).

It must be emphasized that this structural change in the glass-ionomer fissure sealant only occurs in the base of the fissures. The rest of the glass-ionomer typically disappears within a few months. The modified glass-ionomer tends to show integration with the adjacent enamel, with excellent sealing. There is no occurrence of caries and every appearance of strong adhesion, though no bond strength data have yet been reported. These findings are similar to those previously discussed for glass-ionomer restorative materials, which also develop strong adhesive bonds with time and show elevated calcium and phosphate levels in the surface following prolonged contact with saliva.

---

## 57.14 Bonding in Orthodontics

Orthodontics is that branch of clinical dentistry concerned with correctly aligning crooked teeth. This is typically carried out during the teenage years, and involves applying brackets to several of the teeth, and connecting them with high-tensile strength wires. Successive visits to the orthodontist are made, and in each the tension in the wires is increased, thus applying a force that causes the tooth to move within the socket and to be retained there permanently. This is due to changes in the shape of the supporting bone around the socket. Brackets are typically retained on the tooth, either mechanically, or by bonding.



The earliest attempts to bond orthodontic brackets used epoxy resins. However, these adhesives were difficult to use, and so this approach did not find much support within the dental profession. In modern orthodontic practice, bonding agents similar to those used in other parts of dentistry are used. This means the deployment of either bonded composite resins or glass-ionomer cements.

Direct bonding of orthodontic brackets uses the acid-etch technique, with phosphoric acid gel to etch the surface and deliver the initial pretreatment (Kitayama et al. 2007). This is followed by the application of bonding agents or of lightly filled or completely unfilled resins to the surface. These form attachments to the surface mechanically by flowing into the irregularities created in the etching step.

A clinical problem with this technique is that brackets bonded by composite resins in this way have a tendency to develop regions of demineralization around them. This leads to the formation of white spots on the tooth surface. Typically where white spot lesions develop, they affect several teeth of a patient.

Another problem is that, when the time comes to remove the brackets, damage may occur to the surface of the tooth. This is because the bond strength generated by this technique is so high that the enamel shears in preference to debonding.

To overcome the problems of “white spot” lesions, and also to exploit the lower inherent bond strength, glass-ionomer cements are increasingly being used for this application. Their ability to release fluoride ensures that there are no sites of demineralization, hence no white spot formation. There is also much less damage when the brackets are removed (Charles 1998).

---

## 57.15 Conclusions

This chapter describes the principal uses of adhesives in clinical dentistry, and covers both the materials and the clinical techniques involved. The subject is of enormous importance in modern dentistry and is connected with the growing interest in the use of tooth-colored repair materials.

The two types of tooth-colored material, namely, the composite resin and the glass-ionomer cement, are described, together with their current variations. Composite resins are bonded with specific bonding agents, and these substances may be used in either etch-and-rinse or self-etch modes. This technology continues to evolve rapidly, and recent advances in the field are covered in detail. Surface pretreatment is critical for the success with bonding and current understanding of this topic is reviewed as well.

Glass-ionomers are naturally adhesive to both dentin and enamel, though some sort of surface pretreatment is necessary prior to their use. Typically this consists of conditioning the freshly cut tooth surface with dilute aqueous polyacrylic acid, followed by rinsing away the products. Glass-ionomers then bond firmly to the tooth, partly through the development of a mechanically strong ion-exchange layer at the interface that develops with time. This bonding ability is exploited in the important technique of ART, created for use in Third World countries to treat the



growing problem of tooth decay. Glass-ionomers are also used as bonding agents for orthodontic brackets.

Zinc polycarboxylate cement, the first adhesive dental restorative material, is also described in this chapter, though it now has only niche applications in dentistry.

---

## References

- Akinmade A, Nicholson JW (1995) Effect of adhesive layer thickness on the bond strength of a zinc polycarboxylate dental cement. *Biomaterials* 15:149
- Al-Ehaideb A, Mohammed H (2000) Hear bond strength of “one-bottle” dentin adhesives. *J Prosthet Dent* 84:408
- Antoniazzi BF, Nicolos GF, Lenzi TL, Soares FZM, Rocha RO (2016) Selective acid etching improves the bond strength of universal adhesive to sound and demineralized enamel of primary teeth. *J Adhes Dent* 18:311
- Brantley W, Eliades T (2001) Orthodontic materials, scientific and clinical aspects. Thieme, Stuttgart
- Breschi L, Mazzoni A, Ruggeri A, Cadenaro M, Lenarda R, De Stafano DE (2008) Dental adhesion review: aging and stability of bonded surfaces. *Dent Mater* 24:90
- Bouillaguet S, Wataha JG, Virgillito M, Gonzalez L, Rakich DR, Meyer JM (2000) Effect of sublethal concentrations of HEMA (2-hydroxyethyl methacrylate) on THP-1 human monocyte macrophages in vitro. *Dent Mater* 16:213
- Buonocore MG (1955) A simple method of increasing the adhesion of acrylic filling materials to enamel surfaces. *J Dent Res* 34:849
- Burgess JO, Norling B, Summit J (1994) Resin ionomer restorative materials: the new generation. *J Esthet Dent* 6:207
- Carvalho RM, Manso AP, Geraldini S, Tay FR, Pashley DH (2012) Durability of bonds and clinical success of adhesive restorations. *Dent Mater* 28:72
- Charles C (1998) Bonding orthodontic brackets with glass-ionomer cement. *Biomaterials* 19:589
- D’Hoore WRA, Gonthier S, Degrange M, Dejoui J (2001) Reliability of in vitro microleakage test: a literature review. *J Adhes Dent* 3:295
- De Munk J, Van Landuyt K, Peumans M, Poitevin A, Lambrechts P, Braem M, Van Meerbeek B (2005) A critical review of the durability of adhesion to tooth tissue: methods and results. *J Dent Res* 118:132
- Dunn JR (2003) iBond™: the seventh generation, one-bottle dental bonding agent. *Compen Cont Dental Educ* 24(Suppl 2):14
- El Kalla IH, Garcia-Godoy F (1998) Bond strength and interfacial micromorphology of four adhesive systems in primary and permanent molars. *J Dent Child* 65:169
- Frencken JE, van’t Hof MA, van Amerongen WE, Holmgren CJ (2004) Effectiveness of single-surface ART restorations in the permanent dentition: a meta-analysis. *J Dent Res* 83:120
- Frencken JE, Leal SC, Navarro MF (2012) Twenty-five-year atraumatic restorative treatment (ART) approach: a comprehensive overview. *Clin Oral Invest* 16:1337
- Geukins S, Goossens A (2001) Occupational contact allergy to (meth)acrylates. *Contact Dermatol* 44:153
- Greenwood NN, Earnshaw A (1984) The chemistry of the elements. Pergamon, Oxford
- Hamid A, Hume WR (1997) Diffusion of resin monomers through human carious dentin in vitro. *J Oral Rehabil* 24:20
- Hanabusa M, Mine A, Kuboki T, Momoi Y, Van Ende A, Van Meerbeek B, De Munck J (2012) Bonding effectiveness of a new multi-mode adhesive to enamel and dentine. *J Dent* 40:475
- Hume WR, Gerzina TM (1996) Bioavailability of components of resin-based materials which are applied to teeth. *Crit Rev Oral Biol Med* 7:172

- 886 Kanca J (1996) Wet bonding: effect of drying time and distance. *Am J Dent* 9:273
- 887 Katsumo K, Manabe A, Itoh K, Nakamura Y, Wakumoto S, Hisamitsu H, Yoshida T (1996) Contact  
888 dermatitis caused by 2-HEMA and GM dentin primer solutions applied to guinea pigs and  
889 humans. *Dent Mater J* 15:22
- 890 Kidd EAM (1976) Microleakage: a review. *J Dent* 4:199
- 891 Kitayama S, Nikaido T, Ikeda M, Foxton RM, Tagami J (2007) Enamel bonding of self-etch and  
892 phosphoric acid-etch orthodontic adhesive systems. *Dent Mater J* 26:135
- 893 Koibuchi H, Yasuda N, Nakabayashi N (2001) Bonding to dentin with a self-etching primer: the  
894 effect of smear layers. *Dent Mater* 17:122
- 895 Lenzi TL, Soares FZM, Raggio DP, Pereira GKR, Rocha RO (2016) Dry-bond etch-and-rinse  
896 strategy improves bond longevity of a universal adhesive to sound and artificially-induced  
897 caries-affected primary dentin. *J Adhes Dent* 18:475
- 898 Manolea H, Antoniac J, Miculescu M, Rica R, Platon A, Melnicenco R (2016) Variability of the  
899 composite resins adhesion with the dental substrate penetration and the used adhesive type.  
900 *J Adhes Sci Technol* 16:1754
- 901 May KN, Swift JR, Bayne SC (1997) Bond strengths of a new dentin adhesive system. *Am J Dent*  
902 10:195
- 903 McCabe JF, Walls AWG (2008) *Applied dental materials*, 9th edn. Blackwell, Oxford
- 904 McLean JW, Nicholson JW, Wilson AD (1994) Proposed nomenclature for glass-ionomer cements  
905 and related materials. *Quintessence Int* 25:587
- 906 Mitra SB (1991a) Adhesion to dentin and physical properties of a light-cured glass-ionomer  
907 liner/base. *J Dent Res* 70:72
- 908 Mitra SB (1991b) In vitro fluoride release from a light-cured glass-ionomer liner/base. *J Dent Res*  
909 70:75
- 910 Mount GJ (1991) Making the most of glass ionomer cements. *Dent Update* 18:276
- 911 Mount GJ (1994) *A color atlas of glass ionomer cements*, 2nd edn. Dunitz, London
- 912 Mount GJ (2002) *A color atlas of glass ionomer cements*, 3rd edn. Dunitz, London
- 913 Mount GJ, Hume WR (2005) *Preservation and restoration of teeth*, 2nd edn. Knowledge Books and  
914 Software, Middlesbrough
- 915 Mount GJ, Tyas MJ, Ferracane JL, Nicholson JW, Berg JH, Simonsen RJ, Ngo H (2009) A revised  
916 classification for direct tooth-colored restorative materials. *Quintessence Int* 40:691
- 917 Munoz M, Sezinando A, Luque-Martínez I, Szesz A, Reis A, Loguercio AD, Bombarda NH (2013)  
918 Immediate bonding properties of universal adhesives to dentine. *J Dent* 41:404
- 919 Nakabayashi N, Kojima K, Masuhara E (1982) The promotion of adhesion by the infiltration of  
920 monomers into tooth substrates. *J Biomed Mater Res* 16:265
- 921 Nakabayashi N, Saimi Y (1996) Bonding to intact dentin. *J Dent Res* 75:1706
- 922 Ngo H, Mount GJ, Peters MRCB (1997) A study of glass-ionomer cement and its interface with the  
923 enamel and dentin using a low-temperature, high-resolution scanning electron microscope  
924 technique. *Quintessence Int* 28:63
- 925 Nicholson JW (2000) Adhesive dental materials and their durability. *Int J Adhes Adhes* 20:11
- 926 Nicholson JW (2006) Polyacid modified composite resins ("compomers") and their use in clinical  
927 dentistry. *Dent Mater* 23:615
- 928 Nicholson JW, Czarnecka B (2008a) Fluoride in dentistry and dental restoratives. In: Tressaud A,  
929 Haufe G (eds) *Fluorine and health*. Elsevier, Amsterdam/Boston
- 930 Nicholson JW, Czarnecka B (2008b) Biocompatibility of resin-modified glass-ionomer dental  
931 cement. *Dent Mater* 24:1702
- 932 Nicholson JW, Czarnecka B (2016) Dental adhesives. In: *Materials for the Direct Restoration of*  
933 *Teeth*. Woodhead Publishing, Duxford
- 934 Ogata M, Harada N, Yamaguchi S, Nakajima M, Periera PN, Tagami J (2001) Effect of different  
935 burs on bond strengths of self-etching primer systems. *Oper Dent* 26:375
- 936 Pardi V, Periera AC, Mialhe FL, Meneghim MC, Ambrossana GM (2003) A 5-year evaluation of  
937 two glass-ionomer cements used as fissure sealants. *Community Dent Oral Epidemiol* 31:386
- 938 Pashley DH, Carvalho RM (1997) Dentine permeability and dentine adhesive. *J Dent* 25:355

- 939 Perdigao J, Kose C, Mena-Serrano AP, De Paula EA, Tay LY, Reis A, Loguercio AD (2014) A new  
940 universal simplified adhesive: 18-month clinical evaluation. *Oper Dent* 39:113
- 941 Peumans M, De Munck J, Van Landuyt KL, Poitevin A, Lambrechts P, Van Meerbeek B (2010)  
942 Eight-year clinical evaluation of a 2-step self-etch adhesive with and without selective enamel  
943 etching. *Dent Mater* 26:1176
- 944 Roulet J-F, Vanherle G (2004) Adhesive technology for restorative dentistry. Quintessence, Chicago
- 945 Sano H, Takatsu T, Ciucchi B, Horner JA, Matthews JA, Pashley DH (1995) Nanoleakage: leakage  
946 within the hybrid layer. *Oper Dent* 20:18
- 947 Sezinando A (2014) Looking for the ideal adhesive – a review. *Rev Port Estomatol Med Dent Cir*  
948 *Maxillofac* 55:194
- 949 Smith DC (1968) A new dental cement. *Br Dent J* 125:381
- 950 Takamizawa T, Barkmeier WW, Tsujimoto A, Endo H, Tsuchiya K, Erikson RL, Latta MA,  
951 Miyazaki M (2016) Influence of pre-etching times on fatigue strength of self-etch adhesives  
952 to enamel. *J Adhes Dent* 18:501
- 953 Tay FR, Gwinnett AJ, Wei SHI (1998) Relation between water content in acetone/alcohol-based  
954 primer and interfacial ultrastructure. *J Dent* 26:147
- 955 Tay FR, Pashley DH (2001) Aggressiveness of contemporary self-etching systems. I: Depth of  
956 penetration beyond dentin smear layers. *Dent Mater* 17:296
- 957 Tay FR, Pashley DH (2003) Water treeing: a potential mechanism for degradation of dentin  
958 adhesives. *Am J Dent* 16:6
- 959 Van Duinen RNB, Davidson CL, De Gee AJ, Feilzer AJ (2004) In situ transformation of glass-  
960 ionomer into an enamel-like material. *Am J Dent* 17:223
- 961 Van Meerbeek B, Vargas M, Inoue S, Yoshida Y, Peumans M, Lambrechts P, Vanherle G (2001)  
962 Adhesives and cements to promote preservation dentistry. *Oper Dent* 26:S119
- 963 Wagner A, Wendler M, Petschelt A, Belli R, Lohbauer U (2014) Bonding performance of universal  
964 adhesives in different etching modes. *J Dent* 42:800
- 965 Wang Y, Spencer P (2003) Hybridization efficiency of the adhesive/dentin interface with wet  
966 bonding. *J Dent Res* 82:141
- 967 Williams DF (1987) Definitions in biomaterials. Elsevier, Amsterdam
- 968 Wilson AD (1990) Resin-modified glass-ionomer cements. *Int J Prosthodont* 3:425
- 969 Wilson AD, Kent BE (1972) A new translucent cement for dentistry. The glass-ionomer Cement.  
970 *Br Dent J* 132:133
- 971 Zander-Grande C, Ferreira SQ, da Costa TRF, Loguercio RA (2011) Application of etch-and-rinse  
972 adhesives on dry and rewet dentin under rubbing action: a 24-month clinical evaluation. *J Am*  
973 *Dent Assoc* 142:828

Robin A. Chivers

**Contents**

58.1	Introduction .....	1730
58.2	Mechanical Fastening .....	1730
58.3	Adhesives Technologies for Internal Applications .....	1731
58.3.1	Overview .....	1731
58.3.2	Requirements of an Adhesive for Internal Use .....	1732
58.3.3	Categories of Adhesives .....	1734
58.3.4	Synthetic Adhesives .....	1734
58.3.5	Biological Adhesives .....	1739
58.3.6	Laser Welding and Soldering .....	1744
58.4	Adhesives for External Application to the Skin .....	1744
58.5	Conclusions .....	1747
	References .....	1747

**Abstract**

Adhesives are increasingly being used in medicine for repairing cuts and tears in the body as an alternative to mechanical fixation such as sutures. There are very strict regulations controlling the application of adhesives within the body and this means that there are only a limited number of chemistries which are approved for clinical use. The principal internal adhesives in current use are those based on fibrin, gelatin, and poly(ethylene glycol) (PEG) hydrogels and function largely as sealants, though do bond to the tissue surfaces. Cyanoacrylates are approved, mostly only for application to the surface of the skin for wound closure, but are quite widely used in a range of other applications. There are many requirements of an adhesive for internal use and this has led to large number of further systems being proposed. A number of those currently being evaluated for internal

R. A. Chivers (✉)  
York, North Yorkshire, UK  
e-mail: [chiversfamily@waitrose.com](mailto:chiversfamily@waitrose.com)

indications are described. Some are based on synthetic chemistry, some from biological sources such as marine creatures, and some are akin to welding or soldering.

Pressure-sensitive adhesives are widely used for securing dressings and devices to the skin surface. Most of these are now based on acrylic or silicone chemistries.

---

## 58.1 Introduction

In simplest terms, the human body is made up of organs and tissues held together in a way which maintains their mechanical integrity and ability to function correctly. However, there are occasions when, due to accident, surgery or wear, some of these tissues or organs fail. In many cases, the body is capable of repairing naturally but sometimes needs assistance with this. Surgery has developed to such an extent that it is frequently possible to refasten or repair the failure such that the tissue can repair itself and regain its normal function, albeit in a scarred state. Initially, these surgical procedures consisted of provision of a mechanical fixation, but more recently a range of adhesive products and techniques have been developed to replace or augment these, analogously to the substitution of adhesives for nails, screws, bolts and rivets in engineering. This chapter aims to summarize the current state of this technology – adhesion and adhesives for repairing the human body. These may be adhesives for repair of internal organs, or for topical application to the skin, alone or on dressings. They are distinguished as adhesives for contact with body tissue, applied for the most part by medical professionals, though with one exception: dentistry is not included. The use of adhesives is well established in dentistry and will not be covered further here as it is the subject of ► [Chap. 57, “Adhesive Dentistry.”](#)

There are a number of other aspects of adhesion in medicine which will only be touched on here. Adhesives are used widely in the manufacture of medical devices. Some of these applications require the adhesive to be in contact with body material, such as recirculating blood, and are therefore subject to some of the strict regulations which are imposed on products with body contact (Tavakoli et al. 2005). Other aspects of adhesion include the aggregation of cells and proteins onto foreign surfaces within the body, forming biofilms, the desired adhesion of cells in culture onto scaffolds for tissue engineering in the regeneration of organs, and the undesirable adhesion, known as “adhesions” between scarred tissues which can produce serious complications after surgery.

---

## 58.2 Mechanical Fastening

Traditionally, repair of damage to the body has been performed by surgeons using mechanical means. The most familiar of these is the suture, a thread of resorbable or non-resorbable polymer, which is stitched through soft tissue using a specially designed needle. Pulling the tissue edges together encourages the formation of a

bond between them as the tissue regrows. When repair is complete, the surgeon may return to remove the sutures or they may degrade and eventually be excreted by the body. Suturing is usually fairly straightforward and medical professionals are trained in its use. It can also be easily removed and reapplied should there be a problem. It has the disadvantage, though, of only holding the tissue at discrete points, leaving less well-secured gaps between these which may be susceptible to leakage (see, e.g., Fig. 1a). More recent developments in soft tissue fixation include metallic staples and barbed polymeric darts, and when fixation is required to hard tissue, there are ranges of interference screws available. Securing pieces of bone mechanically is usually done using plates, held in place with screws, or by the use of long intramedullary nails which can be inserted down the medullary canal in the long bones, and then held fast by transverse screws at the ends. Metallic repair means may be surgically removed after the tissue has healed, but are frequently left in place if they do not cause a problem for the patient.

Externally, the skin may be sutured or bandaged to give support during natural healing. However, crude adhesives, such as tar, have long been used to protect sites of severe damage.

## 58.3 Adhesives Technologies for Internal Applications

### 58.3.1 Overview

From the time of the introduction of the first adhesive used in an internal application, fibrin sealant, some clinicians have been seeking adhesive solutions to problems in the internal repair of the body, aiming to achieve excellent performance without the problems related to the use of the traditional mechanical means of repair such as localized fixation and the need for removal. Chemists and biologists have been keen to support them in this quest and have produced a wide range of different materials

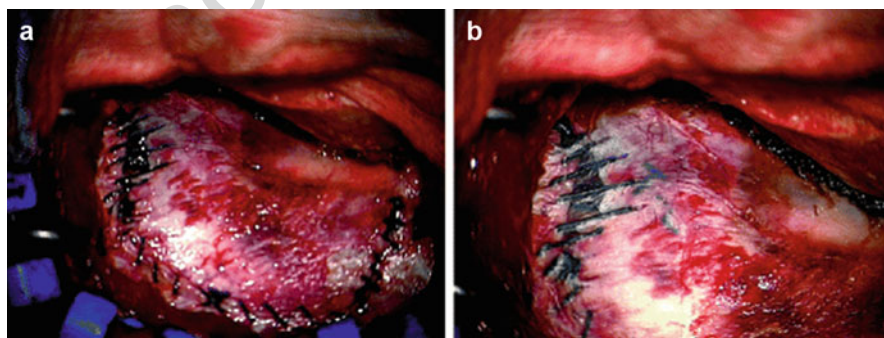


**Fig. 1** Surgical repair of the dura. (a) Mechanical fastening, suturing, does not result in a watertight closure. (b) Adjunctive use of a patch to the closure seals the gap (Images provided courtesy of Tissuemed Ltd.)

with the ability to bond one or more tissue types. Initial experimentation is performed on ex vivo tissue and many materials show some promise in that environment. The ability to bond is, naturally, essential, but is not the only requirement, and many systems which showed initial promise proved not to work when applied in vivo or gave too many undesirable side effects to be permitted for human use. Beyond that, other systems may be successful technically but not be of wide-enough application, or appeal to enough clinical users and purchasers, to be a commercial success and so may be withdrawn from the market. The technical, techno-commercial, and medical literature has many examples of initially promising materials which are not available for clinical use.

This section aims to describe some of the requirements for a tissue adhesive for internal application and then to give further details on the principal materials which are commercially available and clinically used (though not necessarily permitted in all countries). All materials are described generically as chemical species, without brand names and manufacturers' details as these can frequently change and may also differ between countries, potentially leading to confusion. In addition, some of the more promising and distinct developments of potential novel surgical adhesives are described, though usually in less detail. There can be no guarantee that any of these will ever be successful, but it is to be hoped that some will and that further inventors may be inspired to come forward and test new ideas as the subject is still very much alive and there are still many unmet needs for this technology within the clinical community.

### **58.3.2 Requirements of an Adhesive for Internal Use**

The body provides a very distinct environment in which to apply adhesives. There are therefore many special requirements placed on any material considered for this application. Internal use requires stricter provisions than for adhesives which are purely in contact with intact skin. First and foremost they have to be safe. Materials sticking to the body cannot contain chemicals which are toxic to the body or to the cells in their vicinity. In addition, the material must not cause sensitization either for the patient or for the user. Nor must it produce an immune response – rejection – from the body. Safety testing must be comprehensively performed before new chemicals are permitted in these applications.

As with any device or material intended for use in medicine, medical adhesives cannot be sold for clinical use without regulatory clearance from the relevant national authority. This is to ensure, as far as possible, the safety of the product for the designated indication or indications. Different countries impose different requirements on products, which also depend on the nature of the device or material and its intended use. These frequently require extensive testing, both preclinically on animals and clinically in carefully controlled studies on humans, as well as the provision of other safety data. Because of the different regulations, products may be found on sale in one country but restricted in others.

The material must not introduce organisms which might be harmful for the body or for the repair. It must therefore be intrinsically sterile (as produced) or capable of being adequately sterilized. Sterilization is performed by heat (autoclaving), chemical and heat (ethylene oxide), or ionizing radiation (gamma rays), all of which involve the application of much energy. This energy will often be sufficient to initiate chemical reactions, such as the curing of adhesives, so developers of medical adhesives have to include means of ensuring that the adhesives are protected from any possibility of this.

Clearly, a medical adhesive must be capable of reliable secure bonding of the tissue that is to be bonded. Not all tissue is the same. An early misapprehension in the development of medical adhesives was that one adhesive would work everywhere. Subsequent experience has proved that this is not the case. Different formulations have been developed for different tissue types. The moisture content, the fat content, and the protein and polysaccharide content differ, and bone also has mineral content (Duck 1990). It has been found that the strongest bonds occur when there is true chemical bonding to the substrate material (Wilson et al. 2005). Almost universally, the area to be bonded is wet, which is a challenge for many conventional adhesives, and even if it can be temporarily dried at the time of application, the bond will soon be wet again.

The bond must form rapidly as it is unsafe and inefficient for surgery to take longer than strictly necessary. In most cases, a surgeon will opt for a quick action rather than a prolonged surgery. However, it is possible for bonding to occur too rapidly, leading to fixation of an incorrect placement. Related is the concern over adhesive spills or leakage from the joint. It should ideally be possible to see and remove safely any adhesive which gets in the wrong place, though the nature of the adhesive and means of dispensing it should be designed so as to avoid this happening at all. Adhesive products are sometimes colored (usually with a shade of blue), so that they may be distinguished from the surrounding tissue. Figure 5 shows an example of this.

The purpose of most tissue adhesives is to hold the tissue together so that fluids (e.g., blood) do not leak and it is able to heal naturally. Healing may be a slow process, taking several days, so the bond must last as long as the process, ultimately degrading as the tissue is able to regain the necessary strength. Healing, though, will only occur if the adhesive has not formed a barrier to its progress. Several medical adhesives are therefore applied as “patches” or “sleeves,” bridging the gap in tissue, while not penetrating between the tissue surfaces (Fig. 1b). The breakdown products of the adhesive must be safe to the patient and not harmful to the repair process. In general, this requirement is more likely to be met by adhesives of a biological origin, but synthetic and semisynthetic adhesives may also be safe, or the small quantities of material and slow release rate may lead to breakdown products being present in such small concentrations as not to be a problem. In a few cases, it may be necessary for the medical adhesive to provide a permanent fixation, and not to degrade away, if the tissue is not capable of regeneration.

As has already been indicated, packaging and delivery of the adhesive is of key importance. The packaging must keep the material sterile and, for multicomponent



materials, separate. It must be easy to use, and, to remove the possibility of cross-infection by multiple uses, contain the volumes needed to achieve a single repair on one patient, although a second application may be needed in some cases. Application must be foolproof, simple (surgeons' hands may be required to perform many functions), and permit accurate delivery with minimal spillage. Where two components are concerned, the way in which they are mixed, for example, through a mixing nozzle, multi-jet spray, or by sequential delivery, must be reliable and not lead to problems, such as premature setting, clogging the delivery.

### 58.3.3 Categories of Adhesives

Medical adhesives may be categorized in various ways. Clinicians would probably choose listing by the indications for which they may be used. In this chapter, adhesives have been divided into different groups depending on the similarities of the chemistry and technology. There are separate sections below for adhesives which are produced entirely by synthetic chemistry and for those of biological origin. Naturally, there is some crossover where synthetic molecules are used with biological products, and some "biological" materials are being produced by identification of the functional components of a natural product and then reproducing these by a synthetic route. Laser welding and soldering are somewhat different means of producing adhesion between tissues and are covered in a separate section.

### 58.3.4 Synthetic Adhesives

#### Cyanoacrylates

Cyanoacrylates are widely used in a range of engineering applications where instant strong bonding is required when using a minimum of adhesive material. The adhesive only requires a small amount of water on the surfaces in order to set off the polymerization reaction that forms the bond. These features are clearly attractive in a medical context, so it is not surprising that the use of cyanoacrylates in surgery (of small blood vessels) was attempted before 1960. A number of problems were then discovered which have led to only slow adoption over the intervening years, though recently this has gathered pace, particularly after 1998, when the US Food and Drug Administration (FDA) first approved cyanoacrylate products for specific indications, initially external to the body and, more recently, for a few very specific internal applications.

The fundamental structure of a cyanoacrylate is given in Fig. 2. The R group can be one of many different species, though usually alkyl, giving rise to a large family of different molecules with different properties. The adhesive is a low viscosity liquid which cures by anionic polymerization, and the process is exothermic. The reaction can be set off by hydroxyl ions, or similar chemistry, such as hydroxyl or amine groups present in proteins in the tissue surface. Thus, cyanoacrylate is capable of bonding covalently to the tissue surface (Wilson et al. 2005) which contributes, along with its

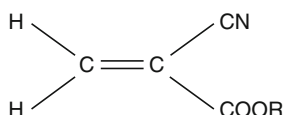


**Fig. 2** The structure of a cyanoacrylate monomer. R can be selected from many different species; see text for details

ease of penetration into the structure of the surface before curing, to the very strong bonds which it can make to most tissue types (Chivers and Wolowacz 1997). The choice of alkyl group in the molecule is very important. Domestic and industrial “superglues” are usually methyl or ethyl cyanoacrylates. These were initially tried in medical applications and found to be unsatisfactory. The curing reaction was too fast, leading to tissue necrosis due to overheating and the rate of subsequent degradation was also too rapid (Woodward et al. 1965). Larger alkyl groups were found to be more successful and the most commonly used medical cyanoacrylates are currently *n*-butyl-2-cyanoacrylate and octyl-2-cyanoacrylate. In addition to these molecules, formulations include stabilizers to permit sterilization and to reduce the likelihood of polymerization during storage, and thickeners, usually poly(methyl methacrylate) (PMMA) or polymerized cyanoacrylate. The hardness and inflexibility of cured cyanoacrylate can be reduced by the use of other additives. Low curing rates of the octyl- monomer, which otherwise has the advantage of giving a more flexible polymer, can be improved by adding accelerators at the point of delivery.

In the early days of their use, medical cyanoacrylate adhesives received bad publicity due to tissue damage at the site of use. This may have been due to the exothermic curing reaction but may also have been due to the degradation products of the polymer (Leonard et al. 1966). Cyanoacrylates degrade hydrolytically by a reverse Knoevenagel reaction to formaldehyde and alkyl cyanoacetate. Concerns about formaldehyde released into the body have led to many considering it as the major cause of the problem, and several routes have been attempted to reduce the likelihood of its release by altering the chemistry or adding agents to capture it (e.g., Leung and Clark 1994). However, as formaldehyde release is only a potential problem *within* the body, cyanoacrylates have become widely used and approved as a topical means of skin closure in accident and emergency situations, where the adhesive is delivered across the laceration (not in between opposing edges) using careful control of the flow. This process is shown in Fig. 3. The result can be good secure holding of the wound, excellent sealing to provide a barrier to microbial ingress, and also a good cosmesis after the adhesive has sloughed off the surface and the wound is healed (Quinn et al. 1997). Figure 4 shows a comparison of wounds from laparoscopic surgery closed using sutures and using cyanoacrylate. It is only recently that the US FDA has approved this application as a Class III device, for topical use only, initially in 1998 for octyl-2-cyanoacrylate and later (in 2002) for *n*-butyl-2-cyanoacrylate (Mattamal 2005).

Cyanoacrylates have been widely used experimentally in a great number of surgical procedures, particularly in eye and ear surgery, which are largely external to the body

**Fig. 3** Application of a cyanoacrylate adhesive to close a skin wound (Published with permission of MedLogic Global Ltd.)

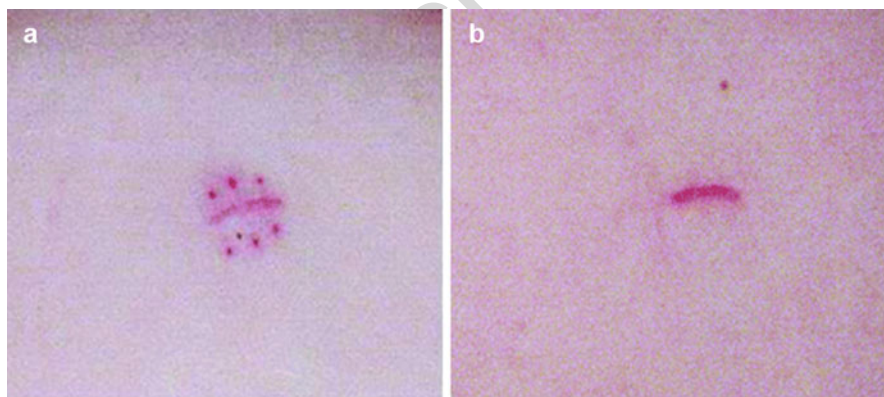


**Fig. 4** Comparison of wounds post laparoscopic surgery closed (a) using sutures and (b) with cyanoacrylate (Published with permission of MedLogic Global Ltd.)

(Quinn 2005). One internal application has also been approved by the US FDA. This is for a formulation of which the major ingredient is *n*-butyl-2-cyanoacrylate. The application is for neurologic embolization in the skull (Mattamal 2005). A cyanoacrylate adhesive, with a special delivery device, has recently been launched in several countries as a fixation means for polypropylene hernia mesh. It is believed that cyanoacrylate adhesives are used off-label for a range of other internal conditions.

## Modified Gelatin

An early commercial medical adhesive was made from gelatin, resorcinol and formaldehyde and is therefore known as GRF (Braunwald et al. 1966). The gelatin is a bioresorbable polymer which can be cross-linked with formaldehyde, and this may also crosslink to the tissue surfaces. Resorcinol can also be cross-linked by formaldehyde, making a stronger bond. However, on enzymatic degradation, the formaldehyde is released. The issues with formaldehyde which are perceived with cyanoacrylates are therefore also present here, but this has not stopped the material from being widely used, though not in the USA, particularly in aortic dissection repairs and also in liver and kidney surgery. The gelatin-resorcinol mixture is a viscous paste which has to be heated to 45°C before application and then mixed with an aqueous solution of formaldehyde, usually containing some glutaraldehyde as well, as it is delivered to the tissue.

Concerns about the formaldehyde have led to several modifications of this system. In a prominent commercial product, it is replaced by a mixture of glutaraldehyde (pentane-1,5-dial) and glyoxal (ethanedial) (Ennker et al. 1994a, b). This formulation is also used for aortic dissections.

A further alternative is to replace the gelatin with another protein, albumin, and an adhesive sealant is commercially available containing 45% albumin solution which is mixed with 10% glutaraldehyde solution as it is delivered to the repair site. This is successful particularly for hemostasis in cardiac and vascular surgery (Chao and Torchiana 2003).

## Polyurethanes

Polyurethanes are formed from the reaction of diisocyanates and diols to make a prepolymer, usually a paste, which can then further polymerize in moist conditions to give a cross-linked strong material. As the body provides a moist environment for bonding, it is not surprising that many groups have attempted to make polyurethane adhesives for medical applications. Indeed, these were some of the earliest surgical adhesives to be explored and were considered particularly for bonding bone. Obviously, the materials have to be able to degrade to safe products, and therefore lactides and caprolactones have featured in the formulations. However, these have not made a commercial success, because of adverse reactions and because of difficulties in obtaining suitable reaction rates. Most are found to cure too slowly.

Recently, several new urethane systems have been developed with chain extenders derived from lysine or other hydrolyzable, bioresorbable molecules (Gilbert et al. 2008). These are now approved for sale in Europe and the USA for the approximation of tissue layers where subcutaneous dead space exists between the tissue planes in abdominoplasty.

## Synthetic Hydrogels

Much body tissue is effectively a hydrogel. Any adhesive used in the body has to be compatible with the high water content and mechanical properties of tissue, so it is not surprising that hydrogels have been widely used for tissue bonding and

sealing. Many of these are based on poly(ethylene glycol) (PEG), which may be cross-linked by a number of means after derivatization to make these reactive, for example, with tetra-succinimidyl and tetra-thiol residues (Wallace et al. 2001), to give the necessary cohesive strength. Two-component systems have been commercialized for sealant applications, such as for incisions in the dura mater, lungs, and blood vessels (Bennett et al. 2003). The two components, PEG and a cross-linker, trilycine, both with reactive end groups and in separate solutions each with very low viscosity, are delivered together, often by spraying. The reaction is very rapid, producing a film which seals over the defect and bonds mechanically to the tissue surface by penetration of the precursors into its crevices, followed by curing. Figure 5 shows the result of application of such a system during lung surgery. The material breaks down over time in the body and the components are excreted.

Hydrogels may alternatively be cross-linked by derivatization with photocurable monomers. This has the advantage of curing only when the light is shone and the disadvantage of working only in “line of sight” of the light source (Sawhney et al. 1993).

A further series of experimental systems use an aminated star PEG cross-linked with dextran aldehydes. The aldehyde not only cross-links the PEG but also bonds chemically to the tissue surface, so varying the aldehyde content can give a range of bond strengths. It is claimed that this chemistry can thereby be tailored to create adhesives for different tissue types (Artzi et al. 2009).

Several workers have been attempting to mimic the performance of fibrins without the need to use blood-based materials with their attendant risks. These formulations include gelatin cross-linked with a calcium-independent microbial transglutaminase (McDermott et al. 2004) and other gelatin-based materials.

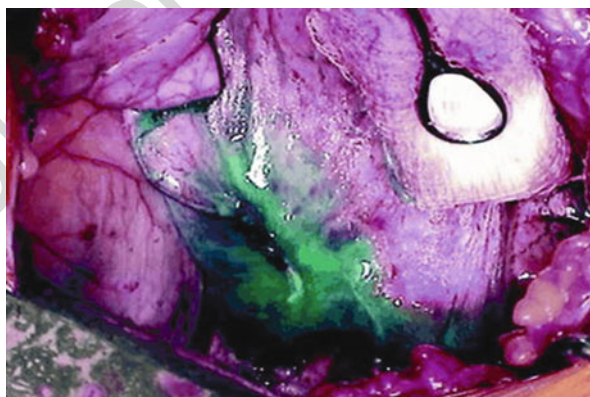


**Fig. 5** Use of a sprayed two-component hydrogel sealant during lung surgery. The sealant (in the lower middle of the picture) contains blue dye to enable the surgeon to see where it is and to judge the thickness of the application (Copyright © 2010 Covidien. All rights reserved. Used with the permission of Covidien)

## Other Synthetic Adhesive Materials

Most of the adhesives discussed here for surgical use are delivered in the form of one or more fluids which cure (react) on the tissue surface to produce a bond and also cross-link to develop cohesive strength. An alternative approach is to make a dry film which already has mechanical integrity and which is coated with materials which react on contact with the wet tissue surface to give a strong bond (Thompson 2009). This therefore has some similarities with the wound dressings which are discussed later in this chapter, but there are numerous differences as these commercial “patches” are intended for internal application for sealing leaks of fluid, for example, air leaks in the lungs, blood leaks and cerebrospinal fluid leaks through the dura, but not for holding the tissue in place. An example of its application to seal the dura is shown in Fig. 1b where the sutures holding the tissue together may also be clearly seen through the film. A resorbable biocompatible film of poly(DL-lactide-co-glycolide) is coated with a layer of a terpolymer of polyvinylpyrrolidone (PVP), polyacrylic acid (PAA) and N-hydroxysuccinimide (NHS). This layer becomes rapidly hydrated on making contact with the tissue surface due to the presence of PVP. The PAA gives tack to the film, producing rapid adherence to the tissue, while the NHS is capable of covalent bonding to the tissue surface. A patch like this will degrade in the body over time with the degradation products being excreted, so leaving no residue.

Bone contains inorganic material, mostly calcium-containing minerals such as hydroxyapatite. Bone defects are often surgically filled with cements made of a variety of calcium phosphates which are found to enhance the healing of the bone. The bonding of the filler to the bone is mostly by mechanical interlocking, and therefore not very strong, but it has been found that some magnesium-containing mineral compounds can be used as adhesives, making stronger bonds to help with the initial fixation of the bone. These have been used, for example, in the fixation of bone-tendon grafts for the reconstruction of the anterior cruciate ligament (ACL) (Gulotta et al. 2008).

Glass ionomer cements have been used for some years in dentistry for bonding restorations to teeth. It has been found in certain circumstances that these can also be used for bonding bone, though as the current formulations contain acrylic polymers, these are not resorbable and can only be used in situations where the bond is intended to be permanent and not replaced by regrowth of the tissue. One such commercial application is for repair of the tiny bones in the ear (Tysome and Harcourt 2005).

## 58.3.5 Biological Adhesives

### Fibrin

Fibrin adhesives have been used for longer than any other tissue adhesive, being first applied in the mid-twentieth century, although they were not sold commercially until 1978. Frequently referred to as fibrin sealants as their ability to seal leaks is more significant than their mechanical strength, they are widely used in a variety of surgical procedures, and more so in recent years after the approval by the US FDA



of one product in 1998 for certain indications and a second product in 2003 (Spotnitz et al. 2005).

Fibrin adhesives contain several constituents. These are fibrinogen, thrombin, factor XIII and calcium ions (usually as calcium chloride) as well as fibrinolytic inhibitors, such as aprotinin, tranexamic acid, or aminocaproic acid (Sierra 1993). The fibrinogen and factor XIII are typically prepared from human blood sources, usually pooled from carefully screened donors and then treated to inactivate any viruses present (MacPhee 1996) either by cryoprecipitation and freeze drying or by solvent detergent cleaning, heat pasteurization and nanofiltration (Spotnitz et al. 2005). The thrombin and aprotinin are sometimes from human and sometimes from bovine sources. Recombinant processes are being sought for these materials. Some products contain the components as lyophilized powders and solutions that have to be mixed just prior to application, while others are supplied as a liquid to be stored at or below  $-18^{\circ}\text{C}$  and then gently thawed before use. Fibrinogen may also be obtained by extraction from the patient's own blood. This is known as autologous fibrin, and is prepared during surgery by taking blood before the operation and centrifuging it to extract fibrinogen. This is naturally somewhat time consuming but has the advantage of eliminating any chance of virus transmission. The viscosity of the preparation and low strength of the resulting adhesive are limitations of material from this source.

The chemistry of the process of formation of the adhesive material from the ingredients is given in Fig. 6 and resembles the final stages of the coagulation (clotting) of blood. Essentially, the thrombin cleaves fibrinopeptides A and B from the fibrinogen molecule to leave fibrin. This polymerizes to form a soft clot, which is cross-linked by the transglutaminase factor XIIIa, which is produced by the action of thrombin on factor XIII in the presence of calcium ions (Marx 1996; Webster and West 2001). The initial soft clot formation is relatively quick but produces a weak material. The cross-linking is a slower process, taking typically about 2 h, giving rise to a considerable increase in strength by formation of covalent bonds and possibly contributing some bonding to collagen in the tissue surfaces (Marx 1996;

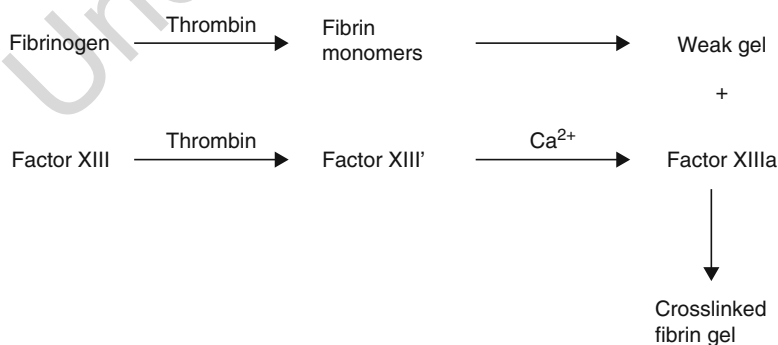


**Fig. 6** Schematic of the formation of fibrin adhesive from its ingredients. This occurs in-situ at the time of use

Donkerwolke et al. 1998). In addition, the cross-linking stabilizes the clot to proteolytic degradation by plasmin. It has been found that different concentrations of the different components can affect the time to cross-link and the strength of the resulting bond (Marx 1996). However, as the materials are of natural origin, it is not always possible to control the ratios precisely.

As a pure biological adhesive resembling blood clots, the fibrin adhesive is able to break down naturally in the body on a timescale resembling that for the tissue to heal (Lontz et al. 1996). Degradation typically occurs in about 2 weeks (Lauto et al. 2008).

Since the bond strength of fibrin adhesives to tissue is not very high (Chivers and Wolowacz 1997), the material is usually used as an adjunct to mechanical fastening such as sutures, hence frequently being referred to as a sealant. It has the advantage of excellent hemostasis and is hence very useful in applications where blood leakage is a problem. In the USA, regulatory approval has been given for several applications where its primary purpose is for hemostasis during surgery on internal organs such as the spleen and liver. It is, however, also used for controlling blood loss during many types of surgery, including orthopedic, and is excellent for sealing blood vessels after suturing and before the blood is readmitted. It may be used for sealing other vessels which do not contain blood, such as lymphatic vessels and the dura containing cerebrospinal fluid, and can be applied to seal an anastomosis (reconnection) of the colon and also air leaks in the lung, although the low strength of fibrin means that special care has to be taken in the latter case when preparing and monitoring the seal. As an adhesive, fibrin has found application in plastic surgery, where it can be used to attach skin grafts to the underlying tissue, though care has to be taken to ensure that it does not act as a barrier to tissue integration under the graft. In these various applications, the bond is most effective if the tissue surfaces are as dry as possible when the fibrin is used, and care must be taken that the bond not be disrupted while cross-linking as pre-cross-linked fibrin can be effective as an antiadhesive (Spotnitz et al. 2005). One of the first applications of fibrin adhesive, one which is still used, is in nerve anastomosis.

An additional application of fibrin is as a delivery means for a variety of pharmaceuticals such as antibiotics, because of its ability to adhere to tissue and so deliver the drug locally, as well as its safe degradation pathways (MacPhee et al. 1996; Webster and West 2001).

### Modified Fibrin

Attempts have been made by several workers to overcome the limitations of fibrin adhesives while maintaining the basic fibrin chemistry. These retain the basic components, unlike those synthetic mimics which have been mentioned above. One way of doing this is to mix fibrillar type I collagen into the fibrinogen/factor XIII solution. When formulated correctly, this enhances the viscosity of the initial solution and therefore its ability to stay at the site where needed, though still permitting easy delivery. In addition, the stiffness and strength of the cross-linked adhesive are enhanced, giving the material greater toughness and ability to withstand loads in use. Effectively it is a fibre-reinforced composite (Sierra 1996). This



technology has been commercialized in a number of formats including: collagen and thrombin to mix with the autologous fibrinogen thus enhancing the otherwise poor properties of autologous fibrin adhesives, collagen fleece coated with lyophilized fibrin adhesive components ready to soak to activate as a patch, and collagen (gelatin) with thrombin which acts as a hemostat with the patient's own blood (Oz et al. 2003).

### Adhesives from Shellfish

The ability of shellfish, such as mussels and barnacles, to stick to underwater structures and remain stuck despite considerable mechanical disturbance, such as due to waves and tides, has long attracted scientists looking for candidate adhesives suitable for medical application where the substrates are wet, the temperature may be up to or over 37 °C, and there is mechanical stress. Since many synthetic adhesives suffer from an inability to stick underwater, an adhesive material which clearly works in wet conditions becomes particularly attractive. Many shellfish-based systems have been assessed, but the most studied has been the byssus, or attachment thread, of several species of mussel, including *Mytilus edulis*. This thread of solidified adhesive ends in an adhesive plaque complex which forms a very strong bond to the substrate surface (Waite 1987; Silverman and Roberto 2007; Forooshani and Lee 2017). Adhesives (known as mussel adhesive proteins or MAPs) can be extracted from the mussels, but it takes a huge number to produce sufficient material for commercial use. Various groups have therefore worked on the identification and synthesis of the essential components of the natural protein in an attempt to be able to produce a MAP without resorting to mussels. It has been found that one of the protein residues essential for bonding (initial chemisorption to the surface and then cross-linking of the adhesive) is 3,4-dihydroxy-L-phenylalanine (DOPA). Any material which resembles MAP will contain this. Genetic engineering may be a route to large-scale production of suitable proteins, but so far this has only succeeded in producing DOPA-containing peptides, not the full sequences of native MAPs. Synthetic analogs are being developed by several groups, for example Yu and Deming 1998 prepared simple copolypeptides of DOPA with L-lysine which, when mixed with certain oxidizing agents, gave good bond strengths to several nonbiological surfaces. An alternative approach has been developed (Lee et al. 2006; Burke et al. 2007), in which the DOPA residues are chemically coupled to PEG molecules and crosslink these rapidly when in the correct oxidation state. The PEG makes up about 80–95% of the formulation which can lead to undesirable side-effects as it swells considerably in an aqueous environment. Further developments include a DOPA-containing block copolymer gel which exhibits a sol-gel transition between room and body temperature and a DOPA-containing monomer (with an acrylate group) which can be photopolymerized (Lee et al. 2006). Recent work has concentrated on putting a wide variety of functional groups onto the catechol to modify the crosslinking and hence control swelling and the mechanical robustness of the structure while altering its ability to bond to surfaces. Different oxidation states of catechol have been found to be needed for bonding to organic tissues from those required when the substrate, such as bone, contains mineral particles (Forooshani and Lee 2017).

## Other Adhesive Technologies

The use of biological molecules has a number of potential advantages in resorption and biocompatibility, though not necessarily in immunogenicity. There is therefore an interest in finding and developing new adhesive systems from biological sources. Many of these are still in the research stage, far from commercialization, and are summarized below to give an idea of the range of ideas being considered.

Attempts are being made to produce proteins (resembling silk and elastin) using recombinant technology from synthetic genes. In this way, specific molecular structures can be constructed to have the desired biological effects, such as good elasticity and bonding to tissue surfaces in the body, while, it is claimed, not having the potentially undesirable side effects which can be shown by wholly natural materials (Cappello 1991).

A number of organisms produce adhesive materials that serve them in a variety of ways, including defense, attack, and to help create protection. As they are naturally produced, they are biocompatible and usually naturally degrade to safe molecules. They are also able to stick in wet environments. Several of these materials have been assessed for use as medical adhesives with promising results.

The sticky secretion from the back of frogs from the genus *Notaden* has been explored by workers in Australia (Graham et al. 2006). This exudate was extracted by stimulating the backs of the frogs and tested in peeling on ex vivo meniscal tissue. Bond strengths exceeded those produced by GRF and fibrin adhesives but not *n*-butyl-2-cyanoacrylate, and it was found that the adhesive functioned primarily as a pressure-sensitive adhesive (PSA) in that the strength was largely unaffected on breaking and reforming the joint.

Shellfish are not the only organisms using adhesives to ensure that they remain in place despite battery from waves and tides. Red and brown algae also produce adhesives, based on polyphenols, which can bond nonspecifically to both hydrophobic and hydrophilic surfaces under water. These have also been investigated, and synthetic analogues have been made which can successfully mimic this performance and are postulated as a soft tissue adhesive (Bitton and Bianco-Peled 2008).

A challenge with any of these is the ability to obtain sufficient for commercial use. These materials are usually made by the organism in very small quantities and harvesting in bulk would be difficult. Preferred approaches are therefore either to identify the essential active molecules and synthesize these (as with mussel adhesion) or to find a way of producing these by using genetic engineering processes.

The mechanism of reversible adhesion used by geckos to walk on walls and ceilings is of interest to several research groups which would like to develop applications using synthetic mimics of this. Unfortunately, gecko adhesion, which is the result of van der Waals interactions between large number of nanoscale pillars and a surface, has been found not to be very effective in the wet, reducing its potential in medical applications. A possible way of overcoming this is being developed in which the nanoscale pillars, made of poly(dimethyl siloxane) (PDMS), are coated with a synthetic mimic of mussel adhesive: poly(dopamine methacrylamide-co-methoxyethyl acrylate) (Lee et al. 2007). The inventors believe that this could have applications as a temporary adhesive for use in the wet in medical settings.

### 58.3.6 Laser Welding and Soldering

The use of light to activate adhesives has been mentioned above offering the advantage that the time of activation is precisely controlled, but the disadvantage of only working in the beam of light. Alternative applications of “light” (including infrared and ultraviolet radiation) have been developed for the clinical bonding of tissue. These are known as welding when light alone is used and soldering when a material is cured with the light (Bass et al. 1996; Lauto et al. 2008).

When tissue is heated, the proteins in it coagulate to form a hard sticky mass. This is similar to the cooking of egg-white. A laser can provide a precise beam of infrared radiation to the edges of two pieces of soft tissue and can weld these together. This is a quick procedure and does not produce the damage that sutures can, but a hazard of this is that the tissue may become too hot and cells could be damaged. This can be reduced by applying a chromophore, which can preferentially absorb the radiation, converting it to heat. For the usual medical infrared laser wavelength of 808 nm, indocyanine green (ICG) is an approved, safe molecule with a maximum absorbance at the same wavelength.

Clinicians have generally found it preferable to apply a solder, a viscous solution of a protein such as albumin or fibronectin (Bass et al. 1996; Chivers 2000; Lauto et al. 2008). When mixed with ICG, this solder is applied over the tissue edges to be bonded and the area is irradiated with an infrared laser beam which is usually pulsed to reduce the net power delivered to the tissue. The enhanced absorption of the ICG enables the solder to reach the coagulation temperature of 65–70 °C well before the tissue has become warm, and the proteins are believed to intermingle with the collagen in the tissue to give a relatively strong repair which can degrade naturally over a clinically acceptable timescale. Concerns over the difficulty of applying a runny liquid and keeping it in place and the possibility of it being diluted by water at the surgical site have led to the development of solid solders, strips and patches of high (>53%) albumin concentration, which can be laid on the tissue surface or placed as a short tube over a cut vessel to be resealed and then irradiated to create the bond. As an alternative to proteins, a similar material has recently been created using chitosan, a polysaccharide (Lauto et al. 2008).

Other, solder-free welding techniques have been reported. One uses Rose Bengal dye activated by laser light at a wavelength of 514 nm, and another a dye made of 1,8 naphthalimide which can be activated by blue light and bonds to tissue seemingly without any heating.

## 58.4 Adhesives for External Application to the Skin

Although cyanoacrylates are now being widely used in the clinic for the closure of skin incisions, as described above, the principal adhesives used on the external surface of the body are pressure-sensitive adhesives. These are the only significant adhesives used on the body in which the application is

frequently not made by a clinician, as they are on first aid dressings and other products for home use.

Pressure-sensitive adhesives (PSAs) have long been used to hold tapes, dressings (Fig. 7), and other devices (e.g., electrodes and ostomy pouches) onto the skin. A further application of PSAs for skin contact is to deliver pharmaceutical agents by a transdermal route. Unlike most other applications of adhesives mentioned here, these are purely for topical use and are normally only in contact with intact skin. This greatly simplifies the regulatory approval process and permits a wide range of materials to be used in comparative safety. There are nevertheless some people who are sensitive to chemicals which may be used in adhesives and care must be taken to watch out for this in clinical practice.

Early PSAs were usually rubber based, containing natural rubber which needs to be modified by the addition of tackifiers, lanolin, and mineral filler to optimize performance. A traditional tackifier is colophony resin (gum rosin), another natural material. A disadvantage of these materials is that they are very poor at handling moisture. These adhesives have to be physically modified, usually by perforation, so that there is not an excessive moisture build-up under a dressing coated with rubber-resin adhesive. Other disadvantages include the lack of resistance to shear, and a tendency to fail in the adhesive mass (cohesive failure), resulting in adhesive



**Fig. 7** High performance wound dressings can be held securely in place on the skin using a pressure sensitive adhesive (Image copyright by Smith & Nephew April 2010)

residues being left on the skin around a dressing while being worn, and after removal. A variety of materials have since been used to make more “skin-friendly” adhesives with better mechanical and moisture-handling capabilities. These include, principally, acrylics and silicones, but there are also poly(vinyl ether)s and poly(vinyl pyrrolidone)s for certain specialist applications (Webster and West 2001). Formulations are continually being developed to attempt to improve these further.

The process of assessing a PSA for use on skin is extremely complex and relies a lot on subjective assessment. Many properties must be considered and have been widely discussed in the literature (Satas and Satas 1989; Chivers 2001). These include the ability to stick securely and yet be easily and safely removed, the ability to stay in place for several days despite the movement of the underlying skin, and the ability to handle moisture and to “breathe” with the skin. Naturally the adhesive is not used alone and must perform successfully when coated on a suitable backing material, usually a film or fabric.

The ability to stick is obvious, as patient health, wound protection and cleanliness can be compromised by a lifting dressing. In contrast, a skin PSA must be able to be removed easily, minimizing discomfort to the patient and risk of damage to skin which may be fragile, as well as ensuring that the adhesive residue is not left on the skin. While it may be thought that the pain experienced when a dressing is removed would be related to the force required to peel the dressing from the skin, it is by no means clear that this is the case. Peeling frequently removes a layer of dead skin cells from the skin surface. It is not known whether this contributes to the discomfort of dressing removal, but it can compromise the ability of the dressing to be repositioned as it can mask the adhesive. Frequent removal of dressings from the same site can cause reddening and even damage to the skin. For that reason, adhesives and systems have been developed which make removal easier (Chivers 2001). Some skin-friendly solvent products are available to help with this, particularly in difficult cases such as ostomy.

Shear of the adhesive is also undesirable as it can lead to dressings sliding from the site of attachment and leaving sticky residues exposed on the skin. These can fasten to clothing or bedding.

As already mentioned, the moisture handling is important, since human skin loses moisture in the form of water vapor at, typically, 200–500 g/m<sup>2</sup>/24 h and inability of any skin covering to cope with this leads to maceration, overhydration, of the skin. In extreme cases the dressing can come off if too wet, which it may also become if immersed in water, since the adhesives cannot stick in very wet conditions. Various ways of handling moisture are available – the formulation of the adhesive can help, but how it is spread on the backing is also important. Gaps may be deliberately produced in the adhesive film – by pattern spreading or perforations.

Developers of new formulations for medical PSAs have a range of in vitro testing methods which they use to help to evaluate these requirements. Ultimately, though, the performance of PSAs on skin is so subtle and subjective that only testing using the correct backing and on humans from the target population will give a true assessment of the acceptability of a new material.

## 58.5 Conclusions

Adhesives technology has two main applications in medicine as considered in this chapter: for internal fixation of tissues usually after surgery, and for use on the skin, primarily to hold dressings in place. There are many differences between the requirements of the technology for these applications.

Internal application is very carefully regulated as there is a need for extreme caution on safety grounds. Adhesives for this have to pass a series of tests before approval, and this may not be universal. Many chemical and biological systems have been tried and several are now in widespread clinical use. The appeal of an adhesive over the current mechanical means of fastening tissue has led many developers to attempt to create new materials from a range of sources. Some of these may be successful, but there is a long way to go in many cases.

Adhesive technology for external application is, by contrast, mature and many successful systems are available as the regulatory requirements are fewer. This has not stopped developers working to improve the existing products, and indeed to modify them for use on further dressing types and for other applications, such as for transdermal drug delivery.

---

## References

- Artzi N, Shazly T, Baker AB, Bon A, Edelman ER (2009) Aldehyde-amine chemistry enables modulated biosealants with tissue-specific adhesion. *Adv Mater* 21:3399–3403
- Bass LS, Libutti SK, Kayton ML, Nowygrod R, Treat MR (1996) Soldering is a superior alternative to fibrin sealant. In: Sierra DH, Saltz R (eds) *Surgical adhesives and sealants current technology and applications*. Lancaster, Technomic, pp 41–46
- Bennett SL, Melanson DA, Torchiana DF, Wiseman DM, Sawhney AS (2003) Next-generation hydrogel films as tissue sealants and adhesion barriers. *J Card Surg* 18:494–499
- Bitton R, Bianco-Peled H (2008) Novel biomimetic adhesives based on algae glue. *Macromol Biosci* 8:393–400
- Braunwald NS, Gay W, Tatroles CJ (1966) Evaluation of crosslinked gelatin as a tissue adhesive and hemostatic agent: an experimental study. *Surgery* 60:857–861
- Burke SA, Ritter-Jones M, Lee BP, Messersmith PB (2007) Thermal gelation and tissue adhesion of biomimetic hydrogels. *Biomed Mater* 2:203–210
- Cappello J (1991) Protein engineering for biomaterials applications. *Curr Opin Struct Biol* 2:582–586
- Chao H-H, Torchiana DF (2003) BioGlue: albumin/glutaraldehyde sealant in cardiac surgery. *J Card Surg* 18:500–503
- Chivers RA (2000) In-vitro tissue welding using albumin solder: bond strengths and bonding temperatures. *Int J Adhes Adhes* 20:179–187
- Chivers RA (2001) Easy removal of pressure sensitive adhesives for skin applications. *Int J Adhes Adhes* 21:381–388
- Chivers RA, Wolowacz RG (1997) The strength of adhesive-bonded tissue joints. *Int J Adhes Adhes* 17:127–132
- Donkerwolke M, Burny F, Muster D (1998) Tissues and bone adhesives – historical aspects. *Biomaterials* 19:1461–1466
- Duck FA (1990) *Physical properties of tissue – a comprehensive reference book*. Academic, London

- Ennker J, Ennker IC, Schoon D, Schoon HA, Dörge S, Meissler M, Rimpler M, Herzler R (1994a) The impact of gelatin-resorcinol glue on aortic tissue: a histomorphologic evaluation. *J Vasc Surg* 20:34–43
- Ennker J, Ennker IC, Schoon D, Schoon HA, Rimpler M, Herzler R (1994b) Formaldehyde-free collagen glue in experimental lung gluing. *Ann Thorac Surg* 57:1622–1627
- Forooshani PK, Lee BP (2017) Recent approaches in designing bioadhesive materials inspired by mussel adhesive protein. *J Polym Sci A Polym Chem* 55:9–33
- Gilbert TW, Badylak SF, Gusenoff J, Beckman EJ, Clower DM, Daly P, Rubin JP (2008) Lysine-derived urethane surgical adhesive prevents seroma formation in a canine abdominoplasty model. *Plast Reconstr Surg* 122:95–102
- Graham LD, Glattauer V, Peng YY, Vaughan PR, Werkmeister JA, Tyler MJ, Ramshaw JAM (2006) An adhesive secreted by Australian frogs of the genus *Notaden*. In: Smith AM, Callow JA (eds) *Biological adhesives*. Springer, Berlin/Heidelberg, pp 207–223
- Lauto A, Mawad D, Foster JR (2008) Adhesive biomaterials for tissue reconstruction. *J Chem Technol Biotechnol* 83:464–472
- Lee BP, Dalsin JL, Messersmith PB (2006) Biomimetic adhesive polymers based on mussel adhesive proteins. In: Smith AM, Callow JA (eds) *Biological adhesives*. Springer, Berlin/Heidelberg, pp 257–278
- Lee H, Lee BP, Messersmith PB (2007) A reversible wet/dry adhesive inspired by mussels and geckos. *Nature* 448:338–341
- Leonard F, Kulkarni RK, Brandes G, Nelson J, Cameron JJ (1966) Synthesis and degradation of poly(alkyl  $\alpha$ -cyanoacrylates). *J Appl Polym Sci* 10:259–272
- Leung JV, Clark JC (1994) Biocompatible monomer and polymer compositions. US Patent 5328687
- Lontz JF, Verderamo JM, Camac J, Arikan I, Arikan D, Lemole GM (1996) Assessment of restored tissue elasticity in prolonged in vivo animal tissue healing: comparing fibrin sealant to suturing. In: Sierra DH, Saltz R (eds) *Surgical adhesives and sealants: current technology and applications*. Lancaster, Technomic, pp 79–90
- MacPhee MJ (1996) Commercial pooled-source fibrin sealant. In: Sierra DH, Saltz R (eds) *Surgical adhesives and sealants: current technology and applications*. Lancaster, Technomic, pp 13–18
- MacPhee MJ, Singh MP, Brady R Jr, Akhyani N, Liau G, Lasa C Jr, Hue C, Best A, Drohan W (1996) Fibrin sealant: a versatile delivery vehicle for drugs and biologics. In: Sierra DH, Saltz R (eds) *Surgical adhesives and sealants: current technology and applications*. Lancaster, Technomic, pp 109–120
- Marx G (1996) Kinetic and mechanical parameters of fibrin glue. In: Sierra DH, Saltz R (eds) *Surgical adhesives and sealants: current technology and applications*. Lancaster, Technomic, pp 49–59
- Mattamal GJ (2005) US Food and Drug Administration perspective on class I, II and III cyanoacrylate medical devices. In: Quinn JV (ed) *Tissue adhesives in clinical medicine*, 2nd edn. BC Decker, Hamilton, pp 159–168
- McDermott MK, Chen T, Williams CM, Markley KM, Payne GF (2004) Mechanical properties of biomimetic tissue adhesive based on the microbial transglutaminase-catalyzed crosslinking of gelatin. *Biomacromolecules* 5:1270–1279
- Oz MC, Rondinone JF, Shargill NS (2003) Floseal matrix: new generation topical hemostatic sealant. *J Card Surg* 18:486–493
- Quinn JV (2005) Clinical approaches to the use of cyanoacrylate tissue adhesives. In: Quinn JV (ed) *Tissue adhesives in clinical medicine*, 2nd edn. BC Decker, Hamilton, pp 27–76
- Quinn J, Wells G, Sutcliffe T, Jarmuske M, Maw J, Steill I, Johns P (1997) A randomised trial comparing octyl-cyanoacrylate tissue adhesive and sutures in the management of lacerations. *JAMA* 277:1527–1530
- Satas D, Satas AM (1989) Hospital and first aid products. In: Satas D (ed) *Handbook of pressure sensitive adhesive technology*, 2nd edn. Van Nostrand Reinhold, New York, pp 627–642

- 734 Sawhney AS, Pathak CP, Hubbell JA (1993) Bioerodible hydrogels based on photopolymerised  
735 poly(ethylene glycol)-co-poly( $\alpha$ -hydroxy acid) diacrylate macromers. *Macromolecules*  
736 26:581–587
- 737 Sierra DH (1993) Fibrin sealant adhesive systems: a review of their chemistry, material properties  
738 and clinical applications. *J Biomater Appl* 7:309–352
- 739 Sierra DH (1996) Fibrin-collagen composite tissue adhesive. In: Sierra DH, Saltz R (eds) *Surgical*  
740 *adhesives and sealants: current technology and applications*. Technomic, Lancaster, pp 29–39
- 741 Silverman HG, Roberto FF (2007) Understanding marine mussel adhesion. *Mar Biotechnol*  
742 9:661–681
- 743 Spotnitz WD, Burks SG, Prabhu R (2005) Fibrin-based adhesives and hemostatic agents. In: Quinn  
744 JV (ed) *Tissue adhesives in clinical medicine*, 2nd edn. BC Decker, Hamilton, pp 77–112
- 745 Tavakoli SM, Pullen DA, Dunkerton SB (2005) A review of adhesive bonding techniques for  
746 joining medical materials. *Assem Autom* 25:100–105
- 747 Thompson I (2009) Technical bulletins. Tissuemed Ltd. Available at <http://www.tissuemed.com>
- 748 Tysome JR, Harcourt J (2005) How we do it: ionomeric cement to attach the stapes prosthesis to the  
749 long process of the incus. *Clin Otolaryngol* 30:458–460
- 750 Waite JH (1987) Nature's underwater adhesive specialist. *Int J Adhes Adhes* 7:9–14
- 751 Wallace DG, Cruise GM, Rhee WM, Schroeder JA, Prior JJ, Ju J, Maroney M, Duronio J, Ngo MH,  
752 Estridge T, Cocker GC (2001) A tissue sealant based on reactive multifunctional polyethylene  
753 glycol. *J Biomed Mater Res (Appl Biomater)* 58:545–555
- 754 Webster I, West PJ (2001) Adhesives for medical applications. In: Dumitriu S (ed) *Polymeric*  
755 *biomaterials*, 2nd edn. Marcel Dekker, New York, pp 703–737
- 756 Wilson DJ, Chenery DH, Bowring HK, Wilson K, Turner R, Maughan J, West PJ, Ansell CW  
757 (2005) Physical and biological properties of a novel siloxane adhesive for soft tissue applica-  
758 tions. *J Biomater Sci Polym Ed* 16:449–472
- 759 Woodward SC, Herrmann JB, Cameron JL, Brandes G, Pulaski EJ, Leonard F (1965) Histotoxicity  
760 of cyanoacrylate tissue adhesive in the rat. *Ann Surg* 162:113–122
- 761 Yu M, Deming TJ (1998) Synthetic polypeptide mimics of marine adhesives. *Macromolecules*  
762 31:4739–4745



Chiaki Sato

## Contents

59.1	Introduction .....	1752
59.2	Impact of Adhesion Bonding in the Environmental Issues .....	1753
59.2.1	Categories of Environmental Issues .....	1753
59.2.2	Greenhouse Gas Emission .....	1754
59.2.3	Use of Finite Resources .....	1754
59.2.4	Basic Strategies to Meet the Challenge for Environmental Issues .....	1754
59.3	Types, Characteristics, and Applications of Dismantlable Adhesives .....	1757
59.3.1	Thermoplastic Adhesives and hot-Melt Adhesives .....	1757
59.3.2	Adhesives Including Blowing Agents or Expansion Agents .....	1758
59.3.3	Adhesives Including Chemically Active Materials .....	1764
59.3.4	Adhesives to Which an Electrochemical Reaction on Interfaces Is Applied .....	1764
59.3.5	Miscellaneous Methods .....	1766
59.3.6	Recent Advances .....	1768
59.3.7	Future Seeds .....	1771
59.4	Conclusion .....	1773
	References .....	1773

## Abstract

Recycling and environmental aspects of adhesion technology are discussed in this chapter. Adhesively bonded adherends should be often separated before they can be recycled. For this purpose, dismantlable adhesives, which can be separated with stimulations, have been developed recently. There are lots of technical processes to realize such adhesives. For example, softening of adhesive, expansion force due to blowing agents or thermally expandable microcapsules, chemical degradation, electrochemical reaction, and taking advantage of interfacial

C. Sato (✉)

Precision and Intelligence Laboratory, Tokyo Institute of Technology, Midori-ku, Yokohama, Japan  
e-mail: [csato@pi.titech.ac.jp](mailto:csato@pi.titech.ac.jp)

phenomena can be applied to dismantlable adhesives. These adhesives have many applications such as temporary joints of work materials, shoe making, integrated circuits (IC) chip fabrication, electronics, housing construction, car fabrication, and so on. The most used trigger to start the separation of these adhesives is heating. Many kinds of methods including infrared, induction, and microwave heating are recently available. In addition, novel dismantlable adhesives, which have anisotropy in strength or are triggered by electric currents, have been presented.

## 59.1 Introduction

Since adhesive bonding has many advantages such as low cost, light weight, easy application, etc., it is increasingly being used by modern industries. Adhesive bonding is more desirable than the other joining methods in terms of energy saving, so that its environmental load is small. However, the consumption of adhesives has been increasing drastically due to the industry globalization and the recent fast-growing of developing countries, and the total environmental load of adhesive bonding is also increasing. To meet environmental issues, the total environmental loads, although they are small, have to be reduced by all possible means.

Adhesive bonding has many aspects related to the environmental issue. One of them is energy consumption in some processes such as production, transportation, application, and curing of adhesives. Another one is recycling of adhesively bonded materials. Strictly speaking, there are other aspects such as recycling of adhesive itself and environmental contamination including vaporized organic chemical compounds (VOC). This chapter treats the recycling issue of adhesively bonded materials. The recycling of the adhesive itself is not dealt with because it is very difficult so far.

Adhesively bonded joints are not easy to separate if they are bonded with strong adhesives or the bonded area is large. Therefore, dismantlability of the joints is not required contrarily to the other joining methods such as mechanical fastening. The fact leads to scarce use of adhesion for substrates that have to be separated. However, a new type of adhesive called a “dismantlable adhesive” has been recently required to meet the demands to separate the adherend for recycling. For instance, a dismantlable design for a product is essential because the materials bonded together become bad wastes difficult to be recycled. However, if the materials can be separated, they become resources. The separation of parts is important even if they are bonded adhesively. Thus, dismantlable adhesives, which can be separated when and as we like, are increasingly required. An advantage of adhesive bonding is the ability to join dissimilar materials. However, it becomes a disadvantage if such materials cannot be recycled. Dismantlable adhesives are also appropriate to solve this problem.

Dismantlable adhesives, however, are thought difficult to realize because a good adhesive has been apprehended as strong and not being able to separate so far. The

effort to realize a good adhesive has been concentrated into this point. The capability to separate when we like is a totally different concept from the past efforts.

As a matter of fact, dismantlable adhesives, if they are weak in strength, have been present since fairly early times. Hot-melt adhesives, for instance, can be separated by heating. However, strong adhesives, especially structural adhesives, present a high technical hurdle to be dismantlable. The trend has been changing for the last decade and many dismantlable adhesives have been proposed as a kind of novel functional adhesives. Although their applications are mainly temporary joints of works or product reworks so far, adherend recycling has become an issue recently. In addition, the adhesives are applied to make separation mechanisms for aircrafts, space crafts, or robots. This chapter deals with dismantlable adhesives, whose development has proceeded very fast recently, and shows the results of recent research and technical trends.

---

## **59.2 Impact of Adhesion Bonding in the Environmental Issues**

### **59.2.1 Categories of Environmental Issues**

The main environmental issues can be categorized in three following items:

1. Hazardous material emission
2. Greenhouse gas emission
3. Use of finite resources

In this chapter, hazardous material emission is not treated (see ► [Chap. 39, “Environment and Safety”](#)). However, these items are not independent from each other and it is difficult to discuss them separately. Thus, the first item will be shortly referred in this chapter too.

Global warming is the most serious and important issue among environmental issues. There is a lot of theory or controversy on the effect brought by the problem and the time limit that we have for preventing vital results. However, it is certain that the final result is devastating to the global environment unless we can reduce, or sustain in the worst case, greenhouse gas emission. In this case, irreversible warming must occur within some decades. Although it is very rare for adhesives to emit greenhouse gases directly, the gases, mainly carbon dioxide, are possibly emitted during their production, application, curing, or disposal processes.

The third item, use of finite resources, may seem different from environmental issues. However, this should be included in environmental issues because the most important finite resource is fossil fuels such as petrol, and their combustion causes carbon dioxide. In addition, avoiding the use of finite resources without their recycling is indispensable to realize sustainable society. From this viewpoint, this item is also discussed in this chapter.

### 59.2.2 Greenhouse Gas Emission

The main greenhouse gas emitted during the processes of adhesive production, use, and disposal is carbon dioxide. In the production process of adhesives, energy due to fossil fuel may be used and this causes carbon dioxide. Energy should be used in the curing process of adhesives too. Since the raw materials of adhesives are mainly made from petrol, carbon dioxide should also be produced by incineration in the disposal process. In addition, the other greenhouse gases such as hydrocarbons or organic solvents may be emitted to the atmosphere during the production or application process of adhesives. Such greenhouse gases have higher warming effects per unit than carbon dioxide. Therefore, even their total amount of emission is small, attention should be paid.

### 59.2.3 Use of Finite Resources

Some raw materials of adhesives are derived from petrol. Therefore, if petrol resources are depleted, the production of adhesive cannot be maintained. This depletion is an ultimate situation, but even the price rise of petrol can give serious and negative impact to adhesive industries. An alternative option is the use of other fossil carbon resources such as coal. Coal is more abundant than petrol in terms of reserve. However, its carbon dioxide emission per unit is larger than that of petrol. Anyway, true sustainable societies cannot be realized while finite fossil resources such as petrol or coal are widely and often used. Energy consumed in the production process of adhesive and its curing process may be derived from fossil fuels too.

### 59.2.4 Basic Strategies to Meet the Challenge for Environmental Issues

The basic strategies to solve the environmental problems can be categorized as follows:

1. Use of eco-conscious materials
2. Provide reworkability or dismantlability to adhesives
3. Recycling of adhesives itself
4. Optimization of the bonding process
5. Design optimization and lifetime cycle assessment of adhesively bonded joints

In this section, they are explained respectively.

#### Use of Eco-Conscious Materials

Selection of raw materials for adhesives is very important to reduce environmental loads. At first, the raw materials should be environment friendly. Synthetic polymers

have relatively larger energy consumption in this production process than other materials such as fillers, including alumina powders, silica aerogels, calcium carbonate or talc consisting of minerals. Therefore, the composition of an adhesive is influential to the total environmental loads. In addition, if an adhesive is burned in the disposal process of the product bonded with it, carbon dioxide is emitted. As seen above, the presence of fillers can help to reduce the carbon dioxide emission because the portion of polymer in the adhesive decreases.

In order to reduce more effectively the environmental loads, use of recycled materials or carbon-neutral natural materials should be considered. Reclaimed rubbers are often used as the raw material of Pressure Sensitive Adhesive (PSA). Polystyrene foam used as shipping supplies can be solved with solvents and used as a raw material for adhesives. As such, recycled materials can be used to produce adhesives for the purposes of reducing environmental impacts and costs.

Use of carbon-neutral natural materials is another option. Since they absorb carbon dioxide from the air during their growing, the total amount of carbon dioxide in the atmosphere is not changed even if these materials are burned. Historically, natural materials are mainly used as raw materials for adhesives. For instance, glue, lacquer, and casein have been widely used to make adhesives (Fay 2005). They are natural materials and carbon-neutral. The other example of natural material use is the case of PSA. To make PSA, natural rubbers for the main component and rosins for tackifiers, which are derived from plants, are often used. They are also carbon-neutral. Recently, other natural materials have been investigated for raw materials of adhesives. For example, polylactide resin can be applied to the main components of adhesives (Viljanmaa et al. 2002). Lignophenolic resins derived from lumber (Kadota et al. 2004) and chitosan resin from exoskeleton of crustacean are other examples (Yamada et al. 2000; Umemura et al. 2003). Soy beans oils can be epoxidized and used for adhesive main components (Ratna and Banthia 2000). The powder of lumbers such as cork is promising as fillers for adhesives because it can give ductility to the cured bulk of adhesive (Jos and Leite 2007).

### **Reworkability or Dismantlability of Adhesives**

The key word “3R” is often referred when environmental issues are discussed. This word means “reduce,” “reuse,” and “recycle.” In order to reuse or recycle adhesively bonded materials, joint separation is often required. To meet this demand, a new type of adhesive called “dismantlable adhesive,” which can be separated on demand, has been invented.

Defective products due to malfunctioned parts bonded adhesively or to inappropriate adhesion are very bad in terms of environment protection because they become a waste without any use. Therefore, dismantlable adhesive can be used to avoid the situation because bonded parts or inappropriate bonded areas can be separated in order to be repaired. This process is called “reworking” of defect products and involved in the processes of “reducing” wastes and “reusing” other nondefective parts in terms of 3R. This topic will be discussed in more detail in Sect. 2.2.

### **Recycling of the Adhesive Itself**

Actual cases of adhesive recycling are still very rare because the amount of adhesive used in a product is much smaller than that of the adherend materials. In addition, adhesives consist usually of various kinds of materials. On the other hand, removing an adhesive layer from substrate is very difficult. Resolving obtained adhesive wastes by any solvent is also not easy because they are fully cured and cross-linked. However, the needs of sealant recycling are recently becoming important because the total amount of its use is huge. Thus, we should start to consider seriously the method to recycle sealant wastes.

### **Optimization of the Bonding Process**

If the bonding process is not optimized, large environmental loads occur. For instance, although the surfaces of adherends often need pretreatment before bonding, there is room to reduce environmental loads. The use of oil accommodating adhesives is effective for the purpose because degrease and chemical treatments of adherends are not necessary. Otherwise, if solvents are used for degreasing, they are hazardous and their atmospheric release is undesirable. Collection systems of solvent vapor are useful for reducing the atmospheric release. The collected solvent vapor can be used again after condensation or thermally recycled, although carbon dioxide is emitted in this case.

It is also effective to reduce sub materials used in adhesion processes such as wiping cloths, gloves, masking tapes, removing agents, mixing cups, brushes, and static mixing nozzles. Since most of them are disposable, much waste is made unless the bonding process is optimized. In addition, release sheets of PSA become a waste too.

Energy consumption to cure adhesives is also a problem. Capabilities of ambient temperature curing or relatively low temperature curing are desirable to be installed for adhesives. Some acrylic adhesives can be cured quickly at room temperatures and they are strong and tough enough to be used for structural applications. A promising epoxy adhesive for structural use, which is ambient temperature curable and heat resistant due to nano-fillers, has been recently presented (Sprenger et al. 2004).

### **Design Optimization and Life Cycle Assessment of Adhesively Bonded Joints**

Design optimization of adhesively bonded joints can contribute to environmental issues in a broad sense because it reduces the used materials and the weight of the joints. Precise knowledge of adhesives strength, modulus, and stress distribution in joints is helpful for designers, and it leads to rational design of the joints to minimize environmental loads. This point of view is likely to be missed, but very important. Adhesive making companies ought to provide positively the data to design joints appropriately. This is important not only for the optimal design, but also for preventing the duplication of basic tests that may be carried out by the adhesive maker and each user.

The other obligation of adhesive makers is disclosure of information for Life Cycle Assessment (LCA) of adhesively bonded joints. If these data are provided, the users of an adhesive can calculate the environmental impact associated with equivalent energy consumption or equivalent carbon dioxide emission. The later is called “carbon footprint” whose requests by users is recently increasing, and adhesives are not an exception. The users can evaluate the environmental impacts by LCA, and make rational decision to employ adhesive joining or not considering the total tradeoff of the whole life-cycle environmental loads of their products.

### **59.3 Types, Characteristics, and Applications of Dismantlable Adhesives**

The main purpose of dismantlable adhesives is reworking of parts or recycling of materials in a product. Temporary joining of works also needs dismantlable adhesives. Reworking of parts is a process in which defective parts are removed and exchanged by normally functioning parts. If the parts are vitally important, defects of the parts have a huge influence on the product value. If the parts are joined with a dismantlable adhesive, they can be separated and exchanged easily, and that leads to an increased yield ratio of the product. Electronic devices have integrated circuit (IC) chips on their circuit boards bonded with epoxy adhesives called under fillers. Recently, reworkable underfillers, which are softened by heating and can be separated easily, are commercially available. Such reworkable adhesives are very promising because all devices are getting gradually complicated and the probability of error is increasing.

Dismantlable adhesives can be categorized as follows:

1. Thermoplastic adhesives, i.e., hot-melt adhesives
2. Adhesives including blowing agents or expansion agents
3. Adhesives including chemically active materials
4. Adhesives to which an electrochemical reaction on interfaces is applied

#### **59.3.1 Thermoplastic Adhesives and hot-Melt Adhesives**

Thermoplastic adhesives, i.e., hot-melt adhesives can be separated. They are softened by heating. For instance, solid wax has been used for temporary joints of work materials. The work materials are joined and fixed on the bed of a machine tool with the melt solid wax, and separated by heating. The wax is usually used for many materials such as glass, ceramics, and silicones which are nonmagnetic and cannot be fixed with a magnetic chuck. The amount of the wax used is increasing, although it is a relatively old material. In electronics applications, several types of dismantlable adhesives are used for making IC chips. At first, silicone ingots are fixed with an adhesive and cut into wafers with a dicing saw. The adhesive can be

softened by heating. The residue of the adhesive on the wafers can be washed off using a particular solvent or an alkali solution. Next, the wafer is fixed with another type of adhesive which can be separated mechanically using a scraper. The residue of adhesive on the wafer's surface can also be washed off with an alkali solution.

Hot-melt adhesives began to be used for housing applications in order to recycle the materials. Figure 1 shows a bonding method of wall boards or ceiling boards on beams using a hot-melt tape and an induction heating machine. The method is called the "Allover Method" and has been utilized already by Japanese construction companies (Sekine et al. 2009). A key point is that the tape has a conductor layer made of aluminum alloy in it. To bond the boards on the beam, the tape is inserted between them. The process is easy because the tape has a weak tackiness. After that, the layer can be heated using the induction heating machine, and the board and beam are joined together. They can also be separated by heating because it is totally reversible.

Combining thermosetting plastics and thermoplastics, reworkable adhesives having high strength, stability, and good utility, can be realized. Epoxy adhesives, which are thermosetting resins, are used often for electronics packaging. The introduction of a thermoplastic property to the epoxy adhesive leads to a novel function where the adhesive can be cured and melted by heating. This is called "thermally molten epoxy resin" and has become an important object for research recently (Nishida and Hirayama 2006). The resin is used as an under-fill adhesive to bond IC chips on circuit boards. If the IC chips are out of order, they can be removed and replaced by other chips. Such chips are usually bonded with an adhesive and solder, and both of them can be softened by heating. Therefore, the chips can be separated from the boards easily. The process is called "IC chip rework" (Fig. 2) and it is not frequent but occasional.

**59.3.2 Adhesives Including Blowing Agents or Expansion Agents**

Mixture of blowing agents or expansion agents into an adhesive is frequently used as a method to provide dismantlability. For instance, thermally expandable microcapsules (TEMs) are used often, as shown in Fig. 3. The TEMs expand by heating and an internal stress occurs in the matrix resin of the adhesive. The stress causes an

**Fig. 1** Principle of the Allover method using induction heating (IH) and hotmelt adhesives (Sekine et al. 2009)

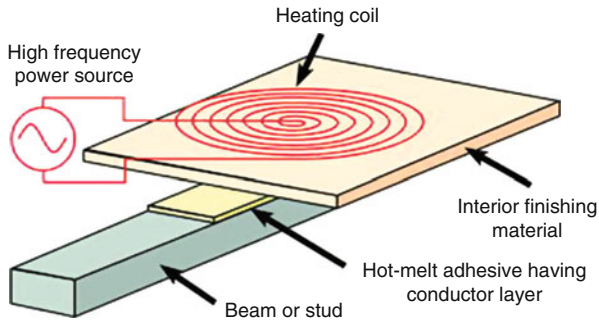




**Fig. 2** Reworkable underfillers used for integrated circuit (IC) chip bonding

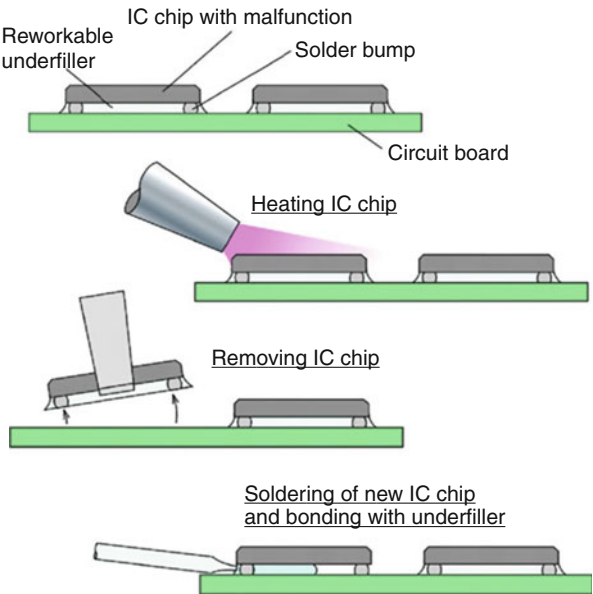
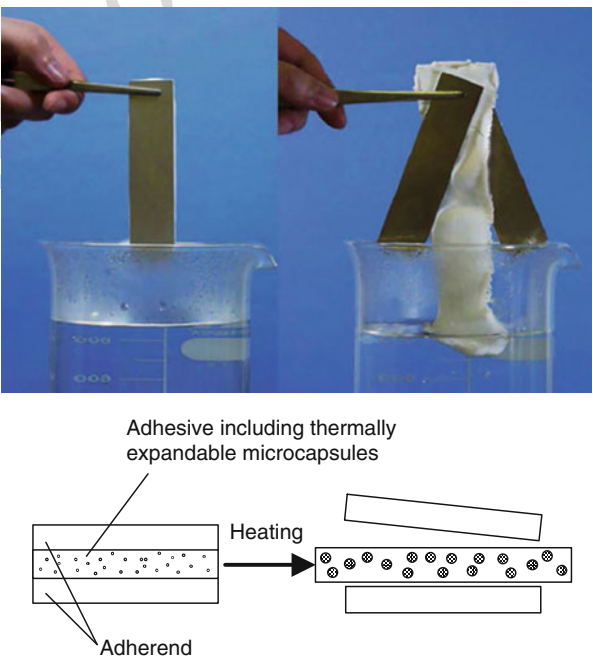


**Fig. 3** Dismantlable adhesive including thermally expandable microcapsules (TEMs)



interfacial separation between the adhesive and the adherend. The type of the matrix resin is important because the internal stress depends on its modulus and strength. Thermoplastic resins are suitable for the adhesive. They can deform much at high temperatures. The expanding force of TEMs induces large deformation in the matrix resin and that leads to interfacial fracture between the adhesive and the adherend (Ishikawa et al. 2005). In addition, the separated surface of the adhesive becomes rough because of the TEMs' expansion, and the roughness becomes a barrier for the adhesive to stick again to the adherend. Therefore, the separated interface cannot be joined again even after the temperature decreases. In the case of a thermoplastic adhesive, the resin is softened over its glass transition temperature, and a similar phenomenon happens also in the case of thermosetting adhesives. Epoxy resins, for example, can be applied as a matrix of a dismantlable system, and they can be used for a wide variety of applications because of the high strength and heat resistance.

As an example of application of this technique, a commercially available tape including TEMs can be shown, which has been used for temporary joints of IC chips die-cutting. The tape has double sided coats of a pressure sensitive adhesive (PSA). The bonding strength and modulus of the PSA are low, so that the tape can expand much with a small amount of TEM inclusion, and the expansion leads to an interfacial separation between the IC chips and the tape. Similar methods are applied to other applications such as adhesives or sealants for housing. A vinyl emulsion adhesive including TEMs is used to join fiber-reinforced plastics (FRP) or decorative steel sheets to plaster boards for fabrication of unit-bath structures in Fig. 4. A silicone sealant including TEMs is used for sealing of kitchen sinks, etc., as shown in Fig. 5. In both the cases above, the joint can be dismantled by heating (Ishikawa et al. 2004).

The technique has been applied to strong adhesives too. A project called "ECODISM," which is the abbreviation of "Ecological and economical development of innovative strategy and process for clean maintenance and dismantling further recycling," was carried out in Europe aiming at the bonding of car structures using dismantlable adhesives or primers (Papon et al. 2008; Alcorta et al. 2004; Bain

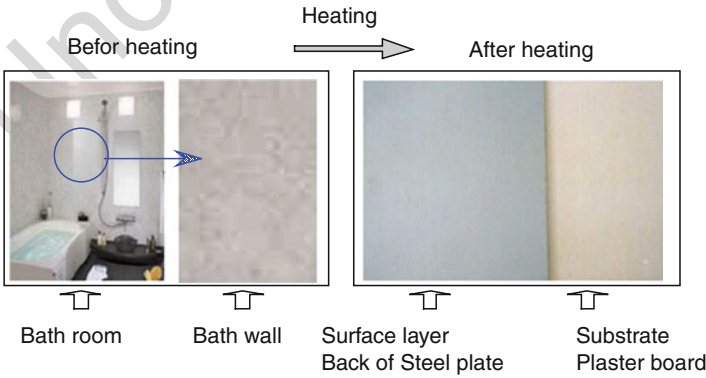


**Fig. 4** Wall panels for a unit-bath room consisting of plaster boards and steel plates bonded with a dismantlable adhesive of vinyl emulsion including TEMs (Ishikawa et al. 2004)

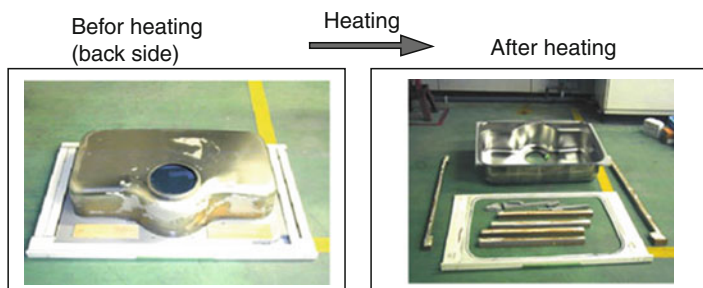


**Fig. 5** Bonded and dismantled parts of a kitchen sink bonded with a dismantlable adhesive of silicone resin including TEMs (Ishikawa et al. 2004)

**Fig. 6** Application of a dismantlable adhesive with thermally expandable microcapsules and blowing agents in the car industry, the ECODISM project (Papon et al. 2008)



and Manfre 2000). A urethane adhesive including TEMs and blowing agents (pTSH) was applied to joints between a windscreen and the body structure, as shown in Fig. 6. A rear hatch having polymer-alloy panels and a glass was also fabricated with the dismantlable adhesive. Infrared (IR) lamps were used to heat the structure in order to separate it, and the structure could be dismantled within 150 s.

Epoxy adhesives are also targets for separation using TEMs, although these adhesives are very strong. For instance, a type of TEMs, shown in Fig. 7, is mixed into an epoxy resin to be used as a strong dismantlable adhesive (Nishiyama et al. 2003). The microcapsules have a structure with a core and a shell. The shell consists of polyvinylidene, and the core is filled by isobutene. The average diameter of the TEMs is about 20  $\mu\text{m}$ . The TEMs can expand due to temperature increases because the shell becomes soft and the inner pressure of the TEMs increases. The expansion starting temperature of the TEMs depends on the material characteristics of the shell and the filling hydrocarbon. There are a lot of commercially available grades having different temperatures of expansion beginning and maximum expansion volumes. The TEMs, shown in Fig. 7, have an expansion starting temperature of 80  $^{\circ}\text{C}$  and a maximum expansion volume of 70 times. Therefore, the temperature of dismantlement of an adhesive is selected as a function of the TEMs. Generally speaking, a grade of TEMs having a high expansion starting temperature has a smaller expansion volume than that

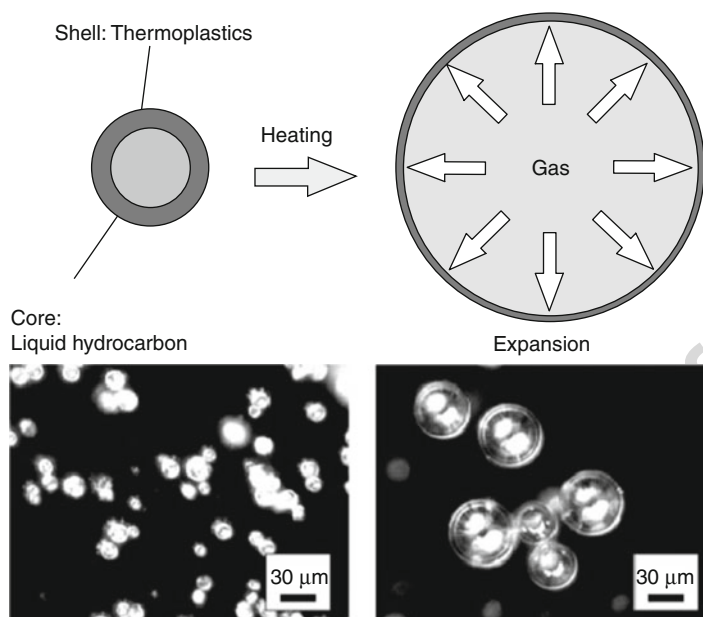


**Fig. 7** Structure of thermally expandable microcapsules (TEMs) (Nishiyama et al. 2003)

of low temperature expansion TEMs. Therefore, an increase of the dismantlable temperature of an adhesive may induce a decrease of dismantlability because the expansion volume is vitally important to separate the bonded joints.

As mentioned before, since the stresses caused by the TEMs expansion is the main driving force for joint separation, the expansion characteristics should be known to improve the performance of a dismantlable adhesive. Several experiments have been carried out to investigate the expansion performance of a type of TEM (Nishiyama and Sato 2005). For the purpose, Pressure-Volume-Temperature tests (PVT tests) were conducted using an experimental set up called “PVT measurement equipments.” In these tests, TEMs are contained in a flexible vessel under hydrostatic pressure with silicone oil under different temperature conditions. The hydrostatic pressure is caused using a pump and the temperature increases using a heater. The volume change of the TEMs was measured using a differential transformer. Therefore, the volume change of TEMs under different conditions of pressure and temperature could be measured and the P- V- T relation could be determined by the tests. For instance, the TEM mixed in the epoxy resin can expand 8 times in volume at 100 °C. The pressure,  $P$ , caused by the TEM for a volume expansion of 800% and  $T = 100\text{ }^{\circ}\text{C}$  could be determined as 1–2 MPa. The result is strange because the pressure is much lower than the strength of the epoxy resin. In other words, the pressure is too small to deform the epoxy matrix resin enough for dismantlement. However, the resin becomes soft enough to deform at the temperature of the TEMs expansion. Thus, the combination of the resin softening and the TEM expansion is the key for the adhesive’s large deformation and internal stress occurrence. In order

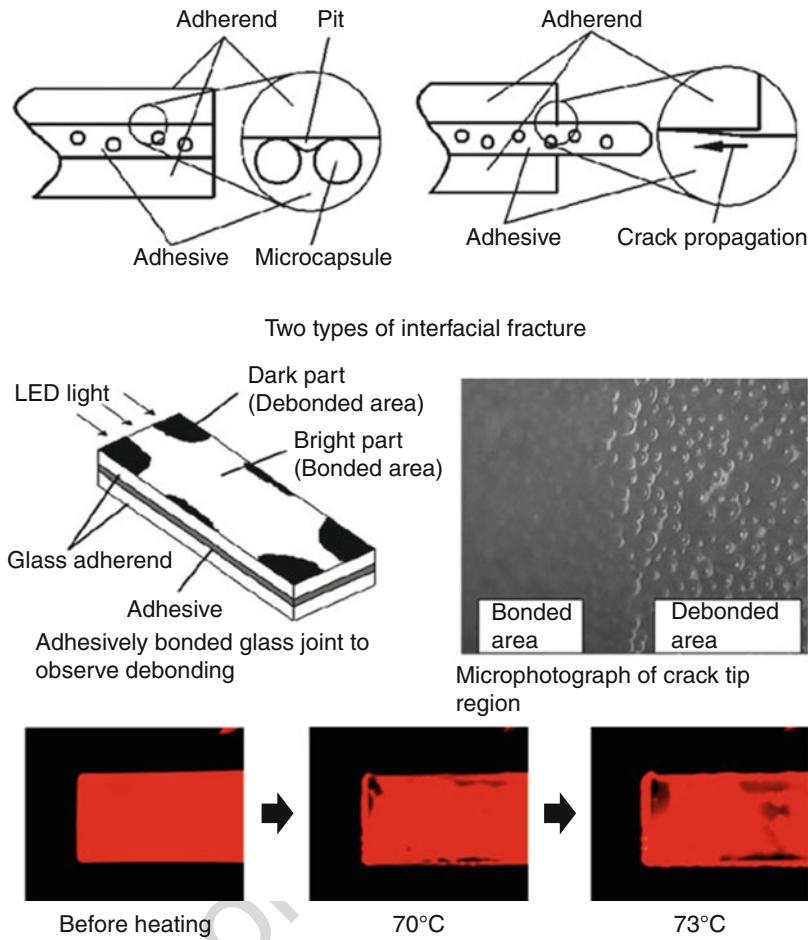


**Fig. 8** Dismantling experiments to observe the interfacial debonding caused by TEMs in an epoxy adhesive; debonded regions in the joint can be seen as the dark parts in the images at the bottom of the figure, and they are expanding with respect to temperature

to provide dismantlability to an adhesive by mixing TEMs, not only the expansion force of the TEMs is important, but also the low strength and modulus of the matrix resin at high temperatures. A resin, whose  $T_g$  is close to the volume expansion temperature of the TEM, whose modulus and strength decreases drastically around the  $T_g$ , and which is soft enough not to suppress the expansion of the TEM in its rubber plateau, has to be selected as the matrix for a dismantlable adhesive.

Two mechanical models of the interfacial debonding of dismantlable adhesives are proposed in Fig. 8. One of them is the local crack generation model, in which the expansion of a TEM causes a small interfacial crack nearby the contact point between the TEM and the adherend. The crack expands to the neighbor cracks, and the cracks join and lead to the total fracture of the joint. The other model is the global stress

generation model, in which the expansion of TEMs induces volume increase of the adhesive layer, leading to joint fracture due to the global residual stress concentrating around the tip of the adhesive layer or interfacial cracks. An experimental verification of the models has been carried out using a glass joint bonded by an adhesive, including TEMs. In this test, optical and microscopic observation was conducted through the glass adherend. No gas generation was observed. Small circumferential cracks around each TEM were observed as explained by the local crack generation model. However, global cracks occurred at the edges of the joint and propagated inside the joint. This implies that the global stress generation model is also valid. Thus, the results support both models, which happen simultaneously, although the contribution ratio of each effect is still unknown.

### 59.3.3 Adhesives Including Chemically Active Materials

Mixture of chemically active materials is an effective method to dismantle adhesives. For example, expandable graphite and aluminum hydroxide can be used for the purpose. Expandable graphite is a flaky carbon having a layer structure of planar crystals. Chemicals such as acids are intercalated between the crystal layers. The acid is vaporized by heating, and water included in the acid is also vaporized. Therefore, the vaporized acid and the vapor can expand the layer structure as an accordion being pulled, increasing the volume drastically, as shown in Fig. 9. Since the vaporized acid and vapor are hot, they can attack the resin. Aluminum hydroxide consists in a fine powder that is transformed into aluminum oxide and vapor at high temperature. The hot vapor can not only expand the resin, but also attack the resin in the same manner as the expandable graphite does. Water becomes superheated vapor over 100 °C in the atmospheric pressure. The superheated vapor can cause chemical decomposition of the resin. An application of the technique is double-side PSA tapes that include aluminum hydroxide and which used for the joining heat sinks to large-size plasma display panels. They have to be dismantled in their recycling process because they are dissimilar materials. The joint can be separated applying a weak force because the PSA tape can be degraded by heating and the bonding strength decreases very much. Other types of chemicals, oxidizing agents such as ammonium perchlorate, can be used to attack the resin too.

### 59.3.4 Adhesives to Which an Electrochemical Reaction on Interfaces Is Applied

A novel adhesive: Electrelease (EIC Laboratories, MA, USA), which can be separated electrically, is already commercially available (Welsh et al. 2003). The interface between the adhesive and the anodic adherend becomes so weak by applying a DC current that the joint can be broken by hand, as shown in Fig. 10. The adhesive was developed to bond sensors on the wing of aircrafts, and has been tested to be applied to a separation mechanism for space applications. The application of this

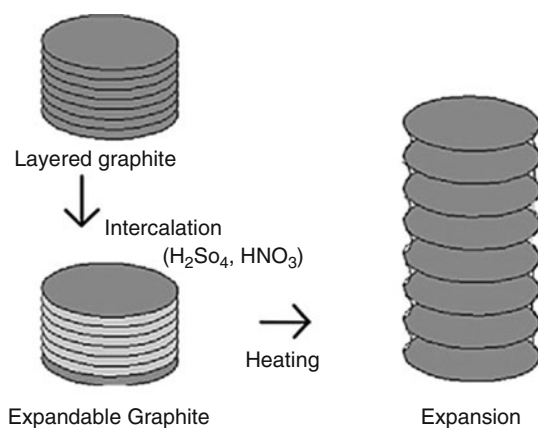


**Fig. 9** Expandable graphite

technique weakens the joint, but not completely. Therefore, some external force has to be applied to separate the joint even after the electric voltage is imposed. For instance, if a weak load is applied continuously using bias springs to the joint, applying only an electric voltage causes the spontaneous separation of the joint. As just described, a one-time separation mechanism triggered electrically can be realized easily using this adhesive as shown, in Fig. 11 (Shiote et al. 2009). The reason why the adhesive can be weakened by electric currents is not completely understood. It is supposed that an electric current transmitted to the adhesive layer causes electrochemical reactions on the surface of the anodic adherend, and this leads to erosion of the metal-oxide layer of the adherend. A similar mechanism of delamination induced by electric currents is known as “cathodic delamination,” in which



**Fig. 10** An electrically dismantlable adhesive (Electrelease<sup>®</sup>, EIC Laboratories) where PEG and PDMS denote polyethyleneglycol and polydimethylsiloxane, respectively (Shiote et al. 2009)

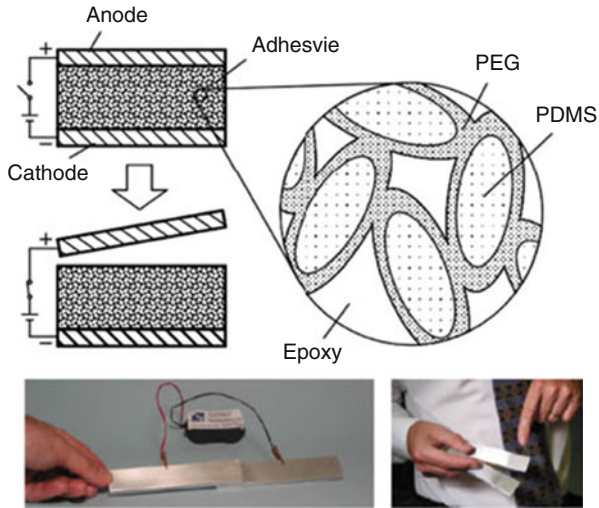
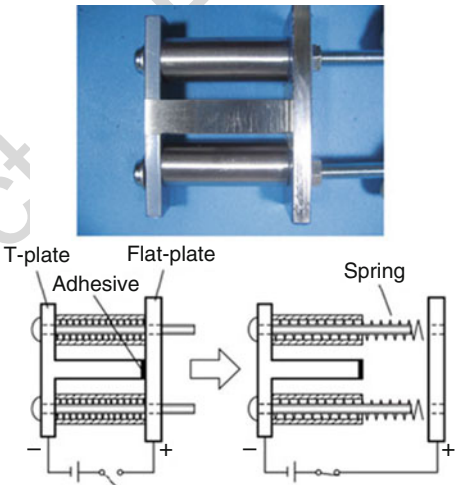


**Fig. 11** One-time separation mechanism using an electrically dismantlable adhesive (Shiote et al. 2009)



alkali materials precipitate at the interface and attack the resin (Horner and Boerio 1990). These delamination mechanisms are quite novel and very promising in terms of expanding the variety of dismantlable adhesives.

### 59.3.5 Miscellaneous Methods

PSAs are promising materials to realize dismantlable joints because separation capabilities are built in already. Recently, strong PSAs have been commercially available, and they have enough strength to be applied for semi-structural uses.



However, it becomes a problem in terms of dismantlability if the strength is too high. To avoid this problem, new types of PSAs, which are strong enough but can be separated easily, have been developed.

Command Tab<sup>®</sup> (3M, MN, U.S.A.) and PowerStrip<sup>®</sup> (TESA, Hamburg, Germany) are examples. Tackiness of PSAs depends on the modulus. If the modulus is out of a particular range known as Chang's "viscoelastic window," the PSA loses the tackiness or the bonding strength (Chang 1991). For instance, the PSA of PowerStrip comprises block-copolymer molecular chains having soft and hard segments, and the modulus depends on the deformation (Krawinkel 2003). If the PSA is pulled enough, the modulus increases and the tackiness decreases. Therefore, the PowerStrip tape can be removed easily, as shown in Fig. 12.

This theory of the viscoelastic window can be applied to other materials. Mixture of cross-linkers is another way by which PSAs can be hardened by heating or UV irradiation and the tackiness decreased. Recently, many kinds of tapes that can be separated by this method are used for dicing of IC chips.

Brittle adhesives have high shear and low peel strength. It is possible to take advantage of this aspect to make a kind of anisotropic adhesive. For example, a temporary joint adhesive, Lock n' Pop<sup>®</sup> (Illinois Tool Works (ITW), WA, U.S.A.) is commercially available. The adhesive is strong enough to fix cardboard boxes due to the high shear strength during their transportation, but is easy to separate by applying vertical forces because of its low peel strength, as shown in Fig. 13.

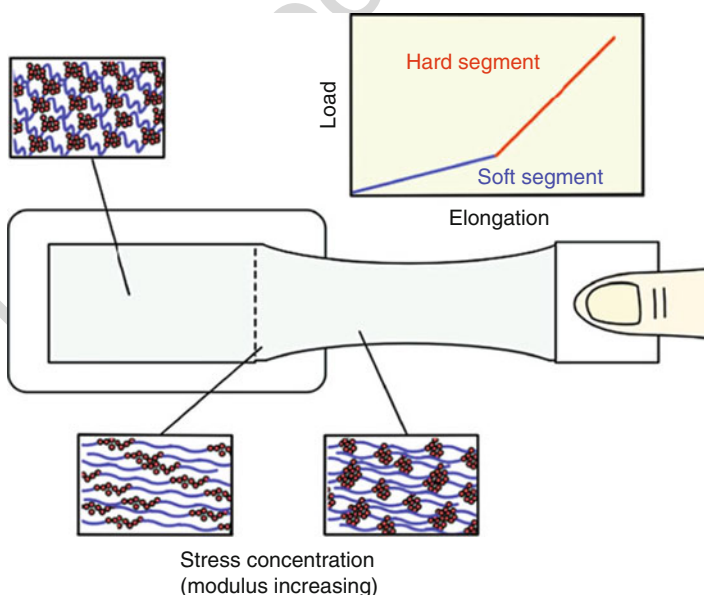


**Fig. 12** High strength strippable PSA tape (PowerStrip<sup>®</sup>, TESA)

**Fig. 13** Anisotropic strength adhesive for a temporary joint of cardboard boxes (Lock n' Pop<sup>®</sup>, Illinois Tool Works (ITW))

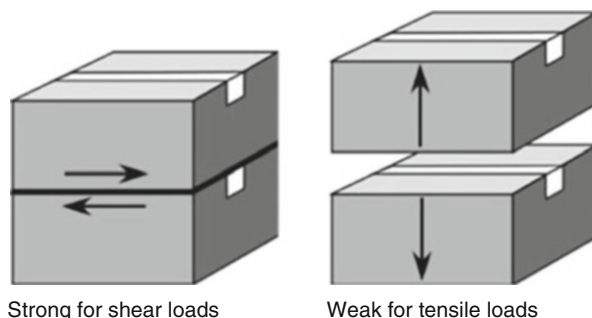
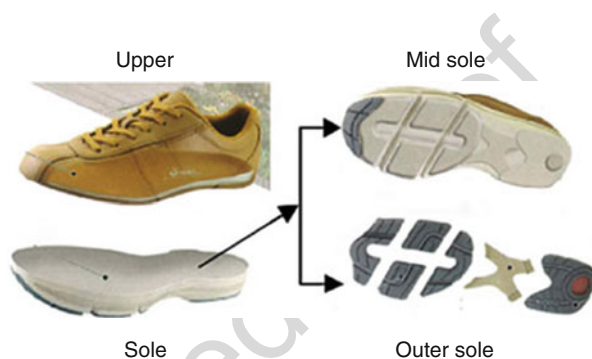


**Fig. 14** A dismantlable adhesive application for shoe industry (Mori and Harano 2009)



### 59.3.6 Recent Advances

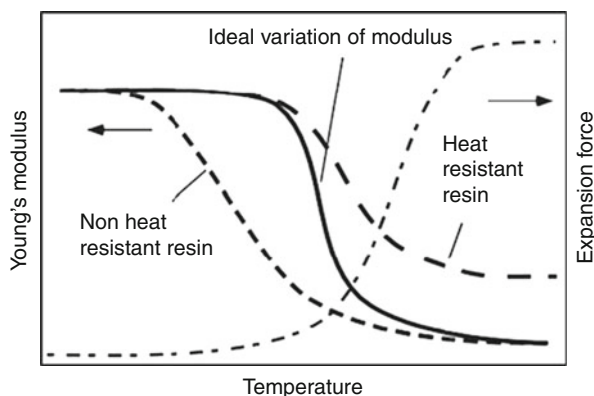
The use of adhesives including TEMs has been expanding in many applications. For example, an adhesive has been introduced for shoe fabrication to bond uppers and soles (mid soles and outer soles) as shown in Fig. 14 (Mori and Harano 2009). The adhesive includes TEMs as expansion agents and diethylene glycol or ethylene glycol as heat-generation agents. Since diethylene glycol is a high-dielectric material, the temperature can be risen by microwave irradiation heating. The temperature rise can induce the expansion of TEMs and finally leads to the separation of the uppers and soles. Microwave irradiation has advantages such that low energy loss, and the necessary equipments have become inexpensive recently. For instance, even a home microwave oven can be used to dismantle the shoes. Requirements for adhesives used in sport shoes are many and severe. Bond strength, flexibility, and heat resistance are indispensable. To meet these requirements, a formulation, which includes an urethane resin, 5 wt% of TEMs, and over 20 wt% of high-dielectric materials, is typically used. At the moment, the adhesive is only applied to expensive shoes for top athletes because they want to reuse the uppers when the soles have to be replaced. However, the adhesive is ready to be used in ordinary shoe markets in terms of performance and price. Shoe industries have huge markets in which adhesives have to be used essentially because dissimilar materials are bonded. Since the total mass of production is enormous and has been increasing, the use of recyclable joining techniques is of significance, especially in the future.

The use of TEMs is convenient to provide adhesives with dismantlability, but it is not versatile because of some disadvantages. One of them is the small expansion forces produced by TEMs, by which a weak adhesive can be separated but strong ones such as rubber modified ductile epoxy adhesives cannot be separated because they have high strength and ductility suppressing interfacial fracture even at a higher temperature than its  $T_g$ . To overcome this disadvantage, there are two alternative ways: changing the expansion agents or modifying the matrix resin. As alternative expansion agents, expandable graphite and aluminum hydroxide are promising, as mentioned above. They are not only chemical attack agents, but also expansion agents having larger expansion capabilities than TEMs.

Modification of matrix resins is also important, but this is the next step and it has not been investigated often so far. A strategy is to modify the resin to be softer than the previous ones at high temperature so that the resin can deform due to the TEMs' expansion. A problem is that the heat resistance of the resin might be damaged if the resin's  $T_g$  becomes too low. Thus, a good compromise of heat resistance and dismantlability must be pursued.

Kishi et al. has tried to develop a heat resistant dismantlable adhesive for joining composite materials and metals, and modified the composition of an epoxy adhesive accordingly (Kishi et al. 2006). This research was conducted as part of the national project "R&D of Carbon Fiber-Reinforced Composite Materials to Reduce Automobile Weight" supported by New Energy and Industrial Technology Development Organization (NEDO) in Japan. As mentioned above, the resin should be soft at the temperature of the TEMs' expansion. A problem is that typical heat resistant resins have moduli and strengths enough to suppress the TEMs' expansion even at high temperatures, over their  $T_g$ . In other words, such heat resistant resins are not soft enough for TEMs to expand even at high temperature. Therefore, a kind of resin which has a high  $T_g$  and enough low modulus and strength above the  $T_g$  is necessary for heat resistant dismantlable adhesives. In addition, steep change of the modulus and strength of the resin around the  $T_g$  is also important to increase the maximum allowable temperature of the adhesive, as shown in Fig. 15.

**Fig. 15** An idealistic variation of modulus for dismantlable adhesive's matrix resin



Kishi et al. aimed a target for the adhesive as:

1. The maximum temperature for use is 80 °C. Under this temperature, the resin has a modulus and a strength high enough to bear the applied loads.
2. Over 100 °C, the resin has a steep decrease of the modulus and strength.
3. In the temperature range over 150 °C, in which the resin is in rubbery condition, the resin should have a modulus and strength low enough for TEMs expansion.

For the adhesive, they proposed a formulation, shown in Fig. 16, including diglycidylether of bisphenol A (DGEBA) 828, DGEBA 1001, and glycidylphthalimide (GPI) as the base resins cured with hardeners dicyandiamide (DICY) and 3-(3,4-dichlorophenyl)-1,1-dimethylurea (DCMU) that can increase the Tg of the resin. An important point of the formulation is the inclusion of GPI that has high polarity and can form strong bonds between the main molecular chains. The bonds work as if the cross-linking density of the resin increases at low temperatures. However, the bonds are dissociated at high temperatures, decreasing the substantial cross-linking density. The low modulus at high temperatures and the steep decrease of the modulus around the Tg are due to the destruction of the bonds. Thus, the resin has high modulus and strength in low temperature ranges, high Tg, steep decrease of the modulus, and low modulus over Tg, which are suitable characteristics for heat resistant dismantlable adhesives. For instance, the resin has a modulus higher than 3 GPa in the glass condition range around the ambient temperature. However, the modulus decreases to 2 MPa over 150 °C.

The resin was combined with an expandable graphite and was used to bond metal parts to carbon-fiber-reinforced plastics (CFRP) plate. The joint could be separated within 5 min at 250 °C, as shown in Fig. 17. The adhesive includes 10 wt% of the expandable graphite and it begins to expand around 200 °C, which is much higher than the Tg of the resin. The margin between the expansion temperature of the expandable graphite and the Tg of the resin was decided considering the chemical stability of the expandable graphite at high temperatures. The temperature of 250 °C

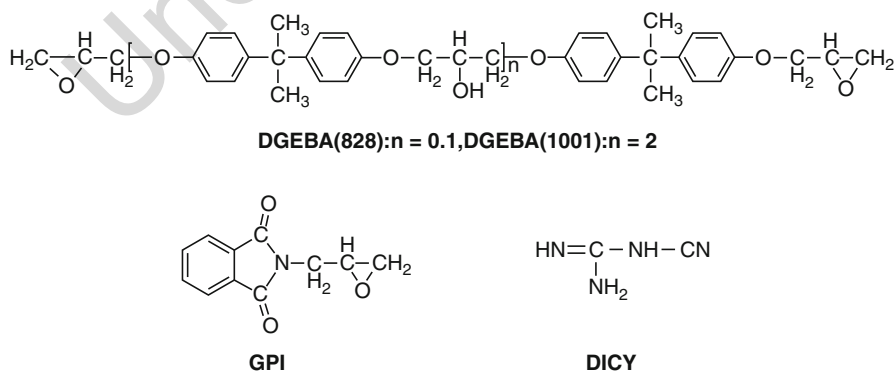


**Fig. 16** Components of the heat resistant dismantlable adhesive (Kishi et al. 2006)

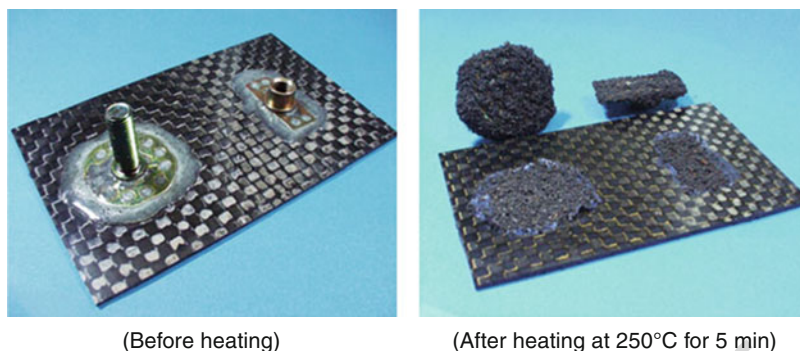


**Fig. 17** Specimen of metal parts bonded on a carbon reinforced plastic (CFRP) plate with a heat resistant dismantlable adhesive

in the dismantlable test was decided as a compromise between time and temperature of separation.

### 59.3.7 Future Seeds

One of the promising seeds to realize novel types of dismantlable adhesives is the use of degradable polymers. Polyperoxide-polymers, for instance, can be applied for that purpose because the resin can be cured and re-liquefied reversibly by heating (Matsumoto and Taketani 2006). Adhesives using the resin can be separated and bonded many times. Another kind of polymer having weak points such as Azo groups in the molecular chains is also promising for heat-degradable dismantlable adhesives. A type of rubber such as thermoreversible hydrogen bond cross-linked (THC) rubber, shown in Fig. 18, can be re-liquefied by heating, has been proposed recently (Chino et al. 2002; Chino and Ashiura 2001; Chino 2006). Such rubbers are also applicable for dismantlable adhesives.

Since almost all recent dismantlable adhesives need heating to be separated, heating methods are also important to improve the efficiency of the dismantling process. The necessity of heating will remain even in the future. Heating the whole structure including the adhesively bonded joints is not efficient. Local heating of the joints is more convenient. Induction heating and microwave heating methods are appropriate in terms of efficiency. A new method of microwave heating using nanoferrite particles, shown in Fig. 19, has been proposed and it can be applied for the heating process of joints bonded with dismantlable adhesives (Sauer et al. 2004).

Other stimulations except heating should be investigated in the future. Magnetism, radiation (neutron beams, gamma ray), hydrostatic pressure, compressive stress, UV irradiation, and high voltage discharge are candidates for the stimulation. Dry adhesion, which has been attracting attention recently, is another possibility to provide new ideas for joint dismantlement (Lee et al. 2007). Further investigation and research on interfacial phenomena must be conducted to obtain further

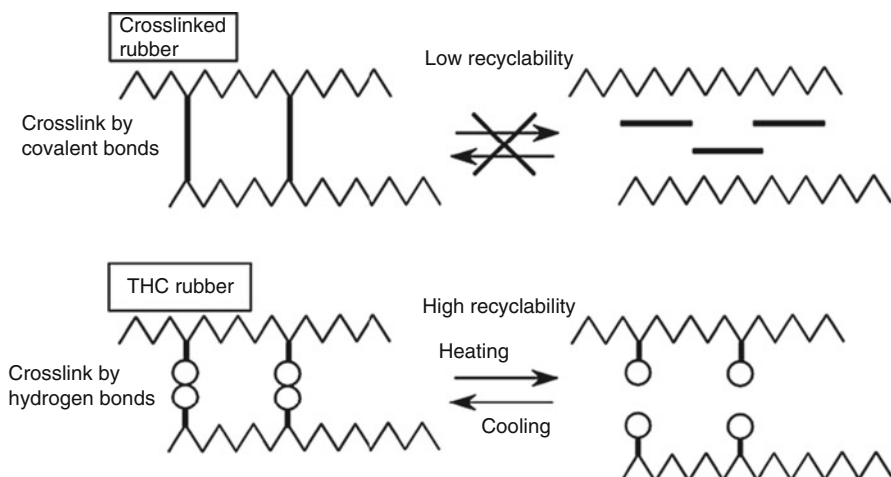
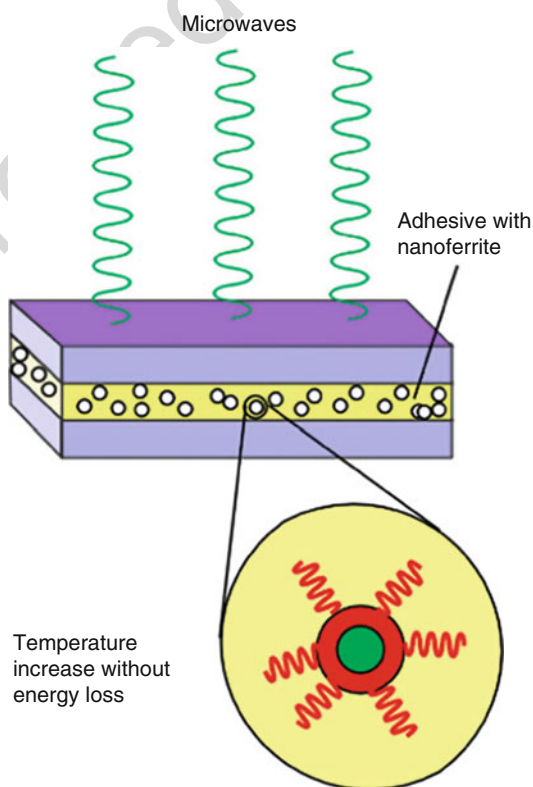


**Fig. 18** Schematic illustration of thermoreversible hydrogen bond cross-linked (THC) rubber principle

**Fig. 19** Microwave heating using nanoferrite as dipole conductors (Sauer et al. 2004)



knowledge because the ultimate dismantlable adhesive must be an adhesive with which its interface can be separated easily and completely with a small amount of energy used for the separation.

---

## 59.4 Conclusion

To promote the use of adhesives, eco-friendly attitudes of both adhesive makers and users are indispensable. Reducing carbon dioxide and energy consumption is the main topics of environmental issues. Recently, alternative options, such as the use of carbon-neutral or recycled materials for making adhesives, can be taken to meet the demands derived from the environmental issues. The optimization of bonding process and joint design is also very important and effective to reduce energy consumption and wastes. Recently, dismantlable adhesives have been available for joining the materials that have to be separated on demand. These adhesives can be applied to adherend recycling or product reworking.

There are many technical seeds for dismantlable adhesives already. Since dismantlable adhesive technology has still some minor problems such as low heat resistance or low durability, they should be solved soon by researchers or industries, and then the use of the adhesives will expand to many applications. Dismantlable adhesive technology has contradictory aspects: good bonding and easy separation. High bonding strength tends to induce difficult separation. Therefore, it is also important to clarify the minimum bond strength necessary for each application instead of pursuing high performance in strength.

---

## References

- Alcorta J, Papon E et al (2004) WO Patent 2004/087829
- Bain PS, Manfre G (2000) WO Patent 2000/75254
- Chang EP (1991) Viscoelastic windows of pressure-sensitive adhesives. *J Adhes* 34:189
- Chino K (2006) Thermoreversible crosslinking rubber using supramolecular hydrogen bonding networks. *Kautschuk Gummi Kunststoffe* 2006, April:158
- Chino K, Ashiura M (2001) Thermoreversible cross-linking rubber using supramolecular hydrogen-bonding networks. *Macromolecules* 34:9201
- Chino K, Ashiura M et al (2002) Thermo reversible crosslinking rubber using supramolecular hydrogen bonding networks. *Rubber Chem Technol* 75:713
- Fay P (2005) History of adhesive bonding. In: Adams R (ed) *Adhesive bonding – science, technology and applications*. Woodhead, Cambridge, pp 3–22
- Horner M, Boerio J (1990) Cathodic delamination of an epoxy/polyamide coating from steel. *J Adhes* 32:141
- Ishikawa H, Seto K et al (2004) Dismantlable adhesive and evaluation of practical uses for building materials. *J Soc Mater Sci Japan* 53:1143. (in Japanese)
- Ishikawa H, Seto K et al (2005) Bond strength and disbonding behavior of elastomer and emulsion-type dismantlable adhesives used for building materials. *Int J Adhes Adhes* 25:193
- Jos H, Leite L (2007) MSc thesis, Faculty of Engineering of the University of Porto (in Portuguese)
- Kadota J, Hasegawa K et al (2004) Adhesive of lignophenols/polyacrylate for wood. *J Adhes Soc Japan* 40:101. (in Japanese)

- 604 Kishi H, Inada Y et al (2006) Design of dismantlable structural adhesives with high temperature  
605 performance. *J Adhes Soc Japan* 42:356. (in Japanese)
- 606 Krawinkel Th (2003) In: *Proceedings of Swiss bonding 03*, Rapperswill, pp 225–233 (in German)
- 607 Lee H, Lee B et al (2007) A reversible wet/dry adhesive inspired by mussels and geckos. *Nature*  
608 448:338
- 609 Matsumoto A, Taketani S (2006) Regiospecific radical polymerization of a tetra-substituted ethyl-  
610 ene monomer with molecular oxygen for the synthesis of a new degradable polymer. *J Am*  
611 *Chem Soc* 128:4566
- 612 Mori S, Harano K (2009) Shuzu no seikei kakou. *Seikei kakou* 21:305. (in Japanese)
- 613 Nishida H, Hirayama N (2006) PCT/JP2006/309543 Patent
- 614 Nishiyama Y, Sato C (2005) Behavior of dismantlable adhesives including thermally expansive  
615 microcapsules. In: *Possart W (ed) Adhesion – current research and applications*. Wiley,  
616 New York, pp 555–568
- 617 Nishiyama Y, Uto N et al (2003) Dismantlement behavior and strength of dismantlable adhesive  
618 including thermally expansive particles. *Int J Adhes Adhes* 23:377
- 619 Papon E, Olive M et al (2008) In: *Proceedings of the 31st annual meeting of the adhesion society*,  
620 Austin, pp 296–297
- 621 Ratna D, Banthia A (2000) Epoxidized soybean oil toughened epoxy adhesive. *J Adhes Sci Tech*  
622 14:15
- 623 Sauer H, Spiekermann S et al (2004) Accelerated curing with microwaves and nanoferrites.  
624 *Adhesion. Adhes & Sealants* 2003(2004):48–50
- 625 Sekine T, Tomita H et al (2009) An induction heating method with traveling magnetic field for long  
626 structure metal. *Electr Eng Japan* 168:32
- 627 Shiote H, Ohe M et al (2009) Effects of electrical treatment conditions on dismantlable properties of  
628 joints bonded with electrically disbanding adhesive. *J Adhes Soc Japan* 45:376. (in Japanese)
- 629 Sprenger S, Eger C et al (2004) Nano-modified ambient temperature curing epoxy adhesives.  
630 *Adhesion. Adhes & Sealants* 2003(2004):20–23
- 631 Umemura K, Inoue A et al (2003) Development of new natural polymer-based wood adhesives I:  
632 dry bond strength and water resistance of konjac glucomannan, chitosan, and their composites. *J*  
633 *Wood Sci* 49:221
- 634 Viljanmaa M, Sodergard A et al (2002) Lactic acid based polymers as hot melt adhesives for  
635 packaging applications. *Int J Adhes Adhes* 22:219
- 636 Welsh J, Higgins J et al (2003) Evaluation of electrically disbonding adhesive properties for use as  
637 separation systems. In: *AIAA 2003–1436 (44th AIAA/ASME/ASCE/AHS structures, structural*  
638 *dynamics, and materials conference)*, Norfolk, pp 1–3
- 639 Yamada K, Chen T et al (2000) Chitosan based water-resistant adhesive. Analogy to mussel glue.  
640 *Biomacromolecules* 1:252



# Adhesion Technology Recap: Current and Emerging Areas

60

Lucas F. M. da Silva, Andreas Öchsner, and Robert D. Adams

## Contents

60.1	Theory of Adhesion .....	1776
60.2	Surface Treatments .....	1776
60.3	Adhesive and Sealant Materials .....	1777
60.4	Testing of Adhesive Properties .....	1777
60.5	Joint Design .....	1778
60.6	Durability .....	1779
60.7	Manufacture .....	1780
60.8	Quality Control .....	1780
60.9	Applications .....	1781
60.10	Emerging Areas .....	1782
60.11	Conclusions .....	1783

## Abstract

This chapter gives a brief description of the subjects and chapters that are included in this second edition of the handbook and the most important changes in relation to the first edition. The handbook is organized in ten parts: theory of

L. F. M. da Silva (✉)

Department of Mechanical Engineering, Faculty of Engineering, University of Porto, Porto, Portugal

e-mail: [lucas@fe.up.pt](mailto:lucas@fe.up.pt)

A. Öchsner

Faculty of Mechanical Engineering, Esslingen University of Applied Sciences, Esslingen, Baden-Württemberg, Germany

e-mail: [andreas.oechsner@gmail.com](mailto:andreas.oechsner@gmail.com)

R. D. Adams

Department of Mechanical Engineering, University of Bristol, Bristol, UK

Department of Engineering Science, University of Oxford, Oxford, UK

e-mail: [r.d.adams@bristol.ac.uk](mailto:r.d.adams@bristol.ac.uk)

© Springer International Publishing AG, part of Springer Nature 2018

L. F. M. da Silva et al. (eds.), *Handbook of Adhesion Technology*,

[https://doi.org/10.1007/978-3-319-55411-2\\_59](https://doi.org/10.1007/978-3-319-55411-2_59)

1775

adhesion, surface treatment, adhesive and sealant materials, testing of adhesive properties, joint design, durability, manufacture, quality control, applications, and emerging areas. A total of 58 chapters are presented covering all aspects of adhesion and adhesives. In addition to the information contained in each chapter, an extensive list of references is given (approximately 4000 references).

---

## 60.1 Theory of Adhesion

In ► [Chap. 2, “Theories of Fundamental Adhesion”](#) by Packham, the historical development and current status of the four classical theories of adhesion (mechanical theory, adsorption theory, electrostatic theory, and diffusion theory) are reviewed. The role of weak boundary layers is also discussed with emphasis on the importance of careful investigation of the locus of failure of an adhesive bond. Next, Brogly in ► [Chap. 3, “Forces Involved in Adhesion”](#) describes the main forces responsible for adhesion, from strong covalent bonds to weak van der Waals forces, also considering specific interactions such as acid-base or capillary forces. ► [Chapter 4, “Wetting of Solids”](#) by Shanahan and Possart considers thermodynamic aspects of wetting, which involves intimate contact between the two phases and the environment. A short overview of the relevant processes and parameters in the spreading of liquids on substrates is presented in ► [Chap. 5, “Spreading of Liquids on Substrates”](#) by Reiter. In a simplified view, the dynamics of these processes can be understood as being controlled by the balance of driving forces and resistance due to dissipative processes. Finally, in ► [Chap. 6, “Thermodynamics of Adhesion,”](#) Possart and Shanahan show that wetting data may be used to estimate the thermodynamic, or Dupré, energy of adhesion, provided certain assumptions are made and suitable models constructed for, in particular, interfacial tensions.

---

## 60.2 Surface Treatments

The use of surface treatments to optimize adhesion has been well-established. In ► [Chap. 7, “General Introduction to Surface Treatments,”](#) Critchlow considers the main treatment methods for metals and polymers in terms of how such processes are carried out and their influence on surface physical and chemical properties. Consideration has been given to a range of treatments from simple degrease options to the more highly complex multistage processes. Davies, in ► [Chap. 8, “Surface Treatments of Selected Materials,”](#) discusses high-performance surface treatments for several metals and other materials. Surface treatment of aluminum and other metals is used to illustrate how proper surface preparations meet these requirements. ► [Chapter 9, “Surface Characterization and Its Role in Adhesion Science and Technology”](#) by Watts reviews a variety of methods of surface characterization that have been found to be useful in the study of adhesion. The methods considered can conveniently be considered in three groups: surface topography, surface free energy of a material, and surface-specific chemical analysis. Next, Watts in

► [Chap. 10, “Use of Surface Analysis Methods to Probe the Interfacial Chemistry of Adhesion”](#) explores the manner in which the surface analysis methods of X-ray photoelectron spectroscopy (XPS) and time-of-flight secondary ion mass spectrometry (ToF-SIMS) can be used to extract information regarding the interfacial chemistry of adhesion from polymer/metal systems such as adhesive joints. The last chapter of this section, ► [Chap. 11, “Organosilanes: Adhesion Promoters and Primers”](#) by Abel, describes organosilanes from their genesis to their chemistry. The necessary interactions that such molecules have to develop on materials in order to fulfil their main role as adhesion promoters are explained. The use of silanes as primers particularly where the user aims to improve adhesion or protect from corrosion is also considered. Some other organic or nonorganic adhesion promoters are also discussed.

---

## 60.3 Adhesive and Sealant Materials

The first chapter ► [“Classification of Adhesive and Sealant Materials”](#) (Chap. 12) by Sancaktar classifies adhesive and sealant materials. For this purpose, various categories are considered depending on the polymer base, functionality in the polymer “backbone,” physical forms, chemical families, functional types, and methods of application. Next, in ► [Chap. 13, “Composition of Adhesives,”](#) Kim et al. give information about various ingredients that may appear in an adhesive or sealant: primary resins, hardeners, solvents, fillers, plasticizers, reinforcements, and various additives. In the third chapter of this section, Papon (► [Chap. 14, “Adhesive Families”](#)) classifies adhesives and sealants in three broad groups. First, there are adhesives where the polymer is pre-existing (and must be placed beforehand in fluid form: solution, emulsion, or “melt” state). Second there are adhesives where the polymer is formed during the course of a reactive process (polymerization). Third, Papon describes the particular category of pressure-sensitive adhesives where the polymer exhibits viscoelastic properties able to develop adhesion during the bonding step. The basic concepts, formulations, and test methods for pressure-sensitive adhesives are presented in ► [Chap. 15, “Pressure-Sensitive Adhesives \(PSAs\)”](#) by Paul, stressing the importance of interfacial interactions, viscous loss, and extensibility. Selection of the correct adhesive for an application can be a daunting task due to the many types commercially available ranging from different chemistries through different forms to an almost continuum of material properties. Kellar in ► [Chap. 16, “Selection of Adhesives”](#) gives a logical approach to this task and selection criteria.

---

## 60.4 Testing of Adhesive Properties

The first chapter by Dillard ► [“Physical Properties”](#) (Chap. 17) addresses several relevant physical properties of adhesives, including viscosity, density, and stress-strain behavior, quantities that are often thought to be intrinsic properties of a material. The thermal properties of adhesives are described next by Comyn.

Consideration is given to the shelf life, the hardening process, the glass transition temperature, the thermal conductivity and thermal expansion, and the thermal breakdown of adhesives. In ► [Chap. 19, “Failure Strength Tests,”](#) da Silva et al. describe the major failure strength tests used to determine the intrinsic adhesive properties. Tensile, compressive, and shear tests are described with reference to the major international standards. Bulk and in situ (adhesive in a joint) tests are discussed and related. ► [Chap. 20, “Fracture Tests”](#) by Blackman considers first the fracture in a bulk adhesive specimen under mode I, i.e., tensile opening loading conditions. Mode II (in plane shear) and mixed-mode I/II testing of adhesive joints are also considered. There is often the need to measure the resistance to fracture in a joint with flexible substrates. One such test is the peel test, and some variants of the peel test are considered in that chapter. Goglio, in ► [Chap. 21, “Impact Tests,”](#) describes the main tests used to assess the impact strength of adhesives and joints. The main tests used in the experiments are pendulum, falling weight, and Hopkinson bar loading conditions or evolutions of these. The last chapter of this section by Dillard and Yamaguchi deals with ► [Chap. 22, “Special Tests.”](#) This chapter gives a brief description of special mechanical tests for various types of material and sample geometries, such as blister tests, tensile tests and shear tests for sealants/foam adhesives, indentation tests, scratch tests, tack tests, and tests for the evaluation of residual stresses.

---

## 60.5 Joint Design

This section starts with ► [Chap. 23, “Constitutive Adhesive and Sealant Models”](#) by Sancaktar. The chapter includes deformation theories and viscoelasticity with linearity and nonlinearity considerations, rubber elasticity, singularity methods, bulk adhesive as composite material, damage models, the effects of cure and processing conditions on the mechanical behavior, and the concept of the “inter-phase.” ► [Chapter 24, “Analytical Approach”](#) by Tong and Luo presents an analytical approach for determining stress and strength of adhesively bonded joints. Various closed-form solutions for adhesive stresses and edge bending moment for balanced single-lap joints are presented and compared. In ► [Chap. 25, “Numerical Approach: Finite Element Analysis,”](#) Ashcroft provides first a general background to the development and application of the finite element (FE) method. Then he discusses some of the practical aspects of FE modeling and gives applications of the FE method to adhesively bonded joints. FE analysis is currently the only technique that can comprehensively address the challenges of modeling bonded joints under realistic operating conditions. However, a reliable and robust method of using FE analysis to model failure in bonded joints is still to be developed. Öchsner, in ► [Chap. 26, “Special Numerical Techniques to Joint Design,”](#) introduces special numerical techniques to analyze adhesive joints. The first part covers special FE techniques which reduce the size of the computational models. The second part of this chapter introduces alternative approximation methods, the boundary element method and the finite difference method. In ► [Chap. 27, “Design Rules and Methods to Improve Joint Strength,”](#) da Silva et al. describe the main factors influencing joint

strength. Methods are then proposed to improve the joint strength by using fillets, adherend profiling and other geometric solutions, and hybrid joining. Repair designs are also discussed. Finally, configurations are recommended for several types of joint. ► [Chapter 28, “Design with Sealants”](#) by Anderson describes the many factors to go into the design of reliable sealant joints. The various joint types are discussed and illustrated, and their critical dimensions and materials are described. Sato, in ► [Chap. 29, “Design for Impact Loads,”](#) discusses design methods for adhesively bonded joints subjected to impact loading. Methodologies to treat the dynamic responses of structures are shown. Some examples of stress analysis are shown, where closed-form approaches and dynamic FE analyses are explained. The last chapter of this section ► [“Vibration Damping of Adhesively Bonded Joints”](#) (Chap. 30) by Adams et al. discusses the general concept of vibration damping in vibrating structures and how it can be used to limit vibration amplitudes. Simple equations for calculating the damping of a lap joint in tension and bending have been developed. As there is very little experimental data available, the damping of a variety of adhesively bonded single-lap joints has been measured by the authors.

---

## 60.6 Durability

In ► [Chap. 31, “Effect of Water and Mechanical Stress on Durability,”](#) Ashcroft and Comyn discuss the effect that absorbed water has on the strength of adhesively bonded joints. The influence of adherend surface treatment, applied stress, and adhesive type on the environmental degradation of bonded joints is demonstrated. Methods of modeling the environmental degradation of adhesively bonded joints using coupled hygro-mechanical finite element (FE) analysis are then described. Chapter “Radiation and Vacuum” of the first edition has been substituted by ► [“Adhesives in Space Environment”](#) (Chap. 32) by Dagrás et al. In the first part, a description of the different uses and needs related to adhesives on spacecraft is given. Then, the characteristics of space environment are explained. Once in orbit, the adhesive has to withstand constraints as particles radiations, UV, and atomic oxygen that are not present on Earth. Before spacecraft launch, the adhesives have to be validated and tested on ground with conditions as representative as possible of the space environment. Finally, the impact of this space environment on adhesives and the associated degradations are described. ► [Chapter 33, “Fatigue Load Conditions”](#) by Ashcroft discusses some of the main factors when considering fatigue, with particular reference to issues applicable to bonded joint. The main methods of characterizing and predicting the response of bonded joints to fatigue loading are described. Finally, there are sections on the special cases of creep-fatigue and impact fatigue. In ► [Chap. 34, “Creep Load Conditions,”](#) Geiss considers viscoelastic models, superposition principles, experimental testing procedures, and predictive methods. In the last chapter of this section, ► [“Durability of Nonstructural Adhesives”](#) (Chap. 35) by Palmer, methods evaluating durability and test regimes, including exposure to elevated and reduced temperatures, UV radiation, moisture,

181 saline solutions, stress, and fatigue, both individually and combined in cycles are  
182 considered.

---

## 183 **60.7 Manufacture**

184 The first subject in this section is ► [“Storage of Adhesives”](#) (Chap. 36) by  
185 Engeldinger and Lim. A major part of this chapter focuses on the shelf life and  
186 safety aspects. Adhesives are divided into four categories, solvent-based, water-  
187 based, hot-melt, and reactive adhesives. In ► [Chap. 37, “Preparation for Bonding,”](#)  
188 Lutz discusses each item of the process chain: the storage of adhesives, transfer  
189 to the application area, different metering and dispensing technologies, mixing  
190 equipment used, substrate preparation, and quality control. Proposals are made  
191 regarding education of personnel and how to create a safe working environment.  
192 In ► [Chap. 38, “Equipment for Adhesive Bonding,”](#) Peschka describes the equip-  
193 ment required for manual adhesive bonding processes. Automation and robotics are  
194 outlined with a special emphasis on parameters affecting accuracy. Accelerated  
195 curing using such devices as UV radiation and inductive heating is also treated.  
196 The last chapter of this section, ► [“Environment and Safety”](#) (Chap. 39) by van  
197 Halteren, deals with the different aspects of consumer, work, and environmental  
198 protection, including health and safety information, related to the use of adhesives in  
199 industrial and domestic areas.

---

## 200 **60.8 Quality Control**

201 This section starts with ► [Chap. 40, “Quality Control of Raw Materials”](#) by  
202 Wakabayashi. The main components of adhesives are first described, and then  
203 quality control procedures are discussed such as chemistry, impurity content, molec-  
204 ular weight, viscosity, density, and quality control of raw materials in storage. Next,  
205 in ► [Chap. 41, “Processing Quality Control”](#) by Haraga, the processing quality  
206 control of adhesively bonded joints in actual production lines is discussed. Topics  
207 such as control of environmental conditions and materials, inspection of surface  
208 treatment of adherends, adhesive selection for easy process control, and education  
209 and training of operators are treated. In ► [Chap. 42, “Nondestructive Testing”](#) by  
210 Adams, the types of defect encountered in adhesive joints and the nondestructive  
211 testing techniques available to detect them are reviewed. Several techniques are  
212 available for void detection, the most commonly used being ultrasonics and different  
213 types of bond tester. The detection of poor cohesive properties is more difficult but  
214 can be achieved with ultrasonic or dielectric measurements. The last chapter of this  
215 section, ► [“Techniques for Post-fracture Analysis”](#) (Chap. 43), was rewritten by  
216 Créac’hcadec. This chapter presents three types of measurement systems: micros-  
217 copy, compositional analysis, and mechanical observations. A table sums up an  
218 exhaustive list of the major observation devices. Then, the main methods are detailed

with macroscopic and mesoscopic observations, microscopic observation, physico-chemico analysis, and mechanical observations.

## 60.9 Applications

The first application treated is the “Aeronautical Industry” by Hart-Smith. The following topics are treated: basic needs, adhesive characteristics, surface preparation, design of adhesive joints, durability, defects, thermal effects, quality control, composite structures, repairs, and examples of use. ► Chapter 45, “Aerospace Industry” was extensively revised by Pérès and Larnac. The chapter introduces some of the specific bonding-related issues that face those responsible for bonding operations in space applications such as extremely high mechanical loads over a short time, with the launcher and its payloads subjected to gravity magnified by about 20, followed by exposure to extremely high temperatures over a very long period, with the observation and telecom satellites under zero gravity. Dilger and Fraunhofer updated ► Chap. 46, “Automotive Industry.” Typical applications for automobiles are shown. Additionally, suitable adhesive properties and surface treatments are discussed. ► Chapter 47, “Adhesive Bonding for Railway Application” is next treated by Suzuki. It is shown that adhesives are an indispensable joining technology for railway industries. Adhesives are used for the fabrication of almost all rail cars. For example, in the steel main structure of conventional rolling stock, adhesives are applied for bonding decorated aluminum sheets of wall and ceiling to frames, bonding of floor covering to the floor plate, and fixing heat insulating material to the inside of the carriages. ► Chapter 48, “Marine Industry” by Davies describes the use of adhesive bonding to assemble structures in the marine industry. The marine environment is extremely aggressive, and this has resulted in widespread use of fiber-reinforced composite materials. Adhesive bonding is a lightweight and corrosion-resistant means of joining these materials. Three industrial applications are used to illustrate the use of adhesive bonding, small pleasure boats, high-performance racing yachts, and bonded structures in the offshore industry. In the well-revised chapter ► “Civil Construction” (Chap. 49), Böhm et al. describe adhesive bonding applications in the civil construction sector, specific requirements, and adherends. The execution of bonding and properties of adhesive bonded civil constructions are also treated. Jung and Kim, in ► Chap. 50 “Electrical Industry,” explain the mechanisms underlying the electrical conduction in adhesive joints, and the thermal and mechanical parameters that should be measured are introduced. In terms of the evaluation of the reliability of adhesives in electronics, the basic test procedures, including several specific test methods and analysis techniques, are explained. ► Chapter 51, “Shoe Industry” by Martín-Martínez constitutes one of the very few reviews in the existing literature on shoe bonding and gives an updated overview of the upper to sole bonding by means of adhesives. The surface preparation of rubber soles and both the formulations of polyurethane and polychloroprene adhesives are described. The preparation of adhesive joints and adhesion tests are also revised. Another chapter was added to this section on ► “Oil Industry” (Chap. 52) by de Barros et al. due to the increase adhesives application that field,



especially for repairs. The main advantage by using adhesive bonding is to avoid the fire risk concerning the traditional weld process. Adhesives also feature protection against corrosion which is a main concern in offshore installations. This chapter shows that the use of composites has become a real alternative to structural repairs in situ as these materials become more and more reliable.

---

## 60.10 Emerging Areas

► [Chapter 53, “Molecular Dynamics Simulation and Molecular Orbital Method”](#) by Zhao et al., various simulation methods pertaining to adhesion technology are introduced, such as molecular dynamics, quantum mechanics, the molecular orbital method, and the density functional theory. Some examples are proposed investigating adhesion issues using various simulation methods. ► [Chapter 54, “Bioadhesives”](#) was rewritten by Richter. It gives an overview about natural adhesives and biological adhesives leading to bioinspired applications. Biological and microbiological adhesives have an enormous potential for industrial applications. The most prominent ones are constructional, packaging, and medical applications. Gorb, in ► [Chap. 55, “Biological Fibrillar Adhesives: Functional Principles and Biomimetic Applications,”](#) reviews functional principles of biological systems in various animal groups such as insects, spiders, and geckos with an emphasis on insects and discusses their biomimetic potential. Data on ultrastructure and mechanics of materials of adhesive pads, movements during contact formation and breakage, the role of the fluid in the contact between the pad and substrate are presented. ► [Chapter 56, “Adhesives with Nanoparticles”](#) are discussed by Taylor. This chapter outlines the principal types of nanoparticles and the methods that may be used to disperse the particles in a polymer matrix. It discusses how nanoparticles can alter the mechanical properties (stiffness and fracture), electrical properties (conductivity), and the functional properties (permeability, glass transition temperature) of thermoset polymers. In ► [Chap. 57, “Adhesive Dentistry,”](#) Nicholson describes the principal uses of adhesives in clinical dentistry, covering both the materials and the clinical techniques involved. The two types of tooth-colored material, namely, the composite resin and the glass-ionomer cement, are described, together with their current variations. Surface pretreatment is critical for the success of these systems, and the current state of the understanding of this aspect of the subject is described. ► [Chapter 58, “Adhesion in Medicine”](#) is covered by Chivers. Adhesives technology has two main applications in medicine as considered in this chapter, for internal fixation of tissues usually after surgery and for use on the skin, primarily to hold dressings in place. The last chapter by Sato concerns ► [“Recycling and Environmental Aspects”](#) (Chap. 59). Adhesively bonded adherends should be often separated before they can be recycled. For this purpose, dismantlable adhesives, which can be separated with stimulations (softening of adhesive, expansion force due to blowing agents or thermally expandable microcapsules, chemical degradation, and electrochemical reaction), have been developed recently. These adhesives can be applied to adherend recycling or product reworking.



## 60.11 Conclusions

The preparation of this second edition has been an interesting experience for the editors. The review process gave a deeper insight into the various aspects of adhesion from basics to applications. Authors come from every background (chemistry, physics, mechanics) and work in either academia or industry, proving that adhesion is a truly multidisciplinary and widely applied subject. The editors would like to thank the authors for their patience with the preparation of this handbook. Finally, the editors especially thank Dr. Christoph Baumann, Ms. Tina Shelton, and Ms. Monika Garg, Springer editors, who helped enormously toward the success of this handbook.